सत्यमेव जयते

INDIAN AGRICULTURAL
RESEARCH INSTITUTE, NEW DELHI

I.A.R I.6.
GIP NLK—H 3 I.A.R.I. —10-5-55—15,000

THE
REVIEW OF SCIENTIFIC
INSTRUMENTS

EDITOR
Gaylord P. Harnwell

ASSOCIATE EDITORS
D. W. Bronk
F. K. Harris
P. H. Miller, Jr.
W. A. Wildhack

EDITORIAL BOARD

Term ending December 31, 1950
W. Fowler
S. A. Korff
F. N. D. Kurie
C. D. Montgomery
L. S. Taylor
R. E. Zirkle

Term ending December 31, 1951
W. Bleakney
J. B. H. Kuper
T. Lauritsen
J. R. Pappenheimer
L. B. Snoddy
C. H. Townes

Term ending December 31, 1952
Kenneth S. Cole
Bernard T. Feld
W. K. H. Panofsky
R. S. Shankland
C. F. Squire
J. H. Williams

VOLUME 21, NEW SERIES
JANUARY-DECEMBER, 1950

A publication of the
AMERICAN INSTITUTE OF PHYSICS
57 East 55 Street, New York 22, New York

SUGGESTIONS FOR CONTRIBUTORS

Send **manuscripts** to Gaylord P. Harnwell, Randal Morgan Laboratory of Physics, University of Pennsylvania, Philadelphia, Pennsylvania. Textual material (abstract, body of the paper, tabular material, references, and figure captions) must be in English, typewritten (except mathematical expressions) double spaced with wide margins on a durable, white paper, preferably letter size. The original copy, not the carbon, should be submitted. For general style, spellings, abbreviations, and form, consult recent issues of this journal.

An **abstract** must accompany each article. It should be adequate as an index and as a summary.

All but the simplest **mathematical expressions** should be carefully printed in by hand. Be sure to distinguish between capital and small letters. Indicate clearly superscripts and subscripts by inverted carets and carets, respectively. Avoid complicated superscripts and subscripts. Avoid repetition of a complicated expression by representing it by a symbol. Identify in the margin Greek letters and unusual symbols. Use fractional exponents instead of root signs. Use the solidus (/) for fractions wherever its use will save vertical space.

References should appear as footnotes, numbered consecutively, and arranged thus:

[1] A. B. Smith, Phy. Rev. 41, 852 (1932).

[2] H. Lamb, *Hydrodynamics* (Cambridge University Press, Teddington, England), sixth edition, pp. 573, 645.

Tables may be typewritten on sheets separate from the running text. Each table must have a caption which will make the data in the table intelligible without reference to the text. Avoid complicated column headings.

Wherever possible **figures** should be planned for the width of a column (3 in.). A convenient reduction ratio is about 2:1 or 3:1. Lettering should be large enough on the original that when reduced it shall not be less than about $\frac{1}{16}$ in. (~1.5 mm.). Line drawings must be in *India ink* on white paper or tracing cloth. Coordinate paper is not desirable but if used must be blue lined and the coordinate lines which are to show must be inked over. Photographs should have maximum black and white contrast. Identify each original drawing or photograph on the back with the author's name and the figure number. Figures should be numbered consecutively. Captions should be typed on a separate sheet of paper.

A limited number of **alterations** in proof are unavoidable, but the cost of making extensive alterations after the article has been set in type will be charged to the author.

Proof and all correspondence concerning papers in the process of publication should be addressed to the Publication Manager, American Institute of Physics, 57 East 55 Street, New York 22, New York.

INFORMATION FOR SUBSCRIBERS

THE REVIEW OF SCIENTIFIC INSTRUMENTS is a monthly journal published by the American Institute of Physics and devoted to scientific instruments, apparatus, and techniques. Its contents include original and review articles on instruments in physics and allied sciences and sections on laboratory practices, book reviews, new instruments, new materials, news, and current literature of physics. One volume is published annually.

Subscriptions and orders for back numbers should be addressed to the American Institute of Physics, 57 East 55 Street, New York 22, New York.

Subscription Price

	U. S. and Canada	Elsewhe
To members and associate members of the American Institute of Physics	$5.00	$6.00
To all others	7.00	8.00

Back Number Prices

Yearly rate when complete year is available	$10.00
Single copies	$ 1.00

Advertising rates will be supplied on request.

American Institute of Physics

57 East 55 Street **New York 22, New York**

CONTENTS

JANUARY, 1950

New Method for Surface-Temperature Measurement . . . Nobuji Sasaki 1
Improved Schlieren Apparatus Employing Multiple Slit-Gratings . . . Tage A. Mortensen 3
Design Study for a Three-Bev Proton Accelerator . . . M. S. Livingston, J. P. Blewett, G. K. Green, and L. J. Haworth 7
Simple Pressure Balance . . . C. A. Swenson 22
Versatile Pneumatic Instrument Based on Critical Flow . . . W. A. Wildhack 25
Design and Use of Piezoelectric Gauges for Measurement of Large Transient Pressures . . . A. B. Arons and R. H. Cole 31
Background Eradication in Thick-Layered Nuclear Emulsions . . . Martin Wiener and Herman Yagoda 39
Choice of Suitable Gap Forms for the Study of Corona Breakdown and the Field Along the Axis of a Hemispherically Capped Cylindrical Point-to-Plane Gap . . . Leonard B. Loeb, James H. Parker, E. E. Dodd, and William N. English 42
Coincidence Experiments for Noise Reduction in Scintillation Counting . . . Hartmut Kallmann and Carl A. Accardo 48
Note on the Detection of Coincidences and Short Time Intervals . . . Robert Hofstadter and John A. McIntyre 52
Large Dempster-Type Double-Focusing Mass Spectrograph . . . Henry E. Duckworth 54
Diaphragm Cell for Thermal Diffusion Measurements . . . E. S. Huse, D. J. Trevoy, and H. G. Drickamer 60
Investigation of the Possible Use of the Glow Discharge as a Means for Measuring Air Flow Characteristics . . . F. D. Werner 61
Small Milligaussmeter . . . G. D. Adams, R. W. Dressel, and F. E. Towsley 69
High Speed Synchroscope . . . C. G. Kelley 71
Design and Construction of Universal Function Generating Potentiometers . . . Granino A. Korn 77

PHYSICAL INSTRUMENTS FOR THE BIOLOGIST

Small Probing Geiger-Müller Counters . . . C. V. Robinson 82
Book Reviews . . . 85
  Author Index to Books Reviewed . . . 93
  Other Books Received . . . 93

Laboratory and Shop Notes:

  Units of Radioactivity . L. F. Curtiss, R. D. Evans, Warren Johnson, and Glenn T. Seaborg 94
  Temperature-Controlled Resistance Furnace for High Temperature Measurements . . . W. G. Schneider and N. R. S. Hollies 94
  Behavior of Rectangular and Square Section Transparent Beta-Counters . . . L. M. Silver and J. B. Warren 95
  New Type Mass Spectrometer . . . Larkin Kerwin 96
  Improved Method of Directing Liquid Flow in a Closed System . L. G. Stang, Jr., and G. J. Selvin 97
  Measurement and Amplification of Minute Displacements by Frequency Modulation . . . P. A. Bricout and M. Boisvert 98
  Scintillation-Type Ion Detector . . . Paul I. Richards and E. E. Hays 99
  Method of Supplying Low Pressure Gases on a Vacuum System . . . Raymond H. McFee 100
  Convenient Gas Sample Tube Holder and Break-off Applicable to Mass Spectrometers . . . Frederick Highhouse and Julius White 101
  Simple Contamination-Free Electron Gun . . . H. E. Farnsworth 102
  Bent Crystal X-Ray Monochromators . . . B. E. Warren 102
  Motor for Use in Vacuum Systems . . . C. P. Butler and F. E. Carpenter 103
New Instruments . . . 103
New Materials . . . 107
Index to Advertisers . . . xxxiv

FEBRUARY, 1950

Precision Faraday Effect Apparatus . . . Samuel Steingiser, George J. Rosenblit, Robert Custer, and Chas. E. Waring 109
Velocity-Acceleration Response from a Seismic Pick-Up via Controlled Damping . . . Robert J. Jeffries 115
Variation of Grain Density with Temperature of Exposure in Nuclear Emulsions . . . Elsie M. Dollmann 118
Design and Construction of a Stark-Modulation Microwave Spectrograph . . . A. Harry Sharbaugh 120
Vortex Thermometer for Measuring True Air Temperatures and True Air Speeds in Flight . . . Bernard Vonnegut 136
Wire Recorded Magnetic Pulse Timing Circuit . . . C. R. Emigh 142
Wide-Band Audio Phasemeter . . . John R. Ragazzini and Lotfi A. Zadeh 145

CONTENTS

Positive Displacement Pump for Corrosive Fluids . . . E. E. GLENN, JR., AND NORMAN HACKERMAN 148
Frequency Modulation Pressure Recording System . . . J. H. HETT AND R. W. KING, JR. 150
Analog Computers for Servo Problems . . . DONALD MCDONALD 154
Gas Phase Counting of Low Energy Beta-Emitters . . . W. BERNSTEIN AND R. BALLENTINE 158
Measurement of Fast Neutron Energies by Observation of Li$^6(n, \alpha)$H^3 in Photographic Emulsions . . . GEORGE R. KEEPIN, JR., AND JAMES H. ROBERTS 163
Automatically Synchronized Electronic Switch . . . W. A. BUDLONG AND BRUCE C. LUTZ 167
Recording Microwave Refractometer . . . GEORGE BIRNBAUM 169
Integrator for Small Beam Currents . . . T. A. HALL, S. D. WARSHAW, AND J. DORSEY 177
Electronic Circuit Which Extracts Antilogarithms Directly . . . F. CURTIS SNOWDEN AND HAROLD T. PAGE 179
Magnetic Suspension for Small Rotors . . . J. W. BEAMS 182

PHYSICAL INSTRUMENTS FOR THE BIOLOGIST

On Adapting a Powder X-Ray Diffraction Camera for Reflection Patterns . JONATHAN PARSONS 185

Laboratory and Shop Notes:

- **Experimental KVAH-Meter** . . . G. M. PETROPOULOS 187
- **Simple Low Power Electronic Relay** . . . WILLIAM P. RATCHFORD AND M. L. FEIN 188
- **Point-Focus X-Ray Monochromators for Low Angle Diffraction** . . . JESSE W. M. DUMOND 188
- **Ultrasonic Tissue Disintegrator** . . . F. F. BIRD AND K. S. LION 189
- **Reprojection Method for Studying Cloud-Chamber Photographs** . . . D. A. BROMLEY AND R. D. BRADFIELD 190
- **Nomogram for G-M Counter Resolving-Time Corrections** . . . HOWARD L. ANDREWS 191

New Instruments . . . 192
New Materials . . . 198
Index to Advertisers . . . xxxviii

MARCH, 1950

High Resolution Recording with Soot . . . K. R. ELDREDGE 199
Ratio-Recording Double Beam Infra-Red Spectrophotometer Using Phase Discrimination and a Single Detector . . . ABRAHAM SAVITZKY AND RALPH S. HALFORD 203
Focusing Properties of a Generalized Magnetic Spectrometer . . . DAVID L. JUDD 213
Scintillation Counter as a Low Resolution Gamma-Ray Spectrometer . . . ROBERT W. PRINGLE, KENNETH I. ROULSTON, AND HARRY W. TAYLOR 216
Radiofrequency Spectrograph and Simple Magnetic-Field Meter . . . R. V. POUND AND W. D. KNIGHT 219
On the Use of Photographic Plate Detectors in Neutron Experiments . . . J. C. ALLRED, A. N. PHILLIPS, L. ROSEN, AND F. K. TALLMADGE 225
Analog Computer . . . J. G. BAYLY 228
Photographic Methods of Measuring Slow Neutron Intensities . . . M. BLAU, I. W. RUDERMAN, AND J. CZECHOWSKI 232
Microcalorimeter Suitable for Study of Easily Absorbed Nuclear Radiations . . . C. V. CANNON AND G. H. JENKS 236
Study of Plateau Slopes in Self-Quenching Geiger-Müller Counters . . . SANBORN C. BROWN AND CLAUDINE MARONI 241
Time Lags in Geiger Counters . . . ARTHUR R. LAUFER 244
Electric Field in a Geiger Counter . . . ARTHUR R. LAUFER 252
Laboratory Modifications in the RCA Model EMC Electron Microscope . . . S. G. ELLIS 255

Laboratory and Shop Notes:

- **Degassing Extended Glass Systems** . . . ALBERT B. STEWART 258
- **Liquid Air Level Control** . . . MARK S. FRED AND EVERETT G. RAUH 258
- **Series Parallel Linear Thermopile with Interchangeable Receiving Units** . . . ROBERT A. CRANE AND FRANCIS E. BLACET 259
- **Low Temperature Gasket** . . . A. WEXLER, W. S. CORAK, AND G. T. CUNNINGHAM 259
- **Simple Method to Seal Liquids of High Vapor Pressure into Glass or Quartz Capillaries** . . . Z. V. HARVALIK 260
- **Simple Recording Manometer** . . . FRASER P. PRICE AND PAUL D. ZEMANY 261
- **High Pressure Fitting for Scintillation Counting** . . . K. D. TIMMERHAUS, E. B. GILLER, L. H. TUNG, R. B. DUFFIELD, AND H. G. DRICKAMER 261
- **Automatic Equipment for Electrolyzing Heavy Water** . . . RALPH W. WANIEK 262
- **Optical Centering System for X-Ray Diffraction Samples** . . . EUGENE L. PERRINE 262
- **Electronic Water-Level Control** . . . R. D. MILLER AND J. S. HOPKINS 263
- **Manometer Leveling Procedure** . . . JOHN E. WERTZ 263

Errata:

- **A High Speed Synchroscope** . . . G. G. KELLEY 264
- **Note on Sealing Nylon Films to Geiger Counters** . . . ROBERT A. BECKER 270
- **Formation of Insulating Layers by the Thermal Decomposition of Ethyl Silicate** . HAROLD B. LAW 270

New Instruments . . . 264
New Materials . . . 269
Index to Advertisers . . . xl

April, 1950

Direct Reading Phasemeter . . . L. H. O'Neill and J. L. West 271

An Electron Tube Potentiometer Method for Use in Circuits Involving Very High Resistance . . . H. Bloom and G. W. Butler 274

Method for Increasing the Safe Power Input of X-Ray Tubes . . . Arthur I. Berman 275

RaDEF Standard Sources for Beta-Disintegration Rate Determinations . . . Theodore B. Novey 280

Construction and Performance of a Multiple Gamma-Ray Counter of High Efficiency . . . Tibor Gráf 285

Calcium and Cadmium Tungstate as Scintillation Counter Crystals for Gamma-Ray Detection . . . R. H. Gillette 294

Low Frequency Sinusoidal Voltage Source . . . Louis A. Rosenthal 302

Photo-Multiplier Gamma-Ray Detector . . . J. D. Graves and G. E. Koch 304

Dust Electricity Analyzer . . . W. B. Kunkel and J. W. Hansen 308

Spectral Sensitivity of Two Commercial X-Ray Films between 0.2 and 2.5 Angstroms . . . Herman E. Seemann 314

Decade Pulse Counter for Geiger-Müller Tubes . . . Björn Aström 323

Null-Coil Pendulum Magnetometer . . . C. A. Domenicali 327

Electron Component in Geiger Discharge . G. G. Kelley, W. H. Jordan, and P. R. Bell 330

Design of Logarithmic Voltage Dividers . . . F. V. Hunt and O. D. Sledge 332

Erratum: A Slide Rule for Radiation Calculations . . . M. W. Makowski 336

Pentode Counting or Control Ring . . . Benjamin L. Moore 337

Low Temperature X-Ray Diffraction Apparatus . . . Donald F. Clifton 339

Pulse Type Regulated High Voltage Supply for G-M Tubes . . . Richard J. Watts 342

Thermistors. Part I. Static Characteristics . . . Otto J. M. Smith 344

Thermistors. Part II. Dynamic Characteristics . . . Otto J. M. Smith 351

Monitor for Low Intensity Gamma-Rays . . . J. B. H. Kuper and R. L. Chase 356

PHYSICAL INSTRUMENTS FOR THE BIOLOGIST

Stainless Steel Micro-Needle Electrodes Made by Electrolytic Pointing . . . Harry Grundfest, Robert W. Sengstaken, Walter H. Oettinger, and R. W. Gurry 360

Automatic Isodose Recorder with Scintillation Counter as Gamma-Ray Detector . . . G. J. Hine, M. Berman, and M. M. Elkind 362

D.C. Amplifier for Biological Application . . . P. O. Bishop and E. J. Harris 366

Volumetric Plastic Micro Respirometer . . . P. F. Scholander 378

Book Reviews . . . 381

- **Author Index to Books Reviewed** . . . 392
- **Other Books Received** . . . 392

Laboratory and Shop Notes:

- **Tungsten Helical Spring Balance** . . . Samuel L. Madorsky 393
- **New Porcelain Rod Leak** . . . H. D. Hagstrum and H. W. Weinhart 394
- **Data on Porcelain Rod Leak** . . . J. P. Molnar and C. D. Hartman 394
- **Rubber Tubing Pump** . . . John W. Weigl and Donald W. Stallings 395
- **Scintillation Counter for Neutrons** . . . Kuan-Han Sun and W. E. Shoupp 395
- **Device for Measuring the High Voltage for a Photo-Multiplier Tube** . . . Ingvar Nilsson 396
- **Further Techniques in Single-Crystal X-Ray Diffraction Studies at Low Temperatures** . . . S. C. Abrahams, R. L. Collin, W. N. Lipscomb, and T. B. Reed 396
- **An Instrument for Mechanically Differentiating Curves** . . . Arnold H. Scott 397
- **High Power Pulsed Magnetron with Replaceable Cathode** . M. F. Amsterdam and W. E. Danforth 398
- **Method of Making Glass-Metal Seals** . . . N. A. Eckstein, J. W. Fitzgerald, and C. A. Boyd 398
- **Improved Double-Crystal Spectrometer for Small Angle Scattering Measurements** . Leo Broussard 399
- **Apparatus and Method for Testing Radium or Thorium Capsule Seals** . . . R. J. Beale 400
- **Automatic Level Controller for Liquid Nitrogen** . . . E. H. Quinnel and A. H. Futch 400

New Instruments . . . 401

New Materials . . . 405

Index to Advertisers . . . xl

May, 1950

Some Properties of the Parallel Plate Spark Counter II . Leon Madansky and R. W. Pidd 407

Differential Analyzer for the Schrödinger Equation . . . R. L. Garwin 411

Design and Operation of Liquid Nitrogen-Cooled Solenoid Magnets . . . James J. Fritz and Herrick L. Johnston 416

Trigonometric Computer with Electrocardiographic Applications . . . Richard McFee 420

Vibration Studies: Related to Electron Microscopy . . . F. A. Hamm and F. C. Snowden 426

Rotating Specimen Mount for Use with X-Ray Spectrometer in Measuring Crystallite Orientation of Cellulosic and Other Textile Fibers . . . Leon Segal, Joseph J. Creely, and Carl M. Conrad 431

Synchrotron Radiofrequency System . . . Mitchell H. Dazey, Jack V. Franck, A. C. Helmholz, Craig S. Nunan, and Jack M. Peterson 436

X-Ray Determination of Slip Planes and Slip Directions . . . R. W. Turner, T. L. Wu, and R. Smoluchowski 440

Electron Pair Spectrometer of Lens Type for Hard Gamma-Radiation . . . Kai Siegbahn and Stig Johansson 442
Focusing Device for the External 350-Mev Proton Beam of the 184-Inch Cyclotron at Berkeley . . . W. K. H. Panofsky and W. R. Baker 445
Relation between Apparent Shapes of Monoenergetic Conversion Lines and Continuous Beta-Spectra in a Magnetic Spectrometer. II . George E. Owen and Henry Primakoff 447
Theory of the Capture Process in a Betatron-Injected Synchrotron . . . David C. de Packh and Milton Birnbaum 451
Apparatus for Recording Fluctuations in the Refractive Index of the Atmosphere at 3.2 Centimeters Wave-Length . . . C. M. Crain 456
Combination Two-Circle Goniometer and X-Ray Spectrometer . . . Morton L. Baron and A. deBretteville, Jr. 458
80-Mev Model of a 300-Mev Betatron . . . D. W. Kerst, G. D. Adams, H. W. Koch, and C. S. Robinson 462
New Mechanical Autocorrelator . . . H. R. Seiwell 481

PHYSICAL INSTRUMENTS FOR THE BIOLOGIST

Design of a Simple Microflowmeter for Biological Perfusion Experiments . . . Alan C. Burton and James T. Nichol 485

Laboratory and Shop Notes:

Best Arrangement of Resistors in a Series Group . . . Herbert B. Brooks 491
Test of Rupture Strength of Thin Plastic Films . . . Joses J. L. Chen 491
New Method for the Measurement of Inhomogeneous Magnetic Fields . . Peter M. Weinzierl 492
High Megohm Bridge . . . F. M. Glass and R. K. Abele 493
High Speed Electronic Scaler . . . W. M. Sessler and A. V. Masket 494
New Pirani-Type Vacuum Gauge . . . E. Blasco and L. Miranda 494
Detaching Device for Balloon Flights . . . Louis G. Collyer 496
Suppressing Mercury Vapor in Vacuum Systems . . . Frederick Ayer II 496
Metal Dewar for Liquid Helium . . . Warren E. Henry and Richard L. Dolecek 496
Power Supply for the Cenco Concentrated-Arc Lamp . . . James M. Mitchell 497
Precision Selector for Voltage-Regulator Tubes . . . O. B. Rudolph 497
Use of Secondary Electrostatic Focusing in a Magnetic Beta-Ray Spectrograph . . . R. D. Hill, J. W. Mihelich, and M. T. Pigott 498
Convenient Cell-Stage for Fluid Profile Measurements . . . William Fox 499
Method of Preserving Specimen Grids for Electron Microscopy . . . Jennie E. Shapiro 500
New Instruments . . . 501
New Materials . . . 505
Index to Advertisers . . . xliv

June, 1950

Vacuum Furnace for Use in the Temperature Range 1000–2000°C . . . J. W. Tomlinson and J. O'M. Bockris 507
High Intensity Ultraviolet Continuum Source for Use in Spectrophotometry . . . Nisson Ascher Finkelstein 509
Rotary McLeod Gauge . . . M. Axelbank 511
Multiple Kerr-Cell Camera . . . A. M. Zarem and F. R. Marshall 514
Method of Neasuring Spurious Counts in Geiger-Müller Counters . . . D. Willard and C. G. Montgomery 520
Measurement of the Magnetic Field in a Nuclear Spectrometer . . . L. M. Langer and F. R. Scott 522
Tests of Flowing Junction Diffusion Cells with Interference Methods . . L. G. Longsworth 524
Balloon-Borne Instrumentation for Neutron Detection . . . Melvin Pavalow, William O. Davis, and William P. Staker 529
Announcement . . . 533
Nuclear Emulsions and the Measurement of Low Energy Neutron Spectra . . . Norris Nereson and Frederick Reines 534
High Resolution Beta-Ray Spectrometer . . . Joseph A. Bruner and F. R. Scott 545
Velocity of Propagation of the Discharge in Geiger-Müller Counters . . . H. Saltzmann and C. G. Montgomery 548
End and Wall Corrections for Absolute Beta-Counting in Gas Counters . . . A. G. Engelkemeir and W. F. Libby 550
Scintillation Type Alpha-Particle Detector . A. S. Goldin, E. R. Rohrer, and R. L. Macklin 554
Theory and Properties of Low Voltage Radiation Counters . . . J. A. Simpson, Jr. 558

Laboratory and Shop Notes:

Useful Fast Coincidence Circuit . . . R. L. Garwin 569
Effective Vacuum Cut-off . . . G. W. Sears and E. R. Hopke 570
Remote-Control Method of Opening Ampoules of Active Materials . . . Jesse E. Sherwood 570
Regulated Low Voltage Power Supply . . . A. K. Solomon 570
Extension of the Low Pressure Range of the Ionization Gauge . . . Robert T. Bayard and Daniel Alpert 571
Circumferential Recording Microphotometer . . . T. C. O'Connell and A. G. Barkow 573
Water-Proofing Rocksalt for Infra-Red Absorption Cells . . . Scott Anderson, William J. Anderson, and Martin Krakowski 574

Improved Electrode Cutter for Spectrographic Laboratories . . . Esther W. Claffy and Joseph G. Schumacher 575

Pulsed Air Core Series Disk Generator for Production of High Magnetic Fields . . . Robert I. Strough and Erwin F. Shrader 575

New Instruments . . . 576

New Materials . . . 581

Index to Advertisers . . . xxxvi

July, 1950

Transfer Device for Low Boiling Liquids . . . Aaron Wexler and William S. Corak 583

Sector-Type Double-Focusing Magnetic Spectrometer . . . Earl S. Rosenblum 586

Linear Preamplifier for Driving a Long Coaxial Cable . . . Lloyd G. Lewis, James G. Robinson, and John Toll 593

New Vacuum Gauge . . . R. Havens, R. Koll, and H. LaGow 596

4π-Radiometer . . . T. Benzinger and C. Kitzinger 599

Recording Torque Magnetometer . . . D. S. Miller 605

Molecular Diffraction Attachment for RCA Microscope . . . B. O. Heston and P. R. Cutter 608

Apparatus for Rapid Measurement of Internal Friction . . . Herbert I. Fusfeld 612

Observations on Some Properties of Ultra-High Frequency Gas Discharges . . . Charles F. Robinson 617

Microwave Power Stabilizer . . . Ivan K. Munson 622

Recording Fluxmeter of High Accuracy and Sensitivity . . . P. P. Cioffi 624

Simple Variable Space Infra-Red Absorption Cell . . . John U. White 629

Duration of Scintillations from Organic Phosphors . . . J. O. Elliot, S. H. Liebson, R. D. Myers, and C. F. Ravilious 631

Instrument for Directional Studies of Cosmic-Ray Intensity . . . H. W. Boehmer and J. E. Coolidge 633

Measurement of Secondary Electron Emission from Dielectric Surfaces . Howard L. Heydt 639

High Speed Expansion Valve for Cloud-Chamber Control . R. P. Shutt and W. L. Whittemore 643

Single Element Verniers Reading Two or Three Dimensions . . . Robert E. Lewis 647

Coincidence Circuit for a Scintillation Detector of Radiation . . . W. C. Elmore 649

100,000,000-Frame-per-Second Camera . . . M. Sultanoff 653

Book Reviews . . . 657

  Author Index to Books Reviewed . . . 667

  Other Books Received . . . 668

Laboratory and Shop Notes:

  Energy Dependence of the Naphthalene Scintillation Detector . . . Jack C. Smeltzer 669

  Modification of Electron Microscope for Electron Optical Shadow Method . . . J. Arol Simpson and Alan Van Bronkhorst 669

  Microtome Knife Sharpness . . . Oscar W. Richards 670

  Glass Variable Microleaks for Gases . . . John J. Hopfield 671

  Ultra-High Vacuum Ionization Manometer . . . J. J. Lander 672

  All-Metal Ionization Gauge . . . F. M. Kelly 673

  Convenient Leak for Testing Helium Leak Detectors . . . G. H. Jenks 674

  Preparation of Unbacked Metallic Films . . . F. E. Carpenter and J. A. Curcio 675

  Comments on "Velocity-Acceleration Response from a Seismic Pick-Up via Controlled Damping" . . . A. J. Hermont 675

New Instruments . . . 675

New Materials . . . 679

Index to Advertisers . . . xxx

August, 1950

Measurement of Rates of Flow of Gases by Wet Test Meters . . . Robert L. Burwell, Jr., Max Metlay, and Frank W. Pfohl 681

Solution of Simultaneous Equations through Use of the A.C. Network Calculator . L. M. Haupt 683

Arithmetic Operations in a Binary Computer . . . Robert F. Shaw 687

Recording Polarimeter . . . Gabor B. Levy, Philip Schwed, and David Fergus 693

High Pressure Ionization Chamber Counters and Their Use . . . R. Wilson, L. Beghian, C. H. Collie, H. Halban, and G. R. Bishop 699

Chalk River Single Crystal Neutron Spectrometer . . . D. G. Hurst, A. J. Pressesky, and P. R. Tunnicliffe 705

Ring Focus in a Thin Magnetic-Lens Beta-Ray Spectrometer . . . Joseph M. Keller, Ernest Koenigsberg, and Arthur Paskin 713

Lens Tester for Photographic Lenses . . . F. G. Back 722

Improvements in Mass Spectrometers for the Measurement of Small Differences in Isotope Abundance Ratios . . . C. R. McKinney, J. M. McCrea, S. Epstein, H. A. Allen, and H. C. Urey 724

Vacuum Tests of Rubber, Lead, and Teflon Gaskets and Vinyl Acetate Joints . . . Robert W. Cloud and Sanborn F. Philp 731

Boron Trifluoride Proportional Counters . . . . I. L. Fowler and P. R. Tunnicliffe 734
Design of a Magnetic Focusing Coincidence Spectrometer . . . . C. M. Fowler and R. G. Shreffler 740
High-Low Temperature Microscope Stage . . . . R. E. Cech 747
Random Coincidence Rates with Unsteady Sources . . . . R. M. Littauer 750
Absolute Determination of the Emission Rate of Beta-Rays . . . . R. K. Clark 753
Electronic Pile Simulator . . . . P. R. Bell and H. A. Straus 760

PHYSICAL INSTRUMENTS FOR THE BIOLOGIST

Infra-Red Microspectrometer for Biological Research . . . . Darwin L. Wood 764
Modification of the Apparatus Used for the Baldes Thermoelectric Method of Measuring Osmotic Pressure . . . . V. Everett Kinsey 767

Laboratory and Shop Notes:

Temperature Coefficient of Resistance of Tin Oxide-Coated Electrically Conducting Glass between 1° and 300°K . . . . D. N. Lyon and T. H. Geballe 769
Improving Differential Amplifier Rejection Ratios . . . . Richard McFee 770
Voltage Stabilizer for 200-Kv Acceleration . . . . J. T. Dewan 771
Mass Indicator . . . . V. J. Caldecourt 772
Packless Valve Flow Regulator . . . . Walter Rose 772
New Instruments 773
New Materials 777
Index to Advertisers xxx

September, 1950

Machine for Synthesizing Two-Dimensional Fourier Series in the Determination of Crystal Structures . . . . H. Shimizu, P. J. Elsey, and D. McLachlan, Jr. 779
Scintillation Efficiency of Anthracene for Low Energy Electrons . . . . W. J. Ramler and M. S. Freedman 784
Fabrication of a High Power Resonant Wave-Guide Window . E. V. Edwards and K. Garoff 787
Erratum: Regulated Low Voltage Power Supply . . . . A. K. Solomon 789
Improved Resolving Time Measuring Device . . . . B. W. Roberts, Jr., K. E. Perry, and R. G. Fluharty 790
500-Kilovolt Linear Accelerator Using Selenium Rectifiers . . . . Wayne R. Arnold 796
Electronic A.C. Differential Voltmeter . . . . L. A. Rosenthal and H. S. Zablocki 799
Microtome Specimen Holder Advanced by Thermal Expansion . . . . M. Eden, A. W. Pratt, and H. Kahler 802

PHYSICAL INSTRUMENTS FOR THE BIOLOGIST

Differential Vectorcardiograph . . . . Stanley A. Briller, Nathan Marchand, and Charles E. Kossmann 805

Laboratory and Shop Notes:

Expansion Valve for Triggered Cloud Chambers . . . . Jacob L. Zar 812
Waterproof Cable Connectors . . . . K. Feldman 812
Motion within a Vacuum System . . . . Fred A. McNally 813
Self-Triggering Cloud-Chamber Counter . . . . E. L. Fireman and G. M. McHaney 813
Diamond Bomb for Obtaining Powder Pictures at High Pressures . . . . A. W. Lawson and Ting-Yuan Tang 815
Resistance-Temperature Relation for Low Temperature Thermometry . . . . . Harold J. Hoge 815
Note on Reduction of Background Fog in Nuclear Emulsion Plates . . . . P. K. S. Wang 816
New Instruments 817
New Materials 821
Index to Advertisers xliv

October, 1950

Chart Recording of Microsecond Pulse Amplitudes . . . . J. T. Dewan and K. W. Allen 823
Technical Apparatus for Determining Thermal Conductivity of Steels up to 500°C . . . . Z. Horák and F. Krupka 827
Polarimeter for the Study of Low Frequency Radio Echoes . . . . A. H. Benner and H. J. Nearhoof 830
Design of Neutron Counters Using Multiple Detecting Layers . . . . R. D. Lowde 835
System for the Collection and Purification of Radon by Remote Control . . . . Chester H. Shiflett, Mark E. Steidlitz, and Wallace Davis, Jr. 842
Precision Thermostat for High Temperatures . . . . William R. Eubank 845
Magnetic Analyzer for Charged-Particles from Nuclear Reactions . . . . C. W. Snyder, S. Rubin, W. A. Fowler, and C. C. Lauritsen 852

PHYSICAL INSTRUMENTS FOR THE BIOLOGIST

Vibrating Probe Electrometer for the Measurement of Bioelectric Potentials . . . . O. Blüh and B. I. H. Scott 867

Book Reviews 869

- **Author Index to Books Reviewed** 880
- **Other Books Received** 880

Laboratory and Shop Notes:

- **Stark Effect Absorption Cells for Microwave Spectroscopy** . . . . D. H. Baird, R. M. Fristrom, and M. H. Sirvetz 881
- **Apparatus for Cutting Metals Strain-Free** . . . . Robert Maddin and W. R. Asher 881
- **High Speed Short Resolving Time Coincidence Circuit for Use with Scintillation Counters** . . . . E. F. Shrader 883
- **Ultraviolet Photon Counting with an Electron Multiplier** . . . . A. H. Morrish, G. W. Williams, and E. K. Darby 884
- **Preparation of Carbon Targets** . . . . G. C. Phillips and J. E. Richardson 885
- **Scintillation Counter for Fast Neutrons** . . . . H. B. Frey 886
- **Making Small Metal Tubes by Electrodisposition on Nylon Fibers** . . . . Rolf J. E. Gezelius 886
- **Volumetric Displacement Flask** . . . . S. D. Snyder, C. J. Craven, and D. B. Trauger 887

New Instruments 887

New Materials 891

Index to Advertisers xlii

NOVEMBER, 1950

Magnetic Tape Recorder for Very Low Frequency Phenomena . . . . Paul E. Green, Jr. 893

Apparatus for the Study of Electrets . . . . Larry A. Freedman and Louis A. Rosenthal 896

Transmission of Beta-Rays by Nylon and Formvar . . . . R. B. Heller, E. F. Sturcken, and A. H. Weber 898

Pulse Generator for the Millimicrosecond Range . . . . R. L. Garwin 903

Erratum: D.C. Amplifier for Biological Application . . . . . P. O. Bishop and E. J. Harris 904

Method for Measuring the Thermal Conductivity of Small Samples of Poorly Conducting Materials such as Optical Crystals . . . . Stanley S. Ballard, Kathryn A. McCarthy, and William C. Davis 905

Synchrotron-Oscillation Resonance . . . . Nelson M. Blachman 908

Electrostatic Beta-Spectrograph . . . . Donald R. Hamilton and Leonard Gross 912

Note on the Geometry of Geiger Counter Telescopes . . . . Homer E. Newell, Jr. and Eleanor C. Pressly 918

Erratum: The Scintillation Efficiency of Anthracene for Low Energy Electrons . . . . W. J. Ramler and M. S. Freedman 922

PHYSICAL INSTRUMENTS FOR THE BIOLOGIST

Continuous Flow Respirometer Utilizing the Oxygen Cathode . . . . Francis D. Carlson, F. Brink, Jr., and D. W. Bronk 923

Laboratory and Shop Notes:

- **Improvements in the Li^6 Technique** . . . . George R. Keepin, Jr. 933
- **Slide Rule for Nuclear Emulsion Calculations** . . . . Arthur Beiser 933
- **Geiger Counter Mounting for Continuous Counting of Gas-Phase Radioactivity** . . . . Francis Bonner and Alfred Weinstein 934
- **Reliable Pirani Vacuum Safety Circuit** . . . . W. Franzen and H. Horton 935
- **Ejection of the Electron Beam from a Betatron** . . . S. L. Fawcett and E. C. Crittenden, Jr. 935
- **Design and Performance of a Joule-Kelvin Helium Liquefier** . . . . J. G. Dash, D. B. Cook, M. W. Zemansky, and H. A. Boorse 936
- **Simple Automatic Recording Microphotometer** . . . . R. M. Fisher and D. S. Miller 938
- **Simultaneous Photography of Self-Luminous and Non-Self-Luminous Effects** . John S. Rinehart 939
- **Two Beta-Gamma-Counters for Gas Samples** . . . . Rodman Jenkins 940
- **Ultrasonic Projector Design for a Wide Range of Research Applications** . . . . E. J. Fry 940
- **Float for Liquid Helium** . . . . Julius Babiskin 941

New Instruments 941

New Materials 943

Index to Advertisers xliv

DECEMBER, 1950

Beta-Ray Spectroscopes . . . . E. Persico and C. Geoffrion 945

Orbit-Bender to Assist Injection into Betatrons . . . . Leverett Davis, Jr. 971

Improved Electrical Network for Determining the Eigenvalues and Eigenvectors of a Real Symmetric Matrix . . . . Abraham Many 972

Distributed Coincidence Circuit . . . . Clyde Wiegand 975

Continuously Sensitive Cloud Chamber . . . . T. S. Needels and C. E. Nielsen 976

Semi-Automatic Device for Analyzing Events in Nuclear Emulsions . . . . Marietta Blau, Robert Rudin, and Seymour Lindenbaum 978

Double Thin Lens Beta-Spectrometer . . . . C. M. Van Atta, Sydney D. Warshaw, Joses J. L. Chen, and Samuel I. Taimuty 985

Continuously Sensitive Diffusion Cloud Chambers . . . . E. W. Cowan 991
Rapid Method for Calculating and Using Platinum Thermohm Tables . . R. A. Buerschaper 996
Electronic Recording Analytical Balance . . . . Idas W. Lohmann 999
Capacitance Bridge for High Frequencies . . . . J. S. Mendousse, P. D. Goodman, and W. G. Cady 1002
Transmission Line Reflection Doubling Amplifier . . . . John Marshall 1010
Frequency Meter for Microwave Spectroscopy . . . . John D. Rogers, Henry L. Cox, and Paul G. Braunschweiger 1014
Apparatus for Concentration of He^3 by Thermal Diffusion . . . . O. F. Schuette, Jr., A. Zucker, and W. W. Watson 1016
Gas Flow through the Mass Spectrometer Viscous Leak . . . . R. E. Halsted and Alfred O. Nier 1019
Erratum. Tektronix Advertisement 1021

PHYSICAL INSTRUMENTS FOR THE BIOLOGIST

Detection of Tritiated Compounds in Paper Chromatography . . . . Irving Gray, Saburo Ikeda, Andrew A. Benson, and David Kritchevsky 1022

Laboratory and Shop Notes:

Simplified Percent Transmission Computer . . . . . . A. L. McClellan and G. C. Pimentel 1023
Note on Crystals Suitable for Double Crystal X-Ray Spectroscopy in the Region 3 to 15A . . . . S. T. Stephenson and D. L. Martin 1023
Greaseless Gas Flow Valve . . . . R. E. Honig 1024
Zero Inefficiency Anticoincidence Circuit . . . . M. Degallier 1025
Varying Nuclear Emulsion Sensitivity with Altitude . . . . Arthur Beiser 1025
Cathode-Follower Fallacies . . . . Paul I. Richards 1026
Electron Optical Disk . . . . L. Marton and J. Arol Simpson 1027
New Method for the Measurement of Hall Coefficients . . . . B. R. Russell and C. Wahlig 1028
Electrical Resistance of Platinum at High Temperatures . . . . H. E. Bennett 1029

New Instruments 1029
New Materials 1032
Author Index to Volume 21 1034
Analytic Subject Index to Volume 21 1040
Volume Table of Contents III
Index to Advertisers xlii

THE
REVIEW OF SCIENTIFIC
INSTRUMENTS

VOLUME 21, NUMBER 1 *JANUARY, 1950*

A New Method for Surface-Temperature Measurement

Nobuji Sasaki
Chemistry Institute, Department of Science, Kyoto University, Japan
(Received April 29, 1948)

The surface temperature of a body is equal to the temperature of the measuring junction of a thermocouple, if this temperature has been, by heating or by cooling, so adjusted that the meter in the couple circuit does not deflect when the measuring junction makes a brief contact with the surface being measured. The validity of this principle was confirmed experimentally by measuring a surface whose *true* surface temperature was known independently. The new method does not sensibly affect the surface conditions as long as the junction is very small in comparison with the object being measured and the contact is short and light. It was shown that the temperature rise due to the proximity of the measuring junction was negligible in the case of a 0.4-mm thick glass sheet or the human skin. The new method can give the correct surface temperature even when radiation comes from above or from below. Consequently the opacity of the surface layer does not matter as in the case of the radiation pyrometry.

THE knowledge of surface temperature of living and inanimate objects has become increasingly important in science and industry. But the method of measurement seems not to have been well standardized.[1]

The method presented here makes use of a thermocouple[2] whose measuring junction can be adjusted to any temperature. The temperature of the junction indicated by a millivoltmeter in the couple circuit is also the temperature of the surface, if the junction temperature has been so adjusted that the needle of the meter shows no deflection, when the junction makes a light brief contact with the surface.[3]

The temperature of the measuring junction may be adjusted by means of a fine heating coil put round the thermocouple wire near the junction. To measure the temperature lower than the room temperature the junction must be overcooled by contact with a suitable constant cold source and adjusted by heating.

The temperature jump the junction undergoes during its short contact with the surface can be made large with a suitable design of the thermojunction. The meter in the thermocouple circuit may be a millivoltmeter (less exact), a potentiometer (more exact but awkward), or both a millivoltmeter in the full e.m.f. circuit and a zero instrument such as a sensitive, short-period galvanometer in an extra circuit in which the e.m.f. has been either partly compensated by keeping the reference junction near the temperature of the measuring junction or almost completely compensated by a symmetrically-connected secondary thermocouple.

To be precise, the temperature of the measuring junction which has been adjusted to T at some distance from the surface, will change to $T+\Delta T$ just before the contact is made.[4] Obviously $T+\Delta T$ is then equal to the surface temperature if no deflection occurs. To minimize this inconvenient ΔT, the adjustment of the thermocouple should be made just in front of the surface, if this does not sensibly affect the surface temperature (see below).

The validity of the new method can be tested by comparing the *true* temperature of the surface being measured with the surface temperature as measured by the new method. What is important is to get a surface whose *true* surface temperature is exactly known. As such a surface we may use a metallic surface at the junction of a thermocouple of rather large diameter,

---

[1] Reference is made to two articles in the book, *Temperature, Its Measurement and Control in Science and Industry* (American Institute of Physics, Reinhold Publishing Corporation, New York, 1941) (1) "Measurement of Surface Temperatures," F. C. Houghten and H. T. Olson, p. 855. (2) "Temperature of Incandescent Lamps," W. E. Forsythe and E. M. Watson, p. 1188.

[2] In principle a resistance thermometer or even a liquid-in-glass thermometer can be used as well.

[3] For a wet or liquid surface a non-wetting junction should be used.

[4] This is caused by the temperature gradient in the ambient air and to the radiation from the surface, apart from the irregular air draughts. ΔT depends on the speed of approach and apparently also on the quickness of response on the part of the meter.

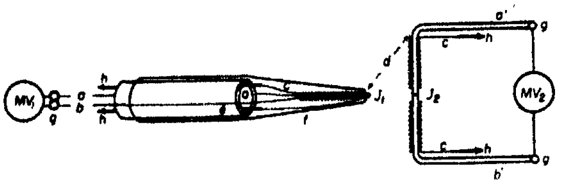

FIG. 1. *a*: Iron wire, diam. = 0.19 mm; *a'*, diam. = 1.17 mm; *b*: constantan wire, diam. = 0.15 mm; *b'*, diam. = 1.00 mm; *c*: heating nickel wire, diam. = 0.08 mm; *d*: thin glass tubings; *e*: ebonite tube; *f*: glass cap; *g*: cold junctions, in a water-ice Dewar vessel; *h*: to a constant a.c. source through a regulator; *J*: hot junctions; and *MV*: millivoltmeters.

which can be electrically heated with two coils on both sides of the junction (J_2 in Fig. 1). Let us suppose that the junction is heated in air and shows a certain e.m.f. Then the *true* surface temperature at the junction may be put equal to the easily measurable temperature of the oil of a bath, in which J_2, with the coil currents off, shows the same e.m.f. In the oil bath the temperature throughout the cross section of the wire at J_2 is uniform, but when the wire is heated in air, there will arise a small temperature drop from the center to the surface of the wire at J_2. It should, however, be negligible, because only a narrow surface is left bare between the heating coils.

The thermocouple J_2 was made by soldering end to end the squared ends of a larger iron wire (a') and a constantan wire (b'), with a heating coil round the glass-covered wire extending 12 mm long on either side of the junction where a narrow collar of surface is left free for measurements.

Thus far the description has concerned the standard surface whose *true* temperature is exactly ascertainable. The following description deals with the measuring junction proper. This junction J_1 (Fig. 1) for the measurement of the surface temperature is made by soldering end to end the flattened and widened (by hammering) ends of an iron wire (a) and a constantan wire (b), each in a fine glass tubing. Both wires are then so bent to the form of a hair pin that both glass tubings now in parallel position touch each other. A coil of fine nickel wire is then formed round these tubings. By finely adjusting the heating current through the coil J_1 can be given any desired temperature without much delay. The thermal capacity of the assembly as described is about 0.0017 cal./deg. The coil is protected against air draughts by a conical glass cap f. The shape of the wire at J_1 as mentioned just before favors the quick establishment of the thermal equilibrium, when J_1 is touched by or removed from the surface being measured.

Now the couple wires of J_1 and those of J_2 are all held in a horizontal plane, the former being perpendicular to the latter (Fig. 2), the junction point J_1 being about 0.5 mm apart from J_2. In *this* configuration the surface temperature of J_2 is measured by means of J_1 by adjusting the heating current of J_1 and noting the e.m.f. on the millivoltmeter MV₁ when the needle ceases to deflect as J_1 touches J_2, while the *true* surface temperature of J_2 is given by the millivoltmeter MV₂.

The surface temperature thus obtained shows deviations from the *true* surface temperature, which are as likely positive as negative, so that the algebraic mean of these deviations, 0.08°C for 12 measurements,* is relatively very small as compared with the individual deviations. This satisfying result is, however, only valid as far as we are concerned with the surface temperature at J_2 *in the presence of* J_1 just in front of it, because on removing J_1 the *true* surface temperature of J_2 drops by about 0.2°C. Theoretically we must always expect a systematic error of this sort, for it is due to the heating effect of the measuring junction brought in proximity to the surface to minimize ΔT mentioned earlier. But the error should be small if the accumulating heat at the point on the surface being measured be rapidly conducted away therefrom. Any significant error will arise, if the specific thermal conductivity of the surface material is very low, or if the object being measured is a free thin film without a massive support, a fine wire, or a small particle.

The heating effect on the surface being measured can roughly be estimated in the following way. About 5 mm apart two points A and B at nearly the same temperature are chosen on the surface. The thermocouple is always held perpendicular to the surface, J_1 being kept about 0.5 mm from it. The temperature of point A is measured as usual and then, without changing the heating current, the junction is shifted to the position just in front of point B and kept there for some minutes until the possible heating effect at A would disappear. Now the junction is rapidly shifted back and made to touch A. If the needle does not move at this moment the suspected heating effect at A did not exist. If it moves to the lower temperature it did exist. This time the glass cap f (Fig. 1) has been replaced by a brass one to prevent

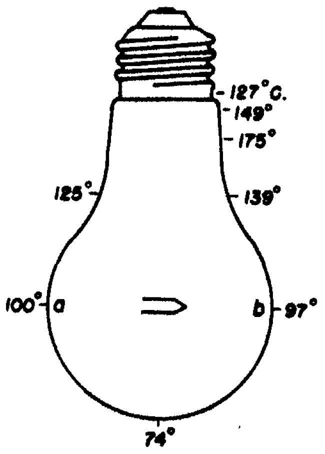

FIG. 2.

---

* These measurements were carried out at several temperatures between 33–65°C in a room at 32°C. Since the magnitude of the deviation is roughly constant throughout this temperature range, the probable error for a single observation was calculated from these 12 deviations, giving ±0.2°C.

the radiation from the hot heating coil from falling directly on the surface. This experiment was made with a burning 20-watt lamp bulb. The surface temperature of the bulb glass about 0.4 mm thick was 92°C. Though the dissipation of heat along the glass sheet and to the air was bad, no heating effect was observed within 0.05°C.† The same was also found true with the human skin.

Some earlier results of surface temperature measurement with a Mazda gas-filled 40-watt electric lamp bulb in a porcelain socket burning at 400 ma are shown in Fig. 2, the room temperature being 30°C.[6] The figures are exact within ±1.5°C. That the point *a* is hotter than *b* indicates a complicated gas current inside the bulb.

It is to be emphasized that, unlike ordinary methods, the measurement should in no way be affected by the intense radiation from the hot filament, because the way of heating the measuring junction to the surface temperature, whether by radiation, by electric current, or by both, is immaterial. To prove this the surface temperature of J_2 is measured with J_1 just above a burning 40-watt electric lamp. To keep the air current steady these are placed inside a vertical cylinder loosely fitting the lamp bulb. When the lamp is lighted, the temperature of J_1 rises from 35 to 63°C or the heating current 120 ma with the lamp off, must be reduced to 45 ma to keep J_1 at 63°C. The algebraic mean of the errors of 6 measurements carried out in the range 54–75°C is +0.07°C and the probable error of a single observation ±0.4°C. So also the measurement may be performed in a high frequency electric field. The surface temperature of a finger nail was found about 0.5°C higher than that of the neighboring skin. The validity of this result is not affected by the degree of opacity of the nail to any heat radiation from the underlying tissue.

In order to see how the accuracy depends upon the nature of the surface being measured, special measurements were made at the point *a* and on the brass skirt of a 40-watt electric lamp burning with the base down. The mean temperature from 8 measurements and the probable error of a single observation are respectively 109.6°C and ±0.3°C at *a* and 50.0°C and ±0.1°C on the base skirt. The measurement can be performed more easily and rapidly with the metallic surface than with the glass surface. The accuracy seems to depend, among others, on the thermal conductivity, the thermal capacity per unit volume, and the deformability, the smoothness, and the size of the surface. The replacement of the inconvenient trial and error method by an automatic one is planned.

---

† 20 scale divisions of the 0.2-sec. period galvanometer now in use correspond to 1°C.

[6] Forsythe and Watson obtained for the base temperature 105°C and for the maximum bare bulb temperature 127°C. With an iron-constantan couple of 0.05-mm wire diameter we found after the method suggested by the authors the temperature always somewhat 10°C lower than that obtained by the new method.

THE REVIEW OF SCIENTIFIC INSTRUMENTS VOLUME 21, NUMBER 1 JANUARY, 1950

An Improved Schlieren Apparatus Employing Multiple Slit-Gratings

TAGE A. MORTENSEN
Midwest Research Institute, Kansas City, Missouri

(Received May 30, 1949)

In the schlieren apparatus described in the following, the conventional knife-edge elements are replaced by multiple slit-gratings. The main advantage gained by this design is the fact that larger-sized working fields can be achieved with an objective lens of given aperture. Also, in some cases, greater intensity of image illumination is obtained, and usually the over-all length of the system is reduced.

1. OPERATING PRINCIPLE OF SCHLIEREN APPARATUS

FIGURE 1 shows a widely used knife-edge arrangement employing a lens as the image forming element. It consists of a light source *C*, a set of condenser lenses *D*, a screen *S* with a narrow slit *Q*, an objective lens *L*, a screen *K* with a straight horizontal boundary, the so-called knife-edge and, finally, an observing screen (or a photographic plate) *B*. The working field is located in the plane *A*, and the system will record the density variations in the points of the working field as changes in light intensity at the corresponding points of *B*.

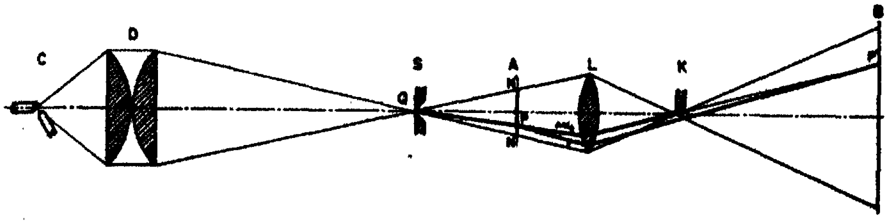

FIG. 1. Schlieren apparatus employing knife edges.

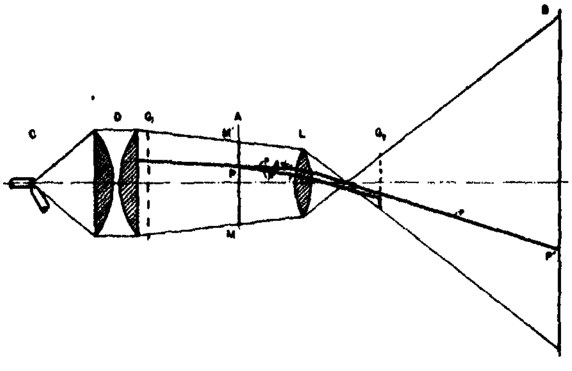

FIG. 2. Schlieren apparatus employing gratings.

The new type of schlieren apparatus is shown on Fig. 2. It employs, as before, a light source C, a condenser D, an objective lens L, and an observing screen B. But the slit Q and the knife-edge K (Fig. 1) are now replaced by two gratings G_1 and G_2. The first grating G_1 is located immediately after the condenser in the direction of the light rays. It is a ladder-like device with rungs or bars and clear spaces in between. The width of the clear spaces is of the same order of magnitude as that of the bars. The second grating G_2 is in the plane where the image of G_1 is formed and is, in fact, a photographic negative of G_1. Therefore, with a certain vertical position, G_2 will completely cover the image of G_1 and no light will pass through G_2. The "slices" of light formed by the first grating all will be intercepted by the opaque bars of G_2 (except stray light caused by diffraction). The ratio of the sizes of G_1 and G_2 will depend on their location relative to L. Normally, the grating G_1 will be larger than G_2, as shown on the figure. The working plane is located between G_1 and L and its image is formed in the plane B.

The operating principle of the set-up is, of course, the same as that of a knife-edge arrangement. In Fig. 2, a heavy line indicates a pencil of light rays p. It is passing through one of the clear spaces of G_1 and a point P of the working field. We assume that the second grating is in such a position vertically that p is allowed to pass through and arrive at the screen B at the point P' which is the image point of P. If now the local index of refraction at P is different than along the rest of the path of p, then the pencil will be deflected an angle $\Delta\alpha$ and will assume the path indicated by p'. In this position, part of p' or all of it (as in the figure) may be stopped by one of the opaque bars in G_2, and the illumination of P' will be correspondingly smaller. Through P will pass rays from other parts of G_1 but, in all cases, the effect of the deflections will be as described for p. There is a possibility that some of the rays will be refracted so much that, instead of being stopped at one of the opaque bars of G_2, they will pass through the next clear space between two bars. With a proper selection of the dimensions and location of G_2, this possibility is only remote. With a different deflection $\Delta\alpha$ at P, rays that would ordinarily have been intercepted by G_2 might now pass through a clear part of G_2, thus resulting in a greater illumination of P'.

All points of the working field will have their image points in B. For all of them, the situation will be as described above. A change in the index of refraction at any point will be transformed into a change of light intensity at the corresponding point in B.

The sensitivity of a schlieren apparatus may be defined as the relative change in light intensity produced by a given angular deflection of the rays at the point P. It will be proportional to the focal length of the objective lens L and inversely proportional to the width of the bars of the grating G_2. These values must therefore be selected according to the desired sensitivity. But the sensitivity will depend also to some extent on the vertical position of G_2 relative to G_1 (for the knife-edge setup, on the vertical position of K relative to Q). Therefore, the grating G_2 (respectively, the knife edge K) shall be adjustable in a vertical direction. This also will provide a regulation of the over-all illumination of the screen B. Since both the illumination of B and the sensitivity vary with the position of G_2 (but not in the same manner), there are certain positions where there is maximum contrast in the schlieren picture.

Both the schlieren systems described are sensitive only to changes in the index of refraction which deflect the rays in a vertical direction or, more correctly, in a plane perpendicular to the knife-edge (respectively, the direction of the bars in the gratings).

2. COMPARISON OF THE KNIFE-EDGE SYSTEM AND THE GRATING SYSTEM

The two schlieren systems described above are alike in operating principles, but they differ in several respects.

In the knife-edge system, the cone of light formed by the condenser lenses is focused on the screen S before it arrives at the objective lens. At the other side of the

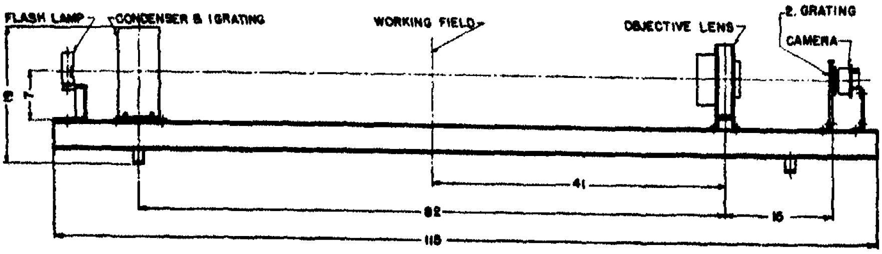

FIG. 3. Side view of schlieren apparatus built at Midwest Research Institute.

FIG. 4. The second grating.

lens, the light cone is again intercepted at its focus by the knife edge *K*. In the grating system, the light cone is focused at a point between the objective lens and the second grating. Instead of being intercepted at its foci, as in the knife-edge system, the light cone encounters the gratings at two planes conjugate to each other with respect to the lens *L*. Also, where the knife-edge system employs one slit *Q* and one knife edge *K*, the grating system uses a number of slits in G_1 and a corresponding number of knife edges in the form of the edges of the rungs in G_2.

By this arrangement a notable advantage has been attained: The size of the working field in comparison to the size of the objective lens has been increased. In Fig. 1, the area in which density changes will be recorded by the apparatus is represented by its diameter *NN'*, which must always be smaller than the diameter of the objective lens. For the grating apparatus this is no longer the case. Here, with the convergent light rays, the diameter *MM'* is greater than that of the lens *L*. With the schlieren apparatus described in the beginning of Section 3 a working field of 17.5 sq. in. has been obtained. This is almost 2½ times as large in area as what could have been effected with a knife-edge setup. The objective lens for any type of schlieren apparatus must be of high quality in all respects. Such a lens is difficult to obtain with a large diameter, and is always very expensive. The fact that a given objective lens permits a larger working field when used in a grating apparatus constitutes, therefore, a considerable advantage. Excepted from this are the cases where parallel light through the working field is required. For many applications, however, slightly convergent light will suffice.

The need for a schlieren apparatus that would effect a greater intensity of illumination of the screen *B* was one of the factors that originally led to the design of the grating apparatus. This requirement was met very satisfactorily. The apparatus built proved to be superior to a comparative knife-edge setup, and in particular to be excellently suited for projection of schlieren pictures for an audience.

From Fig. 2, it will be seen that the grating setup is somewhat shorter in over-all length than the knife-edge system shown. This may not always be the case. It is possible to move the light source itself to *Q* (Fig. 1), provided it has sufficiently small dimensions and well defined boundaries.

FIG. 5. General view of schlieren apparatus built at the Technical University of Denmark, Copenhagen.

3. DESCRIPTION OF A SCHLIEREN APPARATUS EMPLOYING GRATINGS

A schlieren apparatus operating according to the principles described in Section 1 has been built at the Midwest Research Institute. The instrument is for photographic use, recording a working field of 3½"×5" on 35 mm film. Figure 3 is a side view of the apparatus giving its main dimensions. By comparison of Fig. 2 and Fig. 3, it will be seen that they correspond element for element, except for the camera which is not shown on the schematic Fig. 2.

To the left in Fig. 3 is the light source, in this case a flash lamp of 100 microseconds duration. Next follows the condenser unit, consisting of two 12-in. diameter condensing lenses and the first grating, mounted together in a cylinder. The objective lens shown to the right in the figure is an f:3.5, $f=13\frac{1}{2}''$ Eastman Kodak anastigmat lens. The second grating which is seen at the right end of the apparatus is also shown on the photograph Fig. 4. It has been mentioned previously that this type of schlieren apparatus is sensitive to pressure gradients in one direction only. Therefore, to be able to employ the sensitivity of the apparatus in all directions, provisions are made for rotating both gratings about the optical axis of the apparatus. Figure 4 shows a screw adjustment for moving the second grating in a direction perpendicular to the bars in the grating.

Immediately behind the second grating follows the camera with the secondary objective lens. The use of such a lens has not previously been explained. It was assumed that the schlieren image would be recorded by replacing the screen *B* with a photographic plate or film. Some advantage is gained, however, by introducing another objective lens behind the second grating. Normally the schlieren image formed by an arrangement as shown on Fig. 2 would be considerably larger than the working field itself. This would require a large size of film, and—because of the large area to be exposed—a high intensity of the light source. Furthermore, it would leave only a small depth of field. The working field will always in practice have some depth in the direction of the optical axis, and all points in this three-dimensional field must be reproduced with sufficiently good definition in the plane of the film. A secondary objective lens can eliminate the disadvantages mentioned above. It will give a suitable size of the schlieren image, reduce the amount of light required for exposure, and increase the depth of working field.

The diameter of the secondary objective lens must be nearly equal to the diagonal of the second grating. Because the lens works under favorable conditions, it need not be of high quality. An achromatic lens is to be preferred; it is not necessary, however, especially if monochromatic light is supplied.

The body of the camera is that of a standard 35-mm camera. A Packard shutter is mounted between the lens and the camera. The shutter is operated by hand. It is synchronized with the flash lamp so that the flash occurs when the shutter is fully open. Instead of this arrangement, it is possible for photographing transients to get a signal from the transient itself which can trigger the flash.

The critical part of the apparatus is the relative position of the first grating, the main objective lens, and the second grating. Therefore, these elements are supplied with sturdy supports. The base for the optical elements is an I-beam. Once the apparatus has been assembled and adjusted, there are only a few adjustments to be made during the operation. These are the direction of the bars in the gratings which changes the direction of the sensitivity, and the crosswise position of the second grating which changes the size of the sensitivity and the background illumination. The base and the supports for the optical parts are made in an ordinary machine shop since no extremely accurate parts are required.

Figure 5 shows another schlieren apparatus of the grating type. The apparatus was built at the Laboratory for Technical Physics at the Technical University of Denmark in Copenhagen. It is used mainly for projection, demonstrating the operating principle of an acoustic air jet generator which is seen as the second element from the left on the photograph. Since it is designed with a view to easy transportation to other laboratories the light source is not included in the apparatus. A standard carbon arc lamp or a projection lamp is normally used in connection with the apparatus. On Fig. 5 the two gratings and the objective lens, an $f{:}4.5$, $f = 15$ cm Zeiss Tessar anastigmat, will be easily recognized. The figure shows the apparatus as used for projection, and therefore, of course, no secondary objective lens or camera appear in the picture. The apparatus also differs from that shown on Fig. 3 in the fact that the gratings cannot be rotated about the optical axis of the system. Instead of this the air jet generator can be rotated if various directions of the pressure gradient are to be accentuated. This feature eliminates the necessity of adjusting the bars in the two gratings so that they are parallel each time the direction of the sensitivity (relative to the object investigated) has been changed. The total length of the apparatus is about 30 inches.[1]

4. ACKNOWLEDGMENTS

The schlieren apparatus employing gratings instead of knife edges was invented by Mr. F. Larris of the Laboratory of Technical Physics at the Technical University of Denmark in Copenhagen. The apparatus described above was developed at the suggestion of Dr. Jul. Hartmann, the head of the laboratory, who has made extensive use of the schlieren method during his experimental work on acoustics. The writer wishes to express his sincere thanks for the fine cooperation with Dr. Hartmann and Mr. Larris which made this paper possible.

---

[1] For a description of this schlieren apparatus the reader is referred to Jul. Hartmann, "Den Akustiske Luftstraalegenerator," Fysisk Tidsskrift (Copenhagen), No. 3–4 (1940) (in Danish).

THE REVIEW OF SCIENTIFIC INSTRUMENTS VOLUME 21, NUMBER 1 JANUARY, 1950

Design Study for a Three-Bev Proton Accelerator*

M. S. Livingston,† J. P. Blewett, G. K. Green, and L. J. Haworth
Brookhaven National Laboratory, Upton, New York

(Received March 22, 1949‡)

A design study is presented for a proton synchrotron (to be called a "Cosmotron") to accelerate protons to energies of the order of three billion volts. Protons are injected from a four-million volt Van de Graaff machine. They are deflected electrostatically into a racetrack orbit including four quadrants of thirty-foot radius of curvature, and four straight sections ten feet long. The energy gain per revolution supplied by the radiofrequency system will be about 1000 ev. Acceleration will continue to 1.0 seconds to a final energy of about three Bev. Construction of this machine is now in progress.

1. INTRODUCTION

THE synchrotron principle of phase-stable acceleration in a magnetic field can be used to accelerate protons to energies well in excess of one billion volts (Bev). Energies of this magnitude are needed in order to study the processes of formation of mesons. From such studies it is anticipated that much can be learned regarding the role of mesons in nuclear forces. The simplest nuclear process—the bombardment of single protons by other, highly energetic protons—will be the most informative; in this process less than half of the kinetic energy is available for meson formation. The threshold for production of π-mesons (about 300 times electron mass) by this process would be about 300 Mev, and for adequate intensities an energy of 600 Mev is desirable. Production of multiple meson showers or of possible heavier mesons (such as the 700 mass mesons reported in some cosmic-ray observations) would require even higher energies. Furthermore, an energy greater than the 2-Bev theoretical threshold for heavy particle creation is certain to yield interesting and significant results. Accordingly, the design energy for the first Brookhaven proton accelerator (to be called a Cosmotron) has been set at 3.0 Bev. The AEC has approved the program, construction is now proceeding and the accelerator is scheduled for completion in late 1950. This paper is a report of the present design status, and a discussion of the factors leading to the design.

Magnetic accelerators for electrons, such as the betatron or the synchrotron, have a practical energy limit of the order of 1 Bev due to the rapid onset of radiation losses. Linear accelerators are in too early a stage of development to permit prediction of their possibilities in the Bev range. The synchro-cyclotron requires a solid core magnet which, at these energies, becomes exorbitant in weight and cost. A ring magnet is indicated to reduce cost, and protons can be used to avoid the radiation loss limitation. Under these conditions, the synchrotron principle provides a practical method of acceleration of particles to energies of several Bev.

The first proposal of a proton accelerator using a ring magnet, in which both magnetic field and frequency of the accelerating electric field are varied, was made by Professor M. L. Oliphant of the University of Birmingham, England, to the Directorate of Atomic Energy in 1943. This is reported in a detailed design study published in 1947,[1] accompanied by a theoretical analysis of orbit stability.[2] Construction of this accelerator, which will produce protons of 1.3 Bev, is in progress and it should be completed in 1950. Meanwhile the principle of phase stability in synchronous accelerators was announced independently by McMillan[3] at the University of California and Veksler[4] in the U.S.S.R. in 1945; both papers describe the possibility of acceleration of protons in a synchrotron by means of a variable frequency accelerating field.

Designs for super-energy accelerators have been in progress concurrently during the past two years at Brookhaven National Laboratory[5] and at the University of California.[6] These design studies show that energies of 10 Bev are attainable although the cost and time required for development are formidable. The simpler design problems, lower cost, and earlier completion date influenced our decision to start at 2 to 3 Bev. At some later time, when results on the first proton synchrotron justify it, the 10-Bev design may be reactivated.

2. THE PROTON SYNCHROTRON

The proton synchrotron uses a ring magnet to produce a magnetic field over an annular region, in which a doughnut-shaped vacuum chamber is located. Protons produced at low energy in an external source can be focused and deflected into the vacuum chamber. The magnetic field guides the particles in a circular orbit of constant radius, and is modulated from low to high intensity as the protons gain energy. An electric field to accelerate the protons is provided at one point in the circular path, so that the particles acquire an increment of energy on each revolution; this accelerating field must be oscillatory in nature and synchronized with the motions of the ions. Since proton velocity increases with energy, the frequency of the applied electric field must be varied during the acceleration to match the increasing angular velocity of the particles. This frequency must be precisely controlled to provide the correct phase of the accelerating field, so as to maintain constant orbit radius and prevent loss of particles by striking the walls.

---

* Work done under the auspices of the AEC.

† Now at M.I.T.

‡ Revised November, 1949.

[1] Oliphant, Gooden, and Hide, Proc. Phys. Soc. London 59, 666 (1947).

[2] Gooden, Jensen, and Symonds, Proc. Phys. Soc. London 59, 677 (1947).

[3] E. M. McMillan, Phys. Rev. 68, 143 (1945).

[4] V. Veksler, J. Phys. U.S.S.R. 9, 153 (1945).

[5] M. S. Livingston, Phys. Rev. 73, 1258 (1948).

[6] W. M. Brobeck, Rev. Sci. Inst. 19, 545 (1948).

The protons being accelerated in the vacuum chamber are bunched by the phase focusing inherent in the synchrotron. Across a gap at one point in the orbit, is applied a sinusoidal accelerating electric field with a peak voltage about double the value required per revolution to maintain constant radius. The radius, R, which at any moment satisfies the relation $v/2\pi R=$ frequency of accelerating signal, for the protons of velocity v, is known as the "equilibrium radius." If protons traveling on the orbit which has this radius arrive at the correct or "equilibrium" phase they will continue to circulate in the same orbit and to arrive at the correct phase. Protons arriving at other phases will oscillate in phase about the equilibrium phase provided their initial phase and radius do not differ too much from the equilibrium phase and radius; otherwise they will enter unstable orbits and be lost. Associated with the oscillations in phase are radial oscillations. The theory of these oscillations has been developed elsewhere.[2-4,7] The limitations on initial phase and radius are discussed further in Section 7 below. The frequency of the oscillation in the present case varies between about 2600 cycles per second at injection, and 1300 cycles per second at the end of the accelerating cycle. Initially, if the field is rising linearly with time, the amplitude of the radial oscillations will be inversely proportional to the magnetic field. In the extreme relativistic range, the amplitude will decrease as the inverse three-quarters power of the field.

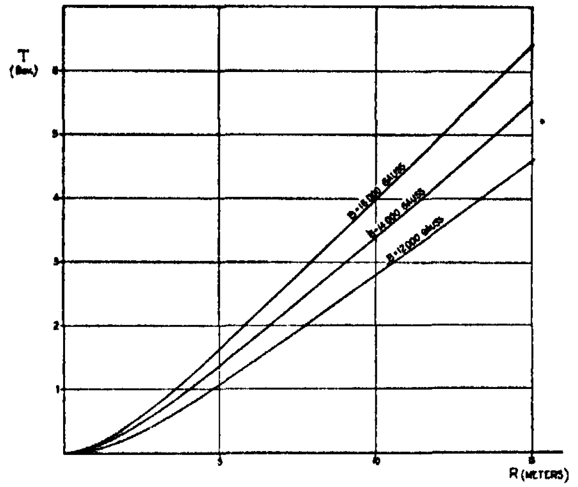

FIG. 1. Proton kinetic energy T *vs.* orbit radius R for several values of magnetic field B.

The magnetic field is not strictly uniform, but must decrease with increasing radius to provide restoring forces for particles which deviate from the equilibrium orbit or the median plane. These forces set up vertical and radial oscillations about the true orbit, known as "betatron" or "free" oscillations, with a frequency of 0.1–1.0 of the ion revolution frequency. These high frequency vertical and radial oscillations are superimposed on the lower frequency synchrotron oscillations to produce a flattened sausage-shaped envelope enclosing the rotating ions. At the start of the cycle when ion energy and magnetic field are low this envelope may extend halfway around the vacuum chamber and be limited in transverse dimensions by the internal size of the chamber. As energy increases, the oscillation amplitudes are rapidly damped to smaller dimensions centered on the equilibrium orbit.

Under ideal conditions the equilibrium orbit would remain fixed at the center of the vacuum chamber. However, the applied frequency may deviate from the value required to maintain a constant radius, and so cause radial displacements of the equilibrium orbit. One of the chief design problems of the proton synchrotron is to provide a control system to limit the frequency deviations and keep the resulting radial displacements within the useful aperture of the chamber.

3. TIME CYCLE

The time of acceleration, during which the magnetic field increases from about 300 to 14,000 gauss, is influenced and limited by several factors:

(a) peak kva required to excite the magnet,
(b) average power consumption—primarily heat developed in the magnet windings,
(c) volts-per-turn requirement for the accelerating electric field,
(d) loss of intensity by gas scattering.

A long acceleration time reduces the peak kva and the volts-per-turn; a short time decreases average power and loss of ions by gas scattering. The design value chosen to balance these several factors is 1.0 second, although the allowable range extends from 0.5 to 2 seconds. The reasons for this choice will be more evident in the discussion to follow.

After the protons have reached top energy and have been ejected, the current in the windings must be reduced to zero, and then the cycle is repeated. The high energy protons will be emitted in bursts over a period of a few microseconds at the end of each 1-second acceleration interval. The repetition rate is limited by the average power rating of the power supply, with a maximum of 12 per minute. The power supply and the techniques to be used for re-cycling the energy stored in the magnet are discussed in a later section.

---

[7] N. H. Frank and R. Q. Twiss, Rev. Sci. Inst. **20**, 1 (1949).

4. ORBIT RADIUS

The product of magnetic field and orbit radius (BR) is a measure of proton energy. A practical limit on the field in iron magnets is set by saturation of the iron, at roughly 18 kilogauss. Depending on the quality of the iron and the design of the magnet, this will establish an allowable maximum field in the gap between poles. Our design of a simple "*C*" magnet structure with wedge-shaped spaces between iron plates results in average fields in the gap between poles of about 14 kilogauss for fields in the iron of 17 to 19 kilogauss. Alternate magnet designs with closer packing of iron would result in higher fields in the air gap, but would involve a more complex structure and greater expense. The design choice is essentially one of minimizing cost for a desired BR value. Our choice has been a relatively large radius and a low field.

The dimensional relation between maximum kinetic energy T_m, magnetic field B_m, and radius R is given (in m.k.s. units) by:

$$T_m(T_m+2E_0)=c^2e^2B_m{}^2R^2. \quad (1)$$

Here T_m is the kinetic energy and E_0 the rest energy of the particle being accelerated and e is the charge of the particle. This expression has been evaluated for protons and is plotted in Fig. 1, with proton kinetic energy (in Bev units) a function of radius for several values of magnetic field. The orbit radius of 30 ft. chosen for the Brookhaven accelerator, at 14 kilogauss, would allow acceleration of protons to 3.1 Bev, deuterons to 2.5 Bev, or He^{++} ions to 5.0 Bev.

5. MAGNET DESIGN

The magnet design chosen after a careful study of alternate structures involves several unusual features. It is basically a "*C*" section with minimum size "window" for the windings. Choice of the *C* shape was influenced by the desire to provide ready access on one side of the magnet gap along the entire periphery. Pump leads can be located as frequently as desired along the length of the vacuum chamber, a valuable feature when vacuum requirements are severe and chamber cross section is small. Access to the chamber for inspection and maintenance is also simplified. When the slot opening of the *C* is on the outer face of the ring, high energy ions or neutrons will emerge tangentially from the accelerator around the entire circumference. To be sure, every effort will be made to eject a concentrated beam in a narrow angle; however, this deflected beam may be limited to a small fraction of the total circulating current. The external slot is thus good insurance that the high energy ions can be utilized to the maximum for experiments. This "poleless" *C*-shaped magnetic circuit has minimum dimensions and weight and requires only two accurately machined surfaces (the pole faces), effecting a significant saving in cost of construction. The octagonal shape is a compromise between a square and the ideal circular shape, and is achieved by cutting off the corners of square plates in manufacture. The magnet cross section is shown in Fig. 2.

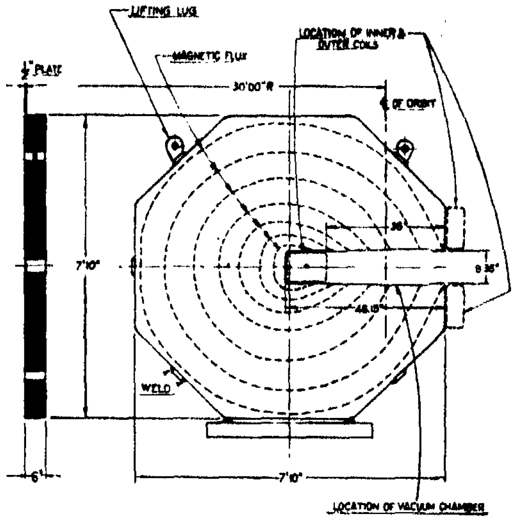

FIG. 2. Cross section of "*C*" magnet and assembly of blocks of ½-inch plates.

Since magnetic field will increase at an average rate of 14 kilogauss/sec. during the acceleration interval, lamination of the iron is essential. Detailed analysis of the eddy currents (see Section 13) has justified a choice of ½-inch plate, which has the advantage of being readily available in large dimensions and at a low base price. The material chosen is equivalent to SAE 1010 mild steel and has magnetic properties closely approaching those for soft iron.

In order to simplify the problems of machining and handling the thousands of half-inch steel plates, a procedure has been devised in which the plates will be pre-formed into bundles for handling and machining. Plates will be rough cut to the octagonal shape, fish paper insulation will be inserted, and then the plates will be stacked into bundles of 12 and welded together by tie-bars at the outer edges. These tie-bars do not link appreciable magnetic flux and so do not introduce an eddy current problem.

Since the plates are welded together, it is no longer possible to test for interlamination short circuits which might be serious if they occurred near the magnet gap. To make a short circuit test possible the insulation between laminations consists of a sandwich of two layers of 7-mil fish paper separated by a 1-mil sheet of aluminum foil. It is expected that any metallic connection which appears between blocks such as, for example, a metal chip, will puncture the aluminum foil and can be detected by a resistance measurement between aluminum foil and steel plate.

Each bundle of laminations will weigh about 5.7 tons, and will be machined as a unit to the precise dimensions and pole shape determined from model tests. There will be 288 such bundles, each about 6 inches thick,

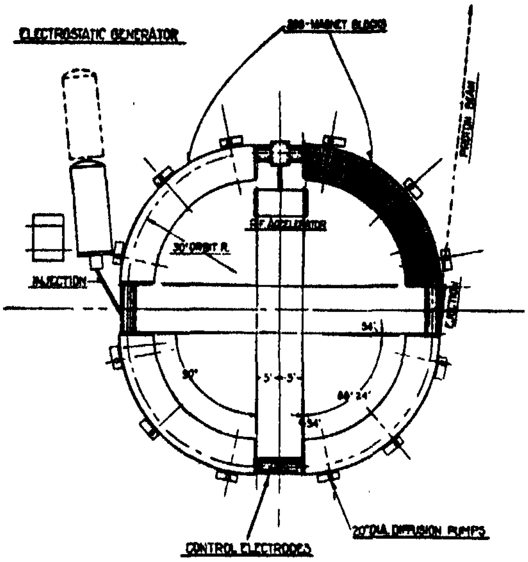

FIG. 3. Plan view of Cosmotron magnet and assembly.

assembled and joined together to form the ring structure and mounted on an accurately aligned base. The base plates will be adjustable in elevation to allow for possible settling of the foundation, and accurate instruments will be used to observe and correct for such settling.

As the design studies at Brookhaven have developed, it has become evident that there are several reasons for desiring sectors of the ion orbit which are free from magnetic field. Such a field free region is essential to accommodate the induction accelerator to be described later; it also simplifies the problem of ion injection and ejection. These considerations have led to a "racetrack" structure for the ring magnet, in which four quadrants are separated by straight runs across which the vacuum chamber extends. These straight sections will be 10 feet in length. The racetrack design was first proposed by Crane[8] and has been investigated theoretically by Dennison and Berlin[9] for the Michigan synchrotron. In this study the authors showed that four or more symmetrically placed short gaps in the magnetic field will not cause defocusing or set up excessive ion oscillations. Higher frequency angular perturbations in the field such as those caused by the magnet laminations or bundles of plates are insignificant in their effect on ion oscillations. Figure 3 is a plan view of the racetrack magnet. As indicated in Fig. 3 the quadrants will each subtend an angle slightly less than 90° at their centers of curvature. This is because the stray fields at the quadrant ends will be appreciable. Model measurements indicate that the ion beam will undergo a 90° deflection for a "quadrant" of 88.4°.

In principle a winding located in a slot of the *C* magnet can provide the necessary excitation. However, this coil of large diameter would produce magnetic fields in the air both inside and outside the circular magnet. External fields (well beyond the iron) would be of the order of hundreds of gauss when the field in the gap is 14 kilogauss. Such external magnetic fields are objectionable from the point of view of operation of instruments nearby and also represent a large stored energy in the air external to the iron of the magnet. In our first model studies the external stored energy with such a slot winding was observed to be approximately 40 percent of the stored energy in the magnet gap itself. The obvious way to reduce this stored energy and eliminate the external fields is to have return windings around the outer periphery of the magnet. Further model tests with such a return winding split symmetrically above and below the slot showed a reduction of the external stored energy to 13 percent of that in the gap. The final choice of exciting coils is indicated in the perspective drawing of the end of a quadrant shown in Fig. 4. In order to minimize the fringing magnetic field in the straight sections, the exciting coils are to be wound around each quadrant separately, but powered in series to obtain identical currents in the four quadrants.

The shape of the winding in the gap can be made to provide a uniform magnetic field in the neighborhood of the winding. Computations of the appropriate winding shape lead to a crescent-shaped cross section. Adjustment of an arbitrary parameter in the cross section leads to a special case in which the winding has a simple rectangular cross section. These theoretical predictions have been supported by model measurements.

The slot windings are made as small as practical in order to minimize the size of the "window" and thereby to reduce magnet weight, stored energy and power requirements. Water cooling will be used rather than forced air or oil immersion cooling. The conductors will be fabricated from rectangular copper tubing of $\frac{3}{4}$ inch by $1\frac{7}{8}$-inch cross section having a $\frac{3}{8}$-inch diameter hole for water cooling. There will be 48 conductors in the slot, arranged in four layers.

The return windings, located above and below the gap on the outside of the magnet, do not have as severe a space limitation, and so have been designed with a 50 percent larger cross section than the slot windings. They will consist of two bundles of 24 turns each, in which each turn will be $\frac{3}{4}$ inch by $2\frac{13}{16}$ inch in cross section and will have a $\frac{3}{8}$-inch water-cooling channel. Connectors joining the inner and outer windings at the quadrant ends will have the same cross section as the outer windings and will also be water cooled.

Water cooling leads for the conductor bars will be brought out in parallel to water manifolds located at the ends of the quadrants, as shown in Fig. 4. Insulation of the $\frac{3}{8}$-inch cooling water pipes will be provided by

---

[8] H. R. Crane, Phys. Rev. 69, 542 (1946).

[9] D. M. Dennison and T. H. Berlin, Phys. Rev. 70, 58 (1946).

5-foot lengths of rubber or plastic hose located between the manifolds and the conductors. The temperature rise in the conductors will be limited to 10°F to minimize thermal expansion and reduce the resulting abrasion of insulation. This requires a total water flow of 500 gal./min. through the 384 parallel cooling tubes, and will be supplied by a pressure head of about 20 lb./in.^{2}. The water will be recirculated through a heat exchanger and a purifier system to maintain an adequately low electrical conductivity.

6. MAGNET POWER

The power supply for the magnet must provide a pulsed current rising approximately linearly with time to a maximum in 1 second, then the current must be reduced to zero as rapidly as possible. This cycle will be repeated at 5-second intervals. The most critical design decision is on the method of energy storage and cycling. At 14,000-gauss field in the magnet gap the total energy stored in the magnet is 1.2×10^7 joules. An electrical capacitance large enough to store so much energy would be prohibitively expensive. The use of batteries would introduce insoluble switching and maintenance problems. On the other hand it is relatively easy to store large quantities of energy in a flywheel. The decision has been in favor of a motor-flywheel-a.c. generator-rectifier unit which will transfer energy to the magnet during one second and then return the magnetic stored energy to the flywheel.

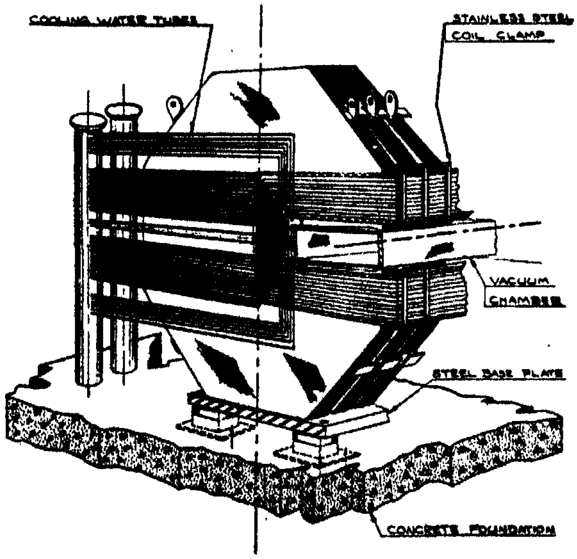

FIG. 4. End view of magnet quadrant with exciting coils and water cooling.

Advice from manufacturers indicates that a reasonable voltage rating for such a power supply would be of the order of 5000 to 6000 volts, dropping by 30 percent or so under full load. The choice of voltage fixes the number of turns in the magnet winding. The pertinent parameters have been computed and checked by measurements on scaled models. At 14,000 gauss, for example, we require a current I in an N turn coil where

$$NI=3.36\times10^5 \text{ ampere turns.} \tag{2}$$

At 14,000 gauss field the total flux in the gap, in the winding, and in the stray field is

$$\phi=88 \text{ webers,} \tag{3}$$

and its rate of change

$$\partial\phi/\partial t=58 \text{ webers per second.} \tag{4}$$

From coil dimensions the resistance of the coil is

$$R=4.95\times10^{-5}N^2 \text{ ohm.} \tag{5}$$

We can now derive the number of turns in the winding from the relation

$$V=N(\partial\phi/\partial t)+RI \tag{6}$$

$$=75N \text{ from (2), (4) and (5).} \tag{7}$$

If we assume that, at 14,000 gauss the supply voltage V has dropped to about 3600 volts, we obtain

$$N=48 \text{ turns.} \tag{8}$$

At 14,000 gauss the peak current in a 48-turn coil will be

$$I_{\max}=7000 \text{ amperes.} \tag{9}$$

The resistance of the magnet winding will be 0.14 ohm. Model measurements show that its inductance will vary from an initial value of 0.47 henry to a maximum of 0.80 henry at about 1000 gauss; as the iron saturates the magnet inductance drops to a final value of about 0.25 henry.

The power supply, which is on order, consists of a wound-rotor induction motor rated at 1750 hp direct connected to a large flywheel and a twelve-phase alternator feeding a bank of ignitron rectifier-inverters. The alternator has a nominal rating of 20,000 kva, specially designed to withstand rectifier service; it will deliver 6000 volts at no load and a peak of 7000 amp. at 4200 volts under full load. The rectifier inverter bank has 24 ignitrons in a 12-phase circuit, with grids and igniters controlled to rectify the alternator output during the 1-second acceleration interval, and then to switch to inverter action to return the stored energy in the magnet (less heat losses) to the alternator-flywheel. The flywheel will be reduced in speed by about 6 percent at the peak of the cycle, representing a 12 percent decrease in the energy stored in the rotating flywheel. The motor will bring the speed back to the original value in the interval between power cycles. This operating cycle can be repeated at a maximum rate of 12 times a minute. The average power demand by the motor at 12 cycles per minute is estimated at 1000 kw; a control system for the motor will limit line surges to 2000-kva peak. Protection against faults is obtained by removing ignitron excitation and closing a fast acting shorting switch across magnet terminals. Under these

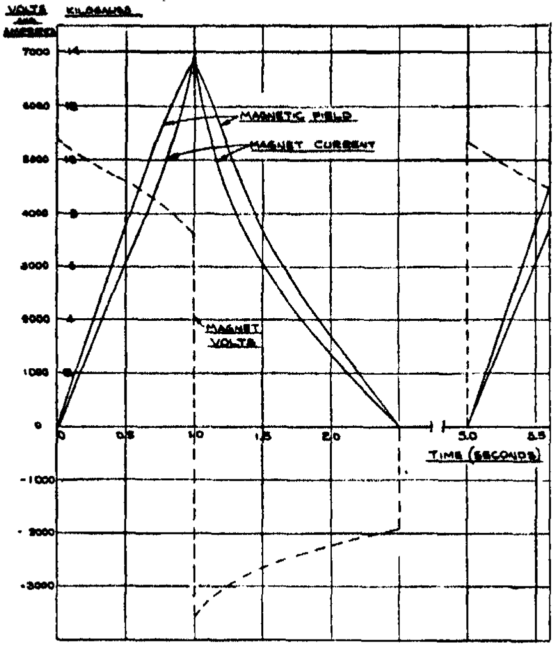

FIG. 5. Time cycle of applied voltage and current in magnet exciting coils, and of magnetic field at the proton orbit.

conditions the magnet windings have adequate thermal capacity and cooling to discharge the peak stored energy for one cycle. Frequency of arc-backs or other faults in the ignitrons is estimated at 1 to 2 per week under full power operation.

The peak current rating of 7000 amperes provides 3.36×10^6 ampere turns, permitting operation to fields of about 14,000 gauss. The magnetic field rise will be non-linear, starting at 16.5 kg/sec. and falling to 9.8 kg/sec. at 1 sec. The time cycle for V and I has been derived from model measurements and is illustrated in Fig. 5, and the variation of dB/dt along with the resulting curve of volts-per-turn required for acceleration at constant radius is shown in Fig. 6.

7. APERTURE DIMENSIONS

Most theoretical studies of particle oscillations in the magnetic field of a synchrotron have been applied only to electrons. At the Massachusetts Institute of Technology Frank and Twiss,[7] in collaboration with the Brookhaven design group, have studied orbital stability specifically for a proton synchrotron. The equations of motion were analyzed to determine frequency, amplitude and damping of phase oscillations and the necessary conditions for stability. Similar calculations were made by the British investigators.[2] As in the electron synchrotron, the oscillations have their maximum amplitude near the start of the motion when the particles are injected and are damped as the energy and magnetic field increase. The limits of stable phase oscillation during injection establish a "phase acceptance angle." For protons of 3-Mev energy, injected in a narrow bundle at the position of the equilibrium orbit for particles of this energy, the phase acceptance angle is approximately 180°. This means that for a beam of constant intensity 50 percent of the ions will be bunched and accelerated synchronously; the remainder will be phase unstable and will be lost to the walls. As the particles oscillate in phase they also oscillate in energy, and so traverse orbits of varied radius. Those ions which are injected at the extremes of the acceptance phase angle will deviate most from the equilibrium energy and will have the maximum amplitude of about ±8 inches; this will be reduced to a fraction of an inch by the time the ions have reached a few hundred million volts energy.

Ions which are injected at an angle to the equilibrium orbit will oscillate about this orbit with the familiar "betatron" type oscillations. The same is true of ions injected parallel to the orbit but displaced from it, such as would result from mistiming of injection. The frequency and amplitude of the betatron oscillations are determined by the "shape" of the focusing magnetic field.

The magnetic index "n" used to define the shaping of the field is given by:

$$B = B_0(r_0/r)^n \tag{10}$$

where B_0 is the field at the central orbit of radius r_0, and B is the field at radius r. By differentiation:

$$n = -r_0/B_0 dB/dr. \tag{11}$$

For circular machines the range of values of n for stability of both vertical and radial oscillations has been shown[10] to be: $0<n<1$, and the angular frequency

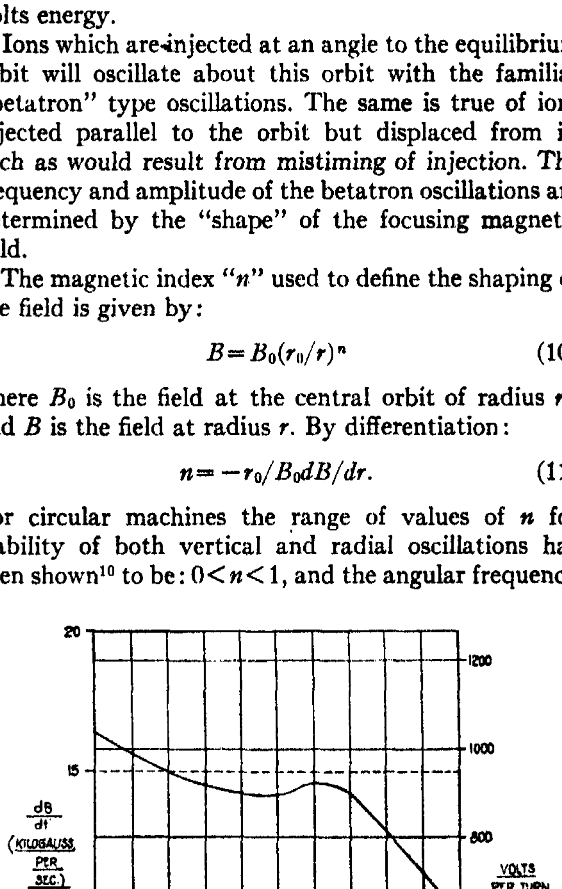

FIG. 6. Rate of change of magnetic field, and accelerating voltage per turn required during acceleration.

---

[10] D. W. Kerst, Phys. Rev. 60, 47 (1941).

of vertical and radial oscillations is a simple function of n:

$$\left.\begin{aligned}\omega_z &= (n)^{\frac{1}{2}}\omega\\ \omega_r &= (1-n)^{\frac{1}{2}}\omega\end{aligned}\right\} \tag{12}$$

where ω is the particle angular rotation frequency. Amplitudes are determined by the initial conditions of displacement and also are affected by the value of n. For large n (near unity) when the decrease of field with radius is greatest, the vertical restoring forces are a maximum and vertical oscillation frequency is essentially equal to ω; the converse is true for small n. Economy in magnet design demands the minimum practical air gap (vertical coordinate) and so a high value of n. A reasonable choice from such simple considerations would be in the range: $0.5<n<1$.

With four straight sections each of length L, the magnet quadrants of radius R, the betatron frequencies are to a first approximation:

$$\begin{aligned}\omega_z &= [1+L/(\pi R)](n)^{\frac{1}{2}}\omega,\\ \omega_r &= [1+L/(\pi R)](1-n)^{\frac{1}{2}}\omega.\end{aligned} \tag{13}$$

The corrective factor, $L/(\pi R)$ is about 10 percent for 10-ft. straight sections and 30-ft. radius. The limits of betatron oscillation stability are unchanged. However, the change in frequency is significant in the analysis of ion orbits at injection, in determining whether the ions will be intercepted by the injector electrodes in the first few revolutions.

Other limitations on choice of n involve possible resonances which might feed excessive energy into one mode of oscillation. The most familiar is the resonance between radial and vertical betatron oscillation frequencies at $n=0.2$ which has been observed in the synchro-cyclotron. For circular machines other possible resonances exist of which the most significant are at $n=0.5$, 0.75, and 0.80 and 1.0. With our racetrack design these same resonances occur at $n=0.5$, 0.80, 0.80 and 0.81. The resonance at $n=0.81$ is for $\omega_z=\omega$ and will cause large amplitude vertical betatron oscillations.

Damping of synchrotron phase oscillations is a slowly varying function of n. With protons the damping becomes positive only for $n>0.67$ (circular) or $n>0.72$ (racetrack) so this would appear to set a lower limit to n. However, the anti-damping for n smaller than this limit is not serious, and results in only a 5 percent increase in amplitude for n as small as 0.4. It may also be compensated by other techniques such as increasing the amplitude of the radiofrequency accelerating voltage.

Eddy current distortion of the magnetic field at the time of injection and saturation effects near the end of the cycle are treated in detail in Section 13. However, the general conclusion can be drawn that such effects will tend to produce an anomalously high value of n. This suggests an n value as low as is compatible with other limitations such as the vertical aperture. From the above considerations a figure of $n=0.6$ has been chosen, with an acceptable range: $0.50<n<0.80$. A certain amount of fluctuation in n may be desirable, to avoid dwelling too long on a specific value characteristic of a high order resonance.

A detailed analysis of the oscillations during injection is given in Section 8. It is shown that the energy spread, angular divergence, pulse length of the injected ions, and gas scattering result in a flattened sausage-shaped envelope for the accelerated ions soon after injection, of about 180° angular length, ±10 inch radial width and ±3.5 inch height. This envelope would be centered about an equilibrium orbit, ideally at the center of the chamber. Errors in frequency of 0.1 percent will cause radial displacements of the equilibrium orbit of about 1 inch at injection, decreasing to smaller displacements at later times. Control of frequency to 0.3 percent is considered to be straightforward, and a precision of 0.1 percent is possible with further development. The radial aperture taken up by the ion envelope might thus be increased to 23 inches for frequency errors of ±0.15 percent.

The gross radial aperture chosen is 36 inches, which is 10 percent of the orbit radius. The net aperture inside the vacuum chamber and within the useful region of magnetic field ($n<0.80$) is about 30 inches. Vertical clearance between magnet poles is 9.35 inches, resulting in a usable vertical aperture of more than 7 inches. A direct comparison with the apertures used for betatrons and electron synchrotrons is difficult, since in these machines injection is at much lower magnetic field, the electron beam from the gun is poorly collimated and injection efficiency depends on betatron acceleration at the start. Radial apertures used in such machines vary from 25 percent of the orbit radius in early designs to 10–15 percent in more recent designs. Most of the difficulties experienced with electron accelerators are associated with the very low magnetic fields at injection, as low as 7 gauss in some instances. The much higher injection energy of the Cosmotron, resulting in fields of about 300 gauss at injection, and the improved collimation available from an electrostatic generator source, justify the choice of a minimum size aperture. The savings in size and cost of magnet iron and the reduction of power demands with the small aperture, were the influencing factors in making the decision.

The discussion above illustrates the difficulty of defining a minimum aperture. Injection pulse length will be adjusted in practice to give maximum intensity, in which case the ions at the extremes will be lost to the walls. Oscillation amplitudes may be greater than those estimated in this study, due to factors such as high order resonances, gas scattering or magnetic inhomogeneities which cannot be anticipated. However, the consequence will be loss in intensity due to ions on the periphery of the envelope striking the walls. Our best estimate is that the final intensity will not be reduced below 10 percent of the number accepted into resonant orbits at injection.

8. INJECTION

All considerations point to the desire for high injection energy. The initial frequency increases with injection energy, thereby reducing the range of frequency sweep required; uniformity of magnetic field at injection improves with increasing field; gas scattering decreases with increasing energy. These factors indicate an injection energy of a few million volts. However, there are practical limits on the energy available from existing types of low energy accelerators which are adaptable to this purpose. The electrostatic generator seems to us to fill the requirements for a source of ions more adequately than other types; it has already been developed to provide the voltage uniformity and small divergence required and the ion source can be pulsed if desired. The cyclotron is a possible alternate which would give higher energies but the focusing of the emergent beam is notoriously poor and its energy uniformity cannot be made comparable with the electrostatic generator except by serious reduction of intensity.

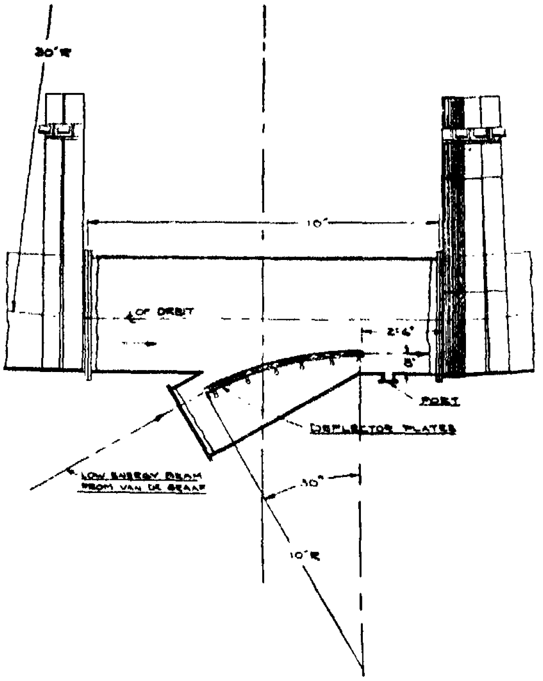

FIG. 7. Electrostatic deflecting system for injection at periphery of vacuum chamber.

Electrostatic generators in the 3–4-Mev range have been developed in several laboratories, with difficulties increasing rapidly toward the top of this range. We have chosen to utilize proven designs and existing knowledge rather than attempt new designs for still higher energy. A "4 Mev" generator will operate reliably at 3 Mev, but usually requires considerable conditioning to operated at its rated voltage. Accordingly, our design parameters are chosen for injection at a minimum of 3 Mev, capable of adjustment to higher injection energy when desired. These parameters are:

Injection energy	3.0 Mev	4.0 Mev
Magnetic field	271 gauss	311 gauss
Ion rotation frequency	0.35 Mc	0.40 Mc
Volts/turn (acceleration)	1040 volts	1040 volts
Time after $B=0$	0.014 sec.	0.017 sec.

Judging from past experience with electrostatic generators, the ion beam at 3 Mev will have an energy spread of less than ±10 kilovolts and an angular divergence smaller than $\frac{1}{4}$ inch in 10 ft. The synchrotron oscillations will require 50 or more revolutions to build up and so have small significance for injection. At these energies and anticipated beam intensities the effects of space charge can be neglected.

A number of methods of injection have been proposed,[7] to minimize loss of ions on subsequent revolutions by striking the injection electrodes or the chamber walls. Some of the methods involve the use of internal electrodes to provide electric fields which will damp the oscillations adiabatically; others propose rapid changes of phase of the accelerating electric fields or a distorted frequency modulation cycle.

The method chosen for injection into the Cosmotron depends on the decrease in radius of path associated with the increasing magnetic field. If particle energy remains fixed (no acceleration during the first few revolutions) the decrease in radius of the equilibrium orbit proves to be: $\Delta R=0.18$ inch/turn. Protons will be injected at one of the straight sections, parallel to the equilibrium orbit at the outer edge of the chamber, at a time when the equilibrium orbit for 3.0-Mev protons is, say, at 2 inches inside the radius of the injector. The ±10-kilovolt energy will result in a band of equilibrium orbits ±1.5 inches wide centered on the mean orbit. The radial betatron oscillations will have initial amplitudes varying between ±0.5 and ±3.5 inches. For a magnetic field index $n=0.6$, the frequency of these radial oscillations is (Eq. (13)):

$$\omega_r=[1+L/(\pi R)](1-n)^{\frac{1}{2}}\omega=0.70\omega. \qquad (14)$$

Hence the maximum positive amplitudes for subsequent revolutions are displaced in angle from the injector position by: 150°, 300°, 90°, 240°, etc. The average particle will make 5 to 10 revolutions before the phase of the maximum amplitude coincides with the location of the injector. If, during this time (15–30 μsec.) there has been no change in energy, the equilibrium orbit will have moved inward 1 to 2 inches, sufficient for a large fraction of the ions to miss the injector.

Angular divergence adds to the radial oscillation amplitudes and also introduces vertical oscillations, with a frequency (at $n=0.6$) of 0.86ω, centered on the median plane. Due to this effect alone, the maximum dimensions of the ion envelope have been computed to be ±0.5 inch vertically and ±0.75 inch radially. Vertical oscillations can be used to advantage by injecting at a position above (or below) the median plane and depending on the mismatch of frequencies to cause the ions to pass below the injector when the radial oscillations alone might cause a hit. So the number of free revolutions can be increased to 10 or 20 and the effective shift in equilibrium orbit radius doubled.

Loss of ions due to impact on the back of the injector or against the walls can be estimated from the considerations above. A short pulse lasting for only a few revolutions, timed for the optimum location of the mean equilibrium orbit (about 2 inches inside the injector), should lose no more than 10 percent during injection. In principle a long pulse could be used, timed to overlap the entire interval during which the equilibrium orbit moves from the injector radius into the center of the chamber, at which point the betatron oscillations fill the chamber. A much larger total number of ions could be thus injected, but the fraction lost would be larger. In practice a variable pulse length and variable injection timer will be used to pick the optimum conditions experimentally.

The electrostatic generator will be so located that the beam is directed at a small angle toward the straight section used for injection. The ions can then be deflected electrostatically so as to enter the first quadrant at the chosen radial position. A field of 50 kilovolts/inch is sufficient to deflect 3-Mev protons on a 10-ft. radius. This deflecting electrode is shown schematically in Fig. 7. Provisions will be made to adjust the radial and vertical location of the deflecting channel and the beam. A channel $\frac{1}{4}$ inch wide will contain the beam, so the minimum orbit shift required to miss the injector is of the order of $\frac{1}{4}$ inch.

The injection scheme described above is most efficient if the ions are not being accelerated during injection. The radiofrequency accelerator can be turned on when the mean equilibrium orbit approaches the center of the chamber, and brought up to full voltage in a few cycles. Within a few hundred cycles synchrotron oscillations will be set up and about half of the uniformly distributed protons will be accepted and trapped in stable synchrotron orbits. The maximum amplitude of the radial synchrotron oscillations is ±8 inches, and on this will be superposed the betatron oscillations whose amplitude will increase due to gas scattering to a maximum of about ±4 inches. This maximum, occurs, however, after the synchrotron oscillations have been damped to some extent. The net oscillation amplitude has, therefore, a maximum value of about ±10 inches.

The beam intensity or number of protons accepted and accelerated during each cycle, depends first on the output of the electrostatic generator. The output desired is a high intensity pulse, of about 100 μsec. pulse length (corresponding to an orbit shift of 7 inches). A development program is under way to provide an ion source for the electrostatic generator which can be pulsed (at 5-second intervals) to provide the highest possible peak intensity. The present estimate of the best peak intensity achievable is 1.0 milliampere of protons accelerated to 3.0 Mev; under these conditions the energy spread and angular divergence will probably be considerably larger than the values obtained for low intensity steady beams. If 10 percent of the protons injected during 100 μsec. are within acceptable oscillation amplitude limits, we could expect 5×10^{10} protons to be successfully injected. Consideration of the scattering due to residual gas in the chamber, and other factors causing loss of intensity, indicate a beam of the order of 10^9 protons per pulse at 3 Bev.

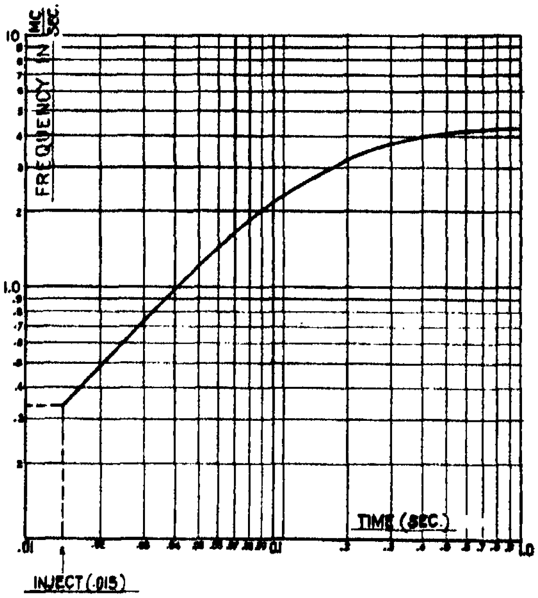

FIG. 8. Cosmotron frequency cycle.

9. RADIOFREQUENCY ACCELERATOR

Ions will rotate in a circular orbit in a uniform magnetic field at a frequency f given by:

$$f=\frac{\omega}{2\pi}=\frac{eB}{2\pi m}=\frac{c^2eB}{2\pi(E_0+T)}. \tag{15}$$

With the racetrack orbit having four straight sections each of length L and four quadrants of radius R, the frequency is decreased by the ratio:

$$\frac{f_i}{f}=\frac{2\pi R}{2\pi R+4L}=0.824. \tag{16}$$

A plot of ion rotation frequency, f_i as a function of time is given in Fig. 8 for the 1-second acceleration cycle. For protons at the injection energy of 3 Mev and the magnetic field of 271 gauss, this frequency is 0.35 Mc, rising to 4.20 Mc at the maximum energy of 3 Bev.

In order to maintain constant radius the ions must be

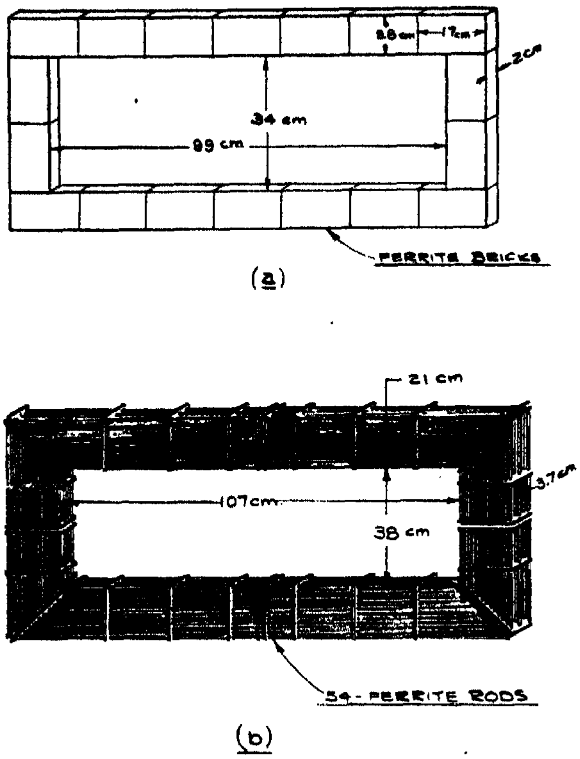

FIG. 9. Typical sections of ferrite core for accelerating transformer.

accelerated on each turn by an amount determined by the rate of change of magnetic field with time, dB/dt. This function of "volts per turn" is plotted in Fig. 6, and shows a value of 1180 volts at injection falling to 680 volts at 1.0 sec. A radiofrequency voltage synchronized with the ion rotation frequency will be applied to the accelerating gap. In order to maintain stable synchrotron oscillations over a wide range of phase and energy the peak r-f voltage should be materially higher than the average "volts per turn" required. A theoretical study[7] shows that a peak voltage double the average requirement will maintain phase oscillations of 0.86π-total amplitude. In this situation the equilibrium phase for protons of the correct energy will be displaced from the voltage peak by 60° and such particles will receive the correct "volts per turn."

The r-f accelerator must supply a potential of about 2400 volts across the accelerating gap at 0.35 Mc, dropping to 1400 volts at 4.20 Mc, following the frequency schedule illustrated in Fig. 8. The precision in frequency required to keep the orbit radius within reasonable limits is of the order of 0.3 percent. The wide frequency sweep and the requirement of following a predetermined schedule, are unique features of the proton synchrotron and pose some of the most difficult problems.

Several methods have been suggested and tested for generating the variable frequency signal. In view of the required precision of the timing and frequency control, electronic tuning appears decidedly preferable to mechanical tuning. The signal generator which has given the most promising results is an LC oscillator in which the inductance is varied by saturation of a ferromagnetic core. The core consists of two toroids of a ferromagnetic ferrite having an initial permeability of the order of 1000. The oscillator tank circuit winding threads both cores, while the control winding has a figure eight configuration around the cores so that no coupling exists between the two windings. The required tuning has been covered with some latitude with this oscillator. When the temperature of the ferrite is held constant to 0.1°C, the oscillator frequency is stable and reproducible at any control current to better than 0.1 percent.

Amplification of the output from the oscillator will proceed in a 4-Mc band width power amplifier. Amplitude control during the cycle will be provided from a pick-up on the accelerating unit.

The proton accelerating system for the Cosmotron presents several new problems. A fixed frequency resonant system, such as the resonant cavity circuit used for electron synchrotrons, would draw excessive power when off resonance. Either the accelerating system must be continuously tuned over the desired frequency sweep, or its impedance must be high enough that it can operate untuned without requiring excessively high power levels. We have chosen the latter approach and have investigated the use of ferromagnetic loading materials to give the desired high impedance accelerating system. This has led to a design which consists of a ferromagnetic core surrounding the vacuum chamber, located in one of the straight sections between magnet quadrants where the magnetic fringing field is negligible. A winding of a few turns excites the core. This winding is supplied from the r-f power amplifier. Evidently the system is a transformer in which the proton beam constitutes a one-turn high impedance secondary.

The input impedance of this system will be:

$$Z = 4\pi\omega N^2(A/d)(\mu/\mu_0)(1/Q+j)\times 10^{-7}\text{ ohm} \quad (17)$$

where $\omega = 2\pi f$, N is the number of turns in the exciting winding, A is the cross section of the core in square meters, d is the length of core in meters, μ/μ_0 is the ratio of permeability of the core material to that for free space and Q is the usual figure of merit of the exciting winding including the effects of core losses.

TABLE I. Comparative properties of magnetic core materials at 1 megacycle.

Material	μ/μ_0	Q
4-79 Mo Permalloy (1 mil lam)	600	0.6
Fe powder (80 mesh grade B)	35	2.0
81 Permalloy powder (120 mesh)	75	1.6
2-81 Mo Permalloy powder (120 mesh)	125	3.0
Typical ferrite	1000	6.0

If, for example,

$$f=1.0\text{ Mc},\quad N=1\text{ turn},\quad A=0.05m^2,\quad d=3m,\quad \mu/\mu_0=1000:$$

$$Z=133(1/Q+j)\text{ ohms.} \qquad (18)$$

The applied voltage on a one-turn winding must equal the peak r-f potential needed for accelerating the proton beam. If this is 2400 volts and Q is 5, the r-f current required would be 18 amperes peak. An alternative arrangement would be for $N=4$ turns in which case the applied r-f potential would be 9600 volts and the r-f current 3.5 amperes. Currents of this magnitude can be supplied by a conventional amplifier using commercially available transmitting tubes. The power requirements for the amplifier are of the order of 100 kw.

The primary problem in this system is the choice of the ferromagnetic core, which must have a sufficiently high permeability at 4.2 Mc to provide efficient flux linkage and which does not introduce unreasonable losses in this frequency range. If the Q of the core is greater than 0.5 up to 4.2 Mc, it will be satisfactory. Fortunately, new materials have been developed during the past few years which have the required properties. These are non-metallic ferrites which have high permeabilities at high frequencies and also have high resistivity so that fine lamination is unnecessary. The components of metallic ferrites are ground, mixed in proper proportions, formed into shapes under high pressure, and then sintered and annealed under controlled temperatures which favor re-crystallization in such a manner that the material acquires ferromagnetic properties. Ferrites having different compositions and treatment show a wide range in properties. In general, high permeability goes with a narrow frequency range and vice versa. Permeabilities of 500 or greater can be obtained with materials having $Q>0.5$ at 4.2 Mc.

A number of ferrites have been investigated and tested. Laminated sheet material such as Permalloy tape in thicknesses of less than one mil, and powdered iron and permalloy have also been tested for comparison. Comparative data on μ/μ_0 and Q for ring core samples of the several materials are given in Table I. The ferrites appear by far the most promising at these frequencies.

The resistivity and dielectric constant of the ferrites are such that eddy current effects will be rendered negligible by lamination to a maximum thickness of about 2 cm.

Two fabrication techniques have been tested, both of which appear to be satisfactory. One procedure involves stacking of "picture frames" of ferrite. The individual frames are assembled as shown in Fig. 9(a) by cementing together 18 ferrite blocks 2×17×9.8 cm. This frame will surround the vacuum envelope with sufficient clearance to allow for insertion of exciting windings. The other procedure uses round, extruded rods about 1 cm in diameter. These rods are stacked and cemented into mycalex supports. The ends of the stacks are ground flat so that, when the core is assembled as shown in Fig. 9(b), series air gaps are less than one mil. Units of both types will be employed in the final core which will have an area of cross section of about 750 sq. cm and will include about 2000 lb. of ferrite. The winding will be effectively a one-turn winding although it will consist of two physical turns so that it can be driven by a push-pull class B power amplifier.

The accelerating field will appear across a short insulating section of the vacuum chamber. The core will be enclosed, except for this gap, in a copper shield. The core sections will be separated by air spaces which will permit forced air cooling and will suppress undesired modes of oscillation. Further suppression of undesired modes can be accomplished by insertion of copper sheets between the core sections.

10. FREQUENCY CONTROL

In order to limit radial excursions of the equilibrium orbit and minimize loss of particles to the walls of the chamber, the frequency of the accelerating r-f must be held to within 0.3 percent of the scheduled value. The scheduled frequency cycle is derived from the magnetic cycle, and can only be determined with precision after magnetic field measurements on the full scale magnet are available. It is possible that the magnetic cycle will be reproducible to a precision better than the above limits. If so, the frequency variation can be programmed. It will be necessary to trigger the start of the frequency cycle from the magnetic field. A signal derived from a back-biased "peaking strip" can be used to initiate the r-f cycle. This time can be varied at will by varying the peaking strip bias. Similar peaking strips can be used to time injection of ions from the electrostatic generator, or any other synchronized operations.

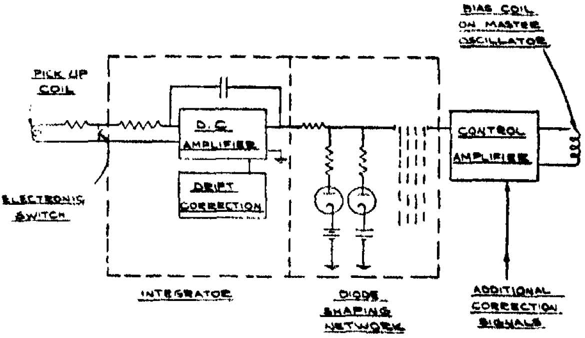

FIG. 10. Block diagram of frequency control system.

Since, in the Cosmotron, the magnetic field is the true independent variable, a preferable frequency control system would be one in which the magnetic field is measured continuously and the frequency is automatically adjusted to the correct value. This is the system which has been adopted for use in the Cosmotron. As shown in the block diagram of Fig. 10 the frequency control system has three essential components —first, an integrating circuit which converts the signal from a pick-up coil in the Cosmotron magnet to a signal directly proportional to magnetic field; second, a network which converts the magnetic field signal to the appropriate frequency control signal; and, finally, an amplifier which applies the control signal to the winding on the ferromagnetic core in the master oscillator. Prototypes of these components have been built and tested. Over periods of several weeks each component is stable and reproducible to about 0.1 percent.

The integrator is a conventional electronic integrating circuit with provision for automatic compensation of zero drift. The conversion circuit is a diode network which automatically switches in successive voltage supplies through adjustable series resistors. This circuit has the virtue that any change made in the relation between output and input at a given time in the cycle affects only the subsequent part of the cycle. This makes adjustment of the circuit a straightforward procedure. To match any possible cycle to 0.1 percent will require about 15 diodes with their associated circuits. The final control amplifier is simple in design since the signal from the control network is already at a high level of about 100 volts. Provision is made in the control amplifier for insertion of correcting signals from other possible sources. For example, an error signal can be derived from a comparison of the outputs of a proton moment magnetic field indicator and of a preset frequency discriminator.

An alternative frequency monitoring method which depends on the radial position of the proton orbit has also been considered in some detail. In principle, an error in frequency will result in a radial shift of the equilibrium orbit. For example, too high a frequency results in a phase shift of the r-f accelerating potential so that the ions get less than the theoretical acceleration per turn and the radius of the equilibrium orbit becomes steadily smaller. To observe this shift in radial location of the ions, a pair of electrodes can be mounted radially inside and outside of the chamber, and the magnitude of the voltage pulses induced on these electrodes by the passage of the bunch of ions can be compared. Electrostatic models of such "pick-up" electrodes have been studied in the laboratory, with a charged wire simulating the beam. Shapes have been developed which have a response linearly proportional to the displacement of the beam from the central orbit. Calculations of the expected induced voltage pulses indicate difference potentials of a few millivolts for a long sausage-shaped bundle containing 10^9 protons located halfway between center and edge of the chamber. It is possible to amplify this difference potential to obtain a signal capable of modulating the frequency of the oscillator so as to correct the ion beam drift. This system suffers from two draw-backs which may be serious. First, it is sensitive to stray pick-up from the main r-f system. Second, during the early stages of tuning up the machine, the beam may not be sufficiently intense to provide a signal detectable above noise and stray pick-up. However, one of the straight sections is allotted to these electrodes, and the control system can utilize this type of signal if it is available.

Another proposal involves the insertion of counters located about the tube so as to pick up a fraction of the scattered ions. In principle, the relative numbers of ions detected by counters one inside, and one outside of the orbit will give a measure of the frequency error.

The more general aspects of the controls needed for the Cosmotron need not be described in detail. All of the usual features of a cyclotron or synchrotron control system will be involved as well as the special requirements of frequency programming. Engineering is now in process on the vacuum pumps and gauges, cooling circuit indicators and interlocks, magnet power supply and time cycling, electrostatic generator (injection timing and pulsing), ion source, r-f oscillator, amplifier and power supply, ejection timing, and the many other circuits required to maintain and operate such a machine by remote control. The combination of high r-f power, a wide frequency range and the sensitive circuits needed for control will require the ultimate in electrical shielding. Personnel hazards and the requirements for remote operation are being carefully considered in designing the circuit interlocks. A large control console in the control room will bring together all of the functions required for operation. This part of the development program will be a continuing one, which cannot be considered completed until the machine is operating at full ratings.

11. VACUUM SYSTEM

Scattering by the residual gas in the vacuum chamber during the 1-second acceleration interval will result in some loss of ions. A theoretical study of this problem[11] shows that the significant scattering all occurs within the first few thousand revolutions or the first 10 milliseconds when ion energy is small and oscillation amplitudes are large. The result of the calculation is that $\mathfrak{X}^2$, the mean square angular divergence due to scattering of the ions from a true orbit is a linear function of proton energy T and gas pressure P:

$$\mathfrak{X}^2 = kP/T. \qquad (19)$$

Vacuum chamber geometry, combined with computed oscillation damping in the synchrotron, can then be used to establish a pressure corresponding to the loss to the walls of any given fracture of the ions. The numerical results are:

$P_{0.5}$ (50 percent proton loss) $= 1.8\times 10^{-6}$ mm of Hg.
$P_{0.1}$ (10 percent proton loss) $= 1.1\times 10^{-5}$ mm of Hg.

---

[11] N. M. Blachman and E. D. Courant, Phys. Rev. 74, 140 (1948).

In the design of the pumping system, the figure chosen as a maximum acceptable pressure is 1.0×10^{-5} mm of Hg. This is to be achieved with 12 or more pumping stations around the periphery of the chamber, each consisting of a 20-inch oil diffusion pump and equipped with refrigerated baffle, close-off valve, and the necessary valves and gauges. Four centrally located fore pumps will supply the rough backing vacuum for the twelve diffusion pumps. Speed at the entrance to the vacuum chamber spout will be about 2500 liters per second at 10^{-5} mm of Hg for each pump unit. The units will be interchangeable for ease in maintenance and testing. They are shown in the plan view of the Cosmotron, Fig. 3.

The method of fabrication of the vacuum envelope is the subject of an experimental program which has not yet arrived at the most satisfactory solution. To avoid induction of eddy currents in the wall of the vacuum envelope, a non-conducting vacuum wall would be preferable. The chamber must however, fit in a space roughly 9×36 inches and must waste as little as possible of this aperture. Strength tests have been made on ceramic sections of roughly elliptical cross sections having outside dimensions 34½×9 inches. The walls were one inch thick, increased to 1¼ inches at the ends of the long axis. These sections collapsed under pressure of about one atmosphere and so are obviously unsatisfactory for this application.

The elliptic cross section of the ceramic chamber was rather wasteful of space and this design has now been superseded by a chamber of rectangular cross section constructed partly of metal and partly of an insulating plastic. Metal foil will be bonded to the inside of the chamber so that no plastic is exposed to the vacuum. Mechanical strength will be obtained by supporting the chamber walls from the magnet structure. Model tests on various configurations of this type indicate that satisfactory mechanical and vacuum properties can be attained without undue disturbance of the magnetic field by eddy currents in the chamber walls.

In the straight sections where magnetic fields are low, solid metal can be used for the vacuum envelope. In the accelerating section, an insulating ring will be introduced across which the radiofrequency accelerating fields will appear.

12. EJECTION

The basic design of a "C" magnet with the slot for the vacuum chamber on the outside provides a favorable situation for obtaining an emergent beam of protons. Another advantage of the Cosmotron over electron synchrotrons is the long acceleration time after injection; during this 1-second interval ejection electrodes or magnetic peelers which might distort or interrupt the beam at injection, can be inserted. By 0.1 second the ions will have reached an energy of 300 Mev and the radial oscillations will be damped to small amplitudes around the central orbit.

A movable "peeler" or magnetic shield has been designed which can be located well outside the ion orbits at injection and then inserted to the proper radius for ejection before the ions have reached final energy. The peeler is a simple magnetic shield formed of a block of iron with a slot or channel through which the ions can travel. A similar device has been used to obtain an emergent beam of electrons from the betatron. The peeler will be located in a vacuum housing with sliding seals to allow radial motion. The external position will be determined by magnetic model tests so as not to distort the magnetic field at the orbit.

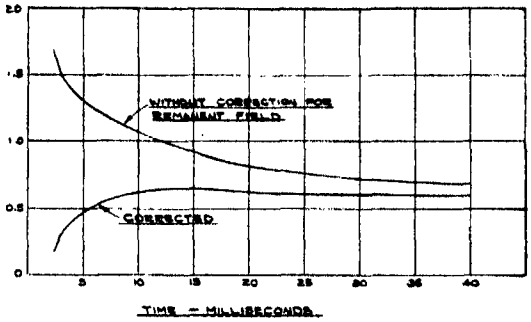

FIG. 11. Model measurement of n value (exponent for radial variation of magnetic field) for short times, showing the effect of eddy currents in the ½-inch laminations. (Injection occurs at 14 milliseconds.)

When using the peeler the ion beam, normally following a central orbit, can be expanded by changing the frequency and hence the phase of the accelerating electric field. A reduction of 1 percent below the resonant frequency will cause the orbit to expand by 9 inches, sufficient to throw the beam into the slot of the peeler. This frequency shift can be timed to eject ions at any desired energy. While passing through the weak field in the peeler channel (about 50 percent of normal) the ions will travel on a larger radius path. The azimuthal location of the peeler is chosen to eject the ions from one of the straight sections, so that a vacuum beam pipe can emerge tangentially to contain and collimate the ejected protons. Pulsed electrostatic fields can be used if necessary to excite radial oscillations and throw the ions out into the peeler channel within a few revolutions.

The efficiency of such an ejection scheme cannot be predicted. Up to the present time only a small fraction of the circulating electrons in a betatron have been ejected. The emergent beam from the Berkeley 184-inch synchro-cyclotron contains about 10 percent of the resonant ions. Assuming a similar success for the Cosmotron, we might expect as much as 10^8 protons per pulse in the ejected beam. With electrostatically pulsed ejection this number might be emitted within about 1.1 μsec.; with the magnetic peeler alone the protons would probably be distributed over a sequence of 10–20 pulses at 4.1-Mc frequency. Both forms of the ejected beam have their advantages for specific detec-

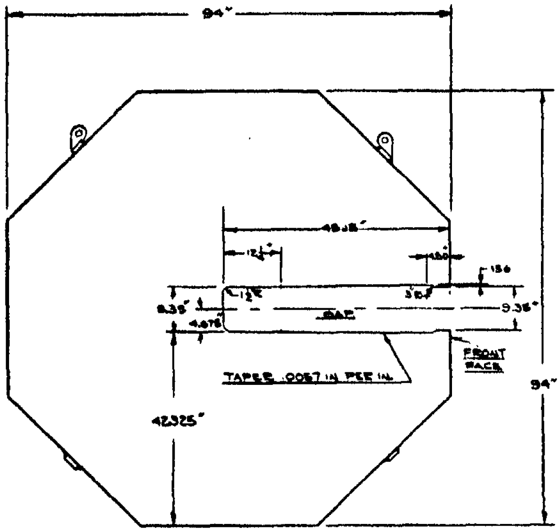

FIG. 12. Magnet lamination showing shape of gap contour.

tion instruments; the single pulse might be desirable for cloud chambers and the multiple pulses for electronic coincidence counters.

Many experimental detection techniques do not require an emergent beam. Photographic film can be mounted on probes at any position around the circumference with vacuum locks to expedite removal. High speed neutrons will emerge tangentially from the periphery, at whatever points the expanding orbits intersect probes or walls. A specific "neutron spout" has, in fact, been designed, consisting of a *T* section in which a probe target can be mounted, with a tangential spout through which the neutrons will emerge. These alternate methods of employing the high speed ions multiply the usefulness of the instrument for research.

13. MAGNETIC PROBLEMS

a. Eddy Current Effects

Dynamic measurements of magnetic field performed on a one-quarter scale model of a short sector of the magnet show that eddy current effects in the ½-inch magnet laminations will be appreciable during the first 30 or so milliseconds. Qualitatively the effect of eddy currents is to reduce the magnetic field at the mid-portion of the gap as compared with the field near the exciting windings. As a result, the rate of field decrease with radius or "n" value (see Eq. (11) above) is increased. The magnitude of this increase in n value has been measured by observing the difference in induced voltage in two coils spaced a short distance apart radially, and located at various positions across the gap. Photographic recordings of the integrated difference voltage displayed on a cathode ray tube have been analyzed to obtain the n value as a function of time. "Δn" or the increase in n over steady state conditions is found to have a large value at very short times; but to be down to about 0.4 at the time corresponding to injection, when the magnetic field is 271 gauss. In Fig. 11 a time plot of n at the central orbit position is given to illustrate the magnitude of this effect before and after injection.

A theoretical study[12] of eddy currents in the ½-inch plates checks the experimental findings and allows extrapolation beyond the extent of the experiments.

If required, this variation of n could be corrected by auxiliary windings distributed across the pole faces. A 48-turn winding (24 on each pole face) would require a current of less than 1 ampere during the first 30 milliseconds in order to compensate for the eddy current effects.

b. Remanent Field

The remanent field resulting from unidirectional operation has also been measured. It is found to have a value of about 30 gauss and to increase almost linearly by about 25 percent from the face of the inner exciting coil to a point near the outer end of the air gap.

The initial negative Δn due to the remanent field decreases with increasing field, and almost completely compensates for the positive Δn at short times due to eddy currents. The maximum resultant Δn measured as the sum of both effects at injection time and over the useful width of pole face is the order of ± 0.1. This is considered to be sufficiently small to make further corrections for eddy currents unnecessary. The variation of n after correction for remanent field effects is shown in Fig. 11.

c. Saturation Effects

At high fields, the permeability of the magnet iron decreases and an appreciable fraction of the magnetomotive force appears in the iron. Due to the *C* shape of the magnet and the resulting large difference in iron path length for flux crossing at the two ends of the gap, the effect of decreasing permeability is to cause an increase in n value at high fields. Results from model tests indicate a measurable rise in n value, starting at about 9000 gauss in the gap, increasing to a Δn of about 0.7 by the time the field reaches 14,000 gauss.

This large change in n value due to saturation effects cannot be permitted, and must be compensated by auxiliary windings. Accordingly designs are in process for a single layer winding on the surface of each pole face adequate to supply the necessary correcting field. These windings will each have 24 turns of 1×⅛-inch copper bar, wound flat with suitable insulation between turns and to the pole. The space required for these windings will probably be reduced to a minimum by imbedding them in the upper and lower walls of the vacuum chamber. To provide correction for a Δn of 1.0 at 14,000 gauss the peak current in these windings would be about 800 amperes. The corrective cycle would require zero current up to about 0.6 sec., an increase of current to a maximum at 1.0 sec., and then a reduction to zero current as rapidly as possible. The time constant of these windings is about 0.1 times that of the main windings, so this condensed time cycle should be possible with applied potentials no higher than required for the main windings. The short cycle and sharp peak call for average power levels of only a few hundred kw.

---

[12] M. H. Blewett, Phys. Rev. 75, 1288 (1949).

d. Pole Face Shaping

To attain a value of $n=0.6$ requires a taper shaping of the pole faces. The pole contour has been derived from model experiments and is shown in Fig. 12. A straight taper cut starting about 4 inches from the front of the main winding produces a 3 percent maximum increase in air gap. At the periphery a lip of iron is retained to extend the region of uniform field to the maximum possible radius. This contour yields a usable field at injection over a radial distance of about 31 inches.

e. Mechanical Problems

Magnetic forces on the coil system and on the iron laminations will be considerable and must be taken into account in the magnetic design. The force on the central winding is inward and tends to compact the coil; that on the return windings is out and away from the gap, requiring closely spaced heavy brackets. The laminations repel one another and tend to spread apart into the air spaces between blocks. This force will be retained by hardwood wedges driven between magnet blocks in the air spaces near the pole face. The laminations of the end blocks of the quadrants will be held together by several insulated bolts. Blocks will be welded together externally to make a rigid unit. Mechanical tests on models have shown these to be satisfactory procedures to prevent lamination spreading.

f. Magnetic Testing Program

The magnetic properties of each magnet block will be checked in detail in order to determine the order of their arrangement in the final magnet which gives the best azimuthal uniformity of remanent field, magnetic median plane, n value, and any other parameter which appears to be important. This will be done by measurements on a full scale three-block model in which the block under test is set between two standard guard blocks. The model will be magnetized to full field using a one-second cycle which duplicates as closely as possible the final operating cycle.

14. SHIELDING AND BUILDING

The radiations from the Cosmotron may be a serious hazard to personnel. The maximum expected beam intensity, of 10^9 protons at 3-Bev energy 12 times a minute, is equivalent to an average power output of 0.1 watt. This may be compared with the 2 microampere time average beam of 200-Mev deuterons from the Berkeley 184-inch synchro-cyclotron, equivalent to 400 watts, or the 4 kilowatt beams for 60-inch standard cyclotrons. After the high energy radiation has been scattered and distributed among secondary radiations, the intensity is to a good approximation proportional to the beam power. On this basis the intensity of scattered radiation from the Cosmotron should be about 2.5×10^{-4} that from the synchro-cyclotron or 2.5×10^{-5} that of a 60-inch cyclotron. The shielding for scattered radiation adequate for the 184-inch machine is 2 ft. of concrete (overhead), providing an attenuation of 10^{-2}; that for a 60-inch cyclotron is 3 ft. for an attenuation of 10^{-3}. On this basis the overhead scattered radiation from the Cosmotron without overhead shielding is $0.025=1/40$ the intensity from these two machines with shielding. Conclusions from this analogy may not be legitimate, however, since the initial energies involved are materially higher than those produced by cyclotrons. An interpretation has been attempted of available data on cosmic-ray absorption and the results, based on several reasonable but uncertain assumptions, indicate the possibility of a dangerously high level of scattered radiation. Moreover, the possibility exists that a higher beam intensity than that mentioned above may follow from ion source developments. The Cosmotron building has, therefore, been designed so that the machine can be enclosed in a concrete housing having walls ten feet thick and a roof four feet thick. This housing will not be set up until the machine has been operated and the intensity of the scattered radiation has been measured.

The penetrating 3-Bev protons and their high energy

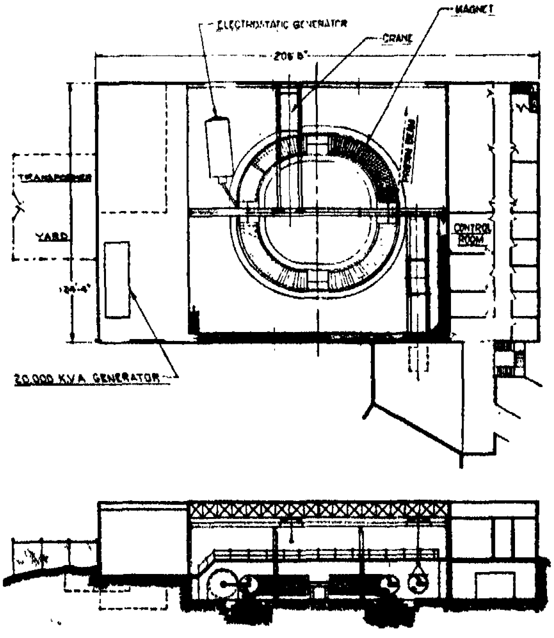

FIG. 13. Building plan and elevation for the laboratory to house the Cosmotron.

secondaries will be severely collimated in the horizontal plane. In this narrow band 4½ feet off the floor, the intensity will be dangerous. The Cosmotron is to be located in an excavation so that this radiation impinges on earth on three sides. The fourth side, in the direction of the ejected beam, is left open so the beam can shoot out across a flat area for experimentation at a distance from the machine, if desired. This area is unoccupied and fenced so that personnel cannot gain access during operation. Operators and maintenance personnel are located on an upper floor, overlooking the Cosmotron pit.

Build-up of contaminating radioactivities will also be approximately proportional to the average power level, and so will be negligible as compared with cyclotrons.

The building design is based on the shielding requirements described above, with control rooms, laboratories, offices and power house on the upper level. Two 10-ton traveling cranes will cover the working floor area. The power house for the magnet power supplies and auxiliaries occupies another large area. Control rooms, both for Cosmotron operation and for experiments, overlook the ejection quadrant and emergent beam run. A plan view of the building is shown in Fig. 13. Construction has started and the laboratory should be ready for occupancy early in 1950. Schedules for erection of the iron, winding the exciting coils, installing power equipment, and assembly of the vacuum chamber and auxiliary equipment indicate that the machine should be assembled late in 1950.

This design study represents the collaborative efforts of some 30 members of the Accelerator Project of the Brookhaven National Laboratory and also of several consultants. Each member has assisted in the progress of the design, but it is impractical to attempt to identify the individual contributions. The authors wish to recognize and credit these contributions to the joint effort. The present stage could not have been attained without the wholehearted assistance of many members of the Brookhaven Laboratory Staff and their Scientific Advisors.

THE REVIEW OF SCIENTIFIC INSTRUMENTS VOLUME 21, NUMBER 1 JANUARY, 1950

A Simple Pressure Balance

C. A. Swenson*
The Clarendon Laboratory, Oxford University, England

(Received August 1, 1949)

Precise pressure measurement in the range from 5 to 100 atmos. is quite a difficult problem. A set of high pressure mercury manometers is very unwieldy and difficult to use, while Bourdon gauges require frequent recalibration and are inherently inaccurate. The most likely solution for this problem is to use a simple piston-in-cylinder pressure balance, which, for these pressures and for accuracies of the order of 0.05 percent, can be relatively crude, and does not require excessively precise machining or care in use. A simple pressure balance was constructed for use in the pressure range from 25 to 35 atmos., and used for both pressure measurements and density change determinations. It proved perfectly satisfactory, giving pressures reproducible from day to day to about 0.01 atmos.

THE accurate measurement of pressure in the range from 5 to 100 atmos. offers quite a serious problem. For low pressures, quite accurate and reproducible pressure measurements can be obtained by means of a mercury manometer of sufficient length. However, above roughly 5 atmos. the mercury column becomes rather long (well over ten feet) and the set-up becomes unwieldy and difficult to use.

An alternative is to use a Bourdon gauge. Here, while the instrument is compact and easy to use, it is accurate at best to only one-half percent of its full-scale reading, unless the gauge is specially built and calibrated against a standard over the range of pressures in which it is to be used. There is always the danger of drift, and frequent recalibration is necessary.

The usual method used for the calibration of a Bourdon gauge is to compare it with a pressure balance. A pressure balance is essentially a piston which fits closely into a cylinder filled with oil, and a schematic diagram of a very simple model is shown in Fig. 1. Since the pressure on the oil is given by the weight of the piston (W) divided by its area (A), this is an absolute rather than secondary means for measuring pressure. In practice, the weight, W, is slowly increased (or, preferably, decreased) until the unknown pressure, P, is "balanced" by W/A, and the piston "floats" at some intermediate position between the top and bottom of the cylinder. Less weight would cause it to rise out of the cylinder, while more weight would cause it to sink to the bottom.

While this forms a very convenient method for calibrating a gauge, there is no reason why a pressure balance should not be used to measure an unknown pressure directly, instead of using an intermediate secondary standard. Pressure balances have been used directly at very high pressures and to very great accuracies, particularly by Michels of Amsterdam, and for this work a great deal of skill and experience is necessary.[1]

---

* Now at Harvard University.

However, for moderate accuracies, say 0.05 to 0.1 percent, and for pressures up to 100 atmos., the set-up need not be complicated at all. The weight can be of moderate size, and the piston large enough so that sufficient accuracy in the machining and the measurement of the diameter is easily obtained. For these accuracies and pressures, most of the difficulties, such as thermal expansions, deformations of the cylinder with pressure, etc., encountered in the more accurate and high pressure work, are negligible. While the above-mentioned accuracies are easily obtained, if another factor of five or ten were desired in the accuracy, a great deal of skill, patience and hard work would be required to produce a satisfactory instrument. Above 100 atmos. the weight becomes quite large for moderate sized pistons, and the balance either becomes very clumsy, or very precise machining is necessary.

The pressure balance can also be used as a means for measuring changes in density at constant pressure, while, for instance, the temperature of a substance is varied. Variations of density are shown by the rise or fall of the pressure balance piston as it increases or decreases the volume of the system to maintain the pressure at its constant value. Thus, direct measurements of density changes can be obtained by observing the change in the height of the piston. Probably the most elementary application of this would be to measure the change in volume of a gas upon liquefaction under pressure.

These conclusions led to the construction of a very simple pressure balance at this laboratory for use in some experiments on the melting curve of helium, and it has proved so satisfactory, both as a pressure measuring device and as a means for determining density changes, that it was thought worth describing in some detail.

DESCRIPTION OF THE APPARATUS

A sketch of the pressure balance cross section and set-up is given in Fig. 2. The pressure balance consists of a silver steel piston, *A*, 1.152 cm in diameter, which has been lapped into a mild steel cylinder, *B*. The piston is about 15 cm long to allow for volume changes of the order of 10 cc. The piston is set into a re-entrant cavity in the mild steel weight, *C*, to make the center of gravity of the weight as low as possible. This is quite important when it is realized that by using this size piston to produce an absolute pressure of 24 atmos. (which was used as a minimum pressure for this work), a weight of about 25 kg is needed. It probably would have been better to place the center of gravity of the weight below the end of the piston; however, the present set-up seems quite satisfactory.

The pressure is transmitted to the gas through vacuum pump oil to an oil reservoir, *D*, of about 200 cc capacity. This oil also acts as a lubricant between the piston and cylinder walls, and the oil that escapes through the separation between the walls is replenished periodically through an opening not shown. This leakage oil is collected in the flask, *E*. The space above the oil surface in *D* is filled with helium under pressure—the pressure determined by the weight and cross section of the piston. The valve, *F*, is a needle valve to either high pressure helium (to raise the piston) or to the atmosphere (to drop the piston). The valve, *G*, goes to the cryostat. A large Bourdon manometer is also in the system to indicate the pressure roughly, although all pressures are calculated from the diameter of the piston and the weight.

To insure that there is a continuous film of oil between the piston and the cylinder walls, the piston is rotated at about 30 r.p.m. by a small electric motor, *H*. The contact, *J*, is made as frictionless as possible by having a roller on the arm attached to the weight and a roller on the arm from the motor. While it is considered very desirable to have the pressure balance rotating freely while taking a reading, often the density changes that were measured took place in a half-hour, while the system would rotate freely for only five minutes or so. To give a semi-free rotation the center of rotation of the arm on the motor is placed slightly off the center of rotation of the piston-cylinder combination. This gives the motor arm a variable speed relative to the weight, and contact at *J* is made only for a short interval during each revolution; that is, when the motor arm is closest to the weight. The rest of the time the weight is rotating freely. A circular disk is placed on the motor arm to prevent the piston from rising out of the cylinder.

The pressure is changed by adding weights to the top of *C*, and, roughly, 10 g=0.01 atmos. Changes in height

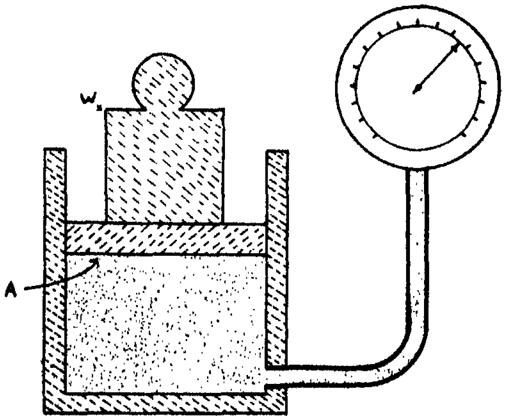

FIG. 1. Schematic diagram of a very simple pressure balance.

---

[1] See, for example, D. M. Newitt, *High Pressure Plant and Fluids at High Pressure* (Oxford University Press, New York, 1940), p. 113.

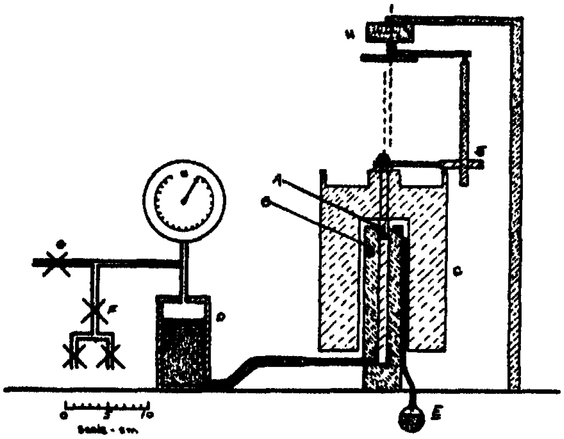

FIG. 2. Cross section of the pressure balance and oil reservoir.

are measured by a stationary centimeter scale placed beside a pointer on the rotating weight.

PERFORMANCE

Since a more standard means of measuring pressure was not available in the laboratory, the absolute pressures determined by the pressure balance are not known to better than 0.2 percent. However, no special effort was made to obtain exact absolute pressures, since for this work the main interest was in dp/dT and the important factors were reproducibility and sensitivity to pressure differences. Thus, in all calculations, it has been assumed that the pressure generated is that obtained by dividing the weight of the piston-weight combination by the area of the piston as calculated from its measured diameter. Absolute pressures are obtained in any given instance by adding barometric pressure to this value, plus the additional pressure due to any weights placed on the top of the piston.

Because there was some possible inaccuracy in the measured value for the piston diameter, the area of the piston was roughly checked by replacing the large weight by a much smaller one and calibrating the result against a two-meter open mercury manometer. The resulting effective area (1.042 cm^2) agreed with the calculated one to 0.1 percent. The final uncertainty was determined by the reproducibility of the pressure balance at these low pressures and the accuracy to which the difference in oil level between the reservoir and cylinder could be determined. This shows that there is little deformation of the cylinder with pressure, as would be expected at these relatively low pressures. Since the weight was known to about 0.05 percent, absolute pressures are known to approximately 0.2 percent.

The reproducibility of the pressure balance, however, is much greater than this, and was checked by repeating melting point determinations on different days for the same cryostat temperature. These results have shown that the pressures are reproducible to ±0.01 atmos. at 25 atmos. The same criterion shows that no variation of pressure with height greater than this exists, so that the balance seems to be working as well as had been hoped.

No precautions need be taken to insure this accuracy, except that a supply of oil be present, and that the rotation is continuous. Thermostating is not necessary, since any error introduced into the effective area and hence into the pressure by thermal expansion is less than 0.01 percent for temperature changes of the order of five degrees centigrade. While it is desirable to have the weight placed as symmetrically as possible, asymmetries seem to have no noticeable effect.

For density changes this pressure balance is not quite as satisfactory, although it does everything that is required of it in our experiments. While the normal rate of fall of the piston is a direct function of the viscosity of the oil, the speed of response of the setup depends inversely on the viscosity. Since the instrument is used in a dynamic manner, this is quite important. So, a compromise was made between oil leak (which should be very small) and speed of response. Shell Box Pump Oil was found to be quite satisfactory, with the piston dropping rather slowly (about 2 cm/hour), and responding to changes in pressure fairly rapidly. This correction to the observed data for normal rate of fall is usually about ten percent for our work, so if the leakage rate is known to 20 percent (changes in room temperature, length of time the balance has been running, height of piston, all seem to have slight effects), the results should be good to about 2 percent. They are definitely as reproducible as this. It has been found that the pressure balance must rotate for an hour or so before it will give reproducible rates of fall, and this is probably the time necessary to insure proper lubrication. In using the balance to measure density changes, however, care must be taken to insure that room temperature does not change during a run, or that the reservoir, *D*, and other large volumes are thermostated.

I wish to thank Professor F. E. Simon for his interest and advice. I also wish to express my appreciation to Mr. A. Charters for his technical assistance. This work was made possible in part by a Parker Fellowship in Physics from Harvard University, and in part by a grant from the Carnegie Fund for Overseas Students.

THE REVIEW OF SCIENTIFIC INSTRUMENTS VOLUME 21, NUMBER 1 JANUARY, 1950

A Versatile Pneumatic Instrument Based on Critical Flow

W. A. Wildhack
National Bureau of Standards, Washington, D. C.

(Received June 20, 1949)

Gas flows through two restrictions in series, the second one or both being a nozzle operating with sonic throat velocity so that discharge is independent of the downstream pressure. For fixed restrictions, the ratio of entrance pressures at the two restrictions depends on their relative sizes and the ratio of entrance temperatures. After calibration, the pressure ratio may be used to measure temperature with a sensitivity of 1°C or better over a range of 2000°C. With the same arrangement, the temperature being constant, the intermediate pressure is a direct measure of mass flow. A sensitivity of better than 0.1 percent is possible in this measurement. For given temperatures, the device can be used as a "pressure divider," with the intermediate pressure controlled by adjusting the restrictions, or as a pneumatic micrometer. Gas analysis is accomplished by removing one component of the gas flow between nozzles. A vacuum pump is used, if necessary, to ensure critical discharge through one or both nozzles; divergent cones on nozzles may be used to minimize pressure drop.

WHEN gas flows through a properly shaped restriction (a nozzle) with the ratio of throat or exit pressure to the entrance or upstream pressure being less than a so-called critical value (roughly 0.5 for air), sonic velocity is attained at the throat, and the mass discharge no longer depends on the value of the downstream pressure. If a divergent cone is used after the throat of the nozzle, a considerable recovery of pressure is obtained at the exit of the cone, although the critical ratio still obtains between the pressure at the throat of the nozzle and the entrance pressure.

These phenomena have been utilized in the design of a new instrument, or family of instruments, for measurement and control of various quantities, such as pressure, temperature, flow, humidity, gas composition, or mechanical displacement. In the simplest form, critical flow is maintained through two nozzles in series. Variations in flow through the first nozzle, occurring with changes of pressure, temperature, or size, are reflected as a change in absolute pressure at the entrance to the second nozzle. The value of this absolute pressure serves as a measure of the variable causing the change. Similarly, a change in composition of the gas stream occurring between the two nozzles is likewise reflected as a change in the absolute pressure at the entrance to the second nozzle.

Essentially the same results are obtained if an orifice-nozzle series is used, although the sensitivity is somewhat reduced. Fairly simple quantitative expressions may be derived relating the absolute pressures and temperatures under the various conditions of use.

FLOW THROUGH NOZZLES AND ORIFICES

The essential characteristics of gas flow through orifices and nozzles are shown graphically in Fig. 1, in which the relative flow is given as a function of pressure ratio.

For a nozzle, the volume flow, Q_e, measured at the entrance pressure, P_e, is related to the ratio, r, of throat to upstream pressure by the expression

$$Q_e=CA\left(\frac{2n}{n-1}\right)^{\frac{1}{2}}r^{1/n}(1-r^{(n-1)/n})^{\frac{1}{2}}\left(\frac{P_e}{\rho_e}\right)^{\frac{1}{2}}, \qquad (1)$$

where n is the ratio of specific heats, A is nozzle throat area, C is a discharge coefficient (between 0.95 and unity), P_e and ρ_e are upstream, or entrance, pressure and density. This holds for values of r between unity and the critical pressure ratio

$$r_c=\left(\frac{2}{n+1}\right)^{n/(n-1)}. \qquad (2)$$

Beyond the critical pressure ratio, r_c, the volume flow as measured at the entrance pressure, P_e, is independent of changes in r. Under these conditions, the *characteristic critical flow* of the nozzles, F_e, for the entrance temperature, T_e, in terms of volume at the upstream, or entrance, pressure is

$$F_e=CA\left(\frac{2n}{n+1}\right)^{\frac{1}{2}}r_c^{1/n}\left(\frac{P_e}{\rho_e}\right)^{\frac{1}{2}}=KAT_e^{\frac{1}{2}}. \qquad (3)$$

For air at 0°C and $C=1$, this *characteristic critical flow* is

$$F_0=1114\text{A}, \qquad (3a)$$

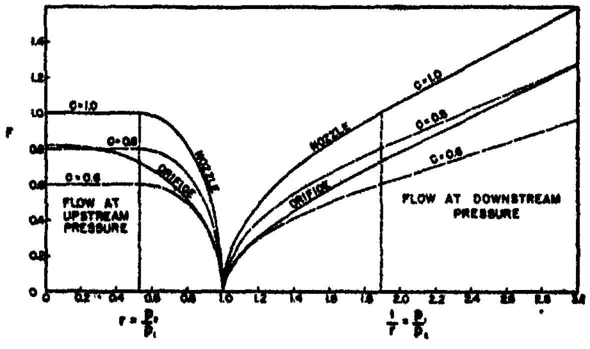

FIG. 1. Flow chart for nozzles and orifices.

when F_0 is in liters per minute and A is in square centimeters. The mass flow through the nozzle is

$$M_N=\rho_eF_e=K_NP_eT_e^{-\frac{1}{2}}, \tag{4}$$

where the factor K_N includes the first two factors in Eq. (3), the gas constant, and appropriate conversion factors for the units chosen. There are certain corrections required to Eq. (4), particularly at high pressures or low temperature, because of deviation of gases from ideal behavior.

Careful calibration of the nozzle under the expected operating conditions can obviate much tedious computation and is, in any event, a desirable check on computed characteristics.

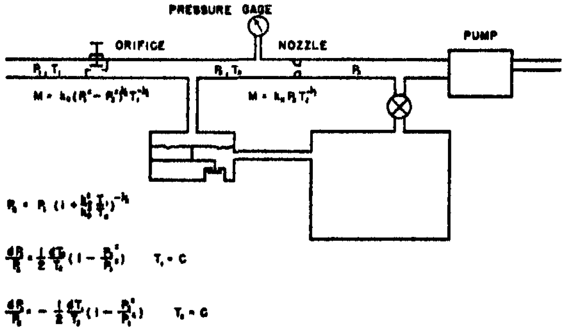
PRESSURE GAGE
ORIFICE
NOZZLE
PUMP
P_1, T_1
P_2, T_2
P_3
$M = K_0(P_1^2 - P_2^2)^{\frac{1}{2}}T_1^{-\frac{1}{2}}$
$M = K_N P_2 T_2^{-\frac{1}{2}}$
$P_2 = P_1\left(1+\frac{K_N^2}{K_0^2}\frac{T_1}{T_2}\right)^{-\frac{1}{2}}$
$\frac{dP_2}{P_2} = \frac{1}{2}\frac{dT_2}{T_2}\left(1-\frac{P_2^2}{P_1^2}\right)$ $T_1 = C$
$\frac{dP_2}{P_2} = -\frac{1}{2}\frac{dT_1}{T_1}\left(1-\frac{P_2^2}{P_1^2}\right)$ $T_2 = C$

FIG. 2.

The flow equation for sharp-edged orifices, in plates no thicker than the diameter and for pressure ratios near unity, is roughly approximated by the nozzle formula, Eq. (1), multiplied by a discharge coefficient of about 0.6. However, this approximation becomes worse for lower pressure ratios. The orifice discharge does not become constant but continues to increase at decreasing pressure ratios. The orifice curve shown on the chart of Fig. 1 for air, is based on the experimental work of Bachmann.[1] This curve may be fairly well approximated over the entire range by the same equation which applies closely for orifices (or tubing) at pressure ratios near unity, with the density assumed proportional to the mean pressure:

$$M_0=K_0(P_1^2-P_2^2)^{\frac{1}{2}}T_1^{-\frac{1}{2}}, \tag{5}$$

where K_0 includes the area, an "effective" discharge coefficient, and normalizing factors. M_0 is the mass discharge through the orifice, P_1 and P_2 are upstream and downstream pressures, and T_1 is upstream temperature. The actual values of C appropriate for different orifices may differ by several percent, but the form of the flow curves is presumably the same.

Both nozzle and orifice equations have corrections for velocity of approach, if the gas stream is moving at a high velocity before entering the restriction. This may be taken into account, approximately at least, by taking the entrance pressure and temperature of the gas as that which would be obtained if the gas were brought to rest at the entrance.

OPERATING PRINCIPLES OF THE INSTRUMENT

The device to be described consists basically of two restrictions in series, through which gas is drawn by suction or forced by pressure, and a pressure-measuring instrument connected to the line between the two restrictions. Figure 2 shows one embodiment of the device, in which the first restriction is a variable orifice, the second a nozzle, and the gas is drawn through the system by a vacuum pump of sufficient capacity to ensure critical discharge.

The mass flow through the two restrictions must be the same at equilibrium conditions. By equating the appropriate flow equations for the two restrictions, we may obtain expressions for the intermediate pressure (between restrictions) in terms of the geometry of the restrictions, one or both of the pressures beyond the restrictions, and the temperatures of the gas at the entrances to the restrictions. For an orifice followed by a nozzle, we equate Eqs. (4) and (5) and obtain

$$P_2=P_1\frac{K_{O_1}}{K_{N_2}}\left(\frac{T_2}{T_1}\right)^{\frac{1}{2}}\left[1-\left(\frac{P_2}{P_1}\right)^2\right]^{\frac{1}{2}}, \tag{6}$$

which may also be expressed: (after squaring, rearranging, and solving)

$$P_2=P_1\left(1+\frac{K_{N_2}^2}{K_{O_1}^2}\frac{T_1}{T_2}\right)^{-\frac{1}{2}}, \tag{6a}$$

where the sub-subscripts indicate the first or second restriction.

For a nozzle followed by an orifice:

$$P_2=P_1\frac{K_{N_1}}{K_{O_2}}\left(\frac{T_2}{T_1}\right)^{\frac{1}{2}}\left[1-\left(\frac{P_3}{P_2}\right)^2\right]^{-\frac{1}{2}}. \tag{6b}$$

For two orifices:

$$P_2=P_1\frac{K_{O_1}}{K_{O_2}}\left(\frac{T_2}{T_1}\right)^{\frac{1}{2}}\left[\frac{1-(P_2/P_1)^2}{1-(P_3/P_2)^2}\right]^{\frac{1}{2}}. \tag{6c}$$

For two nozzles:

$$P_2=P_1\frac{K_{N_1}}{K_{N_2}}\left(\frac{T_2}{T_1}\right)^{\frac{1}{2}}. \tag{6d}$$

For any of these arrangements in which the pressure ratio for a nozzle is sub-critical, the equation which applies is approximately the same as that for an orifice replacing the nozzle, except that the coefficients K_N (sub-critical) would be from 1/0.7 to 1/0.6 times the K_0 corresponding to the same diameter (as may be seen by inspection of Fig. 1).

---

[1] Bachmann, "Messung von Luffmengen," Doctoral Dissertation, (Published by C. Pfeffer, Darmstadt, 1912). Recently translated by Lyman M. Van der Pyl, Rockwell Manufacturing Industries, Pittsburgh 8, Pennsylvania.

It is clear that with these arrangements for which the absolute pressure P_2 is a function only of P_1, the temperatures T_1 and T_2, and the areas A_1 and A_2, it may be taken as a measure of any one of these quantities if the others are constant, or known.

The device can thus serve as:

(1) A wide-range, sensitive thermometer (with fixed areas, P_1 and T_1 (or T_2), known or constant, and T_2 (or T_1) variable, P_2 is a function of the variable temperature).

(2) A pressure divider (with area and temperature ratios constant, P_2 is a constant fraction of P_1).

(3) A pressure controller (with the areas of one of the restrictions adjustable, the pressure ratio changes with the area ratio).

(4) A flowmeter (with temperature T_2 and area A_2 constant, and other factors varied arbitrarily to vary the flow, P_2 is a direct measure of the mass flow).

(5) A micrometer (with temperature and P_1 constant, variation of A_1 or A_2, as by displacement of an object near the nozzle, or by a sliding or rotating valve, will cause a corresponding variation in P_2). When connected to other devices for translating various physical quantities into displacement, this gives an alternative method of measurement and control of very wide scope.

(6) A gas analyzer (with one component of the gas being removed, or changed, by chemical action between the nozzles, the change in P_2 is a measure of the fractional change in the mass flow). Using two nozzles, both operating at critical discharge, with some difference between the normal value of P_2 and its permissible upper design limit (which is set by the requirement of critical discharge through the first nozzle), some further resistance to flow may be permitted between the two nozzles without changing the "normal" value of P_2. This allows a long connecting line, or the inclusion of a chemical scrubber or reactor of one type or another.

It has been stressed that for accurate measurements, calibration is essential. The "errors" or deviations from predicted performance, particularly with both nozzles under critical flow conditions, arise mainly from the equation of state for the gas. Information may therefore be obtained on the equation of state by study of the variation of the pressure ratios from predicted values under various conditions of pressure and temperature. Studies with various gases under the same conditions should yield information on *relative* thermodynamic properties.

The schematic arrangement shown in Fig. 2 will be referred to in further describing the several different uses. The vacuum pump maintains the pressure P_3 sufficiently low for critical discharge through the nozzles at the lowest value of P_2 to be used. To decrease the pump capacity required, a nozzle with an expanding cone may be used to obtain critical discharge at higher values of P_3. The first restriction is shown as a valve, which may be regarded as a variable orifice. A nozzle here would obviously not change the operation in principle, although in practice, variable-area nozzles are rather difficult to make.

APPLICATION IN SPECIFIC MEASUREMENTS

1. As a Flowmeter

With critical discharge at the nozzle, regardless of the nature of the upstream restriction,

$$M = K_{N_2} P_2 T_2^{-\frac{1}{2}} \tag{4}$$

so that, for this condition, P_2 is a direct measure of the mass flow, T_2 being known, whether gas is drawn or forced through the nozzle and whether P_2 is below or above atmospheric. In the arrangement shown, the flow may be adjusted by varying the upper restriction, and is drawn through the nozzle by suction developed by the pump. However, if the gas to be measured is at a sufficiently high pressure upstream of the first restriction, proper choice of nozzle size may keep P_2 enough above atmospheric so that the pump may be dispensed with.

The *sensitivity* of this device as a flowmeter is just that of the associated pressure measuring instrument (approximately 1×10^{-4}), and the absolute *accuracy* is as close to this as the calibration of the nozzle. Since the characteristic *volume* flow is independent of the entrance pressure (except for compressibility corrections), a calibration at only one pressure may suffice, which may justifiably be done carefully and exactly.

The single critical-flow nozzle has been used for flow measurement for many years, but not as widely as its advantages would seem to warrant. This type of flowmeter is simply and ruggedly constructed, is easily adapted to multi-range operation, and, once calibrated, is more accurate than most rate-indicating meters now available.

2. As a Pressure Controller

It is clear that if the upstream restriction is adjusted to a given opening, P_2 will come to some corresponding equilibrium value, as given by Eq. (6a) or (6d) for the orifice-nozzle or nozzle-nozzle combinations, respectively. If the upstream pressure P_1 is constant, and if the temperatures are constant or change in the same ratio, then P_2 will remain constant, independent of variation of P_3 below the critical value. The value of P_2 may be varied by adjustment of the area of either of the restrictions (varying either K_N or K_0). Practically, it is simpler to adjust the "orifice," since any valve will usually behave like an orifice, unless specially designed to behave like a nozzle.

A chamber in which pressure is to be controlled, or pressure instruments are to be calibrated or compared, may be connected to the system between the two restrictions. The rapidity of approach to equilibrium pressure is, of course, dependent on the volume associated with this part of the system. It is therefore more practicable, if large volumes are to be controlled, to use an auxiliary pneumatic relay or admission valve as shown in Fig. 2, which regulates the flow into the chamber in which the pressure is to be controlled, from which air is drawn by the same, or a different, pump. If desired, a second relay with reversed valve action could be connected in the pump line to control outflow from the chamber as well. For minimum response time, not only the fixed volume of the line in the system associated with the pressure P_2, but also the active volume or displacement of the diaphragm in the admission valve, must be minimized.

3. As a Pressure Divider

It is seen from Eqs. (6a) and (6d) that P_2 will vary in approximately direct proportion to P_1 with either the orifice-nozzle or nozzle-nozzle combinations. When used as a reduced pressure controller, with P_1 the ambient atmospheric pressure, the variations of P_2 are only proportional to those of the barometer. These are negligible for many purposes, at least over short periods (seldom more than 0.1 percent in 10 minutes). If, however, the device is connected to a region where a variable pressure P_1 is to be measured, then the variations are reproduced proportionally over a smaller range and at the smaller pressure P_2. This is of some convenience in extending the range of utility of a standard manometer or barometer, for example. For accuracy of the degree desirable for calibrating pressure gauges at the pressure P_1 in terms of the standard barometer or manometer at P_2, the orifice, or preferably the nozzle, used between P_1 and P_2 should have been calibrated at that pressure, although for nozzles, calibration at one pressure may be sufficient if computed corrections for deviation from the gas law are applied.

When it is recalled that accuracy of the order of 10^{-4} atmosphere is easily possible in pressure measurement by mercury columns, it is clear that engineering accuracy (1 percent) can be attained in calibrating gauges up to 100 atm. by this method, using a standard of only 1 atm. range.

4. As a Thermometer

Referring again to Eqs. (6a) and (6d), it is apparent that if P_1, K_N and K_0 (or K_{N_1} and K_{N_2}) remain constant, P_2 will be a function of the ratio of the temperatures T_1 and T_2. If, then, either T_1 or T_2 is held constant, or otherwise measured, measurement of P_2 will suffice to determine the other temperature. For this application, the device is best used with a fixed orifice, or preferably a nozzle, as the upstream restriction. Obviously, the range of temperatures over which it may be used extends up to the melting point of the materials used. The sensitivity of the device as a thermometer, and therefore the possible accuracy over its calibrated range, is quite good. Differentiating Eq. (6a) (orifice-nozzle combination),

$$\frac{dP_2}{P_2}=-\frac{1}{2}\frac{dT_1}{T_1}\left(1-\frac{P_2^2}{P_1^2}\right)(T_2=C) \tag{7}$$

or

$$\frac{dP_2}{P_2}=\frac{1}{2}\frac{dT_2}{T_2}\left(1-\frac{P_2^2}{P_1^2}\right)(T_1=C). \tag{8}$$

For optimum sensitivity, using an orifice, P_2 should equal $P_1(\frac{1}{3})^{\frac{1}{2}}$, as may be seen by differentiating dP_2, as given by Eqs. (7) and (8), with respect to P_2. For this condition,

$$(dP_2)/P_2=\pm\tfrac{1}{3}[(dT)/T]. \tag{9}$$

For two nozzles, both operating under conditions of critical discharge, the corresponding equation (from differentiation of Eq. (6d)) is

$$(dP_2)/P_2=\pm\tfrac{1}{2}(dT)/T. \tag{10}$$

An accuracy of 0.1 millibar is routine in pressure measurement with mercury columns, so that with $P_1=1$ atm., P_2 approximately 0.6 atm. at the temperature of interest, the temperature variation corresponding to 0.1 mb variations in P_2 would be approximately 3/6000 by Eq. (9) or 2/6000 by Eq. (10). If the maximum sensitivity for the orifice-nozzle combination were at room temperature, this would correspond to 0.15° per 0.1 mb, and the sensitivity at 1650°C would be, by Eq. (9), 3/3000 or 1.6° per 0.1 mb. The maximum sensitivity at 1650° would be 0.9° per 0.1 mb with the relative areas of the orifice and nozzle adjusted for this condition, and the corresponding sensitivity at room temperature would be about 0.4° per 0.1 mb. Corresponding maximum sensitivities for the two-nozzle combination would be 0.6° per 0.1 mb at 1650°C, 0.1° at 300°C.

At extremely low temperatures, a sensitivity of 0.005° per 0.1 mb could theoretically be obtained, using helium, in the range 5° to 10°K.

Sensitivities of this order over such a wide range make the device of wide applicability in measuring gas temperatures in presently developing fields, such as high temperature turbines and jets. The computed sensitivity is, of course, not exact, since deviations from the gas law may either decrease or increase the sensitivity, depending on the particular gas and the range of temperature and pressure involved.

The speed of response of the dynamic thermometer, like the controller, is dependent on the line volume between the two restrictions and that associated with the pressure measuring device.

If two nozzles are used, an expression for the "characteristic time lag" of the instrument may be derived simply.

Applying Eq. (4), the difference in mass flow in and out of the intermediate volume, V, is:

$$M_{\text{in}}-M_{\text{out}}=K_{N_1}P_1T_1^{-\frac{1}{2}}-K_{N_2}P_2T_2^{-\frac{1}{2}}. \tag{11}$$

The rate of change of pressure P_2 in this volume is given by:

$$\frac{dP_2}{dt}=\frac{M_{\text{in}}-M_{\text{out}}}{V}\frac{P_0}{\rho_0}\frac{T_2}{T_0}$$

$$=\frac{K_{N_1}P_1T_1^{-\frac{1}{2}}-K_{N_2}P_2T_2^{-\frac{1}{2}}}{V}\frac{P_0}{\rho_0}\frac{T_2}{T_0}. \quad (12)$$

At equilibrium, $P_2=P_{2eq}$, so that

$$K_{N_1}P_1T_1^{-\frac{1}{2}}=K_{N_2}P_{2eq}T_2^{-\frac{1}{2}}.$$

Substituting and integrating,

$$(P_{2eq}-P_2)_t=(P_{2eq}-P_2)_0\exp-\frac{K_{N_2}P_0T_2^{\frac{1}{2}}}{\rho_0VT_0}t, \quad (13)$$

where the subscript 0 refers to the time of start of approach to equilibrium, the subscript t refers to any time t later. The approach to equilibrium is thus exponential, with a "time constant" given by

$$\frac{\rho_0V}{K_{N_2}P_0}\frac{T_0}{T_2^{\frac{1}{2}}}.$$

By Eqs. (3) and (4) this time constant is just the ratio V/F_2, where F_2 is the characteristic critical flow of the second nozzle, for the temperature T_2.

In an experimental setup, the tubing and associated pressure gauge (an aircraft altimeter) had a total equivalent volume of 250 cc, and the characteristic flow was about 1.5 liters per minute, giving a pneumatic lag constant of 10 seconds. The same arrangement with a different gauge had an effective volume of only 20 cc and a time lag of only 0.8 second. The pneumatic lag can be readily determined by closing off the inlet restriction, then suddenly opening it and noting or recording the time variation of P_2. The thermal lag of the instrument may differ slightly from the pneumatic lag, depending on how much of the gas in the intermediate volume changes in temperature. Since the downstream nozzle must be kept at a known temperature, which may require a long tube, or fins, or a water jacket for heat interchange, it may not always be possible to make the volume as small as would be desirable.

If the temperature to be measured is that of hot gases produced by combustion, the condensation of water vapor presents a problem. Under some conditions, it may be possible to design for P_2 sufficiently low so that the vapor pressure is reduced below the saturation value at room temperature. Maintaining T_2 at an elevated temperature by a thermostatted heater and insulation is another way to avoid this difficulty. With either of these arrangements, the hot gases may blow directly on, and enter, the upstream restriction, and the "thermal time lag" will be the same as the "pneumatic time lag." Alternatively, the hot gases may pass over and around the restriction and a tube leading air to it. With this arrangement, corrections must be deduced for the discrepancy between the temperature of the hot gases and that of the air entering the restriction, which will generally be lower. The thermal lag is increased, since the lead-in tube and restriction must come to equilibrium temperature.

The arrangement with two orifices, corresponding to Eq. (6c), has been used for temperature measurement as long ago as 1893.[2–4] In a recent adaptation of this arrangement,[5] ingenious means are provided for control of A_2 by T_2, and the pressure drop across the second orifice is kept constant by a suitable regulator. In all the work with two orifices, differential pressures must be measured. As far as is known, the measurement of gas temperature by absolute pressures in a dynamic system has not been done heretofore, although Stuart and Yarnell[6] have used the two-restriction arrangement with hot water under pressure for automatic control of a condensate drainage value. In this device T_1 and T_2 were equal. The variation in P_2 with T was due to changes in phase following pressure reduction through the first restriction.

5. As a Gas Analyzer

With two nozzles in series, both may operate at critical discharge if: (a) the area of the second nozzle is greater than that of the first, in a ratio greater than the critical pressure ratio for the first nozzle, and (b) the over-all pressure ratio is sufficiently large.

If the "normal" value of P_2 (under equilibrium conditions with the same mass flow through both nozzles) is, say, $0.3P_1$, and critical discharge through the first nozzle occurs with any downstream pressure less than $0.5P_1$, it is clear that additional pressure drop between the nozzles may be permitted, up to $0.2P_1$, without affecting the performance. With much less pressure drop, the gas may be forced through a liquid air trap, a chemical bubbler, a saturator, or a canister of desiccant or other reagent, to remove or modify one of the components of a gas mixture. The flow may be directed first through and then around the reactor, with the difference in P_2 indicating the fraction removed or added. Allowance must be made in calibration for changes in humidity if bubblers or desiccants are used. Also, for greatest accuracy, the calibrations should not be used with a gas mixture greatly different from the one used in calibration.

To obtain a direct indication of the difference in P_2 due to change in the gas stream, four restrictions may be arranged in two parallel circuits, somewhat analogous

---

[2] E. A. Uehling and A. Steinbart, German Patent 77091 (1893).

[3] M. Chopin, Comptes Rendus 186, 1830 (1928); Ann. de physique 16, 101–149 (1931).

[4] H. Schmick, Zeits. f. Tech. Physik 10, 146 (1929).

[5] D. W. Moore, Jr., "A Pneumatic Method for Measuring High-Temperature Gases," Aeronautical Eng. Rev. 7, 30 (1948).

[6] M. C. Stuart and D. R. Yarnall, "Fluid Flow through Two Orifices in Series," Mechanical Engineering 58, 479 (1936).

to a Wheatstone bridge, with a differential manometer indicating the difference between the entrance pressures at the two downstream nozzles. Switching the reactor in and out of the circuit, or from one circuit to the other, will permit corrections for slight differences in the nozzles.

The sensitivity of the device is great enough to promise utility for humidity measurements (1 percent change in relative humidity at room temperature gives a change of about 0.04 percent P_2—between 1 and 2 mm of water). Because water vapor differs from air in density and also in the value of n, the change in P_2 on removal of water vapor is not a direct measure of the vapor pressure, but the slight corrections may be made on the basis of theory or calibration.

6. As a Micrometer or Gauge

Pneumatic gauges have come into fairly wide use in recent years, particularly in industrial inspection and automatic gauging. Gauges of this class all consist of a pneumatic circuit in which a restriction is determined, or varied, by the displacement, or clearance, to be measured. In the several types in current use, the dimension indication is related to: (a) the change in flow, with a given differential pressure across the variable restriction (gauging head); (2) the change in differential pressure, with a constant flow through the gauging head; or (3) the change in differential pressure across the gauging head (or the fixed restriction), with a constant differential pressure across the two restrictions.

When the critical flow device described here is used as a gauge, the gauging pressure is the *absolute* pressure, P_2. Referring to Fig. 2, it is clear that, after calibration, the value of P_2 is a measure of the position of the valve lid at the first restriction. Other gauging heads such as tapered plugs, needle valves, or sliding or rotating ports, or holes partially blocked by the part being gauged—all these are equally adaptable to critical-flow gauging when used with the fixed nozzle downstream. When the gas is forced, by a constant absolute pressure, first through the fixed nozzle at critical flow, then through the gauging head, true critical flow will not be obtained through the gauging head unless the geometry of the variable restriction is such that it behaves like a "nozzle."

DESIGN FEATURES

In all the various uses of this instrument, it is not necessary that a vacuum pump be used, if it is possible to maintain the pressures P_1 and P_2 at high enough values to ensure critical discharge through the nozzle, or nozzles. It may be convenient or sometimes necessary to arrange for this type of operation in metering flows of gas to be added to a process, for example, or in measuring temperature of a gas or liquid in which the nozzle is immersed and exhausts.

The dimensions of the nozzles and orifices used are, in principle, of little importance—only their ratios; but since a large flow requires a large pump and a small flow increases time lag, some compromise must be made. A nozzle of diameter 0.3 mm (No. 80 drill; 0.0135 in.) gives a characteristic flow of about one liter per minute. With this, a small vacuum pump is adequate; e.g., one of 12 liters per minute capacity, for instance. For larger sizes, a larger pump with a capacity of perhaps 100 liters per minute at 0.1 atm. is required, but the pump used need not be capable of attaining extremely low pressure. The limits of performance can be increased, or pump capacity decreased, as noted previously, by designing nozzles with a divergent exit cone to reduce over-all pressure loss.

Although the smallest nozzle so far used in this work was 0.3 mm, it is possible that even smaller ones could be successfully used under certain conditions. However, viscosity effects may be expected to cause trouble in using the smaller nozzles. A recent paper by J. W. Andersen and R. Friedman[7] reports pressure-proportional flow with small sapphire "orifices" as small as 0.05 mm in diameter at entrance pressures from 2 to 5 atmospheres when discharging at atmospheric pressure.

Since in this instrument pressure changes are associated with a change in the measured quantity, mechanical power is available for initiating control of the variable. This fits directly into automatic control systems responding to mechanical signals; pressure transducers may be used as a link when other systems are to be used.

ACKNOWLEDGMENT

This instrument was developed during the war for the Bureau of Aeronautics, Department of the Navy, mainly for experimental use in pressure measurement and control. The investigation of the other applications, and the preparation of this report were supported by the Office of Naval Research, under a project on "Basic Instrumentation for Scientific Research."

It is a pleasure to acknowledge the cooperation of present and former colleagues, especially L. W. Honea, J. M. Davis, A. S. Iberall, and D. S. Goalwin, in constructing and testing the instrument and in elucidating its behavior.

---

[7] J. W. Andersen and R. Friedman, Rev. Sci. Inst. **20**, 61 (1949).

THE REVIEW OF SCIENTIFIC INSTRUMENTS VOLUME 21, NUMBER 1 JANUARY, 1950

Design and Use of Piezoelectric Gauges for Measurement of Large Transient Pressures[*]

A. B. Arons[†] and R. H. Cole[‡]
Underwater Explosives Research Laboratory, Woods Hole Oceanographic Institution, Woods Hole, Massachusetts

(Received June 22, 1948)

This report discusses the design and use of piezoelectric gauges for the measurement of rapidly varying hydrostatic pressures of large amplitude in gaseous and liquid media. Reasons are given for the selection of tourmaline in preference to other types of crystal. Fundamental principles of design are stated, and gauge construction is described in the light of these principles. A simplified theoretical analysis of transient response characteristics is presented.

I. INTRODUCTION

THE original suggestion that transient pressure waves could be recorded as functions of time by observing the trace of a cathode-ray oscilloscope as it was deflected by the signal from a piezoelectric crystal has been credited to J. J. Thomson. Early experiments using such apparatus to record shock waves from under water explosions of TNT were described by Keys in 1921.[1] Since that time, the technique has been applied to several types of large amplitude pressure measurement, the most common being pressure-time phenomena in internal combustion engines and in shock waves due to explosions in air and water.

During World War II, a group at the Underwater Explosives Research Laboratory of the Woods Hole Oceanographic Institution made a number of contributions to the technique of shock wave measurement, utilizing tourmaline crystal gauges. A discussion of the present status of this technique will be given in this report. The type of gauge developed at the Underwater Explosives Research Laboratory will be referred to in the following as the UERL gauge.[¶]

II. BASIC REQUIREMENTS FOR A PRESSURE-SENSITIVE DEVICE

It is illuminating to outline first the criteria which an ideal electromechanical pressure-measuring device should satisfy. Although in principle these criteria should apply to any magnitude or duration of applied pressure, in practice their relative importance depends on both characteristics. In this paper, we consider primarily the measurement of transient pressures lasting a fraction of a second at most and with amplitudes from one to hundreds of atmospheres, as opposed to static pressures or acoustic waves. The requirements for such purposes can be summarized as follows: linearity, freedom from hysteresis, thermal stability, freedom from extraneous signals, adequate high and low frequency response, minimum distortion of the pressure field, ruggedness, and simplicity.

The efforts of the UERL group were directed toward the development of a gauge affording a practicable compromise among these requirements.

III. SELECTION OF THE GAUGE MATERIAL

Of the many known piezoactive crystals, those that have been used and investigated most extensively are rochelle salt, ADP, quartz, and tourmaline. More recently, crystals such as barium titanate and its various modifications, lithium sulfate, and certain tartrates have been successfully prepared and utilized.

The most sensitive of these materials are rochelle salt, barium titanate, and ADP. The first two do not appear to be suitable for measurement of fairly large pressure amplitudes owing to a relaxation or hysteresis effect which causes them to produce a rising signal upon application of a step pressure. Rochelle salt and ADP exhibit further disadvantages in that they are not hydrostatically sensitive and not sufficiently rugged for the applications here intended. The other "synthetics" present various difficulties due to their solubility or the presence of water of crystallization.

An extensive survey of piezoelectric activity of minerals has been reported by Bond.[2] It is interesting to note that after listing all the known piezoactive, naturally occurring minerals, Bond concludes that only quartz and tourmaline are practical for any extensive piezoelectric work. All the other active minerals are very rare, occur in the form of exceedingly small crystals, or are very weak mechanically.

Quartz was rejected because of its lack of hydrostatic sensitivity. Because of its ruggedness, linearity, insolubility, and hydrostatic sensitivity, tourmaline appeared to offer most promise for the construction of small, simple gauges and was selected accordingly.

IV. DESIGN AND CONSTRUCTION OF TOURMALINE GAUGES

A. Basic Considerations of Design

Since the criteria listed in Section II are not all mutually consistent, the design of a gauge for a particular application resolves itself into a search for a suitable compromise among these factors, and sometimes the final design cannot satisfy all the requirements to the extent desired. It has been established that tourmaline is satisfactory with respect to linearity, freedom from hysteresis, and stability of its pressure sensitivity, but there remains the problem of arriving at a design adequate from the points of view of sensitivity, frequency response, and ruggedness—all factors which are to some extent under the control of the designer.

---

[*] The work described in this report was initiated under contract with the OSRD in 1941 and after 1945 was continued under contract with the Navy Department, Bureau of Ordnance. Contribution from the Woods Hole Oceanographic Institution, No. 437.

[†] Present address: Department of Physics, Stevens Institute of Technology, Hoboken, New Jersey.

[‡] Present address: Department of Chemistry, Brown University, Providence, Rhode Island.

[1] D. A. Keys, Phil. Mag. 42, 473 (1921).

[¶] These gauges are now being produced commercially by the Cambridge Thermionic Corporation, Cambridge, Massachusetts.

[2] W. L. Bond, Bell System Tech. J. 22, 145 (1943).

Piezoelectric crystals develop polarization *charge* when subjected to pressure changes. This charge distributes itself over the capacitance which is in parallel with the gauge element, and consequently the amplitude of the voltage appearing at the amplifier input is not only directly proportional to the applied pressure change but also inversely proportional to the total capacitance parallel to the gauge element in the input circuit.

The necessary gauge sensitivity must therefore be evaluated in terms of the following controlling factors: (1) magnitude of pressure variations to be recorded, (2) total capacitance of the gauge circuit (this depends principally upon the length of cable required to connect the gauge to the amplifier or preamplifier), and (3) amplifier sensitivity.

A lower limit is sometimes placed upon the required sensitivity by the presence of spurious signal arising in the cable or the mounting of the gauge. In many applications, a piezoelectric gauge is connected to recording equipment by means of shielded cable, a certain length of which may be unavoidably exposed to the pressure wave as the latter advances from its source. Spurious signal arising in such cases is an integrated effect which generally introduces little error into the determination of initially discontinuous or rapidly changing pressures, but adds progressively more signal as the wave encounters more cable. It is evident that measurements of small pressures behind an initial high pressure region may thus become highly inaccurate and an effort to obtain reliable values of impulse by integration of the pressure-time curves may be entirely vitiated.

Experience has demonstrated that most ordinary commercial rubber microphone cables and polyethylene cables are completely inadequate since the signals they develop when subjected to pressure variations are very large and may even be, under some conditions, larger than those which would be produced by the gauge elements themselves.

A number of cables were developed which proved to be adequate, and one type—a copper tubing cable, originated at the David Taylor Model Basin—was used successfully for several years in under water studies. More recent developments have led to the production of a polyethylene cable (designated F.O. 5879 by the Simplex Wire and Cable Company) which appears to be superior to any other cables previously available and which is equally satisfactory for measurements in both gaseous and liquid media. However, even in this cable, the signal has not been completely eliminated (although it has been very greatly reduced) and one must always make sure that the gauge signal is large relative to the residual cable signal in each application.

Although much work in the past has been done with single-ended systems using coaxial cables,[3] it is well known that push-pull or balanced systems effect material reduction in residual cable signal by canceling out components which are symmetrical about ground. It seems unlikely, however, that such a system would eliminate the difficulty entirely, since there is no reason to expect the cable signal to be a perfectly symmetrical phenomenon.

The sensitivity of a piezoelectric gauge is directly proportional to the available sensitive area of crystal. In cases where spurious signal due to cable or gauge mounting is a significant factor, the permissible lower limit of sensitivity imposed by such signal places a lower limit upon the size of the gauge. On the other hand, the discussion of high frequency response and pressure-field distortion given in Section V shows that higher fidelity is obtained with *smaller* linear dimensions of the sensitive unit. Specific requirements as to accuracy with respect to high frequency response consequently put an upper limit on the linear dimensions of the gauge, particularly the dimension along the direction of propagation of the wave, and this upper limit must be reconciled with the lower limit indicated by the necessity of swamping spurious signal. In some cases the two requirements cannot be reconciled, and one or the other must be compromised in designing the gauge. This is particularly true where it is desired to measure very rapid pressure variations in liquid media. In gaseous media where the high frequency response requirements are usually less stringent, large gauges can be used and the above requirements can generally be reconciled.

In the actual construction of gauges, a given sensitivity can be obtained and the linear dimensions minimized by stacking two or more crystal plates in parallel. This feature has been utilized in all UERL gauges, but, except for a few special cases, it has not proved practicable to use gauges having more than four plates in the pile.

B. Construction of Gauges

The object of the UERL group was to develop a unit suitable for measurement of explosion-produced shock waves in air and water. Many of the basic principles, however, apply to measurement of transient pressure waves in general, and properly modified UERL-type gauges should be useful under a wide variety of circumstances.

The principal difficulties with the early gauge designs proved to be lack of stability of pressure sensitivity and prevalence of large systematic discrepancies between gauges used on the same measurement, even when the sensitivity of each gauge appeared to be stabilized. These difficulties were largely overcome by adoption of an improved construction technique, the governing principle of which was to prevent disturbance of the electrodes during the later stages of gauge assembly and during subsequent use.

---

[3] R. H. Cole, "The use of electrical cables with piezoelectric gauges." OSRD Report No. 4561.

An assembly drawing of a single-ended UERL gauge is shown in Fig. 1, and a picture of the different stages of construction is shown in Fig. 2. Properly lapped tourmaline disks receive a coat of electrode material, such as Du Pont liquid silver No. 4391, and are baked for about an hour at 550°C. Four disks are then assembled in a pile, two on each side of a steel tab as shown in Fig. 1, and the pile is sweated together into a single homogeneous unit by being placed in a spring clamp and again heated in an oven. Provision is made in this operation for electrode connection to the intermediate crystal faces.

The peripheral edges of the pile are insulated by the application of a thin layer of dielectric material such as pure latex which can be painted around the edges and cured *in situ* by baking at *ca.* 120°C. With the periphery properly insulated, contact can now be made between the outermost crystal faces and the grounded central tab. Originally this was accomplished by direct soldering to the electrodes, and the technique was revised because of the deleterious effect on the intimacy of electrode-crystal contact. The present technique is to make contact by means of a conducting silver paint which can be baked on at temperatures low enough to be compatible with the insulating material used around the edges of the unit.

In connecting a unit of this type to a length of electrical cable, it is only necessary to solder the central tab to the cable shield and spot solder the high electrode leads to the cable conductor. These connections can be made quickly, with a minimum of heating of the gauge element. In this manner the electrodes are afforded the greatest possible protection during mounting of the unit. (Elements of this type have also been mounted in threaded inserts which can be screwed into the wall of a container in which pressure variations are to be studied.)

Gauges of this design have been used to measure pressure, impulse, and energy flux in waves ranging in amplitude from 0.5 to 100,000 lb./in.^{2}.

It was originally feared that the introduction of the metal central tab might tend to introduce spurious mechanical oscillations on the pressure-time records. However, there has so far been no evidence of the presence of oscillations more serious than those ordinarily observed with gauges of earlier design which were not provided with central tabs.

The central tab principle is also vitally important because of the strength it gives the completed unit, particularly where measurements are to be made in gaseous media in which stresses caused by the exceedingly high particle velocities are capable of causing severe damage to unreinforced gauges.

The gauge design described is also well suited to the construction of push-pull units. If one pair of tourmaline disks is arranged with positive faces connected to one high potential lead while the pair on the opposite side of the central tab has negative faces connected to another high potential lead, the central tab and outer pair of faces can all be grounded to the shield of a two-conductor cable while the two high potential leads are connected to the two center conductors, respectively. This results in a perfectly symmetrical, completely shielded unit which develops signals balanced about ground. A less symmetrical, but more efficient push-pull gauge can be made by connecting a single-ended-type unit to the center conductors of a two-conductor cable without grounding any point within the gauge.

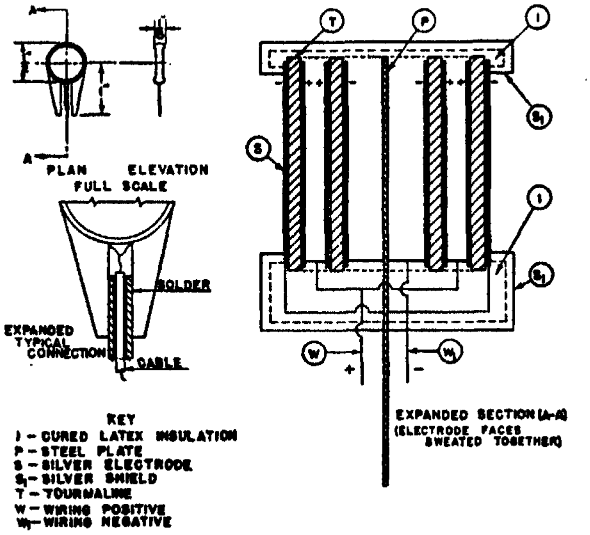

FIG. 1. Assembly drawing of UERL-type tourmaline gauge.

In the case of gauges intended for measurements in gaseous media, the serious effects of perturbation of the flow around the gauge[4] can be minimized by surrounding the gauge element with a streamlined housing or baffle of suitable shape and proportions. Various aspects of this design problem are still under investigation in several laboratories.

C. Coating of Gauges

After the gauge element is assembled and mounted, it is necessary to apply a waterproof coating, since contact with even minute quantities of moisture results in low gauge resistance with consequent impairment of the low frequency response.

Numerous coating techniques have been tested by the UERL group, and only a few have proved satisfactory. The most useful method has been the application of a

---

[4] J. K. L. MacDonald and S. A. Schaaf, "On the estimation of perturbations due to flow around blast gauges," OSRD Report No. 5639.

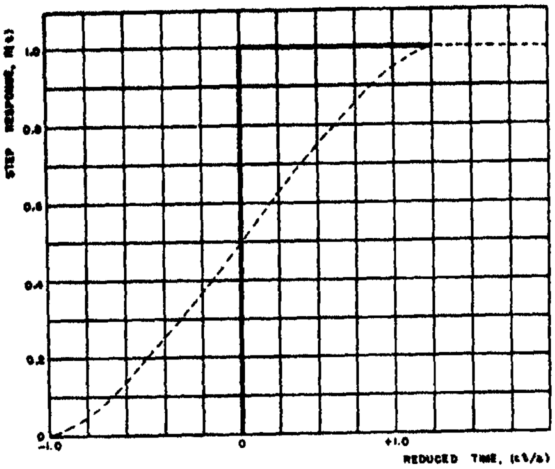

FIG. 5. Response of a gauge of radius a to a progressive step wave of velocity c.

time required for the gauge to give maximum response, this time being theoretically equal to $2a/c$.

The validity of such a correction involves the assumptions that distortion due to diffraction effects dies out sufficiently rapidly not to affect the curve after the maximum, and that the true pressure curve is sufficiently simple for a linear decay law to be a good approximation. It is reasonable, however, to expect that any diffraction effects will have the general character of damped transient oscillations about the gradual rise as the gauge is covered by the advancing wave and should not be significant after the gauge is covered. Whether or not the pressure curve is sufficiently simple to be represented by a straight line or smooth curve, depends, of course, on experimental conditions. Unless appreciable interference or reflections are combined in the resultant wave, the corrected maximum pressure may well be used as a significant measure of the wave.

This principle has been extensively applied by the UERL group in the interpretation of underwater shock wave records and the estimation of true peak pressures under conditions where the gauge size introduced appreciable error. It was found that the simplified theory provides adequate correction for amplitude effects up to about 10 to 15 percent, but then begins to show serious departures from observed values. It has also been found empirically that the gauge radius a which must be used in the theory is not the radius of the element alone, but rather the radius of the *complete* gauge *including* coating material.

B. Interference Effect

The analysis of the effect of gauge size on transient response neglected any disturbance of the pressure wave due to presence of the gauge in the field. Actually, of course, the gauge material is a medium through which sound waves can be transmitted. As a result, one can expect interference effects due to repeated internal reflections of the incident wave at the interfaces of the crystal. This would have roughly the character of a damped saw-tooth oscillation. The frequency of this oscillation cannot be calculated accurately, but it is probably of the order of 100 kc/sec. for the types of gauges described in this paper.

In order to examine the effect of interference on response of an actual gauge, we might consider a circular disk in either of two orientations: face-on and edge-on to the approaching pressure front. The Coulomb sensitivity of a disk of tourmaline depends only on the face area, not on the thickness, and, as a result, the travel time is obviously minimized and the natural frequency highest if a thin disk is oriented face-on. It is to be expected, however, that Bernoulli effects[4] will be much less if the same disk is edge-on.

To the extent that a single very thin disk is practical, the face-on orientation may appear preferable because of the inherently higher frequency characteristic. In actual practice there is a limit to the thinness possible, and in the interest of greater sensitivity, it is desirable to construct a gauge from a pile of disks; thus multiplying the effective area and sensitivity and obtaining a better electrical and mechanical design. Under such circumstances the face-on orientation would have much larger interference oscillations than the edge-on orientation and comparable transit time and flow effects.

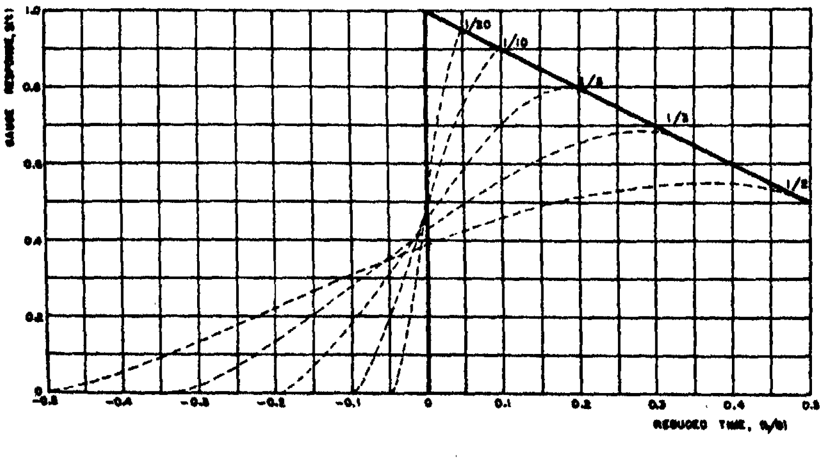

FIG. 6. Response of a gauge of radius a to a progressive saw-tooth wave of decay constant θ and velocity c. Solid line represents incident wave. Dotted curves show response for various values of $a/c\theta$.

Comparing the two possibilities, one might expect the edge-on gauge to have a much smoother rise in response to a step pressure, taking a longer time, but approaching the true curve more smoothly. Experimental tests have roughly indicated this state of affairs, and practical experience has also shown that records obtained with gauges in the edge-on orientation give about as much usable high frequency resolution as face-on gauges and are much cleaner and easier to analyze empirically.

C. Low Frequency Response

(1) Internal impedance. Although a piezoelectric crystal under ideal conditions develops a potential difference between its faces which persists as long as a force is applied to it, in practical use unavoidable leakage resistance and input resistance of recording equipment afford conducting paths by which the piezoelectric charge is gradually neutralized. As a result, the response to applied pressure falls off as the rate of change of pressure decreases. The electrical properties of a piezoelectric crystal are represented with sufficient accuracy for the present discussion by an e.m.f., V_0, proportional to applied pressure, in series with the capacitance, C_0, of the crystal. In actual use the gauge will be shunted by lead capacitance C and leakage or other resistance R.

The response of such a circuit to a step pressure P_0 is a negative exponential:

$$V_t=[KA/(C+C_0)]P_0\epsilon^{-t/\tau}, \qquad (6)$$

where V_t = terminal voltage; KA = gauge sensitivity expressed as charge developed per unit pressure change; and $\tau=R(C+C_0)$.

From Eq. (6) it is evident that the response in the limit of low frequencies or long times approaches zero. The useful lower limit is obviously increased by increasing the time constant τ. Therefore the input impedance and other resistances represented by R should be made as large as other considerations (for example, amplifier stability) permit. Likewise, the time constant can also be increased by use of larger values of C. (In practically all applications $C_0 \ll C$, and increase of crystal capacitance would have no appreciable effect on τ.)

Unfortunately, an increase in the value of the padding capacity C reduces the output voltage by the same proportion. If one is limited in allowable gauge sensitivity by high frequency considerations or by low pressure amplitudes, improvement of low frequency characteristics in this way requires increased sensitivity of the recording system. The best solution in difficult situations requires a compromise between gauge size, resistance of the circuit, and sensitivity of the recorder.

(2) Pyroelectric effect. A second factor that may affect the low frequency response of a piezoelectric gauge is the development of charge as a result of temperature changes in the crystal. Such charges can arise either directly from increased temperature due to adiabatic compression of the crystal, or, indirectly, from temperature changes in the surrounding medium or from radiation such as sunlight, explosion flashes etc.

The first effect has been shown to be negligible by Keys.[5] The second effect depends upon the amount of heat developed external to the crystal and the rate at which it can raise the crystal temperature by thermal conduction or radiation.

The pyroelectric sensitivity of tourmaline is such that a change in temperature of 1°C produces a charge equivalent to that developed by a pressure change of 200 lb./in.^{2}. In liquid media, however, the pressure wave durations are usually very short, and although the adiabatic temperature change of the liquid is appreciable, a gauge can hardly undergo more than a small fraction of the ultimately possible temperature change during such intervals, particularly in view of the thermal insulation afforded by the gauge coating.

In gaseous media, however, radiation effects, temperature changes due to adiabatic compression of the medium, and effects due to variations of ambient temperature become very much more pronounced. Special care must be taken to provide adequate thermal insulation by using coatings of sufficient thickness for the particular application. Excessive thickness of coating, however, has been found to affect the gauge properties by introducing spurious oscillations and other undesirable effects, and a suitable compromise must be found in difficult cases. Radiation effects can largely be protected against by the use of a bright coating, such as silver paint, on the outside of the gauge.

The longer the duration of the signal being measured, the more difficult it becomes to combat interference due to pyroelectric effect, and thus the applicability of the tourmaline gauge is more severely limited by its pyroelectric sensitivity than by the other natural limitations of input impedance, time constant, and piezoelectric sensitivity.

VI. REQUIREMENTS OF ASSOCIATED RECORDING EQUIPMENT

Detailed discussions relative to the design and construction of oscillographic recording equipment and cables for use with piezoelectric gauges will be found elsewhere.[5,6,7] It is the purpose here to discuss briefly only certain requirements of such equipment which are intimately associated with the selection and use of the piezoelectric gauges themselves.

From the foregoing considerations, it is obvious that the low frequency characteristics of an amplifier should be such that its over-all time constant is long relative to the duration of the phenomenon being recorded. In extreme cases this might require a d.c. amplifier. Input

---

[5] D. A. Keys, Phil. Mag. **46**, 999 (1923).

[6] Cole, Stacey, and Brown, "Electrical instruments for study of underwater explosions and other transient phenomena," OSRD Report No. 6238; NDRC No. A-360.

[7] G. K. Fraenkel, "Apparatus for measurement of air-blast pressures by means of piezoelectric gauges," OSRD Report No. 6251; NDRC No. A-373.

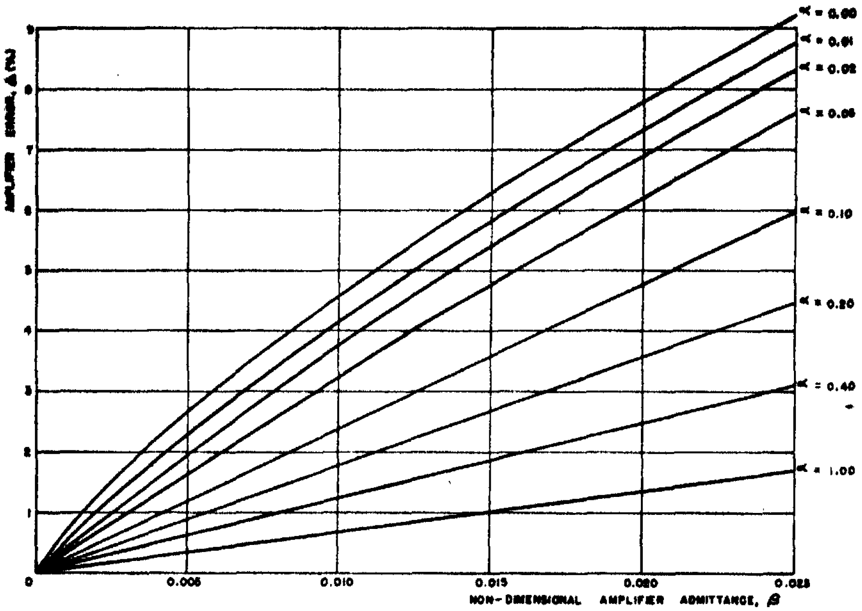

FIG. 7. Amplifier error *vs.* non-dimensional amplifier admittances β for incident waves of various α. (See text for explanation of notation.)

impedance can generally be made sufficiently high by use of cathode follower preamplifiers.

The situation with respect to high frequency requirements is slightly more complex in that a certain amount of high frequency distortion is unavoidably present because of the geometry of the gauge. (This effect was computed for some simple wave forms in Section V.)

In general, therefore, the demand upon amplifier response will be conditioned by the gauge response, and a useful quantitative calculation can be made for the special case of steep-fronted waves, where high frequency considerations are most important.

We assume that a saw-tooth wave is incident at the gauge and that the shape of the signal reaching the amplifier can be represented to a first approximation by a linear rise to a peak value followed by a linear decay, i.e.:

$$F(t)=\begin{cases}0 & \text{when } t<0\\ t/\gamma & \text{when } 0<t<\gamma,\\ 1-(t-\gamma)/\theta & \text{when } t>\gamma\end{cases} \tag{7}$$

where θ is the decay constant of the wave and $\gamma=2a/c$, the transit time of the shock wave across the gauge.

The step response of the amplifier is assumed to have the form:

$$R(t)=1-\epsilon^{-t/\kappa}. \tag{8}$$

Expressing the above relations in terms of dimensionless parameters with θ as the scaling factor ($\alpha\equiv\gamma/\theta$, $\beta\equiv\kappa/\theta$), and applying the superposition integral, it is shown that:

$$\Delta=\beta\ln[1+(1-\epsilon^{-\alpha/\beta})/\alpha], \tag{9}$$

where Δ represents the fractional error introduced by the amplifier in reproducing the peak of the applied function, $F(t)$. $F(t)$, however, already contains an error $\alpha/2$, with respect to the peak pressure of the incident shock wave. Thus the total error introduced by the combined effects of gauge size and amplifier high frequency response is:

$$E=\Delta+\alpha/2 \tag{10}$$

with respect to the incident shock wave peak pressure.

Figure 7 is a representation of Eq. (9) which should prove useful in estimating error due to a given frequency response for various gauge conditions or for design purposes where one seeks to find the frequency response necessary to keep the error below a certain selected limit.

The problem of calibrating piezoelectric gauges is a vital one, involving rather highly specialized instruments and techniques. Owing to fairly recent developments in the field, calibration will be discussed in a separate paper at some future date.

VII. ACKNOWLEDGMENTS

The knowledge and experience upon which this report is based could not have been accumulated were it not for the cooperative effort of a large number of individuals who participated in the work of the Underwater Explosives Research Laboratory. The authors are pleased to acknowledge in particular the significant contributions of Professor E. B. Wilson, Jr., Dr. W. D. Kennedy, Dr. W. G. Schneider, Dr. A. M. Shanes, and Dr. W. E. Gordon, and regret that space does not permit a more adequate identification of the contributions of each individual to the fundamental understanding of the use and design of piezoelectric gauges. Much credit for development of techniques of construction of the present gauge design is due Professor C. Frondel of the Department of Mineralogy, Harvard University. Earlier construction techniques were developed by Dr. D. Silverman and Mr. H. M. Lang of the Stanolind Oil and Gas Company.

Background Eradication in Thick-Layered Nuclear Emulsions

MARTIN WIENER
National Bureau of Standards, Washington, D. C.

AND

HERMAN YAGODA
National Institute of Health, Bethesda, Maryland

(Received August 1, 1949)

A method for eradication of accumulated background on Ilford C-2 plates, 100–200μ thick, without reducing their sensitivity to medium ionizing particles, is described. The method involves a mild oxidation of the emulsion by air saturated with water vapor at 35°C for a period of about 16 hr. The plates are then dried and are ready for experimental exposure. Analysis of grain counts shows no loss of sensitivity in proton tracks over their last 200μ range when the plates are developed with a mild hydroquinone developer. Complete eradication of background alpha-tracks and stars is secured as well as destruction of latent images of the less ionizing proton recoils instigated by external neutron bombardment. Grain density studies on proton tracks located at different depths in the emulsion indicate substantially uniform sensitivity after eradication except for the uppermost 50μ which develop with about a 10 percent reduction in mean grain density as compared with tracks deep within the recording medium.

IN recording the tracks of ionizing particles arising from feeble radioactive sources or induced nuclear reactions of low cross section, it is advantageous to destroy the accumulated background of latent images originating from internal radioactive impurities and incident cosmic radiation. This is particularly important in recording the trajectories of low energy protons that originate from photo-disintegration processes in deuterium-loaded emulsions, as old latent images of alpha-particles develop with a reduced grain density and may be confused with protons of equal range.

Yagoda and Kaplan[1] have demonstrated that the background can be destroyed by exposing the plates above three percent hydrogen peroxide at 25°C. With plates having coatings 25–50μ thick, the process is completed in about 4 hr. When this method is applied to thicker emulsions (100–200μ), however, the oxidation process must be extended in order that the vapor has the opportunity to diffuse through the entire layer. The prolonged oxidation (about 16 hr.) causes a reduction in sensitivity as evidenced by tracks of alpha-particles subsequently produced in the dry emulsion which develop with reduced grain density.

This partial desensitization can be avoided by eradicating the plates with a milder oxidant, such as moist air, and conducting the operation at 35±2°C to accelerate the process. To test the efficiency of this procedure, an old (134 days) Ilford C plate, coated 200μ thick, was cut into three portions, A, B, and C. All three were exposed simultaneously to fast neutrons from a 5-mc Po-Be source. Portion A was then developed so that a record would be had of the knock-on protons and background alpha-tracks in an uneradicated portion of the plate. Portions B and C were exposed to air saturated with water vapor at 35±2°C for 16 hr. After drying the eradicated portions for 1 hr. over anhydrous calcium chloride, Plate B was re-exposed to fast neutrons and then developed, together with the control plate, C. Development was identical with that given Plate A. In this manner, Plate B would give us proton tracks, free of alpha-background, whose grain density could be checked against the proton tracks in Plate A, and Plate C could be examined for the efficiency of the eradication of both the proton tracks and the background.

The development consisted essentially of a 1-hr. immersion in a freshly prepared solution composed of: 2 g hydroquinone, 20 g Na_2SO_3, 1 g KBr, and 10 g Na_2CO_3 per liter of distilled water chilled to 8°C, followed by dilution with an equal volume of water at 25°C, warming the mixture to 22°C, and maintaining, without subsequent agitation, at 22±1°C for 1 hr. Studies of this method[2] indicate that the procedure

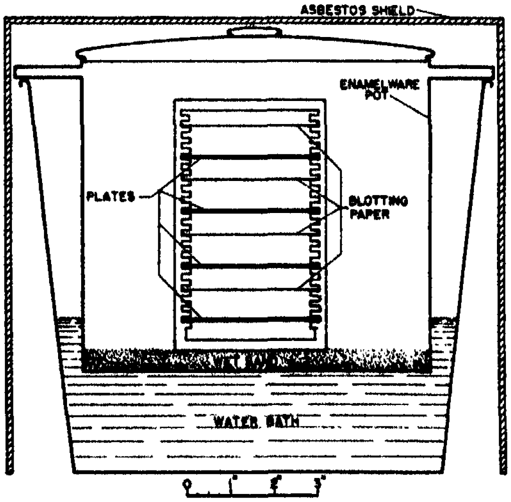

FIG. 1. Arrangement for eradication of plates by means of air saturated with water vapor.

---

[1] H. Yagoda and N. Kaplan, Phys. Rev. 73, 634 (1948).

[2] H. Yagoda, Nucleonics 4, 5, 134 (1949). The processes of fixation and washing are essentially the same as those described in

produces uniform depth development in emulsions 100 to 250μ thick. More powerful elon-hydroquinone developers such as D19 cannot be employed, as the long development time necessary in processing thick emulsions causes the reappearance of eradicated alpha-tracks with, however, greatly reduced grain density.

The apparatus used for eradication consists of a water bath controlled at 35°C, an enamelware pot containing a layer of wet sand, a rack for supporting the plates horizontally, and an asbestos insulating shield as shown in Fig. 1. It is important to avoid metals, particularly aluminum, inside the eradicator vessel, as moist air acting on freshly abraded metallic surfaces produces traces of hydrogen peroxide.[3] The wooden rack employed as a support for the plates should be well aged and impregnated with hard paraffin wax. The alternate layers of blotting paper prevent droplets of condensed water from falling onto the emulsion surface. The paper should be examined periodically for mold growth and replaced as needed.

Microscopic examination of the control plate, C, showed complete absence of proton recoil tracks, demonstrating that the treatment caused total destruction of latent images formed by 0.4 to 11 Mev proton tracks. Background alpha-tracks were observed only in the non-eradicated piece. A count of the alpha-stars on this plate, A, showed a population of about 2800 alpha-stars per cc of emulsion of which 1300 originated in the emulsion itself, the remainder starting in the glass backing. As the emulsions were 134 days old at time of development, this indicated an approximate rate of formation of 10 stars per cc per day originating in the emulsion layer. Only the stars (two to five alpha-branches) were counted, not single alpha-tracks. The latter are about six times as numerous as stars so that about 70 alpha-stars and -tracks were formed per cc per day in this particular Ilford C-2 plate. The population is dependent chiefly on the quantity of thorium and radium present as variable impurities in the components of the plate.

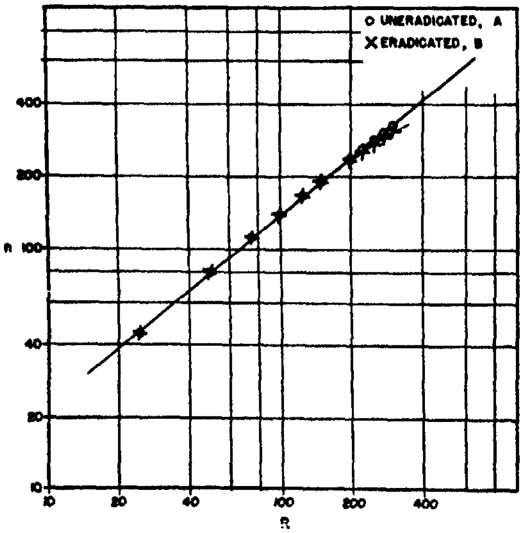

FIG. 2. Comparison of grain development before and after eradication, based on all tracks measured.

In order to detect any small variations in sensitivity produced by the eradication process, grain counts (n) were made along 25μ portions of the proton tracks recorded in Plates A and B, selecting tracks in all levels of the emulsion with a maximum slope of 30° with the plane of the emulsion, and with a range of about 200μ or greater.

The resultant data was evaluated by plotting $\log n$ against the residual range, $\log R$ (Fig. 2) as this function is essentially linear and independent of particle energy. The plot shows no noticeable variation in sensitivity between the eradicated and uneradicated plates over the first 200μ of range from the slow end. Beyond 200μ, the eradicated plate exhibits a slight, but increasing, desensitization. The graph was drawn from the average of 32 tracks on Plate A and 35 tracks on Plate B. The majority of the tracks were about 200μ long, the maximum range in which we were interested for purposes of subsequent photo-disintegration studies, so that the average for the range beyond 200μ is based on fewer grain counts than for the range below.

A further breakdown was made of the tracks in each plate into groups of tracks at different levels in the emulsion. Tracks were chosen at 10–69μ from the top of the emulsion (Group 1), 70–139μ (Group 2), and at depths greater than 139μ (Group 3). Figure 3 shows that

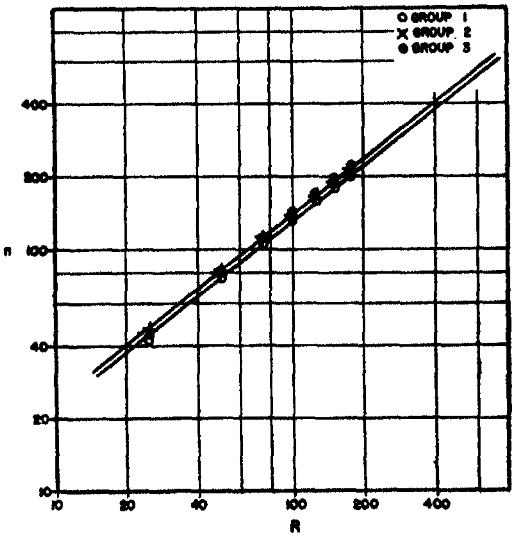

FIG. 3. Variation of grain count with residual range for knock-on protons resident in different layers of an old non-eradicated emulsion (A).

Method VII (reference 3, p. 62–63). When old plates are fixed, the tendency toward emulsion frilling can be minimized by washing the developed plate in five percent sodium sulfate for 20 min. The residual alkali is then neutralized by a 5-min. rinse in two percent boric acid prior to immersion in the 30 percent sodium thiosulfate bath.

[3] H. Yagoda, *Radioactive Measurements with Nuclear Emulsions* (John Wiley and Sons, Inc., New York, 1949), p. 9–12.

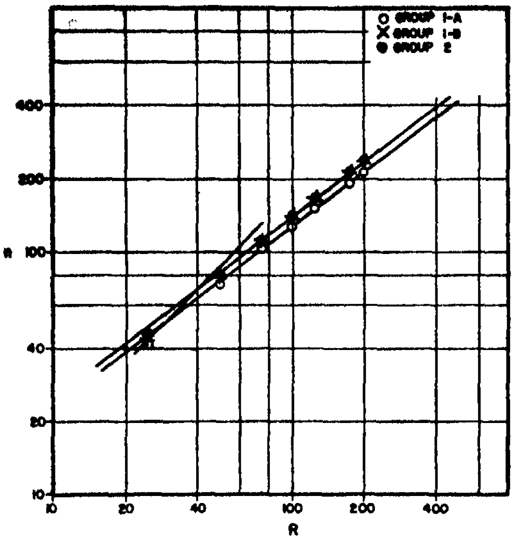

FIG. 4. Breakdown of Group 1 tracks in Plate A exhibiting large reduction in developed grain density in the emulsion layer in contact with air.

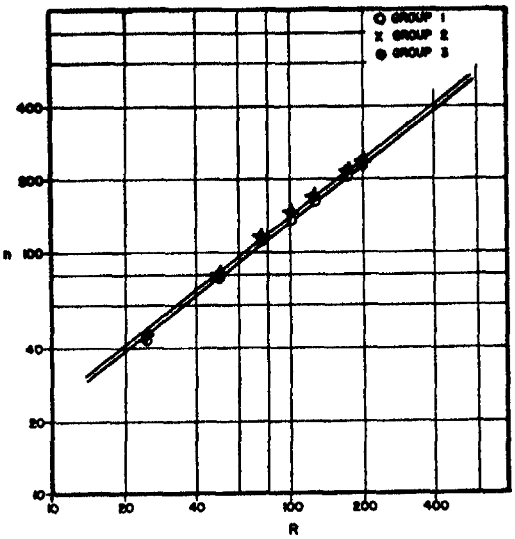

FIG. 5. Variation of grain count with residual range for knock-on protons resident in different layers of an old, but eradicated emulsion (B).

in Plate A (uneradicated) there is a definite desensitization of the upper portion of the emulsion, Group 1, with practically no variation in sensitivity between Groups 2 and 3, indicating, incidentally, uniform depth development at those levels. The reduction in grain density exhibited by Group 1 is caused almost entirely by the tracks in the uppermost 35μ of the emulsion as shown by subdividing Group 1 into 1A (10–35μ) and 1B (36–69μ), as shown in Fig. 4. These two subsections are compared with Group 2, and it is seen that Group 1B is practically coincident with Group 2.

Two possible explanations for this phenomenon present themselves. One is that the surface of the plates lost some sensitivity due to oxidation by the air enclosed in the package. The other is that the plates were not uniformly developed at the upper surface due to the mechanism of development. The portion of the development procedure in question is the dilution of the chilled developer with distilled water. Very little development occurs during the diffusion period at low temperature. The subsequent dilution with water may tend to reduce the rate of development at the surface as compared to the rest of the emulsion after the developer is warmed. Possibly both the oxidation and development factors are involved. Figure 5 shows the same effect for the eradicated plate, B, but to a lesser extent due to the fact that the majority of the tracks in Group 1, in Plate B, occurred below 35μ from the surface.

The eradication procedure appears practical for use in unloaded, Ilford C-2 plates, recording tracks of medium ionizing particles in the absence of background accumulated since time of manufacture. For lightly ionizing particles, loss of sensitivity will be encountered. While the behavior of the process was not investigated for very fast protons or meson particles, the study indicates that the initial portion of the trajectory would probably either not record at all or would be outlined by a smaller number of grains. The eradication method is entirely suitable for recording tracks of alpha-particles and low energy protons without appreciable change in track structure. The investigation also indicates the importance of carefully noting the level of the plate in which the track is found if mass determinations are to be made by grain counts. As indicated by Fig. 4, a proton track recorded in the upper layer of an old emulsion might be confused with a heavy meson particle of about 1300 m_e on the basis of grain counts.* If the plate is old, as it is of necessity in prolonged cosmic-ray exposure, care must be taken in mass estimates that the unknown and comparator tracks are resident at about the same depth.

---

* The 45° line intersects the curves at points of equal grain density. In evaluating the masses of nuclear particles of the same charge by grain counts it is well known that the masses are directly proportional to the residual ranges measured from the points of common grain density. The same method is here employed to evaluate the apparent changes of mass actually due to desensitization of the emulsion.

The Choice of Suitable Gap Forms for the Study of Corona Breakdown and the Fiel Along the Axis of a Hemispherically Capped Cylindrical Point-to-Plane Gap*

LEONARD B. LOEB, JAMES H. PARKER, E. E. DODD, AND WILLIAM N. ENGLISH†
Department of Physics, University of California, Berkeley, California

(Received August 1, 1949)

The various corona gap forms suitable for the convenient investigation of corona phenomena of both signs in the laboratory that are capable of yielding quantitative data involving the Townsend integral for the thresholds of the manifold phenomena are discussed. For laboratory study the most convenient form of gap is the hemispherically capped cylindrical point-to-plane system. Analysis of the potential fall along the axis in such gaps by means of electrolytic model studies indicates that the essential parameter is L/r, the ratio of gap length, L, from point surface to plane relative to the point radius, r. The model study potentials are, however, incapable of giving accurate values of the field strength. These fields must be obtained by computation. Laboratory studies of corona indicate the desirability of relatively large values of L/r. Practical considerations based on studies at atmospheric pressure indicate point radii r of 0.025 and 0.05 cm with a ratio $L/r=160$ to be those giving the greatest flexibility and most widely separated thresholds at convenient potentials. The use of such point systems to standardize data is recommended. On this basis the field along the axis for the hemispherically capped cylindrical point-to-plane gap as computed by E. E. Dodd is given and here applied to the calculation of the point-to-plane Townsend integral for pre-onset burst pulse thresholds in air as observed by H. W. Bandel. The value is compared with the values obtained by W. N. English for confocal paraboloids where the fields are accurately known. The results are satisfactorily consistent. Discrepancies in the fixing of burst pulse thresholds by various observers are discussed.

THE investigation of gaseous discharges using asymmetrical electrode arrangement offers exceptional opportunities for a study of breakdown phenomena. The reason for this lies in the high field concentration at one electrode which, coupled with space-charge accumulations in the lower field regions of the gap, permits one to extend over a considerable voltage range the phenomena leading to breakdown. The discharges with asymmetrical electrodes initiate with the appearance of luminous glows and brushes of diverse forms which can be characterized by the general term coronas. Corona discharges, aside from their scientific interest, have importance in industry in generators for ions of unique sign, in "noiseless" electrical discharges, in electrical valves and control circuits, and as an important source of power loss on high voltage lines.

Laboratory study has now reached the stage where quantitative data in testing basic theory are urgently required and it is important that future studies be made under appropriate conditions. Past investigations have been carried on with the most diverse assortment of electrode systems, and correlation of data has been impossible. The work to be reported here eliminates certain geometries and sets limitations which will assist future workers and lead to better coordination of data.

Modern *basic* corona mechanism studies have shown the desirability of obtaining the data listed:

1. Knowledge of the potential and field distribution across the gap. Such knowledge permits evaluation of the first Townsend coefficient, α, as a function of distance, x, from the point surface, which permits quantitative studies of onset conditions.
2. Convenience for visual, photographic, and oscillographic study. This includes opportunity for direct photographic, telemicroscopic, and spectroscopic observation without distorting the field. Such study is facilitated by concentration of phenomena at one point so that oscillographic records are not complicated by several independent localized coronas on the same system, or by the spread and diffusion of phenomena.
3. Mechanical convenience and simplicity as well as accuracy and ease of adjustment.
4. Uniformity in dimensions to facilitate comparison of data.
5. Proper dimensioning to permit observations of large ranges of pressure and potential change without introducing difficulty with achievable potential supplies or inordinately large dimensions for convenient study.

Possible geometries that have been used are:

1. Concentric cylindrical electrodes.[1]
2. Hyperboloid against plane.[2]
3. Confocal paraboloids.[3,4]
4. Hemispherically capped cylindrical point-to-plane.[5]

All of these, except the hyperboloids, have been used by the Berkeley Laboratory at some time. Hyperboloids were used by Bennett.[2] It is of interest to discuss these geometries in regard to their convenience for basic corona studies.

1. The coaxial cylindrical systems permit accurate knowledge of the fields, especially if equipped with guard rings. They are inconvenient for observation in that discharges may vary from radially symmetrica

---

* This research was assisted by a grant from the ONR.

† Currently at National Research Council, Chalk River, Ontario, Canada.

[1] This geometry has been used in countless studies and is use currently in Geiger counter studies. Until recently, no one has attempted a comprehensive survey of the various threshold mechanisms and a complete accumulation of data for a wide range of pressures and gases compared to other gap types. This has recently been achieved in a Ph.D. thesis by C. G. Miller, University of California, July, 1948, which is now being prepared for publication.

[2] W. H. Bennett, Phys. Rev. 60, 714 (1941).

[3] A. F. Kip, Phys. Rev. 54, 139 (1938), and W. N. English reported here.

[4] K. E. Fitzsimmons, Phys. Rev. 61, 175 (1942).

[5] G. W. Trichel, Phys. Rev. 54, 1078 (1938); 55, 382 (1939). W. N. English, Phys. Rev. 74, 170 (1948).

fans to sectors of such fans and are often diffused down the length of the wire. The regions adjoining the axial wire are usually obscured by supports such that visual observation is difficult. Luminosities at the outer cylinder are hard to see. Several corona events may simultaneously appear at different points on the same inner electrode and the discharge spreads and wanders along the electrode, complicating oscillographic study. The outer cylinder walls play a very important role with the positive wire discharge, especially if the outer radius is small, since the system conserves photons and carriers that are lost in other systems. Such a system is fairly convenient mechanically, adjustment is simple, and outgassing easy. Visual observation is hampered by diffusion and visual aspects appear only at higher currents. Properties of concentric cylindrical coronas must in any case be studied since they furnish important instrumentation such as Geiger counters and other devices, even though they obscure phenomena.

2. Hyperboloids have not been used extensively.[5] It is probably difficult to achieve sufficient field uniformity to permit accurate calculations without using hyperboloid points extensive in space, shorter gaps, and large planes. Fabrication is difficult, especially for sharper points.

3. Confocal paraboloids give accurately calculable fields, if extensive enough. Observation is obscured. They are not easy to fabricate and are awkward to adjust.

4. The fields along the axis for hemispherically capped cylindrical point-to-plane gaps have not to the present been amenable to theoretical calculation. Laborious calculations made on the basis of various studies to be indicated yield a satisfactory solution for the field along the axis near the point for only one ratio of point radius to gap length. The point-to-plane gaps, once the fields are known, are ideal for observation. Localization and observation are excellent. The convenience of fabrication and the accuracy of adjustment are ideal for quick studies. The plane electrode interferes less with the point discharge than any other arrangement. In fact, no marked effect has been noted even in outgassed systems. To date, no studies have been made to indicate the best dimensioning of these systems for laboratory study, and a wide diversity of gaps have been used making comparison difficult. It has been owing to the properties of these gaps that observations of most of the phenomena leading to a knowledge of the basic mechanisms such as burst pulses, streamers, and Trichel pulses were made.

In view of the advantages of the point-to-plane system, it is the purpose of this investigation to study it in order to indicate the most suitable dimensions for experimental application on a laboratory scale, to evaluate the fields along the axis, and to compare corona threshold data for such a system with that for other systems. The cumulative results of these investigations allow of positive recommendations to be made for the future conduct of corona investigations in the laboratory.

The experimental model studies used a tank of wood lined with painted canvas 109 cm along the direction of the axis, 122 cm perpendicular to the axis, and 55 cm deep. The plane was a semicircular disk of Duralumin fastened vertically with its diameter of 116‡ cm along the surface of the electrolyte at one end of the tank. Various hemispherically capped cylindrical brass rod points were used. They emerged from the opposite end of the tank parallel to the water surface with one-half the rod immersed in the electrolyte. The meniscus of the capillary film produced no severe distortions except very close to the point. The rod projected at least 20 cm from the end of the tank. The range of point and gap diameters was limited by the size of the tank. The electrolyte was a 0.02 molal solution of NH_4Cl in water. Later only tap water was used with a higher potential. The potential source consisted of a 1000-cycle oscillator giving 10 v. Later 100 v from a 500-cycle generator was used. The measurements used the conventional potentiometer arrangement common to such studies. A cathode-ray oscillograph was used as null indicator. Potentials along the point axis were determined with a 0.3- and a 0.1-mm diameter probe projecting 1 mm into the liquid. Positioning was achieved by micrometer screw and guide. The observed potentials are shown in column 5 of Table VI, while those calculated are shown in column 4 of Table VI. In view of the inaccuracies of the fields derived from differentiating the curves for potential relative to distance from the point, such fields were not used in calculation. However, the data on potentials and fields led to important considerations in regard to the suitable geometry for use in point-to-plane discharge studies.

The preliminary measurements indicated, as one would suspect, that the principle of similitude was applicable and that the important parameter in the gap was L/r, the ratio of L the gap length from the point surface to the plane, relative to the point radius r. Data obtained for L equal to 76.4 cm, 50.8 cm, and 31.8 cm with point diameters of 0.953 cm, 0.635 cm, and 0.397 cm, gave identical curves for the ratio of potential V at any distance x from the point surface to the total applied potential V_0, when V/V_0 was plotted against the ratio x/L, of x to gap length L within the limits of accuracy of measurement.

Having established the importance of the L/r ratio in such gaps, it was next desirable to indicate the favorable values for corona studies. The work with various corona gaps in this laboratory indicates that the point phenomena are more prominent and the various thresholds are more widely separated in potential the larger the ratio of L/r. These studies also indicate that relatively lower potential gradients at the point surface are needed to start corona at larger point radius, since the critical Townsend integral $\int_{a+r}^{r} \alpha dx$ requires lower values of α

---

‡ In order that the diameter of the disk should lie in the surface of the electrolyte, 4 cm were cut off the curved end of the disk at the bottom.

if the distance $x=a$ from the point radius where ionization ceases can be increased. The larger the point radius the larger the value of a. Thus, except for studies whose specific purpose is to investigate coronas with decreasing point radius, the choice of a conveniently large point radius r within the limitations of available potential sources is indicated.

These factors impose physical limitations of other sorts on the desirable gap radii to be used, as well as fixing the ratio L/r. For example, if it is desired to study the whole range of corona phenomena with one point from onset to spark breakdown, the available high voltage supply becomes important. For $r=0.025$ cm, the threshold in air begins at about 5000 v and ranges to about 40,000 v at breakdown. For $r=0.05$ cm, the threshold is of the order of 8000 v with breakdown correspondingly higher. If potential sources are limited, then smaller values of r are required. In general, the two values given set a limit for comfortable and accurate laboratory control of stabilized potential sources. Thus for convenient work, a value of r given by $0.025\text{ cm}<r<0.05$ cm is indicated if the higher surface fields are to be avoided. Again, since large values of L/r are desirable, further limitations are set by practical considerations in laboratory study. If $L/r=160$ and $r=0.05$ cm, then $L=8$ cm. Now such studies as have been made in this laboratory indicate that if the ratio of plane radius R to gap length L is greater than $R/L=1$, the variation of the plane radius produced no serious change in onset potentials. Theoretical studies further indicate that the length of the point should likewise be at least of the order of the gap length for best results. If $R=8$ cm, the chamber for corona studies must have a diameter in excess of 24 cm so that its electrically screened and grounded walls shall not materially influence the field. This sets an upper limit on values of L/R of 160 for the largest point. The gain obtained by increasing L/r with the $r=0.025$-cm point to 320 with an 8-cm gap is not sufficient to warrant using the longer gap. It is thus recommended that point-to-plane gaps, being used for study in general, be either gaps with $r=0.025$ cm and $L=4$ cm, or $r=0.05$ cm and $L=8$ cm, in order to standardize data. If available potential sources are low, smaller values of r must be used. In any case, irrespective of the value of r chosen, *the ratio of $L/r=160$ appears to present a convenient value.* Accordingly, in setting up the computations for the point-to-plane gap, this ratio of L/r was chosen.

The calculation of the field along the axis and near the point for such a gap is as follows:

The axial electrostatic field intensity at and near the point electrode is expressed in cylindrical coordinates, (r, z), with the plane electrode grounded and at $(z=0)$. Letting $\Phi(r, z)$ be the electrostatic potential for a point electrode of unit radius starting at $(z=160)$ with unit potential difference across the gap, the axial field intensity is:

$$\begin{aligned} X(0, z) &= (\Delta V/\rho)d\Phi(0, z)/dz \\ &= (\Delta V/\rho)E_z, \end{aligned} \tag{1}$$

where ΔV and ρ are, respectively, the actual gap potential and point radius used. E_z will be referred to as the axial field intensity factor.

$\Phi(r, z)$ is approximated by the potential of an axial point charge at (0, 161) followed by an axial charge distribution in $(0, z\geq 161)$ which along with their images in the $(z=0)$ plane produce a unit equipotential surface suitably close to the point electrode boundary. (The $(z=0)$ plane will be at zero potential due to the image charge, but the point electrode boundary cannot exactly be obtained.) Then the axial charge distribution is represented[6] as a step function by a combination of semi-infinite constant axial line charges starting at various values $(z=a)$ so that

$$\Phi(r, z)\approx A_pP(r, z)+\sum_a A_aV(r, z; a), \tag{2}$$

where

$$P(r, z)=([r^2+(161-z)^2]^{-\frac{1}{2}}-[r^2+(161+z)^2]^{-\frac{1}{2}}), \tag{3}$$

and

$$V(r, z; a)=\text{const.}\cdot\int_a^\infty ([r^2+(\xi-z)^2]^{-\frac{1}{2}} - [r^2+(\xi+z)^2]^{-\frac{1}{2}})d\xi,$$

or

$$V(r, z; a)=\log_{10}\frac{a+z+[r^2+(a+z)^2]^{\frac{1}{2}}}{a-z+[r^2+(a-z)^2]^{\frac{1}{2}}}. \tag{4}$$

The total point charge, A_p, and the charge per unit length of any line change, A_a, also contain all necessary proportionality constants and are evaluated by selecting values for $(z=a)$ and imposing upon Eq. (2) the following conditions, which will establish a set of linear simultaneous equations in A_p and the A_a:

On the cylindrical portion of the boundary,

$$\Phi(1, z_i)=1, \tag{5}$$

where z_i are selected values of $z\geq 161$. On the hemispherical portion of the boundary, letting $\Phi(r, z)\rightarrow\Phi(c)$, where c is the great circle displacement from $(c=0)$ at (0, 160),

$$\Phi(0)=\Phi(0, 160)=1 \tag{6}$$

and

$$\Phi_{nc}(0)=d^n\Phi(0)/dc^n=0, \tag{7}$$

where

$$n=2, 4, \cdots.$$

Conditions (5) and (6) make the resulting unit equipotential surface coincide with the point electrode boundary at the points $(1, z_i)$ and (0, 160). The deviation between these points is small and in alternate directions and its effect is neglected. Conditions (7) make the resulting unit equipotential surface have unit curvature at (0, 160) and lie close to the hemispherical portion of the point electrode boundary.

---

[6] This procedure is illustrated for polynomial representations by Crout, J. Math. and Phys. 19, 34 (1940), with general ideas contained in Sections 4A, C, E, F, 5, and 8C. The present representation of the charge distribution is made to simplify the integration and admit a semi-infinite range of (z).

TABLE I. Values of $V(r, z; a)$ from Eq. (4).

a	$V(0, 160; a)$	$V(1, 161; a)$	$V(1, 162; a)$	$V(1, 165; a)$	$V(1, 175; a)$	$V(1, 200; a)$	$V(1, 300; a)$
161	2.50650503	2.80888691	3.19300924	3.72397072	4.27508116	4.75070400	5.40878185
161.1	2.46524762	2.76566438	3.16165444	3.71344489	4.27210512	4.74970965	5.40856350
161.2	2.42759429	2.72286656	3.12869617	3.70265944	4.26910675	4.74871240	5.40834490
161.5	2.33108972	2.60057312	3.01989296	3.66861575	4.25997431	4.74570308	5.40768764
162	2.20682588	2.42745787	2.81157604	3.60532003	4.24427523	4.74062816	5.40658726
170	1.51851394	1.56425222	1.61636247	1.82179656	3.84812921	4.64750435	5.38810812
185	1.13987909	1.15867739	1.17839744	1.24276776	1.55522165	4.36409446	5.34850824
250	0.65854135	0.66443875	0.67040116	0.68861477	0:75330897	0.95419962	5.04143647
400	0.36797679	0.37056340	0.37315779	0.38097896	0.40748351	0.47711884	0.84508740

According to Eqs. (2) and (7), $V_{nc}(0; a)$ and $P_{nc}(0)$ are needed. $V(r, z; a) \rightarrow V(c; a)$ and $P(r, z) \rightarrow P(c)$ by $r = \sin c$ and $z = (161 - \cos c)$, whence, after some calculation,

$$\left.\begin{aligned} V_{2c}(0; a) &= M(-0.5[(a-160)^{-2}-(a+160)^{-2}] \\ &\qquad +[(a-160)^{-1}+(a+160)^{-1}]), \\ V_{4c}(0; a) &= M(+2.25[(a-160)^{-4}-(a+160)^{-4}] \\ &\qquad -6[(a-160)^{-3}+(a+160)^{-3}] \\ &\qquad +5[(a-160)^{-2}-(a+160)^{-2}] \\ &\qquad -[(a-160)^{-1}+(a+160)^{-1}]), \\ &\text{etc., where} \\ M &= \log_{10}e = 0.43429\cdots, \end{aligned}\right\} \quad (8)$$

and

$$\left.\begin{aligned} P_{2c}(0) &= -[(161-160)^{-3}-(161+160)^{-3}] \\ &\qquad +[(161-160)^{-2}+(161+160)^{-2}], \\ P_{4c}(0) &= +9[(161-160)^{-5}-(161+160)^{-5}] \\ &\qquad -18[(161-160)^{-4}+(161+160)^{-4}] \\ &\qquad +10[(161-160)^{-3}-(161+160)^{-3}] \\ &\qquad -[(161-160)^{-2}+(161+160)^{-2}], \end{aligned}\right\} \quad (9)$$

etc.

The set of equations in A_p and A_a obtained from Eqs. (2), and (5)–(7) is

$$\left.\begin{aligned} & A_pP(0, 160)+\sum_a A_aV(0, 160; a)=1 \\ & A_pP(1, z_i)+\sum_a A_aV(1, z_i; a)=1, \quad z_i \geq 161 \\ & A_pP_{nc}(0)+\sum_a A_aV_{nc}(0; a)=0, \\ & \qquad\qquad n=2, 4, \cdots. \end{aligned}\right\} \quad (10)$$

Values of $V(r, z; a)$, $P(r, z)$, $V_{nc}(0; a)$, and $P_{nc}(0)$ as calculated, respectively, from Eqs. (4), (3), (8), and (9) for various values of (r, z) and $(z = a)$ and for $n = 2$ and 4 are listed, respectively, in Tables I–IV. A solution for A_p and A_a obtained by substituting any of these values into Eqs. (10) establishes an expression for $\Phi(r, z)$ by Eqs. (2)–(4) which is compatible with the conditions used, and the axial field intensity factor of Eq. (1) is then

$$\left.\begin{aligned} E_z &= d\Phi(0, z)/dz \\ &= A_p[(161-z)^{-2}+(161+z)^{-2}] \\ &\qquad +\sum_a A_a[2Ma/(a^2-z^2)]. \end{aligned}\right\} \quad (11)$$

An examination of various solutions indicates that the resulting unit equipotential surface fits the point electrode boundary best with one of the arbitrary values $(z = a)$ somewhere between two successive values of z_i with the remaining values of $(z = a)$ close to $(z = 161)$, a variation in the exact values of $(z = a)$ varying E_z by only about ±0.2 percent. Increasing n from 2 to 4 for a given set of z_i varies E_z by only about 0.02 percent, and n greater than 4 are not used.

The solution of Eqs. (10) for the conditions $n = 2$ and 4; $z_i = 161$, 162, 165, 175, and 200; and $a = 161$, 161.1, 161.2, 161.5, 162, 170, and 185 is listed in Table V, column 1, along with the resulting axial field intensity factor at the point surface, E_{160}. Adding $z_i = 300$ and $a = 250$ yields the solution listed in Table V, column 2.

Beyond the last value of z_i used, the resulting unit equipotential surface diverges from the cylindrical boundary due to the axial charge distribution remaining constant beyond the last value $(z = a)$ used, and the resulting axial field intensity factor will be too small. Table V, columns 1 and 2, show how using larger values of z_i increases the resulting axial field intensity factor. An examination of various solutions indicates that one might obtain E_z quite accurately by adding about two more values of z_i and a, extending the conditions to the region of $(z_i \approx 600)$. But since the solution of Eqs. (10) becomes increasingly difficult with additional values of z_i and a, the following approximation is made:

Adding the condition that the axial charge distribution is to be zero beyond an additional value of $(z = a)$ modifies any solution so that the resulting unit equipotential surface converges within the cylindrical boundary beyond the last value of z_i used, and the resulting axial field intensity factor will be too large. In this manner the solutions listed in Table V, columns 1

TABLE II. Values of $P(r, z)$ from Eq. (3).

(r, z)	$P(r, z)$
(0, 160)	0.99688474
(1, 161)	0.99689442
(1, 162)	0.70401082
(1, 165)	0.23946815
(1, 175)	0.06827087
(1, 200)	0.02286256
(1, 300)	0.00502487

TABLE III. Values of $V_{nc}(0; a)$ from Eq. (8).

a	$V_{2c}(0; a)$	$V_{4c}(0; a)$
161	+0.21850229	+0.10719953
161.1	+0.21670726	+0.10808243
161.2	+0.21246958	+0.11065858
161.5	+0.19437271	+0.09513796
162	+0.16421127	+0.05970290
170	+0.04257601	−0.02555883
185	+0.01828506	−0.01533882
250	+0.00585923	−0.00563318
400	+0.00258201	−0.00255451

TABLE IV. Values of $P_{nc}(0)$ from Eq. (9).

$$P_{2c}(0) = +\ 9.735108\times 10^{-6}$$
$$P_{4c}(0) = -10.008905\times 10^{-6}$$

TABLE V. Solutions of Eqs. (10) with E_{160} for the conditions: $n=2, 4$; $z_i=161, 162, 165, 175, 200$; a = values shown in A_a column. Further conditions shown at head of each column.

	1.	2.	3.	4.
	—	(also $Z_i=300$)	(also $\Sigma A_a=0$)	(also $z_i=300$ and $\Sigma A_a=0$)
A_p =	−0.060512	−0.064314	−0.093390	−0.076447
A_{161} =	+32.802649	+33.396195	+37.986009	+35.617700
$A_{161.1}$ =	−45.858086	−46.655654	−52.820437	−49.665187
$A_{161.2}$ =	+7.451914	+7.562661	+8.413206	+7.994968
$A_{161.5}$ =	+7.415526	+7.537521	+8.484869	+8.004021
A_{162} =	−1.534702	−1.558715	−1.745101	−1.651670
A_{170} =	−0.042289	−0.042419	−0.043428	−0.043557
A_{185} =	−0.029465*	−0.028035	−0.016935	−0.026207
A_{250} =	—	−0.029465	−0.258183	−0.012930
A_{400} =	—	—	—	−0.217138
E_{160} =	0.58875	0.59788	0.66869	0.63371

* Round downward.

and 2, become, respectively, those listed in columns 3 and 4.

The solutions listed in Table V, columns 2 and 4, establish fields which provide limits for the true potential and field intensity values, which are represented approximately by the intersection of the linear extrapolations of the values established by these four solutions. For example,

$$E_{160}\approx\frac{0.59788(0.66869-0.63371)+0.63371(0.59788-0.58875)}{(0.59788-0.58875)+(0.66869-0.63371)}=0.60530.$$

Values of E_z and $\Phi(0, z)$ obtained in this way for various values* of (z) are listed in Table VI.

The unit equipotential surfaces resulting from the solutions listed in Table V fit the boundary to within about 0.02 unit up to the last point of coincidence, which is comparable to usual fabrication tolerances for laboratory scale electrodes. The major source of error is the deviation from the boundary at large distances from the point. The results of the solution listed in Table V, column 2, are probably accurate to within two percent (field intensity values too small, potential values too large), and the approximations listed in Table VI are probably accurate to within ±1 percent. Further accuracy is not obtained here since in practice the field may vary somewhat from that of the isolated infinite plane and semi-infinite point electrode system.

A check on the reliability of the result comes from an evaluation of the Townsend integral for the appearance of the positive burst pulse corona in room air at atmospheric pressure and temperature 22°C, with the relative humidity about 50 percent. Measurements were made for this purpose by W. N. English and give the data for the threshold of pre-onset burst pulses and streamers for the nine different confocal paraboloid combinations shown in Table VII. For hemispherically capped cylindrical points of 0.0125, 0.025, and 0.050 cm radius and gap lengths of 2, 4, and 8 cm to the plane, the pre-onset burst pulse threshold observed by H. W. Bandel under the same conditions were 3540, 5280, and 7910 volts, respectively. The theory of Loeb[7] for the threshold of pre-onset burst pulses leads to the relation of $\beta f \exp\int_{a+r}^{r}\alpha dx=1$. Here f is the fraction of the avalanche electrons which collide to give photons capable of photo-ionizing the gas before they enter the anode point. The quantity β is a geometrical factor which gives the fraction of these photons that are absorbed beyond a region of radius at $r+a$ that will produce avalanches equal in magnitude to the first one and so sustain the burst pulse. In gaps as similar as those

TABLE VI.

z in units of ρ	x/r, ratio of axial distance, x, from point surface to radius r	Calculated electrostatic field intensity, E_z, in units of V_0/r	Calculated electrostatic potential, V, in units of V_0	Tank model electrostatic potential, V, in units of V_0
160.0	0.0	0.6053	1.0000	1.000
159.9	0.1	0.5009	0.9450	0.933
159.8	0.2	0.4224	0.8990	0.897
159.7	0.3	0.3597		
159.6	0.4	0.3142		
159.5	0.5	0.2760	0.7968	0.824
159.4	0.6	0.2449		
159.2	0.8	0.1976		
159.0	1.0	0.1639	0.6910	0.725
158.8	1.2	0.1389		
158.6	1.4	0.1197		
158.4	1.6	0.1048		
158.2	1.8	0.09275	0.5931	0.631
157.6	2.4	0.06806		
157.0	3.0	0.05306	0.5098	0.556
156.0	4.0	0.03822		
155.0	5.0	0.02957	0.4318	0.483

---

* (Selected for adaptation to Weddle's and Simpson's quadrature formulas in applications where integration is indicated.)

[7] L. B. Loeb, Phys. Rev. 73, 798 (1948).

studied, βf should be nearly constant so that the threshold set by $\beta f \exp\int \alpha dx = 1$ should yield sensibly the same value of $\int \alpha dx$ for the three paraboloids and the capped cylinder if the theory is correct. Calculating the field as a function of distance x from the expression

$$E_x = \frac{V}{\log_e(f/F)} \frac{1}{x+f}$$

for the confocal paraboloids with focal lengths f and F for the small and large paraboloids used, respectively, and for the point-to-plane by Table VI, it is possible to evaluate Townsend's α as a function of x from the data of Sanders.[8] Plotting α as a function of distance x, $\int_{a+r}^{r} \alpha dx$ can be evaluated by graphical integration or numerical quadrature. Combinations of focal lengths $f = 0.009$ cm, 0.019 cm, and 0.028 cm, with $F = 1.1$ cm, 3 cm, and 5 cm, showed that as theory demands, E_x is independent of F but varies critically with f. The values of the integral obtained were 11.3, 10.4, and 10.0 for focal lengths $f = 0.009$, 0.019, and 0.028 cm, respectively, while the point-to-plane data gave 10.2, 10.3, and 9.1, respectively. It will be noted that the paraboloid and point-to-plane integrals are in relatively good agreement. The agreement is the more remarkable because of the extreme sensitivity of the integral to the shape of the potential curve. Thus one can have some confidence in the accuracy of the point-to-plane field calculations. The collective results yield an average value of the integral of 10.2 so that the avalanche consists of 2.7×10^4 ions. This makes $\beta f = 3.7 \times 10^{-5}$. It will be noted that the integrals seem higher for the smaller radii or focal lengths. In some measure, this may be accidental and not a real variation, since aside from uncertainties in measuring thresholds which may be in the order of two or three percent, the accurate shaping of small points and measurements of radii on these is not easy, even under the microscope. It is also possible that the low values for the larger points may follow from inadequate lengths of the point and plate diameter or paraboloid depths and thus from improper dimensioning of the apparatus. Dodd observed a strong influence of the shank of the point in his calculations of point-to-plane. If this is correct, care must be exercised in future measurements with points of 0.05 cm radius or larger to insure proper point length as well as plate radius. This effect of point length was not investigated experimentally. If Dodd's inferences are correct, it may make use of the smaller point radii desirable under most conditions, since the larger point radii may require inconveniently large chambers.

TABLE VII. f in cm.

		0.009		0.019		0.028	
F in cm		V_g burst pulses	Streamers	V_g burst pulses	Streamers	V_g burst pulses	Streamers
F in cm 1.1	Obs. potential	6075	6175	8025	8175	9425	9550
	V_0 reduced potential	1264	1285	1977	2014	2568	2602
3	Obs. potential	7425	7526	10075	10300	11900	12150
	V_0 reduced potential	1278	1296	1990	2035	2546	2599
5	Obs. potential	8075	8200	11100	11350	13075	13375
	V_0 reduced potential	1278	1297	1992	2037	2522	2580
	Average reduced potential	1273	1293	1986	2029	2545	2594

The values of the potentials and fields marking the burst pulse threshold as given here, and hence the values of the $\int \alpha dx$ here given, are at variance with the values reported by Fitzsimmons[4] for pre-onset burst pulses using the same paraboloids and air of the same character. Fitzsimmons reports the appearance of what *he calls burst pulses* at potentials about half those given here, even for dry air. For moist air, he got values still 20 percent lower. The values of $\exp\int \alpha dx$ in those cases corresponded to 4.46 and 1.86 for a 0.009-cm point. It is clear that such small avalanches could not possibly have been creating self-perpetuating pre-onset burst pulses. Observed on the oscilloscope were *pulses* of some amplitude and it is unlikely that avalanches of five electrons could trigger the observed pulses. The only explanation is that in the large volume available, Fitzsimmons must have used such a strong source of triggering ionization (10 μg of $RaBr_2$ at 3 cm) that he observed pulses caused by the statistical fluctuations of many unresolved avalanches of the magnitude observed. This conclusion is justified in the light of the present work in that Fitzsimmons observed pre-onset *streamers* to begin at values of the potentials yielding $\int \alpha dx$ of around 11 to 12.6. Since, as seen from Table VII, pre-onset streamer thresholds occur at potentials about three percent above burst pulse onset, this would place the values of $\int \alpha dx$ for Fitzsimmons' real burst pulses very close to the values computed from English's data. Thus, Fitzsimmons' results are really in relatively satisfactory agreement with those of English.

---

[8] F. H. Sanders, Phys. Rev. 41, 667 (1932); 44, 1020 (1933).

THE REVIEW OF SCIENTIFIC INSTRUMENTS VOLUME 21, NUMBER 1 JANUARY, 1950

Coincidence Experiments for Noise Reduction in Scintillation Counting

HARTMUT KALLMANN* AND CARL A. ACCARDO
Signal Corps Engineering Laboratories, Fort Monmouth, New Jersey

(Received August 1, 1949)

A method is described which permits discrimination between noise pulses and pulses of small light flashes. The arrangement consists of three multipliers facing the three faces of one and the same crystal. One multiplier acts on the "Y" axis, another on the X axis and the third one on the Z (intensity) axis of an oscilloscope. Light flashes induce pulses in all multipliers simultaneously, whereas noise-pulses occur at random and produce triple-coincidence pulses only very rarely. Triple coincidences are easily recorded with the scope. Pictures are presented illustrating the operation of the arrangement. The original noise being of the order of three thousand per second was dropped to one noise pulse in three seconds.

THE main difficulty in scintillation work is that when light flashes of small intensity are recorded, the counting rate is limited by the number of noise pulses of comparable size occurring in the multiplier tube itself. These pulses are caused by single electrons released from the photo-cathode by thermal collisions; their multiplication in the tube creates a pulse. It has been found by Morton and Mitchell[1] that these single electron pulses are not of equal size but exhibit a whole distribution of pulse sizes. Thus, it may occur that pulses produced by a single electron are even ten times larger than the average pulse size produced by single electrons. On the other hand, a pulse induced by the simultaneous emission of ten electrons from the photo-cathode by a light flash undergoes fluctuations, and it may be that its actual pulse height is considerably less than its medium pulse height; therefore, even pulses originating in the simultaneous emission of several electrons cannot be distinguished with certainty from noise pulses.

I. DISCRIMINATION BETWEEN NOISE PULSES AND LIGHT FLASHES

In this paper, two methods are described which make it possible to distinguish between noise pulses and pulses produced by light flashes from a crystal. For this purpose a crystal was used which emitted its light to three multipliers simultaneously as illustrated in Fig. 1. The faces of the crystal are chosen so that all light proceeding from them can geometrically enter the multiplier window. The multipliers of Type 931A are operated as shown in Fig. 1. One multiplier, called the "Y" multiplier, is connected to the Y axis of the scope and causes deflections of the cathode-ray beam in this direction. The second, the X multiplier, is connected to the X axis of the scope and causes deflections in this direction. This deflection may be produced by the pulse itself which is directly fed into the X plates through an amplifier; then the X deflections are proportional to the pulse intensity (arrangement B) or the pulse may be used to trigger a sweep in this direction giving deflections independent of the pulse intensity (arrangement A). The third, the Z multiplier, is connected to the Z axis amplifier of the scope and regulates the cathode-ray beam intensity according to the size of its pulses.

The cathode-ray beam operates simultaneously in all three directions only if all three multipliers produce a pulse at the same time and only then a deflection of the beam in the Y direction is to be seen when using method A. Noise pulses occurring in the multipliers are entirely distributed at random and are independent of each other. If the duration of a pulse is given by τ, and if the number of noise pulses per second is described by n, the probability of noise pulses occurring in two multipliers simultaneously is given by $n\tau$ and that of noise pulses coinciding in all three multipliers is given by $(n\tau)^2$.

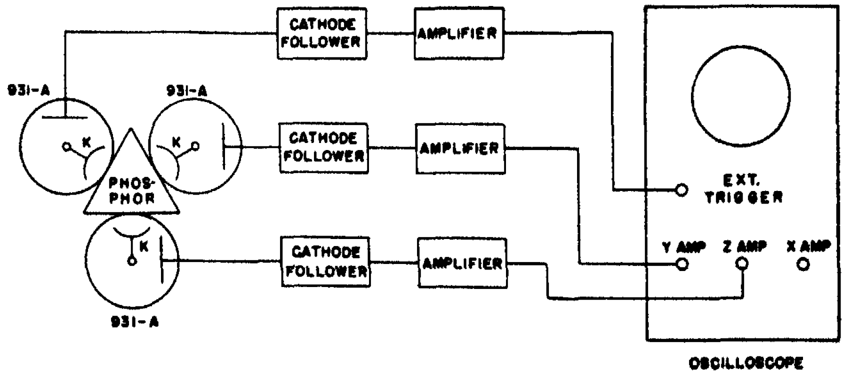

FIG. 1.

---

* Now at Washington Square College of Arts and Science, New York University, New York.

[1] G. A. Morton and J. A. Mitchell, Nucleonics 4, 16 (1949).

FIG. 2. 1/100 sec. exposure of noise pulses from a single photomultiplier.

From this it follows that the number of accidental triple coincidences or the number of events caused by noise pulses in which all three multipliers operate simultaneously is given by $n\cdot(n\tau)^2$, with $n\tau$ sufficiently small, as is usually the case. The number of triple coincidences caused by noise pulses is therefore much smaller than the noise number in one single tube.

If, however, some exterior radiation induces a light flash in the crystal this will induce pulses in all multipliers at the same time, therefore the number of light flashes counted is not reduced by this device. By this method light flashes of small intensity proceeding from the crystal can easily be counted even if noise pulses are much more frequent than the light flashes. With a pulse duration of 10^{-6} second and a noise number of 1000 per second, the number of counted noise pulses is reduced by a factor of 10^{-6}. This means that only after 1000 seconds one accidental triple coincidence occurs in the device. Exterior radiation with such a small counting rate could be detected by this device.

II. EXPERIMENTAL RESULTS

Experiments were carried through according to arrangements A and B and with a small stilbene crystal operating on all three multipliers. The crystal was not very transparent but exhibited considerable light scattering, therefore, the light flashes excited within the crystal did not emit equal light intensities to all multipliers, nevertheless, the pulses of gamma-photons were always indicated by the operation of all three multipliers. Gamma-intensities which were difficult to detect with one multiplier tube since they were covered by noise pulses were easily detected with this triple coincidence arrangement. The counting of pulses was performed photographically.

A. Recording of γ-Pulses in Arrangement A

With arrangement A, the fluorescent screen of the scope was shielded and only a small strip of the screen parallel to the Y axis was visible, on which the pulses produced by light flashes occur. The film was made to run continuously parallel to the X axis. The oscilloscope used had a frequency limit of about 0.5 microsecond and a sweep duration of 5 microseconds. According to these limits the duration of the pulses was chosen of the order of half a microsecond. If, for instance, a light flash starts a sweep, a deflection of the cathode-ray beam is seen half a microsecond after the beginning of the sweep since the Y pulses were delayed by half a microsecond to make them appear fully on the scope. With a high noise rate it is possible that an accidental noise coincidence in the Y and Z multiplier will occur during the 5 microsecond duration of a sweep started by a light flash or a noise pulse in the X multiplier. Such an accidental coincidence pulse in the Y and Z multiplier is registered on the scope by a visible deflection of the cathode-ray beam, however, this deflection does not generally occur at the same position on the scope as the gamma-pulses but appears on another position since they are randomly distributed over this time interval. These pulses were canceled by the described shielding of the scope.

To begin with the noise pulses of the tube were counted by connecting one multiplier to all three axis and were found to be of the order of 3000 per second. Then this arrangement was adjusted in such a way that all pulses excited by light photons were also recorded. Figure 2 describes a "still picture" of these noise pulses with an exposure time of 1/100 of a sec. Numerous small pulses are hidden by the strong intensity at small deflections. Figure 3 demonstrates a similar experiment with an additional exterior gamma-radiation of about 10,000 absorbed quanta per minute. On the other hand Figs. 4 and 5 show still pictures with the triple coincidence arrangement A with an exposure time of $\frac{1}{10}$ of a second. Figure 4, without exterior radiation, is blank since the noise counting rate with the triple coincidence arrangement is very low. Figure 5 shows pulses induced by exterior gamma-radiation.

Visual counting and counting with a running film

FIG. 3. 1/100 sec. exposure of a single photomultiplier with a gamma-source.

FIG. 4. 1/10 exposure (without a gamma-source) (using the triple coincidence method A) (noise pulses not observable).

showed one noise pulse every 4 or 5 seconds. With a pulse duration of a microsecond and with 3000 noise pulses per second one triple coincidence would have been expected every 25 seconds according to the above described equations. The difference between the observed number of accidental triple coincidence and the calculated one may be due to a difference in the number of noise pulses occurring in the different multipliers. Besides this, the width of the visible strip on the scope was a little wider than the width of the pulses, as can be seen in Figs. 2, 3, and 5. As a result such accidental coincidences could also be seen or recorded which occurred during a time duration somewhat longer than that of the actual pulse. A part of the coincidences observed without exterior gamma-radiation are undoubtedly real light flashes from the crystal caused by contamination of the counting chamber or by cosmic-radiation particles. If the triggering of the beam intensity was switched off and if the cathode-ray beam intensity turned on so high that the beam could be permanently seen, 50 pulses per second were approximately counted. These were accidentally occurring noise pulse coincidences in the X and Y circuits.

B. Recording with Arrangement B

The investigations according to method B are described in Figs. 6 through 10. Figures 6 and 7 check the experimental arrangement. They give a picture of the screen when only one multiplier was connected to all three axis. In Fig. 7 not only the pulses produced by the exterior radiation but also the noise pulses cause deflection of the cathode-ray beam. Since the amplifiers in the Y and X axis were adjusted to equal amplification the deflection of the pulse gives straight lines in the 45° direction, in these pictures each pulse is recorded by curves with two traces, a bright trace and one not quite so bright. These two curves occur from the rise and the decay of the pulse (the latter part the bright trace.) That they do not coincide is due to a small difference in the amplifiers used. In this picture, Fig. 6, again only noise pulses of larger intensity can be seen clearly, due to strong intensities of the cathode-beam traces at small deflections. Figure 7 describes a picture in which pulses of exterior radiation as well as noise pulses are seen. It is hard to distinguish between noise or light pulses as observed in Figs. 6 and 7.

Figure 8 describes a photographic picture with the same arrangement but with a pulse running over the Y axis delayed by half a microsecond. For this reason the pulse does not start in the 45° direction but starts from the X axis and then exhibits a sharp deflection in the Y direction corresponding to the sharp rise of the pulse, and then the pulse decays not in a 45° direction but in the direction the tangent of which is given by $e^{\Delta/\tau}$ where τ is the decay time of the pulses and Δ describes the time delay impressed on the Y axis. These curves show how easily coincidence or small time differences between pulses can be determined by this method.

Figures 9 and 10 describe the same operation with the triple coincidence arrangement B; in this case in all three directions different multipliers are operating. It is seen from the photographic pictures that the rise curve and the decay curve do not even nearly coincide in this case; this is due to the fact that the preamplifiers used for this work were not identical but exhibited a little difference in rise times. It is further noted that the decay curve is not represented by a straight line but by an inflected curve and the tangent of the angle of inclination varies along the curve. But it is found that the curves start from the same point; this means that there is no time delay between the X and Y pulses. The inflection of the curve is completely due to small difference in time constants of the multiplier and preamplifier circuits used. If this difference in time constants is given by Δ the tangent varies as $e^{-t/\Delta}$.

These pictures, Fig. 9 and Fig. 10, further indicate that the intensity ratio between the Y and the X pulses is not the same for different pulses but varies from pulse to pulse proving that the intensity of the light flashes proceeding from the crystal to the different multipliers is not the same. This intensity ratio can be determined by connecting the point of largest deflection with the origin. If the same pictures were taken without exterior radiation, they were again completely blank, all noise pulses were eliminated, since noise pulses coinciding in the Y and Z circuit or the X and Z circuit respectively

FIG. 5. 1/10 sec. exposure (with a gamma-source) (using the triple coincidence method A).

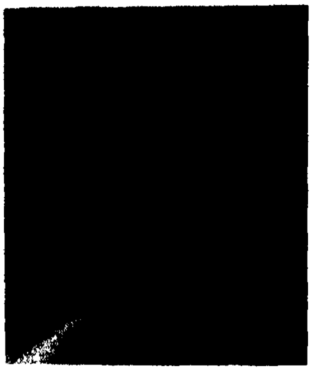

FIG. 6. Exposure of noise pulses from a single photo-multiplier connected to both X and Y amplifiers of the oscilloscope.

FIG. 7. Exposure of a single photo-multiplier with a gamma-source.

FIG. 8. Same as Fig. 7 with Y input delayed.

FIG. 9. Exposure using triple coincidence (method B) with a gamma-source (noise pulses not observable).

FIG. 10. Same as Fig. 9.

are generally deflected only in the Y or X direction but not under a definite angle between the Y and X axis. The method developed makes it possible to compare the light emission of a crystal through the different faces of this crystal.

III. CONCLUSIONS

These methods are not only operable with one single crystal but also with different crystals excited by the same radiation. In this case each multiplier is excited by a different crystal. The noise pulses are eliminated in the same ratio as previously described since only pulses are recorded in which all multipliers operate simultaneously. In this case not only three but a great number of crystals may be used and connected to the Y axis over delay lines with different time delay. Using arrangement A all these multipliers excite deflection in the Y direction which are seen on the screen with different fixed distances on the driven sweep. In this way one photographic picture of the light emission of different crystals energized, for instance, by one event of cosmic radiation can be taken. A similar arrangement can be used for many crystals in case of arrangement B; the pulses of different crystals are then fed to the plus and minus Y and plus and minus X axis with equal time delays. In this way the light flashes proceeding from nine crystals can be recorded simultaneously on one picture.

The limit of this method is given by the intensity of the light which hits the photo-cathode of the different multipliers. If the light intensity hitting the photo-cathodes from one light flash is so small that each light flash does not release one electron, then the number of counted light flashes will decrease. Only when the light flashes release at an average at least one electron is there no decrease in the number of counted light flashes. If the probability that one light flash releases one electron is given by P and if this number is smaller than one, then the number of counted light flashes is diminished by a factor of P^2. Nevertheless, this method of triple coincidence will be advantageous as long as the factor P which diminishes the number of counted light flashes is larger than the factor $n\tau$ which diminishes the number of noise pulses.

THE REVIEW OF SCIENTIFIC INSTRUMENTS VOLUME 21, NUMBER 1 JANUARY, 1950

Note on the Detection of Coincidences and Short Time Intervals

ROBERT HOFSTADTER AND JOHN A. MCINTYRE*
Palmer Physical Laboratory, Princeton University, Princeton, New Jersey

(Received August 1, 1949)

A flexible method of detecting coincidences and short time intervals has been devised in which a photo-multiplier tube views the screen of a cathode-ray tube. By using one pulse as initiator of a sweep and the other in vertical presentation, coincidences can be observed in a fixed portion of the screen while the remainder of the screen is masked off. In present use the method is limited only by the pulses available (5×10^{-9} sec.). The method appears to be capable of extension to time intervals of the order of 9×10^{-10} second or smaller.

A METHOD has been briefly reported by which coincidences in the Compton effect have been studied both visually and photographically on the screen of a cathode-ray oscilloscope.[1] The purpose of this note is to describe how this method can be extended to resolving times of the order of 10^{-9} or 10^{-10} second and otherwise improved by employing a photo-multiplier tube to view the screen of the cathode-ray tube.

The new method for detecting and counting coincidences is described below where we shall make reference to the schematic drawing of Fig. 1.

Pulse I of the coincidence pair is used to trigger the sweep and intensifier gate of the oscilloscope.[2] Pulse II is delayed by a coaxial line B, amplified and brought to the vertical plates of the cathode-ray tube. A mask, having the shape shown in Fig. 1, cuts from view the horizontal sweep trace. Therefore only a vertical pip, appearing in the unobstructed portion C of the mask, illuminates the visible portion of the cathode-ray screen. A camera lens throws a real image of the pip on the window of "viewing" photo-multiplier tube A, which is placed behind an opening in a small light tight box D. This photo-multiplier observes a light pulse only when both a triggered sweep and a vertical pulse are correlated together in time so that the pip appears in region C of the screen. If the length of the delay line B is adjusted to match the time lag required for the triggered sweep to start and run the spot to the region C, each light pulse observed by photo-multiplier A corresponds to a true coincidence. It can be seen that (a) the horizontal position of the vertical pulse will, in general, be correlated with its delay (±) with respect to the triggering pulse and (b) the width of region C determines the resolving time of the coincidence method.

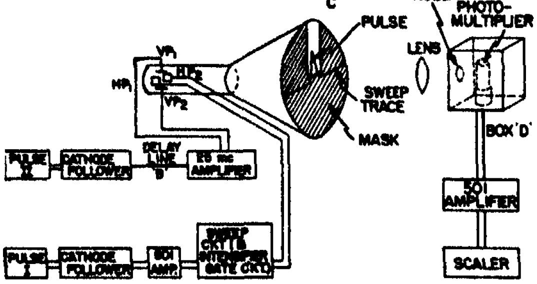

FIG. 1. Schematic diagram for detecting coincidences.

Any pulse II, regardless of shape, which fills the entire width of the open space of the mask above its lower edge, is associated with the same production of light on the screen. Therefore the photo-multiplier light pulse is constant and independent of pulse shape. It is implied that the upper part of the trace does not escape beyond the photo-multiplier's field of view and that the normal statistical spread of photo-multiplier pulse size is small. Both conditions are readily met in practice.

Table I lists typical operating conditions which we have used in detecting coincidences by this method. The coincidence pair has been: I—Compton scattered photon, II—Compton recoil electron pulses in separate luminescent stilbene crystals.[1]

From Table I it may be seen that the method offers the following advantages: (a) The allowable range of pulse sizes is very large for either pulse I or II. (b) The output pulse is constant. (c) The resolving time may be made quite small. (d) One large pulse by itself cannot possibly produce a (spurious) coincidence. We have been unable to employ a coincidence scheme offering an equivalent performance. In recent work we have detected triple coincidences by employing the third pulse as a trigger for the intensifier grid of the oscilloscope tube, as in the accompanying paper by Kallmann and Accardo.

With regard to point (a) the smallest pulse II we have detected above the masked-off-sweep is approximately as large as two line widths of the sweep, or somewhat less than $\frac{1}{16}$ inch. With better focus this figure can be made smaller. Since very large pulses II merely overload the amplifier there is no upper limit to the pulse size. Similarly the only limitation on pulse size I is that it be not so large that it produces two sweeps. In our experience this behavior does not occur. The lower limit of pulse size I is determined by somewhat less than the noise of the pulse source, amplifier, or trigger circuit. Items 12, 13, 14 of Table I show that considerable noise may be associated with pulse I and yet be discriminated against. Smaller resolving times will, of course, aid in cases where the noise pulses are more numerous.

---

* NRC predoctoral fellow.

[1] R. Hofstadter and J. A. McIntyre, Phys. Rev. 76, 172 (1949).

[2] The general methods of high speed electronics are described by W. C. Elmore, Nucleonics Vol. 2, No. 4, 43 (1948).

Referring to item 10 of Table I, we have made a simple test to see how small the resolving time may be made with our relatively crude equipment. The open space C of the mask was made 1 mm wide; we have observed that photo-multiplier A pulse size is still 3.5 times larger than the pulses due to background illumination in the cathode-ray tube. This background is produced partially by tube filament glow and partially by scattered light due to fluctuations in phosphorescent screen glow produced by the large number of noise-triggered sweeps. The background is not the noise of photo-multiplier A, although such noise will provide the fundamental limit of resolving time of this method. Cooling of the photo-multiplier will help to remove this limitation. Using the given sweep speed, 1 mm corresponds to 3.2×10^{-9} second. The slit width may therefore be made at least 3.5 times smaller than 1 mm, or the sweep speed increased by the same factor, so that the resolving time can be made 9×10^{-10} sec. or smaller. Success in eventually employing this method for such small time intervals obviously depends on obtaining pulses of correspondingly small durations and on the accuracy, or lack of "jitter," with which all sweeps are initiated in time. The latter depends on the quality of the linear sweep generator and the triggering amplifier.

The useful resolving time of this method is affected to a small extent by the variable size of the trigger pulse. A small trigger pulse will start the sweep later than a large trigger pulse. Hence the vertical pip will appear in slightly different positions for small and large pulses. In order to avoid missing coincidences the slit should be opened up to accept such early and late pulses. In using a 501 amplifier to generate trigger pulses, the slit should be opened up to 0.1 microsecond to accept all pulses. A fast amplifier, of the type used to amplify pulse II, allows a smaller resolving time.

The ultimate resolving time of this method is probably considerably smaller than the figure given above. Several evident improvements on the method outlined are: placing the photo-multiplier directly at the screen; improvements in cathode-ray tube phosphor with respect to afterglow; obtaining a better focused spot, etc. It is conceivable that a secondary emitting surface might be placed within the cathode-ray tube. The fluorescent screen would then be unnecessary.

The repetition rate of coincidences is limited by the decay time of the phosphor of the oscilloscope screen. Although we have not examined this point in detail, the oscilloscope screen pulse appears to decay to a low value in two to three microseconds. Thus coincidence counting rates of the order of 50,000 per second appear to be possible with suitable phosphors.

A variation of the method given above may be used when it is desired to measure a small variable time interval. In this case several photo-multipliers would simultaneously view adjacent portions of the cathode-ray screen, or a single tube would be moved horizontally along the screen. In the former case each individual photo-multiplier would be associated with a given time delay.

TABLE I.

1. Pulses—Stilbene scintillation counters, 1P21 photo-multipliers; 25 megacycle (upper half-power point) amplifiers. Duration of pulses about 5×10^{-8} second; heights vary between limits of zero and 70 volts (the latter, amplifier overload).
2. Cathode-ray oscilloscope—"Laboratory Oscilloscope"[a]—5CP11A tube.
3. Electron gun accelerating voltage—900 volts.
4. Post acceleration voltage—3600 volts.
5. Sweep speed—0.08 microseconds per inch.
6. Vertical deflection sensitivity—40 volts per inch.
7. Screen—lens distance—16.5 cm.
8. Viewing lens—Biotar $f/1.4$.
9. Width of unobstructed region of screen has been varied between minimum of 1.0 mm and 50 mm corresponding to resolving times of 3.2×10^{-9} to 1.6×10^{-7} sec.
10. Smallest resolving time (see discussion)—9×10^{-10} second.
11. Smallest pulse II detected above blanked-out sweep line .... 2.5 volts.
12. Rate of random occurrence of pulse I as high as . . 1000 per sec. when using resolving time of 5×10^{-8} sec.
13. Rate of random occurrence of pulse II......... 2000 per sec. when using resolving time of 5×10^{-8} sec.
14. Rates of occurrence of true coincidences at various Compton scattering angles..................... 0.2 to 1.0 per second when using resolving time of 5×10^{-8} sec.

[a] V. Fitch and E. W. Titterton, Rev. Sci. Inst. 18, 821 (1947).

If there is a variation in triggering time, in other words if jitter is present, it is advantageous to portray the initiating pulse on the screen and register its position with one or more of the photo-multipliers. We have put both pulses I and II on the screen by bringing each to its own vertical plate. For example, the initiating pulse I is delayed by a fixed amount, amplified and finally brought to the lower vertical plate. The second, variable delayed, pulse II is delayed by a longer fixed time than I, amplified and brought to the upper vertical plate. Hence the initiating pulse I appears as a "down" trace at the left of the screen and the pulse II as an "up" trace at the right of the screen. A properly shaped mask to blank the sweep trace is employed in this method.

We may finally mention that large deflection sensitivities are possible in these methods since the electron beam of the tube need only be accelerated through a voltage drop sufficient to obtain good focus. The viewing photo-multiplier A requires a fluorescent screen pulse only as large as the light equivalent of a single beta-particle scintillation—which is quite small.

An account of a use of the coincidence method in an experimental test of the Klein-Nishina theory at 1.2 Mev has been published in *The Physical Review*.[3]

This work has been partially supported by the Joint Program of the ONR and AEC.

---

[3] R. Hofstadter and J. A. McIntyre, Phys. Rev. 76, 1269 (1949).

THE REVIEW OF SCIENTIFIC INSTRUMENTS VOLUME 21, NUMBER 1 JANUARY, 1950

A Large Dempster-Type Double-Focusing Mass Spectrograph*

HENRY E. DUCKWORTH
Scott Laboratory, Wesleyan University, Middletown, Connecticut

(Received August 1, 1949)

A description is given of a large Dempster-type double-focusing mass spectrograph. The dispersion of the instrument is 2.3 mm for one percent mass difference. The theoretical resolution for a 0.001-in. principal slit is 7000 and has been experimentally realized. The performance of the instrument is illustrated by a mass spectrum showing doublets formed by singly-charged Cu and Zn and triply-charged Pt.

INTRODUCTION

THE first double-focusing mass spectrographs,[1-3] which were completed in 1935 and 1936, were designed primarily for precision mass measurements. Since that time several other double-focusing mass spectrographs have been constructed.[4-11] Because of their velocity-focusing feature, such instruments are well suited for use with hetero-energetic ion sources. Some such sources, notably the "hot spark" type, possess unique advantages in analytical work (both isotopic and chemical), and consequently double-focusing instruments are powerful research tools in fields other than that of precision mass measurement. When plans were being made for the construction of mass spectroscopic equipment at Wesleyan University, a double-focusing design was chosen in order to secure the versatility which it offered. The completed instrument, which is a Dempster type, has been in operation for several months and it is felt that it possesses certain novel features which warrant a published description.

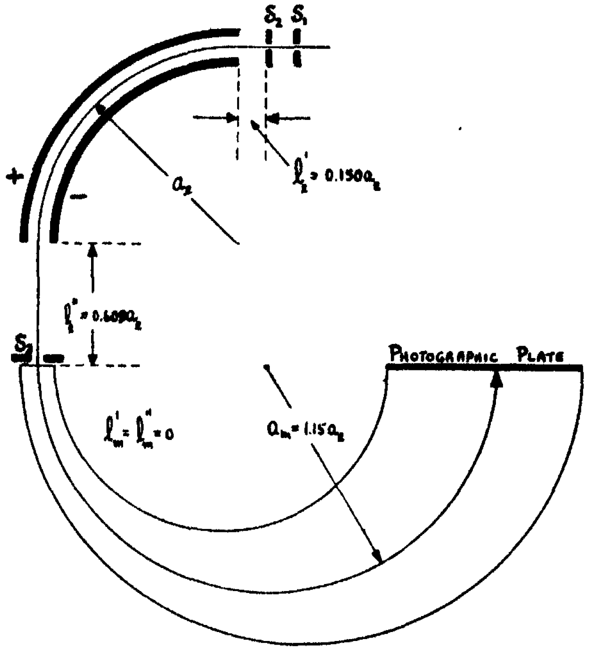

FIG. 1. The Dempster double-focusing arrangement. A $\pi/2$ radial electric field is followed by a π-homogeneous magnetic field.

GENERAL DESCRIPTION OF THE INSTRUMENT

The geometry of the instrument, shown in Fig. 1, follows Professor A. J. Dempster's well-known design.[1] The necessary theory has been worked out by Dempster and others.[12-15] The symbols in Fig. 1 are those employed by R. Herzog,[12] who first solved the problem of the focusing conditions for the general case of a steady electromagnetic field.

The mean radius of curvature of the $\pi/2$ electrostatic analyzer is 7.900 in. The principal slit, S_2, is located $0.150\times 7.900=1.185$ in. ($l_e'=0.150a_e$) in front of the effective boundary of the electric field. The image formed by the electrostatic analyzer is $0.609\times 7.900=4.811$ in. ($l_e''=0.609a_e$) beyond it, and is located at the effective boundary of the magnetic field ($l_m'=0$). For velocity-focusing, the radius of the path in the magnetic field is 9.1 in. The final image is formed at the exit boundary of the magnetic field ($l_m''=0$), at the lower surface of a photographic plate. The slit, S_3, located at the entrance to the magnetic field, allows only those ions, whose energies lie in a narrow range, to enter the magnetic analyzer.

The theoretical resolving power of the instrument, with a 0.001-in. principal slit, is calculated to be 7000. The dispersion, at the position where velocity-focusing obtains, is 2.3 mm for one percent mass difference. This position is located at the center of the 10-in. photographic plate. This plate is long enough to cover on a single exposure the mass spectrum from M to $2.6M$.

The completed instrument is shown in Fig. 2.

---

* This paper is partially based on work done at Wesleyan University under Contract AT(30-1)-451 with the AEC.

[1] A. J. Dempster, Proc. Am. Phil. Soc. **75**, 755 (1935).

[2] K. T. Bainbridge and E. B. Jordan, Phys. Rev. **50**, 282 (1936).

[3] J. Mattauch, Phys. Rev. **50**, 617 (1936).

[4] W. Bleakney and J. A. Hipple, Jr., Phys. Rev. **53**, 521 (1938).

[5] H. A. Straus, Phys. Rev. **59**, 430 (1941).

[6] E. B. Jordan, Phys. Rev. **60**, 710 (1941).

[7] C. Reuterswärd, Arkiv. f. Mat. Astr. o. Fys. **30A**, No. 7, 1 (1944).

[8] H. Ewald, Zeits. Naturforschung. **1**, 131 (1946).

[9] A. E. Shaw and Wilfred Rall, Rev. Sci. Inst. **18**, 278 (1947).

[10] Nier, Roberts, and Franklin, Phys. Rev. **75**, 346 (1949).

[11] T. Mariner and W. Bleakney, Rev. Sci. Inst. **20**, 297 (1949).

[12] R. Herzog, Zeits. f. Physik **89**, 447 (1934).

[13] J. Mattauch and R. Herzog, Zeits. f. Physik **89**, 786 (1934).

[14] A. J. Dempster, Phys. Rev. **51**, 67 (1937).

[15] R. G. E. Hutter, Phys. Rev. **67**, 248 (1945).

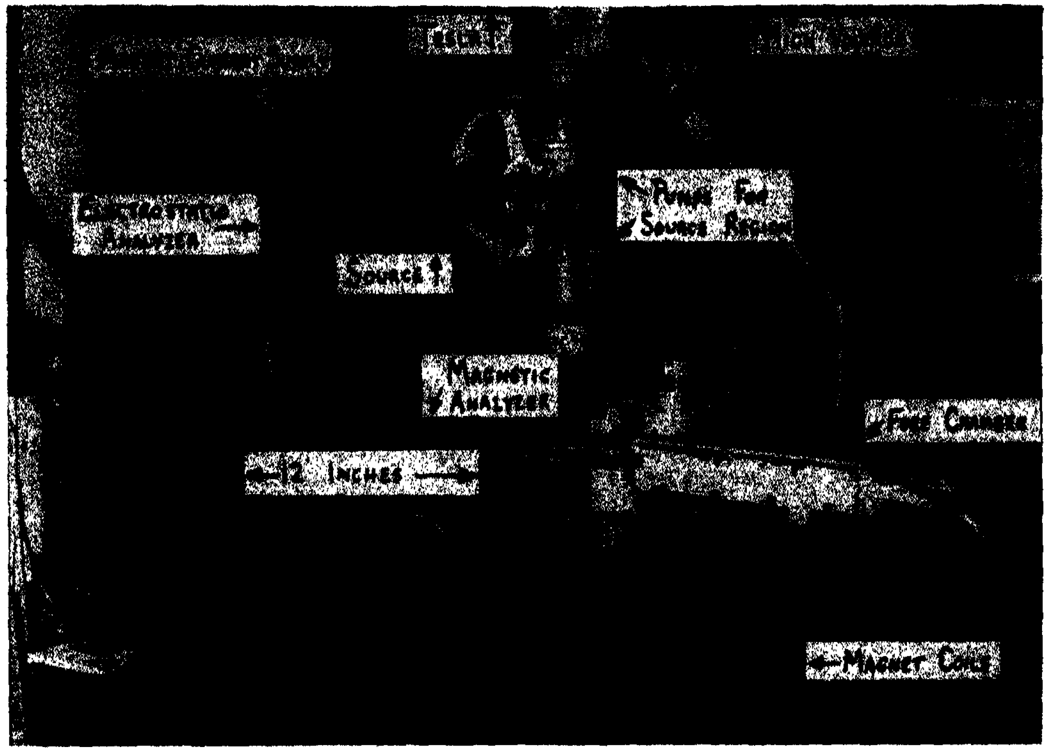

FIG. 2. Photograph of the completed Dempster-type mass spectrograph.

SOURCE AND SLIT SYSTEM

Positive ions are produced in a high frequency spark[16] between two electrodes. The spark is energized by a Tesla circuit of four megacycles frequency. In Fig. 3, which is a sketch of the source and slit region, one electrode is seen to be a rod, while the other is a cylinder inserted in a brass diaphragm. This combination of electrodes was suggested to the author by Professor Dempster. The diaphragm is positioned ⅛ in. away from the unit holding the slits by two ceramic insulators, ¼ in. in diameter and tapped at each end. These were obtained from the American Lava Corporation. The ⅛-in. space constitutes the acceleration region.

The rod electrode is adjusted and fed in by a combination bellows and Wilson[17] seal arrangement of the type described by Shaw and Rall.[9] This unit is waxed

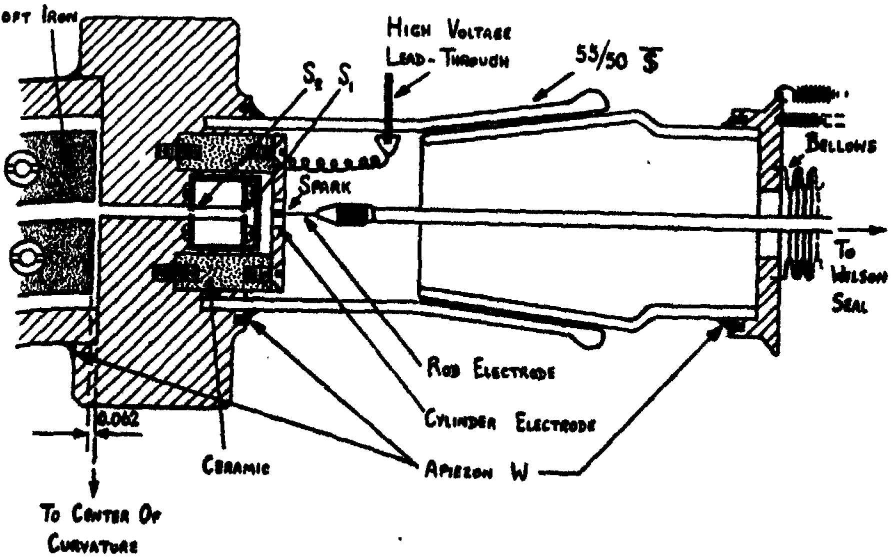

FIG. 3. Source and collimating slits. The striped parts are made of brass.

---

[16] A. J. Dempster, Rev. Sci. Inst. 7, 46 (1936).

[17] R. R. Wilson, Rev. Sci. Inst. 12, 91 (1941).

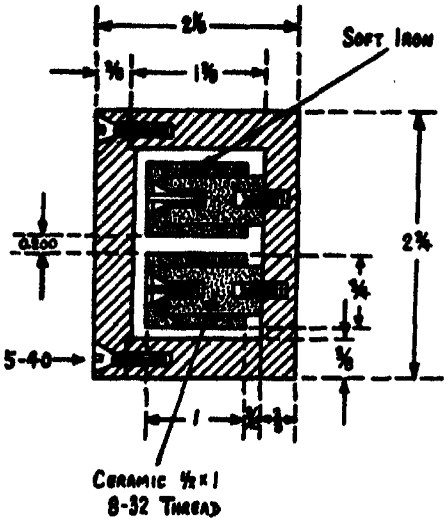

FIG. 4. Sectional view of the electrostatic analyzer showing the soft iron condenser plates supported on ceramic insulators. All dimensions are in inches.

to a male 55/50 standard taper providing a convenient ground joint to be opened when electrodes are to be changed. The ground joint, which is not vacuum-lapped, is made vacuum-tight with Celvacene Heavy, obtained from Distillation Products Incorporated. The joint is readily opened after gentle heating.

The unit holding the slits is removable to permit cleaning or adjustment. The slits are aligned by a method devised by Dr. A. E. Shaw of the Argonne National Laboratory. It is to be hoped that he will publish an account of his scheme. The distance between S_1 and S_2 is 1 cm, S_2 being the principal slit. The distance from S_2 to the front edge of the condenser plates is 1.248 in. This allows, as is Dempster's practice, for the effective electric field to extend $\frac{1}{16}$ in. beyond its physical boundary.

The slit system effectively isolates the source region from the analyzing region. This is highly desirable because of the amount of vapor released when the spark is operating. It, of course, requires that the source region be pumped separately.

THE ELECTROSTATIC ANALYZER

It is important that the curved condenser plates of the electrostatic analyzer be accurately parallel. In order to secure such parallelism, the roughed-out condenser plates were fastened in their final position before their inner surfaces were finished on a lathe. Figure 4 shows how the condenser plates are supported in their housing on ceramic insulators. These insulators, bought from the American Lava Corporation, are very uniform in size. It was possible to select a number, from among twice as many, which were interchangeable. The condenser plates were themselves made of soft iron in order to shield magnetically the ion path. The plates were nickel-plated before the final assembly.

The vacuum chamber, which houses the electrostatic analyzer, was made from a sheet of 2-in. brass. The fourth side is a close-fitting lid held in position by screws. Flanges were attached to each end of this chamber in the manner shown in Fig. 5, and the whole made vacuum-tight with Apiezon *W* wax. It is felt that the extra heavy condenser plates, vacuum chamber walls, and flanges have resulted in a precision which will be permanent.

Positive ions with charge e will acquire kinetic energy $\frac{1}{2}mv^2 = V_ae/300$ ergs in being accelerated by V_a volts. Passing into the electrostatic analyzer they will be subjected to a deflecting force $mv^2/r = Ee \doteq V_de/300b$ dynes, where V_d is the voltage across the curved con-

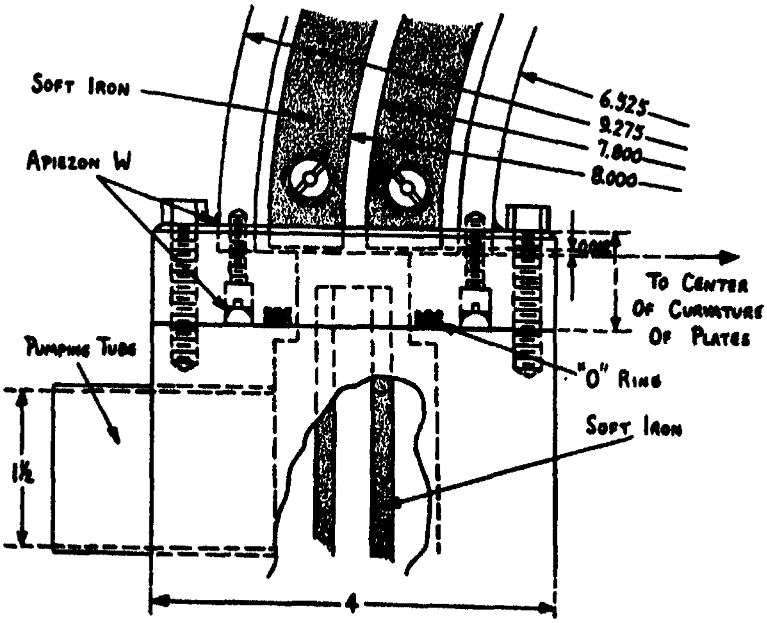

FIG. 5. View showing the joint between the flange at the bottom of the electrostatic analyzer and the spacer between the two analyzers. Two dowels, part of the joint, are not shown.

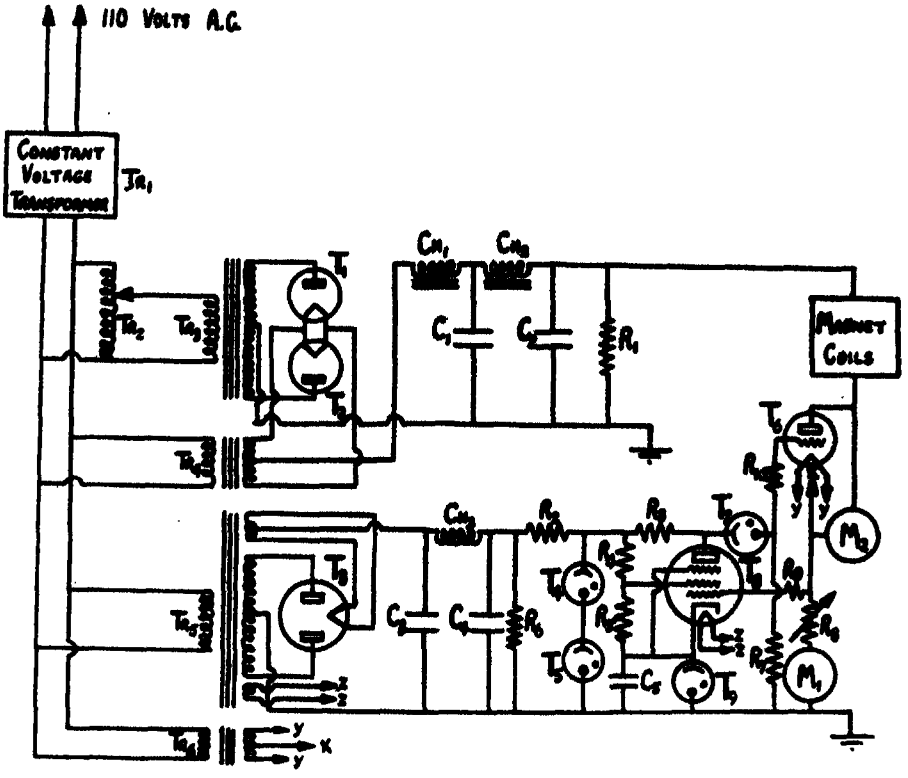

T_1	866A/866
T_2	866A/866
T_3	5R4GT
T_4	VR-150
T_5	VR-150
T_6	2A3
T_7	Ne-2
T_8	6AC7
T_9	VR-150
TR_1	Sola constant voltage transformer, 500 watts
TR_2	G. R. Variac, type 100-Q
TR_3	Thordarson 21P79
TR_4	UTC S-57
TR_5	Navy type CAY 301164
TR_6	2·5 volt, 10 amp.
CH_1	UTC S-38
CH_2	UTC S-37
CH_3	10 henries, 0.2 ampere
C_1	G. E. Pyranol, 14 μfd, 2000 v.d.c.
C_2	G. E. Pyranol, 14 μfd, 2000 v.d.c.
C_3	10 μfd, 600 v.d.c.
C_4	10 μfd, 600 v.d.c.
C_5	0.1 μfd, 600 v.d.c.
R_1	eight 7000∼, 10 watts
R_2	15,000∼, 10 watts
R_3	600,000∼, 1 watt, low temperature drift
R_4	25,000∼, 10 watts
R_5	50,000∼, 10 watts
R_6	120,000∼, 2 watts
R_7	2.2 megohms, ½ watt
R_8	0–5000 ohms, high wattage, low temperature drift
R_9	10,000∼, 1 watt
R_{10}	47∼, 2 watts

FIG. 6. Power supply and stabilizer for magnet current.

denser plates and b is the condenser spacing. From these one can obtain the proper ratio $V_a/V_d \doteq r/2b$. Since the condenser spacing is 0.200 in. and the mean radius is 7.900 in., the ratio $V_a/V_d \doteq 20$. In practice, when the positive ions are being accelerated by 12,000 volts, the appropriate electrostatic field is established by 550 volts, that is, the ratio V_a/V_d is experimentally 22. V_d is provided by B-batteries.

It has been found that the mass spectral lines are sharpest when the negative condenser plate is at ground potential, and they deteriorate steadily as ground is moved toward the positive plate. It is necessary to shield completely the leads to the electrostatic analyzer from the Tesla radiation.

THE MAGNETIC ANALYZER

Two pole pieces, contoured to provide a field of the shape shown in Fig. 1, are held ⅛ in. apart by a brass spacing ring and cover. These pieces, bolted and waxed together, constitute the vacuum chamber of the magnetic analyzer. This unit fits into a 3-in. gap in the large electromagnet, as can be seen in Fig. 2. The brass cover houses a Shaw and Rall[9] mechanism whereby the photographic plate can be moved laterally to allow seven exposures. The motion is got by a rack and pinion action, the rotation of the pinion being accomplished through a Wilson seal.

The magnet is made of Armco iron and has pole faces, before the insertion of the vacuum unit, 18 in.×9½ in. It is excited by approximately 220,000 turns of No. 26 heavy Formvar wire, wound on six coils by the Gramer Company of Chicago, each coil having 8500 ohms resistance. The six coils are connected in parallel and are supplied with current from the power supply and stabilizer shown in Fig. 6. A current of 100 ma establishes, in the ⅛-in. gap, a field of 12,000 oersteds, while a current of 500 ma establishes a field of 17,500 oersteds.

The circuit shown in Fig. 6 provides steady magnet current. T_6, shown in the diagram as a single tube, actually represents four 2A3's, connected identically in

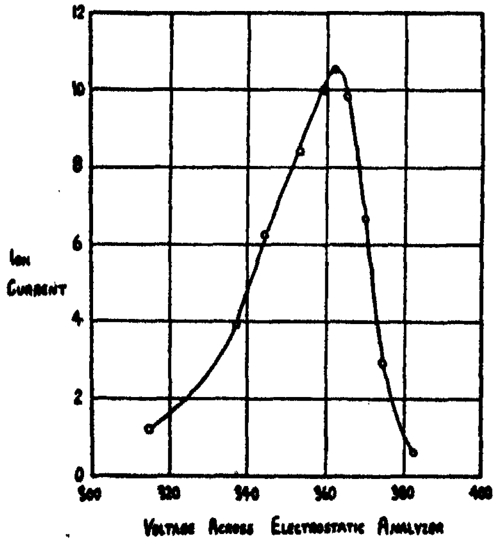

FIG. 7. Ion current emerging from the electrostatic analyzer as the voltage across the electrostatic analyzer is varied. The accelerating voltage has been kept constant.

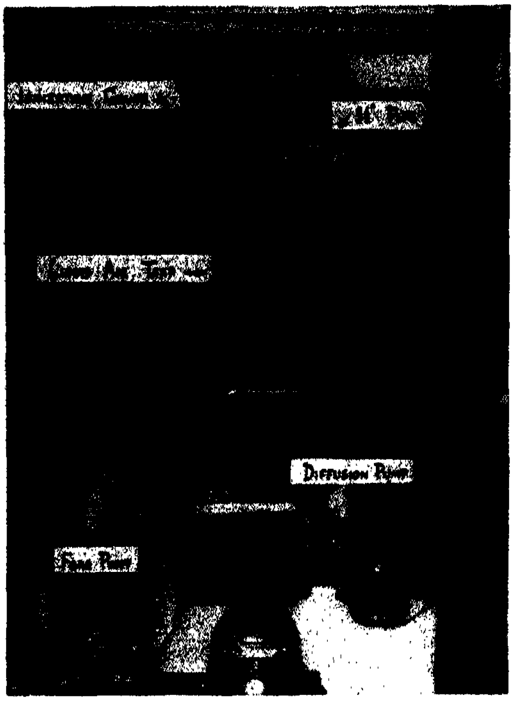

FIG. 8. View showing the vacuum system for the analyzer region. The trap is described in the text.

parallel. The 0–500 voltmeter, M_2, measures the plate voltage of these current carrying tubes. The circuit regulates when this voltage is between 60 and 140 volts. The milliammeter, M_1, measures the current through the reference resistor, R_8, which is also the magnet current. R_8 is a large wattage, low temperature drift, variable resistor. The stability of the magnet current is undoubtedly aided by the large inductance of the magnet coils, which suppresses short time fluctuations. The time constant of the magnet coils is about seven seconds.

ACCELERATING VOLTAGE

Accelerating voltage is got from a 0–40,000 V.D.C. power pack, style No. FW-D, bought from the Moss X-Ray Company of Chicago. The half-wave rectified d.c. is filtered with a 40-megohm resistor shunted by 2.25 microfarads of capacity. The high voltage lead to the source contains a 100-megohm resistor which renders the voltage relatively innocuous.

Figure 7 is a curve showing the ion current emerging from the electrostatic analyzer as the voltage across the electrostatic analyzer is varied. While the data for this curve were being obtained, the principal slit was 0.004 in. and S_3 was replaced by a collector $\frac{1}{4}$ in. wide. It can be seen that although the ratio V_a/V_d is not very critical, intensity can be gained by working with the proper value. In order to stay on the peak of this curve it has been necessary to insert a constant voltage transformer between the high voltage power pack and the a.c. line. Figure 7 shows clearly the energy spread

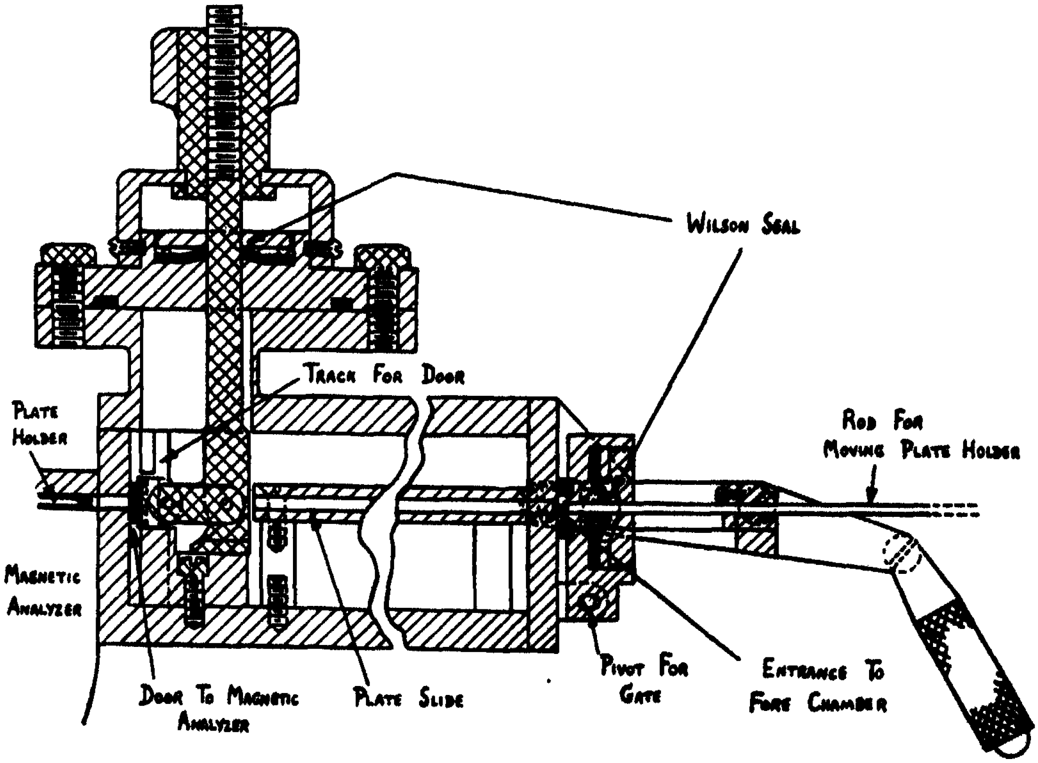

FIG. 9. Diagram of the fore chamber which permits insertion and removal of photographic plates without destroying the vacuum.

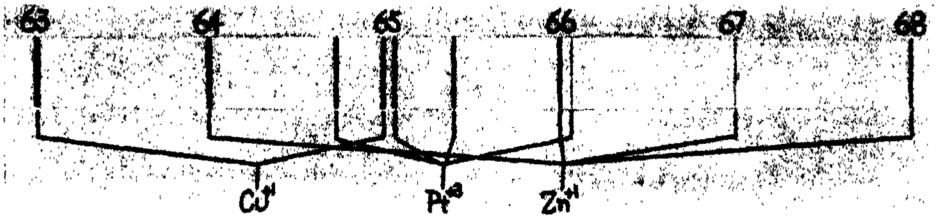

FIG. 10. Doublets formed, at mass numbers 65 and 66, by singly-charged copper and zinc and triply-charged platinum. Magnification 6×.

existing among the ions from the spark source. When ions from the spark have been allowed to enter the magnetic analyzer without first traversing the electrostatic analyzer, the resulting mass spectrum has possessed very broad and poorly defined lines.

VACUUM SYSTEM

As mentioned earlier, the source region is pumped independently of the analyzing region, the slits defining the boundary. The source is pumped by a Distillation Products VMF-10 oil diffusion pump while the analyzing region is evacuated by a Distillation Products MC-275 oil diffusion pump. Both pumps are backed by Welch Duo-Seal, Type 1405H, mechanical pumps. The recommended diffusion pump oil has been replaced with silicone pumping fluid DC 703, obtained from the Dow Corning Corporation, with splendid results. Several accidental and intentional exposures of the hot silicone to atmospheric pressure have apparently not lowered its pumping efficiency, or caused it to "crack."

In both systems liquid air traps have been inserted. These traps are simple in design and appear to be well suited for use with metal systems. As can be seen in Fig. 8, which pictures the pumping system for the analyzers, a standard sweat-fitting *T* is slotted anglewise across the throat, and a metal baffle, which extends well below the bottom end of the *T*, fitted and soldered into the slot. A glass test tube of the appropriate size, in this case $3\frac{5}{8}$ in. in diameter, is waxed into the open end of the *T*, with the metal baffle extending almost to the bottom. The glass end, which fits up into the *T*, is protected from abrasion by a cushioning lead gasket. The design offers a large pumping cross section and permits easy removal of the traps for cleaning.

Exposures are normally taken with a pressure in the analyzers of about 5×10^{-6} mm as measured with an ionization gauge. Prolonged pumping has reduced the pressure to less than 10^{-6} mm. During exposures the pressure in the source region may exceed 10^{-4} mm.

FORE CHAMBER

Figure 9 shows the scheme of the fore chamber, which permits insertion and removal of photographic plates without breaking the vacuum. When it is to be opened, the door between the fore chamber and the magnetic analyzer is raised by a rod sliding through a Wilson seal. The door is held in tracks during the raising by vertical ridges on front and back edges. When the rod is screwed down, the rubber gasket on the face of the door is firmly compressed. The plate holder is meanwhile inserted or removed by the rod which screws into the end of it. The fore chamber is evacuated, using an appropriate system of stop-cocks, by the fore pump which pumps the source end. Immediately after a plate has been inserted, the pressure in the analyzing region has been found to be 2×10^{-5} and rapidly dropping.

PERFORMANCE

With a principal slit, S_2, of width 0.001 in., and S_1 about three times as wide, the measured resolution for faint lines, in the position of sharpest focus, equals the theoretical value of 7000. Since this resolution is more than adequate for the mass comparisons which are currently being made, no attempt has been made to reduce the size of the principal slit. Figure 10 shows two typical doublets formed by singly-charged copper and zinc and triply-charged platinum. For this exposure the slit S_3, between the electrostatic and magnetic analyzer, was set at 0.75 mm. The exposure time was about fifteen minutes.

With S_1 and S_2 both equal to 0.004 in. and $S_3=2.0$ mm, mass spectra of the abundant isotopes of most elements can be got with exposures of a second or less. Ilford Q II plates have been used almost entirely.

ACKNOWLEDGMENTS

The author is grateful to Professor A. J. Dempster for his frequent advice on matters pertaining to mass spectroscopy and for many ideas which the author has unconsciously absorbed during visits to his laboratory. He also appreciates several helpful conversations with Dr. A. E. Shaw of the Argonne National Laboratory.

Thanks are due to the author's senior colleagues, Professor Karl S. Van Dyke and Professor Vernet E. Eaton, for their interest and encouragement during the construction of the instrument. Much help has been given by Benjamin G. Hogg, Robert F. Black, Richard F. Woodcock, Richard S. Preston, Howard A. Johnson, Bertram A. Calhoun, John S. Handloser, and Donald R. Little. Mr. Clifford Gieselbreth, toolmaker, has been responsible for much of the design and construction.

Most of the cost of construction was met by a special grant from the Board of Trustees of Wesleyan University. This grant is gratefully acknowledged. Also, the current support of the AEC is appreciated.

A Diaphragm Cell for Thermal Diffusion Measurements

E. S. Huse, D. J. Trevoy, and H. G. Drickamer
Department of Chemistry, University of Illinois, Urbana, Illinois

(Received August 19, 1949)

A diaphragm cell for thermal diffusion using a fritted glass disk like those used for ordinary diffusion is described. The results obtained are consistent with those obtained for other cells, and the operation of this cell is simpler and shorter than for most other methods.

NOMENCLATURE

ΔN = Normality HCl cold side minus normality HCl hot side.

$100\Delta n$ = (mole fraction benzene cold side minus mole fraction benzene hot side) × 100.

$$q=\left[\frac{\text{mole fraction hot side}}{\text{mole fraction cold side}}\right]_{\text{light component}}\times\left[\frac{\text{mole fraction cold side}}{\text{mole fraction hot side}}\right]_{\text{heavy component}}.$$

T_h = temperature of hot side.

T_c = temperature of cold side.

α = thermal diffusion ratio defined by $1_nq=\alpha 1_n(T_h/T_c)$. The sign of α was arbitrarily determined so that it was positive if the heavy component concentrated on the cold side.

A GLASS diaphragm cell for measuring thermal diffusion in liquids (the pure Soret effect) has been developed. The cell is modeled after the diaphragm cells commonly in use in ordinary diffusion experiments. The device is shown in Fig. 1. The cell is mounted in the wall between the hot and cold baths as shown in Fig. 2. The magnets proved to have considerable effect on each other during operation, therefore the pulley belt was lapped so that the magnets in rotating would always remain in phase. Temperature profiles were measured throughout the cell and over the surface of the disk both with and without stirring. Without stirring, vertical and horizontal temperature gradients within the cell and particularly along the disk were quite uniform; however, the ΔT across the disk was eight percent less than the ΔT between the thermowells. This correction was made in all calculations. Two series of runs were made, one with dilute HCl mixtures analyzed by titration, one with benzene-heptane mixtures, analyzed with the use of a Zeiss water interferometer. The results are shown in

TABLE I.

Thermal diffusion constants obtained with a diaphragm cell, for aqueous solutions of hydrochloric acid

Solution	T_h	T_c	Time (hr.)	ΔN	$\log q$	α
0.100N	306.3	299.4	18–24	0.00293	0.0127	1.28
0.100N	315.9	306.0	38–48	0.00402	0.0179	1.27
0.200N	315.7	306.4	51–106	0.00706	0.0153	1.18
0.200N	311.3	305.6	51–59	0.00471	0.0102	1.275
0.300N	315.8	305.5	75–98	0.0114	0.0165	1.265
0.300N	311.2	305.9	50–61	0.00612	0.0089	1.185

Thermal diffusion constants for aqueous solutions of hydrochloric acid obtained by previous experimenters

Experimenter	Solution	T_c	T_h	Time (hr.)	ΔN	q	α
Chipman	0.5N	293.1	303.1	336	0.0140	1.028	0.84
	0.2N	293.1	303.1	240	0.00418	1.021	0.62
	0.1N	293.1	303.1	168	0.00209	1.021	0.62
Tanner	0.5N	299.4	313.6	24	0.0477	1.099	2.03
	0.32N	298.0	311.9	24	0.0262	1.085	1.80
	0.25N	299.5	313.7	24	0.0195	1.080	1.67

Thermal diffusion constants obtained with diaphragm cell, for 50–50 mole percent benzene-heptane mixtures

T_h	T_c	Time (hr.)	Interferometer reading	$100\Delta n$	$\log q$	α
317.4	306.0	59.5	94.5	0.340	−0.00591	−0.371
317.5	305.8	48.0	89.0	0.319	−0.00557	−0.342
317.5	305.9	65.7	89.0	0.319	−0.00557	−0.345

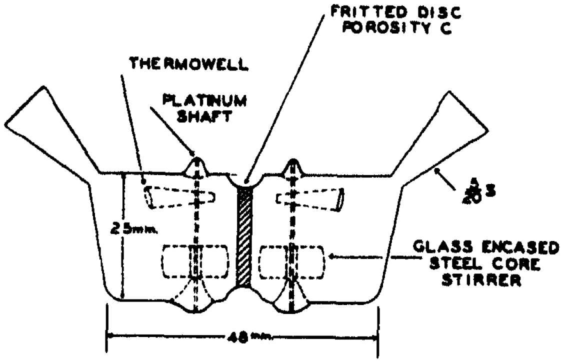

FIG. 1. Thermal diffusion cell.

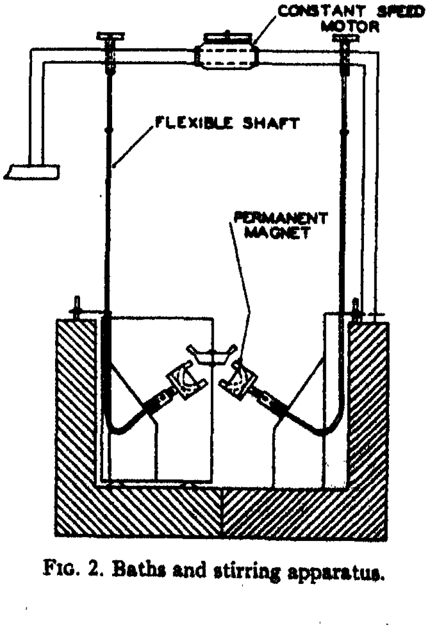

FIG. 2. Baths and stirring apparatus.

Table I, compared with the results of Chipman,[1] who used an open tube supported between two baths, and Tanner,[2] who used two flat plates and an optical method of analysis. As can be seen, the results are more nearly in agreement with Tanner's data which are generally conceded to be more reliable. Also, the time to steady state of this apparatus is less than 48 hours which is shorter by a factor of 5–10 than Chipman's. It is felt that a further substantial reduction in time is possible by using a thinner disk and a smaller cell volume.

[1] J. Chipman, J. Am. Chem. Soc. 48, 2577 (1926).
[2] C. C. Tanner, Trans. Faraday Soc. 23, 75 (1927).

THE REVIEW OF SCIENTIFIC INSTRUMENTS VOLUME 21, NUMBER 1 JANUARY, 1950

An Investigation of the Possible Use of the Glow Discharge as a Means for Measuring Air Flow Characteristics*

F. D. Werner
Aeronautical Laboratory, University of Minnesota, Minneapolis, Minnesota

(Received August 22, 1949)

The glow discharge in air at atmospheric pressure from a point of fine platinum wire has been experimentally investigated in its sensitivity to variations of pressure, velocity, temperature, and humidity, as well as such variables of the instrument as needle point characteristics, location and shape of the other electrode, and magnitude of the discharge current. It has been concluded that the glow current is markedly pressure sensitive, has low velocity sensitivity, is only slightly humidity sensitive, and is negligibly sensitive to ordinary temperature variations. The device offers a significant improvement over conventional pressure measuring instruments by the small size of its sensitive portion (of the order of 0.001-inch diameter wire and 0.002-inch glow diameter) and in its response to high frequency variations (more than 10^6 c.p.s. has been demonstrated experimentally). It suffers from high background noise in the present arrangement. A workable instrument is not presently described, but rather, some promising possibilities are shown to exist. The successful application to measurement of instantaneous pressures in very high frequency sound has been made, however; and the instrument will be reported as soon as possible.

INTRODUCTION

An instrument for measuring such air flow characteristics as very rapid variations in pressure and velocity should be of small size for high resolving power and for some purposes, should respond to variations as rapid as several hundred kc/sec. or higher. Considerable work on glow discharge has been done by several investigators[1–3] toward the end of measuring velocity and pressure variations. The "Diaphragmless Microphone" developed by Thomas[1] was perhaps the first effort in this direction. He made use of two relatively large, blunt end copper electrodes with a small separation between the ends. The arc was started by suitable means, and a high impedance limited the current to values between 1 and 20 ma at voltages of a few hundred to 1000. He found the device sensitive to pressure and useful as a microphone over the audible range. He reported a decrease in sensitivity with increasing frequency, and some trouble from background noise.

This type of discharge was placed in an airstream and successfully used for turbulence measurements by Lindvall.[2] He found good agreement between hot wire turbulence measurements and his glow discharge when both were subjected to the well-known turbulence behind a cylinder in subsonic flow. The two relatively large electrodes were placed normal to the airflow and were possibly interfering aerodynamically somewhat with the glow. The response to high frequency variations was probably fairly good, but apparently did not extend so high as in the case of the glow discharge from a slender point, as described here. Several other experimenters[3] have extended his work but have had generally similar results. Also, they investigated certain other electrode arrangements and other discharges as dark discharge, and experimented with radioactive pre-ionization.

It appeared that the glow discharge from a point of fine wire offers certain advantages over previous devices in the smaller size of its sensitive portion and in its response to very high frequency variations. It was decided to investigate the effects of pressure, velocity temperature humidity, and the rapidity of response. In addition, variables of the instrument itself were important, such as needle point characteristics, location and shape of the other electrode, magnitude of the discharge cur-

---

* This work was supported in part by the ONR and was in part taken from the author's Master of Science thesis. It was presented as a paper at the meeting of the Fluid Dynamics Division of the American Physical Society, July 1, 1949 at Washington, D. C.

[1] P. Thomas, J. A.I.E.E. 42, 219 (1923).

[2] F. C. Lindvall, Trans. A.I.E.E. 53, 1068 (1934).

[3] W. Fuchs, Unclassified German Documents obtained from Air Materiel Command, ATI-37424, ATI-27009, ATI-19032, ATI-37077, ATI-32278, ATI-45549, ATI-36650, IP-4764 R-8243 F-4764, ZWB/THA/1944 R-8039 F-518, ZWB/THA/70, R-8037 F-831, ZWB/THA-54/R-3650 F-629, and others; L. Agostini, paper presented to Seventh International Congress of Applied Mechanics, London, 1948; Dipl. Ing. Oertel, paper presented to Aerody. Conf. St. Louis, France, July, 1947; G. R. R. Bray, prepared by K. R. Eldredge, ONR, London Branch, Tech. Report OANAR-13-48.

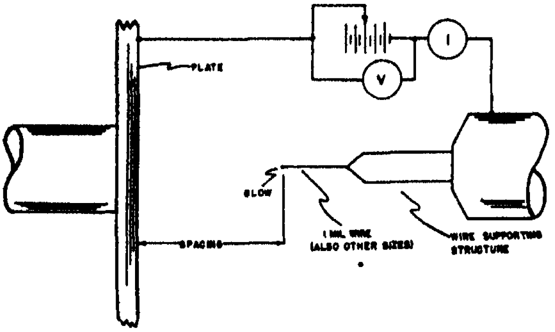

FIG. 1. Electrode arrangement for measuring pressure, temperature and humidity effects. The proportions are approximately correct. This apparatus was placed inside a glass container in the experiments. A schematic diagram of the measuring circuit is also shown. No ballast impedance was necessary due to the rising characteristic of current *versus* voltage.

rent, and polarity. The main purpose of this study was to determine if such a device held promise.

In the discussions which follow, the word, "characteristics," will refer to the curves of current *versus* voltage for the point discharge. This terminology has its origin in the literature on vacuum tubes where curves of current *versus* voltage are widely referred to as "characteristic curves." "Plate" will refer to the electrode opposite the point, even though it is not a plane in all experiments.

EXPERIMENTAL INVESTIGATIONS

Preliminary Investigations

The experimental work was begun with the idea of using as a needle point the tip of a short length of the smallest practical wire size. The smaller size should give more rapid response for reasons which will appear, and should give higher resolution, i.e., should better approximate measurements at a point. Platinum was chosen as the most promising needle material because it is not subject to oxidation and can be obtained in very small sizes. A flat plate was chosen as the plate electrode as shown in Fig. 1, with the assumption that it would give results representative of those encountered in applications requiring somewhat different plates.

In order to estimate the size of the active portion of the discharge, namely the glowing portion, the tip of the wire was examined under the microscope for various currents and wire sizes. Figure 2 presents some photomicrographs showing some of the results of this examination. In the figure are shown the glows from the tip of a negative 1-mil (0.001 inch) platinum wire for currents of 5, 10, and 20 microamperes. Also shown is the glow from a negative platinum wire of diameter 4×10^{-5} inch, for a current of 0.3 microampere. It is interesting to note that the bright glow close to the wire tip is not apparent in this case. It may be that here the wire is so small and, therefore, the electric field so high that high field emis-

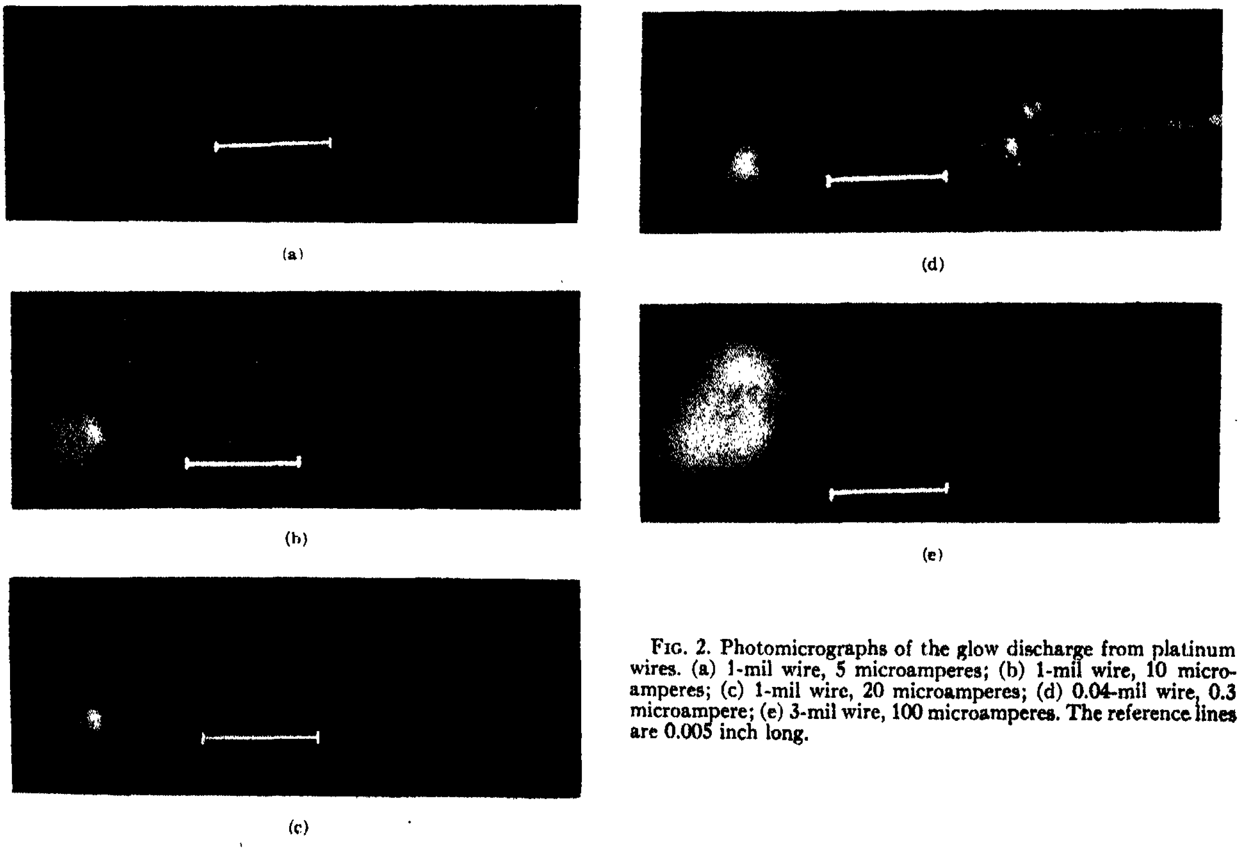
(a) (b) (c) (d) (e)

FIG. 2. Photomicrographs of the glow discharge from platinum wires. (a) 1-mil wire, 5 microamperes; (b) 1-mil wire, 10 microamperes; (c) 1-mil wire, 20 microamperes; (d) 0.04-mil wire, 0.3 microampere; (e) 3-mil wire, 100 microamperes. The reference lines are 0.005 inch long.

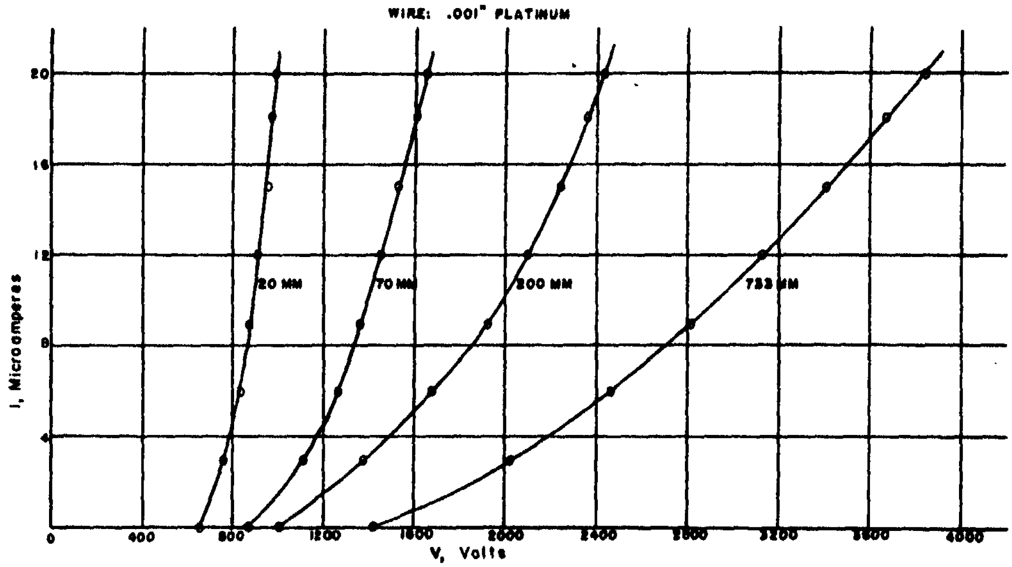

FIG. 3. General effect of pressure on the characteristics for a negative 1-mil wire in dry air for absolute pressures between 20 mm and 733 mm of mercury. These measurements were made with the apparatus of Fig. 1, with constant spacing.

sion of electrons is taking place. Also in Fig. 2 is a photomicrograph of 3-mil platinum wire and is a good example of an irregularity which occurs at a current rather low for the wire size. In this case, the glow is too small to cover the surface of the tip as it does in the other cases, as can be seen in the various photos. The result is that the glow migrates from place to place and gives unsteady characteristics. In this picture it has moved about 3 times during the exposure. This can be corrected by increasing the current. It requires more than 100 microamperes at about 5000 volts for the 3-mil wire.

When the wire is positive, the discharges are somewhat smaller, more intense and more uniformly luminous. Under certain conditions the discharge streams out toward the plate. When the wire is negative, greater pressure sensitivity has been found, so this condition has received somewhat greater emphasis.

Dust can be seen sticking to the wires in the photomicrographs. Since the dust is a poor conductor, it appears to disturb the field very little and therefore causes no noticeable effects on the characteristics unless it appears at the tip where it mechanically interferes with the glow.

The characteristics are quite sensitive to the shape of

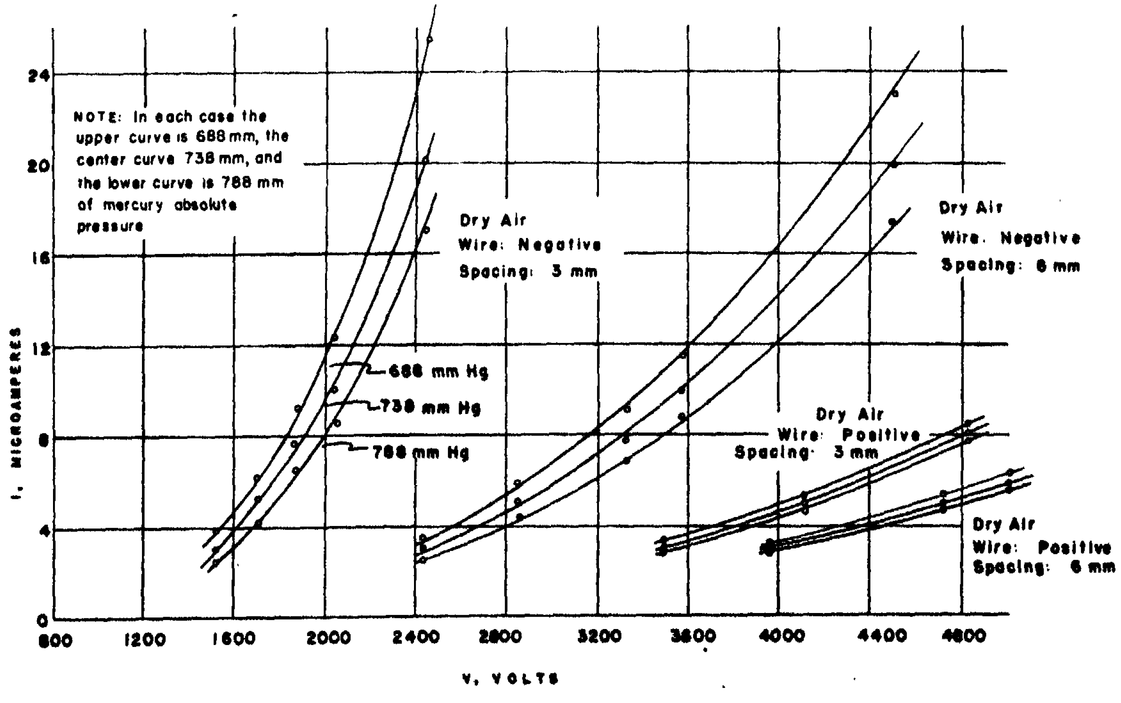

FIG. 4. Dependence of the characteristics on pressure in the vicinity of one atmosphere for 1-mil platinum wire in $CaCl_2$ dried air. Positive currents extend no higher than shown because sparking occurred.

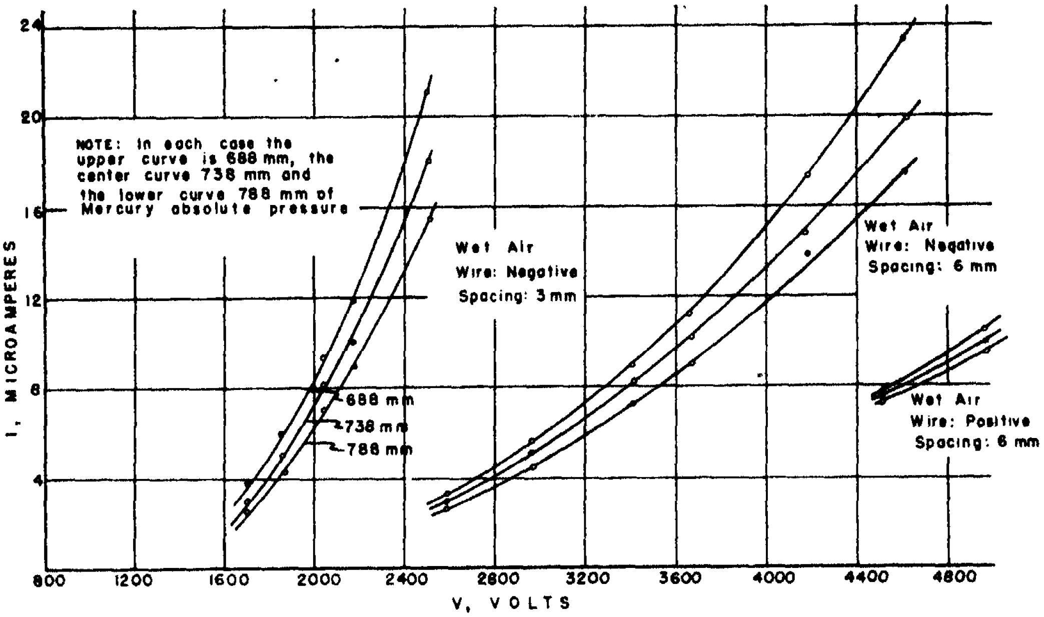

FIG. 5. Dependence of the characteristics on pressure for 1-mil wire in wet air. For positive wire, 3-mm spacing, no data could be taken because the spacing was too small for a measurable differential between onset of glow and onset of spark.

the wire tip, and for this reason it is necessary for good measurements to wait before a reading until the action of sputtering produces the equilibrium shape on the wire tip for the current under consideration before measurements are made. This can be accelerated by preliminary breaking in at somewhat higher current. It has been found desirable to make very frequent examinations of the wire under a microscope of about 100 power to detect any irregularities of the tip.

Tests made in a small glass enclosure gave results which appeared identical to those made in the open. Thus, it was considered safe to perform experiments inside the enclosure. It is believed that the immediate vicinity of the glow is normally so rich in ozone, oxides of nitrogen, and ions, that the use of an enclosure causes a negligible rise in the concentration of these materials at the glow.

The upper useful limit of current was qualitatively

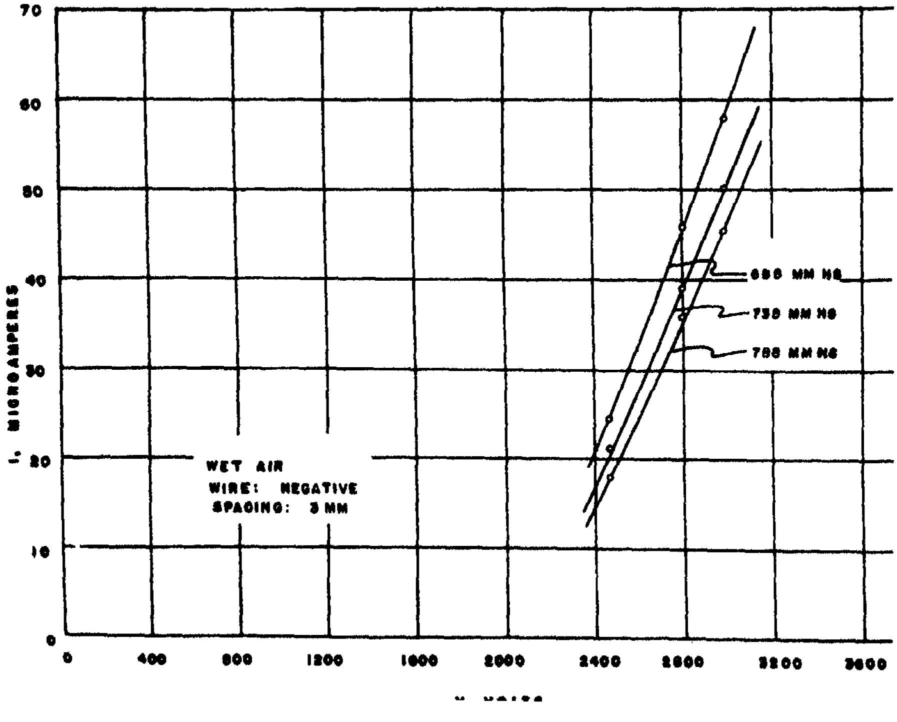

FIG. 6. Dependence of the characteristics on pressure for 3-mil wire in wet air.

determined as the current for which disintegration of the wire became objectionable. This value of current was roughly 1, 5, 40, and 300 microamperes for 0.04-, 0.1-, 1-, and 3-mil wires, respectively. If the gap is too small, a spark will occur before maximum current is reached.

Pressure Dependence

It would be expected that pressure changes would have a marked effect on the glow current if the voltage is held constant, since the mean free path is highly pressure dependent. It is not clear whether electron emission (in the case of negative point) occurs as a result of secondary emission, thermionic emission, or high field emission. Perhaps it is a combination, but in any case, the glow will be very sensitive to changes in the mean free path.

The dependence of the characteristics upon pressure was determined experimentally with electrodes arranged as shown in Fig. 1. These electrodes were mounted inside a glass container in which the pressure could be varied.

The general effect of pressure on the characteristics is shown in Fig. 3. It shows such pressure dependence as to suggest that the device could be useful as a pressure indicator. Another important feature of this discharge is that it should be able to adjust itself very rapidly to changes in pressure. This can be inferred from knowledge that the ions are present primarily in the glow where the field is very high, and that, therefore, the ion drift velocity is high. Since the glow is very small and the drift velocity is high, excess ions present when the pressure increases are quickly removed. On the other hand electron mobility is so high that electrons probably play no part in determining the limiting rapidity with which the glow can adjust itself to a change in pressure.

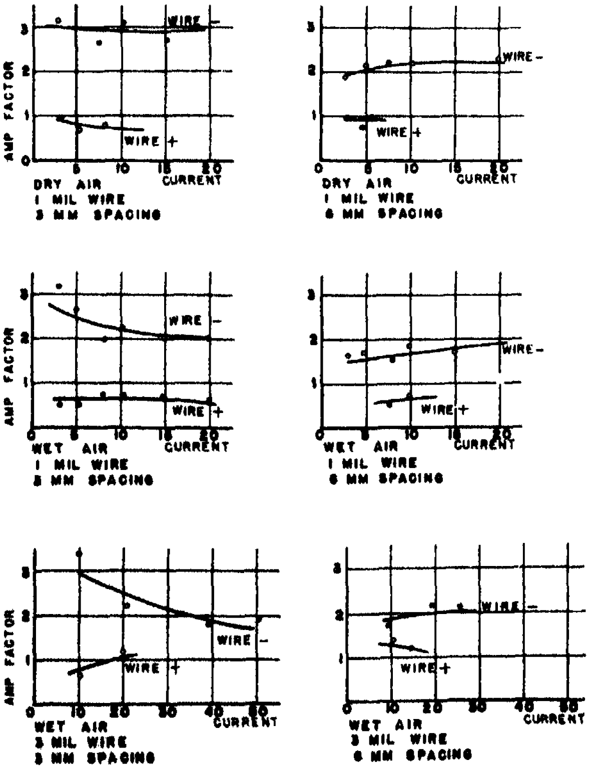

FIG. 7. Pressure sensitivity (amplification factor) of the glow discharge under various conditions. This data is taken from data like that of Figs. 4–6. The amplification factor is defined $P\partial I/I\partial P$.

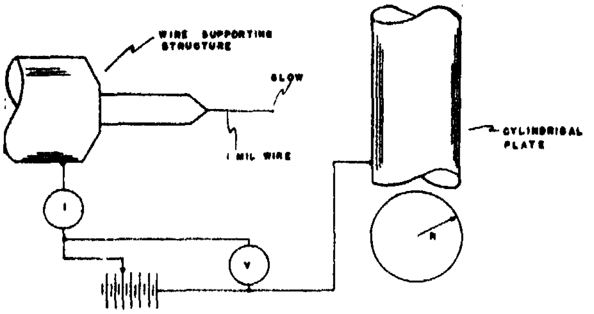

FIG. 8. Electrode arrangement for determining the effect of plate radius on the characteristics. The glow to plate spacing was 3 mm.

Together, these two features of this glow discharge, pressure sensitivity and rapidity of response, suggest that the device might be useful as a microphone for very high frequency sounds and for measuring other rapid pressure variations. Other things which make it interesting in this connection are its very small size, its lack of any mechanical resonance, and its smooth electrical impedance.

With the application of measuring very rapid pressure variations in mind, the pressure dependence in the vicinity of 1 atmosphere was examined in some detail as shown in Fig. 4. Here, the pressure was varied up and down 50 mm of mercury from atmospheric pressure and the voltage across the glow was maintained constant at various values. The various families of curves illustrate the effect of spacing and polarity on the characteristics and on the pressure dependence of the characteristics. Figure 5 shows the same measurements in air saturated with water vapor at 72°F. Apparently, humidity has only a small effect on the characteristics. Figure 6 shows the characteristics for 3-mil wire. The general character is unchanged, but there is a considerable shift to higher current and voltage as would be expected.

These graphs for various pressures bear a striking resemblance to vacuum tube characteristics for various values of grid voltage. This suggests a method for expressing the sensitivity of the device to pressure which is analogous to that used for the vacuum tube. In the case of a vacuum tube, the sensitivity is measured by the amplification factor, and is defined by $\mu=\partial e_b/\partial e_c$, where e_b is the voltage from cathode to anode and e_c is the voltage from cathode to grid. A similar dimensionless coefficient for the pressure sensitivity of the glow discharge may be written $\mu_p = p\partial I/I\partial p$, where I and p are current and gas pressure, respectively. That is, for the glow discharge, the amplification factor is the ratio of

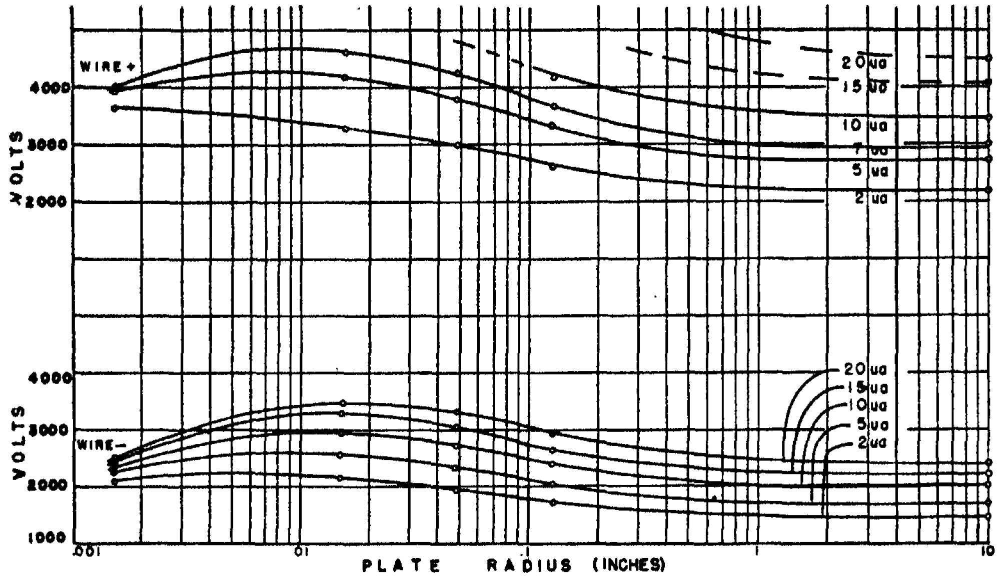

Fig. 9. Effect of variation in plate radius on the characteristics. These curves were taken from characteristic curves for the various radii. The major effect is for small diameter plates, where at high currents a small increase in voltage causes a relatively large increase in current. The upper family is for positive wire tip and the lower is for negative.

the percentage change in current to the percentage change in pressure at constant voltage. Figure 7 gives the relationship between this amplification factor and current as affected by spacing, wire size, humidity, and polarity. This figure was prepared from such data as that in Figs. 4, 5, and 6. The points on these curves depend on the differences between large quantities, and the quantities were not measured with high precision, so considerable scatter results. Nevertheless, they suffice to show that the sensitivity is consistently less for positive than negative wires. Also, there appears to be a small reduction in sensitivity with increasing humidity, and a decrease of sensitivity with increasing spacing. These conclusions must be regarded as tentative until careful quantitative measurements are undertaken.

The current measurements were made with a galvanometer having a 3-sec. period and considerable unsteadiness was evident at low currents. At high currents, the galvanometer stabilized, but radiofrequency noise was generated. It is expected that much of this noise is due to Trichel pulses which are of frequency proportional to the current. Starr[4] reported that no radiofrequency noise was present for discharges from sharp slender points, but this has been observed only for the 4×10^{-5}-inch wire and then only intermittently. Work is being done to reduce this background noise. One interesting possibility is the use of radiofrequency voltage of period shorter than the deionization time instead of d.c. This would appear to eliminate the mechanism for formation of the troublesome Trichel pulses. The signal would appear as amplitude modulation in this case. More will be reported about the background noise later.

Effect of Plate Shape and Size

The effect of changes in the shape of the plate was investigated by using long cylinders of various radii as plates. Figure 8 shows the electrode arrangement for

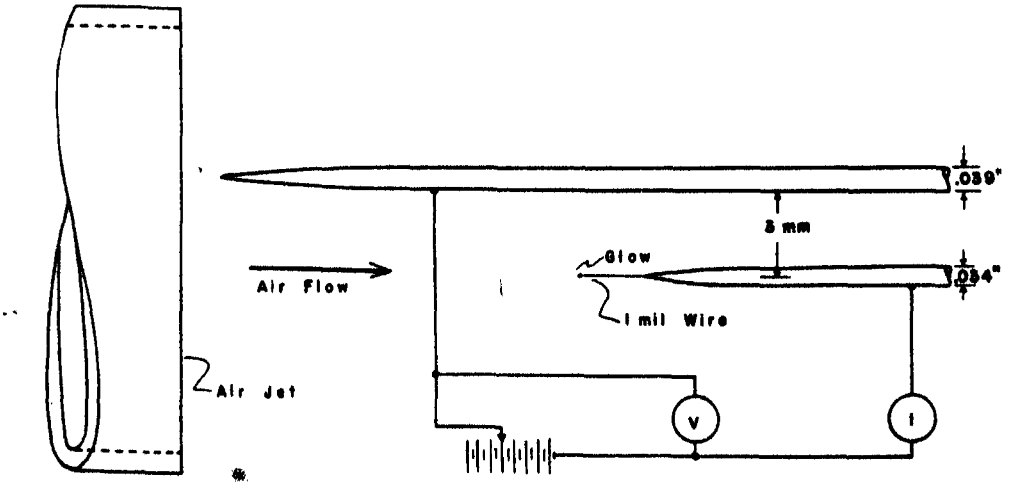

Fig. 10. Electrode and air jet arrangement for determining the velocity sensitivity of the glow discharge. The proportions are approximately correct.

---

[4] E. C. Starr, Trans. A.I.E.E. 60, 356 (1941).

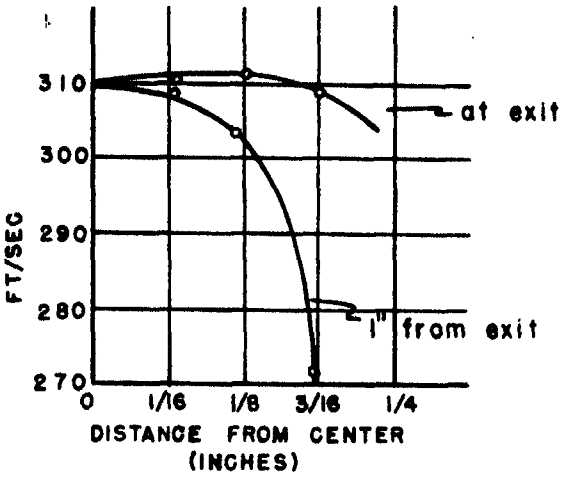

FIG. 11. Velocity distribution for the jet of Fig. 10.

this test. The radius of the cylinder was varied from ∞ to 0.0015 inch. A cross plot of the characteristics for each radius yielded the results of Fig. 9. It shows that for plates of radius greater than about 0.2 inch the radius is insignificant. No great change occurs for radii greater than about 0.03 inch, and for smaller radii the change is not noticeable at low currents, but becomes very marked at high currents. It was noted that a glow appeared at the surface of the plate in this case of small radius and high currents.

The size of the flat plate was found to be immaterial provided the plate was wider than about $\frac{3}{2}$ times the spacing and the edges of the plate were well rounded.

Velocity Dependence

Dependence of the characteristics on velocity might be expected because the wire tip is cooled by the air flow and thermionic emission would be reduced. An effect due to velocity might be partly due to the increase in pressure at the surface of the upstream side of the wire tip caused by impact of the air flow. Probably only a very small portion of the glow is in this region of elevated pressure. It was noted in analyzing the experimental results that the velocity dependence was much less than would have been accounted for by the effect of the impact pressure on the entire glow, and also, when the wire was changed from pointing upstream to a position normal to the airflow, almost no change in the characteristics resulted. When air at the needle point is in motion, a few ions on the downstream side may be carried out of the influence of the electrodes and so cannot contribute to the current, resulting in a decrease in current as constant voltage. At very high velocity, it might be expected that the velocity dependence might become quite marked for this reason.

The effect of velocity was investigated with electrodes arranged as shown in Fig. 10. The 1-mil platinum wire was soldered to the end of a common sewing needle as is the practice and another sewing needle was chosen as the plate, since the data of Fig. 9 indicates characteristics generally similar to those of a flat plate. This arrangement of electrodes is nicely streamlined for air flowing as shown and it is expected that no appreciable change in the air flow in the immediate vicinity of the glow resulted from the presence of these electrodes. A jet of air $\frac{1}{2}$ inch in diameter was used as shown in Fig. 10. The velocity distribution for this jet is shown in Fig. 11, and since it was fairly good near the center of the jet at distances up to 2 diameters, the glow was inserted at one diameter.

The velocity dependence was determined by taking characteristic curves at 0, 255, and 411 feet per second. The results are given in Fig. 12. It is seen that velocity has a definite effect on the glow. If an amplification factor is defined in this case as for pressure dependence, as $\mu_v = V\partial I/I\partial V$, it is found that the velocity sensitivity is about one-twenty-fifth as great as the pressure sensitivity at 255 ft. per sec.

The glow at the tip of the wire was observed under the microscope in this experiment. At zero velocity, it had the same appearance as the photomicrographs of Fig. 2. As the velocity increased at constant voltage, the glow was observed to shrink slightly in size and intensity as would be expected for a decrease in current, without air flow. The tentative conclusion is that the appearance of the glow is not affected by air flow of these velocities, other things being constant. This seems to disprove the idea that the reduction in current with increasing velocity, is due ions being "blown" out of the glow region because in this case the glow intensity would have

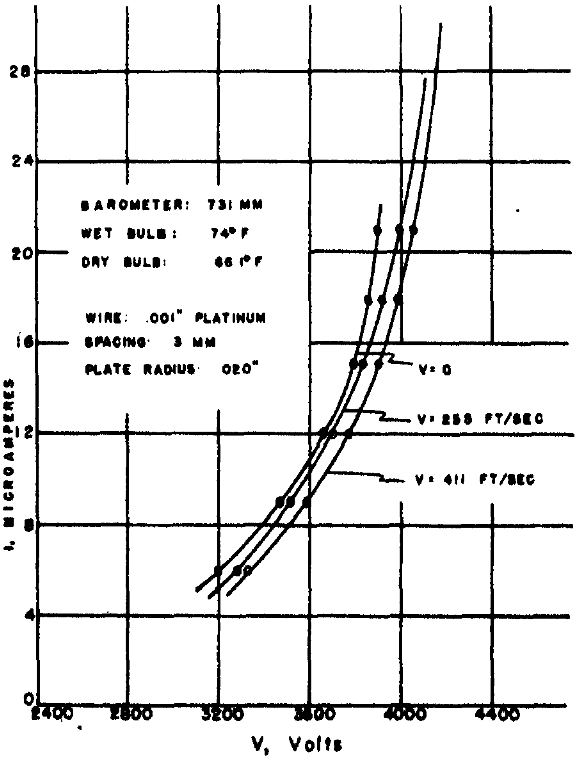

FIG. 12. Velocity dependence for room air at atmospheric pressure for a negative 1-mil wire.

been unchanged, and there would have been a slight distortion of the shape of the glow. While the distortion might escape detection, the change in over-all intensity seems to be a real clue, since this always occurs when the current decreases, whether air is flowing or not. It therefore appears that the effect of reduction of thermionic emission by the cooling effect of the wind, probably plays the most important role in the velocity effect. It is suggested that the voltage for starting the discharge may be very nearly independent of the velocity.

Effect of Humidity

The presence of water vapor can be expected to have an effect on the characteristics, because water molecules have different weight and affinity for electrons than the various molecules making up air. The effect of humidity has been observed by other experimenters for various types of discharges. The findings are similar to those reported here, even though the types of discharge investigated were somewhat different. Generally, the effect is to shift the characteristics to somewhat higher voltages, as seen by comparing Figs. 4 and 5. The effect of humidity on pressure sensitivity is tentatively believed to a reduction of sensitivity with increasing humidity as shown in Fig. 7.

Rapidity of Response

The rapidity with which the glow can adjust itself to new values of pressure or velocity may be roughly estimated theoretically. Consider for example, a small increase in pressure (negative needle). As long as the time for the change to take place is much greater than the time required for the few excess positive ions to migrate to the cathode, the pressure change will be faithfully reproduced by a corresponding current change. This assumes that the excess of electrons can as quickly reach the anode and that negative ions are present in negligible concentration. Considering the 1-mil wire with about 20 microamperes current, the outermost positive ions must move at most only about 0.005 cm to reach the cathode. Since the field is highest at the needle tip, it is reasonable, perhaps, to estimate 500 volts drop over this distance, giving a field of 10^5 volts per cm. Taking the mobility for ions in air as 1.6, the transit time would be about 3×10^{-8} sec. On this basis, pressure or velocity changes having frequency components as high as 10 megacycles or more would be faithfully reproduced by current changes. This estimate neglects the transit time for any negative ions near the outer border of the glow to reach the anode. An estimate for this time would give about 10^{-6} sec. Since the population of negative ions is probably small compared to positive ions, it may be reasonable to neglect the effect of this relatively long transit time.

The velocity dependence experiment gives some experimental support to the belief that very rapid response exists. At an air velocity of 411 ft./sec., a molecule of air moves through the glow region (about 0.002 inch in diameter) in about ½ microsecond. Since the glow was not appreciably distorted in shape, the time of transit for positive ions appears to be short compared with the time for a molecule or ion to be transported by the air flow.

The use of this device as a very high frequency microphone will be reported soon, but at present it might be stated that response to a 1-megacycle acoustic signal has been observed.

Temperature Sensitivity

The ambient temperature was elevated from 74°F to 158°F at constant pressure and no noticeable change in the characteristics was observed. Also there was no change in the pressure sensitivity.

It is concluded that the ionic temperatures are much higher than the ambient temperatures of the experiment, and therefore no appreciable change in the mean free path in the glow resulted. This is evidence that the glow is the only sensitive region of the discharge.

Comparison Between Pressure and Velocity Sensitivity

Consider the equations which define μ_p and μ_v, the "amplification factors" for pressure and velocity, respectively. It is apparent that μ_v decreases smoothly to zero as the mean velocity approaches zero. This condition is readily obtainable in practice. On the other hand, μ_p as can be determined from Fig. 3, changes but little as the mean pressure is reduced. The value of μ_p is, of course, indeterminate as the mean pressure approaches zero, because the glow ceases to exist at moderately low pressures. Summing up, μ_v varies with velocity, decreasing to zero, with decreasing velocity, and μ_p is roughly independent of pressure within the limit studied. Also μ_v is much smaller than μ_p even for rather high velocity.

In any specific application of this glow discharge to measurements where both velocity and pressure are subject to variation, the mean values and amount of fluctuation expected of each must be known before the problem can be solved of determining whether glow current fluctuations represent essentially pressure or velocity variations, or a mixture. For the general case where effects of both pressure and velocity are felt, no generally valid means of distinguishing the effects has yet been found. A specific example of this problem is the application to measurements of instantaneous pressures in a sound wave as mentioned above. Here velocity effects have been found negligible.

This glow discharge is receiving considerable attention at present in the author's laboratory in the application of sound measurements.

Acknowledgments

Professors John D. Akerman and William G. Kubicek deserve much gratitude for advice and suggestions. The support of the ONR is gratefully acknowledged.

A Small Milligaussmeter

G. D. Adams, R. W. Dressel, and F. E. Towsley*
Physics Department, University of Illinois, Urbana, Illinois

(Received September 2, 1949)

Means are described for measuring magnetostatic fields from the order of one milligauss to 100 gauss. The operation consists of measuring the second harmonic content of the exciting current for a ferromagnetic strip which is normally excited to partial saturation. The second harmonic component appears when the strip is biased by an external magnetic field and the amount is directly proportional to this field over the bulk of the useful range. Methods of use are described.

During the course of the model work leading toward the construction of the 300-Mev betatron at Illinois, it became apparent that an instrument capable of making measurements in the milligauss range would be needed. The following is an account of an instrument developed to fill this need.

During the development of this device, the existence of a similar unit designed for the Navy during the war was called to our attention. The physical size of this instrument was prohibitive for model work.

The operation of this instrument depends on the saturation characteristics of the hysteresis loop for a ferromagnetic material. If the magnetic material is field free in the absence of exciting current and if a given sine wave voltage per turn of exciting coil is impressed, then the hysteresis loop will be similar to Fig. 1(a) and the exciting current will be peaked with respect to the sine wave voltage as in Fig. 1(b). Now, if the material be placed in an external field, it will be biased by an amount ΔB. Impressing the same voltage per turn, as in Fig. 1(b), requires the same swing with respect to the unbiased H axis, the loop having been displaced by the amount of the bias, ΔB. This means that the loop has become asymmetrical, as in Fig. 1(c), and changes the exciting current accordingly, as in Fig. 1(d). A Fourier analysis of the unbiased current wave form shows fundamental and odd harmonics. The wave form in the biased case also contains even harmonics. The instrument discussed here measures the second harmonic content of the current wave.

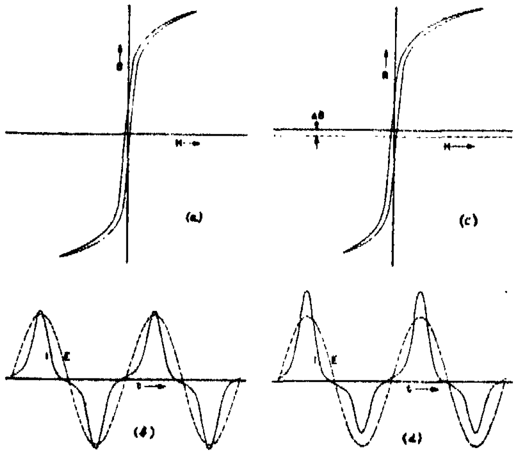

Fig. 1. (a) Hysteresis loop for unbiased ferromagnetic material. (b) Current and voltage wave forms from the hysteresis curve in (a). (c) Hysteresis loop for a biased ferromagnetic material. (d) Current and voltage wave forms from the hysteresis curve in (c).

The magnetic material used in the probe unit is a strip of Hypernik, $0.005\times\frac{1}{16}\times1\frac{1}{2}$ in. The strip is threaded through the center of a spool on which are wound 1000 turns of No. 40 enameled copper wire. The ends of the strip are then overlapped about $\frac{1}{4}$ in. and separated $\frac{1}{16}$ in. with paper. The gap reluctance so formed is about 10 times the strip reluctance. A cross section through a probe is shown in Fig. 2.

In practice, two probes are used in a bridge circuit (Fig. 3), P_1 being the search probe and P_2 the comparison probe. The comparison probe is housed in a thick magnetic shield. The function of the d.c. loop including P_1 is to bias the strip in that probe. How this bias may be used will be described. The capacitors C

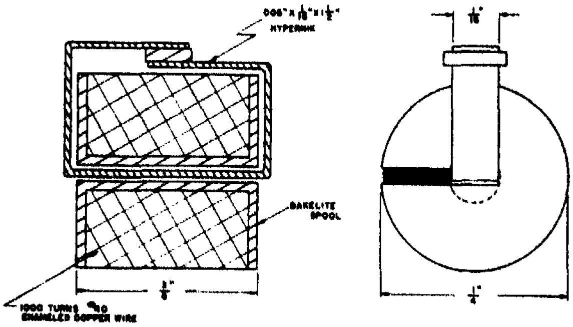

Fig. 2. Construction of typical probe unit.

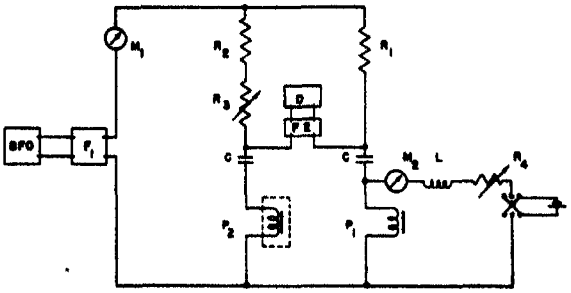

Fig. 3. Bridge circuit using a search and comparison probe.

---

* Now with the Dow-Chemical Company, Midland, Michigan.

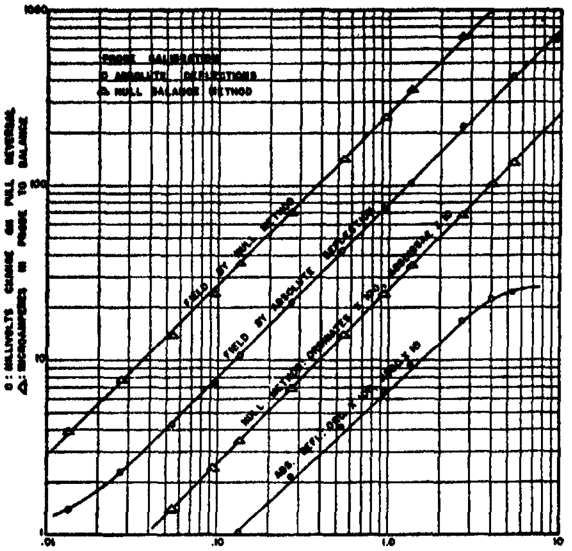

FIG. 4. Calibration of a typical probe unit.

isolate this d.c. from the remainder of the bridge. Each probe is loaded with a close-fitting copper shield to make the loading independent of surroundings.

The bridge excitation is derived from an oscillator (*BFO*) and amounts to 40 ma (M_1) at 5000 c.p.s. The operation of the instrument is sensitive to the excitation and nearly insensitive to frequency, providing this is in the kilocycle range. At 5000 c.p.s., the impedance of the probes is about 500 ohms; the whole circuit is designed around this impedance. F_1 and F_2 are *m*-derived filters with a characteristic impedance of 500 ohms. F_1 is low pass with maximum attenuation frequencies at 10 and 15 kc.p.s.; cut-off is between 7 and 8 kc.p.s. F_2 is band pass with maximum attenuation frequencies at 5 and 15 kc.p.s. and cut-off frequencies near 7 and 12 kc.p.s. The purpose of these filters is to minimize distortion in the input and output wave forms by attenuation of undesirable frequencies which are known to be present. The output detector (*D*) is an harmonic wave analyzer.

In a typical wave analyzer, a few stages of amplification occur before the frequency selection is made. Balancing the fundamental frequency voltage by using a bridge eliminates early stage saturation in the analyzer. The optimum bridge adjustment is made by R_3, the adjustment being for a minimum second harmonic indication when P_1 is in zero magnetic field.

The unit may be used in two ways to measure magnetic fields. The more rapid of these is to use the millivolt indication of the wave analyzer when calibrated against the field of a standard solenoid. It happens that the response is nearly linear up to 40 gauss. The second method is slower but more precise. In this method a null balance is used, the null being achieved by biasing the strip of P_1 with d.c. in the proper direction from the bias supply of Fig. 3. This bias current must also be calibrated against a standard solenoid. Figure 4 shows a set of typical calibration curves. The calibration has varied less than ±5 percent over two years and four different search probes.

It is seen that the null method gives better linearity over a larger range. The device is probably not useful above 100 gauss. On the other hand, the lower limit depends on the sensitivity of the wave analyzer. The analyzer used most in this work had a maximum sensitivity of 0.3 mv full scale which is about 4 milligauss by absolute deflection.

If one desires to measure small detail on a relatively large field, the bulk of the field can be biased out and the remaining detail examined by absolute deflection. In this case, the detail can be examined more precisely than with the null method alone although absolute field value is not known as accurately. This method has proved very valuable in evaluating radial and azimuthal variations of magnetostatic fields.

The probe strip can retain permanent magnetism after exposure to fields appreciably above 10 gauss. This results in an apparent second harmonic unbalance in the bridge. This balance may be restored by increasing the 5000-c.p.s. excitation typically to 150 ma and reducing slowly. In our case, it was necessary to remove F_1 to obtain this much current.

This instrument has also been used for tracing magnetomotive force demand lines at an air-iron interface. In our case the iron was the betatron yoke which is biased during operation. To minimize the leakage flux, it was desired to place the bias winding wires as required by the iron. From the air, the *mmf* surfaces plunge into iron nearly normally. Thus, if a probe of the kind described above be used to measure fields parallel to the iron surface, the direction of the *mmf* surface intersection is indicated by a null reading. This can be made quite sensitive. Following this direction completely around the iron body affords means of evaluating and correcting index errors in direction. For a magnetic circuit containing a window, the relative density of bias ampere-turns required anywhere in the window can be estimated from the indicated peak value of B when measuring parallel to the iron surface.

A High Speed Synchroscope*

G. G. Kelley
Oak Ridge National Laboratory, Oak Ridge, Tennessee

(Received October 4, 1949)

Described is an instrument for observing or photographing fast voltage transients. It consists of a sweep generator with sweep speeds ranging from 30 cm per microsecond to 0.05 cm per microsecond, a vertical deflection amplifier having a rise time of 0.005 microseconds and a preamplifier which, when used with the deflection amplifier, produces an over-all rise time of 0.0063 microseconds with a gain of about 1,000. These units are used in conjunction with a type 5XP cathode-ray tube using 20 kilovolts accelerating voltage.

INTRODUCTION

RECENT work at the Oak Ridge National Laboratory on several phases of the problem of nuclear instrumentation, e.g., the study of scintillation phosphors, Geiger discharge, and the use of high speed coincidence circuits, has led to the need for a synchroscope with features not found in present commercial instruments. The synchroscope to be described was developed to meet this need. The problem in general is the study of randomly occurring events, manifested as voltage variations, practically always of less than 200 microseconds total duration, but with significant fluctuations occurring sometimes in less than 0.01 microseconds; thus a vertical amplifier having a rise time considerably better than 0.01 microseconds is required and since each event is unique the intensity of individual traces should be great enough to be recorded photographically. The signal itself must be used to initiate the sweep, then delayed before presentation upon the cathode-ray tube screen. There are one or more companies developing instruments of this general type, indicating the probability that such an instrument soon may be available.

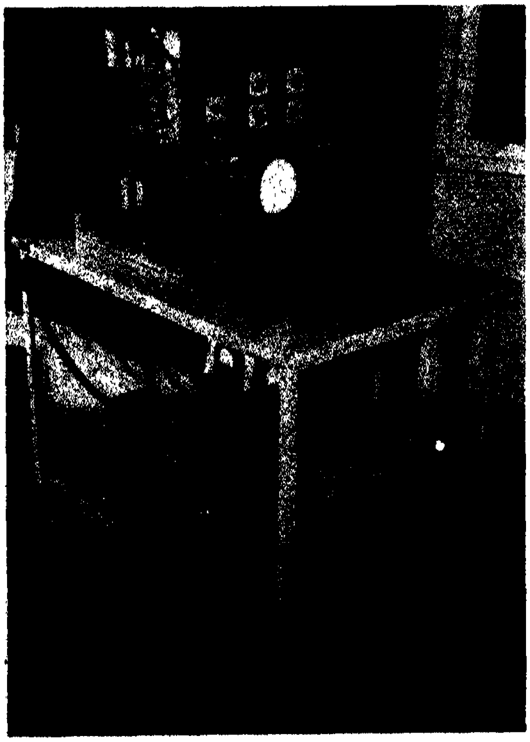

Fig. 1. A general view of the synchroscope and its associated equipment.

GENERAL DESCRIPTION

This instrument, to be called the Model S-1 Synchroscope, has been built around a Dumont type 281-A indicator and type 286-A high voltage power supply, which units house a type 5RP- or 5XP-cathode-ray tube and provide the d.c. voltage necessary for its operation. The complete assembly is shown in Fig. 1. On the shelf, to the left, is the unit which supplies the various voltages used by the sweep generator and vertical amplifier.

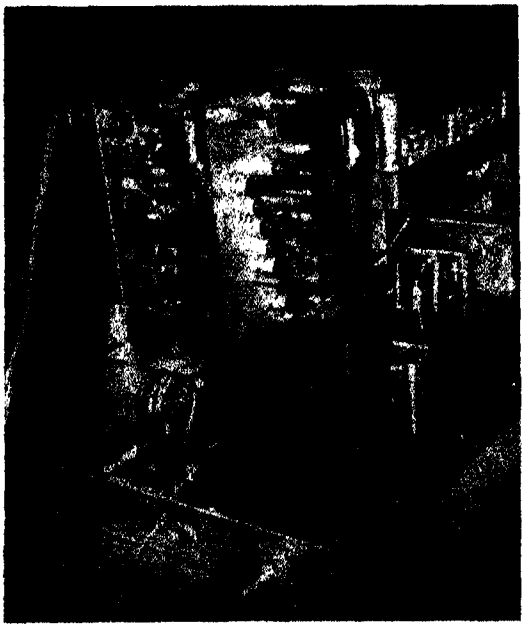

Fig. 2. The rear of the synchroscope. Part of the sweep generator is visible at the left. The delay line connecting the preamplifier, at right, to the deflection amplifier in the center of the picture is coiled in a frame under the table top.

---

* This document is based on work performed under Contract No. W-7405, eng. 26 for the AEC at the Oak Ridge National Laboratory.

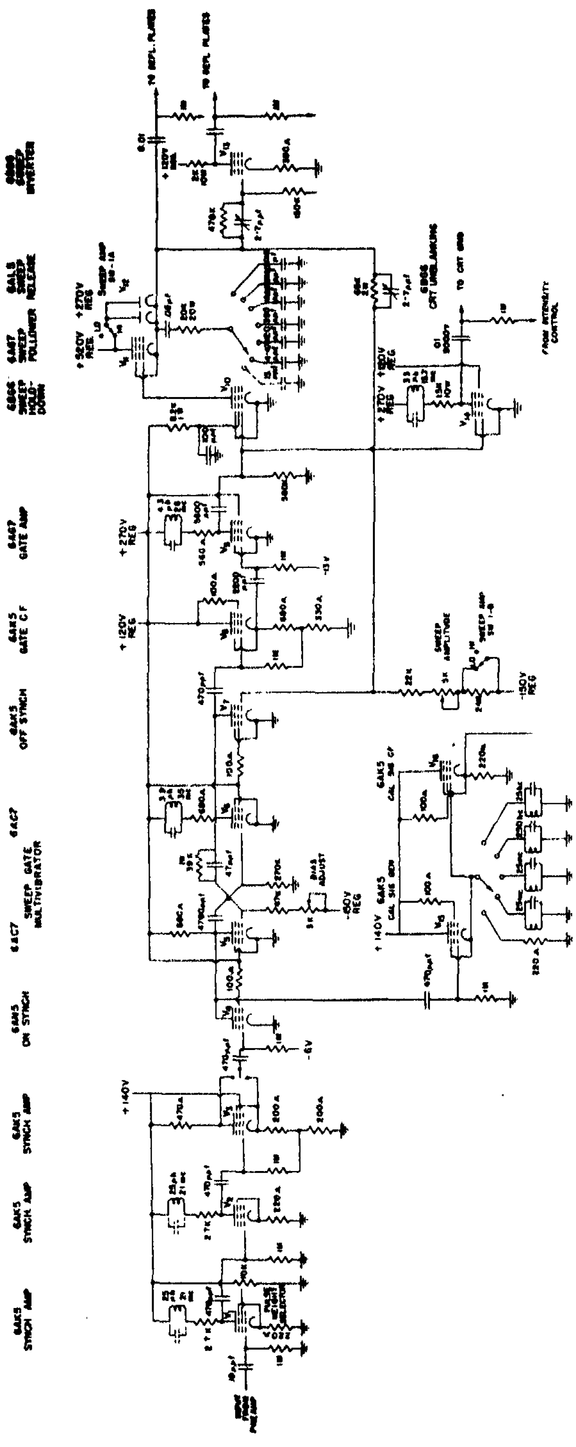

Fig. 3. The sweep generator for Model S-1 Synchroscope.

Beside it is the Dumont type 286-A high voltage power supply. Sitting above is a unit which supplies one of the voltages used in the sweep and amplifier itself. Its function will be included in the main power supply in any future models. The sweep generator, deflection amplifier, and preamplifier are mounted on and above the Dumont type 281-A indicator. Figure 2 shows the arrangement of these units. The sweep generator is on an L-shaped chassis with tubes extending toward the front and right side. At the right in the photograph, mounted vertically, is the deflection amplifier, and the long narrow chassis on the extreme right is the preamplifier. The delay line, which is 133 feet of Amphenol 72–30 coaxial cable, is coiled under the table top.

THE SWEEP GENERATOR

The sweep generator uses fairly conventional techniques and will not be described in detail. It was designed before the vertical amplifier was built, under the assumption that the vertical amplifier would have a band pass of 40 or 50 megacycles, and as a consequence the synch amplifier has a band width of only 13 megacycles. A faster synch amplifier would be advantageous where a shift in the position of the pulse on the base line, depending on its amplitude and duration, is undesirable. There is no noticeable horizontal jitter, however, when the sweep is triggered by uniform fast pulses or by random pulses whose rise time is 0.03 microseconds or greater. An input of about 0.06 volts is required to

Fig. 4. View of the inner side of the deflection amplifier. The clips at the bottom connect to the vertical deflection plates of the cathode ray tube.

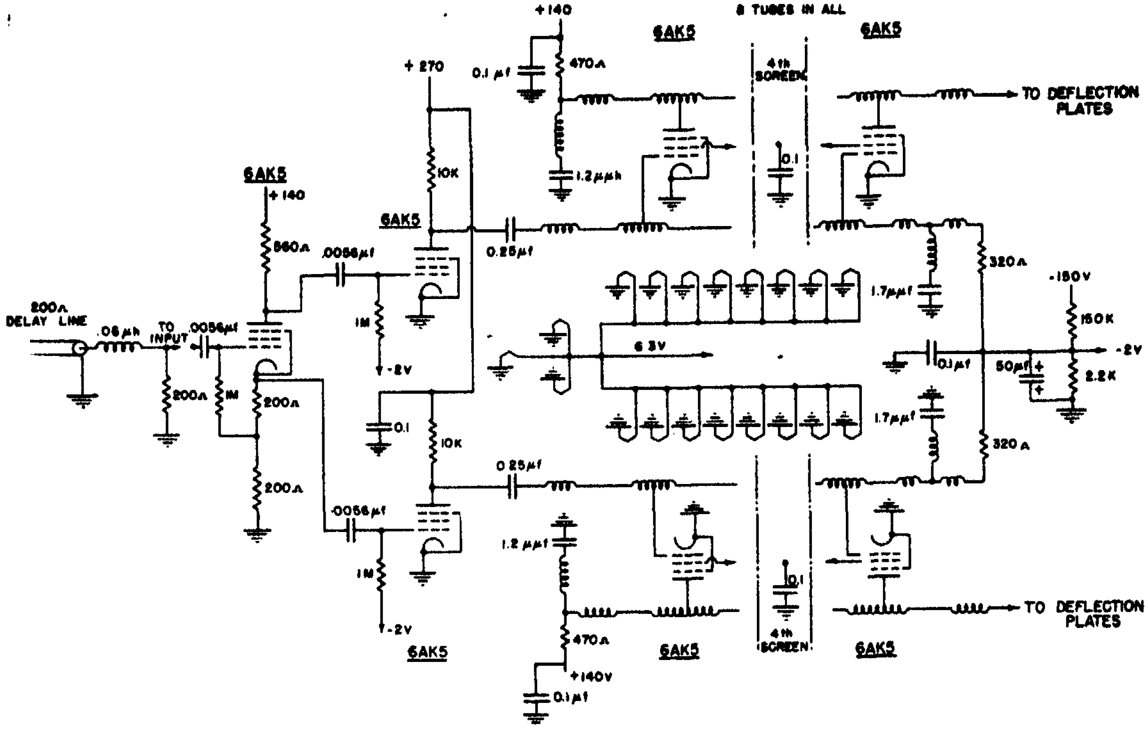

FIG. 5. Schematic diagram of the deflection amplifier for Model S-1 Synchroscope. All screen grids are at +140 v.

trigger the sweep multivibrator. The trace is moving at a uniform rate and the tube is illuminated within 0.01 microseconds after the trigger has arrived. Sweep speeds range from about 0.3 microsecond to 200 microseconds in total duration. Figure 3 is a schematic diagram of this unit.

THE DEFLECTION AMPLIFIER

The deflection amplifier uses the principle of distributed amplification. This principle has been discussed in detail by Ginzton *et al.*[1] and will not be elaborated on here. The amplifier was designed to have a pass band of about 90 megacycles, corresponding to a rise time of about 0.005 microseconds. A voltage swing of at least 60 volts in either direction was desired at the output. Figure 4 is a close-up view of the inner side of the amplifier, and Fig. 5 is the schematic diagram of this unit. The delay line enters through a type "*N*" fitting and is terminated by a 195-ohm 0.5-watt carbon resistor in series with a small inductance. This inductance is very effective in reducing high frequency reflections that arise from the capacitive component of the load. The inverter tube socket may be seen just below the input jack. This type of inverter has proved to be completely satisfactory within the frequency band involved and the amplifier response is not slowed noticeably by this cir-

FIG. 6. Looking up at the under side of the preamplifier.

---

[1] Ginzton, Hewlett, Jasberg, and Noe, "Distributed amplification," Proc. I.R.E. 36, No. 8 (1948).

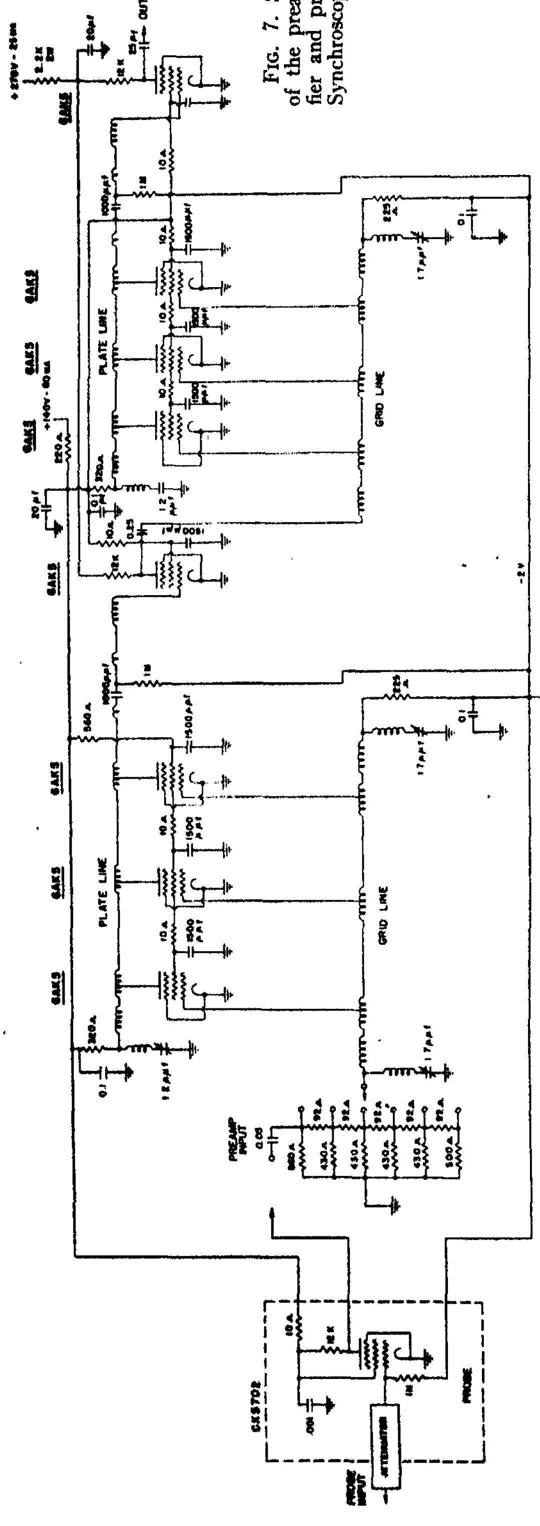

FIG. 7. Schematic diagram of the preamplifier. Preamplifier and probe for model S-1 Synchroscope.

cuit. Following the inverter are the two tubes which drive the grid lines of the eight-tube distributed stages. As may be seen from the diagram, the grid lines themselves form the load impedance for these coupling tubes and these lines are unterminated at their input ends. No termination is needed here if the output ends are sufficiently well terminated, and the gain is a factor of 2 greater. Also, the time constant involved in the low frequency response can be made satisfactorily large because it depends primarily on the current-supplying resistor from the plate of the coupling tube to $B+$. The plate lines of the output stages are terminated only on the input end. Here again only one termination is necessary and the gain is twice as great. Adjustment of the termination is more critical but it is felt that this disadvantage is greatly outweighted by the increased gain.

It will be noticed that the screen grids are paralleled and bypassed only at the center of each stage. This arrangement has proved perfectly satisfactory. The shielding between grid and plate lines was found to be necessary because of the large difference between the amplitude of the plate and grid signals near the output end, which coupled plate signal over into the grid lines.

PREAMPLIFIER

Figure 6 is a photograph of the preamplifier and Fig. 7 is its schematic diagram. Input to the unit is through a 195-ohm ladder type attenuator which may be seen at the right in the photograph. A probe is provided for high impedance input, using a type CK5702 pentode as a plate amplifier. Plug-in capacity-type attenuators are used to prevent overload of this tube. The attenuator in the main unit has a maximum attenuation of 20 db in steps of 4 db. The signal leaving the attenuator enters the grid line of a 3-tube distributed stage having a gain of about 5 and a design cut-off frequency of 118 megacycles. The plate line of this stage is coupled to a second similar stage through a buffer tube which allows the plate line to be unterminated. The second stage is coupled in like manner to the delay line and to the input of the synch amplifier.

No shielding was necessary in the preamplifier, and several components were used that had not been available when the deflection amplifier was built. These were adjustable low capacity condensors for use in the terminations, and feed-through ceramic condensors for transferring most of the wiring to the top side of the

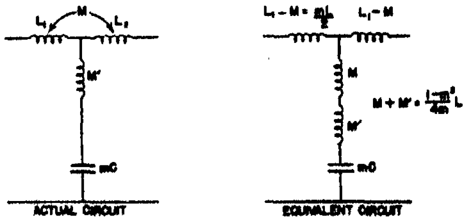

FIG. 8. See text.

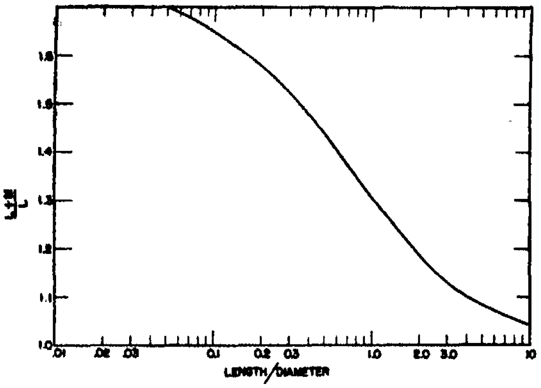

FIG. 9. See text.

chassis, reducing the clutter around the plate and grid lines.

DESIGN

All of the lines used in the amplifier are of the "*m*" derived type. Kallmann discusses this type line in connection with the construction of high fidelity delay lines.[2] He shows that best results are obtained with an "*m*" of 1.27 and points out that negative mutual inductance may be used to eliminate the need for any inductance in the shunt arm. The method of design proceeds as follows: First, a compromise is arrived at in determining the characteristic impedance of the plate line, between gain per tube and pass band desired in the amplifier. The high frequency cut-off of a delay line varies inversely with the line impedance and is given by the equation $f_c = 1/(2\pi Z_0 C)$ where Z_0 is the impedance of the line considered to be a pure resistance, and C is the unavoidable shunt capacity of each section divided by the value of "*m*." The grid line must be designed for the same cut-off frequency as the plate line because the delay per section of both lines must be equal. The required value of L and M, corrected for lead inductance, then may be calculated when Z_0, C, and the value of lead inductance M' are known.

In the equivalent circuit in Fig. 8:

$$Z_0 = 1/(\omega C),$$
$$L = \omega^2 C,$$

and in the actual circuit, setting $m = 1.27$;

$$L_1 = L_2 = 0.515L - M',$$
$$|M| = 0.121L - M'.$$

The experimentally determined values of mC and M' are 4.9 micro-microfarad and 0.021 microhenries for a 6AK5 plate line and 0.028 microhenries and 7.2 micro-microfarads for a 6AK5 grid line. M is required to be a negative mutual inductance because $1 - m^2$ is negative. L_1 and L_2 are wound as one continuous center-tapped coil which gives M the proper sign, and permits its magnitude to be controlled easily. The inductance of the two sections in series is increased by a factor $(L_1 + M)/L_1$ by the mutual inductance between them. This ratio is fixed in a continuous-wound coil by the ratio of length to diameter. It has been computed for the range of values applicable to the design of distributed amplifiers and is plotted in Fig. 9. The coils may be close wound if the proper size wire is selected to give the required length. This method was used and the coils then were checked on a "Q" meter and adjusted to the nearest half-turn. Specifications are given in Fig. 10 for the completed lines.

In every case the plate lines drive a larger capacity than their normal shunt capacity. It is always possible, however, to join two lines so long as they have the same characteristic impedance; therefore the load capacity is connected to the last regular section of a line through an inductance whose value is given by $L = \frac{1}{2}R^2C$. Wherever the capacity in a shunt leg is greater than the normal shunt capacity, the half-section involved will have a lower cut-off frequency than the rest of the line but the attenuation of one half-section is not severe and, while it does reduce the pass band, the alternative of padding all sections of the line up to the value of the maximum capacity and then reducing the line impedance to achieve the same pass band is much less economical of tubes and equipment.

ADJUSTMENT

The terminations for the grid and plate lines in the deflection amplifier were adjusted with the aid of a pulse generator using 2050 type thyratrons, and having a rise time of about 0.002 microseconds. First a negative signal was applied directly to the grids of one stage, of sufficient amplitude to cut off the tubes. The deflection plate ordinarily connected to the other stage was grounded and the observed wave form was assumed to be a function only of the plate line. With a wrong value of terminating resistors the output signal will change stepwise from a value $\Delta i_p Z_0$ to a value $\Delta i_p R$, (each step lasting for twice the delay of the line).

It was found that Sprague NIT non-inductive wire wound resistors, shunted with carbon resistors to the correct value, were very satisfactory in this application.

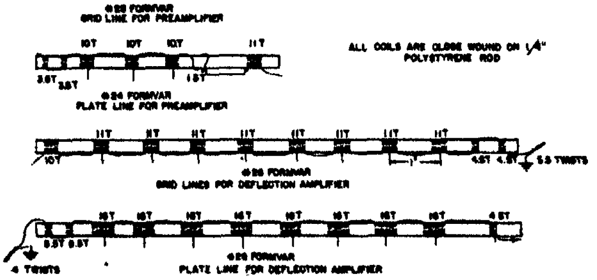

FIG. 10. Specifications of completed line.
Coils for S-1 Synchroscope.

---

[2] H. E. Kallmann, "Equalized delay lines," Proc. I.R.E. 34, No. 9 (1946).

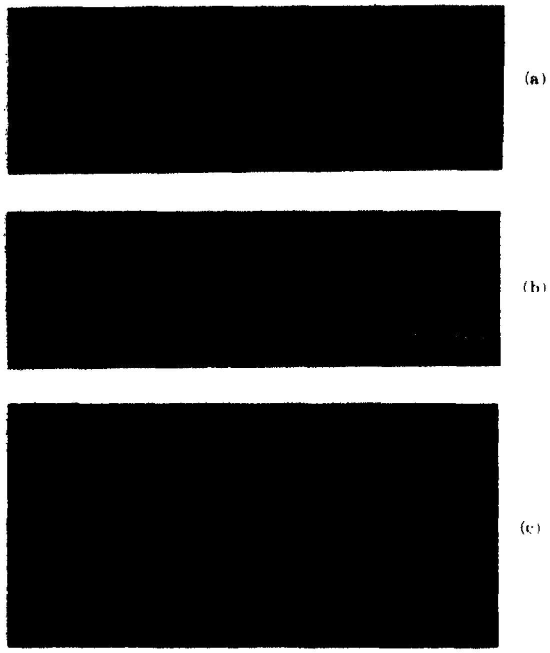

Fig. 11. Response of (a) the deflection amplifier to a step function input, and (b) the deflection amplifier and preamplifier to a 0.1 μsec. pulse. A 30 calibrating signal is given (c),

After the plate line had been adjusted, the stage was returned to normal operation and the grid termination corrected. This problem proved to be a bit more difficult because of the appreciable effect of grid loading. Dissipation along a line requires an inductive component in the termination. This fact, along with the unavoidable presence of capacitive reactance made it necessary to add a small inductance in series with the terminating resistor. Since the grid loading apparently varies with the bias, a compromise had to be made. The best value proved to be about 0.1 microhenries (11 turns of number 26 wire on a 0.1 inch form).

PERFORMANCE

Photographs of the response of the deflection amplifier alone and of the deflection amplifier plus the preamplifier are shown in Fig. 11, along with a 30-megacycle calibrating signal. The rise time as measured from these pictures is slightly less than 0.005 microseconds for the deflection amplifier alone and about 0.0063 with the preamplifier added. The pictures were obtained using about 1.2 volts of signal at the input to the deflection amplifier and 0.05 volts into the preamplifier.

Gain of the deflection amplifier is about 40 and that of the preamplifier is about 25.

All of the 6AK5 tubes used on the vertical amplifier were selected for high mutual conductance on the basis of high plate current at a given value of grid bias. About one-third of the tubes tested were accepted. The selection also gives fairly uniform inter-electrode capacities because there seems to be a rough correlation between mutual conductance and grid-to-cathode capacity.

ACKNOWLEDGMENT

The author wishes to express his appreciation to Dr. W. H. Jordan and Mr. P. R. Bell of this laboratory for many discussions helpful in the development of this instrument.

THE REVIEW OF SCIENTIFIC INSTRUMENTS VOLUME 21, NUMBER 1 JANUARY, 1950

Design and Construction of Universal Function Generating Potentiometers*

GRANINO A. KORN
Lockheed Aircraft Corporation, Burbank, California

(Received September 2, 1949)

The design and construction of a new type of function generating potentiometer, whose output voltage may be made proportional to a wide variety of functions of the shaft rotation, is described. Voltages corresponding to the desired function values are set up at will at the taps of a linear potentiometer, which then interpolates linearly between these values. The new device combines remarkable flexibility with relatively low cost.

I. THE UNIVERSAL FUNCTION GENERATOR

A CONSIDERABLE number of industrial, research, and military applications require a voltage divider or potentiometer whose attenuation varies as a prescribed non-linear function of the shaft rotation.[1] The output voltage of an ordinary linear potentiometer is simply proportional to the shaft rotation. Several types of non-linear relationships between output voltage and shaft rotation may be approximated by various methods of resistance loading of such linear potentiometers.[1] For more exacting requirements, several manufacturers produce potentiometers with non-linear characteristics obtained through the use of tapered cards or windings of variable density. Potentiometers generating square, sine, and logarithmic functions are available on a limited production basis, and special function potentiometers for other functions are made to order in some instances. In all but a few cases, however, the delivery times are prohibitively long if quick tests involving empirically obtained functions are desirable, and the prices are often out of all proportion to those of associated equipment.

In view of these facts, it would be desirable to have a function generating potentiometer which could be easily made up in the laboratory at reasonable cost and which could be set up for a wide variety of desired functions, including functions obtained from empirical data. The following is a description of a new type of function generating potentiometer which is believed to satisfy these requirements.

An inexpensive linear potentiometer is tapped 19 to 39 times. A set of adjustment networks permits the voltages at each tap to be adjusted to correspond to the values of the desired function for the respective angular displacements. The potentiometer output voltage will be correctly set up for the desired function values at the taps. Moreover, the potentiometer will interpolate approximately linearly between the function values set up at the taps, and accuracies better than one percent are possible for reasonable gradient changes. The adjustment networks contain small variable potentiometers or rheostats, so that the function to be generated may be changed at will. If no such changes are desired, fixed resistors may be substituted for the variable ones.

The principle of the universal function generator is illustrated in Fig. 1, while Fig. 2 shows the actual circuits of the adjustment networks for a number of typical cases.[2] The "parallel" arrangement of the adjustment potentiometers shown in Fig. 2(a) is the most flexible one and permits a wide variety of functions to be set up. Its disadvantages are (1) the low impedance presented to the source by the parallel potentiometers and (2) the danger of burning out the main potentiometer winding if the full source voltage appears across a small section of the winding. Both these disadvantages are overcome by the "series-parallel" arrangement of Fig. 2(b) at the expense of flexibility. In this arrangement, the adjustment potentiometers are essentially connected in series across the source, so that each tap voltage can be varied only through a fraction of the source voltage without rewiring. This arrangement is particularly well suited for fixed function potentiometers. The arrangement of Fig. 2(c) presents an even higher impedance to the source, but it is not as easily adjusted as that of Fig. 2(b).

The following advantages of the new function potentiometers should be noted:

1. Relatively low cost potentiometers, such as General Radio potentiometers or Helipots, can be adapted. Five percent accuracy with respect to the linearity of the card and the location of the taps is ample, since the final accuracy is not seriously affected by this.
2. The effect of potentiometer loading on the taper of potentiometers is largely eliminated, since the tap voltage adjustments may be made with the load connected. This results in considerable savings and design simplifications in many cases.
3. The new function potentiometer possesses a high degree of flexibility. Different characteristics can be set into instruments, computers etc. by simply changing the tap voltage adjustments. Tables of these adjustments giving desired functions may be compiled for reference, or complete, interchangeable adjustment networks may be retained for re-use (see below).

The choice of resistance values for the tapped potentiometers and adjustment networks, as well as the effects of loading, will be discussed.

---

* Originally Boeing Report D-10041.

[1] Greenwood, Holdam, and Macrae *Electronic Instruments*, M.I.T. Radiation Laboratory Series (McGraw-Hill Book Company, Inc., New York, 1948), p. 95.

[2] G. A. Korn, "The general difference analyzer," Curtiss-Wright Report P 537-V-46 (1948).

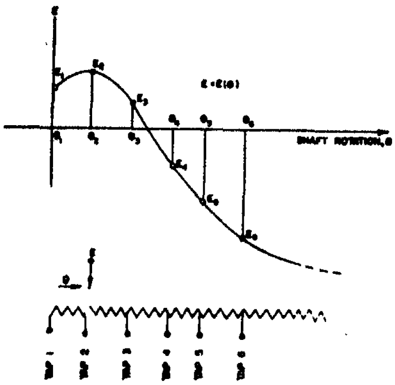

FIG. 1. Linear interpolation by means of tapped potentiometers.

II. DESIGN CONSIDERATIONS

It was seen in Section I that the choice of resistance elements for the tapped potentiometer and its associated networks must satisfy several requirements, which will be taken up in turn.

1. It must be possible to establish the desired voltages at the tap points, with the load connected and without exceeding the power ratings of any of the resistance elements. Any of the arrangements of Fig. 2 may be made to satisfy this requirement if the derivative (slope) of the function to be generated does not change too much over the interval of any one tap segment. This question may be decided very simply by drawing a rough graph of the desired function with the tap points indicated, as in Fig. 1. The points on the graph corresponding to adjacent taps may then be joined by straight line segments as in Fig. 1, and it will be easy to decide whether the interpolation error exceeds a specified percentage. It is clear that, for a given error percentage, functions with rapidly changing derivatives will require potentiometers wih greater numbers of taps than functions whose derivatives vary more slowly.

2. If, as in Fig. 3(a), the function value changes appreciably between adjacent taps (large derivative), care must be taken in order not to exceed the power rating of the potentiometer in question. It is also clear that the rate at which the output voltage can change is limited by the fact that the voltage must vary linearly over the interval of each tap segment. An increase in the number of taps will, thus, permit the generation of more rapidly changing functions. Potentiometers with *split tapped windings*, of which two typical examples are shown in Figs. 3(b) and 3(c), permit the representation of *step functions* as well as better approximations of functions having steep slopes for certain values of the argument. The arrangement of Fig. 3(c) is more flexible than that of Fig. 3(b) but uses twice as many adjustment potentiometers.

3. The output voltage must vary linearly between taps within a specified percentage, with the load connected. This requirement will be satisfied automatically by any of the circuits shown in Fig. 2 if the function generator in question is working into a load of very high impedance, such as a vacuum tube amplifier. If, however, a load of finite resistance R_e is connected between the output terminal of a function potentiometer and ground, the load will draw current from the potentiometer. The resultant voltage drop in the potentiometer winding and networks tends to make the absolute value of the output voltage smaller than that corresponding to linear interpolation. Figure 3(d) shows a graph of output voltage *vs.* shaft rotation for a case with relatively low load resistance and illustrates an extreme instance of the loading effect.

The proper design of the tapped potentiometers and adjustment networks involves the determination of the minimum load resistance in relation to the other resistance elements, which will still yield tolerably linear interpolation. For the analysis of this basic design problem, use is made of the fact that Thevenin's theorem[3] permits the representation of the tapped potentiometer and its associated networks by the *equivalent circuit* of Fig. 3(e).

Let E' be the open-circuit voltage measured between the potentiometer output terminal and ground if the load resistance R_l is removed. According to Thevenin's theorem, the potentiometer circuit is then equivalent to a voltage source of voltage E' connected in series with the resistance R_i' seen by the load if all real voltage sources are replaced by short circuits.

Consider now the variation of the internal resistance R_i' and the open-circuit voltage E' as the sliding contact is moved through any one segment of the tapped winding. Let x denote the fraction of the segment in question traversed by the wiper, with $x=0$ at that tap for which the value of R_i' is lower. It is possible, for each winding segment, to consider R_i' as the sum of a fixed term R_i and a term $r(x)$ variable with the shaft rotation measured by x. Thus,

$$R_i' = R_i + r(x), \quad \text{with } r(x) \geq 0, \quad r(0)=0, \quad 0 \leq x \leq 1. \quad (1)$$

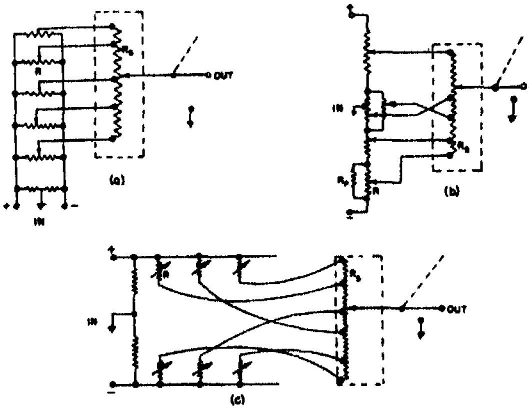

FIG. 2. Universal function generator circuit diagrams.

---

[3] W. R. Smythe, *Static and Dynamic Electricity* (McGraw-Hill Book Company, Inc., New York, 1939), p. 129.

If the tapped potentiometer is a linear one, it is, moreover, clear that the open-circuit voltage E' must be a linear function of x:

$$E'(x)=(1-x)E'(0)+xE'(1). \qquad (2)$$

With reference to Fig. 3(e), Ohm's law yields the output voltage E of the function potentiometer with the load connected, *viz.*,

$$E=(E'R_l)/(R_i'+R_l)=[E'(x)R_l]/[R_i+R_l+r(x)]. \qquad (3)$$

Since E' varies linearly with x, it is seen that, for reasonably linear interpolation, r will have to be made small compared to (R_i+R_l). This will now be discussed on a quantitative basis. Since, in all practical cases,

$$0\leq r(x)<(R_i+R_l),$$

it is possible to expand (3) into an alternating power series in terms of $r(x)$:

$$E=\frac{E'(x)R_l}{R_i+R_l}\left\{1-\frac{r(x)}{R_i+R_l}\pm\cdots\right\}$$
$$=\frac{E'(0)(1-x)+E'(1)x}{R_i+R_l}\left\{1-\frac{r(x)}{R_i+R_l}\pm\cdots\right\}R_l. \qquad (4)$$

It will be remembered that the tap voltages are adjusted with the load connected, so that the output voltage assumes the correct values for $x=0$ and $x=1$. The result of an ideal linear interpolation between these values is

$$E_{\text{lin}}=(1-x)E(0)+xE(1). \qquad (5)$$

Using (1), (2), and (4), this becomes

$$E_{\text{lin}}=\frac{R_l}{R_i+R_l}\left\{(1-x)E'(0)+xE'(1)-xE'(1)\times\left[\frac{r(1)}{R_l+R_i}\pm\cdots\right]\right\}$$
$$=\frac{R_l}{R_i+R_l}\left\{E'(x)-xE'(1)\left[\frac{r(1)}{R_l+R_i}\pm\cdots\right]\right\}. \qquad (6)$$

The error due to the load is given by the difference of (4) and (6), or

$$E-E_{\text{lin}}=\epsilon=\frac{R_l}{R_i+R_l}\left\{xE'(1)\left[\frac{r(1)}{R_i+R_l}\pm\cdots\right]-E'(x)\left[\frac{r(x)}{R_i+R_l}\pm\cdots\right]\right\} \qquad (7)$$

which is seen to vanish for $x=0$ and $x=1$ because of (5).

An attempt will now be made to estimate an upper bound for the error (7). The right side of (7) cannot decrease in absolute value if the full value R_s of one winding segment is substituted for both $r(x)$ and $r(1)$. Since $0<R_s<R_i+R_l$ in all practical cases, moreover, the absolute value of the right side will not be decreased by terminating the power series after the first term. The resulting inequality

$$|\epsilon|\leq\frac{R_l}{(R_i+R_l)^2}R_s[xE'(1)-E'(x)]$$

may be further simplified through the use of (2),

$$|\epsilon|\leq\frac{R_l}{(R_l+R_i)^2}R_s(1-x)E'(0)\leq\frac{R_lR_s}{(R_l+R_i)^2}E'(0). \qquad (8)$$

Equation (8) serves as an estimate of the error due to the load.

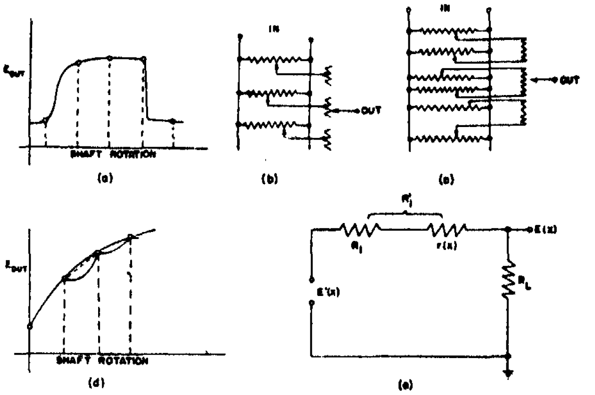

FIG. 3. Design considerations.

The error given by (7) or (8) may be compared to the full source voltage E_i or, more conservatively, to the tap voltage $E(0)=(R_l/R_l+R_i)E'(0)$. In the latter case the percentage error P is given by

$$P\leq\frac{100R_s}{R_l+R_i}(1-x)\leq\frac{100R_s}{R_l+R_i}. \qquad (9)$$

The use of (9) as a convenient design formula is illustrated by the following example. For all the arrangements shown in Fig. 2, the lowest possible value R_{min} of R_i is $R_i=0$, so that (9) yields

$$P\leq 100R_s/(R_i+R_l)=100R_s/R_l. \qquad (10)$$

It should be kept clearly in mind that (10) is *not* a necessary condition which applies to all special cases of function generating potentiometers; it is merely a rather general *sufficient* condition which will hold for many different circuits and a wide range of functions to be generated. If it should be desirable to find optimum design values for special cases, and in particular for the representation of one fixed function, Eq. (7) should be referred to for each winding segment of the potentiometer in question. In many cases such a procedure will lead to much higher values of the ratio R_s/R_l than those given by (10).

In practically all cases the loading errors, as given by (7), may be reduced by introducing resistors in series with either the load or the voltage source supplying the function potentiometer. This will increase R_l or R_i, respectively, at the expense of the output level. *A better scheme is to introduce series resistors between certain taps and the corresponding adjustment networks.* This procedure decreases only the maximum voltage available at the taps in question and may also help to increase the input impedance of the potentiometer and to prevent excessive currents in the winding segments.

4. *The function generator should present a specified impedance to the voltage source.* Since the formulas (7)–(10) for the loading error all involve resistance *ratios* referred to the given load resistance R_l, the input impedance is determined by the network arrangement chosen and by the load resistance R_l. The choice of networks has been discussed in Section I; it may, however, not be possible to obtain input impedances as high as required if the load resistance R_l is necessarily too low. In such cases it may be necessary to sacrifice the output level in order to isolate the function from either the source or the load by means of series resistors. Vacuum tube amplifiers will, of course, serve the same purpose without sacrificing output level.

Apart from these considerations, an intelligent choice of resistance elements for the tapped potentiometer and its associated networks will often involve a preference for types of components which are readily available commercially.

III. CONSTRUCTION OF TAPPED POTENTIOMETERS

At the present time several manufacturers of wire-wound potentiometers will tap their windings on special order, but for small production runs and large numbers of taps the cost of this operation may be quite high. If the demand for tapped potentiometers should increase, however, there is little reason why the cost per tap should exceed fifty cents on orders of 25 or more potentiometers. In any case, the operations involved in tapping potentiometers in the laboratory are not too difficult and will be described in the following.

Figures 4 and 5 illustrate two possible methods for tapping several types of wire-wound potentiometers. At this writing, only wire-wound potentiometers were considered to have the resolution necessary for adaptation as universal function generators.

Figure 4 shows an exploded view of a General Radio type of potentiometer which has been modified by tapping. This type of potentiometer has a cylindrical card or mandrel wound with resistance wire. At each desired tap location part of a single turn of wire has been lifted off the card. This wire was then separated from the rest of the winding by an insulating strip of plastic or cellulose tape, and scraped free of insulation. Contact to these free portions of the winding is then made by (preferably silver-plated) rivets or screw heads fastened to the outer Bakelite housing of the potentiometer in the proper locations. It can be seen from Fig. 4 that this thin outer potentiometer housing is attached to the inner shell by screws which also serve to hold the card in place. Since these screws alone may not effect sufficiently firm contact between the rivets and the winding, it is suggested that an insulated strap, also shown in Fig. 4, be fitted over the rivets and secured tightly by means of a turnbuckle.

Figure 5 shows an alternative method for tapping wire-wound potentiometers and is suited to potentiometers having a thick outer or inner Bakelite shell. The card and winding are first removed from the shell. Holes corresponding to the desired tap locations are drilled in the shell; it will be remembered that the location of the taps is not critical. The holes are then tapped with a fine thread. After the winding has been replaced in the shell, it may be contacted by silver-tipped screws screwed firmly into the tapped holes. Wires may be soldered to these screws, after which the screw heads are secured in position by a layer of sealing wax.

This last method of tapping is especially applicable to potentiometers of the helical card type (Helipots), some of which have shells with thick ribs admirably suited for drilling and tapping. The proper location of the holes for such a helical potentiometer is easily found by placing the shell in a lathe and cutting a very light thread of the proper pitch. This thread, which need only barely score the ribs in the shell, may be located so as to indicate accurately the location of the helical winding inside the shell. The function potentiom-

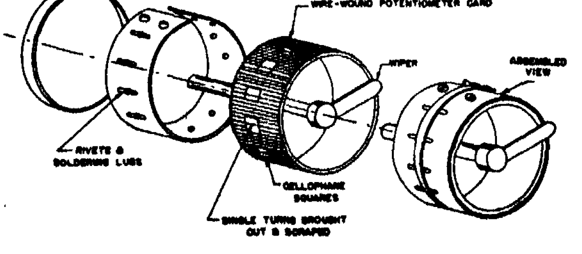
INSULATED STRAP & TURNBUCKLE
WIRE-WOUND POTENTIOMETER CARD
WIPER
ASSEMBLED VIEW
RIVETS & SOLDERING LUGS
CELLOPHANE SQUARES
SINGLE TURNS BROUGHT OUT & SCRAPED

FIG. 4. Exploded view of tapped potentiometer.

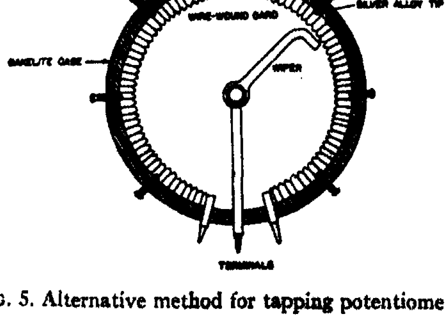

FIG. 5. Alternative method for tapping potentiometer.

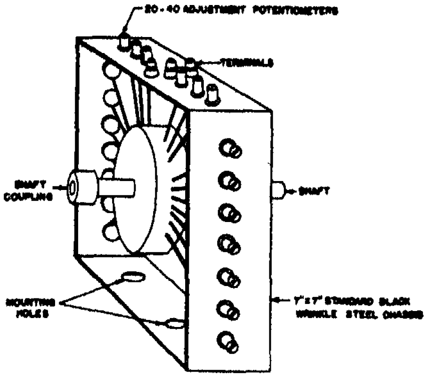
20-40 ADJUSTMENT POTENTIOMETERS
TERMINALS
SHAFT COUPLING
SHAFT
MOUNTING HOLES
7"x7" STANDARD BLACK WRINKLE STEEL CHASSIS

FIG. 6. Arrangement of adjustment shafts.

eter shown in Fig. 5 was constructed in this manner, and the locating scores may still be seen on those ribs not used for tapping.

Figure 6 illustrates one of several methods of locating the adjustment potentiometers and networks around, above, or beside a tapped potentiometer. The most accessible location of the adjustment shafts may have to be chosen separately for each application.

A more sophisticated arrangement is applicable wherever shortness of leads is not a paramount consideration. The tapped potentiometer is mounted in a box. The leads from the taps are brought out to a Jones connector. The adjustment networks are arranged in a separate metal box fitted with a multiple plug in such a manner that it can either be plugged into the potentiometer box directly or connected to it by means of a suitable cable. This arrangement permits the interchanging and filing of several function networks for each tapped potentiometer. This makes it possible to set up several frequently needed function networks once and for all and to interchange them at will. Since the tapped potentiometer proper constitutes a major part of the total cost of the function generator, this may result in considerable savings. This arrangement also permits more convenient location of the adjustment shafts (e.g., on the front panel of a computing machine) for easier adjustments and function changes.

IV. HISTORY AND ACKNOWLEDGMENTS

To the best of the writer's knowledge, tapped potentiometers, with only fixed resistors connected across the taps, were first used by the Arma Corporation of Brooklyn, New York, in connection with computing equipment. The universal function generating potentiometers were developed by the writer's group in the research laboratories of the Curtiss-Wright Corporation, Airplane Division, in Columbus, Ohio. Credit for the circuits shown in Figs. 2(a) and 2(b) is due Mr. D. Kahn of that organization. The split tapped winding was invented by Mr. R. Muirhead, formerly with the Curtiss-Wright Corporation. Several units of the type shown in Fig. 6 were built in the electrical laboratory of the Curtiss-Wright Corporation and were tapped as indicated in Fig. 4 under the direction of Mr. R. Lemon. This work was sponsored by the Applied Physics Laboratory, Johns Hopkins University, Silver Spring, Maryland, under a contract with the Curtiss-Wright Corporation. Figures 1, 2, and 6, as well as part of the accompanying text, were taken from Curtiss-Wright reports written by the present writer.

A number of potentiometers of the type illustrated in Fig. 5, were built in the laboratory of the Physical Research Unit, Boeing Airplane Company, Seattle, Washington, the writer being on loan to that organization under a temporary arrangement with the Curtiss-Wright Corporation. The plug-in network arrangement was conceived by Mr. G. Brown of the Boeing Airplane Company; the mechanical design is due Mr. W. Dillman. The writer wishes to thank Messrs. Brown, Dillman, Kates, and Cosby of the same organization for their able assistance in the construction of universal function generating potentiometers.

The writer also wishes to express his gratitude to Dr. E. H. Gamble of the Curtiss-Wright Corporation, Dr. R. Kershner of the Applied Physics Laboratory, and Mr. G. Stoner of the Boeing Airplane Company for their interest in, and encouragement of, this project; and to Mr. E. C. Wells of Boeing and Mr. R. Blaylock of Curtiss-Wright for their permission to publish this material.

Physical Instruments for the Biologist

Detlev W. Bronk
Associate Editor in Charge of this Section
Eldridge Reeves Johnson Foundation for Research in Medical Physics,
University of Pennsylvania, Philadelphia, Pennsylvania

Small Probing Geiger-Müller Counters

C. V. Robinson
Biophysical Laboratory, Harvard Medical School, Boston 15, Massachusetts

(Received September 2, 1949)

Experiments with argon-ethyl acetate mixture in small counters are described. Details of construction are given for two designs of brain probing counters of 3- and 2-mm diameters.

SEVERAL small probing counters have been built by the author and used at the Massachusetts General Hospital during the past year for the localization of brain tumors with the aid of radioactive phosphorous.[1] The first counters constructed were filled with ether-argon mixtures.[2] Subsequently ethyl acetate-argon was found to be a better mixture (see comparison below). For localization of brain tumors the neutro-surgeon requires a counter which has a probing tube of 3 mm diameter or less and a length of 7 cm or more.[1, 3] For precise localization it is desirable that the sensitive volume be small and located near the tip of the counter. Since, in general, a smaller sensitive volume gives a slower counting rate in a given region, a practical compromise must be reached between speed of counting and precision of localization. The 2-mm diameter probing counter described below is considered to be near the optimum for this application.

I. EXPERIMENTS WITH MIXTURE AND GEOMETRY

Experiments to ascertain suitable mixtures and geometry for small counters were carried out with an experimental multiple counter on the filling system. This apparatus consists of four counter frames enclosed in a metal envelope with five lead-through connections (Fig. 1). Each frame permits a cylinder and wire to be readily screwed into position and the four frames are connected independently to the plate. The plate is screwed to the envelope and the four counters may then be operated with a common gas mixture. Data on ethyl acetate-argon mixtures obtained with this apparatus are shown in Table I. The cathodes are of copper treated with CrO_3 solution activated with H_2SO_4 except for numbers 2 and 13 which are stainless steel No. 304 degreased with acetone. These cathode materials are found to be interchangeable when used with ethyl acetate-argon or ether-argon. The counter wires are shielded with Pyrex capillary except for a central length of 15 mm in order to give a sharply terminated sensitive volume. The threshold readings in numbers 3–12 were

TABLE I. Plateau data for ethyl acetate argon mixtures.

Counter No.	Cathode diam. mil	Wire diam. mil	Ethyl acetate pressure mm	Argon pressure atmospheres	Threshold volts	Plateau length volts	Plateau slope %/100 v
1	228	1	25	2	1120	275	2
2	112	1	25	2	1025	150	5
3	67	1	15	1	710	70	17
4	67	1	25	1	850	80	13
5	67	1	25	2	910	100	3
6	67	1	30	3	1000	125	3
7	67	1	35	4	1065	110	1
8	67	0.4	15	1	670	60	16
9	67	0.4	25	1	780	100	9
10	67	0.4	25	2	830	100	3
11	67	0.4	30	3	890	150	3
12	67	0.4	35	4	960	175	2
13	30	1.5	30	8	870	30	1

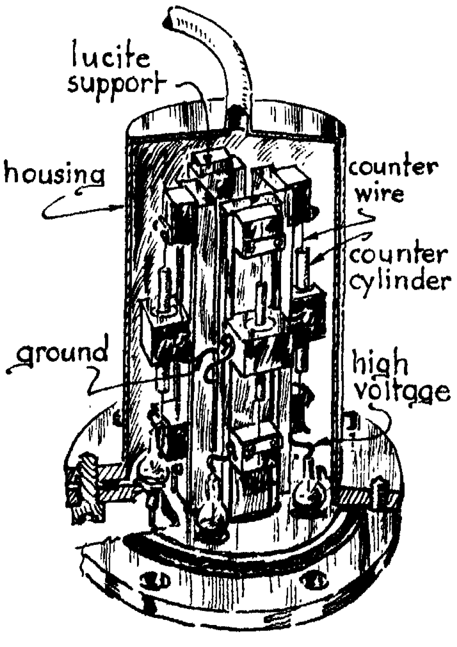

FIG. 1. Experimental counter.

---

[1] Selverstone, Solomon, and Sweet, J. Am. Med. Assn. **277**, 140 (1949).

[2] C. V. Robinson and R. E. Peterson, Rev. Sci. Inst. **911**, 19 (1948).

[3] Selverstone, Sweet, and Robinson, Annals of Surgery (October, 1949).

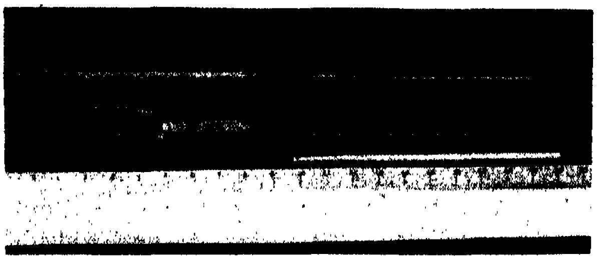

FIG. 2. Probing counters.

made with the same voltmeter so that their relative values are significant, although the absolute values are less accurate.

The effect of cathode diameter on plateau length, other things being equal, is illustrated by counters 1, 2 and 5. The necessity for using a sufficiently high argon pressure is illustrated by a comparison of the plateau slopes of counter 4 with 5, 6, or 7 and counter 9 with 10, 11, or 12. The effect of wire diameter on plateau length is seen by comparing counters 4 with 9, 5 with 10, etc.

It is of interest to compare ethyl acetate-argon with ether-argon,[2] previously tried for small counters. The optimum mixture of ether-argon in an experimental counter which had a geometry almost identical with that of counter 12 gave a plateau length of 80 volts as compared to 175. Even with a larger wire in the same diameter of cylinder, the ethyl acetate gives a longer plateau (counters 6 and 7).

In the author's experience, ether-argon counters are more likely to be permanently damaged by excessive voltage than ethyl acetate-argon counters. Although no systematic breakdown studies were made, a number of ether-argon counters were runied by breakdown, whereas of several ethyl acetate-argon counters which broke down, all recovered.

Although probing counters with both kinds of mixture have served for periods of six months or more, insufficient life test data are available for a comparison. Life tests on a small ether-argon counter without a gas reservoir gave 5×10^7 counts.[2] It has been shown that the life of ethyl acetate-argon counters is limited by depletion of the quenching vapor.[4] Hence a gas reservoir should serve to extend the life of counters with this filling. A reservoir has been incorporated in the designs shown in Figs. 2 and 3.

If helium is used as the noble gas rather than argon, larger wires may be used. Ether-helium mixtures show stable operation with experimental counters having 0.067-in. and 0.030-in. cathodes with 0.005-in. and 0.0025-in. wires respectively. The counting characteristic is short and steep but these counters, like the ethyl acetate-argon counters, were apparently not injured by excessive voltage. The same experimental counters were also operated with a quenching circuit, described elsewhere,[5] using helium plus an impurity,[6] thought to be mercury vapor. The 0.067-in. counter with four atmospheres pressure operated stably and passed a good Chi Square Test.[7,8] The counting characteristic extended from 540 volts to 600 volts. Over this voltage range the counting rate increased 25 percent. The 0.030-in. counter with 8 atmospheres behaved similarly with a threshold of 490 v. From these results with helium, it appears feasible to build small counters with a simple gas filling and hence with an indefinite life.* Since small self-quenching counters need to be used with a cathode follower or preamplifier, the necessary quenching circuit for helium counters does not represent much, if any, additional complication.

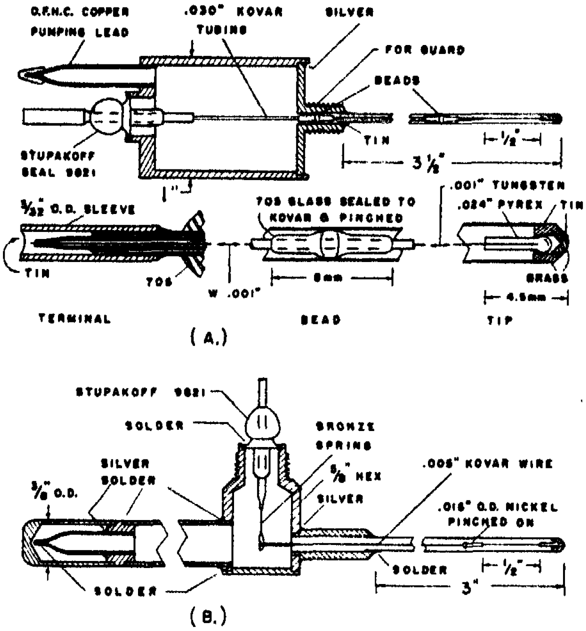

FIG. 3. Details of construction: (A) 2-mm diameter probing counter, (B) 3-mm diameter probing counter.

II. CONSTRUCTION OF PROBING COUNTERS

A pair of 3-mm probing counters including the one shown in the upper half of Fig. 2, have operated satisfactorily for several months. The probing tube is 0.121 in. O.D. with 0.004-in. wall stainless steel 3 in. long.† The sensitive volume coincides with a 12-mm length of 0.001-in. tungsten wire near the tip of the counter (see Fig. 3B). The filling is 25 mm of ethyl acetate and 2 atmospheres of argon. The thresholds are 1050 volts and the backgrounds 4 or 5 counts per minute, unshielded.

---

[4] S. S. Friedland, Phys. Rev. 74, 898 (1948).

[5] C. V. Robinson, Rev. Sci. Inst. 20, 750 (1949).

[6] S. C. Brown, Phys. Rev. 244, 62 (1942).

[7] A. B. Willoughby, Phys. Rev. 75, 1461 (1949).

[8] Strong, *Procedures in Experimental Physics* (Prentice-Hall, Inc., New York, 1946), pp. 302–304.

* Halogen mixtures have also been used for small counters with some success. M. L. Griem, private communication.

† Superior Tube Company, Norristown, Pennsylvania.

A pair of 2-mm probing counters including the one shown in the lower half of Fig. 2 have more recently been put into service. The tube is of stainless steel 0.081 in. O.D.×0.0025 in. wall, 3½ in. long. Since this tube is more flexible, the center conductor is supported with three glass beads, as shown in Fig. 3A. These counters are filled with 35 mm of ethyl acetate and 4 atmospheres of argon, which gives a threshold of 900 v. The plateaus were examined for a range of 60 volts and showed slopes of 7 percent and 12 percent/100 v. The backgrounds were 3 or 4 counts per minute unshielded.

These counters produce pulses considerably smaller than the average counter, because the exposed length of wire is short. To obtain as much life as possible a cathode follower, preamplifier or quench circuit is used, and the operating voltage kept near threshold.

III. ACKNOWLEDGMENTS

This work was supported in part by the Massachusetts General Hospital, the ONR, the United States AEC, and by the American Cancer Society. The author wishes to thank Dr. B. Selverstone of the Massachusetts General Hospital for his close collaboration in the applied aspects of this work, S. C. Brown of the Massachusetts Institute of Technology for his helpful suggestion, especially in regard to the use of helium, and A. K. Solomon for advice and encouragement.

Book Reviews

Atomic Energy Levels, Vol. I, $^{1}H-^{23}V$

By Charlotte E. Moore. Pp. 309+xliii, 23×28 cm. Circular of The National Bureau of Standards 467, 1949. For sale by Superintendent of Documents, U. S. Government Printing Office, Washington 25, D. C. Price $2.75.

In 1932 a compilation of atomic energy values by Bacher and Goudsmit was published in a volume entitled *Atomic Energy States*. This brought together with a uniform notation the results of all of the analyses of atomic spectra that had been made up to that date. This collection has been of very great assistance to all physicists and astronomers concerned with spectroscopic problems. Unfortunately for its present usefulness this compilation was made at about the middle of the great period of spectroscopic analysis in the nineteen twenties and thirties and as a result contains only about one-fifth to one-fourth of the material which is now available. Every user of spectroscopic techniques will therefore welcome a new compilation by Charlotte E. Moore, the first volume of which has just appeared with the title *Atomic Energy Levels*.

Departing from the alphabetical arrangement of the elements of the earlier collection, the present compilation lists the elements in order of atomic number. The volume which has just appeared tabulates the energies of the levels of the elements from hydrogen to vanadium. The form of the present tables follows closely that adopted by Bacher and Goudsmit. Each term is defined in three columns giving the generally accepted notation for the configuration, the designation of the level and the value of J. This is followed by columns listing the energy of the level and the multiplet separations in wave number units. In cases where the original author has used a notation differing appreciably from the generally accepted one, an additional column has been added with this notation. This, combined with an extensive bibliography of the literature for each ion, makes it easy to correlate the tabulated terms with the observed lines listed in the original literature. All energy values in the present volume are given with respect to the lowest level in the ion. The present tables include one new feature namely the series limit for each ion. With the aid of this the energy necessary to remove an electron from any given level to infinity can be rapidly calculated. This is of importance to anyone using isoelectronic sequences for the prediction of terms in ions that have not been analyzed.

In the cases for which detailed Zeeman patterns have been obtained, the observed g value is listed for each level. Theoretical Landé g values for all types of terms are given at the beginning of the volume. Additional tables in the introductory chapter list all terms that are predicted for all ions tabulated in the present volume.

Through the co-operation of various spectroscopists the author has been able to include a substantial amount of unpublished material. Thus, the term values of the hydrogen-like ions from H_{I} to D_{VIII} and including D, T, and $He^{3}{}_{II}$ are based on recent calculations by J. E. Mack. A substantial number of new observational energy values have been supplied prior to publication especially by the Swedish spectroscopists working with Edlen.

The importance of this compilation of atomic energy levels and of Miss Moore's earlier *A Multiplet Table of Astrophysical Interest* can hardly be overestimated. By bringing together on a uniform basis and with a uniform notation the data from the truly enormous literature of spectroscopy of the last few decades, Miss Moore has made it possible for the average astronomer or physicist to effectively apply these spectroscopic results to his researches where hitherto this could only be done by a few spectroscopic specialists. Astrophysical research in particular should be greatly expedited by these compilations.

I. S. Bowen
California Institute of Technology

Introduction to Radiochemistry

By Gerhart Friedlander and Joseph Kennedy. Pp. 412. John Wiley and Sons, Inc., New York, 1949. Price $5.00.

With the rapidly expanding use of radioactive materials by investigators in every branch of science, an increasing demand for instruction within these fields on the general subjects of Radioactivity and Nuclear Physics arises. Some question as to who should give this instruction is certain to appear.

There is a certain reasonableness in the principle of the "division of labor." Any physics department which insists on teaching its own students mathematics and/or chemistry should rightfully be made to justify such procedure. Similarly, the teaching of physics to chemistry students by the chemistry department or the teaching of physics to biologists by the biology department might leave something to be desired.

In an *Introduction to Radiochemistry*, the authors offer a text comprising thirteen chapters, ten of which deal with atomic physics, radioactivity, and nuclear physics. Only three of the chapters, 56 pages in all, deal with chemical phenomena, such as the identification, the concentration, and the isolation of radioactive species, the chemistry of low concentrations, and tracers in chemical applications. Surely the wealth of material dealing with the modern relationship between radioactivity and chemistry warrants a more exhaustive treatment. For example, complete texts can and have been written on the reactions of carbon alone.

Physics departments that would like to have their graduate students take a substantial course in "radiochemistry" could not but feel neglected if most of the time is spent on subject matter more adequately treated in their own department.

There can be no doubt that the eminence of the authors entitles them to discuss authoritatively the material presented in this text. The only reservation of the reviewer is to question the wisdom of such a superficial treatment. For example, wave mechanics is covered completely in one page, and Bose statistics, Fermi statistics, and the Pauli exclusion principle in one paragraph.

At the end of the text a table of isotopes, covering 92 pages, is included. While this table should prove to be useful, it is completely lacking in references to the original investigations. Users of a particular radioactive isotope will usually not be satisfied until they have reviewed the original literature and, to find this, they must consult some other table of isotopes.

The publishers have done an excellent job in making the text attractive in appearance and in legibility. At the end of each chapter is a set of problems of varying difficulty, whose solution should aid the student in understanding the text material. Some 53 figures consisting of line drawings and half-tones help elucidate the expositions.

For a brief, readable survey of modern physics and radiochemistry the text is highly recommended.

J. M. Cork
University of Michigan

An Introduction to Criminalistics

By Charles E. O'Hara and James W. Osterburg, Staff Members, Police Laboratory, New York City Police Department. Pp. 705+xxii, Figs. 314, 24.5×16 cm. The Macmillan Company, New York, 1949. Price $10.00.

The true nature and scope of the applications of the physical sciences to crime detection are something of a mystery to scientific workers generally. The applications are many and varied. The procedures draw heavily on chemistry, physics, and mathematics, with emphasis on microchemical and optical methods of exploration. The objective is accurately to define a physical fact and to determine its usefulness as legal evidence.

Information along these lines has been available for many years in scattered form, but here at last we have a book in which both the familiar and the new applications are assembled. Here are the descriptions of the procedures and the instruments, accurately detailed, that disclose instructively how the scientist in the laboratory, operating in the support of police tactics, goes about it in making his finds of the evidence of forces incongruously applied, the traces of the lethal bullet, the identity of a clot, the source of a fiber, the telltale fingerprint, the differing ink, the flaw in the metal, the slip of the pen, upon which, in the dramatic setting of our courts, turn the liberty of individuals or the rightful titles to property.

The book contains 48 chapters, 46 of which are highly useful. The 47th and 48th chapters are a plug for a centralized institute for the study and development of police laboratory procedures. The inclusion of such a debatable project mars an otherwise unbiased presentation of scientific method as applied to police problems. But the reader can skip these. Forty-six chapters deal with laboratory design and resources; physical measurements; tracks and impressions; photographic explorations; physical tests, mechanical and optical; semimicro- and microchemical testing and analysis, and finally special applications of recent advances in instrumentation in the field of light waves, more particularly the wave-lengths shorter than the visible wave-lengths. Useful references are appended to each chapter, of which about half are in print and are generally easily available.

The authors have titled their book *An Introduction to Criminalistics*. It is more than an "introduction." It comes nearer to being a manual for the indoctrination of a chemist or physicist in crime detection. The general reader should have substantial grounding in the basic sciences. The special reader will need a sound knowledge of the physics of light, since optical methods are stressed throughout the book. All of the topics and methods of procedure treated are within the ready adaptation of a graduate chemist familiar with microchemical analysis; or of a graduate physicist familiar with the spectrographic field. While not encyclopaedic, it covers well the segment of criminal traces chosen to be investigated. Some gaps in the available literature of crime detection are filled. The text is well written. It is instructively supplemented with good illustrations. What is omitted is available elsewhere and may be located from the references given. It has both table of contents and comprehensive subject index.

Obviously, here is something different from the ordinary conception of a textbook. The various modern optical, photographic, and chemical procedures that are requisite for the most satisfactory results in scientific crime detection are gathered here. The worker or student occupied with the search for unequivocal legal evidence scientifically obtained will find it an introduction into the world of ideas. It is excellent and well worth having.

Edward Oscar Heinrich
Berkeley, California

Laboratory and Workshop Notes

Compiled and Edited by Ruth Lang. Pp. 272, Figs. 195. Longmans, Green and Company, Inc., New York, 1949. Price $5.25.

This book is a compilation of selected notes which have appeared in the *Journal of Scientific Instruments* during the past twenty-five years. The selection suffers, as the Foreword states, from the paper restrictions in Great Britain, and because of this only approximately half of the selected notes were published. Readers in this country will also feel that it suffers even more from having been selected only from the *Journal of Scientific Instruments*. Also, since the selection period extends over the past twenty-five years, some of the notes raise nostalgic memories of the "string and sealing-wax" era of physics. Since all the notes from which this is a selection are not available to the reviewer, it is difficult to say whether this selection was the best that could have been made under the restricted conditions of publication. Some of the notes, such as No. 39, entitled, "3-in-1 Oil" (for delicate mechanisms), seems to indicate that at least in some cases it was not.

The work also suffers from being merely a selection without any continuity or critical comparison of methods. It must be pointed out in justification, however, that the author makes no pretense of its being anything more than a verbatim transcript of published material.

In the field of physics represented by these notes, the dissemination of knowledge still depends largely on the "father-to-son" method. There are only isolated efforts at compilations such as this one and *Procedures in Experimental Physics* by John Strong. The latter, although having been of immense value, suffers from representing the experience, if not of one man, at least of a very small school. The following is suggested as a workable method of overcoming these limitations. A publication should be started in the form of a handbook in which the chapters cover fields, such as, for example, vacuum techniques, to be written by one or more experts in the particular field, the chapters to be bound individually, and in turn to be brought together in a loose-leaf cover. This procedure is suggested to permit bringing up-to-date individual chapters where advances in the field make it necessary. These new chapters could then be bought to replace the old ones without the necessity of purchasing a whole new edition.

To return to *Laboratory and Workshop Notes*, it is felt that in spite of the previous discussion, this compilation will prove highly useful, and it is hoped that, as suggested in the Foreword, more volumes of this kind will be published.

L. A. Delsasso
Aberdeen Proving Ground, Maryland

Isotopic Tracers and Nuclear Radiations with Applications to Biology and Medicine

By William E. Siri. Pp. 653, Figs. 136. McGraw-Hill, Book Company, Inc., New York, 1949. Price $12.50.

The title of this very important addition to nuclear physics literature is misleading. It more properly fits the description of a handbook of nuclear physics. The articles on isotopic tracers, while interesting and well written, comprise only about 70 pages of the whole 600 odd. The remainder is divided between a bibliography of tracer work (about 90 pages) and the handbook of nuclear physics (about 500 pages). This short remark is made, not in any critical spirit, but because the title may not make clear to the general nuclear physicist that he has now a handbook available to him.

The first two-thirds of the book are given to a statement of the fundamental facts and relations of nuclear physics. Chapters on nuclei in general, gamma-rays, beta-particles, protons, deuterons, neutrons, etc., are plentifully loaded with equations and tables of all kinds. The ability to convey any kind of explanation in a book so full of material content is naturally limited and no great attempt has been made in this direction. Thus by the end of 200 words we have been told that nuclei are stable when the binding energy is a maximum or when the lowest proton and neutron levels are filled. Further, that if this is not so, K-capture or positron emission may result and so on. Such an approach is clearly that of a handbook and a biologist who is not too sure of such things as K-capture needs considerable supplementary reading before he can make good use of the material in the text.

Granted this approach, the choice of material is admirable, very carefully prepared, and is a book which should definitely be on hand wherever reference material in nuclear physics is needed. The compact statement of the facts of particle absorption is particularly good as is the chapter on Geiger-Müller counters. A very welcome chapter on the theory of tracer methods is also included.

There are several important deficiencies. There is no adequate account of the method of photographic detection, which with the new electron emulsions promises to be a powerful weapon in research. Also scintillation counters are not mentioned. From the biological point of view, there is no discussion of the mechanism of the action of radiation on the living organism, a field of work in which such rapid and interesting progress is being made. In a book which is primarily a handbook, one can also ask more of the index than is here.

In spite of these few criticisms, the reviewer has already made excellent use of the book in courses both in nuclear physics and biophysics and it is a great relief to have a single volume to which a student can be sent in place of the mass of scattered references hitherto available. No one whose work goes along with the tide of postwar physics will regret possessing the book.

E. C. Pollard
Yale University

Seismicity of the Earth

By B. Gutenberg and C. F. Richter. Pp. 273, Figs. 34, Tables 19, 8×11 in. Princeton University Press, 1949. Price $10.00.

This book occupies a unique place in the literature of seismology. It supplies the only uniform as well as systematic analysis now available of a great volume of instrumental observations of earthquakes accumulated since the turn of the century.

The authors, who developed the scale now universally used for assigning a magnitude to earthquakes on the basis of instrumental records, have selected their material scientifically with reference to the magnitudes, hence the energies, involved. This includes deep, intermediate, and shallow earthquakes. Thus, for the first time in the history of seismology, truly significant statistics have been distilled from the chaos that previously resulted from simple tabulations of varying samples of the estimated million earthquakes per year around the globe.

This book bears little resemblance to Special Paper No. 34, of the Geological Society of America, 1941, and a supplementary paper in 1945, under the same title by the same authors. It is completely revised, expanded, and reorganized, in addition to including for the first time statistical results for deep-focus shocks on the same basis as for shallow shocks.

Seismicity of the Earth evaluates the present relative seismicity of the globe, discusses the geography and the geological character of the areas of seismic activity, and correlates earthquake locations with alignments of active volcanoes, gravity anomalies, oceanic deeps, mountain structures, and the mechanism of crustal folding and block faulting. Tsunami, or seismic sea-waves, popularly known as tidal waves, are discussed and a list of 450 active volcanoes is included, with latitude, longitude, date, and type of latest reported activity. According to the authors, "All shocks prior to 1946 which have been located are included in regional tabulations. Of great shallow shocks, 98 have been identified between 1904 and 1947; 361 major shallow earthquakes of less magnitude have been identified for 1918–1946. These are given in separate chronological lists which are believed to be practically exhaustive. Over 2000 shallow shocks, and about 1000 deep-focus shocks, 266 with magnitude greater than seven were selected for study because of magnitude or geographical location."

The authors have calculated that the annual average of energy released by earthquakes between 1904 and 1945 was 12×10^{26} ergs, a value comparable to the annual flow of heat from the interior to the surface, which is 66×10^{26} ergs. In terms of annual values, the energy released by earthquakes varied from a high of 59.7×10^{26} ergs in 1906 to a low of 1.5×10^{26} ergs in 1930. No correlations with such phenomena as sunspots stand up over the interval for which data are available, although 1905–07 were years of high numbers.

Every library in the world that wishes so much as a single book on the subject of earthquake occurrence, distribution, and significance, should have *Seismicity of the Earth* on its shelves. It is a true classic in the field.

L. Don Leet
Harvard University Seismograph Station

Advances in Catalysis and Related Subjects, Vol. I

By W. G. Frankenburg, V. I. Komarewsky, and E. K. Rideal (Editors). Pp. 289+xiii, Illustrated. The Academic Press, Inc., New York, 1948. Price $7.80.

This is the first volume of a projected series, to be published annually. It is the intention of the editors that this series shall eventually "present a compilation of papers, written by competent specialists, which should enable anybody to obtain a fairly complete concept of the practical achievements of current and new methods and of the various theoretical approaches to the manifold problems."

It should be emphasized that the present volume is in no sense a compendium of catalytic information but more closely approximates a series of reviews dealing with specialized and limited fields and summarizing the current state of knowledge in those fields. A work of this kind is clearly not suitable as a text but will be highly appreciated by specialists, who have felt for many years the pressing need for systematization in this rapidly advancing and technologically important field. The contributors to the present volume are all men of outstanding ability in their specialities and the generally high quality of the book is a reflection of their competence. If these standards are maintained in future volumes the plan of the editors will be well fulfilled.

This volume contains eight sections; two deal with methods and techniques of quite broad interest over the whole field of heterogeneous catalysis, two more discuss fundamental theoretical questions, again of wide interest, and the remaining four deal with restricted classes of reactions. Heterogeneous catalysis receives the greatest attention "in view of its particular problematic aspects and its preponderant practical importance." The following specific topics are discussed:

"The Heterogeneity of Catalyst Surfaces for Chemisorption" by H. S. Taylor, Frich Chemical Laboratory, Princeton University, Princeton, New Jersey. (25 pp.) This section presents a brief review of the older literature dealing with this subject and much new data demonstrating the existence of centers of varied activity on a number of important catalysts.

"Alkylation of Isoparaffins" by U. N. Ipatieff and Louis Schmerling, Universal Oil Products Company, Riverside, Illinois. (36 pp.) Following a general introduction, the mechanism of catalytic alkylation, side reactions, and the behavior of particular catalysts are discussed.

"Surface Area Measurements. A New Tool for Studying Contact Catalysts" by P. H. Emmett, Mellon Institute, Pittsburgh, Pennsylvania. (25 pp.) A brief but comprehensive survey of the history, limitations and application of this essential method for the study of solid catalysts.

"The Geometrical Factor in Catalysis" by R. H. Griffith, The Gas Light and Coke Company, London. (23 pp.) A remarkably concise summary of the role of the geometrical arrangement of atoms in solid catalysts in effecting a variety of reactions. This is one of the aspects of catalysis which has been very incompletely developed, and at the same time it is one which promises to be most rewarding in the future.

"The Fischer-Tropsch and Related Processes for Synthesis of Hydrocarbons by Hydrogenation of Carbon Monoxide" by H. H. Storch, Synthetic Liquid Fuels Research and Development Branch, Bureau of Mines, Pittsburgh, Pennsylvania. (41 pp.) This is a detailed discussion of the past and present research on a problem of great practical importance. The need for such a compilation is sufficiently indicated by the large number of references (91) to published work.

"The Catalytic Activation of Hydrogen" by D. D. Eley, University of Bristol, Bristol, England. (42 pp.) The wide participation of hydrogen in catalytic reactions, as well as the controversial status of some of the interpretations of experimental results, makes this survey especially valuable. Chemisorption, dissociation and recombination, the parahydrogen conversion, exchange reactions, and a number of specific reactions are discussed. A brief recapitulation of present theories is given.

"Isomerization of Alkanes" by Herman Pines, Universal Oil Products Company, Riverside, Illinois. (54 pp.) A detailed account of the experimental results and mechanisms of isomerization of butanes, pentanes, and hexanes. Some data on higher hydrocarbons.

"The Application of X-Ray Diffraction to the Study of Solid Catalysts" by M. H. Jellinck, Linde Air Products Company, Tonowanda, New York and I. Fankuchen, Polytechnic Institute of Brooklyn, Brooklyn, New York. (32 pp.) The use of this powerful tool for catalyst studies is discussed as it applies to identification of components, determination of lattice constants, and estimation of crystallite and particle sizes. Examples of applications are given, and techniques are briefly outlined.

The book has good subject and author indexes.

K. A. Krieger
University of Pennsylvania

Introduction to Statistical Mechanics

By G. S. Rushbrooke. Pp. 334+xiii, Figs. 47. Oxford University Press, London, 1949. Price $5.50.

The aim of this book is to provide the student of physical chemistry with a working knowledge of the basic formalism of statistical mechanics. By using the device of proving certain theorems only for special cases and bridging gaps by lucid plausibility arguments, a surprisingly wide ground is covered with a modest mathematical equipment.

The first method used is essentially Boltzmann's, in which the number of complexions is maximized. The discussion of assemblies of localized and non-localized systems demonstrates the procedure. The first one leads to the Einstein model of a solid consisting of independent oscillators, the second to the theory of the perfect Boltzmann gas.

The counting of microstates is carried out from the point of view of quantum mechanics. This is considerably simpler than the approach from the classical phase space. The latter is introduced, however, as a limiting case of the quantum treatment.

On the other hand, the case of ideal quantum gases (Fermi-Dirac and Bose-Einstein statistics) is mentioned only cursorily.

The results obtained up to this point provide the opportunity for a wealth of applications: The specific heat of diatomic and polyatomic gases including a chapter on ortho- and parahydrogen, a discussion of Nernst's heat theorem, dielectric constant of polar and non-polar gases, mixtures of gases, the law of mass action and phase equilibria of one- and two-component systems.

The discussion of Nernst's theorem in the literature is frequently characterized by objectionable overstatements. In trying to avoid this mistake the author gives a very careful discussion of the question of zero-point entropy but finally rather understates the importance of Nernst's law. We read on p. 145: "Applied to a single substance it (Nernst's law) has no meaning. We exclude from consideration here changes in the environment of the assembly, due, for instance, to changing an external magnetic field." It seems somewhat misleading to state that a law has no meaning if one arbitrarily ignores the conditions under which it has one. Still in the same context it is hard to concur with the statement on p. 139: "In practice, measurement of the specific heat may be made, calorimetrically . . . down to, perhaps, 10°K, but thereafter measurements become impracticable." Actually, extensive calorimetric studies have been carried out in the liquid helium range and at magnetic temperatures down to a few thousands of a degree and the Debye extrapolation is hardly the only means of gaining information on the low temperature entropies.

In the above-mentioned discussion on phase equilibria, the relevant thermodynamic conditions of equilibrium are always derived from purely statistical considerations. This leads to a certain amount of redundency compared to a combined use of thermodynamic and statistical methods. Whether or not this is justified by a better insight into the phenomena is largely a matter of opinion.

The last part of the book deals with the explanation of the methods of canonical and grand canonical partition functions and their application to such difficult problems as the Ursell-Mayer theory of imperfect gases and the theory of regular, but non-perfect, solutions including order-disorder transformations. In the latter problem particularly Guggenheim's method is followed. In view of the elementary nature of the book, the ample application of the powerful grand canonical method must be considered most remarkable.

The reviewer feels that a short discussion of fluctuations would have been appropriate and would have helped to give a physical basis for the transition from the microcanonical to the canonical method.

The usefulness of the book is increased by problems and examples following the majority of chapters. Mathematical and thermodynamic formulas are derived in Appendices.

The book is a most welcome addition to the literature of statistical mechanics on an intermediate level.

L. Tisza
Massachusetts Institute of Technology

Engineering Optics—The Principles of Optical Methods in Engineering Measurement

By K. J. Habell and Parker Cox. Pp. 411+xiv, Figs. 182. Pitman Publishing Corporation, New York, 1948. Price $7.50.

The subject matter of this book is described more accurately by the second part of the title than by the first. In the United States particularly the term engineering optics has come to have a broader meaning than optical methods in engineering measurement.

The first chapter deals with the fundamental properties of optical systems, laws of image formation and the like, without consideration of lens defects. The second chapter gives a brief but fairly adequate treatment of the principal aberrations of lenses together with the influence of diffraction in limiting the performance of an optical system. This is followed by a short section on the eye and its performance which is brief, but of far better quality than usually encountered in a book of this sort. Chapters three through six deal with light sources and the optical instruments of particular interest in engineering measurement, including microscopes, telescopes, and optical projection systems. Chapters seven and eight deal with profile measuring systems and miscellaneous optical methods including interferometers. The last chapter of the book considers briefly certain construction features of optical parts and their mounts.

Within its scope the work is well planned and executed. Although many of the descriptions tend to omit important details (perhaps for the sake of brevity), they are in the main clear and accompanied by excellent diagrammatic illustrations. One could wish that certain sections had been expanded, particularly that on interferometry, but in the main the relative space devoted to the several portions of the subject appears a good compromise. The work is a contribution to the subject of optics, and should prove of particular value to one who wishes to apply some of the very powerful methods of optics to problems of engineering measurement.

Brian O'Brien
University of Rochester

Electric Resistance Strain Gauges

By W. B. Dobie and Peter G. Isaac. Pp. 114+xiv, Figs. 89. MacMillan Company, Ltd., London, 1949. Price $3.50.

This fine work by two British authors is in quintessence a handbook devoted in its entirety to the tools for experimental stress analysis. The text is rudimental but the student and engineer will never the less find it extremely useful, for in its hundred odd pages it touches upon stress analysis, strain gauge techniques, electronics, and a smattering of brittle lacquer coating science. The references gathered throughout the book are outstanding and do much in making this book a fine reference source.

The introduction credits Lord Kelvin with the metal wire strain-resistance relationship upon which the entire electrical resistance strain gauge theory is based.

Chapter One, "Guage Characteristics," derives the strain gauge sensitivity factor and the cross sensitivity factor. Considerable emphasis is placed on the technique and the "do's" and "don't's" one should rigorously follow in applying the strain gauge. An itemized table is included disclosing American and British gauges available on the market and the characteristics of each. Some space is given to gauge stability and the effects of high temperature on gauge sensitivity.

Chapter Two, "The Determination of Static Strains," interjects the common Wheatstone bridge and the deviation thereof. Bridge circuits of the series, slide wire, and shunt balancing are shown in detail. The Kelvin form of bridge is derived and although extremely sensitive the authors point out that it is expensive to set up. There is a dissertation on temperature compensation, however the authors refrained, until Chapter three under "Gauge Arrangements," from mentioning the full bridge, which on a bending beam is fully temperature-compensated besides having twice the sensitivity of a single gauge and dummy combination. Another scheme not mentioned in the text is mounting the temperature gauges at right angles to the measuring gauge on the specimen under observation, which automatically compensates for temperature and makes use of Poisson's ratio to give greater sensitivity.

In Chapter Three, "The Fundamentals of Stress Analysis," the authors attempt to give a rather comprehensive outline of elementary tensile, compressive and shear stress and strains. Full derivations are given for complex stresses, ellipse of stress, principal stresses, and Mohr's stress circle. The method for analytical determination of principal stresses and strains for use in stress analysis from experimental results is well executed. Such equations can be utilized in the determination of stress from equilateral and rectangular rosettes. A small section is devoted to gauge arrangements for determination of direct tension or compression, bending, shear and torque.

Chapter Four, "Elementary Electronics," an excellent chapter, touches on cathode-ray oscilloscopes, their fluorescent screen focusing arrangements, and timing circuits; galvanometer oscillographs, their limitations, and the construction of the galvanometer. A very unique discussion of amplifiers, oscillators, and rectifiers gives a rather complete picture of the operation of the electron tube and circuits.

Chapter Five, "Electronic Bridge Circuits," is a carefully written presentation offering highlights of the d.c. bridge and modulator, the carrier wave as it is applied to a.c. circuits, and the common Maxwell's impedance bridge, a modified Wheatstone bridge to determine individual capacitance or resistance. The chapter describes two strain gauge instruments made in the United States for Baldwin-Southwark by the Foxboro Company.

Chapter Six, "Problems in Measuring Dynamic Strain," is concerned with calibrating the apparatus electrically by inserting a known resistance change in the circuit, or by mechanical means such as deflecting a beam a predetermined amount. There is a discussion involving materials used in slip rings and brushes and the effect of their position in the bridge circuit.

Chapter Seven, "Applications of Strain Gauges," some of the uses mentioned; measuring residual stresses trapped inside materials during manufacturing processes such as heat treating, forging, etc. The complicated problem of measuring torque in a shaft is quite easily accomplished with the strain gauge. Measurement of the loads in ships upon launching has been successfully accomplished by the use of strain gauge accelerometers and portable weighting cells for aircraft use, pressure indicators, reinforced concrete measurements, flight test of aircraft, are but a few of the more obvious applications.

Chapter Eight, "Brittle Lacquer Method of Stress Estimation," is a brief resume of the application of brittle lacquer, its uses, limitations, and calibrations.

G. L. Rogers
McDonnell Aircraft Corporation

Constructive Uses of Atomic Energy

Edited By S. C. Rothmann. Pp. 258+ix, Figs. and halftones 48. Harper & Brothers, New York, 1949. Price $3.00.

Fourteen essays on the constructive uses of atomic energy are presented for the interested layman who still wonders whether atomic research is good for anything but to make bombs. These essays are for the most part reprints of papers written for various professional journals, and the array is impressive by reason of the diversity of fields represented: aeronautics, industry, chemical engineering, metallurgy, ceramics, soil research, biology, medicine, and pharmacy.

The series opens with a contribution by Arthur H. Compton on "Atomic Energy as a Human Asset," based upon a paper read in 1945 before the American Philosophical Society at a time when the future of the new atomic age was rosy. This great force was to make men demonstrate greater humanity (perforce). Now, after four years, the need is still there. Next, an elementary exposition of atomic structure is given by L. W. Chubb, and there follow twelve other essays on applications of tracer techniques and atomic radiations to various fields. These essays differ greatly in value and effectiveness. Some exhibit a high degree of analytical thought in which optimism is kept firmly in check by a critical review of the state of the art at the present time. Some authors admit frank skepticism, even pessimism, about the value of the new tools in their fields. Now and then, one can detect the presence of *bullonium* as a contaminant, but fortunately this defect does not dominate the book. On the whole, conjecture is kept under cautious control. That the by-products of the atomic pile have made available large supplies of inexpensive radioactive elements, that these can be used for investigations with tracer techniques, that there are dangers inherent in their use and that experimenters must exercise caution, that there are possibilities for power from atomic energy, and that there is promise of important advances in all fields—such conclusions are not surprising to any intelligent person in these days. However, this group of articles points out somewhat more specifically the limitations of these promises as of the present time.

Your reviewer found most interesting some of those chapters dealing with fields on the borderline of physics in which the details of experimental researches and findings opened to him new vistas and showed the manner in which tracer elements have been employed in such fields as medicine, metallurgy, and soil research. The chapter on "Atomic Energy for Aircraft," by Andrew Kalitinsky, was enlightening and provocative. Anyone who, within this lifetime, expects to have his private plane with plutonium-driven motor may be disappointed to read the analysis which the writer gives to this subject. The chapter by Blau and Carlin on "Industrial Applications of Radioactivity" was stimulating to the imagination with its numerous smart applications of radioactive materials to problems of control. The economics and feasibility of atomic power are discussed by H. Etherington.

At the end of the book there is an Appendix containing a brief chronological list of significant events in the development of atomic energy, a glossary of terms for the uninitiated, and a bibliography of 323 articles on atomic energy. A breakdown of this bibliography shows that the papers are selected from the publications of the Atomic Energy Commission (31), *Chemical and Engineering News* (12), *Nucleonics* (11), and the *Bulletin of Atomic Scientists* (9), with a scattering from 120 other publications, not including the *Physical Review* but including *Coronet*, *Colliers*, and *Popular Science*.

The book gives a good sampling of the fields of human endeavor that are now being touched by the possibilities of radioactive isotopes as a tool for research. It shows where progress has already been made, where lack of promise is apparent, and (as might be expected) how much work remains to be done before the promise of atomic energy as a constructive element in our civilization can be fully realized.

In the meantime, we still have the atomic bomb! What to do about?

Richard M. Sutton
Haverford College

Elektrische Messgeräte und Messeinrichtungen

By A. Palm. Pp. 284, Figs. 232. Verlag. Julius Springer, Berlin, 1948.

This book presents a very complete summary of electrical apparatus used in physical measurements. Since the book is of modest size the material is necessarily mostly descriptive. But adequate references to more detailed treatments are given throughout the text.

The book is divided into two parts of which the first is devoted to a description of electrical meters and the second to other electrical instruments and devices. The scope of the material presented is easily seen from the Table of Contents: Part I (Electrical Meters): Moving Coil Meters, Meters with Crossed Coils, Moving Magnet Meters, Moving Iron Meters, Watt Meters, Meters using Electromagnetic Induction, Hot Wire Meters, Electrostatic Meters, Vibration Type Meters, Relays, Recording Meters, Electricity Meters, Series and Shunt Resistances, Transformers, Summary of Characteristics of Electrical Meters. Part II (Electrical Instruments and Other Devices): Precision Resistors, Inductors and Capacitors, Bridges, Compensating Newtorks, Vacuum Tube Instruments, High Voltage Meters, Ohm Meters, Temperature Meters, Telemetering Systems, Miscellaneous Meters (Piezoelectric Pressure Indicator, Illumination Meter, Liquid Level Indicator, Gas Concentration Meter).

In the foreword to the book the author mentions that much of the recent foreign literature was not available to him. This probably explains why only one chapter is concerned with vacuum tube instruments, whereas nowadays vacuum tubes can be found in most electrical measuring instruments. Similarly much recent work done on telemetering systems is not mentioned in the text.

On the other hand especially the first part of the book is written with care and the book is worth while reading for anybody who would like to familiarize himself with the construction and operation of electrical meters and other instruments which were in use before the last war.

W. E. Meyerhof
Stanford University

Theory of Dielectrics

By H. Frölich. Pp. 179+vi, Figs. 47. The Clarendon Press, Oxford, 1949. Price $4.50.

The book is intended to give a systematic account of the theory of dielectric constant and of dielectric loss. The treatment, based on classical statistical mechanics, is rigorous and methodical. Controversies on the subject which have left it until recent years in the literature are analyzed and clarified in the light of modern investigations by Van Vleck, Onsager, Kirkwood, and the author himself.

The book begins with an exposition of the properties of the electrostatic field in dielectric media and of the thermodynamics of systems in external electric fields. The theory of the static dielectric constant is then treated in detail on the basis of certain general theorems developed by the author, from which the Onsager-Kirkwood theory of polar dielectrics is deduced as a special case. A critical discussion of the Clausius-Mossotti formula is presented from the macroscopic and the microscopic points of view. The limitations of the microscopic formula are discussed in the light of the work of Van Vleck and Kirkwood.

Anomalous dispersion and dielectric loss are treated from the standpoint of the Debye equations with a single relaxation time. Models for the Debye equations are discussed and generalizations are considered. In the final chapter the relationship between structure and dielectric properties is treated in detail, both for non-polar and polar substances. The dielectric behavior of dipolar substances in the gaseous state, in dilute solution, and in the liquid and solid state is reviewed. The book concludes with a discussion of ionic crystals.

The book can be recommended without reserve, not only to specialists in the field of dielectrics but also to all physicists, chemists, and applied scientists who wish to gain a clear and comprehensive grasp of this important field.

John G. Kirkwood
California Institute of Technology

Principles of Electricity and Electromagnetism

By Gaylord P. Harnwell. Second Edition. Pp. 670+xvi, Figs. 398, 16×23½ cm. McGraw-Hill Book Company, Inc., New York. Price $6.00.

Harnwell's book is an important book. Its roots lie right in the laboratory, its approach is modern, it is remarkably up-to-date in the choice of material, and it is written with vigor. It covers a great variety of topics in electricity and magnetism, all of them topics that every physics student today must somehow find the time to learn. This book should help to convince the budding experimentalist that certain equations, obstruse as they may seem at first sight, are not just frills but are essential for the understanding of electromagnetism. In the case of a theoretically inclined reader, this book should help to put across the idea that physics is made in the laboratory. I am sure that, both directly as a student's textbook and indirectly as an instructor's reference book, Harnwell's book has during the past ten years done a great deal toward making college courses in electricity and magnetism more interesting and more vital. With the appearance of the second edition, this important influence of Harnwell's book should become even more widespread.

The breadth of scope of Harnwell's book is shown by the chapter headings: Electrostatics (44 pages in the first edition, now 47 pages); Electrostatic Energy and Dielectrics (31 pages, now 34); Physical Characteristics of Dielectrics and Conductors (27 pages, now 29); Direct-Current Circuits (32 pages, now 34); Non-ohmic Circuit Elements and Alternating Currents (30 pages, now 36); Chemical, Thermal and Photoelectric Effects (33 pages, now 39); Thermionic Vacuum Tubes (38 pages, now 40); Electrical Conduction in Gases (35 pages); Electromagnetic Effects of Steady Currents (34 pages, now 37); Changing Electric Currents and Electromagnetic Reactions (34 pages, now 42); Magnetic Properties of Matter (41 pages, now 43); Electromagnetic Machinery (37 pages); Simple Circuits Containing Inductance, Capacitance and Resistance (35 pages); Coupled Circuits, Filters and Lines (37 pages); Vacuum Tube Circuits (38 pages, now 43); Radiation (46 pages, now 55); Mathematical Appendix (30 pages). The number of problems, most of which are of the more substantial sort, has risen from 381 in the first edition to 431 in the second. The text has been rewritten in a large number of places. The most important new topics added in the second edition are electron structure of crystals (including a brief description of the P-type and N-type semiconductors), magnetic induction accelerators, nuclear induction, very high frequency oscillators, and the propagation of electromagnetic waves in metallic enclosures.

The imposing list of chapter headings given above points up the fact that Harnwell's book is not only a comprehensive textbook, but also a valuable reference book for practicing physicists as well as for the growing group of electrical engineers whose work borders upon physics. This is especially so because, for a book written primarily as an orderly presentation of electromagnetism, this book lends itself unusually well to looking up individual bits of information. Also, one will find here thorough accounts of several important topics that are often slighted in books written primarily for physicists—one example is the excellent discussion of circuit theory. A most important feature of the author's style is that he somehow makes what he writes about especially interesting—as one turns the pages of this book, the various topics not only develop in a logical sequence, but also come to life.

Harnwell's book cuts across the lines of the usual undergraduate physics courses, such as the "E. & M." course, the electronics course, and the atomic physics course; its plan thus serves to emphasize the interdependence of the ideas involved in these branches of physics, and to tie them up with experimental techniques. This very fact would ordinarily make it difficult to fit Harnwell's book into the undergraduate program of a physics major; but I believe that, whether or not this book is used as a text in any of his courses, a student majoring in physics will do well to get a copy of "Harnwell" for his bookshelf—it should prove useful to him for many years to come.

My few criticisms of this book are minor and rather subjective. The equations are not punctuated; in my opinion this fact makes it harder to grasp the organization of the mathematical arguments and is therefore regrettable. The symbols grad and curl are printed **grad** and **curl**, in order to emphasize the fact that they stand for vector fields; to my mind this practice mars the appearance of the printed page to such an extent as to outweigh the small advantage that it may offer to a reader who is at all prepared to read a book as advanced as this book (strictly speaking, the symbol $\mathbf{A}$ for a vector is needed only because the symbol A is needed for another purpose). Volume density of charge is denoted by q_v and current density by $\mathbf{i}_v$; I think that, while in the case of q_v the subscript v suggests the correct units, it suggests incorrect units in the case of $\mathbf{i}_v$. (Some of the sentences in the book are too long; but since more than one sentence in this review has over 50 words, I am making this comment only parenthetically!)

By writing this book and by preparing ten years later this second edition, Professor Harnwell has done an important service to physics; he is to be congratulated heartily.

V. Rojansky
Union College

Our Sun

By Donald H. Menzel. Pp. 326+viii, Figs. 178. The Blakiston Company, Philadelphia, 1949. Price $4.50.

With the exception of the English translation of Abetti's book on the sun in 1937 there has been no new book on this subject for too long a time. The only place where one could look for new developments in the field of solar research was in the literature which though not too unpleasant is a time consuming task. Now a book of this type has appeared as the final number in the Harvard books on astronomy series. Delayed by the war the book has been enhanced by incorporating the war researches done by solar observatories under the sponsorship of the United States Navy. The author is Dr. Donald H. Menzel, Professor of Astrophysics at Harvard College, a recognized leader in the field of solar research.

It is rather curious that books on the sun are so rare. Of the 100,000 million stars in our galaxy there is only one whose surface can be studied in detail and that is the sun. In a sense the sun is the only cosmic laboratory where stellar theories can be formulated and tested for validity.

Since 1937 our knowledge of the sun has expanded through the introduction of powerful research tools like the spectroheliokinematograph, the coronagraph, and the skillful use of electronics in the fabrication of monochromatic filters and the use of electronics as operating and guiding aids. As a result there is found in the literature an enormous amount of detail about the sun which is difficult to trace. This book obviates the necessity of using many references in solar study.

In the planning of the book, Dr. Menzel seems to have pursued a definite pattern. He has glossed over some of the details of sunspots such as their distribution, use in the determination of the solar rotation, temperatures, law of polarity, proper motion, and other features in comparatively few pages. The above information is static and may be found in most textbooks on astronomy. He has reserved the book for the elements of new interest such as the newer theories for the formation of sunspots; the motion, classification and structure of prominences; and he has dealt in detail with the mystery of the solar corona a puzzling feature where the ionization of some of the atoms indicate a temperature in excess of a million degrees yet the photosphere has a temperature of but 6000 degrees. He has discussed the source of the sun's energy in terms of nuclear reaction. He has developed the interrelation of solar phenomena with short wave radio communication, to geophysics of the upper atmosphere and to meteorology. These subjects are fresh, dynamic, and in this reviewer's opinion the author is a dominant figure in this field and knows of no one better qualified to write about them.

Dr. Menzel has been very clever in his choice of analogies to strike home the essential features of a presentation. His comparison of atoms with radio transmitters and the development of this idea is striking in its impact as a device for interpretation. The effectiveness of a good writer lies in his ability to translate from the abstruse to the level of the general reader. Dr. Menzel has developed this skill to a high degree.

The addition of a table of eclipses for the 20th century is a welcome addition and at least for this reviewer it will relegate Oppolzer to the library.

There is one disturbing feature of the book and that is the rather high price. The Harvard series were originally published to sell for $2.50 and now for the same size book the cost has practically doubled. This increase in price simply means that it has been priced out of the range of some people who would want a copy. By careful examination of the book it seemed possible that the cost of the book could be cut by a decrease in the number of illustrations and a subsequent decrease in the number of pages. For instance, in *Our Sun* there are 19 photographs on the solar corona. Many of these could be eliminated without detracting in any way from the excellence of the book. As an example, in Dyson and Woolley's book *Eclipses of the Sun and Moon* there are four coronal illustrations. In this book there seems to be no justification for more than eight or nine. Further, the illustrations and tables tend to cover the larger part of a page or an entire page. It is this procedure which has helped make the cost of the book rise sharply. It is hoped that in the second edition these features will be closely examined to see whether a reduction in the cost of the book is a possibility.

Our Sun compares most favorably with the other books in the Harvard series. It is an invaluable source of up-to-the-minute solar information and it is highly recommended as an excellent addition to the library of both the astronomer and the general reader.

I. M. Levitt,
The Fels Planetarium of The Franklin Institute

Experimental Physics for Colleges

By Walter A. Schneider and Lloyd B. Ham. Pp. 411+xiv, Figs. 182. The Macmillan Company, New York, 1949. Price $3.80.

Experimental Physics for Colleges is a revision of a book first published in 1932. With the experiences gained and with opportunities provided for trying out many new experiments in the interim, the original text has undergone considerable change.

This book, while it is supposed to be used as a laboratory text with any general college physics text seems to be almost a general text in itself as well as a laboratory text. There are seven parts to the book including Units and Measurements, Mechanics, Sound, Heat, Electricity, Light, and Notes and Tables. Each part is divided into chapters making 33 in all and the chapters are divided into a total of 56 experiments plus four optional ones.

A chapter consists of experiments dealing with a common idea, includes a clear explanation of the general theory of the idea, and good directions for the specific experiments. Chapter XXI, Measurement of Resistance and Simple Circuits, for example has eight pages of theory and three experiments-measurement of the resistance of resistors in series and parallel by the ammeter-voltmeter method, Kirchhoff's laws, and measurement of resistance with a slide wire Wheatstone bridge.

The authors have written the book in such a simplified and explicit fashion that most students should be able to study the majority of the theory and experiments themselves, and be ready to go to work upon entering the laboratory. The experiments are designed for at least a two-hour experimental period. In the early chapters sample data are given and tabular forms suggested, but as the experiments progress the student is left more to his own ingenuity.

All the chapters include problems and questions for each experiment. The problems may be worked out by the students in preparing for laboratory but the questions are such that they must be answered after doing the particular experiment.

An idea the authors kept in mind was the use of inexpensive equipment as much as possible so that a laboratory without too large a budget could use the even front procedure. Good examples of this idea may be found in the experiments dealing with centrifugal force, impedance, and index of refraction. In the case of impedance instead of recommending a commercial piece of apparatus, the authors suggest using an inductor wound with No. 16 wire, a capacitor of about 10 microfarads, and a lamp of about 100 ohms. Then in the case of index of refraction, instead of requiring an expensive refractometer, the basic piece needed is a semicircular disk of glass.

Valuable suggestions are offered from time to time throughout the book such as the difference between totally and partially immersed thermometers, how to reason out certain equations rather than just memorizing them, and formulas for cleansing solutions.

The text concludes with notes on useful instruments and procedures, and the usual tables necessary for carrying out experiments in elementary college physics. The notes are especially good. Here can be found bits of information which can be of much help to the student. For example, one set of notes explains the differences between double beam trip scales, ordinary triple beam trip scales, and the better triple beam trip scales used for determination of specific gravity.

Experimental Physics for Colleges deserves careful consideration by anyone looking for a laboratory text for elementary physics. Part one may be a little disappointing but after that the book is interesting, clear, and challenging. A picture of a *fine balance* (analytical balance) might have been included in part one and the theory of the vernier could perhaps be improved.

ROBERT N. JONES
Philadelphia College of Pharmacy and Science

Industrial Rheology and Rheological Structures

BY HENRY GREEN. Pp. 311, Figs. 76. John Wiley and Sons, Inc., New York, 1949. Price $5.50.

This excellent rheological guide will be of decided interest and value to the experienced industrial rheologist and should also provide outstanding assistance and stimulation for the perplexed novitiate in the confused but important field of industrial rheology.

The book is divided into four parts entitled, respectively, "A Rheological System", "The System Applied to Laboratory Measurements", "The Particle—the Basis of Rheological Structure", and "Particle Groups Rheological Structures."

In the first seven chapters constituting Part 1, it is convincingly demonstrated that the position of the proponents of single point so-called "viscosity" determinations is absolutely indefensible, and that complete rheological diagrams must be established for non-Newtonian materials to provide the necessary information to define the system under examination. Anything less is not only useless but frequently is dangerously misleading. The author progressively leads the reader from Newton through Bingham, Buckingham and Reiner, and Rivlin, to his own contributions and those of his associates, based upon microscopic observations in combination with rotational viscometer determinations, particularly on thixotropic materials. The theoretical background, explanation of fundamentals, definition of various and sometimes confusing rheological concepts and nomenclature such as yield value, plastic viscosity, thixotropy, dilatancy, psuedoplasticity, and the like, and descriptions of previously suggested systems, are all extremely well presented.

In Part 2, Chapters 8 to 11, are given detailed information on the rotational and parallel plate viscometers, and instructions, with detailed examples on their use. Other types of viscometers frequently encountered in industrial laboratories are also briefly described.

In Part 3, Chapters 12 to 16, the value of the microscope in studying crowded particle systems is maintained and demonstrated. Definite rules are suggested in connection with detectability, size, shape, preparation of mounts, and finally precautions on the use of the electron microscope.

Part 4, Chapters 17 and 18, contains a tabular summary and discussion of discontinuous and connected structures, together with descriptions and comments on various classes of rheological materials.

Appendices, references, and author and subject indices complete this worth-while work. This book is recommended to all interested in industrial rheology from either the control or the research point of view.

W. F. FAIR, JR.
Koppers Company, Inc.

Author Index to Books Reviewed

Cox, Parker—see Habell, K. J. 88

Dobie, W. B. and Peter G. Isaac. *Electric Resistance Strain Gauges* 88

Frankenburg, W. G., V. I. Komarewsky, and E. K. Rideal. *Advances in Catalysis and Related Subjects, Vol. I* 87
Friedlander, Gerhart and Joseph Kennedy. *Introduction to Radiochemistry* 85
Frölich, H. *Theory of Dielectrics* 90

Green, Henry. *Industrial Rheology and Rheological Structures* 92
Gutenberg, B. and C. F. Richter. *Seismicity of the Earth* 87

Habell, K. J. and Parker Cox. *Engineering Optics—The Principles of Optical Methods in Engineering Measurement* 88
Ham, Lloyd B.—see Schneider, Walter A. 91
Harnwell, Gaylord P. *Principles of Electricity and Electromagnetism* 90

Isaac, Peter G.—see Dobie, W. B. 88

Kennedy, Joseph—see Friedlander, Gerhart 85
Komarewsky, V. I.—see Frankenburg, W. G. 87

Lang, Ruth. *Laboratory and Workshop Notes* 86

Menzel, Donald H. *Our Sun* 91
Moore, Charlotte E. *Atomic Energy Levels. Vol. I,* $^{1}H-{}^{23}V$ 85

O'Hara, Charles E. and James W. Osterburg. *An Introduction to Criminalistics* 85
Osterburg, James W.—see O'Hara, Charles E. 85

Palm, A. *Elektrische Messgeräte und Messeinrichtungen* 90

Richter, C. F.—see Gutenberg, B. 87
Rideal, E. K.—see Frankenburg, W. G. 87
Rothmann, S. C. *Constructive Uses of Atomic Energy* 89
Rushbrooke, G. S. *Introduction to Statistical Mechanics* 88

Schneider, Walter A., and Lloyd B. Ham. *Experimental Physics for Colleges* 91
Siri, William E. *Isotopic Tracers and Nuclear Radiations with Applications to Biology and Medicine* 86

Other Books Received

Practical Spectroscopy. C. Candler. Pp. 190+iv, Illustrations over 100. Hilger and Watts, Ltd., London, 1949. Price $6.10.

Elementary Modern Physics. Gordon Ferrie Hull. Pp. 503+xvi, Figs. 243. The Macmillan Company, New York, 1949. Price $5.25.

Infrared Determination of Organic Structures. H. M. Randall, R. G. Fowler, N. Fusion, and J. R. Dangl. Pp. 239+v, profusely illustrated. D. Van Nostrand Company, Inc., New York, 1949. Price $10.00.

Ionization Chambers and Counters. B. B. Rossi and H. H. Staub. Pp. 243+xviii, Figs. 113. McGraw-Hill Book Company, Inc., New York, 1949. Price $2.25.

Elements of Sound Recording. J. G. Frayne and H. Wolfe. Pp. 686+vii, Numerous figures. John Wiley and Sons, Inc., New York, 1949. Price $8.50.

Theory of Oscillations. A. A. Andronow and C. E. Chaikin. Pp. 358+ix, Figs. 313, Princeton University Press, Princeton, New Jersey, 1949. Price $6.00.

Acoustic Measurements. L. L. Beranek. Pp. 1914+vii, Figs. 519. John Wiley and Sons, Inc., New York, 1949. Price. $7.00.

Spectroscopic Properties of Uranium Compounds. G. H. Dieke and A. B. F. Duncan. Pp. 290+xvii. McGraw-Hill Book Company, Inc., New York, 1949. Price $2.75.

Luminescent Materials. G. F. J. Garlick. Pp. 254+viii, Figs. 127. Oxford University Press, New York, 1949. Price $5.50.

Two Lectures. W. Heisenberg. Pp. 51. Cambridge University Press, New York, 1949. Price $1.00.

Crystals and X-Rays. K. Lonsdale. Pp. 199+viii, Figs. 138. D. Van Nostrand Company, Inc., New York, 1949. Price $3.75.

Electrical Engineers' Handbook of Electric Power, Vol. 1. H. Pender and W. A. Del Mar. 1949. Price $8.50.

Theory and Design of Electron Beams. J. R. Pierce. Pp. 197+xii, Figs. 104. D. Van Nostrand Company, Inc., New York, 1949. Price $3.50.

Introduction to Theoretical and Experimental Optics. Joseph Valasek, Pp. 454+x, Figs. 211. John Wiley and Sons, Inc., New York, 1949. Price $6.50.

Laboratory and Shop Notes

Units of Radioactivity

L. F. Curtiss, R. D. Evans, Warren Johnson,
and Glenn T. Seaborg
National Research Council, Washington 25, D. C.

November 10, 1949

In November, 1947, a joint committee of the Divisions of Chemistry and Chemical Technology and of Mathematical and Physical Sciences of the National Research Council was appointed to make recommendations regarding standards and units of radioactivity. This committee unanimously adopted the recommendations quoted below. The committee would like to point out that these recommendations effectively divorce the curie from the disintegration rate of radium by assigning to the former an arbitrary magnitude (3.7×10^{10} dis./sec.) approximately equal to the disintegration rate of radium. This arbitrary figure is therefore not influenced by any future revisions of the generally accepted disintegration rate of radium. This recommendation has been submitted to the Joint Commission on Standards, Units, and Constants of Radioactivity of the International Unions of Chemistry and Physics for the purpose of obtaining international agreement.

This changes, slightly, the meaning of the curie when applied to radium. For example 1 curie of radon is no longer, on the basis of these recommendations, the amount in equilibrium with 1 gram of radium, but is the amount undergoing 3.7×10^{10} disintegrations per second. Similarly, 1 mg and 1 mc of radium are no longer rigorously synonomous. This distinction has a number of precedents in physics; for example the international ampere, now abolished, was not quite equal to the absolute ampere and the angstrom unit is nearly, but not quite, equal to 1000 x units.

> "*curie.*—The curie should be defined as that quantity of any radioactive species (radioisotope) undergoing exactly 3.700×10^{10} disintegrations per second.
>
> "*rutherford.*—The rutherford should be defined as that quantity of any radioactive species (radioisotope) undergoing 10^6 disintegrations per second.
>
> "*r.h.m.*—For the quantitative comparison of radioactive sources emitting gamma-rays, for which disintegration rates cannot be determined, the *roentgen per hour at one meter* (r.h.m.) is recommended. This is not essentially a new unit since all units involved are well established, explicitly defined, and are in common usage."

The recommendation of this latter unit is a practical step to insure that, by its use, gamma-ray measurements are so made with instruments and under such conditions that measurements on a given isotope (nuclear species) made in any laboratory will be directly comparable with similar measurements made in other laboratories. This will result, if the procedures used comply with the definition of the unit; that is, a source is 1 r.h.m. if it produces 1 roentgen per hour at a distance of 1 meter.

A Temperature-Controlled Resistance Furnace for High Temperature Measurements

W. G. Schneider and N. R. S. Hollies
National Research Council, Ottawa, Canada

August 1, 1949

Several temperature controllers for resistance furnaces have been described.[1-3] In these the temperature sensitive control element is either a thermocouple (or a resistance element) placed in the center of the furnace, or alternatively, the heating wire itself. The first of these methods is not sufficiently sensitive for larger furnaces due to the lag of the thermocouple (or resistance thermometer) in responding to small changes in heating current. The second method lacks stability, and hence also sensitivity, when operated from a power line with large voltage fluctuations. The present control system was developed for a furnace which was required to maintain a platinum gas pipet at a uniform temperature to within 0.05°C over a working temperature range from 600°C to 1200°C. The temperature control element is a small platinum resistance wire which is wound between turns and on the same core as the heavier heating wire. In this manner intimate thermal contact between the control element and the heating wire is achieved, resulting in a rapid response and a high degree of sensitivity to small changes in heating current. Stability in the control circuit is obtained by using a d.c. Wheatstone bridge fed from a 6-volt storage battery.

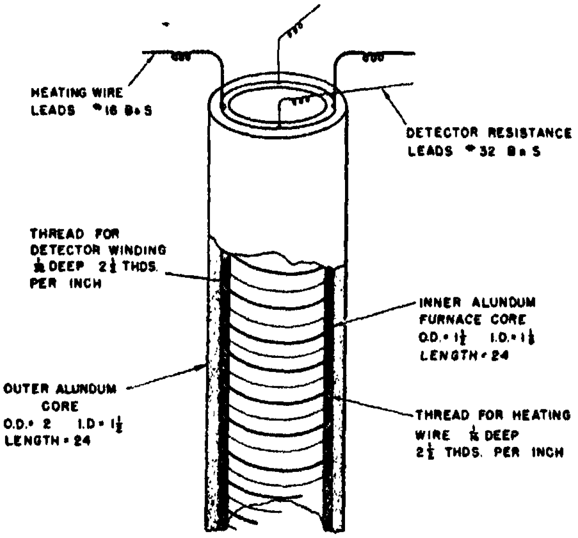
HEATING WIRE LEADS #16 B&S
DETECTOR RESISTANCE LEADS #32 B&S
THREAD FOR DETECTOR WINDING 1/32 DEEP 2½ THDS. PER INCH
INNER ALUNDUM FURNACE CORE O.D.=1½ I.D.=1⅛ LENGTH=24
OUTER ALUNDUM CORE O.D.=2 I.D.=1½ LENGTH=24
THREAD FOR HEATING WIRE 1/16 DEEP 2½ THDS. PER INCH

Fig. 1.

The assembly of the furnace core is illustrated in Fig. 1. It consists of two separate alundum* tubes which were specially selected free from warp and "kiln burn." The smaller tube with inside diameter 1⅛ in., wall thickness 3/16 in., and length 24 in., was ground down so that it fitted snugly inside the second and larger tube which had the same length and an inside diameter of 1½ in. and a ¼-in. wall thickness. To grind down the outer diameter of the smaller tube, the tube was fitted on a brass mandrel and waxed at both ends to prevent turning. Thus mounted the tube could be ground on a lathe using an ordinary grinding wheel and a stream of water flowing over the tube to catch the abrasive dust. After this operation four separate threads were cut on the inner tube, each with a pitch of 2½ threads per inch. Two of the threads, which were started 180° apart, were cut with an abrasive cut-off wheel† 1/16 in. in thickness, to a depth of 1/16 in. The remaining two threads were started at 90° and 270° and were cut with a wheel of 1/32 in. in thickness, to a depth of 1/32 in. The purpose of cutting the grooves in this manner was to allow for bifilar winding of both the heating wire and the resistance wire.

The heating wire consisted of 46 ft. of No. 16 B and S gauge platinum-10 percent rhodium wire, and the control resistance wire was a No. 32 pure platinum wire. The wires were wound on the tube while the latter was still held on a mandrel in the lathe, the heating wire being wound bifilarly in the 1/16-in. grooves, and the control wire in the 1/32-in. grooves. At room temperature the resistance of the heating wire measured 2.2 ohms and that of the control winding approximately 48 ohms. The wires were anchored at both ends by threading through small holes which were bored in the inner alundum tube with an ordinary high speed drill. After the wires were wound the tube was slid into the larger alundum tube.

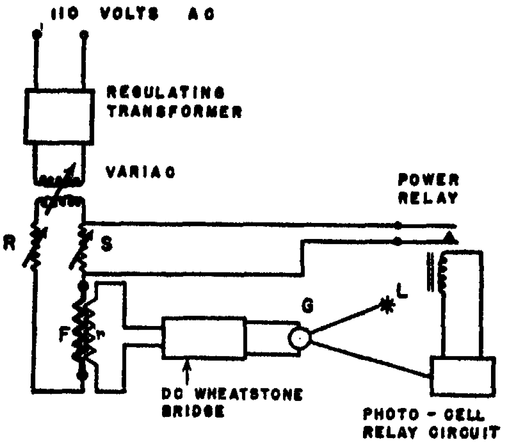

FIG. 2.

The latter served the double purpose of protecting the windings from impurities in the insulation material used around the core and of providing easy access to the furnace windings without disturbing the rest of the furnace assembly. Fitted cylindrical alundum bricks* were used on the ends of the furnace core and the whole assembly was surrounded with 4 in. of powdered aluminum oxide for insulation.

The heating and control circuit are shown schematically in Fig. 2. The furnace winding *F* is heated from a 110-volt a.c. line through a 3-kw Sola regulating trnsformer. A Variac and a variable one-ohm resistance *R* provide for adjusting the heating current of the furnace to a few degrees below the desired working temperature when the one-ohm variable shunt resistance *S* is in the circuit. The control resistance *r* completes a d.c. Wheatstone bridge circuit, the out-of-balance current of which is indicated by a sensitive mirror galvanometer *G*. The sensitivity is further increased by means of a 20-ft. optical lever on the galvanometer, which actuates a photo-cell relay circuit using an RCA No. 931A photo-multiplier tube. The relay circuit in turn operates a power relay which when closed shorts out the shunt resistance *S*. The latter, after the heating current has been properly adjusted and equilibrium reached, can be adjusted to a small fraction of an ohm to reduce the "on-off ripple" to a small value.

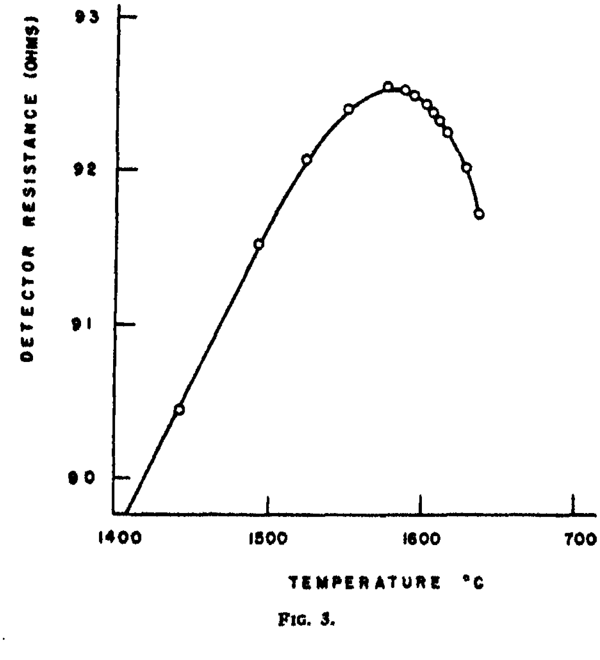

FIG. 3.

The temperature of the present furnace could be controlled at any temperature up to 1500°C. At temperatures above 1000°C the maximum ripple (as measured by a platinum, platinum-10 percent rhodium thermocouple in the center of the furnace) amounted to ±0.04°C and the average ±0.02°C. At lower temperatures the ripple was somewhat less. The resistance of the detector coil showed a slow but perceptible downward drift. For example, at 1000°C this amounted to approximately 0.2°C per hour, which was compensated for manually by adjusting the lowest resistance decade on the Wheatstone bridge. This drift is probably due to a slow recrystallization of the platinum wire. Above 1500°C an additional property of the platinum wire, shown in Fig. 3, was observed; the temperature coefficient of resistance of the detector winding (in this case a No. 28 platinum wire of "commercial" purity) became negligibly small around 1575°C and thereafter became negative. This behavior was also observed with a coil of No. 32 platinum wire procured from Johnson, Matthey, and Mallory Company and specified to be of "thermocouple purity." The coil was wound on a grooved alundum rod and supported in the center of the furnace. Accordingly the maximum temperature at which the control method described here could ordinarily be employed would appear to be approximately 1550°C. However there is a limited temperature range above 1600° in which the negative temperature coefficient of resistance could be utilized.

---

[1] H. S. Roberts, J. Opt. Soc. Am. 11, 171 (1925); see also *Temperature*, (Reinhold Publishing Corporation, New York, 1941), p. 604.

[2] R. F. Proctor and R. W. Douglas, J. Sci. Inst. 9, 192 (1932).

[3] R. M. Zabel and R. R. Hancox, Rev. Sci. Inst. 5, 28 (1934).

* Supplied by Norton Company, Worcester, Massachusetts.

† "37 Crystolon" abrasive cut-off wheels (Norton Company).

The Behavior of Rectangular and Square Section Transparent Beta-Counters

L. M. SILVER AND J. B. WARREN
Department of Physics, University of British Columbia, Vancouver, Canada

October 17, 1949

FOR some experiments it is necessary to use a Geiger counter through which beta-rays of moderately low energies may pass. Counters have been constructed as shown in Fig. 1, using rectangular section (1 in.×⅜ in.) and square section (⅞ in.×⅞ in.) brass tubing envelopes in the sides of which apertures up to 1 in.×⅜ in. have been milled and covered with mica windows. In this way with 2 mg/cm² windows the stopping power of the counter may be kept to 4 mg/cm² as compared to the 60 mg/sq. cm needed for a conventional cylindrical thin-walled glass counter with 30 mg/cm² wall thickness.

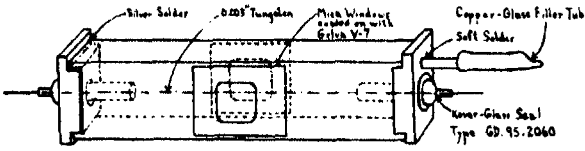
Silver Solder
0.005" Tungsten
Mica Windows sealed on with Glyptal V-7
Copper-Glass Filler Tube
Soft Solder
Kovar-Glass Seal Type GD.95.2060

FIG. 1.

The virtues, such as short dead time, of counters with rectangular envelopes as described by Curran and Reid,[1] have been substantiated. However, we have found that while square section envelopes give satisfactory Geiger operation over a range of 100 volts with plain mica windows ⅝ in.×⅝ in. and the usual argon/alcohol mixtures, it is necessary to make the inside surface of the mica conducting (with graphite or evaporated metal) when rectangular envelopes are used, since otherwise the central region of the counter behaves much as if the wire were beaded in the center.

Even when this precaution was taken with rectangular envelopes at the onset of the Geiger region over a range of 30 volts or so, two distinct size pulses were obtained, while if the counter was made with the windows placed asymmetrically, three pulse sizes were visible. In this last case it was possible to check that the two smaller sizes corresponded respectively to one or the other end of the counter discharging and the large size to those occasions when the discharge spread through the whole length of the counter.

Calculation showed that this failure of the discharge to spread at the start of the Geiger region and consequent lower efficiency in the window region can be explained by the reduction in the electrostatic field at the "critical" radius (taken as three times the wire radius) due to the small inevitable misalignment of the window with the inside surface of the envelope which, in this construction, amounted to less than $\frac{1}{32}$ in. Thus, for the maximum length plateau, it is preferable to use square section tubing. Rectangular envelope counters demonstrate clearly that it is important to avoid even small variations in the electrostatic field in the vicinity of the wire along its length.

We wish to thank the National Research Council of Canada for a grant and bursary held during the period in which this work was done.

[1] S. C. Curran and J. M. Reid, Rev. Sci. Inst. 19, 67 (1948).

A New Type Mass Spectrometer

Larkin Kerwin
Department of Physics, Laval University, Quebec, Canada

October 4, 1949

Of late a certain interest has been shown in improving the focusing properties of magnetic lenses. Bainbridge[1] has proposed the use of circular field boundaries to eliminate second-order aberrations, giving the radii which should be used, while Spighel[2] has also determined these radii. Hintenberger[3-5] has developed a more general theory which includes not only all circular fields, but also the "inflection" field developed in our own work.[6,7] In these latter papers is developed a theory which permits calculating the properties of lenses of any symmetric or assymetric shape, or conversely of designing a lens of any required order of focusing. The circular and inflection lenses are two of the several particular cases of this theory which appear to be of some practical value.

A mass spectrometer utilizing an inflection lens has recently been completed and tested in this laboratory. Although the mechanical appearance of the analyzing field is about the same as for conventional spectrometers, the use of the new focusing principle[5-7] has resulted in the achieving of third-order focusing. The appearance of the ion beam trajectory may be seen in Fig. 1. The shaded section represents the magnetic field of the available magnet, corrected for fringe effect.[8] The pole pieces constitute a magnetic sector of 90°, so that α is 45°. From Table I of reference 6, we see that a 90° magnetic sector may be used as a third-order inflection field if θ is made equal to about 30°. The geometric constants were calculated as follows.

From the given shape of the pole pieces, x was measured as 16.6 cm (corrected for fringe field effect). α was given as 45°. This angle must equal the slope of the ideal focusing boundary, which may be obtained by taking the derivative of Eq. (1).[6] Inserting the values of x and α given above and the relation between x, R, and a at the inflection point,[6] we find that $a = 51.8$ cm. Equation (7)[6] then permits us to calculate R, equal to 33.9 cm. Finally, from the relation $x = R \sin\theta$ we get $\theta = 29.3°$.

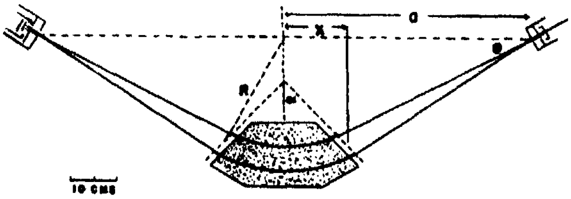

FIG. 1. Geometry of ion beam trajectory.

The magnet design resulted in a very compact instrument which is completely a.c. operated. The various circuits servicing the spectrometer are in the main similar to those described in the excellent paper by Thode, Graham, and Harkness.[9]

In operation, the spectrometer has a resolving power equal to that predicted by the third-order focusing theory, within the experimental error due to measurement of slit widths, etc. Second-order aberrations would thus appear to have been eliminated in practice. As pointed out previously, this advantage is used mainly to increase the beam intensity by increasing the beam divergence.

The magnet's field strength of 6000 gauss, ion beam trajectory radius of 33.9 cm and accelerating voltage of about 2000 volts permit the spectrometer to handle ions up to mass 800. The resolving power is set to the desired value by adjusting the slit widths.

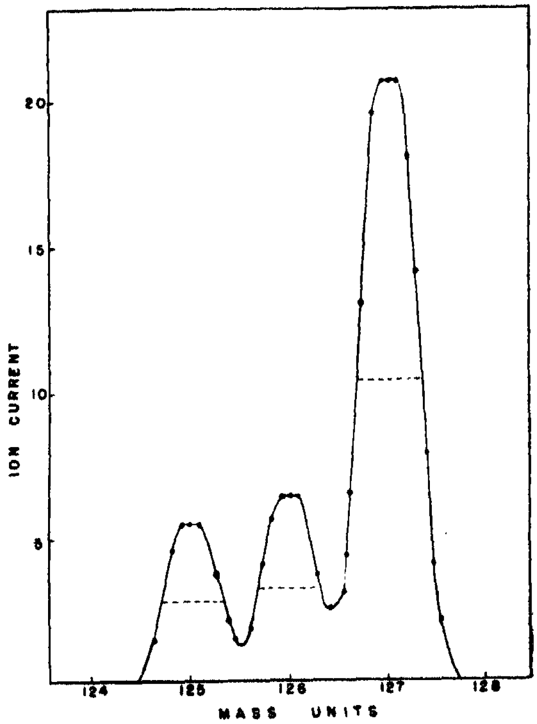

FIG. 2. Iodine peak in presence of naphthalene.

A typical spectrogram is shown in Fig. 2. For this run the slit widths were adjusted so as to give flat-topped peaks. (From the geometric constants of the spectrometer, Eq. (12)[6] enables us to calculate the dispersion per unit mass as equal to 1.8 mm at mass 126. The exit slit was made 1.4 mm wide, so as to be larger than the beam width. It can be shown that for a flat-topped peak, the width of the peak measured at half its height should equal the exit slit width. From the spectrogram, this width is measured to be about 1.3 mm. The beam width at the collecting slit was composed of the entrance slit image, the third-order aberration, and the velocity dispersion. The first is theoretically equal to the entrance slit width,[6] which was set at 0.3 mm. The second may be calculated from Eq. (9)[6] and for the beam spread of about 8° given here is equal to 0.2 mm. The velocity dispersion was set at 0.4 mm, permitting the use of wide electron ionizing beam to increase intensity. This gives a total image width of 0.9 mm. Since this is 0.5 mm smaller than the exit slit width, the flat top should be about 0.5 mm wide. From the spectrogram this is seen to be about 0.3

mm. Regardless of the shape of the ion peak due to intensity distribution, the width may be accurately calculated as being equal to twice the width at half-intensity (exit slit width) minus the top width. This method is often more accurate than direct measurement at the base, if the peak "tails" are difficult to measure. Theoretically this gives a total base width of 2.3 mm while the measured value is also 2.3 mm.

The resolving power for the inflection case may be calculated from the dispersion, aberration, and other image width components. It is given by:

$$RP=(2\times R)/(3\times W),$$

where R is the radius of curvature, and W the total apparent image width, including exit slit. In this case it should be about 96. Measurements on the spectrogram give a resolving power of 98, which thus verifies the prediction. These measurements are taken at half the peak heights. The usual practice of measuring peaks at the base, or of extending the peak sides to the base does not appear to be exact; due to the lack of knowledge concerning the exact intensity distribution in the ion beam, and consequent uncertainty regarding the shape of the curved tails on the peaks. These are often too small to be measureable, and it is this effect which causes some peaks to appear wider than others, although in the same mass vicinity they are the same size, could the exact extent of these tails be measured. Measurements at the apparent peak base, neglecting these tails, will give a higher resolving power than is theoretically obtained.

It is interesting to compare this type of spectrometer with one of the normal type. The same pole pieces used in the usual fashion would give a radius of curvature of only about 20 cm instead of about 34, and the magnet would have to be much heavier to supply the higher field necessary to bend the ion beams in this trajectory. The resolving power and intensity would have been correspondingly lower. A 90° sector normal instrument of the same resolving power and intensity would require a magnet of six times the weight.

It is to be noted that there is still room for improvement. In a recent paper[10] Geoffrion has shown how the optimum relationship between source height and width may be calculated for a 180° spectrometer. This technique may be extended to other instruments, such as this one.

The writer acknowledges with pleasure the encouragement of Professor Enrico Persico and Professor Paul Koenig during the construction of the spectrometer, as well as many fruitful discussions with his associate, Professor Claude Geoffrion. Skillful assistance was also generously given by Mr. Edward Leger of the Chemistry Department, and Mr. Robert Roy, Department Technician.

---

[1] K. T. Bainbridge, 7th Solvay Congress (1947).
[2] M. Spighel, J. de phys. et rad. 10, 207 (1949).
[3] H. Hintenberger, Zeits. f. Naturforschg. 3a, 125 (1948).
[4] H. Hintenberger, Zeits. f. Naturforschg. 3a, 669 (1948).
[5] H. Hintenberger, Rev. Sci. Inst. 20, 748 (1949).
[6] Lar[illegible] Kerwin, Rev. Sci. Inst. 20, 36 (1949).
[7] L. Kerwin and C. Geoffrion, Rev. Sci. Inst. 20, 381 (1949).
[8] Norman [illegible] Coggeshall, J. App. Phys. 18, 855 (1947).
[9] Thode, Harkness, and Graham, J. Sci. Inst. 24, 119 (1947).
[10] Claude Geoffrion, Rev. Sci. Inst. 20, 638 (1949).

An Improved Method of Directing Liquid Flow in a Closed System*

L. G. Stang, Jr. and G. J. Selvin
Brookhaven National Laboratory, Upton, New York

October 27, 1949

A REMOTELY operated closed system for chemical processing requires, if it is to be flexible, a device for directing the flow of liquid into any one of several lines. A manifold from which lead several lines each containing a stopcock or valve is not con-

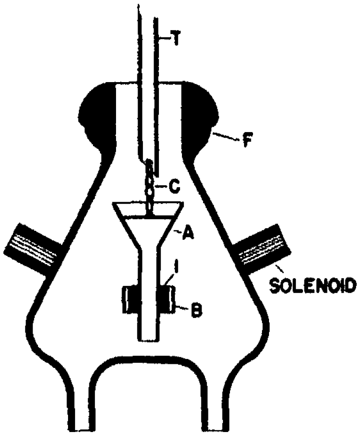

Fig. 1.

sidered appropriate for use with radioactive solutions for a variety of reasons: (1) Such a system invariably has some hold-up in it, and, as a rule, in handling radioactivity both total volumes and held-up volumes should be kept at a minimum. (2) Valves are usually made of metal and are, therefore, subject to corrosion and are sources of contamination. (3) Stopcocks, including even the so-called "No-Lube," require some grease which tends to adsorb activity from a solution. (4) Both stopcocks and valves require more maintenance than may be conveniently given them when they are part of an apparatus operated remotely from behind a concrete wall.

During the war, one of us (L. G. S.), in collaboration with D. Richardson and R. Ballard at Clinton Laboratories, Oak Ridge, Tennessee, solved this problem satisfactorily by constructing the all-glass "Magnetic Cow" shown in Fig. 1. This consists of a stationary flask, F, sealed into the system. Entering the top of the flask is a liquid-inlet tube, T, on the end of which is suspended a glass funnel, A, by means of a glass chain, C. Surrounding the stem of A is a soft iron cylinder, I, completely enclosed by a glass sheath over which is placed a plastic bumper, B. Around the periphery of the bottom of F are sealed any number of liquid-outlet tubes and against the outside of the flask in positions corresponding to the outlet tubes are placed solenoids, one for each outlet tube. By actuating the proper solenoid the funnel is inclined so as to divert liquid into any outlet. This device was quite successful and, with a little care in the design, could be made so as to give 100 percent diversion with no apparent splashing into other lines.

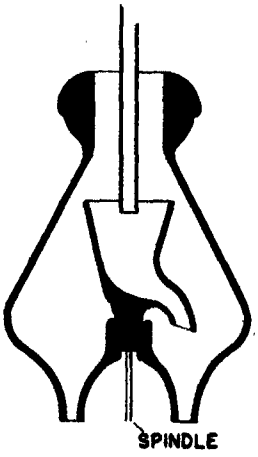

Fig. 2.

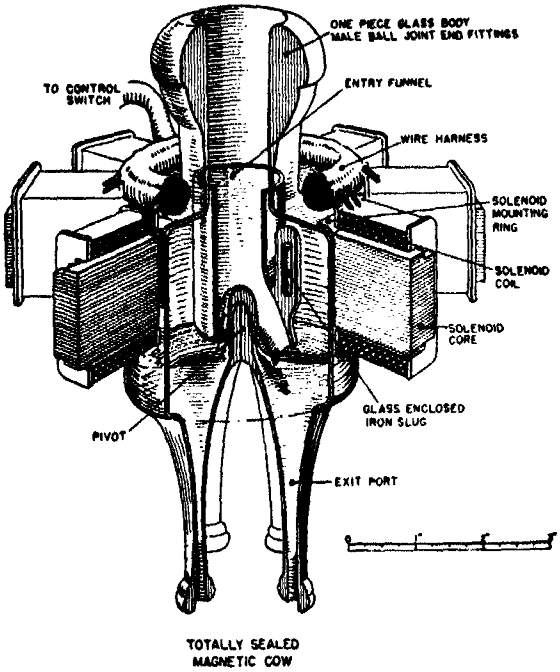

FIG. 3.

A previous model tried, the "Mechanical Cow," is shown in Fig. 2. In this case the funnel stem is offset and rotates about the center of the flask. Rotation is effected by a suitable mechanical connection to the spindle attached to the funnel extending through the joint in the center. This device was not successful since when the remainder of the system was evacuated, the joint in the center of the flask tended to leak even when held by a spring clamp, and when the system was put under pressure the joint stuck. Passage of a thermally warm solution through the funnel softened the grease used to lubricate the joint and aggravated both of these faults.

The authors have combined the above two principles into a third device, shown in Fig. 3. In this device the funnel rotates about a pivot as in Fig. 2. As in Fig. 1 solenoids are placed around the outside of the flask—one for every outlet. If these solenoids are too far apart for smooth operation auxiliary solenoids may be placed in between them. For a device using X solenoids an X-point rotary control switch is connected to the solenoids so that rotating the switch through a given angle rotates the funnel through an equal angle.

This device has numerous obvious advantages over the one shown in Fig. 2, and two important advantages over that shown in Fig. 1: (1) This device avoids the swinging of the funnel which occurred in the case shown in Fig. 1, and the consequent possibility of breakage each time the funnel hit the flask. (2) In the new device current is supplied to the solenoid only when changing position of the funnel. This avoids the necessity of having to dissipate heat from the solenoid and makes the device foolproof in case of power failure. Of course in case of power failure the funnel could not be rotated until power is restored but power failure itself would not cause a change in funnel position as in the case shown in Fig. 1.

Tests made at Brookhaven National Laboratory on a four-outlet glass cow sized as shown in Fig. 3 have proved the new device successful. It is obvious that this same device could be made of plastic instead of glass.

We are indebted to Mr. Paul Roman for the actual construction of the model.

Measurement and Amplification of Minute Displacements by Frequency Modulation

P. A. Bricout and M. Boisvert
Faculté des Sciences, Laval University, Quebec, P. Q., Canada

May 14, 1949

USE of f-m for detection of small changes of capacity is well known but the plain wiring of our apparatus seems noteworthy. All functions are performed using only two tubes: an oscillator and a discriminator, to which can be added an amplifier stage when the sensitivity of the recorder is insufficient. The displacement to be measured is secured to the moving plate of a condenser, which is part of an oscillating circuit and produces changes of frequency. As the *relative* one variation of capacity is always very small, say less than one or two percent, relative frequency shifts are of the same order of magnitude.

Use of a high-frequency is therefore necessary to obtain an *absolute* frequency change that can be easily detected. We have chosen a central frequency equal to about 10 mc so that a relative variation equal to one percent of this value will give a frequency shift of 100 kc, corresponding to the normal range of the discriminators used in f-m receivers.

Principle of apparatus.—The core of the apparatus is a variable condenser consisting of a pressure box (Fig. 1) closed by a thin diaphragm, D, and containing an adjustable insulated plate, B. The plates of the condenser are the envelope with the diaphragm and the inner disk. Capacity is adjusted by changing the distance from the diaphragm to the insulated plate which is firmly pressed by a spring, R, against the tips of three micrometric screws, V. For normal operation, a typical value of the capacitance is approximately 24 mmf. Any flexing of the diaphragm by reduced or increased pressure in the box will produce a capacitance variation, which is detected by a frequency shift of an oscillator connected to the plates of the pressure box. For a given flection, the variation of capacitance is the largest when inner plate and diaphragm are the nearest, hence an easy adjustment of the sensitivity.

Frequency modulation and amplitude modulation.—A basic point in the design of the apparatus is the possible interference between a-m and f-m. It is difficult in practice to obtain a perfect steadiness in the output of the oscillator and a change in amplitude may affect the discriminator in the same way as a change in frequency. As the displacements to be measured control only the changes of frequency, it is very important to make the discriminator insensitive to a-m. Use of pentodes as limiters in connection with resonant circuit discriminators is a conventional solution but it introduces one or two more tubes on the chassis.

A new discriminator described by W. Bradley in *Electronics* (November, 1946) is practically insensitive to a-m if the input e.m.f. exceeds a critical value (about 0.6 volt). It uses only one tube, the new Philco Pentagrid f-m 1000. We thought that this discriminator was fit to meet our requirements and we designed the apparatus to admit it.

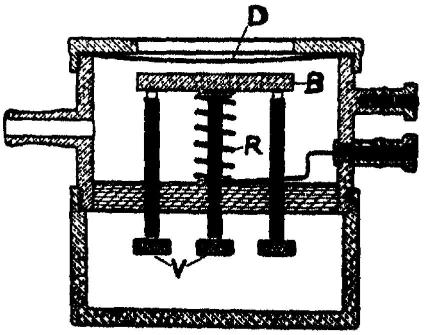

FIG. 1. A cross section of the pressure box.

---

* The device described herein was developed at Brookhaven National Laboratory under the auspices of the AEC.

Description of apparatus.—The pressure box is the capacitor, K, for a Hartley oscillator using tube 6J5 working class A (Fig. 2). A variable condenser is used to adjust the frequency of the oscillator within the range of the discriminator. The oscillator is coupled to the discriminator by a r-f stepdown transformer which applies the frequency to be measured between the cathode and the third grid of tube f-m 1000.

The discriminator can be considered as a T.P.T.G. oscillator with a plate circuit highly dampened by a shunt resistance and tuned to the main frequency. The grid tuned circuit, which is inductively coupled to the plate circuit, feeds the first grid of the heptode. This grid has a large negative bias. The triode part of the tube, made of the first two grids, works as a class C oscillator with a highly pulsating plate current. When the frequency to be measured is applied to the heptode mixing grid, the two frequencies tend toward synchronism. This may occur because the resonant frequency of the f-m 1000 oscillator is not critical due to the high damping of its plate circuit. The change in frequency varies the impedance of the plate and associated circuits, producing a variation of the direct component of the plate current.

By a suitable adjustment of the discriminator circuits, this component can be made proportional to frequency deviation within a range of 75 kc. It is also possible to give a slight curvature upwards or downwards to the response curve of the discriminator. Plate current flows through a 44,000 ohm resistor so that the output of the discriminator is a d.c.; e.m.f. proportional to the frequency deviation, i.e., to the displacement to be measured. The r-f component of the plate current (at 9.1 mc) is not registered by the measuring instrument. When this latter has a poor sensitivity, as in the case of electromagnetic oscillographs, it is necessary to use a d.c. amplifier stage. A 6L6 triode delivering 100 to 150 mA has proved satisfactory.

Adjusting.—It can be seen that one of the great merits of the equipment is its many adjustments which render it suitable for measurements of many kinds. (a) Sensitivity adjustment: The relative variation of capacitance of the pressure box for a given displacement of the diaphragm is greater when the internal part is close to the membrane. A very simple adjustment of the sensitivity is obtained by use of the micrometric screws. (b) Adjustment of the scale position: The discriminator is adjusted in a final position for a given main frequency. The variable condensor, C, of the oscillating circuit is adjusted to change the frequency of this circuit. If a series of tests is taken within a certain range of diaphragm movement and it is required to carry out further tests in another range, it is only necessary to adjust C to bring back the oscillator frequency within the working range of the discriminator. (c) Linear adjustment of scale: Though the diaphragm displacement may not be proportional to a physical dimension to be measured, an output proportional to the physical dimension may, however, be obtained to some extent by correcting the response curve.

Characteristics of apparatus.—The apparatus is of high fidelity and is stable if the tubes are in operation for approximately ten minutes before measurements are taken. The apparatus should be supplied with constant voltage having no alternating current components. Many measurements taken in the laboratory have shown that the output current was not showing sudden changes larger than 1/150 its normal value. If a sensitive oscillograph were used eliminating the need of an amplifying stage, the stability would be enhanced. In its present form, the relative error is less than one percent.

Applications.—The apparatus, due to its flexibility, has many applications. We will mention here a few of the uses it has had.

1. Manograph: An over pressure and an under pressure at the interior of the pressure box produced a displacement of the diaphragm which is measured. Using a steel diaphragm whose diameter and thickness are respectively two inches and 10 mils, the maximum amplitude of the apparatus (110 milliamperes at the output stage of the amplifier) was obtained for a difference in pressure not exceeding 20 millimeters of mercury. With the oscillograph paper traveling at the speed of 50 centimeters per second, variations in pressure were measured for durations of approximately 1/2000 of a second.

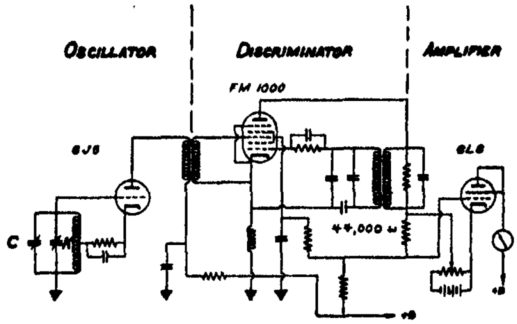

FIG. 2. Wiring schematic of the apparatus.

The following uses, as a graphic manometer, were made: (a) detection of muzzle shock wave in fire arm; (b) study of vibrations of a sound pipe; (c) study of a sudden entrance of gas in pipe; (d) in collaboration with Professor C. Ouellet, measurement of pressure created by a mixture of ether vapor and oxygen at low pressure (cold flame).

2. Vibrometer: In inserting the pressure box between the flange of a beam and a fixed support, it was possible to register the vibrations generating in the beam by an impact. It was possible to study the propagation of sound waves along the beam and their reflection at the end.

3. Seismograph: The vertical and horizontal movements of the mass of a seismograph can be registered by means of three pressure boxes mounted at right angles. The sensitivity of the apparatus allows the mass to be reduced in size.

Scintillation-Type Ion Detector*

PAUL I. RICHARDS AND E. E. HAYS
Brookhaven National Laboratory, Upton, New York

September 19, 1949

THE time-of-flight mass spectrometer[1] being constructed at this laboratory requires a sensitive detector to indicate the *time* of arrival of low energy ions and capable of working in a magnetic field of about 500 gauss. It was felt that one possibility worth investigating was the following: When the ions reach the detector, they are accelerated to relatively high energy and projected upon a luminescent material. The resulting photons are then piped along a quartz rod out of the vacuum system and away from the magnetic field, where they in turn may be detected by a conventional photo-multiplier tube and amplifier.

While the physical processes are rather redundant, the method has the advantage of simplicity, utilizing only commercially available or easily constructed elements; also, relatively little space and material are required within the vacuum system. Since a single energetic ion can produce many photons, there is even a possibility of a gain in signal-to-noise ratio over a simple electron multiplier. Against these advantages must be weighed the need for optical shielding and the finite emission time of the phosphor; our application requires a recovery time of less than one microsecond.

The ions from the mass spectrograph entered the detector through a grid and were accelerated around a corner as shown in order to facilitate optical shielding (Fig. 1). The 30 kv accelerating voltage was obtained from a television-type r-f high voltage supply with a voltage-doubler rectifier arrangement. Both the 1P21 and 5819 photo-tubes were used; the latter appeared to be only slightly more sensitive than the former in our arrangement. Cementing the

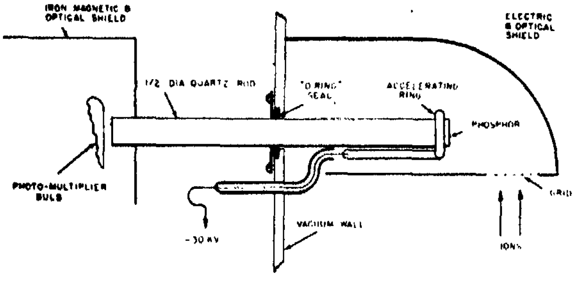

FIG. 1. Scintillation ion detector.

quartz rod to the bulb of the photo-tube with Canada balsam produced no appreciable improvement. The sensitivity of the detector was found to increase with increasing accelerating voltage up to at least 30 kv. Detection of the larger pulses (10^3 to 10^4 ions in about ½ microsecond) starts near 1 kv followed by a rise at first more than linear (up to about 10 kv) and thereafter tapering off to a more linear relation. These large ion currents could, of course, easily be detected by other means, such as an electrometer tube; our application, however, requires extremely rapid response. The only other possibility seems to be an electron multiplier designed to work in the magnetic field.[2]

Three phosphors were studied: silver-activated zinc sulfide, thallium-activated sodium iodide, and anthracene. The sensitivities of these three materials to positive ions appeared to be equal within a factor of about two, rough measurements indicating that, in our arrangement, each ion releases about one photo-electron from the cathode of the multiplier tube. Although a 30 kv ion probably produces 1000 or more photons, the efficiency of the multiplier cathode is only one percent, and the optical system is probably about ten percent efficient.

The synchroscope pictures shown in Fig. 2 were obtained with the preliminary model of the mass spectrograph described in reference 1. The ion source was pulsed during ½ microsecond at an arbitrary repetition rate. The magnetic field was about 600 gauss, so that the time of flight for one revolution was slightly more than one microsecond per mass unit. The sweep shown is 100 microseconds long, starting at the instant the source is pulsed. The peaks, from left to right, as seen in Fig. 2c, are K^{39}, K^{41}, K^{39} twice around, K^{41} twice around, Rb^{85} and Rb^{87}.

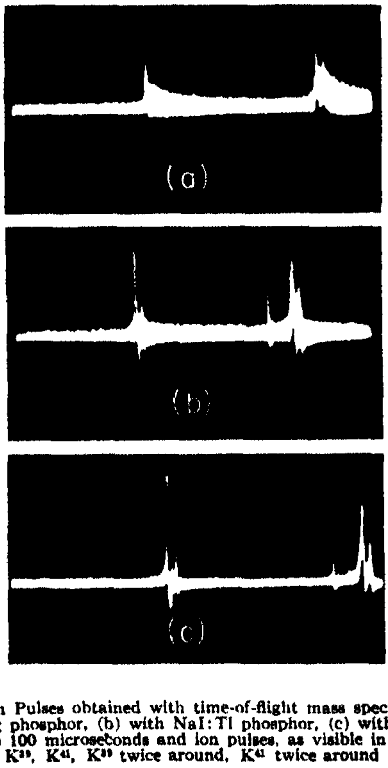

FIG. 2. Ion Pulses obtained with time-of-flight mass spectrograph: (a) with ZnS:Ag phosphor, (b) with NaI:Tl phosphor, (c) with anthracene. The sweep is 100 microseconds and ion pulses, as visible in (c) are from left to right K^{39}, K^{41}, K^{39} twice around, K^{41} twice around (weak), Hb^{85} and Hb^{87}.

Of the three materials investigated, ZnS:Ag is the most conveniently used. It is unaffected either by humidity or vacuum, and the powder will adhere to the end of the quartz rod after the latter has merely been rubbed in the hand. Because the material must be extremely pure, it cannot conveniently be made in the laboratory, but it is commercially available either in the form of a powder or a screen (Patterson-Type D x-ray intensifier screen). The principal disadvantage from our point of view is the long decay time of about 25 microseconds (Fig. 2(a)), which tends to mask small ion bunches following closely on larger ones. For measurement of d.c. ion current, however, ZnS:Ag is probably the most convenient of the three.

NaI:Tl[3] has a much shorter recovery time (Fig. 2(b)) than ZnS:Ag and, like the latter, will withstand the vacuum indefinitely. It is, moreover, extremely simple to prepare and ordinary reagent-grade chemicals are of sufficient purity. We have found the following method most convenient: NaI and TlCl are dissolved in distilled water roughly in the proportion 100 to one-or-more by volume. As the water is boiled off, the solubilities of the salts control the proportion of thallium "impurity" in the final powder, and an excellent phosphor is produced.[4] (TlI may be substituted for TlCl with almost as good results.) A convenient way of placing the phosphor on the quartz rod consists of heating the latter well above 100°C and painting the solution on it. The great disadvantage of NaI:Tl for ion detection, however, is its extreme deliquescence, which requires that it be placed in the vacuum system while still hot and renewed each time the system is opened. Also, it will be seen from Fig. 2(b) that there is evidence of a long-period component which might cover weak ion bunches.

Anthracene, of the three materials investigated, probably has the best combination of properties for our particular application. The recovery time is very short, and there is little evidence of a long-period component (Fig. 2(c)). The crystals were attached to the end of the quartz rod by imbedding them in a thin layer of Dow-Corning silicone stopcock grease. Although the material evaporates in a vacuum, the process is quite slow; in one case, 0.028 g of a 0.044-g crystal evaporated during 60 hours at 5×10^{-6} mm Hg, and its presence did not appear to affect the limiting pressure. Anthracene is not deliquescent and, for this application, need not be in the form of a single crystal. The commercial product, however, must be purified further before it will perform properly.

---

* Research carried out at Brookhaven National Laboratory under the auspices of the AEC.

[1] S. A. Goudsmit, Phys. Rev. 74, 622 (1948). P. I. Richards, E. E. Hays, and S. A. Goudsmit, Phys. Rev. 76, 180 (1949).

[2] Lincoln G. Smith (to be published).

[3] *Robert Hofstadter, Phys. Rev. 75, 796* (1949).

[4] Depending on the chemicals used, however, the efficiency may be as much as a factor of ten below that of a commercial "pure" crystal.

Method of Supplying Low Pressure Gases on a Vacuum System*

RAYMOND H. MCFEE
Photoswitch, Inc., Cambridge, Massachusetts

August 22, 1949

FREQUENTLY it is desired in connection with the treatment of work on a vacuum system to supply a gas to the manifold at a controlled low pressure. In a process which involves absorption of or reaction with the gas, a supply of the gas is required which is

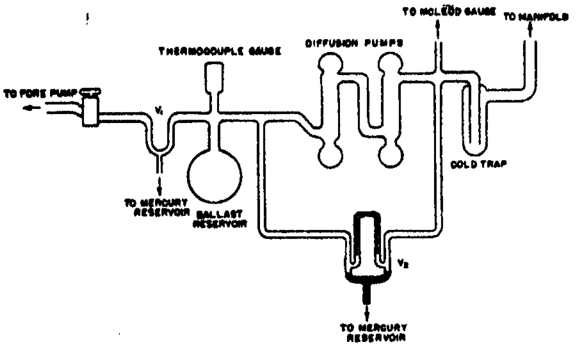

FIG. 1. Typical vacuum system with a double-range feed-back line with mercury valve control.

greater than that afforded by merely filling and closing off the system at the desired pressure. A reservoir of the gas could be connected to the system through a calibrated leak, while pumping on the system, but this is wasteful of gas, which may be of importance where a limited supply of expensive, high purity gases is available.

The method to be described has been in use for many months for the supply of a controlled, low pressure atmosphere to the vacuum system manifold for the purpose of processing photoconductive cells. A diagram of the system is shown in Fig. 1. It is essentially a standard, all-glass mercury diffusion pumping system with the addition of a feed-back line connected between the fore-vacuum manifold and the high vacuum end. A mercury valve is used to cut the feed-back line off, so that normal evacuation may take place. When the line is open the gas in the fore-manifold is pumped back through the feed-back line by the diffusion pumps, establishing a pressure differential between the fore-manifold and high vacuum manifold which is determined by the pumping speed of the diffusion pumps and the impedance of the feed-back line. Such a differential pressure scheme has been used by Monk[1] for the purpose of low pressure measurement by intermediate pressure gauges.

A double section feed-back tube is used, one section of which contains a length of capillary tubing, offering high pumping impedance. This allows two ranges of calibration of the pressure differential. The calibration curves for dry air in a typical system are shown in Fig. 2.

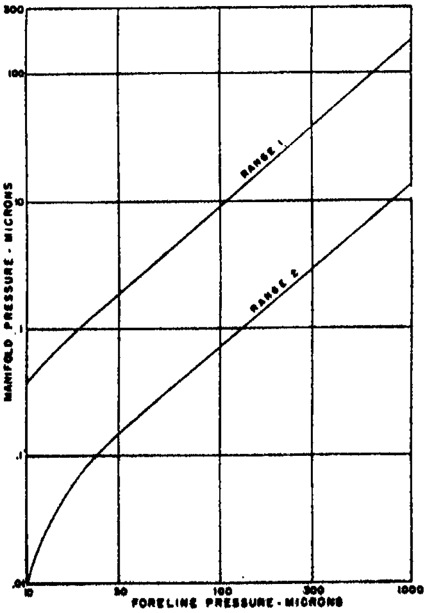

FIG. 2. Calibration curves for dry air for two feed-back line impedances.

The system in Fig. 1 is used as follows: The high vacuum end is pumped out thoroughly with the forepump and diffusion pumps. The forepump is then cut off and the pure gas introduced into the fore-vacuum manifold, its pressure determined by means of a thermocouple gauge. The mercury cut-off valve, V_2, in the feed-back line is opened, allowing the gas to circulate. After the pressure adjustment has been completed, the fore line cut-off, V_1, is closed, isolating the system from all stopcocks. The pressure in the manifold may be changed rapidly from one pressure to another, or to the high vacuum level simply by manipulating the valve V_2.

The advantages of both the closed, static system, and the leak flow system are present because a fixed, small quantity of gas is used with the flowing of the gas at constant pressure produced by the pumps. By the use of variable impedance feed-back lines, a system could be constructed which would allow rapid changing from one manifold pressure to several others without adjustment of the total quantity of gas in the system. The advantages of such an arrangement are obvious when applied to a set-up used for a large number of routine procedures.

---

* Based on work performed under Air Materiel Command Contract No. W33-038-ac-15639.

[1] G. W. Monk, Rev. Sci. Inst. 19, 396 (1948).

A Convenient Gas Sample Tube Holder and Break-Off Applicable to Mass Spectrometers

FREDERICK HIGHHOUSE AND JULIUS WHITE
National Institutes of Health, National Cancer Institute, Bethesda, Maryland

November 1, 1949

IN conducting biological experiments using stable isotopes, many samples are collected for analysis. It has become necessary at times to store these samples for a considerable period before actual analysis in the mass spectrometer. In this laboratory these samples are conveniently collected and stored in sealed glass ampules. To transfer the gas from the ampule to the mass spectrometer, it became necessary to devise a gas sample tube holder and break-off which could be used directly on the spectrometer.

Figure 1 is a full scale illustration of the tube holder. Except for the rubber gasket *C*, the standard taper joint *F* (which leads into the spectrometer), and the windows at *G* the entire unit is constructed of stainless steel. By means of the screws *H* the entire tube holder is rigidly supported to a fixed bracket in the rear. Joint *F* is made air tight with sealing wax. Tube *A* which contains the sample to be analyzed is made of 10-mm tubing about

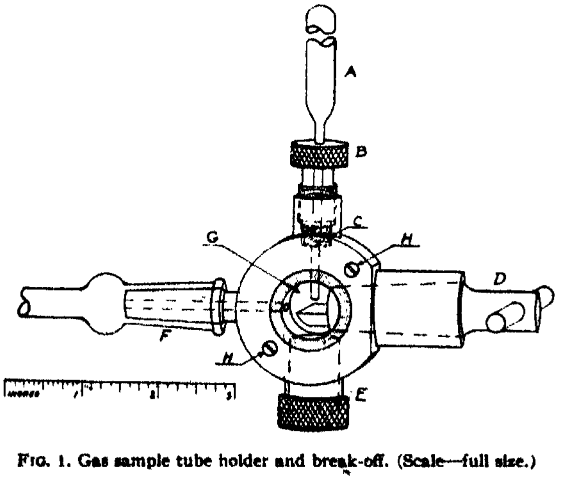

FIG. 1. Gas sample tube holder and break-off. (Scale—full size.)

6 inches long and joined to 3-mm tubing about 6 inches long. Before inserting the tube *A* into *B* a fine scratch is made near the 3-mm end (to facilitate breaking and prevent shattering). After tube *A* is inserted into *B* it is gently forced through the rubber gasket *C* into the well *G* and above the flat surface of the stopcock *D*. The knurled screw *B* is then tightened firmly (to prevent leakage of sample). After the assembly has been completely evacuated by the manifold pump of the spectrometer and the standard background reached, the stopcock of *D* is turned. As the flat edge of the stopcock in the well *G* turns it comes into contact with the 3-mm tube and breaks it releasing the gas into the spectrometer. This operation can be seen through the windows sealed in on both sides of the well *G*. The glass tip which has broken off drops down into *E*. After 20–30 samples, *E* can be unscrewed and the small glass tips which have accumulated drop out. After the sample has been analyzed, *B* is loosened, tube *A* removed and another sample tube inserted.

The advantages of this system are simplicity, ease of maintenance and removal of glass tips and old sample tubes, the relatively small internal volume and loss of little time in evacuation of the system between samples.

A Simple Contamination-Free Electron Gun[*]

H. E. FARNSWORTH
Brown University, Providence, Rhode Island

November 8, 1949

IN the usual type of electron gun, with the cathode mounted on the axis, evaporated material from the hot cathode produces observable contamination of a solid target in the course of several hours. This may be eliminated by mounting the cathode off the axis and deflecting the electron beam by magnetic or electrostatic fields. However, there are many applications in which the presence of a magnetic field is objectionable. Although the electrostatic method does not separate negative ions of different masses, and hence does not prevent them from following the path of the electrons, this method is adequate if one uses a cathode made of electropositive metal which does not evaporate in the form of negative ions. A thorough outgassing of the cathode before applying the deflecting voltage eliminates the possibility of contamination by negative gas ions.

A gun of the electrostatic type which uses only one deflecting electrode and produces an electron beam of high current density over a wide range of energies is illustrated in Fig. 1. This gun is similar to that previously described by the writer[1] except for the deflecting electrode G_2 and the off-axis cathode arrangement. Electrons emitted by *F* are accelerated and pass through G_1, are deflected by a suitable voltage on G_2, and pass along the axis of A_1 and A_2. G_2 is mounted so that its center of curvature lies on the circle passing through the center of *F* and the aperture in A_1, the circle being centered at the lower edge of G_1. None of the dimensions or adjustments appears critical, although no detailed study of this has been made.

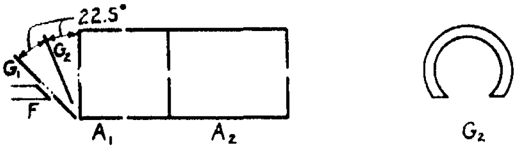

FIG. 1.

To simplify conditions, G_1 and A_1 are connected together. With an accelerating potential difference of 70 volts between *F* and G_1, the required potential on G_2 with respect to *F* is between −100 and −200 volts. The net energy of the electron beam is varied by altering the potential of A_2 with respect to A_1. Satisfactory results have been obtained for beam energies in the range 0 to 8000 ev with no indication that the upper limit has been reached. For the higher energies a slight readjustment of the potential of G_2 is required due to interpenetration of the fields. A guard ring *R*, surrounding A_2 and connected to G_2, prevents electrons from passing outside the electrode A_2.

To date the gun has been used with tantalum and tungsten cathodes, heated by conduction. A gun with a tungsten cathode has been used in a low speed electron diffraction tube which is sensitive to small amounts of contamination. No observable contamination occurred in a period of several hours. Because this gun possesses some velocity selection, the homogeneity of the electron beam is somewhat better than that of the conventional gun.

Financial aid has been received from the ONR and the Research Corporation of New York.

[*] The contamination referred to is from the cathode only. It is assumed that contamination from other sources is not present. This gun has been tested in all-glass systems which were outgassed by baking or torching and in which the residual gas pressure was less than 10^{-7} mm Hg. A cold trap surrounded by dry ice and acetone mixture was placed between the experimental tube and oil diffusion pumps in each case to eliminate oil vapors, and no grease or wax joints were present on the high vacuum side of the pumps.

[1] H. E. Farnsworth, J. Opt. Soc. Am. and Rev. Sci. Inst. **15**, 290 (1927).

Bent Crystal X-Ray Monochromators

B. E. WARREN
Department of Physics, Massachusetts Institute of Technology, Cambridge, Massachusetts

November 17, 1949

PLASTCALLY bent rocksalt and elastically bent quartz are used a great deal in x-ray diffraction work as focusing monochromators. To eliminate half-wave-length components, a bent 111 face of fluorite is often desirable. However, fluorite like many other crystals which might be used as monochromators is difficult to bend without breaking.

A crystal slab breaks on bending because the convex face is put into tension, and brittle substances are weak in tension. One way of avoiding this trouble is to grind the slab so thin that the tension developed is not excessive. This may involve grinding so thin that the slab will break in grinding and handling. A simpler method is to grind as thin as convenient, and then minimize the tension by superimposing a compression.

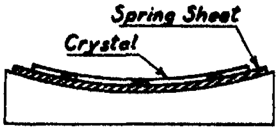

FIG. 1. Crystal mount.

A simple method for doing this is illustrated in Fig. 1. The thin slab of crystal is ground down to some convenient thickness, say 0.012–0.020 inch. It is then cemented to a flat strip of spring sheet metal such as steel or phosphor bronze. Duco cement has been satisfactory for this purpose. The spring sheet is then bent by screws along the side of the crystal slab and forced to fit a block having the desired curvature. Under these conditions, the concave side of the metal sheet is in compression and this diminishes the tension which would otherwise develop in the convex face of the crystal. By this method it is a simple matter to bend 111 slabs of fluorite, or to get good uniform bends in any of the other crystals commonly used.

A Motor for Use in Vacuum Systems

C. P. Butler and F. E. Carpenter
Naval Research Laboratory, Washington, D. C.

November 28, 1949

IN problems where evaporation techniques are used there is often a need for a motor which can be operated inside the vacuum chamber. Here the problem was that of turning a sectored disk in making an evaporated step wedge.

The most important requisite of any motor operated in a high vacuum system is that there shall be no outgassing from the coils, the armature or the bearings even at temperatures up to 100°C. This requirement precludes the use of any motor where insulated wire is exposed to the vacuum system. This requirement has been met by the use of a solid armature motor, whose field coils are hermetically sealed in a brass can.

A Model 61,115 volt a.c. 50/60 cycle 1550 r.p.m. 1/25 h.p. motor made by ILG Electric Ventilating Company, Chicago, Illinois was modified to operate in vacuum. The armature was removed and a brass can made to enclose the field coils. The inner sleeve of the can was of 1¾-inch O.D. brass tubing, and was press-fitted to the inside of the armature. The outer sleeve was of 3½-inch O.D. tubing. Two annular rings were cut to enclose the ends and soft soldered to the two sleeves, thus sealing the coils at atmospheric pressure. Two Kovar glass sealed lead-ins were fitted and soldered to one of the end plates, to which were connected the two wires from the coils. The separate units are shown in Fig. 1.

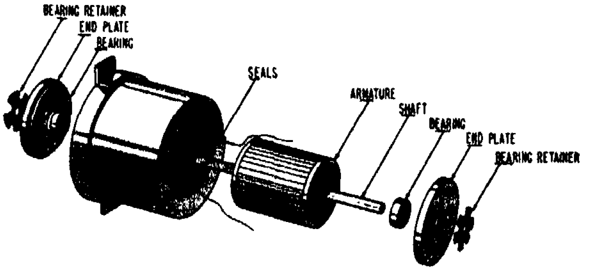

FIG. 1.

The armature of the Model 61 motor is made of laminated iron held together with a soft metal, and it can be easily turned on a lathe from its diameter of 1¾ inch to one of 1$\frac{11}{16}$ inch which gives ample clearance between the armature and the inside brass sleeve. Two end plates were cut to bolt onto the annular rings to support ball bearings for the motor. After completion, the ball bearings were removed from their mounts and the remaining assembly first immersed for 30 seconds in a "bright dip" solution, made with 2 parts sulfuric acid and 1 part nitric acid, and then thoroughly washed in water. The ball bearings were cleaned in acetone. The motor was reassembled and oiled with "Octoil."

In operation the motor was mounted in the bell jar and bare copper wires from the base plate terminals were clipped to the motor leads. A variac was used to control its speed.

The insertion of a brass sleeve between the field and the armature reduces the efficiency of the motor as well as increasing the heat developed when running at full speed. However, the temperature rise at full speed in vacuum was only 35°C during 2 hours operation.

This motor is currently being used to turn a sectored disk in making step wedges. It has been in operation for 4 weeks and no leaks have developed. After long usage, aluminum, chromium, nickel and other metals which have been used in evaporation form a deposit on all metal parts. This can be easily removed by repeating the "bright dip" operation.

New Instruments

W. A. Wildhack: Associate Editor
in Charge of this Section
National Bureau of Standards, Washington, D. C.

These descriptions are based on information supplied by the manufacturer and in some cases from independent sources. THE REVIEW *assumes no responsibility for their correctness.*

Ultrasonic Equipment

The Brush Development Company has announced production of ultrasonic units of laboratory and industrial capacity to be sold under the trade name Hypersonic.

Included in this line of ultrasonic equipment are a variety of titanium ceramic transducers of special shapes for controlling the concentration of the sonic energy.

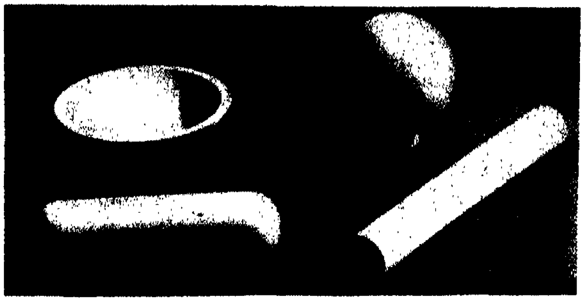

The ceramic transducers have the marked advantage over piezoelectric crystals previously used in that the electrical driving voltage does not have to be applied in a fixed direction relative to crystal axes; nor is the mechanical motion produced subject to this limitation. In ceramic elements, the direction of the mechanical direction is determined by a polarizing electric field applied during manufacture, and its direction may be made to vary at will from one point of the transducer to another. For example, in a tubular transducer element, the polarizing direction may be at all points directed toward the central axis of the tube, thus obtaining on the axis a high concentration of sound energy.

Write for detailed information on various models of Hypersonic equipment.—BRUSH DEVELOPMENT COMPANY, *Cleveland, Ohio.*

Oscillograph

Two new instruments, DuMont Types 304 and 304-H cathode-ray oscillographs, were announced recently as replacements for the famous Type 208-B cathode-ray oscillograph. The new units contain all the features of Type 208-B, plus others new to the low-priced field. Except for the somewhat higher accelerating potential of Type 304-H, Types 304 and 304-H are identical.

Stable, high gain a.c. and d.c. amplifiers are provided for both X and Y axes. Circuit design permits instantaneous recovery from signal overload, even at high gain.

Recurrent and driven sweeps are variable from two to 30,000 cycles per second. Through an arrangement of switches, extremely slow sweeps, of ten seconds or more, are available by the connection of external capacitors between the X-input terminals on the front panel.

Vertical deflections on these instruments may be expanded to four times full-screen diameter; horizontal deflections, to five times full-screen diameter. Positioning controls have sufficient range that any portion of a fully expanded pattern may be centered on the screen, with no on-screen distortion present.

Stabilized synchronization of the pattern is maintained in Types 304 and 304-H by a sync-limiting circuit, so the sweep length and synchronization are unaffected by variations in signal voltage level.

In Type 304, the cathode-ray tube is operated at an over-all accelerating potential of 1780 volts. In Type 304-H, an additional intensifier power supply increases this potential to 3000 volts. The higher accelerating potential of Type 304-H facilitates the use of long-persistence screens so that fullest possible advantage may be taken of the slow recurrent sweeps, the high speed driven sweeps, and the d.c. amplifiers of the instrument. Writing rates as high as 2.8 inches per microsecond may be photographed from the screen of Type 304-H using DuMont Type 314-A oscillograph-record camera with an $f/1.5$ lens.

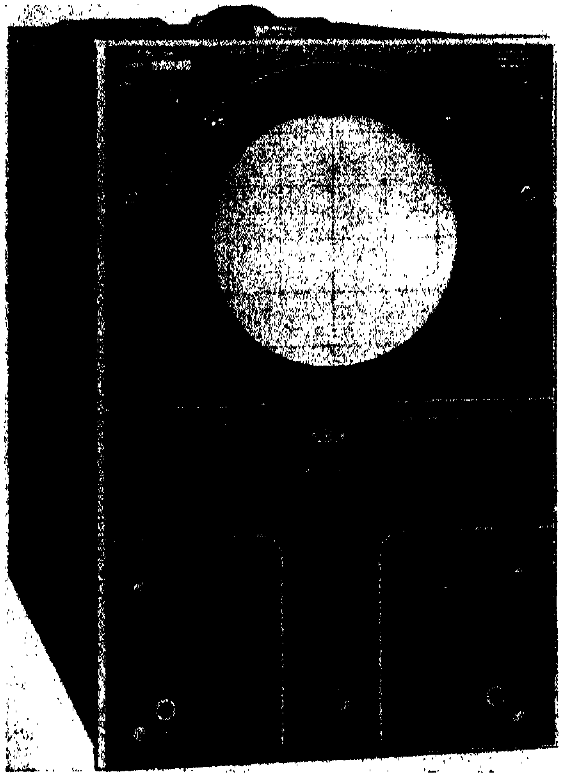

In every dimension Types 304 and 304-H are smaller than Type 208-B, making them even more portable than was their predecessor.—INSTRUMENT DIVISION, ALLEN B. DUMONT LABORATORIES, INC., *1000 Main Avenue, Clifton, New Jersey.*

Ultrasonic Generator

The Type E.7562 Mullard ultrasonic generator is designed as a laboratory tool for research.

The r-f output is generated directly by a silica triode capable of producing one kilowatt of r-f power. Four plug-in coil assemblies, which are rapidly interchangeable—are provided for operation around nominal frequencies of 250 kc, 500 kc, 1 mc, and 2 mc.

The output tube is matched to the crystal impedance by tapping the anode down the coil in the output circuit. Fine tuning of the output circuit and adjustment of grid coupling are effected by means of variometers.

The quartz crystal is contained in a metal case. It is connected to the generator by means of a coaxial cable. The crystal has silver electrodes fired on both sides to which the driving voltages are applied.

To give the maximum ultrasonic output in the forward direction, the generating crystal is air-backed. The limitations on the temperature at which the transducer can work are set by the polythene of the cable and the rubber sealing rings. If silastic rubber is used and the back of the holder is adequately cooled, the crystal can safely be immersed in liquids at temperatures up to at least 150°C.—MULLARD ELECTRONIC PRODUCTS, LTD., ABOYNE WORKS, *Aboyne Road, Tooting, S.W. 17, England.*

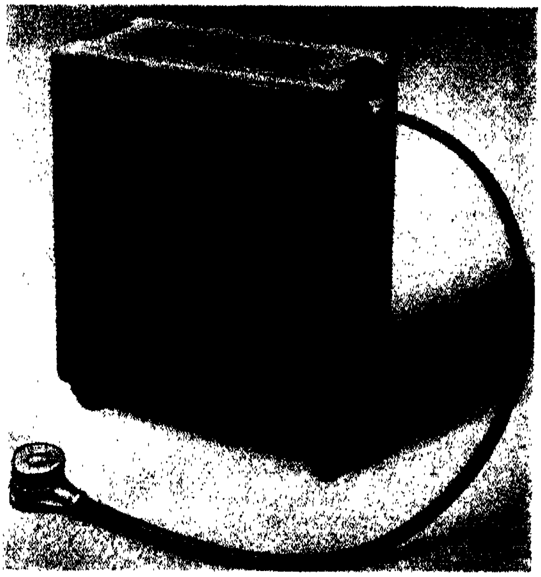

Universal Monochromator

The first true universal monochromator, which covers the ultraviolet, visible, and infra-red regions of the spectrum (0.18 to 40μ) when suitable prisms or gratings are used, is now in production at the Glenbrook, Connecticut, plant of The Perkin-Elmer Corporation.

Designated as the Model 83 monochromator, it consists essentially of the company's present Model 12 infra-red spectrometer optics from entrance slit to exit slit, with the wave-length and slit controls under a standard cover but on a new base assembly. The optics are totally reflecting so that the instrument can be focused with visible light for use in ultraviolet or infra-red as well.

The result is a new type monochromator, 14 in. long, 14 in. wide, and 9 in. high, completely enclosed with an entrance window before the entrance slit and a space 13×4 in. behind the exit slit for mounting detectors. There is also an exit hole in the cover behind the exit slit.

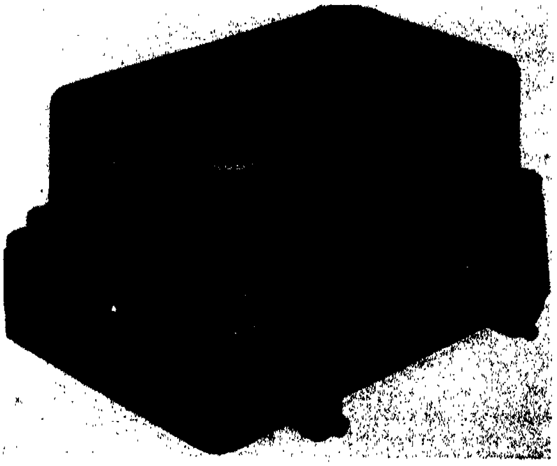

The collimator is an 18° off-axis parabola of 270-mm focal length, and the effective aperture of the Littrow mount is $f/4.5$. The prisms available are fused quartz, crystal quartz, glass, LiF, CaF_2, NaCl, KBr, or KRS-5. Where it is desired, a 14° parabola can be supplied to reflect directly to the Littrow mirror. Fifteen thousand and 7200 lines per inch replica gratings are available to mount in place of the Littrow mirror to furnish a Littrow grating monochromator. The slits are bilateral with entrance slit curvature of 5.59 in., and are adjustable to 0.5μ. The Littrow mirror has a coarse setting adjustment and can be moved through an angle of 9° with a fine micrometer marked with 2000 divisions.

Available for use with the new monochromator are many of the standard Model 12 infra-red spectrometer accessories, such as cell mounts, special covers, and a mirror assembly which permits the beam from the exit slit to be deflected at right angles or allowed to pass out the special cover.

Price of the monochromator without prisms, prism table, or entrance windows, is $1340.00.—The Perkin-Elmer Corporation, *Glenbrook, Connecticut.*

Vacuum Gauge

A new Hastings vacuum gauge is now available for measurements in the range 1 to 1000μ, which embodies a noble-metal thermopile and a dependable bridge circuit similar to those used in the Hastings precision air meter. The gauge consists of an accurate electrical indicator and a small rugged pick-up which screws into a ¼-in. tapped hole in the vacuum system. Fast response, interchangeability of pick-ups without recalibration, freedom from outgassing and corrosion, and freedom from damage by exposure to atmospheric pressure are outstanding features of this new gauge. Simplicity in installation and operation, rugged dependability, and laboratory accuracy are features of the instrument. Calibration is not affected by connecting cable length, thus allowing remote indication and recording. The unit operates at 115 volts a.c.

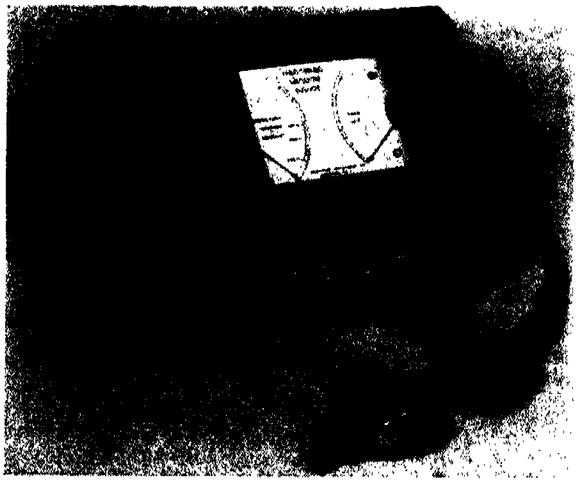

The physical and operating characteristics of the gauge make it adaptable to all vacuum processes in the micron range, such as vacuum tube manufacture, vacuum distillation, automatic exhaust machines, refrigeration service, vacuum dehydration, and laboratory and production processes involving high vacuum systems.

The prices of the control box and indicator and the pick-up are $90.00 and $10.00, respectively (f.o.b. Hampton, Virginia).—Hastings Instrument Company, Inc., *Box 1275, Hampton, Virginia.*

Film Tape Sound Recorder

The Recordall is a long-time permanent recording device in which sound records up to 3½ hr. can be made on each face of an endless plastic band of safety film known as Sonaband. The Sonaband is automatically self-aligning and can be removed or replaced within two seconds. By turning a vernier knob, any point in the recording can be located within a few seconds. Sonaband may be marked with pencil or ball-point pen and may be filed, stored, or mailed.

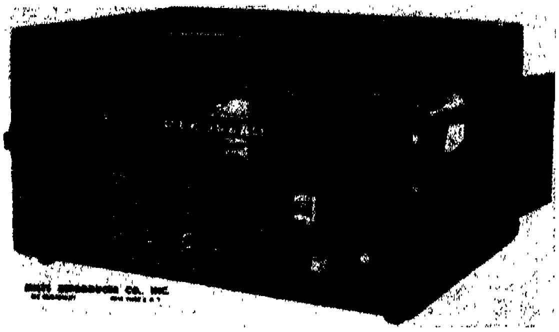

Other features of the recorder are automatic voice activation, automatic stop when within a few seconds after the cessation of sound, automatic volume control, automatic equalization of incoming and outgoing voices when recording telephone conversations, and instantaneous and permanent play-back at any desired speed. Foot controls facilitate the transcribing from a combination recorder-transcriber or from a separate transcriber.

The Recordall recorder-reproducer weighs only 15 lb.—Miles Reproducer Company, Inc., *812–814 Broadway, New York 3, New York.*

Improved RCA-1P21 Multiplier Photo-Tube

RCA tube engineers have been able to reduce the "equivalent noise input" of the Type 1P21 multiplier photo-tube to 5×10^{-13} lumen—a value showing six times improvement over that of 1P21's previously available. In addition, the improved 1P21 features a combination of extremely high photosensitivity, very high secondary-emission amplification, and very small d.c. dark current.

Because of its superior features, the improved 1P21 is recommended for applications involving extremely low light levels. Such applications include the use of the 1P21 in specialized scientific equipment of a laboratory nature represented by (1) photoelectric spectrometers, (2) astronomical telescopes, (3) scintillation counters utilizing "light piping," and (4) other types of equipment employing a collimated light beam.—Tube Department, Radio Corporation of America, *Harrison, New Jersey.*

Super-Brilliant Light Source

Light intensities of 90,000 candles per square centimeter are reached at maximum brilliance with the new Huggins Ames Type-A mercury arc lamp. Shown in the illustration are the lampholder with lamp extracted and, in the background, the fully controllable a.c. power supply. Light output is 65 lu/w; power input 2 kw (1.2 amp. at 1750 v).

Arc dimensions are 2.85 cm (1.125 in.) by 1 mm (0.039 in.). Cooling is accomplished with ordinary tap water, 2½ gal./min. being required; alternatively, a closed-circuit distilled-water system can be used. Average life at rated maximum brilliance is 5 hr., appreciably more at reduced voltages.

In the standard model, 100 percent intensity is reached at 4358A, with an 80 percent peak at 5461A, and a 73 percent peak at 4047A,

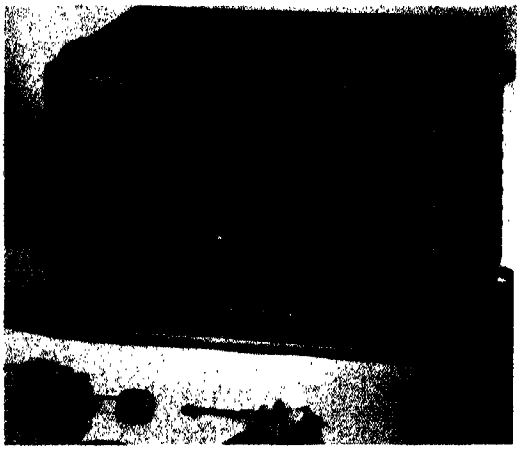

with a maximum radiation of 0.08 w/sterad./A. Intermediate areas average approximately 35 percent. Quartz accessories can be supplied for operation in the ultraviolet region. Direct-current, flash, and stroboscopic power supplies are under development for special applications.

These units are being used for light sources in interferometers, schlieren optical systems, shadowgraphs, monochronometers, and in high speed photography. As high powered ultraviolet sources, they are being used in the production of chemical, biochemical, and ionization changes in substances under study or processing. Numerous applications exist throughout the chemical-, physical-, aeronautical-, and biological-research fields.—HUGGINS LABORATORIES, *712 Hamilton Avenue, Menlo Park, California.*

Temperature Pick-Up The Trans-Sonics Type 17-2 temperature pick-up is designed for the measurement of transient and steady-state gas temperatures for the range of 0 to 315°C. The sensing element is a platinum grid, the resistance of which varies between 5.5 and 11.5 ohms. The total circuit resistance (including the constantan leads for low temperature coefficient) is 8 ohms at 0°C.

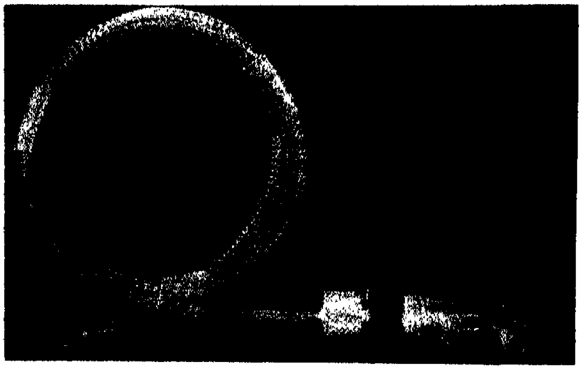

The thermal time constant of the instrument is less than 0.5 sec. in an air velocity of 5 ft./sec. When used with a Type 16-5 resistance bridge, the output varies between 0 and 5 mv/v applied over the temperature range. A 7/16-20 thread is provided for insertion of the pick-up into ram pressure tubes.

In conjunction with its balancing bridge, the Type 17-2 temperature pick-up is suitable for use with standard recording oscillographs and telemetering equipment.—TRANS-SONICS, INC., *Bedford Airport, Bedford, Massachusetts.*

Manufacturers' Literature

Electro-Chemograph—4-page illustrated brochure entitled, *An Advanced Electro-Chemograph Type E,* describes an equipment providing unusual stability, precision, and operating convenience for a wide variety of polarographic analyses in research, and industrial-process control laboratories.—LEEDS & NORTHRUP COMPANY, *4934 Stenton Avenue, Philadelphia 44, Pennsylvania.*

Stress Analysis—14-page booklet explains the services rendered by the Armour Research Foundation in the field of stress analysis.—ARMOUR RESEARCH FOUNDATION OF ILLINOIS INSTITUTE OF TECHNOLOGY, *Technology Center, Chicago 16, Illinois.*

Industrial Thermometer Data—Bulletin "E" gives complete data on liquid-in-glass industrial thermometers in an easy-to-use tabular and sectionalized form.—PRECISION THERMOMETER AND INSTRUMENT COMPANY, *1583 Brandywine Street, Philadelphia 30, Pennsylvania.*

Instrumentation—32-page house organ, Vol. 4, No. 2, contains articles of interest on measurement, control, and recording of industrial processes.—MINNEAPOLIS-HONEYWELL REGULATOR COMPANY, BROWN INSTRUMENTS DIVISION, *Philadelphia 44, Pennsylvania.*

Special Products Digest—4-page illustrated house organ, Vol. VII, No. 5, contains articles on various G.E. equipments, including winding-insulation tester, yarn tension tester, portable harmonic generator demonstrating wave shapes, leak detector, electron diffraction instrument, and ball-bearing grease tester.—GENERAL ELECTRIC COMPANY, *1 River Road, Schenectady 5, New York.*

Wattmeters—*Electrical Measurements,* 8-page house organ, is devoted to various types of low power factor wattmeters and reference standard wattmeters, and general testing single phase wattmeters, giving ranges, prices, and other pertinent information.—SENSITIVE RESEARCH INSTRUMENT CORPORATION, *9-11 Elm Avenue, Mount Vernon, New York.*

The Experimenter—8-page General Radio bulletin, Vol. XXIV, No. 6, features a description of a simple standard-signal generator for f-m broadcast use, amplitude modulator for v.h.f. standard-signal generators and a transformer for 300-ohm balanced output from standard-signal generators.—GENERAL RADIO COMPANY, *275 Massachusetts Avenue, Cambridge 39, Massachusetts.*

CEC Recordings—10-page house organ, Vol. 3, No. 4, features the new Consolidated Titrilog, an instrument for recording traces of quantities of sulfur compounds, also contains descriptions of a new high capacity oscillograph record magazine, a leak detector adaptable as a continuous monitor, a special recording oscillograph for non-standard frequency operation, a new galvanometer, new antifog developer for recording paper, and an analog-type electrical computer, and other items of general interest.—CONSOLIDATED ENGINEERING CORPORATION, *620 North Lake Avenue, Pasadena 4, California.*

Mica Capacitors—1949-50 catalog, 9 pages, lists El-Menco capacitors, with prices.—ARCO ELECTRONICS, INC., *135 Liberty Street, New York, New York.*

High Frequency Voltage Measurement—National Bureau of Standards Circular 481 (illustrated) presents an up-to-date account of fundamental principles and techniques used for voltage measurements primarily for frequencies in the upper audio and radiofrequency ranges and including part of the u.h.f. range. Subject matter limited to principles and methods that have met with some degree of success for both high and moderate precision, emphasizing those developed and applied for primary standard work in this frequency range at the National Bureau of Standards. This paper is intended to give professional workers and graduate students a more comprehensive picture of the methods employed with regard to this subject than is presently available in textbooks and handbooks. Price 20 cents.—SUPERINTENDENT OF DOCUMENTS, U. S. GOVERNMENT PRINTING OFFICE, *Washington 25, D. C.*

Machine Computation—New 12-page, illustrated brochure entitled, *Engineered Machine Computation* describes available engineering-computing service and specialized equipment, of automatic graph readers, electronic graph recorders and novel vibration frequency pick-up.—TELECOMPUTING CORPORATION, *2901 Hollywood Way, Burbank, California.*

Instrument News—Vol. 1, No. 1, 8-page house organ, is devoted to the use of various electro-optical instruments in industry and research; tricks of technique, resumes of new research in optical analysis.—THE PERKIN-ELMER CORPORATION, *Glenbrook, Connecticut.*

Pulverizers—New 6-page bulletin entitled *For Better Testing and Small Scale Reduction* describes applications of laboratory crushers, grinders, and shredders for the reduction of coal, by-products, chemicals, clays, and many other products in testing laboratories.—AMERICAN PULVERIZER COMPANY, *1249 Macklind Avenue, St. Louis 10, Missouri.*

RCA Tubes—Technical bulletins on available new RCA tubes: 6CB6 sharp-cut-off pentode (miniature type); 202K5 converter transformer; 202K6, -7, -8, -9, and -10 picture-IF transformers; 202K11 cathode-circuit trap; 206K1 sound-IF transformer; 207K1 sound-discriminator transformer; and 5675 "pencil-type" triode, a triode of the miniature medium-mu-type for use at frequencies up to 3000 mc, with a power output of 475 mw at 1700 mc.—RADIO CORPORATION OF AMERICA, RCA VICTOR DIVISION, *Harrison, New Jersey.*

Megohmmeter—Bulletin No. 1029 describes the Model 29, a British-made 20 million megohmmeter for measurement of electrical resistance over the range 300,000 to 20,000,000 megohms. Said to exceed in range anything presently available on the American market.—HERMAN H. STICHT COMPANY, INC., *27 Park Place, New York, New York.*

Microphotometer—Bulletin describes the Romicron C. G. Grand microphotometer, especially designed for use with the microscope. Can be used as a microphotometer in general, for densitometry, or for determination of exposure time in photomicrography.—PAUL ROSENTHAL, *505 Fifth Avenue, New York 17, New York.*

Frequency Meters—New catalog describes a complete line of hermetically sealed, direct reading, precision frequency meters for use over the band from 500 to 40,000 mc/sec.—POLYTECHNIC RESEARCH AND DEVELOPMENT COMPANY, INC., *202 Tillary Street, Brooklyn 1, New York.*

Instrument Notes—No. 11, September–October, 1949, 8 pages, summarizes an article on "Electromagnetic determination of wire stress" and describes the Model TC-1 temperature test chamber, a compact temperature-controlled chamber for the rapid performance of ambient temperature variation tests from −65° to +275°F.—STATHAM LABORATORIES, *9328 Santa Monica Boulevard, Beverly Hills, California.*

New Materials

Forest K. Harris: Associate Editor
in Charge of this Section
National Bureau of Standards, Washington, D. C.

Centrifugal Bronze Castings

X-ray quality centrifugally cast bronze bushings are guaranteed to be completely free from porosity, blow holes, sand inclusions, pits, and to have excellent surface finish. These bushings are available in diameters from 2 in. to 18 in. and in lengths up to 12 in. Minimum production quantity is 100 units, and no pattern or mold charge is made.—INDUCTION PROCESSING COMPANY, *3319 West Fifth Street, Tulsa 6, Oklahoma.*

Precision Casting Alloy

Cerrocast, a non-eutectic alloy of bismuth and tin, has negligible shrinkage, extensive melting range, and reasonable hardness. Some of its physical properties are: Melting range, 281–338°F; Yield temperature, 302°F; weight, 0.296 lb./cu.in.; shrinkage, 0.0001 in./in.; Brinell hardness, 22.

This alloy is stated to be especially suitable for use in precision casting by the Lost Wax process. Because of its long melting range it will accurately reproduce the shape, dimensions, and fine surface details of the master pattern. It also works satisfactorily in spray guns and for low temperature soldering of pretinned metal parts. Further information may be obtained from the manufacturer.—CERRO DE PASCO COPPER CORPORATION, *40 Wall Street, New York 5, New York.*

Rust Preventive

Nox-Rust vapor wrapper, a chemical impregnant in wrapping paper, releases a vapor which inhibits the formation of rust on metal parts. The manufacturer has now developed a process for incorporating this chemical in chip-board and corrugated cartons. This development is designed for packaging of metal parts, tools, and appliances, and is stated to eliminate the need for temporary rust-preventive coatings. Full information concerning the paper and cartons can be obtained from the manufacturer.—NOX-RUST CHEMICAL CORPORATION, *2431 South Halsted Street, Chicago 8, Illinois.*

Fluoride Lens Coating

Transkote is a fluoride coating deposited on special glass surfaces, such as those of lenses and prisms, to improve light transmission and reduce reflection. A common fault of conventional fluoride coating is that the film is relatively soft and wears off under normal handling. An improved coating technique, operated under conditions of very high vacuum, is stated to result in a film which is less easily damaged. The process produces a film of the same thickness and with the same optical properties as are found in the conventional film. Information concerning the application of Transkote to specific surfaces may be obtained from the manufacturer.—PANCRO MIRROR, INC., *2958 Los Feliz Boulevard, Los Angeles 26, California.*

Casting Resin

Melpak IV is a casting resin designed specifically for encapsulating subminiature electronic circuits, wherever size, weight, temperature, moisture, or rough handling is a problem. Its dielectric constant is 4.76 at 8.4 mc and its power factor 6.4 percent at 34 mc. Operating temperature range of potted units is from −65°C (ambient) to +170°C (hot spot). Its curing time is 48 to 72 hr. and its shrinkage 6–8 percent. Further information is available from the manufacturer.—MELPAR, INC., *452 Swann Avenue, Alexandria, Virginia.*

New Organosilicons

Three new silanes (vinyltrichlorosilane, diethyldichlorosilane and phenyltrichlorosilane) have become available as "building blocks" which react easily with other organosilicons, alkyd resins, intermediates, and some unsaturated organics to produce liquid or solid polymers (used in hydraulic fluids, mold-release resins, electrical insulation, paint vehicles, and rubber-like materials). The new silanes, soluble in most organic solvents are colorless, fuming liquids. The great variety of useful polymers possible with them is due largely to the very reactive Si-Cl groups, which are readily converted to Si-O, Si-N, Si-S, and other groups. All chlorine atoms in the compounds are replaceable. Hydrolysis and condensation

reactions (with suitable catalysts) yield polymers whose composition and properties can be completely controlled. It is of special interest that the vinyl group is available for reaction either before or after polymerization. These materials are now in pilot production. Information and prices can be obtained from the manufacturer.—NEW PRODUCTS DIVISION, LINDE AIR PRODUCTS COMPANY, *30 East 42 Street, New York 17, New York.*

Fluorocarbons

In many particulars the fluorocarbons resemble the hydrocarbons of organic chemistry, with the important difference that the bond between fluorine and carbon is very much stronger than the corresponding one between hydrogen and carbon. For example, fluorocarbons are non-flammable. They can, however, be used in the formulation of various types of synthetics (lubricants, fibers, rubber-like materials, etc.) of extreme durability. During the early stages of the development of fluorocarbons high manufacturing costs prohibited most applications, but the development of a new electric-cell process now promises an effective solution to the economic problem. Feasibility of large-scale production by the electrical process is currently being demonstrated in pilot plant operation.—PENNSYLVANIA STATE COLLEGE, *State College, Pennsylvania.*

"Teflon" Coatings

Teflon, tetrafluoroethylene resin, is characterized by extreme resistance to corrosion and ability to withstand high temperatures. These properties have also made it difficult to fabricate into usable forms, except in relatively simple shapes with limited usefulness. It has recently been found that, when made up as a suspensoid (35 to 65 percent resin) it could be used as a spray finish, dipping enamel, compounded for extruding insulation on wire, for coating glass fabrics and tapes, and for fabricating unsupported film.

The spray-coating, after being dried at temperatures below 200°F, is brought to a temperature of 750°F, where the resin fuses to a continuous film. This finish will adhere to many metals, such as steel, stainless steel, aluminum, copper, brass, and to sandblasted glass, porcelain, and brick. Where damage occurs in use, the finish may be patched by cleaning down to the metal, applying more spray finish, and fusing with a blowtorch or gas flame. Such repairs can be made in 15–20 min. Spray finishes have chemical and heat resistance and moderately high resistance to wear or erosion. Indicated uses are coatings for chemical pipes and fittings, for agitators and rupture disks in chemical process vessels, for laboratory benches and hoods, and for insulation of equipment in electrolytic processes.

The fusing of Teflon wire enamels is comparable to that of spray finishes, although application is by dipping. **It has been demonstrated that a motor or transformer insulated with Teflon may be operated continuously at 400–500°F. Extrusion compounds have been developed for heavier insulation than is possible with enamel. Coatings from 5 to 20 mil thickness have been applied with a ram extruder, the resin being fused (after evaporation of the suspension liquid) at 700°F. The heavier coatings have exceptional dielectric** properties at high frequencies, and applications in radar and television installations are anticipated. They are also expected to be used for aircraft ignition, thermocouple leads, and in electrical equipment.

Coated glass fabric and unsupported films will complement the wire enamels and extruded coatings in electrical equipment, as slot liners, layer insulation, and possibly as a substitute for sheet mica. In the chemical industry, the fabrics may be used in protective clothing, gaskets, conveyor belts, and flexible ducts for hot, corrosive gases.

In effect, the coated fabrics are simply sheets of Teflon resin reinforced with glass cloth, and these may be laminated into strong, solid material of almost any desired thickness by bonding under heat and pressure.

The new forms of Teflon—spray finishes, enamels, and the raw suspensoid—are available in experimental quantities, and the film and tapes are being manufactured for testing purposes.—E. I. DUPONT DE NEMOURS AND COMPANY, ***Wilmington 98, Delaware.***

Rare Gases

The chemical inertness of the rare gases has led to commercial applications for all of them. The use of neon in electric signs, of helium as a lifting gas, and of argon for Heliarc welding and for filling incandescent lamps, indicates their wide fields of usefulness. Xenon and krypton occur in such small percentages in the atmosphere that their separation and purification has presented complicated problems. These difficulties have been overcome and spectroscopically pure gases are now available in quantity at reasonable prices. Krypton has been introduced as a gas filler for fluorescent lamps, and in some miniature lamps. Because of its low thermal conductivity, it permits the use of higher temperatures in tungsten-filament lamps. Xenon has been used in place of mercury vapor in certain types of thyratrons, since it does not condense at low temperatures. There are rare gas applications in the refining, alloying, and welding of metals. Argon may be used in the refining of calcium, lithium, titanium, chrome alloys, and other metals capable of combining with nitrogen. Another important application of the rare gases is in the filling of Geiger-Müller counter tubes.

Neon, helium, argon, krypton, and xenon are now available in 1-liter lead-glass bulbs containing approximately 1.1 liters of gas of high spectroscopic purity at normal pressure and temperature. —FISHER SCIENTIFIC COMPANY, *717 Forbes Street, Pittsburgh 19, Pennsylvania.*

THE
REVIEW OF SCIENTIFIC
INSTRUMENTS

VOLUME 21, NUMBER 2 *FEBRUARY, 1950*

A Precision Faraday Effect Apparatus[1]

Samuel Steingiser,[2] George J. Rosenblit, Robert Custer, and Chas. E. Waring
Department of Chemistry, University of Connecticut, Storrs, Connecticut

(Received March 28, 1949)

As a result of the improvements made in the Faraday Effect Apparatus as described, our results indicate an attainable precision of ±0.02 percent for visual measurements. Comparing this value with those reported by other investigators, indicates that a definite increase in precision has been achieved. As soon as our method for making measurements photoelectrically is fully developed, it is expected that the precision will be still higher. This will be especially true in the shorter wave-lengths where the eye is insensitive, and also where eye fatigue in general would be eliminated.

THE Magneto-Optic rotation, more commonly called the Faraday effect, is exhibited by all substances. This effect is becoming an increasingly powerful tool for research and analysis. In many cases, it is capable of producing results and giving information about various properties of these substances that are not readily obtainable by other means. In others, it serves as a useful confirmation of, or perhaps to question, conclusions arrived at by other methods. However, since the great amount of work done in the nineteenth century by Perkin and others, its use in the last forty years has been markedly restricted due to lack of sufficiently refined apparatus and also to lack of knowledge of structural effects.

In order to explore more completely the research possibilities of this tool, we have attempted to refine the experimental technique to such a degree so as to produce results of the highest precision possible. It is felt that, in preparation for publication of the results of our researches, a complete description of the apparatus should be given here, showing in what way advantage has been taken of modern equipment to re-establish the usefulness of the Faraday effect in chemical research.

When a plane polarized monochromatic beam of light is passed through a transparent isotropic liquid or solid, placed in a magnetic field and parallel to the lines of force of the field, the plane of vibration of the light beam is turned through a definite angle.

The rotation is proportional to the length of the light path in the medium and its direction is determined by the direction of the magnetic field only. If R is the total angle of rotation in minutes, l the length of the substance in centimeters through which the light beam passes, H the magnetic field strength in gauss, θ the angle between the direction of the magnetic field and the path of light, and V the proportionality constant known as the Verdet constant, then

$$R = V \cdot l \cdot H \cdot \cos\theta.$$

This Verdet constant varies with the nature of the substance through which the light is passing. In addition, it varies with the wave-length of the incident light and the temperature of the material. A more useful term actually employed is the molecular Verdet constant, which is the Verdet constant multiplied by the molecular weight and divided by the density.

It is thus apparent that a reliable determination of the Verdet constant involves the measurement of the angle of rotation of the polarized light, the wave-length of the light, the magnetic field strength and the temperature, to rather a high precision. In addition, subsequent calculations require the measurement of the refractive index and the density.

APPARATUS

Briefly, the major items of apparatus and their interrelationships are as follows. A large solenoid magnet,

---

[1] The work described herein has been supported in part under contract N6ori-216, Task Order 1, with the ONR, and in part by a Frederick Gardner Cottrell Grant-in-Aid from the Research Corporation, New York.

[2] This paper is abstracted from a thesis submitted in partial fulfillment of the requirements for the Ph.D. at the University of Connecticut, Storrs, Connecticut.

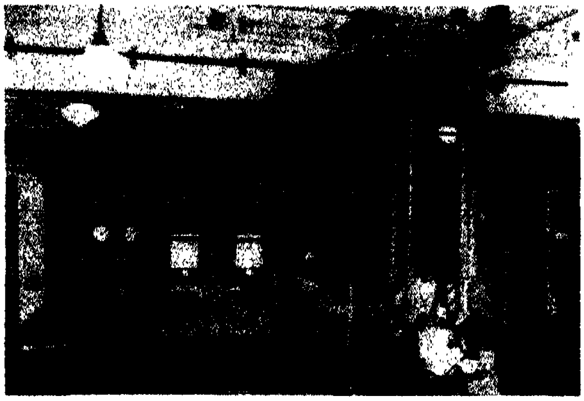

Fig. 1 (a).

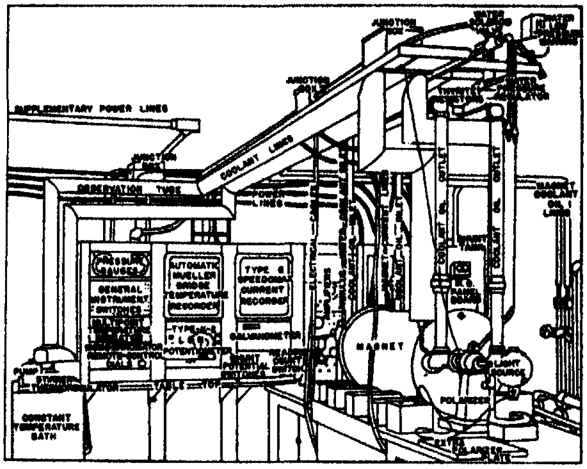

Fig. 1 (b).

surrounding the sample to be investigated, produces the rotation of the plane polarized light as determined by the polarimetric system. The dispersion of the light is produced by a monochromator placed in the light path. The current actuating the magnet is measured and recorded on a Speedomax recorder by means of a calibrated shunt-potential system. An indication is also made on this current record when the balance point of the light intensity of the two halves of the field in the split-field Lippich polarimeter is reached. This may be done visually or by a specially designed photoelectric comparator system. Thus, when for a specified value of the rotation angle, a balance of light intensities is reached, we have a record of rotation *versus* current, or in other words, rotation *versus* magnetic field strength. These are obtained at the exact same moment, the time lag being well within the precision of the measurements. This process can be repeated for any predetermined number of times, e.g., nine or thirty-six, etc., to produce a deviation measure of approx. ±0.01 percent.

Figures 1, 2, 3, and 4 are photographs of the completed apparatus. Outline legends are given with each photograph to identify the various portions of the apparatus. The apparatus as a whole may be subdivided for a more detailed description into three

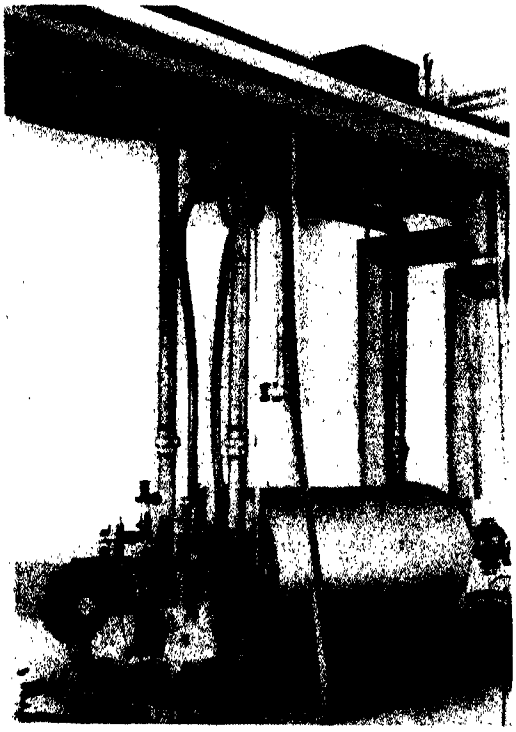

Fig. 2 (a).

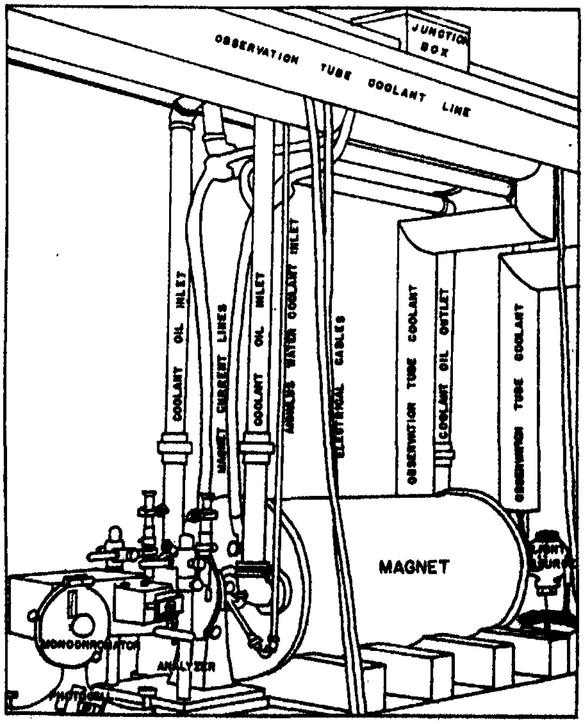

Fig. 2 (b).

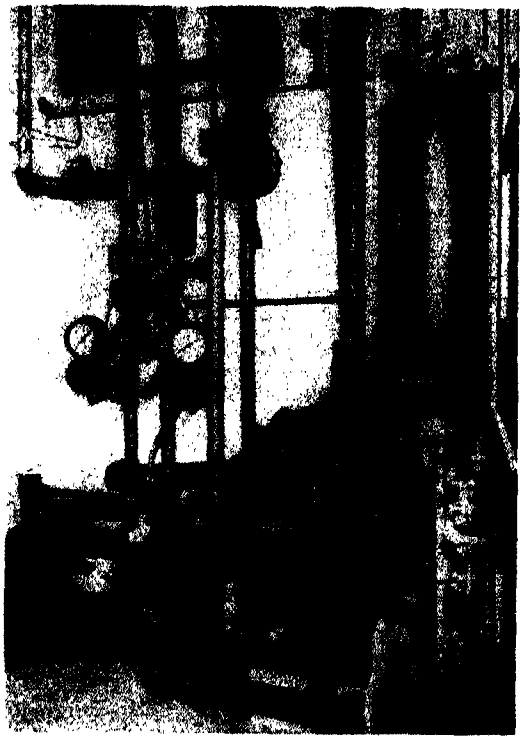

FIG. 3 (a).

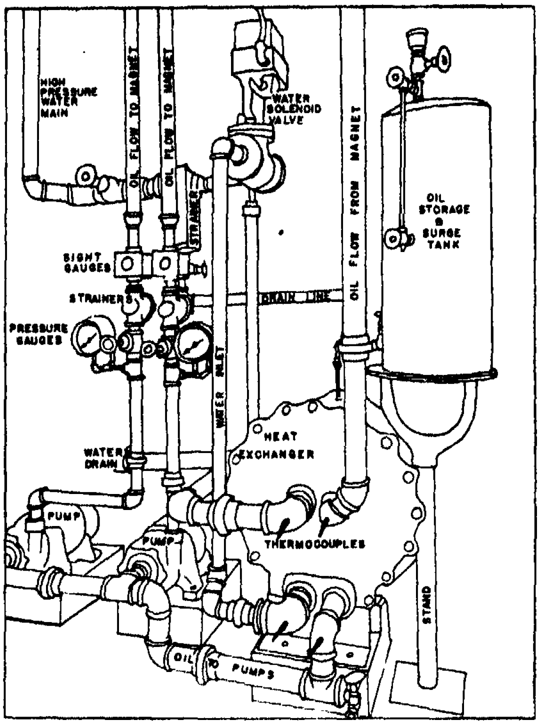

FIG. 3 (b).

sections: The electrical system (Fig. 5), coolant systems (Fig. 6), and the optical-null system (Fig. 7).

ELECTRICAL SYSTEM

The solenoid magnet is of the type described by Campbell and Houston,[3] as used by them for measurements of the Zeeman effect. It is 36 in. long, 18 in. in diameter, and is wound with No. 4 B and S gauge square copper wire, fiberglas insulated. Total weight of the magnet is approximately 1250 pounds. A d.c. motor generator set provides up to 200 amperes at 300 volts for maximum current through the magnet. At this value of current, the field generated is about 7200 gauss over each centimeter of length or close to half a million gauss cm over the entire length of the magnet. Thyrite resistors are inserted across the magnet lines as protective devices to prevent burnout of the coil due to high voltage arcing upon opening the circuit. The voltage and current through the magnet are controlled by means of 'fine' and 'coarse' adjustable field rheostats operating on the d.c. generator. The 'fine' rheostat is controlled by a geared motor device which drives for a definite period in one direction and then in the other direction causing the current to oscillate slowly about any preset value. The polarity of the direct current is

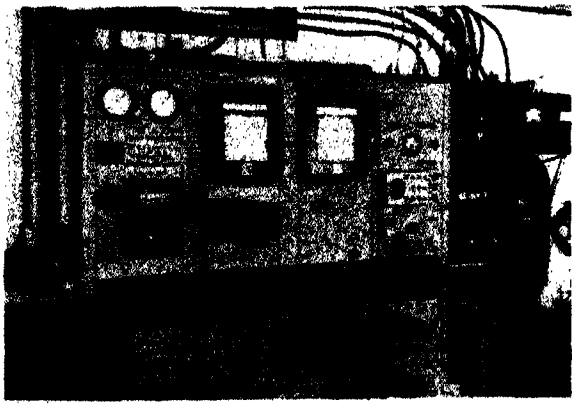

FIG. 4 (a).

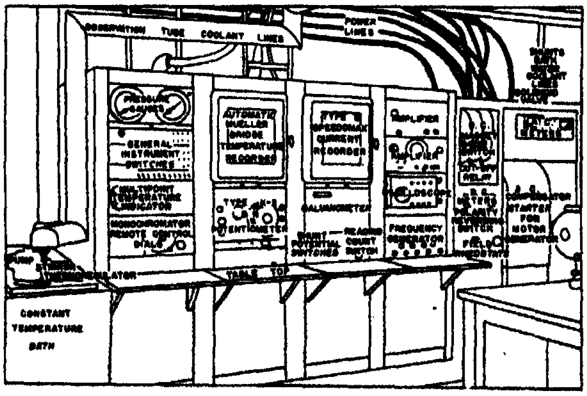
OBSERVATION TUBE COOLANT LINES
POWER LINES
PRESSURE GAUGES
GENERAL INSTRUMENT SWITCHES
MULTIPOINT TEMPERATURE INDICATOR
MONOCHROMATOR REMOTE CONTROL DIALS
AUTOMATIC MUELLER BRIDGE TEMPERATURE RECORDER
TYPE K-2 POTENTIOMETER
TYPE S SPEEDOMAX CURRENT RECORDER
GALVANOMETER
SHUNT POTENTIAL SWITCHES
READING COUNT SWITCH
AMPLIFIER
AMPLIFIER
OSCILLOSCOPE
FREQUENCY GENERATOR
CUT-OFF RELAY
D.C. METERS
POLARITY REVERSING SWITCH
FIELD RHEOSTATS
STARTER FOR MOTOR GENERATOR
PUMP
THERMOREGULATOR
TABLE TOP
CONSTANT TEMPERATURE BATH

FIG. 4 (b).

---

[3] Campbell and Houston, Phys. Rev. 39, 601 (1932).

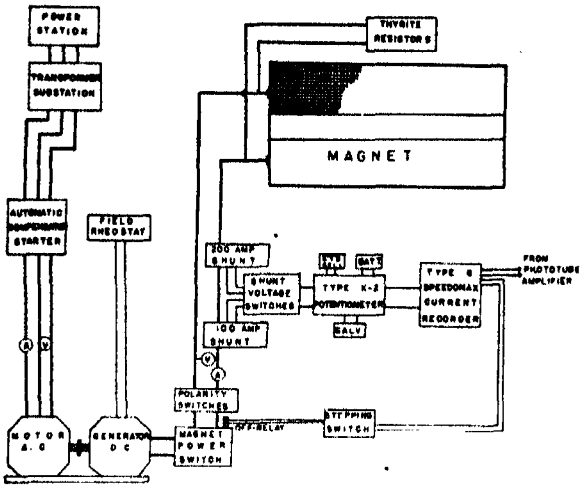

FIG. 5. Electrical system.

changed by means of a set of polarity switches operating through the field coils of the generator. The current is measured by means of a shunt-potential system using two large precision Leeds and Northrup shunts. For currents up to 100 amperes, the 0.01-ohm shunt, and for currents between 100 and 200 amperes, a special 0.005-ohm shunt is used. These are calibrated to ±0.04 percent and by placing them both in a thermostated oil bath to prevent any temperature rise, a precision of ±0.01 percent is attainable in their values. This is the limit of precision we are attempting to set for the overall instrument. Upon passage of current, these shunts will generate a voltage, which is bucked by a slightly lower voltage from a Type K-2 Leeds and Northrup potentiometer. This potentiometer is also precise to ±0.01 percent operating from a double set of large-capacity long-life Willard batteries, kept at a uniform temperature, and a standard cell newly standardized in absolute voltage units. The slightly excess potential which has not been bucked out by the potentiometer is then placed on a Leeds and Northrup Type G Speedomax 'current' recorder. This is a 10-millivolt unit, which in conjunction with the shunts used, will place 1 or 2 amperes across full scale. The speed of travel of the recording pen is $\frac{3}{4}$ seconds across the chart. There are 100 ruled divisions on the chart allowing all measurements of the current to be made to ±0.01 percent, with further estimates being made to ±0.001 percent. The chart speed of the Speedomax has been stepped up to 360 inches per hour or $\frac{1}{10}$ in. per second, producing a very precise continuous determination of the current. An auxiliary pen, mounted on the side of the chart, indicates by a pip, the optical-null point of the polarimeter. This null is obtained either visually or photoelectrically. This then gives us, for any angle set on the polarimeter, a definite value of the current and thus, since the current is directly proportional to the field strength, we have the value of rotation *versus* magnetic field strength. The number of pips or readings is automatically counted on a relay stepping switch which can be preset for any number of readings: 1, 4, 9, 16, 25 or 36, at which time a solenoid plunger relay, mounted with the large magnet power switch, is activated. This power switch is thus thrown off, the magnet is deactivated and a set of readings is completed.

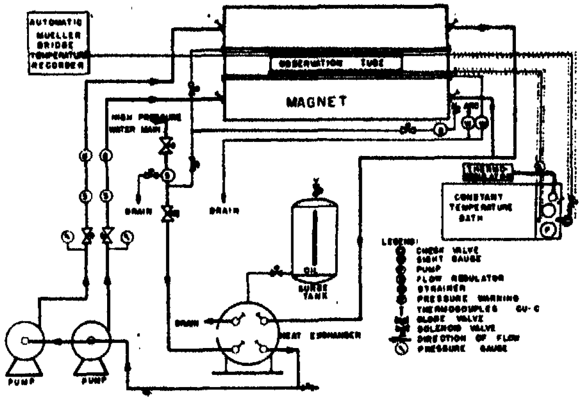

FIG. 6. Coolant systems.

COOLANT SYSTEM

Approximately 65,000 watts are generated each second of the run and this heat must be removed rapidly and uniformly to prevent overheating of the magnet and to allow closer control over the current being supplied to it.

The coolant system has three major divisions whose functions are the cooling of the magnet proper, cooling of the internal core into which the observation tube is set, and the maintenance of a constant temperature around the observation tube itself.

The magnet proper is cooled by pumping Westinghouse Wemco C transformer oil longitudinally through spaces so arranged that the upper and lower face of each winding is in contact with the transformer oil. Two centrifugal pumps, connected in parallel, pump the oil through the magnet at the rate of 100 g.p.m. and then through a heat exchanger after which it is recycled. The heat is transferred in the exchanger to the cold water supplied from a high pressure building main. The

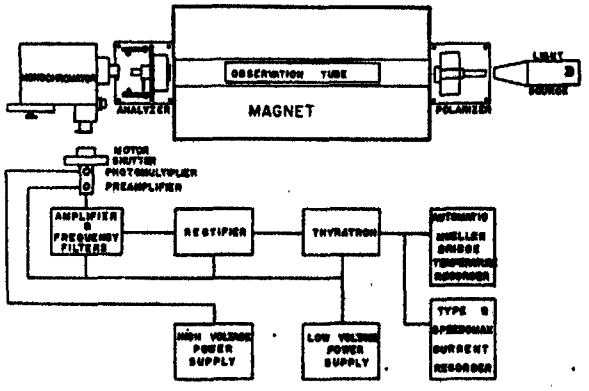

FIG. 7. Optical-null system.

TABLE I. Measured data for acetone-chloroform solution No. 1A.

Run	Angle read	Current	Current deviation	Wave-length	Average tempera-ture	Tempera-ture range
418*D*	75.000	136.856	±0.040	5893	20.01	±0.02
419*U*	75.000	132.182	0.034	5893	20.00	0.02
420*U*	75.000	126.814	0.040	5780	19.93	0.05
421*U*	75.000	112.512	0.032	5461	19.98	0.03
422*U*	150.000	137.758	0.018	4358	19.95	0.04
423*D*	150.000	140.062	0.014	4358	19.89	0.03
424*D*	75.000	115.952	0.028	5461	20.17	0.03
425*D*	75.000	131.072	0.034	5780	20.12	0.05
426*D*	75.000	131.854	0.044	5780	24.82	0.10
427*D*	75.000	116.826	0.028	5461	24.92	0.02
428*D*	150.000	141.076	0.020	4358	24.99	0.06
429*U*	150.000	138.790	0.026	4358	25.10	0.10
430*U*	75.000	113.230	0.030	5461	25.07	0.05
431*U*	75.000	127.692	0.042	5780	24.94	0.03
432*U*	75.000	133.130	0.034	5893	24.95	0.03
433*D*	75.000	137.844	0.046	5893	24.84	0.03

flow of water through the exchanger is about 5000 gallons per hour. An oil expansion and surge tank is provided at the heat exchanger. With this coolant system, the magnet runs at room temperature with currents up to 150 amperes. At 200 amperes, a 10°C rise is produced in the magnet with a 1°C maximum differential from one end of the magnet to the other.

The internal core is cooled by passing an ⅛-in. annulus of cold water through it, regulated by a constant pressure valve. A Fischer-Porter Ratosight alarm flowmeter is used to indicate proper water flow and to sound an alarm at any water failure.

The temperatures of the inlets and outlets of the heat exchanger and inlets and outlets of the magnet and of the annulus core coolant are measured by means of miniature pipe-type copper-constantan thermocouples connected through a multipoint switch to a 0–200°C Wheelco pyrometer reading to ±1°C.

The third division of the coolant system is for the control of the observation tube. A condenser-type brass jacket is built around a quartz observation tube with inlet and outlet tube coming out of one side of the magnet core. The brass jacket is covered with an ⅛-in. asbestos coating for further heat insulation. A large Aminco refrigerated constant temperature bath, controlled to at least ±0.03°C, pumps a water-prestone solution via heavily cork-insulated lines through the observation tube jacket. A flowmeter alarm indicates the flow through the system and sounds an alarm if the values differ from the preset ones. A platinum resistance thermometer is inserted in a well in the brass jacket of the observation tube and is connected to an automatic Mueller Bridge temperature recorder[4] reading to ±0.01°C. An auxiliary pen, which produces a series of pips each time a reading is made, is also mounted on this temperature recorder. Thus, we know the mean temperature of the cell to ±0.01°C as each reading is made.

Another coolant line is available for use with the Hanovia hydrogen arc used as a light source. This line is also protected by a water regulating valve and a flowmeter alarm unit.

OPTICAL-NULL SYSTEM

Various light sources are used including the sodium and mercury arcs for the line bands, a Cenco tungsten lamp, a Hanovia hydrogen arc and a Western Union concentrated arc for the continuous range from the ultraviolet to the near infra-red.

The polarimetric unit, made especially for this Laboratory by the Gaertner Scientific Company, allows the

TABLE II. Calculation of data for acetone-chloroform solution No. 1A.

Run	λ	$\overline{\text{Temp.}}$	$\overline{\text{Rot}}_{\text{Tot}}$	I_{Tot}	$\bar{R}/\bar{I}=k_T$	$k_Q \times 10^5$	k_T-k_Q	Δt	$\Delta k_s \times 10^5$	$\frac{\Delta k_s}{\Delta t}\times 10^5$	$t-t^*$	t^*	$\Delta k_s^* \times 10^5$	k_s^*	$k_s^*\lambda/k_s^*D$
432*U* 433*D*	5893	24.90	75.000	135.487	0.55356	277	0.55079	4.90	398	81	−0.10	25	−8	0.55071	
418*D* 419*U*	5893	20.00	75.000	134.519	0.55754		0.55477				0.00	20	0	0.55477	
426*D* 431*U*	5780	24.88	75.000	129.773	0.57793	281	0.57512	4.86	372	77	−0.12	25	−9	0.57503	1.0442
420*U* 425*D*	5780	20.02	75.000	128.943	0.58165		0.57884				+0.02	20	+2	0.57886	1.0434
427*D* 430*U*	5461	25.00	75.000	115.028	0.65202	304	0.64898	4.92	454	92	0.00	25	0	0.64898	1.1784
421*U* 424*D*	5461	20.08	75.000	114.232	0.65656		0.65352				+0.08	20	+7	0.65359	1.1781
428*D* 429*U*	4358	25.04	150.000	139.933	1.07194	525	1.06669	5.12	790	154	+0.04	25	+6	1.0668	1.9370
422*U* 423*D*	4358	19.92	150.000	138.910	1.07984		1.07454				−0.08	20	−12	1.0745	1.9368

---

[4] See D. R. Stull, Rev. Sci. Inst. 16, 318 (1945).

measurements of the angle of rotation to be made to a precision of 0.001°. The analyzer and polarizer sections are so constructed as to permit their removal for the insertion of the observation cell into the magnet and for the subsequent return to their original optical alignment. The polarizer is a Lippich half-shadow type, made with Glan-Thompson prisms. The analyzer scale has an optical vernier consisting of a filar microscope and micrometer.

The observation tube in the magnet core is about 22 in. long and was made by the American Instrument Company to our specifications. The entire body and end plates are of fused quartz made within the usual specifications of absorption cells. A ground stoppered opening is provided at one end of the tube for emptying and filling. The entire cell is of one piece construction with no cement in any portion.

The light beam which has passed through the polarizer and the sample in the magnetic field and the analyzer, is now passed through a monochromator and then to the observer's eye or to an automatic photoelectric scanning device. Two monochromators, both built by Gaertner, are used interchangeably. One is a precision quartz long range unit from 1850–20,000A and the other a precision visual monochromator from 3900–8200A. Measurements are being made of the Faraday effect with a band width of 20A units. The range of the monochromators is greater at present than that of the polarimeter, which has optics only for the visual wave-lengths. Plans are being drawn up for ultraviolet and infra-red polarimetric units so as to extend studies to these spectral ranges.

The photo-multiplier device for indicating matched intensities or the "null" of the polarimeter is so arranged as to fire a thyratron tube which then activates the two relay pens, one located on the current Speedomax and the other on the Mueller Bridge temperature recorder. The circuits involved in this photo-multiplier scanning device will be published at a later date.

TYPICAL DATA

In Table I are given the measured data for a typical solution run in this apparatus. It is a binary mixture of acetone and chloroform. The letters *D* and *U* in the run number signifies the polarity of the current through the magnet. The correct combination of runs is that having a *D* and a *U* for the same conditions of temperature and wave-length, producing the average rotation. The angle read is the angle set on the polarimeter scale for that run. The current is the mean of 18 individual settings of equal intensity of the polarimetric field as described earlier. The current deviation gives the actual average deviation of the mean, A.D. The wave-length is that set on the monochromator for that run. The average temperature is the mean temperature during the entire run as shown on the Mueller Bridge temperature recorder. The temperature range is one-half the spread of the temperatures furthest apart during a run. In Table II are given the calculations for the data shown in Table I. Two runs are combined, one for each polarity at the same temperature and wave-length. $\overline{\text{Temp.}}$ is the mean temperature of the two runs, $\overline{\text{Rot}}_{\text{Tot}}$ is the average rotation of the sample including that for the tube windows, etc., $\bar{I}_{\text{Tot}}$ is the average current for the two runs, and $\bar{R}/\bar{I}=k_T$ is the ratio of these two factors. k_Q is the same ratio for the quartz tube windows as determined earlier. k_T-k_Q is the value of the ratio for the sample only. Δt is the difference in temperature between the two measured k's at the two temperatures used, Δk_s is the difference in the k's for the same temperatures, $\Delta k_s/\Delta t$ is the value of this difference per degree C, $t-t^*$ is the difference in the experimental temperature and the whole number temperature t^*, and Δk_s^* is the difference to be added or subtracted to k_T-k_Q to give the final value of the ratio k_s^* at the uniform temperature intervals of 20.00° or 25.00°C. It is this value of k_s^* which, when multiplied by the apparatus constant, K, of 0.028030, will give the Verdet constant of the material under investigation.

THE REVIEW OF SCIENTIFIC INSTRUMENTS VOLUME 21, NUMBER 2 FEBRUARY, 1950

Velocity-Acceleration Response from a Seismic Pick-Up via Controlled Damping

ROBERT J. JEFFRIES*
Department of Engineering Research, North Carolina State College, Raleigh, North Carolina

(Received June 30, 1949)

The basic theory of the seismic pick-up is developed and interpreted to show that it is theoretically possible to make a simple seismic system directly amplitude-sensitive to velocity as well as acceleration and/or displacement. This is accomplished by appropriate control of the damping.

INTRODUCTION

SPRING-SUPPORTED seismic masses are used to detect and measure various dynamic characteristics of vibratory motions. Figure 1 illustrates the basic form and application of such a pick-up having "viscous" damping. The relative motion, $s=y-x$, between the seismic mass and the case to which it is connected through a supporting spring system, is usually utilized as being proportional to the quantity to be measured. This relative motion may be detected by mechanical or electrical means. The case (shown partially in cross-section) is securely fastened to the member whose vibratory motion is to be studied.

Numerous pick-ups of this type are available commercially. They are frequently used for both root-mean-square and instantaneous measurements of the displacement and acceleration of vibrating members. In such applications they are known respectively as vibrometers and accelerometers. The theory permitting these applications is well known and will not be repeated here.[1]

An output signal approximately proportional in amplitude to the velocity of the vibrating member is frequently derived from the relative motion, s, in commercial equipments, by generating a voltage in a coil of wire moving with the motion, s, through a magnetic field, the voltage thus induced being proportional to ds/dt, and hence approximately proportional to dx/dt.

It is the purpose of this paper to show that a basically different technique for obtaining a velocity-sensitive response is theoretically possible. The method proposed makes it possible to design for a relative motion. s, which is directly proportional to *either* velocity or acceleration of the vibrating member over a given frequency range, by appropriate control of the damping.

PICK-UP CHARACTERISTICS REQUIRED FOR VELOCITY AND ACCELERATION-SENSITIVE RESPONSE

Given a steady-state displacement function represented by

$$x=A\sin\omega t \tag{1}$$

there is associated both a velocity and an acceleration, represented respectively, by the following expressions:

$$\text{velocity}=dx/dt=\omega A\cos\omega t=\omega A\sin(\omega t+90°), \tag{2}$$

$$\text{acceleration}=d^2x/dt^2=-\omega^2 A\sin\omega t =\omega^2 A\sin(\omega t+180°). \tag{3}$$

Figure 2 illustrates, in wave form, the phase relations of these quantities. Figure 3 illustrates, in terms of amplitude and phase, the characteristics required of a pick-up for exact velocity and acceleration-response.

PERFORMANCE CHARACTERISTICS OF A SEISMIC ELEMENT AS A FUNCTION OF FREQUENCY

The amplitude- and phase-response-*versus*-frequency characteristics of a simple seismic system of the type illustrated in Fig. 1 are shown in Fig. 4 with damping as a parameter. The abscissae for these curves are the various ratios of the frequency of the impressed displacement function of the pick-up case to the natural mechanically-resonant frequency, ω_n, of the seismic system. The damping is expressed as the ratio of the actual damping present to the critical value.[2]

A qualitative inspection of the amplitude-response characteristics reveals that for relatively small values of the damping ratio ($0.5<\delta<1.0$) and for frequencies between zero and the natural resonant frequency of the mechanical system, the peak variation in relative motion, s, with frequency of the displacement function, approximates a square law relation. This approximates, then, the required amplitude characteristic for ac-

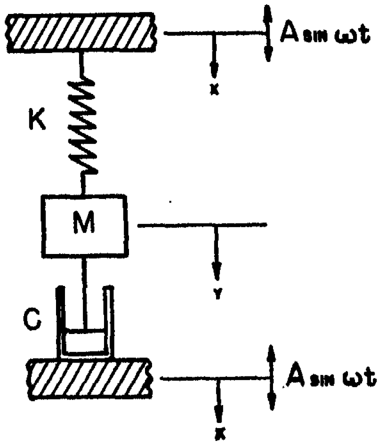

FIG. 1. Fundamental form of a seismic pick-up.

---

* Research associate.

[1] See, for example, W. T. Thomson, *Mechanical Vibrations* (Prentice-Hall, Inc., New York, 1948), pp. 94–97.

[2] For definition and interpretation of the critical damping factor, see, for example, reference 1, p. 64.

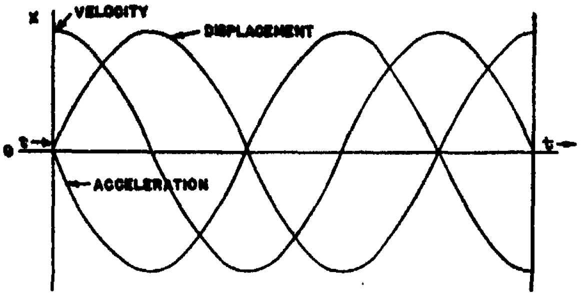

FIG. 2. Phase relations of the dynamic characteristics of a simple harmonic displacement.

celeration-response. However, reference to the phase-response characteristics for values of ω/ω_n between zero and one reveals no value of δ in this range for which the characteristic even approximates the desired 180° phase shift, corresponding in this plot to an indicated constant phase angle of zero degrees.[8] A value of δ between 0.5 and 1.0 will, however, yield an approximately linearly increasing phase angle, and it is a well-known fact that any system possessing a phase characteristic such that the output phase angle is directly proportional to the

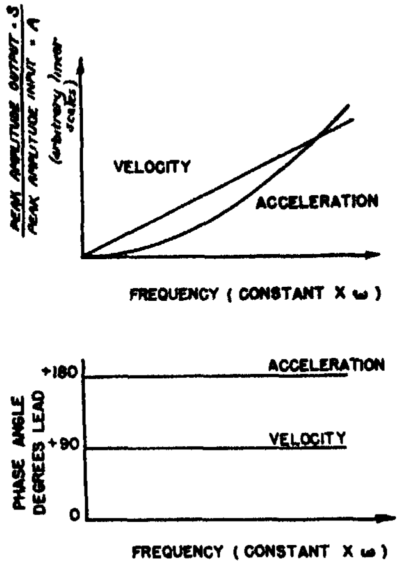

FIG. 3. Amplitude and phase-response characteristics of an ideal velocity and acceleration-sensitive pick-up.

input frequency will transmit a function without distortion but with phase delay. A selection of $\delta \simeq 0.7$ for acceleration response is, therefore, a necessary compromise which yields a reasonably good square-law amplitude-response characteristic over a wide frequency range, and a phase-response characteristic which will delay, but not distort the output wave form.

From qualitative observation of both the amplitude and phase-response characteristics, it is apparent that for large degrees of damping ($\delta \gg 1$) the amplitude-response characteristic approximates the linearly increasing function required for velocity response, and the phase-response characteristic closely approximates the required 90° phase shift, lead, over a substantial frequency range between $\omega/\omega_n = 0$ and $\omega/\omega_n = 1$. These observations lead to the conclusion that the same seismic system may be made either acceleration or velocity-responsive by proper selection of the damping. Because the amplitude of the output decreases with increased damping, it is desirable to use the minimum amount of damping consistent with the accuracy desired.

Desirable values of δ for both velocity- and acceleration-response may be readily selected by reference to a plot of the actual and required amplitude-response characteristics on log-log paper. If the required amplitude-response *versus* frequency characteristics are plotted on log-log paper, they appear as straight lines, the velocity characteristic having a slope of one and the acceleration characteristic a slope of two. By superposing the actual characteristics one may easily select the degree of damping which will yield either velocity- or acceleration-response, over any desired frequency range, to the accuracy desired. Figure 5 shows such a super-

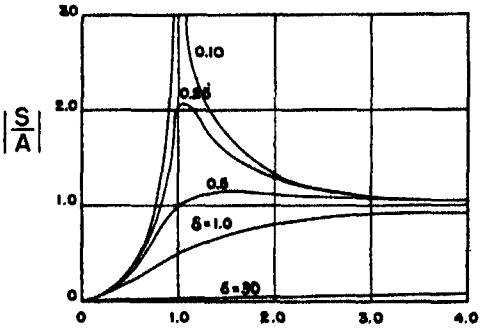

RELATIVE AMPLITUDE RESPONSE
(a)

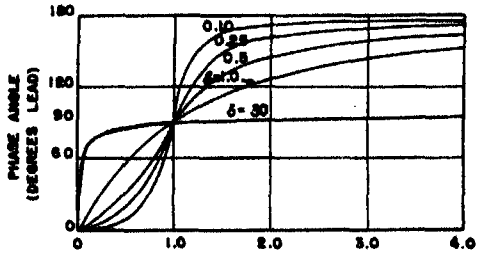

RELATIVE PHASE RESPONSE
(b)

FIG. 4. Amplitude and phase-response characteristics of a seismic pick-up.

---

[8] The correspondence of a constant phase characteristic angle of 0° in Fig. 4(b) to the ideal constant phase characteristic angle of 180°, lead, for true acceleration response is a result of the sign of the solution of the differential equation arising from the assumption of an impressed *displacement* function.

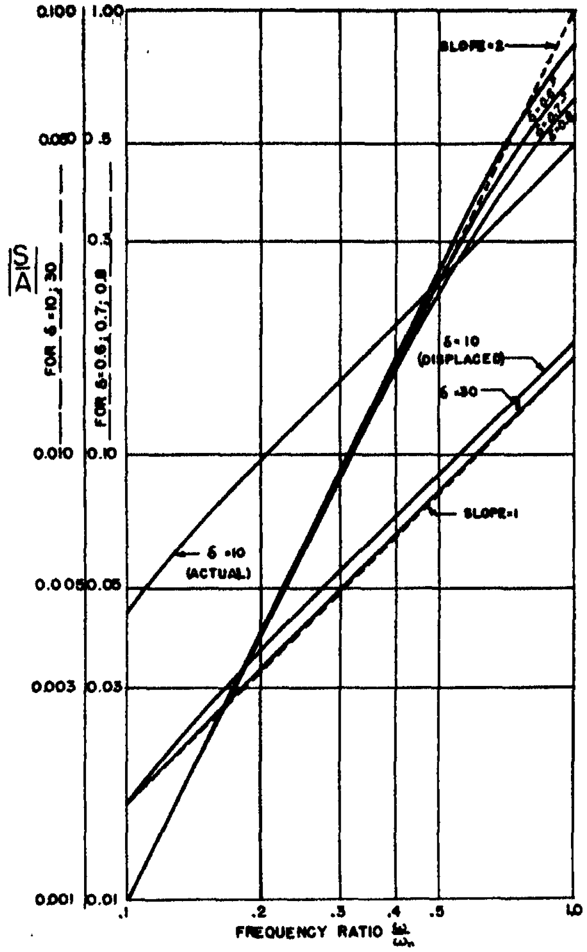

FIG. 5. Amplitude-response characteristics of a seismic pick-up with various degrees of damping.

position. It is readily apparent that a damping factor of 0.7 will give a near-perfect acceleration-response while a damping factor of 30 will yield a near-perfect velocity-response. The reduction in sensitivity (of the order of 10:1) occasioned by the greater damping required for the velocity-sensitive characteristic is not excessive.

It is suggested that the two values of damping required might conveniently be achieved by electrical "drag-type" damping, in which the strength of the magnetic field through which a conducting sheet moves (with motion s) might be controlled by a two-position switch, the switch positions corresponding respectively to velocity and acceleration-response.

CONCLUSIONS

It is theoretically possible to make the output of a seismic pick-up directly proportional to either velocity or acceleration of an impressed displacement function by appropriate control of the damping. A value of damping factor, $\delta = 0.7$, represents a compromise between the available amplitude and phase-response characteristics, and will yield a near-perfect acceleration-responsive pickup. A value of the damping factor, $\delta = 30.0$, yields a near-perfect velocity-responsive pick-up in which both the amplitude and phase-response characteristics closely approximate those required for perfect velocity-response. The control required on the damping to effect either velocity or acceleration-response might conveniently be achieved by electrical damping.

ACKNOWLEDGMENT

The author wishes to express his appreciation to Dr. G. B. Hoadley of this Institution's Department of Electrical Engineering for his careful reading of the manuscript and his valuable suggestions, and Mr. E. H. Tompkins of the Department of Engineering Research for his assistance with the illustrations.

Variation of Grain Density with Temperature of Exposure in Nuclear Emulsions[*]

ELSIE M. DOLLMANN
Brookhaven National Laboratory, Upton, New York

(Received August 1, 1949)

Ilford C-2 unloaded and C-2 boron loaded plates, subjected to temperature changes varying from −66°C to +66°C, were bombarded with 10-Mev neutrons. The recoil protons showed that the temperature change had caused an increase in grain density which varied as much as ⅓ from −66°C to +25°C. Although the C-2 boron loaded plates showed a greater initial grain density than the unloaded plates, the ⅓ increase was preserved.

WHEN scattering and grain density measurements of a number of prongs from stars found in nuclear emulsions exposed to cosmic radiation were compared, an inconsistency was found to exist. In order to examine the possibility that the inconsistency was due to the fluctuation in temperature during the balloon flights, a preliminary survey of temperature-controlled neutron-irradiated plates was made. The results indicated that temperature change had caused a reduced grain density which varied as much as ⅓ between −66°C and +25°C. A temperature correction caused the inconsistency to disappear.[1]

Two groups of experiments were performed in which Ilford C-2 unloaded and C-2 boron loaded plates were subjected to various temperature changes before being exposed to a beam of 10-Mev neutrons from the cyclotron at Columbia University.

Wide mouth glass test tubes, each holding Ilford plates wrapped in black paper, a thermometer, and a mixture of rice and silica gel, were immersed in Dewar flasks containing various cooling and heating mixtures having temperature ranges from −77°C to +66°C. The rice and silica gel was used to maintain a constant relative humidity of 67 percent throughout the experiment. In the first trial each tube contained two Ilford C-2 unloaded 50μ plates, three old Ilford C-2 boron loaded 50μ plates, and three new Ilford C-2 boron loaded 50μ plates. For the second run two Ilford C-2 unloaded 100μ plates and two new Ilford C-2 boron loaded 100μ plates were placed into each tube. The plates remained in the Dewar flask for four hours during which time a temperature equilibrium was reached.

The thermally insulated Dewar flasks were then opened in the cyclotron room; the plate containers were removed and exposed to a beam of 10-Mev neutrons. The temperature before and after each exposure in each case is given in Table I. The variation in temperature in the second group is small due to greater care in handling the plate containers during exposure and better insulation. After exposure the plates were allowed to return to room temperature before being developed according to the standard method recommended by Ilford.

A microscope having a 90× oil immersion objective with a 12.5× compensating eyepiece was used for grain counting. The observers counted the number of grains in 150-eyepiece scale divisions starting 100 divisions from the end of the track. Each division is equivalent to 1.13 microns. Only those recoil proton tracks more than 300μ long and ending in the emulsion were considered. The results are given in Figs. 1 and 2.

Each point on the curves represents the average grain count of many (from 15 to 20) recoil proton tracks. Figure 1 shows two curves. Curve 1 represents the values obtained from Ilford C-2 unloaded 100μ plates. The grain density of the recoil proton tracks shows about a ⅓ increase from −66°C to +25°C, after

TABLE I.

Type of plate	Temperature in degrees centigrade Before exposure	 After exposure	 Average
Group 1			
New and old Ilford C-2 boron loaded 50μ	−75.0	−57.0	−66.0
	−43.0	−22.0	−32.5
	−31.0	−18.0	−24.5
	−10.0	− 2.0	− 6.0
	1.0	7.0	4.0
	21.0	21.0	21.0
	39.0	34.5	36.8
New Ilford C-2 unloaded 50μ	−77.0	−57.0	−67.0
	−41.0	−26.0	−33.5
	−33.0	−22.0	−27.5
	−10.0	− 1.0	− 5.5
	0.5	2.0	1.2
	21.0	21.0	21.0
	40.0	35.0	37.5
Group 2			
Ilford C-2 unloaded 100μ, Ilford C-2 boron loaded 100μ	−66.0	−64.5	−65.2
	−61.0	−59.0	−60.0
	−48.0	−46.0	−47.0
	−40.0	−38.0	−39.0
	−30.0	−29.0	−29.5
	−25.0	−23.5	−24.2
	−14.0	−13.5	−13.8
	− 2.0	− 2.0	− 2.0
	2.0	2.5	2.2
	11.0	12.0	11.5
	25.0	24.5	24.8
	29.5	29.5	29.5
	42.0	41.0	41.5
	46.0	44.0	45.0
	56.0	54.5	.55.2
	58.5	58.0	58.2
	66.0	65.0	65.5

---

[*] Research carried out at the Brookhaven National Laboratory under the auspices of the AEC.

[1] Salant, Hornbostel, and Dollmann, Phys. Rev. 74, 694 (1948).

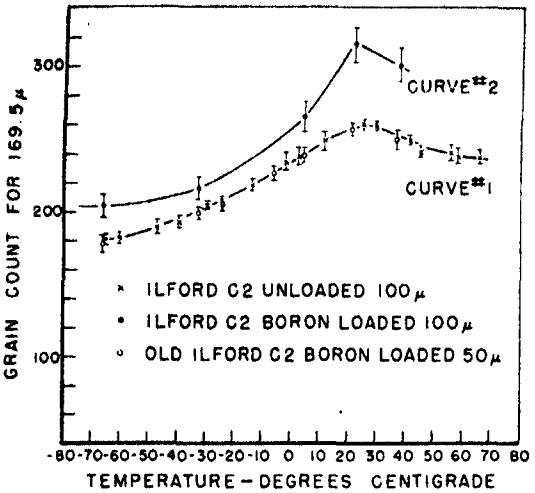

FIG. 1. Temperature *versus* grain density for 3 groups of Ilford plates.

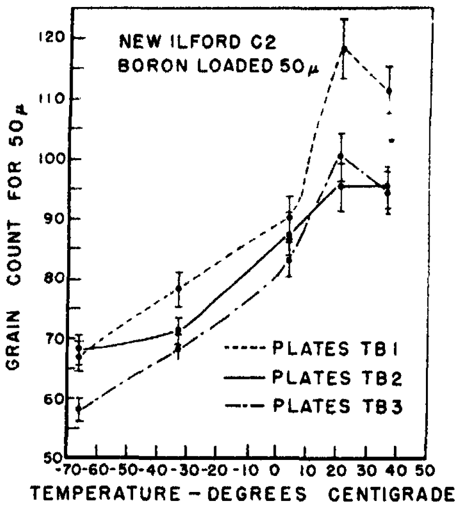

FIG. 2. Temperature *versus* grain density for new Ilford C-2 boron loaded 50μ plates.

which temperature there is a decrease that is primarily due to a photo-chemical change occurring in the emulsion as the temperature is increased. Beyond +40°C a simple interpretation can no longer be given to the curve. A second group of points which fall close to Curve 1 is from Ilford C-2 boron loaded 50μ plates. These plates, however, had been lying around the laboratory for almost a year before exposure. It is likely that they did not possess their full sensitivity at the time of exposure. These plates have been designated as "old". It is well known that, for the same development, tracks in boron loaded plates are on the average much heavier than those in unloaded plates. This is seen in Curve 2 where a fresh batch of Ilford C-2 boron loaded plates was used. Although the intrinsic grain density is heavier, the increase of $\frac{1}{3}$ in grain count for −66°C to +21°C is still preserved. Due to the irregular concentration of boron in the plates the grain density shows a variation as seen in Fig. 2. The three curves show the average value plotted for three sets of plates. Here only fifty microns were counted, starting, as before, 100 divisions from the heavy end of the track.

Similar interpretations were obtained by Cosyns, Dilworth, and Occhialini[2] in their experiments on reducing background tracks by storing the plates at low temperatures. Kodak NT2A plates were exposed to gamma-rays from a radium source between the temperatures of −87°C to +20°C.

Due to decrease in grain density of tracks at low temperatures and the possibility of mistaking low temperature protons for mesons, thereby increasing the apparent meson yield, it is advisable to include temperature recorders or controls in all flights where these nuclear emulsions are used.

I am indebted to Dr. M. Blau for arranging the exposures at the Columbia University cyclotron, and to Dr. C. W. van der Merwe of New York University and Mr. Joseph E. Smith of Brookhaven National Laboratory for helping with the grain counting and to Dr. E. O. Salant for suggesting this problem.

---

[2] Cosyns, Dilworth, and Occhialini, "Obturateur thermique pour plaques nucléaires," Université Libre de Bruxelles, Note n°6 (January, 1949).

THE REVIEW OF SCIENTIFIC INSTRUMENTS VOLUME 21, NUMBER 2 FEBRUARY, 1950

The Design and Construction of a Stark-Modulation Microwave Spectrograph

A. Harry Sharbaugh
General Electric Research Laboratory, Schenectady, New York

(Received August 10, 1949)

A detailed description of a Stark-modulation (see reference 1) microwave spectrograph which has been designed and constructed in this laboratory is given. Circuit diagrams and values of the components are given for all the custom-built equipment. The frequency range is from 17 to 28 kmc/*s*. Peak Stark-modulation voltages up to 1500 volts sine wave and 800 volts square wave are used. The sensitivity is better than 1×10^{-8} cm^{-1}. The absorption lines are about 300 kc wide at half-power and the practical limit of resolution is between ½ and 1 mc. Frequencies may be measured to better than ±0.08 mc.

A. INTRODUCTION

In postwar years the field of spectroscopy in the microwave frequency region has grown with tremendous rapidity. This growth has been stimulated chiefly by the great advances in microwave techniques during the last war and the fact that the method provides the molecular structure investigator with a new source of valuable information. Microwave spectroscopy permits precise evaluation of absorption frequencies (to about one part per million) and resolving powers thousands of times better than the best infra-red spectrometers; thus contributing to a more complete knowledge of the spatial arrangement of atoms in the molecule as well as a study of nuclear spins and quadrupole moments. As evidenced by the wide use of optical spectrometers in industry, the future of the microwave instrument as an analytical tool promises to be a great one.

One of the most successful approaches used for detecting weakly absorbing lines in this high radiofrequency region is that devised by Hughes and Wilson[1] and is usually referred to as the Stark-modulation method. This paper will be concerned with the design and construction details of a microwave spectrograph using this principle.

Briefly, the Stark-modulation scheme makes use of the change in the absorption frequency of a gas molecule when the molecular energy levels are perturbed by an external electric field, i.e., the so-called Stark effect. Referring to Fig. 1, microwave energy from a source is passed through the gas-to-be-studied which is confined in a wave guide cell by transparent mica windows at each end. If the source is tuned to an absorption frequency then a diminished amount of power will be received at the crystal detector. However, the absorption frequency of the gas is being alternately switched between two frequencies corresponding to the peaks and troughs of an externally applied 100 kc square or sine wave electric field based on zero voltage. This field is applied between an insulated electrode strip running down the center of the wave guide and the wave guide itself. Hence the signal reaching the crystal detector is amplitude-modulated or, as we may say, Stark-modulated, at a 100-kc rate and may be amplified and presented on the vertical plates of an oscilloscope. In order to examine a finite region of the spectrum at one time, a frequency axis is provided on the oscilloscope by frequency-modulating the source with a lower frequency saw-tooth voltage and applying this same voltage to the horizontal plates of the oscilloscope (refer to Fig. 1). Figure 1a shows a complete block diagram of the system and the components will be discussed individually in the ensuing sections.

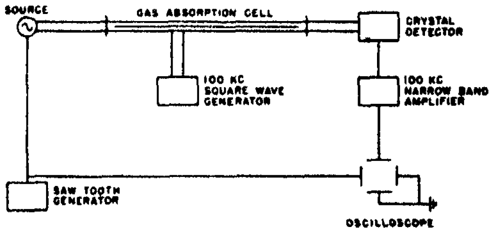

FIG. 1. Simplified block diagram of a Stark-modulation spectroscope.

The main advantages of this system over straight detection and amplification at audiofrequencies without any Stark-modulation are: (1) By detecting and amplifying at a frequency of 100 kc, one avoids the lower frequency region where there is high crystal and source noise. At higher frequencies the impedance of the wave guide cell becomes so low that it is difficult to obtain a good high amplitude square wave modulation voltage. Also, if one uses modulation frequencies higher than about 100 kc, the true absorption line shape becomes distorted (see reference 6). Consideration of these factors thus lead to the adoption of an optimum Stark-modulation frequency somewhere in the neighborhood of 100 kc; (2) Commercial receivers having a very narrow and variable band width may be used as the 100-kc amplifier; (3) Spurious responses caused by standing waves and other frequency sensitive devices in the wave guide system are eliminated. It is evident that, with this scheme, that a 100-kc response is obtained only when one tunes the source through an absorption line; (4) The Stark patterns of the absorption lines are omnipresent and are often useful in identifying the transition and for measuring dipole moments. The disadvantages are that absolute intensity meas-

---

[1] R. H. Hughes and E. B. Wilson, Jr., Phys. Rev. 71, 562 (1947). K. B. McAfee, Jr., R. H. Hughes, and E. B. Wilson, Jr., Rev. Sci. Inst. 20, 821 (1949).

TABLE I. Base connections.

	Z-668	2K33
Pin 1	cavity (ground)	1st focus
2	heater-cathode	heater
3	no connection	no connection
4	reflector	no connection
5	no connection	no connection
6	no connection	no connection
7	heater	heater
8	1st focus	cathode
cap	none	reflector
shell	cavity (ground)	cavity (ground)

urements are difficult to make (though relative measurements may be made with reasonable accuracy) and, under some conditions, the observed lines are sufficiently broad as to limit the ultimate resolution.

It is the purpose of this article to give a rather minute account of an instrument built in the General Electric Research Laboratory in the hope that it may facilitate construction by other interested workers in the field. Wherever special circuits have been designed, these will be reproduced together with circuit constants in order to be of greatest usefulness.

B. SPECIFICATIONS OF THE SPECTROMETER

The frequency range which may be covered with selected tubes is from 16.6 to 28.0 kmc/*s*. This range will be referred to as the "*K*" band throughout this paper. The Stark-modulation voltage may be varied continuously from 0 to 1500 volts sine wave; or from 0 to 800 volts square wave. The factor for converting these voltages to e.s.u./cm is 0.00691. The maximum sensitivity is estimated to be better than 1×10^{-8} cm^{-1}. This figure is based on the fact that the weaker $N^{15}H_3$ lines, present in about 0.4 percent concentration in ordinary ammonia, have been readily observed with a one-foot absorption cell. The absorption lines are about 300 kc/*s* wide at half-power points and the practical ultimate limit of resolution is between $\frac{1}{2}$ and 1 mc/*s*. Frequencies may be measured to an accuracy of ±0.08 mc/*s* over this range. Measurements have been made from room temperature down to −78°C.

C. DESCRIPTION AND DISCUSSION OF COMPONENTS

1. Wave Guide Components and Sources

Sources: The most commonly used power source has been the "*K*"-band radar 2K33 tube (also referred to as 2K33A and QK33). Although the normal frequency coverage is 22.0–25.0 kmc/*s*, these tubes have been used from 16.6 to 28.0 kmc/*s*. By selecting tubes, this range has been usually covered with three tubes. Operation at the extreme ranges has been improved by a 10 percent decrease or increase of the diameter of the external cavity peculiar to this tube. The external cavity appears to be sufficiently closely-coupled to the inner frequency-determining cavity so as to "pull" its frequency slightly. Other operating hints that have been noticed are that low beam currents and voltages favor the generation of low frequencies and *vice versa* at high frequencies. The high frequency limit may be sometimes extended by increasing the heater voltage 10 or 20 percent and operating the tube with beam currents as high as 15 ma. It is realized that such operation represents considerable abuse of the manufacturer's ratings but was considered justifiable in the limited use here. For reference, the base connections are given in Table I and, in Table II, the nominal ratings of this and other microwave tubes which are now being manufactured by the Raytheon Manufacturing Company, Waltham, Massachusetts.

Another type tube which is also used on this spectrometer is the G.E. Z-668.* Unfortunately, this tube was not produced commercially and only a few laboratory samples are available. Since it was designed originally for use in the "*K*" radar band, it covers essentially the same range as the 2K33. In sweeping over wide ranges of frequency, it is easier to keep the Z-668 in a state of oscillation, since there is no external cavity to keep in adjustment as with the 2K33.[2]

Directional couplers: These are essentially of two types; *viz.*, narrow and wide band. The latter is to be preferred, although the demands are not very stringent as used here and both types have been used successfully. A Type TPK-16HU was purchased as surplus

TABLE II. Pertinent data for some microwave klystrons.*

Type	*E* (volts)	*I* (amp.)	Beam volts (max.)	Reflector volts (max.)	Beam current (max.)	Average power output (mw.)	Frequency range	Wave guide output
RK-2K33	6.3±10 percent	0.725	2300	−500	10 ma	40	22 –25 kmc	0.250 in.×0.500 in.×0.040 in. wall
QK-277	6.3±10 percent	0.650	2500	−400	15 ma	18	27.27–30.0	0.140 in.×0.280 in.×0.040 in.
QK-140	6.3±10 percent	0.650	2500	−400	15 ma	18	28.58–33.52	0.140 in.×0.280 in.×0.040 in.
QK-141	6.3±10 percent	0.650	2500	−400	15 ma	10	33.52–36.25	0.140 in.×0.280 in.×0.040 in.
QK-142	6.3±10 percent	0.650	3600	−400	15 ma	5	35.1 –39.7	0.140 in.×0.280 in.×0.040 in.
QK-226	6.3±10 percent	0.650	3600	−400	15 ma	5	37.1 –42.6	0.112 in.×0.224 in.×0.040 in.
QK-227	6.3±10 percent	0.650	3600	−400	15 ma	5	41.7 –50.0	0.112 in.×0.224 in.×0.040 in.

* Available from Raytheon Manufacturing Company, Power Tube Division, Waltham 54, Massachusetts.

---

* The author gratefully acknowledges the loan of several of these tubes from the designer, Dr. J. M. Lafferty, of this laboratory.

[2] A. H. Sharbaugh and R. L. Watters, August, 1946 QST. See also G. E. Research Lab. Report dated March 21, 1945 by J. M. Lafferty.

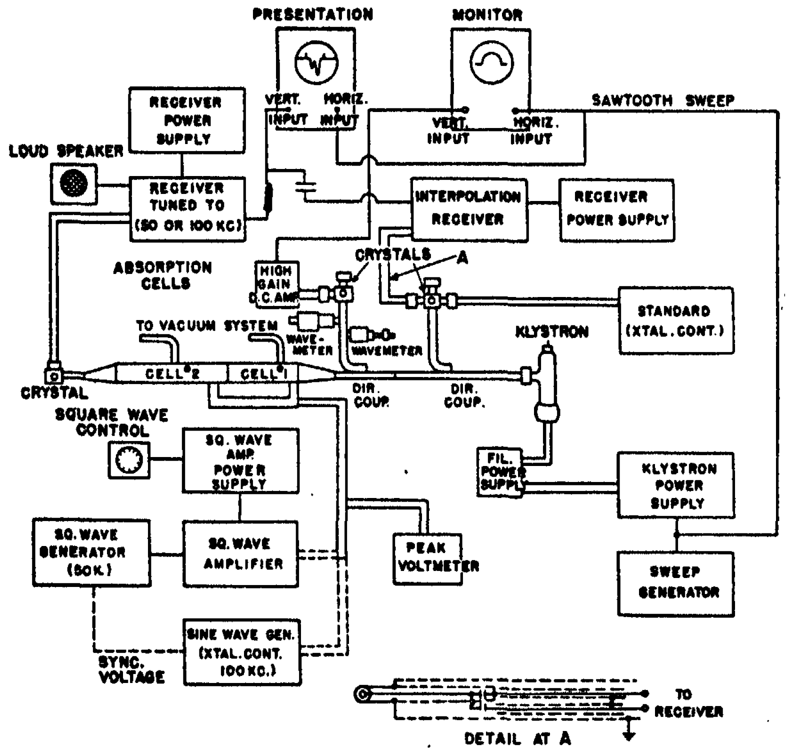

FIG. 1a. Complete block diagram of the microwave spectroscope electronic gear.

from the Humble Oil Company at a very reasonable price. Other couplers were designed according to the procedure outlined by W. W. Mumford[3] with good results.

Wave meters: A Type TFK-2 absorption wave meter[4] utilizing the TE_{111} mode, is used in the range 21–28 kmc/*s*. This wave meter is self-calibrating and, with care, one can measure frequencies to an accuracy of ±7 mc. Such accuracy may be obtained only by narrowing the swept frequency range and measuring the two half-wave responses without changing the wave-meter coupling.

Below 21 kmc the TFK-2 wave-meter response becomes quite broad and is not satisfactory. For this range, a wave meter using the TE_{011} mode was designed using the coupling scheme suggested by Bleaney *et al.*[5] The critical dimensions are indicated in Fig. 2 where all the shaded parts are to be made of high conductivity copper. A wave meter constructed according to this design has been satisfactorily used in the range 16.6–22.0 kmc/*s*.

Crystals and crystal mounts: 1N26 silicon crystals have been used almost exclusively as detectors for the 1-cm energy. There is a wide variation in their performance and great improvement in sensitivity and noise figure can be obtained by using selected crystals. Comparable detector performance could be obtained by using biased germanium crystals but, in general, the silicon crystals, without bias batteries, were more convenient. One precaution, which may be appropriately mentioned here, is always to remove the crystals from the wave guide equipment and shield them before using a sparking coil on the vacuum equipment. Failure to do this will result in burned-out crystals.

The crystal mounts which are used are of the "cross-bar" type shown in Fig. 3. These mounts are designed so as to terminate the wave guide in a matched load

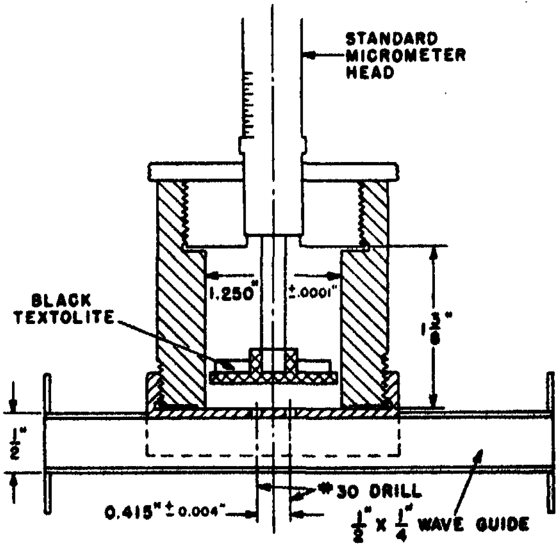

FIG. 2. Cavity wave-meter dimensions; range 16–22 kmc/*s*.

---

[3] W. W. Mumford, Proc. I.R.E. 35, 160 (1947).

[4] C. G. Montgomery, *Technique of Microwave Measurements* (McGraw-Hill Book Company, Inc., New York, 1947), Rad. Lab. Series 11, p. 327.

[5] Bleaney, Loubser, and Penrose, Proc. Phys. Soc. 59, 185 (1947).

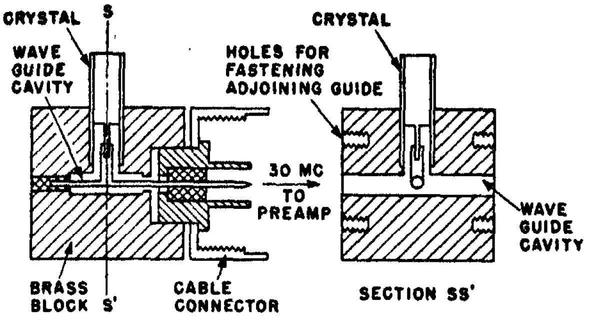

FIG. 3. Construction of the crystal mounts.

when an average crystal unit is inserted. The mounts are tuned to give optimum performance at 24.0 kmc/*s* but are very broadband and work well over the entire tuning range. If it is desirable to obtain a more perfect match at the extremes of the tuning range, a tuning screw and adjustable short circuit can be added to the circuit.

Transformer sections: The transformer sections which are used to join smoothly the $\frac{1}{4}$ in.×$\frac{1}{2}$ in. wave guide to the $\frac{1}{2}$ in.×1 in. size were fabricated in the machine shop. The four sides of the taper were first soft-soldered together and a jig used to align a short length of standard guide to each end. These final joints were made with a lower melting solder so as not to disturb those already soldered. The taper was made three inches long to insure a minimum of reflected energy. From the point of view of reflections, a somewhat smoother taper could be obtained by an electroforming process.

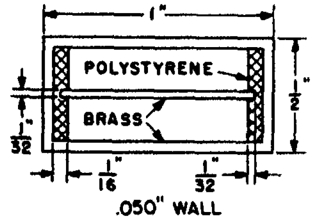

FIG. 4. Cross section of the wave-guide absorption cell.

Wave-guide absorption cell: The absorption cell was constructed of two 16 ft. lengths of $\frac{1}{2}$ in.×1 in. brass wave guide. The lengths are arranged side-by-side on a 2 in.×6 in. board and are made as independent units so that either one or both may be used at a time. The connecting "*U*" is bent out of similar guide and has an inside radius of $1\frac{1}{4}$ in. The two cells are thus sufficiently close to permit enclosure by a wooden box (made of 1 in. boards) to house dry ice refrigerant. The box terminates 6 in. away from the wave-guide windows in order to avoid cracking the beeswax. When it is desirable to chill the gas, the insulation is sufficiently good to allow a single daily filling with crushed dry ice.

The dimensions of the cross section of the cell are shown in Fig. 4. The polystyrene strips were stacked and milled as 6-in. lengths. The center electrode was made by rolling up oversized $\frac{1}{32}$-in. brass strip and cutting to the desired width on a lathe. The strip was unrolled and fed into one end of the wave guide along with the polystyrene strips. It was found convenient to pass a wire down the guide and pull the electrode through rather than push it. The tolerances on the polystyrene strips and brass electrode must be held as closely as possible so as to insure uniform spacing of the electrode since this is the limiting factor in the precision with which the applied Stark field is known. Also, a cell with a slightly off-center septum will cause a doubling of the Stark pattern and thus make their interpretation very difficult. Care should be exercised

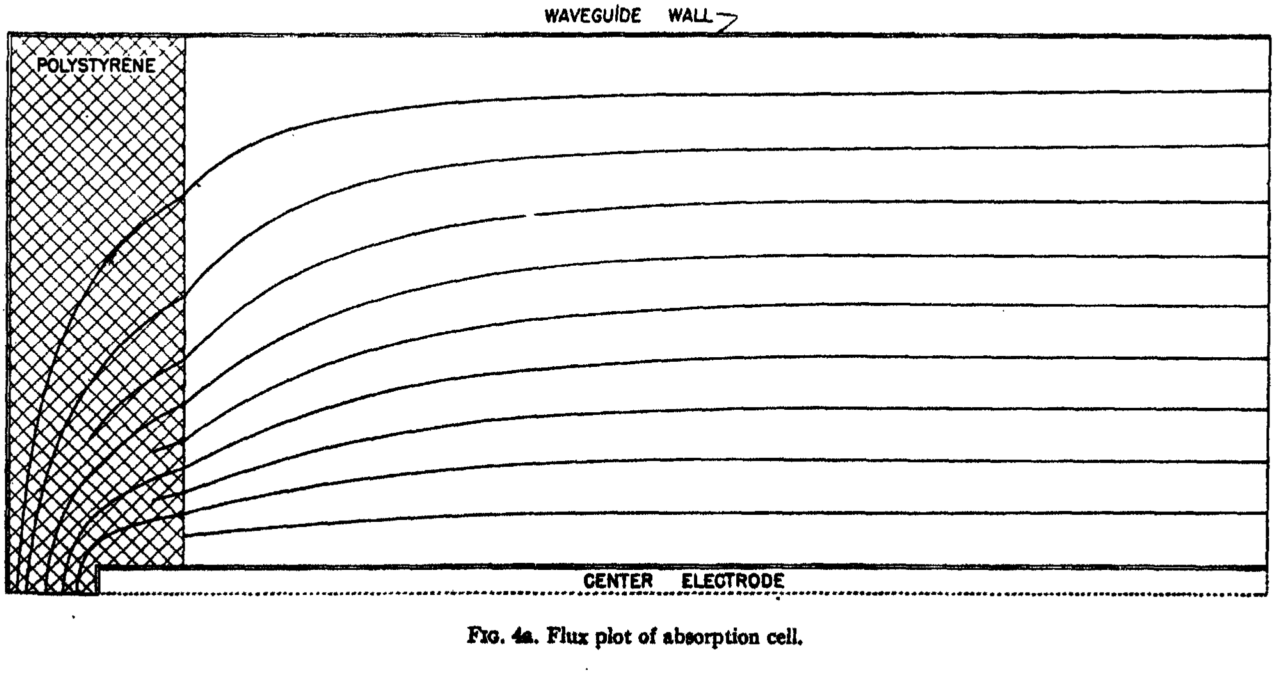

FIG. 4a. Flux plot of absorption cell.

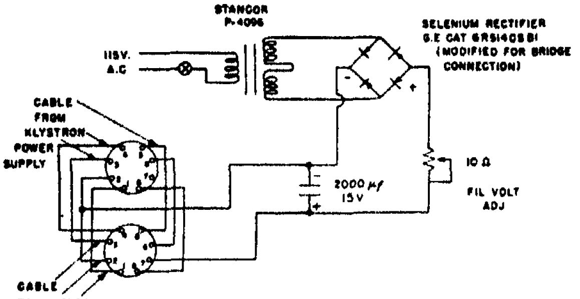
STANCOR P-4096
SELENIUM RECTIFIER G.E CAT 6RS14OSBI (MODIFIED FOR BRIDGE CONNECTION)
115V. A.C
CABLE FROM KLYSTRON POWER SUPPLY
2000 µf 15V
10 Ω
FIL VOLT ADJ
CABLE TO KLYSTRON

FIG. 5. Klystron filament supply.

to obtain pure polystyrene since a plastic which is loaded with a volatile plasticizer may cause much difficulty in obtaining a good vacuum.

When measuring dipole moments, it is desirable to know the Stark electric field as accurately as possible. One possible source of error is the fringing caused by the presence of the dielectric which supports the Stark electrode inside the wave guide. To determine the magnitude of this effect, a flux plot was made in an electrolytic tank.** The difference in dielectric constants was simulated by a difference in tank depth; the dielectric ratio being directly proportional to the conductance. A line of small insulated wires served to define the interface boundary. Figure 4a shows the equipotential flux plot so obtained and demonstrates the exact amount of fringing. Advantage was taken of the symmetry and so only one-quarter of the wave guide cross section was actually plotted. To find out the field distribution, the flux plot was divided into 170 squares and the field strength estimated for each square. The square of the field strength was then plotted against number of squares having the same field; the envelope of which gave a rather smooth distribution curve. The peak of this envelope coincided with the field computed neglecting inhomogeneity and was sufficiently sharp as to demonstrate the inconsequential nature of the fringing at the dielectric boundary. In actual practice, this distribution would have a $\sin^2(\pi x/l)$ weighting factor (l is guide width), which would even further decrease the importance of the fringed regions.

The $\frac{1}{2}$ in.×1 in. wave-guide size was selected in preference to $\frac{1}{4}$ in.×$\frac{1}{2}$ in. size for several reasons: 1. it is easier to fabricate into a cell; 2. percentwise, closer tolerances could be maintained and hence the Stark-field is known more accurately; 3. the chances of saturation and consequent broadening and weakening of the lines is diminished because of the greater cross-sectional area; 4. the attenuation is smaller. A disadvantage is that higher modulation voltages are required to obtain equivalent field strengths. No serious trouble was experienced with the expected higher order modes although their presence was demonstrated by the detection of electric field components at right angles to that in the normal TE_{10} mode. The capacity per foot is about the same with either $\frac{1}{2}$ in.×1 in. or $\frac{1}{4}$ in.×$\frac{1}{2}$ in. wave guide; *viz.*, 60 µµfd./ft. The attenuation is about 1 db/foot which is very high compared to a similar guide without an inner electrode. A brass wave guide having the dimensions $\frac{1}{2}$ in.×1 in. and operated at 24 kmc. in the TE_{10} mode should have about 0.07 db/ft. attenuation. One may readily compute that in the geometry used here, only about 1 percent of the power flowing down the wave guide goes through the di-

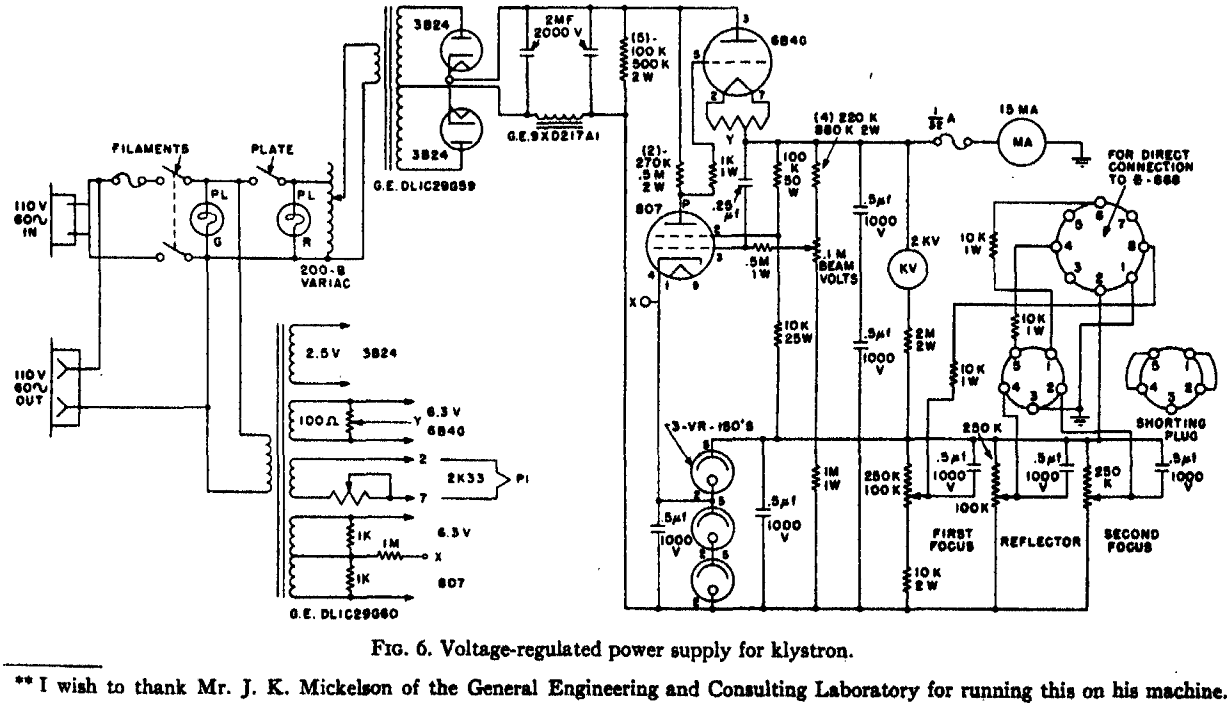

FIG. 6. Voltage-regulated power supply for klystron.

** I wish to thank Mr. J. K. Mickelson of the General Engineering and Consulting Laboratory for running this on his machine.

electric, so this cannot contribute heavily to the losses even if it were a poor dielectric. Because of the division of the absorption cell by the Stark electrode, we actually have energy transmission down two wave guides having the electrode as a common wall. The attenuation by a guide of these dimensions is about twice that previously computed on the basis of the outer geometry. The remainder of the high attenuation is likely due to window reflections and conversion of power to the several other modes of propagation which may be supported by a guide of these dimensions and which are not detected at the crystal mount. The voltage standing wave ratio is of the order of 2 to 1.

The electrical connection to the insulated strip was made with a Fernico wire-glass seal, the Fernico eyelet being soft-soldered to the wave guide. It is well to provide ample clearance of the connecting wire (or, better yet, insulate it) from the outside wave guide so as to avoid short circuiting caused by relative movement when the guide is being chilled. A Type N connector was mounted externally for convenient connection and thorough shielding.

Other variations in construction would be to use a thicker electrode (tapered at the ends to avoid reflections) and hence obtain higher field strengths. To make measurements at elevated temperatures, one could use a ceramic or Teflon spacer instead of polystyrene.

Absorption cell windows: A very satisfactory wave-guide window was made by sealing a thin piece of clear mica with beeswax. The following procedure proved to be the best way of making them vacuum-tight: 1. cut a piece of mica about $\frac{1}{32}$ in. or less in thickness to a size so as just to clear the holes in the coupling flanges; 2. paint around the edges with melted wax before applying the mica; 3. hold mica sheet against the flat coupling flange with a slight positive pressure while heating the entire coupling to melt the wax; 4. hold in place until the wax solidifies; and, 5. paint around the edges with melted wax.

2. Electronic Circuits

Filament Power Supply: When the amplifiers were used at highest gain, a rather troublesome 60-cycle ripple was experienced. This was cured by supplying the klystron heater with d.c. voltage. The circuit given in Fig. 5 was built into a 6 in.×6 in.×6 in. metal box and had a range of 3.5 to 9.5 d.c. volts when working into a ten ohm load. The ripple at 6.3 volts is less than 0.1 volt.

Klystron power supply: The power supply for the klystron is necessarily voltage-regulated in order that the operating frequency of the klystron remain steady. The schematic diagram for the supply used is given in Fig. 6 and follows the conventional design. This circuit supplies 1500–2000 volts of regulated voltage with less than 35 millivolts ripple. The controlling potentiometers for the various electrode voltages are sub-mounted as a safety precaution. A five-prong plug provides a ready access to the reflector electrode to superimpose a modulating voltage. When the modulation is not desired, the shorting plug may be inserted. Early models of the

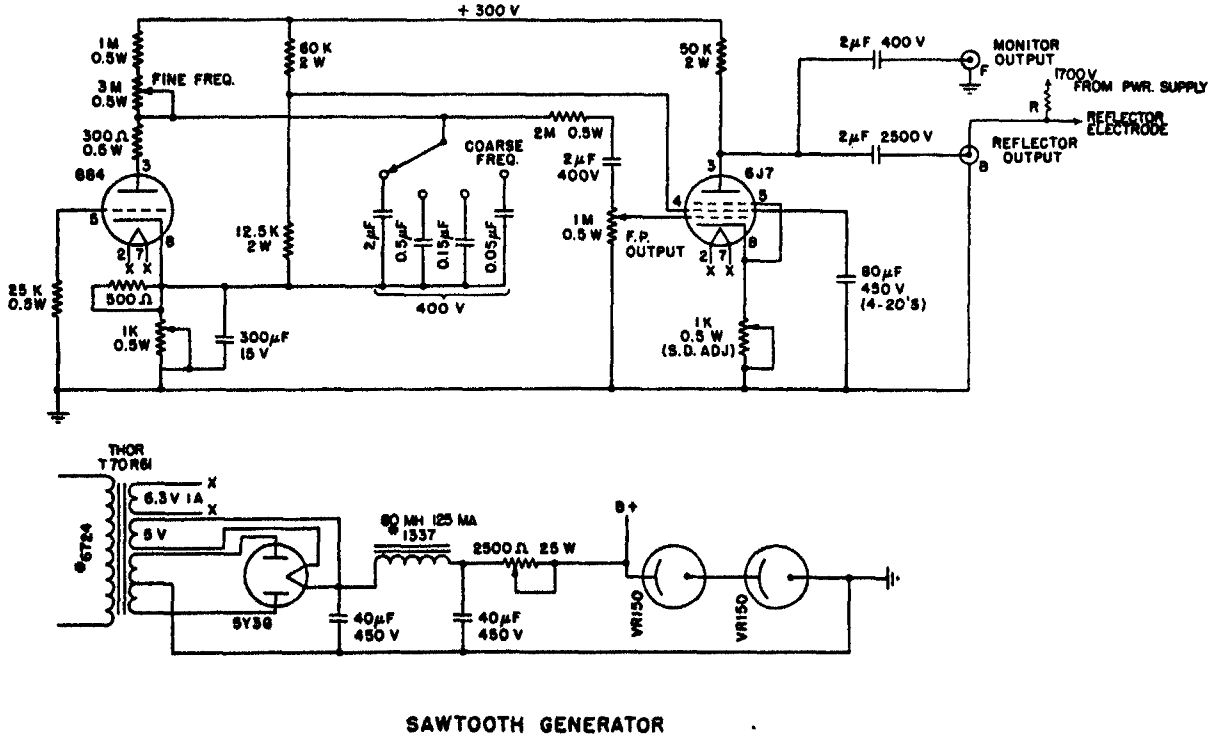

FIG. 7. Sawtooth generator schematic.

Z-668 used a second focus control which accounts for its appearance on the diagram. Furthermore, it is considered good practice to insert 10,000 ohm resistors as current limiters in series with the reflector and focus voltage leads and these have been included in the circuit. The output voltage plug is shown in the circuit schematic for connections to the Z-668. The base connections are different on the 2K33 and hence the connecting cable for this tube will have several transposed leads. (See Table I for base connections.)

Saw-tooth generator: The saw-tooth generator is designed to generate the rather low sweep frequency of two cycles per second. Low sweep rates favor good resolution and more accurate reproduction of the absorption line shapes. Since the band width of the 100-kc amplifier is of the order of 200 c/s (at ten times down in voltage), the lowest sweep rates are necessarily used to avoid amplifier distortion. Suppose, for example, a band 50 mc wide is examined at certain sweep rate f and that an absorption line is 1 mc wide. It would thus require $(1/50)(1/f)$ mc to sweep over a line and the required band width of the amplifier Δf would be of the order $50f$. Equation (6) of Section E shows that Δf should be kept as small as possible for best sensitivity; consequently, the sweep frequency f is adjusted to comply with the narrowest band width attainable. Of course, one could achieve even greater sensitivity by going to a pen recorder where Δf would be of the order of 30 c/s. Although one would have to tune the source through a line at a still slower speed (1/30 sec.), it would only require a minimum of 6 minutes to cover the full range of 10,000 mc.

The reflector electrode, to which the sawtooth output voltage is applied, is at a high potential with respect to ground; consequently, the most convenient way is to couple in with a high voltage condenser or an isolation transformer. Condenser coupling (see Fig. 7) was selected as being the most convenient in this application. Resistor R in Fig. 7 is preferably 1 megohm so as to present a high impedance across the saw tooth generator output, but with some klystrons the gas and leakage reflector current is sufficiently high as to cause the reflector to swing positive with respect to the cathode. This may damage the tube and not permit oscillation. To remedy this, R may be decreased, or, in severe cases, a series connection of three G.E. G-5 germanium diodes has been substituted successfully.

A total range of 2 to 160 c/s is covered with a good wave shape as viewed on an oscilloscope. The output voltage may be varied from zero to 100 volts. In Fig. 7 the circuit is seen to consist of a standard relaxation oscillator with a single stage of amplification.

Sine wave generator: A source of sine wave modulation voltage was designed to give continuously variable voltages from 0 to 1500 volts with a good wave shape. The circuit is given in Fig. 8 and consists of a Pierce crystal oscillator coupled by a cathode-follower circuit to an easily driven 829B beam power tube. The oscil-

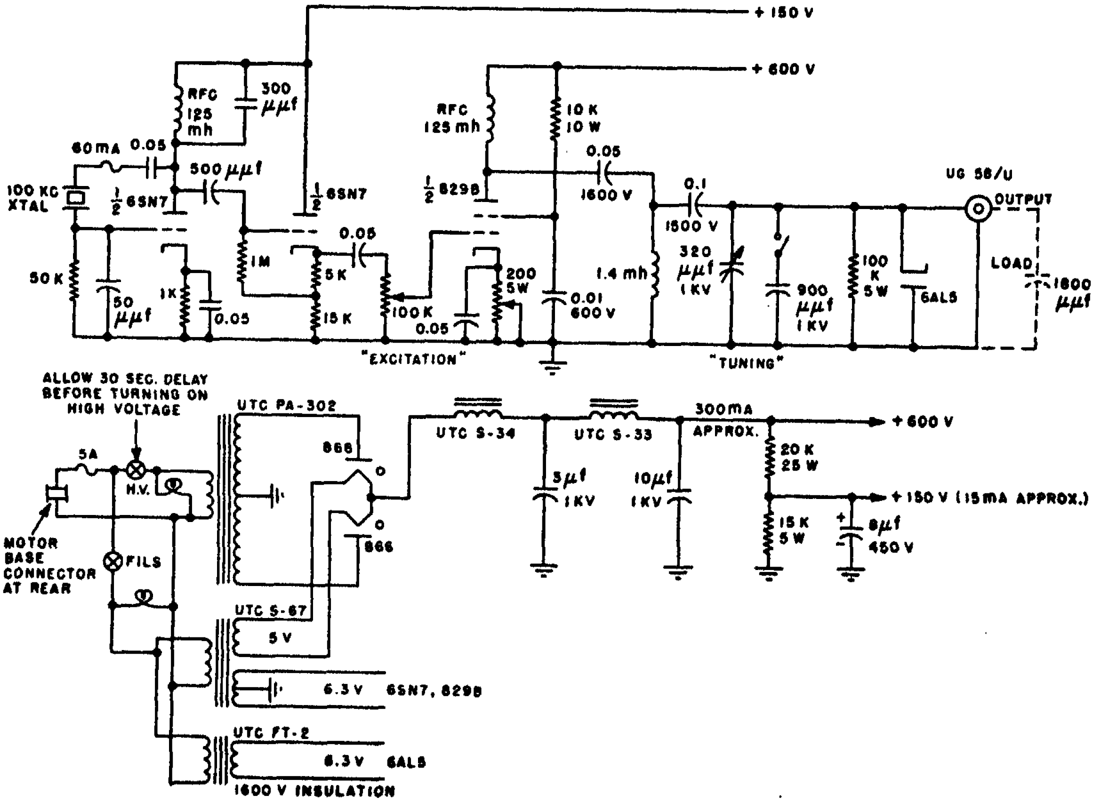

FIG. 8. Sine wave modulation source.

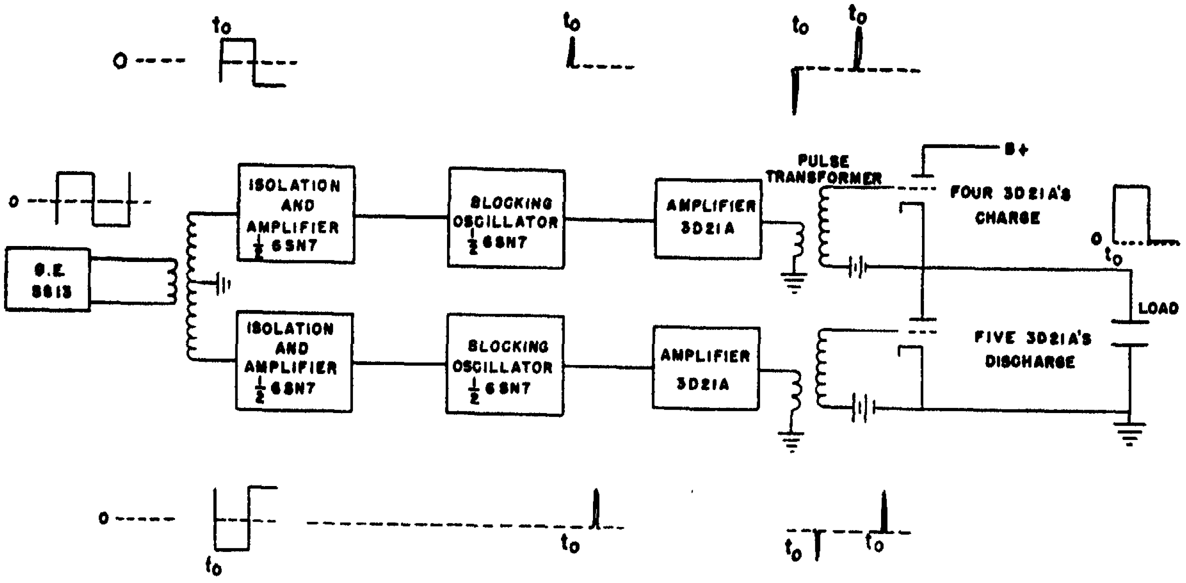

FIG. 9. Block diagram of square wave generator.

lator is crystal-controlled to insure a constant frequency and hence maintain correct tuning of the narrow-band amplifier. It also serves as a convenient source of synchronization voltage to hold the square wave modulation source on frequency. The capacity formed by the Stark electrode and surrounding wave guide serves as the tank capacitor of the 100 kc/*s* amplifier stage. This capacity is shunted with a 320-$\mu\mu$fd trimmer capacity to resonate it precisely and also a fixed capacity equal in magnitude to one of the wave-guide absorption cells. Switching in this latter capacity permits the use of only one of the two wave-guide cells when this is desired. In order to double the available sine wave modulation voltage and to study conveniently Stark effects as a function of voltage, an automatic bias circuit (a 6AL5 tube and 100,000 ohm resistor) was incorporated which always keeps the troughs of the sine wave at zero voltage. It would be necessary to tune the amplifier to twice the modulation frequency if no bias were used.

Square wave generator: If one wishes to make a careful study of line shapes and obtain the Stark effect pattern of degenerate transitions, then it is necessary to use square modulation.[8] The price to pay for a high voltage square wave generator at these frequencies is rather high; consequently, sine wave modulation was used where extremely high fields were required in searching (e.g., on molecules known to have a small dipole moment). Having found a line, one may then switch over to the square wave field for a detailed examination of the Stark pattern. A careful comparison was made between sine and square wave modulation and equivalent shifts of the Stark images were found in the case of the $J=0\rightarrow1$ transition of methyl chloride. However, in the case of more complicated Stark patterns, such as encountered in the $J=1\rightarrow2$ transition of chlorosilane, better resolution and hence more detail was observed when using square wave modulation.

The requirements of the square wave generator are rather stringent; *viz.*, (1) a maximum of 800 volts amplitude based on zero, (2) 50 percent duty cycle at 100 kc/*s* frequency, (3) rise and fall time of less than 0.25 μsec., and (4) a pure capacitative load of about 2000 $\mu\mu$fd. This means that the charging currents are of the order of 6 amperes and the best way to achieve such is to use a bank of high emission tubes to charge the condenser load and another bank to discharge it. To understand more fully the operation of this generator, it will be instructive to refer to the block diagram of Fig. 9 where one complete cycle is traced through the circuit. Referring to the figure, a G.E. SG13 square wave generator is used to trigger a blocking oscillator whose output pulse is amplified and then inverted by a pulse transformer. These positive pulses are fed into the grids of the charge and discharge tubes connected in cascade and alternately charge and discharge the condenser load formed by the Stark electrode. It is seen that the charge and discharge circuits are identical except that the voltage forms are 180° out of phase with respect to each other. The detailed diagram with circuit constants is presented in Fig. 9a where the SG13 triggering generator is to be connected to the input terminals.

A block diagram of the power supply is given in Fig. 10 as an aid in interpreting the detailed schematic diagram of the supply in Fig. 10a. It is to be noted that the charge tubes are self-biased while the discharge tubes use fixed bias from a selenium rectifier. This was done so that the high voltage B^+ would not be shorted through both the charge and discharge tubes when the amplifier was shut down. The 1-V rectifiers are used to

---

[8] Robert Karplus, Phys. Rev. 73, 1027 (1948).

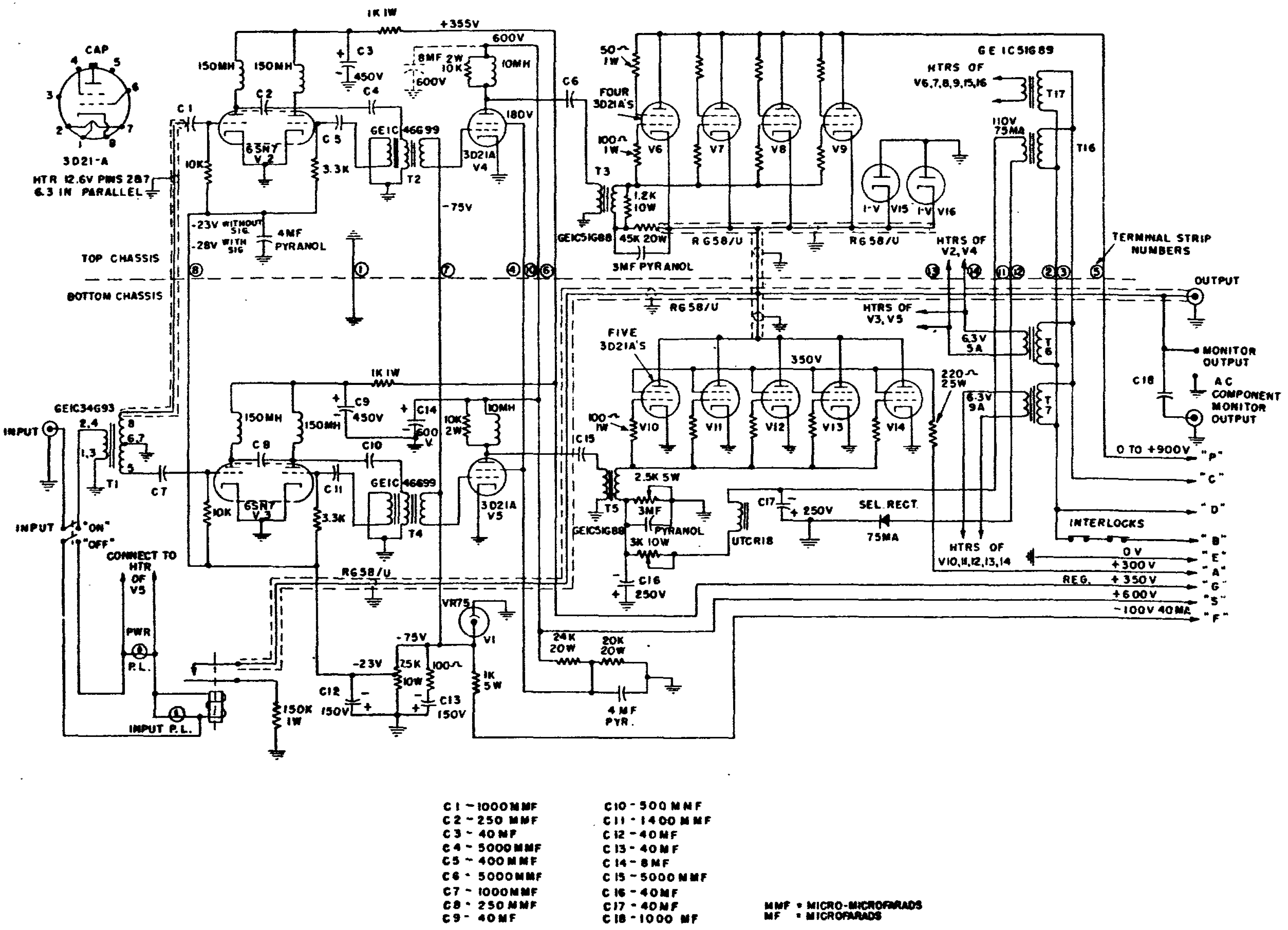

C1 - 1000 MMF
C2 - 250 MMF
C3 - 40 MF
C4 - 5000 MMF
C5 - 400 MMF
C6 - 5000 MMF
C7 - 1000 MMF
C8 - 250 MMF
C9 - 40 MF

C10 - 500 MMF
C11 - 1400 MMF
C12 - 40 MF
C13 - 40 MF
C14 - 8 MF
C15 - 5000 MMF
C16 - 40 MF
C17 - 40 MF
C18 - 1000 MF

MMF = MICRO-MICROFARADS
MF = MICROFARADS

FIG. 9a. Detailed schematic of square wave generator.

clamp the base line of the square wave on zero, should the square wave trough try to go negative.

In the finished generator the square wave was continuously variable between 25 and 800 volts. For observing first-order Stark effects which require less than 25 volts, a resistance-capacity divider is used which extends the low voltage limit down to about ½ volt. The top of the square wave is flat to less than ½ percent and the bottom edge remains constant to within 2 percent. This sort of performance is obtained over the frequency range 25 to 100 kc/*s*.

Peak voltmeter: Since we are concerned with the peak values of the Stark field when using either sine wave or square wave voltages, it seemed advisable to construct a peak reading voltmeter with a direct reading scale. A 5Z4 tube was used as a diode rectifier as indicated in the circuit of Fig. 11. For calibration at 60 cycles, the 0.1-μfd condenser should be shunted with several microfarads of capacity to increase the time constant of the circuit. The use of a large scale DP2 instrument as indicator facilitated accurate reading of the voltages.

Narrow-band amplifier: A National HRO-5RA receiver is used as the narrow-band amplifier. When the crystal filter is in the maximum selectivity position, little distortion of the lines is noted at sweep rates of 2 cycles per second. At higher sweep rates it is necessary to use wider band widths to avoid distortion and hence a sacrifice in signal-to-noise ratio is made. The input to the HRO receiver was modified to use a shielded coaxial connector to avoid stray pick-up and also the audio stages were by-passed so as to avoid possible distortion. The receiver performs satisfactorily at both 50 kc/*s* and 100 kc/*s* although the gain is considerably higher as the latter frequency.

Oscilloscopes: The output from the narrow-band amplifier is fed into a Dumont 208-B oscilloscope. This instrument is admirably suited for this application because of its high *Y*-axis gain and exceptionally good low frequency response. A long persistent Type P-7 fluorescent screen tube is used which enabled sweep rates of 1–2 *c/s* to be used.

For the monitor oscilloscope, a Dumont 241 instrument is used. There is considerable distortion at sweep frequencies below 30 *c/s*; however, since any curvature of the trace indicates power output from the klystron, it may be satisfactorily used to indicate a state of oscillation. A 450A Hewlett-Packard booster amplifier with 40 db gain was used in conjunction with this oscilloscope. In some respects the Dumont 208-B would be a better choice here, but it is convenient to have on hand an oscilloscope with a good high frequency response (as does the Model 241) with which to check occasionally the 100 kc square and sine waves supplies.

Crystal-controlled frequency standard: If one uses an absorption cavity wavemeter as previously described, the absorption lines may be measured with an error of less than ±7 mc over the range of the spectrometer. However, this is not sufficiently accurately to study fine structure of lines which are spaced only tenths of a megacycle apart. Therefore, a crystal-controlled oscillator is used to produce standard marker pips whose frequencies are known to better than one part per million. These markers are produced by beating the crystal standard output (containing 20, 40, 120, and 360 mc and their harmonics) against a fraction of the klystron power derived from the main wave guide with a directional coupler. A single crystal is used both for mixing and harmonic generation; there being continuous harmonics of the standard signal present in the mixing block at least through *K*-band. Since the standard signal harmonics are fixed in frequency, and the klystron signal is continuously swept in frequency, the mixing action of the crystal will cause a continuum of difference frequencies to be generated as the klystron signal frequency approaches, equals, and then passes the standard marker signal. Referring to the block diagram of Fig. 1a, these difference frequencies are fed into the input of a communications receiver (Hammarlund SPX400), and thence to the presentation oscillo-

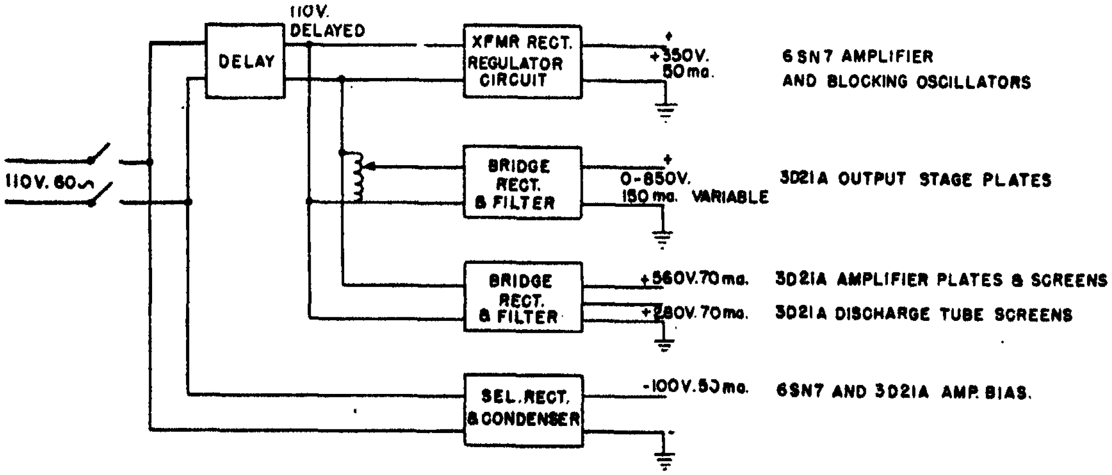

110V. DELAYED
DELAY
XFMR RECT. REGULATOR CIRCUIT
+
+350V. 50ma.
6SN7 AMPLIFIER AND BLOCKING OSCILLATORS
110V. 60∽
BRIDGE RECT. & FILTER
+
0-850V. 150ma. VARIABLE
3021A OUTPUT STAGE PLATES
BRIDGE RECT. & FILTER
+560V.70ma.
3D21A AMPLIFIER PLATES & SCREENS
+280V. 70ma.
3D21A DISCHARGE TUBE SCREENS
SEL. RECT. & CONDENSER
-100V.50ma.
6SN7 AND 3D21A AMP. BIAS.

FIG. 10. Block diagram of square wave generator power supply.

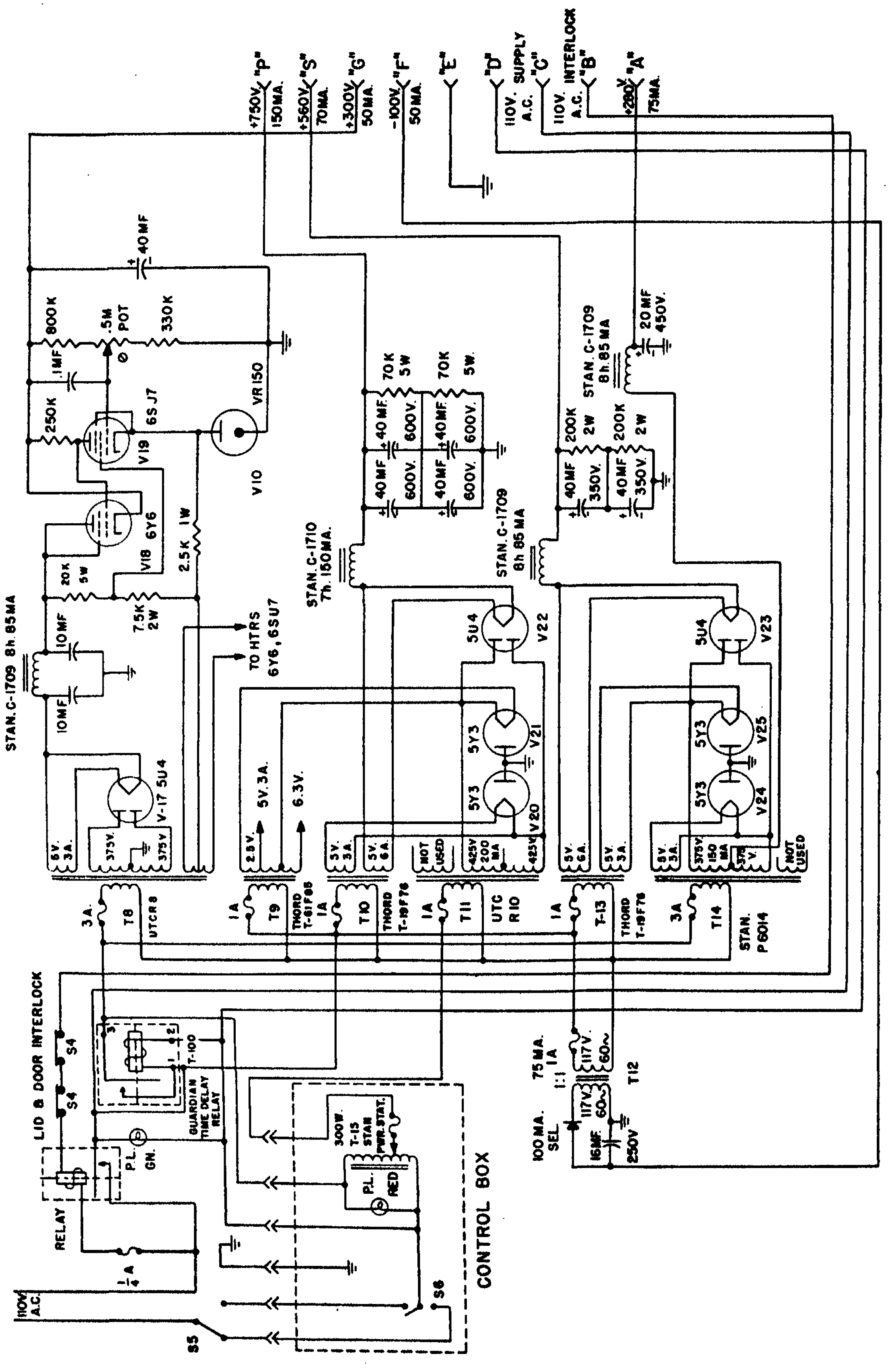

FIG. 10a. Detailed schematic of square wave generator power supply.

scope. When the difference frequency passes through the frequency to which the receiver is tuned, a "pip" occurs on the oscilloscope screen. Thus, for each *K*-band harmonic this gives rise to two markers which are separated by twice the receiver frequency; and by tuning the receiver, a marker may be superposed exactly on an unknown absorption line. The frequency is computed from the relation

$$f=nf_1\pm f_r,$$

when n is an integer, f_1 is the lowest frequency introduced into the crystal mixer; *viz.*, 20 mc in this case, and f_r, the setting of the receiver. In this manner one may continuously interpolate between the standard marker pips. The cavity wave meter is used to determine the value of n in the above equation and so identify the harmonic of the standard generator.

The crystal-controlled standard is similar to one described by Talpey and Goldberg[7] and consists of a crystal-controlled 10-mc oscillator, a buffer stage, two doubler, and two tripler stages with output on 360 mc. As noted on the circuit diagram of Fig. 12, link coupling is made to the 120-mc and 360-mc stages only, but there is sufficient stray coupling to the lower frequency stages to cause harmonics to appear in the crystal harmonic generator every ten megacycles. Since it was difficult to identify positively the markers this close together, a ten megacycle wave trap was incorporated in the output circuit leaving only markers every twenty megacycles.

A frequency trimmer allows the oscillator circuit to be zero heat with *WWV* and the frequency remains constant for days to ±10 cycles or 1 part per million at the used harmonic frequency.

Since the crystal standard output and receiver are in parallel across the crystal, it is desirable to prevent the standard from offering a low impedance to the difference frequencies. A circuit resonating near 4 mc was connected as shown in Fig. 1a and helped to increase the difference frequency signal seen by the receiver. Likewise, the receiver was prevented from absorbing the standard signal by using a quarter wave-length choke. The dimensions of the choke were chosen to present a high impedance at 40, 120, and 360 mc. The multiple shield shown as Detail *A* of Fig. 1a helped to reduce noise pick-up.

Germanium crystals, as expected, were found to be more efficient, harmonic generators than silicon crystals. Their use, combined with the fact that a single crystal was used as both mixer and harmonic generator, probably accounts for the fact that the usual high frequency tripler following the 360-mc stage could be entirely eliminated from the circuit.

More recent experiments show that a butterfly circuit is superior to the lumped constant, 360-mc tank circuit shown in Fig. 12.

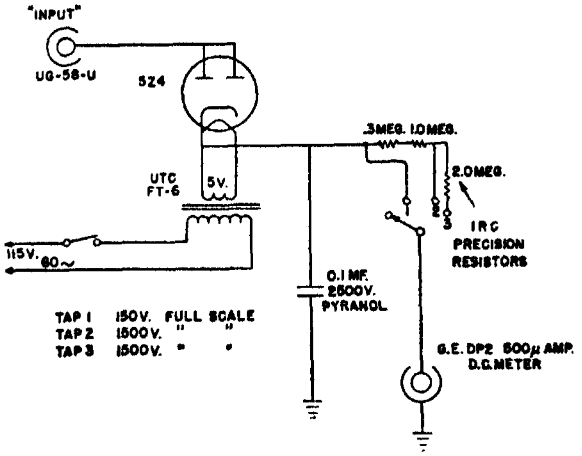

FIG. 11. Peak voltmeter circuit.

3. Vacuum System

A block diagram of the essentials of the vacuum system is shown in Fig. 13. The manifold is equipped with a number of stopcocks for maximum convenience in handling the gases. The remainder of the diagram is self-explanatory. Each sample bulb has a small reservoir for "freezing out" the gas. The stopcocks are all the precision hand-ground variety which insures trouble-free operation.

The circuit diagram for the Pirani gauge is reproduced in Fig. 14. The variable resistance arm in the bridge circuit consists of the G.E. FA-13 tube with a matched FA-14 tube as a compensator. In order to increase the sensitivity, a special low resistance movement micro-ammeter (72 ohms) is used to read the unbalance voltage developed across the bridge as a result of pressure changes. With the circuit constants given, the full scale reading in microns of air is given for the different positions of the sensitivity switch. For greater accuracy at lower pressures a more sensitive meter with still lower internal resistance could be used. Six volts d.c. is normally applied across bridge and may be adjusted with resistor *R*. The other variable resistances are screwdriver adjustable potentiometers which may be permanently set when the meter is calibrated.

The thermocouple gauge circuit is given in Fig. 15. The thermocouple gauge tube may be obtained with either a hard or soft glass bulb. Of course, both of these gauges will respond differently with gases having different convection cooling factors so the pressure readings are only approximate.

D. OPERATIONAL NOTES

The general operating procedure when searching for unknown absorption lines is as follows: The gas sample is "frozen out" with liquid air and pumped down to insure the removal of all the non-condensibles. These non-condensibles tend to dilute the sample and cause a weakening and broadening of any desired lines. The

---

[7] R. G. Talpey and H. Goldberg, Proc. I.R.E. 35, 965 (1947).

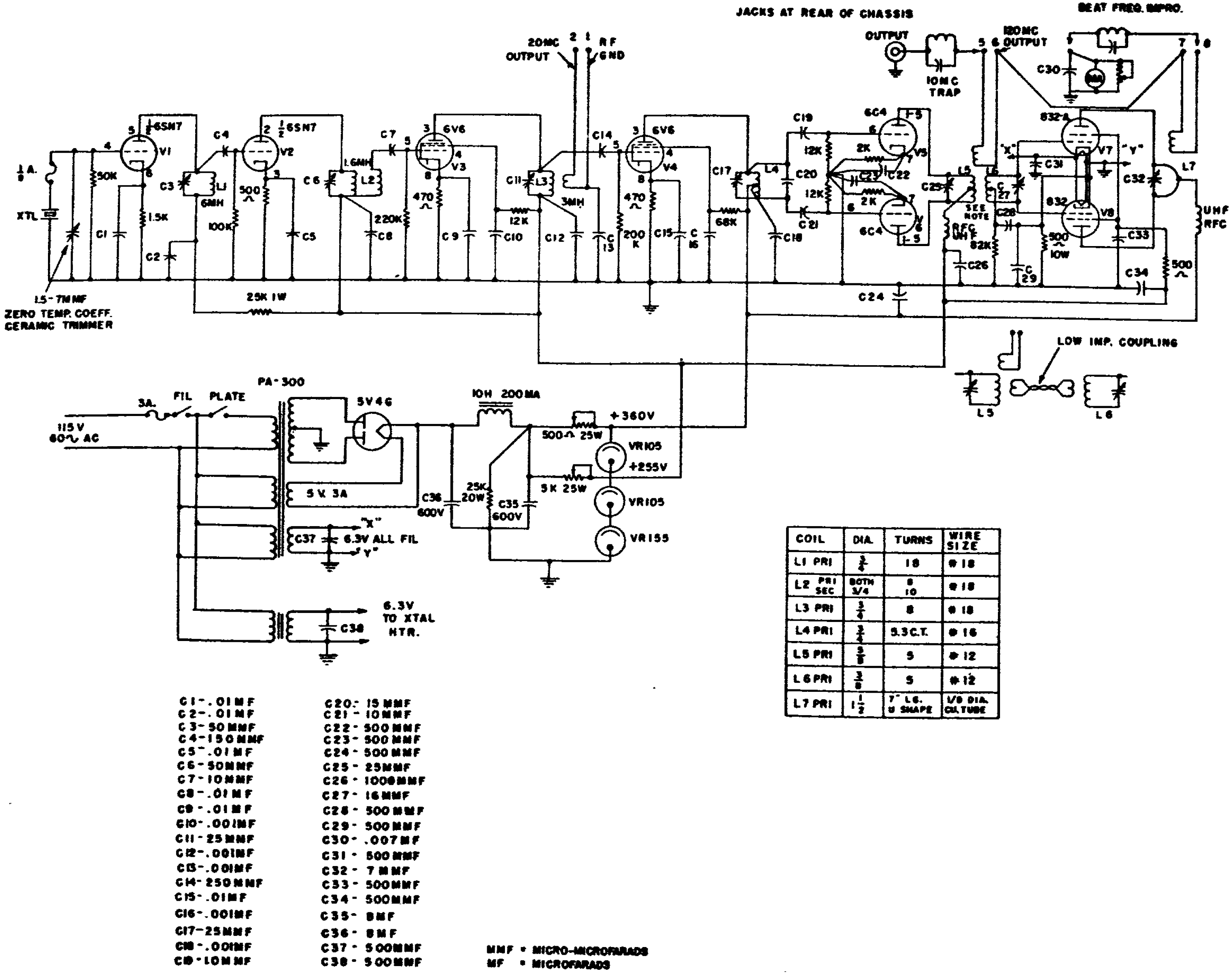

COIL	DIA.	TURNS	WIRE SIZE
L1 PRI	3/4	18	# 18
L2 PRI SEC	BOTH 3/4	8 10	# 18
L3 PRI	3/4	8	# 18
L4 PRI	3/4	5.3 C.T.	# 16
L5 PRI	5/8	5	# 12
L6 PRI	3/8	5	# 12
L7 PRI	1 1/2	7" LG. U SHAPE	1/8 DIA. CU. TUBE

C1 - .01 MF
C2 - .01 MF
C3 - 50 MMF
C4 - 150 MMF
C5 - .01 MF
C6 - 50 MMF
C7 - 10 MMF
C8 - .01 MF
C9 - .01 MF
C10 - .001 MF
C11 - 25 MMF
C12 - .001 MF
C13 - .001 MF
C14 - 250 MMF
C15 - .01 MF
C16 - .001 MF
C17 - 25 MMF
C18 - .001 MF
C19 - 10 MMF

C20 - 15 MMF
C21 - 10 MMF
C22 - 500 MMF
C23 - 500 MMF
C24 - 500 MMF
C25 - 25 MMF
C26 - 1000 MMF
C27 - 16 MMF
C28 - 500 MMF
C29 - 500 MMF
C30 - .007 MF
C31 - 500 MMF
C32 - 7 MMF
C33 - 500 MMF
C34 - 500 MMF
C35 - 8 MF
C36 - 8 MF
C37 - 500 MMF
C38 - 500 MMF

MMF = MICRO-MICROFARADS
MF = MICROFARADS

FIG. 12. Crystal-controlled frequency standard.

wave-guide cell is then flushed out three or four times with the gas and between ten and fifty microns finally admitted to the cell. Searching is usually done with about 500 volts of sine wave Stark field and with the smallest band width of the HRO. Having found a line, if it is desired to study its fine structure, then one can optimize the gas pressure and Stark square wave voltage. For linear and symmetric top molecules the approximate expected absorption frequencies may be computed from Eq. (3) and thus guide one as to which region to sweep initially. In searching, it is necessary to tune the tube slowly and maintain a state of oscillation at all times by adjusting the reflector electrode voltage. Oscillation is indicated by the trace on the monitor oscilloscope and by the amount of noise emanating from the receiver crystal. This latter noise appears as "grass" on the Dumont 208 screen when the gain is increased. The edges of the tube mode are also defined by a sharp response on the oscilloscope due to the reception of the 100-kc harmonic component of the sweeping frequency.

The intensity of some weak lines may be enhanced by chilling the guide with dry ice. The expected amount of increase in intensity may be readily computed with the aid of Eqs. (1) and (2).

In order to check the performance of the spectroscope, one may introduce ammonia in the one-foot cell. Since the ammonia spectrum is so rich in accurately known lines, it may be allowed to remain in the cell to provide visual checks over the entire frequency range. However, after the operator becomes familiar with the instrument, it is usually preferable to pump out the ammonia because its lines are so intense that they become annoying when the amplifier is adjusted to a high gain. To help stabilize the oscilloscope trace against sudden large variations in signal input, a crystal diode limiter was connected across the input terminals to the oscilloscope.

One must avoid introducing ammonia gas into the long wave guide cell because it is very difficult to pump out. On one occasion this accidentally happened and ammonia lines appeared for weeks afterward in spite of constant pumping.

In some parts of the tuning range certain rather broad 100-kc responses are obtained which resemble absorption lines in their behavior. They increase in strength with the Stark field and are not present when the Stark field is zero. It has been suggested[8] that this effect may be caused by electric polarization saturation effects in the polystyrene supports for the Stark electrode or of surface deposits on them. If there is any doubt as to whether one has a spurious response or not, the gas may be pumped out (or frozen out) and, of course, a real absorption line will disappear. Conversely, an increase in pressure will cause a broadening of a real absorption line.

Voltage should be removed from the Stark electrodes when the pressure of the gas is being adjusted because of possible arcing in the wave guide. This will cause a decomposition of the gas and hence ruin the sample.

E. USEFUL EQUATIONS

Several general equations which have been found useful in microwave spectrograph studies will be reproduced here without derivation. These will apply only to linear and symmetric top molecules, since the asymmetric cases are usually more complicated and do not reduce to such simple form.

For pure rotational absorption the intensity ration to be expected by changing the gas temperature from T_1 to T_2 may be shown to be:

$$\frac{I_{T_2}}{I_{T_1}}=\left(\frac{T_1}{T_2}\right)^{5/2}\exp\left[\frac{-E_j}{k}\left(\frac{1}{T_2}-\frac{1}{T_1}\right)\right]\quad\text{for linear molecules}\quad(1)$$

$$\frac{I_{T_2}}{I_{T_1}}=\left(\frac{T_1}{T_2}\right)^{3}\exp\left[\frac{-E_j}{k}\left(\frac{1}{T_2}-\frac{1}{T_1}\right)\right]\quad\text{for symmetric top molecules,}\quad(2)$$

where E_j is the energy of the jth rotational state. Thus, if one uses dry ice as a refrigerant ($T_2 \cong 200°\text{K}$) and ($T_1 \cong 300°\text{K}$), for the case of the usual microwave absorptions the exponential will be very nearly unity. For this special case $I_{T_2}/I_{T_1} \cong 2.8$ and 3.4 for linear and symmetric top molecules, respectively. It must also be remembered that in order to keep the number of molecules a constant, the gas pressure must be reduced as the temperature is lowered when comparative intensity measurements are made.

Prediction of Absorption Frequencies

The expected absorption frequencies for both linear and symmetric top molecules are given approximately by[9]

$$\nu=\frac{1010\times 10^3(J+1)}{I_B}\quad(\text{mc}/s,\ \text{atomic wt.}-\text{Å}^2)\quad(3)$$
$$J=0,\ 1,\ 2,\ \cdots$$

$$\nu=\frac{167.8\times 10^{-36}(J+1)}{I_B}\quad(\text{mc}/s,\ \text{g-cm}^2).$$

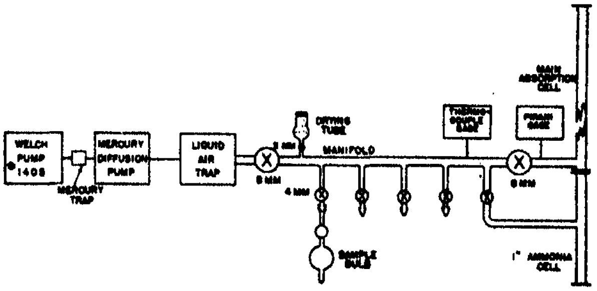

FIG. 13. Block diagram of vacuum system.

---

[8] C. H. Townes and S. Geschwind, Quarterly Report, Columbia Radiation Laboratory, September 30, 1948, p. 21.

[9] See for example G. Herzberg, *Infrared and Raman Spectra of Polyatomic Molecules* (D. Van Nostrand Company, Inc., New York, 1945).

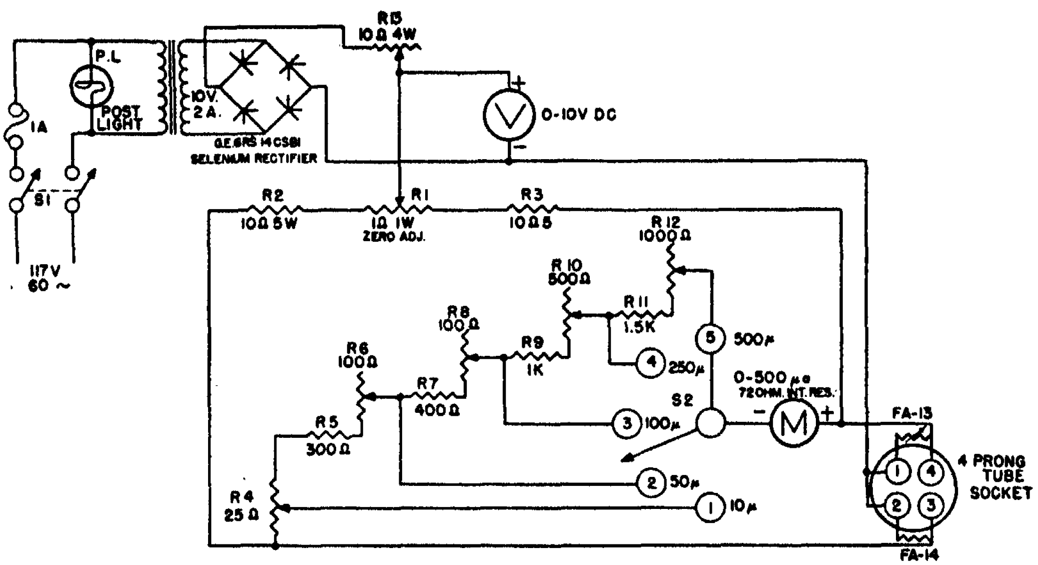

FIG. 14. Pirani gauge circuit diagram.

I_B is the moment of inertia taken about an axis perpendicular to the internuclear or symmetry axis and going through the center of mass. Mathematically it is defined as

$$I_B=\sum_i m_i r_i^2,$$

where r_i is the perpendicular distance of the ith nucleus of mass m_i from the axis passing through the center of mass. Two simple examples will best illustrate the computation of I_B.

For a linear molecule of the X-Y-Z type shown in Fig. 16

$$I_B=M_z(d_{yz}-x)^2+M_yx^2+M_x(d_{yz}+x)^2. \tag{4}$$

The center of gravity is defined by the relation

$$M_x(d_{xy}+x)+M_yx=M_z(d_{yz}-x), \tag{5}$$

where M_i is the mass of the ith atom in appropriate units. The internuclear distances are taken as the sum of the covalent radii as found, for example, in Pauling's book *Nature of the Chemical Bond*.

For symmetric rotor molecules of the type X_3-Y-Z as illustrated in Fig. 17, the computation of I_B may be computed in the following manner: the approximate moment of inertia is obtained by treating the molecule as a linear one with the mass of the three X atoms concentrated at the point defined by the intersection of the symmetry axis and the plane defined by them. In other words, assuming a tetrahedral angle of 110°,

$$d_{y3x}=0.328d_{yx}$$

and Eqs. (3) and (4) are then used as for an X-Y-Z molecule, where M_x is now $3M_x$. When the masses of the X atoms are appreciable, a consideration of the mechanics of this system of point masses shows that I_B may be corrected by adding to it the quantity $1.31M_xd_{yx}^2$. This latter correction is the moment of inertia of two X atoms about the axis aX in Fig. 17.

Computation of Expected Intensity of Absorption

To compute the absolute absorptions, the following equations given by Kisliuk and Townes[10] are useful:

Linear molecules

$$\gamma_{\max}=2.19\times10^{-18}\mu^2\nu^3 \text{ (debye, mc/}s\text{, cm}^{-1}).$$

Symmetric top molecules

$$\gamma_{\max}=4.83\times10^{-22}(A)^{\frac{1}{2}}\mu^2\nu^3\{1-(K^2/(J+1)^2)\}.$$

A is the reciprocal moment of inertia in megacycles

$$A=(10^{-6}h)/(8\pi^2I_A)=(84.0\times10^{-36})/(I_A).$$

J is the quantum number of total angular momentum $=0, 1, 2, 3, \cdots$.

K is the quantum number of the component of angular momentum along the symmetry axis; thus $K=J$, $J-1$, $J-2$, $\cdots$, $-J$.

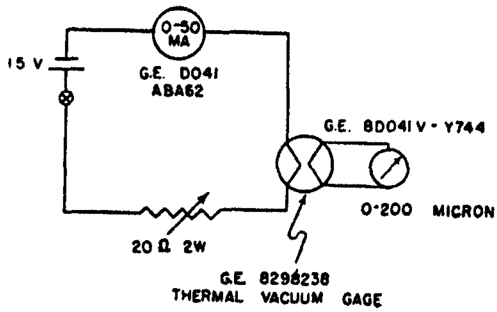

FIG. 15. Thermocouple gauge circuit diagram.

---

[10] P. Kisliuk and C. H. Townes, "Molecular microwave spectra tables," Nat. Bur. Stand. J. Research (to be published).

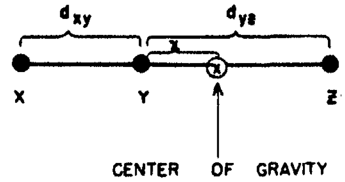

FIG. 16. Linear molecular model.

I_A is the moment of inertia (g-cm^2) about the internuclear or symmetry axis.

Computation of the Optimum Cell Length and Sensitivity[11]

The optimum cell length ($l_{\text{opt.}}$) is given by the simple relation

$$l_{\text{opt.}} = 2/\alpha_c \ (\text{cm}^{-1}).$$

If one uses this optimum length, then the minimum detectable gas absorption coefficient ($\alpha_{0\ \text{min.}}$) is given by

$$\begin{aligned}\alpha_{0\ \text{min.}} &= 2e\alpha_c(2kTN\Delta f/P_0)^{\frac{1}{2}} \qquad (6)\\ &= 50\times 10^{-11}\alpha_c(N\Delta f/P_0)^{\frac{1}{2}},\end{aligned}$$

where e = natural logarithm base = 2.72, α = attenuation coefficient of wave guide (cm^{-1}), k = Boltzman constant = 1.38×10^{-16} (ergs/degree), T = absolute temperature, N = noise figure of detector or receiver, Δf = band width of detector or receiver (c/s), P_0 = power input (watts), 1 neper/cm = 8.7 db/cm = 2 cm^{-1}.

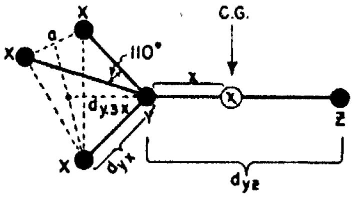

FIG. 17. Symmetric top molecular model.

F. ACKNOWLEDGMENT

The author gratefully acknowledges the assistance of the following rotating engineers, each of which has made many valuable contributions during his assignment to this project: E. Paul Diehl, Robert G. Day, C. Burton Crumly, Richard V. Prucha, Stanley G. Lemon, and John Mattern. I owe thanks also to Frederic C. Billingsley for his cooperation in the construction of the square wave generator and particularly to Dr. Robert Karplus for acquainting me with the field of microwave spectroscopy and rendering invaluable aid during the early stages of the spectroscope construction. I should like to express my gratitude to Dr. A. L. Marshall, director of the Chemical Section of the General Electric Research Laboratory, for his constant interest in the microwave program.

---

[11] C. H. Townes and S. Geschwind, J. App. Phys. 19, 795 (1948).

THE REVIEW OF SCIENTIFIC INSTRUMENTS VOLUME 21, NUMBER 2 FEBRUARY, 1950

Vortex Thermometer for Measuring True Air Temperatures and True Air Speeds in Flight

BERNARD VONNEGUT
General Electric Research Laboratory, Schenectady, New York

(Received October 17, 1949)

The aerodynamic heating experienced by thermometers exposed from airplanes can be very nearly eliminated over a wide range of operating conditions by mounting the thermometer in the center of an air vortex created by a simple housing. This method has been found to simplify air temperature measurements over the operating range of a B-17 airplane. The instrument has promise for measuring temperatures in clouds.

True air speeds can be measured by the difference between the temperature of the vortex thermometer and a thermometer exposed in the usual manner. Designs and flight data are presented for several vortex thermometers and a simple true air speed indicator.

INTRODUCTION

THE measurement of true air temperatures from an airplane is greatly complicated by the heating effect of the moving air. At a true air speed of 200 m.p.h., a thermometer exposed to the air stream indicates a temperature that is about three or four degrees higher than the true air temperature. E. Pohlhausen[1] has shown that the temperature correction ΔT which must be subtracted from the reading of a thermometer exposed in the usual way is expressed by an equation of the sort:

$$\Delta T = CV^2 \tag{1}$$

where V is the true air speed. If temperatures are expressed in degrees centigrade and true air speeds in miles per hour, the constant C is about $+0.8\times 10^{-4}$ for the usual thermometer.

K. Terada and G. Yamamoto[2] report that they have succeeded in greatly reducing aerodynamic heating by mounting a thermometer element in the wall of a small venturi tube exposed in the air stream. They found in a flight experiment made with this thermometer at an altitude of 4000 meters that a change of indicated air speed of from 250 to 400 Km/hr. resulted in an increase of the temperature reading of 0.7°C. An ordinary thermometer would be expected to show a temperature increase of about 5°C for the same change of air speed. If their thermometer data can be expressed by Eq. (1), then the constant C should be about $+0.12\times 10^{-4}$ when their air speeds are corrected for altitude and expressed in miles per hour.

In this work, it has been found possible to eliminate the heating effect of the moving air in a somewhat different way by utilizing Ranque's[3] discovery that a temperature lowering occurs in the center of an air vortex.

The refrigeration which is obtained by mounting a thermometer in a vortex can be used to balance out aerodynamic heating in such a way that the constant C in Eq. (1) becomes very nearly zero and large temperature corrections are no longer necessary.

EXPERIMENTAL

Laboratory Tests.—Laboratory experiments were carried out to determine whether the refrigeration obtained in a vortex was large enough to counterbalance aerodynamic heating. These tests were carried out by drawing air with a vacuum cleaner through various simple vortex creating housings and measuring the temperature in the vortex. The temperature lowerings observed in these tests were of the same order of magnitude as the aerodynamic heating effects which might be expected with similar air velocities.

Flight Test, M-2 Housing.—The first flight tests were made on a preliminary design of the housing which was found to reduce aerodynamic heating to about one-third of its usual value. On the basis of the results of these tests, a second unit (designated as M-2) was designed and constructed. This housing, which is shown in Fig. 1, was provided with a valve shown in the drawing which could be used to regulate the air flowing into the vortex. By adjusting this valve, the refrigeration produced by the vortex could be regulated.

The results of a flight made at 3000 feet with this unit are shown in Fig. 2. Two dial-type thermometers were used in this test. One thermometer was mounted in the housing, while the other was exposed at right-angles to the air stream. The data in Fig. 2 have been plotted relative to a true air temperature computed from the readings of the thermometer exposed in the usual fashion. It can be seen that with the valve wide open, the thermometer in the housing reads far below the true air temperature. With this valve setting, the constant C in Eq. (1) has a value of about -0.7×10^{-4}.

The valve was then adjusted to reduce the air flow so that the thermometer read the computed true air temperature. The observed thermometer readings with this valve setting do not vary appreciably with airplane speeds from about 120 m.p.h. to 225 m.p.h.

Flight Test, M-3 Housing.—Following the successful tests with the second housing, it was felt desirable to make direct comparisons between measurements made with the vortex thermometer and those made with a standard airplane thermometer. The ML-313 psychrometer is in general use for measuring air temperatures and humidities from U. S. A. F. airplanes. Accurately calibrated L-shaped mercury thermometers with 0.1°C divisions are used in this apparatus. The M-3 vortex housing shown in Fig. 3, was designed for use with these thermometers. The valve on this housing is controlled by a screw which moves it in or out and permits fine adjustment. Once the valve has been properly adjusted, it is locked permanently in position with a set screw which can be seen in Fig. 3.

---

[1] E. Pohlhausen, Zeits. f. angew. Math. Mech. 1, 111–121 (1921).

[2] K. Terada and G. Yamamoto, J. Meteorology 4, No. 6, 201–202 (1947).

[3] G. J. Ranque, Bulletin—Bi Mensuel de la Societe Francaise de Physique, 1125–1155 (June 2, 1933).

In the first flight made with this housing, the valve was adjusted to read a true air temperature computed from the reading of the ML-313 dry bulb thermometer using $C=+0.87\times10^{-4}$ which has been determined for this thermometer. With this valve setting, runs were made at 4000 feet, 8000 feet, and 12,000 feet with two observers taking simultaneous readings, one on the ML-313 and the other on the vortex thermometer. The temperatures measured are shown in Figs. 4 and 5. It was apparent from this data that the valve was in a little too far. A slight adjustment was then made, and a second run was made at 4000 feet which is shown in Fig. 6. The variation of temperature with speed with this setting was very small, and this setting of the valve has been used in all subsequent measurements.

The data taken on the M-3 housing are somewhat anomalous in that the readings taken with the two thermometers do not always extrapolate to the same value at zero velocity. When the thermometers are tested in the laboratory, they agree to within 0.1°C. One possible explanation for this discrepancy which is observed in much of the data is that the vibration of the airplane may cause separation of the mercury column. This separation has occasionally been observed with these thermometers.

Further runs have been made on the M-3 housing to determine how well it operates over the range of speeds and altitudes of which the Project CIRRUS B-17 airplane is capable. Figure 7 shows the results of one of these flights. The data have been plotted to show the departure of the readings of the vortex thermometer from a true air temperature computed from the readings of the ML-313 dry bulb.

The mercury thermometer used in the above tests had a scale which went down to −20°C. For tests at higher altitudes and lower temperatures, it was necessary to use another thermometer with a lower range. The physical dimensions of the new thermometer differed slightly from the old, which might be expected to necessitate a slight adjustment of the valve. However, no changes were made. The data obtained using the new thermometer are shown in Fig. 8. These data do not include simultaneous readings taken with the ML-313 thermometer because its mercury column separated.

The air temperatures at a constant altitude were

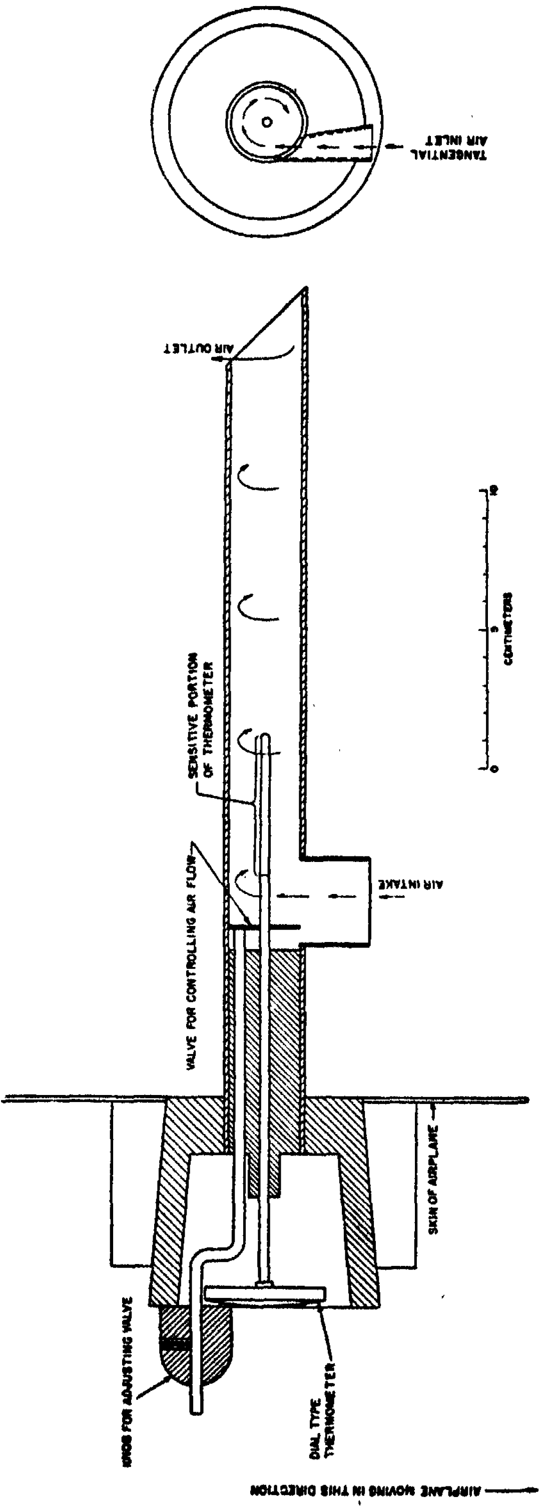

FIG. 1. M2 thermometer housing.

fairly uniform during this flight, and the readings of the vortex thermometer showed a maximum variation of 0.5°C over changes in air speed that would cause the usual thermometer to change at least two degrees. It appears that the vortex housing reduces errors from aerodynamic heating to less than 0.5°, at least up to speeds of 260 m.p.h. and altitudes up to 25,000 feet.

Vortex Thermometer for Measuring True Air Speeds.—Because the aerodynamic heating is a function of the true air speed, it is possible to measure true air speeds by the difference in temperature between a thermometer exposed in the usual way and one exposed in a vortex. In the thermometer tests just described, it was possible to make a fairly close estimate of air speed from the difference in reading of the two thermometers.

A simple true air speed meter was made which consisted of two No. 14B thermistors mounted in a vortex housing. One of these was mounted in the center of the vortex, while the other was mounted on the periphery. The difference in temperature between the thermistors was measured by a microammeter in a simple bridge circuit. A flight was made in which the readings of the microammeter were compared with the true air speed computed from the readings of the usual air speed indicator. The results of this flight show that the instrument may have promise as a true air speed indicator.

SIMPLIFIED THEORY

An adequate theoretical treatment of the vortex would be a formidable task. It is possible, however, to make some simplifying assumptions and arrive at an approximation of what may be the true state of affairs.

If one assumes that the air in the vortex is rotating with uniform angular velocity and that its periphery is moving with the true air speed of the plane, one finds that at 200 m.p.h. the air is revolving at about 45,000 r.p.m. in a $1\frac{1}{2}$-inch diameter tube.

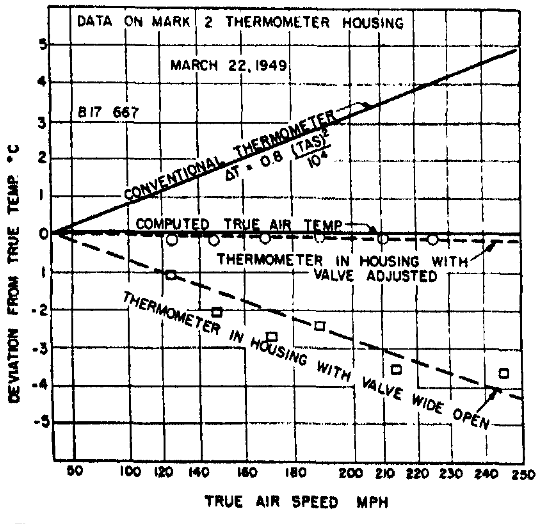

FIG. 2. M2 housing flight data taken at 3000 ft. altitude.

This high speed of rotation sets up a pressure difference between the center and outside of the revolving air. One can regard the temperature lowering in the center of the vortex as being produced by the adiabatic expansion of the air as it passes from the periphery to the center. On the basis of the above assumptions, it can be shown that the difference in pressure, Δp, between the outside and the center of the vortex is given by

$$\Delta p = p(mw/RT)\cdot V^2/2, \tag{2}$$

where p is the pressure of the atmosphere, mw is the molecular weight of the air, R, the gas constant, T the absolute temperature, and V, the true air speed of the airplane. This is the identical expression for the increase in pressure caused by the motion of the airplane through the air. Aerodynamic heating can be regarded as resulting from an adiabatic compression of the air. The vortex can be looked upon as a simple method by which air from the atmosphere is accelerated to the speed of the airplane and adiabatically expanded to its original pressure and temperature. The air in the center of the vortex is at true air temperature and pressure, and because it is moving along with the airplane, its temperature can be easily measured without need of corrections.

If the pressure difference available from the motion of the airplane were limited to the pitot static difference, it is doubtful whether the air could be cooled all of the way back to its original temperature by this system. A certain amount of frictional heating must take place. Fortunately, about double the pitot static pressure difference is available between the ram air pressure and a tube opened downstream, and, therefore, ample cooling is available.

Temperature Measurements in Clouds.—It is believed that the vortex thermometer will be of value in measurements in clouds. The rotational velocities are sufficiently large that it is believed that the high centrifugal force will prevent cloud particles from depositing on the thermometer in the center of the vortex. This would eliminate any errors which might be caused by evaporation or freezing of water on the thermometer. Should any cloud-water drops deposit on the thermometer bulb, they would not be expected to cause evaporation cooling such as is experienced with the usual thermometer. Because the thermometer in the vortex and the air around it are at the true temperature of the cloud, any water on the thermometer would be in equilibrium with the saturated air around it and could not evaporate. When the airplane flew out of the cloud into unsaturated air, measurements would, of course, be in error until the water dried off.

The flights which have thus far been made in clouds have been of such short duration that the thermometers have not had time to reach equilibrium. These flights have shown that the temperature difference between

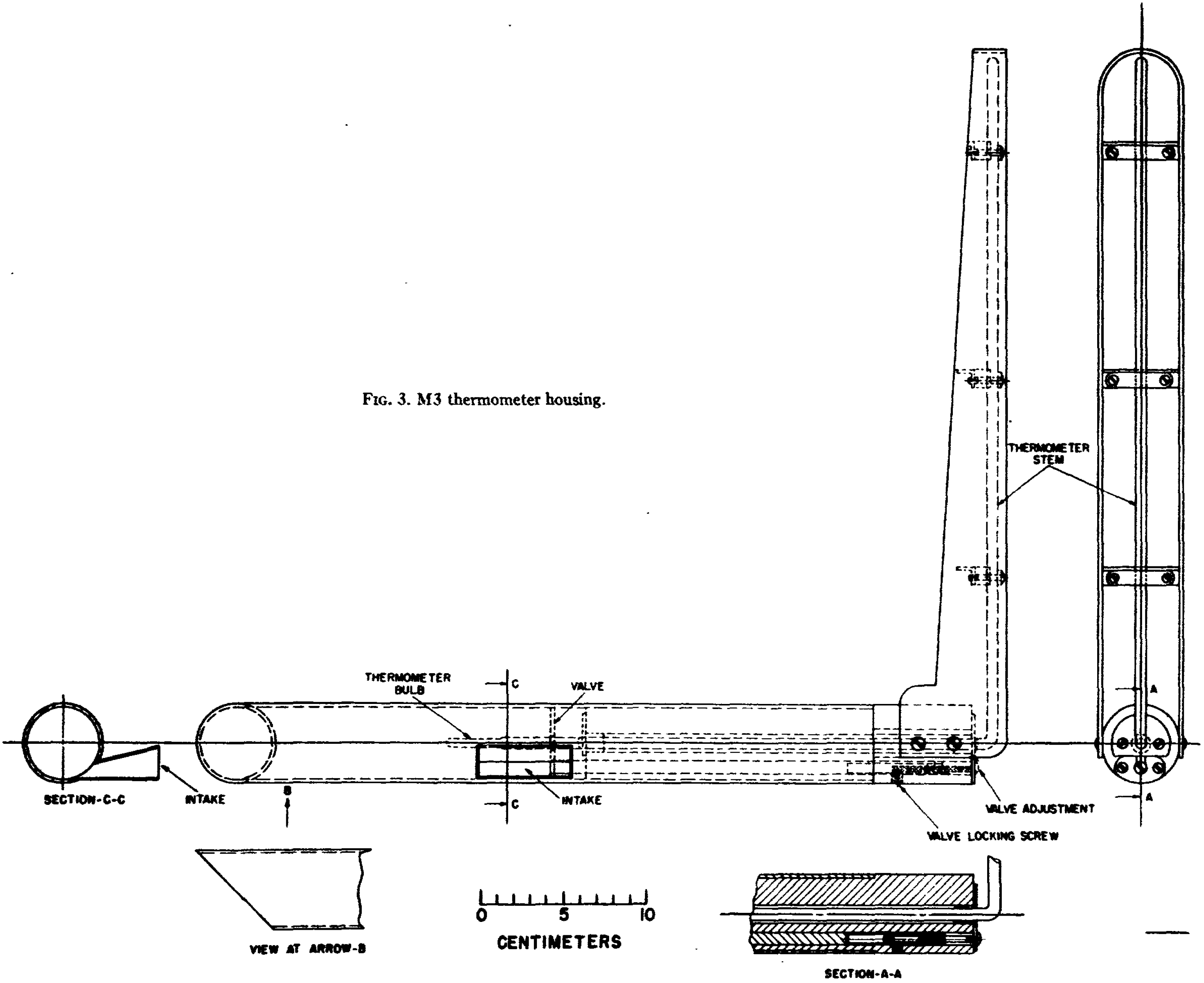

Fig. 3. M3 thermometer housing.

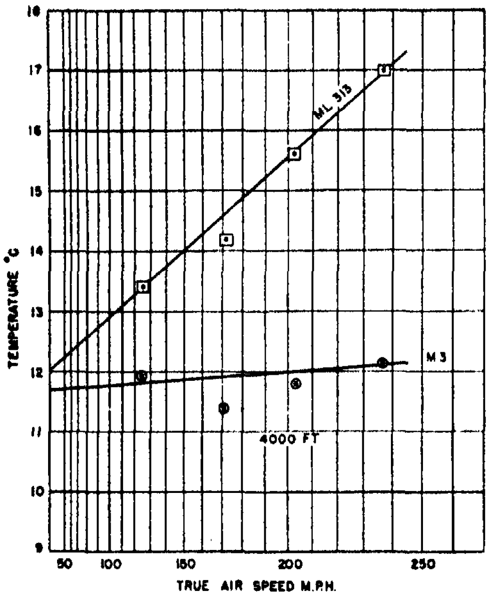

FIG. 4. Data taken with M3 housing at 4000 ft. altitude using preliminary valve setting.

the thermometers decreases somewhat as would be expected.

In the few flights which have been made in icing conditions, rime ice was observed to build out on the leading edges of the air intake of the housing. This deposition of ice did not appear to have any marked effect. It should be possible to use some non-volatile deicing liquid to prevent the formation of ice on the housing.

Effect of Clouds on True Air Speed Meter.—A short flight through clouds has been made using the true air speed meter which has been described. Upon flying into a cloud at constant air speed, the meter reading dropped by a factor of two and upon leaving the cloud, returned to its normal value. This was doubtless caused by deposition and evaporation of water on the high temperature thermistor.

Inasmuch as the air speed is to be measured by the temperature *difference* between the thermistors, there is no reason why the liquid water cannot first be removed either by a system of baffles or by heating and evaporation. This should enable the air speed meter to operate satisfactorily even in clouds.

When the vortex thermometer is used to measure air speed, there is no particular reason that the cold thermistor should be exactly at the true air temperature. It is important, however, that the cold thermistor always be operated above the dew point of the air. At temperatures below the dew point, heating takes place because of condensation of the water to form a cloud. This heating would, of course, make the instrument very unreliable.

CONCLUSIONS

The tests thus far indicate that the vortex thermometer should be quite useful in temperature measurements made from airplanes. There is little doubt that readings obtained with the thermometer deviate to some extent from the true air temperature depending on altitude, pressure, and air speed.

However, from the data obtained thus far, it can be seen that in the range of conditions investigated these corrections are quite small. The data are not sufficiently accurate to give a clear indication whether the thermometer adjusted at low altitude reads too high or too

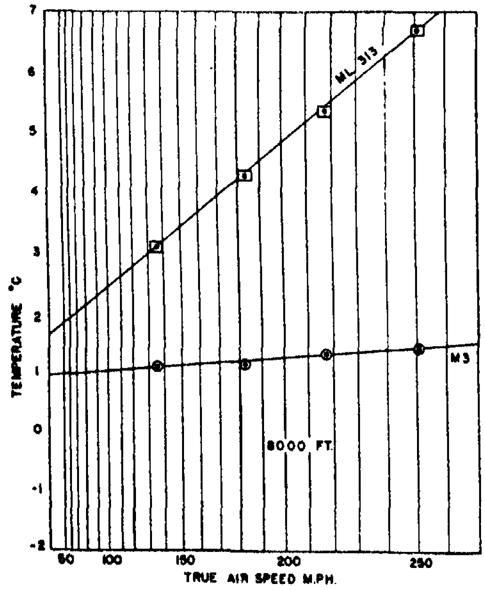

FIG. 5. Data taken with M3 housing at 8000 ft. altitude using preliminary valve setting.

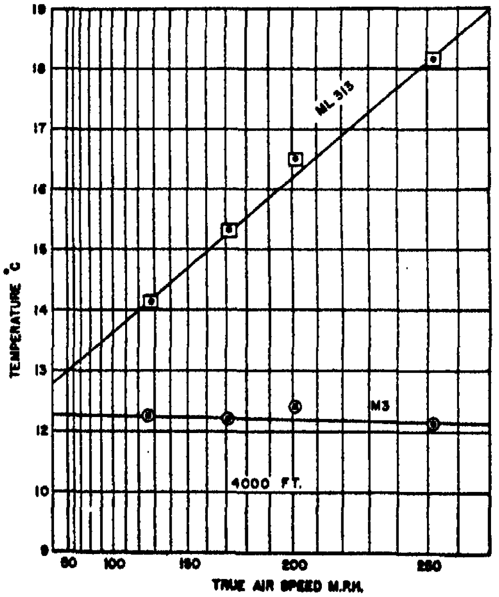

FIG. 6. Second run at 4000 ft. altitude with M3 housing after making slight adjustment of valve.

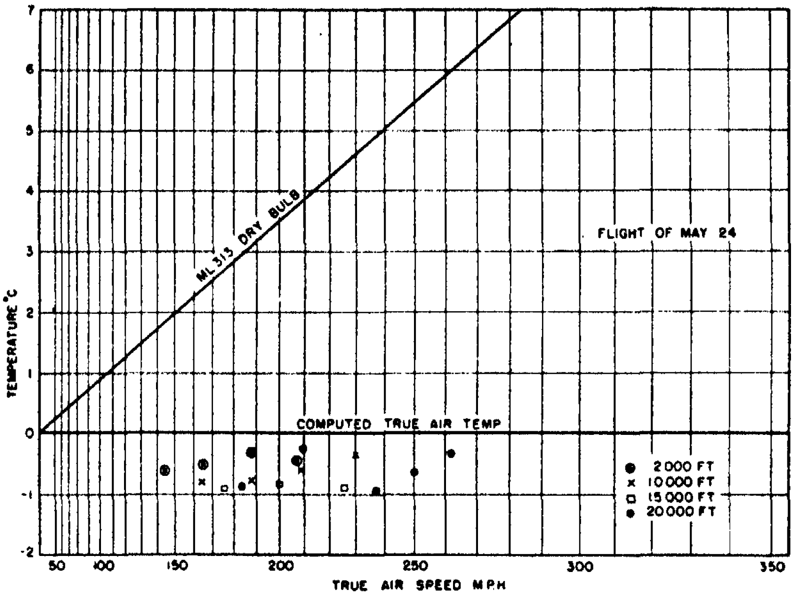

FIG. 7. Deviation of temperatures measured with M3 housing from true air temperature computed from ML313 dry bulb readings.

low at high altitude. The data of Fig. 8 give a slight indication that at high altitude, because of low pressures or temperatures, the vortex may slightly overcompensate for aerodynamic heating by a small fraction of a degree.

Measurements made at higher air speeds and greater altitudes will give a much better picture of the limitations of the device.

The design of the housing does not seem to be at all critical in the range of conditions which have been investigated. Because of this latitude in design, it may be possible by changing the housing to reduce any deviations which may be found to exist.

ACKNOWLEDGMENTS

The author wishes to thank the following for their invaluable cooperation in this work: Mr. A. Parr, who constructed the thermometer housings; Mr. T. Rich and Mr. J. E. Bigelow of the General Electric General Engineering and Consulting Laboratory, who suggested and built the thermistor temperature measuring device on the air speed indicator; S. Rush and associates who prepared the drawings; U. S. N. aerographers, C. Remscheid and R. F. Ryan, and D. Blanchard of the General Electric Research Laboratory who took much of the flight data; and the personnel of Project CIRRUS who cooperated in organizing and carrying out the flight tests.

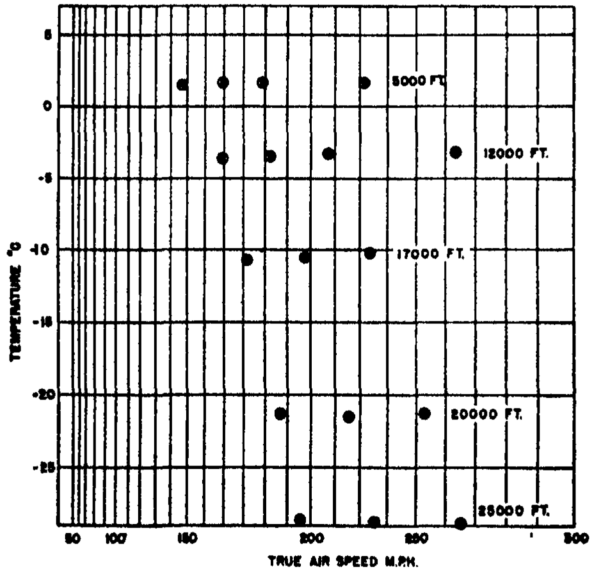

FIG. 8. Temperatures indicated by M3 thermometer as function of altitude and true air speed.

The research reported in this document was made possible through support extended the Research Laboratory of the General Electric Company jointly by the Signal Corps and the Navy Department (ONR) under Signal Corps Contract No. W-36-039-SC-38141. Acknowledgment is also made of assistance from the U. S. Air Forces in providing aircraft and associated personnel.

Wire Recorded Magnetic Pulse Timing Circuit*

C. R. EMIGH
Physics Department, University of Illinois, Champaign, Illinois

(Received August 29, 1949)

A time delay circuit is described for timing and sequencing the operations of a cloud chamber. By magnetizing a moving section of recording wire and at a later time using the magnetized section to actuate a sensitive relay, delays from 0.01 to 0.25 second are obtained. The delay can be adjusted visually to an accuracy of 0.001 second.

INTRODUCTION

THE magnetic pulse timing circuit was developed to synchronize accurately the operations of a cloud chamber to the 80-Mev University of Illinois pulsed betatron.[1,2] This report concerns itself only with the initiation and subsequent operation of the timing circuit. The general operation of cloud chambers in relation to their timing circuits has been described adequately in previous articles.[3,4]

The range of the magnetic pulse timing circuit is from 0.01 to 0.25 second delay with a variation of less than 0.001 second as determined by an oscilloscope. The variation is independent of the delay.

The magnetic pulse timing circuit has several advantages over previously reported cloud-chamber timing circuits.[3–6] It may be initiated by a trigger signal at any arbitrary time, which for the present application is a necessary advantage over the mechanical cam type of timing circuit. The mechanical system, consisting of cam operated micro-switches, has in addition the disadvantages that the time delay is somewhat dependent on the mechanical wear of the cam and the desired delay can be adjusted to an accuracy of ±0.01 second only by an auxiliary timing circuit. The electronic type timing circuit usually incorporates either an RC or R/L type time delay, which is to be preferred for delays less than 0.01 second. However, for delays of the order of 0.01 to 0.25 second the magnetic pulse timing circuit offers greater accuracy and ease of adjustment. Once the pulse timing circuit is calibrated, the magnitude of delay may visually be set to an accuracy of approximately ±0.001 second without any auxiliary equipment. The pulse timing circuit also inherently incorporates a second time delay which allows the cloud-chamber controlling relays to stay energized for a prescribed length of time. The second delay is also variable. The apparatus has the disadvantage of obtaining accuracy and simplicity of operational alignment at the expense of simplicity of construction.

BASIC OPERATION

The cloud-chamber magnetic field coils are energized periodically with a cycle time of the order of 10 seconds, depending on the recovery time of the cloud chamber used. As the current builds up in the field coils, the magnetic field rises proportionally. When the magnetic field passes through a predetermined value, a proton magnetic moment detector[7] (see Fig. 1) produces a signal which is amplified and channeled to the magnetic pulse time delay circuit. (By the use of the proton magnetic moment detector the field can be determined in time to an accuracy of ±0.1 percent at the probe.)

At the pulser unit the signal from the proton magnetic moment detector connects a charged condenser across an inductance. The unidirectional pulse field produced in the iron core of the inductance is used to magnetize horizontally a section of magnetic recording wire wound on the periphery of a disk. The disk is driven by an a.c. synchronous motor and gear reducer such that one revolution of the disk represents 0.267 second.

Located on a platform around the disk are six small pick-up coils. As the magnetized portion of the recording wire passes near a pick-up coil, a voltage signal is induced across the terminals of the coil. The signal triggers a one-shot multivibrator delay circuit which in turn energizes a high sensitivity relay for a period depending on the cycle time of the multivibrator. The relays control the cloud-chamber expansion, turn off the sweep field, trigger the pulsed betatron, open the camera shutters and trigger the pulse lights in their properly timed sequence. At the completion of one revolution of the disk, with respect to the triggering of the pulser unit, the magnetized wire is demagnetized by a d.c. magnet.

The amount of time delay depends on the number of degrees the pick-up coil assembly is rotated about the center of the disk from the pulser unit. The platform is graduated every 13½° (0.01-second intervals). Interpolation between 0.01-second interval marks is done visually.

---

* This work was assisted by the Joint Program of the ONR and the AEC.

[1] Kerst, Adams, Koch, Robinson, Phys. Rev. 75, 330 (1949). Abstract of paper presented at American Physical Society Meeting, November, 1948.

[2] Kerst, Adams, Koch, and Robinson (to be published).

[3] C. C. Jones, Rev. Sci. Inst. 8, 319 (1937).

[4] F. L. Allen, Rev. Sci. Inst. 19, 24 (1948).

[5] J. R. Richardson, Rev. Sci. Inst. 9, 152 (1938).

[6] I. A. Getting, Rev. Sci. Inst. 10, 323 (1939).

[7] Mr. I. Janney is developing the detector for use with cloud chambers from a basic circuit originated by Dr. R. V. Pound.

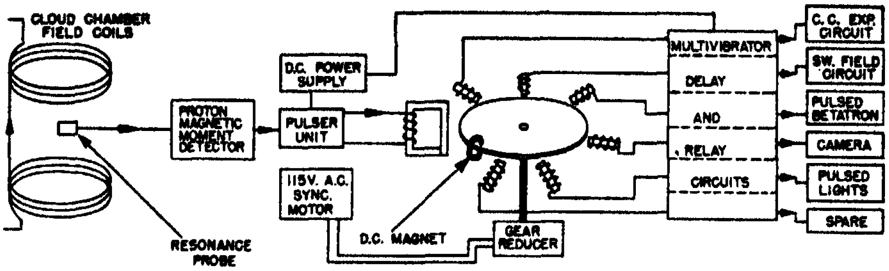

FIG. 1. A block diagram showing the general layout of the delay system as used for cloud-chamber operation.

CIRCUIT DETAILS

Power Supply

The power supply is shown in Fig. 2. It is designed to supply power to the pulser unit and the multivibrator circuits. The power supply is a full-wave bridge type rectifier with one corner of the bridge grounded. Therefore, between ground and the center-tap of the power transformer, approximately +450 volts d.c. are developed by ordinary full wave rectification. The 5W4 in the pulser unit acts as a conventional cascade doubling circuit with the full wave rectifier and supplies the pulser unit at +900 volts d.c.

Pulser Unit

The 16-μfd capacitor is charged by the cascade doubling circuit to +900 volts through a 0.1-megohm resistor and the 4.4-millihenry inductance. The inductance consists of 150 turns of No. 16 enameled copper wire wound on a core of laminations stacked to a cross section of $\frac{3}{4}$ in. by $\frac{1}{2}$ in. The laminated core is shaped such that its ends do not butt up against each other, but overlap by $\frac{3}{4}$ in. (Fig. 2). The overlapping portions are separated by a $\frac{1}{8}$-in. copper sheet. This thickness is of the same order of magnitude as the skin depth of copper at the frequency of operation

$$f=\frac{1}{2\pi(LC)^{\frac{1}{2}}}\quad(C=16\ \mu\text{fd},\ L=4.4\ \text{mh}).$$

When the 4C35 hydrogen filled triode is triggered by the signal from the proton magnetic moment detector, the charged 16 μfd capacitor is essentially shorted across the 4.4-millihenry inductance. The resulting current through the inductance has a sinusoidal wave shape for the first half-cycle. At the end of the half-cycle the 4C35 is extinguished and no further current flows through it. Because of the copper shield between the poles of the core, the sinusoidally varying flux is forced from one pole face around the shield to the other pole face, which produces a concentration of horizontal flux in front of the poles. The peak value of current is roughly 50 amperes, corresponding to an estimated 4000 gauss of horizontal magnetizing field produced at the magnetic recording wire.

Disk and D.C. Magnet

The disk is a 12 in. diameter $\frac{3}{8}$ in. thick piece of red Bakelite with a $\frac{1}{4}$ in. wide, $\frac{3}{16}$ in. deep slot machined around the circumference. All of a commercial 30-minute spool of recording wire is wound in the slot.

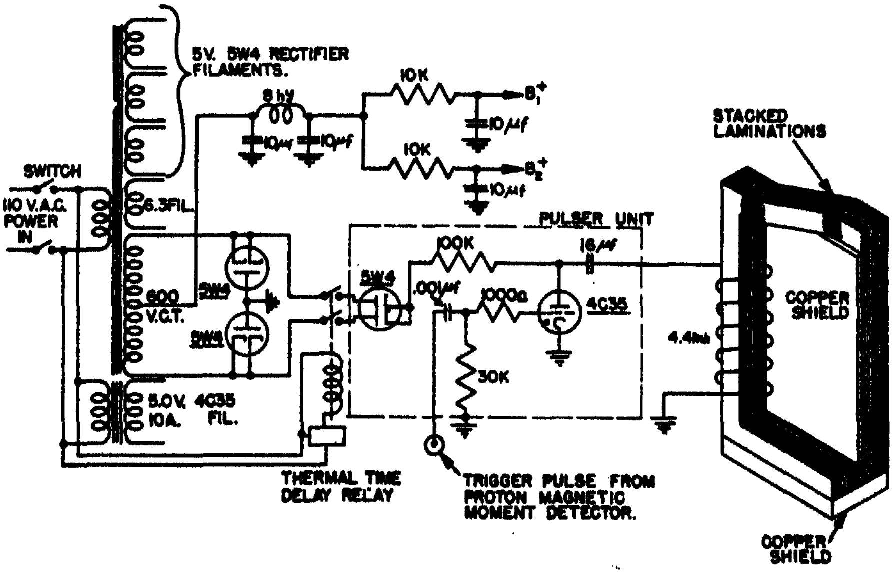

FIG. 2. Power supply and pulser unit.

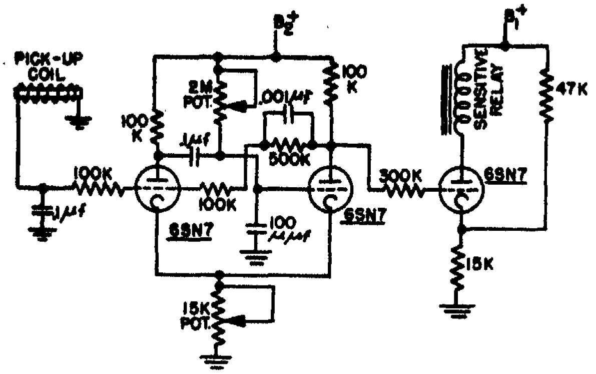

FIG. 3. Multivibrator and sensitive relay circuit.

The above described horizontal pulse field magnetizes a 13° arc of the recording wire (magnetized along the wire's length). After the magnetized section completes nearly one revolution, a d.c. magnet of 5000 gauss magnetizes the wire in a vertical direction (magnetized in the direction of the wire's vertical diameter), thus demagnetizing the horizontally recorded pulse.

Multivibrator Delay Circuit and Relay

The circuit shown in Fig. 3 is a conventional type one-shot multivibrator. The first grid circuit contains the pick-up coil which consists of 10,000 turns of No. 38 wire wound on a solid iron core. The inductance of the coil is 1.5 henry. The resistor in the cathode circuit is adjusted so that the grid containing the pick-up coil is biased below cut-off. Therefore, a 10-volt positive signal from the pick-up coil will trigger the multivibrator. The cycle time of the multivibrator is varied by the potentiometer in the second grid circuit.

The plate of the second section of the multivibrator is coupled through a resistor to the grid of the relay switch tube. Thus the relay is energized during the cycle time of the multivibrator. The relay used is a high-sensitive relay rated at 0.005 ampere for closing. By exceeding this value appreciably for short times, the mechanical delay due to the relay can be reduced to less than 0.002±0.0005 second.

ACKNOWLEDGMENT

The writer wishes to acknowledge the encouragement and helpful criticisms of Professor H. W. Koch regarding the development of this work.

THE REVIEW OF SCIENTIFIC INSTRUMENTS VOLUME 21, NUMBER 2 FEBRUARY, 1950

A Wide-Band Audio Phasemeter

JOHN R. RAGAZZINI AND LOTFI A. ZADEH
Columbia University, New York, New York

(Received August 8, 1949)

The problem of measuring the phase angle between two sinusoidal voltages is an important one in laboratory procedure. Phasemeters which can make this measurement accurately over a substantial frequency range have heretofore been bulky and relatively stationary. This paper describes a circuit which results in a phasemeter which is accurate to about 30 minutes, has a dial adjustment which is independent of frequency, operates over a range of from 20 c.p.s. to 100 kc and is relatively small and inexpensive. The principle used is to match the phase shift between the unknown voltages with a calibrated phase shift in the meter channel. This phase equalization is observed on a standard oscillograph which is used only as a comparison instrument. The oscillograph amplifier phase shifts are balanced out with an uncalibrated phase shifter cascaded in the meter channel and do not affect the measurement.

1. INTRODUCTION

An increasingly common and yet difficult problem that confronts one in the laboratory is that of measuring the phase difference between two sinusoidal voltages. Many methods have been devised for this purpose but few, if any of them, are satisfactory for accurate measurement of phase angles over a wide range of frequencies with relatively simple circuits and equipment. Some are highly accurate but operate over a restricted range of frequencies, while others are of the convenient direct-reading type but lack accuracy. A few such as the ones constructed at the Royal Institute of Technology in Sweden,[1] L. M. T. Laboratories in Paris,[2] Post Office Research Station in London[3] and the Bell Telephone Laboratories in New York[4] combine high accuracy with width of operating range. These, however, are usually very bulky and should be classified as stationary equipment. Few phasemeters except those of the stationary type are commercially available at present.

To be useful in the laboratory as an instrument, a phasemeter should have none of the deficiencies mentioned above and should be relatively simple and inexpensive. A design has been devised and is described in this paper which fulfills the following specifications:

1. The phasemeter should be operative over a frequency range of from 20 c.p.s. to 100 kc.
2. The error should not be in excess of 30 minutes of arc over the entire operating range.
3. The burden of accuracy of the meter should be placed on a few non-inductive linear circuit elements.
4. The dial indication of the meter should be independent of frequency.
5. The meter and associated equipment should be relatively simple and inexpensive.
6. The power supply for the meter should operate from a.c. mains.

A meter has been constructed in accordance with these specifications by the authors. A detailed description of this phasemeter is given in the following sections.

2. PRINCIPLE OF MEASUREMENT

Referring to the block diagram of Fig. 1, it is seen that the phasemeter consists essentially of two channels, C_1 and C_2. The first channel contains two phase shifters, P_c, which is calibrated, and P_{nc}, which is uncalibrated. The calibration of P_c is independent of frequency over the range of operation of the meter (20 c.p.s. to 100 kc). The second channel is a direct connection and is inserted only for convenience in making connections. The output voltages of the phasemeter are connected to the horizontal and vertical inputs of a standard oscillograph.

The meter will measure the phase angle between the voltages E_1 and E_2 by observing the trace on the oscillograph. The general process of measurement consists of first setting the calibrated phase shifter, P_c, to zero and applying the same voltage E_1 to both channels. The uncalibrated phase shifter, P_{nc}, is then adjusted until the oscillograph indicates by its trace that the

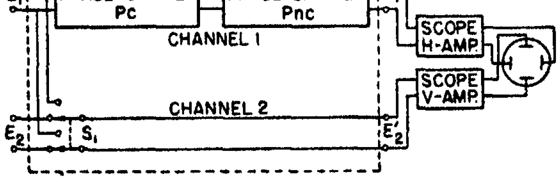

FIG. 1. Block diagram showing principle of phasemeter.

---

[1] H. Werthen and B. Nillson, "An automatic impedance meter," Trans. Roy. Inst. Tech., Stockholm, Sweden, No. 8 (1947).

[2] M. Levy, "Methods and apparatus for measuring phase distortion," Elec. Comm. 18, 206–228 (1940).

[3] R. F. J. Jarvis and E. F. S. Clarke, "Apparatus for the measurement of insertion phase shift at radio frequencies," P.O. Elec. Eng. J. 33, 162–171 (1941).

[4] D. A. Alsberg and D. Leed, "A precise direct reading phase and transmission measuring system for carrier program systems," Bell Syst. Tech. J. 28, No. 2 (1949).

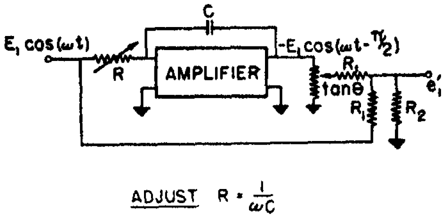

FIG. 2. Block diagram of calibrated phase shifter.

phase shift of both channels is equal. The null indication consists of reducing the ellipse which appears on the screen to a straight line. High degrees of accuracy can be achieved by this process if the trace is amplified so that only a small part of the ellipse actually falls on the screen. Under these conditions, the process of collapsing the ellipse is observed as the bringing together of two straight lines, the remainder of the trace being off the screen.

After the channel phase shifts have thus been equalized, the switch S_1 is thrown to a position which impresses E_1 on channel 1 and E_2 on channel 2. The oscillograph will now indicate a phase shift between the two voltages. This is once again brought to zero only this time by adjustment of the calibrated phase shifter P_c. The reading of this phase shifter dial is the phase angle between the two voltages E_1 and E_2. The measurement is seen to be essentially a null technique and the oscillograph is used only as an indicator to show phase coincidence. The phase shift in each of the channels or associated equipment is cancelled so that inequality in the amplifiers of the oscillograph has no effect.

3. CIRCUIT DETAILS

The basic unit in the calibrated phase shifter P_c is required to shift an applied voltage by an adjustable angle θ. Thus, if the input voltage has the form:

$$e_1=E_1\cos\omega t, \qquad (1)$$

the output voltage should have the form:

$$e_2=E_1'\cos(\omega t+\theta), \qquad (2)$$

where the magnitude is of no consequence but the phase angle θ must be known and should have a value ranging from 0 to 45 degrees. This range, in conjunction with certain switching arrangements shown in Fig. 3, is sufficient to accommodate all possible phase relationships between the unknown voltages.

The method used to transform e_1 into e_2 is summarized in the trigonometric relation:

$$E_1\cos(\omega t)+[E_1\tan\theta]\cos(\omega t+\pi/2)$$
$$=\left[\frac{E_1}{\cos\theta}\right]\cos(\omega t+\theta). \qquad (3)$$

The operations called for in Eq. (3) are mechanized in the following steps:

a. Generation of a voltage $E_1\cos(\omega t+\pi/2)$ which is in quadrature with the voltage $E_1\cos(\omega t)$.

b. The adjustment of this voltage to a magnitude $E_1\tan\theta$ by means of a calibrated linear potentiometer.

c. The addition of the two components in Eq. (3).

The first operation involving a shift of phase of 90 degrees is accomplished by a stabilized feed-back amplifier as shown in Fig. 2. The feed-back amplifier shown is an integrator whose gain is very closely $-1/j\omega RC$ if the gain of the base amplifier is high. If R and C are interchanged, a differentiator results whose gain is $-j\omega RC$. In practice, the latter has been found more desirable and is the type incorporated in the meter.

In the actual circuit shown in Fig. 3, this unit is seen to consist of tubes V_2, V_3, and V_4, capacitances C_6, C_7, C_8, and C_9 and resistors R_5, R_6, and R_7. In the actual unit, a gain of well over 1000 is maintained in the base amplifier over a frequency band of from 20 c.p.s. to 100 kc so that a very accurate 90-degree phase shift is obtained over this band width.

It is evident that, as in the case of any minimum phase shift network, the amplifier produces a gain rise (or loss) with frequency of 6 decibels per octave of frequency. To prevent the gain (or loss) of the amplifier from ranging over too wide limits, a switch S_3 is used to choose the value of capacitance which, in combination with the adjustable bridging resistor R_6, will result in an over-all gain of unity at the frequency of the test voltage. In this manner, the voltages at the input and output of the feed-back amplifier are equal in magnitude but have a phase angle between them of exactly 90 degrees.

The second step in the mechanization is carried out by means of the potentiometer R_{16} whose output has the magnitude $E_1\tan\theta$. This potentiometer is a linear wirewound unit with a dial whose face is calibrated in angle θ, the phase angle which is being measured. Finally, the third step is carried out by the simple adder circuit consisting of two precision resistors, R_{18} and R_{19}, and the common resistor R_{20} across which appears the sum of the two components in Eq. (3). With this circuit, therefore, the operations called for in Eq. (3) are carried out and a voltage which has been shifted by an angle θ with respect to the input voltage is available. The burden of accuracy is placed on resistive components and since the calibration is carried out only to 45 degrees, the dial scale is nearly linear.

The uncalibrated phase-shifter for channel equalization is made up of the subtractor tube V_6 and the RC bridge made up of R_{25}, R_{30}, C_{16}, C_{20}, and the other condensers in the same switching circuit. The switches S_6 and S_7 are used to obtain easily adjustable phase shift at the various frequency ranges. With the calibrated phase-shifter, whose maximum phase shift is only 45 degrees, the switching system made up of S_2, S_3, S_4, S_6, and S_7 makes possible the measurement of

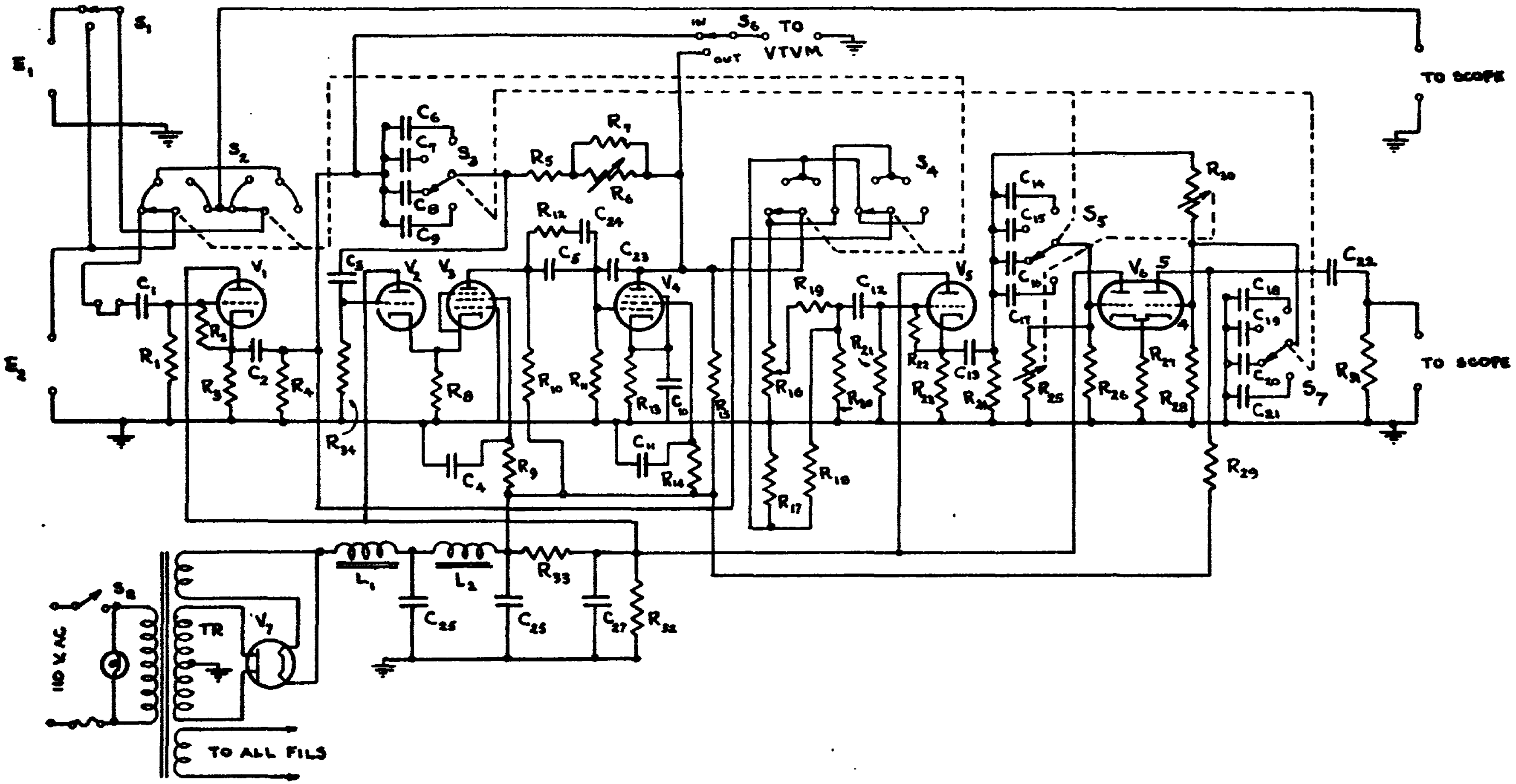

FIG. 3. Circuit diagram of phasemeter. C_{23}—5 μμf; C_6—100 μμf; C_7—500 μμf; C_{14}, C_{18}—0.001 μf; C_8—0.005 μf; C_{15}, C_{19}—0.01 μf; C_3, C_9, C_{12}—0.05 μf; C_1, C_5, C_{16}, C_{20}—0.1 μf; C_2, C_{13}, C_{17}, C_{21}, C_{22}, C_{24}—1 μf; C_4, C_{11}, C_{25}, C_{26}—16 μf; C_{27}—30 μf. R_{13}—350; R_8—500; R_{27}—2*K*; R_{23}—5*K*; R_4, R_5, R_{24}—10*K*; R_{20}—20*K*; R_{15}—25*K*; R_3, R_{17}—50*K*; R_{16}—50*K* (pot.); R_2, R_{10}, R_{11}, R_{22}, R_{25}, R_{29}, R_{30}—100*K*; R_{31}—200*K*; R_6, R_{21}, R_{26}, R_{28}, R_{34}—500*K*; R_9, R_{14}—250*K*; R_{18}, R_{19}—200*K* (Precis.); R_1, R_7, R_{12}—1 Meg.; V_1, V_2, V_5—6*J*5; V_3—6*SJ*7; V_4—6*AC*7; V_6—6*SL*7; V_7—5*U*4*G*; *L*—15*H*, 120 ma; *TR*—440-0-440, 120 ma.

phase angles over a range of ±90 degrees. To cover the remaining 180 degrees, the slant of the collapsed ellipse is noted. If, after adjustment with the calibrated phase-shifter, the slant of the line changes from that noted at the time of channel equalization, 180 degrees is added to the dial reading. As constructed, the phase-meter gives consistent precision of 30 minutes over a frequency range of from 20 c.p.s. to 100 kc.

THE REVIEW OF SCIENTIFIC INSTRUMENTS VOLUME 21, NUMBER 2 FEBRUARY, 1950

Positive Displacement Pump for Corrosive Fluids

E. E. Glenn, Jr. and Norman Hackerman
Department of Chemistry, The University of Texas, Austin, Texas

(Received September 14, 1949)

A positive displacement-type pump in which there are no metal parts exposed to the fluids has been built and tested. Gases, liquids, or mixtures of both can be pumped without any corrosive effects on the pump.

In the course of a laboratory investigation of the corrosion of metals, the need arose for a positive displacement-type pump which could circulate mixtures of corrosive gases and liquids. It was necessary that the pump operate continuously over relatively long periods of time. Several types of commercial pumps were considered. A positive displacement pump using a rubber impeller presented internal lubrication problems; for example, lubrication of the contact between the pump housing and the impeller by the liquid being pumped. This was undesirable since a high gas to liquid ratio in the pumped fluid was required. A liquid by-pass line from the discharge to the suction side of the pump could be used in order to furnish this lubrication, but this was not acceptable since the volume of gas pumped would be greatly reduced. To overcome this, the pump speed could be increased, but this would cause excessive wear of the rubber impeller, housing, and bearings, since tolerances are small in positive displacement pumps. Gear-type pumps were considered, but again, lubrication of the gears by the fluids being pumped presented a problem.

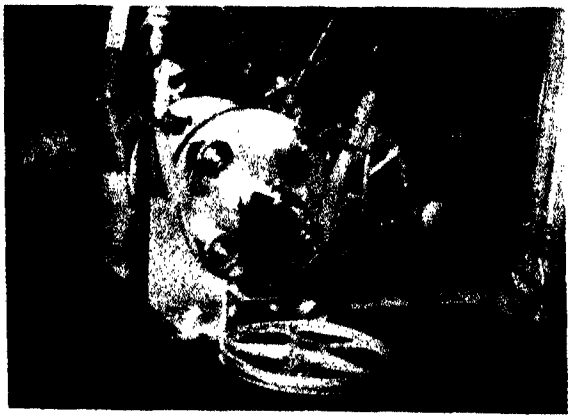

Fig. 1.

A major complication arising from contact of metal pump parts with the fluids was the corrosive attack which not only increased the likelihood of failure of the pump parts, but also introduced undesirable contaminants into the fluid. Neoprene was substituted for the rubber impeller mentioned above, but was unsatisfactory because it was extracted by liquid hydrocarbons in the system. It also swelled sufficiently to cause binding in the pump housing.

Since none of the types of pumps considered showed promise of withstanding deterioration because of the corrosive fluids and long operating periods, a pump to meet these qualifications was designed and built. Figure 1 is a photograph of the pump and Fig. 2 shows the principal components schematically.

The principle of operation of the pump is simply the squeezing of a flexible tube to cause the discharge of its contents. As shown in the diagram this was done by causing four rollers, mounted on a disk, to roll along a flexible tube lying in a semicircular track. As each roller moves along the tube, the fluids contained therein are forced ahead, since the rollers are so mounted as to cause complete flattening of the tube. After a roller passes any point, the tube returns to its circular cross-sectional shape, the volume increase causes a pressure drop, and the pressure gradient so produced forces additional fluids into this portion of the tube. The sizes of the rollers, disk, flexible tubing, and track are purely arbitrary, depending only on the volume to be pumped. In general, only one size tubing can be used with one particular size track and roller mounting; however, volumes may be varied by varying the disk speed.

Tygon tubing, ½ in. i.d., was selected for the system being studied, since it was found to be resistant to the corrosive fluids and to extraction by the hydrocarbons. The Tygon tubing was slipped into a ⅝-in. i.d. rubber tube. The rubber case takes the wear of the rollers and helps the Tygon return to its normal shape after the passage of a roller. The recovery time for Tygon is slower than that for rubber, so use of the latter increases the efficiency of the pump.

The rollers were made of brass, 2 in. in diameter, and mounted on a shaft through double-sealed ball bearings. These roll freely during their period of travel when not in contact with the tube and thus do not cause excessive wear at the point of first contact at the suction end of the tubing. These rollers were mounted perpendicular to and ½ in. inside the periphery of a 10-in. diameter steel disk.

Clamps were mounted on the suction and discharge ends of the tube. The suction end clamp held the tubing to prevent creep along the track in the direction of motion of the main disk, while the discharge end clamp served merely to hold the tube aligned with the rollers.

The flow was, of course, pulsating, which may prove advantageous in many cases. The system for which the pump was designed included a hydrocarbon-water mixture which had to be in the form of an emulsion immediately after it left the pump. By extending the discharge tube upward about 2 ft. the pulsating action, together with the large gas volume, caused sufficient agitation to emulsify the mixture at the desired point in the system.

This design may also be used to feed a given quantity of liquid or gas into a system at definite intervals of time, by regulating the speed of the main disk and the number of rollers mounted thereon. Perhaps the use of a check valve on the discharge end of the pump would be necessary in this case. With the design in the diagram, the rollers act as their own check valve, and, therefore, flow can be only in one direction.

The main disk was mounted on a shaft in such a manner that the rollers moved over the tubing track with just sufficient clearance to allow for the thickness of the flattened tube. The shaft was driven by V-belts and pulleys arranged to give a disk speed of about 100 r.p.m. Various arrangements of pulleys and motor speed could be made to yield almost any speed desired.

The tubing track was a semicircle of such dimensions that the rollers compressed the tubing at all points of contact. In cross section the track resembled a shallow channel iron, the lips preventing sideward movement of the tubing.

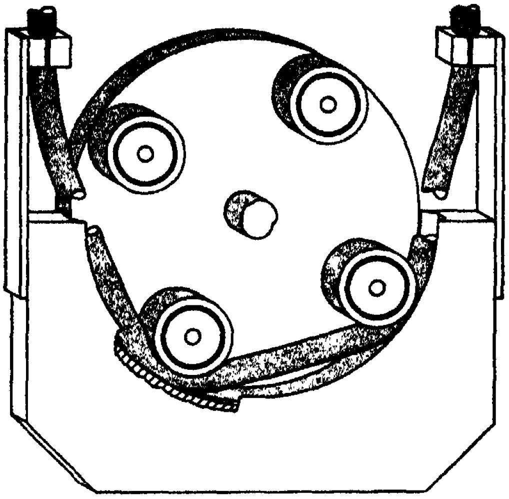

FIG. 2.

Some of the characteristics of the pump are:

(1) Speed—1 g.p.m. of water against a 3-ft. head.
(2) Pressure ratio achieved—pump suction at 14.7 p.s.i.a. discharge at 36.7 p.s.i.a.
(3) End vacuum achieved—0.83 p.s.i.a. (43 mm Hg).
Time to produce end vacuum—1 min.
Lowest end vacuum possible—0.58 p.s.i.a. (30 mm Hg) since water was used to wet the tube.
(4) Average tubing life under given conditions—about 120 hr. continuous operation.

The pump can be used for gas as well as liquid, so long as the tubing is first wetted by liquid. Thus, as a gas pump, some inert liquid would be required as the wetting fluid to provide complete sealing as the roller flattens the tubing. It seems probable that even liquids of fairly high viscosity could be pumped with this design. Solid particles should be avoided because of erosive effects on the tubing.

THE REVIEW OF SCIENTIFIC INSTRUMENTS VOLUME 21, NUMBER 2 FEBRUARY, 1950

A Frequency Modulation Pressure Recording System*

J. H. Hett and R. W. King, Jr.
Research Division, New York University, University Heights, New York

(Received September 23, 1949)

A simple frequency-modulated pressure gauge employing a variable capacity pick-up element has been devised to measure the oscillating pressures of burning gases. It has been used to measure pressures in pulse jet engines ranging from −5 to +60 p.s.i. gauge, under conditions where the gas temperatures ranged from approximately 300°K to 2450°K and the gauge mount vibrated with an amplitude of approximately 0.125 inch. The fundamental frequencies of temperature variation, pressure variation and mechanical vibration were 40 cycles and 220 cycles per second. Under these conditions the pressure response is essentially linear from 0 to 5500 cycles per second.

INTRODUCTION

THE pressure recording system described in this paper was devised to fulfill the following conditions:

1. To give a frequency response extending from static to at least 5000 cycles/sec.
2. To obtain a high stability to take advantage of static response.
3. To respond linearly over selected pressure range.
4. To operate in flame temperatures rapidly fluctuating over a range of 2000°K.
5. To operate with as few microphonics as possible in very high noise fields, and at vibration amplitudes of 0.125 inch, frequency of vibration 40 to 220 cycles/sec.
6. To obtain an apparatus which is electronically simple, easily portable and rugged enough for field use.

Many different systems have been investigated and have failed to fulfill these specifications for the reasons indicated as follows;

The tourmaline crystal gauge has a very high temperature response.

The quartz crystal gauge does not give a static response and for use with cables has a low ratio of signal to cable noise in the range of pressures of interest here.[1]

The various types of strain gauges suffer either from temperature dependence or low frequency response.

The frequency response of the variable inductance gauge is limited by the necessity of using a relatively low carrier frequency.

Magnetostriction gauges have no static response.

The work of various investigators since 1940 indicated that a condenser-type gauge, when used with a suitable circuit, would fulfill our conditions.[2] During the war, many special applications of condenser gauges were devised in this country and in England but references to this literature are still classified.

The general operation of our system is as follows: A pressure sensitive condenser element, shielded from high temperatures by placing it behind a specially designed cooling chamber is part of a tuned circuit which controls the frequency of an oscillator. The output of the oscillator is fed through a cathode follower to the receiver, which contains a "frequency discriminator" consisting of a fixed tuned resonant circuit combined with a phase detector. Changes in the oscillator frequency due

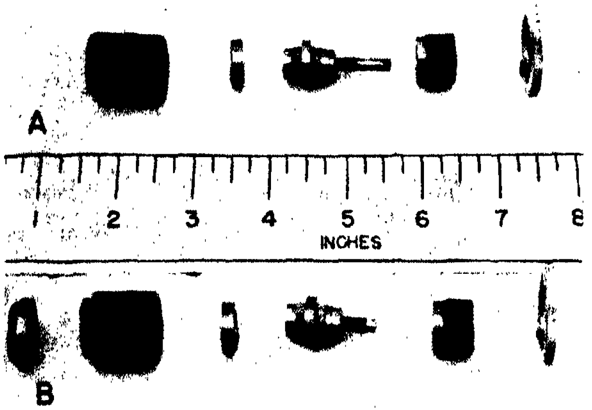

FIG. 1. Model *A* shows the gauge head with the diaphragm integral with the main body. Model *B* shows a gauge head with a diaphragm separable from the main body.

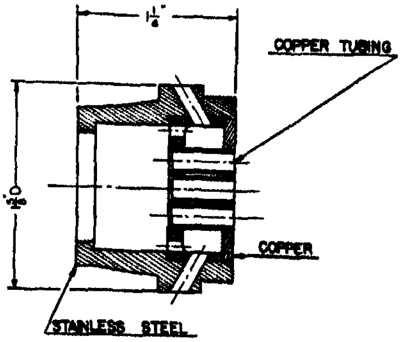

FIG. 2. The cooling chamber in which water is circulated about the fire tubes and in contact with the edge of the pick-up element.

---

* This research was conducted under the auspices of Project Squid, sponsored by ONR, Contract N6Ori-II.

[1] M. A. Greenfield and M. M. Shapiro, "Instrumentation for the Measurement of Underwater Explosion Pressures," TMB Report No. 523, September 1944.

[2] L. C. Roess, Rev. Sci. Inst. 2, 183 (1940). Grinstead, Frawley, Chapman, and Schultz, SAE Journal 52, No. 11, 534–535 (November, 1944). L. G. Smith, OSRD 6320 (February 21, 1946). C. K. Fraenkel and W. D. Kennedy, Naval Ordnance Report 100, 46 (January 25, 1947).

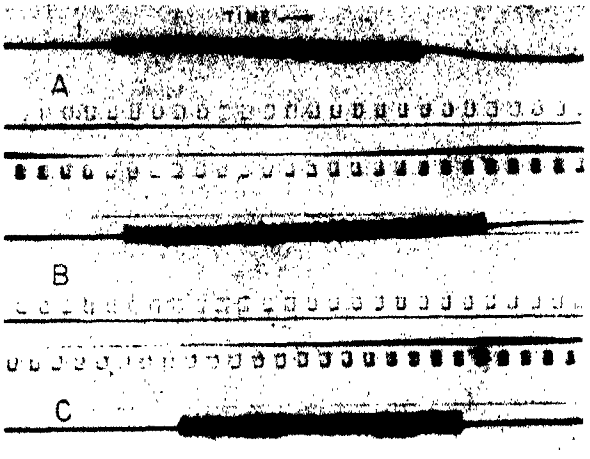

FIG. 3. These records give a comparison of the effectiveness of three differently designed cooling chambers in preventing a temperature drift of the zero level of the record. All were mounted successively on a 3-inch diameter pulse jet, and each tested from 9 to 10 seconds. A. The record given by the cooling chamber and condenser pick-up element made by Southern Instruments for the Royal Aircraft Establishment at Farnsborough, England. B. N. Y. U. Model *A* gauge head and cooling chamber with 1-inch fire tubes but no contact cooling of the gauge. C. N. Y. U. Model *A* gauge head and cooling chamber with 1-inch fire tubes and contact water cooling of the gauge. The thin horizontal line just above the record in B and C is the 20 p.s.i. line.

to changes in condenser capacity cause a relatively large shift in phase between the voltage and the current in the fixed tuned circuit. This phase difference is detected by the phase detector and the resulting signal is fed through another cathode follower to the recording equipment. The transmitter and receiver are connected by a cable 75-feet long. In the following the circuit, consisting of the oscillator and cathode follower, is called the transmitter, and the circuit consisting of frequency converter, amplifier, discriminator, and cathode follower is called the receiver.

THE GAUGE HEAD AND COOLING CHAMBER

The gauge head is a carefully machined unit containing the pick-up element, which is essentially an elastically deformable Invar diaphragm attached to a threaded hollow Invar cylinder which forms the main body of the gauge head. Two different gauge heads are shown in exploded view in Fig. 1. Model *A* shows a gauge head in which the diaphragm is an integral part of the main body. Model *B* shows a gauge head in which the diaphragm and the main body are separable. The diaphragm is 0.500 inch in diameter and 0.020 inch thick for the pressure range −5 to +60 p.s.i. Its interior surface is ground and polished and is spaced 0.001 inch from the end face of a central electrode which fits into, but is insulated from, the main body. A mica disk 0.0007 inch thick is cemented to the end face of the electrode. The condenser element is thus made up of the diaphragm, air space, mica and the central electrode. The use of mica produces a smaller equivalent air gap thereby increasing the electrical sensitivity. This permits the use of a smaller diaphragm movement to obtain the same signal for the same pressure, and thus improves the linearity of response. The natural frequency of the diaphragm is 25,000 cycles per second as determined by bouncing a small steel ball off the diaphragm and observing the resulting vibrations. The sensitivity of the condenser element is about 0.25 mmf/p.s.i., but the sensitivity of the gauge as a whole can be varied over a considerable range by changing the shunted capacity across the condenser element.

When measuring the pressures of hot gases, the gauge is screwed down into a water-cooled chamber, one design

FIG. 4. Gauge head, Hartley oscillator and cathode follower mounted integrally with the cooling chamber.

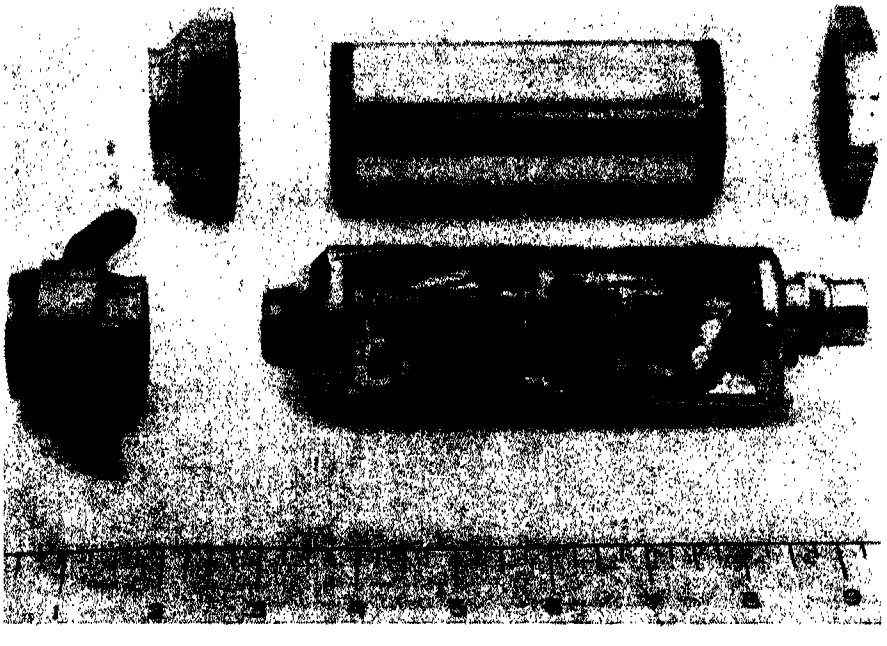

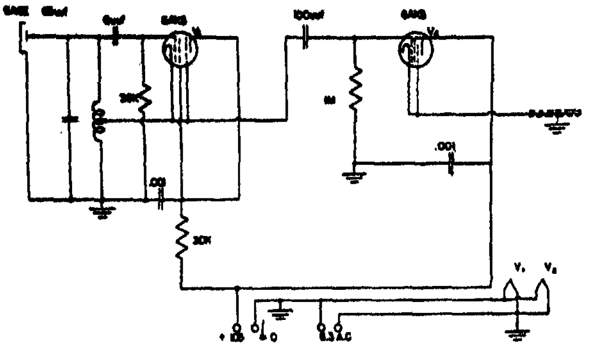

FIG. 5. The transmitter unit circuit diagram.

of which is sketched in Fig. 2. Note that this design of the cooling chamber gives direct water cooling of the perimeter of the diaphragm, as well as cooling of the gases passing through the fire tubes. When the fire tubes are ½ inch in length, the response is essentially linear from 0 to 5500 cycles per second. Figure 3 shows a comparison of the effectiveness of this type chamber with both another N. Y. U. cooling chamber, which did not have direct water contact with the diaphragm, and a cooling chamber and pressure gauge made by Southern Instruments, England.

THE TRANSMITTER UNIT AND RECEIVER

When low pressures are to be measured and maximum sensitivity is necessary, the transmitter unit is mounted directly on the gauge head. A view of the oscillator side of the unit and the mounting case is shown in Fig. 4. When very high shock and vibration are present, the transmitter may be separated from the gauge head by a five foot cable. Either type of transmitter is usually connected by a 75-foot coaxial cable to the receiver.

A circuit diagram of the transmitter is given in Fig. 5. The circuit is a conventional grounded-plate Hartley oscillator capacitively coupled to a cathode follower output tube. The cathode resistor of the cathode follower is located in the receiver. The tubes used are 6AK5's chosen for their relatively low microphonics and long life.

A diagram of the receiver circuit is shown in Fig. 6. The receiver is designed to accommodate signals of frequencies from 2 to 4 megacycles. The intermediate frequency amplifier operates at a center frequency of 430 kilocycles, with a band width of 80 kilocycles. The discriminator is linear within 2 percent over 40 kilocycles and the output voltage varies by 100 volts for this frequency deviation.

The input circuit of the receiver approximately matches the cable impedance of 50 ohms to the grid of the converter stage. The series condenser C_4 and shunt resistor R_2 provide grid leak bias and a certain amount of limiting for large input signals. The first two grids of the converter stage act as a grid and anode of a Hartley oscillator which modulates the space current in the tube. The incoming signal on the third grid further modulates the electron stream. The net current flows from the plate through the resonant load which is tuned to the difference between the local oscillator and signal frequencies. The signal is further amplified by the second tube which drives the discriminator.

The coefficient of coupling of the input intermediate frequency transformer is increased beyond the manufacturer's critical value by sliding one winding along the form closer to the other. The Q of the output winding is reduced with the 33K resistance R_5. This gives 80 kilocycles band width. Amplitude limiting in the intermediate frequency amplifier removes the peaks and gives uniform response. The resistor, R_5, in conjunction with the condenser C_7, in the grid of the intermediate frequency amplifier V_2, causes grid leak biasing in proportion to the incoming signal level. This process provides much of the limiting action of the stage to

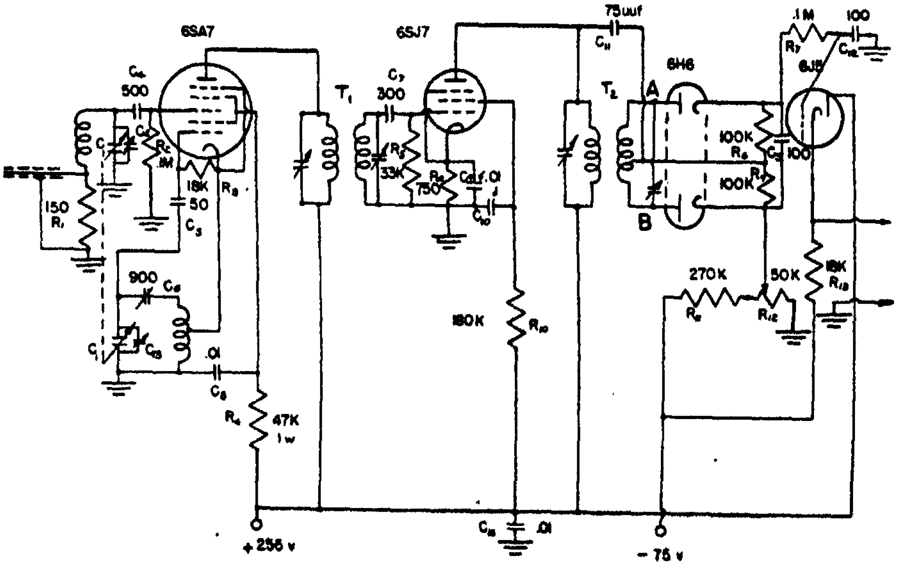

FIG. 6. Receiver circuit diagram.

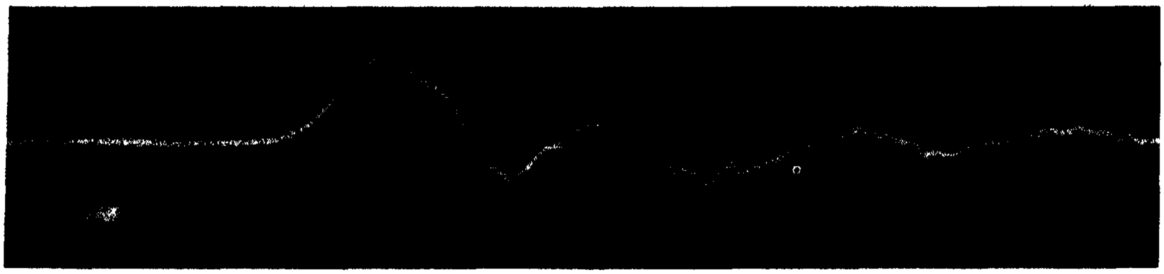

FIG. 7. Low pressure response of the gauge without the use of a cooling chamber. Range +3½ to −1½ p.s.i.

FIG. 8. Response of the gauge to pressures +12 to −7 p.s.i. with a cooling chamber without edge cooling. The horizontal line represents the pressure level of the atmosphere.

which the low screen voltage also contributes. The plate circuit contains a Seeley-Foster discriminator. The output of this discriminator goes to the cathode follower which provides a low impedance source feeding the signal into the recording equipment. The recording is done by a strip camera from a cathode-ray tube.

TYPICAL PRESSURE RECORDS

Figure 7 shows a low pressure record obtained with the circuit adjusted for high sensitivity. This is the record of the pressure near the closed firing end of a 6-foot, half-open flame tube, taken without using the cooling chamber. The first peak and valley measure respectively +3½ p.s.i. and −1½ p.s.i. The length of the trace shown represents 70 milliseconds.

Figure 8 shows 6 pressure cycles recorded 6 inches downstream from the valves in the 21-inch diameter combustion chamber of a large pulse jet. Peaks are +13 p.s.i. and −7 p.s.i. for a low throttle setting of the fuel control. The horizontal line gives the atmospheric pressure level. The superposition of three cycles on the other three is achieved by allowing the oscilloscope recording camera to rotate more than one revolution. It is reasonably certain that there is no appreciable drift during the observation since the atmospheric level was recorded just before the run and coincides with the level of the steps in the pressure cycles which indicate the closing of the valves.

ACKNOWLEDGMENT

The original development work on this instrument was suggested by the late Dr. J. K. L. MacDonald who had a keen interest in the theory and instrumentation of pulse jets.

THE REVIEW OF SCIENTIFIC INSTRUMENTS VOLUME 21, NUMBER 2 FEBRUARY, 1950

Analog Computers for Servo Problems

DONALD McDONALD*
Aeronautical Research Center of the University of Michigan, Ypsilanti, Michigan

(Received September 26, 1949)

The exact equations are derived for operational amplifiers used in analog computers. These exact equations are replaced by simpler equations based upon certain approximations. These approximations are discussed and it is shown, when applied to servo mechanism problems, the operational amplifiers may be designed with greater ease and less complexity than those to be used for more general problems.

INTRODUCTION

IN the last few years, a great deal of interest has been centered on the use of high gain, operational amplifiers in analog computers for the study of dynamic problems.[1-4] One of the major applications for such analog computers has been in the field of servo mechanisms. The transient equation of motion of even the simpler servo mechanisms is difficult and tedious to solve, and therefore, analogs of servo mechanism systems are being used extensively to facilitate the study and design of such systems.

Analog computers for general dynamic studies normally use operational amplifiers having very high gain, some as high as one million. When analog computers are applied to servo mechanism problems, certain important characteristics of the servo problem tend to reduce the required gain and the resulting complexity of the operational amplifiers and power supplies used in the computer. Gains as low as several hundred yield very satisfactory performance for servo problems. In the analysis and synthesis of servo mechanisms, the dynamic response and stability and the steady-state response are the major factors to be determined. The differential equations of motion of the servo mechanism, which are needed to set up the servo analog on the computer, yield the steady-state response quite easily without the aid of the computer. Hence, only the dynamic response of the servo mechanism need be determined with the computer. As will be shown, the dynamic response accuracy of analog computers can be made much higher than their steady-state response accuracy for comparatively low values of the operational amplifier gain.

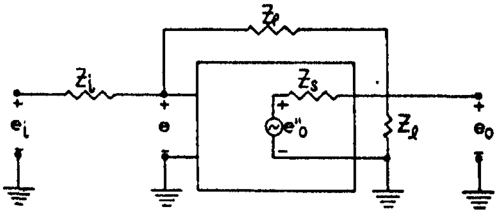

Z_i = input branch impedance.
Z_f = feed-back branch impedance.
Z_s = output stage source impedance.
Z_l = output load impedance.
K = amplifier internal gain.
e_i = input signal voltage.
e = amplifier input voltage.
e_0 = output voltage.
e_0'' = open circuit or no load output voltage, i.e., if $Z_f=\infty$ and $Z_l=\infty$ then $e_0''=e_0$.

FIG. 1(a).

BASIC OPERATIONAL CIRCUITS

Figure 1(a) is a schematic diagram of the basic operational amplifier circuit. In order to more easily analyze the operation of this circuit, it has been transformed by the use of Thevenin's theorem as shown in Fig. 1(b).** Equation (e) of Fig. 1(b), which is obtained by the simultaneous solution of Eqs. (a)–(d), of Fig. 1(b) states the response of the operational circuit. This basic circuit, when employed in analog computers, is usually required to perform the three operations of differentiation, integration, and addition.

Differentiation is achieved by setting Z_i and Z_f equal to $1/jwC_i$ and R_f, respectively; Eq. (e) of Fig. 1(b)

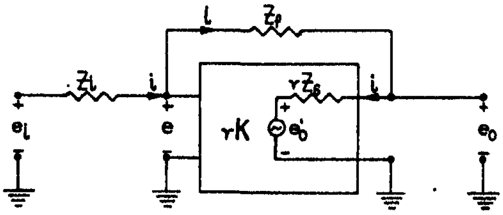

$r=Z_l/(Z_s+Z_l)$; rK = equivalent amplifier internal gain.
The equations for this system are

$$e_i=iZ_i+e \tag{a}$$
$$e=iZ_f+e_0 \tag{b}$$
$$e_0=irZ_s+e_0' \tag{c}$$
$$e_0'=-rKe. \tag{d}$$

Solving these equations simultaneously for e_0/e_i yields:

$$\frac{e_0}{e_i}=-\frac{Z_f}{Z_i}\left[\frac{rK}{rK+1}\right]\left[\frac{1-Z_s/KZ_f}{1+(Z_f+rZ_s)/(rK+1)Z_i}\right]. \tag{e}$$

FIG. 1(b).

---

[*] Present address: Cook Research Laboratory, Division of Cook Electric Company, Chicago, Illinois.

[1] Ragazzini, Randall, and Russell, "Analysis of problems in dynamics by electronic circuits," Proc. I.R.E., 444–452 (May, 1947).

[2] Seymour Frost, "Compact analog computer," Electronics, 116–122 (July, 1948).

[3] F. C. Williams and F. J. U. Ritson, "Electronic servo simulators," J. Inst. Elec. Eng. 94, Part IIA, 112–124 (1947).

[4] Hagelbarger, Howe, and Howe, "Investigation of the utility of an electronic analog computer in engineering problems," University of Michigan Engineering Research Institute, External Memorandum No. 28 (April 1, 1949).

[**] Equation (d) of Fig. 1(b) infers that an odd number of phase inversions take place in the amplifier. The use of the same circulating current i in all branches of the circuit implies the input impedance of the amplifier is infinite.

becomes

$$\frac{e_0}{e_i}=-jwR_fC_i\left[\frac{rK}{rK+1}\right]\times\left[\frac{1-R_s/KR_f}{1+jw(R_f+rR_s)C_i/(rK+1)}\right]. \quad (1)$$

In Eq. (1) and in all later equations, Z_s has been set equal to R_s.

If the input and feed-back branches are a resistor and a condenser, respectively, then

$$Z_i=R_i \quad \text{and} \quad Z_f=1/jwC_i,$$

and the operational circuit becomes an integrator. For an integrator Eq. (e) becomes:

$$\frac{e_0}{e_i}=-\frac{1}{jwR_iC_f}\left[\frac{rK}{rK+1}\right]\times\left[\frac{jw(rK+1)R_iC_f(1-jwR_sC_f/K)}{1+jw[(rK+1)R_i+rR_s]C_f}\right]. \quad (2)$$

The operation of addition or summation implies the existence of two or more input signals; hence the circuit of Fig. 1(b) is shown modified in Fig. 2 with three separate inputs. In Fig. 2, the input and feed-back branch impedances have been made resistive and Eq. (h) of Fig. 2 demonstrates the summation properties of the circuit.

It may be noted, if only one input is used and $R_f/R_1=1$, the circuit of Fig. 2 degenerates to the special case of a sign changer. Of course, the differentiating, integrating, and adding circuits in their most general form also perform a sign change.

DISTORTIONS OF THE EXACT OPERATIONS

The three basic Eqs. (1) and (2), and (h) of Fig. 2 for the operations of differentiation, integration, and addition all have the same general form and all are composed of three similar terms. For each of these equations the first term represents the exact operation while the remaining two terms in brackets distort the exact operation. The first of these distortion terms is common to all of the basic operation equations and will be denoted by A. A may be rewritten as follows:

$$A=rK/(rK+1)=1-1/(rK+1). \quad (3)$$

The distortion produced by A is simply that of multiplying the basic operation by a scale factor dependent only upon the effective gain rK.

The second distortion term is different for each operation and therefore shall be denoted by B_d, B_i, and B_a for differentiation, integration, and addition, respectively. For the case of addition, B_a is also only a scale factor but it is dependent upon all the parameters of the operational circuit as follows:

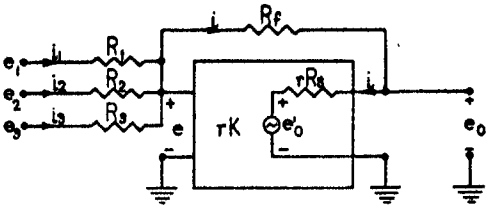

$$e_1=i_1R_1+e \quad (a)$$
$$e_2=i_2R_2+e \quad (b)$$
$$e_3=i_3R_3+e \quad (c)$$
$$i=i_1+i_2+i_3 \quad (d)$$
$$e=iZ_f+e_0 \quad (e)$$
$$e_0=irZ_s+e_0' \quad (f)$$
$$e_0'=-rKe. \quad (g)$$

Solving (a)–(g) inclusive simultaneously yields:

$$e_0=-\left(\frac{R_f}{R_1}e_1+\frac{R_f}{R_2}e_2+\frac{R_f}{R_3}e_3\right)\left[\frac{rK}{rK+1}\right]\left[\frac{1-R_s/KR_f}{1+R_f+rR_s/(rK+1)R_p}\right] \quad (h)$$

where

$$R_p=R_1R_2R_3/(R_1R_2+R_1R_3+R_2R_3)$$

and is the resistance of all three input resistors in parallel.

FIG. 2.

$$B_a=\frac{1-R_s/KR_f}{1+(R_f+rR_s)/(rK+1)R_p}. \quad (4)$$

For differentiation, B_d has both magnitude and phase:

$$|B_d|=(1-R_s/KR_f)\times[1+(wC_i)^2(R_f+rR_s)^2/(rK+1)^2]^{-\frac{1}{2}} \quad (5a)$$

$$\angle B_d=-\tan^{-1}[w(R_f+rR_s)C_i/(rK+1)]. \quad (5b)$$

Similarly, for integration, B_i is

$$|B_i|=w(rK+1)R_iC_f[1+(wR_sC_f/K)^2]^{\frac{1}{2}}\times\{1+(wC_f)^2[(rK+1)R_i+rR_s]^2\}^{-\frac{1}{2}} \quad (6a)$$

$$\angle B_i=\tan^{-1}\{1/wC_f[(rK+1)R_i+rR_s]\}-\tan^{-1}[wR_sC_f/K]. \quad (6b)$$

For satisfactorily designed operational amplifiers, some of the quantities in the distortion terms may be small compared to other quantities in the distortion terms. If the amplifier gain is above several hundred and the input, feed back, and load impedances are large compared to the source impedance, the following approximations in the distortion terms may be made:

$$A\cong 1-1/K \quad (7)$$

$$B_a\cong 1-R_f/R_pK \quad (8)$$

$$\angle B_d\cong-\tan^{-1}[wC_iR_f/K]\cong-wC_iR_f/K \quad (9a)$$

$$|B_d|\cong[1+(wC_iR_f/K)^2]^{-\frac{1}{2}}\cong 1-(1/2)(wC_iR_f/K)^2=1-(1/2)(\angle B)^2 \quad (9b)$$

$$|B_i|\cong KwR_iC_f[1+(wC_fR_s/K)^2]^{\frac{1}{2}}\times[1+(KwR_iC_f)^2]^{-\frac{1}{2}} \quad (10a)$$

$$\angle B_i\cong\tan^{-1}[1/wKR_iC_f]-\tan^{-1}[wR_sC_f/K]\cong 1/KwR_iC_f-wC_fR_s/K. \quad (10b)$$

OPERATIONAL AMPLIFIER

Figure 3 is a schematic diagram of an operational amplifier designed for servo application.† It uses only two tubes, two regulated B supplies, and an a.c. filament supply regulated by a conventional constant voltage transformer. The first stage of the amplifier is a twin stage with the amplification of one-half of a 6SL7. This twin stage has been used primarily to minimize the drift produced by variations in cathode emission. The second stage operates at higher voltage levels and thus is a simple amplification stage. The third and last stage is a cathode follower stage used to minimize R_o. This circuit shows an equivalent input drift of the order of 1 millivolt over four to six hours.

For the circuit of Fig. 3, $K \cong 700$, $R_o \cong 700$, and the output stage has been designed to deliver ±40 volts to a load having a resistance not less than 25,000 ohms. Hence the minimum value of r is $r = 0.97$ or $1 > r > 0.97$ and for all practical purposes $r = 1$.

The circuit of Fig. 3 is only one example of a number of elementary basic circuits which may be used to obtain medium gain amplification.

If the power output of this circuit is not sufficient, a 7F8 may be substituted for the second 6SL7.‡ This substitution will result in approximately a 30 percent reduction in K and an increase in power output by a factor of 2.

The amplifier of Fig. 3 has been designed for values of R_f, R_i, C_f, and C_i, as follows:

$$100{,}000 \text{ ohms} < R_f < 1{,}000{,}000 \text{ ohms}$$
$$100{,}000 \text{ ohms} < R_i < 1{,}000{,}000 \text{ ohms}$$
$$0.1\ \mu f < C_f < 1\ \mu f$$
$$0.01\ \mu f < C_i < 1\ \mu f.$$

Therefore

$$R_f \gg R_o \quad \text{and} \quad R_i \gg R_o.$$

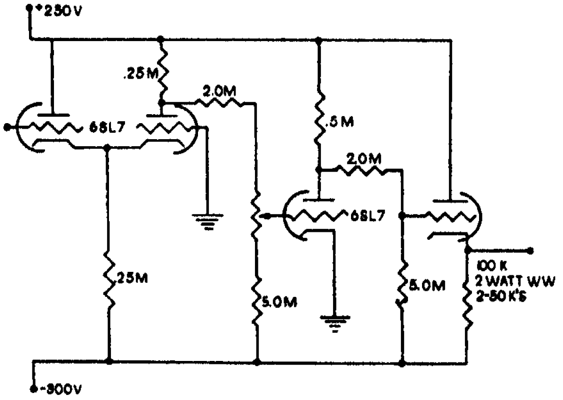

Fig. 3.

EVALUATION OF THE DISTORTION TERMS FOR THE AMPLIFIER OF FIG. 3

Using the values of K, R_o, and r given for the amplifier of Fig. 3, the approximate distortion terms can be evaluated as follows.

The distortion term A, which is common to all of the operations, affects only the magnitude of the exact operation reducing it by one-seventh of one percent.

For the case of addition, if the several inputs are summed but not amplified, the ratio R_f/R_p will have a maximum value equal to the number of input signals summed. Attenuation of the sum will reduce this ratio. Amplification of the sum will increase R_f/R_p but it is not necessary that amplification be done in the summing amplifier. Consequently, B_a, which also affects the magnitude of the exact summation, reduces it by less than one-seventh times the number of input signals times one percent.

In differentiation, B_d produces a negative phase shift as well as a reduction in the magnitude of the exact operation. This phase shift is more important than the magnitude change and for satisfactory servo applications should not exceed a maximum value $\angle B_{d_m}$ for all frequencies below a certain frequency w_c. Therefore, from Eq. (9a)

$$R_f C_i < 700/w_c \angle B_{d_m}. \tag{11}$$

For example, if $\angle B_{d_m}$ is to be kept less than 3° or 1/20 radian up to 50 c.p.s., then

$$R_f C_i < 0.1$$

will satisfy this requirement. This restriction on $R_f C_i$ is very easy to achieve because R_f is usually chosen around 100,000 to 500,000 ohms and hence, C_i must be less than about 1 to 0.2 μf. The choice of 3° for $\angle B_{d_m}$ also limits the magnitude reduction produced by $|B_d|$ to less than one-eighth of one percent.

For the case of integration, there are two phase shifts in B_i, one a positive phase shift occurring at low frequencies and the second a negative phase shift occurring at relatively high frequencies. These two phase shifts occur at such widely separated frequencies that they may be considered separately. The maximum permissible value of $\angle B_i$ at low frequencies and at high frequencies will be denoted by $\angle B_{i_l}$ and $\angle B_{i_h}$, respectively. The frequencies corresponding to these two values of $\angle B_i$ are w_l and w_h, respectively. From Eq. (10b)

$$\angle B_{i_l} \geq 1/700 w_l R_i C_f \tag{12a}$$

$$\angle B_{i_h} \geq w_h C_f. \tag{12b}$$

If the same high frequency specifications are imposed upon the integrator phase shift as upon the differentiator and $C_f < 1\ \mu$f, then

$$w_h \leq 50{,}000 \text{ rad./sec.}$$

or

$$f_h \leq 8000 \text{ c.p.s.}$$

---

† Mr. K. C. Mathews, a member of the Controls Group of the Aeronautical Research Center of the University of Michigan, was responsible for the design and development of these amplifiers.

‡ Usually the loads requiring appreciable power are the multiplier servo potentiometers in the analog computer. Precise potentiometers for such purposes are commercially available with at least 25,000 ohms resistance.

Reasonable maximum values for R_i, C_f, and R_iC_f are 1,000,000 ohms, 1 μf, and 1, respectively.¶ Consequently, if $\angle B_{il}$ is also chosen to be less than 3°

$$w_l \geq 1/35 \text{ rad./sec.}$$

or

$$f_l \geq 1/200 \text{ c.p.s.}$$

Thus from 1/200 c.p.s. to 8000 c.p.s., the phase shift of the distortion term B_i will be less than 3°.

Substitution of Eqs. (12) into Eq. (10a) yields the following form for $|B_i|$:

$$|B_i| \cong w/w_l 1/\angle B_{il}[1+(w/w_h \angle B_{ih})^2]^{\frac{1}{2}} \times[1+(w/w_l 1/\angle B_{il})^2]^{-\frac{1}{2}}. \quad (13)$$

From Eq. (13) it can be shown that $|B_i|$ reduces the magnitude of the exact operation by less than one-eighth of one percent over a frequency range from 1/200 c.p.s. to 8000 c.p.s.

The fractional reduction in magnitude and the phase shift caused by the several distortion terms may be summarized as follows:

Summation:

$$1-AB_a \leq 1/700 \text{ (1+number of inputs).}$$

Differentiation:

$$1-A|B_d| \leq 1/400 \quad 0<f<50 \text{ c.p.s.}$$
$$\angle B_d \leq 3°.$$

Integration:

$$1-A|B_i| \leq 1/400 \quad 1/200<f<8000 \text{ c.p.s.}$$
$$\angle B_i \leq 3°.$$

The reduction in the magnitude of the exact operations produced by the distortion terms of the operational amplifier of Fig. 3 is comparable to the error produced in the exact operation by the use of 0.1 percent resistors and condensers in the input and feed-back branches. For integration, differentiation, and addition, 0.1 percent resistors and condensers will produce an error of as much as 1/500 in the quantities R_iC_f, R_fC_i, and R_f/R_i in the exact operation terms.

Thus low gain operational amplifiers have more than satisfactory dynamic accuracy for servo problems and are less sensitive to drift, are simpler in construction, and require fewer and less regulated power supplies than do high gain operational amplifiers. The magnitude errors in the dynamic response of the operations are less than those obtained (1) in measuring or estimating the coefficients of the differential equations of motion of the servo and (2) in recording the solution of the problem. Similarly, the small distortion phase shifts produced by the integrator and differentiator occur at frequencies which have negligible effect upon the dynamic response, i.e., the effective natural frequency, damping ratio, etc.

On the other hand, the steady-state or zero frequency accuracy of integrators is lower for the low gain operational amplifiers.

STEADY-STATE ACCURACY OF INTEGRATORS

The zero frequency responses of an integrator for different values of operational amplifier gain may be compared by studying its response for a step input

$$e_i = 1. \quad (14)$$

Equation (2) may be rewritten as follows:

$$e_0/e_i \cong -K/1+pKR_iC_f, \quad \text{where} \quad p=d/dt. \quad (15)$$

The approximations used in (15) are the same as used in the previous section with the additional approximation that

$$1-jwR_iC_f/K \cong 1$$

at the frequencies under consideration.

Substituting (14) into (15) and integrating yields

$$e_0 = -K(1-e^{-t/T}), \quad (16)$$

where

$$T = KR_iC_f. \quad (17)$$

Substituting a power series in t/T for $e^{-t/T}$ into Eq. (29) and rearranging terms gives

$$e_0 = -t/R_iC_f[1-1/2(t/T)+1/6(t/T)^2-\cdots] \quad (18a)$$

or

$$e_0 \cong -t/R_iC_f[1-1/2(t/T)] \quad \text{for} \quad t/T \ll 1. \quad (18b)$$

An ideal integrator would have an output $-t/R_iC_f$. Hence the term $1/2(t/T)\times 100$ is the percentage by which the output of a real integrator deviates from the output of an ideal integrator for short periods after being subjected to a step input of voltage. In other words, $50/T$ may be referred to as the initial rate of percent deviation of an integrator. This rate of deviation is dependent upon T. Inasmuch as the maximum value of R_iC_f is essentially independent of amplifier gain K, the minimum initial rates of percent deviation of integrators is dependent upon only K. Therefore, higher gain operational amplifiers will have a smaller rate of deviation than have low gain operational amplifiers. This smaller rate of deviation is very important in many studies such as trajectory studies and requires gains as great as 1,000,000. Such high values of gain increase the number of tubes, power supplies, components and the care that must be exercised in the design of them to minimize drift effects.

¶ These values of R_f and C_i can be increased several-fold but have been chosen for convenience.

Gas Phase Counting of Low Energy Beta-Emitters*

W. Bernstein and R. Ballentine†
Brookhaven National Laboratory, Upton, New York and Rutgers University, New Brunswick, New Jersey

(Received October 4, 1949)

A proportional counter has been designed to detect soft beta-emitters in the gas phase. Data is presented to illustrate the applicability of the counters to the detection of C^{14}, S^{35}, and H^3. Various partial pressures of $C^{14}O_2$ have been investigated to determine the effects on the counter properties. Corrections have been made for the counter ends and the memory effects are described. An energy spectrum is presented for H^3 to determine the low energy limit of the instrument.

THE radioactive assay of very soft beta-emitters such as H^3, C^{14}, and S^{35} is an important problem in both chemical and biochemical research. Assay of solid samples is difficult because of the self-absorption of the samples, and the absorption by the windows or walls of the detector. In the case of tritium, with a maximum energy of 18.9 kev, no practical method of solid counting is available.

Both of these difficulties can be avoided if the samples are counted in a gas phase as part of the counter filling. Such procedures have been developed in the past, using ion chambers[1] or gas filled Geiger-Müller tubes.[2] The G-M tube technique, developed by Brown and Miller, provides the most practical method for the detection of C^{14} (as CO_2) to date, but has the disadvantage of using G-M tubes with a variable filling. The difficulty in obtaining reproducible behavior of G-M tubes under varying conditions is well known.

The ionization chamber method possesses the advantage of handling a relatively large amount of gas sample in the event that the specific activity is low. Also, the background contribution from high energy particles (cosmic rays) is less than in a counter which detects individual events. However, there are statistical fluctuations of both energy and events in an ionization chamber, and, in general, the detection of individual events is preferable.

Counting in the proportional region appears to be a method which can avoid many of these disadvantages. With proper circuits, proportional counters can count extremely active samples accurately, and with negligible coincidence losses. They are also preferable to G-M tubes at low counting rates because there are no spurious counts originating in the detector and the background counting rate is low because they are less sensitive to gamma-rays. Spurious counts may come from the amplifier or high voltage supply but can be eliminated without too much difficulty.

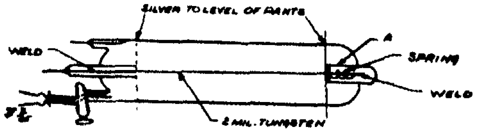

FIG. 1. Cylindrical proportional counter with one end which may be immersed in liquid air.

Proportional counters are also only moderately sensitive to changes in the filling mixtures.[3] This permits a simple, rapid filling technique, and the samples may be counted in different gaseous states. For instance, tritium may be counted as hydrogen gas, sulfur as hydrogen sulfide, carbon as carbon dioxide, acetylene and presumably carbon monoxide. The stability, with respect to the character of the filling, permits a wide range of sample sizes without any serious effect on the counter properties.

The design of the standard counter used in these investigations is shown in Fig. 1. The dimensions may be varied over wide limits. The counter radii vary from 2½ to 10 cm, and the cathode lengths from 10 cm to one meter. The standard counter is 2 cm in diameter and 30 cm long. These counters all show similar operating characteristics, although they have different thresholds. The cathode material used for most of this work is chemically deposited silver, although evaporated chromium or gold cathodes may be used. The center wire is 2-mil tungsten. Since the filling procedures require that one end of the counter be immersed in a liquid nitrogen trap, this end is kept free of glass to metal seals, as shown by *A* in Fig. 1. The successful use of the counter[4] shown in Fig. 2 indicates that the technique is not limited to counters of cylindrical geometry. This spherical cathode is chemically deposited silver and the center wire consists of a 2-cm loop of 2-mil tungsten. The other features of the design of this counter are adapted for a special sampling technique which will be described more fully elsewhere.[5]

---

* This work was done under the auspices of the USAEC.

† Now at McCollum-Pratt Institute, Johns Hopkins University, Baltimore, Maryland.

[1] W. P. Jesse *et al.*, "Ionization chamber techniques in measurement of C^{14}." MDDC 622.

[2] S. C. Brown and W. W. Miller, "Carbon dioxide filled G-M counters," Rev. Sci. Inst. 18, 496 (1947).

[3] The introduction of electronegative gases, in very small amounts, results in a marked distortion of the output pulse heights as a function of energy. Such counters are impractical for energy measurements, but are satisfactory for use as relative activity detectors. At high amplifier gain and high gas multiplication factors, total activity measurements can be made.

[4] H. G. Salvini, "Some G-M and proportional counters of spherical shape," Rev. Sci. Inst. 19, 494 (1948).

[5] R. Ballentine and W. Bernstein, "Method for monitoring $C^{14}O_2$ air contamination," Brookhaven National Laboratory report, BNL T-5.

$C^{14}O_2$ or H_2S^{35} gas samples are obtained with the vacuum system shown in Fig. 3 and the procedure described below. Either barium-carbonate precipitates or sodium carbonate solutions are converted to carbon dioxide gas by adding 40 percent lactic acid under vacuum. H_2S is obtained from sodium sulfide solutions by adding saturated magnesium chloride. The gas sample, after generation, is dried with a dry-ice chilled trap which removes water from the gas stream. The gas is then separated from any carrier air which may be present by freezing out the sample in a trap chilled with liquid nitrogen. At this temperature only a negligible fraction of the gases present in the air are condensed and consequently the separation is quantitative. After collection in the liquid nitrogen trap, the sample is transferred to the evacuated counter by distillation with liquid N_2 on the counter. The counter is then cut off from the gas line, the gases allowed to expand by warming to room temperature, and the counter is filled to about one atmosphere with tank methane. The total elapsed time for the preparation of the gas sample and filling of the counter for either CO_2 or H_2S is about seven minutes. A vacuum line, giving pressures of ten to one hundred microns, available from an ordinary mechanical pump, is satisfactory.

In the case of tritium, the sample is transferred to the counter tube with a Töpler pump, as shown in Fig. 4. Following the complete transfer of the sample into the counter, the pressure in the counter is brought to one atmosphere with tank methane.

Methane is selected as the counter gas to permit rapid recovery of the samples for later gravimetric analysis. This is not possible if argon-CO_2 fillings are used, or if the counters are filled to a predetermined carbon dioxide pressure by adding carrier CO_2. Therefore, the counting gas contains only the analytical sample, together with the added methane. Argon-methane or neon-argon-methane mixtures might reduce the operating voltage, but have not been investigated to date.

The electronic equipment used in this work consists of the Nuclear Instrument and Chemical Company Model 162 Scaler and Model 1092 5000 volt power supply. This scaler has an amplifier with a gain of 1000, an attenuator, and a pulse height discriminator with a maximum sensitivity of 1 volt. Some difficulty was encountered with multiple pulses caused by overloading the amplifier with large input signals. A 1N34 crystal diode, used to clip positive overshoots, at the input to the second loop eliminated this problem. Spurious counts are encountered now only when the first loop is overloaded. The pulse is differentiated with a 1-μsec. time constant at the input to the amplifier which reduces the duration of the overshoot and gives a shorter dead time. The presence of double counts may be checked with a synchroscope.

A non-overloading amplifier, designed by the late H. G. Brewer, Jr. at this Laboratory, which can handle an input pulse height distribution of 7000 to 1 without overloading, has also been used in this investigation.

Figure 5 is a plot of counts per minute against counter voltage for three samples of identical activity, but with different partial pressures of inert CO_2 added. It is apparent that high partial pressures of CO_2 raise the threshold of the proportional region and broaden the pulse height distribution. At 3900 volts the results are summarized in Table I.

The slope of the operating region is not over 3 percent per 100 volts. The overlapping of the operating regions permits the counting of any sample up to 100 mm partial pressure of CO_2 at a constant voltage and gain. In first calibrating the system, it is advisable to select a counter with a low partial pressure of CO_2 and to operate at a point high on its characteristic for standard analysis. Figure 6 is a plot of counting rate against amplifier gain for several different voltage settings.

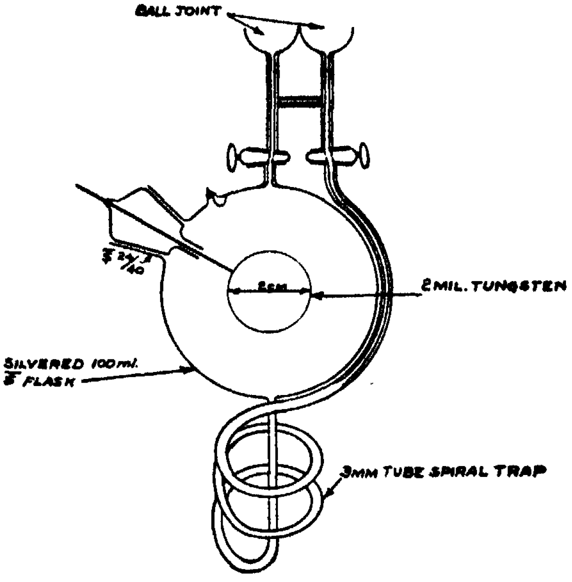

FIG. 2. Spherical proportional counter with spiral trap.

It is apparent from the design of the counter shown in Fig. 1 that some of the gaseous sample lies outside of the sensitive region of the counter. The correction for end effects is determined by one of the following procedures: 1. The ratio of the volume enclosed by the cathode to the total volume of the counter is determined by filling the counter with measured volumes of toluene to the appropriate levels; 2. A series of counters with similar ends but with different cathode lengths are filled with identical samples of $C^{14}O_2$. The counting rates are plotted against the reciprocal of the cathode length and the curve is extrapolated to infinite cathode length.

Two counters which have an effective geometry as determined by the first procedure of 78.7 percent and 90.4 percent gave corrected counting rates for identical samples of 37,400 counts/min. and 36,400 counts/min.

respectively. The extrapolated value (method 2) for the same sample of carbon dioxide was 37,300 counts/min. In a similar run six months earlier the same two counters, filled with the same carbon dioxide samples but using a different scaler, gave corrected counting rates of 36,700 counts/min. and 36,900 counts/min. respectively. This demonstrates that the volume correction is well within the over-all errors of handling samples, and that there is a high degree of reproducibility, not only in a given run but over long periods of time.

Figure 7 is a dilution curve in which the logarithm of the counting rate is plotted against the logarithm of the micromoles of Oak Ridge barium carbonate taken as a sample. The counts at each point done with the two counters, corrected for end effect, did not differ from the best straight line by more than a standard error of ±0.56 percent. The counting rates range from 1000 to 200,000 counts per minute. Failure to show any decrease from the expected counting rate at 200,000 counts per minute indicates that for all practical samples no coincidence correction need be applied. This gives an effective dead time of less than 3 μsec. in agreement with synchroscope observation. The absence of spurious counts from external sources is shown by a standard deviation of ±0.12 percent for ten repeated counts on the same counter, compared to a calculated standard deviation of ±0.11 percent.

Dilution experiments have also been carried out with tritium. The counting rate per cm³ of a tritium gas sample is constant and independent of the counter or the amount of gas taken for the count within sampling error over a range of 20,000 to 40,000 counts/min. Dilution experiments have not been run with H_2S^{35}.

The background count in the standard counter, which has a sensitive volume of 100 cm³, is 140 counts per minute unshielded. Shielding with 2 in. of lead lowers this background count to approximately 100 counts per minute.

Memory effects have been investigated for $C^{14}O_2$ and it was found that even for a sample giving as much as 500,000 counts per minute, pumping for a period of 5 minutes with a mechanical oil pump is sufficient to reduce the counting rate essentially to the background count. Carbon monoxide at a pressure of 70 millimeters and H_2S at a pressure of 85 millimeters were added to mixtures of carbon dioxide and methane, and the expected count was obtained with both of these additional gases present, although the operating region was shifted 100 to 150 volts higher. Sulfur dioxide at 41-millimeters partial pressure and dry anhydrous HCN gas at 65-millimeters pressure both attack the silver cathode and result in a complete loss of the operating region. Radioactive acetylene behaves similarly to carbon dioxide-methane mixtures when the CO_2 is at a low partial pressure.

The satisfactory behavior of H_2S-methane-$C^{14}O_2$ mixtures encouraged the use of radioactive H_2S as a counting gas for sulfur. It seemed probable that sulfide formation with silver cathodes would lead to very large memory effects, and evaporated chromium cathodes were used. A counter containing 21,000 counts of S^{35} at

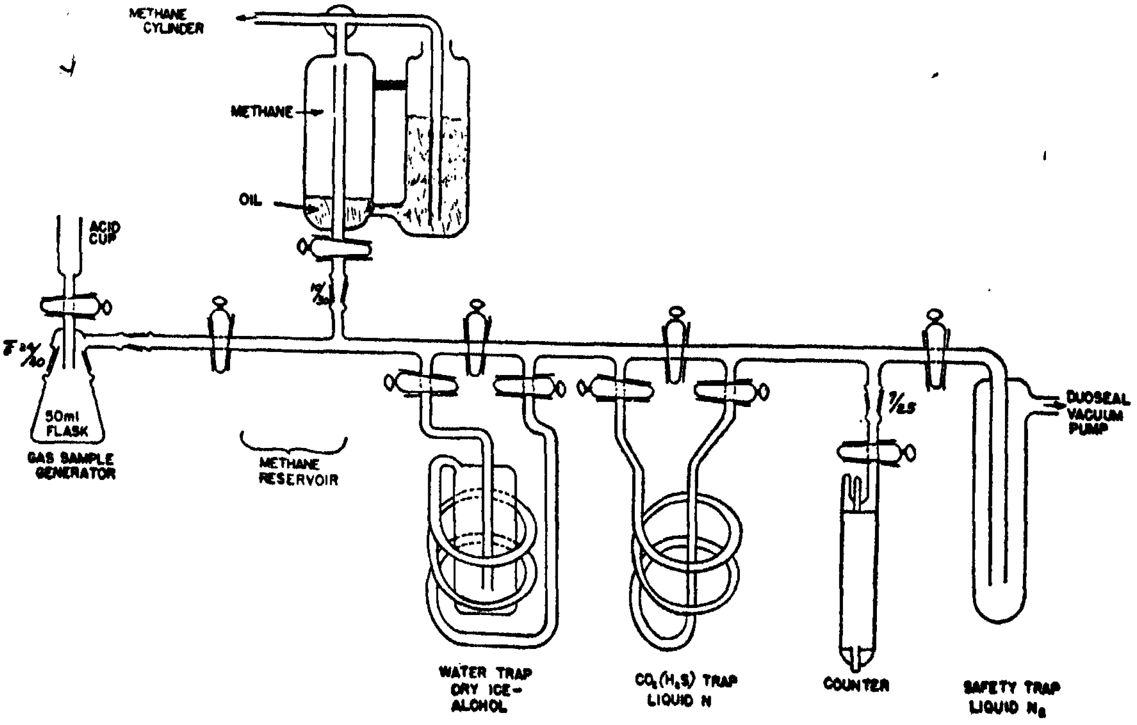

FIG. 3. Filling line for CO_2 and H_2S samples.

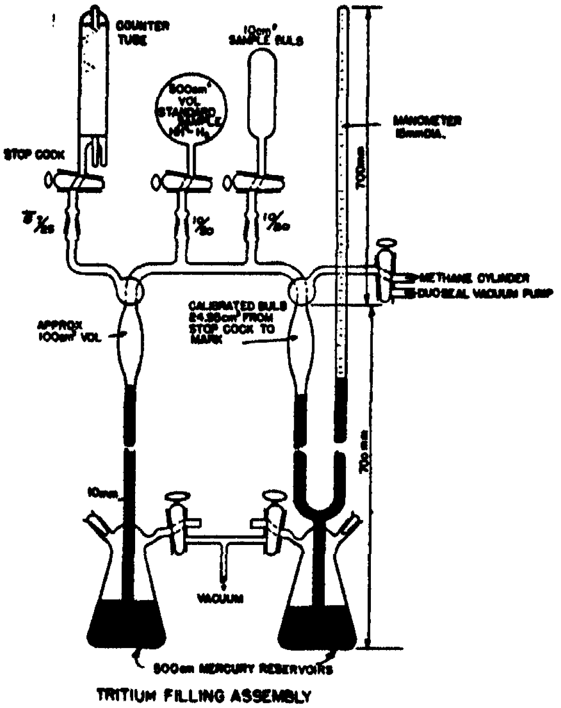

FIG. 4. Filling line for H^3 samples.

34-millimeters partial pressure of H_2S is reduced to background after a few minutes pumping with an oil pump.

Both silver plated cathodes and evaporated gold cathodes show a large memory effect with tritium. A silvered counter filled to 40 millimeters partial pressure of H^3, containing 136,000 counts per minute, gave 145 counts per minute above background, even after long, repeated pumping. Another silvered tube filled with H^3 at 4.5 millimeters pressure giving 409,000 counts per minute gave 50,000 counts per minute above background after having been pumped for an hour. This is a 12 percent memory effect. The same counter, after prolonged flaming and pumping, showed a decrease in the counting rate to 244 counts above background, but even this memory effect would be serious if low level counting were desired. The gold cathode, which was expected to show less absorption of hydrogen, was not better than the silver cathode, so apparently the difficulty lies more in the glass surfaces of the tube than in the cathode material itself. It is hoped that the conversion of tritium water to ethane (via ethyl Grignard) will be perfected shortly, which should permit counting tritium without memory difficulties.

One of the important properties of a counter is the ratio of the detected counting rate to the actual disintegration rate occurring within the sensitive volume of the counter. This ratio may be defined as the efficiency of the counter. An operating region of low slope in a proportional counter, as in Fig. 6, indicates that very few disintegrations are being missed. The length of the region of low slope is determined by the signal to noise ratio, and, if all disintegrations were detected, the slope of the characteristic would be zero.

Contributing factors to the slope in Fig. 6 are wall and end effects which cause an excess of small pulses in the distribution. The efficiency of counting these small pulses increases with voltage (or gain). To check this possibility we were kindly provided with a sample of $BaC^{14}O_3$ assayed by Dr. Warren Miller in his gas filled G-M tube. On this sample we obtained a 13.9 percent higher count than Miller did. It is doubtful that so large a discrepancy could be caused by spurious counts, since synchroscope observations show no appreciable number of multiple pulses or pulses due to electrical interference, and long delayed spurious pulses due to metastables or negative ions would be expected to have very small amplitudes. Another explanation to account for this discrepancy might be over-quenching of the G-M counter with a significant loss of counts in Miller's experiment. In this event the comparison is

TABLE I.

Partial pressure of CO_2	Counts/min.
20 mm	32,850
100 mm	32,700
300 mm	28,300

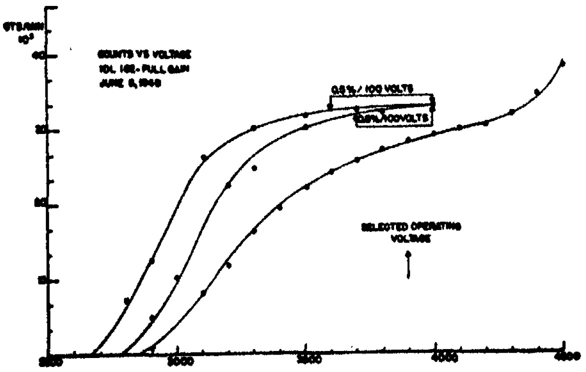

FIG. 5. Effect of CO_2 partial pressures on counting rate *vs.* voltage curves.

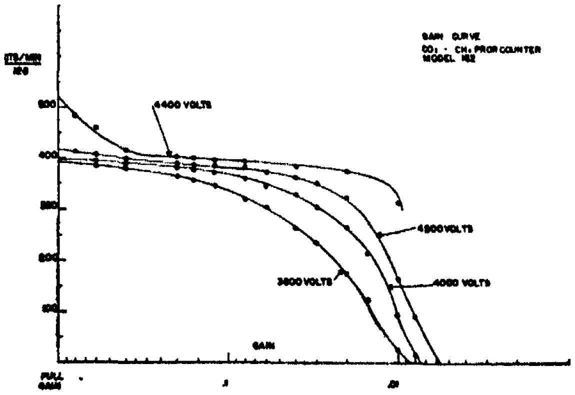

FIG. 6. Effect of high voltage on counting rate—amplifier gain curves.

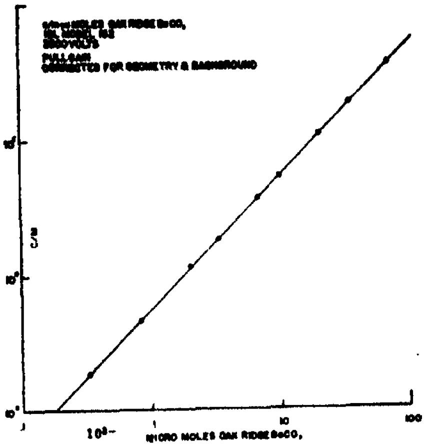

FIG. 7. Dilution curve for $C^{14}O_2$.

not significant. Therefore, the beta-spectra of both tritium and Carbon[14] have been investigated to provide an estimate of the counter efficiency. Figure 8 shows a plot of the spectrum of H^3 run with a counter 10 cm in diameter, the non-overloading amplifier and a single channel pulse height analyzer. If the value of 18.9 kv given by Hanna and Pontecorvo[6] for the maximum energy is assumed, the maximum intensity peak occurs at 3.5 to 4 kilovolts. It is apparent from the curve that the spectrum extends well below this energy. Conservatively, the minimum energy for counting is about 1 kilovolt.

A carbon spectrum has not been obtained to date because none of the counters constructed could encompass the beta-path length. The wall effects and pulse height distortion by the gas are sufficient to distort the spectrum to resemble a continuous distribution. However, if the counter is able to detect 1 kv as shown by the H^3 spectrum, then calculating from the Fermi theory[7] less than 1 percent of the C^{14} disintegrations are lost.

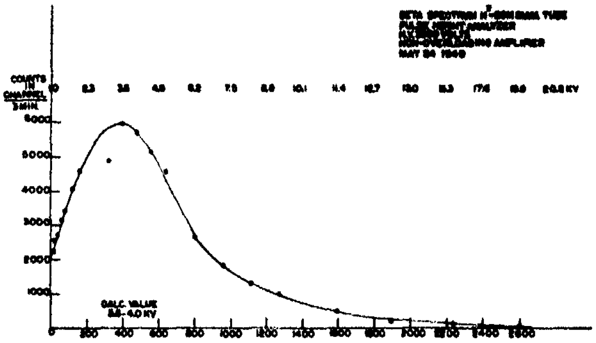

FIG. 8. Beta-spectrum of H^3.

The statistical behavior of the counter, both as far as background counts are concerned and for repeated counts on the same sample, provides strong evidence that the counting rate is not significantly disturbed by spurious counts caused by external disturbances. Since energies of about 1 kilovolt may be detected, we conclude that the efficiency of the counter is about 98 percent for C^{14}.

We have not been able to obtain the most precise energy distribution data on the tritium spectrum for several reasons. We are not equipped to carry out absolute energy calibrations of our counter tubes as was done by Hanna and Pontecorvo. Further investigations, both of the behavior of the counter with various gas mixtures and of the effect of the walls in distorting the beta-spectrum, would be required. Further work on the development of proportional counters for precise energy and absolute activity measurements is in progress. However, at present we feel that the described counter is entirely satisfactory for the routine assay of soft beta-emitters in the gaseous state.

The authors wish to express their appreciation to many members of the Brookhaven National Laboratory, especially to Dr. J. B. H. Kuper and W. A. Higinbotham, for their assistance and suggestions. The authors are indebted to the late H. G. Brewer, Jr. for the design of the amplifier and for his constant interest in this work.

---

[6] G. C. Hanna and B. Pontecorvo, "Beta-spectrum of H^3," Phys. Rev. 75, 983 (1949).

[7] We are indebted to Dr. R. W. Dodson of Brookhaven National Laboratory for this calculation.

THE REVIEW OF SCIENTIFIC INSTRUMENTS VOLUME 21, NUMBER 2 FEBRUARY, 1950

Measurement of Fast Neutron Energies by Observation of $Li^6(n, \alpha)H^3$ in Photographic Emulsions

GEORGE R. KEEPIN, JR.*† AND JAMES H. ROBERTS
Department of Physics, Northwestern University, Evanston, Illinois

(Received October 10, 1949)

A new technique of neutron energy measurement not requiring neutron collimation is described. The method employs the nuclear reaction $Li^6(n, \alpha)H^3$ ($Q=4.64$ Mev) observed within photographic emulsions impregnated with enriched Li^6. Results on monoenergetic neutrons indicate a resolution of at least ±0.1 Mev in the region studied (from thermal energies up to 1.3 Mev). To extend the method to measurement of continuous neutron spectra, both the excitation function and the angular distribution of the Li^6 disintegration process should be known. However, for immediate practical application, the method may be calibrated with a well-known spectrum. The Li^6 technique is particularly well suited to energy measurements on neutrons within a material medium where perturbations introduced by the detector must be minimized and where collimation is clearly impossible.

I. INTRODUCTION

THIS research evolved from the need for a neutron spectrometer which does not require collimated neutrons and whose detector could be placed within a material medium without thereby introducing an appreciable perturbation of the distribution being studied. A photographic plate, due to its small size is well suited to these requirements except that the usual technique, the recoil proton method, requires collimation of the neutrons. This difficulty may be resolved if one can employ a neutron induced reaction disintegrating by a single mode into a small number of ionizing particles whose ranges and directions can be measured from which both neutron energy and direction can be determined. Almost the only possibility is the reaction $Li^6+n\rightarrow\alpha+H^3$ with an average cross section the order of 0.1 barn in the region of interest. Commercial (normal) lithium loaded plates are not satisfactory because the small percentage of Li^6 results in a prohibitively low ratio of disintegrations to recoil protons. To enhance this ratio the use of emulsions heavily loaded with Li^6 was suggested.[1] The Eastman Kodak Company impregnated 50μ NTA emulsions obtaining approximately 0.2 mg/cm² of Li^6. Results of preliminary studies with these plates have been previously reported.[2] Exposures have been made to thermal neutrons and to a Po−Be source at the Argonne National Laboratory and to monoenergetic neutrons produced by the $H^3(p, n)He^3$ reaction with the Van de Graaff generator at the Los Alamos Scientific Laboratory.

II. EXPERIMENTAL PROCEDURE

For an accurate analysis of the data it is necessary to obtain good discrimination between the alpha- and triton tracks as well as to distinguish between disintegrations and a background of proton tracks. A number of methods have been suggested to obtain such discrimination: (1) underdevelopment; (2) the use of a very fine-grained developer; (3) differential fading of the latent image resulting from delayed development; and (4) the use of reducers and desensitizing solutions. A combination of (1), (2), and (3) were used in this work. The plates were processed as follows:

1. Presoaked in H_2O for two minutes with slight agitation.
2. Developed in Microdol diluted one to four for 12 minutes at 68°F.
3. Fixed until clear, washed and dried slowly.

Plates were enclosed in a light tight cadmium box during exposure (except to thermal neutrons) and oriented at an angle of 5° to the direction of the neutron beam. Exposure times were calculated to give two or three disintegrations per field of view.

A Leitz ortholux microscope fitted with binocular body tube and a precision mechanical stage was used. Linear measurements were made with a calibrated Spencer micrometer disk No. 410. Compensating eyepieces of magnification 6× or 12.5× were used in conjunction with a 2 mm apochromat oil-immersion objective (90×, N.A. = 1.32). For this arrangement one division (R.U.) on the micrometer disk was equivalent

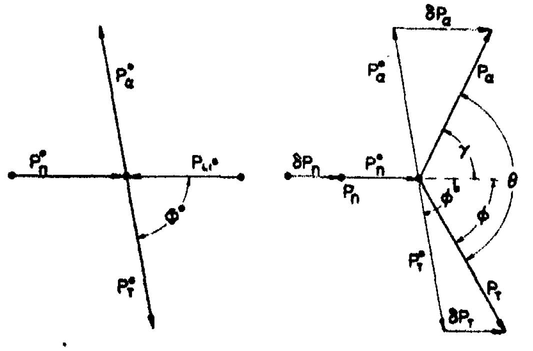

CENTER OF MASS SYSTEM LABORATORY SYSTEM

FIG. 1.

---

* Part of a dissertation presented in partial fulfillment of the requirements for the degree Doctor of Philosophy at Northwestern University.

† Now at the Radiation Laboratory, University of California, Berkeley, on an AEC Postdoctoral Fellowship.

[1] J. H. Roberts, Los Alamos Report, LADC 586 (1948).

[2] G. R. Keepin, Jr. and J. H. Roberts, Phys. Rev. 76, 154 (1949).

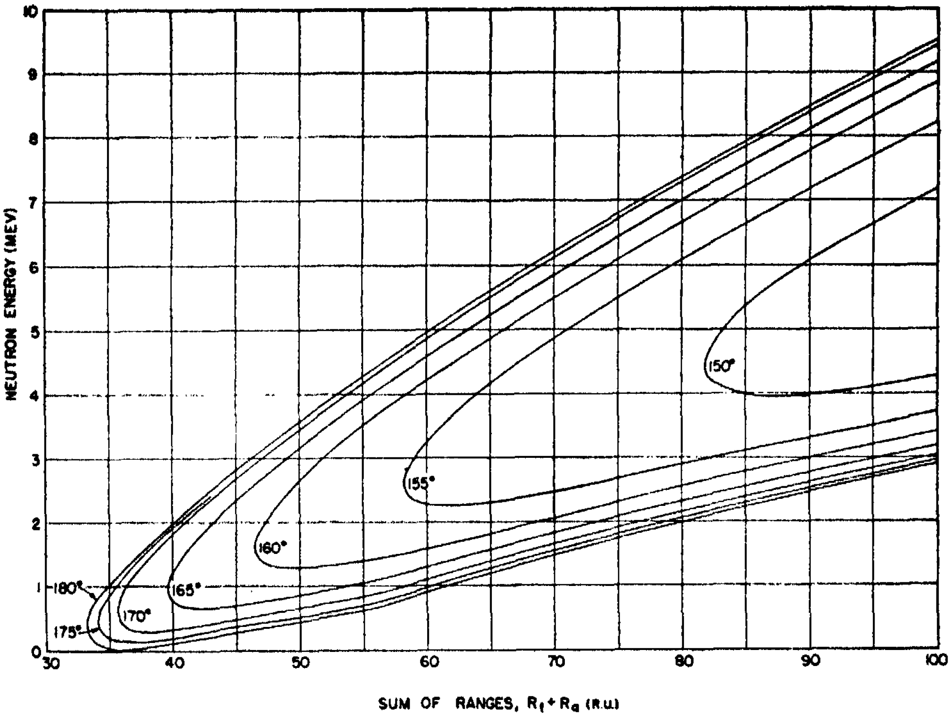

FIG. 2. Neutron energy *vs.* the sum of alpha-particle and triton ranges, parametric in θ.

to 1.25 microns. Angles were measured to an estimated accuracy of ±0.7° with a Gaertner goniometer eyepiece. A depth of focus scale calibrated in microns gave vertical distances in the emulsion. Only those tracks which were entirely within the emulsion and in or near the focal plane were selected for measurement. Points were established on range-energy curves for alphas and tritons in these Li^6 impregnated emulsions and were found to agree within experimental error with Ilford's range-energy relations for protons** and alpha-particles in Ilford C.2 emulsions.[3]

III. KINETICS OF THE DISINTEGRATION PROCESS

Consider the disintegration of a Li^7 compound nucleus into an alpha-particle and triton of energies E_α and E_T, respectively. These are assumed entirely kinetic energies since there are certainly no excited states of tritium in the present energy range. If we let m be the neutron mass and M the mass of the Li^6 target nucleus there is in the center of mass system an energy $\mathcal{E}=E_n+Q-[m/(m+M)]E_n$ available to the disintegration products, the remaining energy $(m/m+M)E_n$ going into kinetic energy of the center of mass. The alpha-particle and triton divide $\mathcal{E}$ in their inverse mass ratio so that

$$P_\alpha^0=P_T^0=\left\{\frac{2m_\alpha m_T}{m_\alpha+m_T}\left(\frac{ME_n}{m+M}+Q\right)\right\}^{\frac{1}{2}}. \tag{1}$$

Motion of the center of mass as seen in the laboratory system adds, in effect, the components δP_α, δP_T and δP_n whose magnitudes are given by particle mass times velocity of center of mass.

From the geometry we have

$$\tan\phi=\frac{P_T^0\sin\phi_0}{P_T^0\cos\phi_0+\delta P_T};\quad \tan\gamma=\frac{P_T^0\sin\phi_0}{-P_T^0\cos\phi_0+\delta P_\alpha}. \tag{2}$$

Therefore

$$\tan\theta=\tan(\phi+\gamma)=\sin\phi_0/A+B\cos\phi_0, \tag{3a}$$

with

$$A=\frac{\delta P_\alpha\delta P_T-(P_T^0)^2}{P_T^0(\delta P_\alpha+\delta P_T)},\quad\text{and}\quad B=\frac{\delta P_\alpha-\delta P_T}{\delta P_\alpha+\delta P_T}, \tag{3b}$$

functions of the neutron energy alone.

Again from the geometry, Fig. 1, we have the vector relation

$$\mathbf{P}_T=\mathbf{P}_T^0+\boldsymbol{\delta}\mathbf{P}_T$$

or, squared,

$$E_T=\frac{1}{2m_T}[(P_T^0)^2+(\delta P_T)^2+2P_T^0\delta P_T\cos\phi_0]. \tag{4}$$

Eliminating ϕ_0 from Eqs. (3) and (4) we obtain a quadratic relation between neutron energy and triton energy for constant θ. Thus a plot of E_n *vs.* E_T with θ as a parameter shows that for each E_n and θ there are two possible values of E_T. We define the larger of these values as the f_T case (favoring the triton) and the

---

** For particles of the same velocity and atomic number but different mass, the ranges are proportional to their masses. This was used in relating range-energy curves for tritons and protons.

[3] G. Lattes, P. Fowler, and P. Cuer, Proc. Phys. Soc. 59, 883 (1947).

smaller as the f_α case (favoring the alpha). Using our established range-energy curves and this E_n *versus* E_t relation, a plot of E_n *versus* $R_\alpha+R_T$, the sum of alpha-particle and triton ranges, was developed (Fig. 2). The two cases f_α and f_t are similarly defined for this sum of ranges curve.

IV. SELECTION AND ANALYSIS OF DATA

Without the restriction of neutron collimation there are four quantities which may be observed for each disintegration: R_T, R_α, θ, and $R_\alpha+R_T$. At least two of these must be measured to determine the energy of the incident neutron. Consider the following combinations of measurements: I—R_α, R_T; II—R_T, θ; III—R_α, θ and IV—$R_\alpha+R_T$, θ. The first method determines E_n uniquely while the methods involving measurement of θ determine E_n as one of two values. If R_α and R_T are measured, E_n is determined directly from range-energy data and energy conservation: $E_n=E_\alpha+E_T-Q$. However, alpha-straggling and the steepness of the R_α *vs.* E_α curve at low energy renders a large error in the determination of E_α and hence E_n. Furthermore, the point of disintegration must be accurately located; this is often difficult especially for $E_n<2$ Mev where straight line disintegrations ($\theta\simeq 180°$) are highly probable. For higher E_n the above objections are no longer serious and we may expect method I to give an accurate determination of neutron energy provided no excited states are found in the triton. When either method II or III is used, many disadvantages are encountered. If $\theta\simeq 180°$, E_n is an insensitive function of θ and θ need not be determined accurately; however, in such cases the point of disintegration is difficult to determine with precision. On the other hand if $\theta\ll 180°$, E_n is a very sensitive function of θ and θ must be determined with a better precision than is experimentally possible.

The major difficulty common to methods I, II, and III is locating the point of disintegration precisely. However, if we measure the sum of alpha- and triton ranges and the angle θ (method IV), E_n will be uniquely determined by deciding between the f_α or f_t case which involves only a rough determination of the point of disintegration. From the sum of ranges curve, Fig. 2, it is clear that the best resolution in neutron energy is obtained by selecting disintegrations which (1) favor the triton and (2) have $\theta\approx 180°$, for under these conditions E_n is the least sensitive function of the two variables being measured. The experimental distributions for monoenergetic neutrons in this low energy region have confirmed this, indicating a resolution of at least ±0.1 Mev. Thus a complete analysis by this sum-of-ranges method of the spectrum (Fig. 3) of 1.3±0.025 Mev neutrons from the Los Alamos Van de Graaff shows that f_α disintegrations give the poorest energy definition, f_t disintegrations with $\theta<175°$ give a somewhat sharper peak and those f_t disintegrations with $175°\leq\theta\leq 180°$ give by far the best resolution in E_n. Note also in Fig. 3 that only method IV is capable of resolving the 0.27 Mev resonance in the Li^6 cross section for neutron capture; this peak is attributed to an unavoidable back-

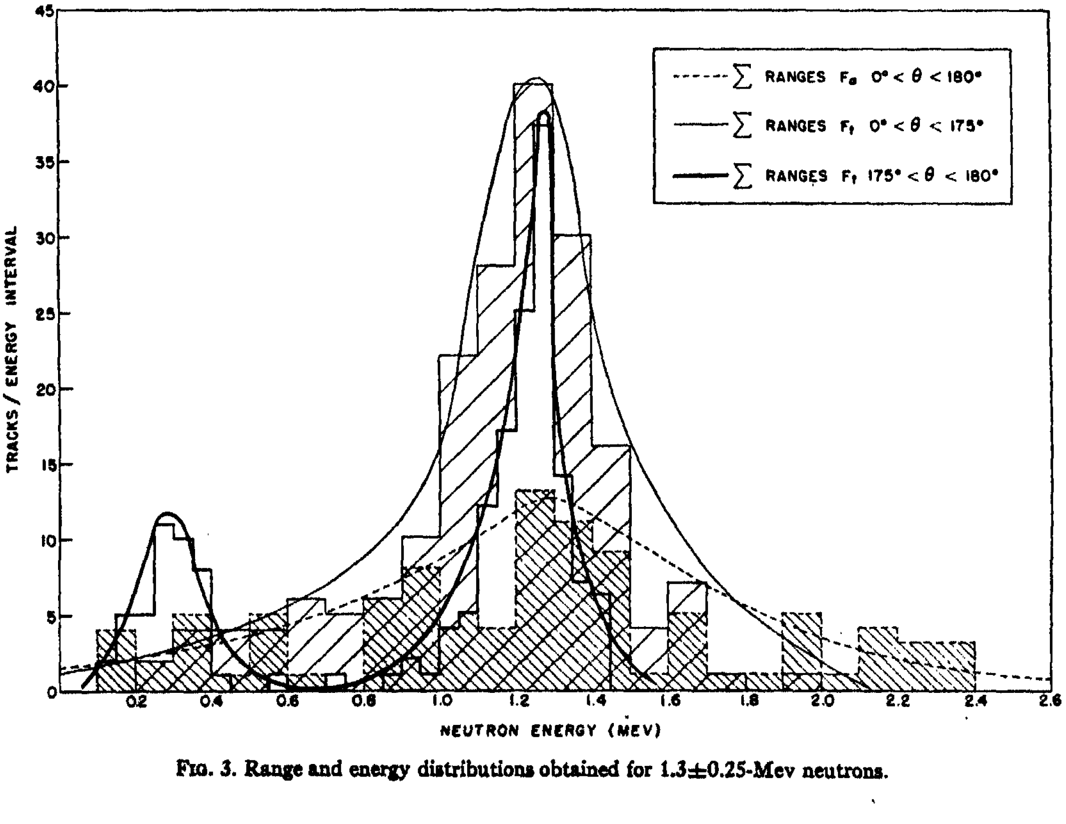

FIG. 3. Range and energy distributions obtained for 1.3±0.25-Mev neutrons.

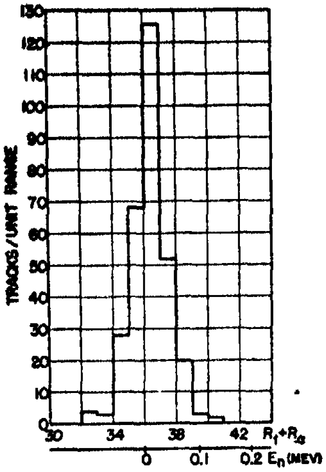

FIG. 4. Range and energy distributions obtained for thermal neutrons.

ground of scattered neutrons around the Van de Graaff. Exposures to neutrons of energy 0.6, 0.3, and ~0 Mev indicate that a resolution of better than ±0.1 Mev is possible all the way down to thermal energies (e.g., see Fig. 4). For $E_n < 3$ Mev there is no danger of confusing a disintegration with the shorter recoil proton tracks (cf. Figs. 5 and 6), whereas for higher E_n the average proton track length greatly exceeds the sum of alpha- and triton ranges, and the best possible discrimination between protons and alpha-triton pairs is required.

V. CONCLUSIONS

We have demonstrated the effectiveness of the Li^6 method for precise energy measurements on monoenergetic neutrons of a few Mev. It is planned to extend the method to measurements of continuous neutron spectra; for this either one may use an accurately known calibration spectrum or appropriate correction must be made for the energy dependence of:

(1) The Li^6 neutron capture cross section which at present is only roughly known up to 0.8 Mev.[4]

(2) The fraction of tracks measured according to geometrical selection criteria. *Viz.* tracks must be entirely within emulsion and approximately parallel to emulsion plane within a depth difference, $\delta = 10\mu$ between track extremities.

(3) The probability that $175° \leq \theta \leq 180°$.

An accurate measurement of the Li^6 cross section over the energy range of interest is being planned. Corrections for (2) have been developed for the case of isotropic and collimated incident neutrons.[5] For the

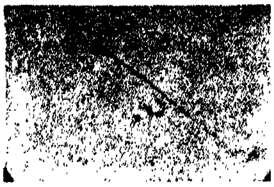

FIG. 5. Photomicrograph of a disintegration produced by a thermal neutron.

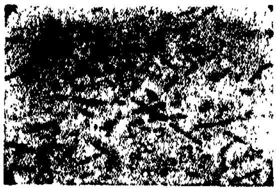

FIG. 6. Photomicrograph of a disintegration produced by a 1.3±0.025-Mev neutron.

angular selection criteria, (3), we ask what is the probability $W(\theta)d\theta$ of θ being in the interval θ, $\theta+d\theta$ for various E_n values. Referring to Fig. 1 we see that a disintegration is uniquely determined by the independent quantities E_n and ϕ_0 so that for each E_n we have:

$$W(\theta)\big]_{E_n}d\theta = \sum W(\phi_0)\big]_{\phi_0(\theta,\,E_n)}d\phi_0.$$

Or

$$W(\theta)\big]_{E_n}d\theta = \sum W(\phi_0)\frac{d\phi_0}{d\theta}\bigg]_{\phi_0(\theta,\,E_n)}d\theta,$$

the sum being taken over the two values of ϕ_0 at a given θ and E_n. $W(\phi_0)$ is of course the angular distribution of the disintegration process in the center of mass system. The quantity $(d\phi_0/d\theta)$ is immediately given by the geometry of Fig. 1, leaving only $W(\phi_0)$ to be determined. For *s*-capture of the incident neutron we have $W(\phi_0) = \frac{1}{2}\sin\phi_0$. However, since we have found definite indications of the presence of *p*-capture at energies considerably lower than would be expected, the angular distribution of the $Li^6(n,\alpha)H^3$ reaction should be measured. A method for doing this using Li^6 loaded plates has been proposed[6] and is now being applied. Pending the determination of these correction functions we should have then a fast neutron spectrometer which extends the photographic method beyond present limits set by recoil-proton techniques.

The authors are indebted to Professor A. J. F. Siegert of Northwestern University for many valuable suggestions, and to G. A. Linenberger and the Van de Graaff group of Los Alamos for the neutron irradiations. Finally, we thank Mr. R. S. Dike of Los Alamos for work on the illustrations.

---

[4] Goldsmith, Isber, and Feld, Rev. Mod. Phys. 19, 259 (1947).

[5] A. J. F. Siegert and G. R. Keepin, Jr., Los Alamos Report, LAMS 937 (1949).

[6] G. R. Keepin, Jr., Los Alamos Report, LAMS 924 (1949).

THE REVIEW OF SCIENTIFIC INSTRUMENTS VOLUME 21, NUMBER 2 FEBRUARY, 1950

An Automatically Synchronized Electronic Switch

W. A. Budlong* and Bruce C. Lutz
Physics Department, University of Delaware, Newark, Delaware

(Received October 10, 1949)

An electronic switch has been developed which eliminates the difficulties with frequency adjustments usually encountered in existing electronic switches. This is done by developing a switching square wave synchronized by either input signal. Therefore this switch is very much easier to use as the control settings are not critical.

THE purpose of an electronic switch is to view simultaneously two different signals of equal or multiple frequencies on the screen of an oscilloscope. This is accomplished by using a pair of amplifiers which are permitted to function alternately. The square wave causing the switching must have a frequency which is a sub-multiple or multiple of that of the examined wave. For switching after each cycle it should have a frequency of one-half that of the examined wave. Therefore to view phenomena of any frequency it is necessary to have a continuously variable switching frequency, which is usually supplied from a free-running multivibrator. There are now two frequency adjustments to be made simultaneously, the multivibrator and the oscilloscope sweep, which is usually tedious and difficult. The chief feature of the automatically synchronized electronic switch is a scale-of-two circuit, synchronized by either of the two input signals. This entirely eliminates one frequency control and provides a switching frequency one-half that of the examined wave. In addition a positive pulse is produced at the start of each cycle of the examined wave which is fed to the synchronization terminal of the oscilloscope making operation possible over a wide range of settings of the oscilloscope sweep frequency control.

Another feature is the use of transformers isolating the two input circuits and making possible the examination of any two portions of a circuit without the danger of shorting part of it. A block diagram of the switch is shown in Fig. 1 and a complete circuit diagram in Fig. 3.

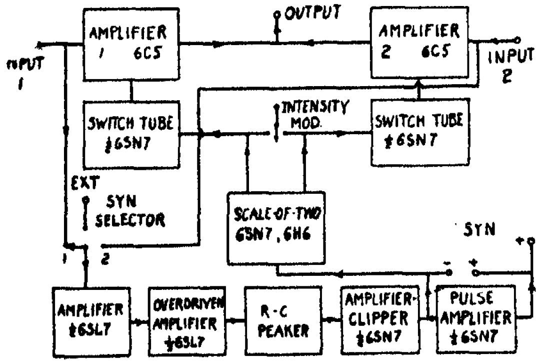

Fig. 1. Block diagram of automatically synchronized electronic switch.

AMPLIFIERS AND SWITCHING

The switching and amplifier circuits are based on those of Schultz and Anderson.[1] Symmetrical square waves 180° out of phase are put on the grids of the switch tubes thus causing them alternately to conduct and cut-off. This action through the common cathode resistors changes the bias on the two amplifier tubes making them function alternately as amplifiers. A potentiometer adjusts the balance of the bias and thus controls the vertical spacing of the two amplifier outputs on the screen. The output is taken over a common plate resistor and put on the vertical plates of the oscilloscope.

WAVE-SHAPING AND SCALER

The synchronization of the scale-of-two is provided from a wave-shaping circuit consisting of an amplifier, an overdriven amplifier, an R-C peaker, an amplifier-clipper, and a pulse amplifier-inverter.

The overdriven amplifier provides an essentially square wave output having the same frequency as that

Fig. 2. Oscilloscope and electronic switch showing two waves 180° out of phase.

---

* Now at Agricultural and Mechanical College of Texas, College Station, Texas.

[1] E. H. Schultz and L. I. Anderson, *Experiments in Electronics and Communication Engineering* (Harper & Brothers, New York, 1943), pp. 186–8.

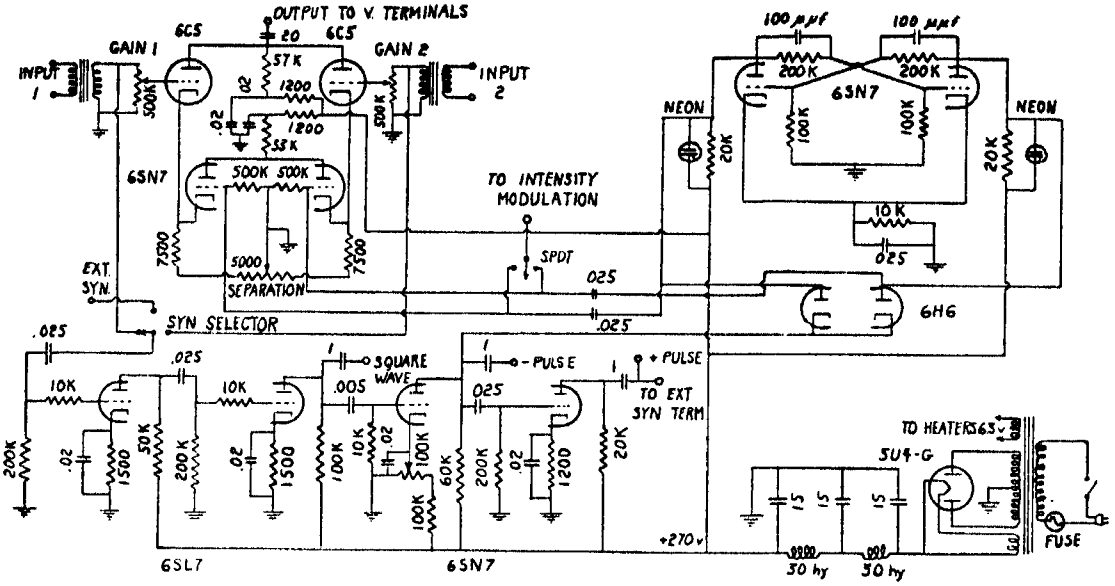

FIG. 3. Complete circuit diagram of the electronic switch. All resistance values are in ohms, all condenser values in microfarads. (K = 1000.)

of the observed signal which may be of almost any shape. This is transformed into a series of positive and negative pulses by the R-C peaker. The amplifier-clipper is biased to cut-off so that it is only sensitive to the positive pulses. The inversion action of the amplifier provides negative pulses superimposed on the plate potential. These operate a Higinbotham scale-of-two circuit,[2] which is simply a diode-triggered flip-flop.

The pulse amplifier-inverter provides positive pulses that are used to synchronize the oscilloscope sweep.

From the plates of the scale-of-two two symetrical square waves 180° out of phase are obtained and put onto the grids of the switch tubes. Thus a switch occurs at the beginning of each cycle of the examined wave. If desired the wave from either plate of the scale-of-two may be temporarily fed to the intensity modulation of the oscilloscope thereby blanking out either of the two waves as is often useful in demonstration work.

OPERATION

The electronic switch is shown at the right of Fig. 2. On the front left-to-right are input 1 terminals, gain 1 control, separation control, gain 2 control, input 2 terminals, synchronization selector switch, blanking control switch, neon lights, off-on switch. The neon lights indicate proper operation of the scaler circuit. On the left side are the outputs for the vertical input, external synchronization, and intensity modulation terminals of the oscilloscope. On the right side are outputs for square wave, negative, and positive pulses.

The switch operates satisfactorily from 25 to 15,000 cycles/sec. with any input over 1.5 volts. Although it operates most satisfactorily for viewing a single cycle, several cycles can be shown by appropriate adjustment of the sweep frequency and synchronization controls. This type of operation will cause small breaks in the pattern where the switch occurs, however this is kept to a minimum by the short switching time. Additional scalers could be used to avoid these breaks and to automatically show any even number of cycles.

This instrument is particularly well adapted for the demonstration and study of phase relations in alternating current circuits. In conjunction with a calibrated audio oscillator it provides a method of frequency measurement especially useful in those cases where the waveform is not readily adaptable to the Lissajou figure method, for example, pulses. Also it may be used as a square wave generator, or a pulse generator giving both positive and negative pulses.

---

[2] W. A. Higinbotham, F. Gallagher, and M. Sands, Rev. Sci. Inst. 18, 708 (1947).

THE REVIEW OF SCIENTIFIC INSTRUMENTS VOLUME 21, NUMBER 2 FEBRUARY, 1950

A Recording Microwave Refractometer*

George Birnbaum
National Bureau of Standards, Washington, D. C.

(Received October 12, 1949)

An instrument designed to measure and record a small difference in frequency between two cavity resonators is described. A sweep frequency technique is used to generate the resonance responses of the cavities. These responses are sharpened and made to control the operating time of a trigger circuit, whose average output is metered. A sensitivity equal to 200 c.p.s. is obtained in the measurement of the frequency difference between two high Q cavities, whose resonance frequencies are equal to 9000 Mc. Applications of this instrument are discussed, especially those relating to measuring changes in dielectric constant. A simple extension of the present instrument is suggested for simultaneously recording changes in dielectric constant and loss.

INTRODUCTION

IN the measurement of the dielectric constant of gases or changes in the dielectric constant of solids and liquids in the microwave region, the need arises for the accurate determination of small changes in the resonance frequency of a cavity resonator. An instrument, designed to measure and record such changes in frequency, is described in this paper. The use and adaptation of this instrument for measurements other than dielectric constant are also mentioned. In its present form, the recording microwave refractometer is especially suitable for investigating phenomena causing small changes in the dielectric constant of lossless gases and very low loss solids and liquids as a function of time.

Two basic methods present themselves for developing a recording microwave refractometer. One involves the use of a cavity as the frequency-controlling element of an oscillator; this is the well-known heterodyne-beat method.[1] The other approach is to employ a cavity as a circuit element to which either a cw or f-m signal is applied; this method is often employed for the determination of the dielectric constant of solids.[2] In this work, the second method was explored, and an instrument was developed which gives a sensitivity of 200 c.p.s. in the measurement of frequency difference between two high Q cavity resonators. In addition, the present instrument combines the following features: (1) relative simplicity of construction and adjustment; (2) flexibility with respect to operation over a wide band of frequencies in the microwave region; (3) availability of a wide range of sensitivities; and (4) ready adaptation to the simultaneous recording of changes in dielectric constant and loss.

DESCRIPTION OF CIRCUITS

Figures 1 and 2 illustrate the method by which a difference in the resonance frequencies of two cavities is measured by the microwave refractometer. A klystron oscillator is frequency-modulated by a saw-tooth voltage, applied to its reflector. The r-f power from the f-m oscillator is applied to two cavities, one functioning as a test cavity, the other as a frequency reference. When the outputs of the cavities, with slightly different resonance frequencies, are applied to the crystal detectors, resonance responses displaced in time are obtained. After amplification and sharpening, one of these pulses turns on a modified Eccles-Jordan trigger circuit, known in this application as a "flopover" circuit, and a short time later, the other pulse turns it off. The output of this circuit is a rectangular wave form with a constant amplitude, but variable width. The average value of this wave form is directly proportional to the frequency difference between the two cavities, provided that the "on-time" of the trigger circuit is directly proportional to frequency difference.

The circuit functions indicated in Fig. 1 may be developed in several different forms. Nevertheless, any satisfactory arrangement should provide for a linear relation between time and frequency. Not only is this desirable for metering purposes, but also for reasons of stability. The latter point is amplified in a separate section. Linearity between time and frequency is attained if the following holds: a linear modulation voltage is supplied by the sweep circuit; this is applied in the linear region of the klystron's electronic tuning characteristic; frequency pulling of the klystron due to high Q loading is avoided; and hum modulation of the klystron and the amplifiers is prevented.[3]

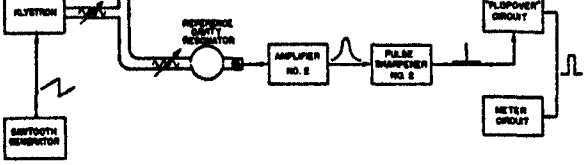

FIG. 1. Arrangement of components of the refractometer.

---

* A preliminary report of this work was presented at the Washington Meeting of the American Physical Society, Phys. Rev. 74, 1212(A) (1948).

[1] An example of this method for measuring the dielectric constant of gases at 3.2 cm has been given by C. M. Crain, Phys. Rev. 74, 691 (1948). Two stabilized oscillators [R. V. Pound, Rev. Sci. Inst. 17, 490 (1946)] were employed.

[2] See, for example, Works, Dakin, and Boggs, Trans. A.I.E.E. 63, 1092 (1944).

[3] *Since a recurrence frequency of 120 c.p.s. is employed, instability in the refractometer output due to hum is eliminated.*

The first of these conditions is realized by the circuit shown in Fig. 3. A cathode follower, with properly adjusted feedback, insures a constant charging current for the 0.01-μf capacitor; this arrangement therefore gives a linear sweep voltage. By firing the thyratron with a wave form obtained from the power supply, the repetition rate of this voltage is maintained at 120 c.p.s. The sensitivity of the refractometer is controlled by the amplitude of the sweep voltage. Although not included in the present equipment, it seems worth while to replace the variable potentiometer in the output cathode follower by a step potentiometer, in order to obtain a range of sensitivities which can be easily and accurately reproduced.

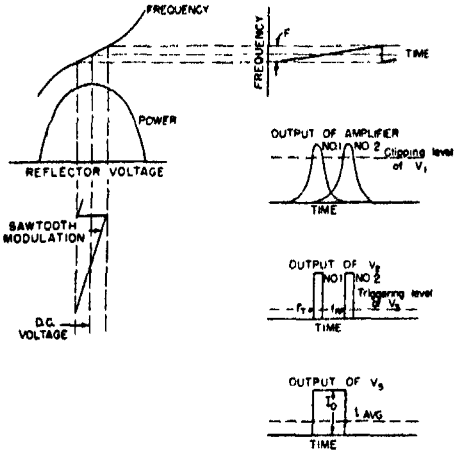

Fig. 2. Wave forms illustrating operation of equipment.

Among the factors contributing to hum modulation, attention was given, of course, to minimizing the amount of ripple in the klystron power supply. In addition, precaution was taken against cable pick-up. This was reduced by the use of a braided shield surrounding the cable to the klystron, with a ground connection at only one end. If this shield is to be effective, a high impedance should not be inserted in any lead at the power-supply end of the cable. Finally, hum modulation in the amplifiers was reduced by destroying the path for ground currents via the wave guide. This was accomplished by the use of insulated wave-guide joints between the klystron and the detectors.

In the wave-guide circuit, a "tee" junction divides the f-m signal between two similar circuits. Attenuators are included between the cavities and the klystron to prevent coupling between the cavities[4] and reaction back on the klystron. Some provision for controlling the matching of the klystron into the wave guide may be advantageous, since the klystron's electronic tuning rate and linearity depend upon its loading.[5] The present instrument, which operates in the 9000-Mc region, employs cylindrical cavities operating in the TE_{011} mode, whose Q-factors are approximately 10^4. The cavities are constructed of either Shelby steel or brass, and are plated with silver. Type 1N23A crystals, in tunable mounts, are employed as the detectors. A 6-db attenuator is included between each cavity and detector.

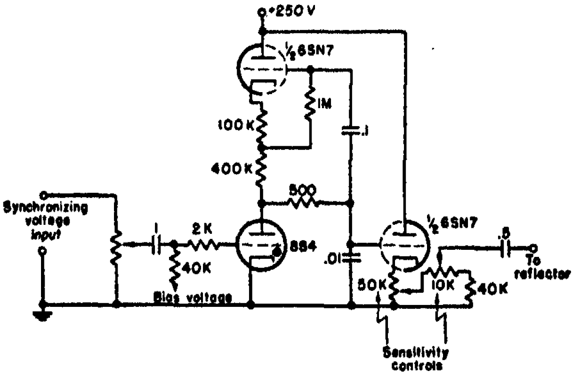

Fig. 3. Sweep circuit.

The broad, continuous form of the resonance pulse, as well as the fact that exact reproduction of this wave form is not essential, permits the use of amplifiers whose band-width requirements are not very critical. Conventional RC-coupled amplifiers with a gain of 10^4 and a pass band extending from 35 to 2000 c.p.s. were found to be adequate. After amplification, sharpening the resonance pulses is accomplished by the circuits shown in Fig. 4. The top of the resonance pulse is clipped at approximately 90 percent of its peak amplitude and amplified by V_1. For a given input into this stage, the clipping level is adjusted by varying the screen voltage. The grid leak arrangement of V_1 and the low screen grid voltage operate to maintain a constant plate circuit output over a limited range of input pulse amplitude. Further amplification of the peak of the resonance pulse is accomplished by V_2. When the output of V_2 triggers the blocking oscillator, V_3, a very sharp negative wave form is produced, which is suitable for firing the "flop-over" circuit, V_5. The diode, V_4, is used to decouple V_5 from the positive overshoot of V_3. The triggering level of V_3 is controlled by the cathode bias. The rectangular voltage output from the "flop-over" circuit is applied to V_7, a differential amplifier, which drives either an ammeter or a recorder. The grid of this circuit is clamped to ground by the d.c. restorer, V_6. In the present instrument it was found useful to provide the ammeter with the following ranges: 50 μa, 1 ma, and 10 ma. When the duration of the rectangular pulse is approximately one-tenth the duration of one sweep, the meter circuit supplies a current of 1 ma. For reasons which are given in the section on stability, pulse durations greater than this were not used. One ma is sufficient to operate directly an Esterline-Angus Recorder. A 20-μf condenser was placed in parallel with the ammeter or recorder to

---

[4] For a discussion on frequency-pulling of cavities due to reactive loading, refer to C. G. Montgomery, *Technique of Microwave Measurements*, Radiation Laboratory Series (McGraw-Hill Book Company, Inc., New York, 1947), Vol. 11, Section 5.3.

[5] A. E. Harrison, *Klystron Tubes* (McGraw-Hill Book Company, Inc., New York, 1947), Chapter 7.

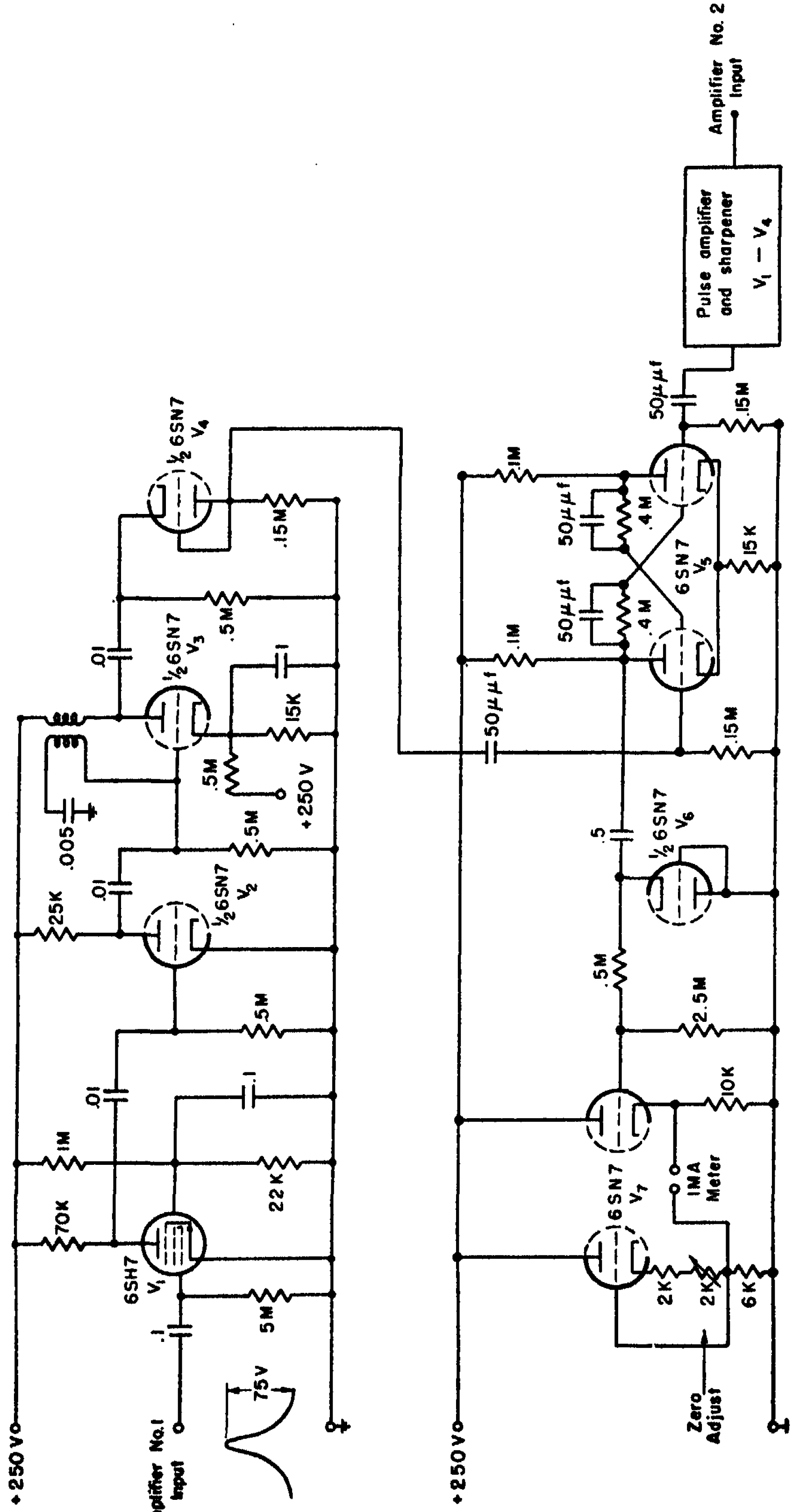

FIG. 4. Sharpening, "flop-over," and meter circuits.
]

shunt the a.c. components in the rectangular wave form. When using the recorder without this condenser, it was observed that the shape of the rectangular wave form across the 10 K resistor of V_7 was distorted; the addition of the condenser remedied this condition. The averaging of the rectangular wave form is performed by the ammeters.

Two electronically regulated power supplies are employed; one furnishes voltages for the Type 723A/B klystron[6] and the other for the electronic circuits. By making suitable changes in the microwave components, with the klystrons now available, the refractometer can be operated over a wide range of frequencies in the microwave region. The operation of the present instrument was checked at 3000 Mc by using a Type 707B klystron and a microwave circuit of the coaxial type, which included cavity resonators operating in the TM_{010} mode.

INITIAL ADJUSTMENT

Initial adjustment of the refractometer was accomplished with an oscilloscope for viewing the wave forms shown in Fig. 2. After a warming period, the cavity resonance pulses were made to appear on top of the klystron mode curve, by mechanically tuning the klystron. This adjustment insured that the modulation voltage was applied to the linear region of the electronic tuning characteristic. To observe this pattern, a directional coupler was inserted between the klystron and the "tee" junction, and the attenuation in front of the cavities was reduced. The d.c. reflector voltage was set for the klystron mode which gave the greatest power output and simultaneously the lowest electronic tuning rate (in Mc/v). Hence, a given amount of hum and instability in the reflector voltage had the smallest effect on the linearity (and ultimately the stability) of the refractometer. Next, the gain of the amplifiers, and the bias of the blocking oscillators, if necessary, were adjusted to trigger properly the blocking oscillators. Then the frequency of the reference cavity was varied with attention fixed on the output wave form of that blocking oscillator which was triggered by the resonance pulse of the test cavity. If the position of the pulse remained fixed, there was sufficient padding between the cavities and the klystron to prevent coupling among these components. The amount of attenuation necessary for operation in the manner just described was approximately 12 db preceding each cavity. For the purpose of checking the time-frequency relation, the position of the rectangular wave form on the oscilloscope trace was varied by adjusting the d.c. klystron reflector voltage. In this test, a constant current on the output meter of the refractometer indicates linearity. For this particular instrument, a constant current was obtained for a variation in the position of the rectangular wave form equal to one-fifth the distance occupied by one sweep. The width of the rectangular wave form was one-twentieth the distance occupied by one sweep. A very high sensitivity (5 ma/Mc) was employed with the idea of emphasizing any effect due to hum modulation.

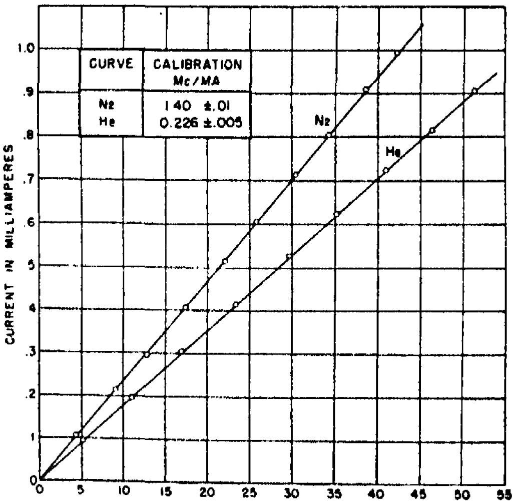

FIG. 5. Typical calibration curves. The calibration error was calculated from the uncertainty attached to the slope of the line, and the quantities in Eq. (1).

The sensitivity was adjusted by varying the amplitude of the sweep voltage applied to the klystron and/or varying the sensitivity of the ammeter. Small sweep amplitude corresponds to large expansion of the frequency scale and hence to high sensitivity in ma/Mc. In connection with adjusting the sensitivity of the instrument, it should be noted that the largest useful frequency change is governed by the extent of the linear region of the klystron's electronic tuning characteristic, while the greatest usable sensitivity depends upon the stability of the refractometer. Procedures for ascertaining the sensitivity are given in the following section.

CALIBRATION PROCEDURE

It is well known that $(\epsilon-1)/(\epsilon+2)$ is accurately proportional to density for non-polar gases. In the present application, the susceptibility $\epsilon-1$ is always less than 10^{-3}; consequently, with negligible error, $\epsilon-1$ is taken proportional to density.[7] Then assuming the ideal gas law,[8] it follows that

$$\epsilon-1=(\epsilon_0-1)(P/760)(273.2/T), \qquad (1)$$

where ϵ_0 is the dielectric constant for $P_0=760$ mm Hg and $T_0=273.2°K$. For a gas filling the entire cavity, the fractional change in resonance frequency, $\Delta f/f$, is given by[9]

---

[6] The klystron power supply is a slightly modified Browning Laboratories, Inc., Type TVN-7 BL. See reference 5, p. 205. A coarse and fine control for the reflector voltage was found to be useful. A d.c. voltage was used for the klystron filament.

[7] Of course, the frequency should be sufficiently far from any resonance absorption by the gas. This is certainly the case for non-polar gases in the microwave region. Unpublished experimental results by Birnbaum, Kryder, and Lyons, on N_2 at 9000 Mc verify that $\epsilon-1$ is directly proportional to density.

[8] If N_2, for example, were an ideal gas, its measured pressure at one atm would be too small by less than 0.1 percent.

$$\epsilon-1=2\Delta f/f. \tag{2}$$

Therefore, a measurement of the output current of the refractometer as a function of gas pressure for a gas whose ϵ_0 is known gives the calibration as well as the over-all linearity. Values of $(\epsilon_0-1)10^4$ equal to 5.87 ± 0.02 for N_2, and 0.710 ± 0.009 for He were taken from previous work at 9100 Mc.[10] Figure 5 shows the results of a typical calibration. The r.m.s. deviations of the measured values from the straight lines which best fit the data for N_2 and He are 0.002 ma and 0.004 ma, respectively. The curve for N_2 demonstrates a linearity over a range of 1.4 Mc, but this does not represent the maximum value, which is determined by the linearity of the klystron's electronic tuning characteristic. Each determination, conducted at room temperature, was completed in approximately 18 min. It is estimated that during these intervals, the temperature difference between the test and reference cavities varied by no more than 0.01°C. By using N_2 and He for the 1.40 Mc/ma and 0.226 Mc/ma calibrations, respectively, the changes in gas pressure were large enough to be read with sufficient accuracy on an ordinary mercury manometer. However, care was exercised to insure against distortion of the test cavity due to a difference in pressure between the atmosphere and the gas in the cavity. Such distortion was avoided by enclosing the test cavity in a metal chamber equipped with gas and wave-guide outlets, as shown in Fig. 6.

Since the accuracy of the calibration depends on the accuracy of the value of ϵ_0, it is desirable to use the rare gases whose dielectric constants have been measured at optical frequencies, where the precision is one or two orders of magnitude better than what is obtained by present radio frequency and microwave techniques. Careful work by Jelatis[11] shows impressive agreement between the dielectric constant of the rare gases as extrapolated from optical frequencies by the Sellemeier dispersion formula, $\epsilon-1=c/(f_0^2-f^2)$, and his own measurements at 1 Mc. Therefore, the rare gases may be used confidently as accurate calibration standards throughout the microwave region.

Greater convenience in the calibration procedure was obtained by using the refractometer as a null-indication instrument, where one cavity contained the gas and the other was equipped with a low tuning-rate plunger whose displacement was measured as a function of gas pressure. Once this measurement was done, the refractometer calibration was readily checked by noting the ammeter reading for a known displacement of the tuning plunger. This procedure may be used as an accurate check on cavity perturbation theory[9, 12] to aid in the design of such tuning plungers. A low tuning rate was obtained by displacing a small part of the cavity wall. Some of the TE_{011} reference cavities in the present equipment are tuned by a concentric cylindrical post, consisting of a micrometer tuning head ground to a small diameter, and protruding slightly into the cavity.

STABILITY CONSIDERATIONS

In discussing the problem of refractometer stability, in terms of output current or frequency difference, it is convenient to distinguish between a long-time stability which refers to the slow drifts occurring during one hour or more, and a short-time stability which refers to the rapid fluctuations occurring in less than a second. The long-time stability of the refractometer depends chiefly upon the variation of the center frequency of the klystron with temperature, the variation of the temperature difference between the two cavities, and the variation of the dielectric composition of the reference cavity. If the relation between frequency difference and the "on-time" of the "flop-over" circuit is linear, changes in the center frequency of the klystron merely shift the position in time when the resonance curves are traced out, without changing the frequency difference indication between them. However, the cavity responses cannot be permitted to wander over the entire length of the sweep, since this time-frequency relation is not everywhere linear. Also, for sensitive operation of the instrument, say at 5 ma/Mc, the entire sweep represents 3 Mc, a range insufficient to trace out completely the tails of the resonance pulse, even for a cavity with a O equal to 10^4. As the resonance pulses drift from the center of the trace, the amplitude (and eventually the shape) of the wave form nearest the end of the trace begins to change. Since the time of firing of the "flop-over" circuit depends upon the shape, and to a smaller extent upon the amplitude of the resonance

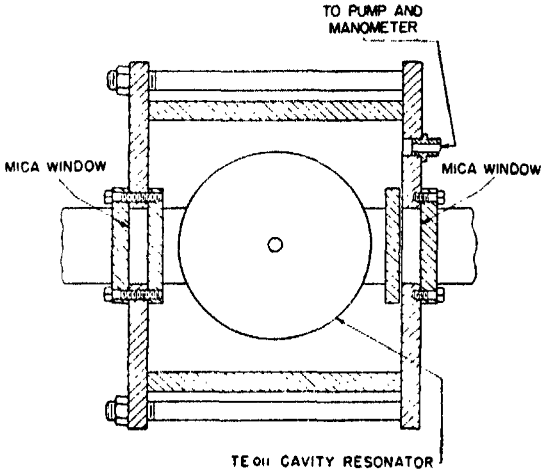

FIG. 6. Chamber for evacuating the cavity resonator without distortion. The cavity is secured to only one side. The gap on the other side is 0.01 in.

---

[9] Equation (2) is obtained with negligible error from $\epsilon=(f_1/f_2)^2$; J. C. Slater, Rev. Mod. Phys. 18, 480 (1946).

[10] Lyons, Birnbaum, and Kryder, Phys. Rev. 74, 1210(A) (1948).

[11] J. G. Jelatis, J. App. Phys. 19, 419 (1948).

[12] H. A. Bethe and J. Schwinger, N.D.R.C. D1-117 (March 7, 1943).

pulse, an error in output current is obtained. Nevertheless, this effect does not seriously limit the stability of the refractometer. Experience has shown that even for sensitive operation at 5 ma/Mc, the allowable drift in the unmodulated frequency of the klystron is as much as ±0.2 Mc. Long-time constancy in klystron frequency was improved by shielding the klystron from changes in ambient temperature. From the foregoing discussion, it is evident that the maximum separation in time (or frequency) between the resonance pulses should be limited to a small fraction of the duration of one sweep. In the present case this fraction was taken equal to one-tenth. Small and rapid changes in the unmodulated frequency of the klystron are caused by fluctuations in the voltages applied to it. In view of the foregoing discussion, this should cause no instability in refractometer output.

When a homogeneous cavity undergoes thermal expansion, the fractional change in frequency with temperature is given by $\Delta f/f = -\alpha$ per degree C, where α is the linear coefficient of expansion for the material.[13] For a temperature change between two steel cavities, which is equal to 10^{-2} °C, Δf is approximately 10^{-3} Mc for $f = 9\times 10^3$ Mc, if α is taken to be 10^{-5}, an average value for steel. Improvement in temperature stability may be obtained by constructing the cavities from invar, for which $\alpha \simeq 2\times 10^{-6}$ per °C, or by temperature compensating the cavities. However, a dual cavity unit, which is a single block of metal, hollowed out for two cavities, proved to be adequate in the stability tests. Such a unit, fabricated from brass, and silverplated, is shown in Fig. 7. A factor affecting the frequency stability of the reference cavity is the change in composition of dielectric in the cavity due to the changes in temperature, pressure, and especially moisture content of the atmosphere.[14] Therefore, the cavity should be isolated from the atmosphere by vacuum seals, and either evacuated or filled with a non-polar gas. Precaution against distorting the cavity due to changes in gas pressure may then be necessary.

FIG. 7. Dual TE_{011} cavity unit. The Q-values are 11,000. The upper cavity is tuned by the micrometer.

The relation between the short-time stability and the factors upon which it depends may be formulated as follows. Subject to the requirements that the detector operates as a square-law device, that the amplifiers pass undistorted the signals applied to them, that the transmission cavity has a high Q, and that the frequency modulation is linear, the shape of the cavity resonance curve is given by[15]

$$V/V_0 = [1 + 4Q^2(f_0 - f)^2/f_0^2]^{-1}, \tag{3}$$

where V and V_0 are the output voltages of the amplifier at frequency f and at the resonance frequency f_0, respectively. For $V/V_0 = \frac{1}{2}$, Eq. (3) gives

$$Q = f_0/\Delta f, \tag{4}$$

where Δf is the band width of the cavity between half-power points. Suppose that some r.m.s. noise voltage, e, is added to the resonance pulse. If V_1 is considered to be some fixed operating level for the trigger circuit (see Fig. 2), the resonance pulse plus the noise will operate this circuit at some new value of f, say f'. Then the fluctuations in firing, in units of frequency, $\delta f = f' - f$, due to some r.m.s. value of noise voltage is found to be

$$\delta f = (\alpha f_0/4Q)(e/V_1). \tag{5}$$

The factor $\alpha = [(V_1/V_0)(1 - V_1/V_0)]^{-\frac{1}{2}}$ shows essentially the dependence of the stability on the slope of the resonance curve at the firing point. Provided that operation does not occur too near the peak, the value of this factor varies slowly. It is readily shown that α/V_1 is minimum for $V_1 = (3/4)V_0$. Since each resonance curve operates the trigger circuit, the total frequency fluctuation, as manifested by jitter in both sides of the rectangular pulse is $(2)^{\frac{1}{2}}\delta f$.

The ratio e/V_1 represents the effective output noise-to-signal voltage ratio of the crystal detector and amplifier, and is expressed as[16]

$$e/V_1 = (4kTB)^{\frac{1}{2}}/MP. \tag{6}$$

In this equation, k is Boltzmann's constant, T is the absolute temperature, B is the effective noise band width of the amplifier, P is that r-f power absorbed by the crystal which corresponds to voltage V_1, and M is the figure of merit for the crystal. The substitution of

---

[13] Reference 4, pp. 384–90.

[14] *The magnitude of this effect is given by the empirical equation,*

$$(n-1)10^6 = 79/T[P + (4800e/T)],$$

where n is the index of refraction, T is the absolute temperature, P is the barometric pressure, and e is the water vapor pressure, both pressures being expressed in millibars; Radiation Lab. Report No. 551 (April 6, 1945).

[15] Reference 4, Section 5.2.

[16] H. C. Torrey, and C. A. Whitmer, *Crystal Rectifiers*, Radiation Laboratory Series (McGraw-Hill Book Company, Inc., New York, 1948), Vol. 15, pp. 344–8.

Eqs. (4) and (6) in Eq. (5) gives

$$\delta f=[\alpha\Delta f/4][(4kTB)^{\frac{1}{2}}/MP], \tag{7}$$

which shows the dependence of the frequency instability δf caused by noise on the resonance pulse as a function of the parameters of the instrument. If the band width, for a given value of Δf and frequency swept out per unit time, is reduced to the point where some minimum requirement for satisfactory reproduction of the resonance pulse is reached, then δf, calculated from Eq. (7) represents a minimum value. Assuming a recording system with a sufficiently small time constant, the value of the frequency swept out per unit time determines the fastest rate of change of frequency that the refractometer can resolve.

If P is increased beyond the microwatt range, or if d.c. bias is applied to a silicon crystal rectifier, M is no longer a constant. The rectified voltage of the crystal, for a given incident power, now has noise components whose fluctuations are proportional to $(f)^{-\frac{1}{2}}$, where f is in the audio frequency range.[17] A similar kind of fluctuation in grid to cathode voltage in the amplifier circuit occurs due to cathode emission changes.[18] Little benefit in suppressing noise is obtained in this case by the usual method of decreasing the sweep frequency so that the amplifier band width can be narrowed. The low frequency cut-off of the amplifier must be accordingly lowered, consequently, bringing in high amplitude noise due to the $(f)^{-\frac{1}{2}}$ law. Where the greatest sensitivity, and hence stability, is required, an alternative procedure consists in integrating the effect of as many sweeps as may be necessary. This was accomplished by adding a resistance-capacitance integrator to the grid circuit of V_7 (Fig. 4). Such an arrangement operated satisfactorily with the present meter circuit, which in this case supplied direct current to the ammeter. Of course, the time constant of the additional RC circuit now controlled the rapidity with which the refractometer was able to follow changes in frequency.

From the wave forms of Fig. 2, it can be seen that the average meter current is given by

$$i_M=(f_T-f_R)(I_0/F), \tag{8}$$

where I_0/F in ma/Mc is the sensitivity, and (f_T-f_R) is the frequency difference between the test and reference cavities. The effect of small variations in (f_T-f_R), F, and I_0 on i_M can be determined by examining the total differential of i_M, which is obtained from Eq. (8). It is then evident that di_M/i_M depends only on the instability in (f_T-f_R) for small values of (f_T-f_R), and when (f_T-f_R) becomes large enough di_M/i_M depends also on the instability in I_0 and F. The instability in (f_T-f_R), see Eq. (7), was discussed in the preceding paragraphs. The fluctuations in I_0 depend upon variations in the plate voltage applied to V_6 and V_7. The value of F, the frequency swept out in one period, is inversely proportional to the sweep rate, which in the present arrangement is controlled by the power line frequency. Where this frequency is not sufficiently stable, or when it is necessary to control the sweep rate, it is profitable to incorporate in the equipment a stable but variable frequency sweep generator.

While no special effort has been made to achieve ultimate stability in the present instrument, the results of some tests are indicative of what may be attained. In the calibration performed with He (Fig. 5) and in other tests, the short-time stability was 0.001 ma, or approximately 200 c.p.s. It is interesting to note that Eq. (7) gives $(2)^{\frac{1}{2}}\delta f\simeq 60$ c.p.s.[19] by taking $M=20$,[20] and using the following equipment parameters: $\Delta f=10^6$ c.p.s., $T=290$°K, $B=2000$ c.p.s., $\alpha=3$, and $P=5\times 10^{-6}$ w. The long-time stability was checked by using the dual cavity unit with each cavity sealed and evacuated. The klystron was shielded from changes in room temperature. With this arrangement, a recording of the refractometer output current revealed that the maximum current fluctuation over a period of 90 min. amounted to 0.004 Mc, and during several 15-min. intervals, the fluctuations were less than 0.001 Mc.

METHODS FOR MEASURING DIELECTRIC CONSTANT

Some methods for employing the refractometer in measuring the dielectric constant of gases were given in the section on "Calibration." In addition to the techniques discussed there, it is advantageous, in some investigations, to employ a flow technique. To effect this modification the end plates of the TE_{011} cylindrical cavity were perforated (the location and size of the holes were chosen for negligible effect on the Q of the cavity) so that a continuous stream of gas could be drawn through the cavity. In this form, the instrument was used in some preliminary experiments to record the variation in the dielectric constant of an artificially controlled atmosphere. The agreement was reasonably good between the measured changes in dielectric constant and the changes calculated from the temperature, pressure, and humidity of the atmosphere.[14] Further, the instrument in this form might be applied, for example, to measure the variations of the dielectric constant of the atmosphere as a function of time.[21]

In working with solids and liquids, great sensitivity to small changes in dielectric constant can be obtained by filling the entire cavity with the material. However, except for dielectrics possessing very small power factors, for example, 2×10^{-4} or less, the procedure would seriously decrease the Q of the cavity. But, the Q is hardly influenced by filling a small fraction of the cavity volume with a low loss dielectric while sufficient sensitivity to changes in dielectric constant is maintained. In this case, the fractional change in frequency is given by[9, 12]

---

[17] See reference 16, pp. 189–94. Similar considerations in relation to the sensitivity of a crystal video receiver for microwave spectroscopy have been discussed by W. Gordy, Rev. Mod. Phys. 20, 677 (1948).

[18] E. B. Moullin, *Spontaneous Fluctuations of Voltage* (Oxford University Press, London, 1938), Chapter VI.

[19] Since the integrating effect of the ammeter is neglected, the calculated frequency instability of the equipment should be lower than this value.

[20] Reference 16, p. 357.

[21] Such measurements are of interest in studies relating to radio propagation and meteorology. See, for example, "Meteorological factors in radio-wave propagation," Phys. Soc. London (1947); W. E. Gordon, Proc. I.R.E. 37, 41 (1949).

$$\Delta f/f = G(\epsilon - 1), \tag{9}$$

where G is a constant depending on the geometry of the sample and the electric field distribution in the cavity. If a cylindrical sample with a small diameter is inserted parallel to the electric field at the position of maximum intensity, in a rectangular cavity operating in its fundamental mode, $G = 2v/V$, where v and V are the volumes of the dielectric and cavity, respectively.[22] The dielectric constant of liquids can be measured by such a small-sample technique by containing the liquid in a thin-walled quartz tube. This and similar small-sample arrangements are recommended as being particularly suited to the refractometer. The advantages of such an arrangement are linearity in $\epsilon - 1$ of the refractometer output, and a rapid method for changing the sample.

The minimum detectable change in $\epsilon - 1$ for gases and for solids and liquids is calculated from Eqs. (2) and (9) by letting $f = 9\times10^3$ Mc, δf = short-time stability $= 2\times10^{-4}$ Mc, and $v/V = 10^{-4}$. The results are 4×10^{-8} for gases, and 1×10^{-4} for solids and liquids.

Because of the recording feature of the refractometer, as well as the convenience of reading frequency difference on a calibrated ammeter, the emphasis in this discussion has been, thus far, on the measurement of frequency changes which are no greater than the linear portion of the klystron's electronic tuning characteristic. Nevertheless, larger changes in the resonance frequency of the test cavity were measured by using the refractometer as a null-indication instrument, where the change in frequency was read from the calibrated tuning control of the reference cavity. Employing the refractometer in this manner, where the frequency change is substituted in Eq. (9), would make it convenient to measure the dielectric constant of low loss solids and liquids.

METHOD FOR MEASURING CHANGES IN Q

So far, the effect of changes in cavity-Q on the operation of the refractometer has been neglected; such changes are caused, for example, by dielectric loss. If the Q decreases, the amplitude of the resonance pulse decreases, and the width increases. Evidently, this can result in an error in the measurement of frequency difference, although the error can be decreased by triggering the blocking oscillator near the peak of the resonance pulse. This is the expedient which is used in the present instrument. A simple modification however, should enable one to reduce this error to a negligible value. Suppose that the amplified peak of the resonance pulse of the test cavity is differentiated to yield two very sharp pulses. Next, two rectangular wave forms can be generated, the width of each representing the time interval between the reference cavity pulse and each of the pulses resulting from the differentiation. Then the average value of the sum of these rectangular wave forms measures the frequency difference between the reference and test cavities, independent of changes in Q of the test cavity.[23]

Examination of Eq. (3) shows that the points of inflection are identical with the ¾-power points of the resonance curve. If the resonance pulse of the test cavity is differentiated, two pulses are obtained whose frequency separation, Δf, equals $1/\sqrt{3}$ times the band width of the cavity. Use of these pulses to generate a rectangular wave form which is then averaged gives a measure of $1/Q$. These pulses, in conjunction with the one obtained from the reference cavity, could be also used in the manner described in the previous paragraph to measure frequency difference. Therefore, both the frequency difference and $1/Q$ could be simultaneously measured and recorded by a slight extension of the present techniques. Since $1/Q$ is measurable, the loss tangent, $\tan\delta$, for dielectrics can be calculated from the equation

$$\tan\delta = (G/\epsilon)(1/Q_2 - 1/Q_1),$$

which holds for gases filling the entire volume of the cavity ($G = 1$), or for solids or liquids occupying a small fraction of the cavity volume ($G = \frac{1}{4}V/v$), for the arrangement of sample and cavity given in connection with Eq. (9).

Other applications, mentioned by *Pound*[1] for his heterodyne-beat method, can also be made with the refractometer. These are the use of the refractometer as an ultra-micrometer, or for the measurement of the thermal expansion of cavity materials. Both applications are possible because of the great sensitivity of the resonance frequency to cavity dimensions.

ACKNOWLEDGMENTS

The author thanks Mr. S. J. Kryder for assistance in the tests and for several valuable suggestions in connection with the circuits, Dr. H. Lyons for suggesting the development of a recording microwave refractometer using cavity resonators, and Mr. D. M. Kerns for several valuable discussions.

---

[22] G. Birnbaum and J. Franeau, J. App. Phys. 20, 817 (1949).

[23] A technique very similar to this was independently developed by Mr. B. F. Husten in connection with work on the stabilization of oscillators by spectral lines in the microwave region.

THE REVIEW OF SCIENTIFIC INSTRUMENTS VOLUME 21, NUMBER 2 FEBRUARY, 1950

Integrator for Small Beam Currents

T. A. Hall, S. D. Warshaw, and J. Dorsey
Institute for Nuclear Studies, University of Chicago, Chicago, Illinois

(Received October 17, 1949)

A simple circuit is described which integrates approximately beam currents of 10^{-14} amp. or larger. It consists of a d.c. amplifier, which converts the current into a voltage signal, and a voltage integrator circuit. Integration is approximate primarily because of slow circuit response to fluctuations; under usual conditions of high voltage accelerator work, one can expect integration accuracy of about one to five percent.

THE usual method of integrating a beam current—repeatedly charging a condenser connected to the beam target to some critical discharge voltage—is quite accurate for currents of 10^{-10} amp. or more, but for smaller currents this method demands impractically low capacitances. We describe here an integrator consisting of a simple d.c. amplifier, which converts the beam current into a change of voltage on the plate of an electrometer tube, and a standard circuit[1] which integrates this change in plate voltage. For most applications the range and accuracy of this integrator are determined by the d.c. amplifier's sensitivity, drift, and linearity. One can couple any appropriate d.c. amplifier to the circuit of the integrator proper. Essentially, any current that can be measured by the d.c. amplifier can be integrated.

The d.c. amplifier tube we have used is the Victoreen VX41-A, which is small and has a grid resistance of 10^{15} ohms. This tube plus a set of high resistances and a selector switch are housed in a steel can close to the beam target. A long shielded cable running between can and integrator circuit carries tube power and the d.c. signal. The circuit is arranged so that the target may be easily held near ground, −150 or −300 volts, in order to reduce secondary electron effects at the target if that is desired.

The VX41 plate connects to the grid of the integrator tube (5691, the more stable version of the 6SL7) through a battery and a potentiometer used to adjust the 5691 no-beam grid voltage. The operation of the regenerative, condenser-feedback integrator circuit is described in reference 1; its main advantage is that the amplifier must be linear over a plate swing of only a few volts, instead of the swing of about 50 volts required with the simplest integrator circuits, and that there is almost no voltage swing at the input grid. The output of the 5691 is the integral of the input signal; as it reaches a certain level the relay in the next stage closes, snapping the input grid back to the voltage of buss line C (Fig. 1) and restarting the cycle. Simultaneously, the normally closed contacts of the relay are used to pulse a register circuit (6SA7, 6V6).

The maximum counting rate could be raised, if desired, by pulsing into a scaler and by using a thyratron or Schmitt circuit instead of the General Electric mechanical relay (G.E. reference number K27J853).

A conventional vacuum tube voltmeter is installed to measure the plate voltage change of the VX41, which is proportional to the beam current. The ammeter itself may be switched from terminals 1 and 2 to a and b to measure the grid bias of the relay tube (6SN7).

In operation one makes three preliminary adjustments: First, with the count switch closed (5691 input grounded) and with the ammeter reading the bias of the relay tube, the regeneration potentiometer r_3 is adjusted so that the relay current is almost critical (6SN7 grid bias about −12 volts). Secondly, with count switch open and no beam, the 22½-volt battery potentiometer (r_1+r_2) is adjusted so that the relay current is again almost critical; the exact optimum for this setting is discussed below. Finally, the VTVM is set to zero with potentiometer r_4 if it is desired to read beam current during operation. The integrator is then ready to work. If absolute integration is desired, a 1½-volt cell is installed, attached to the selector switch in the d.c. amplifier can, so that the counting rate produced by a 1½-volt signal on the VX41 grid can be observed.

In the design of the integrator circuit, several factors limit the allowable sizes of the circuit elements. The counting rate is approximately

$$F = \frac{e_s}{e_f RC(1+A)}, \tag{1}$$

where A is the gain of the two-stage 5691 amplifier, e_s is the change in VX41 plate voltage due to the beam, and e_f is the voltage swing of the 5691 input grid during each cycle; $R \equiv r + r_1 r_2/(r_1+r_2)$ (see Fig. 1). Equation (1) is quite accurate if $e_s \gg e_f$. In order to satisfy this condition without excessive counting rates, A, R, and C should be large. This is not unconditionally possible. First, if C is too large, the voltage at the 5691 output will not be free to recycle quickly as the relay closes. Secondly, A is largest when the 5691 input grid has approximately zero grid bias, but in this bias region, grid current changes rapidly with voltage, acting as a false signal, especially if R is large. It is better to run the tube with slightly negative bias and reduced gain; then the grid current stays almost constant and produces no error. Thus for the circuit in Fig. 1 there is not much latitude in the choice of r, C, and amount of regenerative gain (r_3).

It is worth while to study the integrator in some detail, in order to obtain a condition for optimum inte-

---

[1] MIT Radiation Laboratory Series, Vol. 21, pp. 79–82.

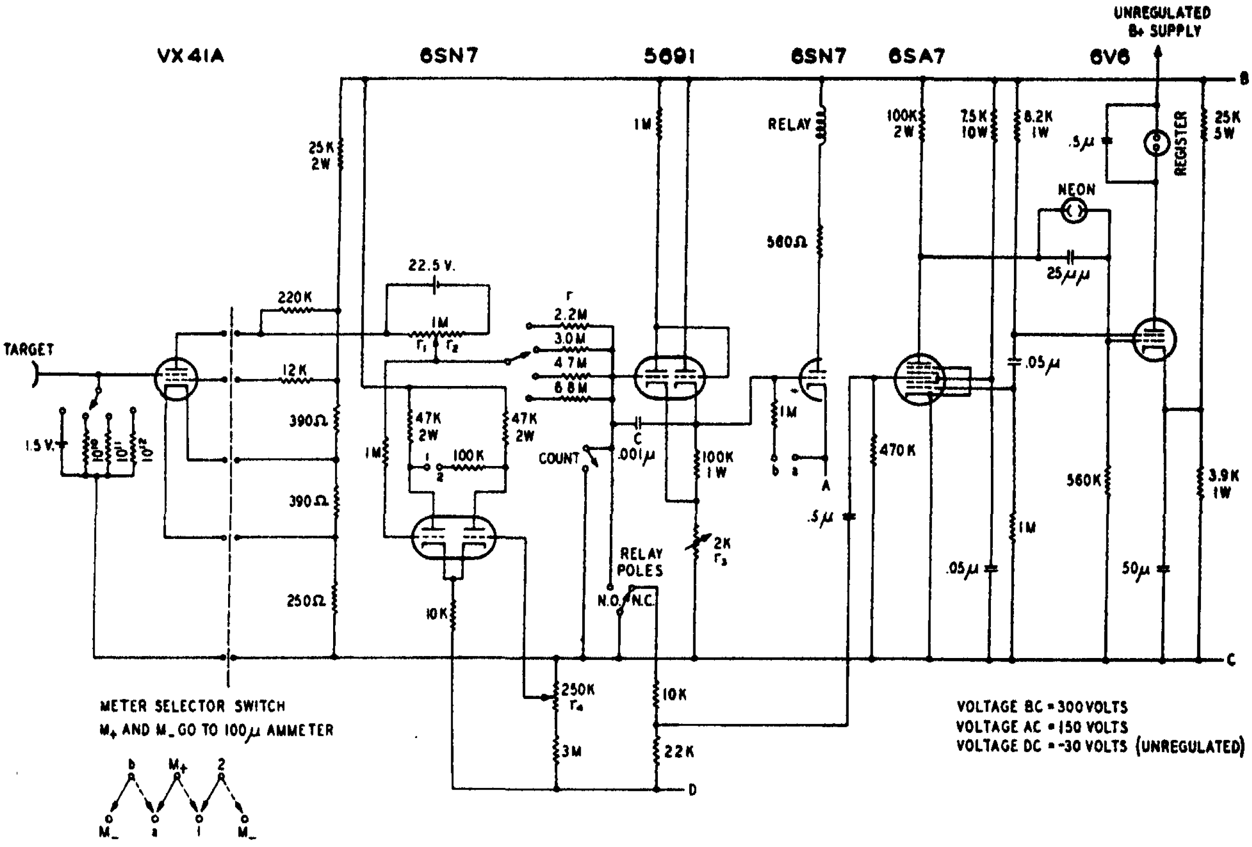

FIG. 1.

gration that applies to almost all voltage integrator circuits. Let e_g be the voltage at the 5691 input grid, and e_0 the value of that voltage when there is no beam; "ground" is defined presently as the value of e_g at the start of each counting cycle. During each cycle e_g obeys the equation

$$e_g=(e_s+e_0)(1-e^{-t/\tau}),\quad \tau\equiv RC(1+A) \tag{2}$$

in the case where e_s is constant. Then the time per cycle T is

$$T=-\tau\ln\left(1-\frac{e_f}{e_s+e_0}\right). \tag{3}$$

A power series expansion yields

$$T\approx\tau\left[\frac{e_f}{e_s}+\frac{1}{e_s^2}(-e_fe_0+\tfrac{1}{2}e_f^2)+\frac{1}{e_s^3}(e_fe_0^2-e_f^2e_0+\tfrac{1}{3}e_f^3)\right]. \tag{4}$$

It follows that the counting rate is most accurately proportional to e_s when $e_f=2e_0$. In other words, at the end of each counting cycle the grid should be returned *not* to its no-beam voltage but to a voltage twice as far from the firing point. This eliminates the quadratic term in Eq. (4) and, for a given counting rate (fixed e_f and varied e_0), reduces the cubic term by a factor of four. The condition $e_f=2e_0$ can be accurately satisfied in making the two preliminary relay tube adjustments described above since the values e_f and e_0 are accurately reflected in the bias of that tube. Its fulfillment considerably extends the range of accurate integration.

Aside from imperfect integration of a constant signal, as displayed in Eq. (4), there are these other inherent errors: Non-linear gain of the VX41, voltage drift in the d.c. amplifier circuit, slow response of the VX41 plate to a change in beam and imperfect integrator response to a non-constant signal e_s. The last two factors arise from the fact that neither d.c. amplifier nor integrator circuit can respond properly to fluctuations shorter than their own time constants. While all these factors prevent precision integration of the sort enjoyed with larger currents, the instrument is still a valuable beam monitor for most uses where great accuracy is not needed. If it is used to monitor a beam in high energy accelerator work, the integrator will function quite accurately, except for those isolated instants when the beam suddenly fluctuates; this means in practice an integration accuracy of about one to five percent in such work.

THE REVIEW OF SCIENTIFIC INSTRUMENTS VOLUME 21, NUMBER 2 FEBRUARY, 1950

An Electronic Circuit Which Extracts Antilogarithms Directly

F. CURTIS SNOWDEN AND HAROLD T. PAGE
General Aniline and Film Corporation, Central Research Laboratory, Easton, Pennsylvania

(Received October 27, 1949)

It has long been established that variable-μ tubes of types such as the 6SK7 were capable of outputs which were proportional to the logarithm of the input over a specified range of bias voltages. The use of inverted triodes, and related circuits, is also widely known. It was decided to combine these two older techniques in the hope of developing a new one. Accordingly, a 6SK7 was hooked up as an inverted triode, i.e., the plate was used as the controlling element, and the control grid was employed as the output element; the results obtained with this arrangement were then plotted and investigated. As reported herein, a circuit capable of extracting antilogarithms over a fairly extended range of input voltages was developed.

THE application of vacuum tubes in the direct extraction of the logarithms of the applied grid voltages has been recognized for some time.[1,2] Circuits developed for this purpose employ vacuum tubes of a variable-μ type, such as a 6D6, 6SG7 or 6SK7. The $i_p - e_g$ characteristic of such tubes is logarithmic over a certain range of grid potentials; that is, within the specified range of grid voltages, the plate current is proportional to the logarithms of the input grid voltages:

$$\log e_g = k i_p. \tag{1}$$

This property of these tube types has rendered them useful in applications such as photoelectric densitometer and colorimeter circuits,[2] where the desired output is to be proportional to the logarithm of the input.

Figure 1 shows a circuit which may be set up to confirm this property of the variable-μ tubes. Measurements were made on both the 6SG7 and the 6SK7 types. The critical range of grid voltages mentioned above differed, of course, for the two types, and the useful range also varied with different values for the cathode resistor, R_2.

Points on the $i_p - e_g$ curve for the tube may now be taken with this circuit. Note that the circuit of Fig. 1 provides for the initial bucking out of the plate current at the starting grid potential. This is done so that a more sensitive meter may be used in the plate circuit, and correspondingly greater accuracy achieved. Battery B_3 provides the bucking potential, and the necessary adjustments are made with the potentiometer R_3. Figures 2 and 3 represent families of $i_p - e_g$ curves for a 6SG7 and a 6SK7 respectively, with the various cathode resistors as indicated. The older 6D6 is not considered here, since its adaptability to circuits of this nature has been discussed elsewhere.[2] Each of the individual curves of Figs. 2 and 3 is the resultant average of five nonconsecutive check runs made under the conditions indicated. Similar families of curves were made on several tubes of each type. The range of grid potentials over which the $i_p - e_g$ characteristic was logarithmic varied somewhat from tube to tube. However, it was observed that *in all cases*, the 6SK7 characteristic was logarithmic between grid potentials of -10 to -20 when a cathode resistance of 10,000 ohms was used; the 6SG7 characteristic was similarly logarithmic between grid potentials of -4 to -10.

The curves of Figs. 2 and 3 also clearly demonstrate that the greater the cathode resistance, the greater the useful logarithmic range of the $i_p - e_g$ characteristic. However, the use of too large a cathode resistance causes the changes in plate current to be too small for useful purposes without additional amplification, which should be avoided whenever possible. Consequently cathode resistors of 10,000 to 12,500 ohms are generally chosen for optimum results in most applications.

The background of an old and tried application of vacuum tubes has now been presented briefly, along with some new data for more recently developed variable-μ tube types which can be used in conjunction with this application. Since these tubes have proven extremely valuable wherever the extraction of logarithms is desired, it can be easily imagined that an equally helpful circuit would be one which performed the reverse function, namely the extraction of antilogarithms. Inasmuch as the $i_p - e_g$ characteristic of the variable-μ tubes had been proven to be logarithmic over a specified range of input potentials, there was no valid reason to suspect that this same characteristic would not be antilogarithmic if these tubes were used in an inverted fashion.

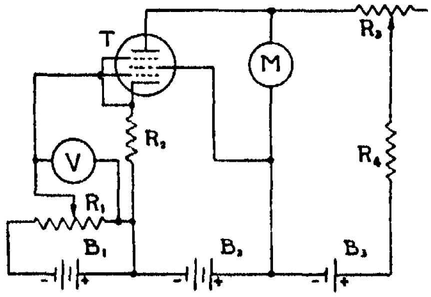

FIG. 1. A circuit which extracts logarithms directly.

B_1, 22½ volts
B_2, 90 volts
B_3, 1½ volts
M, 0–1 milliammeter
R_1, 50,000 ohms
R_2, 2500–15000 ohms
R_3, 50,000 ohm potentiometer
R_4, 1000 ohms
T, 6SG7 or 6SK7
V, 0–30 voltmeter.

---

[1] R. H. Müller and G. F. Kinney, J. Opt. Soc. Am. 25, 342 (1935).

[2] R. H. Müller, R. L. Garman, and M. E. Droz, *Experimental Electronics* (Prentice-Hall, Inc., New York, 1945), pp. 232–233.

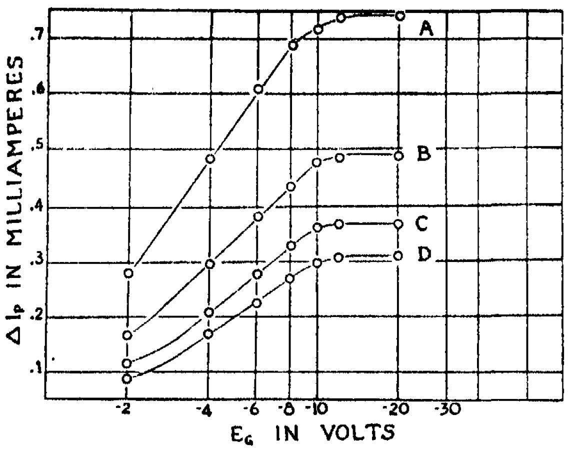

FIG. 2. I_p-e_g characteristic for 6SG7.

A, R_2 = 2500 ohms
B, R_2 = 5000 ohms
C, R_2 = 7500 ohms
D, R_2 = 10,000 ohms.

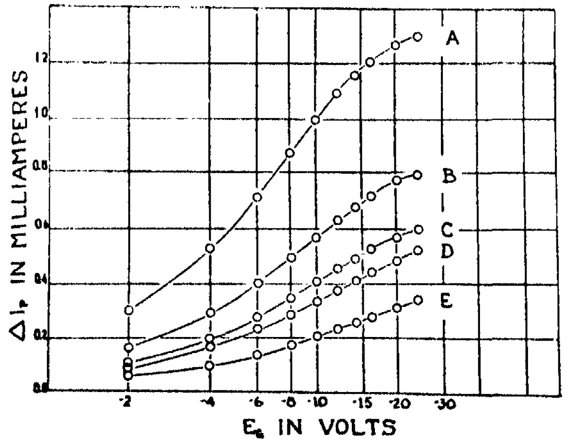

FIG. 3. I_p-e_g characteristic for 6SK7.

A, R_2 = 2500 ohms
B, R_2 = 5000 ohms
C, R_2 = 7500 ohms
D, R_2 = 10,000 ohms
E, R_2 = 15,000 ohms.

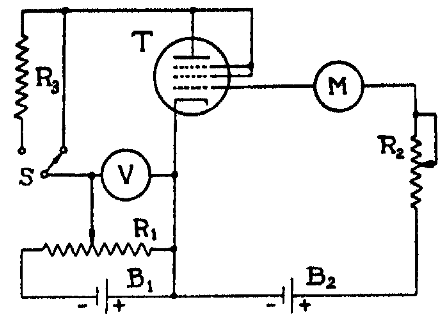

FIG. 4. A circuit which extracts antilogarithms.

B_1, 45 volts
B_2, $1\frac{1}{2}$ or 2 volts
M, 0–1 milliammeter
R_1, 50,000 ohm potentiometer
R_3, 300 megohms
S, SPDT switch
T, 6SK7
V, 0–50 voltmeter
R_2, 2500 ohm calibrated potentiometer.

The data plotted in Figs. 2 and 3 show that the 6SK7 is logarithmic over a more extended range than the 6SG7; as a result it was decided to investigate the properties of the former in an inverted circuit. Figure 4 is a diagram of the circuit used to determine the tube constants and characteristics of a 6SK7 connected up as an inverted triode; the screen and suppressor of the tube are connected directly to the plate. In an inverted tube circuit the signal is applied to the plate, which acts as the grid, and the output current is drawn from the grid element, which in this case acts as the plate; consequently to avoid unnecessary confusion we shall speak hereafter only of input voltage and current, denoted by e_s and i_s, and of output current, denoted by i_0.

The results desired from this circuit are the reverse of the conditions expressed by Eq. (1). We can express this desired result by:

$$\log k_0 i_0 = k_1 e_s \tag{2}$$

or, in terms of the antilogarithm of the input,

$$k_0 i_0 = \text{antilog} k_1 e_s, \tag{3}$$

where k_0 and k_1 are simply constants of proportionality.

TABLE I.*

	B_2 of Fig. 4 = $1\frac{1}{2}$ volts		B_2 of Fig. 4 = 2 volts	
e_s	R_2 = 500Ω I_0 in milliamps	R_2 = 1000Ω I_0 in milliamps	R_2 = 500Ω I_0 in milliamps	R_2 = 1000Ω I_0 in milliamps
−8.3	—	0.780	—	—
−9.6	1.042	0.747	—	1.000
−14.8	0.861	0.638	—	0.873
−20.3	0.704	0.533	—	0.753
−23.0	0.638	0.485	0.925	0.695
−25.8	0.578	0.445	0.845	0.647
−28.7	0.519	0.405	0.767	0.598
−30.2	0.492	0.388	0.730	0.573
−36.0	0.401	0.323	0.615	0.492
−41.9	0.335	0.273	0.518	0.425

* The values in each column above are again the average values of five non-consecutive check runs.

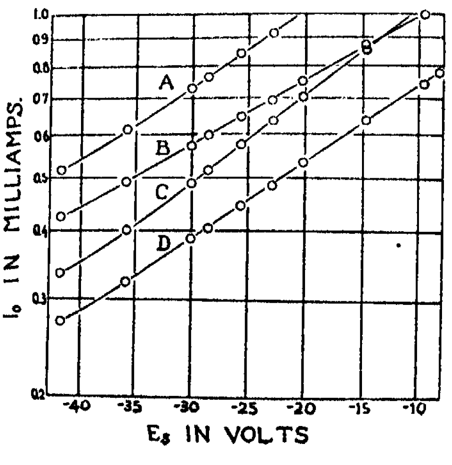

FIG. 5. i_0-e_s characteristic of the inverted 6SK7.

A, B_2=2 v., R_2= 500 ohms
B, B_2=2 v., R_2=1000 ohms
C, B_2=$1\frac{1}{2}$ v., R_2= 500 ohms
D, B_2=$1\frac{1}{2}$ v., R_2=1000 ohms.

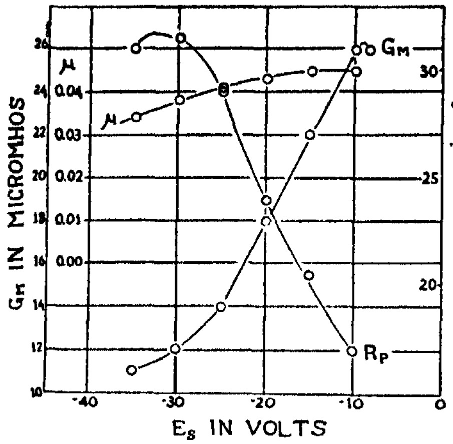

FIG. 6. $G_m-R_p-\mu$-characteristics of the inverted 6SK7.

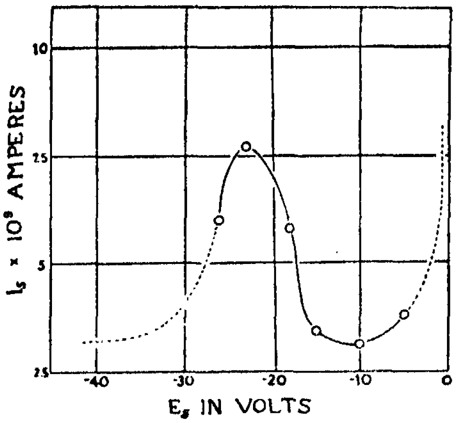

FIG. 7. Input current (L_s) curve for the inverted 6SK7.

The input voltage, e_s, was now varied by means of the potentiometer, R_1, its value being set with the aid of the voltmeter V. A 0-1 milliammeter was placed in the grid circuit for reading the output current. The output load was adjustable with the calibrated potentiometer R_2. Table I is a compilation of the output currents observed at the indicated grid supply voltages, input voltages and load resistances. Figure 5, the plot of these data, clearly shows that the logarithm of the output current is proportional to the input voltage, or conversely, that the output is proportional to the antilogarithm of the input. Thus the conditions of Eqs. (2) and (3) are satisfied, and the desired result achieved.

Similar results obtained with other 6SK7 tubes were equally satisfactory. The extent of the range of input voltages over which the i_0-e_s characteristic was antilogarithmic varied slightly; however, it was observed with all the tubes tested, that the plot of the data was antilogarithmic between input voltages of -18 to -30, when a load resistance of 1000 ohms was used. It was noted that tubes with metal envelopes were somewhat inferior to those with glass envelopes. If the data for the former type of envelope are rejected, the useful antilogarithmic range is extended to include all input voltages between -15 and -30, when a load resistor of 1000 ohms is used in the output circuit.

Figure 6 presents plots of the μ, g_m and r_p characteristics of the inverted 6SK7 as approximated from information available in the curves of Fig. 5. It is readily observed that μ and g_m are extremely low and that r_p is considerably less than the values obtained for a normal triode. However, these results are entirely normal for an inverted tube. It should also be kept in mind that these tube parameters are of secondary and rather irrelevant importance in this circuit since its primary function is to extract antilogarithms. The output of this circuit has been successfully amplified with a d.c. amplifier of conventional design. A useful output signal is then obtained. That amplification of the circuit output would be mandatory is obvious from the values for μ (*ca.* 0.04) and from the actual voltage amplification resulting in the circuit, which varied from about 0.011 to 0.027, depending upon the location on the input voltage axis. These values for voltage amplification correspond to an output load of 1000 ohms. It can also be seen from the results of Fig. 6 that the variable-μ characteristic of the 6SK7 is retained when the tube is inverted, μ changing by more than 25 percent over the range plotted.

The input currents are of more than usual interest in this circuit in view of the rather low output currents. Figure 7 is a plot of the input current *vs.* the input voltage when a load of 1000 ohms has been placed in the output circuit, and an output supply voltage of 1½ volts. These currents were measured in standard fashion by utilizing the drop across the 300 megohm resistor R_s of Fig. 4 when it was placed in the input circuit with the switch S. This voltage drop was derived from the curves of Fig. 5 by noting the output currents on the meter M, both with the 300 megohm resistor in the circuit, and again with this resistor bypassed. Knowing the resistance and the drop across the resistance, the input currents are then easily calculated.

A simple circuit for the extraction of antilogarithms has thus been presented along with a few of its more important characteristics. It is hoped that many applications will be found for this circuit, and that it will prove of definite benefit to the instrument designer.

ACKNOWLEDGMENT

The authors wish to acknowledge the helpful suggestions given them by Dr. R. H. Müller and the encouragement extended them by Dr. L. T. Hallett during the work leading to the results reported upon here.

THE REVIEW OF SCIENTIFIC INSTRUMENTS VOLUME 21, NUMBER 2 FEBRUARY, 1950

Magnetic Suspension for Small Rotors*

J. W. Beams
University of Virginia, Charlottesville, Virginia

(Received November 15, 1949)

A magnetic suspension for small rotors has been developed which employs scattered light to regulate the vertical height of the rotor. Upon entering a horizontal beam of light the rotor scatters or reflects light into a photo-electron multiplier cell. This cell actuates an electronic circuit which in turn regulates the current through the supporting solenoid in such a way as to maintain the ferromagnetic rotor at the desired vertical position. Rotors with diameters down to 0.004″ have been stably supported. A $\frac{1}{64}$″ rotor was spun to an estimated speed of 800,000 r.p.s. which gave a centrifugal field in excess of one-half billion times gravity. Besides providing a support for rotors, the apparatus may be used as an analytical balance for weighing materials inside a vacuum chamber. It detects changes in mass of from 10^{-8} to 10^{-9} gram. Other uses also are indicated.

IN order to produce high centrifugal fields it is necessary to use as small rotors as possible. This results from the fact that for a homogeneous elastic rotor of a given shape the bursting speed depends upon the square of the peripheral speed and is independent of the radius. In other words, for a given shape of rotor made of an elastic material $v^2 = w^2r^2 = K$ where w is the angular velocity, r is the radius of the rotor, v is the maximum peripheral speed and K is a constant. Consequently, the maximum centrifugal field $w^2r = K/r$ and thus increases as r becomes smaller.

In previous reports methods of spinning rotors of various diameters to their bursting speeds have been described.[1] The rotors were suspended in a vacuum by an axial magnetic field and spun by a rotating magnetic field. In this method the vertical stability of the rotor is maintained by the effect of the rotor on the impedance of a small "pick-up" coil placed below or above the rotor and connected in the grid circuit of a high frequency oscillator which in turn regulates the current through the supporting solenoid. As the rotor moves upward or downward, the current through the supporting solenoid is automatically decreased or increased respectively by the proper amount to maintain the rotor at the desired vertical position. Such a magnetic suspension is extremely stable and in practice has a resistance to rotation much smaller than the air friction on the rotor even when the air surrounding the rotor is at a pressure the order of 10^{-6} mm of Hg. However, when the size of the rotor becomes very small (below 0.02″ in diameter) the effect of the rotor on the impedance of the pick-up coil is reduced and consequently the adjustments of the circuits required to maintain vertical stability of the rotor become increasingly difficult. In this paper a magnetic suspension is described in which the vertical height of the rotor is determined by the amount of light scattered by the rotor into a photoelectric "pick-up". With this arrangement much smaller rotors can be suspended and spun than with the previous method.

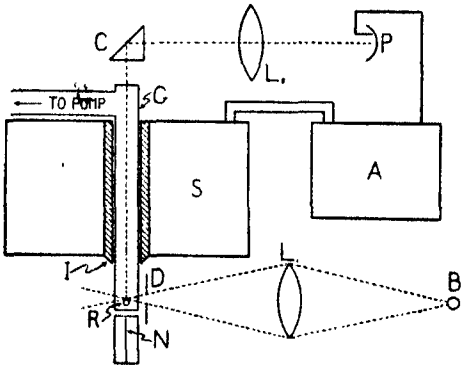

Fig. 1.

Figure 1 shows a schematic diagram (not to scale) of the method. The rotor R is surrounded by an evacuated glass tube G which is mounted coaxially with the supporting solenoid S. Light from a lamp B with a straight incandescent filament perpendicular to the page is brought to focus by a moderately long focus lens L_1 along a diameter of the glass tube in such a way that a thin horizontal beam or sheet of light crosses the glass tube. As the rotor R is pulled upward by the magnetic field of the solenoid S, it enters the light beam and scatters or diffusely reflects light upward through the glass tube, right angle prism C and lens L_2, which concentrates the light on the photo-electron multiplier cell P.

The current signal in P is amplified by the electronic circuit A and made to regulate the current through the solenoid S. When properly adjusted the current in S is automatically regulated so that the vertical position of the rotor remains constant. The horizontal stability is of course provided by the axial magnetic field of the supporting solenoid. A small iron wire N surrounded by a damping fluid and placed below and outside the vacuum chamber G served to damp out any horizontal motion of the rotor.

The solenoid S consisted of 23,000 turns of No. 28 copper wire wound on an insulated Bakelite frame. Its resistance is approximately 1300 ohms and its inductance with the iron core B is about 30 henrys. The iron

---

* This work was supported by the Bureau of Ordinance, U. S. Navy, under Contract NOrd 7873.

[1] Beams, Young, and Moore, J. App. Phys. 17, 886 (1946). See J. W. Beams, Wash. Acad. Sci. 37, 221 (1947) for other references.

core is a cold rolled steel tube 4 inches long, 0.5 inch internal diameter, and 0.1 inch wall thickness. In the first experiments, it had a very narrow vertical slit to prevent eddy currents but this was later found unnecessary. In most of the experiments the current through the solenoid varied from 30 to 70 milliamperes depending upon the size and desired position of the rotor. It was found that the number of turns in the solenoid is not critical, as several different solenoids with varying numbers of turns, resistances and inductances were used successfully. In most of the experiments 500 to 1500 ohms resistance was placed in series with the solenoid described above.

In the majority of the experiments a 1P28 photo-electron multiplier tube was used at P to pick up the light signal although both 931A and 1P21 tubes were used successfully. With most of the circuits used it was an advantage to select photo-multiplier tubes with as low a dark current as possible. Also for the smallest rotors it was found desirable, although not necessary to keep the tube at dry ice temperature in order to maintain the "noise" or current fluctuations at a minimum.

Figure 2 is a diagram of an electronic circuit (A. Fig. 1) which has operated very satisfactorily for long periods of time without adjustment. Also it has been used for supporting rotors over a wide range of sizes and weights. It is composed of ordinary standard parts and is easy to adjust. The signal from the photo-electron multiplier cell P is first amplified by T_1 (6J5) and then applied to the grid of the cathode follower T_2 (6J5) which, in addition to reproducing the signal, generates a derivative of the signal. The signal which occurs across R_7 is applied to the grid of T_4 (6SJ7) while its derivative produced by the circuit R_8C_2 is applied to T_3 (6SJ7) in parallel with T_4. The two signals are mixed and applied to the grid of T_5 (6J5) which is a second cathode follower and then on to the grid of the power tube T_6 (6L6) which regulates the current through the solenoid. The resistance capacity combination $R_{11}C_5$ is not necessary although it makes possible somewhat easier adjustments. The resistances R_8, R_{11} and R_2 and the capacities C_2 and C_5 should be variable in order to facilitate adjustment. The filaments of T_2 and T_5 were each heated by separate insulated storage batteries.

It will be observed that as the rotor rises into the light beam the scattered light falling on P is increased and the current through the supporting solenoid consequently decreased. As a result the rotor falls and scatters less light into P which in turn increases the current through the supporting solenoid S and raises the rotor. Clearly this would give rise to oscillations were it not for the derivative signal generated by the C_2R_8 combination. The phase of this derivative signal is adjusted to be from 70° to 90° out of phase with that of the original signal and hence damps the oscillations. When this adjustment is made properly no vertical motion of the rotor is observable even through a microscope focused on scratches on the rotor. The values given in Fig. 2 were for supporting a 15-mil steel spherical rotor about 1.45 cm below the end of the tubular iron core, but they are not critical with rotor size.

The support circuit (Fig. 2) was found to operate just as satisfactorily with the first stage of amplification T_1 removed. This, of course changes the phase relations so that as the rotor moves out of the light beam the current through the supporting solenoid is decreased and *vice versa* so that the rotor is positioned on the top edge of the light beam rather than on the bottom edge as in the case of the first arrangement. With the first amplification stage out of the circuit it is necessary to increase the signal by increasing the resistance R_3 or the potential on P or both. In practice it is usually found more convenient to use the whole circuit as shown in Fig. 2.

The rotor was spun by a rotating magnetic field produced by an alternating current in two pairs of coils (not shown in Fig. 1) surrounding the rotor but outside the glass vacuum chamber. The frequency of the rotating magnetic field or the a.c. current in the coils is set equal to the desired running speed of the rotor and is controlled piezoelectrically. The rotor is accelerated in a way similar to that of an armature of an induction motor. It should be noted that although the "slip" is large, the comparatively high electrical resistance of the steel rotor gives a satisfactory starting and accelerating torque. It has been shown previously[1] that the frictional drag on a spinning rotor supported magnetically in a high vacuum is so small that the rotor accelerates to speed as an induction motor and then "locks in" and spins in synchronism with the rotating magnetic field without hunting. Except for the piezoelectric control, the driving circuit is similar to that used previously. The power supplied to the coils is about 10 watts and it is necessary to cool them with air circulated by an electrically driven blower. The acceleration of the rotor varied with the size of the rotor but it usually took several hours to bring the rotors up to full speed. The temperature of the rotors was a few degrees above room temperature.

The rotor speed was measured by a photoelectric pick-up for rotor diameters of 20 mils and above. For rotors below 20 mils in diameter no satisfactory direct method has been found for measuring the highest rotor speeds so they must be estimated by indirect methods. However, in all of the experiments if the rotors are accelerated for a long enough period they will "lock in" and spin in synchronism with the rotating magnetic field so that the maximum speeds of the smaller rotors are determined by the respective frequencies of the driving circuits which of course are determined quite accurately by a frequency meter calibrated against W.W.V. With a 1/64-inch diameter steel spherical rotor kindly furnished by Mr. W. S. Pierce, Jr., Miniature Precision Bearing Company, estimated rotor speeds of 800,000 r.p.s. were obtained without exploding the rotor. This gives a centrifugal field on the periphery of over a half-billion time gravity.

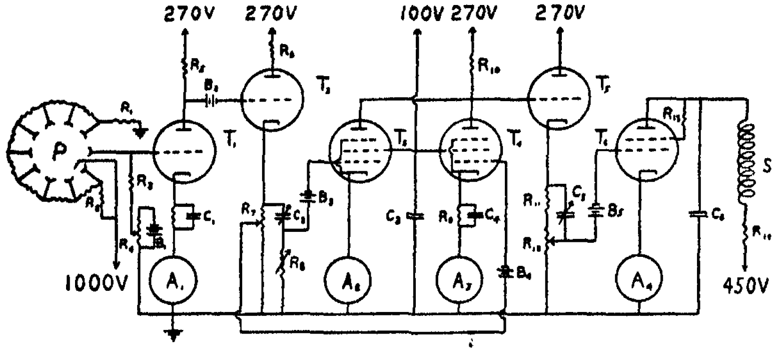

FIG. 2.

$R_1=R_2=R_4=R_7=10^6$ ohms
$R_3=10^8$ ohms
$R_5=2\times10^5$ ohms
$R_6=10^3$ ohms
$R_8=5\times10^4$ ohms max.
$R_{10}=2.7\times10^5$ ohms
$R_{11}=5\times10^4$ ohms max.
$R_{12}=3\times10^4$ ohms max.
$R_{13}=2\times10^4$ ohms
$R_{14}=1500$ ohms max.
$T_1-T_2-T_5-6J5$
T_3-T_4-6SJ7
T_6-6L6

$B_1=2.1$ v
$B_2=135-225$ v (variable)
$B_3=4.6$ v
$B_4=10$ v
$B_5=45-135$ v (variable)
$C_1=C_4=C_6=0.1$ mf
$C_2=0.03-0.1$ mf
$C_3=0.3$ mf
$C_5=0.03-0.15$ mf
$S=30$ h and 1300 ohms

As the diameter of the rotor is reduced below about 20 mils, it becomes more difficult to adjust the damping needle *N* (Fig. 1). The diameter of the steel or alloy needle *N* is made smaller than the rotor and usually is surrounded by water. So far, the requisite damping has been obtained by a tedious process of trial and error. It should be noted that any sudden vertical motion of a rapidly spinning rotor may set it into horizontal oscillation especially if the axis of the magnetic field is not exactly vertical so the power supplies to the electronic circuits must be well stabilized and the spinning rotor should be kept free of vertical motion.

The distance of the rotor below the core of the solenoid varies with the size of the rotor and shape of the core. For rotors below $\frac{1}{8}$ inch in diameter, a satisfactory working distance with the solenoid described above is about 1.5 cm. It will be observed that for rotors with dimensions small in comparison to their distances below the solenoid core, the force F on the rotor is approximately $M(dH/dX)$ where H is the magnetic field, X the distance along the axis of the field, and M the magnetic moment induced in the rotor by the field H. For soft iron (but not necessarily for hard steel) M is roughly proportional to μH so the lifting force $F\propto \mu H(dH/dX)$ where μ is the permeability of the rotor material. Consequently the proper rotor distance below the solenoid is determined by the shape and intensity of the magnetic field and may be varied over considerable ranges.

RESULTS

As mentioned previously the apparatus described in this paper was developed primarily for obtaining high centrifugal fields for use in a number of different studies. So far a series of experiments have been carried out on the bursting speeds of steel spherical rotors of different diameters. These results show that for the particular steel used, the maximum peripheral velocity obtained was approximately the same (10^5 cm/sec.) for all sizes of rotors tried. However, the probability that a given rotor would reach maximum peripheral speed increased markedly as the diameter of the rotor decreased. The explanation of this seems to be that as the rotor diameter is decreased the amount of material around the center of the rotor which is under maximum stress is decreased and consequently the probability of finding a flaw or crack in the stressed part of the smaller rotor is decreased.

Observations also have been made on the centrifugal fields necessary to pull films off of the periphery of the rotor. Since the thickness and density of the films are known the forces on the films can be calculated. In the highest centrifugal fields some of the "trash" laid down on the surface during the polishing process apparently was thrown off although further observations must be made before this can definitely be established. Attempts to use the apparatus for the study of possible molecular orientations by centrifugal fields also are in progress.

In one of the experiments a very narrow slit was placed at *D* in Fig. 1 in order to cut down as much light background as possible. However, in addition to cutting down the background it gave rise to a diffraction pattern the result of which was to give in effect a slow increase of light intensity as the beam was approached from the bottom or top. A 1/64-inch rotor was carefully supported in the lower region of the light beam. The pumps were then started and the system quickly evacuated to less than 10^{-6} mm of Hg. During this evacuation, the rotor was observed through a 30-power microscope and found that its height was considerably decreased. This was repeated several times and traced to the buoyancy of the air. The volume of the rotor was 3.36×10^{-5} cm^3 and its weight 2.6×10^{-4} gram. Further experiments were then carried out to determine the sensitivity of this balance and it was found that between 10^{-8} and 10^{-9} gram change in weight could be observed. Clearly this observation indicates that with the proper design the apparatus may be used as a most sensitive balance. Magnetic suspension balances have been used previously[2] but the present method affords much greater sensitivity and stability and the weighing can be carried out in vacuum, i.e., during a chemical reaction on surfaces, for osmotic pressure measurements, etc. A more detailed description of this application will be described later.

The lower limit to the diameter of rotor that can be supported by the above apparatus has not as yet been reached. The smallest rotor so far used was about 4 mils in diameter.

The writer wishes to express his appreciation and indebtedness to Mr. J. Dillon and Mr. W. Lucke for help with the electronic circuit.

---

[2] John W. Clark, Rev. Sci. Inst. 18, 915 (1948).

THE REVIEW OF SCIENTIFIC INSTRUMENTS VOLUME 21, NUMBER 2 FEBRUARY, 1950

Physical Instruments for the Biologist

Detlev W. Bronk
Associate Editor in Charge of this Section
Johns Hopkins University, Baltimore, Maryland

On Adapting a Powder X-Ray Diffraction Camera for Reflection Patterns

Jonathan Parsons
Edsel B. Ford Institute for Medical Research, Detroit, Michigan

(Received October 12, 1949)

A method is described by which a commercial x-ray diffraction powder camera, designed to take rod or tubular mounts, may be easily adapted to accommodate small, flat mounts. Provision is made to change the customary continuous rotation to that of 10° rotary oscillation. A diffraction pattern of the core of a large renal calculus is shown as being illustrative of the patterns obtained from this modified camera.

SOME powder x-ray diffraction cameras are available commercially which will take reflection patterns from fairly large slabs of material as well as the usual powder diagrams. Others like the North American Philips 114.59-mm camera are designed solely for use with powdered specimens. It has been found possible to adapt the Philips camera[1] fairly easily for use with flat samples without interfering in any way with its accurate and efficient use in powder studies. The parts required can be made without recourse to an expensive machine shop. Flat sections of bone, renal calculi, teeth, and other substances may be studied by the method and their surfaces "mapped" analytically with the adapted camera which may be returned in several minutes to its original state for powder studies.

To adapt this camera for use with flat samples, four modifications in design are required: (1) A sample platform to support flat samples with their surfaces on the axis of rotation, (2) rotary-sample oscillator to replace continuous rotation, (3) a smaller pinhole insert to fit the sample end of the collimating tube snugly, and (4) a lead-lined cap to replace the regular beam-receiving tube.

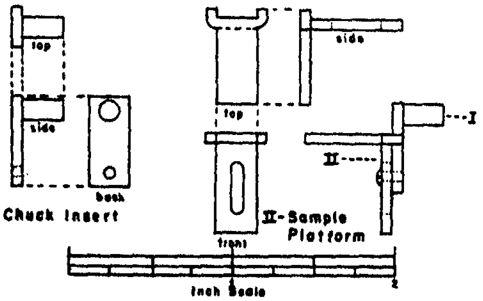

FIG. 1. Specimen mount.

A flat specimen mount has been constructed according to the details shown in Fig. 1. This mount consists of a chuck insert and a sample platform which are clamped together by a screw. The rod end of this unit fits into the camera chuck in place of the standard brass specimen rod. In use a flat sample is attached to the platform, which is then adjusted by means of the screw so that the axis of oscillatory motion is tangent to the surface of the sample. The assembly detailed in Fig. 1 will accommodate samples up to $\frac{1}{4}$ inch in thickness. Thicker samples could be mounted if the arm of the chuck insert were lengthened and one or more threaded holes added.

The rotation axis of the powder camera is given an oscillatory motion of 10° by means of a heart-shaped cam and follower-arm, constructed to fit over the regular motor and camera axis pulleys, respectively.

FIG. 2.

---

[1] W. Parrish and E. Cisney, "An improved x-ray diffraction camera," Philips Tech. Rev. 10, 157–167 (1948).

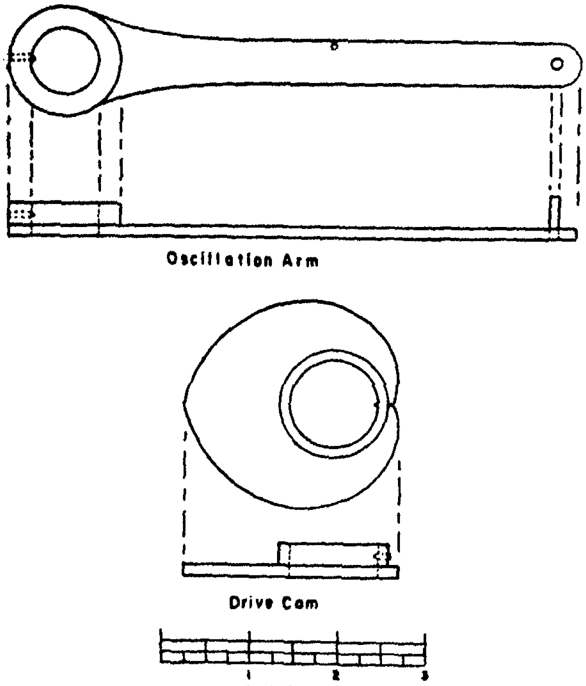

FIG. 3. Oscillation attachment.

Figure 2 is a photograph of the completed assembly and Fig. 3 is a scale drawing of the oscillation arm and drive cam. The cam and arm are secured to these pulleys by Allen head screws. A tension spring holds the arm against the cam as the latter rotates. The shape of the cam was determined empirically to give a uniform oscillatory motion of 10° to the specimen mount.

Since the x-ray beam strikes the sample at an oblique incident angle, the area irradiated is considerably larger than the beam cross section. To reduce the size of this area and increase line resolution, a brass insert has been made for the small end of the collimating tube. This insert is 4 mm long, has a bore of 0.013 in. on the inner end and a guard bore of about 0.016 in. at the sample end. A flange prevents this insert from being pushed too far into the end of the collimating tube.

The oscillation range of a flat sample must be as low as possible in order to keep the blocking of low Bragg angle lines to a minimum. However, this oscillation range should not be set so low that the area upon the sample becomes elongated more than twice the beam diameter. Oscillation ranges of from 15° to 25° without this insert have been used. In order to register low Bragg angle lines a tube with a long K_α wave-length target material should be used.

A diffraction pattern obtained by reflection is single. This necessitates mounting the sample so as to reflect downward, since the film must be loaded into this type of camera with its continuous surface at the bottom.

A further consequence of the one-sided diffraction of flat samples is that a different method must be used to obtain the position at which the direct beam strikes the film. A lead-lined cap has been substituted for the regular beam-receiving tube. By using such a cap it is not necessary to punch the film on the receiving tube side. At the end of each exposure the camera is opened, with only safe light illumination, and the specimen mount removed. The x-ray beam is turned on at low voltage and tube current for a fraction of a second, in order to register the direct beam position.

A pattern shown in Fig. 4, which was obtained with the camera adapted as described, was taken from the core of a large renal calculus. The flat surface was obtained by bisecting the stone with a fine jewelers' saw. Upon analysis of this pattern calcium oxalate proved to be the principal constituent.

FIG. 4. Pattern of renal calculus core.

By using this special sample mount with its oscillatory axis motion it is possible to analyze selectively small inclusions or narrow layers in sample surfaces without altering their crystalline arrangements. Information about possible orientations in the structure may also be obtained. This method is not as easy to use as the straight powder analysis but when used in conjunction with the latter, additional information about the crystalline nature of the sample, particularly about the variations in composition through the volume of the substance, is often found.

Laboratory and Shop Notes

An Experimental KVAH-Meter

G. M. Petropoulos
National Technical University, Athens, Greece

November 28, 1949

PRINCIPLE.—Figure 1 shows the principle of the KVAH-meter. The voltage of the a.c. circuit is rectified[1] by a suitable metal rectifier and then smoothed by an electrolytic condenser. The current flowing through the pressure circuit of the d.c. KWH-meter is thus quite proportional to the a.c. circuit voltage. The primary of a transformer is installed in series to the a.c. circuit. Its core has an air-gap in order to secure an approximately constant inductance. The voltage induced in the secondary, which contains a considerable number of turns, is rectified and smoothed as in the case of the voltage circuit. The d.c. thus obtained is passed through suitable windings installed in the place of the current coils of the d.c. KWH-meter.

The ripple of the unidirectional currents passing through the meter elements can easily be smoothed to a value of the order of 5 percent. Thus, the torque produced by the alternative components of these currents will not exceed 0.25 percent of the torque due to the product of the d.c. components. Consequently, the dependence of the meter constant (rev./KVAH) from the a.c. circuit power factor will be practically negligible.

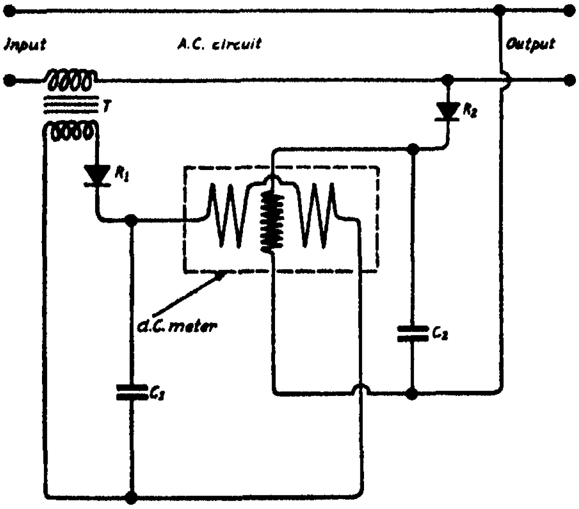

FIG. 1. Principle diagram of the KVAH-meter.

Application.—A single-phase KVAH-meter has been arranged in accordance to the above principle with the following data. The current coils of a motot type, 10A, 110-v d.c. meter have been replaced by two coils with 8500 turns each, of 0.15-mm enameled copper wire. The resistance of both coils in series was 3750 ohms and the total resistance of the potential circuit of the meter, 5800 ohms. The original d.c. meter constant was 2850 rev./KWH.

Each of the rectifiers of Fig. 1 consisted of 30 elements of the selenium type, 18 mm in diameter. Non-conductive and conductive resistances were, as measured under working conditions through a C.R.O., about 0.5 megohm and 1300 ohms respectively. Each smoothing capacitor consisted of three 40-μF, 150-v electrolytic condensers in parallel.

The core and the arrangement of the windings of the transformer (T) are shown in Fig. 2. The primary, wound over the secondary, consisted of 16 turns, 1.5 mm in diameter cotton insulated copper wire. The secondary had 4000 turns of 0.25-mm enameled copper wire. A 0.51-μF condenser was connected across the secondary, causing an increase of the secondary voltage, due to the leakage reactance of the windings.

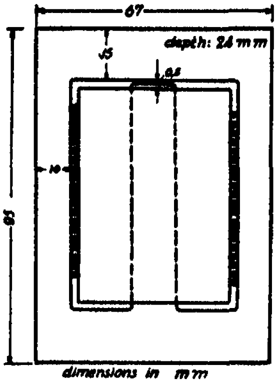

FIG. 2. Core and windings of the transformer.

Figure 3 shows the results finally obtained in trying to secure linearity[2] between the current of the a.c. circuit and the d.c. voltage across the final current coils of the meter. The ripple of the d.c. voltages across the coils in question and the voltage circuit of the meter was, as measured through a C.R.O. under full load, less than 2.5 percent of the d.c. components.

Results.—The KVAH-meter described above has been tested with a rotary meter testing set at 220 v. The results obtained are given in Fig. 4 and seem to be quite satisfactory. The values of the meter constant at 0.1, 0.5, and unity power factor are very closely together so that the performance under these conditions is represented by the common curve. The meter constant is roughly 1000 rev./KVAH at full load, i.e., about one-third of the original constant of the d.c. meter (2850 rev./KWH). It may be concluded that if the adaptation of the d.c. meter was carried out so as to bring the number of revolutions per KVAH closer to its original constant, the faults under small loads would be comparable to the normal d.c. meter faults.

Practical considerations.—In the case of a symmetrical three-phase load, an adequately adapted single-phase meter would be able to measure the number of KVAH consumed. For an unbalanced three-phase load, the meter should have a special design: as the voltages are about the same in all three phases, the potential circuit of the meter could be connected, after rectification and

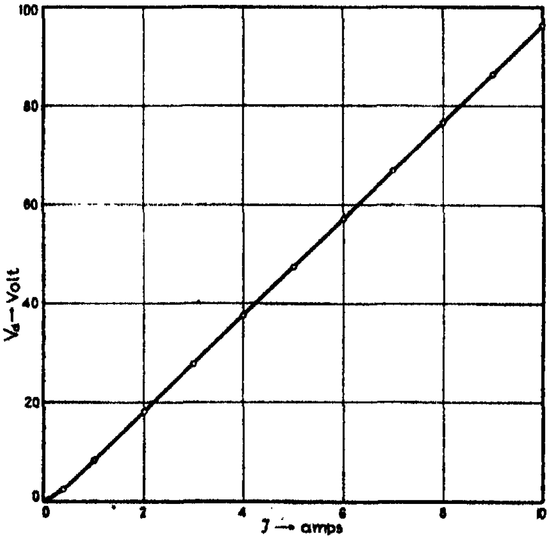

FIG. 3. Current circuit characteristics.

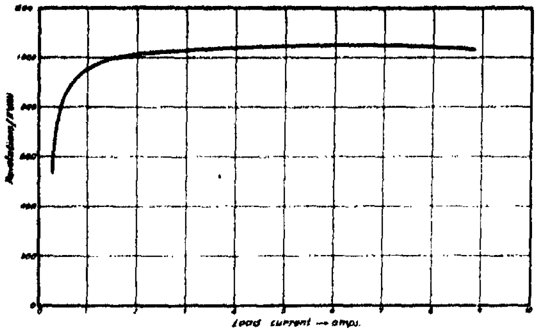

FIG. 4. Meter characteristics at 220 volts a.c.

smoothing, across any one pair of line conductors. Due to the differences in the line currents, three separate current circuits had to be used, each supplying one-third of a triple winding occupying symmetrically the space provided for the two current coils of the d.c. meter.

Regarding the stability of the KVAH-meter described, one can object to the use of metal rectifiers. They suffer, as it is well known, from a resistance variation due to aging. This would result in a slow variation of the meter constant with time. However, modern metal rectifiers seem to maintain their characteristics over long periods without any appreciable variation. Another question arises in connection with the considerable temperature coefficient of the rectifiers. As this coefficient is negative, a temperature compensation of the total circuit seems practicable.

In presenting the above results, the author is not suggesting a device ready for practical use. However, a further investigation as regards the stability of its performance, which seems to be a question of metal rectifiers construction, may lead to a possibly cheap solution of the KVAH-meter problem.

Acknowledgment.—The author expresses his best thanks to Messrs. Ferranti Ltd., Hollinwood, England, for valuable information.

[1] A KVAH-meter using rectification is described in the British Patent Specification 357,347. Its principle is substantially different, due to the lack of a smoothing device and of an air-gap in the transformer core. In order to reduce power factor influence, the single-phase meter described in the patent should have at least two potential circuits, out of phase.

[2] The design of a device transforming an a.c. into a proportional d.c. has been the subject for the Mech. and Elec. Engineering degree thesis, of Miss. D. Kokkinou.

Simple Low Power Electronic Relay

WILLIAM P. RATCHFORD AND M. L. FEIN
*Eastern Regional Research Laboratory, Philadelphia, Pennsylvania**
November 28, 1949

THE recent note of Linnel and Haendler[1] describing a simple thermostat relay in which an *FG* 57 thyratron controlled several hundred watts prompts us to describe a similar inexpensive low power circuit (Fig. 1), which we have used for about a year with a precision manostat.[2] This relay used a 2050 thyratron.

In order that the signal grid shall remain in control when the anode is positive, terminal (2) of the secondary must be 180° out of phase with terminal (1) of the primary. This is conveniently determined by trial after the relay has been assembled. If the tube fires continuously, the leads from the secondary should be reversed.

The relay has satisfactorily operated the air inlet valve of the manostat; L is the 750-ohm solenoid of the valve. When an increase in pressure closes the regulator contacts, the filament voltage is applied across R_1 and is thus impressed on the signal grid out of phase with the anode voltage. The tube does not fire, and the air inlet closes. When the pressure falls and opens the contacts, the signal grid is no longer biased to cut-off and loses control. The tube fires and energizes the solenoid, thus opening the air inlet, and the cycle repeats. R_2 limits grid current.

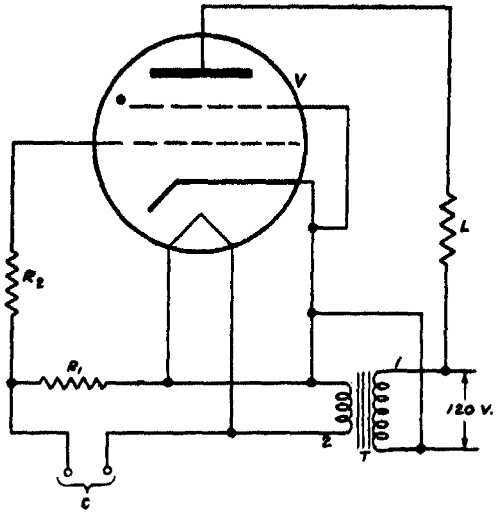

FIG. 1. Low power relay. $T=6.3$ volt a.c. 1 amp. $R_1-R_2=1$ megohm, 1 watt. $V=2050$ thyratron. $L=750$–800 ohm solenoid. C = connection to regulator.

Although suitable for controlling only low power (10 watts or less), the relay has replaced a commercial unit costing five times as much.

We wish to thank Dr. C. R. Eddy of this Laboratory for helpful suggestions.

* One of the Laboratories of the Bureau of Agricultural and Industrial Chemistry, Agricultural Research Administration, United States Department of Agriculture.

[1] R. H. Linnel and H. M. Haendler, Rev. Sci. Inst. 20, 364 (1949).

[2] W. P. Ratchford and M. L. Fein (to be published).

Point-Focus X-Ray Monochromators for Low Angle Diffraction

JESSE W. M. DUMOND
California Institute of Technology, Pasadena, California
November 21, 1949

GUINIER[1] has applied the principle of the reflection type curved crystal focusing *x*-ray monochromator[2] to improve both intensity and angular resolution in low angle *x*-ray diffraction studies. In Guinier's method, a thin sample is placed in the convergent monochromatic *x*-ray beam and the low angle diffrac-

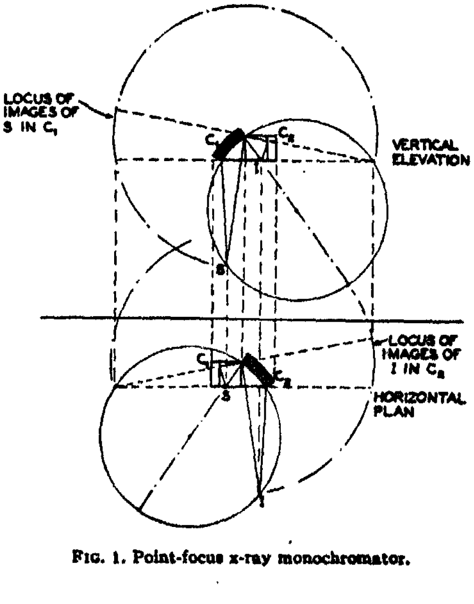

FIG. 1. Point-focus x-ray monochromator.

tion pattern is formed as a diffuse distribution symmetrically disposed on either side of the central primary line focused by the crystal.

An x-ray monochromator capable of forming a beam converging to a *point* focus would have the following important advantages. (1) The scattered intensity incident in the focal plane would be increased (relative to the line focus monochromator) in the ratio of the feasible line height to the line width, perhaps several hundred fold. (2) The awkward and complicated analytical procedure[3] for transforming the line focus diffraction pattern distribution into the point focus distribution would be completely avoided. (3) In the case of the two crystal monochromator described below, the residual factor limiting the sensitivity of the method, namely the background fog from incoherent scattering of the continuous x-ray spectrum incident on the first crystal, would be greatly reduced because practically only monochromatic radiation reaches the second crystal.

The type illustrated in Fig. 1 can be made of two monocrystalline quartz lamina cut to a cylindrical shape in the unstressed state, the concave surface being of radius R. The lamina should be cut so that the (310) planes ($d \cong 1A$) are parallel to the plane tangent to the cylinder *at one end of the cylindrical arc*. The lamina must then be elastically bent in a precisely profiled holder so that the surface which had radius R now has a radius $R/2$. This will fulfill the condition for monochromatization and exact focusing for all points on the cylindrical crystal arc. The full line circles are the loci of real focal points (both source and image) for each crystal. The foci shown are approximately those for Cu-K radiation. The dot-and-dash circles are the loci on which lie *the images of each focal point mirrored in the different (310) planes along the bent crystal arc*. The generators of the two cylindrical crystal surfaces *are mutually at right angles*. Thus, each crystal causes the final beam to converge in one of the two dimensions normal to its direction of propagation. Figure 1 shows the disposition of the components in both horizontal and vertical projection. The crystals are disposed so that the pertinent short arc of the dot-and-dash circle, on which the image of S (or I) lies, is in each case projected upon the plane of the other view approximately *as a point coincident with I (or S)*. The (thin) scattering sample is to be placed near the second crystal in the final doubly converging beam, and for best focusing, it should coincide nearly with the polar region of the surface of a sphere whose opposite pole is at the final focus of the beam.

In the second type of point-focusing monochromator illustrated in Fig. 2, use is made of a mica crystal which is bent by cementing it (under pressure with a rubber cushion) to the carefully figured concave surface of a metal block having two different principal radii of curvature, R_1 and R_2. The dot-and-dash line CC is the axis of rotation of the lathe in which such a concave surface is generated. It is easy to show that $R_2/R_1 = \sin^2\theta$ where θ is the Bragg angle. The figure shows the approximate geometry for monochromatizing fluorine K radiation from a fluoride target. The permissible crystal arc of radius R_1 is limited by a well-known aberration[4] but *for the production of a point focus*, there is no limit whatever to the extent of the arc of radius R_2 (about the axis CC). The arc may be a complete circle if convenient. To insure good homogeneity of scattering angle, however, it would be preferable to use the complete circle design only for a much shorter wave-length and smaller Bragg angle.

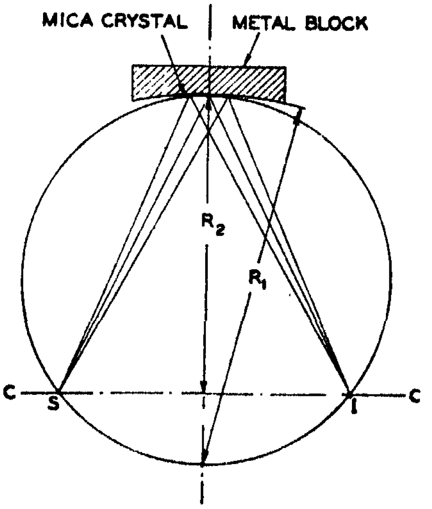

FIG. 2. Point-focusing x-ray monochromator.

The circularly symmetrical low angle diffraction patterns thus obtained could be studied very conveniently by direct G-M counter methods. To do this, an opaque concentric circular stop of *variable* radius r would be inserted in the pattern and the counter would measure the intensity associated with that part of the pattern *outside* the radius r.

[1] A. Guinier, Ann. de physique 12, 161 (1939).

[2] J. W. M. DuMond and H. A. Kirkpatrick, Rev. Sci. Inst. 1, 90 (1930), see Fig. 2.

[3] J. W. M. DuMond, Phys. Rev. 72, 83 (1947).

[4] J. W. M. DuMond, Rev. Sci. Inst. 18, 629 (1947), see Fig. 3.

Ultrasonic Tissue Disintegrator

F. F. BIRD AND K. S. LION
Laboratory of Applied Biophysics, Department of Biology, Massachusetts Institute of Technology, Cambridge, Massachusetts

December 8, 1949

THE ultrasonic disintegration of organic matter for electron microscopic and other investigations requires a high concentration of energy in the treated substance. This energy is frequently conveyed from a crystal transducer through an oil bath

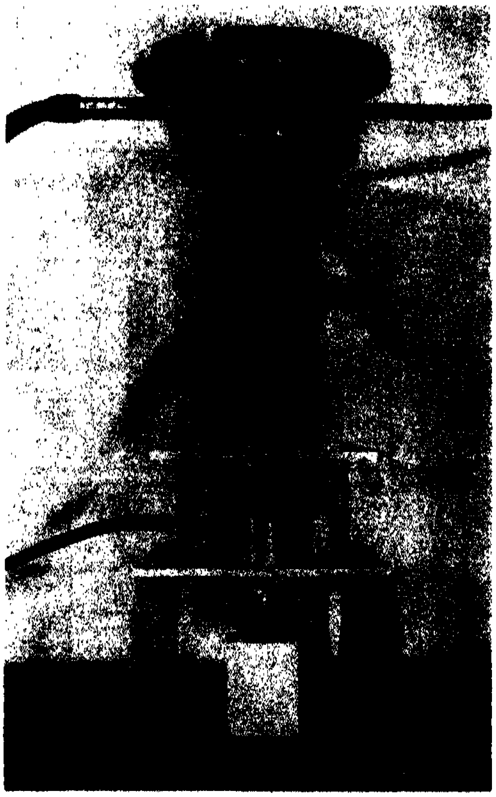

FIG. 1.

to the substance which is usually a suspension in a glass beaker. This often causes reflections and standing waves in the walls of the beaker so that the efficiency of the treatment is much reduced. Direct contact of the treated substance with the oscillating crystal surface is seldom possible because of the difficulty of cleaning and sterilizing these surfaces. Electrode surfaces on crystals, or bending membranes from magnetostrictive generators also tend to disintegrate so that metal particles are likely to get into the suspension.

These disadvantages are considerably reduced by using a method whereby an oscillating rod dips from above into the glass beaker filled with the suspension to be treated. Figures 1 and 2 show a Raytheon 10-kc magnetostrictive transducer adapted for this purpose. This transducer has a laminated nickel rod which drives a diaphragm acting as an impedance transformer. In normal use the diaphragm serves as the oscillating bottom of a container for the substance to be treated. For the above described purpose an aluminum rod is fastened in the center of the diaphragm, and the unit is mounted upside down. This requires a change of the water cooling duct as indicated in Fig. 2. The aluminum rod has never caused any trouble through disintegration, although for some special purposes it may be covered with glass.

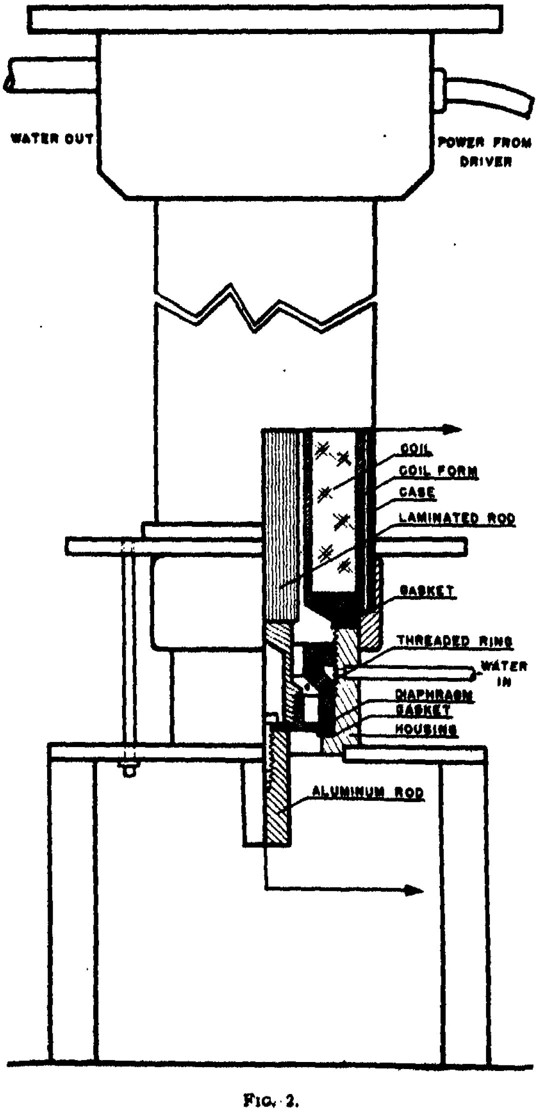

FIG. 2.

The instrument is mounted in the following way: First a quarter-inch hole is drilled through the center of the diaphragm. This is best done by grinding since the Stellite surface resists conventional drills. The aluminum rod is fastened to the diaphragm by a machine screw, and the laminated rod is screwed into place. The diaphragm and the rod are held in position in the brass housing by the threaded ring. Cooling water enters through the holes in the threaded ring, flows through the space between the laminated rod and the coil form and out the tube at the top of the coil. To bring pressure upon the gaskets the whole assembly is held between two aluminum plates which are connected by brass rods. An appropriate stand constructed of wood elevates the instrument so that a small sample in a beaker can be placed under the rod for treatment.

A Reprojection Method for Studying Cloud-Chamber Photographs

D. A. BROMLEY* AND R. D. BRADFIELD
Department of Physics, Queen's University, Kingston, Ontario, Canada

August 3, 1949

A SIMPLE reprojection system for use in studying stereoscopic cloud-chamber photographs has been assembled and used in this laboratory. Much more elaborate apparatus of this general type has been described elsewhere[1,2] but it is hoped that the relatively simple design described here will be of service to others.

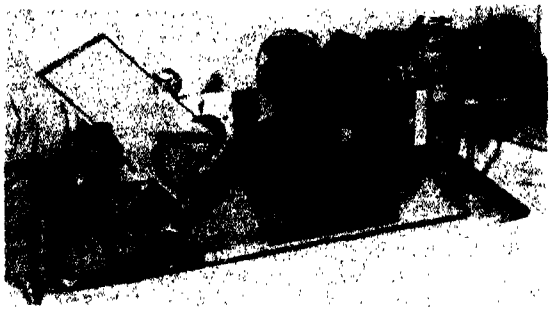

FIG. 1. The reprojection unit using the ground glass screen.

The stereoscopic photographs are obtained in the usual way, using two 35-mm cameras rigidly mounted on an aluminum casting. The films are automatically advanced for each exposure by small electric motors. A cam arrangement, driven from the film itself, opens the motor circuit and locks the film accurately in position.

Spring mounted Plexiglas windows were set into alternate backs for the cameras coincident with the position of the 35-mm frame during exposure in order to hold the film accurately in the focal plane of the lenses and permit reprojection.

The camera unit is removed from above the cloud chamber and is mounted with the optical axes horizontal as shown in Fig. 1.

Magnetic screen clamping devices have been used throughout for ease and speed of operation. A 15×12-inch section of boiler plate was machined and attached to the plywood base on which the entire unit is mounted. One side of the magnetic circuit of a 10-henry choke coil was removed, the resultant poles were machined to rest on the boiler plate, and to increase the stability of lead-weighted plate was fitted flush with the base of the magnet.

The screen shown in Fig. 1 consists of a 10×12-inch ground glass plate, free to rotate about a horizontal axis which in turn is fastened to, and moves with, the base. A second choke coil unit mounted over the screen axis and an iron disk armature fixed to the axis permit clamping at any angle. A graduated circle on the disk and a grid system ruled on the boiler plate are used to assign coordinates.

The screen assembly shown in Fig. 2 is considerably more flexible in use and consists of a 12-inch circular aluminum plate finished with white enamel on the working surface. A 3-inch mild steel hemisphere was attached rigidly to the screen with its center of curvature coincident with the center of the front surface of the screen and an iron-clad magnet was assembled to hold this screen in any position while permitting rotation in all directions. In order that the residual magnetism should be sufficient in itself to hole the screen in position the core was turned from mild steel. The 1¼-inch iron pipe which formed the external section of the magnetic circuit and the core face were turned to a spherical profile to match the screen hemisphere closely. The dimensions used are such that the screen can take any position outside of an approximately 30 cone about the support magnet. This magnet is mounted as shown, using a heavy aluminum frame. A selenium rectifier with a 0–130-volt d.c. continuously variable output is used to energize the holding coil.

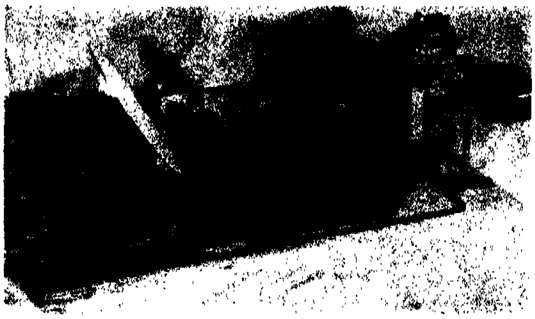

FIG. 2. The reprojection system using the disk screen. The selenium rectifier is shown in the background.

The films are rewound after processing in the cassettes and replaced in their respective cameras. For each frame the screen is moved to bring the images of the top and bottom of the chamber into coincidence and the distances from the film planes to the screen are checked against the original distances. This serves as a check on the film positioning. Angle and range measurements are made directly on the screen surface; when permanent records are desired, photographic paper is clipped to the screen and exposed.

To avoid distortion caused by the plate glass chamber roof a similar plate was inserted in the proper position between the screen and cameras during reprojection.

The writers wish to express their appreciation of Dr. J. A. Gray's helpful interest in this project.

---

* Holder of a National Research Council Scholarship and a Shell Oil Fellowship 1948–1949.

[1] Brueckner, Hartsough, Hayward, and Powell, Phys. Rev. 75, 557 (1949).

[2] Dee and Gilbert, Proc. Roy. Soc. A163, 265 (1937).

A Nomogram for G-M Counter Resolving-Time Corrections

HOWARD L. ANDREWS
Laboratory of Physical Biology, Experimental Biology and Medicine Institute, National Institutes of Health, Bethesda, Maryland

November 21, 1949

IT is well known that a G-M counter tube fails to respond to all primary ionizing events within it because of the finite time required to recover sensitivity after each discharge. Because of this recovery time an observed counting rate *n* will be lower than

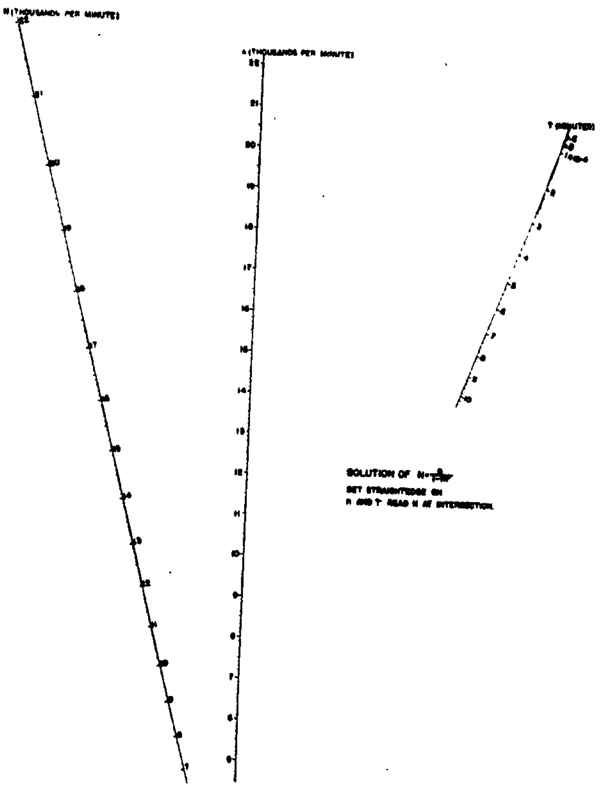

FIG. 1. Nomogram for determining resolving-time corrections.

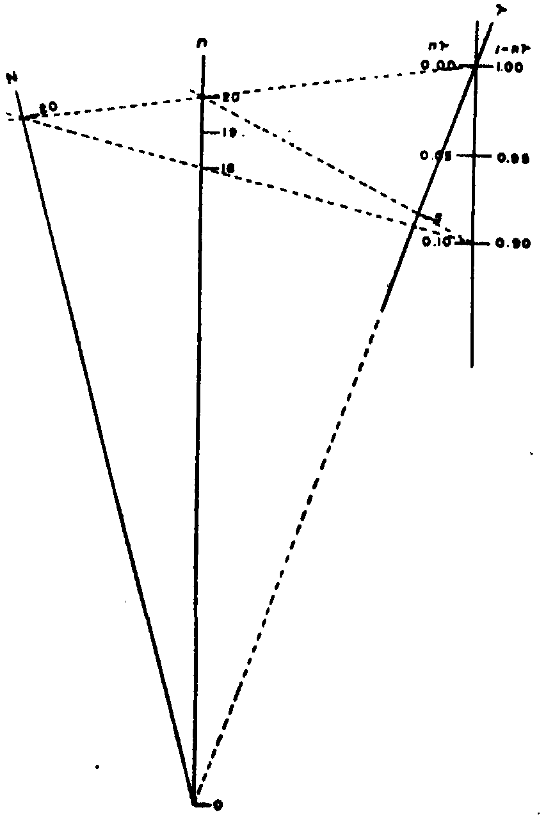

FIG. 2. Constructional details of nomogram.

the true counting rate N by an amount which increases with n. It can be shown[1] that

$$N = n/(1-n\tau), \tag{1}$$

where τ is the resolving time of the counter tube. τ is most usually determined by using two radioactive sources and determining the counting loss.[2]

When large numbers of observations must be corrected the time involved becomes appreciable and the possibility of computational errors is not negligible. The nomogram shown in Fig. 1 was devised to provide a solution of Eq. (1) which can be carried out rapidly and accurately by relatively untrained personnel.

To construct this nomogram the linear n scale is first laid off. The τ-scale is then drawn from the zero of the n scale at a convenient angle. At a convenient point on the τ-scale the auxiliary ($n\tau$) and ($1-n\tau$) scale is drawn parallel to the n scale and appropriate values are laid off linearly. Reasonable values of n and τ are chosen and $n\tau$ is computed. The non-linear τ-scale is now constructed by laying a straight edge across the chosen values of n and $n\tau$ and plotting values of τ at the intersection, Fig. 2. To determine the slope of the N scale two values of n and τ are so chosen as to yield the same value of N from (1). Then

$$\frac{n}{n'} = \frac{1-n\tau}{1-n'\tau'}. \tag{2}$$

Since the linear $n\tau$-scale is also a ($1-n\tau$) scale two lines can readily be drawn through the two chosen values of n and ($1-n\tau$). The intersection of these lines determines the N scale which must pass through the zero of the n scale. With the slope of the N scale determined the graduations are obtained by projecting the n scale using $n=0$ as a center.

The nomogram is based on two successive applications of the basic product-nomogram with non-logarithmic scales.[3] Reference to Fig. 2 shows that the n, τ, and $n\tau$-scales form the first product nomogram which will also give values of ($1-n\tau$). Equation (1) can obviously be solved by a simple product-nomogram formed with n, N, and ($1-n\tau$). If the ($1-n\tau$) scale is continued to zero the N scale extended will be found to intersect at this point and thus the basic requirement for the construction is fulfilled. Since given values of n and τ serve to determine both $n\tau$ and ($1-n\tau$) the ($1-n\tau$) scale is not required explicitly and a single straight edge application is sufficient to obtain N.

To determine the accuracy obtainable a series of 50 problems were computed by (1) and compared with the solutions obtained with the nomogram by a variety of personnel. The average error of 0.2 percent obtained with an 8 in.×10 in. reproduction includes both the errors of drawing and reading. This is quite adequate for correcting most counting data.

---

[1] R. E. Lapp and H. L. Andrews, *Nuclear Radiation Physics* (Prentice-Hall, Inc., New York, 1948), p. 235.

[2] A. E. Ruark and F. E. Brammer, Phys. Rev. **52**, 322 (1937).

[3] D. S. Davis, *Empirical Equations and Nomography* (McGraw-Hill Book Company, Inc., New York, 1943), p. 722.

New Instruments

W. A. Wildhack: Associate Editor
in Charge of this Section
National Bureau of Standards, Washington, D. C.

These descriptions are based on information supplied by the manufacturer in some cases from independent sources. THE REVIEW *assumes no responsibility for their correctness.*

D.C. Magnetic Amplifier

This amplifier, developed in London by Electro Methods Ltd., is designed for the amplification of small d.c. voltages in measurements work. The gain is constant to ±½ percent with a ±10 percent change in line voltage, and the zero drift over a period of several weeks is less than ±50 μv referred to the input terminals. Max. power gain—14,000; max. voltage gain—27; max. transconductance—5×10^6 micro-mhos; load resistance = 3 ohms; power line—117 v, 60 cycles; max. output current—300 ma.

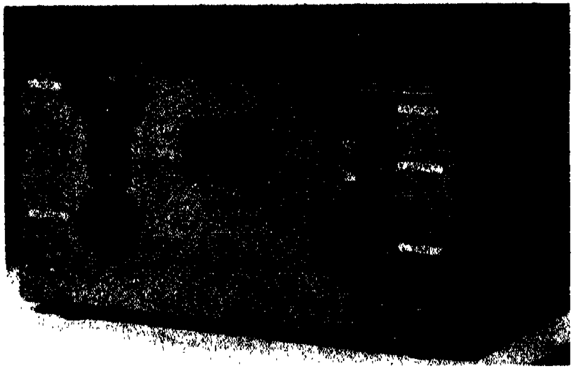

The amplifier is intended for use in measurements and control and, when used with thermocouples or strain gauge pick-ups, makes possible the recording of temperatures, pressure, accelerations, etc., on standard recording milliammeters. The excellent reliability of magnetic amplifiers makes the unit suitable for standby application when the reliability of vacuum tube amplifiers would not be adequate.—TRANS-SONICS, INC., *Bedford, Massachusetts.*

D.C. Power Supply

This regulated power supply is a laboratory source of stable, ripple-free d.c. power. It is continually variable in output voltages from 0–500 v. The ripple is less than 10 mv.

Power input is 105–125 v, 60 cycle. A.c. output is 6.3 v at 10 amp. (non-regulated). Regulation between 10 and 30 v is two percent, between 30 and 500 v it is one percent. The unit is mounted in relay rack or cabinet, and is compact in size.—CHATHAM ELECTRONICS CORPORATION, *475 Washington Street, Newark 2, New Jersey.*

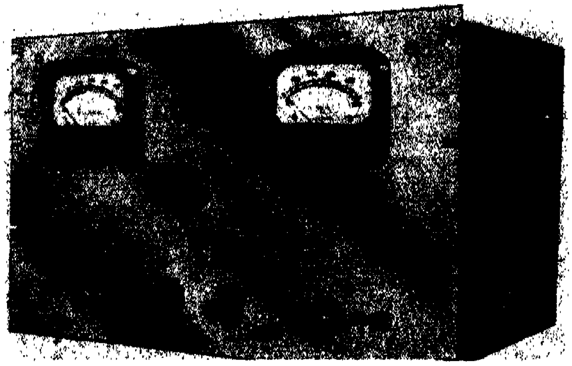

Gamma-Survey Meter

A five-range ionization chamber-type gamma-survey meter covering the unusually wide range from 0–5 mr/hr. to 0–50,000 mr/hr. is the only instrument of its type offering a scale changing meter with only one range visible at a time. The instrument is unusually rugged for field work, yet highly accurate for laboratory use. The large 4-in. scale changing meter is shockproof for added protection. There are separate scales for the five ranges: 0–5, 0–50, 0–500, 0–5000, and 0–50,000 mr/hr.

The instrument has a hermetically sealed ion chamber and the entire instrument is immersion proof. The instrument can be set

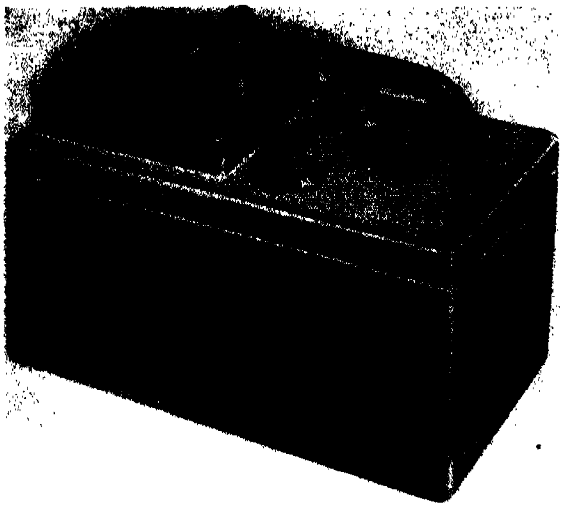

to zero in a radiation field of any strength; this setting is maintained . . ., there is no zero drift.

Built to strict military specifications, the K-350 has a ±10 percent accuracy over an operating range from −10°F to 125°F. Warm-up time is negligible. This instrument is non-microphonic. The K-350 has a sturdy steel case and convenient shoulder strap. One thousand-hour batteries furnish power for the instrument.

Further details including complete description of this unit and other Kekeket electronic instruments for the detection and measurement of radioactivity are available on request.—The Instrument Division, The Kelley-Koett Manufacturing Company, *12 East 6 Street, Covington, Kentucky.*

Alpha-Counter

The Model 501 alpha-counter is a nuclear instrument for the detection of alpha-particles from any source. All uranium and thorium ores may be quickly, qualitatively, and quantitatively analyzed, when the radioactive content is as low as a fraction of one percent. The device is stable in operation so that it may be calibrated against known sources and samples.

The Clarkstan alpha-counter utilizes a highly efficient optical system and a newly developed phosphor screen. From these it provides a statistical count of alpha-particle scintillations. Unlike the spintharascope, which must be used in the dark, the Model 501 alpha-counter may be used under subdued white light or red light illumination.

The Clarkstan alpha-counter has wide use and applications for the prospector, assayer, nuclear physicist, teacher, and mineralogist. It comes complete with luminescence-quenching filter, radioactive samples, aluminum carrying case, and complete instructions. The net price is $5.00.—The Nuclear Division, Clarkstan Corporation, *11927 West Pico Boulevard, Los Angeles 34, California.*

Volometer

Some of the special features of this rugged and flexible 20,000-ohm/v meter include a 4⅜ in. square meter—50 μa—Alnico magnet—three a.c. current ranges to 3 amp.—three resistance ranges to 20 meg. Weighing only 2 lb. and 5 oz., and housed in a high impact round-cornered Bakelite case with carrying strap, it measures $5\frac{1}{4}\times6\frac{3}{4}\times2\frac{7}{8}$ in.

Specifications: five d.c. voltage ranges at 20,000 ohm/v to 3000 v; five a.c. voltage ranges to 3000 v; three resistance ranges to 20 meg. Also three a.c. and d.c. current ranges to five db ranges.

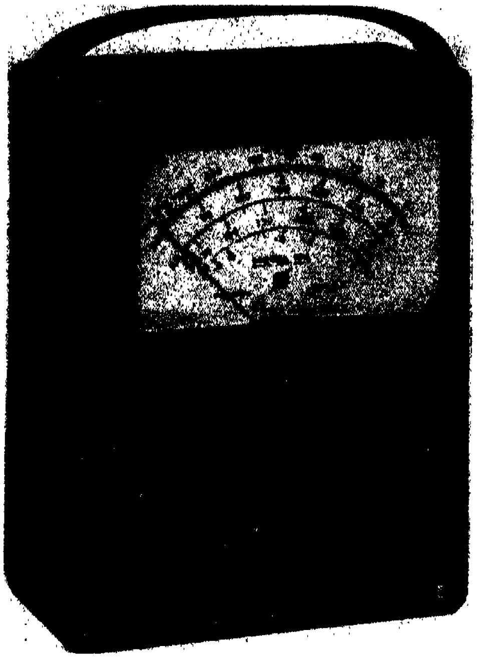

The new Model 104 volometer is a product of precision standards, but is priced at only $24.95.—Electronic Measurements Corporation, *423 Broome Street, New York 13, New York.*

Aerolog Wind Recording System

A new method of recording the wind movement and its direction is based on pneumatic impulses rather than electrical impulses. This method enjoys entire freedom from an external source of power which fails so often during those critical times when the record is most important, or is entirely absent in remote locations.

The system comprises a transmitter, support, recorder, and connecting hose. The transmitter contains a propeller-driven bellows-type air pump housed in a streamlined wind vane identical in size and shape to the Aerovane transmitter. This transmitter includes a distribution valve to direct the pressure impulse into one (or two) channels of a four-channel tube, according to the direction of the wind vane. The propeller is geared to the pump in such a ratio that each unit (mile, knot, or kilometer) of wind passing the propeller causes a single pressure impulse.

The support of this transmitter is of the conventional steel tube type with a tripod base.

The recorder is of the continuous strip chart type, with spring-driven clock drive. The receiving mechanism is composed of four diaphragms, each connected to one of the four channels in the

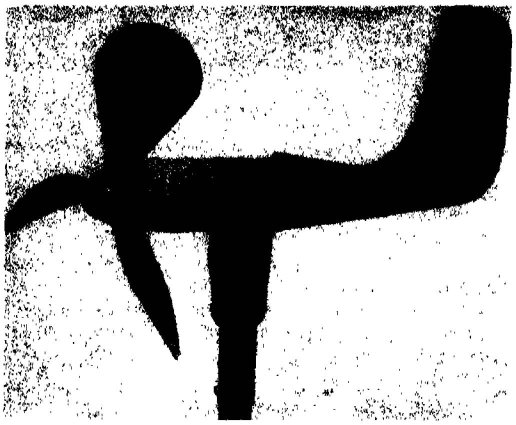

connecting hose. To each diaphragm is connected a pen which normally draws a straight line on the chart but upon receiving an impulse is deflected momentarily about ¼ in. sidewise. Thus a record of the four cardinal directions can be made. When the impulse is channeled through two of the tubes simultaneously, an intercardinal direction is indicated.

The mechanism also contains a slide bar which is actuated by any one of the above pen motions. This slide bar in turn actuates a fifth pen whose mechanism is so arranged that each tenth stroke is longer than the preceding nine, thus making possible counting wind movement by decades.

This system will operate with as much as 60 ft. of connecting hose.—Friez Instrument Division, Bendix Aviation Corporation, *Baltimore 4, Maryland.*

Air-Cooled High Vacuum Pump

A self-cooled high vacuum pump for laboratory use has been developed to form a simple, handy, reliable, and economical evacuation tool for applications both where large or small receptacles have to be kept under constant vacuum for long periods and where small systems shall be repeatedly evacuated.

The air-cooling principle offers a considerable simplification in installation and service, as no special cooling medium supply and no protection devices in connection therewith are necessary.

The three-stage mercury diffusion pump produces a high vacuum pressure of 10^{-4} mm Hg against as high a forepressure as 20 mm Hg. This feature simplifies and reduces the cost of the necessary pump equipment on the forepressure side, and even a water jet pump may be used as a forepump.

The great compression capacity of the pump has also made it possible to equip the unit with a mercury trap on the forepressure side. This trap prevents a backflow of gas from the forepressure to the high vacuum side if the pump should stop for some reason, such as failure in the power supply.

The patented design of the pump also offers easy dismantling for cleaning purposes and ensures correct assembly.—Aros Electric, Inc., *16 East 71st Street, New York, New York.*

Industrial Electron Tubes

Three new electron tubes suitable for a wide range of industrial services where dependable operation and a service life up to 10,000 hr. is required, feature of exceptional uniformity, stability of characteristics during 10,000-hr. rated life and specially designed mounts to withstand shock and vibration.

Structural specifications include ability to resist impact shocks of 100 G for prolonged periods, 500 G for short periods, and 2½ G during continuous vibration at 20 cycles per second, while being operated at maximum rated voltages.

The three new types include 5691, a high mu twin triode recommended for voltage amplifier use and supplied with series-unit heater; 5692, a medium mu twin triode with series-unit heaters suitable for balanced d.c. amplifier, multivibrator, blocking oscillator and resistance coupled amplifier applications; and 5693, a sharp cut-off pentode designed particularly for high gain resistance coupler amplifier service. The 5693 may be operated with No. 1 grid resistance values up to 40 meg.—Sylvania Electric Products, Inc., *Emporium, Pennsylvania.*

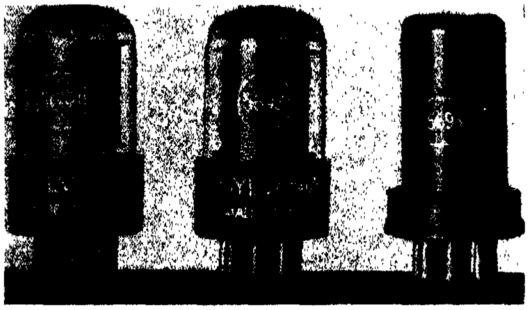

Proportional Counters

The phenomenally low alpha-background of less than one count per hour makes the PC-2A an outstanding instrument in the nuclear field. It is no longer necessary to struggle with background when counting low activity samples. With the wide range

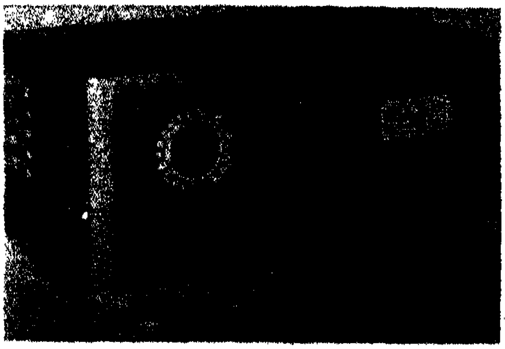

of sample types and sizes which the PC-2 accommodates, sampling time is greatly reduced. Excellent reproducibility and stability is obtained and complete automatic operation reduces operation time to an absolute minimum.

The types of samples counted are evaporated salts, precipitates, compressed pellets, loose soils, and ashed samples. The maximum sample size that the chamber accepts is 2¼ in. diameter by ¼ in. thick.

The PC-2 takes the fullest advantage of automatic operation, thus reducing the operating cycle to recording the data, exchanging the sample, and pressing a lever. A scaling factor of 8, 16, and 32 is provided and the maximum counting rate is 15,000 c/min. Gas flow control is automatic and timing is automatic up to 20 hr. A flush panel mounting, a register with lever-type reset, and illuminated leakproof bubbler are provided. All that is needed to put the PC-2A in operation is a cylinder of commercial argon, available in most any city.—NUCLEAR MEASUREMENTS CORPORATION, *3339 Central Avenue, Indianapolis 5, Indiana.*

Labmarkers

The Berkshire Labmarker is essentially a wave-shaping device used to produce time marks in cathode-ray oscillography. A sinusoidal input voltage (maximum amplitude 30 v r.m.s.) is converted by the Labmarker into a series of sharp unidirectional pulses. These pulses may be displayed directly on the face of a cathode-ray tube by connecting the output of the Labmarker to the vertical input. Timing marks consisting of short breaks in the oscillograph trace are obtained by connecting the output of the Labmarker to the "*Z*" input terminals of the oscilloscope. Both of these timing methods are shown in the photographs. The records shown are unretouched actual photographs showing spike potentials in giant internuncial fibers of the cockroach, with 1000-cycle time marks.

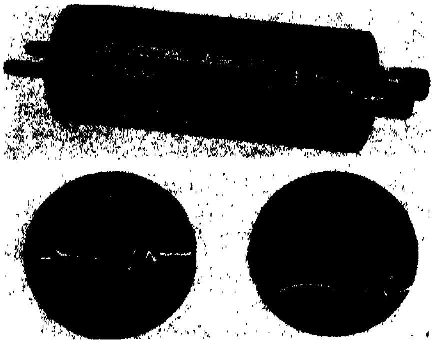

The Labmarker is a compact self-contained unit which may be plugged into the terminals of an audiofrequency oscillator. No other power source is required. The output binding posts of the Labmarker may be used with leads having single or double banana plugs, spade tips, phone tips, or plain wire ends.

Two types of Labmarker are available, the Model 1N, giving negative pips; and the Model 1P, giving positive pips. The price is $10.00 f.o.b. Concord, Massachusetts, for either model.—BERKSHIRE LABORATORIES, *P. O. Box 70R, Concord, Massachusetts.*

Vacuum Gauge

A new recording vacuum gauge for recording total pressure in the extremely useful range from one micron to 10 mm of mercury has been made possible by circuit modifications in the standard Alphatron cold-emission ionization gauge permitting connection to a Brown ElectroniK recorder, and it possesses the same continuous linear response to total pressure as does the Alphatron itself. Ionization is provided by means of alpha-particles emanating from an enclosed radium source.

Incorporating either strip or circular chart recorders, and full-scale sweeps of 24, 12, or 4½ sec., the recording Alphatron provides versatility to meet a demand for continuous recording of either slowly changing pressures or rapidly fluctuating pressures.

The total pressure range of 1 micron to 10 mm is covered in three separate ranges provided by the Alphatron, 0–0.1 mm, 0–1 mm, 0–10 mm. Normally, recording occurs on whichever of these three ranges the Alphatron is set. Optionally, a two-position switch can be provided to record normally in one position and in the other position to record only a single specified range. In this position the Alphatron indicates but does not record in the other two ranges.

Control of an external circuit can be provided at option also, by a mercury switch on the recorder which can be set to open or close as the pressure rises above or falls below a given value, with an accuracy of ±2 percent of the full-scale value.

The recording Alphatron is calibrated at the factory and arrives as a complete unit comprising a complete Alphatron gauge, a Brown ElectroniK recorder and a ten-foot connecting cable.

The upper scale is usually set for 0–10 mm, but can be factory-set for 0–20 mm at option without loss of linearity.—NATIONAL RESEARCH CORPORATION, *70 Memorial Drive, Cambridge, Massachusetts.*

Ultrasonic Soldering Iron

The soldering of aluminum and other light metals and alloys is made easy by means of an ultrasonic soldering iron, Type E7587, which consists essentially of a removable copper soldering bit and a magnetostriction transducer. The soldering bit, which is heated by means of a conventional resistance winding, is secured to a brass block held in firm contact with the nickel core of the transducer. The ultrasonic power necessary to drive the transducer is supplied by an electronic amplifier comprising the power supply unit.

In this new soldering iron the problem of temporarily destroying the refractory oxide film, which forms on most light metal and alloys, is solved by ultrasonic stimulation. This provides a clean surface and greatly facilitates the soldering of aluminium and other metals which form refractory oxides.

The soldering iron is simple to use, and has the advantage that no flux is required, and that standard soft solders may be employed. To avoid electrolytic action, however, it is advisable to use a solder with a tin-zinc base instead of the usual tin-lead alloy.

In application, the soldering bit is allowed to heat to the usual operating temperature. The transducer is then energized, and the bit is tinned by applying a soft solder. After this, soldering is carried out in the normal way, care being taken to maintain a good liquid contact between the bit and the work. This ensures the maximum acoustic efficiency and enables positive and uniform joints to be obtained.

The ultrasonic frequency chosen to operate the bit is well above the normal audible range, so that no discomfort is experienced by the operator.

This new ultrasonic soldering iron, which is the first commercial model of its kind in the world, should prove of particular value in the aircraft, civil engineering, shipbuilding, and hardware industries, and in fact in all manufacturing industries where the successful soldering of aluminum and its alloys has for so long been a pressing production problem.—Mullard Electronic Products Ltd., *Century House, Shaftesbury Avenue, London, W.C. 2, England.*

Variable Electronic Filter

The Model 300 single-section and the Model 302 dual-section variable electronic filters have a continuously variable cut-off from 20 c.p.s. to 200 kc. Each section has an attenuation rate of 18 db per octave, and sections can be cascaded to provide 36, 54, etc. db attenuation. A range switch selects the type of section desired—high pass or low pass—as well as four decade frequency ranges. In addition, the Model 302 dual-section filter can be switched to a band pass position so that any band width between 20 c.p.s. and 200 kc can be selected.

Compact in construction and reliable in operation, the—SKL—Series 300 filters fulfill a long-felt need in sound analysis in conjunction with sound level meters, psycho-physical and physiological measurements. To the communications, radio broadcasting, recording, and moving picture industry, these new filters bring a convenience and flexibility not hereto available.—Spencer-Kennedy Laboratories, Inc., *186 Massachusetts Avenue, Cambridge 39, Massachusetts.*

"CO-AX" Very Low Capacitance Cables and Flexible Feeders

CO-AX articulated-air-insulated coaxials by Transradio Ltd. are extensively used on account of their exceptionally low capacitance and/or attenuation values and their great flexibility.

The following new types have now been added to this range of highly specialized cables: 1. *Type C34 low capacitance cable:* O.D. 0.85 in.; capacitance 4.8 mmf/ft.; impedance 231 ohms. 2. *Type C344 very low capacitance cable:* O.D. 0.85 in.; capacitance 4.3 mmf/ft.; impedance 259 ohms. 3. *Type A34 highly flexible medium power transmission line:* O.D. 0.85 in.; impedance 73 ohms. At 100-Mc attenuation is 0.65 db/100 ft. and loading 1.5 kw. Bending radius 3 in. 4. *Type A344 flexible 51.5-ohm medium power transmission line:* O.D. 0.85 in.; nominal impedance 51.5 ohms; bending radius 4 in. Loading 2.3 kw and attenuation 0.78 db at 100 Mc/sec.—Transradio Ltd., *138a Cromwell Road, London, S.W. 7, England.*

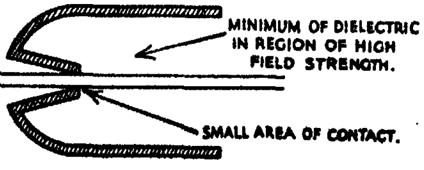

BASIC PRINCIPLE OF CO-AX AIR-SPACED CABLES

Diffusion Pump

A new fractionating oil diffusion pump, superior to previous pumps of the same size, has been developed by Distillation Products, Inc. Known as the MCF-300 pump, the new model provides a speed of approximately 300 liters per second in the range 10^{-5} to 10^{-4} mm Hg, the highest ever achieved with a 4-in. I.D. pump casing. An ultimate vacuum of 5×10^{-7} mm Hg at 25°C is attainable without cold traps.

The MCF-300 embodies three-stage concentric-cylinder type of fractionating jet assembly fitted into an enlarged boiler. The larger boiler area not only provides sufficient vaporizing surface to insure adequate fractionation and jet power, but also permits the use of external electrical heating units without danger of burn-out. The unusually powerful vapor jets are capable of pumping hydrogen one and one-half times faster than air and, with Octoil as the pump fluid, will operate against a forepressure of 0.150 mm Hg or more, depending on the heater input.

Important features are the compact size of the water-cooled casing and the ease of removal of the jet assembly for cleaning. A new, improved method of centering the jet assembly in the casing is employed. Backstreaming is low and thermal efficiency high because of the streamlined double-wall jet design.

The MCF-300 pump is recommended to the experimental physicist and research engineer for evacuation of continuously pumped electronic devices, such as, electron diffraction cameras, electron microscopes, mass spectrometers, small cyclotrons and synchrotrons, Van de Graaff machines, linear accelerators, and UHF power tubes. The new pump may also be used on vacuum coaters and other kinetic systems when unusually low pressures are required.—Distillation Products, Inc., *755 Ridge Road West, Rochester 13, New York.*

"Infinite Life" Counters

Research at Radiation Counter Laboratories, Inc. has discovered that a combination of the gas argon admixed with a small amount of xenon, oxygen, and nitrogen, yields a self-quenching Geiger counter of essentially infinite life. Data on counters with this admixture was presented recently at the symposium on Geiger counters held at the Naval Research Laboratory. These counters, like ordinary counters, operate with any standard scaler whose high voltage can go up to 1800 volts or more. No perceptible change in counter characteristics has been found up to 4×10^{9} counts. The useful counting life appears to be at least 100 times longer than for conventional Geiger counters filled with chemically decomposable organic quenching gases. Since these thin window counters have a near atmospheric pressure filling they should not be used or shipped to higher altitudes.

The counters are available with a mica window thickness of 3–4 mg/cm². For those experimenters using less energetic emitters such as C^{14} and S^{35}, mica window thicknesses of less than 2 mg/cm² are available.

Each counter tube is checked twice before it leaves the laboratory and complete threshold and plateau curves are provided with each unit tube.—RADIATION COUNTER LABORATORIES, INC., *1844 West 21 Street, Chicago 8, Illinois.*

Audiomatic Generator Model 282-A audiomatic generator is an audio sweep generator. This instrument has a low distortion beat-frequency oscillator with a manually adjustable range of 0–32 kc. Automatic frequency variation is applied to the normally fixed r-f oscillator of the BFO, and this variation is continuously adjustable by means of a dial calibrated in 500-cycle increments from 500 cycles to 10 kc.

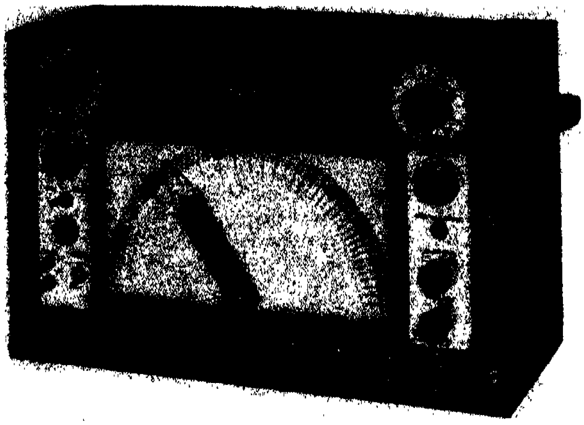

An internal saw-tooth generator drives the frequency variation circuit at a linear time rate, and the same saw-tooth wave is made available for use as an oscilloscope deflection voltage, for the x axis amplifiers. By this means, the time base of the oscilloscope starts at the setting of the "start frequency" dial and portrays the frequency range to which the "swept band" dial is set. The time rate of the sweep circuit is adjustable from 2 to 10 sweeps per second. By adjustment of the "start frequency" dial, discontinuities in a response curve may be spread out and examined in great detail.

The purity of output waveform has been kept to rigid standards to eliminate the portrayal of spurious responses in testing band pass and high pass filters. In addition to its function as an audio sweeper, this instrument is a high quality beat-frequency type of oscillator, with less than one-half percent distortion at frequencies above 100 cycles.

The output impedances are 4000 ohms single-ended, or 600 ohms balanced to ground. Separate jacks are provided for these impedances; the center of the 600-ohm output transformer may be grounded but is also accessible for connection to the circuit under test.

Dimensions are 19 in. wide, 12¼ in. high, and 8¼ in. deep. Power consumption is 50 watts, from a 115-volt, 50–60-cycle power line.—THE CLOUGH BRENGLE COMPANY, *6014 Broadway, Chicago, Illinois.*

Manufacturers' Literature

Cenco News Chats—No. 66, winter 1949–1950 issue, contains portrait and comments on the life of Sir Isaac Newton, description of the American Petroleum Institute, performance data on laboratory gas burners, and description of an automatic vacuum and pressure controller.—CENTRAL SCIENTIFIC COMPANY, *1700 Irving Park Road, Chicago 13, Illinois.*

Metal Powders—Bulletin 567 illustrates and describes some of the more important applications for the iron, steel, nickel, manganese and silicon powders produced by the company, such as in the making of gears, bearings, bushings, magnets and magnetic cores, and also as reagents and catalysts in the chemical and process industries.—THE NATIONAL RADIATOR COMPANY, PLASTIC METALS DIVISION, *Johnstown, Pennsylvania.*

Special Films and Plates—A new 8-page booklet describes special sensitized plates and films for the scientific and industrial laboratory, and includes a description of emulsions available for spectrographic work, photomicrography, and nuclear track studies, with complete information regarding the sensitivity of these emulsions.—INDUSTRIAL PHOTOGRAPHIC DIVISION, EASTMAN KODAK COMPANY, *Rochester 4, New York.*

Adherometer—Catalog sheet illustrates and describes the Adherometer, designed to measure the stripping force required to remove a paint film from the surface of a metal test panel. —HENRY A. GARDNER LABORATORY, INC., *4723 Elm Street, Bethesda 14, Maryland.*

SR-4 Strain Gauges—Bulletin 279-B, "How to Apply SR-4 Strain Gages," includes instructions for preparing the surface and applying gauges to various test items. Bulletin 279-A, "SR-4 Strain Gauges for Stress Analysis," tells how to select and use the strain gauges for stress analysis and explains the fundamentals of strain gauge circuits and instruments.—THE BALDWIN LOCOMOTIVE WORKS, *Philadelphia 42, Pennsylvania.*

GE Temperature Indicators—Bulletin GEC-565, 8 pp., describes the operation and applications of the GE line of resistance thermometers (up to 300°F) and thermocouple thermometers (to 3000°F).—GENERAL ELECTRIC COMPANY, *Schenectady 5, New York.*

Constant Temperature Baths—4-page catalog leaflet illustrates and describes low cost general-purpose temperature baths.—HENRY A. GARDNER LABORATORY, INC., *4723 Elm Street, Bethesda 14, Maryland.*

Frequency Adjustment of Quartz Crystals—National Bureau of Standards Circular No. 480, entitled "Fundamental Techniques in the Frequency Adjustment of Quartz Crystals," presents in detail the methods of changing the frequency of high frequency thickness-shear quartz crystals. Literature references are also given for those who may wish to pursue the subject more extensively. Price: 10 cents.—SUPERINTENDENT OF DOCUMENTS, U. S. GOVERNMENT PRINTING OFFICE, *Washington 25, D. C.*

Experimenter—December 1949 issue features an attenuator having a wide frequency range.—GENERAL RADIO COMPANY, *275 Massachusetts Avenue, Cambridge 39, Massachusetts.*

Oscillographer—Volume 11, No. 4 (October–December 1949) describes construction and performance of Types 304-H and 304 cathode-ray oscillographs.—ALLEN B. DU MONT LABORATORIES, INC., *1000 Main Avenue, Clifton, New Jersey.*

Tracerlog—No. 23, December 1949, describes new radioactive ore detector (SU-7), with a discussion of prospecting for radioactive ores.—TRACERLAB, *130 High Street, Boston 10, Massachusetts.*

Ring Balance Meters—4-page leaflet shows how ring balance meters may be compensated for pressure and temperature.—HAGAN CORPORATION, *Hagan Building, Pittsburgh 30, Pennsylvania.*

Circuit Panels—4-page catalog leaflet describes circuit panels and charts for electronic instruction and experimentation. Various charts are applied over the basic panel, illustrating the connections to be made for hook-ups appropriate for certain electronic experiments.—KEPCO LABORATORIES, INC., *Flushing, Long Island, New York.*

The Laboratory—Volume 19, No. 2, contains an article on chemical accomplishments in respect to food flavor and descriptions of a direct-reading viscometer, improved Fisher burner for natural gas, instruments for recording temperature and pressure, and an improved dropping mercury electrode instrument.—FISHER SCIENTIFIC COMPANY, *717 Forbes Street, Pittsburgh 19, Pennsylvania.*

Precision Spectrometer—Bulletin 165–50, 4 pp., describes Model L124 Precision Spectrometer, reading to one second of arc. The instrument is used principally for precise determinations of refractive indices and dispersion and for measurement of prism and wedge angles.—THE GAERTNER SCIENTIFIC CORPORATION, *1201 Wrightwood Avenue, Chicago 14, Illinois.*

New Materials

Forest K. Harris: Associate Editor
in Charge of this Section
National Bureau of Standards, Washington, D. C.

Copying Film

Autopositive is a sensitized film designed to produce a positive copy directly from a positive drawing without an intermediate negative step. It can be handled in normal room light and may be exposed on blueprint equipment employing a high intensity light source. The emulsion, on a translucent base, is silver-sensitized and will retain fine lines and minute detail. Material printed on opaque stock or on both sides of a page can be copied, and a right-reading print obtained by reading through the back of the film. A matte surface on both sides of the film permits making ink or pencil corrections or additions. A standard 2-solution eradicator is employed for erasing. The film can be used as an overlay in combination with cloth or paper for drawing revisions. Thirty- and 100-ft. rolls are available in widths ranging from 24 to 44 in.—EASTMAN KODAK COMPANY, *Rochester 4, New York.*

Printed Circuits

A process has been developed for supplying specified circuit layouts on ceramic, plastic, paper, and wood-base surfaces. The deposited material is normally conductive but non-conducting outlines can also be deposited. The bond is permanent, the outline is dimensionally accurate, and the deposit does not appreciably raise the surface. Soldered connections can be made as required by the user.—ELECTRO PATTERNS, INC., *68-39 79 Street, Middle Village, New York.*

Woven Glass Fabric

Soft-Flex is a processed glass fabric with crepe or herringbone weave in a 51-in. width and 6-oz. weight. It is stated to have an excellent "hand," and to be flexible without wrinkling. It is available in colors or white, plain or in patterned finishes. The material is odorless, translucent, and flameproof, and can be washed. Applications include draperies, filtering, dust collecting, and laminates.—WATERWAY PROJECTS, INC., *1008 North Highland Avenue, Los Angeles 38, California.*

Surface-Active Chemical

Rada, rosin-amine-D-acetate, is a surface-active amine salt in water-soluble form which is being used by the petroleum industry. In some oil fields the extraction of crude petroleum depends largely on secondary recovery methods, one of which is water injection. The new chemical provides control of bacterial action and affords protection against corrosion in water-flooding systems. It also acts to reduce turbidity in the flood-water, preventing plugging of oil-bearing sands.—HERCULES POWDER COMPANY, *Wilmington, Delaware.*

Rust Inhibitor

Santolene C, a hydrocarbon-soluble, water-insoluble nonmetallic organic material, is designed as a rust inhibitor for gasoline, fuel oil, kerosene, and similar light oil products in pipe lines and static storage. A dosage of 0.002 percent is effective when tested against distilled water, while 0.01 percent is required for protection against sea water. In these concentrations there is no effect on the usual specification items for gasoline, kerosene, and No. 2 fuel oil, except that the ASTM test on gasoline shows a moderate increase in gum at the higher concentrations, not more than 1 mg per 100 cc per 0.002 percent of inhibitor.—MONSANTO CHEMICAL COMPANY, *St. Louis 4, Missouri.*

Cellulose Acetate Cement

Acetate cement for bonding cellulose acetate assemblies is a solvent mixture designed to replace acetone which is highly flammable and which is considered to be a dangerous fire hazard even when stored in very small quantities. The new solvent is less volatile than acetone, and can be safely stored in unlimited quantities. In contrast with acetone, which often evaporates before it has an opportunity to soften, penetrate, and weld a cellulose acetate assembly, the new cement evaporates slowly enough to prevent blushing, has good penetration, and provides an excellent bond, according to the manufacturer. It is water-white, free-flowing, and is stated to be nontoxic.—SCHWARTZ CHEMICAL COMPANY, *326 West 70 Street, New York 23, New York.*

Pipe Insulation

K-Shield, made of foamed polystyrene, is a light-weight, rigid insulation for segmental application on vessels, pipes, and pipe fittings. It is made in three thicknesses in sizes for pipe from ¾ to 36 in., and in specified shapes for curved surfaces. It weighs from 1¼ to 1¾ lb. per cu. ft. and has a thermal conducting factor of 0.27 Btu/sq. ft./min./deg. F/in. at 70°F. it has high moisture vapor resistance and is not subject to mold growth, rot, or decay. It is nonirritating to the skin, and has no food value for insects and rodents. It is rigid, has a compression strength of 20 lb. per sq. ft., and can be cut and fitted with ordinary tools. It is designed for applications in the temperature range −250°F to 170°F.—ROBINSON INDUSTRIES, *3049 Curtice Road, Coleman, Michigan.*

Core Material

Ferroxcube, ferromagnetic ferrite, has been announced as a new transformer core material suitable for components of r-f electronic circuits. The material has a permeability more than 10 times that of powdered iron and a high electrical resistivity 10^7 times as great as that of iron. Eddy current losses are reduced as a consequence of this high resistivity.—NORTH AMERICAN PHILIPS COMPANY, *100 East 42 Street, New York 17, New York.*

Conducting Rubber Vee-Belts

Rubber, leather, canvas, and other types of belting generate static charges and, under low humidity conditions, can build up very high voltages. While the charge can be bled off by point or brush contacts on the belt surface, this device is not completely satisfactory. The accumulation of charge can be prevented by "loading" the belt with conducting material. While excessive loading will act adversely on the mechanical characteristics of the material, it has been found that normal belt life is retained when sufficient conducting material is incorporated in the belting to make it static-proof. The resistance of this belt is approximately 10 meg. when measured between disk electrodes at a spacing of 8¼ in., as determined with a 500-v megger. It may be noted in this connection that a resistance of 75 meg. for a 4-in. spacing, determined under the same conditions, is stated by one of the industrial fire insurance companies to eliminate static when operated between grounded metal pulleys.—B. F. GOODRICH COMPANY, *Akron, Ohio.*

THE
REVIEW OF SCIENTIFIC
INSTRUMENTS

VOLUME 21, NUMBER 3 *MARCH, 1950*

High Resolution Recording with Soot

K. R. Eldredge*
Research Laboratory on the Physics and Chemistry of Rubbing Solids, Department of Physical Chemistry, University of Cambridge, England

(Received November 15, 1949)

The treatment of a soot coating with a hydrocarbon solvent compacts the coat so that fine lines may be drawn in it with little force. The line resolution available is somewhat better than that of ordinary photographic films. Enlargements up to fifty times the size of the original record may be usefully employed.

I. INTRODUCTION

During the course of an investigation of the mechanism of the friction of rolling it was desirable to have a simple method for recording the frictional data. It was also necessary that the method use very little force for operation since any recording force would be added to the coefficient of friction for the rolling system, which might be of the order of 0.0001.

The method using an ordinary soot film on glass or other backing was tried for recording. It was found that the coefficient of friction was high and that the lines drawn were quite jagged and wide. For soot coats that were thick enough to make good photographic reproductions, the line widths drawn were seldom less than 0.1 mm wide and were generally more. A fluffy soot coat is rather sticky and tends to pile up irregularly on the writing point.

It was found that treating the soot coat with a solvent markedly altered and improved its character for recording purposes. Sooted plates were easily made in which the necessary recording force was about one milligram, the coefficient of friction less than one, and which had a line resolution exceeding 500 lines per centimeter.

II. PREPARATION OF THE SOOT COATS

Microscope slide glass, measuring three inches by one inch, was chosen for the record material because of the ready availability and ease of storage. From five to twenty complicated records have been made on each plate. After recording the plates were lacquered and served as negatives for the production of final enlarged photographic prints.

Ground edge microscope slides which are flat and fairly free from scratches are used. Small scratches do not seem to interfere with the writing point although the soot is not cleaned from the scratch and a black speck is left on the record. The plates are cleaned so that they are fairly free from dirt but small amounts of residual grease and dust are of little importance.

The simplest source of smoke is a wax candle. The cheap, smoky varieties with a wick size large enough to support a flame of a height of two or three centimeters are the best. The soot deposited is slightly uneven but sufficiently uniform. Liquid fuels burned from a wick were also tried but with much less satisfactory results. It was found that the soot usually deposited with a string or rope-like appearance which was completely unsatisfactory for recording purposes. Burners may be devised which will produce proper soot coats but they are unnecessarily complicated for the present purpose.

During the sooting process the glass slide is gripped along the edges, near one end, with a pair of laboratory tongs with grooved jaws. The glass is held flat or nearly flat in the upper one-third of the candle flame. As the soot deposits the glass is moved back and forth until the candle flame just ceases to be visible through the soot coat. After treatment the optical density of this thickness of soot allows the easy production of black and white prints on photographic paper of any grade of contrast. Thinner soot coats will produce better line resolution but will be more difficult to print.

After the glass is sooted it is put aside for cooling. It may be cooled very quickly if it is laid flat on a metal plate. At this stage the soot is fragile and a strong puff of air or a drop of liquid on the soot surface will ruin its uniformity. The solvent may be introduced by condensation or by capillary action and, after wetting, the surface becomes much stronger. Any of a large number of ordinarily water-free hydrocarbon solvents may be used. The presence of any appreciable amount of water weakens the bond between the soot and the glass so that patches of the soot may float away.

---

* At present with the London Office of the ONR.

The condensation treatment was done by immersing the cool glass slide in the vapor phase over a solvent boiling in a large beaker. The process is finished as soon as the surface is wet with the condensed liquid. Carbon tetrachloride may be used but care should be observed to prevent the production of poisonous gases with open flames.

The three methods which have been used to introduce the solvent into the soot by capillary action are as follows:

1. The slide is tipped up at a small slope of about 1:100 and 6 or 8 drops of kerosene are put on the slide at the high end.
2. The slide is placed vertically in a closed box with the lower end in the solvent. The solvent will creep up for a considerable distance at the rate of a centimeter in 5 to 10 minutes.
3. The slide is dipped vertically and progressively into the solvent at such a rate that the capillary line in the soot is always one or two mm above the liquid surface.

The third method produces the most uniform result. The first method was generally used, but the first centimeter of the coating is spoiled where the liquid first touches the slide.

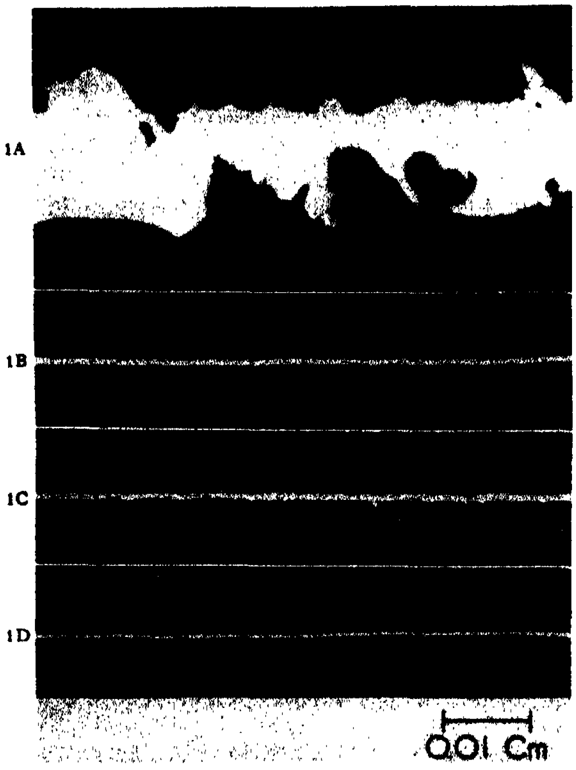

FIG. 1. Lines produced in a soot layer on a glass plate. All lines drawn with the same stylus in the same soot layer. 1A. Fresh candle soot. 1B. Soot layer treated with kerosene and line drawn while plate was still wet with kerosene. 1C. Kerosene removed with carbon tetrachloride and line drawn in dry soot layer. 1D. Soot layer re-wet with kerosene and line drawn while wet.

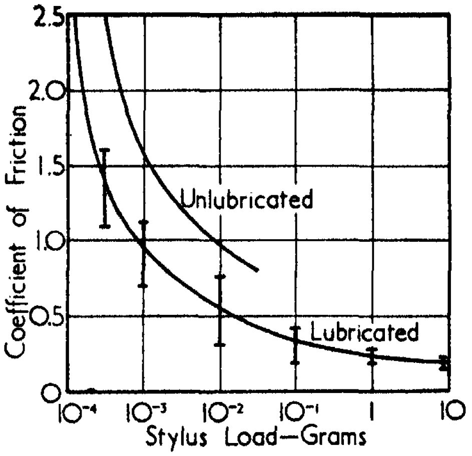

FIG. 2. Friction curves for a metal stylus moving through a soot layer deposited on glass.

The character of the soot changes markedly during the solvent treatment. The initial deep brown color of the coat changes to a neutral gray. Tar-like materials are washed out. The most striking change is the decrease of optical density. The final density obtained can be gauged by the distance of capillary wetting ahead of the liquid. If the distance is three or four mm the layer will be optically thin. If it is one-half mm or less the layer will be nearly as dense as before treatment. This applies for low viscosity liquids such as acetone as well as for higher viscosity materials such as an SAE 20 lubricating oil.

During the wetting a particle re-orientation seems to take place in the form of a vertical structure growing up from the glass surface. The granularity of the coating increases as the optical density decreases. The probability of the vertical growth arrangement in the optically thin coatings is shown by the fact that very lightly loaded writing points, which do not cut through the soot layer, produce black lines. This is apparently the result of crushing the carbon into a more compact layer.

After the initial wetting, liquid can be poured over the slide quite freely without disturbing the soot record. The slides are cleaned after recording with carbon tetrachloride in order to remove oils and particles of soot detached by the stylus. If the room humidity is high the slide should be warmed to remove any water condensed by the evaporation cooling of the carbon tetrachloride.

In order to make the slides permanent, they are lacquered after the record is made. A satisfactory cellulose lacquer may be made as follows:

Thick cellulose cement	2 parts
Amyl acetate	1 part
Acetone	4 parts.

This is poured on the sooted surface and allowed to run around by tilting the slide. It will dry in a few minutes. Sufficient lacquer should be used to produce a shiny coat since a thinner mat finish is much less resistant to handling.

III. FRICTION AND LINE CHARACTER

The force required to record in the soot or the fineness of line obtained can be favorably influenced by the treatment given to the coating, either before use or during use. Results obtained at various stages of treatment are outlined.

A. Fresh, Untreated Candle Soot

The coefficient of friction may be over two. The vertical force required to produce a line is very small but the lateral force may be many milligrams because of the stickiness of the particles. In Fig. 1 the white line shows the erratic character of the soot removal in the untreated layer compared with the lines obtained with treated soot.

B. Soot Treated with Kerosene and Used While Still Wet

The coefficient of friction of this lubricated layer, as shown in Fig. 2, varies between 0.2 and 1.0 but 0.7 is a reasonable average at light loads. The force required is very small, and stylus loads down to one milligram have given good records. The line of Fig. 1B is typical of the results achieved. The debris removed by the writing is rather fluffy in appearance.

C. Soot Coat Treated with Kerosene, Washed with Carbon Tetrachloride and Used Dry

With this treatment the coefficient of friction again reverts to the high value and writing loads of the order of ten milligrams or more are necessary to break through the soot layer. The line width, such as is shown in Fig. 1C, is, however, almost as good as that obtained in lubricated layers.

D. Soot Treated with Kerosene, Washed with Carbon Tetrachloride, Allowed to Dry and Then Re-Wet with Kerosene

This soot coat is harder and more brittle than that from method IIIB. The coefficient of friction drops to that of the lubricated value, but the minimum writing force is nearer to ten milligrams. Figure 1D is a typical result. The debris removed is quite flaky in appearance. This method produces the finest lines.

A reproduction of a small portion of a grating made in one of these coatings is shown in Fig. 3. The left side of the grating is 400 and the right side is 200 lines per centimeter in the original. The width of the individual lines is approximately 10 microns.

The frictional data shown for the lubricated soot layers in Fig. 2 are the results from over a hundred measurements made during the course of an investigation. The vertical limit lines on the lubricated soot curve include over 95 percent of the results from diverse methods of preparation and thickness of soot coats. The dry friction is exceedingly variable but the curve shown is a reasonable average of the results.

The lubricated soot curve of Fig. 2 is shown as extending to loads lighter than one milligram. This part of the curve is not ordinarily practical for use because the capillary force holding a fine writing point to the oiled soot coat is of the order of one milligram. The data were obtained by applying a negative mechanical force to the stylus.

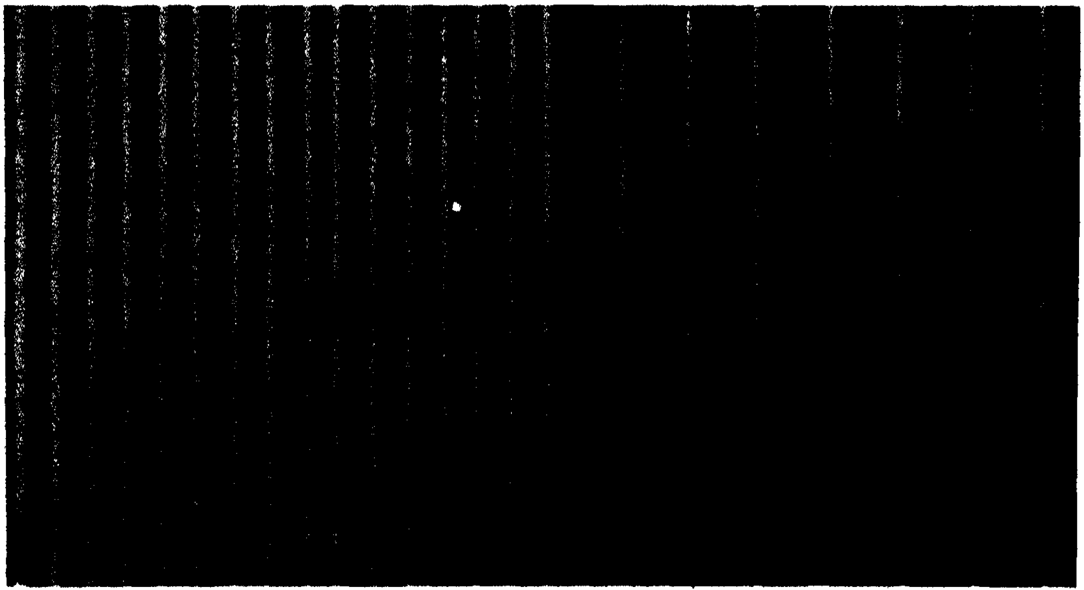

FIG. 3. Enlarged portion of a grating ruled in a treated soot layer.

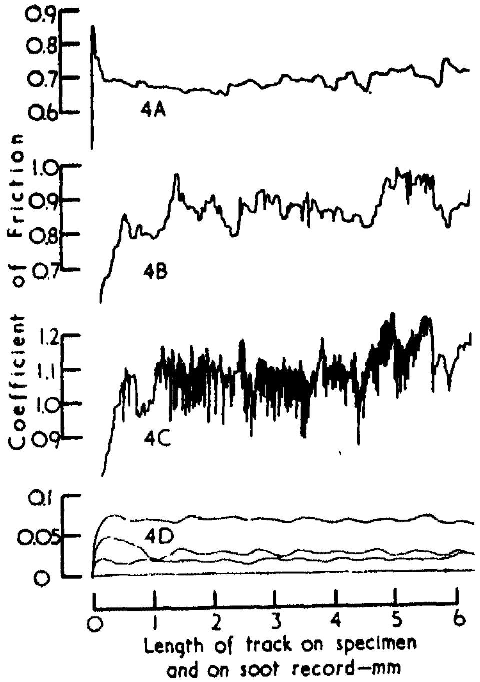

FIG. 4. Typical coefficient of friction records obtained with the soot recording method. 4A. Sliding, steel on copper, first passage. 4B. Sliding, steel on copper, second passage. 4C. Sliding, steel on copper, third passage. 4D. Rolling, steel on copper. A decrease of rolling resistance occurs after each passage over the same track.

The lubricants referred to in the above sections have been kerosene or other oils of higher viscosity. In any event it has been found that better results are obtained if the surface is actually wet and not just damp. If the record can be made within a period of a half an hour, kerosene is highly satisfactory. If longer times are necessary light lubricating oils may be used to obtain equally good records.

IV. THE STYLUS AND ITS SUPPORT

For many purposes the use of too fine a writing point may be a disadvantage. For any purpose where the record is enlarged less than about twenty times, a line width such as that of Fig. 1D may produce poor results. It will be found that such lines are so narrow that ordinary photographic enlargers will not resolve them satisfactorily.

Since the load on the writing point is very small, even copper is hard enough to serve as a durable material. Steel wire, however, of 20 B.S. gauge or smaller has generally been used. The wire is clipped off diagonally with a pair of pliers and then ground by hand to a point which is suitably fine for the purpose. The writing points used to make the records for the illustrations were prepared with little effort in a few minutes.

The complexity of the mounting for the stylus will depend upon the application. The side force required to move the stylus will be about three-fourths of the load on the stylus, if inertia forces are not considered. In general, a considerable amount of motion in the direction normal to the sooted surface will have to be allowed in order to be able to lift the stylus to change the records. If the stylus is spring mounted and not hinge mounted the lateral rigidity should be 10 to 100 times greater than the rigidity in the direction normal to the surface to prevent the tip of the stylus from lagging too far behind the writing arm. The small size of the records and the small forces required make it possible to design quite high frequency systems.

V. RESULTS

A number of typical friction records are shown in Fig. 4. These records are direct enlargements from the soot records and the lines obtained are black. The stylus used was somewhat coarser than that used for the previous illustrations in order to permit satisfactory results with 10× enlargements. The full length of the original records was 1.5 to 2 cm. After enlargement a convenient record length of 15 to 20 cm was obtained.

The records in Fig. 4 show a comparison of sliding and rolling friction under similar conditions. Both sets of records were made with a load of 600 grams on a 1.58-mm diameter steel ball sliding or rolling on an unlubricated annealed copper surface. During sliding there is an increase of friction and the development of the "stick-slip" phenomenon with successive passages over the same track. During rolling, each passage of the ball over the same track showed a decrease of friction. The friction continued to decrease measurably after twenty or more passages.

VI. ACKNOWLEDGMENT

Grateful appreciation is extended to members of the staff of the Laboratory of Physics and Chemistry of Rubbing Solids who contributed suggestions and much help in the construction of apparatus. The continued encouragement by Dr. F. P. Bowden was of great assistance.

THE REVIEW OF SCIENTIFIC INSTRUMENTS VOLUME 21, NUMBER 3 MARCH, 1950

A Ratio-Recording Double Beam Infra-Red Spectrophotometer Using Phase Discrimination and a Single Detector[*, **]

ABRAHAM SAVITZKY[***] AND RALPH S. HALFORD
Department of Chemistry, Columbia University, New York, New York

(Received June 30, 1949)

A simple modification is described for converting a Perkin-Elmer Infra-Red Spectrophotometer to double beam operation for direct recording of percent transmission *versus* wave-length. A phase discrimination system is used, requiring no changes in the optical system, and no sacrifice of versatility or ease of prism interchange. A complete spectrum over the rocksalt region may be obtained in 25 minutes with good resolution, and with no attention from an operator. Samples as small as 1×6 mm can be studied. The system is readily adaptable to other spectrophotometers, including those in the visual and ultraviolet range, the only limitation being sufficiently rapid response by the detector.

INTRODUCTION

THE desirability of using direct ratio instruments for the recording of infra-red spectra is immediately obvious when one considers the labor involved in taking energy curves with sample in and sample out, and then carrying out the point by point division to obtain a spectrum of percent transmission *vs.* wave-length. There is also the attendant difficulty that there may be variations in source intensity or in atmospheric absorption between the two runs. An instrument which performs this function automatically must be capable of viewing the radiant energy passing through both sample and standard simultaneously.

As recently described by Williams,[1] present double-beam automatic percent recording spectrophotometers may be generally divided into two types: (a) The beams which have passed through sample and reference cells are passed through the entrance slit of the spectrometer alternately. Any difference in intensities of the two beams is seen by the detector as an a.c. signal, the phase of which determines the direction of movement of a "comb," or diaphragm to produce an optical null.[2–4] The position of the diaphragm is recorded as percent transmission. (b) The two beams pass separately through the spectrometer, and fall on separate detectors. The ratio of the two signals can be obtained by placing the reference signal across the slidewire of a recording potentiometer and balancing against the sample signal.[5–7]

In the latter system, it is necessary to contend with problems of drift, and differences in sensitivities and spectral response of the two detectors. These difficulties are not present in the former case; since it is an a.c. system, there are no drift problems and the null method eliminates errors which might arise in the detecting and amplifying system. It does, however, use a rotating mirror at one point in the optical system, with the possibility of undesirable motions amplified over the long optical path of the monochromator, and of spurious a.c. signals arising from inhomogeneities in the moving reflector. Commercial instruments based on the above systems are available but expensive.

In planning the construction of the percent recording instrument described in this paper, the authors wished to take account of the following requirements, in addition to the utmost economy:

1. Conversion of the Perkin-Elmer Model 12B Monochromator[8] in our laboratories with the minimum of changes in the optical system.
2. There should be no moving parts with critical functions in the optical system; especially no moving mirrors.
3. There should be no interference with the use of the spectrophotometer as a direct deflection instrument when desired.
4. The two beams should be as close together as possible, for ease in thermostating reference and sample cells at very low or high temperatures.
5. The high speed of response and the sensitivity of the Golay detector[9] employed in the instrument should be used to best advantage.

The instrument to be described below makes use of the phase discrimination characteristics of the breaker or commutator rectifying system. It requires no change in the basic spectrometer other than the addition of a removable superstructure containing a rotating sector, motor, and breakers. Since the sector acts merely as an on-off device, its positioning is not critical, and its

---

[*] From a dissertation submitted to the Faculty of Pure Science at Columbia University by Abraham Savitzky in partial fulfillment of the requirements for the degree of Doctor of Philosophy.

[**] Publication assisted by the Ernest Kempton Adams Fund.

[***] Allied Chemical and Dye Corporation Fellow at Columbia University 1947–48.

[1] V. Z. Williams, Rev. Sci. Inst. **19**, 155 (1948).

[2] E. Lehrer, Zeits. f. tech. Physik **23**, 169 (1942).

[3] N. Wright and L. W. Herscher, J. Opt. Soc. Am. **37**, 211 (1947).

[4] Baird, O'Bryan, Ogden, and Lee, J. Opt. Soc. Am. **37**, 754 (1947).

[4a] J. U. White and M. D. Liston, J. Opt. Soc. Am. **40**, 29, 36, 93 (1950).

[5] J. D. Hardy and A. I. Ryer, Phys. Rev. **55**, 1112 (1939).

[6] G. B. B. M. Sutherland and H. W. Thompson, Trans. Faraday Soc. **41**, 178 (1945).

[7] R. F. Wild, Rev. Sci. Inst. **18**, 436 (1947).

[8] Barnes, McDonald, Williams, and Kinnaird, J. App. Phys. **16**, 77 (1945).

[9] Marcel J. E. Golay, Rev. Sci. Inst. **18**, 347, 357 (1947).

construction requires no more than ordinary care. Figure 1 is a photograph of the complete instrument.

PRINCIPLE OF OPERATION

The great selectivity, in many respects similar to that of sharply tuned amplifiers, afforded by the use of the breaker-type rectifying system has been adequately recognized and reported.[10–12] Of particular interest in the present instance is the fact that this system also acts as a phase discriminator, such that signals 90° out of phase with the breaker operation do not contribute to the d.c. component of the output signal.

The operation of the breaker system is shown in Fig. 2. The signal (a frequency of 10 c.p.s. is used in this instrument) passes from the amplifier through a phase inverter and impedance matching system, appearing at points *A* and *B* as a pair of signals (2*a* and 2*b*) 180° out of phase. The switching motion of the center point of the breaker is synchronized to be either exactly in phase, or exactly 90° out of phase, with the signal. When in phase, as shown by curve 2*c*, the output is a d.c. signal whose magnitude is proportional to that of signal entering the amplifier. When the breaker is set 90° out of phase with the square wave, as shown in curve 2*d*, the output is a square wave having twice the frequency of the input signal, and having no d.c. component to appear at the output of the filter.

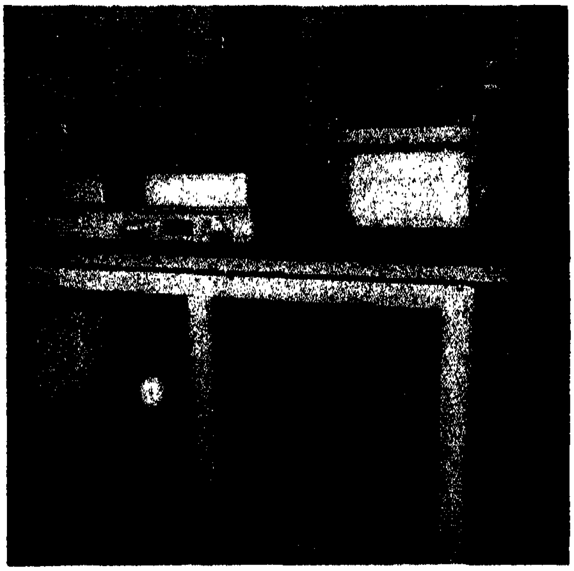

FIG. 1. The complete spectrophotometer. The amplifier is mounted behind the upper panel of the rack beneath the table, the second panel contains a standby amplifier, the third is a dummy. The control panel, providing for the functions enumerated in the text, is mounted above the Brown recorder. Test points on the front panel of the amplifier are used for monitoring the signal with the oscilloscope.

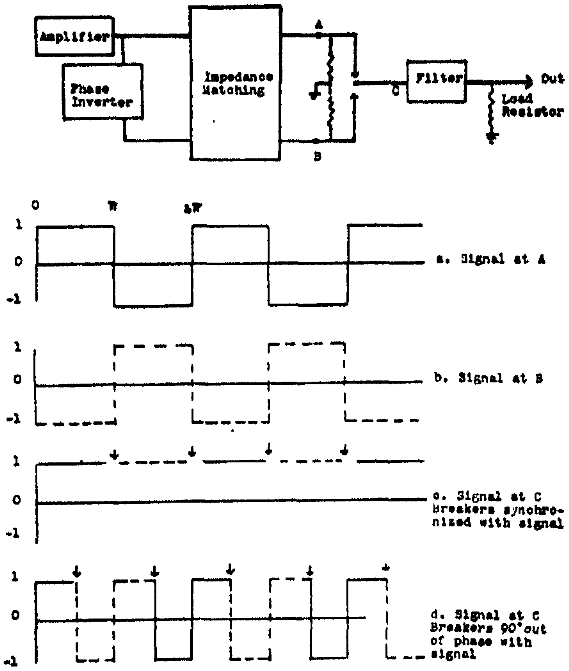

FIG. 2. Operation of breaker system.

If the signal entering the amplifier is a composite of two waves differing in phase by 90°, a pair of breakers can be used, set so that upon rectification each produces a d.c. component proportional to one of the signals, while the a.c. component due to the other signal is removed by filters.

Although the above analysis of breaker operation makes use of square waves these may be resolved by Fourier methods into a sum of sine waves consisting of the fundamental and its odd harmonics:

$$F(x)=4/\pi[\sin x-\tfrac{1}{3}\sin 3x+\tfrac{1}{5}\sin 5x-\cdots].$$

The breakers may be considered to be acting on each of these components individually. Thus, the method is applicable when one has only the fundamental frequency present, or any combination of fundamental and odd harmonics. The breaker operation is such that even harmonics of the breaker frequency do not contribute to the d.c. output in either the in phase or the 90° out of phase case. In our application of the principle we have, however, used a sharply tuned amplifier, which eliminates all harmonics but the fundamental.

The operation of the complete ratio system can be illustrated by the block diagram of Fig. 3. Radiation from the source housing passes the rotating sector which can be seen in Fig. 4, through the absorption cells, and falls on the entrance slit. The sector is shaped so that it divides the radiation beam into upper and lower halves each interrupted at 10 cycles per second, with a 90° phase difference. The beam then passes through the monochromator and falls on the detector which converts the radiant energy into a composite electrical signal of the type discussed immediately

---

[10] R. Gunn, Rev. Sci. Inst. 9, 267 (1938).

[11] Liston, Quinn, Sargeant, and Scott, Rev. Sci. Inst. 17, 194 (1946).

[12] Charles B. Aiken and W. C. Welz, Electronics 20 (October, 1947).

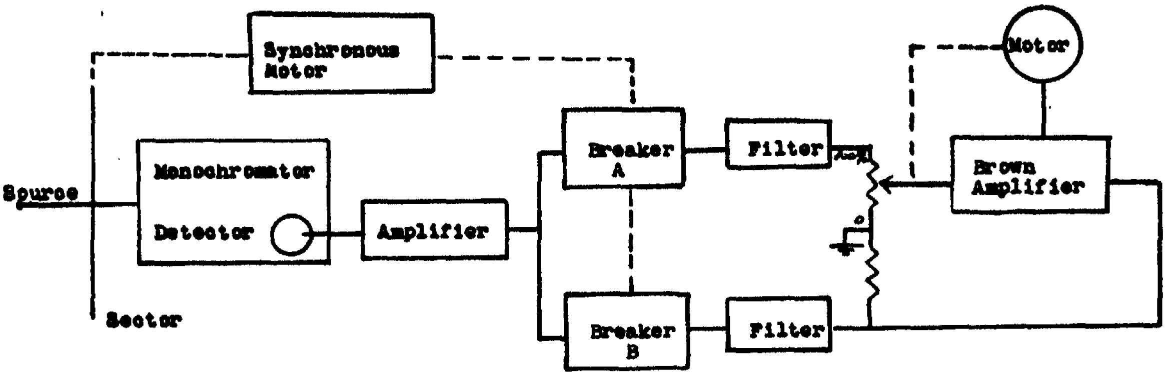

FIG. 3. Block diagram of complete ratio system.

above. After amplification, the signals are separated by a pair of breakers, 90° out of phase, and filtered. The reference signal is placed across a slidewire in a Brown recorder, and finally, the sample signal balanced against it. The position at balance is the ratio of the two signals, and is continuously recorded by a pen mechanically connected to the variable arm of the slidewire. The optical portion of the system is illustrated in Fig. 4.

THE MECHANICAL SYSTEM

The "superstructure," above the source housing in Fig. 4, contains the sector disk, synchronous motor, and breakers. In order to achieve good mechanical balance one revolution of the sector corresponds to two electrical cycles and so it is driven at only 300 r.p.m. Connection is made to the breakers by a 2 to 1 bevel gear. The breakers themselves are a war surplus item† and, since they are designed to be run at 1800 r.p.m. in both the input and output ends of a 30-megacycle receiver, are remarkably sturdy, free of noise, and provided with all necessary phasing adjustments. The entire superstructure can be raised or lowered, varying the proportion of energy in the sample and reference beams as desired. It can be raised till the entire beam passes through only the outer portion of the sector, for direct deflection records requiring the maximum energy. Moreover, the assembly can be moved parallel to the optic axis in the space between housings, permitting the use of large or small cells at will. The cell must, of course, be placed close to the rotating sector.

If desired, when recording directly, the superstructure can be removed entirely. An auxiliary on-off disk run by a 600-r.p.m. synchronous motor is placed directly in front of the globar. The motor is rotated until the sector interrupts the light in phase with one of the two breakers on the superstructure.

THE DETECTOR

Since the successful operation of this instrument depends in no small part upon the fast response and high sensitivity of the Golay cell, a description of its operation is given here. The position of the detector is shown in Fig. 4. The energy from the exit slit is focused on the detector by a silver chloride lens. The detector itself[9] consists of the pneumatic cell, in which radiant energy falling on an absorbing membrane heats the gas in the cell. The pressure change due to this heating is transmitted through a small constriction to a second chamber where it distends a flexible mirror. The motion of this mirror is amplified by an optical lever system of line grids. Changes in light intensity are observed by a thalofide (thallous sulfide) photo-conductive cell.[13]

Extensive studies have been made on the sensitivity of our detector which has an air filled cell. At present the equivalent noise input (ENI) of the detector-am-

FIG. 4. Optical system of spectrophotometer. The Golay detector and silver chloride lens are at the right of the monochromator partition. On the superstructure, at the top of the photograph, are the double breaker, motor and sector. One rotation of the sector is equivalent to two electrical cycles.

---

† Yagi Antenna switching motor from SCR 521 or similar airborne radars. This component is available at many war surplus outlets complete with a 24-volt d.c., 1800 r.p.m. motor. It is labeled "Autolite Part No. SWB4002 manufactured for Philco Corporation. Part No. 451-1084."

[13] R. J. Cashman, J. Opt. Soc. Am. 36, 356A (1946).

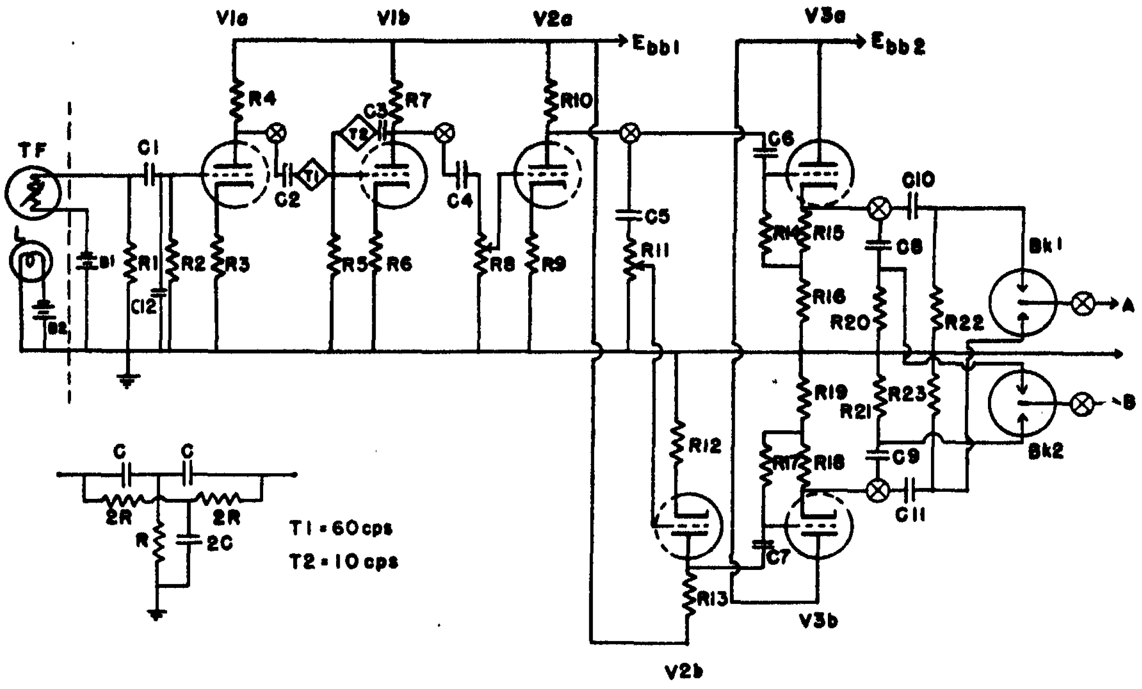

C_1 = 0.02 mfd
C_2, C_3, C_6, C_7 = 1.0 mfd
C_4 = 0.05 mfd
C_5 = 0.15 mfd
C_8, C_9, C_{10}, C_{11} = 10 mfd
C_{12} = 0.01 mfd
R_1 = 1.0 megohm
R_2, R_5 = 1.5 megohms
R_3, R_6, R_9 = 1000 ohms
R_4, R_7, R_{10}, R_{13} = 30,000 ohms
R_8 = 1.5 megohms

R_{11} = 500,000 ohms
R_{12} = 5,000 ohms
R_{14}, R_{17} = 220,000 ohms
R_{15}, R_{18} = 400 ohms
R_{16}, R_{19}, R_{20}, R_{21}, R_{22}, R_{23} = 10,000 ohms
*T*1, Twin-*T* Plug-in unit
  2*R* = 1 megohm
  C = 0.0026 mfd
*T*2, Twin-*T* Plug-in unit
  2*R* = 1 megohm
  C = 0.0157 mfd

L = Exciter Lamp
TF = Thalofide Photo-conductive Cell
V_1, V_2, V_3 = 6SN7GT
Bk 1, *Bk* 2 = Breakers
*B*1 = 45 V
*B*2 = 6 V
*Ebb*1, *Ebb*2 = +135 V
⊗ = Test Points

FIG. 5. Amplifier circuit diagram.

plifier system is believed to be $\pm 1\times 10^{-10}$ watt R.M.S. for an amplifier time constant of 2.3 seconds.[††, 14]

At least a $\sqrt{5}$-fold improvement would be expected if the air were displaced by xenon.[15] However, replacement of the Golay cell and optical grid by a plane mirror causes no more than 25 percent reduction in the noise level, if any, indicating that at least the major part of the noise originates in the optical amplifier, either in fluctuation of lamp intensity or movement of the lamp filament, since extinguishing the lamp removes practically all noise from the system. This leads us to conclude, subject to the reservation concerning the energy standard employed, that the intrinsic ENI of the Golay detector is less than $\pm 5\times 10^{-11}$ watt R.M.S. in our arrangement. In this circumstance an even greater improvement is to be expected from the substitution of xenon, which causes five-fold increase of response at the expense of $\sqrt{5}$-fold increase in that part of the noise only which originates in the Golay cell. We have not sought this improvement since we have already attained the operating condition wherein the prism itself usually constitutes the major limit of resolving power and since, for ratio measurement, we preferred the more rapid response of the air cell.

The noise level is not altered perceptibly by removal of the superstructure, although the mechanism is audible when operating.

THE AMPLIFIER

The output of the thalofide cell is transmitted to the amplifier (Fig. 5) through a coupling network[16] which acts as a filter having a pass band approximately 30 cycles wide. The amplifier proper consists of three resistance-coupled triode stages. Further narrowing of the amplifier passband is achieved by use of a twin-*T*

[††] The sensitivity of this detector was not measured directly. Dr. Van Zandt Williams of the Perkin-Elmer Corporation has kindly supplied the information that, measured with a thermocouple of known sensitivity, the energy at the exit slit of a Perkin-Elmer spectrophotometer, with Globar at 250 watts, at 955 cm^{-1} and slit of 0.085 mm, is about 2.7×10^{-8} watt. The above result for our Golay cell is obtained from the observation that, for a deflection of 80 percent of full scale, the noise level is 1 percent to 1.5 percent, peak to peak, measured over an interval of at least 15 minutes. A factor of 4.6 is used for conversion of peak to peak values to R.M.S. (see reference 14). The above sensitivity measurement is offered primarily for comparison with other detectors installed in Perkin-Elmer instruments.

[14] Carroll Creitz, Analytical Chem. **20**, 707 (1948).

[15] See reference 9, p. 351.

[16] E. A. Johnson, Physics **7**, 130 (1936).

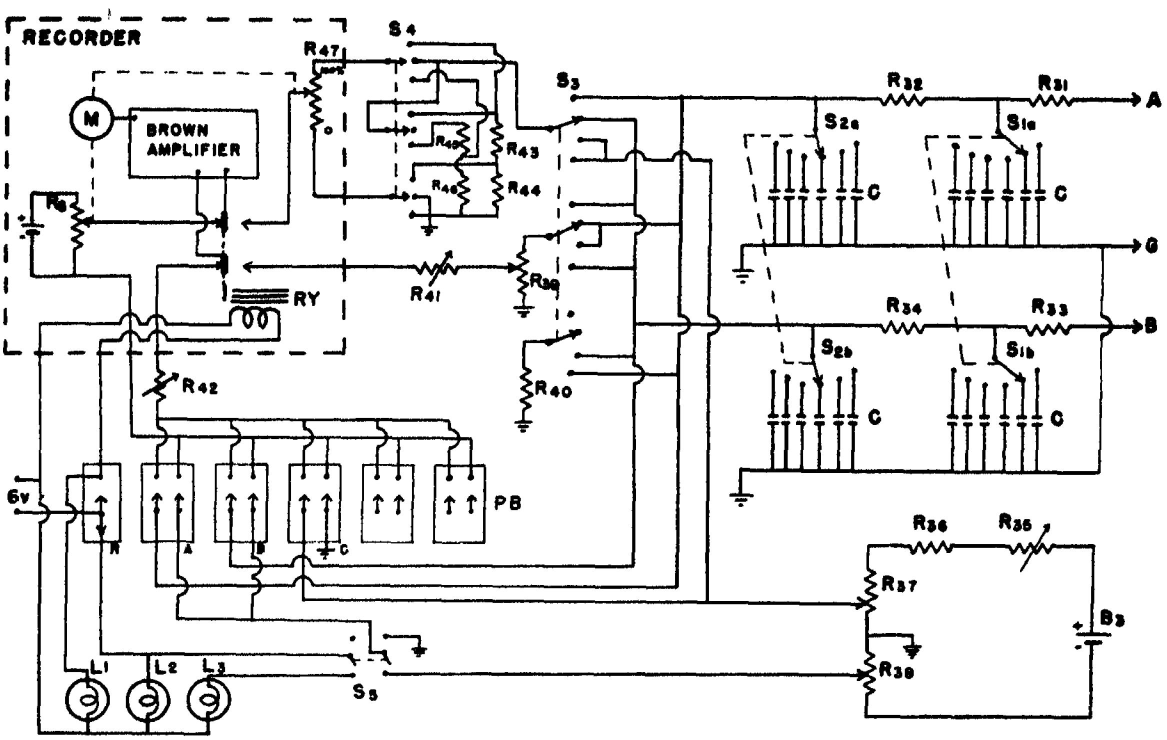

R_{31}, R_{32}, R_{33}, R_{34} = 5,000 ohms
R_{44}, R_{45} = 500 ohms
R_{36}, R_{40}, R_{43}, R_{46} = 1000 ohms
R_{35}, R_{39}, R_{41}, R_{42}, R_{47} = 1000-ohm Potentiometers
R_{37} = 50-ohm Potentiometer
R_{38} = 10-ohm Potentiometer
R_s = Recorder measuring slidewire

S_1, S_2 = 2-pole 6 position switches
S_3 = 3-pole 4 position switch
S_4 = 3-pole 3 position switch
S_5 = *DPDT* switch
PB = Push button switch assembly
RY = *DPDT* relay
M = Balancing motor
L_1, L_2, L_3 = Pilot lights

B_1 = 1.5 V
C = Each condenser bank
Position 1 = 400 mfd
2 = 200 mfd
3 = 150 mfd
4 = 100 mfd
5 = 50 mfd
6 = 20 mfd

FIG. 6. Schematic diagram of control panel and recorder modifications.

negative feed-back network[17–22] in the second stage. Gain is controlled in the conventional manner at the input to the third stage. Unbypassed cathode resistors provide grid bias. Cathode followers are used for impedance matching between the amplifier-phase inverter plate circuits, and the low impedance filters. Since the signals from the two cathode followers must have the same amplitude, a balance control is provided at the phase inverter input.

Most of the amplification of the detector signal occurs in the optical amplifier preceding the thalofide cell, reducing the gain requirements for the electronic amplifier so that Johnson noise and other random effects in it are completely negligible. This greatly decreases the restrictions on the first triode stage, so that no more than ordinary precautions[23] must be observed in construction. However, because of the unusually high capacities of the cathode coupling condensers, C_8, C_9 C_{10}, and C_{11}, leakage resistance becomes of great concern, requiring the use of 600-v oil filled paper capacitors. The resistance-capacitance filter system (Fig. 6) has been furnished with variable capacities to provide a wide range of response times.

Filament power is obtained from 6-v storage batteries. For greater stability, the exciter lamp used in the Golay optical amplifier is supplied from a set of No. 6 dry cells. To avoid undesirable feedback across the *B*-battery plate supply, it was found necessary to provide a separate supply for the cathode followers. While this might have been avoided by the use of decoupling filters in the early amplifier stages, these are quite difficult to construct for this low frequency.

To allow for the use of an oscilloscope in locating troubles in the amplifier, and for monitoring purposes, test points, marked by ⊗ in the circuit diagram, have been connected to banana jacks on the front panel.

CONTROL PANEL AND RECORDER

The circuit of the control panel, located above the recorder in Fig. 1, is shown in Fig. 6. The signals from the pair of breakers and the filter system are now completely independent, and can be called signal *A* and signal *B*. These, together with a constant signal, *C*, obtained from potentiometer R_{37}, appear at the selector

---

[17] H. H. Scott, Proc. I.R.E. 26, 226 (1938).
[18] J. M. Sturtevant, Rev. Sci. Inst. 18, 124 (1947).
[19] M. P. Givens and Saby, Rev. Sci. Inst. 18, 124 (1947).
[20] M. P. Givens, Rev. Sci. Inst. 18, 802 (1947).
[21] A. H. Hastings, Proc. I.R.E. 34, 126P (1946).
[22] G. E. Valley and H. Wallman, *Vacuum Tube Amplifiers* (McGraw-Hill Book Company, Inc., New York), M.I.T. Radiation Laboratory Series, Vol. 18, p. 384 ff.
[23] L. C. Roess, Rev. Sci. Inst. 16, 172 (1945).

TABLE I. Calculated resolving power of ratio system. These slits give a peak noise of 1 percent for filter time constant of 2.5 seconds.

Frequency cm^{-1}	Slit mm	Resolution cm^{-1}
3400	0.023	22.3
1600	0.059	9.4
1185	0.095	4.6
920	0.157	3.0
747	0.287	2.5

switch, S_3, which allows one to take the ratio of B/A, A/B, A/C, or B/C.

Switch S_4 permits "expansion" of the ratio scale so that the full range of the ratio potentiometer can be used to record ratios from 0–50 percent, or 50–100 percent, as well as the normal 0–100 percent. The position of the "100 percent" mark is completely arbitrary, since it is determined by the relative amounts of energy in the reference and sample beams. A rough setting can be made by raising or lowering the sector. Potentiometer R_{39}, acting in the same manner as a gain control, is used for a fine setting of the ratio maximum.

The ratio slidewire R_{47} is mounted at the rear of the recorder chassis, Fig. 7, and is coupled mechanically to the cable drum which drives the pen and variable arm of the recorder slidewire. The ratio slidewire acts as the load resistor for the reference circuit, except when recording the ratio of A/C or B/C. The ratio fine control, R_{39}, is the load resistor for the sample circuit. The potentiometer used for R_{47} should have the same useful angle of rotation as the recorder cable drum; the General Radio type 214-A can be made to match closely by filing the end stop.

Rapid change of the recorder functions is provided by the use of push buttons. The shift from normal recording to ratio recording is made by a relay actuated by Button 1. The relay is mounted underneath the Brown amplifier. Pressing any other button releases the relay, allowing the recorder to function normally. Thus signals A, B, or C may be recorded directly at any time. In addition, positions have been provided for recording signals from any other equipment which might be used with the spectrometer, such as heater thermocouples.

FIG. 7. Ratio slidewire at rear of recorder chassis.

The characteristics of the rectifier system are such that the output signals are referred to a ground or zero potential, which always places the signal zero at the zero of the recorder. When desired, such as when observing detector performance by signal to noise ratios, the signal zero for direct deflection from either channel can be placed at any other point on the paper by means of switch S_5 and potentiometer R_{38}.

The Brown recorder is modified electrically only by the addition of the relay and slidewire mentioned above. The automatic standardization has been mechanically disconnected.

SLIT CONTROL

Although the ratio recording system will compensate for most variations in the energy entering the spectrometer, such as the water vapor and carbon dioxide absorptions, the response of the Brown amplifier tends to fall off when the reference signal falls below 4–5 millivolts. Because of the enormous variations of globar energy with wave-length[24] some method of slit adjustment must be provided.

At present, continuous slit control is achieved by use of the Perkin-Elmer slit cam. This device is unfortunately quite inflexible, allowing for only one set of operating conditions, such that it can be used only with the NaCl prism and even then it affords only one slit schedule, suitable for use with liquids and gases. Solids and slurries that scatter appreciably, as well as single crystals whose apertures are likely to be small, require larger slits, especially when examined with polarized light, than are obtainable with the device. Some helpful variations can be attained by using drums of various diameters on the slit micrometer in addition to the one provided. Table I shows slit widths obtained with the standard drum. The peak noise to signal ratio with these slits amounts to about 1 percent on the ratio scale for a filter time constant of 2.5 seconds.

Ideally, of course, slit control should be based on the amplitude of the signal in the reference channel. Two methods are suggested, one manual, the other automatic:

1. The amplifier signal may be monitored by means of an oscilloscope plugged into one of the breaker test points. The slits are reset manually when the signal falls below a specified level on the oscilloscope screen.

2. Figure 8 shows a suggested‡ automatic slit control

---

[24] See reference 1, p. 146.

‡ We have been informed by Professor D. F. Hornig that he has been using a mechanism of this kind with success.

system, which has not yet been tested. The breaker shown is operated by an auxiliary synchronous motor, which is adequate to keep the breaker phased properly once it is set to select the reference signal. A filter of very long time constant should be selected to prevent rapid changes in slit width when passing through the water vapor region. The desired reference signal level is selected by adjustment of the potentiometers R_L and R_B.

ABSORPTION CELLS

A typical cell for non-volatile liquids consists of a round rocksalt plate, on which is placed a semicircular plate. The sample is placed between the semicircular and circular plates and the assembly clamped in a brass cell holder. The single thickness of NaCl acts as the reference cell.

To make a cell for volatile liquids, the half-plate may be heated, Saran thread[25] allowed to flow around the edges, and a heated round plate pressed on. The Saran acts as a cement, so that no holder is necessary. Holes drilled in the half-plate allow filling by hypodermic needle. A cell for solution *vs.* solvent records can be made in a similar manner, with the Saran melted around the edge of the full plate, and across the diameter to divide the cell into two sections. Alternatively, cells have been made with metal spacers. A good seal is achieved with stopcock lubricant of the glycerol sugar type.[26]

Solids may be studied in Nujol suspensions smeared on half of a circular rocksalt plate. To compensate for the effect of scattering and of Nujol absorption, a paste of sulfur in Nujol can be used on the other half of the plate. Single crystals and fibers have been placed near the slit on one side of a horizontal, reflecting tongue that extends out to the sector, the latter being near the monochromator housing.

Gas cells may be constructed by soldering a highly polished brass plate between the two halves of a brass cylinder so that four semicircles of rocksalt can be fastened to the ends. The reflecting partition will return to the beams all rays that normally would cross the optic axis along its length and thus reduce light loss to a negligible level.

An opaque strip is placed across all cells to define sharply the two halves. This greatly increases the tolerances in machining the edge defining the inner and outer portions of the sector, yet can be made narrow enough to intercept not more than a very small fraction of the beam.

PERFORMANCE

One of the chief reasons for constructing this double beam instrument was the desire to eliminate from the spectra the effect of absorption by atmospheric water vapor and carbon dioxide. However, when first tested, the instrument fluctuated violently when passing through the regions of atmospheric absorption. Investi-

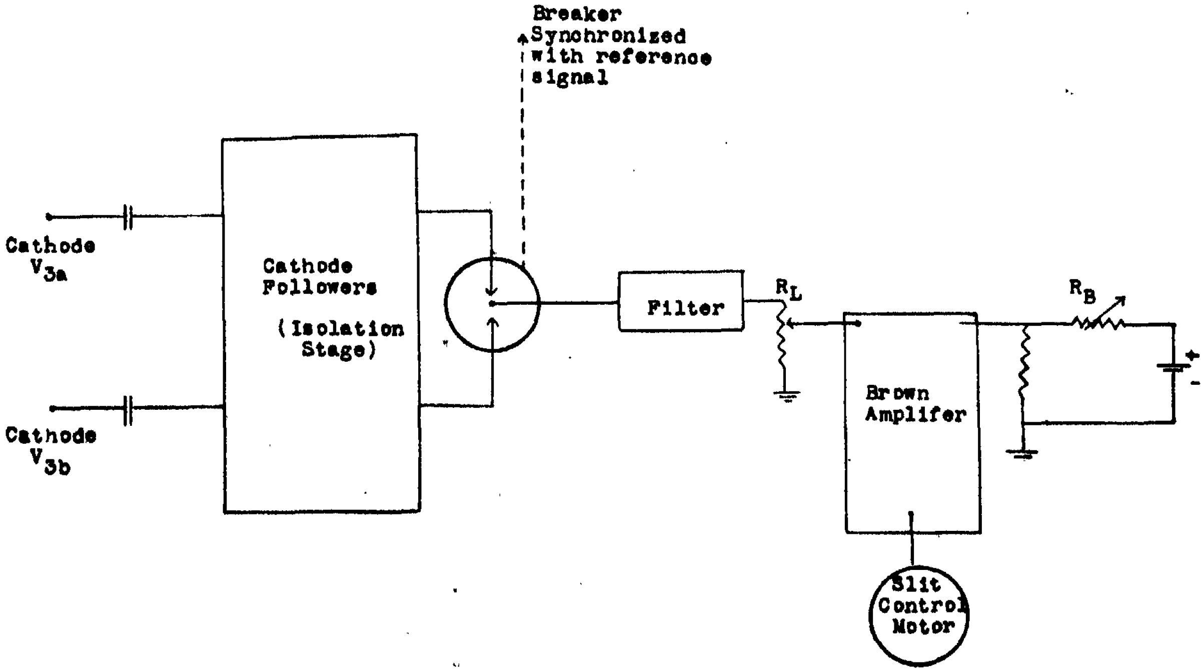

FIG. 8. Block diagram of proposed automatic slit control system. Input is taken from the cathodes of V_{3a} and V_{3b}, Fig. 5, through 1-mfd condensers. The cathode follower stage and breaker connections are exactly similar to those of V_{3a} and V_{3b}. An auxiliary Brown amplifier and control motor must be used. Slit widths are determined by the settings of R_L, R_B and the amplifier gain control.

---

[25] H. R. Broadly, Rev. Sci. Inst. 19, 475 (1948).
[26] C. C. Meloche and W. G. Frederick, J. Am. Chem. Soc. 54, 3264 (1932).

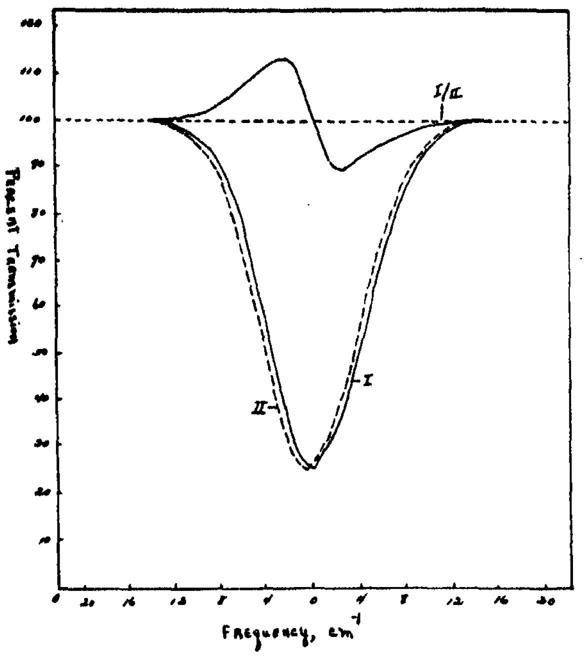

FIG. 9. I and II, Gauss error curves; half-width 10 cm⁻¹, centers displaced by 0.5 cm⁻¹, illustrating the effect of spectral displacement on the ratio I/II.

gations showed that this failure of the ratio device was due to misalignment of the spectrometer optics, in that the two beams pass through the spectrometer on slightly different paths, and the upper and lower portions of the exit slit were receiving slightly different regions of the spectrum. The effect of such displacement of the two spectra is shown in Fig. 9, where, for illustration, Gauss error curves have been drawn with half-amplitude widths of 10 cm^{-1} and with their centers displaced by only 0.5 cm^{-1}. An important characteristic of such curves is a cross-over point where the ratio passes rapidly through unity, giving rise to the violent fluctuations referred to above. Records obtained before adjustments were undertaken are quite similar to curve I/II in Fig. 9. Since the resolving power of the instrument in the water vapor region is about 10 cm^{-1} with the slit normally used, the criteria of adjustment for removal of this effect must be far higher than for ordinary operation of the spectrometer. We have found the most effective adjustment to be the tilt of the small exit mirror which is mounted at the rear of the prism table. The mirror is spring loaded against an adjusting screw which was not designed for the fine adjustment required here. However, once adjusted a prism may be removed and replaced without seriously affecting the setting of the mirror, which has had to be readjusted only once in 5 months of operation, immediately after moving the spectrometer and its accessories to a new location.

The degree of success in removal of the water vapor bands is demonstrated in Fig. 10, which shows the signal in the reference channel (I), sample channel containing anisole (II), the ratio of these two signals (III), and the ratio of reference to sample signals without an absorber in the sample beam (IV). These spectra were taken with the CaF_2 prism, which has a much higher resolving power in this region than the NaCl prism,[27] thereby exaggerating the difficulty of compensating for atmospheric absorption by sharpening the individual bands, under the scanning conditions employed. While the water bands may not have been completely eliminated, any residual bands are small, and so could be allowed for in the evaluation of the anisole spectrum without the necessity of the point by point division which would be required in the case of the direct deflection spectra. Figure 11 allows one to judge results obtained with the NaCl prism.

A part of the fluctuation in curve IV must be ascribed to increased noise to signal ratio due to the large water

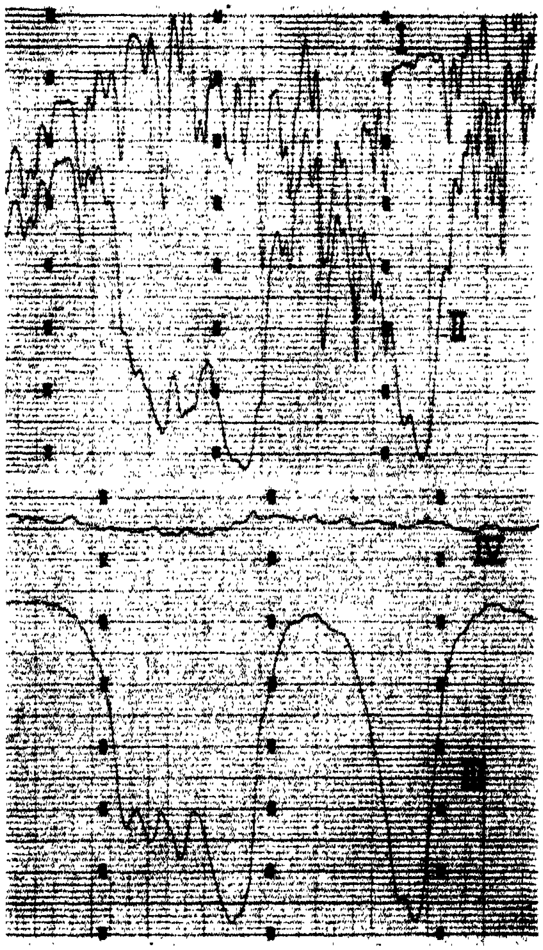

FIG. 10. Upper-half, direct deflection spectra using CaF_2 prism. I. Atmospheric water vapor absorption in the reference channel. II. Spectrum of anisole superimposed on water vapor absorption in sample channel. Lower-half, ratio spectra using CaF_2 prism. III. Spectrum of anisole *vs.* blank. IV. "100 percent" curve, anisole removed from sample beam.

---

[27] Gore, MacDonald, Williams, and White, J. Opt. Soc. Am. 37, 23 (1947).

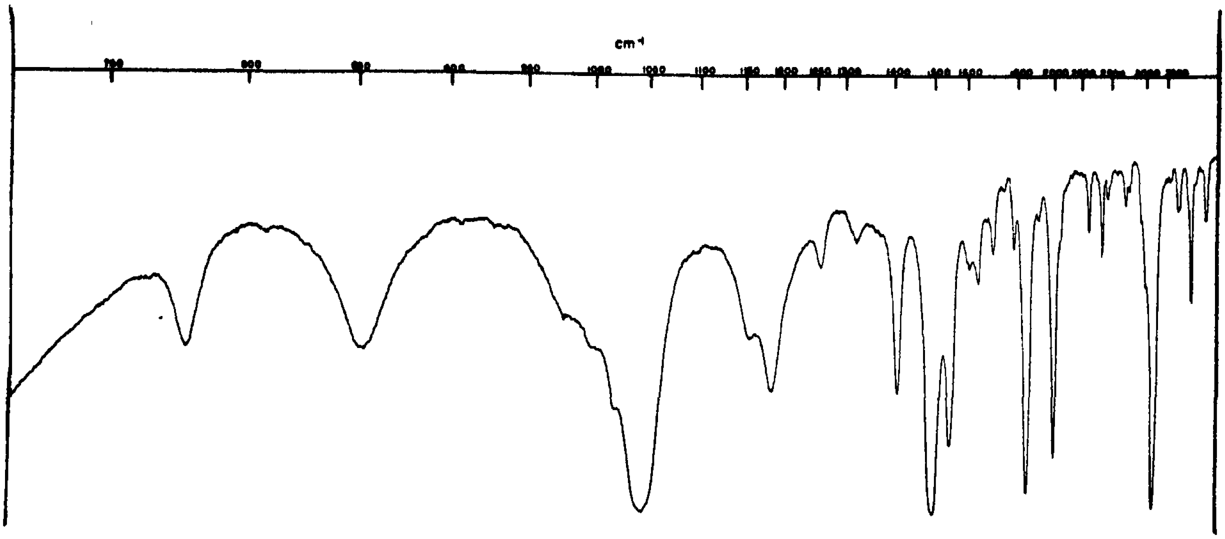

FIG. 11. Spectrum of liquid benzene in sealed cell, 0.1-mm spacer, recording time 50 minutes, time constant 2 seconds. Slit schedule is $\sqrt{2}$ times that shown in Table I.

vapor absorptions. This effect will appear whenever there is atmospheric or solvent absorption in the reference channel. Because the noise level is determined by the amplifier gain setting, the noise in the sample channel will be equal to the noise in the reference channel when the Ratio Fine Control is at its maximum setting, and less than the reference channel noise at any other setting of this control. If n is the noise level in signals s and s', and r the noise level in the ratio $R = s/s'$, then the noise, expressed as fraction of the ratio scale, is $r = n/s'(1+R^2)^{\frac{1}{2}}$, showing that (1) the noise for percent recording will never exceed $\sqrt{2}$ times the percent of noise in the reference channel, and (2) for a given ratio, R, the noise in the ratio is inversely proportional to the reference signal.

The foregoing relations governing propagation of noise into the ratio have been verified experimentally within the limits imposed by the difficulty of measuring noise. Moreover, for $R \leqslant 1$, $s' \geqslant (s+s')/2$, and it follows that $r \leqslant 2\sqrt{2}n/(s'+s')$. That is to say, the noise on the ratio scale should not exceed $2\sqrt{2}$ times the noise to signal ratio observed when the instrument is used in the conventional manner with a single beam including the entire aperture at the same gain and slit. The factor of 2 arises from division of the aperture into two parts while the factor of $\sqrt{2}$ comes from the usual statistical multiplication of noise in the quotient of two equally noisy signals. We have verified experimentally that the observed noise r has this theoretical value, again within the limits of error involved in any measurement of noise. The observed, theoretical noise on the ratio scale in our instrument is thus not more than twice the corresponding theoretical noise in one using the optical null method,[2–4] where each beam includes the entire aperture. On the other hand, if undesirable motions of the moving mirror, or inhomogeneities of its surface, or misalignment of the beams intersecting upon it, introduce any noise in an optical null instrument its theoretical advantage may be offset in this way. We cannot say from our own experience how the actual noise in such instruments compares with the theoretical value, inasmuch as the commercial instruments we have examined do not include provision for their use as single beam direct deflection instruments.

The amount of cross talk between channels is determined by the accuracy of phasing the breakers. Channel A is blocked, and the signal in channel B set to full scale on the recorder. Doubling the slit then gives a signal which is four times full scale. Channel A is connected to the recorder and its breaker is adjusted so that the signal is less than 1 percent of full scale, although the signal in channel B is still four times full scale. The procedure is repeated for the other channel, leaving a maximum cross talk in each signal of less than 0.25 percent.

A complete spectrum of liquid benzene from 5000 cm^{-1} to 700 cm^{-1} (the NaCl region), Fig. 11, was recorded in 50 minutes. This can be compared with spectra published by Wild[7] and the American Petroleum Institute with the National Bureau of Standards.[28] The 100 percent line (ratio blank without absorber) under the same conditions remains steady between 800 and 2500 cm^{-1}, but rises through a few percent at longer and shorter wave-lengths. The rise at short wave-lengths is caused by differential absorption in the imperfectly positioned silver chloride lens, at long wave-lengths, by stray light which is unequally distributed between the two beams. The first effect can be eliminated by substitution of reflecting optics for the lens, the second one by the use of filters.

Survey spectra are ordinarily run in 25 minutes with

---

[28] American Petroleum Institute Research Project 44 at the National Bureau of Standards. Catalog of Infra-Red Spectrograms, Serial No. 307 and Serial No. 498.

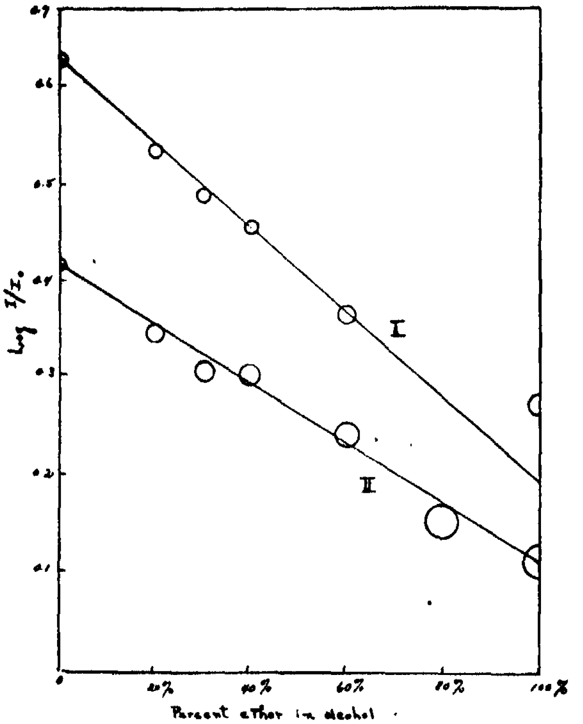

FIG. 12. Infra-red analysis of mixtures of methylethylisobutyl carbinol and its methyl ether.

slight loss of resolution in the region from 5000 cm^{-1} to 2000 cm^{-1} with the response time used here. All the resolution shown in Fig. 11 may be retained at the higher scanning speed by increasing the speed of response, with consequent increase in the noise level. The compromise between recording speed and response time is entirely at the discretion of the operator and is selected to suit the problem. Time constants (time to reach 63 percent of full deflection) of the ratio system range from 1.2 to 2.25 seconds. The lower limit is imposed by the maximum rate at which the pen can be driven (3.8 sec. for full scale deflection[14]). The accuracy of the ratio measuring device was checked by comparing calculated and measured ratios of A/B, A/C, and B/C in the range 15 percent to 90 percent, with applied signals of 1.6 to 10 millivolts. Maximum error was found to be 1.1 percent with an average deviation of ±0.4 percent, which was well within the peak to peak noise level of 1 percent. Further evidence, less accurate, but included for the sake of completeness, of the fidelity of the ratio measurement, as well as of the separation of the sample and reference signals, is given in the Beer's Law curves of Fig. 12, in which the logarithm of I/I_0 is plotted for various solutions of methylethylisobutyl carbinol and its methyl ether.[29] Curve I is based on an ether band at 810 cm^{-1}, curve II is based on an ether band at 840 cm^{-1}. The data are rough because solutions were made up by dropper to a total volume of 20 drops. Spectra were observed using a sealed cell with 0.1-mm aluminum spacer *versus* a single rocksalt plate in the reference half of the beam. The circles indicate only ±0.5 percent in transmission, while the maximum peak to peak noise level of the records was 1.5 to 2 percent.

We have verified experimentally that the ratio remains independent of slit width and amplifier gain over the whole range of adjustments available to us. The noise on the ratio scale also is observed to be independent of gain.

SUMMARY

A ratio-recording double beam infra-red spectrophotometer has been described which can be constructed with no changes in the optical system of the commercial monochromator and with no sacrifice of versatility and ease of prism interchange. There are no very exacting requirements in either the mechanical or the electrical design. Its cost is little, if any, more than the cost of conversion of a d.c. instrument to ordinary a.c. operation. Percent-transmission spectra over the complete rocksalt region can be obtained in 25 minutes with good resolution, and with no attention from an operator. With the sector moved very close to the slit, samples less than 1×6 mm in size can be studied. In the extreme cases where it is necessary to work at the limit of resolution of the monochromator, the instrument can be immediately converted to direct deflection operation but with a gain in the signal to noise ratio of at most a factor of two. Any rapid response detector, such as the nickel-strip bolometer, the Thermistor detector,[30] or fast thermocouple could be substituted for the Golay cell with appropriate changes in the amplifier, although there might be some loss in signal to noise ratio, depending on detector speed.

It should be emphasized here that this system is readily adaptable to visible and ultraviolet spectrophotometers, as well as to any infra-red instrument. Where photo-tube operation is possible, fast response of the detector is not a problem, and the signal frequency can be increased to some more conveniently handled value than 10 cycles per second.

---

[29] W. von E. Doering and H. H. Zeiss, J. Am. Chem. Soc. 72, 147 (1950).

[30] See reference 1, pp. 158–159.

THE REVIEW OF SCIENTIFIC INSTRUMENTS VOLUME 21, NUMBER 3 MARCH, 1950

Focusing Properties of a Generalized Magnetic Spectrometer

David L. Judd*
California Institute of Technology, Pasadena, California

(Received August 1, 1949)

The first-order focusing properties of a magnetic spectrograph similar to that of Siegbahn and Svartholm, but differing in that both source and collector lie outside the field, are investigated. The parameters of the analogous thick lens optical system are derived. General expressions for image distance, astigmatism, magnification, solid angle, dispersion, and resolution of lines with a spread in momentum are obtained. Factors affecting the compromise between intensity and resolution are discussed. The possibility of increasing resolution without loss of intensity by introducing some astigmatism is considered. Second-order effects have not been included since they are thought to be of the same order as corrections for the fringing field. The first approximation proved adequate for the design of an instrument in which satisfactory focusing was obtained by simple empirical adjustments.

I. INTRODUCTION

In the double-focusing or anastigmatic magnetic spectrometer developed by Siegbahn and Svartholm,[1] both source and collector are located in the magnetic field. This arrangement is experimentally inconvenient, especially if the source is to be activated by artificially accelerated particles. For this reason, a study was made of the focusing properties of a modified arrangement in which both source and collector are located outside the field, as a guide to the design and construction[2] of such an instrument. The first-order theory of images formed by particles whose paths are paraxial to an optic axis, in analogy with Gaussian optics, can easily be developed from simple geometric considerations; the deviations from the equilibrium trajectory are known to be sinusoidal[3] to first order inside the field region, and rectilinear outside it. It was not considered worth while to calculate the more involved second-order aberrations since they will be of the same order of magnitude as other aberrations resulting from the effects of the fringing field[4] and other discrepancies between ideal and practically attainable fields. This opinion was justified by the fact that satisfactory focusing of the spectrometer finally constructed[2] was attained through simple empirical adjustments of source and collector positions.

II. THE MAGNETIC FIELD

The field is assumed to exist only in the wedge-shaped region between the planes $\vartheta=0$ and $\vartheta=\theta$ of a cylindrical polar coordinate system r, ϑ, z. In this region it is assumed to be symmetric about the plane $z=0$ and to be independent of ϑ. If its components are expanded in double Taylor series about the values at $r=r_0$, $z=0$, and only constant and first-order terms retained, Maxwell's equations and the symmetry conditions yield

$$H_z \approx H_{z0}[1-n(r-r_0)/r_0]; \quad H_r \approx -nH_{z0}z/r_0$$

where H_{z0} is a constant; $H_z \propto r^{-n}$ near $r=r_0$, $z=0$. The two field parameters of importance in the first-order theory are θ and n; there is no focusing unless $0<n<1$. The fringing fields near $\vartheta=0$ and $\vartheta=\theta$ are neglected since they lead to second-order corrections.

III. FOCAL DISTANCES

Let a point source of monoenergetic charged particles of rest mass m_0, velocity v, mass $m=m_0[1-v^2/c^2]^{-\frac{1}{2}}$, and charge e be placed in the plane $z=0$, outside the field at a distance d_0 from the plane $\vartheta=0$ on a line tangent to the circle $r=r_0$, $z=0$ at the edge of the field [Fig. 1(a)]. If $H_{z0}=-mv/er_0$, a particle whose path is normal to the plane $\vartheta=0$ outside the field will be bent in a circle of radius r_0 in the field, and will emerge normal to the plane $\vartheta=\theta$. Its path will lie in the plane $z=0$, and will be called the optic axis of the system. Particles following paraxial trajectories lying in the plane $z=0$ will focus on the optic axis at a distance d_r beyond the plane $\vartheta=\theta$; particles following paraxial trajectories whose projections onto the plane $z=0$ lie on the optic axis will focus on this axis at a distance d_z beyond the plane $\vartheta=\theta$ [Fig. 1(b)]. We shall measure all distances in units of r_0 to simplify the notation.

To find d_z and d_r we note[3] that inside the field $z=A\sin n^{\frac{1}{2}}(\vartheta-a)$; $r-1=B\sin(1-n)^{\frac{1}{2}}(\vartheta-b)$, where A, B, a, and b are constants. Also

$$\partial \log z/\partial\vartheta\,|_{\vartheta=0}=d_0^{-1}; \quad \partial \log z/\partial\vartheta\,|_{\vartheta=\theta}=-d_z^{-1},$$

and similarly for r; hence

$$\tan[n^{\frac{1}{2}}\theta+\tan^{-1}n^{\frac{1}{2}}d_0]+n^{\frac{1}{2}}d_z=0,$$

and d_r is obtained by replacing $n^{\frac{1}{2}}$ by $(1-n)^{\frac{1}{2}}$. We may thus obtain d_z and d_r for given d_0, θ, and n from the two equations (obtained by taking either subscripts r or z)

$$\phi_{r,z}+\phi_{r,z}'+\theta_{r,z}=\pi,$$

where

$\tan\phi_z=n^{\frac{1}{2}}d_0$, $\tan\phi_z'=n^{\frac{1}{2}}d_z$, and $\theta_z=n^{\frac{1}{2}}\theta$, and quantities

---

* Now at the RAND Corporation, Santa Monica, California.

[1] K. Siegbahn and N. Svartholm, Nature 157, 872 (1946); Arkiv. f. Mat. Astr. o. Fys. 33A, No. 21 (1946); F. B. Shull and D. M. Dennison, Phys. Rev. 71, 681 (1947), as corrected in Phys. Rev. 72, 256 (1947).

[2] Snyder, Lauritsen, Fowler, and Rubin, Phys. Rev. 74, 1564 (1948); C. W. Snyder, doctoral thesis (California Institute of Technology, 1948).

[3] D. W. Kerst and R. Serber, Phys. Rev. 60, 53 (1941).

[4] N. D. Coggeshall, J. App. Phys. 18, 855 (1947).

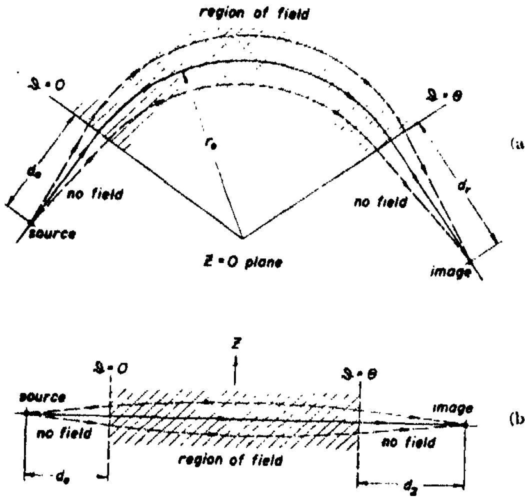

FIG. 1. (a) Radial focusing; (b) vertical focusing.

with subscripts r can be obtained by the same substitution. These equations have the simple geometric interpretation of Fig. 2. They are quite general, and include as special cases the results of Stephens[5] in which $n=0$ (uniform field) and of Siegbahn and Svartholm[1] in which $n=\frac{1}{2}$, $d_0=d_r=d_z=0$, and $\theta=2^{\frac{1}{2}}\pi$. In Stephens' case, Fig. 2(b) becomes the physical diagram of field, object, and image. The well-known semicircular focusing method comprises a special case of Stephens' result when $d_0=d_r=0$ and $\theta=\pi$. If $n=\frac{1}{2}$, Figs. 2(a) and 2(b) become identical and we have a point image for paraxial particles. The equations are not applicable to negative d's. For double-focusing, the first-order astigmatism is

$$d_z-d_r=\{d_z+(1+d_z^2/2)[\theta+d_0/(1+d_0^2/2)]\}(1-2n)$$

for n near $\frac{1}{2}$, and approximately equals $5(1-2n)$ for $d_0\sim d_z\sim d_r$ and $\theta=\pi$.

Since the system acts like a thick lens, focal points and unit planes may be located in analogy with the usual optical treatment.[6] The nodal points coincide with the unit points due to the symmetry of the lens. The principal foci are found by setting $d_0=\infty$; for vertical focusing they lie outside the field edges by distances $\Delta_z=(n^{\frac{1}{2}}\tan n^{\frac{1}{2}}\theta)^{-1}$, and Δ_r is obtained by replacing $n^{\frac{1}{2}}$ by $(1-n)^{\frac{1}{2}}$. The focal length f_z is found from the equation $(d_0-\Delta_z)(d_z-\Delta_z)=f_z^2$, yielding $f_z=(n^{\frac{1}{2}}\sin n^{\frac{1}{2}}\theta)^{-1}$, and similarly for f_r. The unit planes lie inside the field edges by distances $u_{z,r}=f_{z,r}-\Delta_{z,r}$;

$$u_z=n^{-\frac{1}{2}}(\csc n^{\frac{1}{2}}\theta-\cot n^{\frac{1}{2}}\theta)=n^{-\frac{1}{2}}\tan 2^{-1}n^{\frac{1}{2}}\theta,$$

and u_r is similarly obtained. All of these relationships are illustrated in Fig. 3. The unit planes always lie inside the field region for cases of practical interest, but the principal vertical (or radial) foci may lie either outside or inside according to whether $n^{\frac{1}{2}}\theta$[or $(1-n)^{\frac{1}{2}}\theta$] is less or greater than $\pi/2$. The Siegbahn instrument represents a limiting case in which $\Delta=f=\infty$, $u=0$.

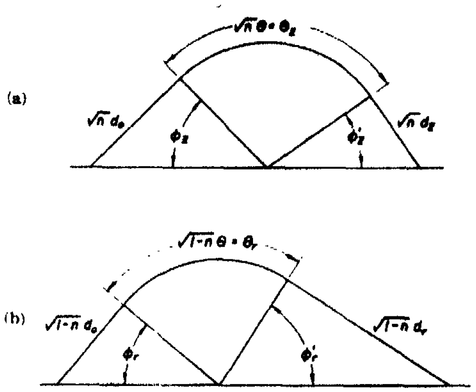

FIG. 2. Geometric relations for (a) radial focusing; (b) vertical focusing.

IV. MAGNIFICATION

The vertical magnification M_z is defined as the ratio of image height to object height measured normal to the plane $z=0$; the lateral magnification M_r is similarly defined. We define M_r and M_z to be positive if the image is inverted in the respective directions; they can be found from the equation $M=f/(d_0-\Delta)$, which results in the two equations

$$M_{r,z}=(\tan\phi_{r,z}\sin\theta_{r,z}-\cos\theta_{r,z})^{-1}.$$

These give $M_r=M_z=1$ for the Siegbahn arrangement and for any other symmetric arrangement of object and image.

V. SOLID ANGLE

If the paraxial beam of particles attains its maximum cross-sectional dimensions in the radial and vertical directions inside the field regions (i.e., if d_r and $d_z\leq\infty$, corresponding to converging or parallel outgoing beams) and if the available cross-sectional area Ar_0^2 is independent of ϑ, then the solid angle Ω in which emitted particles reach the focal points is independent of the field angle θ and of the values of ϑ at which the maxima are attained. It can be shown that

$$\Omega/A=[(1+d_0^2)/n(1-n)+d_0^4]^{-\frac{1}{2}}$$

subject to the usual cosine approximation for beams of small divergence. This function is plotted in Fig. 4;

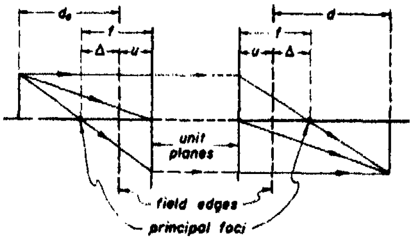

FIG. 3. Thick lens analogy.

---

[5] W. E. Stephens, Phys. Rev. 45, 513 (1934).

[6] For example, P. Drude, *Theory of Optics* (Longmans, Green and Company, New York, 1939), Chapter II.

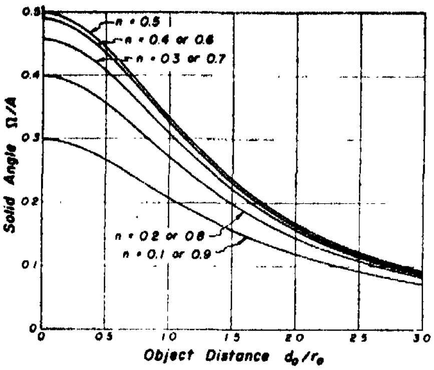

FIG. 4. Solid angle *versus* object distance for different n.

$\Omega/A=\frac{1}{2}$ for the Siegbahn case. If $n=\frac{1}{2}$,

$$\Omega/A=(d_0^2+2)^{-1}.$$

VI. DISPERSION

Suppose that the field H_{z0} is adjusted for focus of particles of momentum $p=mv$, as described previously; then, if particles of momentum $p+\delta p$ are emitted from the same point source, their focal distances d_r and d_z will increase by amounts δd_r and δd_z, and their radial focus will move outward normal to the optic axis by an amount δx. This distance is a measure of the dispersion D, defined here as $D\equiv\delta x/(\delta p/p)$. It is given by the simple formula

$$D=(1+M_r)/(1-n).$$

This reduces to $D=4$ for the Siegbahn case and to the well-known result $D=2$ for semicircular focusing. It can be shown that

$$\delta d_r/(\delta p/p)=\tfrac{1}{2}\left(\frac{n}{1-n}\right)\left[d_r+\{d_0+\theta[(1-n)d_0^2+1]\}M_r^2\right]$$

and

$$\delta d_z/(\delta p/p)=\tfrac{1}{2}\left[d_z+\{d_0+\theta[nd_0^2+1]\}M_z^2\right].$$

Both reduce to $2^{-\frac{1}{2}}\theta$ for the Siegbahn case; in semicircular focusing there is no d_z, and $\delta d_r=0$.

VII. RESOLUTION

In principle, the resolving power is a function of the size and shape of the image of a point source formed by the particles emitted in a finite solid angle; these depend on the deviations from the linearized theory, which in turn depend on the values assigned to higher derivatives of the field strength than the first, and on effects of the fringing fields. A calculation of these effects would form a generalization of the work of Svartholm[7] and of Shull and Dennison,[1] and would be qualitatively similar. In general, it will be possible to make the image very small in either the radial or vertical direction, but not in both simultaneously, by proper choice of the higher field derivatives and by appropriate shaping of the pole piece ends. However, it is believed that an empirical approach to this problem is more practical, since a second-order calculation including fringing effects would become very cumbersome.

In practice, the necessity for use of source and collector apertures of finite size for particles with broad-line momentum spectra modifies the problem of resolution. A practical criterion of resolving power is obtained by computing the fractional change in momentum required to move an image out of the collector slit so that it will not be confused with an adjacent image. If we assume that the collector slit width s' is adjusted so as to just receive the image of the source slit formed by the spectrograph, the required momentum change $\delta p/p=s'/D$; we define its reciprocal as the resolving power R. If there are no aberrations, $s'=M_rs$, where s is the source width. Actually, $s'=\alpha M_rs$, where α is a number somewhat greater than unity depending on the aberrations; we then have

$$R=(1+M_r^{-1})/\alpha s(1-n).$$

VIII. DISCUSSION

The design objectives are to attain maximum solid angle Ω and resolving power R for reasonable values of the d's; the available parameters are d_0, θ, and n. An inspection of the results obtained above shows that to maximize Ω one must take $d_0=0$ and $n=\frac{1}{2}$. These are the choices of Siegbahn, and any departure from them will decrease Ω, so that the price paid for a conveniently accessible source and collector is a reduction in intensity. However, to maximize R one must take n as large as possible and use small magnification (which requires large d_0). These requirements both conflict with those for large Ω, so the usual compromise must be made, based on the relative importance of these criteria.

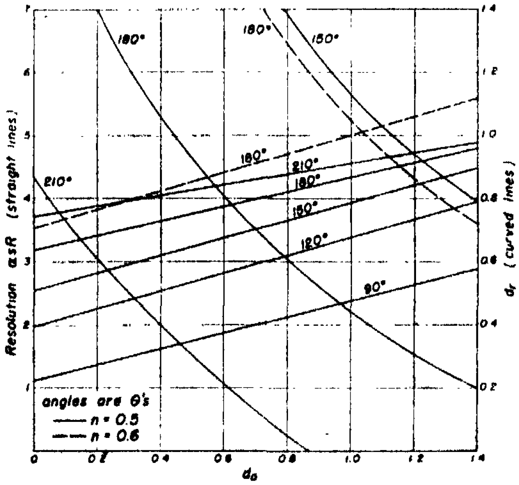

FIG. 5. Resolution and image distance for radial focusing *versus* object distance, for different n and θ.

---

[7] N. Svartholm, Arkiv. f. Mat.-Astr. o. Fys. 33A, No. 24 (1946).

We must have $n=\frac{1}{2}$ for double-focusing,* but for other values of n a point source becomes a vertical line image at d_r for a paraxial beam, as in uniform field focusing, but perhaps much shorter. By use of a line collector at this point, momentum separation could be achieved; however, some types of detectors are not appropriate for line collection. Ω is much less sensitive than R to small changes in n, which indicates that there may be an advantage in choosing n somewhat greater than $\frac{1}{2}$ for applications requiring large R, if a line collector can be used.

The general effect of decreasing θ is to weaken the power of the lens and thus to increase the d's and decrease Ω. For given d_0 and n (and hence Ω), R is increased by increasing θ, which brings the image nearer the field edge. If we require d_0 and $d_r>0.5$ to keep source and collector well out of the field, and $n=0.5$ for double-focusing, we must have $\theta<200°$. By taking $\theta=180°$, we satisfy this and leave room for some flexibility; there is the additional advantage that both pole pieces may be symmetrically machined at once, as was done in reference 2. The resolving power may then be increased by 14 percent by increasing d_0 from 0.5 to 1.0, at a loss of 18 percent in intensity. The use of smaller θ merely results in less intensity for the same resolution, or vice versa.

If we abandon double-focusing, we may improve resolving power somewhat at almost no cost in solid angle. For example, if $\theta=\pi$, $d_0=0.7$, we have 12 percent larger R with $n=0.6$ than with $n=0.5$ (see Fig. 5); it can be shown that a point source produces a line image about 0.9 times as high as the pole piece clearance in this case. The principal difficulty in devising arrangements with larger n or θ to gain further in R lies in holding down this height. The disadvantages of a line collector probably outweigh the gain in R; R can always be raised in the double-focusing instrument by stopping down to reduce the aberrations, if necessary.

IX. ACKNOWLEDGMENTS

The author wishes to express his gratitude to Dr. R. F. Christy, who suggested this investigation, and to Dr. W. A. Fowler and Dr. C. C. Lauritsen for their encouragement and helpful discussion.

---

* There exist exceptional cases in which an intermediate radial or vertical focus, but not both, occurs inside the field region, but these are uninteresting since they require a particular d_0 for given θ, and occur only for $\theta>n^{-\frac{1}{2}}\pi$ or $(1-n)^{-\frac{1}{2}}\pi$; focusing forces are widely different in the radial and vertical directions, and the system lacks flexibility.

THE REVIEW OF SCIENTIFIC INSTRUMENTS VOLUME 21, NUMBER 3 MARCH, 1950

The Scintillation Counter as a Low Resolution Gamma-Ray Spectrometer

Robert W. Pringle, Kenneth I. Roulston, and Harry W. Taylor
Physics Department, University of Manitoba, Winnipeg, Canada

(Received October 10, 1949)

A scintillation gamma-ray spectrometer has been developed, which is of particular use for the study of isotopes of low specific activity and in which the energies of the gamma-rays are identified from the pulse height distributions of the recoil electrons produced in an activated NaI crystal. The Compton distributions are easily recognized, and a study of the gamma-radiation of Co^{60} and I^{131} shows a proportionality to exist between the total light output per scintillation and the energy of the corresponding secondary beta-ray particle. The noise level of the RCA 5819 photo-multiplier, as used in this test, corresponded to an energy on the pulse height scale of less than 20 kev. A brief description is given of a new type of differential pulse height analyzer which has been developed for work of this type.

FOR some time work has been going on in this laboratory to develop a scintillation gamma-ray spectrometer in which the energies of the gamma-rays could be found from the Compton distributions of recoil electron energies which, it was anticipated, would be identified in the differential pulse height distribution curve obtained with a suitable scintillation counter[1] exposed to the gamma-radiation. The assumption is made of a proportionality between the total light output per scintillation and the energy of the secondary beta-particles. However, for a given energy of beta-particle there will be fluctuations in the number of quanta which are emitted and which actually reach the photo-sensitive surface. This effect will determine the upper limit to the resolution of the spectrometer. Consideration must also be given to the fluctuations in the photo-multiplier amplification due to events in the first one or two stages, but with these limitations the device was expected to behave as a proportional counter. It was not anticipated at the present stage that the resolution obtainable would therefore be equal to that of the best beta-ray spectrometer measurements, but the method is unique in its extreme efficiency for counting and its obvious

---

[1] For earlier work on scintillation counters see: H. Kallmann, Natur und Technik (July, 1947); J. W. Coltman and F. H. Marshall, Phys. Rev. 72, 528 (1947); M. Deutsch, Nucleonics 2, 58 (1948); P. R. Bell, Phys. Rev. 73, 1405 (1948); R. J. Moon, *ibid.*, 1210; R. Hofstadter, *ibid.* 75, 796 (1949); P. R. Bell, Oak Ridge Conference.

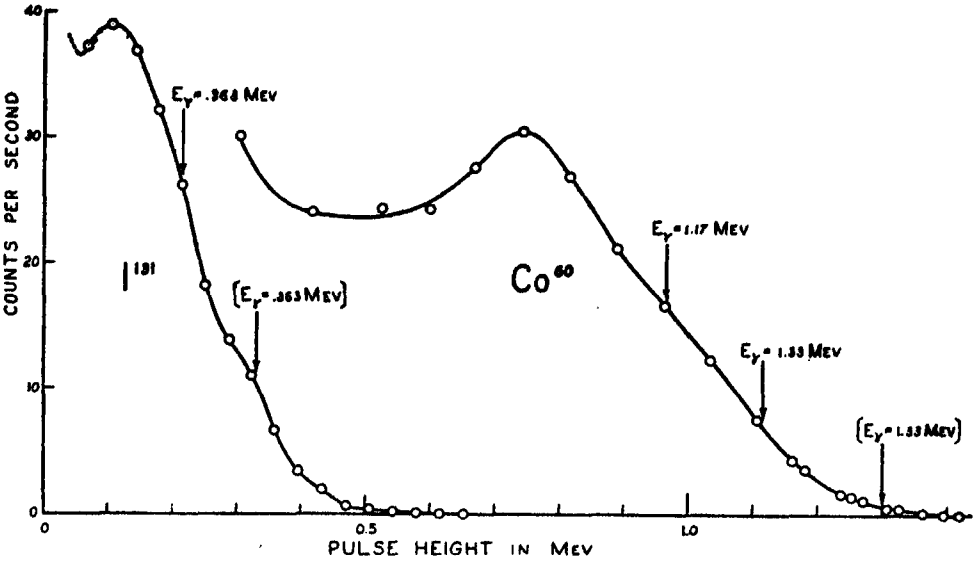

FIG. 1. Recoil electron spectra in NaI crystal. Distribution with pulse height (in Mev) of the pulses in a given range of energies.

use in the study of isotopes of low specific activity, quite apart from the relative simplicity and compactness of the equipment. Further, the ability of such a device to resolve gamma-ray energies opens up new possibilities in the study of gamma-gamma-coincidences and beta-gamma-coincidences for the elucidation of nuclear energy level schemes, where the limitations of the Geiger counter are already well known.*

The advantages of choosing a very dense crystal with a large light output per pulse lie in increased counting efficiency, higher resolution of energies and increased signal to noise ratio, but a disadvantage is the problem of light gathering owing to effects of total reflection in the crystal. It is obvious that large single crystals are desirable as the relative effect due to the secondary beta-particles which leave the surface of the crystal must be kept small, and the effective solid angles (for the collection of quanta) which are subtended at the photo-sensitive surface by the different parts of the crystal should be substantially the same—as they would not be were a polycrystalline mass used. With these considerations it was decided that the best crystal to employ was sodium iodide activated with thallium iodide. A single crystal of this material, with 1 percent thallium activation, was cut in the form of a truncated cone of maximum diameter 1¾ inches, ½ inch thick, with sides designed to throw the maximum amount of light onto the photosensitive surface. The surfaces of the crystal remote from the photo-multiplier were highly polished and covered with a reflecting layer of tinfoil. The surface adjacent to the multiplier was slightly roughened to reduce effects of total reflection and hence improve the light transmission. A good contact with the surface of the photo-tube was obtained with Canada balsam. The necessity of a maximum gathering of light limits the choice of photo-tube to the new RCA 5819 wide-angle photo-multiplier which has a 1¾-inch diameter flat transparent cathode. A multiplier voltage of 870 was used in the experiments. It is essential to integrate with the amplifier as completely as possible over the average duration of a scintillation, about ½μsec.,[2] and yet retain sufficient resolution at the counting rates involved.

Figure 1 shows the distributions with pulse height of the number of pulses in an arbitrary range of pulse heights, which were obtained with collimated gamma-rays from sources of Co^{60} (gamma-ray energies 1.17 Mev and 1.33 Mev)[3] and I^{131} (principal gamma-ray energies 80 kev, 284 kev, 363 kev, and 600 kev).[4] The probable error in the counting statistics is better than 2 percent for any of the observed points, and the counting rate for points near the peak of the Co^{60} curve is of the order of 2000/min. As no very prominent photoelectric effect was obtained with the iodine atoms in the crystal lattice the question arises as to the best procedure to adopt for the identification of gamma-ray energies. It was decided on the basis of earlier experience,[5] to associate the upper energy limit of the Compton distribution, or the limit corresponding to $\theta=0$ in the Compton formula, with the inflection point of the energy distribution curve. The inflection point may be obtained by plotting the second differential curve as the differences between the successive readings for the first differential curve. Where two Compton distribution curves are superimposed as, for example, in the Co^{60} curve, the positions of the inflections on the combined curve will not necessarily coincide with the positions of the inflections on the separate curves. If an approximate separation can be made better values can be obtained. This has been done using the results of Fig. 1 and employing a simple graphical separation of the effects near the end point on the assumption of the existence of two gamma-rays of energies 1.17 and 1.33 Mev in equal intensities. It is not suggested that the results would have been accurate enough in themselves to resolve adequately the effects of these two energies. On this basis it was possible to calibrate the pulse height in terms of beta-particle energy as in Fig. 1. All the values indicated in this figure are of known energies placed according to the calibration. The values indicated in brackets refer to possible photoelectric effects with the iodine atoms in the crystal lattice. There is no such effect very evident with the Co^{60} radiations, but with the lower energy I^{131} radiations there seems to be a partially resolved photo-electron line due to the strong 363-kev component. The weak 600-kev component produces a small Compton effect only and the inflection point for the main distribution corresponds well to that expected for the Compton effect with the 363-kev component.

---

* *Note added in proof.*—A number of natural isobaric nuclei of neighboring atomic number have been tested for possible gamma-ray activity, and the purest materials have been sought for this purpose. Lanthanum (39 g La_2O_3) showed an activity of 0.7±0.1 quanta/second/g which could not be attributed to a naturally occurring radioactive impurity, and the gamma-ray energy was estimated at 1.05±0.05 Mev. An upper limit to the half-life of La^{138} of 1.2×10 in. years is thus obtained [Phys. Rev., to be published]. The energy of the gamma-ray emitted in the disintegration of K^{40} has been estimated at 1.47±0.03 Mev [Phys. Rev. 76, 841 (March 15, 1950)], using 90 g of KCl. Sharply resolved lines due to photoelectric effects with the iodine atoms in the crystal lattice have been obtained with low energy gamma-rays (e.g., the Au^{198} 411 Mev line). A rare high energy gamma-ray of energy 1.1 Mev has been found with Au^{198}, present in less than 1 percent of the disintegrations.

In recent comparisons of gamma-ray energies it has sometimes been found easier to use the approach to the pulse height axis, rather than the inflection point of the distribution as described above. The single channel differential discriminator will shortly be replaced by a five-channel "hicksorter." A gamma-ray coincidence scintillation spectrometer has just been constructed.
R. W. P.

[2] W. C. Elmore and R. Hofstadter, Phys. Rev. 75, 203 (1949).
[3] D. A. Lind *et al.*, Phys. Rev. 76, 591 (1949).
[4] F. Metzger and M. Deutsch, Phys. Rev. 74, 1640 (1948).

Thus we see that there is no evidence to disprove the anticipated proportionality between beta-ray energies and scintillation light output in the range of energies involved. The rise in counting rate below 0.4 Mev for Co^{60} appears to be due to the presence of degenerate radiation as well as to the loss of secondary beta-particles from the surfaces of the crystal. Part of the rise below 90 kev with I^{131} is, of course, due to low energy components. The noise level in the photo-tube corresponds to an energy on our scale of less than 20 kev for beta-particles, and it is only below this level of pulse heights that the signal to noise ratio deteriorates. This is an important result inasmuch as it indicates the lower limit of beta-particles energy which can be studied effectively in this arrangement with the photo-tube operating potential of 870 volts.

The electronic equipment consists of a conventional linear amplifier and scaler, and a pulse height differential discriminator built in this laboratory. This functions as a one channel "kicksorter" and consists essentially of two Schmitt trigger circuits followed by an anticoincidence system. The bias voltages used in each trigger circuit can be adjusted with precision potentiometers and thus the minimum amplitudes of pulses necessary for triggering can be selected in each case. In practice the levels of the two circuits are set some 2–5 volts apart, and with the incoming pulses from the linear amplifier up to approximately 100 volts in magnitude this implies a subdivision of the range into 20–50 steps. The output pulses from the trigger circuits are obtained by loading the second tube in each with an inductance in parallel with an I N 34 crystal diode. This gives positive-going pulses of approximately $\frac{1}{2}$-μsec. duration.

The discriminator is required to pass a triggering pulse to the scaler when only one of the Schmitt circuits operates, but not to pass a pulse when neither operates or both operate. Thus an anticoincidence circuit is required. The circuit used here is a simple differential amplifier consisting of two tubes cathode coupled. The two Schmitt circuits are coupled to the two grids and the output for the scaler is obtained from the plate of one of the tubes.

Owing to the finite rise time of the amplifier, pulses from the Schmitt circuits caused by the same input pulse do not occur simultaneously. But they are required to cancel each other in the differential amplifier. To overcome this difficulty the tube to which the earlier pulse is applied is biased beyond cut-off so that only the center portion of the pulse is used. By this means adequate cancellation is obtained. Wire-wound and stabilized carbon resistors are used where desirable to maintain d.c. levels as constant as possible. The stability of the triggering level appears to be better than 0.1 volt and the discriminator could not have reduced the resolving power of the spectrometer by any appreciable amount.

More recent work, to be published soon, has concerned the disintegration scheme of K^{40}, and the development of new highly efficient gamma-gamma- and beta-gamma-coincidence apparatus in which the energies of the gamma-rays are analyzed by the method which has been described. Attempts are also being made to develop the measurement of fast neutron energies with the above technique using the recoil protons formed in crystals of anthracene. In particular, a study is being made of the energies of the neutrons from a Po—Be source, but the presence of gamma-radiation of high energy from the excited C^{12} nucleus makes the interpretation of the results difficult. Further work with gamma-rays is centered on the development and use of crystals containing heavy atoms, so as to render much more significant the photo-electron lines in the pulse height distribution curves.

---

[5] K. Siegbahn, Proc. Roy. Soc. A189, 527 (1947).

THE REVIEW OF SCIENTIFIC INSTRUMENTS VOLUME 21, NUMBER 3 MARCH, 1950

A Radiofrequency Spectrograph and Simple Magnetic-Field Meter*

R. V. POUND
Lyman Laboratory, Harvard University, Cambridge, Massachusetts

AND

W. D. KNIGHT**
Trinity College, Hartford, Connecticut

(Received November 21, 1949)

A simple oscillating circuit with a special feed-back circuit is employed as a tool for the search for and detailed analysis of nuclear paramagnetic absorption lines. The sensitivity approaches the optimum for a given noise band width and particularly useful is the ease of conducting slow, continuous changes of frequency while recording the output data. Spectra having several components at scattered frequencies are thus displayed. Line shapes are unambiguously recorded because of the absence of sensitivity to dispersion. Using protons in water, or solutions containing Li^7, the device can be used as a versatile and extremely precise meter for measuring magnetic field strengths in the range from about 100 to 25,000 oersteds with a minimum of auxiliary equipment.

INTRODUCTION

THE apparatus used for observing the absorption[1,2] or the dispersion associated[2–4] with nuclear paramagnetic resonance in matter has most frequently taken the form of a radiofrequency bridge circuit supplied with a fixed frequency signal from a master oscillator. Variations in the amplitude of the signal transmitted through the bridge, that occur as the magnetic field is moved through the resonance, are observed on an oscilloscope. For many of the weaker lines in solids and particularly for observation of line shapes, observation is made with a meter fed from a phase sensitive detector. To facilitate the observation of resonances of complex character and for searching for unknown lines, a spectrometer that operates with a varying frequency, while the magnetic field is held constant, is of considerable utility. Because the nuclear resonance effect is very weak in crystalline solids, any device for this use must be so designed that the available signal-to-noise ratio is very nearly achieved and it is in this respect that the device to be described here is thought to represent a useful innovation.

Others have devised devices for observing nuclear resonance using oscillators[5,6] and super-regenerative detectors.[5,7] These have been used principally for determining gyromagnetic ratios with liquid samples having short relaxation times. Little information has been given, however, on the adaptability of these devices to a range of relaxation times and line breadths, and on the degree of attainment of the signal-to-noise ratio theoretically available. The super-regenerative scheme, because of its complex signal spectrum, seems ill-fitted to the study of line breadths or shapes in crystalline samples, although, judging from the large number of nuclei for which gyromagnetic ratios have been reported,[8,9] it must approximate the optimum sensitivity.

BACKGROUND CONSIDERATIONS

Unfortunately a genuinely versatile r-f spectrometer should be variable over a wide range of r-f signal power levels and scanning rates as well as of frequencies because the nature of the resonance lines varies widely with the kind of a sample. Consider two equations taken from reference (2). First, Eq. (64)

$$A_s/A_n = 1.6\times 10^{-4} V_c^{2/3} \eta A h^2 N_0 \gamma^{11/4} \times H_0^{7/4} T_2^{*\frac{1}{2}} I(I+1)/kT(kTBF)T_1^{\frac{1}{2}} \quad (1)$$

gives, approximately, the maximum available amplitude ratio of signal-to-noise as a function of the various parameters descriptive of the sample and the conditions of the experiment. The number that results if one is concerned with a resonance in a solid having a thermal relaxation time T_1 of several seconds, a spin-spin relaxation time T_2 of, say, 10^{-4} sec. (line breadth of approximately 10 kc/sec.), a γ of 5000 radians per second per gauss (nuclear magneton, spin of one), N_0 of 10^{22} (fairly rich in the subject nuclei), in a field of 5000 gauss, for a 1-cc sample at room temperature is about $4/(FB)^{\frac{1}{2}}$ where FB is the effective noise figure[10] times the effective noise band width. Thus, this case, typical of many solid samples, requires for detection with the optimum noise figure of unity a noise band-width of only about 1 c.p.s. This may be compared with the signal available from a liquid sample containing the same nuclei where T_1 may easily be reduced to be about equal to T_2 by adding paramagnetic ions, and one obtains a 100-fold increase in available signal-to-

---

* An early version of this device was described at the Montreal Meeting of the American Physical Society, June 1947. R. V. Pound, Phys. Rev. 72, 527 (1947).

** Work performed by W.D.K. at Brookhaven National Laboratory, under contract with the AEC.

[1] Purcell, Torrey, and Pound, Phys. Rev. 69, 37 (1948).

[2] Bloembergen, Purcell, and Pound, Phys. Rev. 73, 679 (1948).

[3] Bloch, Hansen, and Packard, Phys. Rev. 70, 474 (1946).

[4] W. W. Hansen, Phys. Rev. 70, 4 (1946).

[5] A. Roberts, Rev. Sci. Inst. 18, 845 (1947).

[6] N. J. Hopkins, Rev. Sci. Inst. 20, 401 (1949).

[7] J. R. Zimmerman and D. Williams, Phys. Rev. 73, 94 (1948).

[8] J. R. Zimmerman and D. Williams, Phys. Rev. 76, 350 (1949).

[9] W. H. Chambers and D. Williams, Phys. Rev. 76, 638 (1949).

[10] H. T. Friis, Proc. I.R.E. 32, 419 (1944).

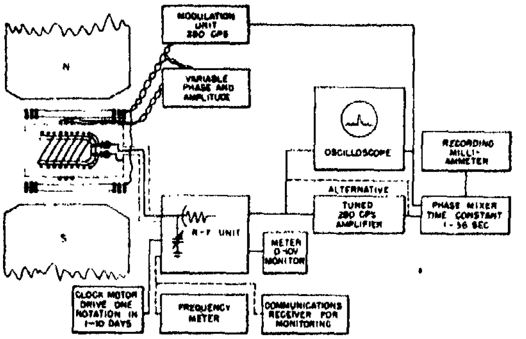
N
S
MODULATION UNIT 280 CPS
VARIABLE PHASE AND AMPLITUDE
OSCILLOSCOPE
RECORDING MILLI-AMMETER
ALTERNATIVE
TUNED 280 CPS AMPLIFIER
PHASE MIXER TIME CONSTANT 1-36 SEC
R-F UNIT
METER 0-10V MONITOR
CLOCK MOTOR DRIVE ONE ROTATION IN 1-10 DAYS
FREQUENCY METER
COMMUNICATIONS RECEIVER FOR MONITORING

FIG. 1. Block diagram of the arrangement of components as an r-f spectrometer.

noise ratio. The often observed proton line in water or mineral oil can be another factor of about 1000 stronger because of the sixfold larger γ and eightfold larger N_0.

The calculation assumes, however, that the optimum r-f signal amplitude is employed, if the absorption effect is being observed, and this cannot be known in advance of knowing values for T_1 and T_2. The condition to be met is [Eq. (59) of reference (2)]

$$\gamma^2 H_1^2 T_1 T_2 = 1, \qquad (2)$$

where H_1 is the amplitude of one of the two circularly polarized signals of which the oscillating r-f field may be considered composed, or is thus one-half the amplitude of the r-f field. At a given value of γ, one might be concerned with the product T_1T_2 in a range from perhaps 10^{-2}, for very sharp lines in liquids, to 10^{-8} for broad, quickly relaxed lines in solids and liquids, a range of 10^6. Such a range cannot be accommodated in the present apparatus, but its level of operation has been found suitable for a wide variety of samples in spite of this.

PRINCIPLE OF OPERATION

As in other methods, the sample is contained in a cylindrical coil placed in the magnetic field with its axis perpendicular to the field lines. A short cable of low capacity (15 $\mu\mu$fd) connects this coil in parallel with a variable condenser forming a shunt resonant circuit. The r-f signal is supplied to this circuit by connecting it to an electronic circuit that forms a two-terminal negative resistance and thus sustains oscillations in the resonating circuit. To just sustain oscillation the magnitude of the negative resistance must be just equal to the positive shunt resistance of the tuned circuit. If it is less than this the level of oscillation rises to a point where curvature of the tube characteristics increases the magnitude of the negative resistance, averaged over a cycle, to the value of the shunt resistance, and equilibrium between the rate of generation and of dissipation of energy is obtained. The magnitude of the negative resistance used here is kept just below the level at which oscillations are sustained and, because the curvature of the tube characteristics is small for such a small voltage swing, the level of oscillation is sensitive to the small changes in shunt resistance resulting from passing through a nuclear resonance. Such variations in level are observed as variations in the amplified r-f voltage after rectification. In the region below saturation of the nuclear resonance, the signal-to-noise ratio should be proportional to the r-f voltage, if the effective noise figure were a constant independent of level. Because the tube characteristics are more non-linear at high levels, one would expect noise components originating in a wider range of frequencies to become mixed with the r-f signal, with a corresponding increase of the noise figure. The effective gain of the circuit, of course, varies widely with the operating level and is highest at the oscillation threshold. That the level of oscillation is sensitive to the shunt impedance, however, results in a very large change in level, soon reaching the limit level, as the frequency is varied, unless a special circuit is employed. The circuit feeds back, through an RC filter a long time constant (2 sec.), the d.c. rectified voltage in such a way as to control the value of the negative resistance and holds the level of oscillation constant at the level far below natural limiting. Variations of amplitude occurring at audiofrequencies are not removed.

Figure 1 is a block diagram showing the method of use of the spectrometer for weak resonances. The required small band width is obtained by modulation of the magnetic field at an audiofrequency with amplitude of a fraction of the anticipated line breadth. As the resonance is passed through by the changing frequency of the oscillator, the level of oscillation varies coherently with the modulation in a phase that reverses at the center of the line. The tuned audio-amplifier and phase sensitive detector, fed also directly with the modulating signal in the right phase, produce a d.c. output which therefore is proportional to the first derivative of the absorption line with respect to field strength. The

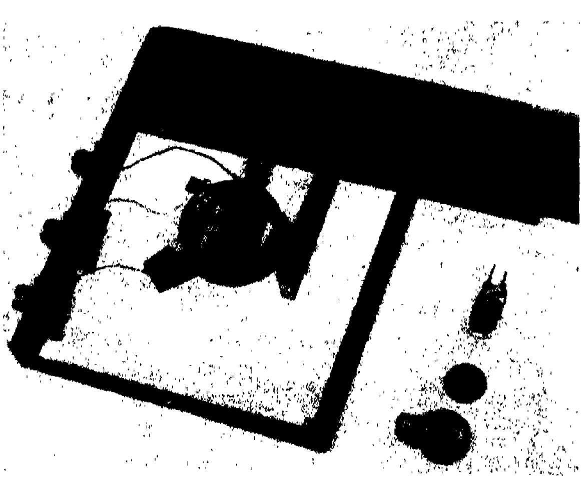

FIG. 2. Photograph of modulation coils, shielding box, and a plug-in r-f coil. At the right is a small unit used for the application as a field meter.

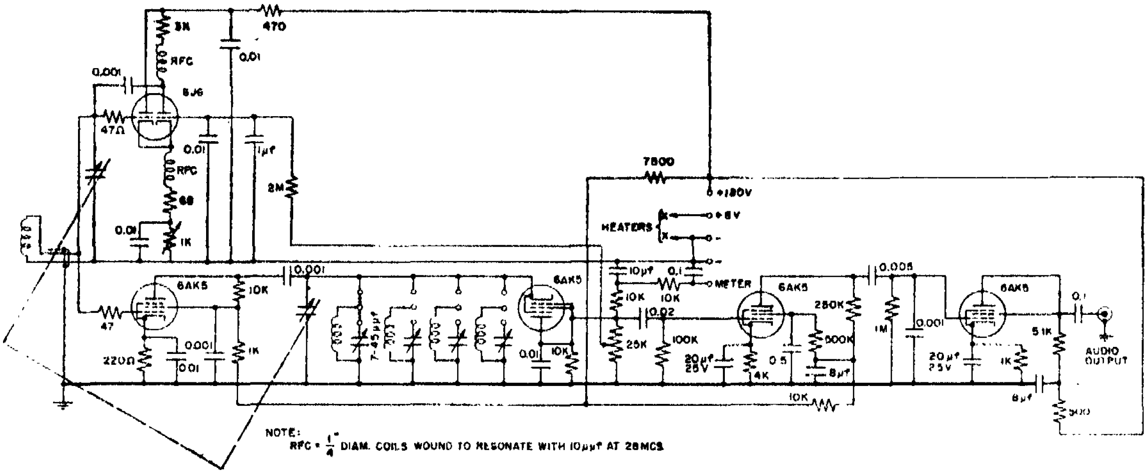

FIG. 3. Circuit diagram of an oscillator unit.

effective noise band width is approximately the reciprocal of the time constant of an RC circuit before the indicating meter. Time constants of 1 sec. and 20 sec. have most commonly been used.

One must not sweep through the resonance in a time less than several times the time constant. Therefore, a very extended search for a narrow but weak line might consume a considerable period of time. With the 20-sec. time constant and a line of 2 kc/sec. width, a sweep rate of about 1 kc/sec./min. would seem desirable. A factor of two in frequency from 6 to 12 mc/sec. can thus be covered in not less than 6000 minutes or 4 days. A 1 r.p.m. synchronous motor and a train of reduction gears is used to obtain one of several rates in this region. Visual observation of the meter would be tedious, and a recording milliammeter is used instead, allowing 24-hour-a-day operation. In this way one is enabled to search for lines without previous clues as to their frequencies.

A serious difficulty is encountered in the fact that a small amount of voltage at the modulation frequency is induced in the r-f coil even though it is ostensibly at right angles to the magnetic field. Such a voltage mixes in the oscillator and produces a strong signal in the phase sensitive detector in the absence of the nuclear resonance. Its amplitude and phase change with tuning of the oscillator, causing serious zero drift in the output indicator. The effect increases with increased modulation frequencies. Because it is found desirable, in order to avoid similar difficulties with flicker effect noise, to use a modulation frequency of several hundred cycles (280 c.p.s.) instead of the 30 c.p.s. common with bridge circuits, this becomes the most troublesome aspect of the system. Several schemes have been used to reduce the effect. One of these was to have adjustable relative positions of the r-f coil and the modulating Helmholtz coils. Two parameters were necessary to get a null in the pick-up; one coil relative to the other and the pair relative to the shield walls of the containing box. This is needed because there are eddy currents in these walls producing an out-of-phase component in the modulation field which cannot be compensated by a single-parameter adjustment. At large modulation amplitudes, the box walls and the modulation coils tend to vibrate in the field and this causes instability in the compensation. A better scheme has been found to be to shield the r-f coil with a thin-walled copper shield supported on a Bakelite form inside the modulation coils. Another coil is wound on the outside of the shield, coaxial with the r-f coil, and supplied with a current of completely variable phase and amplitude derived from the voltage supplying the principal modulation. In this way a stable null in the pick-up can be achieved. Figure 2 shows the parts of the spectrometer, with one of the plug-in r-f coils outside the unit. These are thin-wall

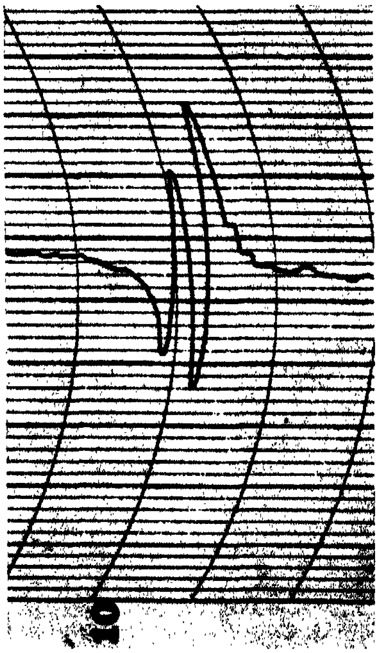

FIG. 4. Record of resonance of Li^7 in aqueous solution with modulation frequency higher (1400 c.p.s.) than line breadth.

glass forms $\frac{1}{2}$ in. i.d. with tungsten prongs fitting a standard miniature tube socket. The 0.003-in. thick copper r-f shield also serves to prevent the r-f voltage from coupling into the modulation system. Such coupling has been found to result in strong false resonances associated with the modulation circuit elements.

THE OSCILLATOR UNIT

Several circuits have been used for the oscillator, that in Fig. 3 being the most recent and most flexible so far tried. The oscillator itself is a cathode coupled 6J6[11] with a peaking coil in the cathode circuit and the second plate circuit to hold up the gain to 45 mc/sec. A one-stage r-f amplifier follows this, with its grid directly connected, except for a small parasitic suppressor, to the oscillator grid. The load circuit of the amplifier is tuned in tandem with the oscillator tuning and a 6AK5 as a diode is used as a rectifier. Two stages of audio amplification are included and r.m.s. noise in a 5 kc/sec. band width at the output is about 0.1 volt. In this version the normally grounded grid of the second half of the 6J6 is used to control the level of oscillation and with 300 μμfd-max. tuning condensers a factor of about 2.3 in frequency can be covered with each set of coils. Thus 1.5 mc/sec. to 45 mc/sec. are covered with four coils. Straight-line-capacity condensers are used. Originally a crystal rectifier was used but it was found to add noise at the higher levels of oscillation. Hence the diode detector was added.

The r-f voltage across the coil can be varied, by variation of the feedback potentiometer and of the cathode bias resistor, from less than about 0.1 v to 1.5 v r.m.s. Because the time average energy stored in the condenser is, in a resonating circuit, equal to the energy stored in the magnetic field, one can compute the region of T_1T_2 for which optimum signal results for this range of voltages with a coil of given volume.

By using Eq. (2), one finds the optimum r.m.s. r-f voltage V_1 to be

$$V_1=(V_c/2\pi\gamma^2T_1T_2C)^{\frac{1}{2}}$$

in electrostatic volts, where V_c is the volume of the coil in cc, and C is the tuning capacitance in centimeters. This leads to values of V_1 for γ in the region of 6000 (gauss sec.$^{-1}$), taking C as 200 cm, and V_c as 2 cc,

$$V_1=1/(2.5\times10^5T_1T_2)^{\frac{1}{2}},$$

where V_1 is now expressed in volts. A level of 0.065 volts is desired if $T_1=1$ sec. and $T_2=10^{-3}$ sec. for these conditions. For shorter values of T_1 a larger voltage is required to get the optimum signal-to-noise ratio but, unless one is working with a diluted sample, or a very small γ, it is not necessary to obtain the maximum signal-to-noise ratios in these cases. Note that as one uses smaller and smaller values of γ, the voltage for optimum signal increases as $1/\gamma$. In the range of small γ's, the method of detection has a strong practical advantage over a bridge method because a bridge must have a very high stability to accommodate large applied r-f voltages, which in turn necessitates a very high degree of balance. The oscillator described is thus seen to provide optimum signal level for samples having T_1T_2 in the approximate range 10^{-3} to 10^{-6} for the conditions described.

Direct measurements of noise figure were not made with this oscillator circuit. An earlier pentode circuit*

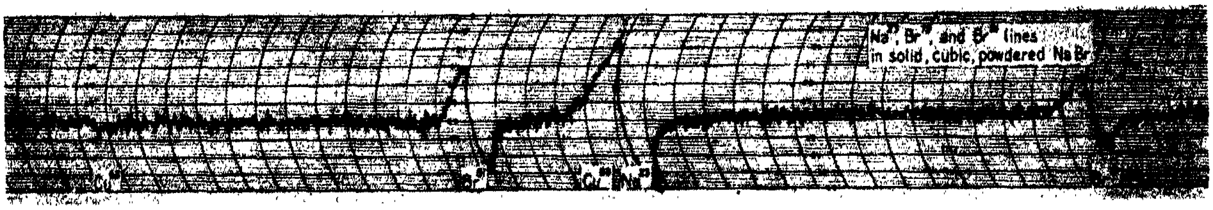

FIG. 5(a). Spectrum of NaBr, showing weak Cu^{63} and Cu^{65} lines as well as those of Na^{23}, Br^{79}, and Br^{81}. About 15 percent frequency range is covered, at 3 mc/sec. The time scale is 15 minutes per division and the 20-sec. time constant is used.

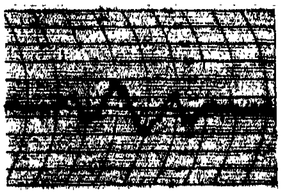

FIG. 5(b). Li^7 resonance in $Li_2SO_4\cdot H_2O$ as a single crystal showing splitting caused by electric quadrupole coupling.

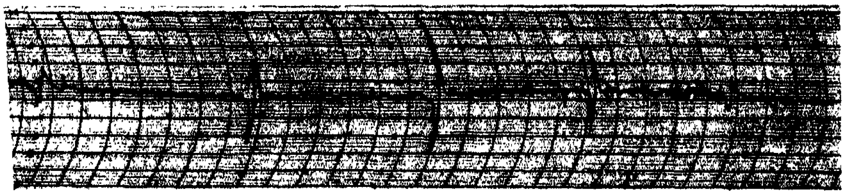

FIG. 5(c). Five-line spectrum of Al^{27} resonance in Al_2O_3. The spectrum covers 1440 mc/sec., centered at about 7 mc/sec. The time scale is 30 minutes per division.

---

[11] G. C. Sziklai and A. C. Schroeder, Proc. I.R.E. **33**, 701 (1945).

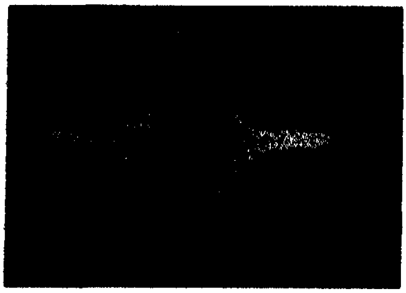

FIG. 6(a). Trace on an oscilloscope of proton resonance in 0.5 cc of mineral oil in 6400-gauss field, illustrating use as field meter. Total sweep here is about 0.5 gauss. "The Wiggles" are very prominent, owing to the good homogeneity of the field over the sample. Sweep amplitude is about 0.5-gauss peak-to-peak.

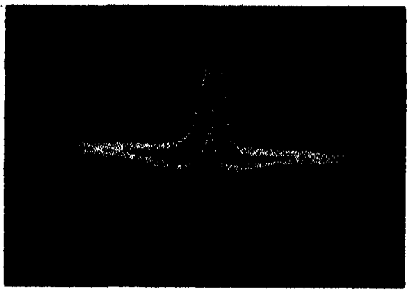

FIG. 6(b). Resonance in same magnet as (a), but in aqueous solution with added paramagnetic, $MnSO_4$. Sweep amplitude is about 5 gauss, peak-to-peak.

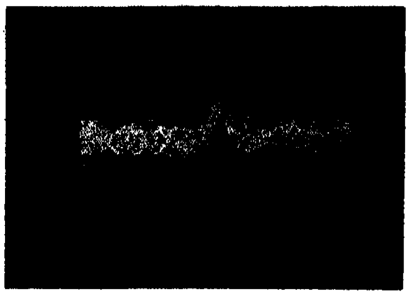

FIG. 6(c). Oscilloscope trace in field of 360 gauss, with about 0.5-gauss inhomogeneity over the sample. Sweep amplitude is about 10 gauss, peak-to-peak.

used at frequencies below 4 mc/sec. was equipped with a tungsten filament diode so arranged that shot noise current caused by a temperature limited anode current developed noise voltages across the input tuned circuit of which the shunt resistance was known. Comparison of the recorded noise amplitudes for the diode current at zero and then at a suitable small value allowed computation of the noise figure. This was found to be less than about 5 at 0.5 mc/sec. using a 30 c.p.s. phase sensitive detector but it rose sharply at higher radiofrequencies. A higher modulation frequency of 1400 c.p.s. resulted in a noise figure of about 3 at 4 mc/sec. With the present circuit, signal-to-noise ratios are as large as expected with a system of small noise figure and are as large as with bridge circuits operating under similar conditions and known to have noise figures of about 2. The modulation frequency does have to be kept high, for detection with the phase-sensitive detector, a 30-c.p.s. system having been found definitely inferior in signal-to-noise ratio.

Two disadvantages accompany the use of a high modulation frequency. First, difficulties with pick-up of the modulation frequency are enhanced and second, lines are sometimes broadened or distorted. This happens if a line has a breadth in frequency of less than the modulation frequency, which happens easily with liquid samples of small gyromagnetic ratio in a homogeneous field. Figure 4 shows a lithium line of distorted shape resulting from this effect with a 1400-c.p.s. modulation frequency. The effect may be thought to occur because the separate side bands of the modulation frequency (which, because the modulation results in frequency modulation of the precession frequency, may be thought to represent a number of discrete simultaneous precession frequencies of relative amplitude and phase determined by the modulation) interact individually at separated radio-frequencies. Thus one gets a number of lines superimposed. This effect has been observed by Brown and Purcell[12] as setting a practical artificial limit to the sharpness of resonance lines in very weak fields. R. Karplus has given an analytical treatment[13] of the effect.

OPERATION AND TYPICAL RESULTS

In conducting a search for an unknown resonance, the adjustment of the modulation level, power level and sweep rate must be so made as to fit the characteristics of the sample. A few typical spectra are shown in Figs. 5 (a), (b), and (c). In Fig. 5 (a) is a spectrum for NaBr as a solid with the resonances of the two Br isotopes and the Na all occurring in a frequency range of 10 percent. Weak lines thought to be caused by Cu^{63} and Cu^{65} in the coil can also be seen. Figure 5 (b) shows a spectrum of Li^7 in a single crystal of $Li_2SO_4 \cdot H_2O$, where a definite structure is observed in the line, this being caused by the nuclear electric quadrupole interaction with the crystalline field. Finally a spectrum of Al^{27} in a single crystal of Al_2O_3 shows five lines widely separated, again caused by the quadrupole interaction. For spectra of this last kind, the variable frequency aspect of the apparatus is almost indispensable for quantitative measurements, because the range covered is so large that it would be difficult to make known, large, changes in the field, and the spectrum one would obtain, if the field were varied, would be harder to interpret. A large permanent magnet, with a field strength of 6400 gauss, in a $1\frac{3}{8}$-in. gap of 6-in. diameter is currently being used with the spectrometer, all variations then being made in the frequency.

For somewhat reduced sensitivity compared to the phase sensitive detector but considerably greater than that obtained with direct observation of the audio output on the oscilloscope, the oscilloscope may be connected to the output of the tuned audio amplifier, as indicated by the broken lines in the block diagram. This amplifier has the effect of narrowing the noise band width to that of the amplifier (about 5 c.p.s.) and, with a modulation amplitude about equal to the line breadth, one observes the resonance as a sinusoid, synchronous with the modulation frequency. This reverses phase as the frequency of the oscillator passes through exact resonance and the associated null signal gives an accurate measurement of the point of maximum absorption. The amplitude is, of course, just the quantity to which the phase sensitive detector responds, but one avoids possible errors associated with the integrating time of the detector and the response time of the meter. The null is, on the other hand, less precisely specified because the noise band width is greater.

---

[12] R. M. Brown and E. M. Purcell, Phys. Rev. 75, 1262 (1949).

[13] R. Karplus, Phys. Rev. 73, 1027 (1948).

Frequency measurements are made by making marks on the chart of the recorder as the oscillator passes through zero beat with a heterodyne frequency meter. Actually, if a small amount of the frequency meter signal is allowed to leak into the oscillator, marks are made by the spectrometer itself. A crystal oscillator with multivibrators could be used to provide marker signals throughout a large frequency interval, obviating the necessity of returning to the resonance for quantitative measurement after it is found, as is done at present.

The oscilloscope connected to the tuned audio amplifier can assist in accurate frequency measurements as well because the signal that actuates the phase sensitive mixer can be observed on it. In fact, the instant of zero beat can be observed.

USE AS A METER FOR MAGNETIC FIELDS

For use as a meter for magnetic fields, the oscillator has been equipped with a small probe coil containing as a sample an almost saturated aqueous solution of LiCl with about 1N $MnSO_4$ to shorten the relaxation times. A $\frac{3}{4}$-in. copper tube, $\frac{3}{4}$ in. long has been used as a shield box around the coil containing about 0.5-ml sample. Modulation coils have been wound around each end of the tube and supplied with 60-c.p.s. current. An oscilloscope is connected directly to the output of the oscillator unit and very strong proton resonances are found in homogeneous fields, that in Fig. 6 (a) being found in the above described permanent magnet. With a sample of shorter relaxation time, the "wiggles,"[2] prominent in Fig. 6 (a), are damped out sooner. Figure 6 (b) shows a H^1 resonance in an aqueous solution of $CrCl_3$, in the same magnet. Probe coils have been used to cover a range from 45 to 1 mc/sec. thus allowing very accurate measurement of fields from 10,000 gauss to about 250 gauss. The resonance photographed in Fig. 6 (c) illustrates the line found in a field of about 360 gauss (1.5 mc/sec.) with an inhomogeneity of about 0.5 gauss over the $\frac{1}{4}$-in. diameter, $\frac{1}{2}$-in. long sample. A more uniform field increases the signal-to-noise ratio proportionately. With larger samples, in uniform fields, one can go to fields. A good signal-to-noise ratio has been observed on an oscilloscope at 350 kc/sec., or about 80 gauss, using a 20-cc sample. For fields above 10,000 gauss, the Li^7 resonance may be used. This is not nearly so strong but, by using it only in the strong fields, one obtains quite adequate signal strengths so long as the field is uniform to less than 1 gauss over the sample. For less uniform fields, the narrow-band phase sensitive detector, or perhaps just the tuned audio amplifier with oscilloscope, would have to be used. The Li^7 resonance extends the range up to about 25,000 gauss with the same set of coils. The accuracy of measurement of the field is, in practice, limited only by the homogeneity over the sample and the accuracy of the frequency measuring equipment. Conversion of the measured frequency into field strength may be done only to the precision that the absolute value of the gyromagnetic ratio is known.[14] With the phase sensitive detector, an error voltage is obtained and this has been used to provide precise regulation of an electromagnet in a standard manner.

CONCLUSIONS

It is felt that for a large variety of samples the spectrometer achieves very nearly the ultimate sensitivity determined by thermal agitation noise in the resonant circuit, consistent with its band width. It has a very great advantage over both bridge and nuclear induction techniques for studying line shapes because the device is sensitive only to the absorption part of the resonance and one always obtains records showing the derivative of the absorption. In contrast, both the electrical bridge, and the induction apparatus, are responsive to either χ'' or χ' or any mixture of the two depending on very critical and hard to make adjustments. For this same reason, the present device, especially when used in association with a permanent or proton-regulated magnet, is useful for making precision gyromagnetic ratio measurements because the centers of the lines can be so precisely designated. The dispersive part of the resonance may be shown to exist by observing the frequency modulation resulting[6] but, for the weaker resonances, this is not easily detectable. To observe this while varying frequency would require a tracking receiver, one of the parts of a more conventional scheme that has been avoided in the preferred arrangement.

As a field-strength meter, the two most serious limitations are that the field must be rather homogeneous (say, one part in 10^3 over the sample) if one wishes to use the oscilloscope as an indicator, and that the cable from the probe to the unit is only about 18 in. in length. If one were interested in observing only small changes in field in a large magnet, the wide tuning range could be temporarily discarded, allowing the addition of a one-half wave-length cable to the existing one. One would then separately control the tuning condensers and almost any magnet could be investigated in this fashion. If care were taken to avoid use of ferromagnetic materials, one could perhaps place the unit close to, or even inside, a large magnet. At low fields, and correspondingly low frequencies, one can use a longer cable of lower capacity per unit length, but at high frequencies one begins to get rather serious impedance transformations from the cable. The oscillator could probably be made to operate up to 85 mc/sec. by changing the peaking coils, allowing use of protons for field measurement up to 20,000 gauss.

---

[14] Thomas, Driscoll, and Hipple, Phys. Rev. **75**, 902 (1949).

It should finally be noted that in all oscillator circuits tried, a power supply of very low ripple and noise (about 1 mv) and d.c. heater supply were required, to avoid a large (compared to noise) a.c. component in the audio output. For field-meter use, battery operation is convenient, the total plate current drain being about 25 ma.

THE REVIEW OF SCIENTIFIC INSTRUMENTS VOLUME 21, NUMBER 3 MARCH, 1950

On the Use of Photographic Plate Detectors in Neutron Experiments*

J. C. ALLRED, A. N. PHILLIPS, L. ROSEN, AND F. K. TALLMADGE
Los Alamos Scientific Laboratory, Los Alamos, New Mexico

(Received July 12, 1949)

A technique is discussed for utilizing photographic plate detectors in an evacuated camera, containing an appropriate radiator, to make precise determinations of the range distributions of the disintegration products of slow neutron reactions. The same technique is applied to the problem of measuring neutron energies by making range measurements on the forward recoil protons projected by fast neutrons from a thin polyethylene radiator. As an indication of the accuracy attainable with photographic plates when used in this manner, determinations have been carried out for the Q values of the $\mathrm{Li}^6(n,\alpha)\mathrm{H}^3$ reaction and the $\mathrm{B}^{10}(n,\alpha)\mathrm{Li}^7$ reaction.

IT is now well established that photographic emulsions can be used to advantage in many experiments for making, simultaneously, determinations of the energy distribution and angular intensity distribution of the products of nuclear reactions. In the case where collimated charged particles are to be detected, one essentially has in a photographic plate a "coincidence" detector in space; i.e., the tracks must originate on the surface of the emulsion and must travel in vertical and horizontal directions with respect to the surface of the emulsion as defined by the collimating system. When used in this manner a great deal of the background and track measuring difficulties are eliminated and precise results are made possible.

It would obviously be desirable to be able to do neutron experiments with the same accuracy and facility as is now attainable in charged particle experiments. This turns out to be possible if one can maintain and successfully utilize photographic emulsions in vacuums for reasonable periods of time.

We have recently found that photographic emulsions can be kept at pressures in the range of 10^{-3} mm Hg for periods of more than 20 hours without prohibitive effects, and this is ample time for many neutron experiments. In order to determine whether prolonged exposure to a vacuum changes the resolution or stopping power of photographic emulsions, the range distributions of plutonium alpha-particles were obtained as a function of time spent by photographic plates in a vacuum. Figure 1 shows the range distribution for one hour, 6½ hours, and 16½ hours of exposure to plutonium alphas while in a vacuum of 1.1×10^{-3} mm Hg. (Ilford C-2 emulsions were used in all of the experiments discussed in this paper.) It is seen that the vacuum produces no significant effect on the resolution or stopping power. (The energy of the alphas, as determined from the extrapolated range** and the range

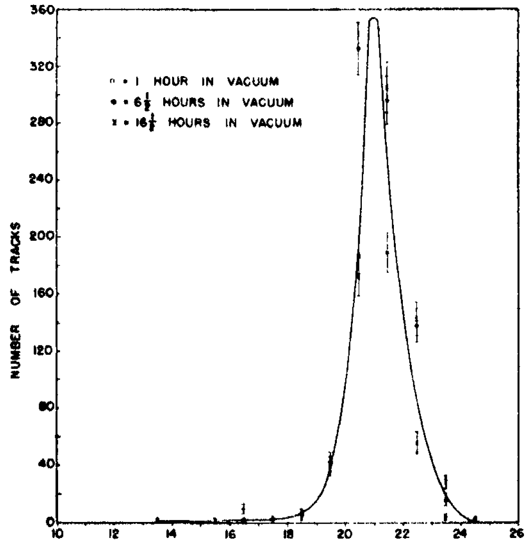

FIG. 1. Range distribution of plutonium alpha-particles as determined from photographic plates exposed in a vacuum for one, 6½, and 16½ hours.

---

* This document is based on work performed at Los Alamos Scientific Laboratory of the University of California under Government Contract W-7405-eng-36.

** The procedure followed to determine the mean range from the extrapolated range of the integral curve was identical to that outlined by Livingston and Bethe in Rev. Mod. Phys. 9, 283 (1937). Errors in the measurement of track lengths were treated as additional straggling.

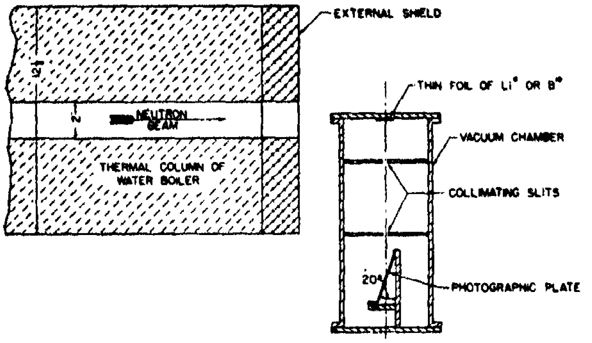

FIG. 2. Source-detector geometry for determination of energy spectra of charged particles from thermal neutron reactions.

energy relations of Lattes, Fowler, and Cuer,[1] is 5.10±0.14 Mev, in good agreement with the prevailing average value of 5.14 Mev.[2]) Having established this point, we were ready to attempt some neutron experiments using the same collimation techniques[3] heretofore reserved for charged particle experiments.

Figure 2 shows the experimental arrangement employed to determine the range distributions of charged particles from thermal neutron induced reactions, the Los Alamos slow neutron reactor being utilized as the neutron source in these experiments. The function of the slit system is to permit only those particles to enter the emulsion the angle of whose trajectories will not vary by more than eight degrees with respect to the surface of the emulsion, thus eliminating the necessity for making depth measurements. In the case of short tracks, an eyepiece scale is used to make length measurements. Thus, even if the track makes a large angle in the horizontal plane (looking down on surface of emulsion) with respect to the line between the radiator and the center of the photographic plate, no error is introduced. However, when long tracks are to be measured, it is much more convenient to measure the projection of the tracks along the line from the center of the plate to the radiator, and for this case it is necessary to collimate the particles to be detected so that only particles traveling in a cone of small angle are accepted. This can be done either by a slit system as shown in Fig. 2, or by moving the plate a sufficient distance from the radiator. The maximum error introduced in length determinations by the above method is approximately two percent for tracks which do not suffer appreciable scattering in the emulsion, and this can be in large part corrected for. An important feature of this arrangement is that the detector can see the radiator without seeing the source of neutrons, thus considerably reducing the gamma-ray and neutron-induced background on the plate.

Figure 3 gives the range distribution of the alphas and tritons from the $Li^6(n, \alpha)H^3$ reaction. Li^6 as Li_2SO_4 was converted to $LiNO_3$ by adding $Ba(NO_3)_2$ to the Li_2SO_4 and precipitating out $BaSO_4$. The $LiNO_3$ in Zapon-alcohol solution was then painted on platinum and converted by heating to Li_2CO_3. The Li_2CO_3 layer had an average thickness of 0.11 mg per cm².*** The Q for this reaction is 4.67±0.21 Mev, as again determined from the extrapolated ranges, which were determined by using the integral number *vs.* range curves for the two groups of particles and the range energy relations of

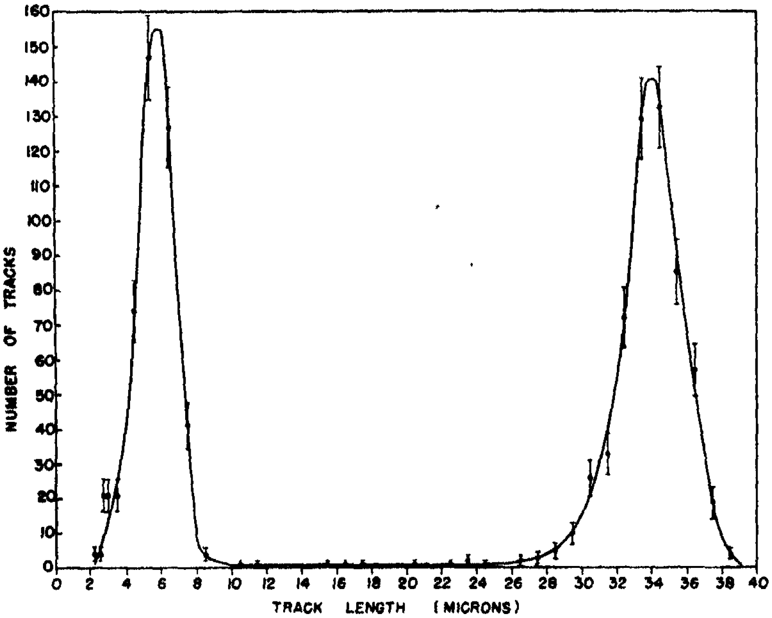

FIG. 3. Range distribution of tritons and alphas from $Li^6(n, \alpha)H^3$ reaction for thermal neutrons.

---

[1] Lattes, Fowler, and Cuer, Proc. Phys. Soc. 59, 884 (1947).

[2] G. T. Seaborg and I. Perlman, Rev. Mod. Phys. 20, 638 (1948).

[3] Rosen, Tallmadge, and Williams, Phys. Rev. 76, 1283 (1949).

*** All foils used in these experiments were made by John Povelites and Jane Evans of the Chemistry Division of the Los Alamos Scientific Laboratory.

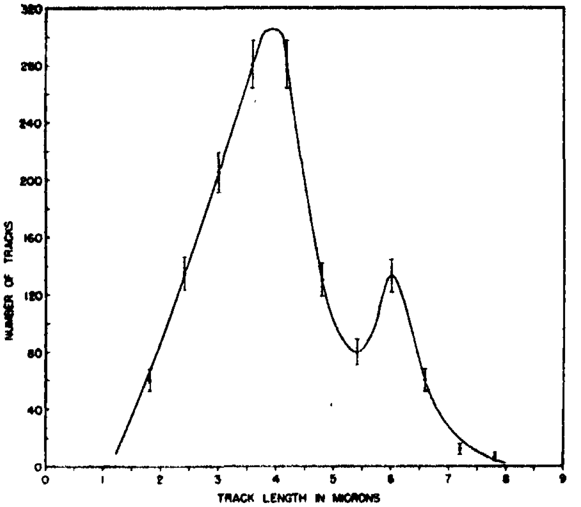

FIG. 4. Range distribution of alphas from $B^{10}(n, \alpha)Li^7$ reaction for thermal neutrons.

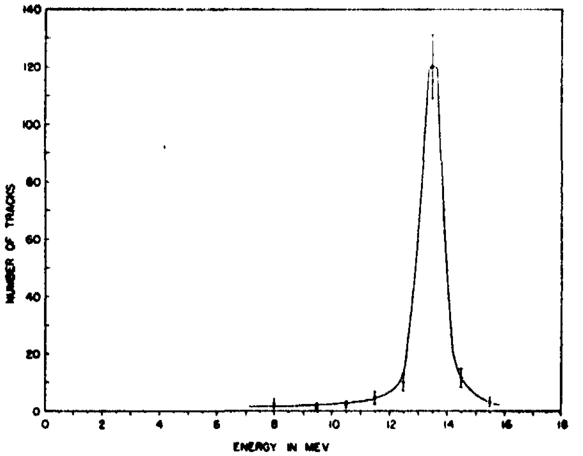

FIG. 6. Infra-Red energy distribution of 14 Mev neutrons as determined from ranges of recoil protons.

Lattes, Fowler, and Cuer. This appears to be in good agreement with previously determined values of 4.86 Mev[4] and 4.97 Mev.[5]

Figure 4 gives the range distribution of the alphas from the $B^{10}(n, \alpha)Li^7$ reaction. A slurry of B^{10} powder in alcohol was carried through successive decantations until a fine suspension was obtained. This was then painted on platinum and heated under an infra-red lamp to drive off the alcohol. The B^{10} was deposited on the platinum to an average thickness of 0.012 mg per cm^2. The peak of short range alphas, which comprise about 90 percent of the total number of alphas, is due to the well-known excited state in Li^7. The energy of the alphas giving rise to the short range group was determined to be 1.45±0.10 Mev by the method referred to above. This implies a Q value of 2.28±0.20 Mev for this group. This value is also in good agreement with previous determinations.[6] A determination of the energy of the alphas giving rise to the high energy peak would not be reliable due to interference from the group of lower energy.

An obviously important application of the above technique is to be found in the investigation of neutron energy spectra. For such experiments the radiator consists of a hydrogen or possibly deuterium containing material. In order to keep to a minimum errors in energy determinations produced by finite angular resolution, the axis of the vacuum chamber is so aligned as to make a sufficiently small angle with respect to the line from the center of the photographic plate to the neutron source. The advantage of this method for such experiments, as well as for experiments as the one described, over the method of using the plate as both radiator and detector arises chiefly from the fact that one has only to scan the surface of the emulsions for tracks; and, if proper geometry is used, those tracks starting at the surface and produced by particles originating in the radiator have a known and convenient orientation. This greatly facilitates the search for and measurement of the tracks. This technique also eliminates large corrections (especially when high energy neutrons are being investigated) arising from the fact that long tracks have a lower probability of ending in the emulsion and hence of being counted in their proper energy interval than shorter tracks.

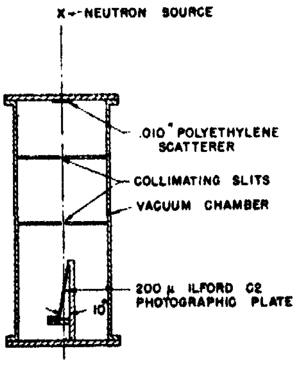
X←NEUTRON SOURCE
.010" POLYETHYLENE SCATTERER
COLLIMATING SLITS
VACUUM CHAMBER
200 μ ILFORD C2 PHOTOGRAPHIC PLATE
10°

FIG. 5. Source-detector geometry for neutron energy spectra determinations.

Figure 5 gives the experimental arrangement for determining the energy spectrum of a high energy source of neutrons. In the case of a low energy neutron source, one might well use the arrangement of Fig. 2 with an appropriately thin radiator and with the axis of the vacuum chamber making a small angle with the direction of the neutron beam so that the plate is not subjected to bombardment by the primary neutron beam.

Figure 6 gives the energy distribution of the recoil protons projected from a 0.005 inch polyethylene radiator by a monoenergetic beam of 14 Mev neutrons. Only protons making an angle of less than eight degrees with the incident neutron direction were recorded. The low energy straggling is probably due to slit penetration of the recoil protons and to the detection of recoil protons from neutrons which do not come directly from the source. Here again the slit system could have been dispensed with by sufficiently increasing the distance between the radiator and detector.

---

[4] M. S. Livingston and J. G. Hoffman, Phys. Rev. 53, 227 (1938).
[5] Rumbaugh, Roberts, and Hafstad, Phys. Rev. 54, 657 (1938).
[6] W. F. Hornyak and T. Lauritsen, Rev. Mod. Phys. 20, 204 (1948).

The errors shown on the experimental points of all curves only represent the statistical probable error based on the number of tracks counted for each point. Additional uncertainties are introduced in the measurement of the absolute ranges traversed by the particles in the emulsion as well as by the finite radiator thickness and finite angular resolution. The above effects manifest themselves as an apparent range straggling and are responsible for the fact that in Fig. 4, for example, the two peaks are hardly resolved. The various experimental factors which produce the finite widths in the number *vs.* range curves do not carry equal weight at every range. In the region above 100 microns, for example, the absolute range of a particle can be determined to better than ±3 percent and this accuracy depends for the most part on the accuracy with which one can measure the projected length of the track, the effect due to finite grain spacing being relatively small. In the region of 5 microns on the other hand, the range of a particle cannot easily be determined to better than ±15 percent due in no small part to the finite spacing between the individual grains comprising the track.

This technique would be especially useful for high energy neutron spectra determinations where much thicker radiators could be used.

ACKNOWLEDGMENTS

The Li^6 used in the above described experiment was produced by Carbide and Carbon Chemicals Corporation, Y-12 Plant, Oak Ridge, Tennessee, and obtained on allocation from the Isotopes Division of the AEC.

THE REVIEW OF SCIENTIFIC INSTRUMENTS VOLUME 21, NUMBER 3 MARCH, 1950

An Analog Computer

J. G. Bayly
Atomic Energy Project, National Research Council of Canada, Chalk River, Ontario, Canada

(Received November 28, 1949)

An integrator has been constructed which is capable of computing the yield of nuclear reactions produced by radiation of intensity that varies arbitrarily with time. By combining the appropriate number of such machines the yield resulting from a series of consecutive reactions may be found.

While the emphasis in this paper is on applications involving the yield of radioactive isotopes produced by a pile or other source of radiation, the instrument may be used to calculate temperatures in thermodynamic problems, voltages and currents in electrical networks, and so on, wherever the quantity (x) to be determined is governed by the differential equation

$$dx/dt = -\lambda x + f(t),$$

$f(t)$ being a given function of the time, and λ a known constant.

I. INTRODUCTION

THE calculation of the yield of a radioactive nuclide produced by the irradiation of another nuclide, as in a pile, cyclotron, etc., becomes very laborious if the radiation intensity is altered often during the experiment. Unavoidable changes in intensity result from the variations in power level and complete shut-downs required for experiments, routine maintenance, and emergency conditions. To economize time and effort a need was felt for a computer which was flexible enough to solve the different types of problems with better than 1 percent accuracy, capable of being set up and operated by non-mathematicians either manually, from a record of the radiation intensity, or automatically, from a signal produced by an instrument such as an ionization chamber. The instrument described in this paper satisfies all these requirements.

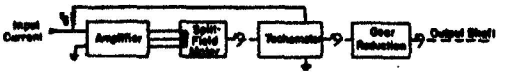

FIG. 1. Velocity-servo.

II. THE DIFFERENTIAL EQUATIONS

The simplest type of integration, i.e., the solution of the differential equation

$$dQ/dt = P, \tag{1}$$

where P is a given finite, single-valued real function of time t, may be performed automatically by a servo whose angular velocity, dQ/dt, is proportional to a current which in turn is proportional to P. The actual integration is performed by the shaft of the servo, the value of the integral being read from a dial driven by the shaft.

By modifying the servo so that the angular velocity is proportional to the difference between two currents, one of which is proportional to P and the other proportional to the yield, Q, the instrument will solve equations of the type

$$dQ/dt = P - \lambda Q. \tag{2}$$

In the computers of this type that have been built at Chalk River, P is generally made proportional to

FIG. 2. Circuit for solving $dQ/dt = P - \lambda Q$.

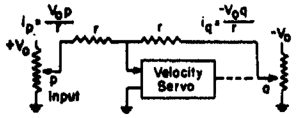

the neutron flux, and Q represents the yield of a neutron induced reaction, usually a radioactive isotope. The quantity λ is then the disintegration constant of this isotope.

More complicated problems arise when the yield is determined by two simultaneous equations. These may be solved by using two computers, the output of the first determining the function P for the second, or in many cases by recording the output of one computer on the graph of a recording voltmeter and subsequently using this graph as the function P with the computer set up to solve the second differential equation.

When the target material is appreciably reduced by the reaction, the equations are of the form

$$dQ_t/dt = -PQ_t, \tag{3}$$

$$dQ/dt = PQ_t - \lambda Q, \tag{4}$$

where Q_t represents the number of target nuclei. Here the function PQ_t is obtained first from Eq. (3), and used as the input to solve Eq. (4).

A reaction for which the computer has been frequently used is one in which two nuclear reactions take place, the yield nucleus of the first providing the target for the second. The instantaneous yield of the first reaction is found from Eq. (2) or (4), and the product PQ, which is proportional to the rate of production for the second reaction, is used as the function P for a second calculation. An example of this type of reaction is discussed in Section V.

These problems, involving addition and multiplication, represent a few of the more useful applications of the computer. Many other differential equations may be solved using the well-known circuits[1] for dividing, squaring and generating sine, cosine, logarithmic, etc. functions of quantities available as shaft rotations or voltages.

III. PRINCIPLE OF OPERATION

The integration involved in the calculation is performed by a dial driven by a velocity-servo which produces an angular shaft velocity accurately proportional to an applied current. The servo, the velodyne of Williams and Uttley,[2] Fig. 1, consists of a high gain, stable d.c. amplifier controlling a reversing motor-tachometer-generator. The tachometer voltage produces a current determined by r_g, which except under transient conditions reduces the net amplifier input current to the very small value required to overcome friction in the mechanical system. During transients caused by rapid changes in the demanded speed of the servo, the error in this current balance, occurring while the motor is accelerating or decelerating, is stored in a memory circuit in the amplifier. This remembered error is applied as a correction to the speed of the motor, so that the resultant error is zero after the transient is over. An extensive analysis of this type of servo has been given by Williams and Uttley.

FIG. 3. Circuit for solving $dQ_t/dt = -PQ_t$.

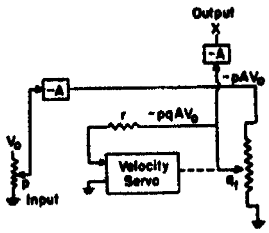

The motor also drives a gear reduction unit which is coupled, through a friction clutch, to the shaft of a helical potentiometer carrying the dial upon which the solution of the calculation is read. For simplicity, the amplifier, motor generator, gear box, and feedback portions of the calculator will be shown as a single unit with an input current connection and an output shaft, and labelled a velocity-servo in subsequent figures. The action of the velocity-servo is simply to convert an input current into an angular shaft velocity, which may be integrated by the dial.

The function P may take the form of a current from an ionization chamber monitoring the radiation intensity, or it may be given in a chart or table of intensities *versus* time. While the current, suitably amplified, may be used directly to control the computer it is generally more practical to use a chart or table of intensities. In this way the entire calculation may be performed in a small fraction of the time required for the irradiation. For this purpose an auxiliary unit has been built in which a chart of the type used in Esterline-Angus recording meters is motor driven at a constant velocity. The curve on the chart is followed manually by means of a stylus which rotates the moving arm of a potentiometer, producing a voltage proportional to P. If the curve consists of a series of radiation pulses of constant amplitude, a "square input" control is used to switch this voltage between zero and the value corresponding to the constant amplitude.

A circuit appropriate to the problem to be solved must be used to synthesize the velocity-servo input current from P, Q, λ, etc. Several examples of circuits that have been found useful in pile yield problems are given below.

IV. TYPICAL CIRCUITS

The simple calculation of the yield of an active isotope indicated by Eq. (2) is performed by the circuit shown in Fig. 2. The two potentiometers are calibrated from 0 to 1; the values p and q read on the calibrated scales are then the normalized equivalents of P and Q, the

---

[1] M.I.T. Radiation Lab. Series, Vol. 21, p. 32.

[2] F. C. Williams and A. M. Uttley, J. Inst. Elec. Eng. 93, IIIA, 1256 (1946).

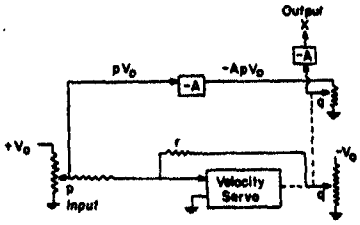

FIG. 4. Circuit for obtaining PQ from $dQ/dt=P-\lambda Q$.

maximum values of these, P_m and Q_m, corresponding to $p=1$ and $q=1$.

The angular velocity of the output shaft is proportional to the input current, which is i_p+i_q, or

$$dq/dt=c(i_p+i_q)=\lambda p-\lambda q.$$

The magnitude λ playing the role of disintegration constant is directly proportional to the voltage V_0 and the resistance r_0 (Fig. 1); inversely proportional to the resistance r, the strength of the magnetic field of the tachometer, and the gear reduction factor; and independent of the d.c. amplifier, provided only that the amplifier gain is high and the zero drift of the amplifier is negligible during the calculation.

The following information must be supplied to the calculator:

1. A record of the time variation of $p=P/P_m$, where P is the intensity of the radiation, and P_m is the maximum intensity occurring during the irradiation;
2. The disintegration constant λ of the radioactive isotope produced;
3. The saturation yield, Q_m, which would have been produced had the intensity remained constant at P_m for an indefinitely long period of time.

The yield at any time during the experiment may be found from the reading of the q dial at the corresponding time during the calculation,

$$Q=qQ_m.$$

Equation (3) may be solved by means of the circuit shown in Fig. 3. The units labeled $-A$ are current amplifiers which reverse the sign of the applied voltage and have high input and low output resistances. Their voltage amplification factor A is approximately unity. The output at x may be used as the pV_0 voltage in a second computer, or this output may be recorded on an Esterline-Angus recorder for use in a second calculation, using the circuit of Fig. 2 to solve Eq. (4).

When the yield to be calculated results from a reaction involving the yield of a previous reaction, the "p" function for the second integration may be determined from the circuit in Fig. 4. The output from the point x is proportional to the radiation intensity and to the number of target nuclei and is used immediately or stored as a chart as in the previous example.

V. USES OF THE COMPUTER

The analog computer has been used to find the yields of Ba^{139} and Ba^{140} produced when Ba^{138} is irradiated by a neutron flux.[3]

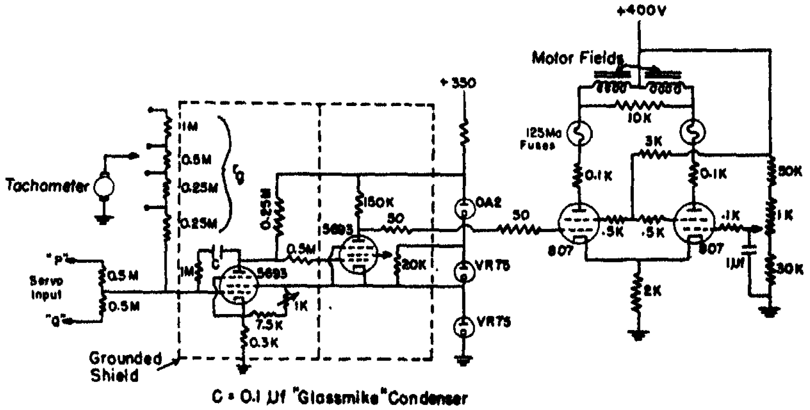

FIG. 5. Servo amplifier.

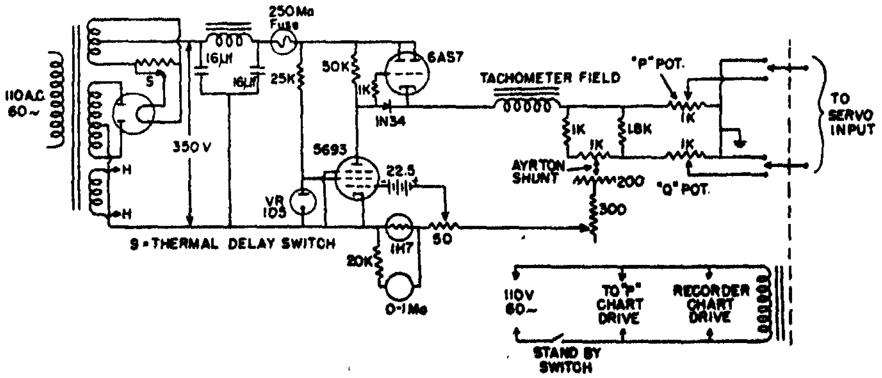

FIG. 6. Tachometer field supply.

---

[3] Yaffe, Sargent, Kirsch, Standil, and Grunlund, Phys. Rev. 76, 617 (1949).

$$\begin{tikzcd}
\mathrm{Ba}^{138} \arrow[d, "n"', "\gamma"] & & \\
\mathrm{Ba}^{139} \arrow[r, "\beta", "85\text{ min.}"'] \arrow[d, "n"', "\gamma"] & \mathrm{La}^{139} \arrow[d, "n"', "\gamma"] & \\
\mathrm{Ba}^{140} \arrow[r, "\beta", "12.8\text{ day}"'] & \mathrm{La}^{140} \arrow[r, "\beta", "40\text{ hr.}"'] & \mathrm{Ce}^{140}.
\end{tikzcd}$$

The differential equations for this chain of reactions are:

$$dQ/dt = P - \lambda_Q Q - aPQ, \quad \lambda_Q = 1.36 \times 10^{-4}\text{ sec.}^{-1}$$
$$dR/dt = aPQ - \lambda_R R, \quad \lambda_R = 6.27 \times 10^{-7}\text{ sec.}^{-1},$$

where Q is the yield of Ba^{139}, λ_Q the disintegration constant of Ba^{139}, R is the yield of Ba^{140}, λ_R the disintegration constant of Ba^{140}, and a is proportional to the capture cross section of Ba^{139}. Since aP was negligible compared with λ_Q, the circuit shown in Fig. 4 was used to give a graph of the product PQ as well as the instantaneous values of Q. The calculation of R was performed by using the PQ graph with the circuit in Fig. 2.

The amount of La^{139} present may be obtained by integrating Q, since the amount destroyed by neutron capture is small. If, during this calculation, the product of P and the yield of La^{139} is recorded, a second calculation will give the contribution to the La^{140} yield due to the chain through La^{139}. In a similar way the La^{140} yield from the Ba^{140} may be found.

VI. INSTRUMENTAL DETAILS

1. The Servo Motor

The Velodyne motor-generator Type 74 is used.[2] The motor armature is supplied with a constant direct current of 3 amperes, obtained from the 110-volt d.c. mains, using an incandescent lamp load to obtain a high dynamic resistance (constant current) characteristic. Since this current is not appreciably reduced by the back e.m.f., the motor acceleration remains at its maximum value until the demanded speed is reached.

2. Servo Amplifier

The amplifier which drives the split-field motor is shown in Fig. 5. Zero drift is made negligible by supplying the tube filaments from a stabilized power supply, and by heating the filaments for 15 minutes before applying the high voltage. It was found necessary to use a "Glassmike" condenser[4] in the memory circuit to prevent zero drift due to the variable leakage current present in ordinary condensers. As a precaution, the zero error is checked daily, but corrections are necessary only about twice per month.

3. Tachometer Field Supply

The disintegration constant is proportional to V_0, and inversely proportional to the generator field. Since, to a first approximation, the generator field is proportional to the field current, a circuit was used in which the field current and potentiometer voltage V_0 were proportional to one another. Thus, to a first approximation, the disintegration constant is independent of small changes in the supply.

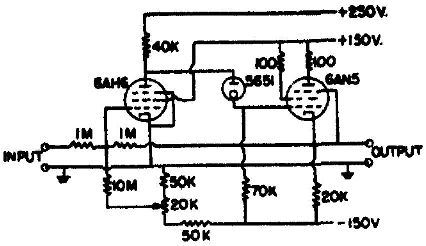

FIG. 7. Current amplifier.

Changes in the supply current were made very small by regulating the current as shown in Fig. 6. The ballast tube, 1H7, with a dynamic resistance of approximately 2500 ohms, and a static resistance of 110 ohms, produces a considerable stabilizing action, which is amplified by the pentode-series triode circuit. The internal impedance of the supply is greater than 10^6 ohms, so that changes in the generator field resistance due to the heating of the windings gives a negligible error.

Since a control whose setting was linear with the disintegration constant was desired, an Ayrton shunt was used to provide the voltage V_0 which is proportional to λ. The center-tapped rheostat ganged to the Ayrton shunt provides a rough compensation for the changes in resistance of the shunt.

To avoid hysteresis effects the field current is never allowed to exceed its normal operating value. To this end, the current is made to build up slowly after the stabilizing amplifier (5693 and 6AS7) has heated up. A thermal delay switch turns on the rectifier filament voltage 1½ minutes after the amplifier heaters are turned on, and the field current then builds up slowly as the rectifier filament heats and the filter condensers charge up. The field current is finally adjusted upward to its normal operating value by reducing the series field rheostat. A voltmeter connected to read the voltage across the 1H7 provides a very sensitive indication of the current, a change of 2 percent from the normal operating point representing a current change of 0.1 percent.

4. Current Amplifiers

A satisfactory design for these units, of which two were built, is shown in Fig. 7. These amplifiers are indicated by the symbol $-A$ in Figs. 3 and 4. By applying the methods used to minimize zero drift in the servo amplifier and by using the highly stable 5651 constant voltage tube, these amplifiers are made so stable that zero adjustments need only be made about once a week.

VII. ACKNOWLEDGMENTS

The author is indebted to Dr. B. W. Sargent for his stimulating interest and to Mr. T. Hughes for assistance in the design and construction of the first model.

---

[4] Condenser Products Company, Chicago, Illinois.

THE REVIEW OF SCIENTIFIC INSTRUMENTS VOLUME 21, NUMBER 3 MARCH, 1950

Photographic Methods of Measuring Slow Neutron Intensities

M. Blau, I. W. Ruderman, and J. Czechowski
Pupin Physics Laboratories, Columbia University, New York

(Received December 1, 1949)

The relative slow neutron sensitivities of β-sensitive emulsions, x-ray film-indium foil combinations, and boron-loaded plates were investigated. Since the detection efficiency depends upon the neutron energy, experiments were made with epithermal, thermal, and cold neutrons. β-sensitive emulsions and x-ray-indium combinations are about equally useful for the detection of epithermal neutrons. B^{10} loaded plates, which are best for the detection of thermal and cold neutrons, have the following advantages: very low neutron intensities can be measured by microscopic counting of α-tracks, neutrons can be counted in the presence of β- and γ-radiation, the number of α-tracks is essentially independent of the development conditions, and a wide range of neutron intensities can be measured with a single plate.

INTRODUCTION

For neutron diffraction and scattering experiments, it is desirable to be able to measure neutron intensities simultaneously and continuously over large areas. When large changes in neutron intensity occur within small regions, such as is the case in crystal diffraction patterns, the use of conventional BF_3 neutron counters entails the disadvantages of poor resolution and long scanning times. If photographic plates could be made sufficiently neutron sensitive, they would not be limited by these disadvantages and would constitute a valuable tool for neutron experiments. A study of various photographic emulsions suitable for slow neutron detection was therefore initiated, with the dual objective of evaluating the techniques which have already been reported in the literature and seeking, if possible, to improve these techniques for our purposes.

The following classification of neutrons according to energy will be used in this paper: fast, >10,000 ev; slow, 0–10,000 ev; epithermal, 0.3–10,000 ev; thermal, 0.01–0.3 ev; and cold, <0.01 ev.

EXPERIMENTAL METHOD

The following methods of achieving neutron sensitivity in photographic emulsions were considered: (a) utilization of the capture cross section of the elements normally present in emulsions, (b) addition of high cross section elements to the emulsion, or (c) use of a combination of a neutron absorbing metallic foil and a photographic emulsion.

Method A

The only elements in emulsions that need be considered are nitrogen and silver. The usefulness of the $N^{14}(n, p)C^{14}$ reaction is limited by its low cross section (1.7 barns at 0.025 ev),[1] which makes it relatively insensitive to slow neutrons. Silver has nuclear resonances at 56, 41, 31, 16, and 5.1 ev, and has a fairly high capture cross section for neutrons ($\sigma=6.6+9.05E^{-\frac{1}{2}}$).[2] It is therefore useful for detecting thermal and cold neutrons as well as neutrons having energies in the neighborhood of its resonances. Furthermore, Ag^{108} and Ag^{110}, which are formed from normal isotopic silver by the n, γ reaction, are β^{-}- and β-, γ-emitters with short[3] half-lives of 2.3 min.[4] and 24.2 sec.,[5] respectively. The high energy (2.6 and 2.8 Mev) β-rays emitted by these isotopes can produce tracks in the recently developed β-sensitive emulsions. Since the β-rays are produced directly in the emulsion, they should contribute more to the darkening than the γ-rays, which must first produce secondary electrons. The following types of β-sensitive emulsions were investigated: Ilford *G*5, 200μ, 37.0 mg Ag/cm²; Kodak Ltd. *NT*4, 200μ, 39.4 mg Ag/cm²; Eastman Kodak *NTB*3, 65μ, 11.0 mg Ag/cm²; and Eastman Kodak pellicles, 250μ, 42.3 mg Ag/cm².

Method B

X-ray film covered on one face by a thin sheet of indium has been successfully utilized by Wollan and Shull[6] to record neutron Laue patterns. Since no other available metallic foil appeared to offer any large advantage over indium, our experiments were conducted with *K*-type, double coated, acetate base x-ray film covered on both sides with 0.5-mm indium foil (368 mg In/cm²).

Method C

The use of B or Li loaded plates for neutron dosage measurements has recently been described by Shapiro and Barnes[7] and by Titterton.[8] Increased sensitivity may be achieved by the use of B^{10} instead of normal isotopic boron. Furthermore, if the boron is incorporated in relatively insensitive emulsions such as the Ilford D_1, the additional advantage of γ-ray insensitivity may be achieved.

---

[1] K. Way and G. Haines, CNL-33 (July, 1948).

[2] Rainwater, Havens, Wu, and Dunning, Phys. Rev. **71**, 65 (1947), and recent unpublished work by Havens and Rainwater.

[3] An isomeric state of Ag^{110} having a 225-day half-life is also formed, but it decays too slowly to be useful. See, for example, M. Goldhaber, Phys. Rev. **70**, 89 (1946).

[4] Amaldi, D'Agostino, Fermi, Pontecorvo, Rasetti, and Segrè, Proc. Roy. Soc. (London) **A149**, 522 (1935).

[5] M. L. Pool, Phys. Rev. **53**, 116 (1938).

[6] C. G. Shull and E. O. Wollan, Science **108**, 69 (1948).

[7] M. M. Shapiro and J. R. Barnes, Phys. Rev. **73**, 1243 (1948).

[8] E. W. Titterton, Nature **163**, 990 (1949).

The importance of achieving the highest possible concentration of boron (preferably as B^{10}) is illustrated by Fig. 1, in which the neutron transmissions of boron loaded plates containing various grams B^{10} per cm^3 of emulsion are plotted as a function of neutron energy. Ilford D_1 plates, which were used in our experiments, contain 23 mg normal boron per cm^3 emulsion, although this quantity can be doubled with special treatment.

In exploratory experiments carried out in this Laboratory, 100μ Ilford D_1 nuclear plates were soaked for one hour with agitation in a solution containing 5 g of $Na_2B_4{}^{10}O_7 \cdot 10H_2O$ per 100 ml of water. Comparison of the α-track density of these plates with Ilford B loaded plates of known boron content, after exposure to the same neutron flux, indicated B^{10} uptakes of $\sim$20 mg per cm^3 of emulsion. Experiments were carried out with these B^{10} loaded plates, without further attempts to increase the boron content. Yagoda and Kaplan[9] have recently reported that a concentration of $\sim$15 mg B^{10} per cm^3 of emulsion can be obtained by soaking 200μ Ilford C_2 plates for two hours in a solution of normal isotopic lithium borate. One could therefore expect to obtain a concentration of $\sim$80 mg B^{10} per cm^3 of emulsion if $Li_2B_4{}^{10}O_7$ were used. Plates containing such high boron contents approach conventional BF_3 proportional counters in neutron detection efficiency, as indicated in Fig. 1.

Exposures to neutrons were made in the collimated beam of the Columbia neutron velocity spectrometer.[10, 11] The photographic plates were mounted on one face of a 5-in. diameter disk of paraffin-boron carbide mixture 1 in. thick, from which several sectors had been cut (Fig. 2). The disk was placed in the neutron beam so that the face not covered with plates was perpendicular to, and facing, the neutron beam. The disks were rotated intermittently during exposure in order to minimize neutron flux variations. Because the cyclotron efficiency varies considerably with time, the exposure periods were made in terms of the number of counts from a neutron fission counter placed within the cyclotron enclosure.

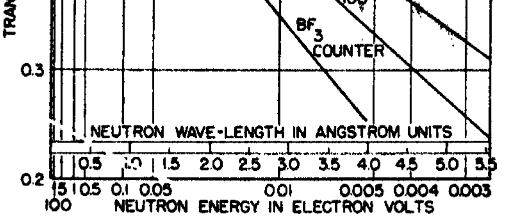

FIG. 1. The transmission as a function of neutron energy of 200 μB^{10} loaded plates containing various mg B^{10} per cm^3 of emulsion. The cross section of B^{10} was taken to be $\sigma = 627E^{-\frac{1}{2}}$. The transmission of a conventional BF_3 proportional counter, 10 cm long and filled to 50-cm pressure with pure $B^{10}F_3$, is included for comparison.

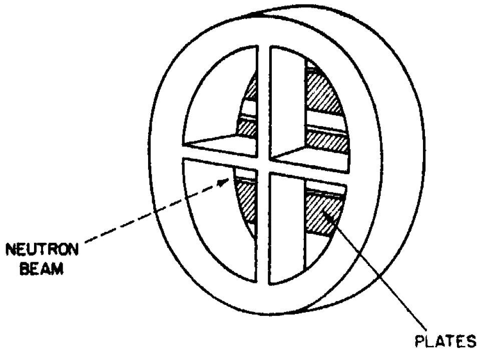

FIG. 2. Arrangement of photographic plates on paraffin-boron carbide template and position of the latter relative to the neutron beam.

Since the detection efficiency depends markedly on neutron energy, the relative merits of the different types of emulsions were determined by separate exposures to epithermal, thermal, and cold neutrons. This was accomplished by the use of a Cd filter to cut out the thermal and cold neutrons, and Be plus BeO filters to reduce the epithermal and thermal neutron flux. Figure 3 shows the different neutron energy distributions in the collimated beam obtained in this way. In all cases, the fast neutrons leaving the internal beryllium target in the cyclotron were first slowed down to an essentially thermal distribution by a 6.5-cm thick slab of paraffin placed at the beginning of the collimating system.

Development of each particular type of emulsion was carried out in the standard manner, taking care to obtain reproducible results. The optical density of the patterns produced in the plates was determined by a Baird Associates' non-recording densitometer, measurements being made both of the blackened parts and the background in their immediate neighborhood, and of unexposed plates. In the case of the boron loaded plates, the density of α-tracks was also measured by microscopic examination using magnifications up to 90×15. Curves of optical density *vs.* neutron exposure were also obtained for each of the emulsions, exposures being made with an unfiltered neutron beam.

RESULTS

The β-sensitive emulsions were rated on the basis of the gross observable blackening due to β-tracks, rather than on the detailed structure of the tracks. The sensitivity thus depends not only on the number of grains produced for equal values of the energy loss, but also on the grain size. A preliminary survey of the various β-emulsions now available led us to the conclusion that the *NT*4 emulsion (Kodak Ltd.) is the most sensitive for our purposes, although the differences between the various types are not very large. Our experiments were therefore carried out principally with *NT*4 plates.

---

[9] H. Yagoda and N. Kaplan, Phys. Rev. **76**, 702 (1949).

[10] J. Rainwater and W. W. Havens, Jr., Phys. Rev. **70**, 136 (1946).

[11] W. W. Havens, Jr. and J. Rainwater, Phys. Rev. **70**, 154 (1946).

High humidity was found to decrease seriously the sensitivity of the β-plates, just as has been found to be the case in the use of these plates for the detection of lightly ionizing particles. The loss in sensitivity results from the decrease in the number of grains corresponding to equal values of the energy loss per unit length of track.

Figures 4a and 4b give optical density curves (for full neutron beam exposure) for *NT*4 plates and for x-ray film with and without indium foil. In Fig. 4a the density is expressed as the difference between the optical density, D, of regions exposed to the neutron beam and the density, D_b, of the film shielded by the boron-paraffin disk. This defines an effective density such as is useful in neutron diffraction work when absolute intensities are required. By plotting the density as the difference between D and the density, D_0, of completely unexposed plates, as shown in Fig. 4b, an over-all density uncorrected for stray radiation is obtained. Comparison of Figs. 4a and 4b shows that, except in the case of x-ray film without indium foil, the blackening due to neutrons was much greater than the stray radiation background. The latter was mostly due to γ-radiation.

X-ray emulsion is less sensitive to high energy β-particles than is β-sensitive emulsion, and also contains much less silver than the latter. The neutron sensitivity of x-ray film is hence much less than that of a β-sensitive plate such as *NT*4 (Figs. 4a and 4b). However, when x-ray film is covered with a thin sheet of indium foil, a very large increase in sensitivity is obtained. Indium, which has a high neutron capture cross section, emits γ-radiation from the n, γ reaction and both β- and γ-rays from the radioisotopes In^{114} [12] and In^{116} [4] which are formed. That the principal contribution of the indium is the γ-radiation was demonstrated by exposing to neutrons a stack of twelve x-ray films covered only on the front face with an 0.5-mm thick indium foil. It was found that there was little attenuation in the optical density from film to film, a result which would not be the case if the β-rays from the In^{114} and In^{116} contributed significantly to the density.

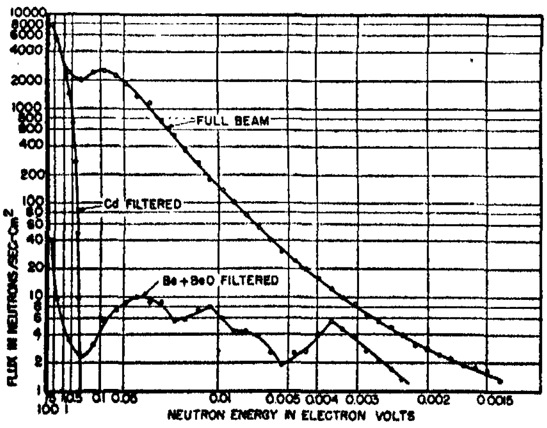

FIG. 3. Energy distributions of the full, Cd filtered, and Be plus BeO filtered neutron beams. The neutron fluxes were calculated from data obtained with the neutron velocity spectrometer.

The density curves in Figs. 4a and 4b should be considered as only roughly quantitative because the known inhomogeneity of the neutron beam probably did not permit equal exposures of all the plates that were simultaneously exposed. In addition, the *NT*4 plates used for these density curves were not fresh, and had suffered some loss of sensitivity because of exposure to high humidity. In other experiments, fresh, dry *NT*4 plates were found to be somewhat more sensitive than x-ray film plus indium foil (for unfiltered neutrons).

The two triangular points in Fig. 4a and in Fig. 4b represent the total densities of a combination consisting of two *NT*4 plates placed and exposed emulsion to emulsion. It is seen that considerable improvement in effective density, without appreciable sacrifice in resolution, may be achieved in this way.

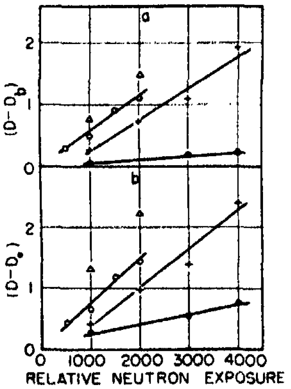

FIGS. 4a and 4b. Optical densities for different neutron exposures of x-ray film with (○ *points*) and without (● points) indium foil, and of *NT*4 emulsion (+ points). The two points in each figure indicated by Δ represent the combined densities of two *NT*4 plates placed and exposed emulsion to emulsion. D, D_b, and D_0 refer to the optical densities of the directly exposed areas, exposed background areas, and unexposed plates, respectively. Exposures were made with the full (unfiltered) neutron beam.

The results of the experiments on the dependence of detection efficiency on neutron energy are given in Table I. The x-ray-indium combination appears better, relative to the *NT*4 emulsion, for cold neutrons (Be plus BeO filtered) than for thermal and epithermal neutrons. This is reasonable in view of the higher indium absorption cross section[13] for slow neutrons and the larger amounts of indium present, compared with the silver in the β-plates. The performance of the *NT*4 plates, particularly when fresh and dry, is remarkably good, a result which may be attributed to the excellent β-sensitivity of these plates.

---

[12] S. W. Barnes, Phys. Rev. 56, 414 (1939).

[13] At 0.025 ev the absorption cross section of indium is 194 barns (see reference 1), compared with 69 barns for silver.

TABLE I. The effect of neutron energy on the relative detection efficiency of an x-ray-indium combination and *NT*4 β-sensitive emulsion.

Neutron beam	Exposure, neutrons/cm^2	Type of emulsion	Emulsion density $(D-D_b)$	Emulsion density $(D-D_0)$
Full beam	3.2×10^7	x-ray+In	1.02	1.24
	3.2×10^7	*NT*4	0.94	1.34
Filtered with 13 g/cm^2 Be plus 11 g/cm^2 BeO	1.9×10^5	x-ray+In	Not measurable	
	1.9×10^6	*NT*4	Not measurable	
Filtered with 13 g/cm^2 Be plus 11 g/cm^2 BeO	4.1×10^5	x-ray+In	0.32	0.71
	4.1×10^5	*NT*4	0.22	0.55

TABLE II. Some experiments with 100μ Ilford D_1 plates loaded with 23-mg normal boron per cm^3 emulsion. The exposures in neutrons per cm^2 were calculated from the data in Fig. 3; the corresponding counts as recorded with BF$_3$ counters were obtained with the neutron velocity spectrometer.

Neutron beam	Exposure, neutrons/cm^2	Number of α-tracks per mm^2	Number of counts in BF$_3$ counters; full beam = 100
Full Beam	3.2×10^7	3355	100
Filtered with 13 g/cm^2 Be plus 11 g/cm^2 BeO	1.9×10^5	49	1.1
Filtered with 0.48 gm/cm^2 Cd	1.5×10^7	548	13

In order to determine whether improved sensitivity of β-plates might be achieved by the use of supplementary indium foils, Ilford *G*5 plates covered on the back face (away from incident neutrons)[14] with 0.5-mm indium foil were exposed, along with control plates, to the full neutron beam. The effective optical density, $(D-D_b)$, of the *G*5 indium combination was 0.10, compared with an average value of 0.08 for the control *G*5 plates. That only such a small improvement was observed may be explained by the relatively poor sensitivity to γ-radiation of the *G*5 plates (the grain diameter is only about one-tenth as large as the grain diameter in *K*-type x-ray emulsion). Furthermore, a considerable fraction of the β-rays produced by the In^{114} and In^{116} are absorbed in the In foil. Even apart from these considerations, it does not appear to be practical to use indium foil with β-plates because these plates are very sensitive to pressure effects[15] which distort the homogeneity of the image. Improvement in sensitivity for low neutron fluxes might be achieved by counting β-tracks, and it was indeed found possible to count tracks microscopically when the track density was low. However, this method is tedious, and the accuracy is seriously limited by the cosmic-ray background.

Shull and Wollan have suggested[6] the use of fluorescent screens in conjunction with x-ray film plus indium in order to improve the sensitivity. Such an improvement might be expected for the β-radiation emitted by the indium. However, as has already been pointed out, it is mainly the γ-radiation which is responsible for the blackening effect in the x-ray-indium sandwich; and for γ-rays the intensifying effect of fluorescent screens is low. For example, the use of a calcium tungstate screen (which is perhaps the most effective for penetrating radiation) in conjunction with *F* type x-ray film can be expected to give a maximum amplification of about four over no-screen film.[16] It is assumed here that the exposure time is optimum with respect to reciprocity law failure. At the same time, however, the screen would reduce the resolution by a factor of perhaps 5 to 10.

The possibility of using an organic fluorescent material such as naphthalene or anthracene to improve the intensity of x-ray film does not appear too feasible. The large screen thickness which would be necessary for the effective use of such a screen would probably result in a prohibitive reduction in resolution. The same consideration is valid for fluorescent screens in which are incorporated elements having high cross sections for (n, α) or (n, p) reactions. Here there is the further difficulty of introducing large concentrations of such elements without impairing the luminosity of the screen.

Table II gives some results obtained with boron loaded emulsions. The ratio of the measured α-track density for unfiltered neutrons to that for Be plus BeO filtered neutrons to that for Cd filtered neutrons is seen to agree fairly well (considering the fluctuations in neutron flux) with the ratio of the respective neutron fluxes as determined with BF$_3$ proportional counters. The smallest track density which can be measured without undue effort and loss of accuracy is ~50 tracks per mm^2; the maximum density which it is convenient to measure is $\sim6\times10^4$ tracks per mm^2. Since 9.1×10^4 tracks per mm^2 was found to correspond to an effective optical density $(D-D_b)$ of 0.16, while 2.3×10^4 tracks per mm^2 gave an effective density of 0.03,[17] it would appear (as is to be expected) that the optical density is essentially linear with respect to the track density at least in this high track density region where it is feasible and convenient to measure the density with a densitometer. Boron loaded plates thus offer the distinct advantage of being useful over a very wide range of slow neutron fluxes.

Perhaps the most important thing to note is that, after an exposure of 1.9×10^5 neutrons (Be plus BeO filtered) per cm^2, no measurable darkening was produced in the *NT*4 plates or x-ray film plus indium foil

---

[14] By covering only the back face of the plate with indium, only neutrons not captured in the G5 emulsion were available for absorption by the indium.

[15] H. Yagoda, *Radioactive Measurements with Nuclear Emulsions* (John Wiley and Sons, Inc., New York, 1949), p. 14.

[16] G. M. Corney, Nondestructive Testing 7, 17 (Winter, 1948–49).

[17] This experiment was carried out by exposing simultaneously to the same neutron flux an Ilford D_1 normal boron loaded plate and a D_1 plate impregnated with pure B^{10} in this Laboratory. Both plates contained roughly the same concentration of boron, but they differed in their sensitivity by a factor of 5.3 because of the different B^{10} contents.

(Table I). However, this same exposure produced a measurable density of 49 tracks per mm^2 in the Ilford D_1 plates loaded with normal boron (Table II). Boron loaded plates therefore offer a large advantage over β-sensitive plates and the x-ray-indium combination for the measurement of low thermal and cold neutron intensities. This advantage can be increased several fold by the use of higher boron concentrations in the emulsion and by the substitution of B^{10} for normal isotopic boron. Thus, if the quantity of boron was doubled (from 23 to 46 mg per cm^3 of emulsion), and pure B^{10} was used, a total exposure to only 2×10^4 neutrons (Be+BeO filtered) per cm^2 would be necessary to give a measurable number of tracks per mm^2. This high neutron sensitivity should make it more feasible to carry out neutron scattering and diffraction experiments.

A further very valuable advantage of boron loaded plates lies in their specific sensitivity to neutrons, provided that the density is measured by α-track counting. By selecting the proper type of emulsion, such as Ilford D_1, the sensitivity to β- and γ-radiation can be kept relatively low. Thus, after an exposure of a D_1 plate to ~80 r of γ-radiation (from a Ra source), the γ-ray background was still low enough to allow short alpha-, or even proton, tracks to be counted readily.

Another important advantage of boron plates lies in the fact that the recognition of α-tracks is largely independent of the development conditions, contrary to other photographic methods based on the density of the image.

The disadvantage of boron plates for low neutron fluxes lies in the necessity for microscopic scanning. However, in scattering experiments where accurate position and intensity measurements of the scattered neutrons are required, the additional time spent in counting tracks (0.5–2 hours depending on the track density and the required accuracy) is not too serious.

ACKNOWLEDGMENT

We wish to thank the AEC who supported this work both through a direct contract with Columbia University and subcontract S-62 with Brookhaven National Laboratory.

THE REVIEW OF SCIENTIFIC INSTRUMENTS VOLUME 21, NUMBER 3 MARCH, 1950

A Microcalorimeter Suitable for Study of Easily Absorbed Nuclear Radiations*

C. V. CANNON† AND G. H. JENKS
Chemistry Division, Oak Ridge National Laboratory

(Received December 5, 1949)

A microcalorimeter suitable for measuring the energy of easily absorbed nuclear radiations is described. The calorimeter is an isothermal type operating at the temperature of liquid nitrogen and using the rate of vaporization of nitrogen under constant pressure as a measure of the heat input. The calorimeter is fairly simple to construct and to operate and has a short equilibration period. Heat inputs to the calorimeter as low as 7×10^{-6} cal./sec. can be measured with an accuracy of one percent.

INTRODUCTION

CALORIMETRIC measurement of the heat evolved upon absorption of nuclear radiations is a method for exact determination of the total energy of the radiations and may be applied to the study of radioactive isotopes in several ways. For example, calorimetric measurements may be employed in checking and correlating information on the energetics of decay derived from more sensitive though less absolute instruments, in exact determinations of average β-ray and γ-ray energies, and in standardization of other instruments. However, a great majority of the isotopes of interest are available in only small quantities, and it is generally necessary to employ microcalorimetric methods in studies of this nature.

A microcalorimeter which is of relatively simple construction and operation and which may be applied to the measurement of nuclear radiation energies has been developed at this Laboratory. The calorimeter is an isothermal type operating at the temperature of liquid nitrogen. Heat from a source within the calorimeter volatilizes nitrogen, and the volume of nitrogen gas evolved is measured at a constant room temperature. The relationship between the rate of vaporization and the heat input is determined with a resistance heater.[1]

The sensitivity which can be achieved with this calorimeter, as with others, is limited by two factors: (1) the uncertainty in the measurement of the quantity of heat entering the calorimeter, and (2) the uncertainty existing as to what fraction of the heat entering the calorimeter is due to the source and what fraction is due to thermal leakage from the surroundings.

---

* This document is based on work performed under Contract Number W-7405 eng 26 for the Atomic Energy Project at Oak Ridge National Laboratory.

† Present address: Physics Department, Antioch College, Yellow Springs, Ohio.

[1] Calorimetric methods involving the volatilization of nitrogen have been described by (a) J. W. Stout and W. M. Jones, Phys. Rev. 71, 582 (1947) and (b) James Dewar, Proc. Roy. Soc. A76, 325 (1905), but no previous attempt to use the technique with calorimeters of very high sensitivity has been reported.

The first of these factors is determined mainly by the accuracy with which the quantity of vapor evolved corresponds to the quantity of heat which has entered the calorimeter. Were there no temperature fluctuations within the calorimeter during a measurement, the heat absorbed would determine completely the volume of vapor evolved. In practice, of course, the temperature does not remain perfectly constant but varies as the pressure of vapor within the calorimeter varies. Condensation or vaporization of liquid independent of the rate of heat flow can then occur, introducing an uncertainty into a measurement which is equivalent to the product of the values for the temperature fluctuation and heat capacity of the calorimeter. In order to minimize temperature fluctuations, the nitrogen vapor pressure within the calorimeter was held constant within close limits.

The other factor affecting the sensitivity, i.e., the uncertainty as to the source of heat, was minimized by two procedures: (1) the calorimeter proper was insulated by a vacuum jacket to reduce thermal exchange with the surroundings, and (2) the jacket was immersed in a bath of liquid nitrogen the temperature of which could be regulated and maintained close to that of the calorimeter. As with the calorimeter proper, temperature regulation in the bath was effected by control of vapor pressure.

Two calorimeters of this type have been constructed and their working characteristics investigated. One of the instruments contained considerable mass and was used in the study of γ-rays of moderate energy. The other contained only a small amount of mass and was used for measuring easily absorbed radiations such as β-particles. Only the latter calorimeter will be described here.

DESCRIPTION OF APPARATUS

Calorimeter

The calorimeter assembly was constructed entirely of glass and consisted basically of three concentric Dewar-type flasks. The innermost of these was the calorimeter proper. It contained the heat source to be measured together with some liquid nitrogen. The intermediate flask served as a container for the calorimeter bath. The outer Dewar held liquid nitrogen and was used to prevent excessive influx of heat to the bath region. Both the inner and intermediate flasks were connected with external pressure regulating systems. The calorimeter connecting tube was enclosed by a silvered vacuum jacket in the region which passed through the surface of the outer liquid bath in order to minimize changes in temperature gradients along the tube. Ground glass joints were used to permit access to the two inner flasks.

The arrangement of this apparatus is shown in the scale drawing, Fig. 1. The three flasks mentioned are identified in the drawing as *A*, *B*, and *M*, respectively, and the closures for flasks *A* and *B* are shown at *E* and *F*. The tube connecting the calorimeter with the external system is shown at *C* and the tube leading from the bath region at *D*. Electrical leads which consisted of 36-gauge copper wire were passed into the calorimeter through tungsten-glass seals at *G* and *E*.

The volume of the calorimeter bulb was about 10 ml and a heat source 2.5 cm in length could be accommodated. Restrictions imposed by the neck limited the diameter of a source to 6 mm or less. In operation the bulb was almost filled with liquid nitrogen. The heat

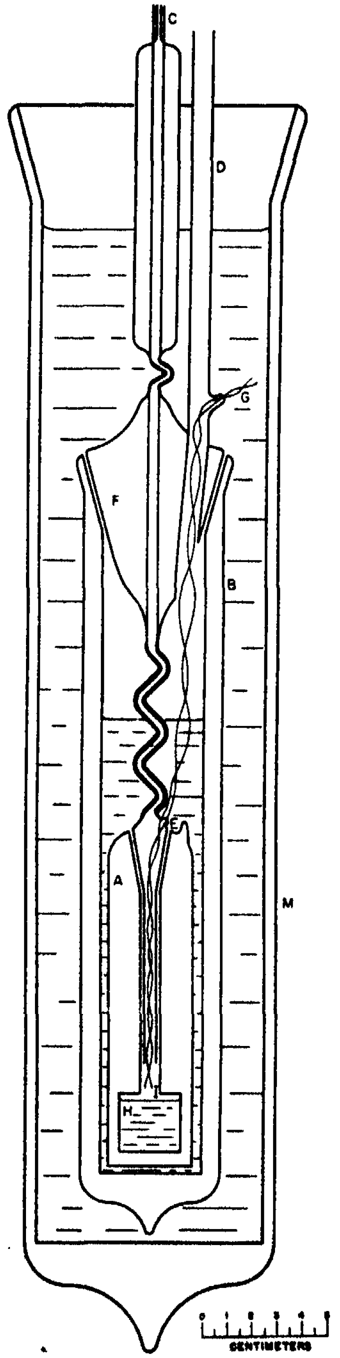

FIG. 1. Calorimeter assembly.

capacity of this liquid plus that of the glass walls made up the total heat capacity of the calorimeter, about 6 cal./deg.

The procedure adopted in assembling the calorimeter was the following: The heat source to be measured was placed in bulb *H* or, in the case of the resistance heater, attached to the lead wires at *I*. About 10 ml of liquid were then transferred into the bulb, and the flask placed on the ground joint *E*. A tight seal was made at this joint using a cement which consisted of a mixture of rubber cement, Apiezon *N* lubricant, and toluene.[3] When frozen, the cement served also to hold the flask in place. Flask *B*, filled with sufficient liquid to bring the level to the approximate height indicated, was next placed in position and the joint then sealed as above. To complete the assembly flask *M* was brought into place and filled with liquid nitrogen.

Maintenance of Pressure and Metering of Gas Evolution Rate

A fixed pressure within the calorimeter was maintained by adjusting the external volume of the system to counteract deviations from the desired pressure. In the apparatus designed for this purpose, the net increase in the external volume of the system represented the volume of gas evolved during the given period and served as a measure of the rate of gas evolution.

A sketch of the apparatus employed to control pressure and meter the gas evolution is shown in Fig. 2. The volume-adjusting device pictured at the right was made up of the glass syringe *D*, the split-phase motor *E*, and the mercury column *B*. The shaft of the motor was coupled to the plunger of the syringe so that rotation of the shaft would displace the plunger and thus change the level of mercury in *B*. This system responded to pressure deviations detected by the mercury manometer-metallic probe arrangement at *A*. The manometer contact and the motor were connected through an electronic relay and a Brown amplifier so that the motor would rotate in a forward or reverse direction depending on whether the contact was made or broken. Thus as a deviation in pressure altered the height of mercury in the manometer, the level of mercury in *B* would be changed to counteract the deviations.

The sensitivity of the mercury-metal contact was, of course, very important in getting close pressure control. It was found that a platinum wire prepared by heating to redness and then coating with a thin layer of Aqua-Dag was exceedingly sensitive, and that it would remain so for several days of operation if the current through the relay were kept to less than a micro-

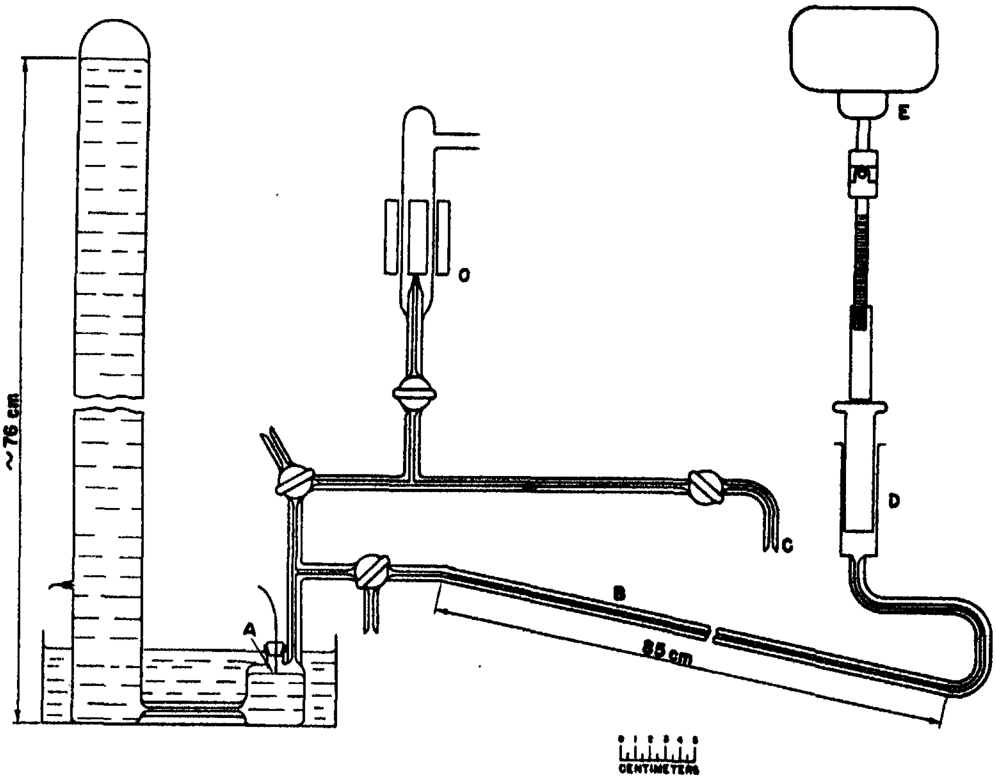

FIG. 2. Apparatus for controlling pressure and measuring gas evolution.

---

[3] Stout and Jones, see reference 1(a), have reported the successful use of rubber cement diluted with toluene as a sealing agent at liquid nitrogen temperature. We have found that the addition of Apiezon lubricant to the mixture increases the reliability of forming a gas-tight seal.

ampere. It was also found that if a slight vibration were imposed on the mercury surface, the sensitivity of the control was increased. With the vibration occurring, the mercury-metal contact was made and broken many times a second. However, the motor would appear to remain stationary when no change in the quantity of gas within the system was taking place. When the quantity of gas was changing, the motor would rotate slowly in the direction necessary to compensate for the change.

In addition to the volume adjusting system, a solenoid operated gas outlet at 0, Fig. 2, was also provided. This valve, which could be controlled by the contact at *A*, was used when only a relatively rough control of the pressure (±0.1 mm) was required. A similar system consisting of a manometer and solenoid valve was used in regulating pressure over the calorimeter bath.

OPERATION OF CALORIMETER

The procedure for setting the calorimeter into operation was fairly simple. The source to be measured was placed in the calorimeter Dewar and the whole Dewar system assembled as previously described. The calorimeter was then connected to the pressure control system from which air had been previously excluded. To complete the assembly, the bath region was joined to its pressure regulating system. This assembly procedure was repeated for each series of measurements on a given source, and of course whenever a new source was substituted.

When the calorimeter was first assembled, its temperature was far from the equilibrium temperature, and the rate of gas evolution was high. The solenoid valve arrangement was then used to control the pressure until the rate had become sufficiently low to permit the convenient use of the volume-adjusting system. After the calorimeter had reached the equilibrium temperature, as indicated by the rate of gas evolution, measurements were started.

To carry out a measurement the mercury in tube *B*, Fig. 2, was first brought to the top by allowing gas to leak from the solenoid valve at a constant slow rate which the volume adjusting system could follow without disturbing the pressure. The solenoid valve was then closed, and the time required for the mercury level to be lowered through a given distance, usually the length of the capillary, was observed. To repeat the measurement, the mercury level was returned to the top as before, and the rate of depression of the level again measured.

To preclude the possibility of condensation within the calorimeter system, the pressure regulator for the bath was set to maintain a pressure approximately 1 mm greater than that within the calorimeter. No change in this relative pressure was made between calibration determinations and measurements on an unknown source. The pressure at which the calorimeter was operated was about 2 cm below average atmospheric pressure at this Laboratory.

TABLE I. Calibration data.

Calorimeter assembly no.	Power level watts ×10^4	Rate of N_2 production arbitrary units 1	2	Computed	Percent deviation of average
1	2.498	1.22	1.21	1.218	+0.41
1	1.800	0.898	0.892	0.888	−0.79
2	1.100	0.562	0.558	0.556	−0.71
3	0.662	0.347	0.347	0.349	+0.57
4	0.200	0.129		0.130	+0.77

The liquid nitrogen which was used in all work was obtained from the Linde Air Products Company. Although only customary precautions to prevent oxygen contamination of the liquid were observed, an added precaution was taken to insure that the compositions of liquids in the calorimeter and bath were the same. In filling the flasks they were first pre-cooled to the temperature of liquid nitrogen and then refilled with liquid taken directly from the shipping tank.

PERFORMANCE

Studies of the performance of the calorimeter as well as calibration determinations were carried out using a resistance heater to produce precisely known power levels within the calorimeter. The resistance used was a ½-watt, Allen-Bradley, carbon resistor measuring ∼5700 ohms at room temperature and ∼11,000 ohms at the low temperature. The resistance of the small copper lead wires could therefore be neglected. The power developed in the resistor was determined by measuring, with a Type *K* potentiometer, the voltage drops across the heater and across a standard resistor in series with the heater.

The results of a representative series of studies which were carried out with the heater are presented in Table I. The energy input is given in the second column and the observed rates of gas evolution for successive measurements are given in the next two columns. Column five contains a list of rate values computed from the equation,

$$R = 0.4732 \times 10^4 W + 0.0358,$$

(R = rate in arbitrary units and W = power level in watts), which was determined from the experimental data by the method of least squares. The percentage deviation of the measured from the computed values is shown in the final column.

Additional calibration data are tabulated in Table II. These data were obtained using a capillary which differed slightly in cross-sectional area from that previously used and thus cannot be directly correlated with those shown in Table I.

The calibration data exhibit a reproducibility of better than ±1 percent for any energy input within the range calibrated. Because of the directness of the electrical calibration and the accuracy with which the power may be measured, it is believed that the probable error

TABLE II. Calibration data.

Calorimeter assembly no.	Power level watts $\times 10^4$	Rate of N_2 production arbitrary units		
		1	2	Average
1	2.200	1.179	1.185	1.182
2	2.200	1.171	1.183	1.177
3	2.200	1.164	1.164	1.164
4	2.200	1.167	1.174	1.170
5	0.3600	0.212		
6	0.3600	0.207		
7	0.3600	0.213		

of determinations on any source falling within the calibrated range is less than ± 1 percent.

Some conclusions regarding the degree of pressure control and the magnitude and reproducibility of the heat leakage may also be drawn from the calibration data. Each rate value reported is the average rate at which a total of 3.0 to 3.5 ml of nitrogen gas were evolved. Since the heat of vaporization of nitrogen is such that 1 ml of gas is evolved by 0.06 cal., the data indicate reproducibility to $\pm 2\times 10^{-3}$ cal. Assuming that all variations between consecutive measurements during a single assembly of the instrument were produced by fluctuations from the given temperature of the calorimeter, and using the value of 6 cal./deg. for the heat capacity of the calorimeter, it may be estimated that the maximum variation in temperature was $\pm 3\times 10^{-4}$ deg. From this value it follows that the maximum detectable variation of the pressure within the calorimeter was $\pm 2\times 10^{-2}$ mm. Actually the pressure control was probably somewhat better than this since a part of the observed deviation between consecutive measurements could be accounted for by a small variation of the temperature at which the gas volume determinations were made.

By reference to the equation relating the experimental data, it can be seen that at zero power the calorimeter still exhibited an appreciable rate of gas evolution. This background rate was undoubtedly caused by heat flowing into the calorimeter from the bath region. The precision of the calibration data show that the uncertainty introduced by any change in the background between different assemblies of the calorimeter was at least as small as that arising from temperature fluctuations within the calorimeter.

If fluctuations of the calorimeter temperature were the only source of uncertainty, still smaller power levels could be measured by extending the observation period. However, the total uncertainty arising from the background would not be affected by longer measurements, and the percentage error would increase as the power of the source decreased. Several attempts were made to reduce the magnitude of the background by reducing the pressure difference between calorimeter and bath. These attempts usually failed because of the occurrence of condensation within the calorimeter before the background was decreased appreciably. This phenomenon was probably caused by the large depth of liquid nitrogen within the bath and the low thermal conductivity of the liquid and of the materials in contact with the liquid. In the absence of stirring it was possible, if heat entered the bath by any path which did not lead through the surface, for liquid surrounding the calorimeter to be warmer than the surface liquid. The tube which conducted vapor from the calorimeter was in contact with the surface and vapor could therefore be condensed at that point while heat was being transferred into the calorimeter from a lower region of the bath.

The length of time required to carry out a measurement with the calorimeter depended upon the power generated by the source under investigation. As noted above, a total of 3 to 3.5 ml of nitrogen gas, corresponding to a total heat input of ~0.2 cal., were evolved during each measurement. Thus the duration of a measurement ranged from ~60 min. for the highest power level calibrated to ~500 min. for the lowest. The time required for the equilibrium temperature to be established after the calorimeter was assembled was independent of the source and was usually 1.5 to 2 hr. In passing from one power level to another after the calorimeter was at the equilibrium temperature, a constant rate of gas evolution was achieved within less than 10 min.

DISCUSSION

The described calorimeter has several characteristics which recommend its use in measuring the heat from nuclear radiations. The sensitivity of the instrument is such that 10 mC of an activity decaying with an energy of 1 Mev form a conveniently measured source. The short period required for equilibration after changing the power level enables study of fairly short-lived activities (>10 hr.) without the necessity of correcting for "lag." Furthermore, no difficulty arises in obtaining good thermal contact between the source and the calorimeter.

This instrument has been used[3,4] in a study of the half-life of tritium and the average β-energy released in its decay. It has also been used in connection with an absolute β-disintegration rate study, using P^{32}. The former of these measurements will be reported in detail elsewhere.

The calorimeter employing the same principle of operation but containing considerably more mass has been used for gamma-absorption measurements at this Laboratory. The sensitivity which could be achieved with the instrument was less than that of the one described here by a factor proportional to the increase of heat capacity, and its use was limited to the measurement of relatively large activity levels.

---

[3] Jenks, Ghormley, and Sweeton, Phys. Rev. **75**, 701 (1949).

[4] Zumwalt, Cannon, Jenks, Peacock, and Gunning, Science **107**, 47 (1948).

THE REVIEW OF SCIENTIFIC INSTRUMENTS VOLUME 21, NUMBER 3 MARCH, 1950

A Study of Plateau Slopes in Self-Quenching Geiger-Müller Counters*

SANBORN C. BROWN AND CLAUDINE MARONI†
Department of Physics and the Radioactivity Center of the Laboratory for Nuclear Science and Engineering, Massachusetts Institute of Technology, Cambridge, Massachusetts

(Received December 12, 1949)

A study of plateau slopes of self-quenching Geiger-Müller counters shows that no quenching vapor tested produced flat characteristics. On the assumption that the slopes were given by spurious counts arising from the gas discharge phenomena, a study was made of the controlling factors. Neither the quenching gas nor the vehicular gas positive ions were found to be significant. A study of the negative ions produced by molecular dissociation of the quenching gas at the cathode, and electron attachment in the body of the gas shows that these factors are directly correlated with the slopes of the plateau characteristics.

IT is a well-known fact that the slopes of the plateau curves of Geiger-Müller counters are markedly affected by the nature of the gas filling. It is not obvious from theoretical studies of the discharge mechanisms why the plateau characteristics of counters incorporating an organic quenching agent are not flat. After the discharge has broken down, having been initiated by an external charged particle, the electric field of the anode falls below threshold and remains so until the positive ion sheath has moved from the anode to allow the field to return to a value sufficient to support a discharge once more. During this period of so-called dead time, the counter is insensitive. The positive ions continue to move toward the cathode making collisions on the way such that if the counter is behaving properly, the positive ions of the vehicular gas will, before reaching the cathode, have transferred their charge by collision to neutral quenching agent atoms, forming quenching agent ions and neutral vehicular gas atoms. By this mechanism, no vehicular gas ions reach the cathode. A proper quenching agent will be one whose ions will produce no secondary electrons or negative ions on collision with the cathode wall. If electrons or negative ions were produced at any time after the dead time, the counter would break down in a spurious count, since it would be the result of an internal mechanism and not an indication of the arrival of an external ionizing particle. In the present study, the assumption is made that the cause of the slope of a plateau curve is spurious counts arising from mechanisms involved in the counter discharge, and that a study of the causes of the plateau slopes gives information on the causes of spurious counts.

EXPERIMENTAL PROCEDURE

An experimental procedure was evolved for obtaining reproducible and consistent results. Two identical counters were constructed with tantalum cathodes. These cathodes were five inches long and one inch in diameter. The anode wires, 0.006 inch in diameter, had an effective length slightly shorter than that of the cathode. This was accomplished by having the large tungsten leads which sealed through the glass envelope extend within the cathode, the anode wire being hard soldered between these two leads. The two counters were connected to an evacuating and filling system which was free from mercury. The low pressure was measured with thermocouple and ionization gauges, and filling pressures were measured with a mechanical Bourdon gauge. Between runs the counters were pumped to a pressure of 10^{-6} mm of mercury by an oil diffusion pump. Whenever the system was let up to air, or any vehicular gas change took place, the counters were outgassed by baking at 400°C for several hours at a pressure of 10^{-6} mm of mercury. To obtain reproducible results, it was found essential to use spectroscopically pure vehicular gas and carefully distilled organic vapors.

Both counters were filled together, and the data were considered significant only if the results from both counters were the same. Whenever the counters began to give erratic results, they were removed from the system and their cathodes cleaned chemically. Unsatisfactory behavior of the counters was tested in two ways: the plateau characteristics of both counters had to be the same within the experimental error, and the normalized slope had to be independent of counting rate. The normalized slope is defined as the ratio of the change in counting rate divided by the total counting rate, to the change in voltage divided by the total voltage at the onset of the plateau. These criteria lead to an average of steeper plateau slopes than the customary practice of accepting only the flattest plateaus, but since this study was directed toward an understanding of the spurious count mechanism and not toward producing good counters, this procedure seemed more significant.

POSITIVE ION EFFECTS

A study was first made of the effect of changing the relative concentration of the polyatomic quenching gas. Although the plateau slope changes for small concentrations of the quenching agent, it was found that after a certain minimum concentration, the plateau slope was independent of the amount of polyatomic gas present. This is interpreted in the following way. The role of

---

* Assisted by the Joint Program of the ONR and AEC.

† Now at Tracerlab Inc., Boston, Massachusetts.

TABLE I. Average normalized plateau slopes.

	Benzene	Acetone	Methyl alcohol	Ethyl alcohol	Iso-amyl acetate
Helium	1.1	0.9	1.1	0.8	0.4
Neon	0.9	0.9	1.0	1.0	0.4
Argon		0.8	0.8		0.5

the quenching gas is to serve as a trap to prevent the vehicular gas ions from reaching the cathode and producing secondary electrons. The trapping is achieved through a charge transfer mechanism in which the ionized vehicular gas transfers its charge on collision to the polyatomic gas molecule, causing a polyatomic ion and a neutral vehicular gas atom. In order for this mechanism to be successful, two criteria must be met: first, the ionization potential of the vehicular gas must be greater than that of the polyatomic gas; and, second, the polyatomic ion must dissociate on or before collision with the cathode to prevent its ionization energy from releasing a secondary electron from the wall.

With this picture of the operating mechanism, we can see the reason for the observed behavior of the plateau slope with polyatomic gas concentration. If an insufficient number of polyatomic atoms are present, too few charge transfer collisions occur to prevent some vehicular gas ions from reaching the cathode. If this occurs, spurious counts are caused by the resulting secondary electrons from the vehicular gas ions colliding with the cathode. After the concentration of polyatomic molecules is sufficient to act as a complete trap for the vehicular gas ions, the number of spurious counts caused by the vehicular gas should be zero, and the slope should be independent of quenching agent concentration, as observed.

If the above description of the mechanism is correct, it would strongly suggest that the vehicular gas should have no effect on the plateau slope, provided that the polyatomic gas concentration is sufficient. This has been checked by an extensive series of tests using helium, neon, and argon gas with several polyatomic quenching agents. The results of this study are shown in Table I. The numbers tabulated are the average normalized slopes of the plateau curves. Each value is the average of between twenty- and thirty-plateau determinations with widely differing quenching gas concentrations.

The charge transfer mechanism, upon which we are relying to remove the vehicular gas ions from the discharge, is dependent upon the ionization potentials of the ions and atoms involved. The transfer can occur only when the ionization potential of the vehicular gas is higher than the ionization potential of the quenching gas. Furthermore, the probability of the transfer occurring on collision is greater when the ionization potentials are almost equal than when they are far apart. The ionization potentials for the vehicular gases vary from 24.5 volts for helium to 15.7 volts for argon while the quenching vapors have ionization potentials between 9 and 11 volts. If the charge transfer were not complete, the greater probability of transfer from argon than helium would be expected to be a significant factor. Since this is not the case, we have further evidence of the completeness of charge transfer. These data strongly support the conclusion that we have eliminated the noble gases as a source of spurious counts. If we make the assumption that the probability of producing a significant number of secondary electrons by positive polyatomic ion collision with the cathode is negligible, all positive ions are eliminated as a source of spurious counts.

NEGATIVE ION TESTS

A study of the literature does not show that any of the quenching agents used in the positive ion tests have been analyzed for negative ions produced by electron bombardment. Therefore, the negative ion part of the study was made with different quenching vapors from the positive ion studies. Negative ion measurements have been made[1] in carbon tetrachloride, freon-12, ammonia, and methane. The result of a study of the normalized plateau slopes using these gases as quenching agents is plotted in Fig. 1 as a function of the intensity of the most abundant negative ion referred to the most abundant ion of either sign, as determined by mass spectroscopic studies.[1] These values of the normalized slopes are average values determined as described in the positive ion studies, the slopes being independent of quenching agent concentration in a given mixture.

It is obvious from an examination of the data in Fig. 1, that a definite correlation exists between the normalized plateau slope and the relative intensity of the negative ions produced in an electrical discharge. Since the normalized slope is independent of the quenching agent concentration in a given mixture, one can

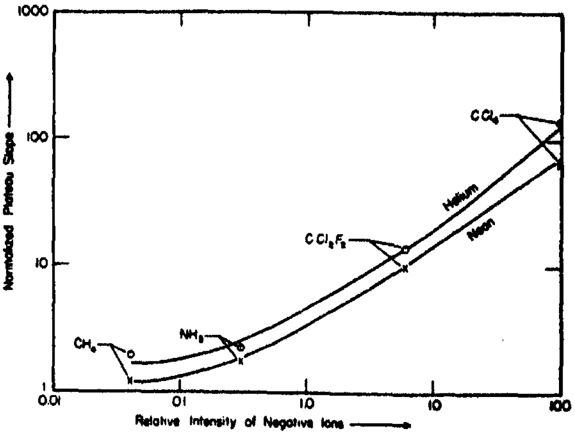

FIG. 1. Average normalized plateau slopes are plotted as a function of mass spectroscopically measured relative intensities of negative ions, for helium and neon vehicular gases.

---

[1] L. G. Smith, Phys. Rev. 51, 263 (1947)—(CH_4); Mann, Hustrulid, and Tate, Phys. Rev. 58, 340 (1940)—(NH_3); R. F. Baker *et al.*, Phys. Rev. 53, 683(A) (1938)—(CCl_4) and (CCl_2F_2).

conclude that a constant number of negative ions is produced independent of the concentration of quenching gas. This is evidence that the negative ions in these quenching gases are produced in the dissociation of the positive molecular ion on collision with the wall, since apparently only the ions produced by charge transfer with the vehicular gas affect the production of negative ions. If the negative ions were produced either by direct attachment or by electron bombardment in the body of the gas, increasing the concentration of the attaching gas should increase the negative ion population, and this is found not to be the case.

Another phenomenon apparent in these negative ion tests, and in which they differ from the positive ion tests, is the fact that the normalized plateau slopes are dependent upon the vehicular gas. We are unable to offer a definite explanation for this observation, although one can examine in more detail the behavior of negative ions in producing a spurious discharge. A spurious count will only be produced when a negative ion arrives in the high field region after the counter has recovered from its dead time. If the negative ions are produced by molecular dissociation at the cathode, they all would produce spurious counts, since the positive ion space charge does not reach the cathode until after the dead time is over. Thus, the mobility characteristics in the vehicular gas of the negative ions produced at the cathode should not be a significant variable. This is consistent with our observations. The ions will have their highest mobility in helium and, therefore, if they could be swept out before the end of the dead time, they would have the greatest chance of doing so in this gas. Yet, we find that the greatest number of spurious counts occur in helium showing that the mobility characteristic is not significant. It has been found experimentally[2] in the noble gases that the second Townsend coefficient increases with increasing ionization potential, the possible mechanisms for the second Townsend coefficient in these experiments being the production of secondary electrons produced either at the walls or in the gas due to photons created in the discharge. It is possible to explain the increased production of spurious counts in helium over neon by the photo-ionization in the gas since this would increase the population of positive vehicular gas ions, and hence by charge transfer, the number of quenching agent ions which will subsequently dissociate into negative ions. The ionization potential of helium is 24.5 volts and that of neon 21.5 volts, and, therefore, these gases are in the correct relation to each other for this explanation to be valid, but no check of this hypothesis is available.

The halogen gases show quenching characteristics and the atomic ions are known to have high electron attachment probabilities; therefore, studies were made using chlorine as a quenching gas. This gas was chosen, since its behavior would be expected to differ from those gases producing negative ions by molecular dissociation. Negative ion attachment in the volume of the gas is known to occur, and so far as is known, negatively charged ions are not produced in the molecular dissociation at the cathode which gives rise to the self-quenching properties. Since the negative ions are not associated with a charge transfer mechanism, but are produced by direct attachment to chlorine atoms in the discharge, one would expect the number of ions produced would depend on the chlorine concentration. This is in fact the case, as shown in Fig. 2.

Although electron attachment to the atom has a high probability, it does not occur to the chlorine molecule. Therefore, one would expect the negative ions to be formed only close to the discharge region. Since the negative ions would not move very far before losing their electrons in the high field, one might expect that very few would be left by the time the counter dead time is over. It is because the residual number is small, that chlorine can make a practical self-quenching counter. Those negative ions which produce spurious counts will be only those that have not been swept out by the electric field before the dead time has elapsed, and hence the number of spurious counts produced by these ions should depend upon the ionic mobility in the vehicular gas. The mobility of chlorine ions in argon is lower than the mobility in neon, and hence more negative ions are left at the end of the dead time in argon than in neon. This offers an explanation for the behavior of the data shown in Fig. 2, where the normalized slopes in argon are greater than in neon.

CONCLUSION

The quenching agents that we have studied fall into three groups. The first group are those for which we could find no information concerning their negative ion production. These gases include most of the common quenching agents and show low normalized plateau slopes which are independent of the quenching agent concentration and independent of the vehicular gas.

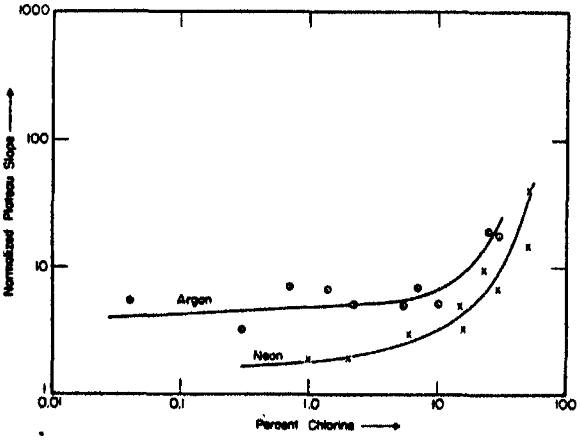

FIG. 2. Normalized plateau slopes are plotted as a function of percent chlorine quenching gas for argon and neon vehicular gases.

---

[2] M. J. Druyvesteyn and F. M. Penning, Rev. Mod. Phys. 12, 110 (1940).

The gases in this group which we studied include benzene, acetone, methyl and ethyl alcohol, and iso-amyl acetate. These quenching vapors show plateau curves of low but not constant slope and it seems probable that these gases exhibit very small negative ion production by dissociation of the positive ions at the cathode.

The second group of quenching gases are those which form negative ions by dissociation of positive ions at the cathode. These gases show increasing normalized plateau slopes with increasing negative ion production, independent of the quenching agent concentration but dependent upon the type of vehicular gas. These gases include methane, ammonia, freon, and carbon tetrachloride.

Only one gas, chlorine, of a third group was studied; this group contains those which form negative ions by electron attachment in the gas. Gases of this group are characterized by increasing normalized plateau slopes with increasing quenching gas concentration and the slopes are dependent on the type of vehicular gas.

None of the plateau characteristics were flat, and the variation in plateau slopes for the cases of the usual quenching agents shown in Table I might be the result of such factors as the changes in sensitivity from gas to gas and the end effects of the electric field. These factors, however, account for only small variations in the plateau slopes and not the large variations illustrated in Figs. 1 and 2.

THE REVIEW OF SCIENTIFIC INSTRUMENTS VOLUME 21, NUMBER 3 MARCH, 1950

Time Lags in Geiger Counters

ARTHUR R. LAUFER[*]
New York University, University Heights, New York

(Received December 5, 1949)

Light from a spark was used to produce a primary ionizing event in a Geiger counter by means of the photoelectric effect. The time lag between this event and the detection of the pulse on the counter wire was studied as a function of counter filling, pressure, and overvoltage. The measured lags, ranging from tenths of microseconds to many microseconds, were used to calculate electron mobilities, sheath spread velocities, and electron attachment coefficients. The lags appear to be the result of the transit time required by the initial electrons to move from their point of origin to the high field region, and the time required by the sheath to spread laterally along the wire and to move radially outward far enough to produce an electrical pulse which can be detected.

INTRODUCTION

Several investigators[1] have reported the observation of a time lag between the time at which a primary ionizing event occurs in a Geiger counter and the time at which the electrical pulse is detected. The magnitudes of such delays appear to range, in different reports, from several hundredths to many tens of microseconds. It has been suggested that the causes of these delays are the transit time required by the initial electrons to move from their point of birth to the avalanche region near the wire,[2] and the capture of electrons to form negative ions[3] which require an even longer transit time. However, lags are obtained[4] even when the initial electrons are formed close to the wire surface in counters containing fillings which do not form negative ions.

In all but one of the previous investigations, only relative lags could be observed, since measurements were made of the differences in the firing times of two counters actuated by the same primary ionizing event. In the one case[5] of observation of absolute delays, the technique used did not permit the detection of very short lags, and only a negative-ion-forming gas (oxygen) was studied.

Such time lags may limit the counting rate in high speed counting, and may cause real coincidences to be missed in the method of coincidence counting. In addition, a fuller understanding of the causes of the lags may give further insight into the processes involved in Geiger counter action. For these reasons a study of the magnitudes and causes of time lags in Geiger counters was undertaken in the present investigation.

EXPERIMENTAL TECHNIQUE

The central problem in the determination of the absolute time lag in a Geiger counter is the production of a primary ionizing event in the counter at a known instant. The use of a second Geiger counter to determine this instant can give only the relative lag between the two counters and not the absolute lag.

The procedure employed in the present work can be simply stated. Each Geiger counter used had one or

---

[*] Now at the University of Missouri, Columbia, Missouri.

[1] B. Rossi and N. Nereson, Phys. Rev. 62, 417 (1942); Montgomery, Ramsey, Cowie, and Montgomery, Phys. Rev. 56, 635 (1939); H. K. Ticho, Rev. Sci. Inst. 18, 271 (1947).

[2] Den Hartog, Müller, and Verster, Physica 13, 251 (1947).

[3] M. E. Rose and W. E. Ramsey, Phys. Rev. 59, 616 (1941).

[4] C. Sherwin, Rev. Sci. Inst. 19, 111 (1948).

[5] C. G. Montgomery and D. D. Montgomery, Rev. Sci. Inst. 18, 411 (1947).

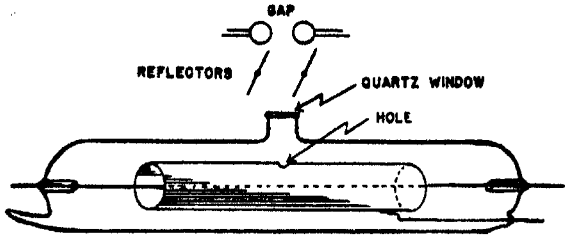

FIG. 1. Spark gap, reflectors, and Geiger counter.

more small holes drilled in the cylinder wall, and light from a fast spark[5] was admitted to each hole through a quartz window, as indicated in Fig. 1. The spark light, which ejected photo-electrons from the inner wall of the cylinder, was taken to be the primary ionizing event. At the same instant some of the spark light fell upon a vacuum photo-tube. Since no time lag has ever been observed in a vacuum photo-tube, the electrical pulse from the tube was taken to be coincident with the time of ejection of the photo-electrons in the Geiger counter. The time interval between the photo-tube pulse and the electrical pulse from the counter was measured with a fast-sweep synchroscope, and was taken to be the absolute time lag in the Geiger counter.

The spark light was obtained from an overvolted spark gap with a 3-ohm resistance in series to damp the oscillation critically. The time of duration of the spark light was measured to be less than 0.1 μsec. by viewing the photo-tube pulse on the synchroscope, and was independently checked by measuring the blurring of the cannelure of a bullet in flight photographed with the light of the same spark.

The counter used for most of the work had a 4-mil wire and a 2.5-cm diameter copper cylinder, 20 cm in length. A series of $\frac{1}{16}$-in. holes was drilled in a straight line along 18 cm of the cylinder length. The quartz windows, transparent to radiation down to about 1500A, permitted the ejection of photo-electrons from the cylinder, which has a work function of about 4.4 volts (2800A). Photo-ionization of the counter gases used, however, was quite improbable,[6] since this process requires radiation of at least 1100A.

In the main recording circuit, Fig. 2, part of the pulse from the photo-tube was differentiated and used to trigger the sweep of the synchroscope. The remainder of the pulse passed successively through a cathode follower, a delay line, and a one-stage, low gain, wide-band amplifier. The Geiger counter pulse passed through an almost identical circuit, and the amplifier stages of the two circuits were coupled by the use of a common plate load resistor. This coupling mixed the photo-tube and Geiger pulses to give a single output which was applied to the vertical deflecting plates of the synchroscope. The multivibrator section of a Sylvania P4

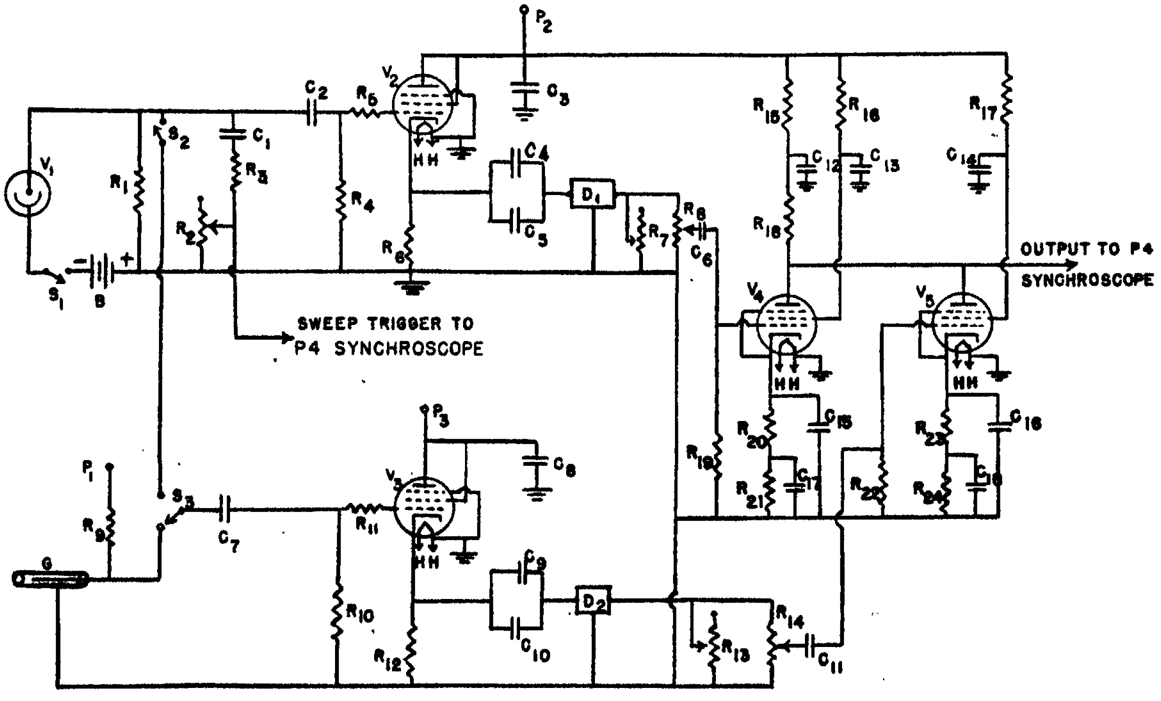

FIG. 2. Main recording circuit. G, Geiger counter; V_1, RCA 917; V_2, V_3, V_4, V_5, 6AG7; S_1, S_2, SPST; S_3, SPDT; B, Eveready, 300 v; P_1, 0—2 kv; P_2, P_3, 400 v; D_1, 0.5 μsec. delay line; D_2, 1.0 μsec. delay line; C_1, 150 μμf; C_2, C_7, 0.001 μf, 2500 wv; C_3, C_8, 0.5 μf; C_4, C_9, 100 μf; C_5, C_{10}, 1000 μμf; C_6, C_{11}, 0.01 μf; C_{12}, C_{13}, C_{14}, 2 μf; C_{15}, C_{16}, 0.004 μf; C_{17}, C_{18}, 40 μf; R_1, 1.5 MΩ; R_2, 20 kΩ; R_3, R_{19}, R_{22}, 100 kΩ; R_4, R_{10}, 1 MΩ; R_5, R_{11}, 50Ω; R_6, R_{12}, 820Ω; R_{15}, 500Ω; R_{16}, R_{17}, 2 kΩ; R_{18}, 1 kΩ, 4 w; R_{20}, R_{23}, 10Ω; R_{21}, R_{24}, 330Ω; R_7, R_{13}, 500Ω; R_8, R_{14}, 10 kΩ; R_9, 1.5 MΩ for self-quenching counter, or 3×10^9Ω for non-self-quenching counter.

---

[6] Hughes and DuBridge, *Photoelectric Phenomena* (McGraw-Hill Book Company, Inc., New York, 1932).

TABLE I. Measured values of time lags.

Counter filling		Total pressure (cm)	Over-voltage (volts)	Operating voltage (volts)	Total lag (μsec.)	Transit lag (μsec.)
% argon	% ethyl alcohol					
90	10	6	100	910	0.39	0.24
90	10	8	100	975	0.48	0.27
90	10	10	100	1065	0.56	0.27
90	10	12	100	1110	0.56	0.31
90	10	14	100	1160	0.60	0.32
90	10	16	100	1230	0.58	0.35
90	10	18	100	1290	0.66	0.34
90	10	20	100	1340	0.70	0.39
95	5	10	100	950	0.54	0.31
90	10	10	100	1065	0.56	0.27
85	15	10	100	1180	0.50	0.28
80	20	10	100	1260	0.48	0.27
75	25	10	100	1355	0.47	0.27
70	30	10	100	1420	0.45	0.25
90	10	10	40	1005	1.16	0.29
90	10	10	80	1045	0.60	0.27
90	10	10	120	1085	0.46	0.28
90	10	10	160	1125	0.39	0.29
90	10	10	200	1165	0.35	0.28
% argon	% amyl acetate					
90	10	6	100	920	0.46	0.25
90	10	8	100	990	0.53	0.28
90	10	10	100	1085	0.55	0.28
90	10	12	100	1140	0.62	0.32
90	10	14	100	1195	0.66	0.33
90	10	16	100	1270	0.68	0.36
90	10	18	100	1330	0.72	0.35
90	10	20	100	1380	0.76	0.36
95	5	10	100	950	0.58	0.29
90	10	10	100	1085	0.55	0.28
85	15	10	100	1200	0.55	0.29
80	20	10	100	1290	0.54	0.27
75	25	10	100	1390	0.53	0.26
70	30	10	100	1450	0.53	0.27
90	10	10	40	1025	1.34	0.31
90	10	10	80	1065	0.68	0.30
90	10	10	120	1105	0.52	0.28
90	10	10	160	1145	0.42	0.29
90	10	10	200	1185	0.37	0.29
Hydrogen						
		4	100	915	0.23	0.22
		6	100	1060	0.27	0.25
		8	100	1180	0.28	0.25
		10	100	1310	0.33	0.29
		12	100	1400	0.32	0.31
		14	100	1520	0.37	0.30
		16	100	1610	0.38	0.33
		18	100	1720	0.43	0.34
		20	100	1800	0.42	0.36
		10	40	1250	0.43	0.30
		10	80	1290	0.34	0.29
		10	120	1330	0.31	0.26
		10	160	1370	0.29	0.28
		10	200	1410	0.29	0.27

synchroscope was rebuilt to provide an externally triggered, single-sweep arrangement, with sweep speeds of 0.5, 2, 6, and 25 μsec. per in. A 2-Mc crystal oscillator was built and employed to calibrate the synchroscope. It was also possible to pass a given photo-tube pulse alone through both the photo-tube circuit and the counter circuit to obtain a measure of "zero lag."

Part of the data was taken photographically, and part visually, the results proving reproducible to within experimental error. A DuMont oscilloscope camera was refitted with a xenon $f{:}2$, 50-mm, coated lens. This lens, together with Linagraph Pan film and Kodak SD19a developer, permitted satisfactory photography of the traces on the synchroscope screen.

Figure 3 presents several typical photographs. The differentiated part of the photo-tube pulse triggered the synchroscope and started the motion of the cathode-ray beam toward the right. After a fixed delay, the remainder of the photo-tube pulse caused the initial rise in the pattern. This rise was taken to correspond to the instant at which photo-electrons were released in the Geiger counter. The photo-tube pulse was "limited" in size by the cathode follower, and since the photo-tube charge was allowed to leak off through a high resistance, the pulse maintained its height and served as a base line for the succeeding Geiger pulse. Then, after another fixed delay of 0.5 μsec., if there had been zero time lag in the Geiger counter, the second rise in the trace would have indicated the arrival of the counter pulse. The *increase* in this time was taken to be a measure of the absolute lag in the counter.

By rotating a pair of cardboard reflectors mounted between the spark gap and the counter, the intensity of spark light incident upon the counter could be varied. With zero intensity the synchroscope trace exhibited the initial rise due to the photo-tube pulse, but did not show the second rise since no electrons were produced in the counter and no counter pulse was generated. One trace of this kind is shown in Fig. 3. When the intensity was increased, some of the sparks ejected electrons in

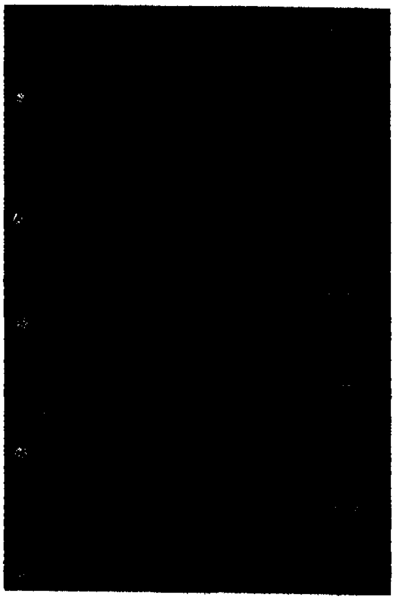

FIG. 3. Photographs of time-lag traces on synchroscope.

the counter and therefore a certain fraction, ρ, of the traces showed Geiger pulses. At full intensity all traces exhibited Geiger pulses.

EXPERIMENTAL RESULTS

Tables I and II present the averaged data obtained in this experiment. The gases used were of 99.8 percent purity, and the organic vapors were of C.P. grade. For the counters used, it was found that the pulse size was very nearly equal to the overvoltage on the counter. For most of the measurements the gain of the recording circuit was set at unity, at which gain the pulse on the counter wire had to be at least six volts in magnitude before it could be detected.

Measurements were made in the following manner: First, black masking tape was used to block the spark light from all the holes of the cylinder except one at its midpoint, and the lags thus observed were named "total" lags; second, the spark light was admitted through all the holes of the cylinder and the (different) lags thus obtained were named "transit" lags. For all counter fillings, sets of measurements were made using the full spark light intensity.

In addition, with argon-oxygen and oxygen fillings and with only the hole at the cylinder midpoint open, the intensity of the light incident upon the counter was reduced until the ratio of the number of sparks yielding a Geiger pulse to the total number of sparks was $\rho = 0.45$. Using this intensity, which produced few enough electrons in the counter to permit all of them to be captured, the ratio of the number of sparks resulting in time lags greater than 5 μsec. to the total number of sparks was measured under various conditions.

Inasmuch as all of the processes involved in a Geiger counter discharge are statistical in nature, the measured time lags also gave a statistical distribution. Therefore, for the determination of the lag in each case, one hundred measurements were made and the arithmetic mean was taken to be the time lag. In a typical case, the measured distribution of lags had a mean value of 0.56 μsec. and a root-mean-square deviation of 0.04 μsec. The root-mean-square deviations in the various cases exhibited no significant trend.

THEORETICAL ASPECTS

When a primary ionizing event takes place in a Geiger counter the initial electrons produced are accelerated toward the wire, near the surface of which Townsend avalanches[7] produce a large number of additional free electrons. By means of photo-ionization, photons produced in the avalanches cause the discharge to spread with a measurable velocity[8] along the entire length of the wire, and the collection of the electrons by the wire anode leaves behind a positive ion sheath closely surrounding the wire. The radially outward motion of the sheath produces a drop in the potential of the wire.[9]

TABLE II. Measured values of time lags.

Counter filling		Total pressure (cm)	Over-voltage (volts)	Operating voltage (volts)	Total lag (μsec.)	Transit lag (μsec.)	Percent of lags >5 μsec.
% argon	% oxygen						
95	5	10	100	1130	0.33	0.16	1.5
90	10	10	100	1360	0.27	0.13	3.5
80	20	10	100	1430	0.29	0.14	5.9
60	40	10	100	1540	0.28	0.14	11.8
40	60	10	100	1610	0.26	0.13	17.6
20	80	10	100	1690	0.28	0.12	22.6
0	100	10	100	1740	0.27	0.13	27.6
90	10	10	40	1300	0.78	0.15	3.2
90	10	10	80	1340	0.38	0.14	3.6
90	10	10	120	1380	0.26	0.14	3.1
90	10	10	160	1420	0.21	0.13	3.9
90	10	10	200	1460	0.19	0.15	3.4
Oxygen							
		4	100	1090	0.16	0.10	10.2
		6	100	1160	0.20	0.12	17.9
		8	100	1580	0.23	0.13	22.3
		10	100	1740	0.28	0.15	27.6
		12	100	1910	0.29	0.13	30.7
		10	40	1680	0.60	0.13	26.6
		10	80	1720	0.31	0.11	26.1
		10	120	1760	0.22	0.14	27.3
		10	160	1800	0.21	0.13	29.2
		10	200	1840	0.17	0.12	28.4

The time lags observed in Geiger counters appear to be the result of the transit time required by the initial electrons to move from their point of origin in to a point at which the field is great enough to produce avalanches, and the time required for the sheath to spread laterally along the wire and to move radially outward far enough to produce an electrical pulse which can be detected. In order to analyze these hypotheses, mathematical expressions are required for the electron transit time and for the rate of fall of the potential of the wire, i.e., for the pulse shape.

Consider an electron ejected by the spark light, at a time $t=0$, from the cylinder wall, at a distance $r=b$ from the wire axis, where b is the cylinder radius. Assuming a constant "mobility," k_e, for the electron in the gas of the counter at the existing pressure, the drift speed of the electron toward the wire is

$$dr/dt = -k_e E, \tag{1}$$

where the field intensity is given by

$$E = V_0/(r \ln b/a). \tag{2}$$

Here V_0 is the operating potential across the counter, and a is the wire radius. At a time t_t the electron reaches the high field region, effectively at the wire surface where $r=a$. Integration of (1), with the aid of (2), between the given limits, yields

---

[7] S. A. Korff, *Electron and Nuclear Counters* (D. Van Nostrand Company, Inc., New York, 1946).

[8] Alder, Baldinger, Huber, and Metzger, Helv. Phys. Acta **20**, 73 (1947).

[9] W. E. Ramsey, Phys. Rev. **57**, 1022 (1940).

$$t_t=\frac{\ln b/a}{2k_eV_0}(b^2-a^2) \tag{3}$$

as the "transit time" of the electron, a result similar to that obtained by Den Hartog *et al.*[2]

Assume that the electron produces the initial avalanche at a time $t=0$ on a new time scale, and at a distance D from the nearer end of the counter wire. Then the sheath spreads with a speed v toward both ends of the counter simultaneously. Assume also that the sheath is formed at the wire surface, and that the positive charge per unit length in the sheath is q_1. If the output capacitance of the counter is C, the energy of the counter before a discharge takes place is $\frac{1}{2}CV_0^2$. Consider an element of charge q_1dx situated at a distance x along the counter wire from the position of the initial avalanche. In moving the charge q_1dx from $r=a$ to $r=r$ the field does work on the charge in the amount $\int_a^r(q_1dx)Edr$, the energy of the counter drops to the value $\frac{1}{2}CV_t^2$, and the wire potential drops to the value V_t.[10] Hence,

$$\tfrac{1}{2}CV_t^2=\tfrac{1}{2}CV_0^2-\int_a^r(q_1dx)Edr. \tag{4}$$

The pulse size, or drop in potential of the wire, due to the outward motion of this element of charge is $dV=V_t-V_0$. Using (2) and the fact that the pulse size is small compared with the operating voltage, (4) becomes

$$dV=-\frac{q_1dx}{C\ln b/a}\ln\left(\frac{r}{a}\right). \tag{5}$$

As the sheath spreads along the wire from the position ($x=0$) of the initial avalanche, it reaches the point $x=x$ at the time $t=x/v$ and immediately thereafter the element of charge, q_1dx, begins to move radially outward. Therefore, $r=a$ at $t=x/v$, and $r=r$ at $t=t$. The outward drift velocity of the element of charge is given by $dr/dt=KE$, where K is the mobility (here assumed constant) of the positive ions in the gas used and at the pressure existing in the counter. Integration between the given limits gives

$$r^2=a^2+\frac{2KV_0}{\ln b/a}\left(t-\frac{x}{v}\right),\quad \text{for } 0\leqslant x\leqslant vt. \tag{6}$$

Since, for $t\leqslant D/v$, the sheath is spreading simultaneously toward both ends of the counter, there is another element q_1dx at a distance x on the other side of the position of the initial avalanche. Therefore, doubling (5), combining with (6), and integrating from $x=0$ to $x=vt$, we can obtain the total pulse size, V, as a function of t. If L is the length of the counter wire, the maximum pulse size is $V_m=-Lq_1/C$. Then the fractional pulse size is given by

$$\frac{V}{V_m}=\frac{v}{L\ln b/a}\left[\left(t+\frac{a^2\ln b/a}{2KV_0}\right)\ln\left(\frac{2KV_0t}{a^2\ln b/a}+1\right)-t\right], \tag{7}$$

for $t\leqslant D/v$.

This analysis may be easily extended to the time ranges $D/v\leqslant t\leqslant (L-D)/v$ and $t\geqslant (L-D)/v$. The pulse shapes for several special cases are plotted in Fig. 4. If the primary ionizing event produces initial electrons at more than one point along the wire length, the sheath spread begins almost simultaneously at all of these points. Therefore, as indicated by curve C in Fig. 4, the initial rise of the pulse is much more rapid.

The contribution of the electron collection by the anode to the pulse magnitude has here been assumed to be negligible. If we assume that the center of gravity of the ion sheath when initially formed is at a distance d from the wire surface, then the average electron moves in to the wire from $r=a+d$ to $r=a$. Applying the above theory to the electron motion, the ratio of the electron pulse, V_-, to the positive sheath pulse, V_+, is found to be

$$V_-/V_+=\ln[1+(d/a)]/\ln[b/(a+d)]. \tag{8}$$

The center of gravity of the initial ion distribution can be roughly assumed to be one and one-half mean free paths from the wire surface. Using the Ramsauer curve for argon, we find $d=6\times10^{-6}$ cm. Hence, $V_-/V_+=0.2$ percent, and the neglect of the electron contribution is justified.

If the initial electrons produced by the primary

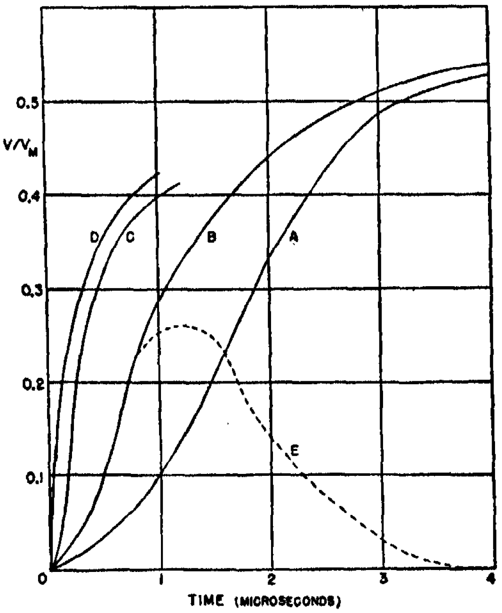

FIG. 4. Calculated pulse shapes for a 90 percent argon-10 percent ethyl alcohol Geiger counter at 10 cm pressure. $a=0.0051$ cm, $b=1.25$ cm, $V_0=1165$ v, $L=20$ cm, $v=8$ cm/μsec., $K=8.3$ cm²/(v-sec.). A. One initial electron at one end. B. One initial electron midway between ends. C. Five initial electrons spaced along wire length. D. Proportional counter pulse for one initial electron, $V_0=500$ v. E. Curve B clipped with a short time constant (RC).

---

[10] D. R. Corson and R. R. Wilson, Rev. Sci. Inst. 19, 207 (1948).

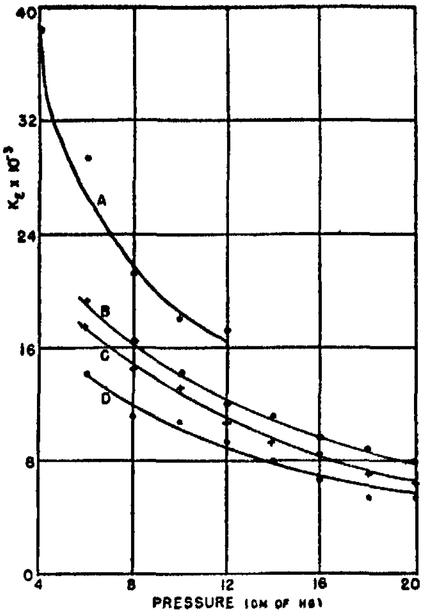

FIG. 5. Electron mobilities, k_e, as a function of the total counter pressure. A. Oxygen. B. 90 percent argon-10 percent ethyl alcohol. C. 90 percent argon-10 percent amyl acetate. D. Hydrogen.

ionizing event are captured, as they travel toward the wire, by molecules with a high electron affinity, the low mobility of the negative ions thus formed may result in a time lag of many microseconds. When the ions reach the high field region, at about $E/p=90$ according to Loeb,[11] the electrons are torn away from the ions and then produce the usual avalanches and pulse. The total time required for the electrons and ions to reach the high field region will be called the "ion lag."

In the present experiment a large number of photons from the spark are incident upon the counter cylinder, and the probability of the ejection of a photo-electron by a given photon is very small (about 10^{-4}). To this situation Poisson's probability density law applies. If n is the average number of electrons ejected per spark, then $P=\epsilon^{-n}n^k/k!$ is the probability that k electrons be ejected per spark, and n is also the mean value of k. Then the probability that *at least one* electron be ejected is $\rho=(1-\epsilon^{-n})$. It may be assumed that if at least one electron is ejected by the spark, a counter pulse will result. Therefore, the ratio of the number of counter pulses to the number of sparks is merely ρ.

In order that an "ion lag" be produced, all n electrons ejected by a given spark must be captured. Call q the probability that a given electron be captured to produce an ion lag equal to or greater than t_i, where t_i is the sum of the times required by the electron to move from $r=b$ in to the point of capture, $r=R$, and by the ion to move from $r=R$ in to $r=a$. If the electron is captured at $r\geqslant R$, then the resulting ion lag will be $\geqslant t_i$. Then it can be shown[6] that the probability that a given *spark* give an ion lag $\geqslant t_i$ is

$$P_q=\epsilon^{-n}(\epsilon^{qn}-1). \tag{9}$$

Since ρ and P_q may be observed experimentally, q may be calculated. Also, the probability that an electron be captured to give an ion lag $\geqslant t_i$ is equal to the probability that the electron be captured within a distance $(b-R)$ of the cylinder wall. Hence,

$$q=1-\exp[-N_1A(b-R)], \tag{10}$$

where N_1 is the number of gas molecules per unit volume, and A is the effective capture cross section of a molecule for an electron. If σ is the collision cross section of the molecule for an electron, and if h is the probability of capture per collision, or attachment coefficient, then $A=\sigma h$. Equation (3) may be used for ion transit times if k_e is replaced by the mobility of the negative ion, and if b is replaced by R. The equation may then be used to compute R, which may in turn be used in (10) to compute A. From the Ramsauer curve for a given gas and electron energy, σ may be obtained, and it is therefore possible to calculate h, the attachment coefficient.

COMPARISON OF THEORY WITH EXPERIMENT

Each "total lag" listed in Tables I and II, observed with the use of a single cylinder hole and the full spark light intensity, is presumed to be the sum of the "transit lag," or the time required by the electron to move from the cylinder wall in to the avalanche region, and the "sheath lag," or the time required for the sheath

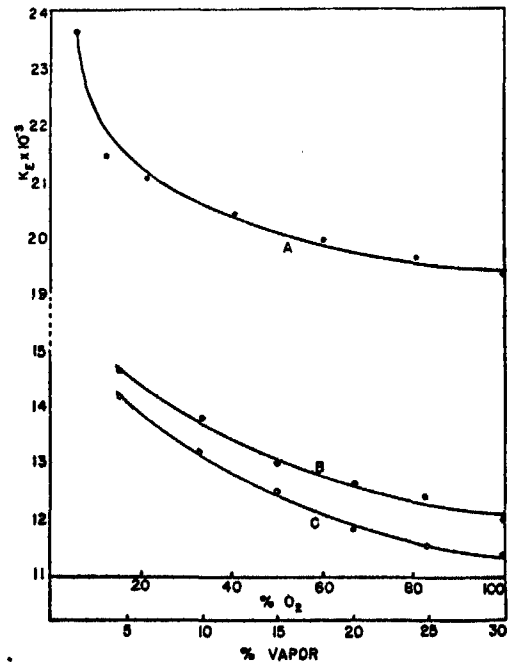

FIG. 6. Electron mobilities, k_e, as a function of percentage constitution at 10-cm total counter pressure. A. Argon-oxygen B. Argon-ethyl alcohol. C. Argon-amyl acetate.

---

[11] L. B. Loeb, Phys. Rev. 48, 684 (1935).

to spread laterally along the wire and radially outward far enough to permit detection of the pulse. The use of many cylinder holes and the full light intensity, producing photo-electrons all along the cylinder length, effectively eliminates the sheath lag, and the lags observed in this manner are presumed to be the transit lags alone, as listed in Tables I and II. The difference between each total lag and the corresponding transit lag should thus be the sheath lag alone. It has been observed elsewhere[12] that lightly ionizing particles give delays which are substantially longer than those found with heavily ionizing particles, which appears to confirm the hypothesis that the lags depend in part on the initial ionization produced by the primary ionizing event.

Using the measured transit lags and counter data of Tables I and II, and Eq. (3), the electron mobility, k_e, was calculated for each case and the results graphed in Figs. 5 and 6. The values so obtained are of the same order of magnitude as the mobilities observed by other investigators. Considering the fact that, strictly speaking, there is no real electron "mobility constant," and the fact that almost imperceptible traces of unrecognizable "impurities" have an enormous power over the electron "mobility," this agreement appears to be fortuitous.

For a given gas mixture, the electron mobilities appear to be inversely proportional to the square root of the product of pressure and operating voltage. The mobility in hydrogen appears to be *lower* than that in the mixtures of argon and organic vapors, which may result from the fact that the drift velocity and mobility of an electron in a gas are inversely proportional to the average thermal agitation velocity of the electron. The organic vapors, with many low lying energy levels, hold the electron's thermal energy to a low value and thereby increase the mobility. Therefore, although the mobility of an electron in pure hydrogen is greater than that in pure argon, a vapor added to the argon increases the mobility of the mixture to a value higher than that in hydrogen.[13] In oxygen, which has several low energy levels, the electron mobility appears to be higher than that in either hydrogen or the mixtures.

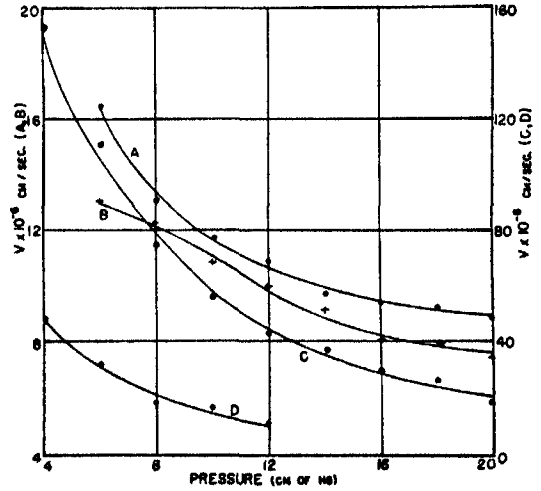

FIG. 7. Sheath spread velocity, v, as a function of total counter pressure. A. 90 percent argon-10 percent ethyl alcohol. B. 90 percent argon-10 percent amyl acetate. C. Hydrogen. D. Oxygen.

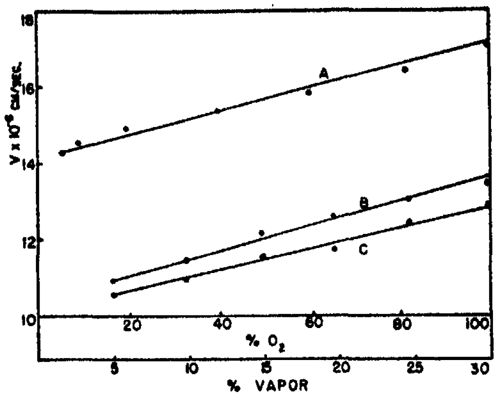

FIG. 8. Sheath spread velocity, v, as a function of percentage constitution at 10-cm total counter pressure. A. Argon-oxygen. B. Argon-ethyl alcohol. C. Argon-amyl acetate.

The sheath lag was computed for each case from the data of Tables I and II. In this experiment the sheath lag is the time required for the pulse, once it has begun, to reach the fractional size $V/V_m = 0.06$. Using reasonable values for the ion mobilities, K, Eq. (7) was employed to calculate the sheath spread velocity, v, for each case, and the results are graphed in Figs. 7–9. The values obtained in this way are of the same order of magnitude as those obtained by the more direct methods of other observers.[14] Figure 7 indicates that for all counter fillings v decreases as the total pressure increases, and Fig. 9 indicates that v increases rapidly as the overvoltage increases. Figure 8 is particularly interesting in that it indicates an increase in v as the percentage of quenching vapor is raised.

While an avalanche is being formed, photons of various energies are emitted by the return of excited and ionized molecules to their ground states. This radiation is composed of two types of photons: photons which are energetically capable of ionization (11 to 15 volts, or more); and lower energy photons which are incapable of ionization but have enough energy (about five volts) to eject photo-electrons from the cylinder wall. The ionizing radiation is highly absorbable in all counter fillings, in noble gases as well as in vapors. Jaffe *et al.*,[15] find that 99 percent of this radiation is absorbed within a distance of 1 mm. The photons of lower energy are only slightly absorbed by noble gases, but are strongly absorbed by polyatomic molecules with subsequent predissociation.

---

[12] H. L. Schultz and R. Beringer, Rev. Sci. Inst. **19**, 424 (1948).

[13] J. S. Townsend and V. A. Bailey, Phil. Mag. **43**, 593 (1922). J. Allen and B. Rossi, LADC 177, Los Alamos Technical Series.

[14] J. Hill and J. Dunworth, Nature **158**, 833 (1946); Knowles, Balakrishnan, and Craggs, Phys. Rev. **74**, 627 (1947); D. H. Wilkinson, Phys. Rev. **74**, 1417 (1948); also see reference 8.

[15] Jaffe, Craggs, and Balakrishnan, Proc. Phys. Soc. **62**, 39 (1949).

The ionizing photons, absorbed within a millimeter or two of the wire surface, serve to propagate the discharge along the wire by producing new electrons which in turn produce new avalanches. The average new electron produced by photo-ionization is born within a millimeter or two of the wire surface. This electron then travels in to the high field region, which begins at less than half a millimeter from the wire surface. The travel time of the photons themselves, and the time required to complete an avalanche once it has begun, are very small.[16] It is therefore likely that the major part of the time required for a given step in the propagation process is the 10^{-9} sec. or so occupied by the new electron in traveling in to the high field region.

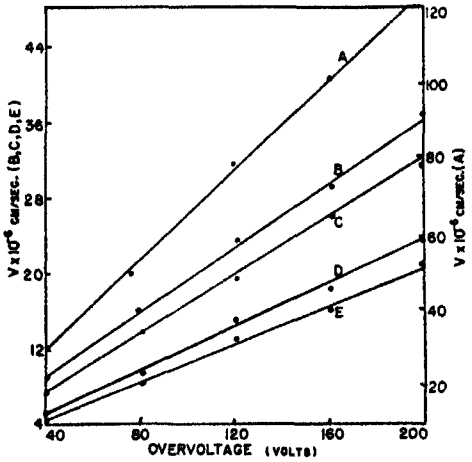

FIG. 9. Sheath spread velocity, v, as a function of overvoltage at 10-cm total counter pressure. A. Hydrogen. B. Oxygen. C. Argon+10 percent oxygen. D. Argon+10 percent ethyl alcohol. E. Argon+10 percent amyl acetate.

Therefore the sheath spread velocity, v, should depend primarily upon the electron velocity, v_e, in the particular counter filling and field. If it is assumed that $v_e=k_eE$, where E is proportional to V_0, the curves of Figs. 7–9 appear to be consistent with the above hypotheses. As the percentage of quenching vapor increases, the electron mobility decreases (Fig. 6), but the operating voltage required for a given overvoltage increases by a bigger factor. Therefore v_e increases, and we find that v increases as the percentage of vapor increases.

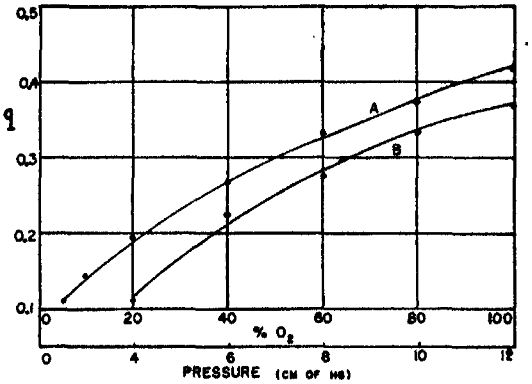

FIG. 10. Probability, q, that an electron be captured to give an ion lag $\geqslant 5$ μsec. A. 10-cm total pressure of argon-oxygen, as a function of percent of oxygen. B. Oxygen, as a function of total counter pressure.

For a given percentage constitution, an increase in total pressure decreases the mean free path for ionization of the high energy photons, reduces the length of each step, and lowers v. As the overvoltage is raised, the radius of the high field region and thus of the sheath about the wire increases. More photons of a longer mean free path for ionization are produced per avalanche, each step is lengthened, and v increases. Although k_e has been found to be lower for hydrogen than for the vapor mixtures, V_0 is materially higher for a hydrogen counter than for the vapor counters. Therefore, $v_e=k_eE$, and v are higher for hydrogen.

Using the value $t_i=5$ μsec., and Ramsauer's values for σ, for each case in Table II a value of q was computed and the results are graphed in Fig. 10. The curves indicate that q rises more slowly than linearly as the oxygen constituent increases, which is to be expected from Eq. (10). For each case a value of the attachment coefficient, h, was also calculated. These values showed no trend and had a mean value of 3.3×10^{-4}, which is at least of the correct order of magnitude.

CONCLUSIONS

The satisfying simplicity of the direct observation of the absolute counter time lags on the synchroscope screen gives the measured values a certain measure of reliability. Although the calculation of electron mobilities, sheath spread velocities, and attachment coefficients had only an indirect bearing on the purposes of this investigation, the fact that the theory and the measured time lags yielded results of the correct orders of magnitude for these quantities permits some confidence to be placed in the proposed mechanisms.

The results suggest the procedure to be used in order to minimize time lags in Geiger counters. The particles to be detected should be introduced as close to the wire as possible, and in a direction as nearly parallel to the wire as possible. The counter filling should not contain any constituents which possess high electron affinities. A high overvoltage and a fairly high gain, wide-band amplifier should be employed. These precautions should make it possible to determine the instant of passage of a particle through the counter to within a few hundredths of a microsecond.

ACKNOWLEDGMENTS

The author is indebted to Drs. S. A. Korff and L. H. Fisher of New York University for many illuminating discussions of the problems involved in this investigation, and also to Dr. C. G. Montgomery of Yale University for some helpful correspondence and conversation.

---

[16] S. A. Korff, Phys. Rev. 72, 477 (1947).

THE REVIEW OF SCIENTIFIC INSTRUMENTS VOLUME 21, NUMBER 3 MARCH, 1950

The Electric Field in a Geiger Counter

Arthur R. Laufer
University of Missouri, Columbia, Missouri

(Received December 1, 1949)

The mechanism of the reduction and recovery of the electric field in a Geiger counter is discussed, and the role of the series resistance is analyzed. The contribution of the collection of the electrons to the total pulse size is shown to be negligible.

THE literature contains a large number of papers dealing with Geiger counter action, but certain aspects of the reduction and recovery of the electric field intensity around the wire, though implied in some of them, are not treated explicitly. An analysis of these aspects may therefore serve a useful purpose.

In its usual form the Geiger counter consists of a pair of concentric cylindrical electrodes mounted in a glass or metal envelope which contains a gas at relatively low pressure. The central electrode, normally operated as the anode, is a wire of small diameter, whereas the concentric cathode is a hollow cylinder of much greater diameter. For this geometry, with a voltage source supplying a difference of potential V_0 between the electrodes, the radial field distribution is given by

$$E=\frac{V_0}{r\ \ln b/a}, \tag{1}$$

where a and b are the wire and cylinder radii respectively, and r is the distance from the wire axis. Hence, as indicated in Fig. 1 by the curve ABC, the field is of low value throughout most of the counter volume, but rises very sharply to a high value as the wire surface is approached.

Suppose that a primary ionizing event produces a free electron somewhere within the sensitive volume of the counter. This electron is accelerated toward the high field region near the wire surface, where it can gain enough energy in a free path to initiate the cumulative process of ionization by collision known as a Townsend avalanche. Photons emitted from the avalanche produce photo-ionization at other points in the counter, resulting in a spread of the discharge laterally along the wire. For a "Geiger" counter, the probability is unity that the discharge will spread along the entire length of the wire. The free electrons produced in the avalanches are rapidly collected by the wire anode, leaving behind a cylindrical shell of positive ions which closely surrounds the wire. It will presently be shown that the collection of the electrons makes only a negligibly small contribution to the final pulse size delivered by the counter. It is the relatively slow subsequent outward motion of the low mobility positive ion sheath which permits the wire potential to drop, and which therefore produces the Geiger pulse which is normally observed.

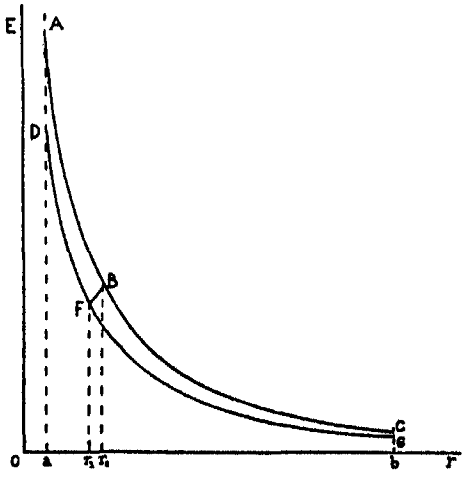

Fig. 1. The electric field in a Geiger counter.

The collection of the free electrons reduces the field between the wire and the positive ion sheath to a value below the critical value required for avalanche production. If a new primary ionizing event were now to occur in the counter, no further avalanches could be formed and the event would not be detected. The counter is now said to be "dead," or insensitive to new ionizing events. Therefore, immediately after the electrons have been collected, the wire potential has not been altered by any appreciable amount, the positive ion sheath has moved outward through only a negligible distance, and the field around the wire is reduced below the critical value. The occurrence of the primary ionizing event has, as yet, produced no change in the counter which could be detected by an external recording circuit, and the counter is in the "dead" condition. It is the outward motion of the positive ion sheath which *may* permit the wire potential to drop, producing an externally detectable pulse, and which *may* permit the field around the wire to recover, restoring the counter to its former sensitivity. The italics are used advisedly, inasmuch as both the drop in potential of the wire and the recovery of the sensitivity of the counter depend entirely upon the magnitude of the resistance R, Fig. 2, in series with the counter.

If the counter has a sensitive length L and a capacitance C, prior to a discharge the positive charge per unit length on the wire is $q=CV_0/L$, and the electric field intensity at a distance r from the wire axis is given by $E=2q/r$. This field distribution is represented by curve ABC in Fig. 1. When a discharge subsequently occurs, the collection of the electrons reduces the net positive charge per unit length on the wire to some lower value, q'. The positive ion sheath, of course, plays no part in the reduction of the field intensity near the wire, inasmuch as the field inside a long cylindrical shell of charge, due to the shell itself, is zero. The field reduction is the result of the collection of the electrons by the wire, reducing the charge per unit length from q to q'. Hence the field between the wire and the sheath is reduced to $E'=2q'/r$. If the sheath is located between $r=r_1$ and $r=r_2$, Fig. 1, then the reduced field distribution between the wire and the sheath is represented by curve DF. The field *outside* a cylindrical shell of charge is determined by the total charge within the shell. Therefore the field rises from F to B in passing through the sheath, and maintains its initial distribution, BC, outside the sheath. It may be noted in passing that even though the sheath contains about 10^{10} positive ions, these ions constitute only one part in 10^7 of the total number of gas molecules in the region occupied by the sheath.

Now suppose that the series resistance, R, is infinite. This condition may be attained by merely disconnecting the source of V_0 from the counter wire. Since potential is a scalar quantity depending on charge distribution, as the positive sheath moves outward the wire potential, V, drops below V_0 and continues to drop until the sheath is collected at the cylinder, at which time the wire potential has attained its minimum value. The wire potential for this case is plotted as a function of the time in Fig. 3. As the sheath moves outward, the field surrounding the wire *does not recover at all.* Since the wire is isolated, the charge, q', per unit length on the wire cannot change as the sheath moves outward. Hence, the reduced field, $E'=2q'/r$, around the wire remains reduced, and after the sheath has been collected at the cylinder the field distribution in the counter is represented by curve DFG, Fig. 1. With an infinite series resistance, therefore, if a primary ionizing event occurs in the counter the wire potential drops, yielding a pulse which can be detected by an external recording circuit, but at the same time the counter becomes permanently insensitive to new ionizing events.

Suppose, next, that the series resistance is zero. In this case the wire potential must remain fixed at the value V_0. As the positive ion sheath moves outward, the wire potential tends to drop, but since the potential must remain fixed, the net result is that electrons flow off the wire into the source of the applied voltage. Thus the net positive charge, q', per unit length on the wire gradually increases as the sheath moves outward, and the field, $E'=2q'/r$, gradually recovers. When the sheath reaches a certain critical distance from the wire axis, the field near the wire is far enough recovered so that a new primary ionizing event would be capable of just barely producing a new avalanche. The time of duration of the previous insensitive condition is known as the "dead time" of the counter. At the time that the sheath reaches the cylinder, the field is fully recovered, and a new primary ionizing event would be able to produce another full discharge. The time interval between the end of the dead time and the time of full recovery is called the "recovery time" of the counter. Hence, with zero series resistance the electric field in the counter can achieve full recovery, but since the wire potential is fixed at V_0, the counter discharge cannot be detected by an external recording circuit. This constant wire potential is also indicated in Fig. 3.

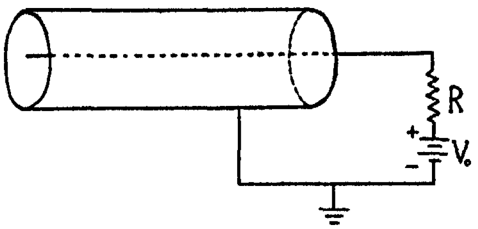

FIG. 2. Geiger counter circuit.

Thus an infinite series resistance permits the delivery of a counter pulse but does not permit recovery, whereas a zero series resistance permits full recovery but does not permit the delivery of any pulse at all. Of course, neither of these extreme cases is ever used. A series resistance of about 10^6 ohms will permit both the delivery of a pulse and the recovery of the counter, but the pulse size is smaller in this case than that obtained with an infinite series resistance. As indicated in Fig. 3, for a resistance of 10^6 ohms the wire potential begins to drop as in the case of infinite resistance. At the very beginning of the pulse the rate of fall of the wire potential due to the motion of the sheath is greater than the rate of rise due to the electrons leaking off the wire. Therefore the wire potential drops. At some later time when the rate of fall due to the sheath motion has decreased, the two rates become equal and the wire potential reaches its minimum value. Even later, the rate of rise of the wire potential due to the electrons leaking off exceeds the rate of fall due to the sheath motion, and then the wire potential rises back to its initial value, V_0.

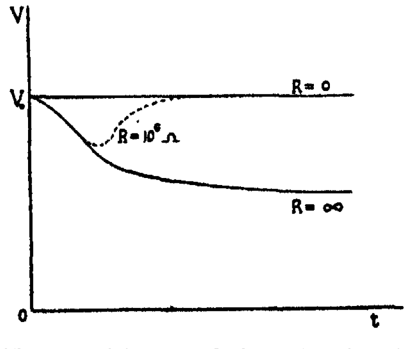

FIG. 3. Wire potential, V, graphed as a function of the time, t, for various values of the resistance, R, in series with the Geiger counter.

From this time on, the wire potential remains at the value V_0 and the counter action simulates the case of zero resistance, permitting full recovery to obtain.

In the case of a counter filled with a self-quenching gas mixture, collection of the sheath at the cylinder completes the counter action and leaves the counter ready for the next primary ionizing event. In the case of a counter employing a non-self-quenching gas, however, collection of the sheath at the cylinder results in the ejection of secondary electrons from the cylinder, and these secondaries initiate another discharge even though no new primary ionizing event has occurred in the counter. Thus the counter goes into a state of intermittent, self-perpetuating discharge. In order to use a counter containing the latter type of filling, "external quenching" must be invoked. Effectively, the counter wire must be isolated from the power supply, as in the case of an infinite series resistance, until some time after the positive ion sheath has been neutralized at the cathode. Thus the counter is not permitted to recover its sensitivity until after the act of neutralization is completed. The secondary electrons produced during this act are produced during the period of insensitivity and therefore are incapable of producing additional avalanches and spurious counts.

The required temporary isolation of the counter wire from the power supply can most easily be achieved through the use of a series resistance of the order of 10^9 ohms. For a counter having a typical capacitance of 10^{-11} farad, this means a time constant of 10^{-2} second. Since the time required for the collection of the positive ion sheath is of the order of 10^{-4} second, the need for a time constant as long as 10^{-2} second to quench the discharge may require explanation. The time constant, RC, of the counter circuit is the time required for all but $1/e$ of the free electrons deposited during the discharge to flow off the wire. If this time constant were 10^{-4} second, at the time of neutralization of the sheath at the cylinder the field at the wire would have recovered by an appreciable amount and the counter would be in a sensitive condition. Secondary electrons from the cylinder would be able to produce a spurious discharge. However, if the time constant is 10^{-2} second, at the time of neutralization of the sheath at the cylinder only $1-\exp(-10^{-4}/10^{-2})$, or about one percent, of the electrons have leaked off the wire and the field about the wire is too low to permit a spurious count. Hence, the time constant of the circuit must be made much longer than the time actually required for the collection of the sheath. The use of an electronic quenching circuit instead of the high resistance, though not as simple, is usually desirable since it eliminates the need for a long time constant and therefore permits more rapid counting.

Corson and Wilson have shown[1] that the drop in the potential of the wire due to the motion of a positive ion in the sheath from a point at $r=r_0$ to a point at $r=r$ is given by

$$-\frac{1}{V_0C}\int_{r_0}^{r} eEdr, \tag{2}$$

where e is the charge on the ion. Suppose that the center of gravity of the ion distribution in the sheath, when initially formed, is at a distance d from the wire surface, i.e., at $r_0=a+d$. Then the drop in the potential of the wire produced by the m positive ions in the sheath as a result of their radially outward motion to the cylinder, where $r=b$, may be obtained by performing the integration in (2), with the use of (1), between these limits. This integration yields

$$V_+=-\frac{me}{C\ln b/a}[\ln b-\ln(a+d)]. \tag{3}$$

The mean electron collected by the wire must move from $r_0=a+d$ in to the wire surface, where $r=a$. A similar integration yields, for the drop in the potential of the wire due to the collection of the electrons,

$$V_-=-\frac{me}{C\ln b/a}[\ln(a+d)-\ln a]. \tag{4}$$

The total pulse size, of course, is merely $V_m=V_++V_-=-(me)/C$. The ratio of the electron pulse to the positive ion pulse is

$$\frac{V_-}{V_+}=\frac{\ln[1+(d/a)]}{\ln[b/(a+d)]}. \tag{5}$$

The kinetic theory value of the mean free path, l_e, of an electron in a gas can be calculated from

$$l_e=\frac{1}{\pi N_1\sigma^2}, \tag{6}$$

where N_1 is the number of gas molecules per unit volume and σ is the radius of a gas molecule. For argon at a pressure of 10 cm of Hg, $N_1=3.54\times10^{18}$, and σ can be taken to be 1.5×10^{-8} cm, giving $l_e=4\times10^{-4}$ cm. According to the Ramsauer curve for argon, as reproduced in Loeb,[2] at electron energies of about 16 volts (the electron energy in the avalanche region) the mean free path is roughly one-tenth of the kinetic theory value. Therefore the mean free path of the electrons in this region can be taken to be 4×10^{-5} cm. The center of gravity of the initial ion distribution may be assumed to be roughly one and one-half mean free paths from the wire surface. Therefore the value $d=6\times10^{-5}$ cm is obtained. Using the dimensions of a typical counter, the ratio V_-/V_+ is found to be 0.2 percent. Therefore the assumption that the electron pulse is a negligible fraction of the total pulse size was a valid assumption.

---

[1] D. R. Corson and R. R. Wilson, Rev. Sci. Inst. 19, 207 (1948).

[2] L. B. Loeb, *Kinetic Theory of Gases* (McGraw-Hill Book Company, Inc., New York, 1934).

THE REVIEW OF SCIENTIFIC INSTRUMENTS VOLUME 21, NUMBER 3 MARCH, 1950

Laboratory Modifications in the RCA Model EMC Electron Microscope

S. G. Ellis
RCA Laboratories, Princeton, New Jersey

(Received December 8, 1949)

The anode opening was reduced to reduce thermal expansion in the specimen stage. The asymmetry of the objective lens was compensated. Working at the lowest possible angular aperture of illumination and focusing critically (by using a carefully settled fluorescent screen and a high magnification viewer) a resolving power of approximately 50 A.U. was demonstrated on suitable specimens.

INTRODUCTION

In the course of experiments made to test the performance of a standard RCA model EMC electron microscope, it became apparent that some minor modifications of the column would result in improvement of the performance of the instrument. Since the modifications could be made in any laboratory machine shop, they are described here for the benefit of other operators. It is believed that these modifications bring the resolution of the instrument close to its ultimate value, approximately 50 A.U.

It is worth emphasizing that the work described here was done on only one instrument. If one repeated the work on other instruments, it is not unlikely that the problems encountered would differ in degree from those described here. It is believed however, that the major problems have been discussed below, and that if the basic principles are grasped, there should be no great difficulty in repeating this work in other laboratories. To facilitate this end, the experimental work is described below in the order in which it was done.

EXPERIMENTAL WORK

The microscope on which this work was done had been in use in another laboratory. As a first step, it was thoroughly cleaned and the fluorescent screen was replaced.

The cleanliness of an electron microscope may be tested in the following way: Employ as a specimen, a filmless mount of carbon on a rigid copper mesh so that thermal drifting of the specimen is minimized. Obtain a focused image at top magnification (×5000 approximately) and vary the intensity of illumination either by changing the filament temperature or by moving the gun tilt screws. If the column is clean, an *accurately* focused image will move by much less than one-thirty-second of an inch, as measured on the fluorescent screen. It will be seen from what is said later, that it may not always be easy to distinguish between thermal drifting of the specimen and a deflection of the imaging beam by the charging up of dirt or contamination in the column.

In cleaning the electron microscope, dirt and contamination must be removed from all surfaces which can "see" the electron beam, until only the bare, polished, substrate metal remains. Cleanliness is more important in regions close to the imaging beam, particularly so where the beam current density is high. Surfaces which are not machined with high precision, may be cleaned with steel wool.[1] These include: the grid-cylinder (or shield), the anode aperture holder, and the specimen stage. When it is necessary to clean such parts, they should be removed from the column, and when they have been cleaned, all shreds of steel wool should be removed from them with a strong bar magnet.

Critically machined surfaces, such as the pole-pieces, should be cleaned with a very thin paste of Linde *B* polishing powder in water.[2] This paste may be taken up on soft tooth-picks,[3] or on suitably shaped sticks of soft wood. Orange sticks are too hard to be used safely on the soft iron of the pole-pieces. The pole-piece openings should be gently cleaned with a rotary motion until they shine. The polishing powder should be removed by washing with hot water and soap. The pole-pieces may then be polished dry with a lint-free lens tissue.[4] They should not be dried by allowing the water to evaporate from them.

In the work reported here, both the objective and projector apertures were removed. No completely satisfactory method is known for cleaning these apertures, and it would therefore seem imperative to remove the objective aperture in the preliminary tuning-up of the microscope.

A settled fluorescent screen was made using 33Z607 phosphor,[5] following the directions of Sadowsky.[6]

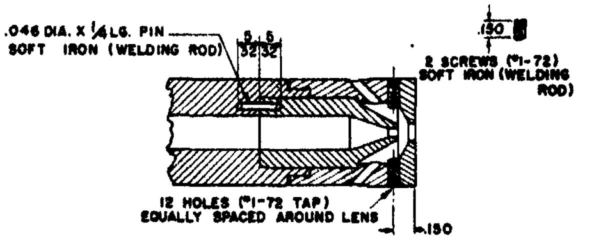

FIG. 1.

---

[1] Such as grade 0000 from American Steel Wool Mfg. Co., Long Island City 1, New York.

[2] Linde Air Products Co., East Chicago, Indiana.

[3] Round, "World's Fair" polished wood toothpicks, Forster Manufacturing Company, Strong, Maine.

[4] Ross-Adams Lens Tissue, Clay Adams Co., Inc., New York, New York.

[5] Available from RCA Victor Division, Lancaster, Pennsylvania. (Also available as Stock No. 51579 from RCA Victor Division, Camden, New Jersey.)

[6] M. Sadowsky, J. Electrochem. Soc. 95, 112 (1949). (See page 125 for details.)

It is extremely important to have an efficient fine grain fluorescent screen, since the screen limits the accuracy with which the microscope can be focused and also the precision with which image shifts and other defects can be examined. In all the work with this microscope, the fluorescent screen has been examined through a reversed ×10 eye-piece, from a light microscope, used as a high magnification viewer. Under these conditions, the grain has been barely visible, and the out-of-focus Fresnel fringes at major discontinuities in the specimen, have been seen easily.

The filament in the electron gun was pinched-up to give the minimum radius of curvature at its apex so that it would provide a small effective source of illumination. The filament height was set by trial and error until it gave the minimum saturation beam current consistent with adequate intensity of illumination. The procedure finally adopted, was to turn the grid cap until the filament apex was in the plane of the grid hole. The grid cap was then turned off (anti-clockwise) four turns. This gave a beam current of less than 100 micro amps, the bias resistor being 700,000 ohms. Bias resistors between 0.5 and 1.0 megohm are probably satisfactory but their value will determine the best filament height. In the trial and error determination of the filament height to be used, it is best to start at the smaller filament heights (corresponding to the higher beam currents) since if the filament height is greater than a certain, rather critical amount, the intensity of illumination becomes completely inadequate. The filament should always be run hot enough for the saturation beam current to be reached.

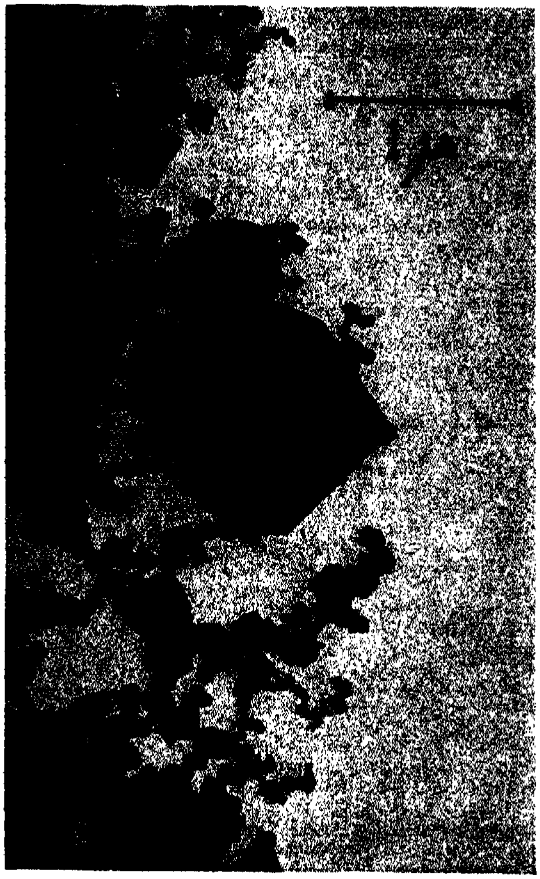

FIG. 2. Magnesium oxide smoke. Filmless mount.

These preparations having been completed, the instrument was run using carbon on a copper mesh as a test specimen. The images were acceptable in quality but it was noticed that for a short time after the instrument was turned on, and for a short time after the specimen was changed, there were thermal drifts in the image. In the particular model EMC electron microscope under test, the diaphragm which limits the beam current reaching the specimen, was mounted on the same posts which carry the snubbing springs for the specimen stage. Heat generated in this diaphragm, was causing thermal expansion of the specimen stage. To overcome this difficulty, a plug with a central 0.5 mm diameter knife edged aperture, was pressed into the opening of the anode. This reduced the current reaching the movable beam limiting diaphragm and no further trouble was encountered with thermal drifts. On days when the microscope was to be used, the low voltage circuit was turned on at the beginning of the day and allowed to run continuously.

At this stage of the work, it became apparent that the objective lens asymmetry was the major remaining defect in the instrument. The asymmetry was reduced by a modification of the method of Hillier and Ramberg.[7] As shown in Fig. 1, twelve holes were drilled and tapped in the objective section of the pole-pieces, and two tightly fitting soft iron screws were made to fit them. The holes should be accurately radial and the tips of the screws should not wander when the screws are advanced, but should move radially. The procedure for correcting the asymmetry is then:

(i) With no screws in the lens, switch the lens on and off several times to standardize its magnetic state, align the microscope and take a picture of a filmless mount of carbon which will demonstrate the asymmetry. Project this picture onto a screen so that it appears in the same orientation as it did on the fluorescent screen. Mark the direction of the natural lens asymmetry, N, as a double ended vector, perpendicular to the high side Fresnel fringes.

(ii) Put the pair of screws into the lens in opposite holes and advance them as far as possible towards the axis, so that the asymmetry they produce will swamp the natural lens asymmetry. Put the lens back in the microscope in the same orientation as before and determine the direction of the new asymmetry T.

(iii) From the angle between T and N deduce the pair of holes into which the screws must be put, in order to introduce a correcting asymmetry C most nearly perpendicular to N. Put the pair of screws into these holes and advance them by trial and error until the asymmetry is minimized.

---

[7] J. Hillier and E. G. Ramberg, J. App. Phys. 18, 48 (1947).

In the least favorable case, where the desired direction is midway between two available pairs of holes, theory shows that the natural lens asymmetry should be reducible to half its initial value. In the work reported here, the asymmetry was rapidly reduced until it was no longer detectable. In a less favorable case, it is possible that a second pair of screws would have to be inserted to complete the correction.

PERFORMANCE

When the lens asymmetry had been compensated, the instrument demonstrated a resolving power of approximately 50 A.U. on suitable specimens. This resolving power was maintained during several months of intermittent operation. At the end of this time, the objective was becoming slightly contaminated.

By observing the fluorescent screen with the magnifier, it was possible to focus the microscope accurately with very good consistancy. This does, however, require experience of the nature of the contour phenomena, and of the changes in contrast on going through focus.

Some further attempts were made to improve the performance of the instrument, since micrographs taken on an RCA model EMU electron microscope, operated at an accelerating voltage of 30 kv showed crisper images. This observation indicated that the accelerating voltage was not the limiting factor in the model EMC microscope. It was concluded that the angular aperture of the illumination was the parameter that was restricting the resolution to 50 A.U. Since, in the absence of a condenser lens, the aperture of illumination could only be reduced by increasing the filament to grid-cylinder spacing, and since, as has been said above, this reduces the intensity of illumination to less than an acceptable level, it is believed that the resolution reported here is close to the ultimate resolving power of an instrument of this design.

Figures 2 and 3 demonstrate the performance of the instrument.

OPERATION AND MAINTENANCE

The reduced size of the anode opening makes the instrument somewhat more tedious to align. If, however, one starts by removing the gun and placing a flash-light bulb in the position of the filament to obtain mechanical alignment of the beam limiting diaphragm by looking along the column from the camera end and then proceeds to the electronic alignment at low magnification, the whole alignment procedure will not be found difficult. Once the gun traverse adjustment has been made and locked, it should be possible to change filaments and rapidly realign the microscope with the tilt controls alone. The alignment is not too critical; it will usually be sufficient to bring the current center onto the final viewing screen. To have the current center near the center of the screen, does however, facilitate focusing, since the image does not sweep on changing the lens strength.

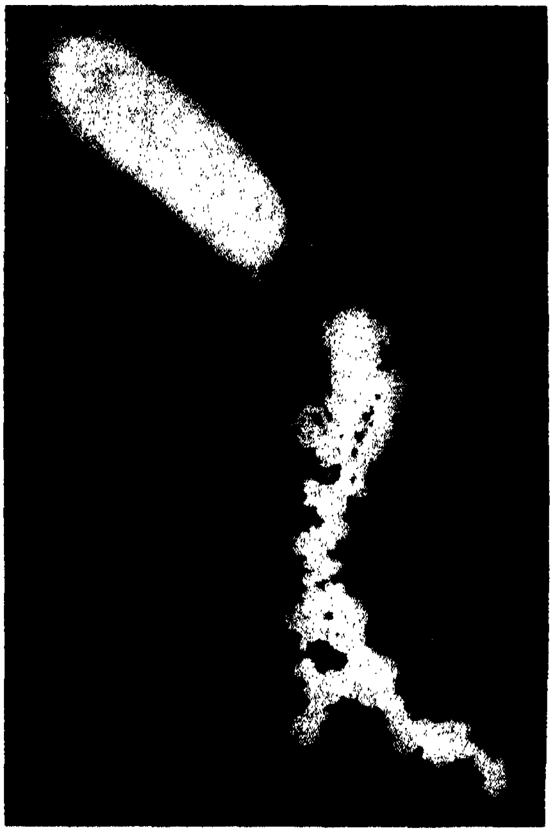

FIG. 3. Proteus bacterium and carbon, shadowed with chromium.

No objective apertures were used in the work reported here. Their use might be justified in the examination of thick specimens where the specimen lowers the resolution in any case. It is desirable to use a projector aperture since without it, the electrons which pass through the peripheral parts of the projector strike the walls of the viewing chamber and are scattered into the final image causing an appreciable loss of contrast.

Laboratory and Shop Notes

Degassing Extended Glass Systems

Albert B. Stewart
Antioch College, Yellow Springs, Ohio
January 11, 1950

By using infra-red heating it is possible to degas an extended glass vacuum system without building a large oven to enclose the entire apparatus. In preparing tubes for studying glow discharge phenomena* the writer has found the following procedure very satisfactory.

The glass tubing to be degassed is painted with a suspension of lampblack in water, the suspension being obtained with the help of a wetting agent. Stopcocks and other parts of the system that should not be heated are left unpainted and covered with aluminum foil. A battery of 375-watt reflector-type infra-red bulbs is placed a centimeter or so from the tubing and the bulbs and tube surrounded with aluminum foil which effectively traps the radiation. A mercury thermometer with bulb blackened records a temperature of about 400°C within five minutes after the bulbs are turned on. One to two hours of application of heat suffices to degas the glass to the point that an ionization gauge in the system reads the same pressure with the bulbs on as off. The infra-red bulbs can be left in place or removed and the glass tubing cleaned with a damp rag.

---

* This work is supported by a grant from the Frederick Gardner Cottrell Fund of the Research Corporation.

Liquid Air Level Control

Mark S. Fred and Everett G. Rauh
Argonne National Laboratory, Chicago, Illinois
January 25, 1950

A simple device has been designed and constructed which automatically maintains within predetermined limits the level of liquid air or liquid nitrogen in a bath. Control is based on the large negative temperature coefficient of resistance of an ordinary carbon resistor. By incorporating the resistor in a voltage divider there is obtained, with a change of temperature of the resistor, a large voltage change which actuates an electronically controlled liquid air pump. In Fig. 1 the grid controlled thyratron will fire during the positive half-cycle of the line voltage if the starting anode is sufficiently positive with respect to the cathode. When the thyratron is conducting, the relay opens a solenoid valve which admits air pressure to a liquid air reservoir and forces liquid air into the Dewar until *R*1 is immersed. The resistance of *R*1 increases and lowers the fraction of the line voltage applied to the starting anode to a value below the firing potential, closing the solenoid valve. The resistance increase for a change +20°C→−180°C is about a factor of 1.7, causing a change of voltage of about 15 volts. Since a change of a few volts is sufficient to control the thyratron, some choice in the lower limit to which the liquid air falls is possible by adjustment of *R*3.

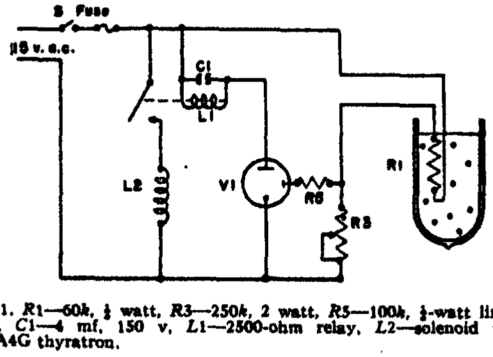

Fig. 1. *R*1—60*k*, ½ watt, *R*3—250*k*, 2 watt, *R*5—100*k*, ½-watt limiting resistor, *C*1—4 mf, 150 v, *L*1—2500-ohm relay, *L*2—solenoid valve, *V*1—OA4G thyratron.

The upper level for the liquid air is fixed fairly sharply at the lower edge of the resistor, and the lower level can be set by *R*3 at several millimeters to several centimeters below the resistor. However, for a larger swing, the resistor must warm to nearly room temperature and control becomes uncertain. Hence the system shown in Fig. 2 was devised with independent resistors and thyratrons for controlling the upper and lower levels. Permitting a larger change in level while retaining positive control leads to a greater economy of liquid air.

*R*1 and *R*2 form with *R*3 and *R*4 voltage dividers which determine the potential of the starting anodes of *V*1 and *V*2. *R*3 and *R*4 are adjusted so that the starting anodes vary below and above the firing potentials as *R*1 and *R*2 are and are not immersed in liquid air. Examination of the circuit shown in Fig. 2 will show that *L*1 is closed only by *V*1 and opened only by *V*2. Therefore *R*1, the lower resistor, must warm slightly before pumping begins, and *R*2, the upper resistor, must become immersed before pumping ceases.

*R*3 and *R*4 are adjusted in the following manner: *R*3 is set at minimum resistance, *R*4 to maximum, and *S* is opened momentarily to insure *L*1's being open. *R*3 is increased until the relays close and pumping begins. Pumping is allowed to continue until the liquid air level reaches *R*2, then *R*4 is decreased until the relays open.

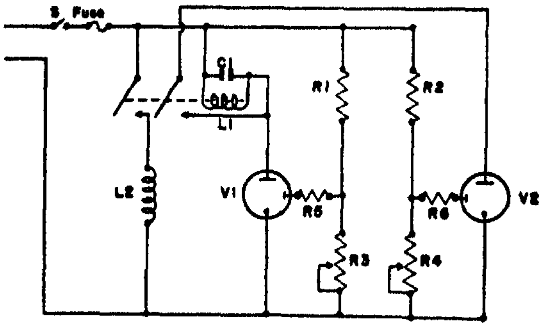

Fig. 2. *R*1, *R*2—60*k*, ½ watt, *R*3, *R*4—250*k*, 2 watt, *R*5, *R*6—100*k*, ½-watt limiting resistor, *C*1—4 mf, 150 v, *V*1, *V*2—OA4G thyratrons, *L*1—2500 ohm relay with DPST normally open contacts, *L*2—solenoid valve (Asco Type P32X, manufactured by the Automatic Switch Company, Orange, New Jersey).

Should it be desirable to maintain a level varying only a few millimeters, it is only necessary to set *R*4 at zero resistance. *R*1 then controls both the opening and closing of *L*1.

This control principle can be used with many tube types. The OA4G thyratron, however, is convenient because it is of the cold cathode type requiring no heater supply and its firing potential is near the mean for the voltage divider swing which is a maximum when $R3=(R1R1')^{\frac{1}{2}}$, where $R1'$ is the resistance of *R*1 at −180°C. Furthermore, the OA4G requires no d.c. supply and permits complete a.c. operation which is an advantage in itself in that it allows the starting anode to regain control after each cycle. If a vacuum triode is used, a battery is required to obtain proper grid bias and still retain the maximum voltage change.

An Asco type P32x solenoid valve, manufactured by the Automatic Switch Company of Orange, New Jersey, was found suitable because it operates on 115-v a.c. and allows venting the pressure created by evaporation of liquid air in the reservoir. The ports are marked *A*, *B*, and *C* on the commercial item. *A* was led to the reservoir, *B* to the line pressure, and *C* was left open to the atmosphere.

The chief advantage of this system is its flexibility obtained because the controlling elements require very little space and may be adjusted for a wide range of requirements. Control has proved to be positive and reliable.

A Series Parallel Linear Thermopile with Interchangeable Receiving Units

Robert A. Crane* and Francis E. Blacet
Chemistry Department, University of California, Los Angeles 24, California

September 14, 1949

In order to determine the quantum yields of certain photochemical reactions it was necessary to measure the absolute intensity of ultraviolet light passing through a reaction cell 30 mm in diameter. Examination of the existing literature did not disclose a suitable instrument for this purpose. The thermopile type described by Leighton and Leighton[1] and previously used in these laboratories was not as sensitive as desired and the design by F. A. Firestone[2] did not cover a large enough area.

Figure 1 gives a perspective view of one of the receiver elements which are the basic units in the thermopile which was constructed to meet our needs. As many of these units as required in order to cover a given area may be held together by means of insulated bolts placed through the two holes, *C*. The receivers in this way are connected in a series parallel manner reducing the total resistance for the thermopile considerably below that for the same number of units arranged in a series manner.

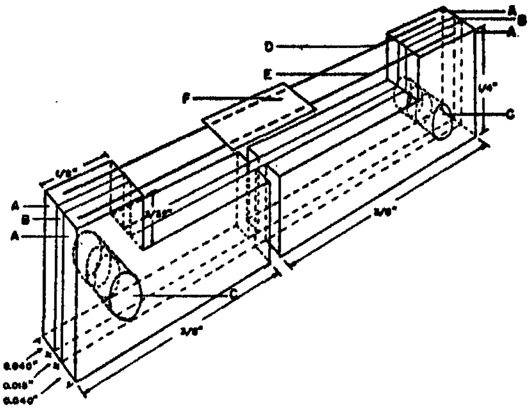

Fig. 1. Perspective view of a single thermopile unit. A. Brass cold junction, B. fiber insulator, C. assembly rod hole, D. bismuth wire, E. bismuth-tin wire, F. platinum receiver.

The cold junctions consist of four "*L*" shaped brass pieces, *A*, cemented to a fiber board insulating piece, *B*, in such a manner that each "*L*" is electrically insulated from the others. The brass pieces were cut from 18-gauge sheet brass, drilled and machined in a group to make them of uniform size. The topmost edges of the brass "*L*" 's were tinned using Wood's metal as a solder.

The radiation receivers were made from platinum foil, 0.0005 inch thick, in the following manner. Using a soldering iron, one side of the platinum foil was covered uniformly with a thin layer of tin. To remove small irregularities, the tinned foil was rolled until the combined thickness of the tin and platinum was about 0.0007 inch. Receivers about 2.4 by 4.0 millimeters were cut from this material. Pure bismuth and 95 percent bismuth-5 percent tin wires 0.004 inch in diameter, obtained from Baker and Company, Inc., Newark, New Jersey were cut to three-quarters of an inch, and soldered to the tinned backs of the platinum receivers in the following way. A receiver was laid on a glass plate, tinned side up, and one of each type of wire placed the long way of the receiver about one-half millimeter from each edge. A thin mica sheet, having on its under side a small drop of zinc-hydrochloric acid flux, was then laid over the wires so as to wet the entire receiver and wires. Heat was applied by means of a miniature soldering iron pressed directly on the mica sheet until the wires fused to the tin layer covering the platinum. The completed receiver and wires were washed in warm water to remove the excess flux.

The receivers next were soldered to the "*L*" shaped cold junctions making use of the Wood's metal previously applied. Heat was administered with extreme caution to avoid melting the wires at the point of contact with the cold junctions.

The shiny platinum surface was plated using a solution of 0.025N hydrochloric acid containing 0.3 percent platinum chloride and 0.025 percent lead acetate.[3] A sufficient amount of this plating solution was placed in a small platinum boat so that the solution, due to surface tension, extended a little above the edges. The thermopile unit was suspended platinum face down and then lowered by means of a screw device until the platinum just touched the surface of the plating solution. It was important to cover the entire surface of the platinum but yet not to allow any of the solution to cover the back side of the unit because the platinizing solution would react with the tin causing poor electrical connections where the wire was bonded to the tinned platinum. Plating for approximately five minutes with a current of about 2 milliamperes resulted in a uniform velvety black surface. The plated units after rinsing in warm water and drying were ready for testing and final assembly.

Two linear thermopiles were assembled from units of this design each with an exposed area of 3 mm by 30 mm and consisting of 14 and 16 receiving junctions. The total resistance of the thermopiles was 27 and 32 ohms respectively. The sensitivity of each of these thermopiles was nearly double that of a thermopile covering the same area but constructed following the design described by Leighton and Leighton[1] and using bismuth and silver wires. The response of the most sensitive thermopile was 0.068 microvolt for a radiation intensity of one microwatt per square centimeter. This figure was calculated from the galvanometer characteristics and the deflections obtained using standard lamps from the Bureau of Standards. The time constant for the maximum response was less than four seconds, under the conditions used.

The response of the thermopiles was linear over the range of intensities covered, from 0 to 300 microwatts per square centimeter. The surface linearity of the instruments was checked by moving a 4-mm slit along the sensitive receivers so that only this portion was exposed at one time. In both the variation in surface sensitivity was less than 5 percent compared with about 15 percent for the silver-bismuth thermopile. Thus, the bismuth-bismuth alloy thermopiles represent a decided improvement over the silver bismuth thermopile both in increased sensitivity, which is expected in view of the more favorable thermal e.m.f. of the metals used in their construction, and in more uniformity of the absorbing surface attained by the platinum black plating process, as well as by interchanging and matching the individual units making up the complete instrument.

---

* Charles A. Coffin Fellow, awarded by General Electric Company (1948–1949) and (1949–1950).

[1] P. A. Leighton and W. G. Leighton, J. Phys. Chem. 36, 1882 (1932).

[2] F. A. Firestone, Rev. Sci. Inst. 1, 630 (1930).

[3] G. Jones and D. M. Bollenger, J. Am. Chem. Soc. 57, 280 (1935).

Low Temperature Gasket

A. Wexler, W. S. Corak, and G. T. Cunningham
Westinghouse Research Laboratories, East Pittsburgh, Pennsylvania

November 17, 1949

In the assembly of low temperature apparatus the closure technique presents several problems. In the first instance, securing a reproducible vacuum-tight seal is complicated by the fact that joints which are tight to helium gas may not be tight to superfluid He II.[1] Second, in some cases the necessity of heating the apparatus, when a standard soldering procedure is used, is detrimental to the materials it contains. Finally, the presence of ordinary solder, which becomes superconducting, and hence strongly diamagnetic, interferes with magnetic measurements that may be made at low temperatures.[2]

From the room temperature thermal expansion coefficients, it appeared that gold should function satisfactorily as a gasket in copper containers, which are most frequently used. Gold gaskets have been used previously in these Laboratories in high temperature apparatus.[3] The use of a gold gasket in a low temperature

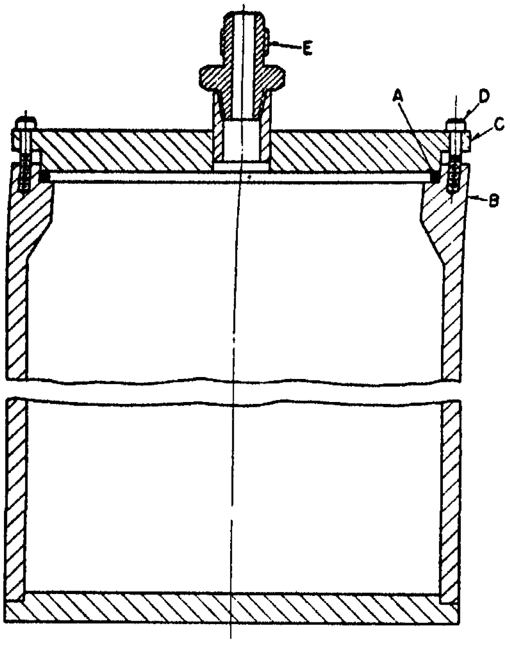

Fig. 1. Low temperature gasket.

container is indicated in Fig. 1. The gold wire, *A*, 0.020 in. in diameter, sealed the copper container, *B*, which in this application happened to be 8×4 in. (diameter), when the copper cap, *C*, was forced down onto it by twenty-two 4–40 Allen-head screws. The initial tightening of the cap caused the gold to flow and to take up any irregularities in the sealing surfaces. At the same time it became work-hardened and elastic. The gasket adhered well to the container and was not removed during subsequent disassembly operations. In the application in which this arrangement was used, the presence of magnetic bodies was not objectionable; hence standard steel screws were used. For experiments in which this is a consideration, strong, non-magnetic screws will be employed; beryllium copper screws appear to be a good choice for this purpose.

The arrangement was checked for tightness with a helium mass spectrometer leak detector.[4] Preliminary measurements, made with the leak detector operating in routine fashion, that is, with the diffusion pump associated with the device open to the system under test, gave a conservative lower limit to the size of leak detectable equal to 5×10^{-6} (micron-liter)/sec., measured at room temperature. Within this limit, no leak was detectable with the apparatus exposed to helium gas at one atmosphere in the temperature range room temperature to *ca.* 4.2°K, or to liquid helium between *ca.* 4.2° and 1.92°K.

Because of the general interest in the tightness of the gasket when the seal is exposed to superfluid helium, the test method was elaborated so as to decrease the lower limit to 5×10^{-9} (micron-liter)/sec. with the apparatus immersed in liquid helium below the λ-point. The container was filled with a machined piece of aluminum which decreased the gas space in the container practically to zero. The container communicated with a 1.5-liter volume at room temperature by way of the pumping line. When the liquid helium in which the container was immersed reached the λ-point, the container was isolated from the pumping system of the leak detector, and any helium leaking in was allowed to collect in the room temperature volume. The collection time was 100 min., during which time the liquid helium, whose vapor was being pumped away continually, reached a vapor pressure of 18.2 mm, corresponding to 1.92°K. At the end of the collection time, the system was quickly opened to the mass spectrometer, and, from independent calibrations, the lower limit already noted could be deduced. There exists the possibility that the actual leakage rate is higher than the value given because of the adsorption of helium gas on the low temperature surfaces of the container. No further work was done on this possibility.

There was no ambiguity associated with the temperature measurement. It was determined from the vapor pressure as indicated by both an ordinary mercury manometer and a Dubrovin gauge having a ninefold amplification factor and readable to ±0.1 mm Hg. The gauges were connected to a tube having an I.D. of 0.175 in. and immersed in the liquid helium. The attainment of the λ-point was indicated by a discontinuity in the slope of the vapor pressure, time relation for the evaporating liquid and corresponded accurately to the λ-point pressure as read on the gauges.

The assembly survived 12 cooling-heating cycles between room temperature and 77°K, as well as six separate openings and closures, with no evidence of leakage. Parenthetically, it is interesting to note that the leak test included any possible contribution by the S.A.E. brass to copper flare fitting which was therefore free of leaks to the limit and under the conditions described.

It is evident that the seals described here are sufficiently tight to permit the use of the practice widely employed in the case of glass Dewar vessels.[5] Thus it would be possible to rough pump a copper vacuum container using a gold gasket and to allow the pressure to drop to a negligible value when low temperatures are reached. In other words, no kinetic diffusion pump system need be used.

In conclusion, the authors are happy to acknowledge the cooperation of Dr. R. E. Fox and Mr. D. J. Grove in certain phases of the use of the mass spectrometer leak detector.

[1] Giauque, Stout, and Barleau, J. Am. Chem. Soc. 61, 654 (1939).
[2] Giauque, Fritz, and Lyon, J. Am. Chem. Soc. 71, 1657 (1949).
[3] W. M. Hickam, Rev. Sci. Inst. 20, 472 (1949).
[4] Thomas, Williams, and Hipple, Rev. Sci. Inst. 17, 368 (1946).
[5] W. F. Giauque, Rev. Sci. Inst. 18, 852 (1947).

Simple Method to Seal Liquids of High Vapor Pressure into Glass or Quartz Capillaries

Z. V. Harvalik
University of Arkansas, Fayetteville, Arkansas

August 1, 1949

A SIMPLE method of sealing a liquid of high vapor pressure (water, ethyl ether, ethyl alcohol, carbon disulphide) into heavy-walled glass or quartz tubes and capillaries is described as follows.

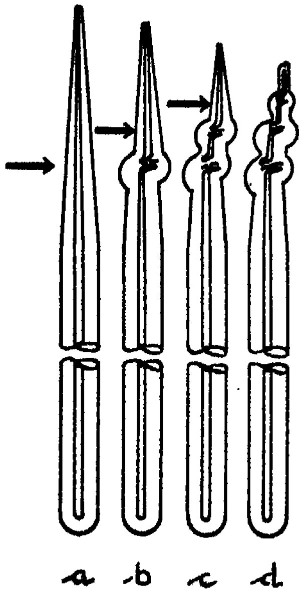

Fig. 1.

The glass or quartz tubing or capillary is drawn into a heavy-walled capillary of tapering bore of approximately 10 to 15 cm length, and filled with the liquid to be sealed in. Then the beginning of the capillary is carefully heated (see arrow in Fig. 1a) until the glass (or quartz) becomes soft. Compress gently and dislocate the compression bulb laterally 2 to 3 mm. Figure 1b shows the seal after compression and dislocation. Then heat the capillary about 5 to 10 mm above the first compression seal (see arrow in Fig. 1b) until glass becomes soft, compress and dislocate laterally again. This second compression seal (Fig. 1c) will prevent any escape of vapor of the liquid of large amounts through the capillary. By heating the end of the capillary 5 to 10 mm above the second compression seal, a perfect closing of the tube can be achieved (Fig. 1d).

Capillaries have been filled with liquids to two-thirds of the length of the tube, and sealed by using the method described above. The capillaries are heated electrically in a tube-like furnace to the critical temperature of the liquids. When the critical temperature was reached the meniscus disappeared.

As testing liquids, water (critical temperature, 374°C; critical pressure, 218 atmospheres), ethyl ether (193°C, 35 atmospheres), ethyl alcohol (243°C, 63 atmospheres), and carbon disulphide (273°C, 75 atmospheres) were sealed into Pyrex and quartz capillaries of 2- to 3-mm original bore.

Carefully annealed seals withstand pressures of the magnitude of the critical pressures of the liquids mentioned above.

During the testing the disappearance of the meniscus was observed through a shield of safety glass. It is recommended not to attempt to heat the capillary in an open flame while holding it in the hand.

A Simple Recording Manometer*

Fraser P. Price and Paul D. Zemany
Research Laboratory of the General Electric Company, Schenectady, New York

January 5, 1950

In the course of some work on gas reactions the problem of obtaining a record of pressure changes of the order of 100 mm Hg occurring over periods of 10–20 seconds was encountered. The problem was solved in a simple and as we believe novel manner, since no reference to a similar device could be found in the literature. A diagram of the apparatus is presented in Fig. 1.

It consisted of a conventional *U*-type mercury manometer in the evacuated side of which was stretched a length of 20-mil nichrome wire (*C*). This was kept taut and centered by two tungsten wire springs (*B*) which were connected to heavy wire leads (*A*) sealed through the glass, all metal-metal connections being spot welded. The two ends (*A*) were connected to a 1.5-v dry cell in series with a resistance of about 500 w. In this manner the current through the wire was kept constant and the voltage drop (about 1 mv) across the portion of the wire untouched by the mercury was a function of the height of the mercury in that limb.

This voltage drop was amplified by a G.E. self-balancing potentiometer which in turn actuated a G.E. photoelectric recorder. The short limb of the manometer was about 1¼ in. I.D. while the long limb was of ⅜ in. I.D. tubing. Thus more than 90 percent of the pressure rise was effective in changing the voltage drop. Also the relatively large diameter of the long limb prevented the wire from coming too close to the side thus giving rise to undesirable wall effect.

In order to get reproducible results it was found necessary to use scrupulously clean mercury and to flash the nichrome wire several times in about 3 mm of H_2, pumping out to about 20 microns between flashings. With these precautions two such manometers, one 1 meter long and one 100 mm long have functioned without discernable change in calibration over periods of months.

The calibrations of the smaller one taken every day for the period of a month were plotted on the same graph. They all fell on the same line showing no hysteresis and were reproducible to within the error in reading the recorder chart, i.e., ±2 percent. Since this was sufficient for the problem at hand, no attempt was made to find whether or not this error could have been reduced by a more precise recorder.

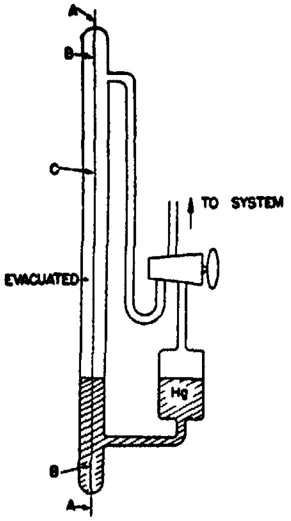

Fig. 1.

In preliminary models of this instrument, in order to get the change of resistance per unit length as high as possible, attempts were made to use very fine (about 0.5 mil) tungsten wire as the filament. However it was found that it was not possible to get good calibrations presumably due to the inability of the mercury to make reproducible contact with so fine a wire. Also since the filament apparently has to be in the evacuated limb a manometer having a wire in each side connected to a bridge circuit so as to accentuate the unbalance probably would not prove feasible.

With the manometer described here no attempt was made to use a.c. on the manometer filament, principally due to the fact that the d.c. amplifier and recorder were available. However we can see no reason why the use of a.c. should not be possible and perhaps even desirable as the problems connected with amplification and recording would probably be simpler.

---

* This work supported in part by a contract from U. S. Army Ordnance.

A High Pressure Fitting for Scintillation Counting

K. D. Timmerhaus, E. B. Giller, L. H. Tung,
R. B. Duffield, and H. G. Drickamer
University of Illinois, Urbana, Illinois

January 5, 1950

The use of a scintillating crystal with a photo-multiplier has opened up a number of new techniques in tracer work. It is now possible to make continuous analyses without sampling. This is especially advantageous in high pressure systems, particularly near the critical point where sampling would considerably disturb conditions. For these cases the crystal is placed inside the apparatus and the light is conducted out by a Lucite or quartz rod.

Figure 1 shows a high pressure seal for the operation. The seal is made with *O*-ring, and the shoulder and nut are merely to keep the rod from sliding out. The rod goes to a photo-multiplier tube in a cooled box. Considerable care is necessary to make the whole system light tight.

The above system has been pressure tested to 2000 p.s.i.a., and would probably go considerably higher. With Lucite rods, a temperature of 55°C has been maintained for five days with no appreciable effect on the seal or light conducting properties. At 60°C some softening takes place, and at 65° the rod deforms and loses seal in less than 24 hours. There is no apparent temperature limitation on the quartz, within the limits permissible for *O*-rings.

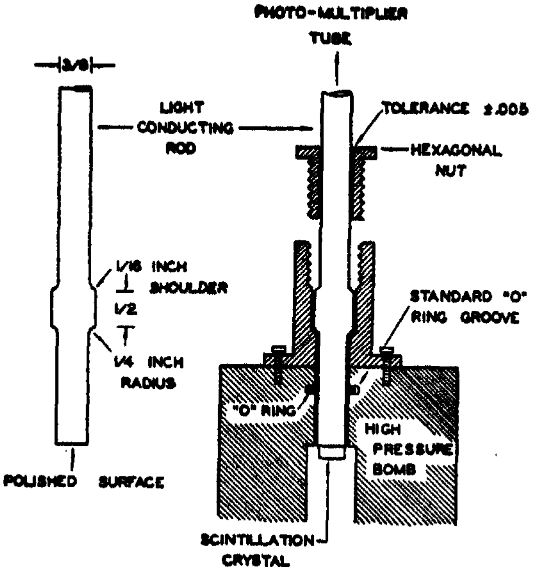

FIG. 1. Fitting for high pressure scintillation counter.

The crystal can be sealed to the rod with a glue made from Lucite dissolved in ethylene dichloride. This also makes an effective coating for anthracene crystals to prevent attack by paraffin hydrocarbons without significantly decreasing the counting rate even for such weak beta-emitters as C^{14}.

Automatic Equipment for Electrolyzing Heavy Water

RALPH W. WANIEK
Institut fuer Radiumforschung, Akademie der Wissenschaften, Vienna, Austria

January 5, 1950

FOR the production of deuterium necessary for the supply of the ion source of a neutron generator, we devised a very simple and automatically working equipment. The apparatus avoids the heated palladium tube which might be very difficult to obtain and is much simpler than the unit described by Slack and Ehrke.[1] Figure 1 shows the construction of the V-shaped cell made of Pyrex glass which contains about 5 cc of heavy water. We employed, as electrodes, 0.5-mm thick platinum wires which were sealed into the glass walls, and produced the necessary electrical contact by means of small mercury columns. Thus, the whole cell can be easily dipped into a beaker with water to produce the right cooling. The shape of the cell permits keeping the "dead volume" (i.e., the quantity of electrolyte which cannot be reached by the electrodes) at a minimum.

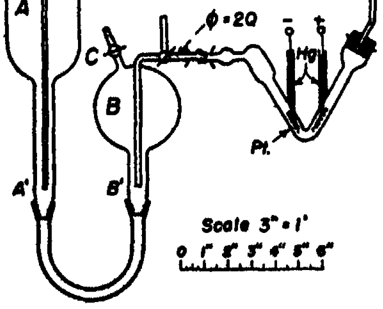

FIG. 1.

The problem of equalizing the different pressures on the two sides of the electrolyzing apparatus was solved as shown in Fig. 1. The cross section of the glass tubing of the deuterium line is twice that of the oxygen tubing. Before a run is started, bulb B is filled completely with a special liquid which does not show a too accentuated exchange effect between heavy and light component. High vacuum oils or benzene may therefore suit the purpose. During the production, deuterium is stored in bulb B and the liquid rises in A. Thus, the same hydrostatic pressure is to be expected at both points A' and B' which are at the same height. The oxygen escapes through A. By means of stopcock C, deuterium can be filled into an evacuated bulb which provides the ion source with gas through a needle valve. Voltage and current of the equipment can be controlled accurately. The apparatus works automatically for hours and represents a satisfactory solution in all cases of this kind.

---

[1] C. M. Slack and L. F. Ehrke, Rev. Sci. Inst. 8, 39 (1937).

Optical Centering System for X-Ray Diffraction Samples

EUGENE L. PERRINE
Armour Research Foundation of the Illinois Institute of Technology, Chicago, Illinois

January 16, 1950

WHEN samples are to be rotated during exposure to a narrow beam of x-rays, as is frequently done when x-ray diffraction studies are made, it is necessary to place the sample on the axis of rotation so that it does not move in and out of the x-ray beam during exposure. This positioning is frequently done by observing the sample with a low power microscope while it is rotated manually and placed on the proper axis. This results in correct placement, but it is inconvenient because the positioning operation must be carried out while the worker is looking through the microscope. He is unable to watch what he is doing with his hands.

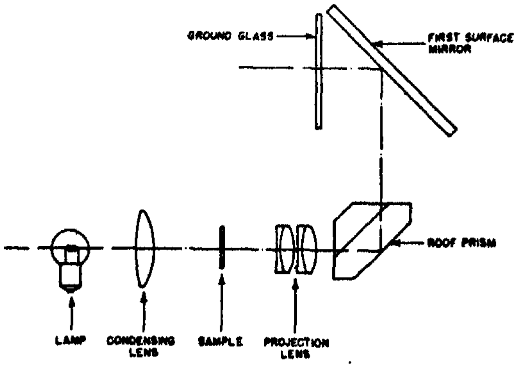

FIG. 1.

The instrument described was constructed to avoid this difficulty (see Figs. 1 and 2). The device consists of a light source, a condensing lens, a folded projection system, and a viewing screen. The light source is a six-volt lamp which is powered from the line by means of a transformer. The light from this lamp is concentrated on the sample by a single condensing lens which is focused slightly beyond the projection lens. The projection lens itself is a petzval with a focal length of one inch. With the path length provided it gives a magnification of approximately four and one-half times. The optical path is folded by a roof prism and a first surface mirror. The roof prism corrects the left to right transposition of the projection lens and the folding of the optical system corrects inversion which is also produced by the projection lens.

FIG. 2.

With these compensations the image produced is erect and correct with respect to left and right. It is, therefore, easy to position the sample because all movements are in the same direction when viewed through the optical system as they are when viewed directly. The ground glass viewing screen is placed above and slightly behind the sample so that the sample and the image can be viewed simultaneously. A vertical line on the ground glass shows the axis of rotation and a horizontal line indicates the point at which the x-ray beam intersects this axis. The same pilot pins which are used to position the sample holder on the x-ray diffraction camera are used to position it on the alignment unit.

Electronic Water-Level Control

R. D. Miller and J. S. Hopkins
Division of Soils, University of California, Berkeley 4, California

October 18, 1949

In the construction of a recirculating, constant volume soil permeability apparatus, it was necessary to devise a means of producing and maintaining a controlled hydraulic gradient across the sample chamber and flow meter. This reduced to a matter of pumping water from one arm of a manometer to the other at such intervals as were necessary to maintain the water-level in one arm within narrow limits. An electronic control was used to direct the action of the pump (see Fig. 1).

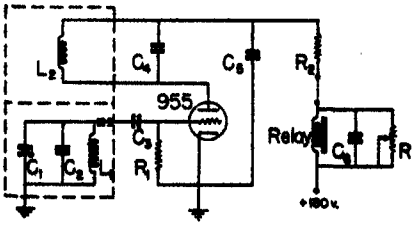

FIG. 1. Circuit of electronic water-level control. The distributed capacities of the shielded lead and of the coils are not indicated. C_1 2–10-mmf variable air condenser; C_2 2-mmf silvered ceramic; C_3 150-mmf mica; C_4 10-mmf silvered ceramic; C_5 500-mmf silvered mica button; C_6 16-mf paper; R_1 100 K ½ watt carbon; R_2 5 K 1 watt carbon; R_3 10 K w.w. pot; L_1, L_2 32 turns No. 32-scc enameled wire, open wound on ½ in. i.d., 1/16-in. wall polystyrene tubing; relay d.c. resistance 4000, 4 ma to close, open at 2.5 ma. Observed operating frequency: 10.5 megacycles.

The high dielectric constant of water suggested that if a manometer arm passed through the coil of a tuned circuit, its resonant frequency would be altered by a change in water-level within the coil. A tuned-plate tuned-grid oscillator was constructed in which a manometer arm passed through the plate coil. If the water-level subsided, resonance between plate and grid circuits was destroyed, and the resultant increase in plate current closed a relay, starting the pump. Pumping continued until the water-level in the manometer arm rose to a point at which oscillation was resumed and the relay opened.

By careful shielding of plate and grid coils to minimize coupling, a control cycle was obtained in which the maximum displacement of the water surface was less than 2 mm. The pressure control range was reduced to less than 0.5 mm of water by using USP white oil as the manometer fluid in an inverted manometer. Any desired head could be obtained by sliding the unit to the appropriate point on the manometer arm.

A Manometer Leveling Procedure

John E. Wertz*
The George Herbert Jones Chemistry Laboratory, University of Chicago, Chicago, Illinois

November 21, 1949

In numerous gasometric procedures it is necessary to balance gas pressures against one another, making use of a manometer as a null instrument. To establish the point of equality of levels of manometric liquid without reading their positions on a scale, the following procedure is found to be rapid and probably as accurate as is possible with the unaided eye.

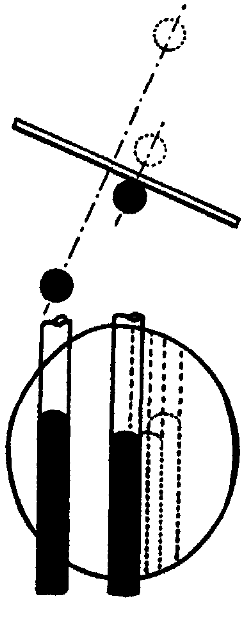

FIG. 1. Monometer leveling procedure using a mirror.

A plane mirror is held vertically against the back of one leg o the manometer, but at an angle to the plane of the latter, as in Fig. 1. (It is essential that this leg be truly vertical.) To avoid parallax, the eye is adjusted to such a level that the meniscus and its image are superimposed. By rotating the mirror about the leg of the manometer, the image of the other meniscus can be brought into juxtaposition with the first, so that any inequality in levels is easily discernible. This permits equalization to within 0.1 mm.

---

* Present address: School of Chemistry, University of Minnesota, Minneapolis, Minnesota.

Erratum: A High Speed Synchroscope

[Rev. Sci. Inst. 21, 71 (1950)]

G. G. Kelley
Oak Ridge National Laboratory, Oak Ridge, Tennessee

SEVERAL errors occur in Fig. 3 of the above article. A corrected diagram of the sweep generator appears below.

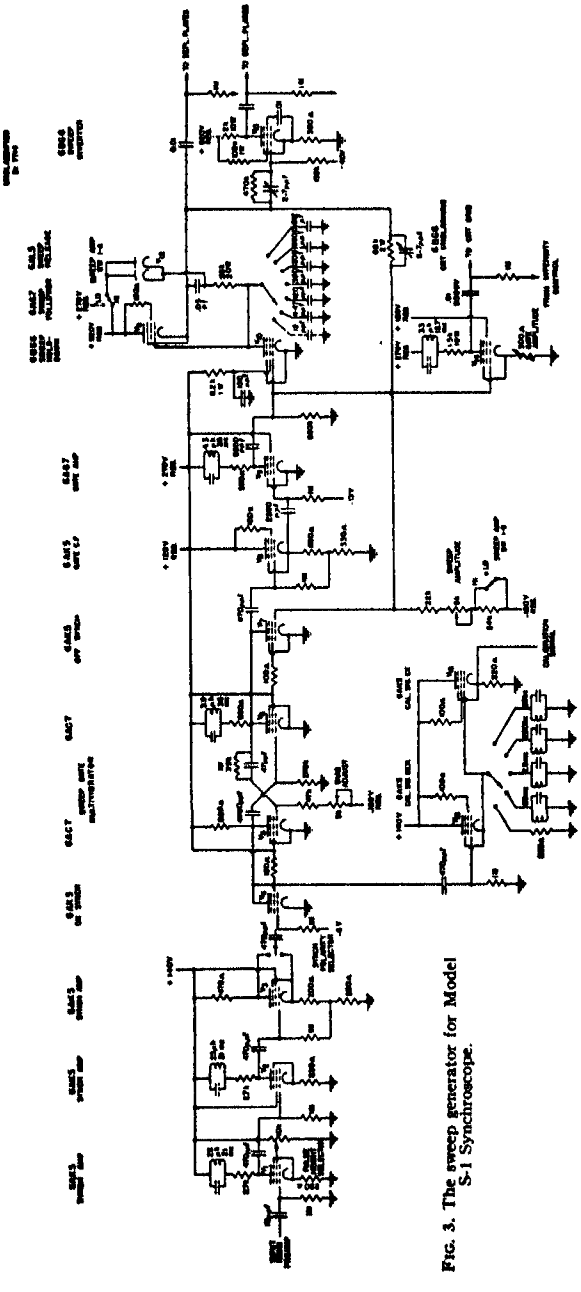

FIG. 3. The sweep generator for Model S-1 Synchroscope.

New Instruments

W. A. Wildhack: Associate Editor
in Charge of this Section
National Bureau of Standards, Washington, D. C.

These descriptions are based on information supplied by the manufacturer and in some cases from independent sources. The Review *assumes no responsibility for their correctness.*

Spectrophotometer

The new Beckman Model B spectrophotometer is a low-priced instrument designed for rapid, convenient, and accurate measurements in the wave-length range 320 to 1000 mμ.

The instrument is applicable to a wide variety of measurements and carries convenient provisions for attaching accessories. It features: direct-reading absorbance, transmittance and wave-length scales; a simple, inexpensive optical system of high resolution, high wave-length accuracy and minimum stray light; a variable slit mechanism of novel design insuring smooth operation, reproducibility and freedom from lost motion and backlash; high photometric sensitivity; and an accurate, stable d.c. amplifier of rapid response.

The low cost of this new instrument will enable the rapid, accurate methods of spectrophotometry to be used for a large number of routine analyses now accomplished by colorimetry or by gravimetric, titrametric, or other tedious methods.

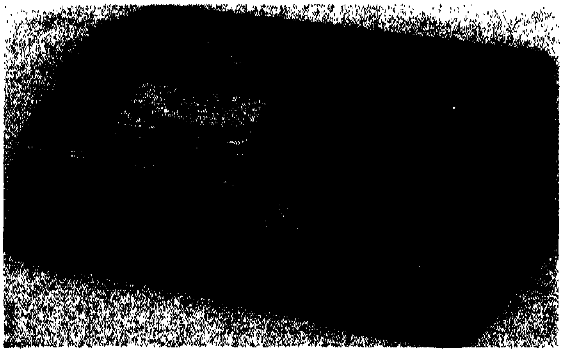

The dispersive element of the Model B spectrophotometer is a borosilicate glass prism with curved faces, of the type first described in 1910 by Charles Féry. The auto-collimating action of the prism eliminates the need for a collimating mirror, thereby simplifying the monochromator optical system.

The effect of the natural astigmatism of the Féry prism is overcome in the Model B spectrophotometer by employing a curved entrance slit. The exit slit is straight. This slit design also enables narrower absorption cells to be used and reduces exit beam deflections caused by test tube type cells. The prism is subject to a simultaneous rotational and translational motion by means of a compact quadrilateral framework hinged with beryllium copper spring reeds, which accommodates for the change in focal length with wave-length.

The high resolution of the Model B allows the spectral range 320 to 1000 mμ to be covered with maximum effective band widths of 5 mμ.

The amplifier is a.c.-operated, employing miniature and subminiature tubes in a negative feed-back circuit. An electronic regulator compensates for the effect of line voltage variations on the amplifier. Lamp power is provided through the built-in transformer, but for the most accurate work, the lamp should be operated from a battery or auxiliary voltage regulator.

Two interchangeable photo-tubes are available for measurement: a red-sensitive photo-tube for the range 600 to 1000 mμ, and a blue photo-tube supplied with the instrument for the range 320 to 700 mμ. A Corning No. 9863 filter is provided for use below

400 mμ, reducing stray light to less than 1.5 percent at 320 mμ. Stray light decreases at longer wave-lengths.

Readings on the transmittance scale can be reproduced to 0.3 percent. The scale can be expanded, by use of a precision amplifier sensitivity control, to further increase measurement accuracy.

Presently available accessories for the Model B are the integrating sphere reflectance accessory and the test tube holder. The monochromatic light beam may also be brought outside the instrument to accommodate longer cells, or for special uses requiring a high grade monochromator.

Other Beckman spectrophotometers are the well-known Model DU, for ultraviolet through near-infra-red work; and the Model IR-2 for the infra-red region.—National Technical Laboratories, *South Pasadena, California.*

F-M Generator

The Type 202-*D* f-m signal generator, designed for use with telemetering receiver equipment and in other associated applications, covers the frequency range from 175 to 250 mc and is provided with three continuously adjustable deviation ranges, 0–24 kc, 0–80 kc, and 0–240 kc. In addition, amplitude modulation up to 50 percent may be obtained using the internal audio oscillator, and modulation to 100 percent using an external audio oscillator.

The internal audio oscillator provides eight fixed frequencies between 50 c and 15 kc, any one of which may be conveniently selected by a rotary-type switch for frequency modulation or amplitude modulation.

The deviation sensitivity of the f-m system is within ±0.5 db from d.c. to 200 kc. The a-m system is substantially flat from 30 c to well above 100 kc.

A front panel jack permits direct connection of an external modulation voltage source to the screen element of the final stage for pulse and square-wave amplitude modulation. Under these conditions, the rise time of the modulated carrier envelope is less than 0.25 μsec. and the decay time less than 0.8 μsec.

A monitoring meter is used to standardize the output level of the signal generator in order to make the mutual inductance (piston type) r-f attenuator direct-reading over the range 0.1 μv to 0.2 v. The output impedance (with cable attached) is 26.5 ohms.

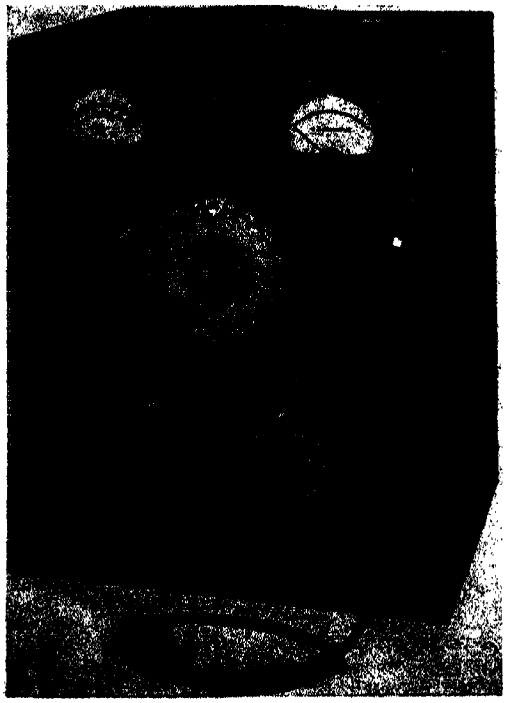

The instrument is self-contained, with power supply, and is designed for use on 115 v, 60 c.—Boonton Radio Corporation, *Boonton, New Jersey.*

Square Wave Generator

Type 105 square wave generator is continuously variable in frequency from 25 c.p.s. to 1 mc. The unusually fast rise time of approximately 0.02 μsec. (10 to 90 percent) is maintained at all frequencies without overshoot.

The Type 105 is essentially a square wave current generator with maximum current capability of 160 ma to output load. When used with the 93-ohm output cable, as furnished, approximately 15 volts are available. In the event that higher output voltages are desired, they may be had by the use of higher impedance output cables with a proportional increase in rise time.

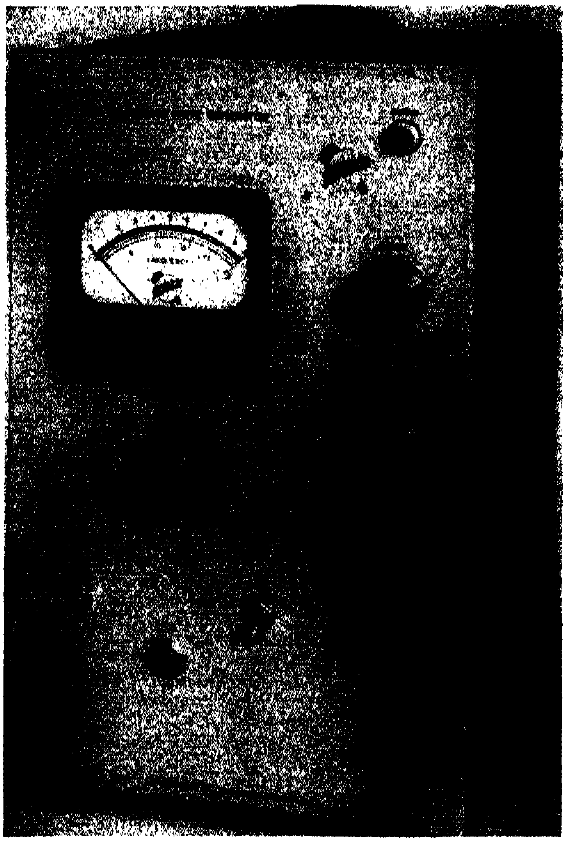

This instrument provides an ideally suitable signal for quickly and accurately testing the amplitude and phase response of amplifiers, filters, etc., having pass bands of a few c.p.s. to 20 mc.

The price of the Type 105 is $395.00 f.o.b. Portland, Oregon. Detailed specifications available upon request.—Tektronix, Inc., *712 S.E. Hawthorne Boulevard, Portland 14, Oregon.*

Microphotometer

The "Romicron C. G. Grand microphotometer" represents an instrument especially designed for use with the microscope. The photometer may be left on the microscope at all times. Readings may be obtained by operating a lever which will move the photoelectric cell into the path of rays. Indicator is a microammeter with arbitrary scale of ten divisions. A range switch mounted on the side of the housing permits a change of sensitivity and, by means of a female plug, an amplifier or galvanometer may be attached to increase scope of instrument. Also available will be a diaphragm eyepiece with observation telescope and beamsplitter

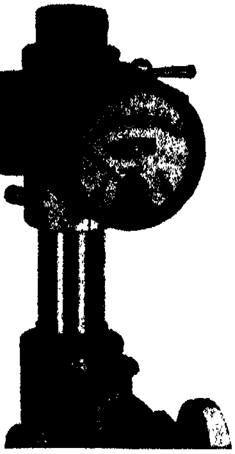

for measuring small areas and specific sections of a specimen.—Paul Rosenthal, *505 Fifth Avenue, Room 900, New York 17, New York.*

Cartesian Manostat

Designed for automatic pressure and vacuum control in the laboratory, pilot plant, and industry, the Cartesian manostat eliminates the use of complicated electrical and mechanical systems or extra equipment.

The operation is based on sealing off a given amount of gas at the control pressure desired inside a Cartesian diver floating in a pool of mercury. At equilibrium, the diver normally rests against the upper, adjustable orifice sealing it shut, but an increase in pressure in the system will cause it to sink, allowing the excess gas to escape from the system through the orifice to a source of pressure lower than the control pressure. The system pressure will then drop until the control pressure is reached, when the diver again seals the orifice. A small bleed into the system from a source of higher pressure insures that the system pressure will never go below the control point.

Model No. 5 industrial has a maximum capacity of 20 CFM for a system pressure of 100 p.s.i.a. with the largest orifice size, and a maximum sensitivity of 0.025 percent at 10 p.s.i.a. with the smallest orifice size.

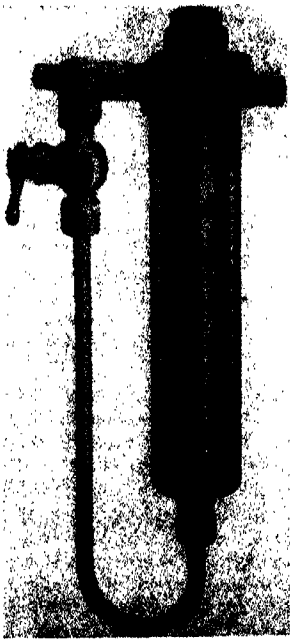

Model No. 6 (illustrated) does not have the large capacity of the No. 5, but it has a feature that once a vacuum has been set in the instrument, the system may be shut down without disturbing the setting. When operated under vacuum, the quantity of gas maintaining the control pressure is sealed inside the diver even when the system is restored to atmospheric pressure, since the excess pressure forces the diver down upon an internal central tube, closing it and protecting the mercury seal.

Suggested applications include precise vacuum distillations or evaporations and physical chemical measurements such as vapor-liquid equilibrium determinations.—Emil Greiner Company, *20–26 North Moore Street, New York 13, New York.*

Vacuum Fusion Apparatus

In the vacuum fusion apparatus in use at National Research Corporation, Cambridge, Massachusetts, impurities in metals can be detected even when the percentage of a given element is as small as 10^{-5} (0.00001) percent or one part in ten million.

During the various stages of preparation, all metals retain or pick up small quantities of oxygen, hydrogen, nitrogen, and carbon. It has long been known that even minute amounts of these impurities may produce marked effects on the final properties of the metals. The above-mentioned elements may be contained as gaseous occlusions in structural faults, in solution or held in actual chemical combination as oxides, hydrides, nitrides, and carbides of various composition and degree of stability. Among the properties which have been found to be markedly affected by gaseous impurities are drawing characteristics, ductility at both elevated and room temperatures, tendency toward strain embrittlement, and heat-treated properties as affected by the degree of effective utilization of reactive alloy additions. As the demand for special alloys containing reactive metals and for highly purified metals is rapidly increasing, it becomes more and more important to determine the exact relationship between the amount of an impurity and its ultimate effect on the properties of a given metal or alloy.

Ordinary analytical procedures for the determination of the elements in question are impracticable in the percentage range encountered. Hence, vacuum fusion and vacuum combustion methods were developed specifically to handle this problem.

Under proper melting conditions under high vacuum, metals may be made to give up their gases quantitatively. The combined oxides react with the graphite crucible in which the melting is conducted, and the oxygen is released in the form of carbon monoxide. The hydrides and nitrides are decomposed, and the hydrogen and nitrogen are liberated directly. The choice of a correct temperature is highly important; it must be sufficiently high

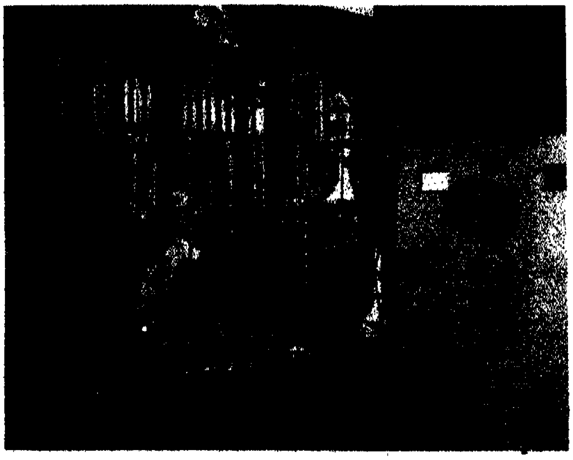

to decompose the chemical compounds and at the same time not so high that the metal being analyzed will volatilize and coat the inside of the apparatus. Sometimes it is necessary to add a flux to assist in achieving these results. The mixture of hydrogen, nitrogen and carbon monoxide is pumped by means of a mercury diffusion pump into a vacuum chamber of known volume. The pressure of gas collected is measured by a McLeod gauge, which is simply a device intended to measure very low gas pressures.

After the total pressure of the gases is determined, they are circulated through a tube containing copper oxide. Here the hydrogen and carbon monoxide take oxygen from the copper oxide and are converted to water vapor and carbon dioxide, respectively. All the gases are allowed to circulate also through a cold trap cooled to −196°C by liquid nitrogen. Here the carbon dioxide and the water vapor are frozen out, while the nitrogen remains gaseous. The nitrogen is then returned to the McLeod gauge, where its pressure is determined.

The cold trap is then warmed up to about −80°C with a mixture of dry ice and acetone. At this temperature, the CO_2 is set free, and its pressure plus the pressure of the nitrogen is measured. By this means, the weight of each gas present may be determined.

The apparatus itself is necessarily complicated. It is constructed entirely of glass, and the few ground glass joints present are carefully sealed with a special high vacuum wax having an exceedingly low vapor pressure. Since the pressure in the system should be in the order of 0.01μ, the smallest leak will vitiate the results.

The main system is evacuated by the combination of a diffusion pump and an efficient mechanical pump. The gases are circulated through the system by means of two small, high speed diffusion pumps.

Since it would be impracticable to place a heater inside a high vacuum system, the metals are heated from outside the system by means of a high frequency induction coil.

The time for a single analysis, exclusive of the preparation of the sample, is about an hour and a half. Accuracy depends a good deal on the individual system and the operator, but with care, determinations may be made with a high degree of reproducibility. The quantities detectable may be as low as 10^{-5} percent, as is the case with hydrogen in many metals.

The vacuum combustion system used to determine small amounts of carbon is similar in nature but considerably simpler. Here the sample is heated in a ceramic crucible in the presence of oxygen under about 16 cm pressure. The carbon in the sample burns in the oxygen and is converted to carbon dioxide. The mixture of carbon dioxide and the excess oxygen then pass through a freezing chamber where the carbon dioxide is frozen out. The gaseous oxygen may then be pumped from the system. After the oxygen has been removed, the carbon dioxide is allowed to warm up and its pressure measured. By applying the same principles as outlined previously, the weight of carbon dioxide may be readily determined and hence the percentage. Analyses by this method give good results, and checks are consistent to 0.001 percent C.—National Research Corporation, *70 Memorial Drive, Cambridge, Massachusetts.*

"Ruggedized" Electrical Instruments

Improved performance has been attained with a completely new, internally shock-mounted, D'Arsonval type of panel instrument. The low mass movement is carefully designed to provide improved electrical accuracy, as well as resistance to severe abuse. The rubber shock mounts, movement, frame structure, fasteners, hair springs, bearings, pointer, and panel mount have all been designed for maximum resistance to shock and vibration and electrical overloads. Hermetic sealing has also been provided for weather protection in any climate.

Ruggedization has not been at the expense of any of the electrical and other performance requirements for electrical indicating instruments. Thus the instrument user and equipment designer are granted a new freedom of application, since the use of electrical instruments is permitted in fields previously limited by the essential fragility of the conventional electrical instrument.—Marion Electrical Instrument Company, *Manchester, New Hampshire.*

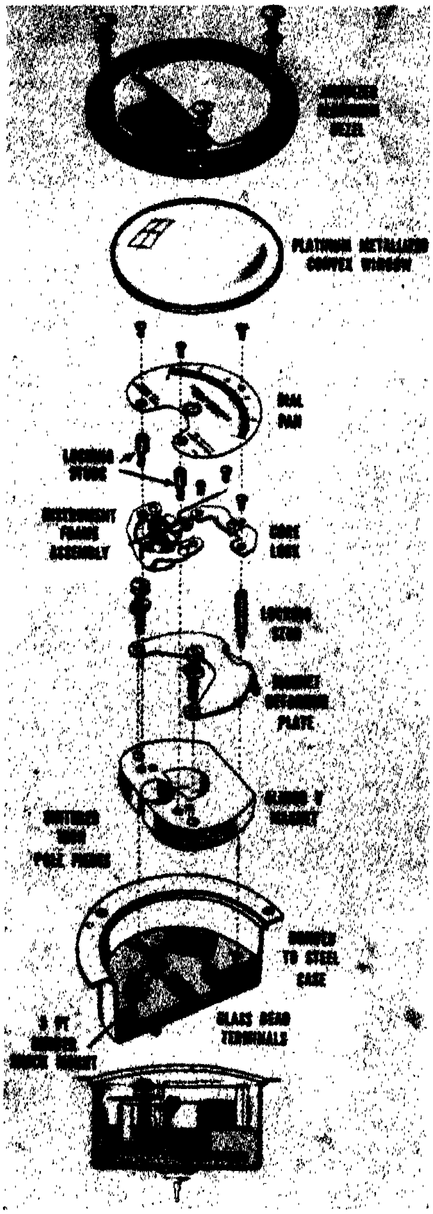

TV Amplifier

The Model 212TV amplifier, specifically designed for television use, is a single untuned amplifier having a band width of 40 to 240 Mc and a gain of 20 db into a 72-ohm unbalanced load, and 25 db

into a 300-ohm balanced line. Capable of replacing up to 12 single channel TV or f-m amplifiers, it has a transmission characteristic of ±2 db over the band width and an impedance of 200 ohms. In addition to an integral power supply, transformers can be supplied to match 52-, 72-, and 93-ohm unbalanced, and 300-ohm balanced lines.

Owing to the traveling wave circuit used, a tube failure does not mean amplifier failure, but only a loss of 0.7 db in gain. Compact and simple in construction and reliable in operation, the Model 212TV amplifier can safely be left unattended over long periods of time in television distribution systems, in hotels, apartment houses, restaurants, sales rooms, and television sets in fringe areas. —Spencer-Kennedy Laboratories, Inc., Department SI, *186 Massachusetts Avenue, Cambridge 39, Massachusetts.*

Synchronous Camera

New 16-mm synchronous cameras (Model 111) are used for photographing events taking place at two or more remote stations with exact shutter synchronization. Model 111 is supplied with shutter speeds of 5, 10, and 20 or 4, 8, 16, and 32 frames per second. The cameras may be used with standard AN-A-6 magazines or with Syno-Pack magazines which are specially designed to eliminate film stoppages.

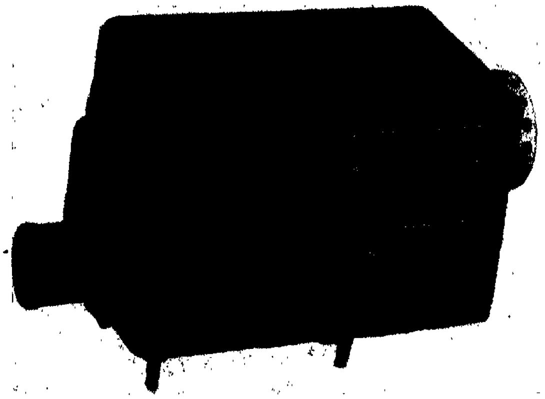

Provision is made for single exposure operation, if desired. Timing and coding lights mark film to facilitate the location of any given sequence or any marked frame without counting. External synchronization pulse circuit is provided, permitting shutter synchronization accurate to 1 msec. Any number of synchronized cameras may be used in a parallel gang.

Some of the more obvious applications of the camera include flight testing, guided missile flight records, fire control system evaluation, and the study of industrial process controls and instrumentation. If a timer is used for taking one frame per minute, 33 hr. may be recorded on one magazine load of film. Price is $950.00, with six weeks' delivery.—Flight Research Engineering Corporation, *P. O. Box 1-F, Richmond, Virginia.*

Electronic Blackboard

For a long time the efficiency of electronic training programs has been hampered by the lack of sufficiently large display of oscilloscope wave forms. The new T-602 projection oscilloscope provides an excellent solution to this problem. Called the "electronic blackboard," it delivers pictures either 18×24 in. on a built-in screen, or 8×10 ft. with an external screen for larger audiences. The great light-gathering power of its Bausch and Lomb $F/1.9$ refractive optical system provides the largest, brightest cathode-ray tube display now commercially available.

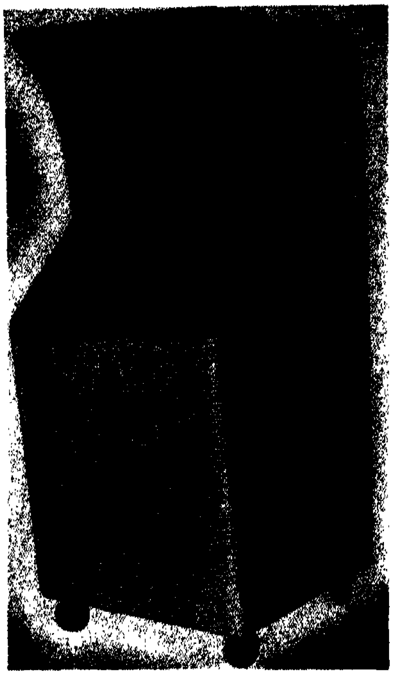

To facilitate the instructor's use, the instrument is housed in an attractive integral assembly. It meets all the performance requirements for high grade general purpose oscilloscope work. Its advanced circuit design and moderate price make it particularly attractive in any application where large screen display of electronic circuit phenomena is needed.

Particular new features such as functional centering controls, improved calibration circuit, driven and recurrent sweeps, line frequency deflection and phasing, as well as novel brightening and Z axis intensity circuits greatly increase the basic usefulness of the T-602. Although essentially a high gain, medium band width unit, it is also available on special order in a wide band version for more involved applications.—Television Equipment Corporation, *238 William Street, New York 7, New York.*

Manufacturers' Literature

Aluminum Products—Booklet contains descriptive information and illustrations of the various forms in which Revere aluminum is fabricated. Also included is a chart with comprehensive tables giving the properties and characteristics of most of the wrought aluminum alloys.—Revere Copper and Brass, Inc., *230 Park Avenue, New York 17, New York.*

Leak Detector—16-page catalog describes the Model 24-101A leak detector for the location and measurement of leaks in evacuated or pressure systems. Examples of both probe and envelope techniques are discussed, and accompanying schematic diagrams show the testing equipment necessary.—Consolidated Engineering Corporation, *620 North Lake Avenue, Pasadena 4, California.*

Leak Detector—Bulletin LD-6 describes typical applications of the Model MS-2 mass spectrometer leak detector. Principle of operation, features, and pertinent data pertaining to vacuum testing and pressure testing with explanatory illustrations are included.—Vacuum-Electronic Engineering Company, *316 37th Street, Brooklyn 32, New York.*

Sound Level Meter—Catalog leaflet describes the Type 410-A sound level meter, a lightweight, pocket-size instrument meeting ASA requirements. Included are specifications and list of accessories, with prices.—Hermon Hosmer Scott, Inc., *385 Putnam Avenue, Cambridge 39, Massachusetts.*

Cathode Press—Vol. 7, No. 1, Winter, 1949–50, 33 pp., contains articles on the first ceramic x-ray tube, a coaxial power triode for higher power at the higher frequencies, new techniques for superficial therapy with beryllium window x-ray tubes, the twenty-four million volt betatron, methods of evaluating x-ray screen quality and performance, and other articles of interest.—MACHLETT LABORATORIES, INC., *Springdale, Connecticut.*

Panalarms—Bulletin 400, 4 pp., describes Series 400 Panalarms, signals for hazardous and corrosive atmospheres. White and red lights are dim in normal operation; bright when off-normal. Sound signals may also be included.—PANALARM PRODUCTS, INC., *7216 North Clark Street, Chicago 26, Illinois.*

Selenium Rectifiers—4-page pamphlet on design, application, and servicing of selenium rectifiers, information on trouble-shooting methods for the half-wave circuit, and rectifier repair and replacement technique.—RADIO RECEPTOR COMPANY, INC., SELETRON DIVISION, *251 West 19th Street, New York 11, New York.*

Experimenter—Vol. XXIV, No. 8, January, 1950, features a simple, complete coaxial measuring equipment for the u.h.f. range, and includes description of equipment for standing-wave measurements, for power measurements, for voltage measurements; fixed-line and adjustable-line elements; terminations; attenuators; filters; external coupling elements; and foundation elements.—GENERAL RADIO COMPANY, *275 Massachusetts Avenue, Cambridge 39, Massachusetts.*

Optical Bench Assembly—Bulletin 174–50, 4 pp., describes and illustrates the Model L360N precision optical bench assembly, consisting of a collimating system with light source, targets and filters, a nodal slide, and a viewing microscope, all mounted on a lathe bed type bench.—THE GAERTNER SCIENTIFIC CORPORATION, *1201 Wrightwood Avenue, Chicago 14, Illinois.*

Coordinate Comparator—Bulletin 181–49 describes and illustrates the M1225–37 coordinate comparator, for measuring star photographs, spectrograms, x-ray plates, charged particle tracks, and any similar records made on $3\frac{1}{4}\times4\frac{1}{4}$-in. photographic plates.—THE GAERTNER SCIENTIFIC CORPORATION, *1201 Wrightwood Avenue, Chicago 14, Illinois.*

Tracerlab—Catalog B, 100 pp., illustrated, presents the complete line of Tracerlab instruments. Included are applications, specifications, and prices on scalers and scaler accessories, preamplifier and tube accessories, counting rate and survey meters, Geiger-Müller tubes, radioactive reference sources, general equipment, lead shields, dosage meters, industrial instruments, etc.—TRACERLAB, INC., *130 High Street, Boston 10, Massachusetts.*

Polarographic Literature—Leeds and Northrup Bibliography of Polarographic Literature [Bibliography E-90(1) 1950] is an up-to-date listing of all available literature on the polarographic method of chemical analysis. Listed are a total of 2208 references, by 1310 authors, on 903 principal subjects. Articles are listed in chronological order, from the earliest associated work in 1903 up to the middle of 1949. All references are cross-indexed alphabetically by authors and by subjects.—LEEDS AND NORTHRUP COMPANY, *4934 Stenton Avenue, Philadelphia 44, Pennsylvania.*

Pressure Transducers—4-page temporary catalog, December, 1949, describes various types of transducers, including information on ranges and resistances, and prices.—STATHAM LABORATORIES, *9328 Santa Monica Boulevard, Beverly Hills, California.*

Spectrographic Outfits—Catalog H-1, on Hilger equipment, discusses the process of spectrochemical analysis and some of the advantages of prism instruments. Complete technical data are given for each instrument. Applications for each type instrument are indicated.—JARRELL-ASH COMPANY, *165 Newbury Street, Boston 16, Massachusetts.*

Instrumentation—Vol. 4, No. 3, 32 pp., fully illustrated, contains articles concerning measurement and control of industrial processes.—MINNEAPOLIS-HONEYWELL REGULATOR COMPANY, BROWN INSTRUMENT DIVISION, *Wayne and Windrim Avenues, Philadelphia 44, Pennsylvania.*

Oscillograph—Bulletin B-641-A describes the construction and performance of a Duddell-type oscillograph employing an oil-damped bifilar suspension required to operate at frequencies up to 1000 c.p.s.—MUIRHEAD AND COMPANY, LTD., *Beckenham, Kent, England.*

New Materials

Forest K. Harris: Associate Editor
in Charge of this Section
National Bureau of Standards, Washington, D. C.

Electrosensitive Recording Paper

Alfax is an electrosensitive paper for permanent, instantaneous recording at high speeds. Papers are available in three types. Type A is the most sensitive high speed paper. It records a sepia brown trace on a white background and is being used at speeds up to 18,000 in. per min. Types OO and NO record a black trace on a white background and are used at writing speeds up to 700 in. per min. Paper impedance varies from approximately 500 ohms at low writing speeds to 200 ohms at the highest writing speeds. The power required to mark the paper depends on the writing speed and the density required in the mark. At low speeds a current of a few milliamperes will produce a legible trace. At 28 sq. in. of area per min. 2–3 watts at 20–30 volts will produce dense solid areas, while at a speed of 180 sq. in. per min. 25–30 watts may be required for solid dense recording. The paper may be used with conventional recorders using a positive stylus or roller on the paper and a negative metal platen or edge under it. Inertialess recording is obtained by using a helix type of recorder. A cylindrical drum with a raised spiral turn forms the negative electrode. The paper passes between this helix and a narrow-edged strip of metal used as a positive electrode. Current passing from this strip through the paper to the helix marks the paper with a small spot. The helical drum can be driven synchronously or through a servo mechanism where scanned information is to be recorded. The system is thus available for copying or for facsimile recording as well as for the recording of any phenomenon which can be translated into an electrical impulse. Experimental rolls are available from the manufacturer for one dollar, or paper of special sizes and characteristics can be made.—ALFAX PAPER AND ENGINEERING COMPANY, *40 Riverside Avenue, Brockton, Massachusetts.*

Molybdenum Lubricant

Molybdenum has been used in recent years either in place of or supplementing regular oils and greases in the lubrication of high speed, high temperature, high pressure bearings. It is an extremely "greasy" metal, is practically indestructible at high temperatures, and in certain forms has the property of "plating out" on a friction surface to form a friction-supporting film which cannot be "squeezed out" by pressure. Thus the bearing is protected against scoring or seizing even after all the oil has been burned out.

Liqui-Moly is a molybdenum-based lubricant designed for use in any conventional lubrication system. It can be used alone or added to crank-case or other oils which carry it to the friction surface where it "plates out" forming a permanent low friction coating. Tests reported by the manufacturer show that friction surfaces running at high speed under heavy pressure will heat from 300 to 500 percent faster with ordinary lubricating oil than when running dry with Liqui-Moly, and moreover that the temperature-rise with oil is continuous until failure and seizure, whereas with Liqui-Moly it reaches a stable point and then recedes. This material has high chemical stability and is unchanged in its properties by extreme temperatures, operating effectively from sub-zero to red-heat. Typical applications, in addition to conventional uses, are the lubrication of deep-drawing dies; elimination of "run-in" time on precision bearings and slides; as a pipe-fitting compound, to insure quick disassembly regardless of age, heat, or corrosion; reduction of friction and seizure in press-fitting; to prevent sticking in tightly wound flat coil springs; as a lubricant for guns; and in the permanent factory-lubrication of products. It is available in experimental quantities direct from the manufacturer at $2 per pound.—THE LOCKREY COMPANY, LUBRICANTS DIVISION, *College Point 1, New York.*

Silver Storage Battery

Silvercel is an alkaline storage battery using silver and zinc as the active materials. The electrolyte is absorbed into active material so that there is no tendency to leak or spill. There are no plates or separators and resistance to mechanical shock is limited only by the strength of the case which can be selected to meet various requirements. The ampere-hour efficiency is nearly 100 percent and the energy efficiency nearly 85 percent. Heavy discharge does not injure the battery and no fumes are released on either charge or discharge. The battery is stated to compare favorably with all present-day storage batteries on the basis of life, size, weight, and number of recharging cycles. Five sizes are available ranging from a ½-amp.-hr., 1½-v battery in a case 1×½×1½ in. to a 40-amp.-hr., 1½-v battery in a case 4¼×1½×4 in. Larger capacity units are in the development stage.—YARDNEY ELECTRIC CORPORATION, *105 Chambers Street, New York 7, New York.*

Flexible Stainless Tubing

Carpenter No. 20 stainless steel is used in manufacturing a new line of flexible tubing in sizes from 1 to 2½ in. inside diameter, and in various gauges. It is intended for use where flexibility and corrosion resistance are major considerations. Fittings can be welded to it or the ends can be supplied in rigid standard tube sizes for use with flanges.—CARPENTER STEEL COMPANY, *131 Springfield Road, Union, New Jersey.*

Hydrophobic Starch

Dry-Flow is a hydrophobic (water-repellant) derivative of corn starch. It is a finely divided powder with a silky texture, and is free-flowing to such an extent that it behaves like a liquid in many ways. The presence of hydrophobic groups makes it extremely difficult to wet with water under ordinary conditions. It can, however, be wet with water if a wetting agent is used or if the dry material is first wetted with alcohol or other water-miscible solvents. Potential applications listed by the manufacturer include rubber dusting, flatting agent for lacquers, detackifying agent for rubber articles formed by the dip method, antihalation powder for the back of photographic films, prevention of sticking of viscous materials to container walls, lubricating agent, and cosmetic powders.—NATIONAL STARCH PRODUCTS, INCORPORATED, *New York, New York.*

Nylon Thread-Lock Plug

A service is available through which Nylon locking plugs may be fitted to threaded screw-machine parts, or the completed part will be made to specification. The threaded part is drilled through the side in which a small Nylon plug is inserted and secured by upsetting the outer end of the drilled hole. The inner end of the plug extends to the crest of the internal threads. When turned onto a stud or screw the Nylon compresses and causes the nut and stud threads to grip each other. It is not affected by oil or grease, does not age, and can be used repeatedly. A minimum length of ¾ in. is required to allow room for the plug, and the wall thickness of the part should be at least 0.1 in. Steel or aluminum parts are preferable but brass or zinc can be used.—NYLOK CORPORATION, *475 Fifth Avenue, New York 17, New York.*

Silicone Sealing Compound

G-E 81083, a silicone dielectric compound, is a smooth homogeneous mixture designed to provide a chemically stable, waterproof, dielectric seal for aircraft ignition systems and electronic equipment. As a dielectric, it is used to waterproof exposed surfaces on plastics and ceramic insulators. It will wet and adhere to both metallic and non-metallic surfaces, and is non-corrosive and relatively inert chemically. It is substantially unchanged by temperatures from −70 to +450°F, and has good resistance to steam, hot water, and hot air. In appearance and consistency it resembles medium heavy translucent grease. As a dielectric it prevents arcing due to moisture condensation on spark plugs, coils, etc. It is available in 8-oz. tubes, and in 1-, 5-, and 30-gal. containers.—GENERAL ELECTRIC COMPANY, *Pittsfield, Massachusetts.*

Sapphire Gauge Points

A line of contact points with sapphire or carbide tips is available to fit any specified dial indicator. Shapes may also be made to specification. They are characterized by resistance to wear and by a dense surface that will not charge or pick up foreign matter.—PRECISION SUPPLY AND MACHINE COMPANY, *1 East 42nd Street, New York 17, New York.*

Errata

Note on Sealing Nylon Films to Geiger Counters

[Rev. Sci. Inst. 20, 966 (1949)]

ROBERT A. BECKER
Physics Research Laboratory, University of Illinois, Champaign, Illinois

Formation of Insulating Layers by the Thermal Decomposition of Ethyl Silicate

[Rev. Sci. Inst. 20, 958 (1949)]

HAROLD B. LAW
RCA Laboratories, Princeton, New Jersey

BECAUSE of an unfortunate error, the figures of these two Laboratory and Shop Notes were interchanged.

There is also a typographical error in the title of Mr. Becker's article. The word "Nylons" should be "Nylon."

THE
REVIEW OF SCIENTIFIC
INSTRUMENTS

VOLUME 21, NUMBER 4 *APRIL, 1950*

Direct Reading Phasemeter

L. H. O'Neill and J. L. West
Department of Electrical Engineering, Columbia University, New York, New York

(Received August 29, 1949)

This paper describes a simple and accurate method for the measurement of the phase difference between two sinusoidal voltages and an instrument for making the measurement. It is shown that measurement accuracy sufficient for most ordinary purposes can be obtained through the use of very simple circuitry, and that measurement errors can be made arbitrarily small by resorting to more complex circuitry. The instrument is compact and convenient in use.

THE method described in this paper for measuring the difference in phase between two sinusoidal voltages takes advantage of the fact that the amplitude of the sum or difference of two sinusoids of equal amplitude provides a convenient and accurate measure of the magnitude of the phase difference.

Consider two sinusoids having the common amplitude E_0. The amplitudes Σ and Δ of their sum and difference, respectively, are given by:

$$\Sigma = 2E_0 \cos\theta/2 \tag{1}$$

and

$$\Delta = 2E_0 \sin\theta/2, \tag{2}$$

in which θ is the magnitude of the difference in phase between the voltages. It is evident that if the prescribed amplitude E_0 is chosen as that causing a half-scale deflection of a voltmeter used to measure Σ and Δ, an "on scale" reading corresponds to every value of θ. It is therefore possible to establish a scale or scales on the voltmeter expressing either or both of the relationships (1) and (2), and thus obtain a directly read measure of the angle θ. However, because the slopes of the sine and cosine functions are small when their arguments are in the vicinity of 90 and 0 deg., respectively, Eq. (1) yields a scale which is quite compressed when θ is near 0 deg. while Eq. (2) yields a compressed scale for values of θ near 180 deg.

Excessive scale compression can be avoided by restricting the use of the difference method to cases in which θ is between 0 and 90 deg., and the sum method to cases in which θ is between 90 and 180 deg. Since, when this is done, Σ and Δ never exceed $\sqrt{2}E_0$, it is possible, and evidently desirable, to choose E_0 as the voltage causing a meter deflection of $\sqrt{2}/2$ of full scale. Thus, "on scale" readings correspond to all values of θ, and full use of the scale is made.

ELEMENTS OF THE SYSTEM

Evidently, in order to measure phase by the previously described method, it is necessary to provide the following devices: (a) A means of adjusting the amplitudes of the two voltages to the prescribed value E_0. (b) A method of forming the sum and difference of the two sinusoids. (c) A voltmeter provided with the previously described scales and a mark at $\sqrt{2}/2$ of full scale. These devices will be described in the above order. Since it is frequently desired to measure phase difference as a function of frequency, these devices must perform their respective operations accurately over as wide a frequency range as is desired.

(a) Adjustment of Amplitudes to the Prescribed Value

Since E_0 is expressed in terms of a corresponding meter deflection, one of the voltages can be made to yield the required deflection by adjusting the sensitivity

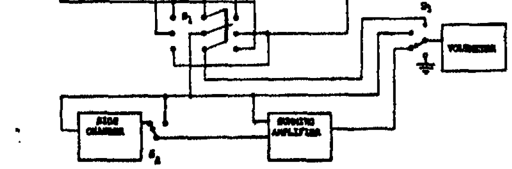

Fig. 1.

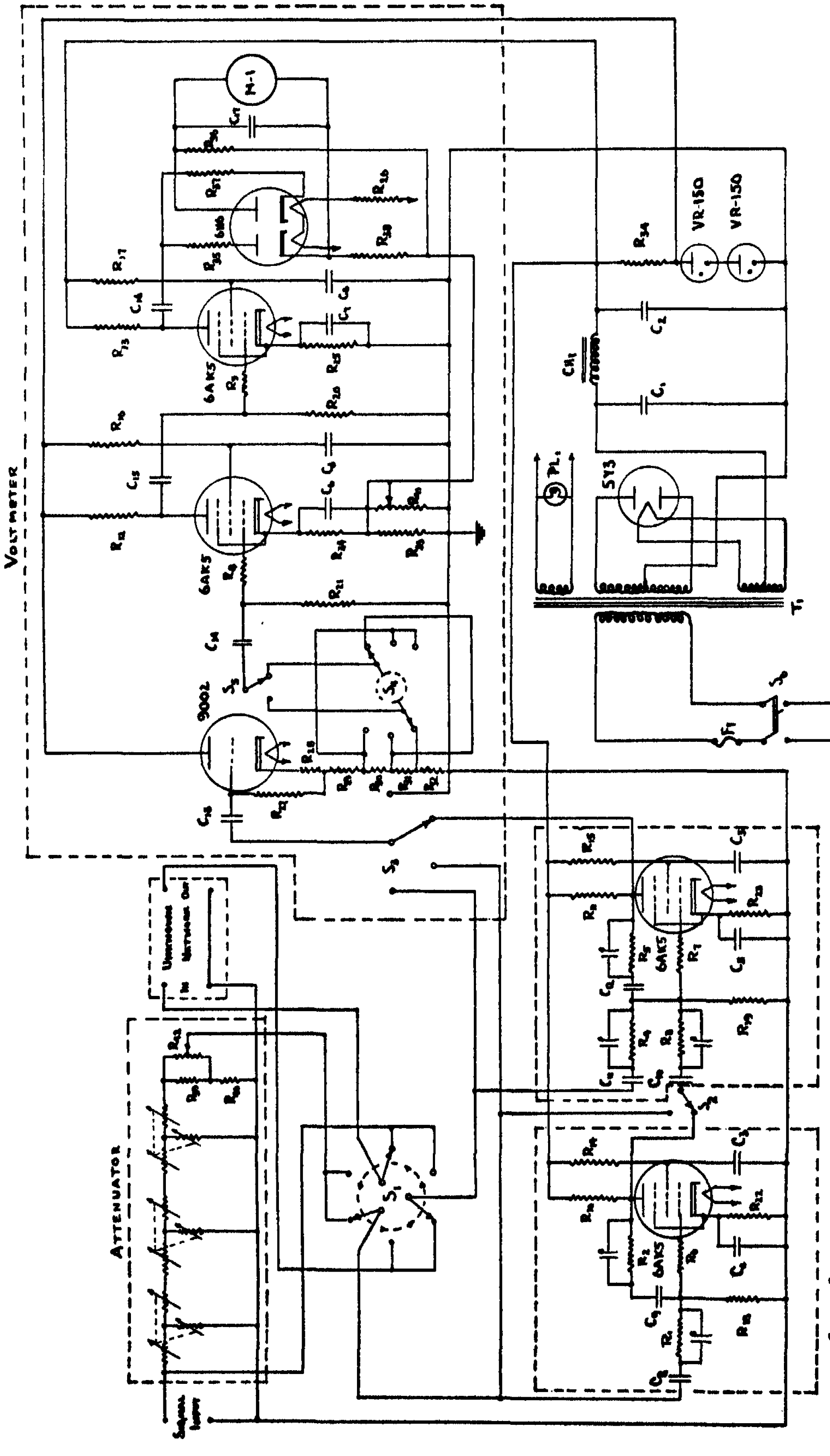

FIG. 2. Gain and Phasemeter.

of the voltmeter used to measure its amplitude. If this operation is performed with respect to the smaller of the two voltages, the larger voltage may be attenuated in a conventional attenuator until it has the required amplitude. The attenuator used for this purpose must be designed to avoid the imposition of significant phase shift upon the sinusoid transmitted through it. Appropriate attenuators for operation over frequency ranges as large as several megacycles are manufactured. The attenuator design problem is not considered here.

(b) Formation of Sum and Difference

Since the sum or difference amplitude is the measure of the phase angle, the formation of the sum or difference must be accomplished accurately in order to avoid appreciable errors in the measurement of θ. This can be accomplished through the use of a "summing amplifier" similar in principle to those used in electronic analog computers.[1] When simple, single stage amplifiers are used for this purpose, it is possible to limit phase measurement errors due to summing and subtraction errors to as little as 0.25 deg. over the frequency range from 7 c.p.s. to 100 k c.p.s. The use of multistage amplifiers makes possible the obtaining of improved accuracy. In general, the only limit on accuracy in this respect is imposed by the degree of complexity in the amplifiers which may be tolerated.

(c) Voltmeter

A voltmeter which has a deflection sensitivity essentially independent of the amplitude of the voltage applied to it has been used in the instrument which will be described. This characteristic is desirable because it avoids the compression of the scale at low amplitudes which sometimes occurs in diode probe-type meters. However, any voltmeter which has a reasonably linear scale and does not become excessively insensitive over the frequency range in which it is desired to make measurements may be used.

THE INSTRUMENT

The block and wiring diagrams of an instrument based upon this method of measuring phase difference are shown in Figs. 1 and 2, respectively. In addition to the elements previously described, the instrument includes a power supply for the purpose of providing the operating voltages for the system, and required switching systems.

The instrument shown in Figs. 1 and 2 is designed to facilitate the measurement of the phase shift through any four-terminal linear system. The instrument may be used with systems having gains greater than or less than unity. The switch *S*-1 interconnects the elements properly for these two cases.

The switch *S*-2 inserts or removes the sign changing amplifier from the system. Thus, either the sum or difference method may be used. The switch *S*-3 is used to connect the voltmeter input terminals to the input and output voltages of the system tested and to the output voltage of the summing amplifier.

The switch *S*-4 is used to adjust the voltmeter sensitivity in decade steps.

The attenuator is for the purpose of adjusting the amplitude of the larger voltage to E_0.

The instrument thus contains all the elements necessary for making the phase measurement. It is compact in form (the entire system being mounted in a 10×12-in. chassis) and has been found to be convenient in use. The over-all obtained accuracy is plus or minus one degree over the frequency range from 7 c.p.s. to 100 k c.p.s. Most of the error is imposed by the attenuator. Improved accuracy can be obtained through the use of a wider band attenuator and multistage summing and sign changing amplifiers.

As shown, the instrument measures only the magnitude of the phase difference. A simple resistance-capacitance circuit may be cascaded with the system tested to obtain an additional phase shift of known sign. The sign of the system phase shift may be determined by observing whether θ increases or decreases when such a network is inserted.

---

[1] Ragazzini, Randall, and Russell, "Analysis of problems in dynamics by electronic circuits," Proc. I.R.E. 35, 444–453 (May, 1947).

An Electron Tube Potentiometer Method for Use in Circuits Involving Very High Resistance

H. Bloom and G. W. Butler
Chemistry Department, Auckland University College, Auckland, New Zealand

(Received July 15, 1949)

The construction and use of an electron tube potentiometer designed for circuits involving high resistances to the order of 100 megohms are described.

IN the investigation of electrokinetic potentials of systems involving organic liquids, by the streaming potential method (see Briggs,[1] Bull,[2] Bull and Gortner[3]) it is necessary to measure potentials of the order of 10 to 2000 millivolts, the resistance of the streaming cell being often as high as 100 megohms. As the electrodes are easily polarized thus leading to spurious results, no d.c. must flow during the measurements. The circuit described below and shown diagrammatically in Fig. 1 was devised to replace the commonly used quadrant electrometer, and *p*H meter as null-point detecting instruments in the usual Poggendorf compensation method for measuring potential.

The principle of the method is similar to that of Kreielsheimer[4] and Macnamara[5] who used a pair of tubes (with identical grid voltage—plate current characteristics) operated in push-pull as null-point detecting instruments for a Wheatstone's bridge network used for measuring impedances. In the present circuit, the arrangement shown in the figure is utilized for the measurement of potential in a Poggendorf compensation circuit.

The tubes T_1 and T_2 have a galvanometer G connected across their load resistors $R_1-R_2-R_3$ to detect differences in the plate currents. The negative side of the potentials to be balanced (one from the streaming cell and the counter-potential from the Leeds and Northrup measuring potentiometer) are connected to the respective grids, the positive ends being earthed. If the potentials are not equal, the two grids will be at different potentials to ground with the result that the plate current is different for each tube provided that the tubes used have equal characteristics. As the potential drop across each load resistor will then be different, the galvanometer will register a deflection. When the voltage applied from the measuring potentiometer is adjusted to be equal to that of the streaming cell, both grids will be at the same potential and the galvanometer will show no deflection. The reading of the measuring potentiometer will then give the value of the potential drop across the streaming cell under the conditions of balance. The operation of the potentiometer is not affected by the introduction of large resistances into one or the other of the grid circuits, even with resistances as high as 100 megohms. On using the apparatus for the measurement of electrokinetic potentials in systems involving non-polar liquids, constant and reproducible results were obtained showing that there was no polarization of the electrodes and hence no passage of grid current during the measurements.

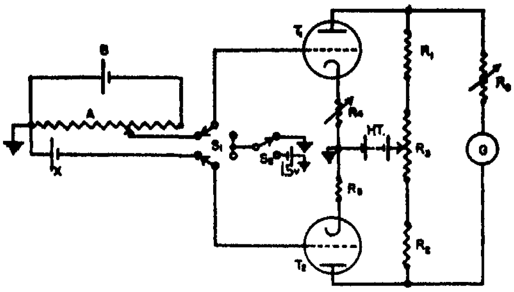

Fig. 1. S_1 = D.P.D.T. switch; S_2 = S.P.D.T. switch; $R_1=R_2$ = 10,000 ohms; R_3 = 2000-ohm radio potentiometer; R_4 = 1200 ohms (variable); R_5 = 1000 ohms; R_6 = 250,000 ohms (variable); A = Leeds and Northrup measuring potentiometer; B = accumulator (2-volt); X = streaming cell; T_1, T_2 = RCA tubes, type 955; G = medium sensitivity galvanometer.

To use this circuit as a potentiometer in measurements involving very high resistances, extremely good insulation is necessary. Hence all-glass tubes, RCA Type 955 (Acorn) triodes having the necessary high transconductance and electrical insulation were used, the circuit being built up on a paraffin-wax block. Tubes with identical grid voltage-plate current characteristics are desirable, but in practice those with closely similar characteristics can be used by adjusting cathode and load resistors (R_4 and R_3) alternatively until their characteristics coincide over the range in which the measurements are to be made (in this case 0–1500 millivolts). To enable such adjustment and streaming potential measurements to be made alternatively, use is made of the switches S_1 and S_2. The grids are disconnected from the potentiometer circuit and connected together by means of S_1. R_3 and R_4 are adjusted so that there is no deflection of the galvanometer when the two grids are connected by means of S_2 directly to earth or to the negative pole of a 1.5 volt battery, the positive pole of which is earthed. Provided that the grid voltage-plate current characteristics of the two tubes are sufficiently similar (or preferably identical), these tubes will now be operating on the same grid voltage-plate current characteristic over the desired range. This was checked experimentally by the following tests:

---

[1] D. R. Briggs, J. Phys. Chem. 32, 641 (1928).
[2] H. R. Bull, J. Am. Chem. Soc. 57, 259 (1935).
[3] H. R. Bull and R. A. Gortner, J. Phys. Chem. 35, 309 (1931).
[4] K. S. Kreielsheimer, Ann. d. Physik 5, 293 (1933).
[5] Macnamara, Rev. Sci. Inst. 2, 343 (1931).

(1) A number of stable potentials from 0 to 1.5 volts (from a Leeds and Northrup potentiometer with low internal resistance) were measured using the apparatus described.

(2) The results were compared with those obtained by using a contentional Poggendorf compensation potentiometer with a galvanometer as null-point detector. These sets of results then agree to within 0.1 millivolt over the entire range. The initial adjustment of the two tubes to be on the same plate current-grid voltage characteristic was carried out by trial and error, the process being fairly lengthy, but once a satisfactory adjustment had been made for a given pair of tubes, it was necessary only to adjust R_4 before all subsequent measurements. This could be carried out rapidly.

S_1 is then moved so as to break the connection between the grids and connect them into the potentiometer circuit. A regulated voltage power supply (250-volt) was used for the high tension. The filament supply was 5.5 volts d.c. supplied from lead accumulators (with voltage divider). This suppply was found to be perfectly satisfactory for stable operation.

The higher the transconductance of the tubes the greater will be the sensitivity of the detector. With 955 tubes (transconductance approx. 2000 micromhos), potential measurements could be made to 0.1 millivolt, but as this accuracy was not required a series variable resistance R_6 was included in the galvanometer circuit. It was adjusted to decrease sensitivity so that the potential of the streaming cell could be measured to within 0.5 millivolt.

The main advantages of this electron tube electrometer over others (e.g. quadrant electrometer, tube *p*H meter) commonly used are:.

1. Ease and rapidity of operation.
2. Much higher stability. No measurable drift of the galvanometer could be detected during 1 or 2 hours and only a slight drift during a day.
3. Higher sensitivity.

The authors wish to express their appreciation for the advice and encouragement received from Dr. K. Kreielsheimer of the Physics Department, Auckland University College.

THE REVIEW OF SCIENTIFIC INSTRUMENTS VOLUME 21, NUMBER 4 APRIL, 1950

A Method for Increasing the Safe Power Input of X-Ray Tubes

ARTHUR I. BERMAN*
Stanford University, California

(Received September 26, 1949)

A method for cooling x-ray tubes was devised, based on the principle of relative motion between the target and focal spot. The electron beam is deflected by a rotating magnetic field so that the focal spot moves in a circle upon the target face. Simultaneously, the tube itself is gyrated (without rotation about its axis) so that any point on the target describes an equal circle. The two rotations are equal in frequency but phased 180 degrees from each other. Thus the focal spot remains stationary in laboratory space. The advantages are (1) it is adaptable to most x-ray tubes with target face perpendicular to the tube axis, and target diameter twice that of the longest focal spot dimension, without any modification of tube design; (2) it combines the benefits of a rotating target, water-cooled target, and line focus without the need for rotating joints or vacuum connections. Tubes, operating continuously for hours at a time at a gyrating frequency of 6 r.p.s. have been cooled successfully by this method without observable shifting of the focal spot in laboratory space.

I. INTRODUCTION

A. Limitation on Power Input

THE fact that only about 1 percent of the kinetic energy of the electron beam evolves as x-radiation and the remaining energy is present as heat makes it imperative that an adequate cooling mechanism be incorporated in the operation of the tube. The efficiency of this cooling device will set an upper limit to the anode voltage and current permitted.

If the temperature of the target material is allowed to exceed its melting point, not only will the target be permanently damaged but even more serious consequences may arise. The metallic vapor atoms may become ionized through collision with the electron beam and change the tube resistance inducing erratic tube behavior. In addition, the metallic vapor may deposit on the glass walls, absorb x-rays, and provide a conducting path between the cathode and target. High temperatures may drive gas from the tube wall, or even crack the glass if heated non-uniformly.

B. Cooling by Radiation and Conduction

The simplest method for removing heat from the focal spot is by direct radiation into the air from the

---

* Now at the Los Alamos Scientific Laboratory, Los Alamos, New Mexico.

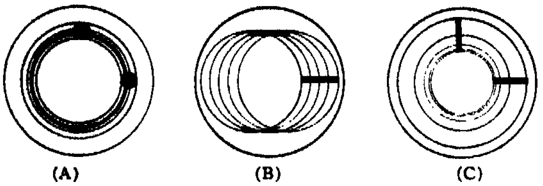

FIG. 1. (A) Path of circular focal spot on surface of gyrating or rotating target. (B) Path of rectangular focal spot on surface of gyrating target. (C) Path of rectangular focal spot on surface of rotating target. (Hottest regions shown by closest spacing of lines.)

spot and the surrounding target. Also, the heat may be conducted down the body of the anode, stored in a mass of large heat capacity, and radiated at the end of the tube.

If the tube is designed for continuous operation, the heat may be conducted from the target directly to a moving current of water. Oil is often used because of its insulating properties despite its much lower specific heat and thermal conductivity.

C. Cooling by Target Motion

By permitting an element of target material to be periodically rather than continuously irradiated, the focal spot energy is, in principle, distributed over a much larger area. This provides much more effective radiation and conduction cooling. The method was suggested as early as 1897 by Wood, and in 1914 Thomson developed a tube in which the target rotated by means of an electric motor. Coolidge and Bouwers both have built tubes of this type,[1] and they now have come into wide commercial use after difficulties in lubricating the internal bearings were surmounted. In 1931 Müller succeeded in combining water cooling with target rotation using a drive shaft passing through a special stuffing box and evacuating continuously with pumps.[2] This feat has been accomplished also by Fournier, Gondet, and Mathieu at speeds of 3 or 4 revolutions per second using a "well-greased ground conical joint."[3] Coolidge eliminated the need for internal bearings by rotating the entire tube and bending the electron beam with a constant magnetic field.[1]

A line (Benson) focus is often used to increase the effective x-ray output for a given apparent focal spot area seen by the observer. The principle is that when viewed from the side (at a grazing angle 15° or more), the projected spot will radiate about as much energy as when viewed normal to the surface. This is in direct opposition to the Lambert law of thermal radiation by which the energy would decrease by the cosine of the angle between the direction of propagation and the normal to the surface.

The rotating target tube will permit the use of this fact if the long dimension of the focal spot is set along a target radius (see Fig. 1(C)). A focal spot set in a sector of the target circle would be most efficient in minimizing local heating. The Coolidge rotating tube may use the line focus provided the target is designed in the form of a cone so that the electron beam, falling on one side, will produce an elliptical spot projected as a circle when viewed at the proper angle during rotation. This tube would require an x-ray window which extends around its girth. The filament current would be supplied by means of slip rings.

DuMond and Youtz achieved the same result as rotation by gyrating the target in a circular path (without rotation).[4] This tube, designed for continuous operation, was water-cooled. The motion was transmitted through a metal bellows. Circular symmetry is required in the focal spot for maximum cooling efficiency since a non-symmetric spot will produce local hot areas as the spot sweeps through its long dimension on the target face.

II. A NEW METHOD

A. Theory

In the writer's method the tube itself is gyrated without rotation so that a point on the target describes a small circle. Simultaneously, the electron beam is deflected by a rotating magnetic field so that the focal spot rotates in synchronism with, but phased 180 degrees from, the mechanical gyration. The strength of the field is adjusted until the circle which the focal spot traces on the target face equals the target circle. Thus the focal spot remains stationary in laboratory space while rotating on the face of the target.

It may be mentioned that the danger of tube breakage while undergoing the gyrating motion is very slight. Thin-walled glass tubes fifteen inches long have been gyrated at one end with an amplitude of one-half inch at six revolutions per second with no visible sign of strain. Actually it can easily be seen that the radial centripetal force encountered by the tube at this speed and amplitude is less than one times its weight.

It is not necessary that the x-ray window extend around the girth of the tube, but merely be somewhat larger than necessary for stationary operation. This necessity might be avoided by gyrating the tube in such a manner that the window remains in the line of sight.

B. Efficiency

The ratio of the safe power input while moving, W_m, to the power input permitted in normal stationary tube operation, W_s, is a function of the speed of rotation, the ratio of the duration of the heated part of the thermal cycle to the period of the entire cycle (approximately the focal spot diameter, for a circular spot, divided by the circumference of its path over the target face) which we call r, and specific target constants.

---

[1] W. D. Coolidge, Gen. Elec. Rev. 33, 612 (1930).

[2] A. Müller, Brit. J. Radiology 4, 127 (1931).

[3] Fournier, Gondet, and Mathieu, J. de phys. et rad. 8, 160 (1937).

[4] J. M. DuMond and J. P. Youtz, Rev. Sci. Inst. 8, 291 (1937).

These constants are: target thickness from face to fluid, d, specific heat of the target material, σ, conductivity, c, and the target density, ρ. Curves showing W_m/W_s for a circular spot, as a function of a variable called

$$\theta^2\left(=\frac{\pi d^2\rho\sigma}{c}\times\text{r.p.s.}\right)$$

for different values of r have been computed by DuMond, Watson, and Hicks and are reproduced in Fig. 2.[5] All the curves equal the value $1/r$ in the limit of infinite tube velocity.

It is obvious that the tube should be gyrated at high speed to increase the efficiency since, by decreasing the time increment during which each element is irradiated we tend, in effect, to distribute the focal spot energy in an annular ring.

C. Desirable Tube Characteristics

As in the DuMond and Youtz gyrating target tube, the focal spot should have circular symmetry to prevent local heating. A drive which permits the use of a line focus is discussed in Section IIIB.

It is desirable that the interelectrode spacing be at least 1 cm. The target diameter should be at least twice as large as the focal spot, and it should be cut perpendicular to the tube axis. To see this, the dependence of the magnetic field strength on the interelectrode distance for a desired deflection and anode voltage will be discussed below.

The following assumptions are made: (1) Space charge is absent, or at any point in interelectrode space the potential difference between the point and the filament is proportional to the axial distance to the filament. (2) The initial velocity of the electron beam is negligible. (3) The magnetic field at any moment is uniform throughout the interelectrode region. (4) The force on the electron beam by the magnetic field is perpendicular to the tube axis since the deflecting angle is small. (5) Relativistic effects are negligible.

Reference is made to Fig. 3. The equation of motion of an electron acted upon by a magnetic induction of strength B is (in m.k.s. units):

$$\ddot{y}=\frac{d}{dt}\left(\frac{dy}{dt}\right)=B\frac{e}{m}v_x,$$

where x is measured along the axial direction, y is the displacement of the beam in the direction $-(\hat{x}\times\bar{B})$, and e/m is the charge to mass ratio of an electron.

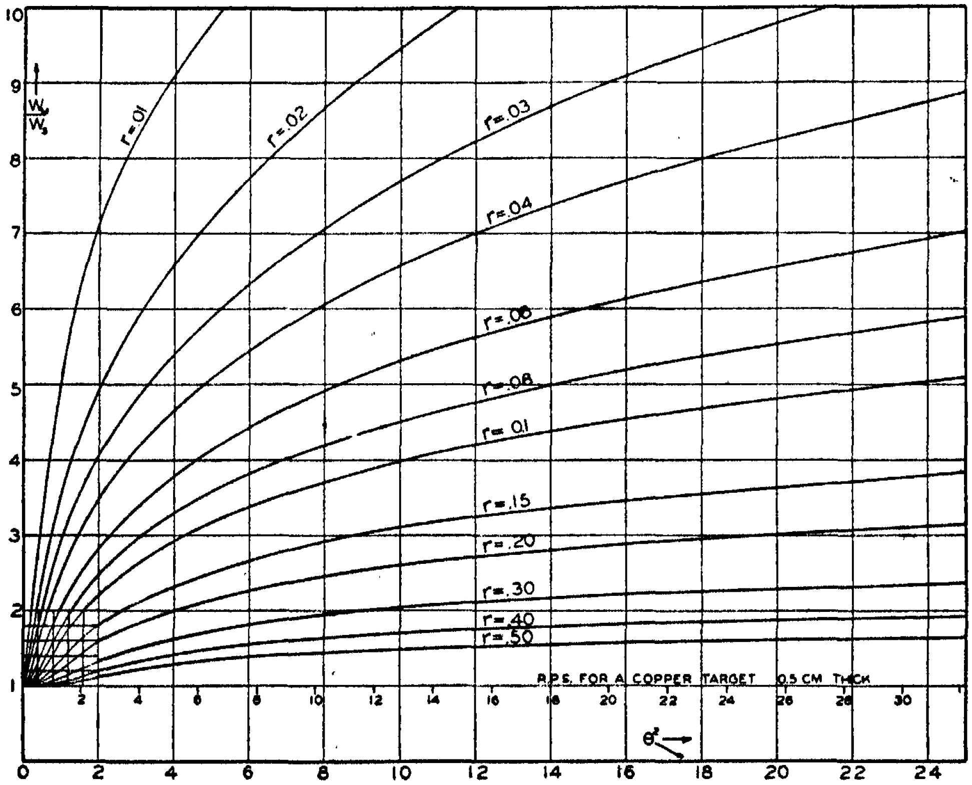

FIG. 2. Multiplication of permissible power input by virtue of tube gyration for different speeds, θ^2 = const. ×r.p.s., and for different sizes of focal spot relative to path swept out (r). (Reproduced from Rev. Sci. Inst. 6, 191 (1935).)

---

[5] DuMond, Watson, and Hicks, Rev. Sci. Inst. 6, 183 (1935).

We write:

$$\frac{d}{dt}\left\{v_x\frac{dy}{dx}\right\}=B\frac{e}{m}\frac{dx}{dt},$$

where $v_x\equiv dx/dt$ is the component of electron velocity along the x axis. The differential equation becomes

$$d\{v_x(dy/dx)\}=B(e/m)dx.$$

Since the potential difference between a point at distance x and the filament, $V=k_1x$, and since $eV=\frac{1}{2}mv_x^2$, therefore $v_x=k_2x^{\frac{1}{2}}$, where k_1 and k_2 are constants.

The solution of the differential equation is, after substituting for v_x,

$$k_2x^{\frac{1}{2}}(dy/dx)=B(e/m)x+k_3.$$

k_3, the constant of integration is found to be zero on substituting initial conditions. Solving between limits:

$$\int_0^D dy=\frac{B}{k_2}\frac{e}{m}\int_0^s x^{\frac{1}{2}}dx.$$

D, the deflection of the electron beam at the target, is therefore

$$D=\frac{2}{3}\frac{Be}{k_2m}s^{\frac{3}{2}}.$$

k_2 is found by noting:

$$v_{x=s}=\{(2e/m)V_p\}^{\frac{1}{2}}=k_2s^{\frac{1}{2}},$$

where V_p is the target to filament voltage and s is the interelectrode spacing. Therefore

$$k_2=\{(2e/sm)V_p\}^{\frac{1}{2}}.$$

Inserting this result for k_2, we obtain the magnetic induction necessary to produce the deflection D:

$$B=\frac{3}{2}\frac{D}{s^2}\left\{2\frac{m}{e}V_p\right\}^{\frac{1}{2}}$$

or

$$B=5.05(D/s^2)(V_p)^{\frac{1}{2}}\times10^{-4}\text{ weber/meter,}^2$$

where V_p is in volts and D and s are in centimeters.

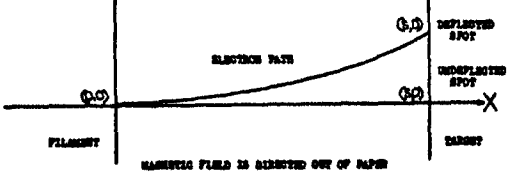

FIG. 3. Path of electron beam from filament to target under a uniform magnetic field directed out of paper.

As an example, if the tube potential is 40 kilovolts and interelectrode spacing is 3 centimeters, the magnetic induction required to deflect the beam 0.5 centimeter is 56×10^{-4} weber/meter^2 (or 56 gauss).

The relativistic derivation begins with the equation of motion

$$F_y=(d/dt)(mv_y)=Bev_x,$$

where

$$m=m_0\{1-[v_x/c]^2\}^{-\frac{1}{2}}$$

(m_0 is electron's rest mass and c is velocity of light). The result obtained differs from the non-relativistic derivation above by less than 3 percent for plate voltages as high as 100 kilovolts so the simpler expression may be accurate enough for most purposes.

Since the beam deflection is a function of the interelectrode spacing, this distance should be constant for all deflections, requiring the target face to be perpendicular to the tube axis.

To minimize the magnetic field strength required for a given deflection and tube voltage, the interelectrode spacing should be as large as possible, as indicated above.

D. Design of the Apparatus

A photograph of the experimental apparatus is shown in Fig. 4. The rotating field is supplied by a toroid surrounding the tube at the interelectrode space. The toroid, one foot in diameter, is divided into 12 segments of 250 turns each, around a core of transformer iron strips. A magnetic induction of 0.01 weber/meter^2 is produced in the center with a current of 8 amp. fed across opposite ends of the toroid (4 amp. through each half). The field is perpendicular to the axis and directed along the line connecting the points at which the current is applied. A smaller coil would, of course, produce a greater field strength at the center.

To gyrate the tube, a d.c. motor whose speed may be varied is used. A hard rubber insulating shaft is connected, through a universal joint, to a disk upon which a self-aligning ball bearing is set. A clamp connects the bearing to the anode. The filament end of the tube is held by a light socket connected to a coil spring which permits free swivel motion and allows for tube expansion. During the entire operation, the target is water-cooled through the hoses shown.

Each of the twelve toroid divisions leads to a segment of a twelve-part stationary commutator which surrounds the motor shaft. The current is fed across opposite commutator segments, and thence across opposite toroid segments, by means of two opposing carbon brushes rotating with the motor shaft and fed from the 120 volt d.c. supply by slip rings and stationary brushes. Sparking is removed with condenser-resistor circuits, not shown, connected across the segments. As successive segments receive current, the field rotates in synchronism with the gyration.

FIG. 4. Experimental model of the tube gyration apparatus.

III. RESULTS AND FUTURE POSSIBILITIES

A. Results

Figure 5 is a pinhole photograph (adjusted to show the view normal to the target face) of (A) focal spot in normal stationary operation, (B) gyrating focal spot without compensating magnetic field, (C) gyrating focal spot with compensating field. The tube is continuously operated and water-cooled. The target to filament voltage is 50 kilovolts, the magnetic induction is 16×10^{-4} weber/meter^2, the deflection of the 0.49 cm diameter focal spot is 0.36 cm, and the interelectrode spacing is 4.8 cm. The gyrating frequency is 6 revolutions per second, and the tube is an old type thin-walled molybdenum target Coolidge tube.

By extrapolating the curves of Fig. 2, it can be seen that if the target were large enough so that the deflection could be increased by a factor of say 5, and the tube designed with say a 1 mm focal spot, then the ratio of permissible power input when moving, to that when stationary is 20 to 25 times.

B. Line Focus

The line focus target may be cooled efficiently by this tube gyration method by driving the tube at an angular velocity which varies during the cycle. Thus, if the length of the focal spot is four times its width (so that at 15 degrees grazing angle the spot appears square), it should be moving four times as fast during the horizontal part of its path than during the vertical part. The path is shown in Fig. 1(B). This motion could be realized with elliptical gears. If the major axis is twice the minor axis, a constant velocity drive on one would transmit the required angular velocity to the other.

C. Slant Anode Tube

The two problems which must be solved in applying the tube gyration method to non-right angled tubes are: (1) non-symmetric deflection of the beam during the cycle, (2) defocusing of the beam as its length is varied during the cycle. The first problem could be solved by varying the toroid current and hence the magnitude of the field strength during the cycle with suitable resistors in the toroid circuit having different values when carrying current in one direction than in the other. The focusing problem may not be too serious for in general the size of the spot will not change appreciably during the cycle even though its outline may be blurred slightly.

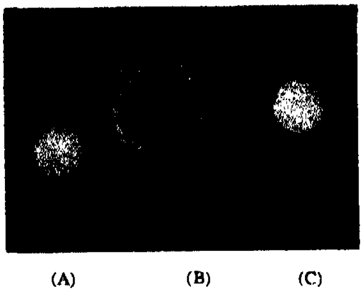

FIG. 5. Pinhole photographs of the focal spot of a water-cooled continuously operated x-ray tube. (A) Focal spot with tube in normal stationary operation. (B) Focal spot gyrating with target at 6 r.p.s. but without compensating magnetic field. (C) Focal spot gyrating with target at 6 r.p.s. and compensated with rotating magnetic field. Exposure was one minute for each picture at 50 kilovolts and 20 milliamp.

D. Application to Radiography and X-Ray Microscopy

The observation of detail in radiographs depends directly upon the minuteness of the focal spot. The concentration of energy upon a small region of the target necessitates low power input resulting in difficulties in photographic and fluoroscopic observation unless means for removing the heat rapidly are applied.

The inchoate field of x-ray microscopy begun at Stanford by P. H. Kirkpatrick requires an intense point source of x-rays at the focus of a condensing and objective lens system for high resolution microscopic analysis.[6] The tube used could be continuously operating and cooled by both water and tube gyration.

ACKNOWLEDGMENT

The writer wishes to thank Professor Paul H. Kirkpatrick for the very valuable aid given him in the successful completion of this project. His many helpful suggestions are sincerely appreciated.

---

[6] P. H. Kirkpatrick and A. V. Baez, J. Opt. Soc. Am. 38, 766 (1948).

THE REVIEW OF SCIENTIFIC INSTRUMENTS VOLUME 21, NUMBER 4 APRIL, 1950

RaDEF Standard Sources for Beta-Disintegration Rate Determinations

THEODORE B. NOVEY
Argonne National Laboratory, Chicago, Illinois

(Received October 17, 1949)

The preparation and use of calibrated RaDEF equilibrium sources for absolute beta-counting is described. The sources are essentially weightless and are mounted on a thin backing to reduce self-absorption and back-scattering correction problems. Calibration was done by determination of the alpha-disintegration rate of RaF in a parallel plate alpha-ionization chamber. No secondary standards are required and the sources can be recalibrated at any time.

As an example of the application of such standards, details of the calibration of a P^{32} solution distributed by the Bureau of Standards for intercalibration in February 1949 are given. The final result is 88.8 mrd/ml at 8 A.M.C.D.T. March 1, 1949. The precision of the measurement is 0.3 percent. The accuracy is estimated to be 1–2 percent.

I. INTRODUCTION

FOR most work with beta-active radioelements there is no need for an absolute measure of the number of radioactive nuclei. Relative activity measurements are sufficient. For a few fundamental measurements, however, some of the best methods depend upon a measurement of the disintegration rate of a source. Examples are the determination of neutron absorption cross sections by the activation method,[1] the determination of neutron flux by the activation of gold,[2] the determination of fission product yields,[3] and the determination of radioactive decay constants.[4]

Absolute activity measurements can be made fairly readily with an accuracy of ten or twenty percent; however, when it is desired to carry the determinations to one or two percent accuracy many difficult problems arise, mainly problems of correction for absorption and scattering of the radiation.

This paper describes the preparation and use of a RaDEF equilibrium standard which is readily recalibrated and is mounted so as to minimize the absorption and scattering correction and thus the uncertainty in the result.

II. BASIS FOR RaDEF STANDARD SOURCE

The usefulness of the RaDEF equilibrium,

$$\mathrm{RaD}\xrightarrow[22-y]{\text{soft }\beta}\mathrm{RaE}\xrightarrow[5.0-d]{\text{hard }\beta}\mathrm{RaF}\xrightarrow[138.4-d]{\alpha}\mathrm{Pb}^{206},$$

for beta-activity measurements depends upon the fact that alpha-disintegration rates can be determined quite accurately through the use of parallel plate alpha-counters which basically have a counting geometry of 2π or "fifty percent." From the alpha-activity of the source the beta-activity can be calculated. This has been done in several ways. (1) A pure RaD source is prepared and from the rate of growth of alpha-activity the beta-disintegration rate is calculated.[5] (2) A pure RaE source is prepared and the beta-disintegration rate calculated at any time from the alpha-activity growth curve.[6] (3) RaD and stable lead are electrolytically deposited from a standard pitchblende sample and the resultant equilibrium RaE activity is calculated from a knowledge of the radium content of the ore. This method was used by the Bureau of Standards in preparing beta-standards. It was subsequently found[7] that the unavoidable weight (*ca.* 1 mg) of stable lead in the source caused an eight percent error in activity determinations using the sources due to scattering.

The method chosen for this work was to prepare the sources from a solution of RaDEF in transient equilibrium decaying with the RaD half-life of 22 years. The RaF alpha- and RaE beta-activities are in the ratio of $T_1/(T_1-T_2)$ or 1.0175 and the standard sources may be checked for recalibration at any time by alpha-counting. The activity decays at a rate of 3.2 percent per year.

III. PREPARATION OF STANDARDS

For the comparison of sources of different radioactive nuclides it has been found desirable to use "weightless" sources mounted on very thin backing. In this way large back-scattering, self-scattering and self-absorption corrections are avoided.[8] This is necessary due to the uncertainties of ten or twenty percent associated with these corrections. "Weightless" in this case means a weight of material that will cause an absorption effect much less than the accuracy desired in the standards. Taking one to two percent for this accuracy it turns

---

[1] Seren, Friedlander, and Turkel, Phys. Rev. 72, 888 (1947).

[2] T. Novey, "The fission products," *Radiochemical Studies*, National Nuclear Energy Series, Division IV (McGraw-Hill Book Company, Inc., New York, 1950), Vol. 9, No. 10.

[3] Anderson, Fermi, and Grosse, Phys. Rev. 59, 52 (1941); Engelkemeir, Novey, and Schover, N.N.E.S., Division IV (McGraw-Hill Book Company, Inc., New York, 1950), Vol. 9, No. 205.

[4] Engelkemeir, Hamill, Inghram, and Libby, Phys. Rev. 75, 1825 (1949).

[5] H. Anderson and E. Fermi, Plut. Proj. Rep. CPA-2, J. H. Roberts, Plut. Proj. Rep. CP-1156 (January 4, 1944).

[6] Novey, Engelkemeir, and Levy, N.N.E.S., Division IV (McGraw-Hill Book Company, Inc., New York, 1950), Vol. 9, No. 9.

[7] B. Burtt, Nucleonics 5, 28 (August, 1949).

[8] Engelkemeir, Seiler, Steinberg, Winsberg, and Novey, N.N.E.S., Division IV (McGraw-Hill Book Company, Inc., New York, 1950), Vol. 9, Nos. 5 and 6.

TABLE I.

Source No.	Low geom. activity	Calculated dis. rate	High geom. activity	Geometry
7	1183.5±0.7 c/m	440,940±260	221,050±110	0.5013±0.0004

out that for RaE for example, the source may weigh one hundred micrograms per square centimeter. Similarly the source backing should not contribute more than one percent backscattering effect to the counting rate. Any difference in the amount of backscattering for different energy sources will not cause an appreciable effect when all sources are mounted on identical thin supports.

The active material consisted of a solution of RaDEF in one normal nitric acid. The solution was several years old and thus was within a tenth of one percent of equilibrium. No residue could be seen on evaporating aliquots of the size used for the standards. Fractionation of the polonium in the mounting procedure could not be detected. Normal decay was observed over a period of a year.

Tygon films (*ca.* 0.7 mg/cm^2) were used as backing for the sources. These were prepared by dipping glass plates into a suitably diluted solution of clear Tygon paint. The films were stripped off when dry and were cemented with Aquadag to aluminum rings (Fig. 1c). A thin layer of Aquadag was applied to the film surface to make it slightly conducting. This avoids alpha-counting irregularities caused by charging up of the films if they are insulated from the plate on which they are placed.

The active solution was spread on the films by the use of insulin solution.[9] A drop of the insulin solution was touched to the film and spread over an area of one square centimeter. Most of the solution was then removed. The RaDEF solution (*ca.* 50 microliters) was then placed on the film and the source dried in a vacuum desiccator. The insulin solution was forty units or ten milligrams per cc. About a quarter of a drop remained spread over the source area giving a weight of about 125 μg/cm^2, well below the point where source self-absorption is appreciable.

Six standard sources were prepared with activities of about 8000 dis./min.

IV. CALIBRATION BY ALPHA-COUNTING

The standard sources were alpha-counted in a parallel plate ionization chamber filled with a 3 percent carbon dioxide-argon mixture at one atmosphere pressure. The chamber is operated at 1450 v. A fast high gain amplifier is required to provide the necessary pulse size for the scaling circuit. This counter has a very low counting loss, about 1 percent at 200,000 c/min. whereas ordinary air chamber counters have a loss of about 1.25 percent per 1000 c/min. The low loss of the A-CO$_2$ counter was useful in the calibration of the alpha-chamber. The efficiency of the chamber is very close to 50 percent when a source is mounted on a low atomic number backing as these were, but for a check an alpha-source was prepared of considerably higher activity (*ca.* 400,000 dis./min.) and was counted in the 50 percent chamber and then in a low geometry (0.2684 percent) vacuum chamber in which the beam from the source was collimated by an accurately machined circular diaphragm and passed into a carbon dioxide-argon ionization chamber through a very thin mica window.[10] The low geometry was calculated using the formula given by Kovarik and Adams.[11] The ratio of the activities—corrected for counting loss—gave the ratio of the geometries. Table I gives the results of the determination with standard errors.

V. BETA-COUNTING PROCEDURE

Mica end-windowed (*ca.* 3 mg/cm^2) G-M tubes were used with a shelf arrangement as shown in Fig. 2 for all beta-counting. The mica windows were made conducting with a thin layer of Aquadag. The apparatus fits inside a vertical lead shield with 1½-in.-thick wall. Standard commercial Higginbotham type scaling circuits were used.

All of the determinations were made in the top shelf position with the source three millimeters from the window. No attempt was made to use more distant

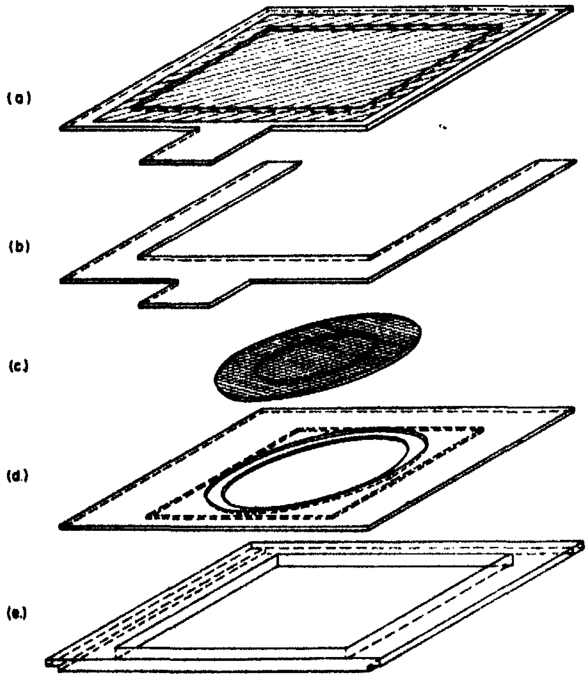

FIG. 1. Exploded view of source mounting arrangement. (a) Absorber holder. (b) Wedge to lift absorber against counter flange. (c) Source mounting ring with attached Tygon film. (d) Source mounting ring positioner. (e) Movable shelf.

---

[9] L. M. Langer, Rev. Sci. Inst. 20, 216 (1949).

[10] A. Jaffey, USAEC-MDDC-1336 (February, 1947).

[11] Kovarik and Adams, Phys. Rev. 40, 718 (1932).

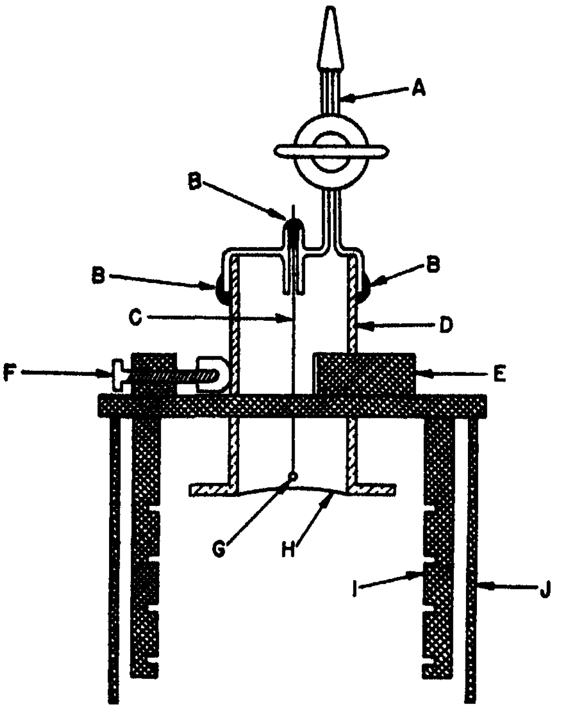

FIG. 2. Geiger-Müller tube and shelf arrangement.

A. Gas filling tube
B. Apiezon seals
C. Kovar wire anode
D. Brass cathode
E. Tube holder (Lucite lined)
F. Set screw (Lucite tip)
G. Pyrex bead
H. Mica window (sealed to tube flange with Gelva cement)
I. Aluminum shelves
J. Aluminum supporting rod.

positions as the absorption corrections rapidly become more uncertain.

The source rings were placed in a special support (Fig. 1d). This support slid onto a shelf support (Fig. 1e) which in turn fits closely into the slots in the shelf holder of Fig. 2. The positioning was then reproducible for beta-counting and the source rings were removable for insertion into the alpha-counter chamber. The beta-geometry is very sensitive to source position at the high geometries used, a change of one millimeter being sufficient to cause about ten percent change in the counting rate.

In order to correct for absorption of the beta-particles in the air layer and in the mica window, absorption curves were taken using mica absorbers supported on a $\frac{1}{16}$-in. thick aluminum frame (Fig. 1a). The absorbers were lifted against the tube flange by inserting a wedge (Fig. 1b) between the absorber holder and the source support. It is important that the absorbers be as close to the window as possible. Reasons for this are discussed in the next section.

VI. BETA-COUNTING RATE CORRECTIONS

1. Absorption Correction

The absorption correction is the largest and most difficult correction to determine accurately. For RaDEF sources it amounts to about 25 percent due to the fact that the sources must be counted through sufficient absorber to absorb the alpha-rays of RaF. A total absorber thickness of about 11 mg/cm², is more than sufficient for this purpose as seen in Fig. 3, curve *A*. The extrapolation to zero absorber would seem to require the use of a 40.4 mg/cm² half-thickness; however, when a pure RaE source was prepared and an absorption curve taken to thinner absorber (Fig. 3, curve *B*) the curve was observed to change slope at around 15 mg/cm². The initial slope was 33.3 mg/cm². A similar absorption curve on another source yielded a slope of 34.0 mg/cm². For the standard correction the average, 33.6±0.3 mg/cm², was used requiring an absorption correction factor of 1.255±0.0028 for 11.0 mg/cm² total absorber; i.e., 3.0 mg/cm² mica G-M tube window. 0.5 mg/cm² air and 7.5 mg/cm² added mica absorber.

The absorption curves are very sensitive to the relative positions of the source and absorbers. Figure 4 shows, curves where the source is 3 mm from the tube flange and the absorbers are 1 mm from the flange (curve *A*) and against the flange (curve *B*). Even with the latter arrangement, the initial point where no absorber has been added does not fall exactly on the exponential curve due to the fact that there is still a small air space between the curved mica window and the flat mica absorbers; however, the difference is small and will partly cancel in the similar correction to be applied when another source is to be calibrated against the standard and the same absorber and source positions are used.

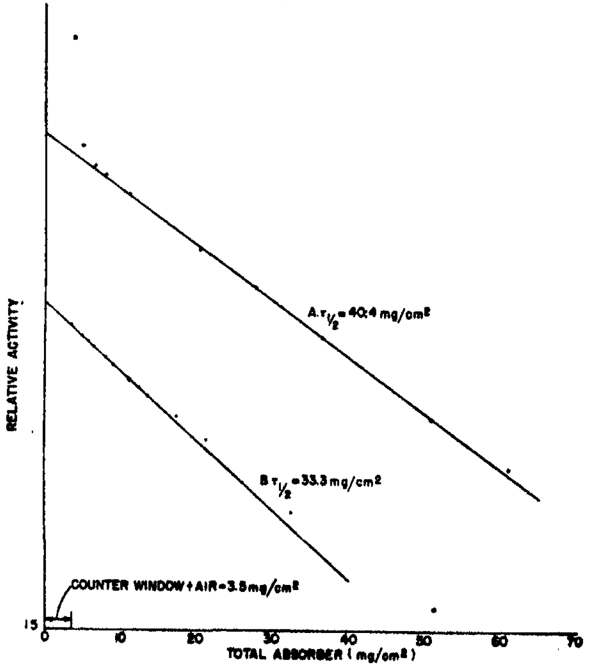

FIG. 3. Initial slope of RaE mica absorption curve as determined from RaDEF equilibrium source absorption curve, *A*, and separated RaE source absorption curve, *B*. Source is 3 mm from counter flange. Absorbers are against the counter flange.

2. Counting Loss Correction

Beta-counting rates were a few thousand counts per minute causing a counting loss of about 1 percent. This will cancel if the standard source counting rate and the unknown source counting rate are the same. For our purposes we applied a correction of 0.5 percent per 1000 c/min. of counting rate. This is an average value for our G-M tubes and will not cause a large error in the result. For the calculations of standard error in the beta-counting results we assume the counting loss correction to be 0.50±0.25 percent per 1000 c/min. of counting rate. As counting rate differences were at most 1400 c/min. between the standard sources and the unknown sources the uncertainty due to counting loss is less than 0.4 percent.

VII. APPLICATIONS TO P^{32} STANDARDIZATION

The standard sources were used to determine the specific activity of a P^{32} solution distributed by the Bureau of Standards in March, 1949.

Two 0.050-ml and two 0.100-ml samples of the P^{32} solution were mounted on Tygon films in the same manner as the standards. The absorption correction is smaller for P^{32} as there is no soft radiation to be masked out so the extrapolation to zero absorber is made from about 3.5 mg/cm². The initial half-thickness is 157 mg/cm² corresponding to an absorption correction factor of 1.016.

The four P^{32} sources and the six RaDEF sources were counted at the shelf 1 positions on two different counters designated *A* and *B*.

The RaDEF source counting rates were corrected for absorption and counting loss and divided by the previously determined beta-disintegration rate to give the "geometry." This geometry is presumably the solid angle of the source subtended by the sensitive volume of the counter excluding the small back-scattering correction. The values obtained by the six standards in the two tubes are shown in Table II with their standard errors as determined by the method of propagation of errors.

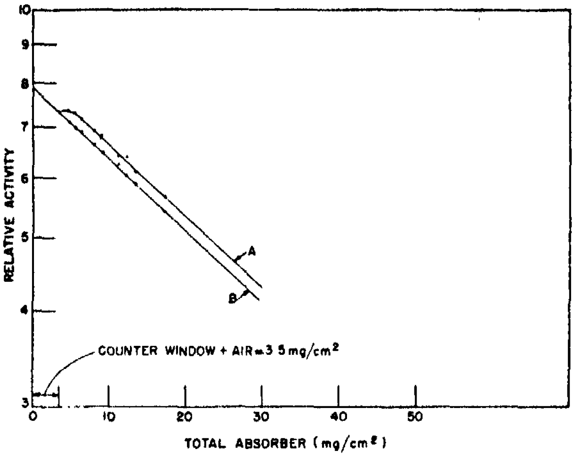

Fig. 4. RaE mica absorption curves showing curves where the mica absorbers are 1 mm from Mica counter flange, *A*, and where mica absorbers are against the counter flange, *B*. Source is 3 mm from counter flange.

The averaged geometries were then applied to the corrected counting rates of the P^{32} samples to give the disintegration rates. These are shown in Table III together with the sample volumes and the activity per milliliter of original solution corrected using a half-life of 14.30 days to the comparison time 8 A.M. E.S.T. March 1, 1949 with appropriately calculated errors.

This value is about 8 percent higher than the best value given by the Bureau of Standards for the P^{32} solution. The reason for the error in their measurements was mentioned in Section II of this paper. The value is in excellent agreement with that obtained by B. Burtt by the RaEF method.[7]

Table II. Alpha- and beta-counting and correction data involved in beta-geometry determinations.

Standard No.	G-M tube	Alpha c/min.	Alpha-geom	Alpha dis./min.	Beta dis./min.	Beta c/min.	Counting loss corr.	Absorption corr.	Beta dis./min.	Beta-geom.
1	*A*	4312	0.501	8606	8458	1557	1.0079	1.255	1954	0.2310±0.0014
	B					2180	1.0109		2736	0.3235±0.0020
2	*A*	4325		8633	8484	1558	1.0080		1956	0.2306±0.0014
	B					2222	1.0111		2788	0.3286±0.0020
3	*A*	4332		8648	8499	1558	1.0080		1956	0.2302±0.0014
	B					2233	1.0112		2802	0.3297±0.0020
4	*A*	4333		8649	8500	1541	1.0079		1934	0.2275±0.0014
	B					2235	1.0112		2804	0.3299±0.0020
5	*A*	4329		8642	8493	1553	1.0079		1950	0.2295±0.0014
	B					2185	1.0109		2742	0.3228±0.0020
6	*A*	4293		8570	8422	1560	1.0080		1958	0.2325±0.0014
	B					2219	1.0111		2785	0.3307±0.0020
Av	*A*									0.2302±0.0011
	B									0.3275±0.0028

TABLE III. Beta-counting and correction data involved in the determination of specific activity of P^{32} solution.

Source No.	Sample volume	G-M tube	Beta c/m	Counting loss corr.	Decay corr. to 10 A.M.C.D.T. 5/23/49	Absorption corr.	Beta geom.	Beta dis./min.	Beta mrd/ml	Beta mrd/ml 8 A.M.C.D.T. 3/1/49
1	0.0500_6	*A*	1085	1.0054	1.001	1.016	0.2302	4821	1.607	90.00±0.80
		B	1432	1.0072	1.049		0.3275	4693	1.565	87.60±0.75
2	0.0500_6	*A*	1080	1.0054	1.003			4807	1.602	89.73±0.80
		B	1437	1.0072	1.052			4723	1.574	88.15±0.76
3	0.1000_2	*A*	2107	1.0105	1.006			9454	1.575	88.26±0.79
		B	2850	1.0142	1.055			9460	1.577	88.29±0.89
4	0.1000_2	*A*	2120	1.0106	1.008			9528	1.587	88.90±0.82
		B	2878	1.0144	1.057			9570	1.594	89.29±0.91
Av.										88.8 ±0.3

VIII. PRECISION AND ACCURACY

Tables II and III show a precision of 0.6 percent for the individual geometry determinations and 0.3 percent for the P^{32} activity determinations. The precision of the geometry determination is also indicated by the average deviations given for the average geometries. This is less than the standard error of the individual geometries.

The accuracy of the method depends upon systematic errors not shown in the corrections thus far used. These errors may be estimated as follows:

1. Possible Difference in Back-Scattering Coefficient of P^{32} and RaE from the 0.7 mg/cm^2 Tygon Films

As the total backscattering is less than 1 percent for this thickness of backing the difference due to energy difference of RaE and P^{32} is not more than a few tenths of a percent.

2. Non-Uniformity of Sources

Activity measurements on RaDEF and P^{32} sources showed some concentration of the activities at the periphery of the area. This effect if totally uncompensated by the source to be determined could cause a systematic error of several percent. For this reason it is important that the standard and unknown sources be prepared the same way.

3. Change of Geometry with Energy

If the sensitive volume of a counter depends strongly upon the energy of the incident beta-particle, then it might be expected that a geometry determined for one energy spectrum would not hold for another spectrum. The fact that geometries determined over a wide range of energies by various methods agree within a few percent,[12] i.e., within the accuracy of those determinations, sets an upper limit to the possible inaccuracy due to this factor.

A reasonable estimate of the accuracy of the method thus seems to be 1–2 percent.

IX. RANGE OF APPLICATION OF THE METHOD

The accuracy of the standardization depends upon the energy of the beta-spectrum and upon some knowledge of the decay scheme of the nuclide. Low energy beta-spectra will require the use of thinner windows on the counter tubes to avoid large absorption corrections. Atmospheric pressure flow type counters either in the proportional or Geiger region can be built with window thicknesses easily down to 50 μg/cm^2. Air absorption becomes the dominant factor here. This can be helped by substituting helium or hydrogen for the air in the counting apparatus.

If the decay involves gamma-radiation then a correction for the gamma-counting efficiency must be made. Conversion electrons are the most serious source of trouble as they are usually soft and make the absorption correction very difficult. Harder electrons such as those produced by Au^{198} amount to usually only a few percent and can be more easily accounted for.

Within these limitations this method of standardization seems at least as simple and accurate as the three other main methods of specific activity determination, "4π" counters, coincidence counters and gas counters.[4] The first method has recently been investigated by C. Borkowski and co-workers at Oak Ridge National Laboratory[13] using atmospheric proportional counters. Here gamma-rays, beta-rays, and conversion electrons only cause one count in general as they are emitted within the resolving time; however, there is a small slope to the plateau curves of ½ to 1 percent per 100 volts. As the counters have a plateau of from 300 to 1500 volts, this represents a considerable uncertainty in the disintegration rate.

Accurate activity determination by coincidence counting requires a knowledge of the decay scheme. If the scheme is simple then an accurate determination can be simply made with a source that is thin for its gamma-rays. To calibrate a counter position, however, in order to determine the disintegration rate of another source again requires an absorption correction to zero absorber. Angular correlations of emitted particles may also interfere.

---

[12] L. R. Zumwalt, USAEC MDDC-1346.

[13] Private communication.

Active gas counting seems to be an accurate method and is suitable for materials which can be prepared in a gaseous form that will not impair counter action.

X. SUMMARY

A procedure has been presented for the preparation of essentially weightless RaDEF equilibrium standard sources mounted on a very light backing for use with end-windowed type counters. This type of mounting avoids the necessity of dealing with self-absorption and backscattering problems. The standards have the advantage of being relatively permanent, can be recalibrated by alpha-counting at any time, and in many cases can be used to determine the activity of other radionuclide sources with an error of <2 percent. The method loses accuracy when the beta-spectra are of low energy so that the absorption corrections are large and less reliable or when an unknown amount of conversion electrons are present.

XI. ACKNOWLEDGMENTS

The author is grateful to A. Jaffey, J. Lerner, and W. Bentley for the use of the carbon dioxide-argon alpha-counting instruments, and to P. Fields for the equilibrium RaDEF solution.

THE REVIEW OF SCIENTIFIC INSTRUMENTS VOLUME 21, NUMBER 4 APRIL, 1950

Construction and Performance of a Multiple Gamma-Ray Counter of High Efficiency

TIBOR GRÁF
L. Meitner Laboratory, Royal Institute of Technology, Stockholm, Sweden

(Received October 18, 1949)

A multiple gamma-ray counter is described, composed of 24 counter tubes connected in parallel. The tubes have Bi-plated brass screen cathodes and are placed inside the same envelope. Relative and absolute values for the efficiency of the counter were determined experimentally in the range 0.28 to 2.62 Mev. Compared to a single brass counter of similar dimensions, the multiple counter shows for gamma-rays of, say, 0.7 Mev energy a tenfold increase in efficiency. Its starting voltage is 5–600 volts lower.

The "effective resolving time" of the multiple counter appears to be 3 to 4 μseconds.

The counting rate curve seems to follow the inverse-square law down to the shortest counter-source distances. The solid angle subtended by the multiple counter for sources, placed in its middle, is nearly 4π.

I. INTRODUCTION

THE problem of measuring the gamma-radiation of substances of very low specific activity led the author to a counter design incorporating several features, all tending to increase the efficiency of the counter for gamma-rays. The high efficiency values obtained in the energy range 0.28 to 2.62 Mev, as well as other desirable properties of the counter, revealed in the course of some investigations of the author,[1] seem to warrant publishing some details of its construction and performance.

Quite generally, the efficiency of a G-M counter for gamma-rays can be improved by increasing the absorption of the gamma-rays in the material of the counter in such a way that the greatest possible number of the resulting secondary electrons should enter into the sensitive volume of the counter. This can be achieved, in principle, by making the counter of a solid metal cylinder provided with a number of counter cavities. The walls between these cavities should be thin so that a large proportion of the secondary electrons produced in them should be able to reach the counter volumes. If the individual counters have the same threshold voltage then all the wires can be connected in parallel, so that an automatic addition of the pulses initiated in the different cavities becomes possible.

In practice it is more convenient to take, instead of a solid cylinder provided with cavities, a number of hexagonal or rectangular tubes,[2] and place them inside a single envelope, in close contact with each other. Also stacks of circular tubes, of the usual G-M counter type, can be used, though there always remains a small dead space between such tubes, reducing somewhat their efficiency.

In spite of this, the use of tubes with circular cross section seemed to be preferable in the present case. The reason was greater simplicity of construction, and the advantage procured by the cylindrical symmetry of the assembly. In fact, this symmetry makes the counter useful for quantitative measurements also in cases when the sources, on account of their low specific activity, must entirely surround it in order to give a sufficient counting rate.

A further improvement in the gamma-ray efficiency of G-M counters may be obtained by making the cathodes of a material of high atomic number and presenting a large effective surface, such as a wire gauze.[3] The absorption coefficient of gamma-rays increases with the atomic number of the absorber, and the use of wire gauze seems to increase the probability of the secondary electrons reaching the sensitive volume of the counter.

---

[1] T. Gráf, "On the radioactivity of K^{40}," to be submitted for publication in Arkiv f. Fysik.

[2] The use of rectangular tubes for this purpose was first suggested by S. C. Curran and J. M. Reid, Rev. Sci. Inst. 19, 67 (1948).

Recently, counter constructions of the multicellular type, consisting of several pill-box shaped counter cells, have been applied with success to problems related to the measurement of approximately parallel gamma-ray beams of fairly large cross section. Counters specially designed for such applications were made by several workers.[4–6]

While the present work was progressing, several short papers have also appeared on the use of parallel-connected gamma-ray tubes,[7–9] showing the current interest in this type of gamma-counters.

An attempt of increasing the gamma-ray efficiency of G-M counters, though by a different method, was also made by H. Slätis.[10]

II. CONSTRUCTION

General Design

The increase of efficiency obtainable with stacks of parallel-connected tubes may be estimated by comparing the counting rates produced by a large beam of gamma-radiation, in the stack, on the one side, and in a single counter of identical size, on the other. For a cylindrical stack of 7 tubes, for instance, in which 3 tubes are on a diameter, the counting rate is about 7 times that produced in a small tube, the counting rate of the single large counter being about 3 times this counting rate. In fact, the cross section of three small tubes together equals that of the single counter. Thus, the counting rates, and the efficiencies, are, in this case, approximately in the ratio 7 to 3. For a total number of 19 or 37 tubes, easily built up in rings around a central tube, the corresponding increase of efficiency may be expressed approximately by the ratios 19/5 and 37/7, respectively.

In the present design an open passage of 1.7-cm diameter was left along the axis of the entire assembly, allowing small sources to be introduced into its center. For this reason, the disposition, shown in Fig. 1(a), of the

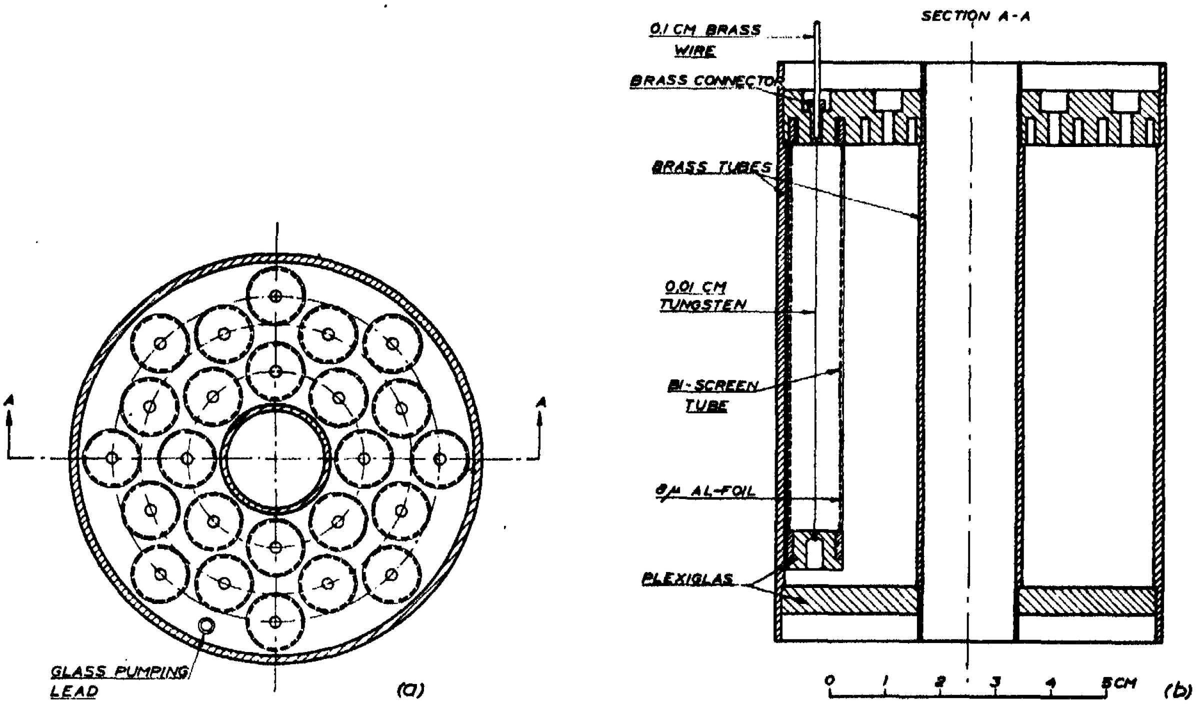

FIG. 1. Schematic diagram of the multiple counter. (a) The 24 counting tubes disposed in 3 concentric rings, as seen through the end plate. (b) Sectional view, with only one of the 24 tubes.

---

[3] R. D. Evans and R. A. Mugele, Rev. Sci. Inst. 7, 441 (1936).
[4] J. W. M. DuMond, Rev. Sci. Inst. 18, 626 (1947).
[5] J. R. Beyster and M. L. Wiedenbeck, Rev. Sci. Inst. 19, 819 (1949).
[6] D. A. Lind, Rev. Sci. Inst. 20, 233 (1949).
[7] R. W. Pringl, J. Sci. Inst. 25, 423 (1948).
[8] H. Friedman, Nucleonics 4, No. 1, 36 (1949).
[9] J. L. Putnam, J. Sci. Inst. 26, 198 (1949).
[10] H. Slätis, Rev. Sci. Inst. 20, 353 (1949) and Ark. f. Mat. Ast. o. Fysik 36A, No. 17 (1948).

24 tubes used, is somewhat less compact than in the arrangements mentioned above, and the improvement due to the use of a stack of tubes alone may, in this case, hardly be expected to exceed a factor of 3. Further increase of efficiency, as was actually revealed by subsequent measurements, was probably due to the other causes mentioned in the introduction.

On the other hand, the presence of a free passage in the middle constitutes an advantage in many applications on account of the large solid angle ($\sim 4\pi$) subtended by the counter for a central source. Also a single beta-counter, to be used in coincidence with the multiple counter, may be placed together with the source in the central channel. The envelope of the counter was made of 7.0-cm brass tubing of 0.15-cm wall thickness.

The anodes consisted of 0.01-cm tungsten wire mounted as shown in Fig. 1(b). A small piece of copper wire was squeezed onto one of the ends of the tungsten wire, to prevent it from slipping through the fine hole made in the lower Plexiglas plug. At the upper end of the counter, the wire passes through a brass connector, set tightly in the Plexiglas plug. To fix the wire, it is held stretched while it is blocked in position by a tapered brass pin.

This method of fixing the counter-wire was found to facilitate the construction of the multiple counter. It has previously been used with success in assembling a number of counters of various design.

After assembly, the end plates were sealed with Apiezon *W* wax.

Cathode Tubes

Bismuth was chosen as material for the cathode tubes. Bi has the highest atomic number of all the stable elements, is free from radioactive impurities, and is much less expensive than either Pt or Au. The use of lead in the counter does not seem advisable, since lead almost invariably contains RaD, and consequently also RaE and RaF, in radioactive equilibrium with it. The presence of the beta-rays of RaE is especially disturbing as they cannot be stopped by a protective surface layer, without also absorbing many of the secondary electrons produced in the lead by the gamma-radiation to be measured.

The Bi had to be electroplated on tubes which in the present case were made of brass wire gauze. For the electroplating process, the technique described by Good, Kip, and Brown was used.[11] These authors recommend a plating solution made by dissolving 9 gram of Bi_2O_3 in 100 cc of 70 percent perchloric acid, and diluting to 1000 cc of solution. The gauze mesh was 0.2 cm, the diameter of the brass wire being 0.035 cm. The tubes made of this gauze had an inside diameter of 0.8 cm, and a length of 8.5 cm. Satisfactory results were obtained when the tubes were plated with an initial current of 40 milliamp. As a result of the gradual increase of the cathode surface during the plating process, the current had to be increased after the first 22 hours. It was then maintained at 60 milliamp. for another period of 22 hours. The corresponding value of the current density was somewhat less than 2 milliamp. per cm^2 of cathode surface.

In order to reduce the time necessary for the plating of a large number of tubes, a special plating apparatus was constructed. This device made possible the simultaneous plating of four tubes, which were rotated continuously in order to obtain a smooth surface and a Bi layer of uniform thickness.

The Bi electrodes were cast from pure Bi crystals in a graphite mould which was placed inside an evacuated Pyrex tube. Four Bi electrodes, 0.4 cm in diameter, were soft soldered to small brass rings mounted into the Bakelite base plate of the plating apparatus. Connections to the Bi electrodes were brought through the Bakelite tubes which supported the upper plate. All brass or copper parts in the solution were coated with paraffin wax. The cathode tubes were guided in their rotation around the Bi electrodes by small Plexiglas rings, of 0.7-cm diameter, embedded in the wax at the foot of each electrode. Half of the total current passed through a Bi electrode of 0.8-cm diameter which was suspended in the middle of the solution and had the purpose of furnishing metal to the outside surface of the tubes.

After electroplating, the diameter of the wire attained 0.07 cm, the weight of Bi deposited on each tube being between 5 and 6 grams. The mechanical strength of the screen tube was greatly increased by the plating procedure. One of the reasons being that the brass wire ends, which had merely been twisted, became actually soldered together with Bi.

The ends of the tubes which were not covered with Bi, were cut away after the plating process. Two cylindrical brass rings were soft soldered to the remaining 7.0-cm length. The upper ring was pressed into one of the cylindrical grooves machined into the upper Plexiglas end plate of the counter, whereas the other ring held the lower insulating plug of the tube, as shown in Fig. 1(b). In order to prevent the passage of the discharge from one tube to another, an Al foil, 8μ in thickness, was wrapped around each tube. All the cathodes were electrically connected to the wall of the inner brass tube of the multiple counter.

Only straight tungsten wire lengths and cathode tubes free from points were used. With moderate care in cleaning and in assembling the different parts of the counter, it was possible, practically straight away, to secure normal operation for all the 24 tubes. After observing that the Bi cathodes were light sensitive, the transparent end plates were covered with sealing wax.

Gas Filling

While a more permanent counter construction, containing no organic materials, is quite feasible, the present design appears to serve its purpose well. The multiple discharges which appear in the counter, usually a few months after its filling, as they do in all counters containing wax, and plugs made of organic matter, disappear as soon as the counter is filled anew. This seems to indicate, that multiple discharges in the present case are mainly due to a decrease of the amount of alcohol in the gas, caused probably by its diffusion into the sealing wax and the end plates.

---

[11] Good, Kip, and Brown, Rev. Sci. Inst. 17, 262 (1946).

Also, in order to obtain good counter characteristics, the pressure of the ethyl-alcohol quenching vapor used had to be increased to 1.8 cm of mercury, from the usual value of 1.0 cm, the total pressure of the argon-alcohol mixture being 20 cm of mercury. The quenching of the counter discharge appeared to be insufficient with a lower alcohol pressure, probably owing to the small cathode diameter.

It was found that the useful life of the counter could be increased by allowing alcohol vapor, at a relatively high pressure (3–4 cm of mercury), to stay a few hours inside the counter, and diffuse into its different parts, before the definitive filling of the counter. This treatment reduced at the same time the large initial variation of the threshold voltage which was previously often observed with newly filled counters.

III. PERFORMANCE

General Characteristics

The characteristic curve of the multiple counter was found to be essentially similar to that of one of the small tubes. The plateau had a slope of 5–6 percent per hundred volts. Though the slope increased somewhat with use, as it always does with counters which cannot be outgassed properly, yet several times 10^7 pulses could be counted with the same filling. The starting voltage of the multiple counter was less than 900 volts, as compared to 1500 volts for a single counter of the same overall size filled to a pressure of only 10 cm of mercury. The starting voltage of the individual tubes was the same within 2–3 volts.

Background

The background of the unshielded counter was about 1400 counts/min. It was mainly due to gamma-radiation from the ground and the walls of the building. Indeed, a cylindrical lead shield of 10-cm wall thickness, with 10 cm of lead on the top, and 7.8 cm under the counter, reduced it to only 63 counts/min. Since the sum of the background pulses in the 24 individual counters, surrounded by the same lead shielding, was $24\times4.8=115$ counts/min., most of the background pulses with 10 cm lead must have been due to particles which each produced ions in more than one tube. Thus, whereas the connection in parallel of a number of tubes greatly improves the gamma-ray efficiency of the counter, its background due to cosmic rays will not increase in the same proportion.

TABLE I.

Energy in Mev	Ratio of the efficiency of the multiple counter to that of a conventional brass counter
0.28	21.0±0.6
0.51	13.7±0.8
0.68	10.2±0.2
1.25	6.6±0.5
2.62	5.8±0.5

Furthermore, owing to the ionizing nature of these particles, many of the pulses produced by them may be eliminated by the use of anticoincidence counters. A very simple and effective anticoincidence arrangement, especially for sources placed at the center of the counter, would consist in using the 8 central tubes of the multiple counter for the measurement, the other 16 tubes being connected in anticoincidence. The background of the 8 central tubes with 10 cm of lead was found to be 26 counts/min., whereas a determination of the number of coincidences between the central group and the group of 16 counters of the outer rings yielded 19 coincidences/min. Thus, an effective anticoincidence circuit should reduce the background of this arrangement to only 7 counts/min. This is 9 times less than the value of the background found with all the 24 tubes connected in parallel. Since for an internal source the central group of 8 counters has about half the efficiency of the whole assembly, an improvement by about a factor of five in the ratio (source activity)/(background counts) may be expected. This improvement would be especially important in the case of weak gamma-emitters giving a counting rate of the same order as the background. Experiments are being planned in order to obtain a very low background with the help of a suitable anticoincidence amplifier.

Resolving Time*

Attempts were made to determine the resolving time of the multiple counter by investigating the form and the distribution of the counter pulses. This investigation was made with an oscilloscope, the horizontal sweep of which was triggered by the counter-pulse itself.

The pulse heights observed on the oscilloscope screen were in the ratio 1:2:3:4:5, much like in the case reported by Lind.[6] The larger pulses, which were less numerous, were obviously due to discharges produced simultaneously in several individual tubes, either by secondary electrons which passed through the screen-openings of the tubes, or by cosmic-ray particles, or even by scattered gamma-quanta which became absorbed or scattered once more. The pulses due to one of the parallel-connected tubes were about 8 times smaller than those observed with a single tube disconnected from the others. This reduction of pulse height results obviously from the large capacitance of the counter wires ($=60$ $\mu\mu f$). While pulses of this magnitude are quite sufficient to operate the usual G-M tube amplifiers, they are so small that the anode voltage of the multiple counter will practically never be lowered to a value near the threshold.

---

* The author is indebted to Mr. G. von Dardel, Mr. C. Taylor, and Mr. N. Voghera for discussions on the subject of this section.

Consequently, after a discharge in one of the tubes, the other 23 tubes, in which no positive ion sheath has been formed, remain fully sensitive to radiation. Since the probability that two subsequent discharges of the multiple counter occur in the same individual tube is quite small ($\cong 1/24$), the multiple counter will almost always count an ionizing particle, even when this particle follows the previous ionizing event in an interval much shorter than the deadtime of a single tube. Hence, no deadtime, in the accepted sense of this expression can be associated with the multiple counter. In fact, intervals as short as 4 μsec. between successive pulses were observed on the oscilloscope screen. However, an "effective resolving time" τ_0 may be considered, at least when the number of pulses n per second in the different individual tubes may be assumed to be approximately the same. τ_0 may be defined as being equal to the resolving time of a single counter which at a counting rate $N=24n$ would suffer the same relative loss as the multiple counter. This latter loss is approximately the same as the relative counting loss $n\tau$ in one of the individual tubes, for the counting rates, and hence also the losses, are supposed to be the same in all the tubes. Since, for $N\tau_0 \ll 1$ the relative loss in the single counter is $N\tau_0$, and by definition $N\tau_0=n\tau$, it follows that $\tau_0=(n/N)\cdot\tau$. Thus, for not too high counting rates, the effective resolving time of the multiple counter should be about 24 times shorter than that of an individual tube. For unequal distribution of the counting rates between the individual tubes, this time would obviously be somewhat longer.

A measurement of the resolving time of the multiple counter was kindly made, at the author's request, by Mr. G. von Dardel, with a 20-channel time interval analyzer constructed by him. For this measurement the pulses generated by the multiple counter across a 500 ohms load were amplified by a fast linear amplifier of gain 10^4. Although the smallest interval between pulses that could be measured with this arrangement was of the order of 4 μseconds, no minimum interval between successive pulses of the multiple counter could be detected. For intervals shorter than about 60 μseconds the number registered by each channel of the analyzer was 3 or 4 percent less than for intervals exceeding this value. This decrease in the number of intervals is attributed to the fact that two subsequent discharges separated by an interval smaller than the deadtime of an individual tube,—though they may occur in two different tubes of the multiple counter,—may not take place in one and the same tube. Hence, the probability that the second of two such discharges will actually take place is reduced in the ratio 23/24. This interpretation is confirmed by a measurement made with the interval analyzer which for the deadtime of the individual tubes of the multiple counter gave a value of 60 μseconds.

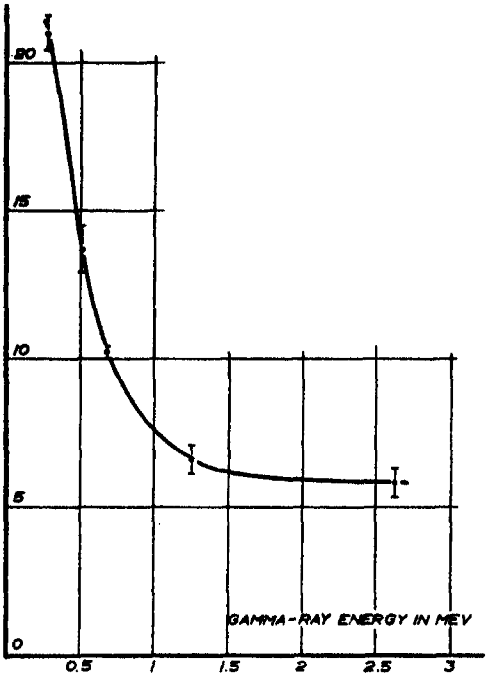

FIG. 2. Experimentally determined ratio for the efficiency of the multiple counter to that of a single brass counter of the same size, as a function of quantum energy.

According to what was said previously the effective resolving time of the multiple counter should be about 24 times smaller than this value, i.e., about 2.5 μseconds. To this should be added the time of spread of the discharge along the wire,[12] estimated at 0.5 to 1 μsecond.

Thus, compared to a conventional counter of the same over-all size as the multiple counter, for the deadtime of which a value of 760 μseconds was obtained, the multiple counter exhibits an about 200 times smaller resolving time.

Relative Efficiency

The efficiency of a G-M counter for a beam of monoenergetic gamma-rays is defined as the ratio of the quanta counted to the number of quanta passing through the counter. Consequently, the efficiency of two counters of identical size may be compared, by comparing, under the same geometrical conditions, the counting rates produced in each counter by a distant source emitting a single gamma-ray.

The counting rate of the multiple counter was compared to that of a conventional brass counter which had the same diameter and the same wire length (7.0 cm). For these measurements the counter was placed on a wooden table, with its axis vertical. A small size source was disposed in the median plane of the counter, at a

---

[12] See, for example, Huber, Alder, and Baldinger, Helv. Phys. Acta 19, 204 (1946).

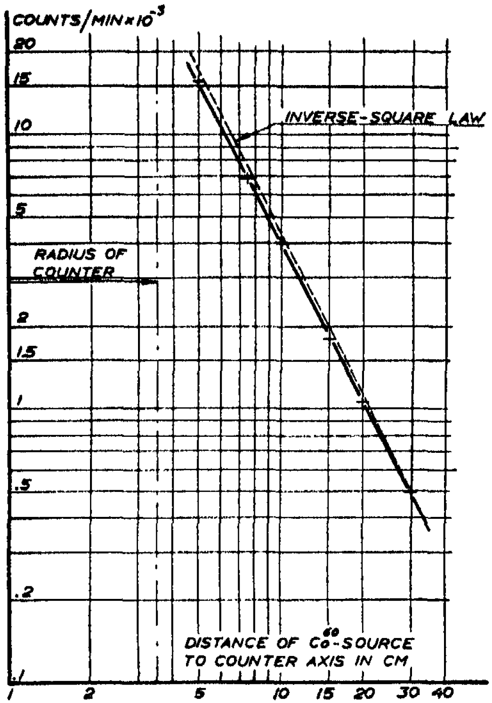

FIG. 3. Double logarithmic plot of counting rate *vs.* distance of source from counter axis. For comparison, a dashed straight line, representing the inverse-square law, was drawn through the experimental point at 30 cm.

distance of 20 to 100 cm from the counter axis, depending on the intensity of the sample. The amount of scattered radiation reaching the counter was kept at a negligible value.

The following gamma-ray sources were used:† Hg^{203} (0.28 Mev[13]), Cu^{64} (0.51 Mev), Cs^{134} (0.68 Mev[14]), Co^{60} (1.25 Mev[15]), and ThB+C+C″ (2.62 Mev).

Co^{60} and Cs^{134} emit several gamma-rays, of not very different energy. The energies quoted for these two sources are weighted mean values.

For Cu^{64} the contribution of the 1.35 Mev weak gamma-radiation[16] was determined through absorption measurements and was corrected for in the results. Similar corrections were made for the low energy gamma-quanta emitted by ThB+C+C″.

The final results of the comparison, given in Table I, show that the efficiency of the multiple counter for 0.28 Mev quantum energy is 21 times larger than that of the brass counter. This ratio diminishes for larger energies, as can be expected, and, above about 1.5 Mev becomes approximately equal to 6. The experimental points lie on a continuous curve, shown in Fig. 2, representing the efficiency ratios for all quantum energies between 0.28 and 2.62 Mev.

In order to determine the influence of the source-counter distance in measurements made with comparatively thick sources placed near the counter, the counting rate produced by the gamma-rays of Co^{60} was measured for distances between 5 and 30 cm. The results of these measurements are plotted on double logarithmic scale on the graph of Fig. 3. Following calculations of F. Norling,[17] the solid angle subtended by a counter of conventional design varies much less rapidly at short distances than would be indicated by the inverse-square law. According to the experimental points of Fig. 3, however, this law seems to apply rather closely for the multiple counter, even for distances comparable to its radius.

This behavior may partly be due to the fact that the length of the multiple counter is approximately equal to its diameter. Another possible cause is the fact that the secondary electrons are ejected from points more evenly distributed throughout the volume of the multiple counter than in a counter of the usual design.

The influence of the relative position of the source around the counter was investigated by measuring the counting rate produced by a sample of Cu^{64} placed directly on the surface of the counter, at different points of its "equatorial circle." No deviation exceeding the limits of the experimental error (±0.5 percent) was found, although any asymmetry should have the greatest effect for the shortest distance between source and counter. Hence, this result may be taken as an indica-

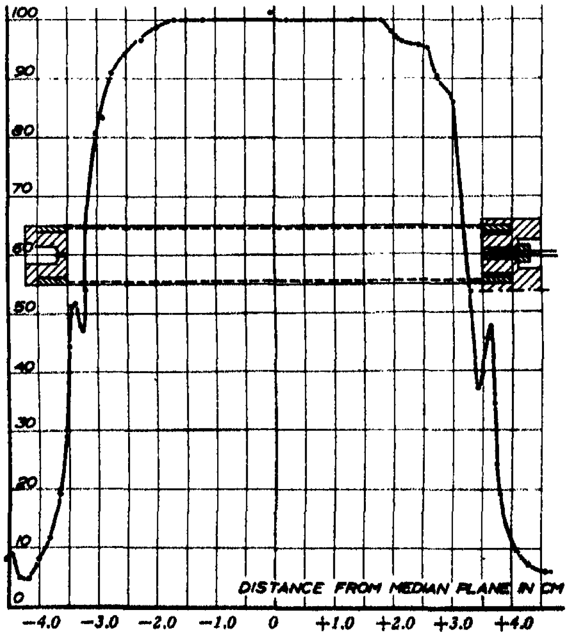

FIG. 4. Relative efficiency values along the axis of the multiple counter. The relative position of one of the counting tubes is indicated.

---

† The author is greatly indebted to Dr. K. Siegbahn who made these sources available to him.

[13] H. Slätis and K. Siegbahn, Ark. f. Mat. Ast. o. Fysik 36A, No. 21 (1949).

[14] K. Siegbahn and M. Deutsch, Phys. Rev. 73, 410 (1948) and L. G. Elliott and R. E. Bell, Phys. Rev. 72, 979 (1947).

[15] Lind, Brown, and DuMond, Phys. Rev. 76, 591 (1949).

[16] M. Deutsch, Phys. Rev. 72, 729 (1947).

[17] F. Norling, Ark. f. Mat. Ast. o. Fysik 27A, No. 27 (1941).

tion of the good cylindrical symmetry of the multiple counter.

The counting rate for a Cu^{64} source placed at the center of the counter was found to be about twice that obtained when the same sample was applied directly against the outer envelope of the counter. This increase is mostly due to the much larger solid angle (nearly 4π) subtended by the counter. However, for a central source, the losses due to the absorption in the counter walls are also smaller. On the other hand, a gamma-quantum coming from the center of the counter may only pass through three tubes, at the most, instead of six, and its probability of being counted is correspondingly smaller.

The variation of efficiency over the cross section of the counter was investigated by using the gamma-radiation from a Co^{60} source placed at 40 cm from the counter. A horizontal fan-shaped beam of gamma-radiation was employed, the position of which remained unaltered during the measurements. Its vertical dimension was limited to 0.15 cm. Its horizontal extension was greater than the length of the counter.

In a first series of measurements the counter was placed vertically at different heights above the table. The counting rates obtained furnished, after correction for the background and for scattered radiation, a relative measure of the efficiency along the counter wire. These relative values are plotted in Fig. 4, against the distance of the beam from the median plane of the counter. There appears to be a fairly large region of constant efficiency.

In a second series of measurements the counter was disposed horizontally. The direction of incidence of the beam was perpendicular to the counter axis and parallel to a diameter of the counter passing through two tubes only (see Fig. 1(a)). The counting rates obtained with the counter at different levels above the table were plotted, after corrections, in Fig. 5, against the distance of the beam from the counter axis.

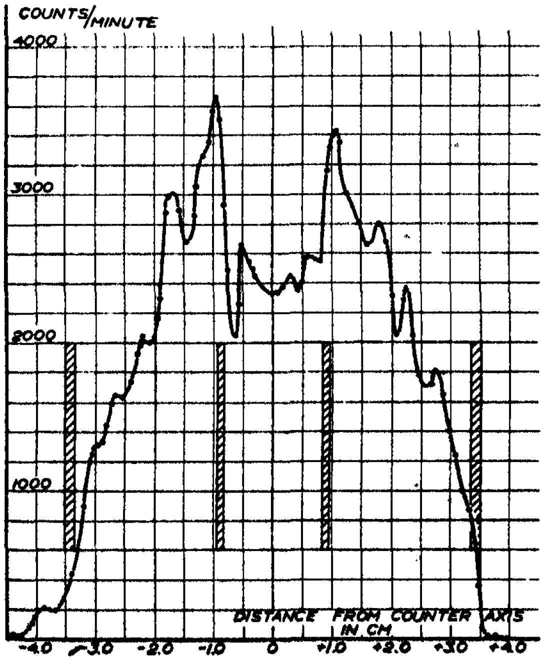

FIG. 5. Counting rate *vs.* distance of beam from the axis of the multiple counter. Incident beam normal to the schematic cross section shown.

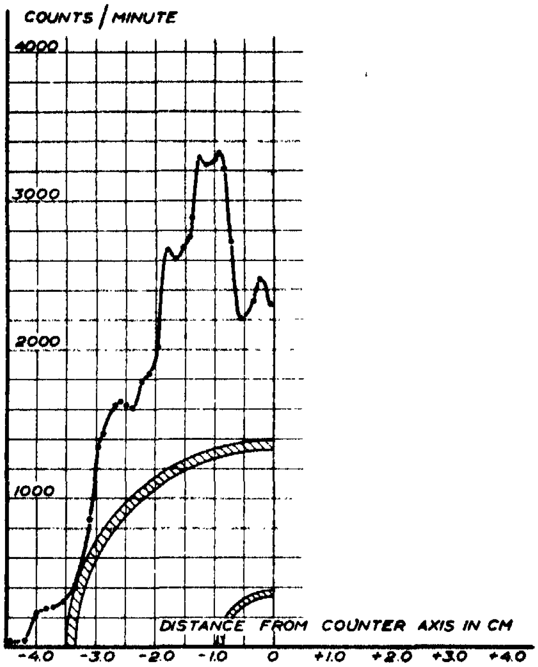

FIG. 6. Counting rate due to a beam parallel to the counter axis, as a function of its distance from the axis. Area encountered by the beam can be deduced from the diagram.

The peaks of the curve obtained indicate the increase in the number of secondary electrons produced in the walls of the individual tubes on the point of entering the beam. The depression in the middle of the curve is, of course, due to the presence of the open channel along the counter axis. The corresponding loss of efficiency may be estimated from the curve at about 10 percent.

Finally, the counter was placed with its axis parallel to the direction of the beam, its center being at the same distance from the source as for the previous measurements. The net counting rates, obtained with the counter at various heights, are plotted in Fig. 6 against the distance of the beam from the counter axis. The curve drawn through the experimental points corresponds to only half the cross section of the multiple counter. It is interesting to note that the area under the entire curve, which was assumed to be symmetrical with respect to the counter axis, is nearly equal to the area of the curve in Fig. 5. This means that a parallel beam of gamma-radiation from Co^{60} (1.25 Mev), irradiating the whole counter, would produce the same counting rate, whether the counter axis is parallel or perpendicular to the beam. Since the circular cross section of the counter is smaller than its rectangular cross section, the efficiency of the counter for an axial beam is about $(4/\pi)$ times greater. Also, in order to reduce the counting rates observed to the same solid angle, the ordinates of the curve in Fig. 6 should be multiplied by the ratio of the counter diameter and the chord length corresponding to each ordinate. It may be seen then that for a beam of sufficiently large cross section (a few cm^2), the efficiency over the annular face of the counter is much more uniform than the curve of Fig. 6 would indicate it.

Clearly, a more uniform response would be obtained by disposing the tubes in parallel rows, instead of in concentric rings.

However, as was mentioned in the introduction, for measurements with nearly parallel gamma-rays, where uniform efficiency over a large counter area is desirable, counter designs of the multicellular type, such as those described by DuMond,[4] Lind,[6] and Beyster and Wiedenbeck,[5] appear to be more appropriate.

Absolute Efficiency

The absolute efficiency of the multiple counter for different quantum energies was obtained by multiplying the experimentally determined efficiency ratios, read on the curve of Fig. 2, with the efficiency of the brass counter used for the calibration.

The curve connecting the experimental points, which in Fig. 7 are indicated by crosses, represents the efficiency curve of the multiple counter in the range 0.28 to 2.62 Mev. For the efficiency of the brass counter, the values measured by Bradt *et al.*[18] were assumed. The lower curve of Fig. 7 shows the one obtained by these authors, after correction for the absorption of the gamma-rays in the 0.15-cm thick counter wall.

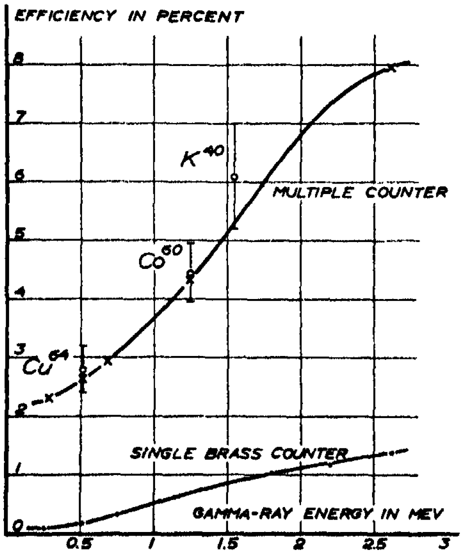

FIG. 7. Absolute efficiency of multiple counter *vs.* gamma-ray energy. Beam normal to counter axis. Lower curve: Absolute efficiency of single brass counter, following Bradt *et al.*, corrected for absorption in the counter wall.

The efficiency of the multiple counter varies, as is seen, from 2.3 percent at 0.28 Mev to about 8 percent at 2.62 Mev. The uncertainty in the determination of the individual points is estimated at about 10 percent.

In order to provide a check on the efficiency curve obtained in this way, the absolute efficiency of the multiple counter was also measured directly for three different quantum energies.

In the case of the 0.51 Mev annihilation radiation, from Cu^{64}, the coincidence method was used. For 1.25 Mev quantum energy the gamma-radiation from Co^{60}, and for 1.55 Mev the radiation from K^{40} was employed, the counting rates produced by known source intensities being measured under well determined geometrical conditions.

The coincidence method allows a determination of the efficiency of the counter for the annihilation radiation without the necessity of knowing exactly the source intensity or the solid angle subtended by the counter. The reason for this is that the two annihilation quanta are emitted in opposite directions. The efficiency of one of two coincidence counters, placed symmetrically with respect to the source, will simply be given by the ratio of the coincidence rate to the counting rate of the other counter. Corrections must, of course, be made for chance coincidences, for the background, for the absorption of the radiation in the source, and for the possible presence of other gamma-rays.

A Cu^{64} source, in the form of a 0.5-cm long activated Cu wire of 0.16-cm diameter, was placed between the multiple counter, and a conventional brass counter of the same wire length and of 3.5-cm inside diameter. The counters were placed vertically, at 20 cm from each other, with the source in the middle of their center line.

The value furnished by this method for the efficiency of the multiple counter, 2.8±0.4 percent, appears to be in good agreement with the corresponding value of 2.6 percent taken from the curve of Fig. 7. However, the value yielded by the coincidence method does not represent the average efficiency over the entire counter cross section, as do the values obtained by calibration with the brass counter. It corresponds to a smaller sectional area subtending a solid angle equal to that subtended by the brass counter. When the distance of the brass counter to the source was increased to 20 cm, that of the multiple counter remaining 10 cm, the somewhat higher value of 3.2±0.3 percent was obtained for the efficiency. The reason for this increase is clear from the curve of Fig. 4, since the quanta giving rise to coincidences in this second arrangement are passing through a region of the multiple counter which extends only about halfway between its median plane and the ends of the wires, and in which the efficiency has its maximum value. As a matter of fact, this increase of efficiency was partially compensated by the fact that in the second arrangement the lateral extension of the effective solid angle was limited to a region situated within less than one cm from the axis of the multiple counter. As shown by the curve of Fig. 5, the average value of the efficiency is somewhat less in this region than in the twice wider region corresponding to the first arrangement.

---

[18] Bradt, Gugelot, Huber, Medicus, Preiswerk, and Scherrer, Helv. Phys. Acta 19, 77 (1946).

An attempt was also made to justify experimentally the use in the present investigation of the results obtained for the efficiency of a brass counter by Bradt *et al.*, by measuring the efficiency of the brass counter for the annihilation radiation. The solid angle for coincidences was defined by the multiple counter. It covered the diameter of the brass counter exactly, but only the middle half of its wire length. After correction for absorption in the counter wall a value of 0.23±0.03 percent was obtained for the efficiency of the brass counter. This result agrees well with the value of 0.215±0.007 percent obtained by Bradt *et al.*

The determination of the efficiency at 1.25 Mev was made with a Co^{60} standard, the intensity of which at the time of the measurements was 0.62±0.06 microcuries, as deduced from data furnished with the standard by Tracerlab, Inc. With the source in the median plane of the multiple counter, at 30 cm from its axis, a net rate of 490±14 counts/min. was found. The corresponding value of 4.45±0.5 percent, obtained for the efficiency of the multiple counter at 1.25 Mev, is seen to fit well the efficiency curve of Fig. 7.

With counters of high efficiency even a substance of as low specific gamma-activity as natural potassium may conveniently be used as a standard.

Potassium is readily available, its activity suffers practically no decay, and its gamma-radiation is composed of a single gamma-ray. This gamma-ray has an energy of 1.55 Mev[19,20] and is emitted at a rate for which a new computation of the author yielded the value of 3.4±0.5 quanta per second per gram of potassium. This value is thought to be somewhat more precise than the value published previously.[20]

About 315 g of K_2SO_4 was placed around the counter, in an annular box which was in its turn surrounded by 7.0 cm of lead. The mean distance of the source from the counter axis was 6.0 cm. Minor corrections had to be applied to account for self-absorption and for a certain reduction in the counting rate caused by the axial extension of the source (7.0 cm). A net counting rate of 139 counts/min. was obtained, corresponding to a value of 6.1±0.9 percent for the efficiency of the multiple counter at 1.55 Mev. This value agrees, within the limits of the error, with the value which was determined by calibration. A more precise determination of the gamma-emission rate of potassium seems, however, to be desirable before potassium may become a useful gamma-ray standard in connection with detectors of high efficiency.

A comparison of the efficiency values obtained for the present counter with those of the multicellular counter reported by Lind[6] and by Lind *et al.*[21] seems to indicate that the values published by these authors are overestimated.*

IV. CONCLUSIONS

The multiple counter described combines the advantage of high gamma-ray efficiency and of short resolving time with the simplicity and reproducibility of operation of the conventional G-M counter. In measurements with large beams of extremely weak gamma-radiation, or in coincidence measurements, when large solid angles are desirable (as in connection with beta-spectrometer work, for example), the multiple counter may prove to be more advantageous even than a scintillation counter.

At low energies, in the range 0.2 to 1 Mev, it may prove difficult to attain an efficiency comparable to that of a good scintillation counter. At an energy of 2.6 Mev, however, the average efficiency of the present construction for a large *axial* beam of gamma-rays is already about 10 percent. It appears comparatively easy to improve this value by a factor of 2 or 3, by increasing the length and the number of the tubes.

For still higher gamma-ray energies, it should be possible to attain an efficiency of 40–50 percent in this way.

V. ACKNOWLEDGMENTS

The author is greatly indebted to Professor Lise Meitner for her continued interest in this work and for stimulating discussions. Thanks are also due Mr. H. Johansson for his excellent machine work in the construction of the multiple counter.

The loan by Dr. S. Eklund and Mr. G. von Dardel of part of the equipment used in this investigation is gratefully acknowledged.

---

[19] O. Hirzel and H. Wäffler, Helv. Phys. Acta 19, 216 (1946).

[20] E. Gleditsch and T. Gráf, Phys. Rev. 72, 640 (1947).

[21] Lind, Brown, Klein, Müller, and DuMond, Phys. Rev. 75, 1544 (1949).

* Dr. Lind has kindly informed the author of his essential agreement with him as to the efficiencies to be expected for the multicellular counter.

THE REVIEW OF SCIENTIFIC INSTRUMENTS VOLUME 21, NUMBER 4 APRIL, 1950

Calcium and Cadmium Tungstate as Scintillation Counter Crystals for Gamma-Ray Detection

R. H. GILLETTE
Laboratory of the Linde Air Products Company, Tonawanda, New York

(Received November 17, 1949)

The high density, transparency, and chemical inertness of calcium and cadmium tungstates, together with their reasonable luminescent efficiencies when stimulated with high energy radiation, strongly suggest their use as phosphors in scintillation counters for gamma-ray detection. Some of the properties of these crystals are reported and compared with anthracene. It is shown that with proper design, the total anode current produced by a given source is several times greater with the tungstates than with anthracene, although the latter has a more favorable pulse size distribution. Cadmium tungstate has a zero temperature coefficient of luminescence up to 40°C and shows no afterglow after exposure to intense radiation.

SHORTLY after the announcement by Moon[1] that a single crystal of natural Scheelite ($CaWO_4$) gave a considerable response as a scintillation counter phosphor for gamma-ray detection, experiments were started in this Laboratory to synthesize and test crystals of this material for scintillation counter applications. Subsequently it was found that cadmium tungstate has certain advantages for this application and consequently both crystals have been prepared and studied. It is the purpose of the present communication to summarize the results of these tests and to compare the performance of these tungstates in gamma-ray detection with some of the other currently interesting materials.

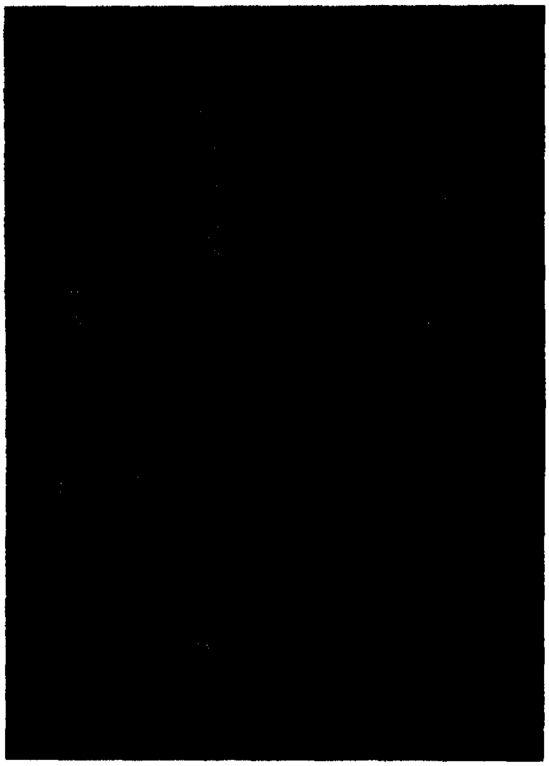

FIG. 1. Some "as grown" and fabricated forms of $CaWO_4$ (right half) and $CdWO_4$ (upper left). Rods of both materials are seen and a boule and a boule section of $CdWO_4$. The last named shows a cloudy region. Polished rods and a mosaic of $CaWO_4$ are presented.

NATURE AND PROPERTIES OF THE CRYSTALS

The crystals used in this investigation were prepared by the Verneuil technique and have been grown mainly as rods about one-eighth inch in transverse dimension and up to five inches in length, although some other shapes and sizes have also been prepared experimentally and tested. Calcium tungstate is obtained as a water-clear crystal of tetragonal structure usually with the crystallographic C axis oriented along the growth axis of the rod. Some of the earlier crystals showed clouds of precipitated CaO but it was found possible to eliminate this completely. Cadmium tungstate grows as a clear, yellowish green monoclinic crystal showing very marked (010) cleavage, although cloudy crystals have also been prepared. In fact, unless special precautions are taken to prevent it, the material cleaves much like mica. The crystal structure does not vary much from tetragonal and generally the "unique" (b) axis is oriented perpendicular to the growth axis of the rod; in this way cleavage occurs along the rod. The exact color is very sensitive to trace impurities. The physical and chemical properties of the two materials are summarized in Table I, and Fig. 1 displays a photograph of typical as grown and fabricated forms. Optical transmission curves throughout the visible, near ultraviolet, and infra-red are shown for calcium and cadmium tungstate, respectively, in Figs. 2 and 3. These were obtained with a Beckman DU spectrophotometer and a Perkin-Elmer Model 12C infra-red spectrometer. The transmission of a slab of natural Scheelite, kindly loaned us by Professor Moon, is also shown in Fig. 2. This material had a considerable number of opaque inclusions so that it was not possible to find a field entirely free of them for the transmission measurements, although they constituted not more than 5 percent of the irradiated area.

The fluorescent emission peaks listed in Table I were obtained by direct visual observation of the fluores-

---

[1] R. J. Moon, Phys. Rev. 73, 1210 (1948).

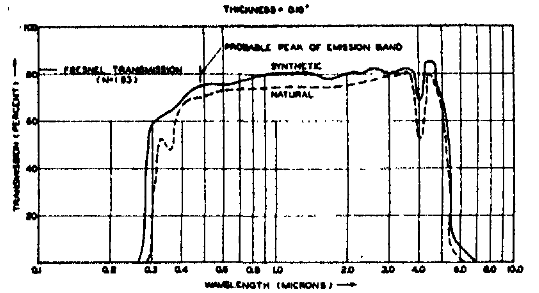

FIG. 2. Transmission curves of synthetic and natural calcium tungstate. The latter contained a number of opaque inclusions. The Fresnel transmission of a slab and the probable peak of the emission band when stimulated with gamma-rays are indicated.

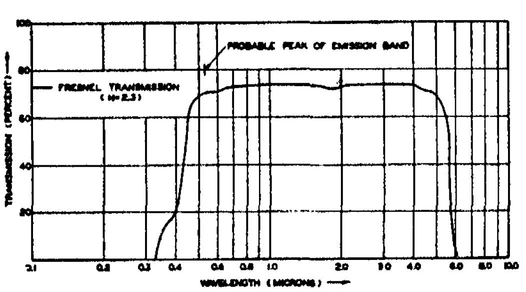

FIG. 3. Transmission curve for pale yellow-green cadmium tungstate. Coloring by trace impurities can change this curve very appreciably and may introduce serious absorption of the luminescent radiation.

cing crystal using a Bausch and Lomb spectroscope. The hardness measurements, specific gravity determinations, and the data on chemical resistivity were obtained in this Laboratory as were also the crystal parameters of $CdWO_4$; the remaining data are taken from the literature.

Because of the high density of the crystals and the presence of a high concentration of tungsten ($Z=74$) very considerable absorption of gamma- and x-rays is to be expected. The absorption coefficients have been calculated on the assumption that the different ions present in the crystal absorb independently of one another. In the gamma-ray region the absorption coefficients due to photo-electron production (τ_{PE}), Compton scattering (τ_C) and a pair production (τ_{PP}) were calculated from the corresponding values[2] for Pb by use of the formulas:

$$\begin{aligned}(\tau_{PE})&=4.07\times10^{-7}(\rho Z^4/A)(\tau_{PE})_{Pb}\\(\tau_c)&=0.224(\rho Z/A)(\tau_c)_{Pb}\\(\tau_{PP})&=2.72\times10^{-3}(\rho Z^2/A)(\tau_{PP})_{Pb},\end{aligned}\qquad(1)$$

where ρ is the density of the material in question in the crystal, A is its atomic weight, and Z its atomic number. The results of these calculations are shown in Table II where the contributions from the three processes are listed separately. It is interesting to note in this connection that the contribution of oxygen atoms to the Compton coefficient is not negligible, a typical value being 0.086 cm^{-1} for 1-Mev gammas. For comparison, the values of τ_c for anthracene calculated on the assumption that only the carbon absorbs are also presented in Table II; τ_{PE} and τ_{PP} are negligible for this substance over the range covered. The data are plotted in Fig. 4. In the x-ray region standard mass absorption coefficient data[3] were used in the usual way. The data are presented in Table III where both the mass and linear absorption coefficients at a number of useful wavelengths are given. The thickness of crystal necessary to reduce the incident beam to 0.1 of its initial intensity, ($2.303/\mu$), is also given.

A quantity of considerable interest in the design of scintillation counters is the refractive index of the phosphor crystal since this governs the amount of luminescent radiation which escapes from the crystal. This arises from the fact that the light is generated in a medium of refractive index $\eta>1$ but, at least in the 931A type photo-multiplier tube, it must traverse a region of refractive index $\eta=1$ in getting to the photosensitive cathode. It is well known that light traveling from an optically dense medium to a less dense one suffers partial reflection; the fraction reflected varies with angle of incidence on the surface and becomes 100 percent at angles equal to or greater than the critical angle α which is given by $\alpha=\sin^{-1}(1/\eta)$. In order to make these results more nearly quantitative, let us consider the somewhat idealized case of a com-

TABLE I.

Property	$CaWO_4$	$CdWO_4$
Crystal system	Tetragonal $a=5.246$A $c=11.349$A $c/a=2.1634$	Monoclinic $a=5.00$A $b=5.83$A $c=5.08$A $\beta=88°40'$
Melting point	1535°C	1325°C
Hardness:		
Moh	4.5–5.0	4.0–4.5
Knoop	390	200–280
Specific gravity	6.12	7.90
Refractive index (n_D)	$\omega=1.9368$ $\epsilon=1.9200$	2.2–2.3
Luminescence under ultraviolet	Blue	Green
Peak of emission curve (x-ray stimulation)	4300A	5300A
Cleavage	Weak or none	Marked (010)
Chemical resistance	Unattacked by cold water, slowly etched by boiling water. Attacked slowly by cold, concentrated HCl and by diluted HCl or NaOH at the boiling point. Boiling NaCl solutions shows no attack.	

---

[2] See, for example, R. G. Fluharty, Nucleonics 3, 46 (July, 1948).

[3] Internationale Tabellen zur Bestimmung von Kristallstruktur, (Bornträger, Berlin, 1945), Vol. II, Chapter XI, compiled by W. L. Bragg *et al.*

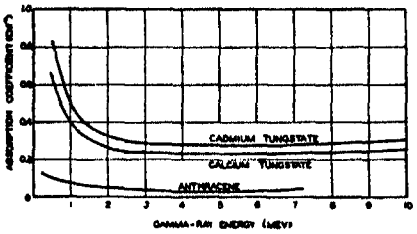

FIG. 4. Gamma-ray absorption coefficients.

pletely transparent, isotropic crystal in the form of a rectangular parallelepiped which is free from scattering material and which has optically polished faces. (Actual crystals of scintillation counter interest are not isotropic, but the indices are so close together that no serious error is introduced by neglecting the anisotropy.) Consider any volume element in the crystal in which light is being isotropically generated and drop perpendiculars from it to the six faces. If now the index of refraction be $\geqslant\sqrt{2}$, and this covers all crystals of scintillation counter interest, the only light which can escape from the volume element will be that emitted into the six cones of half-angle α which have the above perpendiculars as axes. The solid angle subtended by a whole sphere is 4π while that subtended by a cone of half-angle α is $2\pi(1-\cos\alpha)$, hence the fraction of the light from the volume element emitted into each cone is $\frac{1}{2}(1-\cos\alpha)$. It follows that a fraction of the light given by $1-3(1-\cos\alpha)=3\cos\alpha-2$ is permanently entrapped in the crystal. In Table IV the percentage of light escaping from each face and the percentage entrapped under the above assumptions is listed for a number of crystals of scintillation counter interest. It is evident that very serious losses may occur with the higher index materials. Similar results hold for other geometric forms although the quantitative calculation may become extremely difficult in some cases. For example, it is not difficult to show that the fraction of light permanently entrapped in a sphere with an optically smooth surface is $(\cos\alpha)^3$. This quantity is also listed in Table IV and shows a sphere to be a somewhat less favorable shape than a rectangular prism of comparable volume.

Some of the light emitted into the favorable cones above will also be reflected in accord with Fresnel's laws. The fraction of the incident light transmitted may be computed as a function of angle of incidence by use of well-known formulas,[4] and is given by $(T_{\parallel}+T_{\perp})/2$ where $T_{\parallel}$ is the transmission coefficient for light the electric vector of which is in the plane of incidence and $T_{\perp}$ is that for light having its electric vector perpendicular to the plane of incidence. This function is plotted in Fig. 5 for materials which span the range of refractive indices of scintillation counter interest. Consider, however, a ray of light emitted into that favorable cone which has its axis perpendicular to the "front" face. A fraction of it, given by the above function, will be transmitted; the remainder will be reflected and strike the back face at the same angle of incidence either directly or after total reflection from a side face. The same fraction will be transmitted and the remainder will hit the front face again, still at the same angle of incidence. Because of the assumption of complete transparency, all the light will eventually emerge as this process is repeated. Furthermore, the amount lost through the back face will be exactly compensated by a corresponding fraction of the light originally directed into the favorable cone based on the back face. Hence all the light in the favorable cones escapes in the case considered; none of that not emitted into these cones. It is also of interest that light directed toward the "front" face can never escape from a side face. In practice, of course, there is always some scattering material present which changes the direction of a portion of the light allowing it to escape and there is always some absorption which degrades the remainder into heat.

It is possible, by suitable design, to avoid the above losses to a considerable extent. When using the 5819 photo-multiplier tube this can be done by cementing

TABLE II. Calculated gamma-ray absorption coefficients for $CaWO_4$, $CdWO_4$, and anthracene. τ_{PE}, τ_C, and τ_{PP} are the absorption coefficients for photoelectric effect, Compton effect, and pair production respectively.

		Energy of gamma-rays (in Mev)						
		0.5	1.0	1.5	2.0	3.5	5.0	10.0
$CaWO_4$—	τ_{PE}(cm^{-1})	0.254	0.058	0.029	0.019	0.010	0.006	0.003
	τ_C(cm^{-1})	0.410	0.346	0.280	0.237	0.170	0.135	0.084
	τ_{PP}(cm^{-1})	—	—	0.004	0.011	0.054	0.088	0.164
	τ_{total}(cm^{-1})	0.664	0.404	0.313	0.267	0.234	0.229	0.251
$CdWO_4$—	τ_{PE}(cm^{-1})	0.299	0.065	0.034	0.022	0.012	0.007	0.005
	τ_C(cm^{-1})	0.504	0.431	0.349	0.295	0.213	0.168	0.104
	τ_{PP}(cm^{-1})	—	—	0.005	0.014	0.071	0.116	0.218
	τ_{total}(cm^{-1})	0.803	0.496	0.388	0.331	0.296	0.291	0.327
Anthracene	τ_C(cm^{-1})	0.102	0.074	0.062	0.050	0.030	0.026	0.025

---

[4] See, for example, J. A. Stratton, *Electromagnetic Theory* (McGraw-Hill Book Company, New York, 1941), p. 496.

TABLE III. Absorption coefficients for x-rays. μ/ρ and μ are the mass and linear absorption coefficients respectively.

	Wave-length of x-rays (A) energy of x-rays (Mev)	0.5604 0.0220	0.7097 0.0174	1.5392 0.00803	1.9344 0.00638	2.2869 0.00540
$CaWO_4$	(μ/ρ)(cm^2/g)	36.42	70.38	145.7	256.2	370.7
	μ(cm^{-1})	223	431	890	1570	2270
	$(2.303/\mu)$(microns)	103	54	26	15	10
$CdWO_4$	(μ/ρ)(cm^2/g)	32.60	63.24	162.3	297.4	428.8
	μ(cm^{-1})	258	500	1280	2350	3390
	$(2.303/\mu)$(microns)	89	46	18	9.8	6.8

the crystal to the tube envelope so that the light never passes through air (or vacuum). Under these circumstances the refractive index of the crystal in the formulas for trapped radiation is replaced by the ratio of this index to that of the tube envelope. This is a smaller number than η and hence a larger fraction of the light can escape. In fact, it can be shown that if this ratio becomes less than 1.225 all the light escapes. Under these circumstances the light from a rectangular prismatic crystal cemented to the 5819 tube and silvered on the other five sides would be almost completely funneled to the photo-cathode. If, however, the ratio were still 1.414 or greater not more than one-third of the total light would strike the photo-cathode—i.e., that directed toward the front and back faces.

The methods of the last paragraph are not applicable to the 931A type tube because the light must traverse a region of refractive index $\eta=1$ in reaching the photo-cathode. It may be shown that attaching a film or a plate of different refractive index between the crystal and air (or vacuum) would not change the over-all critical angle and hence the amount of light entrapped. Under these circumstances it is probably best to introduce a non-absorbing, scattering medium into the crystal or to roughen one or more of its surfaces to produce diffusion. In this way the direction of the light rays is changed and, in the absence of absorption, all the light can eventually escape since it will ultimately reach a surface at an angle less than the critical angle. Precipitation of a cloud of transparent particles of different refractive index in the body of the crystal, controlled introduction of many very fine bubbles, and rough grinding of the surfaces have all been found to be very efficient for this purpose. A mosaic made up of several crystal bars, the adjacent surfaces of which have been rough ground before cementing together with a transparent cement of different refractive index, makes a particularly favorable arrangement for a coincidence device in which two photo-cells look at the same crystal.

When working with a 931A type photo-multiplier tube some care must be taken in the selection of the mirror arrangement to be used if the maximum gain is to be obtained. Marshall, Coltman, and Bennett[5] have shown that the photo-cathode in this tube is effectively 12 mm×5 mm in linear dimensions and it is situated behind a focusing grid at some distance inside the envelope. This fact limits the solid angle of radiation which can be accepted by the photo-cathode to a rather small fraction of that of a hemisphere. The light emitted by each face of the phosphor, on the other hand, is spread into a whole hemisphere but that emerging near grazing refraction is somewhat decreased in intensity due to the falling off of the curves of Fig. 5 as the critical angle is approached and hence the longer path of these rays in the crystal. If the crystal is much larger than the photo-cathode, the light from the four side faces is inevitably lost (for $\eta \gtrsim 1.414$) and hence not more than one-third of the total light can be used even if the crystal be silvered. If the crystal is smaller than the photo-cathode, there will be a small loss attendant upon silvering the side faces because a portion of this light would, in the absence of the silvering, reach the photo-cathode. Evidently silvering the back face would about double the light reaching the photo-cathode. However, the most favorable mirror arrangement for a small crystal is probably similar to that of Marshall, Coltman, and Bennett who use a hemispherical mirror the diameter of which is large relative to the crystal. In this way, instead of the approximately two-fold gain realized by the silvered crystal, a gain approaching sixfold is possible. Crude experiments with aluminum foil have indicated the essential soundness of this approach.

TABLE IV. Percentage of generated light emitted from each face of a rectangular prism$^{(A)}$ and percentage entrapped in such a prism$^{(B)}$ and in a sphere$^{(C)}$ on the assumption of polished, optically smooth faces, no scattering, and no absorption. $\alpha=\sin^{-1}(1/\eta)$ where η is the refractive index.

Crystal	η	(A) $100(1-\cos\alpha)/2$	(B) $100(3\cos\alpha-2)$	(C) $100(\cos^3\alpha)$
$CdWO_4$	2.3	4.98 percent	70.0 percent	73.0 percent
$CaWO_4$	1.93	7.23	56.2	62.6
NaI	1.77	8.74	47.5	56.2
KI	1.68	9.86	40.8	51.9
Anthracene	1.59	11.05	33.9	46.5
Naphthalene	1.58	11.22	32.8	46.4

TOTAL ANODE CURRENT MEASUREMENTS

In most of the experiments to be reported a single 1.67-mg radium source was used. It was shielded with steel and, after shielding, gave 1.4 mr per hour at 1 meter with a standard survey-meter. The photo-multiplier tube was a selected 1P21 type operated at

---

[5] Marshall, Coltman, and Bennett, Rev. Sci. Inst. 19, 744 (1948).

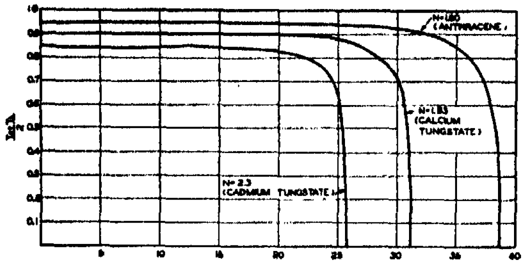

FIG. 5. Fresnel transmission function.

115 volts per dynode obtained from Eveready Mini-Max Batteries (No. 493) by means of a suitable voltage divider. The voltage drop in the load resistor in the anode circuit of the photo-multiplier tube was bucked out as indicated by a Leeds and Northrup Model 2420C galvanometer having a sensitivity of 0.019 μA/mm, and the potential across the bucking network was read. The photo-multiplier tube, attached crystal and voltage divider were mounted in an aluminum box which had a very thin aluminum cover which could be removed to change crystals and so arranged that the crystal was irradiated through the cover. As a matter of practice the response was measured with the source at a series of distances from the phosphor and the data were plotted on log—log paper. Because of the finite size of the source compared to the distances of separation the inverse square law was replaced with an inverse 1.7 power law. Typical plots are shown in Fig. 6.

A number of preliminary experiments were carried out with crystals of different size to find the permissible range of positions with respect to the photo-cathode over which no significant variation in response could be detected. When these had been found great care was taken in centering the crystals studied to insure comparable results. Finally to correct for changes in response due to aging of the photo-multiplier tube, temperature variations, and drift of the voltage supply batteries, and thereby secure day to day reproducibility, a number of crystals were selected and maintained as standards so that they could be checked from time to time and slight adjustment of circuit elements made to secure a constant response. The variation in response to the standards was always less than 7 percent over any experiment. Whenever possible crystals being compared were ground and polished to the same shape and size. If this was not possible the relative responses were corrected to the same volume basis, although in most cases the correction was a minor one.

A series of nine identically shaped $CaWO_4$ pieces fabricated at different times and under different conditions were carefully intercompared. The anode currents with the source at 5.5 cm from the phosphor crystal ranged from 16.6 to 23.8×10^{-8} amp. with an average of 17.7×10^{-8} amp. Inspection of the samples, however, showed excellent correlation between response and the degree of cloudiness of the crystals—probably from precipitated CaO. These particles serve as diffusing media and permit escape of a larger portion of the generated light. The completely clear crystals all showed responses close to 17×10^{-8} amp. Comparison of a clear $CaWO_4$ crystal with a high quality anthracene crystal of the same shape and size prepared at the University of Rochester showed that the tungstate gave a response 3.15 times as great as the anthracene. When a clear $CdWO_4$ crystal was tested under the same circumstances, the response was 4.28 times that of anthracene. A similar comparison between crystals of $CaWO_4$ and KI(T1) showed about equal response, but it was not possible in this case to make the conditions exactly comparable.

The data of the last paragraph can be used to make a very rough comparison between the number of visible quanta emitted by the tungstates and by anthracene under identical conditions of gamma-ray stimulation. This is done by correcting for differences in gamma-ray absorption ($[1-e^{-\tau d}]$ where τ is taken from Table II and d is the crystal thickness), the amount of entrapped light $\frac{1}{2}(1-\cos\alpha)$, and the differences in response of the photo-multiplier tube to the fluorescent radiation.[6] When these corrections are applied and the above data substituted, it is found that the same number of fluorescent quanta are generated in $CaWO_4$ as in anthracene and twice the number in $CdWO_4$. However, these results may be uncertain by perhaps a factor of two because of failure of the crystal to stop the recoil electrons, etc.

The expected increase in response of $CdWO_4$ when a diffusing medium is added has also been observed. Three crystals of this material of the same color but respectively clear, partially cloudy, and entirely cloudy were compared with an anthracene crystal of identical size and shape. The relative responses to the gamma-ray source as measured by the total anode current were 4.28, 5.00, and 6.25, respectively. Use of an aluminum foil reflector somewhat more than doubled the anode current from each but left the relative response substantially unchanged. The composition of the material producing the clouds in the crystals is not known with certainty.

It has been shown in considerable detail by Kröger[7] that the tungstate phosphors show a considerable temperature dependence of luminescent output when stimulated with ultraviolet light. As may be seen from Fig. 27 of reference 7 each of these phosphors tends to approach a limiting low temperature efficiency which is maintained over a considerable range. On heating, however, a characteristic temperature of the phosphor is reached at which the response begins to decrease and this decrease continues gradually and non-linearly toward zero with further heating. The same behavior is observed when the crystals are used for gamma-ray counting as is seen in Fig. 7 where the fraction of the response at 30°C is plotted against temperature. These data were collected by placing the crystals in an oven at some distance from the photo-multiplier tube and "piping" the light to it through a Pyrex rod. In this way only the temperature of the crystal was varied. The data agree quite closely with those of reference 7. The temperature of half-response is 86° for $CaWO_4$ and 118°C for $CdWO_4$. Below 40°C the temperature coefficient of the latter is seen to be zero.

---

[6] R. W. Engstrom, J. Opt. Soc. Am. 37, 420 (1947).

[7] F. A. Kröger, *Some Aspects of the Luminescence of Solids* (Elsevier Publishing Company, Amsterdam, 1948).

A further significant difference between calcium and cadmium tungstate is associated with the afterglow following exposure to intense radiation. A sample of the former was placed near a 20 millicurie Sr^{90} beta-ray source for a period of sixty hours after which it was quickly removed and placed in front of the photo-multiplier tube in the device for measuring anode current. Strong phosphorescence was observed which decayed as shown in Fig. 8. At the two breaks in the curve the crystal was removed from the container and exposed to the room light for the indicated period of time. In each case the emission was considerably enhanced in this way but this extra luminescence rapidly decreased to the slower rate of decay characteristic of the darkened crystal. The light storage properties are rather remarkable in that the above sample still showed appreciable phosphorescence (in the form of a considerably enhanced "background" count) more than nine months after exposure to the Sr^{90} source.

When the above experiment was repeated with samples of cadmium tungstate no phosphorescence was observed after the few seconds necessary to transfer the crystals from the Sr^{90} source to the photo-multiplier tube compartment. The same relative behavior of calcium and cadmium tungstate has been observed after exposure to an intense x-ray beam ($\approx 10^6$ roentgens). So far as the writer is aware, cadmium tungstate is the only useful scintillation counter crystal which shows this complete absence of afterglow following exposure to intense radiation.

A few preliminary experiments were performed to test the response of the tungstates to x-rays. The Geiger counter on a North American Philips x-ray Spectrometer was replaced with the crystal and a 1P21 photo-multiplier tube the output of which was fed into a counting rate meter and the counts per second recorded with a Brown Recorder. The spectrum from the copper target x-ray tube was scanned by placing a cleaved single crystal of rock salt in the specimen holder. Both tungstate phosphors showed very similar behavior and both showed increased sensitivity at the shorter wave-lengths. The minimum intensity detectable at 1.54A gave 10,000 counts per minute with the Geiger tube, while the minimum detectable intensity at 0.5A gave 600 counts per minute with the Geiger tube; but part of this difference is the result of decreased efficiency of the Geiger counter at the shorter wave-lengths.

PULSES FROM THE TUNGSTATES

For some purposes the total anode current measurements are inadequate and it is necessary to count individual pulses. The electron released by the gamma-ray probably excites the phosphor in a very short time and the decay following excitation is probably exponential, although there are few enough luminescent quanta involved so that considerable statistical fluctuations are to be expected. If it be further assumed that a constant fraction of the light emitted each instant reaches the photo-cathode, the current pulse in the load resistor will be of the same form. This seems to be confirmed by the few studies that have been made with very fast oscillographs. The only amplifiers available for the present work, however, had rise times of about 0.15 microseconds which is of the same order of magnitude as the probable time constant of the exponential phosphor decay. Investigation of the transient response of broad-band amplifiers to such pulses indicates that the pulse observed will have a characteristic shape which will allow the time constant for phosphor decay to be estimated if the rise time of the amplier is known.

Many pulses from the tungstates have been photographed using an Atomic Instrument Company Model 204B Linear Amplifier and a DuMont Model 248A Oscillograph. The traces observed using a triggered sweep of 2.5 microseconds duration are consistent with a time constant of phosphor decay of about 0.5 microseconds. In addition, calcium tungstate tended to show one or more smaller peaks on the same trace. In general, these had less than one-third the amplitude of the triggering pulse and were observed much less frequently with cadmium tungstate and with anthracene. In view of the long afterglow of the calcium compound mentioned earlier, these subsidiary peaks may represent energy stored in the phosphor and released compara-

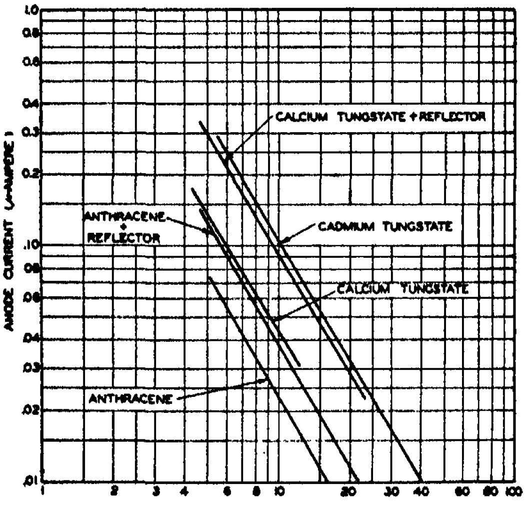

FIG. 6. Total anode current at various crystal to source distances.

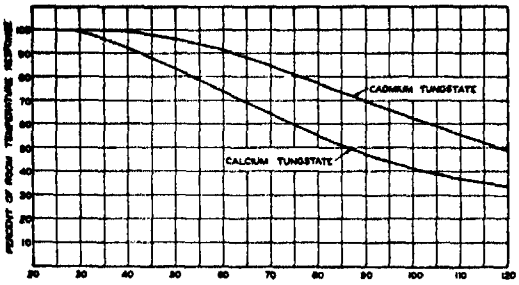

FIG. 7. Temperature dependence of luminescent output.

tively slowly, perhaps by some phosphorescent mechanism distinct from that for the main luminescence. In effect, the pulses have long, low tails. In cadmium tungstate and anthracene the small peaks observed can probably be accounted for by noise and by direct response of the photo-multiplier tube to gamma-rays which is by no means negligible. Possibly this "tail" of phosphorescent emission would account for the observation by Bell[8] that the decay time of scheelite is about 10 microseconds. It is hoped that data with more suitable recording equipment can be obtained soon which will settle this question.

Anthracene, in common with NaI(Tl), has an especially favorable pulse height distribution curve showing a considerable fraction of large pulses.[9] In order to compare the pulse height distribution from this material with that from the tungstate phosphors, the discriminator circuit of the Model 204B Amplifier was used in connection with a scale of 64 scaler and impulse register to count the pulses at various discriminator settings. It proved to be desirable for this purpose to cool the photo-multiplier tube to dry ice temperatures. In one set of experiments the crystals were also cooled while in another the crystal was kept at room temperature and the light "piped" to the cooled photo-multiplier tube through a Pyrex rod. The results are shown in Figs. 9 and 10 where counts per minute above background are plotted against the grid bias of the discriminator. Previous experiments had proved that these grid bias values were accurately proportional to the height of the pulses in volts which triggered the multivibrator of the discriminator; although the actual height, of course, depends on amplifier gain. It is evident from these curves that the behavior of these phosphors is only slightly affected by the decrease in temperature and that the anthracene shows a considerably greater proportion of large pulses. However, extrapolation to zero pulse height would give a decidedly larger count rate for the tungstates than for anthracene in agreement with the total anode current measurements reported above.

CONCLUSIONS

Calcium and cadmium tungstate crystals show some very interesting properties as scintillation counter phosphors. They are high melting materials, chemically inert toward most of the reagents with which they are likely to come in contact, and in general they are not difficult to fabricate. The pronounced cleavage of $CdWO_4$ may be advantageous in some applications. Because of their high density and because of the presence of elements of relatively high atomic number they show strong absorption of gamma-radiation. This has a corollary that they show a considerable energy dependence as gamma-ray detectors, but this can probably be minimized by suitable methods.

Although the pulse height distribution of the tungstates is seen to be less favorable than that of anthracene, the total response to the gamma-rays of radium as measured by the anode current of the photo-multiplier tube is greater than that of anthracene by factors of 2 to 6 and undoubtedly could be made even greater by proper design. The light yield of the tungstates is probably not greatly different from that of anthracene. The total anode current from the tungstates is about the same as that from thallium activated potassium iodide. Cadmium tungstate shows a zero temperature coefficient of luminescent output in the vicinity of room temperature, and is probably unique in showing no afterglow after exposure to extremely intense radiation.

The pulses from the tungstates while well under a microsecond in duration are undoubtedly considerably

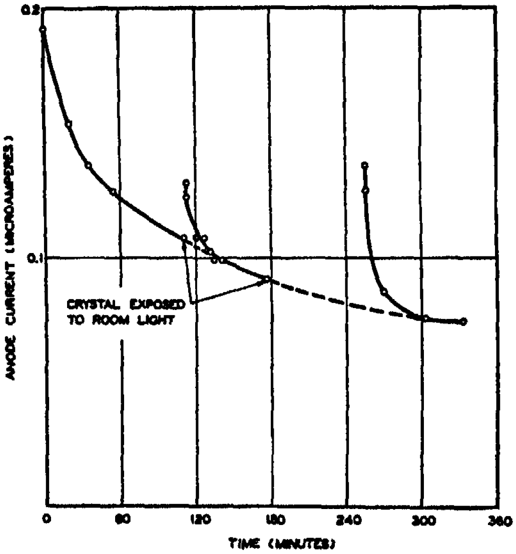

FIG. 8. Decay of calcium tungstate phosphorescence after 60 hours' exposure to a 20 mc SR^{90} source. At the two points indicated by the beginning of the broken line the crystal was removed from the photo-multiplier tube chamber and exposed to room light. When replaced in front of the photo-multiplier tube and measurements resumed the points on the solid line following the break were obtained. Note especially the greatly enhanced emission produced by the exposure to light. A portion of the initial slope may have been caused by the brief exposure of the crystal to room light during transfer to the photo-cell chamber.

---

[8] Bell, Oak Ridge Conference on Scintillation Counters (June 3 and 4, 1949); W. H. Jordan and P. R. Bell, Nucleonics 30 (October 1949).

[9] P. R. Bell, Scintillation Counting with Anthracene, AECD 1889.

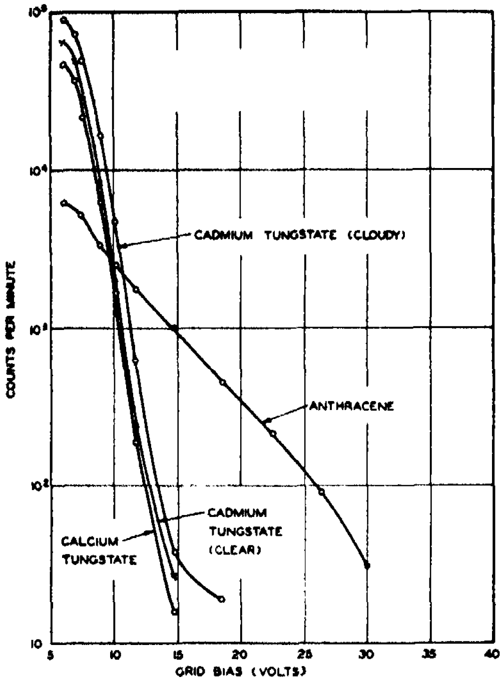

FIG. 9. Integral bias curves for a number of crystals at dry ice temperature. The background count obtained by removing the source has been subtracted from each point as well as the contribution due to direct response of the photo-multiplier tube to gamma-rays. The photo-multiplier was cooled to dry ice temperature.

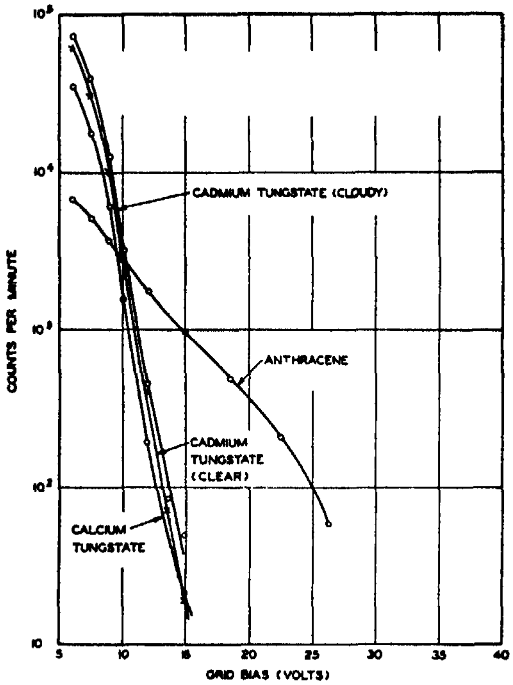

FIG. 10. Integral bias curves for a number of crystals at room temperature. The background count obtained by removing the source has been subtracted from each point as well as the contribution due to direct response of the photo-multiplier tube to gamma-rays. The photo-multiplier was cooled to dry ice temperature.

longer than those from the organic phosphors. Kröger[7] has shown that the characteristic emission of the tunstates is associated with the $WO_4^=$ ion and probably approximates an atomic emission line broadened by lattice vibrations. It seems reasonable that this is the only effect observable in $CdWO_4$ where the pulse appears to be less than 0.8 μsec. in duration. In Scheelite, however, the long phosphorescence following exposure to intense radiation and the photo-sensitivity during this phosphorescence, together with the delayed peaks seen on the oscillograph traces of the pulses, suggest that a typical phosphor mechanism associated with lattice imperfections and electron traps may also be operative. Randall and Wilkins[10] have reported photoconductivity in pressed $CaWO_4$ powders, but this result was not confirmed by the single crystal measurements of Klick and Schulman.[11] However, it appears that the lattice effect, if present, represents a rather small part of the total luminescence and hence may not have been detectable in these measurements.

In conclusion the writer wishes to acknowledge the very competent assistance of Mr. Ontario H. Nestor of this Laboratory who carried out many of the measurements reported, and to thank Dr. W. G. Eversole and his co-workers for supplying the crystals. To Dr. L. I. Dana and Dr. J. M. Gaines he is deeply indebted for many very helpful discussions of the problem and for permission to publish this work. Professor Brian O'Brien has given much valuable advice on the optical problems.

---

[10] J. T. Randall and M. H. F. Wilkins, Proc. Roy. Soc. (London) 184, 347 (1945).

[11] C. C. Klick and J. H. Schulman, Phys. Rev. 75, 1606 (1949).

A Low Frequency Sinusoidal Voltage Source

LOUIS A. ROSENTHAL
Rutgers University, New Brunswick, New Jersey

(Received December 1, 1949)

The low frequency range of an audio oscillator can be extended to d.c. by means of a heterodyning circuit using power line frequencies as a reference. The voltage wave forms are essentially sinusoidal and can be used for certain novel tests. A theoretical discussion of the beating phenomenon is included with particular applications and observed results.

A NUMBER of interesting applications exist for a low frequency sinusoidal voltage source. Frequencies extending from 20 c.p.s. to near d.c. can be obtained with the circuit described and the range of the normal audio oscillator is thus extended. The method is essentially a beating method in which an audio oscillator is heterodyned with a stable frequency source. The 60-cycle power line is excellent for the reference frequency and a Hewlett-Packard oscillator (200 B), after a sufficient warm-up period, is a very stable variable frequency source.

Wave forms can be observed on a recording-type meter such as an Esterline-Angus or Brush recorder and the period can be ascertained by knowing the chart speed. Figure 1 is a recording of some wave forms that can be obtained. Since the recorder used* has a -3-db response at approximately 1 cycle per second, the range of usable frequencies was limited. Any variable frequency test must take into account the response of the recorder.

It is worth while to mathematically describe the behavior of the modulator.[1, 2] The circuit is shown in Fig. 2. A voltage of frequency "ω_1" feeds the two peak rectifiers 180° out of phase. In addition, another signal "ω_2" is fed in phase to both rectifiers. If either signal goes to zero, the output will likewise be zero. Figure 3 shows the vector voltage addition that takes place. The locus of the vector voltage "ω_2" is a circle and its relative angular velocity is "$\omega_2-\omega_1$." Since the detectors are essentially peak detectors, the actual output voltage should be the difference between the amplitudes E_1 and E_2.

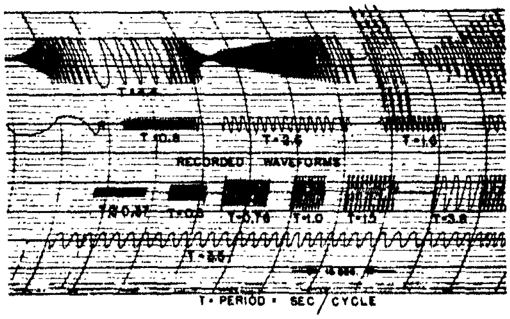

FIG. 1. Some typical recorded voltage wave forms. The frequency and amplitude can be controlled independently.

The magnitude of the voltage applied to the upper diode is

$$|E_1|=(A^2+B^2+2AB\cos\theta)^{\frac{1}{2}},$$

and that of the lower diode,

$$|E_2|=(A^2+B^2-2AB\cos\theta)^{\frac{1}{2}},$$

where $\theta=(\omega_2-\omega_1)t$. If a modulation factor is intro-

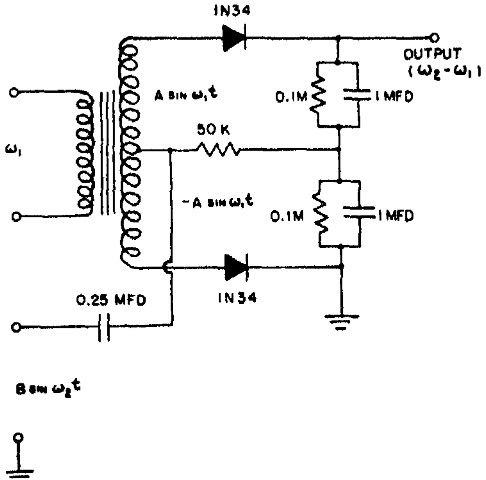

FIG. 2. The modulator circuit. The transformer is a center-tapped filament transformer; 4 volts r.m.s. on each side of center-tap.

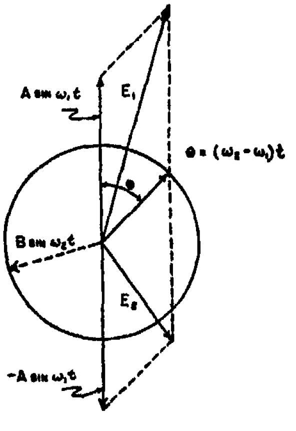

FIG. 3. The vector addition of the two voltages of different amplitude and frequency. The voltages E_1 and E_2 are the amplitudes to be detected.

---

* Esterline-Angus 1-ma 1600-ohm recording milliammeter.

[1] H. J. Reich, *Theory and Application of Electron Tubes* (McGraw-Hill Book Company, Inc., New York), first edition, p. 140.

[2] D. A. Alsberg and D. Leed, "A precise direct reading phase and transmission measuring system for video frequencies," Bell Sys. Tech. J. XXVIII, p. 237 (1949).

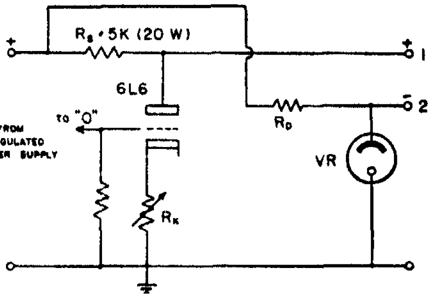

FIG. 4. The power stage driven by the modulator (see text).

duced as

$$m=\frac{2AB}{A^2+B^2},$$

then

$$|E_1|=(A^2+B^2)^{\frac{1}{2}}(1+m\cos\theta)^{\frac{1}{2}}$$
$$|E_2|=(A^2+B^2)^{\frac{1}{2}}(1-m\cos\theta)^{\frac{1}{2}}.$$

The RC filter and peak rectifier can produce a voltage that follows the magnitude, provided the modulation factor is not its maximum of 1 and the RC time constant is properly chosen.

The voltage across the two filter networks is

$$\begin{aligned}E_0&=|E_1|-|E_2|\\&=(A^2+B^2)^{\frac{1}{2}}[(1+m\cos\theta)^{\frac{1}{2}}-(1-m\cos\theta)^{\frac{1}{2}}].\end{aligned}$$

Expanding the result in a series there results

$$\begin{aligned}E_0=(A^2+B^2)^{\frac{1}{2}}\bigg[1&+\frac{m\cos\theta}{2}-\frac{(m\cos\theta)^2}{8}\\&+\frac{3}{48}(m\cos\theta)^3\cdots-1+\frac{m\cos\theta}{2}\\&+\frac{(m\cos\theta)^2}{8}+\frac{3}{48}(m\cos\theta)^3\cdots\bigg].\end{aligned}$$

Collecting terms there results

$$E_0=(A^2+B^2)^{\frac{1}{2}}[m\cos\theta+1/8(m\cos\theta)^3\cdots].$$

Thus, there is some distortion present which decreases rapidly for small values of "m." The maximum possible value for "m" is 1 where $A=B$. If one of the injected voltages is twice the other then $m=0.8$, while for a three to one ratio, $m=0.6$. The output amplitude to be expected is

$$|E_0|=m(A^2+B^2)^{\frac{1}{2}}=\frac{2AB}{(A^2+B^2)^{\frac{1}{2}}}$$

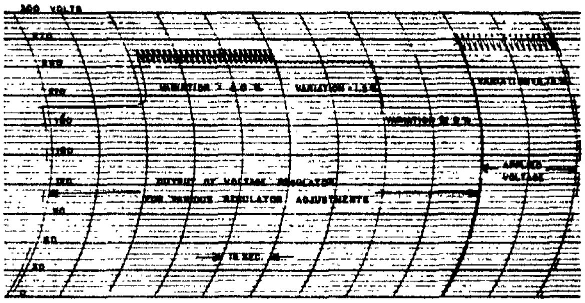

FIG. 5. The low frequency ripple before and after the regulator is observed for various regulator adjustments.

and the frequency is essentially the difference frequency "$\omega_2-\omega_1$."

The modulator, being of high internal impedance, can drive a power tube and the low frequency output can be obtained with or without a d.c. component. Figure 4 is such an arrangement. A well-regulated power supply is shunt modulated by the 6L6 as a triode. The output of the low frequency modulator is applied to the grid, and an adjustable R_k allows various d.c. voltages to appear between terminal 1 and ground. If a signal "e_g" is applied at "0," a voltage variation of

$$\frac{uR_se_g}{(1+u)R_k+R_p+R_s},$$

where u, R_p = tube parameters, will appear at terminal 1. The d.c. component can be altered by adjusting "R_k." To cancel out the d.c. component a voltage reference tube or battery can be used. Thus the amplitude of oscillation, frequency, and average value can be controlled independently. Other circuits might suggest themselves depending upon the particular application in mind.

As a typical application, consider the testing of a voltage regulator circuit. The recording milliammeter is converted to a recording voltmeter by a proper series resistance. A d.c. voltage with a superimposed alternating component is applied to the regulator, and the voltage before and after the regulator is recorded (see Fig. 5). A quantitative evaluation of the regulation properties can be made.

My thanks are extended to Mr. W. Kurylo and Mr. H. Borkan of the Department of Electrical Engineering, who assisted in the preparation of this report.

A Photo-Multiplier Gamma-Ray Detector

J. D. Graves and G. E. Koch
Naval Radiological Defense Laboratory, San Francisco, California

(Received December 1, 1949)

The sensitivity of the RCA 1P21 photo-multiplier to gamma-radiation has led to the investigation of the characteristics of this tube as a gamma-ray detector. The range, linearity, directional dependence, temperature dependence, applied voltage regulation requirements, and radiation energy dependence were determined for several tubes. Preliminary results concerning the ability of the tube to maintain a calibration are given. A basic circuit for such a detector is given.

In many high intensity measurements (order of 10 r per hr.), where the scintillating phosphor must necessarily be diminished in size or efficiency to limit the total current from the photo-multiplier, the main contribution to this current proved to be due to the action of the gammas directly upon the tube. This led to the investigation of the RCA 1P21 photo-multiplier tube without a phosphor as a possible detector of high intensity gamma-radiation. For high gamma-radiation fields such a detector would incorporate many of the desirable features of an integrating-type scintillation counter without the difficulties usually accompanying the use of a phosphor.

To determine the extent to which such a device could be applied as a gamma-radiation detector, the following characteristics of the 1P21 photo-multiplier were studied:

(a) the extent of the detectable range of gamma-radiation intensity from a radium source;
(b) the linearity of response as a function of radiation intensity;
(c) the response of the tube as a function of the direction of the impinging gamma-radiation;
(d) the temperature effect on the sensitivity from −196°C to +70°C using a fixed radiation intensity;
(e) the signal current output as a function of the total voltage applied to the tube;
(f) the response of the tube to equal roentgen intensities in the energy range from 40 to 180 kv as compared to 1.2 Mev.

APPARATUS AND EXPERIMENTAL METHODS

The detector is shown schematically in Fig. 1. The "probe" consists of a blacked-out 1P21 photo-multiplier in a metallic container to eliminate non-penetrating radiations and to provide electrical shielding and protection from shock. A negative battery supply was used to operate the photo-multiplier. Two stages of direct coupled amplification were used. To insure operation in a region where the amplifier tube characteristics are linear, and to obtain greater sensitivity, it was desirable to use a sensitive meter (0–20 μa) in the plate circuit. Metering the output of the photo-multiplier was achieved by initially shunting the meter, adjusting the grid bias for linearity of the plate current over the 20-μa range, and finally balancing out this plate current by adjusting the current flow from the meter battery. In this manner any negative voltage developed across the anode load resistor of the photo-multiplier gives a positive indication on the meter. In the most sensitive position a radium gamma-flux of 1.2 mr per hr. gave full-scale deflection at room temperature.

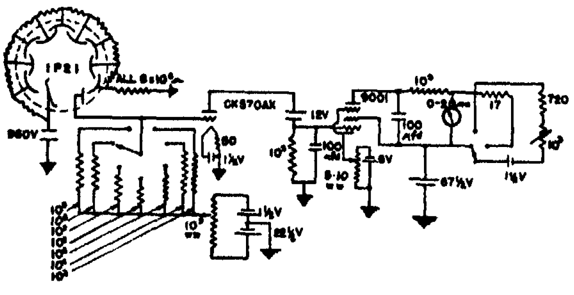

Fig. 1. Schematic diagram of the circuit used in the determination of the gamma-radiation detection characteristics of the 1P21 photo-multiplier.

The linearity of response and intensity range of the detector were determined by placing a 100-mg radium pill at various distances from the photo-multiplier, observing the plate current, and calculating the gamma-intensity at the photo-multiplier.

The response of the detector as a function of the direction of the impinging radiation was measured by moving a 1-mg radium pill around a circular path 40 cm in radius in planes perpendicular to and containing the axis of the tube.

The effect of temperature on the response of the photo-multiplier was measured with the photo-multiplier mounted in a special container designed to allow operation throughout the temperature range from −190°C to +70°C. This container was first heated to 70°C and kept at this temperature until temperature equilibrium was established as indicated by a constant output. The temperature of the container was then rapidly lowered approximately 5°C, and temperature equilibrium was again established. This procedure was repeated until liquid-nitrogen temperature was reached. After reaching liquid-nitrogen temperature equilibrium, the container was allowed to warm to room temperature at a rate which required about 8 hr. By a similar gradual process the container was then heated to 70°C. The entire temperature cycle required about 18 hr.

The energy dependence of the photo-multiplier or the response of the tube to equal roentgen intensities of varying energy was determined in the region from

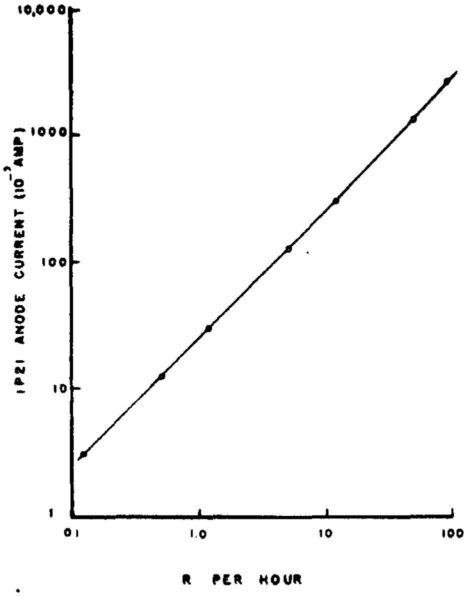

FIG. 2. 1P21 anode current as a function of gamma-radiation rate from a radium gamma-source.

40 kv effective to 180 kv effective and at 1.2 Mev by exposing the photo-multiplier to the radiations from a commercial 250-K.V.P. x-ray machine and a 200-mC cobalt 60 gamma-source. The K.V.E. output of the x-ray tube was varied by variation of the peak voltage applied and filtration, and was determined by the conventional measurement of the half-value layer of copper. Intensities were measured in the x-ray region by observing the discharge rate in thimble chambers exposed at the actual time of photo-multiplier exposure. The intensity of the cobalt 60 gamma-radiation incident upon the photo-multiplier was calculated. A total of five tubes were tested. The results presented are for one of these tubes.

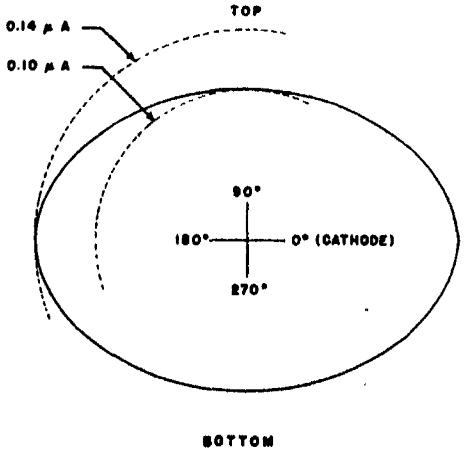

FIG. 3. Directional response of the 1P21 to a point source of radium gamma-radiation 40 cm from the center of the tube and in a plane containing the axis and intersecting the cathode of the tube.

DISCUSSION OF RESULTS

Detectable Range of Radiation Intensities

With the fixed voltage supply used, the detectable range of gamma-radiation was from 0.12 mr per hr. to 100 r per hr. The lower limit of this range is a function of the total amplification available and could theoretically be extended. When that portion of the total current from the photo-multiplier contributed by the action of the gamma-radiation is comparable to the fluctuations in the dark current, the meter time constant must be increased to minimize the effect of these fluctuations as observed on the meter. This time constant is the factor determining the lower practical limit of the detector. With the 0.1-sec. time constant used here, 0.12 mr per hr. was the lowest gamma-flux detectable. This lower limit varies by a factor of about two for the five tubes tested due to the variations in the dark current fluctuations from tube to tube.

The upper limit of this instrument, 100 r per hr., is not the true upper limit of the instrument but is determined by the fixed circuit parameters used. At this gamma-radiation intensity, the current output from the photo-multiplier was comparable to the maximum current available, as limited by the 8-megohm voltage-dropping resistors used in the photo-multiplier power supply. By reducing the values of these resistors and reducing the voltage applied to the photo-multiplier, it would be possible to extend the upper limit of this instrument manifold.

Linearity of Response

The current output of the photo-multiplier as a function of radiation intensity is shown in Fig. 2 for the range of intensities from 0.1 to 100 r/hr. The response of the photo-multiplier is seen to be linear throughout this range. The output of the amplifier was linear on every range with the same slope, so that only a single scale multiplier was required for each range. As a matter of convenience the photo-multiplier anode load

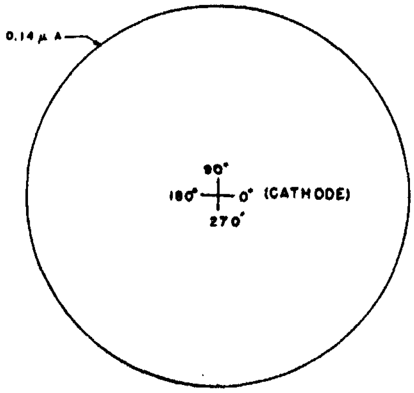

FIG. 4. Directional response of the 1P21 to a point source of radium gamma-radiation 40 cm distant from the center of the tube and in a plane perpendicular to the axis and bisecting the cathode of the tube.

resistors were adjusted so that the multiplier increased by a factor of ten with successively increasing ranges. All tubes tested exhibit a linearity in response; however, a slight shift in applied voltage is necessary to maintain a calibration between tubes.

Directional Response

The directional properties obtained are shown in Figs. 3 and 4. For all five tubes, a 40 percent change in current is observed when the source is moved from a point on the axis of the tube 40 cm above or below the center of the cathode to a point equally distant in a plane perpendicular to the axis and through the center of the cathode (Fig. 3). There is no observable difference in the response of the tube to equal radiation flux from the top or the bottom of the tube. It may be seen from Fig. 4 that the response of the tube is independent of the direction of the impinging radiation in a plane perpendicular to the axis of the tube and passing through the center of the cathode.

Effect of Temperature

The temperature dependence of the current output of the tube is indicated in Fig. 5 for increasing temperatures and for decreasing temperatures. The slight difference in appearance of the two sets of data may be due either to a difference in the physical position of the dynodes, because of expansion and contraction, or to a lag in the emission properties of the surfaces. Figure 5 shows these temperature characteristics to be independent of applied photo-multiplier voltage. It may be seen that the contribution of the dark current to the total current from the photo-multiplier increases rapidly with increasing temperature above 25°C. Above about 70°C the dark current is still rising rapidly, but the contribution due to the signal remains essentially constant. The effect of applied voltage upon these two contributing factors at 70°C is shown in Fig. 6. The temperature dependence curves were found to maintain a similarity of shape from tube to tube, but the temperature at which the decrease in sensitivity with increasing temperature began (in this case −10°C) shifted as much as 20°C in either direction. The general shape of the dark current curve with temperature was also similar, but its value at a given temperature showed 100-fold variations in magnitude from tube to tube. The choice of a photo-multiplier for maximum signal to dark current ratio throughout a temperature range should be made through consideration of the temperature at which the sensitivity of the tube begins to decrease as well as the initial signal-to-noise ratio.

Sensitivity as a Function of Voltage

The output of the tube as a function of voltage is shown for two constant temperatures in Fig. 6. In both cases the percentage change in current output is greater at the low voltage portion of the curve than it is at the high. The actual magnitude of the change, however, is greater at high voltage than at low voltage. It is significant to note that the percentage increase in dark current at the higher temperature is far greater than the corresponding increase in signal current. For example, at 1040 v, dark current is less than 50 percent of the total current, while at 1140 v, the dark current represents more than 80 percent of the total current. There is no measurable dark current present in the output at −80°C. In both cases a one percent increase in applied voltage causes a 10 percent increase in current output. Although the signal-to-noise ratio, and therefore the relative sensitivity of the signal and dark current to voltage, varies greatly from tube to tube, the sensitivity of the total current output to the applied voltage is essentially the same for all five tubes.

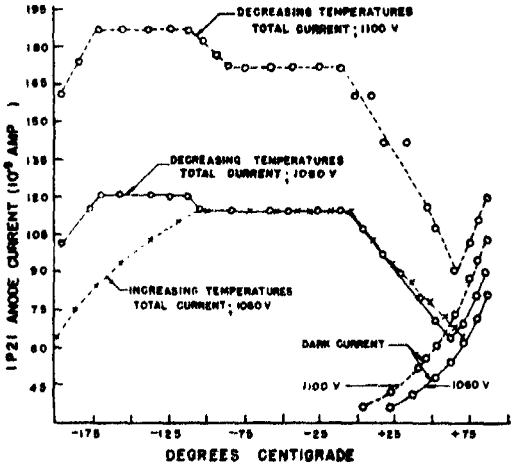

FIG. 5. The effect of temperature on the signal current and dark current output of the 1P21 for 1060 and 1100 total tube voltage. The response of the tube with increasing and decreasing temperatures is shown at 1060 v. A constant intensity of gamma-radiation was used.

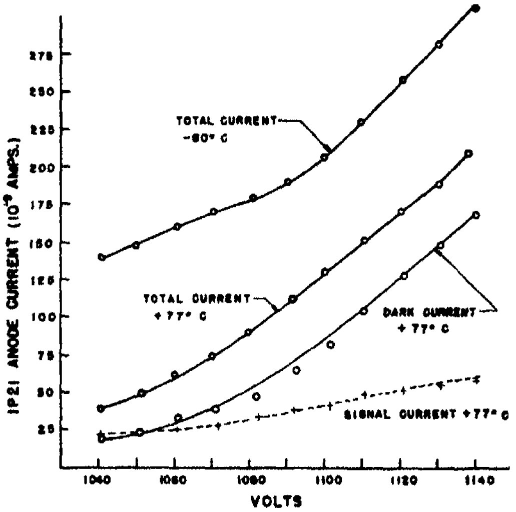

FIG. 6. The effect of applied voltage upon the total 1P21 anode current at −80°C, and the total current and dark current at 77°C.

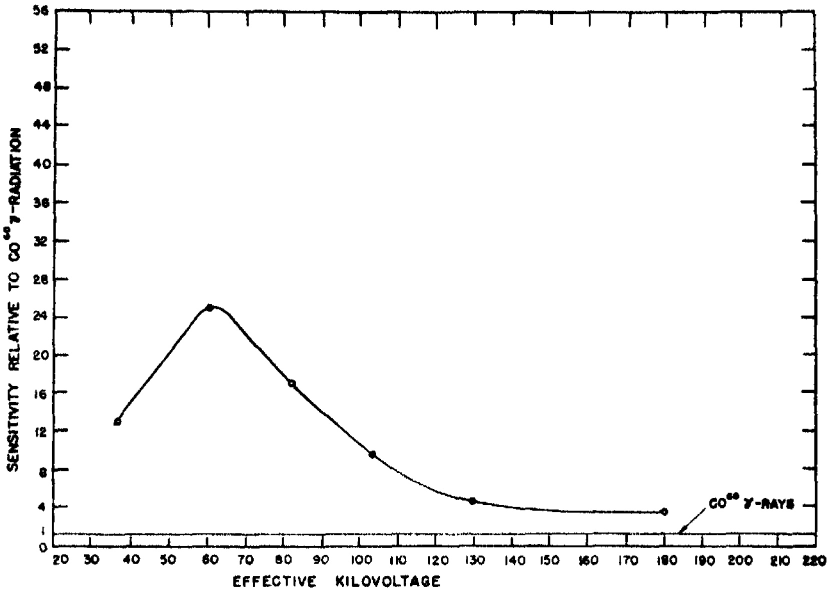

FIG. 7. The sensitivity of the 1P21 photo-multiplier to x-radiation relative to Co^{60} gamma-radiation as a function of the x-ray energies expressed in effective kilovolts.

Energy Dependence

The sensitivity of the photo-multiplier to x-radiation in the range from 40 to 180 K.V.E., relative to cobalt 60 gamma-radiation, is shown in Fig. 7. This curve is for constant roentgen radiation intensity and is therefore the ratio of current output of the tube to the ionization in air, as a function of energy.

The sensitivity of the tube to 60-K.V.E. x-radiation is seen to be 24 times its sensitivity to the 1.2-Mev gamma-radiation. At 130 K.V.E. the sensitivity is only five times that at 1.2 Mev. Although this dependence upon energy appears rather extreme, it is similar to that of other heavy-walled counters and less than that of some of the inorganic scintillation counters.

The ability of the photo-multiplier to maintain a constant anode current over long periods of time when irradiated by a constant source is being investigated at the present time. The detailed results of this investigation will be presented at some future date. It has been observed, however, that some photo-multipliers operated at a constant temperature of 0°C, a constant applied voltage, and exposed to a constant radium gamma-flux exhibit an initial decay in output current varying in time from several hours to several days and in magnitude from a few percent to 50 percent. Several of the tubes showed a constant current output for two months after the initial decay. With a few of the tubes the initial rapid decay was followed by a continued linear decay. Removal of the constant temperature conditions produced extreme variations in the output current, presumably due to the variation in room temperature.

CONCLUSIONS

The wide range, linearity of response, and directional properties of the photo-multiplier appear to make it a suitable gamma-radiation detector. The pronounced energy dependence below 0.5 Mev can introduce serious errors in measurement of radiation fields unless the energy distribution of the radiation is known and the detector calibrated for it. The use of shielding around the photo-multiplier can reduce this energy dependence considerably over wide ranges of gamma-energy. Although the use of shielding accentuates the energy dependence in the low energy region below the peak (60 K.V.E.) and tends to move the peak to higher energies, the energy dependence in the high energy region above the peak will be diminished.

In applications where the temperature range of expected use is in the region of changing sensitivity of the tube, it is necessary to provide some compensation for this effect in order to obtain a quantitative measure of the radiation field. Compensating thermistors in the metering circuit and the dark current bucking-out circuit can be used successfully over given temperature regions to minimize this temperature dependence.

The effect of applied voltage on the response of this detector presents a similar disadvantage. As a one percent change in total applied voltage causes a ten percent change in response, some degree of regulation would be required for quantitative results.

The extreme speed possible with this type of detector is of value in measurements of rapidly changing high gamma-flux.

A Dust Electricity Analyzer*

W. B. Kunkel and J. W. Hansen
Department of Physics, University of California, Berkeley, California

(Received November 15, 1949)

An apparatus is described by means of which the size and the charge of large numbers of microscopic particles can be simultaneously determined. The method is based on Hopper and Laby's work on the determination of the electronic charge, i.e., horizontal deflection of particles settling under gravity recorded photographically. The procedures involved are given in some detail, and the nature and limitations of the general results are discussed. Simplicity of operation and design are emphasized to render the instrument a workable tool in industrial research.

THE electric charges of the particles in dust clouds and aerosols are of increasing interest, both practically and theoretically. In the first place, all industrial processes in which materials in powder form are used are affected by the electrical behavior of the particles; occasionally direct use is made of the charges acquired by them.[1] On the other hand, it is obvious that the analysis of the electric charges generated at the surfaces of microscopic particles by contact and friction represents a powerful method in the study of surface phenomena because the areas involved are large compared to the volumes and because the charges that can be measured are extremely small. For these reasons, it was considered desirable to describe here a relatively simple arrangement by means of which the charges and sizes of the individual particles of a sample of a dust cloud can be determined in a single experiment.

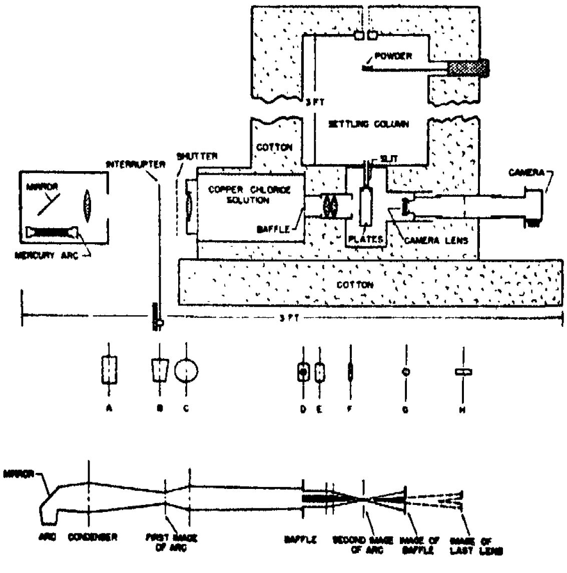

FIG. 1. Sketch of apparatus, drawn to scale in most details. Specifications of the optical elements used in our arrangement were (from left to right): mirror $d=57$ mm, $f=\infty$, first and second lens $d=56$ mm, $f=52$ mm, third and fourth lens (coated) $d=39$ mm, $f=63$ mm, fifth lens Leica objective $f=50$ mm set at $d=f/4.5$. Note: The third and fourth lens are considerably closer to the deflecting plates than shown in the diagram. All lenses are double convex.

THE APPARATUS

The apparatus is basically that designed by V. D. Hopper and T. H. Laby[2] for use in their determination of the value of the electron. Since these authors, however, did not describe their arrangement in sufficient detail for duplication, and since for the dispersion of dust clouds a large volume was needed, the system had to be redesigned and adapted to the proposed use. The apparatus required was built and put into operation in 1947.[3] As the measurements achieved by it were, however, still fairly crude and not accurate for particles below 3 microns in diameter, it was found necessary further to develop and refine the arrangement. The final successful design and operation of the device is the topic of the present article.

PRINCIPLE

The main feature of this method is to record photographically successive positions of the particles as they settle under the influence of gravity in a horizontal electric field. From the observed rate of fall, it is simple to calculate the Stokes' law diameter,[4] and from the simultaneous horizontal deflection one can thus calculate the approximate charge of the particles. Such an arrangement, however, calls for a rather special optical system to obtain a strong dark field illumination. Clearly the light cannot be introduced at right angles to the direction of observation since the plates needed to set up the field have to be vertical and solid. Illumination at acute angles introduces great difficulties of construction. Thus, observation in the direction of propagation of the light is the only practical solution. The dark field is obtained by cutting out the central cone of the highly divergent light beam so that no direct light strikes the lens of the camera. Only light scattered into this dark cone will be caught by the camera lens and thus reach the film. The complete arrangement is perhaps best explained by a simplified sketch (Fig. 1).

---

* This research was supported by ONR funds.

[1] E.g., in "Xerography," see Chem. Eng. News 26, 3264 (1948).

[2] V. D. Hopper and T. H. Laby, "The electron charge," Proc. Roy. Soc. A178, 243 (July, 1941).

[3] J. W. Hansen, Phys. Rev. 72, 741 (1947), and 73, 532 (1948); also, "The electrost. charge on insecticidal dusts," thesis (1948), unpublished.

[4] W. B. Kunkel, J. App. Phys. 19, 1056 (1948).

The optical system was designed to yield optimal contrast, i.e., maximum intensity with minimum scattered background, using the lenses at our disposal at the time of construction. It should be noted, however, that it seems possible to improve the performance of the instrument by proper changes in the dimensions indicated in Fig. 1. The following description, therefore, emphasizes the important features of the arrangement, rather than the exact dimensions. In this description items will be referred to by their letter designations in Fig. 1.

DESCRIPTION

A high pressure mercury arc, water cooled, G. E. Type A-H6, serves as light source. It has to be operated in a horizontal position, so that a prism or a front silvered mirror is needed to tilt the virtual source into an upright position. The beam is first focused at a short distance by a large lens of short focal length. Near this first image of the source, a rotating disk interrupter which is driven by a synchronous motor is introduced. The interrupter, 12 inches in radius, was geared to run at 450 r.p.m. by a motor running at 1800 r.p.m. It carried four openings of 6° (*B*), two or three of which could be closed according to the time intervals to be observed. Since the intensity emitted by the arc fluctuates with 120 maxima per second, it is essential to line the shutter disk up so that maxima occur whenever an opening crosses the optical axis. Behind the disk a hand operated shutter is mounted. It is opened only during an actual observation. This shutter keeps all light and heat out of the system when no illumination is needed. A second large lens, similar to the first, condenses the light into a slightly converging beam which passes through a large volume of aqueous solution of $CuCl_2$, reducing the infra-red intensity by about 95 percent without appreciably affecting the strong green and blue light. Directly behind this heat filter, an opaque circular baffle (*D*) of $\frac{1}{2}$-inch diameter is interposed at the center of the beam. The light that passes, mainly above and below the baffle, is admitted by an oblong aperture (*E*) to the actual analyzing chamber. At the entrance of the analyzing chamber, a system of two lenses serves to focus the beam at the center between the vertical plates to form a second and reduced image of the source. The dimensions are so chosen that the image of the opaque spot has the size of and falls on the iris diaphragm (*G*) of the camera lens (set at *f* 4.5) which is detached from the camera body and brought close to the vertical plates. The position of the camera body should be adjustable in order to make it possible to bring into focus particles that are displaced along the optical axis. It is desirable although not essential that the camera operate with a focal plane shutter. We have been using a Leica camera. If no focal plane shutter is available, the exposures can be timed by hand by means of the flange shutter between the first and second lens. A copying attachment by means of which the camera can be replaced by a ground glass plate enables visual observations to be made. Particles reaching the region of the second image which is very bright scatter much light in the forward direction, i.e., into the dark cone subtended by the camera diaphragm. However, light scattered from the last lens surfaces also reaches the camera lens and appears as background on the film. In order to reduce this disturbance, a baffle (*H*) is introduced between the camera and its iris diaphragm at the image plane of the last lens. Although it is true that this additional limitation of the solid angle reduces the intensity received by the film in some parts of the focal plane, the gain in contrast is appreciable, since most of the background is caused by the last lens (despite its being coated).

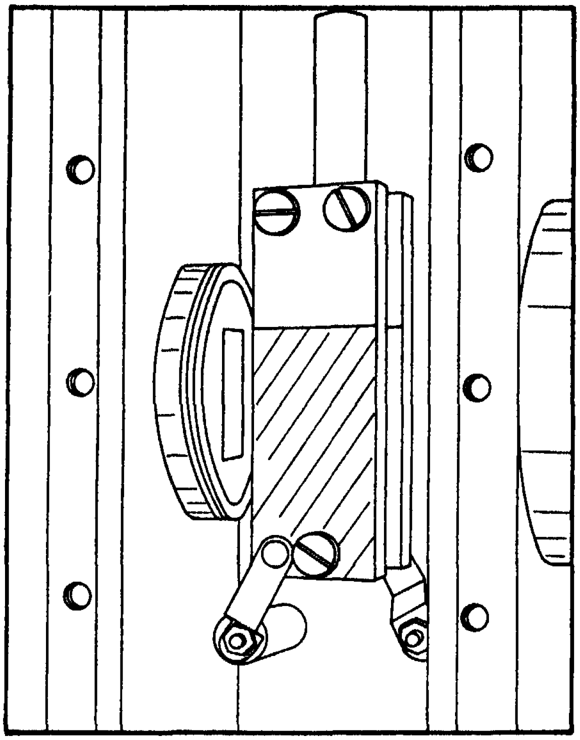

FIG. 2. View of vertical plates inside analyzing chamber. Note that the graphite coating does not reach far above the optical axis because of Eq. (5) in spite of loss of accuracy of field strength.

The sketch is drawn to scale and so are the apertures and the outline of the beam indicated under it. The dust is introduced at the top of the settling column either by blowing it through a tube or by mounting a small thimble-like container, as shown in Fig. 1, and applying a measured short blast of air from above. In either case, the volume of air blown in should be small compared to the volume of the tower in order not to cause a violent disturbance in the system. The cloud thus produced will settle under gravity and partly enter the analyzing chamber through the slit right above the region of the second arc image. The slits used were made mostly of microscope cover glass edges

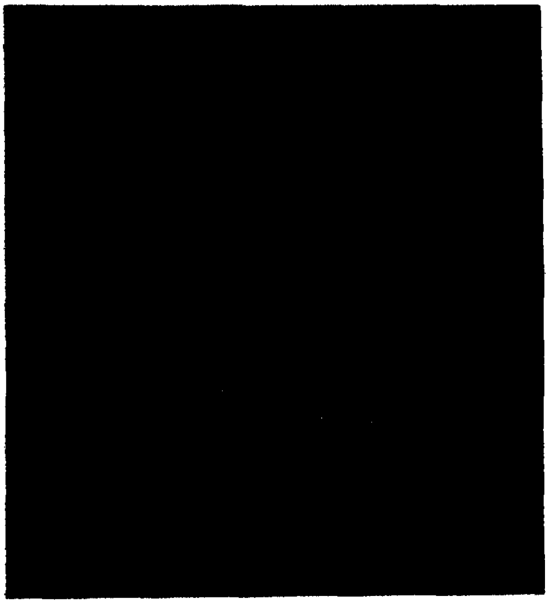

FIG. 3. Quartz particles of various sizes (2 to 9μ) settling without horizontal field. 30 flashes/sec.

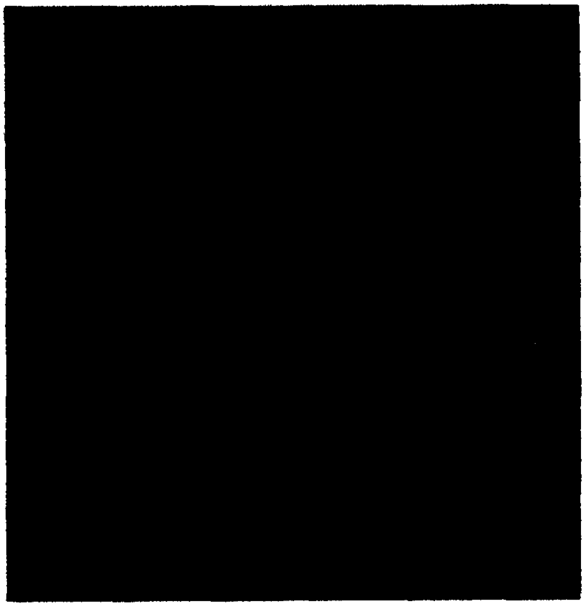

FIG. 4. Quartz smoke (mostly less than 1μ diameter) settling without field. Note how many are out of focus and how many deviate from the vertical. 7.5 flashes/sec.

which were 0.2 mm thick, 5 mm long and spaced approximately 1 mm apart. The dimensions and material of the slit are important as will be shown later.

For the observation of fine dusts, it proved advantageous to lower the slit as far down as possible to reduce the loss of particles by diffusion. The vertical plates are made of glass and coated with colloidal graphite. They are held very accurately 8 mm apart by three carefully ground quartz spacers and mounted electrically insulated parallel to the vertical walls of the chamber. Thin wire leads connect the plates through insulators to a reversing and grounding switch outside the apparatus near the camera. Ordinarily both plates are grounded, the voltage supplied by B-batteries, chiefly 180 volts, being turned on only during the actual exposures. The chamber itself is made of heavy brass mounted on a bottom plate carrying set screws and a level indicator. All surfaces inside are coated with a highly absorbing flat black paint, and all parts touched by light at grazing incidence are covered with black velvet. Since in this arrangement it is impossible to avoid light striking certain areas inside the chamber, the total time of exposure to radiation has to be limited to the utmost minimum. Only during an actual observation is filtered light admitted at the rate of at most 30 flashes, of 1/450 second each for an exposure of 1 second duration, i.e., a total illumination of not more than 1/15 second. If this illumination is not repeated after too short intervals, the absorbed energy will spread rapidly over the whole metal chamber so as not to cause any noticeable heating. After prolonged exposures, however, heating of the metal parts will result, followed by convection, rising at the walls and funneling down between the plates, increasing the apparent rate of fall of the particles. The apparatus without an elaborate thermostated heating system to maintain constant temperatures, therefore, has its limitations. If great accuracy and easy operation with long exposures are required it will be necessary to surround the entire settling tower and analyzing chamber by a thermostatic heat bath. In general, however, as in our case, wrapping the whole structure in two to three inches of cotton and keeping the room temperature constant to within a degree centigrade is all that is necessary. Under these conditions the temperature inside the system usually stayed constant within 1/100 of a degree centigrade for several hours, and the convection setting in near the end of the observation, at most, falsified the measurements on particles smaller than 1 micron in diameter. Great care should be taken to see that the camera is not shifted or tilted during a measurement. Since vibrations and shocks should be prevented from reaching the apparatus, the motor driving the rotating shutter is mounted on rubber supports resting on lead bricks, which in turn are imbedded in a large box of dry sand. No vibrations made themselves felt through this filter. A sketch of the analyzing chamber is shown in Fig. 2.

PROCEDURE

Before the actual experiments begin, the vertical as well as the correct position of the camera and the associated magnification are determined by photographing first a weighted hair hanging freely through the slit and then a small calibrated scale held in the plane of observation. To accomplish this, the apparatus has to be opened. If the same slit is used repeatedly, and if neither the camera lens nor the camera holder are moved, these operations, of course, need not be repeated. After reassembling the apparatus, sufficient time must be allowed to let the system come to complete thermal equilibrium. We actually let at least one night pass before runs were made. A long stem thermometer graded in 1/20 of degrees, the bulb of which touched the metal of the chamber, served as a check on the inside temperature.

After equilibrium is reached and all convection presumably has died down, the cloud is generated in the manner desired inside the tower near the top or it is introduced through a hole at the top of the settling column. If rapidly falling particles are expected to be present, the arc is turned on and pictures are taken at once at short intervals of, say, 10 seconds. The polarity of the horizontal *field is reversed between successive exposures to reduce the loss of particles by a steady drift toward one of the sides* caused by the bulging of the field beyond the ends of the plates. After about two minutes, when the largest particles have settled out, the intervals between pictures are gradually increased, roughly in inverse proportion to the average velocity of the particles. When after 10 to 30 minutes, the sizes and thus the rates of fall get very small, the time of exposure is increased to two, three, and finally four seconds, and the number of flashes per second is reduced by closing some of the shutter openings. This enables the measurement of particle sizes down to below two microns in diameter (depending on the density of the material). The tracks of the smallest particles of about one micron diameter and less cannot be resolved at this shutter speed. In this case the presence of completely resolved traces in the same picture are relied on to serve as a time scale. If no such traces are visible, then the scale is taken from the timing of the complete camera exposure. It would, of course, also be possible to arrange for a slower interrupter speed when these fine smoke particles are to be observed. Test runs must be made in order to determine and adjust the cloud density if possible, or to adjust the slit width so that the number of particles reaching the analyzer is neither too large nor too small for a good evaluation of the cloud properties.

Examples of tracks obtained are shown in Figs. 3 to 7. All of them are due to quartz particles. The first two pictures are taken without a field. They show that the trajectories of these particles are neither necessarily vertical nor straight. If they are very small, Brownian motion and unequal radiative heating causing photophoresis may interfere. If the particles are too heavy, their shape may cause them to skid sideways.† Figures 5 to 7 show particles of various sizes and charges. The vertical dimension of the field of view is approximately 5 mm. Since we are using the camera lens, which is corrected for distant objects, as a projector lens, particles slightly too far away will appear as circles, the diameter of which is proportional to the displacement out of focus. Similarly, point objects too close to the camera appear as blurred stars or hexagons caused by the hexagonal iris diaphragm of the camera lens.

In order to calculate the sizes and charges of the particles photographed, the negatives of the pictures

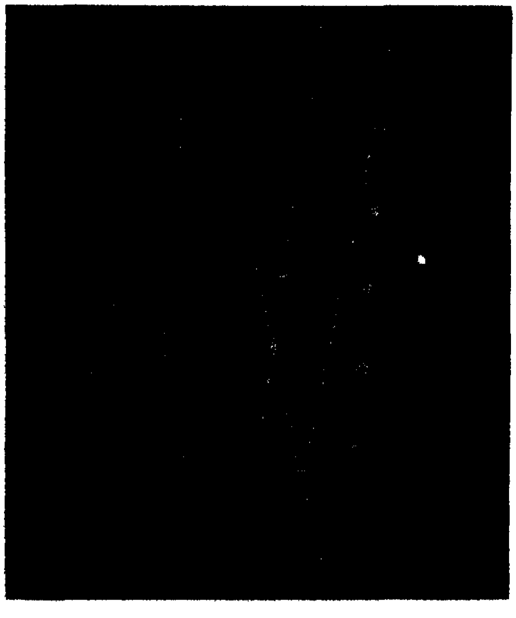

FIG. 5. Tracks of fairly large quartz particles (5 to 16μ) in a field of 225 volts/cm. 30 flashes/sec. Note the stars and circles due to particles too close and too far from the lens. Also note how the images are partially eclipsed near the upper and lower edges of the picture due to the aperture *H* in Fig. 1.

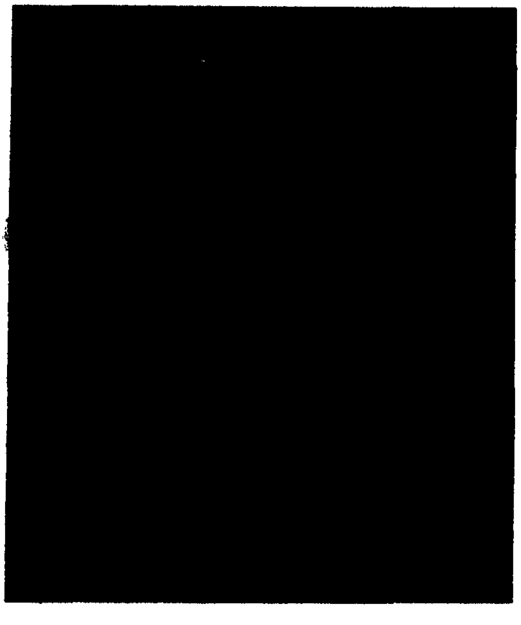

FIG. 6. Tracks of highly charged quartz particles of medium size in a field of 225 volts/cm. 7.5 flashes/sec.

---

† In a previous article it was shown that wedge-shaped platelets will appear to drift laterally as if charged. This is owing to a short time observation of the well-known helical paths of such platelets under viscous free fall.

are projected to a standard total magnification of, say, 50 onto a screen on which the vertical and horizontal displacements are easily measured. If the vertical length of a certain trace is denoted by Y and the horizontal displacement by X, the corresponding velocities are given by

$$V_x = \nu X/MN \quad \text{and} \quad V_y = \nu Y/MN,$$

where M is the magnification, ν the number of flashes per second, and N the number of intervals between dots of the trace. Using Stokes' law to estimate the particle size, we have for the diameter:

$$d = \left[\frac{18\eta V_y}{(\rho_1 - \rho_2)g}\right]^{\frac{1}{2}} = \left[\frac{18\eta\nu}{(\rho_1 - \rho_2)gM}\right]^{\frac{1}{2}} \times \left[\frac{Y}{N}\right]^{\frac{1}{2}} = A\left(\frac{Y}{N}\right)^{\frac{1}{2}}; \quad (1)$$

similarly for the charge

$$q/d = \frac{3\pi\eta V_x}{E} = \frac{900\pi\eta l\nu}{VM} \cdot \frac{X}{N} = B\frac{X}{N}, \quad (2)$$

where η is the coefficient of viscosity of the medium (air), $g = 981$, ρ_1 and ρ_2 the densities of the material and the medium respectively, and V and l the voltage (in volts) and the distance between the plates respectively. All quantities are expressed in c.g.s. units. It should be kept in mind, however, that for solid particles these formulas in general are only very approximate, since mostly we are not dealing with spheres. Both values will, at least as long as the analogy with the viscous flow holds, appear smaller than they actually are.[4] The magnitude of the error will depend on the shape and may easily exceed 10 percent, but it will hardly ever falsify the order of magnitude. This is also the reason why it is in general not necessary or justified to apply the Cunningham correction. Only for particles smaller than 1 micron, which often do not deviate appreciably from the spherical shape, will any such correction have to be considered. It should also be pointed out that the Cunningham correction opposes the shape correction, the first letting the particles fall faster than Stokes' law predicts, and the latter slowing them down again. For the same reason, the density of air can, in general, be neglected relative to the density of the material as can the temperature variation and uncertainty in the coefficient of viscosity. There is little sense in attempting to use accuracies better than 1 percent in any of the constants involved. For the objectives of these applications greater accuracy is usually not required.

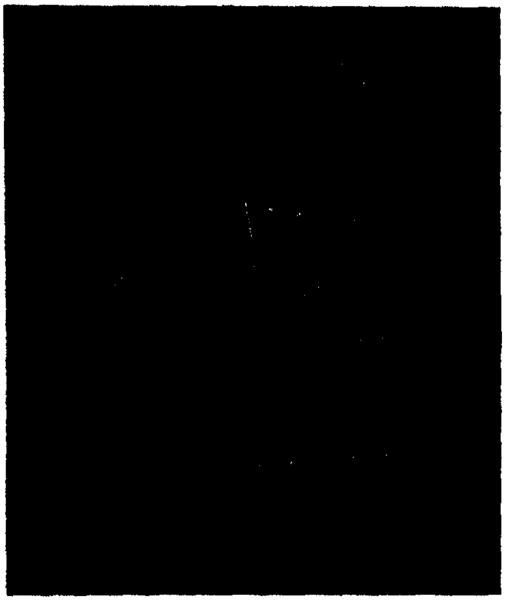

FIG. 7. Tracks of highly charged small quartz particles in a field of 225 volts/cm. 7.5 flashes/sec.

The constant B in Eq. (2) depends on the experimental conditions only, while A in Eq. (1) also varies with the density of the material involved. Both, however, will usually not change in the course of one experiment, except, perhaps, for the factor ν, the flash frequency, which might be intentionally decreased (preferably by a factor of 4) when the fast particles have settled out and only the slow small ones are being observed. The evaluation of the quantities q/d and d will then simply consist in multiplying the velocities and, respectively, the square root of the velocities, as given by X/N, and by $(Y/N)^{\frac{1}{2}}$, into these constants. This can be done by slide rule if N is counted and X and Y are measured in centimeters, but it is usually faster to employ a combined multiplying nomogram measuring tool. It is easy to see how such a device should be constructed. It should give the same reading for constant ratios Y/N etc.; e.g., by plotting N at right angles to the displacement and drawing in lines of constant slope each carrying the appropriate value of d. Taking into account the polarity on the plates and the sense of the deflection, a complete analysis of the charge and size distribution of the sample observed is obtained.

LIMITATIONS

It is essential to investigate some of the numerous instrumental limitations of the method. The most serious shortcoming of the arrangement described here is the tendency to develop convection currents inside the analyzer. If the convection has a horizontal component, it is easily detected and the experiment can be declared invalid. But it so happens that the convection currents most often are vertically upward or downward in the region that is photographed because the walls of the chamber are either cooler or warmer than the plates. In the former, the small particles whose settling rate is less than the air velocity are swept out, while those larger particles that reach the field of vision are slowed down and appear smaller than they really are. Usually this difficulty quickly becomes apparent by the general dearth and rather sudden cut-off of particles of small size. The vertically downward convection however, is not only the most likely convection, as pointed out before, but also the one most easily overlooked. All that happens is that the particles settle faster than in still air, thus appearing too large, an effect counteracting the shape correction. When the average velocities of the particles seem to increase with time, increasing downward convection is the most probable cause.

The most definite check on the reliability of the size measurement and thus indirectly on the charge estimates is a comparison of the observed size distribution with a microscopically determined one.[5] Especially convincing is a check against the dust that is collected on a cover glass placed below the region observed in the measurement. This should be done in every crucial experiment. When the size frequency curves for the photographed and collected samples show great similarity, the effect of convection can be considered negligible. Figure 8 shows an example of good agreement.

Another critical factor is the width of the slit. It will be desirable to make the slit as narrow as possible in order to admit the particles that are falling very close to the focal plane only. On the other hand, it is clear that highly charged small particles will have less chance of passing through a narrow slit than those with lower charge or larger diameter because of the attraction by the induced charges in the slit material. In order to keep this disturbing variation of the effective slit width below 10 percent for a reasonable upper limit of charge on the smallest particles to be studied, the slit will have to have a minimum width. A crude calculation giving a first approximation appears to be very simple. Consider a particle of charge q approaching the slit very much closer to one edge than to the other. Assume now that the slit material is not only conducting but that the total image charge $-q$ is concentrated on the very edge at the point of closest approach of the particle trajectory. Then the effective collision radius of the charged particle provided q is large is given by:[6]

$$a' = 2(C/V)^{\frac{1}{2}}, \tag{3}$$

where $C = q^2/3\pi\eta d$ is due to Coulomb's and Stokes' laws and $V = g\rho d^2/18\eta$ is the settling rate of the particle. Thus

$$a' = \left(\frac{24}{\pi g}\cdot\frac{q^2}{\rho d^3}\right)^{\frac{1}{2}}.$$

If this is required to be less than 5 percent of the slit width S, we have

$$S > 20a' \cong 0.001\frac{q}{\rho^{\frac{1}{2}}d^{\frac{3}{2}}}, \tag{3}$$

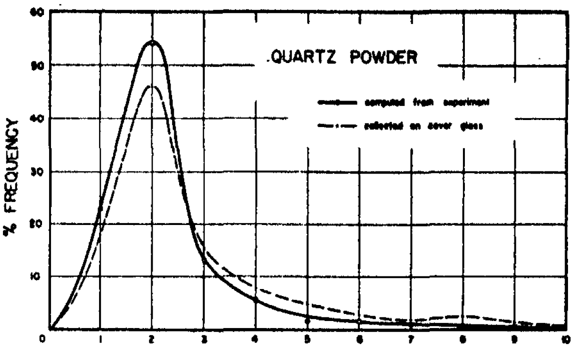

FIG. 8. Size distribution of quartz dust. Case of negligible convection; particles appear smaller in the experiment than they actually are. Sample photographed: 2500 approx., sample counted by microscope. 500 approx.

where q is now to be expressed in electrons and d in microns. For $q = 200$ and $d = 1$

$$S > (0.2/\rho^{\frac{1}{2}})\ \text{cm},$$

i.e., in general of the order of 1 mm. From this it is also clear how important it is to use a material of low dielectric constant to form the slit, since in that case the attraction will be much smaller than here calculated. In addition, it sets an upper limit for the density of the clouds to be studied. Since it would not be desirable to obtain more than N tracks per picture and since the volume visible at any time is AS where A is the area of the field of vision, we must require a density

$$n \leq N/(AS). \tag{4}$$

In our case, $A = 0.2$ cm², $S = 0.1$ cm, and taking $n = 50$, we find $N \leq 2500$ cm^{-2}, a number which is at the same time small enough to make any agglomeration during settling highly improbable.[6]

The third limitation to be considered is due to the effect of the electric field which makes itself felt at some distance above the plates. In order not to lose small highly charged particles which will drift sideways under influence of the field above the plates during an exposure, the polarity is reversed for successive observations and the time between pictures is chosen long enough to select the particles coming from a region relatively unaffected. This minimum interval T will depend on the charge q and the size of the particles, i.e., their settling rate V_0, the duration of the previous exposure τ, and the dimensions involved. As a first approximation, we find for large q and a permitted displacement $l/4$ of particles of diameter d

$$T = \frac{l_0}{V_0} + \frac{l}{2V_0}\cot\frac{3\pi^2\eta l^2 d}{2V\tau q}, \tag{5}$$

where l_0 is the distance between the observed region and the upper edges of the conducting plates. l is again the distance between plates and V their potential difference.

---

[5] For microscopic size determinations, see J. M. Dalla Valle, *Micromeritics* (Pitman Publishing Corporation, New York, 1943).
[6] W. B. Kunkel, J. App. Phys. 19, 1053 (1948).

As an example for one of our cases, we give $l=0.8$ cm, $l_0=0.5$ cm, $V=180$ volts, $\tau=4$ sec., $q=200$ electrons, $d=1$ micron, and for quartz, $V_0=0.008$ cm/sec., which yield $T=110$ sec. This means that 4-sec. exposures at 2-min. intervals will include all particles with $d\geq 1$ micron and $q\leq 200$ electrons, but may lose particles exceeding one of the limits. The relation between the critical values of q and d that will be just admitted is implied in (5) but is rather complicated as V_0 is proportional to d^2.

CONCLUSION

The apparatus described here has been used with considerable success in the study of the electrification of dusts in general and under different conditions of dispersion. It has proved to be a very workable instrument, efficient, reliable and easy to operate. The results have been reproducible, quantitative, and unambiguous, which is rare in the literature on tribo-electricity. The great advantage of the method lies in the fact that large samples can be measured, permitting reliable statistics and significant conclusions. In general it proved amply sufficient to make measurements on random samples ranging from 300 to 2000 particles, depending on how pronounced the effects were and on the accuracy required. The labor involved is not prohibitive once a method of measurement and tabulation is worked out. These features may very well make the apparatus a tool that could be employed to advantage in various branches of industrial research, and it is hoped that this description will be of some help to whoever has to investigate the charges on small particles.

We wish to express our gratitude to Professor L. B. Loeb who started us on this method of study and whose active support and helpful suggestions were essential to the development of this work.

THE REVIEW OF SCIENTIFIC INSTRUMENTS VOLUME 21, NUMBER 4 APRIL, 1950

Spectral Sensitivity of Two Commercial X-Ray Films between 0.2 and 2.5 Angstroms*

Herman E. Seemann
Kodak Research Laboratories, Rochester, New York

(Received December 12, 1949)

The spectral sensitivities of Kodak No-Screen and Kodak Industrial Type K X-Ray Films were determined in the region between 0.2 and 2.5A using the filtered K fluorescence of several irradiated elements as approximately homogeneous radiation. Exposures in roentgens were obtained with an air ionization chamber designed especially for the purpose. Curves are given showing the number of roentgens incident on the film which will give a developed photographic density of 1.0 above fog for the various wave-lengths. The K limits of silver and bromine are prominent. The maximum sensitivity in terms of roentgens occurs at about 0.4A, but the marked decrease found by other observers at shorter wave-lengths is probably obscured by inaccuracies. From the energy value of the roentgen, the sensitivity of the films is expressed as the incident ergs per square centimeter required to produce a density of 1.0 above fog. Computations from these results show that as the wave-length increases the films utilize the *absorbed energy* more efficiently. On the other hand, high energy *quanta* are more efficient than low energy quanta but not in proportion to their energy. In addition to the more or less gradual change with wave-length of efficiency of utilization of absorbed energy, there is evidence for sudden jumps at the K limits of Ag and Br. Qualitative explanations are given for the observed changes in efficiency.

INTRODUCTION

Most diffractionists are familiar with the general appearance of a photographic film which has been used to record the continuous x-ray spectrum diffracted by a crystal. In general, there is an increase in photographic response in going toward longer wave-lengths until the K absorption edge of the silver in the silver bromide emulsion introduces a sudden drop. The film density again increases to the K limit of bromine, at which another drop in density occurs. When compared with the absorption curve, such a record indicates that there is a connection between the x-ray energy absorbed and the amount of silver in the developed image. Figure 1 illustrates this point, but is subject to qualitative interpretation only since the intensity distribution in the diffracted spectrum was not known. For such a record to yield quantitative information, the energy distribution incident on the film must be known, as well as the characteristic curve (density-exposure relation) of the film and whether or not the latter relation is independent of wave-length. If separate monochromatic beams are obtained by diffraction from a crystal, the exposed areas are small and this may introduce errors due to development effects, to inaccurate densitometry or to difficulties inherent in silver analysis.[1] Thus, the experimental difficulties probably account for the scarcity of information in the literature† on the x-ray spectral response of photographic emulsions.

---

* Communication No. 1300 from the Kodak Research Laboratories.

[1] C. E. Kenneth Mees, *The Theory of the Photographic Process* (The Macmillan Company, New York, 1942), pp. 230 and 879.

† Since the completion of this manuscript, a paper on the same general subject by H. Hoerlin has been noted: J. Opt. Soc. Am. 39, 891 (1949).

In preparing data sheets on properties of Kodak x-ray films for industrial radiography,[2] it was noticed that these films did not have the same relative spectral response in the radiation quality range commonly used. The explanation for this variation was not obvious and there was little hope of obtaining adequate information by merely using the filtered continuous spectrum from a tungsten target tube.

In view of the difficulties associated with spectral-sensitivity determinations with x-rays monochromatized with a crystal, the possibility of using the *K* fluorescence from several elements was considered. Irradiating an element with continuous spectrum x-rays excited at a suitable potential and utilizing the *K* fluorescence for various experiments is an old expedient dating back to the early history of x-rays. The use of fluorescence radiation was particularly popular before the discovery of crystal diffraction since it was then the only method for obtaining a reasonably pure spectrum. Preliminary filtration-curve data supported the fact[3] that there is indeed very little continuous background associated with the *K* fluorescence. Later absorption tests comparing the radiation from a molybdenum target x-ray tube with that from a molybdenum secondary radiator showed that electron bombardment of molybdenum resulted in much more background than did x-irradiation. Both x-ray tubes were supplied with 30 kv electrically filtered to give essentially constant potential.[4] The additional facts that the fluorescence can be further purified by reducing the proportion of $K\beta$-radiation with a suitable filter and that by proper disposition of the apparatus the intensity was sufficient for exposures to be made on "fast" x-ray films in a reasonable time lent encouragement to the practicability of utilizing the $K\alpha$-fluorescence of several elements to determine spectral sensitivity of x-ray films.

Determination of spectral sensitivity required the use of some instrument with which the intensity of the x-rays could be measured. The increasingly wide use of the international roentgen‡ caused us to investigate the possibilities of instruments which would give indications in roentgens. Commercial instruments available, however, were deficient in two important respects: They were not suited for measuring in the long-wavelength region, and their construction made them unsuitable for use with our "x-ray fluorescence sensitometer," a device of special construction designed primarily for film exposures. After some experimental work, an air ionization chamber was developed[5] which had a sufficiently transparent window for the longer wavelengths, was mechanically suited for use with the sensitometer, and could be conveniently used in conjunction with the electrometer of a sturdy commercial instrument. This instrumentation made it possible to expose films to known amounts of radiation expressed in roentgens and, since the roentgen represents a certain amount of energy absorbed in air,[6] the results could also be expressed in terms of energy.

Occasional inquiries from diffractionists about the properties of x-ray films prompted us to delay work on the main problem in order to obtain information which might be of immediate practical value. Accordingly, *relative* "speeds" of several x-ray films were determined using the unfiltered *K* fluorescence from chromium, copper, and molybdenum. The work was restricted to these elements since they represent commonly used targets in diffraction tubes. No attempt was made to obtain absolute measurements, but instead, one of the films was chosen as a standard of reference for the others. *The results showed clearly that films which are quite similar in atomic composition and therefore absorb x-rays similarly do not maintain the same relative speeds at different wave-lengths.*[7]

APPARATUS AND METHOD

The low intensity of fluorescence x-rays compared with the exciting radiation necessitates careful planning and disposition of the apparatus as well as operation of the x-ray tube near its load or current limit. The schematic diagram in Fig. 2 illustrates the arrangement

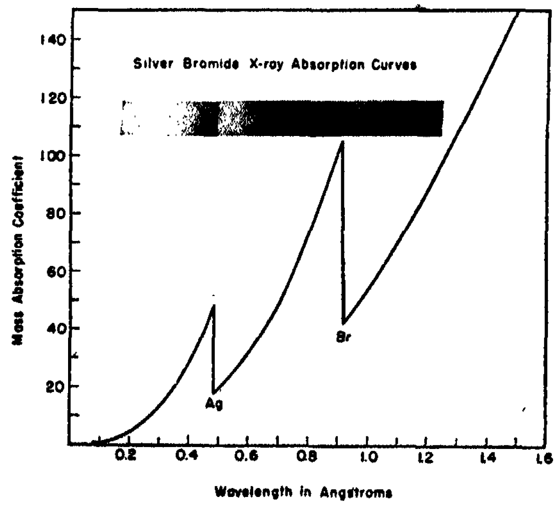

FIG. 1. Comparison of a spectrogram taken on a silver bromide emulsion with the silver bromide absorption curves. (Courtesy of *Non-Destructive Testing*.)

---

[2] "Kodak films for industrial radiography," data sheet released by the Eastman Kodak Company, Rochester, New York (April, 1945).

[3] S. K. Allison and W. Duane, Proc. Nat. Acad. Sci. 11, 485 (1925).

[4] See also A. H. Compton and S. K. Allison, *X-Rays in Theory and Experiment* (D. Van Nostrand Company, Inc., New York, 1935), p. 589.

‡ The *roentgen* is the quantity of x- or gamma-radiation such that the associated corpuscular radiation per 0.001293 gram of air produces, in air, ions carrying 1 e.s.u. of quantity of electricity of either sign. (International Committee for Radiological Units, 1937.)

[5] Details of this instrument are given in Rev. Sci. Inst. 20, 903–907 (1949).

[6] W. V. Mayneord, Brit. J. Radiol. 13, 235 (1940).

[7] "Kodak Films for X-Ray Diffraction," data sheet released by the Eastman Kodak Company, Rochester, New York (October, 1947).

of the fluorescence sensitometer and x-ray source as used in this study.

The x-ray tube was especially designed by the Dunlee Corporation, of Chicago, to operate at the high currents and low voltages necessary for this work. It had a projected focal spot about 4.5 mm square. Condensers were connected across the rectified high voltage supply to give nearly ripple-free power. This was found to furnish a steadier output of fluorescence radiation than when pulsating potential was used. It is well known that the intensity of fluorescence varies rapidly with the potential applied to the exciting x-ray tube when this potential is above the critical value required for excitation. Consequently, changes in high voltage wave form due to heating of the transformer, for example, might change the quality of the exciting x-rays enough to alter the fluorescence output. There was evidence in favor of this explanation but it was not tested to the point of conclusive proof.

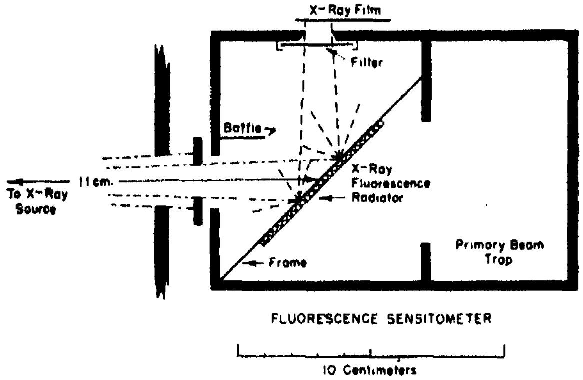

FIG. 2. Schematic diagram of x-ray fluorescence sensitometer. Heavy lines represent lead protection.

Several elements were chosen as x-ray fluorescence radiators whose $K\alpha$-emissions would permit sensitivity determinations to be made on both sides of the K absorption limits of silver and bromine. For each radiating element, another element of lower atomic number was used as a filter to isolate the $K\alpha$-doublet by absorbing the $K\beta$-doublet preferentially. A sheet of each radiating element or a suitable compound was supported by a light aluminum frame which could be placed in a compartment of the sensitometer, resting at an angle of about 45 degrees to the central ray of incident x-rays. Thus, the "fluorescence focal spot" as "seen" by the film was a disk about 2 cm in diameter. The baffle was arranged to prevent lead fluorescence emitted by the limiting diaphragm from reaching the film. The primary beam trap served a similar purpose (see Fig. 2).

For exposure, the x-ray film was placed in a cassette having a window made of a No. 87 Wratten filter. This is an infra-red gelatin filter which furnished adequate protection for the film in subdued room light but, unlike black paper, does not have a fibrous structure which would be recorded radiographically with soft radiation. The cassette was moved in a series of automatically timed steps in a direction perpendicular to the plane of the diagram. Times of exposure were $\frac{1}{16}$, $\frac{2}{16}$, $\frac{3}{16}\cdots\frac{7}{16}$ min., and the intensities were sufficient to give an adequate range of densities on Eastman No-Screen X-Ray Film, Code No. 5133, and on Kodak Industrial X-Ray Film, Type K, Code No. 5135. Both of these films are "fast" direct x-ray types. One film strip of both types exposed to each radiation, and the ionization readings taken before and after, made one run. A total of three runs was made several days apart. Considerable preliminary work was done to establish the reliability of the method. Exposed areas on the film strips consisted of a row of 1-cm squares separated by about 1 mm of unexposed film. No systematic variation in density in a square could be detected, thus proving that the fluorescent beam was sufficiently uniform in section.

Good uniformity of development was assured by developing in a machine which is a small modification of one designed for routine sensitometric testing.[8] All of the film strips for a single run were developed together for 4 min. at 68°F in Kodak Rapid X-Ray Developer. They were then rinsed in an acetic acid stop bath for a few seconds, fixed, washed, rinsed in Kodak Photo-Flo (a water-spot preventive), and dried. Densities were read on a densitometer calibrated in diffuse density.

Exposure of films in a timed series of steps made it possible to plot a density-exposure curve for each radiation and thus to interpolate to find the exposure required to produce an arbitrarily chosen density of 1.0 above fog. These data, as well as some obtained in preliminary work, have shown no systematic difference in the shape of the density-log exposure curve in the wave-length range covered[*][9] except for some uncertainty at the longest wave-length (Cr $K\alpha$) where the absorption in the "front" emulsion and film base materially affected the intensity of x-rays reaching the "back" emulsion. Thus, it would have been reasonable to have determined the characteristic curve with one radiation and to have used this as a calibration curve for *single* exposures made with the other radiations. This method would certainly save time in the exposing of films of low sensitivity, but for accuracy in the present work on films of high sensitivity there was little to choose between interpolation from single sensitometric runs and the arithmetical average of several equal exposures to each radiation, with subsequent reference of this value to one calibration curve.

For each sensitometric series, an ionization measure-

---

[8] Jones, Russell, and Beacham, J. Soc. Mot. Pict. Eng. 28, 73 (1937).

[*] Several experimenters have shown that the shape of the photographic characteristic curve is independent of x-ray wave-length (reference 9).

[9] W. Friedrich and P. P. Koch, Ann. d. Physik 45, 399 (1914); R. Glocker and W. Traub, Physik. Zeits. 22, 345 (1921); G. E. Bell, Brit. J. Radiol. 9, 578 (1936); W. Busse, Zeits. f. Physik 34, 11 (1925).

TABLE I.

Radiating element	Filtering element	Wave-length of $K\alpha$-lines of radiating element (angstroms)	Kilovolts required to excite K spectrum	Kilovolts constant potential used	Tube current in ma	Form of radiator	Form of filter	Percent absorbed by filter
24 Cr	23 V	2.29	5.98	20	40	Heavy plating	Powder,[a] V_2O_5	63
29 Cu	28 Ni	1.54	8.86	20	20	Sheet	Sheet, 0.0075 g/cm^2	38
35 Br	34 Se	1.04	13.5	28	20	CBr_4, cast slab	Powder[a]	65
38 Sr	37 Rb	0.88	16.1	28	10	Powder, $SrCO_3$	Powder,[b] $RbCO_3$	54
42 Mo	40 Zr	0.71	20.0	30	10	Sheet	Sheet, 0.029 g/cm^2	50
48 Cd	46 Pd	0.54	26.7	40	10	Sheet	Sheet, 0.031 g/cm^2	53
51 Sb	50 Sn	0.47	30.4	45	10	Powder[a]	Sheet, 0.058 g/cm^2	39
53 I	51 Sb	0.43	33.2	55	10	Powder,[a] NaI	Powder[a]	71
57 La	56 Ba	0.37	38.7	55	10	Powder,[a] La_2O_3	Powder,[a] $BaSO_4$	63
74 W	72 Hf	0.21	69.3	90	20	Sheet	Powder,[a] HfO_2+0.091 g/cm^2 copper	96
78 Pt	74 W	0.19	78.1	95	20	Sheet	Powder,[a] $CaWO_4$	98

[a] Powdered material bonded with a minimum of cellulose nitrate cement somewhat in the manner used in the manufacture of intensifying screens.
[b] Water solution with gelatin, dried to make a thin sheet.

ment[5] was made so that the x-ray intensity in the plane of the film could be expressed in roentgens per minute. Therefore, film sensitivity could be expressed in incident roentgens or in incident ergs[6] required to produce a chosen density. A No. 87 Wratten filter was placed over the ionization chamber diaphragm so that the chamber truly measured what the film received through a similar window in the cassette. The back of the cassette consisted of a plate of aluminum 0.3 cm thick covered with black felt. The scattering from the back was considered negligible compared with the incident radiation.

Table I is a summary of the conditions used in these experiments. Most of the previously published data were taken from the tables in Sproull's book.[10] Impurities or unwanted elements in the radiators and filters were deemed to be insignificant for the purpose intended.

If it is assumed that the ratio of fluorescence intensities $K\alpha/K\beta$ is the same as when these lines are emitted by a tube target,[11] i.e., about 6, it is easy to calculate what amount of filtering element will change the ratio to some chosen value, say, 20. This proposed reduction of the $K\beta$-intensity to about five percent of the intensity of the $K\alpha$ was a compromise between having a really negligible proportion of $K\beta$ and too low an intensity of $K\alpha$ for practical exposing conditions. The filtering elements used in the form of foils were a little greater in thickness than necessary to obtain this reduction of $K\beta$, but for those made up from powders and powdered compounds which were bonded together, only the crudest estimate of their efficiency was possible. The amount of filtration was necessarily an integral number of layers of the particular filter stock at hand. Final tests of spectral purity were made by absorption measurements. When it was found that the *log intensity versus mass per unit area* curve was a straight line and gave the same absorption coefficient that the $K\alpha$-radiation should give, within experimental limits, the selective filtration was considered adequate. Sufficient analyzing filtration was used to reduce the intensity to the order of one tenth of its original value, thus providing a range sufficient to give a reasonable sensitivity to departure from linearity. The radiation from 74 W and 78 Pt were found to be inhomogeneous according to the linearity criterion, but this point will be discussed later.

RESULTS

The graphs in Fig. 3 show the relation between the incident number of roentgens required to produce a density of 1.0 above fog, and the wave-length. The vertical lines at 0.485 and 0.918A represent the silver and bromine K absorption edges. Since breaks are to be expected at absorption discontinuities, it seemed proper to draw them in and to extrapolate the curves to these limits. The existence of a maximum in sensitivity (minimum incident roentgens) at about 0.4A is in general agreement with the findings of other observers[12] but no detailed comparison is justified, inasmuch as they used other kinds of film and different degrees of homogeneity of radiation. In the present work there is considerable uncertainty about the sensitivity values for the two points at the shortest wave-lengths, *viz.*, 0.19A (Pt $K\alpha$) and 0.21A (W $K\alpha$), since these radiations were definitely not as homogeneous as assumed and, what is probably more significant in the present case, the calibration of the ionization chamber was most doubtful in this region.[5] Judging by the earlier work,[12] these points should be higher.

Since the roentgen represents a certain amount of energy absorbed in air, it is also possible to calculate film response in terms of incident ergs or in terms of ergs absorbed per square centimeter. From the exponential absorption law, $E=E_0\exp[-(\mu/\rho)\rho x]$, it follows that $E_a = E_0[1-\exp(-(\mu/\rho)\rho x)]$, where E_a is the energy absorbed in a layer of air x units thick, E_0 is the incident energy, and μ/ρ is the mass absorption coefficient. But μ/ρ is an absorption coefficient which includes photoelectric or true absorption and absorption by scattering. In evaluating the roentgen, absorption by scattering must be excluded because it does not contribute appreciably to the ionization, but since the Compton recoil electrons which are associated with scattering do cause ionization, their contribution is significant for short wave-lengths. The equation is therefore rewritten,

---

[10] W. T. Sproull, *X-Rays in Practice* (McGraw-Hill Book Company, Inc., New York, 1946).

[11] See reference 4, p. 640. Y. H. Woo, Phys. Rev. (2) **28**, 427 (1926).

[12] H. Hoerlin and V. Hicks, Non-Destructive Testing **6**, 15 (1947). G. E. Bell, see reference 9. R. B. Wilsey, unpublished results obtained in Kodak Research Laboratories.

$$E_a = E_0\left(1-\exp\left[-\left(\frac{\tau}{\rho}+\frac{\sigma_a}{\rho}\right)\rho x\right]\right),$$

where τ/ρ is the coefficient for photoelectric absorption, and σ_a/ρ is the coefficient for true absorption associated with Compton scattering.

Figure 4 shows the results of this computation in terms of incident energy in ergs per square centimeter per roentgen as a function of wave-length. The value of 33 ev was taken as the approximate average energy required to produce one pair of ions in air leading to a value of 0.110 erg absorbed in 0.00129 gram of air, the energy equivalent of a roentgen.[6] Since, for 1 roentgen, $E_a = 0.110$ erg,

$$E_0 = \frac{0.110}{1-\exp[-(\tau/\rho+\sigma_a/\rho)0.00129]}$$

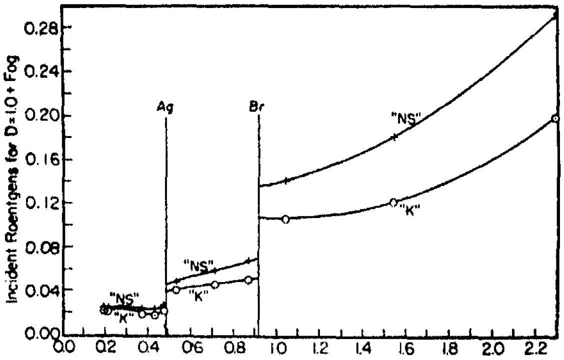

FIG. 3. Spectral sensitivities of No-Screen and Type K X-Ray Films in terms of incident roentgens required to produce a developed density of 1.0 above fog.

for wave-lengths greater than about 1A; or

$$E_0 = \frac{0.110}{0.00129[(\tau/\rho)+(\sigma_a/\rho)]} \text{ approximately,}$$

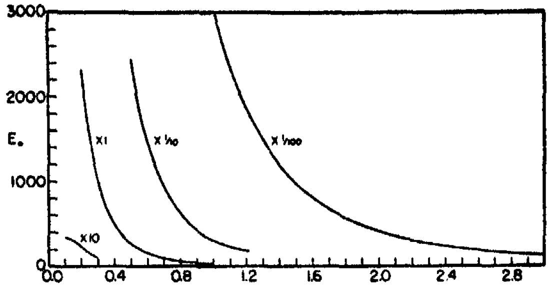

FIG. 4. The energy, E_0, per square centimeter cross section of an x-ray beam per roentgen as a function of wave-length.

for shorter wave-lengths, where the total absorption is quite small. Equation (3.185) in Compton and Allison's book[13] gives the true absorption per electron caused by scattering. From this we find that

$$\sigma_a/\rho = \sigma_{e0}N_0(Z/A)\frac{\alpha}{(1+2\alpha)^2},$$

where σ_{e0} is the classical scattering per electron, $N_0(Z/A)$ is the number of electrons per gram of air, and $\alpha = h\nu/mc^2$. The numerical values necessary to compute E_0 for different wave-lengths were taken from Victoreen's paper on mass absorption coefficients.[14] The results shown in Fig. 4 are from 10 to 20 percent higher than Mayneord's.[6] Mayneord does not give any details of his computation. Figures 5 and 6 show sensitivities in terms of the incident energy per square centimeter required to produce a density of 1.0 above fog. The single-coated films are the same exposed strips but the "back" emulsion was removed after the total densities were read. It is interesting to note that these two films, with almost identical chemical composition and amount of silver bromide per unit area but different grain characteristics, have the same sensitivity only at the shorter wave-lengths.

The results of Fig. 7 were obtained by computing the energy absorbed per square centimeter in the "front" emulsion. The mass absorption coefficients for silver bromide were calculated from the absorption data for silver and bromine in the Compton and Allison tables.[15] Because of the high absorption of silver bromide and the heavy coating on these x-ray films, the exponential absorption law rather than its linear approximation was used to calculate the absorbed energy, but no correction was applied for scattering within the film.

Although it is obvious that the data in Fig. 7 do not justify the drawing of a smooth curve through the short-wave-length region, it is also quite apparent that there is a large change in efficiency of utilization of the absorbed x-ray energy—a factor of about three times. Bouwers[16] found a trend in the same direction. It is to be expected that the photographic effect of x-rays is due largely to the ionization caused by photo- and

---

[13] See reference 4, p. 260.

[14] J. A. Victoreen, J. App. Phys. 14, 95 (1943).

[15] See reference 4, p. 800 ff.

[16] A. Bouwers, Acta Radiol. 4, 368 (1925).

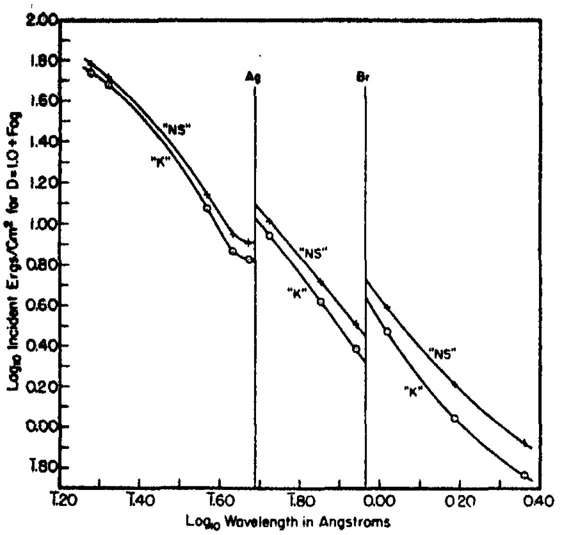

FIG. 5. Spectral sensitivities of No-Screen and Type K X-Ray Films in terms of incident ergs required to produce a developed density of 1.0 above fog.

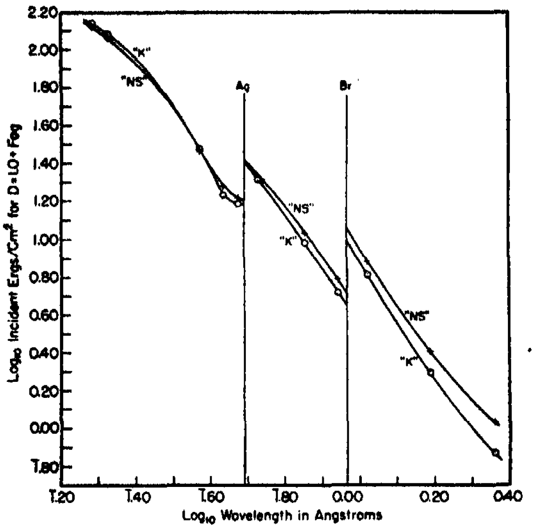

FIG. 6. Same as Fig. 5 but for the "front" emulsion only.

Compton electrons.[17–20] At long wave-lengths, the photo-electrons do not have much energy and therefore ionize primarily within the grain where they originate and render it developable. Some, of course, lose their energy in the gelatin of the emulsion if they happen to originate at the surface of a grain and travel outward. While it cannot be assumed that high energy electrons are more likely to lose a greater proportion of their energy in the gelatin than in the silver bromide, such might be the case.

From studies of nuclear emulsions,[19] however, it is known that high velocity particles expose (ionize) grains much more efficiently near the end of their paths than at the beginning. Presumably, the same principle operates for other emulsions. This means that as the wave-length decreases and the photo-electrons acquire greater and greater energies, they are less efficient in producing latent image. Although a high energy electron may have sufficient energy to expose several grains, it will lose much of its energy at such low concentration per unit length of path that it is not very effective, i.e., at high velocity there will be insufficient ions per grain to expose it. In the recent work of Bromley and Herz,[18] it was found that a water-swollen emulsion was less sensitive to hard x-rays than it was in the dry state. Thus, for the same x-ray absorption in the silver halide of the swollen emulsion, the same number of photo-electrons could not, on the average, reach and expose as many grains, because of their absorption in the increased amount of matter separating the grains. While this picture of the initiation of latent image by x-rays accounts qualitatively for the trend shown in Fig. 7, another idea which has been accepted for some years also points in the same direction.

It is generally considered that one x-ray quantum is sufficient to render a silver bromide grain developable.[21] A large number of silver atoms are liberated by one x-ray quantum but the number is much smaller than would be expected, considering the energy of the quantum. It has been estimated that only five to six percent of the absorbed x-rays which are converted to electron energy are utilized in liberating silver atoms.[22]

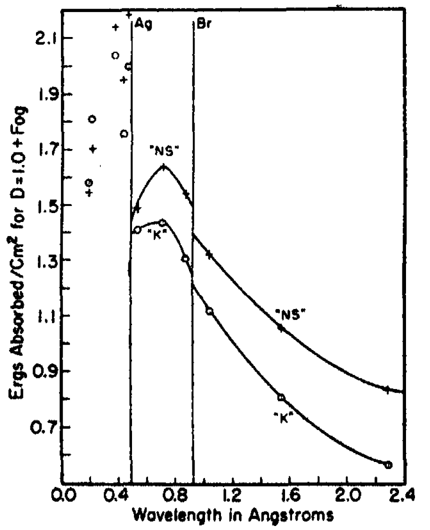

FIG. 7. Spectral sensitivities in terms of ergs absorbed per square centimeter required to produce a developed density of 1.0 above fog in the front emulsion of No-Screen and Type K X-Ray Films.

---

[17] J. Eggert and E. Schopper, Zeits. f. wiss. Phot. 37, 221 (1938).

[18] D. Bromley and R. H. Herz, Proc. Phys. Soc., London (to be published). (The author was privileged to read this paper in manuscript form. The present experimental work was initiated and carried out independently, however.)

[19] J. H. Webb, Phys. Rev. 74, 511 (1948), p. 530, Fig. 21.

[20] R. H. Herz, Phys. Rev. 75, 478 (1949).

[21] J. Eggert and W. Noddack, Zeits. f. Physik 43, 222 (1927). L. Silberstein and A. P. H. Trivelli, Phil. Mag. 9, 787 (Suppl. Number, May, 1930).

[22] P. Günther and H. Tittel, Zeits. f. Elektrochemie 39, 646 (1933).

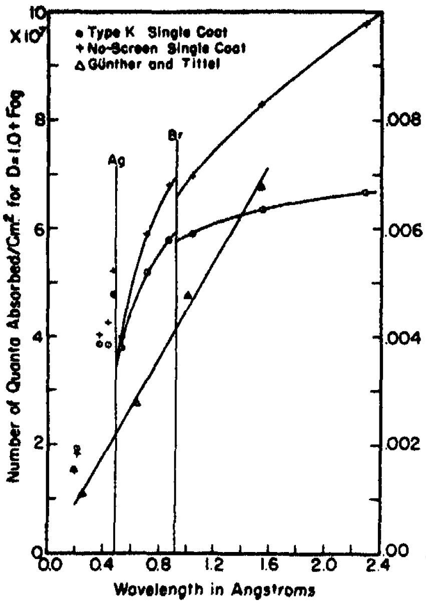

FIG. 8. Similar to Fig. 7 but expressed in terms of number of quanta absorbed per square centimeter. Data of Günther and Tittel included for comparison. Their results are the number of quanta per silver atom freed by the radiation.

The decrease in efficiency with increasing quantum energy shown in Fig. 7 may be explained in part by the idea that if an x-ray quantum of a certain low energy is sufficient to expose a grain, energy is wasted if a larger quantum exposes a similar grain. The ionizing power of electrons as a function of energy and the absorption of electrons by the gelatin must also be important contributory factors in this decrease of efficiency with decrease in wave-length.

In Fig. 8 the results are given in terms of the number of quanta absorbed for a developed density of 1.0 above fog. For the sake of comparison, data of Günther and Tittel[22] are included. In their experiments, they exposed the emulsion to the point of solarization and analyzed it for the amount of silver *photolytically* freed. Their results are expressed here as the number of quanta absorbed per silver atom freed. With due regard to the risk involved in comparing results obtained on different photographic materials, and in extrapolating from exposures producing solarization to those required to give a density of 1.0, we suggest that the graphs of Fig. 8 indicate proportionality between the amount of latent-image silver and the developed density in the shorter wave-length region where it may be assumed that several grains are rendered developable by one quantum.[16] At wave-lengths longer than the Br *K* limit, our results for Type K Single Coat show a tendency toward parallelism with the wave-length axis. Since density is proportional to the number of developed grains (see reference 1, p. 229), this would indicate a trend toward the one-grain-per-quantum condition. A slight suggestion of this is apparent for No-Screen Single Coat in the same wave-length interval. It appears that with the materials examined here the exposure of more than one grain per quantum extends to longer wave-lengths than in the case of materials studied by other experimenters.

Comparison of Figs. 7 and 8, which show different aspects of the same thing, indicates that while short-wave-length x-ray energy is less efficient than long-wave-length energy, the high energy quanta are more efficient than the low energy quanta, *when considered as quanta*. The high energy quanta simply are not as efficient as they should be, considering their energy. Some reasons for this are mentioned in the preceding paragraph. Pelc[23] concluded that the same absorbed energy always renders the same number of grains developable, regardless of wave-length. Our results are quite contrary to this.

The closest approach to the present method of investigation of x-ray spectral sensitivity was that of Berthold, and Berthold and Glocker.[24] They used the radiation from x-ray tube targets of various elements filtered by an element which would tend to isolate the $K\alpha$-lines. It is our opinion, expressed earlier, that this does not give as homogeneous a radiation as the filtered fluorescence. Furthermore, considering the date of their work (1923–24), absorption data for air and silver bromide may not have been sufficiently accurate. Also, there is some question as to whether or not their air ionization chamber gave readings proportional to roentgens, i.e., proportional to the energy absorbed in air. All of this, in addition to the differences in photographic emulsions which probably exist, practically eliminates a valid comparison of the two experiments. Later, however, Glocker recomputed his results using more reliable absorption data[25] and observed sudden breaks in the sensitivity curve at the Ag *K* and Br *K* limits when the sensitivity was expressed for the *same energy absorbed in the emulsion* at the different wave-lengths. The change at Ag *K* was about 10 per cent but was quite small at Br *K*. In general, the efficiency of utilization increased with increasing wave-length, in qualitative agreement with our results.

Recent work by Sandström[26] showed that for two different photographic materials, the sensitivity ratio between the short- and long-wave-length sides of the Ag *K* limit did not agree with the sensitivity ratio computed on the basis of absorbed energy. He only measured the response for the immediate vicinity of Ag *K* and used density ratios obtained from microphotometer records of exposures to the diffracted continuous spectrum. This is probably a legitimate procedure for his low density exposures. Sandström's average for the two materials he used is only about eight percent higher than the average of 1.65 obtained from column 2 in Table II. (Sandström expressed the ratio as the reciprocal of the ratio used here.) No conclusive explanation was offered for the difference in efficiency of utilization of absorbed energy, but the experimental fact is in good agreement with that found in the present work.

---

[23] S. R. Pelc, Proc. Phys. Soc. **57**, 523 (1945).

[24] R. Berthold, Ann. d. Physik **76**, 409 (1925). R. Berthold and R. Glocker, Zeits. f. Physik **31**, 259 (1925).

[25] R. Glocker, Zeits. f. Physik **40**, 479 (1926). R. Glocker, Zeits. f. tech. Physik **7**, 571 (1926).

[26] A. E. Sandström, Arkiv. f. Math. Astr. o. Fys. **34B**, 1 (1947).

The results summarized in Table II show the pronounced difference of 40 to 49 percent between computed and observed values for sensitivities at the K limit of Ag, and only one to four percent at the K limit of Br.

On referring again to Fig. 7, it appears that a small break occurs at the Br K limit and a larger one at the Ag K limit, similar to the results obtained by Glocker in his revised computations.[25] The result obtained by Sandström[26] at the Ag K limit is equivalent to ours. Although the accuracy of our data is not great and the values are obtained by extrapolation, the agreements noted are strong evidence for the breaks noted in Fig. 7. Glocker ascribed these discontinuities to sudden changes in the relation between fluorescence and photoelectric emission. With this point we agree, but we shall now consider it in more detail.

The true absorption of an x-ray quantum, $h\nu$, results in the emission of a photo-electron whose kinetic energy, E_{kin}, is given by the Einstein photoelectric equation,

$$E_{\text{kin}}=h\nu-W_K,$$

where W_K is the energy required to remove the electron from the K level, for example, of the atom. The K fluorescent emission resulting from the return of an electron to the K level of a silver or bromine atom is not necessarily absorbed in the surrounding emulsion, since the absorption coefficient for this radiation is not exceptionally high, although it is more than twice as great for the bromine fluorescence as for the silver fluorescence.

A moderate difference, however, between $h\nu$ and W_K yields a photo-electron which is effective in exposing. However, just at the absorption limit where $h\nu=W_K$ there will be no exposure from a K electron and, since the utilization of the corresponding fluorescence is not complete, a drop in efficiency may occur. The greater absorption of the bromine fluorescence by the silver bromide may account in small part for the observation that the sensitivity change in the film corresponds more nearly to the absorption change at the bromine K limit than it does at the silver K limit. Furthermore, the K fluorescence yield of silver is about one-third greater than the K fluorescence yield of bromine.[27] Thus a greater proportion of the absorbed energy on the short wave-length side of Ag K results in fluorescence than is the case with Br K. Conversely, there will be relatively more Auger electrons (internal conversion of photon energy) than from the silver. Since the Auger electrons are much more strongly absorbed than the fluorescence, the greater Auger electron yield of bromine increases its efficiency of utilization of absorbed energy. The greater break (see Fig. 7) at Ag K than at Br K is explained therefore by (1) the lesser absorption of the Ag K fluorescence, and (2) the greater Ag K fluorescence yield. Whatever the over-all efficiency of the photographic emulsion in utilizing absorbed x-rays, a small decrease may be expected just at the short-wave-length side of an absorption edge. (This over-all efficiency has been estimated to be only five or six percent.[22])

CONSIDERATION OF ERRORS

From previous experience in the photographic photometry of x-rays, we believe that the measurements of relative exposure on the films fall within the limits of an error of ±3 percent. Uniform development of film strips is the most essential factor in attaining accuracy as good as this, and the machine mentioned earlier[8] has been found very satisfactory in this respect. All the films of one kind were taken from the same box, thus keeping film variation at a minimum.

An ionization-chamber reading was made before and after the film exposures for each kind of radiation. They were very consistent. In only a single instance was there a difference as great as six percent between the "before" and "after" readings. The ionization chamber had a scale of ten divisions so that tenths of a division were estimated. The fiber was in good focus, and the scale divisions were of such a size that estimating of tenths could be done with reasonable accuracy. The exposure in roentgens was taken as the mean of the two readings. Relative sensitivities of the two films studied are believed to be fairly well established but measurement of absolute values involves several uncertainties.

Referring to Fig. 5, it will be noted that the first point on the short-wave-length side of the K limit of silver causes the curve to approach the limit in a very different manner from the corresponding approach to the K limit of bromine. It may also be noted that this radiation ($K\alpha$ of antimony) is nearer an absorption limit than is any other radiation used. Therefore, sufficient spectral impurity could have just the effect observed, while equivalent impurity in the other radiations near the K limits might have a negligible effect.

As mentioned before, the radiations used were tested for homogeneity by their absorption curves in aluminum or copper. While this method is not extremely sensitive, the alternative of photographing the spectrum diffracted

TABLE II.

Spectral region	Ratio of film sensitivities (from Fig. 6)	Computed ratio of absorbed energy	Ratio $\frac{\text{computed}}{\text{observed}}$
K limit of Ag	Type K 1.70 No-Screen 1.60	Both films 2.38	Type K 1.40 No-Screen 1.49
K limit of Br	Type K 2.24 No-Screen 2.19	Both films 2.27	Type K 1.01 No-Screen 1.04

---

[27] A. H. Compton and S. K. Allison, loc. cit., p. 489.

by a crystal requires great care in interpretation. A *very faint* background density near a spectral line of moderate density must be *integrated* with respect to wave-length before its value with respect to the line can be properly assessed since, as in our exposing arrangement, the spectrum is not spread out, but line and entire background both fall on the same area.

Although the absorption test did not indicate good purity for the $K\alpha$ of 74 W and 78 Pt, we do not believe that this alone introduces a serious error, inasmuch as there are no absorption edges for AgBr near these wave-lengths. Rather, the calibration of the ionization chamber[5] in this region is uncertain because its sensitivity was found to change on a continuous spectrum basis and we used it here on a homogeneous spectrum basis. Under these conditions, therefore, we do not have great confidence in the exact number of roentgens per scale division of the instrument.

Each point on the curves in Figs. 3 and 5–8, inclusive, represents the average of three separate determinations, i.e., the experiment was performed three times, for each of which the films were developed together. This procedure introduced a development variation between runs, since temperature and strength of developer could not be controlled as accurately as in a more elaborate apparatus. To give a truer picture, therefore, of the accuracy of determination of relative sensitivity to the different radiations, the runs were reduced to a common development basis. This was accomplished by determining the ratio, r_1/r_2, of the roentgens to give a density of 1.0+fog at each wave-length for runs 1 and 2, for example, and multiplying all of the values of r_2 by the *mean ratio*. The largest value of the mean ratio which it was necessary to use was 1.11, thus indicating a maximum development difference of 11 percent. While this procedure was used to correct for development differences, it also includes any other systematic differences which may have been associated with a given run. It is most likely, however, that development conditions were the only significant differences between runs. On making corrections for development differences, it was found that the average spread of data is 4.7 percent. This was calculated as follows: Since there were three runs, there were three values to be averaged for each datum point in Figs. 2 and 3. The values of maximum percentage spread of all data were averaged, giving the average spread of 4.7 percent. The greatest spread found for any datum was 12.5 percent. Energy relations given in Figs. 6–8 were derived from these averaged data.

CONCLUSIONS

(1) X-ray films of nearly the same atomic composition and therefore having similar x-ray absorptions do not necessarily have similar relative spectral sensitivities.

(2) X-ray energy absorbed in an emulsion is more efficiently used at long than at short wave-lengths. Large x-ray quanta are more effective than small quanta but, as the energy efficiency indicates, not in proportion to their energy.

(3) The sudden change in sensitivity of film to incident x-rays in crossing the K limit presumably cannot be computed simply on the basis of absorbed energy. This apparent discrepancy may be due to the negligible value of kinetic energy of K photo-electrons just on the short-wave-length side of the absorption edge and to the loss of fluorescence radiation.

(4) A photo-electron may render a single grain developable and also waste some of its energy in the gelatin. Or it may expose several grains near the end of its path after losing some of its energy at such high velocity that the ions formed are widely separated and the grains penetrated are therefore not exposed. If an incident quantum has only sufficient energy to remove an electron from its energy level, this electron can do no exposing and the fluorescent quantum resulting from its return may not be absorbed. Thus, some x-ray energy may be absorbed without producing latent image. The relative importance of these various factors will depend upon grain size, grain-size distribution, and proportion of gelatin. Hence, different x-ray emulsions may vary in relative spectral sensitivity even though they absorb similarly.

ACKNOWLEDGMENTS

We should like to express thanks to several colleagues for valuable contributions: to R. L. Griffith for the spectrogram in Fig. 1; to G. Kornfeld for the opportunity to discuss certain phases of the work; to H. J. Dietz for making some of the radiators; and particularly to E. J. Hunemorder (now with the Dow Chemical Company) for his painstaking care in preparing various filters and in holding the x-ray tube to constancy of output during exposures.

THE REVIEW OF SCIENTIFIC INSTRUMENTS VOLUME 21, NUMBER 4 APRIL, 1950

Decade Pulse Counter for Geiger-Müller Tubes

BJÖRN ÅSTRÖM
Nobel Institute for Physics, Academy of Sciences, Stockholm, Sweden

(Received December 20, 1949)

A pulse counter of decade type, which does not require any components with narrow tolerances, has been designed. A direct reading system for the total count has been used, which eliminates all calculations. Several instruments of the type described here have been put to daily use for more than half a year without any failure.

INTRODUCTION

COUNTING of pulses from Geiger-Müller tubes has in general been made by using scalers of the binary type consisting of a number of scale-of-two circuits.[1,2] The reading of the total number of pulses registered by such a pulse counter is often troublesome and tedious and mistakes may easily be made in the computations of the interpolations required by such a system. For a long time it has, therefore, been felt desirable to design a pulse counter of the decade type, where it should be possible to read directly the figures of the number of pulses counted. Several such counters have already been published.[3-7]

The pulse counter, to be described here, has the following features: (1) The number of pulses counted is directly indicated on the front panel. Units and tenths in illuminated figures and hundreds in a five figure mechanical register. (2) The register and the electronic circuits can easily be reset to zero. (3) All resistances and condensers have standard values with 10 percent tolerances. (4) The instrument has proved to be very reliable and insensitive to power line fluctuations. (5) The sensitivity is high, which gives better plateaus, specially when small Geiger-Müller tubes are used. (6) The mechanical construction is such that all parts are easily accessible for control and service. (7) The

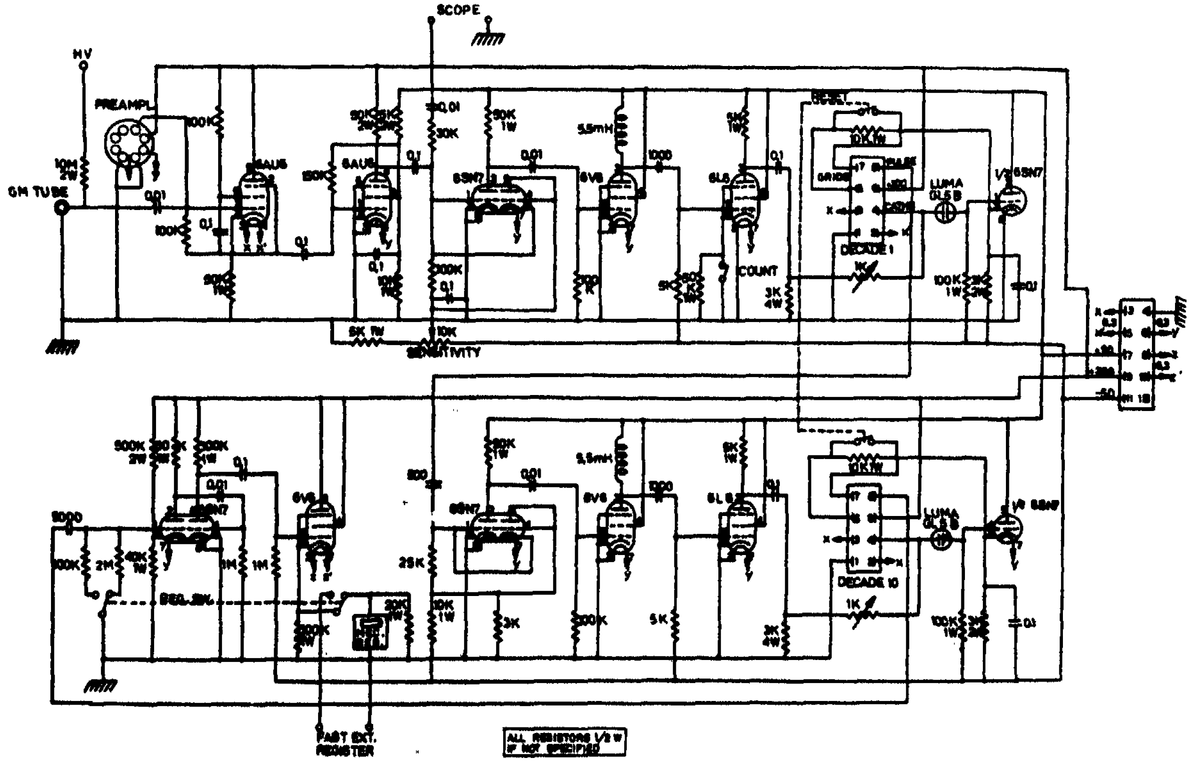

FIG. 1. Circuit diagram of the pulse counter, showing the pulse amplifier, pulse forming circuits, stabilizing circuit for the decade cathode to grid voltage, and register driving circuit. Decade units fit into the two eight-terminal plugs.

---

[1] W. Eccles and F. Jordan, Radio Rev. 1, 143 (1919).
[2] H. Alfvén, Proc. Phys. Soc. 50, 358 (1938).
[3] J. Potter, Electronics 17, 110 (June, 1944).
[4] V. H. Regener, Rev. Sci. Inst. 17, 185 (1946).
[5] T. K. Sharpless, Electronics 21, 122 (March, 1948).
[6] Rotblat, Sayle, Holt, and Thomas, J. Sci. Inst. 25, 33 (1948).
[7] R. Weissman, Electronics 22, 84 (May, 1949).

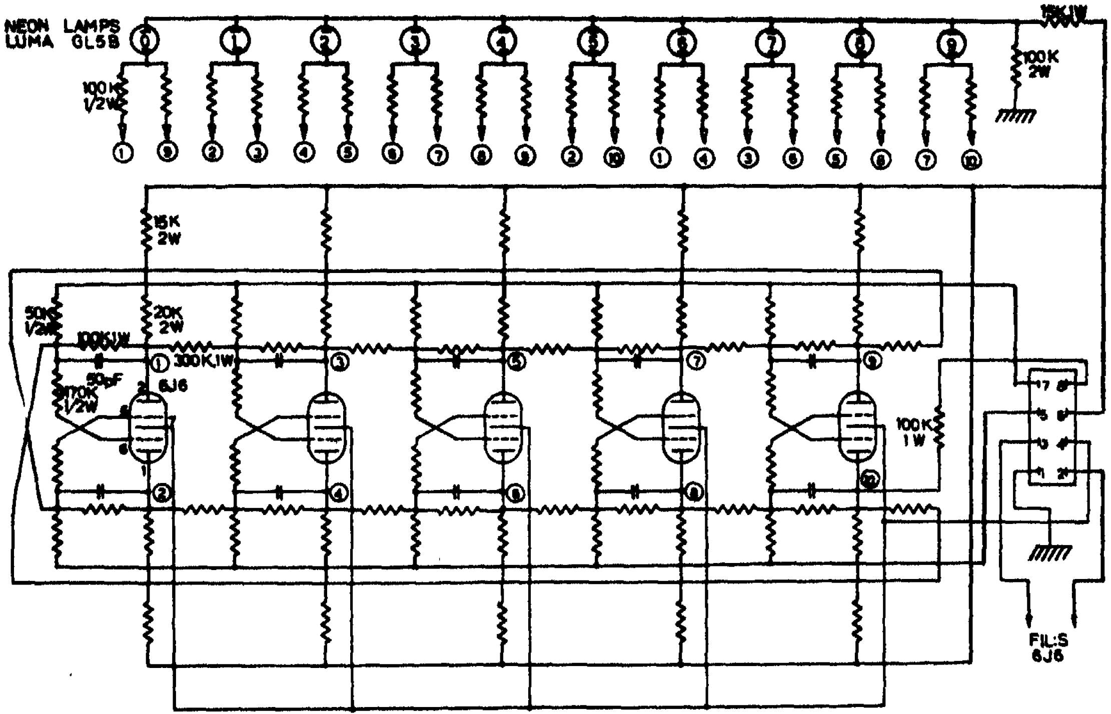

FIG. 2. Circuit diagram of the decade units. The neon lamps used are of the 0.1-watt type with a starting voltage of about 85 volts.

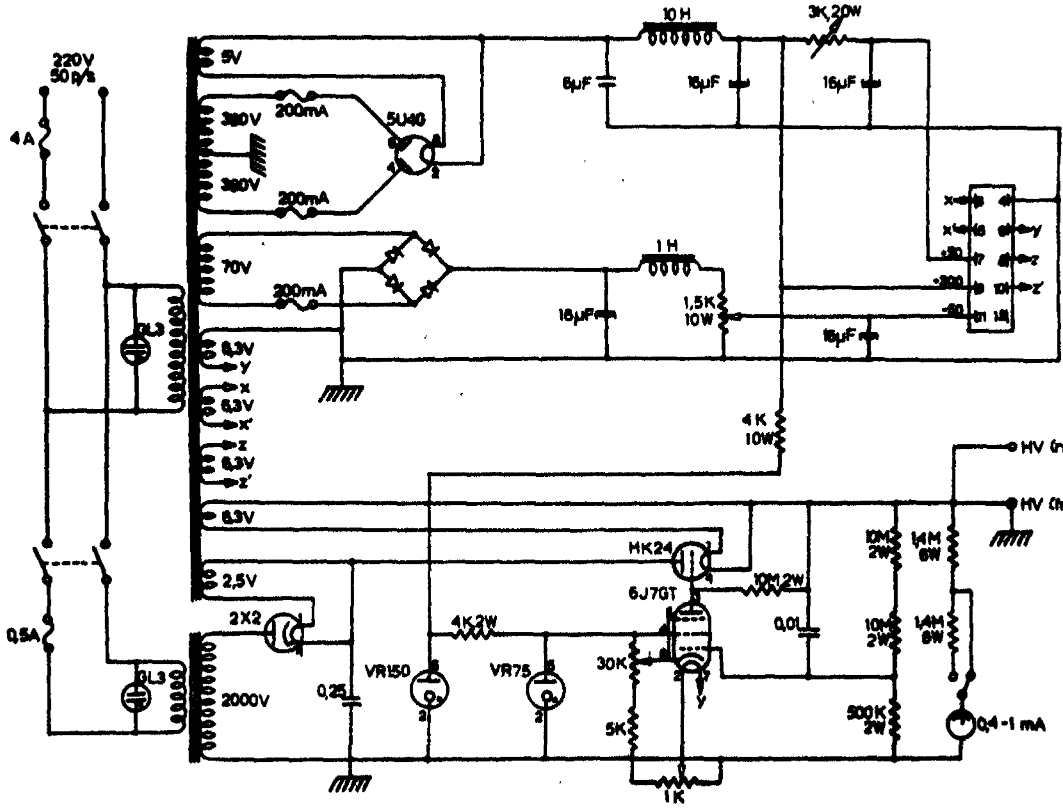

FIG. 3. Circuit diagram of the power supply.

high voltage supply for the G-M tube is capable of supplying enough current for a quenching circuit of the Neher-Pickering type.

CHOICE OF DECADE SYSTEM

After some preliminary experiments it was decided to use the decade principle outlined by Baker.[8] In this circuit only five double triodes are needed for a scale-of-ten and the two triode systems in one tube may have a common cathode, which makes it possible to use the inexpensive miniature tube 6J6. Indication of the number of counts stored in the decade can easily be realized with ten miniature neon lamps, and the circuit is not critical when grid current limiting is introduced.

BLOCK DIAGRAM

As seen from Fig. 1 and Fig. 3 the pulse counter consists of the following main parts: pulse amplifier with discriminator, two decades with their respective pulse-forming circuits, the driving circuit for the mechanical register, and the power supply with a stabilized high voltage rectifier for the G-M tube. An external quenching circuit can be connected and there is also an output plug for operating an oscilloscope or a counting rate meter. Finally there is another plug for connecting a fast external mechanical register or a loud speaker.

PULSE AMPLIFIER AND DISCRIMINATOR

The pulse counter is generally used without a quenching circuit for the G-M tube and thus the first tube in the pulse amplifier is a cathode follower. The connection to the G-M tube is made through a 150-ohm coaxial cable, which may be made as long as 100 cm without introducing any harmful attenuation when normal G-M tubes are used. The second tube is a conventional pentode amplifier, with the grid return to a positive voltage to decrease the sensitivity to positive pulses. Discriminator action is realized by varying the grid bias of the first tube in the pulse forming circuit of the first decade. At maximum sensitivity, the pulses counted are 0.15 volt or larger and at minimum sensitivity, the corresponding pulse amplitude is 1.0 volt.

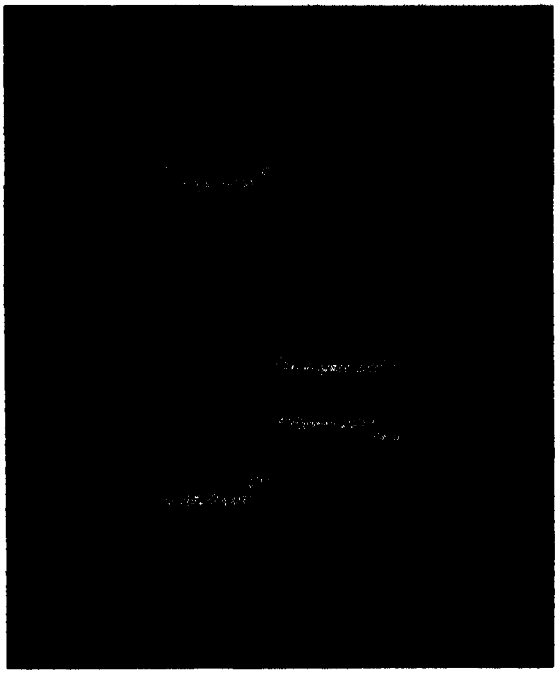

FIG. 5. Oscilloscopic picture of the plate (upper curve) and grid voltage (lower curve) of one triode system when ten successive pulses are fed to the decade. Initial condition is with the tube non-conducting. Plate current is started by the fifth pulse.

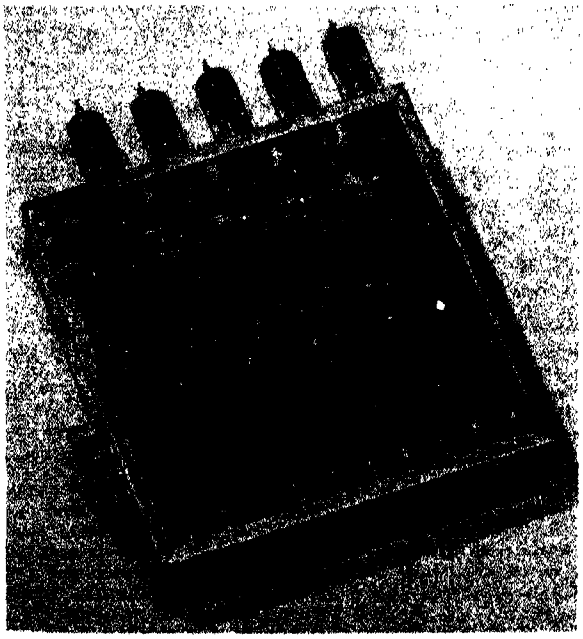

FIG. 4. Mechanical construction of the decade unit. Two units are used, mounted on the main chassis with the neon lamps close behind a window in the front panel.

PULSE FORMING CIRCUIT

To make sure that the decades work properly it is necessary to feed them with pulses that are equalized, and this is made by means of two pulse forming circuits of the type used in Eniac and described by Sharpless.[6] This type of pulse-forming circuit has been chosen because of its reliability; but it may be possible to design a pulse-forming circuit, good enough for this purpose, containing fewer components and with less power consumption. The pulses, from the pulse former used, have 70 volts amplitude and a length of 3 μsec.

DECADES

The circuit of the decades is given in Fig. 2 and the mechanical lay-out can be seen in the photograph in Fig. 4. They are constructed as separate units and are connected to the instrument by means of an eight-terminal plug.

The working principle of the decades can be described as follows. Each double triode is connected in a scale-of-two circuit with the grid potential of the non-conducting system far below cut-off. The connection between the five scale-of-two stages is made through a coupling resistor, as a result of which the plate potential of the tube proceeding contributes to the grid potential of the tube following. Starting with upper triodes conducting, the grids of four of the non-conducting triodes are connected to the plates of four conducting triodes, which have a low plate voltage, and thus only increase the grid voltage very little. The grid of the fifth non-conducting triode on the other hand is connected to the plate of a non-conducting tube and in this case the grid potential is raised almost to the cut-off value. The tube, which contains this grid, will thus be triggered when a negative pulse of limited amplitude is fed to the common cathode bar. Successive pulses will trigger the five scale-of-two circuits from one stable condition to the other, and the next five pulses will trigger them back again one after another. After ten pulses, the decade has completed one cycle of operation and has returned to the initial condition.

---

[8] G. T. Baker, J. Sci. Inst. 25, 127 (1948).

The indicating lamps are so connected that the starting voltage is reached only when both the limiting resistors are connected to the plates, which are in a conducting state, and that happens only to one lamp in each part of the cycle.

Figure 5 shows an oscilloscope picture of the grid voltage and the plate voltage in one triode system when ten pulses are fed to the decade. The diagram of the plate voltage in particular gives a very good indication that the decade works properly.

The resistances used in the decades have all values with 10 percent tolerances and it has proved appropriate to make an adjustment of the whole system after the resistors are soldered in place. This is easily made in the following way. Before the tubes are put in their places pin number 6 of the decade plug is connected to a stabilized voltage of +150 volts (VR 150). Pins 5 and 7 are grounded. The voltage between ground and the ten grid points (the connection of the resistances 50 K, 100 K, 300 K, and 470 K) is measured and adjusted by shunting the grid resistors (50 K) with large resistors, so that the measured voltage for the ten points does not vary more than 1 volt. The voltage is about 45 volts and generally about five resistances of the value 800 kohms, 1 megohm or 2 megohms, will be necessary for one decade.

The plate current in the two halves of the 6J6 tubes used, should not differ more than 0.3 mA for the combination $E_b = 230$ volts, $R_a = 35$ kohm and $E_g = 0$. The current is about 5 mA. This requirement is fulfilled by about 90 percent of unsorted tubes from the manufacturer. When the decades are placed in the counter, pulses are fed from a pulse generator to the input and the cathode potentiometers (1 k) are adjusted to a point between the two positions where the decade starts to work improperly. The interval between these two positions should be about half the value of the potentiometer, if everything is in order.

The tube 6SN7 to the right in Fig. 1 is not essential for the functioning of the circuit but serves to increase the reliability by stabilizing the voltage between the grids and the cathodes of the decade tubes, if the tubes used do not all have the same plate current.

The complete instrument can resolve pulse pairs of 10 μsec. separation, and for the electronic circuit the maximum counting speed for uniformly spaced pulses is about 40 kc/sec. without any adjustment and about 80 kc/sec. after some readjustment of the cathode resistor.

REGISTER DRIVING CIRCUIT

The built-in register is of the telephone type with zero reset. It has a maximum counting speed of about 20 pulses/sec. but the driving circuit has been so designed that a special register with ten times higher counting speed can also be used. The cathode follower circuit has been used to make it possible to ground one side of this external register.

POWER SUPPLY

All voltages that are necessary for the pulse counter and the G-M tube are delivered from a conventional power supply, the circuit of which can be seen in Fig. 3. The high voltage stabilizer has coarse and fine controls and the voltmeter has a depressed zero point and two ranges, extending between 600–1400 volts and 1200–2800 volts. Ten percent line fluctuations will change the high voltage less than 0.2 percent at 1000 volts and has no other effect on the functioning of the counter. After a warming-up period of 15 minutes the temperature drift is negligible.

MECHANICAL CONSTRUCTION

The pulse counter with the decades is mounted on a 17-in. standard chassis made of 3-mm Al sheet and the power supply is mounted on another chassis of the same type. Both chassis fit into a box made of angle-bar-iron and iron sheet. All resistors and condensers are mounted on boards and more attention has been paid to a surveyable and reliable layout than to compactness.

RESULTS

A number of pulse counters have been built of the type described, and they have all behaved very well without any adjustments other than those described. The oldest one has been in daily use for more than a year without any repair other than replacement of one rectifier tube.

ACKNOWLEDGMENTS

The author wishes to thank the Director of this Institute Professor M. Siegbahn under whose supervision this work has been carried out. G. Hillerup and B. Nyquist assisted in the design and assembly of the instrument.

THE REVIEW OF SCIENTIFIC INSTRUMENTS VOLUME 21, NUMBER 4 APRIL, 1950

A Null-Coil Pendulum Magnetometer*, †

C. A. DOMENICALI‡
Laboratory for Insulation Research, Massachusetts Institute of Technology, Cambridge, Massachusetts

(Received December 20, 1949)

A null-method magnetometer is described for the measurement of magnetization of small single crystals of polycrystalline specimens of ferromagnetic materials. It may also be used for measurements on para- and diamagnetic materials. The specimen is placed in an inhomogeneous magnetic field inside a "null-coil" of known geometry, and the current through the coil is adjusted so as to reduce the net magnetic moment of coil and specimen to zero. This coil is rigidly attached to the lower end of a sensitive pendulum and the null-position of the pendulum is observed with the aid of a projection-microscope. This method eliminates the necessity of measuring the force on the specimen and the gradient of the magnetic field. The conditions are discussed under which the absolute error may be reduced to arbitrarily small values. The secondary field arising from the current in the null-coil is, in general, negligible; however, a simple method is described for its elimination.

INTRODUCTION

CONSIDER a region in space having a non-homogeneous magnetic induction field $\bar{B}$ with cylindrical symmetry with respect to a z axis. A small specimen of magnetic moment m_s placed on the axis of symmetry and oriented parallel to the z direction experiences a force parallel to this direction**

$$(f_z)_s = m_s(dB_z/dz)_s. \qquad (1)$$

The subscript on the derivative refers to the effective gradient throughout the volume of the specimen. The magnetization of the specimen, derivable from the magnetic moment m_s, is obtained from a knowledge of the force and the field gradient; this relation is the basis of a number of magnetometers.[1, 2]

If the specimen is replaced by a coil with a current producing a magnetic moment m_c parallel to the z axis, this coil experiences a force

$$(f_z)_c = m_c(dB_z/dz)_c. \qquad (2)$$

If now the specimen is fastened inside the coil with the moments in opposition the force is the difference between Eqs. (1) and (2). By varying the coil current, the coil-specimen combination may be restored to its original equilibrium position in the magnetic field, if the forces $(f_z)_c$ and $(f_z)_s$ are made equal and opposite. If the effective field gradients acting on the specimen and coil are equal, the return to the equilibrium position implies that

$$m_s = m_c = iAN, \qquad (3)$$

where i is the current through the coil, A its effective cross-sectional area, and N the number of turns on the coil.

Obviously the effective gradients acting on the coil and on the specimen will not, in general, be equal, so that even if the forces $(f_z)_s$ and $(f_z)_c$ are equal and opposite, the magnetic moments m_s and m_c are not necessarily equal and opposite. There are two ways of circumventing this difficulty: The pendulum magnetometer may be calibrated with a specimen of known magnetic properties and the same shape and size as the specimens to be measured; or one may obtain a magnetic field geometry in which the "effective gradient" is the same for specimen and coil. The first method was applied to the present instrument. Both methods will be discussed.

I. THE MAGNETOMETER

The most important component of the null-coil pendulum magnetometer (Fig. 1) is the balancing or

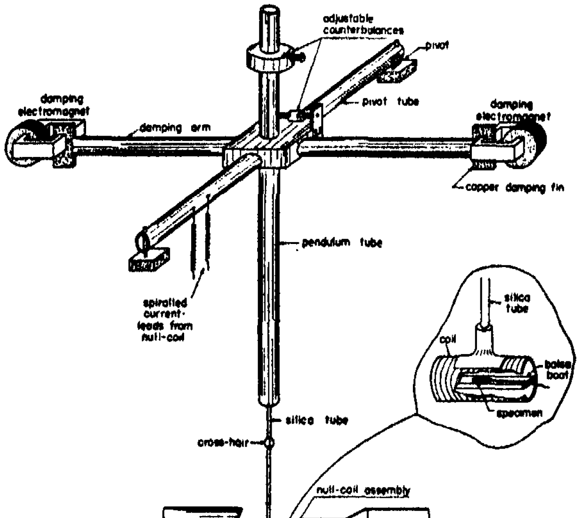

FIG. 1. Schematic diagram of magnetometer and null-coil assembly.

---

* Sponsored by the ONR, the Army Signal Corps, and the Air Force under ONR Contract N5ori-07801.

† From a thesis submitted in partial fulfillment of the requirements for the degree of Doctor of Philosophy in Physics at the Massachusetts Institute of Technology.

‡ Now at Alfred University, Alfred, New York.

** M.k.s. units will be used unless otherwise specified.

[1] Cf. L. W. McKeehan, Rev. Sci. Inst. 5, 265 (1934). Several months after the construction of a preliminary instrument, the writer learned that a similar device had been suggested by A. R. Kaufmann, Rev. Sci. Inst. 9, 369 (1938).

[2] R. Buehl and J. Wulff, Rev. Sci. Inst. 9, 224 (1938).

null-coil. In the present instrument this consists of 302 turns of No. 36 double-silk-covered copper wire, wound in six layers on an aluminum cylinder 10.8 mm long and 11.68 mm diameter. The mean diameters A_1, A_2, $\cdots$ and numbers of turns N_1, N_2, $\cdots$ of each layer were recorded, and their products N_1A_1, N_2A_2, $\cdots$ added to give an over-all effective constant $NA=392.7$ cm^2. The coil is inserted into a thin cylindrical copper shell to which is soldered a smaller diameter thin wall copper tube to form a T-joint (Fig. 1). The resistance of the coil, exclusive of leads, is approximately 15 ohms; the null-coil currents had to be kept <250 ma at room temperature to avoid undue heating.

In designing a null-coil for a given application it is convenient to calculate the magnetic moment in terms of the mean coil diameter, the number of turns, resistance of wire, and power dissipated as

$$m=\left(\frac{1.96\times10^{-3}Wd^3N}{r}\right)^{\frac{1}{2}}, \tag{4}$$

where m is the magnetic moment of the coil in c.g.s. units, W the power dissipated in watts, d the mean diameter in cm, N the total number of turns, and r the resistance of the wire per unit length in ohms/cm.

The specimen was cemented with neutral Canada balsam into a cavity in the center of a small, balsa wood "boat" (Fig. 1). The boat, made slightly larger than the hole in the aluminum coil form, was forced into place inside it. The thermocouple, attached to the null-coil, was placed in direct contact with the specimen. The 25-cm silica tubing, fitted at its upper end into a thin wall, brass tube (the "pendulum tube"), was joined to the "pivot tube" as shown in Fig. 1. Two hard steel needles at the ends of this "pivot tube," resting in a hole and groove, respectively, in two glass beads, formed the pivots for the pendulum. A damping arm consisting of a brass tube at right angles to both the pivot tube and the pendulum tube, carried a copper rectangle at each end which fitted into the narrow gap of a small electromagnet. Thus the motion of the pendulum could be damped electromagnetically. Attached to the tubes were two adjustable counterbalancing weights. The complete pendulum system could be rotated about a vertical axis.

Displacement of the pendulum was observed by the position of a cross hair fastened to the silica tube of the pendulum. This cross hair, illuminated with an intensely bright microscope lamp, was projected onto a ground-glass screen rigidly attached to the magnetometer stand. A small lateral displacement of the hair was thus magnified 40 times.

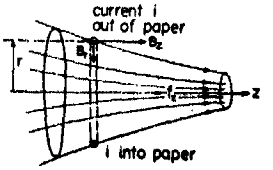

FIG. 2. Loop in non-homogeneous field of cylindrical symmetry.

The electromagnet could be used under steady load at a maximum induction field of *ca.* 0.5 weber/m^2 (5000 gauss); the pole pieces were shaped to give a gradient (gauss/cm) of approximately $3\frac{1}{2}$ percent of the total induction, a percentage found to be fairly constant for all intensities. The pole pieces, which were different in diameter (6.68 and 6.22 cm), had concave pole faces; the amount of concavity required was determined by trial and error. At the time that the magnetometer was built the Laboratory did not possess a large electromagnet; consequently, because of the large gap (6.5 cm) required for the experiments, the methods outlined for calculating the appropriate pole face shape could not be used.

II. PERFORMANCE OF THE INSTRUMENT

With specimens of magnetic moments of the order of 3×10^{-3} amp. m^2 (3 c.g.s.) the relative sensitivity of the magnetometer at intermediate fields is of the order of 0.05 percent of this value, that is, much higher than the accuracy with which the null-coil current can be read. The absolute sensitivity depends upon the geometry of the magnetic field, the size of null-coil, and other factors as indicated. If the null-coil was located in the center of the gap, the absolute value of saturation magnetization of a nickel sample of the same shape and size as the magnetite specimens later investigated was found to be correct to within one percent, if calculated according to Eq. (3). This was checked by measuring ballistically the saturation magnetization of a nickel cylinder from which the small sample was later taken.

The variation of the *indicated* value of magnetization with the axial position of the null-coil in the electromagnet gap was found to be almost linear, and to amount to ±4 percent for a ±5-mm axial displacement of the null-coil.

The coil itself and other parts of the pendulum in the vicinity of the electromagnet gap contained traces of ferromagnetic impurities. Consequently, upon application of a magnetic field with no specimen inside the null-coil, the pendulum showed a deflection which increased slowly with field. The maximum null-coil current necessary to restore the pendulum to its zero position was only 0.5 ma, however, whereas the current required for compensation of a magnetite specimen [magnetic moment $\simeq3\times10^{-3}$ amp. m^2 (3 c.g.s.)] was of the order of 200 ma. This maximum value of 0.5 ma was found to be independent of temperature over the range from $+24°$ to $-186°$C.

III. ELIMINATION OF NULL-COIL FIELD

Although the field caused by the null-coil is, in general, small compared with the applied field, a simple method of reducing it to an arbitrarily small value may be used, if required, by employing two coaxial coils with currents in opposite directions. If the two coils, of equal length, are long compared with their diameters and have cross-sectional areas A_1 and A_2, and if the coils are wound with the same total number of turns N, the field at the common center of the coils is zero for all values of current if they are connected in series and traversed by the same current I in opposite directions. The magnetic moment is now

$$m_c = (NI/10)(A_1 - A_2) \tag{5}$$

when I is measured in amp., A_1 and A_2 in m², and m_c in amp. m².

IV. ANALYSIS OF MAGNETOMETER FIELDS

It was stated in the Introduction that if the effective magnetic field gradients for the null-coil and specimen are made equal by choosing the proper field geometry, the desired magnetic moment of the specimen can be found simply from the coil current and the known characteristics of this coil. We have investigated the conditions under which these effective gradients are equal for coil and specimen, and ways in which such conditions can be met by a proper design of the electromagnet pole pieces. Two particular cases of field symmetry in the magnet gap are of interest here; namely, a magnetic field (Fig. 2) of cylindrical symmetry about the longitudinal axis of the magnet poles, and a field (Fig. 3) symmetrical with respect to a plane, which to a first approximation may be treated as a two-dimensional field.

The mathematical procedure is as follows.†† We consider only a single turn of the null-coil. We replace the specimen by an equivalent surface current of density $\mathbf{J}_s = \mathbf{M} \times \mathbf{n}$, where $\mathbf{M}$ is the magnetization vector (assumed uniform), $\mathbf{n}$ is an outward-pointing unit vector normal to the surface of the magnetized body, and again we consider only an element of this surface current of axial length dz.

The axial force acting on the coil loop and that acting on the specimen loop are equated, and this expression involves the radial field component B_r. Introducing the magnetic moments of the two current loops, we investigate the conditions necessary for the equality of the moments. In the case of cylindrical symmetry this leads to the field components $B_r = Ar$ and $B_z = -2Az + C$, and to a potential function $\psi = A(z^2 - \frac{1}{2}r^2) - Cz + G$, where A, C, and G are constants. A similar calculation for the case of a two-dimensional field gives $B_z = Az$, $B_x = -Ax + C$, $\psi = \frac{1}{2}A(x^2 - z^2) - Cx + G$.

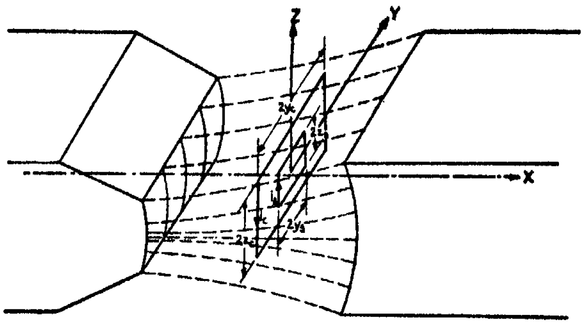

FIG. 3. Magnetic field non-homogeneous in two dimensions.

The procedure for finding the shape of the pole faces is as follows. Having decided upon the desired (and available) values of the field components, we establish the reference point for the coordinate system, and then calculate the values of the constants A, C, and G. In this way we find the shape of the equipotential surfaces in the electromagnet gap. The pole faces are now cut out so as to coincide with the appropriate equipotential surfaces.

It is clear that the analytical method outlined will not give an exact solution of the problem of pole-face shape since the solution given assumes that the pole faces are infinitely large and accurately represent equipotential surfaces. However, if the distance between the pole faces is small compared with their diameters, our solution should give a good first approximation to the solution, thereby serving as a time-saver in the operation of turning these pole faces on the lathe.

---

†† Details of the analysis are given in Technical Report XXIV, ONR Contract N5ori-07801, Lab. Ins. Res., M. I. T. (October, 1949).

Electron Component in Geiger Discharge*

G. G. Kelley, W. H. Jordan, and P. R. Bell
Oak Ridge National Laboratory, Oak Ridge, Tennessee

(Received December 27, 1949)

Observation of the wave form of current during a Geiger discharge indicates the presence of a component due to electron collection ammounting to as much as 50 percent of the total energy involved in the discharge. It appears, therefore, that the initial ion sheath can have a mean radius of the order of 10 to 15 times the radius of the center wire. Apparatus is described, wave forms are shown and the method used to evaluate electron component and mean radius of ion sheath is indicated. Results for two tubes with different quenching vapors are tabulated.

INTRODUCTION

INVESTIGATORS of Geiger discharge have been of the opinion that the ion sheath formed about the center wire during a discharge is initially so thin that its electrons are collected without making an appreciable contribution to the pulse. Alder *et al.* performed an experiment which seemed to confirm this view, and Wilkinson, ignoring space-charge effects, arrived at a figure of three percent for the electron contribution.[1,2]

Using an experimental procedure similar to that described by Alder *et al.*, but with a faster amplifier, we have obtained evidence that as much as 50 percent of the energy involved in the discharge is used to collect electrons. The first work done along this line was reported at the 1948 annual meeting of the American Physical Society in January, 1949. Recently the experiment has been repeated with considerably faster equipment.

APPARATUS

The equipment used in the recent work consists of a Geiger tube, with variable voltage power supply, connected directly to the 200-ohm input of a high speed synchroscope which has been developed at the Oak Ridge National Laboratory.[3] The vertical amplifier in this instrument has a maximum gain of 1000 and a rise time of about 6.5×10^{-9} sec. A built-in delay line allows the sweep to be triggered 0.15 μsec. before the signal appears at the vertical plates. The fastest sweep is 0.28 μsec. in total duration. The voltage across the Geiger tube is held essentially constant during the discharge by a 0.1-μf condenser from cathode to ground. The voltage developed across the input terminals of the synchroscope in series between the anode of the tube and ground is therefore a measure of discharge current which in turn may be seen to be a measure of the rate at which electrical energy is being used by the discharge. Traces from individual discharges appearing at the face of the cathode-ray tube were photographed, using a moving film camera, with the film moving fast enough to separate individual traces.

METHOD

On the assumption of an infinitesimal ion sheath starting from the surface of the counter wire, an expression may be easily obtained for the shape of the discharge pulse. A development of this expression is given by Alder *et al.* and by others. The shape of any particular pulse depends, of course, on the location and direction of the path of the initial radiation. The discharge will burn in both directions along the wire until it reaches one end of the counter and will continue then in only one direction until it burns out at the other end. The curves shown in Fig. 1 were plotted for a discharge starting at one end of the tube. The parameter t_0 is the time required for the ion sheath to travel from $r=0$ to the actual effective initial radius of the ion sheath and t_s is the duration of the burning time; that is, the time required for the whole ion sheath to be formed. These

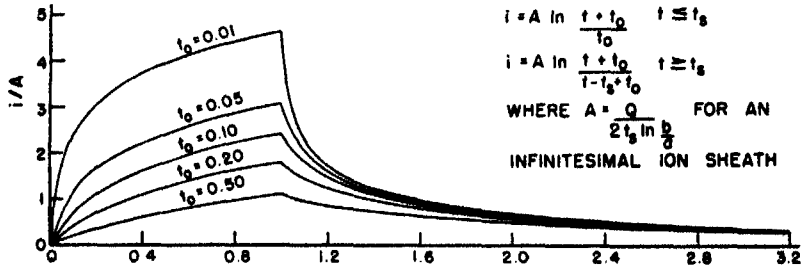

FIG. 1. Curves of ion current obtained from theoretical formula for various values of t_0 and a fixed value of t_s.

---

* This document is based on work performed under Contract No. W-7405, eng. 26 for the Atomic Energy Project at Oak Ridge National Laboratory.

[1] Alder, Baldinger, Huber, and Metzger, Helv. Phys. Acta **20**, 73 (1947).

[2] D. N. Wilkinson, Phys. Rev. **74**, 10 (1948).

[3] G. G. Kelley, Rev. Sci. Inst. **21**, 71 (1950).

FIG. 2. Photograph of a series of pulses from tube B with an overvoltage of 115 v. The source was about one foot from the center of the tube and was uncollimated.

curves also apply to discharges which start at the center of the tube since t_e is halved in this case.

A series of pulses obtained using the apparatus described is shown in Fig. 2. It will be seen that the pulses are quite different from the curves of Fig. 1. They are somewhat distorted because of the non-linearity of amplifier gain but even when corrected they cannot be made to fit the curves of positive ion contribution. A tracing of one of the pulses, one in which the burning originated near the center of the tube, is shown in Fig. 3(a). Figure 3(b) is the pulse corrected for amplifier gain, and Fig. 3(c) is a curve obtained from the formula with constants adjusted to give the best fit after the burning time. There is no measurable difference between the curve and the pulse for times more than just slightly greater than the burning time. When this theoretical curve is subtracted from the pulse there is obtained a relatively rectangular remainder of considerable amplitude, shown in Fig. 3(d). Just such an effect would be expected from electron collection. Due to the fact that the mobility of electrons is very much greater than that of positive ions, the electrons are collected essentially instantaneously as they are produced and give rise to a constant current, building up as fast as the beginning of the ion sheath can be established, and lasting only during the burning time.

The mean radius of the initial ion sheath may be evaluated from the ratio of electron collection energy to the total energy involved. This is the ratio $(i_e t_e)/Q$ where i_e is the magnitude of the electron component of the current. This ratio represents the portion of the total potential, V_T, through which the mean electron has fallen. Thus,

$$\frac{V}{V_T}=\frac{i_e t_e}{Q}=\frac{\ln r/a}{\ln b/a} \quad \text{or} \quad r=a\left(\frac{b}{a}\right)^{i_e t_e/Q}.$$

The value of Q, the quantity of ion pairs formed, in coulombs, was determined by electrically integrating the discharge current. A cathode follower was added

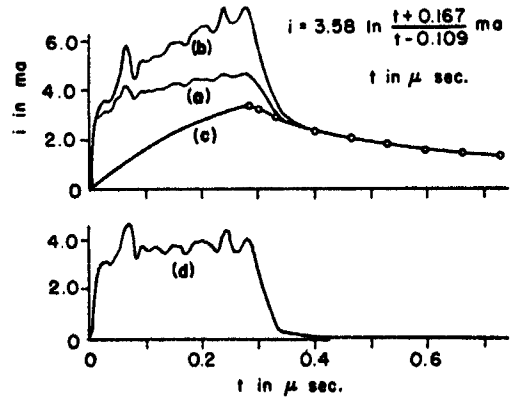

FIG. 3. (a) A tracing of one of the pulses in the photograph. (b) The pulse corrected for the non-linearity of the amplifier. (c) The computed positive ion pulse which coincides with the observed pulse after the discharge. (d) The difference between (b) and (c) and represents the current due to electron collection.

TABLE I.

Counter voltage V_T (volts)	Overvoltage	Electron current i_e (ma)	Burning time t_e (μsec.)	$i_e t_e$ (coulombs)	Ion pairs formed Q (coulombs)	Electron energy / Total energy	Mean radius of ion sheath (cm)
				Tube A			
860	14	0.34	2.38	0.81×10^{-9}	2.13×10^{-9}	0.38	2.6×10^{-2}
870	24	0.58	1.90	1.10	3.05	0.36	3.2
890	44	0.87	1.34	1.16	4.93	0.23	1.7
910	64	1.15	1.05	1.20	6.8	0.18	1.3
930	84	1.62	0.88	1.44	8.7	0.16	1.1
950	104	2.13	0.72	1.62	10.6	0.15	1.1
				Tube B			
1275	0	1.38	1.11	1.53	2.40	0.58	10.0
1290	15	1.56	0.92	1.43	2.71	0.53	6.0
1310	35	1.88	0.80	1.50	3.27	0.46	5.4
1330	55	2.08	0.69	1.43	3.60	0.39	3.8
1350	75	2.26	0.60	1.35	4.07	0.34	3.0
1370	95	2.50	0.54	1.35	4.32	0.29	2.3
1390	115	2.95	0.46	1.35	4.59	0.22	1.6

between the tube and synchroscope to provide a high impedance input, which input was shunted by a condenser large enough to integrate the discharge current. Then $Q=e_{\max}/C_T$ where C_T is the added capacity plus the tube and circuit capacity.

RESULTS

With the equipment used originally, which involved an amplifier with a rise time of 2.5×10^{-8} sec., the corners of the wave forms were rounded to the extent that there was some ambiguity as to the magnitude of the electron component. For this reason it was necessary to apply the process just described (that of fitting the theoretical curve to the tail of a pulse and determining the remainder during the pulse) for each evaluation. With the newer equipment, however, the electron component could be measured directly, subject to small statistical fluctuations which could be accounted for easily by eye. Results for two tubes are given in Table I. Both were thin-wall glass tubes with cathode dimension 7×0.7 in. using 4-mil center wires. Tube A was filled with 9.6 cm of neon and 0.6 cm of amyl acetate. The Geiger threshold was at 846 v. Tube B was filled with 8.2 cm of neon and 2 cm of ethyl alcohol. Its threshold was at 1275 v. It will be noticed that the electron component of the energy does not increase as rapidly with overvoltage as the total energy and in fact in tube B appears to decrease, although the differences may be within the experimental error.

The pulse rise time of tube A was measurable and decreased with overvoltage from 2.3×10^{-8} sec. at 870 v to 0.5×10^{-8} at 950 v. The rise time of the pulse from tube B was too fast to be measured at all values of overvoltage with the amplifier available. It is estimated from the fact that it appeared slightly slower than the step function response of the amplifier that the rise time of this tube lies somewhere between 0.3×10^{-8} and 0.5×10^{-8} sec. The fall time of the electron component was in all cases slower than the rise, probably due to the fact that the ends of the anode are not sharply defined.

THE REVIEW OF SCIENTIFIC INSTRUMENTS VOLUME 21, NUMBER 4 APRIL, 1950

Design of Logarithmic Voltage Dividers

F. V. Hunt and O. D. Sledge*
Cruft Laboratory, Harvard University, Cambridge, Massachusetts

(Received January 11, 1950)

Suitably shaped electrodes attached to a thin sheet of isotropic conducting material, such as one of the newly developed conducting plastics, can make available a specified distribution of potential at a contact sliding along an edge of the sheet. Electrode contours are evaluated for the assumption of a logarithmic potential distribution along the straight-line edge of a voltage-divider strip cut out of the conducting sheet. The ratio of the total length for contact travel to the maximum width of the strip controls the attenuation rate. For a specified attenuation rate (db/in.), the three non-straight edges of the divider strip can be scribed or punched by repeated use of a single curved template or die. Alternative electrode configurations for attachment to rectangular strips of material offer simplification of construction at some sacrifice of linearity of the logarithmic scale.

In the spring of 1937, as a part of the graduate study program for one of us (ODS), we undertook the analytical problem of finding what disposition of fixed electrodes on a thin, plane sheet of conducting material would produce a logarithmic variation of potential along a straight-line edge of the material. Although an exact solution of the problem proved not too difficult, it appeared to have little more than academic interest at that time since available materials had conductivities that were either too high or too low to yield useful values for the overall resistance of the voltage divider. Since conducting plastic materials have now been developed which appear to have values of resistivity appropriate for such service, it seems worth while to present the results of a restudy of this problem.

METHOD OF ATTACKING PROBLEM

The general design problem is attacked in the following way. Two-dimensional current flow is assumed in an infinite plane sheet of conducting material. The desired variation of potential along some particular straight or curved line is expressed mathematically and taken as a boundary condition on the current flow. A secondary boundary condition is expressed by requiring that one of the current flow lines be the straight or curved line along which the variation of potential is prescribed. All the equipotential lines and current flow lines compatible with these boundary conditions are then determined. The desired voltage divider is then extracted from the infinite sheet by making four cuts, two along equipotential lines and two along current flow lines. Electrodes can be attached to the edge surfaces exposed by the equipotential cuts, perhaps most easily by electroplating since the material is conducting, and are to be maintained at appropriate fixed potentials. The divider strip is left free and insulated along the edges exposed by the flow line cuts. The desired variation of potential is then available at a contact sliding along one of these flow line cuts, provided no current is drawn from the movable contact. The latter restriction is seldom serious in practice since the variable potential is usually to be applied to the very high resistance grid circuit of a succeeding amplifier stage.

---

* Now at Central Radio Propagation Laboratory, National Bureau of Standards, Washington, D. C.

DETAILS OF EXACT SOLUTION

It will be assumed that the x axis of the coordinate system of Fig. 1 is to represent the straight line along which the potential is to vary logarithmically. Then the first boundary condition is expressed by the requirement

$$V(x, 0) = V_0 e^{-kx}, \tag{1}$$

in which V_0 represents the potential at the origin and k is the prescribed attenuation scale-factor in nepers per unit of length along the x axis. In order that the x axis also be a line of current flow, it is necessary that the normal component of the electric field vanish along the axis; thus

$$\partial V/\partial y = 0 \quad \text{for} \quad y = 0. \tag{2}$$

Equations (1) and (2) represent, therefore, the boundary conditions which are to be imposed on an otherwise-general solution for two-dimensional current flow in the conducting sheet represented by the x,y plane.

If a solution of Laplace's equation is assumed in the form of a product of two functions—one of x alone and one of y alone—the variables can readily be separated and the solution cast in the form

$$V = f_1(x)f_2(y) = e^{kx}(A_1 \sin ky + A_2 \cos ky) + e^{-kx}(A_3 \sin ky + A_4 \cos ky), \tag{3}$$

where the A's are arbitrary constants. Three of these constants vanish conveniently when the boundary conditions (1) and (2) are imposed on (3), leaving the equation for the potential distribution in the form

$$V(x, y) = V_0 e^{-kx} \cos ky. \tag{4}$$

By setting $V(x, y)$ equal to various constant values, this relation determines the shape of the equipotential lines in the x,y plane.

An equation for the current flow lines in the x,y plane can be found by setting up a function $W(x, y)$ which is conjugate to $V(x, y)$. The form of this function is established by differentiating Eq. (4) and substituting the derivatives in the Cauchy-Riemann relations $\partial V/\partial x = \partial W/\partial y$ and $\partial V/\partial y = -\partial W/\partial x$. After integration, the conjugate function emerges as

$$W(x, y) = V_0 e^{-kx} \sin ky + W_0. \tag{5}$$

Typical flow lines are then determined by assigning various constant values to Eq. (5). Since W_0, the value of W at the origin, can be merged with these arbitrarily assigned constant values, it is apparent that the flow lines are geometrically similar to the equipotential lines since the sine and cosine functions are complementary. This similarity turns out to be very useful in the actual construction of voltage dividers.

Several typical flow lines and equipotential lines are shown in Fig. 1. In one sense these complete the formal solution of the problem since, as suggested above, the desired voltage divider "strip" can be lifted out of the infinite plane by cutting along these lines. However, several practical questions influence the choice of the lines along which cuts are to be made. For example, it is to be noted that the potential of a line passing through the ordinate that makes $ky = \pi/2$ is zero for all values of x. A cut along this line parallel to the x axis can serve as a site for the attachment of a zero-potential electrode. Then if the high potential electrode is applied to the edge exposed by a cut along the line $OA''A'A$, and if the conducting strip lying between the x axis and edge BWC extends indefinitely to the right in Fig. 1, a strictly logarithmic variation of potential will appear along the entire x axis as required by the design specifications. However, it is more common to

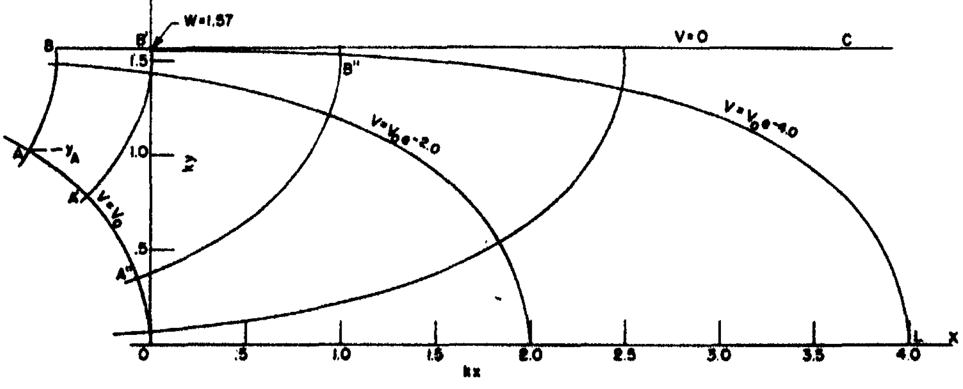

FIG. 1.

require only that some specified maximum of attenuation be reached within a specified distance along the x axis. This condition will be satisfied if the upper edge of the conducting strip is cut along the particular curved equipotential line corresponding to the maximum required attenuation. An electrode attached to this surface can then be maintained at the appropriate not-quite-zero potential by introducing a small external "wing" resistor between this electrode and ground.

In order to make the final cut which will free the finite divider strip from the infinite x,y plane, it is only necessary to choose among flow lines of which AB, $A'B'$, and $A''B''$ in Fig. 1 are typical. The potential distribution along the x axis is the same whichever of these cuts is selected for the left-hand edge of the divider strip, but the total resistance between the electrodes is profoundly affected by the choice. Since the total resistance is a primary design parameter, it is important to determine its magnitude in terms of the electrode geometry and the specific resistivity of the conducting sheet. If the current density at any point x,y is resolved into two components, these currents can be written at once in terms of the resistivity and the potential gradient. Thus

$$u_x = -(1/\rho)(\partial V/\partial x), \quad u_y = -(1/\rho)(\partial V/\partial y); \qquad (6)$$

where u_x is the component of current density (amperes/cm^2) flowing along the $+x$ axis, u_y is the corresponding current density component along the y axis, and ρ is the specific volume resistivity of the conducting material in ohm-cm. Substituting Eq. (4) in (6) gives

$$\begin{aligned} u_x &= u_0 e^{-kx} \cos ky, \\ u_y &= u_0 e^{-kx} \sin ky. \end{aligned} \qquad (7)$$

where $u_0 = kV_0/\rho$ is the current density at the origin. The resultant of these two components of current density is just

$$u = u_0 e^{-kx}, \qquad (8)$$

which leads to the interesting conclusion that the total current density at any point is independent of the y ordinate or distance from the contact surface of the divider. Equation (8) also indicates that the current density is attenuated along the x axis at the same rate as is potential, as might have been anticipated in view of the assumed uniform resistivity of the conducting material.

The total current supplied by the external circuit is to be found by integrating the current density over the surface of the high potential electrode. This can be set up in the form

$$I_{\text{total}} = t \int_{0-A} u ds, \qquad (9)$$

where t is the (uniform) thickness of the conducting sheet (cm) and ds is an element of path length along the high potential electrode. The result of this integration is

$$I_{\text{total}} = \frac{tu_0}{k} \tan ky_A \qquad (10)$$

where y_A is the ordinate of the point A (Fig. 1) or tip of the high potential electrode. When the value of u_0 is introduced, the total resistance between the high potential electrode and "ground" ($V=0$) is given as

$$R_{\text{total}} = \frac{V_0}{I_{\text{total}}} = \frac{\rho}{t} \cot ky_A. \qquad (11)$$

When the divider strip is cut along the equipotential corresponding to maximum attentuation, and terminating at $x=L$, the total resistance is reduced by $R_{\text{total}}e^{-kL}$ which must then appear in the wing resistor, connected as indicated by R in Fig. 2a.

It was mentioned above that the distribution of potential along the variable contact surface is independent of the choice of flow line (e.g. AB or $A'B'$) along which the plate is cut. The three flow lines indicated in Fig. 1 were drawn so as to intersect the V_0 equipotential through the origin at ordinates which would make $\cot ky_A$ equal to $\frac{1}{2}$, 1 or 2. This freedom of choice gives the designer an independent parameter with which to control the overall resistance of the divider, and is the more convenient because all the flow lines are geometrically similar. Moreover, the equipotential lines are also similar to each other and (with an inversion around the x axis) to the flow lines. Thus all the curved lines appearing in Fig. 1 can be drawn by using a single template. Alternatively, sheet material could be punched in any of the various allowed shapes by using a single curved die, the inversion being handled by punching equipotentials from one side of the sheet and flow lines from the other.

ENGINEERING DESIGN

In laying out a template or die for the required curvilinear cuts, it is useful to rewrite Eq. (4) explicitly for the equipotential representing the maximum attenuation N_L. This may take the form

$$\frac{L-x}{L/N_L} = -20 \log \cos\left(0.1151 \frac{y}{L/N_L}\right), \qquad (12)$$

in which N_L is in decibels and the numerical factor $0.1151 = (20 \log_{10} e)^{-1}$. Equation (12) can then be solved for a unique set of associated numerical values of $(L-x)$ and y (see Table I), each measured in terms of an arbitrary unit of length, L/N_L, representing the distance of contact travel per decibel change in attenuation.

Figures 2a and 2b illustrate the shape of divider strips for values of L/N_L of 0.1 inch per decibel and 0.2 inch per decibel respectively. For each of these the electrode profile BDL is derived from Table I. The procedure in laying out such a divider strip is as follows:

TABLE I. Equipotential template layout.
Unit of length $= L/N_L$.

$L-x$	y	$L-x$	y
0	0	10	10.85
1	4.09	15	12.09
2	5.62	20	12.77
3	6.81	30	13.37
4	7.71	40	13.557
5	8.46	60	13.635
7	9.62	∞	13.644

the specified length of contact travel OL is marked off in units of L/N_L, which is equivalent to marking off on OL the desired decibel scale. The electrode profile BDL is then plotted from the data of Table I and a template prepared to lie within $BDLO$. The high-potential electrode profile OA can then be drawn congruent to the lower portion of BDL by sliding the template along the line OL until L coincides with O. The insulated cut AB can then be drawn by turning the template over about the straight edge OL and shifting it upward and to the left so that the straight edge OL lies along a horizontal through the point W, the ordinate value that makes $ky=\pi/2$. According to the last entry in Table I, W has the ordinate value 13.644 L/N_L. This is, incidentally, the maximum width of material required for a divider strip to yield any specified rate of attenuation. If the resistance multiplier term, $\cot ky_A$, is to be unity, the proper AB line will be obtained when the vertex of the template L lies vertically over the origin O thus placing the tip of the high potential electrode A at $y_A=6.82$. For resistance multipliers of ½ or 2, the template should be moved to the left or right as required to bring the intersection at A to the ordinate value 9.62 or 4.03 respectively as determined from the relation

$$\frac{y_A}{L/N_L}=8.686\cot^{-1}(R_{\text{total}}t/\rho). \qquad (13)$$

The examples shown illustrate the general characteristic that dividers for a small attenuation range tend to be relatively wide and short while those for a large attenuation range appear long and narrow. The minor role played in the design by thickness of the material would suggest that a surface distribution of conducting material could be employed. If a homogeneous material is used in very thin slabs, a strip shaped as in Fig. 2a might be wrapped around a cylindrical form to provide for angular rotation of a contact arm.

FIG. 2a.

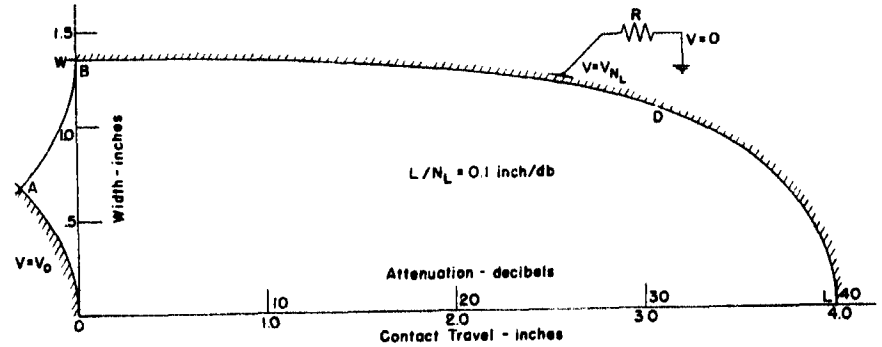

FIG. 2b.

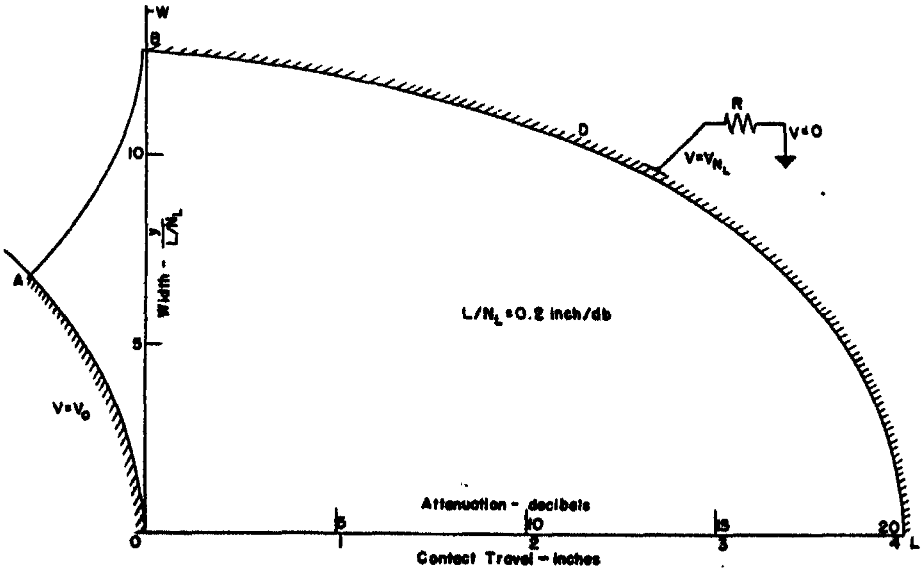

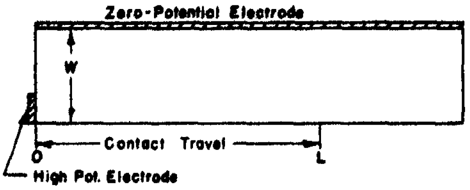

FIG. 3.

APPROXIMATE SOLUTIONS

The shapes of the boundary surfaces prescribed by the foregoing exact solution are so relatively simple as to make approximations for further simplification of marginal value. One configuration illustrated in Fig. 3 was studied, however, and may be useful under some circumstances. The conducting material was assumed to be available in the form of a rectangular strip to which electrodes could be attached along the straight line edges. A zero-potential electrode was applied along the full length of the upper side at a distance from the origin corresponding to W of Fig. 2. The high potential electrode was applied along a portion of the vertical OW and extended from 0 to an ordinate $A=0.32W$. Under these conditions a decibel scale of attenuation, linear within about one per cent, was found to be available for a distance OL, which is less than the total length of the strip by about $1.5W$. The attenuation *rate* is determined by the width of the strip ($W=13.6L/N_L$) as in the exact solution requiring curved electrodes. Also as in the exact solution, the resistance multiplier is primarily determined by the length of the high-potential electrode, although this length can probably not exceed one-third of the width without adversely affecting the linearity of the scale for small values of attenuation. The "price" paid for the rectilinear disposition of electrodes is the overhang of material beyond the range OL within which the decibel attenuation scale is linear. The accuracy limits quoted for linearity of the attenuation scale were assessed by tests on this configuration in an electrolytic tank.

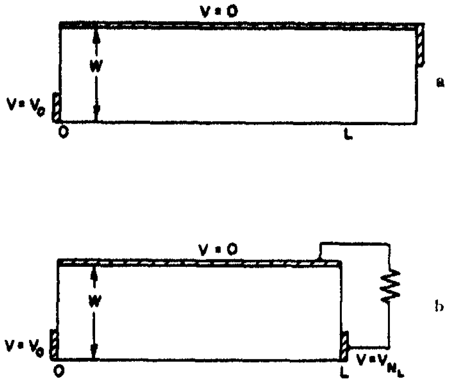

FIG 4.

It seems likely that the amount of overhang might be substantially reduced if the low potential electrode were extended around the corner and along part of the free edge as indicated in Fig. 4a. In fact it seems likely that a rectangular configuration of this type, when used in conjunction with a suitable wing resistor, might be capable of eliminating the overhang entirely. Another electrode configuration that seems to approximate the ideal somewhat more closely is shown in Fig. 4b. In this case the zero-potential electrode extends only along the upper surface. A third electrode, similar to the high potential electrode of Figs. 3 and 4a, is attached at L and approximates by a straight line the lower portion of the equipotential corresponding to maximum attenuation N_L. In the absence of the conducting material to the right of L, this electrode would assume a potential higher than that corresponding to N_L, but it can be brought back to the correct potential by connecting in shunt a suitable external resistor as indicated. No experimental data are available yet for establishing tolerance limits on the linearity of attenuation afforded by the arrangement of Fig. 4b.

EXTENSIONS OF THE SOLUTION

The case of straight-line motion of a contact arm has been worked out above in some detail because this conformed to the requirements of a voltage divider for use in a high speed power-level recorder. It should be possible, however, to introduce a transformation of coordinates that would permit these results to be carried over to cases involving circular symmetry. The general nature of the required configuration of electrodes can usually be inferred qualitatively by inspection, but the exact shapes required will be influenced by additional boundary conditions imposed by constructional requirements.

Erratum: A Slide Rule for Radiation Calculations

[Rev. Sci. Inst. 20, 876 (1949)]

M. W. MAKOWSKI

A footnote should have been added to the paper stating that the work was carried out at Admiralty Research Laboratory, Teddington, Middlesex, England.

THE REVIEW OF SCIENTIFIC INSTRUMENTS VOLUME 21, NUMBER 4 APRIL, 1950

Pentode Counting or Control Ring*

BENJAMIN L. MOORE
The Computation Laboratory, Harvard University, Cambridge, Massachusetts

(Received January 15, 1950)

The 6AS6 pentode has been used in a very stable counting or control ring whose input is essentially independent of amplitude and wave shape. Values of supply voltages and circuit parameters are not critical. Control voltages corresponding to one or more stable states of the ring may be obtained very easily.

INTRODUCTION

IN the past a number of ring or counting circuits have been described. The operation of many of these circuits depends to a large extent on the amplitude, wave shape, and pulse repetition rate. Some of the circuits require careful selection of vacuum tubes for successful operation. In this paper is described a very stable 6AS6 pentode counting or control ring[1] whose operation is essentially independent of the amplitude, wave shape, and repetition rate of the incoming pulses, and does not require a careful selection of tubes.

RING CIRCUIT

The 6AS6 pentode, whose suppressor grid has essentially the same control of the plate current as the control grid, is the basic element of the ring. Two of these pentodes are connected as a direct coupled trigger pair, as shown in Fig. 1, using the screens of the tubes as "plates." The important feature of this trigger pair to be noted is that the suppressor grid has control of the plate current of the tube whose screen is conducting, and has no control of the plate current of the tube whose screen is not conducting. It is this characteristic which is used to operate the ring.

Figure 2 is a schematic circuit of a ring of ten pentodes. Opposite tubes are connected as the trigger pair in Fig. 1, and for clarity the voltage divider resistors and filament wiring have been omitted. Normally all suppressor grids are biased to cut-off, those of the odd-numbered tubes being connected to one input, and those of the even-numbered tubes to a second input. The plate of each tube in the ring is connected to the screen of the next tube.

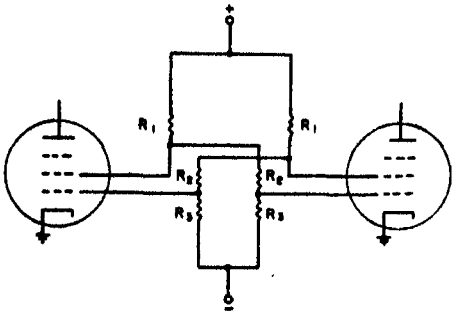

FIG. 1. 6AS6 pentode trigger pair using the screens as plates.

As each tube is one of a trigger pair, half the tubes in the ring will always be conducting. Assume that tubes one through five are initially conducting. A positive pulse on input 1 will result in plate current in tubes 1, 3, and 5. As the screens of tubes 2 and 4 are already conducting, the additional currents through the plates of tubes 1 and 3 will not change the conducting states of these tubes. The plate current in tube 5, however, will lower the screen voltage of tube 6, thus cutting off tube 1 and causing tube 6 to conduct. A second pulse on input 2 will similarly cut off tube 2 and turn on tube 7. Thus alternate pulses applied to inputs 1 and 2 will cause the ring to step once for each pulse.

When power is first applied to the ring, the order of the conducting tubes is random. There are several methods of setting the trigger pairs, so that the proper sequence of tubes is conducting initially. One of the simplest ways of doing this is to insert momentarily, by means of a manual switch, a high resistance between R_3 and the negative power supply in half the voltage dividers.

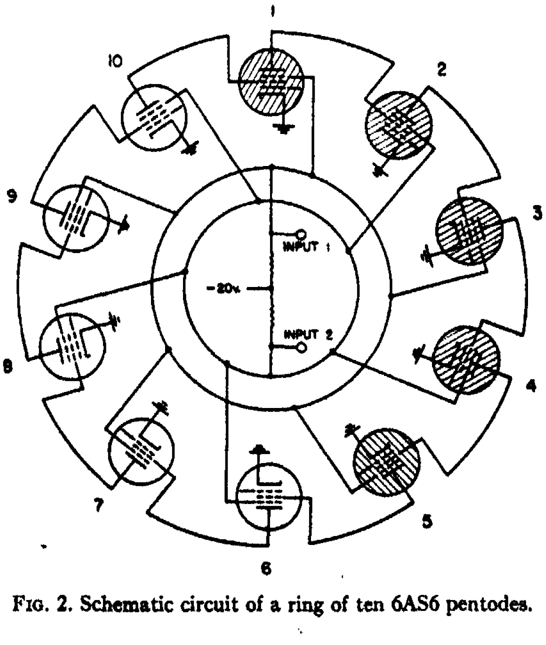

FIG. 2. Schematic circuit of a ring of ten 6AS6 pentodes.

---

* This work was supported by Section Re3d of the Bureau of Ordnance, U. S. Navy, under contract NOrd 8555.

[1] A preliminary report on this work was given at the June, 1949, meeting of the American Physical Society at Cambridge, Massachusetts [Phys. Rev. 76, 465 (1949)].

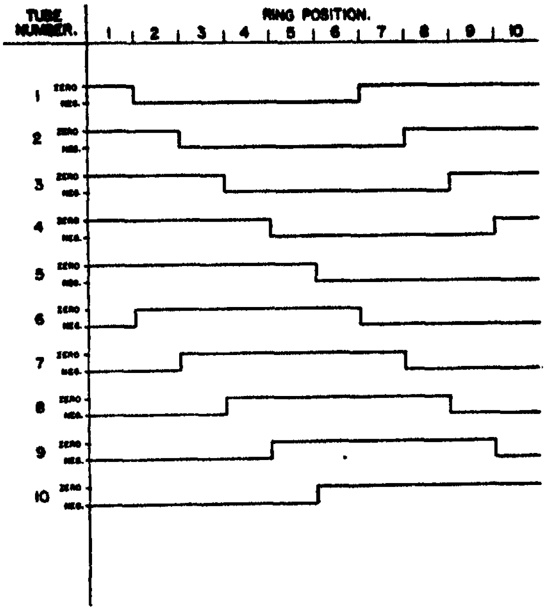

FIG. 3. Grid voltages as a function of ring position.

There are no limitations on the wave shape or maximum width of the input pulses. In fact, the only limitations placed on these pulses are that they do not occur simultaneously on both input lines, and that each pulse raise the suppressor grids above a minimum threshold potential for a sufficient length of time to permit the trigger pair to trip.

The circuit has proved to be very stable in operation. Tube characteristics and values of resistances and supply voltages are not critical. No difficulty has been experienced with five percent tolerances on the latter two items, and careful selection of vacuum tubes has not been necessary. It should be noted, however, that maintaining a close tolerance on resistance and voltage values will permit more variation in tube characteristics, which are more difficult to control.

Using only reasonable care to minimize wiring capacitance, with values of $R_1 = 22{,}000$ ohms, $R_2 = 39{,}000$ ohms, $R_3 = 75{,}000$ ohms, and positive and negative supply voltages of 150 volts each, the circuit has operated reliably with pulses of one microsecond duration at repetition rates of several hundred kilo-pulses per second on each input. This circuit was developed as a component of the Mark III computing machine, and no attempt has been made to extend the operating range to higher pulse repetition rates. Consequently, the repetition rate mentioned above is not necessarily an upper limit. By-passing resistor R_2 with a small condenser will speed up the trigger action or permit operation at the same speed with somewhat larger values for the resistances. For example, approximately the same operating characteristics as above can be obtained with $R_1 = 39{,}000$ *ohms*, $R_2 = 75{,}000$ *ohms*, and $R_3 = 150{,}000$ ohms, using a 25 micromicrofarad condenser to by-pass resistor R_2. These larger resistors reduce the power required, and make the tolerances on both the resistances and tubes even less critical.

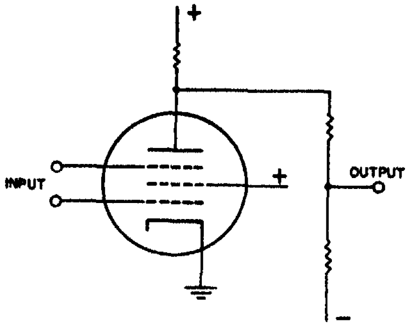

FIG. 4. 6AS6 pentode gate.

The number of tubes in the ring is essentially limited by the power available to drive the suppressor grids. In general, for a larger number of states than, say, 10, it is more economical to use two smaller rings coupled together such that the second ring moves one position for each complete cycle of the first. For example, a ring of 4 and 6 would give 24 stable states.

CONTROL VOLTAGES

In many applications, it is desirable to obtain control voltages corresponding to one or more positions of the ring. Figure 3 shows the potentials of the various control grids for each stable state of the ring. By connecting the control grid and suppressor grid of the pentode gate shown in Fig. 4 to grids of two tubes of the ring, it is possible to make the gate conduct or not conduct for one or more stable states of the ring. For example, by connecting to grids of tubes 1 and 5, the gate will conduct for stable state 1 only, and by connecting to grids 6 and 7 it will conduct for states 3 through 6. The output of the gate, by means of a voltage divider, can be made to operate between zero and some negative voltage which can be used to operate another gate directly.

ACKNOWLEDGMENTS

The author wishes to thank Professor Howard H. Aiken, Dr. Morris Rubinoff, Mr. Charles A. Coolidge, Jr., and Mr. Harrison Fuller for valuable suggestions and assistance in this work.

Low Temperature X-Ray Diffraction Apparatus

DONALD F. CLIFTON
Institute for the Study of Metals, University of Chicago, Chicago, Illinois

(Received January 23, 1950)

When studying transformations at sub-zero temperatures it is often convenient to be able to carry out treatments such as cold-working and annealing and to transfer the specimen, at temperature, to the x-ray diffraction camera. Several cameras have been designed, primarily for the x-ray spectrometer, in which this is easily done. For constant temperature work a flask, having a nozzle which allows cold liquid to flow over the specimen, is used. The holder is such that the specimen can be put in, in correct alignment, while in a cold bath. Two types of cameras giving variable temperatures are described. One, using cold gas blown over the specimen for cooling, permits putting the specimen in place under liquid nitrogen and keeping it at this temperature while it is aligned in the spectrometer. Rapid changes and accurate control in the range up to nearly room temperature are possible. A more versatile camera with a working range from 77°K to over 375°K uses liquid nitrogen as a coolant. Temperature control is by balancing the heat conduction along a tube with a heater near the specimen. This camera allows inserting the specimen at any chosen temperature in the working range but does not allow as rapid temperature changes in the cold gas camera.

INTRODUCTION

WHEN studying transformations at sub-zero temperatures it is often convenient to be able to carry out treatments such as cold-working and annealing and to transfer the specimen, at temperature, to the x-ray diffraction camera. Several cameras have been designed, primarily for the x-ray spectrometer, in which this is easily done. They have proved convenient for x-ray spectrometer studies of transformations and photographic studies of lithium and other polymorphic samples.[1]

CONSTANT TEMPERATURE TYPE CAMERA

For experiments where a constant temperature, such as the boiling point of a liquid gas or the temperature of a mixture such as dry ice and ether, is satisfactory, a stream of the coolant may be flowed over the specimen[2–4] or sprayed on it.[5, 6]

A simple flask to flow a stream of coolant over a specimen that meets the requirement for putting a sample in cold, and is adaptable to both the spectrometer and film cameras is shown in Fig. 1. The nozzle is of large diameter for most of its length so gas bubbles do not block it. It is insulated with a plastic sleeve. The small outlet tube extends through the bottom of the large tube and well up into it to form a trap for solid particles, such as ice, which settle out. A rod with a long taper on the end fitting into the outlet tube is adjustably supported by an arm at the top of the flask giving control of the coolant flow which is kept slow to minimize x-ray scattering by the coolant.

Nozzle A has a plate and spring to hold a stationary specimen in correct alignment. Nozzle B is for rotating powder specimens and oscillating single crystals. The outlet tube in nozzle B is off center and inclined to direct the coolant stream at the specimen. The rod which carries the specimen passes through the center of the nozzle in a fairly closely fitted bearing which is nearly liquid tight and through another bearing on the arm at

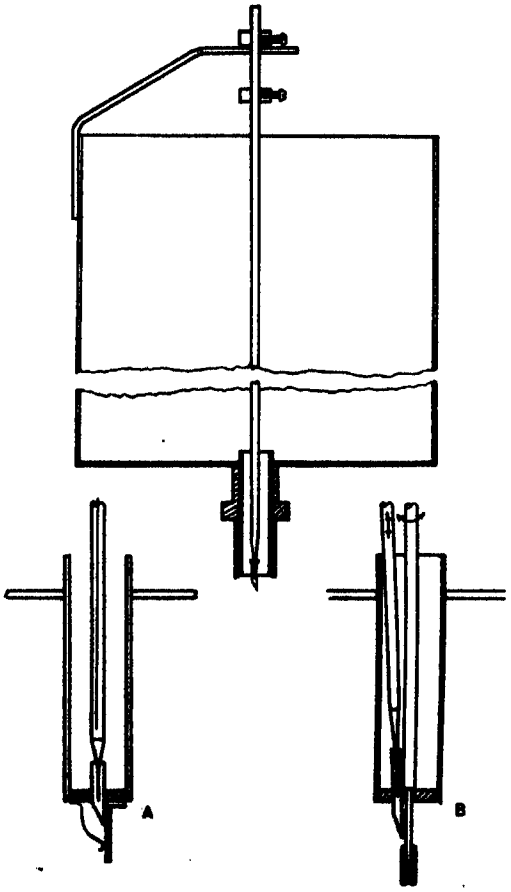

FIG. 1. Dropping flask. A. Nozzle for stationary specimen. B. Nozzle for rotation specimen.

---

[1] C. S. Barrett and O. R. Trautz, Trans. A.I.M.E. 175, 579 (1948); C. S. Barrett, "Transformations in Metals," Cornell Symposium on Transformations in Solids of National Research Council (1948).

[2] Hengstenberg and Mark, Zeits. f. Krist. 69, 271 (1928).

[3] N. W. Taylor, Rev. Sci. Inst. 2, 751 (1931).

[4] K. Lonsdale and H. Smith, J. Sci. Inst. 18, 133 (1941).

[5] A. Goetz and R. C. Hergenrother, Phys. Rev. 40, 643 (1932).

[6] J. A. Santos and J. West, J. Sci. Inst. 10, 219 (1933).

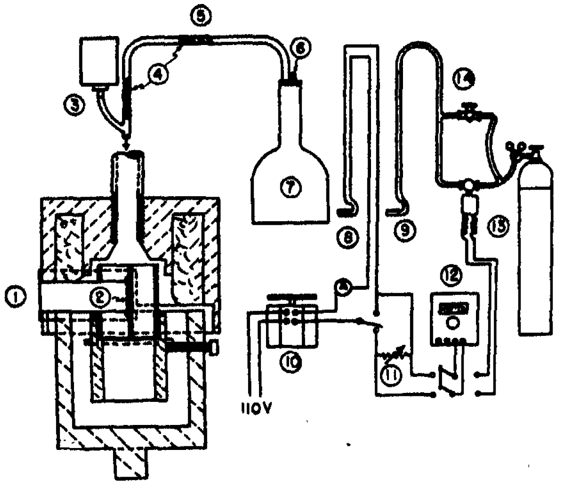

FIG. 2. Gas cooled camera. 1. Camera. 2. Specimen. 3. Dropping flask. 4. Flexible stainless steel hose. 5. Insulated tube for cold gas. 6. Heater or gas coil. 7. Dewar flask. 8. Heater coil. 9. Gas inlet coil. 10. Variac. 11. By-pass variable resistor. 12. Temperature controller. 13. Solenoid valve. 14. By-pass and manual control valve.

the top of the flask where it is connected to the drive mechanism.

The flask itself is of thin metal insulated with ¾ inch of Styrofoam[7] which keeps evaporation loss of liquid nitrogen to about ¼ liter per hour. A glass vacuum flask with a Kovar[8] seal at the nozzle could be used[9] but it is doubtful if the saving of coolant would be worth the loss of simplicity and ruggedness.

Specimens are easily put in the proper position in nozzle A under liquid nitrogen or other coolant. Loading nozzle B under a coolant is simplified by a sleeve on which the specimen can be aligned before it is put on the rod. The flowing coolant protects the specimen from ice during transfer to the camera.

The spectrometer camera is a 1½-inch diameter tube mounted on cross slides for centering the specimen in the x-ray beam. The camera top[10] is an easy fit in the tube and has a hole in the center in which the flask nozzle is a close fit. The windows for the x-ray beam are cellophane kept free of ice by warm air from a hair dryer. A drain is provided for non-volatile coolants.

For work with film a commercial 71.6 mm powder camera[11] is used. The specimen table shaft is removed from its bearing and the flask nozzle fits in its place. A coolant drain has a length of rubber tube to make it light tight.

With a liquefied gas as coolant the drain can be partially blocked and a dry atmosphere automatically maintained protecting the specimen from ice. With other coolants a slow stream of dry gas is introduced into the camera.

Normal film speed can be maintained by warming the outside of the camera without affecting the specimen temperature.

GAS COOLED VARIABLE TEMPERATURE CAMERA

Blowing cold gas over the specimen is a convenient method of cooling with control of the temperature.[12-14] The cold gas camera for the spectrometer is shown in cross section in Fig. 2.

The hood, which directs the cold gas over the specimen, is clamped to a vertical rod so it can be lifted to allow the base cup and specimen to be put in under it with cold gas flowing. The flexible joints in the cold gas transfer tube are of stainless steel flexible hose.

The base of the camera is a plastic cup with a short boss on the bottom to locate it in the spectrometer. An aluminum sleeve, extending from about 5 mm from the bottom of the cup to flush with the top is supported on three centering screws and carries the specimen holder on an internal shoulder. The specimen holder is a copper tube about 40 mm long by 25 mm diameter with a 15

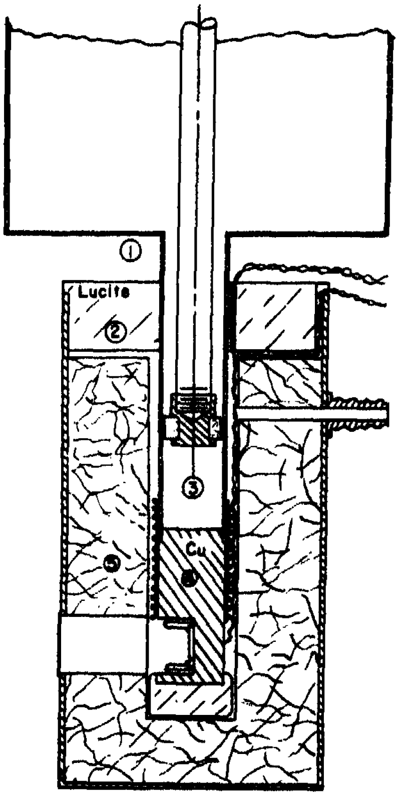

FIG. 3. Conduction cooled camera. 1. Stainless steel tube. 2. Plastic collar. 3. Copper piston with Styrofoam washer. 4. Copper block holding specimen. 5. Heating coil.

---

[7] Manufactured by Dow Chemical Company.

[8] Manufactured by Stupakoff Ceramic & Manufacturing Company.

[9] E. M. McNatt, Rev. Sci. Inst. 10, 42 (1939).

[10] The methyl methacrylate plastics have been very satisfactory where good low temperature mechanical properties and low thermal conductivity are required.

[11] Picker X-Ray Corporation.

[12] L. W. McKeehan and P. Cioffi, Phys. Rev. 19, 444 (1922).

[13] R. F. Mehl and C. S. Barrett, Trans. A.I.M.E. 89, 577 (1930).

[14] H. S. Kaufman and I. Fankuchen, Rev. Sci. Inst. 20, 733 (1949).

mm high opening extending slightly over half around for the x-ray beam window. The specimen is held by two springs to a copper plate behind the window opening. There are fins on the back of this plate to give better cooling.

A cold specimen can easily be put in the holder under liquid nitrogen. Then with the base cup full of nitrogen the specimen holder is placed in the aluminum sleeve and will keep cold by conduction long enough to get it under the hood. The flask from the constant temperature camera can be used, as in Fig. 2, to introduce liquid nitrogen through the hood during adjustment thus saving the nitrogen in the large Dewar flask for controlled temperature work. The evaporating nitrogen keeps a dry atmosphere around the specimen preventing icing during the preceding steps.

Using liquid air or nitrogen as a coolant the source of cold gas can be either tank gas cooled by running through the liquid gas or gas evaporated from the liquid. The first method uses only about one-half as much liquefied gas as the latter but does not give as sensitive temperature control.

Control circuits for the two types of cooling are shown in Fig. 2. Control of the temperature is conventional in both cases: manually by the Variac controlling the current in a heating coil in the liquefied gas or by the stopcock controlling the flow of tank gas or automatically by a temperature controller operating a relay or a solenoid valve with part of the input bypassed to minimize overshooting. The regulator keeps the temperature within about ±1°C and manual control can keep it well within ±0.5°, especially with the heating coil. The temperature can be changed rapidly and stabilized quickly at the new value which is the chief advantage of this type cooling. About 4 liters of liquid nitrogen per hour are required with the heating coil for operation at 120°K.

CONDUCTION COOLED VARIABLE TEMPERATURE CAMERA

A third method of cooling is by conduction through a metal block with the coolant at a distance from the specimen.[15,16] To get variable temperature the block supporting the specimen can be reduced in cross-section area, reducing its heat conductivity so the specimen temperature can be raised by a heater on the block near it.[17,18]

A cross section of the conductivity camera is shown in Fig. 3. The temperature range of the camera is from about 70°K (evacuating over the liquid nitrogen in the flask) to a maximum dependent on the temperature the camera materials will stand. The flask for the coolant is of metal insulated with Styrofoam. A ¾-inch tube of stainless steel extends from the bottom of the flask and pressed into its lower end has a copper block with a flat surface milled on one side for the specimen, which is held in place by springs. The heating coil around the copper block is electrically insulated from it with thin mica. A copper piston with a Styrofoam washer gives control of the level of the coolant in the tube for varying the heat conductivity. This makes it possible to get fairly rapid cooling yet keep liquid nitrogen consumption reasonably low when near room temperature. Icing of the specimen is prevented by introducing a slow stream of dry nitrogen near the top of the camera.

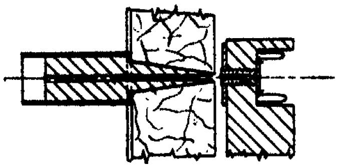

FIG. 4. Pinhole system for conduction cooled camera.

The plastic collar on the tube is held in place by a set screw, so the position of the specimen in the camera can be adjusted, and is a close fit in the camera. The leads to the heater are brought through the collar and the leads for the thermocouple, which is usually embedded in the specimen, through a slot on the side.

The camera is a 3-inch diameter metal tube closed at the bottom and mounted on cross slides on the spectrometer. A Styrofoam block inside the tube has window openings matching those in the tube and a 1-inch diameter central hole for the specimen holder. A foot on the specimen holder closely fitting this hole keeps the specimen centered in the camera. Cellophane windows, one inside the Styrofoam and the other on the outside of the tube, are shellaced to slow the diffusion of moisture through them.

To transfer a specimen at any desired temperature from the air or liquid bath in which it was prepared to the camera the specimen holder is brought to temperature in the camera, taken to the bath, the specimen put in place in the holder, and returned to the camera. The temperature cannot be controlled exactly during the transfer ±10° being about the practical limit. At low temperatures a little ice is picked up during the transfer and will gradually form in the camera but ice lines have not been detected on the spectrometer charts.

For use with film the camera is made with a larger window and for better insulation the inner cellophane window replaced by fairly thick Styrofoam as the slightly greater x-ray absorption is less serious with film. For back reflection pictures a conventional cassett and pinhole system can be used. For transmission the pinhole system is shown in Fig. 4. The front pinhole in the copper specimen holder keeps to a minimum the area of the specimen not in contact with the copper. The back pinhole, separate from the front, gives a reasonably long collimator yet conducts a minimum of heat to the specimen. A ¾-inch square lead shield behind the specimen holder protects the film from x-rays scattered by the air between the pinholes and any diffracted rays

---

[15] M. Wolf, Zeits. f. Physik 53, 72 (1929).

[16] R. L. McFarlan, Rev. Sci. Inst. 7, 83 (1926).

[17] H. Mark and F. Halla, *Roentgenographische Untersuchung von Kristallen*, (J. A. Barth, Leipzig, 1937), p. 149.

[18] A. Eisenstein and N. S. Gingrich, Phys. Rev. 62, 261 (1942).

from the back of the front pinhole. The plastic collar on the specimen holder is keyed to the camera to keep the pinholes aligned.

The temperature of the camera is readily controlled by the position of the plunger and the heating current. The piston may be removed to obtain maximum cooling rate and replaced when the temperature is to be raised. With correct positioning of the piston liquid nitrogen consumption can be held to about 1½ liters per hour over most of the sub-zero temperature range. Constant heating and cooling rates can be maintained over the entire temperature range.

If long runs are to be made on either the constant temperature or the conductivity cameras, automatically refilling the flasks from a large storage dewar is convenient.[19, 20]

ACKNOWLEDGMENT

The cameras were developed under the supervision of Dr. C. S. Barrett and grateful acknowledgment is made for suggestions made by him and by Dr. O. R. Trautz.

---

[19] B. B. Scott and H. C. Howard, Rev. Sci. Inst. 6, 329 (1935).

[20] J. A. Cambell and H. C. Hildebrand, J. Chem. Phys. 11, 334 (1943).

THE REVIEW OF SCIENTIFIC INSTRUMENTS VOLUME 21, NUMBER 4 APRIL, 1950

Pulse Type Regulated High Voltage Supply for G-M Tubes*

Richard J. Watts
The Los Alamos Scientific Laboratory, Los Alamos, New Mexico

(Received January 16, 1950)

A pulse type 1000-v variable high voltage supply is described. This supply utilizes a 6BG6 tube to interrupt the current through a standard inductance. Rectification is by means of a CK1013 cold-cathode rectifier which eliminates a well-insulated filament transformer. The output is shunt regulated by means of a 2C53 tube. An advantage of these supplies is the small size 5×5×6 in. and the economy in cost. Standard parts are used throughout. Ripple at 1000 v is 80 mv. Regulation curves are given.

INTRODUCTION

Despite the wide use of G-M tubes, there is as yet to the author's knowledge no variable regulated high voltage supply commercially available suitable for incorporating in a chassis with other equipment. The use of commercial r-f equipment entails the necessity for adding additional regulation, or if a regulated supply is used the equipment is in general too large to permit room for other components on the chassis. The following instrument is an attempt to rectify these difficulties. A paramount consideration is reliability since G-M tubes are often operated for many hours consecutively.

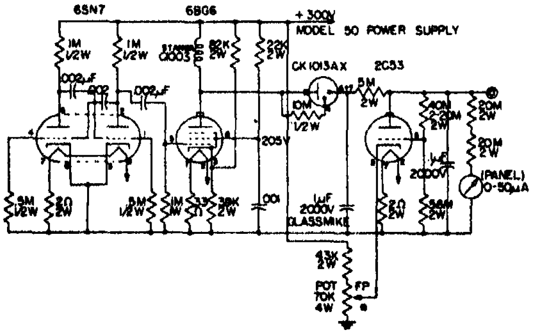

Fig. 1.

CIRCUIT

The pulse type high voltage supply has been investigated in a very adequate manner by Siezen and Kerkhof.[1] These supplies are based upon the periodic interruption of current through an inductance L. Assuming that this inductance is shunted by a stray capacitance Cp, the peak voltage V_m of the transient oscillation caused by the interruption can be deduced from the energy equation

$$\tfrac{1}{2}Li_m^2=\tfrac{1}{2}C_pV_m^2;$$

hence,

$$V_m=i_m(L/cp)^{\frac{1}{2}}.$$

Thus, if $i_m=12$ ma, $L=50$ henrys, $C_p=50$ μμf, $V_m=12$ kv. The advantages of this type of supply can be enumerated as follows:

(1) The interruption frequency can be made high enough so that there can be a substantial reduction in the size of the filter.

(2) The frequency can be made low enough so that no interference is generated.

(3) The inductance L may be small enough so that stray magnetic fields are eliminated.

(4) Insulation requirements on the a.c. side are less severe because of the transient nature of the oscillations.

(5) V_m is a function of i_m, hence, V_m can be adjusted by varying the bias.

(6) The high voltage generation by a tube limits the output. Hence, the output may be shorted with no injury to the circuit.

---

* This document is based on work performed at Los Alamos Scientific Laboratory of the University of California under Government Contract W-7405-Eng-36 and the information contained therein will appear in the National Nuclear Energy Series as part of the contribution of the Los Alamos Scientific Laboratory.

[1] G. J. Siezen and F. Kerkhof, Proc. I.R.E. 36, 401 (1948).

FIG. 2.

Figure 1 is a schematic of the circuit used. A multivibrator has been chosen for the repetition frequency although a blocking oscillator or other means could have been used. This was done in the interest of economy. The repetition frequency was measured to be 200 c.p.s. By means of a Tektronix oscilloscope the usual multivibrator wave pattern was observed. The wave shape on the grid of the 6BG6 showed a 170-v drop in 2 μsec. followed by an exponential rise of 100 v in about 2.5 msec. followed by a square wave of about 2.5-msec. duration. It is necessary to place a large negative voltage on the grid of the cut-off tube in order that it does not conduct during the time the large transient voltage is on the anode.

In order to eliminate the need for a well-insulated filament transformer for the rectifier, a cold-cathode high voltage rectifier was used. If voltages higher than 1200 v are needed, it is necessary to replace this cold-cathode rectifier with an 8016. This, combined with a change in bias on the 6BG6, permits a 3-kv output provided the Stancor C1003 choke is immersed in transformer oil.

Regulation is obtained in the conventional manner by means of a 2C53 tube shunt regulator. At 1000-v output the drop across the anode load of this regulator is 500 v.

To obtain a variable output voltage the bias on the cathode of the 2C53 tube is varied. This bias is obtained from the 300-v supply. The control for this bias plus the 0–50 microammeter is mounted on the front panel of the associated equipment.

PERFORMANCE

Figure 2 illustrates the manner in which this supply is laid out. The performance of the instrument will depend to some extent on the supply voltage used with it. The curves in Fig. 3 were taken with a Model 50 supply. This supply is similar to the circuit described by Higinbotham, Gallagher, and Sands[2] with the exception that more current output is provided.

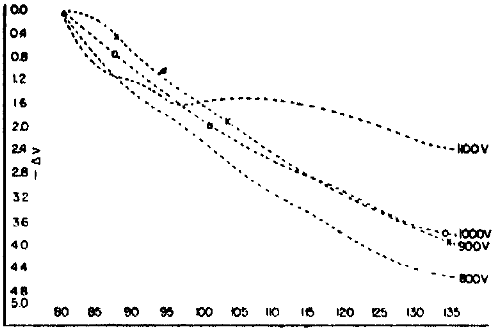

FIG. 3. Line voltage.

To obtain some idea of the regulation the following method was used. By means of a Variac the line voltage input to the low voltage power supply was set at 80 v a.c. The output of the high voltage supply was set at 800 v. 800 v of bucking batteries were then employed so that a general radio 728-A high impedance voltmeter could be set on the 10-v scale. The line voltage was then varied in steps of 5 v and the change in the voltmeter reading was noted. The process was repeated at 900, 1000, and 1100 v. This information is plotted in Fig. 3. It will be noted that the supply is stabilized to 0.1 percent change in output d.c. voltage per ten percent change in the line at 115 v a.c. Of course, this good performance should be attributed to the well-regulated low voltage supply. However, since this supply is one commonly used with scaling circuits the results are germane.

To improve reliability and insure long life it should be noted that all the filament voltages have been reduced by means of resistors. The filament supply is 6.3 v a.c. taken from the associated low voltage supply. The efficiency of the supply is not good, being of the order of four percent. However, since G-M tubes require very small currents (usually less than 3 μa), the efficiency is relatively unimportant since one can afford to waste power provided the input power is not a serious drain on the low voltage supply.

The input power in this case is 3.6 w or 300 v at 12 ma. Since this is easily furnished by most supplies used in conjunction with this circuit no attempts were made to improve the efficiency.

Ten of these circuits have been built and operated continuously for six months with no failures from any cause whatever. Output ripple voltage is about 80 mv as measured with a Ballantine Model 300 voltmeter. This was considered sufficient for the purpose in hand. However, this value can be reduced by inserting an appropriate condenser between the plate and the grid of the 2C53.

---

[2] Higinbotham, Gallagher, and Sands, Rev. Sci. Inst. 18, 714 (1947).

THE REVIEW OF SCIENTIFIC INSTRUMENTS VOLUME 21, NUMBER 4 APRIL, 1950

Thermistors. Part I. Static Characteristics

OTTO J. M. SMITH
Division of Electrical Engineering, University of California, Berkeley 4, California

(Received January 5, 1950)

The fundamental thermistor equations are presented as functions only of electrical quantities and constants, and independent of temperature measurements. The universal curves allow one to predict the static characteristics of thermistors as circuit elements. The two most significant characteristics are the power coefficient of resistance, and the negative incremental resistance. These can be computed, or read from the universal curves, if the resistance and four parametric constants are known. These five values can be determined from six convenient measurements: the resistance and change of resistance with current at very low current, at the maximum voltage point, and at maximum current.

INTRODUCTION

A THERMISTOR has a large negative resistance-temperature characteristic, and is a sensitive conversion element for the measurement of fluid flow, vacuum, radiant energy, and temperature. It can be used as a circuit element, displaying high positive resistance at high frequency simultaneously with low negative resistance and high inductance at low frequency. It can be used as a time-delay lock-in or lock-out device, and as a variable-mu element in volume controls and dynamic volume expanders.

The static curves of the W.E. 1-B thermistor are shown in Fig. 1. At low power, the resistance decreases with increasing temperature, causing the family of curves to intercept the origin at different slopes. For a single ambient temperature, as the thermistor temperature increases due to its internal losses, the rate of resistance decrease becomes so great that the voltage reaches a maximum near 30°C rise, and then decreases again. For high sensitivity to energy, either radiant or losses within the thermistor, it is usually operated below the maximum voltage point. For a circuit element with negative incremental resistance, it is operated above this point.

PREVIOUS WORK

Becker, Green, and Pearson[1] of the Bell Telephone Laboratories have published a comprehensive treatment of the electrical and thermal properties of thermistors and semiconductive material. They defined the temperature coefficient of resistance, a, as

$$a=(1/R)(dR/d\theta). \qquad (1)$$

They showed that this coefficient decreased with increasing temperature in the following manner:

$$-a=(D/\theta^2)+(c/\theta).$$

The term (c/θ) is a correction to account for the fact that the logarithm of the resistivity is not quite proportional to the reciprocal of the absolute temperature. The previous work has used temperature as the independent parameter. If an electrical quantity such as resistance or current is to be used, then the thermal dissipation constant becomes a very significant factor.

CONSTANTS

θ_0 Absolute ambient temperature in degrees Kelvin,
$\Delta\theta$ temperature rise above θ_0 in degrees centigrade,
a_0 temperature coefficient of resistance at θ_0, ohms per ohm per degree centigrade,
K dissipation constant in watts per degree centigrade rise, $W/\Delta\theta$,
k incremental dissipation constant, $dW/d\theta$,
m power coefficient of resistance in ohms per ohm per watt, $(1/R)(dR/dW)$,
n dimensionless correction exponent, equal to $c/a_0\theta_0=-cs$,
R resistance of thermistor, V/I,
r incremental resistance of thermistor, dV/dI,
W watts dissipated in thermistor, VI,
s parametric constant for each thermistor, $=-1/a_0\theta_0$,
x independent variable, $=W/K\theta_0=\Delta\theta/\theta_0$,
g correction exponent for dissipation constant.

The subscript $_0$ refers to values at the ambient temperature. The subscript $_1$ refers to values at maximum voltage. The constant s is positive, and varies from 0.073 for W.E. D-159923 which has a temperature coefficient of 0.046 ohm per ohm per degree, to a maximum s of 0.112 for W.E. 1-A, a bead type for time delay applications, which has a temperature coefficient of only 0.030. The correction exponent n has values that usually lie between $+3$ and -3.

The temperature coefficient a is about minus four

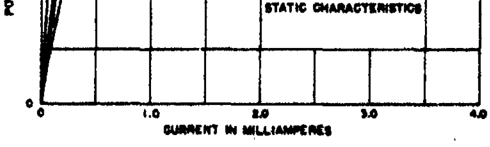

FIG. 1.

---

[1] See Bibliography.

percent per degree at room temperature, and decreases to about 1.3 percent at 200 degrees. The power coefficient of resistance diminishes to 0.1 or 0.01 of its cold value, at elevated temperatures, but its actual value depends upon the physical size of the thermistor. The largest change is in the resistance, which can diminish by a factor greater than one thousand.

The dissipation constant K in watts per degree rise does not vary until the temperature is sufficient to cause increased convection or radiation losses. Figure 2 shows the power required by four typical thermistors, and Fig. 3 shows the manner in which the dissipation constant varies. D-159923 was designed for a circuit element, and is enclosed in an evacuated bulb. It requires only 0.2 milliwatt to reduce the resistance to $1/e$ of its ambient value. The 1-B thermistor is mounted in a fiber tube. It has an a of only -0.031 and requires 10 mw to reduce R to $1/e$ of R_0.

The rapid rise of power at high temperature, if caused by increased radiation, should be a function of the fourth power of the absolute temperature. Actually, the exponent is different for different units, and for D-159923, it is approximately

$$W=K_0((\Delta\theta)+k''(\Delta\theta)^6).$$

k'' is of the order of 3×10^{-12}. Differentiation yields the incremental dissipation constant:

$$k=dW/d\theta=K_0(1+6k''(\Delta\theta)^5).$$

An expression that will hold for all thermistors will be given later.

By definition, the product of the incremental dissipation constant times the power coefficient of resistance is the temperature coefficient of resistance:

$$a=km. \tag{5}$$

At room temperature, with negligible losses in the thermistor,

$$K_0=k_0. \tag{6}$$

$$a_0=K_0m_0. \tag{7}$$

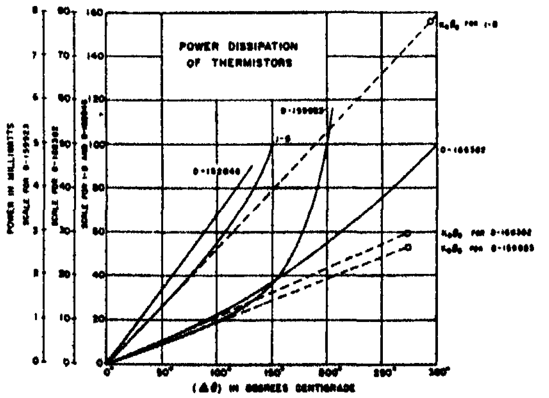

FIG. 2.

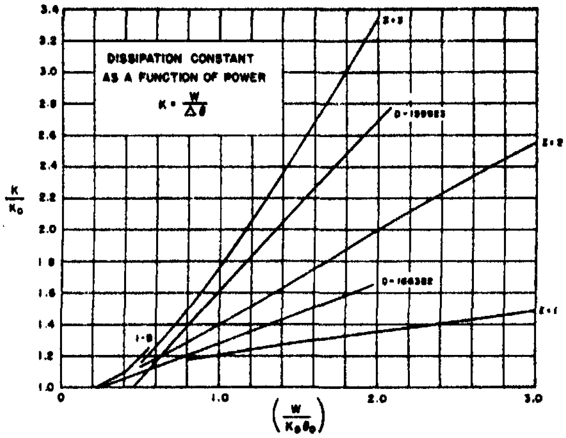

FIG. 3.

Even at the maximum voltage point, k_1 is only a negligible fraction of a percent greater than K_1.

At the maximum voltage point, $R_1=V_1^2/W_1$. Differentiating R to obtain the power coefficient, it becomes,

$$m_1=dR/RdW=-1/W_1. \tag{8}$$

The power coefficient is therefore the negative reciprocal of the measured power at the maximum voltage point. The temperature coefficient at the maximum voltage is similarly simple:

$$a_1=-k_1/W_1. \tag{9}$$

APPROXIMATE RELATIONS

A few rule-of-thumb approximations can be generalized from the fact that the temperature coefficient is almost inversely proportional to the absolute temperature squared. The logarithm of the resistance is inversely proportional to the absolute temperature. At 30°C rise, the voltage reaches its maximum, the incremental resistance becomes zero, and the direct-current resistance has decreased to 0.3 times its ambient value. At 300°C rise, which is possible with only the most rugged elements, $R=R_0/1000$, and the incremental resistance $r=-R_0/2000$.

UNIVERSAL TEMPERATURE COEFFICIENT CURVES

Figure 4 shows the manner in which the temperature coefficient of resistance decreases with increasing temperature. This is a plot of the equation,

$$a/a_0=(1-nW/K\theta_0)/(1+W/K\theta_0)^2, \tag{10}$$

which was derived* from Eq. (2) by algebraic substitutions. The maximum voltage restriction Eq. (9) above can be expanded to read

$$a_1/a_0=-1/a_0\theta_0(W_1/k_1\theta_0). \tag{11}$$

If k_1 is considered equal to K_1,

$$a_1/a_0=s_0/x_1. \tag{12}$$

---

* The derivations are given in the Appendix.

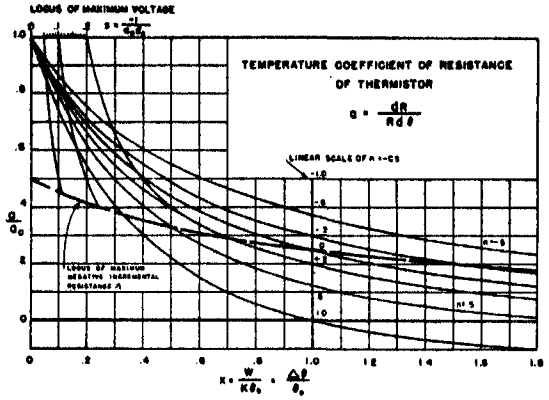

FIG. 4.

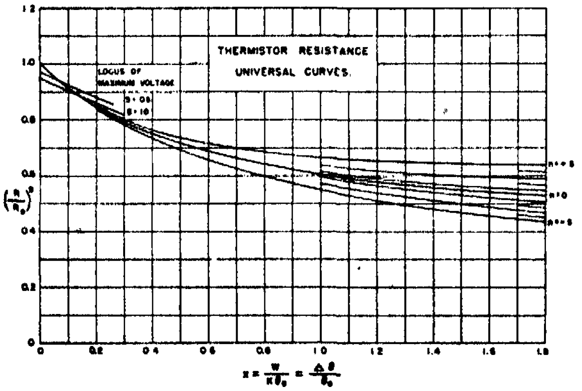

FIG. 5.

This is the auxiliary equation plotted in Fig. 4, whose intercepts with Eq. (10) determine the maximum voltage points. Figure 4 can be used to determine the sensitivity of a thermometry application.

To design temperature compensation circuits, Fig. 5 is more convenient. It shows the decrease in thermistor resistance with increasing power. These curves are plots of

$$(R/R_0)^s=(1+x)^{+n}\exp[-x(1+n)/(1+x)]. \quad (13)$$

A set of loci for maximum voltage intercepts are also shown. These are plots of the auxiliary equation

$$(R/R_0)^s=(1+x)^{-((1+x)^2s/x-1)/x} \times\exp[((1+x)s/x-1)]. \quad (14)$$

To use Fig. 5 for any given thermistor, the constants n, s, and K_0 must be known. These can be determined from the following measurements:

R_0 resistance at ambient temperature, with internal temperature rise less than 0.1 degree, or else corrected back to ambient temperature using Eq. (13) with $n=0$.

θ_0 measured ambient temperature.

m_0 power coefficient of resistance from a measurement of the current necessary to decrease the resistance about two percent, (0.5°C rise); since m_0 is decreasing 4 percent of its value per degree *rise*, *it is therefore important* to correct it back to the ambient temperature, in this case an increase of about one percent.

R_1, W_1 both measured at maximum voltage; to prevent burning out the thermistor, when it reaches the negative resistance region, a fixed series resistance must be used which is at least half as big as R_0. A 100-volt d.c. supply is usually adequate.

$$s_0/x_1=a_1/a_0=m_1/m_0=-1/W_1m_0. \quad (15)$$

Equation (14) could be solved for x_1 using the measured R_1/R_0 and s/x_1 from (15), but this is difficult analytically. A graphical solution for x_1 and s is provided in Fig. 6, a maximum voltage nomograph for Eq. (14). The correction exponent n can be read from either Fig. 4 or 5. K_0 is $W_1/x_1\theta_0$. Since s and n vary approximately as the absolute temperature, it is important to record the room temperature θ_0 at which the tests were made. c is $-n/s$; D can be computed from Eq. (2) if it is desired.

If these curves are to be used for a thermistor with an arbitrary elevated ambient temperature θ_a, the new constants can be determined as follows:

$$s_a/s_0=n_a/n_0=(\theta_a/\theta_0)(1-n_0\theta_0/s_0)/(1-n_0\theta_a/s_0). \quad (16)$$

$$s_a/s_0=\theta_a/\theta_0(1-n_0\Delta\theta/\theta_0). \quad (17)$$

INCREMENTAL RESISTANCE

Above the maximum voltage point, the resistance decreases so quickly that the incremental resistance becomes negative. In this region, the resistance to high frequency is positive, but it is negative to frequencies less than about one-fourth the reciprocal of the thermal time constant. This is occasionally a useful function to

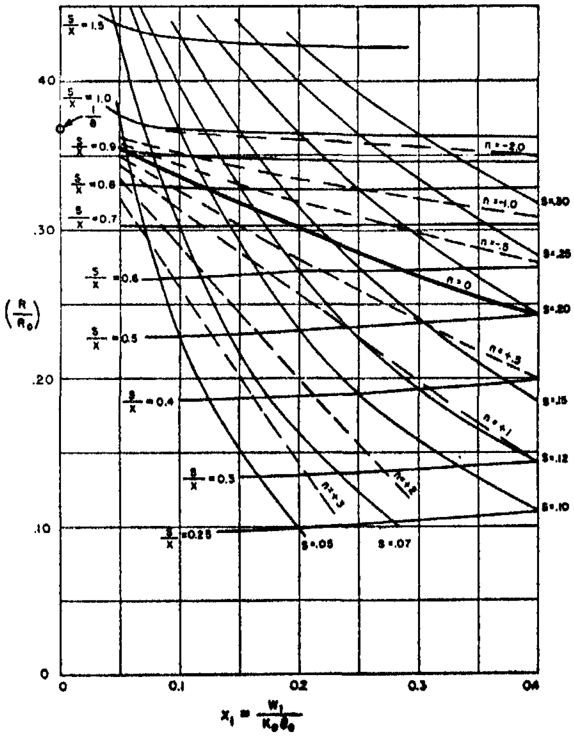

FIG. 6. Maximum voltage nomograph.

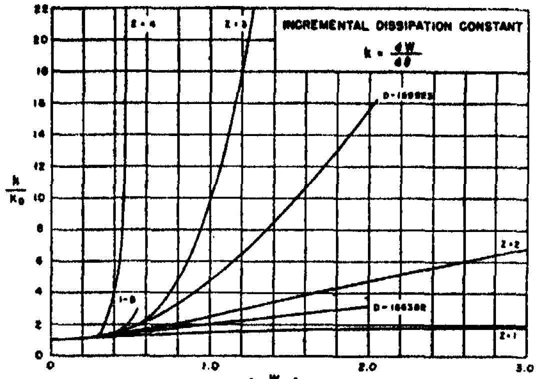

FIG. 7.

have in a d.c. control system. The volt-ampere curve is moderately linear in the vicinity of the maximum incremental resistance. When biased in this region, the a.c. resistance (V/I) might be one-tenth of the cold resistance R_0. The incremental, or resistance for d.c. changes, (dV/dI) might be minus one-fourth of the a.c. value. The bias supply must have an internal impedance greater than $r=dV/dI$ for the current to be stable in this region.

The incremental resistance and the power coefficient of resistance are related by definition.

$$Wm=Wa/k=(r/R-1)/(r/R+1). \tag{18}$$

With this, one can compute the power coefficient from a measured incremental resistance. This equation is indeterminate at zero dissipation, and consequently m_0 has to be measured directly as previously mentioned.

The incremental resistance is

$$r/R=(1+Wm)/(1-Wm). \tag{19}$$

With Eq. (19), r/R can be computed if m is known as a function of the power. This relationship is

$$m/m_0=(1-nW/K\theta_0)/(1+W/K\theta_0)^2(k/K_0). \tag{20}$$

Both of the dissipation constants are variables for which an analytic expression would be desirable. Figure 3 shows the manner in which K/K_0 has been observed to vary experimentally, and Fig. 7 illustrates the same thing for k/K_0. The equation to represent this additional loss at high temperatures should preferably be a function of W and not of the temperature, as unfortunately are Figs. 4 and 5. The form which seems to fit best is

$$(K/K_0)^y=1+k'(W/K_0\theta_0)^z. \tag{21}$$

Substituting W/θ for K, and differentiating, one obtains

$$k/K_0=\frac{(1+k'(W/K_0\theta_0)^z)^{(y+1)/y}}{1+k'(W/K_0\theta_0)^z-(zk'/y)(W/K_0\theta_0)^z}. \tag{22}$$

The relationship between the two constants is

$$k/K_0=\frac{(K/K_0)^{(y+1)}}{z/y+(1-z/y)(K/K_0)^y}. \tag{23}$$

The last form is particularly well-suited for choosing the value of y which matches the observed phenomena. Figure 8 is a plot of the experimental curves, along with Eq. (23) for $y=3$, which appears to be the best value. The parametric variable z is fixed for a given thermistor, and is a measure of the rate of increase of the dissipation constant. The arbitrary constant k' influences only the low wattage part of the curve. An approximation for Eq. (22), which is satisfactory for low values of heating is

$$k/K_0=1+k'(z+1)(W/K_0\theta_0)^z/3. \tag{24}$$

From Eq. (23), and experimental values from the curves in Fig. 8, z can be computed to be 3.595 for the 1-B, and 2.61 for the D-159923. Substituting these values plus points from the curves in Fig. 7 into Eq. (24), it can be computed that both curves go through the point $(k/K_0=1.145;\ W/K_0\theta_0=0.289)$. Substituting these values into Eq. (24) gives an analytic expression for k':

$$k'=0.435/(z+1)(0.289)^z. \tag{25}$$

The incremental resistance is therefore analytically determined by Eqs. (19), (13), (20), (21), and (22), and (25). It can be expressed as a function of power only, and independent of temperature rise. The power coefficient of resistance is plotted in Fig. 9 from Eq. (20). These curves allow one to make a single measurement of incremental resistance at maximum current, compute the power coefficient from Eq. (18), and read off the value of the correction exponent z, from Fig. 9.

The basic curve, marked $K=K_0$, is for a massive thermistor whose dissipation constant does not vary.

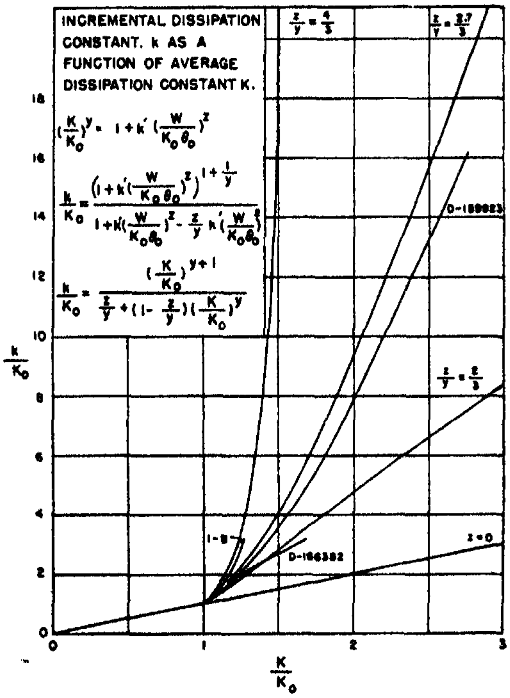

FIG. 8.

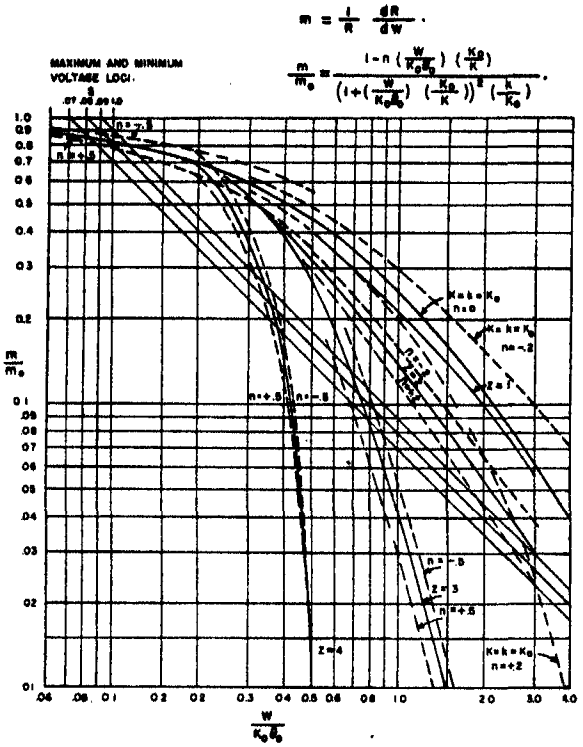

FIG. 9. Thermistor power coefficient of resistance.

The usual element, however, follows a curve like $z=3$. It can be seen that the value of n determines the curve for low wattages, and that z, which has no effect below 60°C rise, has a marked effect at higher wattages.

The incremental resistance Eq. (19) can be rewritten as

$$r/R=\frac{1-(W/K_0\theta_0)(m/m_0)/s}{1+(W/K_0\theta_0)(m/m_0)/s}$$

$$=\frac{1+(Wa_0/K_0)(m/m_0)}{1-(Wa_0/K_0)(m/m_0)}, \qquad (26)$$

or

$$r/R=\frac{s(1+x)^z k/K_0-x(1-nx)K/K_0}{s(1+x)^z k/K_0+x(1-nx)K/K_0}. \qquad (27)$$

Equation (26) includes the three parameters s, n, and z, as well as the independent variable $(W/K_0\theta_0)$, which is proportional to watts only, and therefore is more convenient than the variable x. The manner in which the incremental resistance varies with n and s is shown in Figs. 10 and 11 respectively.

The maximum ratio of negative to positive resistance is found in a thermistor with an almost constant dissipation constant K, high temperature coefficient of resistance (low s), and n slightly negative (−0.2 or −0.3). It occurs at a temperature rise of about 300°C, and r/R has a value of approximately one-half. The effect of the rapidly increasing dissipation constant K in some thermistors (z equals 3 or 4), is to cool the thermistor so effectively that the power coefficient of resistance is very low, and the change in resistance is small. This effect is shown in Fig. 12. It is possible to operate a thermistor so that it will not have a negative incremental resistance. In Fig. 9, it is seen that this would happen when the maximum voltage locus is tangent to the curve. This situation exists if the room temperature is elevated. Since s and n increase with ambient temperature, if the thermistor were operated at 200 degrees centigrade, the constants might be $s=0.12$, $n=0.5$, and $z=4$, and there would be no negative V-I slope.

Figure 12 shows the manner in which the negative incremental resistance varies with the dissipation exponent z. For high negative resistance circuit efficiency, r/R should be large, and z should not exceed 2.

These characteristics which have been presented are useful in predicting the transient response of a thermistor. The time constant is a function of the dissipation constant, and the equivalent inductance and critical frequency (at which the series a.c. resistance becomes

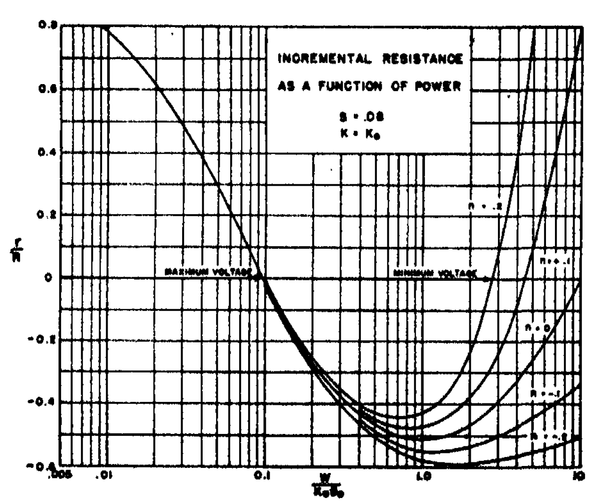

FIG. 10.

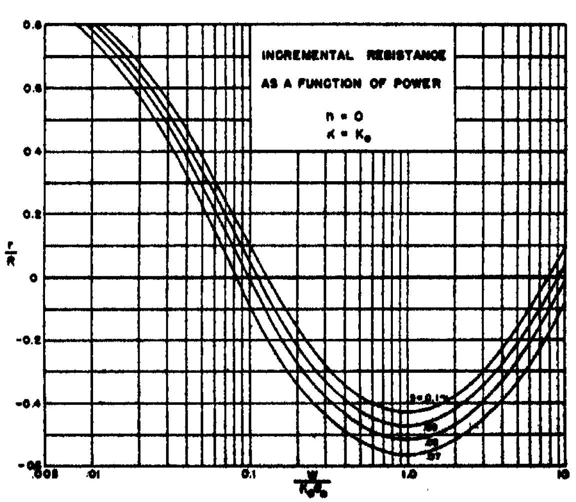

FIG. 11.

zero) are functions as well of r/R and R_0. Figure 7 shows increases in the incremental dissipation constant of over ten times the cold value, and correspondingly large changes in time constant have been observed.

SUMMARY

Curves have been presented of the temperature coefficient, dissipation constants, d.c. and incremental resistance, and power coefficient in terms of three constants, n, s, and z, and low power values of R_0, K_0, and m_0. An examination of all these curves indicates that it is possible to satisfactorily represent all of the effects of the constant n by appropriate small changes in the constants s and z. At low powers, n can be assumed zero, and s computed as though it were. At high powers, where the effect of n is significant, changes in z have an even greater effect, and therefore an equivalent z can be determined again upon the assumption that n is zero. This will give correct electrical characteristics, but computed temperature rises will differ from the actual values.

APPENDIX

Temperature Coefficient.

$$-a=(D/\theta^2)+(C/\theta). \qquad (2)$$

$$D=-a\theta^2-c\theta$$

$$a\theta^2+c\theta=a_0\theta_0^2+c\theta_0$$

$$a=\frac{a_0\theta_0^2-c(\theta-\theta_0)}{\theta^2}=\frac{a_0-c(\Delta\theta)/\theta_0^2}{(\theta_0+\Delta\theta)^2/\theta_0}$$

$$c=na_0\theta_0$$

$$W/K=\Delta\theta$$

$$a/a_0=(1-nW/K\theta_0)/(1+W/K\theta_0)^2$$
$$=(1-nx)/(1+x)^2. \qquad (10)$$

Resistance.

$$D=-a_0\theta_0^2-c\theta_0=-(1+n)a_0\theta_0^2=(1+n)\theta_0/s.$$

$$a=dR/Rd\theta=-D/\theta^2-c/\theta \qquad (2)$$

$$a=-(1+n)\theta_0/s\theta^2+n/s\theta. \qquad (28)$$

Substituting $\theta/\theta_0=(1+x)$,

$$a=-(1+n)/s\theta_0(1+x)^2+n/s\theta_0(1+x). \qquad (29)$$

Integrating Eq. (28),

$$\ln R=(1+n)\theta_0/s\theta+(n/s)\ln\theta+\text{constant},$$

at $\theta=\theta_0$, $R=R_0$,

$$\ln(R/R_0)=(1+n)(\theta_0-\theta)/s\theta+(n/s)\ln(\theta/\theta_0)$$
$$=(1+n)(-x)/s(1+x)+(n/s)\ln(1+x).$$

$$(R/R_0)^s=(1+x)^n\exp[-x(1+n)/(1+x)]. \qquad (13)$$

At the maximum voltage point,

$$a_1=-k_1/W_1. \qquad (9)$$

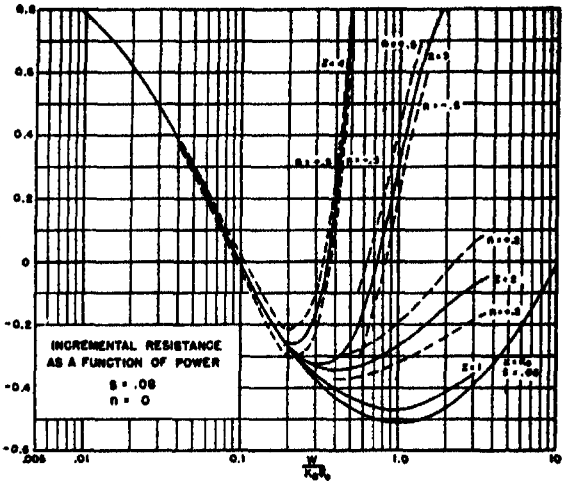

FIG. 12.

If $k_1=K_1$,

$$a_1=-1/x_1\theta_0. \qquad (30)$$

Setting Eqs. (29) and (30) equal will yield the value of n at maximum voltage.

$$-(1+n)+n(1+x)=-s\theta_0(1+x)^2/x\theta_0$$

$$n=(1-(1+x)^2s/x)/x. \qquad (31)$$

$$(1+n)x/(1+x)=1-(1+x)s/x. \qquad (32)$$

The locus of maximum voltage on resistance scales would be:

$$(R/R_0)^s=(1+x)^{[(1-(1+x)^2s/x)/x]}$$
$$\times\exp[-1+(1+x)s/x]. \qquad (14)$$

The solution for x in Eq. (14), if (s/x) and (R/R_0) are known, is best performed by assuming values of s and x and computing R/R_0. This can then be plotted as a nomographical solution. Five-place accuracy must be maintained in the computation.

The value of s is almost indeterminate, because it is not particularly important for the low wattage part of the curve whether the change in resistance is attributed to the correct values of s and n, or whether n is quite inaccurate or assumed to be zero, and the value of s slightly altered to compensate. To measure experimentally the maximum voltage point, a small very low frequency current should be superimposed upon the d.c. bias, and the bias adjusted for a null in the measured low frequency voltage across the thermistor. Frequencies with periods less than six times the thermal time constant, or incremental step changes in the d.c. bias cannot be used because the thermistor will appear initially as a linear resistance, and then the voltage will change transiently to its final value, as the temperature of the thermistor changes. For very precise values of s and K_0, a_0 should be determined at room temperature by mounting the thermistor next to a thermometer bulb, wrapping the whole with cotton tape, and measuring the resistance for a few degrees C rise. This value of a should be corrected back to a_0 in the same manner as the m_0 measurement. Then $K_0=a_0/m_0$, s can be computed from Eq. (15), and n from Eq. (31).

Variation of constants with ambient temperature.

$$s_0=-1/a_0\theta_0$$
$$s_a/s_0=a_0\theta_0/a_a\theta_a.$$

Substituting Eq. (10),

$$s_a/s_0=\theta_0/\theta_a(1+\Delta\theta/\theta_0)^2/(1-n_0\Delta\theta/\theta_0)$$
$$n_a/n_0=s_a/s_0=\theta_a/\theta_0(1-n_0\Delta\theta/\theta_0). \qquad (17)$$
$$n_a/n_0=\theta_a/(\theta_0(1+n_0)-n_0\theta_a).$$

Incremental Resistance

$$I=V/R$$
$$dI=dV/R-VdR/R^2$$
$$(V/R^2)(dR/dI)=dV/RdI-1=r/R-1.$$
$$I^2R=W$$
$$2IRdI+I^2dR=dW$$
$$2RdI/IdR=RdW/WdR-1=1/Wm-1.$$

Eliminating dI/dR.

$$r/R-1=2Wm/(1-Wm)$$
$$r/R=(2Wm+1-Wm)/(1-Wm)$$
$$=(1+Wm)/(1-Wm). \qquad (19)$$

Solving for Wm,

$$r/R-rWm/R=1+Wm$$
$$Wm=(r/R-1)/(r/R+1). \qquad (18)$$

Power Coefficient

$$m=dR/RdW=dR/Rd\theta(dW/d\theta)=a/k. \qquad (5)$$

$$m/m_0=(a/a_0)(K_0/k).$$

From Eq. (10)

$$m/m_0=(1-nW/K\theta_0)/(1+W/K\theta_0)^2(k/K_0). \qquad (20)$$

This is plotted in Fig. 9 as

$$m/m_0=(1-n(W/K_0\theta_0)(K_0/K))/(1+(W/K_0\theta_0)(K_0/K))^2(k/K_0).$$

From Eqs. (19) and (5)

$$r/R=\frac{1+(Wa_0/K_0)(m/m_0)}{1-(Wa_0/K_0)(m/m_0)}$$
$$=\frac{1-(W/K_0\theta_0)(m/m_0)/s}{1+(W/K_0\theta_0)(m/m_0)/s}. \qquad (26)$$

The maximum voltage restriction can be easily derived from Eq. (26) by setting $r/R=0$.

$$m_1/m_0=s/X_1. \qquad (15)$$

BIBLIOGRAPHY

1. Becker, Green, and Pearson, "Properties and uses of thermistors," Bell Sys. Tech. J. **76**, 170–212 (1947); Elec. Eng. Transactions **65**, 711–725 (1946).
2. Ashworth, Needham, and Sillars, "Silicon-carbide, non-ohmic resistors," J.A.I.E.E. **93**, Part 1, No. 69, 385 (1946).
3. F. Ashworth, "Resistance/temperature coefficients of metals and semi-conductors," J.A.I.E.E. **92**, Part 1, No. 59, 412–3 (1945).
4. J. A. Becker and W. H. Brattain, "Thermistor bolometer," J. Opt. Soc. Am. **29**, 148–62 (1939).
5. J. H. Bollman, "A Pilot-channel regulator for the K-1 carrier system," Bell Lab. Record, **20**, No. 10, 258–62 (1942).
6. W. H. Brattain, "Copper oxide varistors," Bell Lab. Record **19**, No. 5, 153 (1941).
7. J. Ewles, "Fast and sensitive dielectric bolometer of new material and construction," J. Sci. Inst. **24**, 57–61 (1947).
8. Lawrence Fleming, "Thermistor-regulated low-frequency oscillator," Electronics **19**, No. 10, 97–9 (1946).
9. R. S. Goodyear, "Thermal resistor elements for electrical circuit applications," Product Engineering **16**, No. 2, 93–5 (1945).
10. R. A. Gund, "Automatic temperature control for aircraft," Trans. A.I.E.E. **64**, 730–4 (1945).
11. E. M. Hickin, "Bolometers for V.H.F. power measurement," Wireless eng. **23**, No. 278, 308–13 (1946).
12. E. J. Iverson, "Copper oxide and silicon carbide varistors," Product Engineering **17**, No. 11, 121–3 (1946).
13. J. C. Johnson, "Thermistor technics," Electronic Industries **4**, 74–7 (1945).
14. R. C. Jones, "Steady-state load curves for semi-conductor bolometers," J. Opt. Soc. Am. **36**, 448–54 (1946).
15. R. J. Maurer, "Electrical properties of semi-conductors," J. App. Phys. **16**, 563–70 (1945).
16. L. A. Meacham, "The bridge-stabilized oscillator," Proc. I.R.E. **26**, No. 10, 1278–94 (1938).
17. C. D. Niven, "Organic thermistor bolometer," Can. J. Research **24**, No. 6, 93–102 (1946).
18. J. R. Pattee, "Temperature compensation of instruments with negative coefficient resistors," Electronics, **16**, 102–5 (1943).
19. G. L. Pearson, "Thermistors—their character and use," Bell Lab. Record **18**, No. 4, 106 (1940).
20. G. L. Pearson, "Physics of electronic semi-conductors," Electrical Engineering **66**, No. 7, 638–42 (1947).
21. R. L. Shepherd and R. O. Wise, "Variable-frequency bridge-type frequency-stabilized oscillator," Proc. I.R.E. **31**, 256–68 (1943).
22. J. N. Shive, "Heating and cooling of bolometer elements," J. App. Phys. **18**, 398–405 (1947).
23. J. A. Weller, "Volume limiter for leased-line service," Bell Lab. Rec. **23**, No. 3, 72–5 (1945).
24. J. E. Stone, "An ultra-low frequency oscillator," Electronics **23**, No. 1, 94–5 (1950).
25. J. H. Bollman and J. G. Kreer, "The application of thermistors to control networks," Proc. I.R.E. **38**, No. 1, 20–26 (1950).

THE REVIEW OF SCIENTIFIC INSTRUMENTS VOLUME 21, NUMBER 4 APRIL, 1950

Thermistors. Dynamic Characteristics. Part II

OTTO J. M. SMITH
Division of Electrical Engineering, University of California, Berkeley 4, California

(Received January 1, 1950)

The thermistor sinusoidal and transient response characteristics are presented, as a function of the dissipation constant and incremental resistance. Equations are given for time constant, critical frequency, equivalent inductance, and Q. The construction of a low frequency oscillator is discussed, as well as possible non-linear filter applications.

INTRODUCTION

THE first part of this paper presented universal curves of thermistor static characteristics as a function of easily measurable electrical quantities.

The dynamic response to sinusoidal and step functions of current are given here.

THERMISTOR APPLICATIONS

A thermistor is a resistance with a high negative temperature coefficient of resistance. They are semiconductors similar to Thyrite except that their resistance changes with temperature instead of applied voltage. They are usually made of fused oxides of manganese, nickel, and cobalt, and are extremely stable for long lengths of time.

Thermistors can be used for sensitive temperature indicating devices because the resistance changes about 4 percent per degree C. They can be used as sensitive bolometers for microwaves or visible light, if connected in a bridge circuit to balance out ambient temperature changes. A thermistor can be used as a non-linear circuit element in many of the same applications as a carbon-filament light bulb. For example, the output of a bridge using thermistors in opposite arms is sensitive to applied voltage, and will have a null at a specified voltage. This can be used as the reference and sampling circuit in a voltage regulator.

A thermistor in the feed-back circuit from the output of an oscillator will change temperature with the amplitude of oscillation, increasing the negative feedback for an increased output voltage. In this application it is an amplitude stabilizer.

A thermistor network in series with a loud speaker will perform the function of a volume expander with the time constant determined by the thermal lag of the thermistor. This can be chosen to give fast expansion and slow compression at rates most pleasing to the ear.

A thermistor can be used as a volume-control device or a controlled a.c. impedance in a function generator. The a.c. signal is capacitively coupled at low level through the thermistor, and a large d.c. bias current is passed directly through the thermistor to control the magnitude of the output a.c. signal. If the output is taken across the thermistor, it varies approximately as ϵ^{-14I}, where I is the d.c. bias current. This has the distinct advantage over variable-mu tubes of not introducing distortion in the a.c. signal.

LOW FREQUENCY OSCILLATIONS

Time delays of seconds and minutes are realizable with thermal transients. They seem to be inherently capable of long time delays, for with good thermal insulation, it is not difficult to obtain a time constant of an hour in a physical space of only a few inches. The thermal time constant of a thermistor no larger than a one-watt resistor can duplicate the effect of 100,000 henries.

The sizes of the frequency-determining elements in a low frequency oscillator are usually excessive. An L−C oscillator to generate 0.005 c.p.s. might have 10,000 henries and 100,000 microfarads, though a phase shift circuit to perform the same function would need only two 30-microfarad condensers and two one-megohm precision resistors.

Very low frequency oscillations occur not only on transmission lines and bridges, but also in mechanical and electrical servo mechanisms. There is a need for a laboratory low frequency oscillator for testing the "soaking" effect or interfacial capacity of condensers, and the response characteristics of servomechanisms, process control analogs, and structural analogs.

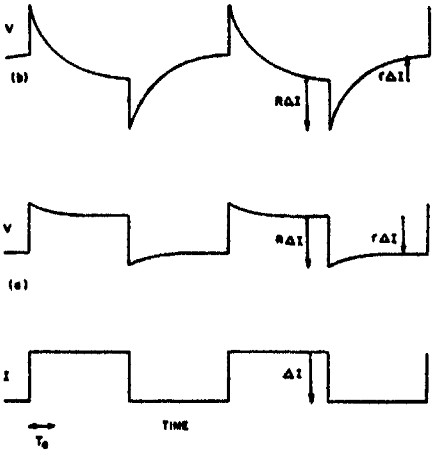

FIG. 1. Transient response of thermistor.

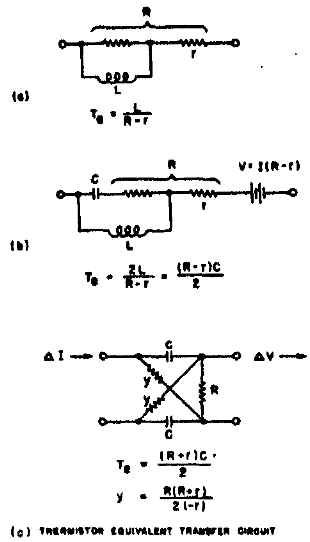
R
r
L
(a)
$T_e = \frac{L}{R-r}$
C
R
V = I(R-r)
r
L
(b)
$T_e = \frac{2L}{R-r} = \frac{(R-r)C}{2}$
ΔI
C
ΔV
y
y
R
C
$T_e = \frac{(R+r)C}{2}$
$y = \frac{R(R+r)}{2(-r)}$
(c) THERMISTOR EQUIVALENT TRANSFER CIRCUIT

FIG. 2. Thermistor equivalent circuits.

TIME CONSTANT

A thermal reservoir surrounded by thermal insulation has a logarithmic time constant for small temperature changes, of $T_\theta = H/k$, where H is the heat capacity in watt-seconds per degree centigrade, and k is the incremental dissipation constant in watts increase required per degree centigrade rise. In Part I of this article curves were presented showing how the thermistor dissipation constant varied with the thermal power being radiated. The thermal time constant T_θ decreases markedly with increasing power, because of the increase in k.

The electrical time constant T_e is less than the thermal time constant for increasing temperatures (decreasing resistance), and is greater than the thermal time constant for decreasing temperatures. Since the electrical quantities are complicated functions of the thermal transient, the electrical time constant cannot be applied blindly to a logarithmic transient.

If the thermistor is heated slightly above the equilibrium temperature for the operating bias, and allowed to cool again, $\Delta\theta = \Delta\theta' e^{-t/T_\theta}$, where $\Delta\theta'$ is the initial temperature rise above the final value in degrees centigrade. The resistance equation is

$$(R/R_0)^s = e^{-x/(1+x)}. \tag{1}$$

The variable x is equal to $\Delta\theta/\theta_0$, and s is a constant about 0.07. Substituting the temperature transient into Eq. (1), and differentiating with respect to time, gives an initial rate of

$$dR/dt = R'\Delta\theta'/s\theta_0 T_\theta. \tag{2}$$

If the electrical time constant is defined with reference to the initial conditions, it is the resistance change divided by the rate.

$$T_e = (R_0 - R')/(dR/dt) = T_\theta(R_0/R' - 1)/\ln(R_0/R'). \tag{3}$$

$$T_e = T_\theta(e^{x/s(1+x)} - 1)/(x/s(1+x)). \tag{4}$$

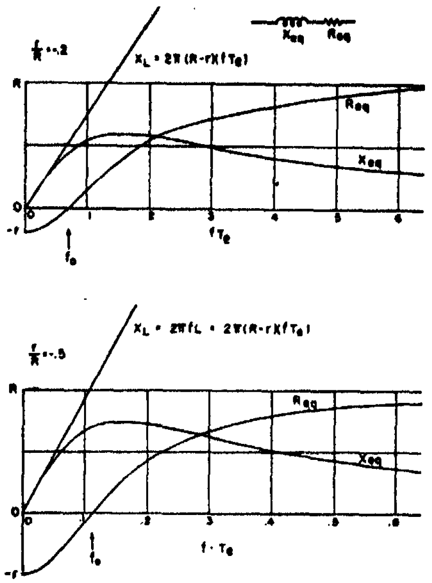

FIG. 3. Thermistor equivalent series constants.

If the change is only a few degrees, an adequate series approximation is

$$T_e = T_\theta(1 + x/2s(1+x) + x^2/6s^2(1+x)^2). \tag{5}$$

Typical values for a transient drop in temperature of 10 degrees are 55.5 percent increase in resistance, and $T_e = 1.26 T_\theta$. If the transient involves only a small percentage change in temperature or resistance, then the two time constants are equal. If the transient is a rise in temperature, x should be considered negative. For a large rise in temperature due to a sudden increment in current, most of the resistance change occurs at the beginning, and the electrical time constant is very short. A 100 degree rise (factor of 30-resistance drop) has an electrical time constant of one-half of the thermal constant. A 400 degree rise (factor of 10,000 resistance drop) has an electrical time constant of 0.06 times the thermal constant.

If the transient is a drop in temperature, the initial change in resistance is very slow, and reaches a maximum rate as the temperature nears its final value. For a drop of 100 degrees, the initial rate corresponds to an electrical time constant of three times the thermal value, a maximum rate is reached at about one thermal time constant, and the resistance has made 68 percent of

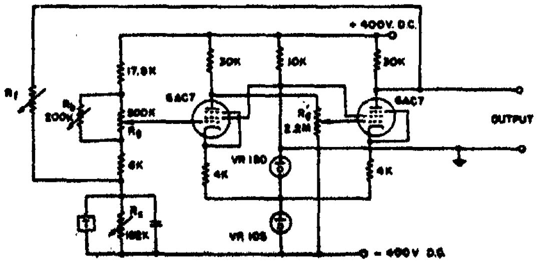

FIG. 4. Thermistor oscillator.

its change in 1.3 thermal time constants. For a drop of 400 degrees (increase in resistance of 10,000 times), the initial change in resistance corresponds to an electrical time constant of 120 times the thermal time constant, but the resistance change increases so rapidly that the resistance is up to 68 percent of its final value in 3½ time constants. This has the characteristics of a time delay circuit with "snap action."

TRANSIENT RESPONSE

The transient response of a thermistor depends upon the steady d.c. bias. At zero bias, the a.c. and d.c. resistances are equal. A square wave of current would produce a square wave of voltage. If a d.c. bias current is superimposed, however, the voltage wave will have the shape shown at (a) in Fig. 1. When the current increases, the voltage increases instantaneously an amount $R\Delta I$, but as the thermistor heats and the resistance drops, the voltage decreases a small amount $(R-r)\Delta I$ at a rate given by the equivalent electrical time constant. R is the total voltage divided by the total current, while r is the incremental resistance or dV/dI. If the bias current is increased until the incremental resistance is negative, then the voltage response to a current square wave will have the shape shown at (b) in Fig. 1.

Equivalent circuits for thermistors are given in Fig. 2. Circuit (a) is valid only for the transient component, but holds even if the incremental resistance r is negative. If the percentage current change is small enough that the transient is logarithmic, then the equivalent inductance is

$$L=(R-r)T_e. \tag{6}$$

For the W.E. 10-A thermistor, biased to maximum per unit negative incremental resistance, T_e is 100 seconds, R is 1000 ohms, r is -300 ohms, and L is 130,000 henries. Circuit (b) represents correctly both the transient and the steady-state current. The self-impedance of the thermistor has the same form as the transfer impedance of circuit (c) in Fig. 2.

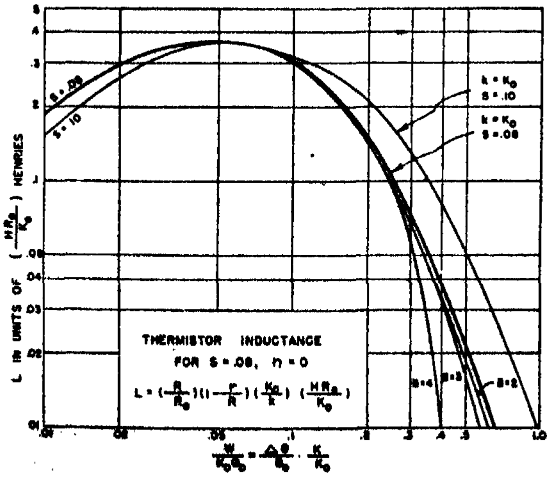

FIG. 5.

SINUSOIDAL RESPONSE

The sinusoidal response for small current amplitudes matches exactly the same equivalent circuit as for transients [(a) in Fig. 2]. The total impedance of this circuit is

$$Z=R_{eq}+jX_{eq}.$$
$$Z=r+(R-r)(\omega L)^2/((R-r)^2+(\omega L)^2)$$
$$+j(R-r)^2(\omega L)/((R-r)^2+(\omega L)^2). \tag{7}$$

Both the resistive and reactive components vary with frequency. This variation is shown in Fig. 3 for two typical bias settings, giving percentage negative resistances of 20 percent and 50 percent respectively. The value of L in circuit (a) is constant, and at very low frequencies, the shunting resistance $(R-r)$ is so large compared to the reactance that the entire L appears in the series equivalent circuit, as shown by the correspondence of X_L and X_{eq} in Fig. 3 for low frequencies. At very high frequencies, X_L is so great in comparison to $(R-r)$, that it is effectively shorted out, so that the resultant X_{eq} is only $(R-r)^2/X_L$, which diminishes hyperbolically with increasing frequency.

The equivalent resistive component is $R=V/I$ at high frequencies and $r=dV/dI$ at very low frequencies. If the bias is sufficient to make r negative, then there is some intermediate frequency at which R_{eq} is zero. This is called the critical frequency, f_0.

$$2\pi f_0=(R/L)(1-r/R)(-r/R)^{\frac{1}{2}}. \tag{8}$$

$$f_0=[(-r/R)^{\frac{1}{2}}]/2\pi T_e. \tag{9}$$

Near three times the critical frequency, the Q of the circuit is one, and as the frequency is reduced, Q increases until it becomes infinite at the critical frequency. Typical values for a $1-B$ thermistor are $R=6000$ ohms, $r=-1500$ ohms, $L=5150$ henries, $T_e=0.7$ seconds, and $f_0=0.11$ c.p.s.

LOW FREQUENCY OSCILLATOR

If the thermistor is paralleled with a condenser whose reactance is less than X_{eq} at f_0, the combination will oscillate continuously. If the capacity is increased, the

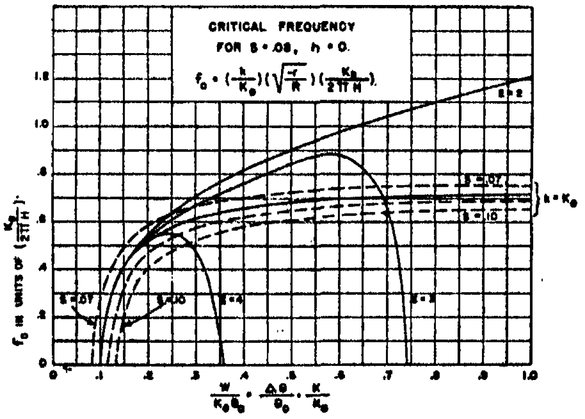

FIG. 6.

frequency will diminish, and the amplitude will rise because of the increase in the series negative resistance. The amplitude of oscillation stabilizes at the point where the a.c. energy dissipated in the internal impedance of the constant-current bias supply is just equal to that generated by the negative resistance. The series impedance $R_{eq}+jX_{eq}$ can be replaced by equivalent parallel values, R_p and X_p, the condenser C, and the parallel loading resistance R_c. Their values for frequency f are:

$$R_p=R_{eq}(Q_p^2+1), \tag{10}$$

$$X_p=X_{eq}(Q_p^2+1)/Q_p^2, \tag{11}$$

where

$$Q_p=X_{eq}/R_{eq}=R_p/X_p. \tag{12}$$

For sustained oscillations at the frequency f, the capacity must be

$$C=1/2\pi fX_p=Q_p^2/2\pi fX_{eq}(Q_p^2+1). \tag{13}$$

The amplitude must be small for the output to be sinusoidal. This is fulfilled when R_c, the loading resistance, is just equal to $-R_{eq}$. Since the negative resistance varies with frequency, R_c must be adjusted by the tuning control.

A word of caution concerning the adjustment of experimental oscillators is in order. If the frequency is set for much less than f_0, and if loading is not provided in the form of high series resistance in the condenser circuit, or high parallel conductance, then when the switch is first turned on, the condenser will charge slowly, and the thermistor will remain cold. As the thermistor begins to heat when the condenser is fully charged, it goes through a large temperature transient as described before, with a very short time constant. The condenser discharges suddenly and the thermistor burns up.

The oscillator can be tuned to frequencies above f_0 by supplying a small amount of positive feedback with a two-stage d.c. amplifier. One satisfactory design is shown in Fig. 4 for a W.E. 1−B thermistor. Since the inductance decreases almost hyperbolically with increasing frequency (constant reactance), the oscillator can be tuned over a ten-to-1 frequency range with a ten-to-1 instead of a 100-to-1 capacitor. The variable resistor R_b adjusts the d.c. bias current; R_a adjusts the d.c. level of the output signal, and is usually set to give zero volts d.c. output. R_f controls the positive feedback, and R_s provides loading for controlling the starting transient. The gain of each stage is limited to 10 by negative feedback. This oscillator will deliver 40 volts peak-to-peak with 14 percent second harmonic and no measurable third harmonic.

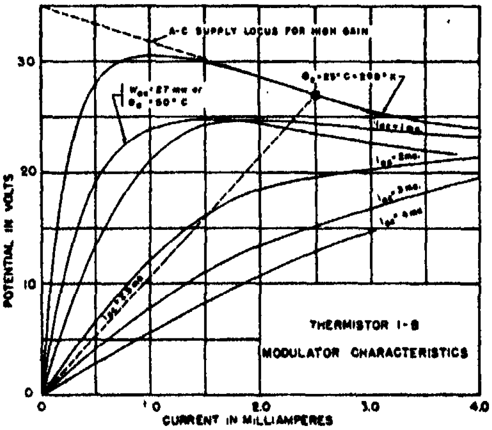

FIG. 7.

Bias tuning can be used on a thermistor oscillator either with or without feedback. The reason for this is apparent from Fig. 5, which shows that the inductance diminishes in the same manner as the resistance for increasing bias power dissipated, above the maximum voltage point.

$$L=(R/R_0)(1-r/R)(HR_0/K_0). \tag{14}$$

$$f_0=[(-r/R)^{\frac{1}{2}}](k/K_0)(K_0/2\pi H). \tag{15}$$

Figure 6 shows the variation in critical frequency with bias. It indicates the region in which feedback is not necessary. Between $W/K_0\theta_0$ of 0.11 and 0.3, the critical frequency increases by a factor of 6, and in the same region, from Fig. 5, the resonant frequency also increases, but only by a factor of two, for fixed parallel capacitance. In the same region, the incremental resistance increases by a factor of nine. The effective negative resistance, therefore, increases markedly, and the amplitude of oscillation rises with bias. Above $W/K_0\theta_0$ of 0.3, however, the rate of change of critical frequency becomes small, the incremental resistance begins to decrease, and the resonant frequency rises at a more rapid rate, all three effects tending to keep the amplitude constant independent of the bias tuning, and eventually to decrease the amplitude at very high bias.

Notice that the inductance is independent of bias for $W/K_0\theta_0$ of 0.05, which is just before the voltage reaches the peak of its curve (15° rise). Here the incremental resistance is changing quite rapidly. On the other hand, the negative resistance reaches a peak at about $W/K_0\theta_0$ of 0.3, (90° rise) and here the inductance is decreasing quite rapidly. It is difficult, therefore, to adjust a simple capacitively-tuned oscillator so that both amplitude and frequency are independent of bias changes.

FILTERS

A biased thermistor can be operated as a filter element near its critical frequency, but its characteristics are different from an ordinary inductance. The reactance is almost constant over a wide range of frequencies, and if used in an R−L network, phase shifts could be obtained which would be relatively independent of frequency.

It is interesting to note from Fig. 5 that the inductance is more than one-half of its maximum possible value for a range of $W/K_0\theta_0$ of 0.01 to 0.17, corresponding to temperature rises from 3 degrees to 50 degrees. The parallel resistance which the equivalent internal inductance L sees is $R-r$ ohms for a constant-current (infinite impedance) source. The internal Q is therefore

$$Q_i = k/\omega H = 1/\omega T_\theta. \qquad (16)$$

This has the units of power dissipated in watts per degree divided by thermal energy stored in watt-radians per degree. The external series Q_s for the same condition is X_{eq}/R_{eq} or

$$Q_s = (R-r)Q_i/(R+rQ_i^2). \qquad (17)$$

At low bias currents, r is almost equal to R, and Q_s is very low. At the maximum voltage point, $Q_s = Q_i$.

MODULATOR

If the thermistor is common to both an a.c. and a d.c. circuit, variations in d.c. can change the a.c. impedance and voltage. It can therefore be used as a modulator, in single units or bridge circuits, but the modulating frequency must be less than the critical frequency.

If the a.c. supply is high impedance and delivers constant current, the conversion voltage gain for a small alternating current and a large direct-current bias is

$$A = de_{ac}/de_{dc} = i_{ac}(R-r)/I_{dc}(-r). \qquad (18)$$

This is negative. At low bias levels when $r=R$, A is almost zero. At maximum voltage $r=0$, and A approaches a very large gain, but this is not realizable because the input impedance r goes to zero for changes in E_{dc}.

Figure 7 shows the d.c. V−I curves for a 1−B thermistor for several a.c. bias currents. These curves are reversible; that is, they are valid a.c. V−I curves for a set of d.c. bias currents. The equations given in Part I of this paper hold for modulator applications if W represents the total watts dissipated, $(i_{ac}^2+I_{dc}^2)R$. If the a.c. power, W_{ac}, were constant, then the curves in Fig. 7 would look just like the set for different ambient temperatures, the correspondence being $\theta_a = \theta_0 + W_{ac}/k$. Since the a.c. current is constant in Fig. 7, the slope r is more positive than for the constant-power curves.

Figure 8 represents a practical form of modulator circuit. For maximum power gain, the d.c. input impedance should equal the thermistor impedance for changes in current, which is the initial slope of the curves in Fig. 7, or R. The total output impedance is also R, and can be matched with a transformer to a rectifier, amplifier, or other device. (The incremental output impedance is r.) If the d.c. input increases, the output current and the output voltage will each increase by the factor $1/(1+dR/2R)$, where dR is negative. The change in output power will be approximately

$$dW_{ac} = -W_{ac}(1-3dR/4R)dR/R. \qquad (19)$$

The a.c. power dissipated internally in the thermistor does not change if the output load r' is equal to R. The change in d.c. power input required is

$$dW_{dc} = dR/mR. \qquad (20)$$

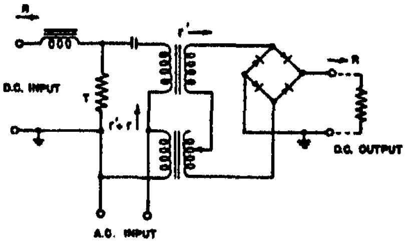

FIG. 8. Basic thermistor modulator.

This follows from the definition of m as the power coefficient of resistance. The power gain for matched impedances is approximately

$$G = dW_{ac}/dW_{dc} = -W_{ac}m = (r/R-1)/(r/R+1). \qquad (21)$$

The d.c. input should be small to make dR/R in Eq. (19) negligible. If the a.c. bias is too small, the gain will be low because of insufficient current to vary. If the bias is too high, G will again be low because m will be small due to small changes in input power having negligible effect on the resistance. The maximum possible gain occurs when the product of $W_{ac}m$ is a maximum. This maximum product corresponds to a line tangent to the curves in Fig. 9, Part I, with a slope of −45°. The value of $W_{ac}/K_0\theta_0$ is 1 for $k=k_0$, and 0.2 for $z=4$. The corresponding values of m/m_0 are 0.25 and 0.65.

The maximum gain occurs at the same values of bias power as the maximum negative incremental resistance, as can be seen by comparison with Fig. 12, Part I. The a.c. bias supply is stable, however, because of the external loading resistor r'.

The power gain for $k=K_0$ and $n=0$ is approximately

$$G = -W_{ac}m_0/(1+W_{ac}/K_0\theta_0)^2. \qquad (22)$$

The maximum possible power gain is

$$G_{\max} = -K_0\theta_0 m_0/4 = -a_0\theta_0/4. \qquad (23)$$

This is about three for the ordinary thermistor. For $Z=4$, this gain drops to 0.13 $a_0\theta_0$ or about 1.66.

The thermistor appears as a negative incremental resistance to the a.c. bias supply. This can be used to supply thermal positive feedback by reducing the output resistance r' until it is just slightly greater than r, the slope of the a.c. V−I curve for the power W_{ac} (top curve in Fig. 7). r' will be one-half to one-fourth of R.

If the resistance changes an amount dR, then the change in output power will be

$$dW_{ac} = -2dRW_{ac}r'/R^2(1+r'/R). \qquad (24)$$

The increase in a.c. current increases the losses within the thermistor. The internal feed-back power is

$$dW_i = W_{ac}dR(r'/R-1)/R(r'/R+1). \qquad (25)$$

The change in resistance is due to the total input watts,

$$dW_{dc} + dW_i = dR/mR. \qquad (26)$$

The power gain is

$$G' = dW_{ac}/dW_{dc} = -2W_{ac}mr'/R((r'/R+1) - W_{ac}m(r'/R-1)). \quad (27)$$

The numerator term ($W_{ac}m$) can be replaced by the matched impedance gain G. The same denominator term can be replaced by the function of r given in Eq. (21). Simplifying:

$$G' = G(r/R+1)/(r/r'+1). \quad (28)$$

If $r' = -r$, the a.c. system is critically unstable, and the gain becomes infinite. The gain can be made as arbitrarily large as one dares, the price being an increasingly longer time constant because of the thermal delay on the feedback. The bias current and load resistance fix the input a.c. voltage.

$$V_{ac} = i_{ac}(R+r') = (R+r')(W_{ac}/R)^{\frac{1}{2}}. \quad (29)$$

In a high gain system, the input voltage has to be adjusted carefully, because small changes in it are just as serious as small changes in r'.

Mr. Jay Stone, Engineer at the Ames Laboratory, Moffett Field, California, designed and built the low frequency oscillator described in this paper as an M.S. thesis.

THE REVIEW OF SCIENTIFIC INSTRUMENTS VOLUME 21, NUMBER 4 APRIL, 1950

A Monitor for Low Intensity Gamma-Rays*

J. B. H. Kuper and R. L. Chase
Brookhaven National Laboratory, Upton, New York

(Received January 23, 1950)

A recording monitor for low intensity gamma-radiation has been developed, using a simple and inexpensive form of dynamic condenser electrometer in connection with an ionization chamber and a commercial recording potentiometer. Use of a rate of drift method at relatively low voltage sensitivity eliminates difficulties with contact potentials and grounding key kicks. The instrument gives an indication and recycles when 5 microroentgens have been received. Normal gamma-background current is 4 to 5×10^{-15} amperes and at this sensitivity the instrument is extremely rugged and operates outdoors in all weather.

THIS instrument has been developed in response to the need for a device to record gamma-rays of low intensity, of the order of 2 mr per week, continuously and without requiring attention over long periods of time. A major requirement was that the instrument be rugged and capable of outdoor operation in all weather conditions. Considerations of energy dependence dictated the choice of a Bakelite wall ionization chamber operated at atmospheric pressure. Since the current to be expected in a chamber of reasonable size, say 5 liters capacity, is only of the order of 4 or 5×10^{-15} amperes, it was felt that the usual vacuum tube electrometers would give excessive trouble with grid current and drifts when left unattended over periods of several days. Therefore, it was decided to use a simple form of dynamic condenser or vibrating reed electrometer.[1] This type of electrometer lends itself exceptionally well to use in connection with a recorder of the electronic self-balancing potentiometer type such as the Brown "Electronik" or Leeds & Northrup "Speedomax."

Since we are interested in determining the integrated dose of radiation, we used a rate of drift method with automatic recycling after a definite amount of charge has been accumulated. As indicated in the simplified schematic, Fig. 1, the charge accumulated in the ionization chamber is fed to the dynamic condenser and the resulting a.c. signal is removed through the coupling condenser and fed to the amplifier of the potentiometer recorder in place of the signal normally furnished by a chopper. The signal is amplified and used to drive the pen and potentiometer slide wire. The d.c. voltage appearing on the moving contact of the potentiometer is fed back to the coupling condenser and serves to bind on the latter all the charge collected except the residual necessary to furnish an error signal. Given sufficient amplifier gain, the voltage on the potentiometer slide wire contact will be equal to that on the coupling condenser to within a single convolution of the potentiometer slide wire. In the case of the Brown recorder this is 1/1400 of full scale.

In the actual instrument, of course, there is a contact potential difference across the dynamic condenser, and in order to obtain a vanishing error signal the potential applied by the feed-back line must equal the contact potential. This, however, appears only as a zero correction, provided the contact potential does not drift.

A convenient value for the coupling condenser is in the neighborhood of 10 $\mu\mu$f. It is possible to use a comparatively large voltage on the potentiometer, of the order of one volt, and thus minimize the effects of contact potential drifts and kicks due to grounding and

---

* This work was done under the auspices of the U. S. AEC.

[1] Palevsky, Swank, and Grenchik, Rev. Sci. Inst. 18, 298 (1947).

ungrounding the circuit. This greatly reduces the cost of the electrometer.

The recording potentiometer is arranged to trip a switch when near the upper end of the slide wire. This actuates a grounding key which is held down by a synchronous motor timer for a period of 30 seconds in order to allow ample time for the recorder to return to zero, and is then released. Thus, the instrument is insensitive for 30 seconds out of each cycle and at high dosage rates a suitable correction would have to be made for this fact.

Under normal conditions of background in our location, one cycle takes about 35 minutes and represents about 5 microroentgens of gamma-radiation. In routine operation a message register is used to count the number of cycles and it is not necessary to use the recorder itself. The chart record is useful for observing changes in gamma-ray intensity and for diagnosis in case trouble is experienced.

As indicated in the photograph, Fig. 2, the ionization chamber, dynamic condenser, coupling condenser, and preamplifier are mounted together in a housing suitable for outdoor installation. The recording potentiometer, power supplies, and other accessories are mounted together indoors, and the cable between them may be of any desired length.

The housing for the dynamic condenser and preamplifier was purposely made much larger than necessary in order to provide some shelter for the ionization chamber from direct rainfall. The dynamic condenser was made by modifying the modulation condenser of a surplus AN/APN-1 radio altimeter.[2] The original ceramic insulator supporting a pair of stator plates was removed and discarded and a new stationary electrode supported with Teflon or fluorethene insulation was provided. Silver plating of this electrode was found to reduce the contact potential drifts to an acceptably low value.

A half-inch brass tube connects the stationary electrode of the dynamic condenser to the ionization chamber with a 1000-megohm resistor interposed to prevent loss of signal into the ionization chamber capacitance, and to reduce the effects of hum picked up by the chamber center electrode. The coupling condenser consists of a length of brass tubing mounted coaxially with the one mentioned above on three Kovar glass seals. The use of air dielectric for this condenser avoids difficulties with insulator soakage. The dynamic condenser is driven with about one-half volt 60-cycle a.c. obtained from a small stepdown transformer and the 60-cycle error signal is fed to the two stage preamplifier. To minimize hum pick-up the "grounding pin" actuator and preamplifier heaters are operated on direct current. In all probability sufficient gain could be obtained from a single stage of amplification at this point, but it was felt safer to provide a second stage and thus reduce the danger of hum pick-up in the cable between the preamplifier and the recorder. The output of the amplifier was stepped down to an impedance level of a few hundred ohms before being placed on the line. The recording potentiometer was modified to have a full scale range of one volt, and the drive voltage was removed from the mechanical chopper. The signal from the preamplifier was fed directly to the input step-up

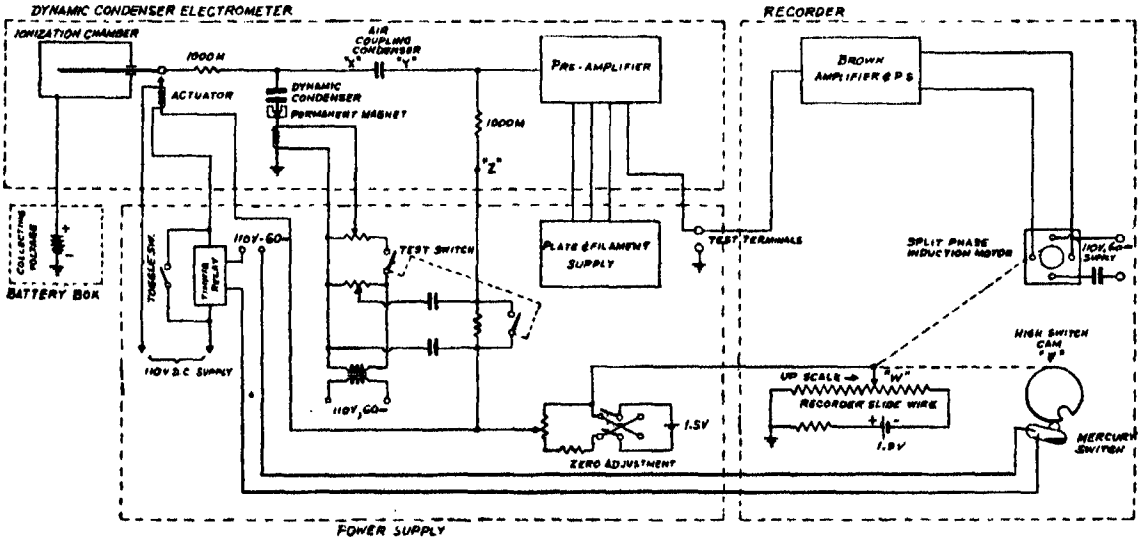

FIG. 1. Simplified schematic of the dynamic condenser monitor. Charge is collected on the insulated line "X" and is bound on the air coupling condenser by an equal and opposite charge at "Y" produced by feeding back the slide wire voltage at "Z." When the recorder reaches a preset point on scale the mercury switch closes, energizing the "grounding pin" actuator and discharging the coupling condenser. After a predetermined time, long enough for the recorder to return to zero, the actuator is released and a new cycle started.

---

[2] We are indebted to Dr. R. J. Moon of the University of Chicago for the suggestion of using the altimeter condenser for this purpose.

FIG. 2a. Photograph of the complete assembly, including power supplies and recorder.

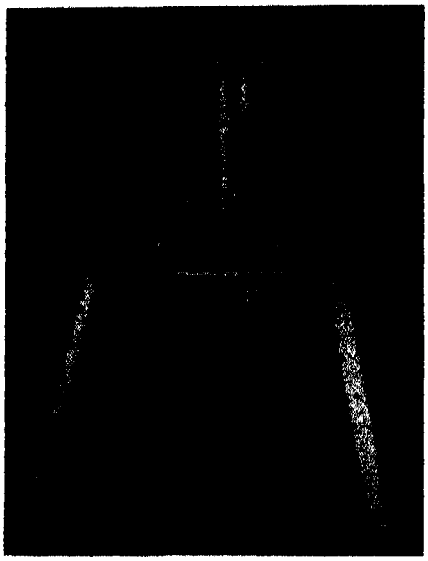

FIG. 2b. Inside view of the electrometer head showing the dynamic condenser, preamplifier and the grounding pin and actuator used for recycling.

transformer of the Brown amplifier. The mechanical chopper was not removed since it is used for the automatic standardization of the working current in the potentiometer. Feed-back voltage from the potentiometer slide wire is applied to the coupling condenser through a 1000-megohm resistor.

The use of 60 cycles for the working frequency in the dynamic condenser is convenient from the standpoint of the potentiometer drive motor which acts as a phase detector in this application. However, if it were not for this consideration a much higher frequency would have been chosen. Not only does the use of 60 cycles seriously complicate the hum problem,[3] but also it requires the use of very high impedances in the input to the amplifier in order to obtain a reasonable conversion efficiency from the dynamic condenser. The first stage of the preamplifier is operated at low screen voltage in order to reduce the grid current as far as possible. Even so, an occasional 6AK5 has so large a grid current as to bias itself into an unfavorable region because of the 1000-megohm grid leak.

In order to simplify servicing of these instruments in the field, suitable test points have been provided. A rough over-all check for satisfactory operation can be obtained by turning the zero adjust knob a definite number of divisions corresponding to a known voltage increment, and checking that the recorder pen moves correspondingly. The pen should move promptly and positively as though to indicate that the control is "stiff." If the over-all gain is too high, overshooting or hunting will be observed in this test. Since there is more than enough gain in both the preamplifier and the main amplifier, it is not sufficient to know that the over-all gain is correct. The gain must be divided between the two parts of the amplifier so that neither is overloaded. This is done by feeding a known a.c. signal to the preamplifier by means of the test signal switch and observing with a high impedance voltmeter or with a calibrated oscilloscope that the correct output voltage is obtained from the preamplifier. The conversion efficiency of the dynamic condenser may be checked by applying a known d.c. voltage through the zero adjust control and observing the preamplifier output. For this test the potentiometer drive motor must be stopped and heater voltage removed from the recorder amplifier. Excessive drive voltage applied to the dynamic condenser will cause it to short occasionally. This will cause recognizable distortion of the wave form at the preamplifier output. Once the conversion efficiency and preamplifier gain have been set to the correct values, the main amplifier gain can be adjusted to give the correct over-all gain.

Because of the feed-back connection variations in gain can be tolerated so long as the gain is somewhat greater than the minimum value necessary to start the potentiometer drive motor when the unbalance signal exceeds that due to one convolution of the slide wire. This makes the whole instrument relatively tolerant of line voltage fluctuation. Nevertheless, we have found it good practice to operate the equipment from a Sola voltage regulating transformer to stabilize the dynamic condenser drive voltage. This is desirable because the zero position depends somewhat on hum pick-up, in addition to the contact potential, and, therefore, is a function of conversion efficiency.

Collection voltage for the ionization chamber is obtained from ordinary B batteries. Since changes in this voltage will appear directly in the record, it is advisable to protect the batteries from sudden temperature changes.

The principal difficulty encountered in building a group of sixteen instruments was, as might be expected, with the insulators. The insulator for the ionization chamber is protected by a guard ring so that none of the high insulation is ever subjected in normal circumstances to a voltage greater than the contact potential of the dynamic condenser. Insulator leakage may appear to accelerate or decelerate the rate of drift, depending on the sign of the contact potential. The sign and approximate magnitude of the contact potential can be determined from the setting of the zero-adjust potentiometer required to bring the recorder to zero.

---

[3] Hum pick-up will cause a displacement of the zero position, and may cause the amplifier to overload, so precautions should be taken to minimize it.

Insulator leakage, provided it is not too severe, may be determined by the behavior of the error signal observed at the output of the preamplifier with the slide wire drive motor turned off. In the absence of leakage the error signal will increase indefinitely as ionization current is collected, until, of course, the preamplifier saturates. If an insulator leak becomes appreciable with respect to the ionization current of a few times 10^{-15} amperes, the error signal will rise to some value and remain constant. Given a knowledge of the ionization current and the contact potential, it is possible to compute the insulation resistance, if one determines the d.c. voltage on the dynamic condenser corresponding to the observed error signal.

We have made satisfactory insulators of molded or polished polystyrene or of machined fluorethene. In some cases machined Teflon has been quite satisfactory, but occasional samples of this material appear to have inclusions which increase the conductivity.

Far more troublesome, however, than ordinary leakage effects, have been difficulties with surface charges on insulators. We have found it of the utmost importance not only to coat with conducting material as much as possible of any exposed insulator surfaces, but also to coat those portions which are supposedly in contact with metal. Neglect of this precaution leads to extremely annoying drifts which appear whenever the ambient temperature is changed suddenly. If an instrument which has been in thermal equilibrium is suddenly moved to a new environment, the apparent ionization current may increase for a period of time followed by a reversal in which the "current" is either greatly diminished or even reversed, and ultimately, after the instrument has come into equilibrium with its new surroundings, a return to the normal rate of drift.

Our explanation for this effect is as follows: The contact surface between the insulator and the metal part supported by the insulator is by no means perfect, especially since in our case both surfaces are machined and not highly polished. Thus, it is possible for charges on the surface of the insulator almost but not quite in contact with the metal to remain indefinitely. Any slight relative displacement of the two surfaces occasioned by differential thermal expansion will change the capacitance across the gap and hence result in an apparent flow of charge. Because of the very small clearances involved, this flow may be surprisingly large. We suspect that a phenomenon of this sort may be at the bottom of many reported cases of stress currents or pyroelectric effects in insulators. Effects of the sort postulated here will presumably disappear in time and their disappearance can be hastened by exposure to a strong gamma-ray source. However, we have found it preferable to eliminate them at the start by careful treatment to insure good contact between the insulator and the adjacent metal part. Teflon and fluorethene are exceedingly difficult to wet with aqueous solutions. We have found it possible to get a satisfactory conducting coat by using Lubrifilm, an alcohol suspension of colloidal graphite.

Another problem which has given us some difficulty is that of alpha-particle contamination of the ionization chamber itself. The ionization current due to gamma-rays of the order of 4 or 5×10^{-15} amperes is equal to that which would be produced by one alpha-particle of average energy every four or five seconds.

Some of our chambers were found to be contaminated to the extent of something like six alpha-particles a minute. Fortunately this was a surface contamination and could readily be removed by cleaning and recoating the chamber with graphite.

The ionization chamber and preamplifier are sealed up, with drier inside, and provision is made for accommodating changes in atmospheric pressure and temperature through a breather balloon. Thus, for the most accurate work it would be necessary to apply a correction for pressure and temperature in the ionization chamber. The joints in the ionization chamber are sealed with Glyptal lacquer and we have so far experienced no trouble with moisture seeping in. The chambers have been operated with a hose played on them with no apparent ill effects. An important advantage of the type of ionization chamber described here is its extreme ruggedness. The instrument is quite insensitive to microphonics. In fact, it is possible to pound on the ionization chamber-preamplifier assembly without causing any effect on the record. Also, on one occasion during a severe windstorm, an instrument was blown loose from its fastenings on the roof of a building and tipped over on its side. This, too, resulted in no appreciable effect on the record.

With a given ionization chamber, coupling condenser, and potentiometer range, the maximum intensity that can be measured is limited by the speed of the recorder drive motor. Making correction for the insensitive time during recycling, we can measure up to about 100 times the normal background intensity without alterations.

It is a pleasure to acknowledge the contributions of our colleagues in the Electronics Division, and particularly Mr. Lloyd Davis.

THE REVIEW OF SCIENTIFIC INSTRUMENTS VOLUME 21, NUMBER 4 APRIL, 1950

Physical Instruments for the Biologist

Detlev W. Bronk
Associate Editor in Charge of this Section
Johns Hopkins University, Baltimore, Maryland

Stainless Steel Micro-Needle Electrodes Made by Electrolytic Pointing

HARRY GRUNDFEST, ROBERT W. SENGSTAKEN, AND WALTER H. OETTINGER
Department of Neurology, College of Physicians and Surgeons, Columbia University, New York

AND

R. W. GURRY
Research Laboratory, U. S. Steel Corporation of Delaware, Kearny, New Jersey

(Received November 28, 1949)

Micro-needle electrodes of any desired taper and sharpness for insertion into living tissue can be made quickly by electrolytic etching. For stainless steel wire the electrolyte is a mixture of sulfuric and ortho-phosphoric acids. The wire to be pointed is made the anode of a circuit initially carrying about 0.03 amp. Gross shaping of the needle is done by repeatedly immersing the wire and withdrawing it slowly from the bath. Fine shaping of the point is carried out with reduced current. The electrodes are finished by insulating all but the fine tip with a baking enamel. The process described is adaptable to making a batch of micro-needles at one time.

MANY physiological studies require insertion electrodes of a size that will cause minimal damage when they are introduced into neural tissue and which are insulated to record or stimulate only at a very fine electrode tip. Such electrodes have been constructed (Grundfest and Campbell)[1] by shaping thin steel needles with a special grinding technique and then insulating them by dipping in a baking varnish. Electrodes can be made with tips of 5–10μ, but when examined microscopically, the points are somewhat blunt and rough. The chief disadvantage of the procedure, however, is that the electrodes are individually made with a time-consuming technique.

The present paper describes a technique of electropointing of a non-corroding stainless steel wire in an acid bath to produce needle electrodes relatively uniformly and quickly. This technique is similar to that used for electropolishing specimens for microscopic examination. Many needles can be made at one time. Microscopically smooth sharp points can be made any desired shape, size, and taper suitable for the specific application (Fig. 1). The point found most practical for work in the intact mammalian nervous system is shaped like a narrow "V." However, needles have been made with a thin, microscopically sharp, hair-like tip less than 0.2μ in diameter for 1 mm and then coming to a heavier shank. These have been used in tissue cultures.

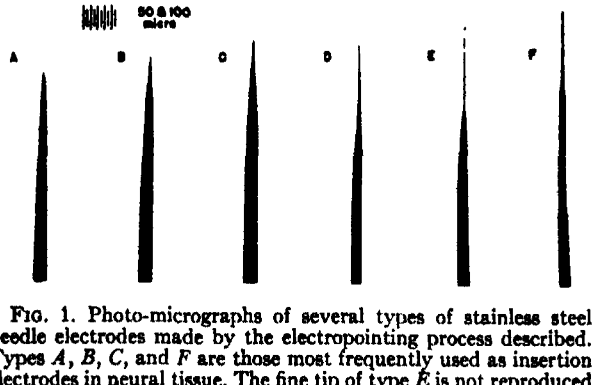

FIG. 1. Photo-micrographs of several types of stainless steel needle electrodes made by the electropointing process described. Types *A*, *B*, *C*, and *F* are those most frequently used as insertion electrodes in neural tissue. The fine tip of type *E* is not reproduced adequately because of bubbles in the mounting medium. The needles shown are without insulation.

Various stainless steels, in the form of 0.25-mm (0.01-in.) diameter wire, were used for constructing the micro-needle electrodes. The most satisfactory is hard-drawn 18-8 wire. We have found stainless steel and particularly the 18-8 composition superior to a carbon steel wire in respect to corrosion in living tissue and preservation of the point after multiple insertions within neural tissue.

The needles are pointed by dipping in an acid made as follows: 34 cc concentrated sulfuric acid (sp. gr. 1.84), 42 cc ortho-phosphoric acid (sp. gr. 1.69), and 24 cc of distilled water to total 100 cc of solution. A portion of this solution is placed into a small metal beaker which is connected to the negative side of a 6-v d.c. source. The wire to be pointed is made the anode. A switch, variable resistance, and milliammeter are included in the circuit. A microscope of low magnification is fitted in front of the beaker so that the stage of electrolytic pointing may be observed at any time by raising the needle out of the acid solution.

The pointing process is carried out by immersing the wire in the acid solution and passing a current through it. At first, the electrolytic action is carried on rapidly to produce a general tapering of the needle. A current of 0.03 amp. per needle produces an optically smooth finish in a satisfactory time. Higher current will cause pitting and such rapid electrolysis that control of the shape of the point is difficult. During the electrolytic pointing process, about 15–20 mm of the wire is repeatedly immersed and withdrawn slowly from the acid to produce the desired taper. Toward the end of the procedure, when shaping of the tip is done, the current is reduced, to make the pointing more easily controlled. Various tapers and points may be obtained by varying the depth of immersion, time of electrolytic action, and current strength. Microscopic examination during this stage is essential. Following electrolytic pointing, the needle should be dipped into 10 percent hydrochloric acid in order to prevent staining of the wire, and then thoroughly washed.

---

[1] Harry Grundfest and Berry Campbell, "Origin, conduction and termination of impulses in dorsal spino-cerebellar tracts of cats," J. Neurophysiol. 5, 275–294 (1942).

Care must be taken with the acid solution used for electrolytic pointing as its concentration is critical. If a small volume of solution is used or if many needles are made at one time the water content of the acid will decrease by electrolytic action, ultimately increasing the electrical resistance of the solution to the point where no pointing will occur. Since the acid is hygroscopic, it must be made freshly as a too dilute acid will not work despite a low electrical resistance.

After the point has been produced, the blunt end of the needle is electroplated with copper in order to present a surface which can be used to solder the needle into a holder rod. The plating is necessary, since the stainless steel would otherwise have to be fixed to the heavier rod either by clamping, silver soldering, or welding. Clamping presents hazards of poor and variable electrical contact while we have found that high heat applied to the fine stainless steel wire often causes softening of the needle shank.

Copper sulfate is employed for the plating process with a copper plate and the blunt end of the needle immersed in the solution. About 20 ma of current per needle (which is connected to the negative pole) and about 2 min. produce a satisfactory well-bonded plating of copper.

Following this, the needle is cleaned with alcohol, dried, and insulated. It is dipped into and then very slowly removed from General Electric Formvar Enamel No. 9825. The enamel is baked for 30 min. at 125°C. The enamel is usually diluted to obtain a thin, uniformly deposited coating on the needle. Several coats may be necessary to produce satisfactory insulation. In the insulating process all but the blunt, copper-plated end of the needle is immersed in the enamel, and during the drying the needle is held vertical, with the tip up. This aids retraction of the enamel film from the extreme tip, so that usually the tip is open even after several coats of enamel have been baked on. If it has become insulated, one or two gentle strokes of the tip against very fine abrasive will remove sufficient insulation to permit use as an electrode.

There are several special steps in this procedure worthy of mention. The first is that stainless steel wire as supplied to us on a roll has to be straightened to obviate a curved or bent needle. Such a process, requiring cross rolling, has been done for us by the Art Wire and Stamping Company of Newark, New Jersey. The second is that it is preferable to have a smooth and flawless enamel coating of the needle. Attention must be given to the prevention of dust and other foreign materials from getting on the needles during the enameling and baking processes.

The procedure described in the foregoing is easily adaptable to making a large number of needles simultaneously. All that is needed is to assemble an array of wires on the needle holder, in such a way that they all make contact with the positive input terminal, but do not touch each other. When properly assembled the array can also be plated and insulated as a unit, and stored until needed.

The steps in the manufacture of the microelectrodes are: (1) pointing by an electrolytic process in acid; (2) copper plating of the other end of the needle; and (3) insulation by dipping in an insulating enamel. This technique has produced over one thousand needle microelectrodes for use in the study of bioelectric potentials observed in the mammalian nervous system. They have been made in a variety of shapes and sizes for various studies and have proved satisfactorily durable so that one needle can withstand use in a number of experiments. They cause minimal tissue trauma and permit recording from areas as small as one neural cell.

We wish to express our sincere gratitude to Dr. J. B. Austin, Director of the Research Laboratory of the United States Steel Corporation for his interest and assistance; to Mr. N. C. Beese, Research Department, Westinghouse Electric Corporation, Bloomfield, New Jersey, for samples of wolfram wire and electrolytically pointed wolfram needles which were tried early in the development of the procedure described; and to Dr. Joseph Greenspan, Process and Instruments, Brooklyn, New York, who informed one of us (H.G.) of the existence of the electrolytic pointing process.

Automatic Isodose Recorder with Scintillation Counter as Gamma-Ray Detector

G. J. Hine,* M. Berman, and M. M. Elkind**
Division of Physics and Biophysics, Sloan-Kettering Institute for Cancer Research, New York, New York

(Received November 28, 1949)

This paper describes an instrument for investigating the radiation field of any type of gamma-ray source. A small calcium tungstate crystal together with a light-conducting quartz rod and a 1P21 photo-multiplier tube is used as gamma-ray detector. The lines of constant radiation intensity in a selected plane (isodose curves) are recorded automatically with a good accuracy in a short period of time.

INTRODUCTION

THE use of extended gamma-ray sources for therapeutic purposes requires knowledge of the dosage due to the gamma-radiation. Therefore, the three-dimensional radiation field of gamma-ray emitters has to be determined thoroughly. For practical applications, the lines of constant radiation intensity within a given plane (isodose curves) are frequently the most desirable information.

Based on some ideal assumptions[1] the isodose curves for sources of simple geometric configurations, such as linear sources, can be constructed mathematically. However, the limited account for the absorption in the walls of the linear radium tubes and the radium salt itself prevents accurate calculations of the regions close to the sources and around their ends. For odd assemblies of several linear gamma-ray sources, calculations become extremely difficult, tedious, and time-consuming.[2] Therefore, it is practically impossible to determine for each patient individually the applied or even the most effective radiation distribution. For the use of extended gamma-ray sources, such as Co^{60} where fabricated shapes have been activated in a pile,[3] little information can be obtained by computations.

Several attempts have been made to determine isodose curves experimentally. Radioautographs can be made only for a few simple source arrangements, and the results obtained are not very accurate. An isodose recorder similar to the one described here had been developed by L. D. Marinelli and one of the present authors.[4] However, the ionization chamber employed as a radiation detector could supply only an average radiation intensity over its volume. Leakage and amplification problems have kept the volume of the chamber too large in comparison with the field region of interest; the resolution obtained was therefore rather poor. Furthermore, the usefulness of the instrument was limited for practical purposes by the great amount of activity required for the application of a small ionization chamber. The recent development of scintil-

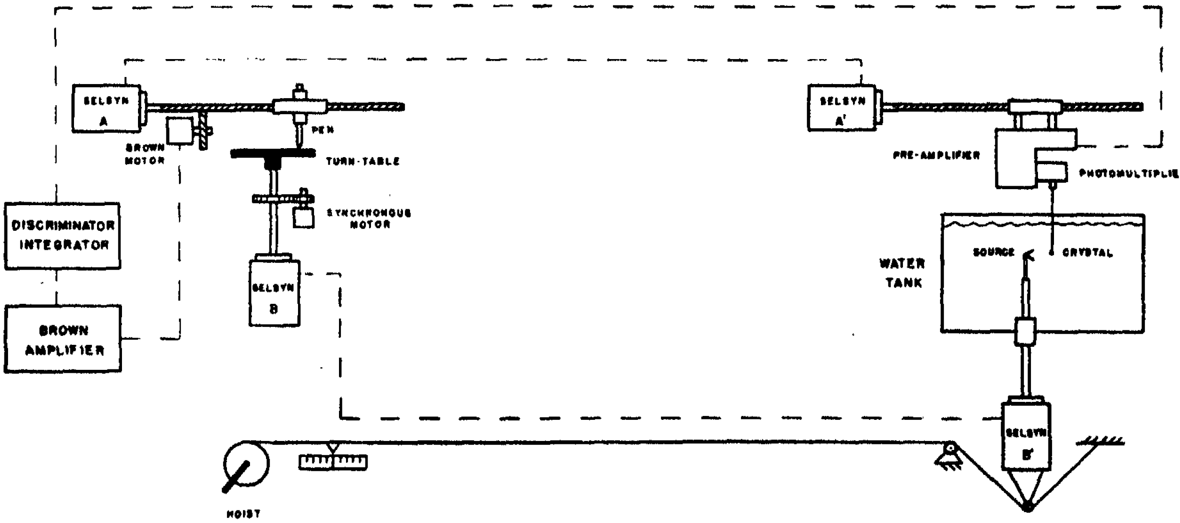

Fig. 1. Block diagram of the isodose recorder.

---

* At present Research Fellow of the National Cancer Institute at the Massachusetts Institute of Technology, Cambridge, Massachusetts.

** At present at the National Cancer Institute, Biophysics Section, Bethesda, Maryland.

[1] B. S. Wolf, Am. J. Roentg. and Ra. Therapy 54, 296 (1945).

[2] R. Paterson and H. M. Parker, Brit. J. Radiology 11, 252 (1938).

[3] W. G. Myers, Am. J. Roentg. and Ra. Therapy 60, 816 (1948).

[4] L. D. Marinelli and G. J. Hine, Phys. Rev. 74, 1245(A) (1948).

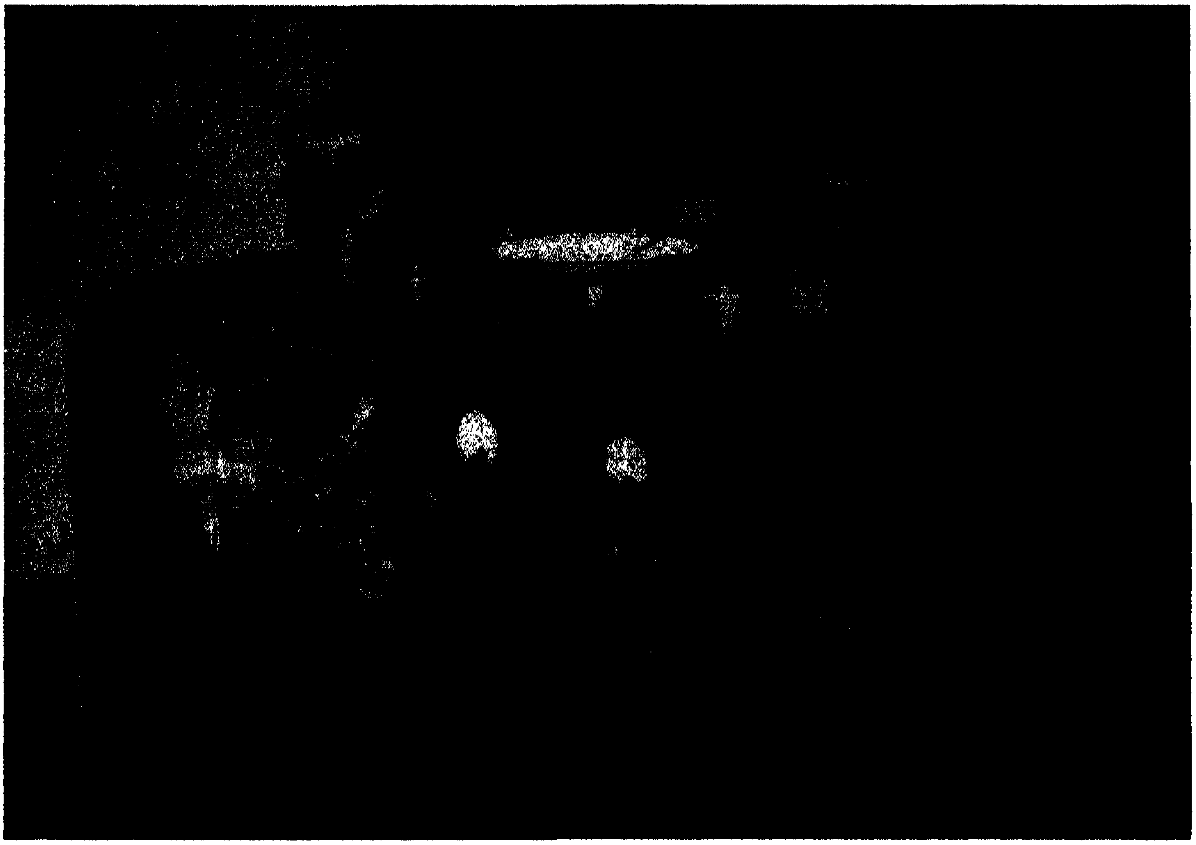

FIG. 2. Recording assembly. On the top plate of the cabinet are shown turntable with recording pen, and Brown motor driving pen leading screw and selsyn *A*.

lation counters provides a small detector with a high gamma-ray efficiency.[5]

The automatic isodose recorder to be described satisfies the demand for tracing radiation fields with a good accuracy in a short length of time. Careful construction of this instrument insures simple and reliable operation.

GENERAL OPERATION OF THE ISODOSE RECORDER

The instrument records a line of constant radiation intensity (isodose curve) within a gamma-ray field for any selected plane. The source is rotated about an axis perpendicular to the selected plane. The detector moves within the plane radially with respect to the rotating source. The radiation intensity as seen by the detector controls its movement through a servomechanism. An increase in radiation intensity due to the rotation of the source causes the detector to move away from the source; a decrease in intensity brings it closer to the source. Hence, the detector is always forced to follow a line of constant radiation intensity. A turntable rotating synchronously with the source and a pen translating simultaneously with the detector permit the continuous recording of the isodose curves.

Isodose curves representing different field intensities can be selected within a plane. Furthermore, by recording isodose curves in various planes one can obtain corresponding three-dimensional isodose surfaces.

Figure 1 gives the working diagram of the complete instrument. In order to minimize any danger of radiation exposure to the operator, the instrument is separated into two groups of asemblies. Electric cables and the hoist cable which is used for raising and lowering the source relative to the scintillation crystal are the only connections between both groups. Two selsyn systems permit remote and synchronous operation. Selsyns *A* and *A'* simultaneously translate the detector and the recording pen, while selsyns *B* and *B'* driven by a synchronous motor rotate both source and turntable.

In order to compare isodose curves obtained in air with those in a scattering medium, the source and detector can be surrounded by water in a tank. The selsyn shaft on which the source is mounted enters the tank through its bottom. A mercury seal preventing water leakage permits vertical translation of the selsyn shaft, as well as rotation with negligible retarding torque.

The recording assembly of the instrument is shown in Fig. 2.

---

[5] G. J. Hine, Science **110**, 380 (1949).

SCINTILLATION COUNTER AND ELECTRONIC CIRCUITS

A small cylindrical calcium tungstate crystal $\frac{1}{8}$ inch in diameter and $\frac{1}{8}$ inch high (volume 0.03 cm^3) used as a gamma-ray detector shows equal efficiency for radiation incident from any direction. Its high gamma-ray sensitivity[5] provides a sufficiently high counting rate even at intensities as low as 10 roentgens per hour. The light flashes from the crystal are conducted through a quartz rod ($\frac{1}{8}$ inch in diameter and 15 inches long) to a 1P21 photo-multiplier tube. The amount of light reaching the photo-tube is further increased by aluminum foil surrounding the crystal as a reflector. The crystal, quartz rod, and 1P21 tube surrounded by a light tight Al cover are assembled together with the preamplifier.

The input and output *RC* time constants of the preamplifier equal that which yields a good signal-to-noise discrimination[6] for this particular crystal. A cathode follower stage provides a low impedance output for the transmission of the pulse through a cable from the detector to the discriminating and integrating circuit (Fig. 3). The amplifier stage (V_1) with the potentiometer R_1 is used as pulse height discriminator. The output of V_1 is fed into a one-stroke multivibrator stage (V_2) for pulse equalization. The integration of the pulses is accomplished by a diode (V_3) and an integrating circuit R_3C_3 whose time constant is approximately 0.5 second. A negative signal is obtained across the integrating circuit as pulses are collected. This signal is opposed by a positive voltage in order to provide zero output from the cathode follower stage (V_4). Potentiometer R_2 sets the positive voltage necessary.

While the detector is on any selected isodose curve, the counting rate is constant (this is accomplished by discriminator R_1), and the output of V_4 is zero. Any deviation from the isodose curve results in either a positive or negative d.c. voltage. This is fed into a "Brown" amplifier[†] driving a motor, the direction of rotation of which depends on the polarity of the input. The motor, in turn, controls the movement of the detector relative to the source (Fig. 1) in such a manner as to bring it back to the isodose curve.

The statistical fluctuation of the output signal is a function of the counting rate and the time constant of the integrating circuit. For a statistical accuracy of about 3 percent, a counting rate of 2000 counts per second was chosen as a minimum. The same degree of accuracy is obtained for all isodose curves by setting potentiometer R_1 in such a position that only 2000 counts per second will pass. This is possible since a wide pulse height distribution is provided by the photomultiplier tube. R_1, then, can be calibrated for the different radiation intensities for any radiation source and subsequently used as isodose selector. The operation of the instrument on 2000 counts per second (or any other selected value) enables the operation of the multivibrator, integrator, and cathode follower stages at the same characteristics regardless of the isodose curve traced.

There are other ways whereby different dose levels could be selected; the grid bias of the last stage could be varied, or the integration time changed. By using one of these methods, the total energy spectrum could always be included. However, independent of the electronic system applied, the instrument has to be recalibrated for each different gamma-ray emitter.

DISCUSSION

Isodose curves can be traced at different speeds, completing one revolution of the source and turntable in 1, 2, 4, or 6 minutes. The 1- and 2-minute speeds can be used only for isodose curves close to the center of rotation. The results are reproducible with an accuracy

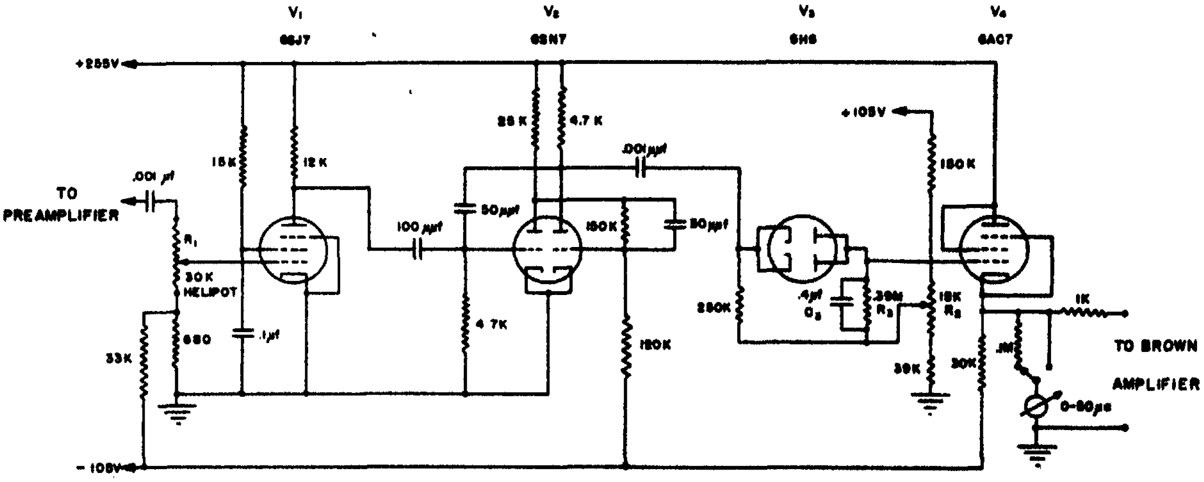

Fig. 3. Discriminating and integrating circuit.

---

[6] Marshall, Coltman, and Bennett, Rev. Sci. Inst. 19, 744 (1948).

[†] This amplifier and motor are parts of standard Brown recorder.

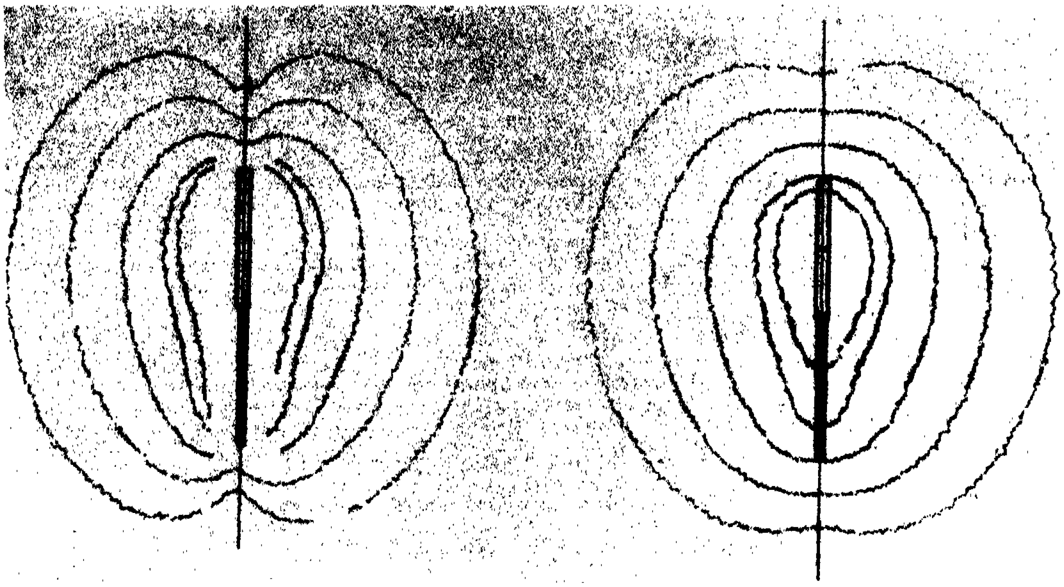

FIG. 4. Isodose curves for 250, 500, 1000, 2000, and 3000 roentgens per 1000 mg-hours of radium (0.5-mm Pt filtration) for a tandem of two 12.5 and two 25 mg sources. Each tube has an active length of 1.2 cm. (a) Isodose curves in center plane of the four tubes. (b) Isodose curves in a parallel plane 0.7 cm above the center plane.

of about ±5 percent, limited by the stability of the electronic circuits and the response of the servomechanism. Both the speed of the isodose tracing and the accuracy obtained are quite adequate for practical clinical requirements. This represents great improvements in comparison with previous methods, but without having reached the ultimate limit. A reduction in crystal size would increase the resolution and would permit the recording closer than 5 mm from the source.

The scintillation counter applied in its present form cannot be calibrated in roentgens so its calibration will hold for the gamma-radiation of different isotopes. The integrating circuit registers the number of pulses produced in the crystal whose height exceeds a certain selected size. No account is given to the amount of ionization produced in the crystal by gamma-rays of various energies. Whereas this would be an advantage for low molecular-weight crystals, the pulse height distribution in the heavy calcium tungstate crystal is not comparable with the ionization in an air-equivalent medium. Therefore, the instrument has to be calibrated for each isotope by means of a standard point source, for which the radiation intensity falls off with the inverse square of the distance.

Since in a scattering medium the radiation field of even a point source has not yet been determined, the response of the scintillation counter cannot be expressed in roentgens for any other medium than air. The amount of light produced in various crystals by gamma-rays of different energy, as well as the change in dosage due to a scattering medium, has to be investigated.

The isodose curves obtained with linear radium sources agree with the calculated results for those regions where accurate calculations are possible. As an example, the isodose curves for a tandem of four linear radium tubes of two different intensities are presented. Figure 4a shows the isodose lines in the center plane of the four sources, and Fig. 4b those obtained in a parallel plane 7 mm above the first one. The absorption around the axis of the tubes is of special interest. Detailed results for a great number of problems will be reported elsewhere.

ACKNOWLEDGMENTS

The authors wish to express their gratitude to Mr. L. D. Marinelli for suggesting the instrument and his interest during the course of its development. They are indebted to Mr. R. J. Zabelicky and his group of the SKI Instrumentation Shop for the excellent production of the mechanical assemblies, and they further acknowledge the assistance of Mr. S. Vacirca in setting up the instrument. The work was supported in part by a grant from the ONR.

THE REVIEW OF SCIENTIFIC INSTRUMENTS VOLUME 21, NUMBER 4 APRIL, 1950

A D.C. Amplifier for Biological Application

P. O. Bishop*
Anatomy Department, University College, London
AND
E. J. Harris
Biophysics Research Unit, University College, London

(Received November 1, 1949)

The limitations of direct-coupled valve amplifiers are discussed and a method is given for assessing their performance. A multichannel high gain direct-coupled amplifier is described. This was designed for use in biological applications requiring a high input impedance. The input impedance at the grid is greater than 100 MΩ at 10 kc/sec. The frequency response is flat from zero to over 10 kc/sec. Alternative condenser coupling is provided so that the large amplitude very low frequency noise elements may be eliminated. When the amplifier is direct-coupled the zero shift is of the order of 100 μv peak-to-peak over a period of 30 min. Sufficient voltage gain is available for the limit of useful amplification to be set by the noise generated in the input circuit and first amplifying valve. A parallel balanced circuit is used giving a very high discrimination against in-phase signals. Both the input and output are at earth potential.

AN instrument was required to measure both steady potentials and variations in potential in the nervous tissue which makes up the brain. In the particular application for which the instrument was designed these potentials are led off from discrete microscopic regions in the interior of the brain of an experimental animal by means of microelectrodes which may have a resistance of the order of 10 MΩ or more. The potentials are very small and the amplifier must have sufficient gain to permit recording. It is also desirable to be able to record simultaneously from several different positions in the brain, which means that a suitable number of separate channels of amplification should be available. The main requirements as far as the amplifier is concerned are:

(1) A high input impedance, not falling below 10 MΩ in the frequency range 0–10 kc/sec.

(2) Only differences of potential between the electrodes (neither being earthed) should be amplified and there should be a high discrimination against in-phase changes.

(3) The amplifier should deal with frequencies from zero up to 10 kc/sec.

(4) Input potentials of the order of microvolts are to be amplified sufficiently to operate an oscilloscope for photographic recording, or alternatively to operate a pen recorder (in the frequency range 0–80 c/sec.).

(5) The sensitivity to external disturbances, both electrical and mechanical, should be a minimum without the use of bulky screening.

(6) The d.c. level about which the output is obtained should not be excessive.

(7) The setting-up procedure should be simple.

(8) The apparatus should, as far as possible, be mains operated.

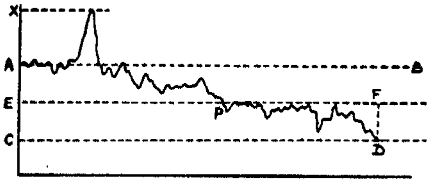

Fig. 1.

It was decided to limit the number of channels to four. Multichannel recording made the additional requirements desirable:

(9) There should be no interaction between channels.

(10) It should be possible to use any particular channel in the absence of any of the others or any combination of channels up to a total of four.

AMPLIFIER LIMITATIONS

The requirements outlined made the use of a valve amplifier essential. The limitations to the amplification of small alternating potentials are well known, but the limitations to the amplification of small direct voltages by a valve amplifier are imperfectly understood. The authors have made a general review of this subject elsewhere[1] so that only a brief treatment is needed here. The spectral intensity of both thermal agitation noise and shot noise is constant and independent of frequency provided allowance is made for the changing impedance of the circuit. A source of frequency-dependent noise was first observed by Johnson[2] and the term "flicker effect" was applied to this phenomenon by Schottky.[3] At very low frequencies, flicker noise becomes considerably greater than anode current shot noise and thermal agitation noise, but not greater than the shot effect of the grid current when the resistance in the grid circuit is made extremely large (i.e. $>10^{12}\Omega$). Under the conditions which are being considered, however, flicker noise is likely to be the determining factor to the useful sensitivity.

Attempts have been made (Macfarlane[4]) to derive mathematical expressions for the flicker effect, but insufficient quantitative information is available for it to be possible to calculate the intensity of flicker noise under any given conditions. An attempt, therefore, was

---

* Post graduate Fellow in Medicine of the University of Sydney, Sydney, Australia.

[1] E. J. Harris and P. O. Bishop, Electronic Eng. 21, 332 (1949), also p. 355.

[2] J. B. Johnson, Phys. Rev. 26, 71 (1925).

[3] W. Schottky, Phys. Rev. 28, 74 (1926).

[4] G. G. Macfarlane, Proc. Phys. Soc. 59, 366 (1947).

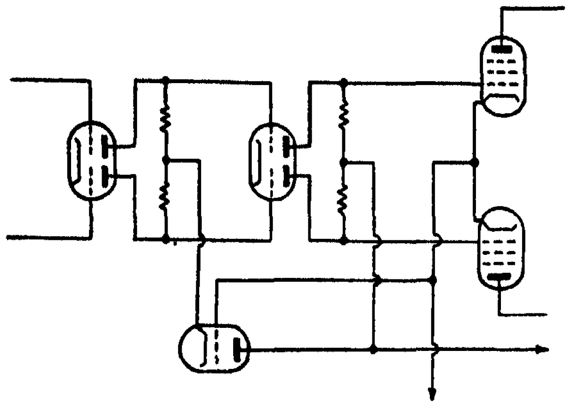

FIG. 2(a).

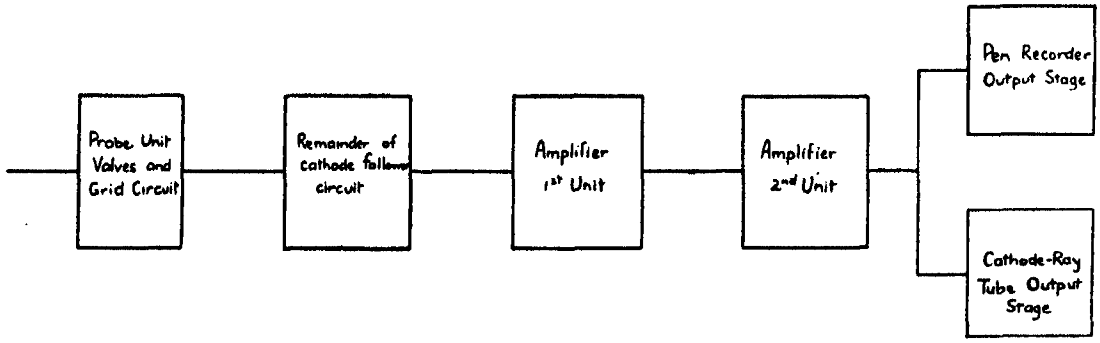
Probe Unit Valves and Grid Circuit
Remainder of Cathode follower circuit
Amplifier 1st Unit
Amplifier 2nd Unit
Pen Recorder Output Stage
Cathode-Ray Tube Output Stage

FIG. 2(b).

made to arrive at some estimate of the ultimate sensitivity of d.c. amplifiers from a survey of the literature. This survey revealed widely divergent claims to useful sensitivity, and with the exception of a few papers the methods of expressing the degree of stability attained were unsuitable for any comparative assessment to be made. The lack of agreement is a consequence of the arbitrary distinctions drawn between noise and drift. The term "drift" has never been precisely defined and is rather vaguely applied to undesired fluctuations in the output which occur relatively slowly compared with "noise" fluctuations. Drift used in this sense thus includes very low frequency noise elements, as well as variations due to changes of the operating conditions of the valve (e.g., supply voltages, temperature, etc.).

In the absence of any precise criteria for enabling the distinction to be made, it would appear best not to attempt to differentiate between noise and drift but to regard all the fluctuations of the output balance of the amplifier from whatever cause as though they were noise. Consider a record such as depicted in Fig. 1. The maximum peak to peak fluctuation ($X-C$) may give an entirely erroneous idea of the stability, for with the exception of one large peak the practical performance of the amplifier would be much better than the peak-to-peak figure. What appears to be the correct method for expressing the performance is as follows: A line (CD) is drawn parallel to the original zero (AB) and passing through the point of maximum departure (D) from the zero position. The area between the curve and the line (CD) is measured and divided by the length (CD) to obtain a mean level (say EF). We then obtain the mean fluctuation amplitude over the time considered by division of the total area included between the record and EF [i.e., the area ($APE+FPD$)] by CD. Similarly, the mean fluctuation intensity can be derived from the area included under a plot of the squares of the instantaneous deviations from the base line divided by the time interval. The lower limit of the passband of the amplifier is set by the period of observation; that is, the period over which the record is taken sets an arbitrary limit to the lowest fluctuation frequency which is observed.

Unfortunately, the records given in the literature are unsuitable for the method described above to be applied. Indeed, it would be very difficult to publish a suitable record even if it were available, and such an analysis would be extremely laborious. A possible practical method for obtaining the required figure would be to apply the output to integrating watt meter, such as an ice calorimeter containing a resistance coil, and a reversible electrochemical Coulombmeter in series. The ice calorimeter gives a measure of mean off-balance power, measured from the original zero and the Coloumbmeter provides a measure of the mean off-balance current. By subtracting the product of the square of the latter times the resistance of the watt meter coil, from the former expressed in the proper units, the mean off-balance power, measured from the most favorable zero (the level EF in Fig. 1) is obtained. For the present purpose, however, it was decided to use the maximum peak-to-peak deviation observed in a given period, bearing in mind the limitations of this method. The original balance setting at the commencement of the record remains the point of reference, for it is not admissible to use a time-dependent base line when the usefulness of the apparatus for long-term direct-coupled measurements is in question.

The older papers describing circuits for electrometer valves followed by a sensitive galvanometer have been useful because they usually give figures for the long-term drift of the zero position. The best performance appears to be that of Hafstad[5] who reports an equivalent

---

[5] L. R. Hafstad, Phys. Rev. 44, 201 (1933).

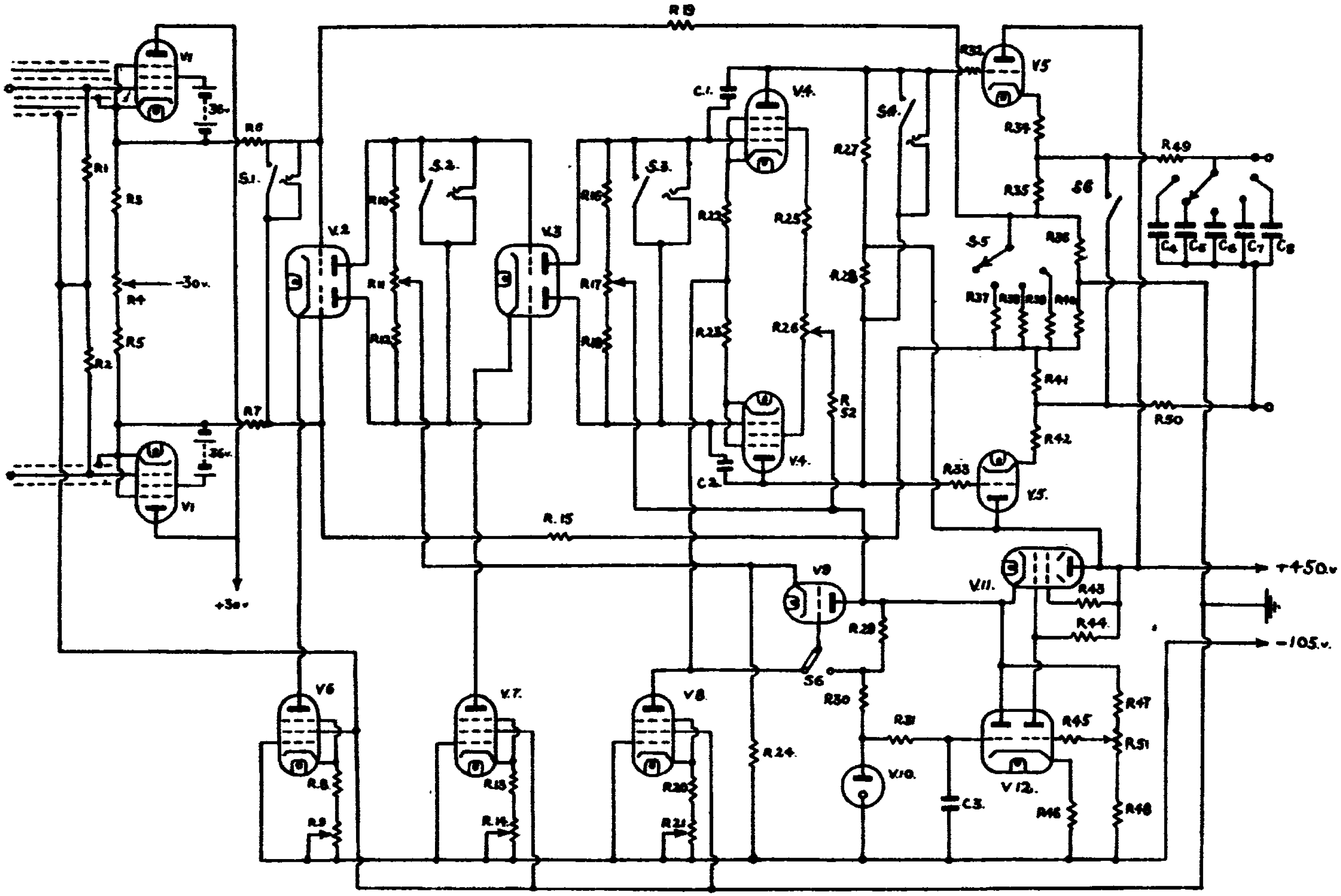

FIG. 3.

R1, R2—1000 megohm
R3, R5—500 kohm
R4—100 kohm W.W. pot.
R6, R7—50 kohm
R8—1.5 kohm
R9—1 kohm W.W. pot.
R10, R12—100 kohm
R11—25 kohm W.W. pot.
R13—470 ohm
R14—400 W.W. pot.
R15, R19—50 kohm
R16, R18—100 kohm

R17—25 kohm W.W. pot.
R20—1 kohm
R21—500 ohm
R22—100 ohm
R23—100 ohm
R24—100 kohm
R25—33 kohm
R26—50 kohm W.W. pot.
R27, R28—500 kohm
R29–28 kohm
R30—22 kohm
R31—2.2 megohm

R32, R33—10 kohm
R34, R42—20 kohm
R35, R41—15 kohm
R36, R40—330 ohm
R37—680 ohm
R38—150 ohm
R39—33 ohm
R43—47 ohm
R44—200 kohm
R45—100 kohm
R46—22 kohm
R47—250 kohm

R48—100 kohm
R49, R50—50 kohm
R51—25 kohm W.W. pot.
R52—133 kohm

C1, C2—200 μμf
C3—0.5 μf
C4—0.1 μf
C5—0.05 μf
C6—0.02 μf
C7—0.002 μf
C8—270 μμf

V1—954
V2—6J6
V3—6J6
V4—12SH7
V5—12J5
V6—12SH7
V7—12SH7
V8—12SH7
V9—12J5
V10—85A1
V11—12A6
V12—12SC7

Note: 1. The switch S1 should be shown on the input side of R6 and R7 so that feedback is applied in either position of the switch. 2. The high frequency filter (R49 and R50 and C4–8) should be shown at the input of the circuit in Fig. 4. This enables the connecting link between the two units to be at a relatively low impedance to ground.

fluctuation to 30 μv r.m.s. over a period of 40 min. In arriving at this estimate Hafstad used an arbitrary base line which enabled him to neglect a considerable unilateral drift of his zero position. From this base line ordinates were taken every 30 sec. and the root-mean-square fluctuation is determined. When expressed as a peak-to-peak value the shift of the zero position was probably nearer 100 μv for the 40-min. period.

Among the many papers on direct-coupled amplifiers[6–18] that of Buchthal and Nielsen[6] appears to have been overlooked in the literature. The residual instability of the amplifier described by these authors is given as 100-μv shift of the base line over a three-hour period. This paper was published in 1936 and there does not appear to have been any very significant improvements in the performance of direct-coupled amplifiers in subsequent years. In 1948, the authors[19] published figures relating to the performance of a direct-coupled amplifier similar to that described here, the residual instability being of the order of 60 μv peak-to-peak over a period of 30 min.

Thus, it would appear that in the absence of further knowledge concerning the nature of the flicker effect, the limit to the useful sensitivity of a direct-coupled amplifier is set by a probable residual instability of the order of 100 μv peak-to-peak over a period of 30 min. Although short-term (i.e., taking place over several seconds) fluctuations are much less than this, depending on the input resistance and band width, it is evident that the ultimate sensitivity of direct-coupled amplifiers is necessarily inferior to that of condenser-coupled amplifiers in which low frequency noise elements are more or less eliminated. Accordingly, it was decided to provide alternative condenser coupling in the amplifier to be described. A source of long-term instability lies in the aging of the cathode coatings of valves. This is discussed briefly by Gray.† It appears that a correlation exists between the behavior of the two parts of twin valves but the data presented do not allow an estimate to be made of the heater and anode potential stabilities over the term of the observations. If the supplies used when making the observations were subject to any variation, the results might only indicate a similar performance of the two parts of the valve with respect to the potentials rather than similar aging effects.

TABLE I.

V_{g1}	−1.4 v
Heater	4 v
Ia	50 μa
g_m	170×10^{-6} mhos
Ra	>5 MΩ
I_{g1}	5×10^{-13} amp.
Input capacity	0.05 μμf

THE COMPLETE UNIT

The unit, complete except for the duplication of the channels of amplification, is shown in block schematic form in Fig 2(b). Only two channels have so far been constructed, although the main power supplies are sufficient for four channels. Double triode, 6J6, valves heated from a low tension power unit have been used in the first two stages of amplification of each channel. It is, however, likely that other types could be used without loss of performance, and this is discussed later. Each amplifier has a separate electronically stabilized 150-ma supply for series-heating the remaining valves associated with the early stages. This is necessary if an amplifier is to be used in the absence of any or all of the other channels. A further stage of high tension voltage stabilization is also included in each amplifier; this serves to decouple the supplies to the various channels and to stabilize the positive supply with respect to the negative supply. In a differential amplifier it is more important for the positive and negative supplies to be stable with respect to one another than with respect to earth (Johnston[20]). The description of the amplifier which follows refers to a single channel.

THE INPUT CIRCUIT

In order to obtain a high input impedance a cathode follower stage was used. The circuit shown in Fig. 3 has been described in detail elsewhere.[21] Acorn pentodes type 954 are used and the operating potentials and characteristics are shown in Table I, the values given being for one valve.

The valves may be used without grid leaks as the brain tissue provides an earth connection for the grids. The input resistance to the cathode follower is then determined by the insulation resistance between the grid and cathode. The input capacity given in Table I is the calculated value. In practice, stray capacities associated with the pick-up electrode system are of a higher order than the input capacity to the valve. The output impedance of the cathode follower is about 5 kohm, which will not limit the frequency response of the following amplifier in the band width 0–10 kc/sec. The potentiometer $R4$ in the cathode circuit enables the d.c. levels of the two cathodes to be balanced. The valves and grid circuits are included in a probe unit connected by screen cable to a chassis which houses the remainder of the circuit associated with the cathode follower. This chassis also houses the corresponding portions of the other four channels, an arrangement which effects a considerable economy in wiring. Screened leads then provide appropriate connection to the various amplifier channels. The 954's are heated from the 150-ma d.c. supply, resistors in parallel with each valve being provided to ensure the correct heater potential. The high tension supplies to the cathode followers are obtained from batteries. Apart from the floating batteries which provide the screen potentials the high tension supplies could have been obtained from the main power supply by means of cathode followers but in view of the low anode currents it is much simpler to use batteries.

---

[6] F. Buchthal and J. O. Nielsen, Skand. Arch. Physiol. 74, 202 (1936).
[7] Forbes and Grass, J. Physiol. 91, 31 (1937).
[8] H. Goldberg, Trans. A.I.E.E. 59, 60 (1940).
[9] W. H. Huggins, Elec. Eng. 60, 437 (1941).
[10] C. W. Goodwin, Yale J. Biol. Med. 14, 101 (1941).
[11] S. E. Miller, Electronics 14, 27 (1941).
[12] S. E. Miller, Wireless World 48, 111 (1942).
[13] H. Goldberg, Proc. I.R.E. 32, 330 (1944).
[14] E. L. Ginzton, Electronics 17, 98 (March, 1944).
[15] G. R. Mezger, Electronics 17, 106 (July, 1944).
[16] M. Artzt, Electronics 18, 112 (August, 1945).
[17] H. S. Anker, Electronics 20, 138 (June, 1947).
[18] W. G. Shepard, Electronics 20, 138 (October, 1947).
[19] E. J. Harris and P. O. Bishop, Nature 161, 971 (1948).
† See reference 23, p. 730.

[20] D. L. Johnston, Wireless Eng. 24, 231 (1947).
[21] P. O. Bishop, Electronic Eng. 21, 469 (1949).

THE MAIN AMPLIFIER

The main amplifier conveniently divides into two separate units; the first of these is required to be highly stable and provide a voltage gain of some 50 to 60 db. The maximum gain of the first unit is 100 db but this is reduced by negative feedback so that the second unit provides the final amplification. With the exceptions of a balance potentiometer and a gain control the adjustments required during operation are included in the second unit. Cathode followers are used as output stages in both units. All the valves in the second chassis are a.c. heated; those in the first are d.c. heated, the 6*J*6's from a floating accumulator, and the others from a stabilized 150-ma supply.

1. The First Unit

The circuit shown in Figs. 2(a) and 3 was derived from one published by Johnston[20] and subsequently modified by the authors.[22] It uses feedback of the mean anode potential of the second stage (which sets the cathode potential of the third stage) onto the anodes of the first stage. This system has the advantage that the mean level of the second stage output is self-stabilized. It was not found practicable to employ this method of feedback to the later stages on account of the curvature of pentode characteristics. When the Ia-Vg relation is non-linear the mean of the two anode potentials of a stage, after an unbalance signal has been applied to the grids, is not equal to the values holding originally. That is, a signal generates a change in the mean d.c. level and this proves to be in the positive direction. If the mean level is fed back to an earlier stage, a component which varies with the signal is also fed back. If now there is any curvature in the characteristic of the preceding stage, the impedances of the individual valves will be unequal when a signal is applied even if they were equal for the zero signal condition. The results would be that the fed-back component from the succeeding stage will be injected more into the side with the lower anode impedance than into the other side and as a lower impedance obtains in the side to which a positive going signal has been applied it will be to this side that the greater proportion of the feed-back potential becomes injected. This will lead to instability and the system cannot be held in a balanced state, it will deviate to and remain at whichever side of balance it is sent by the applied signal.

The output from the first unit was tapped off the load resistors of the cathode followers. This involves about 7-db loss of gain, but reduces the mean d.c. level of the output to about 70 v. The output impedance is about 9000Ω (18,000Ω push-pull).

a. Gain Control and Frequency Response

The maximum voltage gain of the first unit is 100 db and this is reduced by negative feedback from the output to about 48 db. This provides the maximum stability for low frequencies (including d.c.), but of course does not improve the ratio signal-to-"noise," where noise includes all the variations arising between the grid and cathode of the first valve. A stepped gain control is provided by a series of shunting resistors, *R*37, *R*38, and *R*39. It has been found impracticable to increase the feedback more than that required to reduce the gain by the above amount, because, owing to unavoidable phase shifts at higher frequencies self-oscillation occurs. To prevent this, Miller feed-back capacitors *C*1, *C*2, have been applied to the third stage. The frequency response of the whole unit is thereby made 6 db down at 15 kc/sec. However, when less feedback is applied the capacity may be omitted and under these conditions the frequency response is flat to over 15 kc/sec.

If the maximum benefit is to be achieved, feedback in direct-coupled amplifiers should be degenerative for mean d.c. level changes as well as for the differential voltage changes. This is discussed in greater detail elsewhere.[1] When the feed-back factor is large, precautions have to be taken to avoid disturbing the d.c. working voltages of the stage into which the feedback is introduced. This occurs if the feedback is taken from a point at a potential considerably higher than that of the earlier stage. To avoid this the feedback is taken from a tapping on the cathode load resistor of valves *V*5 at which the potential is equal to that of the grids of the first amplifying valve. This arrangement has the added advantage that relatively low valued wire-wound resistors can be used in the feed-back loops. To avoid producing unbalance it is desirable that the resistors should be closely matched in each feed-back circuit.

The feedback is introduced into the grid circuits of the valves *V*2. It will be seen that the output impedance of the valves *V*1 forms part of the feed-back potential divider network. The swamping resistors *R*6 and *R*7 have been introduced to avoid alterations in the feedback factor which would otherwise occur if the input valves are changed. If the output impedances (Zo) of the cathode followers were left to determine the feed-

---

[22] P. O. Bishop and E. J. Harris, Wireless Eng. 24, 375 (1947).

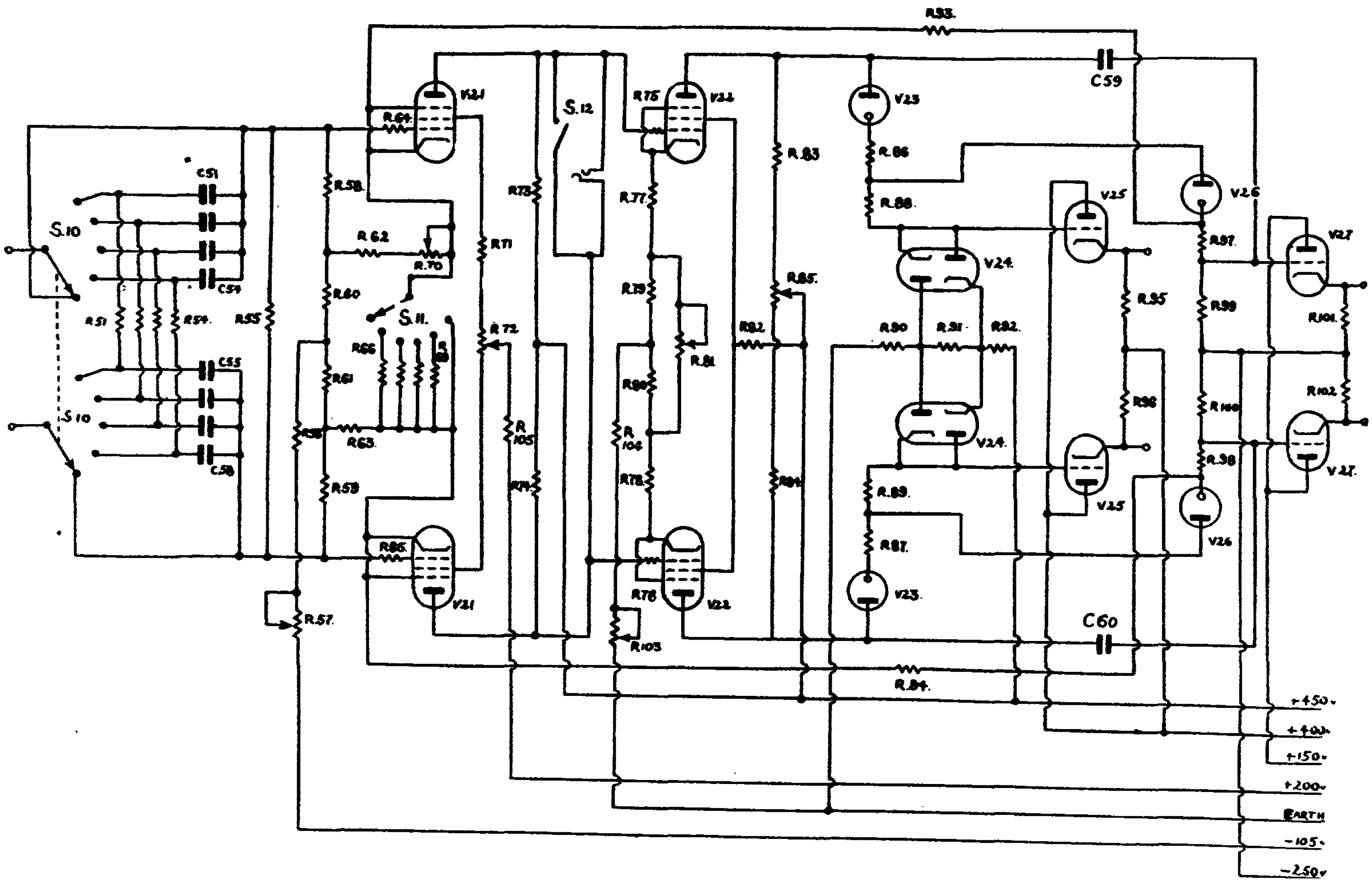

R51, R52, R53, R54—33 megohm
R55—2 megohm
R56—50 kohm
R57—25 kohm W.W. pot.
R58, R59—1 megohm
R60, R61—68 kohm
R62, R63—1.5 kohm
R64, R65—50 kohm
R66—100 kohm
R67—22 kohm
R68—6.8 kohm

R69—1.5 kohm
R70—1 kohm W.W. pot.
R71—33 kohm
R72—50 kohm W.W. pot.
R73, R74—400 kohm
R75, R76—10 kohm
R77, R78—100 ohm
R79, R80—1 kohm
R81—5 kohm pot.
R82—200 kohm
R83, R84—68 kohm

R85—15 kohm
R86, R87—250 kohm
R88, R89—470 kohm
R90—100 kohm
R91—150 kohm
R92—270 kohm
R93, R94—2.2 megohm
R95, R96—6.8 kohm
R97, R98—100 kohm
R99, R100—2 megohm
R101, R102—68 kohm

R103—15 kohm
R104—33 kohm
R105—100 kohm

V21—6SH7
V22—6AC7
V23—VR 150
V24—6H6
V25—6V6 (triode connected)
V26—VR 150

V27—6SN7

C51, C55—0.01 μf
C52, C56—0.25 μf
C53, C57—1.0 μf
C54, C58—4.0 μf
C59—0.01 μf
C60—0.01 μf

FIG. 4. Correction. The lead from the junction of R95, R96 should be shown connected to the earth line, *not* to the + 400 V line.

TABLE II. Current requirements.

(1)	+600-v smoothed supply (→+450-v stabilized supply)	
	Main stabilizing unit	16 ma
	Four amplifiers including second voltage stabilizing units	140 ma
	Total	156 ma
(2)	+150-v, −250-v smoothed supply (→−250-v and −105-v stabilized supplies)	
	6 *SN7* output cathode followers, four amplifiers	32 ma
	Main stabilizing unit	24 ma
	Four amplifiers including second voltage stabilizing unit	72 ma
	Total	128 ma
(3)	+400-v smoothed supply	
	6*V*6 output cathode followers, four amplifiers	200 ma

back factor of the system, the considerable variability (by a factor of as much as 2) of conductance, and therefore of Zo, from valve to valve would be inconvenient. By introducing 50 kohm in series with Zo (which lies between 3.5 and 7 kohm) this effect is swamped. The fact that the resistance of the electrodes varies very considerably makes the introduction of feedback into the input circuit impracticable.

b. Second Voltage-Stabilizing Circuit

Each amplifier channel has a separate voltage-stabilizing circuit (Figs. 3 and 5) to provide the positive and negative high tension supplies to the first two stages. The stabilizer is located on the same chassis as the first amplifier. The shunt valves in the stabilizer are heated from the 150-ma supply and the effects of any fluctuations in this supply are reduced by a simple form of cathode compensation[11] in the shunt valves. This circuit also stabilizes the positive and negative high tension supplies with respect to one another. These features make it possible to relax the requirements for the performance of the main stabilizing unit so that a.c. heating can be used for the shunt valves in the latter. In other respects the circuit of this additional stabilizer is similar to that used in the main power supply.

c. Alternative First Amplifier Valves

The electrode arrangement of the 6*J*6, from the point of view of balancing out the effect of changes in heater potential, is preferable to that of the 12*SC*7. The latter and similar types have, however, the distinct advantage that they can be heated from a supply of only 150 ma (instead of 450 ma) which is easily stabilized by electronic means. As the 12*SC*7 has only recently become available to us, experiments are now being carried out to determine the relative performance of the amplifier using 6*J*6's heated from accumulators and that of an exactly similar amplifier employing 12*SC*7's heated from 150-ma stabilized supply.

The 12*SC*7 is probably no more favorable from the point of view of obviating changes in heater potential than a double triode, such as the 12*SL*7, in which the cathodes are separate. However, the fact that 150-ma heater current can be stabilized more effectively than the supply to the 6*J*6's may offset this disadvantage. A 12*SC*7 specially selected for balance is available under Type No. RCA 1634. Since the development of this apparatus a new valve, the 6*SU*7, which is a 6*SL*7 specially selected for balance and low grid current has become available and this valve is recommended in the Radiation Laboratory Series Handbooks[23] for balanced amplifier applications. A disadvantage is that the heater current is 0.3 amp. There does not appear to be an exactly corresponding 12-v 0.15-amp. valve, the 1634 being the nearest, the latter type is not discussed in the reference.

It is evident that a careful comparison of different valves is desirable, although it is likely that by careful selection comparable performances can be obtained from any twin valve. The criticism of the 6*J*6 made by Valley and Wallman[23] may have been the result of a lower proportion of these valves having such good characteristics as the majority of 6*SU*7's. When selecting valves attention should be paid to the grid current. The 6*J*6, 6 or 12*SL*7, and the 12*SC*7 often have a rather high grid current, up to 1 μa.

The compensating circuit described by Miller[11] was not used in the first stages of the present amplifier because it was considered more desirable to preserve the common cathode load so as to achieve a high discrimination against in-phase signals. Compensation for splitting the cathode load would have meant a considerable increase in the complexity of the circuit.

2. The Second Unit

The second amplifier unit (Fig. 4) includes a high frequency filter, the alternative condenser coupling circuits and output stages as well as two stages of voltage amplification. Jack points and an anode shunting switch are provided for *V*21. The input grids are at about +75 v with respect to earth and the final anodes are at approximately +310 v. The main gain control for the whole channel is obtained by the switch *S*11 in steps of 6 db and a fine gain control is provided by a variable resistor *R*81. The maximum gain of the second unit is about 80 db and a linear output of 200 v peak-to-peak is obtainable. The frequency response is flat to over 10 kc/sec.

a. High Frequency Filter

Several values of high frequency response can be selected by switching capacitors differentially across the input of the second amplifier. The swamping resistors

---

[23] Valley and Wallman, *Vacuum Tube Amplifiers* (McGraw-Hill Book Company, Inc., New York, 1948). See also Vols. 17 and 21 of Radiation Laboratory Series.

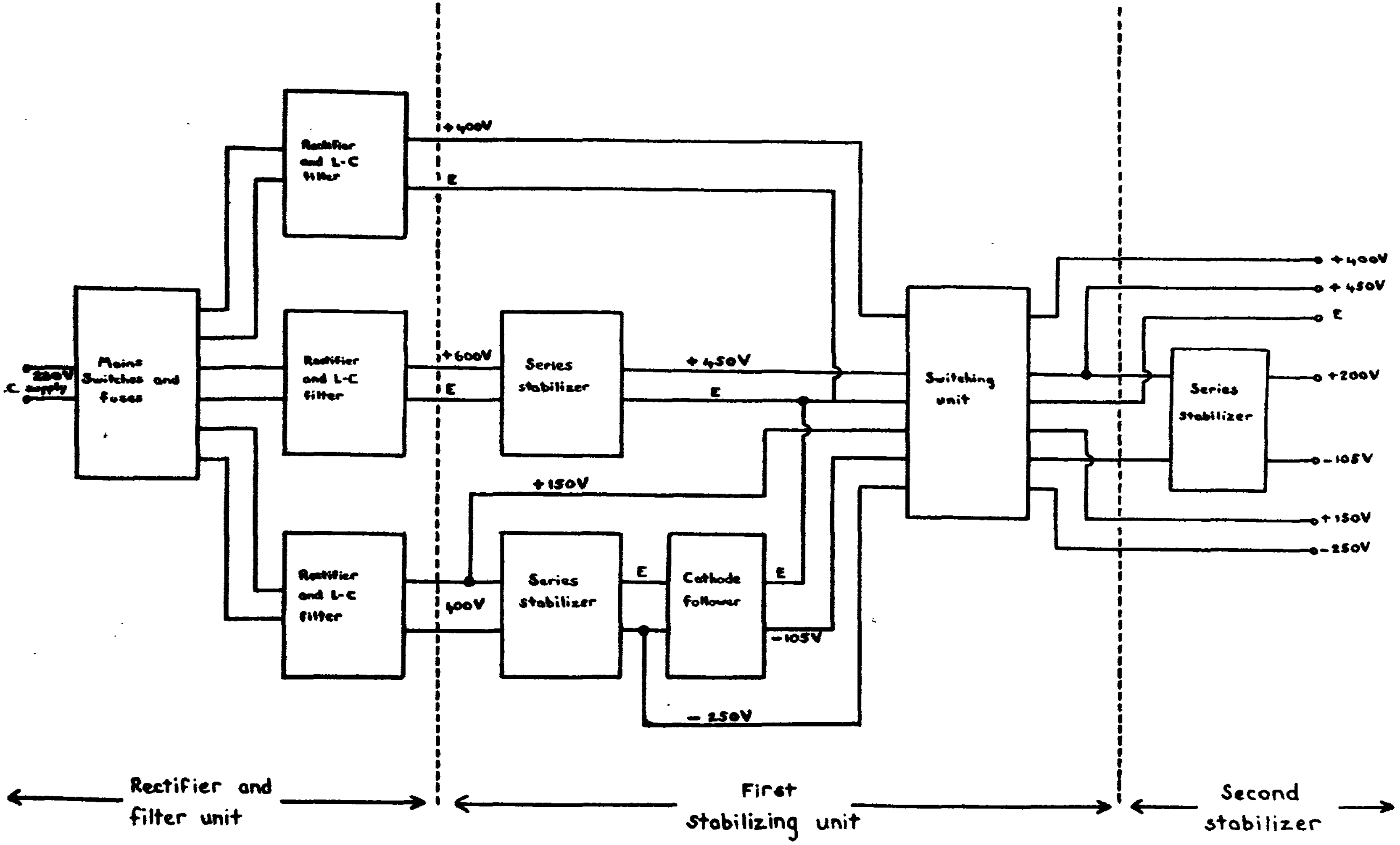

230V A.C. supply
Mains Switches and fuses
Rectifier and L-C filter
Rectifier and L-C filter
Rectifier and L-C filter
+400V
E
+600V
E
400V
Series stabilizer
+450V
E
+150V
Series stabilizer
E
Cathode follower
E
−105V
−250V
Switching unit
Series Stabilizer
+400V
+450V
E
+200V
−105V
+150V
−250V
Rectifier and filter unit
First stabilizing unit
Second stabilizer

FIG. 5.

TABLE III. Voltage stabilities.

Supply	Voltage change	Equivalent signal at input of amplifier
+450 v	1 v	0.3 mv
−105 v	1 v	1.7 mv

*R*49 and *R*50 isolate these capacitors from the feed-back loops of the first amplifier.

b. *Alternative Condenser Coupling*

As pointed out, considerable improvement in the signal-to-noise ratio can be achieved by limiting the low frequency response by means of capacitative coupling. By placing the coupling condensers between the two amplifier units the effective values of the coupling condensers are not affected by the adjustment of the feedback in either amplifier.

Several values of time constant can be selected by the switch *S*10. The pairs of capacitors are connected differentially by resistors sufficiently high in value not to alter the time constant appreciably. The pairs of capacitors are, therefore, kept at equal potentials. This avoids a switching surge when the time constant control is operated. In order to reduce stray capacities the capacitor cans have been insulated from earth and from one another. This arrangement has been found satisfactory if the capacitor assembly is well screened. Owing to the cathode feedback in the fourth stage of amplification, the input impedance is much greater than that of the 1 MΩ grid leaks. It is desirable to limit the input impedance to a definite value and this is done by placing a 2-MΩ resistor differentially across the input to the stage. The over-all time constant is then numerically equal to the value of the coupling condensers expressed in microfarads.

c. *The Output Stages*

Two cathode follower output stages are used; one at 150 v provides sufficient current to drive a pen recorder and the other at earth potential gives the full voltage swing provided by the last amplifying stage. The moving coil pen recorder has a 5000-ohm center-tapped coil requiring 120 v across it for the maximum usable deflection from the central zero position. In order to avoid a large standing current in the coils a bridge circuit is used. The 6*V*6's used in the cathode follower circuit have a standing current of about 25 ma which is provided from a separate smoothed supply. By taking the pen recorder output at 150 v it is possible to avoid using a negative high tension supply.

If it is desired to feed a single cathode-ray tube, the plates may be driven directly from the output of the amplifier, which is capable of a peak-to-peak voltage swing of about 200 v. The potentiometer in the anode circuit of the first 6*J*6 stage provides the *Y* shift. When the amplifier is condenser-coupled it will be necessary to use the potentiometer in the screen circuit of the 6*SH*7 stage of the second unit. In the latter case the disadvantage arises that at the lower gain settings the potentiometer becomes relatively ineffective owing to the large negative feedback. This is, however, offset by the fact that the amplifier described here was designed to feed simultaneously into several display units each with its own output amplifier and shift arrangements. For this reason it was desirable that the output of the amplifier should have a mean level at about earth potential. These additional amplifiers and shift controls are included in the display unit and will not be described here.

Gas discharge tubes (*VR* 150) running at 120 μa are used to drop the voltage down to the appropriate levels for the two output cathode followers. Although the actual voltage drop per tube is some 12 v less than with the rated current (5–30 ma), the arrangement has been found to be quite satisfactory at the relatively high level involved.

THE POWER SUPPLIES

1. The High Tension Supplies

Table II shows the approximate current requirements. The main positive and negative high tension supply is shown in block schematic form in Fig. 5 and the circuit details are given in Fig. 6. It is built in two units, the first consisting of the three separate transformer, rectifier, filter circuits and the second of the two series-valve stabilizing circuits together with the switching arrangements for the various channels. The 600-v smoothed supply is subsequently stabilized at +450 v with respect to earth. The +150-v smoothed supply is used for the cathode follower providing output about earth potentials in each amplifier channel, and the negative potential is stabilized with respect to earth to give −250 v and −105 v.

Table III shows the effect of a 1-v sudden change in the output voltages of the respective supplies expressed as an equivalent signal at the input of the amplifier. The effect of a very much smaller change is probably somewhat less than that calculated from the figures as there is less likelihood of non-linearity. It is difficult to ensure that the high tension supplies do not occasion irregularities in the amplifier greater than, say, 50 μv, expressed as an equivalent signal at the input. If it is desired to make the signal equivalent of a change in the high tension less than 50 μv, the effect of slow changes in the output of the stabilized supplies due to changes in the heater current of the shunt amplifying valves become of increasing importance. The effect of these slow changes are of course eliminated by making the amplifier condenser-coupled with a suitable time constant. Thus, the demands on the stability of the high tension supplies never become a limiting feature in the design of the amplifier. The ripple level of the +450-v and −250-v supplies is 2 mv peak-to-peak, and less than 1 mv peak-to-peak, respectively.

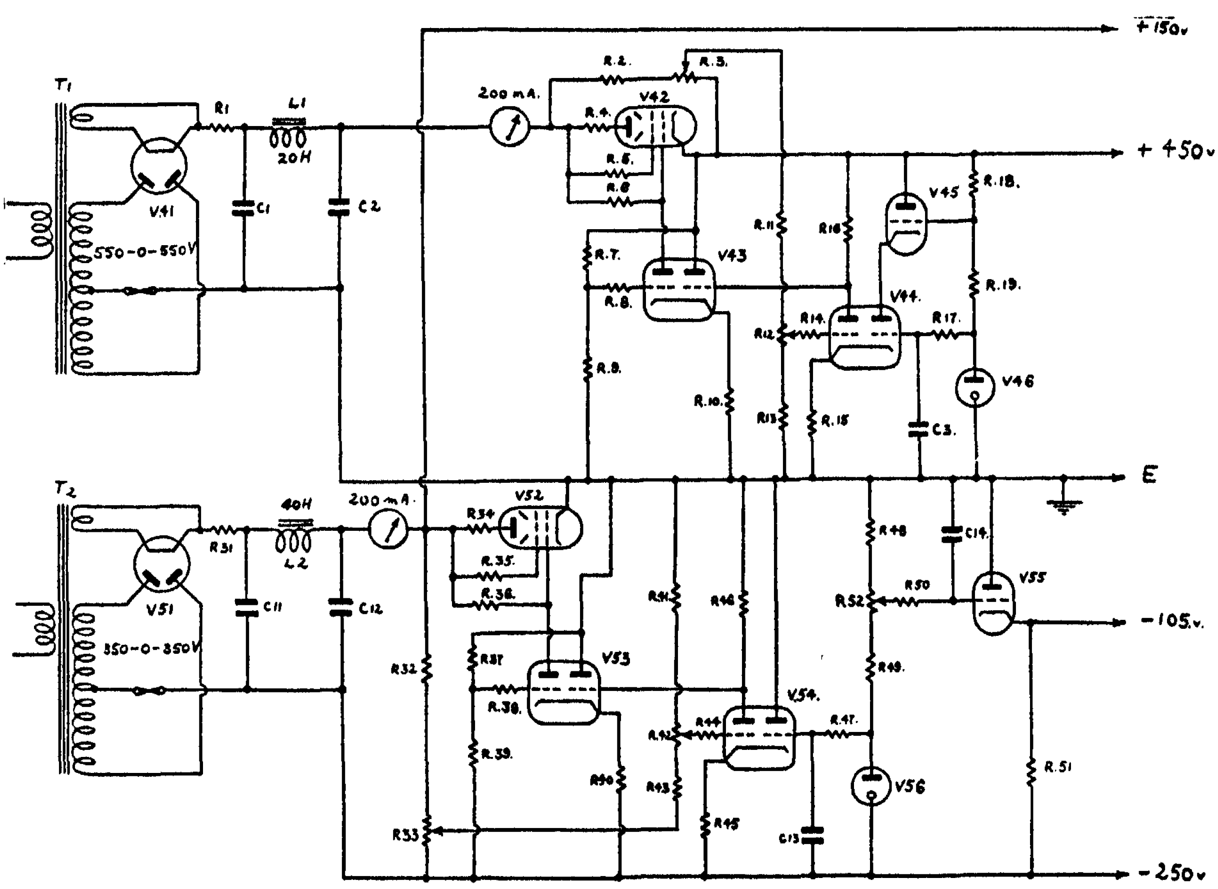

*R*1—47 ohm
*R*2—200 kohm
*R*3—1 kohm W.W. pot.
*R*4, *R*5—47 ohm
*R*6—200 kohm
*R*7—100 kohm
*R*8—100 kohm
*R*9—125 kohm
*R*10—68 kohm
*R*11—200 kohm
*R*12—25 kohm W.W. pot.
*R*13—68 kohm

*R*14—100 kohm
*R*15—22 kohm
*R*16—200 kohm
*R*17—220 kohm
*R*18—50 kohm
*R*19—33 kohm
*R*31—47 ohm
*R*32—400 kohm
*R*33—2 kohm W.W. pot.
*R*34, *R*35—47 ohm
*R*36—200 kohm
*R*37—50 kohm

*R*38—100 kohm
*R*39—133 kohm
*R*40—68 kohm
*R*41—100 kohm
*R*42—10 kohm
*R*43—50 kohm
*R*44—100 kohm
*R*45—33 kohm
*R*46—200 kohm
*R*47—220 kohm
*R*48—22 kohm
*R*49—10 kohm

*R*50—220 kohm
*R*51—3150 ohm
*R*52—5 kohm W.W. pot.

*C*1—4 μf
*C*2—8 μf
*C*3—2 μf
*C*11—4 μf
*C*12—8 μf
*C*13—2 μf
*C*14—0.5 μf

*V*41—5*R*4
*V*42—12*E*1
*V*43—6*J*6
*V*44—6*J*6
*V*45—6*J*5
*V*46—85*A*1
*V*51—5*U*4*G*
*V*52—12*E*1
*V*53—6*J*6
*V*54—6*J*6
*V*55—6*V*6
*V*56—85*A*1

FIG. 6.

The Philips-Mullard 85*A*1 stabilizing valve is free from the sudden discontinuities in the current voltage characteristics found in most glow discharge tubes[24] and has a relatively low temperature coefficient.[25]

The result of changes in the output of the filter circuit of the power supply is practically reduced to zero by feeding a portion of the unstabilized supply on to the grid of the shunt amplifying valve. In the case of the positive supply this was done by the parallel bridge arrangement across the series valve,[26] while in the case of the negative supply a small fraction of the unstabilized voltage was taken from the negative side of a resistance network across the smoothed supply.

Perhaps the most difficult feature in the design of the main high tension supplies is the provision of a stable source of heater current to the shunt amplifying valves. When only one amplifying channel is to be constructed the best solution is to use shunt valves of 12.6-v 150-ma heater rating, the heater current being obtained from the 150-ma stabilized supply. Unfortunately, it is inconvenient to adopt this arrangement when several channels are to be used. Various other methods have been tried though none have been found to be very satisfactory. Perhaps the best arrangement is the use of a voltage regulated transformer of the three-limbed type, regulation being obtained by iron saturation. They are designed for constant load and provide some compensation for changes in frequency but have the disadvantage of a considerable stray field. The effects of fluctuations in the heater supply are reduced by the use of the cathode compensation circuit in the shunt amplifying valves.

2. Switching Arrangements

Four switches, one for each amplifier, are provided on the second chassis. When an amplifier is not being used dummy resistive loads keep the current drain on the stabilized high tension supplies constant. The

---

[24] E. W. Titterton, J. Sci. Inst. 26, 33 (1949).
[25] T. Jurriaanse, Philips Tech. Rev. 8, 272 (1946).
[26] V. Attree, J. Sci. Inst. 25, 263 (1948).

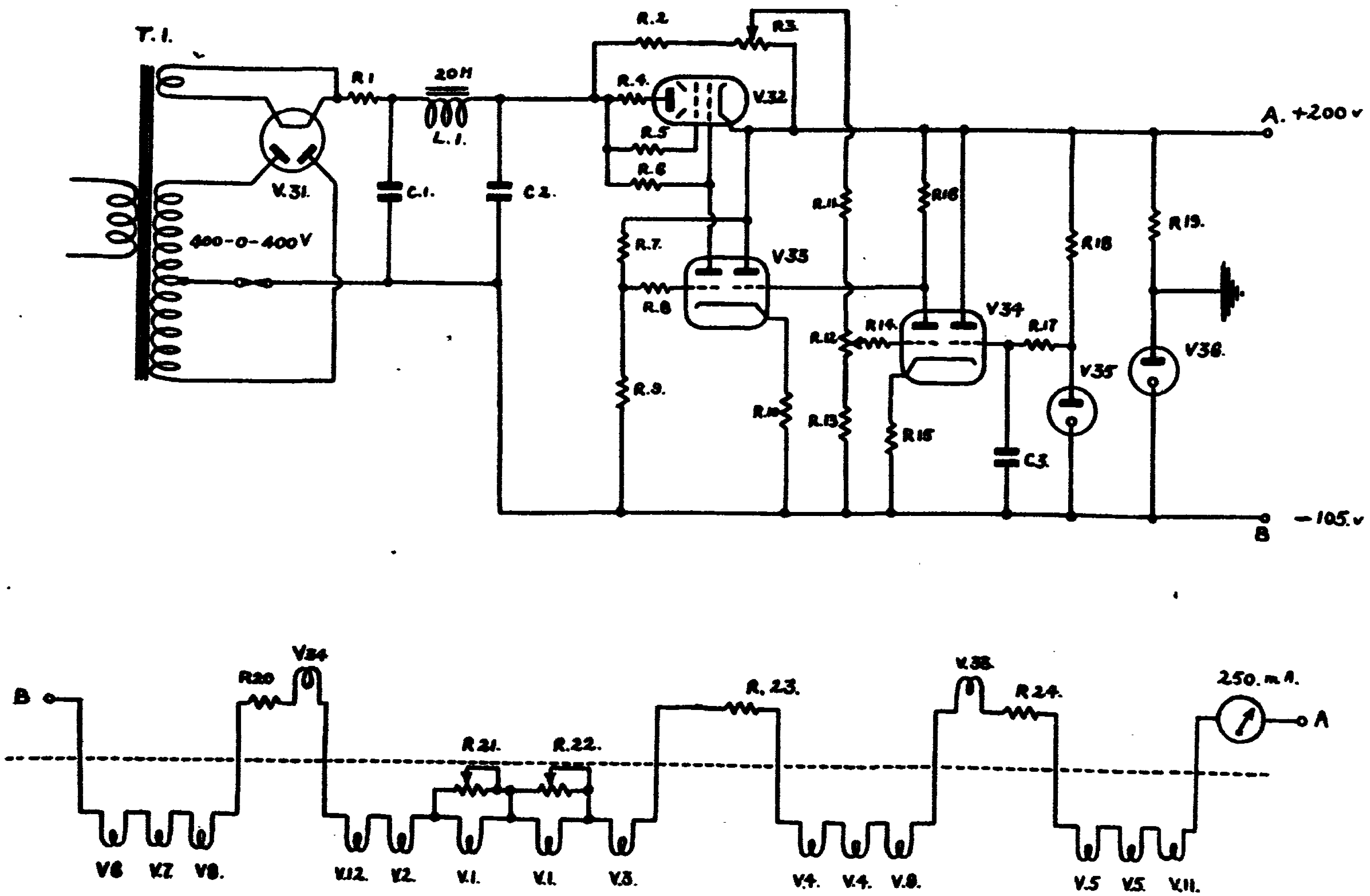

FIG. 7.

R1—47 ohm
R2—200 kohm
R3—1 kohm W.W. pot.
R4—47 ohm
R5—47 ohm
R6—200 kohm
R7—68 kohm

R8—100 kohm
R9—100 kohm
R10—68 kohm
R11—100 kohm
R12—25 kohm W.W. pot.
R13—168 kohm
R14—100 kohm

R15—25 kohm
R16—200 kohm
R17—2.2 megohm
R18—50 kohm
R19—33 kohm
R20—220 ohm
R21—300 ohm W.W. pot.

R22—300 ohm W.W. pot.
R23—220 ohm
R24—440 ohm

C1—4 μf
C2—8 μf
C3—0.5 μf

V31—5U4G
V32—12E1
V33—12SC7
V34—12SC7
V35—85A1
V36—VR105

Note: The transformer should be rated 450—0—450 v.

switching arrangement also enables the heater current to the amplifier to be established before the high tension is applied, and for the reverse to be the case when the use of the channel is discontinued.

3. Stabilized Heater Supply

In an amplifier with 6*J*6 balanced stages without cathode compensation it has been found that a 10-mv change in heater potential is equivalent to a signal of about 0.7 mv at the input. The provision of a sufficiently stable supply of heater current is, therefore, rather difficult and becomes the most critical feature in the design of the amplifier as far as long-term stability is concerned. The use of 6*J*6 valves in the first two amplifier stages makes a separate source of heater current necessary. This supply becomes unnecessary if 150-ma 12.6-v valves are used.

a. Heater Supply Unit

This includes the 150-ma stabilized supply and the low tension transformers for heating the valves of the second amplifier unit. The stabilizing circuit shown in Fig. 7 is very similar to that used in the high tension supply unit except that 12*SC*7 valves are used as the shunt amplifying valves so that they can be heated from their own stabilized supply. The 305-v floating output is held with respect to earth by a *VR* 105 gas discharge tube to give +200 v and −105 v. The valve heaters are placed in series across the output in such a way that the respective heater cathode potential differences are minimal. In the amplifier described in this paper 6*J*6 valves were used in the first two stages of amplification and the valves *V*34 and *V*33 shown in the heater chain in Fig. 7 were replaced by equivalent resistors. The heater chain shown in Fig. 7 represents the arrangement when the 12*SC*7 valve is used in the first two stages.

b. Heater Supply for the 6J6 Valves

The current for heating the 6*J*6 valves used in the first two stages of amplification was derived from lead accumulators of large storage capacity. This supply was earthed by means of the center tap of a resistance network across the terminals. To achieve long-term stability it was found necessary to place the accumulators across the output of a charging unit adjusted so that the net charge current was zero. Even the charging current needs stabilization and this is best done by means of a series-transformer electronic stabilizer.[20]

SETTING-UP PROCEDURE

The link *S*6 (Fig. 3) is connected so that the grid of valve *V*9 is set from the resistance network *R*29 and *R*30. The mean anode potential of the various stages, beginning with *V*2 and progressing toward the output, may now be adjusted to the appropriate level. In the first three amplifying stages this is accomplished by varying the grid bias on the cathode load valves by means of the potentiometers *R*9, *R*14, and *R*21 and in the case of the later stages by means of the potentiometers *R*57 and *R*103 (see Fig. 4). The latter enables the output provided by *V*27 to be adjusted to approximately earth potential. The actual mean anode potential of the amplifying stages in order are 30, 70, 170, 170, 310 v. Having adjusted the mean anode levels, the link *S*6 may now be returned to the common cathode of *V*4 so as to apply mean d.c. level feedback to the grids of *V*2. The mean anode levels may be checked from time to time by means of jacks but should not need adjustment except at relatively long intervals. The adjustment for balance between the two sides of the amplifier should, however, be done each time the amplifier is used. This is quickly done by shunting the anodes of the various stages in turn by means of the switches provided, beginning at the output and working toward the input of the amplifier. Each stage may then be balanced by the potentiometer in the anode or screen circuits so that the trace is brought to the middle of the cathode-ray tube screen each time. When the amplifier has a condenser coupling between the two units the feedback used in the first unit prevents non-linearity in the output even when the differential unbalance is the maximum allowed by the potentiometer *R*4, *R*11, *R*17, and *R*26. In these circumstances the amplifier can be used with condenser coupling without any danger of non-linearity arising from slow drift in the first amplifier unit.

PERFORMANCE

The performance as regards long-term shift of the zero position to be expected from the amplifier is of the order of 100 μv peak-to-peak over a period of 30 min. It is difficult to stabilize the heater current sufficiently to make valve-matching relatively uncritical. In these circumstances the performance will vary from valve to valve within a given type.

THE REVIEW OF SCIENTIFIC INSTRUMENTS VOLUME 21, NUMBER 4 APRIL, 1950

Volumetric Plastic Micro Respirometer[*]

P. F. SCHOLANDER
Marine Biological Laboratory, Woods Hole, Massachusetts

(Received September 22, 1949)

A simple plastic micro respirometer is described based on a direct reading volumetric principle. The respiration chamber with CO_2 absorber is balanced against a compensating chamber through a manometer drilled in Lucite. As oxygen is used it is replaced from a syringe so as to maintain balance with the compensating chamber. The oxygen consumed is read directly on the syringe. Two sizes have been made covering a range of oxygen consumption from 10 mm^3 to 10 cc per hour.

A SIMPLE and direct volumetric principle of micro respirometry was introduced by Winterstein, 1913,[1,2] and was later adopted by Tyler and Berg[3] and Dixon.[4] Scholander[5,6] introduced oxygen replacement in the system and the principle in its final form can hence be stated as follows: The respiration chamber with CO_2 absorber is balanced against a compensating chamber through a manometer. As oxygen is used it is replaced from a measuring device so as to maintain balance with the compensating chamber. The oxygen consumed is read directly on the measuring device.

The system offers considerable advantages. The oxygen consumption is read directly in volume units and is independent of the gas content of the apparatus. The only calibrated part is the measuring device for the introduction of oxygen. Each respirometer is compensated and therefore relatively insensitive to external temperature and pressure changes. The oxygen tension does not drop in the respiration chamber which can therefore be kept small with a corresponding gain in sensitivity.

The respirometer to be described consists of a plastic manometer block connected to an oxygen measuring device (syringe) and to a respiration chamber and a compensating chamber. The shape, size and position of these components are not critical and may be varied to suit individual requirements (see Scholander[7]). Two sizes have been made covering a range of oxygen consumption from 10 cubic millimeters to 10 cc per hour. The apparatus are easy to make, they are almost unbreakable and have been used on a large variety of animals and plants in field and laboratory studies.

A. STANDARD SYRINGE APPARATUS

One or several manometers are drilled into a rectangular piece of $\frac{3}{8}$ inch Lucite, using a jig and a long No. 24 drill (Fig. 1A). The openings of the bores are tapered to fit a standard syringe nozzle. To accomplish this a brass taper like the syringe nozzle, but slightly longer, is put on a file handle, heated and pressed into the manometer bore. The taper is cooled under the faucet and removed. Tapered Lucite plugs (D) or plugs drilled out from neoprene stoppers fit the other end of the manometer bore. For student use it is desirable to furnish the manometers with a lower opening (Fig. 1, manometer 2) through which a rod can be introduced to dislodge broken syringe tips stuck in the manometer opening. Screw top or other standard vials make excellent respirometer chambers (Fig. 1B). They are connected to the manometer block by means of neoprene stoppers or pieces of Tygon tubing which fit on Lucite buttons cemented to the block (Fig. 1B). The absorption bucket is made from the bottom portion of a small vial, and is forced into a few loops of stainless steel wire spiral; the other end of the spiral is bent into a V and fits removably into the bore of the Lucite button (Fig. 1B). The manometer block is suspended over the edge of the water-bath window with two brass hooks. 1 cc to 10 cc syringes furnished with arresting clips are used for the oxygen delivery. A wooden or metal thermoregulated tank with Lucite windows makes a satisfactory water-bath.

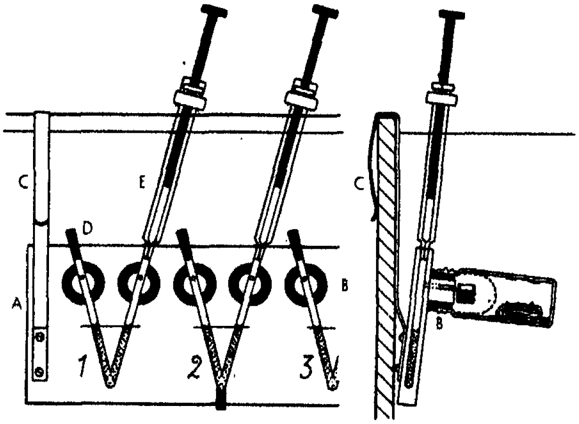

FIG. 1. A—Part of manometer block with two syringe respirometers. B—Neoprene stopper on Lucite button, attaching the respiration chamber. C—Suspension hook. D—Taper plug. E—Syringe for oxygen delivery.

---

[*] Developed in 1947 at the Arctic Research Laboratory, Point Barrow, Alaska under contract with ONR.

[1] H. Winterstein, Biochem. Zeits. 46, 440 (1912).

[2] H. Winterstein, Zeits. f. Biol. Technik und Methodik 3, 246 (1913).

[3] A. Tyler and W. A. Berg, Science 94, 397 (1941).

[4] M. Dixon, *Manometric Methods* (Cambridge University Press, London, 1943).

[5] P. F. Scholander, Rev. Sci. Inst. 13, 32 (1942).

[6] P. F. Scholander and G. A. Edwards, Rev. Sci. Inst. 13, 292 (1942).

[7] P. F. Scholander, Rev. Sci. Inst. 20, 885 (1949).

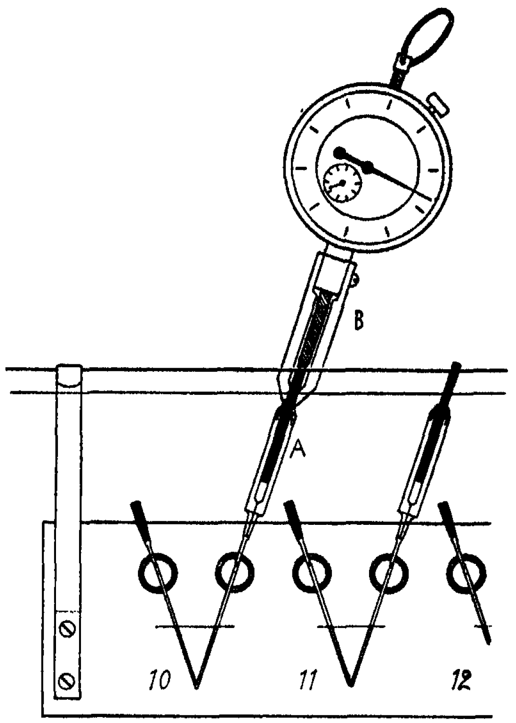

FIG. 2. Part of manometer block showing two complete micro syringe respirometers. A—Plastic micro syringe. B—Dial indicator with plastic sleeve, in measuring position.

Reagents

The manometer fluid consists of methyl-orange colored water containing enough liquid potassium soap to make the solution run easily in the manometer bore. For carbon dioxide absorption 10 percent or stronger KOH solution is used, or, in case of especially high respiratory rates, Ascarite (A. H. Thomas Company, Philadelphia). Syringe tips, taper plugs and plungers of micro syringes are greased lightly with XX heavy Nevastane grease (Keystone Company, Philadelphia).

Operation

The manometers are filled to the mark with manometer fluid. The compensating chambers, wet on the inside, are firmly pressed on to the stoppers. The respiring material is placed in the moist respiration chambers and is, if necessary, kept away from the absorption bucket by means of a screen diaphragm. This is a square of plastic fly-screening cut diagonal to the weave and pushed into the vial (Fig. 1B). KOH solution or Ascarite is placed in the absorption buckets and the respiration chambers are firmly connected to the manometers and placed without delay in the water bath, keeping the chambers completely submerged but the manometer openings dry. In this position the suspension hooks of the manometer block must be clamped securely to the water-bath with a pair of rubber tubing screw clamps. After a short time for thermo equilibration the manometer openings on the compensating side are closed, and the syringes are, one at a time, filled with oxygen from a rubber bladder and immediately inserted into the other end of the manometers. The respirometer bank is now lowered until all the gas-volumes are under water. A drop of glycerine is placed around the syring bearing for tightness. At suitable time intervals the syringes are adjusted and read when the manometer fluid is back to the mark. The difference between two readings gives the volume of oxygen consumed during that time, uncorrected for S.T.P.

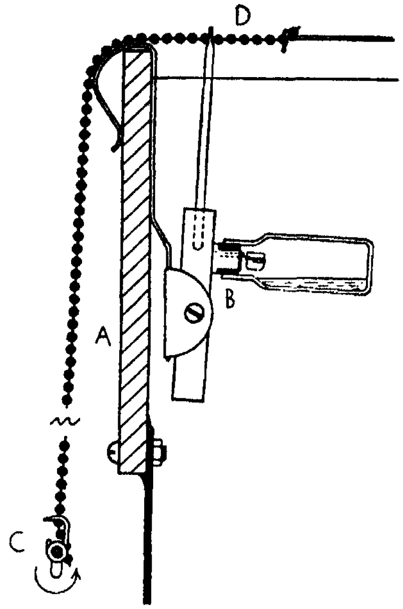

FIG. 3. Shaking device. A—Suspension hook hinged on to manometer block. B—Respiration vial attached by means of Tygon tubing to connecting button on manometer block. D—Ball-chain engaging rocking pin and rubber band. C—Hook engaging ball chain and crank.

Accuracy

With a known calibration of the syringes the sensitivity and accuracy of the apparatus depends mainly upon the capacity of the chambers; small respiration chambers and large compensating chambers increase the sensitivity. For any combination the accuracy (stability) of the apparatus is found by blank runs, i.e., runs without respiratory material. Through a temperature range of 0 to 40 degrees centigrade, using 20 to 25 cc chambers and a 1 cc tuberculin syringe, the method is stable within 10 mm^3, an hour.

B. MICRO SYRINGE APPARATUS

This is essentially a small edition of A, using special plastic micro syringes. These are made from $\frac{1}{4}$ inch Lucite rod (Fig. 2A). The open end of the barrel is machined down to a neck, which tapers to a sharp edge at the opening. A $\frac{1}{8}$-inch Lucite rod selected for size, and with ends machined straight, serves as a plunger.

Air-tightness is obtained by means of a short sleeve of thin-walled Tygon tubing which maintains a slight pressure against the plunger. The ends are cut off straight and paralleled on a brass mandrill which is held in the lathe. The plunger is operated manually by a screw motion and the position measured by means of a dial indicator, introduced by Gilmont.[8] The indicator is provided with a Lucite sleeve (Fig. 2B) which during measurements lightly rests against the straight edge of the plastic sleeve of the syringe. The spring tension is removed from the feeler rod and is substituted by a wire ring for finger control. We have been using Ames model 282 M dial indicator with one inch travel divided into 1000 parts. The plunger position can be manipulated and read within 0.003 inch, where 0.005 inch is equal to 1 cubic millimeter, which is also the stability of the instrument per hour as determined by blank runs using 3–4 cc vials for compensating and respiration chambers.

Rocking Device

A simple hinge device which does not change the described procedure of operation is given in Fig. 3. The lower end of a ball-chain engages adjustably with a crank device. The chain runs in a groove on the suspension hook and is stretched across the water tank by means of a rubber band. The respirometer bank is engaged to the chain by means of the split head of a rod (D), which is loosely stuck into the manometer block. The crank is run by a geared-down motor, e.g., a small electric hand drill, controlled by a Variac.

ACKNOWLEDGMENTS

I wish to express my gratitude to Dr. Laurence Irving, Director of the Arctic Research Laboratory, Point Barrow, Alaska, for encouragement and helpful criticism; and to Mr. Walter Flagg and Dr. R. Wennesland at the same laboratory for assistance in testing of the apparatus, and to Mr. Otto Hebel, Swarthmore College, for suggesting the use of the dial indicator.

---

[8] R. Gilmont, Analytical Chemistry 20, 1109 (1948).

Book Reviews

Matrix Analysis of Electric Networks

By P. Le Corbeiller. Pp. 112+xi, Figs. 49. Harvard University Press, Cambridge; John Wiley and Sons, Inc., New York, 1950. Price $3.00.

This book is the first of a series of Harvard Monographs on Applied Science. We are promised that the emphasis in this series will be on the applied *physical* sciences especially "on topics that involve intellectual borrowing among academic disciplines." If the other volumes of this series conform to the standard set in this first volume, the literature in applied science will be significantly enriched.

The aim of this book is to present a simplified version of Gabriel Kron's stationary network analysis. We are told that an understanding of the present work will enable the reader to avail himself without difficulty of the greater amount of information contained in Kron's *Tensor Analysis of Electric Networks* (John Wiley and Sons, Inc., New York, 1939). Due to the rather abstruse nature of the mathematical concepts Kron employs, his work has not as yet received the recognition it deserves among communication engineers and applied physicists. This abstruseness is necessary in Kron's treatment of rotating machinery, but with reference to stationary networks, as Le Corbeiller says, "it should not be necessary to use such a tremendous sledgehammer to crack this rather small nut." The nutcracker Le Corbeiller employs is simple matrix algebra combined with two elementary formulas borrowed from topology, giving the number of independent meshes and node-pairs of a network in terms of the number of nodes, branches, and subnetworks.

Although this monograph may serve as an introduction to Kron's more extensive work, it is actually complete in itself and its mastery will provide the reader with very general and powerful tools for the solution of the most complex networks. Before launching into a description of its contents it should be said at once that this little book is, with a few minor reservations noted below, a masterpiece of pedagogical exposition as well as an intellectual treat. One scarcely knows which to admire the more: the facile clarity of the presentation or the continual delights and surprises found on nearly every page. The author's method is to teach by example and to this end the book is amply supplied with well-chosen illustrations. A number of exercises selected to amplify and illuminate the text are scattered throughout the book.

It is assumed that the reader has a knowledge of elementary algebra including determinants and of elementary alternating current theory. The first chapter entitled "Preliminary Concepts" gives all the extra mathematical background required for an understanding of the later chapters. It consists for the most part of a very clear development of matrix algebra with illustrative examples drawn from simple circuits and from geometry. The chapter concludes with an intuitive proof of the topological results mentioned above.

In Chapter 2 "The Mesh Method of Kron" is described as an extension of the familiar Maxwell mesh method. Kron's extension seems almost trivial at first sight. The final result is a matrix equation giving the branch currents in terms of the series branch e.m.f.s. This equation involves the impedance matrix of the network and also the transformation matrix which operating on the mesh currents transforms them into branch currents. The transformation matrix depends only on the topology of the network and on the choice of the M independent meshes. The full power of the method is realized when there is coupling between two or more of the branches. The Kron method involves no additional complexity even if every branch is coupled with every other, or if the coupling is symmetric (magnetic) or asymmetric (triode). The reader is introduced to the Kron method via an example on the Wheatstone bridge network. Unfortunately, the directions and polarities assumed in the network diagram of this example do not check with the subsequent equations. This is especially a pity since a novice may be tempted by this stumbling block to give up the whole enterprise at the start. Actually, the equations are self-consistent and what needs to be done is to reverse all e.m.f.s. and branch currents in Fig. 14 save those in branch f.

Chapter 3 "The Node-Pair Method" gives Kron's extension of the conventional node-pair method in which the data are given in terms of constant current sources instead of e.m.f.s. The result is again a matrix equation relating the node voltages to the current sources in terms of a transformation matrix and the network admittance matrix.

A truly amazing development is presented in Chapter 4, "The Mixed Method." It is shown here how Kron is able to analyze a network not only with all possible couplings but in which both constant current and constant voltage sources may be connected internally and externally in every possible way. The trick here is to use the external sources to provide sufficient additional meshes to make the transformation matrix non-singular. If there are too few such sources, a number of voltmeters are judiciously added to make up the difference; if too many, the effects of the extra ones can be considered separately. Corresponding to the dual nature of current and voltage there is a second possible treatment making use of node-pairs instead of meshes. This chapter is considerably more difficult to read than the others, doubtless owing to the relative complexity of the networks treated. Still, one cannot help but feel that the discussion in parts of this chapter could be profitably expanded.

There are a number of additional misprints, most of which are obvious and should cause no trouble. In Fig. 46, the two current sources should be interchanged and the direction of current in branch C should be reversed to make this diagram conform to Eqs. 53–1. The physical significance ascribed to the current j^i on p. 85 seems to be incorrect since if all the sources mentioned as contributing to it were absent, it is evident that it would not vanish in general.

Professor Le Corbeiller has done much more than just to enliven a traditionally dull subject. All physicists and electrical engineers owe him a debt of gratitude for this very ingenious, stimulating and useful book.

H. C. Torrey
Rutgers University

Vacuum Equipment and Techniques

Edited by A. Guthrie and R. K. Wakerling, Radiation Laboratory, University of California. Pp. 264+xvii, Figs. 102, 23×15 cm. McGraw-Hill Book Company, Inc., New York, 1949. Price $2.50.

This book is one of the National Nuclear Energy Series, being Vol. I of Division I (Electromagnetic Separation Project). It is an outgrowth of the developments carried out at the Radiation Laboratory, University of California, of high vacuum equipment and techniques for use in electromagnetic separation plants. Routine production of high vacuum in large systems on the scale necessary for the electromagnetic separation process never before had been done and, as a consequence, the problems involved were of a magnitude which required considerable amount of pioneering work on both equipment and testing. The results of and the methods used in this work are reported in this volume. The body of the book is divided into five chapters. The chapters have been written by individuals originally connected with the actual work, except Chapter 5 on leak-detection techniques and procedures which was prepared by the authors from existing reports.

Chapter 1, "Fundamental Considerations in Vacuum Practice," by Robert Loevinger (58 pages), presents those parts of the kinetic theory of gases essential to modern industrial and laboratory vacuum practice. The material for the chapter is well selected and prepared. Impedance and conductance of vacuum plumbing, the flow of gases and vapors in the viscous, molecular and transition regions, system speed, pumping speed of vacuum pumps, methods for the measurement of pumping speed, evacuation rate, and pumping speed of cold traps are discussed quite adequately. For example, in the section on molecular flow through pipes, Knudsen's formula is used in the fundamental equation from which the conductance of a long circular pipe and a circular annulus is obtained. The combination of these results in the conductance of a short pipe with aperture. The rectangular duct, the equilaterally triangular duct, the thin slit-like tube, ducts of other shapes, bends and elbows are described as elements of a vacuum system and formulas expressing their conductances are developed. Other sections are treated similarly. Sample calculations are given. An appendix summarizes in tabular form the formulas most frequently used in vacuum design work. These formulas are given in two types of units—the metric laboratory units and the mixed metric and English laboratory units. This table will be found most useful to those engaged in the design of high vacuum systems.

Chapter 2, "Elements of the Vacuum System," by William E. Bush (46 pages), gives material on rotary, oil-sealed mechanical pumps, oil booster pumps, and oil diffusion pumps. Precautions to be observed in the successful operation of vacuum pumps are discussed at some length. The procedure to be followed in the selection of a pumping system where both mechanical and diffusion pumps are involved is outlined. Contamination of mechanical and diffusion pump oils, and oil migration problems are considered. Methods of testing the performance of diffusion pumps are given. Refrigerated traps, a subject which is overlooked in many books on this subject, is given brief consideration at the end of this chapter. In the appendix there are two tables listing mechanical pump oils and diffusion pump oils, and some of their properties. These tables are not complete, but they list several oils which are used as pumping fluids.

Chapter 3, "Vacuum Gauges," by Kenneth M. Simpson (41 pages), includes the usual low pressure gauges that have found extensive use in the laboratory and in production. The McLeod gauge (mercury and oil types), Pirani gauge, thermocouple gauge, Knudsen gauge, and ionization gauge (hot cathode, Phillips, and Alphatron) are the principal ones described. Several control circuits and special designs of these gauges developed at the Radiation Laboratory are reviewed at some length. The question, "What is measured by vacuum gauges?" is asked and an answer given.

Chapter 4, "Vacuum Materials and Equipment," by William E. Bush (44 pages), summarizes in some detail the methods of gasketing and the techniques employed in the flanges used for making high vacuum connections between pumps and vacuum plumbing and other connections within the system. Gasket materials and their properties are set forth in tables and discussed in the text. The methods used by the Radiation Laboratory in adapting standard gate and globe valves for use as vacuum valves is described in a very complete manner, including good illustrations of several types. There are several tables in the appendix listing vacuum greases, cements, solders, and brazing alloys useful in building up and maintaining a vacuum system.

Chapter 5, "Leak Detection Instruments and Techniques," by R. Loevinger, and A. Guthrie (53 pages), is a summarization of the classical techniques and the more recently developed ones. The vacuum analyzer, an instrument which provides information regarding the nature of the gases and vapors inside a vacuum system, and the helium leak detector, the dean of leak detection instruments, are given full discussions. Several pages are devoted to the construction of a helium-type leak detector since it is stated that the cost of these units makes them prohibitive for many laboratories and the simple cold cathode leak detector developed at the Radiation Laboratory can be built by the laboratory personnel. Theories of leak detection and general leak-hunt procedures are included.

The editors have achieved a unified volume. Each chapter may be read independently of the others, which is perhaps an advantage in using the volume as a reference work. Throughout the work abundant reference has been made to the published literature. *Vacuum Equipment and Techniques* is a book to be recommended to those working with vacuum systems to give a better understanding of vacuum processes.

H. M. Sullivan
Central Scientific Company

An Introduction to the Luminescence of Solids

By Humboldt W. Leverenz. Pp. 569, Figs. 140. John Wiley and Sons, Inc., New York, 1950. Price $12.00.

This book is written by one of the internationally outstanding experimental investigators in the field of crystal luminescence. It represents a summary of nearly twenty years of continuous and precise work and as a result has a prominent and unquestioned position in the literature of the subject. It should be on the shelves of anyone who has a serious interest in the subject. The hard core of the book centers about the vast work on inorganic phosphors carried out at the RCA laboratories by Leverenz and his associates; however, all material closely related to it is included with careful evaluation. It is precisely within the period of time that Leverenz has been working in the field that luminescent materials have achieved a prominence which makes them an indispensable part of the broader field of electronics. This coincidence is not an accident, for he has been responsible for many of the outstanding advances in development, such as the discovery of the zinc beryllium silicate system, which played a key role in the luminescent lamp industry for a decade.

The first quarter of the book deals with the descriptive and theoretical background of the subject: A survey of atomic and crystalline structure, the processes by which crystals are formed in practice and the imperfections they may contian, the general techniques employed to synthesize phosphors and the energy level diagrams applicable to solid systems. The latter part of this develops the general theory of luminescent systems and is written in a straightforward and unimpassioned way. Leverenz treats the theory as a useful rack or set of pigeonholes for classifying ideas and materials and does not offer a particular viewpoint as a nostrum for curing all ills. The reviewer regards this as an exceedingly healthy outlook since there is a strong tendency on the part of many investigators in the field to make extravagant claims about their own insight into the workings of particular complex systems, whereas the truth seems to be that only one or two simple materials have been studied with sufficient thoroughness to permit even the beginnings of quantitative theoretical analysis.

Chapter V, "Luminescence of Phosphors," which comprises nearly half the volume, represents the heart of the subject. It contains a detailed summary of all of the practically interesting properties of a large number of prominent inorganic materials and a few organic ones that have current interest. Discussed here are such subjects as means of excitation, emission spectra, decay times, stimulation and quenching, absolute and relative efficiency, poisoning agents and the influence of factors such as activator concentration, operating temperature and current density and voltage for cathode-ray operation. This chapter contains about 100 illustrations which summarize important experimental observations.

The remainder of the book represents a general review of special topics that are possibly of more specialized interest than the parts described above, but which should be presented in a book of this type. There is, for example, a chapter in which subjects such as photolysis, "burning" and the effects of milling are discussed, along with sundry other subjects of comparable importance. Finally, there is a chapter on "Uses of Phosphors" which contains a detailed description of the many ways in which luminescent crystals have been used both commercially and in research and the manner in which the existing materials are suited for such application.

In the appendix Leverenz provides additional specialized information including advice on the preparation of the ingredients for sulfide-type materials which require great care if reproducible results are to be obtained.

The bibliography contains at least 1000 entries and should make a similar survey unnecessary for some time to come. I doubt if any contributor to the field can claim that he has been neglected.

The reviewer also noted with some amusement that Leverenz' well-known periodic chart of the elements appears in removable form in a flap in the back cover. This chart contains so much data that I must confess that I become dizzy if I look at it very long. On the other hand, many of my friends find it very useful. In addition it must be admitted that it is tame compared with the nuclear charts that are being evolved at the present time.

FREDERICK SEITZ
University of Illinois

Basic Theories of Physics: Mechanics and Electrodynamics

BY PETER G. BERGMANN. Pp. 280+viii. Prentice-Hall, Inc., New York, 1949. Price $3.75.

This book is an important attempt in presenting the structure of classical theoretical physics in coherent form. It covers the basic theorems of classical mechanics and electrodynamics with special emphasis on presenting results leading to modern theory.

A special feature of this book is the emphasis on the transformation character of all quantities involved. This emphasis leads the author to write all fundamental relations in tensor notation from the very outset, a practice which is very recommendable. Axial vectors like angular momentum, magnetic field, etc., are introduced immediately as second rank tensors which makes a later discussion of the distinction between tensors and tensor densities much simpler.

The first half of this book is devoted to a survey of classical mechanics. After a critical discussion of the point particle concept and of Newton's laws and the associated conservation laws the book gives a brief but concise outline of Hamiltonian dynamics. The generalized dynamics section is written with special regard to demonstrating the relations which led to quantum-mechanical concepts. A section then follows on the mechanics of continua which is one of the most useful parts of the book, since it summarizes in compact notation the basic theorems of hydrodynamics, elasticity and acoustics usually not found in a single place. Again the material is given totally in tensor notation and most of the theorems useful in the section on electricity are developed.

The transition from classical mechanics is made by a discussion of the meaning of a field theory *vs.* action at a distance theory. In this respect this reviewer feels that the author has not done full justice to the basic concepts of a field theory. The author emphasizes the "field" mainly in terms of its continuity properties but does not critically discuss the field concept in terms of cause and effect separation or study the equivalence between action at a distance and field concepts which has so recently become of importance.

Electrostatics is developed in the customary manner from Coulomb's law. The treatment given to the mechanics of continua makes it possible to introduce the Maxwell tensor and similar material in a much easier manner than is usually possible. Polarization, multipoles, etc., are introduced in the usual manner.

The subject of magnetastatics is introduced by the use of magnetic poles. The author's principal points in the introduction of the magnetastatic interaction are: (1) That this is the first time that a velocity dependent interaction is encountered. (2) That Newton's third law is apparently violated. The latter point is unfortunately much confused by the use of the single magnetic pole in describing the interaction. It is true that the magnetic interaction between single moving charges does not obey the third law; this is due to the non-stationary character of the fields and the consequent changes of electromagnetic momentum. In the case of stationary current interactions (including magnetic materials) the third law is always obeyed as can easily be demonstrated. The point is thus an important one but the means of demonstrating it are not too properly chosen. In the section on the general electromagnetic field the magnetic interaction between moving charges is discussed with the correct explanation of the apparent breakdown of the third law. The general electrodynamic equations are introduced in essentially the classical way with an excellent discussion of the conservation laws. The solutions of the equation in terms of retarded and advanced potentials are discussed only briefly and so are the actual radiation fields. A very brief discussion of the basic postulates of special relativity is given and the covariance of Maxwell's equations is demonstrated by direct substitution into the Lorentz transformation.

The book concludes with a general discussion of some of the results of electromagnetic theory in the field of optics. An unusual feature is a good discussion of the eiconal equations and the relation of Fermat's to Hamilton's principle. This chapter will be particularly useful to the student studying the physical foundations of quantum mechanics.

This is an excellent book for the serious student who is interested in the structure of classical theoretical physics rather than principally in its applications. It will acquaint him with the fact that even in classical physics there are many questions of a controversial nature. The book will be found a valuable text in schools where theoretical physics is taught in a single course.

WOLFGANG K. H. PANOFSKY
University of California

Aerials for Metre and Decimetre Wave-lengths

BY R. A. SMITH. Pp. 218, Figs. 125. Cambridge University Press, London, 1949. Price $3.75.

In about 200 pages of relatively easy reading, the author includes a great deal of information of interest to the experimental research man and the design engineer. This has been accomplished by limiting the depth of the book to a scanty framework of simple theory in which the results of experiment and of the more elaborate theories are presented. The scope of the book is necessarily restricted, not only by the wave-length regions specified in its title, but also by the fact that typically microwave antennas are treated in another volume of the series "Modern Radio Technique" (General Editor: J. A. Ratcliffe).

The first two chapters contain a factual statement of the performance characteristics of resonant dipoles and dipole arrays. The next two chapters present a simple theory based on four-terminal network relations and sinusoidal current distributions in linear antennas. In addition, a very instructive graphical comparison is drawn between experimental values for the impedance of center-fed dipoles and the several values predicted by simple sinusoidal theory and by the more sophisticated theories of Schelkunoff, King and others.

Chapter 5 describes the impedance and pattern characteristics of driven elements combined with reflectors and directors. The next two chapters consider the more specialized problems associated with arrays of such units when used as high power transmitting antennas and as receiving antennas for wave-lengths of a few meters. Problems of supporting, insulating, feeding, and switching these antennas are treated.

Chapters 8 through 11 are devoted to several important fields of practical application. The radiation characteristics of long wires are described and are used to predict the performance of terminated wires, V antennas, inverted V antennas, and rhombic antennas. Solutions are offered for the matching, feeding, and switching problems encountered with broadside arrays for 1.5-meter ground radar. The specialized art associated with Yagi antennas is outlined. The aircraft antenna problems in this frequency range are recognized and a number of particular solutions—mainly exposed antennas—are offered.

The principles underlying broad-band antennas and slot antennas are discussed in Chapters 12 and 13, including an exploitation of the Booker-Babinet principle for the interpretation of slot radiation characteristics. In the next chapter these principles find application to antennas for decimeter wave-lengths.

The final chapter makes an interesting analysis of the sources of antenna noise. Directional and frequency factors are considered and related to the noise factor of the receiver.

In considering specialized fields of application, the author largely avoids engineering detail and emphasizes general design techniques. In some cases, as might be expected, the book does not reflect the advance in the art which has occurred since the war. The treatment of many subjects is a bit sketchy, to the extent that the reader will want to turn elsewhere for more complete information. However, this additional information will usually be found in the well-selected original sources to which frequent reference is made.

The author's practical experience is evident in a number of passages noteworthy not because they are startling, but because they are so very true. The reviewer can not refrain from quoting some of these which come closest to his own experience. Past measurement and theory are left on about an equal footing by the following two statements. "In view of the lack of consistent measurements covering a wide range of dipoles a designer who needs a very accurate estimate of the impedance of a half-wave dipole must measure it under the conditions of use." "Summarizing, one may say that in view of the difficulty in realizing the ideal conditions assumed by theory the agreement between theory and experiment is remarkably good, and the difference between Schelkunoff's values and those obtained from the later treatments of Hallen's equation are not very significant in practice. . . . In any case the final adjustments due to the presence of insulators, etc., are likely to be even larger than the discrepancies between theoretical and actual values for the free aerial."

The following statements may seem to be self-evident, but the first has been actively questioned in this country and the second ineffectively applied. "It is much easier to produce a good 'all-round' polar diagram for vertical polarization than for horizontal polarization, . . ." "Moreover, it will be almost essential to decide where such slot aerials are to be placed in the early stages of the design of aircraft in order that the structural design may take account of their presence."

The book is not recommended as a classroom text or for study by one with no previous knowledge of antennas, since basic assumptions and restrictions to simplified developments are not always made clear. It is recommended, however, to the experimentalist and the design engineer as a convenient and helpful reference.

L. G. Van Atta
Naval Research Laboratory

Engineering Supersonic Aerodynamics

By E. Arthur Bonney. Pp. 264+xi, Figs. 180. McGraw-Hill Book Company, Inc., New York, 1950. Price $4.00.

Engineering Supersonic Aerodynamics by E. Arthur Bonney is a textbook of applied aerodynamics designed to provide an undergraduate engineer who has already become acquainted with the classical phases of applied aerodynamics with the additional background information needed for the design of supersonic aircraft. Since a wide range of topics is covered and since the mathematical techniques necessary for the theoretical development of these topics is beyond the ability of those students who might use the text, no attempt is made to derive the results from fundamental principles; however, adequate references to the basic literature are included for the use of those who require more complete details.

The first chapter describes the basic phenomena of compressible fluid flow including shock waves, Mach waves, oblique shock waves, expansion waves, and wave interactions. The second chapter covers the one-dimensional steady flow theory of nozzles and diffusers. Chapter three presents the oblique shock and Prandtl-Meyer expansion theory, the approximate two-dimensional linear theory and Busemann's second- and third-order expansion theory. Tables of the results of the oblique shock and Prandtl-Meyer expansion theory which are complete enough for most practical applications are included. Chapter four covers two-dimensional airfoil theory, the theory of the rectangular wing and of delta-wings, and the downwash fields behind finite wings. Chapter five treats bodies of revolution. This chapter could be strengthened by reference to the Stone-Kopal calculations of the lift and drag of cones. Chapter six discusses the design and instrumentation of supersonic wind tunnels. Chapter seven, the last chapter, discusses some of the problems of composite design including interference and performance analysis.

The only important theoretical error noted by the reviewer occurs in the treatment of the rectangular wing (p. 143) where it was assumed that the wave drag of the rectangular wing is reduced from the two-dimensional drag in the same ratio as the lift reduction. The correct theory was given by von Kármán [J. Aero. Sci. 14, 373 (1947)] and shows that the formula given by Bonney is in error by a factor of two (for the zero lift wave drag) at the Mach number where the Mach line from each tip of the leading edge touches the opposite trailing edge tip. In addition the use of the Busemann second-order theory to correct the lift in the tip region of a rectangular wing is of questionable value since the correction has no sound theoretical foundation and cancels out in the two-dimensional region where it is valid and since the final correction so deduced is of a very small magnitude.

There are two items of notation which are, perhaps, unwise. First, the word "characteristics" is used freely in the usual dictionary sense. Since the use of the word in its technical sense applicable to the mathematics of hyperbolic partial differential equations is never mentioned, its use is perfectly correct; however, it may lead to confusion in the minds of immature readers unless there is some comment on the technical use. Second (p. 141), the term acceleration is used to refer to a finite velocity increment. In addition there are several of the minor errors of a proof-reading nature which are inevitable in any new text. Figure 4–13 (the lift/drag ratio of two-dimensional airfoils) is mistitled and improperly referred to in the text. The only other correction worth noting occurs in Fig. 4–61 (the downwash infinitely far behind a delta-wing) where the ordinate scale is cut short so that the downwash behind the wing in the plane of the wing is not shown.

Since the mathematical difficulties of the theories of compressible fluid flow are too great for the vast majority of the undergraduate engineering students, it seems to be impractical to develop completely any extensive portion of this theory in undergraduate courses. On the other hand, the very great importance of compressible flow phenomena in modern aerodynamics makes it essential that some basic education in this field be obtained. The approach used by Mr. Bonney appears to present a reasonable solution of this problem.

H. J. Stewart
California Institute of Technology

Spectra of the Rare Metals and Some Metalloids

By A. Gatterer and J. Junkes. Vol. 3 of the Atlas of Spectral Lines. Vatican Observatory.

Volume 3 of the Atlas of Spectral Lines has been received from the Astrophysical Laboratory of the Vatican Observatory. This handsomely bound and printed volume completes the series on the spectra of the elements assembled to aid in chemical analysis. Volume 1 contained the spectra of 30 chemical elements, Vol. 2 the rare earth metals, and Vol. 3 contains the spectra of As, Au, Be, Br, Cb, Cl, Ga, Ge, Hf, Hg, I, In, Ir, Os, Pd, Pt, Re, Rh, Ru, S, Sb, Se, Ta, Te, and U. There are 42 photographs, 30 x 40 cm in size, of the arc and spark spectra of these elements from 6400-2100A. The same dispersion was used for all the elements and each photograph has six elements adjacent to each other to help in identifying the lines. The normal iron arc or spark spectrum is photographed with the spectrum of each element for comparison. The platinum metals Ru, Rh, Pd, Os, Ir, Pt appear together as do the metalloids Cl, Br, I, S, Se. The other elements are grouped alphabetically with Hf by itself as it was photographed later than the others.

The photographs are enlarged 20 times from the original plates and have a dispersion ranging from 0.80 to 27.28A/mm. The dispersion is given for wave-length ranges of 50A which enables the displacement of lines measured in mm on the photographs to be converted to angstroms.

There are tables giving the wave-lengths of the lines of each element, the wave-lengths of the strong lines (*raies ultimes*) suitable for analysis and the lines of the principal impurities. The tables are accompanied by some text that describes the material used, electrode form, purity, mounting, and general characteristics of the spectrum obtained. The table of intense lines has also been reprinted on heavy paper for more convenient use in analysis. The tables give the state of ionization, the wave-length, and the visual intensity in arc and spark on a scale of 1 to 10 with 15 and 20 for intense lines. The tables are not meant to be exhaustive and no new lines were sought although some of the lines were measured by the authors. Most of the wave-lengths were taken from tables by Kayser-Ritschl, the *M.I.T. Wavelength Tables* of G. R. Harrison, Tables of Exner and Haschek, special tables in Kayser's *Handbuch* and special monographs. New iron standards had to be found in the ultraviolet region 2300–2100A. This Atlas should be a great boon to those doing spectrochemical analysis.

C. W. Ufford
University of Pennsylvania

Earth Waves

By L. Don Leet. Pp. 122, Figs. 58. Harvard University Press, Cambridge; John Wiley and Sons, Inc., New York, 1950. Price $3.00.

This book presents selected information concerning elastic waves which are propagated through the earth. It is written for readers with training in the fundamentals of some branch of engineering, physical, or geological science, and deals with first principles with only elementary mathematics. It is not intended for use as a textbook in seismology or seismic prospecting, but rather as a compact summary of the state of our knowledge, for a newcomer in the subjects covered. A relatively large portion of the information provided is taken from material published in periodicals with limited circulation. The book is based on eight lectures of the author on "Application of seismological techniques for engineering problems." This latter title very well describes the content of the book.

The first 38 pages deal with the recording and measurement of elastic waves which have traveled in the earth. It gives an excellent presentation of the principles of recording instruments and the characteristics of the records they write. Diagrams of specific seismographs are well selected.

In the second chapter (20 pages) the known types of earth waves are described. The author considers mainly waves recorded from artificial explosions but he also discusses the types found in seismograms of distant earthquakes and a record written by a field seismograph located near the atomic bomb exploded in New Mexico on July 16, 1945. This is the record in which the author discovered the so-called "hydrodynamic wave," a term not too well chosen, since—except for the form of motion during the passage of the wave—there seems to be no relation to actual hydrodynamic waves.

The third chapter contains a summary of the transmission characteristics of earth waves in seismic prospecting over various wave paths determined by layers having different elastic properties. About 14 pages are devoted to the transmission of elastic waves through the earth, including calculation of the wave velocity in the earth's interior, typical seismograms from various epicentral distances in shallow earthquakes, wave paths through the earth's interior and time-distance curves. The next 18 pages give similar information about seismic prospecting.

In the last chapter (10 pages) the author discusses some aspects of microseisms, or ground unrest, recorded continuously by sufficiently sensitive instruments. He deals mainly with the problem of locating the source of microseismic storms and the direction of travel by the use of three stations, located at the apices of a triangle with separations of approximately one mile. He also discusses possible improvements of this method.

Throughout the book, the author has provided excellent illustrations; most of the 58 figures are derived from his own work.

Dr. B. Gutenberg
Seismological Laboratory
Pasadena, California

Giant Brains, or Machines That Think

By Edmund C. Berkeley. Pp. xvi+270, illustrated. John Wiley and Sons, Inc., New York; Chapman and Hall, Ltd., London, 1949. Price $4.00.

The high speed sequence-controlled computing machines such as the ENIAC and the Harvard Mark I, Mark II, and Mark III machines are certainly among the most pregnant and suggestive developments of recent years. It seems clear that their applications will be numerous and significant. In *Giant Brains*, Berkeley has offered a primer of these devices and of their uses, so far as the latter can now be visualized.

It is genuinely a primer. Its prose has been, as the author explains, carefully examined to make sure that the little steps it presents are not too difficult for little feet. He says: "Every word of two or more syllables was continually checked: is it needed? can it be replaced by a shorter word?" One gets the impression that the sentence structure was similarly examined for elaboration and complexity; at any rate, only straightforward and rather short sentences have survived. I found the resulting prose repellent, but the author may have achieved his goal of making understanding easy.

The book deals with a remarkably wide variety of computing mechanisms, including IBM punched-card machinery, the M.I.T. differential analyzers, the Harvard Mark I machine, the ENIAC, the Bell Telephone Laboratories relay calculators, a machine for examining logical propositions, and some remarkable new machines suggested in outline, for illustrative purposes, by the author. It has a chapter on language, and another which explains how the reader can make a simple computer in his basement, provided he can secure the tape-reading mechanism from an old teletype machine.

Berkeley chooses to treat these machines in very considerable detail as concerns coding, information transfer, and the like, while refraining almost altogether from dealing with the devices used to realize the functions of the machine, at least when these grow more complicated than gear trains or relays. This is probably an inescapable choice for one who intends to write for a large public mostly ignorant of electronics, but it has the unfortunate result that it permits no discussion of the ways in which the properties of computer components dictate computer design. Undeniably, the characteristics of the new computing machines now nearing completion in several U. S. and overseas laboratories have been determined at least as much by the strengths and deficiencies of the computer components currently available, as by the wishes of the designers.

A strong anthropomorphic flavor pervades the book. The homemade computer recommended to the reader is called Simon (for Simple Simon), the ENIAC is constantly referred to either as "Eniac" (without the article), or as "he," computing machines are almost always called "mechanical brains," and so on. This confers on the work an air of naivete which is somewhat revolting at best, and misleading at worst. The title, for example, is misleading; the "mechanical brains" we now know how to build are "giant brains" only in the sense of being monstrosities in comparison with physiological brains. The ENIAC, with a million times less complexity than the human central nervous system, occupies a space several thousand times bigger, dissipates a thousand times the power, and is a good deal less reliable.

With its defects, which are probably mostly visible to the scientist, and may not be so objectionable to the lay reader, *Giant Brains* has virtues. It contains a useful bibliography, its descriptions of existing machines probably include some facts unknown to any reader, and the discussions of future possibilities, though incomplete, may be suggestive.

Louis N. Ridenour
University of Illinois

Introduction to Theoretical & Experimental Optics

By Joseph Valasek. Pp. 454+x, Figs. 211. John Wiley and Sons, Inc., New York, 1949. Price $6.50.

This book is a text and laboratory manual for a full year course in optics for advanced undergraduate students. Until now only one comparable modern text, Monk's *Light*, has been available so that the appearance of Professor Valasek's book doubles the number of possible choices for instructors of courses in optics on the intermediate level who wish to use a *single* text for geometrical, physical and radiation optics and an accompanying laboratory course.

The treatment of geometrical optics follows the general pattern used in Drude's classical book. It is clear and concise with sufficient emphasis on basic concepts such as Fermat's principle and the collinear transformation. Particularly clear, though brief, are the chapters on apertures and illumination. One might wish that more subjects had been expanded to the same extent as the optics of the eye, stereoscopy, and the prism spectroscope but it is apparent that the author intends that a reading of the text be supplemented by working the problems. These problems—there are 87 on geometrical optics alone—are excellent and adequately serve to emphasize and amplify principles and methods described only briefly in the text.

In the section on physical optics the principles of interference and diffraction are thoroughly developed from wave theory and diffraction of x-rays in crystals is treated. Mention is made of the limitations of the Fresnel theory when applied to microwaves. Polarization and optical activity are discussed on the basis of electromagnetic theory, which leads to treatments of refraction, dispersion and reflection. The use of advanced calculus is not avoided. A comparison is made between the classical and quantum theory expressions for dispersion.

In the third section on radiation and spectra a wide range of topics including thermal radiation, atomic, molecular, and x-ray spectra, Zeeman, Stark, photoelectric, Kerr and Raman effects, chromaticity, and scattering are condensed into 79 pages. The treatment is necessarily much less thorough and is of a more descriptive nature than that used in the first two sections, but the important equations and relationships are presented and briefly described. Here one could, without detriment to a course in classical optics, omit some chapters on topics which might be more appropriately and extensively treated in an advanced undergraduate course in atomic physics.

The last section of the book describes twenty-four experiments in geometrical and physical optics, spectroscopy, and photometry. Most of these are, of course, similar to those found in Monk or in Taylor's *Manual of Optics*, but included are interesting experiments in spectrochemical analysis, spectrophotometry, x-rays, and a valuable discussion of the photographic process. The principles involved and the use of the apparatus are fully described with frequent references to the body of the text for additional theoretical background, but explicit step-by-step experimental procedure is not usually given. Thus the student must acquire a real understanding of the experiment in order to perform it properly.

The book is carefully written and the numerous excellent line drawings are well thought out. The author's teaching experience has enabled him to introduce new subjects in such a way that salient points are clearly brought forth in a few well-chosen sentences.

Robert B. King
California Institute of Technology

Spectroscopic Properties of Uranium Compounds

By G. H. Dieke and A. B. F. Duncan. National Nuclear Energy Series, Manhattan Project Technical Section, Division III, Vol. 2. Pp. xviii+290. McGraw-Hill Book Company, Inc., New York, 1949. Price $2.75.

This book is devoted chiefly to a discussion of the visible and ultraviolet absorption and fluorescence spectra of several dozen uranyl compounds. These compounds have the general formula $M_xUO_2N_y$, where M is a positive ion, usually a monovalent metal, and N a negative ion (halide, nitrate, sulfate, etc.). The spectra were studied in the crystalline state, and were measured with both low and high resolving power, at various temperatures down to 14° K, and in the presence of magnetic fields up to 24,000 oersteds. They are interpreted in detail with respect to the vibrational fine structure and other characteristics of molecular electronic spectra in crystals. In the interpretation frequent use was made of the vibrational isotope effect obtained by substitution of O^{18} for O^{16}. The spectra are summarized in some 40 tables constituting Appendix 1.

In addition the volume contains a chapter on the x-ray crystallography of uranyl compounds and four chapters on various aspects of the chemical preparation of the compounds. An extensive bibliography is included. It is divided into spectroscopic and non-spectroscopic parts, and the references are listed year by year. The reader is warned (in the Preface, however, not at the heading of the Bibliography) that the spectroscopic bibliography includes nothing that was referenced by Nichols and Howe in their 1919 monograph on the fluorescence of uranyl salts, and that the non-spectroscopic part should be regarded as an extension of the literature cited in Part 55 of *Gmelins Handbuch der anorganischen Chemie* (1937). The authors point out that the new elements neptunium and plutonium may have compounds with properties like those of the uranyl compounds. The present volume should be a useful compendium for investigators of the spectra of such new substances.

Richard C. Lord
Massachusetts Institute of Technology

Luminescent Materials

By G. F. J. Garlick. Pp. 254+viii, Figs. 127. Clarendon Press, Oxford, 1949. Price $5.50.

Dr. Garlick has provided a book which will give a reader with prior knowledge of solid state physics an opportunity to become acquainted with some of the main characteristics of luminescence in solid materials together with associated descriptive theory in a minimum of time.

The content of the book is divided into eight chapters. The introductory chapter gives a brief survey of the phenomenon of luminescence together with examples and indicates the main characteristics which must be adequately explained. In Chapter II a review of the fundamental mechanisms that play a role in luminescence are reviewed. These include a brief and somewhat terse presentation of the theory of optical absorption and the luminescent processes based on the Block electron-energy band theory of perfectly periodic crystals together with additional impurity centers and assumed electron traps. The discussion probably indicates that with the present knowledge of the subject it is not possible to give a detailed treatment of the nature of luminescent centers and a quantitative treatment of electron transitions.

Chapter III is quite long and provides in the main a catalog of the luminescence characteristics of impurity-activated phosphors with some attempt to connect them with the theories presented in the previous chapters. Ample examples of these characteristics in various phosphors are given with the help of a large number of illustrative curves.

Chapter IV is devoted largely to the luminescence processes in zinc sulfide. The material presented here is mainly recent and covers more detailed investigations by the author and collaborators done in order to provide information which would establish a more precise theoretical description of phosphorescence and thermoluminescence.

Chapter V contains interesting material on the electrical properties of phosphors associated with luminescence. The principle electrical effects discussed are the electrical conductivity during luminescence, the change in dielectric constant and dielectric loss during luminescence and the production of luminescence when a strong field is applied to some phosphors. One of the most interesting features is the change in dielectric properties from which it is concluded that electron retrapping is negligible in luminescence and that the electron traps have a large effective size.

A description and theory of the effect of infra-red radiation in enhancing and quenching luminescence is given in Chapter VI.

Cathodoluminescence is covered in Chapter VII. The main characteristics of luminescent phosphors when excited by incident, moderately high energy electrons is treated. The theory of this type of excitation is given in a qualitative way which only serves to make one wish for a really quantitative description of the fate of an electron entering the phosphor.

The final chapter covers certain aspects of luminescence from organic molecules. A thorough understanding of the phenomenon in such molecules would go far in providing a basis for understanding certain phenomena in more complicated solids. The reviewer had the mild wish that the subject could have been begun with a comprehensive discussion of this topic as a prelude to the treatment of luminescence in more complex solids.

Lloyd P. Smith
Cornell University

Electrical Engineers' Handbook of Electric Power

Edited by H. Pender and W. A. Del Mar. Fourth edition, pp. 1650+xii. John Wiley and Sons, Inc., New York, 1949. Price $8.50.

Reviewing a book implies that someone has read it. When the book in question happens to be a handbook, and if perchance that the volume contains some 1650 pages, the implication is staggering and in this case untrue. Fortunately, for this reviewer's peace of mind, a handbook is not designed to be read but rather to be used as a reference. When tested in this way, the fourth edition of the now famous Pender-Del Mar *Electrical Engineers' Handbook on Electric Power* comes through with flying colors.

The chief objection to the book is its size. This may not be as much a criticism of the editors and authors as it is of the ever increasing informational demands which our civilization places upon the engineering profession. Still, on leafing through the book, one is struck by the relatively high fraction of the volume occupied by textual matter as contrasted with tables and graphs. One is inclined to suggest that some of this material be omitted or abridged or, if this is not desirable, that the book be enlarged still more and called an encylopedia rather than a handbook.

Some 71 different authors have contributed to the present edition, which in turn is the outgrowth of earlier editions to which still others have contributed. While this procedure insured a degree of competence on the part of the authors of specific sections which could not otherwise have been obtained, some variations in style and level of treatment and some redundancy are evident.

Certain features of the volume stand out and justify special mention. The format of the tables and particularly of the conversion tables is pleasing and convenient. In fact, the format and typography are uniformly excellent. By way of contrast, the paper stock, although of the now favored off-white color, verges on the poor quality side—a few thin and frayed pages being noted in the reviewer's volume as received. The binding is also a bit light for a book intended for hard usage.

Another notable feature is the inclusion of extensive bibliographies at the end of each section. The listing of the references by subjects and in chronological order within sub-divisions rather than alphabetical by authors would seem preferable. As a final feature to be mentioned, one is struck by the all-inclusive nature of the material covered. It is hard to think of any handbook type information that a self-respecting electric power engineer might admit needing that is not contained in the book.

For a reference work of this size, the index is rather small and none too useful, at least as judged by a few simple tests. The rather extensive Table of Contents and the division of the book into sections offsets this deficiency although the use of heavy weight and perhaps colored separators for section headings would be a distinct aid. There appears to be no real difficulty in locating any desired information.

The fourth edition of Pender's handbook is evidently destined to uphold the reputation established by the earlier editions and, accordingly, it deserves a place on the electrical engineer's bookshelf.

A. L. Samuel
International Business Machines Corporation

Acoustic Measurements

By Leo L. Beranek. Pp. 914+vii, Figs. 519. John Wiley and Sons, Inc., New York, 1949. Price $7.00.

This is not only an exceptionally comprehensive book, but one that is very well organized and shows the results of great care in the selection and treatment of the whole range of modern techniques for acoustical measurements. There are many complete circuit diagrams and detailed descriptions of recommended laboratory set-ups for measurements or microphones and loudspeakers and for the use of the audiometer and the sound level meter. Excellent discussions are given of methods for the determination of frequency, the steady-state and transient analysis of sound, articulation tests and the response of systems to noise. Proper emphasis is placed on the importance of devising testing and evaluation methods applicable to a complete acoustical system, and not merely for the measurement of certain components. The work has a fine historical introduction and is to be commended for its clear presentation of recent agreements in the difficult matter of terminology.

Workers in this field will be grateful for the inclusion of a considerable amount of basic acoustical theory needed for a thorough understanding of measurement techniques. There are sections on the attenuation of sound in air under a variety of conditions. Mention is made of the attenuation of sound in water, but here one wishes that more adequate notice had been given of the recent work, both theoretical and experimental, of Eckart and Lieberman relating to Stokes absorption, compressional viscosity effects, and attenuation in chemically active media. It is proper that the work of Eyring on the effects of temperature gradients in "jungle acoustics" is recorded and one can only wish that space had permitted similar mention of the related problems studied by Spitzer, Eckart and many others on the paths of sound waves in the sea. On pp. 103–05 it is gratifying to see reproduced the beautiful but almost completely unknown measurements on diffraction made during the war at Orlando, Florida by the Underwater Sound Reference Laboratories.

Chapter 4 is an excellent piece of writing. Here the reciprocity method of calibration is explained in complete detail. This section of the book should banish any lingering doubts in the minds of workers in acoustics that the reciprocity principle is the primary technique for acoustical calibrations. It includes the important wartime developments in this field not only in air acoustics, but also in underwater sound. The book has a most scholarly treatment of both the Rayleigh disk and the thermophone. For the former the author not only gives a modernized theoretical discussion of this classic device, but also presents a concise summary of recent

British work with this standard, perhaps not generally available in this country. The discussion of the thermophone and especially the clear unraveling of the long controversy between the results obtained with this instrument and those found both by reciprocity and the Rayleigh disk is most enlightening. We are especially indebted to the author for making generally available the results of the beautiful experiments on the thermophone of Geffeken and Keibs.

The chapters dealing with the measurement of acoustic impedance and its relation to acoustical materials are very well done. Here Dr. Beranek writes of a field in which his own contributions have been outstanding. His work, together with that of Morse and Bolt, Hunt and many others, has now nearly if not quite brought this subject to the place where standard specifications and practice for architectural acoustics can be stated in terms of the acoustic impedance of materials rather than in the language of the pioneering days of acoustics.

Workers in all branches of acoustics are indebted to Dr. Beranek for this excellent book, and we may hope that he will be able to revise it as the art progresses so that it will remain an authoritative treatise. The Office of Naval Research is also to be complimented for wisdom and vision in providing support for such a worth while endeavor.

Robert S. Shankland
Case Institute of Technology

Practical Spectroscopy

By C. Candler. Pp. 190+iv, over 100 illustrations. Hilger and Watts Ltd., London, 1949. Price $6.10.

This book is essentially an expanded manual for use with the Hilger wave-length spectrometer, and as such it serves its purpose admirably. The wave-length spectrometer is a well-known and very versatile instrument: in its standard form with a constant deviation glass prism it is suited either for visual observation or for use with a photographic camera. The length of the visible spectrum from 4000 to 7000A is about three inches. With the help of various pieces of auxiliary equipment the instrument can be converted into a grating instrument, an ultraviolet monochromator, an infra-red spectrometer, or can be used with an interferometer or an echelon.

The author describes a considerable number of experiments that can be performed with the instrument which would be appropriate to an elementary laboratory course in spectroscopy or physical optics. The content is as follows: Chapter I. Measurement of wave-length, adjustment of instrument, visual and photographic measurements, lining up of the light source. Chapter II. Qualitative Spectrochemical Analysis: arc, spark, flame, examples. Chapter III. Quantitative Spectrochemical Analysis: visual estimates, photographic method with internal standard, microphotometer, with special emphasis on flame methods. Chapter IV. Absorption Spectra: spectrophotometers, visual and photographic techniques, applications to organic compounds and metallic ions. Chapter V. Infra-red: quartz, fluorite, rocksalt, sylvine prisms; sources; thermopiles and galvanometers; influence of slit width; organic compounds; residual rays. Chapter VI. Raman Spectra. Chapter VII. The Ultraviolet Monochromator. Chapter VIII. The Structure of Line Spectra. Chapter IX. Interferometers: Fabry Pérot etalon, adjustment and use, Lummer plate, echelon grating.

Each chapter contains a general discussion of principles and applications and specific short instructions for the experiments. The treatment is elementary and clear.

For someone interested in an elementary course in practical spectroscopy who has available only the wave-length spectrometer or a similar instrument, this book will be very useful and, in fact, practically indispensable.

According to the publisher's preface, however, this book is also intended to serve as an introduction to general spectroscopy, and as such it is open to a number of criticisms. Since the title is *Practical Spectroscopy*, one might expect it to provide the reader with a general idea of the methods now in use by practical spectroscopists, as apart from what can be accomplished with the use of the Hilger wave-length spectrometer. So long as Mr. Candler confines himself to this one instrument, his treatment is good and convincing. But when he goes beyond these limits, there are some omissions and misleading statements which might leave the student with a wrong impression of the more general aspects of the subject. A few examples may serve to illustrate this. For absorption photometry the visual and photographic methods are treated. The first is of very limited use only, the second cumbersome and not very accurate. Nothing is said in this chapter of the photoelectric spectophotometer which at least in the United States can now be found in every laboratory where absorption measurements are made. Some mention of the photoelectric spectrophotometer would have been particularly easy, since the foundation for it is laid in Chapter VII.

The advances that have been made with infra-red receivers, notably the lead sulfide cell, have revolutionized and simplified the technique in the near infra-red and have made it possible to use many instruments in this region with increased accuracy and sensitivity. One would expect to find some mention of this method in a book published in 1949, but there is none.

At meetings of spectroscopists in this country during the thirties, there were frequent and often quite heated discussions as to the relative merits of grating and prism spectrographs. The arguments were not always marked by great objectivity, but they gradually subsided with the realization that well-designed instruments of either kind are quite equivalent in performance, provided that they have the same resolving power, dispersion and speed, and that the relative advantages and disadvantages are dictated by convenience rather than by any fundamental differences. A statement such as the following by Mr. Candler is, therefore, very surprising: "A major fault of the grating is the low intensity of the spectra produced, in round figures a grating needs an exposure 60 times as long as a prism.—A weak source, such as a helium lamp, produces hardly any lines which are visible, and when the spectrum is photographed the exposure may well stretch to 8 hours." He states further that when a grating is used the necessary exposure times in the photographic infra-red become impossibly long. In general, nothing could be further from the truth. It is, of course, quite possible that Mr. Candler's grating had these properties. If so, he should have thrown it away and obtained a better one.

The chapter on the structure of line spectra also contains some misleading statements. The width of a spectrum line is not usually determined by the Doppler effect as stated on page 160. In all the commonly used light sources, such as arcs, sparks, and ordinary discharge tubes, the width of the line is controlled by pressure or resonance broadening. The mechanism of self-reversal is, therefore, not the one given by the author. On the next page (161) one finds the statement: "Only lines which arise in transitions ending in the ground term appear self-reversed." Anyone can convince himself without too much difficulty that all strong lines, no matter on what state they end, may appear self-reversed.

Shortcomings such as these do not seriously impair the usefulness of the book as a manual for the wave-length spectrometer. They would, however, be serious pitfalls in an introduction to general spectroscopy for the beginning student or for the inexperienced science teacher who would rely chiefly on the information contained in this book.

G. H. Dieke
Johns Hopkins University

Infrared Determination of Organic Structures

By H. M. Randall, R. G. Fowler, N. Fuson, and J. R. Dangl. Pp. 239+v, profusely illustrated. D. Van Nostrand Company, Inc., New York, 1949. Price $10.00.

The title of this book is somewhat misleading in the sense that the work deals largely with related compounds of but one class.

This limitation is pointed out in the preface: ". . . the authors formed one of the . . . research groups . . . whose objective was to determine the structure of penicillin. . . . In order to become sufficiently oriented for effective work, it was necessary to study spectra of many compounds, not all directly related to the penicillin molecule in structure, but largely all of [a] common family. . . . Because of this trend in the choice of compounds, no claim is made to a complete treatment of the present status of infra-red spectroscopy, *even in its application to molecular structure.*" (Reviewer's italics.)

Chapter I is a short account of the application of infra-red spectroscopy to chemical analysis. The reviewer was surprised to find the unqualified intimation that optical isomers could be identified by usual infra-red techniques. The discussions of the interpretation and recognition of specific structure groups in Chapter II are largely confined to the functional groups of acids and acid derivatives (amides, imides). The treatment for these groups is empirical and based on a large number of compounds; here is given a detailed account of the position of the absorption maxima to be expected from the carbonyl ($C=O$) group when it is flanked by OH, OC, or NH groups. The phenyl group and conjugation effects, in general, are also treated.

Chapters III and IV contain most of the meat of the book. Here are included a chart of positions of absorption regions for various structure groupings causing the absorption, a detailed table (over 600 entries) of various groups which cause absorption in the "double bond" region (4.8–6.9 microns) and a catalog of absorbing groups occurring in 135 "theoretically analyzed" molecules. Chapter V cites several specific (practice) examples of the application of the infra-red method to qualitative analysis. Chapter VI on "Instruments and Experimental Techniques" confines itself largely to a very detailed description and performance characteristics of the University of Michigan spectrometers which were used to obtain the spectra reproduced in Chapter VII. In this last chapter (VII) are presented the spectra (original records) of 355 compounds. It is unfortunate that no indication of purity is given for any. About 200 of the compounds are acid and acid derivatives, the remainder are spread among alcohols, ketones, ethers, organic salts, thiazoles, and miscellaneous.

An error of fact has been pointed out to the reviewer by R. A. Friedel and D. S. McKinney. The spectra for liquid morpholine (Plate 257) is actually that for liquid nitromethane (Plate 247). Thus the discussion (p. 7) of hydrogen bonding in morpholine based on Plate 257 is not applicable.

Related to the restriction of the discussions to "amide type" compounds is the further restriction of the text to that portion of the spectrum between 2.8 and 7.8 microns. In view of the trend (by spectroscopists) in reporting measurements as frequencies (wave numbers), it is encouraging to find that, while wave-lengths are used exclusively in the text, the important tables do have both the frequencies and wave-lengths entered.

The book itself is quite handsome, made of high quality paper and the print is large and clear. The content should be very useful to those working with the class of compounds described here and to a larger group for the catalog of spectra of the 355 compounds.

Raymond L. Arnett
American Petroleum Institute

Theory of Oscillations

By A. A. Andronow and C. E. Chaikin. Pp. 358+ix, Figs. 313. Princeton University Press, Princeton, New Jersey, 1949. Price $7.50.

This is an introductory text to what is commonly known as non-linear mechanics. The original, of which this is an abbreviated version, appeared in Russian in 1937. Translation and editing was done by a group directed by S. Lefschetz in Princeton. The authors of this volume are outstanding members of the Moscow Institute of Oscillations founded by Mandelstam in the early 1930's. The American public has become familiarized with the now famous work in mathematical physics of this school by the well-known treatise of Minorski.

The book will greatly appeal and can most heartily be commended to all those who wish to become familiar with non-linear mechanics, but do not care to be burdened with very elaborate analytical machinery. The mathematical tools have been carefully limited; they go nowhere beyond calculus of real variables and some simple theorems in ordinary differential equations. The book does not presuppose much knowledge of conventional mechanics of linear system, rather it builds the subject up from the beginning by means of an approach adapted to the later developments. The general principles are introduced at a leisurely pace and each step is illustrated by several concrete examples that are always analyzed in detail and are profusely illustrated. As a consequence of this, relatively little space is taken up in the book by the general theorems and their proofs, but this in no way diminishes continuity and logical organization. The methods are mostly those of analytical geometry that aim at finding graphically the trajectories of the system. Only the last chapter, IX, is devoted to some purely analytical methods. Most research on non-linear oscillations has been on systems of one degree of freedom, and so the book and its technique is restricted to these, with the notable exception of coupled relaxation oscillations (flip-flop circuits) which also can be treated by the standard methods developed. The exposition culminates (Chapter V) in the theorem, due mainly to Poincaré, that the only steady regimes of systems of one degree of freedom are equilibria (stationary currents) or limit cycles (self-sustained oscillations) and the main objective of the analysis is the development of criteria for the existence and stability of these particular solutions. The practical examples taken from pure mechanics are few and not the most significant; but the fundamental types of non-linear electric oscillations are thoroughly covered, including grid-tuned oscillators, arcs, multivibrators, trigger circuits, parasitic oscillations in generators, and others.

Given the broad nature of the treatment, the matter covered inevitably had to be limited. The major restriction is that to systems called "autonomous," i.e., the omission of all forced oscillations, non-linear resonance, etc. The editor's preface states, moreover, that a great simplification of the original has been achieved by cutting out most of the general analytical theory while retaining the examples. The result is gratifying and attractive. Furthermore, one never has the feeling that the mathematical authors "talk down" to the engineer or are not conversant with the somewhat more practical aspects of circuitry. The book would have gained by the inclusion of an up-to-date selected bibliography, replacing the rather poor "reading list" given; this seems to be the only major flaw of an otherwise consistently excellent job of the American editors. Might some economy in the illustrations have substantially reduced the price of the book?

W. M. Elsasser
University of Pennsylvania

Elementary Modern Physics

By Gordon Ferrie Hull. Pp. 503+xvi, Figs. 243. The Macmillan Company, New York, 1949. Price $4.25.

Elementary Modern Physics, a revision of *An Elementary Survey of Modern Physics*, has an all-inclusive title which allows the author to range widely over the developments of the last 60 years. The historical method is used in which discoveries are traced chronologically from the early experiments. No chance is missed to emphasize the drama of the action which is done even in the style of a reporter, especially in connection with the work in which the author had a hand. This makes for some interesting reading. In addition to atomic and nuclear physics there is an extensive chapter leading to the modern developments in electronics which include military applications to radar and the proximity fuse. Another application of wartime developments is a stimulating account of cosmic-ray experiments with VII rockets.

Subjects are discussed from several points of view with stress on the fundamental idea, thereby giving the students a broad understanding. The ideas are illustrated by up-to-date examples from the student's experience or by simple situations which he can visualize. A can of molecules is thrown off a cliff. The random motion is not increased until they hit the bottom. The Edison effect is illustrated by an experiment with a 50-watt lamp. In discussing a subject the author does not lose sight of other topics with which it is connected or which obey similar laws. The equation $I = I_0e^{-\lambda t}$ applies to light, radioactivity, and the law of atmospheres. The author has given considerable thought to simple derivations. Some of these derivations are admittedly crude but stress the possibility of their being understood rather than the rigor they achieve. The more complicated ones are relegated to appendices. Many equations are stated without derivation, an unfortunate situation that faces any author of an elementary modern physics text but one about which he must make his own compromise.

The historical approach and emphasis on the broad connections of the subject also have their pitfalls. In trying to analyze the confusing picture that certain developments leave in the mind of the reader, it seems as though the author with his vast background and experience has a tendency to include many sidelights, related items, and links with other phenomena which interrupt the argument and confuse the issue for the uninitiated. For example, into the middle of a section on the scattering cross section for neutrons are put three lines on the scattering cross section for electrons. More continuity could be gained by finishing up one topic without interrupting the train of thought and then comparing it with other phenomena after the first point has been thoroughly grasped.

A second confusing feature of the broad historical approach is that it leaves the reader wondering what exactly is accepted gospel at present and what is apocryphal. The present status of the ether is vague as is also the value of h. For the student of 1950 with a crowded curriculum, it is a question of whether pumpkins and parabolas are worth the time their discussion requires, even if it makes a fascinating story of the structure of the atom and the measurement of its mass. Elliptic orbits, Bragg x-ray doublets, hydrogen introduced through the walls of x-ray tubes, and Maxwell's distribution of electron velocities in metals are among the delicacies offered to titilate the intellectual appetite, whose omission would cause no undernourishment of the mind. The chronological presentation is cluttered up with historical errors in the pursuit of knowledge.

Elementary Modern Physics by Gordon Ferrie Hull with its many interesting illustrations from the experience of the author will be of most use to those interested in the historical approach to modern physics.

C. W. UFFORD
University of Pennsylvania

Ionization Chambers and Counters

BY BRUNO B. ROSSI AND HANS H. STAUB. National Nuclear Energy Series. Pp. 243+xviii, Figs. 113. McGraw-Hill Book Company, Inc., New York, 1949. Price $2.25.

At the end of the war the Manhattan Project and Atomic Energy Commission laid plans for the writing of no less than 60 volumes of declassified technical material for publication. This huge work was to make available as much as possible of the specialized scientific knowledge gained in the numerous laboratories concerned with the wartime development of atomic energy. While the intentions are still good, the writing has evidently progressed slowly, as might have been expected, knowing how anxious most of the scientists were to turn their minds to other kinds of work, and knowing the tediousness of the declassification process. The amount of effort involved in the latter process is indicated by the display of prefaces and forewords in the volume we are about to discuss—seven in all. But whatever the effort required, the authors of these books perform an extremely valuable service in making knowledge available which would otherwise have to be rediscovered at the cost of much time and money. *Ionization Chambers and Counters: Experimental Techniques* by Bruno Rossi and Hans H. Staub has just been published as one of a set of three volumes on experimental techniques. Of the two others, *Electronics* by Elmore and Sands, and *Miscellaneous Physical and Chemical Techniques* by Graves *et al.*, the first has appeared and the second is to appear during the coming year.

Ionization Chambers and Counters should perhaps have been titled *Ionization Chambers and Proportional Counters*, to be more accurately descriptive of its content. The first three chapters (71 pages) give a thorough treatment of the problem of ion production and collection in ionization chambers when there is no multiplication by collision. The theoretical derivations of the drift of electrons and ions through gases under an electric field are followed by numerous experimental curves of the drift velocities, mean agitation energies and electron attachment in the particular gases and mixtures of gases which are of interest in fast ionization chamber work. The next part of the discussion leads into the consideration of the time variation of the ionization chamber current under the condition of transient or pulsed ionization, which is of course the condition which is of most interest when individual particles are to be counted. Here, again, experimental curves and data are given which have been obtained at Los Alamos and at other laboratories.

Following the discussion of ion collection a chapter (28 pages) is devoted to gas multiplication, consisting mostly of the presentation and discussion of experimental curves and data. A number of different gases and gas mixtures, and different geometrical conditions, are considered, with attention paid to transient effects. Many of the data will be new to those who were not members of the wartime project. In the remaining 140 pages the application of the ionization chamber and proportional counter to special problems—alpha-, beta-, gamma-, and fission counting—is taken up. Drawings of a great many of the counters which were built in the Manhattan Project laboratories are reproduced, together with experimental data on their performance. The volume is replete with practical drawings, curves, and data, and should prove to be of great value to all who are working with ionization chambers and proportional counters.

H. R. CRANE
University of Michigan

Elements of Sound Recording

BY JOHN G. FRAYNE AND HALLEY WOLFE. Pp. 686+vii, profusely illustrated. John Wiley and Sons, Inc., New York, 1949. Price $8.50.

The authors have, in their own words, directed their efforts "to writing a book that will give useful information on basic sound problems to the practical designer, operating engineer, or technician," a book that will be "useful to the practising sound engineer as well as the student in college or vocational school." In one sense, their efforts have been extremely successful: the resulting volume should serve as an excellent text for students of engineering who wish to learn the details of sound recording theory and practice, with particular emphasis on film recording. For the practising sound engineer, this book will prove useful in many ways, although the well-informed engineer in this field should already be familiar with much of the material included. It will still serve him as a convenient compilation of the current literature in his field. The physicist will find this volume an impressive account of intricate engineering problems and the ingenuity with which they have been solved.

The first 12 chapters provide the student with a speaking acquaintance with the tools of the craft: sound waves and hearing, electronic components and circuits, recording systems, and electrical measurements. It might be argued that the material presented in these chapters is already available in standard journals, texts, and handbooks, but the student will be grateful to the authors for providing so useful and brief a compilation and for their careful documentation of original sources. The utility of the material to the student is enhanced by the inclusion of numerical examples to illustrate the application of various design formulas.

Despite their brevity, the chapters on disk and magnetic recording are reasonably comprehensive, and a considerable number of references are provided from which the student may obtain more detailed information. It is perhaps unfortunate that these references do not include any of the several bibliographies currently available in these fields [Alfred Jorysz, "Bibliography of Disk Recording," Tele Tech (June, 1947). N. M. Haynes, "Bibliography of Magnetic Recording," Audio Engineering (October, 1947)], but the references provided are probably adequate for the authors' immediate purposes.

The degree of specialization of this text may be deduced from the relative number of chapters devoted to each of the several recording media: disk recording is treated, for the most part, in two chapters, and magnetic recording in one chapter, while film recording methods and systems provide material for the greater part of fourteen chapters. The less specialized reader may find this degree of emphasis on film recording somewhat unexpected, but it is amply justified by the authors' professional experience and by the circumstances under which the material was originally compiled. Over a period of years, the authors have been intimately connected with the film industry and its problems, to the solution of which they have made outstanding personal contributions.

The treatment of film recording is comprehensive and carefully documented. Five chapters are devoted to a discussion of the principles and techniques of variable-density and variable-area recording. Measurement techniques, drive mechanisms, production processes, and reproducing systems are the subjects of other chapters, some of which are applicable to disk and magnetic recordings as well as to film. The authors conclude with brief but useful discussions of loudspeakers, room acoustics, and stereophonic recording.

Engineers engaged in sound recording will welcome this volume as a survey of current practice and literature, while the student of sound engineering should find it a helpful and stimulating guide.

John A. Kessler
Massachusetts Institute of Technology

Histopathology of Irradiation from External and Internal Sources

By William Bloom. Pp. 808, Figs. 516. McGraw-Hill Book Company, Inc., New York, 1948. Price $8.00.

This book is a systematic study of the effects of radioactive elements administered to animals, as compared to the well-known effects of x-ray treatment. The lesions due to radioactive bombardment are illustrated by hundreds of remarkable photographs, while numerous autoradiographs make it possible to visualize the localization of the radio-element. Knowing the sites of origin of the radioactive particles, it becomes possible to deduce whether the lesions are the results of a local bombardment rather than a generalized, unspecific effect. Besides this ambitious aim, the authors had the more practical purpose of recognizing the type of lesions due to radio-elements with the view of eventually giving them medical attention, since the work was started during the war at a time when the possibility of an atomic war was looming in the near future.

The authors set out to achieve these goals by a considerable series of experiments. The immediate goal of describing the pathology of the organs is very well done. It is apparent from the outset that the director of the group responsible for this work is an histologist. He is, in fact, the author of the well-known textbook of histology: Maximow and Bloom. After a chapter on the cell, the various organs of the body are examined, one by one, and their response to the various radioactive agents is thoroughly described. Thus, the skin was found to be greatly damaged by external applications of radio-elements but not by internal treatment. The hemoietic organs and gastro-intestinal tract, which are very sensitive to both, showed lesions which are remarkably well illustrated in this book. The chapters on kidney, vascular system and nervous system are among the most original of the volume.

The authors used considerable restraint in the interpretations of the results, a fact which may be somewhat disappointing, in view of the excellent material available. Often, the possible physiological and pharmacological significance of the autographic pictures is not mentioned. Of course, the rather crude autographic method, which had to be used because of the urgency of the work, often made it difficult to assign a precise localization to the radio-elements. Lacking this knowledge, many of the lesions could not be interpreted.

The summary is devoted to the fundamental mechanisms playing a role in the action of radiation on living tissues. Thus, it was emphasized that the effects of irradiation are not unlike those of intoxication with mustard gas and other damaging agents. Furthermore, there were no qualitative differences in the reaction of animals to comparable doses of x-rays, gamma-rays, fast and slow neutrons and (for the skin) external beta-rays. These various agents at approximately the $LD_{50}/30$ days cannot be differentiated on the basis of their histological effects. Furthermore, the main difference between radiation from internal and external sources lies in the fact that internal radiation will usually be more prolonged.

In addition, the effects tended to be more localized when the short-ranged alpha-particles were used, while rather diffused responses were obtained with beta-emitters. This is partly due to the fact that the biological beta-emitters, such as Na_{24}, C_{14} and P_{32}, are fairly widely disseminated in the body. Therefore, the effects of such substances will be quite similar to those of an external source, irradiating the whole body.

At the other extreme are a few isotopes, such as $Ba_{140} - La_{140}$, Sr_{89}, Y_{11} and Ra_{229} which produce obvious damage only to those radio-sensitive organs in which they localize.

A stimulating discussion of radio resistance and the causes of radio-sensitivity (primitiveness of cells, mitosis, acquired resistance, etc.) supplies many new points of view on the matter.

Presumably, much of the future work on the subject will be inspired by this book. As it is, it is indispensable, not only to those concerned with the damaging effects of radio-elements, but also to those who are applying radio-elements to the solution of physiological problems and must constantly be careful to avoid the use of harmful doses.

C. P. Leblond
McGill University

Author Index to Books Received

Andronow, A. A. and C. E. Chaikin—*Theory of Oscillations* 389
Beranek, Leo L.—*Acoustic Measurements* 387
Bergmann, Peter G.—*Basic Theories of Physics: Mechanics and Electrodynamics* 383
Berkeley, Edmund C.—*Giant Brains, or Machines That Think* 385
Bloom, William—*Histopathology of Irradiation from External and Internal Sources* 391
Bonney, E. A.—*Engineering Supersonic Aerodynamics* 384
Candler, C.—*Practical Spectroscopy* 388
Chaikin, C. E.—see Andronow, A. A. 389
Dangl, J. R.—see Randall, H. M 388
Del Mar, W. A.—see Pender, H. 387
Dieke, G. H. and A. B. F. Duncan—*Spectroscopic Properties of Uranium Compounds* 386
Don Leet, L.—*Earth Waves* 385
Duncan, A. B. F.—see Dieke, G. H 386
Fowler, R. G.—see Randall, H. M 388
Frayne, J. G. and H. Wolfe—*Elements of Sound Recording* 390
Fusion, N.—see Randall, H. M 388
Garlick, G. F. J.—*Luminescent Materials* 386
Gatterer, A. and J. Junkes—*Spectra of the Rare Metals and Some Metalloids* 384
Guthrie, A. and R. K. Wakerling—*Vacuum Equipment and Techniques* 381
Hull, G. F.—*Elementary Modern Physics* 389
Junkes, J.—see Gatterer, A. 384
Le Corbeiller, P.—*Matrix Analysis of Electric Networks* . 381
Leverenz, H. W.—*An Introduction to the Luminescence of Solids* 382
Pender, H. and W. A. Del Mar—*Electrical Engineers' Handbook of Electric Power* 387
Randall, H. M., R. G. Fowler, N. Fusion, and J. R. Dangl—*Infrared Determination of Organic Structures* . . 388
Rossi, B. B. and H. H. Staub—*Ionization Chambers and Counters* 390
Smith, R. A.—*Aerials for Metre and Decimetre Wave-Lengths* 383
Staub, H. H.—see Rossi, B. B 390
Valasek, Joseph—*Introduction to Theoretical and Experimental Optics* 386
Wakerling, R. K.—see Guthrie, A 381
Wolfe, H.—see Frayne, J. G 390

Other Books Received

Electromagnetic Theory (Proceedings of Symposia in Applied Mathematics, Vol. 2), Pp. 91. American Mathematical Society, New York, 1950. Price $3.00.

Introduction to the Theory of Probability and Statistics. N. Arley and K. R. Buch. Pp. 236+xi, Figs. 21. John Wiley and Sons, Inc., New York, 1950. Price $4.00.

The Meaning of Relativity. Albert Einstein. Pp. 150. Princeton University Press, Princeton, New Jersey, 1950. Price $2.50.

Electronics: Experimental Techniques. W. C. Elmore and M. L. Sands. Pp. 417, Figs. 182. McGraw-Hill Book Company, Inc., New York, 1949. Price $3.75.

The Characteristics of Electrical Discharges. Edited by A. Guthrie and R. K. Wakerling. Pp. 376, Figs. 234. McGraw-Hill Book Company, Inc., New York. 1949. Price $3.50.

Electronics in Engineering. W. R. Hill. Pp. 274, Figs. 205. McGraw-Hill Book Company, Inc., New York, 1949. Price $3.50.

Physiology of the Eye, Vol. 1—Optics. Arthur Linksz. Pp. 334+xii, Figs. 137. Grune and Stratton, Inc., New York, 1950. Price $7.50.

Piezoelectric Crystals and Their Application to Ultrasonics. Warren P. Mason. Pp. 508+xi, Figs. 203. D. Van Nostrand Company, Inc., New York, 1950. Price $7.50.

The Physical World. Paul McCorkle. Pp. 450+vii, Figs. 291. The Blakiston Company, Philadelphia, 1950. Price $4.25.

Physical Principles of Oil Production. Morris Muskat. Pp. 922, profusely illustrated. McGraw-Hill Book Company, Inc., New York, 1949. Price $5.00.

Albert Einstein: Philosopher-Scientist. Edited by P. A. Schilpp. Pp. 781+xvi. Library of Living Philosophers, Northwestern University, Evanston, Illinois, 1949. Price $8.50.

The Transuranium Elements (2 parts). G. T. Seaborg, J. J. Katz, and W. M. Manning. Pp. 1529, numerous figures. McGraw-Hill Book Company, Inc., New York, 1949. Price $15.00.

Electron-Tube Circuits. Samuel Seely. Pp. 529+ix, Figs. 469. McGraw-Hill Book Company, Inc., New York, 1950. Price $6.00.

Trilinear Chart of Nuclear Species. William H. Sullivan, John Wiley and Sons, Inc., New York, 1949. Price $2.50.

Lehrbuch der Theoretischen Physik. Walter Weizel. Pp. 771, Figs. 270. Springer-Verlag, Berlin, 1949.

Der Ultraschall. L. Bergmann. Pp. 748, Figs. 460. L. Hirzel Verlag Zurich, 1949.

Quantitative Ultramicroanalysis. Paul L. Kirk. Pp. 310+vii, Figs. 113. John Wiley and Sons, Inc., New York, 1950. Price $5.00.

Laboratory and Shop Notes

Tungsten Helical Spring Balance

Samuel L. Madorsky
National Bureau of Standards, Washington, D. C.

November 15, 1949

A SIMPLE tungsten helical spring balance has been developed in connection with a study of rates of thermal decomposition of polymers in a vacuum. This balance was designed for a range 0 to 100 mg, exclusive of a platinum bucket weighing 368.3 mg. It was found to give reproducible results within ±2μ of elongation of the spring which is equivalent to about ±0.013 mg of weight. Previously quartz springs have been used in connection with vacuum work; for example, in the McBain-Bakr sorption balance.[1] However, quartz springs are very fragile and involve loss of time in calibration due to frequent breakage.

A diagrammatic view of the tungsten spring balance is shown in Fig. 1. The spring *A* is made from 3-mil annealed tungsten wire and consists of 45 turns, each turn having an outside diameter of 6 mm. The total weight of the spring including extensions at both ends is about 100 mg. The spring is enclosed in a Pyrex tube and is suspended from a Pyrex rod attached to a ball joint at the top of the tube. The ball joint serves to center the spring in the Pyrex tube *H*. A platinum crucible *G*, weighing 368.2 mg, is suspended from the lower extension of the spring. The spring proper, when hanging free, i.e., without the crucible, is 4 cm long, but with the crucible suspended from it, it is 9.5 cm long. Friction clasps, *B*, serve to hold the spring in place and stretched to its normal length (9.5 cm) when the balance is moved around or when the crucible is removed. The clasps consist of two small brass plates, B^1, padded on the surfaces facing the tungsten wire with thin sheets of rubber. The clasps are attached to brass rods held rigidly in ball joints *C* by means of hard Apiezon wax. By keeping the clasps in a vertical position and sliding the ball joints in opposite directions in a horizontal plane, the spring can be either clasped or released. Crossline *E* consists of 1-mil phosphor bronze wire held to the tungsten extension wire by means of a drop of hard Apiezon wax. The lower part of the glass housing, *K*, is held to the upper part, *H*, by means of a waxed ground joint *F*. A sensitive cathetometer reading to 1μ and provided with a microscope capable of moving in a vertical and horizontal direction was used in connection with the tungsten spring balance.

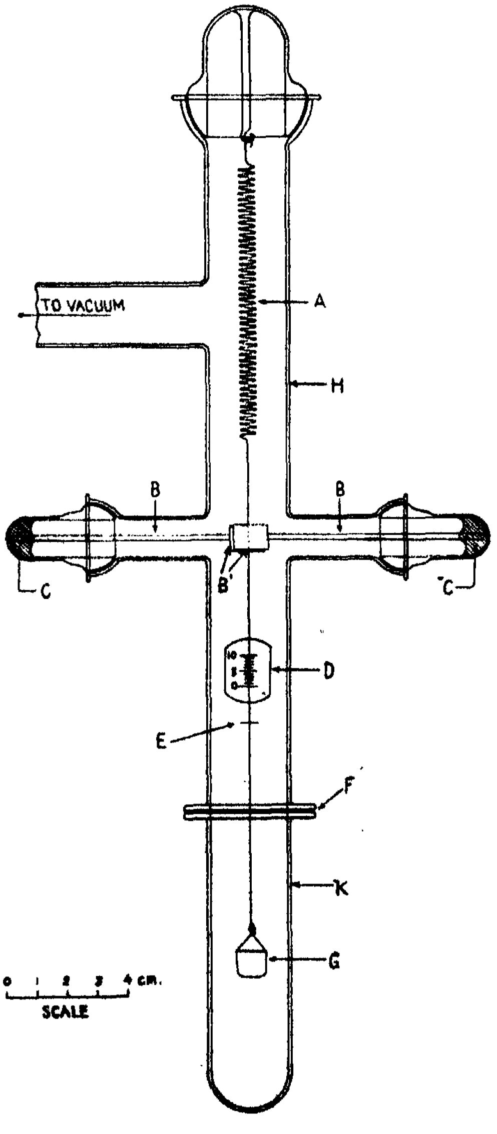

FIG. 1. Tungsten helical spring balance.

Unless the balance is operated in a constant temperature room, the problem of the effect of temperature changes on the tungsten spring balance requires careful consideration. A maximum variation of 10°C will be assumed in this discussion. This variation will affect, in the first place, the rigidity of the spring. The thermal coefficient of modulus of rigidity of tungsten is -6.6×10^{-6} per 1°C.[2] For a 10° change the modulus will change by -6.6×10^{-4}, i.e., by about 0.07 percent, which is negligible. The problem of thermal expansion is more complicated. Here the thermal effect not only on the spring but on the housing of the spring, if the balance is to be used in a vacuum, and on the cathetometer, should be considered. The most suitable material for construction of a housing for the spring is Pyrex glass. It so happens that the linear coefficient of expansion of Pyrex is about the same as that of tungsten:

Tungsten	4.3×10^{-6} per °C[3]
Pyrex	3.6×10^{-6} per °C.[4]

In view of this the position of the crossline *E* will not change appreciably with respect to any reference point on the glass tube *H* because of thermal expansion. However, differences in the linear thermal expansion of the cathetometer and balance housing supports will affect the position of crossline *E* on the tungsten spring with respect to the cross hair in the cathetometer and will introduce appreciable errors in the readings. This source of error is eliminated in this balance by fastening a micro-scale *D* to the inside of the glass tube *H* back of the tungsten extension wire at about the level of the crossline *E*, with the crucible suspended from the spring. This scale is made of glass and consists of 1 cm divided into 0.1-mm unit. By measuring the vertical distance of the crossline *E* to some point on the scale *D* before or after reading the position of this crossline with respect to the cross hair and scale of the cathetometer, any error due to thermal expansion of the cathetometer and balance housing supports will be reduced. The microscope can be focused alternately on the scale *D* or on the crossline *E*.

In order to determine the amount of elongation of the spring per unit weight, calibrated weights of 25, 35, 50, 70, and 100 mg were placed in the platinum crucible and the elongation was noted in each case after 5 min. from the time the weight was put on and after 24 hours. Elongation in microns per mg, on the 5-min readings, varied from 152μ for the 25-mg weight to 151μ for the 100-mg weight. The additional elongation, or elastic creep, during the interval between 5 min. and 24 hours after the start of weighing, was 0.4 percent of the original elongation. Beyond the 24-hour period the creep was very small.

A suspended spring is sensitive to all kinds of vibrations which will interfere with the reading of a reference point on it. In a vacuum the only damping force is the internal friction or viscosity of the material of the spring. In this respect, tungsten with a coefficient of internal viscosity of about 10^{10} poises is by far superior to fused quartz with a coefficient of internal viscosity of only about 10^{6} poises. In a test in a vacuum of about 10^{-6} mm of Hg, the tungsten spring came to rest, after disturbance, in about 10–20 min., while a similar quartz spring, under similar conditions, continued to swing for several hours.

---

[1] J. W. McBain and A. M. Bakr, *J. Am. Chem. Soc.* **48**, 690 (1926).

[2] W. G. Brombacher, Rev. Sci. Inst. 4, 688 (1933).

[3] Charles D. Hodgman and Harry N. Holmes, ***Handbook of Chemistry and Physics*** (Chemical Rubber Publication Company, Cleveland, 1941–2), p. 1650.

[4] See reference 3, p. 1651.

A New Porcelain Rod Leak

H. D. Hagstrum and H. W. Weinhart
Bell Telephone Laboratories, Murray Hill, New Jersey

March 6, 1950

FOR a number of years we have been using in this laboratory a porcelain leak of the type first described by Smythe.[1] As shown at (A) in Fig. 1 it is made entirely of glass and porcelain and incorporates the side mercury by-pass tube, suggested by Bazzoni,[2] for indicating the mercury level inside the porcelain tube. We have found it an excellent leak for our purposes but at best a difficult one to make. The main difficulty arises in the necessity of shrinking the glass into intimate contact with the porcelain tube over the lengths demanded for a reasonably slow leak.

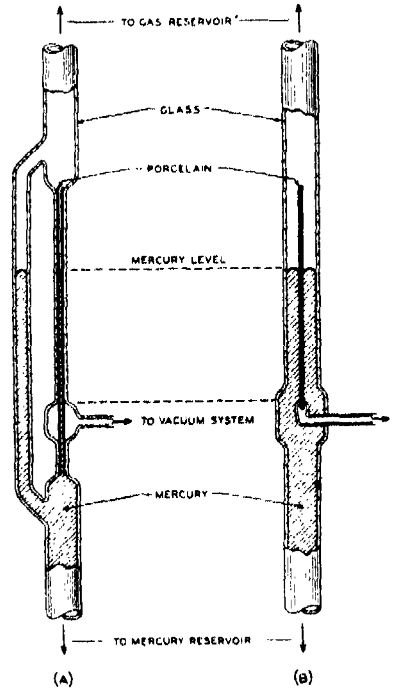

FIG. 1.

The purpose of this note is to present a new form of porcelain leak, shown at (B) in the figure, which, although its principle of operation is the same as the old, possesses several advantages over the old. Here the porous member through which the gas leaks is in the form of a rod rather than a tube.[3] The mercury column surrounds the rod as shown. The leak may be shut off by raising the mercury above the top end of the porcelain and the leak rate increased by increasing the distance of the mercury level below the top of the porcelain as before.

The advantages of this new arrangement are: (1) The glass need be wetted to the porcelain over only a very short length; (2) no side tubing is needed to indicate the mercury level; (3) the porcelain to glass seal is not exposed to the outside thus making it less likely that the seal will crack due to thermal shock if the leak is torched; (4) the glass connection to the vacuum system, which may be subject to strain, here connects to the glass wall of a strong tube and thus cannot transmit strain to the porcelain-glass seal as in the old form. There thus appears to be definite advantages both as regards fabrication and use of the new leak. The rod leak has been used with gas reservoirs filled to 400-mm pressure.

---

[1] W. R. Smythe, Rev. Sci. Inst. 7, 435 (1936).

[2] C. B. Bazzoni, Rev. Sci. Inst. 8, 171 (1937).

[3] The rod used in this leak is No. 1646 standard refractory ceramic, 0.050 in.–0.060 in. in diameter and 5 in. long, obtained from Stupakoff Ceramic and Manufacturing Company, Latrobe, Pennsylvania. The porcelain is *sealed to a very short section of No. 542 Blue Glass which in turn is sealed to* the standard No. 774 EJ Pyrex.

Data on Porcelain Rod Leak

J. P. Molnar and C. D. Hartman
Bell Telephone Laboratories, Murray Hill, New Jersey

March 6, 1950

WE have found the porcelain rod type of leak described in the preceding note to work very satisfactorily in the arrangement shown in Fig. 1. The lower Y cut-off permits pumping out the connecting tubing between the gas bottle and leak before the break-off tip is shattered. The upper Y cut-off permits a sudden shut-off of gas flow from the leak. If the flow is shut off only by covering the porcelain rod completely with mercury, the gas which is still trapped in the rod will continue to flow for several minutes longer.

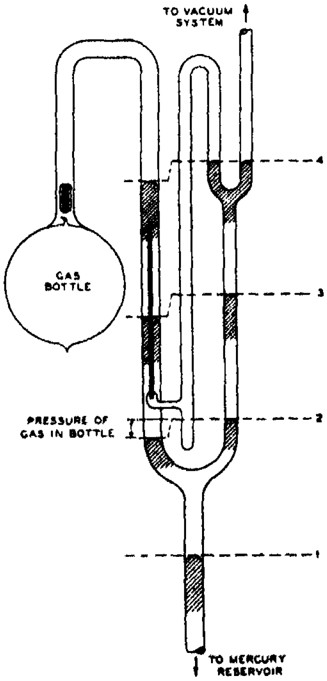

FIG. 1.

Four levels are indicated for the mercury column. The height of the mercury reservoir is so adjusted that when the reservoir is at atmospheric pressure the mercury column rises to level 2. During the bake-out and exhaust of the leak and connecting tube, the mercury is pumped down to level 1. When the leak is in use, pressure is applied to the reservoir (by means of a squeeze-bulb of the kind used in a physician's blood pressure-measuring equipment) to raise the mercury to some level as indicated by 3. Level 4 indicates the condition of cut-off. With this arrangement, if the applied pressure is inadvertently removed, say by a leak in a stopcock, the gas cannot be lost through the lower Y cut-off.

The resistance offered to gas flow by this leak is proportional to the length, l, of the porcelain rod wetted by the mercury and glass seal at the bottom of the rod. For a rod 0.055 in. in diameter we measured a leak rate of (1.0×10^{18}) p/l molecules per second for nitrogen gas, where l is expressed in cm and p is the pressure in millimeters of mercury in the gas bottle. (The pressure on the other end of the leak is, of course, negligible in comparison with p.) Our porcelain rods are 13.1 cm long (max. value of l), while the length of the glass seal is 0.33 cm (min. value of l). Thus we have a controllable range of 40 to 1 in leak rate with our units.

Rubber Tubing Pump*

John W. Weigl† and Donald W. Stallings
Radiation Laboratory, University of California, Berkeley, California

January 30, 1950

ALTHOUGH rubber tubing pumps appear to be used for gas circulation in a number of laboratories, it seems that each group has had to invent one for itself. For this reason, a brief description of a useful model is presented here.

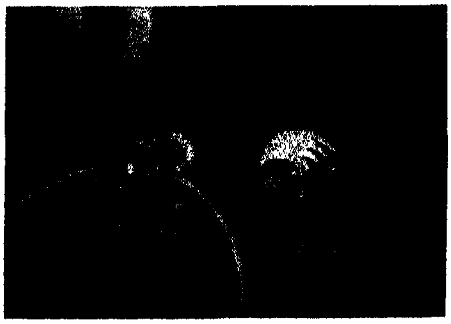

FIG. 1a.

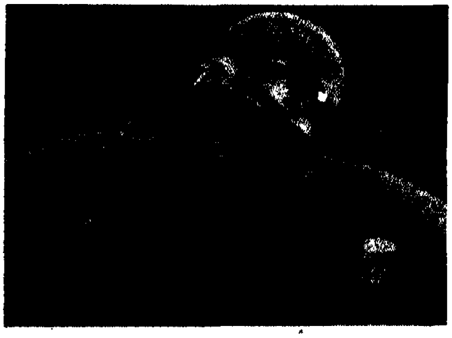

FIG. 1b.

Its mode of operation may be recognized from Fig. 1. One after another, the four rollers at the corners of the square rotor compress a piece of rubber suction tubing, pushing the gas ahead of them, each roller blocking a new gas pocket before the last has been lifted off. The speed may be controlled from about 100–1500 cc/min. by means of a set of step pulleys, as well as by adjustment of the hinged tubing race, and by changing the size of tubing used. If the rollers run smoothly, a piece of amber pure gum suction tubing outlasts between ten and thirty hours of operation.

The main virtues of this type of circulating pump are the smooth flow and negligible hold-up, the lack of metal parts and lubricant in contact with the gas, its rugged construction and ability to withstand evacuation without leakage around shafts and bearings. It may be used for pushing or re-cyling gas, or for the well-controlled evacuation of a closed system to less than one millimeter pressure.

---

* This work was supported by the United States AEC.

† Now at the University of Minnesota, Minneapolis, Minnesota.

Scintillation Counter for Neutrons

Kuan-Han Sun and W. E. Shoupp
Westinghouse Electric Corporation Research Laboratories, East Pittsburgh, Pennsylvania

January 30, 1950

DURING the development of the scintillation counter for α-, β- and γ-particles at these Laboratories, it was immediately apparent that the scintillation counter may be used for detecting neutrons in the same manner, though not with the same efficiency, as is used for α-particles provided that certain materials which intercept neutrons to yield energetically charged particles are introduced into the phosphor. The first qualitative test was carried out in April, 1947 by using a powdered mixture of Patterson D, ZnS phosphor and anhydrous B_2O_3 mixed in polystyrene dope and painted on a 931A photo-multiplier tube. The neutron pulses observed were about the same order as those of α-particles from uranium on the same phosphor. In the subsequent experiments, a powdered mixture of ThO_2 and ZnS phosphor, or $UO_2(NO_3)_2 6H_2O$ and ZnS phosphor painted on the surface of a 931A photo-multiplier tube was used to observe the scintillations due to fission by neutrons. The photo-multiplier was operated with a circuit similar to that used by Coltman.[1] Visual observation on an oscilloscope indicated that fission pulses due to fast neutrons from the cyclotron deuterons (15 Mev) on a thick Cu target, were several times higher than those due to α-particles from uranium, and somewhat higher than the highest pulses from proton recoils from the polystyrene

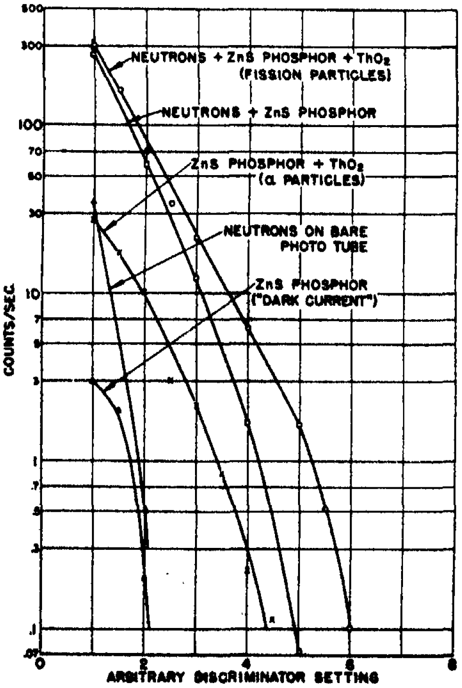

FIG. 1. Pulses from scintillation counter for fast neutrons.

dope and protons and α-particles produced in the phosphor (without fissionable components) by the fast neutrons. In observing fission pulses, it was found necessary to set the gain of the amplifier below the saturation limit. The gradual decrease of light transmission with increasing thickness of powdered phosphor, however, results in a continuous distribution of the pulses. These are shown in Fig. 1 which indicates that the number of counts decreases continuously with the raise of negative bias voltage or discriminator settings. Figure 1, however does reveal that (1) fission pulses can be distinguished from proton recoils or protons and α-particles formed due to fast neutrons on ZnS phosphor or carbon; (2) ZnS phosphor with hydrogeneous materials (polystyrene dope) also may be used for detecting fast neutrons. Knowing the number of α-counts per unit weight of ThO_2 used through other experiments, it was possible to deduce the "effective" weight of Th in the phosphor by measuring its total number of α-pulses. By assuming a fission cross section, 0.15 barn for Th by fast neutrons based on data by Ladenburg *et al.*[2] and Agens *et al.*,[3] it was found that the neutron flux at 181 cm in the forward direction from the Cu target by 15-Mev deuteron bombardment was 1.5×10^4 and 7.5×10^4 neutrons/cm²/sec./μa deuteron for arbitrary discriminator settings 3 to 1 respectively (Fig. 1). A corresponding value of the neutron flux deduced from the $S^{32}(n,p)P^{32}$ neutron threshold detector of a later date[4] gave 1×10^4/cm²/sec./μa deuterons. The agreement is favorable considering the complexities involved in the response of Th and S threshold detectors for various energies of fast neutrons and also in the different schemes of detection. The scintillation counter for detecting neutrons has low efficiency because of the poor light transmission of the powdered ZnS phosphors. The above work, however, indicates that a quantitative counter, perhaps using a thin layer of ZnS with U^{235} or Pu^{239}, may be constructed without any interference from background due to intense γ-rays, or other energetic charged particles.

The authors would like to express their appreciation to Dr. J. W. Coltman for his constructive criticisms and to Dr. A. J. Allen for the use of the University of Pittsburgh cyclotron.

---

[1] Marshall, Coltman, and Bennett, Rev. Sci. Inst. 19, 744 (1948).

[2] Ladenburg, Kanner, Barschall, and Van Voorhis, Phys. Rev. 56, 168 (1939).

[3] Ageno, Amaldi, Bocciarelli, Cacciapuoti, and Trabacchi, Phys. Rev. 60, 67 (1941).

[4] Allen, Nechaj, Sun, and Jennings, Phys. Rev. 76, 188, 463 (1949).

A Device for Measuring the High Voltage for a Photo-Multiplier Tube

INGVAR NILSSON
Laboratory for Nuclear Chemistry, Chalmers Institute of Technology, Göteborg, Sweden

February 13, 1950

WHEN using a photo-multiplier tube as a scintillation counter, it is necessary to hold the high voltage constant within 1 volt. This can be accomplished by using an electronic voltage regulator. It is, however, of great importance that the voltage can be measured with the same accuracy.

It is possible to construct a device fulfilling this requirement by comparing the unknown voltage with the voltage from a RCA 5651 voltage reference tube. This tube is guaranteed to hold the voltage constant within ±0.1 volt. By this method it is possible to subdivide the interesting interval, say 500–1000 volts, in intervals of for instance 100 volts, each interval giving full scale deflection on a meter. The error introduced by the uncertainty in the reference voltage will be of the order 0.1 percent, e.g., 1 volt at 1000 volts.

In order not to overload the meter, it is necessary to know the voltage approximately and to set the voltage selector for the meter at a correct position. This difficulty may be overcome by combining the selector with the voltage control.

The basic circuit is shown in Fig. 1. The values of the components R_1, R_2 and R_3 may be obtained from the equations

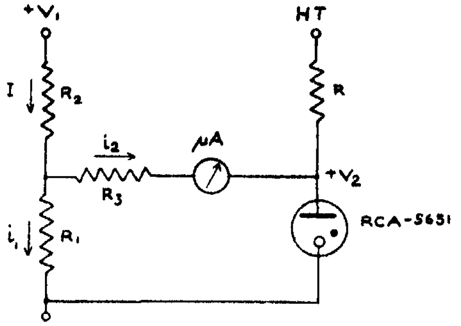

FIG. 1.

$$V_2=R_1i_1-R_3i_2 \qquad (1)$$

$$V_1=[R_2+R_3((R_2/R_1)+1)]i_2+V_2(1+(R_2/R_1)). \qquad (2)$$

In Eq. (1) R_1 may be chosen so that $i_2=0$. Then $R_1=V_2/i_1$, where i_1 is given a suitable value. The values of R_2 and R_3 are obtained from Eq. (2) by requiring that for a certain value of V_1 the meter should read zero, and for a voltage a certain amount higher the meter should have full scale deflection.

As an example a voltmeter using a 100 μa meter and covering the range 600–1100 volts is given in Fig. 2.

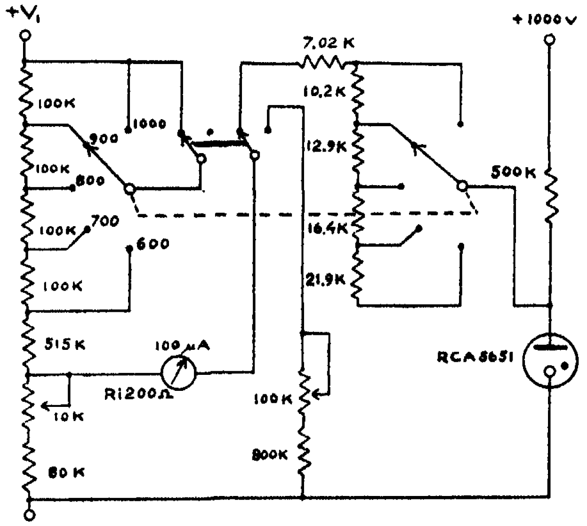

FIG. 2.

The work was performed under the auspices of Atomkommittén, Stockholm.

Further Techniques in Single-Crystal X-Ray Diffraction Studies at Low Temperatures*

S. C. ABRAHAMS, R. L. COLLIN,† W. N. LIPSCOMB, AND T. B. REED
School of Chemistry, University of Minnesota, Minneapolis, Minnesota

January 23, 1950

IN the course of some recent studies of the structure of a series of crystals melting in the range 0° to −40°C, it became necessary to extend the techniques already in use.[1] The resulting methods have enabled us to grow rapidly good single crystals, and to preserve them for sufficient lengths of time to record nearly all the possible (hkl) reflections.

The general method is very similar to that described by Kaufman and Fankuchen. The liquid to be examined is sealed into a glass capillary and maintained solid by blowing a stream of cold air over it. We have now applied this method for use both with Weissenberg and Buerger precession cameras. The capillaries are of uniformly drawn out Pyrex tubing less than 1 mm in cross section with wall thickness about 0.05 mm. The liquids are introduced into the capillaries either by direct distillation from a vacuum line, or by immersing the whole capillary, which is about 1 cm long and has one end previously sealed off, and which has a longer and very fine capillary tube inserted into it, in the liquid. It now readily fills, and then the other end is sealed after cooling the remainder of the capillary tube in a block of dry ice.

The cooling air is taken directly from a compressed air line, passed through a series of drying agents, and then passed through a copper spiral tube immersed in a dry ice-sec. butyl alcohol mixture. It is then led to the capillary through a vacuum jacketed glass tube, as shown in Fig. 1. The pressure of air just before entering the heat exchanger is about 1 cm Hg, and this arrangement permits a steady stream of cold air to be delivered without further attention for periods up to ten hours. A uniform temperature is maintained close to the specimen by mounting the capillary at the apex of a 120° cone, which is made from a Plexiglas block: this holder is readily attachable to the goniometer head. The thermocouple junction is placed about 2 mm from the tip of the specimen, to obtain an accurate measure of its temperature.

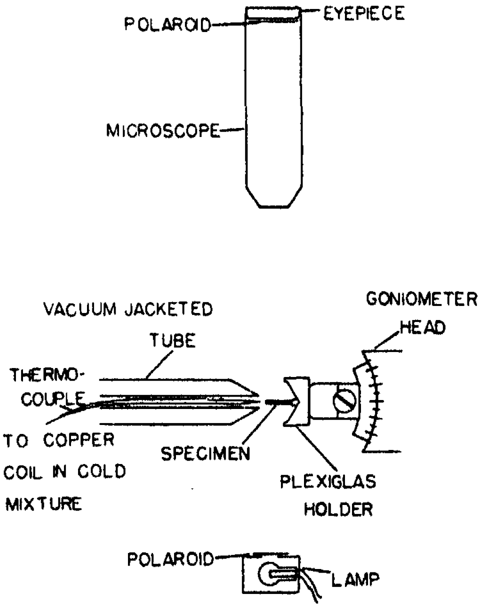

FIG. 1. Low temperature single crystal arrangements.

The crystal is grown by the following procedure, in which the progress of crystal growth may be continuously viewed through a simple polarizing microscope, of about 6–10 magnifications. The specimen may sometimes be solidified by lowering the temperature to about 5° below its melting point, but frequently the liquid supercools to such an extent that a thermal-shock must be applied, either by touching the side of the tube with a piece of dry ice, or even by pouring liquid nitrogen over the specimen. The temperature is then raised to just beneath the melting point, and the solid in the tip of the capillary is then melted by directing a fine controllable jet of dry warm air on to it. On removing this local source of heat, crystal growth will occur until the tip is again solid, and if the temperature is adjusted so that the rate of growth is only just discernible, it is very likely that the newly grown portion will consist of several single crystal fragments. The remainder of the microcrystalline solid is then melted in the same manner with growth now originating from the tip. This often gives rise to a good single crystal immediately, but if not, the procedure is repeated by again melting the tip, followed by fresh growth from the resulting crystal. In this manner, a good single crystal will usually be obtained in a matter of minutes.

To avoid condensation of ice on the capillary, the room in which this work was carried out was dehumidified, so that the vapor pressure of water was about 5 mm. With this condition satisfied, temperatures as low as −55°C have been maintained for extended periods, with a very small amount of ice formation, and this could readily be brushed away, thus doing away with the use of troublesome shields. This technique was developed in conjunction with a Buerger precession camera, which has the advantages that the specimen is very easily accessible, and that once a single crystal is obtained, a large volume of the reciprocal sphere is readily explorable, using MoK_α radiation. With the present cooling arrangement, the precession angle has a maximum of about 23°, corresponding to about $\sin\theta = 0.4$. It is found advantageous to obtain preliminary unit cell and space group data in this way, and then to regrow the crystal on, or transfer to, a Weissenberg camera for a more complete record of the reciprocal lattice. The camera we used is similar to that described by Buerger,[2] for which it was found necessary to construct a new film holder of radius about 4.5 cm, and with a portion subtending about 70° cut out of the back reflection area on the lower side of the holder, so that it could be slipped over the glass vacuum jacket without having to disturb the crystal.

These methods have been successfully applied to hydrazine, hydrogen peroxide, and thiophene, and their crystal structures will be published in detail elsewhere.

The present cooling system may readily be adapted to give a supply of air at temperatures down to −120°C by the use of a second cooling coil immersed in liquid nitrogen. At such temperatures, some shielding device becomes necessary to prevent ice formation on the specimen. It appears possible to construct a set of thin cellulose acetate shields which could be easily removed and so retain access to the capillary. At least certain convenient developments of low temperature techniques appear to lie in such directions, and also in increasing the present precession angle of the Buerger camera, so as to obtain the maximum range from this instrument.

* This research is being supported by the ONR Contract N8onr 66203.

† Now at Department of Research in Chemical Physics, Mellon Institute, Pittsburgh, Pennsylvania.

[1] H. S. Kaufman and I. Fankuchen, Rev. Sci. Inst. 20, 733 (1949).

[2] M. J. Buerger, *X-Ray Crystallography* (1942), p. 224.

An Instrument for Mechanically Differentiating Curves

ARNOLD H. SCOTT
National Bureau of Standards, Washington, D. C.
November 17, 1949

DURING the late war, a group at the National Bureau of Standards, working on the internal ballistics of guns, differentiated displacement-time curves to get velocities and then differentiated the velocity-time curves to get accelerations. These differentiations were made using a protractor to measure slopes, obtaining the tangents of the angles, multiplying by their proper factor, and plotting the results. In an effort to eliminate a large part of this work, a Coradi integraph[1] was modified by the writer so that it could be reversed to differentiate curves and plot the derivative ordinates directly on graph paper.

The modification consisted in removing the pen (*A*) (Fig. 1) and attaching to the pen holder (*B*) a frame (*I*) which had an index glass taken from a slide rule attached to its feet. A short line was ruled perpendicular to the long line to indicate the point of

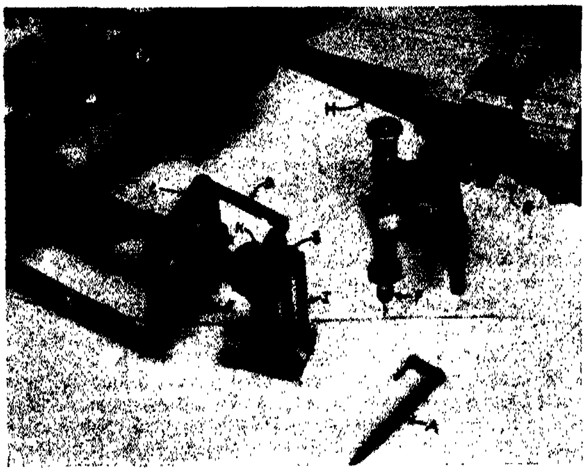

FIG. 1.

measurement. The index frame is rotated with the guide wheel frame (*C*) by means of the link (*D*) so that the long line on the index glass is always parallel to the plane of the guide wheel (*E*). Its angular position is controlled by the position of the pointer (*F*) and the position of the clamp (*G*) on the graduated arm (*H*).

To differentiate a curve the instrument is adjusted so that it rolls parallel to the abscissa of the curve, the guide wheel (*E*) being held off the paper by the lifting screw. With the carriage of the graduated arm (*H*) locked in its zero position the pointer is adjusted to zero and the index frame is adjusted until the long line is parallel to the abscissa. The carriage is then released and the instrument and carriage are moved until the intersection of the index lines is at the point where the differentiation is desired. The pointer is then moved until the long index line is parallel to the curve as viewed through the pen opening (*K*). The pointer is then pressed into the paper to constitute one point of the plot.

The distance (*X*) along the graduated arm at which the clamp (*G*) should be set is computed from

$$X=Q/PR,$$

where P is the value per unit distance of ordinate for the derivative curve, and Q and R are the values per unit distance of ordinate and of abscissa respectively of the curve being differentiated. Since the scale on the graph paper may be slightly different from that on the instrument the setting should be checked by setting the pointer on an ordinate value equal to X. If the long index line is not parallel to a line having a slope of 45° then adjustment of the setting of the clamp (*G*) on the graduated arm must be made.

To test the accuracy of this method a selected curve was integrated using the Coradi instrument as an integraph. The resulting integral curve was then differentiated using both the present reversed-integraph method and the previously mentioned protractor method. The error was assumed to be the difference between the original curve and the derivative curve. This included the errors of integrating the original curve. The average error was 2.10 percent for the reversed-integraph method and was 3.08 percent for the protractor method. The main error is probably in setting the index line tangent to the curve and this problem is common to both methods.

The advantage of the reversed-integraph method is that it is much faster than the protractor method. A disadvantage is that the slope which it can differentiate is limited to about 66 degrees and that range can only be obtained if the clamp is set at eleven cm or less. The most practical range for the clamp setting is between 15 and 25 cm. If the clamp is set at 25 cm the maximum slope is 45 degrees.

High Power Pulsed Magnetron with Replaceable Cathode

M. F. AMSTERDAM AND W. E. DANFORTH
Bartol Research Foundation of The Franklin Institute, Swarthmore, Pennsylvania

January 16, 1950

A NEED has been felt for some time in this laboratory for a magnetron whose cathode would be readily replaceable. The specific type of magnetron involved is the 4J32, a 12-vane high power pulsed tube of 10-cm wave-length, a tube which is normally supplied with a radial cathode mounting.

In order to achieve cathode demountability it seemed that an axial mounting would be more practical and Fig. 1 shows the general plan of our first attempt in this direction. Having secured encouraging performance with the present design, future effort will be directed toward greater compactness which will probably call for a permanent magnet rather than the present cumbersome electromagnet.

The cathode is of the thoria sleeve type with tungsten heating coil inside the sleeve. Heater power is brought in axially by a rod and concentric pipe which go through one pole-piece and also serve to support the cathode. The tube is continuously pumped through one of the holes in the anode block originally intended for a radial cathode lead.

Pole pieces are brazed to the anode block, and the cathode assembly is passed through the hole bored in the pole-piece, the seal being made with a rubber gasket.

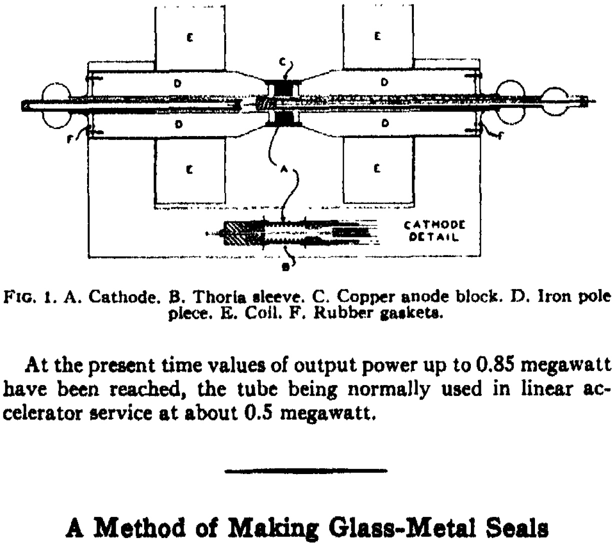

FIG. 1. A. Cathode. B. Thoria sleeve. C. Copper anode block. D. Iron pole piece. E. Coil. F. Rubber gaskets.

At the present time values of output power up to 0.85 megawatt have been reached, the tube being normally used in linear accelerator service at about 0.5 megawatt.

A Method of Making Glass-Metal Seals

N. A. ECKSTEIN, J. W. FITZGERALD, AND C. A. BOYD
The University of Wisconsin, Naval Research Laboratory, Department of Chemistry, Madison, Wisconsin

February 13, 1950

GLASS to metal seals have been made at this laboratory by an electroforming process. These seals have been found to be vacuum tight and reasonably insensitive to thermal shock.

The essential features of the method are illustrated in Fig. 1 which shows the steps involved in making a joint between a Pyrex glass tube and a copper tube.

In Step 1 the glass tube is coated on one end with a ceramic type silver paint.[1] This is then fired on the tube to produce a strong glass-silver bond and to make the coat conducting.

In Step 2 a wax form is inserted in the coated end of the tube. This form will determine the shape of the connecting copper tube.

The wax form is then made electrically conducting[2] as illustrated in Step 3, and then a layer of copper is electro-plated over the entire surface. The current density is adjusted so as to produce a smooth surface and the thickness of the copper tubing so formed is

---

[1] Manufactured by G. Coradi, Zurich, Switzerland.

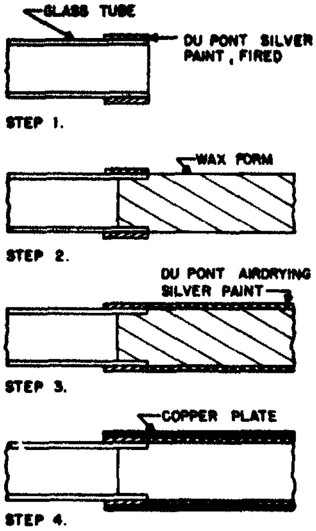

FIG. 1. Steps involved in making a glass-copper joint.

determined by the plating time. The net result after this treatment is illustrated in Step 4. The wax form can then be removed by heating the copper-glass joint which melts the wax.

Joints between Pyrex and copper tubing made in this manner have been heated up to 300°C without breaking. They have also been found to be vacuum tight.

This same general method has been used successfully to electroform quartz crystal electrodes and mounts for ultrasonic apparatus and to seal glass windows on metal cells. Joints between quartz tubing and Pyrex tubing have also been made by electroforming a short copper tube between the two.

---

[1] Obtainable from the E. I. du Pont de Nemours and Company, Inc., Electrochemicals Department, Wilmington 90, Delaware as Ceramic Silver Paint No. 4666.

[2] This may be accomplished in several different ways. However, it has been found convenient to use an air-drying conducting silver paint obtainable from the du Pont Company.

Improved Double-Crystal Spectrometer for Small Angle Scattering Measurements

LEO BROUSSARD
Esso Laboratories, Esso Standard Oil Company (Louisiana Division), Baton Rouge, Louisiana

November 3, 1949

IN experiments dealing with small angle scattering of x-rays the important measurement to be made is the determination of the resulting angular spread of intensity of a monochromatic beam of x-rays after this beam traverses the specimen. The field of interest in this type of work is usually less than 2 degrees on each side of the central undeviated beam. In using an ordinary double-crystal spectrometer for this work, one crystal is fixed in position to produce a monochromatic beam which is directed through the specimen. The angular divergence of x-rays produced by the sample is then determined by rotating the second (or analyzing) crystal through the range of angles required to allow these divergent rays to strike the second crystal at the proper angle of incidence to produce reflection. The reflected x-rays are usually detected with a Geiger-Müller counter. Because of the small angles involved, the counter is sometimes fixed in a permanent position and sometimes moved through twice the angle through which the analyzing crystal is rotated. It is the purpose of this paper to indicate a simple method for overcoming the disadvantages of the present methods.

It is important to remember the difference between the type of reflection occurring when x-rays are reflected by crystals and that of ordinary light reflecting from a plane mirror. In the case of light reflecting from a plane mirror, reflection occurs at all angles of incidence in such a way that the angle of incidence equals the angle of reflection. For monochromatic x-rays reflecting from one set of crystal planes, the angle of incidence still equals the angle of reflection, but reflection will take place for only one particular angle of incidence for a first-order reflection. This fixes the angle of reflection for a given wave-length and a given set of crystal planes, so that the counter tube should be rigidly attached to the crystal in order to maintain a constant angle of reflection between crystal and counter. In this manner the counter is always at the proper position to receive reflected radiation provided the crystal is oriented at the proper angle of incidence for the particular divergent ray being measured.

Reference to Fig. 1 indicates in an exaggerated way the manner in which reflections from the second crystal take place. *MO* represents the main undeviated beam striking the second crystal at its axis of rotation *O*. Another ray *MA* scattered by the specimen strikes the crystal at *A* and does not reflect because the angle of incidence is not correct. Rotating the crystal to the new position (dotted) allows ray *MA* to strike the crystal at *B* making the proper angle of incidence and reflecting to the counter along *BC*. As shown the counter should be coupled directly to the crystal. Now it can be seen that the ray *MOC* does not reflect from the same region of the crystal as ray *MBC*. This displacement requires that the surface characteristics of the crystal be taken into consideration. Also, this displacement can cause the reflected ray *BC* to strike a portion of the counter tube which is different from that portion struck by reflected ray *OC*. This effect can give rise to erroneous readings of intensity since the sensitivity of counter tubes is affected by the point of incidence and the direction of the x-ray beam striking the counter.

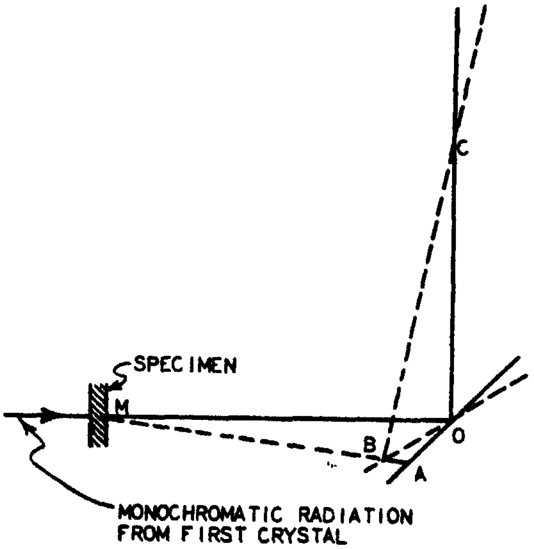

FIG. 1. Reflections from second crystal.

In order to eliminate these difficulties the second crystal is rotated about *M*, the center of the specimen, instead of about *O*. In this way the ray *MA* will strike point *O* when the crystal is brought around to the proper position for optimum angle of incidence. The same portion of the analyzing crystal is used for measurements of all rays and all the reflected rays strike the same portion of the counter.

This improved instrument consists of these main parts. A first crystal is used to produce a monochromatic beam of x-rays. A

Geiger counter is permanently coupled to the second crystal at the proper angle of reflection for this monochromatic radiation. The second crystal and the Geiger counter, as a unit, rotate about the center of the specimen in order to analyze the angular divergence of x-rays emerging from the specimen.

Apparatus and Method for Testing Radium or Thorium Capsule Seals

R. J. Beal

Health Radiation Branch, National Research Council, Atomic Energy Project, Chalk River, Ontario

February 6, 1950

SEALED radium capsules, after equilibrium has been reached, contain radon and radon decay products. Similarly, thorium capsules contain thoron and thoron decay products when equilibrium conditions have been established. In both cases the decay products or active deposits are solids which attach themselves to dust particles. The active deposits are strongly alpha-active, the radium active deposit having a half-life of about 50 minutes and the thorium deposit a half-life of 10.5 hours.

The method here described depends upon the fact that the source capsule while under test, will expel a part of the emanation and accompanying decay products, if the seal is faulty. The expulsion of the emanation is achieved by heating the capsule by a steam jacket to about 100°C. It has proved convenient to collect the active deposit by carrying out the heating with the source placed in the collecting volume of an electrostatic precipitator. The particulate activity precipitates on the inner surface of a removable cylinder, which forms the outer electrode of this precipitator assembly. The activity could no doubt be collected by the long established method of collection on an electrode charged negatively to a few hundred volts. Counting has been done by making the collecting cylinder the outer electrode of a methane-filled cylindrical proportional counter. A very high counting efficiency is thus secured.

The apparatus, as shown in Fig. 1, consists of a cylindrical precipitator with a central electrode at 10 kv positive potential relative to the collecting cylinder. The source under investigation is placed in a cup which slides into position at the base of the cylinder. The complete precipitator and source assembly is surrounded and supported in a steam jacket. The steam jacket is carefully sealed from the precipitator assembly to ensure that moisture does not interfere with precipitation.

The first step in the procedure consists of placing the source in the source cup which is then elevated and locked in position in the precipitator base. Then the steam is turned on and allowed to circulate during the entire time of the test. High tension is applied to the h.t. electrode for 90 minutes. The equipment described above requires about 30 minutes to reach operating temperature of 90°–100°C and a total testing time of 90 minutes is used so that an hour of precipitation occurs at maximum temperature of the test. The collector as used fits into a methane proportional chamber for counting.

Some typical results secured with the method outlined above are given.

(*a*) *A radium-beryllium source of 200-mc nominal value.*—This source gave a precipitation which counted 1500 alpha-c.p.m. It is interesting to note that when this source was held in the apparatus at 10 kv for 24 hours *at room temperature*, only 30 c.p.m. were collected on the tube.

(*b*) *A radium needle of 1-mc nominal value.*—This source gave a precipitation which counted 77 alpha-c.p.m.

(*c*) *Sources ranging in value from 1 mg to 1.2 g.*—A number of sources, ranging in value from 1 mg to 1.2 g, were checked and most of these, when subjected to the test, gave counts within 10 c.p.m. of the normal background of the counter, indicating a satisfactory source seal.

(*d*) *Effect of radium contamination on the exterior of the capsule.*—Monel metal cylinders approximately the same size as a source capsule were prepared with surfaces varying from a high polish to an extremely rough, pitted surface. These monel cylinders were heavily contaminated with radium sulfate. On precipitation only the cylinder with the roughest surface gave any appreciable counts above the normal background, namely 5 c.p.m. Thus, it would appear that surface contamination under normal capsule conditions has little or no appreciable effect on the results of the test.

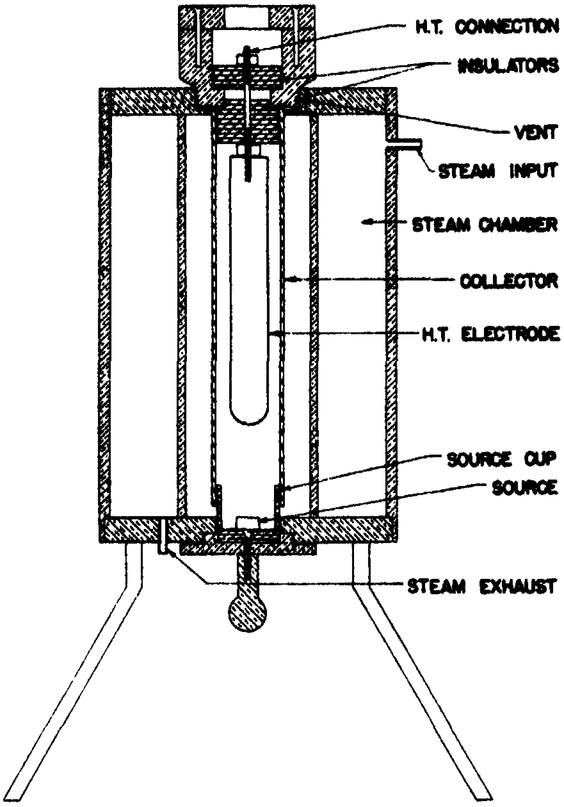

FIG. 1. Radium and thorium capsule seal tester.

Automatic Level Controller for Liquid Nitrogen

E. H. Quinnel and A. H. Futch

Naval Research Laboratory, Washington, D. C.

January 30, 1950

ON many occasions there is a need for an automatic level controller in cryogenic research involving low temperature liquid baths. It is desirable that such a device be simple in construction, positive in operation, occupy as little space as possible, and in case of malfunction, will be fail-safe.

Level controllers utilizing floats,[1] vacuum systems,[2] or vapor pressure thermometers[3] as the sensitive elements have been developed but space requirements limit the application of these devices. The controller to be described uses a resistor as the sensitive element and, therefore, has nominal space requirements.

The controller utilizes the difference in heat dissipation of a liquid and its vapor to establish a large change in the temperature of a resistor dissipating power when its environment changes from liquid nitrogen to the gaseous nitrogen immediately above the liquid. With a five-watt input to a small copper coil, the temperature change for the conditions described above results in a resistance change of a factor of about six. This resistance change is sufficient to operate a low resistance relay in a constant voltage circuit.

The circuit diagram for the controller is given in Fig. 1. The sensitive element C, a coil of approximately 24 feet of A.W.G. 40 copper wire, is connected in series with a six-volt storage battery E and a normally closed relay R. When the sensitive element C is above the level of the liquid nitrogen in Dewar D_2, the resistance of C is large (order 18 ohms) and the current in the circuit is too small to actuate the relay R. Thus, the relay contact completes the 110-volt circuit, supplying power to the heater H[4] and closing valve V. Pressure builds up in the Dewar D_1, and liquid nitrogen is transferred to Dewar D_2.

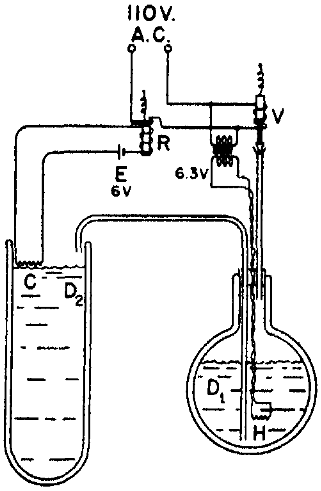

FIG. 1.

When sufficient liquid nitrogen has been transferred to immerse the sensitive coil C, the resistance of C becomes small (order 3 ohms) and the current in the circuit is now sufficient to actuate the relay R. Actuation of the relay breaks the 110 volt circuit thus cutting off the power to heater H and opening valve V. The pressure in Dewar D_1, is reduced and transfer of the liquid ceases until the liquid level again falls below coil C. If it is desired to protect the controller against an accidental opening of the battery circuit, a minimum current relay controlling the 110-volt power input to the system can be installed.

The level controller as built has operated satisfactorily for periods of 48 hours and maintains the desired level of the liquid nitrogen to within ±3 millimeters.

---

[1] R. B. Scott and F. G. Brickwedde, Rev. Sci. Inst. 2, 171 (1931).
[2] G. O. Jones and C. A. Swenson, J. Sci. Inst. Phys. Ind. 25, 239 (1948).
[3] G. O. Jones, J. Sci. Inst. Phys. Ind. 25, 239 (1948).
[4] H. Grayson-Smith and J. C. Findlay, Chem. Rev. 39, No. 3, 397 (1946).

New Instruments

W. A. Wildhack: Associate Editor
in Charge of this Section
National Bureau of Standards, Washington, D. C.

These descriptions are based on information supplied by the manufacturer and in some cases from independent sources. THE REVIEW *assumes no responsibility for their correctness.*

Interference Color Filter

Wide application in the fields of color television, photography, refractometry, and astronomy are foreseen for this new development. The filter consists of two semi-

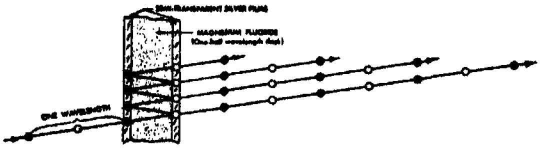
SEMI-TRANSPARENT SILVER FILMS
MAGNESIUM FLUORIDE (One-half wavelength thick)
ONE WAVELENGTH

TRANSMISSION TYPE INTERFERENCE FILTER

transparent, silver films separated by a magnesium fluoride film of a given thickness. As a light ray passes through the filter, part of it is reflected back and forth between the silver films with some of it emerging at each reflection. Wave-lengths equal to twice the thickness of the magnesium fluoride film emerge in phase, and therefore maximum transmission occurs for that particular wave-length; at the same time interference occurs for other wave-lengths and effectively monochromatic transmission is obtained. The color transmitted is determined by the distance the multiple reflections must travel which, in turn, is determined by the thickness of the fluoride film and the angle of incidence of the light. Both transmitting and reflecting type filters are available.—BAUSCH & LOMB OPTICAL COMPANY, *Rochester 2, New York.*

Improved Ultra-Sensitive D.C. Amplifier

This new and improved d.c. amplifier of the General Motors breaker type offers many advantages in the measurement of d.c. and low frequency a.c. voltages in the microvolt and fractional level thermocouple voltages, infra-red detectors, photovoltaic cells and the like. It can be used to replace suspension galvanometer systems.

This new amplifier (Model 10) features very high immunity to the effects of a.c. pick-up in the input circuit. The discrimination ratio against 60-cycle pick-up is over 1000. It has an improved life breaker. Convenient and accurate coarse and fine gain controls, zero position controls and calibration signals are provided.

This instrument has a zero stability of better than 0.005 μv per day after warm-up. The noise level approaches the limit imposed by the Johnson noise of the external circuit. This amplifier is available for operation with input circuits from 0 to 1 megohm. The d.c. output of the amplifier is sufficient to operate standard recorders, milliamperemeters and d.c. relays. For 110 volts, 60-cycle operation. Price $580.00.—LISTON-FOLB, *Department M, Box 1334, Stamford, Connecticut.*

Ultra-Low Frequency Oscillator

A new, wide range, ultra-low frequency oscillator Model 410-A combines the sub-audio with the normal audiofrequencies and provides both sine and square wave outputs over the entire frequency range from 0.02 to 20,000 c.p.s. Six frequency bands are provided, each covering a full decade, with continuous control of frequency. A single, 11-in., illuminated, direct reading logarithmic scale is used on all bands.

The sub-audio range of frequencies makes the unit especially useful for design and test of servomechanisms, control instruments and feed-back amplifiers, for vibration checks and medical research, and in conjunction with timing and production controls. The square wave output is useful for low frequency switching and triggering operations and for checking the frequency or transient response of audio circuits.

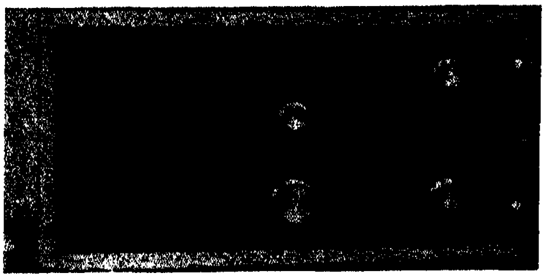

This instrument features low distortion and hum level, constant output impedance, excellent frequency stability and amplitude constancy over the entire frequency range. An important feature of a sub-audio electronic oscillator is its ability to recovery quickly from band-switching and similar disturbances. The sine wave output of the 410-A recovers to 90 percent of its steady-state amplitude in less than two cycles of the dial frequency.—Krohn-Hite Instrument Company, *580 Massachusetts Avenue, Cambridge 39, Massachusetts.*

Industrial Rouy-Photrometer

Designed to speed routine processing analyses, the new Industrial Rouy-Photrometer provides the highest accuracy obtainable in colorimetric absorption analysis. This greatly improved type of photoelectric colorimeter gives concentration readings in which inherent functional error is cut to within 0.1 percent. Such a high degree of accuracy is made possible for the first time by careful matching of the photoelectric cell and the microammeter, which results in strict linearity of current *vs.* light energy.

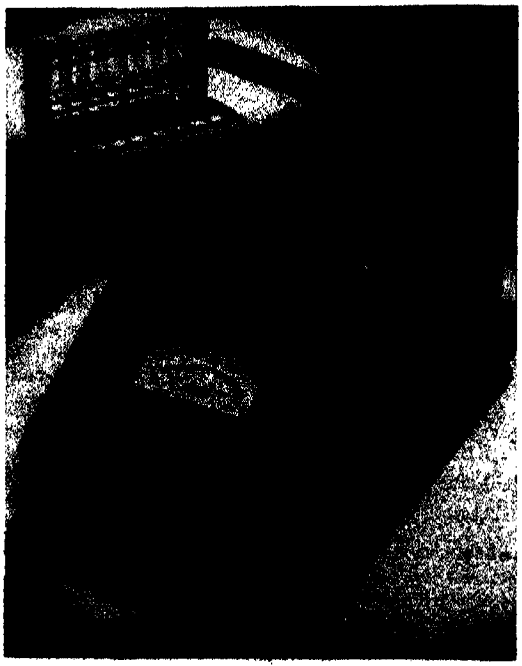

Operation of the Rouy-Photrometer is rapid and simple, with a single control for all adjustments, and once calibrations have been set up, no special skill or calculation is required of the operator.

Maximum reproducibility, so important in efficient process control, is assured for identical readings on the same specimen can be obtained by different workers, even on different Photrometers.

Highest selectivity over the entire visible spectrum is another outstanding Photrometer advantage. Each instrument is equipped with a set of ten compound compensating glass filters. The filters are mounted in one rotating plastic disk which rotates within the Photrometer. Two blank spaces are provided for filters required in special work. Each filter and filter element is controlled in production and matched to produce identical transmission curves.

The Rouy-Photrometer is a single cell, line-operated instrument. On special order, it is adaptable to 6-volt d.c. operation. It is available complete with four absorption cells, one sealed H_2O absorption cell, plastic insert, dust cover, and handbook.—E. Leitz, Inc., *304 Hudson Street, New York 13, New York.*

Variplotter

The Model 205 variplotter is designed to record one variable as opposed to another in any application where the functions may be represented by varying d.c. voltages, such as electron tube characteristics, temperature-pressure curves, wind-tunnel data, industrial processes, etc. The plotting surface is a back-lighted, 30-in. glass square over which the plotting paper is positioned.

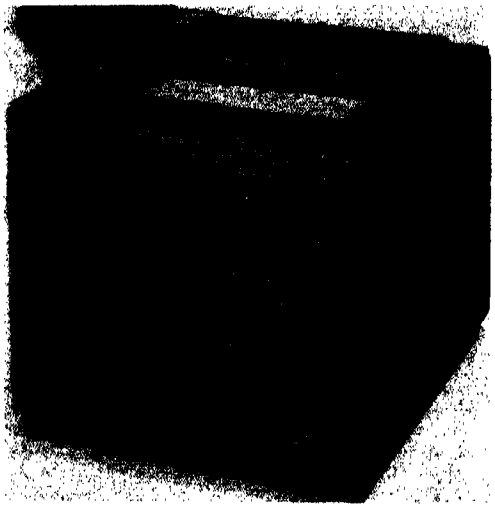

Sensitivity is 50 mv/in. with other ranges also available, and the pen can traverse the board in either X or Y direction within three seconds. Accuracy is 0.05 percent of full scale at a temperature of 68°F for static conditions and 0.1 percent for dynamic conditions. —Electronic Associates, Inc., *Long Branch, New Jersey.*

Thermocouple and Ionization Type Vacuum Gauge

Designed to fill all the needs of the laboratory or plant high vacuum installation, this new instrument has two thermocouples for the range from 1 mm Hg abs. to 10^{-3} mm and an ionization head for five ranges covering pressures between 5×10^{-3} and 10^{-8} mm Hg abs. Outstanding features of this instrument include a specially designed, low leakage, shielded connecting cable which eliminates errors at pressures below 10^{-6} mm where the ionization currents are less than 10^{-4} ma, and a protective relay with very short time delay which automatically turns off the ionization gauge filament when the pressure in the system exceeds 1½ times the full-scale

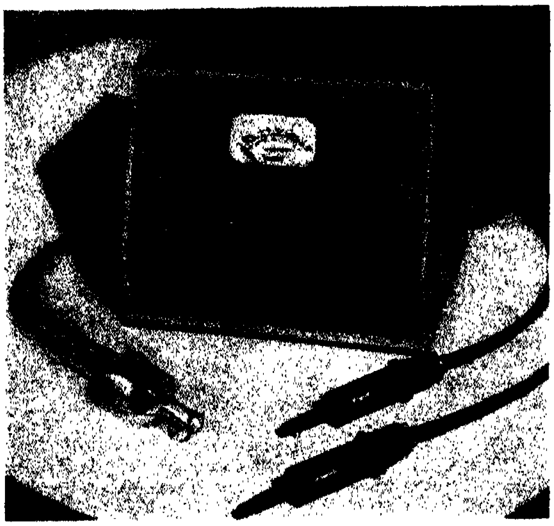

pressure for which it is set; in preliminary tests gauges have survived more than 100 instantaneous pressure bursts from 10^{-3} mm to atmospheric pressure. In addition, the filament emission is automatically regulated at 1, 5, or 10 ma at the operator's choice; the indication of small pressure changes without readjustment of emission is particularly useful for leak detection.—NATIONAL RESEARCH CORPORATION, *70 Memorial Drive, Cambridge, Massachusetts.*

Earth Resistivity Apparatus

Intended for use by contractors, engineers, and students, who require data on sub-surface conditions at comparatively shallow depths, 300 ft. or less, the Type LLR earth resistivity apparatus is a modification of the Gish-Rooney instrument, but is considerably less expensive. It is a moderately priced, compact apparatus which measures earth resistivities by the Wenner four-electrode method. Certain types of rock, ores, sand, and gravel have characteristic resistances, and by applying the principles of the Wenner method of data evaluation, it is comparatively simple to determine the depth at which such deposits occur as well as their horizontal and vertical extent.—GEOPHYSICAL INSTRUMENT COMPANY, *Arlington, Virginia.*

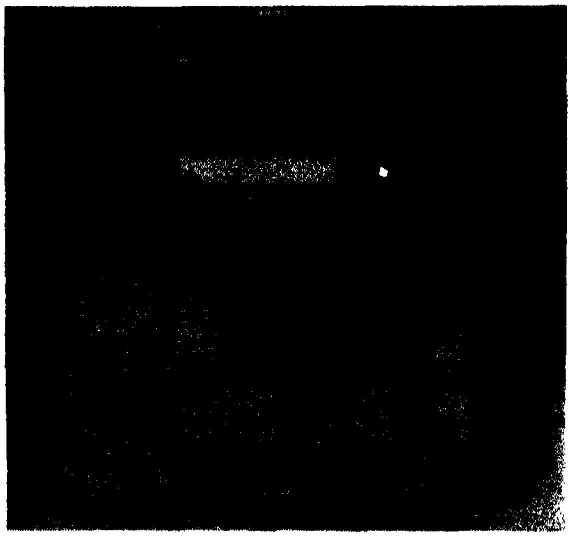

F-M Signal Generator and Amplitude Modulator

The Type 1022-A f-m standard signal generator (illustrated) is designed specifically for testing f-m broadcast receivers. Carrier frequency range is 88 to 108 Mc and I-F range 10 to 11.5 Mc. The r-f oscillator is modulated directly by a reactance tube, thus eliminating the difficulties caused by spurious beats or "birdies" that occur in beat-type systems. Modulation system is flat from 20 cycles to 15 kc, and internal modulating frequencies of 60 and 400 cycles are provided. Deviation range is 0 to 200 kc, with less than five percent incidental amplitude modulation. Open circuit output voltage is continuously variable from below 0.1 μv to more than one volt. Leakage is completely negligible. Output impedance is 50 ohms and is practically constant over the operating range.

The Type 1023-A amplitude modulator is designed for use with the f-m signal generator as well as with other signal generators for receiver tests where amplitude modulation is desired with negligible incidental f-m. It modulates the signal generator output after attenuation, so that reaction on the oscillator frequency, which produces f-m, is eliminated.

Modulation up to 80 percent at 60 cycles, is provided internally. External modulating frequencies between 20 cycles and 15 kc can be used. Input and output impedances are 50 ohms.

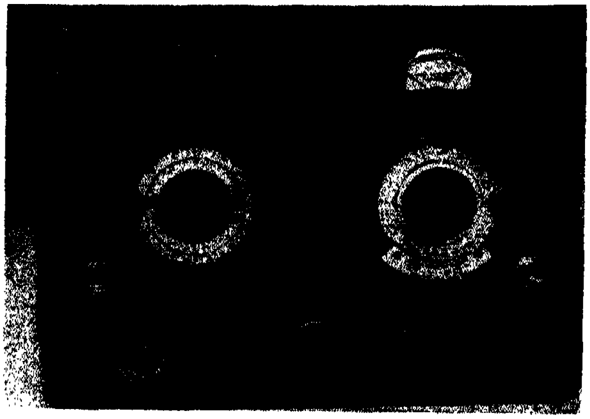

Radiofrequency range is 10 to 150 Mc with a gain of 0.1 and 10.1 to 11.3 Mc with a gain of 10.—GENERAL RADIO COMPANY, *275 Massachusetts Avenue, Cambridge 39, Massachusetts.*

D.C. Integrator Motor

An integrator motor is now available for applications requiring the time integral of a d.c. voltage. Speed of the motor is proportional, within half of one percent, to applied voltages between −15 and +15 volts. Speed is actually proportional within a quarter of one percent through all of the range except near zero voltage, or reversal point. Angular shaft displacement over any given period, therefore, is proportional to the integral of applied voltage during that period. The output shaft may be geared or directly coupled to an indicator or other

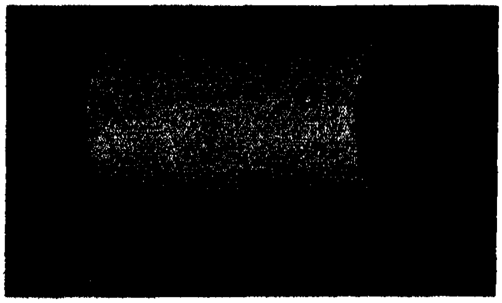

instrument load. In the model illustrated, the armature is geared to a single output shaft at a ratio of 500 to 1. An alternate model can be supplied with the armature geared to two output shafts, at ratios of 100 to 1 and 1000 to 1.

Unique design, precision workmanship, and jewel bearings provide the extremely high torque-to-inertia ratio of 400,000 to 1 at 1 volt applied. The integrator motor consistently starts and runs on the energy supplied by a photo-cell exposed to sunlight. Weight of the motor is 12 ounces, and the greatest over-all dimension is 3¾ in.—Specialties, Inc., *Skunks Misery Road, Syosset, New York.*

Miniature Speed Changes

Gear reductions as high as 750,000 to 1 are now practical and available. These special units are made up by adding one or two additional gearing sections to the standard 3-section units having ratios up to 3375 to 1. This provides several hundred ratios between 1000:1 and 750,000:1 in addition to (500 or more) standard 1-, 2-, and 3-section units.

Input speeds as high as 50,000 r.p.m., and output torques up to 2 lb.-in. are permissible. Weights of 4- and 5-section units are approximately 6 and 7 ounces, respectively. Body diameter is 1.050 in.; body lengths are 3$\frac{15}{16}$ in. for 4-section unit and 4⅝ in. for 5-section units.

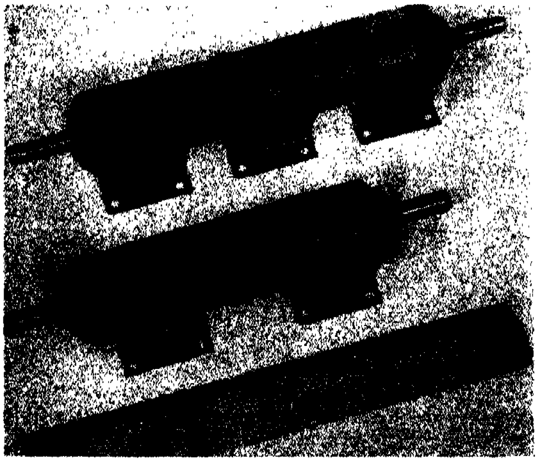

The addition of still another section with a maximum ratio of over *11 million to 1* is structurally practical, but so far no application for such extremely high gear reduction has been found.

▶ Very high ratios in hobbed gears and "zero backlash" construction can be furnished at reduced torque rating. Zero backlash is obtained by the use of a torsional spring and two parallel gear trains built into each gear section. One gear train is spring loaded against the other so that backlash is taken up continuously. Torsion spring is initially wound up to provide a zero backlash output torque of 1 lb.-in. in either direction, but may be unwound to any extent desired.—Metron Instrument Company, *432 Lincoln Street, Denver 9, Colorado.*

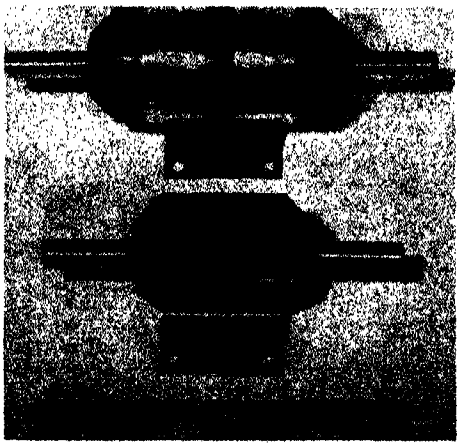

Logarithmic Attenuator

The new Kay-Lab logarithmic attenuator, Model 511, has internal thermostatic control to maintain temperature at 100°F. This feature eliminates temperature dependence of non-linear circuits in the attenuator and permits use at temperatures from freezing up to 100°F.

The non-linear circuit elements are adjusted to give an output which is accurately proportional to the logarithm of input voltage. A.c. Logatens operate on both halves of the wave and are substantially flat from d.c. to 100 kc. Both a.c. and d.c. Logatens are available, and it is recommended that d.c. Logatens be used for d.c. applications, due to contact potential and other effects. D.c. Logatens are half-wave devices which have been adjusted for a specific polarity.

Suggested applications for the use of a Logaten are in a decibel meter, in dynamic compression, in electronic computing and control amplifiers, and in acoustic studies. Plug-in units with either octal plug or banana terminals are available.—Kalbfell Laboratories, Inc., *1076 Morena Boulevard, San Diego 10, California.*

Model F-1 Oscillograph

The complete instrument consists of an amplifier and strip chart recorder which are also available separately. The amplifier has a 2000 to 1 maximum gain in four stages with a single 6V6 final stage. Its frequency response is flat from ½ to 100 c.p.s. and allowable input voltages range from 0.010 to 275 volts. Impedances are 10 megohms input and 50 ohms output. The recorder has a magnetic pen drive with a sensitivity of 1.1 mm/volt and 1.5 mm/ma with a 3-in. pen, and the frequency

response is flat from ½ to 70 c.p.s. The ink well may be refilled through an opening in the top of the case, and a Plexiglas door provides access to the chart so immediate notations may be made on the chart paper while the instrument is in operation. Dimensions of both instruments are 15×7×7 in.—PHOTRON INSTRUMENT COMPANY, *6516 Detroit Avenue, Cleveland 2, Ohio.*

Manufacturers' Literature

Titrilog—4-page illustrated bulletin on new Consolidated Titrilog describes the Titrilog application for the continuous recording of trace quantities of sulfur compounds.—CONSOLIDATED ENGINEERING CORPORATION, *620 North Lake Avenue, Pasadena 4, California.*

Magnetic Storage Systems—8-page brochure describes magnetic storage systems for use in computing inventory and automatic control systems to replace storage relays, stepping switches, punched tape and other bulky forms of storage.—ENGINEERING RESEARCH ASSOCIATES, INC., *1902 West Minnehaha Avenue, St. Paul, Minnesota.*

Tracerlog—No. 24, February, 1950, 12-page house organ, features a description of the SC-13 radioactive ore analyzer. Included also are revised data on LKB mechanical register and an index of Tracerlog articles for the year 1949.—TRACERLAB, *130 High Street, Boston 10, Massachusetts.*

The Oscillographer—Vol. 12, No. 1, 24-page house organ, includes a discussion of the new Type 292 cathode-ray oscillograph and an article entitled, "Transducers—A review of the design and applications of transducers for oscillography."—ALLEN B. DUMONT LABORATORIES, INC., INSTRUMENT DIVISION, *1000 Main Avenue, Clifton, New Jersey.*

Announcer—No. 50-1-37, 16-page house organ, features an article on "Phase contrast microscopy," and includes other equipment items.—EBERBACH AND SON COMPANY, *Ann Arbor, Michigan.*

Technique—8-page house organ, illustrated, includes articles on "Constant-impedance attenuators and faders," "Some specialized applications of the miniature standard cell," and "Phototelegraphy and medicine."—MUIRHEAD AND COMPANY, LIMITED, *Beckenham, Kent, England.*

Laboratory Mixer—Brochure describes a new laboratory mixer, in which an annular rather than a circular flow is produced by two concentric oppositely rotating propeller-equipped shafts. With this device, laboratory mixing is accomplished in exceptionally short mixing times. In addition, centrifugal effect is minimized, no vortex is caused, and the liquid level remains essentially constant, allowing the use of nearly filled containers without danger of slop-over.—BROOKFIELD ENGINEERING LABORATORIES, INC., *Stoughton, Massachusetts.*

Resistance Percentage Bridge—Brochure S142 illustrates and describes the operation of a resistance percentage bridge having an accuracy better than 0.01 percent throughout its range of indication. The instrument is used for quick, accurate calibration of high precision potentiometers.—SPECIALTIES, INC., *Skunks Misery Road, Syosset, New York.*

Fluid Pressure Cell—Bulletin 306, 2 pp., on SR-4 resistance wire strain gauge-type pressure cells of eight capacities from 200 to 50,000 lb. per sq. in.—**Load and Pressure Cells**—Bulletin 307, 2 pp., describes compression Type SR-4 load cells in which SR-4 resistance wire strain gauges bonded to a column are the load sensitive elements. Cell capacities range from 2000 to 200,000 lb. in seven sizes. Also included are specifications.—THE BALDWIN LOCOMOTIVE WORKS, *Philadelphia 42, Pennsylvania.*

Radioactivity Measurement Instruments—4-page brochure includes illustrations and descriptions of various radioactivity measurement instruments, including a safety sample carrier, a mobile safety shield.—RADIATION COUNTER LABORATORIES, INC., *1844 West 21st Street, Chicago 8, Illinois.*

Nuclear Isotope Chart—16×20-in. color chart showing atomic weight, atomic number, and radioactive transitions of elements from thallium to americium in the thorium, neptunium, uranium, and actinium series. Free on request.—W. M. WELCH MANUFACTURING COMPANY, *1515 Sedgwick Street, Chicago 10, Illinois.*

Nucleometers—4-page folder illustrates and describes basic complete laboratory for radioactivity research. Also illustrated are scaler-type nucleometer and nucleometer without scaler.—RADIATION COUNTER LABORATORIES, INC., *1844 West 21st Street, Chicago 8, Illinois.*

Pycnorator Instruments—Catalog 76, 8 pp., illustrates and describes Pycnorator instruments for measurement and control of fluid density and specific gravity.—FISCHER AND PORTER COMPANY, *76 County Line Road, Hatboro, Pennsylvania.*

Recorders—New illustrated catalog provides technical data concerning direct writing recorders and industrial amplifiers.—SANBORN COMPANY, INDUSTRIAL DIVISION, *39 Osborn Street, Cambridge 39, Massachussetts.*

Magnetic Counter—Leaflet describing small, lightweight three- or four-digit precision counter, one inch high. The additive or subtractive counter wheels record a maximum of 1200 counts per minute on 24 or 110-volt a.c. or d.c.—ABRAMS INSTRUMENT CORPORATION, *Lansing 1, Michigan.*

The Chronotest—(Electronic millisecond timer), 4-page illustrated folder on Chronotest, a British instrument for measuring short-time intervals between 0.1 and 10,000 msec. with an accuracy of one to two percent, useful in measuring the operating times of relays, fuses, switchgear and overloads, for timing chemical, physical and biological reactions, for testing camera shutters and for making psychological investigations. —HERMAN H. STICHT COMPANY, INC., *27 Park Place, New York, New York.*

New Materials

Forest K. Harris: Associate Editor
in Charge of this Section
National Bureau of Standards, Washington, D. C.

Mercury Filter

The Type "F" gold adhesion mercury filter consists of a reservoir with a discharge aperture at the bottom. A gold ring surrounds the aperture and constitutes the filter element. Mercury wets the ring, forming a metallic bond which results in a seal against anything that is not soluble in the mercury. The walls of the container are not wet by the mercury, so that liquids and fine particles of solids are drawn downward along the interface between the mercury and the wall by capillary action and agitation, but are stopped upon reaching the wetted ring. The filter allows a rapid flow of mercury and filters out dirt, oxide scums, oil, water, and acid, delivering dry mercury. It does not remove fine gold in suspension, or dissolved metals. These are usually removed by distillation. The seal is a noble alloy of gold which is more durable than pure gold and will last for several months of active operation. It is in the form of an easily replaceable disk. All other metal parts of the apparatus which come into contact with mercury are of stainless steel and are resistant to nitric acid.—BURRELL CORPORATION, *1942 Fifth Avenue, Pittsburgh 19, Pennsylvania.*

Teflon Gaskets

Chemiseal Snap-on Teflon (tetrafluorethylene) molded gaskets are designed to seal connections in glass pipe assemblies. Gaskets are stocked to fit Corning Pyrex conical-end pipe measuring 1, 1½, 2, 3, and 4 in. inside diameter. An annular ring construction insures correct centering and provides an efficient seal that is not subject to attack by any known chemical, and that will not contaminate any fluid being handled. The gasket compensates for misalignment and does not restrict the flow area at the pipe joint.—UNITED STATES GASKET COMPANY, *610 North 10th Street, Camden, New Jersey.*

Synthetic Mica

Synthetic mica, with essentially the properties of natural mica but able to withstand much higher temperatures, has been crystallized successfully at the National Bureau of Standards by Insley, Van Valkenburg, and Pike. The synthesis was carried out at atmospheric pressure with the aid of a fluorosilicate as a crystallizing agent. The other raw materials needed are quartz, magnesite, and bauxite. The mixture is placed in a platinum crucible and melted in an electric furnace at about 1400°C. As the furnace cools, mica crystals grow from a seed at the bottom of the crucible. The most satisfactory synthetic mica developed so far has the formula $K_4Mg_{12}Al_4Si_{12}O_{40}F_8$ and is equivalent to a form of natural mica in which the hydroxyl radical has been replaced by fluorine. Its physical properties compare favorably with those of natural mica. The largest crystals grown so far have a surface area of four square inches.

Satisfactory synthesis depends largely on the crucible lining. Ceramic linings are badly corroded by a fluorine-bearing melt. Carbon and silicon carbide crucibles are better but fluorine escapes through the porous walls and fine carbon particles become imbedded throughout the mica. Crucibles lined with platinum foil give the best results. The shape of the crucible is also important. Flat-bottomed crucibles are undesirable since they offer a large surface for formation of seed crystals which grow in different directions and limit the development of large crystals. If a crucible with a cone-shaped bottom is used the number of seed crystals is reduced and the direction of growth tends to be upward. Experiments are in progress to find ways of predetermining crystal growth more closely.—NATIONAL BUREAU OF STANDARDS, *Washington 25, D. C.*

Aluminum Thermal Insulation

Infra Type 6 consists of three aluminum sheets spaced 1½ in. apart by fiber partitions which are stated to be flame, mold, and vermin proof. Thus six reflective surfaces (two external and four internal), having emissivity and absorption of only three percent, are made active by fully effective reflective spaces. Permeability to water vapor is zero, and the material will not support or store condensation. It is installed in a single operation requiring no special skill, at a speed of 2000 sq. ft. per day. It may be installed in floors or ceilings, over or under radiant heating panels, concrete slabs, etc.

A 44-page brochure entitled "Simplified Physics of Thermal Insulation," containing descriptions and data on aluminum and mass insulation, is available on request from the manufacturer.—INFRA INSULATION, INC., *10 Murray Street, New York, New York.*

Glass Building Blocks

PC "55" glass blocks consist of seven new types designed to permit a more uniform panel appearance and better brightness control. Functional features include opal glass fused into the block junction to diffuse light which would otherwise be directly transmitted through the block edge, fibrous glass inserts to further diffuse light transmitted by the block and special prisms on interior faces of certain patterns. These features are combined in accordance with the use for which the specific block has been designated. Some are designed for south elevations, others for north elevations. Light-directing and light-diffusing blocks are available for these special applications. The blocks with fibrous glass inserts increase light diffusion on extremely sunny exposures. In addition to functional qualities the blocks have a new face pattern which permits easy cleaning.—PITTSBURGH CORNING CORPORATION, *307 Fourth Avenue, Pittsburgh 22, Pennsylvania.*

THE
REVIEW OF SCIENTIFIC
INSTRUMENTS

VOLUME 21, NUMBER 5 *MAY, 1950*

Some Properties of the Parallel Plate Spark Counter II

LEON MADANSKY[*] AND R. W. PIDD[†]
Brookhaven National Laboratory, Upton, New York

(Received September 2, 1949)

The delay error distribution of the parallel plate spark counter has been measured and the average delay is found to be 6×10^{-9} sec. The counters are, therefore, applicable to the measurement of lifetimes as short as 10^{-9} sec. Auxiliary circuits, including a fast synchroscope, for short time interval measurements are described, and the resolution limitations of the counters and circuits are discussed.

INTRODUCTION

A PARALLEL plate spark counter has been developed[1] which is satisfactory for coincidence counting, and the time resolution of a coincidence detecting system has been measured. The time resolution concerns the accuracy with which time intervals can be measured, while the maximum counting rate of the system, limited by a 0.001-sec. counter quench time, determines how quickly data may be accumulated. The resolution in time interval measurements is determined by the random delay errors in the counters and errors introduced by the recorder.

The delay error distribution for a counter is defined as the distribution of the time delays between the passage of a detected particle through the counter and the appearance of the counter pulse. In practice, the time at which the particle passed through the counter is detected by a second counter which will also have a delay error. Thus the measured distribution is the combined delays of the two counters. Constant delays are not important, since they can always be balanced by delay lines. However, the random delays introduce an error into time measurements. The shape and half-width of the delay distribution function present one of the limiting factors in the shortness of time intervals which can be measured by counters. For example, it can be shown that for a Gaussian delay distribution the shortest lifetimes which can be measured with counters in coincidence is of the order of 0.2 the width at half-value of the delay error curve.

The parallel plate counters were developed in order to obtain shorter delays than are observed in the cylindrical Geiger counter. The reason for the parallel plate design is that, since the electric field is uniform and the discharge is a spark, the initiation and propagation of the gas discharge should occur much more quickly than in the Geiger counter. It will be shown that the half-width of the delay error distribution is 6×10^{-9} sec.

THE EXPERIMENTAL METHOD

In the following experiments, beta-particles from a P^{32} source traverse two parallel plate counters. The counters have 98 percent efficiency for detecting beta-rays and operated with 0.001-sec. quench time. Figure 1 shows the experimental arrangements. The particles pass through the copper foil electrodes of each counter, producing an instantaneous coincidence. The solid angles are such that half the counting volume of counter *I* and all of counter *II* is utilized. The voltage pulse from counter *II* triggers a blocking oscillator which provides a brightening pulse for the scope. The same pulse is also delayed through 50-ohm coaxial cables and fed to one of the vertical deflection plates. The pulse from counter *I* is delayed and then triggers a sweep circuit. This delay amounts to about 3×10^{-8} sec. The pulse from counter *I* is also delayed in another channel and appears on the other vertical deflection plate. The vertical delays are adjusted to have the pulses from counter *I* and counter *II* appear displaced from one another on the sweep. The pulses are easily distinguished since they appear with opposite polarity. The time between these pulses is fixed so that the

---

[*] On leave from The Johns Hopkins University, Baltimore, Maryland.

[†] Now at the University of Michigan, Ann Arbor, Michigan.

[1] The technique of preparing the counters has been improved since the publication of Part I, Phys. Rev. 75, 1175 (1949). The details will be described elsewhere.

"tail" on the first pulse does not overlap the rise of the second. This arrangement provides that only pulses which occur within the sweep time will appear on the scope as a "coincidence." Events of this sort are photographed with a camera having continuously moving film. With a suitable calibration of the sweep one can measure the time delays between pulses and plot the distribution. A typical trace is reproduced in Fig. 2 together with a calibration which was a 106-Mc/sec. signal.

DESCRIPTION OF APPARATUS

The construction and preparation of the foil counters are described elsewhere.[1] The counters are shown in Fig. 3. It is important to shield the counters from one another, since the ultraviolet from the spark discharge in one counter can cause a discharge in the other. These spurious coincidences can be observed by their characteristically long time delay (~0.1 μsec.). A copper box is constructed around each counter, shielding it optically in order to avoid this effect. By placing a lead wall between the counters, thus preventing true coincidences, one could look for spurious coincidences. It was found that the shield was entirely effective and no spurious coincidences existed.

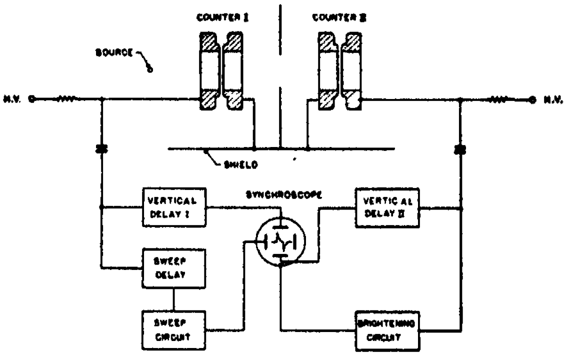

FIG. 1. Schematic diagram of experimental arrangement.

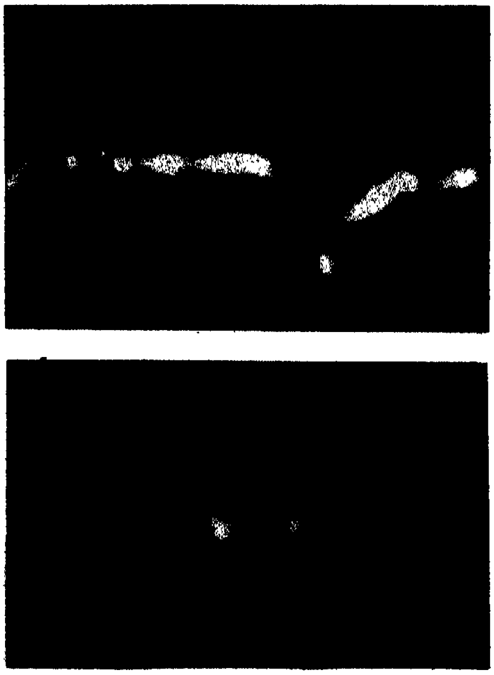

FIG. 2. A typical oscilloscope trace showing a coincidence. Lower figure is 106 Mc/sec. calibration signal.

FIG. 3. Photograph of foil counters.

The signals from the counters that are used to trigger circuits (about 200 volts) are coupled into 50-ohm coaxial cables, which act as delay lines, by 50-μμf condensers. The signals for the vertical pulses are coupled with 10-μμf condensers. The cables are matched at both ends to avoid reflections in the lines. Both counters are supplied with negative 4000 volts through 88-megohm resistors, which act as the quenching resistors.

The brightening circuit is a blocking oscillator having a pulse of 0.2 μsec. duration. The sweep signal is produced by charging a 50-μμf capacitor through an 807 tube that has been brought up to conduction from cut-off. The positive pulse that supplies the 807 grid comes from a blocking oscillator similar to the brightening circuit. The sweep has a duration of 5×10^{-8} sec. and occupies 3 inches of the scope face. All the voltages for these circuits are regulated to minimize random delays in starting times. The variation in starting time of the sweep circuit is about 1×10^{-9} sec. However, measurements are made on the intervals between the pulses from each counter, avoiding this error. The scope tube is a Dumont 5RP11 operated with 35-kv accelerating potential. A typical coincidence trace and the accompanying calibration is shown in Fig. 2.

The sweep is recorded on linagraph pan film with the use of a special Schmidt optics camera. The Schmidt mirror and lens system was obtained from the Edmund Salvage Company. The Schmidt camera has a f. 0.9 optical system and is provided with a continuously moving film feed. The line width of a typical trace with such a recording system is 5×10^{-10} sec. so that intervals of 10^{-9} sec. are clearly distinguishable.

ERRORS

The precision with which one can determine the delay errors are limited by two factors. First of all, the accuracy of the determination of the "break" of the pulse from the sweep base line is limited by the inherent curvature of the initial part of the spark pulse. Although the shape of the pulse is fairly constant, small changes in the slope and initial curvature do exist and produce small errors in determining the position of the pulse on the sweep. With these counters this error is $\pm 5\times 10^{-10}$ sec. The shape of the pulse is a function of counter spacing[2] and the resulting error must be determined for each particular design.

Since the sweep is non-linear, equal space intervals on the sweep trace represent different time intervals, depending on where in the sweep the intervals occur.

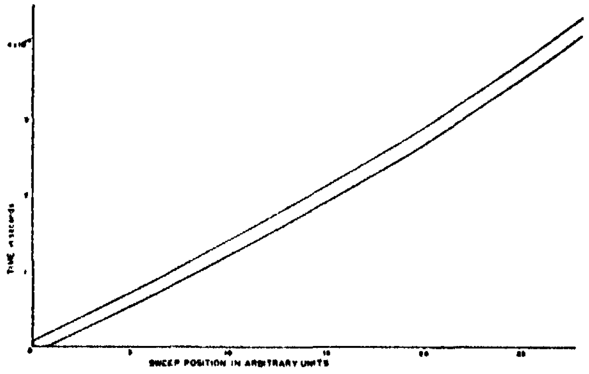

FIG. 4. Limits of calibration curves of sweep.

A curve can be plotted from which time intervals can be read as a function of the position of two pulses on the sweep. This curve is obtained by calibrating the sweep with a known signal (106 Mc/sec. in our case) on the vertical plates. The shape of the sweep signal, or the non-linearity, varies somewhat from sweep to sweep, so that the measured time intervals are uncertain by a small amount. Figure 4 shows two curves which represent the limits of any sweep calibration. About 90 percent of the sweeps fall well within these limits. At most, errors introduced by changes in the shape of the sweep signal amount to no more than $\pm 10^{-9}$ sec. The measured distributions of delay errors include the inherent counter delays as well as the effect of sweep error.

DISCUSSION OF THE RESULTS

The random time lags are measured as deviations of the time between pulses on the sweep from a fixed time interval, which represents true zero. This true zero time is measured by having a pulse from a single counter feed all four channels. The delay error distributions were obtained for several values of overvoltage. Some typical delay error curves are plotted in Fig. 5. These are for operation at 300 volts, and 1000 volts above the threshold for sparking. The width of the curves at half-value decreases with overvoltage until at 1000 volts one obtains a value of 6×10^{-9} sec. These results are in good agreement with the values of delay errors given by J. W. Keuffel.[3] The long delays that he describes ($>10^{-8}$ sec.) are probably due to sparking at the edges where the field is not uniform.[4] This was absent in our case, since the edges of the counters were well shielded by a collimator. In each of the cases the delay error distributions show a negligible probability for a pulse after a certain time. This cut-off is a true one, since no pulses were ever observed beyond this point in a total of 5000 counts. The curves are symmetrical, indicating that the counters are indeed alike with respect to time lag in spark initiation.

CONCLUSIONS

The results of these measurements may be analyzed in terms of the measurement of a lifetime of an excited state and time of flight of an elementary particle. A lifetime measurement involves first the detection of a particle that has left the nucleus in the excited state we wish to observe, and second, the emitted particle from the decay of this state. In many cases the first particle is the electron from beta-decay and the second is the internal conversion electron from the transition to the next lower state. Let $P(t)dt$ be the probability that the pulses from each counter will appear a time t apart on the sweep. We assume here that the delays of the cables and circuits have been subtracted out and that t is measured from a zero time. Thus, for simultaneous coincidences $P(t)$ is the delay distribution. This function is important in that it places a limit on the smallest life-

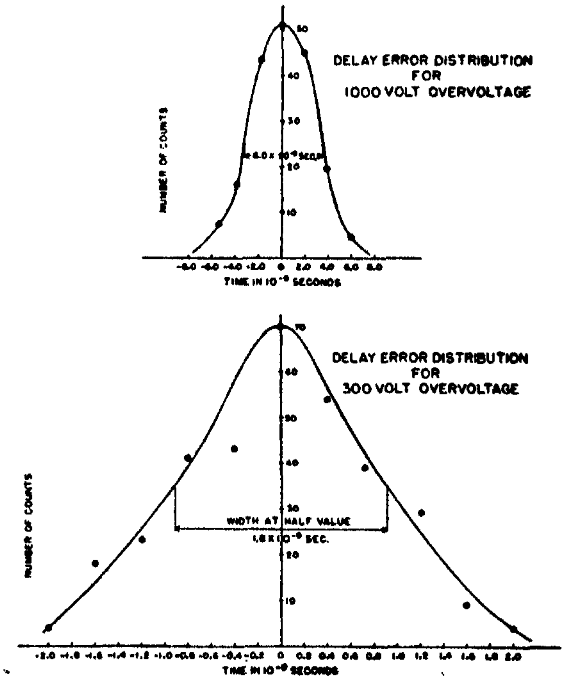

FIG. 5. Typical delay error distributions for spark counters with 300 volt and 1000 volt overvoltages.

---

[2] R. W. Pidd and L. Madansky, Phys. Rev. 75, 1178 (1949).

[3] J. W. Keuffel, Rev. Sci. Inst. 20, 202 (1949).

[4] Private communication.

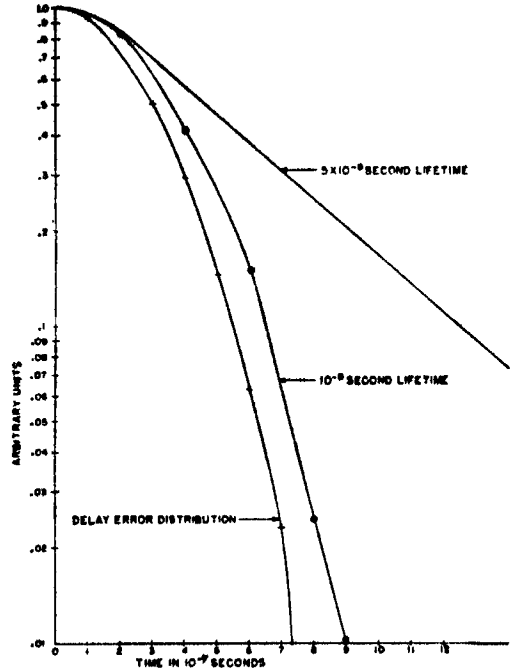

FIG. 6. Expected lifetime distributions for a delay error distribution with 6×10^{-9} sec. width at half-value.

times one can measure. It is easy to find the effect on this function $P(t)$ if the coincidences are not simultaneous but are a result of a true delay distribution in the source itself due to a short lived excited state. Figure 6 shows a typical random delay distribution curve for an experiment with the P^{32} source and counters operated at 1000 volts overvoltage. Additional curves illustrate the distributions one expects for states whose lifetimes are 10^{-9} and 5×10^{-9} sec. The fact that the delay error curves do cut off at a fixed limit allows one to consider the exponential tail on the observed distribution to be due to a lifetime and not to long time delay errors in the counters. It is clear that with 1000 volts overvoltage one can measure a lifetime of 10^{-9} sec. without much difficulty.

A second example is the measurement of times of flight. It may be assumed that the error in detecting a time delay is equal to the half-width of the delay error distribution. At beta $=0.75$ the time of flight of a particle between two counters spaced 10 meters apart is 4.45×10^{-8} sec. An error of 5×10^{-9} sec. in the time interval measurement would introduce a 13 percent error in the measurement of beta. In terms of a μ-meson the energy of a 50-Mev particle could be measured with an 8 percent error. The use of more than 2 counters in coincidence would sharpen the combined delay distribution and make an experiment of this sort more accurate.

There are two indications that improvement in the time resolution of spark counters may be obtained. Time lags of the order of 1 μsec. have been observed in the initiation of a spark at overvoltages of 5 volts.[5] Our data show that an increase in overvoltage from 300 to 1000 volts reduces the half-value width of the delay error distribution from 1.8×10^{-8} sec. to 6×10^{-9} sec. It would appear then that higher overvoltages would yield better counters. Although it is not practical to operate the present counters at more than 1000 volts above threshold with a 1-msec. recovery time, there may be counter preparation techniques which make it possible to operate at 3000 volts above threshold. Such counters have been made with the same technique of preparation but cannot as yet be systematically duplicated.

A second improvement in the counter resolution can probably be achieved by reducing the electrode spacing. Observations of the structure of the spark pulse displayed on the fast synchroscope show a time lag of 3×10^{-9} sec. in the development of the fast spark pulse when the electrode spacing is 4 mm. This time lag is reduced to 10^{-9} sec. when the electrode spacing is made 1 mm, hence reducing the error in reading the position of the initial rise of the pulse on the sweep. Time lags which are due to inhomogeneities of the electric field can also be reduced by better counter construction. The electric field in our counters was uniform in the counting region to within 1 part in 500. Further improvements in the recording circuits are in progress, with particular emphasis on the reduction of sweep errors.

ACKNOWLEDGMENT

The authors wish to thank Dr. J. B. H. Kuper for the courtesy of his laboratory and to express appreciation to his technical staff for their excellent cooperation. This work was done under the auspices of the U. S. Atomic Energy Commission.

---

[5] L. Fisher and B. Bederson, mimeographed abstract of papers at Brookhaven Gas Discharge Conference, 1947.

THE REVIEW OF SCIENTIFIC INSTRUMENTS VOLUME 21, NUMBER 5 MAY, 1950

A Differential Analyzer for the Schrödinger Equation*

R. L. Garwin
Department of Physics, University of Chicago, Chicago, Illinois

(Received August 29, 1949)

A rapid differential analyzer of accuracy about 0.5 percent is discussed and its performance reviewed. Extensions to differential equations other than that of Schrödinger are mentioned.

INTRODUCTION

For some time there has been a need for a small, simple differential analyzer. For example, in nuclear physics it is most convenient to have available a rapid method of solution of the one-dimensional Schrödinger equation,

$$(\partial^2\varphi/\partial x^2)+[E-V(x)]\alpha\varphi=0, \qquad (1)$$

for a large variety of functions $V(x)$. The problem undertaken in this research was primarily to design and build a machine capable of solving this equation, and, secondarily, to develop methods to be used in extending the usefulness of the machine to other problems. For most purposes an accuracy of solution of the order of one percent is sufficient, but 0.1 percent is desirable, and, as will be seen, readily achieved.

METHOD OF ATTACK

There are, in general, at least two overlapping classes of computing machines; analog and digital computers. In the Schrödinger problem either type may be used; for instance, a moving needle galvanometer with zero friction and zero restoring torque, the axis of whose coil coincides with the axis of the magnetized needle in the zero position, obeys the Schrödinger equation in the sense that if the current through the coil is made to vary in proportion to $[E-V(t)]$, the angular position of the needle as a function of time will be the solution of the equation

$$(\partial^2\theta/\partial t^2)+(K/I)[E-V(t)]\theta=0$$

over a considerable range of θ. This analog of the Schrödinger particle was not employed as a computer because of its severely limited scope.

A general analog differential analyzer (Bush type) adapted to the problem at hand has the form schematized in Fig. 1. Here a, b, c, and d are variables of the physical form required for the operation of the machine, i.e., shaft rotations, voltages, etc., and b_0, c_0 the initially given or assumed values of b, c. Now, from the nature of the individual units

$$a=db/dx,\quad b=dc/dx;\quad a=d^2c/dx^2$$
$$d=[E-V(x)]\alpha c=a;$$

so:

$$(d^2c/dx^2)+[E-V(x)]\alpha c=0, \qquad (2)$$

which differs from (1) only by a simple change of variable.

In a certain sense, a digital computer is the ideal type for almost any problem, especially if adapted to take data in the form of tables, graphs, or even rough sketches, but in the present state of the subject a small digital computer, though a powerful tool, is not available for this purpose. It should be noted, however, that if, as seems likely, storage mechanisms are improved, a small immensely flexible digital computer would certainly be a possibility.

It was desired to perform the required operations electrically insofar as possible to dispense with the usual gears, shafts, servos, etc. With the electrical methods available, however, a great simplification is achieved by making the independent variable the time, (t). Electrical methods have the advantage of flexibility, accuracy, economy, but suffer from limitations, the most severe of which restricts the most straightforward machine to linear differential equations.

The heart of the analyzer is the integrator unit which is derived from the simple resistance-capacitance integrator of Fig. 2 as follows.

The voltages in this circuit are connected by the relation $dE_0/dt=(Ei-E_0)/\tau$ where $\tau=RC$. Considering the voltages as variables, this network would be a perfect integrator if the term E_0/τ could be removed. Physically this term arises because the junction of the resistor and condenser is not always at ground potential, or in other words, τ is non-infinite. Evidently τ itself cannot be made infinite without losing a large factor in voltage in each integrator, so another method is employed; namely, to keep this junction at ground poten-

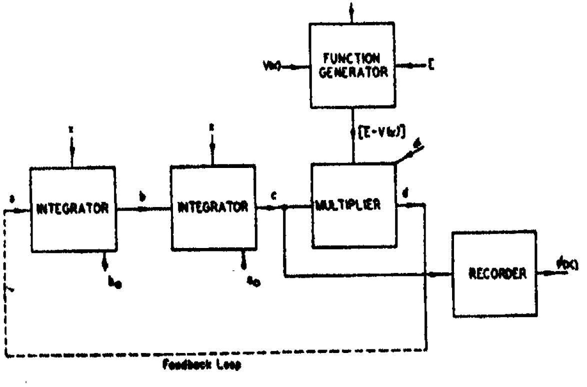

Fig. 1. Bush type Schrödinger differential analyzer.

---

* Part of this work was performed under an AEC Predoctoral Fellowship.

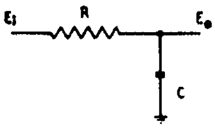

FIG. 2. Prototype electrical integrator.

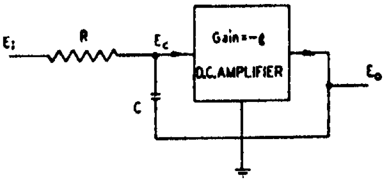

FIG. 3. Basic compensated integrator.

tial by using a feed-back amplifier to vary the potential of the bottom terminal of the condenser (Fig. 3).

Now the continuity equations for current give

$$\frac{E_i-E_c}{R}=\frac{-d(E_0-E_c)C}{dt}=-\frac{d}{dt}\left(\frac{g+1}{g}CE_0\right)$$

and for g large (in our case at least 10^6)

$$\frac{-dE_0}{dt}=\frac{E_i}{RC}+\frac{E_0/g}{RC}\approx\frac{E_i}{RC}.$$

It is to be noted that accuracy of integration depends only on the minimum variational g during the integration period, as well as on unwanted components of E_i, τ.

The major difficulties were three. It was found that most resistors of the value necessary are violently non-linear, but certain sputtered film or deposited carbon resistors afford a convenient solution to the problem.[1] The restriction is really quite stringent since for 0.1 percent accuracy in each integrator and 200 v applied to the resistors, a voltage coefficient of resistance less than 10^{-5}/v is required.

The second problem was non-ideal behavior of the condenser. Most condensers are satisfactory as regards leakage (it is evidently only terminal-to-terminal leakage that counts, since leakage to ground enters only as it affects g), but it is difficult to find a condenser which does not possess some dielectric "soak-in." A quite satisfactory solution to the difficulty was found in polyethylene film condensers[2] with leakage time constants $>10^6$ sec. and dielectric soak-in about 10^{-4}.

The third and by far the most difficult problem was the input behavior of the d.c. amplifier, that is, grid current and grid-cathode potential changes. It was felt that the use of standard receiving tube types was an important advantage worth considerable effort to achieve. Grid current was finally reduced to less than 10^{-9} amp. without tube selection by using a 6AK5 at 100-μa plate current. The grid-cathode potential was stabilized by regulating the average heater power to better than 0.1 percent by the scheme[3] illustrated in Fig. 4. In this circuit the filament of the first diode is operated at such current that the emission is temperature-limited. It is then easily shown that the sensitivity of the space current to heater voltage variation gives about 2 v change in plate potential for 0.1 percent heater voltage change. This error signal is then amplified and applied through the power output tube and transformer so as to maintain constant heater voltage.

After testing many circuit designs, several of which operated with considerable success (cascodes), the amplifier sketched in Fig. 5 was standardized. The amplifier pictured is connected as an integrator by the feed-back

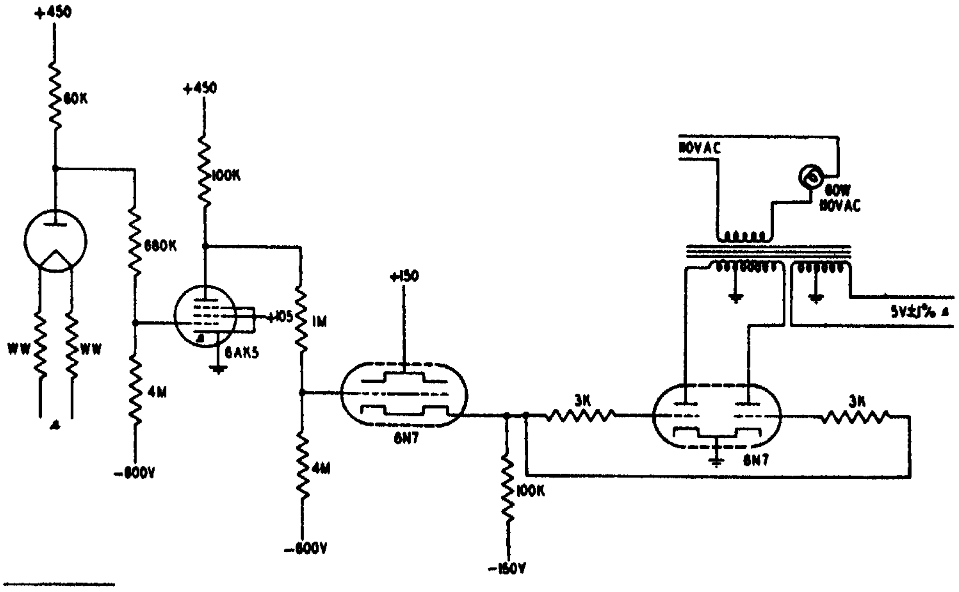

FIG. 4. An a.c. r.m.s. voltage regulator.

---

[1] *IRC* type *DCH*, linear to 10 parts/million/volt.

[2] Condenser Products Company, Chicago, Illinois, Type *LAC*.

[3] Independently developed, but similar to that mentioned by M. M. Hubbard and P. C. Jacobs, *Radar System Engineering* (McGraw-Hill Book Company, Inc., New York, 1947), p. 564.

condenser C. An important point to note is that because the non-fed-back gain of the amplifier is greater than 10^6, the grid of the first tube is always within 0.2 mv of ground, for an output voltage of -150 to $+150$ v. This fact allows the use of a simple method of setting initial conditions for integrators: If the input is grounded and the switch S_2 is closed, the output potential of the amplifier must adjust itself so that the first grid potential is zero. This can only be done by seeking a well-defined output potential for each setting of the coarse and fine initial condition potentiometers in the lower left-hand corner. (The initial condition is, of course, set by observing the output potential with the machine's accurate servomechanical d.c. voltmeter and adjusting the potentiometers to give the desired voltage.)

On opening S_2 no potential change larger than 0.1 mv is expected or observed. The switch must, however, be so modified by filing that the grid contact "makes" last and "breaks" first, for obvious reasons.

The properties of the amplifier, in view of its practically infinite gain, can be characterized by the behavior of the input circuit: grid current is always negligible, while grid-cathode potential changes (which may be compensated by varying the $5K$ cathode resistor) are less than 1 mv/hr. after a few minutes warm-up. It may be remarked that a grid potential change of 10 mv would be produced by a leakage resistance to the grid of 5×10^{11} ohms from a 500-v source. The trick is that the grid circuit is entirely separated from points at different potential by a grounded "guard ring," i.e., on S_2 only half the contacts are used, the others being grounded, while all grid wiring is enclosed in shielded cable. Thus the problem is simplified to that of keeping grid-to-ground leakage above 10^6 ohm, which is readily done. The only adjustment needed or possible in the amplifier is the compensation of grid-cathode potential changes by means of the variable first cathode resistor. This is accomplished by setting the input switch to $1M$ with input grounded. Any grid-cathode unbalance E then produces a rate of rise of the output voltage E v/sec. (for a 1-mf condenser) which is to be reduced to zero by varying the cathode resistor. The lack of grid current may be checked by observing that zero drift rate on $1M$ means also zero drift with the input switch at $10M$. Drift rates at high output voltages were checked by observing the output voltage with a 50-mv meter and a bucking battery. This drift rate is equal to that at zero output voltage because of the high amplifier gain.

For the usual integrating period of 30 sec., the amplifier characteristics are such that drift errors are held to 0.1 percent of full scale even on the shortest

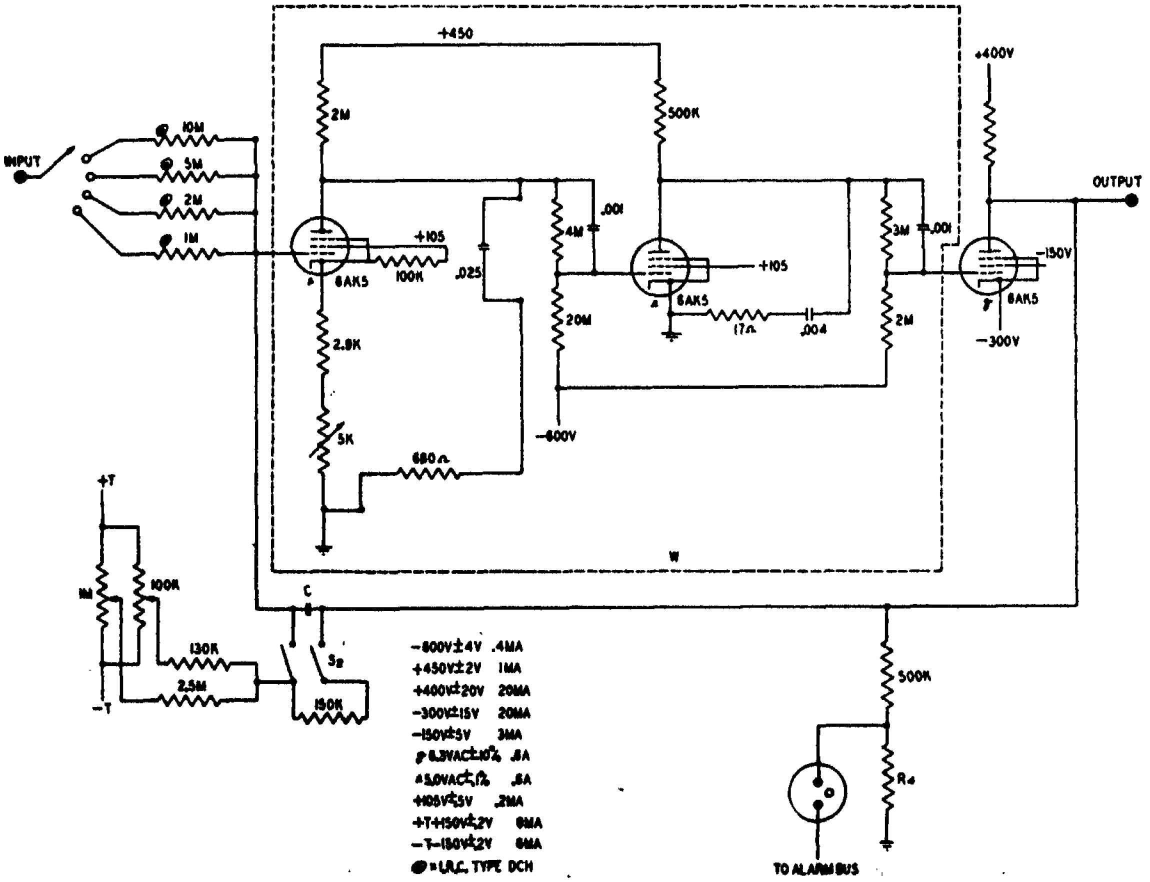

FIG. 5. Standardized d.c. feed-back amplifier.

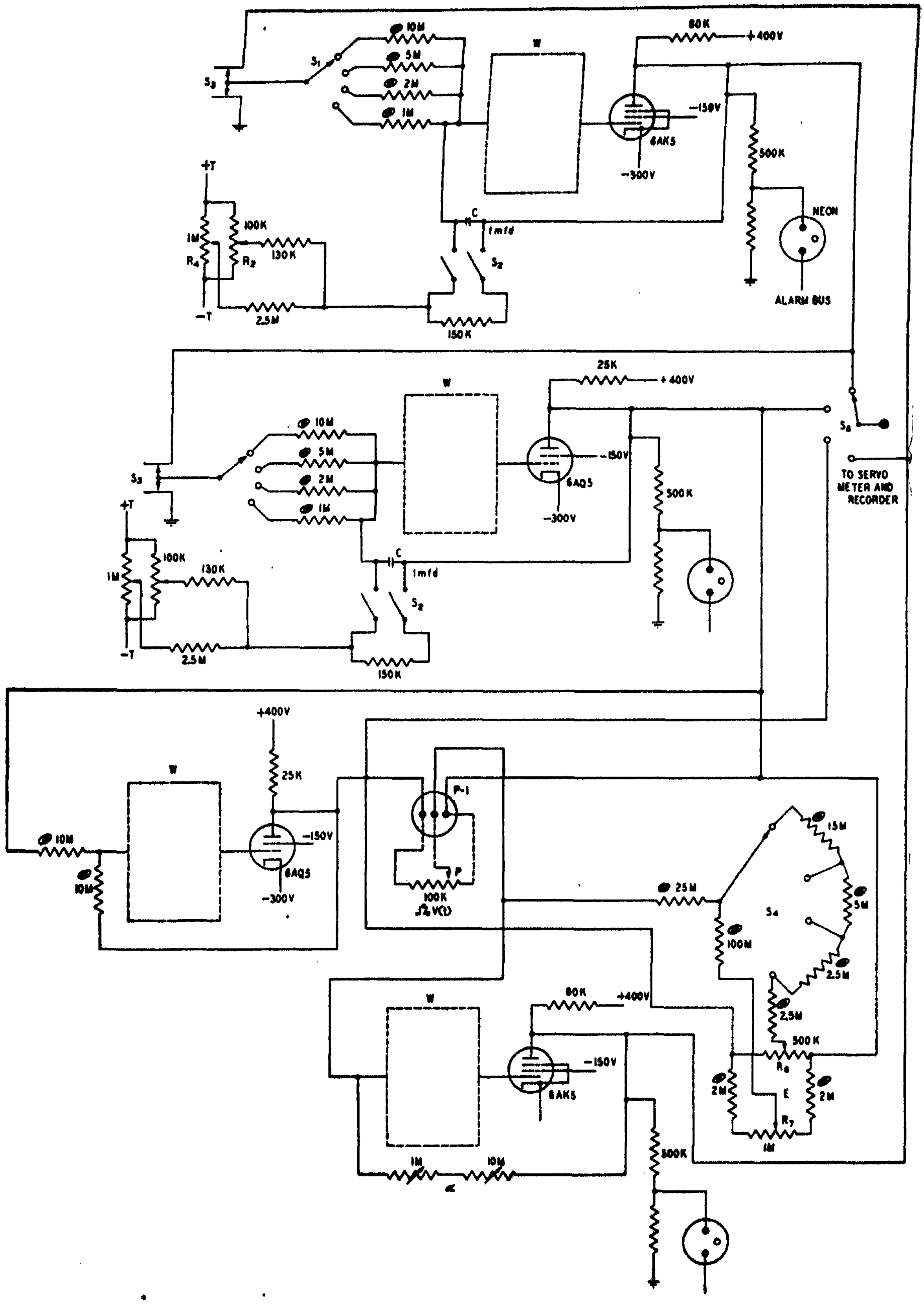

Fig. 6. Computing section.

time constant. The networks between first and second and between the second and third stages serve to stabilize the amplifier against high frequency oscillations, while low impedance (non-regulated) and separate power supplies for the first two and last stages serve to prevent low frequency instability. A power supply yielding many voltages was chosen rather than a more complicated integrator since the power supply may be used for a much larger differential analyzer without undue current requirements. With the proper output tube (6AQ5) and plate resistor, the amplifier is capable of an output voltage range of plus 150 to minus 150 v into a 10,000-ohm load, with, of course, negligible effective output impedance. Relays between units maintain isolation until the desired instant, and an overload signal is available from the neon lamp. The same amplifier may be used with a feed-back resistor in place of the integrating condenser to give an inverting amplifier, impedance changer, etc.

The overloading of any amplifier automatically turns off the multivibrator-controlled relays S_3 (Fig. 6), thus allowing the operator to adjust the various multiplying factors and initial conditions so as to keep the variables within range. This multivibrator is operable also from a start-stop foot switch and from contacts bearing on pencil lines marked on the graph carrying the potential function, allowing precise control of the integrating period. The scheme of the entire machine except for power supply and servos is shown in Fig. 6. Not shown in Fig. 6 are 20-mmf condensers across the feed-back resistors in the amplifier and multiplier sections. These, together with parallel combinations of 2200-ohm resistors and 0.01-mf condensers in the cathode of each of the four output tubes, effectively stabilize the system against phase shift oscillations caused by the capacitance to ground in shielded cables.

The machine thus consists of four "package" amplifiers identical except that two have polyethylene condensers as the feed-back elements, while two have linear resistances. The purpose of the integrators is seen from Fig. 1. The third unit is used as a phase inverter to give a voltage equal to and of polarity opposite from that appearing at the output of the second integrator. These two equal and opposite voltages are then added in varying proportion by means of the linear potentiometer P and the stable potentiometers R_6 and R_7. Thus if y is the voltage appearing at the output of the second integrator, $-y$ appears at the output of the phase inverter and $[E-V(x)]y$ at the input to the fourth unit. This fourth amplifier is really an impedance changer, its output completing the differential analyzer feed-back loop by being connected to the input of the first integrator.

During operation the finger of the linear potentiometer (P) is constrained, by hand or with a photo-cell +servo system, to follow the graph of $V(X)$ carried on a rotating drum, while another linear potentiometer and servo record the solution $\varphi(t)$ on a synchronously rotating cylinder.

PERFORMANCE

In order to find an eigenvalue and eigenfunction of a given Schrödinger potential, a trial E is chosen and a solution computed on the machine, with convenient initial conditions. By node counting and interpolation, a better trial value is found and the process repeated until the desired accuracy is achieved. Usually five repetitions (30 sec. per integration, 10 min. total) suffice for 0.1 percent accuracy in E.

Three identical brass scales are used with the machine: one on the servo output meter (equipped also with a switch increasing the sensitivity ten times), one on the pointer connected to the linear potentiometer P, and one for use in drawing input potential functions. The first step in the solution is to draw the potential function as large as will allow it to fit on the input graph, and to any convenient abscissa $x(t)$.

Next, one has to adjust the individual sections of the machine. This is done by throwing relays S_3 into the "rest" position by means of the foot switch and varying the cathode resistor in the first integrator until no drift is apparent. Evidently the switch S_1 should be set at $1M$ for this purpose. The same is done for the second integrator. Now with the output of the second integrator at zero potential the cathode resistor in the inverter is adjusted to give zero output voltage. With the output of the second integrator (and thus the inverter output) held at zero, the cathode resistor of the fourth unit is now adjusted until its output is zero. The only remaining adjustment consists of choosing the free oscillation period of the machine so as to make the analog "mass" of the analyzer equal to that of the Schrödinger particle. The mass of the particle is entirely fixed by wave-length at some energy E_0. The input potentiometer P is thus set at E_0 on the graph and the switches S_1 adjusted to give approximately the right period. The machine is then allowed to make an oscillation at this frequency, and the wave-length is measured. Any discrepancy between the Schrödinger wave-length and the period of the machine is then removed by changing the multiplying factor α in proportion to the square of the ratio of the wave-lengths. This also can be done without calibrated dials by using the servo voltmeter.

After this has been accomplished the physical analogy is complete and one can search for eigenvalues without the necessity of readjustment except at intervals of some hours.

A very rough estimate of the desired eigenvalue is made. The machine is then allowed to perform its solution of the differential equation for this trial eigenvalue. If, for instance, the ground state is desired, one counts the number of nodes in the trial solution. If the trial solution has a node a lower trial eigenvalue is selected and the solution drawn by the machine. By a simple process of extrapolation a better trial eigenvalue is found, two more trial solutions usually being sufficient to give 0.1 percent sensitivity in the eigenvalue.

The machine may be relied upon, when used properly, to give solutions of absolute accuracy 0.2 percent in not unfavorable cases. Of course, the machine solution must often be supplemented by asymptotic analytic solutions, especially at infinities in the potential.

This differential analyzer is also immediately suited to the solution of the paraxial equations for the path of charged particles in cylindrically symmetric magnetic fields and affords a considerable saving in time. Indeed, any second-order differential equation $y''+X_1y'+X_2y=0$ may be solved on this machine after first making the substitution $y=u\exp(-\frac{1}{2}\int X_1dx)$ to give $u''+[X_2-\frac{1}{2}X_1-\frac{1}{4}X_1^2]u=0$.

It is hoped to use the analyzer for the computation of nuclear potentials for nuclear shells. By adding two more input graphs the present model may be adapted to the solution of the relativistic Dirac equation where its main purpose may well be to provide experience and intuition as to the behavior of the solutions.

By the use of magnetic clutches[4] or hydraulic servo mechanisms operating on control powers of only a watt or so, it should be possible to perform multiplication, and hence all processes necessary to solve non-linear differential equations with linear circuits and potentiometers. Because of the use of linear elements, these solutions should be accurate to perhaps 0.1 percent with care.

ACKNOWLEDGMENT

The writer takes this opportunity to thank Professor E. Fermi for much help and encouragement in the prosecution of this project.

---

[4] Similar to those described by E. S. Bettis and E. R. Mann, Rev. Sci. Inst. 20, 97 (1949).

THE REVIEW OF SCIENTIFIC INSTRUMENTS VOLUME 21, NUMBER 5 MAY, 1950

Design and Operation of Liquid Nitrogen-Cooled Solenoid Magnets*

JAMES J. FRITZ[1] AND HERRICK L. JOHNSTON
Cryogenic Laboratory and Department of Chemistry, Ohio State University, Columbus, Ohio

(Received December 20, 1949)

This paper describes the design and construction of compact iron-free solenoid magnets cooled by immersion in liquid nitrogen. Construction details and performance data are given for two such magnets, which produce a magnetic field of 4000 gauss with a power expenditure of 2.7 to 3.3 kw. Heat transfer coefficients between copper wire and boiling liquid nitrogen have been measured for temperature differences between the wire and the liquid of 2 to 11°K.

FOR many types of magnetic measurements, it is desirable to obtain large magnetic fields by use of an iron-free solenoid. This is particularly true for measurements at the temperatures of liquid helium, where differential magnetic susceptibilities are often required. If such measurements are to be made precisely, hysteresis in the magnet must be eliminated, and the interaction between the magnet and small measuring fields must be reduced to a minimum. These conditions are best met by the use of a magnet which contains no ferromagnetic material.

TABLE I. Design requirements for liquid nitrogen-cooled magnets.

Magnetic field at full power	4000 to 5000 gauss
Variation of magnetic field along axis	No more than one percent over 1 cm from center
Maximum power expenditure	4 kw
Maximum consumption of liquid nitrogen	1200 cm^3/min.
Available voltage	190 v
Maximum current (for convenience)	30 amp.
Inside diameter	3 in.
Maximum outside diameter	6 in.

In designing a solenoid magnet, it is desirable to obtain as large a magnetic field as possible for a given amount of power under given conditions of working space and homogeneity. To achieve this, the magnet should be constructed from wire of as low resistivity as possible. It should be as compact in size as other conditions permit, and the space enclosed by the windings should be filled, insofar as possible, by the wire itself. Adequate provisions must be made for electrical insulation and for the removal of heat produced during operation. Wire size, total resistance, and the nature of electrical connections depend mainly upon the current or voltage characteristics desired, and do not greatly affect the power expenditure.

For most installations, these conditions can be met by a multilayer winding of relatively large wire, preferably of square or rectangular cross section, with spacings between turns and layers smaller than the wire size. Cooling can be accomplished by circulation of a non-polar liquid of low viscosity.

---

* This work was supported in part by the ONR under contract with The Ohio State University Research Foundation.

[1] Now at Pennsylvania State College.

DESIGN OF A LIQUID NITROGEN-COOLED MAGNET

It is obvious that the power consumption of a solenoid magnet can be reduced if the resistivity of the metal is lowered by cooling it to low temperatures. If this is done by immersion of the coil in a refrigerant such as liquid nitrogen, certain other advantages are gained. In the first place, the electrical energy can be removed by boiling the refrigerant. The rate at which liquid coolant must be supplied is considerably reduced, in comparison with that required for an ordinary cooling cycle. If a sizable reservoir of refrigerant is used, this will automatically supply the amounts required and needs only to be refilled periodically. Furthermore, heat transfer to a boiling liquid is excellent, and the viscosity of the liquid is at a minimum. Because of these factors, the area required for heat transfer and the spacing needed for liquid circulation are minimized.

The use of a magnet cooled by liquid nitrogen proves especially advantageous for work involving liquid helium, since the liquid helium container must be surrounded by liquid nitrogen or liquid air in any event. In a typical installation, a magnet immersed in liquid nitrogen can have an inside diameter of about 3 in., instead of a minimum of about 6 in. required for one operating at room temperature about the same apparatus. This affords a considerable increase in compactness.

Previous operations of solenoid magnets in liquid refrigerants has been reported by de Haas and Westerdijk,[2] who produced fields up to 250,000 gauss for periods of about 0.1 sec. with coils immersed in liquid hydrogen and in liquid helium. They extended methods previously used by Kapitza[3] for production of very large magnetic fields. For continuous operation at smaller magnetic fields, liquid nitrogen would appear to be a more efficient and less costly cooling medium than the lower boiling gases. However, if wire with a sufficiently low residual resistance (e.g., highly purified gold or copper) were used, it would be quite feasible to operate a magnet in liquid helium for moderate periods of time.

DESIGN DATA FOR LIQUID NITROGEN-COOLED MAGNETS

The design requirements set up for the present magnets are given in Table I. The conditions in Table I called for a winding which would produce at least 140 gauss per ampere at the center, and which would have a resistance between 4 and 10 ohms under operating conditions.

The length of the magnet was determined by the requirement for homogeneity of the magnetic field. Table II gives calculated values of the magnetic field per ampere turn per centimeter for several solenoids having dimensions of 7.6 cm (3 in.) I.D. and 14.0 cm (5½ in.) O.D. Values are given for the center of the magnet and for a point along the axis 2 cm from the center.

TABLE II. Field homogeneity for solenoids of various lengths.

Length of solenoid		Magnetic field per amp. turn per cm Gauss cm/amp. turn		Change in field over 2 cm from center
cm	in.	at center	2 cm from center	percent
10	3.9	1.388	1.312	5.5
16	6.3	1.671	1.639	1.9
20	7.9	1.768	1.763	0.3

As is apparent in Table II, a solenoid about 6 in. long produced fields with about the desired degree of homogeneity. Further reduction in length not only reduces the uniformity of the field, but also considerably reduces the current efficiency of the winding.

Commercial copper magnet wire was chosen as the most practical material for the winding. Its resistance was found experimentally to drop by a factor of 8 on cooling from ordinary temperatures to 77°K. This factor was used for design purposes.

It was decided that the turns on each layer should be wound as closely as possible, with spacings between layers to provide for refrigerant circulation. The problem of removing the heat evolved had two aspects. First, there must be sufficient area for heat transfer between the copper and the boiling refrigerant. Second, the spacing between layers must be adequate to provide for exit of nitrogen vapor and entry of fresh liquid.

Heat transfer data for boiling liquid nitrogen were not available. Estimates from the equation of Jakob[4] indicated that the heat transfer coefficient from copper to boiling liquid nitrogen should be about 10 times the corresponding coefficient for water, and should be represented by

$$h=5\times 10^{-2}(\Delta T)^4 \text{ B.t.u. hr.}^{-1}\text{ ft.}^{-2}\ (^\circ\text{F})^{-1}, \tag{1}$$

where ΔT is the temperature difference between the metal and the liquid. On the other hand, Giauque[5] quoted a value of 335 B.t.u. hr.$^{-1}$ ft.$^{-2}$ (°F)$^{-1}$ for liquid oxygen with a ΔT of 3.6°F. This is about 50 times larger than that which would be predicted from Eq. (1). For design calculations Eq. (1) was used, since it certainly gives a very conservative estimate of the heat transfer coefficient for moderate temperature differences.

The heat to be removed at 4 kw power input is 1.4×10^4 B.t.u. hr.$^{-1}$. For wires close-wound on a 6-in. length, the area available for heat transfer would be roughly $A=2\pi nld_{\text{Av}}$, where l is the length of the magnet, n is the number of layers, and d_{Av} is the average diameter. Calculations made with values of h given by

---

[2] W. J. de Haas and J. B. Westerdijk, Nature **158**, 271–2 (1946).

[3] P. Kapitza, Proc. Roy. Soc. (London) **115**, 658–683 (1927).

[4] H. J. Stoever, *Applied Heat Transmission* (McGraw-Hill Book Company, Inc., New York, 1941), p. 63.

[5] W. F. Giauque, Final Report on Liquid Oxygen Trailer Unit, OSRD No. 4141, p. XI-29 (1944).

Eq. (1) showed that the temperature difference required for the dissipation of 4 kw by a single layer coil should be no more than 13°C. For a multilayer coil it would surely be less, and heat transfer to the boiling liquid should present no serious problem.

At high power inputs, however, large amounts of nitrogen gas must be produced inside the windings. Sufficient space had to be allowed for the removal of the gas, since otherwise it might prevent the entry of fresh liquid, with consequent heating of the magnet.

In order to determine the amount of spacing necessary for proper gas and liquid circulation, a small model winding was constructed and tested. This model contained six layers of No. 20 copper wire, close-wound on a 2-in. O.D. form to a length of 3 in.; layers were separated by $\frac{1}{16}$-in. spacers. The coil had a resistance at 77°K of about 0.5 ohm. It was tested with currents up to 26 amp. (325 watts power input). Resistance measurements during operation indicated that the wires heated 1 to 2°K immediately upon application of the maximum current, and did not heat any further. The area of spacing was 18 cm^2; at 325 watts the average velocity of the nitrogen gas must have been about 10 cm sec.^{-1}. From the appearance of the coil under test and the measured resistances, it was concluded that the velocity of the gas could be increased considerably, possibly to as high as 3 meters/sec., without denying the liquid proper access to the windings. Spacings less than $\frac{1}{16}$ in. could probably be used for most solenoids.

For spacings between $\frac{1}{32}$ and $\frac{1}{16}$ in., wire sizes between No. 20 and No. 24 could be used to meet the other specifications. Number 22 was chosen for reasons of convenience.

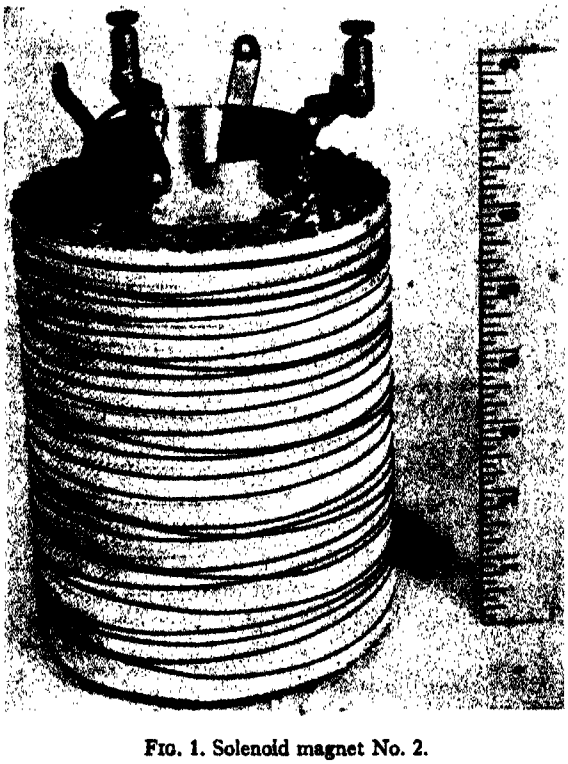

FIG. 1. Solenoid magnet No. 2.

CONSTRUCTION DETAILS AND PERFORMANCE OF LIQUID NITROGEN-COOLED MAGNETS

Two magnets have been constructed and have been operated at nitrogen temperatures. Both were 6 in. long and 3 in. I.D. and were of essentially similar construction. Magnet No. 1 consisted of 17 layers of No. 22 double cotton-covered magnet wire. The wire was wound as closely as possible on each layer; each layer contained 26 turns per inch. The layers were separated by strips of $\frac{1}{16}$-in. glass cord spaced about $\frac{5}{16}$ in. apart. In the process of winding, the strips were flattened somewhat; the average separation between layers was 0.040 in. The cords extended about $\frac{1}{4}$ in. beyond each end of the solenoid and were tightly laced with fish-line for stability. The outside of the solenoid was protected by a wrapping of 1-in. wide glass tape. The over-all outside diameter was $5\frac{1}{2}$ in.

Magnet No. 2 is shown in Fig. 1. It consisted of 16 layers of No. 22 single cotton-covered enameled copper magnet wire, with 30 turns per inch on each layer. In this case the spacers between layers were strips of $\frac{1}{32}$ in. by $\frac{3}{32}$-in. red fiber about $\frac{3}{8}$ in. apart. The average spacing between layers was 0.031 in. As can be seen from the photograph, the strips extended about $\frac{1}{8}$ in. beyond the ends of the solenoid. They were bent outward at the ends almost at right angles, so as to prevent movement of the copper wires. The outside diameter of the solenoid was 5.0 in. The inner brass tube can be seen above the top of the windings. It was 2.99 in. O.D. and $\frac{1}{32}$ in. thick. The tube was insulated by several coats of Formex, and was baked at 150°C after each application of the plastic. The first layer of the solenoid was wound directly on the insulated brass tube.

The details of support and electrical connection can be seen in the photograph. The two ends of the winding are brought to standard brass terminals mounted on brass supports attached to the central tube. They are insulated from the tube by strips of $\frac{1}{8}$-in. red fiber. The four brass strips which extend upward and outward from the top of the central tube permit support of the magnet from above by vertical bars or strips.

The electrical data on the two magnets are given in Table III.

The figures given for power consumption in Table III were calculated by use of the actual resistances of the magnets at currents of 20 to 22 amp. These resistances were slightly higher than the zero-current resistances listed in Table III, due to slight heating of the windings under heavy load. Both magnets have been operated at fields between 4000 and 5000 gauss, and magnet No. 2 has been operated continuously for about 5 hr. at 3700 gauss. No difficulties were encountered. The operation of the magnets was smooth and steady.

Heat transfer and gas liquid circulation in the magnets were extremely good. At 3500 to 3600 watts,

TABLE III. Electrical characteristics of nitrogen-cooled solenoid magnets.

Magnet No.	1	2
Resistance at 300°K	53 ohms	50.4 ohms
Resistance at 77°K	6.4 ohms	6.0 ohms
Gauss/amp. at center	179.5	197.1
Gauss/amp. 1 cm from center	178.5	196.1
Power consumption at 4000 gauss	3340 watts	2720 watts

resistance measurements indicated that the windings heated about 2°K above bath temperature. This pointed to a heat transfer coefficient of about 200 B.t.u. hr.$^{-1}$ ft.$^{-2}$ (°F)$^{-1}$, compared with a value of about 16 predicted by Eq. (1) and that of 335 for boiling liquid oxygen.[5]

The area available for passage of gas upward was about 36 cm^2 in magnet No. 2. At 3600 watts, the total amount of nitrogen evolved was 0.64 mole/sec., or 4100 cm^3/sec. at 77°K. Thus, the average gas velocity over the length of the magnet was about 60 cm/sec. There was no evidence that this was anywhere near the maximum velocity feasible. At high power inputs, the gas streams caused violent agitation of the liquid nitrogen above the magnet. It might be desirable to install a system of baffles or screens in the liquid to absorb the kinetic energy of the escaping gas and thereby reduce the agitation.

The liquid nitrogen was consumed at approximately the rate calculated from the power input, as it should be unless there were serious losses in the transfer system or in the nitrogen Dewar.

HEAT TRANSFER COEFFICIENTS FROM COPPER WIRE TO BOILING LIQUID NITROGEN

As an aid to further design, rough measurements were made of the rate of heat transfer from copper wire to boiling liquid nitrogen. For this purpose, a single layer coil of No. 34 double-enameled copper wire, 2 in. long and 2⅝ in. O.D. was used. The coil was wound on a Dilecto tube ⅛ in. thick, with turns spaced as closely as possible.

The test coil was immersed in liquid nitrogen with its axis vertical. The current flowing through the coil and the voltage drop across it were measured for power inputs from 0.4 to 1200 watts. These measurements were made with multirange meters to a precision of about 0.5 percent. The resistance of the coil between 77° and 90°K was calibrated against a thermocouple in a separate experiment and was thereafter used to determine the temperature of the wire.

Since the wire was wound tightly upon the form, which was a rather good heat insulator, only the outer surface of the copper could be effective for heat transfer. Estimates showed that heat conduction through the form to the inside could at most account for only a few percent of the power dissipated. The area used for calculations was the outside surface of a cylindrical sheet having the dimensions of the coil. Although the outside area of the coil was somewhat larger than this, the portion inside the crevices between turns could hardly be more than slightly effective. The temperature difference used was that between the average temperature of the wire and the bath temperatures, since it could readily be shown that temperature differences inside the wire were negligible, even at the highest power input. The results obtained from a smoothed plot of the data are given in Table IV.

TABLE IV. Heat transfer coefficient from enameled copper wire to boiling liquid nitrogen.

Temperature of bath 77.3°K		Outside area of coil 0.115 ft.^{2} (107 cm^2)	
Temperature difference between coil and bath °K	°F	Heat transfer coefficient (h) B.t.u. hr.$^{-1}$ ft.$^{-2}$ (°F)$^{-1}$	Cal. sec.$^{-1}$ cm^{-2} (°C)$^{-1}$
2.0	3.6	320	0.037
4.0	7.2	780	0.092
6.0	10.8	1350	0.158
8.0	14.4	1675	0.197
10.0	18.0	1880	0.220
11.0	19.8	1915	0.225

As can be seen from Table IV, the heat transfer coefficient was roughly proportional to the temperature head. The value at a temperature difference of 3.6°F was almost identical with that given by Giauque[5] for boiling liquid oxygen.

Certain other observations were made during the experiments. The coil operated quite satisfactorily up to a current of 12.5 amp., but failed suddenly at about 15 amp. The current density at failure was about 5×10^6 amp. cm^{-2}. Later examination of the coil disclosed that in several spots adjacent turns had fused together when failure occurred. On the other hand, the enamel coating elsewhere in the coil showed no evidence of damage either in its appearance or in its electrical properties. It is quite probable that magnets could be operated successfully using enamelled or Formex-covered wire in place of the cloth-insulated wire used in magnets Nos. 1 and 2.

PRECAUTIONS IN THE USE OF LIQUID NITROGEN-COOLED MAGNETS

In the operation of liquid nitrogen-cooled magnets, particularly with high power inputs, it is essential that the liquid nitrogen used contain no appreciable amount of oxygen. Any oxygen present will be concentrated as the refrigerant is boiled off and replaced, and might eventually cause detonation of organic material present in electrical insulation, particularly if a short or a "hot spot" should develop. The fact that in the heat transfer experiments copper was fused in highly purified liquid nitrogen without detonation gives reassurance of the safety of this medium. However, a similar occurrence in refrigerant containing an appreciable amount of oxygen could easily lead to a serious explosion or a bad fire. (It should be noted that the copper fused at a current density about 10 times higher than the maximum used with magnets 1 and 2.) If sufficiently pure nitrogen could not be obtained, it might be necessary to withdraw the refrigerant when the oxygen concentration reached a few percent and replace it with fresh liquid. This hazard could be reduced by keeping the amount of inflammable insulating material to a minimum, but it can hardly be eliminated completely.

It is also essential that provision be made to maintain the nitrogen level safely above the top of the magnet at all times. Safety factors are provided by the large amount of energy required to heat the magnet from nitrogen temperatures even to room temperature and by the large increase of resistance as the temperature increases. In a test run, in which the liquid nitrogen was allowed to boil away completely, no difficulty was encountered so long as the nitrogen made any contact with the coil. However, when the level of the liquid was below the bottom of the magnet, the top heated faster than the bottom and was well above room temperature before the bottom had warmed appreciably.

SUMMARY

The use of boiling liquid nitrogen as a coolant makes possible the design of compact solenoid magnets capable of producing large magnetic fields with relatively moderate expenditures of power. These magnets are especially useful for work involving liquid helium. They can be designed to produce fields of 5000 gauss with currents of 30 amp. or less, so that standard laboratory equipment can be used for control of the electrical circuits. Design and operational data for two such magnets have been presented. As an aid to design, rough values of the heat transfer coefficients from copper wire to boiling liquid nitrogen, have been determined.

We wish to thank Mr. O. D. Gonzales and Mr. L. E. Davis for aid in assembly and test of the magnets and Mr. L. E. Cox for technical assistance in the actual construction.

THE REVIEW OF SCIENTIFIC INSTRUMENTS VOLUME 21, NUMBER 5 MAY, 1950

A Trigonometric Computer with Electrocardiographic Applications

RICHARD McFEE*
Departments of Electrical Engineering and Physics, Syracuse University, Syracuse, New York

(Received October 20, 1949)

An analog computer has been built which determines $(e_1^2+e_2^2)^{\frac{1}{2}}$ and Arc Tane_2/e_1 two thousand times a second with an accuracy of about five percent. Using amplified electrocardiographic voltages proportional to three perpendicular components of the dipole moment of the hearts electric field, a pair of computers of this type will be able to produce other voltages proportional to the magnitude and two directional angles of the dipole. This may simplify considerably the study of fluctuations in the direction of the dipole and the neutralization of the effects of abnormal heart positions.

INTRODUCTION

DURING a study of the character of the electric field of the heart it became apparent that the experimental application of the theory might be considerably simplified if computers of the type described here were available. The practical realization of this possibility required the answers to two questions; first, could apparatus which would meet the specifications be built, and second, what electrode systems on the body would furnish the required voltages? The computer discussed in this paper has answered the first question, but since the answer to the second question is at the moment only partially known, the apparatus cannot be put to immediate practical use. However, it is hoped that its principle of operation and the details of the circuits used, particularly the "baseline clamper," will be of general interest, quite apart from its specific medical application.

The application of a trigonometric computer to electrocardiography stems from an opinion, held by most but not all of those familiar with the situation, that the electric fields set up in the body by the heart may be considered due to a varying electric multipole located at the heart's center of which the dipole moment, or "heart vector" is usually predominant. Unfortunately, this opinion has been of limited practical value, partly because actual calculation of the heart vector is tedious, and partly because the measurement techniques which in actuality define the heart vector were, until recently, specified more or less dogmatically, the result being that its physical significance was debatable. Some recent work in this connection[1] has clarified the situation considerably, and it seems probable that the "best" positions for the electrodes will soon be determined.

The fluctuations of the heart vector are of medical interest chiefly because it is supposed to reflect the vectorial average of all the infinitesmal EMF's generated by the heart, and thus the average direction of the spread of the excitation wave and the relaxation process. At first it might seem that it could be best

---

* Now at the Heart Station, University Hospital, Ann Arbor, Michigan. This paper is based on a thesis submitted in partial fulfillment of the degree of Master of Science in Physics at Syracuse University.

[1] H. D. Burger and J. B. Milaan, "Heart vector and leads," British Heart Journal **8**, 157 (1946); **9**, 154 (1947); **10**, 229 (1948).

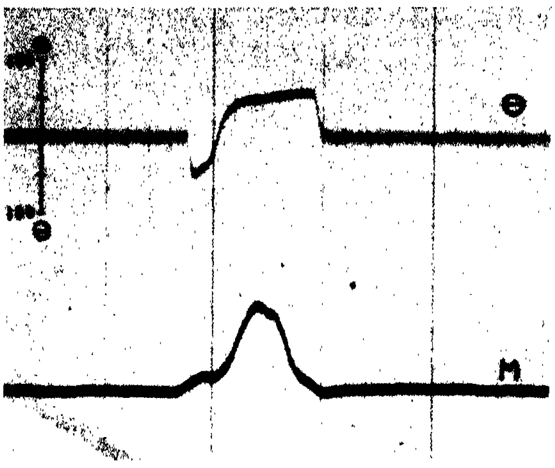

FIG. 1. A typical computer output.

studied in terms of time graphs of voltages proportional to its three components, but unfortunately unimportant changes in the angular position of the heart from individual to individual sometimes completely change the configuration of such records, obscuring other features of its variations which may indicate the presence or absence of heart disease. These "other features" referred to are usually relative angles; for example, the difference between the directions of the dipole during the beginning and end of contraction, or the abrupt changes in the direction of the dipole during the excitation process.

The problem of portraying the fluctuations of the heart vector in a fashion which emphasizes the relative angles has been attacked thus far through the use of the vectorcardiograph.[2] The latter is a cathode-ray tube with one component of the dipole on its vertical plates and another on the horizontal plates. The result is that the spot is displaced from the origin by these voltages and is viewed as a point in a plane, of which the polar coordinates are evident. By obtaining two vectorcardiograms with different pairs of components, it is possible to infer the variations in the direction of the heart vector with considerably less difficulty than with time graphs of the three components.[3] The recent development of the steroscopic cathode-ray tube presentation has enabled considerable extension and refinement of this vectorcardiographic approach.[4, 5]

The application of a trigonometric computer to this problem can now be explained. Such a computer can be used to obtain voltages proportional to the *spherical coordinates* of the heart vector; i.e., to the latitude angle $\phi(-90° < \phi < 90°)$, the longitude angle $\theta(-180° < \theta < 180°)$, and the magnitude M. When recorded on a time graph, these voltages yield information concerning relative angles in a singularly direct fashion. Furthermore, the angle voltages may be applied to the deflection plates of a cathode-ray tube, and the magnitude voltage to the intensity controlling grid, thus producing a simple map-like presentation of the variations of the heart vector throughout the beat.

Such voltages can be obtained with two computers each having two inputs (e_1, e_2) and two outputs (e_θ, e_M) related by the equations

$$\begin{aligned} e_M &= k_M(e_1^2+e_2^2)^{\frac{1}{2}} \\ e_\theta &= k_\theta \operatorname{Arc\,Tan}(e_2/e_1). \end{aligned} \tag{1}$$

The input of the first computer would consist of two amplified components of the heart vector, and the input of the second would use the magnitude output of the first and the third remaining component. The three remaining outputs would be the desired voltages.

A typical record of the output obtained from one computer of this type using only two components of the heart vector is shown in Fig. 1. Since only one computer has been built, similar records showing all three spherical coordinates are not available.

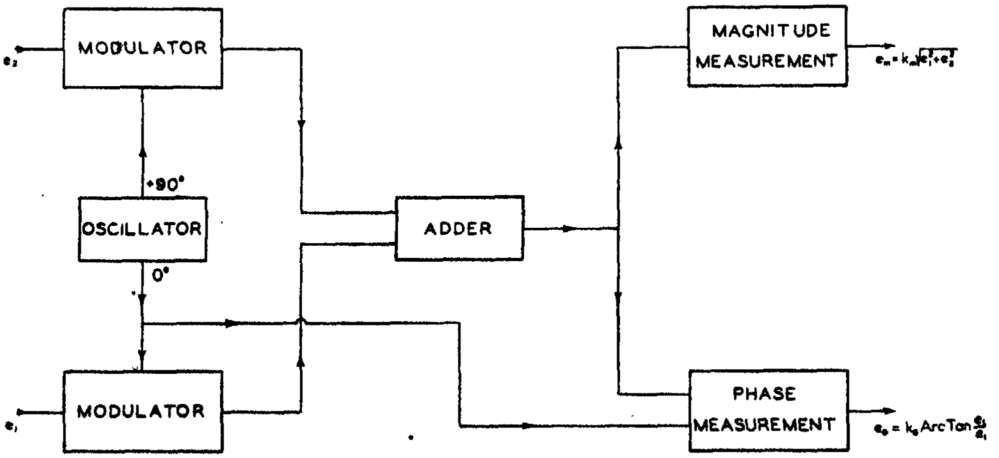
e_2
MODULATOR
+90°
OSCILLATOR
0°
MODULATOR
e_1
ADDER
MAGNITUDE MEASUREMENT
$e_M = k_M\sqrt{e_1^2+e_2^2}$
PHASE MEASUREMENT
$e_\theta = k_\theta \operatorname{ArcTan}\frac{e_2}{e_1}$

FIG. 2. Simplified block diagram.

---

[2] F. N. Wilson and F. D. Johnston, "The vectorcardiogram," American Heart Journal **16**, 14 (1938).

[3] P. W. Duchosal and R. Sulzer, *La Vectorcardiographie* (S. Karger, New York, 1949).

[4] B. Levine and O. H. Schmitt, "Three-dimensional vector-cardiography," a paper read at the Am. Physiol. Soc. Meetings, Detroit (April, 1949).

[5] O. H. Schmitt, "Cathode-ray tube presentation of three-dimensional data," J. App. Phys. **18**, 819 (1947).

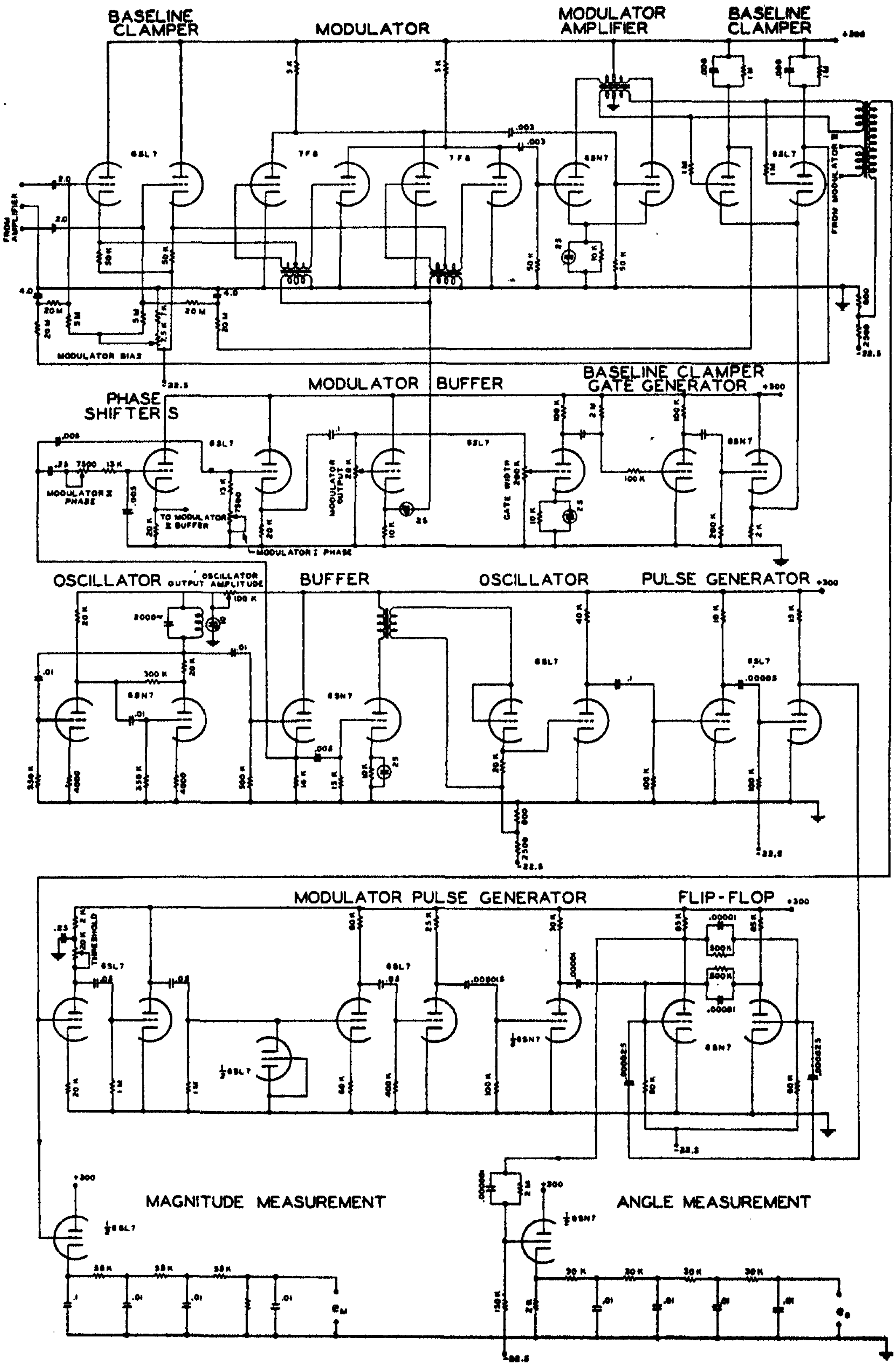

FIG. 3. Circuit diagram (does not show second modulator).

GENERAL DESCRIPTION OF THE COMPUTER

The computer operates by taking advantage of an analog between the equations (1) and the equations giving the phase and magnitude of the sum of two sinusoidal voltages ninety degrees out of phase with each other. In this latter case the well-known result is

$$V_1\underline{/0}+V_2\underline{/90}=(V_1^2+V_2^2)^{\frac{1}{2}}\underline{/\text{Arc}}\,\text{Tan}(V_2/V_1). \quad (2)$$

A similar use of this analog has been made previously in connection with radar ranging apparatus.[6]

In practice the two sinusoidal waves ninety degrees out of phase are obtained from a master oscillator and are separately modulated by the two inputs to the computer. These are added and the amplitude measured by an ordinary detector and the phase determined by comparison with the unmodulated output of the oscillator. A simplified block diagram of the circuits are shown in Fig. 2.

The basic circuits required are two modulators, two pulse generators, two baseline clampers, and an oscillator, a detector, and a phase measuring circuit. The construction of the particular circuits used is shown in the over-all circuit diagram of Fig. 3, and their roles are illustrated in the detailed block diagram, Fig. 4, and the timing diagram, Fig. 5.

The purpose of the baseline clamper is to make the outputs of the modulators zero when their inputs are at the baseline level, which is not necessarily zero. It will be described in more detail shortly. The modulators are more or less conventional, although designed for linearity, small variation in phase, and small harmonic distortion in their output. The harmonic distortion of the oscillator output is also intentionally low. The modulator pulse generator produces a pulse when its sinusoidal input passes through zero going positive, regardless of the amplitude of the latter unless the amplitude is very small, in which case no pulses at all are produced. The oscillator pulse generator produces a pulse when its input passes through zero going negative. The outputs from these pulse generators are applied to the grids of a flip-flop trigger circuit. The pulse from the modulator generator will make the output of this circuit flip up but not down. Oscillator pulses, on the other hand, will cause the output to flip either up or down. When the modulator generator is producing pulses the length of time the output of the trigger circuit is positive is determined by the phase difference between the outputs of the pulse generators. When the modulator generator is not producing pulses, the oscillator derived pulses trigger the flip-flop circuit at half the normal rate and produce a square wave at the output. The average of this square wave is the same as the average of the square wave produced when the magnitude of the heart vector is appreciable (thus causing modulator pulses) and the angle is zero. Thus when the angle is indeterminate, the angle voltage becomes equal to the zero angle value, which is desirable because it thus automatically shows the zero level. The phase measuring method involved here has been described previously.[7]

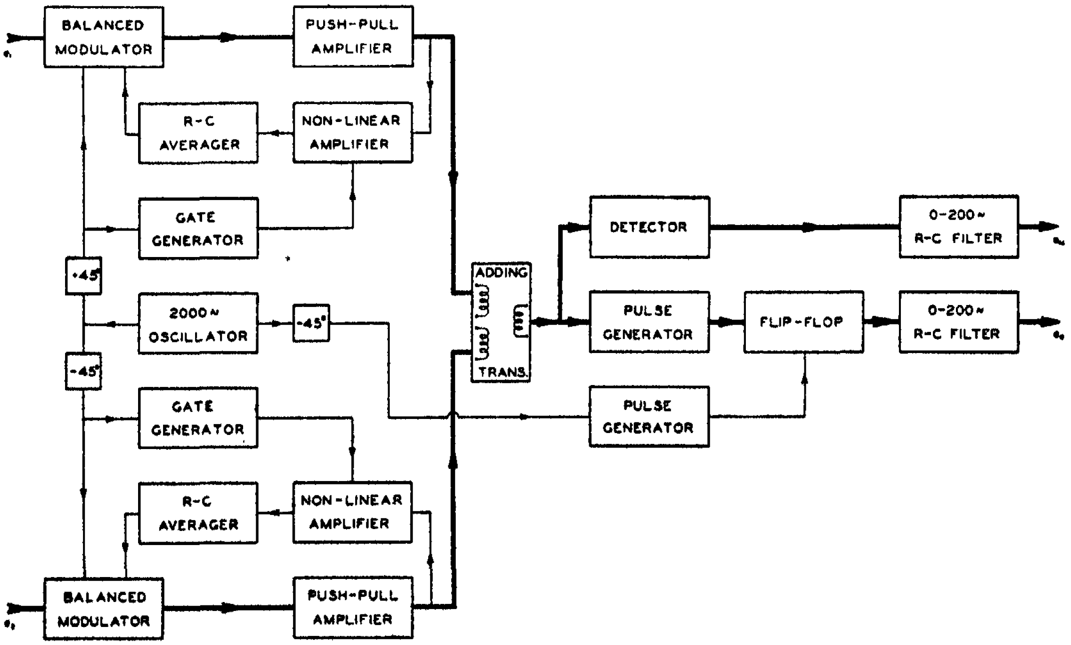

FIG. 4. Detailed block diagram.

---

[6] Greenwood, Holdam, and MacRae, *Electronic Instruments* 21 (McGraw Hill Book Company Inc., New York, 1948), MIT Radiation Series first edition, Chapter 6.

[7] Crufts Laboratory Staff (Harvard), *Electronic Circuits and Tubes* (McGraw Hill Book Company, Inc., New York, 1947), first edition, p. 854–855.

The threshold level at which the change-over occurs is adjustable. When it is set too low, small but rapid changes in the baseline level, sixty cycle pick-up and muscle tremor noise will cause large and erratic variations in the angle voltage output. When it is set too high, the angles associated with small magnitudes are not shown. Some compromise between messy records and more complete information is necessary, and this is made manually with the "threshold" control. This is the only control that needs adjustment during actual operation.

An oscillator frequency of 2000 cycles was chosen as a compromise between the greater difficulty in constructing pulsing circuits at higher frequencies and the modulators and filters at lower frequencies.

In order to avoid building the special low frequency pulse generators required to test the accuracy of the computer with the baseline clampers in operation, accuracy tests were made with the latter disconnected.[8] In one test a series of inputs were applied which corresponded to a heart vector of about three-quarters maximum magnitude rotating in discrete steps from −175 to +175 degrees. The error in the output voltage proportional to the angle did not exceed a value equivalent to five degrees, and the magnitude output voltage (which should have been constant) fluctuated about five percent. It is probable that this was due to changes in line voltage while the readings were being taken. The behavior beyond ±178 degrees became erratic, as would be expected, in view of the discontinuity at ±180 degrees. The second test was run keeping the angle constant at +45 and −135 degrees while varying the magnitude. A "compression" amounting to about four or five percent was noticed at maximum magnitudes. The angle voltage stayed constant within ten degrees down to about ten percent of maximum magnitude and within thirty degrees down to about five percent maximum. The error due to the baseline clamper is naturally uncertain, but the close agreement between plotted graphs of θ and M calculated from measured time graphs of the heart vector, and direct $\theta - M$ time graphs obtained from the same persons with the computer indicate that it is not excessive.

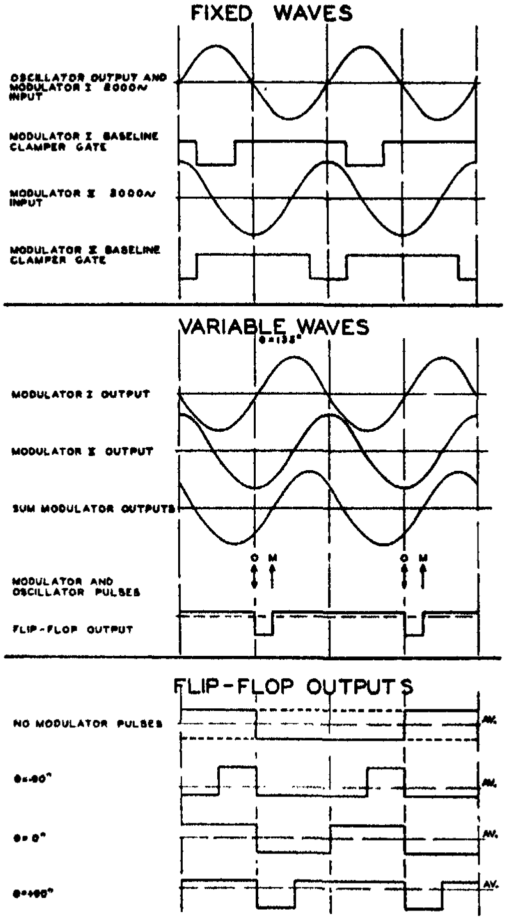

FIG. 5. Timing diagram.

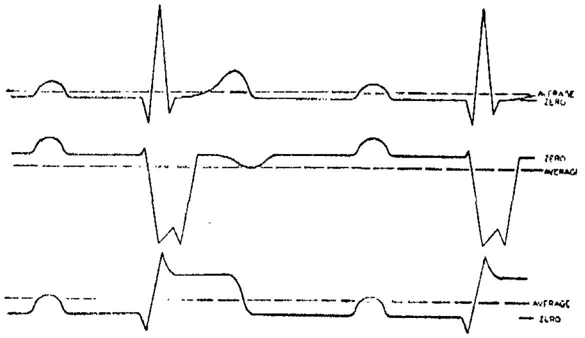

FIG. 6. Baseline and average levels for various electrocardiographic waves.

THE BASELINE CLAMPER

The baseline clamper as used here is a circuit which automatically adjusts the modulator so that its output is zero when its input voltage is at the baseline level. To illustrate what is meant by the baseline it is pointed out in each of the various electrocardiographic wave forms shown in Fig. 6. It has been found experimentally that these voltage levels occur when the heart is electrically inactive and consequently when the components of the heart vector are zero. Thus the baseline clamper circuit insures that the modulator output is zero when it should be.

Such a circuit is necessary because the actual modulator input voltage corresponding to this baseline level is usually *not* zero. Unbalanced electrolytic potential differences at the pickup electrodes produce this effect when d.c. amplifiers are used, and the difference between the average and the baseline levels (also shown in Fig. 6) produce it when low frequency a.c. amplifiers are used.

---

[8] Observation of the modulator output resulting from an amplified electrocardiographic wave applied to the input showed that the automatic adjustment made by the baseline clamper was identical to that which would have been made manually, if it had been necessary. It is difficult to specify any other way for telling whether or not the baseline clamper is "accurate."

Perhaps the simplest way to make the modulator output zero at the baseline level would be to connect an oscilloscope to the modulator output and manually adjust the modulator zero point so that the observed output was zero most of the time. However, such a manual adjustment has obvious disadvantages. Not only does it involve extra equipment and time, it also requires a difficult subjective judgement on the part of the operator. Furthermore, the input wave form will change slightly from one series of cycles to another making frequent and in some cases continuous adjustments necessary. As a result, an automatic adjustment is highly desirable.

The baseline clamper circuit operates by adding to the input voltage a d.c. voltage (which can vary slowly) strongly tending to make the time the modulator output is positive equal to the time it is negative. To see how this property produces the desirable result, consider the output resulting from a modulator input wave having the baseline level *above* the value giving zero output. If the input is at the baseline level for more than half its cycle, then the output will be positive for more than half the time. Similarly, if the baseline level is *below* the zero level, the output will be negative for more than half the time. Thus the baseline clamper will be in equilibrium only when the baseline level and the zero level are equal. The condition that the wave be at the baseline level more than half the cycle is sufficient but not necessary. A more exact statement is that the wave must be at the baseline level longer than the absolute value of the difference between the time it is above and the time it is below that level. This condition is met by nearly all electrocardiographic waves with recognizable baselines.

It is not difficult to construct a feedback circuit having this time equalization property. An amplifier can be gated so that its output is influenced only by the peaks of every other half-cycle of the input and so that it is overdriven by very small signals. Its output will then assume definite but different values for positive and negative (reversed in phase) inputs and its average output, except for a constant factor, will be proportional to the difference between the time its input is positive and the time it is negative. This average value is obtained with an *R-C* low pass filter and is fed back to the input of the modulator so that it tends to reduce itself. The system is essentially an error proportional servomechanism, and its design requires the usual attention to stability conditions. The actual circuit used for the baseline clamper is shown in Fig. 7. The triode amplifiers are gated by negative pulses on their cathodes. The tubes are cut off except during the pulses. During the pulses the large signal on the grid, of the order of fifty volts, either again cuts off the tube or else produces simultaneously grid limiting and plate saturation. The small plate condensers prevent the plate voltage from changing during one or two carrier frequency cycles but are not large enough to interfere with the relatively slow changes associated with variations of the modulator inputs. The *R-C* feedback path has a time constant of about forty seconds. It is felt that about double this value would give some improvement.

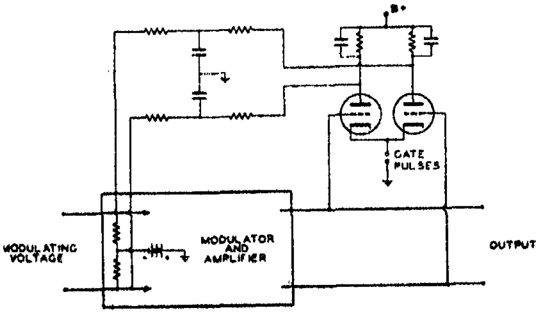

Fig. 7. Baseline clamper circuit.

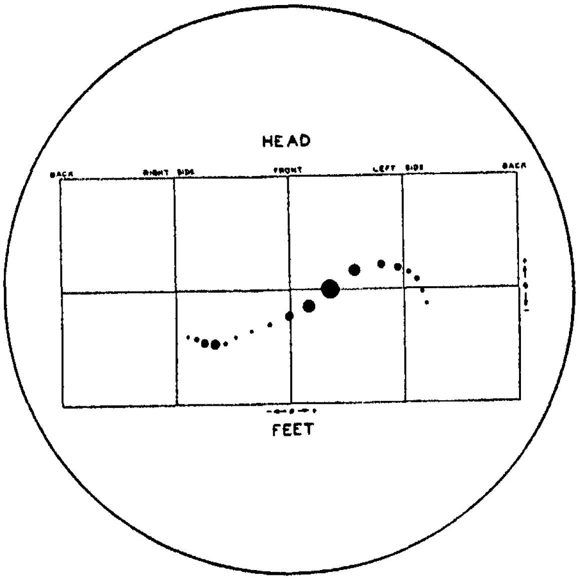

Fig. 8. Hypothetical heart vector map of ventricular excitation.

Even simpler baseline clampers can be constructed to operate with d.c. amplifiers, since they do not require special gating circuits.

THE HEART VECTOR MAP

It is of interest to outline how a maplike display of the three-dimensional heart vector can be achieved, even though this has not yet been done. If two computers are available, they can be interconnected so that one computer determines the magnitude and angle of the projection of the three-dimensional heart vector on one plane, and the second computer uses the "magnitude" output of the first and an additional heart vector component perpendicular to the first plane to determine the three-dimensional magnitude and second angular coordinate. Since the "magnitude" output of the first computer is always positive, the "angle" output of the second never exceeds ±90 degrees.

If the angle coordinate voltages are connected to the vertical and horizontal plates of a C.R.T., and if the magnitude coordinate voltage is used to focus and intensity modulate the spot, the map presentation is attained. To interpret this display we think of the heart as being surrounded by a sphere which is "mapped" onto the face of the cathode-ray tube in such a fashion that the latitude and longitude lines of the sphere form a rectangular grid. The position of the spot on this map corresponds to the place where the heart vector "pierces" the sphere, and the size of the spot corresponds to the magnitude of the heart vector. The spot can be turned on and off regularly, so that the time dependance of the heart vector is also evident. A photograph of the tube taken during the initiation of the contraction of the ventricles would appear similar to the sketch in Fig. 8.

The main purpose of this presentation would be to permit easy compensation for the effects of abnormal heart positions. By rotating the computer reference system it might be possible to reduce most normal map displays to a standard one (normalization). Electrical networks for producing such a rotation are already in use.[5] More careful study of the heart vector could be made by taking time graph records of the three spherical coordinate voltages after it has been normalized with the "map" presentation.

Since it is clear that considerable distortion of the movement of the heart vector would exist near the top and the bottom of the map, the normalization would be made so that the standard trace lay along or near the equator.

OTHER APPLICATIONS

Computers of this type have general application to any situation where Arc Tan(e_2/e_1) and $(e_1^2+e_2^2)^{\frac{1}{2}}$ need be determined rapidly. It is possible that careful design and construction would lead to accuracies within 1 percent for the magnitude output and within 1 degree for angles associated with fairly large magnitudes. The baseline clamper could be used as an automatic centering circuit for vectorcardiographs.

ACKNOWLEDGMENT

I am grateful to the many members of the Departments of Electrical Engineering and Physics at Syracuse University who have helped in the construction of the computer, and in particular to Dr. Wilbur Le Page, whose suggestions and encouragement had much to do with its success. Electrocardiographic tests were made with the space and equipment kindly furnished by Dr. J. S. Robb, of the Syracuse Medical School. The suggestions and criticism of Dr. Franklin Johnston, of the Heart Station at the University Hospital, Ann Arbor, Michigan, were of considerable help in the preparation of this paper.

THE REVIEW OF SCIENTIFIC INSTRUMENTS VOLUME 21, NUMBER 5 MAY, 1950

Vibration Studies: Related to Electron Microscopy

F. A. Hamm and F. C. Snowden
General Aniline and Film Corporation, Central Research Laboratory, Easton, Pennsylvania

(Received December 5, 1949)

This paper describes a convenient scheme for detecting and measuring vibration as related to the performance of an RCA electron microscope (Type EMU). The procedure involves the use of a Webster Model F5P2 phonograph pick-up arm in conjunction with a cathode-ray oscillograph. The cathode-ray oscillograph signal amplitude which represents the vibration of the location being investigated was calibrated by means of a Brush Development Company Type BL-301 vibration pick-up whose voltage output is proportional to the product of the vibration amplitude and the square of the frequency. An audio oscillator was used to calibrate the voltage output of the Webster (rochelle salt) pick-up as a function of frequency. After calibration, these oscillographic measurements may be used to determine absolute mechanical displacements.

Electron micrographs are included to illustrate the image displacements due to several different amplitudes of vibration. Cognizance of vibration is often necessary, especially in high resolution electron microscopy. This scheme may be used as a guide in high resolution electron microscopy.

INTRODUCTION

ELECTRON microscopists are becoming more critical of inherent and accidental instrumental limitations. This is the natural result of several factors—experience, greater interest in high resolution and the instrumentational type of research emanating mostly from the RCA Laboratories,[1] Princeton, New Jersey.

One of the accidental limitations is vibration. In this case the specimen moves, usually with a certain periodicity, with respect to the imaging system of the electron microscope. A resolvable image shift, whose magnitude is dependent upon the instrument magnification and vibration amplitude results.

The electron microscopist may have little choice in the matter of choosing a site for the instrument, thus, the critical investigator should be able to recognize prohibitive specimen vibration and expend some effort to eliminate it.

---

[1] Although many papers have been published, perhaps the one most pertinent to this subject is by James Hillier and E. G. Ramberg, "Magnetic electron microscope objective: Contour phenomena and the attainment of high resolving power," J. App. Phys. 18, 48 (1947).

It is the purpose of this paper to report on a convenient method for *detecting* amd *measuring* vibration as related to the performance of an RCA electron microscope in the hope that the dissemination of this knowledge may aid others. In general, this scheme may be put to the following uses: (1) to identify what combination of machinery is responsible for the vibration in the vicinity of the electron microscope or other instruments adversely affected by vibration, (2) to probe the building for the best location for the electron microscope, preferably before the initial installation, (3) to use as a guide for determining when the vibration amplitude is tolerable, especially when recording high magnification images.

GENERAL DISCUSSION

For several years it has been realized in this laboratory that specimen vibration was periodically prohibitive at high instrument magnification. The trouble was traced to a combination of large vacuum pumps, an air compressor, and a 15-hp air-conditioning unit, all located in the basement almost directly beneath the first floor location of the electron microscope. This service equipment had already been essentially isolated from the building by mounting it on large concrete slabs set in 4-in. cork. Some improvement was effected by remounting the service lines from this equipment to the basement ceiling with commercial vibration shock mounts. These shock mounts consist of rubber in shear bonded to metal.

It was soon realized that the elimination of these floor vibrations was a difficult, if not impossible, task. A careful analysis of the whole vibration problem was then made which revealed: (1) the three principal frequency components were 15, 60, and 300 c.p.s.; (2) the two lower of these components are the more difficult to suppress; (3) the intolerable floor vibrations occurred only periodically, that is, some frequent, but irregularly recurring, combination of heavy laboratory service equipment was responsible for the trouble; (4) the undesirable image shifts were usually observed only at high instrument magnifications above 15,000×.

TABLE I. Absolute vibration data.

Location of vibration	Amplitude in mils with air conditioner on 15 c.p.s.	Amplitude in mils with air conditioner on 60 c.p.s.	Amplitude in mils with air conditioner off 15 c.p.s.	Amplitude in mils with air conditioner off 60 c.p.s.
(1) Floor in front of diffusion pump	0.45	0.09	0.27	0.06
(2) Left side of deck;[a] forepump on	0.62	0.13	0.24	0.06
(3) Left side of deck; forepump off	0.62	0.13	0.15	0.04
(4) Right side of deck; forepump on	2.02	0.48	0.72	0.15
(5) Right side of deck; forepump off	2.31	0.40	1.10	0.12
(6) In hall, 9 ft. from the microscope	0.66	0.13	0.15	0.03
(7) Saturday morning[b]				
(a) Right side of deck			0.14	0.022
(b) Floor in front of diffusion pump			0.05	0.0074

[a] The red colored platform which slides over the instrument panel is referred to as the deck.

[b] All the other data were taken during week-day working hours. The electron microscope and all the service equipment in the basement had been turned off on that Saturday morning.

TABLE II. Vibration data related to electron microscopy.

Figure No.	CRO deflection[a] corrected to a gain set of 100 Max.	CRO deflection[a] corrected to a gain set of 100 Min.	Deflection breakdown by components 15	Deflection breakdown by components 60	Brush pick-up equivalent 15	Brush pick-up equivalent 60	Open circuit voltage r.m.s. 15	Open circuit voltage r.m.s. 60	Vibration amplitude in mils 15	Vibration amplitude in mils 60
2	1.6	0.9	0.34	1.24	0.07	0.72	0.0054	0.023	0.20	0.054
4	10.8[b]	4.5	3.15	7.65	0.66	4.45	0.058	0.14	2.13	0.33
5	9.9	4.5	2.70	7.20	0.57	4.18	0.049	0.134	1.81	0.31
6	3.8	1.3	1.26	2.51	0.27	1.46	0.023	0.047	0.85	0.11

[a] The Webster F5P2 was placed on top of the deck to the right of the column. In all cases the oscillograph *y*-gain was set at 50 except for Fig. 6 where 40 was used.

[b] This is only approximate because of trace length, but is within five percent of real value.

Several attempts to insulate the electron microscope from the vibrations were unsuccessful. A closer examination of points (1) and (2) above reveals why these attempts failed; the low frequency of the principal components of the vibrations observed makes difficult

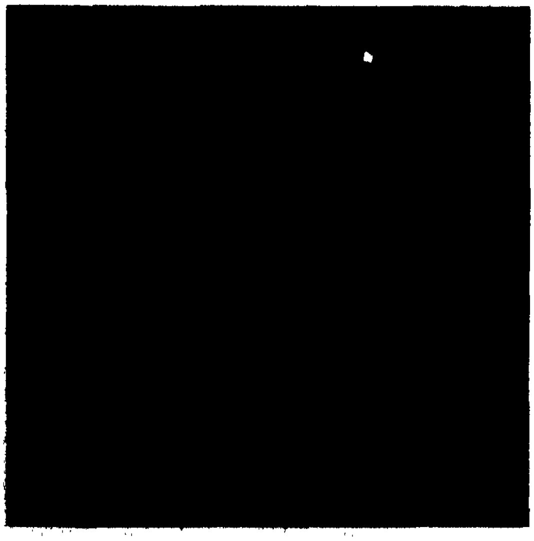

FIG. 1. 80,000×. Diatoms. No significant vibration.

FIG. 2. 80,000×. Camphor carbon black. Forepump on.

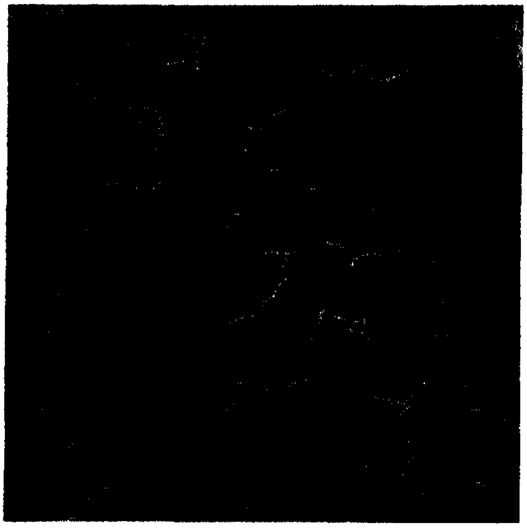

FIG. 3. 80,000×. Same field as Fig. 2. Forepump off.

their effective suppression. This is explained by the fact that for a given material the compression in inches *versus* the load in pounds is a fixed value. Similarly, the natural frequency of an insulating elastomeric mount is an inverse function of the static deflection of the mount under load. Calculations showed that for a 20-fold suppression of the 15 c.p.s. component a vibration mount exhibiting a static deflection of one inch and a natural frequency of 3 c.p.s. had to be found. Such a vibration mount cannot be purchased for a load as light as that of the electron microscope (875 lb.).

It was then decided to devise a technique for continuously measuring these vibrations, using such measurements as a guide for high resolution electron microscopy. It was also decided to move the instrument to a new location within the laboratory, making it necessary to measure floor vibrations at various possible locations. The subsequent section describes the method used. It must be remembered that this scheme does not represent an exhaustive appraisal of the problem, but it does afford a very satisfactory solution from the electron microscopist's point of view. However it is obvious that the data given in Tables I and II cannot be used by other investigators. Unless completely calibrated commercial vibration analyzing equipment is used, the investigator will have to calibrate his own scheme, which may be similar to the one described herein.

OSCILLOGRAPHIC MEASUREMENT OF VIBRATION

The preliminary step taken in the solution of this problem was the probing of the floor area in the vicinity of the electron microscope, and the red deck on the microscope itself, with a Webster Model F5P2 pick-up arm, the output of which was observed on a DuMont Model 208B oscillograph. Three principal frequencies were present in the troublesome vibrations of approximately 15, 60, and 300 c.p.s. The 15 c.p.s. was the envelope for the 60-c.p.s. component, and the 60 c.p.s. the envelope for the 300 component. The same three principal frequencies were observed at various intensities throughout the first floor of the building.

Once the frequencies of the vibrations were known, the horizontal gain control of the oscillograph was depressed to zero facilitating the reading of the maximum and minimum vertical traces. These vertical traces were proportional to vibration amplitude, and it was easily determined in which areas the vibration effects were minimum, and consequently which areas were best suited for the relocation of the microscopy laboratory.

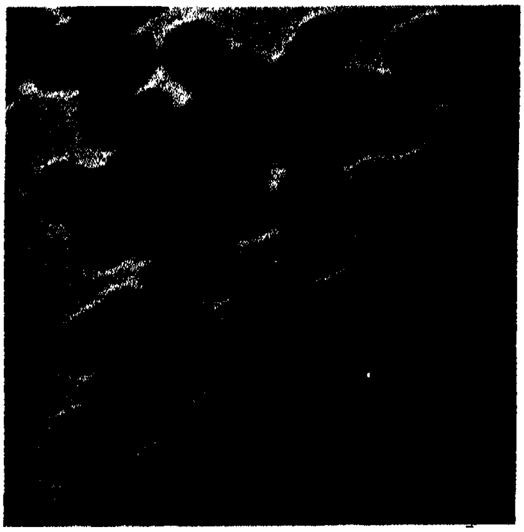

FIG. 4. 120,000×. Camphor carbon black. 200A shift.

However, this data, while useful, gave no information of an absolute nature required for correlation of image quality with actual vibration amplitude and for determining the critical vibration level. Since some indication of this critical amplitude level was desirable, a Brush Type BL-301 pick-up[2] was employed, permitting its calculation.

The Brush BL-301 is an inertia-type pick-up. Such pick-ups generate, piezoelectrically, a voltage which is proportional to the amplitude and the square of the frequency of the vibrations under investigation, when these vibrations are sinusoidal in nature. It was safe to make such an assumption on the basis of the vibration wave-forms as seen on the oscillograph. Thus,

$$e = kaf^2, \qquad (1)$$

where k is some constant of proportionality determined by the pick-up sensitivity. The sensitivity of the BL-301 is given as 30 v (open circuit r.m.s.) per 0.001-in. displacement at 500 c.p.s.[3] Under these conditions

---

[2] Manufactured by the Brush Development Company, 3504 Perkins Avenue, Cleveland 14, Ohio.

[3] This information is given in the manufacturer's data on the pick-up.

Eq. (1) becomes

$$e=0.12af^2. \qquad (2)$$

An investigation into the impedance characteristics of this pick-up reveals that the impedance is very nearly purely capacitative, the capacity of the pick-up at 40°C being 0.0015 μf.[3] This is the value used in subsequent calculations since the calibration measurements were made at ambient temperatures of 34–37°C.

The voltage E_g generated by the pick-up is the vector sum of the internal voltage drop E_i, and the external drop E_0 across the oscillographic input resistance. At the lower frequencies E_0, the actual voltage amplified, will be only a fraction of E_g, the voltage that must be substituted in Eq. (2) for the solution of the amplitude. It must be known, then, what fraction of E_g is represented by E_0 at the pertinent frequencies. These were calculated and found to be 27.8 percent at 15 c.p.s. and 74.5 percent at 60 c.p.s.

Since the Webster F5P2 pick-up is more sensitive at 15 and 60 c.p.s. than the BL-301, it was decided to calibrate the former with the latter. This also permitted the calculation of vibration amplitudes directly from the data already obtained with the Webster. Vibrations of known frequency from an audio oscillator were transferred to a hard table top through a radio speaker. The F5P2 pick-up was calibrated by comparing its output with that of the BL-301. The only assumption made was that the sensitivity provided by the manufacturer for the BL-301 was essentially correct, since we had no means for generating a vibration of known amplitude.

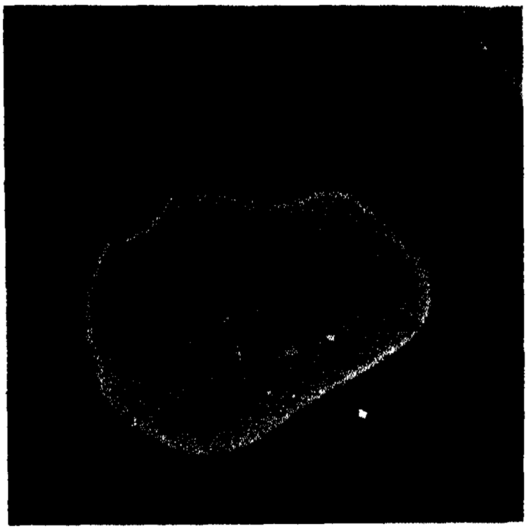

FIG. 5. 120,000×. Diatom. Forepump on.

The results of the calibration showed that at 15 c.p.s. the F5P2 was 4.75 times as sensitive as the BL-301, at 60 c.p.s. 1.72 times as sensitive, but at 300 c.p.s. only 0.33 times as sensitive.

Next the oscillograph sensitivity and amplifier gain were determined by the application of known voltages, first directly to the vertical deflection plates, and then to the amplifier input. The sensitivity was 24 v r.m.s. per 1-in. deflection above and below the normal position. The amplifier gain was 500. From the information now available it is possible to calculate absolute vibration amplitudes, and a list of the results obtained appears in Table I.

From Table I it can be seen that the vibrations are much more severe when a large air conditioner is on. This air conditioner is one floor level below the electron microscope.

It is peculiar to note that the vibration amplitude on the right side of the deck was actually less when the forepump was on than it was when the forepump was off. The authors have no completely satisfactory explanation of this phenomenon. The fact that the vibrations on the microscope deck are considerably greater in amplitude than those on the floor directly beneath it is indicative of the difficulties encountered in any attempt to damp out low frequency vibrations. The vacuum forepump is connected to the microscope valving block. Thus, in general, two sources of vibration must be considered—the forepump and the building vibrations.

Left out of the tables, purposely, were the results obtained for the 300-c.p.s. component present, because under the worst conditions encountered, the amplitude of this frequency was calculated to be only 0.000027 mil, or 0.007 percent of the corresponding 60 c.p.s. component.

Measurements were also made on a Saturday morning with all of the most troublesome machinery turned off. The results showed a spectacular decrease in the amplitude of the vibrations present. No 300-c.p.s. component was noticed at all, and the others were greatly reduced in magnitude. As an example, on the floor in front of

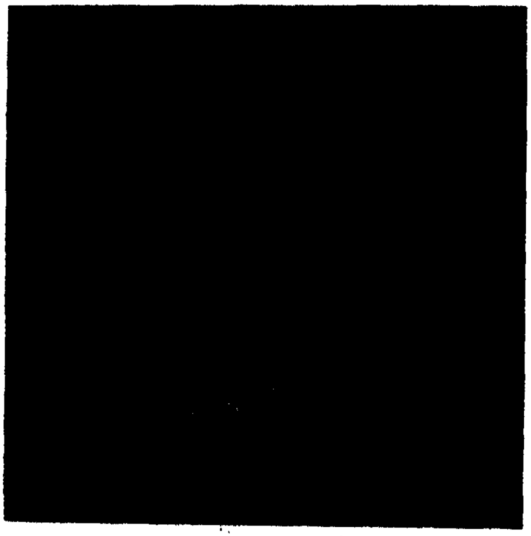

FIG. 6. 120,000×. Same field as Fig. 5. Forepump off.

the diffusion pump column the amplitudes of the 15- and 60-c.p.s. components were only 0.048 and 0.0074 mil, respectively. On the right side of the microscope deck, where the amplitudes always appear to be greatest, the results showed a maximum displacement of only 0.14 mil for 15 c.p.s. and 0.022 mil for 60 c.p.s.

The vacuum forepump (Cenco Hypervac 20) was mounted on thick cork in a coil spring suspension "cradle" bolted to the basement ceiling beneath the microscope. In spite of these precautions prohibitive vibration amplitudes are frequently exhibited by the action of the pump.

Since the detecting and measuring scheme described is admittedly only preliminary in nature, there are several considerations requiring some clarification. First, the piezoelectric crystal in the Webster pick-up is virtually insensitive to vertical vibrations; it is more sensitive to horizontal or twisting vibrations. Thus, the position in which the pick-up is placed with respect to the plane of vibration must be carefully considered. Displacements of the specimen in the horizontal plane, on the other hand, most seriously affect the quality of the final image. The electron microscope possesses a relatively large depth of field (*ca.* 0.5μ) which permits tolerating a fair amount of vibration in the vertical plane.

It is not intended to accept any vibration measurements obtained at places external to the specimen holder in the electron microscope as being representative of, or equivalent to, the actual vibrations extant on the specimen itself. This scheme is intended primarily as a *guide* to critical electron microscopy. Over and beyond the simple monitoring function of this method, however, it should be said that information of a more pertinent nature might well be obtained if a crystal pick-up system were permanently attached to the objective lens where the evaluation of vibration data would undoubtedly have greater significance. Completely absolute data describing the vibration of the specimen itself would be exceedingly difficult to measure. The virtue of the scheme described herein lies in its usefulness.

In order to achieve greater accuracy in relating the frequency and amplitude of vibration with image displacements, a Brush direct inking oscillograph Model BL-211 could be used. This instrument would provide a permanent record of the exact data for the relatively low frequencies usually encountered in the average laboratory. Errors inherent in estimating the length of an oscillographic trace would thus be precluded.

Although the procedure described in this paper enjoys advantages of simplicity and low cost, other methods are applicable. References[4] to these adaptable techniques are cited.

DISCUSSION OF ELECTRON MICROGRAPHS

The use of an auxiliary optical magnifier (RCA EMX-1) facilitates the detection of small image shifts in the electron microscope due to vibration, specimen drift, electrostatic charging, etc. At a total final magnification of 350,000×, image shifts on the order of 20A can be detected.

Although the effects of specimen drift and vibration are both almost invariably directional, a distinction can be made by careful examination of the image. Specimen drift can be detected at once by comparing the relative positions of the image on the five frames of the photographic plate. Conversely, serious vibration may cause the formation of a secondary image which is equally as sharp as the primary image. The displacement of these two images is a function of the vibration amplitude. If the vibration amplitude is small, a distinct "ghost" image may not be observable; instead the resultant 5 or 10A image shift normal to the direction of vibration appears only as a *broadened* white halo in an underfocused image. Fresnel fringes in underfocused images are an indication of good instrument performance. These interference fringes, on the other hand, may be observed in well-focused images which are affected by vibration.

The electron micrographs presented here were taken during periods when the oscillographic vibration data were recorded, with the exception of Fig. 1. The pertinent data are given in Table II. Image quality should be considered in terms of these data. All micrographs were taken at an instrument magnification of 20,000× with an exposure time of 15 sec. In general, the images are all somewhat underfocused. This is of no significance in this study.

Figure 1 is a high quality image of diatoms taken during a period when no oscillographic data were recorded. However, this micrograph was taken under optimum conditions for another purpose, and is presented here as an example of a micrograph in which no directional motions were present to affect the image. It should be used for comparison with subsequent micrographs most of which exhibit image displacements.

Slight specimen drift is illustrated in some of the following figures. This accidental factor is extremely difficult to avoid, and cognizance of this drift has been taken. It does not alter the significance of this vibration study in any sense. The arrows in the micrographs indicate the direction of the vibratory motion.

Figures 2 and 3 represent the first and second frames of the same plate. The mechanical forepump had been turned off during the second and fourth exposures. The level of vibration during the exposure of Fig. 3 was observed to be very low. A very slight specimen drift occurred during the photographing of this series, but it was a constant for each 15-sec. exposure and is of no significance in comparing these micrographs. The oscillographic signal induced by the deck vibrations indicates that there should have been *no* prohibitive vibration for any of the five exposures. Accordingly the presence of mechanical motion in Fig. 2 must be due to forepump action, which has a greater effect on the microscope column than on the deck; the forepump is connected to the microscope column through the valving block. This behavior has been observed repeatedly, although good quality pictures have occasionally been taken with the forepump on. All of the electron micrographs used in this paper were taken only when the effects of the vibration persisted in the instrument for periods of 30 sec. or more. In this way possible accidental effects from other sources than vibration are safely eliminated.

---

[4] W. Jay Kennedy, J. Opt. Soc. Am. 31, 99 (1941); H. H. Scott, J. Acoust. Soc. Am. 13, 46 (1941); R. O. Fehr, Gen. Elec. Rev. 45, 695–699 (1944); H. J. King, J. Inst. Elec. Eng., Part II 93, 435–62 (1946); A. J. Cogman, Electronic Eng. 19, 70–74, 109–13, 152–6 (1947).

The image illustrated in Fig. 4 resulted from an abnormally large vibration (cf. Table II) traced to the moving of a relatively light dolly down a nearby hall. Although this represents an exceptional case, it serves to relate in a semiquantitative way the relationship between image motion, and the mechanical displacement at the microscope deck. This image displacement in Fig. 4 is on the order of 200A.

Figures 5 and 6 depict the same field photographed within a 30-min. period. The vibration level indicated in Fig. 5 is typical of a good portion of the average working day. The seriousness of this condition is quite evident; the image shift is on the order of 100A. In Fig. 6 the same field is shown under somewhat better than average conditions. No attempt is made here to demonstrate high resolution; this micrograph is presented for comparison with that of Fig. 5 only. A first-order Fresnel fringe indicating a somewhat underfocused image suggests good instrument performance.

The decrease in the size of the hole in the diatom with prolonged exposure to the electron beam, which incidentally was never at maximum intensity, is apparent by comparing Fig. 6 with the previously photographed Fig. 5. A subsequent micrograph, not illustrated, exhibited a further decrease in the size of the opening. Specimen contamination alone cannot be held responsible for this change. Presumably silica in this thickness is expanded to a serious degree by the electron beam.

CONCLUSIONS

A convenient scheme for determining the proper location of an electron microscope and for serving as a guide to high resolution electron microscopy, when serious vibration is a factor, has been described. While the technique is only preliminary in nature its usefulness has been demonstrated by its constant use in this laboratory. This oscillographic method is especially useful for detecting relatively minor floor vibrations which may cause an image shift of only 10A.

The relation between image shift and microscope deck vibration is in general only qualitative. At present, the data available suggests that an instrument deck displacement of about 2 mils at 15 c.p.s. can be related to an image displacement of 200A, and a similar displacement of 1.5 mils appears to result in an image displacement of about 100A. This has been illustrated by a series of electron micrographs.

ACKNOWLEDGMENTS

The authors are indebted to L. T. Hallett who made this investigation possible, and to H. T. Page who recorded most of the oscillographic data compiled.

THE REVIEW OF SCIENTIFIC INSTRUMENTS VOLUME 21, NUMBER 5 MAY, 1950

A Rotating Specimen Mount for Use with X-Ray Spectrometer in Measuring Crystallite Orientation of Cellulosic and Other Textile Fibers

Leon Segal, Joseph J. Creely, and Carl M. Conrad
Southern Regional Research Laboratory,[*] New Orleans, Louisiana

(Received January 5, 1950)

The quantitative evaluation of crystallite orientation in textile fibers by x-ray methods is discussed. It is found that photographic recording and photometering of the resulting films can be replaced by automatic recording on a strip chart with the aid of an x-ray spectrometer with Geiger-Mueller counter. The design and details are given for a specimen holder capable of properly positioning and rotating a bundle of fibers in the x-ray beam so that the 002 or other selected diffraction arc passes before the window of the counter. A tentative procedure is outlined for evaluating, with the aid of this apparatus, the crystallite orientation of a bundle of cellulose fibers. Some typical recordings of the intensity curves of the 002 arcs from ramie, cotton, and high tenacity rayon are presented.

INTRODUCTION

SISSON and Clark[1] originally developed and applied the quantitative x-ray method for the estimation of cellulose crystallite orientation which, with some modifications, is largely in use at the present time. It was based on the concept, previously outlined by Weissenberg,[2] that the intensities of the diffraction arcs at any angle to the equator are proportional to the number of crystallites in the fiber at the same critical angle to the fiber axis. They made intensity measurements with a microdensitometer equipped with a rotat-

---

[*] One of the laboratories of the Bureau of Agricultural and Industrial Chemistry, Agricultural Research Administration, U. S. Department of Agriculture.

[1] W. A. Sisson and G. L. Clark, Ind. Eng. Chem., Anal. Ed. 5, 296 (1933).

[2] K. Weissenberg, Zeits. f. Physik 8, 20 (1921).

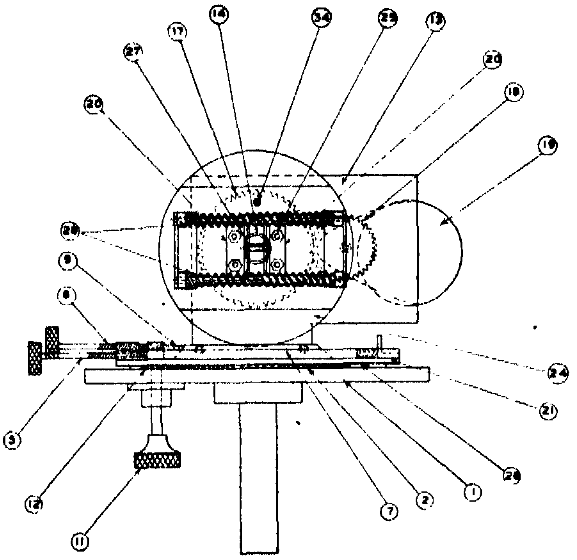

FIG. 1. Front view of assembled rotating specimen holder.

ing stage[1, 3] so that the flat photographic plate could be rotated through 360° while measurements of density were made around the selected diffraction arcs, particularly the 002 arc. The method was considerable refined by Berkley and co-workers[4, 5] who designed and applied a microphotometer for the purpose.

When a bundle of parallelized cotton fibers is placed in and perpendicular to the x-ray beam, the centers of the principal (equatorial) diffraction arcs on the flat plate are found to be located at right angles to the direction of the bundle or fiber axis. Providing the bundle has been well centered and held in a plane normal to the beam, these arcs will be symmetrical and concentric about the spot where the primary x-ray beam irradiates the fibers. It is obvious, then, that if the bundle axis is maintained in the plane normal to the x-ray beam and the bundle itself is rotated about the irradiated area as a center, the diffraction arcs also will rotate.

If, now, an efficient Geiger counter tube is placed at the proper angle to intercept a diffraction ray, then as the bundle is slowly rotated, the counter will actually measure, by counting the x-ray quanta, the changing intensity of the rotating diffraction arcs.

According to Friedman[6] the development of Geiger counter tubes and techniques has progressed to the point where one count is produced for almost every x-ray quantum entering the tube, as compared to the 10^4 to 10^5 quanta required to produce minimum detectible blackening on film. The Geiger counter, then, provides a very sensitive means of directly measuring radiation and when incorporated in x-ray diffraction equipment has been found by Buhler,[7] Decker,[8] Klug[9] and others to remove the limitations imposed by recording diffraction patterns photographically.

In the recording x-ray spectrometer where the Geiger counter output signals are led into a strip chart recorder, the x-ray intensities are plotted directly since the excursions of the recorder pen are proportional to the received intensities. By synchronizing the chart speed with bundle rotation, an automatic recording can be made of the intensities of the diffraction arcs being scanned. If the arcs from the 002 diffraction plane of cotton are selected for scanning in this manner, the resulting trace should be essentially comparable to the photometer curves of photographically recorded diffraction patterns obtained by Sisson[10] and by Berkley.[5]

The introduction of the Geiger tube eliminates in one step the entire problem of photographic recording with its limitations of proper exposure, rigid control of processing, non-linearity of film response, and tedious manual photometering of the diffraction patterns.

The present paper describes a specimen holder for rotating the fiber bundle in the x-ray beam together with suitable controls for centering and other adjustments.

THE SPECIMEN HOLDER

The design of the specimen holder provides the following essential conditions: (1) The size and shape of the entire unit conforms to the limitations imposed by the shape and construction of the spectrometer's x-ray

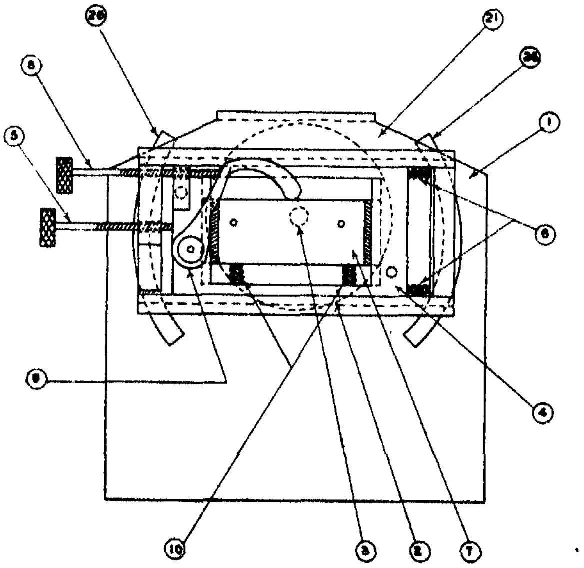

FIG. 2. Top view of adjustable stage.

---

[3] W. A. Sisson, Text. Research 7, 425 (1937).

[4] E. E. Berkley and O. C. Woodyard, Ind. Eng. Chem., Anal. Ed. 10, 451 (1938).

[5] Berkley, Woodyard, Barker, Kerr, and King, U. S. Dept. Agri. Tech. Bull. 949, 3–14, 57–61 (1948).

[6] H. Friedman, Electronics 18, 132 (1945).

[7] J. S. Buhler, Electrical Manufacturing (June, 1945).

[8] Decker, Asp, and Harker, J. App. Phys. 19, 388 (1948).

[9] Klug, Alexander, and Kummer, J. Industrial Hygiene and Toxicology 30, 166 (1948).

[10] W. A. Sisson, Ind. Eng. Chem. 27, 51 (1935).

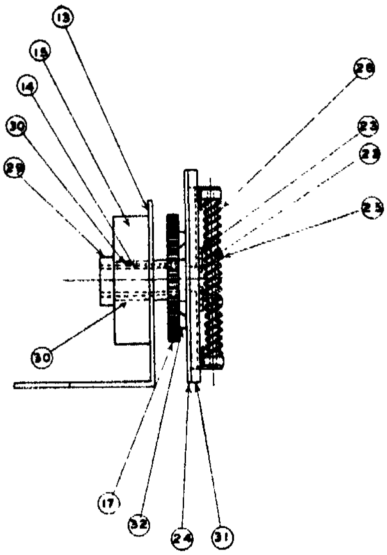

FIG. 3. Side view of rotating mechanism and bundle holder.

unit;† (2) the primary x-ray beam, the diffracted, and the transmitted beams are not blocked or shaded by any portion of the holder; (3) the fiber bundle can be clamped so that it is under constant tension and the fibers are held essentially parallel; (4) the bundle can be rotated at constant speed in a position such that the plane in which the bundle axis lies is always normal to the primary beam; (5) a movable carriage allows the sample bundle to be displaced with respect to the axis of the primary beam for the purpose of properly centering the sample bundle, displacements being made in vertical, transverse, parallel, and angular directions.

The complete mount consists of four parts: (a) the platform, (b) the adjustable stage, (c) the rotating mechanism, and (d) the bundle holder. The assembled mount is shown in Fig. 1, while in Fig. 2 is shown the adjustable stage.

(a) The Platform

The platform, 1 (Figs. 1 and 2), consists of an aluminum plate to which is fastened perpendicularly a steel shaft machined to fit into the specimen post socket located at the center of the graduated quadrant. The center-line of this shaft is considered to be the geometrical center of the system to which the sample is to be brought at all times in order to obtain at the counter diffracted radiation of maximum intensity. The pivot pin, 3 (Figs. 1 and 2), is attached to the platform to furnish the center for the angular adjustment of the stage. Fastened to the platform and concentric with the pivot pin are two outrigger bearing surfaces, 26 (Figs. 1 and 2), which support the adjustable stage at its outer edges and prevent it from tilting.

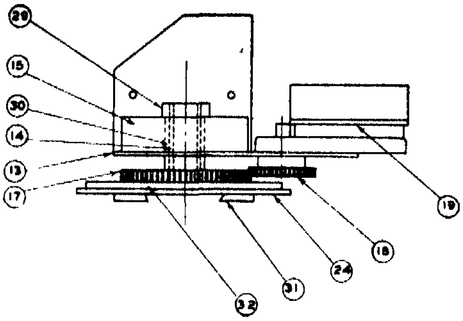

FIG. 4. Top view of rotating mechanism and bundle holder with clamps removed.

(b) The Adjustable Stage

This (Figs. 1 and 2), which permits centering the sample both in the x-ray beam and over the geometrical center, consists of three components which afford angular, transverse, and parallel adjustments.

Fastened to the underside of the brass plate, 21, is the gear, 2, for angular adjustment. This gear rests on the platform and is held centered by the pivot pin, 3, which fits snugly into the bore of the gear. The driving gear, 12 (Fig. 1), is fitted to the shaft and knob, 11, which projects through to the underside of the platform. Rotation of the knob causes the whole stage to rotate about the pivot pin as center, thus swinging the plane of the sample bundle into a position normal to the primary beam.

Transverse adjustment is accomplished by the movement of the transverse slide, 4 (Fig. 2), across the primary beam. This brass slide with beveled edges along its length moves between two brass rails which are fastened to the plate and whose undersides are so beveled that they serve to hold down the transverse slide. The transverse adjustment screw, 5 (Figs. 1 and 2), is threaded through a bar fastened to the plate. The screw presses against the slide and is opposed at the other end by the compression springs, 6 (Fig. 2), which are placed between the slide and a bracket fastened to the plate. The center portion of the transverse slide is open to allow insertion of the parallel adjustment slide, 7 (Figs. 1 and 2).

The parallel adjustment slide moves parallel to the primary beam, and its beveled edges slide in corresponding bevels along the edges of the open section of the transverse adjustment slide. Forward movement is caused by the action of the adjusting screw, 8 (Figs. 1 and 2), bearing against the lever arm, 9, which in turn presses against the back edge of the slide. The lever arm and threaded bracket for the parallel adjusting screw are both mounted on the transverse slide. The compression springs, 10 (Fig. 2), oppose the lever arm and afford backward movement. The purpose of this adjustment, in the direction parallel to the primary beam, is to bring the fiber bundle over the geometrical center.

---

† Although the North American Phillips spectrometer was used here, any appropriate x-ray apparatus may be used, perhaps with slight adaptations.

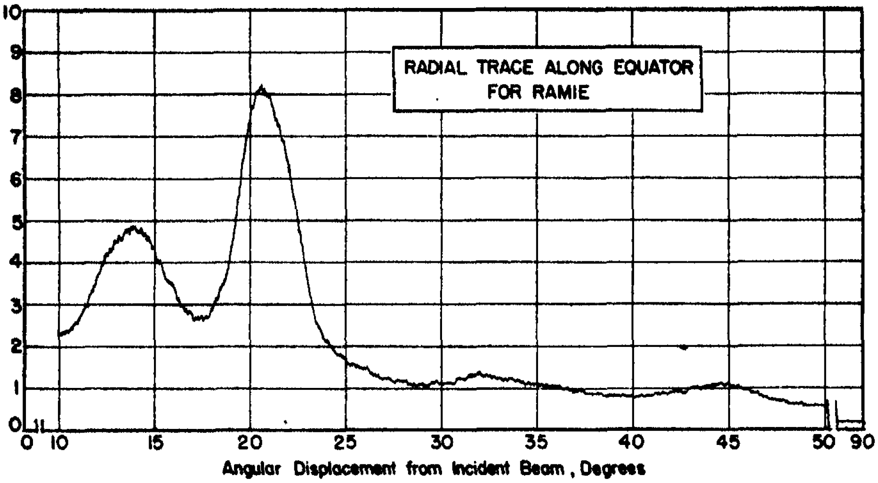

FIG. 5. Radial trace along equator for ramie.

(c) The Rotating Mechanism

The rotating mechanism, shown in Figs. 3 and 4, which also include the bundle holder, is that portion of the unit which rotates the bundle in the x-ray beam, causing the diffraction arcs to move across the window of the Geiger counter tube. An electric timing motor of two revolutions per hour (however, other speeds could be used) with right-hand, one-way friction drive, 19 (Fig. 4), turns the bundle holder through two gears, 17 (Figs. 3 and 4), and 18 (Fig. 4). The driven gear, 17, is securely mounted on a hollow shaft, 14 (Figs. 3 and 4), which turns with very little friction in the bushing, 30. The shaft and assembly are held in place by the hub, 29. The bushing holder, 15, and the synchronous motor are fastened to the upright portion of a 90° bracket, 13. The bottom horizontal portion of the bracket is fastened to the parallel adjustment slide. The primary x-ray beam which strikes the fiber bundle held by the holder mounted on the driven gear, passes through the hollow shaft, 14.

(d) The Bundle Holder

To facilitate loading, the bundle holder is detachable from the rotating mechanism. Attachment is made to the driven gear by means of a dove-tailed tongue and groove, 32 (Figs. 3 and 4). A positioning setscrew, 34 (Fig. 1), through the plate, 24 (Fig. 1), of the holder and bearing against the driven gear prevents sliding as the holder rotates. A dove-tailed groove, 31 (Figs. 3 and 4), on the front face of the plate, but at right angles to the tongue on the back face, holds the slides to which are fastened the clamps, 20 (Fig. 1). The purpose of the tongues and grooves on the back and front faces being at right angles to each other is to supply a further aid in centering the bundle.

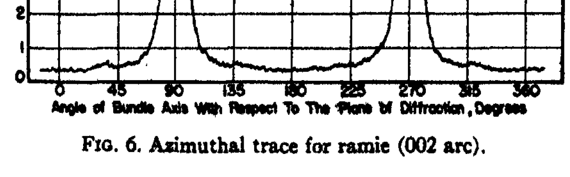

FIG. 6. Azimuthal trace for ramie (002 arc).

The lower jaw, 23 (Fig. 3), of each clamp is bolted to a slide, of which there are two. One of these slides has a set screw which locks it against the plate, while the other is forced outward by means of compression springs, 28 (Figs. 1 and 3), which are held in alignment by the internal, sliding rods and sleeves, 22 (Fig. 3). The steel combs, 27 (Fig. 1), located on the outer edges of the lower jaws serve to keep the fibers in the bundle parallel while under tension. The upper jaws of the clamps are tightened against the bundle by the hexagonal nuts, 25 (Figs. 1 and 3).

Vertical adjustment as such was not embodied in this model. The vertical dimensions of each component were held critical so that in the final assembly the horizontal diameter of the rotating bundle holder coincided with the center of the primary x-ray beam. A vertical adjustment can be incorporated by cutting a suitable thread on the upper portion of the steel shaft for a thin, knurled ring, internally threaded. This ring upon being rotated would raise or lower the entire assembly by bearing against the upper surface of the specimen post socket.

APPLICATION

For evaluating the crystallite orientation of a bundle of parallel fibers, the tentative procedure outlined below has been followed.

With the bundle holder detached and the combs in contact at the center of the opening, the bundle of fibers (weighing about 30 milligrams, combed and prepared in the conventional manner except not tied)

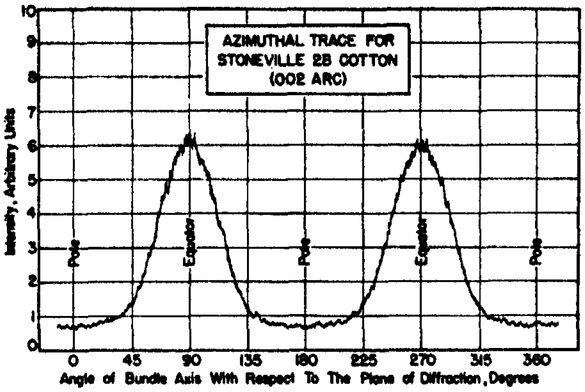

FIG. 7. Azimuthal trace for Stoneville 2B cotton (002 arc).

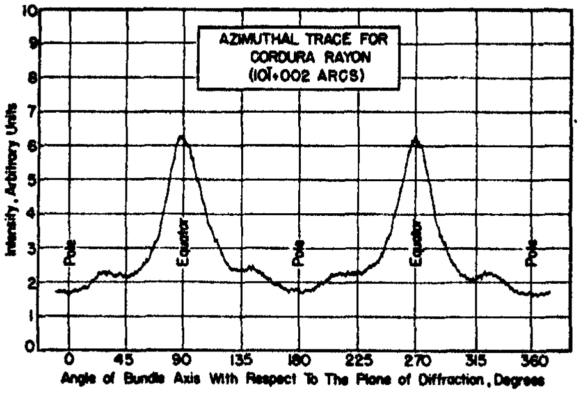

FIG. 8. Azimuthal trace for cordura rayon (10$\bar{1}$+002 arcs).

is inserted perpendicularly across the combs. The movable comb is then displaced to the edge of the opening, thus maintaining the fibers parallel. The jaw is then screwed down on the ends of the fibers, fixing them rigidly in place. The screw of the fixed comb is now loosened, and this comb moved to the other edge of the center opening. The jaw is tightened on the fibers, and the screw again tightened to fix the position of this jaw. The bundle is placed under tension by inserting the springs. The holder is centered on the mount and then rotated so that the axes of the fibers in the bundle are in the vertical plane. The x-ray port is now opened to irradiate the bundle.

For cellulosic as well as most other fibers the position of the diffraction arc to be scanned is located by first operating the scanning arm radially in the usual manner in conjunction with the strip recorder. Figure 5 shows the trace resulting when a bundle of ramie fibers was scanned radially across the equatorial arcs from 70° to within 10° of the primary beam. The chart is set to move at the rate of 1 inch per minute, although other speeds may be selected.

The scanning arm is next moved to the angular position indicated by the peak of the selected diffraction arc, and the exact position for the maximum intensity is found by a series of short scans. The recorded height of the peak may be varied within a considerable range by adjustments made at the recorder. After the counter is positioned at the point of maximum diffracted radiation, the chart of the strip recorder is shifted to bring one of the chart lines under the pen, and the apparatus is ready to scan the selected diffraction arc (azimuthal trace). Since the counter, tube, the primary beam, and the center of the bundle are located in the horizontal plane of diffraction, the equatorial diffractions will be recorded when the bundle axis is in the vertical position. The recorder and the rotating specimen holder are started simultaneously.

Figure 6 shows the recorded intensities of the radiation diffracted by the 002 planes of ramie cellulose while Fig. 7 shows a similar trace for the 002 planes of cotton cellulose. Figure 8 shows the trace received from the combined 10$\bar{1}$ and 002 planes of high tenacity rayon, the close juxtaposition of the two diffraction maxima preventing any appreciable resolution.

The marked differences in the shapes of the recorded intensities are due to the crystallite orientation of the fibers—ramie having the greatest orientation, high tenacity rayon and cotton having somewhat less—and the differences in type of cellulose (native and hydrate). The differences shown in peak intensities are related to factors other than orientation, such as bundle size, intensity of x-ray beam, etc.

It might be pointed out that in the present design one complete, recorded azimuthal scan of the two symmetrical diffraction arcs is obtained every 30 minutes from the time the bundle holder begins to rotate. This is to be compared to the large amount of time, as well as effort, required by the usual photographic method of obtaining similar data. By suitable selection of time motors and chart speeds the rate of recording may be varied.

A thorough study is being made of the variables in the method for the purpose of adapting this technique to a routine basis.

ACKNOWLEDGMENT

The authors wish to acknowledge the work of Miss H. Ziifle and Miss L. Katz who prepared the drawings.

THE REVIEW OF SCIENTIFIC INSTRUMENTS VOLUME 21, NUMBER 5 MAY, 1950

Synchrotron Radiofrequency System

MITCHELL H. DAZEY, JACK V. FRANCK, A. C. HELMHOLZ, CRAIG S. NUNAN, AND JACK M. PETERSON
Radiation Laboratory, Department of Physics, University of California, Berkeley, California

(Received September 14, 1949)

A description of the radiofrequency system of the Berkeley synchrotron is given.

INTRODUCTION

THE electron beam in the Berkeley synchrotron is accelerated to a peak energy of 335 Mev in three steps. The electrons are injected at a voltage of about 100 kv and are then accelerated to about 2 Mev by betatron action. Finally they are accelerated to 335 Mev by a radiofrequency voltage applied across a gap in the beam orbit. This paper will describe the design, construction, and operation of the radiofrequency system now used in the Berkeley synchrotron.*

SPECIFICATIONS

The Berkeley synchrotron has an orbit radius of one meter, with a magnetic gap of approximately $3\frac{3}{4}$ in. The vacuum chamber is a toroid of elliptical aperture. In cross section the outside dimensions are $3\frac{1}{2}$ by $6\frac{1}{4}$ in. and the nominal wall thickness is $\frac{5}{16}$ in. Fused silica (quartz) was the material used for the manufacture of the vacuum chamber or donut.

Space limitations made it desirable to utilize a section of the donut as a quarter-wave resonator, with the open, or high voltage end being the gap across which the acceleration of the electrons takes place. The dielectric constant of fused silica is four, so that one-eighth of the donut was required to form a resonator with the proper frequency. For ease of manufacture and handling it was decided to have the donut made in eight 45° sections. The segment and spares to be used for resonators were ordered with slightly larger wall thicknesses, $\frac{7}{16}$ in., since this would lead to a 40 percent increase in the theoretical Q over a resonator with a $\frac{5}{16}$-in. wall.

The complete donut was assembled by covering the eight joints with 4-in. wide, $\frac{1}{16}$-in. thick butyl rubber bands. A smooth surface under the bands was obtained by baking on the ends of the silica segments a 2-in. wide band of red glyptal. Heavy lubriseal was used under the rubber bands to insure a good vacuum seal. To prevent chipping of the segments and to insulate adjacent sections from each other, the ends were separated by a $\frac{1}{16}$-in. thick teflon gasket. All of the segments except the resonator were coated inside with du Pont No. 4817 air drying silver and grounded so as to avoid the accumulation of static charges. The grounding circuit was designed to distribute uniformly the betatron accelerating voltage over the several gaps between segments. The circuit consists of a ring of eight 1000-ohm resistors tied to ground at the injector; the two ends of each segment (except the resonator) are connected through 10-ohm resistors to a junction between 1000-ohm resistors. The resonator segment is grounded via the transmission line to the oscillator.

The electrical specifications for the radiofrequency system were as follows.

(a) Frequency. The nominal frequency of the synchrotron is 47.7 mc. The desired tuning range is determined by the radial width of usable magnetic field at the orbit. Since the usable field extends from 93 to 106 cm radius, the desired tuning range of the radiofrequency is from 45.0 to 51.1 mc.

(b) Voltage. Assuming a final energy of 341 Mev at the synchronous orbit (6 Mev are lost in collapsing to the target), the instantaneous energy (E_s) of the electrons can be written as a function of time (t), thus

$$E_s = 341\times 10^6 \sin(2\pi 32t)\text{ev},$$

since 32 cycles/sec. is the frequency of the magnetic field and the energies are essentially relativistic throughout. The mean energy gain per turn (V_t) is then

$$V_t = \frac{1}{47\times 10^6}\frac{dE}{dt} = 1450\ (\cos 2\pi 32t)\text{ ev per turn.}$$

The radiation loss, L, which varies as $(E_s)^4$, is 1200 v per turn at peak magnetic field. Adding V_t and L, the minimum accelerating voltage is 1450 v just after the betatron period and is less than 1450 v for the remainder of the accelerating period. Experience with the General Electric 70-Mev synchrotron[1] indicated that a gap voltage of two or three times the minimum is adequate for accelerating the electron beam. For this reason there was specified a voltage of up to 3500 peak volts at the radiofrequency gap in the electron orbit.

(c) Pulse length. Varying the pulse length is a convenient way to change the energy of the output beam, and the pulse length was therefore specified to be variable from zero to greater than 7800 μsec. ($\frac{1}{4}\times\frac{1}{32}$ sec.).

(d) Pulse shape. The envelope of the radiofrequency pulse was specified as a square wave with a rise time to full voltage of about 10 μsec.

(e) Repetition rate. The repetition rate of the radiofrequency system is the same as that of the magnet, which is a maximum of six pulses per second. It was specified that the radiofrequency pulse should be started by a circuit associated with the magnetic field.

---

* A more detailed report is given in the AEC document number AECU-578.

[1] Elder, Gurewitsch, Langmuir, and Pollock, J. App. Phys. **18**, 810 (1947).

(f) Eddy currents. An important requirement is that eddy currents induced in the conducting surfaces of the resonator by the alternating magnetic field be small, both to preserve uniformity of magnetic field and to avoid excessive heating. For ease of compensation it was specified that the mean eddy current field be less than 0.8 gauss; to avoid excessive distortion of the electron orbit, the maximum deviation of the eddy current field from its mean was specified as 0.2 gauss.

THE RESONATOR

A quarter-wave resonator, somewhat similar to the one used in the General Electric synchrotron,[1] was constructed. The rough exterior of the fused silica resonator section† was ground with silicon carbide grinding wheels to obtain a smooth surface and a thickness uniform within $\pm\frac{1}{32}$ in. The resonator section, shown in Fig. 1, was treated by the following procedure.

The section was filled with hydrofluoric acid for about 24 hr. to etch the inner surface glaze. It was cleaned by washing in acetone and then fired at about 1200°F to oxidize any remaining organic matter. When the section had cooled to room temperature, Liquid Bright platinum solution was applied by brush and the section was fired in an amply ventilated furnace. The temperature was brought up slowly to burn out the organic material in the Liquid Bright solution. When most of these materials had been vaporized, the coating was "set" by running the temperature up to about 1150°F for 15 min. Two or three coats give sufficient surface conductivity to allow good electroplating.

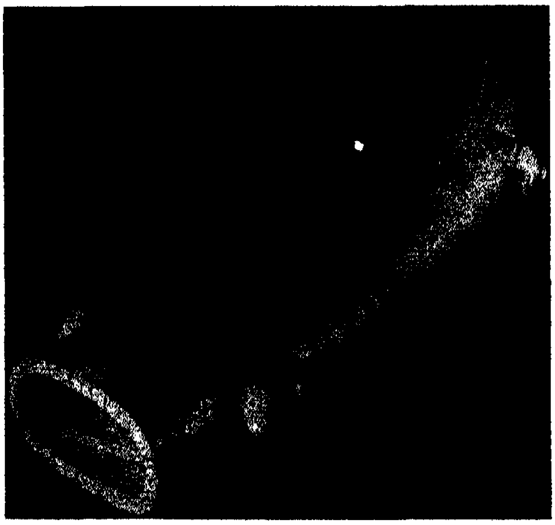

FIG. 1. Resonator. (A) Cross strap. (B) Feedpoint. (C) Accelerating gap. (D) Scribe lines.

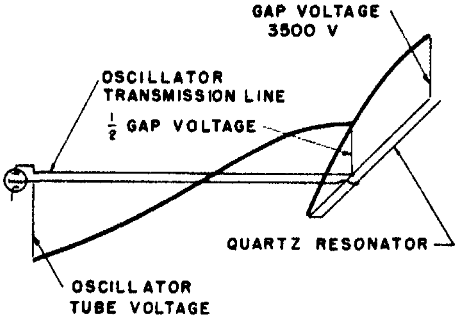

FIG. 2. Oscillator voltage distribution.

Eddy currents in conductors in a magnetic field go up rapidly as the area of the conductor is increased, so it was necessary to scribe "stop-off" lines before electroplating, leaving strips of metal to form the resonator. Scribe lines (see Fig. 1) were laid out by painting glyptal on with a rotating wheel device attached to a long radius arm.

The resonator was placed in a copper sulfate bath. Fixed anodes were shaped so as to be approximately $1\frac{3}{4}$ in. and equidistant from the surfaces to be plated. Copper fingers were added to protrude into the resonator bumps at the feedpoint and near the gap. It was found desirable to flash plate at about 15 amp. total current, using a small movable anode to plate areas which did not plate from the fixed anodes. After the complete surface was covered with a thin coat, the current was reduced to 5 amp. total and the plating was built up uniformly, using movable and fixed anodes. A reverse-plating method was used which consisted of 10 sec. plating, and 2 sec. de-plating. Although it was not possible to measure the thickness of the plating with any accuracy, it was estimated that about 0.003 in. of metal was applied.

After the plating, the glyptal was dissolved from the scribe lines with methyl ethyl ketone. The metal from the Liquid Bright solution was first ground out by an abrasive cut-off disk (carborundum) and then burned out electrically.

After the scribe lines were cleaned up, a coupling strap (A, Fig. 1) was painted around the resonator using du Pont air drying silver solution No. 4817 both on the inside and outside surfaces at a position which experimentally was found to give the highest Q. This strap was then electroplated by the technique mentioned previously.

The resonator has a $\frac{3}{8}$-in. wide accelerating gap (C, Fig. 1) and is driven at the half-voltage point by a coaxial transmission line from the oscillator. The plating on the inside surface is brought out through a hole and a copper-plated quartz plug is soldered into the hole to allow connection to the transmission line inner conductor. The gap in this resonator is not radial, but no difference in operation was observed with a radial gap. The bumps at the gap end are used for ports in other segments but serve no purpose in the resonator.

---

† The quartz sections were supplied by Amersil Company, Inc., Chestnut Avenue, Hillside 5, New Jersey.

When the resonator is installed in the synchrotron there is ⅛-in. clearance top and bottom between the resonator and the magnet pole tips. This small clearance allows considerable radiofrequency power to be dissipated in the pole tips. When the cross-strap was painted at the accelerating gap, the resonator Q was measured as 225 between the pole tips and 409 when away from the pole tips. The optimum position for the cross-strap was found to be about 45 percent of the distance from the gap to the high current end of the resonator. This gave a Q of 445 between pole tips and 545 away from the pole tips. These figures refer to the resonator shown in Fig. 1. Note that at the ends of the resonator the scribe lines connecting inner and outer surfaces are "radial" (i.e., perpendicular to the inner and outer surfaces). This gave a higher Q than "vertical" scribe lines.

The resonator was then placed in an alternating magnetic field and the delay in time of zero field due to eddy currents in the plating was measured with peaking strips. The delays corresponded, when converted to the conditions of operation at injection, to fields of 0.4 to 0.8 gauss over the radial aperture except at the cross-strap, where it was 2.2 gauss. Most of the variation was azimuthal; the maximum radial variation over the 4-in. radial range was measured as 0.15 gauss. The resonator field is compensated along with the rest of the magnetic field by coils around each 45° segment of the pole tips. The eddy current heating is still large enough so that it is necessary to cool the resonator with a blower supplying 200 cu. ft./min. and designed to produce 30 ft./sec. flow of air over the resonator surface. Without cooling, the lubriseal used under the wide rubber bands to make the vacuum seals becomes warm and flows.

ELECTRICAL

In this radiofrequency system, the quartz resonator, the transmission line to the tube, and the tube with its associated circuit components comprise a single resonant circuit. In terms of transmission lines, the resonant circuit is three-quarters of a wave-length long: the quartz section is equivalent to a quarter of a wave-length, and the transmission line with the tube and its associated circuit components is electrically a half-wave-length long. Figure 2 represents, approximately, the voltage distribution along the quartz resonator and the transmission line to the oscillator tube.

Figure 3 is a schematic diagram of the circuit and indicates the approximate location of components. The 2500-watt air-cooled oscillator tube (Eimac 3X2500A3) is connected in a grounded grid circuit across the high voltage end of the transmission line. The tuning capacitor (C_1) controls the frequency of the entire radiofrequency system between 45 and 51 mc. It is located at the top of the oscillator tube housing and is remotely controlled from the synchrotron control desk with a selsyn motor.

The feedback for the oscillator tube is obtained by coupling to the magnetic field in the transmission line with an adjustable loop. A series connected variable capacitor or phasing capacitor (C_2) compensates for the

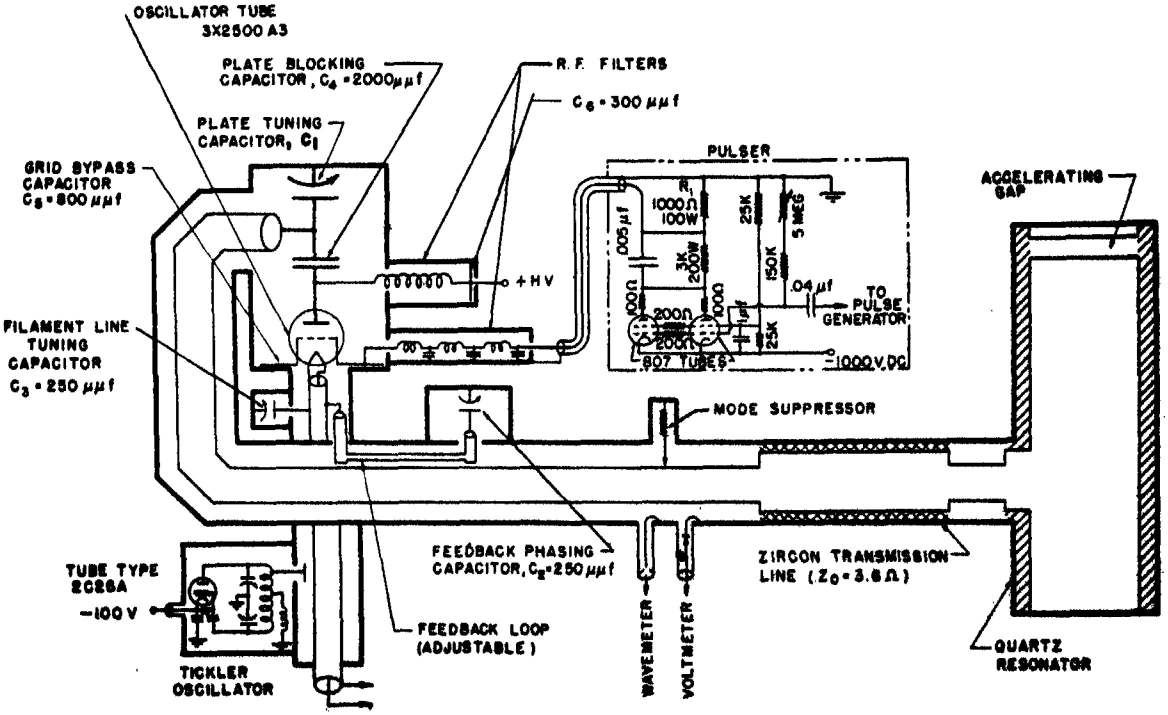

FIG. 3. Schematic diagram of radiofrequency oscillator.

effect of the self-inductance of the feed-back loop. This circuit allows the drive to be adjusted in phase as well as in amplitude. The transmission line is "curled back" upon itself to keep this feed-back circuit as short as possible and at the same time have the loop couple near a magnetic field maximum.

Since the tube filaments are connected to the d.c. ground it is necessary to use a plate d.c. blocking capacitor (C_4) and a grid d.c. blocking capacitor (C_5). A copper-plated disk of titanium dioxide was used as a plate-blocking capacitor since this shape fits into the geometry of the circuit and gives the necessary voltage insulation (6000 v d.c.) and capacity (approximately 2000 $\mu\mu$f). This capacitor is clamped between two rows of spring fingers. The tube rests upon its grid connector which is part of a brass disk forming the grid blocking capacitor. Two pieces of 0.005-in. sheet polystyrene are used as the dielectric to give a capacity of about 800 $\mu\mu$f and to insulate for 2000 v d.c. The grid bias resistor (R_1) for the oscillator is mounted in the pulser chassis about fifty feet away. The tickler oscillator helps initiate oscillations and reduces the jitter time to 0.1 μsec.

When the oscillator was first tested, two spurious modes of oscillation were observed. These were eliminated by installing a 300-ohm globar mode suppressor resistor across the transmission line at the voltage node of the fundamental mode.

The resonator is driven at the half-voltage point rather than at the gap in order to simplify the design of the insulating surfaces at the feedpoint. Between the mode suppressor and the resonator is a section of transmission line (approximately an eighth wave-length) using zircon as the dielectric. This section of low impedance line acts as an impedance transformer to allow the oscillator tube to operate at approximately twice the feedpoint voltage in order to obtain good oscillator efficiency.

The oscillator delivers approximately 6-kw peak power at approximately 60 percent plate efficiency when operating at the maximum gap voltage (3500 volts peak) and the nominal pulse length (7800 μsec.). At the maximum repetition rate (6 c.p.s.) the duty cycle is 1/20. Most of the energy goes into conduction losses in the resonator plating and in the transmission line. Dielectric heating of the quartz is negligible. The forced air cooling mentioned in connection with eddy currents dissipates this heat. Forced air cooling is used to cool the grid-to-plate seal and the plate of the oscillator tube. The filament seals of the tube are cooled by high pressure air supplied through the inner conductor of the filament transmission line.

The oscillator is keyed by controlling the fixed grid bias voltage with the pulser shown in Fig. 3. During the offtime the pulser holds the grid of the oscillator tube at about $1\frac{1}{4}$ times the cut-off voltage. To initiate the radiofrequency pulse, the leading edge of a negative square wave of voltage from a "one-shot" multivibrator cuts off the 807 switch tubes, allowing the bias voltage on the oscillator grid capacitor to discharge through the grid resistor R_1. When the bias rises above cut-off, the tube functions as a class *C* oscillator, establishing its own bias across R_1. To terminate the radiofrequency pulse, the trailing edge of the negative square wave puts the 807's sharply into conduction, which places sufficient negative bias on the grid of the oscillator to stop the oscillations.

The length of the negative square wave of voltage generated by the one-shot multivibrator is varied by a potentiometer adjusted from the synchrotron control desk by means of selsyn motors.

OPERATION

None of the radiofrequency pulse parameters has been found to be critical. In normal operation the electrons are accelerated by betatron action for the first 100 μsec. to 2 Mev. The radiofrequency pulse can be started at any time over a 5-μsec. range without appreciable difference in x-ray beam intensity. The resonator is driven at about 47.1 mc/sec. The beam intensity decreases rapidly when the frequency is tuned beyond 48.1 or 46.6 mc/sec. and is fairly constant between these limits.

At peak magnetic field the electrons lose energy by radiation at the rate of about 1200 volts per turn. When the radiofrequency pulse is ended, the electrons lose energy by radiation and spiral into an internal target. In normal operation at full energy the electrons begin to strike the target about 120 μsec. after the end of the radiofrequency pulse and the x-ray beam lasts for about 10 μsec. For some types of experiments it is desirable to have the x-ray pulse last for a longer period in order to allow counters to function for a longer time during each synchrotron pulse; for a given beam intensity the pile-up of independent counts within the resolving times of the counters is correspondingly reduced. For this purpose the duration of the x-ray pulse has been increased to as much as 2500 μsec. by shaping the oscillator plate voltage so that it decays over the last few milliseconds of the radiofrequency pulse. This type of operation has been of considerable value in experiments involving proportional and scintillation type counters.

We wish to thank Professor E. M. McMillan for advice and encouragement.

The work described in this report was performed under the auspices of the AEC.

THE REVIEW OF SCIENTIFIC INSTRUMENTS VOLUME 21, NUMBER 5 MAY, 1950

X-Ray Determination of Slip Planes and Slip Directions

R. W. TURNER, T. L. WU, AND R. SMOLUCHOWSKI
Metals Research Laboratory, Carnegie Institute of Technology, Pittsburgh, Pennsylvania

(Received December 27, 1949)

An application of x-rays for determination of active slip systems based on a comparison of distortion of Laue spots is described.

WHENEVER they are applicable, direct visual methods offer the simplest approach to the study of slip systems: The orientation of the sample may be determined by study of etch pits with an optical goniometer, and the slip plane may be determined by noting the orientation of the slip line on the surface. Slip direction is more difficult to determine, except in the case of samples having at least two, non-parallel surfaces polished for careful visual observation. However, it is frequently desirable to study slip in samples which are not suitable for these methods. In our laboratory, we came up against the problem in connection with the study of slip in small, thin, flat crystals of aluminum, such that only one surface could be polished for visual studies. The problem was solved using x-rays, and the various methods are here reported.

Aluminum is known to slip on the (111) planes in (110) directions. Hence, since the orientation of the crystal was known, the slip plane was determined in the usual way by noting the direction of the slip lines on the one polished surface and referring to the projection of the crystal.[1] This method, however, did not indicate the slip direction; it was necessary to turn to x-ray methods for this information. As a first step, samples were studied in which the slip plane was known but the slip direction was not. In this case, a Laue exposure offers probably the simplest and most direct method. The crystal was oriented so that the normal to the slip plane was not quite parallel to the x-ray beam. In this orientation, the zone of all planes belonging to this direction was recorded in its entirety, and the reflections were indexed by plotting on a stereographic projection. The planes normal to the direction of the active slip were identified by a distorted or split reflection. This identification of the active slip system is based on the general theory of strain hardening according to which a local curvature appears on the active slip plane in the direction of slip. As a check, it was desirable to reorient the specimen so that two reflections of the same form (*hkl*) in the zone under consideration were located at equal distances from the central spot. These two spots were then compared directly as shown in Fig. 1. Here the beam was almost parallel to $(1\bar{1}1)$, and we compared the $(\bar{1}\bar{1}0)$ and (011) reflections. A further reorientation showed the $(\bar{1}01)$ reflection to be most distorted.

If it is necessary to determine the slip plane by means of x-rays, then a similar method may be used. Here the

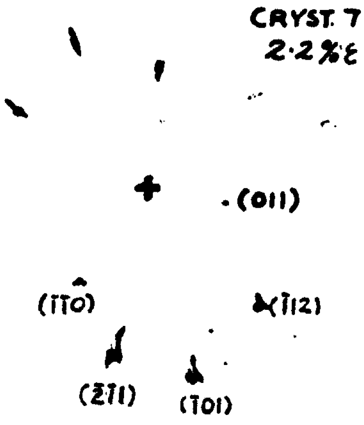

FIG. 1. Laue transmission. Beam roughly parallel to $(1\bar{1}1)$.

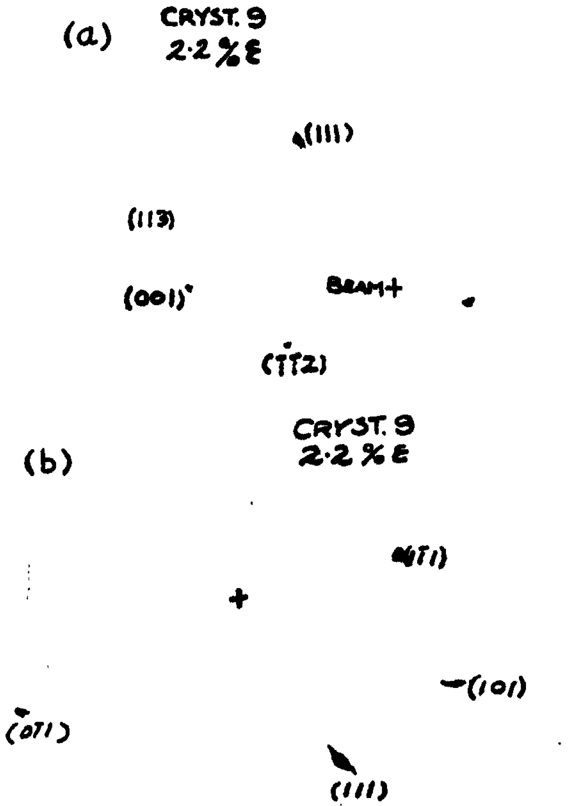

FIG. 2. Laue transmission. (a) General orientation. (b) Beam roughly parallel to $(\bar{1}01)$.

---

[1] C. S. Barrett, *Structure of Metals* (McGraw-Hill Book Company, Inc., New York, 1943).

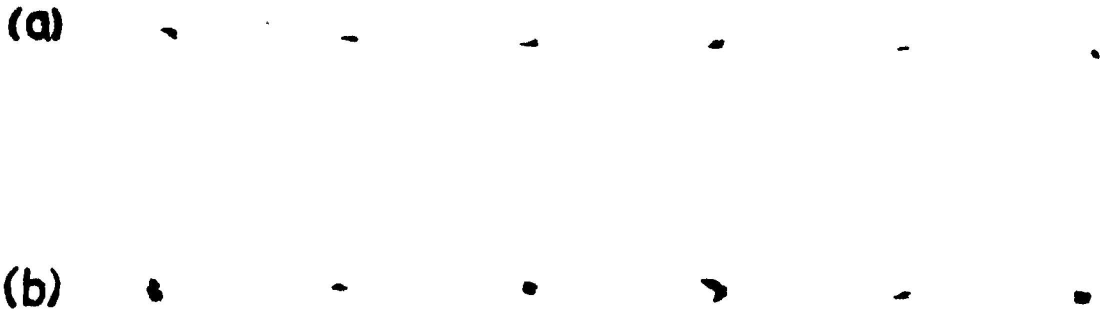

FIG. 3. Weissenberg method. Rotation around (111). Reflections from various {110} planes in an almost strain-free (a) and in a deformed sample (b).

beam is adjusted almost parallel to a (110) direction, and one can compare the various (111) reflections. Figure 2(a) illustrates the results obtained with the crystal in random orientation. Indexing was again done with the aid of a stereographic projection. As before, it was desirable to make a check by an exposure with the sample oriented so that two reflections of the same form were equidistant from the center for comparison. This is shown in Fig. 2(b). Here the beam was almost parallel to ($\bar{1}01$), and we compared the (111) and (1$\bar{1}$1) reflections.

It was our experience that this transmission method represents the simplest and most straightforward approach to the problem. It has the great advantage that the alignment of the specimen is only moderately critical. Furthermore, all exposures are short, and a glance at the film is sufficient to determine whether or not further adjustment is necessary. The back-reflection Laue method may have to be used in certain cases, but it was somewhat limited in usefulness in our problem.

An attempt was made to measure the rotation of the crystal lamellae which occurs during slip: the tensile axis of the specimen makes a smaller angle with the slip direction after slip than before. This method requires precision measurements of orientation or large deformations. In our case the rotations were small, and the results were not conclusive.

Finally, a comparison of reflections in one zone was made using a Weissenberg camera. For this, it was necessary that the slip plane and its orientation be known so as to orient this plane perpendicular to the axis of rotation. The equatorial layer line will now contain the reflections from all the planes perpendicular to the slip plane, and the slip direction will be the normal to those planes which show maximum distortion. In Fig. 3, reflections from "strain-free" and deformed samples are compared. Although the planes normal to the slip direction show the most distortion, almost all reflections show some distortion. This indicates the very high sensitivity of the method. In fact, it is too sensitive if only the directions of slip rather than the general conditions of strain in the sample are to be determined. The time and trouble involved in proper alignment of the sample do not seem to be justified for a simple determination of slip plane and slip direction.

Another variation of the Weissenberg method would be to have the specimen oriented with the slip plane normal to the axis of rotation, and the x-ray beam reflecting from this plane. As the sample is rotated, the reflection would change, and in that direction which corresponds to the active slip direction it will be most distorted. This technique has not been tried.

It appears that for a critical study of the state of strain in the sample, the Weissenberg technique recording the reflections of planes perpendicular to the plane of slip would be the most informative. On the other hand, the Laue technique is more suitable when the problem consists only in determining slip plane and slip direction. In general, transmission Laue is easier and faster than back-reflection Laue. If the sample has been subjected to large deformations, measurement of the rotation of the crystal lamellae may be more convenient than other methods. In all cases, comparison exposures of a strain-free section of the sample help to clarify and establish the interpretation.

THE REVIEW OF SCIENTIFIC INSTRUMENTS VOLUME 21, NUMBER 5 MAY, 1950

An Electron Pair Spectrometer of Lens Type for Hard Gamma-Radiation

KAI SIEGBAHN AND STIG JOHANSSON
Nobel Institute for Physics, Stockholm, Sweden

(Received January 5, 1950)

A new type of pair spectrometer is described. The rotation of the image in a short magnetic lens is used to separate negatrons and positrons by putting the pair converter a little aside from the optical axis of the lens. It is then possible to obtain coincidence "lines." The apparatus has been tried on the 2.62-Mev γ-ray of ThC″ and the 2.76-Mev γ-ray of Na^{24}.

THE γ-radiations emitted during transmutation experiments (by means of particle accelerators or nuclear reactors) are normally much more energetic than those emitted from ordinary radioactive bodies. If one wants to study, β-spectrometrically, the energy of such high energy γ-radiation by means of secondary electrons in order to get good accuracy and possibilities to analyze any complex radiation, one is faced with the difficulty that the line-producing photo-effect (as well as the Compton effect) is getting small at higher energies. Instead, the pair production effect increases. The fact that the whole γ-energy is consumed in the simultaneous emission of the electron positron pair can very conveniently be utilized in two ways: First, the background can be effectively reduced to a minimum by using two detectors in a coincidence arrangement, second, it is possible to obtain coincidence "lines" characteristic of the γ-energies in question. If the electron pair converter is put in a transversal homogeneous magnetic field, the negatron and positron in the pair are bent away in opposite directions. The electrons are normally registered after 180° and a coincidence line occurs at a magnetic field, corresponding to an energy $=\frac{1}{2}(E_\gamma-1.02)$ Mev, where E_γ is the energy of the γ-ray. This device has successfully been used before.[1,2]

It has not yet been tried to use any other type of focusing except the semicircular to register the electron pairs. The lens method, which possesses a much higher transmission power, cannot immediately be used since this type of focusing ordinarily does not separate negatrons and positrons. It is true that this can be made if a twisted shutter system is introduced.[3] If this is done, however, only one type of particles, i.e., either negatrons or positrons, is transmitted and the important condition for obtaining coincidence lines is lost, namely, the simultaneous transmission and registering of both particles in the pair.

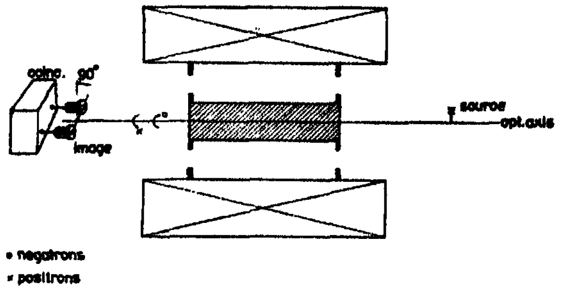

FIG. 1. Principle of the electron pair lens spectrometer.

One can avoid this difficulty in a rather simple way, making use of the property of a short lens of rotating the image. It is well known that a long lens with a homogeneous field has a rotation of image of 360°. A short lens will generally have a rotation of image, which is $\neq 360°$ and it is easy to dimension the lens and the distance between the source and detector so that the angle will be around 90°. If the electron pair converter is placed a little to one side of the optical axis of the lens (see Fig. 1), the negatrons and positrons due to their opposite direction of rotation, will form *two* separated images in a distance from each other, which is twice the distance of the converter from the axis (provided the rotation is 90°). If the rotation is different from 90° the separation will be smaller. Two G-M tubes in coincidence arrangement are then put with their apertures coinciding with the two images.

The correct positions of the two images, when the source was 1.5 cm from the axis, were found experimentally by focusing the ThB *F*-line on to a photographic plate and then changing the direction of the current through the lens. Figure 2 shows the result. As can be seen, the images are fairly well defined on the plate. Due to a small shift in the current during the exposure of the negatron image, this is less sharp. A somewhat better separation can be obtained if the rotation of image were closer to 90°.

The two G-M counters have been designed in one unit with the gas mixture in common. The apertures have a diameter of 10 mm and are situated on the sides of the counters so that the electrons enter the sensitive region directly.

There is especially one important question which has to be considered when further details of the instrument are worked out, i.e., the angular correlation between the photon and the positron and negatron in the pair. This correlation is energy dependent and is approxi-

---

[1] V. Dzelepov, Comptes Rendus U.R.S.S. 23, 24 (1939).

[2] B. McDaniel, G. von Dardel, and R. Walker, Phys. Rev. 72, 985 (1947); R. Walker and B. McDaniel, Phys. Rev. 74, 315 (1948).

[3] M. Deutsch, L. Elliot, and R. Evans, Rev. Sci. Inst. 15, 178 (1944).

mately given by the formula by Bethe and Heitler.[4]

$$N(\theta)d\theta=\frac{\theta d\theta}{(\Theta^2+\theta^2)^2};\quad \Theta=\frac{mc^2}{E_0},$$

$N(\theta)$ = number of electrons making the angle θ with the quantum, E_0 = energy of the electron.

In the actual case the γ-emission takes place in the immediate vicinity of the pair converter, i.e., the particle beam from the accelerator should strike the target in close contact with the converter, or the radioactive material should be put directly behind the converter. Independent of γ-energy we will therefore always have, e.g., negatrons emitted from the converter which can pass the diaphragm system and be counted in the one tube. The positron belonging to one of these negatrons may, however, easily get lost in the shutter if the angle between the positron and negatron is too large. The *average* angle between the negatron and positron may be found by differentiating the formula and is approximately given by $\theta_{\text{Av}}\sim mc^2/E_0$. For high energy γ-radiation ($\gtrsim$10 Mev) this angle is seen to be very small, and a substantial part of the electron pairs may go through the diaphragm system.

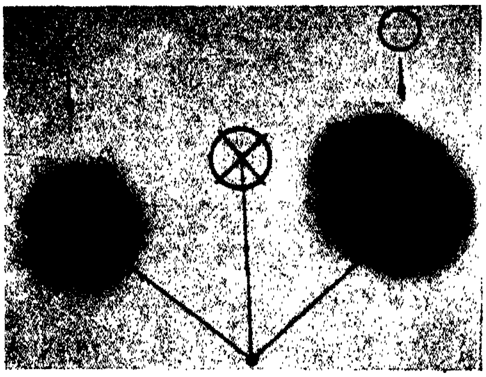

FIG. 2. Photographic investigation of the separation of positrons and negatrons when the sample is placed some distance from the optical axis.

In designing the diaphragm system, attention must be paid to this circumstance. Thus, at lower γ-energies, the shutter system must be rather widely opened, which makes the maximum resolution fairly small. As the γ-energy increases, the number of pairs goes up (a factor of 10 from 2 Mev to 10 Mev), and simultaneously the angle between the negatron and positron makes it possible to increase the resolution by using a more narrow shutter system.

In order to investigate the general properties of the pair spectrometer, its ability of separating and registering positrons and negatrons in the two counters was first studied. In all these measurements the sample was placed 1.5 cm from the axis and with wide-opened shutter system. If the strong F-line of ThB was focused on the one counter, the line could not be observed with the other counter. If the direction of the lens current was changed, the line appeared in the other counter with the same intensity and at the same current as before but could not be observed in the first counter. Next, the continuous spectrum of Na^{24} and Co^{60} was investigated with the two tubes and with different direction of the current. Figures 3(a) and 3(b) show the results for Co^{60}. No window (10 mg/cm^2) correction has been applied. As can be seen from Fig. 3, only a small portion of the spectrum is registered with the "wrong" counter. If the direction of lens current is reversed [Fig. 3(b)], the intensities are almost exactly the same as before when registered with the opposite counters. In all cases the spectra obtained yield Fermi plots, which are straight lines over very large parts of the spectra. The upper limits obtained from these plots agree very well with previously reported values.

Since the ability of registering positrons and electrons is quantitatively known from these experiments, one can also easily use the arrangement to investigate and separate β-spectra consisting of both kinds of particles

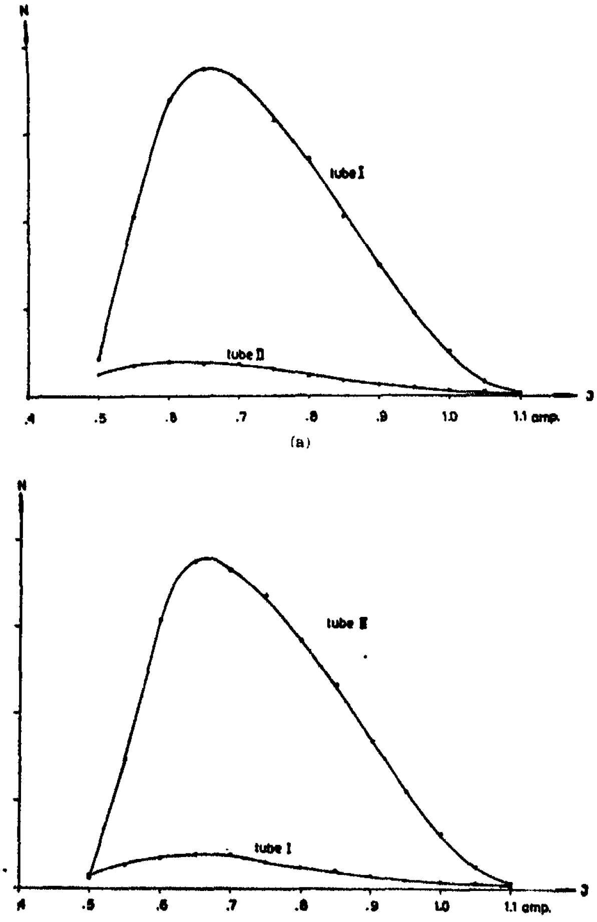

FIG. 3. Co^{60} β-spectrum registered with the two counters. In (b) the current has been reversed compared to (a),

simultaneously, provided the intensity of one of them is more than about five percent of the other. This limit could probably be made much smaller if the sample were put say, 2 cm from the axis and the shutters and G-M-slits were made narrower. If the rotation of image were made closer to 90° than in the present case the separation would also be greater. For the present purpose there is no need for a more complete separation, the only necessary requirement being the ability of registering positrons and negatrons simultaneously in two different tubes.

---

[4] H. Bethe and W. Heitler, Proc. Roy. Soc. 146, 83 (1934).

We have finally tested the pair spectrometer by investigating the electron pairs expelled from a Pb converter by the γ-radiation of ThC'' ($E_\gamma = 2.62$ Mev) and Na^{24} ($E_\gamma = 2.76$ Mev). It should be emphasized that this choice for testing the apparatus is very unfavorable in several respects. Apart from the low pair cross section at these energies, the angle between the positron and negatron is unsuitably large for any kind of pair spectrometer. Furthermore, in order to stop all the primary electrons from the sample the converter had to be chosen thick, which gives rise to pronounced multiple

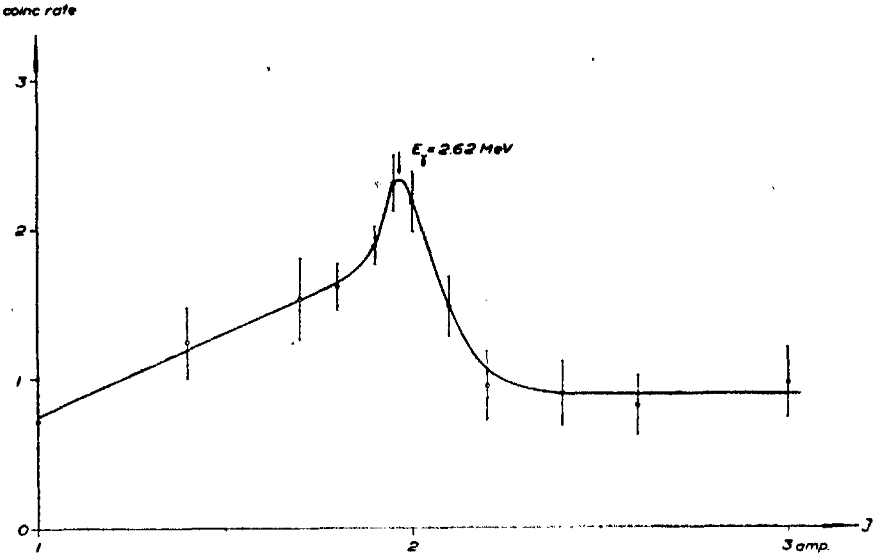

FIG. 4. Coincidence line of the hard γ-ray of ThC''.

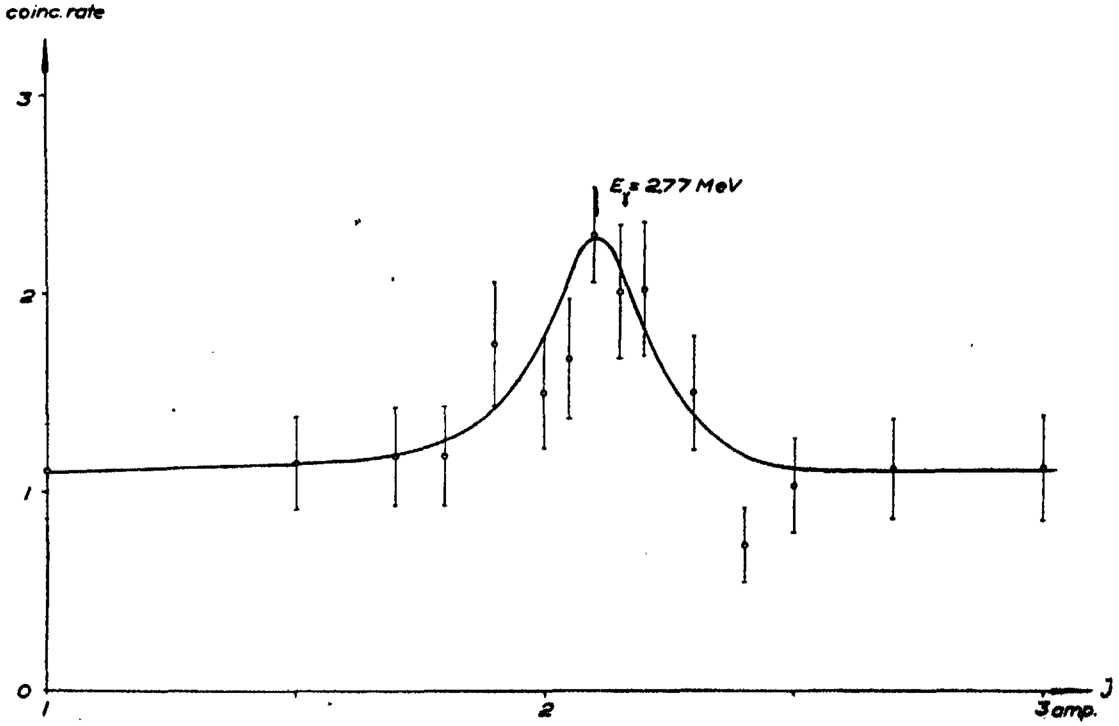

FIG. 5. Coincidence line of the hard γ-ray of Na^{24}.

scattering. The Compton electrons expelled from the thick converter cause a rather high background of the counter registering negatrons and this increases the coincidence background, which otherwise would be very small. Figures 4 and 5 show the coincidence lines obtained for ThC$''$ and Na^{24}. The spectrometer was calibrated by means of some well-known photo-lines in the energy region in question. Using this calibration, the values obtained for the γ-energies of ThC$''$ and Na^{24} from the coincidence lines are 2.62 and 2.77 Mev, i.e., in very good agreement with data obtained by other methods.

Since these experiments in spite of the very unfavorable conditions for a pair spectrometer could give reasonably good results, it seems likely that the instrument may be useful when higher γ-ray energies are available for a similar study.

THE REVIEW OF SCIENTIFIC INSTRUMENTS VOLUME 21, NUMBER 5 MAY, 1950

A Focusing Device for the External 350-Mev Proton Beam of the 184-Inch Cyclotron at Berkeley

W. K. H. Panofsky and W. R. Baker
Department of Physics, Radiation Laboratory, University of California, Berkeley, California

(Received January 11, 1950)

A device has been constructed to focus the external beam of the 184-in. cyclotron at Berkeley. The device consists of a cylindrical tube 4 ft. in length and 3 in. in diameter, which contains a longitudinal arc of nearly uniform current density. Such a device will focus any beam of cylindrical symmetry. Owing to the large power requirements of such a device it is applicable only to very short pulsed beams.

The external beam of the 184-in. synchro-cyclotron[1] is produced by a pulsed electrostatic deflector displacing the cyclotron orbits to enter a magnetic shield which channels the beam to the outside of the magnetic field. The beam thus produced covers an area of approximately 8 sq. in. at the bombarding position (about 46 ft. from the center of the cyclotron). Since the total beam attained thus far is only of the order of 10^{-9} amp., the resultant beam density is insufficient for many experiements or at least leads to long runtimes. Since in most experiments beam density rather than total current is the determining factor a focusing device was considered of advantage.

Both horizontal and vertical focusing is possible by means of a wedge-shaped deflecting magnet.[2] The use of such a device, although practical in principle, was rejected here since it involved re-location of the target facilities and also since the physical size of a focusing magnet at this energy and aperture is very considerable. It was therefore decided to study an "in-line" focusing device, i.e., a device focusing without deflection.

The device chosen consists essentially of a current-carrying cylindrical conductor whose axis is parallel to the beam and which is transparent to the passage of the beam. If the current density is uniform, the magnetic field will increase linearly with the radius, and a linear restoring force on the beam will result (Fig. 1). It can easily be shown that if such a device is effectively a "thin" lens, it will give rise to a focal length

$$F=(a/L)(B\rho)/B_o, \tag{1}$$

where $(B\rho)$ is the momentum of the beam, B_o the magnetic induction at the outer edge of the transparent conductor, and the a and L are dimensions defined in Fig. 1.

A current-carrying conductor transparent to the proton beam was realized physically in the form of an arc inside a cylindrical glass tube 3 in. in diameter and 48 in. in length. The arc was struck between two cylindrical aluminum electrodes protruding into the arc tube. The physical layout is shown in Fig. 2. The entrance of the tube is closed by a $1\frac{1}{2}$-mil dural foil; the foil has to be thin enough such that the multiple scattering in the foil will not produce appreciable broadening

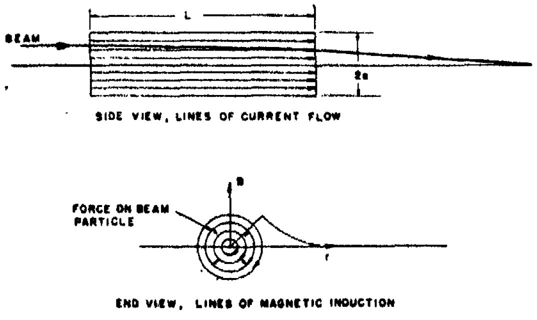
L
BEAM
2a
SIDE VIEW, LINES OF CURRENT FLOW
B
FORCE ON BEAM PARTICLE
r
END VIEW, LINES OF MAGNETIC INDUCTION

FIG. 1. Focusing action of magnetic arc lens. The top figure shows the beam trajectory and the arc current flow; the bottom figure shows the lines of magnetic field and the radial variation of the field.

---

[1] Powell, Henrich, Kerns, Sewell, and Thornton, Rev. Sci. Inst. 19, 506-12 (1948).

[2] Leo Lavatelli, MDDC-350, "Snouting and focusing the cyclotron beam."

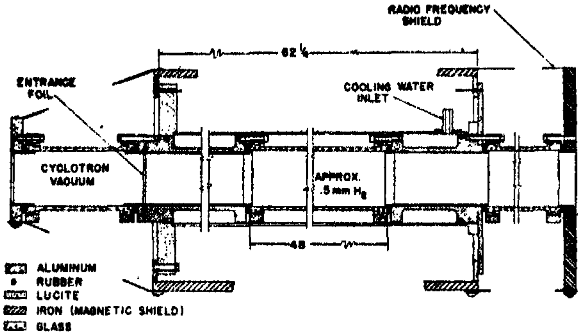

FIG. 2. Cross section of magnetic arc lens.

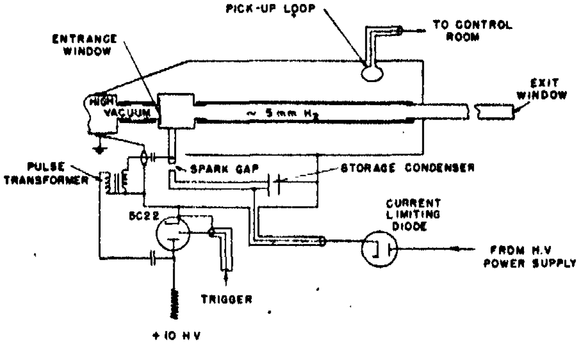

FIG. 3. Diagram of arc lens pulse connections. Note the coaxial connections of the storage condenser in relation to the spark gap and discharge tube.

of the beam. Even at a proton energy of 350 Mev this necessitates the thin foil as indicated owing to the large distances involved. The arc was operated at a pressure of 0.3 to 0.5 mm of hydrogen. The hydrogen was circulated continuously to purify the gas from gases generated from the surfaces of the discharge. The exit foil (0.010 in. Al) which has to stand atmospheric pressure was located near the target to make scattering effects unimportant.

The arc was fed from a condenser bank consisting of sixteen 0.03-μf condensers through a spark gap triggered by a 70-kv pulse transformer. The trigger arrangement is shown in Fig. 3. The arc was operated at a pulse repetition rate of approximately 60 c.p.s., in synchronism with the rotating condenser of the synchrocyclotron. The time sequence of firing the electrostatic deflector and the arc is shown in Fig. 4. At this repetition rate it was found necessary to air-cool the condenser bank and to water-cool the gas discharge tube.

The location of the lens relative to the bombardment position required a focal length of approximately 200 in. and an arc current of 4000 amp. The arc drop under these conditions is 9 kv, principally inductive.

In order to produce a good focal point, two requirements have to be fulfilled: (1) The current density of the arc has to be uniform. (2) The incoming beam must originate from a (real or virtual) point source. Neither of these requirements can be fulfilled accurately in practice. The current distribution in the arc is affected by a number of factors, including the magnetic contraction effect which focuses the beam. There is however, also, at this rate of rise of current, a skin depth effect which tends to keep the arc apart. These and other effects depend on the arc conditions; the arc was thus adjusted empirically to give most uniform current density so judged by end-on photographs of the discharge.

The deflected beam of the 184-in. cyclotron is somewhat astigmatic, i.e., has a different divergence of the

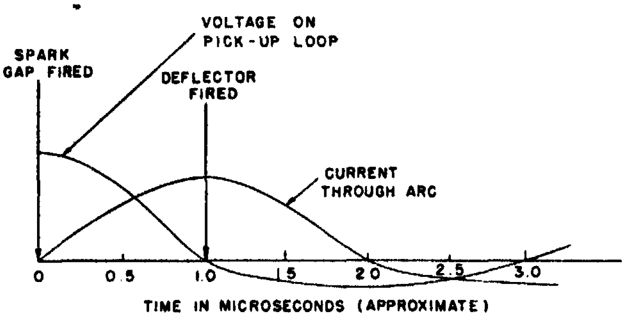

FIG. 4. Time sequence of arc operation. Note the relative firing times of the arc and electrostatic deflector.

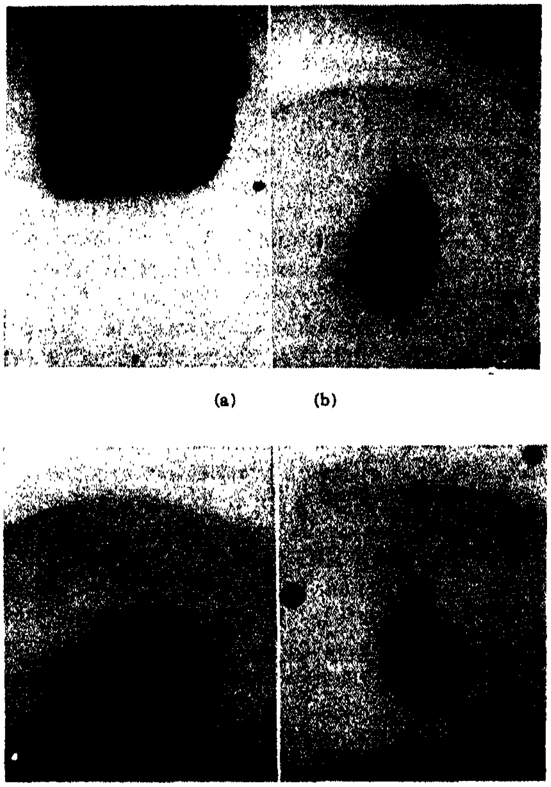
(a) (b)

(c) (d)

FIG. 5. Beam cross sections taken on x-ray film. Operating conditions are as follows: (a). No arc. (b). Arc voltage 7 kv. (c). Arc voltage 12 kv. (d). Arc voltage 8.5 kv; astigmatism corrected. *Note.*—The round marks are fiducial marks and of no significance here.

beam horizontally and vertically. Figure 5(a) shows the cross section of the deflected beam in the external bombardment area of the 184-in. cyclotron with the "arc lens" inoperative. Figure 5(b) shows the beam shape at 7-kv arc voltage and Fig. 5(c) shows the beam shape at 13-kv arc voltage. Note that the optimum focusing conditions for the vertical and horizontal directions are different, indicating astigmatism in the primary beam. An attempt was made to correct the astigmatism with a transverse magnetic field produced by a magnetic quadrupole consisting of two opposed Alnico magnets (see Fig. 6). These magnets, as can be seen by inspection of Fig. 6, produce a vertical focusing and horizontal defocusing force. By choosing magnets of suitable strength (250 gauss at 1½-in. radius for 4-in. depth), the beam astigmatism could be compensated. The resulting beam shape is shown in Fig. 5(d). The ratio in area of Fig. 5(a) (lens not operating) and Fig. 5(d) (lens at optimum) is 8.5. The current density within a central circular area of 1-in. diameter is increased by approximately a factor of five.

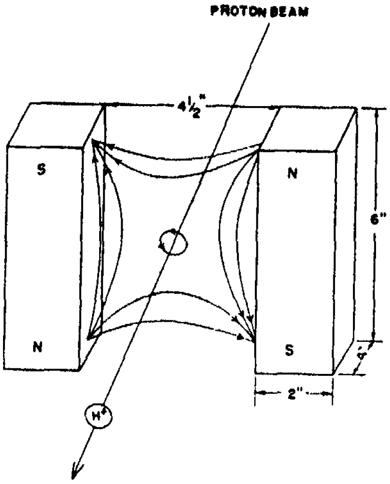

FIG. 6. Geometry of Alnico magnet "quadrupole" to correct astigmatism. Lines of force due to magnets and due to beam are shown to indicate sign of the forces.

The writers are greatly indebted to Messrs. David Vance and Robert Meuser for mechanical design. Mr. Harvey Orrin and Mr. Charles Park aided in the design and installation of the timing and safety circuits. We also owe thanks to Mr. James Vale and Robert Watt and the crew of the 184-in. cyclotron for assisting effectively in these tests. The work was done under the auspices of the AEC.

THE REVIEW OF SCIENTIFIC INSTRUMENTS VOLUME 21, NUMBER 5 MAY, 1950

Relation between Apparent Shapes of Monoenergetic Conversion Lines and Continuous Beta-Spectra in a Magnetic Spectrometer. II

GEORGE E. OWEN AND HENRY PRIMAKOFF
Department of Physics, Washington University,[*] *St. Louis, Missouri*

(Received January 30, 1950)

The method worked out previously for correcting distortions which affect the apparent shape of a continuous beta-spectrum has been further extended. A general solution of the integral equation governing the relation between the true and the observed spectra is given, and is applied to the correction of the experimental spectra from a 1-mg/cm^2 source of Cu^{64}. The kernel of the distortion integral equation is determined from a study of the internal conversion lines of I^{131} (47 and 330 kev) using sources of various thicknesses from 0.042 to 0.840 mg/cm^2. It is found that the discrepancy between the experimental Cu^{64} negatron and positron spectra and those predicted by the Fermi ("allowed") theory can be completely understood as a thick source effect.

I. INTRODUCTION

IN a previous paper[1] written sometime ago, a general method was described for compensating source-thickness and instrumental distortions in continuous β-spectra by means of an analysis of monoenergetic conversion lines. Since then, work[2] with S^{35} and H^3 has re-emphasized the importance of source thickness in producing distortions, while an experimental investigation of distortions introduced by spectrometer chamber scattering[3] has shown that these last can be reduced to a minimum by proper chamber design.

Although the experimental data on line shapes used in I was quite rough, it was indicated, as a consequence of the analysis there developed, that the then existing discrepancies between the Fermi theory and experiment for relatively thick source Cu^{64} positron and negatron spectra could well arise from source-thickness and instrumental distortions. Recent work[4] with Cu^{64}, employing extremely thin and uniform sources prepared by thermal evaporation from a hot filament, has confirmed this suggestion, yielding linear Fermi-Kurie (F-K) plots for both positrons and negatrons down to energies as low as 50 kev.

---

[*] Assisted by the joint program of the ONR and AEC.

[1] G. E. Owen and H. Primakoff, Phys. Rev. 74, 1406 (1948); referred to in the present text as I.

[2] R. D. Albert and C. S. Wu, Phys. Rev. 74, 847 (1948). Curran, Angus, and Cockroft, Phil. Mag. 40, 53 (1949).

[3] G. E. Owen and C. S. Cook, Rev. Sci. Inst. 20, 768 (1949).

[4] Langer, Moffat, and Price, Phys. Rev. 76, 1725 (1949); G. E. Owen and C. S. Cook, Phys. Rev. 76, 1726 (1949).

As a further contribution to the clarification of the source-thickness distortion problem in continuous β-spectra, we have (a) made studies of the dependence of conversion line shapes on variation in source thickness for the I^{131} 47- and 330-kev lines, and (b) employed this data and a somewhat more accurate mathematical treatment in order to analyze the discrepancy between Fermi theory and experiment in the continuous positron and negatron spectra from a 1.0-mg/cm² Cu^{64} source. We found that in both cases the discrepancy can be completely understood as a thick source effect.

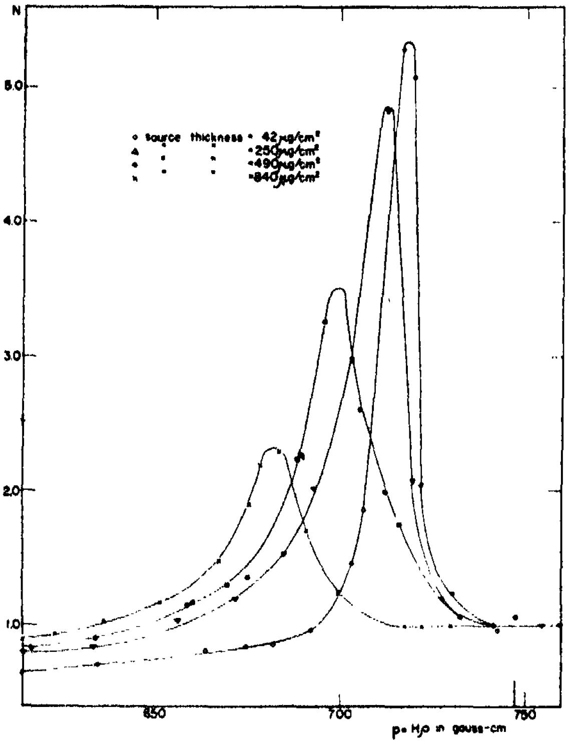

FIG. 1. Line shape at 47 kev (I^{131}) as a function of source thickness.

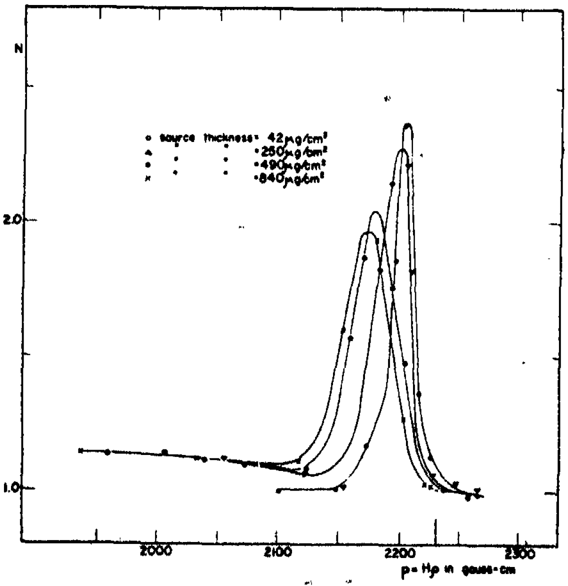

FIG. 2. Line shape at 330 kev (I^{131}) as a function of source thickness.

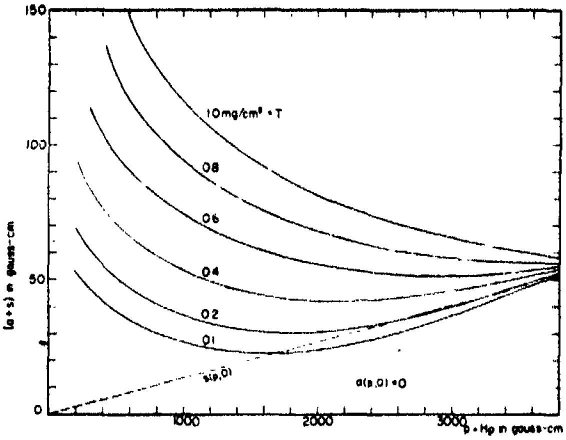

FIG. 3. Coefficient of the first derivative distorting term.

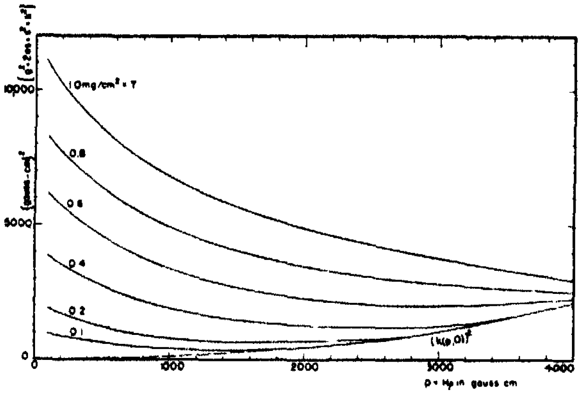

FIG. 4. Coefficient of the second derivative distorting term.

In view of the usefulness of the present technique in the possible analysis of other thick source continuous spectra, the results of the study summarized in (a) and (b) are herewith presented.

II. GENERAL SOLUTION OF THE DISTORTION EQUATION

The distortion problem has been formulated in I, where it has been shown that

$$M(p)=\int_0^\infty N(p')K(p',p)dp', \tag{1}$$

with

$M(p)dp=$ the number of electrons appearing at the spectrometer exit slit with the magnetic field set to admit particles with magnetic rigidity (momentum) lying between p and $p+dp$ (the measured momentum distribution).

$N(p')dp'$ = the number of electrons emitted by the nuclei of the source with an original momentum lying between p' and $p'+dp'$ (the true momentum distribution).

$K(p', p)$, the "kernel" of the distortion (integral) equation; this kernel is determined by the apparent (measured) shape (dependence on p) of a suitably normalized monoenergetic conversion line with a true momentum $= p'$. $K(p', p)$ is therefore a function of the source thickness, T, and the scattering and focusing properties of a given spectrometer.

If $N(p')$ is now expanded in a Taylor series in $p'-p$, the general approximation is obtained

$$M(p)=N(p)\int_0^\infty K(p',p)dp' +\frac{dN(p)}{dp}\int_0^\infty (p'-p)K(p',p)dp' +\frac{1}{2}\frac{d^2N(p)}{dp^2}\int_0^\infty (p'-p)^2\ K(p',p)dp'+\cdots. \quad (2)$$

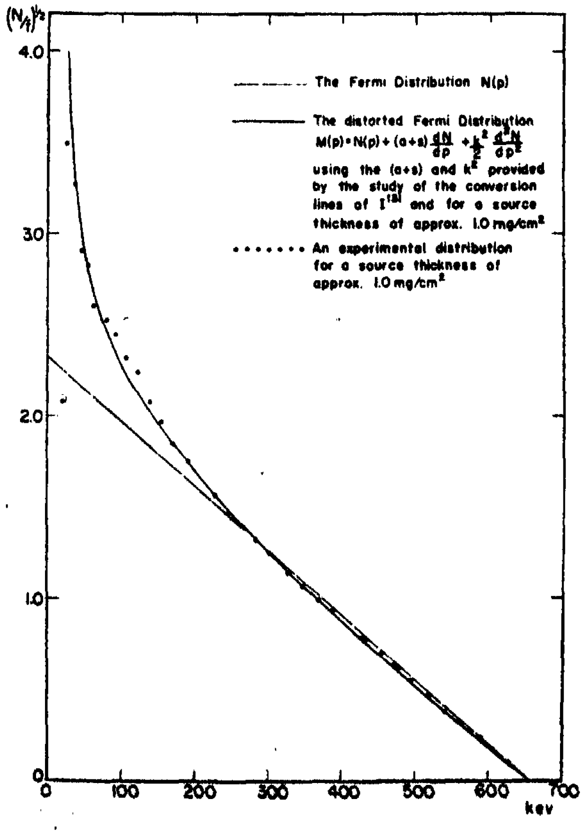

FIG. 5. F-K plot of the positrons from Cu⁶⁴.

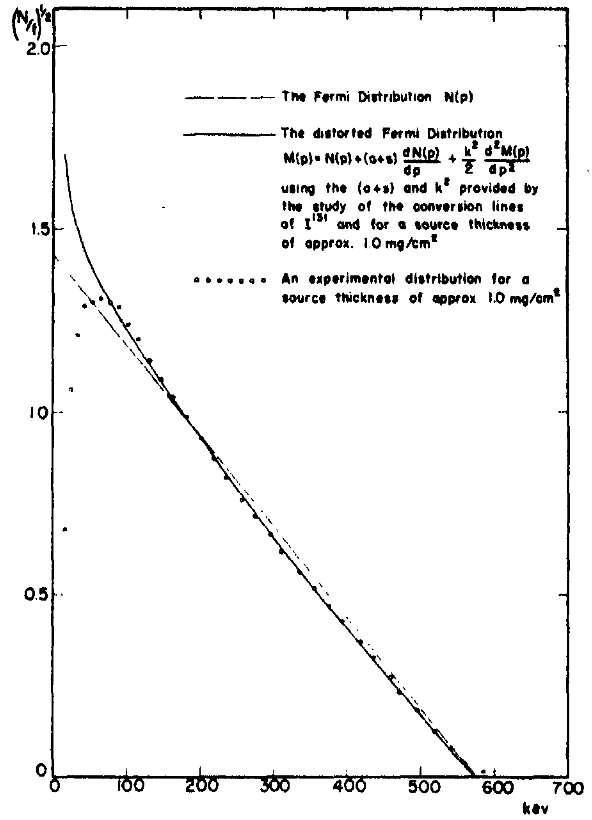

FIG. 6. F-K plot of the negatrons from Cu⁶⁴.

Further, the observed point of maximum intensity of an internal conversion line with a true momentum p' does not lie exactly at p' but rather at $p_m(p', T)$. The quantity $p_m(p', T)$ for a fixed p' decreases with increasing T, i.e., the point of maximum intensity shifts to lower momenta as the source thickness is increased.[5] It is therefore convenient to introduce new variables,

$$s(p', T)=p'-p_m(p', T) \quad (3)$$

and

$$x(p', T)=p_m(p', T)-p=p'-s(p', T)-p\approx p'-p-s(p, T), \quad (4)$$

the last (approximate) equality being a consequence of the relatively slow variation of $s(p', T)$ with p' (compared to the variation of $K(p', p)$). Insertion of Eq. (4) into Eq. (2) then yields,

$$M(p, T)=N(p)+[s(p, T)+a(p, T)][dN(p)]/dp +\tfrac{1}{2}k^2(p, T)[d^2N(p)]/dp^2, \quad (5)$$

where

$$a(p, T)=\int_{-\infty}^{\infty} xK(p+x+s(p, T), p;\ T)dx = \text{the centroid}$$

of the internal conversion line shape about the momentum, p_m, of the maximum intensity. The shape is specified for a given source thickness T by the kernel $K(p', p; T) = K(p+x+s(p, T), p; T)$; also $k^2(p, T) = g^2(p, T) + 2a(p, T)s(p, T) + s^2(p, T)$, with

---

[5] $p_m(p', T)$ will approach a limiting value when T becomes sufficiently thick to stop all electrons originating at the back of the source.

$$g^2(p, T) = \int_{-\infty}^{\infty} x^2 K(p+x+s(p, T), p; T)dx$$

and g^2 = the radius of gyration, squared, of an internal conversion line shape for a source thickness, T, about the momentum, p_m, of the point of maximum intensity.

In general it has been found that the second derivative correction is small and only becomes important near the maximum momentum of the continuous distribution.

III. APPLICATION TO A SMALL 180° SPECTROMETER

The 47- and 330-kev internal conversion lines of I^{131} were studied in a small 180° magnetic spectrometer (5.7-cm radius of curvature).[3] The conversion lines were investigated using four different source thicknesses (42, 250, 490, and 840 μg/sq. cm). The sources were prepared by allowing the solvent containing the I^{131} to evaporate after being placed upon the source backing. This method is known to produce non-uniform crystalization resulting in the actual source thickness for the beta-particles being much larger than the average source thickness as obtained by weighing. In order to minimize non-uniform crystalization small amounts of gelatin were added to the solution. This procedure was found to be quite satisfactory. The average thicknesses of the sources were obtained by weighing.

Figures 1 and 2 show the shapes of the internal conversion lines as a function of the source thickness, T. From the experimental data concerning these lines, values of $s(p, T)$, $a(p, T)$, and $g^2(p, T)$ plus their dependence on source thickness were deduced by interpolation. These values should be accurate to approximately ±20 percent.

Figures 3 and 4 illustrate a summary of this analysis. We have also given, for the sake of comparison, values of $s(p, 0)+a(p, 0)$ and $k^2(p, 0)$ which are to be expected (for an infinitely thin source) from a theoretical analysis of the focusing properties of a 180° magnetic beta-ray spectrometer.[6]

It is significant to note in Fig. 1 that not only does the peak intensity of a line decrease as the source thickness is increased, but that the intensity of the low energy tail grows appreciably with an increase in source thickness. This increase in the intensity of the tail of the line illustrates the degradation of particles to momenta much lower than they originally possessed, and essentially accounts for the type of continuous spectrum distortion which is exhibited as an excess of particles in the low energy region.[7]

To test the accuracy of our method, a comparison was made between the corresponding Fermi allowed shape, $N(p)$, which had been distorted according to Eq. (5) and the values of $a(p, T)+s(p, T)$ and $k^2(p, T)$ for 1.0 mg/cm^2 from Figs. 3 and 4, and, an experimental distribution from a source of approximately 1.0 mg/cm^2 thickness. Experimentally obtained positron and negatron spectra of Cu^{64} were used for this comparison. The $N(p)$ spectra distorted according to Eq. (5), i.e., the $M(p)$, and the experimental spectra were normalized at the value of p where $dN(p)/dp = 0$, since we could expect a minimum distortion at this point.

Figures 5 and 6 present the result of this comparison. The $M(p)$ curve for 1.0 mg/cm^2 obtained from Eq. (5) and Figs. (3) and (4), is represented by the continuous line, and the experimental distributions of positrons and negatrons from a source thickness of approximately 1.0 mg/cm^2 are indicated by the small circles. The agreement is quite good, both in the case of the positrons and in the case of the negatrons.

The greater magnitude of the distortion for positrons as compared to negatrons arises from the higher first derivatives of the positron momentum distribution in the low energy region.[8] In both cases the experimental points at very low energies fall below our $M(p)$ spectra because of absorption in the counter window.

---

[6] G. E. Owen, Rev. Sci. Inst. **20**, 916 (1949).

[7] The line shapes in Figs. 1, 2 were normalized on the high energy side where the thick source distortion is a minimum.

[8] In general because of the sensitive dependence of the corrections to the measured spectrum ($M(p)$) on the derivatives of the true spectral distribution ($dN(p)/dp$, etc.), it is not possible to correct a continuous thick source spectrum by means of a direct comparison with a continuous thin source spectrum, unless the two spectra have the same true shape.

THE REVIEW OF SCIENTIFIC INSTRUMENTS VOLUME 21, NUMBER 5 MAY, 1950

Theory of the Capture Process in a Betatron-Injected Synchrotron

David C. de Packh and Milton Birnbaum
Naval Research Laboratory, Washington, D. C.

(Received September 15, 1949)

The investigation of electrons of all possible initial phases and phase velocities at transition between betatron and synchrotron phases of an electron synchrotron has been undertaken with a view toward determining the effect of different ways of applying the r-f. It has been found that for an average accelerator there is an advantage in a moderately slow increase of the voltage from zero to its final value, while for the extreme case where particles enter the transition region with large phase velocity, an asymptotic final radial oscillation amplitude is reached which is independent of the manner in which the voltage is applied, provided only that it is applied adiabatically.

I. INTRODUCTION

It has been shown by Bohm and Foldy[1] and others that the differential equation governing the phase oscillation in a synchrotron is

$$d/dt(H\dot{\phi})+a^2V\sin\phi=a^2V\sin\phi_s, \tag{1}$$

where H is the orbital magnetic field, V is the r-f voltage envelope, ϕ is the phase of the electron with respect to the rotating wave, and $a^2=\omega_0^2/2\pi R(1-n)$. As usual, R is the stable orbit radius, ω_0 is the angular velocity of the electron in its orbit, and $n=-R\partial H/H\partial R$. ϕ_s is the equilibrium angle of the bunch. Following reference 1, we may take the right-hand side of (1) to be negligible at the transition between betatron and synchrotron phases, since the betatron flux condition is satisfied and since the energy of the electron at transition, W_1, is large in comparison with the rest energy, W_0. The rate at which energy is being added to the particle due to betatron action is assumed to be slow. As a consequence of this assumption, one may divide out the H from the first term of the left-hand side; that is, the percentage change of H during one cycle of the phase oscillation is taken to be small. Consequently, the differential equation is to a sufficient approximation of the form

$$d^2\phi/dt^2+f(t)\sin\phi=0;$$

to make matters more precise, $f(t)$ can be taken as a power of the time and the equation written

$$d^2\phi/dt^2+b^2(t/T)^s\sin\phi=0. \tag{2}$$

The bunching process is taken to be over in a time T dating from the instant of application of the r-f. Accordingly, the power s is a design parameter (a quantity $p=1/(s+2)$ will be used frequently in preference to s for convenience in the analysis), and $b^2=a^2V_T/H_T$, where V_T/H_T is the value of V/H at $t=T$. For the most part T will be sufficiently short so that H can be considered constant, meaning that the voltage envelope increases as the sth power of the time. V_T is supposed to be enough larger than $2\pi c\dot{H}/\omega_0^2$ so that the equilibrium angle of the bunch shifts by a negligible amount after the betatron flux is removed.

In general one can distinguish two limiting types of behavior of the particles subject to (2) according as their initial phase velocity, $\dot{\phi}_0$, is large or small in comparison with the quantity $b\phi_0$, where ϕ_0 is the initial phase displacement. To explain the difference between these two, let us for the moment suppose that the angles involved are small and consequently that $\sin\phi$ can be replaced by ϕ. This is then the equation of a harmonic oscillator of displacement ϕ whose restoring force varies with the time. If the particle is given a large initial velocity, it is plainly of advantage to increase the restoring force as rapidly as possible if the amplitude of oscillation is not to become excessive. If, on the other hand, the particle has an initial displacement but no initial velocity, it is desirable to increase the restoring force slowly in order not to bestow too great a velocity on the particle by the time it first passes through the equilibrium position. If there is a group of particles, all subject to the same restoring force but having varying conditions of initial displacement and velocity, it then appears that there is a certain optimum way of applying the restoring force in order to keep the maximum number of this group confined within a given range of final amplitudes of oscillation.

This qualitative argument fails to do justice to those particles whose initial phase velocities are high because the restoring force is in fact not linear with ϕ but sinusoidal. It will be shown for this type of particle that its final velocity is, in the main, independent of the manner of application of the r-f, provided it is applied slowly; it depends only on the final voltage and the initial phase velocity of the particle.

II. THE "LINEARIZED" EQUATION AND ITS GENERAL SOLUTION

In order to explore the distribution of amplitudes arising from the initial velocity and displacement components, we may examine the "linearized" equation in which $\sin\phi$ is replaced by ϕ; this is of course

$$d^2\phi/dt^2+b^2(t/T)^s\phi=0. \tag{3}$$

---

[1] D. Bohm and L. Foldy, Phys. Rev. 70, 249 (1946).

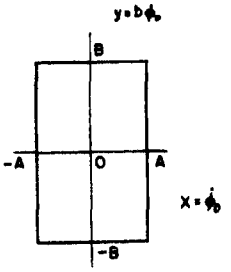

FIG. 1. Rectangle representing possible starting conditions.

The solution of this[2] is

$$\phi=t^{\frac{1}{2}}[a_1J_p(u)+a_2J_{-p}(u)]$$
$$\dot\phi=bt^{\frac{1}{2}}(t/T)^{s/2}[a_1J_{p-1}(u)-a_2J_{1-p}(u)] \qquad (4)$$

in which

$$u=2pTb(t/T)^{\frac{1}{2}p},\quad p=1/(s+2),\quad a_1=\phi_0p!(pTb)^{-p}T^{\frac{1}{2}},$$

and

$$a_2=\phi_0(-p)!(pTb)^{+p}T^{-\frac{1}{2}}.$$

The simplified notation $p!=\Gamma(p+1)$ is used throughout.

We are interested in rise times appreciably greater than one cycle of phase oscillation, so that we may use the asymptotic approximations for the Bessel functions. Since what determines the loss or capture of a particle is whether or not its radial oscillation amplitude exceeds the available aperture, the amplitude in turn depending on the final phase velocity, we accordingly find the asymptotic value of this quantity, using the relation

$$[\dot\phi_a(T)]^2=[b\phi_0\pi^{-\frac{1}{2}}(-p)!(pTb)^{p-\frac{1}{2}}]^2$$
$$+[\dot\phi_0\pi^{-\frac{1}{2}}(p-1)!(pTb)^{\frac{1}{2}-p}]^2+2b\phi_0\dot\phi_0\cot p\pi, \qquad (5)$$

where the subscript a indicates the amplitude of the quantity it follows. The amplitude of the phase velocity is greatest at $t=T$. The two opposing trends mentioned above are clearly in evidence in this expression; the first term vanishes while the second becomes infinite with increasing T.

In order to determine the best way of applying the voltage, one must consider the prior distribution of phase amplitudes and velocities at the instant when the r-f is first turned on. It is apparent that all phases from $\phi=\pi$ to $\phi=-\pi$ are equally probable for a given particle. Following reference 1, we take the energy spread of the beam to be

$$\Delta W=(1-n)(2W_0W_I)^{\frac{1}{2}}(x_1/R),$$

where W_I is the kinetic energy of injection and x_1/R is the relative aperture. The phase velocity at energy $W_I \gg W_0$ is, from (15),[1]

$$[\omega_0(2W_0W_I)^{\frac{1}{2}}/2W_I](x_1/R), \qquad (6)$$

since the energy spread is equally divided about a mean. We may take (6) to be the limit of possible phase velocities and assume that any phase velocity between $-A$ and A, where A is the value of (6), is as probable as any other for a given particle.

We may now construct a rectangle as shown in Fig. 1, taking $y=b\phi_0$ and $x=\dot\phi_0$, extending between the limits $-A$ and A as regards x and between $-B$ and B as regards y; here $B=\pi b$. As indicated in the preceding paragraph, the area of this rectangle has been taken to be everywhere equally densely populated with particles.

The error incurred in extending the linear solution to $\phi=\pi$ and thus of taking the limit B simply as πb in the face of the non-linear character of the original Eq. (2) is not as great as might be supposed. The smallest value of B/A for a conceivable machine is about 20, and the value is usually higher, so that particles having large initial displacements derive most of their energy of oscillation from initial potential rather than kinetic energy. Now one can form a good idea of the behavior of a particle with zero initial phase velocity without making the linearizing approximation (see Appendix I); such a calculation indicates that for $p=\frac{1}{3}$, for example, the ratio of $\dot\phi_a(T)$ as computed in this more accurate way to the approximate "linearized" value from (5) is between 0.91 and 1.00 for any starting angle up to 178°.

In the notation adopted for the rectangle one can put (5) as

$$z=fx^2+gy^2+hxy, \qquad (7)$$

where z is the square of the final phase velocity amplitude and f, g, and h are the corresponding coefficients depending on p and T. An examination of (5) indicates that the discriminant of this expression, h^2-4fg, is constant and equal to -4. Thus it follows that the lines of equal z and consequently of equal final radial oscillation amplitude are ellipses symmetric about the origin.

The greatest interest is in the ellipse $z=z_1$, where z_1 is the particular value of z corresponding to the available aperture; one has $z_1=\omega_0^2(x_1/R)^2$ [see, for example, Saxon and Schwinger,[8] relation (21)]. If a particle lies within the rectangle but outside the ellipse $z=z_1$, then its radial oscillation is greater than the aperture and it is lost. It therefore becomes desirable as nearly as possible to fit the ellipse to the rectangle. In this con-

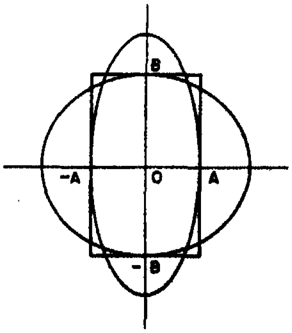

FIG. 2. Ellipses representing approximate limiting values of g.

---

[2] E. Jahnke and F. Emde, *Tables of Functions* (Dover Publications, New York, 1943), p. 147.

[8] D. Saxon and J. Schwinger, "Orbits in magnetic resonance accelerators" (unpublished).

nection it is also desirable that $z=z_1$ be as little tilted as possible, since any dissymmetry with respect to the axes cannot but reduce the area common to the rectangle and the ellipse. In view of the large value of B/A, it is easy to verify that the xy term in (7) can be overlooked, so that this requirement is automatically satisfied. From (5), $fg=\csc^2 p\pi$; thus the equation of the ellipse becomes approximately

$$x^2\csc^2 p\pi/g+gy^2=z_1. \qquad (8)$$

Now one can see (Fig. 2) that there are two approximate limits on g for $z=z_1$; these are tangency at the sides $(x=\pm A)$ and tangency at the top $(y=\pm B)$. Going beyond these limits cuts off particles at the sides and top, respectively, of the rectangle. Tangency at the sides means $g=A^2\csc^2 p\pi/z_1$; tangency at the top gives $g=z_1/B^2$. The best value lies between these limits. Now

$$A=\omega_0[(2W_0W_I)^{\frac{1}{2}}/2W_1](x_1/R)$$

and $B=\pi b=\pi\omega_0(V_T/2\pi RH_T(1-n))^{\frac{1}{2}}$ [see (1), (2), and (6)], so that

$$\csc^2 p\pi W_0W_I/2W_1^2<g<(1/\pi)^2(x_1/R)^2 \times[2\pi RH_T(1-n)/V_T], \qquad (9)$$

unless of course the rectangle is such that $z_1/B^2 \leqq A^2\csc^2 p\pi/z_1$, in which case the common area is greatest if one keeps the ellipse tangent at the sides, its area being contained entirely within that of the rectangle.

The best possible value of g in the range (9) can be found by choosing it such that one of the ellipses of the family, say $z=z'<z_1$, is tangent to the rectangle at both top and sides; this is the value of g which concentrates the greatest number of particles in the amplitude z'. Substituting in (8) gives the best value of g, say g_0, as

$$g_0=A\csc p\pi/B,\text{ from which } z'=AB\csc p\pi. \qquad (10)$$

Remembering (5), we have $g=(-p!)^2(pTb)^{2p-1}/\pi$, whence one finds the rise time corresponding to g_0 to be

$$T_0=(1/pb)[(-p)!^2/\pi g_0]^{1/(1-2p)}, \qquad (11)$$

which is valid only if pT_0b turns out large compared with 1.

The distance along the normal to the two curves z and $z+dz$ is $dz/|\nabla z|$; consequently the area between them is $dz\int ds/|\nabla z|$, the integral being along the curve z. In Cartesian coordinates this becomes $dz\int dx/(\partial z/\partial y)$; in polar coordinates it is $dz\int rd\theta/(\partial z/\partial r)$. If the total number of electrons in the rectangle is taken as unity, then the number dN having oscillation amplitudes between z and $z+dz$ is

$$dN=(dz/4AB)\int dx/(\partial z/\partial y)$$
$$=(dz/4AB)\int rd\theta/(\partial z/\partial r).$$

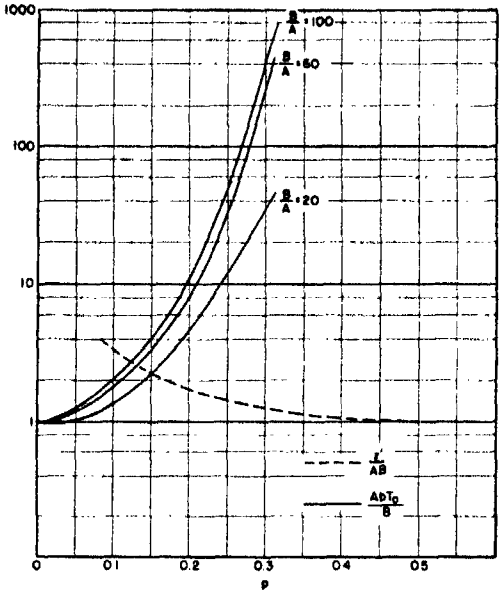

FIG. 3. Variation with p and B/A of the quantities z'/AB and AbT_0/B. The former is proportional to the square of the required aperture and the latter to the rise time.

In order to determine the distribution of amplitudes when the optimum value of g is used, one divides the region into two parts, namely, $0<z<z'$ and $z'<z<2z'$, since $2z'=A^2\csc^2 p\pi/g_0+g_0B^2$ is the largest possible value of z within the rectangle, assuming that z_1 is outside the rectangle. All the ellipses in the first region are complete and lie inside the rectangle; hence, polar coordinates are used, the integration extending from 0 to 2π. This gives

$$dN=\pi\sin p\pi dz/4AB,\quad 0<z<AB\csc p\pi. \qquad (12)$$

This means that the squares of all radial oscillation amplitudes up to

$$x_0/R=\{\pi[(2W_0W_I)^{\frac{1}{2}}/2W_1] \times[V_T/2\pi RH_T(1-n)]^{\frac{1}{2}}\csc p\pi(x_1/R)\}^{\frac{1}{2}}$$

are equally probable and that $\pi/4$ of the total number of particles are in this group. The remainder of the electrons are between x_0/R and $(x_0/R)\sqrt{2}$; by using Cartesian coordinates one can verify without difficulty that the distribution is

$$dN=(dz\sin p\pi/2AB)[\arcsin(z'/z)^{\frac{1}{2}} -\arcsin(1-z'/z)^{\frac{1}{2}}]. \qquad (13)$$

If $z=z_1$ lies wholly within the rectangle, one has again

$$dN=\pi\sin p\pi dz/4AB,$$

where, however, the limits of application are $0<z<z_1$; the distribution is uniform over all amplitudes within the aperture, and the fraction of particles captured is $\pi\sin p\pi z_1/4AB$. The intermediate case in which $z=z_1$ is partly inside the rectangle and partly outside can be worked out without difficulty by the methods already outlined.

To estimate the amplitude if the r-f is applied suddenly one may return to Eq. (3), taking $s=0$. From this it can be seen that if the voltage is applied in one step, the lines of equal oscillation amplitude will be the circles $z=x^2+y^2$; further, if, as before, we impose the circle $z_1=x^2+y^2$ on the rectangle, we can form an idea of the number of particles lost. Two cases can be distinguished: (1) the circle is within the rectangle, under which conditions the fraction saved is simply $\pi z_1/4AB$; (2) the circle is partly outside the rectangle, in which case the number saved is $(z_1/2AB)[q(1-q^2)^{\frac{1}{2}}+\text{arc}\sin q]$ where $q=A/z_1^{\frac{1}{2}}=(2W_0W_I)^{\frac{1}{2}}/2W_1$. This fraction cannot of course exceed 1.

It may be profitable to discuss a numerical example in order to fix these concepts. Consider a machine of the following specifications: $\omega_0=3\times10^8/\text{sec.}$, $V_T=10$ kv, $n=\frac{2}{3}$, $W_I=50$ kev, $x_1/R=3$ percent, $W_1=1.5$ Mev; tentatively we take $p=\frac{1}{3}$, that is, the voltage rises linearly with the time. From (9) we learn that $7.41\times10^{-3}<g<3.70\times10^{-2}$; from (10) $g_0=1.66\times10^{-2}$. It is apparent, however, that the linear rise leads to an excessive rise time; (11) gives $bT_0=1.3\times10^5$ and $T_0=8800$ μsec. The importance of choosing the law of rise so as to keep the rise time within reason is here made clear. Under these conditions it is desirable to form an idea of the dependence of T_0 and the required aperture on p. Figure 3 shows graphs of AbT_0/B and z'/AB as functions of p. From these it may be inferred that the best value of p for most machines lies somewhere between 0.1 and 0.2, somewhat favoring the larger value. Smaller values of p lead to excessive apertures; larger ones to excessive rise times. In this example, one might take $p=\frac{1}{6}$, corresponding to a fourth power law of rise, giving a rise time of 21.3 μsec. Equation (12) indicates that the distribution is uniform up to a relative aperture of 2.64 percent and that 79 percent of the particles are in this group; if the electrons could do so, they would occupy an aperture of 3.74 percent, which exceeds the available space, so that a small number are lost. This number might be computed by integrating (13) between apertures of 3.0 and 3.74 percent; however, it is easier to compute the difference between the area of the rectangle and the portion of $z=z_1$ contained within it; the fraction of particles lost amounts to about 8 percent of the total. Finally, to estimate the number retained if the voltage is applied suddenly, one finds $q=0.075$, so that the total fraction saved is 30 percent.

In general, it may be remarked that any factors in the design which limit the range over which g can vary in (9) are detrimental to the efficiency of capture. This consideration favors values of p not too near zero, high transition energies, and large apertures. The degree to which this affects the ultimate design of the machine must, of course, be weighed against other factors not mentioned here.

III. THE LIMITING CASE FOR PARTICLES OF HIGH INITIAL PHASE VELOCITY

One is justified in applying the results of the last section only because in actual machines the rectangle describing the distribution of initial conditions is tall and narrow. The linear solution is otherwise quite inaccurate. It is therefore of interest to determine the upper limit of oscillation possible in a machine in which, for one reason or another, particles may enter the transition region with large phase velocities. One can immediately see that the prediction arising from the linearized theory of infinite amplitude for an infinite rise time is in error because of the sinusoidal character of the restoring force; in fact, if the rise time is long enough so that the process is truly adiabatic, it would appear probable that the final oscillation amplitude will be independent of the manner of application of the voltage since in this case there is no dependence on the initial phase of the particle; the angular velocity depends merely on the magnitude of the applied voltage and the initial phase velocity.

To show this, let us consider the analogous pendulum of unit length in a slowly varying gravitational field; if the displacement is ϕ as before, then

$$d^2\phi/dt^2+g\sin\phi=0. \tag{15}$$

Two forms of solution for this equation are available according as the pendulum is rotating or vibrating.[4] These are

$$\phi=2\,\text{arc}\sin\begin{cases}k\,\text{sn}(u,k)\\ \text{sn}\left(K\int_0^u kdu/K,\,1/k\right)\end{cases}$$
$$\phi=2kg^{\frac{1}{2}}\begin{cases}\text{cn}(u,k)\\ \text{dn}\left(K\int_0^u kdu/K,\,1/k\right),\end{cases} \tag{16}$$

where the upper quantities refer to the vibrating and the lower to the rotating pendulum. If ϕ_a is the amplitude of the velocity variation, then $k=\phi_a/2g^{\frac{1}{2}}$, $u=\int_0^t g^{\frac{1}{2}}dt$, and K is the complete elliptic integral of the first kind and the appropriate modulus (k or $1/k$). The two cases are thus differentiated according as k is less or greater than one. The integral form of the argument in the rotating case is necessitated by the variation of the period of the function during the course of the motion.

The action integral for the rotating pendulum is readily found to be

$$J=kg^{\frac{1}{2}}E(1/k)=a\phi_0, \tag{17}$$

where a is a constant, since the motion is adiabatic at $t=0$. $E(1/k)$ is the complete elliptic integral of the second kind of modulus $1/k$. Since the total energy at $t=0$ is kinetic and $E(0)=\pi/2$, the constant a is seen to be $\pi/4$ and consequently $\dot{\phi}_a$ can be obtained at any time during the motion of the rotating pendulum from the transcendental equation

---

[4] E. T. Whittaker, *Analytical Dynamics*, 4th ed. (Cambridge University Press, London, 1937), pp. 72–74.

$$kE(1/k)=\pi\phi_0/4g^{\frac{1}{4}}. \tag{18}$$

If g continues to increase, there will eventually be a crossover point at which the pendulum passes from a rotating to a vibrating mode. This of course corresponds to particles which are slipping over the crests of the potential function but which are finally trapped in a valley because of the increase in the height of the crests with time. Accordingly, we must have $\dot{\phi}_c/\phi_0=\pi/2$, where ϕ_c is the amplitude of ϕ at the crossover.

Moreover it has been shown [1, 3] that the solution for the vibrating pendulum can be put in the form

$$\phi=2k_1g_1{}^{\frac{1}{4}}g^{\frac{1}{4}}\mathrm{cn}(u,\, k), \tag{19}$$

where k_1 and g_1 are values of these quantities at some specific time, say t_1. One can now estimate the amplitude at the time T, assuming that the crossover has occurred before this time, by taking $t_1=t_c$, the crossover time. At this instant $k_1=1$ and $g_1=\pi^2\dot{\phi}_0{}^2/16$, so that

$$\phi_a(T)=(\pi\phi_0 g_T{}^{\frac{1}{4}})^{\frac{1}{2}}=(\pi b\phi_0)^{\frac{1}{2}} \tag{20}$$

in the notation of Eq. (2). The condition that the crossover occur in the interval $\frac{1}{2}<t<T$ is $\phi_0<4b/\pi$.

This analysis of course neglects those singular regions in which the crossover occurs when the particle is very near the unstable point $\phi=\pi$. Accordingly, there are certain specific values of ϕ_0 which give rise to these singularities and impose a fine structure on the general behavior indicated by (20). These singularities have been investigated both numerically, by means of a computing machine, and analytically, by joining the adiabatic solution to one in which the restoring force is a triangular rather than a sine wave. The singularities are of a very low order (see Appendix II). It is thus reasonable to suppose that only a very small percentage of the totality of particles of large velocity are affected by this fine structure and that the behavior indicated by (20) is essentially that followed by the great majority of the particles. It is a pleasure to acknowledge the assistance of Mr. C. H. Chrisman in connection with the numerical work performed on the BTL relay computer.

APPENDIX I

To arrive at the solution for the general Eq. (2) for a particle with an initial displacement ϕ_0 but no initial phase velocity, one must investigate the differential equation near $t=0$, where the adiabatic solution previously obtained is no longer valid. An exact solution already exists for the linearized Eq. (3), and consequently a simple way to proceed is to determine the effect on the solution (4) of putting $\sin\phi$ for ϕ for large phase displacements. We do this by considering Eq. (2) as that of a modified harmonic oscillator, in which the "period" of the motion is modified in the same way as the period of a pendulum is changed with large oscillation amplitudes. That is, the period is multiplied by a factor $2K(k)/\pi$, where K is the complete elliptic integral of the first kind of modulus $k=\sin\phi_a/2$, ϕ_a being the amplitude of oscillation; thus one makes the transformation

$$u=\frac{\pi b}{2}\int_0^t (1/K)(t/T)^{s/2}dt$$

instead of

$$u=b\int_0^t (t/T)^{s/2}dt$$

in (3). We shall use this relation to establish the time of the first zero of the displacement, at which time it will be assumed that the motion is adiabatic so that a juncture can be made to the solution (16). If t_0 is the time of the first zero and if we assume that $\phi_0=\phi_a$ for $0<t<t_0$, then one can establish that

$$t_0/T=[K(\sin\phi_0/2)u_0(-p)/\pi pTb]^{2p},$$

where $u_0(-p)$ is the first zero of $J_{-p}(u)$. We can also get the value of the amplitude of the function at the first zero to a reasonable approximation by recalling that at this time the motion is supposed to be adiabatic and of constant frequency with respect to u and therefore that the value of the "amplitude" is equal to the value of the derivative. Using these concepts and (16) one obtains the result

$$\dot{\phi}_a(T)=\sin\{(\phi_0/2)\Lambda'_{-p}[u_0(-p)]\}(\pi pTb/K(\sin\phi_0/2)u_0)^{p-\frac{1}{2}},$$

where $\Lambda_p(u)=p!(u/2)^{-p}J_p(u)$.[5] Λ' is the derivative of this function with respect to its argument. The values for $u_0(-p)$ and $\Lambda_{-p}'[u_0(-p)]$ can be computed from existing tables and formulas.[2] The results obtained from the above expression are in excellent agreement with numerical solutions of (2) obtained from the digital computer.

APPENDIX II

An approximate form of (2) which furnishes a reasonable idea of the behavior of the particles near $\phi=0$ and $\phi=\pi$ is furnished by the two linearized equations $d^2\phi/d^2t+b^2(t/T)^s\phi=0$ and $d^2\theta/dt^2-b^2(t/T)^s\theta=0$, where $\theta=\phi-(2m+1)\pi$, m an integer. The former equation holds for ϕ near $2m\pi$, the latter for θ near zero, the transitions between the domains of application of the two equations being at $\theta=\pm\pi/2$. It is apparent that, by the use of these equations and the indicated boundary conditions, the original motion described by (2) is changed into a motion in which the restoring force as a function of the displacement is in the form of a symmetrical triangular wave with period 2π and a slope of ± 1. This modification preserves the qualitative features of the motion, particularly near $\phi=0$ and $\phi=\pi$.

For the purpose of investigating the crossover in the neighborhood of the singularity at $\phi=\pi$ the second equation is sufficient. If u is defined as in (4) and u_0 corresponds to the value of u at which $\theta=-\pi/2$ and such that the crossover occurs in the immediately following quarter-cycle $(-\pi/2<\theta<0)$, then one may write $\delta=u-u_0$ and form the asymptotic solution to the equation thus:

$$\theta/\theta_0=(1+\delta/u_0)^{p-\frac{1}{2}}[\cosh\delta+(\dot{\theta}_0/\theta_0 b)(u_0/2pTb)^{2p-1}\sinh\delta]$$

$$\dot{\theta}/\theta_0=b(2pTb/u_0)^{2p-1}(1+\delta/u_0)^{\frac{1}{2}-p}$$
$$\times[\sinh\delta+(\dot{\theta}_0/\theta_0 b)(u_0/2pTb)^{2p-1}\cosh\delta],$$

from which one concludes immediately that at the crossover

$$\tanh\delta=(2\dot{\theta}_0/\pi b)(u_0/2pTb)^{2p-1},$$

where θ_0 has been put equal to $-\pi/2$, or $u_c=u_0+\mathrm{arc\ tanh}(2\dot{\theta}_0/\pi b)\times(u_0/2pTb)^{2p-1}$, u_c being the value of u at the instant of crossover. Now from (19)

$$\phi_a(T)\propto g_c{}^{\frac{1}{4}}=\{(\tfrac{1}{2}pTb)[u_0+\mathrm{arc\ tanh}(2\dot{\theta}_0/\pi b)(u_0/2pTb)^{2p-1}]\}^{\frac{1}{2}-p}.$$

Also $\mathrm{arc\ tanh}\,y=\frac{1}{2}\log(1+y)/(1-y)$; if we take y very near 1, we can neglect additive constants, so that in this region

$$\phi_a(T)\propto[-\log(1-h\dot{\theta}_0t_0{}^{-s/2})]^{\frac{1}{2}-p},$$

---

[5] See reference 2, p. 128ff.

where h is a constant depending on p, T, and b, and t_0 is the time corresponding to u_0. The relation of $\dot{\theta}_0 t_0^{-s/2}$ to the initial conditions can be established by recalling the adiabatic theorem in the form $J=\bar{T}\tau=a\phi_0$, where $\bar{T}$ is the mean kinetic energy over one cycle, τ is the duration of that cycle, and a is a constant. Since $\bar{T}\tau\propto\phi_0$ while $\bar{T}\propto\dot{\phi}_0^2$ for a small change in ϕ_0, it follows that $\tau\propto 1/\dot{\phi}_0$, while if the number of cycles is constant, the whole elapsed time t_0 must also be proportional to $1/\dot{\phi}_0$. Now $\dot{\theta}_0\propto\dot{\phi}_0$, and since $t_0\propto 1/\dot{\phi}_0$, one has $\dot{\theta}_0 t_0^{-s/2}\propto\dot{\phi}_0^{\frac{1}{2}p}$, so that

$$\phi_a(T)\propto[-\log(1-h\dot{\phi}_0^{\frac{1}{2}p})]^{1-p}.$$

THE REVIEW OF SCIENTIFIC INSTRUMENTS VOLUME 21, NUMBER 5 MAY, 1950

Apparatus for Recording Fluctuations in the Refractive Index of the Atmosphere at 3.2 Centimeters Wave-Length*

C. M. Crain
Electrical Engineering Research Laboratory, The University of Texas, Austin, Texas

(Received January 16, 1950)

This article describes equipment which is being used for measuring and recording rapid fluctuations in the refractive index of the atmosphere.

RECENT studies[1,2] in microwave propagation have indicated the need for a device which will accurately record small changes in the refractive index of the atmosphere. A block diagram of the equipment which has been used by the Electrical Engineering Research Laboratory at The University of Texas for recording such changes is shown in Fig. 1. The equipment is a modification of that previously used for measuring the dielectric constants of several gases under controlled conditions.[3] The frequency of each of two microwave oscillators is controlled by the resonant frequency of its associated cavity resonator by the method previously described by Pound.[4] The outputs of the two stabilized oscillators are mixed in a crystal detector as shown. The output of the crystal is amplified by a two-stage conventional 10.7-megacycle amplifier and then applied to a limiter and discriminator. The output of the discriminator is used in conjunction with a differential amplifier to deflect a recording milliammeter. Thus, the deflection of the milliammeter is made proportional to the change in resonant frequency of one of the cavity resonators if the resonant frequency of the other cavity remains fixed. TFX-30EC wave meters were used for the cavity resonators. One cavity was sealed off so that its resonant frequency would not change with atmospheric refractive index changes. The second cavity was modified by drilling holes in one end plate as shown in Fig. 2, making about 20 percent of the end plate open. The plunger was reduced in diameter to give approximately the same open area on the other end of the cavity. A small blower was coupled to the cavity by means of a thin rubber hose so that air could be pulled through it. Thus, a change in the dielectric properties of the air being pulled through the cavity causes the output frequency of the oscillator to change accordingly. The 10.7-megacycle amplifier, limiter, and discriminator were built such that the recording milliammeter would be deflected linearly from its normal mid-scale position to either zero or full scale by a frequency change from

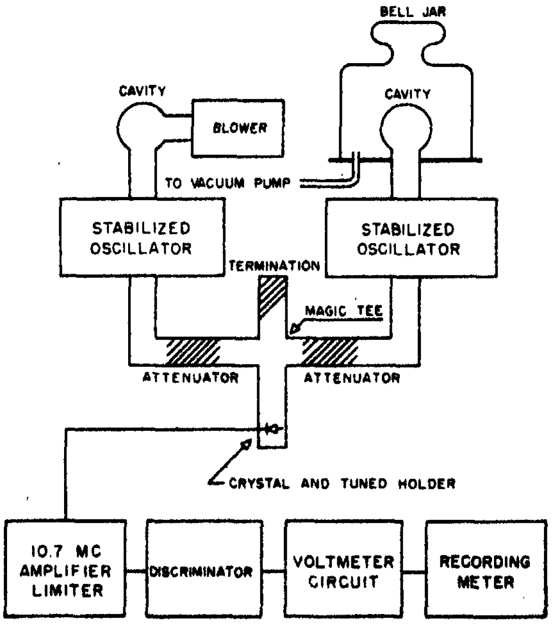

FIG. 1. Equipment arrangement for measuring rapid variations of dielectric constant.

---

* Sponsored by the ONR at The University of Texas under contract N5ori-136, T.O.I.

[1] W. E. Gordon, "A theory on radar reflections from the lower atmosphere," Proceedings of the Institute of Radio Engineers, 37, 41–43 (January, 1949). (Electrical Engineering Research Laboratory Report No. 27, The University of Texas.)

[2] A. B. Crawford, "Radar reflections in the lower atmosphere," Proceedings of the Institute of Radio Engineers, 37, 404–405 (April, 1949).

[3] C. M. Crain, "The dielectric constant of several gases at a wave-length of 3.2 centimeters," Phys. Rev., 74, 6, 691–693 (September 15, 1948).

[4] R. V. Pound, Rev. Sci. Inst. 17, 490 (1946).

10.7 megacycles of ±100 kc. It can be shown that the change in resonant frequency of the cavity resonator in kilocycles is 9.34 $(\Delta N)10^6$, where ΔN is the change in index of refraction of the gas in the cavity resonator, and the normal resonant frequency of the cavity is 9,340 megacycles. Thus, if the index of refraction varies one part in a million, the resonant frequency of the cavity resonator will change 9.34 kc and the recording milliammeter will change deflection approximately 4.7 percent of full scale deflection. The equipment then records changes in the refractive index about a mean value of ±100/9.34 or 10.7 parts in a million or simply 10.7 N units. Changes in one direction only as large as 21.4 N units can be recorded by adjusting the micrometer of the cavity wave meter such that operation is at one end of the discriminator curve. Measurements which have been made to date indicate that such a range is adequate for recording the maximum fluctuations which occur in the refractive index at a fixed point in time intervals less than a minute. The stability of the equipment was such that when both cavities were sealed off, the variation in the indicated index of refraction was never greater than 0.25 N unit in a minute.

Most of the measurements to date have been made from two to ten feet above the ground and surprising results have been obtained. Variations over a period of a fraction of a second greater than 10 N units were recorded when the ground was wet. For drier ground conditions, the variations have been less. A detailed study of these fluctuations for heights above the ground up to 300 feet and for various meteorological conditions is now being made.

The actual changes in refractive index are greater than those recorded as the nature of the equipment is such as to smooth out the peaks in the variations. Obviously the cavity itself will have some smoothing effect due to its volume. In many cases, as is apparent from examining the milliammeter recording, the time response of the meter has limited the magnitude of the change indicated. Changes in refractive index due to changes in the temperature of the air are smoothed out to some extent since air entering the cavity tends to assume the temperature of the walls of the cavity. However, the rate of flow of air has been such as to make this smoothing effect small. Another error can arise from the dimensions of the cavity varying because of fluctuations in temperature. However, since the invar cavity walls are 0.15 inch thick, the temperature time constant of the cavity will be such as to practically eliminate all erratic fluctuations about a mean temperature. The long time variations in temperature will be fairly well compensated for since both cavities will change dimensions approximately the same. Corrections as necessary could be made by recording the temperature difference between the cavity walls. This has not been done in the equipment described as this error has been negligible in the study of rapid fluctuations.

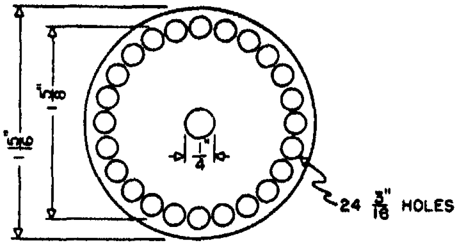

FIG. 2. End plate of cavity resonator.

THE REVIEW OF SCIENTIFIC INSTRUMENTS VOLUME 21, NUMBER 5 MAY, 1950

Combination Two-Circle Goniometer and X-Ray Spectrometer

MORTON L. BARON AND A. DEBRETTEVILLE, JR.
Signal Corps Engineering Laboratories, Fort Monmouth, New Jersey

(Received January 16, 1950)

A combination instrument consisting of a two-circle goniometer and x-ray spectrometer suitable for the study of crystals was designed and fabricated in Squier Signal Laboratory. A crystal can be oriented optically by using the instrument as a goniometer. X-ray techniques can then be used to study the crystal by replacing the collimator and telescope with an x-ray slit system and a Geiger counter. Absolute intensity measurements can be made by fixing the Geiger counter at twice the Bragg angle and rotating the crystal at 8° per hour from $\theta_{\text{Bragg}}-\Delta\theta$ to $\theta_{\text{Bragg}}+\Delta\theta$. Back reflection angles of up to 160° are obtainable. The result of a test on synthetic halite (400) reflection, gave a structure factor 12.7 compared with Max Renniger's value of 12.67. No absorption corrections are required with this technique of measuring intensities.

I. INTRODUCTION

IN the study of single crystals by x-ray diffraction, an instrument was required which could be used for many purposes. To study the mosaic structure, the instrument should be capable of receiving the total reflected intensity. In making absolute intensity measurements, the crystal must be rotated at a low constant angular velocity and the Geiger counter must intercept a large solid angle of reflection; also monochromatic radiation must be used. To obtain high resolution, the instrument must be capable of large back-reflection angles in order to work with the higher orders, although this factor is subsidiary to intensity demands. These requirements are fulfilled by using an optical two-circle goniometer designed for easy conversion to an x-ray spectrometer. Brill *et al.* describe a similar instrument.[1] This is accomplished in this instrument by substituting a Geiger counter for the telescope and an x-ray incident slit system for the light collimator. The counter subtends an angle of 14°, the crystal is rotated at a constant rate of 8° per hour and back-reflection angles of up to 160° are possible. The instrument's inherent characteristics obviate time-consuming x-ray crystal alignment by first pre-aligning the crystal optically and then converting the machine for x-ray work. Time and budget limitations made it necessary to construct the apparatus in an ordinary machine shop using commercially available components; but in so doing, the high degree of accuracy required must not be impaired. For example, we employed camera lenses as our objectives in the collimator and telescope. We also used precision ball bearings in the rotating parts, instead of the conventional instrument design of a conical shaft ending in an optically flat hardened steel block, the thrust being transmitted through a sapphire whose curved surface rests on the steel block. Intensity tests on the instrument proved to be satisfactory, indicating that the required accuracy can be obtained in an apparatus of this type and can be constructed in a machine shop at a labor cost of approximately 500 man-hours.

II. GENERAL DESCRIPTION OF THE INSTRUMENT

Referring to Fig. 1 (some parts referenced appear only in Fig. 2 and/or Fig. 3) the instrument is supported on the leveling screws (1) which are also used to adjust the height of the instrument for alignment with the x-ray beam. The base (2) of the instrument is a heavy bronze casting in which are located the Geiger counter preamplifier, the rheostat (3) for varying the light intensity, the motor and collimator switch (4), the collimator jack (5) and the power cord. The main shaft (6) is a hardened and ground steel shaft firmly affixed to the base. The vertical circle bracket (7) and the telescope or Geiger counter bracket (8) are sturdy annealed aluminum castings. These rotating brackets are supported on the main shaft by means of angular contact precision ball bearings (9) and (10) mounted in tandem. These bearings are preloaded by means of lock nuts (11) and (12). The brackets may be locked in position by means of lock screws (13) and (14). The lock screws pass through tangent clamps (15) and (16) which are conveniently located between the legs of the collimator bracket (17). Tangent screws (18) and (19) acting on these tangent clamps produce slow motion angular adjustment of the two rotatable brackets. The vertical circle bracket (7) contains a housing (20) which is fitted with precision ball bearings (21), and a horizontal hardened and ground steel shaft (22). On this shaft are mounted the vertical circle (23) which is 6 inches in diameter, and the goniometer head (24). The goniometer head is provided with all the usual movements, namely, two perpendicular sliding motions, two rocking motions and a translation along the axis by means of rack (25) and gear (26). This latter motion is locked by means of lock screw (27). The vernier (28) permits the angular setting to be read to 1 minute of arc. The vernier body supports the vertical circle clamp screw (29) and tangent screw (30) for slow motion adjustment. The second rotating bracket (8) may be fitted with either a telescope (31) or a Geiger tube (32).

---

[1] Brill, Grimm, Hermann, and Peters, Ann. d. Phys. 34, 408–409 (1939). These authors describe a similar apparatus but there are no provisions for optical alignment on the instrument itself. The crystal is pre-aligned on an optical two-circle goniometer and then the goniometer head is transferred to their x-ray spectrometer.

The telescope is focused by means of knob (33) and is locked in position by screw (34). The telescope lens system consists of a Zeiss Tessar *f* 3.5 cm, *f*/3.5 objective (35) and a 5× eyepiece. This system has a magnification of 2×. The telescope is focused for infinity and contains an adjustable slit system (36) located in the focal plane of the objective to mask any spurious reflections. By replacing the eyepiece with an adapter and a 10× eyepiece (37), the telescope may be used as a 30 power microscope for examining the surface of the crystal. The telescope orientation is adjustable by means of two groups of three set screws located radially about the telescope 120° apart. After final orientation, these set screws are securely locked. To replace the telescope with the Geiger tube, it is merely necessary to release lock screw (34), slide the telescope out and insert the commercial Geiger tube which is retained in a steel adapter of the same diameter as the telescope tube for interchangeability. The angular relation between the two rotating brackets and/or the collimator is read on the 8-inch horizontal circle (38) in conjunction with the brackets' verniers (39) and (40) to one minute of arc. The stationary collimator bracket (17) is fastened to the base and is a sturdy annealed aluminum casting. It may be fitted with either a light collimator (41) or an x-ray collimator (42). The light collimator is moved forward or back by hand and locked in position by lock screw (43). The lens system consists of a Zeiss Tessar *f* 10.5 cm, *f*/4.5 objective (44) which is focused, for infinity, by turning threaded retainer (45). The aperture system (46) is located at the focal plane of the lens. The apertures consist of the following: pin hole, large and small Maltese crosses, vertical line and horizontal line. They are interchanged by rotating the

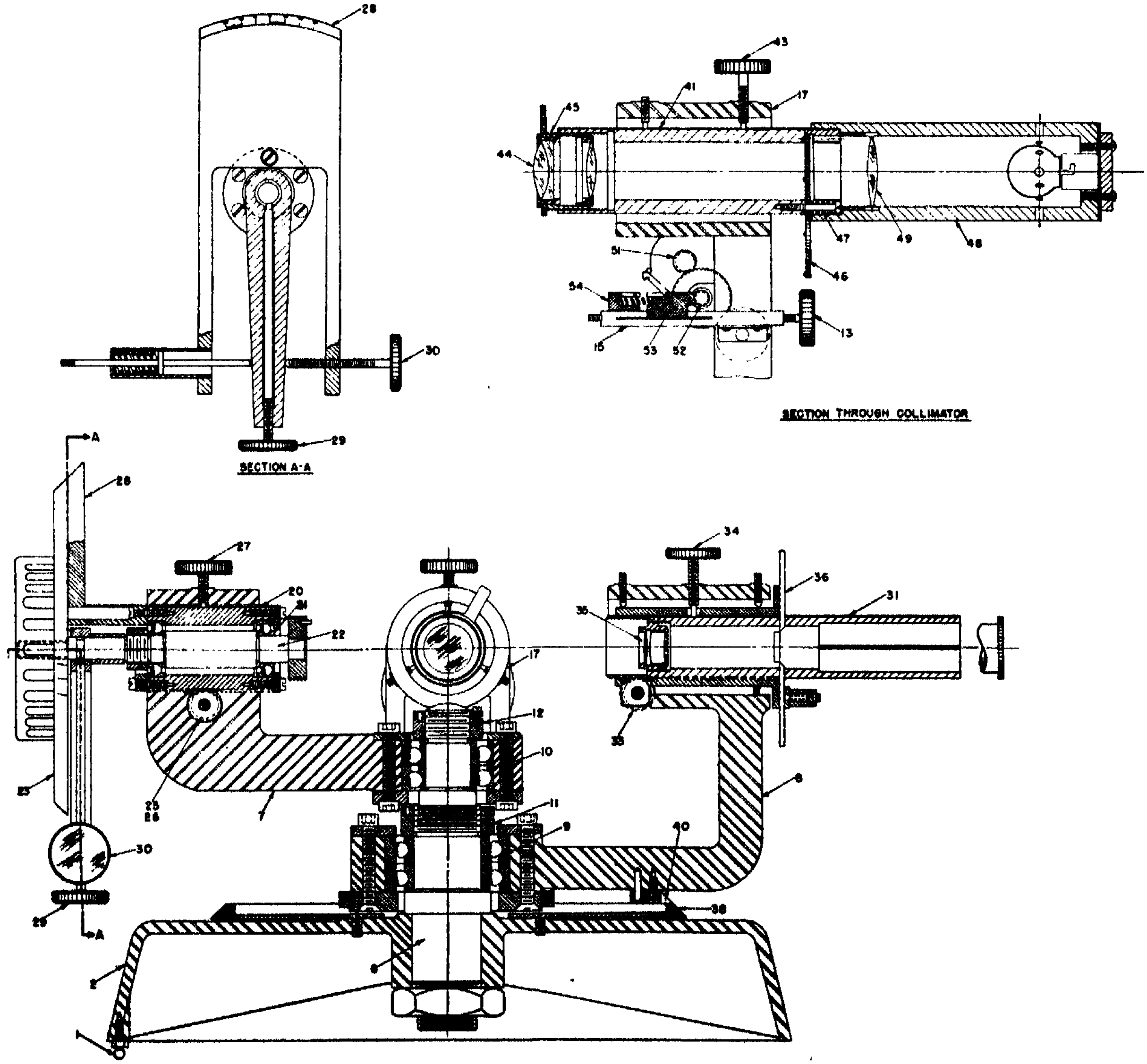

FIG. 1. Cross-sectional drawing of the two-circle goniometer and spectrometer.

holder. A spring device (47) snaps into position when the aperture is correctly located in the center of the tube. The light house (48) is built in and contains a simple condensing lens (49). Current for illuminating the lamp is provided through a transformer and the rheostat (3) located in the base. The lead terminates in a plug which may be inserted in the jack (5) located in the base. The collimator orientation is adjustable by the set screws 120° apart as heretofore.

To replace the light collimator with the x-ray collimator, it is necessary to release lock screw (43), unscrew the lens mounting (45), slide the assembly out and replace it with the x-ray collimator (42). This collimator is made of steel and is fitted with four adjustable shields (50) to produce rectangular windows. These shields are made of Babbitt metal which contains a high percentage of lead and which have the desirable features of being easily machined, relatively sturdy and show little or no wear due to friction. A one-r.p.m. clock motor with a 3 to 1 spur gear reducing train (51) is mounted on one leg of the collimator. A 20 pitch worm (52) is mounted in ball bearings between the legs and is driven by this combination. A segment of a 20-pitch, 10½-inch diameter worm wheel (53) is mounted on a slide on the vertical circle tangent clamp (15). This segment is engaged in the worm by the spring-loaded thumb-latch (54) thus causing the vertical circle bracket and the goniometer head, presenting the crystal, to move across the x-ray beam at a rate of 8° per hour. Back lash or lost motion between the worm and wheel is obviated by constraining the drive to operate against the spring and plunger of the tangent screw slow motion system.

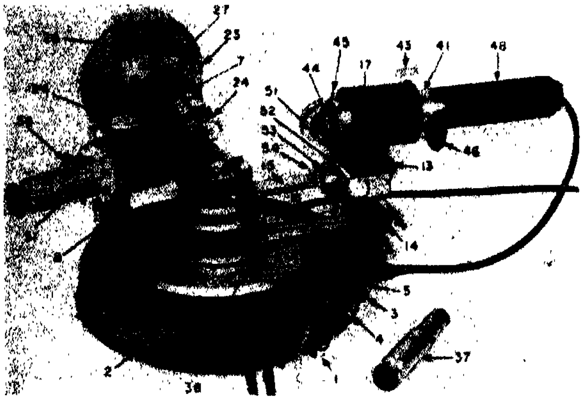

FIG. 2. Over-all view of the two-circle goniometer set up for use as an optical goniometer.

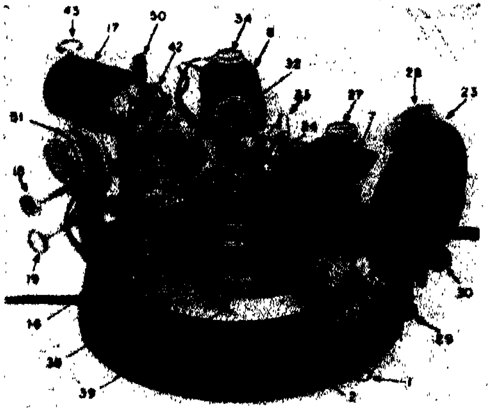

FIG. 3. Over-all view of the two-circle goniometer and spectrometer set up for use as an x-ray diffraction spectrometer.

III. OPERATION

Referring to Fig. 2 it is seen that for operation as an optical goniometer, the instrument is fitted with the light collimator and the telescope. The collimator lead is plugged into its receptacle and the switch thrown to the "collimator" position. The desired aperture is selected and the light intensity is adjusted with the rheostat, while viewing the aperture with the telescope, until the signal is bright with no attendant glare. The crystal is mounted with plasticine or wax on the goniometer head with one face, called the pole face, in a position as nearly perpendicular to the horizontal axis as can be arranged by eye. The vertical circle bracket is placed approximately in an angular position where a reflection from the crystal to the telescope is possible, then locked in position. The telescope is rotated until a reflection is observed and clamp (14) is drawn up. Slow motion tangent screw (18) is then turned until the aperture image is centered in the field of the telescope. The horizontal axis of the crystal is then adjusted with the goniometer head until it lies in the plane of the collimator and telescope. This can be achieved by observing the aperture image reflected from the pole face and rotating the crystal by the hand wheel mounted on the vertical circle. When the image describes a circle with the intersection of the telescope's cross-hairs as a center, the horizontal axis then lies in the plane of the telescope and collimator. The pole face is then adjusted so that the diameter of the circle described on rotating the crystal is as small as possible. When this circle is reduced to the vanishing point, the pole face is then perpendicular to the horizontal axis. The readings of the circles now obtained are the zero readings, denoted by π for the polar angles and ϕ for angles obtained from the vertical circle. The vertical circle and the vertical circle bracket are rotated until the image giving the desired face is received in the telescope. This procedure is repeated for each face in turn and a table of π- and ϕ-angles represents the full data obtained.

For operation as an x-ray spectrometer see Fig. 3. The telescope is removed and replaced with a Geiger counter which is connected to the shielded lead provided. The Geiger counter is used without slits and thus subtends a solid angle of reflection of 14°. The light collimator is removed, its lead to the base jack disconnected and the x-ray collimator is inserted into the housing. The two leads are connected to the electronic recorder and the power supply. The crystal is mounted and adjusted as in the foregoing description. The Geiger counter bracket is then located at θ_{Bragg}, the vertical circle bracket at $\theta_{\mathrm{Bragg}}+\Delta\theta$ and the worm wheel segment is then released from its detent. Upon throwing the switch to the "motor" position and actuating the x-ray beam, the crystal will move across the beam at a rate of 8° per hour. The reflections will be received in the Geiger counter and the integrated output impressed on an electronic recorder or the impulses may be fed to a scaling circuit and counted on an impulse counter.[2]

IV. PERFORMANCE AND TESTS

The results of several tests indicate that the instrument is accurate, capable of obtaining back reflection angles of up to 160°, operates with facility and has good resolution. For example, a test run on synthetic halite (400) reflection, gave a structure factor of 12.70 as compared with Max Renninger's value of 12.67. In Fig. 4 we can see the resolution possible. This is a test run on the 12th-order basal reflection of aluminum phosphate using a penta-erythritrol monochromator. The K alpha-one and the K alpha-two lines, separated by 0.004A, were resolved at a distance of approximately ½ inch on the chart, running at a speed of 20 inches per hour. In Fig. 5 are shown the results of another test which was run to determine the reproducibility. This test was made on the sixth-order basal reflection of aluminum phosphate using the same monochromator. The run was repeated and the resulting curves are shown. They are symmetrical; and using an impulse counter it was found that the difference in the areas under the curves was less than one-half of one percent. (The area is considered proportional to the energy or number of quanta reflected.)

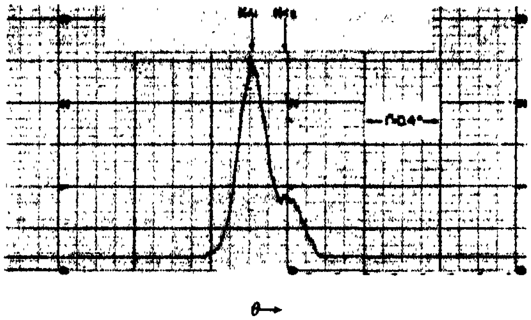

FIG. 4. Curve obtained from basal plane reflection from aluminum phosphate in the 12th order, as a function of the crystal angle. Geiger counter fixed at twice the Bragg angle for the 12th order. (Resolution Run 0012 ALPO$_4$ using penta-erythritrol monochromator.)

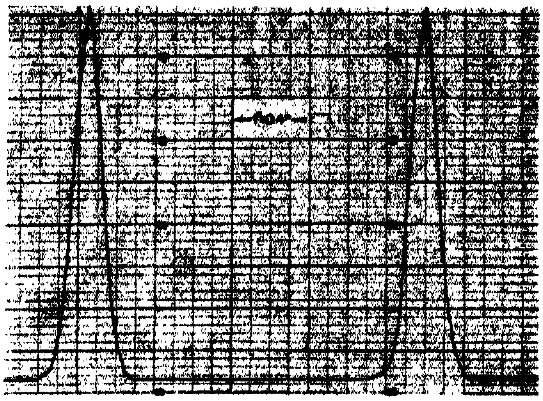

FIG. 5. Curves obtained from basal plane reflection from aluminum phosphate in the sixth order, showing reproducibility. (Run 006 ALPO$_4$ using penta-erythritrol monochromator.)

V. ACKNOWLEDGMENTS

We are indebted to Dr. R. Brill of the Phillips Petroleum Company for his stimulating and helpful interest. We are also indebted to Fred Richardson and Andrew Misko of the Squier Signal Laboratory Shop Section for their skill and careful craftmanship in the construction of the instrument.

---

[2] H. Friedman, Electronics (April, 1945).

THE REVIEW OF SCIENTIFIC INSTRUMENTS VOLUME 21, NUMBER 5 MAY, 1950

An 80-Mev Model of a 300-Mev Betatron[*][†]

D. W. KERST, G. D. ADAMS, H. W. KOCH,[‡] AND C. S. ROBINSON
Physics Department, University of Illinois, Urbana, Illinois

(Received January 16, 1950)

The construction and operation of a flux-biased 80-Mev betatron is described. This betatron was built as a model to test design features later to be incorporated in a 300-Mev betatron. Particular attention is paid to factors influencing design and to considerations of magnetic problems which are common to betatrons and synchrotrons such as the construction of field magnets which are uniform, the testing of fields at injection time, the mechanism of electron capture, and the influence of field inhomogeneities. The dimensions and operating characteristics are included together with many comparisons with the 300-Mev betatron.

I. INTRODUCTION

SINCE the completion of the first betatron in 1940, the University of Illinois has looked toward the construction of an accelerator large enough to produce mesons. By July, 1945, the necessary techniques and ideas were available, and a project was established for building a betatron of about 300-Mev energy. At that time this energy was believed ample to produce meson pairs. The General Assembly of the State of Illinois granted a special appropriation for this project. This paper will describe an 80-Mev model constructed to test the important design features of the 300-Mev betatron.

II. FACTORS INFLUENCING DESIGN

A. Earlier Betatrons

In the design of a large betatron for 300 Mev many improvements can be employed which reduce the size and cost. In the early betatrons the field strength at the orbit was much less than that which can be supplied by iron pole faces. In the first design a flux density of about 1200 gausses was used at the orbit so that the iron structure would not overheat when operated at 600 cycles per second.

In the second machine the flux density is around 3600 gausses at 20 Mev. With this flux density at the orbit, the flux density in the central iron of this betatron exceeds 11,000 gausses and is approaching a magnitude at which the changing permeability of the iron will cause the orbit to shrink in radius.

If the volume of the gap containing the vacuum tube could be reduced in such a machine and the orbit kept close to the central iron, the flux density in the orbit could be increased somewhat above that used in the 22-Mev betatron. This improvement in proportions was incorporated in the 100-Mev conventional betatron at Schenectady.

B. Flux Forcing

The expense of a machine can be greatly reduced by eliminating the air gap in the magnetic circuit which carries the central flux. This saving results from the elimination of the magnetic energy stored in the air gap, and a several fold reduction in size of the capacitor bank. Closing the air gap also simplifies the problem of controlling leakage flux from the central magnetic circuit.

In order to make the central iron of the betatron a closed magnetic circuit with no air gaps, it is necessary to devise some means of insuring that the flux within the orbit and the field at the orbit are always kept proportional in spite of the variable reluctance of iron and the constant reluctance of the air gap. The flux change within the orbit and the field at the orbit must satisfy the equation:

$$\Delta\phi = 2\pi r^2 B, \qquad (1)$$

where $\Delta\phi$ is the change in flux during the time in which the field, B, rises from zero, and r is the orbital radius. This is achieved by "flux forcing," that is, connecting the coil containing the flux linkage of the iron magnetic circuit in parallel with the coil containing the flux in the air gap magnetic circuit (Fig. 2). The number of turns and the geometry of the coils about the poles must be such that these two sets of coils can be placed in parallel and fulfill the relation in Eq. (1) at some usable position in the magnet gap. A fine adjustment of this voltage and hence of the orbit radius can be made by a small auto-transformer on one of the coils.

C. Biased Betatrons

An increase by a factor of two in the flux density allowed at the orbit can be achieved by having the flux in the central iron reversed at the time the field at the orbit is zero. Then during acceleration, the flux in the central iron reverses direction while the flux density at the orbit rises from zero to approximately 9000 gausses. Such a betatron is called a biased betatron.

There are two different types of biasing which allow this increase in energy.[1,2] One is field biasing, and the other is flux biasing. In a field biased machine the magnetic field at the orbit has an alternating and a steady component while the flux in the central iron has only an alternating component. The steady superimposed unidirectional magnetic field at the orbit requires gap windings carrying direct current (Fig. 1a). A flux biased machine requires direct current bias winding on the central iron. A flux biased machine cannot be run on alternating current without seriously saturating the central iron which is already biased nearly to saturation. Consequently such a machine must be excited by unidirectional pulses of current (Fig. 1b).

---

[*] Certain phases of this development were assisted by the joint program of ONR and AEC.

[†] Kerst, Adams, Koch, and Robinson, Phys. Rev. 75, 330 (1949).

[‡] Present Address: X-Ray Section, National Bureau of Standards, Washington, D. C.

[1] D. W. Kerst, Phys. Rev. 68, 233–234 (1945).

[2] W. F. Westendorp, J. App. Phys. 16, 657–660 (1945).

Flux biasing was chosen for the 300-Mev betatron for two reasons.

(1) Fewer bias ampere turns are required because of the complete elimination of the air gap in the central iron core. This advantage is somewhat offset by the fact that the induced voltage in a bias turn around the central iron is approximately three times greater than the induced voltage in one bias turn around the field region. Nevertheless, the choke coil used to prevent a large induced current from flowing in the bias system during the period of changing flux is approximately ten times smaller for flux biasing.

(2) Intermittent unidirectional excitation of the magnet at a low repetition rate is possible with mercury pool tubes and is desirable in order to keep the power consumption low and to reduce the heating of the coils so that coils occupying a small space can be used. By minimizing the space occupied by the coils, useless leakage flux is minimized. The energy stored in this useless leakage flux of an alternating magnet must also be stored in capacitors, and the capacitor cost for a betatron such as we will describe is almost as great as the cost of the iron lamination stock.

It is expected that the yield of the 300-Mev betatron will be sufficiently great that it will be satisfactory to pulse it at a low repetition rate to get integrated results such as those observed in photographic emulsions. Intermittent operation is also needed for cloud-chamber experiments. Although high speed counting techniques which we now have were not yet devised when the repetition rate for our betatron was chosen, it was hoped that improvements in resolving powers of counters would allow one to count several events produced by the same burst of radiation from the accelerator. This hope depended not only upon the development of high resolving power counting techniques but also on the possibility of lengthening the duration of the burst of radiation from the betatron. This lengthening is possible by slightly agitating the beam so that it is intercepted bit by bit by the target. Pulses lasting more than 10 microseconds have been observed from the 22-Mev betatron when this agitation method is used, whereas the normal duration of the x-ray burst can be as small as $\frac{1}{3}$ microsecond.

The repetition rate chosen for the 300-Mev betatron is six pulses per second. The repetition rate of the model described here cannot be this high because of the scaled-down current carrying capacity of the wires. The pulse for each machine is a half of a sixty cycle per second sine wave. The model can run continuously at only one pulse every three seconds.

D. Radiation Loss

One of the important problems which must be faced in high energy accelerators is the energy loss of charged particles by radiation resulting from their acceleration toward the center of a circular orbit.[3] For a particle at radius r (cm) whose energy is proportional to $\sin\omega t$, the fraction of energy which has been lost when the maximum magnetic field has been reached is

$$\Delta E/E = E^3/(300r^2\omega), \qquad (2)$$

where E is the maximum energy of the particle in units of mc^2 and $\omega/2\pi$ is the frequency of the magnetic field in cycles per second. To compensate for this energy loss extra flux must be supplied within the orbit. The fractional increase in the flux needed to hold the orbit at a fixed radius is equal to the fractional energy loss from the orbit at radius r.

In the original betatron, operating at 2.5 Mev and 600 cycles per second, the energy loss according to Eq. (2) is only of the order of five volts. This was not large enough to cause a significant shift or decrease in the orbital radius. The equation is for a single charge, e, in the orbit; but before this early machine was constructed, R. Serber calculated that the energy loss for an isolated electron was in fact the same energy loss that an individual electron would experience although

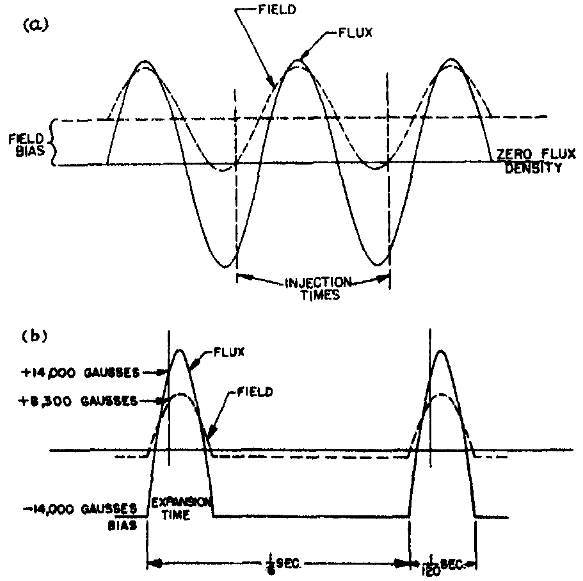

FIG. 1. Field and flux wave forms. (a) Field biased betatron. (b) Flux biased betatron.

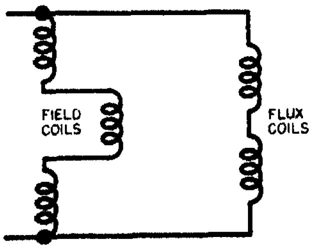

FIG. 2. Elementary flux forcing circuit.

---

[3] D. Iwanenko and I. Pomeranchuk, Phys. Rev. 65, 343 (1944); J. Schwinger, Phys. Rev. 75, 1912 (1949) and included references.

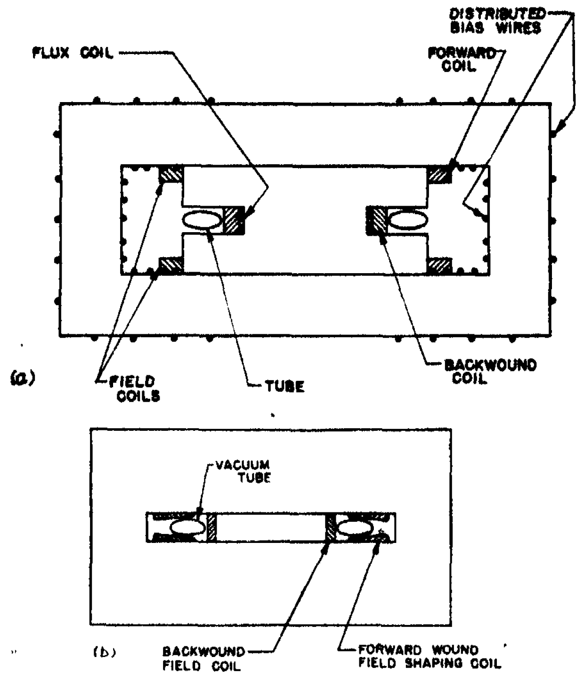

FIG. 3. (a) Single magnetic circuit flux biased betatron. (b) "Poleless" betatron.

accompanied by many other electrons randomly spaced around the circular orbit. It was recognized at that time that a conventional betatron for about 200 Mev would have a serious loss of energy due to orbital radiation. However, the small orbital radius permitted in biased betatrons causes the radiation loss to be serious at a much lower energy. For example, the 80-Mev model discussed here has a computed fractional energy loss, $\Delta E/E = 0.053$. This loss would contract the orbit in about eight percent or two centimeters in radius which would bring the orbit very close to the inner wall of the vacuum tube. This large shift in orbit radius has given an opportunity to experiment with methods of compensating for the radiation loss.

In the case of the 300-Mev betatron the fractional radiation loss will be held to about eight percent by allowing the electrons to remain in the machine for only 75 electrical degrees. The magnetic field at this phase is about 3.5 percent less than the peak field; but removal of the beam at this time results in the maximum energy output of the machine. Retaining the beam longer would require increasing the amount of flux to compensate for radiation loss and consequently this would decrease the amount which is available for acceleration.

In the flux forced betatron the addition of the radiation compensating flux within the orbit can be accomplished by supplying flux which does not link the flux forcing circuit or by destroying the rigid relation between field at the orbit and the flux change within the orbit which is established by the flux forcing circuit. Both of these general methods have been used with the 80-Mev model.

E. X-Ray Production

Moving the high energy beam to the target so that it produces x-rays has been accomplished in two ways. We have used an injector placed at a radius larger than the equilibrium orbit. The beam can be expanded symmetrically to this target by supplying extra flux within the orbit or it can be displaced sideways by decreasing the magnetic field on one-half of the orbital circle and increasing the magnetic field on the other half of the orbital circle.[4] However, the beam does not simply move sideways toward the target when this azimuthal variation in field strength is applied,[5] and with the 80-Mev model it has not been a very satisfactory method for striking the target.

III. MAGNET STRUCTURE

Two magnetic structures were considered in the early design work. One type of structure had one magnetic circuit which carried both the biasing flux and all of the time varying flux. The other structure was composed of two separate magnetic circuits. In the latter case one magnetic circuit carried the central accelerating flux and the biasing flux, while the other magnetic circuit carried only the flux necessary for the field at the orbit. Figure 3 shows two varieties of the one-circuit design, and Fig. 5b shows the separated betatron with two magnetic circuits. Figure 3b might be called a "pole-less" betatron in which the shape of the magnetic field at the orbit was determined by the configuration of the current-carrying coils.

The ampere turns in coil B must be completely cancelled by the ampere turns in coil A (Fig. 5b) so that the large magnetomotive force (mmf) produced by these field coils does not appear across the closed iron core. Coil C of a relatively small number of ampere turns supplies the relatively small mmf for the flux in the central closed core. With an orbital region as large as that necessary for a 300-Mev machine it is possible to put the backwound coil, A, within the air gap. This has the advantage of terminating the mmf planes from coil B in a very uniform way as shown in Fig. 16. Coil A might be said to terminate the field in the air gap with no edge effect, while there is a strong edge effect at the outside pole rim. This position of coil A minimizes the amount of pole rim flux or leakage flux that must be supplied from energy stored in a capacitor bank.

The structures shown in Fig. 3 had the disadvantage of carrying a strong bias flux radially outward under the pole surface. This required a radial mmf drop which seriously distorted the weak magnetic field between poles at the time of injection. If the biasing flux were taken out radially in all directions, it might be possible to shape the iron surfaces or the coils in a way which would compensate for the distorting effect of the strong bias flux.

---

[4] Clark, Getting, and Thomas, Phys. Rev. 70, 562 (1946).

[5] D. W. Kerst and H. W. Koch, Rev. Sci. Inst. 18, 681 (1947).

Tests on d.c. models in 1946 led us to believe that the structures shown in Fig. 3 would be practically hopeless for a 300-Mev betatron, although it might be successful for an 80-Mev betatron. The reason is that at the present stage of development of electron accelerators it is convenient to inject electrons at voltages of about 50 to 100 kilovolts, whatever the size of the instrument. This means that with the usual injection equipment the electrons must be injected into a large betatron when the magnetic field is far smaller than the field at injection time in small betatrons. For this reason the uniformity of the magnetic field must be better for large instruments. Small asymmetries of the field due to the d.c. bias flux would be relatively more serious for large machines. For example, we inject into the 80-Mev betatron at the time the magnetic induction at the orbit is 22 gausses. On the other hand we expect to inject into the 300-Mev betatron at about 7 gausses. The tests with direct current models were sufficiently discouraging with the single magnetic circuit betatron to cause the choice of the separated betatron. This separated structure in Fig. 5 can be thought of as composed of field magnets the same as those necessary for a synchrotron but with a biased pulse transformer passing through the ring of field magnets to supply the accelerating voltage for each revolution of the particles.

Perhaps the most important improvement in magnet design is the structure of the field pieces, or "C's." The structure was devised to carry all laminations through the same magnetic cycle. The path length in iron for the air gap flux is identical at all azimuths around the betatron. Likewise there is no variation in the cross section of the iron flux path at any azimuth in the betatron. This is achieved by punching all laminations with the same die except for a fraction of the laminations which have their ends cut off at different radii on the pole face. They are stacked to form tapered sectors of laminations in a circular pole structure. This radial arrangement of laminations is essentially the same as that used in the earlier betatrons. The back legs of the "*C*" laminations are pulled together into six bundles around the machine (Figs. 4 and 5). These are clamped to form six "*C*'s" with V-shaped crotches between them. By bundling into six "*C*'s" the crotches are wide enough to allow the free passage of an x-ray beam out of the machine without any distortion of the flux path in iron. The size of the window in the "*C*'s" was determined so that on the 300-million volt scale it would be possible for a man to reach any azimuth inside of the "*C*'s" for purposes of experiment or field correction, if this should be necessary.

In order to make six well-constructed "*C*'s" the laminations were bent in a brake so that they fitted closely together. This scheme of having the entire pole face supplied with flux by laminations which are identical (except for the few mixed in whose ends are clipped) insures that residual magnetism distributed over the pole face after a pulse will be precisely the same at all

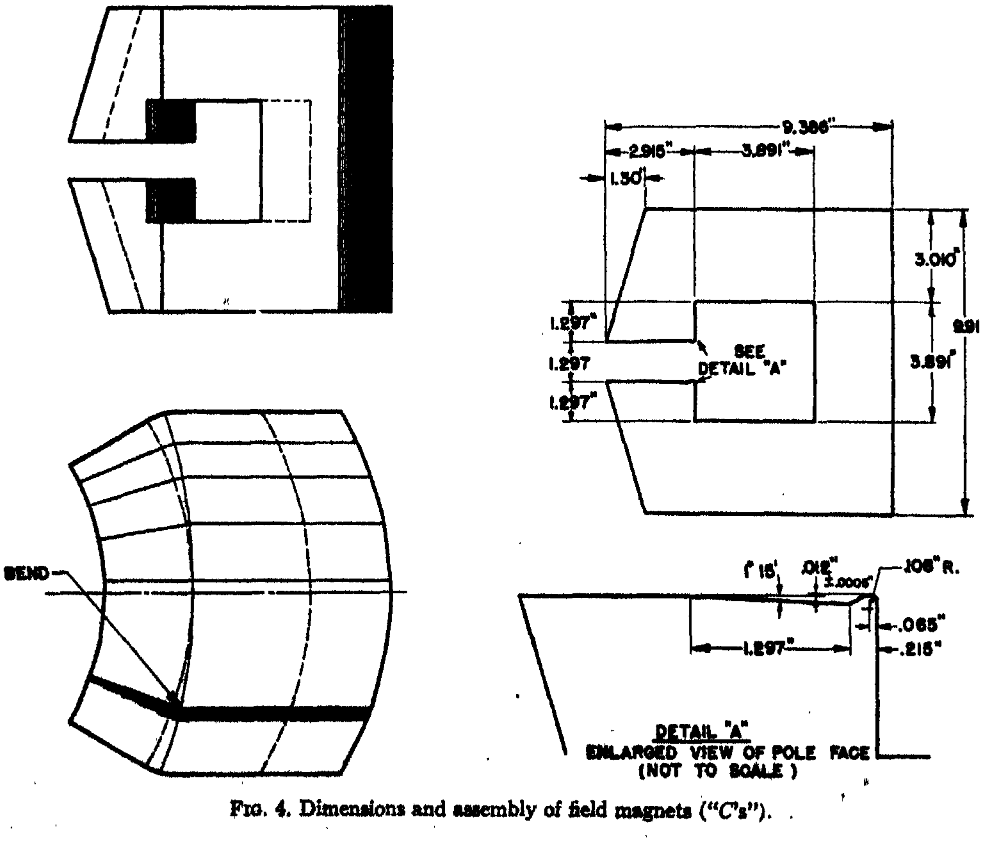

FIG. 4. Dimensions and assembly of field magnets ("*C*'s").

azimuths. It also insures that the time lag of the flux for all azimuths around the pole will be precisely the same at the start of the pulse because the same number of eddy-current ampere turns is required for all flux paths. In addition, the six "C's" fit together snugly so that there is no break in the circular pole piece except a sheet of insulation between "C's." Thus we have avoided a gap between adjacent "C's" which would allow flux to come out of the sides of laminations and which would cause an out-of-phase or lagging flux at the orbit between "C's." Separated pole sections are used in the "race track" type of accelerator, but the ends of each field piece may have to be specially shielded or laminated so that out-of-phase flux sufficient to eject particles will not be produced. The hard problems of field correction are avoided with this magnetic structure; and, as will be described later in the section on field tests, the "C's" produce a field which was two orders of magnitude smoother than the fields of earlier conventional betatrons.

A section of the pulse transformer core is reserved for expansion of the orbit radius when it is desired to cause the beam to strike the target. This section is provided with enough iron so that it can not only move the orbit from its equilibrium position out to the target, but it can also supply the energy lost in the form of central acceleration radiation. In the model about 7 percent of the cross section of the central core is excited late in the acceleration period. In the 300-Mev betatron about 9 percent of the central core is reserved for compensation and expansion.

Figures 4 and 5 show the dimensions of the magnetic circuits. The iron for orbit expansion and radiation compensation is in the sides of the core and it does not link the flux forcing circuit. Except where it passes through the ring of field pieces, this iron is bent away from the central core so that separate windings can be put around this portion of the magnetic circuit. These side packages of iron are wrapped in copper shields to minimize flux leakage into them from the central core throughout the acceleration period. Shielding is also provided on the central part of the pulse transformer to eliminate flux leakage into the space in which the field magnets are installed. Such leakage flux could produce field irregularities at the orbit which might be serious at injection time. The design of these shields will be explained in Section X.

IV. THE FLUX FORCING CIRCUIT

Figure 6 shows the connections of a flux forcing circuit. Coils A and B are in series so that coil A exactly backwinds coil B, while coils C, which are essentially in parallel with the combination of coils A and B, excite the pulse transformer within the orbit. A small transformer, O.P.T., is used for positioning the orbit. Ignoring the effect of this orbit positioning transformer, since it changes the voltage on the core only a small amount, we have equality between the voltage across

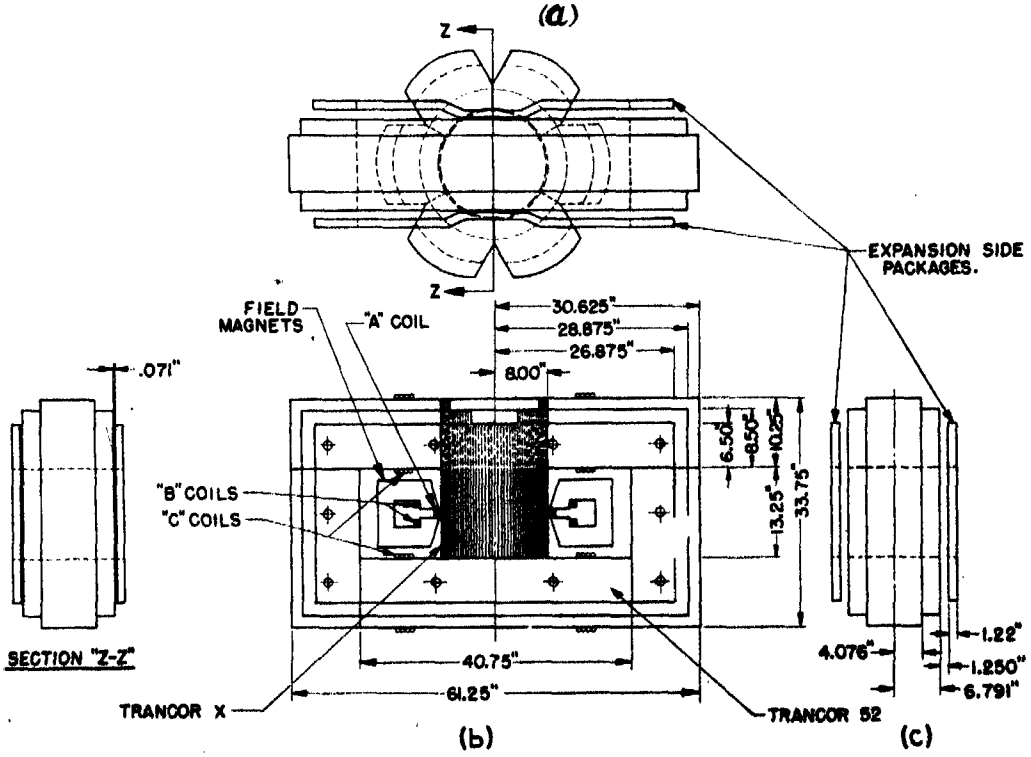

FIG. 5. Assembly of magnetic circuits for 80-Mev model. Coil A is the backwound field magnet coil. Coils B are the forward field magnet coils. Coils C are the excitation coils for the acceleration core.

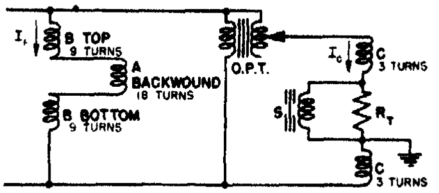

FIG. 6. Pulsed coils and flux forcing connections used. *A*, 19 strands No. 20 enameled. *B*, 19 strands No. 18 enameled. *C*, acceleration core coils, two No. 10 *SN* in parallel. O.P.T., orbit positioning transformer. R_T, trimming resistance for equalizing fundamental I R drop. *S*, saturating reactor which short-circuits R_T at peak current.

the field coils and the voltage across the core coils; thus,

$$N_F\phi_F\times10^{-8}+I_FR_F=N_C\phi_C\times10^{-8}+I_CR_C. \qquad (3)$$

If $I_FR_F=I_CR_C$ at all times, it is clear that flux changes within the orbit are always proportional to field changes at the orbit, and consequently the orbit would remain at a fixed radius except for central acceleration radiation of energy. The current, I_F, through the field coils has almost completely the fundamental frequency of the exciting pulse since the field coils represent a constant inductance and since I_F is large compared to I_C. However, the current passing through the core coils, I_C, has a strong harmonic content. Adjustments of R_T enables the fundamental *IR* drop in the circuit of coil *C* to be made equal to I_FR_F, but the remaining voltage drops in the resistance due to higher harmonics of the current through coils *C* will cause variations in the orbit position. For example, in the 80-Mev betatron, the inductive voltage is close to 1000 volts, whereas I_FR_F reaches a maximum of 1300 amperes $\times R_F$, or 123.0 volts. If the error due to resistive voltage drop were not partially compensated by R_T, then the fractional error in flux within the orbit would be

$$\int_0^t I_FR_Fdt\Big/\int_0^t Vdt$$

where *V* is the voltage across the flux forcing circuit. This is about 12.3 percent in our case at 90 degrees for the 80-Mev model. To supply a compensating voltage drop we set R_C equal to 0.65 ohm. Since the fundamental current through R_C is about 200 amperes peak, the compensating voltage is about 130 volts. Higher harmonic IR drops which cause the variation in orbit position produce about 0.5 percent error in the flux at 75°. This troublesome effect we have eliminated quite well by connecting a saturating reactor, *S*, in parallel with the resistance which balances the first harmonic IR drop. When the large current passes through the core windings, the voltage drop in R_T (Fig. 6) is decreased because the current flows through the saturating reactor. Since the linear scale factor between the 80-Mev and the 300-Mev machines is 4.63, we would expect the flux error without a saturating reactor in the 300-Mev machine to be 0.5 percent $\times 1/(4.63)^2=0.024$ percent. This is a negligible error.

V. PULSE POWER SUPPLY

The pulse power supply, except for some of the auxiliary circuits, is shown in Fig. 7a and the sequence of operations in Fig. 7b. The magnet current pulse is obtained by discharging a capacitor bank through the magnet coils by means of an ignitron. For operation of the model at 80 Mev a capacity of 5000 microfarads is used at an initial voltage of 1130 volts. The pulse is very closely a slightly damped half-sine wave lasting 1/120 second and having a peak current of 1850 amperes. The voltage across the bank reverses during the discharge. Because of dissipation, principally in the coil windings and the ignitron, the final voltage is about 25 percent smaller in magnitude than the initial voltage. This voltage decrease is much larger than that which will be found in the 300-Mev betatron.

After each discharge a mechanical switch is operated to reverse the connections to the capacitor bank. Then, before the next discharge, the 25 percent loss is made up by recharging the bank through a choke coil from a grid-controlled 6-phase rectifier.

Wherever it has been practical, the sequence of operations and the circuits used have been made the same as planned for the 300-Mev machine although many simplifications could have been made in the model. Operation of the model is limited to a rate of about three pulses per second or slower by the speed of the reversing switch. As explained in Section II-C, continuous operation for long periods is limited by heating to one pulse every three seconds. In the 300-Mev design approximately half of the one-sixth second (10-cycle) interval between pulses is available for operation of the reversing switch, and the other half for recharging. In the model the reversing switch takes about 10 cycles, but recharging is accomplished in 5 cycles.

A trigger pulse synchronized with the 60-cycle line is obtained from a frequency subdividing circuit producing 3, 1, or ⅓ pulses per second. This pulse initiates the discharge through the betatron coils. The negative voltage appearing across the capacitors after the discharge actuates the reversing switch. When the reversal is completed, an auxiliary contact triggers two multivibrator gate circuits which allow trigger pulses to reach the grid-controlled rectifier tubes for the following five cycles. During these five cycles the rectifier passes a 1/12-second half-sine-wave current pulse of about 30 amperes peak into the capacitor bank through a 120 millihenry choke chosen to resonate with the capacitor bank at 6 cycles per second. There is a 360-cycle ripple superimposed on this charging pulse, but the 6-phase rectification and the inductance of the charging choke reduce this to about 5 percent peak. If there were no losses in the charging circuit the d.c. power supply voltage should be set halfway between 1130 volts and the capacitor voltage after reversal, or at 990 volts.

Since there are nearly enough losses to critically damp the charging circuit, the power supply voltage must be raised nearly to 1130 volts.

Grid-control of the rectifier is necessary to shut off the charging current completely while the reversing switch contacts are open and to eliminate a large current surge during the time when the capacitor voltage is negative. The rectifier circuit was chosen as six-phase double-way (three-phase bridge) because this required the smallest transformer rating. It has since been found that this choice may have a false economy because of the more complicated excitation equipment required for this circuit.

The reversing switch is constructed from two Allen-Bradley 150-ampere motor-starting contactors using standard cadmium-silver contacts. Auxiliary contacts (not shown) are used to prevent each contactor from being energized while the other is closed. Except for a small current due to the charging and discharging of stray capacity, current flows only while the contacts are completely closed. This allows somewhat higher rating of the contacts. The 150-ampere contacts have operated satisfactorily in air with 300 amperes of steady a.c. for several hours and short tests at 800 amperes r.m.s. showed no damage. The resistance (at 60 cycles per second) of a single contact depends on the applied force, but in practice, at about 10 pounds, it is about 1.5×10^{-4} ohm either in air or in oil. With a high peak current lasting a short time, as in the model, each pulse appears to cause local heating and perhaps welding of the contact, without much dependence on the r.m.s. current. A set of contacts operated in air for 8500 pulses in the model circuit at 1700 amperes peak became deeply pitted and welded together. Another set operated at 700 amperes peak for 290,000 pulses showed no damage except for the slight mechanical wear on the contact surfaces. These tests were made at a rate of 1.5 pulses per second through the contacts. During the last year the model has been operated many hours at about 1800 amperes peak current with the contacts under oil, and no difficulty has occurred.

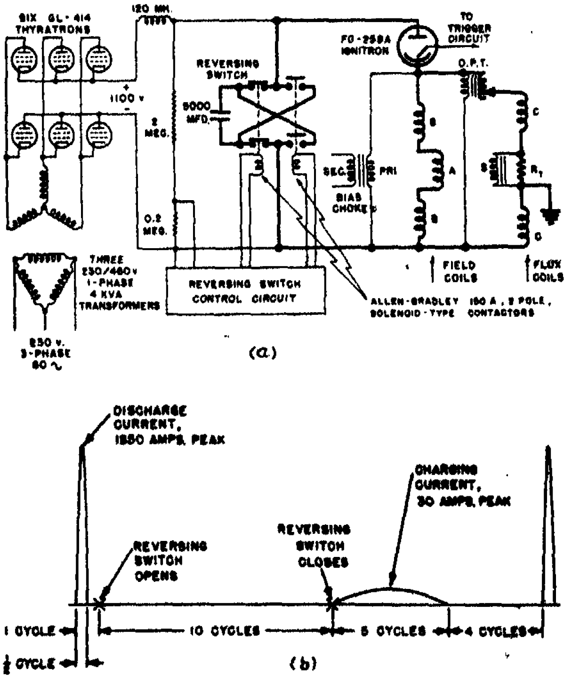

FIG. 7. (a) Pulse power supply. (b) Sequence of power supply operations at 3 pulses per second. The 4-cycle interval is increased for lower repetition rates. 60 cycles = 1 second.

The 5000-microfarad condenser capacitor bank consists of 130 microfarad units rated at 1600 volts d.c.

The fact that the betatron coils are grounded at their electrical center to reduce the insulation requirements introduces fast, high voltage surges into all parts of the power supply when the betatron is pulsed. To prevent these surges from accidentally triggering thyratrons or multivibrators, all sensitive circuits are heavily biased (say, to −100 volt) and supplied with a trigger pulse 200 or more microseconds long which is sent through a low pass RC filter with a 50-microsecond time constant. Each thyratron has a surge-limiting capacitor (0.001–0.003 microfarad) connected between grid and cathode. In addition, certain of the signal transformers are electrostatically shielded.

VI. BIAS CIRCUIT

The central section and the side packages of laminations in the pulse transformer are biased separately. Figure 8a shows the bias supply for the central iron of the core. A choke coil, Fig. 8b, is used to prevent the direct current supply from short-circuiting the voltage pulse which occurs during acceleration. The choke coil is of a special design such that its exciting current does not pass through the direct current source. This exciting current is supplied by a primary winding on the choke coil connected to the main pulsed power line to the betatron. Taps are provided on the primary to assist in adjusting it for a minimum current pulse through the direct current power supply. The resistance of the primary circuit must be chosen so that the IR drop in it is the same as the IR drop across R_T, Fig. 6. Only then will the voltage induced in the choke coil secondary be in step with the voltage induced in the bias winding around the core. A somewhat similar biasing system supplies 275 ampere turns from the same direct current source to the side packages.

Because of the extremely small field at injection time it is necessary that the leakage flux from the central core be made negligible. To do this the direct current bias winding is distributed over the core in a manner such that the ampere turns are placed where they are demanded by the core. This detailed distribution is accomplished in the following way. The tangential component of the field along the iron can be measured by energizing the core without the field pieces in place. The exciting coil is suspended in the middle of the window. The space between this coil and the iron is then free for these measurements. The magnitude of this tangential component is proportional to the ampere-turn density which must be supplied at each point along the iron. The distribution of ampere turns required is found to vary over the surface of the iron in such a way that the wires must be wound in an irregular manner. The direction in which the wires must be placed on the surface of the iron is orthogonal to the direction of the tangential magnetic field. Both the magnitude of the tangential magnetic field and its direction were determined by a conveniently small detector which is capable of measuring fields from several oersteds down to 0.01 oersted.[6] The apparatus is calibrated in a solenoid from time to time.

Special care is necessary in distributing the wires, where the gap in the field pieces is close to the central core. Final positioning of these wires was carried out in the presence of the field pieces while the field detector was placed at the position of the orbit. These bias wires were adjusted until the horizontal magnetic field at the orbit position was less than a calculated tolerance of 0.1 gauss.

VII. VACUUM TUBE

The vacuum tube is made of six glazed porcelain sections which can be maneuvered into the magnet gap through the crotches between "C's." These sections are joined by ¾-in. black Scotch Electrical Tape, Type No. 33, wrapped snugly over the joint. Four of these seals are made with the adjacent sections pulled out into a crotch so that one can examine the seal all around. A small band of No. 1201 Glyptal is painted over the edges of these four seals. The last two seals must be made with the vacuum tube in its final place between the poles. For these two seals the Glyptal painting cannot be completed, but this is not necessary if the seals are made skillfully. However, overlapping ends of the Scotch Tape are exposed so that they can be painted to avoid leaks at the overlap. Another type of seal between sections of the tube was made with rayon taffeta tapes coated with red sealing wax (Dennison's American Express No. 2) and sweated onto the tubes by heating wires; but this method, although it was successfully used for some time, was abandoned because it was more tedious to employ than the Scotch Tape method.

The injector is a very small structure shielded so that the electron beam will not be deflected by the high voltages on the electrodes. Its dimensions are shown in Fig. 12. It was waxed onto a stem in one of the porcelain sections.

The inner walls of the porcelain tubes were coated with Hanovia liquid bright palladium No. 62, and the ends of each section were terminated with Hanovia burnish silver paste No. 38. Silver paste strips were brought out to glass buttons fused to the porcelain glaze for purposes of connection. Mica spacers were inserted at three of the joints. The acceleration voltage appears principally at the insulated joints. Ten ohm external resistances were connected between the coatings of some adjacent sectors, and the total resistance at the insulated gaps was made about 1000 ohms. One of the completely insulated sections was behind the injector section so that it was possible to observe the electron beam passing through this section after it had completed one revolution. This assists in the start-up of such a machine because the injection time can be precisely set by observing the voltage signal from the beam passing through this insulated section. A DuMont 256-D oscilloscope was used to observe the passage of the beam. This helped greatly in adjusting the injection time for first trials.

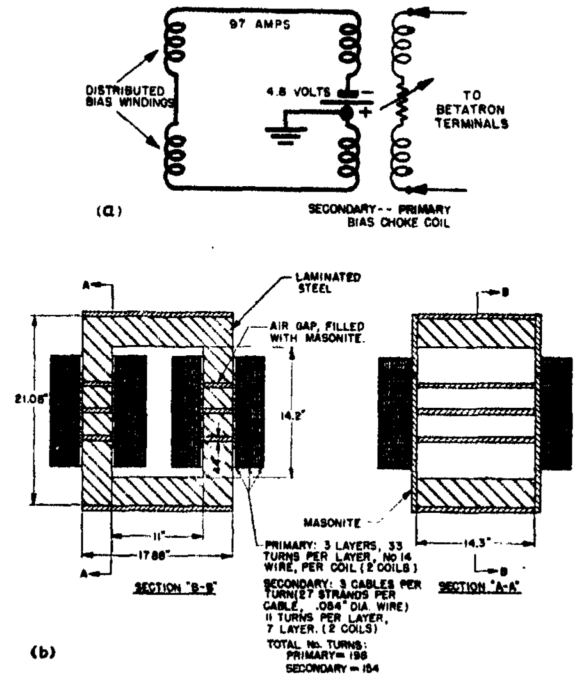
97 AMPS
DISTRIBUTED BIAS WINDINGS
4.8 VOLTS
−
+
TO BETATRON TERMINALS
(a)
SECONDARY- - PRIMARY
BIAS CHOKE COIL
A
B
LAMINATED STEEL
AIR GAP, FILLED WITH MASONITE.
21.08"
14.2"
11"
17.88"
MASONITE
14.3"
PRIMARY: 3 LAYERS, 33 TURNS PER LAYER, No 14 WIRE, PER COIL (2 COILS)
SECONDARY: 3 CABLES PER TURN(27 STRANDS PER CABLE, .084" DIA. WIRE) 11 TURNS PER LAYER, 7 LAYER. (2 COILS)
TOTAL No. TURNS: PRIMARY = 198 SECONDARY = 154
SECTION "B-B"
SECTION "A-A"
(b)

FIG. 8. (a) Bias circuit for central package of accelerating core. The bias winding distributed over the core is composed of 10-parallel 6-turn circuits. (b) Bias choke coil for central package.

It is imperative that the inside of the vacuum tube be coated so that charges cannot accumulate on the surfaces on insulating spots within the tube since charged spots on the wall will deflect the electron beam. In the conventional 22-Mev betatron small insulated areas have been known to prevent successful operation. We experienced the same difficulty in starting up the 80-Mev model, because during several attempts to install a vacuum tube a small amount of insulating material got into the tube. Operation at these times was unsuccessful. Successful operation was achieved later with no change in the magnetic field conditions but with a clean tube.

VIII. AUXILIARY CIRCUITS

The injector circuit employed gives an approximately flat-topped voltage pulse of 60 kilovolts for 5 micro-

---

[6] Adams, Dressel, and Towsley, Rev. Sci. Inst. 21, 69 (1950).

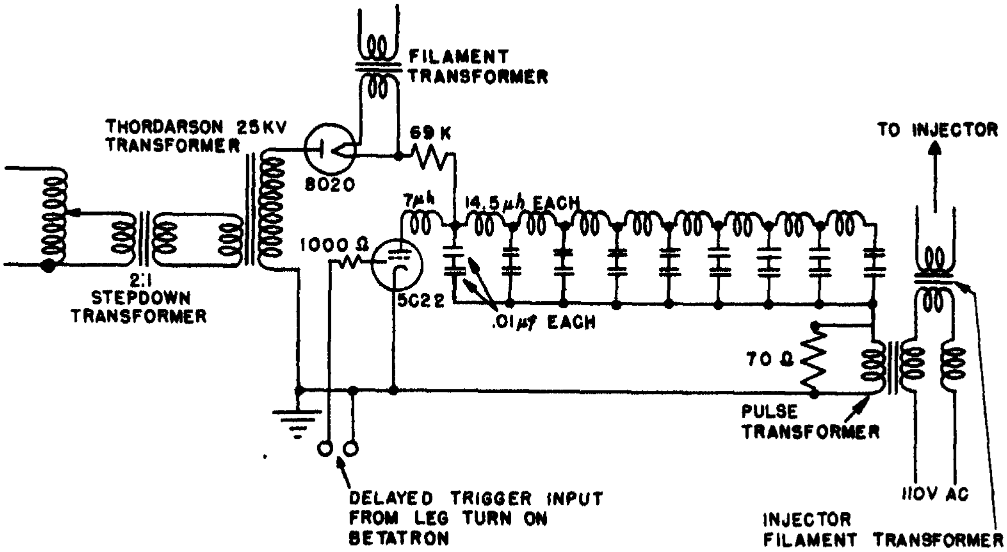

FIG. 9. Injector circuit. The pulse transformer has a 15.7 cm² core cross section. The primary has 19 turns, and the bifilar secondary has 172 turns.

seconds. This duration removes the necessity for precise timing of injection. When the beam is injected, an orbit contraction circuit is excited which suddenly draws a loss current through the backwound coil before the flux forcing circuit can react. The result is that the orbit tends to spiral inward away from the injector. The output of the machine was increased by a factor of 20 by this device.[7] Figure 9 shows the injector circuit and specifications for the associated pulse transformer. Figure 10 shows the contractor circuit.

Since residual magnetism of several gausses remains in the gap of the field magnets after a pulse, the time of injection may occur very close to the time of triggering the main ignitron. Any transients remaining in the flux forcing circuit at injection time will cause the orbit to be at an incorrect radius. To gain time in which the transients can disappear we have used a slight backward bias on the magnetic field so that the field actually comes up through zero after the betatron pulse starts. This biasing will be more important for the larger betatron. It is supplied by the circuit shown in Fig. 11.

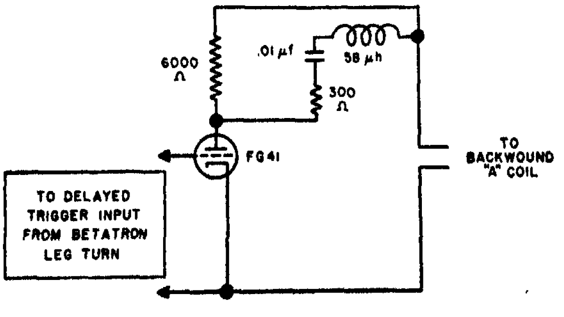

FIG. 10. Contractor circuit. The FG 41 plate circuit components were determined by trial.

The expander circuit is basically a thyratron discharging a 1000-volt 24-μf condenser through 25 turns on the side packages. An additional method of orbit expansion and radiation compensation is now in use which actually increases the flux in the central package of core laminations late in the cycle. This is accomplished by a delay line which produces a voltage on a capacitor in series with the primary of the O. P. T. when the field is approaching its peak value.

The timing circuits for triggering injection, contraction, and expansion are activated by the steep voltage rise generated in a turn around a leg of the yoke. Adjustable delay circuits provide timing controls. The most critical of these is the contraction control.

IX. STARTING TRANSIENTS

When the ignitron is fired the voltage of the capacitor bank suddenly appears across the terminals of the iron magnet and a large sudden rise of current must occur in the circuit. This is the result of the establishment, within a few microseconds, of the peak value of the circulating eddy currents in the iron laminations. Because of the close coupling between the magnet coils and these loss currents a similar working current must circulate in the magnetizing coils. The time of establishment of the eddy currents is important because it can influence the field shape between the poles of a pulsed magnet and because in the case of a betatron it will influence the time taken to establish a strict proportionality between the magnetic field and the changing flux linkage. Since the field magnets have a large air gap in them, it is merely necessary to allow the magnetic field to penetrate a slight distance into the surface of each lamination before the reluctance of the thin flux-carrying surface of the laminations of the field magnet is very small compared to the reluctance of the

---

[7] G. D. Adams, Rev. Sci. Inst. 19, 607 (1948).

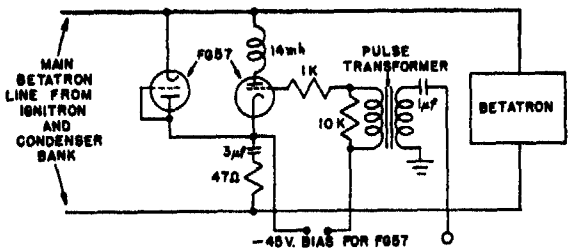

FIG. 11. The field bias circuit.

air gap. Thus in a magnet with an air gap of the proportions used in our betatron, the rate of rise of field in the gap reaches its peak value in less than a microsecond; but the closed-core flux-carrying circuit which links the orbit has no such air gap, and the rate of rise of flux density builds up to a maximum much more slowly. Accurate treatment of flux penetration is described by H. L. Rehkopf.[8] He obtains

$$t=(\pi\mu d^2)/(3\times10^9\rho) \tag{4}$$

for the time required for the eddy currents to reach 95 percent of their full value. ρ is the resistivity in ohm cm, d the thickness in cm, and μ the differential permeability. In our case, the case for heavily biased 0.014-in. silicon steel laminations, $t=7.5$ microseconds for 95 percent establishment of eddy currents. A similar time is required to establish the rate of rise of flux within the iron of the core.

The capacitor voltage is divided between the leakage inductance of the connecting wires and the magnet coils. Presence of leakage inductance will cause an additional delay in establishment of the rate of rise of flux. When one looks closely at the time for establishment of the betatron flux condition in the 80-Mev betatron, it is found that the flux condition is established within 1

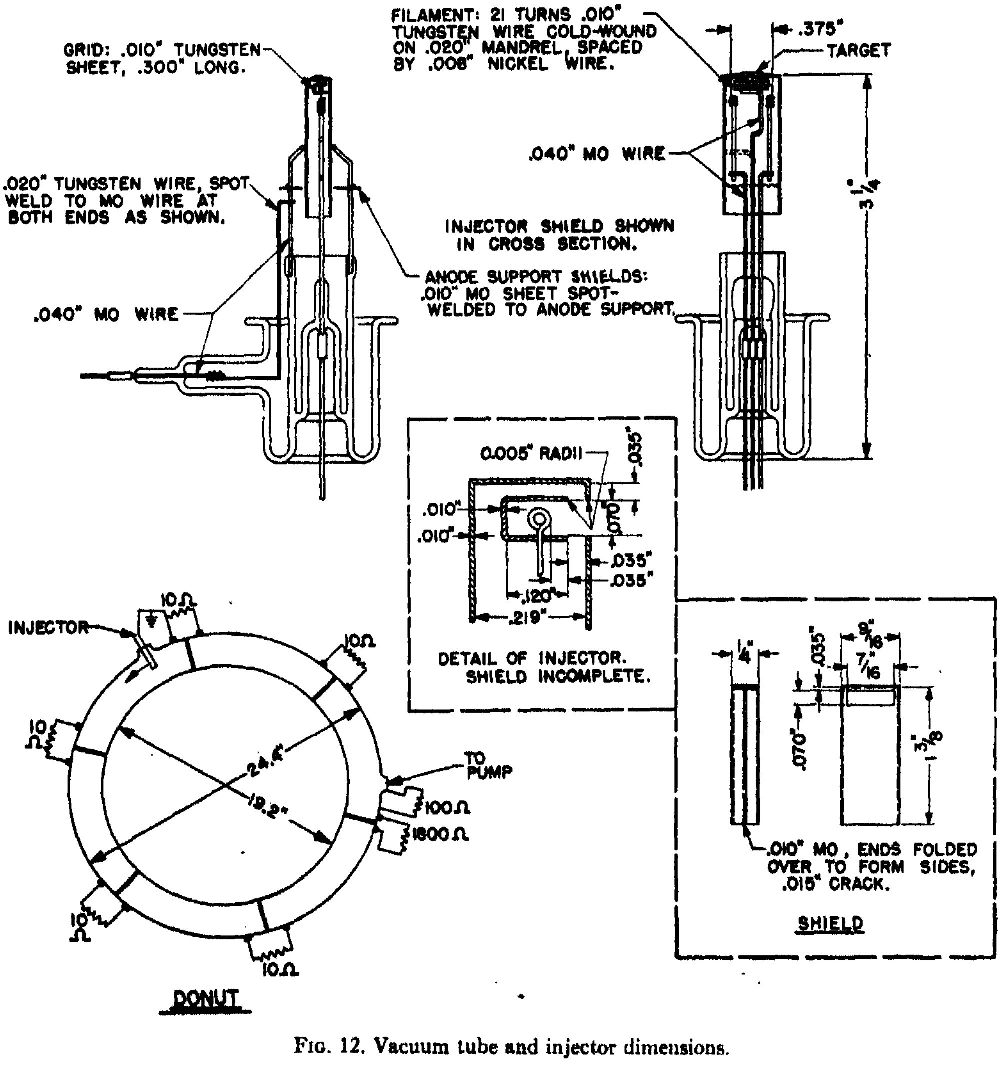
GRID: .010" TUNGSTEN SHEET, .300" LONG.
FILAMENT: 21 TURNS .010" TUNGSTEN WIRE COLD-WOUND ON .020" MANDREL, SPACED BY .008" NICKEL WIRE.
.375"
TARGET
.040" MO WIRE
.020" TUNGSTEN WIRE, SPOT WELD TO MO WIRE AT BOTH ENDS AS SHOWN.
3¼"
INJECTOR SHIELD SHOWN IN CROSS SECTION.
ANODE SUPPORT SHIELDS: .010" MO SHEET SPOT-WELDED TO ANODE SUPPORT.
.040" MO WIRE
0.005" RADII
.035"
.010"
.010"
.070"
.035"
.035"
.120"
.219"
DETAIL OF INJECTOR. SHIELD INCOMPLETE.
INJECTOR
10Ω
10Ω
10Ω
24.6"
19.2"
TO PUMP
100Ω
1800Ω
10Ω
10Ω
DONUT
¼"
.035"
9/16"
7/16"
.070"
1⅜"
.010" MO, ENDS FOLDED OVER TO FORM SIDES, .015" CRACK.
SHIELD

FIG. 12. Vacuum tube and injector dimensions.

---

[8] H. L. Rehkopf, "The equivalent circuit of a pulse transformer core," Radiation Laboratory, Massachusetts Institute of Technology Report 666.

percent of its final value in about eight microseconds. The penetration of flux into the core sets a lower limit on the time of establishment of proportionality between field and flux change.

While the closed core is acquiring its full rate of change of flux, the field in the air gap is increasing with its full rate. Consequently, the field may reach a value requiring an inconveniently high injection voltage before the equilibrium condition is established. To avoid this difficulty the slight reverse field bias is used (Fig. 11). For example, the rate of rise of field is 4 gausses per microsecond in the 300-Mev betatron, and 60-kilovolt injection occurs at 7 gausses. With 8 microseconds for the establishment of the equilibrium condition and with about 3.5 gausses of residual magnetism left in the gap from the preceding pulse the field in the gap would reach about 35 gausses before the flux condition holds. Thus a field bias of about 28 gausses is needed. In the 80-Mev model we use the same rate of rise of field and we inject at about 22 gausses so we need only about 13 gausses of bias.

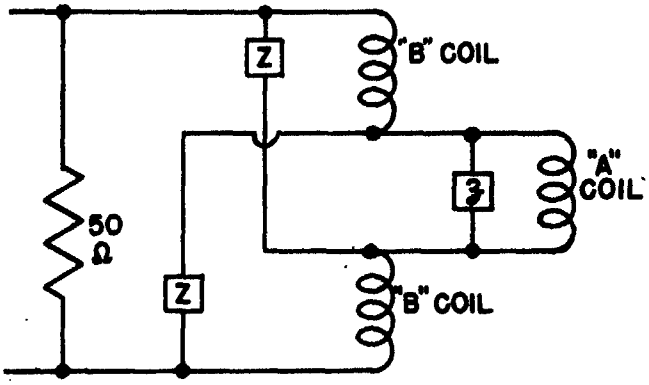

FIG. 13. Location of transient controlling networks.

Some additional transients due to shock excitation of the coils were observed. These were suppressed by increasing the rise time in the line a few microseconds with resistances across the line and by connecting the terminals of the backwound coil to the line with empirically trimmed impedances (Fig. 13).

X. FLUX SHIELDING

Core shielding is necessary for three reasons. First, to insure that the side packages of laminations do not carry an appreciable leakage of pulsed flux from the main core. Such leakage flux would partially fill the side packages which are reserved for expansion and radiation compensation. Second, leakage flux from the core would also disturb the orbit if it passed through the field magnets near the gap. This is especially true for the leakage flux produced at the time of the eddy current inrush. This leakage flux should be prevented from reaching the orbit. Third, unless a distributed pulse winding is wound on the core, shielding is needed to prevent heating of the laminations under the bunched coil which drives the core of the 300-Mev betatron.

A copper shield wrapped around the core with an insulated split to prevent a short circuit about the flux is used. A generous overlap at the split is necessary for an efficient shield. Such a shield placed over or under the bunched driving coil will distribute the magnetomotive force over the core to locations where it is demanded. Currents circulate in the shield to cancel the mmf of the bunched coil and the canceling filaments of current have a return path coincident with the locus of demanded mmf on the core. If this were not so, a leakage flux would pass out through the shield. At the lap these filaments of current run parallel to the edge and a large overlap allows a wide low resistance path for this portion of the circuit. The thickness of the shield at the bunched coil is chosen so that it can carry the canceling current without getting hot, but the thickness elsewhere presents a problem which must be solved so that the leakage flux which escapes is depressed to a tolerable level. The solutions of this problem for both continuous sine wave excitation of the core and for pulsed excitation of a core and estimates of the number of leakage maxwells were determined by S. P. Lloyd. Only $\frac{1}{32}$-inch copper shields were needed.

XI. FIELD DISTRIBUTION, FIELD ERRORS, AND FIELD TESTS

The radial variation of field is described by $1/r^n$. We placed the injector a little outside of the point where $n=1$. n was 0.5 at the normal equilibrium radius and it decreased to 0.2 at the smallest radius within the ac-

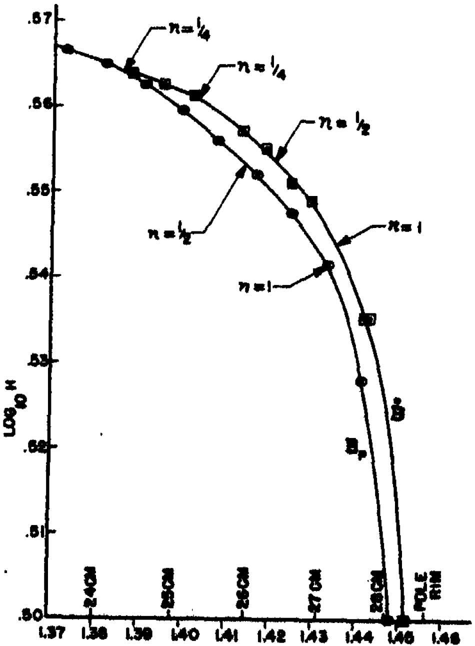

FIG. 14. Magnetic field shapes. $\dot{B}$ is the relative rate of rise of field near zero field and B_p is the residual or permanent magnetic field in the gap left as a result of unidirectional pulsing.

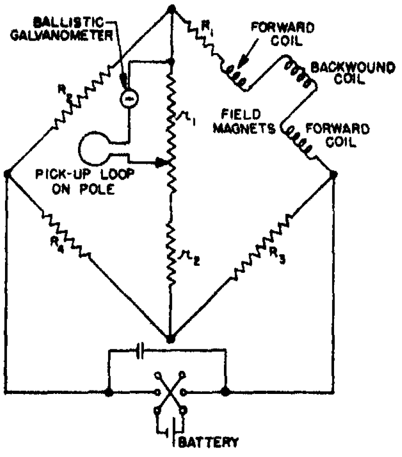

FIG. 15. Bridge for determining orbit position by reversals of direct current. Only the field magnet coils are excited by the bridge current.

celerating region. The field shape obtained is shown in Fig. 14. We have had excellent yield from other betatrons when the injector was placed near $n=1$; this is possible because restoring forces can exist outside the radius at which $n=1$. The reason for using a low value of n over most of the space is that such a field shape minimizes the shrinkage of orbit radius with energy loss due to central acceleration radiation. The contour necessary to provide this field was determined by successive trials with a d.c. model of $\frac{1}{16}$ scale of the 300-Mev machine. This d.c. model had $\frac{1}{8}$-in. laminations. The measurements were taken with a search coil and ballistic galvanometer actuated by the reversal of the field in the d.c. model.

One method of determining the equilibrium orbit position was to use the bridge circuit shown in Fig. 15. This bridge circuit allows a null comparison of the flux picked up in any one of several concentric coils distributed over the pole face with the flux linkage between the field-producing coils A and B. Since in a flux forced betatron these field-producing coils are in parallel with the flux-producing coils wound on the core, there is a fixed ratio between the core flux and the flux linked by the field-producing coils, that is, the mean flux linkage in the "C's" between the forward and backwound coils of the field magnets. One therefore need not excite the core of the pulse transformer with d.c. in this orbit position determination. The orbit is located at the point where the flux linkage divided by the radius of the pick-up loop is a minimum. In our case, the ratio between flux in the core and mean flux linkage between the field coils was chosen to be approximately three to one, that is three times as many turns are used on the field magnets as are used on the core. Thus, in determining the orbit position with the d.c. model, one reads only the flux supplied by the field magnets within the pick-up loop, but to this one adds three times the mean flux per turn linking the field coils in order to compute at what radius the ratio of total flux linkage to radius is a minimum.

An attempt was made to determine the outer radius of the pole rim which would give the proper orbit by the method of hand flux plotting using tubes of flux and the orthogonal magnetomotive force planes. The rules for plotting in the region of the gap and in the region of the current for a three-dimensional magnet with circular symmetry were used. Figure 16 shows the flux plot obtained. Although experience has shown this method of plotting is not capable of giving field details, it is capable of giving a fairly good estimate of integral properties of a magnet such as inductance and orbit

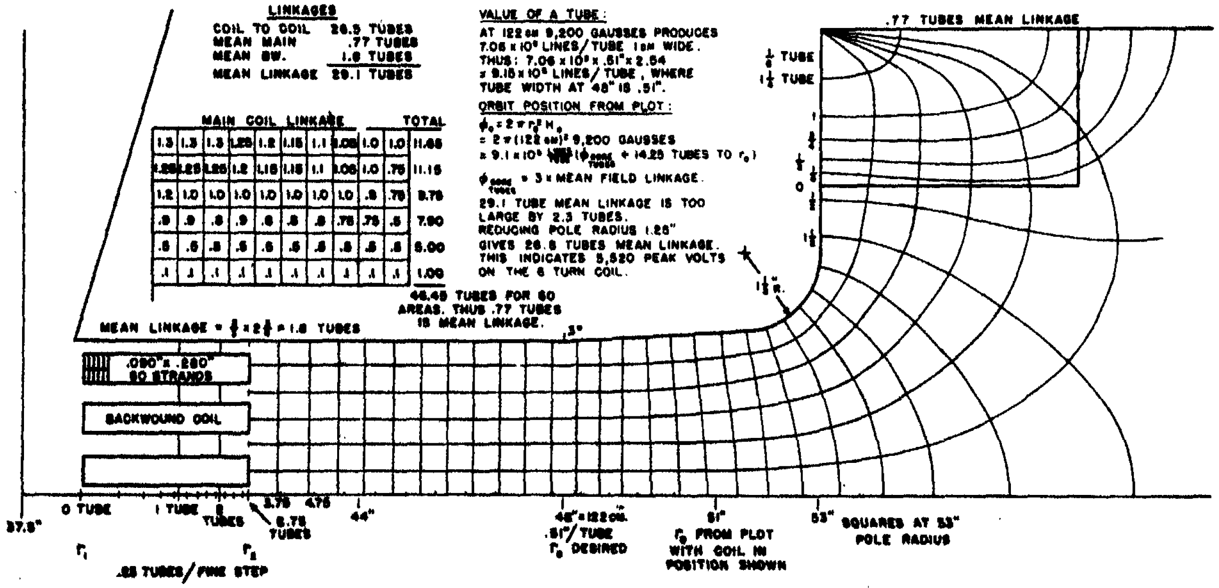
LINKAGES
COIL TO COIL 26.5 TUBES
MEAN MAIN .77 TUBES
MEAN BW. 1.8 TUBES
MEAN LINKAGE 29.1 TUBES
MAIN COIL LINKAGE TOTAL
1.3 1.3 1.3 1.25 1.2 1.15 1.1 1.05 1.0 1.0 11.65
1.25 1.25 1.25 1.2 1.15 1.15 1.1 1.05 1.0 .75 11.15
1.2 1.0 1.0 1.0 1.0 1.0 1.0 1.0 .8 .75 9.75
.9 .9 .8 .9 .8 .8 .8 .75 .75 .5 7.90
.5 .5 .5 .5 .5 .5 .5 .5 .5 .5 5.00
.1 .1 .1 .1 .1 .1 .1 .1 .1 .1 1.00
46.45 TUBES FOR 60 AREAS. THUS .77 TUBES IS MEAN LINKAGE.
MEAN LINKAGE = $\frac{4}{5} \times 2\frac{1}{4} = 1.8$ TUBES
VALUE OF A TUBE:
AT 122 cm 9,200 GAUSSES PRODUCES 7.06 × 10⁶ LINES/TUBE 1 cm WIDE.
THUS: 7.06 × 10⁶ × .51" × 2.54
= 9.15 × 10⁶ LINES/TUBE, WHERE TUBE WIDTH AT 48" IS .51".
ORBIT POSITION FROM PLOT:
$\phi_0 = 2\pi r_0^2 H_0$
$= 2\pi(122\text{ cm})^2\ 9{,}200$ GAUSSES
$= 9.1 \times 10^6 \frac{\text{LINES}}{\text{TUBE}} (\phi_{\text{core tubes}} + 14.25$ TUBES TO $r_0)$
$\phi_{\text{core tubes}} = 3 \times$ MEAN FIELD LINKAGE.
29.1 TUBE MEAN LINKAGE IS TOO LARGE BY 2.3 TUBES.
REDUCING POLE RADIUS 1.25"
GIVES 26.8 TUBES MEAN LINKAGE.
THIS INDICATES 5,520 PEAK VOLTS ON THE 6 TURN COIL.
.77 TUBES MEAN LINKAGE
$\frac{1}{8}$ TUBE
$1\frac{1}{8}$ TUBE
1
$\frac{3}{4}$
$\frac{1}{2}$
$\frac{1}{4}$
0
$\frac{1}{4}$
$1\frac{1}{2}$
$1\frac{1}{2}$" R.
.3"
.080" × .280" 80 STRANDS
BACKWOUND COIL
37.8"
0 TUBE
1 TUBE
2 TUBES
3.75
4.75
5.75 TUBES
44"
r_1
r_2
.25 TUBES/FINE STEP
48" = 122 cm.
.51"/TUBE
r_0 DESIRED
51"
r_0 FROM PLOT WITH COIL IN POSITION SHOWN
53"
SQUARES AT 53" POLE RADIUS

FIG. 16. Trial flux plot for three-dimensional 300-Mev field magnet. This plot shows that the 53-in. trial pole radius should be decreased to 51.75 in. for the orbit at 48 in. and that the field coil voltage is 5520 volts.

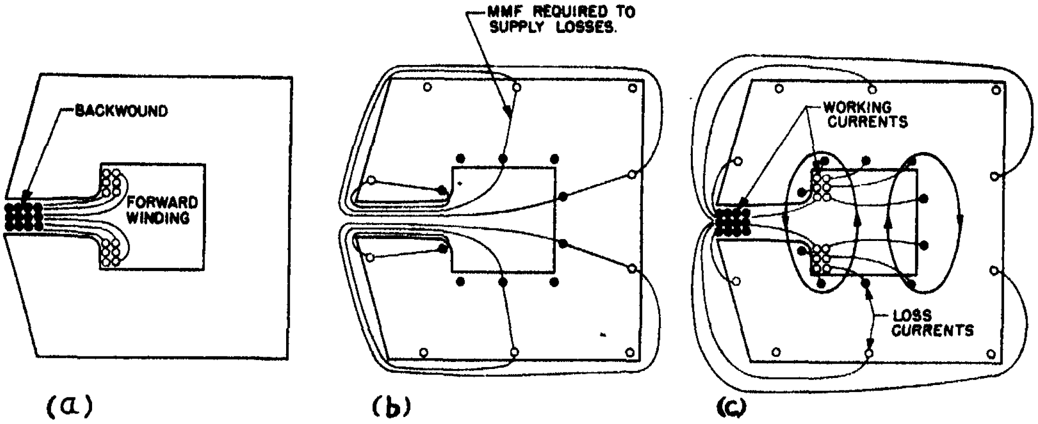

FIG. 17. Flux plot due to working currents and loss currents. a. Working current plot. b. Loss current plot. c. Combination plot near injection time showing reversal of field just outside of pole rim.

position. The flux plot and the bridge tests were used to determine the proper pole rim radius to give the three to one ratio between core flux and field magnet flux with an orbit at about 26.5-cm radius.

Electrical measurements on the pulsed 80-Mev model gave the final determination of orbit position. The measurements were made with a pick-up coil constructed with an accurately known cross section bucked against the pick-up voltage on a loop about the pole face at the position of the orbit. A pair of General Radio decade resistance boxes (Type 602J) with good high frequency characteristics was used as a potentiometer to sub-divide the voltage picked up by the turn at the orbit radius so that it gave a null comparison with the voltage picked up by the search coil. A DuMont 256-B A/R scope was used for a null detector. It is possible to use this coil arrangement to determine the orbit positions as early as a few microseconds after the pulse begins.

Distortions of the magnetic field shape due to errors and imperfections in the pole geometry can be made small simply by care in assembly. However, there are certain other causes for distortion of the magnetic field shape at the time of injection. Leakage flux from the pulsed excitation of the core and leakage flux from the core due to imperfect distribution of bias wires were discussed earlier.

There are reasons for field distortions and inhomogeneities in the magnetic field due not only to the central core but also to the field magnets themselves. First, the residual magnetism left in the gap after a pulse has a distribution depending upon the magnetic properties and the configuration of the iron circuit. This permanent magnetism corresponds to the hysteresis phase shift in a continuously excited betatron. Second, the eddy-current losses in the iron produce field inhomogeneities by time lags, or phase shifts of the magnetism. These depend upon the presence of short circuits between groups of laminations and differences in the proportions of the various iron return paths for flux. Third, time lags are also caused by the natural distribution of the mmf supplied by the eddy currents in the iron combined with the opposite mmf supplied by the eddy-current inrush in the driving coils. These effects all distort the field shape at injection time, but they cause negligible distortion during most of the later acceleration period.

Our observation of the radial distribution of the residual magnetic field in the gap after a pulse showed a fortunate similarity to the distribution of dB/dt. Figure 14 shows the distribution of residual magnetic field as a function of radius. There was also no harmful azimuthal variation of this residual field. Apparently there were no serious variations in the coercive force of the iron used in the "C's." Thus, troubles from the first cause of field irregularities did not exist. The magnitude of the residual field observed was about 3.5 gausses in the gap. This is comparable to the residual field estimated roughly from the dimensions of the field magnet and the coercive force for a symmetrical hysteresis loop of iron (Armco Trancor 52). This residual field is roughly

$$B_r = (L/G)H_c, \tag{5}$$

where L is the effective length of the flux path in the iron, G the dimension of the air gap, and H_c the coercive force. For our magnet L/G was approximately six and for the induction used in the magnet, H_c should be about 0.2 oersted. The calculated residual magnetism in the gap is thus more than one gauss. This calculation is difficult to make precise because the only coercive forces readily available are for symmetrical hysteresis loops. A strange observation which was repeated several times was that the residual field left in the gap was slightly smaller when the magnet was pulsed to its maximum amplitude than when it was pulsed to two-thirds of its maximum amplitude.

The second difficulty mentioned, namely the short circuits between the laminations in the field magnets, was eliminated by the use of 0.005-inch Kraft paper sheets every quarter of an inch in the lamination stack.

We had no evidence of difficulties caused by short circuits between laminations.

The time lag of a flux path caused by eddy current build-up is

$$T=\mathcal{L}d^2l/(4\rho A), \qquad (6)$$

where $\mathcal{L}$ is the power line inductance plus leakage inductance, d is the lamination width, l is the iron flux path length, A is the air gap area, and ρ is the resistivity.

In case the iron return paths for the flux crossing the air gap do not all have the same reluctance, there will be a field bump due to a greater time lag in starting the flux through the high reluctance iron path. The field bump, ΔB, is the difference between the fields in the two paths and is given by

$$\Delta B\sim\dot{B}\tau(1-l_1A_2/l_2A_1)(1-\exp[-t/\tau]), \qquad (7)$$

where l_1, l_2 are the iron path lengths and A_1, A_2 are iron areas for the two path lengths. The time constant, τ, for this field difference to build up is

$$\tau=\pi d^2l/(\rho G10^9), \qquad (8)$$

where G is the air gap. The field error reached is

$$\Delta B=\dot{B}\tau f=5\times10^{-8}\dot{B}fl/G, \qquad (9)$$

where f is the fractional difference in iron reluctance.

In our model

$$\dot{B}=4\times10^6 \text{ gausses per second and } l/G\approx6.$$

Thus $\Delta B\approx f$ gausses. This and the residual magnetism formula show the necessity for designing with nearly identical flux paths at all azimuths. It is important to notice that small l/G results in small residual field and small transient field errors.

The third type of field distortion caused at the time of injection is fundamental, but in our magnet the distortion is present only far out near the pole rim and outside of all positions occupied by the electrons.

To explain this third effect Fig. 17 illustrates the reason for the lagging field at the pole rim.[9] The effect is to increase the value of n at the injection time, and the cause is the presence of a flux distribution due to the inrush ampere turns in the driving coils and the distribution of eddy currents on the surface of the laminations of the field magnet. Magnetomotive force surfaces stretch between the inrush coil current and the eddy current filaments distributed around the iron core. The leakage flux produced at the time of injection is in such a direction in the winding space of the field magnet that it subtracts from the flux fringing out from the pole gap. Since the field at the gap is small at injection, and since the eddy current flux plot has maximum intensity at injection, the superimposed field distributions can cause a zero value of the resultant field close enough to the pole rim to cause a noticeable increase in n just inside the pole rim.

The distribution of this eddy current magnetomotive force was roughly modeled on a d.c. magnet. A dis-

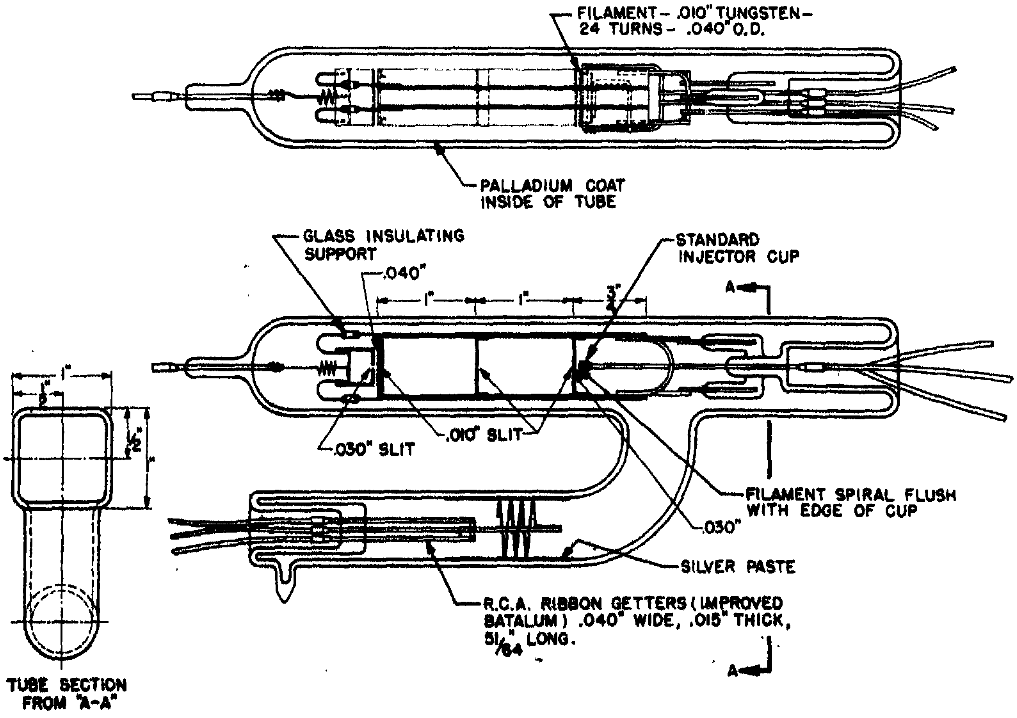
FILAMENT – .010" TUNGSTEN – 24 TURNS – .040" O.D.
PALLADIUM COAT INSIDE OF TUBE
GLASS INSULATING SUPPORT
.040"
1"
1"
3/4"
STANDARD INJECTOR CUP
A
1"
1/2"
1/2"
.030" SLIT
.010" SLIT
FILAMENT SPIRAL FLUSH WITH EDGE OF CUP
.030"
SILVER PASTE
R.C.A. RIBBON GETTERS (IMPROVED BATALUM) .040" WIDE, .015" THICK, 51/64" LONG.
A
TUBE SECTION FROM "A-A"

FIG. 18. Zero field detector. This device enables one to determine the relative times of zero field for various locations.

---

[9] D. W. Kerst, Phys. Rev. 71, 137 (1947).

tributed winding over the surface of the iron imitated a loss current and the working current or eddy current inrush was simulated by a current sent through the main driving coils of the model. The ampere turns in the distributed winding which imitates the distribution of eddy currents on the surface of the iron were made precisely equal to the ampere turns in the coils modeling the driving coils of the field magnet. This model study indicated what was later found on the operating machine, namely that n was affected by the loss currents only out near the pole rim for our injection field.

The 0.1-gauss tolerance for the horizontal component of the magnetic field at the orbit at injection time was chosen because this field would raise or lower the whole orbit about 1.5 inches in the 300-Mev betatron. The oscillations resulting from this shift are sufficient to cause electrons injected near the median plane to strike the tube wall.

The same tolerance was chosen for the variations in the vertical component of the magnetic field at injection time. In this case, 0.1 gauss excessive on one-half of the pole circumference and a deficiency of 0.1 gauss on the other half would shift the orbit enough to remove about 6 percent of the usuable radial space. A similar distribution in horizontal field at the orbit would cause about the same loss of space. These displacements were calculated by the method described in Section XII.

Over-all tests of the uniformity of the field at injection time were made in the following manner. The radial dependence of the rate of rise of magnetic field was determined by pick-up coils at representative azimuths. Then, with the field magnets biased a few gausses opposite to the normal direction, the time at which the magnetic field came through zero was determined for all regions of the pole face. With these data one can calculate the magnetic field at any time after the start of the pulse for any location in the gap. Fortunately, the radial distribution of the rate of rise of magnetic field was the same at all azimuths in the gap except for slight local decreases in the rate of rise at the crotches where the pole faces were separated approximately 0.020 inch extra over a small region at each crotch. The additional necessary observation, namely the time at which the magnetic field goes through zero at every point of the pole, showed simultaneity at all points of the pole face except around the outermost rim of the pole. The simultaneity observation determined that the field at any point in the gap went through zero when it was everywhere less than 0.1 gauss, the limit of the sensitivity of our observing instrument at $\frac{1}{4}$ peak excitation.

Previous experience with peaking strips[10] for the determination of the time when the field in the gap goes through zero led us to distrust peaking strips for observation of the time of zero field as a function of radius. Such an observation is necessary to determine the effective value of n at the injection time. The reason for our difficulty was that the width of the voltage pulse generated in the peaking strip was slightly greater and the wave shape was slightly different when the peaking strip was moved to larger radii where the magnetic field strength was lower. This made it very difficult to choose a correct criterion for the time on the peaker pulse which represented zero field. Our peaker pulses were nine microseconds long and had a flat top. However, we have always had good success using peaking strips to determine the azimuthal variation of magnetic field at injection time since the peaking strip was always placed at the same radius for all azimuths about the betatron.

Since the rate of rise of magnetic field is four gausses per microsecond at the injection time, or about two gausses per microsecond when the machine is run at half-amplitude where we made many of our tests, it is necessary to be able to estimate the time of zero field within one-twentieth of a microsecond if one wishes to observe field errors of 0.1 gauss. Since we were attempting to keep all spurious fields below the 0.1-gauss mark, a tolerance unnecessarily small for the 80-Mev model but one which we have adopted for the 300-Mev machine, it seemed that variations in the width of a peaking strip pulse of the order of one percent would spoil the accuracy. We chose not to use the peaking strip technique but rather to use an entirely different method for determining the time of zero field. We used a short electron gun made from the filament and grid of an injector. It shot a 100-volt beam of electrons through a three-slit collimator into a Faraday cup. The beam could enter the Faraday cup only when the magnetic field was within plus or minus $\frac{1}{2}$ of a gauss of zero. Observation of the pulse on the Faraday cup was made with an A/R scope with its own amplifier. The time of the pulse peak could be estimated to an accuracy equivalent to 0.1 gauss.

Figure 18 shows the zero field detector. It was necessary to bias the cup negatively with respect to the collimator so that stray electrons could not jump over the collimator and enter the cup, giving a wide background pulse. The filament was operated at an emission of about 20 milliamperes, and the synchroscope sweep was started by a trigger circuit driven from the leg of the magnet. Since the zero field detector was sealed off in a small glass tube one inch high which could be placed within the poles of the magnet, it could be moved around by hand while the machine was running. A series of tests showed no variation in the time of zero field at different positions in the gap except for the slight lag near the pole rim beyond the point where electron orbits were to exist.

This zero field detector was the over-all test which showed us that our magnetic field shape was that given by the radial distribution of the rate of change of field shown in Fig. 14. This method of field test includes all effects of eddy currents and residual magnetic fields.

---

[10] A. F. Clark, Phys. Rev. 70, 444 (1946) and Adams, Kerst, and Scag, Rev. Sci. Inst. 18, 799 (1947).

The successful production of a magnetic field with a vertical component uniform within 0.1 gauss was one of the main purposes for the construction of the 80-Mev model.

The determination of the strength of the horizontal component of the spurious magnetic field at injection time was much more difficult than the determination of the vertical component. The contribution of the distributed bias windings on the core to the spurious field has already been explained. An additional horizontal field due to coil transients was found. There was a tendency for the top and bottom main coils around the pole rims to ring differently when the betatron was pulsed. This horizontal flux was observed on a pick-up loop placed vertically at the edge of the gap. Adjustment of the transient trimming network successfully eliminated this oscillation. In addition, studies were made with a 14,000-turn coil placed on edge in the gap against the backwound coil so that any varying horizontal flux leaking from the central core into the air gap could be observed. With this coil in place the betatron was not pulsed since severe shock excitation would result within this multiturn coil. Instead, the machine was run at 1/20 of full amplitude at 60 cycles per second. Adjustment of the position of the coil so that no vertical flux was picked up was exceedingly difficult and had to be done with a hand in the gap. However, since we were searching for flux phase shifted by 90 degrees, it was possible to detect the presence of horizontal a.c. flux. These low amplitude tests extrapolated up to full amplitude showed regions of horizontal field protruding inward or outward at injection time, but only in a very small region was 0.1 gauss exceeded.

One reason for being careful about horizontal fields is that, in the past, horizontal fields have been known to prevent the operation of betatrons. In the conventional betatron the horizontal field can be caused by a phase shift between the top and bottom pole. The original 2.3-Mev betatron was very sensitive to this type of disturbance.

In the 300-Mev betatron the air gap will be sufficiently large so that our zero field detector can be placed first on the bottom pole for a time reading and then moved directly above to the top pole to observe differences in the time of zero field at these poles. Such a difference would be a result of a horizontal magnetic field in the central plane of the air gap, and the time difference for the two poles can be used to evaluate the magnitude of the horizontal magnetic field at the middle of the gap. The observed difference between fields at the two pole faces will be twice the value of the horizontal magnetic field in the central plane of the gap.

XII. METHOD OF STARTING AND GENERAL OPERATING CHARACTERISTICS

After complete tests of the vertical and horizontal components of the field at injection time were finished, the sectional vacuum tube was installed and operation tests were begun. In order to simplify the search for the correct injection timing, filament emission, and orbit position, the magnet was run at 1/20 of normal amplitude on continuous 60-cycle excitation. This allowed continuous operation and the possibility of rapid adjustment of the parameters just mentioned.

Bursts of 60-cycle sine wave excitation at $\frac{1}{3}$ of normal amplitude and lasting about five to ten seconds were also used to allow rapid adjustment during the burst. To eliminate the injection timing parameter the signal produced by the electron beam passing through various insulated sections of the vacuum tube was displayed on a synchroscope. A section about 270 degrees around the machine from the injector shows a brief voltage pulse if the injection timing is correct. We had a flat-topped five-microsecond injection pulse so that the timing was not very critical; but by observing the pulse of current, which was much less than five microseconds in width, passing through an insulated section of the vacuum tube we could positively adjust our injection timing and eliminate this variable.

A great deal of difficulty with the vacuum system was experienced for about four months. The trials for yield in this period were spoiled by the presence of insulating material inside the vacuum tube at locations where this material could be charged by the electron beam.

Successful operation was finally obtained by installing a clean vacuum tube. The yield was found first by a Geiger counter. No corrections of magnetic field or change of operating conditions from those used in the early tests were necessary. During a few days of burst operation at 25 Mev with no bias on the core it was learned that the temperature variation, presumably of the backwound coil, caused a change which moved the equilibrium orbit radius. This made burst operation very difficult because the orbit position would move out of the usable region during a 10-second burst. A Variac in place of the orbit positioning transformer made possible the rapid and continuous positioning of the orbit. It was gratifying to find that the usual disturbing noise of a betatron was negligible with our type of "C" structure. Sine wave operation at 8 Mev is practically inaudible. At 25 Mev the sound is a faint hum.

Operation was quickly changed to pulsing with a biased core, and there was no trouble in obtaining yield at essentially full amplitude within a couple of days. These burst and pulsed tests required about a week at the end of August, 1948. After this successful operation, the assembly of the 300-Mev machine was immediately started.

Numerous tests were subsequently carried out to determine various characteristics of the apparatus. A circular coil had been installed above and below the orbit so that the shape of the magnetic field at injection time could be altered by the passage of a current through this wire. No significant alteration of the yield of the machine resulted as the radial dependence of field strength was changed.

Studies were made on the conventional 22-Mev betatron for the purpose of understanding the action of a so-called contractor which had been in use for several years.[7] It was thought that such a device might be helpful on the 80-Mev model. Some of the facts learned during these tests and their bearing on the use of the contractor on a large accelerator are worth explaining. The contractor is a device which disturbs the flux condition at injection time in a manner such that the radius of the equilibrium orbit rapidly decreases. This is achieved by abruptly starting a loss current around the central flux of a betatron at about the time of injection. It had been observed that in the 22-Mev machine the contractor improved the yield by 33 percent when the machine was operated at maximum yield with an injector emission of 0.51 ampere; but when the emission from the injector was decreased to 0.02 ampere, the contractor was capable of increasing the rather low yield by a factor of eight. This gave encouragement to the idea that injection into conventional betatrons had been successful because of the self-contraction effect of the circulating electron beam within the vacuum tube.[11] An estimate of the self-contraction of the beam was also made by observing signals on a loop of wire around the pole of a 22-Mev betatron under the orbit. It was possible to observe the pulse of flux due to the circulation of the injected electron beam. The circuit to detect this pulse of flux was such that it was shock excited when the injected electron beam changed the flux linkage. There are generally two times during the injection voltage pulse, once on the rising side and later on the falling side, when electrons are injected with acceptable momenta. These two acceptance times could be observed and correlated with the corresponding times on the injection voltage pulse.

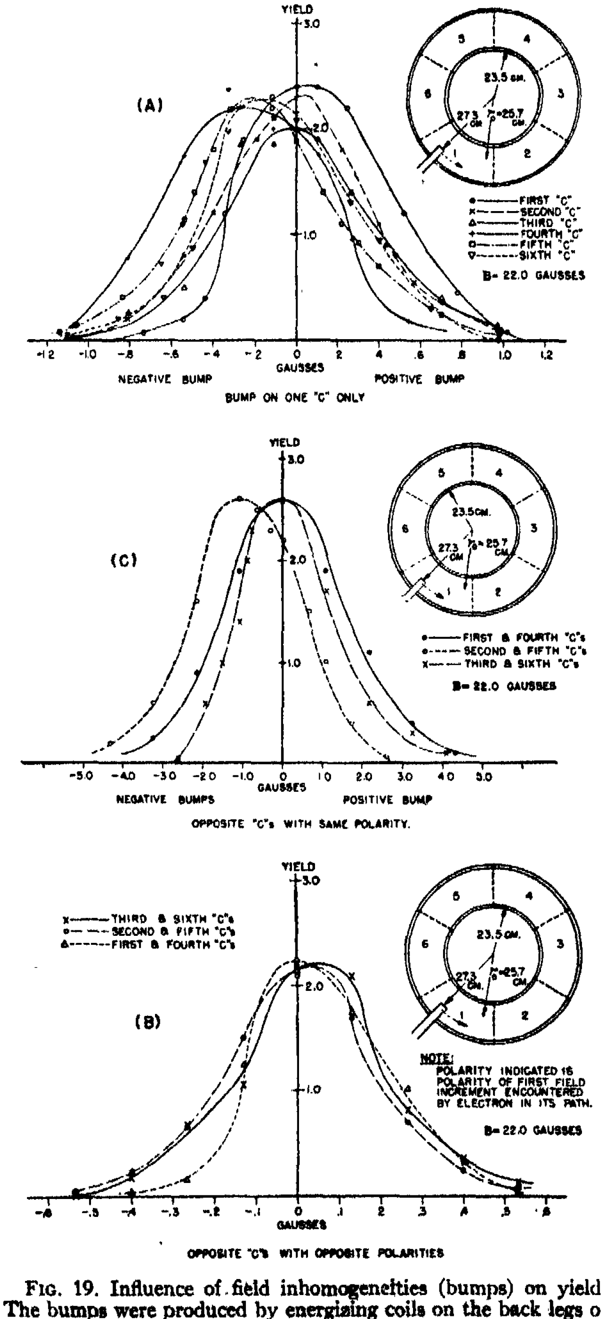

FIG. 19. Influence of field inhomogeneities (bumps) on yield. The bumps were produced by energizing coils on the back legs of each "*C*."

The measurements showed that at least 130 maxwells were withdrawn from the flux within the orbit by the start-up of the circulating beam in the orbit. This circulating current can build up for only about 10^{-7} second (the acceptance time) and the contracting effect of the pulse of negative flux is calculated to be at least 1.1 mm. The amount of circulating current immediately after injection which would be necessary to produce this flux is several times the 0.2-ampere current which we know reaches the target.[12] This is evidence that much of the current injected into the tube circulates for a while and then is lost. We know that some electrons circulate about the machine at least 100 revolutions before being intercepted by the injector structure; this was shown by the effect of firing a contractor circuit as late as one microsecond (about 100 revolutions) after injection. Some electrons destined to be lost after 100 revolutions are saved by this delayed contraction which increases the yield of x-rays.

The sacrifice of some circulating current can produce an expansion of the orbit of electrons injected late in the acceptance time thus making possible injection from a radius smaller than the equilibrium orbit. This same sacrifice of space charge can produce a pinching together of the beam about the equilibrium orbit by the decrease of space charge repulsion. The magnitude of this can be estimated in the following way: If the loss of space charge occurs during the time for many revolutions the process is adiabatic and the action is constant. For an oscillator

---

[11] D. W. Kerst, Phys. Rev. **74**, 503 (1948).

[12] L. Bess and A. O. Hanson, Rev. Sci. Inst. **19**, 108 (1948).

$$J\nu=\tfrac{1}{2}ma^2\omega^2, \tag{10}$$

where J is the action variable, ν the angle variable, m the particle mass, a the amplitude of oscillation, and ω the circular frequency of oscillation which is proportional to ν. Thus ωa^2 is a constant for the period of time considered. So $a\sim\omega^{-\frac{1}{2}}\sim(1-n)^{-\frac{1}{4}}$, where n is the field shape exponent and thus

$$\delta a/a=\delta n/4(1-n) \tag{11}$$

for radial oscillations.

An estimate of δn comes from the magnitude of the circulating current which is sacrificed. Since $\Delta B/B=-n\Delta r/r$, then $(\Delta B+\delta B)/B=-(n+\delta n)\Delta r/r$ and

$$\delta n=-r\delta B/(B\Delta r), \tag{12}$$

where ΔB is the field change caused by the pole shape in the radial span, Δr, and where δB is the part of the magnetic field caused by the beam itself. At a distance Δr from the center of the beam, which is assumed to be cylindrical and of uniform charge density, $\delta B=2I/(10\Delta r)$ where I is the circulating current contained within Δr. In the 22-Mev betatron $r=20$ cm, and at injection $B=45$ gausses and the beam width, $2\Delta r$, is about 2 cm. If we let $I=\frac{2}{3}$ ampere, then $\delta n=-0.06$ (magnetic effect). We know that the Coulomb repulsion of the beam for $v/c=\frac{1}{2}$ is four times as great as this magnetic attraction or $\delta n=+0.24$ (electrostatic effect). The net effect of the beam is $\delta n=0.18$. So $\delta a=2$ mm when $\frac{2}{3}$ ampere is sacrificed. Thus a loss of circulating current of this magnitude has a large damping effect on oscillations. The $\frac{2}{3}$-ampere figure is the calculated space charge limit of the 22-Mev betatron and it is approached at injection time.

The fact that strong self-contraction effects occurred in previous betatrons may have been an important factor in their successful operation. With the newer designs of synchrotrons and betatrons having small tube proportions for radial and axial oscillations it may be very difficult to build up a sufficiently great circulating current to produce the contraction effect. Hence artificial contraction might be expected to be more important with these compressed designs. The improvement of yield by a factor of twenty showed this to be the case with the 80-Mev model. However, in the case of the 300-Mev betatron it may be that a contractor will not have such a beneficial effect, because the voltage per turn in the machine is a much larger proportion of the injection voltage, and therefore the method of capture described in the earlier theory[13] by the damping of radial oscillations and shifting of instantaneous circles should be sufficient. For example, in the 300-Mev betatron with 60-kilovolt injection ordinary beam spiraling would be about 2 mm per turn which would easily allow the particles to pass the injector. Thus contraction is not likely to be so necessary in large instruments.

The x-ray output from the model was roughly measured with several ionization meters. The tests were made while the beam was penetrating the iron of one "C" magnet, and the accuracy of the observation is not good; but it is estimated that the output is at least 0.001r per pulse at one meter. A slight rotation of the vacuum tube is sufficient to bring the x-ray beam out between the "C's" without the necessity of penetrating iron.

It was interesting to make tests on the effect of the azimuthal variation of magnetic field with this six "C" betatron. Since it is possible to wind a coil about the back leg of each "C" and to energize them in different combinations, it is possible to arrange some well-defined variations in the magnetic field. Observations similar to those made earlier with the 22-Mev betatron[6] showed that if the field bumps are created at the time it is desired to produce x-rays, either polarity for the bumps will cause the beam to strike the target. A simple theory of the vibration generated by these bumps indicates that the field should be strengthened at the azimuth of the target and weakened at the opposite side of the orbit. However, it is found that the reverse polarity of the field bumps brings the beam to the target equally well.

In the case of the 80-Mev model the agitation produced in the orbit is not as simple as that produced in the earlier experiments in which the target was well

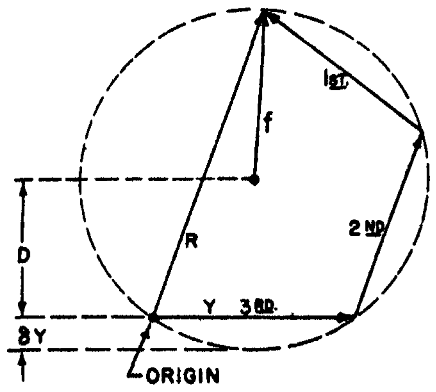

FIG. 20. Vector spiral for summing oscillations produced by the passage of an electron through a bump. Y is the maximum displacement produced by the field inhomogeneity. It is proportional to the deflecting impulse. If the particle passed through the bump only once, the projection of Y on the vertical axis would be the displacement ($Y\sin\omega t$). ω is the free oscillation circular frequency. Subsequent passages through the same bump produce the second and third vectors of magnitude Y. The resultant vector (R) can be decomposed into a free oscillation (f) which rotates with angular velocity ω, a steady displacement (D), and a forced vibration (δY). f and D are not important because they are eliminated by different initial conditions for the injected electrons, but the forced vibration (δY) is the remaining agitation due to the bump. Combinations of bumps and uniform orbit displacement can be treated by adding vector spirals.

---

[13] D. W. Kerst and R. Serber, Phys. Rev. 60, 53–58 (1941).

within the region where $n=1$. The 80-Mev model had the target placed where n was about 1.

Tests were also made of the yield from the betatron as a function of the magnitude of field bumps at the time of injection. Figure 19 shows the results for different combinations of bumps. The curves show that practically no improvement can be produced in the output of this betatron by employing azimuthal variations such as we used in the tests.

The method described below was used to estimate the magnitude of the orbital vibration generated by these bumps. The magnitude of the oscillation thus estimated which brings the yield essentially down to zero is 2 centimeters in these experiments. In estimating the amplitude of such an oscillation the problem involved is that of summing numerous sine functions having frequencies all equal to the frequency of radial oscillation. Each sine function represents a free oscillation generated by one passage over a bump, but the individual sine oscillation produced by each passage has a phase depending upon the ratio of the period of radial oscillation to the period of orbital revolution. The method used in optics to sum sine waves by a Cornu spiral is useful in determining the sum of the oscillations produced by the successive impulses given to the particle on its passages through the field bumps. The vector diagram or spiral for such oscillations is shown in Fig. 20, and the motion described by this spiral can be decomposed into a steady displacement, a forced oscillation, and a free oscillation represented by the vectors D, δY, and F. In the case of two equal and opposite field variations on opposite sides of the machine the formula for the maximum displacement of the beam from the equilibrium orbit is determined by such vector diagrams as

$$\delta Y=\{W\Delta B_Z/[2(1-n)^{\frac{1}{2}}B_Z]\}\tan 2\pi(1-n)^{\frac{1}{2}}/4, \quad (13)$$

where W is the width of the bump, ΔB_Z. Using the data shown in Fig. 19 the formula shows that the orbit moves 1 cm for the yield to cut-off. Approximately the same result is found for all combinations of bumps. This formula is one dimensional and it should hold for a few oscillations. Later coupling mixes the r and Z motions.

Because of the low repetition rate, this 80-Mev betatron is not a versatile instrument. However, it is well suited for use with cloud chambers and photographic emulsions. It has been used both with the x-ray beam penetrating a field magnet and with the tube rotated so that the x-ray beam leaves through an opening between "C's." Many accelerated electrons are scattered on striking the target and leave the machine after one revolution. This electron beam comes out between two "C's" and it has been useful for cloud-chamber studies with electrons.

Other physics department staff members carried out certain phases of the model work. Much vacuum tube work particularly on a 300-Mev size vacuum tube was done by Professor G. M. Almy, and Dr. L. S. Skaggs contributed to the development and testing of the 80-Mev tube. Professor E. M. Lyman initiated the work on excitation for the model and for the 300 Mev unit. Cuttings for both flux yokes were planned by Professor L. J. Haworth. We had the continuous assistance from graduate students R. W. Dressel, C. R. Emigh, E. L. Hahn, S. P. Lloyd, L. G. Mann, G. A. Price, and G. W. Rodeback. Other graduates who contributed considerably were G. R. Briggs, K. R. Ferguson, E. D. Klema, and F. E. Towsley.

THE REVIEW OF SCIENTIFIC INSTRUMENTS VOLUME 21, NUMBER 5 MAY, 1950

A New Mechanical Autocorrelator*

H. R. Seiwell
Woods Hole Oceanographic Institution, Woods Hole, Massachusetts

(Received January 16, 1950)

A relatively simple and inexpensive machine for mechanical computation of the autocorrelation function is described. The original design resulted from a collaboration with Dr. George P. Wadsworth of the Massachusetts Institute of Technology.

The theoretical definition of the autocorrelation function is given. This is followed by an outline of the hand computational procedure as applied in this laboratory to observational (ocean wave) data of finite scope. The machine computation is next compared with the hand process.

1. INTRODUCTION

A RELATIVELY new statistical tool for analyzing time series is the so-called autocorrelation coefficient. It is the coefficient of the product moment correlation between items of a series computed k equal intervals apart. The autocorrelation coefficient is normalized by dividing by the variance of the series, and r_0 equals 1. The diagram obtained by plotting the auto correlation coefficient of order k against k as abscissa is known as the correlogram. It was originally due to Yule.[1]

The theoretical definition of the autocorrelation coefficient assumes stationary conditions. Thus, $\phi(\tau)$ for $f(t)$ is[2]

$$\phi(\tau)=\lim_{T\to\infty}\frac{1}{2T}\int_{-T}^{T}f(t+\tau)f(t)dt. \tag{1}$$

It is normalized by dividing by $\phi(0)$.

2. HAND COMPUTATION OF AUTOCORRELATION FUNCTIONS

The following step-by-step outline of the formulas used in this laboratory for computing autocorrelation coefficients from observational data is given in view of the many inquiries. In practice, certain adjustments are made in the theoretical formulas to fit natural data of finite scope. For a series of N equally spaced discrete observations $(x_1, x_2, \cdots, x_N)$, the autocorrelation coefficients for k equally spaced time intervals are computed as follows.

For the variance we have the observations squared, divided by the number of observations (N) from which the mean squared is subtracted.

$$\sigma_v^2=\frac{\sum_{i=1}^{N}x_i^2}{N}-\frac{\sum_{i=1}^{N}x_i^2}{N}. \tag{2}$$

This gives the variance of the entire series under examination. In practice, the procedure is to compute a running harmonic mean variance. Thus,

$$\sigma^2=\left[\frac{1}{N-k}\sum_{i=1}^{N-k}x_i^2-\frac{1}{(N-k)^2}\left(\sum_{i=1}^{N-k}x_i\right)^2\right]^{\frac{1}{2}}$$

$$\times\left[\frac{1}{N-k}\sum_{i=1}^{N-k}x_{i+k}^2-\frac{1}{(N-k)^2}\left(\sum_{i=1}^{N-k}x_{i+k}\right)^2\right]^{\frac{1}{2}}. \tag{3}$$

The series is next lagged by an amount k. The cross products computed, summed, and divided by N minus k. Thus,

$$\frac{\sum_{i=1}^{N-k}x_ix_{i+k}}{N-k}. \tag{4}$$

FIG. 1. Operation of the mechanical autocorrelator.

---

* Contribution No. 504 from the Woods Hole Oceanographic Institution and the ONR, Contract N6onr-277/I.

[1] M. G. Kendall defines the serial correlations of order k for finite series as corresponding to autocorrelations of infinite series. See: "Contributions to the study of oscillatory time series," Occasional Papers IX, National Institute of Economic and Social Research, Cambridge, 1946. This paper also contains important references to earlier works of Yule and others.

[2] See: Maurice G. Kendall, *The Advanced Theory of Statistics*, (London, 1948), Vol. II. Publisher: Charles Griffin and Company, Limited, 42 Drury Lane.

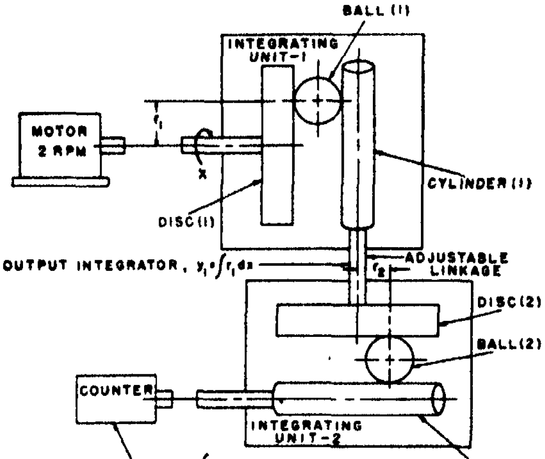

FIG. 2. Ball disk integrator hook-up for mechanical autocorrelation.

The autocorrelation of the lagged series is next obtained by subtracting the product of the mean of each column from Eq. (4). Thus,

$$\frac{\sum_{i=1}^{N-k} x_i x_{i+k}}{N-k} - \left[\frac{(\sum_{i=1}^{N-k} x_i)(\sum_{i=1}^{N-k} x_{i+k})}{(N-k)^2}\right]. \tag{5}$$

The autocorrelation coefficient is normalized by dividing (5) by the variance (3).

$$r_k = \frac{[(\sum_{i=1}^{N-k} x_i x_{i+k})/N-k] - \bar{X}_a \bar{X}_b}{\sigma^2}. \tag{6}$$

In the above, $\bar{X}_a$ and $\bar{X}_b$ are the respective means of the columns [see (5)].

3. THE MECHANICAL COMPUTATION OF AUTOCORRELATION FUNCTIONS

When using the mechanical autocorrelator described in Section 4, the mechanics of the computation differ slightly from the hand procedure, but the final result is the same. For the mechanical autocorrelator, two identical curves of observations are prepared on standard Esterline-Angus six-inch cross-section paper and then lagged in the same fashion as for discrete values in the hand procedure. The machine is so adjusted that the mean of one curve is always zero (running mean as for the hand computation). In this case, we have for the autocorrelation coefficient,

$$r_k\sigma^2 = \frac{\sum_{i=1}^{N-k} (x_i - \bar{x}_a)(x_{i+k})}{N-k}, \tag{7}$$

identical with Eq. (6).

A running harmonic mean variance [Eq. (3)] is first computed at the start of each new operation to determine the workable region of reasonably constant variance.

4. THE MECHANICAL AUTOCORRELATOR

The mechanical autocorrelator permits computation of autocorrelation functions for any length of time series, many times faster than possible by hand computation with electrically operated computing machines, and without loss of accuracy. Two operators are required to follow the duplicate observational curves with styli (Fig. 1).

The essential part of the computer consists of two linked ball disk integrators which perform continuous cross multiplications of the plotted data; their schematic operational principle being illustrated by Fig. 2. Mechanical details of the instrument are shown in Figs. 3–5. As the curves move slowly, the tracing styli transmit motions to the ball of each integrator. The disk of integrator 1 (Fig. 2) is rotated at a constant speed of two revolutions per minute (x) and, as its ball rolls, it rotates its cylinder in the opposite direction. The rate of rotation of the cylinder is proportional to the linear distance of the ball from the center of the disk, r_1, controlled by its curve-following stylus. The

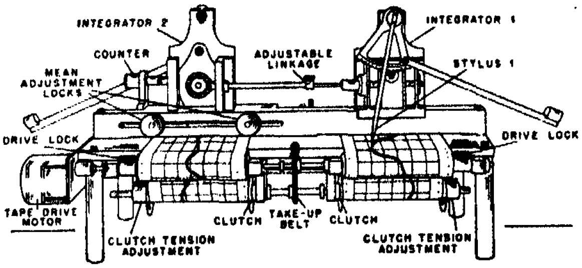

FIG. 3. Rear view of mechanical autocorrelator. This is working position of operator for left side integrator.

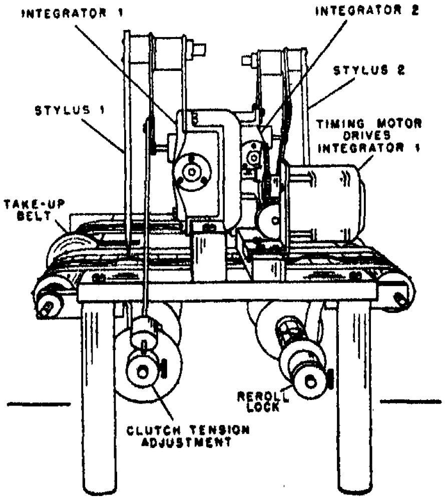

FIG. 4. Left side view of mechanical autocorrelator.

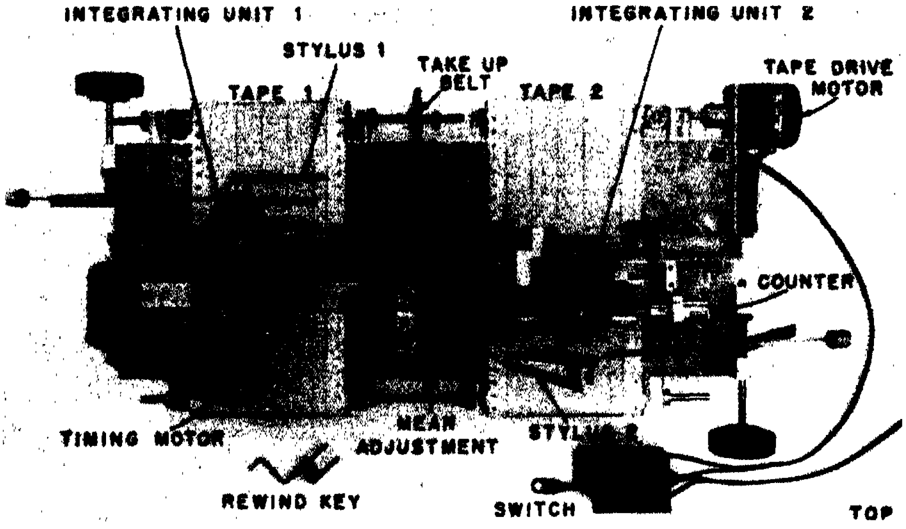

FIG. 5. Top view of mechanical autocorrelator.

output of the cylinder of integrator 1 ($\int r_1 dx$) is geared to rotate the disk of integrator 2. The final output of the second integrator ($\int r_1 r_2 dx$), proportional to the linear distance of its ball from the disk center, r_2 (resulting from its stylus operating on the duplicate curve), is read from a revolution counter (Fig. 3).

The instrument contains two separate chart-feed mechanisms, each consisting of one reroll stick and one drive roll. The two drive rolls are mounted on one axle and rotated by a Holtzer-Cabot a.c. synchronous motor of two revolutions per minute, to produce a chart-feed rate underneath the styli of approximately 9.1 in./min. (Fig. 3). Each chart, securely held by grids, revolves freely and rewinding is done manually. A zero adjustment of one curve is accomplished by changing the relative position of integrator to curve through the sliding coupling linking the two integrators (Fig. 3).

5. COMPUTATIONAL PROCEDURE

(a) A running mean (in absolute units) is computed every k units for the series of N observations, using an auxiliary computing machine.

(b) Based on the above result, one integrator is adjusted and locked at the mean position of its tape. This position may be changed as the computation proceeds to adjust for changes in the mean which exceed the machine sensitivity, e.g., one-half of a one-tenth-inch square on the cross-section paper.

(c) Next, a running harmonic mean variance (in machine units) is computed for the curves in place on the machine [Eq. (3)]. An empirical machine factor K converts to absolute units.

(d) Cross multiplications of the duplicate curves are carried out as previously described; for $\bar{X}_a$ a running mean is used, and σ^2 is an adjusted running variance. The values in machine units are not converted to absolute values for computation of the dimensionless autocorrelation coefficienct, r_k.

6. CALIBRATION

The principle of the integrators used in the autocorrelator consists in transmission of motion from a disk to a cylinder by means of a ball having sufficient friction at each point of rolling contact. The lines of rolling contact of the ball on both the cylinder and the disk are straight and parallel. In the integration of rdx, the distance from the center of the disk to the point of contact of the ball is r, and the angular distance turned by the disk from a fixed position represents x. For computation of the non-dimensional autocorrelation coefficient, the essential values are held in terms of the number of turns read from the revolution counter at the final output. However, for evaluation of the variance and other units in terms of absolute values, the machine values need be multiplied by an empirical constant, K, determined from the machine.

Constancy of the machine output was tested by running at normal procedure 12½-in. tapes for each of the constant styli settings tabulated in Table I-A and I-B; h_1 and h_2 being measured distances (inches) of the styli from zero positions of their respective integrators, and Δ is the integrated output as read from the revolution counter.

For styli settings at both constant product (I-A) and the linear graduated product (I-B), the machine output was consistent within limitation of the revolution counter. Since the latter registers discrete tenths, a reading of the counter at any time may be in error by 0.05 revolution, and the difference between any two readings by 0.10 revolution. This becomes insignificant as the readings become larger, as is usually the case. From the data we compute the evaluation constant K to be ($K\Delta = \text{area} = h_1 h_2$).

$$K = \frac{12.5 h_1 h_2}{\Delta} = 3.472 \text{ (Table I-A) and } 3.436 \text{ (Table I-B).}$$

A second computation of K from a continuous 20-min. operation with h_1 and h_2 values of 2.5 and 2.0, respectively, ($h_1 h_2 = 5.0$) gave nearly identical values of K (3.5).

To test the possibility of slippage of the ball-connecting disk and cylinder with rate of change of radial

Table I.

A				B			
h_1	h_2	h_1h_2	Δ	h_1	h_2	h_1h_2	Δ
1.00	0.50	0.50	1.8	0.25	1.00	0.25	0.9
0.50	1.00	0.50	1.9	0.25	2.00	0.50	1.8
0.25	2.00	0.50	1.7	0.50	1.50	0.75	2.7
2.00	0.25	0.50	1.9	1.00	1.00	1.00	3.7
1.50	0.33	0.50	1.8	1.25	1.00	1.25	4.5
0.33	1.50	0.50	1.7	1.50	1.00	1.50	5.5
			Av. 1.8			Av. 0.875	3.183

Table II.

A				B			
$R-r$	+Diff.	−Diff.	Total	$R-r$	+Diff.	−Diff.	Total
0			8	0			10
0.01	2	5	7	0.01	1	1	2
0.02	1	0	1	0.02	3	1	4
0.03	0	3	3	0.03	2	3	5
0.04	0	1	1	0.04	2	1	3
0.05	0	1	1	0.05	1	0	1
				0.06	4	3	7
	$\sigma^2=0.000294$			0.07	1	1	2
	$\sigma=0.0171$			0.08	0	2	2
				0.09	1	2	3
				0.10	0	0	0
				0.11	0	0	0
				0.12	0	1	1
				0.13	1	0	1
				0.14	1	0	1
					$\sigma^2=0.00328$		
					$\sigma=0.05727$		

velocity, two sine functions were plotted each in duplicate, and their autocorrelation coefficients computed by the machine and compared with theoretical values. For function 1,

$$\sin(2\pi x)/10$$
$$\text{the mean slope: } (2A)/(T/2)=0.4.$$

For function 2,

$$\sin(2\pi x)/4$$
$$\text{the mean slope: } (2A)/(T/2)=1.$$

Differences between normalized theoretical (R) and machine (r) computed values of the autocorrelation coefficient ($R-r$) are tabulated in Table II-A and II-B.

Table II bears out other experience that confidence in the machine computation diminishes as the slope of the traced curve becomes steeper. Experience has shown that curves of time series for this particular machine computation should be arranged so as not to exceed an average slope of 0.4. This is standard operational procedure, and a standard deviation of 0.017 is used to estimate the machine computational error.

7. ACKNOWLEDGMENT

The operational principle of the instrument described originated during discussions with Dr. George P. Wadsworth of the Massachusetts Institute of Technology. The machine (with the exception of the ball disk integrators) was constructed at the Woods Hole Oceanographic Institution by Mr. R. H. Bodman. Calibration of the machine and improvements in technique have been undertaken by Mr. T. C. Duke of the Woods Hole Oceanographic Institution.

THE REVIEW OF SCIENTIFIC INSTRUMENTS VOLUME 21, NUMBER 5 MAY, 1950

Physical Instruments for the Biologist

Detlev W. Bronk
Associate Editor in Charge of this Section
Johns Hopkins University, Baltimore, Maryland

The Design of a Simple Microflowmeter for Biological Perfusion Experiments

ALAN C. BURTON AND JAMES T. NICHOL*
Department of Biophysics, University of Western Ontario,† London, Canada

(Received December 27, 1949)

Various types of flowmeters are discussed with reference to their use at very small flows. The differential pressure type, using rubber membranes, appears most suitable. The steps are outlined in the design of an instrument sensitive to flows as low as 0.01 ml/min. yet with a response time less than 10 sec. In this instrument a completely differential linkage between two membranes is accomplished by the use of an incompressible fluid. The theory of the response is developed. This gives a prediction of the speed of response from the sensitivity and the diameter of the membrane used.

I. INTRODUCTION

NEW types of flowmeters are continually being devised for the measurement of the volume flow of blood or of perfusion fluid in the vascular bed of animals.[1] The devices are so varied and numerous that it is well to attempt a classification so that common disadvantages and advantages can be assessed.

II. TYPES OF FLOWMETERS AVAILABLE

A. Methods That Give a Direct Measurement of Volume Flow in Unit Time

Examples are the classical Ludwig "stromuhr" and its many modifications, in which vessels of known volume are alternately filled and emptied. These are operated manually or by devices of increasing complexity. An excellent review is given by Green.[2] Drop recorders and tilting-bucket recorders come under this classification as does the more recent simple and effective device of the bubble flowmeter.[3]

These methods have the great advantage over all others in that they unequivocally measure volume flow directly and that thus calibration is not affected by other factors such as viscosity. Their limitations are that they do not give *rate* of flow directly but quantity that has flowed in a given time, and they are not well adapted (except for the bubble flowmeter) to flows as low as 0.01 ml/min. (This would only be about one drop each 5 min.)

B. Differential-Pressure Flowmeters

In this group of methods a fixed resistance to flow, usually a short length of capillary tubing or an orifice, is inserted into the flow system and the difference of pressure at the two ends of this resistance is measured and taken as proportional to the rate of flow. This assumption is usually justified where the velocity is below that of turbulence. The variety of flowmeters of this type is due to the great number of ways by which the pressure difference may be observed or recorded, from direct observation of the standing height of liquid in manometers, to optical deflection of mirrors on rubber or metal membranes or the use of electrical strain gauges. Indeed the ingenious rotameter[4] may be regarded as of the differential-pressure type since the support of the floating ball is due to the difference of pressure below and above it.

The whole group of differential-pressure flowmeters suffers from the disadvantage that rate of volume flow is not directly measured. The difference of pressure depends on the resistance to flow of the resistance inserted, and this depends not only on rate of flow of the liquid, but also upon its viscosity. The calibration is different for each liquid used, and if the viscosity of the perfusate, as of blood in a physiological experiment, changes with time, correction must be made for this. However, in many circumstances, as where perfusion fluid of fixed composition and at fixed temperature is used, this is not a great difficulty, and the great adaptability of the differential-pressure type of flowmeter is a strong recommendation. As will be seen, this type can be made to be extremely sensitive and used for very small flows. Also instantaneous rate of flow is measured rather than quantity in unit time and thus rapid changes of flow can be accurately followed.

C. Indirect Methods of Measurement of Flow

A number of ingenious methods have been devised which do not in any sense measure flow directly, but some property which is dependent on flow. The thermostromuhr of Rein[5] and its many improvements is an example, for it measures directly effective thermal conductivity of tissues[6] which depends not only on blood flow, but also on many other factors which may not remain constant in a given experiement. There are also special devices such as the electromagnetic flowmeter[7] and those of the hot-wire anemometer type which essentially measure velocity of flow rather than rate of volume flow. In physiological cases where the diameter of the vascular bed is a variable, these methods are so indirect that they are justified only because of their applicability to specific cases, for which they may possess advantages. Methods which measure volume pulsation of tissues, or pulsation of quantity of haemoglobin (as in photoelectric plethysmography of the skin)[8] are of course still more indirect as measurements of flow.

---

* Holder of a Studentship of the National Research Council of Canada.

† This work was supported by a grant from the Life Insurance Medical Research Fund.

[1] These are reviewed in *Methods in Medical Research* (The Year Book Publishing Company, Chicago, 1948), Vol. 1.

[2] H. D. Green, see reference 1, p. 78.

[3] H. D. Bruner, see reference 1, p. 80.

[4] E. C. Crittenden, Jr. and R. E. Shipley, Rev. Sci. Inst. 15, 343 (1944).

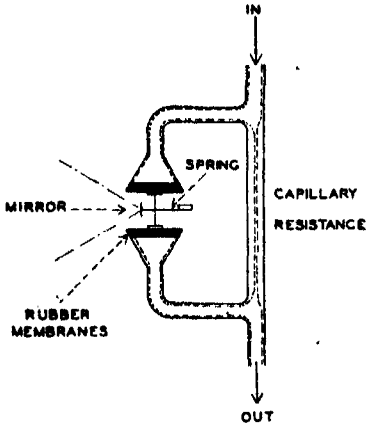

FIG. 1. Simple microflowmeter devised by Bozler.

III. DESIGN OF SENSITIVE MICROFLOWMETERS

Of all these types of flowmeters the differential-pressure group offers the best chance of extreme sensitivity combined with directness and simplicity.

An ingenious simple flowmeter of this type was used by Bozler[9] for measuring the flow in the blood vessels of the frog's hind limb. The principle of this meter is illustrated in Fig. 1. The pressure at the ends of the capillary resistance is measured by the deformation of two thin rubber membranes on the funnels, which oppose each other. The centers of the two membranes are connected by a link, the movement of which tilts a mirror and deflects a light beam. This flowmeter was the starting point in our design and development.

From the point of view of design this simple effective flowmeter has a major fault, in that it makes use of two different rubber membranes. Unless the tensions in these and their distensibilities are identical, the deflection will depend not only on the difference in pressure but on the mean pressure at the flowmeter also. For since the bulging of the first (upstream) membrane will be a function of the pressure there, say $f_1(P_1)$, and the bulging of the second (downstream) membrane will be a function of the pressure there, say $f_2(P_2)$, then the movement of the link will be proportional to $f_1(P_1) - f_2(P_2)$. Unless f_1 and f_2 are identical functions, and this requires identical distensibilities in the two membranes, this will not be a function of $(P_1 - P_2)$, the difference of pressure alone, but also explicitly of P_1 and P_2. Also in the flowmeter there is severe departure from the ideal spherical shape of the membranes under pressure, the central portion being restrained by the link and the rubber bulging between the central attachment to the link and the rim of the membrane. This will not give the optimal conditions for sensitivity.

The first step in improvement was therefore to use one membrane only and to apply the two pressures to opposite sides of this single membrane. The method of measuring the deformation can also be improved. A small mirror placed at the edge of the membrane, which takes up the inclination approximately of the tangent to the spherical shape of the membrane, is in practice much better than the linkage system, connected to the center of the membrane. Simple geometrical considerations show that to achieve the same sensitivity by a linkage, the lever arm to which the mirror in a linkage is connected must be less than the radius of the membrane. Since for speed of response membranes of very small diameter are required, this is not easily achieved.

A simple design incorporating these improvements is illustrated in Fig. 2. This type has been in regular use in our laboratory. Sensitivity of 1-mm scale deflection at a distance of 1 meter, for flows of 0.001 ml/min., is easily achieved, with a time period of response which is

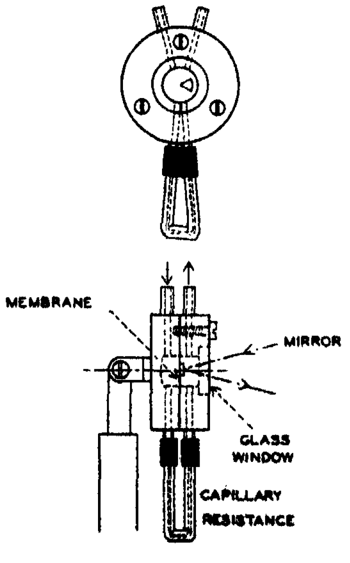

FIG. 2. Modification of Bozler's flowmeter, using one membrane only.

---

[5] H. Rein, Zeits. f. Biol. 87, 394 (1928).

[6] A. C. Burton, J. App. Phys. 9, 124 (1938).

[7] A. Kolin, Proc. Soc. Exper. Biol. and Med. 46, 235 (1941).

[8] A. B. Hertzman, see reference 1, p. 177.

[9] E. Bozler, Am. J. Physiol. 117, 457 (1936).

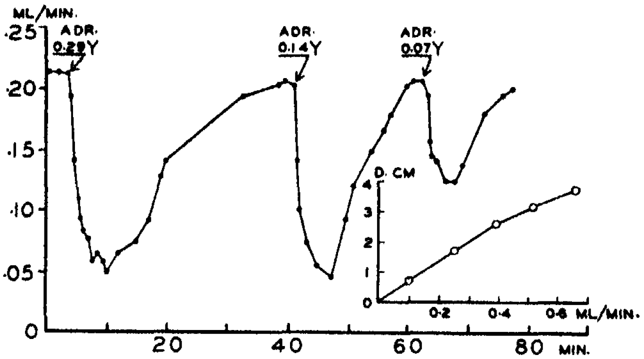

FIG. 3. Results obtained in perfusion of frog's leg with injection of adrenalin. The speed of response and great sensitivity to adrenalin (concentration 1/100,000) is illustrated. Inset: Calibration curve of the flowmeter used.

less than 10 sec. Two practical difficulties had to be surmounted. One is that the very thin latex rubber first used rapidly changes in elastic properties if allowed to stand in oxygenated Ringer's solution (evidently because of oxidation). This may be avoided by using butyl rubber, which has proved to hold its calibration for more than a year. The second difficulty was that silvered mirrors, however we attempted to preserve them by coating with plastic varnishes, quickly deteriorated in saline solutions. This difficulty was met by using mirrors of stainless steel, filed from an old ferrotype plate or knife blade.

Figure 3 shows the record of the change in flow of a perfused leg of a frog when a minute dose of adrenalin was added to the perfusing Ringer solution. It well illustrates the sensitivity and speed of response of these simple microflowmeters.

However, a disadvantage of this type exists. It cannot be used where opaque perfusing fluids (blood, dye solutions, etc.) are used, since the light beam must pass through the front chamber to reach the mirror. A linkage bringing the movement of the membrane to the outside would be impractical. We have succeeded in designing a microflowmeter free from this objection, yet retaining the advantages of the single membrane type.

The final modification is shown in Fig. 4. Two membranes (part of a single butyl sheet) are used, yet the deflection is free from dependence of the mean pressure at the flowmeter, and is dependent only on the difference of pressure in the two chambers. This is accomplished by the use of a "hydrostatic link" between the two membranes. The front chamber is filled with an incompressible fluid (water). Consequently one membrane cannot bulge out without an exactly corresponding inward bulging of the other. The deflection of a mirror on either of the membranes depends on the distensibility of both membranes, not on that of either membrane alone. If there be no flow, and no difference of pressure, both membranes will remain flat whatever the pressure at the flowmeter. Figure 5 shows the components.

This type of microflowmeter has proved completely satisfactory. The volume of the water in the front chamber must be kept as low as possible to avoid the shift of zero that will occur if the temperature changes greatly, but this has been done and changes of zero during a day's experiment were negligible. The front glass window is tilted to throw the direct reflection at the surface off the scale.

IV. SPEED OF RESPONSE AND SENSITIVITY

It is well known that the two requirements often demanded in any instrument, that is, sensitivity and quick response, are mutually antagonistic. For example, sensitivity in these flowmeters can be increased indefinitely by increasing the resistance to flow in the capillary tube of the flowmeter, but the speed of response will be correspondingly decreased. A theoretical investigation has been made (see Appendix) to analyze how the two factors of sensitivity and of speed of response depend upon the tension with which the membrane is applied, upon the resistance to flow of the flowmeter, and, of particular importance, upon the diameter of the membrane used.

This analysis results in a general approximate relation, of very simple form, between sensitivity and speed of response. It is expressed by the equation:

$$t_0 = [(\pi a^3)/8]S,$$

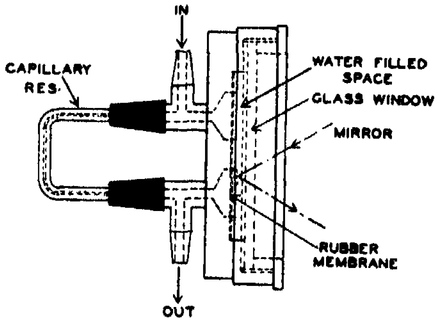

FIG. 4. Schematic drawing of final modification, using two membranes linked by water.

where t_0 is the time constant in minutes (time to reach $1/e$ of the final deflection when flow is abruptly changed), S is the sensitivity in radians for a flow of 1 ml/min., and a is the radius of the membrane in cm. It will be noted that the other variables, the tension in the membrane, and the resistance in the capillary do not appear in this relation. These variables affect the sensitivity and the speed of response in exactly opposite directions. For example, doubling the diameter of the membrane will give (other things being equal) twice the sensitivity, but will also double the time period of response.

Verification of this approximate relation has been made using three different flowmeters with the variables of diameter, tension, and resistance altered over a large range. Figure 6 shows the response curve of one of these instruments when the flow was abruptly changed from a constant value to zero. Table I gives the results for the time constant of response calculated from the theoretical relation and observed from such a response curve (the time to $1/e$ of deflection was employed for this). The correspondence with the predicted values is considered to be satisfactory in view of the obvious approximations in the theory. The bigger discrepancy in the smallest membrane is to be expected, since here the mirror cannot be very close to the tangent at the edge of the membrane.

The theoretical relation is therefore regarded as a reliable guide in design. If the sensitivity required is known, the maximum diameter of membrane that can be used to give the speed of response also required can be calculated. For example, if a sensitivity of 1 radian for 1 ml/min. is needed, and a time constant of less than 10 sec., the relation shows that this cannot be achieved, by any means available, unless the membrane used is of less than 1.5 cm in diameter.

V. SUMMARY AND CONCLUSIONS

(1) Devices for measuring rate of flow of liquids, particularly in biological research, can be classified into three main types, those that measure the volume flowing in unit time, the differential-pressure type that measures instantaneous rate of flow, and a miscellaneous group in which the flow measurement is indirect. The advantages and disadvantages of each are discussed.

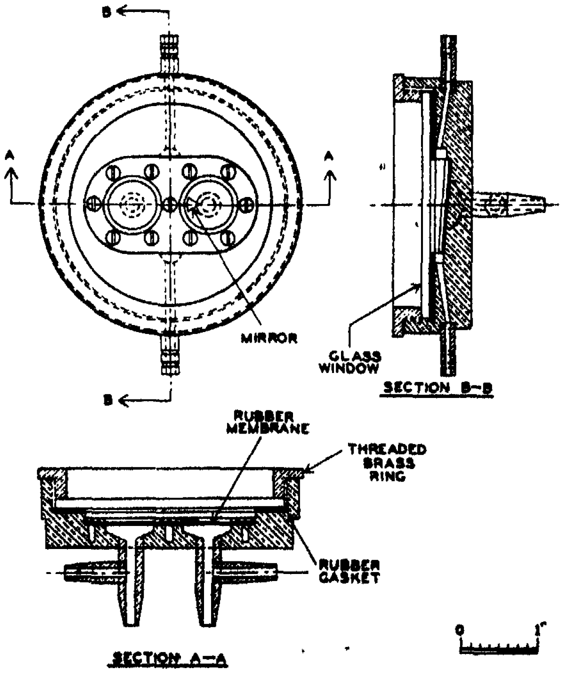

FIG. 5. Scale drawing of final model of flowmeter.

(2) For great sensitivity, simplicity, and adaptability, the differential-pressure type offers the greatest promise. The steps in improving the design of the simple microflowmeter of Bozler are discussed. A single manometric membrane can be used instead of the two in the original apparatus, or the two membranes can be connected by a "hydrostatic link." This ensures that the deflection is independent of the mean pressure in the flowmeter.

(3) Sensitivities of 1-mm deflection at 1 meter for 0.001 ml/min. are achievable with time constants of response less than 10 sec.

(4) The theory of the response curve is developed and a simple approximate formula results which enables the time constant of response to be estimated from the sensitivity and the radius of the membrane.

VI. ACKNOWLEDGMENTS

We gratefully acknowledge our indebtedness to Mr. L. R. Allingham of the Instrument Shop of the Medical School for his patient drafting and construction of the various models in the development, also to the Life Insurance Medical Research Fund and to the National Research Council of Canada whose financial assistance made the work possible.

APPENDIX

SENSITIVITY AND SPEED OF RESPONSE OF DIFFERENTIAL-PRESSURE FLOWMETERS

The following simple analysis applies not only to those particular flowmeters described, but should apply to all of the differential flowmeter type.

A. Sensitivity

Let P = difference of pressure at any time on the two sides of the membrane (or between the two membranes).

Let T = the tension in the membrane. This will consist of a constant tension caused by the stretch with which the membrane was put on, plus a tension which will increase with the degree of deformation, that is, with P.

Let a = radius of the membrane opening.

Let r = radius of curvature of the spherical shape into which the membrane will be deformed.

Then, by the law of Laplace,

$$P=(2T)/r. \tag{1}$$

If the mirror is placed at the edge of the membrane, its tilt (α) will be that of the tangent at the edge (Fig. 8). Then:

$$\begin{aligned}\sin\alpha&=a/r\\&=(aP/2T)[\text{by (1)}].\end{aligned} \tag{2}$$

The deflection will be twice the change in α, and we may define it either as the angle turned through by the light beam, or as the sine of this angle. Where the angle is small there will be little difference. Then:

$$\theta=2\sin\alpha=(aP)/T. \tag{3}$$

The flow F is proportional to the difference of pressure P, unless there be turbulence, or with very low flows with complex liquids, i.e.,

$$P=FR_1, \tag{4}$$

where R_1 is the resistance to flow in the flowmeter. Combining (3) and (4):

$$\theta = (aR_1F)/T. \tag{5}$$

The sensitivity S is the rate of change of θ with F. If we assume that the tension is a constant, and independent of the pressure difference (and therefore of F):

$$S = (\partial\theta)/(\partial F) = (aR_1)/T. \tag{6}$$

Actually T will increase with F and the full differential is:

$$S = \frac{aR_1}{T} - \frac{aR_1F}{T^2}\,\frac{\partial T}{\partial F}. \tag{7}$$

The sensitivity will therefore decrease with increasing flows, and the calibration curve will not be linear. The fact that over the working range of these flowmeters, the calibration is approximately linear justifies taking Eq. (6) for the sensitivity. This equation shows, as was obvious, that the sensitivity is proportional to the resistance in the flowmeter. It also shows that it may be increased proportionally by increasing the diameter of the membrane.

B. Speed of Response

Let us examine the transition from a steady rate of flow to another steady rate, caused by an instantaneous change of resistance to flow in the perfused preparation. See Fig. 7. Assume that the resistance between the reservoir and the flowmeter is negligible, so that, throughout, the pressure on the "upstream" side of the membrane (or that at the upstream membrane when there are two membranes) be P' at any instant. The membrane will bulge towards the downstream side, in a spherical shape. Let V be the volume of the segment of a sphere between the bulging membrane and the flat configuration of the membrane when there is no differential pressure (no flow).

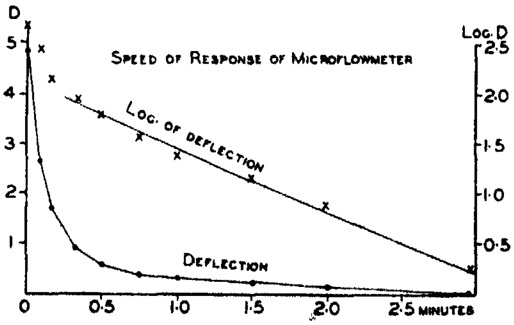

FIG. 6. Speed of change of deflection of flowmeter when flow is changed from a steady value abruptly to zero. The semilog plot shows the curve approximately exponential except for the first few seconds.

Let R_1 be the resistance in the flowmeter between the two pressure chambers and R_2 the resistance in the perfused preparation. If the "exit" pressure at the outlet of the preparation is zero, the instantaneous flow out of the "downstream" chamber will be P'/R_2. The instantaneous flow into this chamber will be $(P'-P)/R_1$. The rate of change of volume of fluid in this chamber will therefore be given by the differential equation:

$$\frac{dV}{dt} = \frac{P'}{R_2} - \frac{(P-P')}{R_1} = \frac{P}{R_2} - (P-P')\left(\frac{1}{R_1}+\frac{1}{R_2}\right). \tag{8}$$

But the volume V depends on the distortion of the membrane, which is related to the difference of pressure $(P-P')$ by Eq. (1). Let us assume that approximately, for small deflection,

$$P-P' = kV, \tag{9}$$

TABLE I. Sensitivity of speed of response of flowmeters.

Type	Radius of membrane cm	Sensitivity radians/ml/min.	Ratio res./tension	Time constant sec. calc.	Obs.
Single membrane	0.47	0.81	0.61	3.4	8
Double membrane (water-linked)	0.78	0.37	0.48	3.7	5
Double membrane (water-linked) resistance increased	0.78	1.10	1.41	11	13

This approximate relation is proved in a later paragraph. Substituting in Eq. (8):

$$\frac{dV}{dt} = \frac{P}{R_2} - k\left(\frac{1}{R_1}+\frac{1}{R_2}\right)V. \tag{10}$$

This is a linear differential equation of the first order, whose solution is:

$$V = A\exp\left[-k\left(\frac{1}{R_1}+\frac{1}{R_2}\right)t\right] + \frac{P}{k[1+(R_1/R_2)]}. \tag{11}$$

The value of A is determined by the initial and final conditions in the usual way.

Equation (11) shows that the approach to the final deflection will be exponential, with a time constant (time to $1/e$ of final deflection) given by:

$$t = \frac{1}{k[(1/R_1)+(1/R_2)]}. \tag{12}$$

The speed of response therefore depends on the distensibility "k" of the membrane, and on the resistance not only in the flowmeter but also that in the "final" state of the preparation. Thus the final deflection will be reached more rapidly when the resistance R_2 is reduced (as by dilation in a vascular bed) than when it is increased (as in vasoconstriction). The slowest speed of response and the longest time constant will be when the resistance in the preparation is increased to infinity, i.e., flow is reduced to zero. This time constant t_0 is given by:

$$t_0 = R_1/k \tag{13}$$

and may be regarded as the time constant of the flowmeter itself. In any actual change of flow the time constant of response will never be greater than this.

It remains to evaluate this distensibility "k" in terms of the tension in the membrane and the radius of the membrane opening, "a." Referring to Fig. 8, the volume of the segment of a sphere of height h is given by:

$$V = (\pi/6)h^2(h^2+3a^2). \tag{14}$$

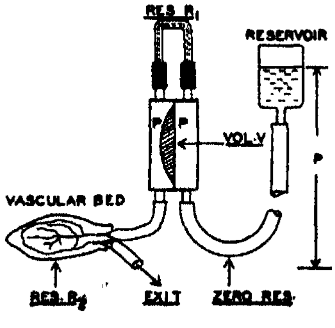

FIG. 7. Schematic diagram of operation of flowmeter.

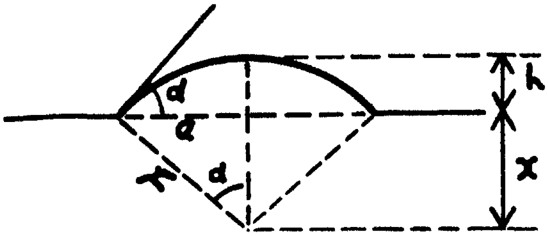

FIG. 8. Geometry of membrane under pressure.

But

$$h = r - x = \frac{a}{\sin\alpha} - \frac{a}{\tan\alpha} = \frac{a(1-\cos\alpha)}{\sin\alpha}. \tag{15}$$

Substituting in (14) we find:

$$V = \frac{\pi}{3}\frac{a^3(1-\cos\alpha)(1-\cos\alpha+\sin^2\alpha)}{\sin^3\alpha}. \tag{16}$$

Further, we may substitute for $\sin\alpha$ since by (3), $\sin\alpha = (aP)/(2T)$ This gives:

$$V = \frac{\pi}{3}\frac{T^3}{P^3}\left[1-\left(1-\frac{a^2P^2}{4T^2}\right)^{\frac{1}{2}}\right]\left[1+\frac{a^2P^2}{4T^2}-\left(1-\frac{a^2P^2}{4T^2}\right)^{\frac{1}{2}}\right]. \tag{17}$$

The final step is to make the approximation, that, for small angles α, $\sin^2\alpha = a^2P^2/4T^2 \ll 1$. Equation (17) then becomes:

$$V = (\pi a^4/8T)P \tag{18}$$

which gives the distensibility "k"

$$k = P/V = (8T)/(\pi a^4). \tag{19}$$

The final expressions for the time constants are then:

$$t = \frac{\pi a^4}{8T[(1/R_1)+(1/R_2)]} \tag{20}$$

$$t_0 = (\pi a^4 R_1)/(8T). \tag{21}$$

Substituting for T its value from Eq. (6), Eq. (21) gives finally:

$$t_0 = (\pi a^3 S)/8. \tag{22}$$

Laboratory and Shop Notes

Best Arrangement of Resistors in a Series Group

HERBERT B. BROOKS
3006 Porter Street, N.W., Washington, D. C.
February 20, 1950

IN his classical book on Electrical Resistance, Price[1] suggests a simple method for determining a preferred arrangement of *n* nominally equal resistors in a series group. In resistors taken at random, the departures from the nominal value or from the group average value will vary from one resistor to another, some being smaller and some larger than the average departure. Price's method arranges the resistors in series to make the error in percent approximately constant, regardless of the number of resistors in circuit. In many years of service at the National Bureau of Standards the writer has found Price's method useful and has recommended it to other workers, none of whom had heard of it. The purpose of this article is to call attention to the simplicity and evident advantages of the method. Price merely illustrated his method in the following manner.

"Again, in constructing a set of coils * * it is often possible to compensate for errors in the several coils by a proper arrangement of the order in which they are placed. To take an extreme case, consider the following set of ten coils, each of which is intended to be 100 ohms:

Coil No.	Resistance	Res. of Sum
1	100.01	100.01
2	99.97	199.98
3	100.05	300.03
4	99.93	399.96
5	100.09	500.05
6	99.89	599.94
7	100.13	700.07
8	99.85	799.92
9	100.17	900.09
10	99.81	999.90

The right-hand column of figures is the resistance of the dial with the corresponding hole plugged. It is seen that a set of coils, all of which are in error by amounts varying from 1 to 19 parts in 10,000, may be arranged so that there is no error in the dial of more than 1 part in 10,000."

For practical purposes Price's method may be outlined as follows. The percentage error of the sum of the resistances of the *n* coils is determining because the method aims to give the same percentage error for 1, 2, 3, ⋯ *n* coils in circuit. If therefore the percentage error of the *n* coils in series is too large for a given purpose because (for example) coils with +errors predominate, some of those having the largest +errors should be replaced with coils having −errors. The error of the entire series group having thus been reduced to a satisfactory amount, divide the resistance of the group by *n* to get the mean resistance of the coils. Select the coil having most nearly this value as the first coil of the group. Subtract the resistance of this coil from twice the mean resistance; the remainder is the most desirable value for the second coil. Choose from the remaining 9 coils the one closest to this value. From three times the mean resistance subtract the sum of the resistances of the selected coils 1 and 2; the remainder is the desirable value for the third coil of the group; and so on. It is evident that this method automatically defers, as long as possible, the selection of coils which have relatively large errors; also, that near the end of the group the effect of their large errors on the accuracy of the settings in which they occur will be relatively small.

As a practical example of the usefulness of the method the following recent case in my work may be cited. It was desired to construct a resistance decade of ten 100,000-ohm coils. Because of high humidity during Washington summers, the coils chosen were pie-wound on ceramic forms and hermetically sealed in glass containers. These units are stated by the maker to be adjusted within 1 percent. A much closer value for the proposed decade was desired. The 10 resistors purchased were "run-of-mine" and in the purchase order no selection for accuracy was requested. The Price procedure showed that with these 10 units a decade could be assembled that would be sufficiently precise at each of the 10 settings if the accuracy of the sum of the resistances of the 10 units could be regarded as satisfactory. It happened, however, that this sum was 0.4 percent higher than the nominal value because the resistances of a majority of the coils happened to be greater than the nominal value. A more accurate value being desired, five more coils of this type were purchased as commercial items without special selection for accuracy. From the total of 15 coils then available were selected 10 coils whose sum was in error at 25°C by only 0.03 percent. With these 10 coils arranged in order by Price's method the error at the other nine settings ranges from a minimum of 0.001 percent to a maximum of 0.064 percent.

To illustrate further the value of the Price selection method, three other possible groupings of these 10 coils were computed. For two of them the order of arrangement of coils in the group was determined by chance by drawing folded numbered slips from a cup. For the third grouping the Price method was used "in reverse" to give the worst possible arrangement. The results for all four arrangements are given in Table I.

TABLE I. Error at each step of a decade for Price's and other arrangements.

Step No.	Error in percent			
	Price	Random 1	Random 2	Reverse Price
1	−0.044	+0.446	+0.071	+0.581
2	+0.014	−0.199	−0.019	+0.513
3	−0.021	+0.061	−0.294	+0.395
4	+0.024	+0.018	−0.231	+0.314
5	−0.020	−0.034	−0.234	+0.243
6	−0.035	−0.036	−0.228	+0.188
7	+0.034	−0.008	−0.208	+0.145
8	−0.001	+0.002	−0.126	+0.102
9	+0.064	−0.020	−0.095	+0.062
10	−0.027	−0.027	−0.027	−0.027

It has been suggested that the Price method might be applied to other cases than resistors in series. Possible cases are: a group of *n* nominally equal capacitors of which any number up to *n* may be put in parallel to give equal increments of capacitance; and a group of *n* nominally equal Johanssen blocks used to obtain very accurate steps of length.

---

[1] William Arthur Price, *A Treatise on the Measurement of Electrical Resistance* (Oxford University Press, New York, 1894). Price is best known today for his guard-wire method for avoiding leakage in the measurement of insulation resistance.

Test of Rupture Strength of Thin Plastic Films*

JOSES J. L. CHEN†
Department of Physics, University of Southern California, Los Angeles, California
March 20, 1950

THE purpose of this note is to describe a simple technique for making direct rupture tests on very thin plastic films and to present a criterion for evaluating the minimum practicable thickness to be used under prescribed conditions. In beta-ray spectroscopy a very thin film backed by an appropriate grille is generally used for the window of the G-M counter. The mechanical factors to be considered are, in general, the limiting differential pressure on the film, the diameter of the window (or the grille holes), the thickness and the material of the film. It has been found convenient to express the results of direct tests in terms of rupture constants so that different materials may be easily compared. The limiting pressure for any window diameter and thickness of film may be readily determined for any of the several materials tested by use of the rupture constants given in this note.

For making rupture tests a test chamber was constructed having a replaceable test plate mounted with a pressure seal at one end of the chamber. The pressure in the chamber was made to increase gradually above atmospheric pressure, the differential pressure being read on an open mercury manometer. On the test plate seven holes were drilled to give diameters from 0.1610 in. down to 0.0135 in. The test plate was carefully weighed before and after attaching the thin film to be tested, and the film thickness thus found in terms of mg/cm², the area of the plate being known.

Thin films of a few materials usually employed in beta-ray spectroscopy were made by the conventional drop technique.[1] The film floating on water was picked up by a semicircular wire loop previously immersed in water. The wire loop was made with handles, which protruded from the surface of the water near the edge of the spreading film while the wire loop rested on the bottom of the tray. This arrangement was found convenient especially when the solvent of some film material took a few minutes to evaporate from a film, such as in the case of Nylon,[2] and when a multilayer film was made by repeated picking up on the same wire loop of a few very uniform thin films.

In making rupture tests single films or multilayer films of thickness from 0.01 mg/cm² to 0.32 mg/cm² were used. After attaching the film and mounting the plate to the test chamber the pressure in the chamber was gradually increased. The limiting differential pressure at which the film ruptured at the largest hole was first observed. After closing the largest hole of the plate from outside, the differential pressure was increased again from zero up and the limiting pressure for the second largest hole was observed, and similarly down to the smallest hole, or up to maximum workable differential pressure.

For each film it was found that the limiting pressure, p, was inversely proportional to the hole diameter, d, so that the product pd was found to have a constant value. Since the total force on the film, $p\cdot\pi d^2/4$, divided by the perimeter of the film, πd, gives $pd/4$, the product pd may be taken as a convenient measure of the strength of the film. It was found that the constancy of this product gave a simple and direct test of the uniformity of thin films. For each material many films of different thicknesses were tested, and the product pd was found to be proportional to the film thickness t as expected. It is thus convenient to express the strength of films in terms of a rupture constant R defined by

$$R=\frac{p(\text{cm}\cdot\text{Hg})\cdot d(\text{cm})}{t(\text{mg/cm}^2)}.$$

Mean values of R found from rupture tests made on thin films of some materials are listed.

Material	Rupture constant R
Formvar E[3]	102
Collodion	74
Nylon	46
LC 600[4]	34
Zapon (Brevon #2)[5]	14.5

The probable error of these results was about 5 to 13 percent. The principal source of error was in the determination of film thickness. These results are compatible with the tensile strengths of 12×10^3 p.s.i. for Formvar E and 2×10^3 p.s.i. for Zapon as given by the manufacturers.

The author wishes to thank Professor C. M. Van Atta and Dr. S. D. Warshaw for their encouragement and advice.

---

* This work was assisted by the joint program of the ONR and the AEC.

† Fellow of the China Foundation for the Promotion of Education and Culture.

[1] J. Backus, Phys. Rev. 68, 59 (1945).

[2] Brown, Felber, Richards, and Saxon, Rev. Sci. Inst. 19, 818 (1948).

[3] Shawinigan Products Corporation, New York 1, New York.

[4] Lithgow Corporation, Chicago 9, Illinois; cf. L. M. Langer, Rev. Sci. Inst. 20, 216 (1949).

[5] Atlas Powder Company, North Chicago, Illinois.

A New Method for the Measurement of Inhomogeneous Magnetic Fields

PETER M. WEINZIERL
I. Physics Institute, University of Vienna, Austria

January 30, 1950

FOR the precise determination of magnetic field strength within strong and inhomogeneous fields, frequently of the greatest importance in electron-optical work, the usual method is to measure the flux. This method requires a very complicated experimental set-up in order to achieve the necessary precision.[1] We used successfully a very small magnetron acting as a probe for the measurement of field intensities in inhomogeneous magnetic fields. At the same time the direction of the field is determined with a high degree of accuracy.

If we calculate the movement of an electron in the electric field of two coaxial cylinders simultaneously superimposing a homogeneous magnetic field along their axis, we find that an electron starting from the inner cylinder cannot reach the outer one, if the magnetic field strength H exceeds the value

$$H=6.72((V)^{\frac{1}{2}}/r)$$

(H in gauss, V voltage between the cylinders in volts, r radius of the outer cylinder in cm; assuming the outer cylinder much larger than the inner one).[2] The drop of the anode current which is to be expected at these field intensities may be used for the measurement of H.[3]

Because of the above relation the magnetic field strength can be measured very accurately as a function of the anode voltage. According to the relation $H\propto 1/r$ it is possible to change the range of H to be measured by varying the outer diameter r. As the anode current in the magnetron will be a minimum, if the directions of the magnetic field and the cylinder axis are parallel, this direction has to be found by varying the direction of the magnetron at the beginning of each measurement.

We tried different tubes, changing diameter and length of the copper anode cylinder from 0.5 to 1.0 mm. As cathode a spiral of tungsten wire (diameter of the spiral 0.1, length 2 mm) was used. These electrodes were placed within a well-evacuated glass tube (diameter 6 mm, length about 200 mm). To avoid magnetron oscillations as far as possible[4] the cables of the electrodes should have a very small mutual inductivity and capacity. A special set-up made it possible to vary position and direction of the tube within the magnetic field.

The calibration of the magnetron, used as measuring instrument, is carried out in the following way. A certain value of the anode current is chosen, for instance the value for $H=0$ and $V=2$ volts (this voltage has to be suitable to the range of H to be measured). Now every variation in this current due to a magnetic field ($H\neq0$) is compensated by varying the anode voltage. So we obtain a calibration plot $H=H(V)$, $i=$ const. The accuracy of this measurement is about ±1 percent. Using a magnetron characteristic $i=i(H)$, $V=$ const., it is possible to measure deviations from homogeneity of magnetic fields with an accuracy of about 2 percent.

By means of one of these magnetrons (anode diameter 0.6 mm, range from 100 to 6000 gauss) we determined point for point magnitude and direction of the magnetic field, especially of the stray field, in a mass spectrometer. (The shape of the stray field depends on the size of the magnetizing current because of the effects of saturation in the iron; therefore an exact calculation of the field, as is possible for an electric condenser,[5] cannot be carried out in our case.) The values of the deflection of charged particles calculated from the measurements of the stray field were in satisfactory agreement with the experimental results obtained from mass spectra.

---

[1] J. Dosse, Zeits. f. Physik 117, 437 (1941).

[2] A. W. Hull, Phys. Rev. 18, 31 (1921).

[3] A. W. Hull, Phys. Rev. 22, 279 (1923).

[4] L. Brillouin, Phys. Rev. 60, 385 (1941).

[5] R. Herzog Physik. Zeits. 41, 18 (1940).

A High Megohm Bridge

F. M. Glass and R. K. Abele
Instrument Department, Oak Ridge National Laboratory,
Oak Ridge, Tennessee

February 6, 1950

THE instrument to be described here is a simple direct reading Wheatstone bridge capable of rapidly measuring resistances up to 10^{13} ohms with 1 percent accuracy and 1.5×10^{14} ohms with somewhat less accuracy. Several of these have been constructed and used at the Oak Ridge National Laboratory during the past two years. The need for them arises out of the fact that almost any device for measuring very small (usually ionization) currents makes use of resistors in the range of 10^{8} to 10^{14} ohms, and the accuracy of the results is only as good as the precision with which the resistance values are known.

As shown in Fig. 1, the circuit consists of a four-arm resistance bridge, balance of which is detected by a simple battery operated vacuum tube electrometer. The meter serves only to establish a null and the value of the unknown resistance R_x is read directly from the duoscale dial of the 15-turn helipot in bridge arm *D*. Two sets of multiplying factors, determined by the positions of switches *S*-2 and *S*-3, establish the decimal point.

It is at once apparent that inaccuracies may result from (1) lack of sensitivity in the null detector, (2) failure to establish a preliminary null (with no voltage on the bridge) having the electrometer plate and grid voltages identical to those of the final balance, (3) lack of linearity or error in the maximum resistance of the helipot *D*, and (4) errors in the values of the known multiplying resistances *A* and *B*. Steps taken to avoid each of these difficulties will be discussed in turn.

(1) As constructed, the vacuum tube voltmeter has a sensitivity of 0.17 volt for mid-to-full scale meter deflection. If the leakage resistance in the grid circuit is then kept above 10^{14} ohms, the sensitivity will be sufficient to determine the null setting on the helipot dial to four significant figures, even when measuring a 10^{13} ohm resistance. The introduction of a parallel leakage path of (say) 10^{13} ohms from any point at grid potential to ground, will seriously reduce the balancing sensitivity but will not otherwise lead to erroneous results.

Insulators with leakage resistance of 10^{15} ohms or higher, require special consideration.[1] Satisfactory materials are Teflon, fluorothene, and polystyrene, although the latter is much more difficult to use. Since such insulators may not be touched with the fingers a metal canopy protects the number 1 feed through insulator which supports one of the binding posts for R_x (see Fig. 2). In use, a metal shield (not shown) is placed over the unknown resistor and the exposed terminals.

Selector switches $S\text{-}1_B$ and *S*-2 must also meet the high impedance requirement. These are Cent-alab Ceramic switches which have been specially treated for minimum leakage.[1]

(2) The switching sequence of the four-deck switch *S*-1 has been arranged so that position 2 applies only filament voltage; position 3 applies plate voltage (this delay is necessary, otherwise the electrometer would drift for hours[2]), shorts the electrometer input, and allows the first zero adjustment to be made. Position 4 allows the second zero adjustment, zero′, to be made with no voltage applied to the bridge, hence the effects of grid current and contact potential may be eliminated and the conditions of balance will be identical to those of the final balance. Preliminary balance is made on position 5 with 1.5 volts applied to the bridge, while final settings are made on position 6 with 24 volts on the bridge.

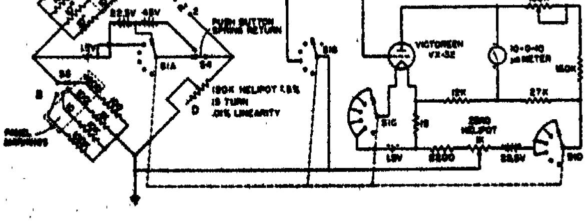
*S1,S2 NON-SHORTING, SPECIALLY TREATED, CERAMIC SWITCH. INSULATION RESISTANCE 10¹⁵ OHMS.
BRIDGE BATTERIES WRAPPED IN POLY FILM FOR BETTER INSULATION.
PANEL MARKINGS
A
B
C
D
S2
S3
1
2
22.5V
45V
1.5V
PUSH BUTTON SPRING RETURN
S1A
S1B
S1C
S1D
S4
150K HELIPOT 1.5% 15 TURN .01% LINEARITY
VICTOREEN VX-32
10-0-10 μa METER
ZERO 150K
150K
15K
27K
ZERO HELIPOT 1K
2200
22.5V
PANEL MARKINGS

FIG. 1.

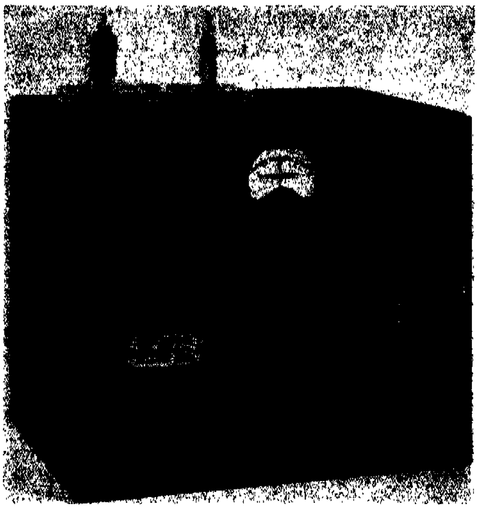

FIG. 2.

(3) The helipot used in arm *D* can be obtained from the manufacturer* with the linearity of 0.01 percent specified. Its maximum resistance at 15 turns must be 150K within the same accuracy as is desired in the use of the instrument.

(4) The standards in leg *B* are precision resistors selected to within 0.1 percent. The standards for leg *A* were worked up, in factors of ten, with the greatest of care from a base of ten one-megohm precision resistors placed in series to form a 10^{7}-ohm standard. The resistor standards to be selected for leg *A* were placed in leg *C* to be measured, and then resistors were interchanged between legs *A* and *C* to check for evidence of polarization and thermal e.m.f.'s. Since it is possible to read any given resistance with several combinations of switch positions of *S*-2 and *S*-3, a ready comparison check on the stability and accuracy of each of the standards is possible at any time.

Resistors used for standards in leg *A* are Victoreen Hi-Meg resistors. In view of the necessity of selecting standards and also because of their cost (approximately $5.00) construction of this bridge is not recommended unless one has a sizable stock from which to choose. Further, these standards may not be handled without altering their values. When constructing the instrument components must be arranged to provide minimum input capacity in the grid circuit in order to keep the time required for balance to a reasonable figure when measuring resistances above 10^{12} ohms.

The voltage coefficient of high meg resistors is a matter of some concern. An indication of this effect may be had by comparing readings with 1.5, 24, and 45 volts applied successively to the bridge. Resistor polarization may be ascertained by reading an unknown, then returning *S*-1 to position 4 and rechecking the zero as a function of time.

Work covered here was performed for the Atomic Energy Project at the Oak Ridge National Laboratory.

---

[1] F. M. Glass, "Methods of reducing insulator noise and leakage," Rev. Sci. Inst. 20, 239 (1949).

[2] J. A. Victoreen, "Electrometer tubes for the measurement of small currents," Proc. I.R.E. 37, 432 (1949).

* The Helipot Corporation, 1011 Mission Street, South Pasadena, California.

High Speed Electronic Scaler

W. M. Sessler and A. V. Masket
Physics Department, University of North Carolina, Chapel Hill, North Carolina

March 6, 1950

In developing a counter chronograph capable of reading time intervals of the order of 0.2 microsecond, it was found that there were few circuits in the literature capable of operating above one megacycle. One of the most promising scalers in this region had been developed by the M. I. T. Radiation Laboratory[1] using British tubes. Using the ideas presented in this circuit, such as diode "grippers," a new circuit was designed (Fig. 1) using tubes and components which were available on the commercial market. Germanium diodes were used as the diode "grippers" because of their low capacity, small physical size, and low forward resistance.

Considerable work was necessary with regard to coupling several of the stages together. In order to keep the power dissipation and number of tubes to a minimum, condenser coupling was used in preference to coupling amplifiers or cathode followers between the stages. The output signal was secured by connecting the diodes, which "grip" when the tubes are conducting, to 105 volts through resistors. The resistors were so chosen that when the diode is drawing current the plate of the diode is at 100 volts and during the no-current period is at 105 volts. This five-volt variation is coupled to the next stage through a condenser. A 1.1-microhenry choke was placed in the 120-volt supply line in order to present a high impedance path to the incoming signal.

The scalers were triggered with a 6-volt negative square wave. The square wave was secured by feeding the sine wave output of a crystal oscillator into a limiter circuit. The limiter circuit was composed of two 1N34 germanium diodes so connected that one eliminated the positive swing while the other limited the negative swing to 6 volts.

The plate, grid, and output signal wave forms are shown in Fig. 2(a), (b), (c) when the input frequency was 4.046 megacycles. Figure 2(d), (e) are wave forms of the plate and output signal at 5.8 megacycles.

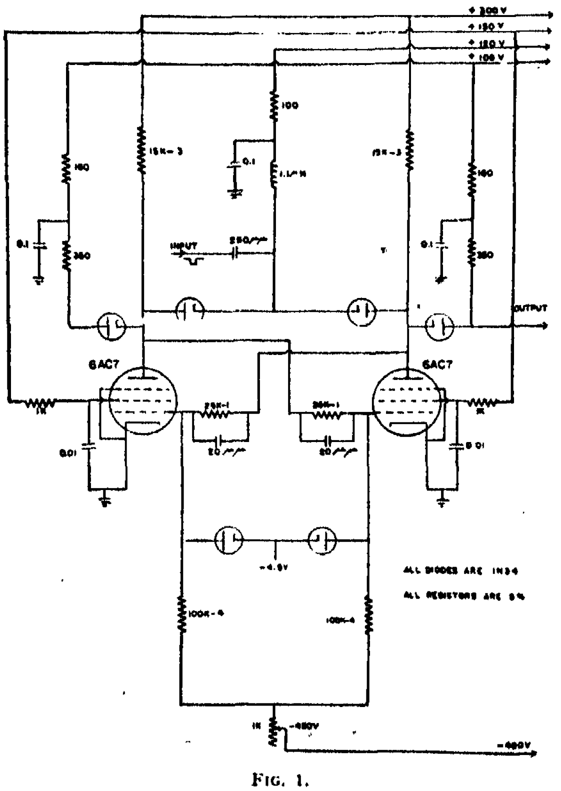

FIG. 1.

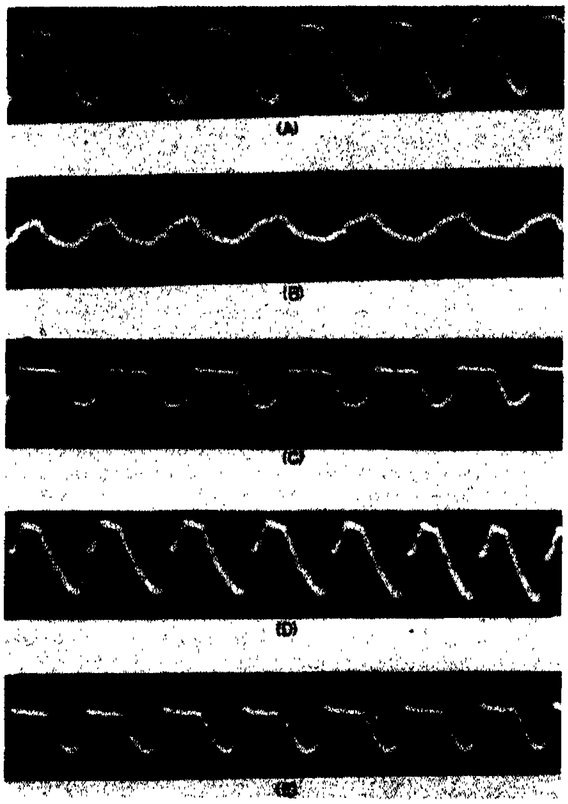

FIG. 2.

As in most high speed scalers the components were matched to within 5 percent or less. The 1000-ohm potentiometer at the bottom of the voltage divider network was provided to facilitate minor adjustments necessary due to small variations in tubes and resistors.

---

[1] Chance, Hughes, MacNichol, Sayre, and Williams, *Waveforms* (M. I. T. Radiation Laboratory Series, McGraw-Hill Book Company, Inc., 1949) Vol. XIX, pp. 606–608.

A New Pirani-Type Vacuum Gauge

E. Blasco and L. Miranda
High Vacuum Section of the Torres Quevedo Institute, Madrid, Spain

February 6, 1950

The following qualities are desirable for a pressure-gauge for use with a high vacuum distillation unit: simplicity of operation; pressure range from 10^{-3} to 1 mm Hg; direct-reading; ruggedness of construction; use in all types of gases; insensitivity to variations of line voltage.

A diagram of the circuit is shown in Fig. 1. The gauge is connected to the a.c. line through the half-wave selenium rectifier R, the output of which is *only partially* filtered by the condenser C^1. The purpose of C^1 will be explained later. The bridge circuit is mounted on the socket supporting the sensitive element which in turn is contained in a 16-mm diameter glass tube which may be connected with the vacuum apparatus by a standard vacuum rubber connection or clamp. The indicating galvanometer with the calibration-curve and the line switch is on a separate panel. The circuit is adjusted so that the galvanometer reads zero when the gauge is evacuated and full scale when at atmospheric pressure. Bulb dimensions are determined so that the air conductivity at 1 mm Hg will only be slightly less than atmospheric conductivity; the Pirani gauge then reaches a maximum of sensitivity in the

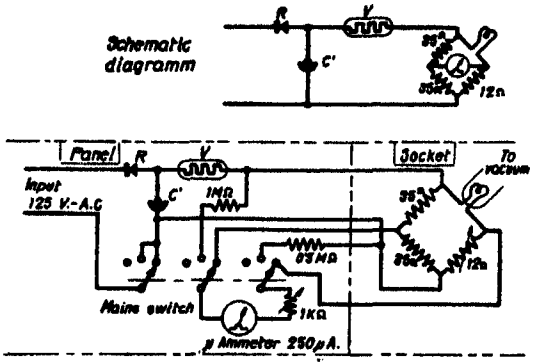

FIG. 1. Electrical connections.

10^{-3} to 10^{-1} mm Hg range. The most important problems to be solved in this type of Pirani gauge are those related to its stability in "dirty" atmospheres and its sensitivity to line voltage fluctuations.

Stability against chemical agents.—The Pirani zero-point shift when working in molecular distillation installations has been pointed out by Hickman.[1] We found the same phenomenon in the case of tungsten filaments either untreated or when covered with a tungsten hydride layer by heating in a wet hydrogen atmosphere as indicated by von Ubisch.[2] The cause of this shift as a result of which the gauge shows a tendency to read a higher pressure than that existing in the apparatus, thus indicating a decrease of temperature or resistance is probably related to the fact that the oil vapor is disintegrated when in contact with the hot wire producing a carbon deposit. As a result the specific emissive power of the filament and the accommodation coefficient (Knudsen) increases and consequently also the thermal loss, whereas the resistance simultaneously decreases due to the conducting layer by which the filament is thickened.

In order to avoid this effect we covered the filament with a fine glass capillary,[3] and worked at temperatures as low as compatible with a negligible influence of ambient temperature variations on the gauge reading. In Fig. 2 different phases of construction are shown. The filament is a tungsten spiral from a 100-watt, 110-volt lamp, with an approximate cold resistance of 8 ohms and working temperature (110°C) resistance of 12 ohms. The capillary tube is melted upon the filament while evacuating from one end in order to avoid bubbles.

All metal parts of the gauge that would be in contact with the interior atmosphere are glass covered, so that the gauge may be used with corrosive gases (excepting HF). A considerable rigidity of the assembly is obtained and the filament is insensitive to vibrations. The zero-point stability obtained by this method is very good. We did not find any appreciable shift after two years of operation in molecular distillation stills.

Of course, by introducing the glass capillary with its corresponding thermal capacity a reading delay is involved showing a small variation when different elements are used but with all of them being less than a minute and a half from the moment when the cold filament is connected till it reaches its maximum temperature corresponding to high vacuum.

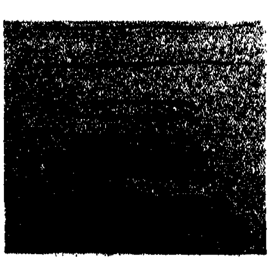

FIG. 2. Construction of the sensible filament. (a) Filament with welded terminals. (b) The same with the stuck capillary. (c) Bent filament. (d) Mounted on glass tube. (e) Complete with socket.

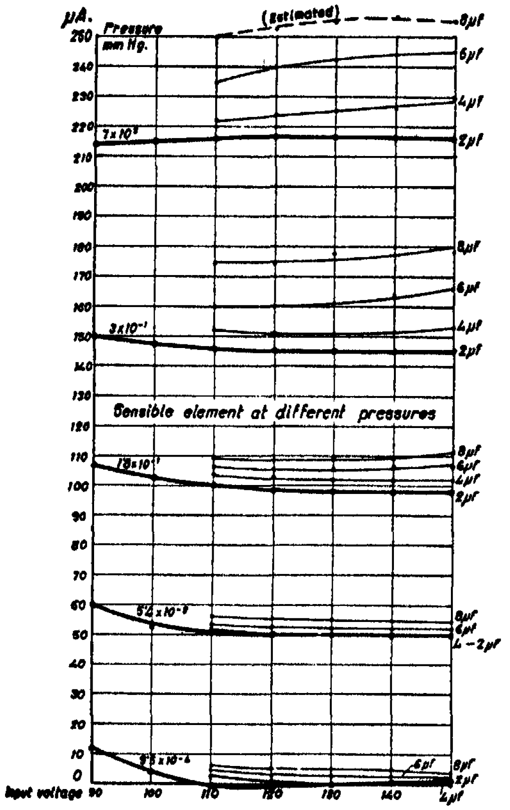

FIG. 3. Variation of μammeter indication with mains voltage.

Stability against variations of line voltage.—In order to reduce the dependence of the Pirani gauge reading on line voltage variations, a current regulating tube—Phillps C 10—(V in the diagram of Fig. 1) is connected in series with the bridge. The regulation provided by the tube is not perfect but it is improved by the effect of the incomplete filtering of supply voltage mentioned earlier.

The partially filtered current is equivalent to the sum of direct and alternating components. An increase in the direct component causes an increase in the unbalance of the galvanometer. This is partly compensated by an increase in wire temperature indicating an apparently higher vacuum, which tends to reduce the galvanometer reading. The first effect prevails over the second. On the contrary, an increase of the alternating component of the voltage is not directly registered by the measuring instrument but produces an additional heating of the wire, tending to return the galvanometer to zero. A relation can be established between the direct-current and the alternating-current components so that the increasing and decreasing effects are nearly balanced, resulting in a pressure reading which is to a certain extent independent of line voltage.

This compensating effect is not independent of gauge tube pressure. It is therefore necessary to decide at what pressure the compensation is desired, and to adjust the ratio of a.c. to d.c. current accordingly. In Fig. 3 are represented the gauge readings *versus* line voltage for different values of C^1 at five arbitrary pressures. The effect is easily seen and the value $C^1 = 2$ μf evidently gives the best compensation over the whole range. It is also seen that the higher the capacity, the lower the compensation point. With the selected value for C^1 a fairly good compensation is observed in the range 110–150 volts.

---

[1] Hickman, Chem. Rev. 34, 52, 1 (February, 1944).

[2] von Ubisch, "An investigation on hot-wire vacuum gauges," Arkiv. f. Mat. Astr. o. Fys. 34A, No. 14 (1947).

[3] Neumann and Pirani, "High vacuum gauges," Electronic Engineering, 277 ff. (December, 1944).

Detaching Device for Balloon Flights

Louis G. Collyer
Department of Physics, New York University, University Heights, New York, New York

August 22, 1949

WHILE conducting cosmic-ray balloon flights it was found to be necessary to terminate the flight after a given time in order to control the overland distance within reason. The most effective means to do this was found by detaching enough balloons from the flight so that the total lift of remaining string is less than the load carried.

In order to effect this detaching, many ways were tried, using heated wires which burned off a cord; squibs to break the cord; spring operated knives and so forth. All were found very uncertain.

The device described herein was found to work without fail. It consisted of a frame carrying a hook and a positive lock for same. A certain number of balloons, say three or four, carried the device with a ring on the hook connected to the rest of the flight below. The actuating device consists of an alarm clock which is set for the number of hours required for the flight to be air-borne. When the alarm trips, the turning of the winding key turns the eccentric and unlocks the hook releasing the mechanism and balloons from the rest of the flight.

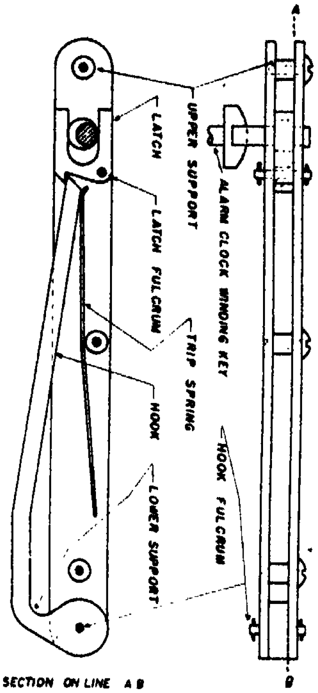

FIG. 1

The locking is very important because tripping too soon would be a serious matter especially over a city. The latch is positive and the lift of the upper balloons has no tendency to unlock it.

Very little machining is necessary and, except for the eccentric, all the work can be done with a saw and drill.

The only uncertainty found was in the clock itself. This uncertainty was found to be caused by the effect of extreme cold on the lubricant used. This may be overcome by washing out all the oil and relubricating by means of graphite or the use of the new molybdenum sulfite lubricants.

Figure 1 is self-explanatory. This device was used successfully in a number of flights in Denver, Colorado; San Juan, Puerto Rico; Bethlehem, Pennsylvania and elsewhere.

Suppressing Mercury Vapor in Vacuum Systems*

Frederick Ayer II
Physics Department, New York University, University Heights, New York, New York

February 27, 1950

IT is sometimes necessary to exclude mercury vapor from vacuum systems which are designed to operate at any pressure between atmospheric and 10^{-4} cm Hg. In such a system, the most convenient combination of pressure measuring instruments is a mercury manometer for pressures down to about two millimeters, coupled with some other device such as a vacuum thermocouple.

Mercury vapor may then be prevented from diffusing from the manometer into the system by floating a layer of some low vapor-pressure oil of the Apiezon "*B*" type on the mercury surface, to a depth of perhaps three centimeters. If the oil is placed in one arm of the manometer only, it will of course cause a lowering of the mercury column. In cases where determination of the absolute pressure in a system is necessary, equal amounts of oil may be floated on both mercury surfaces. However, where the system is being used as a means for filling evacuated vessels with certain gases, oil need be placed only in one arm of the manometer since the difference in level of the mercury column before and after admitting the gas indicates the pressure introduced.

If left to itself without continuous pumping, the system will contain, at equilibrium, both mercury and oil vapors, but as the rate of diffusion of mercury vapor through the oil layer is very slow, its concentration will be greatly lowered when the system is evacuated by large-capacity pumps. Such an arrangement is called a "kinetic system" by Strong.[1] If desired, additional "getters" of gold foil may be placed at those points in the system farthest removed from the pumps. It is assumed, of course, that the system is supplied with liquid-air traps if mercury vapor diffusion pumps are used. It may be argued that an equivalent result may be arrived at by mere substitution of closed-end oil manometers for mercury manometers, but the slowness of response of the former makes pressure readings time-consuming.

A word of caution is necessary. Many gases dissolve in Apiezon "*B*" and similar oils, and if a system is left for a time with an appreciable internal pressure, the oil will boil during evacuation, causing it to spill over into the system proper. The remedy lies in slow evacuation so that long columns of froth do not form, or breaking up the bubbles which do form by running a sparking leak tester up and down the manometer tube at the froth level.

Boron trifluoride tends to darken Apiezon "*B*" in time, but this effect may be minimized by evacuating the system after each use. Furthermore, although the oil reacts slowly with the mercury, the dirty surface does not diminish reading accuracy to any important extent for a long time.

Other investigators in this laboratory have made use of this suggestion and report that with it pressures as low as 10^{-7} cm Hg can be attained in much shorter times than when the mercury column is not sealed off.

---

* This work was assisted by the joint program of the ONR and AEC.

[1] J. Strong, *Procedures in Experimental Physics*, p. 125.

A Metal Dewar for Liquid Helium

Warren E. Henry and Richard L. Dolecek
Naval Research Laboratory, Washington, D. C.

January 30, 1950

EFFICIENT utilization of space is of prime importance in Dewar design for cryomagnetic research where the available working space is restricted by magnet pole separation or solenoid opening. Metal Dewars can be designed for efficient utilization of space. In addition, they are durable, are convenient to manipulate because of one-piece construction, and offer the opportunity of design for electrostatic and magnetic shielding where required.

Metal Dewars have been constructed for use in solenoids of the "Bitter"[1] type having openings 1¼ inches and 4 inches in diameter. A longitudinal cross section of the Dewar constructed for use in the 1¼-inch magnet is given in Fig. 1. A maximum working space (*A*) in the liquid helium is achieved by the use of a common insulating vacuum (*C*) for the helium and nitrogen Dewars, and a radiation shield (*R*) cooled by conduction to the liquid nitrogen vessel (*B*). Axial symmetry is maintained at the top by the perforated annular ring (*S*) and at the bottom by mica spacers (*M*) designed to minimize heat conduction. Stainless steel was used in the construction of the upper portions of the Dewar and to minimize field distortion, non-magnetic materials were used for the cylinders surrounding the working space (*A*). Thus, the lower section of the helium vessel and the outer cylinder were constructed of $\frac{1}{32}$-inch non-magnetic brass, and $\frac{1}{16}$-inch copper was used for the radiation shield (*R*). These cylinders were spaced $\frac{1}{16}$ inch apart. To facilitate assembly both silver soldered and soft soldered joints were employed. For an over-all diameter of $1\frac{1}{16}$ inch, this design yields a $\frac{9}{16}$-inch working space.

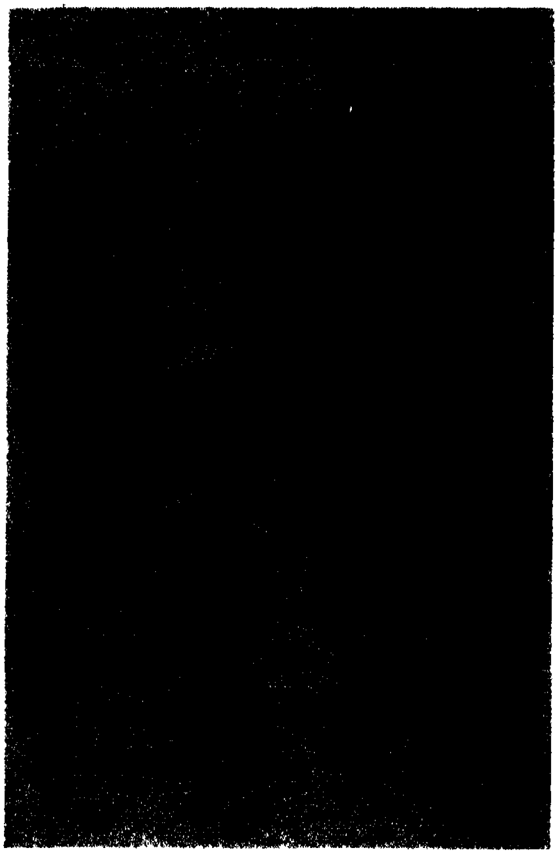

FIG. 1. Metal Dewar for use in "Bitter" type solenoid having 1¼-inch opening.

The Dewar is prepared for use by flushing with dry nitrogen, and to allow rapid precooling[2] of the helium Dewar and sample, only a partial vacuum of the order of 25 microns is established before closing a metal valve soldered to *V*.

The Dewars have proved entirely satisfactory for use in both the helium I and helium II regions. The heat leak at 4.2°K is of the order of 50 cc of liquid helium per hour. As the reservoir has a capacity of approximately one liter, considerable time is available for conducting an experimental investigation.

---

[1] F. M. Bitter, Rev. Sci. Inst. 10, 373 (1939).
[2] C. T. Lane and H. A. Fairbank, Rev. Sci. Inst. 18, 522 (1947).

Power Supply for the Cenco Concentrated-Arc Lamp

JAMES M. MITCHELL
California Institute of Technology, Pasadena, California
March 13, 1950

IN using a Cenco* concentrated-arc lamp with the conventional power supply, it is necessary to hold the starting switch until the lamp fires and then to release the switch upon starting. If the switch, which supplies the high voltage required to initiate the arc, is not released quickly, the high voltage will damage the lamp. In particular applications using the lamp in enclosed spaces where it is impossible to observe when it has started, the conventional power supplies are not satisfactory. Also, in student laboratories where these lamps are used, many are damaged when the power supply is not operated correctly. To eliminate this starting trouble, the power supply shown (Fig. 1) was designed.

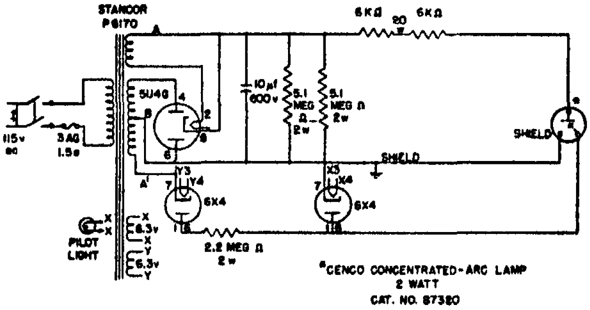

FIG. 1.

The design of this power supply is based on the high impedance of the arc lamp before it has started and the low impedance after starting. The power supply acts as half-wave rectifier across the transformer (*A*–*A*′) when no current is drawn by the circuit. However, as soon as the circuit draws current, the power supply becomes a full wave rectifier with the voltage across the center tap of the transformer (*A*–*B*). The two diodes are used to prevent a closed circuit across the lower half of the transformer (*A*′–*B*).

The values shown in the circuit diagram are for use with the Cenco 2-watt concentrated-arc lamp. However, by suitable choice of values, the circuit is satisfactory for other lamps. Also, the circuit has been used in other applications requiring a high starting d.c. voltage and a lower operating voltage.

*Central Scientific Company, 1700 Irving Park Road, Chicago 13, Illinois.

Precision Selector for Voltage-Regulator Tubes

O. B. RUDOLPH
Carbide and Carbon Chemicals Division, Union Carbide and Carbon Corporation, Oak Ridge, Tennessee
February 6, 1950

VOLTAGE regulation, or the elimination of the ripple voltages from a.c. rectified sources, has achieved such widespread usage that one often thinks of it as a simple procedure. (The term "ripple" as used here embraces transients of not only 60 and 120 cycles, but any frequency that might be reflected in the output of the d.c. supply.) Indeed, laboratory set-ups have been made that give regulated d.c. supplies with extremely low ripple voltages; but these circuits are frequently too cumbersome to be used widely in industrial applications.

The increased usage of d.c. voltages in industrial equipment has resulted in the designing of special regulating (VR) tubes to meet most requirements; however, where an unusually constant voltage is desired, careful tube selection is necessary as tubes vary noticeably in their operating characteristics. This article presents

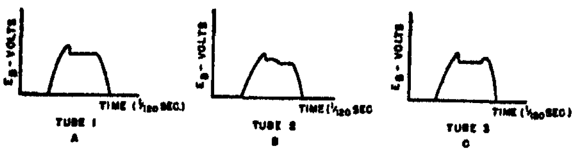

FIG. 1. Various oscilloscope traces obtained.

a simple circuit for predetermining the reliability of VR tube performance.

Since the function of a VR tube is that of an automatic variable resistor which changes its internal resistance to steadily maintain a fixed voltage drop across its two terminals within its rated current range, failure of the tube to function properly will be reflected in the action of the regulator. Particularly where the regulation network output is to be amplified, small transient variations in VR tube action cause difficulty.

Ideally, the voltage drop across the VR tube is constant throughout its rated current range; however, by employing highly sensitive laboratory-type instruments, it has been shown that in any group of tubes chosen at random, many do not give a uniform regulating characteristic. Instead, small transients caused by line variations or other reasons resulted in changes in voltage drop across the tube with consequent changes in regulated output (Fig. 1A, B, C). These results are virtually independent of tube age, and new tubes are sometimes among the worst offenders.

Thus to properly test VR tubes, it is necessary to examine each tube over its entire operating current range, while employing a sensitive detecting device to indicate voltage variations.

The tube selector circuit developed is shown in Fig. 2. By throwing the double-pole, double-throw switch S_1 to position 2, a well-filtered d.c. output will be obtained which can be used for preheating the tube undergoing test if desired and also for checking firing voltage which will be indicated on meter M_2. With switch S_1 in position 1, pulsating d.c. voltage will be applied to the tube for precision checking of the over-all voltage-current characteristic. Since meter M_1 will indicate R.M.S. value of current, care will need to be exercised to prevent the peak value of the current from exceeding 40 ma; current can be adjusted to proper value by potentiometer R_1.

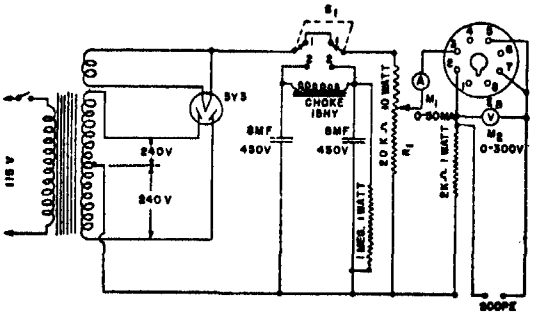

FIG. 2. VR tube selector-elementary diagram.

Shown in Fig. 1A, B, and C are three of the various types of oscilloscope traces which have been obtained from different tubes. "*A*" is ideal and the only one acceptable for many applications.

This "Precision Selector" circuit is very simple. It can be set up in the research laboratory or in industrial servicing shops in a matter of minutes after construction of the individual units; and furthermore, these units need not be "tied down" to this specific use. Pretested VR tubes may be kept on hand for replacements with certain knowledge that each will perform acceptably.

This report is based on research carried out under contract for the AEC, the Isotope Research and Production Division at the Carbide and Carbon Chemicals Division, Union Carbide and Carbon Corporation, Y-12 Plant, Oak Ridge, Tennessee.

The Use of Secondary Electrostatic Focusing in a Magnetic Beta-Ray Spectrograph

R. D. Hill, J. W. Mihelich, and M. T. Pigott
Physics Department, University of Illinois, Urbana, Illinois*
February 27, 1950

In order to detect low intensity conversion lines with a magnetic, 180° focusing, photographic beta-ray spectrograph, our experience is that exposures of many weeks duration are often required. The purpose of this note is to describe a modified spectrograph using secondary electrostatic focusing which reduces the exposure time for conversion lines of the order 100-kev energy by a considerable factor.

A plan of the modified spectrograph insert is shown in Fig. 1. This insert is placed in the field of a permanent magnet so that electrons describe circular orbits and exhibit the well-known 180° first-order magnetic focusing. In addition, a certain amount of focusing in a plane perpendicular to the orbital plane is achieved by the electrostatic lens placed directly across the electron orbits, as is shown in Fig. 1.

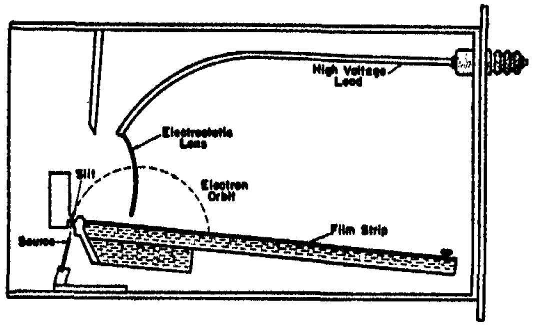

FIG. 1. Focusing insert for 180° beta-ray spectrograph.

We have experimented, using both empirical and ray-tracing methods, with a number of simple forms of electrostatic lenses. Thus far, best results have been obtained with a plane grid of five $\frac{1}{32}$-inch diameter wires, arranged one above the other, and approximately 0.2 inch apart and from the top and bottom plates of the insert. The grid wires were maintained at a constant positive potential with respect to the insert walls. The plane of the grid was placed tentatively at the correct focal distance from the photographic plate for electrons following the 100-kev trajectory, and it was then bent into an arc which was approximately perpendicular to the other electron trajectories. Experimentally, it was found that the maximum grid potential was determined by vacuum conditions in the spectrograph. We were able to attain a potential of only 8 kv, beyond which potential there was a risk of an occasional discharge fogging the photographic film.

The effectiveness of the electrostatic focusing may be appreciated by referring to Table I, where photographic densities of the same 90-kev Ta^{182} line are given for four equal-duration exposures using different focusing potentials. It is clear that at 7 kv the effective intensity of the line is about four times greater than that at zero potential. In actual practice, if a source which decays appreciably during a long exposure is used, the increase of intensity may be even higher than a factor of four. There appears

TABLE I. Photographic densities and intensities of 90-kev Ta^{182} at four focusing potentials.

Focusing potential (kv)	zero	2	5	7
Line density	0.61	0.82	1.00	1.15
Background density	0.43	0.46	0.51	0.58
Line density above background	0.18	0.36	0.49	0.57
Relative line intensity[a] above background	1.0	2.1	3.3	4.4

[a] The intensities were derived from an intensity-density calibration of the photographic emulsion.

to be a further advantage of focusing. As will be seen from Table I, the background for the line does not increase with focusing voltage at as high a rate as does the line intensity. The background is due to both continuous beta-rays and scattered electrons, and it is likely that the scattering from top and bottom plates of the insert is being reduced by focusing of the electrons.

* The work was supported in part by the joint program of AEC and ONR.

A Convenient Cell-Stage for Fluid Profile Measurements

WILLIAM FOX
*U. S. Department of the Interior, Bureau of Mines, Bartlesville, Oklahoma**

February 20, 1950

THE practical utility of profile measurements which permit the determination of contact angles at the mutual line of contact of the interfaces of solid-liquid-gas systems has been demonstrated in the field of flotation.

Although the importance of such measurements has been realized, difficulties which had previously been encountered in making determinations of contact angles through liquid-liquid-gas systems have hindered the use of these constants for an understanding of the wetting and spreading phenomena of such systems.

In the last few years, methods have been described for making direct measurements of the contact angles through mutually saturated three-phase fluid systems.[1,2]

From these measurements the wetting and spreading tendencies of each of the three fluid phases under consideration can be determined. These determinations are important in many practical problems, including those which are involved in the recovery of petroleum.[3]

For use in these investigations a cell-stage of the type shown in Fig. 1 (a) is convenient.

This apparatus is similar to one described[4] for use in flotation experiments. The cell-stage shown in Fig. 1 is a more compact unit than that previously described and can be constructed easily. Details of the construction can be noted from Figs. 1 (b) and 1 (c).

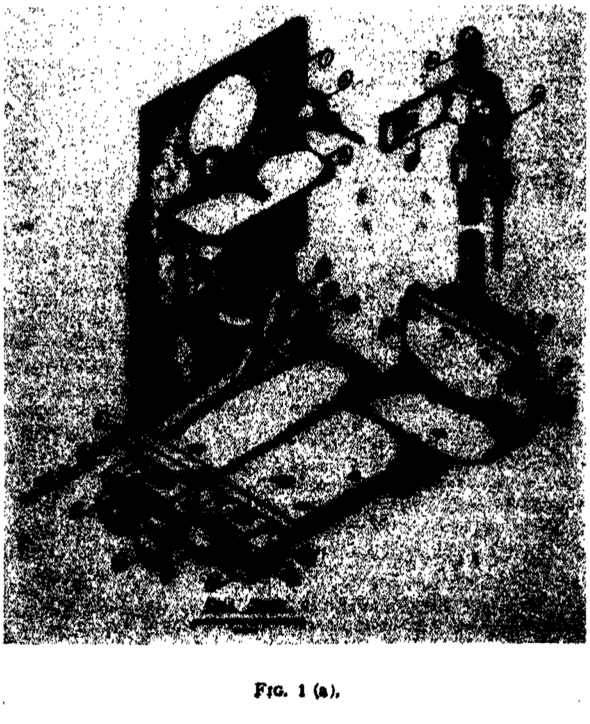

FIG. 1 (a).

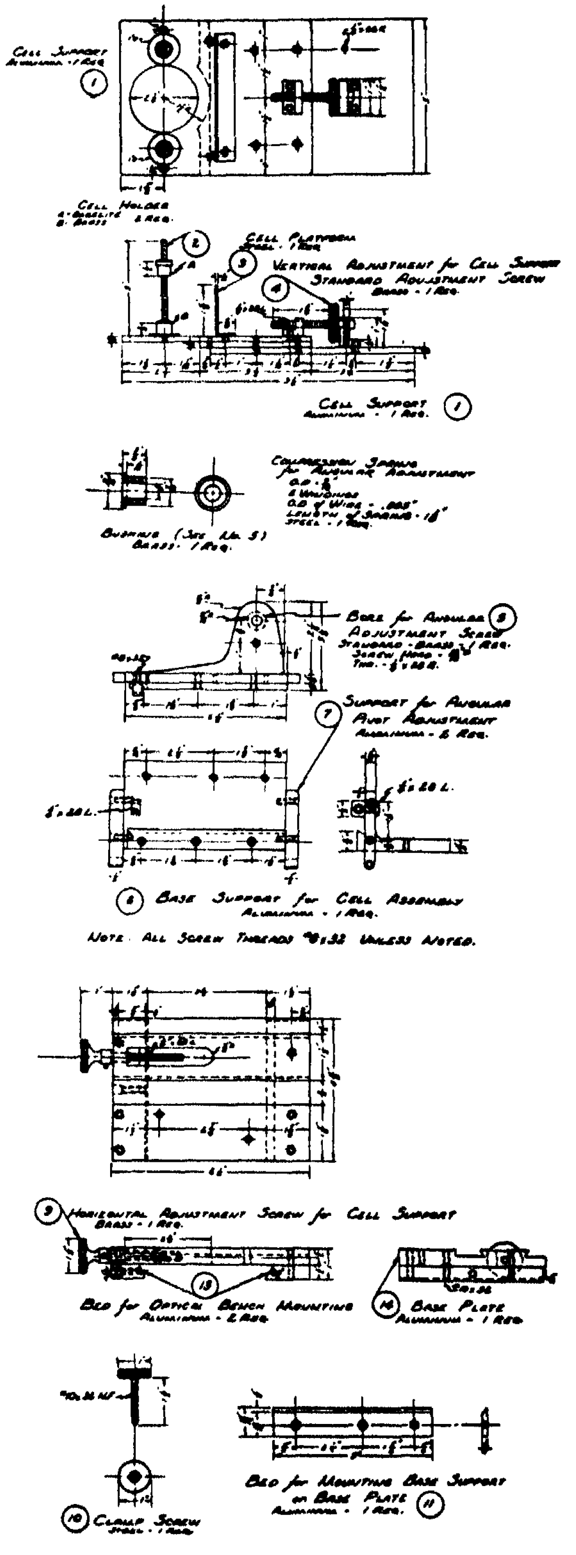
Cell Support Aluminum - 1 Req.
1
Cell Holder A-Bakelite B-Brass 2 Req.
2
Cell Platform Steel - 1 Req.
3
Vertical Adjustment for Cell Support Standard Adjustment Screw Brass - 1 Req.
4
Cell Support 1
Compression Spring for Angular Adjustment
Bushing (See No. 5) Brass - 1 Req.
Bore for Angular Adjustment Screw Standard - Brass - 1 Req.
5
Support for Angular Pivot Adjustment Aluminum - 2 Req.
7
6 Base Support for Cell Assembly Aluminum - 1 Req.
Note All Screw Threads #8-32 Unless Noted.
9 Horizontal Adjustment Screw for Cell Support Brass - 1 Req.
13
Bed for Optical Bench Mounting Aluminum - 2 Req.
14 Base Plate Aluminum - 1 Req.
10 Clamp Screw Steel - 1 Req.
Bed for Mounting Base Support on Base Plate Aluminum - 1 Req. 11

FIG. 1 (b).

The observation cell containing the system under examination can be placed on the cell platform (3) below the circular hole in

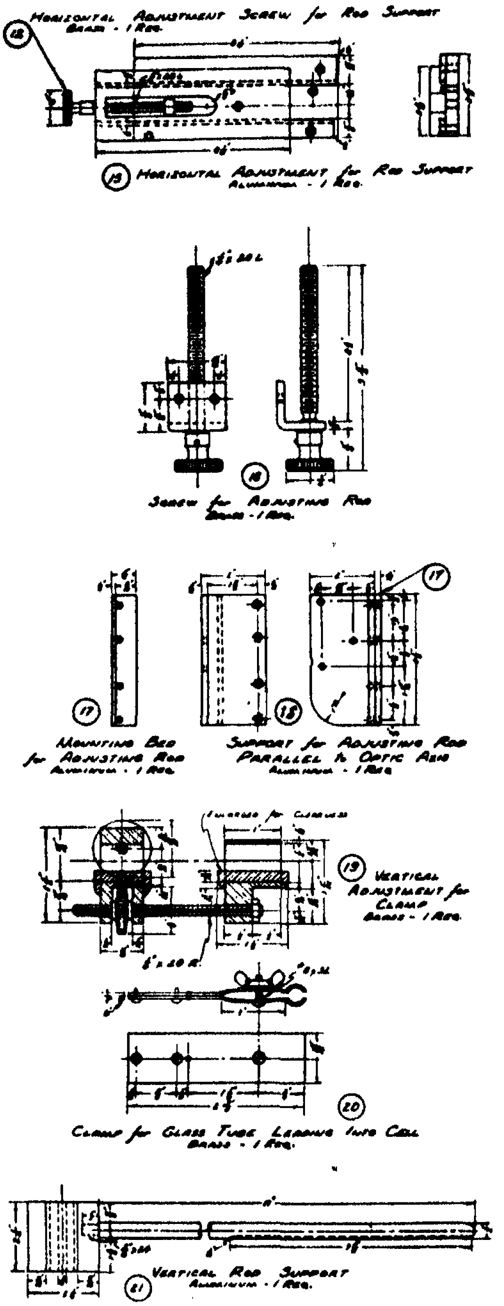
Horizontal Adjustment Screw for Rod Support Beam - 1 Req.
⑮ Horizontal Adjustment for Rod Support Aluminum - 1 Req.
⑯ Screw for Adjusting Rod Brass - 1 Req.
⑰ Mounting Bed for Adjusting Rod Aluminum - 1 Req.
⑱ Support for Adjusting Rod Parallel to Optic Axis Aluminum - 1 Req.
⑲ Vertical Adjustment for Clamp Brass - 1 Req.
⑳ Clamp for Glass Tube Leading into Cell Brass - 1 Req.
㉑ Vertical Rod Support Aluminum - 1 Req.

FIG. 1 (c).

the cell support (1). The cell is held in place by the cell-holders (2) on opposite sides of the circular hole. The cell platform is replaceable, and a larger platform can be mounted on the support to accommodate a thermostat of the type described by Hauser *et al.*,[5] into which the observation cell can be placed conveniently.

Adjustment screw (4) permits vertical adjustment of the cell support, which can also be rotated by (5) on the pivots (8) for angular adjustment.

The base (6) on which the cell support is mounted is adjustable by (9) so that the observation cell can be moved horizontally across the optical axis of the camera.

The clamp (20) is used to hold a glass tube in place in the observation cell. This clamp can be adjusted vertically on the rod support (21) by the vertical adjustment (19). This part of the cell-stage can be moved as a unit parallel to the optical axis of the camera by (16) and perpendicular to the optical axis by (12).

The cell-stage is mounted on the optical bench by (13) and held in place by clamp screw (10). This part of the unit can be modified to fit on any type of optical bed that is available. If the cell-stage is mounted on a base that can be adjusted by leveling screws, the pivots and the screw which permit angular adjustment of the cell support can be eliminated.

Details of the photographic equipment and necessary procedures for securing profiles from which measurements of equilibrium contact angles can be made have been described.[1,2]

The author wishes to thank Mrs. Joanne M. Grindstaff of the Bureau of Mines drafting department for making the drawings, and John O. Greenwalt of the Bureau of Mines machine shop for constructing the apparatus.

---

* Physical Chemist, Petroleum Experiment Station. Present address: Detective Division, New York City Police Department, New York, New York.

[1] W. Fox, J. Chem. Phys. 10, 623 (1942).

[2] W. Fox, J. Am. Chem. Soc. 67, 700 (1944).

[3] W. Fox, "Contact angles and their relationship to the wetting and spreading of liquid-liquid-gas systems," presented before the Division of Colloid Chemistry at the 116th national meeting of the American Chemical Society, Atlantic City, New Jersey (September 20, 1949).

[4] G. R. M. del Giudice, Eng. Min. J. 137, 291 (1936).

[5] Andreas, Hauser, and Tucker, J. Phys. Chem. 42, 1003 (1938).

A Method of Preserving Specimen Grids for Electron Microscopy

JENNIE E. SHAPIRO
Biology Department, Brooklyn College, Brooklyn, New York

March 8, 1950

FREQUENTLY specimen grids prepared for electron microscopy must be used repeatedly or subjected to more than one process in preparation. This poses the problem of storing and filing, in the interim periods, in an easily accessible manner. The method, described here and illustrated in Fig. 1 has been found to be efficient in repetitive handling. In addition to maintaining the grids in excellent condition, specimen side uppermost, the material is in a form which is readily available for preliminary study with the light microscope. Moreover, it may be stored for future reference in an ordinary slide box.

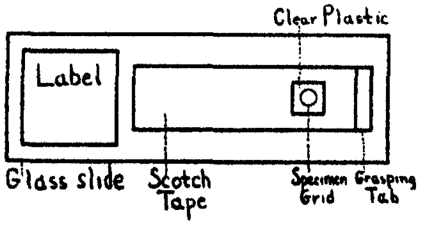

FIG. 1

The grid to be preserved is placed specimen side up on a clean glass microscope slide. A one-quarter inch square of clear plastic or celluloid (approximately the thickness of a No. 2 coverslip) is placed directly above it to protect its surface. The whole preparation is then sealed to the slide with a strip of clear cellulose Scotch Tape, one end of which is folded under to act as a grasping tab for subsequent removal. The specimen is now housed in a small chamber one surface of which is glass, the other clear plastic or celluloid. Specimens prepared in this way can be examined with the light microscope through both the Scotch Tape and plastic which function as coverslips. On peeling the Scotch Tape from the slide, the plastic cover which adheres thereto is raised and the grid with specimen side up is freed for further use.

New Instruments

W. A. Wildhack: Associate Editor
in Charge of this Section
National Bureau of Standards, Washington, D. C.

These descriptions are based on information supplied by the manufacturer in some cases from independent sources. THE REVIEW *assumes no responsibility for their correctness.*

Pulse Generator

Model 212A, a new general purpose instrument, is the first commercial pulse generator to successfully combine broad laboratory usefulness with fast rise time, high power, continuously variable pulse width and other features demanded in radar, television, and nuclear work.

Among the outstanding features of the new instrument are the unusually fast pulse rise and decay time (0.02 μsec.), the high power (50 watts) pulse, and a continuously variable pulse length, 0.07 to 10 μsec. A low internal impedance of 50 ohms or less insures a pulse shape virtually independent of load. This low impedance also makes it possible to deliver accurate pulses at some distance from the instrument if transmission lines are properly terminated.

The instrument has a repetition rate (frequency) continuously variable from 50 to 5000 pulses per second, and pulse rate can be controlled internally, or from an external synchronizing source. Continuously variable synchronization pulses are available either in advance or following the main pulse. An amplifier-attenuator system is provided with low source impedance, making possible either positive or negative pulses with continuously variable amplitude.—HEWLETT-PACKARD COMPANY, *395 Page Mill Road, Palo Alto, California.*

Industrial Television

The small size and weight of this new wired television equipment is chiefly due to the use of a miniature pick-up tube, only 1 in. in diameter and 6 in. long. This tube represents a departure in pick-up tube design in that it operates on the principle of photoconductivity, while the image orthicon and other current pick-up tubes in general employ photo-emissive cells. The camera is as small as the average 16-mm movie camera and is designed to employ regular 16-mm lenses with the standard Type C mount. It weighs 8 lb., is 10 in. long, 5 in. high, 3 in. wide, and requires a scene brightness of 2 foot-lamberts minimum. The Control Monitor contains a 7-in. viewing screen as well as all controls, both for itself and for the camera. Three knobs control the operation of the Monitor itself: (1) brightness, (2) contrast, and (3) blanking (black level). And three controls for the camera are also included on the Monitor panel: (1) beam intensity, (2) electronic focus, and (3) optical focus. The optical focus controls a small reversible motor in the camera which changes the focus of the lens. The Monitor weighs 58 lb. and is 26½ in. long, 17 in. high, and 8½ in. wide. It also has provision for plugging in additional television receivers, and since the scanning frequency and interlacing are the same as that employed for broadcast television, it is possible to use regular broadcast receivers as additional monitors by merely adding a one-tube amplifier. The connecting cable permits the Monitor to be located up to 250 ft. from the camera and greater distances can be covered by use of slave monitors or booster amplifiers. Power requirements are 375 watts at 110 volts, 60 cycles.—RADIO CORPORATION OF AMERICA, *Camden, New Jersey.*

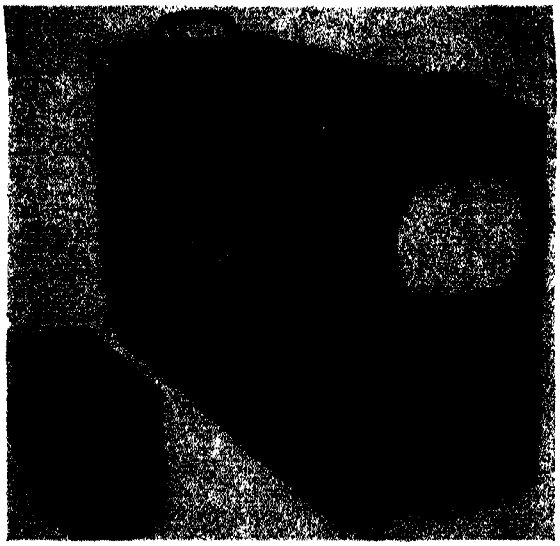

Minature Seismograph

This unit, Type PSU-11, is designed around the GA-11 amplifier, which features performance equal to or better than many of the old type standard amplifiers. The waterproof amplifier case pictured measures 6×13×21 in., weighs approximately 35 lb., and contains twelve Type GA-11 amplifiers plus the control unit. The amplifiers have a gain of 120 db and no preamplifiers are necessary; the AGC operates over an unusually wide range, thus preventing distortion from high input levels. The initial suppression is individually adjustable, and filter selectors are also provided. The amplifiers are of the plug-in type, and no soldering is necessary to replace them in the field. The oscillograph makes 25 traces on 6-in. paper and has barrel-type,

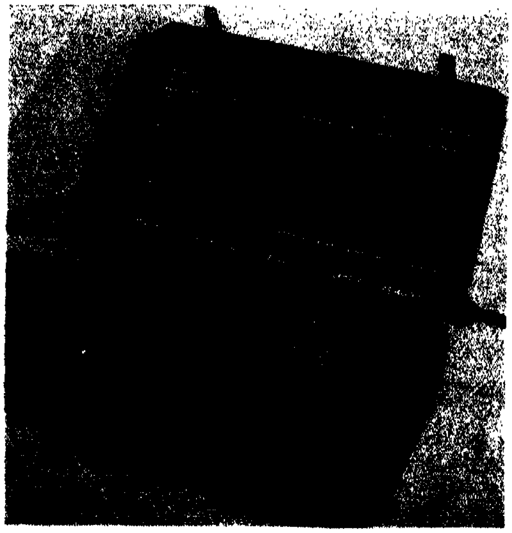

electromagnetically damped galvanometers, a viewing screen, a built-in timing system, removable take-up magazine, built-in paper knife, a governor controlled cranking motor, and dimensions of 8×9×16 in. with a weight of approximately 25 lb.—SOUTHWESTERN INDUSTRIAL ELECTRONIC COMPANY, *P. O. Box 13058, Houston 19, Texas.*

H-42 Strainalyzer

The Strainalyzer is designed for d.c. bridge excitation from self-contained batteries and has the necessary high gain d.c. amplifiers, balance controls, and voltage and calibration controls for each strain gauge bridge channel. The instrument can be used with Baldwin SR-4 strain gauges of either the "A" or "C" type from 60 to 500 ohms and will give excellent linear response. A four-gun cathode-ray tube makes possible the simultaneous observation and recording of electronic traces of four functions in correct time relationship without the necessity of optical alignment. The Strainalyzer is composed of four units: the indicator (illustrated), the indicator power supply, the camera, and the camera speed control. The strain gauge bridge control panel is a removable plug-in unit, and four binding post terminals are provided for each bridge, making all four arms available to allow use of one to four active gauges. Deflection sensitivity is better than 0.002 volt d.c. per in., maximum undistorted deflection is 3 in. peak to peak, and the input is single-ended, capacitive, and has an impedance of 10,000 ohms shunted by 40 $\mu\mu f$. The apparatus weighs approximately 200 lb. and will draw 400 watts at 105–125 volts, 50–60 cycles.—ELECTRONIC TUBE CORPORATION, *1200 East Mermaid Lane, Philadelphia 18, Pennsylvania.*

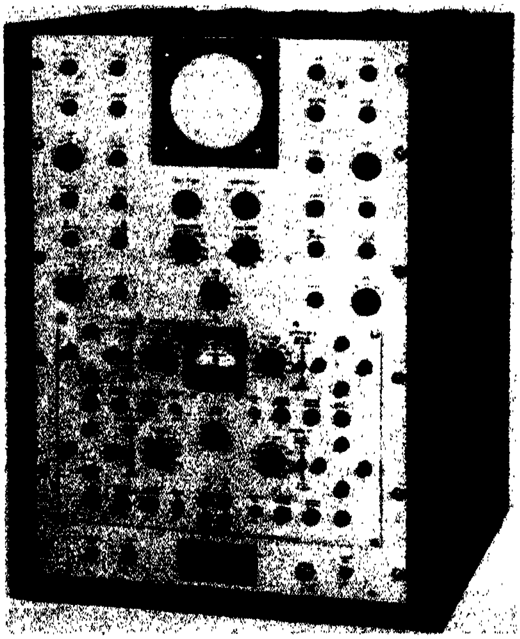

Ionization Gauge

The DPA-38 ionization gauge control circuit is a direct-reading vacuum gauge capable of measuring pressures from 10^{-3} mm Hg on into the 10^{-9} region. It has a voltage-regulated power supply and a two-stage automatic grid control, which has been provided to operate throughout the full life of the DPi VG-1A ion tube. The control circuit automatically shuts off the ion tube whenever the pressure rises above 1.2 times full-scale deflection, and it operates on all of the various ranges. An unusual feature of the DPA-38 is that it permits continuous pressure readings during the degassing of the ion tube. Readings are remarkably easy to make because the decimal negative exponent is read on the range selector and the coefficient is read on the dial gauge. The instrument can be adapted to operate in conjunction with a recording unit, and it draws 175 watts from a 110-volt, 60-cycle line.—DISTILLATION PRODUCTS INDUSTRIES, *Rochester 3, New York.*

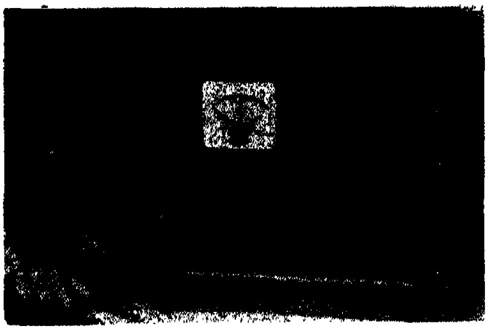

All-Purpose Scaler

Geiger, proportional, or scintillation counting can be accomplished with the Ultra-Scaler by either automatic or manual methods. Facilities for every type of counting are thus included within one instrument.

A built-in timer is provided which may be set for a predetermined length of time and will then turn off the scaling unit automatically. The instrument may also be set for a predetermined number of counts, and the scaling unit will stop at that number of counts and indicate the time on the timer. In addition, a number of features are provided so that the instrument may be operated manually or used for monitoring purposes with a suitable probe.

The Ultra-Scaler incorporates two inputs, one for Geiger pulses and the other for very small proportional pulses requiring linear amplification. The fast Higinbotham-type scale of 128 has a resolution time of only two microseconds. Scale selection is provided to permit the use of smaller scaling factors. Stabilized high voltage is available up to 2500 volts, and a built-in register indicates the total number of counts. A special time delay prevents overvoltage surge on the Geiger tube when the instrument is first turned on.—NUCLEAR INSTRUMENT AND CHEMICAL CORPORATION, *229 West Erie Street, Chicago, Illinois.*

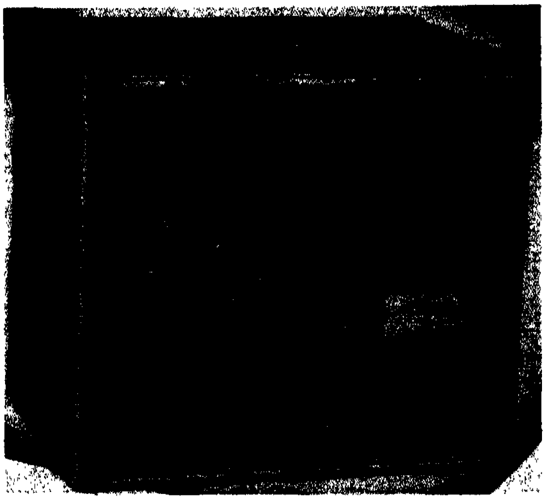

Spectrum Analyzer

The Model LSA spectrum analyzer is a laboratory instrument used to provide a visual indication of the frequency distribution of energy in an r-f signal in the range of 10 to 16,520 mc. Three tuning units cover the bands from 10 to 1000, 940 to 4500, and 4460 to 16,520 mc, with 5-kc resolution at all frequencies. This instrument features continuous, single-dial tuning with direct reading frequency accuracy of one percent, and frequency dispersion can be varied from 250 kc to 25 mc. A frequency marker is provided to measure frequency difference from 0 to 25 mc. The microwave tuning units incorporate broad-band attenuators and use the latest design non-contacting shorts to insure long mechanical life. A 5-in. CRT display unit, a klystron power unit, and a low voltage power unit constitute the remainder of the equipment.—POLARAD ELECTRONICS CORPORATION, *100 Metropolitan Avenue, Brooklyn 11, New York.*

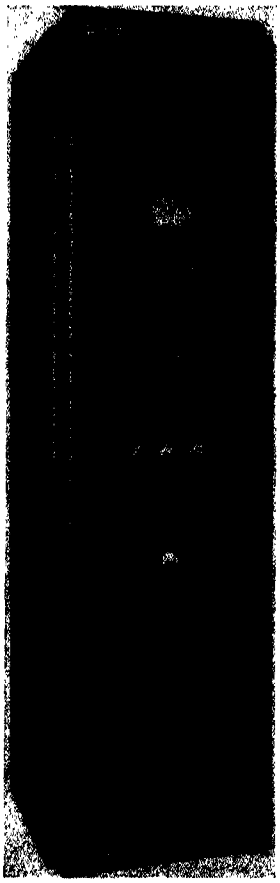

Infra-Red Spectrophotometer

A new double-beam infra-red spectrophotometer, known as the Model 21, with a wider range of operating variables than earlier commercial models, is the first infra-red spectrophotometer that meets the demands of the structural chemist for high resolution and sensitivity and those of the analytical chemist for speed and accuracy.

The Model 21 records directly in percent transmission against a linear wave-length scale on large, easily read charts. Use for this versatile instrument may be found in practically every application of infra-red spectrometry in both academic and industrial laboratories.

The new instrument's resolution is up to the limitations imposed by the Raleigh criterion and Johnson noise. Its speed of scanning ranges from 3 min. to 100 hr. for the rocksalt region. The wavelength drive speed can be suppressed automatically when desired. Time of response varies from a few seconds to more than a minute for full-scale deflections. The over-all range of the instrument is from less than 2 to 15μ in the rocksalt region.

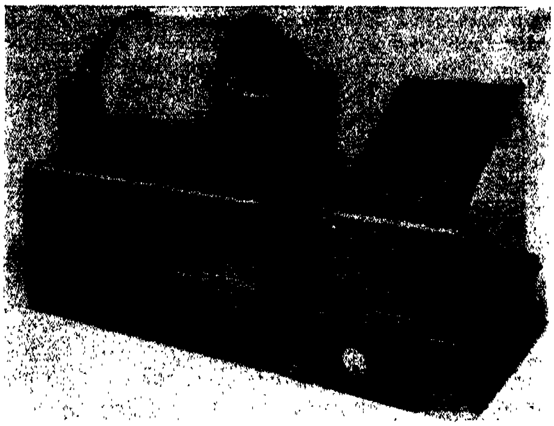

Chart scales of the Model 21 are uniform from 1 to 50 in. per micron by integral factors. The chart size is about 32 by 11 in. The instrument is 40 in. long, 22 in. high, and 20 in. wide. The amplifiers and power supplies are external.—THE PERKIN-ELMER CORPORATION, *Glenbrook, Connecticut.*

Pulse Rise Time Indicator

The Model 632-B pulse rise time indicator is an instrument for the accurate plotting of the rise time of rapidly rising positive voltage pulses. The device employs a specially designed delay line of variable length and a vacuum tube voltmeter. The VTVM reads the peak of the resultant pulse produced by the pulse under test and its reflection; its magnitude is a function of the rise time and the delay of the line. When the delay (total time of propagation) is less than the rise time, the resultant pulse amplitude will be smaller than that of the impressed

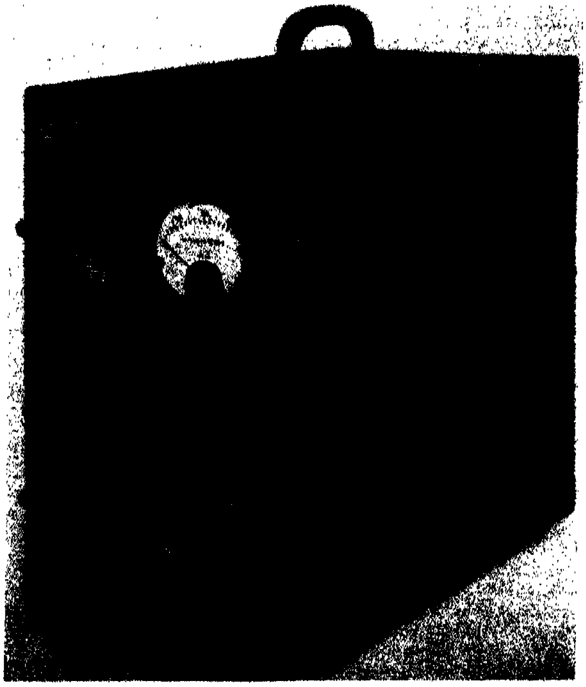

wave; when the delay of the line is equal to the build-up time of the pulse, the VTVM reading will have reached a maximum. Thus the calibrated line is a measure of the rise time and may be used to plot the leading edge. The instrument is also applicable to conditions requiring a shorted variable delay line which will fall into the steps and frequency (*Zo*=50 ohms, *Wc*=160 mc) of this model. An example—a stub tuner.

Specifications: Rise time —0.005 μsec. to 0.1 μsec. in 20 steps. Pulse repetition rate and allowable source impedance—from 30 to 100 ohms, up to 1 mc—from 100 to 200 ohms, up to 0.25 mc—from 200 to 300 ohms, up to 100 kc; voltage sensitivity—positive peak pulses from 1 to 200 volts; accuracy—a maximum error of ±0.005 μsec; weight and dimensions—under 75 lb.—16×12×7 in.; 110 volts—60 cycles 60 watts.

The controls include an on-off switch, zero set and sensitivity selector, speed and direction controls for varying the length of line, and an indicator denoting delay of line.

The 632-B thus features a radical change in the method of analyzing the build-up time of a pulse. However, the most important factor is the range available: 0.005 to 0.1 μsec. in 20 steps. Unaffected by time or voltage jitter, the instrument removes the approximate results obtained from expensive instruments and time consuming set-ups, by giving accurate results in a matter of seconds. Available in other ranges upon request.—ELECTRONIC SYSTEMS COMPANY, *555 East Tremont Avenue, New York 57, New York.*

VHF Signal Generator The Model 608A VHF signal generator (10 to 500 mc) has a master oscillator power amplifier circuit and a directly calibrated output from 0.1 μv to 1.0 v for measuring gain, selectivity, sensitivity or image rejection of receivers, i.f. amplifiers, broad-band amplifiers or other VHF equipment. The 1-v output (into a 50-ohm load) is useful over the entire frequency range for driving bridges, slotted lines, antennas, filter networks, etc. The output circuit is directly calibrated in volts and decibels for fast reading. No charts are necessary.

On this new instrument, frequencies from 10 to 500 mc are covered in five bands, calibrated directly in megacycles on a drum-type dial having effective scale length of 90 in. A single-dial, ball-bearing frequency control insures maximum convenience and accuracy in tuning and resetting. The instrument also offers microsecond pulses, wide modulation capabilities, small residual f-m, and has CW, a-m, or pulsed output.

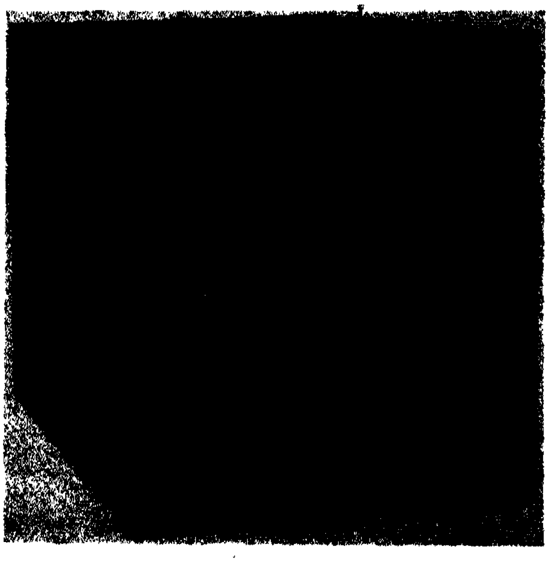

The master oscillator and power amplifier circuits are enclosed in a heavy cast aluminum shield, insuring high stability and minimum electrical leakage. The instrument will sell for $850.00.

A new impedance-measuring VHF bridge, Model 803A (50 to 500 mc) and its companion instrument, the Model 417A VHF detector, are additional components of this line of precision VHF equipment. The bridge determines impedance by sampling the magnetic and electric fields of a transmission line. Phase is measured by determining the point of cancellation of these samples along a second transmission line. This method effectively overcomes the narrow frequency limitations of conventional bridge configurations.

This new instrument offers direct impedance readings from 2 to 2000 ohms. Its primary frequency range is 50 to 500 mc, but it is useful at frequencies up to 1000 mc and down to 5 mc. It can be used for any type of VHF impedance measurement, determining characteristics of transmission lines, antennas, r-f chokes and condensers, connector impedances, standing wave ratios, percentage of reflected power, VHF system flatness, etc. The bridge is priced at $495.00.

The detector is essentially a super-regenerative a-m receiver covering all frequencies between 10 and 500 mc. It offers high sensitivity, quick easy operation, and the customary -hp- direct-reading frequency control. It is thoroughly shielded and suitable for general laboratory work including approximate frequency checks, noise and interference measurement, etc. The detector will sell for $200.00.—HEWLETT-PACKARD COMPANY, *395 Page Mill Road, Palo Alto, California.*

Manufacturers' Literature

Millivolt Meter—Technical Report TR-21, 8 pp., describes instrument for high impedance measurements above 5 mc. Crystal rectifiers are used as "pseudo-thermocouples," combined with a high impedance vacuum tube millivoltmeter for d.c., to make measurements at lower levels than possible with ordinary heater-type thermocouples.—MILLIVAC INSTRUMENTS, *P. O. Box 3027, New Haven, Connecticut.*

Electric Instruments—A new, revised edition of General Electric's "Manual of Electric Instruments" (GET-1087A) describes the fundamentals of construction and operating principles of all major types of electric instruments. Manual is 150 pp., extensively illustrated by photographs and diagrams, and includes a full reference index. Priced at $1.00 per copy.—GENERAL ELECTRIC COMPANY, *Schenectady 5, New York.*

Phototransistor—Press release dated March 30, 1950, announces an entirely new type of "electric eye"—much smaller and sturdier than present photoelectric cells. The sensitive element is a germanium disk with a dimple ground into one side, and the entire apparatus is housed in a tiny cylinder about as large as a .22 caliber rifle cartridge.—BELL TELEPHONE LABORATORIES, *463 West Street, New York 14, New York.*

Spectro Computer—Bulletin 278 describes the Phillips 66 spectro computer, which solves simultaneous linear equations of the type encountered in infra-red and mass spectrometry. This computer, which makes use of d.c. potentials substituted for the unknowns in the equations, solves these equations by a method of iteration. Multiplication, division, addition, and subtraction steps necessary in solving as many as ten simultaneous equations can normally be performed by the computer within 5 to 30 min. Results of spectrographic analysis of hydrocarbon samples have been computed to an accuracy of 0.1 percent with this instrument.—PHILLIPS PETROLEUM COMPANY, SPECIAL PRODUCTS DIVISION, *Bartlesville, Oklahoma.*

Pulp Density Scales—Bulletins S1C-B and S1C-B1 include the Denver pulp density scales, for speed and accuracy in determination of specific gravity of pulps and liquids in routine mill-control work. S1C-B is for specific gravities 1.4 to 3.2, and S1C-B1 is for specific gravities 1.35 to 1.85. Scales can be used wherever metallurgical results are dependent upon water-to-solids relationship in mill pulps, such as: Ball mill discharge, classifier overflow, thickener discharge, condition discharge and agitator circuit. Also included are pulp density formulas and tables.—DENVER EQUIPMENT COMPANY, *1400 Seventeenth Street, Denver 17, Colorado.*

Water Demineralizer—Catalog No. 123 describes in detail the difference between distilled and demineralized water. This 20-p. catalog highlights the advantages of either distilled water or demineralized water as used in manufacturing and processing operations which call for pure water.—BARNSTEAD STILL AND STERILIZER COMPANY, INC., *2 Lanesville Terrace, Forest Hills, Boston 31, Massachusetts.*

Instrument News—Vol. 1, No. 2, 8 pp., features articles on a mobile infra-red spectrometer, mass analyses of plant tissues and soils by means of a flame photometer, the use of electrophoresis apparatus in clinical diagnoses, and includes other items of general interest.—THE PERKIN-ELMER CORPORATION, GLENBROOK, CONNECTICUT.

Experimenter—Vol. XXIV, No. 10, features the Type 1021-A standard-signal generator for frequencies between 50 and 920 mc and also includes description of the Type 100-P6 amplitude modulator for video frequencies. Specifications included.—GENERAL RADIO COMPANY, *275 Massachusetts Avenue, Cambridge 39, Massachusetts.*

Hastings Indicator—March, 1950 issue describes briefly two new Raydist two-dimensional hyperbolic systems constructed for the U. S. Naval Ordnance Laboratory and the U. S. Navy Bureau of Aeronautics, a vacuum gauge, and a miniature temperature compensated non-directional pick-up and contains other items of interest.—HASTINGS INSTRUMENT COMPANY, INC., *Box 1275, Hampton, Virginia.*

Modern Precision—Winter 1949–1950 issue of tabloid-size review of industrial use of Leeds and Northrup control and recording instruments.—LEEDS AND NORTHRUP COMPANY, *4902 Stenton Avenue, Philadelphia 44, Pennsylvania.*

Mercury Manometer Flowmeters—Catalog 37, 12 pp., illustrates and describes the new mercury manometer flowmeters. These flowmeters require no pressure-tight bearings or stuffing boxes; they use the Fischer and Porter magnetic clutch, or the impedance bridge electric transmitter.—FISCHER AND PORTER COMPANY, *Hatboro, Pennsylvania.*

Ratosleeve Flowmeters—Catalog 83, 12 pp., describes and illustrates Ratosleeve meters, suitable for liquids, gases, pulps and slurries.—FISCHER AND PORTER COMPANY, *Hatboro, Pennsylvania.*

CEC Recordings—Vol. 4, No. 1, 12 pp., features the Telereader, which speeds reading of oscillographic records, and includes articles on vibration measuring and recording without amplifiers, studies of ferromagnetic materials, new torsiograph now in production, recording galvanometers, control analysis of methyl mercaptan, and other items of interest.—CONSOLIDATED ENGINEERING CORPORATION, *620 North Lake Avenue, Pasadena 4, California.*

Laboratory Microscopes—Catalog D-185 presents the company's line of laboratory microscopes. Photographs and prices included.—BAUSCH AND LOMB OPTICAL COMPANY, *Rochester 2, New York.*

Kelefax—Vol. 1, No. 1, the first issue of a new bimonthly publication of interest to personnel engaged in radiation and industrial instrumentation, nuclear science and technology. Included in the first issue are useful reference data and tables for working with radiation or radioactivity, information about the complete line of Keleket instruments, equipment and components, announcements of new Keleket products, and other articles of interest.—THE KELLEY-KOETT INSTRUMENT DIVISION, *12 East Sixth Street, Covington, Kentucky.*

Testing Machine—Bulletin 305, 4 pp., gives full details on the Baldwin-Tate-Emery testing machine, having ranges from 0-2 lb. full scale to 5000 lb. capacity. This bulletin illustrates the loading system internally as well as externally, giving an explanation of operation, details on ranges, accuracy, new features, specifications and accessories.—THE BALDWIN LOCOMOTIVE WORKS, TESTING EQUIPMENT DEPARTMENT, *Philadelphia 42, Pennsylvania.*

Hydraulic Weighing Systems—Bulletin 303, 20 pp., dedescribes and illustrates new Baldwin portable hydraulic weighing system components for various applications. Also covered are hydraulic lifting jacks and hand pumps for use with compression-type load cells.—THE BALDWIN LOCOMOTIVE WORKS, TESTING EQUIPMENT DEPARTMENT, *Philadelphia 42, Pennsylvania.*

Coil Checker—Bulletin 19-B provides complete technical data on the new Model 301A coil checker, consisting of a vacuum tube voltmeter, a calibrated variable capacitor and an amplifier tube. When coupled with any r-f oscillator, the 301A measures inductance, distributed capacity, and the "*Q*" of any inductor, as well as the capacity of mica condensers.—CLOUGH BRENGLE COMPANY, *6014 Broadway, Chicago 40, Illinois.*

Radiation Instruments—Information Bulletin No. 9 presents the company's line of radiation instruments.—RADIATION COUNTER LABORATORIES, INC., *Chicago 8, Illinois.*

New Materials

Forest K. Harris: Associate Editor
in Charge of this Section
National Bureau of Standards, Washington, D. C.

Nickel-Clad Copper

Kulgrid, heat-resistant nickel-clad copper wire which combines the electrical conductivity of copper with the corrosion-resistant properties of nickel, is being made in diameters from 5 to 10 mils. These sizes are adapted both for stranding and for lead wire applications where the high temperature working of hard glass frequently renders solid copper wire brittle. Stranded conductors of nickel-clad copper may also be suitable as electrical leads in aircraft, for electric furnaces, jet engines, and a wide range of laboratory and industrial equipment where high temperature or corrosive atmospheres tend to make solid copper conductors brittle and unreliable. A practically uniform ratio of nickel to copper (27 to 29 percent nickel) is maintained throughout the drawing operations and perfect bonding of nickel to copper is obtained. Good workability and electrical characteristics are assured through heat treating or annealing at frequent intervals and after the final draw.—Sylvania Electric Products, Inc., Parts Division, *Warren, Pennsylvania.*

Rolled Gold Plate

Rolled gold plate having a highly finished gold layer more than 10 times as thick as the average gold electroplate is now commercially available at relatively low cost. In the *Inter-Weld Process* used for this purpose a bar of gold is welded to a barrier layer of pure nickel. This dual layer is then silver-soldered to a metal base. The interposition of the nickel layer prevents diffusion of the silver solder to the surface of the gold. The surface texture is further enhanced by the use of a special lapping process applied to the rolls of the mill in which the material is reduced to its final thickness. The rolls are highly polished and their variations are less than 1 microinch. The finish imparted to the plate is protected by a thin plastic coating (less than 0.0005 in. in thickness) which remains in place during blanking and forming operations on the material, but which can easily be removed by stripping at any time. This virtually eliminates the expensive finishing and polishing operations required when gold-electroplated brass is used. Rolled gold plate, having a mirror finish protected by "Filmcote," is available in any ratio of gold to base metal on a variety of base metals such as brass, copper, nickel, nickel silver, beryllium copper, etc. It is made in thicknesses down to 0.005 in. and in widths from ¼ to 4½ in.—American Silver Company, Inc., *Rolled Plate Division, Flushing, New York.*

Interlocking Lead Bricks

Model 3039 interlocking lead bricks, for background shielding, are designed to eliminate the low density "joint space" between ordinary rectangular bricks. The interlocking sections are so designed that a completely dense wall may be obtained by fitting suitably shaped bricks together. Provision is made for corners and similar construction. Standard 4×4×2-in. wall bricks can be assembled with two types of corner bricks, and a triangular filler is available to eliminate the low density area at the bottom of the structure. Complete information and construction suggestions are available from the maker.—Nuclear Instrument and Chemical Corporation, *223 West Erie Street, Chicago 10, Illinois.*

Nuclear Track Emulsions

Two new photographic emulsions for recording nuclear tracks have been developed by Eastman, extending the range of special plates and films available for scientific use.

Kodak Type *NTB2* is intermediate in speed between nuclear plate Types *NTB* and *NTB3*, and is especially useful where stray radiation may produce undesirable background with faster emulsions. Electron tracks to 400 kv have been observed on this emulsion, which will be available in both plate and pellicle form. The second new emulsion, Type *NTC3*, is designed to record low energy alpha-particles and low energy protons to 7 Mev. It is recommended for cyclotrons and synchrotrons where background radiation is of high intensity.

Two additional emulsions, Types *NTB* and *NTA*, are now available in pellicle form along with Types *NTB2* and 3. These pellicles permit an emulsion thickness of approximately 250 microns without the problems of uneven development which may be encountered when emulsions of this thickness are coated on glass.—Eastman Kodak Company, *Rochester 4, New York.*

"Teflon" Tape

"*Teflon*" (tetrafluoroethylene) tape is characterized by heat resistance, toughness over a wide temperature range, excellent electrical properties and chemical inertness. It is capable of continuous service without deterioration at 250–270°C and is therefore suitable for use as Class *H* insulation (180°C hot-spot temperature), and maintains its flexibility to temperatures below −70°C. It is strong, smooth, and conforms well to sharp corners. Furthermore it has "plastic memory" and tends to return to its original shape when heated. Thus the tape tends to recover the stretching caused by the wrapping operation, so that it becomes tighter as the temperature rises. Its power is less than 0.05 percent from 60 cycles to 30,000 Mc; its volume resistivity is greater than 10^{15} ohm-cm after prolonged soaking in water; and its surface resistivity is greater than 10^{13} ohms even at 100 percent relative humidity. Short-time dielectric strengths range between 1000 and 2000 volts/mil at room temperature and are almost as high at 200°C. (The maker recommends working stresses between 50 and 100 volts/mil.) *It is not recommended for use in the presence of corona*, which degrades it slightly. It is attacked only by molten alkali metals, and by fluorine and chlorine-trifluoride at elevated temperatures and pressures. Outdoor weathering has no observable effect.—E. I. du Pont de Nemours and Company, *350 Fifth Avenue, New York, New York.*

Teflon Rods and Tubes

Teflon is now being processed into machinable rods and tubing. It may be used in the electrical and electronic fields as high frequency insulation, and in other applications where complete inertness, resistance to high temperatures, and non-sticking qualities are indicated. Information should be obtained from the maker concerning sizes of rods and tubing that are now in commercial production.—The Polymer Corporation, *Reading, Pennsylvania.*

Silicone Rubber

Two new silicone rubber compounds, *GE#13011* and *GE-#13012*, have been developed for special applications, and are designed for use at extreme temperatures for shock mounts, light spring-loaded gaskets, damping devices and related uses where conventional or silicone sponge-rubber parts either deteriorate or collapse from "compression set."—General Electric Company, *Pittsfield, Massachusetts.*

Vacuum Pump Fluid

Narcoil-20 diffusion pump fluid (di-2-ethylhexyl sebacate) especially treated for high vacuum use is now available in quantity. This ester is capable of attaining as low or lower pressures than any other pump fluid. It is recommended for use in any diffusion pump for service in which pressures less than 0.1 micron are required. It is available in pint, quart, and gallon containers.—National Research Corporation, *70 Memorial Drive, Cambridge, Massachusetts.*

Glass Orifice Plates

While the advantages of dimensional stability and corrosion resistance of glass orifices have long been recognized, use has been limited because of the high cost of production to required standards. By employing a new technique, Pyrex-glass orifice plates can be made economically to extremely close tolerances with sharp square edges maintained where required. Both inside and outside dimensions are ground on a diamond wheel. Glass orifice plates are available in various thicknesses from ¼ in. up, and in sizes up to 16 in. O.D. Further information is available from the maker.—Precision Thermometer and Instrument Company, *1535 Brandywine Street, Philadelphia 30, Pennsylvania.*

THE
REVIEW OF SCIENTIFIC
INSTRUMENTS

VOLUME 21, NUMBER 6 JUNE, 1950

A Vacuum Furnace for Use in the Temperature Range 1000–2000°C

J. W. TOMLINSON* AND J. O'M. BOCKRIS
Department of Inorganic and Physical Chemistry, Imperial College of Science and Technology, London, England

(Received February 27, 1950)

A laboratory vacuum furnace with a glass envelope has been developed, using as a heater a cylindrical grid of tungsten wire enclosed by radiation shields.

The furnace is suitable for physicochemical measurements in the range 1000–2000°C.

INTRODUCTION

A SURVEY of the literature revealed the absence of a record of a vacuum furnace for use in the range 1000–2000°C, suitable for physicochemical measurements, those vacuum furnaces described being of complex design and generally unsuitable for quantitative experiments. A suitable furnace was therefore constructed, the details of which are recorded in this paper.

GENERAL CONSTRUCTION

The envelope and all glass parts are of Pyrex glass; the dimensions shown in Fig. 1 being most suitable, the joints are of standard sizes. The window *A* is of 2 mm optically flat Pyrex glass and is situated at the end of tube *B* to avoid darkening due to condensation of evaporated metal. Connection to the pumping system, which should have a speed of 10–20 liters/sec. at 10^{-4} mm Hg, is via the B29 standard joint at *C*. All joints and the flanges at *D*, are greased with Dow Corning silicone high vacuum grease which retains its viscosity and stability up to 200°C.

The main functional parts of the furnace, shown in Fig. 2, are suspended from tungsten rods which are sealed into joints which fit into joints sealed to the upper flange; from the rods *E* the heater is suspended, and from the rods *F* the crucible, which in the present case is of molybdenum, but which could be fabricated from any desired material. The heater is in the form of a cylinder of twelve 4 cm loops of 0.5 mm diameter tungsten wire, supported by hooks suspended from a silica ring attached to the two rods *G*; this method of support eliminates sagging at high temperatures. The ends of the heater wire are welded into the two molybdenum rods *H*, the length being such that the heater is in the center of the radiation shields *I*. The size and length of wire used are chosen to correspond to the power available and in operation 35 amp. at 40 v were required to maintain a temperature of 2000°C for a heater of the dimensions given; thicker wire might be used with advantage to reduce the applied voltage, thus avoiding the gaseous discharge which occasionally occurred with the present apparatus at low vacuum. The crucible *J* is suspended from molybdenum rods *K* sealed into joints fitting into the flange diametrically opposite to those supporting the heater; contact between heater and crucible and heater and radiation shields must be avoided by accurate centering of these parts relative to each other.

The cylindrical radiation shields *I* are of 0.2-mm molybdenum sheet and are 12 cm in length and have diameters differing by 0.5 cm; the assembly is secured on molybdenum rods and spacers *L*, into which are slotted tungsten rods *M*, these resting in side arms *N* off the main envelope. The function of this type of shield as radiation reflectors is well known and has recently been treated mathematically,[1] indicating an optimum number of four or five.

The furnace is run at a pressure of approximately 10^{-3}–10^{-4} mm Hg after an initial period of outgassing at 10^{-6} mm Hg. Deposition of metal from the heater on the wall of the envelope occurs and is due to evaporation and possibly attack by gases given off from the hot glass; the deposit may be periodically removed and

---

* Now at Massachusetts Institute of Technology, Cambridge, Massachusetts.

[1] A. W. Lawson and R. Fano, Rev. Sci. Inst. 18, 727 (1947); A. E. De Barr, Rev. Sci. Inst. 19, 569 and 574 (1948).

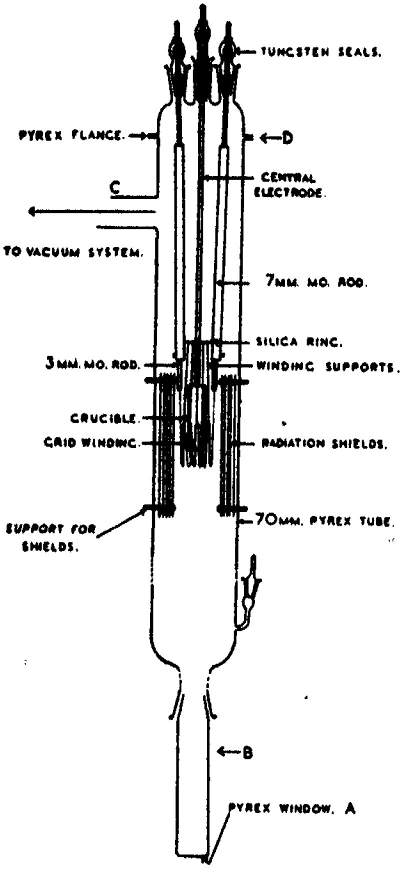

FIG. 1.

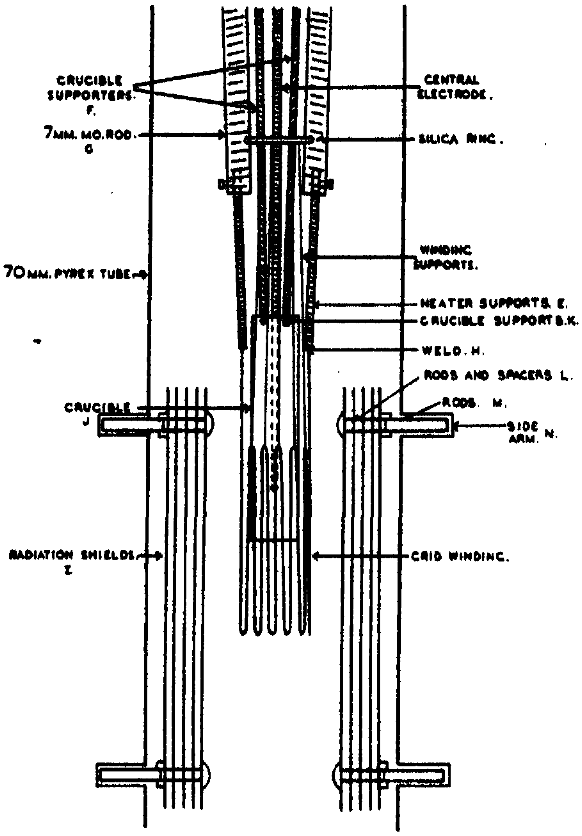

FIG. 2.

constitutes no disadvantage in operation. All metals other than molybdenum and tungsten are rigidly excluded in construction.

TEMPERATURE MEASUREMENT

The temperature is measured by optical pyrometer sighted through the window *A* onto the crucible bottom, and, as the estimation of the blackbody conditions would be extremely difficult, the pyrometer is calibrated over the range up to 1700°C to determine these conditions. Comparison readings are taken against a *Pt/Pt-Rh* thermocouple suspended inside the crucible the leads being sealed through joints in the upper flange. By means of a magnetic device, which enabled the couple to be moved inside the crucible relative to the bottom, the temperature constancy was found to be within 10° over a distance of 1.5 cm.

ADVANTAGES OF THE FURNACE

(i) Ease and rapidity of reaching temperatures of the order of 2000°C. (15 min. or less is sufficient time to reach 2000°C.) (ii) Neutral atmosphere and vacuum. (iii) Possibility of rapid cooling, i.e., quenching. (iv). Higher temperatures attainable; there is no reason why, by the addition of top and bottom shields, etc., the range should not be increased to temperatures of the order of 2500°C. (v) Ease of construction, low cost and ease of replacement of winding. (vi) Possibility of micro-work because of small size.

USES

The furnace was used by the authors for the measurement of electrical conductivities of liquid silicates using a central electrode. The potential uses of the apparatus are many and include investigation of phase equilibria, chemical reactions at high temperatures, solid phase reactions, melting point measurements, high temperature sintering and general measurement of properties at high temperatures.

THE REVIEW OF SCIENTIFIC INSTRUMENTS VOLUME 21, NUMBER 6 JUNE, 1950

A High Intensity Ultraviolet Continuum Source for Use in Spectrophotometry

NISSON ASCHER FINKELSTEIN
Massachusetts Institute of Technology, Cambridge, Massachusetts

(Received November 8, 1949)

A high intensity ultraviolet continuous spectrum d.c. source emitting between 50 and 100 times as much light as comparable commercial sources has been designed and constructed. Transitions between two molecular energy states of hydrogen are induced to produce a continuum from 1850A to 6000A. The arc is run at approximately 14 amperes and 90 volts from a 220-volt d.c. line. A hydrogen pressure of 3 mm of mercury is used. Lifetimes greater than 40 hours have been obtained.

INTRODUCTION

FOR the performance of experiments in ultraviolet reflection spectrophotometry it was found necessary to design a continuous spectrum source emitting radiation through a large solid angle and having a greater intensity than any lamp commercially available. Three possibilities for a continuous spectrum in the ultraviolet are the molecular spectrum of hydrogen, the helium continuum, and the hydrogen atomic Lyman continuum. The helium continuum is above 3000 angstroms and the Lyman continuum below 2000 angstroms. Only the molecular spectrum of hydrogen is in the 2000 to 4000 angstrom ultraviolet region desired. The fact that this spectrum extends up to almost 6000 angstroms facilitates a check with reflection spectrophotometry previously accomplished in the visible.[1]

The source designed is an extension of the work of Munche[2] and Allen,[3, 4] and was constructed with the assistance of Mr. H. Wyckoff of the Massachusetts Institute of Technology Biology Department.

THEORY OF OPERATION

The ultraviolet continuous spectrum of molecular hydrogen[5, 6] results from transitions from a stable upper state to an unstable lower state[*] which immediately dissociates into two unexcited hydrogen atoms with accompanying emission of radiation, any excess energy available being converted into kinetic energy of the dissociated atoms. The initial upper state must be excited by a potential which is a function of the frequency of radiation emitted. The minimum potential for excitation is given by various investigators[5, 6] as lying between 11.6 volts and 12.7 volts. The observed continuum extends from about 6000 angstroms down to the Schumann region (1850 angstroms) with a maximum at about 2500 angstroms. Superposed upon the continuum are the lines of the Balmer series due to atomic excitation in this region. When the source is used with a spectrophotometer having a slit width of about 20 angstroms, the line intensities integrated over this 20-angstrom band produce a signal less than three times as great as that produced by the continuum. No lines are present in the 2000-angstrom to 3700-angstrom region.

DESIGN AND CONSTRUCTION

Figure 1 shows a simplified cross-sectional view of the electrode arrangement inside the source. The discharge passes from the cathode *F* through the localizing orifice *C* to the anode *A*. It is viewed along the axis through a rectangular slit, 3 mm×6 mm, in the anode. The voltage required to start the arc is 220 volts d.c. The operating cathode-anode potential difference is between 80 and 120 volts, depending on what arc current is being drawn. A Tesla high voltage coil is applied to the starting ring, *E*, to facilitate striking the arc.

The cathode, *F*, is constructed of a 1½-in.×14-in. piece of nickel screening folded twice on the long dimension to form a strip ½ in.×14 in. This strip is then folded accordian-wise to assume the shape shown in Fig. 2.

Finally, the cathode is sprayed with a barium strontium carbonate solution to give high electron emission when the cathode is heated by passing an a.c. current through it. The resistance of the cathode at a temperature of 900°K is about 0.1 ohms. The two ends of the cathode are mounted on nickel rods which are brought

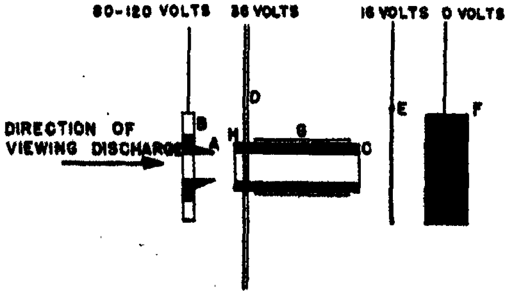

FIG. 1. Simplified cross-sectional view of electrode arrangement inside the hydrogen arc source. Typical operating potentials are shown.

---

[1] A. C. Hardy, J. Opt. Soc. Am. 25, 305 (1935).

[2] R. H. Munche, J. Am. Chem. Soc. 57, 1863 (1935).

[3] A. J. Allen and R. G. Franklin, J. Opt. Soc. Am. 29, 453 (1941).

[4] A. J. Allen, J. Opt. Soc. Am. 31, 268 (1941).

[5] J. G. Winans and E. C. G. Steuckelberg, Proc. Nat. Acad. Sci. 14, 867 (1928).

[6] D. Chalonge, Ann. de physique 123 (1934).

[*] It has thus far not been possible to determine experimentally exactly which pair of molecular levels it is between which transitions are induced to produce the continuum; but a typical pair between which suitable transitions might take place is the upper stable $1s\sigma 2s\sigma\,^3\Sigma_g$ and the lower unstable $1s\sigma 2p\sigma\,^3\Sigma_u$.

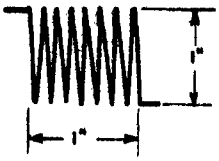

FIG. 2. Nickel screen cathode as seen from direction of anode.

out through the top of the brass can enclosing the electrode system by means of Kovar-glass seals which maintain electrical insulation of the rods from the can. The a.c. source of cathode heating power is applied to these two rods.

The starting ring, *E*, is a 30-mil molybdenum wire bent in a 1½-in. diameter circle and brought out through the can top by a Kovar-glass seal.

The localizing orifice, *C*, is a ½-in. diameter molybdenum rod ¾ in. long through which an axial rectangular slit 4 mm×7 mm has been machined. The arc is forced to pass through this long slit passage, since a 60-mil sheet of molybdenum, *D*, prevents it from passing around the orifice to the anode. The shield is held on to the orifice by a molybdenum nut, *H*, which threads on to the orifice.

The anode, *A*, is made of molybdenum and has a slit 3 mm×6 mm through it, also lined up with the localizing orifice. The orifice slit is machined 1 mm larger in each dimension to make allowance for the arc's "pulling away" from the sides of the orifice as it passes through.

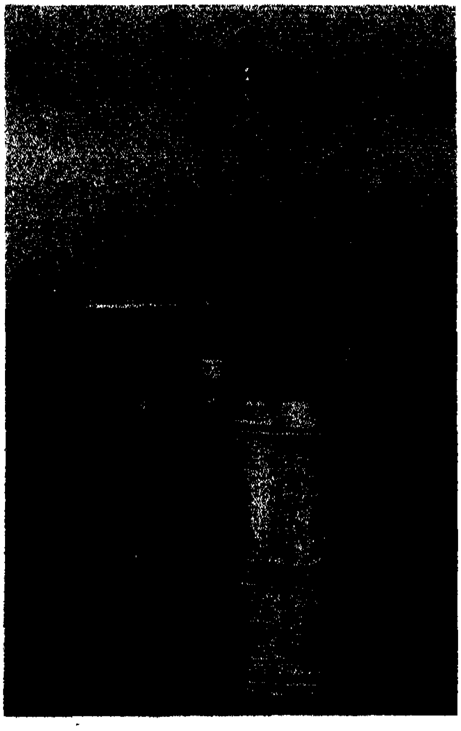

FIG. 3. Ultraviolet source ready for use. 1. Cathode terminals, 2. starting ring terminals, 3. anode terminal, 4. outlet to pump, 5. water cooling tubing, 6. beam port, 7. observation port.

Because of the high current density of the arc, molybdenum was chosen as an electrode material because of its high melting point, 2620°C. It was found necessary, however, to water-cool the anode and orifice to prevent evaporation of molybdenum into the arc and subsequent appearance of molybdenum lines in the spectrum. Since it is not possible to solder to molybdenum or to make any simple welded connection, the anode was set into a copper plate, *B*, to which it was tightly screwed for good thermal contact. In the case of the molybdenum orifice tube, a copper jacket, *G*, was thermally shrink-fitted about the tube by machining the jacket undersized 1½ mil in diameter and heating it while cooling the molybdenum. In this manner a quite satisfactory thermal contact was gained. Copper tubing, $\frac{3}{16}$ in. in diameter, was silver soldered to the anode copper plate and about the orifice copper jacket; this tubing was brought out through the top of the can and water passed through to provide cooling. The copper tubing soldered to the anode plate was brought out through Kovar-glass seals for electrical insulation and the positive d.c. anode potential was applied to this tubing. The tubing also serves to support the anode in position in the can. Since the localizing orifice is hung from the can, the two are at the same potential and the orifice water cooling tubing is not brought out through Kovar-glass seals but through holes in the can cover sealed with silver-solder.

The electrode system is contained in an all brass can with two quartz window ports 1 in. in diameter, one for viewing the discharge and the other for checking operation of the tube. This latter observation port is mounted in such a manner that the cathode, starting ring, and cathode side of the localizing orifice are visible. The brass can and cover are water cooled by means of copper tubing silver soldered on for good thermal contact. The quartz windows are sealed to the ports and the cover to the can with deKhotinsky wax cement. Figure 3 is a picture of the source ready for use.

AUXILIARY EQUIPMENT

The d.c. power for operation of the arc is drawn from a 220-volt d.c. line and the arc current is adjusted by switching 9 Calrod 6-ohm resistors into different series-parallel combinations to vary the resistance in series with the source.

The cathode is heated by an alternating current of approximately 50 amperes to a color temperature of about 850°C as estimated with an optical pyrometer, this being the temperature necessary for satisfactory electron emission. The power is shut off immediately after the arc is struck in order to save excessive wear and tear on the cathode and to prevent 60-cycle oscillations in the light source.

In order to strike the arc an electrostatic field must be passed through the orifice from the cathode to the anode. This is difficult because of the narrowness of the orifice passage, and it is found necessary to touch a high voltage Tesla coil to the starting ring to cause the arc to jump first to the ring and then through the orifice to the anode. If difficulty is experienced in starting the arc the cathode current is increased to provide more electron emission and hence higher ionization.

It is found that the source is quite pressure sensitive with respect to ease of starting. While it can be started immediately at hydrogen pressures of from 2.5 to 3.5 mm of mercury, higher and higher anode-cathode voltages are necessary when pressures above this are existent. As a result of the absorption and emission of hydrogen gas by the brass container and the various electrodes during the processes of cooling and heating it is found most convenient to provide a means of adjusting the hydrogen pressure within the source. A palladium leak hydrogen input is used in conjunction with a fore pump to adjust the pressure, and the pressure is measured with an oil manometer.

PERFORMANCE CHARACTERISTICS

The lamp operates with arc currents between 10 and 20 amperes at arc voltage drops of between 125 and 75 volts.

The radiation emitted originates at the positive column of the discharge situated along the length of the localizing orifice. The angle through which radiation is emitted is such as to fill an $f/4.3$ system in the horizontal plane and an $f/2.2$ system in the vertical plane. In comparison with commercially available sources of this type which fill an $f/35$ system, this source emits radiation through 64 times as great a solid angle.

For operation at arc currents of 14 amperes cathode lifetimes of more than 40 hours have been obtained thus far.

THE REVIEW OF SCIENTIFIC INSTRUMENTS VOLUME 21, NUMBER 6 JUNE, 1950

A Rotary McLeod Gauge*

M. Axelbank**
Distillation Products, Inc., Rochester, New York

(Received November 15, 1949)

The use of the sensitive McLeod gauge is limited by its fragility, bulk, and lack of portability. A new type of McLeod gauge is described which greatly reduces these difficulties. A helix of several turns of glass tubing provides the volume through which the gas is compressed by a small quantity of mercury as the gauge is rotated upon its rotary seal. A model has been constructed which is 16×16×21 cm in over-all dimensions and weighs less than 1 kg. Its gauge constant with a 0.8 mm capillary is 1.4×10^{-6} mm^{-1}.

McLEOD gauges of high sensitivity, intended for accurate measurement of pressures below 10^{-3} mm of Hg, are characteristically non-portable, fragile, cumbersome to operate, and subject to accident. The rotary or swivel form of McLeod gauge[1,2] has provided a satisfactory solution of these problems for measurement in the higher pressure ranges. However, the ordinary rotary type of gauge is not practical for the lower ranges because of the large weight of mercury required.

Among the gauges capable of higher sensitivity, the leveling bulb McLeod[3] is widely used in laboratories because of its simple construction, but it is not portable and is subject to contamination of the mercury by the rubber connecting tube. The original McLeod gauge[4] was of this form. Plunger type gauges[5] are more convenient to operate but are not portable and are subject to accidents in which mercury is thrown into the system

Fig. 1. Front view of the rotary McLeod gauge.

---

* Communication No. 140 from the Laboratories of Distillation Products, Inc.,

** Now attending the University of Paris, Paris, France.

[1] S. Dushman, *Scientific Foundations of Vacuum Technique* (John Wiley and Sons, Inc., New York, 1949), p. 272.

[2] E. W. Flosdorf, Ind. Eng. Chem., Anal. Ed. 10, 534 (1938); 17, 198 (1945).

[3] See reference 1, p. 265.

[4] Phil. Mag. 48, 110 (1874).

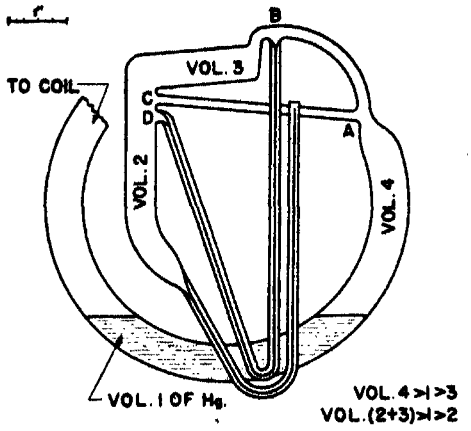

FIG. 2. The "head" of the gauge.

or back out of the reservoir into the room. The short form of McLeod gauge, in which the mercury is raised by atmospheric pressure and lowered with a mechanical pump, has been utilized to provide the greatest sensitivities yet achieved with McLeod gauges. However, if a model is desired which will indicate pressures much below 10^{-5} mm of Hg[5,6] the weight of mercury required exceeds 50 lb. and large cast supports must be built for the bulbs. Such a gauge with its associated mechanical pump is expensive, non-portable, and easily broken by mercury surges.

It is the purpose of this article to describe a gauge developed by the author which obviates many of the difficulties which have previously limited the use of the sensitive McLeod gauge to the laboratory. The gauge is constructed entirely of glass except for the rotary "O" ring vacuum seal (see Fig. 1). For purposes of analysis it may be divided into three sections—the "head" (Fig. 2) which contains the open and closed capillaries, the coil or helix, and the end section (Fig. 3) comprising the reservoir, cut-off, and rotary seal.

In the rest position of the gauge the pool of mercury lies in the lower part of the first turn of the helix which forms the reservoir. Only 300 g of mercury are required for the gauge illustrated. The gauge is free to turn about the rotary seal which is rigidly clamped to a support or to the vacuum system. The fixed part of the rotary seal may be attached to a glass system with a glass-to-metal seal, or soldered directly to a metal system. In the case of a rigid metal system no further support is necessary.

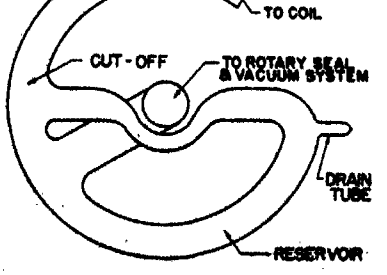

FIG. 3. The end section.

The operation of the gauge proceeds as follows. As the mercury leaves the reservoir and enters the coil, it cuts off the gas in the coil and head from the system. Proceeding through the turns, it compresses the gas into the head. When it reaches point A (see Fig. 2) it flows into the spillway (AC) as well as toward point B. At B it cuts off the upper end of the reference capillary. It then fills volume 3 and cuts off the upper end of the spillway at point C before opening the lower end, since volume 1 is greater than volume 3. When point D is reached, the lower end of the reference capillary is cut off and a certain volume of gas is trapped in the capillary at the pressure existing in the head at this moment. With further rotation the upper end of the reference capillary is opened and the trapped air released to the system. A simple development from Boyle's law shows that this loss of gas does not appreciably affect the final reading. The error is approximately equal to the ratio between the volume of the open capillary and volume 2, which is negligibly small. As the volume (2+3) is greater than volume 1, and most of volume (2+3) is substantially below the reference capillary at this moment, then all of the mercury which entered the capillary flows out at point B into volume 3. When the capillaries are brought to a vertical position, the gas is compressed into the closed capillary and the excess mercury drains through the spillway, leaving the reference column approximately at "zero" level. The gauge is rotated slightly beyond the vertical position, so that when it is returned the mercury in the open capillary is at the proper level. With a little practice this may be done quickly and easily. The pressure is then read directly from a square law scale mounted behind the capillary tubes.

The gauge is reset by counterclockwise rotation. All the mercury drains from the head, as volume 4 is greater than volume 1. If this were not the case, an extra revolution would be required in resetting. The design of the reservoir section makes it impossible for any mercury to escape into the system.

The gauge described is approximately 16×21×21 cm in over-all dimensions. It gives a gauge constant, $C=1.4\times10^{-6}$ mm^{-1}, where $C=\pi r^2/V$ with r, the radius of the capillary, equal to 0.4 mm and V, the volume of the gauge beyond the cut-off point, equal to 3.6×10^5 mm^3. The volume V may be easily measured as follows. In constructing the gauge a drain tube is provided on the reservoir in the position shown in Fig. 3. Initially this tube is open and the end is fire polished. The required amount of mercury is inserted in the reservoir, and with the axis horizontal the gauge is rotated until the mercury level reaches the cut-off point. A line is then drawn around the outside of the glass at the level

---

[5] See reference 1, p. 269.
[6] Rev. Sci. Inst. 10, 131 (1939).

of the mercury with a "glass marking" pencil or crayon. The mercury is poured out through the drain tube and the gauge weighed to the nearest tenth of a gram. The axis of the gauge is placed in a vertical position with the rotary seal end upward, and distilled water is poured in through this open end while the gauge is rocked slowly from side to side until all trapped air bubbles rise to the top and the excess water escapes through the drain tube. The gauge is carefully tilted while keeping the drain tube uppermost until the axis is horizontal, and then the reservoir is rotated upwards and the drain tube downwards until all the water in the reservoir has escaped through the drain tube. The rotation is continued until enough water overflows at the cut-off and escapes through the drain tube to bring the water surface exactly at the position outlined by the "glass marking" pencil. The gauge and its contents are then weighed to the nearest tenth of a gram. The trapped water may also be emptied through the drain tube into a beaker for weighing, but it is difficult to remove all of the water from the narrow tubes in the head of the gauge. After drying the gauge, the drain tube is sealed off as shown in Fig. 3. The calibration constant C can also be determined by calibrating the rotary gauge against a standard laboratory McLeod at two or three points. The pressure in mm of Hg is given by $P=Ch^2$ where h is the depression of the mercury in the closed capillary when the level of the mercury in the open capillary is set to the top of the closed capillary. The length of the closed capillary from the top to the bend is about 15 cm, and the useful range of pressure covered by the scale is from 2×10^{-6} mm to 2×10^{-2} mm Hg.

The weight of the rotating part of the gauge, including the mercury, is less than one kilogram. Thus no undue strain is put on the glass-to-metal seal or the rotary joint. A cylindrical guard of perforated sheet metal or wire mesh may be placed around the glassware to protect the gauge from accidental blows. However, it has been found convenient to use the unprotected gauge without any accessories in the laboratory.

For the design of the rotary "O" ring seal, the author is indebted to Mr. Judd Black of the D.P.I. instrument shop. As shown in Fig. 4 it consists of a single "O" ring of Neoprene and a needle bearing (Torrington B-912X) supported in a brass housing. The rotary member is a brass tube soldered to a glass-to-metal seal which is connected to the gauge. This seal has functioned satisfactorily without any measurable leakage and with negligible outgassing since the first model of this gauge was constructed.

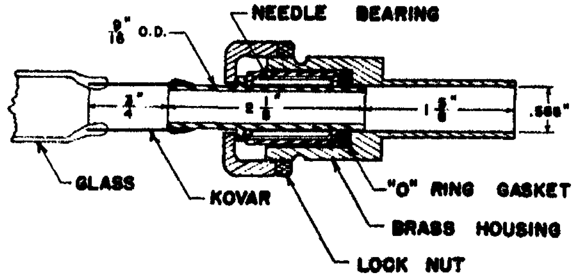

FIG. 4. Details of rotary seal.

It is readily seen that the gauge is nearly accident proof. Should atmospheric pressure be suddenly admitted to the system or the gauge by breakage or inadvertent opening of the wrong valve, the mercury resting in the reservoir would not be displaced. Even should an accident occur while the gauge is in use, with the mercury in the coil, it is unlikely that mercury would escape into the system or break the head of the gauge, as most of the impact of the air on the mercury would be taken up in the turns of the coil and air will by-pass the mercury at the top of each turn.

The rotary seal will admit small quantities of condensable vapors to the system, but probably not more than the stopcock usually placed between a McLeod gauge and the vacuum system. This is generally unimportant, as McLeod gauges are almost invariably trapped.

A somewhat different helical gauge has been described by Reden.[7] It involves a glass spiral ending in a capillary "U" tube. A tapered ground glass joint is used for the rotary seal. Our experience has shown that such joints "freeze up" after a short period of time even with the best of lubricants. Every reading must be computed by multiplying the compression ratio corresponding to the mercury level in the closed arm by the height of the level in the open arm above that in the closed arm. Reden's gauge is not suited for measuring extremely low pressures because the cross section of the coil tube cannot be too large compared with the cross section of the capillary.

---

[7] U. v. Reden, Zeits. f. d. physik. u. chem. Unterricht 24, 50 (1911).

THE REVIEW OF SCIENTIFIC INSTRUMENTS VOLUME 21, NUMBER 6 JUNE, 1950

A Multiple Kerr-Cell Camera

A. M. Zarem* and F. R. Marshall
U. S. Naval Ordnance Test Station, Pasadena Annex, Pasadena, California

(Received January 25, 1950)

The need for new ultra-high speed photographic techniques in studies of brief transient phenomena has led to the development of a multiple Kerr-cell camera designed to take a sequence of three photographs at submicrosecond exposure times. This camera uses shutters of the electro-optical type utilizing the Kerr effect in nitrobenzene. Pulsing networks for the Kerr cells and synchronizing networks for the entire system are described. The system has shown itself to be capable of high shutter speed, high sequence rate, and very good stability of timing. With this camera, studies of electrical discharages at effective exposure times of 0.04 microsecond and framing rates corresponding to 40,000,000 frames per second have routinely been made. It is felt that cameras of this type are valuable research tools that will help open the way for further important studies.

INTRODUCTION

TECHNOLOGICAL advances in the last few years have resulted in renewed interest in the study and investigation of physical phenomena of a transient nature. In the field of photography, particularly, a growing need has been felt for (1) techniques to obtain ultra-short (submicrosecond) exposure times, (2) a means for synchronizing operation of the camera with the phenomenon to be studied.

To date, the shortest exposure times obtainable with mechanical shutters are of the order of a millisecond. Commercial motion picture cameras employing rotating prisms are available when exposure times down to the order of 75 microseconds are needed. For exposure times of a few microseconds, special cameras using rotating mirrors are available. In these mechanical shuttering methods, the problem of precise synchronization between the phenomenon studied and the operation of the camera shutter may be one of moderate difficulty. Flashlamp techniques which overcome this problem have been developed for use when exposures down to a microsecond are required. Such lamps, however, have obvious shortcomings for the photography of self-luminous objects or of objects having very high level background light.

When submicrosecond photographic exposure times are required, one is obliged to seek new methods, since both mechanical means and flashlamp techniques have not yet been commercially developed to be effective in this range. A shutter which can be used in the submicrosecond range is the Kerr-cell shutter, named for the discoverer of electrically induced birefringence. This shutter consists of the cell proper and two suitably positioned, "crossed" polarizers placed before and after the cell along the optical path. The cell is a transparent container of a liquid, usually nitrobenzene, and is provided with electrodes for establishing an electric field in the liquid in a direction perpendicular to the optical path. With no electric field, the crossed polarizers prevent transmission of light; with a field applied, the state of polarization of the light passing through the cell is altered, permitting light to pass through the second polarizer.

The optical transmission of a Kerr-cell shutter for

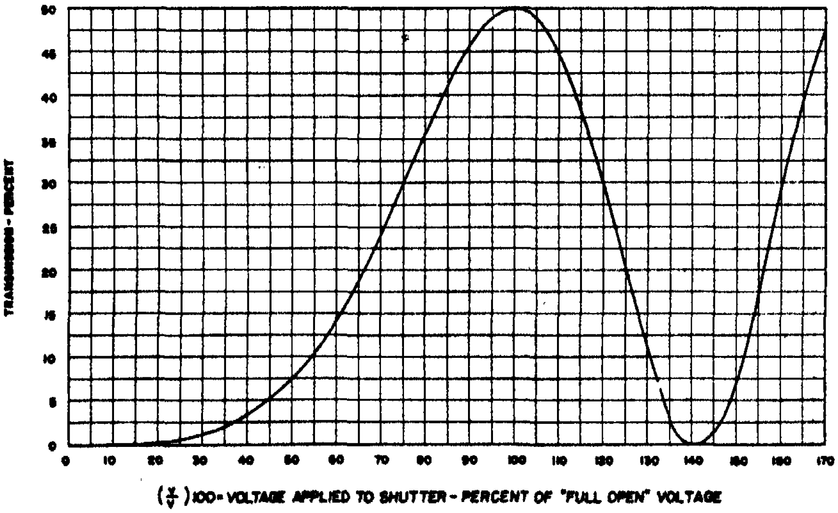

Fig. 1. Optical transmission of ideal Kerr cell shutter.

---

* Consultant to U. S. Naval Ordnance Test Station, is now Director of the Los Angeles Division, Stanford Research Institute and Chairman of the Department of Applied Physics.

axial rays is given by

$$T=A\sin^2[\pi/2(v/V)^2], \qquad (1)^1$$

where v = voltage applied to the electrodes, V = "full open" voltage of the cell, A = a constant which takes into account rejection of one-half of the light by the first polarizer and absorption and reflection losses in all components of the shutter. A plot of Eq. (1) is given in Fig. 1. Attention is directed to the very low transmission at low voltages.

The full open voltage for a Kerr cell may be calculated from the expression

$$V=300d(2lK)^{-\frac{1}{2}},$$

where d = distance between plates, cm, l = length of the electrodes, cm, K = Kerr constant of the cell fluid, c.g.s. e.s.u., V = voltage applied to the electrodes.

Because of its high Kerr constant, nitrobenzene is usually used as the active fluid in these cells. The Kerr cells in the camera to be described in this paper have rectangular electrodes which are 1 cm wide, 2 cm long and are separated by 0.5 cm. Figure 2 shows two models of Kerr cells which were used. For both models the full open voltage is approximately 12,500 volts. J film polaroid was used as polarizer.

The theory of operation of Kerr cells and their application in a wide variety of scientific investigations has been described in the literature. The development of a compact and simply operated shutter of this type for ordinary photographic purposes has taken place only recently. Since the speed of operation of a Kerr-cell shutter is limited intrinsically only by the rapidity with which certain molecular phenomena can occur and practically only by the rate of application of electrical potential to the cell, such cells have been used successfully in obtaining effective exposure times as brief as 0.01 microsecond.[2] The all-electrical operation of such shutters greatly enhances their utility by making possible the application of electronic techniques to high speed photographic shuttering. For such shutters the problem of synchronization of the camera with the phenomenon under study becomes an electrical timing problem of little difficulty.

Much could be said about the general design requirements for a Kerr-cell shutter but it is felt that this subject should be covered in a separate paper. However, brief comments on some of the common problems are pertinent here. The limitations of the Kerr-cell shutter arise from the fact that the design is usually a compromise between two factors—high operating voltage and electrode configuration that tends to restrict the areal and angular aperture of the camera. Details regarding spectral transmission of nitrobenzene and dispersion in the Kerr constant may be found elsewhere.[1] In addition, consideration must be given to the purity of the nitrobenzene used, on which further comment is made in the Appendix.

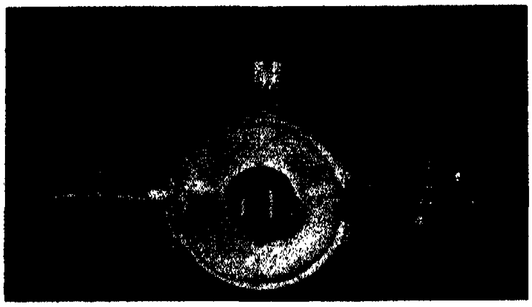

(a)

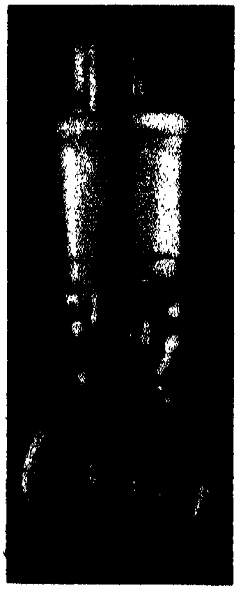

(b)

FIG. 2. Two models of Kerr cells used in multiple-Kerr-cell camera.

THE KERR-CELL CAMERA

A Single-Cell Camera

The essentials of a Kerr-cell camera are (1) a suitable camera, (2) a Kerr-cell shutter, and (3) an electrical circuit capable of delivering voltage pulses to the Kerr cell under suitable synchronization with the phenomenon to be photographed.

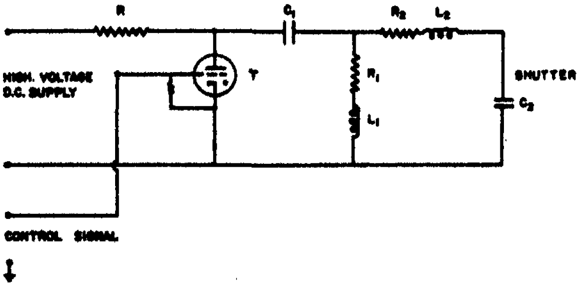

FIG. 3. Circuit diagram of Kerr-cell pulser.

---

[1] Zarem, Poole, and Marshall, "An electro-optical shutter for photographic purposes," Inyokern, U. S. NOTS (May 1948), NavOrd Report No. 1016; "An electro-optical shutter for photography," Elec. Eng. 68, No. 4, 282–288 (April 1949).

[2] W. M. Cady, and A. M. Zarem, "Brief pulses using Kerr cells," Nature 162, No. 4118, 528–529 (October 2, 1948).

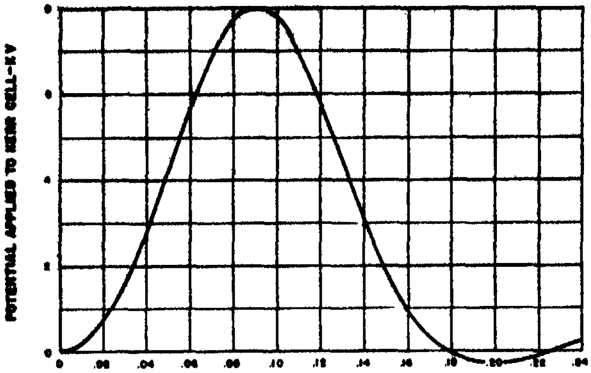

FIG. 4a. Voltage-time curve of Kerr-cell pulser.

There are many methods for obtaining brief electrical pulses of many kilovolts in magnitude, but most of these were thought to be objectionable from the point of view of economy, simplicity, or other technical grounds. The system finally decided upon was quite simple and operated with complete satisfaction. Figure 3 is a circuit diagram of the Kerr-cell pulser[3] used to supply a high potential, short-duration electrical pulse for operation of the Kerr-cell shutter.

When the thyratron T is in a non-conducting condition, capacitor C_1 is charged to supply voltage. Applying a voltage pulse to the grid of thyratron T causes it to conduct, discharging capacitor C_1 and creating a transient disturbance in the network which results in impressing on the Kerr cell (capacitor C_2) a voltage-time wave of the shape indicated in Fig. 4a. Observe that the capacity of the Kerr cell forms part of the network. The thyratron T in Fig. 3 may be any of several types, depending upon the peak voltage it is desired to switch to the Kerr-cell electrodes. The hydrogen thyratron series 3C45, 4C35, and 5C22 were used. Further details are given later.

It should be noted that the peak voltage impressed upon the Kerr cell with this network is approximately equal to the voltage to which the network is initially charged. For this reason, the circuit described has some advantages over the "line" type of pulse-forming networks, which ideally supply to a load only one-half of the voltage to which they are charged.

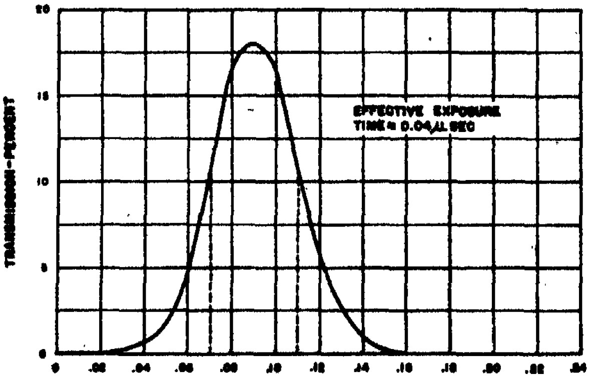

FIG. 4b. Transmission-time curve of Kerr-cell pulser based on Fig. 4a.

The curve of Fig. 4b shows the optical transmission as a function of time for a Kerr-cell shutter pulsed with the voltage-time wave form of Fig. 4a. The transmission characteristics of Fig. 1 indicate that in general the transmission-time characteristic of a Kerr-cell shutter will be briefer than the electrical pulse applied. Attention is called to this fact in Fig. 4, in which the transmission-time characteristic is seen to be much shorter than the voltage wave form. In Fig. 4b, 70 percent of the total exposure occurs in an interval of 0.04 microsecond; this is called the effective exposure time.

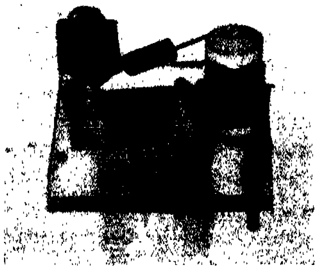

FIG. 5. Plug-in type network.

The electrical parameters of the circuit, Fig. 3, can readily be changed in order to accommodate Kerr cells of different electrostatic capacitance or to vary the duration of the output voltage. Since output voltage is unchanged by change in the impedance of the network as a whole, for Kerr cells of different electrostatic capacitance the circuit parameters are altered as follows:

$$C_1' = [C_2'/C_2]C_1$$
$$R_1' = R_2' = [C_2'/C_2]^{-1}R_1$$
$$L_1' = [C_2'/C_2]^{-1}L_1$$
$$L_2' = [C_2'/C_2]^{-1}L_2.$$

Notation of components is as in Fig. 3. Primes indicate values in the altered circuit.

To alter the pulse duration, thereby varying the effective exposure time, the time constants of the circuit are changed by the ratio of new to original exposure time. When Kerr-cell capacitance is assumed to be constant

$$C_1' = C_1$$
$$C_2' = C_2$$
$$R_1' = R_2' = [t'/t]R_1$$
$$L_1' = [t'/t]^2 L_1$$
$$L_2' = [t'/t]^2 L_2,$$

where t is effective exposure time. Primes indicate values of the altered circuit. When necessary, both of the above transformations can be utilized successively.

Using the above formulas, plug-in-type networks as shown in Fig. 5 were designed and constructed. To change the effective exposure time available with a Kerr cell, one merely substitutes the proper network designed by the equations given above. With such networks, pulse durations corresponding to effective exposure times of 0.007 to 7 microseconds were readily achieved.†

---

[3] A. M. Zarem *et al.*, "Circuit for pulsing capacitive loads," U. S. Patent No. 2,464,279 (March 15, 1949).

The Multiple-Kerr-Cell Camera

Framing—the recording of successive photographic exposures on separate film areas—presents a number of special problems at framing rates in excess of 100,000 per second. However, for a small number of frames, a simple arrangement is obtained by providing a separate Kerr-cell shutter and associated lenses, etc., for each frame in the sequence. Such a system will record slightly different aspects of the phenomenon on the several frames (unless semireflecting mirrors are used), but this limitation may not be serious, particularly if the subject is either distant or has convenient symmetry.

An arrangement of components in a three-frame camera is shown in the line diagram of Fig. 6 and the photograph of Fig. 7. The three frames are recorded on a single 4×5 photographic film of a standard Speed Graphic camera. This arrangement has an equivalent numerical aperture of about f:16 and a total angular field of approximately 5 degrees. It should be noted that a more compact arrangement might be achieved with a Kerr cell of smaller over-all dimensions. Such a cell, recently developed, has a maximum over-all dimension of 1 inch. It will be described in a note to be published soon.

The pulsing network for each of the Kerr cells is mounted above the Speed Graphic camera. More complete discussion of the circuitry is given below.

With the camera design indicated in Fig. 6, the optical paths from object to image are necessarily not equidistant. Difficulties due to this circumstance are avoided by placing the object at the focal point of the first lens and the photographic film at the focal point of the camera lens. The images I_1, I_2, and I_3 then appear in equal focus. The use of two mirrors or prisms on the longer light paths insures that neither of these images will appear reversed. However, the optics of the system is such that images I_1 and I_3 are of lower intensity than image I_2. To remedy this defect a neutral filter can be placed behind the second shutter to equalize the intensities of all three images.

Camera-Synchronizing System

A diagram of the camera-synchronizing system is shown in Fig. 8. This particular arrangement permits timing of the camera operation to be accomplished in two separate adjustments. One adjustment controls the

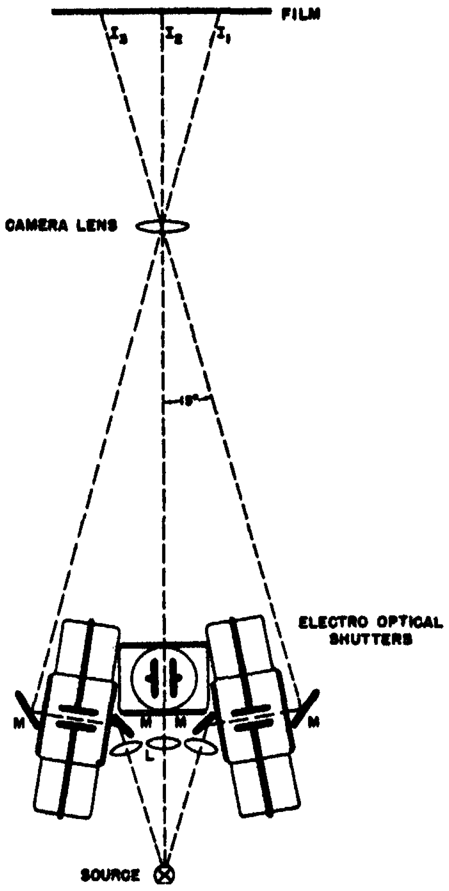

FIG. 6. Line diagram of multiple-Kerr-cell camera.

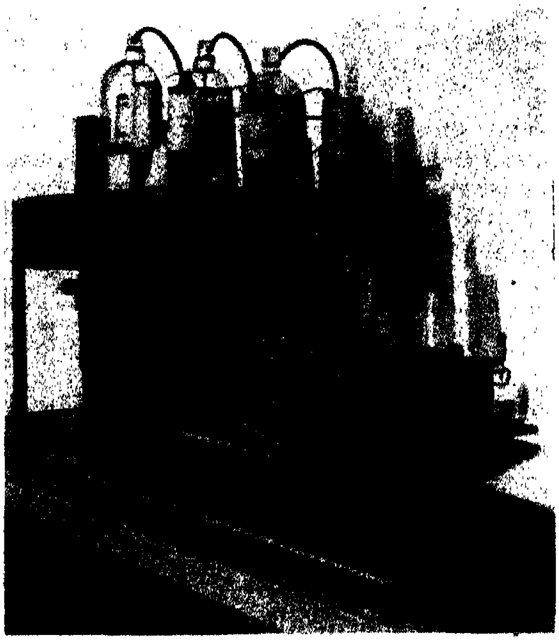

FIG. 7. Photograph of multiple-Kerr-cell camera.

---

† All statements on time intervals were verified with the aid of a high speed oscillograph with resolution time of 0.002 microsecond.

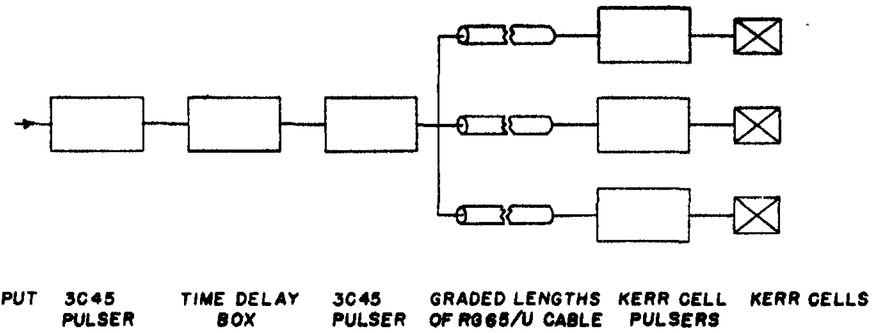

FIG. 8. Block diagram—circuit of triple-Kerr-cell camera.

time at which the shuttering sequence starts; it is effected by the delay box with a range of 2 microseconds in steps of 0.025 microsecond. The other adjustment varies the time interval between the operation of the three shutters; it is made by varying the cable lengths between the second 3C45 pulser and the various Kerr-cell pulsers. The time interval between successive shuttering operations can easily be made as small as 0.01 microsecond, corresponding to a framing rate of 100,000,000 per second.

The circuit diagrams of the 3C45 pulsers and the delay box are shown in Figs. 9 and 10. The cable used in the delay box and elsewhere in the camera-synchronizing system is a spirally wound, high impedance, high delay cable type RG 65/U.

The second 3C45 pulser is not functionally necessary. Its purpose is primarily to insure a more precisely timed sequence of the Kerr-cell pulsers by regenerating (sharpening) the synchronizing impulse at this point. A secondary purpose is prevention of voltage loss that would occur if cables were simply branched at this point.

The synchronizing signal is of much larger magnitude (2,000 volts with rise time approximately 0.01 microsecond) than is necessary to ionize the several thyratrons. The excess voltage serves to decrease the ionization time, thereby eliminating the need of carefully matched thyratrons in the three Kerr-cell pulsers. A fine adjustment of the timing of these thyratrons is provided by means of a 10,000-ohm rheostat in series with each grid.

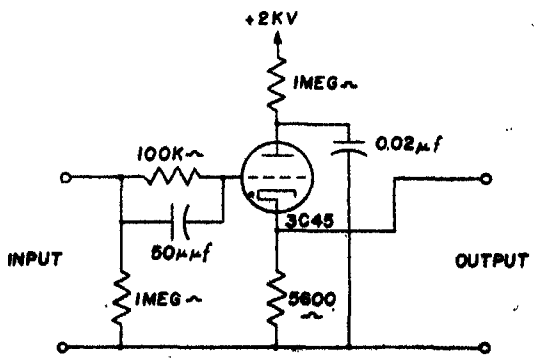

FIG. 9. Circuit diagram of 3C45 pulser.

The synchronizing system is capable of very precise timing. In a recent experiment,[2] in which the time resolution was 0.001 microsecond, no "jitter" could be observed in the time interval between the operation of two Kerr cells.

Oscillographic check on the timing of the multiple-shutter camera was maintained. Figure 11 is an oscillogram showing the three voltage pulses applied to Kerr cells 1, 2, and 3. The timing-wave frequency is 10 megacycles.

APPLICATIONS AND RESULTS

The Kerr-cell shutter is a useful device for obtaining exposure times in the microsecond and submicrosecond ranges. When a few frames are adequate, and in particular when framing rates are greater than 100,000 exposures per second, the multiple-Kerr-cell camera described will be useful. A particular application of this type of camera has been made in the study of microsecond electrical discharges of different types.

Figure 12 is a photographic record taken with the multiple-Kerr-cell camera, showing various stages during the vaporization of a single fine platinum wire. The effective exposure time, as determined by the Kerr-cell pulser, was 0.04 microsecond for each of the Kerr cells. The pulsing rate or interval between pulses was 0.01 microsecond; for this reason, the framing rate is said to be 10,000,000 exposures per second.

Figure 13 is a photographic record showing the vaporization of a single fine gold wire. The exposure time of each frame was 0.04 microsecond and the framing rate 40,000,000 exposures per second.

Using the multiple-Kerr-cell photographic technique, it has been possible to obtain a qualitative depiction of the vaporization process when fine filaments are electrically surged. Photographic record of the fuse action of such filaments continues to reveal interesting results. It is hoped that a more detailed report on this topic can be given at a later date.

CONCLUSIONS

It has been demonstrated that the multiple-Kerr-cell camera is a valuable and versatile device for obtaining photographic sequences of short exposure time and high framing rate. As a research tool it may find addi-

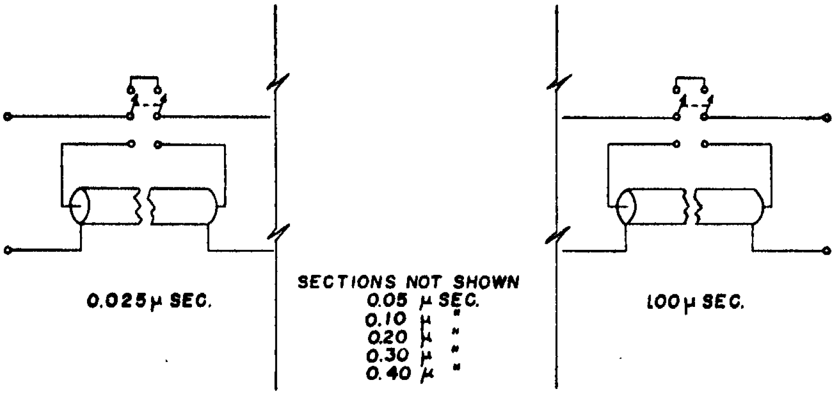

Fig. 10. Schematic diagram of time-delay box.

tional application to studies of ballistic and explosive phenomena.

APPENDIX

Comments on Purity of Nitrobenzene

A question frequently raised in Kerr-cell work concerns the effect of the purity of nitrobenzene on the operation of the Kerr cell. The consensus is that such impurities are important only because of their effect in increasing the electrical conductivity. For this reason the criterion of high purity is usually taken to be low electrical conductivity.

There appear to be three deleterious effects of increased conductivity of nitrobenzene.

(1) The loading effect of the lowered Kerr-cell impedance on the electrical circuits used to operate the Kerr cell needs no detailed comment. Difficulties may be avoided by proper design of circuits to be used.

(2) The heating of the Kerr cell by conduction currents—this is objectionable chiefly because non-uniform heating will cause optical distortion. Additionally, increased temperature lowers the Kerr constant of the nitrobenzene. Heating can be diminished by lowering the conductivity of the nitrobenzene by purification or, as is frequently possible, by short-time or intermittent application of voltage to the cell electrodes. Water jackets can be used to prevent temperature rise.

(3) The distortion of the electric field in the Kerr cell caused by concentration of ions near the Kerr-cell electrodes—this difficulty can be avoided if the potential is applied to the Kerr cell for so short a time that insignificant ion concentrations occur. H. J. White[4] states that this time is of the order of 0.01 second, but does not specify the conditions under which this is true.

Since the Kerr-cell shutters described in this report were operated at exposure times much shorter (i.e., in the order of 0.01 microsecond) than the time necessary for concentration of ions, one would expect the shutter operation to be highly independent of nitrobenzene purity. This expectation has been corroborated in two ways.

(1) It was observed that, over a period of months, the purity of the nitrobenzene in a Kerr cell deteriorates appreciably, but that no detectable difference in photographic results obtained.

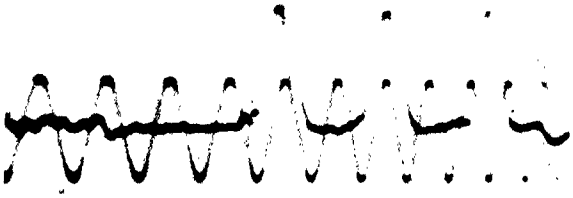

Fig. 11. Oscillogram of timing pulses applied to Kerr cells. The timing-wave frequency is 10 megacycles and the three pips indicate the instant of operation of cells 1, 2, and 3, respectively.

Fig. 12. Three stages during vaporization of a fine platinum wire. Effective exposure time per frame: 0.04 microsec. Framing rate: 10,000,000 exposures per sec.

Fig. 13. Three stages during vaporization of a fine gold wire. Effective exposure time per frame: 0.04 microsec. Framing rate: 40,000,000 exposures per sec.

(2) A measurement of the magnitude and duration of the optical transmission of a Kerr cell when operated at a 60-cycle repetition rate with a pulse duration of approximately 0.01 microsecond was made using two samples of nitrobenzene of widely different conductivity. Again, no difference in operation could be detected, indicating that under such pulsed conditions the purity of nitrobenzene is not a critical factor.

Although these experiments are definitely not critical, the results are in accord with those of White.[4] They are mentioned to provide added emphasis to this subject for those workers who may be considering the use of Kerr cells under pulsed operation.

---

[4] H. J. White, "The technique of Kerr cells," Rev. Sci. Inst. 6, 22-26 (1935).

A Method of Measuring Spurious Counts in Geiger-Müller Counters*

D. WILLARD AND C. G. MONTGOMERY
Sloane Physics Laboratory, Yale University,† New Haven, Connecticut

(Received February 13, 1950)

A counter was excited by a series of x-ray pulses of short duration occurring at regular intervals. Spurious counts were then easily recognized since they occur between the x-ray pulses. The counter pulses were displayed on an oscilloscope screen with a synchronized sweep and the counter deadtime, recovery time, and number of spurious counts determined by inspection. More quantitative information of the time distribution was obtained with an electronic circuit that recorded counts in a small arbitrarily chosen interval. It was found that the interval distribution shows at least two maxima. A mechanism is suggested for the appearance of the second maximum in terms of negative ions formed at the cathode by positive-ion bombardment.

THE principal difference between good and bad Geiger-Müller counters is the relative number of spurious counts, that is, counts caused by the action of no external agent. Nearly all recipes for counter construction were found with this criterion as the deciding factor; a good plateau means few spurious counts. Investigations of counter behavior necessitate a determination of the number of these spurious counts. If spurious counts are numerous, they are of course easily recognized; if they are few in number, it is extremely difficult to distinguish spurious discharges from those which are the desired result of an external agent. The only method by which spurious counts can be recognized is by a measurement of the frequency distribution of intervals between counts. An interval distribution with spurious counts contains more short intervals than a random distribution. Interval distributions have been measured by several observers[1] in the past. This method suffers from the disadvantage, common to all statistical measurements, that a large number of observations must be taken to obtain reasonable accuracy. We have therefore investigated a possible improvement in this method of distinguishing real from spurious discharges.

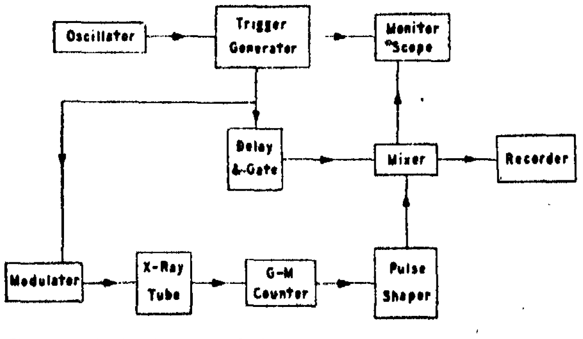

FIG. 1. Block diagram of circuit for counting spurious counter discharges within an interval delayed an arbitrary amount from a genuine discharge.

The number of genuine discharges can be increased at will with suitable sources of radiation, and the spurious counts are also increased. If, however, it is possible to arrange the true counts to occur at regularly spaced intervals and in sufficient numbers, then nearly all counts that take place between true counts are spurious ones and can be recognized readily. Ultraviolet light can be easily produced in pulses but most counters are either not photoelectrically sensitive or have absorbing envelopes. X-radiation, on the other hand, can penetrate most counter envelopes and can excite discharges even though the efficiency is not high. To obtain x-rays a standard tube with a tungsten anode (Type *RW*, General Electric Company) was used. Negative voltage pulses of 15 kv with a duration of 0.5 μsec. were applied to the cathode by means of a radar modulator, nicknamed "vest pocket" from an *AN/APS-2* radar. The pulse repetition frequency could be varied from 500 to 2000 per sec. The filament current was furnished by a low capacitance transformer. X-rays impinged on the counter and produced discharges which were amplified and inspected on the screen of a *P4-E* synchroscope which also furnished the trigger pulse for the modulator. The spurious discharges occurring between the x-ray pulses were easily visible and the screen could be photographed to obtain a permanent record. The size of the pulses was also evident on the screen and the deadtime and time of complete recovery of the counter could easily be observed. It was found in all cases that most spurious counts occurred at the time of complete recovery.[2] That is, spurious counts occurred following a genuine count when the positive ions formed in the genuine count reached the counter cathode and produced electrons which traveled to the anode and there gave rise to a spurious count. Not all spurious counts occurred at this time, however. Some happened before the counter was completely recovered, and others a considerable time after complete recovery.

It was difficult to obtain quantitative measures of the time distribution of the spurious counts from the synchroscope pictures and a counting circuit was devised for this purpose. Since the component parts of this circuit were all commonplace, only a block diagram is reproduced here as Fig. 1. A gate of adjustable length was formed which started at an arbitrary time after the trigger pulse. The number of counts admitted by the gate were recorded. A sample of the results obtained is shown in the curve in Fig. 2. For these data the pulse repetition frequency was 500 per sec., and the gate was 8 μsec. wide. It should be noted that the ordinate is plotted on a logarithmic scale. At the bottom of Fig. 2 is sketched the envelope of pulse heights on a linear scale as a function of time after the x-ray pulse. The counter used had a copper cathode 8 by 1⅝ in. in a glass envelope with a 0.003-in. wire. The filling gas was 1 cm of alcohol plus 9 cm of argon. The counter voltage was high, and the counter was operating above the plateau. It is evident from the figure that the spurious counts are distributed in time with two peaks, the first and larger at the time when the counter is fully recovered after the x-ray pulse and the second at approximately twice this interval. A graphical integration of the area under this curve plotted on a linear scale, resulted in a spurious counting rate of about 100 sec.$^{-1}$, or about one-fifth of the genuine counting rate.

---

* The measurements reported here were presented at the Symposium on Geiger Counters at the Naval Research Laboratory, October, 1949.

† Assisted by the joint program of the ONR and AEC.

[1] A. Ruark, Phys. Rev. 56, 1165 (1939); A. Roberts, Rev. Sci. Inst. 12, 71 (1941); S. C. Curran and E. R. Rae, Rev. Sci. Inst. 18, 871 (1947); J. L. Putman, Proc. Phys. Soc. London 61, 312 (1948).

[2] C. G. Montgomery and D. D. Montgomery, Phys. Rev. 57, 1030 (1940); J. Frank. Inst. 231, 526 (1941).

Putman[1] has analyzed his observations on spurious counts into a whole series of maxima such as this. He has suggested that each peak is composed of spurious counts which are the result of the counts occurring in the preceding peak. We have endeavored to extend our observations to find other peaks, since according to this hypothesis there must be an infinite geometrical series of them. We were unable to prove to ourselves that a third peak existed. Spurious counts do occur after the second peak, but the low counting rates prevented a certain detection of additional peaks.

Although the whole series of peaks of spurious counts undoubtedly occurs, it is possible that the second peak is higher because of another mechanism of production of spurious discharges. It may happen that when the positive ion sheath strikes the cathode after the genuine discharge not only electrons are formed but also some negative ions. These negative ions would travel in toward the counter wire, lose an electron by a collision near the wire and produce a spurious discharge. This discharge would occur at an interval after the genuine discharge equal to two traversal times for ions across the counter. The mechanism of formation of these counts is thus somewhat similar to the production of long time lags by electron capture.[3] It is well known that positive ions striking a metal surface sometimes do produce negative ions. In carbon dioxide gas, this process is apparently rather probable.[4] Counters containing alcohol vapor must eventually contain some CO_2 from the breakdown of the vapor during the discharge.

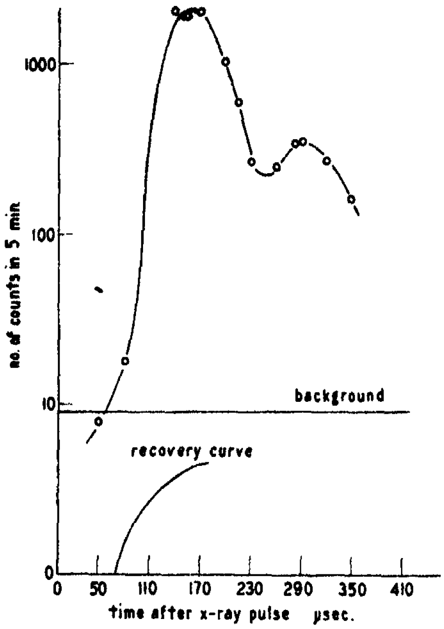

FIG. 2. Time distribution of spurious counts. The gate length was 8 μsec.

---

[3] C. G. Montgomery, and D. D. Montgomery, Rev. Sci. Inst. 18, 411 (1947).

[4] S. C. Brown and W. W. Muller, Rev. Sci. Inst. 18, 496 (1947).

The Measurement of the Magnetic Field in a Nuclear Spectrometer*

L. M. LANGER AND F. R. SCOTT
Physics Department, Indiana University, Bloomington, Indiana

(Received February 27, 1950)

An arrangement is described which gives a continuous measurement of the relative magnetic field strength in a nuclear spectrometer with an accuracy of about 0.1 percent. The method consists of balancing the a.c. voltage picked up by a coil rotating in the field of the spectrometer against that picked up in a standard Helmholtz field.

INTRODUCTION

THE main limitation to taking full advantage of the high resolution available in a large nuclear spectrometer[1] employing iron has been that of obtaining sufficiently accurate determinations of the magnetic field strength. This difficulty can only be fully appreciated when one attempts to determine the shape of a line of internal conversion electrons whose spread in momentum ($H\rho$) at half-maximum is only 0.5 percent or less. Clearly, in order to be able to place ten to twenty points on such a line, one must be able to measure relative values of the magnetic field strength with an accuracy of 0.1 percent or better. It is further desirable to have available a continuous indication of the field strength so that predetermined settings may be made for optimum spacing of the data. The usual method of employing a flip coil and ballistic galvanometer does not readily satisfy either of these requirements. The elegant method of nuclear magnetic resonance is not applicable to the extremely low values of magnetic field which are necessary at low energies with a spectrometer employing a 40 cm radius of curvature.

The scheme to be described has been found to be extremely satisfactory. It is quick and simple to operate and yields results which are reproducible to better than 0.1 percent. Basically, it is a null method whereby the a.c. voltage picked up by a coil rotating continuously in the field of the spectrometer is bucked against a similar voltage picked up in the standard field of a set of Helmholtz coils. Measurements are made in terms of the accurately determined d.c. current through the Helmholtz coils. Although the general idea is straightforward, some of the details of the complete system may be of interest.

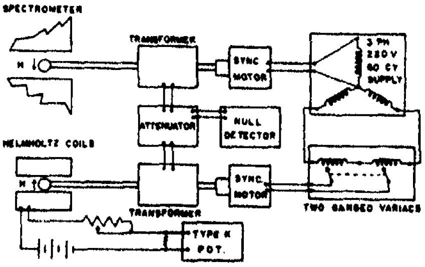

FIG. 1.

METHOD

Figure 1 shows a schematic arrangement of the system. The two pick-up coils are rotated by separate synchronous motors whose relative phase of rotation can be adjusted by means of the Variac arrangement. The voltages induced in the pick-up coils are brought out by means of the special transformers. These transformers have rotating primaries, which are rigidly connected to the shafts of the respective pick-up coils. The secondaries are stationary. By this means, the variable contacts usually associated with slip rings or brushes are avoided. The continuity of the magnetic flux through the core of the transformer is maintained by the means of the precision ball bearings. The transformer outputs are passed through an attenuator and balanced in a null detector. The attenuator is designed to permit operation over the extreme range of spectrometer fields (0–750 gauss) with only a relatively small change in the Helmholtz field. The attenuators offer constant loads to the generators on all settings so that no large phase shifts are encountered in switching scales.

In operation, the Helmholtz current and the phase of rotation are varied until a null is indicated. The magnitude of the Helmholtz current, as read on a type *K* potentiometer, gives a direct measure of the field. It is also possible to pre-set the Helmholtz current to correspond to a given field and then vary the spectrometer field until a null is obtained. This latter procedure is extremely useful in locating narrow electron lines.

DESIGN AND CONSTRUCTION

The Helmholtz coils are of conventional design. Five thousand turns of No. 22 Heavy Formvar magnet wire with a current of 200 milliamperes in each coil yields

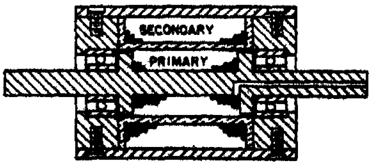

FIG. 2.

---

* This work has been assisted by a grant from the Frederick Gardner Cottrell fund of the Research Corporation and by the joint program of the ONR and AEC.

[1] L. M. Langer and C. Sharp Cook, Rev. Sci. Inst. 19, 257 (1948).

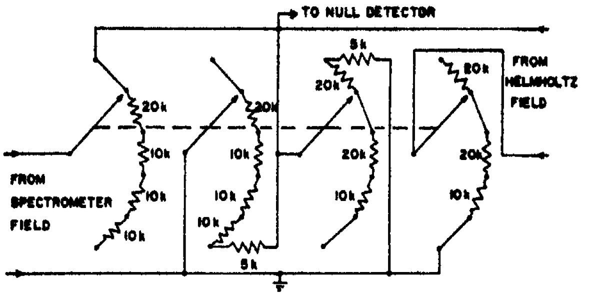

Fig. 3.

a field of 100 gauss at the center. The current for these coils is supplied by a 48-volt bank of storage batteries and is continuously variable by means of several rheostats rated for much higher currents than those employed. As indicated in the figure, the current is measured by means of a standard resistance and a type *K* potentiometer.

The pick-up coils each contain 30,000 turns of No. 40 Formvar covered wire and are wound on Lucite spools 1.4 in. O.D. and 1.1 in. long. The coils are held on brass shafts seven inches from the bearing support. No vibrational difficulties were encountered.

Although the design of the rotating primary transformers is far from ideal, they do serve satisfactorily to bring out the induced voltages with good wave form and without the use of rotating electrical contacts. As shown in Fig. 2, each primary, consisting of 6000 turns of No. 36 Formvar covered wire, is wound on an iron core which is directly coupled to the brass shaft supporting the pick-up coil. The secondary of each transformer contains 11,200 turns and is wound on a stationary brass spool which is supported concentrically around the primary by means of the iron shell. Precision ball bearings are used to complete the iron circuit.

The attenuator circuit shown in Fig. 3 permits balancing the whole range of spectrometer fields with the Helmholtz field varying only between the limits of 50 to 100 gauss. The upper limit is set to preclude any heating of the convection-cooled coils. The lower limit is imposed so as to minimize the effect of the earth's magnetic field on the calibration. The apparatus was calibrated for each step of the attenuator. Since the time constant seen by each generator remains essentially constant as the attenuator is switched, only slight phase shifts result. The exact phase balance is obtained with the Variac arrangement which provides a very sensitive means of shifting the one synchronous motor with respect to the other.

The null detector is a negative feed-back amplifier tuned for 30 cycles and discriminating strongly against 60 cycles. By avoiding the use of chokes and transformers the usable sensitivity of the instrument at 30 cycles is two microvolts. The balance is indicated on a "magic eye" tube.

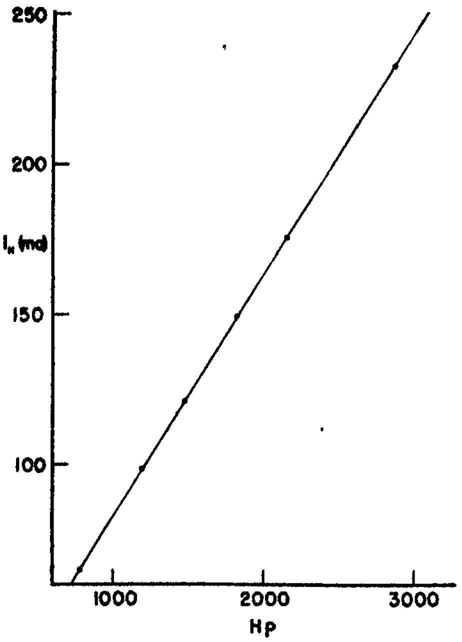

Fig. 4.

For the proper operation of the apparatus, the Helmholtz coils must be isolated from all stray magnetic fields. To minimize the effect of the earth's field, the Helmholtz coils are arranged with their axis horizontal. The vertical component of the earth's field which would give a quadrature component to the pick-up voltage is canceled out by means of an auxiliary set of degaussing coils.

CALIBRATION

For each setting of the attenuator, the spectrometer field was varied and the Helmholtz current required for a balance was determined. At the same time, the relative magnetic field was determined by repeated readings with a flip coil and ballistic galvanometer. The galvanometer was calibrated against a standard mutual inductance at each point. A section of the straight line calibration for one setting of the attenuator is shown in Fig. 4. The absolute calibration is in terms of the Au^{198} internal conversion line. Relative field settings may easily be made to better than 0.1 percent. The absolute calibration seems to remain constant to about the same accuracy.

THE REVIEW OF SCIENTIFIC INSTRUMENTS VOLUME 21, NUMBER 6 JUNE, 1950

Tests of Flowing Junction Diffusion Cells with Interference Methods

L. G. Longsworth
Laboratories of The Rockefeller Institute for Medical Research, New York, New York

(Received February 6, 1950)

The construction and manipulation of two diffusion cells, one of glass and the other of stainless steel, are described. In both cells the initially sharp boundary is formed by allowing solution and solvent to flow together into a narrow horizontal exit slit in the side wall of the diffusion channel. These cells have been tested by diffusion measurements with the aid of the Gouy interference method. Moreover, in the case of the metal cell which is provided with a reference channel in close proximity to that in which diffusion occurs, an interference method that gives the refractive index directly as a function of the height has also been studied.

INTRODUCTION

Although the use of the Gouy interference fringes[1-3] to follow the spreading of a boundary between solution and solvent permits precise measurements of ideal diffusion the available theory does not provide for those cases in which the coefficient is sufficiently concentration-dependent to give skew gradients. It is desirable, therefore, to adopt supplementary interference procedures for skew boundaries. Since the one suggested by Philpot and Cook[4] and by Svensson[5] gives the refractive index directly as a function of the level in the boundary it appears to be well adapted for the study of non-ideal diffusion and some preliminary tests with this method are reported below. Also included in this report is a description of two new diffusion cells, both of which utilize a modification of the siphoning procedure of Kahn and Polson[6] for the formation of an initially sharp boundary between solution and solvent. As in the British work[3] the modification consists in allowing solution and solvent to flow from below and above, respectively, into a narrow horizontal slit in the side wall of the diffusion channel. A boundary formed in this manner will be called a flowing junction boundary in order to distinguish it from one formed by a shearing mechanism as in the Tiselius,[7] Neurath,[8] and Claesson cells.[9] The results of tests of the new cells with the aid of the Gouy method are also described.

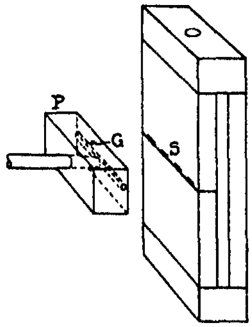

Fig. 1. The essential components of the glass diffusion cell.

THE DIFFUSION CELLS

One of the cells to be described has a stainless steel body with a closable exit slit in the diffusion channel whereas the body of the other cell consists of glass plates cemented together with a corrosion-resistant flux. Thus far it has not been possible to build a glass cell with cemented windows, as in the Tiselius cell, in which the optical quality is comparable with that of clamped windows. Consequently both cells have clamped windows, of 15 mm thickness, the flatness of which before clamping is better than one wave-length and the angle between opposite faces less than 20 sec. of arc. In both cells the cross section of the diffusion channel is 5×50 mm and the height 86 mm.

THE GLASS CELL

In the case of the glass cell the two most essential parts are shown in perspecitve in Fig. 1. The unique feature of this cell is the four colinear slits, *S*, at the center of the left-hand wall of the channel. Each slit is 5 mm in length and the spacing is such that the maximum horizontal distance that liquid must flow in entering one is 6.4 mm, a value only slightly greater than the narrow dimension, 5 mm, of the channel. The vertical dimension of the slits is 0.05 mm. Since the wall thickness is 8 mm, only 8 cu. mm of solution is trapped in these exit slits when the sharpening flow is stopped at zero time. The disturbances that may arise from the contact of this stagnant solution with the diffusing boundary are considered later in this paper.

The flow is stopped with the aid of the take-off plate, *P* of Fig. 1. When the face of this plate con-

---

[1] L. G. Longsworth, J. Am. Chem. Soc. 69, 2510 (1947).

[2] Gerson Kegeles and L. J. Gosting, J. Am. Chem. Soc. 69, 2516 (1947).

[3] Coulson, Cox, Ogston, and Philpot, Proc. Roy. Soc. A192, 382 (1948).

[4] J. St. L. Philpot and G. H. Cook, Research 1, 234 (1948).

[5] Private communication. Cf. Harry Svenson, Acta Chemica Scandinavica 3, 1170 (1949). It is also a pleasure to acknowledge my indebtedness to Dr. Svensson for constructive criticism in cell design. The details of the ones described in this report have been influenced by the examination and tests of a cell brought here from Upsala by Dr. Svensson in February, 1948.

[6] D. S. Kahn and Alfred Polson, J. Phys. and Colloid Chem. 51, 816 (1947).

[7] Arne Tiselius, Trans. Faraday Soc. 33, 524 (1937).

[8] Hans Neurath, Science 93, 431 (1941).

[9] Stig Claesson, Nature 158, 834 (1946).

taining the groove, G, of 2 mm square cross section is greased and pressed against the side of the cell so that the solution from the slits flows into this groove, and hence into the waste flask, F of Fig. 2, a vertical movement of this plate of 2 mm is sufficient to close the slits.

The arrangement for moving the take-off plate and for clamping the windows, W, to the cell is shown in Fig. 2, together with the brass masking plate, A, the solution reservoir, S_1, and the solvent reservoir, S_0. Although not shown in this figure the stopcocks of the reservoirs are provided with handles for operation from outside of the thermostat.

The filling procedure that appears to require the least material is to allow solution to run into the dry channel until the meniscus is just below the exit slit. With the waste flask disconnected, solvent is then slowly pipetted through the exit slit into the channel until it is filled and the meniscus has passed the stopcock of the solvent reservoir. Since some solution is thereby carried into the solvent portion of the apparatus this reservoir is rinsed, filled with solvent and its stopcock opened to allow the contaminating solution to be flushed out through the exit slit. Then with the reservoirs filled to the same level both stopcocks are opened and the boundary sharpened until the exit slit and stopcocks are closed at zero time.

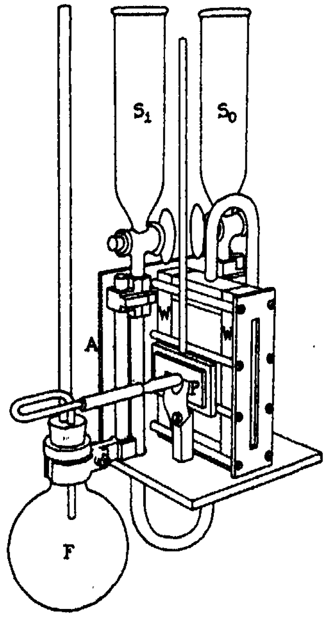

FIG. 2. The assembled glass cell.

THE METAL CELL

A horizontally exploded view of the stainless steel cell is shown in perspective in Fig. 3. When assembled as indicated in the figure the walls of the diffusion channel are formed by the plates A, B, and C whereas those of the reference channel are formed by C and D. Access to the reference channel is afforded by the tubes d and e whereas solution and solvent enter the diffusion channel through b and c, respectively. The tube a connects with the exit slit.

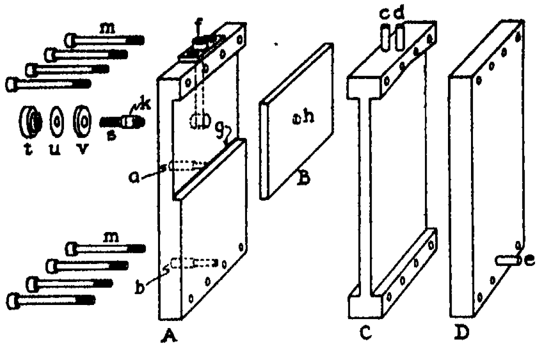

FIG. 3. Horizontally exploded view of the metal diffusion cell.

In this cell the exit slit may be closed, as described below, so that no stagnant solution remains in contact with the boundary. The plate B fits in the recess in A with a vertical clearance of 1 mm. Otherwise its dimensions are those of the recess. It is held with the post, s, that is threaded into a blind hole, h, in B, the thumbscrew, t, and the metal and Neoprene washers, u and v. A small vertical movement may be imparted to this plate by means of the hollow headed screw, f, that is threaded into the hole, k, of the post, s. Rotation, with the aid of an Allen wrench, of the screw f opens, or closes, the exit slit that is formed by the lower edge of B and the lower edge of the recess in A.

In order to insure uniform sharpening of the boundary along its entire length a groove, g, of relatively large cross section, 1.5×1.5 mm, funnels the solution into the tube a. Although not shown in Fig. 3 dowels are used between the screws, m, that hold the cell together and the window faces are ground, after final assembly, to a flatness of about one wave-length. Moreover since the windows serve as guides for the vertical movement of the plate B this plate is always left in the closed position when these windows are removed for cleaning. The filling procedure for the metal cell is similar to that for the glass cell.

OPTICAL METHODS

In testing the diffusion cells described above the Gouy interference method has been used in conjunction with the procedures outlined by Gosting *et al.*[10] and by the British workers,[3] for the determination of the normal slit image position and the fractional part, F, of the

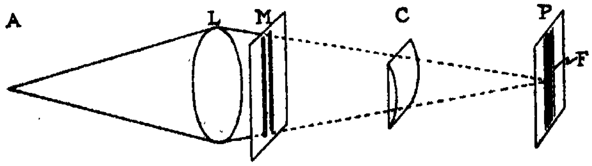

FIG. 4. Optical system of the concentration fringe method.

---

[10] Gosting, Hanson, Kegeles, and Morris, Rev. Sci. Inst. **20**, 209 (1949).

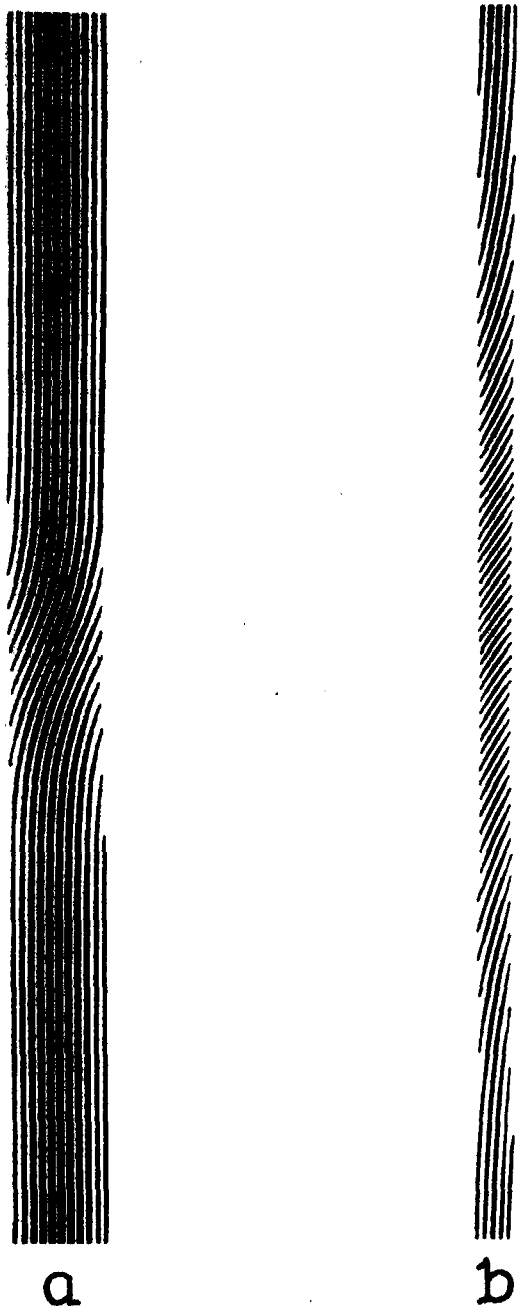

FIG. 5. (a) Photomicrograph of the concentration fringes obtained during the diffusion of 0.008N KCl into water. Slit width = 0.8 mm. Slit separation = 6.5 mm. (b) Photomicrograph of the concentration fringes obtained during the diffusion of 0.05N KCl into water. Slit width = 1.6 mm. Slit separation = 6.5 mm.

total fringe number, j_m. These procedures are clearly superior to those suggested by the author.[1] As in the British work the reference fringes are photographed simultaneously with those from the diffusion channel, superposition of the images being avoided by the use of a displacing plate in the reference path.

In the case of the metal cell it has been possible to supplement the Gouy method with one[4,5] that gives the refractive index directly as a function of the height in the boundary. The principle of this method is shown in Fig. 4 in which A is a point source of monochromatic light, L is a lens that forms an image of this source in the plane at P, M is a plate containing two vertical slits that mask the diffusion and reference channels, respectively, and C is a cylinder lens with its axis horizontal that focuses the cell vertically but does not affect the horizontal spacing of the Rayleigh fringes, F, that are formed at P by the vertical slits. If the liquid in the diffusion channel is homogeneous these fringes are vertical. With a boundary in this channel, however, they are warped, as shown in the photomicrograph of Fig. 5a, into a trace of the refractive index-height curve. With sufficiently narrow masking slits the number of fringes within the central diffraction maximum can be made to exceed the path difference, in wave-lengths, between solution and solvent. As is shown in Fig. 5a at least one of the fringes will then remain within the envelope throughout the transition from solution to solvent. This is the self-plotting procedure suggested by Philpot and Cook.[4] The author prefers, however, to use wider slits and larger concentration differences. As shown in Fig. 5b successive fringes then intersect the envelope diagonally as overlapping segments of the complete refractive index-height curve.

Fringes of the type shown in Fig. 5 will be called concentration fringes in order to distinguish them from the Gouy fringes that afford a measure of the concentration gradients in the boundary. Since the concentration fringes spread as the boundary spreads, whereas the converse is true of the Gouy fringes, the two methods supplement each other. Thus the Gouy fringes may be photographed during the early stages of diffusion, while the concentration fringes are frequently too close together to be resolved, after which the necessary changes in the optical system are made without disturbing the boundary and the concentration fringes then recorded. The changes consist in (a) the superposition of a vertical slit upon the horizontal one[11] that serves as light source in the Gouy method, (b) the insertion of vertical masking slits at the cell, (c) the removal of the displacing plate from the reference path and (d) the introduction of the cylinder lens.

EVALUATION OF THE PHOTOGRAPHS

The procedure for evaluating the Gouy fringe photographs has been adequately described elsewhere.[1,12] In the case of the concentration fringes the plate is aligned in the comparator with the vertical fringes that are conjugate to the homogeneous column of solvent above the boundary[13] parallel to the comparator axis and with the cross-hairs focused on a minimum, say. As the plate is moved the diagonal fringes conjugate to the boundary come under the cross-hairs and their positions are recorded as a function of the fringe number. Since each fringe corresponds to a path difference of one wavelength a plot of the comparator reading against fringe number gives, if the refractive index, n, varies linearly with the concentration, c, the concentration-distance curve in a coordinate system involving only apparatus constants. Moreover, since both maxima and minima can be used a 50-fringe system, for example, affords 100 datum. Using only the minima this is illustrated for a typical experiment in Fig. 6 where the small circles represent the comparator readings and the large circles the reciprocals of the tabular differences of these readings.

---

[11] As Philpot and Cook have noted, a vertically extended source may also be used but the fringe resolution is inferior to that with the essentially point source that is obtained with the crossed slits.

[12] L. G. Gosting and Margaret S. Morris, J. Am. Chem. Soc. 71, 1998 (1949).

[13] If solvent is also present in the reference channel, as is the usual procedure, these fringes are spaced symmetrically about a

When, in the foregoing comparation, the vertical fringes conjugate to the homogeneous column of solution below the boundary are reached, it is generally observed that the cross-hairs are now displaced from a minimum. If the comparator is provided with a graduated cross-axis movement, a value for the fractional part, F, of the total fringe number may be obtained from this displacement. It is better, however, to obtain F from a concentration fringe photograph that is taken during the sharpening process since at this stage the boundary is thin and the alignment of the plate in the comparator is less critical.

Since the comparator readings from a concentration fringe photograph are proportional to heights in the cell corresponding to a constant increment in n, and hence in c, they appear to be well adapted for tabular integration of Boltzmann's equation[14] and hence the evaluation of differential diffusion coefficients as a function of the concentration. However, as will be shown below, the author's present cylinder lens distorts the fringe pattern and no attempt to use the Boltzmann relation will be made until this distortion has been eliminated.

The following procedure for utilizing the data is due in part to L. J. Gosting and assumes that the diffusion is ideal. If, for example, $j_m=50.52$ the comparator reading, Δ, corresponding to the center of the boundary at which $j=j_m/2=25.26$ is determined by interpolation between the positions of the 25th and 26th fringe. This value of Δ is then subtracted from all readings to give the distance, H_j, on the plate of the jth fringe from the level conjugate to the center of the boundary in the cell at $h=0$. Since

$$\frac{\pm 2j}{j_m}\mp 1=\frac{2}{(\pi)^{\frac{1}{2}}}\int_0^{h_j/[2(Dt)^{\frac{1}{2}}]} e^{-y^2}dy,$$

a value of $h_j/2(Dt)^{\frac{1}{2}}$ for each fringe can be interpolated from the WPA "Tables of Probability Functions."[15] If A_j is the ratio of $(h_j/2(Dt)^{\frac{1}{2}})$ to H_j the diffusion coefficient, D, is then given for each fringe by the relation

$$D_j=(1/4t)(h_j/H_jA_j)^2$$

in which H_j/h_j is the magnification due to the cylinder lens, 1/1.533 in the present example.

In Fig. 7 values of D_j for a typical case are plotted against the fringe number and show a drift with that parameter that is probably due, not to boundary skewneww, but to imperfections in the cylinder lens that become evident when this lens is subjected to a Foucault knife-edge test. Moreover, these imperfections introduce a systematic error since the mean value, 2.409×10^{-6}, is 0.4 percent less than the Gouy value of 2.421×10^{-6} obtained earlier in the same experiment. It is clear that the simple plano-cylindrical element now available must be replaced by a corrected lens if the present apparatus is to yield precise results.

DISCUSSION

In testing with the aid of the Gouy method the cells described above the diffusion of 0.05N potassium chloride and of 0.379 percent sucrose into water has been studied. No significant difference between the results in the two cells has been observed. Thus at 1.01° in the metal cell sucrose gave a value of 2.421 $\times 10^{-6}$ while in the glass cell the value was 2.422×10^{-6}. The value reported by Gosting and Morris[12] for 0.5 percent sucrose at 1.00° was 2.418×10^{-6}. After correction to 0° the values for potassium chloride were 9.382×10^{-6} in the glass cell and 9.391×10^{-6} in the metal one. The value given by the Onsager-Fuoss theory is 9.399×10^{-6}.

The zero-time corrections in all of these experiments were 4–6 sec. and may be compared with values of 20–30 sec. observed by Gosting and Morris with a single tipped siphon, or about 10 sec. with a two-prong

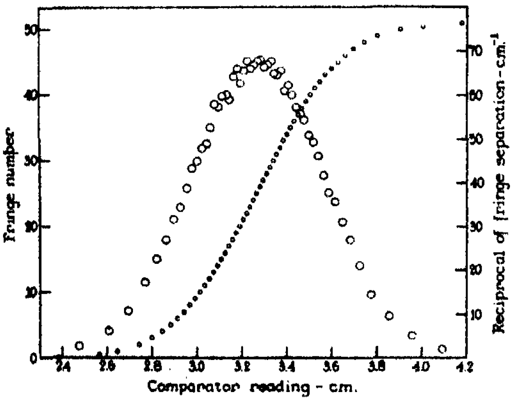

FIG. 6.

---

central maximum. It has been repeatedly observed, however, that this symmetry is lost if solvent is left too long in the reference channel. This is probably due to slow extraction, by the water, of a soluble component of the grease that is used in sealing the windows.

[14] S. Boltzmann, Wied. Ann. 53, 959 (1894).

[15] "Tables of Probability Functions," Federal Works Agency—Works Project Administration, Supt. of Documents, Washington, D. C. (1941).

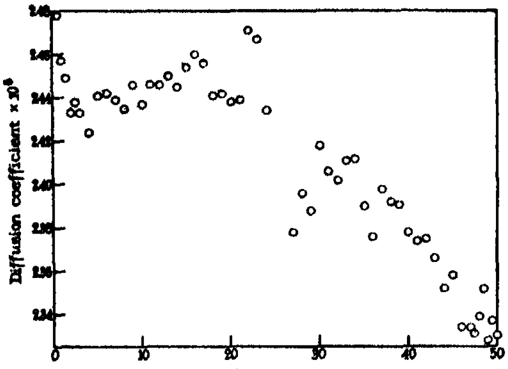

FIG. 7. A plot of the diffusion coefficient computed for each concentration fringe against the fringe number. The drift with this number is due, in part, to imperfections in the cylinder lens.

capillary. The exit slit thus represents an improvement over the Kahn-Polson procedure and yields boundaries whose sharpness is comparable with that of a shearing mechanism.

Except possibly in the case of the lowest Gouy fringes in the early photographs the stagnant solution in the exit slits of the glass cell does not appear to be a source of error. Computations for a 50-fringe system indicate that the path difference over the width of this slit is less than two wave-lengths after 515 sec. in the case of sucrose at 1° and 133 sec. for potassium chloride. At such early times the proportionality between the deflection and the gradient at the center of the boundary probably fails also[16] and the slit error is thus simply superimposed thereon.

Although the metal cell, with its reference channel, is the more adaptable of the two cells it is my impression that it is also more prone to warp. For example, as the metal cell has aged it has become difficult to close the exit slit completely. Although incomplete closure of this slit is not a source of error, if the stopcocks of the two reservoirs are also closed at zero time, it does indicate the difficulties in annealing the steel so that it will retain its shape. Similar experiences with a Claesson-type cell have made me skeptical of stainless steel as a satisfactory material for diffusion cells.

In the case of the optical system shown in Fig. 4 the horizontal spacing of the fringes increases as the separation of the masking slits decreases. In order to obtain precision in the measurement of the fractional part, *F*, of the total fringe number it is essential, therefore, to keep the partition between the reference and diffusion channels thin and in the metal cell it was possible to do this. It is also possible to do this in a glass cell if the windows are cemented but difficulties remain to be overcome if the windows are clamped. In this connection it may be noted that, caused, apparently, by the inhomogeneity of the green line in the *H*4 lamp, interference is not observed if the path difference is excessive. Thus one cannot use a limb of the Tiselius cell as a diffusion channel with the reference path through the adjacent thermostat water unless duplicates of the channel windows are included in this path. When this is done, however, the concentration fringe method may be used with this cell and preliminary experiments indicate that greater precision can be achieved thereby in the electrophoretic analysis of a protein mixture, say, than with the schlieren scanning procedure.

Although the present diffusion measurements were obtained with a twin lens system, i.e., parallel light through the thermostat and cell, the results with a single lens or convergent light system were the same. This affords experimental confirmation of the conclusion[2] that the spacing of the Gouy fringes is the same in both systems if the "optical lever arm," *b*, is determined correctly. In the convergent light system *b* is the optical distance from the center of the diffusion channel to the focal plane of the schlieren lens and was measured directly to the nearest 0.001 in. by means of a 9 in. micrometer, a set of seven 8 in. to 9 in. rods calibrated therewith and shorter telescoping rods. In determining the distance from the photographic emulsion to the thermostat window, for example, the calibrated rods were placed, end to end, in a brass tube whose length was somewhat less than the distance being measured and a telescoping rod set to fill the remaining gap. Its length was then determined with the micrometer and added to that of the rods. In the parallel light system *b* is the distance from the second principal plane of the second spherical lens to the focal plane. In order to avoid locating the principal planes of this lens the displacement of Rayleigh fringes by a prism that had been calibrated in the convergent light system was used in determining *b* for the parallel arrangement.

ACKNOWLEDGMENT

It is a pleasure to acknowledge my indebtedness to Mr. Emil Maier of the Pyrocell Manufacturing Company for his care and ingenuity in the construction of the glass cell and to Dr. D. A. MacInnes of this Institute for his critical review of this report.

---

[16] Harry Svensson, Arkiv f. Kemi. Miu. Geol. 22A, No. 10, 1 (1946).

THE REVIEW OF SCIENTIFIC INSTRUMENTS VOLUME 21, NUMBER 6 JUNE, 1950

Balloon-Borne Instrumentation for Neutron Detection*

MELVIN PAVALOW, WILLIAM O. DAVIS,† AND WILLIAM P. STAKER
Research Division, New York University, University Heights, New York, New York

(Received March 6, 1950)

A description is given of balloon-borne proportional counters and circuitry for telemetering and recording cosmic-ray neutron intensities. The preamplifier, amplifier, scaler, and trigger circuit described all use low drain directly heated battery-type tubes. Methods and reasons for pressurization of high voltage circuits are discussed. Included is a description of a multiple-level flight technique using single large plastic balloons for long time intervals at pre-set altitudes.

INTRODUCTION

To measure the neutron intensity as a function of altitude, BF_3 counters with suitable instrumentation were flown by means of free balloons to very high altitudes. In common with all balloon-borne cosmic-ray instruments it was essential that the circuitry and counters be as lightweight as possible. In addition, atmospheric neutron intensities are in general low, so that special attention must be paid to obtaining adequate statistics when measurements are made. This may be accomplished by using large counters, by increasing the pressure of the counter to increase its efficiency, or by operating the counters for a long period of time. Increasing the pressure of the counter would mean a higher operating voltage, thus using a large power supply and increasing the danger of corona, or alternatively, a high gain amplifier with very good stability which in turn would require more tubes and batteries, thus increasing the weight of the instrument. A compromise was reached by using a reasonable size counter, a medium gain amplifier, and operating for a long time at desired altitudes by means of a two-level balloon technique.

Most previous experimenters[1] have used a cadmium shield to discriminate against background in the measurement of slow atmospheric neutron intensities. In view of recent calculations by Davis[2] which show that a sizeable proportion of neutrons in the atmosphere are captured at energies above the cadmium cut-off, it is seen that such instrumentation will not give a true picture of the neutron intensity. In the present experiment, two counters were used, identical in construction and filled to the same pressure, but with one containing isotopically enriched BF_3 (96 percent B^{10}) and the other one containing isotopically depleted BF_3 (10 percent B^{10}).[3] If counters A and B are exposed to the same neutron flux, containing the same background of recoils and other cosmic-ray events, then the neutron intensity, N, is given by: $N=(A-B)/0.86$, and the background, b, is: $b=B-0.1N$; where A is the counting rate of the enriched counter, B that of the depleted counter, and N is the neutron intensity which would be measured by a counter filled with BF_3 containing only the B^{10} isotope.

This form of instrumentation effectively eliminates the high energy recoils and other background since B^{11} would presumably be as effective as B^{10} in this type of event. It has a major advantage over the cadmium shield method in that all neutrons are counted rather than merely those in the lowest energy region. In addition, there is no cadmium shield around one counter so no correction factor nor auxiliary tin shield is needed around the second counter.

A general block diagram of the circuit used is given in Fig. 1. It will be noted that the counters are operated with the outer cylinder at a high negative voltage and the central wire near ground potential. The purpose of this arrangement was to avoid the necessity of a large blocking condenser between the counters and the amplifier and also to avoid the necessity of bringing a high voltage line out of the pressure shield, or placing a bulky condenser inside. The purpose of the pressure shield will be discussed later.

The leads from the center wires of the counters emerge from the pressure shield through a hermetic seal and feed into the two sides of a single-pole-double-throw microswitch. The microswitch is actuated by a wooden rod, cam-driven by the program motor. The cam is cut for a two-to-one ratio of times. The cam wheel is geared to turn at approximately ⅓ r.p.m., giving approximately 3 min. on one counter and 1½ on the other. At the time of switching from one counter to the other, an auxiliary contact in the switching motor causes the telemetering transmitter to be modulated so that the time of switching may be recorded. This switching signal is different for the two positions so that it is possible to tell at once which counter is being recorded.

The counter pulse, taken from the microswitch, is fed into a simple cathode follower preamplifier and then into a two-stage resistance-coupled amplifier. A scale of four follows which is also a pulse-shaping circuit, and from here the pulse goes to the trigger circuit. Since a relatively low frequency a-m telemetering sys-

---

* Assisted by the joint program of the ONR and AEC, and by the USAF.

† Major, USAF, now assigned to USAF Special Weapons Command, Kirtland Air Force Base, Albuquerque, New Mexico.

[1] Agnew, Bright, and Froman, Phys. Rev. 72, 203 (1947); S. A. Korff and E. T. Clarke, Phys. Rev. 61, 422 (1942); S. A. Korff and A. Cobas, Phys. Rev. 73, 1010 (1948); and L. C. L. Yuan, Phys. Rev. 76, 165 (1949).

[2] W. O. Davis, Phys. Rev. (to be published).

[3] Obtained from the Isotopes Division of the Oak Ridge National Laboratory of the AEC.

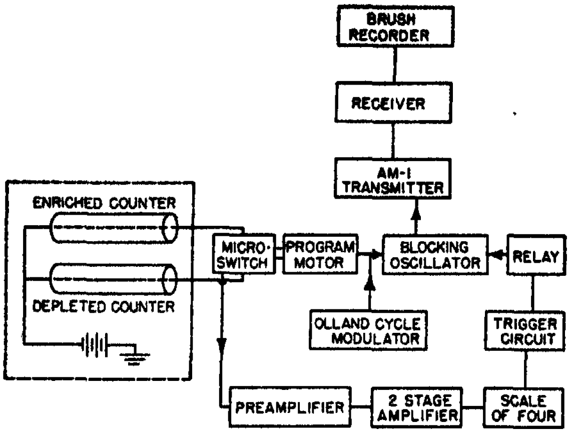

FIG. 1. General block diagram.

tem was used for maximum range (up to 500 miles), it was necessary for each count signal to be lengthened to about 0.2 sec. so that its characteristic modulation might be distinguished from random noise at great distances. Therefore, a scaler was found to be necessary because of the required long time constant of the trigger circuit.

The trigger circuit (a univibrator) contains the primary of a relay in its plate circuit. The relay secondary is in series with a resistor connected between the grid of a blocking oscillator and ground. When the relay closes, the blocking oscillator operates and modulates the transmitter. The auxiliary contact in the program motor and an Olland cycle pressure modulator[4] also cause modulation of the transmitter. The transmitted signal is received on a Hammarlund Super-Pro 400X receiver[5] feeding a Brush pen oscillograph.[6]

APPARATUS

The BF_3 proportional counters used in these experiments were especially filled in this laboratory. Commercial tank BF_3 was found to be unsatisfactory for the purpose. In addition to containing 20 percent B^{10}, a percentage which was not desirable for our purposes, counters filled with this gas were found to exhibit poor plateau characteristics even after multiple distillation. The gas appeared to contain impurities which could not be driven out in the purification process. It was concluded that even a fraction of a percent impurity had noticeable effect on the behavior of the counters.

A complex of $BF_3(BF_3\cdot CaF_2)$ in powder form was obtained both in the 96 percent B^{10} form and in the 10 percent B^{10} form. The powder was heated in an electric oven to drive off the gaseous BF_3, which was then filtered, passed through a dry ice and alcohol trap to remove water vapor and other high freezing-point impurities, and passed into the distillation system. Here the gas was frozen out in a liquid air trap and the system pumped out carefully. The liquid air was then removed and the BF_3 permitted to return to the gaseous state. On the basis of experiment, this process was repeated five or six times to be sure that most impurities were removed. The gas was then stored in a flask from which counters were filled. After pumping out, counters were outgassed in an oven for periods up to 24 hr. and then filled to a pressure of 17.6 cm Hg with the purified BF_3.

Each counter was calibrated in the following manner. First, a plateau check was made to be sure that each counter operated in the correct region and exhibited acceptable plateau characteristics. Counters were then checked for contamination background inside a boron shield. In all cases this background was found to be less than $\frac{1}{4}$ c.p.m. Counters were then given a long run close to a neutron source at their operating voltage using the same amplifier and scaler with which they would be flown. The counting rate was computed and compared with the counting rate of a standard reference counter given a similar run with the same equipment immediately thereafter.

It was not deemed feasible to make an absolute calibration of counters, since the distribution of neutron energies in paraffin or any other usual moderator is not the same as encountered in the atmosphere. Short of using a velocity spectrometer or some other device, it did not seem possible to make a calibration which would be of any value in determining the absolute sensitivity to atmospheric neutrons. Instead, one counter was used as a standard and others checked against it. When counters operated correctly there was never a deviation from the standard greater than the statistical fluctuation.

At the operating voltage deemed most suitable, the average pulse developed by a neutron is approximately 0.01 volt and 10^{-5} sec. in duration. The amplifying

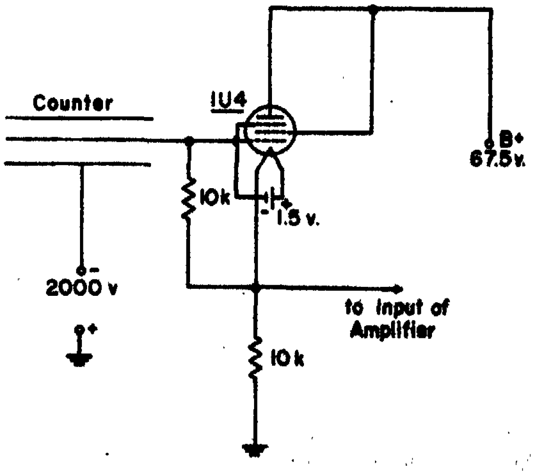

FIG. 2. Preamplifier.

---

[4] K. O. Lange, Bull. Am. Meteor. Soc. 18, 107 (1937); E. T. Clarke and S. A. Korff, J. Frank. Inst. 232, 217 (1941).

[5] Hammarlund Manufacturing Company, New York 1, New York.

[6] Brush Development Company, Cleveland, Ohio.

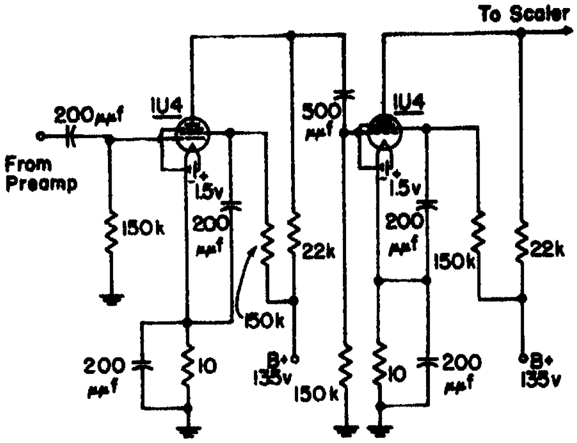

FIG. 3. Two-stage resistance-coupled amplifier.

system must therefore favor pulses of this size and discriminate against smaller and faster pulses.

The preamplifier (Fig. 2) chosen is a cathode follower. It meets the necessary requirements of providing a high impedance match to the proportional counter and a low impedance match to the amplifier. Other advantages of the cathode follower are that the output pulse is almost identical to the input pulse and of the same polarity. In addition, its degenerative feedback results in good stability and improves the circuit performance with respect to the variations in supply voltage. Its one disadvantage, however, is that it has less than unit voltage gain.

With a grid resistor of 10k ohms, an excellent reproduction of the input pulse was found at the output of the preamplifier. If a grid resistor of higher resistance were to be used, the pulses would be lengthened considerably. For example, a one-megohm grid resistor was found to lengthen the pulses by a factor of ten. This caused a large build-up of gamma-ray pulses from the source used for calibration, with the result that even though the bias of the amplifier was set to eliminate gamma-ray pulses, many large build-ups were occurring which rivaled neutron pulses in size.

The cathode follower consists of a 1*U*4 tube with a filament voltage of 1.5 volts and a filament current of 50 ma. The plate voltage is 67.5 volts with a plate current of 0.2 ma, and the over-all gain of the preamplifier is 0.8.

The resistance-coupled amplifier (Fig. 3) consists of two 1*U*4 tubes with plate voltages of 135 volts and plate currents of 0.1 ma. The maximum gain of the amplifier is found at 50 kc with its half-power points at 25 kc and 150 kc.

Because of possible feedback, each section of the amplifier has its own filament supply with the bias voltages developed across the cathode. The rise time of the amplifier is 1.1 μsec. while the delay time is 0.65 μsec. These small time constants are an advantage in that they allow the amplifier to recover quickly from a pulse, thus permitting fast resolving times.

The scaling circuit (Fig. 4) is a form of the Eccles-Jordan circuit consisting of two 3*A*5 tubes which are directly heated 1.5 volt dual triodes. Each tube makes up a scale of two. The filament current is 220 ma and the bias voltage for each section of the tube is developed across a common cathode biasing resistor in the filament circuit. The plate voltage is 135 volts with 1.2 ma flowing in the conducting tube and 0.6 ma flowing in the non-conducting tube. The circuit will handle approximately 10^5 evenly spaced pulses per second.

Without exception, all components in this scaling circuit are very critical. The components which are to be given extra special consideration are the plate resistors which have to be within 10 percent of each other and the grid and feedback resistors which have to be within five percent of each other. Another important factor that was taken into consideration in the design of the scaling circuit is the constant decrease of battery voltage with time during a flight. It was found that the circuit would work efficiently with a decrease of 20 percent in its voltage supply.

The output of the scaling circuit is passed through a differentiating circuit and on to the grid of the univibrator trigger circuit (Fig. 5). The univibrator is used to modulate the transmitter. It consists of one 3*A*5 tube with a plate voltage of 135 volts. The bias voltage is developed across the 2500-ohm resistor in the filament.

Individual trigger units sometimes were found to have a tendency to oscillate. When the mutual coupling between the plates and grids of the univibrator is purely capacitive, the bias voltage for both triodes is developed across the common cathode resistor. If the capacitor only had a resistance of 50 megohms, there was found to be current flow through the grid resistor, thereby adding an additional bias to the grid of the tube. This additional voltage caused the circuit to oscillate. There-

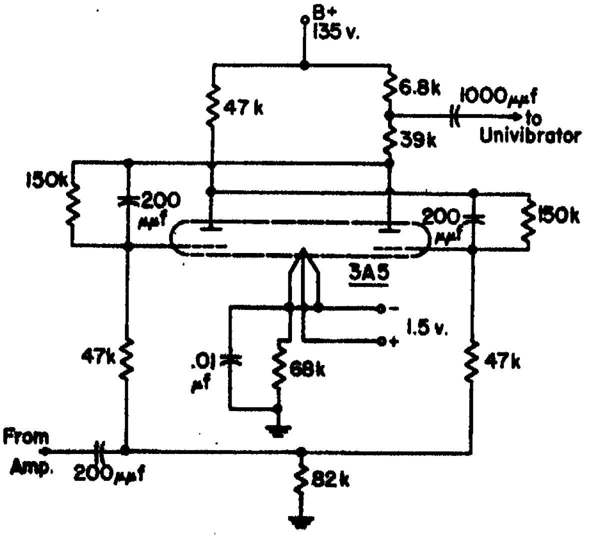

FIG. 4. Scale of two. A scale of four can be made by adding an identical scale of two to the output of the first scaler.

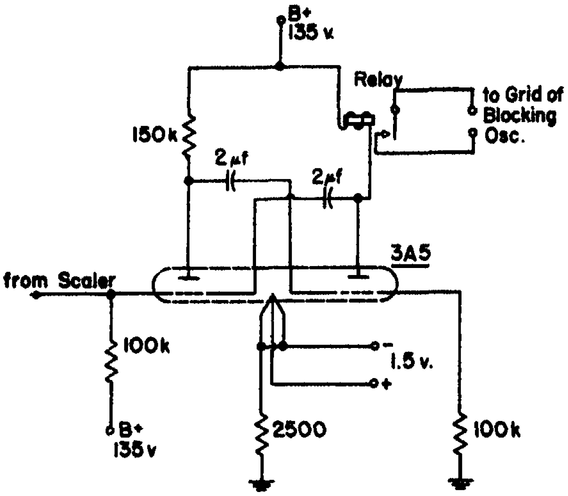

FIG. 5. Trigger circuit (univibrator).

fore only condensers with very high internal resistances, of the order of 1000 megohms, could be used.

A Sigma[7] relay (41*R*-5000G) is placed in the plate circuit of the second triode. The secondary of the relay is connected to the grid circuit of the blocking oscillator. The blocking oscillator is used to audio-modulate the transmitter. The length of time that the transmitter is modulated depends upon the time constant of the univibrator. The lightweight *AM*-1 transmitter used was designed especially for long-range flight by L. Hillman[8] of the New York University, College of Engineering, Research Division.

Two ground stations were used where possible, one at the launching site and one several hundred miles downwind, so that data could be recorded for a maximum possible time. These stations were identical, each consisting of a Hammarlund Super-Pro receiver feeding a Brush oscillograph. It is also necessary to receive information regarding the pressure at every moment during flight. The Olland cycle modulator is used for this purpose. The Olland cycle pressure modulator, as presently designed, contains a standard Signal Corps *ML*-310*E* radiosonde aneroid unit, a rotating cylinder of insulating material with a metal helix wound around the cylinder, and a 6-volt electric motor which rotates the cylinder. There are two contacting pens which ride on the cylinder and conduct electrical current when they touch the helix. One pen is fixed in position and makes a contact at the same time in each revolution of the helix. This contact is used as a reference point for measuring the speed of rotation of the cylinder. The time that the second pen, which is linked directly to the aneroid cell, makes contact with the spiral is dependent on the cylinder speed and on the pen position which is determined by the pressure. By an evaluation chart, the atmospheric pressure can be determined as a function of the relative position of the pressure contact as compared to the reference, thus eliminating all rotation effects other than short term motor speed fluctuations. The advantage of this system of modulation over the conventional type normally used for meteorological observations is that one can detect smaller fluctuations in pressure without ambiguity. The conventional type of Diamond and Hinman[9] apparatus adopted by the U. S. Weather Bureau does not allow one to know, when the balloon has been floating, whether it is ascending or descending until it crosses a reference point, which may be after a considerable length of time.

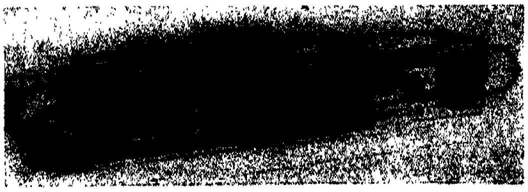

FIG. 6. Flight set.

As a result of a number of tests, it was determined that for consistent results without spurious counts the counters and high voltage system should be pressurized. Lack of this is evidenced by extra counts at atmospheric pressures corresponding to about 40,000 ft. or higher. These spurious counts can be traced to a corona discharge taking place between some point of the high voltage system and the frame. In addition, it has been noticed that within high voltage batteries themselves there appears to be a corona discharge when the pressure of the air surrounding them is less than 185 mb.

The method shown in Fig. 6 was used as the simplest expedient for obtaining a pressure tight system for these units. As it shows, the high voltage batteries are mounted in an aluminum box on the lower shelf of the frame. The circuit batteries are mounted on the same shelf so that all heavy materials are in the center and below the two counters. The pressure system, except for connecting tubing, is constructed of welded aluminum. Pressure gaskets are used to seal the lid on the box and the end plates on the counter containers. The high voltage leads to the counter cylinders from the battery box are contained in copper tubing sealed by means of standard flare pressure fittings. The low voltage leads from the central wire of the counter emerge through pressure fittings sealed by Neoprene gaskets and are fed to the microswitch through metal braid shielding.

The flight frame was designed to provide a minimum of scattering or star-producing material in the hemisphere above each counter, and in addition, the counters are mounted with their longitudinal axes in line so that a minimum solid angle is subtended by one counter upon the other. The entire circuitry is on one shelf above the batteries. Units are mounted individually so that in case of malfunction in the field any element may be removed and replaced without detailed trouble-shooting being required at the time. This precaution has proved invaluable on field trips, enabling changes to be made where necessary without requiring elaborate laboratory facilities on the spot. Batteries are connected to individual components by means of chassis connectors and spare packs are available so that in case of doubt a complete circuit battery change can be made instantly.

---

[7] Sigma Instruments, Inc., Boston 21, Massachusetts.

[8] L. Hillman, Radio-Electronics (December 1948).

[9] Diamond, Hinman, and Dunmore, J. Research Nat. Bur. Stand. 18, 73 (1937); 20, 369 (1938); and 25, 327 (1940).

The frames themselves are of aluminum angle stock and are of all welded construction to insure strength and good electrical bond. A common point is chosen to which all circuits and the counter batteries are grounded. This is essential for proper operation of equipment which cannot be connected to an earth ground.

The transmitter, blocking oscillator, and Olland cycle modulator are a self-contained unit in a separate box which is bolted to the flight frame. The entire unit weighs approximately 57 lb. and is suspended from the balloon by means of four eyebolts on the top of the frame. To shield against outside electrical noise pick-up, the entire circuitry is surrounded by copper screening. Before flight the entire apparatus is wrapped in double Cellophane to maintain batteries at above freezing temperatures by means of the "greenhouse" effect.

MULTIPLE-LEVEL TECHNIQUE

The use of non-extensible balloons has become common in the past three years because of the large load they can lift and their inherent stability when floating at their maximum altitude. A non-extensible open-appendix balloon will tend to float at the altitude where it has just valved enough gas to make the lift equal to the load. In this work, it was desired to utilize this characteristic to obtain long times at two constant levels.

Flights were launched carrying a large amount of liquid ballast in the form of aircraft compass fluid which has excellent low temperature viscosity characteristics. The balloon would then level off at an altitude corresponding to a lift just equal to the total load, including the ballast. After a desired time interval, a chronometric switch would fire electrically operated explosive squibs to open a drain in the bottom of the ballast reservoir and permit ballast to drain out. After all ballast has gone a second squib was used to cut the supporting line and permit the ballast reservoir to descend by parachute. As a result of this loss of weight the balloon would then ascend to a new equilibrium altitude where it would again float.

In this manner it was possible to compare counting rates at two different altitudes with excellent statistics. The spread in altitudes obtainable by this process is about 10,000 to 15,000 ft. at 50,000 ft. with the payloads used in these experiments. For smaller payloads the spread could be made greater. The advantages of this method for application to specific measuring problems are obvious. The major disadvantage is that the launching of large plastic balloons calls for experienced crews, large launching areas, and low surface winds.

The authors would like to express their appreciation for the guidance and assistance of Professor S. A. Korff, Director of the New York University Cosmic-Ray group. In addition, they would like to acknowledge their indebtedness to the New York University Balloon Project, under the technical direction of William Murray and J. R. Smith, for making the balloon flights, and to M. J. Swetnick, H. Neuburg, and L. G. Collyer for assistance in the filling of counters and the construction of flight sets.

Announcement

From time to time, the Institute has received inquiries from subscribers for information as to where and how they may have their copies bound. After investigation the Institute has found that this may be best accomplished by selecting a capable bindery that will work to our specifications and produce a well-bound volume at as low a price as possible. The necessary arrangements have been completed with the Book Shop Bindery, 308 West Randolph Street, Chicago 6, Illinois.

The volumes will be bound in the best grade of washable buckram with facsimile gold stamping on the spine and the subscriber's name in gold on the front cover. A distinctive color for each of the Journals has been selected as listed below. Advertising matter and covers are removed before binding. The price of $3.00 per volume applies to any of these journals regardless of size. Issues, comprising complete volumes, should be sent by prepaid express or parcel post to the Book Shop Bindery. Bound volumes will be shipped approximately 30 days after receipt. Return transportation will be prepaid when remittance accompanies order.

No deviation in color or specification can be allowed in view of the favorable price.

Physical Review	Green
Reviews of Modern Physics	Orange
Journal of the Optical Society	Brown
Journal of the Acoustical Society	Orange
American Journal of Physics	Black
Review of Scientific Instruments	Grey
Journal of Chemical Physics	Blue
Journal of Applied Physics	Red
Physics Today	Purple

THE REVIEW OF SCIENTIFIC INSTRUMENTS VOLUME 21, NUMBER 6 JUNE, 1950

Nuclear Emulsions and the Measurement of Low Energy Neutron Spectra*

Norris Nereson and Frederick Reines
Los Alamos Scientific Laboratory, Los Alamos, New Mexico

(Received March 8, 1950)

An experiment was performed with Ilford Type *C2* nuclear emulsion to determine the usefulness of photographic plates for measuring neutron fluxes and spectra by proton recoils in the region of the low energy limit of the emulsion. The results show that the plates give valid data for neutron flux determinations and energy distributions down to a neutron energy of about 0.5 Mev. Below 0.5 Mev the proton recoils give low values for the number of incident neutrons but approximate results can be obtained down to 0.3 Mev by applying a correction factor in this energy region. The experimental results permit a range-energy curve for protons in *C2* emulsion to be determined for the energy region from 0.2 to 1.5 Mev. Finally, recoil proton energy distributions obtained from neutron irradiations of *C2* plates at various low energy values are presented and discussed.

INTRODUCTION

SEVERAL recent experiments at the Los Alamos Scientific Laboratory have involved the measurement of neutron spectra by means of nuclear emulsions. Frequently, the interesting part of the spectrum has occurred in the 0.1 to 1 Mev energy decade which contains the low energy limit above which nuclear emulsions can be used for measuring neutron or proton energies. Some investigations have been made of the high energy limit of nuclear emulsions but very little information has appeared on the reliability of nuclear plates at low energies. Therefore, the chief purpose of this investigation has been to determine the practical low energy limit of proton recording nuclear emulsions and the reliability of these emulsions at low energies for measuring neutron spectra. The work has been restricted to measurements of proton recoils making a small angle with the direction of the incident neutron.

EXPERIMENTAL TECHNIQUE

In order to ascertain the usefulness of nuclear plates at low energies, the plates were given neutron irradiations at various energies from 0.24 to 1.54 Mev. The Los Alamos Van de Graaff machine and the reaction $H^3(p,n)He^3$ were used for the exposures as shown in Fig. 1. The plates were placed at 0° with respect to the proton beam, with their emulsion surfaces parallel to the beam. Each plate was exposed to the same number of neutrons as monitored by a long counter[1] placed $1\frac{1}{2}$ meters from the target. This type of counter has a response which is flat to within 10 percent over the range of neutron energies used in this experiment.

The spread of neutron energies arising from the target assembly of the Van de Graaff was minimized by having the tritium at a low pressure equal to 15 cm of mercury. This resulted in a tritium thickness to protons of about 30 kev or a proton energy spread of ±15 kev. A thin aluminum foil of 1.4 mg/sq. cm separated the tritium from the proton accelerating tube. The aluminum foil thickness was determined by carefully weighing about ten samples of the foil material used in the target and then averaging these values. The energy spread arising from variations in the thickness of the aluminum foil was difficult to determine; consequences of this phenomenon are mentioned later in the section on Conclusions. Neutron energy degradation and scattering in the target were negligible since the tritium container walls were of 10-mil steel. Since the initial proton energy was accurately known, the average energy of the protons reacting with the tritium could be obtained by subtracting the aluminum foil thickness and one-half the tritium thickness from the bombarding proton energy. The neutron energy is then computed from the conservation of energy and momentum and the known Q of the reaction.

Care was taken to minimize the number of scattered neutrons entering the emulsion by holding the plate at the back with a very light support. Also, the tritium target was well in the clear and distances to large scattering objects were great compared with the distance from the target to the plate. However, in spite of the above precautions, scattered neutrons seem to have slightly influenced the results.

Ilford *C2* plates (batch number *Z2283*) were used in the experiment. The average thickness of the emulsion measured about 85μ before processing and between 34 and 37μ after processing. The plates were analyzed with microscopes using a 90× oil immersion objective (N.A. of 1.3) and a 12× compensating eyepiece. One of the eyepieces contained a suitable measuring scale and the other a 20° angle with bisecting line. The area analyzed on the 1×3-in. plates was restricted to a small section 1 cm long by 2 mm wide about the center line of the plate; this section was started about 5 mm from the front edge of the plate. By confining the area studied to this region, the maximum angle which a neutron from the tritium target could make with the plate center line was 2°. The average angle of the incoming neutron was about 1° and this accuracy is well within the limits of error of the measurements described below.

---

* This document is based on work performed at Los Alamos Scientific Laboratory of the University of California under U. S. AEC Contract W-7405-Eng-36.

[1] A. O. Hanson and J. L. McKibben, Phys. Rev. 72, 673 (1947).

The method of analysis was similar to that used by Richards[2] and consisted of measuring the proton recoil tracks about a small angle in the forward direction. The angle was restricted so that only tracks making an angle of less than 10° with the center line of the plate were measured. Due to film shrinkage during processing, the 10° angle limitation restricts the original azimuthal angle of the proton track to a maximum of 23° to 25°, depending upon the amount of shrinkage.

In order to select data containing a minimum number of tracks which penetrated the emulsion surface, tracks originating in a small thickness of emulsion on the top and bottom were ignored. For energy values above 1 Mev, two microns of emulsion thickness were skipped at the emulsion surface and for values below 1 Mev, the thickness ignored was one micron. Using this procedure, less than one percent of the total tracks measured were observed to leave the emulsion.

The plates measured in this experiment were purposely given a small neutron irradiation so as to present a useful or measurable track density of one to two tracks per microscope field (about 300,000 cubic microns). A small track density aids in several ways: (1) the possibility of obscuring short tracks by longer tracks is minimized; (2) the number of background grains produced by gamma-rays usually present with neutron sources is decreased by a short exposure; and (3) the tendency of observers to select long tracks and overlook short ones is minimized.

The difficulty in analyzing *low energy* (<0.5 Mev) proton tracks by the methods described arises not so much in measuring their lengths as in determining whether or not the azimuthal angle of the track is within prescribed limits. Since one micron is a practical limit[3] for the depth of focus in the microscopes in use here, the decision as to whether any track length less than 5.5μ (or 0.5 Mev) is within the 10° angle limit is subject to error. Therefore, measurements of proton energies below 0.5 Mev by different microscopists might be expected to differ as to the relative number of protons present in each energy interval. This difficulty might be eased by choosing a greater angle limit but such a choice would decrease the energy resolution of the method and the corrections to be applied to the observed proton energy become quite large. However, for spectra which vary slowly with energy, a large angle limit for the tracks is a less serious objection. Another aid for increasing the accuracy in determining the azimuthal angle of short, as well as long, tracks might be a tilting stage microscope.[4]

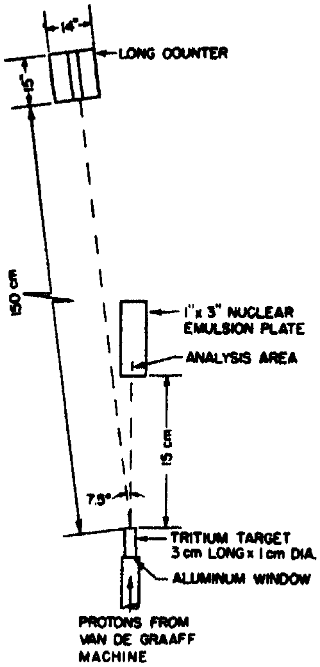
14"
LONG COUNTER
15"
150 cm
1"x 3" NUCLEAR EMULSION PLATE
ANALYSIS AREA
15 cm
7.5°
TRITIUM TARGET 3 cm LONG x 1 cm DIA.
ALUMINUM WINDOW
PROTONS FROM VAN DE GRAAFF MACHINE

FIG. 1. Experimental arrangement.

TABLE I. Experimental data.

Bombarding neutron energy in Mev	Microscopist	Forward proton recoils per 10^6 cubic microns of processed emulsion	σ_p in barns	R_0[a]	R[b]	Uncorrected mean proton range in microns	Proton energy in Mev associated with uncorrected mean range
0.24	1 2	5.1 ±0.3 4.6 ±0.3	9.2	0.46±0.03	0.46±0.03	1.85±0.2 1.85±0.2	0.22
0.35	1 2	4.8 ±0.3 6.0 ±0.4	7.6	0.64±0.04	0.64±0.04	3.15±0.2 3.35±0.2	0.33
0.47	1 2	6.7 ±0.4 6.8 ±0.4	6.4	1.00±0.05	0.93±0.05	4.7 ±0.2 4.5 ±0.2	0.44
0.68	1 2	5.6 ±0.4 5.45±0.3	5.3	1.04±0.05	1.02±0.05	7.9 ±0.2 7.6 ±0.2	0.64
1.06	1 2	4.6 ±0.3 4.4 ±0.3	4.2	1.07±0.05	1.03±0.05	14.2 ±0.5 15.0 ±0.5	1.00
1.54	1 2	4.2 ±0.2 3.8 ±0.2	3.45	1.16±0.04	1.08±0.04	25.2 ±0.5 25.5 ±0.5	1.48

[a] R_0 = Average forward proton recoils (per 10^6 cubic microns of processed emulsion) divided by $\sigma_p \times 10^{24}$. Values obtained for R_0 at 0.24, 0.35, and 0.47 Mev have been multiplied by 0.87, 0.90, and 0.95, respectively, to adjust for the inefficiency of the long counter monitor at these energies.
[b] $R = R_0$ corrected for background (scattering) effect. (See the section on Conclusions.)

---

[2] H. T. Richards, Phys. Rev. 59, 796 (1941).
[3] Some experienced microscopists state that they can discern 0.5μ differences in depth measurements.
[4] I. Barbour, Rev. Sci. Inst. 20, 530 (1949).

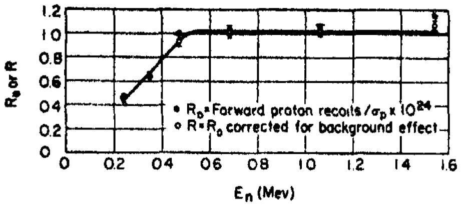

FIG. 2. Response of Ilford *C*2 nuclear emulsion to low energy neutrons.

Since the personal element enters into an experiment of this type, the more important results of the experiment have been based upon the findings of two experienced microscopists working independently.

EXPERIMENTAL RESULTS

1. Application to Flux Measurements and Monochromatic Neutrons

Since all the plates were bombarded with the *same* number of neutrons, each plate at a different energy, the number of recoil proton tracks in the forward direction should also be equal after being corrected for the variation with energy of the *n, p* collision cross section (σ_p) and background effects. These results are tabulated in Table I and are shown graphically in Fig. 2. The solid circles illustrate the nuclear emulsion response (R_0) to neutrons as determined by dividing the number of forward proton recoils (for equal emulsion volumes) by the *n, p* cross section. The open circles provide a better approximation for the emulsion response (R) to neutrons, as these points represent the R_0 values corrected for background effects (see the section on Conclusions). The two high neutron energy values at 1.54 and 1.06 Mev were analyzed in order to provide data in an energy region where the use of nuclear emulsions is known to be valid. However, the reliability of these two points is weakened to a certain extent since the background effect increased with energy. The values obtained below 0.5 Mev have been corrected to take into account the variation in response of the long counter monitor. The long counter used in this experiment had a sensitivity of 95 percent at 0.5 Mev and drops to 85–90 percent in the 0.2- to 0.4-Mev region.

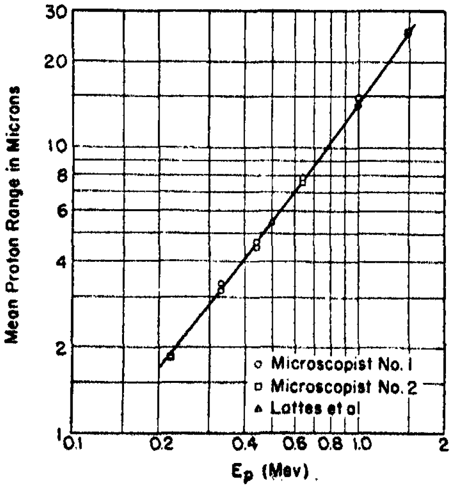

FIG. 3. Range-energy curve for protons in Ilford *C*2 emulsion at low energy values.

Figure 2 provides information on the reliability of nuclear plates for measuring neutron fluxes at various energy values, i.e., the point at a certain energy represents *all* the forward proton recoils, irrespective of their energy, arising from the bombarding neutrons of this energy. The results show that the corrected number of proton recoil tracks remains essentially constant until the 0.47-Mev point is reached. Therefore, one would conclude that nuclear emulsion data provide correct experimental values for the relative number of neutrons arising from monochromatic sources, except below 0.5 Mev. Data taken at neutron energies below 0.5 Mev by the above technique will be in error. It seems satisfactory to utilize as approximate data these low flux values in the energy region from 0.3 to 0.5 Mev if they are appropriately corrected according to Fig. 2. It should be emphasized that these corrected measurements at energies below 0.5 Mev are less reliable and subject to greater error than measurements at higher energies.

The result at 0.24 Mev is low by a factor of two. The agreement obtained here between the two microscopists is considered to be somewhat fortuitous. Comparison of spectral curves from different readers lends support to this contention. The use of the data obtained by the method of analysis employed here cannot be recommended for this low energy. In consequence, microscopists have also found that the determination of track acceptability in this energy range, that is, whether they fall within prescribed angular limits, is very time-consuming. Furthermore, there exists the possibility that the background grains may occasionally give the appearance of very short tracks.

2. Proton Range-Energy Relation

As a by-product of these investigations involving known neutron energies, it was possible to determine a proton range-energy curve in *C*2 emulsion in the region from 0.2 to 1.5 Mev. For each neutron energy, a plot was made of the number of proton recoil tracks (in the forward direction) measured at each division of the microscope eyepiece scale. Each division was equal to approximately 0.5μ. The peak of this curve was taken as an uncorrected mean range. The proton range obtained from this curve corresponds to an energy less than the neutron energy from the Van de Graaff, since most of the proton recoils are measured at a small angle to the incident neutron direction and hence are less energetic than the incident neutrons. The theoretical energy value at which a maximum occurs in a graph of proton recoil tracks per unit energy interval *versus* proton recoil energy is determined in Appendix II.

This energy value is taken to be associated with the uncorrected mean range value as determined above. The results of the analysis show that this energy is 5±1 percent lower than the neutron bombarding energy.

The data for the proton range-energy curve in the region from 0.22 to 1.48 Mev are listed in Table I and a curve is illustrated in Fig. 3. The agreement above 0.5 Mev between values from this experiment and from those of Lattes and others[5] is good. Range-energy values below 0.5 Mev obtained from the curve in Fig. 3 are listed in Table II.

3. Use of $N^{14}(n, p)C^{14}$ Reaction to Check Emulsion

Before discussing the proton recoil distributions obtained from the Van de Graaff exposures, it is appropriate to mention a side experiment which was performed in connection with this investigation as a check on the properties of the emulsion. This experiment consisted of exposing an Ilford C2 100μ plate in the thermal neutron flux of the "water boiler" at the Los Alamos Laboratory. The result should be tracks representing the sum of ranges of the proton and C^{14} arising from the nitrogen in emulsion by means of the reaction $N^{14}(n, p)C^{14}$. The energy of the protons should be 14/15 of the Q of the reaction. If an average Q value of 0.62 ±0.01 Mev is taken for this reaction,[6] 0.58-Mev protons should be observed. Previous calculations indicate that the C^{14} track comprises ~2 percent of the combined proton and C^{14} range.[7] Since the proton range was only measured to an accuracy of ±3 percent, the C^{14} track would hardly be detected in the present experiment. In this experiment, the proton source was unquestionably monochromatic so that any irregularities in the shape of the proton distribution could be traced to properties of or techniques associated with the nuclear emulsion rather than to the source.

The plate was analyzed by measuring all tracks with azimuthal angles in the processed emulsion less than 10°. The horizontal projections were measured rather than the actual track lengths. However, since the average inclination angle of the measured tracks is only 5°, the consequent error in the range is less than 0.5 percent.

The proton energy distribution derived from a measurement of about 400 tracks in this check experiment is shown in Fig. 4. The curve indicates a maximum at 0.58±0.01 Mev which agrees with the expected value. A plot of the number of tracks *vs.* range shows a maximum at 6.7±0.2μ for the combined proton and C^{14} range. This is in good agreement with the combined range value of 6.6μ obtained by Cuer.[7] The proton distribution in Fig. 4 shows a Gaussian-type curve having a half-width at half-maximum of 0.05 Mev. Evidently, this half-width must be accounted for by proton range straggling in the emulsion, the size and spacing of the grains, and observational error. Only the proton range straggling is felt to be important. The curve is quite symmetrical,[8] a result to be expected from natural range straggling. These results indicate that the nuclear emulsion yields the expected distribution curve from a measurement of monoenergetic protons.

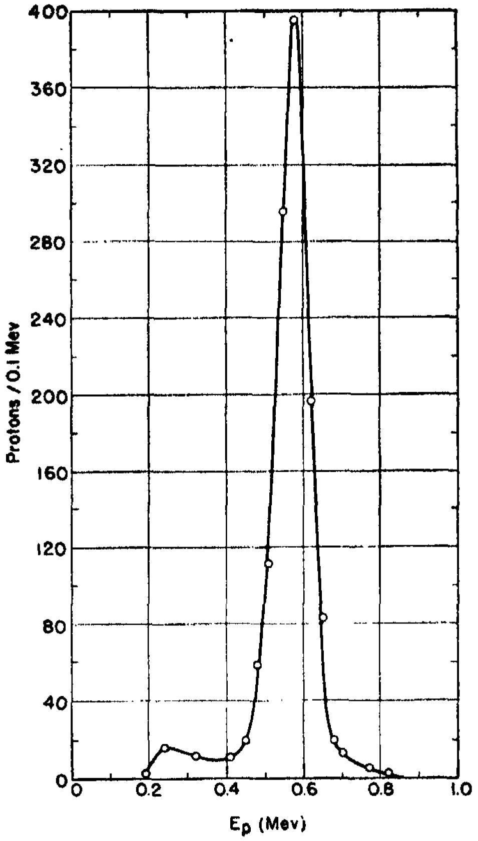

FIG. 4. Proton energy distribution from thermal neutrons on $C2$ emulsion.

4. Proton Recoil Distributions from Van de Graaff Neutrons

Returning again to the primary experiment, the energy distributions of the proton recoil tracks resulting

TABLE II.

Proton energy	Mean range in Ilford $C2$ emulsion
0.5 Mev	5.5 ±0.2 microns
0.4	4.1 ±0.2
0.3	2.8 (5)±0.15
0.2	1.7 ±0.15

---

[5] Lattes, Fowler, and Cuer, Nature **159**, 301 (1941) and Proc. Phys. Soc. **A59**, 883 (1947).

[6] See, for example, the following recent determinations for the Q-value: D. Hughes and C. Eggler, Phys. Rev. **73**, 809 (1948). Shoupp, Jennings, and Sun, Phys. Rev. **75**, 1 (1949). Franzen, Halpern, and Stephens, Phys. Rev. **76**, 317 (1949). P. Huber and A. Stebler, Phys. Rev. **73**, 85 (1948).

[7] P. Cuer, J. de phys. et rad. **8**, 83 (1947).

[8] The reason for the few low energy tracks on the extreme left side of the distribution is uncertain. A possible explanation is that they are alpha-tracks arising from some (n, α) reaction with the oxygen or nitrogen present in the emulsion.

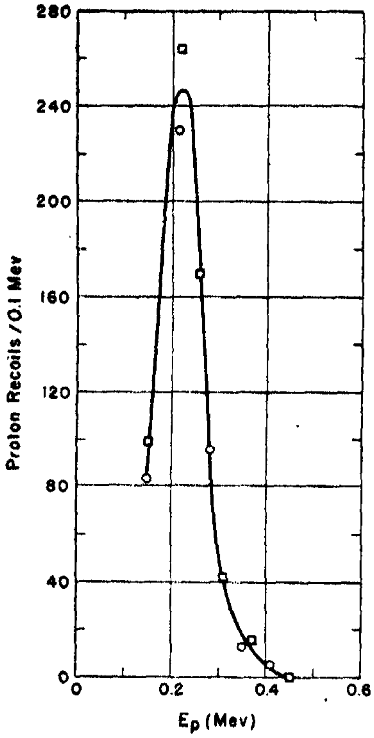

FIG. 5. Proton recoil distribution from $E_n = 0.24$ Mev.

from the Van de Graaff neutron exposures are plotted in Figs. 5 to 10 inclusive. Each graph gives the measured number of recoil proton tracks per 0.1-Mev interval as a function of the proton recoil energy. In each case the results of two microscopists are illustrated. Each set of data from a reader comprises a total of about 300 measured tracks except in Fig. 10, where, due to the larger energy spread, each microscopist measured a total of 600 tracks. Except for Figs. 5 and 6, the general shape of these curves is asymmetrical with a disproportionate number of tracks on the low energy side.

In order to determine whether the above-measured proton recoil distributions are reasonable, it was necessary to know the shape of the proton recoil spectrum admitted by the experimental geometry, i.e., by the prescribed angular limits referred to in the method of analysis. This proton recoil spectrum has been calculated in Appendix I. The result represents the proton recoil spectrum which would be obtained if range straggling or missing grain phenomena discussed below did not exist. However, the experimentally measured spectrum will be the admitted proton recoil spectrum modified chiefly by range straggling. This problem is solved in Appendix II for different straggling magnitudes. It was found that if the straggling is represented by a Gaussian curve, the best fit to the distributions was obtained by using a Gaussian half-width of 0.05 ±0.01 Mev. It is encouraging that this corresponds to the half-width obtained in examining the protons from the $N^{14}(n, p)C^{14}$ reaction (Fig. 4). The calculated spectrum using a Gaussian half-width of 0.05 Mev has been superimposed as a dashed line on the experimental data for the neutron energies above 0.24 Mev. The height of the calculated spectrum was normalized to that of the experimental curve. The agreement between the experimental and calculated distributions is quite good for the lower energy distributions but only fair for the higher energy distributions (i.e., for 1.06 and 1.54 Mev).

In all cases the disagreement occurs on the low energy side of the curve below the half-maximum value. Probable reasons for this discrepancy will be mentioned at the end of this paper.

An examination of the proton recoil distributions for points below 0.5 Mev suffices to show why the values below 0.5 Mev in Fig. 2 are too low. In both of these low energy distributions, the left side of the curves extends into the region below 0.3 Mev or track lengths less than 2.8μ. This region contains tracks consisting of about five grains and less. Track lengths which should consist of five grains may, on account of straggling, result in only two or three grains and such tracks will certainly be missed. Furthermore, as shown in Appendix III, for tracks having less than a nominal five grains, the probability that the track will appear shorter due to the chance absence of grains at either end is not negligible. For example, if the probability that any one grain is missing is[9] x, the probability of observing a

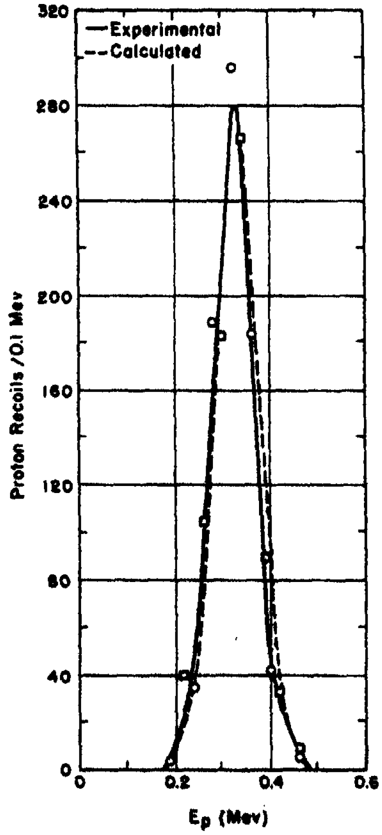

FIG. 6. Proton recoil distribution from $E_n = 0.35$ Mev.

---

[9] Direct evidence on the value of x is not available. However, it appears that in the case of alpha-particles, if development is delayed for 12 hr. as in the present work, the average grain density drops to ~80 percent of the value which obtains for

track shorter than the four-grain length it would have if $x=0$ is (cf. Fig. 17) 11 percent for $x=0.3$ and 20 percent for $x=0.5$.

Therefore, it is to be expected that distributions whose low energy regions extend below approximately 0.3 Mev will show an abnormally low track count. Note that the low energy portion of the proton recoil distribution from 0.47-Mev neutrons begins to extend into this region, and, therefore, might be expected to be in the neighborhood of the lowest energy at which a correct value could be obtained for a neutron flux measurement. Except for the case of the distribution at 0.24 Mev, no serious attempt was made to measure tracks containing less than a few grains because of the difficulty of distinguishing random background grain patterns from true tracks. More detailed study was made in the 0.24-Mev case chiefly to secure a point for the range-energy curve at this value.

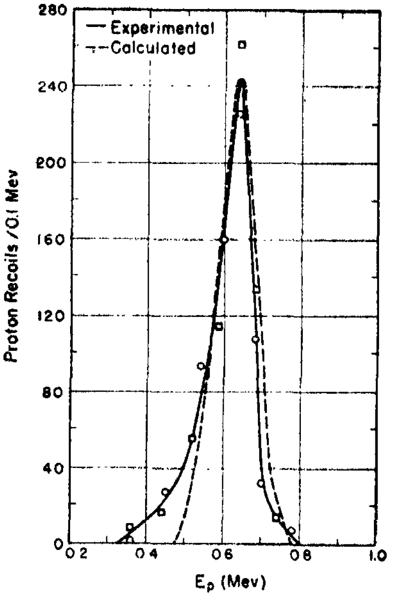

FIG. 8. Proton recoil distribution from $E_n=0.68$ Mev.

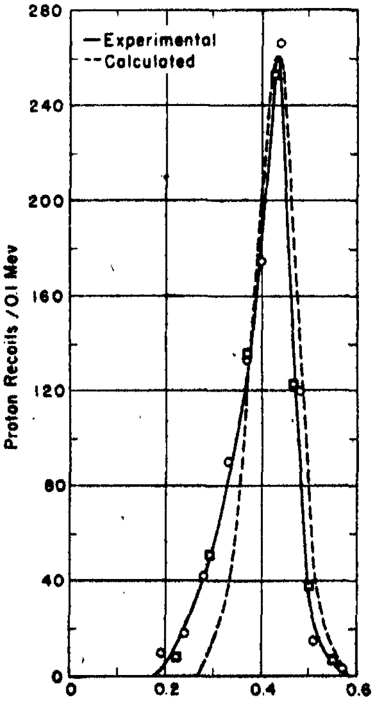

FIG. 7. Proton recoil distribution from $E_n=0.47$ Mev.

5. Application to Neutron Spectra Measurements

The results of this experiment can also be utilized to determine the usefulness of nuclear plates for measuring mixed monochromatic neutron sources or continuous spectra. In order to investigate the reliability of such measurements, suppose that a source consists of neutron groups having energies of 0.35, 0.45, 0.65, 0.85, and 1.05 Mev, with each group emitting the same number of neutrons per second. If a proton plate is exposed to such a source and analyzed by measuring recoils in the forward direction, the individual distributions from each energy value should closely resemble those drawn in Fig. 11; the measured or total proton recoil distribution curve obtained from this analysis should then be the sum of these individual distributions. The solid line distribution curves in Fig. 11 represent the Van de Graaff data (Figs. 4 through 10) which correspond best with the above-listed energies. Small errors arise from the facts that the experimental data do not exactly represent the energies in the assumed source and, where exact representation does occur, the observed maxima are slightly lower than the energies of the incident neutrons. Each of the solid curves in Fig. 11 has been normalized so as to represent data from the *same volume* of processed emulsion. The dashed curve at 0.85 Mev has been guessed, using the shape of adjacent curves as a guide.

One method of obtaining the approximate intensity distribution at the maxima of the neutron source assumed above is to determine the number of proton recoils (corrected for σ_p) occurring in 0.15-Mev[10] intervals taken about the peak of the curves. This number should be equal if the emulsion detector and the associated recording technique are energy independent. Since this is not the case, it is interesting to ascertain the useful energy range of this technique for correctly measuring neutron intensity of continuous spectra.

The number of proton recoils was obtained by summing the areas under *each* curve passing through the particular 0.15-Mev interval containing the energy value as midpoint. These sums are plotted as circles at the midpoint of each energy interval. The odd-spaced distribution at 0.35 Mev was included in order to determine the usefulness of spectrum measurements in the 0.3- to 0.4-Mev interval. The contribution to the

---

immediate development. Cf. H. Faraggi and G. Albouy, Comptes Rendus 226, 717 (1948).

[10] An analysis using 0.1-Mev intervals gave similar results.

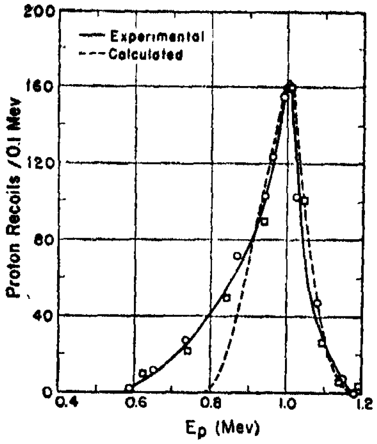

Fig. 9. Proton recoil distribution from $E_n = 1.06$ Mev.

0.35-Mev interval from the 0.55-Mev distribution is drawn as a dotted line at the base of the 0.275- to 0.425-Mev interval.

The numbers of proton recoils divided by σ_p are plotted as triangular points in Fig. 11; this curve exhibits a constant region at the high energy end and drops off at the low energy end. The curve is not plotted beyond the 0.85-Mev interval because the experimental data at higher energies are less reliable. (See the section on Conclusions.) The main point of this analysis concerns the low values obtained at 0.35 and 0.45 Mev as compared to the results at 0.65 and 0.85 Mev; this comparison demonstrates the decreased efficiency of the emulsion for measurements at low energies. In order to give the correct number of neutrons the point at 0.45 Mev should be increased by 10 percent and the one at 0.35 Mev by about 50 percent. Since the long counter has a sensitivity of around 90 percent at 0.35 Mev, this correction should be raised to 55 percent. Although no measured value is available for the point at 0.55 Mev, a reasonable interpolation indicates that this value should be increased by five percent or less. These results are similar to those discussed in connection with Fig. 2. The lack of proton recoils in the low energy distributions is due chiefly to the large straggling effects. These straggling effects produce tracks which will be missed either because they are too short or because they lack too many grains to be recognized as tracks.

6. Comparison of Emulsion with Cloud Chamber

The following independent experiment was conducted to provide additional data on the reliability of nuclear emulsions for measuring continuous neutron spectra in the region of the low energy limit of the emulsion. A well-collimated neutron beam having a spectrum which decreased rapidly with increasing energy in the region from 0.3 to 1 Mev was investigated with *both C2* nuclear emulsion and a hydrogen-filled cloud chamber. A total of 2000 proton recoil tracks taken within 15° of the forward direction were measured in the energy range from 0.1 to 0.8 Mev with the cloud chamber. The nuclear emulsion data covered the energy range from 0.3 Mev and upward and consisted of 4000 proton recoil tracks measured by two experienced microscopists who used the previously described technique. The cloud-chamber data were normalized to the film data in the 0.5- to 0.8-Mev energy region. Good agreement existed between the slopes of the two sets of data in the normalizing or matching region. However, below 0.5 Mev the film data fell below the cloud-chamber results. Table III shows the resulting corrections to be applied to the emulsion spectrum data as derived from a comparison with the cloud-chamber data and from the previous analysis (Fig. 11) using the Van de Graaff data.

Except for the 0.3- to 0.4-Mev interval, the correction factors as derived from the two experiments agree satisfactorily. The correction factors obtained from the cloud-chamber comparison are more reliable since they were derived in a more accurate and direct manner than those obtained from the Van de Graaff results. The influence of scattered neutrons on the Van de Graaff results is commented on in the section on Conclusions. Only the correction value for the 0.3- to 0.4-Mev interval can be appreciably affected by scattered neutrons and, to adjust for this effect, this value might well be increased from 55 to about 70 percent.

7. Straggling

The proton recoil distributions from the Van de Graaff and the proton distribution from the $N^{14}(n, p)C^{14}$ reaction show that a half-width (at half-maximum) of 0.05±0.01 Mev can be expected from straggling effects alone in Ilford C2 emulsion. Within the accuracy of these experiments, this width appears to be energy independent over the 0.5- to 1.5-Mev interval studied. If the half-width divided by the energy is taken as a measure of the straggling, then the proton energy straggling varies from 10±2 percent at 0.5 Mev to 3±1 percent at 1.5 Mev. The *latter value* can be compared with Bethe and Livingston's results[11] and is found to be in agreement within experimental error

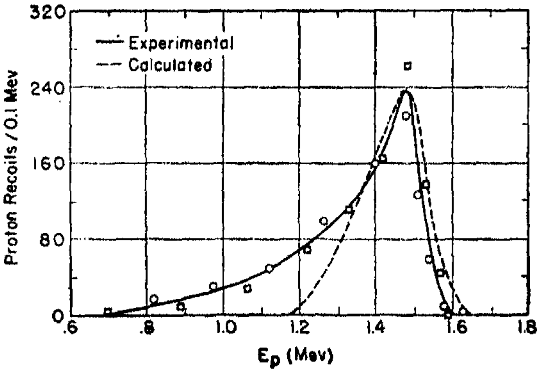

Fig. 10. Proton recoil distribution from $E_n = 1.54$ Mev.

---

[11] H. A. Bethe and M. S. Livingston, Rev. Mod. Phys. 9, 285 (1937).

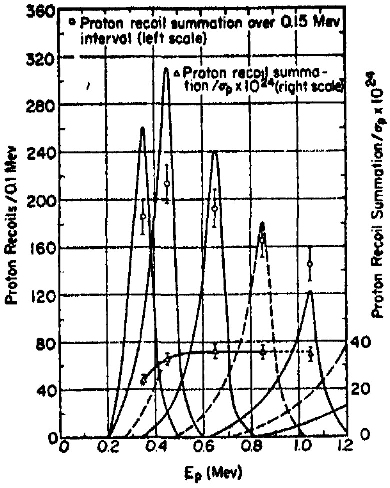

FIG. 11. Application of individual proton recoil distributions to determine usefulness of nuclear emulsion for low energy neutron spectral measurements.

with the energy straggling of ~2 percent as calculated from their curve. The above experimental straggling values are comparable with the results of Lattes *et al.*,[12] who have obtained a half-width of about 0.08 Mev at 3.2 Mev for proton straggling in *B*1 emulsion.

In the type of spectral analysis used in this experiment, that of counting recoils in the forward direction, the energy spread of the proton recoils as admitted by the experimental geometry becomes comparable with the energy spread due to proton range straggling at energies around 1 Mev. This causes the absolute magnitude of the energy width of the distribution curves to increase with energy in this type of analysis. It is, however, customary to express the width as a fraction of the energy or range. This has been done in Fig. 12 where the energy half-width of the distribution curves, expressed as a percentage of the mean proton energy, has been plotted against the energy (solid curve). It must be emphasized that this particular curve is of value for indicating proton recoil energy widths for neutron spectra only if the analysis is performed according to the technique used in the present work. The half-width to be expected from straggling effects alone is shown as a dashed curve in Fig. 12. For the energy range covered in this experiment, the latter curve is merely obtained by plotting 0.05/*E* expressed in percent *vs.* *E*.

TABLE III.

Neutron spectrum energy interval	Percentage increase to be applied to nuclear emulsion data From Van de Graaff results	 From cloud-chamber comparison
0.7–0.8	None	None
0.6–0.7	None	None
0.5–0.6	<5 percent	None
0.4–0.5	10 percent	10 percent
0.3–0.4	55 percent	75 percent

CONCLUSIONS

The present experiment provides information on the accuracy of proton recoil data from nuclear emulsions for determining numbers of neutrons and neutron spectra at low energies. Results show that correct data are obtained for energies above about 0.5 Mev and that approximate data can be obtained down to 0.3 Mev if suitable corrections are applied. The proton range *vs.* energy relation below 0.5 Mev is presented for *C*2 emulsion. Proton recoil distributions obtained from low energy neutron exposures and analyzed by the technique of measuring recoils in the forward direction are presented and discussed.

The experimental distributions from recoils in the forward direction can be approximately described by a function representing the admitted proton recoil spectrum on which is superimposed a Gaussian function of half-width equal to 0.05 Mev. Only the extreme low energy side of the experimental curves is in serious disagreement with the above composite function. A measurement of areas reveals that the experimental curve has an excess area over that of the calculated curve equal to 13 percent at 0.47 and 0.68 Mev, 20 percent at 1.06 Mev, and 25 percent at 1.54 Mev. The exact reason for the excessive number of these low energy tracks is not clear. The fact that the distribution from the $N^{14}(n, p)C^{14}$ reaction was as expected and that the above disagreement occurs consistently throughout the entire energy range would indicate that the surplus low energy tracks probably reflect the spectrum of the neutrons striking the film.

It seems most logical to assume that the excess low energy recoils arise from neutrons leaving the tritium target in the backward direction and then being subsequently scattered into the film by heavy materials surrounding the back of the target. Although the number of neutrons produced in the backward direction is not large,[13] the solid angle subtended for scattering of

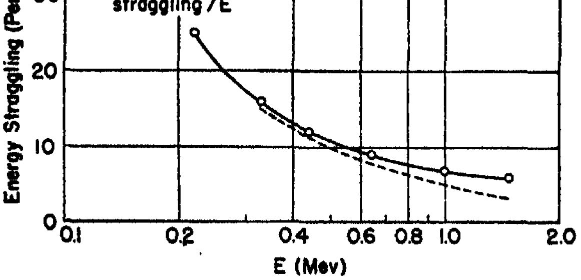

FIG. 12. Proton energy straggling in *C*2 nuclear emulsion at low energies.

---

[12] Lattes, Fowler, and Cuer, Proc. Phys. Soc. A59, 883 (1947).

[13] Hanson, Taschek, and Williams, Rev. Mod. Phys. 21, 645 (1949).

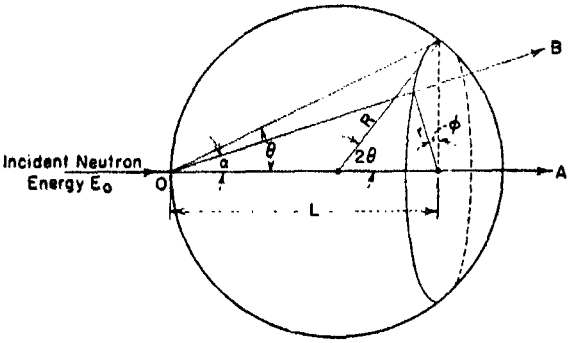

FIG. 13. Reference figure for calculation of proton recoil spectrum.

these neutrons by Van de Graaff components and structures is probably great enough to produce the observed effects. The following subsidiary facts also support this supposition. The disagreement between the calculated and experimental distribution increases with energy. This would be expected, since the yield of the T(p, n)He^3 reaction in the backward direction increases with proton energy.[13] The distribution curves show that the lowest energy is approximately one-half the highest energy observed. This result is consistent with the fact that the reaction produces a neutron in the backward direction with roughly one-half the energy of that produced in the forward direction. It is unfortunate that the nuclear emulsion detector exaggerates the number of scattered neutrons, since the cross section for proton recoil production is more favorable for the scattered low energy neutrons than for the higher energy neutrons coming directly from the target. Approximate corrections can be made for the effect of these scattered neutrons. However, in the important energy region of this experiment, namely, at low neutron energies, the number of scattered neutrons is small compared to the number of neutrons direct from the target.

It might be imagined that the aluminum foil in the target assembly could give rise to the observed straggling. This explanation is rendered unlikely by the reasonable agreement, at the high energy ends of the distribution curves, between the calculated and experimental results.

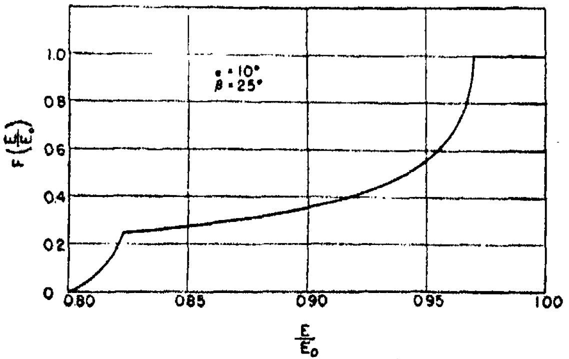

FIG. 14. Proton recoil spectrum, $F(E/E_0)$, admitted by experimental geometry.

In reference to Fig. 2, the corrections to the number of proton recoils due to the presence of the low energy scattered neutrons can be estimated from the following expression:

$$R=R_0\left(1-\frac{p_1}{p}\right)\left[1+\frac{1}{(\sigma_{p1}/\sigma_{p0})((p/p_1)-1)}\right], \quad (1)$$

where R is a measure of the film response; $R_0=p/\sigma_{p0}$ is the uncorrected response; p is the total number of proton recoils per unit volume of emulsion; p_1/p is the fraction of proton recoils ascribed to the scattered neutrons (this factor is estimated from the difference in area between the experimental and calculated curves); σ_{p0} is the $n-p$ cross section for the bombarding neutrons; σ_{p1} is the estimated average $n-p$ cross section for scattered neutrons. The correction is everywhere less than 10 percent.

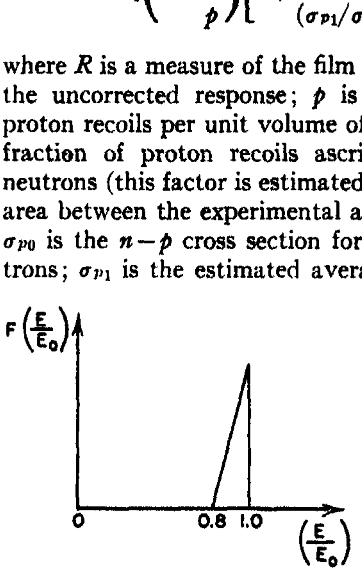

FIG. 15. Approximate proton recoil spectrum admitted by experimental geometry.

The range-energy relation is not influenced by the scattering since the experimental and calculated distribution curves agree well beyond the energy region where the maxima of the curves are located; from this it can be concluded that the peak of the curve is not shifted by the presence of the scattered neutrons.

The spectrum analysis presented in Fig. 11 may be appreciably influenced only in the 0.35-Mev result. The results as presented at the 0.45-, 0.65-, and 0.85-Mev points are derived from distributions which contain about[14] 15±3 percent scattered neutrons. If these spurious neutrons had not been present but instead their number was replaced by neutrons direct from the target, the effect would have been to increase the area in the above three intervals by approximately 15 percent. This area increase would, in turn, raise the portion of the curve marked by triangular points by the same factor, and the ordinates of the 0.45- and 0.55-Mev intervals relative to those for the higher energies would not change appreciably. It is more difficult to estimate the effect of the scattered neutrons on the 0.35-Mev point since the experimental and calculated distributions are in agreement. This agreement may be due either to the fact that the scattered neutrons are too low in energy to be recorded by the film, or because their number may be small (~5 percent) at this energy.

---

[14] Since no experimental measurement was made for the 0.85-Mev interval, an interpolation was used to give the percentage of scattered neutrons in this interval; the result, a value of about 17 percent.

Assuming the first statement is true and employing the same reasoning as given above, the 0.35-Mev point should also be raised but not as much as at the higher energies because of the smaller percentage of scattered neutrons at this energy. In either case, the 0.35-Mev point would not change significantly. Consequently, its value relative to the flat portion of the curve would be decreased, and the correction required to make it agree with the flat portion is raised from the previous 55 to ~70 percent.

The authors wish to thank Jewell Erickson and Dorothy Squires of the microscopy laboratory for their services in reading the nuclear emulsion plates used in this experiment. Appreciation is also expressed to the Van de Graaff group at Los Alamos for their cooperation and the use of their machine.

APPENDIX I. RECOIL PROTON SPECTRUM ADMITTED BY EXPERIMENTAL GEOMETRY

Consider a beam of monochromatic neutrons incident on the photographic emulsion from the left. The geometry employed in this experiment admitted all recoil protons within a vertical angle $\pm\alpha(\pm 10°)$ and a horizontal angle $\pm\beta(\pm 25°)$. We first consider the limitation on the spectrum set by the angle $+\alpha$ (Fig. 13). The angle α is the angle between diametral line OA and the plane indicated by OB.

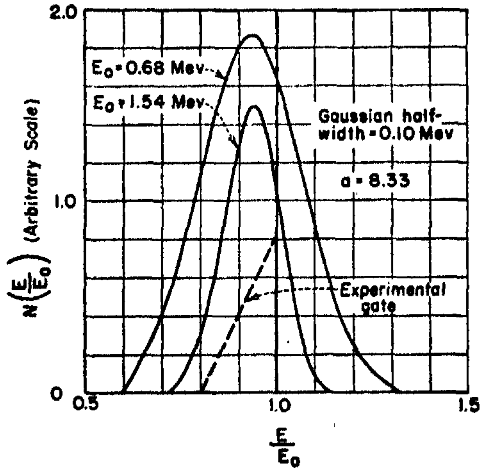

FIG. 16(a). Calculated proton recoil spectrum, $N(E/E_0)$, for a Gaussian half-width of 0.10 Mev at $E_0=0.68$ and 1.54 Mev. (Ordinates of the curves are not normalized.)

From conservation laws, the energy, E, of the recoil proton is

$$E=E_0\cos^2\theta. \tag{2}$$

From Fig. 13, elementary trigonometry, and Eq. (2),

$$\phi=\cos^{-1}\left[\left(\frac{E/E_0}{1-E/E_0}\right)^{\frac{1}{2}}\tan\alpha\right]. \tag{3}$$

The angle ϕ measures the fraction of the solid angle at energy E/E_0 which is excluded by the experimental geometry.

If we consider the intersection by two planes at right angles to each other and passing through point O at angles of α and β, respectively, with diametrical line OA, ϕ becomes

$$\phi=\cos^{-1}\left[\left(\frac{E/E_0}{1-E/E_0}\right)^{\frac{1}{2}}\tan\alpha\right]+\cos^{-1}\left[\left(\frac{E/E_0}{1-E/E_0}\right)^{\frac{1}{2}}\tan\beta\right]. \tag{4}$$

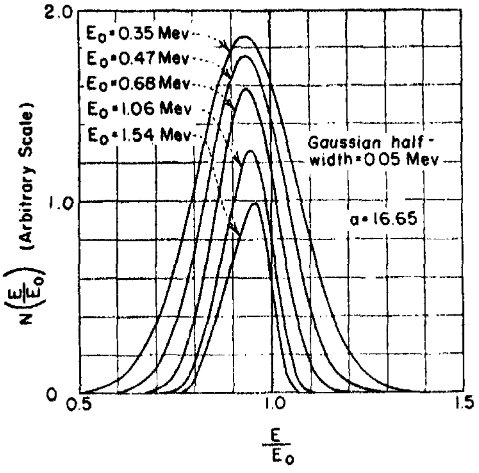

FIG. 16(b). Calculated proton recoil spectrum, $N(E/E_0)$, for a Gaussian half-width of 0.05 Mev at all experimental values of E_0. (Ordinates of the curves are not normalized.)

The fraction of the solid angle admitted by the experimental geometry is

$$F(\alpha,\beta,E/E_0)=1-(2/\pi)\phi. \tag{5}$$

Figure 14 gives the calculated spectrum for $\alpha=10°$, $\beta=25°$.

APPENDIX II. CALCULATION OF THE APPARENT PROTON RECOIL SPECTRUM

The true proton recoil spectrum as admitted by the geometry of this experiment from a monoenergetic neutron source is that given in Appendix I. The apparent or measured spectrum should be expected to differ from this because of the phenomenon of straggling. If the sum total of the straggling effects is taken to be Gaussian, as seems reasonable, it is possible to deduce an observed spectrum for any assumed half-width using the recoil proton spectrum admitted by the experimental geometry given in Appendix I. Judging by the spread of the experimental curves, the Gaussian half-width is about 0.05 Mev. In consequence, it was felt to be reasonable to replace the rather complicated function of Appendix I by a triangle, Fig. 15, so that

$$F(E_p/E_0)=C_1[(E_p/E_0)-0.8], \tag{6}$$

where E_0 = neutron energy, E_p = recoil energy, $1>E_p/E_0>0.8$, and C_1 is a constant.

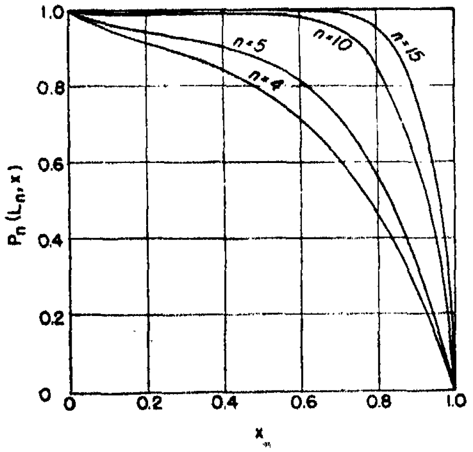

FIG. 17. $P_n(L_n, x)$ vs. x for $n=4$, 5, 10, and 15.

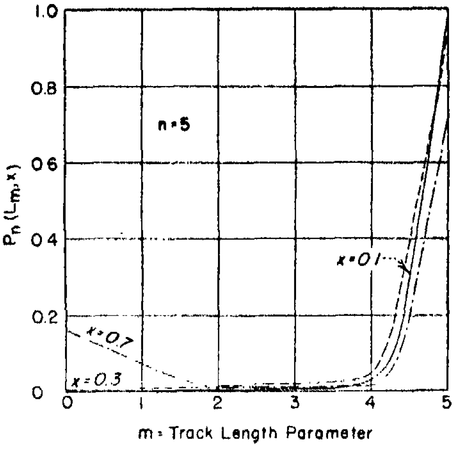

FIG. 18(a). $P_n(L_m, x)$ *vs.* m for $n=5$ and $x=0.1$, 0.3, and 0.7.

The measured spectrum, $N(E/E_0)$, should then be given by

$$N(E/E_0)=C_2\int_{0.8}^{1}F(x)\exp\left[(-a^2E_0^2)\left(\frac{E}{E_0}-x\right)^2\right]dx, \tag{7}$$

where the half-width of the Gaussian is determined by the constant a and C_2 is a normalization constant. Equation (7) has the virtue that it can be integrated in terms of tabulated functions. The result is

$$\frac{N(E/E_0)}{C}=\frac{(\pi)^{\frac{1}{2}}}{2}\frac{[(E/E_0)-0.8]}{aE_0}$$
$$\times\left[\frac{2}{(\pi)^{\frac{1}{2}}}\int_{aE_0[0.8-(E/E_0)]}^{aE_0(1-E/E_0)}\exp(-x^2)dx\right]+(1/2a^2E_0^2)$$
$$\times\{\exp-[aE_0(0.8-E/E_0)]^2-\exp-[aE_0(1-E/E_0)]^2\}, \tag{8}$$

where C is a constant.

The spectrum given by Eq. (8) has been plotted in Fig. 16(a) for two different neutron energies, $E_0=1.54$ and 0.68 Mev used in this experiment, and for a Gaussian with half-width$=0.10$ Mev. Figure 16(b) illustrates Eq. (8) plotted for all the neutron energies used in this experiment and for a Gaussian half-width$=0.05$ Mev. The experimental proton recoil distribution curves have been compared with these calculated curves in Fig. 16(b), i.e., the dashed curves in Figs. 6 to 10.

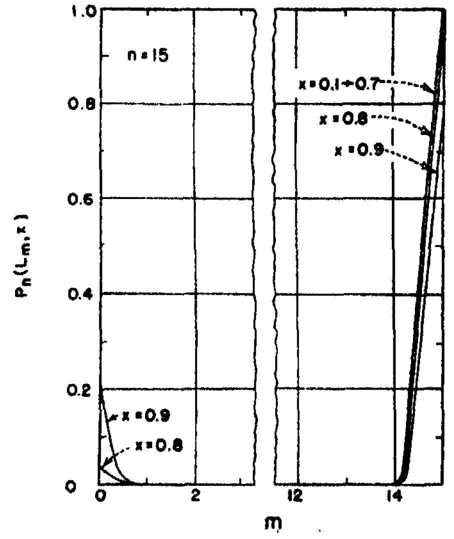

FIG. 18(b). $P_n(L_m, x)$ *vs.* m for $n=15$ and $x=0.1$ to 0.7, 0.8, and 0.9.

The spectrum has a maximum which is located no lower in energy than the center of area of the gate. This result is independent of the gate shape and follows directly from Eq. (7). As the Gaussian half-width is increased the spectrum maximum shifts to the left. From (7) the condition for the maximum as $a\rightarrow 0$ is

$$\int_{0.8}^{1}F(x)\left(\frac{E'}{E_0}-x\right)dx=0$$

so that

$$\frac{E'}{E_0}=\int_{0.8}^{1}xF(x)dx\bigg/\int_{0.8}^{1}F(x)dx. \tag{9}$$

Since for a triangular gate $E'/E_0>0.933$ and $E'/E_0=0.95\pm0.01$ for a half-width of 0.05 Mev, it is seen that the location of the maximum is insensitive to the Gaussian half-width. The lowest value of E'/E_0 is 0.930 for the actual experimental gate given in Appendix I.

We wish to thank the Los Alamos computing group under Bengt Carlson and Max Goldstein for performing the numerical work.

APPENDIX III. CHANGE OF APPARENT PROTON RECOIL SPECTRUM DUE TO LOSS OF GRAINS

It appears from the analysis given below that the apparent increase in the number of short recoil proton tracks due to the probability that a given grain along the track is not rendered developable is negligibly small except in the case of tracks having ~5 grains or less. We assume that the range of the proton in the emulsion is dependent only on its energy. This seems reasonable in view of the approximate equality of the stopping powers of the silver bromide grains and the remainder of the emulsion. Range straggling is neglected in this appendix.

Let $x=$probability of any one grain missing. Assume that x is independent of the number of grains.

Then $(1-x)^{n-\alpha}x^{\alpha}=$probability that α grains are missing and $(n-\alpha)$ grains are present.

Let $C_\alpha(L_m)=$probability that if α grains are missing and $(n-\alpha)$ grains are present, the track length will be $L_m=(m-1)a$. Assume equally spaced grains of spacing a. According to the convention adopted here, the length of a track is defined by the distance between the end grains without regard to the number of grains between them.

Then

$$P_{\alpha,n}(L_m,x)=C_\alpha(L_m)(1-x)^{n-\alpha}x^{\alpha}, \tag{10}$$

where $P_{\alpha,n}(L_m,x)=$probability that the track length will be L_m if x is the probability that any one grain is missing and α out of n grains are missing. Finally,

$$P_n(L_m,x)=\sum_{\alpha=n-m}^{n-2}P_{\alpha,n}(L_m,x), \tag{11}$$

where $P_n(L_m,x)=$probability that a track length L_m is observed when x is the probability that any one grain is absent in an assemblage of, at most, n grains.

Consideration of the combinations involved leads to the following expressions for $P_n(L_{n-\alpha},x)$:

$$P_n(L_{n-\alpha},x)=\frac{(\alpha+1)\alpha!}{n(n-1)(n-2)\cdots(n-\alpha+1)}x^{\alpha}(1-x)^{n-\alpha}$$
$$+\frac{(\alpha+1)(\alpha+1)!(n-\alpha-2)}{n(n-1)\cdots(n-\alpha)}x^{\alpha+1}(1-x)^{n-\alpha-1}$$
$$+\frac{(\alpha+1)(\alpha+2)!(n-\alpha-2)(n-\alpha-3)}{2!n(n-1)\cdots(n-\alpha-1)}x^{\alpha+2}(1-x)^{n-\alpha-2}$$
$$+\cdots$$
$$+\frac{(\alpha+1)r!(n-\alpha-2)(n-\alpha-3)\cdots(n-r-1)}{(r-\alpha)!n(n-1)\cdots(n-r+1)}x^{n}(1-x)^{n-r}$$
$$+\cdots+[2(\alpha+1)/n(n-1)]x^{n-2}(1-x)^2, \tag{12}$$

where $m=n-\alpha$ and $n-2>\alpha>n-m$.

For

$$\alpha = n-1: P_n(L_1, x) = (1-x)x^{n-1}$$
$$\alpha = n: P_n(L_0, x) = x^n.$$

So that

$$P_n(L_n, x) = 1 - \sum_{\alpha=n}^{\alpha=1} P_n(L_{n-\alpha}, x). \tag{13}$$

The results for $P_n(L_n, x)$ and $P_n(L_{n-\alpha}, x)$ are given as a function of x and for selected values of n in Figs. 17, 18(a) and (b).

In the above it was assumed that the length of the track was given only by the distance between the end grains. This assumption is somewhat unrealistic because of the fact that an "empty" track would not be recognized as a track at all and that a partly empty track might be mistaken for two short tracks. Judging from experimental experience, it is estimated that at least three or four grains would have to be missing in order to mistake one long for two short tracks. Given a nominal 10-grain track, the probability that three grains are missing and seven grains are present is much *less* than $(1-x)^7x^3$ because the three missing grains are postulated to occur in sequence and somewhere near the center of the track.

This quantity has a maximum value at $x=0.3$ of 2.2×10^{-4}, and, consequently, the apparent number of short tracks due to this cause is negligible.

The authors wish to thank Miss Lois Foster of the Rand Corporation for checking the derivation of Eq. (12) and assistance with the numerical computations.

THE REVIEW OF SCIENTIFIC INSTRUMENTS VOLUME 21, NUMBER 6 JUNE, 1950

A High Resolution Beta-Ray Spectrometer*

JOSEPH A. BRUNER† AND F. R. SCOTT
Indiana University, Bloomington, Indiana

(Received February 27, 1950)

A relatively inexpensive 180° magnetic focusing beta-ray spectrometer has been constructed, having a principle orbit radius of 15 cm. A radially inhomogeneous field provides essentially perfect focusing of electrons leaving the source within a 33° angle. In operation, with a 1-mm wide source, the transmission is 0.2 percent, the full width at half-maximum of an internal conversion line is 0.4 percent, and the effects of background and scattering are generally inappreciable.

INTRODUCTION

A MEDIUM-size, high resolution, 180° magnetic focusing beta-ray spectrometer has been constructed, patterned in many respects after that described by Langer and Cook[1] (hereafter referred to as the larger spectrometer), but differing in several important features. While the two instruments have transmissions, resolutions, and background counting rates of the same order of magnitude, the new instrument, because of its smaller size, has the major advantage of being easier and less costly to construct and minor disadvantages of necessarily narrower sources, a small (usually negligible) amount of scattering, and a shorter measurable energy range.

Essentially perfect focusing in the median plane is obtained by the use of a radially inhomogeneous magnetic field closely approximating the theoretically required field as determined by Beiduk and Konopinski:[2]

$$H = H_0(1 - 3\delta^2/4 + 7\delta^3/8 - 9\delta^4/16 + 51\delta^5/320 + \cdots),$$

where $\delta = (r - r_0)/r_0$, r_0 is the radius of the principal orbit, and H_0 is the field at $r = r_0$. In addition, a slight amount of axial focusing is obtained by accepting only orbits for which $\delta > 0$[2].

MAGNET

Except for the pole face profile the dimensions of the magnet frame are one-half those of the larger instrument. This fact alone, of course, reduces the cost of the iron by a factor of eight. The shape of the profile was determined by tests on a half-scale model, then applied to the full-size design. As a first approximation in calculating shape changes the pole faces (except near the edges) were assumed to be equipotential surfaces. The theoretically desired profile, as determined by these calculations, was approximated by means of angles and straight lines in order to facilitate the ma-

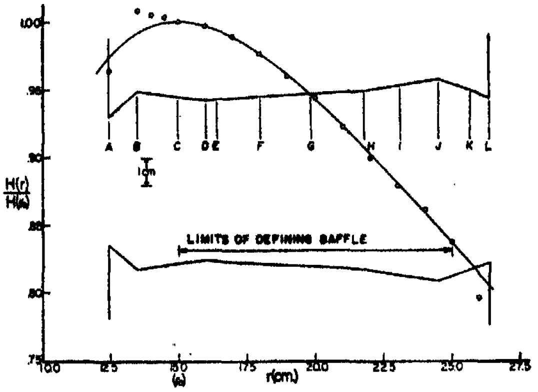

FIG. 1. Pole face profile and magnetic field distribution. The curve represents the field distribution theoretically required for perfect focusing. The points show the actual field. The pole face dimensions are given in Table I.

---

* This work has been supported by a grant from the Frederick Gardner Cottrell Fund of the Research Corporation and by the joint program of the ONR and AEC.

† AEC Predoctoral Fellow.

[1] L. M. Langer and C. S. Cook, Rev. Sci. Inst. 19, 257 (1948).

[2] F. M. Beiduk and E. J. Konopinski, Rev. Sci. Inst. 19, 594 (1948).

chining of the faces in the Physics Department shop. Figure 1 shows the profile of the finished pole faces (see Table I), the resulting field distribution, and a plot of the Beiduk-Konopinski curve for $r_0 = 15$ cm. The agreement is seen to be excellent over most of the region; the defining baffle is set so as to exclude from use the edges, where the agreement is poor.

The convection-cooled coil consists of 14,300 turns of No. 22 heavy Formvar wire and carries a maximum current of about 0.5 amp. This current produces a field in excess of 1000 gauss—sufficient to measure electron energies up to at least 4 Mev.

The magnet current is stabilized by four 807 tubes in parallel in a circuit similar to that described by Elmore and Sands.[3]

The magnetic field is measured by means of a flip coil and a ballistic galvanometer, the calibration of which is frequently checked in terms of a standard mutual inductance. The absolute calibration of the field is in terms of the internally converted 411.2-kev gamma-ray of Au^{198}.

TABLE I. Dimensions of pole face (see Fig. 1). r is the radius to the point in question, and g is the gap at that point.

Point	r (cm)	g (cm)
A	12.45	5.009
B	13.50	6.838
C	15.00	6.401
D	16.00	6.162
E	16.50	6.238
F	18.00	6.421
G	20.00	6.629
H	21.80	6.848
I	23.00	7.219
J	24.50	7.711
K	25.50	7.021
L	26.35	6.335

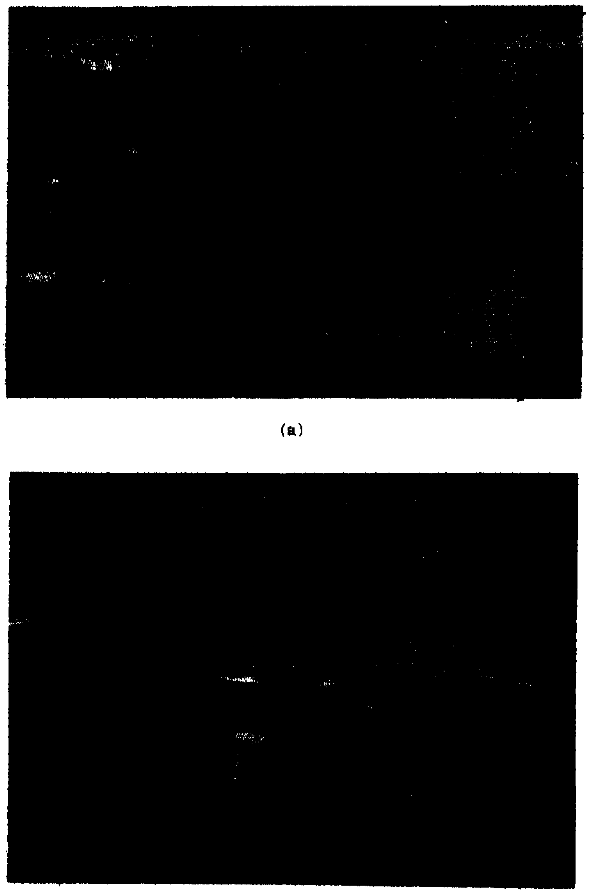

(a)

(b)

FIG. 2. Two views of the completed spectrometer. Points of interest are: (a) A, Source supporting rod; B, G-M counter; C, counter slit control knob. (b) D, Background gate rod; E, exit to vacuum pumps; F, defining baffle control; G, flip coil.

At very low field strengths it is found that a particular cycling of the magnet is necessary in order to retain the desired radial distribution of the field; above 150 gauss, however, this precaution need not be taken.

VACUUM CHAMBER

The aluminum vacuum chamber was cast in a single piece in the form of a "pot," to which a $\frac{1}{4}$-in. sheet aluminum lid is screwed. Incorporated in the casting were several bosses (see Fig. 2) for convenience in attaching a source observation window, flip coil, movable defining baffle, background gate, etc. Fixed aluminum baffles were placed at the 30°, 60°, 120°, 150° positions to help prevent scattering. The edges of the adjustable detector slit were made of tungsten to provide an optimum combination of stopping power and geometrical thinness. Wilson-type vacuum seals were used for the defining baffle, background gate, and detector slit mechanism; and Neoprene gaskets were used for all other seals. No leaks occurred in the chamber.

SOURCES

Sources for measurement of beta-ray spectra are prepared as follows. Upon a 1-in. diameter aluminum ring are placed three 1.5-μg/cm^2 Zapon films. A line of insulin[4] 2 cm long and 1–3 mm wide (depending upon the desired resolution) is ruled on the Zapon by means of a simple machine, then permitted to dry. One or two drops of radioactive solution are then deposited on the same region. Because of the action of the insulin the solution spreads so as to cover completely the desired area. The source is then dried and covered with a single zapon film.

Sources for the measurement of gamma-ray energies are prepared in the manner described by Langer and Cook,[1] using a uranium radiator 2 by 0.3 cm.

The source ring is supported by a skeleton framework on the end of a rod and is inserted into the vacuum chamber through a vacuum gate. Positioning of the ring is accurate to within 0.1 mm both radially and vertically. The orientation of the source is determined by visual alignment with a machined vertical edge of the vacuum chamber.

---

[3] W. C. Elmore and M. Sands, *Electronics: Experimental Techniques* (McGraw-Hill Book Company, Inc., New York, 1949), p. 392.

[4] L. M. Langer, Rev. Sci. Inst. **20**, 216 (1949).

DETECTION

End-window G-M counters, filled to 10 cm pressure with an argon-ethylene mixture, are used to detect the electrons. Two types of windows are employed, depending upon the energy of the particles to be observed: for very low energies a zapon window is used; otherwise, thin mica windows are adequate.

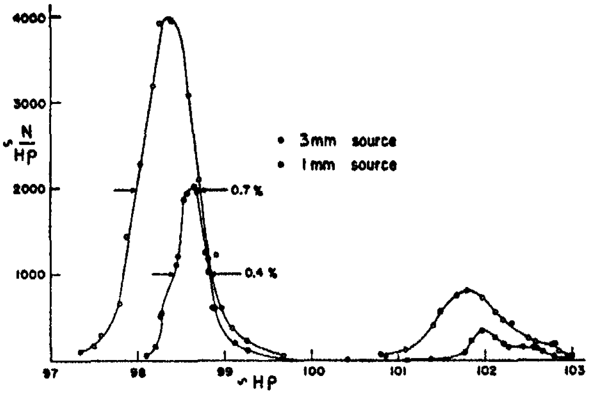

FIG. 3. Internal conversion K and L lines from Cs^{137} as measured using two sources of different widths.

Preparation of the zapon windows has already been described.[1] The supporting grid is made of Lektromesh.[5] Since these windows are unable to support atmospheric pressure, the counters are evacuated simultaneously with the vacuum chamber, then filled from a ballast tank. The connection to the ballast tank is left open during the operation of the spectrometer to maintain constant pressure in the counter against the slight diffusion through the window.

PERFORMANCE

Usually the source and counter slit are set 3 mm wide. The defining baffle is set with its inner edge at a 15-cm radius and its outer edge at a 25-cm radius, thus permitting the passage of a (1 in. high) beam which subtends an angle of 33° at the source, in the plane perpendicular to the field. Under these conditions the transmission[2] is calculated to be 0.2 percent, about twice that of the larger spectrometer. In practice, however, for a given specific source activity the counting rates of the two instruments are very nearly the same because of the difference in source areas.

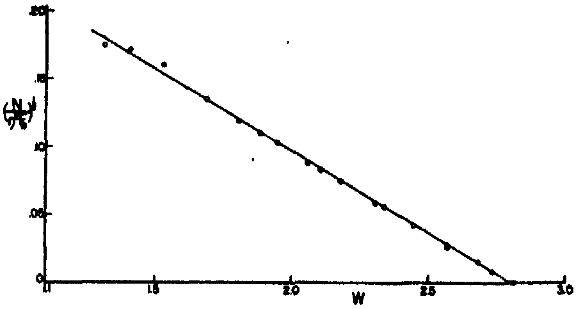

FIG. 4. Fermi plot of Pr^{143} beta-ray spectrum. Deviation from a straight line occurs at about 300 kev because of a relatively thick (0.5 mg/cm^2) source. Source and counter slit widths were each 3 mm.

The resolving power of the spectrometer is demonstrated in Fig. 3 for source widths of 3 and 1 mm. The full widths of the lines at half-maximum are 0.7 and 0.4 percent, respectively. The irregular shape of the narrower line is probably due to the fact that, in the preparation of this particular source, there was an accidental overflow of the source solution slightly beyond the region defined by the insulin.

Figure 4 shows a typical result from the measurement of a beta-ray spectrum. In this case[6] the experimental momentum spectrum of Pr^{143} is compared with that predicted for an allowed transition by the Fermi theory. The theory predicts a straight line when $(N/\eta^2F_b)^{\frac{1}{2}}$ is plotted against W, where N is the number of electrons counted per unit momentum interval, η is the electron momentum, F_b is the Bethe approximation for the Coulomb correction factor, and $W=(1+\eta^2)^{\frac{1}{2}}$ is the electron energy in units of m_0c^2.

The authors wish to express their gratitude to Dr. Lawrence M. Langer for his valuable advice and encouragement.

---

[5] Langer, Motz, and Price, Phys. Rev. 77, 798 (1950).

[6] Bruner, Langer, and Moffat, Phys. Rev. 77, 747 (1950).

THE REVIEW OF SCIENTIFIC INSTRUMENTS VOLUME 21, NUMBER 6 JUNE, 1950

The Velocity of Propagation of the Discharge in Geiger-Müller Counters*

H. SALTZMANN AND C. G. MONTGOMERY
*Sloane Physics Laboratory, Yale University,*** *New Haven, Connecticut*

(Received March 8, 1950)

The velocity of propagation of the discharge in a Geiger-Müller counter has been measured in a counter with a divided cathode by the method of delayed coincidences. The parameters varied were the counter potential and the percentage of ethyl alcohol mixed with argon. The results are compared with Wilkinson's theory. Good agreement is obtained except for high velocities where the theory predicts values much too low.

THE propagation velocity of the discharge along a counter wire has been measured by several observers,[1] and rough agreement has been found among them. Recently Wilkinson[2] has proposed a theory of the propagation and derives a formula for the velocity which can be compared with experiment. Unfortunately none of the observations published are sufficiently detailed to allow a check of the theory. A series of experiments were therefore undertaken with this purpose in mind.

The counter used had a divided copper cathode 1 cm in diameter; one part was 20 cm long, the other part 3 cm in length. The wire was tungsten of 0.003-in. diameter and the envelope was Pyrex glass. A discharge was started at one end of the long cathode by gamma-rays from Co^{60} collimated by a small hole in a lead block. The discharge traveled along the counter wire and after a short time interval reached the short end cylinder. The start of the discharge was recorded by a pulse taken from the long cathode; the arrival of the discharge at the other end produced a pulse from the short cylinder. The two cylinders were shielded from each other to some extent by copper foil wrapped around the outside of the counter and connected to ground. The time interval between the two pulses was measured by delayed coincidences using the circuit described by Schultz and Beringer.[3] The first pulse was passed through a variable calibrated delay line and mixed with the second pulse in a coincidence circuit with a resolving time of about 3×10^{-8} sec. The length of the delay line was varied until a maximum number of delayed coincidences was recorded with a counting-rate meter. Preamplifiers placed next to the counter cathodes were used and hence only a very small initial portion of the counter pulse was necessary to actuate the circuit. The leak resistors were 1 megohm. The counter was permanently connected to a filling system with a manometer and various mixtures of tank argon and ethyl alcohol vapor were used. In addition the average charge produced in each counter discharge was obtained from measurements of the counting rate and the current through the counter. The counter voltage was measured with a potentiometer.

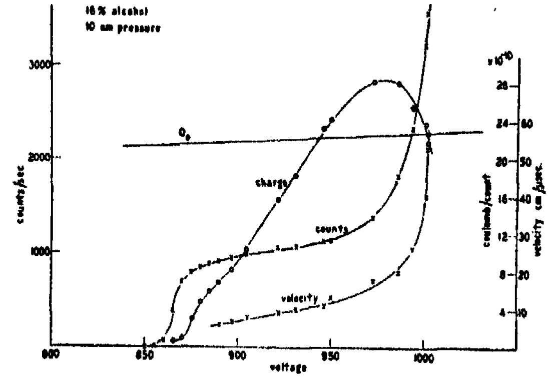

FIG. 1. Typical set of observations.

A typical set of data is shown in Fig. 1. The characteristic curve shows a plateau with a considerable slope and a steep rise just below 1000 volts caused by spurious counts. The charge formed in each count increases linearly with voltage but reaches a maximum at voltages corresponding to the end of the plateau. For higher voltages the charge decreases again. This decrease is also to be attributed to spurious counts which seem to contain, on the average, less charge because of incomplete recovery of the counter. The velocity of propagation of the discharge increases with counter voltage, slowly at first but later with increasing rapidity. The percentage of alcohol vapor in the counter was varied, keeping the total pressure constant at 10 cm Hg. The variation of the velocity that resulted is shown by the curves in Fig. 2. It should be noted that the curve for 14 percent alcohol shows two sets of points. These observations were taken at different times and with different gas in the counter tube. The agreement of the two sets is excellent. Since these four curves have nearly the same shape, but are displaced to higher voltages the higher the alcohol content, the velocity can be regarded as a function of the over-voltage (counter voltage minus starting voltage) alone in the first approximation. Systematic deviations from

---

* These measurements were reported at the Symposium on Geiger-Müller Counters at the Naval Research Laboratory, October, 1949.

** Assisted by the joint program of the ONR and the AEC.

[1] van Gemert, den Hartog, and Muller, Physica 9, 556 (1942); J. M. Hill and J. V. Dunworth, Nature 158, 833 (1946); Huber, Alder, and Baldinger, Helv. Phys. Acta 19, 204 (1946); E. Wantuck, Phys. Rev. 71, 646 (1947); Knowles, Balakrishnan, and Craggs, Phys. Rev. 74, 627 (1948).

[2] D. H. Wilkinson, Phys. Rev. 74, 1417 (1948).

[3] H. Schultz and R. Beringer, Rev. Sci. Inst. 19, 424 (1948).

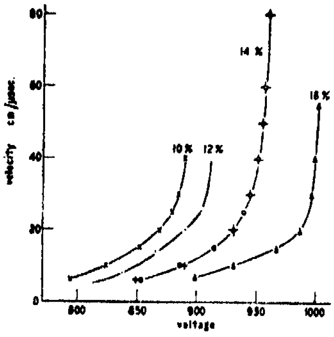

FIG. 2. Discharge velocity as a function of counter voltage for different alcohol percentages. The total pressure is constant at 10 cm Hg.

this approximation are evident, however, particularly in the data for 16 percent alcohol.

The calculations of Wilkinson[2] resulted in the following expression for the velocity v of discharge propagation:

$$v=\frac{4}{\pi}\left[1-(\tfrac{1}{2})e^{m}\right]\left[\frac{e^{m}-1}{\ln(Q_0\epsilon/e')(1-e^{-m})^2}\right]^{\frac{1}{2}}v_e,$$

where the notation is $m=Q/Q_0$, the charge formed in the discharge divided by the charge on the counter wire, e' = the electronic charge, v_e = the mean electron velocity in the immediate vicinity of the wire, and ϵ = the probability per ion that one avalanche give rise to a succeeding one. The quantities v, Q_0, and m are determined from direct measurements and fortunately the expression for v depends insensitively on the value of ϵ. The most probable value of $Q_0\epsilon/e'$, according to Wilkinson, is about 10^4. Since Q_0 varies only slightly (see Fig. 1) it was assumed constant for these computations. Unfortunately too little is known about the velocity of electrons in the extremely high fields near the counter wire to choose an experimentally determined value for v_e. We can regard it as a parameter to be determined from the present observations. It is obvious that the rapid increase of the velocity at high values of the overvoltage is not reproduced by Wilkinson's formula. For lower values, the agreement with the formula is shown in Fig. 3. The three curves have been calculated assuming a value of v_e = 31 cm/μsec. The ordinates in Fig. 3 are plotted on a logarithmic scale so that the theoretical curve corresponding to a different

FIG. 3. Comparison of theoretical curves with the experimental points. The velocity v_e was chosen as 31 cm/μ sec., and the quantity $Q_0\epsilon/e'$ was taken to be 10^3, 10^4, and 10^5 for the three curves, the smallest value pertaining to the uppermost curve.

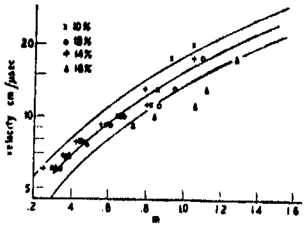

value of v_e can be obtained by a vertical shift of the curves. The parameter $Q_0\epsilon/e'$ was given three values: 10^3, 10^4, and 10^5 for the three curves. For values of m of less than 0.6, the observations are well represented by Wilkinson's formula. At larger values the divergence between the formula and the observations increases more and more. Somewhat better agreement for values of m near 1.0 might be obtained by the choice of a different value of v_e for each pressure, although the agreement between theory and experiment would then be destroyed for low m values. It should be noted that velocities as high as 100 cm/μsec. were observed which are much too large to fit the theory. No very large variations of v_e with counter voltage are to be expected.

Several investigators have derived the velocity of propagation from observations of the build-up of the counter voltage during the discharge. Such determinations do not measure the same velocity as measured by the present experiments. The voltage rise of a counter pulse is determined by the time necessary for the space charge to be formed about a unit length of counter wire. It is not essential that the successive avalanches be contiguous. On the average they will be separated by the mean range of the photons producing them. If a large number of photons are produced in an avalanche, one photon may travel an appreciable distance down the counter wire before it is absorbed. Thus the velocity of propagation as measured by experiments of the type described here should show large fluctuations and yield somewhat greater values than those derived from pulse shape. Such fluctuations in time of traversal of the discharge were observed but no quantitative measurements were made.

The radioisotopes used in this investigation were obtained through the courtesy of the AEC.

THE REVIEW OF SCIENTIFIC INSTRUMENTS VOLUME 21, NUMBER 6 JUNE, 1950

End and Wall Corrections for Absolute Beta-Counting in Gas Counters

A. G. ENGELKEMEIR AND W. F. LIBBY*
Argonne National Laboratory, Chicago, Illinois

(Received February 6, 1950)

A^{37} (2.8 kev Auger electrons) and Kr^{85} (0.74 Mev β) were used to determine end corrections for gas counters with flat ends and brass walls. The corrections were found to agree with those published previously for C^{14} (0.154 Mev). Argon-alcohol fillings were used with small quantities of the active gas being studied. Wall loss corrections were measured for Kr^{85} and calculated for A^{37}, C^{14}, and Kr^{85}. It appears from the results that absolute beta-counting for energies from about 0.01 to 0.8 Mev to an accuracy of one or two percent can be accomplished by the use of flat end Geiger counters applying the corrections indicated.

INTRODUCTION

THE intrinsic limitations to the efficiency of argon-alcohol filled Geiger counters in which the active sample is incorporated in the gas mixture are the weakening of the field near the ends of the counter sufficient to prevent a large part of the ionization formed in that region from starting an avalanche and the possibility that particles from disintegrations occurring near the wall will escape from the counter before forming an ion pair.

During the course of measuring the half-life of C^{14} using brass wall counters with flat Lucite ends,[1] the loss in counting efficiency because of the inhomogeneity of the field, i.e., the end loss, was determined. It was assumed as a first approximation that for a given volume of active gas, the difference between the counting rates of two counters of the same diameter but of different lengths was a measure of the end correction. The results obtained fit this hypothesis and indicated that the end loss is principally a function of the length to diameter ratio of a counter.

Further investigation of the end loss was undertaken with A^{37} and Kr^{85} as the active gases to determine whether particles of different energies would show different end losses and also to determine whether weakly ionizing radiations would show an appreciable wall loss.

PROCEDURE

The same counters were used as in the C^{14} determinations with the exception of two counters of smaller length to diameter ratio which were employed to obtain larger end corrections and greater accuracy. The same counting mixture was used also, 1.2 cm Hg of ethanol and 7 cm Hg of argon. The active samples were introduced into the counters with the argon, the radioactive argon and krypton of high specific activity having been diluted several hundredfold with inactive argon.

The radioactive argon was obtained by bombarding KCl with 8-Mev deuterons in the University of Chicago cyclotron;[2] its decay was followed for slightly more than one half-life to show the absence of contaminant activities. The krypton was obtained by dissolving a 10 g piece of an "old" irradiated uranium slug and condensing the noble gases on activated charcoal at liquid nitrogen temperature. Although the slug had been irradiated so long ago that it could be assumed that all other gaseous fission product activities had completely disappeared, the identity of the radioactive gas was demonstrated by running an absorption curve in Al on a sample contained in a brass cell with a mica window. The curve showed only a single beta-component and no gamma-radiation; a Feather analysis gave an energy of about 0.8 Mev. This is in good agreement with 0.74 Mev obtained by Hoagland and Sugarman.[3]

The counting procedures were similar to those described in the C^{14} work. For each counter filling the counting rate of the sample was determined at 25 volt intervals and the counting rate of an external standard plus the sample measured at 50 volt intervals, thereby providing two criteria of counter behavior.

END LOSS

A. Results

The end correction data obtained may be represented by an equation of the form

$$y = K/(L/D - K),$$

where y is the end correction, L the length and D the diameter of any counter, and K is a constant. This equation may be derived as follows by making the assumption that the effective insensitive length, l, of any counter is proportional to the diameter: Let R = observed counts/min. for any given volume of active gas in any counter of length L and diameter D, ρ = disintegrations/min for the same volume and v = insensitive volume $= l\pi D^2/4$.

If the end correction be called y, then

$$y = (\rho - R)/R,$$

---

* Institute for Nuclear Studies and Department of Chemistry, University of Chicago.

[1] Engelkemeir, Hamill, Inghram, and Libby, Phys. Rev. 75, 1825 (1949).

[2] Operated under ONR Contract N6ori, Task Order III.

[3] E. J. Hoagland and N. Sugarman, National Nuclear Energy Series, Div. IV, Vol. 9, *Radiochemical Studies; The Fission Products*, Paper 69; (McGraw-Hill Publishing Company, Inc., New York, to be published).

TABLE I. Specific counting rates.

L/D	3:1		6:1		12:1	
Counter	1"×3"	2"×6"	1½"×9"	2"×12"	1"×12"	1½"×18"
Part A. Data obtained with A^{37} (c/min./cc cm)[a]						
	3.136±0.040	3.072±0.040	3.292±0.070	3.247±0.020	3.311±0.020	3.384±0.050
	3.290±0.050*	2.947±0.060	3.260±0.030	3.383±0.030	3.348±0.019	3.302±0.050
	3.090±0.028	3.009±0.060	3.252±0.020	3.209±0.065	3.449±0.019	3.440±0.045
	3.143±0.025	3.135±0.055	3.323±0.030	3.227±0.020	3.327±0.020	3.427±0.040
		3.118±0.030	3.298±0.025	3.232±0.018		3.335±0.035
		3.243±0.015	3.289±0.010			3.321±0.035
						3.335±0.020
Average[b]	3.123±0.020	3.087±0.039	3.286±0.010	3.259±0.028	3.359±0.026	3.363±0.020
L/D Average[c]	3.105±0.030		3.272±0.020		3.361±0.023	
Part B. Data obtained with Kr^{85} (c/min./cc cm)[a]						
	7.861±0.118	8.118±0.066	8.355±0.085	8.443±0.151	8.365±0.069	8.328±0.152
	7.963±0.104	8.168±0.041	8.358±0.297	8.372±0.174	8.436±0.084	8.540±0.230
	8.032±0.133	8.117±0.082	8.370±0.178	8.464±0.102	8.446±0.042	8.646±0.112
	7.838±0.202	8.124±0.031	8.292±0.102	8.519±0.119	8.473±0.87	8.386±0.151
	7.648±0.072	8.006±0.085			8.457±0.095	8.718±0.093
	7.679±0.276					8.595±0.091
Average[b]	7.837±0.059	8.107±0.024	8.344±0.015	8.449±0.026	8.435±0.018	8.536±0.057
Average**[b]	8.378±0.059	8.383±0.024	8.728±0.015	8.736±0.026	9.017±0.018	8.929±0.057
L/D Average**[c]	8.380±0.042		8.732±0.020		8.973±0.038	

[a] Errors for individual rates are statistical counting errors.
[b] Errors for average rates are standard deviations.
[c] Errors for L/D averages are averages of standard deviations.
* Omitted in average because of deviation from average.
** Experimental wall loss correction applied.

or

$$y=\frac{l\pi D^2/4}{(L-l)\pi D^2/4}=\frac{l}{L-l}.$$

Assume

$$l=KD.$$

Then

$$y=K/(L/D-K).$$

A consequence of this assumption is that for any counter in which the total gas volume is that volume enclosed by the cathode and flat ends the end correction is a function only of the length to diameter ratio.

The end corrections obtained with A^{37}, C^{14}, and Kr^{85} are almost identical. Table I is a tabulation of the specific counting rates for the counters with A^{37} and Kr^{85}, corrected for coincidence losses, and in the case of the argon, for decay on the basis of a 34.1 day half-life.[4]

Table II consists of the end corrections calculated from the data in Table I. Part A lists the end corrections for individual counters, and Part B the end corrections for counters of the same length to diameter ratio. The wall correction discussed below was applied to the krypton data to make possible the averaging by length to diameter ratio. Part C gives the average of the corrections in Part B together with the average for C^{14}.

Figure 1 shows the average end corrections (Part C, Table II) for each gas as a function of the length to diameter ratio.

B. Discussion

The end loss has been ascribed to a weakening of the field near the ends which makes that region less sensitive. In addition to the bowing or distortion of the field at the counter ends characteristic of a cylindrical condenser, there is probably some effect due to the accumulation of charge on the insulating ends.

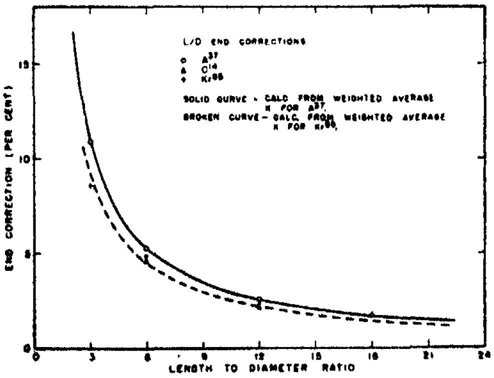

FIG. 1. The end corrections obtained from the average specific activity for counters of the same length to diameter ratio with A^{37}, C^{14}, and Kr^{85}. The curves represent the average corrections calculated for A^{37} and Kr^{85} from the equation $y=K/[(L/D)-K]$, where $K_{A^{37}}=0.298\pm0.014$ and $K_{Kr^{85}}=0.259\pm0.012$.

---

[4] Weimer, Kurbatov, and Pool, Phys. Rev. 66, 209 (1944).

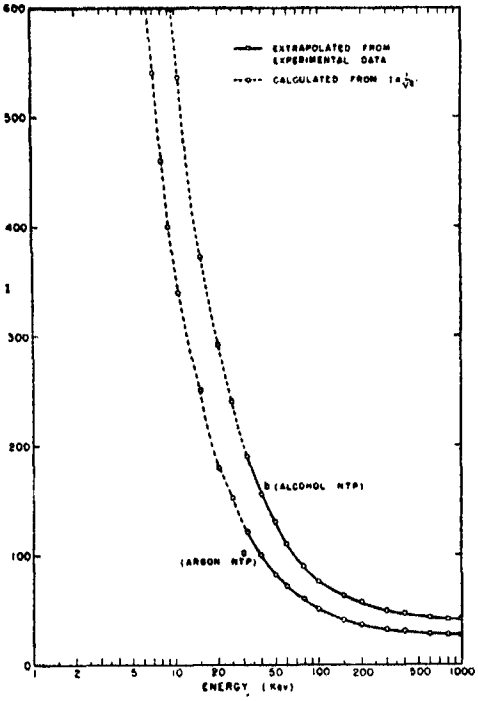

FIG. 2. Primary ionization as a function of energy for argon and ethanol at N.T.P. The solid lines were extrapolated from experimental data on the primary ionization in argon[8] and alcohol[9] on the assumption that I_A and I_{alc} differ from I_{air}[7] by a constant factor independent of energy. The dotted curves were calculated from $I=\alpha/V^2$ with α chosen to fit the solid curves in the region of 50 to 100 kev.

It is by no means obvious that the end losses should be the same for the A^{37} radiations which consist principally of 2.8 kev K-capture Auger electrons[5] as for C^{14} (154 kev, maximum energy of the beta-spectrum)[6] and Kr^{85} (740 kev maximum). The average lengths of the dead volumes, assuming them to be cylindrical, obtained for C^{14} and Kr^{85} are very much less than the range of either radiation in the gas mixture in the counters, whereas the length of the dead volume for even 1 in. diameter counters is of the order of the A^{37} range under these conditions. The ranges of the three radiations are listed in Table III together with the lengths of the dead volumes calculated from the end corrections obtained for each gas.

C. Conclusions

Since all known beta-emitters have ranges greater than that of the A^{37} Auger electrons and since the end effect for even this low energy radiation is essentially identical with that for C^{14} and Kr^{85} one assumes that the present corrections apply for all absolute beta-counting in counters with flat ends for beta-emitters with maximum energies below 0.75 Mev.

TABLE II. End corrections.

	3:1		6:1		12:1	
	1″×3″	2″×6″	1½″×9″	2″×12″	1″×12″	1½″×18″
	Part A. Corrections for counters of same diameter (percent)					
A^{37}	10.1±1.4	11.1±3.1	4.7±1.4	5.3±1.5	2.3±0.3	2.3±0.7
Kr^{85}	10.2±1.0	8.4±1.1	4.6±1.5	4.0±0.5	2.4±0.2	2.2±0.7
	Part B. Corrections for counters of same length to diameter ratio†					
A^{37}	10.8±2.3 11.0±1.6		5.1±1.1 5.4±1.8		2.5±0.4 2.6±0.9	
Kr^{85*}	8.4±1.1 8.8±0.9		4.0±0.5 5.5±1.0		2.2±0.2 2.7±0.5	
	Part C. Average corrections for same L/D					
A^{37}	10.9±2.0		5.3±1.5		2.6±0.6	
C^{14**}			4.7±0.6		2.3±0.5	
Kr^{85*}	8.6±1.0		4.8±0.7		2.4±0.4	

† The two end corrections for counters of the same length to diameter ratios for A^{37} and for Kr^{85} are the corrections obtained with each of the other length to diameter ratios; e.g., for $L:D=3:1$ for A^{37}, 10.8±2.3 percent is the end correction calculated from the difference in observed specific counting rates for the 3:1 and 6:1 length to diameter ratio counters and 11.0±1.6 percent is that calculated from the difference between the 3:1 and 12:1 counter rates.
* Experimental wall loss correction applied.
** Data from reference 1.

WALL LOSS

A. Results

Since the loss for particles escaping from the counter before any ionizing collision approximates a surface effect, it might be expected to vary as the ratio of surface to volume for different counters, or inversely as the diameter. On the basis of this assumption the correction in the krypton measurements was found to be approximately 6.9±1.1 percent for 1 in., 4.6±0.7 percent for 1½ in., and 3.4±0.5 percent for 2 in. diameter counters. No wall loss was observed with A^{37} as the active gas.

B. Discussion

The loss for particles which penetrate the walls before forming a single ion pair was calculated by considering the probability that a particle emitted from a differential element of volume in the gas would reach the wall without causing ionization. An integration of the losses over the entire volume of the counter was carried out to give the total loss. For counters of diameter 1 in. or larger, the fractional loss due to this effect equals $1/ID$ where I is the number of primary ion pairs per unit path length. In obtaining the primary ionization in the gas mixture in the counters, it was assumed that the primary ionization in the mixture used differed from that in air by a factor which was independent of energy. The values of I for air obtained

TABLE III. End loss dead volumes.

Isotope	Energy (kev)	Range in counting mixture (mm)	Average K	l/2 for D=1″ (mm)
A^{37}	2.8	2.7	0.298±0.014	3.8±0.2
C^{14}	154	1.5×10^4	0.269±0.036	3.4±0.5
Kr^{85}	740	1.5×10^4	0.259±0.012	3.3±0.2

---

[5] Kirkwood, Pontecorvo, and Hanna, Phys. Rev. 74, 497 (1948).
[6] P. W. Levy, Phys. Rev. 72, 248 (1947).

TABLE IV. Loss due to non-ionization.

Isotope	Wall loss For $D=1''$	Wall loss For $D=2''$	Compensated wall loss For $D=1''$	Compensated wall loss For $D=2''$
A^{37}	0.3%±0.2	0.15%±0.1	0	0
C^{14}	5.5 ±1.4	2.8 ±0.7	3.1%±0.8	1.5%±0.4
Kr^{85}	10.7 ±2.1	5.4 ±1.1	7.1 ±1.4	3.5 ±0.7

by Graf[7] for energies from 50 kev to 1000 kev were used to calculate the relative primary ionization for the mixture as a function of energy. The absolute values were obtained by using the value for I for argon obtained by Curran and Reid[8] at 420 Kev and the higher value of I calculated for alcohol by Hazen.[9] Curves *a* and *b* of Fig. 2 give the primary ionization of argon and alcohol at N.T.P. as a function of energy.

The wall loss to be expected for the different energy radiations was then calculated by integrating over the beta spectra. Columns 2 and 3 in Table IV give the percent of the total disintegrations in the 1 in. and 2 in. diameter counters which will not cause counts because of their occurring in the vicinity of the walls.

The loss due to "non-ionizing" particles is in some part compensated by the emission of secondary electrons from the cathode. For very low energies the ratio of secondary electrons to primary is about one for a brass or copper surface; for higher energies the multiplication factor is less than unity, approaching 0.3 above 100 kev, so that the wall loss is not completely cancelled. By interpolating between the data recently published by Trump and Van de Graaff[10] for high energy primary electrons and data for the very low energy range,[11] and integrating over the β-particle spectra, ratios of secondary to primary electrons of about 0.4 for C^{14} and 0.3 for Kr^{85} were determined and applied as a correction to the calculated wall losses. The corrected values are given in Table IV, columns 4 and 5.

Figure 3 is a plot of the ratio of secondary electrons to incident primaries *versus* energy for brass surfaces.

C. Conclusions

From these considerations it appears that the wall loss is entirely negligible for counters of 1 in. diameter or greater for β-energies less than 10 kev. For example, the wall loss compensated by secondary emission for H^3 (average energy approximately 6 kev)[12] in a 1 in. counter at 0.1 atmosphere pressure is of the order of a tenth of a percent. For higher energy radiations it should be possible to calculate the wall loss for any brass wall Geiger counter with an argon-alcohol filling from the curves in Figs. 2 and 3 since the wall loss is inversely proportional to counter diameter and to pressure for any energy β-particle and since secondary emission is a function only of energy.

Having completed the calculations for the wall loss for C^{14} it appeared of interest to re-examine the data obtained in the half-life determination, particularly since it had been noticed that the counters of smallest diameter yielded results considerably lower than the average for a given length to diameter ratio. Calculations based on the assumption that the wall loss is inversely proportional to the diameter gave the following results: for 1 in. diameter counters, 3.5±1.2 percent, for 1½ in. counters, 2.3±0.8 percent, and for 2 in. counters, 1.8±0.6 percent. Because the errors in the respective values are large it is possible that the agreement between the experimental and the calculated corrections is fortuitous, although highly suggestive. It is also significant that application of the empirical correction decreases the root-mean-square deviation from the average of the half-life data for all the counters by a factor of two. It is to be noted that applying these corrections to the half-life data lowers the published value of the half-life of C^{14} by about 2½ percent to 5580±45 years.

The principal limitation to the calculated wall loss corrections arises from uncertainties in the values for the primary ionization in argon and in alcohol. While the value for argon is probably approximately correct there may be considerable error in the value for alcohol (cf. Curran and Reid).[8] It is to be seen, however, that even a factor of two change in the absolute value of I_{alc} means a change of less than twenty percent in the calculated corrections because of the small partial pressure of alcohol in the counters.

A second limitation to the calculation of the wall loss is the possibility that the exact nature of the brass surface may exercise some effect on secondary emission. The evidence seems to indicate, however, that the

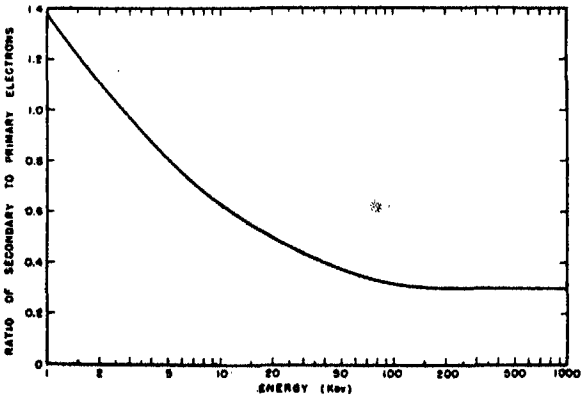

FIG. 3. Secondary emission from brass surfaces as a function of energy. The curve was obtained by plotting secondary emission as a function of atomic number at energies from 0.25 to 2 kev[11] and from 40 to 1000 kev[10] and interpolating in the region between.

---

[7] T. Graf, J. de phys. et rad. **10**, 513 (1939).

[8] S. C. Curran and J. M. Reid, Nature **160**, 866 (1947).

[9] W. E. Hazen, Phys. Rev. **63**, 107 (1943).

[10] J. G. Trump and R. J. Van de Graaff, Phys. Rev. **75**, 44 (1949).

[11] V. K. Zworykin and G. A. Morton, Television (John Wiley and Sons, Inc., New York, 1940), pp. 28–41.

[12] [5.69] Jenks, Ghormley and Sweeton, Phys. Rev. **75**, 701 (1949).

treatment of the surface affects the ratio of secondary electrons to primary greatly only for very low energies, i.e., those below 1.5 kev.

SUMMARY

For flat end brass wall Geiger counters containing active gas samples the end loss presumed due to inhomogeneity of the field has been measured for A^{37} and Kr^{85}. The loss was found to be approximately the same for them as for C^{14} despite the differences in energy, and to be proportional to the length to diameter ratio.

The counting loss for particles which escape from the counter without causing ionization was measured with Kr^{85} and calculated for A^{37} and C^{14} as well as for Kr^{85}. The experimental and calculated losses agree well within the limits of error and show the loss to be inversely proportional to diameter.

THE REVIEW OF SCIENTIFIC INSTRUMENTS VOLUME 21, NUMBER 6 JUNE, 1950

Scintillation Type Alpha-Particle Detector

A. S. Goldin, E. R. Rohrer, R. L. Macklin
Carbide and Carbon Chemicals Division, Union Carbide and Carbon Corporation, K-25 Laboratory Division, Oak Ridge, Tennessee

(Received November 28, 1949)

A portable scintillation detector for alpha-survey work is described. The instrument can detect as few as 16 alpha-counts (32 disintegrations) per minute because of the virtual elimination of spurious background. The upper limit of 50,000 counts per minute is not inherent and can be raised by appropriate circuit changes. The instrument is stable and is unaffected by most atmospheric conditions other than strong sunlight. Gamma-radiation up to 14,000 mr/hr gives no detectable response on this alpha-meter. The probe is the size of a GT type radio tube with a shield, allowing access to relatively small spaces. The sensitive area is about 1 in.×⅜ in. when a 931-A photo-multiplier is used.

INTRODUCTION

DETECTION of ionizing radiation by scintillation counters has been developed by Kallman,[1] Deutsch,[2] Coltman and Marshall,[3] Bell,[4] Hofstadter,[5] and others. Coltman and Marshall,[6] in particular, have developed scintillation counters for alpha-particles.

A scintillation type radiation detector consists essentially of a sensitive screen, a photo-multiplier tube, an amplifier, and a counter or rate-measuring instrument. The detection of alpha-particles differs from that of most other ionizing radiation because of the short range (three to five mg/cm²) and the high specific ionization. The short range makes it necessary to have the alpha-source very close to the instrument and to provide a light-tight window of some material sufficiently thin that the alpha-particles can penetrate it. The high specific ionization makes it possible to use sensitive screens of such materials as commercial zinc sulfide fluorescent powder in very thin layers.

Presently available field alpha-detection instruments are of either the ionization chamber (Zeuto) type or the proportional counter (Poppy) type. The Zeuto types are stable, have satisfactorily low drift rates, and are sensitive to about 100 to 500 alpha-counts per minute. (Throughout this report, the words "counts per minute" are used to refer to a counting rate as measured on a 50 percent geometry ionization chamber.) Poppy types are sensitive to individual alpha-particles, but are also sensitive to moisture, and have backgrounds so high that they are not able to detect with certainty a source of less than 100 counts per minute. Both types are somewhat sensitive to high intensities of beta- and gamma-radiation. Previously, in this section of the laboratory, we have built scintillation counters capable of detecting alpha-particles, but only when the alpha-source was enclosed in the same light-tight housing as the detector. It would be desirable to have a field type alpha-detector which would be sensitive to sources weaker than 100 counts per minute, and which would also be stable, have a low drift rate, and be insensitive to atmospheric conditions and to radiations other than alpha.

CONSTRUCTION

Probe

Because of the high specific ionization of alpha-particles, it was felt that the fairly inexpensive type 931A or type 1P28 photo-multiplier tube could be used rather than the more expensive type 1P21 or type 5819. Also, the rather less efficient commercial zinc sulfide powder could be used in place of crystalline anthracene or similar phosphors. A thin scintillator, such as a zinc sulfide screen would reduce the gamma-ray absorption while completely absorbing the alpha-rays.

It is found necessary to select the tubes used for low background rate. This was done on the regular scintillation counter equipment in this laboratory, consisting of a voltage divider for the photo-multiplier tube, a type A-1 linear amplifier with pulse-height selector,[7] and a scale-of-64 unit. The tube background was measured at several pulse-heights and then the alpha-counting rate was measured at the same pulse heights. If the background was low (e.g., 0.01 sec.$^{-1}$) at a pulse height at which the alpha-counting rate was still high, the tube was accepted.

---

[1] H. Kallman, Natur. u Tech. (July, 1947).
[2] M. Deutsch, Phys. Rev. 73, 1240 (1948).
[3] J. W. Coltman and F. H. Marshall, Nucleonics 1, 58 (1947).
[4] P. R. Bell, Phys. Rev. 73, 1405 (1948).
[5] R. Hofstadter, Phys. Rev. 75, 796 (1949).
[6] Marshall, Coltman, and Bennett, Rev. Sci. Inst. 19, 744 (1948).

After considerable experimentation, it was found to be more satisfactory to use dry adhesives rather than liquid for attaching the phosphor and light shields to the tube. The type of probe now in use was made in the following manner.

Scotch Tape was put around the cylindrical surface of the photo-multiplier tube, sticky side out, and was fastened at the side opposite the cathode. A mask around the cathode area was made by applying Scotch Tape sticky side down, leaving the sticky Scotch Tape surface uncovered over the window itself. A fluorescent screen could then be applied by rolling the tube in Patterson Type "D" fluorescent powder* which adhered to the Scotch Tape in a thin layer. The mask was then removed and the screen covered with aluminum Dutch leaf** having a thickness of approximately 0.16 mg/cm². This thin leaf has pinholes and so it was necessary to use two layers of it as a coating. This double coating was more satisfactory when the two layers were in close contact. Usually a piece was cut large enough for both layers. This was then folded and rolled between two sheets of tissue paper to insure close contact. By rolling the tube over the aluminum, the leaf adhered to the Scotch Tape. It was, of course, necessary to make the outer layer somewhat larger than the inner layer. The tube was then made light-tight with black Scotch electrical Tape and with Apiezon *Q* wax. In the probes so far constructed, the dome-shaped part of the tube was blackened by applying four or five coats of a solution of Apiezon *W* wax in trichloroethylene, allowing thorough drying between coats, but this method failed to give complete opacity and had to be supplemented by use of Apiezon *Q*. In view of this, it is felt that the preliminary coating with Apeizon *W* is unnecessary.

A case was made for the probe by machining out the inside of a 1¼ in. copper solder cap until it was a fairly loose fit for the probe, soldering to this a skirt of 0.012 in. brass to cover the tube except the window area, and then soldering copper screen over the window area. This screen was ordinary copper screen which had been etched in dilute nitric acid until the wires were reduced to about 0.006 in. in diameter. It is desirable to supply this case with a grounding wire.

Circuit

The circuit developed was a five-stage device consisting of an inverter, a discriminator, a second inverter, and a multivibrator. Subminiature tubes of the types CK 571 AX and CK 512 AX were chosen because of their small physical dimensions and tube characteristics, such as low current drain and relatively high amplification factor. The circuit diagram is shown in Fig. 1.

The photo-multiplier tube operates with a negative potential of 600 v. applied to the photo-cathode. A ten-

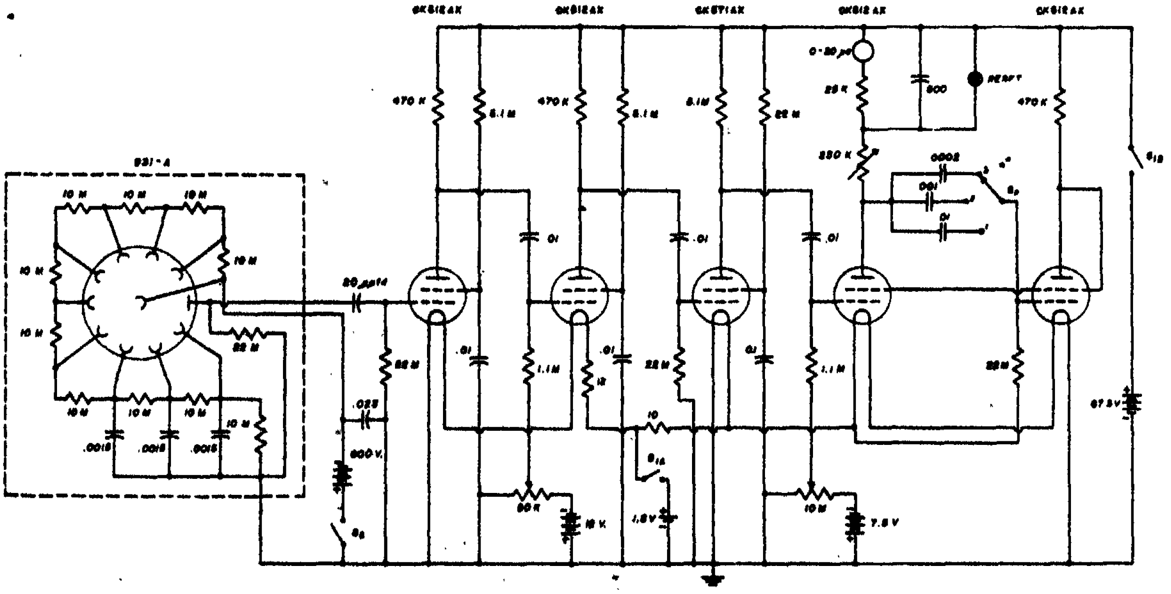

FIG. 1. Portable alpha-detector circuit. (Capacitor values are in microfarads unless otherwise noted.)

---

[7] W. H. Jordan and P. R. Bell, Rev. Sci. Inst. 18, 703 (1947).

* Kindly provided gratis by the Patterson Screen Division, E. I. duPont de Nemours and Company.

** Sherwin-Williams Company.

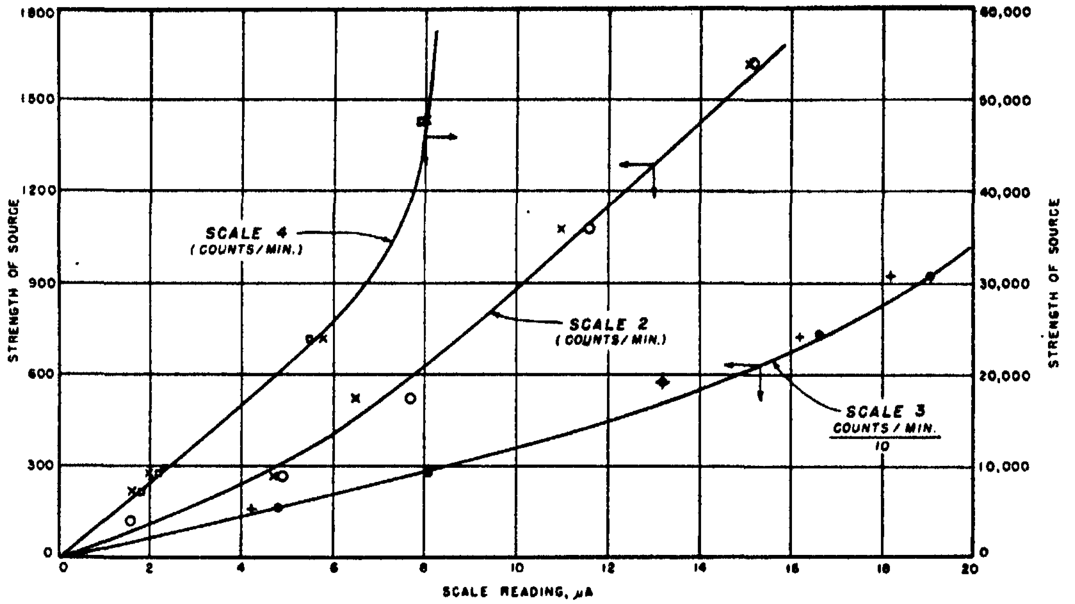

FIG. 2. Calibration curve for portable alpha-detector.

stage voltage divider between this point and ground provides for equal voltage drops between successive deflecting dynodes.

Output pulses are developed across the 22 megohm resistor between the collecting anode and ground. These pulses are negative and need to be reversed in polarity before they reach the discriminator. The first stage provides an amplified signal of the proper polarity to the discriminator grid. The second stage is biased just beyond the cut-off point for applied signals due to photo-multiplier dark current noise. Under this condition, alpha-pulses drive the tube into conduction, producing relatively large negative pulses on the plate. The third stage inverts the pulses from the discriminator and couples them to the grid of the first stage of the multivibrator.[8]

The final two stages make up a one-kick multivibrator which operates statically with the first tube cut off and the second conducting. When a positive pulse initiates the multivibrator action, a constant plate current flows through the meter and charges the shunting capacitor for a period of time determined by the grid leak resistors and coupling capacitors. The time constant can be changed by varying the value of the coupling capacitor. This variability provides the increased range of the rate meter. After the multivibrator has returned to static condition, the charge developed across the 500 μfd capacitor leaks off slowly through the meter and the series 25,000 ohm resistor. The time constant of the meter circuit is such that the current through the meter is proportional to the rate at which pulses activate the multivibrator.

With the low voltage supplies on, the plate load resistance of the first stage of the multivibrator is adjusted to provide a reasonable plate current. This varies with individual tubes and resetting is necessary only when the tubes or tube characteristics are changed. This adjustment is made in conjunction with the setting of the bias of the first multivibrator stage. The bias control is adjusted for cut-off and acts as a zero adjustment for the rate meter. The high voltage is then turned on and the discriminator bias is adjusted so that dark current background pulses are rejected.

PERFORMANCE

The probes were first tested on this laboratory's scintillation counter equipment, previously described. With this equipment, it was possible to set the acceptance level at such a height that background was only 0.001 or 0.002 count per second while the over-all counting efficiency was still about 30 percent as high as a 50 percent geometry ionization chamber. The sources used were disks about 0.5 in. in diameter placed about one-eighth in. from the fluorescent screen, giving a geometry of some 16–28 percent.

When used with the portable rate-meter circuit, the discriminator bias could be set at such a level that background counts occurred at the rate of one every ten minutes or so. Under these circumstances, the meter needle will swing at the occurrence of this background impulse and will slowly return to zero. The *RC* time of the meter circuit is about 18 sec., so that it takes almost a minute for the needle to return substantially to zero. The probability of a second background impulse occurring before the needle has returned to zero can be calculated from the Poisson distribution law. It is the probability of more than one impulse occurring in any minute, and is 0.018 for an average background rate of one impulse in five minutes, or 0.005 for an average background rate of one impulse in ten minutes. It is thus clear that if the background rate is kept to these values, it will be extremely unlikely that the meter reading will exceed the value caused by a single impulse which is about one microampere.

---

[8] The third and subsequent stages of the circuit are essentially the same as the portable alpha-detector circuit developed by Mr. Clyde Warram of the Instrument Engineering Department.

On the other hand, it can also be calculated from the Poisson distribution law that there will be a 95 percent probability of two or more impulses occurring in a single minute if the average rate of impulses is 4.74 per min. Assuming an efficiency of 30 percent compared to a 50 percent geometry counter, this means that a source with a strength of 15.8 counts per minute will give a second impulse, before the needle has returned substantially to zero, 95 percent of the time. A source with a strength of 15.8 counts per minute could, therefore, be detected by the fact that the maximum meter reading would be greater than one microampere.

In actual tests using scale 1, the most sensitive scale, results were obtained at various discriminator settings, as shown in Table I.

The average of the maximum readings for the 16-count-per-min. source is 3.3±0.9 microamperes; for the 40-count-per-min. source, it is 5.8±1.4 (95 percent confidence interval). The ratio of these averages is 1.76, compared with a theoretical ratio of 2.5. Of course, it must be remembered that at these extremely low counting rates, the data are inherently poor.

When used with stronger sources, over the range from about 100 counts per min. to 48,000 counts per min., results were obtained as shown on the accompanying calibration curve (Fig. 2). The scales are numbered in order of decreasing sensitivity.

A ten milligram radium source, within one inch of the probe, did not cause a meter reading; neither did holding wet hand immediately in front of the window.

The detector was checked for sensitivity to light. Its background is not changed outdoors in the shade; however, in the bright sun, the detector could not be used. The light intensities as measured on a G-E photographic type light meter were: indoors 24; outdoors in shade, 180; outdoors in sun, 3000–7000. Probably this light sensitivity could be completely removed by using more layers of aluminum leaf and by making a better light seal between the edge of the aluminum leaf and the tube blackening material. However, for instruments intended for indoor use, it is felt that this is undesirable because of the difficulties in adding more layers of leaf.

TABLE I. Performance of detector at various discriminator settings.

Discriminator setting (volts)	Background		Time for 10 impulses (sec.)	Max. reading (μa)†
	Impulses/min.	Max. reading (μa)		
−6.5	Continuous	20	—	—
−7.0	0.6 (5 min.)	1.2	203 (16 c/min.)	2.3*
			295 (16 c/min.)	1.5
			110 (40 c/min.)	2.7*
			87 (40 c/min.)	3.7*
−7.5	0.2 (5 min.)	1.2	118 (16 c/min.)	3.8*
			150 (16 c/min.)	3.0*
			43 (40 c/min.)	6.2*
			60 (40 c/min.)	5.6*
−7.75	0. (10 min.)		139 (16 c/min.)	5.0*
			147 (16 c/min.)	3.8*
			42 (40 c/min.)	8.2*
			31 (40 c/min.)	6.7*
−8.0	0. (10 min.)		149 (16 c/min.)	3.8*
			122 (16 c/min.)	3.2*
			42 (40 c/min.)	6.7*
			45 (40 c/min.)	6.5*

† In runs marked (*), the meter reading did not return to zero after the first swing.

CONCLUSIONS

A scintillation type alpha-particle detector is now available which is capable of detecting alpha-sources as weak as sixteen counts per min. It is stable, insensitive to gamma-radiation and to atmospheric conditions other than strong sunlight. The probe can be used with various modifications for various types of field service.

THE REVIEW OF SCIENTIFIC INSTRUMENTS VOLUME 21, NUMBER 6 JUNE, 1950

The Theory and Properties of Low Voltage Radiation Counters[*]

J. A. SIMPSON, JR.
Argonne National Laboratory and Institute for Nuclear Studies, University of Chicago, Chicago, Illinois

(Received December 27, 1949)

The behavior of permanent gas mixtures which lead to low breakdown potentials is discussed, and criteria are established for attaining minimum threshold and operating potentials for G-M counters. Curves showing the dependence of counter characteristics upon pressure and electrode parameters have been obtained for various mixtures of neon and argon. The properties of cathode surfaces have been investigated and the criteria for obtaining suitable surfaces for counter operation were found.

Two classes of counters were observed using these permanent gas mixtures. The first class possesses the lowest range of threshold potentials (approximately 115 to 135 volts) at pressures up to approximately 7 cm Hg. They require quenching circuits having relatively long time constants. The second class of counters have threshold potentials in the range of approximately 135 to 210 volts corresponding to pressures from 7 to 50 cm Hg. They operate with fast quenching circuits.

Miniature portable radiation detectors and meters have been made using these detectors.

I. INTRODUCTION

RADIATION counters operating in the proportional and Geiger-Müller counting regions have been prepared and studied[1] which have unusually low operating potentials. Although the original purpose of the experimental investigation was to devise small portable radiation meters for personnel protection, the behavior of permanent gas mixtures at moderately high pressures for producing low voltage counters is of experimental and theoretical interest. Therefore, this paper emphasizes certain aspects of the theory of this class of counter and describes a series of measurements through which the properties of these counters have been determined.

For many years various methods have been used to reduce the operating potentials of Geiger-Müller and proportional counters. These methods may be reviewed briefly as follows:

1. Reduction of Gas Pressure

This method has been widely used,[2,3] but is extremely limited by the rapid decrease in counter efficiency and inadequacy of counter performance[2] with decreasing pressure. Threshold potentials as low as 375 volts have been obtained in helium[2] at pressures of about 1 cm Hg. The well-known minimum in permanent gases such as argon which occurs at about 0.1 to 0.8 cm Hg pressure has been used giving threshold potentials of 300 volts. The efficiency is low, and the counters possess poor characteristics.

2. Changes in the Relative Diameters of the Electrodes

About 20 percent reductions in counter threshold potentials are possible under optimum conditions. The range downward in size of center wires is limited by mechanical difficulties.

3. Triode Counters

By using a screen grid around the counter center wire[4] with the outer cathode 10–200 volts negative with respect to the grid Korff and Ramsey[5,6] have been able to reduce the operating potentials of large counters approximately 40 percent.

4. Mixtures of Permanent Gases

Counters filled to moderate pressures have been used in which the threshold potentials V_t were lower than for the principal gas alone.[7,8] The threshold potentials, however, were not less than 70 to 90 percent those of the principal gases. These mixtures operated as counters down to 400 volts or more. A mixture with V_t of approximately 300 volts at high pressure (53 cm Hg) has been reported[3] using a neon-helium mixture of unstated proportions, but counter performance was not satisfactory. Argon-oxygen,[9] neon-hydrogen, and impure argon have been used extensively as counters at somewhat higher potentials. Attempts have been made to use low voltage neon glow lamps as counters for radiation meters.[10,11] [*Note.*—More recently Present[1a] has proposed the use of halogen plus permanent gas mixtures for self-quenching counters. Liebson[1b] and Friedman[1c] have prepared counters of this type which operate successfully down to at least 250 volts. It would appear that these counters may be superior to permanent gas counters for radiation meters except where an instrument of unusually small size and weight is required.]

---

[*] Most of this work was done under Contract W-7401-Eng-37 for the Manhattan District Project Engineers in 1944–1946, and the information covered therein will appear in the National Nuclear Energy Series. The present paper was declassified April, 1947.

[1] J. A. Simpson, Jr., Metallurgical Laboratory M.U.C.-J.A.S.-52 (1945); -53 (1945); -57 (1945); Phys. Rev. **72**, 181 (1947).

[2] C. L. Haines, Rev. Sci. Inst. **7**, 411 (1936).

[3] S. Werner, Zeits. f. Physik **90**, 384 (1934); **92**, 705 (1934).

[4] W. F. Libby, Phys. Rev. **55**, 245 (1939).

[5] S. A. Korff and W. E. Ramsey, Rev. Sci. Inst. **11**, 267–269 (1940).

[6] S. A. Korff, Phys. Rev. **68**, 53, 284 (1945).

[7] S. A. Korff, Electron and Nuclear Counters (D. Van Nostrand Company, Inc., New York, 1946), p. 77 and references therein.

[8] L. B. Loeb, Fundamental Processes of Electrical Discharge in Gases (John Wiley and Sons, Inc., New York, 1939), p. 495.

[9] G. L. Locher, Phys. Rev. **55**, 675 (1939).

[10] T. A. Chambers, Brit. J. Radiol. **7**, 755 (1934).

[11] P. R. Pallister, Brit. J. Radiol. **10**, 759 (1937).

[1a] R. D. Present, Phys. Rev. **72**, 243 (1947).

[1b] S. H. Liebson, Phys. Rev. **72**, 181(A) (1947).

[1c] S. H. Liebson and H. Friedman, Rev. Sci. Inst. **19**, 303 (1948).

The following discussion will show that it is possible to obtain reproducible permanent gas counters having operating potentials ranging from approximately 130 to 250 volts, representing gas pressures ranging from approximately 5 to over 50 cm Hg.

II. THE THEORETICAL BASIS FOR LOW THRESHOLD POTENTIALS

A considerable amount of information is available on the behavior of the breakdown potentials for gases with different systems of electrodes as a function of the properties of the gases and gas mixtures. The discussion will be limited to permanent gases. The gas discharge regions useful for proportional counting and Geiger counting lie within a few volts of the breakdown potential of a mixture of permanent gases. It is thus desirable to consider the problem of obtaining minimal breakdown potentials using data in the literature before considering the more restrictive conditions for counter operation. It is not to be expected, therefore, that the determination of minimum breakdown potentials will necessarily at the same time determine sufficient conditions for the adequate performance of a counter. These additional conditions for counter operation will be presented later in the discussion concerning the counter tubes and will be supported by experiments.

A

As the potential difference is increased between two electrodes in a gas the current which flows is at first caused by residual ionization in the volume and photoemission at the cathode. This is the ion chamber region in which, under optimum conditions, all ions formed in the volume are collected at the electrodes. By further increasing the applied potential, electric fields may be obtained in which an electron formed in the gas may acquire sufficient energy to produce an ion pair by collision. This may lead to a self-sustaining discharge. The potential for which the discharge current increases by a factor of 10^7–10^8 and becomes self-sustaining is called the breakdown potential V_B for that particular system. This represents the beginning of the corona discharge region. The discharge regions of interest in this paper are: (1) the electron avalanche region near the breakdown potential which determines proportional counter characteristics; and (2) the breakdown potential and the corona current region immediately above V_B which determines G-M counter characteristics.

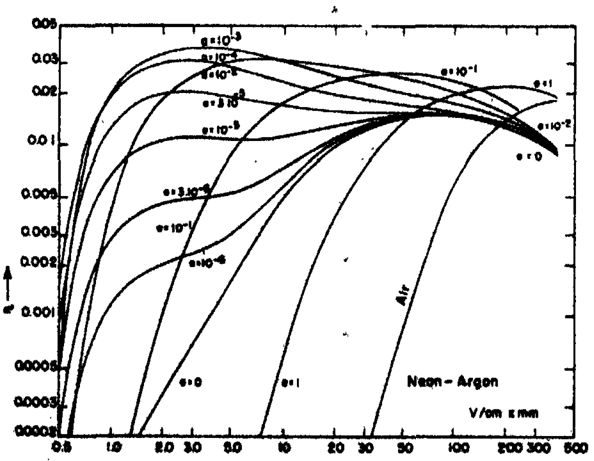

FIG. 1. Values for $\eta=\alpha/E$ as a function of E/P for various gases and gas mixtures. (See reference 14.)

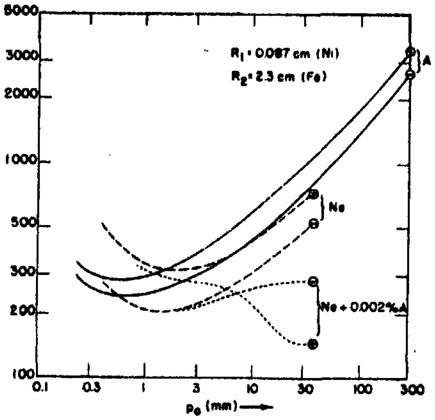

FIG. 2. The breakdown V_B between coaxial cylinders of radius $R_a=R_1$; $R_c=R_2$ in neon, argon, and neon plus 0.002 percent argon. (See references 17–20.)

For a coaxial electrode system it may be shown[12] that the condition for reaching a steady minimum current with a corona discharge beginning around the positive center wire is:

$$\gamma \exp\left(\int_0^{V_B} \eta dV\right)=1 \qquad (1)$$

provided $R_a \ll R_c$; $E_a/P \gg E_c/P$ and $E_c/P<1$ (R_a and R_c are radii of anode and cathode respectively).[13]

Thus, gases or gas mixtures which have high values for η produce low breakdown potentials. Extensive measurements of η have been reported in the literature.[14–16] Figure 1[14] shows the values of η for some gas mixtures as a function of E/P.

---

[12] L. B. Loeb, *Fundamental Processes of Electrical Discharge in Gases* (John Wiley and Sons, Inc., New York, 1939).

[13] For reference, several parameters of electric discharges are defined as follows: α—Townsend coefficient, the number of ion pairs formed per cm path length traversed by an electron in a field E. P—gas pressure in millimeters of mercury. $\eta(E/P)=\alpha/E$—a function of the energy of the ionizing electron; the ionization per cm path length per volt potential difference. i—electron current in amp. i_0—electron current as $V\rightarrow 0$. γ—the number of secondary electrons from the cathode surface per ion pair formed in the gas. This emission is principally caused by: (a) Emission of electrons by positive ion bombardment at the cathode. (b) Photo-electron emission by incident radiation quanta. (c) Emission of electrons by metastable atoms approaching the cathode.

[14] A. A. Kruithof and F. M. Penning, Physica 3, 515 (1936).

[15] A. A. Kruithof and F. M. Penning, Physica 4, 430 (1937).

[16] M. J. Druyvesteyn and F. M. Penning, Rev. Mod. Phys. 12, 87 (1940).

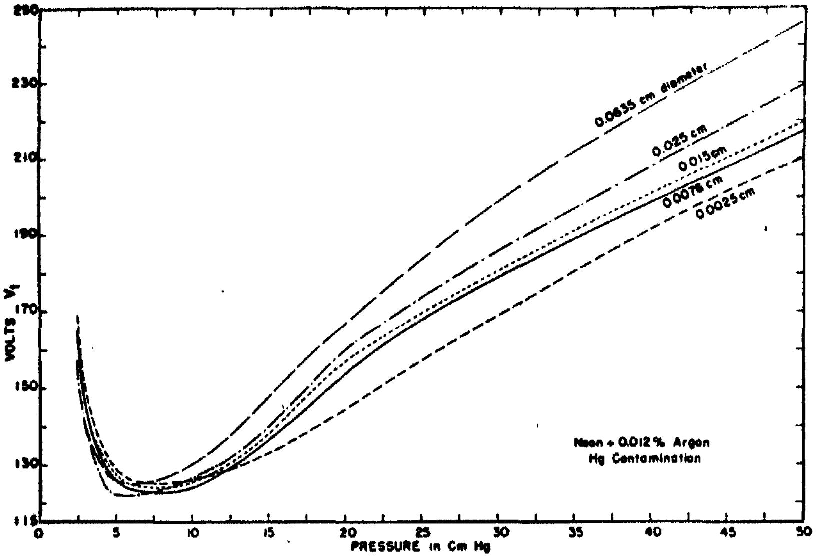

FIG. 3. The G-M pulse threshold potential V_t for a mixture of neon plus 0.012 percent argon as a function of the gas pressure. With a copper cathode radius $R_c=0.61$ cm. V_t was determined for values of $2R_a=0.0025$, 0.0076, 0.0152, 0.0254, and 0.064 cm.

The values of $\eta(E/P)$ for mixtures of pure neon and argon shown at low values of E/P are among the largest experimentally determined. Therefore, these special mixtures should demonstrate unusually low breakdown potentials, and they will be used as representative of this class of gas mixture throughout the discussion which follows.

Penning and his co-workers[17–20] have determined the breakdown potentials for coaxial electrode systems (Fig. 2) as a function of pressure using both pure gases and neon with small admixtures of argon.

B

An examination of the properties of this mixture reveals the reasons for the observed high values of η or low values of V_B.

Electrons in collision with gas atoms G_1 such as pure neon may excite the atoms and leave them in metastable states $G_1{}^m$ for considerable periods of time. Thus, large amounts of energy removed from the electric field by electrons are used to produce excitation and not ionization. This will result in small values of η or large values of V_B for such gases. When, however, a small quantity of a second gas G_2 is admixed with gas G_1 the mean life time of metastable atoms $G_1{}^m$ may be reduced to a very small value.

This will occur provided the second gas has a first ionization potential V_2 which is less than, but close to, the potential $V_1{}^m$ of the metastable state of the principal gas G_1. The following collision process will take place between an atom of kind G_1 in its metastable state $G_1{}^m$ and a neutral atom G_2.

$$G_1{}^m+G_2\rightarrow G_1+G_2{}^+ + \text{electron}; \text{ provided } V_1{}^m > V_2. \quad (2)$$

It is evident that for a given production rate of metastables $G_1{}^m$ in gas G_1 at pressure p_1 there is an optimum amount of G_2, say p_2, to provide for complete removal of metastable states in a time t to give a ***minimum*** breakdown potential $V_{B\text{ min}}$.

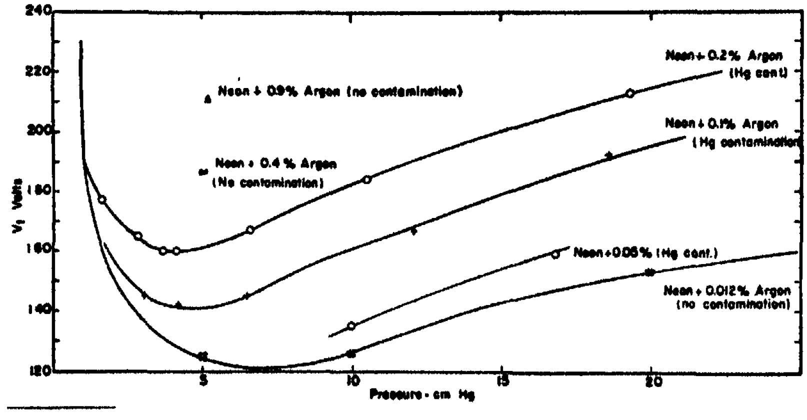

FIG. 4. The G-M pulse threshold potential V_t as a function of pressure for neon mixed with 0.012, 0.05, 0.1, and 0.2 percent argon, respectively.

---

[17] Penning, Moubis and Addink, Physica (old series) **13**, 209 (1933).
[18] F. M. Penning, Phil. Mag. **11**, 961 (1931).
[19] H. F. Boulind, Phil. Mag. **18**, 909 (1934); **20**, 68 (1935).
[20] F. M. Penning, Zeits. f. Physik **46**, 335 (1927).

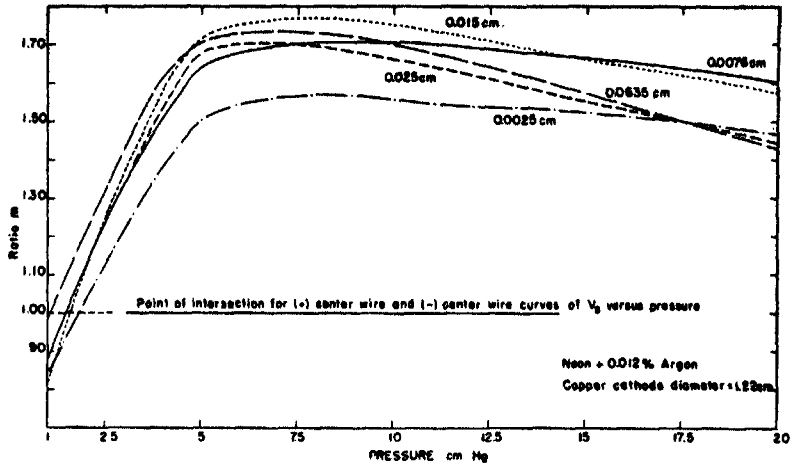

FIG. 5. To demonstrate that the counters are operating in the anomalous low voltage region, the ratio $m=(V_B$ to negative wire$/V_B$ for positive wire) has been determined. Compare these curves with Fig. 2.

For the particular case of neon gas mixed with small amounts of argon,

$$V_1=21.47 \text{ ev.}$$
$$V_1^m=16.6 \text{ ev.}$$
$$V_2=15.7 \text{ ev.}$$

These values satisfy condition (2).[20a] Amounts of argon greater than 0.0004 percent will measurably change the V_B of pure neon gas.

It should be noted that Hg vapor is about ten times more effective than argon in minimizing V_B in neon. At room temperature, however, insufficient amounts of Hg vapor are available for neon above one centimeter Hg pressure.

The very low values for η in Ne-A mixtures at $E/p<1$ are due to electron energy losses resulting from collisions with the atoms.

C

There is an additional, important factor which contributes to the lowering of V_B in the mixtures of neon and argon when the coaxial electrode system is to be used as a pulse counter since the center wire is positive with respect to the outer cylinder. It is apparent from Fig. 2 that at higher pressures the breakdown potential is lower for an anode center wire than for a cathode center wire. The theory of the anomalous lowering of V_B when the potential difference between electrodes approaches V_B has been described by Druyvesteyn and Penning.[16]

III. THE PROPERTIES OF LOW VOLTAGE G-M COUNTERS

A. Experimental Procedures

All counters used in the studies were constructed with Pyrex glass envelopes containing cathodes composed either of thin metal films, or of tubing. The center wires were made of tungsten so they could be heated by an electric current during the outgassing periods on the vacuum system. A group of counters which do not conform to the above specifications will be described later. Sets of identical counters were used for all measurements. The components of the vacuum system included a three-stage oil diffusion pump, a large manifold to which 30 counter tubes could be attached and a manifold on which were sealed flasks of gases to be used for the studies. The manifolds were separated by appropriate liquid nitrogen traps. A large furnace for outgassing the array of counters was provided so it could be rolled around the manifold containing the counters. Constant temperature controls protected the array of counters during the outgassing period. All data on counter characteristics were taken at 21°–24°C, and

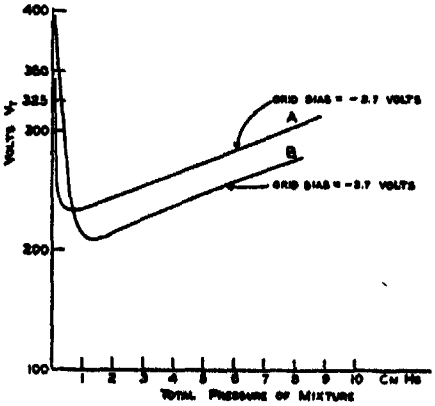

FIG. 6. Values for V as a function of pressure for:
A. He$+1.5\times10^{-2}$ percent A B. He$+1.6\times10^{-3}$ percent Xe

He	A	He	Xe
First ionization			
24.48 ev	15.69 ev	24.48 ev	11.5 ev
Metastables			
19.73 ev	—	19.73 ev	—
20.55 ev	—	20.55 ev	—

[20a] Additional examples of combinations of gases fulfilling condition (2) include:

Vehicular gas potentials in ev		Added gas
Ne ($V_1=21.47$);	($V_1^m=16.6$ ev)	Hg ($V_2=10.39$)
He ($V_1=24.4$);	($V_1^m=20.55$ ev) $=19.73$	Xe ($V_2=11.5$)

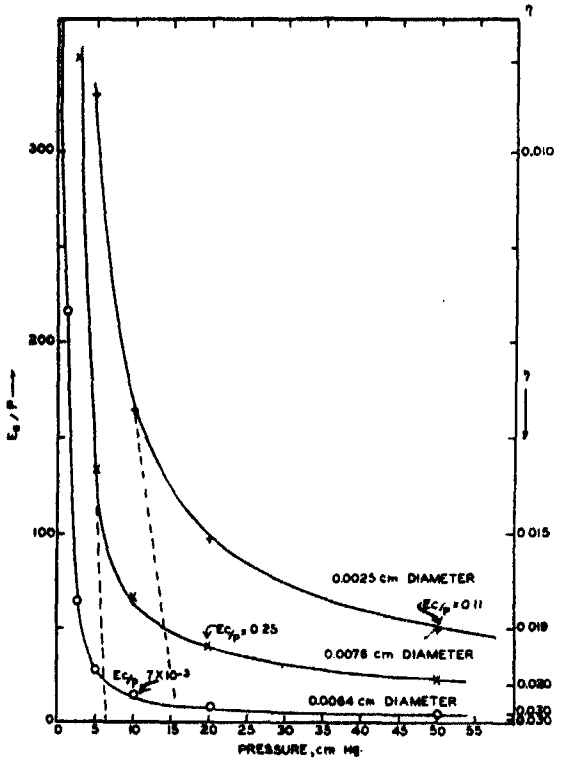

FIG. 7. Values for E_a/P at the surface of the anode have been calculated from experimental data as a function of the gas pressure. Each curve represents a different value for R_a. These values are obtained from Fig. 3. The gas mixture is neon plus 0.012 percent argon.

all data are obtained from the preparation of from 6 to 30 counters for a single measurement.

The outgassing process required at least 4 to 6 hours of pumping with the furnace at 300°C and included the use of an electrical discharge for "clean-up," a baking of the vacuum system parts which were outside the furnace and incandescent heating of the center wires. Liquid nitrogen cooled the traps after the removal of water vapor, air, and organic materials was complete.

Vacuum gauges covering several ranges of pressure were provided. Pirani gauges calibrated for the various gases were used when the gas pressures in the manifold were less than 0.1 cm Hg. Manometers calibrated in mm Hg were used for higher pressures.

All gases used were purified and stated to be "spectroscopically pure" by the manufacturer.[21] Neon gas was an exception since it contained not more than 0.1 percent helium. However, since Penning[15] has shown that helium up to 0.3 percent would leave the breakdown potential of neon unchanged from the value for pure neon the helium impurity was not important for these experiments. Break-off tips on the gas flasks were opened after proper outgassing of the manifold had taken place.

Pulse measurements such as threshold values V_t for the Geiger counting region were made with a conventional Neher-Harper[22] electronic circuit using a subminiature[23] type 512 Raytheon tube.

B. The Threshold Potentials for G-M Counters

With liquid nitrogen around the manifold traps a mixture of neon plus 0.012 percent argon was prepared in the counters. The pulse threshold as a function of pressure appears in Fig. 3 with center wire diameters as a parameter. The cathode was 1.22 cm in diameter and was made of chemically cleaned copper. Some Hg contamination might have been present on the copper surfaces. The change in threshold potential between 4 and 10 cm Hg is relatively small. Similar curves for 0.1 and 0.2 percent argon mixed with neon are shown in Fig. 4.

By determining the ratio $[V_B \text{ (wire negative)}]/[V_B \text{ (wire positive)}] = m$ as a function of pressure as in Fig. 5, it is easily shown that for pressures greater than 1.0 cm Hg the counters are operating in the anomalous low voltage region discussed in the previous section. Compare the position for $m=1$, Fig. 5, with Fig. 2 showing the intersection of the center wire positive and the center wire negative curves. Values for V_B with the center wire *negative* with respect to the outer cylinder may be determined from Figs. 3 and 5 as a function of pressure. (These data are of interest if the counter is to be used in a potential reversing circuit.)[24]

Other gas mixtures obeying condition (2) include He-argon and He-xenon, Fig. 6, and neon-Hg vapor.

Groups of counters with identical cathode diameters and surfaces but having different center wire diameters were used to obtain information on the variation of V_B with different values of R_a. Counters representative of each group were used for Fig. 3. At pressures above 16 cm Hg of neon plus 0.012 percent argon the characteristics are normal, that is, the pulse threshold potential is a direct function of R_a. Below approximately 16 cm Hg and extending down to about 2 cm Hg the V_B-pressure curves for different values of R_a cross to make V_B an inverse function of R_a. Haines[3] has reported such a phenomenon for H_2 and helium at low pressures but with high threshold potentials; no explanation of the effect was given. Brown[25] has predicted this kind of cross-over for helium by developing the theory of breakdown potentials in helium.

It appears that for the case of neon plus argon a satisfactory explanation of the effect may be made. From Fig. 3 it may be seen that the V_B *vs.* pressure curves for concentric electrode systems having different values of R_a cross at low pressures and that it is not the minimum R_a which produces the minimum values for V_B. The explanation of these characteristics depends upon a knowledge of the field intensity E_a near the surface of the anode and the effective mean-free-path λ of the ionizing electrons in neon-argon gas mixtures. Since $\lambda \sim 1/p$ then the ratio E/p may provide information to aid in interpreting the cross-over as a function of p. Using the data from Fig. 3, calculations of E_a, and hence, E_a/p have been made with three different values for R_a covering the pressure range 10 to 500 mm Hg. For a stated R_a the corresponding values of E_a/p are plotted as a function of p in Fig. 7. Values for η are also given for corresponding values of E_a/p. The values of E/p are maximum values at the anode, and since the field varies as $1/r$ the values for E/p only short distances away from the center wire will be much lower. Spot values for E_c/p at the cathode are shown on the graph to emphasize the fact that E_c/p is so low that the corresponding values of η are practically zero.

---

[21] Linde Air Products Corporation, Tonawanda, New York. The neon and argon may contain several parts per million of H_2O, CO_2, H_2 and oxygen. In addition the argon may contain 1–2 parts per million nitrogen. Gases not meeting these specifications were discarded.

[22] V. Neher and W. Harper, Phys. Rev. 49, 940 (1936).

[23] The use of subminiature tubes was desirable since they would find direct use in portable radiation meters.

[24] J. A. Simpson, Phys. Rev. 66, 39 (1944).

[25] S. C. Brown, Phys. Rev. 62, 244 (1942).

With the above information the crossing-over properties of Fig. 3 may be predicted. At pressures above 20 to 25 cm Hg values of E_a/p for all R_a shown are in a region where η has values which are near the maximum for the gas mixture. For example, at E_a/p for $r_c/r_a = 480$ the value for η is low, but a short distance r from the anode still within the avalanche region η will have reached its maximum value. Therefore, at the higher pressures the electrode systems behave normally as predicted in electrical discharge theory where V_B varies *directly* with r_a and r_c.

However, as the pressure is decreased Fig. 7 indicates that observed values of E_a/p begin to increase more rapidly for small values of R_a than for large values of R_a. This upward break occurs because the region of the $1/r$ electric field in which η is large is moving away from the region of the anode. It is, therefore, necessary to increase the field intensity distribution in the region around the anode where the avalanche processes occur to compensate for this average decrease in η. This appears as an increase in V_B. Thus, both decreasing p and increasing E_a results in a large increase in E_a/p. Since this increase of E_a/p begins at higher pressures for small r_a then a cross-over of the V_B-pressure curves for two different but *small* values of r_a should result at a higher pressure than for two different but *large* values of r_a. This is in accord with the experimental results.

An approximate value for the pressure at which cross-over would take place for two values of r_a may be estimated by extrapolating the steep slope portion of the E_a/p *vs.* P curve to intersect the pressure coordinate. Thus, the pressure range for cross-overs is approximately 2.5 to 16 cm Hg for values of r_c/r_a between 10 and 500 with this neon-argon gas mixture.

Figure 7 shows that increasingly great differences in E_a/p at constant P exist between any two values of r_a for pressures below 5 cm Hg. This arises from a continuation of the shift of maximum η away from the avalanche region as already described. As a result V_B in this low pressure region is an *inverse* function of r_a.

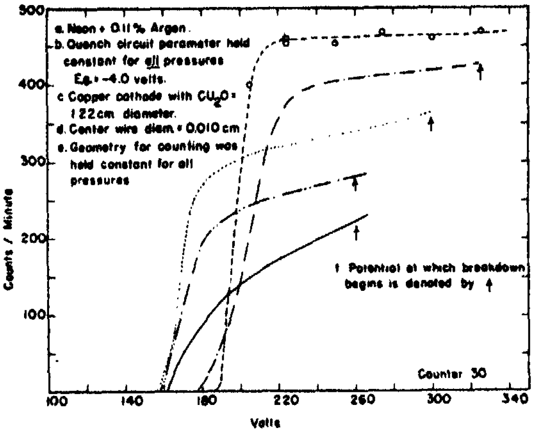

FIG. 8. Characteristic curves of a counter operating with an electronic quenching circuit having parameters which are *not* at optimum values for all counter pressures.

The optimum value of r_a required to achieve minimum V_B for any particular pressure of the neon-argon mixture may be determined approximately from Fig. 3.

It has been shown[22] that near the anode

$$\frac{dE_a}{dr_a} = \frac{V}{r_a^2 \ln(r_c/r_a)}\left[\frac{1}{\ln(r_c/r_a)} - 1\right],$$

and that only for dE_a/dr_a *decreasing* can the corona region exist. This requires that $r_c/r_a > e$, a condition that exists for all the experiments which are being described. It follows that as $r_c/r_a \rightarrow e$ the maximum current drawn by an avalanche discharge will increase.[26] The data presented in Figs. 3 and 7 may be used to further test the validity of Brown's theory[25] for determining

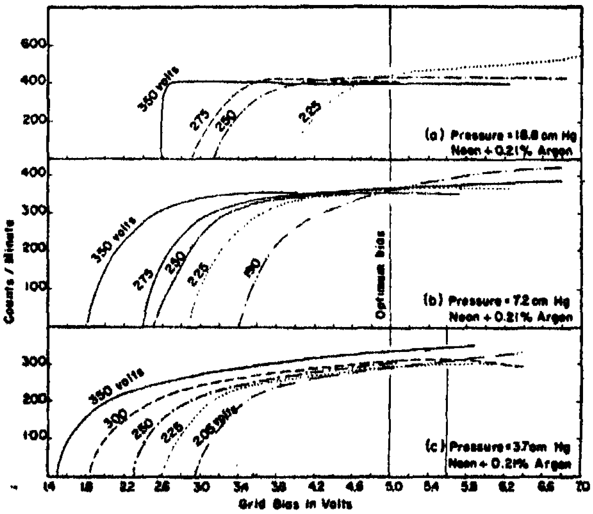

FIG. 9. Family of plate potential curves with counting rate as a function of grid bias, e.g., on the "quenching" tube.

---

[26] S. C. Brown, Rev. Sci. Inst. **17**, 544 (1946).

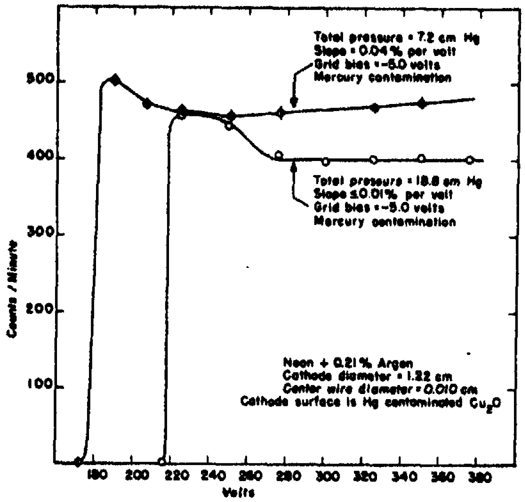

FIG. 10. Characteristic curves determined by using the optimum bias shown in Fig. 9.

the breakdown potential of a helium counter when applied to the case of a *mixture* of permanent gases.

C. Counter Measurements in the Geiger-Müller Region

The principal features of the counter discharge mechanism of permanent gas mixtures have already been described.[27, 28] *A necessary condition* for a counter to return to its operating potential without spontaneously continuing the avalanche process is that the counter remain below V_B for a time t sufficient for the removal of all ions and metastable atoms in the counter gas. This time t is minimized to decrease the insensitive time of the counter.

With the experimental verification of regions of low threshold potentials for Geiger counters it is important to examine the characteristics of these mixtures under counter operating conditions and examine the additional limiting conditions placed upon the choice of gas mixtures and cathode surfaces by the G-M discharge mechanism.

One conventional method for displaying G-M counter characteristics is to determine the counter response in counts per unit time as a function of applied potential. These so-called characteristic curves have been plotted for a variety of pressures and gas mixtures in Figs. 8, 10, 11, and 12. However, since the counter characteristics are not independent of the external electronic "quenching" circuit the indiscriminate use of these curves to study the counter tube alone is meaningless. For example, in Fig. 8 the characteristic curves of a counter filled with neon plus 0.11 percent argon are plotted for pressures of 18.6, 12.1, 6.5, 4.2 and 3.1 cm Hg using an electronic circuit with the *same* parameters for *all* pressures of the gas mixture. The circuit was initially adjusted for the counter operating at the highest pressure. As will be shown below, these changes in counter characteristic curves with decreasing pressure are *not* due alone to changes in the counter pulses but are also due to *improper* use of the electronic quenching circuit.

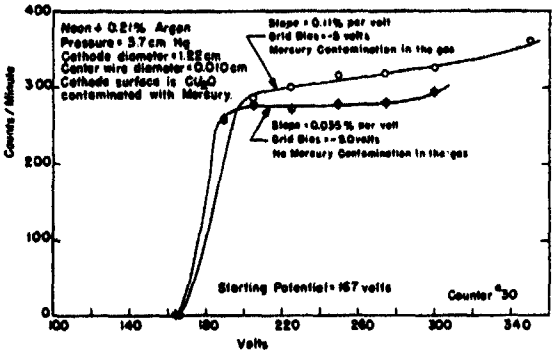

FIG. 11. The effect of mercury vapor and organic vapor impurities on the counter characteristics at a low pressure.

A set of counters was filled with neon plus 0.21 percent argon with Hg contamination to a pressure of 18.8 cm Hg. Counting rates as a function of the grid bias $-E_g$ on the N-H circuit were obtained as in Fig. 9 with plate supply potential as a parameter. This set of curves is more important than the "plateau" curves for determining the characteristics of a permanent gas counter tube. Not only are the slope characteristics of the counting region determined for any grid bias $-E_g$ but also the uniformity of pulse height, freedom from multiple pulses and freedom from momentary corona breakdown determined from these curves. For any given plate supply potential the region in which the counting rate is constant for a range of values of $-E_g$ provides a measure of the uniformity of counter pulse heights. An example of counter performance in which the pulses were of uniform height is shown in Fig. 9a with plate potential = 350 volts.

At high operating potentials permanent gas counters which produce spurious discharges due to impurities in the gas, may break down at random into corona discharges for long intervals of time. Consequently, a low counting rate is observed at high operating potentials. This behavior of counters has been discussed by Neher and Harper[22] and appears as a negative slope on the above curves for high values of $-E_g$. Such an effect is just becoming detectable at a pressure of 3.7 cm Hg for grid biases of about -6 volts as shown in Fig. 9c.

The selection of the optimum bias from Fig. 9 is approximately -5.0 volt. It is to be expected that the counting rate at 225 volts will be high as shown because the over voltage does not produce pulses large enough to operate the quenching circuit hence multiple pulses arise. This peak near the counter threshold potential is observed in Fig. 10. At 18.8 cm Hg the characteristic curve slope was less than one percent for a 100 volt interval. No multiples or discharges were observed even

---

[27] C. G. Montgomery and D. D. Montgomery, Phys. Rev. 57, 1030 (1940); and references therein.

[28] A. Nawijn, Physica, 's Grav. 9, 481 (1942).

at 400 volts. The threshold potential was 214 volts. At 7.2 cm Hg the counting rate slope was 4.5 percent in a 100 volts interval, but otherwise the counter characteristics were the same as at higher pressures. The threshold potential was 167 volts.

A further reduction in pressure to 3.7 cm Hg still with mercury and stopcock grease vapor contamination present resulted in the curves of Fig. 11. At optimum grid bias the counter plateau slope increased to 11 percent in a 100 volt interval. The addition of liquid nitrogen traps for a period of 10 hours left the threshold potential unchanged at 159 volts. However, a remarkable improvement in operating characteristics was found with the slope being reduced to 2.5 percent in a 70 volt interval. Removing the liquid nitrogen traps resulted in the system returning to the original characteristics with the 11 percent slope. Many groups of counters have shown the same shift of characteristics with reduction of pressure whenever these contaminants were present at room temperature.

In all cases the addition of mercury vapor was made by saturation at room temperature; hence as the total pressure in the counters was reduced the proportion of mercury vapor increased in the mixture. In general it was found that only with pressures of neon-argon mixtures below 7 to 10 cm Hg do counter characteristics become seriously dependent on mercury and stopcock grease vapor contamination.

A plateau curve from a counter with neon-argon mixture at 4 cm Hg having a threshold potential of 118 volts is shown in Fig. 12. As will be seen from the more detailed discussion which follows counters with such low threshold potentials require longer recovery times than counters with over approximately 135 volts threshold potentials.

D. Pulse Characteristics

Using a driven sweep circuit,[29] and cathode follower input to a wide band amplifier with an oscilloscope the rise times of counter pulses have been measured for various pressures and amounts of argon in neon. Counters with 0.1 percent or more of argon at pressures of about 10 cm Hg or above had rise times of approximately 2×10^{-6} sec. The formation of the peak of the pulse required 10^{-5} sec., and the total pulse width was 10^{-4} sec.

Counters filled with approximately 4 cm Hg of neon plus 0.1 percent argon had rise times of 10^{-4} sec. and a pulse width of about 3×10^{-4} sec.

However, counters filled with neon plus the order of 0.01 percent argon to about 5 cm Hg pressure producing minimum threshold potentials of 115 to 135 volts have different pulse characteristics. The rise time as measured on the plate of the quench circuit was $1\text{–}3\times10^{-4}$ sec. but the pulses had a recovery time of approximately 10^{-3} sec.

All pulse measurements were made with an overvoltage of 20 to 25 volts; overvoltages higher than this improved rise time characteristics appreciably as predicted by theory.[27] In all cases copper cathodes prepared to give optimum results have been used with the counters described. The determination of these satisfactory cathode surfaces is discussed later.

The constancy of counter characteristics has been determined for several mixtures of neon and argon over a period of two years. Threshold potentials have remained within one percent of their initial value and pulse shapes have remained unchanged. Many small counters were constructed simply by using a 0.95 cm diameter length of Kovar tubing as a cathode with small glass seals on both ends. These counters maintained their initial characteristics over two years with threshold potentials of 115 to 125 volts. See Fig. 12.

The background counting rates for these counters agree well with the number of ionizing events expected per unit volume.

E. Cathode Surface Characteristics in Neon-Argon Counters

Evaluation of the secondary effects at the cathode of permanent gas counters is difficult. The function γ which represents these effects has been defined as the

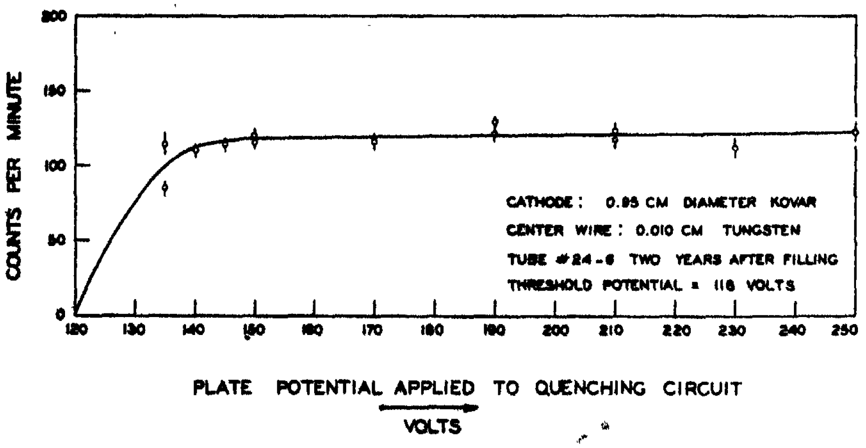

FIG. 12. Characteristic curve of low voltage neon-argon counter using quenching circuit.

---

[29] H. G. Stever, Phys. Rev. 61, 38 (1942).

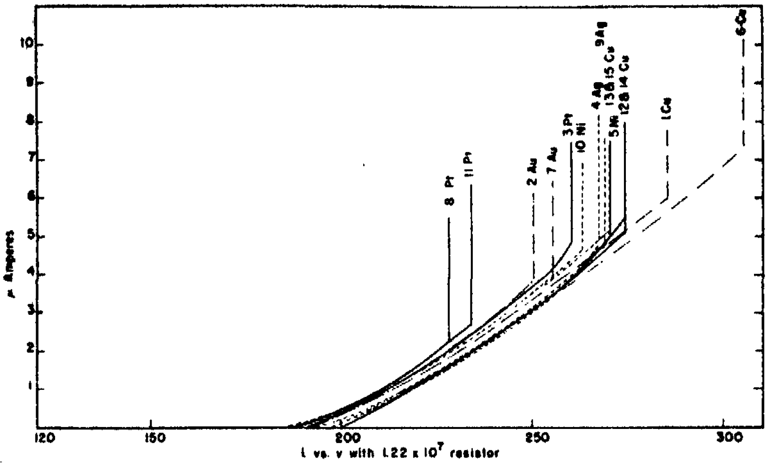

FIG. 13. These curves show the potentials at which the corona current sharply increases. All counters are identical except for the material used for the cathode surface.

number of electrons which are ejected from the cathode per ion pair formed in the gas. Although no attempt has been made to measure this quantity for any cathode surface in these experiments several interesting trends have been observed.

From the approximate expression (1) for a coaxial system of electrodes,

$$\int_0^{V_B} \eta dV = \ln(1/\gamma),$$

and it is seen that the breakdown potential V_B varies inversely with γ. If two electrode systems S_1 and S_2 in the same gas mixture are identical except that their cathode surfaces have values of γ_1 and γ_2, respectively, then since η is almost exactly the same for both gases:

$$\int_0^{V_{B^1}} \eta dV - \int_0^{V_{B^2}} \eta dV = \ln(\gamma_2/\gamma_1).$$

Thus

$$\int_{V_{B^2}}^{V_{B^1}} \eta dV = \ln(\gamma_2/\gamma_1) \approx \eta(V_B{}^1 - V_B{}^2), \qquad (3)$$

if the values for $\gamma_2 - \gamma_1$ are small and $V_B \gg (V_B{}^1 - V_B{}^2)$. Both these assumptions are satisfied in the data presented below.

Expression (3) indicates that even for moderately large differences of γ_1 and γ_2 the value of $(V_B{}^1 - V_B{}^2)$ will be very small. Therefore, the cathode surface cannot contribute appreciably to the lowering of breakdown potentials and from this point of view would not be important in achieving low voltage counters.

TABLE I.

Type of cathode surface	Threshold potential	Relative photo-sensitivity	Counter performance
A Mechanically cleaned	190 volts	11	Unsatisfactory
B (CuO)	189 volts	14	Unsatisfactory
C (Cu_2O)	192 volts	1	Excellent

However, the secondary effects at cathodes *are* important in determining other operating characteristics of G-M counters. An ionizing event within the counter gas is followed by multiplication of the initial ion pairs near the anode center wire. Photons produced in this process may eject electrons from the cathode which then extend the avalanche process at random along the length of the counter. A positive ion sheath[27] soon forms, and the center wire may drop rapidly below V_B. For high values of γ the positive ions or metastable atoms approaching the cathode surface have a high probability for ejecting electrons. These secondary electrons may either continue the discharge so that the counter cannot recover or, if a long-lived metastable atom approaches the cathode, may produce a spurious pulse. Thus it is important to use cathode surfaces with *low* values of γ to insure adequate counting characteristics.

To study the change in V_B with γ and the change in performance of G-M counter tubes with γ a series of different cathode surfaces was prepared from otherwise identical sets of counters. Since all the surfaces were mercury contaminated results cannot be compared with studies of V_B made with clean cathodes. In fact, considerable variations in cathode properties were found among groups of supposedly identical surfaces, and it should be understood that some aspects of the following measurements are little more than qualitative.

Three groups of counter cathodes were prepared.[30] Group *A* had mechanically cleaned copper, group *B* had a thick layer of CuO on copper, and group *C* had a thick layer of Cu_2O (brick red oxide) on copper for cathode surfaces. Table I gives a comparison of the three groups of counters with a gas mixture of neon plus 0.2 percent argon. A mercury light source with slit aperture was used to illuminate the interior of a counter cathode from each group under fixed geometry conditions. The background counting rate was determined for each counter, and then the counting rate with illumination was determined. The values of relative photo-sensitivity should not be considered to show more than the trend in values.

---

[30] These were prepared according to J. Strong, *Procedures in Experimental Physics* (Prentice-Hall, Inc., New York, 1939), pp. 268–270.

The increase of threshold potential with decreasing photo-sensitivity of the cathode is in agreement with the assumption that photo-sensitivity is a function of γ.[31]

A comparison of G-M counter performances for the three types of surfaces shows that spurious and non-uniform pulses occur with group *A* and *B*, and at moderate overvoltages they will break down in random discharges that may last a second or more. Group *C* on the other hand had uniform pulses free from spurious discharges, and the counter overvoltage could be used over a wide range without a breakdown occurring. The dark backgrounds of all three counters were low.

This provides tentative confirmation for the statement made earlier that only counters having a low value for γ will show satisfactory characteristics in the counter operating region.

Another experiment was performed in which groups of two or three cathodes were used having heavy plated coatings of platinum, nickel, gold, silver and two different copper surfaces. All surfaces were originally chemically cleaned, but it must be assumed that some mercury contamination was on the surfaces. These groups of counters were operated under identical conditions. With 1.22×10^7 ohms resistance in series with each counter the potential was increased until an almost discontinuous increase in the corona current was observed. This was apparently the beginning of the glow discharge region. The potential at which this abrupt shift in corona current occurred is dependent on the γ of the cathode surface. The potentials at which these current breaks are observed along with the magnitude and sharpness of the breaks are shown in Fig. 13. The greater the average corona current required to supply photons and metastable atoms at the cathode for breaking into the glow discharge region the lower must be the effective γ of the cathode surface. From Fig. 13 the cathode surfaces tabulated in order of decreasing γ were platinum, gold, nickel, silver, clean copper and Cu_2O. The deviations of a few individual counters in Fig. 13 were probably attributable to unclean surfaces. The counter operating characteristics ranged from severe random breakdowns with the platinum cathodes to normal counter performance for copper oxide cathodes.

In making large numbers of counters it was found useful to use the measurement of the corona current break in predicting satisfactory counter operation before sealing off the counters from the vacuum system.

Assuming that this explanation of the behavior of the breaks in the corona currents is correct, it follows that for any given cathode surface the corona current breakpoint must be a function of E_a/P. Selecting a platinum cathode the corona current at the breakpoint was determined as a function of the gas pressure. The calculated values of E_a/P near the center wire were evaluated for these pressures, and the shapes of these two curves are compared in Fig. 14.

The characteristics of counters employing very thin silver or copper films were highly dependent on film thickness, uniformity and oxides. Many of these counters displayed spurious background effects such as those described by Malter and Roggen and Scherrer.[32]

IV. LOW VOLTAGE PROPORTIONAL COUNTERS

The proportional counting region for noble gas counters lies between the potential at which ion multiplication begins to occur at the center wire and extends to the breakdown potential V_B. Therefore, all discussions of the threshold potential for G-M counters which have been presented also define the approximate

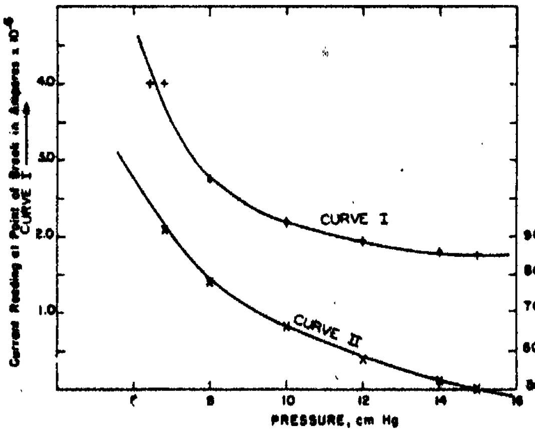

FIG. 14. The two curves show the dependence of the corona current at the breakpoint on the value of E_a/P. The counter cathode was plated platinum.

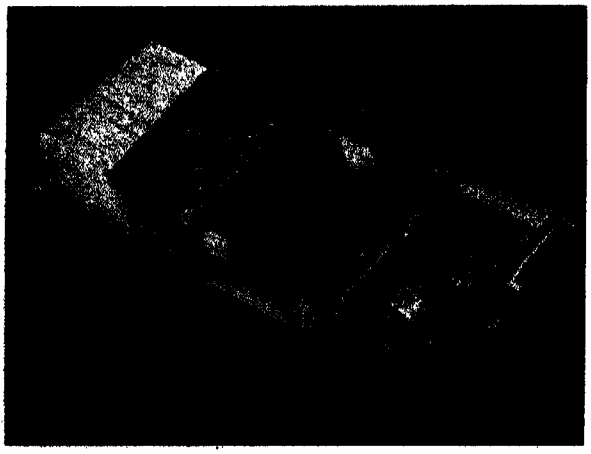

FIG. 15. A complete G-M counter radiation detector, for use with headphones, weighing less than 300 g. Case dimensions are 1×3×6 in.

---

[31] D. H. Hale and W. S. Huxford, J. App. Phys. 18, 586 (1947), and references therein.

[32] F. Roggen and P. Scherrer, Physica 15, 497 (1942).

operating potentials for proportional counter performance.[33] Counters with pure boron films deposited on iron cathodes have been prepared using neon-argon gas mixtures. Their characteristics have been studied by using the alpha-pulses from the $B^{10}(\eta, \alpha)Li^7$ reaction to produce the ionizing events. The maximum usable gas amplification factor[34] is more stable in neon-argon counters when pressures above 10 cm Hg are used, but the amplification factor is critically dependent on operating potential.

V. APPLICATIONS FOR LOW VOLTAGE G-M COUNTERS

Since the operating potential requirements of these neon-argon counters are modest it is convenient to use batteries which have been recently developed for hearing-aids and radiosonde equipment.[35] Several pocket radiation detectors have been constructed[1] using thin-wall counters having a threshold potential of 125 volts. An electronic quenching circuit utilizing a subminiature tetrode or pentode supplied a pulse signal for a high impedance head-phone. The dimensions of the aluminum instrument case were $1\times3\times6$ in., and the total weight was less than 300 g. The detector unit parameters were calculated so that 25×10^{-3} roentgen unit per hour of gamma-radiation produced an output signal in which the individual pulses could barely be audibly resolved. An early design is shown in Fig. 15.

Another type of radiation meter was constructed utilizing approximately 160 to 200 volts threshold counters.[1] The output of the quenching circuit operated a two tube counting rate meter and a single tube vacuum tube volt meter using a 1 in. diameter 0–100 microammeter. A movable absorber over the counter window provided a method for separating beta- and gamma-radiation. The dimensions of the instrument case were $1\times3\times10$ in. and it weighed 600 g.

Boron-coated cathodes used in neon-argon proportional counters produce convenient slow neutron detectors of small size using subminiature vacuum tubes in pulse amplifiers.

VI. SUMMARY

Conditions have been found for the adequate performance of low voltage counters. It is assumed that the additional factors essential for the adequate performance of all G-M counters in general are well known from the literature and need not be described. Thus, it has been shown that neon with small amounts of argon added is at least one combination of a class of gas mixtures which will successfully produce low voltage counters. They have the following counter characteristics: 1. A selection of G-M counter threshold potentials ranging from 115 to above 250 volts depending upon pressure, gas mixture and electrode dimensions is possible. 2. Counters with threshold potentials of 145 volts or more have "plateau" slopes of approximately 1 to 2 percent in a 100-volt interval. These counters have pulse rise times the order of 2×10^{-6} sec. and may be used with fast quenching circuits (Figs. 10 and 11). 3. Counters with threshold potentials *below* 135 to 145 volts require quenching circuits with long recovery times ($\sim5\times10^{-3}$ sec.) (Fig. 12). 4. The counters employ gas mixtures at pressures of 4 cm Hg ($V_t=112$–125 volts) to beyond 50 cm Hg ($V_t=210$ to 250 volts) having high specific ionizations. At pressures of 15 cm Hg or more the counter efficiency for ionizing events is very near 100 percent. 5. The counters appear to be stable for an indefinitely large number of counts and are essentially non-temperature dependent.

Neon-argon tubes with the characteristics described above have many applications in miniature radiation survey instruments. In general, only those counters with threshold potentials above 145 volts are useful for quantitative measurements. Improved electronic quenching circuits contribute greatly to extending the applications of these counters.

ACKNOWLEDGMENTS

The author wishes to convey his sincere appreciation to N. Wood and H. Bryant of the Argonne National Laboratory who have given invaluable assistance in setting up experiments and aid in the collection of the data.

---

[33] M. E. Rose and S. A. Korff, Phys. Rev. 59, 850 (1941).

[34] M. E. Rose and W. E. Ramsey, Phys. Rev. 61, 504 (1942).

[35] For example, Ever-Ready Battery No. 122.

Laboratory and Shop Notes

A Useful Fast Coincidence Circuit

R. L. GARWIN
Institute for Nuclear Studies and Department of Physics, University of Chicago, Chicago, Illinois

February 17, 1950

IN connection with some work on beta-gamma-angular correlation[1] a reliable fast coincidence circuit was needed. It had to satisfy at least three requirements: (1) to be operable at resolving times shorter than 0.02 μsec. (μ=microsecond) and preferably as short as 0.002 μsec.; (2) to be absolutely reliable in rejecting single impulses and to count properly all coincident pulses; (3) to be operable on relatively small pulses so that the driving source for the coincidence circuit need not handle large power.

The circuit depicted in Fig. 1 fulfills all of the requirements and has been operating for more than eight months at resolving times of the order of 0.02 μsec. without failure or necessity of adjustment. The difficulty with the common Rossi circuit (Fig. 1 without the diode (a)) is that a coincident pair of negative pulses lasting 0.01 μsec. will allow the anode capacity to charge through the anode resistor to about 20 volts above the quiescent potential of 60 volts, during the coincidence. The tube characteristics, however, indicate that driving a single grid negative will allow the plates to reach some 90 volts, a 30-volt output pulse. Therefore, a long single pulse gives a larger output than the desired coincident pair. This situation is alleviated by the clamping diode (a) in Fig. 1. When the grids are not pulsed, this diode carries somewhat more than half the total plate current to the double triode, charging the fast ceramic 0.01-μf condenser to a potential determined by the tube characteristics (∼100 volts). The total tube current is then 30 ma, of which 18 ma flows through the diode. Since resistance of the diode in the forward direction is ∼20 ohms (1 Type IN56 or 3 parallel IN34) the positive output pulse arising from driving one grid negative is of amplitude 15 ma×20 ohm or 0.3 volt. The coincidence pulse, however, is not attenuated, remaining ∼20 volts for 0.01 μsec. Therefore, if the crude discriminator is set at one volt, no difficulty is observed with resolving times as short as 0.005 μsec.

In order to be able to use a conventional scaler, the pulse stretcher consisting of the diode (b) and the stray capacities C_s (∼3 mmf) lengthens the coincidence output pulse to 0.5 μsec.

The clamp diode (a) has also the advantage of eliminating active capacities between plate and grid. For fast pulses without the clamp, one may expect the plates to fall some 2 volts in view of the grid plate capacities if the grids are driven 3 volts negative. The charging during the coincidence time may or may not be large compared to 2 volts. The diode (a), however, reduces the initial drop due to capacitive feed-through to less than 0.2 volt, effectively removing this undesirable phenomenon. Little advantage is gained by using two pentodes rather than the triodes, except for somewhat larger output. However, the Type 6AH6 pentode with g∼9000 micromhos allows a considerable reduction in grid pulse amplitude. The flawless operation of the 6J6, however, makes the substitution of pentodes somewhat a matter of taste.

The circuit requires negative pulses of 3-volt amplitude for proper operation and has been tested with artificial pulses from a mechanical switch-coaxial line arrangement[2] down to coincidence times of 0.005 μsec. Since one wants to be able to use the coincidence circuit with fullest flexibility, the input should be transmitted through electrically smooth coaxial cable. The current needed from the driving source is about 15 ma for cable impedance of 173 ohms. It is fortunate that not much current is required since the obtaining of fast negative pulses from a cathode follower requires continuous passage of large currents through the tube. The driver and pulse shaping lines are also indicated in Fig. 1, the shorted stub lines in the grid circuits being 1 meter long for 0.01 μsec. resolving time. The impedance match in the grid circuit is only approximate and may be improved somewhat by placing 200-ohm resistors to ground from the cathodes of the cathode followers.

It should be noted that most photo-multipliers (RCA 5819) may be operated at voltages high enough (1500–2000 volts) to give pulses 3 v high from anthracene crystals with 50-kev ionization loss in the crystal. This enables one to dispense with amplifiers and to get the ultimate resolving times of which presently available photo-multipliers are capable. No refrigeration is used and the noise pulse amplitude is increased only to the equivalent of about 50-kev ionization loss in anthracene. The number of these noise pulses diminishes extremely rapidly with amplitude so that one can count all beta-rays of energy 100 kev with less than one noise pulse per minute. Of considerable help in reducing photo-multiplier noise is the operation of the photo-multiplier anode at only 10 volts positive with respect to the preceding dynode. This causes space-charge saturation on the fast noise pulses to a greater extent than on the slower signal pulse, improving the signal-to-noise ratio. With crystals faster than anthracene, the usefulness of this trick disappears. In cases of very low ionization loss, i.e., say 80-kev gamma-rays detected by Compton recoils in anthracene, distributed amplifiers will be used with lower photo-tube voltage.

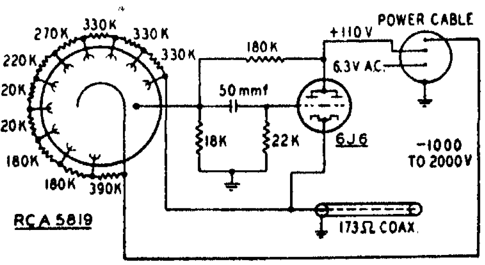

PREAMPLIFIER AT EACH PHOTOMULTIPLIER

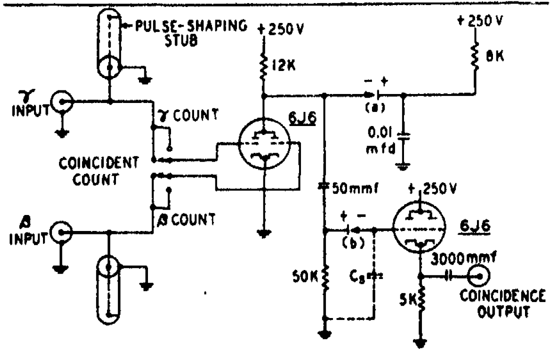

FIG. 1.

Care should be taken in absolute measurements with this coincidence circuit using the photo-multiplier pulses. If single counts are to be taken continuously with the coincidences, the biases should be set to be appropriate for the purpose of the experiment. This type of difficulty is not present with artificially generated (blocking oscillator) pulses.

The circuit of Fig. 1 has proved so trouble-free that it is now much used even in relatively slow coincidence applications. Until better photo-multipliers with less transit time spread and better crystals than stilbene become available, this circuit should be adequate for fast coincidence work.

---

[1] R. L. Garwin, Phys. Rev. 76, 1876 (1949).
[2] To be the subject of a later communication.

An Effective Vacuum Cut-Off

G. W. Sears* and E. R. Hopke
Department of Physics, Duke University, Durham, North Carolina

April 18, 1950

It is frequently necessary to cut off gas flow from one part of a vacuum system to another. Particularly for the manipulation of condensed phases in vacuum a tight closure is demanded to avoid sample losses as well as contamination of the pumping system. A cut-off involving non-volatile components is desirable to facilitate outgassing.

This note describes a cut-off constructed of glass and quartz, which might equally well be constructed solely of either material. The particular form shown here served as a Rodebush gauge[1] for measuring small pressures. The device is shown graphically in Fig. 1.

A circular plate, *C*, of optically flat quartz 1 mm thick and 25 mm in diameter seats against the polished end of an 18-mm Pyrex tube, *B*, to cut off gas flow. A quartz eye sealed to the center of the disk is attached via a quartz fiber, *F*, to a quartz encased iron armature, *A*. This assembly is suspended via a quartz fiber, F^1, from a quartz cantilever spring, *S*, which serves to seat the disk against the opening of the tube.

The upward force of the spring is counterbalanced by a downward force of a solenoid on the armature when the cut-off is to be opened. In closed position a high pressure region outside of the Pyrex tube is sealed off from a low pressure region inside the tube. In fact, it is impossible to open the cut-off under these conditions. The pressure must be nearly equalized to open the cut-off. By weighting the plate the gate may be made to open against a larger pressure difference.

The annular surface of the Pyrex seat was prepared by successive grinding with *F* through *FFFF* carborundum grits. The surface was maintained normal to the tube axis with the aid of a jig. The finely ground surface was polished with a good grade of red rouge on a pitch lap until the surface appeared smooth as observed without magnification. Some care was necessary in sealing the eye on the quartz plate. A region no larger than 8–10 mm in diameter at the center of the plate could be distorted during the operation. The completeness of the cut-off can be judged by the observation that a vacuum of 10^{-5} mm Hg was maintained against a pressure of 1 atmosphere in one test.

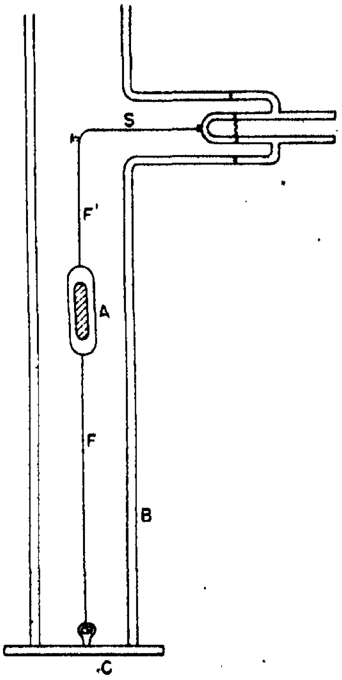

FIG. 1. Apparatus for vacuum cut-off.

---

* Present address: Research Laboratory, General Electric Company, Schenectady, New York.

[1] G. W. Sears and E. R. Hopke, J. Phys. Chem. **52**, 1137 (1948).

A Remote-Control Method of Opening Ampoules of Active Materials

Jesse E. Sherwood
National Bureau of Standards, Washington, D. C.

April 10, 1950

When working with highly reactive materials such as alkali metals, one is likely to require a method for opening an ampoule of such a material in a vacuum or some special atmosphere. In work with molecular beams, for example, such devices as magnetically operated hammers cannot be used because of space limitations. In case heating of the material is permissible, the following procedure may be used. It utilizes the effect of the high thermal expansivity of aluminum as compared to glass.

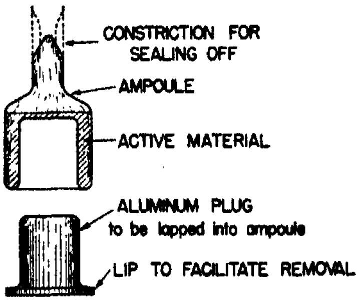
CONSTRICTION FOR SEALING OFF
AMPOULE
ACTIVE MATERIAL
ALUMINUM PLUG to be lapped into ampoule
LIP TO FACILITATE REMOVAL

FIG. 1.

The ampoule is made in the shape shown in Fig. 1. The cavity in the end of the ampoule is made to receive a cylindrical plug which is lapped into place with an abrasive. The plug is then removed and the ampoule filled in the usual way. After sealing off, the plug can be snugly set in place. The ampoule will break when the plug is heated. The ampoule should be placed with the plug uppermost.

In our work, the ampoule is of Pyrex glass and the plug is about 6–7 mm in diameter. The arrangement described has functioned in all cases on being heated to 100°C.

Regulated Low Voltage Power Supply

A. K. Solomon
Biophysical Laboratory, Harvard Medical School, Boston, Massachusetts

March 20, 1950

A regulated low voltage power supply has been designed for use with the direct current amplifiers in a mass spectrometer of the Nier type.[1] It is a series regulator with two stages of amplification; the circuit diagram is shown in Fig. 1. The output is 225 volts at a current of 190 milliamperes. The use of a battery instead of a resistance chain in the feed-back circuit imposes the whole error signal on the input grid of the 12AX7. There is no provision for adjustment of output voltage, since it can be varied by 1.5-volt steps by adjusting the battery potential. In a circuit of this type, any change in tube electrode potentials to alter the output voltage results in departure from the optimum conditions for operation. Should this be essential it would be possible to replace the 226.5-volt battery with a smaller battery and the conventional resistance chain. For best operation it is

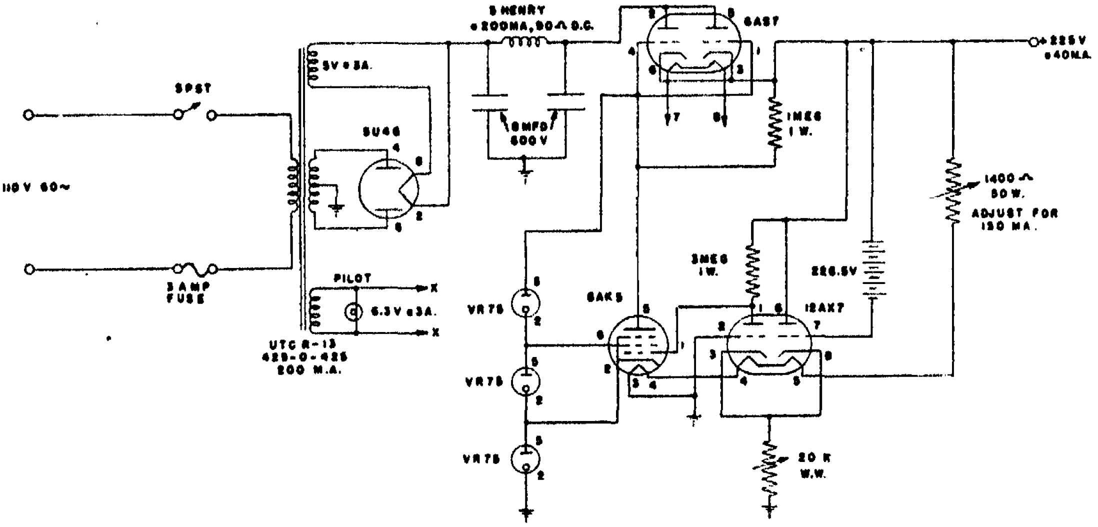

FIG. 1.

necessary to adjust the 20,000-ohm rheostat in the cathode circuit of the 12AX7 to set the voltage between the ground and the right-hand grid to a value between 1.5 and 2.0 volts. Direct current heating of the filaments of the 12AX7 and the 6AK5 improves the performance by a factor of two. The direct current amplifier, for whose power requirements the present circuit was designed, uses 150 milliamperes for filament heaters and 40 milliamperes for plate supply. When used in this connection, the 1400-ohm potentiometer is replaced by the series heaters in the amplifier and a much smaller resistance with which the current is adjusted to 150 milliamperes.

Data on the performance of the power supply follow. A change of input voltage from 108 to 135 volts results in a 10-millivolt change in output; a change from 93 to 135 volts results in a 20-millivolt shift. At 118 volts input, a change in load from 0 to 190 milliamperes results in a 20-millivolt shift in output voltage. Ripple is less than 1 millivolt between 93 and 135 volts.

In order to determine the expected operating characteristics of the power supply in the spectrometer, it was fed from a Sola constant voltage transformer, and the output was bucked by a set of batteries. A load drawing 150 milliamperes was supplied. The difference between the bucked potential and ground was then measured on a 4.5-second Brown Electronik Recorder with a full scale deflection of 10 millivolts. Since the input impedance of the Brown recorder is not high and is a function of the position of the carriage on the slide wire in the recorder, the current drawn from the batteries is not constant and a balance must be achieved between charging and discharging the batteries. This balance is critical and extends over a very narrow range; either side of balance the system rapidly becomes unstable. It will be seen from Fig. 2 that when a balance is achieved, the output voltage is stable to better than 50 microvolts. Any fast fluctuations do not, of course, appear. Standardization pips in the recorder account for the large apparent shifts in voltage; it can be seen that the battery-recorder system does not return to the same position after this momentary disconnection in the circuit.

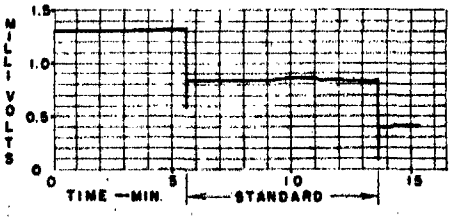

FIG. 2.

The author wishes to express his thanks to Mr. David Caton for his most valuable assistance. This work has been supported in part by the AEC.

[1] A. O. C. Nier, Rev. Sci. Inst. 18, 398 (1947).

Extension of the Low Pressure Range of the Ionization Gauge

ROBERT T. BAYARD AND DANIEL ALPERT
Westinghouse Research Laboratories, and Physics Department, University of Pittsburgh, Pittsburgh, Pennsylvania

April 13, 1950

THE ionization gauge[1] has been generally considered useful for the measurement of gas pressures ranging down to 10^{-8} mm Hg.[2] This low pressure limit is not the lowest pressure attainable with modern vacuum techniques, but has been shown to be a limitation of the conventional ionization gauge itself. An investigation made in this laboratory to determine the cause of this limitation has resulted in a new ionization gauge whose range has been considerably extended. The new gauge has been used to measure pressures of the order of 10^{-10} mm Hg.

The conventional ionization gauge resembles structurally the triode vacuum tube. The grid, however, serves as anode and is operated at a positive potential (100 to 250 v), while the plate is negative (10 to 50 v), both with respect to the cathode. Electrons from the cathode, before being collected at the grid, can create positive ions by collision with gas molecules. The number of ionizing collisions for a given electron current is considered to be proportional to the gas density. The current to the ion collector, or plate, is thus a measure of the pressure.

Dushman[3] has shown that the ion current for a given electron emission is indeed linearly related to the pressure between 3×10^{-6} mm Hg and 10^{-3} mm Hg. On the assumption that this relation continues to hold true, ionization gauges have been used to measure lower pressures. Workers in the field today, however, agree that while currents less than that corresponding to 10^{-8} mm Hg[4] could easily be measured, they are not observed. On the other hand many investigators[5] have had indications that considerably lower pressures than 10^{-8} mm Hg have actually been attained. This suggests the existence of a residual current to the ion collector which is independent of pressure. Nottingham[6] has suggested that this residual current is due to soft x-rays which release photo-electrons from the ion collector, the x-rays being created at the grid by the incidence of the thermionic electrons.

Independent evidence for the existence of a residual current comes from the observed characteristics of the ionization gauge itself. If for a given pressure and electron current, the ion collector current i_c is measured as a function of grid potential v_g, the plot of i_c *vs.* v_g, shown in Fig. 1a, has a characteristic shape for pressures above 10^{-7} mm Hg. The gas ionization curve shown (upper line) is typical of data taken on RCA type 1949 gauges. Note that i_c rises rapidly with v_g up to 200 volts and varies slowly with potential above this value. When the pressure is considerably lowered (ion gauge reading 10^{-8} mm Hg) the curve of i_c *vs.* v_g is radically different as shown (lower line). This residual curve continues to rise with grid potential, the slope on a log-log plot being between 1.5 and 2. In the intermediate range of pressures (10^{-7}–10^{-8} mm Hg) the characteristic corresponds to a superposition of the "gas ionization" curve and the "residual" curve. These results, obtained independently in this laboratory, are in agreement with data published in 1931 by Jaycox and Weinhart[7] and with unpublished findings of W. B. Nottingham.

With the explicit purpose of examining the hypothesis that this residual current is due to x-rays, a design was sought for an ion gauge which would operate in the usual manner but whose ion collector would intercept only a small fraction of the x-rays produced at the grid. The ionization gauge which evolved from these considerations is shown in Fig. 2. The new gauge has the usual three elements, but is inverted from the conventional arrangement; the filament *A* is outside the cylindrical grid *B*, while the ion collector *C*, consisting of a fine wire, is suspended within the grid. The volume enclosed by the grid is made comparable to that between the grid and plate of the ordinary ionization gauge. The positive potential on the grid forms a barrier to the ions formed inside the grid-enclosed volume so that they are eventually collected at the center wire. The ion collection efficiency is thus comparable to that of the conventional ionization gauge. On the other hand, the geometrical cross section of the ion collector to radiation from the grid is approximately one hundred times smaller than that of the conventional cylindrical collector.

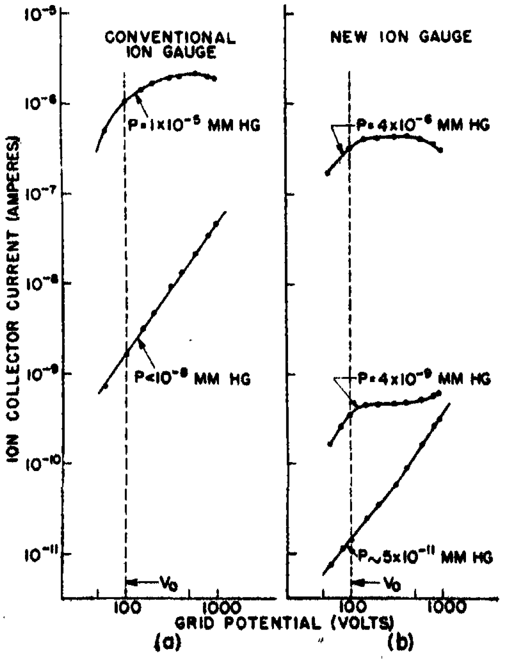

FIG. 1. (a) Typical data for RCA type 1949 gauge. (b) Typical data for the new type gauge. V_0 is the normal operating voltage.

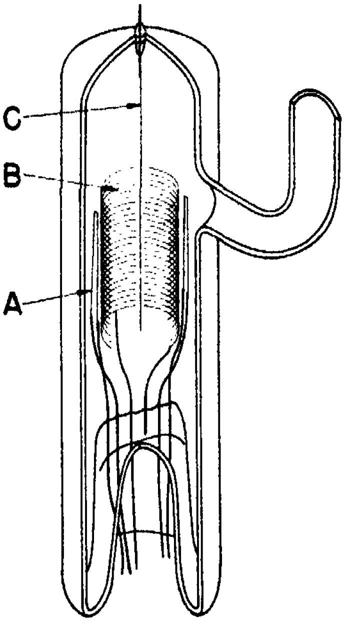

FIG. 2. Cutaway view of the new gauge showing filament *A* (an auxiliary filament is also shown), grid *B*, and ion collector *C*.

The properties of the new ionization gauge are shown by the curves of Fig. 1b. At higher pressures the characteristics of the new gauge are very similar to those of the RCA gauge, but it is evident that the new tube continues to have typical "gas ionization" characteristics at much lower pressures. At 4×10^{-9} mm Hg the collector current is predominantly due to gas ionization, and it is not until the pressure is less than 10^{-10} mm Hg that the residual current predominates.[8] Note that the slope of the residual curve is the same as that for the RCA gauge. On the other hand the value of the collector current for the new gauge, at a given grid voltage, is one hundred times lower than that for the RCA gauge. This ratio of residual currents for the two types of ion gauges is the same as the ratio of their geometrical cross sections to radiation mentioned above. These general characteristics of the new gauge clearly substantiate the x-ray hypothesis and indicate that ionization gauges can be built to measure even lower pressures.

The sensitivity of the new ionization gauge has been measured by calibration with a McLeod gauge at nitrogen pressures in the neighborhood of 10^{-4} mm Hg and by comparison with a standard ionization gauge at various pressures between 10^{-5} and 10^{-7} mm Hg. As seen from the typical curves in Fig. 1, the sensitivities of the two types of ionization gauges are essentially the same. The new gauge gives indication of pressures at least 100 times lower than the standard ion gauge. It has a minimum of metal surface, is easily outgassed, and is operated on a standard power supply. These characteristics make the gauge a useful tool for studies in the field of high vacuum.

---

[1] For a complete discussion of ion gauges see for example S. Dushman, *Scientific Foundations of Vacuum Techniques* (John Wiley and Sons, Inc., New York, 1949), p. 332–366.

[2] Pressures mentioned in this letter are equivalent nitrogen pressures.

[3] S. Dushman, Phys. Rev. 17, 7 (1921).

[4] This current is usually of the order of 10^{-9} ampere for 0.010 ampere electron current and 100–150 v grid potential.

[5] (a) P. Anderson, Phys. Rev. 47, 958 (1935). (b) W. B. Nottingham, J. App. Phys. 8, 762 (1937). (c) I. R. Senitsky, Phys. Rev. 78, 331 (1950). (d) The so-called flash filament method of L. Apker, whereby pressures are estimated from measurements on the rate of accumulation of gas on a clean wire, has been used by several investigators including the author to measure pressures of the order of 10^{-10} mm Hg. (e) The mass spectrometer group in our laboratory has had indications that in a well-baked out spectrometer tube the residual gas pressure is 10^{-9} mm Hg or less.

[6] Reference 1, p. 359.

[7] E. K. Jaycox and H. W. Weinhart, Rev. Sci. Inst. 2, 401 (1931).

[8] The pressure represented by the lowest curve, as judged by the deviation of the lower portion from a straight line, is estimated to be of the order of 5×10^{-11} mm Hg.

A Circumferential Recording Microphotometer

T. C. O'Connell* and A. G. Barkow
Physics Department, Marquette University, Milwaukee, Wisconsin

January 16, 1950

In preliminary experiments on the x-ray diffraction method of determination of fatigue in metals and the change in crystal structure in metals due to impact or shock, the need for a circumferential recording microphotometer was apparent.

The illumination system consisted of a line filament 32-candlepower automobile spotlight bulb which was supplied by a 6.3-volt transformer of heavy current capacity. The input to the transformer was controlled by a Variac to allow for a certain degree of light input variation. A double condensing lens of the Ramsden type was placed in front of the light source.

An adjustable micrometer slit was placed immediately in front of the condensing lens. The image of the slit was then projected forward on to the film by means of a microscope objective of 25.4 mm focal length. This system was used because of its relative simplicity and versatility. The slit width could be varied by placing the microscope objective in a focusing mount. Moving the film carriage back and forth, which was equivalent to changing the slit image distance, allowed the slit length to be varied enough to cover almost any diffraction ring encountered. As a matter of fact the slit could be made as small as necessary by means of a mask.

The film carriage consisted of a shaft mounted on a sheet metal stand which in turn was mounted on a geared track to allow for the centering of the diffraction ring under investigation. The photo-cell housing was located immediately behind the film, the latter being held flat against a flat faced cylinder by means of a pressure plate of highly polished aluminum under slight spring tension. The photo-cell was enclosed in an aluminum housing just large enough to fit over the photo-tube. A Type 917 (RCA) vacuum cell was used in the present equipment. This tube has the advantage of being relatively small in diameter (1.165 inch maximum at the base), allowing for the scanning of diffraction patterns of only 0.75 inch radius. Furthermore, the fact that it has an anode cap rather than an anode base lead, tends to reduce leakage currents. The vacuum photo-cell, in spite of its lack of sensitivity compared to the gas cell, is preferable for light measurement applications because of its higher internal resistance and more constant sensitivity. The cell was placed just far enough in back of the film so that the longest slit produced a spot of light which covered as much area as possible of the cathode element. Such coverage is necessary if maximum stability is to be had in the long time use of the photo-tube.

The socket is of the ceramic type to prevent leakage. The leads from the tube should be shielded and should have as high an insulation resistance as possible. These precautions must be taken if one expects to have response to small amounts of light and at the same time desires to maintain accuracy. The current supplied by the photo-cell developed an IR drop across two portions of a 10-megohm resistance (R_9 and R_{10}). Hence, any shunt leakage resistance is an erratic variable which may cover up the effect of small photo-tube currents. The complete schematic diagram is shown in Fig. 1.

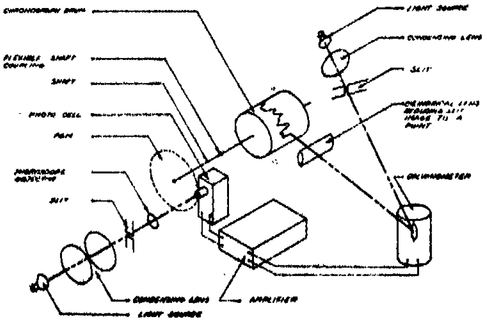

FIG. 1. Complete schematic diagram of the circumferential recording microphotometer.

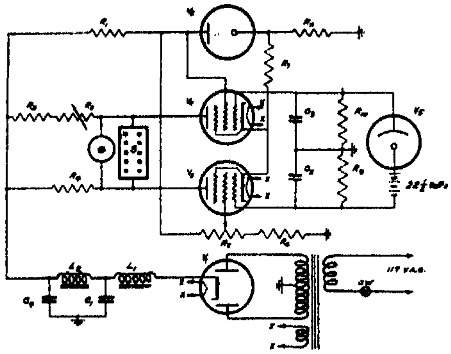

FIG. 2. Circuit diagram of the photo-tube amplifier.

Amplifier Part List

(All resistances in ohms and capacities in microfarads.)

C_1	8	400 v elect.
C_2	0.01	mica
C_3	0.01	mica
C_4	8	400 v elect.
R_1	5600	2 watts
R_2	47000	½ watt
R_3	1000 pot	vernier balance control
R_4	47000	½ watt
R_5	100000 pot	rough balance control
R_6	2400	1 watt
R_7	1200	1 watt
R_8	470	1 watt
R_9	5 meg.	½ watt
R_{10}	5 meg.	½ watt
L_1	10 henrys	
L_2	10 henrys	
S	0–100 shunt box	
T	Power transformer, 550 v C.T. 6.3 volts, 2 amp.	
V_1	6X5	
V_2	VR 105	
V_3	6J7	
V_4	6J7	
V_5	917 (anode cap) or 919 (cathode cap)	

The photo-tube amplifier (Fig. 2) used in this instrument consisted of a Wheatstone Bridge, two legs of which were made up of low μ-tubes. No more than 22.5 volts were applied to the photo-tube at any time. This low anode potential is necessary to prevent ionization of small amounts of residual gas which might lead to erratic operation of the cell.

For quantitative work, the entire system must be regulated to within 0.1 percent as far as applied voltage is concerned for consistent results. A Sola saturable reactor type transformer was used, the line voltage fluctuations being small enough to be kept within the limits suggested. A VR 105-voltage regulator tube was used to stabilize the screen voltage.

The output of the amplifier was supplied to a wall type galvanometer of moderate sensitivity and of a period of about three seconds. Since an amplifier of the type used has a sensitivity of about 0.3 volt full scale with a one-milliampere movement, the galvanometer whose resistance was 126 ohms was shunted by a 0–100-ohm shunt box. This allowed for a very wide range of sensitivity as well as the use of a very narrow slit in scanning.

The deflections of the galvanometer, due to the variations in film blackening, were recorded on the photographic enlarging paper which was fastened to a chronograph drum. This drum in turn was coupled to the film carriage in order that the diffraction ring to be scanned makes one revolution in synchronism with the drum itself. The coupling consisted of two rigid shafts connected to one another by means of a universal joint to prevent any strain on the film carriage. The speed with which the drum rotated was governed by means of a Variac controlled motor. A complete revolution could thus be made in about 20 to 30 minutes, depending upon the spot sizes on the diffraction ring. It should be mentioned that the galvanometer followed all variations in the film.

An astigmatic optical system was used to produce the trace on the enlarging paper (chloro-bromide). This system provided more than ample illumination due to the extreme speed of the paper used.

The procedure for operation of the densitometer was relatively simple. The amplifier was allowed to warm up for about twenty minutes to overcome any possible drift due to temperature changes. The x-ray film was centered on the carriage and the photographic paper placed on the drum.

The amplifier was adjusted to zero by means of the coarse control, R_4, and finally by the fine control, R_3. This adjustment was made with no light falling on the cell, in other words, this represented zero percent transmission. Next, the light source was turned on, and the slit made as narrow as possible. The slit image was then made to fall on a clear background region close to the ring being scanned. The intensity of the light source was then varied in conjunction with the slit and the galvanometer shunt in order to obtain a 100 percent transmission reference. This point was chosen arbitrarily at a particular distance from the zero reference and, of course, was a function of the dimensions of the drum.

The film was then moved so that the ring to be scanned was in the path of the slit image. The motor was then turned on and the trace made.

Applications.—The circumferential microphotometer was applied to the x-ray diffraction study of the changes in metals due to impact or shock. A sheet of Duraluminum, $14\times20\times\frac{1}{8}$ inches, was rigidly fixed at the four corners, or in terms of the coordinates at the points $(7, 10)(-7, 10)(7, -10)(-7, -10)$. An impact hammer capable of imparting 2000 ft. lb. per blow was allowed to strike the fixed plate at the coordinates $(0, 0)$. X-ray diffraction pictures of the plate were taken at two points, $A(3.5, 0)$ and $B(0, 5)$. These are two of several points analyzed by x-ray diffraction in an effort to determine the stresses set up in the metal. In analyzing the conditions, it was assumed that the vibrations set up in the aluminum were similar to those present in a vibrating plate fixed at the four corners. The points A and B were marked so that the plate could be removed from the impact machine, and set up in a frame on the diffraction unit in such a way that the two exact points could be irradiated. Preliminary pictures 1A and 1B were taken of the unstrained sheet while 2A and 2B were taken after the aluminum sheet had been struck forty times by the hammer or after 80,000 ft. lb. of energy were imparted to the plate. The diffraction pictures showed very little as to the nature of the change in the metal plate. In Fig. 3 it is immediately evident that a slight preferred orientation existed in the plate in the no fatigue stage. However, after the forty impacts a definite change in the orientation has manifested itself, especially at point B. These changes were hardly perceptible on the diffraction picture. Traces in Fig. 3 represent 360° or the complete diffraction ring of the second-order reflection from the (111) plane with copper $K\alpha$-radiation. The diameter of the chronograph drum was 6.7 inches; hence Fig. 3 is a reduction from traces approximately 21 inches in length. To check the accuracy of the preferred orientation, four India ink marks were placed at the quadrant marks on the diffraction film. These appeared as large "pips" on the microphotometer traces and help in orienting the pattern.

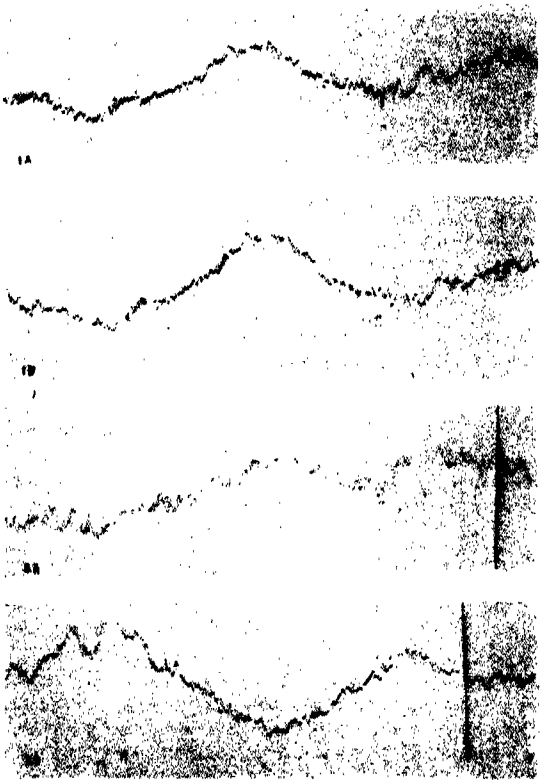

FIG. 3. Microphotometer traces of Duraluminum. 1A and 1B are of two points, 90° apart, of the unstrained plate. 2A and 2B are of the same two points after the plate was subjected to 40 impacts of 2000 ft. lb. each.

---

* Now at the Herlec Corporation, Milwaukee 3, Wisconsin.

Water-Proofing Rocksalt for Infra-Red Absorption Cells

SCOTT ANDERSON, WILLIAM J. ANDERSON, AND MARTIN KRAKOWSKI
The Anderson Physical Laboratory, Champaign, Illinois

March 13, 1950

SOME time ago we had occasion to do some infra-red absorption work with vegetable oils prepared by a steam distillation process. The water content of the oils was sufficient that they attacked rocksalt vigorously. The region of the spectrum of interest to us was between 10–12μ which is beyond the useful transmission limit of CaF_2. Therefore, we sought a means of protecting the salt with a film of material. The requirements on such a film were as follows: it should (1) contain no characteristic absorption of its own between 4 and 14μ, (2) be capable of a highly polished surface, (3) have refractive index low enough that reflection losses would not be excessive, and (4) be uneffected by either water or carbon tetrachloride (or some other solvent that could be used to remove the oil). Evaporated selenium satisfied all these requirements. This note is to describe the technique and precautions necessary for the successful use of these cells.

Rocksalt plates were prepared in the usual manner by polishing with fine Alundum using alcohol for a lubricant. In this connection we found that durable selenium films were formed only when the polishing lap was of high quality hair felt. When a cotton lap was employed to do the polishing, the selenium invariably began to peel off the salt after two or three fillings of the finished cell.

Four salt plates were prepared each time, two plates drilled and two undrilled. This was done so we could make two cells alike and alternate them as standards and unknowns. The plates were mounted close together in the center of a brass plate. After mounting, the plates were rinsed with carbon tetrachloride to remove all dust and lint and placed in the evaporator eighteen inches above the evaporating filaments. These latter were molybdenum ribbons. Two were used to get a uniform coat of selenium on the salt.

Pieces of amorphous selenium were placed on the ribbons and evaporated onto the salt with a vacuum of the order of 10^{-5} mm of Hg. The evaporation was done in two stages. It is our belief that most pinholes in these thin films arise as a result of dust particles being present on the substrate surface. Consequently, the initial evaporation is carried out until the rocksalt plates are a pale orange by transmitted light. The plates are then removed from the holder, rinsed with carbon tetrachloride, and returned to the evaporator. It is hoped that this process removes the dust particles present during the first evaporation and other particles do not settle on the same spot. The second evaporation is carried out at the same pressure in the vacuum system. This evaporation is continued until the rocksalt plates transmit about the same as a Wratten No. 25 filter. Very seldom were pinholes detected in the selenium films.

The liquid absorption cells are assembled in the usual manner with the coated surfaces of the rocksalt plates toward the inside. The lead and tin foil spacer are amalgamated to insure a sealed contact. Care must be exercised not to move the spacer once it is placed on the selenium surface.

Cells prepared in this manner transmit between 80 and 85 percent of the radiation at 12μ. A single cell, made properly (i.e., polish the salt on hair felt and evaporate the selenium at 10^{-5} mm of Hg or better), can be used for between 700 and 1000 filling and rinsing cycles if the water content is below 4 percent. We had one cell that withstood 30 filling and rinsing cycles of water solutions without showing any deleterious effects. Our work with water solutions has not been as extensive as it was with the water-containing vegetable oils so we really can not say how well the properly made cells will withstand pure water.

Carbon tetrachloride is the only solvent we found which was satisfactory for rinsing the cells. Carbon bisulfide and alcohol remove the selenium films very readily and are unsuitable.

If the selenium coat is too heavy and the salt plates are polished plane, a Fabry-Perot effect is encountered. This is convenient for measuring the cell thickness but annoying when attempting to analyze the spectra. This effect can be avoided if the plates are polished slightly convex.

An Improved Electrode Cutter for Spectrographic Laboratories

Esther W. Claffy and Joseph G. Schumacher
Crystal Branch, Naval Research Laboratory, Washington, D. C.

April 13, 1950

CONSIDERABLE difficulty has been experienced in cutting and shaping spectrographic electrodes to uniform size, shape, and wall thickness for quantitative spectrochemical analysis.

Our equipment in the past has consisted of the motor-driven electrode cutter and saw, No. 2380, supplied by Applied Research Laboratories of Detroit, with a cutter-blade modified to produce a small crater with thin, sloping walls. This device is normally fitted with a mandrel having a guide hole of 0.246-in. diameter to accommodate ¼-in. electrodes.

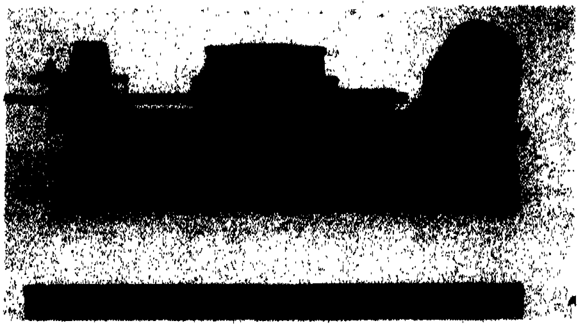

FIG. 1. Photograph of the modified tool, disassembled to show cutter-blade set in holder and chuck mounted on dust hood. "A" is a photographed series of 20 shaped electrodes, chosen at random, to show uniformity of cut.

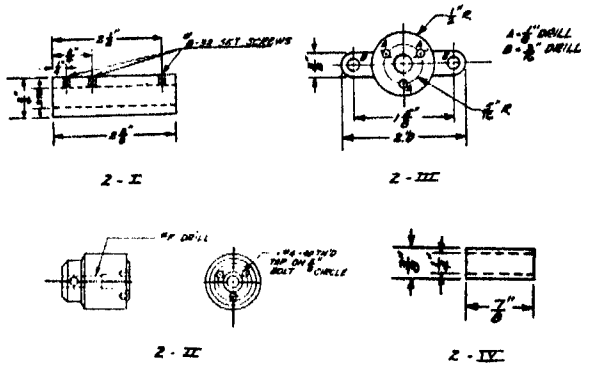

FIG. 2. Machinist's drawings: I, Modified cutter holder, material: drill rod. II, Modification of No. 1A Jacobs drill chuck. III, Support for Jacobs drill chuck, material: brass $\frac{1}{16}$ in. thick. IV, Spacers for Jacobs drill chuck, two required, material: brass tubing.

So-called ¼-in. electrode rods, however, were found to vary considerably in diameter. Some were too thick and became wedged into the opening. Others were thin, and in removing the shaped electrode slight random movements of the hand caused chipping of the crater walls. A certain amount of erratic play inherent in the rotating, axle-borne mandrel also contributed to our difficulties. Thus, there was considerable loss of time as well as waste of material. Moreover, even among the usable shaped electrodes there was noticeable variation.

An extensive but simple modification of the apparatus (Fig. 1) now permits the production of electrodes of remarkably uniform size and shape (Fig. 1A). These can be made with negligible breakage from rods of varied diameters.

The new cutter-blade (seen in Fig. 1) was designed to produce a thin straight-walled crater 3 mm wide and 3 mm deep. The crater holds 20–30 mg of sample. The original mandrel has been discarded and replaced by a small light-weight holder (Fig. 2-I) which is firmly seated on the axle. Cutter-blades can be inserted in the holder without removing it from the axle. Electrode rods are now fed through a modified Jacob's chuck (Fig. 2-II, IV) which is adjustable to the diameter of the rod. The chuck and its support (Fig. 2-III) are permanently attached to the dust hood (Fig. 1). Only the cutter-blade and its holder rotate. The accompanying diagrams are drawn to scale.

Pulsed Air Core Series Disk Generator for Production of High Magnetic Fields

Robert I. Strough and Erwin F. Shrader
Case Institute of Technology, Cleveland, Ohio

February 6, 1950

A HIGH current d.c. generator of the series unipolar type employing no iron in its magnetic circuit has been constructed and tested. The rotor of the machine serves as a flywheel for energy storage and is driven up to speed between current pulses by means of a jet of compressed air acting on turbine buckets cut in the face of the rotor. The present prototype model employing a 5¾ inch diameter forged beryllium-copper rotor weighing 11 pounds has been operated at 20,000 r.p.m. at which speed it stores 29,000 joules of kinetic energy.

The series field "winding" of the machine consists of two circular turns of conductor encircling the rotor and connected in parallel. The conductors are copper castings of 1 by 2 inch cross section. One end of each turn makes contact with the periphery of the rotor by means of a separate brush. The opposite end of each turn is connected by means of a shorting bar to the single center brush. This machine is operated short circuit to produce a large current in the series winding and hence a large useful magnetic field in the vicinity of the series coil of the machine. A separate starting winding consisting of a few turns of small conductor concentric with the rotor and energized by an external battery is also provided to supply the initial field necessary to start the build-up of current in the series winding.

To obtain the negative resistance characteristic required for current build-up in the machine it is essential that the brush resistance be kept extremely small since the e.m.f. generated by the disk per ampere in the series winding is very small (about 50 microvolts per ampere) at 20,000 r.p.m. for the machine described. For this reason a brush arrangement employing mercury flowing between amalgamated surfaces has been developed. The mercury brushes also provide a convenient switch since the series winding may be connected to the disk by starting the flow of mercury through the brushes.

To operate the machine, the rotor is brought up to speed, the mercury flow to the brushes is started, and the starting coil energized. The current in the series coil increases rapidly to a maximum and then decreases to a small value due to the slowing down of the disk as its kinetic energy is drawn off to provide the magnetic field energy and the resistive losses. The mercury flow and starting coil are then shut off and the machine is ready to repeat the cycle.

In preliminary tests the model described above developed a maximum field at the center of the disk of about 4000 gauss when operated at an initial speed of 19,600 r.p.m. This amounts to a total maximum current of about 45,000 amperes through the winding with a resulting current density of 40,000 amperes per square inch at the center brush. The time interval between the switching on of the starting coil and the maximum current is about 0.2 second. A check on the resistance of the series coil revealed a very poor conductivity for the copper castings (about ¼ that for commercial annealed electrical copper). It is estimated that remedying this defect would increase the maximum field obtainable with this particular machine to perhaps 15,000 gauss. The principal limitation on the maximum field obtainable with this machine is still brush resistance, however.

Mapping of the field produced is now in progress to determine the suitability of the machine as a cloud-chamber field supply. Also, the possibility of using such a machine as the source of magnetic field for an air core betatron or synchrotron is being investigated.

New Instruments

W. A. Wildhack: Associate Editor
in Charge of this Section
National Bureau of Standards, Washington, D. C.

These descriptions are based on information supplied by the manufacturer and in some cases from independent sources. THE REVIEW *assumes no responsibility for their correctness.*

Electron Microscope The new RCA permanent magnet electron microscope is expected to broaden greatly the field of application of this most modern tool of science. Employing for the first time permanent magnet lenses requiring no stabilization circuits and controls, this greatly simplified table model stands only 30 in. high and is expected to sell for less than $6000, about one-third the price of the well-known RCA Universal Model. The new instrument has the same 50,000-volt accelerating potential as the larger unit, and is more than 20 times as powerful as the best optical microscope, with a depth of focus 150 times as great. It will provide useful magnifications up to 50,000 diameters by photographic enlargement, with direct magnification in the instrument ranging up to 6000 diameters. Significant advantages of the new instrument are that specimens may be inserted and removed from the evacuated column without breaking the vacuum and photographic plates may be changed without admitting more than a small amount of air; as a result, pumping time between plates is reduced to only 90 seconds, which is just about enough time for the photographic development normally carried out between exposures. The simplicity of operation achieved in the new design, it is claimed, makes the instrument safe for operation in the hands of a high school student or unskilled laboratory personnel. With no more than an hour of instruction an operator generally familiar with the optical microscope should be able to insert specimens and produce well-focused pictures. Widespread application in the fields of metallography, bacteriology, and medicine is foreseen for this instrument, which has now been brought within the means of a much larger number of potential users.—RADIO CORPORATION OF AMERICA, RCA VICTOR DIVISION, *Camden 2, New Jersey.*

Mini-Chopper The Mini-Chopper, weighing 1.3 ounces and having less than one-eighth the volume of d.c.–a.c. choppers previously available, accomplishes all the functions of modulation, demodulation, rectification, and inversion of intelligence signals normally accomplished by electronic or electromechanical choppers. Despite the outstanding reduction in size and weight, all of these functions are accomplished with no loss of efficiency, and the Mini-Chopper has been proved to have a normal life expectancy of over 1000 hr. The Mini-Chopper is designed for installation in a standard seven-prong miniature electronic tube socket and for retention with a standard miniature tube retainer. Its use in airborne and other mobile systems will permit outstanding savings in both space and weight with the assurance of long trouble-free life.

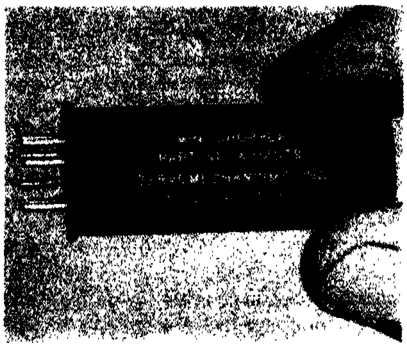

The Mini-Chopper will modulate to frequencies from 60 to 600 cycles at a rated input of 6.3 volts. A very simple provision is made for varying phase shift over an appreciable range during manufacture of these choppers. Extreme temperature tests have shown that the Mini-Chopper is unaffected by ambient temperature from −55°C to +120°C. Hermetic sealing renders it practically impervious to the effects of humidity and pressure.—Servomechanisms, Inc., *Old Country and Glen Cove Roads, Mineola, New York.*

"Printed-Circuit" TV Tuner

The television industry's first "printed-circuit" television tuner is a major development in home-receiver design which provides greatly improved performance, including superior reception in fringe areas as well as in receivers operated with built-in antennas.

A radical departure from conventional wound-coil units, RCA's new "printed-circuit" tuner utilizes a unique photo-etch process to reproduce the critical circuits. The process eliminates the complicated process of mechanically winding separate coils, and at the same time produces precision circuits of superior performance.

The new printed-circuit tuner provides high and substantially uniform gain of between 28 and 35 db on all channels under typical operating conditions. Other features include an excellent noise factor, high rejection of spurious responses, very low oscillator stability, and a low reflection coefficient in the transmission line.

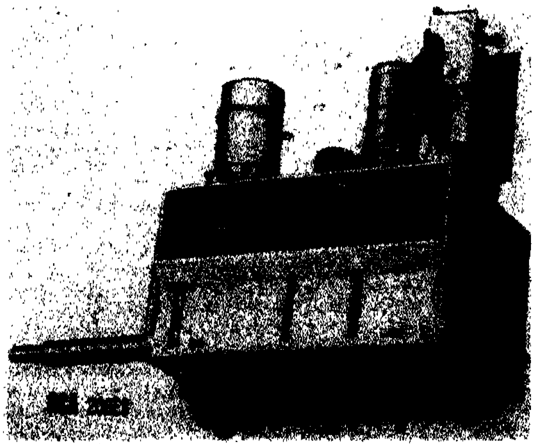

The photo-etch process developed for the RCA printed-circuit tuner begins with the photographing of a circuit drawing. A contact print is then made from the negative in a copper-clad sheet of phenolic plastic which is coated with a light-sensitive material. The print of plastic sheet is next developed and placed in an etching solution. The solution etches away that part of the copper not covered by the pattern of the circuit, leaving the required copper circuit on the plastic sheet. The sheet is then placed in a die and cut into separate sections and pierced.

Especially suited to television-tuner production, the photo-etching process is conducive to continued improvement and circuit development, since all that is necessary when a change is to be made in a circuit is to make a new photographic negative. Reproducibility is excellent, with detail and precision of the lines in the circuit approaching photographic accuracy.—RCA Victor, Division of Radio Corporation of America, RCA Tube Department, *Harrison, New Jersey.*

Subminiature Electrometer Type CK5889

The CK5889 is a new subminiature electrometer pentode having several new mechanical design features which have hitherto been unavailable in any subminiature tube designed for electrometer applications. The more important of these are the 7.5-ma low microphonic filament, the double-ended construction, and the guard ring. The maximum grid current is 3×10^{-15} amp., but the nominal value will be 1×10^{-16} amp., an unusually low value. The electrical characteristics include high transconductance, good emission stability, low drift, and low microphonics.

In the single-stage type of circuit, where the tube must actuate the indicating or recording device, the CK5889 has sufficient reserve emission, notwithstanding the extremely low filament current, to provide operation for several thousand hours. In multi-stage circuits, where the tube is operated at low space

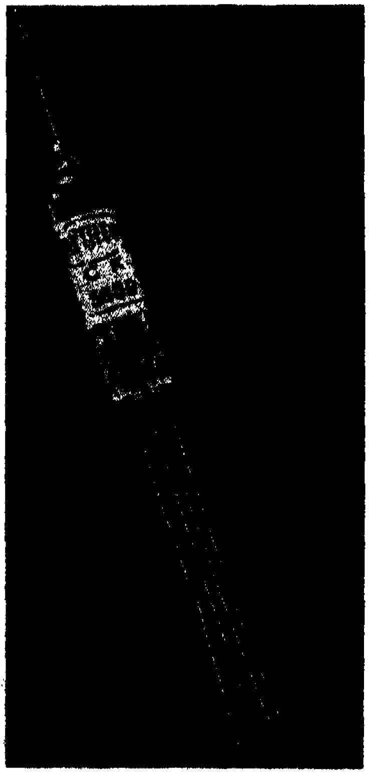

currents in the high gain, pentode connection, the filament power may be reduced to 5 mw, or approximately 6 ma at 0.85 volt, with stable, long-life operation. The external leakage paths from the control grid lead at the top of the tube to the leads from other electrodes are broken by a metallic guard ring which is permanently bonded to the glass bulb.—RAYTHEON MANUFACTURING COMPANY, SPECIAL TUBE SECTION, *55 Chapel Street, Newton 58, Massachusetts.*

A Three-Stage Non-Magnetic Mass Spectrometer

A three-stage non-magnetic mass spectrometer, employing the principle of velocity selection, has been developed by Dr. Willard H. Bennett of the National Bureau of Standards. In the new spectrometer a radiofrequency field replaces the usual magnetic field. Combining unusually simple operation with small size, light weight, and high sensitivity, the instrument has promising applications in several fields of science and industry.

In ordinary mass spectrometers a high intensity beam of ions is bent in the field of a large iron magnet, passed through a narrow slit, and then focused accurately on a narrow receiving slit. The non-magnetic mass spectrometer uses neither bending nor focusing. Ions produced in the ionization chamber travel in parallel paths through the tube, a glass cylinder 8 in. long and 2 in. in diameter. Three sets of three tungsten-wire grids are spaced along the tube to form the three stages. A radiofrequency potential is applied to the middle grid in each stage. An additional grid, with a negative potential applied, follows the final stage and in the absence of r-f potential turns back any electrons that may have arisen anywhere along the tube. Following the final grid is a collector plate whose potential is sufficiently positive to repel all but the desired positive ions.

The distances between grids and between stages are selected very accurately so that for any particular ion mass there will be a single definite frequency of the radiofrequency potential which can speed up ions of that mass as they pass through each stage. The increased speed of these ions enables them to overcome the opposing potential on the collector while all other kinds of positive ions are turned back. Successive distances between stages must be chosen so that the r-f potential will complete an exactly integral number of cycles during the time it takes for an ion of the desired mass to travel between stages, picking up maximum energy in each stage. The best combination of these integral numbers for a three-stage tube turns out to be 7 and 5, and in actual operation the seven-and-five cycle tube has completely separated the isotopes of chlorine. From this observation it is estimated that a four-stage tube, using integral numbers 13, 11, and 7, should resolve masses differing by only one percent.

The spectrometer can make use of all the ions that can be made to emerge through a grid several centimeters in diameter, and a new kind of positive ion source has been developed to take advantage of this. A spiral filament delivers an ionizing electron current of 100 ma through a double grid attached at one end of a hollow metal cylinder 3 cm deep. The far end is closed by a grid and near it is another grid at a negative potential which turns back all electrons and draws positive ions out from the cylindrical enclosure. At a pressure of 4×10^{-5} mm of mercury the source delivers a positive ion current of 100 μa.

By an appropriate change in ion source and reversal of potentials, the spectrometer works well for the study of negative ions, an important feature of the new instrument. Since negative ions are in general much less abundant, when they exist at all, the unusual sensitivity of the Bennett spectrometer is a great advantage in the study of negative ions.

In the development of vacuum tubes as for example power transmitting tubes such a spectrometer can be very helpful in analyzing gases and vapors that are evolved from the heated electrodes.

Surface reactions are another group of processes for which the new spectrometer can be used, separately analyzing the positively or negatively charged components. In gaseous discharges, the instrument can be used for direct analysis of the ions without magnetically disturbing the discharge.

One of the urgent needs of the U. S. Bureau of Mines is an instrument which can be used in the field for the analysis of small percentages of hydrogen in the manufacture of helium. The new spectrometer has already demonstrated adequate sensitivity and resolution for this task, and it can be readily adapted to automatic operation. Similarly, the new instrument could be used for continuous observation of the air in an enclosed space, giving warning of the presence of dangerous components such as hydrogen or chlorine. In addition, an active project is now under way at the National Bureau of Standards to adapt this instrument for use as an extremely sensitive carbon monoxide detector.

The lightness and compactness of the non-magnetic spectrometer offers a way to settle the question of the chemical composition of the upper atmosphere. This is a problem which is directly related to work in radio propagation and stratospheric flight. Arrangements have been made with the Applied Physics Laboratory of the Johns Hopkins University to send one of the new spectrometers aloft in a rocket. Before it is mounted in the rocket, the spectrometer tube will be evacuated and sealed; when the rocket has reached maximum altitude, an arm of the tube will be broken open to the rarefied air. The relative densities of atmospheric components will then be telemetered back to the ground for recording.

The non-magnetic mass spectrometer is now being adapted to the rapid scanning of mass spectra. Present methods permit sweeping twice a second through the mass range from 10 to 50, displaying the measured mass components directly on the screen of a cathode-ray oscilloscope. The scanning is accomplished by sweeping the ion accelerating voltage from 50 to 250 volts while modulating the radiofrequency potential with a 1000-cycle signal. —NATIONAL BUREAU OF STANDARDS, U. S. DEPARTMENT OF COMMERCE, *Washington 25, D. C.*

Electrostatic Generator

Two recently revealed electrostatic generators of 6 and 20 kv are designed to replace cumbersome and short-lived batteries as a high voltage supply for "snooper-scopes," "sniper-scopes," and similar infra-red sighting equipment. In the photograph, the new equipment is shown on the right, and the old, on the left.

The generators are extremely compact, weigh only 10 lb., and are powered by a spring motor. Whereas batteries which were formerly used lasted 3 hr., these units operate indefinitely. One spring winding of the new unit generates for 20 min.

Special problems solved in design included development of new dielectric materials, a pressure-tight transmission and new techniques of hermetic sealing. A special variable speed governor controls the power from the spring motor to provide constant speed.

An interesting point about this type of generator is that, unlike most generators, constant speed results in constant current output rather than constant voltage. Constant voltage output is maintained with a corona discharge regulation tube. This type tube also eliminates the power wasting and extra power requirements of resistance-type voltage divider regulation.—Chatham Electronics Corporation, *Newark, New Jersey.*

Temperature Control

This new unit, named PAKOTEMP, automatically holds fluid temperatures within a range as narrow as plus-minus ½°F by circulating a tempering liquid rapidly through a jacket or tempering panels surrounding the critical fluid. Incorporated in the unit is a radically different stainless steel heat exchanger which automatically provides heat or refrigeration as required to hold the temperature of the critical fluid within pre-determined limits.

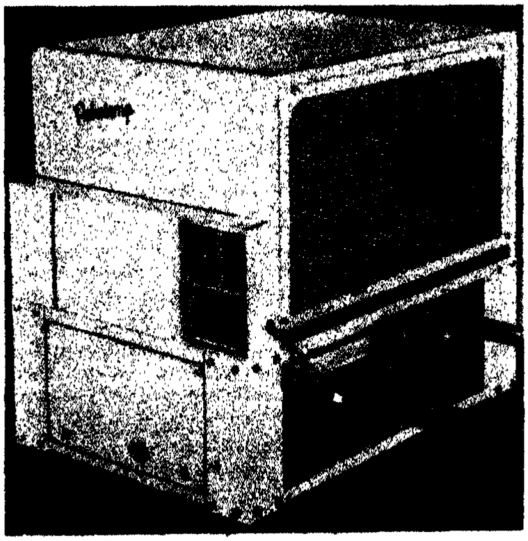

Since the tempering liquid is force circulated through a closed circuit extremely small temperature changes are corrected. This also avoids the setting-up of temperature zones within the critical fluid.

All thermostatic and electrical controls are conveniently located on the PAKOTEMP eliminating the hazards of electrical connections on solution tanks. Complicated mixing valves or manual controls are also eliminated. Only one electrical connection and two simple non-corrosive plumbing connections are required.

In addition to the standard models the PAKOTEMP may be modified for direct tempering and circulation of a critical fluid.—PAKO Corporation, *1010 Lyndale Avenue, N., Minneapolis, Minnesota.*

Diode Modulator for Video Frequencies

Useful in the laboratory, in TV-receiver production testing and in the TV service shop, the General Radio Type 1000-P6 crystal diode modulator converts an oscillator, standard-signal generator, or other r-f source into a test-signal generator for television-receiver testing. It modulates the oscillator signal after attenuation, so that reaction on the oscillator frequency is negligible. Thus it produces an amplitude-modulated signal with no significant incidental f-m.

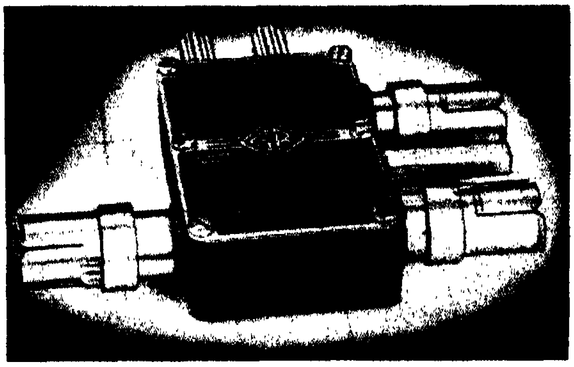

Range of modulating frequencies is 0 to 5 Mc and carrier frequency range is 20 to 1000 Mc, covering the proposed new u.h.f. television bands, as well as all currently used frequencies.

For receiver testing, a video signal can be conveniently derived from a TV receiver tuned to a local channel. With this video signal applied to the modulator, and an oscillator tuned to the desired carrier, a TV picture can be placed on any desired channel merely by tuning the carrier oscillator.

The modulator is small, compact, and inexpensive ($35.00). It is equipped with Type 874 coaxial connectors for r-f input, output, and for modulation input. Adaptors are available for connection to other types of terminals. Impedance is 50 ohms for r-f circuits, and coaxial 50-ohm attenuators and other accessories are available.—General Radio Company, *275 Massachusetts Avenue, Cambridge 39, Massachusetts.*

Ultra-Sensitive D.C. Current Measuring Device

The new PR6-NL 1000 to 1 capacitive d.c. divider is an ultra-sensitive current measuring device to be used with Millivac's d.c. millivoltmeter, Model MV-17b. The minute currents, to be measured, are fed into a 500-mmf condenser for a definite period

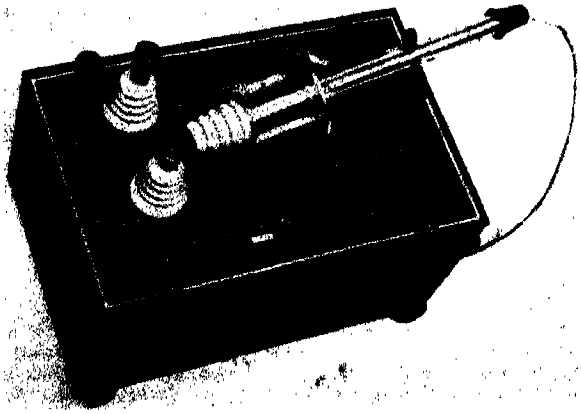

of time. A switch then transfers the charge of the 500-mmf condenser into an 0.5-mf condenser supplying d.c. power to the high impedance MV-17b millivoltmeter. Current measurements down to 5×10^{-13}A can actually be made with a charging time of 50 sec. The PR6-NL can also be used for *infinite impedance* voltage measurements between 1 v and 30 kv. It then replaces sensitive electrostatic voltmeters.—MILLIVAC INSTRUMENTS, *P. O. Box 3027, New Haven, Connecticut.*

Micro-Manometer

The Type 179 micro-manometer is a commercial version of an instrument developed at the National Bureau of Standards by Messrs. Dibeler and Greenough for the purpose of measuring pressures in the micron region in connection with mass spectrometers. It consists of a sensing unit and a separate sensitive and stable electronic indicator which can be mounted at some distance from the sensing unit. The indication of the pressure is independent of condensable vapor in the system and is read directly from the scale of a 4-in. meter calibrated in 1μ steps and having a full-scale value of 50μ.

The sensing unit consists of an exceedingly thin diaphragm contained in an outer chamber which is evacuated to a pressure approximately 1/100 of that to be measured. Pressure from the system to be measured is introduced on the other side of the sealed diaphragm and moves it closer to a radiofrequency transformer. Movement of the diaphragm varies the degree of coupling between the primary and secondary of this r-f transformer, and this effect, in conjunction with the electronic equipment described below, creates the desired indication.

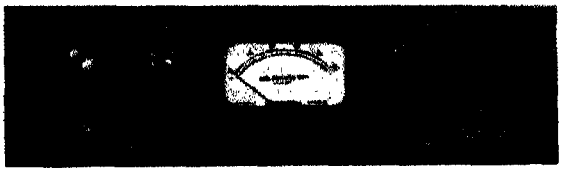

The radiofrequency oscillator, which is automatically controlled in amplitude, supplies radiofrequency current to the primaries of two transformers. These primaries are connected in series, and the same current flows in each. The coupling in one of the transformers is fixed, and a portion of the secondary voltage of this transformer is used as the reference voltage for zero adjustment of the instrument. The second of these transformers is located in the sensing unit in such a way that its coupling is varied by the position of the diaphragm. When the diaphragm moves, the voltage induced in the secondary of this transformer will vary, while the reference voltage from the first transformer remains constant. These voltages are both fed to a 60-cycle chopper or vibrator acting as a single-pole double-throw switch to feed, alternately, one or the other of the two voltages to a diode detector. As long as these two voltages are equal, no audio signal is developed by the detector. However, when they differ, a 60-cycle square wave is developed, the amplitude and phase polarity of which depends upon the magnitude and direction of the inequality of the r-f voltages. This square wave is amplified and rectified by means of the same chopper contacts as are used in the r-f circuit. The rectified output is used to energize the d.c. indicating meter, which is calibrated in terms of pressure on the high pressure side of the diaphragm.

The above arrangement results in a system, having extraordinary stability, which indicates true pressure differentials and is independent of the type of gas being measured. There is no possibility of contamination of the vacuum system by mercury, decomposition or polymerization of vapors by heated filaments, etc. For most applications, calibration curves are not required due to the wide range of linearity.—CLARK INSTRUMENT CORPORATION, *910 King Street, Silver Spring, Maryland.*

Manufacturers' Literature

Cathode Press—Vol. 7, No. 2, 32-page quarterly publication of Machlett, includes articles on a new vacuum bearing system for rotating anode x-ray tubes, a ceramic planar power tetrode, Dynamax motor controls, radiofrequency heating, tubes for 10- to 20-kw induction heaters, the x-ray tube for the 24-Mev betatron, Machlett-Graybar Exhibit at I.R.E. Convention. Price 75¢.—MACHLETT LABORATORIES, *Springdale, Connecticut.*

Research Microscopes—Catalog D-1010, 20 pages, illustrated, presents the company's line of Series E research microscopes, with price list.—BAUSCH & LOMB OPTICAL COMPANY, *Rochester 2, New York.*

Vibration and Stress Analysis—Catalog CGC-206, 12 pages, illustrated, covers recording oscillographs and vibration strain analysis equipment. Specifications included.—CENTURY GEOPHYSICAL CORPORATION, *1333 North Utica, Tulsa 10, Oklahoma.*

Castaloy Laboratory Appliances—New 24-page illustrated booklet describes the company's line of laboratory hardware, including clamps, burette holders and extension clamps for controlling flow, supporting thermometers, and sliding rod attachments, etc. Also illustrated and described is the line of "Flexaframe" supports for holding simple and complex assemblies of glassware.—FISHER SCIENTIFIC COMPANY, *717 Forbes Street, Pittsburgh 19, Pennsylvania.*

Experimenter—Vol. XXIV, No. 11, features a description of the Type 1803-A vacuum-tube voltmeter and includes other articles of interest.—GENERAL RADIO COMPANY, *275 Massachusetts Avenue, Cambridge 39, Massachusetts.*

Cenco News Chats—No. 67, 25 pages, features a portrait and short biographical sketch of Dr. Henry G. Knight, and includes articles on the American Institute of Chemists, equipment for study of laws of optics, Tygon tubing, microprojector for slides, new projection meter, clinical thermometer, spot tests for sugar or acetone, new low-cost autoclave, new induction unit for ignitions, new delineascope, holder for culture plates, evacuating with high speed, instrument for determining optical rotation, research hand torch, latest in culture tubes, vacuum scale demonstration, and other articles of interest.—CENTRAL SCIENTIFIC COMPANY, *1700 Irving Park Road, Chicago 13, Illinois.*

Regulated Power Supplies—Bulletin 81, illustrated, presents Lambda Electronics Corporation regulated power supplies. Prices included.—DUBIN ELECTRONICS COMPANY, INC., *103–02 Northern Boulevard, Corona, New York.*

Instrumentation—Vol. 4, No. 4, 32-page quarterly house organ, includes articles on automatic mass production of television tubes at RCA's Lancaster Plant, textile bleachery controls in processing and air conditioning, continuous specific gravity measurement, world's largest induction furnace, the recording mass spectrometer, electronic control featured in completely new indicating millivoltmeter, instrument shop test panel, control devices.—MINNEAPOLIS-HONEYWELL REGULATOR, *Wayne and Windrim Avenues, Philadelphia 44, Pennsylvania.*

Potentiometer—Brochure describes a new precision electronic potentiometer (Model P-2) for making precise potential measurements on high impedance electrochemical cells or electronic tubes and circuits. The instrument is suitable for the measurement of potentials from zero to three volts in three ranges.—SOUTHWESTERN INDUSTRIAL ELECTRONIC COMPANY, *2831 Post Oak Road, P. O. Box 13058, Houston 19, Texas.*

Radioactivity Measurement—Folder describes and illustrates two recently developed instruments, the RCL alpha-beta-gamma-survey meter and the RCL bismuth wall gamma-counter, and other radiation equipments.—RADIATION COUNTER LABORATORIES, INC., *1844–50 West 21st Street, Chicago 8, Illinois.*

Announcer—No. 50 3 38, 15-page house organ, contains articles on torsion laboratory balance, Coleman photonephelometer, Dyna-Cath magnetic mercury cathode, micropette, Babcock meniscus reader, methyl-purple indicator, water aerator, Neoprene-coated draining rack, Brewer-Petri metal tops, Parafilm, Barnstead laboratory sterilizers, and Temco hot plate. Also included is a brief sketch on John Tyndall and an article on Modern Nephelometry (employing the principle of "Tyndall light").—GREENE BROTHERS, INC., *1812 Griffin, Dallas 2, Texas.*

Electronics Dictionary—64-page illustrated dictionary of electronic terms, including concise definitions of words used in radio, television, and electronics, is available at a cost of 25¢.—ALLIED RADIO CORPORATION, *Chicago 7, Illinois.*

Amplifier—Catalog sheet describes a new wide-band d.c. amplifier (Model 120), designed to serve as a preamplifier in connection with a.c. and d.c. oscilloscopes, vacuum-tube voltmeters and similar instruments to extend their ranges to smaller signals.—FURST ELECTRONICS, *12 South Jefferson Street, Chicago 6, Illinois.*

Nuclear Measurements—40-page Catalog K (1950) presents the company's line of instruments for nuclear measurements.—NUCLEAR INSTRUMENT AND CHEMICAL CORPORATION, *223 West Erie Street, Chicago 10, Illinois.*

Tracerlab Catalog—Catalog B contains 90 pages of detailed information on all Tracerlab products, which are designed for every application of radioisotopes to research, industry, medicine, agriculture, etc. Included is descriptive material on instruments, Geiger-Müller tubes, tagged organic and inorganic chemicals, and industrial beta-ray thickness gauges. Also included is an extensive list of radiochemicals.—TRACERLAB, INC., *130 High Street, Boston 10, Massachusetts.*

Electrical Measuring Instruments—45-page catalog presents the company's line of portable panel and switchboard meters. Prices included.—W. M. WELCH SCIENTIFIC COMPANY, *1515 Sedgwick Street, Chicago, Illinois.*

New Materials

Forest K. Harris: Associate Editor
in Charge of this Section
National Bureau of Standards, Washington, D. C.

Porous Bearing

The *Oil-Well* bearing, of sintered powdered metal, is molded with an annular well or cavity in the form of a ring around the bearing bore. Alternatively the cavity may be filled with sponge iron, or may have a series of small holes. Oil or grease impregnated into the finished bearing will fill the cavity as well as the metal pores to form a reservoir of reserve lubricant. The unit is molded and sintered conventionally, but a special process has been developed to include the cavity which acts as a reservoir. Specific bearing problems should be taken up directly with the company.—MICHIGAN POWDERED METAL PRODUCTS COMPANY, *50 Industrial Street, Northville, Michigan.*

Powdered Stainless Steel

A new stainless-steel powder having excellent compactibility has been developed for use in work involving intricate shapes. Previous stainless-steel powders have been difficult to mold because of their inherent hardness. In contrast parts molded from the new powder have high strength prior to sintering. Analysis resembles chrome and chrome-nickel steels.—AMERICAN ELECTRO METAL CORPORATION, *318 Yonkers Avenue, Yonkers 2, New York.*

Stainless Steel

Armco 17-7 PH is a new precipitation-hardening stainless steel, designed for use in springs, pressure tanks, diaphragms, conveyor parts, and tools in chemical and other plants. This steel is characterized by the fact that its yield strength in compression is equal or higher than yield in tension, that it can be severely formed in the soft-temper state, that it can be wrapped on its own diameter in hard-temper form, and that low temperatures are required in heat treatment. It is available in most gauges and sizes for sheet, strip, and plate in soft-temper form. Wire and certain gauges and widths of sheet material can be obtained in hard-tempered form.—ARMCO STEEL CORPORATION, *701–5 Curtis Street, Middletown, Ohio.*

Knitted Metal

Knitted Wire Mesh, used in certain applications for some time, is now available, because of recently developed processing techniques, for such applications as shields for radio-noise suppression, resilient washers and mountings, high temperature packing, and air or liquid filters. The material is knitted (not woven) into a mesh from wire or ribbon of stainless steel, copper, brass, aluminum, monel, etc. It can be formed into shapes such as disks, strips, and cylindrical tubes that will be resilient and yet possess good mechanical stability. When used for radio-noise shielding, the material is used in the form of cylindrical mesh strip which may be fastened down along joints like weather stripping. Where a flange is provided, the mesh is pressed into resilient conducting gaskets that contain the noise, provide a breather action, and can operate safely at high or low temperature. Anticorrosion properties are determined by the type of material used. Pressure-tight shielding gaskets can be made by combining the mesh with rubber. Formed disks can be used as supporting washers for porcelain insulators.—METAL TEXTILE CORPORATION, *Roselle, New Jersey.*

Heat Treating Material

Hard-N-Deep is the trade name of a powder (containing chromium, carbon, and a catalyst) designed for case-hardening soft steel parts. The process consists in heating parts to a cherry red, dipping them in the powder, reheating, and quenching. The action taking place includes carbonizing, nitriding, and chromizing.—MIRACALOY CORPORATION, *50 Broadway, Room 1907, New York 4, New York.*

Heat Insulation

Alfol Asbestos is a combination of aluminum foil bonded to ¼-in. corrugated asbestos sheet. The corrugations permit fitting the material around edges in ducts and tanks, as well as wrapping it on runs of pipe. The outer surface is smooth aluminum to reflect heat, the ¼-in. thickness is equivalent in insulating value to 1¾ in. of plain air-cell asbestos.—REFLECTAL CORPORATION, *Room 2007, 155 East 44th Street, New York 17, New York.*

Mercury Battery

The *RM-1 Mercury "A" Battery*, latest of a line of hearing-aid batteries, is now available for general applications such as biasing cells in electronic equipment and as a source of constant potential. The unit is compact, having a diameter of 0.625 in. and a height of 0.644 in. It weighs 0.39 oz. and has a capacity of 1000 ma-hr. It is stated to have a very long shelf life, uniform discharge voltage, and a high ratio of energy to volume and weight. The unit operates under extreme pressure and temperature ranges, is leak-proof and dimensionally stable, and has high resistance to humidity and corrosion.—P. R. MALLORY AND COMPANY, *3029 East Washington Street, Indianapolis 6, Indiana.*

Fluorocarbon Plastic

Kel-F, a polymer of trifluorochloroethylene, differs from other fluorocarbon plastics in that inclusion of the chlorine atom in the formula makes the product readily moldable by all standard methods. It is resistant to virtually all corrosives and will withstand operating temperatures up to 390°F. Water absorption is nil and, in addition, the material has high dielectric strength, high insulation resistance, and other properties which are desirable in electronic and electrical equipment. One application is for multi-electrode hermetically sealed terminals in airborne communications equipment where good sealing, resistance to heat and cold, and freedom from "tracking" are important.

A series of dispersions of Kel-F are also available for application to materials and equipment which are not amenable to processing by conventional plastic molding. The general procedure for applying the dispersions is to build up a layer on the surface to be coated, dry out the solvent, and fuse to a continuous film. Coatings of from 10 to 15 mils can be built up in this way.—THE M. W. KELLOGG COMPANY, *P. O. Box 469, Jersey City 3, New Jersey.*

Molding Compound

Plaskon Alkyd 411 is unique among plastics in that it is supplied in the form of a putty rather than the conventional powder or granular form. It can be molded at pressures far lower than any other plastic-pressures as low as 50 p.s.i. being used commercially. For demonstration purposes the material can be molded by hand and cured to a hard, heat-resistant solid by brief heating. Because of the extremely low pressure requirements this material is particularly suited to applications in which a plastic shell must be molded around delicate electrical assemblies that would be crushed by the high pressures necessary to mold other plastics. The molder may preassemble the unit just before molding and produce an integral piece with all components, including wire leads, sealed into a stable moisture- and heat-resistant unit.—PLASKON DIVISION, LIBBEY-OWENS-FORD GLASS COMPANY, *2112 Sylvan Avenue, Toledo 6, Ohio.*

Protective Tape

"Polyken" Industrial Tape is a calendar-oriented polyethylene film with a synthetic adhesive applied to one side. It is designed for corrosion-protective operations, and does not require heat or solvents for application. The tape maintains a permanent pressure around the coated metal equal to the tension with which it was applied, and keeps moisture from reaching the protected metal. The tape is 0.009 in. thick and comes in various widths on 100-ft. rolls. Its insulation resistance is 100 megohms, dielectric strength 1400 volts per mil, moisture absorption 0.1 percent, and operating range −40 to 100°C.—BAUER AND BLACK, *222 West Adams Street, Chicago 6, Illinois.*

Oil-Proof Flexible Conduit

Flexible tubing of galvanized steel covered with *Geon* plastic is designed particularly to carry machine wiring in either stationary or movable positions. In addition to flexibility the conduit has the abrasion resistance, insulating properties and ability to withstand attack by coolants, greases, oils, and moisture associated with the plastic coating. Liquid-tight steel fittings are used in the assembly with standard or water-tight conduit boxes Sizes from ⅜ to 2 in. I.D. are available. —CHICAGO METAL HOSE CORPORATION, *1313 South 3rd Street, Maywood, Illinois.*

Vibration Isolator

Cohrlastic vibration-isolating equipment and instrument mounts employ silicone rubber to provide a unit which will function satisfactorily at temperatures between −100 and +500°F. Units can be designed and supplied for specified service, equipment weight, and vibration frequency.—CONNECTICUT HARD RUBBER COMPANY, *405–9 East Street, New Haven 9, Connecticut.*

Silicone-Treated Paper

A silicone-treated kraft paper has been developed which is non-adhesive to rubber, asphalt, pressure-sensitive tapes (even Scotch Tape), and most other adhesive materials. The non-adhesive qualities are attained by treatment with Dow-Corning's *DC 1107* silicone resin. Appearance, color, and feel of the paper are the same as an untreated paper. Tensile strength, tear resistance, and moisture-vapor transmission are unaltered. However, the new paper is water repellent. The release characteristics of this paper indicate applications such as interleaving sheets for uncured rubber stock, camel-back, tube repair patches, pressure-sensitive rubber tape, and other adhesive tapes. It may also be used to make shipping containers for such materials as asphalt.—CENTRAL PAPER COMPANY, *Muskegon, Michigan.*

THE
REVIEW OF SCIENTIFIC
INSTRUMENTS

VOLUME 21, NUMBER 7 JULY, 1950

A Transfer Device for Low Boiling Liquids

Aaron Wexler and William S. Corak
Westinghouse Research Laboratories, East Pittsburgh, Pennsylvania

(Received February 27, 1950)

The principles involved in the transfer of low boiling liquids under their own vapor pressures are indicated and calculations are presented for the specific case of the transfer of liquid nitrogen. A convenient device for transferring liquid nitrogen by this procedure is described and its operating characteristics are compared with the calculations.

I. INTRODUCTION

SINCE liquid air, oxygen, and nitrogen are so extensively used in research laboratories, the improvement of the transferring technique should be of general interest. It is the purpose of this note to describe a procedure, now generally employed at the Westinghouse Research Laboratories, which permits the convenient transfer of liquid nitrogen from large metal Dewar containers to vessels and apparatus in which immediate use is to be made of the refrigerant.

The standard technique for transferring liquid nitrogen from containers of capacity larger than 15 liters, from which for mechanical reasons it is not wise to pour directly, is to apply pressure above the liquid. The pressurizing gas is usually nitrogen or air. The rate of transfer is controlled by adjusting the pressure above the liquid, and the flow of liquid is stopped by depressurizing to atmospheric pressure. The disadvantages of this procedure are evident from the foregoing description. Thus it is not always convenient to have available a source of pressurizing gas. Moreover, unless pure nitrogen is used, the liquid becomes contaminated. If the pressurizing gas is wet, for example, it is not uncommon for the gas inlet tube to freeze up. In any case, the condensation of the pressurizing gas is reflected in an appreciable loss of liquid in the subsequent depressurization, as will be shown in the following discussion. Finally, this procedure does not permit good regulation of the transfer rate.

The method to be described involves a simple arrangement, which may be fitted easily to standard liquid containers, permitting the controlled transfer of the low boiling liquid under its own vapor pressure. While the principles involved are undoubtedly appreciated by those working primarily with liquefied gases, they seem to have eluded workers using these liquids as refrigerants. The essential point is that the liquid in equilibrium with its vapor at a pressure greater than atmospheric represents a large ballast of gas which tends to maintain the space above it at a relatively constant pressure as the vapor space increases during the transfer operation.

II. PRINCIPLES OF THE METHOD

Given a container full of liquid nitrogen in equilibrium with its vapor at a pressure P_0 atmospheres, one wishes to calculate what the pressure above the liquid will be, under equilibrium conditions, as a function of the fraction of liquid remaining when the liquid is transferred rapidly out of the container. It is assumed that the transfer time is sufficiently small to make the total heat leak negligible compared with the thermal changes accompanying the evaporation process. Let the volume of the container be V_0 liters and let V be the volume of the liquid when the equilibrium pressure has changed to P. The entire system is assumed to be isothermal at a temperature T°K, which is a condition that is met in practice in the case of commercial Dewar-type containers in which the inner vessels are made of copper.

If a small volume dV of liquid is transferred out, the temperature of the liquid will drop to $T=T_0-dT$, as a result of the evaporation of dn moles of the liquid, such that the pressure P above the liquid is just the vapor pressure at the temperature T. Let ΔH_V cal./mole be the latent heat of vaporization of the liquid and C_p cal./mole·degree be its heat capacity. Then, if k is the

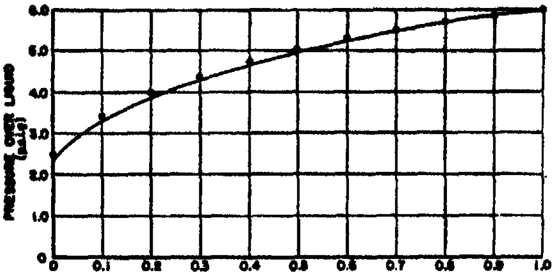

FIG. 1. Pressure over liquid on transferring from a pressurized liquid nitrogen container.

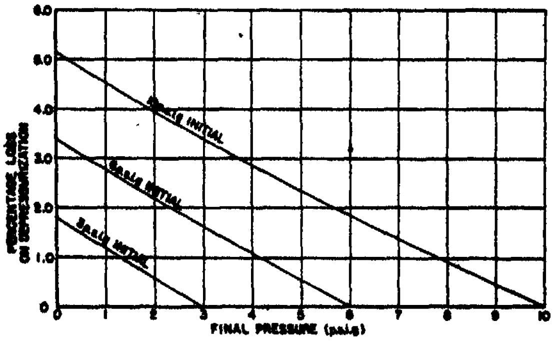

FIG. 2. Theoretical loss of liquid nitrogen when depressurizing liquid from various pressures.

number of moles per liter of liquid,

$$dn = -kVCpdT/\Delta H_V. \tag{1}$$

The changes in the thermodynamic variables of the vapor are obtained from the equation of state

$$Pv = \gamma mRT \tag{2}$$

where $v = V_0 - V$ is the volume of the vapor, R is the gas constant, m is the number of moles of vapor, and γ is the compressibility factor which corrects the ideal gas equation for departure from ideality. Thus,

$$dm = \frac{1}{\gamma RT}\left[(V_0 - V)dP - PdV - P\frac{(V_0 - V)}{T}dT\right]. \tag{3}$$

The equating of (1) and (3) and the substitution of $\alpha = V/V_0$ results in

$$\frac{d\alpha}{dT} + \left(\frac{1}{P}\frac{dP}{dT} - \frac{1}{T} - \frac{k\gamma RTCp}{P\Delta H_v}\right)\alpha = \left(\frac{1}{P}\frac{dP}{dT} - \frac{1}{T}\right). \tag{4}$$

The expressions in the parentheses of Eq. (4) may be expressed as functions of T, so that it takes on the form

$$(d\alpha/dT) + f_1(T)\alpha = f_2(T), \tag{5}$$

whose solution is

$$\alpha = \exp\left[-\int f_1(T)dT\right] \times\left\{\int f_2(T)\exp\left[\int f_1(T)dT\right]dT + C\right\}. \tag{6}$$

The solution of Eq. (6) involves a numerical integration which was performed with the aid of Gauss' mechanical quadrature formula.[1] In this calculation, the following approximations were used for the range of variables considered. The vapor pressure[2] was assumed to be represented adequately by $P = 0.139T - 9.74$. Mean values were selected for the rest of the data: $\Delta H_V = 1320$ cal./mole,[3] $Cp = 15.0$ cal./mole degree,[3] $k = 28.5$ moles/liter,[4] and $\gamma = 0.96$.[5] Figure 1 gives the results of the calculation for an initial pressure of 6 g p.s.i. The vapor pressure relation was used to transform the results obtained from Eq. (6) to give α as a function of the equilibrium pressure above the liquid. It is clear, therefore, that even for the least favorable case of rapid and complete transfer of the contents of a full pressurized liquid nitrogen container, the vapor pressure should be adequate to supply the transfer pressure head.

The losses which result in the depressurizing of a liquid nitrogen container may be estimated from Eq. (1). If β is the fraction of liquid which evaporates when the pressure above it is decreased from P_i to P_f, corresponding to T_i and T_f, then

$$\ln(1-\beta) = -\int_{T_i}^{T_f}\frac{Cp}{\Delta H_V}dT. \tag{7}$$

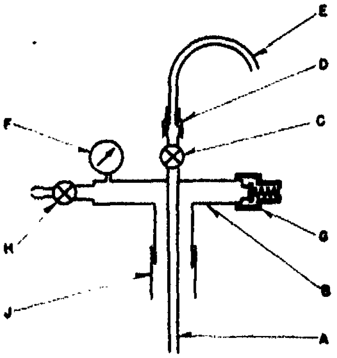

FIG. 3. Schematic diagram of the transfer device. A. Stainless steel tube, ⅛ in. O.D.×0.010-in. wall. B. Brass manifold. C. Crane No. 88 needle-point globe valve. D. ⅛-in. flare fitting. E. Copper transfer adapter. F. 0 to 15 p.s.i. gauge. G. Pressure-regulating and relief valve. H. Same as C. J. Heavy rubber tube connector.

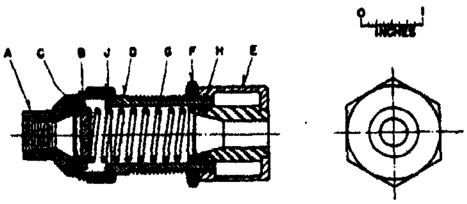

FIG. 4. Pressure-regulating and relief valve. A. Aluminum seat. B. Aluminum valve plate. C. "O" ring. D. Aluminum body. E. Aluminum adjustment nut and spring retainer. F. Brass lock-nut. G. Spring. H. "O" ring. J. Neoprene gasket.

---

[1] Lowan, Davids, and Levinson, Bull. Am. Math. Soc. 48, 739 (1942).

[2] B. F. Dodge and H. N. Davis, J. Am. Chem. Soc. 49, 616 (1927).

[3] R. W. Millar and J. D. Sullivan, Bur. Mines Tech. Paper No. 424 (1928).

[4] *International Critical Tables* (McGraw-Hill Book Company, Inc., New York, 1933), Vol. III, p. 204.

[5] O. Q. Hougen and K. M. Watson, *Chemical Process Principles* (John Wiley and Sons, Inc., New York, 1947), Part Two, p. [illegible], Fig. 103.

The percentage loss accompanying depressurization as calculated from Eq. (7) is shown in Fig. 2 for several initial pressures. Thus, when a liquid nitrogen container is pressurized with nitrogen gas to 6 g p.s.i. for the purpose of transferring liquid and is then depressurized to atmospheric pressure at the termination of transfer, the upper limit to the loss by depressurization is 3.4 percent of the contents of the container. This is an upper limit for the loss for the reason that in most transfer operations, thermal equilibrium is not established throughout the bulk of the stored liquid.

III. DESCRIPTION OF THE DEVICE

A transfer device suitable for permitting the transfer of liquefied gases under their own vapor pressures is indicated schematically in Fig. 3. The details of construction are indicated in the legend associated with the figure. The valve *G*, shown in detail in Fig. 4, is adjustable and has a differential between the opening and closing pressures of less than 1 g p.s.i. It is set so as to open at approximately the desired operating pressure. Valves of this type have been found to be very useful as safety valves for systems containing condensed gases. They are helium leak detector[6]-tight when operated at pressures less than atmospheric. Normally, the container is filled by connecting a suitable tube to fitting *D* and opening valve *H* for venting purposes. The rubber tube *J* is selected to give a gas-tight closure under operating conditions while acting as a vent at higher pressures. At the termination of the filling operation, the container is left with a pressure of 2 to 3 g p.s.i., which is suitable for most transfer operations. Due to the normal heat leak, the pressure builds up until the relief and regulating valve opens to maintain the container at the pre-set pressure. The transfer of liquid is effected by simply opening valve *C*, the rate of transfer being determined by the amount by which the valve is opened. A Crane No. 88 needle-point globe valve is used for this purpose because, among inexpensive commercial valves it appears to have the smallest heat capacity. The transfer device is shown mounted on a standard 50-liter storage container in Fig. 5.

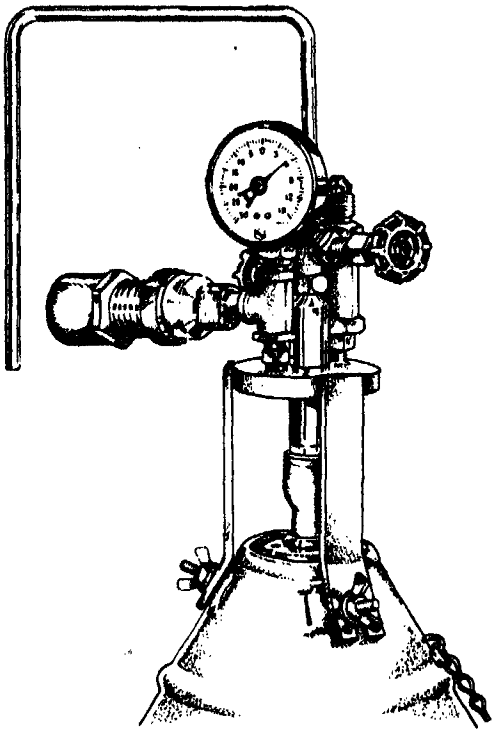

FIG. 5. Transfer device mounted on 50-liter storage container.

The maximum rate of flow permitted by the device is about $2\frac{1}{2}$ liters/min. For the purpose of checking the calculations made according to Eq. (6), a 50-liter container fitted with the device was filled with liquid nitrogen at a vapor pressure of 6 g p.s.i. The liquid was then transferred out at the maximum transfer rate, and the pressure was noted as a function of the fraction of liquid remaining. The experimental points in Fig. 1 indicate excellent agreement with the calculated curve. It was found that under most laboratory conditions, the pressure above the liquid remained very close to the equilibrium vapor pressure as the volume of the vapor space increased during the transfer operation.

IV. ACKNOWLEDGMENTS

The authors' thanks are due Dr. E. V. Somers for pointing out the very convenient method used in integrating Eq. (6). They are also indebted to Mr. G. T. Cunningham for his contributions to the design and construction of the device.

---

[6] Thomas, Williams, and Hipple, Rev. Sci. Inst. 17, 368 (1946).

THE REVIEW OF SCIENTIFIC INSTRUMENTS VOLUME 21, NUMBER 7 JULY, 1950

A Sector-Type Double-Focusing Magnetic Spectrometer

EARL S. ROSENBLUM
Case Institute of Technology, Cleveland, Ohio

(Received May 26, 1949)

An analysis is made of the focusing characteristics of a magnetic spectrometer having an annular magnetic field which varies approximately with $1/r^{\frac{1}{2}}$, thus permitting axial as well as radial focusing of particles of a given energy. By considering the field angle and source location as independently variable, the analysis provides for an instrument more flexible in use than similar existing types.

An optical analogy is developed from which a first approximation to the field shape is made, and from which the source and image location, magnification, dispersion and resolution can be readily obtained. Information thus obtained, combined with the results of an investigation into the image shape based on a series expansion, through second order, of expressions for the field strength and particle coordinates, yields more detailed information on the field shape which gives optimum focusing conditions and resolution for any chosen set of initial conditions.

Comparisons are made with the homogeneous field spectrometer and with the spectrometer of Svartholm and Siegbahn.

INTRODUCTION

A MAGNETIC spectrometer which achieves axial as well as radial focusing of charged particles by means of a magnetic field which varies radially as $1/r^{\frac{1}{2}}$, with both source and image within the field, has been developed by Siegbahn[1] and Svartholm.[1, 2] They showed that simultaneous radial and axial focusing is achieved after the particles have passed through a field angle of $2^{\frac{1}{2}}\pi$ (254.5°). Shull and Dennison[3] developed the path equations by standard perturbation methods, giving results through the second order of approximation, extending the theory to provide for any field whose axial component is expressible as a series representing arbitrary corrections to the field existing at a reference radius, which corrections are functions of powers of the radial displacement from the reference radius.

Snyder, Lauritson, Fowler, and Rubin[4] have built a spectrometer of this general type, but with the field having an angular extent of 180° and with source and image outside the field boundaries, approximately equidistant from the edges of the field.

This paper proposes to develop the path equations for a similar spectrometer, considering both the field angle and source location as independently variable. A set of equations are developed representing the first-order focusing characteristics in terms of an analogous thick lens system in geometric optics.

From these equations, a first-order determination of the field shape is made, information as to the location of source and image, limits on field angle, magnification and dispersion are obtained, and a preliminary estimate made of the resolution. From the second-order equations, choices of a second-order field shape parameter are made, which will cause the instrument to have a high resolution and good focusing characteristics, as computed through second order, for a chosen set of initial conditions.

Comparisons are made, throughout the development, with the spectrometer of Svartholm and Siegbahn, and with the homogeneous field spectrometer.

THEORY

Most of the symbols used in this paper are indicated on Fig. 1. It will be noted that the coordinates r, φ, and z are used within the field, region III, while two sets of x, y, and z axes are used, single primes indicating coordinates in the object space, region I, and double primes indicating coordinates in the image space, region II.

Throughout the paper, all distances will be given in units of the reference radius, which thus does not appear explicitly in any of the equations. Using this convention, Shull and Dennison's equations[3, 5] for the axial and radial components of the field become:

$$H_z=H_0[1-(r-1)\alpha+(r-1)^2\beta+z^2(\alpha/2-\beta)]$$
$$H_r=zH_0[-\alpha+2\beta(r-1)],$$

where α and β are arbitrary constants representing corrections to the field H_0, which is the axial field at the intersection of the reference radius and the plane $z=0$, henceforth called the equilibrium orbit.

The path equations were shown by Shull and Dennison to have the following zeroth-order solutions:

$$r=1;\quad z=0;\quad r\dot{\varphi}=v_0=\omega=-eH_0/m;\quad \varphi=\omega t.$$

To solve the path equations through second order, the mass, velocity, and coordinates of any particle in the field are expressed as their zeroth-order values plus first- and second-order correction terms.

$$\begin{aligned} r&=1+\lambda\rho_1+\lambda^2\rho_2\\ z&=\lambda\zeta_1+\lambda^2\zeta_2\\ \dot{\varphi}&=\omega+\lambda\theta_1+\lambda^2\theta_2\\ m&=m_0(1+\lambda\gamma)\\ v&=v_0(1+\lambda\eta), \end{aligned}\tag{1}$$

---

[1] N. Svartholm and K. Siegbahn, Arkiv. f. Mat. Astr. o. Fys. 33A, No. 21 (1946).

[2] N. Svartholm, Arkiv. f. Mat. Astr. o. Fys. 33A, No. 24 (1946).

[3] F. Shull and D. Dennison, Phys. Rev. 71, 681 (1947).

[4] Snyder, Lauritsen, Fowler, and Rubin, Phys. Rev. 74, 1564 (A) (1948).

[5] F. Shull and D. Dennison, Phys. Rev. 72, 256 (1947).

where λ is a parameter of smallness, ρ_1, ρ_2, ζ_1, ζ_2, θ_1, and θ_2 are functions of the time, and γ and η represent small variations in mass and velocity from reference values. There are no second-order corrections to m and v, as the mass and velocity of a particle remain constant within the field.

When the above values of the variables and the field components are substituted into the path equations, the solution proceeds in a manner similar to that described by Shull and Dennison, with the addition of terms in η and γ. It is convenient at this point to eliminate the time from the equations of motion, so that the particle coordinates r and z are given in terms of the angle φ.

Then, to extend the solutions so as to describe the motion in the image space in terms of the initial conditions at the source, it is noted from Fig. 1 that, if ϵ', κ', ϵ'', and κ'' are considered to be small angles,

$$\begin{aligned} y_1 &= b' - \kappa' t' \\ z_1 &= d' - \epsilon' t' \end{aligned} \qquad (2)$$

$$\begin{aligned} y'' &= y_2 + \kappa'' x'' = (r^* - 1) + \kappa'' x'' \\ z'' &= z_2 + \epsilon'' x'' = z^* + \epsilon'' x''. \end{aligned} \qquad (3)$$

The asterisk is used to indicate the values of r, φ, and z and their functions at the III–II boundary. Also,

$$\kappa'' = (1/r^*)(\partial r/\partial\varphi)^*, \quad \epsilon'' = (1/r^*)(\partial z/\partial\varphi)^*. \qquad (4)$$

Substituting Eqs. (4) and the general relationships, Eqs. (1) into Eqs. (3) give

$$\begin{aligned} y'' = \lambda[\rho_1{}^* + x''(\partial\rho_1/\partial\varphi)^*] \\ + \lambda^2[\rho_2{}^* - x''\rho_1{}^*(\partial\rho_1/\partial\varphi)^* + x''(\partial\rho_2/\partial\varphi)^*] \end{aligned} \qquad (5)$$

$$\begin{aligned} z'' = \lambda[\zeta_1{}^* + x''(\partial\zeta_1/\partial\varphi)^* \\ + \lambda^2[\zeta_2{}^* - x''\rho_1{}^*(\partial\zeta_1/\partial\varphi)^* + x''(\partial\zeta_2/\partial\varphi)^*]. \end{aligned} \qquad (6)$$

The solutions of these equations, after substitution of the path equations within the field and their first derivatives with respect to φ, and Eqs. (2), and letting $\varphi = \Phi$ at the III–II boundary, are

$$\begin{aligned} y'' = \kappa'\Big[& -t' \cos(1-\alpha)^{\frac{1}{2}}\Phi - \frac{1}{(1-\alpha)^{\frac{1}{2}}} \sin(1-\alpha)^{\frac{1}{2}}\Phi \\ & + x''\{(1-\alpha)^{\frac{1}{2}} t' \sin(1-\alpha)^{\frac{1}{2}}\Phi - \cos(1-\alpha)^{\frac{1}{2}}\Phi\Big] \\ & + \frac{\eta+\gamma}{1-\alpha}[-\cos(1-\alpha)^{\frac{1}{2}}\Phi \\ & + (1-\alpha)^{\frac{1}{2}} x'' \sin(1-\alpha)^{\frac{1}{2}}\Phi + 1] \\ & - b'[-\cos(1-\alpha)^{\frac{1}{2}}\Phi + (1-\alpha)^{\frac{1}{2}} x'' \sin(1-\alpha)^{\frac{1}{2}}\Phi] \\ & + \text{higher order terms.} \end{aligned} \qquad (7)$$

$$\begin{aligned} z'' = \epsilon'\Big[& -t' \cos\alpha^{\frac{1}{2}}\Phi - \frac{1}{\alpha^{\frac{1}{2}}} \sin\alpha^{\frac{1}{2}}\Phi \\ & + x''(\alpha^{\frac{1}{2}} t' \sin\alpha^{\frac{1}{2}}\Phi - \cos\alpha^{\frac{1}{2}}\Phi)\Big] \\ & - d'[-\cos\alpha^{\frac{1}{2}}\Phi + x''\alpha^{\frac{1}{2}} \sin\alpha^{\frac{1}{2}}\Phi] \\ & + \text{higher order terms.} \end{aligned} \qquad (8)$$

In order to obtain a perfect first-order focus, all rays from a given point on the source must come to a common focus at the image, whose coordinates are $x'' = t''$, $y'' = b''$, and $z'' = d''$. So, for simultaneous focusing in both the y and z directions, the coefficients of the initial angles κ' and ϵ' and Eqs. (7) and (8) must be zero at the image. Equating these coefficients to zero, and solving for t'' in both cases,

$$\begin{aligned} t'' &= \frac{[t'/(1-\alpha)^{\frac{1}{2}}] \cot(1-\alpha)^{\frac{1}{2}}\Phi + (1/\{1-\alpha\})}{t' - [1/(1-\alpha)^{\frac{1}{2}}] \cot(1-\alpha)^{\frac{1}{2}}\Phi} \\ &= \frac{(t'/\alpha^{\frac{1}{2}}) \cot\alpha^{\frac{1}{2}}\Phi + (1/\alpha)}{t' - (1/\alpha^{\frac{1}{2}}) \cot\alpha^{\frac{1}{2}}\Phi}. \end{aligned} \qquad (9)$$

If α is given the value of $\frac{1}{2}$, this equation is satisfied for any combination of t' and Φ, representing a field shape which permits flexibility in the choice of initial conditions.

Certain other values of α, within the allowable limits of $0 < \alpha < 1$, will satisfy this equation. However, for any such $\alpha \neq \frac{1}{2}$, there is at most one value of $\Phi < 2\pi$ for each $t' \geqslant 0$; an instrument so designed would have an inconveniently arranged geometry, would be inflexible, and its radial focusing characteristics would be different from the axial ones. Such cases will not be considered here.

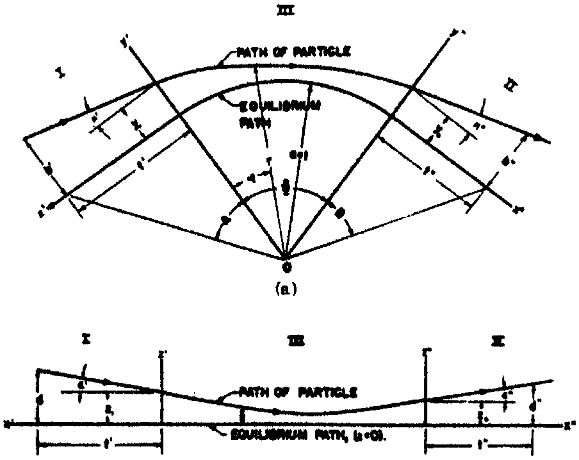

FIG. 1. Path of particle between source and image. (a) Section perpendicular to axis. (b) Axial section taken along a constant radius.

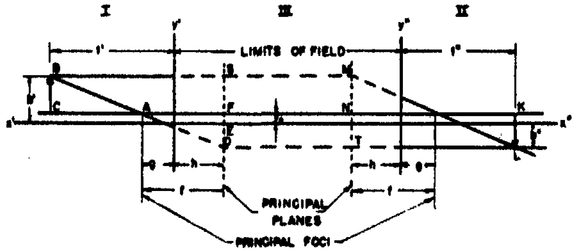

FIG. 2. Radial trajectories, based on optical analogy.

OPTICAL ANALOGY

Letting $\alpha=\frac{1}{2}$ in Eq. (9), either part of the equation, when rearranged, gives

$$2^{\frac{1}{2}}\cot\Phi/2^{\frac{1}{2}}=(t't''-2)/(t'+t'')=g, \tag{10}$$

where g is merely a symbol, for the moment, used to identify this equality. However, if $t'=\infty$ in Eq. (10), $t''=g$; similarly, if $t''=\infty$, $t'=g$. Therefore, g is the location, expressed as a distance from the field edges, where rays from infinity are focused, thus locating the principal foci of an analogous optical system. This parameter, and others derived below, are shown in Fig. 2, in which the equilibrium orbit is considered to be a straight line, for convenience.

The principal planes of the system can be located from the equations for the image coordinates, which are obtained from Eqs. (7) and (8), letting $\alpha=\frac{1}{2}$, using the coordinates of the image, and recalling that the coefficients of κ' and ϵ' vanish at the image.

$$b''=b'M+2(\eta+\gamma)(1-M) \tag{11}$$

$$d''=d'M, \tag{12}$$

where $M=\cos\Phi/2^{\frac{1}{2}}-t''/2^{\frac{1}{2}}\sin\Phi/2^{\frac{1}{2}}$. M, then, is the magnification, and is the same in the radial and axial directions.

For unit magnification, either Eq. (11) or (12), with Eq. (10), show that there is a distance h, given by

$$h=-2^{\frac{1}{2}}\tan\Phi(2^{\frac{1}{2}}2), \tag{13}$$

such that $h=t'=t''$. Therefore, h is the distance from either field edge to the principal planes of the system. Because of symmetry considerations, the nodal points lie on the principal planes.

An incidental result with $t''=h$ is that the coefficient of $\eta+\gamma$ in Eq. (11) becomes identically zero indicating that the dispersion of the instrument is zero at the principal planes. However, the significance of this fact is limited, as explained below.

The focal length f can be determined directly from the values of g and h as, by definition,

$$f=g-h, \tag{14}$$

from which

$$f=2^{\frac{1}{2}}\csc(\Phi/2^{\frac{1}{2}}). \tag{15}$$

The optical analogy is completed by combining Eqs. (10), (14), and (15), resulting in the familiar relations

$$f^2=(t'-g)(t''-g) \tag{16}$$

$$1/f=1/(t'-h)+1/(t''-h). \tag{17}$$

Results Obtained from Optical Analogy

Several items of useful information can be obtained from examination of the equations derived above.

Although the total focusing angle is always an integral multiple of 180°, for a homogeneous field,[6] a comparable relationship does not exist for the present case, and the total focusing angle $A+B+\Phi$ (Fig. 1) is *not* the same for all values of t' and Φ.

Source and image move relative to one another in the same manner as for a thick optical lens; as the object moves toward the field edge, the image moves away, and vice versa.

From Eqs. (11) and (12), information on the magnification can be obtained. At $t''=g$, $M=0$, indicating that a point image is formed at the focus, as expected. As the source moves in from infinity, the image moves out from $t''=g$; from the above equations M is always negative for $\Phi<\pi2^{\frac{1}{2}}$, so that the image is inverted, increasing in size directly with t''. (For $\pi2^{\frac{1}{2}}<\Phi<2\pi2^{\frac{1}{2}}$, the image is erect.)

From Eq. (10), it is seen that object and image distances are equal when

$$t'=t''=t=g\pm f.$$

When $t=g-f$, $t=h$ from Eq. (14), representing unit magnification at the principal planes. When $t=g+f$, $b''=-b'$ and $d''=-d'$, representing an inverted image of unit magnification. The spectrometer of Svartholm and Siegbahn[1] represents a special example of this case, with $t=0$.

Using standard conventions of geometrical optics, a typical path is plotted in Fig. 2 for a particle having momentum slightly greater than that necessary to follow the equilibrium orbit. Referring to Fig. 2,

$$b''=y_f+f(y_f-b')/(t'-g),$$

while, from Eqs. (11), (16), and (17),

$$b''=2(\eta+\gamma)+f[\{2(\eta+\gamma)-b'\}/(t'-g)].$$

Comparing the last two equations,

$$y_f=2(\eta+\gamma).$$

A similar substitution into Eq. (12) shows that for the same particle, $z_f=0$.

This indicates that particles of a given $(\eta+\gamma)$ have an equilibrium orbit in the median plane, displaced from the equilibrium radius by $y_f=2(\eta+\gamma)$.

Herzog[6] has shown that for the homogeneous field spectrometer, $y_f=\eta+\gamma$, representing only half as great a displacement as above. For further discussion of this factor, see the section on Dispersion and Resolution.

---

[6] R. Herzog, Zeits. f. Physik 89, 447 (1934).

Limits of Optical Analogy

The analogy does not describe the motion within the field boundaries, and so is valid only for t', $t'' \geq 0$. Thus, the statement above that unit magnification is obtained at the principal planes is true only if they are outside the field, which is the case only for $\Phi > \pi 2^{\frac{1}{2}}$. Also, the analogy will not account for an image obtained within the field. However, such an image can be located directly from the path equations or by considering that the field is cut off at that point, and letting $t''=0$.

Then, from Eq. (10), additional limits can be set to the location of source and image. That equation shows that source and image distances are negative when, respectively, the image and source distances are less than g. Furthermore, for $g<0$, the maximum values of t' and t'' are obtained for $t''=0$ and $t'=0$, respectively. From Eq. (10), either maximum distance is $-2/g$. For $g \geq 0$, the maxima are infinite.

Within these limits on object and image distances, the location of object and image and the magnification can be determined either graphically by the methods of geometrical optics, or by the use of the optical equations.

Dispersion and Resolution

The momentum of a particle which follows the equilibrium orbit is $p_0 = m_0 v_0$, and the momentum of a particle having slightly different energy is, through first order,

$$p = mv = p_0(1+\eta+\gamma)$$

and, letting $\delta p = p - p_0$, $\delta p/p_0 = \eta+\gamma$. Let $\delta b''$ be the radial change in image coordinates, for a given change in momentum. From Eq. (11),

$$\delta b'' = 2(\eta+\gamma)(1-M),$$

or, letting

$$D = 2(1-M), \quad \delta b'' = D(\eta+\gamma). \tag{18}$$

Then $\delta b''/(\delta p/p) = D(\eta+\gamma)/(\eta+\gamma) = D$, which defines the dispersion of the instrument From Eqs. (18) it is seen that D varies in absolute value directly with t'', so that for best dispersion $t'=0$, or $t'=g$, whichever is greater. The dispersion is zero with the image at a principal plane; $D=4$ for the case where $t'=t''=t=g+h$. This last figure is twice the value determined by Herzog[6] for the homogeneous field spectrometer with equal object and image distances, and checks Shull and Dennison's[3] statement comparing the dispersion of the double-focusing type with the 180° homogeneous field type.

TABLE I. Typical parameters for first-order focusing.[a]

t''	t'	y_0''	D	D_0
g	∞	0	2	∞
∞	g	∞	∞	$2/y_0'$
$g+f$	$g+f$	$-y_0'$	4	$4/y_0'$
h	h	y_0'	0	0
$-2/g$	0	$y_0' \sec\Phi/2^{\frac{1}{2}}$	$2(1-\sec\Phi/2^{\frac{1}{2}})$	$\frac{2}{y_0'}(1-\cos\Phi/2^{\frac{1}{2}})$
0	$-2/g$	$y_0' \cos\Phi/2^{\frac{1}{2}}$	$2(1-\cos\Phi/2^{\frac{1}{2}})$	$\frac{2}{y_0'}(1-\sec\Phi/2^{\frac{1}{2}})$

[a] *Note:* Not all of the quantities tabulated represent real images for all values of the field angle Φ.

The ratio of the dispersion D to the image width y_0'' is the reciprocal of the smallest resolvable percent change in momentum. Defining this ratio as the resolution, D_0, and expressing y_0'' in terms of the object width y_0' by means of Eq. (11),

$$D_0 = (2/y_0')[(1/M)-1]. \tag{19}$$

From this equation it can be shown that D_0 is infinite for $t''=g$ and decreases asymptotically to a magnitude of $2/y_0'$ for $t''=\infty$. At $t''=h$, $D_0=0$. For the particular case where $t'=t''=t=g+f$, $|D_0|=4/y_0'$, compared to the value of $2/y_0'$ determined by Herzog for a comparable geometry with a homogeneous field.

A computation of the resolution based on first-order image coordinates is somewhat deceptive, due to second- and higher-order defocusing; however, these values of D_0 are useful in obtaining a preliminary determination of optimum operating conditions.

Since it may be desirable in certain applications to design an instrument with a predetermined object distance, it will be of interest to select the field angle Φ which will give the best dispersion and resolution at fixed object distance. Expressing D and D_0 in terms of

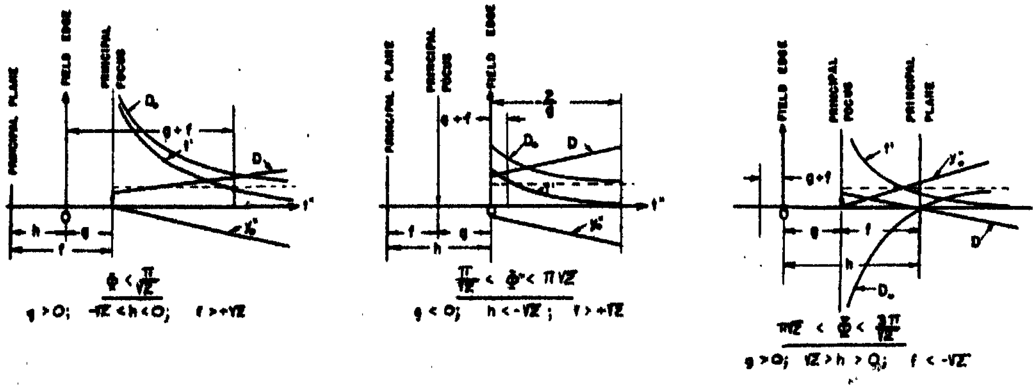
PRINCIPAL PLANE
FIELD EDGE
PRINCIPAL FOCUS
D_0
g+f
t'
D
t''
y_0''
h
g
f
O
$\Phi < \frac{\pi}{\sqrt{2}}$
$g>0$; $-\sqrt{2}<h<0$; $f>+\sqrt{2}$
PRINCIPAL PLANE
PRINCIPAL FOCUS
FIELD EDGE
$\frac{2}{g}$
g+f
D_0
D
t'
t''
y_0''
f
g
h
O
$\frac{\pi}{\sqrt{2}} < \Phi < \pi\sqrt{2}$
$g<0$; $h<-\sqrt{2}$; $f>+\sqrt{2}$
FIELD EDGE
PRINCIPAL FOCUS
PRINCIPAL PLANE
t'
y_0''
g+f
t''
g
f
h
D
D_0
O
$\pi\sqrt{2} < \Phi < \frac{3\pi}{\sqrt{2}}$
$g>0$; $\sqrt{2}>h>0$; $f<-\sqrt{2}$

FIG. 3. Graphical summary of focusing properties. *Note:* t', y_0'', D_0, and D are all plotted as ordinates, to arbitrary scales.

t', and then finding the values of $\partial D/\partial\Phi$ and $\partial D_0/\partial\Phi$ and equating them to zero, the following field angle and object distances are obtained:

$$\Phi=2^{\frac{1}{2}}\tan^{-1}(-t'/2^{\frac{1}{2}})\,;\quad t''=0,$$

which may be an awkward arrangement, physically. Furthermore, the second partials indicate that, while the first-order resolution is a maximum, the dispersion is a minimum. Therefore, nothing can be concluded as to the best field angle at fixed object distance, on the basis of first-order solutions only.

Summary of Parameters for First-Order Focusing

In Fig. 3, values of t', y_0'', D, and D_0 are plotted as functions of t'' for several ranges of Φ. Table I gives numerical values of these quantities at certain values of t'', from which the magnitude of the various ordinates plotted in Fig. 3 can be estimated.

As a special case, $\Phi=\pi 2^{\frac{1}{2}}$. Here, $g=\infty$, so $t''=-t'$, from Eq. (10). The only real solution, then, is for $t'=t''=0$. This is the instrument described by Siegbahn and Svartholm.[1] Note that the first-order magnification, dispersion, and resolution are the same for this instrument and for the sector-type spectrometer with equal object and image distance, $g+f$.

As another special case, $\Phi=\pi/2^{\frac{1}{2}}$. For this case, $g=0$, and the curves are the same as the first illustration of Fig. 3, with the origin of t'' coinciding with g. For this angle, $f=+2^{\frac{1}{2}}$, $h=-2^{\frac{1}{2}}$, and $t't''=2$.

Effect of Non-Radial Field Edges

An attempt has been made to determine whether or not the performance of the instrument could be improved by shaping the field edges so that they are straight lines making arbitrary angles with the y' and y'' axes, respectively (Fig. 1). However, such a modification destroys the flexibility of the instrument, in that there is no value of the field-shape parameter which will allow radial and axial focusing with various object distances. If these angles are considered as small angles, this objection disappears, but the accompanying second-order effects consist of a slight broadening or simply a shift of image position.

Furthermore, although the effects of fringing fields are not discussed quantitatively in this paper, it is probable that their defocusing effects would be as great in magnitude, or greater, than the effects due to this type of field-shape correction.

SECOND-ORDER SOLUTIONS AND CHOICE OF PARAMETER β

If the operations indicated by Eqs. (5) and (6) are performed with $\alpha=\frac{1}{2}$ and if terms in η and γ are neglected, the image coordinates become, in terms of the initial conditions at the source,

$$\begin{aligned}
b''={}&b'\left[\cos\frac{\Phi}{2^{\frac{1}{2}}}-\frac{t''}{2^{\frac{1}{2}}}\sin\frac{\Phi}{2^{\frac{1}{2}}}\right]+\left[(b'-\kappa't')^2\frac{2\beta-1}{3}+\kappa'^2\frac{8\beta-1}{3}+(d'-\epsilon't')^2\frac{3-4\beta}{6}+\epsilon'^2\frac{3-8\beta}{3}\right]\\
&\times\left[\cos\frac{\Phi}{2^{\frac{1}{2}}}-\frac{t''}{2^{\frac{1}{2}}}\sin\frac{\Phi}{2^{\frac{1}{2}}}\right]+\left[\kappa'(b'-\kappa't')\frac{4\beta-2}{3}-\epsilon'(d'-\epsilon't')\frac{4\beta}{3}\right]\left[t''\cos\frac{\Phi}{2^{\frac{1}{2}}}+2^{\frac{1}{2}}\sin\frac{\Phi}{2^{\frac{1}{2}}}\right]\\
&+\left[\{(b'-\kappa't')^2-2\kappa'^2\}\frac{4\beta+1}{12}-\{(d'-\epsilon't')^2-2\epsilon'^2\}\frac{\beta}{3}\right][\cos 2^{\frac{1}{2}}\Phi-t''2^{\frac{1}{2}}\sin 2^{\frac{1}{2}}\Phi]+\left[-\kappa'(b'-\kappa't')\frac{4\beta+1}{3}\right.\\
&\left.+\epsilon'(d'-\epsilon't')\frac{4\beta}{3}\right]\left[\frac{1}{2^{\frac{1}{2}}}\sin 2^{\frac{1}{2}}\Phi+t''\cos 2^{\frac{1}{2}}\Phi\right]+[(b'-\kappa't')^2+2\kappa'^2]\frac{1-4\beta}{4}\\
&+[(d'-\epsilon't')^2+2\epsilon'^2]\frac{2\beta-1}{2}+\frac{t''}{2^{\frac{1}{2}}2}[(b'-\kappa't')^2-2\kappa'^2]\sin 2^{\frac{1}{2}}\Phi+\kappa'(b'-\kappa't')t''\cos 2^{\frac{1}{2}}\Phi. \qquad (20)
\end{aligned}$$

$$\begin{aligned}
d''={}&d'\left[\cos\frac{\Phi}{2^{\frac{1}{2}}}-\frac{t''}{2^{\frac{1}{2}}}\sin\frac{\Phi}{2^{\frac{1}{2}}}\right]+\left[-(b'-\kappa't')(d'-\epsilon't')\frac{4\beta}{3}+\kappa'\epsilon'\frac{6-16\beta}{3}\right]\left[\cos\frac{\Phi}{2^{\frac{1}{2}}}-\frac{t''}{2^{\frac{1}{2}}}\sin\frac{\Phi}{2^{\frac{1}{2}}}\right]\\
&+2^{\frac{1}{2}}\left[-\epsilon'(b'-\kappa't')\frac{4\beta}{3}+\kappa'(d'-\epsilon't')\frac{3-4\beta}{3}\right]\left[2^{\frac{1}{2}}\sin\frac{\Phi}{2^{\frac{1}{2}}}+t''\cos\frac{\Phi}{2^{\frac{1}{2}}}\right]+\left[\{(b'-\kappa't')(d'-\epsilon't')\right.\\
&\left.-2\kappa'\epsilon'\}\frac{3-4\beta}{6}\right][\cos 2^{\frac{1}{2}}\Phi-2^{\frac{1}{2}}t''\sin 2^{\frac{1}{2}}\Phi]+2^{\frac{1}{2}}\left[\epsilon'(b'-\kappa't')\frac{4\beta-3}{6}+\kappa'(d'-\epsilon't')\frac{4\beta-3}{6}\right]\\
&\times[2^{\frac{1}{2}}\sin 2^{\frac{1}{2}}\Phi+2t''\cos 2^{\frac{1}{2}}\Phi]+[(b'-\kappa't')(d'-\epsilon't')+2\kappa'\epsilon']\frac{4\beta-1}{2}\\
&+\frac{t''}{2^{\frac{1}{2}}2}[(b'-\kappa't')(d'-\epsilon't')-2\kappa'\epsilon']\sin 2^{\frac{1}{2}}\Phi+\frac{t''}{2}[\epsilon'(b'-\kappa't')+\kappa'(d'-\epsilon't')]\cos 2^{\frac{1}{2}}\Phi+\frac{t''}{2}(b'\epsilon'-d'\kappa'). \qquad (21)
\end{aligned}$$

The most satisfactory solutions to these equations depend on the uses to which a given instrument is to be put, the space and equipment available, and the economics of the project. The initial conditions and field angles selected below for investigation were based on a desire for the following characteristics, which are enumerated together with their respective somewhat contradictory effects on the instrument design.

1. Source and image should be accessible for use with auxiliary equipment and for easy removal during an experiment. If they can be located in regions where the magnetic field is relatively weak, some difficulties in the use of certain types of sources and detectors are lessened. These requirements are best satisfied by maximum separation of source and image from the field edges. However, design on this basis, besides conflicting with items listed below, may cause undue increase in the volume and complication of the vacuum system.

2. If the instrument is to be used with particles of energies so high as to make collimation of the image within the instrument difficult, it is desirable to work with an image large enough so that the detector itself can act as the exit slit. In this case, the object distance should be a minimum and the image distance a maximum, so that the dispersion will be as large as possible for the limiting image width.

3. The instrument should transmit a maximum amount of the radiation from the source. With a given pole shape and separation, this requires that the source be at the edge of, or within the field. Pole separation is limited by the problem of maintaining the field shape over a large cross section, particularly due to excessive fringing near the inner and outer radii. With a large gap, power consumption will be quite high.

4. The resolution should be as large as possible. The narrowest possible image, together with maximum dispersion make for highest resolution. First-order focusing characteristics are not very helpful here, as second-order defocusing terms may be large enough to cause extremely large changes in the resolution. It has been found that (for a given object size and fixed limitations on radial and axial angles transmitted), when the field shape parameter β is chosen for minimum image width at each object distance, the resolution does not vary greatly with object distance.

The resolution can be increased by decreasing the object width and radial and axial angles, but with a corresponding decrease in intensity. The optimum ratio of these quantities and object length depends somewhat on the actual size of the instrument; a radius in the 10- to 20-cm range is assumed here.

Naturally, all these considerations could not be satisfied simultaneously; one immediate result has been that the object size and other initial conditions have been limited to smaller values than those allowed by Shull and Dennison.[3] In the analysis below, somewhat arbitrary limitations on the design parameters have been chosen; as one compromise combination:

TABLE II. Performance data with selected design parameters.

Φ	t'	t''	g	h	f	D	D_0	$\frac{\delta p}{p_0}=\frac{1}{D_0}$
$\pi/2^{\frac{1}{2}}$	1	2	0	$-2^{\frac{1}{2}}$	$2^{\frac{1}{2}}$	4.83	154	0.0065
π	0.7	0.7	-1.08	-2.86	1.78	4.00	174	0.0057

$$|b'|\leqslant 0.01;\quad |d'|\leqslant 0.05;\quad |\kappa'|\leqslant 0.1;\quad |\epsilon'|\leqslant 0.05;$$
$$0.7\leqslant (t',t'')\leqslant 2.$$

The limitation on angle can be obtained by a suitably shaped baffle placed at $\varphi=\pi/2^{\frac{1}{2}}$; a rectangular-shaped baffle is assumed here. The restriction on object and image distances imposes limits on the field angle which are given roughly by

$$\pi/2^{\frac{1}{2}}\leqslant\Phi\leqslant\pi.$$

Equations (20) and (21) have been solved at these two limits of field angle, and a value of β has been chosen to result in the narrowest possible image, for ($\Phi=\pi/2^{\frac{1}{2}}$, $t'=1$, $t''=2$; $\beta=0.35$) and for ($\Phi=\pi$, $t'=t''=0.701$, $\beta=0.25$).

On Fig. 4 is plotted the image of half of a rectangular source for the two cases, along with a rectangle representing the object size, and sections showing the image of a point object at two positions on the source. The image width is obtained from these plots, and using that width and the optical equations, the information tabulated in Table II is obtained.

With these combinations of initial conditions, about one-fifth to one-fourth percent of the total radiation from an isotropic source is transmitted. This represents a lower intensity than that obtainable with the same gap for the case where $t'=t''=0$, but with other accompanying advantages in flexibility, accessibility, etc.

COMPARABLE PATH EQUATIONS FOR THE HOMOGENEOUS FIELD SPECTROMETER

With a homogeneous field, $\alpha=\beta=0$, the path equations within the field are those given by Shull and Dennison. These path equations can be extended to describe the image coordinates with an arbitrary set of initial conditions and field angle, but this is not done

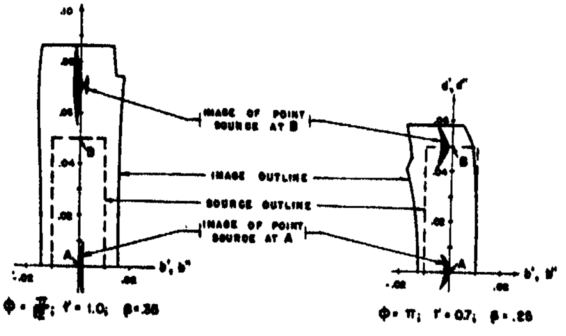

FIG. 4. Image size with selected field shapes and initial conditions.

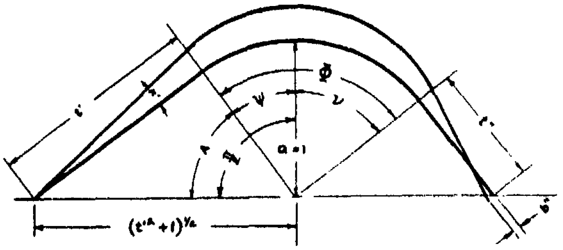

FIG. 5. Path of particle in homogeneous field spectrometer.

in the present paper. However, Stephens[7] has developed an equation for the case represented by Fig. 5. where $b'=d'=\epsilon'=0$. That equation is

$$b''=-\left(\frac{\kappa'^2}{2}\right)(t'^2+1)^{\frac{1}{2}}\left(\frac{\sin^2\psi}{\sin\nu}+\frac{\sin^2\nu}{\sin\psi}\right). \tag{22}$$

Now, substituting the same initial conditions into the path equation gives, at the image,

$$b''=\left(\frac{\kappa'^2}{2}\right)\left[-\frac{1}{t'\sin\Phi-\cos\Phi}+t'\sin 2\Phi\right.$$
$$\left.+\frac{t'^2-1}{2}\cos 2\Phi-\frac{t'^2+1}{2}\right]. \tag{23}$$

When the angles ψ and ν in Eq. (22) are expressed in terms of angles A and Φ, using Fig. 5, that equation becomes identical with Eq. (23), thus affording a check on the two approaches to the problem.

CONCLUSIONS

With suitable choices of initial conditions and field-shape parameters, the instrument described in this paper is one of high intensity and resolution, although the intensity suffers when the source is not at the field edge. However, advantages are gained in flexibility and convenience which allow the instrument to be a useful one.

It has the same advantages over spectrometers of other types as does the Siegbahn spectrometer, the latter being a limiting case of the spectrometer described above, with object and image distance set equal to zero, resulting in a focusing angle of $\pi 2^{\frac{1}{2}}$. This combination transmits a higher intensity than all other combinations, except for those with zero object distance, and does not suffer from possible defocusing effects caused by fringing fields (see below), so probably has as high a resolution as any other combination. However, the source and image are located in a strong field between the poles of the magnet, thus decreasing the flexibility and accessibility of the instrument. The sector-type spectrometer is also more suitable for determining the energy of particles which must originate in other equipment, and which should cross the fringing fields as nearly as possible normal to them, to minimize defocusing.

The effects of fringing fields have not been discussed in detail, but by analogy to Coggeshall's[8] analysis of the edge effects of a homogeneous field, it is probable that these effects will not cause considerable defocusing, if source and image are located either completely within the field or in regions of low field strength, and if the particles enter and leave the field nearly normal to the fringing field.

Although the resolution as computed through second order neglects the defocusing due to higher order terms, the fact that the intensity is not uniform over the image indicates that the computed values of resolution probably can be closely realized. Shull,[9] and Kurie, Osaba, and Slack[10] have shown that the resolution of the instrument does not vary widely with variations of β in the range $\frac{1}{8}\leqslant\beta\leqslant\frac{3}{8}$ for the $\pi 2^{\frac{1}{2}}$ instrument; it is considered likely that the behavior will be similar for an instrument with a different field angle.

The author wishes to express his appreciation of the help of Dr. E. F. Shrader, who supervised the work of this paper, and of Dr. E. C. Crittenden, whose suggestions led to the investigation of the double-focusing spectrometer and some of its more significant properties.

---

[7] W. Stephens, Phys. Rev. 45, 513 (1934).

[8] N. Coggeshall, J. App. Phys. 18, 855 (1947).

[9] F. Shull, Phys. Rev. 74, 917 (1948).

[10] Kurie, Osaba, and Slack, Rev. Sci. Inst. 19, 771 (1948).

A Linear Preamplifier for Driving a Long Coaxial Cable*

LLOYD G. LEWIS, JAMES G. ROBINSON, AND JOHN TOLL
Palmer Physical Laboratory, Princeton University, Princeton, New Jersey

(Received January 23, 1950)

A circuit for driving a long coaxial cable is described. Its response characteristics permit impedance matching of the coaxial line without sacrificing linearity of response, and make possible a relatively long line between the particle detector and the recording apparatus. The circuit was found to be reasonably stable for long periods of time, even under severe outdoor operating conditions.

INTRODUCTION

FAST wide-band amplifiers, such as the Los Alamos Model 100 and Model 500 amplifiers,[1] have found considerable use in nuclear physics and cosmic rays. These amplifiers have stabilized gains of about 10^6, rise times as short as 0.15 μsec. excellent monatonic transient response to step signal, and good linearity of response. Their characteristics have made these amplifiers extremely useful for studying the size and the shape of the pulses produced by particle detectors excited by heterogeneous radiations.

The arrangement of the apparatus is usually such that the particle detector and the preamplifier are located very near each other in order to make the signal lead from the detector as short as possible. The amplified signal is transmitted to the main amplifier and recording circuits by a short piece of coaxial cable. For a cable no longer than about six feet, impedance matching at each end is usually not necessary, and the cable can be considered to be a capacity shunting the output of the preamplifier. Under these conditions the cathode follower that drives the coaxial line can work into a fairly high impedance, and the linearity of the cathode follower can be made to approach that of the rest of the amplifier.

For some experiments it is essential that the preamplifier be located at a considerable distance from the main amplifier. Figure 1 shows an example of such a situation encountered in an experimental arrangement for recording the height and shape of each pulse produced by cosmic-ray events in each of four electron collection ionization chambers. The chambers were located so that they measured the particle density in a cosmic-ray air shower at four points separated by as much as 25 meters. The four cathode-ray tubes were located side by side so that they could be photographed by the same camera. This arrangement was made possible by the 100 ft. long coaxial signal cables between the preamplifiers and the main amplifiers.

A coaxial line 100 ft. long should be terminated in its characteristic impedance to avoid distortion of fast signals by the reflections from the ends of the line.

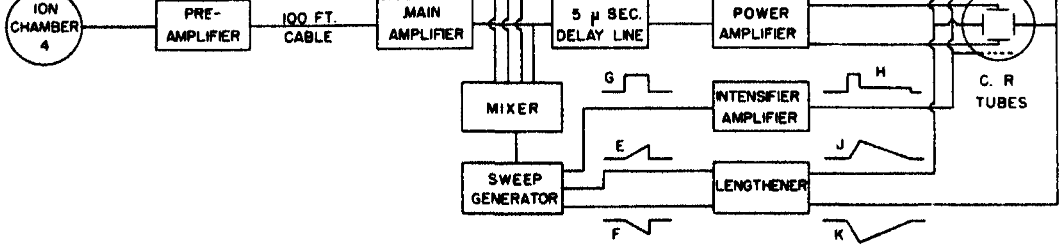

FIG. 1. This figure gives the schematic layout of the several components in a four channel pulse amplifier and recorder. A step signal A and the several amplified signals B, C, D are shown together with the sweep voltage E, F, J, K and cathode-ray intensifier pulses G and H produced by the triggered single-sweep generator. The cathode-ray tube beam is turned on for the fast sweep from left to right and remains on for the much longer return sweep from right to left. In this way coincidences between channels could be studied for resolving times as long as 0.1 sec.

---

* Assisted by the joint program of the AEC and ONR.

[1] W. C. Elmore and M. Sands, *Electronics; Experimental Techniques* (McGraw-Hill Book Company, Inc., New York, 1949), Div. V, Vol. 1 N.N.E.S., pp. 166 and 167.

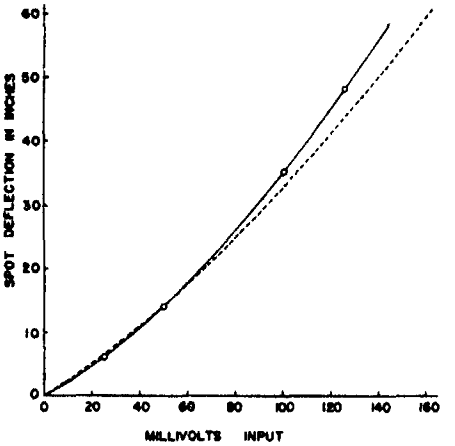

FIG. 2. The solid curve gives the deflections of the cathode-ray tube spot as a function of the signal voltage fed to a preamplifier that contained a simple cathode follower for driving the signal cable. The large deflections plotted were obtained by measuring the deflections on the screen of the cathode-ray tube and multiplying them by factors obtained from attenuators in the main amplifiers. The dotted curve is the response computed assuming all amplifier components linear except for the cathode follower that drives the long 98-ohm coaxial cable.

The 98 ohm characteristic impedance of an *RG7U* cable is so low that the 6*J*6 cathode follower in the Model 500 preamplifier output stage has a noticeably nonlinear response over the range of signals produced by the ionization chambers. This nonlinearlity is illustrated in Fig. 2. The solid curve gives the deflection of the cathode-ray tube spot as a function of the signal placed on the input of the preamplifier. The large deflections plotted were obtained by measuring smaller deflections and multiplying by a factor obtained from an attenuator in the main amplifier. The dotted curve in Fig. 2 is the computed response of the amplifier under the assumptions that all components except the 6*J*6 are linear and have the gains measured for each stage; that the 6*J*6 is biased at $-4V$, works into a 100 ohm load and has the published average characteristics. The similarity between the two curves indicates that almost all of the nonlinear response can be attributed to the characteristics of the 6*J*6.

Considerable gain in linearity can be obtained by replacing the simple cathode follower with a circuit whose gain is stabilized by inverse feedback. The circuit to be described here makes use of well-known principles and may possibly have been worked out independently by others;[2] however, it is presented here to call attention to the obtainable improvement in linearity and to the possible added convenience of a longer cable be-

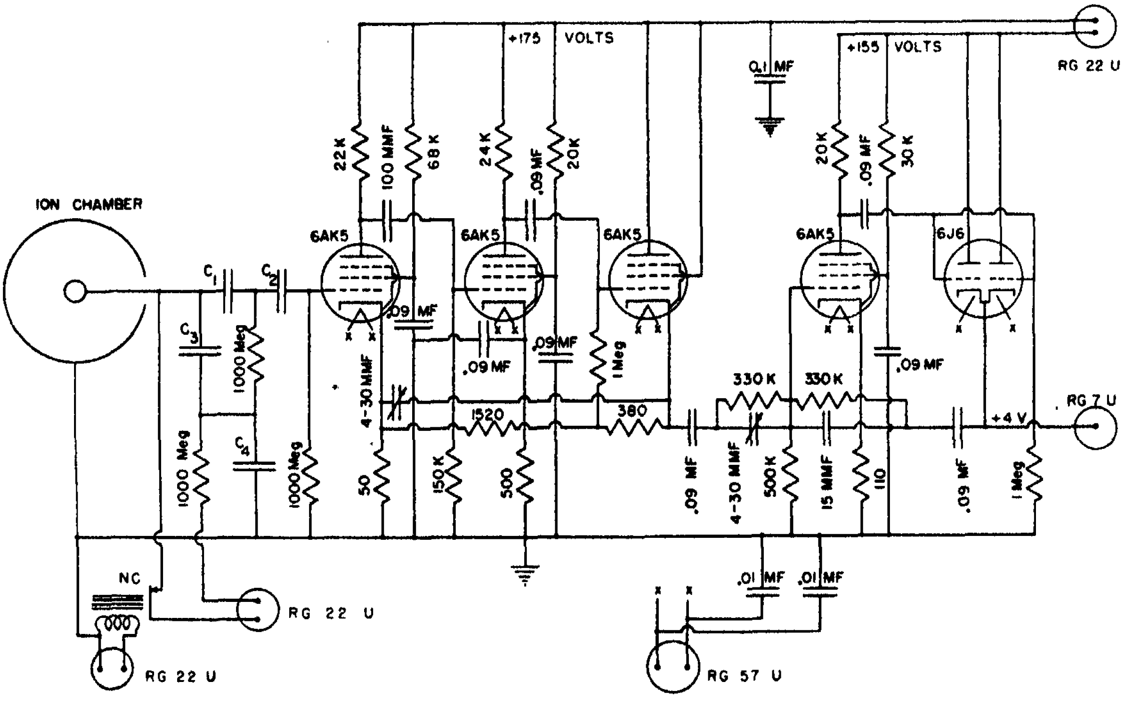

FIG. 3. This figure gives the wiring diagram of the complete pre-amplifier used to drive the long coaxial cable shown in Fig. 1. The three tubes next to the ion-chamber are operated similarly to those in the Los Alamos Model 500 amplifier. The last two tubes are connected so that their gain is stabilized by inverse feedback. The connection shown is for a gain of -1. The cathode of the 6*J*6 is maintained at $+4$ volts with respect to ground by a resistor condenser network across the $B+$ of the main amplifier. C_1 is a 30-$\mu\mu$f air condenser, C_2 is a 50-$\mu\mu$f double cup ceramic condenser, C_3+C_4 are the guard ring stray capacities.

---

[2] A single tube gain of -1 circuit is described by E. W. Titterton and V. L. Fitch, Rev. Sci. Inst. **18**, 639 (1947), for inverting trigger pulses, and V. L. Fitch and E. W. Titterton, Rev. Sci. Inst. **18**, 821 (1947), for inverting a sawtooth to get push-pull cathode-ray tube sweep signals.

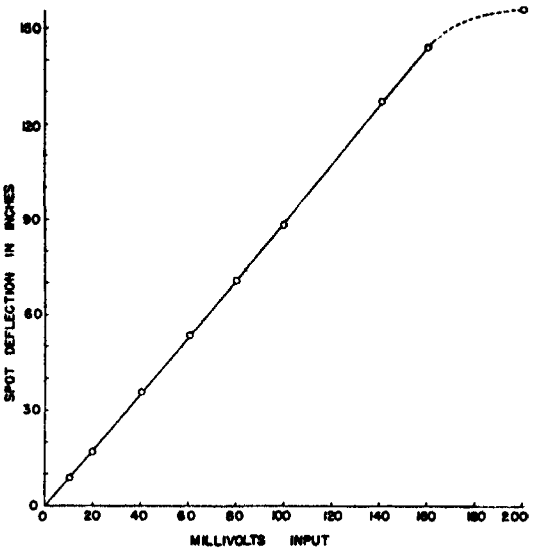

FIG. 4. This figure gives the cathode-ray tube spot deflection as a function of the signal supplied to a preamplifier wired as indicated in Fig. 3. The large deflections plotted were obtained by multiplying the observed deflection by a factor obtained from an attenuator in the main amplifier. The dotted portion of the curve indicates the region of overloading.

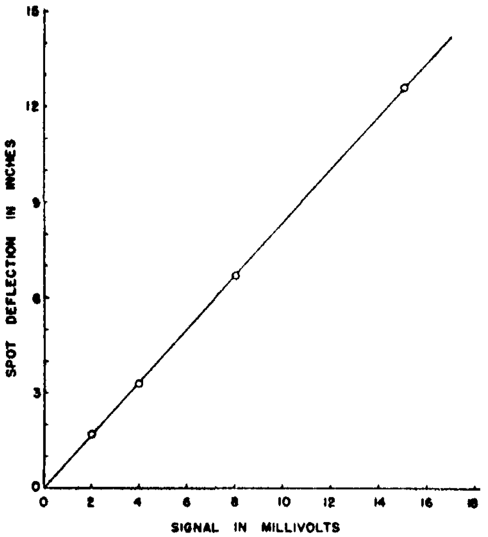

FIG. 5. This graph gives the first part of the curve Fig. 4 in more detail. A comparison of the slope of this curve with the slope of the upper part of Fig. 4 indicates that the non-linearity has been reduced to a few percent.

tween preamplifier and main amplifier. It should be emphasized that the attenuation of a coaxial cable increases with frequency so that the maximum length of the cable will be set by the rise time of the pulses or of the amplifier, whichever is longer, and by the permissible distortion. For our case a 100-ft. *RG7U* cable gave only slight rounding of the corners on a step signal. The amplifier rise time was measured to be about 0.3 μsec.

AMPLIFIER CHARACTERISTICS

The complete preamplifier circuit is shown in Fig. 3. The first three tubes are operated essentially as in the Model 500[1] preamplifier inverse feedback loop except that the rise time has been lengthened by using the larger plate load resistors shown The second inverse feedback loop consisting of the fourth 6*AK*5 and the 6*J*6 is shown connected to give a gain of -1. This inversion of signal is convenient since the ion chamber pulses are negative and it is convenient to have positive pulses at the input to the 6*J*6. Gains different from unity are obtained by choosing other values for the components of the voltage divider network in the grid circuit of the fourth 6*AK*5. The grid bias voltage for this fourth 6*AK*5 can be obtained in a number of ways. The circuit diagram of Fig. 3 shows it obtained by using the 110 ohm cathode resistor. This necessitates the 0.09-μf blocking condensers shown. If the blocking condensers are omitted, the grid bias voltage can still be obtained from a cathode resistor of about 1200 ohms, but this resistor must be suitably by-passed.

Two variable condensers are shown in Fig. 3, one in each of the feedback loops. The adjustment of the condenser in the first feedback loop was found to have very little, if any, effect on the shape of the pulse on the coaxial cable when a step pulse was put into the preamplifier. There was no oscillation of the first preamplifier loop for any possible setting of this condenser, so it was set at minimum capacity and left there. The shape of the pulse on the cable was found to depend on the adjustment of the second variable condenser. The amplifier response to a step signal could be made anything from an oscillatory overshoot to a very slow monatonic rise. The adjustment of this condenser also changed the shape of the response curve, Fig. 4. This response curve was nearest to a straight line when the response to a step signal was a non-oscillatory overshoot that was just visible on careful inspection. The magnitude of this overshoot was less than three percent of the pulse height. Figure 5 gives the spot deflections for small signals. The difference between the slope of the straight line, Fig. 5, and the slope of the curve, Fig. 4, for large signals, shows that there is still a small non-linearity in one or more of the amplifiers between the ion chamber and the cathode-ray tube. Most of this remaining non-linearity may be caused by the cathode follower that drives the delay line.

LONG TERM PERFORMANCE

Each of four preamplifiers, made according to the circuit diagram, Fig. 3, was used for nearly 3000 hours of observation during the period July 1948 to May 1949. The amplifiers were mounted in small tents on the mountainside near Mt. Evans, Colorado. They were exposed to wide variations in temperature and to occasional covering by snowdrifts. The cables were frequently buried in a layer of ice and had to be chopped out when the experimental arrangement was changed.

The apparatus performed satisfactorily under these conditions except when the ends of the high voltage cables were wet from melting snow.

Calibration curves similar to those of Fig. 4 and Fig. 5 were run several times in each 24-hour period. The slope of the curve in Fig. 4 drifted about eight percent during the first few hours after the equipment was turned on. Thereafter, the change in slope of the curve in Fig. 4, between the coldest part of the day (just after sunrise) and the warmest part of the afternoon, was about two percent. The initial adjustment of each of the several condensers in the feedback loops of the preamplifiers was made in July 1948 and did not have to be changed during the whole of the summer's and following winter's work, even though the tubes were changed several times.

In general, we feel that the linear response of the recording apparatus resulted in a great simplification of the analysis of the cosmic-ray data. The effort required to install and adjust the second feedback loop in the preamplifier was so small that the change was very much worth while.

THE REVIEW OF SCIENTIFIC INSTRUMENTS VOLUME 21, NUMBER 7 JULY, 1950

A New Vacuum Gauge

R. HAVENS, R. KOLL, AND H. LAGOW
Naval Research Laboratory, Washington, D. C.

(Received January 23, 1950)

A new vacuum gauge has been developed that is capable of measuring pressures from one atmosphere down to less than 10^{-5} mm Hg. The principle and construction of the gauge and experimental results are given.

A NEW vacuum gauge has been developed that is capable of measuring pressures from one atmosphere down to less than 10^{-5} mm Hg. Although there are many vacuum gauges now available which measure these pressures, usually three different types are required to cover this range completely. In addition, most of these gauges must be checked carefully for proper performance. The new gauge not only covers the complete range of pressures, but is rugged, has a small volume, and requires little attention for high accuracy of measurement.

The new gauge works on the principle that an a.c. signal can be obtained from a normally d.c. pressure gauge by cyclically changing the pressure at a given frequency. Many pressure-sensitive devices develop a d.c. signal as a function of pressure, temperature, applied voltage, and other physical quantities. In the new gauge the pressure changes, while the other physical quantities contributing to the d.c. voltage remain constant during a cycle. Thus, an a.c. signal is developed which is primarily a function of pressure alone, as long as the electrical signal from the gauge is appreciably above thermal and microphonic noise.

A model of the gauge has been constructed in which resistance wires are used as detecting elements and bellows are employed to change the pressure. A schematic drawing of the gauge is shown in Fig. 1, while Fig. 2 is a photograph showing the bellows arrangement. The detecting elements in the gauge are each placed inside a sylphon brass bellows, 6 cc in volume. The eccentric shaft of a small motor drives both bellows, changing their volumes by about 20 percent. With this double bellows arrangement, the shaft is working against the same pressure in each of the bellows independently of the pressure surrounding the gauge. The pressure is communicated to the element inside the bellows through small holes—one of 1-mm diameter and the other of ½-mm diameter—which restrict the flow of the gas. At any pressure the gas cannot escape at a speed greater than one-third of the speed of sound, i.e., about 100 meters per second. For the ½-mm hole, 20 percent of the volume of the gauge cannot escape in

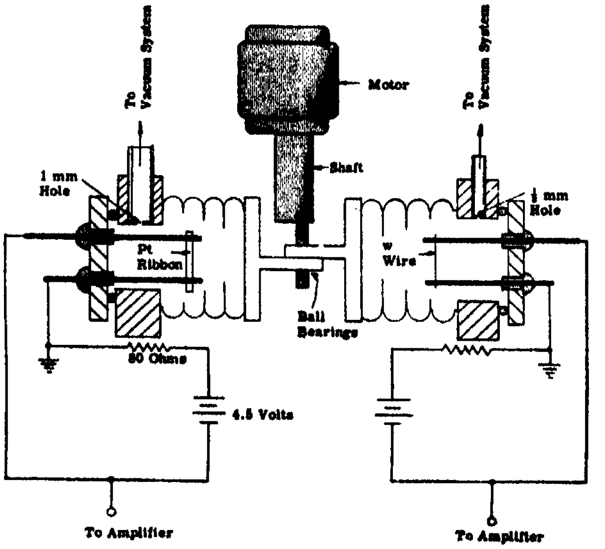

FIG. 1. Schematic drawing of the new gauge showing the arrangement of bellows and motor and the tungsten and platinum elements in their circuits.

less than 0.06 sec. Since the pressure inside the bellows is changed almost every 0.02 second, the greater part of the percent change in volume is realized as a percent pressure change. At low pressures a larger hole is satisfactory, due to restrictions in the tubing to the vacuum system.

One of the detecting elements used in the gauge model is a 1000-ohm tungsten wire, 7μ in diameter, wound around a mandrel with 4-mm spacings between mechanical supports. The signal from such an element can be understood by first considering its calibration curve when it is used simply as a Pirani gauge (Fig. 3A). At a pressure of 0.6 mm Hg, a 20 percent change in the pressure changes the voltage across the wire 0.27 volt. At other pressures this change is different, as Fig. 3B shows. When the pressure surrounding this element is actually changed by the motion of the bellows, an a.c. signal is developed whose magnitude corresponds to the average pressure surrounding the element. A curve of the peak-to-peak a.c. voltage, or d.c. voltage change, across the 7μ-wire as a function of pressure when the bellows is expanded 20 times a second is shown in Fig. 4A. The theoretical values derived from Fig. 3A and partly shown in Fig. 3B are plotted on the semilogarithmic scale of Fig. 4 as a dashed curve. The discrepancy between curves 4A and 4B is due to the time lag of the tungsten wire at low pressures.

At pressures higher than 50 mm Hg the tungsten wire is acting as a simple thermal element and is no longer effective as a Pirani gauge, as Fig. 3A shows. At these pressures the temperature, and correspondingly the resistance, of the wire increases when the gas in the bellows gives up heat under compression, and decreases when the gas expands. The temperature change of the wire is a function of the mass of gas in the bellows and hence of the pressure.

A brief summary of this somewhat involved explanation may perhaps serve to clarify it: There is a large signal across the wire at one atmosphere which decreases as the pressure decreases. When the wire starts acting as a Pirani gauge the signal begins increasing, reaches a peak value, and then decreases, becoming linear at 200μ and indicating extrapolation to 0 signal at 0 pressure. The curve in Fig. 3B shows that the response of the tungsten wire is directly proportional to the pressure at pressures below 200μ. Although the actual signal is less than this theoretical one because of the time lag of the wire, its curve is also linear at pressures below 200μ.

FIG. 2. Photograph of the new gauge in its present form showing the arrangement of bellows and motor and the tungsten element wound on its mandrel.

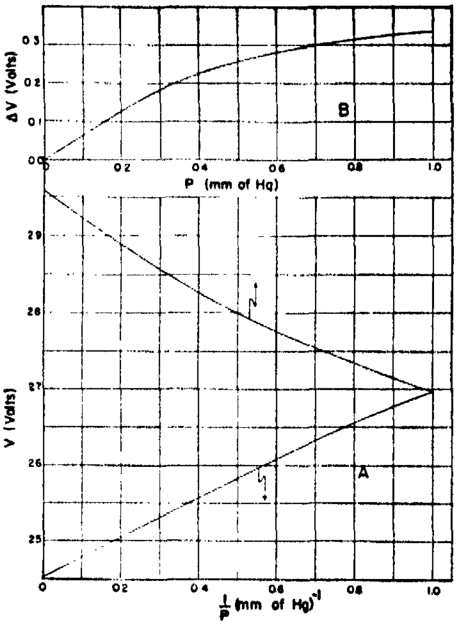

FIG. 3. Curve A is the calibration of the tungsten element used as a Pirani gauge. Curve B shows the change in d.c. voltage for a 20 percent change in pressure as a function of the mean pressure. This curve is derived from curve A.

Another element used in the gauge is a platinum ribbon 0.2μ thick, 0.5 mm wide, and 8 mm long.[1] Data obtained from this element at pressures below 1μ of Hg are shown in Fig. 5. Calibrations were made at two different values of current through the element, one at 27 ma and the other at 13 ma. It should be noted that the curves deviate from linearity below 0.1μ, the signal actually increasing in the case of the higher current. This increase is apparently due to a vibration of the ribbon with respect to the walls, which affects the heat transfer by radiation. This effect may or may not be in phase with the volume change. In designing the gauge no attempt was made to decrease this effect, but it can be greatly reduced by changing the position of the ribbon.

With the gauge just discussed, pressures below 10^{-4} mm Hg could not be measured accurately because of the motion of the ribbon. While this effect can be reduced, there are two other factors that will limit the sensitivity of the gauge—the sensitivity of an a.c. amplifier and the gas coming from the walls of the bellows.

Roess[2] has detected signals as low as 5×10^{-10} volt with an amplifier intended to measure the alternating output of a rapid-response thermocouple in an infra-red

---

[1] This ribbon was obtained from Baird Associates, Cambridge, Massachusetts. It was originally developed for use in sensitive bolometers. Its low heat capacity per unit surface area also makes it a sensitive pressure element.

[2] L. C. Roess, Rev. Sci. Inst. 16, 172 (1945).

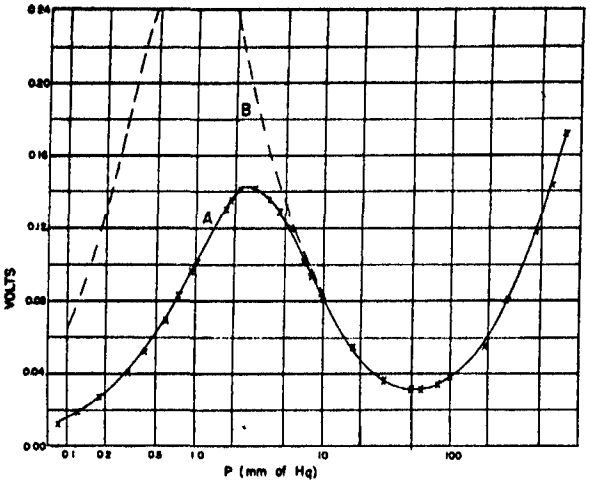

FIG. 4. Curve A is the calibration of the new gauge employing the tungsten element. The peak to peak magnitude of the a.c. voltage is given. Curve B is curve B of Fig. 3, which represents the theoretical calibration of the gauge below 50 mm Hg ignoring the time lag of the tungsten wire.

spectrograph. The only essential difference between Roess' instrument and the vacuum gauge is that in his, radiation is interrupted at 1 to 5 c.p.s. while in the vacuum gauge the pressure change interrupts the energy lost by heat conduction at 20 c.p.s. The inherent noise level of the amplifier described by Roess is less than the thermal noise of either resistance element used in the new vacuum gauge. Roess calculates the thermal noise voltage of a 1000-ohm thermocouple to be 2.5 $\times 10^{-9}$ r.m.s. volts.* A pressure of 10^{-7} mm Hg will give a signal of 10^{-8} volt, which should be above the noise level. Gas from the walls of the bellows will probably maintain the pressure above 10^{-7} mm Hg, so that this will be the main factor in limiting the range of the gauge. If a bellows can be evacuated below the pressure corresponding to the minimum detectable signal from the gauge in its present form, still lower pressures can be measured by creating larger signals in the detecting element. This can be done by increasing the pressure change inside the bellows and by using an element with a larger surface area. For example, the 10-ohm platinum ribbon has an area of 0.05 sq. cm. If the ribbon were ten times as long and ten times as wide, the thermal noise would be the same, but the voltage output would be ten times as large.

If a thermocouple were used in the new gauge in place of the tungsten wire or platinum ribbon, the a.c. voltage developed would be directly proportional to the average pressure, as long as the ratio of the heat capacity of the gas to the heat conduction of the gas was small compared to the period of the gauge or as long as the temperature change did not approach an adiabatic temperature change. By switching from the thermocouple to the resistance element at 200μ the gauge could be made to be linear with pressure from 400 mm Hg or more, down to as low a pressure as can be measured.

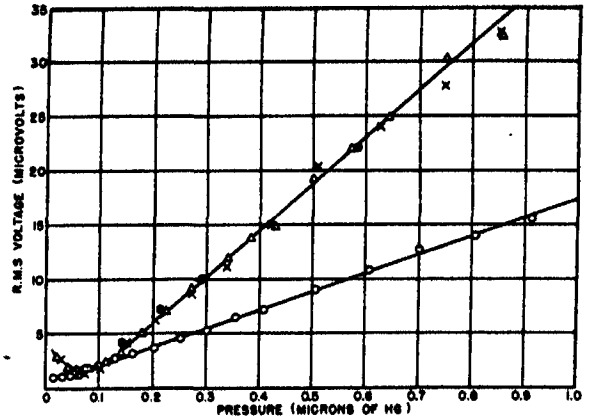

FIG. 5. Calibration curve of the new gauge employing the platinum ribbon. Data represented by the symbol ○ were obtained while operating the element at 13 ma. Data represented by symbols △ and × were obtained at 27 ma through the ribbon.

Another pressure-sensitive device adaptable to the principle of the new vacuum gauge is the ionization gauge. The range of pressures measured by the ionization gauge is limited by a current of photo-electrons from the collector, produced by soft x-rays generated in the tube. For standard ionization gauges the photoelectric current corresponds to 10^{-8} mm Hg. This current, remaining constant during a cycle, will be eliminated from the a.c. signal of the new gauge. With an ionization gauge as the pressure-sensitive element in the new gauge, the factors limiting the lowest detectable pressure, assuming such a pressure could be obtained, are the maximum pressure change that can be made surrounding an enclosed ionization gauge and the minimum measurable current at ten to 20 c.p.s. J. W. Townsend[3] states that with an amplifier with a 100-c.p.s. band pass, a 1000-c.p.s. current of 4×10^{-14} amp. can be measured. A 10- to 20-cycle current can be measured to as low a value. The current in a standard ionization gauge is 10^{-5} amp. at a pressure of 10^{-4} mm of Hg, so that with a one percent pressure change a current of 4×10^{-14} amp. would correspond to 4×10^{-11} mm of Hg.

It has been shown how a resistance element, a thermocouple, and an ionization gauge can be used in the new gauge. It is possible, however, to use any pressure-sensitive device that develops an electrical signal. The gauge can also operate by any means of changing the pressure other than a volume change.

The model of the new gauge, with the tungsten wire, was used to measure pressures at the nose of a Viking rocket fired September 6, 1949. The gauge performed successfully, measuring pressures from 660 mm Hg at ground level to 570μ of Hg at the peak of the flight at 53 km.

---

* This calculation was made for a band width of 0.4 cycles and a temperature of 300°K with the 1000∼ filament at 600°K and a 5-cycle band width. The thermal noise would be 1.2×10^{-8} volt.

[3] J. W. Townsend, Jr., Phys. Rev. 76, 465 (1949).

THE REVIEW OF SCIENTIFIC INSTRUMENTS VOLUME 21, NUMBER 7 JULY, 1950

A 4π-Radiometer

T. BENZINGER AND C. KITZINGER
Naval Medical Research Institute, Bethesda, Maryland

(Received January 25, 1950)

Total radiated heat loss and average surface temperature of living bodies have heretofore required laborious computation from numerous local measurements. The present study introduces the blackbody principle for this objective. Shieldless surface receivers have been designed, and built from identical and symmetrical sets of thermoelectric foil junctions, which were then made different only in their power to absorb or reflect radiation. By means of thermal shunting, they have been rendered stable against air motion up to 8 m/sec. A cavity, when uniformly lined with such receivers, will integrate the measurements of radiated output into every direction of space, permitting a direct recording of the total. The receivers have been developed specifically for application to the human gradient calorimeter now under construction. However, since the laws of radiation apply to cavities of any size or shape, the proper function of blackbody radiometry could be experimentally verified with a smaller number of receivers in a body of $8\times8\times16$ cu. in. The 4π-measurement is practically independent of location, size, or shape of the emittent source. The sensitivity is 76 μv/cal./sec. Full response is attained within 2.4 sec.

BACKGROUND AND OBJECTIVES

RADIANT energy is dissipated by human or animal bodies at different rates from different sites. The shape of the radiant surface of the body is irregular and changeable. The temperature of the radiant body surface is by no means uniform. It is, therefore, difficult to measure the total flux of radiated energy. It is also difficult to determine by integration of single measurements the average temperature of the human or animal skin. It seems even more difficult to follow the temporal variations of human skin temperature or radiant heat loss through continuous recordings, for instance, under various kinds of sudden and transitory stress or stimulation. There is, however, considerable interest in such measurements because in a normal environment the radiant fraction of heat amounts to more than one-half of the thermal output of a living body. Furthermore, skin temperature is essential for the measurement of "conductance," an important factor in blood circulation and in the over-all control of body temperature and heat exchange. Measurements of skin temperature have therefore been attempted by many investigators, with various principles of instrumentation.

Although existing methods have their individual merits, they have certain limitations. The *contact measurement* with mercury, thermoelectric, or resistance thermometers at single points or in special suits is based on the assumption that the thermometers assume the temperature of the skin, which is difficult to verify. Movements of the body under muscular exercise may add to this difficulty. Moreover, contact thermometers, when continuously applied, will unavoidably influence the temperature of the skin. Therefore, our method is based on the direct measurement of *thermal radiation*. Existing radiometers, however, show variations in zero reading because the receiver takes up radiation not only from the source of radiation but also from other parts of the instrument or from the surroundings, or from both. While single measurements are readily corrected for such variations, stability of zero is required for the purpose of continuous recording.

Air movement is a source of error in conventional radiometers, unless they are completely shielded either by contact with the skin or by windows. Contact with the skin tends to influence skin temperature, and windows tend to increase the response time of the instrument and make it susceptible to heat conveyed to the windows by conduction or convection. Furthermore, no method is known to us for a simultaneous integration of radiometric measurements into a total of radiant heat loss or an average of surface temperature. Existing instruments and the methods of evaluation give only approximate average temperatures. The procedures, moreover, are cumbersome. They do not lend themselves to continuous recording.

It has, therefore, been the objective of the present study to develop a radiometer for continuous recording of radiant flux, automatically integrating total radiated heat loss or average surface temperature over a solid angle of 4 π-radians in a manner which does not interfere with the radiant environment of the object. It was essential to avoid contact of any part of the instrument with the object. Moreover, it was necessary to insure that neither movements accompanying exhausting muscular exercise nor air motion would appreciably affect the measurement of thermal radiation. High accuracy and a rapidity of response sufficient to permit study of sudden reflex changes in cutaneous circulation were considered desirable characteristics. With reference to the gradient calorimeter now under construction[1] the simultaneous measurement of the totals and fractions of heat loss including the radiant part, as well as the simultaneous recording of skin and rectal temperatures, was desired. "Conductance" could then be continuously determined.

---

[1] T. H. Benzinger and C. Kitzinger, Rev. Sci. Inst. **20**, 849 (1949).

THEORETICAL PREMISES

Rigorous requirements as outlined above called for a deviation from current concepts of dermal radiometry. Instead of the usual receivers of small size and undefined shape, a blackbody surface receiver entirely enclosing the emitter was introduced.

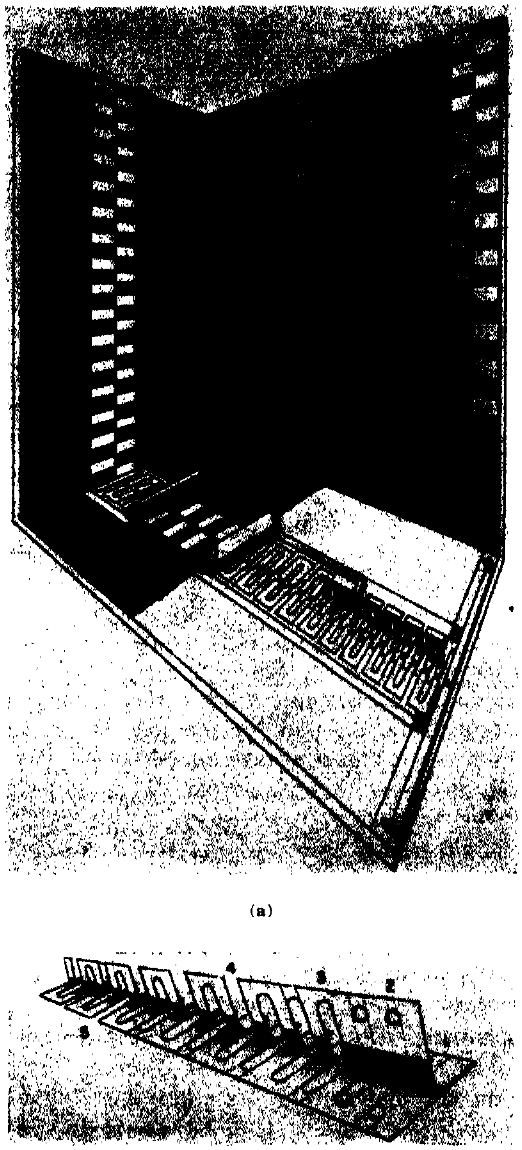
(a)

(b)

Fig. 1. Upper part: Design of thermoelectric receivers. The perpendicular walls at a corner of the blackbody radiometer show the external appearance of the receivers. The receiver at the bottom is partially uncovered and unfolded. Note the symmetrical arrangement in a twin chain which compensates the effect of heat flows in the three directions of space. Note the junctions along the center line of the twin chain, the U-shaped bridges of copper or constantan, the insulating foils, the copper leads (right), the copper bridge between the mates (left), and the covering foil of anodized aluminum with alternate black and shining surfaces. Lower part: Process of making thermoelectric chains. The procedure is shown in subsequent steps: soldered double foil strips of copper and constantan are first marked (1, dotted line), then circular holes are punched (2), then common slits are cut into the copper and constantan foil (3), and last, alternatingly either a copper (4) or constantan (5) bridge is removed.

Let it be assumed that a non-selective thermoelectric surface receiver of uniform temperature and emissivity can be so constructed that every small element of its area will develop a certain potential in response to a unit net rate of incident radiant energy. If the individual potentials from the small elements could be made additive by serial wiring, their sum would represent the net rate of radiant energy falling upon the entire surface of the instrument. When such a receiver is extended to form a boundless surface enclosing the emitter, the limiting edges disappear, and the solid angle of 4π-radians is intersected. The following characteristics of this type of radiometer can be predicted: (a) Disturbing influences from any external sources of radiation will be excluded, (b) the instrument will intercept and measure the total, not a selected fraction, of the rate of energy emitted from a source of radiation. The following factors do not enter into this measurement: *The size of the radiometer*, because the density of radiant flux at the surface will increase or decrease in reversed proportion with the size (or number of sensitive elements) of the surface; *the shape of the radiometer* (defined by the angular inclination of different parts of the surface), because the product of the surface area and the density of the radiant flux received on the same area remains constant, when the surface is turned from the perpendicular to an oblique position with respect to the direction of radiation (Lambert's cosine law); *the geometric size of the source of energy*, because the receiving area intersects a solid angle of 4π-radians at any mean distance from the emitting surface; *the shape of the source of radiation*, because Lambert's cosine law applies to the source as well as to the receiver; *the distribution of temperature and emissivity at the surface of the radiant source*, because the closed surface of the blackbody will correctly integrate the radiation coming from all angles; *the location of the emitter* within the radiometer, because it has no influence upon the average density or mean angle of incidence of radiant flux exchanged between the emitter and the receiver.

For the enumerated reasons, a blackbody radiometer is distinguished from all former radiometers inasmuch as its measurements are practically independent of the relative location of emitter and receiver as well as of their angular positions in space.

Thermal radiation received and measured by the instrument can be written:

$$\Phi = A\cdot\sigma\cdot\epsilon\cdot(T^4 - T_e^4),$$

according to the Stefan Boltzmann law, where Φ = radiant flux [cal./sec.]; A = radiant surface of the source of radiation [cm^2]; ϵ = mean emissivity of the source of radiation [percent of blackbody emissivity]; T_e = temperature of receiving surface [° Abs.]; σ = Stefan Boltzmann constant, 1.373×10^{-12}[cal./(sec. cm^2 deg.^{4})]; = average surface temperature of the source of r

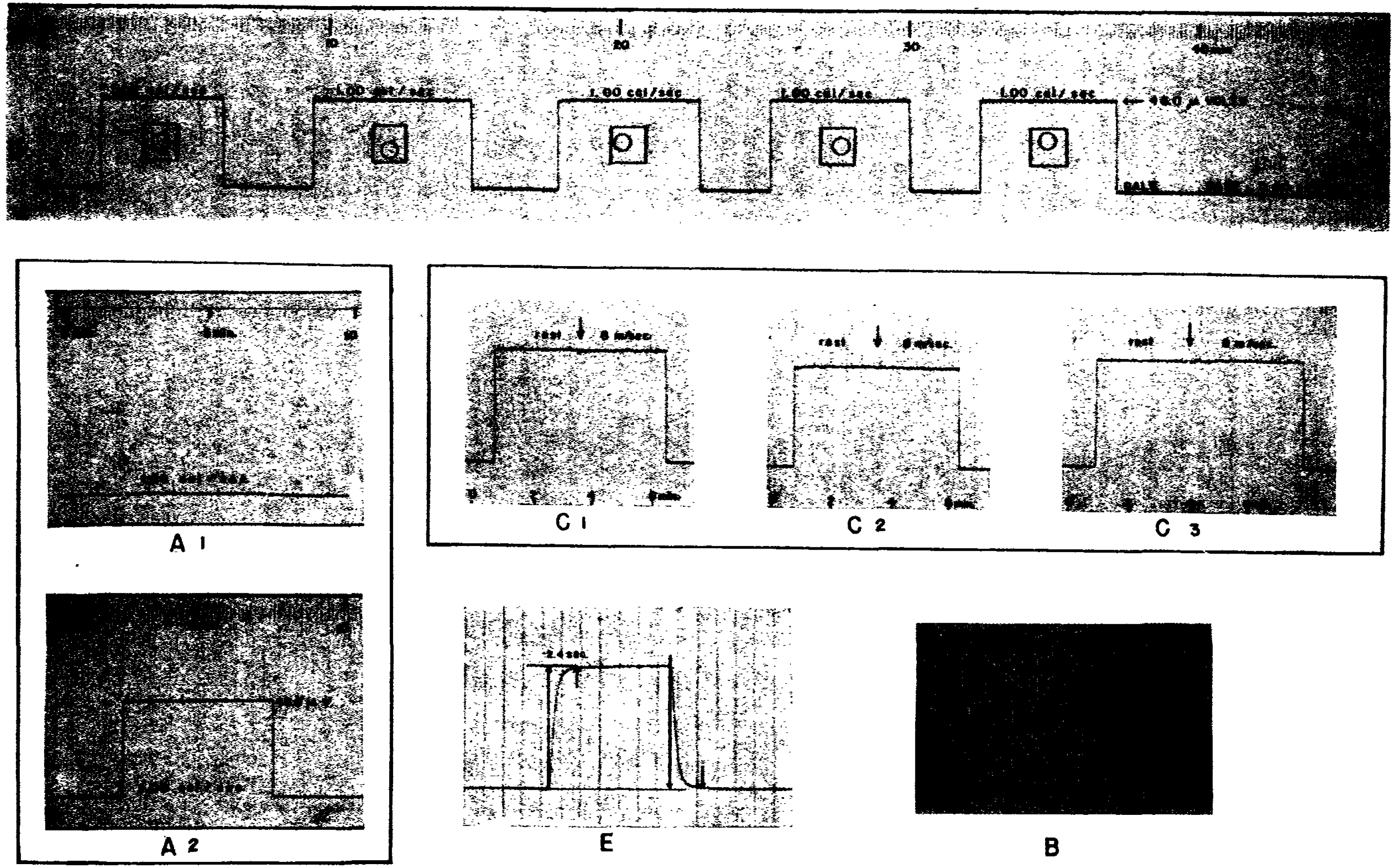

FIG. 2. A. Response specific to radiant heat. Potentials from the surface receivers of the 4π-radiometer have been recorded over time with a mirror galvanometer and slit camera, A.1 before, and A.2 after making every other junction reflective for thermal radiation. The recordings show responses in potential induced by 4.18 watts (1 cal./sec.) of heat loss from an electrically heated resistance coil in the interior of the instrument. The completed receiver responded with 46 μv to the radiant fraction (0.60 cal./sec.) of heat lost from the coil (A.1). The incomplete receiver with its uniformly absorptive surface was relatively unaffected as shown in A.2. B. Characteristics of zero. The galvanometer beam has been recorded over time with a slit camera; the radiometer was switched into or out of the galvanometer circuit. Full scale corresponds to human basal heat output. C. Measurement of thermal radiation in the presence of air motion. Potentials induced by thermal radiation (approximate intensity 1.4 cal./sec. m^2) to a receiving chain have been recorded over time, with a mirror galvanometer and slit camera, in the presence or absence of air movement in the three directions, longitudinally (left), transversely (center), and vertically (right) with respect to the chain. D. Location of heat source in the blackbody, and radiometer response. Potentials induced by the radiant fraction of a constant loss of 4.18 watts (1 cal./sec.) from a heated resistance coil were recorded with the coil moved into five different locations within the blackbody. The locations of the coil relative to the walls are schematically indicated. Shortest distance from the walls: ¼ in. E. Response time of surface receivers. Potentials were recorded over time with mirror galvanometer and slit camera, when a shield was placed between, or removed from between, a source of heat and the radiometer. One side of the radiometer was open.

tion [° Abs.].* Hence, when Φ is measured, and A, ϵ, and T_e are kept constant, changes of T can be observed and recorded in correct proportion. They can be measured in absolute terms, when A, ϵ, and T_e are known. On the other hand, changes of the radiant surface (with changes of bodily posture) can be observed in correct proportion as long as T is constant, or measured, when T is known. The blackbody radiometer may, therefore, be applied to observations of (a) rate of radiant heat loss; (b) average surface temperature of bodies of determined surface area and emissivity; (c) radiant surface area of bodies of known surface temperature and (d) emissivity of bodies when area and temperature of the surface are known.

Problems of a similar nature may arise in physics (emissivity of coatings, determination of radiation constants), or in technology (evaluation of sources of heat, light, or other kinds of radiated energy). In meteorology or astronomy, where the enclosure of radiant sources is out of consideration, there may, however, be applications for a simplified surface receiver. Heavenly or solar radiations can be intercepted on plane surfaces. The measurement of total radiant surrounding would require an inversion of the blackbody, i.e., the closed surface of a body of uniform temperature, uniformly covered with a surface receiver.

CONSTRUCTION OF SURFACE RECEIVERS

The source of thermal radiation to be measured is accommodated in a closed container of high thermal capacity and conductivity, the temperature of which is precisely set and carefully maintained. The inner walls of this "blackbody" are absorptive for thermal radiation. There are, however, numerous small reflecting spots distributed uniformly on the wall in equidistant longitudinal rows (Fig. 1). Beneath these rows, continuous chains of thermoelectric junctions are installed. The chains consist of alternating strips of copper and constantan foil. All copper constantan junctions (sequence in one direction of the electric circuit) are located beneath shining spots. All constantan copper junctions, on the other hand, are located beneath absorptive sites of the radiometer wall. Hence, with a source of radiant energy inside, all the constantan copper links will become slightly warmer than the corresponding copper constantan links, from which thermal radiation is reflected. Every couple of thermojunctions will, therefore, develop a small thermoelectric potential. Serial wiring of the junctions in continuous chains makes these potentials additive. Their sum will, after proper calibration, represent the total of thermal radiation which the wall received from the subject or heat source. 1280 junctions were installed. The details of their serial construction are shown in Fig. 1. The internal resistance of the whole instrument amounts of 35 ohms.

CHARACTERISTICS OF PERFORMANCE

In the design and construction of the radiometer, efforts had been made to obtain reproducible responses (in potential) to radiant energy (in calories per second) regardless of disturbing influences such as air movement or heat flows of other than radiant origin. Linear characteristics of response were desired. Stable zero reading was considered essential for continuous recording. The sensitivity was expected to be adequate to operate commercially available recording potentiometers without preliminary amplification. The response time, on the other hand, should be in the order of seconds only. The following tests have been carried out to evaluate these characteristics of the instrument.

Response specific to radiation.—Absence of response to heat transfer except thermal radiation must be ascertained before the instrument is made sensitive to radiation. For this purpose, a blackened coil of Nichrome tape, $\frac{1}{8}$ in. wide, 3Ω per ft., with a total resistance of 49.0Ω and a surface area of 600.0 cm², was placed within the radiometer before the installation of the reflectors, and heated with an input of 4.185 watts (1 cal./sec.). After a few minutes, the coil reached a final temperature and acted as a constant source of thermal radiation as well as heat for transfer by conduction and convection. It is observed that the total heat flow of one calorie per second does not induce an appreciable potential in the instrument as long as the mates in every pair of thermojunctions are both black (Fig. 2A.1). When, however, one mate in each pair was covered by reflecting aluminum foil, a response toward radiation was obtained as shown in Fig. 2A.2.

Stability of response.—The specific response to thermal radiation is stable as shown by the straight appearance of the line drawn by the mirror galvanometer (Fig. 2A.2). Repeated tests (compare Fig. 3) showed that the responses were identical on any experimental day.

Stability of base.—The base line of the radiometer prior to or following a given heat input was found to be stable and the same as the base line of the galvanometer, the sensitivity of which had been adapted to the range of measurements (Fig. 2B). It can, therefore, be concluded that disturbing galvanic potentials were absent and that thermal potentials were properly compensated in the pile of 1280 junctions.

Negligible influence of air movement.—As a source of thermal radiation, an electrically heated metal rod was placed above a radiometric chain at a distance of 10 in. which resulted in a stable potential of 42 μv from the chain. This potential was recorded over time with a mirror galvanometer and slit camera. In the first part of the recording (Fig. 2C), the air was still. At the point indicated by the arrow, a powerful convection current was established. The air movement came from the open end of a copper tubing of 0.16 cm² diameter which was supplied with compressed air at room temperature. The air left the tubing at an average velocity of 8 m/sec. as computed from diameter of the opening and air volume per unit time. The distance between the chain and the opening of the wind pipe was 1 cm in every instance. Tests were performed with wind blowing in three directions, i.e., longitudinally, C.1, transversely, C.2, or vertically, C.3, with respect to the chain. The wind influence on the measurement shows to be negligible.

---

* The statement of the formula $\Phi = A \cdot \sigma \cdot \epsilon(T^4 - T_e^4)$ presupposes that the temperature and the emissivity are mean values. A more detailed statement would be $\Phi = \sigma \int_s \epsilon_{(dA)}(T^4_{(dA)} - T_e^4)dA$, where $\epsilon_{(dA)}$ is the emissivity of the surface element dA, and $T_{(dA)}$ is the temperature of the surface element.

Linearity of response.—A sphere $3\frac{3}{4}$ in. in diameter was made of solid aluminum. The surface was "anodized" in order to make it sufficiently emissive in a reproducible manner. A soft soldered thermojunction of 36-gauge copper and constantan wires was hammered into a shallow notch chiseled into the surface. The "cold" junction was soldered to a disk of copper sheet 1 in. in diameter and 5/1000 in. thick, which was cemented to the wall of the radiometer. The potential of this pair of thermoelectric junctions was read from a precision null balance potentiometer to determine the difference between the temperature of the receiving surface, T_e, and the temperature of the radiating surface, T. The sphere was heated and suspended on light threads in the interior of the radiometer where it lost its added heat in an exponential manner. Therefore, the readings of both radiometer potential and surface temperature of the sphere needed to be taken quickly. The same potentiometer was used for both measurements. A double-pole double-throw switch was turned to change from one reading to the other. Readings were taken every minute of either radiometer potential or temperature difference, T_1-T_2. Potentials and temperatures were then plotted against the time of the reading, and simultaneous readings of radiometer potential and surface temperature were obtained by graphic intrapolation. Responses in potential were then plotted against values $(T^4-T_e^4)A\sigma$, which represents calories per second of thermal radiation, when A is the surface [cm^2] and σ the Stefan Boltzmann constant, 1.373×10^{-12}[cal./sec. cm^2 deg.^{4}], assuming that the emissivity of the sphere was 100 percent of blackbody emissivity. Actually, it was less than 100 percent, as will be shown later. However, within a narrow range of temperatures, emissivity is a constant. Figure 3 shows that the radiometer responds in a linear manner to radiant heat output. For the measurement of surface temperature, the characteristics deviate from linearity in the degree required to satisfy the Stefan Boltzmann equation.

Sensitivity.—Since the instrument responds in a linear manner to radiant heat loss, its sensitivity can be expressed in microvolts per watt, or calories per second, of radiant energy, after proper calibration. For this purpose, however, the emissivity of the radiant

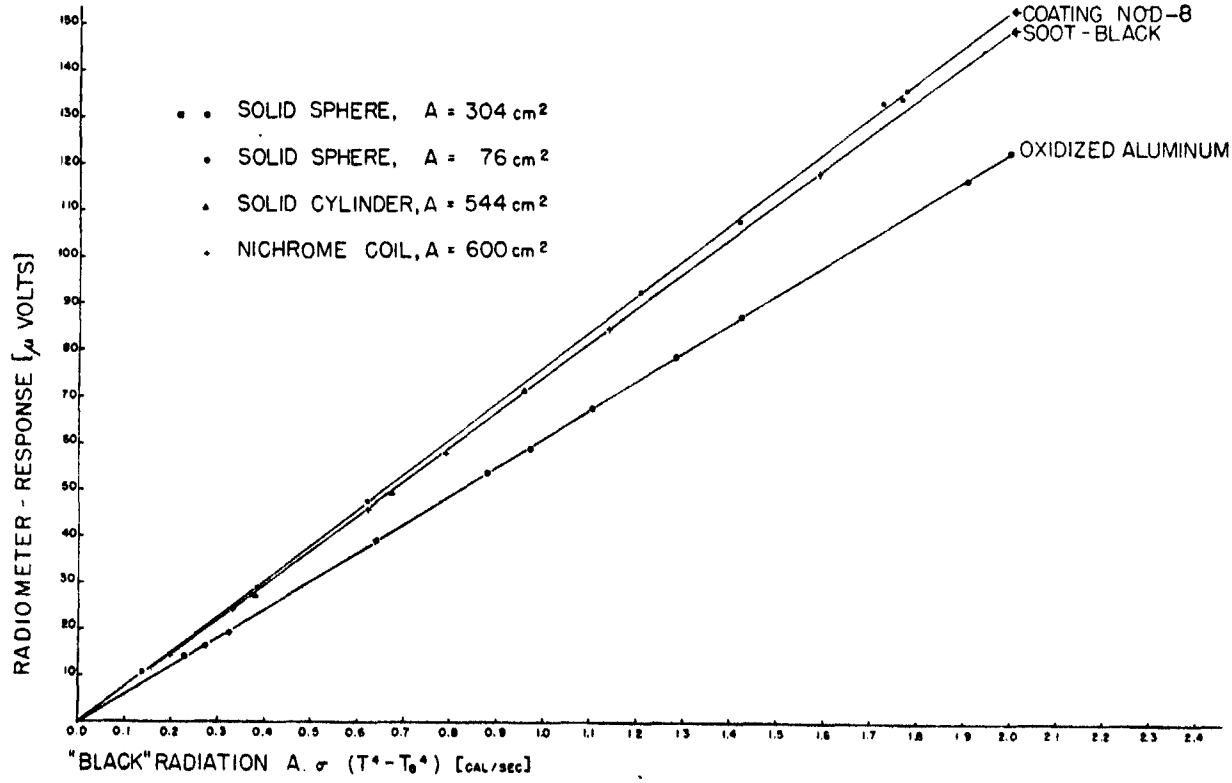

FIG. 3. Calibration of blackbody radiometer. Bodies of various sizes, shapes, and emissivities of surface have been used as source of radiation. Radiometer responses [μV] have been plotted against the radiant flux [cal./sec.], which the source of radiation would emit, when perfectly black, from its surface, A [cm^2] at its temperature T [° Abs.] toward the walls at a temperature, T_e[° Abs.]. σ was assumed to be 5.75×10^{-8}[watt/m^2 deg.^{4}]. The graph shows that size, shape, and material of the source have no appreciable influence on the values observed. The relative emissivities of the surfaces appear from the radiometer responses. Blackbody radiation for a determination of the absolute sensitivity was unavailable. The absolute sensitivity must, therefore, be slightly higher than 76.2 v/cal./sec. as observed with the special coating "air interface absorber N.O.D.—8".

surface must be known, or close to unity. Figure 3 shows calibrations performed on bodies with different coatings. "Air interface absorber N.O.D.—8"† appeared to be 2½ percent better than soot black. It shows the highest emission and can be considered almost completely absorptive, according to recommendations by the National Bureau of Standards. Hence, the sensitivity of the radiometer (Fig. 3) should only slightly exceed 76.2 μv/cal./sec. Ideal blackbody radiation is not directly applicable in the present instance.

Uniformity of response of all receivers in the radiometer.—If the geometrical considerations are correct and if the measuring units of the receiving surface are sufficiently numerous and evenly distributed, the same response to radiated energy will be obtained from large or small sources of radiation, as shown in Fig. 3.‡ The response of the radiometer also is not altered, when a source of radiation is moved from one position to another, up to a distance of ½ in. from the wall (Fig. 2D).

Rapidity of response.—A test was carried out with an electrically heated metal rod mounted above the open radiometer. A shield was placed between the radiometer and the source of radiation. When the shield was removed or replaced, the instrument responded in an approximately exponential manner (Fig. 2E). Half-response was attained within a quarter of a second, approximate equilibrium within 2½ sec. The time of half-response of the galvanometer was 0.1 sec. under the conditions of these experiments.

DISCUSSION

The tests have shown a satisfactory stability of the present receivers against thermal flows of other than radiant origin as well as against air motion. It may be of interest to discuss how these characteristics have been obtained without the use of shields or windows:

Whereas in known thermopiles the "warm" junctions differ from the "cold" junctions by separate location (Moll,[2] Coblentz[3]) or selective shielding (Coblentz,[3] Hardy[4]) or selective thermal insulation in a vacuum (Bohnenkamp[5]), or selective shunt with the instrument body (Moll,[2] Johansen,[6] Harris[7]) the junctions in the present radiometer are identically constructed and symmetrically arranged. They differ only with respect to their absorption of radiated energy. Heat flows of other than radiant origin, coming either from the object, or striking the instrument wall at the outside, will therefore affect the two mates in any couple of adjacent junctions almost simultaneously and with similar intensity, yet with opposite direction of the potentials developed. This compensation applies, for example, to heat conveyed to the receiver by warm air currents.

Convection, however, has a further effect upon a radiation thermopile: even if the moving air does not carry any exchangeable heat, the thermal resistance between the "warm" and "cold" junctions will decrease during air motion, since moving air is more conductive than resting air. This must result in a decrease of the response to radiated energy during air motion. We have attempted to eliminate this source of error on several ways: Translucent windows failed, as they absorb and store heat from various sources and radiate it subsequently towards the radiometer. Establishing a constant maximum convection appeared to be cumbersome and would put limitations on the variability of experimental conditions. Cooling of the warm junctions by the Peltier effect of an attached chain supplied with a measurable current, was insufficient, as the Joule effect interfered. Heating of the cold junctions would disturb simultaneous calorimetric measurements.

While these attempts were generally unsuccessful, the following approach effectively eliminated the convection error: Within certain limitations, the sensitivity of a radiation thermopile is inversely proportional to the thermal conduction between the "warm" and "cold" junctions. The conduction, C, can be considered as the sum of two parts, C_s and C_a, C_s taking place through the solid connections, and C_a taking place through the surrounding air. If C_s is made very large in comparison with C_a, variations in C_a induced by air motion, will have little influence upon the total conduction (C_s+C_a), which determines the sensitivity. In the present radiometer, C_s has been made very large, by close contact between the junctions and the base. An additional thermal shunt was introduced by the covering aluminum foil. By this means, sensitivity is decreased, and stability against air motion is obtained. The loss of sensitivity can be accepted, as the large number of junctions provides more voltage than necessary to operate the recording instruments.

Since the characteristics observed correspond to the requirements already outlined under objectives of the present study, further discussion of the performance does not seem necessary.

---

† Received by courtesy of Dr. J. J. Pittman, Eastman Kodak Company, Rochester, New York.

‡ For computations of radiant flux Φ in Fig. 3, the receiving surface has been considered "black," because of the blackbody condition. In this assumption, however, the finite surface area of the emitter has been neglected. For an emitter the surface area of which equals the surface area of the blackbody receiver, Φ would be smaller by a factor ϵ', namely, the mean emissivity of the wall coating. For small emitters this correction becomes negligible. In the examples of Fig. 3, it would be less than one percent of observed values. The sensitivity of the radiometer to radiant flux, however, does not change when the surface of the emitter increases or decreases.

[2] W. J. H. Moll, "A thermopile for measuring radiation," Proc. Phys. Soc. London **35**, 257 (1922–1923).

[3] W. W. Coblentz, "Radiation," Dict. App. Phys. **4**, 554, and Bull. Bur. Stand. **10**, 7 (1913).

[4] J. D. Hardy, "The radiation of heat from the human body," J. Clin. Invest. **13**, 593, 605, and 615 (1934).

[5] H. Bohnenkamp and H. W. Ernst, "Untersuchungen über die Grundlagen des Energie- und Stoffwechsels. 1. Mitteilung, 2. Mitteilung," Pfluegers Archiv **228**, 40, 63, (1931).

[6] E. S. Johansen, Ann. d. Physik 4, **33**, 517 (1910) and Physik. Zeits. **14**, 998 (1913) cited from Forsythe, *The Measurement Of Radiant Energy* (McGraw-Hill Book Company, Inc., New York, 1937), p. 189.

[7] L. Harris, J. Opt. Soc. Am. **36**, 597 (1946).

A Recording Torque Magnetometer

D. S. Miller
Research Laboratory, United States Steel Corporation of Delaware, Kearny, New Jersey

(Received February 6, 1950)

This instrument produces, automatically, a curve of torque *versus* angle of orientation for a thin iron or steel disk in a strong magnetic field. A resistance strain gauge converts the torque acting on the disk specimen to a small d.c. voltage, which is recorded on a "strip-chart" recording potentiometer. The specimen is rotated in synchronism with the translation of the chart paper, both being driven by synchronous motors. A torque curve is completed in six minutes.

TORQUE magnetometers of various types have been used for many years in laboratory studies of the magnetic anisotropy of single crystals. For instance, such instruments were used by Weiss[1] in the study of pyrrhotine and by Webster[2] in the study of iron crystals. More recently, others[3-6] have used them for the study of both single crystal and polycrystalline iron alloys. N. P. Goss[7] used the same type of device in developing a treatment to produce a high degree of preferred orientation in an iron-silicon alloy.

The torque magnetometers used by these workers were manually operated, readings being made point by point. It has recently been found that the instrument is useful in both development and production where rather large numbers of specimens are to be tested. It was considered, therefore, worth while to devise a modification of the instrument which would record the data automatically and more rapidly than could be done with the manual type of instrument. Ingerson and Beck[8] devised a scheme for generating the torque curve on the screen of a cathode-ray tube, which would provide the speed we wished, but was not exactly suited to our needs since we preferred a directly produced permanent record such as is provided by a pen-driving type of potentiometer-recorder.

In the instrument which we have designed to fulfill these requirements the torque exerted on a disk specimen is converted, by a resistance strain gauge, to a small direct-current voltage. This voltage is applied to the measuring circuit of a "strip-chart" voltage recorder of the proper sensitivity. The disk is rotated about an axis perpendicular to its plane by means of a synchronous motor and reduction gearing. The chart paper in the recorder is also driven by a synchronous motor, so that there is a definite relation between the angular rotation of the disk and the movement of the chart paper. As the disk rotates the torque varies and the pen in the recorder moves in accordance with this variation. By use of the proper conversion factor, the voltage record on the chart paper becomes a plot of torque *versus* angle of orientation of the disk in the magnetic field.

The construction of the torque transducer is shown in Fig. 1. The specimen, a disk one inch in diameter, is held between spring jaws on the holder (*B*), which fits on two taper pins on the cross-head (*J*) of the transducer. The torque on the specimen is transmitted through the cross-head and the shaft (*I*), producing a displacement of the shaft of the strain gauge (*K*) by means of a bronze strip (0.002×0.020 in.) wrapped once around the shaft (*I*) and attached to the two collars (*H*) on the strain gauge shaft. Figure 2 shows the manner in which the strain gauge is coupled to the shaft (*I*). Pivots at the ends of shaft (*I*) ride in *V*-jewels mounted in the supporting rectangular frame.

The strain gauge (*K*), which is a product of the Statham Laboratories of Beverly Hills, California,

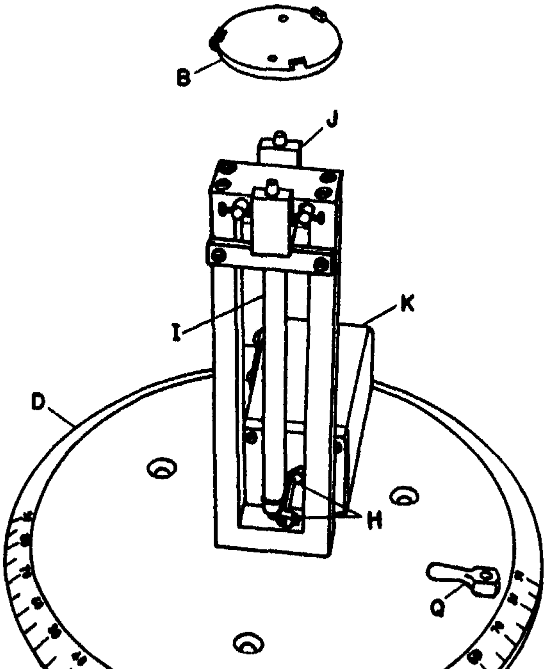

Fig. 1. Torque transducer, showing method of mounting specimen.

---

[1] Weiss, J. de Phys. 4, 469 (1905).
[2] Webster, Proc. Roy. Soc. **107**, 496 (1925).
[3] Dahl and Pfaffenberger, Zeits. f. Physik. **71**, 93 (1931).
[4] K. J. Sixtus, Physics **6**, 105 (1935).
[5] H. J. Williams, Rev. Sci. Inst. **8**, 56 (1937).
[6] F. Bitter and L. P. Tarasov, Phys. Rev. **52**, 353 (1937).
[7] Trans. Am. Soc. for Metals **23**, 511 (1935).
[8] W. E. Ingerson and F. J. Beck, Jr., Rev. Sci. Inst. **9**, 31 (1938).

consists of four resistance strain elements connected as a Wheatstone bridge to which a direct current of not more than 30 ma is supplied. The gauge used here has a range of 4 oz. applied force, producing an output of approximately 20 mv maximum. The torque limit of the transducer is 50,000 dyne-centimeters, which is adequate for practically all of the steels which we have tested, in thicknesses from 0.015 to 0.080 in. To produce curves of usable amplitude from thinner specimens, having thicknesses from 0.010 to 0.015 in., we have made holders to take specimens of 1.5 in. diameter. The graduated scale on the base plate (*D*) provides a measure of the angle between the direction of the applied magnetic field and the orientation of the transducer. It is an approximate measure of the angle between the magnetization in the specimen and a chosen reference direction in the specimen. The errors involved in this reading will be discussed later. The small hand lever (*Q*) controls one stop which operates the limit switch (*Z*). With this stop in the operating position the allowed rotation is 100 degrees. A fixed stop limits rotation to 200 degrees when the lever (*Q*) is in the open position.

The position of the torque transducer between the poles of the electromagnet is shown in Fig. 3. It is attached, by means of three screws through the base plate (*D*), to a drive plate on the base of the magnet yoke. This drive plate connects, through a gear train in the base of the magnet, to a small synchronous motor mounted below and in back of the yoke. The drive rotates the gauge at a rate of 30 degrees per minute. A thumb lever (*E*) disengages the drive so that the gauge may be rotated by hand to set the starting position. Two switches (*F* and *G*) on the right foot of the magnet pedestal control the motors for rotating the torsion gauge and driving the chart paper in the recorder. A limit switch (*Z*) under the right hand magnet coil shuts off both of these motors at the completion of a run. A plug and four wire cable (*U*) connects the strain gauge to its supply battery and to the recorder.

The output terminals of the gauge are connected to the input of the recorder. We have used a Brown strip-chart recorder with a range, −4 to +4 mv. By making the range of the recorder a fraction of that of the gauge we have enhanced the useful range of the instrument. A specimen whose maximum torque is 50×10^3 dyne-cm is kept on scale by setting the gauge input current to 6 ma; a specimen whose maximum torque is 10×10^3 dyne-cm is made to record full scale by setting the gauge current at its maximum, 30 ma. Furthermore, by selection of the gauge current, a convenient factor for the torque scale on the chart can be chosen. The current required for a preselected scale factor can be determined by a simple calculation, using the volume of the specimen to be tested and the constant of the gauge.

The electromagnet is of conventional design. Each coil has approximately 4500 turns of No. 16 wire. With a current of 2.3 amp. the field at the center of the 1.75 in. gap is about 4000 oersted. The heat dissipation at this current is not sufficient for continuous operation but is adequate for short runs. At 2.0 amp. continuous operation is possible. With this current the field is about 3700 oersted.

The recorder and controls for the electromagnet and the recording circuit are mounted in a cabinet 22 in. wide, and 68 in. high. A field-discharge switch, a 50-ohm 200-watt rheostat, and a 3-amp. ammeter provide control of the magnet current. A milliameter (30 ma) and two rheostats (1000 ohm for coarse, and 100 ohm for fine adjustment) for control of the input current to the strain gauge are mounted on a panel above the recorder. On the same panel a 50-ohm potentiometer wired into the recorder measuring circuit provides fine control of the zero point of the recorder. This adjustment is necessary because the strain gauges cannot be so precisely adjusted in manufacture that the output voltage is zero for zero strain.

Within the limits of the useful range the output of the transducer is linearly proportional, to within ½ percent, to the applied torque and to the input current. The transducers were calibrated by using a torsion fiber of known constant, attached, at its upper end, to a graduated circle (a converted optical goniometer), and at its lower end, to the specimen holder (*B*).

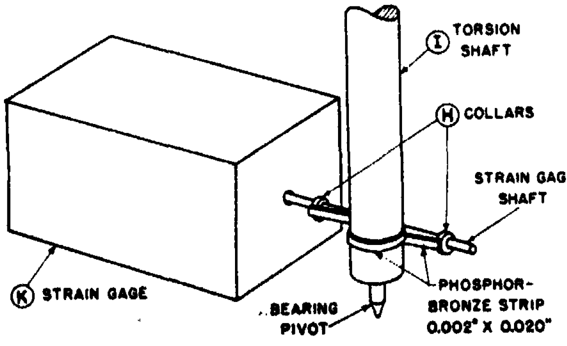

FIG. 2. Method of coupling strain gauge to torsion shaft.

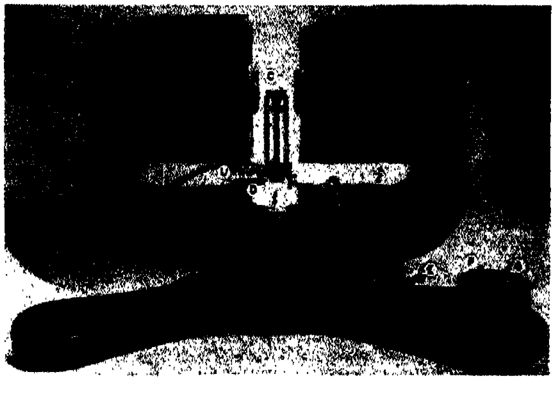

FIG. 3. Torque transducer mounted on electromagnet.

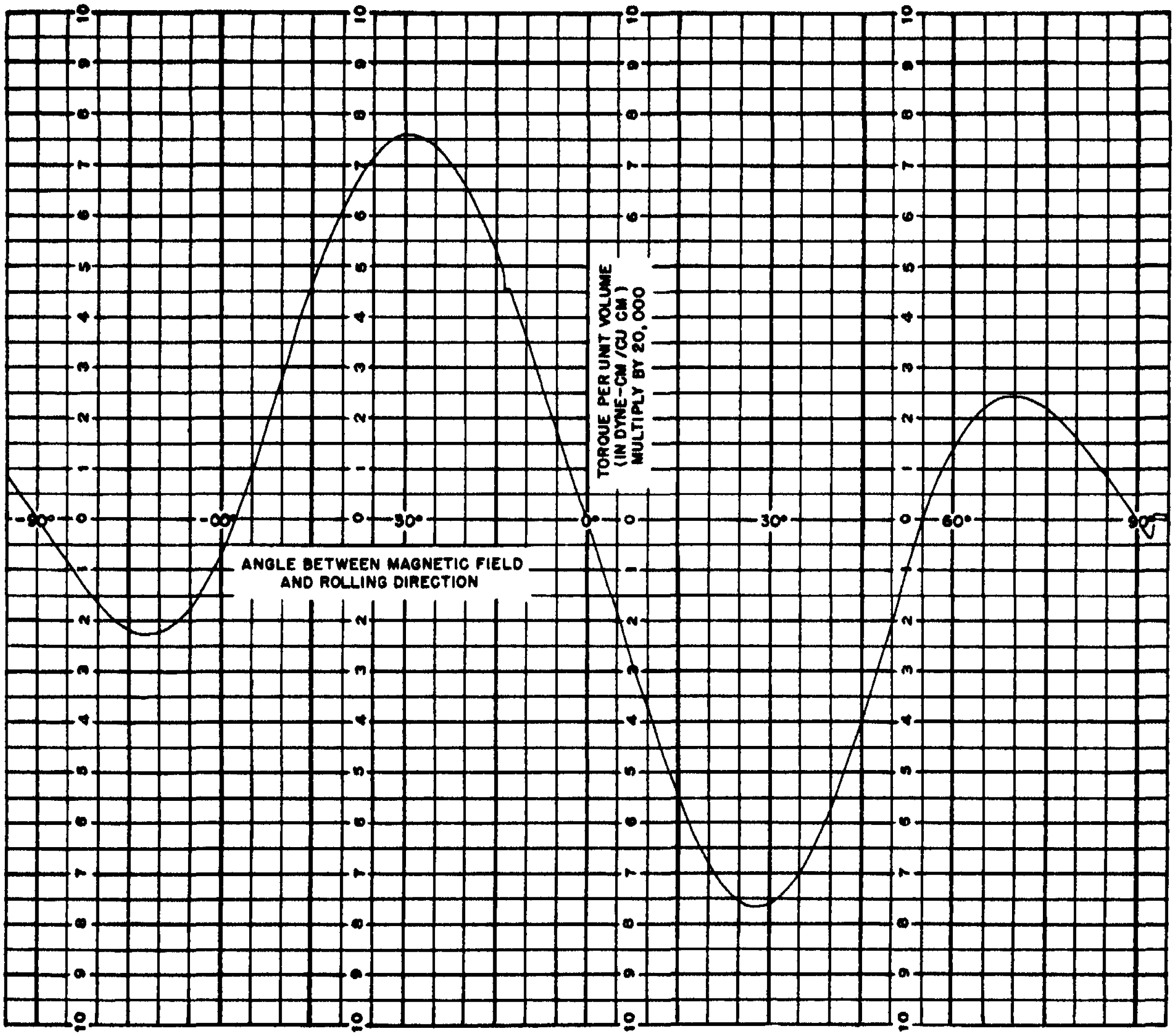

FIG. 4. Typical magnetic torque curve obtained on a specimen of silicon steel having a high degree of preferred orientation.

As stated previously, the plot obtained is an approximation to the true torque as a function of the angle between the direction of magnetization and the reference direction in the specimen. The principal error, which is in the angular measurement, arises from two sources. For any torque other than zero, the specimen must be deflected from its rest position with respect to the torsion gauge. The maximum value of this deflection is 0.7 degrees; for the torque radius of the gauge is 0.125 in. and the limit of displacement of the strain gauge shaft is 0.0015 in. The second source is the deviation of the magnetization in the specimen from the direction of the magnetizing force. Bozorth[9] has calculated this effect and shown that it becomes small at high fields. An error in the torque arises from the fact that in punched disks the edges are not saturated. This could be eliminated by making the specimen ellipsoidal. A more complete discussion of these errors is given in reference 6. In the applications for which we have used the instruments up to the present the errors are not large enough to be significant.

A typical curve obtained on an iron-silicon alloy specimen is shown in Fig. 4. This material was processed in a manner somewhat similar to that developed by Goss.[7] The curve approximates that of a single crystal having a (110) plane in the plane of the specimen and a (100) direction parallel to the reference direction (zero degrees). The step in the curve at about −13 degrees was caused by the operation of the automatic standardizing mechanism in the potentiometer-recorder.

---

[9] Bozorth, Phys. Rev. 42, 882 (1932).

THE REVIEW OF SCIENTIFIC INSTRUMENTS VOLUME 21, NUMBER 7 JULY, 1950

Molecular Diffraction Attachment for RCA Microscope

B. O. HESTON AND P. R. CUTTER
University of Oklahoma, Norman, Oklahoma

(Received February 17, 1950)

A new device for the distribution of vapors across an electron beam for molecular diffraction studies is described. The efficiency of the new method has made it possible to obtain molecular diffraction patterns with an electron microscope without need of alterations.

The vapors are ejected from a circular crest of a diffusion box immediately surrounding the beam to give a heavy concentration of vapors in contact with the beam while releasing a small amount of vapor. The method has been standardized with well known patterns of CCl_4 and CBr_4.

INTRODUCTION

THIS paper describes a molecular diffraction attachment designed to fit an RCA microscope. The attachment consists of a radial diffusion box and needle valve assembly, which is shown unassembled in Fig. 1, and assembled on an RCA diffraction adapter in Fig. 2. Figure 3 gives a cross-sectional drawing of the diffusion box as prepared and used for this study.

The radial diffusion box, Fig. 1, part *A*, and Fig. 3, was used for both distribution of vapors and as a sample box in the study of crystalline organic compounds with vapor pressures of less than 1.0 mm. With organic liquids of higher vapor pressures the diffusion box was used for the distribution of vapors and the needle valve was used as a sample box to give better control on the amount of vapors released.

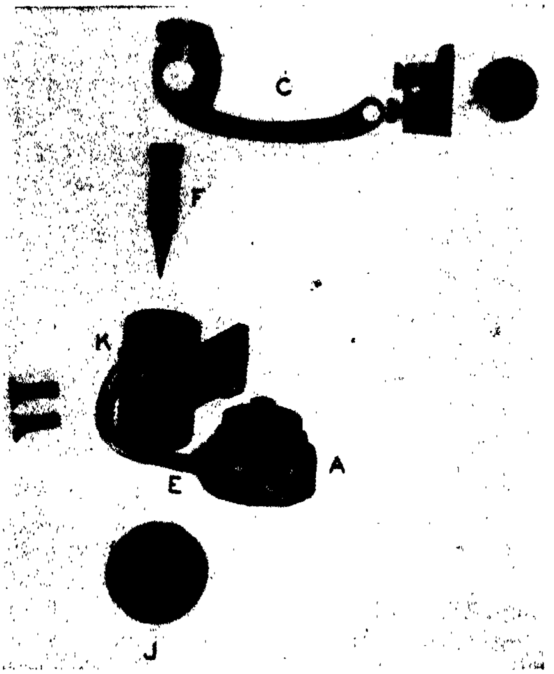

FIG. 1. Unassembled radial diffusion box and needle valve used for molecular diffraction studies with the electron microscope. A. Radial diffusion box. C. Control lever for opening and closing needle valve. E. Tube for transporting vapors from needle valve to box. F. Needle valve. J. Needle valve sample box cover. K. Needle valve body.

The radial diffusion box was so made that when it was placed in a vacuum and opened a fraction of a turn, any vapors present in the box would converge as a thin circular front of increasing density toward a central point in the open cylindrical channel traversing the center of the box. By passing the electron beam of the microscope through this point of greatest density, it was possible to obtain excellent molecular diffraction patterns without overloading the instrument with vapors. The amount of vapors released with the new method was so small that the use of a cold finger[1-5] or rapid auxiliary pump[6] was unnecessary. By using the diffusion box as the sample holder for low vapor pressure compounds, the need of an electrically heated sample box was partially eliminated. The operational technique of the microscope was not altered in any way, and the small amount of vapor going through the vacuum pumps did not hamper their operation. The development of the new device thus introduces a new use for the electron microscope.

APPARATUS

The Radial Diffusion Box

The radial diffusion box, Fig. 1, part *A*, and Fig. 3, was machined from brass and had an O.D. of 9/16 in. and a height of 3/16 in. which was as large as the space in the microscope permitted. The lid, Fig. 3, part *M*, screwed inside the box *Z* and had an O.D. of 7/16 in. with an outer depth of 2/16 in. and an inner depth of 1/16 in. A channel was drilled through the center of both the lid and box 1/16 in. in diameter giving a cylinder 3/32 in. in depth for the concentration of vapors. The box and lid were threaded with 40 threads per inch. When the concave lid was completely closed, then opened 1/5 revolution, a circular crevice 0.005 in. wide and 0.2 in. in circumference admitted vapors toward the centrally located electron beam, Fig. 3, part *e*. The under side of the lid was machined out

---

[1] H. De Laszlo, Proc. Roy. Soc. A146, 672 (1934).
[2] L. R. Maxwell, J. Opt. Soc. Am. 30, 375 (1940).
[3] V. E. Cosslett, Trans. Faraday Soc. 30, 981 (1934).
[4] Hendricks, Maxwell, Mosley, and Jefferson, J. Chem. Phys. 1, 549 (1933).
[5] R. Wierl, Ann. d. Physik 8, 521 (1931).
[6] L. O. Brockway, Rev. Mod. Phys. 8, 231 (1936).

1/16 in. to allow space for organic crystals, Fig. 3, part *E*, when the box was to be used as a sample holder. The box was then soldered on the back side of the RCA orifice designed to hold penetration specimens. When the new assembly was placed on the under side of the RCA diffraction adapter as shown in Fig. 1, part *A*, and Fig. 2, and the entire assembly placed in the instrument, the point of greatest density of vapors or the distance from the circular crevice to the photographic plate was found to be 25.9 cm. To open the box, one end of a small steel chain was soldered on the edge of the lid. By attaching the other end of this chain to a tiny hook which has been soldered to the lower RCA rotating rod, Fig. 2, the box could be opened after being placed within the instrument. The diffusion box alone was sufficient for the study of crystalline compounds with vapor pressures ranging between 0.01 to 1 mm, but with organic liquids the loss of vapor through the threads of the box was too great. For this type of work it was found necessary to design a needle valve assembly as a side attachment to the diffusion box for better control of the amount of vapors released.

Valve Assembly

The needle valve assembly as shown in Fig. 1 was machined from brass with the exception of the needle which was made of Tobin bronze for greater wear resistance. The over-all length of the assembly was made slightly less than one inch in order to fit the limited cylindrical space present in the instrument. The needle used, Fig. 1, part *F*, was 0.81 in. long with a diameter of 0.167 in. The needle valve body Fig. 1, part *K* was 0.625 in. long and cut from a 0.375 in. O.D. brass rod. The needle valve body was brazed to a 0.064 in.×0.20 in.×0.75 in. brass strip for attachment to the RCA adapter by means of two steel screws. The lower end of the needle valve body was machined out for a sample compartment. This compartment could then be sealed by screwing on the cap, Fig. 1, part *J* and closing the needle valve. Lead turnings were melted in the bottom of the cap to give a lead gasket 1/16 in. in depth for proper sealing. The vapors released from the needle valve compartment were transported to the diffusion box through a tiny copper tube Fig. 1, part *E*, soldered into port holes in the side of the needle valve body and diffusion box respectively. The diffusion box was then opened and closed, after placing it in the instrument, by means of attachments, Fig. 1, part *C*. By rotating the upper thumb knob, Fig. 2, the upper rod could be moved in or out thus making it possible to open and close the needle valve within a few seconds.

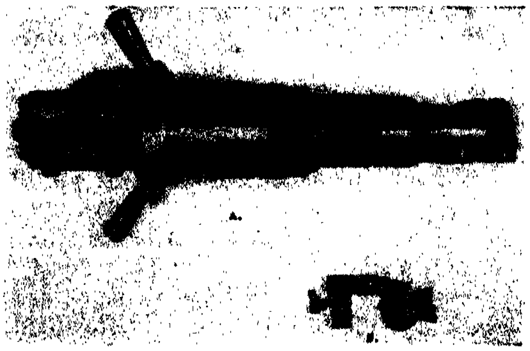

FIG. 2. (A) Radial diffusion box and needle valve attached to RCA electron diffraction adapter. (B) Parts which must be removed from RCA adapter before mounting the molecular attachment.

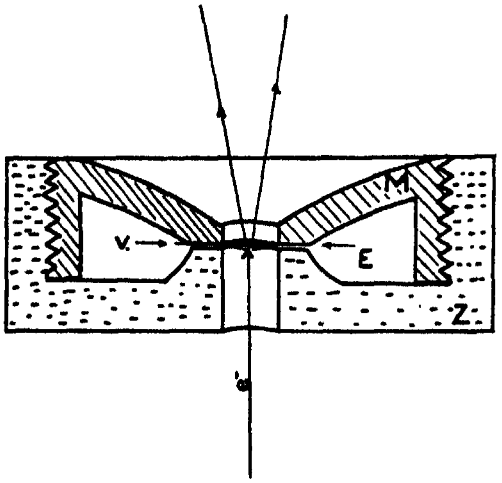

FIG. 3. Radial diffusion box (cross section). E. Sample box. M. Diffusion box lid. Z. Diffusion box. V. Route of organic vapors. e. Path of electrons.

EXPERIMENTAL

Sample with Low Vapor Pressure

Diffraction patterns of vapors derived from organic crystals were obtained using the diffusion box alone. To place the sample in the box, the bottom side of the lid was turned up and a small number of purified crystals were placed in the machined out chamber. The lid was then screwed in place while holding it in the same position. After completely closing the lid, the loose end of the attached chain was fastened to the lower rod before placing in the instrument. When the diffraction attachment had been screwed into the instrument, the microscope was prepared for operation in the same manner as for magnification work. All lenses of the machine were left in turned-off position except the condenser lens which was used to focus the electron beam to give the brightest spot on the fluorescent screen. After the beam was properly adjusted, the box was opened by rotating the lower thumb knob, Fig. 2, until a diffraction pattern appeared on the screen. Five exposures were then made in rapid succession allowing slightly different time for each. As soon as the plate was exposed the instrument was shut off and the diffraction adapter removed. It was unnecessary to close the box after each exposure with low vapor

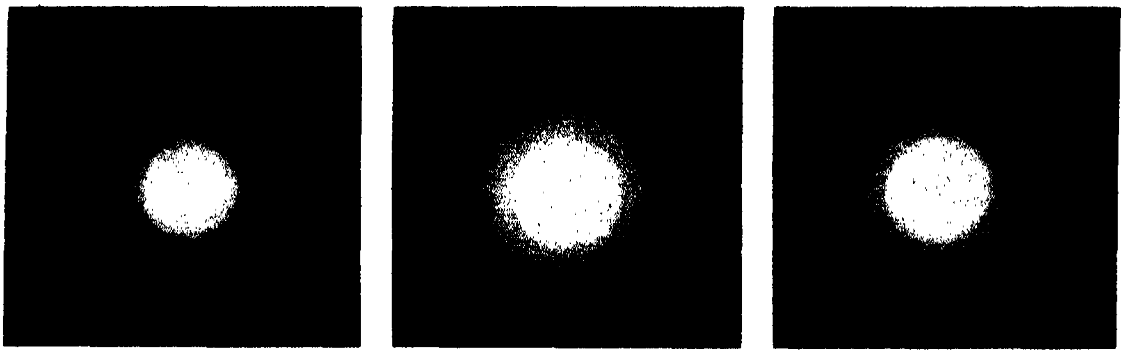

1 sec. 3 sec. 2 sec.

CCl_4

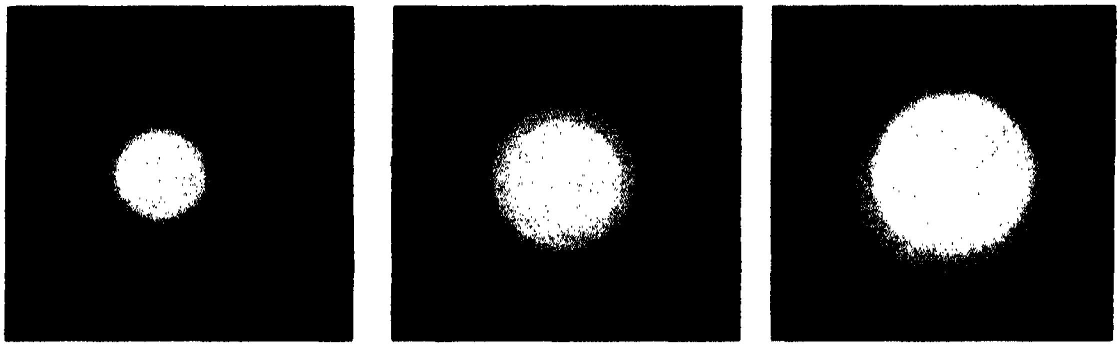

1 sec. 2 sec. 3 sec.

CBr_4

FIG. 4. Electron diffraction patterns of CCl_4 and CBr_4 made with electron wave-length of 0.0534A and a specimen to photographic plate distance of 25.9 cm.

pressure compounds such as CBr_4 as the amount of vapor released was not great enough to disturb the vacuum of the instrument or interfere with the diffraction pattern.

Sample with High Vapor Pressure

The first attempt to run liquid samples such as CCl_4 with the diffusion box alone did not prove successful for when the box was slightly opened, the vapors left through the threads around the outside of the box as well as the circular crevice which resulted in overloading the instrument. To correct this, a needle valve assembly was constructed for a control of these vapors and the threads of the diffusion box sealed with solder after opening 1/4 revolution. When this assembly was placed in operation it was discovered that when the needle was opened slightly in the vacuum of the instrument, instead of a steady stream of vapor coming off the liquid sample, the flow appeared to be intermittent. This was believed to be caused by droplets of liquid coming from the needle valve compartment. To correct this, a small pad of cotton which had been previously freed of any volatile matter by heating to 110°C in an oven was immersed in the liquid sample to be studied. The cotton pad was drained of all surplus liquid by placing it on a dry piece of filter paper. The damp pad was then sealed in the sample box of the needle valve assembly and the instrument made ready for the run. Before turning on the high voltage and electron gun, the needle valve was opened and closed once to be sure that no droplets were present to cause an overload while exposing the plate. With this improved technique, the needle valve could be opened, the diffraction pattern photographed, and the needle valve again closed without any danger of excess vapors. This made it possible to run numerous samples in a single day without operational difficulties. Here again, the time of exposure was varied to bring out different orders of the diffraction pattern.

RESULTS

Although the authors will reserve any detailed discussion of results for another paper, the electron diffraction patterns of CCl_4 and CBr_4 which were used to standardize the method, are shown in Fig. 4, and the corresponding microphotometer tracings are given in Figs. 5 and 6. The pattern of CBr_4 was made using the diffusion box as the sample holder while the pattern of CCl_4 was made using the needle valve compartment to control the amount of vapors released across the electron beam.

Theoretical equations were derived from tetrahedral models for both of the above compounds based on the concept of Debye's[7]

$$I=K\sum_i \sum_j f_i f_j \sin sr_{ij}/sr_{ij},$$

where the symbol I is the intensity of the scattered electrons; r_{ij} is the distance between the ith and the jth atom; s is equal to $(4\pi \sin\theta/2)/y$; $\sin\theta/2$ is equal to one-half the angle between the incident beam and the point of intensity under observation; y is the wavelength in angstroms. For simplification, the symbol f_i and f_j were set equal to the corresponding atomic numbers of the atoms under consideration.

The reduced theoretical scattering equations for CCl_4 and CBr_4, based on tetrahedral models were found to be

$$(CCl_4)\quad I/K=4.25\sin X/X+\sin 0.612X/0.612X,$$
$$(CBr_4)\quad I/K=8.75\sin X/X+\sin 0.612X/0.612X,$$

where X is substituted for sr.

Theoretical values of X found where I/K reached maximum or minimum values, were then divided by corresponding experimental s values derived from corresponding ring diameters to give the desired values of r. For CCl_4 the average value of r, or the Cl—Cl distance, was found to be 2.89±0.02A. By multiplying this value by 0.612, a C—Cl distance of 1.76±0.03A resulted which agrees well with the now accepted value[8] for this

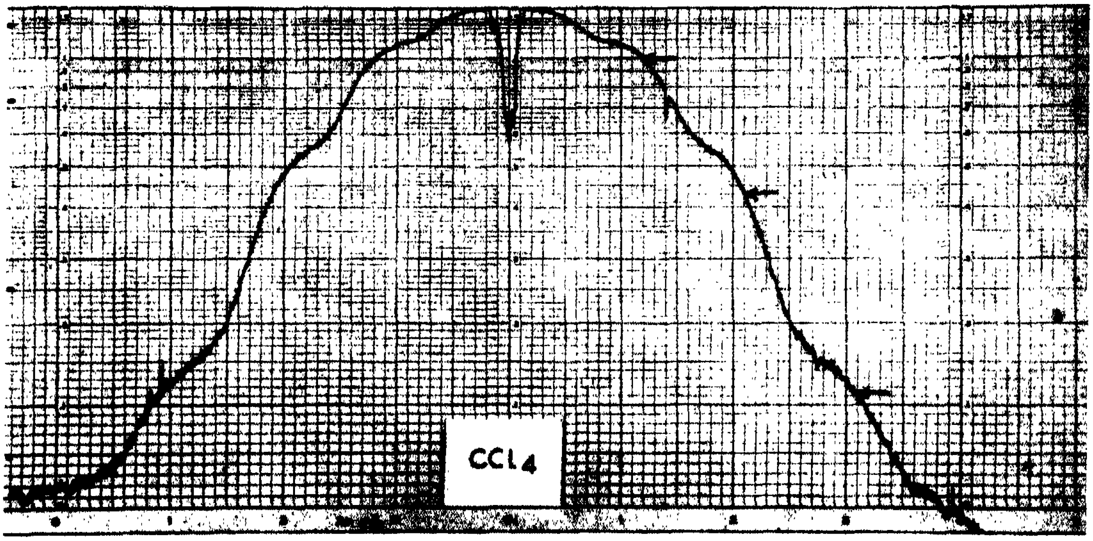

FIG. 5. Microphotometer chart of a CCl_4 diffraction pattern showing the location of the first three maxima.

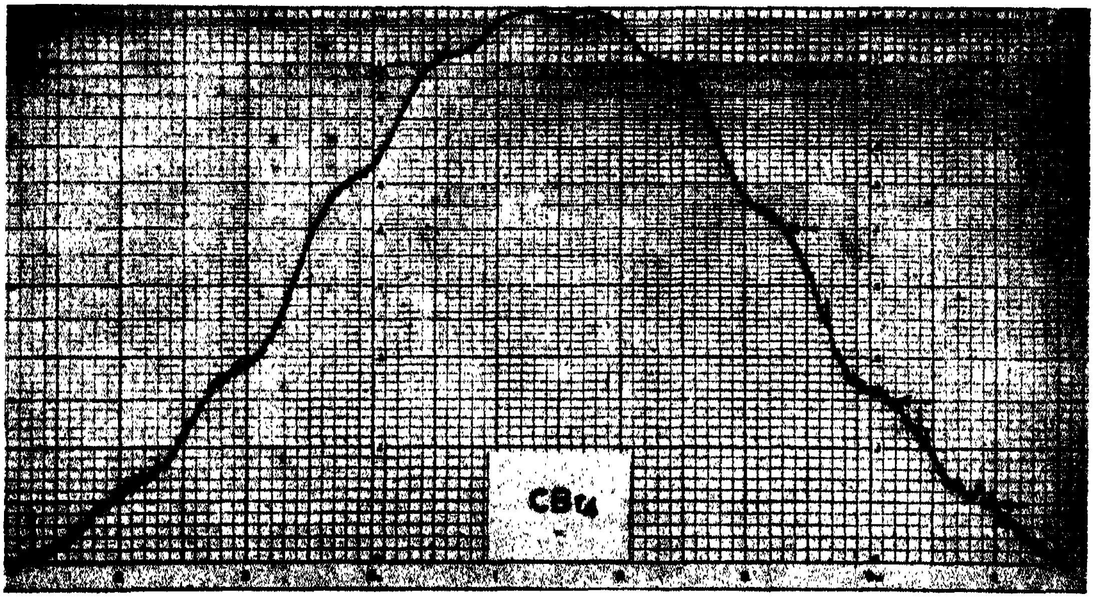

FIG. 6. Microphotometer chart of a CBr_4 diffraction pattern showing the location of the first four maxima.

---

[7] P. Debye, Ann. d. Physik 46, 809 (1915).

[8] L. Pauling and L. O. Brockway, J. Chem. Phys. 2, 867 (1934).

atomic distance. Similarly, analysis of CBr_4 gave an average Br—Br distance of 3.15±0.03A which is within the accepted value of 3.12±0.03A.

From the close agreement with the literature with both compounds, the method was considered sufficiently accurate for analysis of compounds of unknown structure.

ACKNOWLEDGMENT

Due credit is given Mr. Carl Starkey, University of Oklahoma, for his excellent assistance in helping the authors prepare the molecular diffraction attachment described in this article.

SUMMARY

The greatest contribution of this paper is believed to lie in the new technique of distributing vapors for electron diffraction work, first by eliminating any possibility of directional effects, and second, that the efficiency of the method opens a new use for the electron microscope with no alterations or changes necessary. The accuracy of the new method has been established by analysis of the diffraction patterns of CCl_4 and CBr_4.

THE REVIEW OF SCIENTIFIC INSTRUMENTS VOLUME 21, NUMBER 7 JULY, 1950

Apparatus for Rapid Measurement of Internal Friction

Herbert I. Fusfeld
Pitman-Dunn Laboratory, Frankford Arsenal, Philadelphia, Pennsylvania

(Received April 13, 1950)

This paper describes apparatus for measuring internal friction which satisfies the conditions (a) low induced stress amplitude to preclude any plastic flow of the specimen, (b) ability to install specimen within a few minutes after treatment, (c) rapidity of measurement, at a rate of ten to twenty per minute, (d) accuracy of at least one percent.

Longitudinal vibrations are induced by an eddy-current drive, similar to one previously described in the literature, satisfying (a) and (b). Conditions (c) and (d) are obtained by measuring the decay time of free vibrations using vacuum tube trigger circuits and a counter chronograph. Satisfactory measurements can be made with push-button rapidity and simplicity.

INTRODUCTION

In order to investigate certain aspects of internal friction of metals arising from cold-work, apparatus had to be developed embodying the following characteristics: (a) Induced stress amplitudes must be so low that negligible plastic flow occurs due to the measurement itself. (b) Specimen must be properly installed in the apparatus within a few minutes after metallurgical treatment. (c) It should be possible to obtain ten to twenty measurements per minute. (d) An accuracy of about one percent or better should be obtainable.

The first requirement is admirably fulfilled by electromagnetic coupling of the specimen to the driving and detecting units. This method was used by Wegel and Walther[1] utilizing steel armatures cemented to the ends of the specimen, with electromagnets at the driving and detecting units. The second requirement is met by a similar arrangement, but without the added steel armatures, used by Randall, Rose, and Zener.[2] Eddy currents induced in the specimen interacted with a fixed magnetic field to set the specimen into vibration.

The apparatus to be described utilizes this latter eddy-current method, but modifies the measuring equipment to include trigger circuits and a counter chronograph. Shorter times are thus measurable with satisfactory accuracy to meet the last two requirements. A detailed description of the method with accompanying diagrams is presented. These items, though not inherently difficult to workers in the field, do not appear to have been published previously.

The only other semi-automatic method thus far described in the literature to the writer's knowledge is by Förster and Breitfeld.[3] This also measures the decay time of a freely vibrating specimen by arrangement of thyratrons which fire between specific amplitudes of vibration. In their arrangement, condensers are alter-

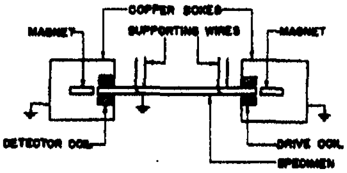

FIG. 1. Schematic arrangement of specimen, drive, and detector units.

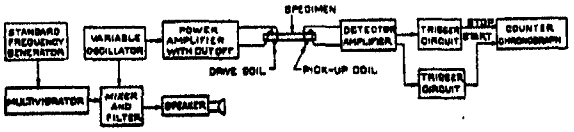

FIG. 2. Schematic diagram of electronic components.

---

[1] R. L. Wegel and H. Walther, Phys. Rev. 6, 141 (1935).

[2] Randall, Rose, and Zener, Phys. Rev. 56, 343 (1939).

[3] F. Förster and H. Breitfeld, Zeits. f. Metallkunde 30, 343 (1938).

nately charged when a thyratron fires, then discharged through a ballistic galvanometer. The total galvanometer deflection is then a measure of the number of cycles of vibration undergone by the specimen during decay, from which the damping is determined. It is believed that the apparatus described in this paper is simpler to operate and more accurate.

METHOD OF MEASUREMENT

A measurement of internal friction or damping capacity is essentially a measure of the energy dissipated internally within the specimen when mechanical energy is applied externally. If a specimen is set into vibration, several possible quantities may be used to evaluate damping: (a) The decrement of the equivalent circuit formed by incorporating the specimen into an electrical circuit through electromechanical coupling. (b) The power input necessary to maintain a constant vibrational amplitude. (c) The relative width of the amplitude *vs.* frequency curve. (d) The time necessary for the specimen to decay a known fraction of some predetermined amplitude while in free vibration at a resonant frequency.

The first method provides the highest accuracy, but requires relatively elaborate installation of the specimen. The last method named has been chosen as allowing the simplest installation of the specimen and, with the use of a counter chronograph, yielding satisfactory accuracy. In principle, all of the last three measurements can be made with the one method of specimen installation and vibrational drive. However, the measurements of power and of frequency width contain somewhat more uncertainties than that of decay time.

The mechanical arrangement of specimen, drive, and detector units is shown in Fig. 1. The specimen is a bar of uniform cross section, supported by two vertical wires. An alternating voltage is applied to the drive coil, which induces eddy currents in the specimen. A bar magnet, placed along the axis of the specimen and adjacent to it, sets up a magnetic field with radial components in the region affected by the eddy currents. These currents flowing circumferentially interact with the radial magnetic field to produce an axial force on the end of the specimen. The resulting motion is transmitted through the specimen with the frequency of the driving voltage and at the velocity of sound in the material. A similar arrangement of coil and magnet is present at the pick-up end. The vibrations of the specimen in the magnetic field now cause eddy currents to be set up in it, which in turn induce a voltage in the coil surrounding the specimen.

The electronic components of the apparatus are shown schematically in Fig. 2. An alternating signal is produced by the variable oscillator and fed to a power amplifier. The drive coil is placed in the plate circuit of the output tube, a 6F6 power pentode. To measure the frequency, the output of a multivibrator is mixed with the oscillator signal to produce beat notes which can be identified with the aid of a speaker.

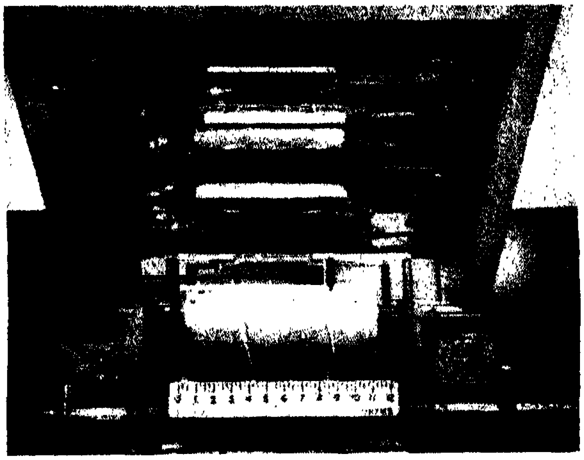

FIG. 3. Photograph of specimen in position; mirror at top gives view looking down on apparatus.

The detector amplifier serves to amplify the pick-up signal and rectify it, giving a d.c. output on the order of 100 to 200 volts. This output is fed to two trigger circuits, each of which is designed to produce a sharp voltage pulse when the d.c. signal from the amplifier drops below some particular value. Both circuits feed into a counter chronograph.

To measure the damping capacity, the driving amplifier is shut off electronically, with a minimum of decay transients, so that the specimen is left in free vibration. As the amplitude of vibration decays, the amplifier output voltage decreases to a value which fires one of the trigger circuits. This "start" circuit feeds into a counter chronograph to initiate the counter. When the vibration decays further, the amplifier output reaches a lower value at which the second trigger circuit has been set to fire. The output of this "stop" circuit operates to stop the counter. The counter thus registers the time interval for the amplifier output to decay between the voltages at which the respective trigger circuits fire. To take into account possible nonlinearities in the amplifier, the values used for computing the damping are obtained by placing known a.c. voltages across the pick-up coil and determining the input voltages which fire the trigger circuits.

The actual operation of the apparatus consists in pressing a button to shut off the driving signal, so that the time interval appears on the counter chronograph. This interval is recorded, a second button pressed to reimpose the driving signal, and a contact on the counter closed to reset that instrument. The cycle of operation can be carried out with manual recording at a rate of about 5 to 10 per minute. Up to 20 readings per minute can be obtained with two operators, or with photographic recording of the time readings and an auxiliary clock.

The damping capacity of the system is related to the measured quantities by the expression:

$$\delta = (\log V_1/V_2)/ft$$

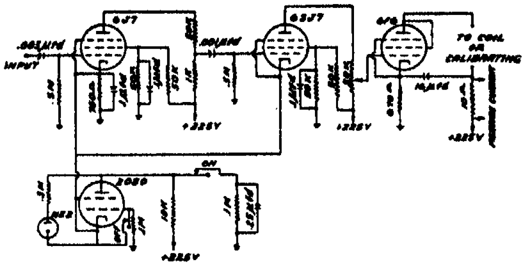

FIG. 4. Circuit of drive amplifier with cut-off.

where δ = damping capacity, V_1 = input voltage to fire "start" circuit, V_2 = input voltage to fire "stop" circuit, f = frequency of vibration, t = time for voltage input to decay from V_1 to V_2.

For most frequencies, the mechanical impedance of the specimen will be so high as to prevent the rod from converting any appreciable fraction of the electrical input energy into mechanical motion. At the natural frequencies of the specimen, however, the mechanical impedance is low and measurable vibrations are induced. Hence, the method described is limited to operate only at a set of discrete frequencies. These frequencies are given by the relation:

$$f_n = nv/l$$

where v = velocity of sound in the specimen, l = length of specimen, $n = 1, 2, 3, \cdots$.

Should measurements be desired at frequencies other than the harmonics corresponding to a particular length of specimen, specimens of different lengths can, of course, be prepared to allow new sets of frequencies.

SPECIMEN ARRANGEMENT AND AUXILIARY COMPONENTS

Figure 3 shows a specimen of 0.220 in. diameter positioned between drive and pick-up units supported in a radiation-type furnace used for tests at elevated temperatures. The mirror allows a top view of the arrangement with the lids removed from the furnace, drive and pick-up units.

The supporting wires are 0.005-in. diameter iron and constantan, respectively. They are utilized as a thermocouple, using the specimen itself as the hot junction. The furnace shown consists of a section of Superex pipe insulation between two aluminum cylinders that were shaped to fit the insulation. About 120° of the cross section was cut out as a lid to be removed for positioning of the specimen. Number 24 (AWG) Nichrome wire wound on lengths of ceramic tubing forms the heating element.

Drive and pick-up coils consist of No. 36 (AWG) wire wound on Lucite forms with $\frac{9}{32}$ in. I.D. Each form is fastened to a bar magnet entering one end of the form. The top view of Fig. 3 shows this connection, but the coils themselves fit into the cylindrical portions of the drive and pick-up boxes in alignment with the specimen and bar magnets. In the pick-up coil, where maximum sensitivity is desired, iron wire is used to increase the radial component of magnetic field in the specimen. Copper wire is used for the drive coil.

The drive and pick-up units, specimen and furnace supports are mounted on brass plate, containing grooves in which the drive unit can slide to allow positioning of the specimen. This plate is mounted on a steel base plate upon which a steel chamber is lowered to permit measurements in a vacuum. All electrical connections are made through spark plugs fitted to the base plate with a close thread. These plugs are covered with specially machined copper shields visible in Fig. 3.

ELECTRONIC COMPONENTS

Oscillator

The driving voltage is supplied by an oscillator with a range of approximately 1 to 100 kc and capable of being tuned to within 0.001 cycle per second. The precision of the setting is limited by a frequency drift of about 0.01 cycle per minute. A method of beat notes is used for frequency determination. The oscillator output is mixed with a standard frequency from a multivibrator, the resulting frequencies then being fed into a speaker. Audible beat notes between the oscillator output and harmonics of the multivibrator can then be identified as kilocycles and fractions of kilocycles.

Drive Amplifier with Cut-Off

The oscillator output of several volts is amplified by the circuit of Fig. 4 to produce about 120 volts across the drive coil, representing a mean power of about six watts. This driving power must be shut off so completely and quickly that no transient decay voltages of the amplifier output can act to drive the specimen while measurements of supposedly free vibrations are under way.

For this purpose, the circuit of Fig. 4 includes an auxiliary 2050 thyratron tube which permits instantaneous cut-off of the output. The "on" and "off" switches shown are merely push buttons, so that both are open in normal use. While the amplifier is in operation, the thyratron is not conducting. The plate is at 225 volts, the grid is at ground potential, and the cathode is tied to the cathodes of the first two tubes (6J7 and 6SJ7) at a few volts above ground, so that the neon lamp in the plate-to-cathode circuit is lit. When the "off" button is momentarily pressed, the grid is shorted to the cathode, and the tube becomes conducting. The plate current thus produced flows through the cathode resistor of 750 ohms in the first two tubes, raising their cathodes by about 16 volts. These tubes are therefore biased well below their cut-off point, and cease to pass any signals. Finally, with the 2050 tube conducting, the small voltage drop between plate and cathode is not enough to keep the neon tube aglow.

The amplifier can be made to function again by pressing the "on" button. This momentarily places the plate of the 2050 tube at ground potential and stops conduction. The current through the cathode resistor is decreased, lowering the cathode potentials on both tubes (6J7 and 6SJ7) and hence elevating the grid bias above the cut-off point. The amplifier is now in normal operation, and the neon lamp in the plate-to-cathode circuit of the 2050 tube is lit due to the rise in plate voltage of that tube.

High Gain Detector Amplifier

The peak signal induced in the pick-up coil is from about fifty to several hundred microvolts. This must be amplified and rectified to a level capable of firing trigger circuits, while keeping the inherent noise level at a negligible fraction of the signal.

The amplifier consists of five stages of amplification, including a tuned plate circuit in the third stage, coupled by an audio transformer to a rectifier-voltage doubler unit. It has a gain of about 7×10^5 d.c. out/a.c. in, and a noise level of about one microvolt. Considerable care in wiring and shielding is necessary to secure a high signal-to-noise ratio. Partitions of copper strip are used to shield the separate stages, while the condensers and coil of the tuned plate circuit are in a separate shielded box. Two power supplies are used, one for the first three stages, a second for the remainder. Both supplies are well regulated, the first having an a.c. ripple of less than 0.001 volt, the second of less than 0.010 volt.

While the tuning is highly effective in reducing the noise level, the quality of the rectified signal is dependent on the choice of *RC* circuit in the cathode circuit of the voltage doubler unit. This rectified signal should provide a smooth envelope through the peaks of the damped sine wave produced by the specimen vibration. If one considers an initial peak voltage V_1 and the succeeding peak voltage V_2, their relation in terms of the damping of the system δ is given by:

$$V_2=V_1e^{-\delta}.$$

Similarly, the voltage on a condenser C discharging through resistance R drops from V_1 to V_2 in time t according to the relation:

$$V_2=V_1e^{-t/RC}.$$

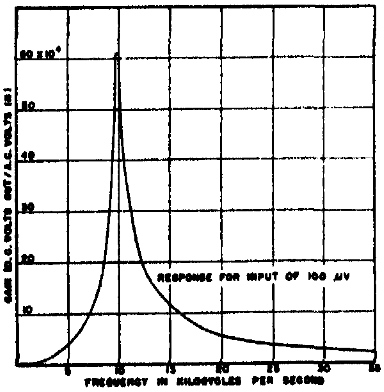

FIG. 5. Frequency response of amplifier for input of 100 μv.

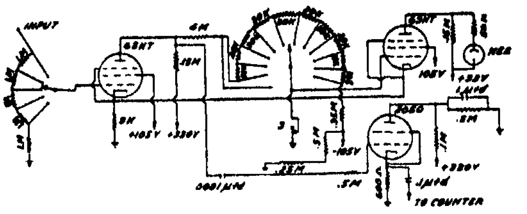

FIG. 6. Trigger circuit used to start and stop counter chronograph.

Hence, the rectified output will reproduce the proper damping characteristics when these two processes are equivalent, or when:

$$\delta=t/RC=1/fRC,$$

where f is the resonant frequency of the specimen. In practice, the condensers of the *RC* circuit are changed when the product $f\delta$ changes by an order of magnitude.

The response of the amplifier when tuned for 9800 cycles per second is shown in Fig. 5. Its gain is reasonably flat from approximately 50 to 350 μv.

Trigger Circuits

When the drive amplifier is shut off, the d.c. output from the detector amplifier decays. It is necessary to obtain a sharp voltage pulse at two values of this decaying voltage to start and stop a counter chronograph. The use of a simple thyratron tube, with grid bias controlled by the d.c. output, was not reproducible to within several percent. A hard vacuum tube trigger circuit, shown in Fig. 6, was therefore designed for this function.

The d.c. voltage from the detector amplifier, or a suitable fraction, is applied to the grid of a 6SH7 pentode. The output of this first tube is coupled through an *RC* circuit to the grid of a 2050 thyratron and, through resistors, to the grid of a second 6SH7 serving as a control tube. Both 6SH7 tubes operate from a common cathode resistor. Before a measurement, the first 6SH7 has a high potential at the grid and is conducting while the 2050 is biased below the firing point. The second 6SH7 has a large negative grid bias and is not passing plate current, hence the neon glow tube in its plate circuit is out.

When the detector amplifier output decays, a value is reached at which the grid of the first 6SH7 drops below the cut-off point. The plate potential suddenly rises to the value of the plate supply, transmitting a positive pulse on the order of 200 volts to the grid of the 2050. This tube now is conducting, its cathode potential rises sharply to several volts, and a pulse of this value is transmitted to the counter chronograph.

The second 6SH7 has its grid raised above the cut-off point by the rise in plate potential of the first tube. It therefore begins to conduct, lighting the neon glow

TABLE I.

Temp.	Av. time ±probable error	Percent probable error
T_1	1.683±0.007	0.4
T_2	1.678±0.020	1.2
T_3	1.204±0.009	0.7
T_4	0.566±0.005	0.9

tube in its plate circuit, raising the cathodes of both 6SH7 tubes above ground. When the signal level on the first 6SH7 grid has been raised by reimposing the driving voltage prior to another measurement, switch *S* is closed. This momentarily grounds the grid of the second 6SH7, stops its conduction, lowers the cathode potentials, and permits the first 6SH7 to conduct. The second grid again becomes negative, and the circuit is set for another operation.

Two trigger circuits are used for starting and stopping the counter chronograph. The output of the detector amplifier is developed across two 100,000-ohm resistors in series, with the "start" trigger circuit actuated by the voltage at the midpoint of this combination and the "stop" trigger circuit operating from the peak voltage across both resistors.

Calibrating Circuit

It is necessary to know the ratio of the input voltages to the detector amplifier corresponding to the decay voltages at which the "start" and "stop" trigger circuits fire. To do this, a calibrating circuit is used which takes the signal from the drive amplifier at the identical frequency used in driving the specimen, and applies a measured voltage in series with the pick-up coil into the detector amplifier.

A switch is used to replace the drive coil in the output plate circuit of the drive amplifier with a resistor. This resistor is coupled through condensers to a microvolter whose output is placed across a 500,000- and 1500-ohm resistor in series. The voltage across the smaller resistor is put in series with the pick-up coil and fed into the detector amplifier. This input voltage is varied by adjusting the microvolter, which can be read to an accuracy of about 0.5 percent.

PERFORMANCE OF EQUIPMENT

Measurements of decay times can be recorded to an accuracy on the order of one percent. A typical series of data that lends itself to statistical analysis can be taken from tests made of the variation of damping with temperature. Ten measurements were recorded at each temperature. The readings of the counter chronograph are summarized in Table I.

As discussed in the section on Method of Measurement, the damping is computed from the log of the ratio of stop and start voltages, the decay time and the resonant frequency. Each stop and start voltage can be read, and is reproducible to, 0.5 percent. Since the logarithm is on the order of unity, the error is less than one percent. The resonant frequency is determined to better than one part in 10^4. The decay times are accurate to about one percent. The total error in the calculated damping is therefore on the order of 1.5 percent.

ACKNOWLEDGMENT

The writer would like to express his sincere appreciation for the initial guidance and suggestions in setting up this work provided by Dr. T. A. Read, School of Mines, Columbia University. Finally, it is desired to thank Mr. Joseph T. Gilbert for his work in wiring and testing the components of the apparatus. His efforts have greatly expedited the program.

THE REVIEW OF SCIENTIFIC INSTRUMENTS VOLUME 21, NUMBER 7 JULY, 1950

Observations on Some Properties of Ultra-High Frequency Gas Discharges*

CHARLES F. ROBINSON†
Norman Bridge Laboratory of Physics, California Institute of Technology, Pasadena, California

(Received March 6, 1950)

A series of experiments designed to yield information on the mechanisms of ultra-high frequency discharges which influence the operation of ion sources employing such discharges is described. The main conclusions are that such discharges exhibit a high negative space charge due principally to secondary emission from the walls of the discharge chamber and that ion production is inhibited by the space-charge trap so formed, that under certain conditions extremely intense electron beams may be obtained from a resonant cavity containing a gas discharge, and that fairly large ion currents may be obtained by the interaction of the emergent gas and the emergent electron beam in the exit orifice of the cavity.

A FREE charged particle having mass m, charge q, placed in an alternating electric field, will exhibit a motion described by

$$z=\frac{qE_0}{m\omega^2}[\sin\theta-\sin(\omega t+\theta)]+\left[\frac{qE_0}{m\omega}\cos\theta+\dot{z}_0\right]t, \quad (1)$$

where the field is given by

$$E=E_0\sin(\omega t+\theta), \quad (2)$$

and $\dot{z}_0$ is the particle's velocity at the instant $t=0$. This is clearly a superposition of two simple motions, the first being a steady drift in the direction parallel to the field, of magnitude

$$V_{\text{drift}}=qE_0\cos\theta/m\omega+\dot{z}_0, \quad (3)$$

and the second being a sinuous motion in synchronism with the field, of amplitude

$$a=qE_0/m\omega^2. \quad (4)$$

In the absence of initial energy ($\dot{z}_0=0$) we have the kinetic energy

$$T=\frac{q^2E_0^2}{2m\omega^2}[\cos\theta-\cos(\omega t+\theta)]^2, \quad (5)$$

which has its maximum value

$$T_{\max}=(q^2E_0^2/2m\omega^2)[1+|\cos\theta|]^2 \quad (6)$$

at the instants given by

$$t=[(n\pi-\theta)/\omega] \quad (n=0, \pm1, \cdots), \quad (7a)$$

$$\cos(\omega t+\theta)\cos\theta>0. \quad (7b)$$

An electron placed in a rarefied gas such that the drift velocity given in (3) vanishes, and exposed to a field such that its amplitude as given in (4) is less than the distance to the nearest wall, may make many oscillations before being collected at one or another surface. In so doing, its probability of ionizing a gas molecule may be much enhanced over that of an electron accelerated by a steady or slowly varying field. Additionally, the presence of m in the denominators of (4) and (6) suggests that ions formed by electrons moving in this way would be relatively very insensitive to such a field so that they might be withdrawn from an enclosure—an ion source—by a comparatively weak steady field. These two facts make it appear that an ion source based on this principle of excitation would operate at lower pressures, and hence at lower gas consumption and pumping load, than conventional sources employing self-sustaining discharges, and that the independence of control over the fields used to form ions and the field used to withdraw them might permit the circumvention of some space-charge effects. It can be anticipated that the superposition of a steady field would inhibit the discharge by imparting appreciable steady velocities to electrons which might otherwise have average velocities of only thermal origin.

The work here to be described was done in an attempt to gain some understanding of the phenomenology of ultra-high frequency discharges in order to permit assessment of the feasibility of constructing practical ion sources based on such discharges.

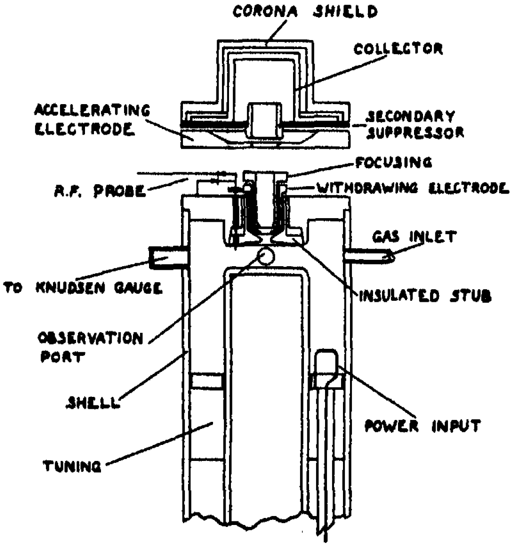

FIG. 1. The basic discharge cavity and ion collector.

---

* Excerpts from a thesis submitted in partial fulfillment of the requirements for the degree of Doctor of Philosophy, California Institute of Technology (1949).

† Now at Consolidated Engineering Corporation, Pasadena, California.

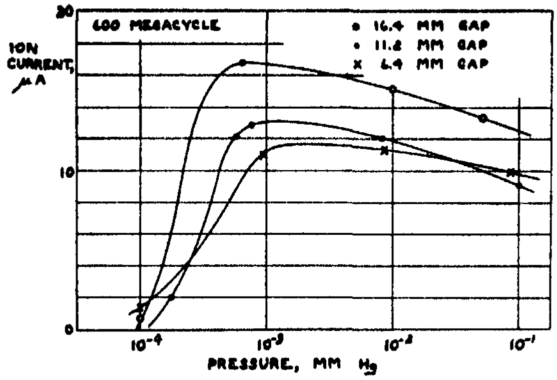

FIG. 2. Ion yields as a function of pressure and gap spacing at 600 Mc.

The theory for such discharges has been developed[1-4] far beyond the derivation given here, but unfortunately under hypotheses on whose validity these results cast grave doubts; these results, far from confirming that secondary emission from the walls of the discharge chamber may be ignored, suggest that secondary electron emission may play a role of governing importance, at least once the discharge has started.

The source of r-f power consisted of a three-stage oscillator-buffer-amplifier system incorporating 2C43, 2C40, and 2C39 high frequency (lighthouse) triode tubes, each one in a conventional double cavity representing the equivalent of a tuned-plate-tuned-grid arrangement. All three stages worked at the same frequency in the range 550 to 900 Mc, coupling was by means of RG8U cables, and impedance matching was obtained by "trombones" of conventional type. Output power delivered to the discharge was estimated at 10 to 20 watts. Although this system worked extremely well it has been rendered obsolete by recently developed CW magnetrons and need not be discussed in detail here.

The basic discharge cavity was of copper-plated steel; it was of the "concentric line" type as shown in Fig. 1, immersed in an evacuated bell jar of essentially conventional construction. Gas was admitted directly to the cavity and pressures were measured by a Knudsen-DuMond gauge connected directly to the cavity. The fixed end stub was insulated from the remainder of the cavity, being pressed into a mica-lined tapered socket. This was done in order to permit the superposition of d.c. and a.c. fields and to permit measurements of d.c. stub currents arising from the discharge.

The central pillar of the cavity could be moved in and out to investigate the effect of changes in gap spacing, and tuning was accomplished from outside the bell jar, without disturbing the vacuum, by means of an O-ring joint. A $\frac{1}{4}$-in. diameter hole, sealed by mica held in place with Scotch Tape, served as an observation port. The bell jar was evacuated by a VMF 100-W oil diffusion pump backed by a Cenco "Megavac" and the pressure in the bell jar was usually in the range $1-5 \times 10^{-5}$ mm Hg. The r-f sensor shown in Fig. 1 was useful principally as an aid to tuning and coupling adjustment in the no-load condition since, with a discharge in the cavity, the probe was shielded by space charge to such an extent as to be essentially useless.

The first stage of the work, done with dry air as the ionized medium, with no magnetic field, and with an all-metal (copper-plated steel) discharge chamber, led to the following conclusions.

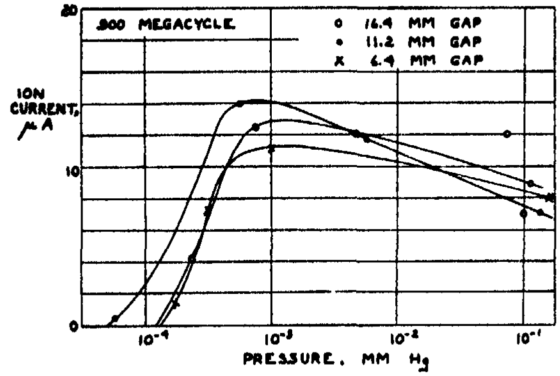

FIG. 3. Ion yields as a function of pressure and gap spacing at 900 Mc.

1. That an ultra-high frequency discharge could be initiated and maintained, in a metal cavity, at pressures ranging from 10^{-4} mm Hg up to several tenths of a millimeter. Only rarely was it possible to initiate the discharge at low pressures; more usually it was necessary to introduce a burst of gas to raise the pressure up to 2 to 3×10^{-3} mm, after which the pressure could be reduced, sometimes as far as 5×10^{-5} mm, and the discharge maintained. It has been mentioned that the electrons which are effective in maintaining the discharge at low pressures are those having very little initial energy; apparently random electrons which have their origin in ionizing events in the laboratory are sufficiently energetic that they are ineffective in initiating a high frequency discharge either directly or through secondary emission at the walls, unless there is sufficient gas in the chamber to provide a mechanism for energy degration. Once the characteristically high frequency (that is to say, low energy) discharge has been started, pressure may be depressed one or two orders of magnitude before the discharge goes out.
2. Neither the ion yields (Figs. 2 and 3) nor the general behavior showed appreciable frequency dependence in the range 600 to 900 Mc, and there was no clear evidence for dependence on gap spacing in the range 6.4 to 16 mm.
3. No ions were ever observed in amounts over 5 μa, and rarely over 1, without an auxiliary withdrawing potential, and the magnitude of the ion currents increased monotonically with withdrawing potential up to some 700 volts (Fig. 4), although electron currents over 100 μa were frequently observed with no steady potentials anywhere, even on the collector.
4. The superposition of a parallel axial steady electric field always depressed the ion yield regardless of polarity, and a steady field strength of 200 to 300 volts per centimeter was sufficient to extinguish the discharge altogether at low pressures.
5. Ion currents to a collecting chamber of conventional type (Fig. 1) tended to be in the range 10 to 20 μa. They showed a

---

[1] H. Margenau, Phys. Rev. 73, 297 (1948).
[2] H. Margenau, Phys. Rev. 73, 326 (1948).
[3] H. Margenau and L. M. Hartman, Phys. Rev. 73, 309 (1948).
[4] L. M. Hartman, Phys. Rev. 73, 316 (1948).

surprisingly small dependence on the r-f field strength. The excitation of a discharge in the cavity changed the resonant point in a direction corresponding to an inductive load.

6. The initial energies of the ion beam, expressed as volts referred to the source chamber, were as high as 120 volts (Fig. 5). This indicates a high positive space charge in the presence of the withdrawing field and conclusion (3) above indicates an even higher negative space charge in its absence.

7. There is essentially no difference in performance when the working medium is changed from air to hydrogen, which suggests that if space-charge effects are present, they are insensitive to the mass of the ion involved.

At the conclusion of this phase of the work it was felt that the results were being influenced by a space-charge effect whose exact nature was unknown. Accordingly an arrangement was provided to inject electrons into the cavity in order to influence this charge. The result of electron injection, as shown in Fig. 6, was to *reduce* the ion current; this indicates that the net space charge is negative and that ion production is inhibited by the potential "trap" caused by this space charge.

It seemed obvious that such a space-charge trap must have its origin in secondary electron emission at the walls of the cavity; consequently the walls were next coated with Aquadag in an attempt to suppress these secondaries. Two effects were noted as soon as this was done, the first being that there was no important change in ion current[‡] and the second being that the d.c. current to the insulated stub *changed sign* when the tuning plug was moved through the resonant position (Fig. 7), being negative when the cavity was off resonance and positive when the cavity was tuned to resonance, although nothing else in the cavity was affected and no d.c. fields except those due to space charge were present anywhere. A series of observations with various d.c. biasing fields on the insulated stub were next made; these results are also shown in Fig. 7. The fact that this current becomes more positive when the stub bias itself is made more positive, and vice versa, indicates that the "primary" stub current is composed principally of electrons and that the sign of the current is a function largely of the electron energy on impacting the stub, being positive when the impact energy corresponds to a secondary emission coefficient greater than unity and conversely.

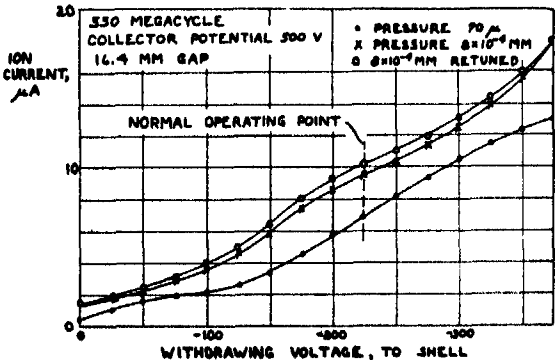

FIG. 4. Collector current as a function of pressure and withdrawing voltage.

The next observations were made with an axial magnetic field in the cavity. These observations showed that at pressures of about 10^{-3} mm and below, a magnetic field of a few tens of gauss would extinguish the discharge altogether; in a few instances such a field would blow the discharge out within the gap but would leave a fringing discharge around the edges of the gap. It was further observed that even magnetic fields not strong enough to extinguish the discharge altogether would impair the ion yield; the degree of impairment depended on pressure and withdrawing voltage, but there was no instance in which the magnetic field increased the ion yield unmistakably and there was always at least one value of the magnetic field whose employment resulted in marked impairment of the ion yield regardless of the withdrawing voltage.

A final measurement in this series was made with an insulated copper sheet on the inner wall of the cavity; the arrangement and the electron current to this sheet, as a function of magnetic field, are shown in Fig. 8.

The explanation of these observations seems to be the following: With no magnetic field in the cavity, secondary electron emission from the walls of the cavity gives rise to an intense negative space charge which traps ions and interferes with their removal. The injection of electrons from below increases the intensity of this space-charge trap and inhibits ion production still further. The stray field from a withdrawing electrode sweeps away some of this space charge and permits the withdrawal of ions in numbers which depend on the magnitude of the withdrawing potential. If the electrons are swept away by a withdrawing field, the positive ions which remain behind by reason of their greater inertia give rise to a positive space charge which may impart anomalous energies to the ions which are removed.

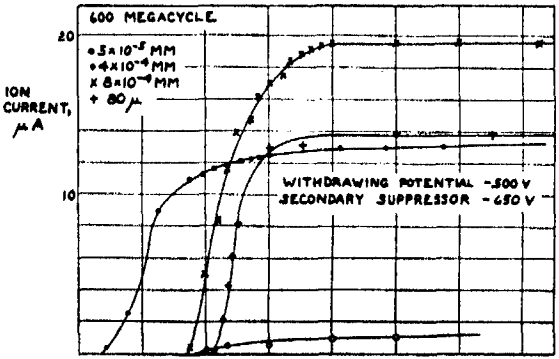

FIG. 5. Collector current as a function of collector potential, showing anomalies in ion energy.

[‡] Data given by Harries (Electronics 17 (2), 100. (1944)) indicate that Aquadag is somewhat overrated as a suppressor of secondary electrons, the secondary emission coefficient being greater than unity through the range of 100 to 500 volts in primary bombarding energy.

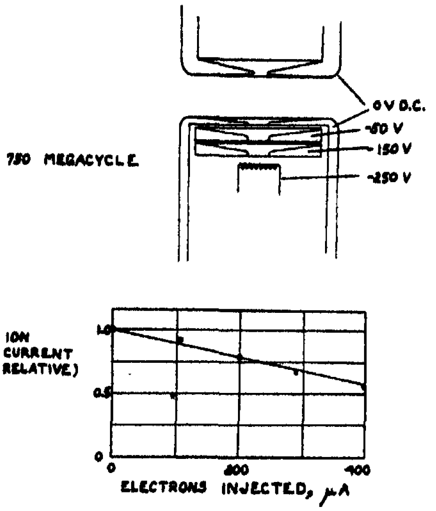

FIG. 6. The depression of ion yield resulting from the injection of electrons into the cavity.

Under a considerable range of conditions the end surfaces of the gap may run at a secondary emission coefficient greater than unity, excess electrons being ejected radially by the space-charge-induced field, collected on the inner radial surfaces of the cavity where the main field is a steady one due to space charge and from where they return to the gap surfaces by conduction through the walls. This phenomenon is at least qualitatively the same whether the gap surfaces are copper, Aquadag, or bare polished steel and there can be little doubt that the emission of secondary electrons is enhanced by the gas present in the cavity.

The imposition of an axial magnetic field inhibits this radial circulation of electrons (Fig. 8) and the resultant space charge increases. At low magnetic fields, the space-charge trap is deepened and ion withdrawal is inhibited, while at higher magnetic fields the space-charge-induced field is strong enough to extinguish the discharge altogether at low pressures, where the discharge is not self-starting. At higher pressures the phenomena are masked by collisions and by the self-starting character of the discharge and the discharge has more of the properties of a low pressure d.c. arc, which is of secondary interest here.

Hall[5] has reported an ultra-high frequency ion source in which ion currents of the order of several hundred microamperes were obtained in a well-focused beam. Inasmuch as such currents are more than an order of magnitude greater than the ones thus far observed here, it was of interest to investigate the behavior of a discharge induced in a Pyrex bottle rather than a metal cavity since this was Hall's arrangement. It was decided to attempt to duplicate Hall's results if possible; several Pyrex bottles of the type described by Hall were obtained[**] and measurements with them begun.

The first measurements indicated that ion current showed the previously observed dependence on withdrawing voltage and that even with a withdrawing voltage of some 700 volts, the ion currents were only about 30 μa. Ion currents showed the previously observed insensitivity to r-f field strength. The intense localized "core" first noted by Hall was observed; the formation of this core *reduced* the ion current by nearly a factor of four. These observations are made with a withdrawing potential of 400 volts (negative, of course, with respect to the body of the cavity). Rapid erosion observed in the Pyrex bottles and occasional sodium color in the discharge made it appear certain that the excitation was as violent as the Pyrex could withstand.

Finally it was observed that in the absence of any steady electrode voltages, electron currents to the collector as high as two or three milliamperes could be obtained; further, by adjusting the obvious parameters to their optimum values, electron currents to the collector as high as 20 to 30 *milliampere* could be obtained; on several occasions, 40 *milliampere* were observed, and on one occasion, 50. This current was enhanced by an axial magnetic field; a plot of current *vs.* magnetic field showed sharp strong maxima, and the current increased monotonically with increasing r-f drive. Under optimum conditions the emergent electron beam formed a well-collimated jet plainly visible in a well-lighted room. It was always necessary to run at high pressure (over 10^{-3} mm Hg) to prevent extinction of the discharge by the magnetic field.

At this time the discharge was being fed gas (hydrogen) produced by an electrolytic generator running at some 200 ma. Visual examination of the Pyrex bottle suggested strongly that electrons were ejected from both ends about equally; taking this into account and making a reasonable allowance for gas leakage within the bell jar, it results that the assumption that the electrons observed came from ionization of the hydrogen requires an over-all conversion efficiency for the process of somewhat more than 100 percent. Consequently it would seem reasonably certain that at least some, and

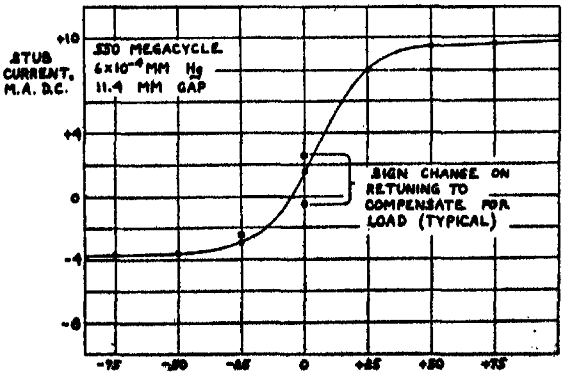

FIG. 7. Stub current as a function of stub voltage, showing stub current to change from negative to positive when the cavity is retuned to match the load introduced by the discharge.

---

[5] R. N. Hall, Rev. Sci. Inst. 19, 905 (1948).

[**] The first one used, which served as a pattern for the remainder, was furnished by Mr. Holloway of the Kellogg Radiation Laboratory at this Institute.

probably nearly all, of the electron currents observed must have had their origin as secondaries within the cavity.

The exit bore of the Pyrex bottle was approximately 1 mm diameter by 0.8 mm long; using Langmuir's[6] ionization coefficient for 100 volt electrons[††] of 0.038 ion per centimeter per electron and assuming an average pressure in the exit bore of 4×10^{-2} mm (based on pumping speed calculations), one finds ions produced in the exit jet at the rate of some 600 μa per mm of jet length per 40 ma of electron current. This agreement with Hall's work is fully as good as could be expected and these data seem to point inescapably to the conclusion that the ion currents reported by Hall were formed not by high frequency ionization within the cavity but by collisions between the emergent gas and the emergent electron stream in the exit orifice.

High ion currents could not be brought to a satisfactory focus with the voltages and geometry available here; a special collector capable of receiving a considerable portion of a widely divergent ion beam was constructed and ion currents of 350 to 400 μa to it could be obtained provided the withdrawing voltage was made zero or slightly *positive.*

The emergent ion beam was not subjected to mass analysis; however, visual spectroscopic examination showed the Balmer lines to be bright and clear compared to the weak band background, which is in general agreement with Hall's measurement of some 60 percent protons in the beam. The chief function served by the Pyrex bottle would seem to be to ensure that the emergent hydrogen is atomic, having been dissociated in the discharge, rather than molecular in form.

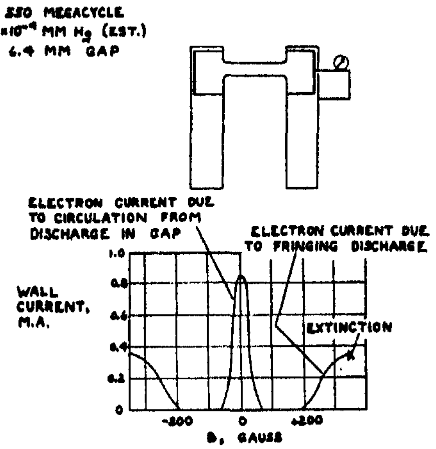

FIG. 8. Showing the circulation of electrons from the discharge to the cavity wall in the absence of an axial magnetic field and the inhibition of circulation by a magnetic field.

CONCLUSION

At frequencies of 500 to 900 Mc and with gap spacings of 7 to 15 mm a self-sustaining discharge can be maintained at pressures well below those where a d.c. or low frequency discharge is no longer possible. Such a discharge is a prolific source of electrons, most of which have their origin as secondary electrons at the faces of the gap. Ions produced in the discharge tend to be trapped by high negative space charge due to these secondary electrons. If a d.c. field sufficient to sweep away these electrons and aid in ion removal is applied, the residual positive space charge may give rise to anomalies in ion energy of several score volts so that such a discharge would appear to have little use as an ion source in applications, such as mass spectrometry, where the ion energy needs to be held to an accurately determinable value. Such a discharge would seem to have interesting possibilities as an ion source in one segment of a sealed-off accelerating column, possibly for work with rare isotopes, since the high frequency discharge would be self-sustaining at pressures below those at which a subsequent series of d.c. accelerating gaps might be expected to break down.

ACKNOWLEDGMENT

A portion of the graduate work of which this research was a part was assisted by a predoctoral fellowship of the National Research Council.

---

[6] I. Langmuir, Rev. Mod. Phys. 2, 123 (1930).

[††] This was approximately the potential to which the electron beam, unaided, would raise the collector and is consequently a rough measure of the electron energy on emergence from the bottle.

THE REVIEW OF SCIENTIFIC INSTRUMENTS VOLUME 21, NUMBER 7 JULY, 1950

Microwave Power Stabilizer

IVAN K. MUNSON
National Bureau of Standards, Washington, D. C.

(Received March 20, 1950)

An apparatus for the power stabilization of medium-level microwave power sources, intended for laboratory use, by means of a degenerative feed-back network connected in tandem with the power source is described. An analysis of the operation of the network is presented, based on obtaining optimum stabilizing action and optimum transmission efficiency for the network. Design of an electrically-operated attenuator (which is a servo device), and its effect on the stabilization characteristics of the network are discussed. A transmission efficiency of 70 percent and a stabilization factor of 21 were obtained in an experimental model.

UNMODULATED microwave power in excess of a few milliwatts for laboratory use is usually obtained from reflex klystron oscillators. The power stability of klystrons is adversely affected by ambient temperature variations, electrode voltage changes (such as may be encountered in an automatic frequency control), and mechanical disturbances. In some cases, these variations can be minimized. However, an oscillator sufficiently isolated for stabilization purposes is not a very useful device. The use of a feed-back network, described in this paper, inserted between the power source and the r.f. load is in general a practical solution of the problem. The network described has a transmission efficiency of 70 percent and a stabilization factor of 21.

THE NETWORK

A block diagram of the network is presented in Fig. 1. A small amount of the output power is fed to a crystal rectifier by means of a directional coupler. The output voltage of the crystal rectifier is compared with a reference voltage and the difference is applied to a d.c. amplifier. The output of the amplifier is coupled to an electrically-operated attenuator thereby completing the feed-back loop.

ANALYSIS

The crystal detector is assumed to be a square law device for small input power. The network equations are then,

$$P_2=(\alpha+mV_2)P_1, \tag{1}$$

$$P_3=(1-R)P_2,\quad 0<R<1, \tag{2}$$

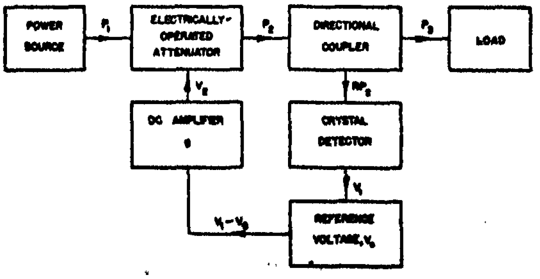

FIG. 1. Block diagram of the stabilization network.

$$V_2=g(V_1-V_0),\qquad g>1, \tag{3}$$

$$V_1=kRP_2,\qquad k>0. \tag{4}$$

The powers P_1, P_2, and P_3 and the voltages V_1 and V_2 are identified in Fig. 1. The coefficients α and m describe the electrically-operated attenuator, α being the attenuation when V_2 is zero and m the derivative of the attenuation with respect to V_2. The sign of m may be reversed by reversing the connections to the attenuator. The amplifier gain is g and the ratio of the power diverted out of the side arm of the directional coupler to the input power P_2 is given by R. The crystal characteristic is k and is defined by Eq. (4).

P_2, the output power of the electrically-operated attenuator may be obtained by the substitution of Eqs. (3) and (4) into Eq. (1) and is found to be,

$$P_2=\frac{(\alpha-mgV_0)P_1}{1-mgkRP_1}. \tag{5}$$

The useful output power, P_3, obtained from Eqs. (2) and (5), may be written,

$$P_3=(1-R)\alpha[(1-(mg/\alpha)V_0)/1-mgkRP_1]P_1. \tag{6}$$

P_3 must, of course, always be positive. R is positive and less than one. Hence, the quantity in the brackets must always be positive.

In practice, the reference voltage, V_0, is adjusted so that V_2 is zero when P_3 has the desired value, $P_3{}^0$. Then $V_0=kRP_2$ and Eq. (6) can be rewritten,

$$P_3{}^0=(1-R)\alpha P_1{}^0. \tag{7}$$

Most laboratory power sources operating in the microwave region provide relatively little power output and it is therefore essential that auxiliary apparatus operate as efficiently as possible. We may express the efficiency of the network as simply:

$$\eta=P_3{}^0/P_1{}^0=(1-R)\alpha. \tag{8}$$

We may also define a stabilization factor as the inverse of the slope of the response curve, evaluated for the selected output power, P_3^0.

$$S=\frac{1}{([dP_3]/[dP_1])_0}=\frac{1-mkgRP_1^0}{(1-R)\alpha}. \tag{9}$$

From Eqs. (8) and (9), we obtain a relation between efficiency and stabilization factor.

$$S/\eta=1-mgkRP_1. \tag{10}$$

It is seen that a value of $(-mgkRP_1)\gg 1$ is necessary for good stability and efficiency. For a given P_1 and a given network, however, it is seen that stability can be increased only at the expense of efficiency. Thus, for a given network and input power, the stability obtainable is dependent upon the output power required.

MODEL DEVELOPED

The design of the apparatus described in this paper was based on a desired transmission efficiency of 70 percent. An *mgkR* product of 50 was estimated for the components used. The calculated stabilization factor was 16 for an input power of 200 mw.

The components comprising the microwave transmission path are shown in Fig. 2.

The electrically operated attenuator is designated *A* in the figure. A directional coupler is shown at *B*, whereby a small amount of the output power is coupled to the crystal rectifier *C*. The amplifier used was a commercial d.c. amplifier[1] having suitable gain and frequency response.

The electrically operated attenuator provides an attenuation of microwave power controlled by an applied d.c. voltage. A commercial D'Arsonval system[2] is used to obtain angular axis displacement proportional to applied voltage. A mica vane is mounted on the system shaft as illustrated in Fig. 3. The mica vane is coated with graphite as indicated by the shaded areas so that angular displacement of the vane about the system axis changes the attenuation of the microwave power. In order to minimize frequency pulling of the power source caused by changes in its load impedance resulting from rotation of the attenuator vane, the vane was made an odd number of guide quarter-wave-lengths long and electrically symmetrical about its axis of rotation. The axis was centrally located with respect to the wave guide. The input voltage standing wave ratio for this arrangement was less than 1.1 to 1 at 9300 Mc, and was nearly independent of the angular position of the vane. This mechanism can be developed for any microwave frequency and any waveguide size.

FIG. 2. Components which form the microwave transmission path.

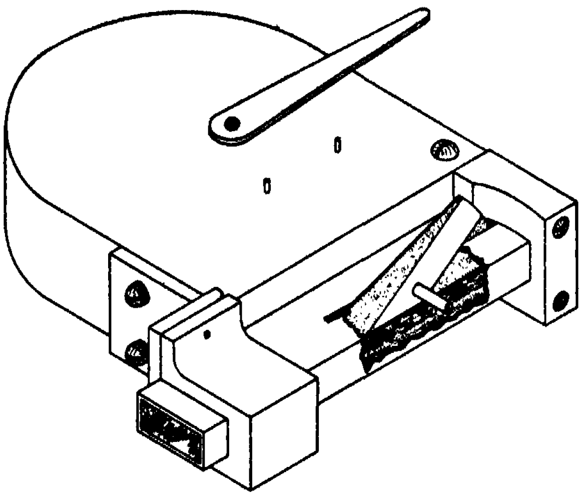

FIG. 3. Cut-away view of electrically-operated attenuator.

STABILIZATION FACTOR AS A FUNCTION OF THE FREQUENCY OF POWER VARIATION

The stabilization factor is given by Eq. (9) and is a function of the frequency of V_2 insofar as the product *mg* is a function of this frequency. The quantity *m* is

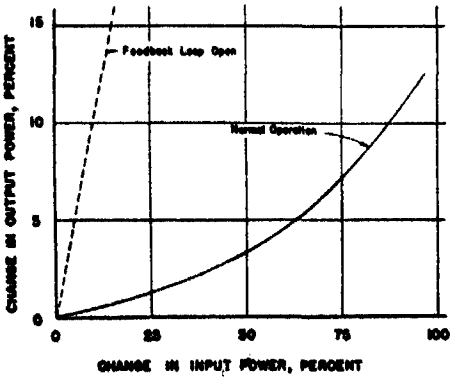

FIG. 4. Measured characteristics of stabilization network.

---

[1] The "Microsen D-C Amplifier," manufactured by Manning, Maxwell, and Moore, Inc., Bridgeport, Connecticut, was considered suitable for this application.

[2] A Brush Magnetic Recording Penmotor, manufactured by the Brush Development Company, Cleveland, Ohio, was found suitable for this application.

descriptive of the dynamic properties of the D'Arsonval system which is a form of servo mechanism. The attenuation-phase relationships for servo transfer functions is discussed in the literature.[3] A sufficient condition for stability of the feed-back system, derived from the Nyquist criterion,[4] is that the gain of the feed-back loop be less than unity for all frequencies for which the phase angle of the transfer coefficient of the feed-back loop is between $(n\pi)/2$ and $(3n\pi)/2$, where n is any integer. It was found experimentally that the phase angle of the transfer coefficient of the D'Arsonval system alone exceeded $\pi/2$ at 25 c.p.s. In order to satisfy the sufficient condition for stability, an amplifier was selected which had a very large voltage gain in the frequency range from zero to 3 c.p.s. and essentially zero gain at all frequencies above 5 c.p.s. Hence, the stabilization factor will have its maximum value in the frequency range of zero to 3 c.p.s. and be very small at higher frequencies.

MEASURED STABILIZATION CHARACTERISTICS

The power input to the network was increased 100 percent in discrete steps and the power output was measured at each step. The results are shown in Fig. 4 and represent the response of the network to variations of zero frequency. The dashed line represents the response of the network with the feed-back loop open. The (Power) stabilization factor at zero frequency for this network is 21, determined from the initial slope of the network response curve.

---

[3] James, Nichols, and Phillips, *Theory of Servomechanisms* (McGraw-Hill Book Company, Inc., New York, 1947), pp. 167–171.

[4] See reference 3, pp. 158–163.

THE REVIEW OF SCIENTIFIC INSTRUMENTS VOLUME 21, NUMBER 7 JULY, 1950

A Recording Fluxmeter of High Accuracy and Sensitivity

P. P. Cioffi
Bell Telephone Laboratories, Inc., Murray Hill, New Jersey

(Received March 6, 1950)

A recording fluxmeter has been developed which employs one or two integrators and a double element L and N Speedomax recorder for tracing magnetization curves directly on standard coordinate paper. The response of the recorder pen drive mechanism is proportional to the flux density, B, and is controlled by the B integrator. The response of the paper drive mechanism is proportional to the magnetizing force, H, and is controlled either by the magnetizing current, when the specimen is in the form of a ring, or by the H integrator when the specimen is in the form of a bar. Ayrton shunt networks provide flexible B and H scale adjustments. High accuracy and sensitivity are obtained by minimizing the causes of drift. At maximum sensitivity, four interlinkages give a deflection of one mm.

INTRODUCTION

FOR many years the ballistic galvanometer has been widely employed for obtaining magnetization curves and hysteresis loops of magnetic materials. The method is reliable, but, because it is slow and laborious, a number of investigators have devised hysteresigraphs for facilitating magnetic measurements.[1] Such instruments have been operated either by slowly changing d.c. magnetization or by a.c. magnetization. The d.c. hysteresigraph[2] generally employs a galvanometer or fluxmeter for the integrating element and inaccuracies result because of uncontrolled galvanometer drift. The a.c.[3] method can only be applied for measurements on thin or laminated materials because of eddy current shielding. With such instruments the curves have been traced directly on photographic paper by a reflected beam of light or have been presented on a cathode-ray tube and subsequently photographed. Such hysteresigraphs, however, are not sufficiently convenient in routine measurements because of the delay in obtaining the photographic record and the necessity of scaling the coordinates of points on the curves to obtain numerical results. Also, depending upon the method of integration, the results may be of questionable accuracy. For these reasons the ballistic method is still the most generally applied method in precise magnetic measurements.

In considering the design of a recording fluxmeter of greater flexibility and accuracy, the objective was to obtain an ink trace of the curves directly on standard coordinate paper and to provide means for readily adjusting the scale of the curves to the paper. In this manner a direct reading scale could be provided and the results could be read from the curves directly after tracing. The attainment of these objectives was dependent upon the availability of a suitable integrating and recording system. The Edgar photoelectric fluxmeter[4] suggested an integrator which could be adapted to a commercial recorder such as the Leeds & Northrup Speedomax.[5] This paper describes the application of these devices in a recording fluxmeter characterized by high accuracy, sensitivity and flexibility of scale adjustment.

---

[1] Valentino Zerbini, L'Elettrotecnica **32**, 182 (1945).

[2] F. E. Haworth, Bell Sys. Tech. J. **10**, 20 (1931).

[3] J. B. Johnson, Bell Sys. Tech. J. **8**, 286 (1929).

[4] R. F. Edgar, Trans. AIEE **56**, 805 (1937).

PRINCIPLE OF OPERATION

To obtain the magnetization curve and hysteresis loop of a ring specimen with this fluxmeter, the specimen is uniformly wound with two coils. The primary winding is used for producing the magnetizing force by energizing it by a direct current which can be changed continuously, by means of a slidewire potentiometer. The magnetizing force, H, for such a specimen is proportional to the magnetizing current. The secondary winding is connected to the integrating element of the fluxmeter which converts the change in flux interlinking the search coil to a change in current proportional to the flux density, B, in the specimen in a manner which will be described later. The two currents, one proportional to B and the other proportional to H, are passed through two separate networks which respectively adjust the scale of the two independent mechanisms of a double element Leeds & Northrup Speedomax recorder. One of these mechanisms, the B element, drives the pen proportionally to B, while the second mechanism, the H element, drives the paper drum proportionally to H. By continuously increasing the magnetizing current from zero to a positive value followed by a cyclic reversal of the same value, the pen and paper drum of the recorder are simultaneously driven proportionally respectively to B and H in the specimen and the magnetization curve and hysteresis loop are traced. If, while tracing a curve, retrogressions of the magnetizing current are made, minor loops are obtained at any desired position, as shown in Fig. 1.

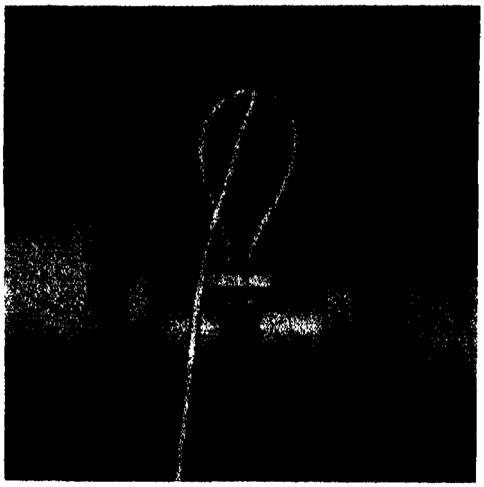

FIG. 2. Arrangement for measuring the magnetizing force in a short bar with the Chattock potentiometer.

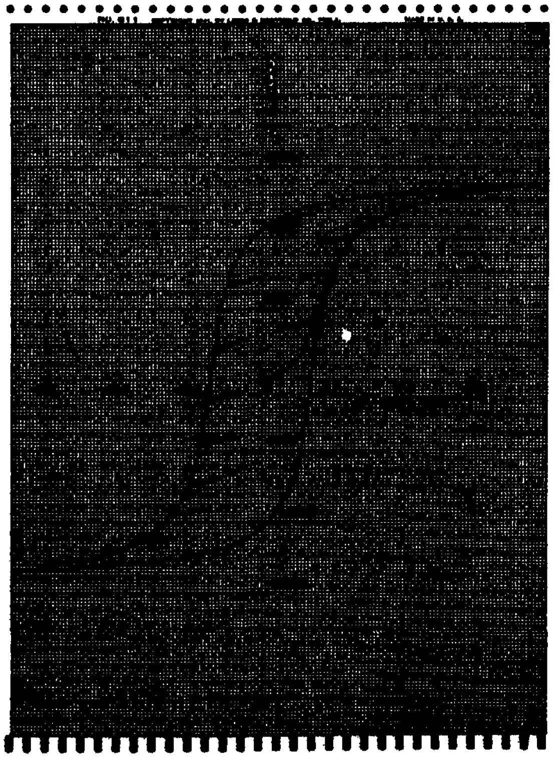

FIG. 1. Magnetization curve, hysteresis loop and minor loops for a ring sample of 45 Permalloy.

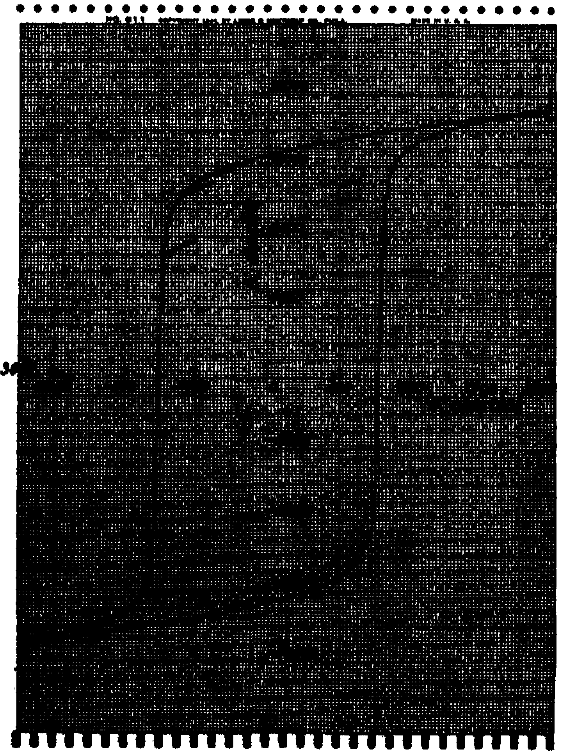

FIG. 3. Major hysteresis loop and minor loops for a cylinder of Alnico V, 0.47 in. diam. × 0.67 in. long. H is measured with a magnetic potentiometer and a second integrator.

---

[5] A. J. Williams, Jr., Trans. AIEE 57, 565 (1938).

For tracing the magnetization curve and hysteresis loops of samples in the form of straight bars, the magnetizing force is supplied by a solenoidal field or the field between the poles of an electromagnet. Since in this case the field in the specimen is not strictly proportional to magnetizing current, the field must be measured independently. This is accomplished by means of a Chattock magnetic potentiometer coil[6, 7] whose ends span the *B* search coil and are in contact with the specimen, as shown in Fig. 2. This potentiometer is connected to a second fluxmeter (*H* integrator) which, like the *B* integrator, converts changes in *H* in the specimen to a current proportional to it. This current is now passed through the *H* control network to drive the paper drum of the recorder. By a slow cyclic change of the magnetizing current the magnetization curve and hysteresis loop may be drawn as simply and accurately as for a toroidal specimen. An example of such a curve for a straight bar is shown in Fig. 3.

Because of the infinite time constant of the integrators, the rate of tracing the magnetization curves and hysteresis loops can be varied from approximately one-quarter minute to 5 minutes or longer, depending upon the specimen. For specimens of high permeability, having loops with steep sides, the eddy currents set up in the specimens cause the flux to lag behind the magnetizing force if its rate of change is too rapid. For this reason, the rate of change of magnetization is always kept slow enough to insure that the motion of the pen is in step with the motion of the chart.

The integrating circuit resembles the familiar ballistic galvanometer circuit in which the search coil is connected in series with a galvanometer and the secondary of a mutual inductance coil. Unlike the ballistic method, however, Edgar showed that the galvanometer can be used approximately as a null instrument by opposing the search coil interlinkages by equal interlinkages from the mutual inductance secondary coil. This is accomplished by splitting the light beam from the galvanometer between two photo-cells connected in a bridge circuit and applying the voltage unbalance, resulting from the change in light distribution as the galvanometer tends to deflect, to the grid of a vacuum tube in the primary circuit of the mutual inductance. The change in primary current so obtained is a measure of the change in search coil interlinkages, which is used to drive the *B* element of the recorder.

The *B* and *H* integrators are housed in individual cabinets approximately 30 in. wide by 18 in. deep and 72 in. high, provided with relay rack mountings for the various control panels. The power supplies are in a standard relay rack size cabinet. The double element recorder and its amplifier circuits are mounted on a separate frame. Since the *B* and *H* integrating circuits

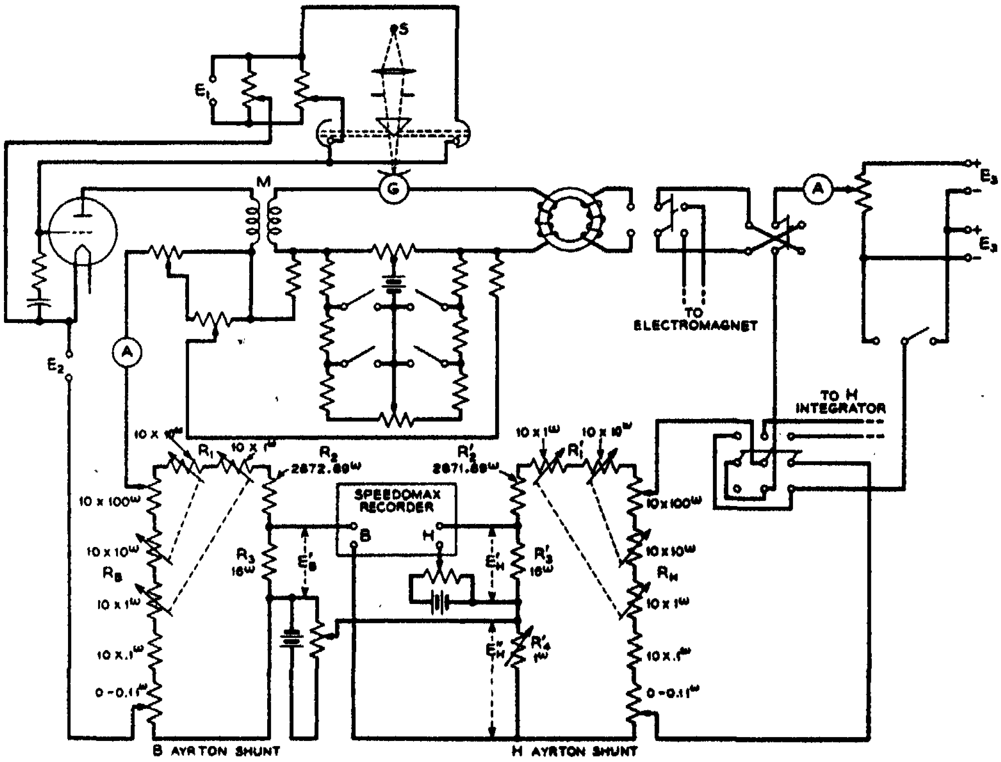

FIG. 4. Diagram of the *B* integrator and the magnetizing circuit.

---

[6] A. P. Chattock, Phil. Mag. 24, 94 (1887), first showed that the magnetic potentiometer coil can be used to measure the line integral of the magnetic field ($\int H dl$) between two points.

[7] L. F. Bates, Phil. Mag. 36, 297 (1945).

are identical, only the *B* integrator, together with the magnetizing circuit, is shown in the diagram of Fig. 4. When bar samples are tested the *H* integrator is connected to the *H* control network of the recorder in place of the magnetizing circuit.

POSSIBLE CAUSES OF ERROR

The fluxmeter is capable of high accuracy, stability and sensitivity. Its successful operation is due to the painstaking care in all details of its design and construction in order to eliminate or compensate drift over the entire scale. Drift of the mutual inductance current, arising from uncontrolled drift of the galvanometer, could result in large errors. In order to maintain a high over-all accuracy the objective was to limit errors due to drift to the order of 0.1 percent in a period of approximately 5 minutes—usually longer than is required to trace a hysteresis loop.

The principal causes of galvanometer drift are as follows: (a) Thermal e.m.f.'s arising in the galvanometer circuit. (b) Mechanical instability due to vibrations. (c) The restoring torque of the galvanometer suspension resulting from the small displacement necessary to initiate and maintain the current change in the mutual inductance. (d) Leakage currents into the galvanometer circuit from the neighboring higher potential circuits.

The method of correcting drift to achieve the required degree of stability is described in the following section.

Other sources of error are in the calibration of the mutual inductance coil and in the recorder and its input control networks.

STABILITY OF THE GALVANOMETER CIRCUIT

The galvanometer or secondary circuit of the integrating system consists of the galvanometer, the search coil, the mutual inductance secondary and a galvanometer control circuit. The procedure in setting up this circuit to prevent instability from thermal e.m.f.'s, was to reduce the number of circuit junctions wherever possible and to prevent significant temperature gradients in the junctions between the various circuit elements which could not be avoided. This is accomplished by providing isothermal enclosures for parts of the circuit where thermal e.m.f.'s are likely to arise.

The galvanometer control circuit is a bridge for balancing out galvanometer drift due to any residual thermal e.m.f. It is also used for the initial adjustment of the primary current of the mutual inductance coil by momentarily unbalancing the circuit in the appropriate direction by the scale shift switches shown in the circuit diagram.

The arrangement of the optical system is shown in Fig. 5. It consists of a lamp, a concave galvanometer mirror, a right angle prism and photo-cells. The mirror and prism are front coated with an evaporated aluminum film. Light from the lamp illuminates a slit in front of the galvanometer mirror which reflects the light beam to the prism. The prism edge between the right angle faces splits the light beam and each part is reflected by a prism face onto the cathode of a photo-cell located at each side of the prism.

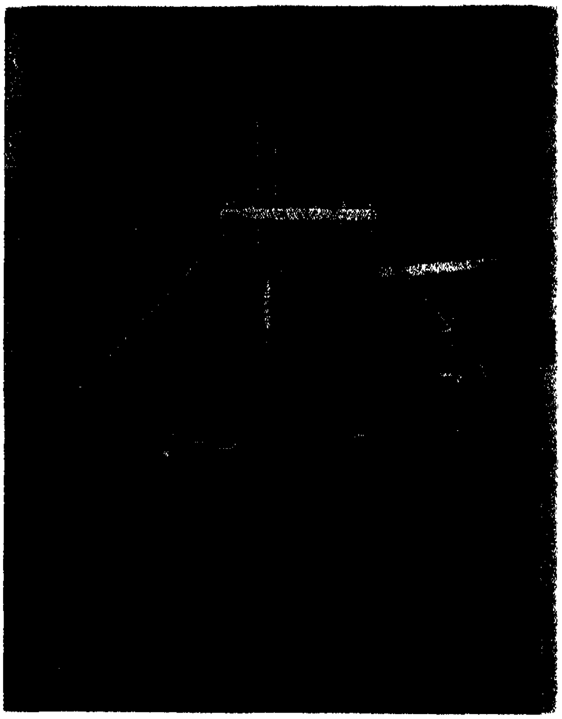

FIG. 5. The optical system of the recording fluxmeter.

The lamp, galvanometer and prism and photo-cell assembly are mounted on a brass plate. Optical bench parts permit easy adjustment and focusing of the optical system. The vacuum tubes for supplying the mutual inductance primary current are also mounted on this plate to permit direct connections between them and the photo-cells.

Mechanical stability of the galvanometer and its optical system is achieved by means of a suspension hung from the cabinet housing. It consists of a damped spring connected through a fine piano wire link, to one point of a framework attached to an extending above the plate. This link assures that the plate remains permanently level. The incoming leads are supported from a terminal block fastened to a second link also attached to the spring suspension. A corresponding terminal block attached to the plate directly below is connected to the circuit elements on the plate and the two blocks are interconnected through flexible coils of fine wire.

Provision is made to anchor the table rigidly so as to avoid setting the system into vibration whenever zero adjustments of the galvanometer are required. This is accomplished by an elevator platform, directly below, which picks up the plate on three adjustable screw supports without change of plate level. The elevator platform is attached to the shaft of a piston which is pneumatically operated. The operation is smooth and gentle and no perceptible disturbance is imparted to the suspension system when it disengages from the plate. Any residual motion is damped out magnetically by means of a copper disk attached at each end of the plate, free to move in the air-gap field of a strong permanent magnet.

Because of the small, but definite, galvanometer deflection necessary for a given mutual inductance current, a slow downward drift will result unless the restoring torque of the galvanometer coil suspension is balanced out. Suitable compensation is provided by an adjustable voltage tapped from the mutual inductance circuit and applied across the resistance in the galvanometer circuit.

THE RECORDER AND AYRTON SHUNT CONTROLLER

The two element Speedomax recorder was specially built by Leeds and Northrup for this application. The units are essentially high speed, self-balancing slide wire potentiometers for measuring unknown voltages. Compensation of slide wire wear is made by an adjustment of the slide wire current. The potentiometer slide wires of the two units are similar and the potential drop is 0.4 millivolt per half-inch or main division, δ, of the coordinate scale.

The networks for adjusting the B and H scales are Ayrton shunts, also supplied by L and N and are shown schematically in Fig. 4. The input side R_B of one network is connected in series with the mutual inductance of the B integrator and the input side R_H of the other is connected in series with the magnetizing coil or the mutual inductance of the H integrator as the case may be. The recorder elements are connected across the 16-ohm output resistances of the shunt arms in series with an adjustable voltage from a battery source to permit scale shifting for locating the curve with respect to the chosen origin on the paper. The corresponding decade resistances in R_B and R_1 and in R_H and R_1' are double decked and connected so that the sum of R_B and R_1 and the sum of R_H and R_1' remain unchanged for all settings. The recorder elements thus operate from a substantially constant input resistance. From the circuit constants, the product of the mutual inductance current I_B and the Ayrton shunt resistance setting R_B is given by

$$I_B R_B = 0.1\delta_B \text{ volt} = E_B. \tag{1}$$

If I_B is the change in primary current of the mutual inductance M caused by a change in interlinkages in a search coil of n turns around a specimen of sectional area A cm^2, the flux density in the specimen is given by

$$B = (M10^8/nA)(E_B/R_B). \tag{2}$$

From Eq. (2) R_H is determined for any scale of B chosen with respect to E_B. Similarly the magnetizing force for a toroidal specimen is given by

$$H = (4N/10D_m)(E_H/R_H), \tag{3}$$

where N is the number of turns of the magnetizing winding and D_m is the mean diameter of the specimen. The resistance setting R_H for the required H scale can be determined from this relationship.

When the magnetic field in a bar sample is measured with the H integrator and a Chattock potentiometer coil, the scale setting is also readily determined and depends upon whether the nA or MMF constant of the potentiometer is given.

The intrinsic magnetization curve, $(B-H)$ *vs.* H, may be obtained by subtracting a voltage E_H'' from E_B' by a predetermined setting of R_4' in terms of known constants.

Any part of the magnetization curve or hysteresis loop may be magnified by appropriate scale expansions.

ACCURACY AND SENSITIVITY

The accuracy is dependent upon the mutual inductance and upon the recorder and its associated Ayrton shunt controllers. The accuracy of the mutual inductance is estimated to be 0.25 percent and the accuracy of the recorder and controller is given as 0.25 percent, giving an over-all accuracy of 0.5 percent. Actually the accuracy is found to be somewhat better than this estimate.

At maximum sensitivity, only 4 interlinkages are required for a deflection of one mm. This is to be compared with sensitivities of ordinary ballistic galvanometers requiring 100 to 500 interlinkages for a mm deflection.

The accuracy and sensitivity are independent of the galvanometer circuit resistance.

CONCLUSIONS

The recording fluxmeter described is an exceptionally sensitive and flexible instrument. It has been very valuable in extensive investigations of magnetic materials. Its maximum sensitivity is many times greater than that of the conventional ballistic galvanometer. The B and H scales can be adjusted for a wide range of sensitivity and constants of the specimen. The calibration is provided simply by the scale settings which are determined in advance from known constants. Magnetization curves and major and minor hysteresis loops of ring and bar samples can be traced in a few minutes compared to the several hours required by the ballistic method.

THE REVIEW OF SCIENTIFIC INSTRUMENTS VOLUME 21, NUMBER 7 JULY, 1950

Simple Variable Space Infra-Red Absorption Cell

JOHN U. WHITE*
The Perkin-Elmer Corporation, Glenbrook, Connecticut

(Received March 8, 1950)

A variable space liquid absorption cell is described for use in the infra-red spectral region. Its range of thicknesses from 5 mm to less than 10 μ makes it suitable for the compensation of absorption by solvents in a double beam spectrophotometer; its accuracy and reproducibility are sufficient for most direct qualitative and quantitative measurements. The minimum volume is approximately one cc, and the leakage is negligible. Its windows of rocksalt may easily be removed and repolished.

VARIABLE thickness liquid absorption cells have been available for use in the visible and ultraviolet parts of the spectrum for many years.[1] More recently descriptions of cells suitable for use in the infra-red have been published by Barr,[2] Smith,[3] and Gordon.[4] Each of these has many good features but none is satisfactory for the present purpose. For use with the Perkin-Elmer Model 12[5] and Model 21[6-8] Infra-Red Spectrometers, the following features were considered important:

(1) angular aperture of f-4 and useful area $\frac{3}{4}$ in. in diameter,
(2) range up to 5 mm,
(3) accuracy of thickness setting within a few μ,
(4) leak-proof for volatile liquids,
(5) windows that are easily removed and repolished,
(6) ruggedness and convenience of use.

The cell described by Gordon and Powell would be satisfactory except for the fragility of the fine thread and the limited range imposed by the flexible diaphragm method of sealing it. The present cell is to a large extent a modification of theirs with the substitution of a double nut employing coarser differential threads and a long cylinder and piston for the liquid seal. It is readily demountable with a design that requires only one flat surface on each window with no precise orientation between it and the other surfaces.

The cell is illustrated schematically in Fig. 1. It has a useful window area three-quarters of an inch in diameter with a clear aperture over this area of f-4. It is 4.88 in. long and 3.25 in. in diameter, excluding the filling needles, *F*. It employs a close fitting cylinder, *C*, and piston, *P*, to keep the windows, *W*, parallel to each other and to minimize leakage between the moving parts. Motion is controlled by the differential nut, *N*, on the two threads, *TC*, and *TF*, with the large compression spring, *S*, to press the windows toward each other and remove backlash. Thread pitches of 1 and 0.8 mm give a differential piston advance of 0.2 mm for every turn of the nut. The precision cylinders and the threads are completely enclosed to protect them from damage. Molycote* is used as a lubricant.

Of the maximum possible separation of 7 millimeters, 5 are calibrated for use. Two additional millimeters are for overrun and for take-up for gradual changes due to repolishing the inner window. The scale may be read to 1μ using millimeter and hundredth millimeter calibrations on the nut, and tenth millimeter and μ-index lines on the outside of the case. To adjust the scale zero, the index lines may be moved until the scale reading agrees with the cell thickness at some measured setting. The small piece with the tenth millimeter index lines may be moved by loosening two screws. To move the μ-index lines the outer case must be loosened and turned. These scales are illustrated in the photograph shown in Fig. 2, where the separation is set to 0.245μ.

The windows are rocksalt, 70×10 mm and 36×8 mm. The large one is held against the ground flat seat, *FS*, on the end of the cylinder by pressure screws on a steel ring. As it is seated on the side facing the inner window, this side must be flat, but there is no

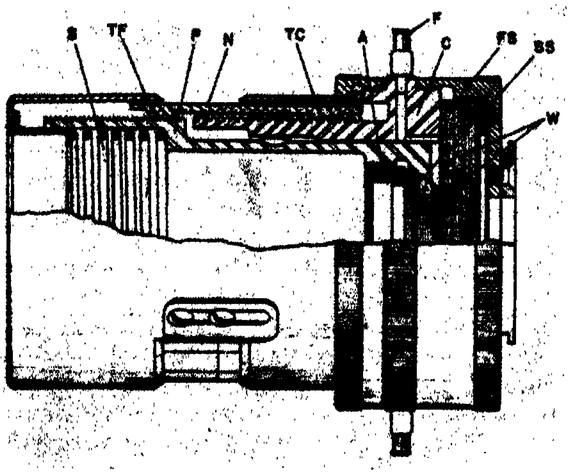

FIG. 1. Cross section of variable space absorption cell.

---

[*] Present Address: The White Development Corporation, 90 Lincoln Avenue, Stamford, Connecticut.
[1] Adam Hilger and Sons, London, England.
[2] E. S. Barr, Rev. Sci. Inst. 12, 396 (1941).
[3] D. C. Smith and E. C. Miller, J. Opt. Soc. Am. 34, 130 (1944).
[4] R. R. Gordon and H. Powell, J. Sci. Inst. 22, 12 (1945).
[5] Barnes, McDonald, Williams, and Kinnaird, J. App. Phys. 16, 77 (1945).
[6] J. U. White and M. D. Liston, J. Opt. Soc. Am. 40, 21 (1950).
[7] M. D. Liston and J. U. White, J. Opt. Soc. Am. 40, 36 (1950).
[8] J. U. White and M. D. Liston, J. Opt. Soc. Am. 40, 93 (1950).

[*] Molycote is the trade name for a molybdenum sulfide dry lubricant manufactured by The Alpha Corporation, Greenwich, Connecticut.

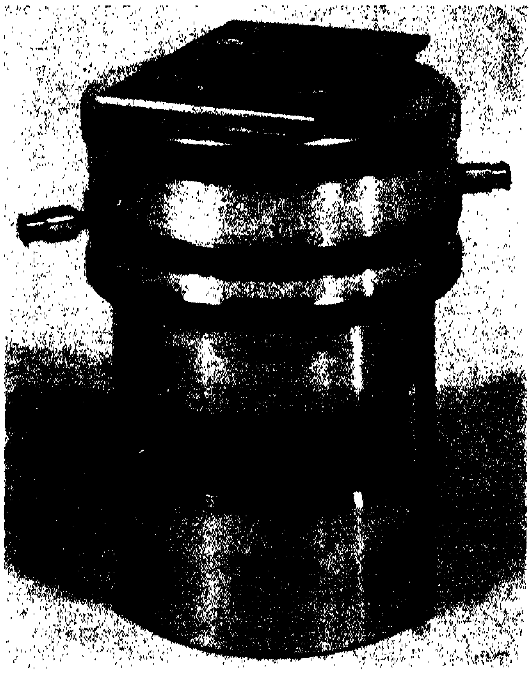

FIG. 2. Photograph of variable space liquid cell.

strict requirement on the flatness of the other side or the parallelism of the two. The small window has a spherical bevel and is held in a mating spherical seat, *SS*, in the piston. Its orientation is adjustable by changing the pressure on its retaining screws, *A*. By loosening one and tightening another, it can be slid slightly in its seat until the visible interference fringes observed under a mercury arc indicate it to be parallel to the outer windows. The windows are enclosed except for the area actually used.

The cell is filled by inserting a hypodermic syringe into one of the needles pressed into the cylinder. It has a minimum volume of about one to two cc in the closed position, depending on how far the small window protrudes through the end of the piston. The windows appear to make tight joints with their lapped seats, and losses of samples along the ground cylinders are small. In tests with the cell filled with carbon disulfide the miniscus had not appeared in the window area after four hours.

The differential thread and double nut were used to make the scale easier to read and to avoid relative rotation between the inner and outer cylinders. If the cylinders were permitted to rotate as they would with a single thread drive, the cell could only be closed if both windows were exactly square on the axis, and any contact between them would result in twisting scratches. The method of mounting salt plates with retaining rings and push screws has been found best to avoid the twisting and scratching that results when a threaded retaining ring is screwed directly against the window.

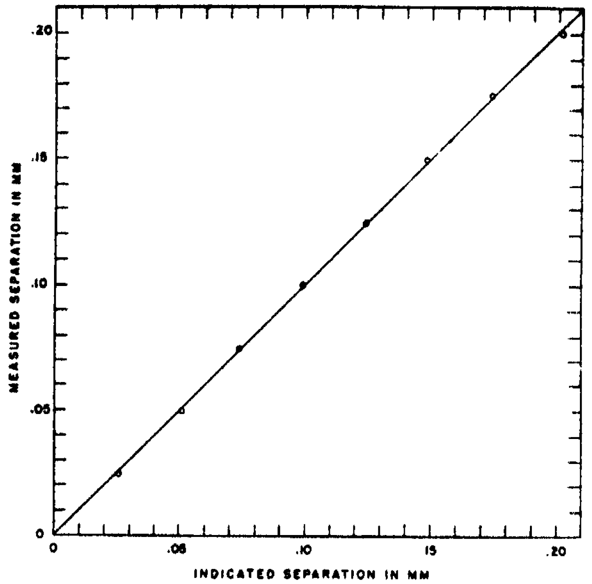

FIG. 3. Calibration curve of variable space liquid cell. An index correction of 0.005 mm has been applied.

The adjustment for parallelism proved adequate during preliminary experiments with an annular ring of rocksalt on the end of the outer cylinder as a seat for the large window. The ring was polished simultaneously with the inner window to make them both parallel and coplanar.

In testing the cell visible and infra-red interference fringes were used. Observation of the reflected fringes in mercury green light indicated that the two windows remained parallel within about two wave-lengths as their separation was changed. The reproducibility of setting over short times was tested by measuring the separation for five repeat settings to the same scale reading from the same direction. The mean departure from the mean was 1.0μ, with a maximum departure of 1.6μ. The difference between the mean separations at the same setting approached from opposite directions was 6.4μ. Over long times the scale must be readjusted to take account of changes in the rocksalt windows. The accuracy of the scale is shown in Fig. 3, where the measured distance between the windows is plotted against scale reading. The calibration is essentially a straight line with a sinusoidal variation of approximately one μ superimposed on it. This performance indicates that the cell is accurate enough for most qualitative and quantitative analyses at thicknesses greater than 0.1 mm. The adjustment is smooth enough to permit accurate compensation for the absorption bands of the solvent in a solution by successive trial and error settings until the bands are eliminated from the record. Approximate compensation is obtainable directly by setting the cell to the thickness calculated to be equivalent to the solvent content of the sample.

Duration of Scintillations from Organic Phosphors

J. O. ELLIOT, S. H. LIEBSON, R. D. MYERS, AND C. F. RAVILIOUS
Electricity Division, Naval Research Laboratory, Washington, D. C.

(Received January 25, 1950)

Measurements have been made on the time of decay of scintillations from organic phosphors irradiated with gamma-rays. Interference between the output pulse from a photo-multiplier and its reflection from a shorted line is used to determine the time constants.

SEVERAL authors[1–4] have reported measurements of the duration of light flashes from organic phosphors when excited by gamma-radiation. In each case a photo-multiplier tube was used as a detector of the light flash and its output pulses were fed either directly to oscilloscopes or through fast amplifiers and then to oscilloscopes. The pulse time was determined from the oscilloscope tracing.

The present investigation employed a shorted line technique to measure pulse decay times. The output of a 931-*A* photo-multiplier was fed into an *RG8U* coaxial cable, with a short-circuited variable length side arm, as shown in Fig. 1; the resultant of each original pulse and its out-of-phase reflection from the shorted line was rectified by a germanium crystal and was fed to a preamplifier, amplifier, and ten-channel discriminator and scaler. Curves of counting rate *vs.* length of shorted cable for a given pulse height setting of the discriminator were taken. These curves should exhibit a steady counting rate for long lines and should show a decreasing counting rate for lines of length less than the critical length corresponding to the beginning of interference between a pulse and its out-of-phase reflection.

Germanium crystals were selected by oscilloscopically observing their rectification properties for pulses using a long length side arm with first an open-circuit termination and then a short-circuit termination. All the diodes tested exhibited similar rectification characteristics. The error introduced by imperfect rectification is well within the the range of the experimental error.

Reflections from the germanium crystal were minimized by keeping the length of line between the crystal and the shorted line junction as small as possible. The load output of the photo-multiplier and the cathode follower input were resistances equal to the characteristic impedance of the lines, so that no reflections occurred at these points.

Oscilloscopic observations[2] have shown the scintillation pulses of organic phosphors to have exponential decays. Due to statistical fluctuations, individual pulses will deviate from the simple exponential shape; however, since the method presented here is a statistical method in principle, the pulse may be assumed to be exponential in character, as shown in Fig. 2. If the amplifier and scaler are peak voltage operated, no change in counting rate for a given discriminator setting should be expected until the reflected pulse detracts from the peak of the original pulse. However, if the time constant of the amplifier is much longer than the width of the input pulses, an integrating effect is obtained and the triggering of the scaler is dependent on the area under the pulse. With such a time constant, no change in count rate should be observed until the reflected pulse starts to overlap the photo-multiplier output pulse.

Since the shape of the output pulse of the photo-multiplier is assumed to be of the form $e^{-t/\tau}$, the over-all

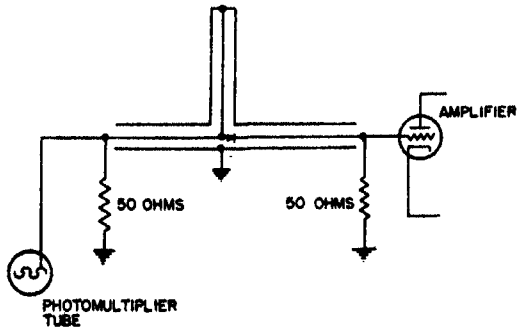

FIG. 1. Diagram of the shorted line and detection circuit.

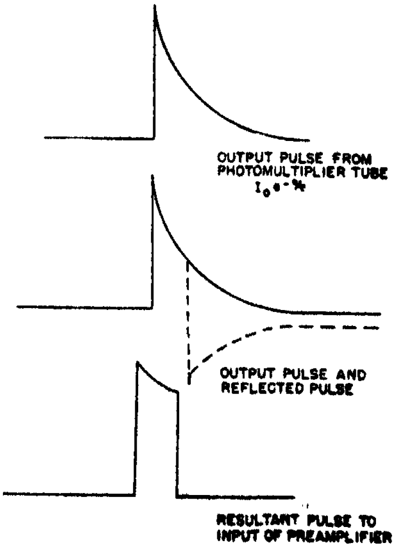
OUTPUT PULSE FROM PHOTOMULTIPLIER TUBE
$I_0e^{-t/\tau}$
OUTPUT PULSE AND REFLECTED PULSE
RESULTANT PULSE TO INPUT OF PREAMPLIFIER

FIG. 2.

---

[1] R. Hofstadter, private communication.
[2] G. T. Kelley, Oak Ridge National Lab. Report No. 366 (1949).
[3] P. R. Bell, IRE-AIEE Conference on Electronic Instrumentation in Nucleonics and Medicine (New York City, October 31, November 1–2, 1949).
[4] W. H. Jordan and P. R. Bell, Nucleonics 5, 30 (1949).

TABLE I. Calculations for anthracene.*

Pulse height (p)	Equivalent pulse height for ∞ line ($p/0.632$)	Corresponding ∞ line counting rate	Critical cable length L_c	$\tau/n = 2L_c/1.98\times10^{10}$
volts	volts	counts/min.	cm	sec.$\times10^{-8}$
10	15.8	18,400	380	3.8
20	31.6	10,100	360	3.6
30	47.4	6300	380	3.8
40	63.2	4100	360	3.6
50	79.0	2900	360	3.6
60	94.8	2200	360	3.6

* Average $\tau/n = 3.6\times10^{-8}$ sec. Constant n for diode used $=0.94$. $\tau = 3.4\times10^{-8}$ sec.

response of the system will be of the form $e^{-nt/\tau}$, where n is a constant describing the non-linearity of the entire rectification and amplification system. A measurement of n over the desired pulse duration range (10^{-9} to 10^{-7} sec.) proved to be quite difficult. A pulse source with accompanying attenuator was substituted for the photo-multiplier in Fig. 1, and n was obtained by measuring the voltage ratio produced at the amplifier output by a known voltage ratio from the pulse source. This pulse source showed n to be a constant for 2.5×10^{-8} sec. pulses and for 2.5×10^{-7} sec. pulses. A reliable determination of n for 10^{-9} sec. pulses was impossible due to the unavailability of such a pulse source. A further check on the accuracy of the determination of n was made by Dr. R. C. Waddel of this Laboratory, who measured the decay constants for the same phosphor samples used in this experiment by oscillographic techniques and whose results agree with the ones presented here within the error indicated in Table II. Dr. Waddel undertook a further verification of n at higher frequencies by measuring twice the mean deviation for the dark noise pulses of a photo-multiplier and obtained 4.5×10^{-9} sec. which agrees fairly well with the value presented below considering the assumptions, as stated below, that must be made to obtain a value for dark noise pulses with the shorted-line apparatus. Subsequent calibrations for different diodes were made by finding the value of n required to obtain the same values for the decay constants of the standard anthracene and stilbene crystals as those presented here.

TABLE II. Decay constants in seconds.

Author	Phosphor Anthracene (%)		Stilbene (%)	
NRL	3.4×10^{-8} sec.	±10	1.3×10^{-8} sec.	±20
Bell[3] and Kelley[2]	3.5	±10	1.0	±20
Hofstadter[1]	3.0	±30	1.5	±30

Referring to Fig. 2, the area that would appear at the discriminator-scaler input due to the original photo-multiplier pulse alone would be proportional to

$$\int_0^\infty e^{-nt/\tau}dt = \tau/n;$$

this is also the area that would appear if the variable length side-arm of Fig. 1 were infinite in length. The desired length of shorted line to measure the decay constant τ/n of this pulse is that line which gives a reflected pulse whose leading edge occurs at a time t' after the leading edge of the original photo-multiplier pulse, where t' is the time required for the amplitude of the original pulse to fall to $1/e$ of its peak value. t' then is τ/n. The resultant area of the original pulse and the reflected pulse from the desired length of shorted line appearing at the discriminator-scaler input

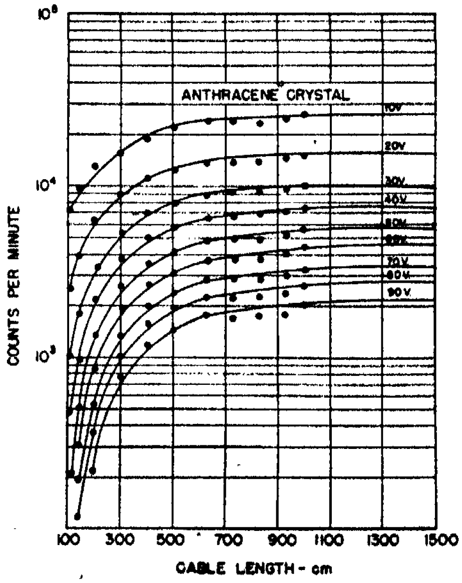

FIG. 3. Anthracene counting rate *vs.* shorted cable length for various pulse height discrimination levels.

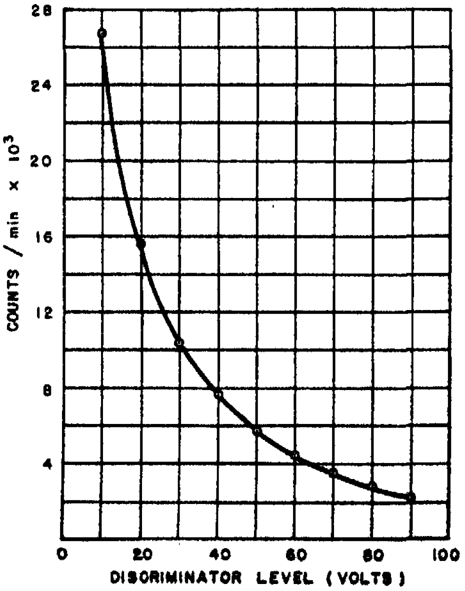

FIG. 4. Anthracene counting rate *vs.* pulse height discrimination level for the infinitely long shorted line.

would be proportional to

$$\int_0^{\tau/n} e^{-nt/\tau}dt=\tau(1-1/e)/n,$$

taking into account the action of the diode (again refer to Fig. 2). The ratio of the areas appearing at the discriminator-scaler input for the desired shorted line and the infinite line is $1-1/e$ or 0.632. Thus the constant τ/n may be determined for anthracene from a curve of the counting rate *vs.* the shorted cable length for different discriminator settings as shown in Fig. 3 and from the data for the counting rate *vs.* discriminator settings for the infinite line as shown in Fig. 4. This determination is made for a given discrimination level of Fig. 3 by finding that length of shorted line which gives the same counting rate as the infinite line gives (Fig. 4) at a discriminator setting 1/0.632 greater. The determinations in the case of anthracene are presented in Table I where it is seen that τ/n is independent of the discriminator setting. From the average value of τ/n, from the constant for the diode used, and from a measured value of 1.98×10^{10} cm/sec. for the velocity of propagation in *RG8U* cable, the duration τ of the scintillations of anthracene may be found. Similar measurements and analyses were made for the scintillations of stilbene. All measurements were made with the phosphors at room temperature using a 10 microcurie radium gamma-ray source. The photomultiplier was cooled to liquid nitrogen temperature to reduce the dark noise. Table II presents the results of these measurements, together with determinations by other authors for the same phosphors using oscillographic methods.

In view of the mechanism of the production of noise pulses, it would seem more reasonable to assume a Gaussian distribution for their time duration. Using the same type of analysis but adjusting the constants to fit a Gaussian shape rather than exponential shape, similar measurements on dark noise pulses yielded a value of 6×10^{-9} sec. for twice the mean deviation.

No attempt has been made to correct the values in Table II for the spread in photo-multiplier time.

The anthracene single crystal samples were obtained from the Harshaw Chemical Company. The stilbene crystals were prepared by Dr. S. Zerfoss and Mr. L. R. Johnson of the Crystal Section of this Laboratory.

THE REVIEW OF SCIENTIFIC INSTRUMENTS VOLUME 21, NUMBER 7 JULY, 1950

Instrument for Directional Studies of Cosmic-Ray Intensity

H. W. BOEHMER AND J. E. COOLIDGE*
Department of Physics, University of Colorado, Boulder, Colorado

(Received March 13, 1950)

In order to obtain a versatile instrument for directional cosmic-ray studies, and to investigate an indicated correlation of the soft component of cosmic radiation with the present cosmic-ray burst studies being carried on at the University of Colorado a dual cosmic-ray telescope was constructed. Each bank of the telescope consists of five counter trays with nine Geiger counters in each tray. The electronic circuits are connected to give three triple consecutive coincidence trains: 1, 2, and 3; 2, 3, and 4; 3, 4, and 5. By the insertion of eight centimeter-thick lead blocks covering the sensitive area of a Geiger tray between trays 3 and 4, and 4 and 5; a separation of the components of the radiation is possible. The telescope is adjustable in zenith in 15 degree intervals from 0 to 75 degrees from the vertical. However, in azimuth, in order to investigate asymmetry characteristics, two positions 180 degrees apart are employed. The control of the telescope is entirely automatic with the recording of data being obtained by means of periodic photographs of the indicating panel, showing the counting rate, zenith and azimuthal positions, and the time and date of the measurement. The telescope changes in zenith and in azimuth every forty minutes; the changes in zenith and azimuth being displaced twenty minutes. A cycle of operation, which consists of the step change in zenith from 0 to 75 degrees with the associated alternate azimuthal changes, requires four hours.

SINCE the initial measurements of the East-West asymmetry of cosmic radiation by B. Rossi,[1] T. H. Johnson and J. C. Street,[2] and T. H. Johnson,[3] many elaborate instruments have been employed to determine the nature of the asymmetry and associated phenomena. One characteristic which is common to many measurements is that the data are obtained over a relatively short time interval. Other measurements have been handicapped by the necessity of manual operation. In order, therefore, to obtain a versatile instrument for directional cosmic-ray studies and to investigate possible correlations of the components of cosmic radiation with the present cosmic-ray burst studies and solar studies being carried on at the University of Colorado, a dual cosmic-ray counter telescope was constructed. The telescope was designed to be fully automatic, requiring only routine checks of its operation and semi-weekly attention to the recording apparatus. This work began in the fall of 1947 and was sponsored by an ONR grant N6onr-231, T.O. V. The instrument began its operation in September, 1948 and ran continuously except for occasional repair and adjustment until June, 1949 at which time it was temporarily shut down because of the termination of the cosmic-ray burst studies.

---

* Now in the Department of Electrical Engineering, Pennsylvania State College, State College, Pennsylvania.

[1] B. Rossi, Ric. Sci. 5, 583 (1934).

[2] T. H. Johnson and J. C. Street, Phys. Rev. 43, 381 (1933).

[3] T. H. Johnson, Phys. Rev. 45, 569 (1934), and Phys. Rev. 43, 703 (1933).

With the help of the voluminous data which were obtained during this nine-month operation, interesting results concerning the over-all characteristics of East-West asymmetry along with its seasonal and daily variations are expected. At the present time only a part of the data has been analyzed and these preliminary results are to be reported elsewhere. The purpose of this paper is to describe the apparatus.

GENERAL DESCRIPTION OF APPARATUS

The instrument (Fig. 1) consists of 2 telescope banks which can be positioned in zenith at 15° intervals from 0–75° by means of a motor driven lead screw. In order to facilitate asymmetry measurements, the telescope is turned back and forth through a 180° azimuthal variation at suitable intervals of time. This arrangement allows each bank of the telescope to divide its recording time equally between each direction at a given zenith angle.

TELESCOPE BANKS

The configuration of the telescope banks is the same as that employed in a vertical dual unit constructed at the Bartol Research Foundation.[4] It consists of 5 trays (designated as trays 1, 2, 3, 4, and 5 numbering from the top down) of Geiger counters spaced 5.5 in. apart, each tray containing 9 counters. The counters are supported by means of polystyrene strips which are grooved to hold the counters in close proximity (Fig. 2). In order to insure a low leakage, the leads from the Geiger counters are brought directly to the coincidence circuits through screw mounts in polystyrene strips. It was originally planned to use a ceresin wax to insure a low surface leakage. The polystyrene alone, however, gave a measured value of leakage current of less than 1 microampere which was deemed satisfactory. The dry climate of Colorado does not present the problem of surface leakage that causes trouble in measurements made in more humid regions.

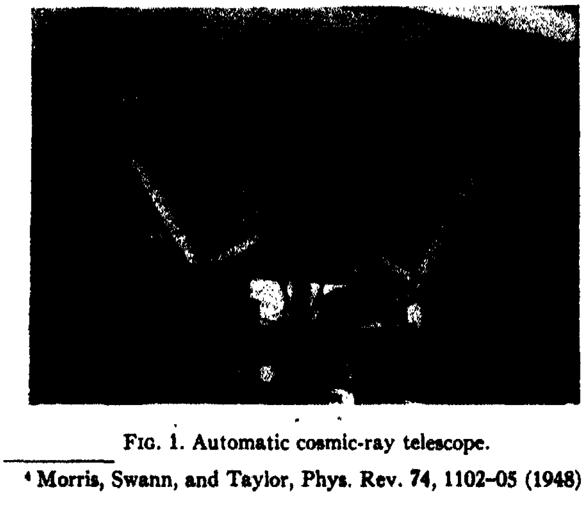

FIG. 1. Automatic cosmic-ray telescope.

The counters used in the telescope were designed and constructed at the Bartol Foundation. The counter consists of a glass cylindrical envelope in which are mounted a thin-walled (0.005 in.) copper tube 4 in. long, 0.395 in. outside diameter, and a three-mil tungsten wire as the anode. The gas employed in the tube is 94 percent argon and 6 percent oxygen at a total pressure of about 14 centimeters of mercury. A standard resistance quenching circuit was employed which results in a recovery time for the counter circuit of approximately 3.5×10^{-3} seconds. (An IRC 500 megohm resistor is used). Because of the relatively low counting rate, this recovery time results in a counter tray efficiency of 99.2 percent when considering the probability of losing counts due to rays passing through a counter during its recovery period.

The directional effect is achieved in the usual manner by use of coincidence circuits—the particular circuit employed being a standard triple coincidence circuit of the Rossi type (Fig. 3). The desirable low capacity in the Geiger circuit and also a compact circuit design is effected by mounting the quenching resistors and associated electronic circuits directly on the Geiger counter trays.

FIG. 2. Tray element of telescope.

In order that the characteristics of the soft, medium, and hard components of the radiation can be investigated, lead blocks 8 cm in thickness are mounted between trays 3 and 4 and trays 4 and 5. The trays are connected in triple coincidence schemes with coincidences 1-2-3, 2-3-4, and 3-4-5 being recorded for each telescope bank. Impulses registered for coincidence 1-2-3 will give a measure of the total radiation striking in the solid angle and tray area of the coincidence at the particular zenith angle of the telescope. In like manner, coincidences registered for 2-3-4 and 3-4-5 indicate the radiation of sufficient energy to pass through 8 cm and 16 cm of lead respectively, striking in the solid angle and tray area defined by the coincidences.

ZENITH POSITIONING

The adjustment in zenith angle is accomplished by means of a motor driven lead screw which pivots the banks around axes through the outer corners of the individual telescope banks. The connections to the lead screw from the individual banks are made by means of two tie rods on the ends of which are connected yokes—the yokes in turn are connected to the drive nut. The importance of this method of construction is the balanced load produced on the lead screw in the horizontal direction. With a common point of support through their individual tie rod yokes at the drive nut steel support pins, the horizontal components of the forces necessary to produce equilibrium exactly balance while the vertical components add. Because of the large mechanical advantage obtained through the screw and bevel gear system employed in the lead screw drive, a torque of only 12 in.-oz is necessary to produce the angular change under its most severe loading conditions. It is interesting to note that when the telescope banks are directed 75° from the vertical, the stress in the tie rods is a maximum, but the loading on the drive screw is very small. This condition is accomplished by means of the mechanical advantage afforded by the horizontal position of the tie rods.

---

[4] Morris, Swann, and Taylor, Phys. Rev. 74, 1102–05 (1948).

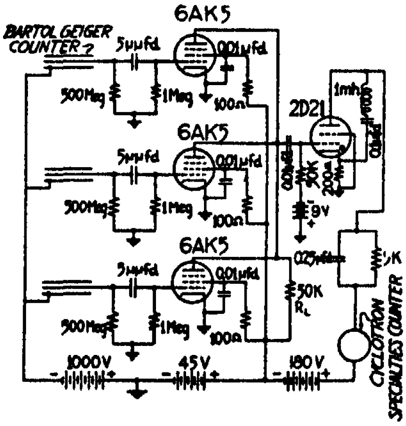

FIG. 3. Coincidence circuit.

The positioning control for zenith is activated by micro-switches connected directly to the base of one of the telescope banks. As the bank is pivoted by the motor driven lead screw an arm connected directly to the bank rotates with the bank and closes the proper set of micro-switches. Alongside each positioning micro-switch is a second switch which indicates the position of the telescope in zenith by lights on the main panel. This indicating contact is displaced slightly forward so as to insure the indication of the position before the control system has stopped the telescope. Such a direct method of controlling and indicating the position of the banks directly from one of the banks leaves no chance for error in the positioning or its indication. A schematic diagram for the zenith control is given in Fig. 4. The heart of the control is the Hayden timing motor (a) which makes one revolution every 40 minutes. A brush contact attached to the drive shaft of the motor closes control contact (b) which in turn activates coils "*c*" and "*d*." Coil "*c*" energizes the camera control circuit while coil "*d*" closes a hold-in contact for the circuit; i.e., allows the original motor-closed contact to open without changing the condition of the circuit and applies voltage to the zenith drive motor through the reversing relay (*e*). Assuming that the initial position of the telescope is vertical, the banks will be driven to the 15° position where the brush attached to the bank will close relay "*f*" through contacts on the zenith control and the contacts of the impulse relay "*g*." On the closing of the relay "*f*," the relay coil "*d*" is deactivated, turning off the motor and closing the coil of the impulse relay through the normally open contact of the relay "*f*." Thus, the impulse relay is switched to its other stable position, which opens the circuit to relay "*f*" and cocks the telescope control for its necessary zenith change. This cocking of the circuit is facilitated by having alternate position contacts with the (0-30-60) and (15-45-75) contacts connected to each side of the single pole double throw impulse relay. Depending then on the position of the impulse relay, the circuit is controlled by that set of zenith contacts corresponding to the position of the relay. As the positioning of the telescope is done in consecutive steps, the operation may be accomplished by switching the impulse relay at each step, setting the circuit for the next change. The time necessary for each zenith change is approximately 45 seconds. The next zenith change occurs 40 min. later when the same cycle of relay operation described above takes place. Following the zenith change, the camera circuit is pulsed through the adjoining contact to that of the main zenith control contact (*b*) by the Hayden motor-driven brush contact approximately 60 seconds after the start of the zenith change.

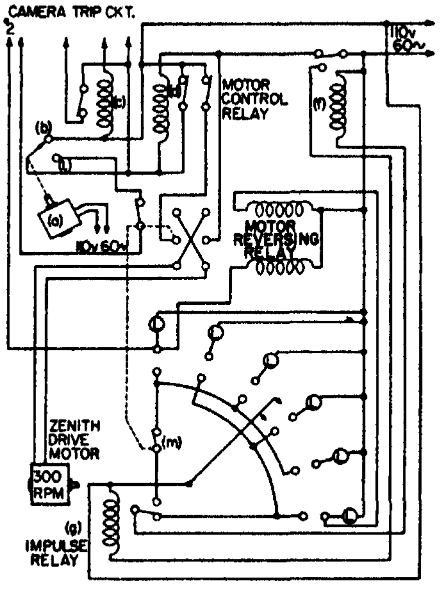

FIG. 4. Zenith control.

This system of change of zenith angle takes place in 15° intervals until a direction of 75° from the vertical is reached. At this position a cycle of relay operation is the same as in other positions but the motor relay is also reversed by the zenith 75° indicator contact which excites the reversing relay coil along with lighting the indicator light. In order that the telescope may return directly to the vertical, it is necessary to have the motor reversing relay interrupt the return to the impulse relay (*m*) which is common to zenith contacts (0-30-60). At the vertical position the system is returned to its normal operation ready for its necessary change to 15°. In order that a picture will not be taken during the return to the vertical (approximately 3 minutes is required for the return), the motor reversing relay also opens the camera control lead adjacent to the main zenith control contact (*b*). At the vertical, however, the camera is pulsed by a parallel circuit to that which is used at other position changes. The latter camera circuit is necessary in order that the main control will be free for operation for the change to 15°.

AZIMUTH POSITIONING

In order to investigate asymmetry of cosmic radiation, the telescope is set alternately in two positions of azimuth 180° apart, the positions of the banks simply being exchanged. This positioning is achieved by means of a worm gear drive which rotates the telescope through the 180° change. In order to avoid the necessity of slip rings and brushes, the telescope is rotated back and forth through the 180° change.

The positioning control in azimuth is accomplished by means of micro-switches operated directly by an arm attached to the telescope which not only controls the relay circuits necessary to the motor drive but also lights the indicator azimuth lamps on the meter panel to indicate the position of the telescope in azimuth. The 180° change is made in approximately 20 seconds.

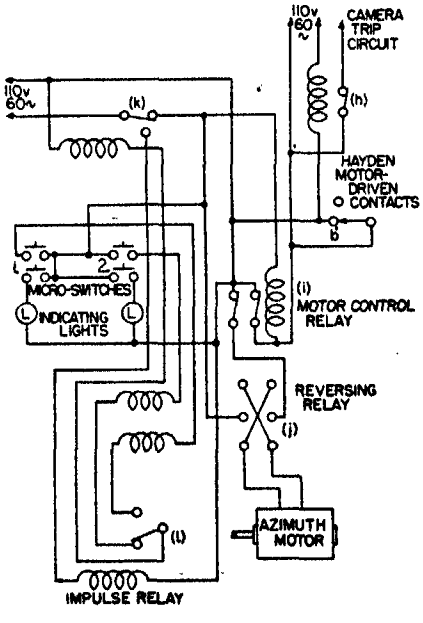

FIG. 5. Azimuth control.

The main control for azimuth is a second set of contacts activated by the Hayden motor driven brush contact. Relay "*h*" (Fig. 5), controls the camera circuit while "*i*" locks the circuit and drives the motor through the reversing relay (*j*). The azimuthal positions at 180° are controlled by micro-switches (1), (2). On contact, "2" being closed, the reversing relay is changed and relay "*k*" is opened. The opening of "*k*" releases the circuit, and on the closing of its normally open contact, relay coil "*l*" is excited. This switches the impulse relay to its other stable position. The relay control system is now set for the return through the 180° interval which occurs 40 minutes later. The camera circuit is pulsed after each azimuthal change.

RECORDING

The recording of coincidences occurring in each telescope bank is made by means of electromechanical counters manufactured by the Cyclotron Specialties Company of California. Together with the indicating lights of zenith and azimuth position and a 24-hour clock, the 6 electromechanical counters are mounted on a panel. The recording of data is accomplished, therefore, by means of a periodic photograph of this panel. As described in the discussions of zenith and azimuth control above, pictures are taken before and after each position change, enabling us to take into consideration the counts registered during the change which therefore could not be used in any calculations of the angular characteristics of the cosmic radiation. The camera employed is a war surplus motor driven gun camera which is pulsed so as to take a 3-frame picture. In order that the film will not be "fogged" in case the internal camera shutter remains open after being pulsed, an external shutter is employed which is pulsed and made to remain open by the same circuit that pulses the camera. This method requires the change of a 50-foot film cartridge every five days.

The camera control is illustrated in Fig. 6. Camera circuit No. 1 is activated by relays "*c*" and "*h*" of the zenith and azimuth control systems respectively. When relay "*a*" of the camera control is closed, the condenser "*c*" discharges by means of its normally open contacts through relay coil "*b*." The length of time that relay "*b*" will remain closed and (thus the time the camera motor will run) is determined by the RC time constant of the condenser and relay coil. The latter discharge time is adjusted so that a 3-frame picture is taken. The advantage of this type of control is that the length of time over which voltage is applied to the camera is independent of the length of time that the control relays in zenith and azimuth are closed. In order that 2 consecutive pictures may be taken at the vertical position, once on the return to the vertical and again just as it leaves that position, a parallel camera circuit is needed. This latter circuit is activated through the vertical indicator light contact on the zenith control.

COUNTING CHARACTERISTICS

Because of the random character of radiation to be measured, a counting rate determined from a finite time of recording is subject to statistical fluctuations which may be calculated from the theory of probability. The application of the probability theory to Geiger counter measurements has been discussed by many investigators.[5,6] All of these discussions are based on the Poisson distribution law which states that if N is the average number of counts in a time interval, T, supposed to be evaluated from an infinitely long period of observation, the probability that the number of counts recorded in any particular interval of duration, T, will be n, is given by

$$P_n=(N^n\times e^N)/N!.$$

Although in actual practice the quantity n is directly measured and the desired quantity is N, Rainwater and Wu[6] show that Poisson's formula is applicable to this problem. The standard deviation, which is defined as the amount by which any given measurement may be expected to be deviated from the mean value, is given by the formula

$$G=n^{\frac{1}{2}},$$

with the probable error given by $P_G=0.6745n^{\frac{1}{2}}$.

In the practice of making telescopic direction readings, the corrections that must be made to the observed counting rate are stated by T. H. Johnson[5] as (1) the difference between the actual and the effective area of the Geiger tube; (2) the variation of "j" (the rate per unit solid angle per second per unit area) over the effective aperture of the counters; (3) the probability that an ionizing ray can pass through the train without producing discharge of all counters; (4) the probability that false counts will occur when nearly simultaneous, but unassociated, rays pass through the counters; (5) the probability that two or more associated rays will pass through the train simultaneously and be recorded as a single count; (6) the probability that a group of associated rays from the side will discharge the counters simultaneously although no single ray has passed through the train; (7) the probability that two or more coincidences will occur within the action time of the mechanical recording device so that only one will be recorded; (8) the absorption of rays within the counter walls. Johnson discusses these considerations in general in his article, and we will discuss their application to the particular problem of the counter telescope described here.

(1) Because of the use of single layer trays of Geiger counters in forming the elements of the telescope, the problem of area efficiency becomes not the difference between the actual and effective area of a single tube, but that of the difference between the actual and effective area of a tray of tubes. The actual area of the tray (the actual area is defined as the area defined by the outer extremities of the tray of counters) is 116 sq. cm, with an effective area (the effective area is defined as that area through which an ionizing particle may pass and produce a discharge in a counter) of only 90 sq. cm. Thus, the active area consists of only 78 percent of the actual area. Each tray is an element of a three-coincidence train resulting in an over-all area counting efficiency of $(0.78)^3$ or 46.5 percent (E_A).

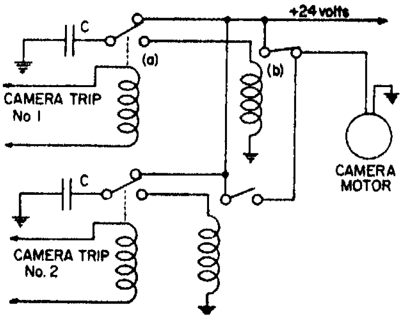

FIG. 6. Camera control.

(2) The variation of "j" over the aperture of the telescope presents no problem in the investigation of asymmetry as only comparative measurements as a function of position and time are required. However, in calculations of direction intensities, the variation of "j" over the aperture of the telescope can be accounted for by use of equations derived by Witmer and Pomerantz.[7] Witmer and Pomerantz calculate the average path length of particles passing through the coincidence train. In this calculation it is necessary to assume the angular distribution of the radiation being measured. If a cosine squared distribution is assumed, the number of counts can be expressed in terms of the intensity $I(0)$ as

$$N=[I(0)L^4A^2]/\lambda^6,$$

where A is the area of a train, L, the length of the train, λ is the average path length through the coincidence train. Therefore, from a measure of N, $I(0)$ can be calculated.

Effect (3) has been discussed in many papers and texts[8] and in this application results in a tray efficiency of 97 percent or an over-all coincidence counting efficiency of 90 percent (E_T).

(4) The probability that false counts will occur when any simultaneous but unassociated rays pass through the counter can be calculated. However, this accidental counting rate may be conveniently included in an experimental determination of the total accidental rate

---

[5] T. H. Johnson, Rev. Mod. Phys. **10**, 193 (1938).

[6] L. J. Rainwater and C. S. Wu, Nucleonics **1** (October, 1947), and Nucleonics **2** (January, 1948).

[7] E. E. Witmer and M. A. Pomerantz, J. Franklin Inst. **246**, No. 4 (1948).

[8] S. A. Korff, *Electron and Nuclear Counters* (D. Van Nostrand Company, Inc., New York, 1947).

due to both unassociated and associated (those due to showers) rays. This latter measurement will be described later.

The probability that a group of associated rays from the side will discharge the counter simultaneously although no single ray has passed through the train is a function of the showers produced in the surrounding structure or frame of the telescope. Due to the complexity of the structure, the number of such showers would be difficult to predict theoretically. However, it is possible to measure experimentally the number of accidental counts due to this shower production; the measurement includes those due to accidentals as discussed in Section 4. The technique consists of connecting trays 1 and 2 in bank number one of the telescope in coincidence with tray number three of bank number two when the telescope is in the vertical position. By this arrangement we have a coincidence train which is out of line and, therefore, can only be discharged by associated rays from the side or unassociated rays that pass through the train elements nearly simultaneously. An accidental counting rate of 0.16±0.008 counts/minute was observed.

As it is desired to keep the background count to a minimum, arrangements can be made to keep accidentals to a low value. One method of accomplishing this, as mentioned by Johnson and employed by the Bartol Foundation, is to shield the tray common to all coincidences (in this application tray No. 3, Fig. 2) with 1 in. lead aprons so as to absorb the soft shower particles. However, this method did not seem to be helpful in this application; in fact, the aprons had a detrimental effect. The greater number of counts obtained with the lead aprons in position indicated that their effect in producing showers was greater than their effect in absorbing shower particles.

A more suitable method of limiting the shower-produced accidentals is to install anticoincidence circuits. The anticoincidence circuits are arranged with anticoincidence Geiger counters lying adjacent to the sides of the common tray; if a tube in the tray and one of the adjacent anticoincidence counters are discharged simultaneously, the coincidence circuit will be prevented from recording a coincidence. This system would have the detrimental effect of increasing the dead time of coincidence, but with an effective anticoincidence area of less than half that of a telescope tray, this effect would be small. At the present time, no anticoincidence circuits are employed in the telescope. In any arrangement for limiting the accidental count, it is still necessary to measure the accidental count as indicated earlier in this section.

Because of the low counting rate of the telescope, the probability of two or more coincidences occurring within the action time of the mechanical recording device is very small. The efficiency of the mechanical counter differs from 100 percent by less than $\frac{1}{10}$ of 1 percent. From these efficiency calculations and measurements of accidentals, an adjusted counting rate can be determined from the measured values of the telescope. Assume that R_r is the rate recorded. Then the adjusted rate is

$$R_T=\frac{R_r-R_a}{E_T\times E_a}=\frac{R_r-0.16}{0.42},$$

where E_T is the efficiency of the coincidence train to count a single pulse (90 percent) and E_a the area efficiency of the train (46.5 percent) and R_a, the shower accidental counting rate as determined by experiment. (0.16 count/minute.)

The over-all counting efficiency $E_T\times E_a$ discussed above was checked experimentally. The experimental method consisted of a measurement with the telescope connected in a four-consecutive tray (1-2-3-4) coincidence followed by a triple coincidence measurement in which tray number three was omitted (1-2-4). In this manner we defined the same solid angle by a four- and three-tray coincidence. The ratio of the two counting rates when so connected gives the efficiency of an individual tray. The over-all counting efficiency of a four-tray coincidence is $E_4=(E_1)^4$ where E_1 is the efficiency of a single tray. In like fashion, the corresponding over-all efficiency of a three-tray coincidence defining the same solid angle as the four-tray coincidence is $E_3=(E_1)^3$. If N_0 is the actual number of rays traversing the coincidence in a given time, the number recorded by the four-tray coincidence would be $N_4=E_4N_0$ while in the corresponding three-tray coincidence, $N_3=E_3N_0$. The ratio of N_4 to N_3 is

$$\frac{N_4}{N_3}=\frac{E_4N_0}{E_3N_0}=\frac{(E_1)^4}{(E_1)^3}=E_1.$$

The single tray efficiency so determined gives a value of 77 percent which when cubed to obtain the triple consecutive tray coincidence efficiency gives a value of 44 percent.

Thus the adjusted rate based on experimental measurements is

$$R_T=(R_r-0.16)/0.44.$$

The authors wish to express their appreciation to Dr. James W. Broxon for his patient guidance in the construction of the telescope.

THE REVIEW OF SCIENTIFIC INSTRUMENTS VOLUME 21, NUMBER 7 JULY, 1950

Measurement of Secondary Electron Emission from Dielectric Surfaces

HOWARD L. HEYDT*
Servomechanisms Laboratory, Massachusetts Institute of Technology, Cambridge, Massachusetts

(Received March 23, 1950)

A technique is developed for the rapid and precise measurement of the secondary electron emission properties of certain dielectric surfaces. The dielectric surface is bombarded by primary electrons having energies which produce a secondary emission ratio greater than unity. This establishes the surface potential at a known value. With the known potential difference between the dielectric surface and primary electron source, the energies of the primary electrons are automatically determined for the first instant of surface bombardment. The net current to the dielectric surface at any moment is measured by using a cathode-ray oscillograph to observe the transient current to a metal plate which backs the dielectric. The method has been used to study metallic surfaces and has yielded results which agree very closely with those obtained using the conventional d.c. method of measurement.

INTRODUCTION

WHEN a stream of electrons strikes the surface of any solid body, some secondary electrons are always released by that body. These secondary electrons may or may not escape from the surface. The path taken depends, at least in part, upon the nature of the electric and magnetic fields in the vicinity of the emission and on the composition of the emitting surface. The average number of secondary electrons released by each primary (incident) electron is known as the secondary emission ratio. Normally, a curve showing the variation of the secondary emission ratio with primary electron energy is used to characterize any surface with regard to the ability of that surface to yield secondary electrons. Surface structure and the angle of incidence of the primary beam, however, are known to affect this curve. In addition, it is believed that the secondary emission from certain complex surfaces may be a function of the previous bombardment of that surface, and it is possible that the emission may also be a function of the current density of the primary beam.

It is readily seen that the secondary electron current available from a particular surface is a function of several factors, some of which may not be known or which cannot easily be controlled. This makes repeatable results difficult to obtain and probably accounts for some lack of published data on the secondary emission properties of various surfaces.

The here-to-be described measurement technique was developed for the purpose of studying the variation of the secondary emission properties of certain surfaces which are dielectric in nature. The surfaces in question were of interest because of their possible suitability as storage surfaces in electrostatic storage tubes which will probably be used extensively as the storage medium in high speed electronic computers. It was assumed that there existed a possibility for a variation of secondary emission properties of certain complex surfaces with time and surface bombardment. Little information pertaining to the variation of secondary emission characteristics is found in the literature. In a few instances, however, it has been implied that certain changes in emitting properties will take place.[1,2]

SECONDARY EMISSION MEASUREMENTS ON DIELECTRICS

Obtaining data for the preparation of a secondary emission curve for any surface necessitates (1) a means for the measurement of the energy of the bombarding electrons and (2) a means for measuring the current to and from the bombarded surface. When a metallic surface is used as the secondary emitter the problem is simply solved by using a voltmeter between the target and the primary electron source and a current meter in series with the target. When a dielectric surface is used as a secondary emitter, however, such a measurement method is obviously not applicable. A "dynamic" measurement method must be employed, in which consideration is given to the charging and discharging of the capacitance between the front surface of the dielectric and the metal back-plate to the dielectric. This back-plate shall be henceforth referred to as the signal plate.

Serious consideration of a method for measuring secondary electron emission from dielectrics has appeared only in the last decade. Two forms of the dynamic method were proposed in 1940.[3,4]

The first phase of the method herein proposed consists of establishing the potential of the dielectric surface at a known value. When the potential of the surface is known with respect to the potential of the primary electron source, the velocity of the primary electrons as they strike the surface is automatically determined. For the case of a dielectric surface, this velocity exists only instantaneously after bombardment by primary electrons begins. To establish the surface potential, use is made of the fact that the surface potential will assume an average value nearly equal to the collector potential provided the surface is bombarded sufficiently long with primary electrons having energies which produce a secondary emission ratio greater than unity.

---

* Now at the University of Connecticut, Storrs, Connecticut.

[1] H. Bruining and J. H. de Boer, "Secondary electron emission," Physica 6, 823–833 (1939).

[2] R. Engstrom, "Photo-multiplier tube characteristics; application to low light levels," J. Opt. Soc. Am. 37, 420 (1947).

[3] H. Salow, "On the secondary emission factor of electron-irradiated insulators," Zeits. f. Tech. Physik 21, 8–15 (1940).

[4] W. Heimann and K. Geyer, "A method of direct measurement of secondary electron emission from insulators," Elek. Nach.-Tech. 17, 1–5 (1940).

If the signal plate, the secondary electron collector, and the primary electron source are connected together through suitable electrical paths, the current to the signal plate will be identical in magnitude to the net current leaving the dielectric surface at any moment. This is made possible since the signal plate and surface are joined by an effective condenser. Observation of the transient signal plate current by means of a cathode-ray oscillograph provides, consequently, an adequate means for measuring the net current leaving the surface.

DETAILED METHOD OF MEASUREMENT

Tube for Testing Surfaces

All measurements were made on surfaces contained in cylindrical glass tubes. Each tube contained an electron gun at one end and a target assembly at the other, as is shown in Fig. 1. During the operation of the tube, the electron beam is positioned into the hole of the circular nickel aperture plate which also serves as the secondary electron collector. A small distance behind the collector, and parallel to it, is the surface to be tested. In this investigation the surfaces studied were composed of a layer of beryllium on a base of aluminum oxide, Al_2O_3. Each surface was produced by evaporating beryllium onto the surface of an anodized aluminum disk. The aluminum disk served as the signal plate and the Al_2O_3 became the dielectric separating the signal plate and surface. A new tube was prepared and sealed off for every surface studied.

Establishing the Dielectric Surface Potential

The method of surface potential stabilization can be illustrated by reference to Fig. 2, in which the circuit associated with the target is shown. Surface potential stabilization for primary velocities at which the secondary emission ratio exceeds unity implies that the flow of secondary electrons from the surface to the collector shall just equal the flow of primary electrons to the surface. Such a situation could be brought about if the stabilized surface potential were to be a few volts positive with respect to the collector potential. A slight retarding action would then be exerted by the collector on the secondaries emitted by the dielectric surface. There is a definite energy distribution of the secondary electrons and only those secondaries with energies greater than the retarding potential could ever reach the collector. Actually, such a retarding potential does exist which so adjusts itself that the net current to the surface does equal zero and the stable surface potential is realized.

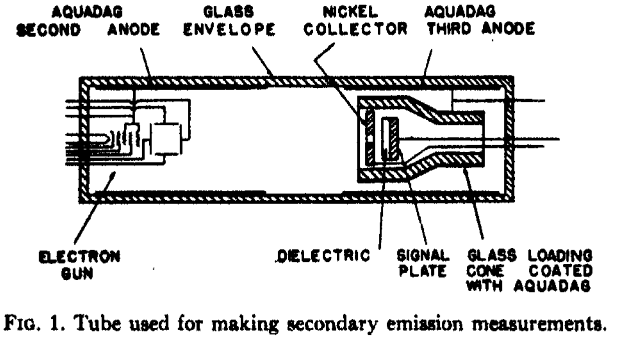

FIG. 1. Tube used for making secondary emission measurements.

After the dielectric surface potential has been stabilized at approximately the collector potential the primary beam may be turned off. If the dielectric is good, the charge on its surface will remain at least temporarily, and the surface potential may be assumed to be at collector potential.

To make an actual secondary emission measurement using the circuit illustrated, the surface potential is stabilized using the method just described, with the signal plate connected to ground (center position of the selector switch). Next, with the primary beam off, the d.c. potential of the signal plate is switched to the more negative value of 50 volts below ground potential. The dielectric surface potential now becomes 50 volts less than its stabilized value, assuming (1) that there has been no appreciable loss of charge from the surface and (2) that the capacitance between the dielectric surface and the signal plate is considerably greater than the capacitance between the surface and all other electrodes in the tube. When the primary beam is again switched on, the primary electrons will instantaneously strike the dielectric surface with energies which are known. The energy of each of the initial primary electrons is fixed by the known initial difference in potential between the dielectric surface and the cathode of the electron gun. This energy is conveniently expressed in volts. It is seen that the energy of these initial primary electrons is equal to

$$\begin{bmatrix}\text{cathode-to-}\\ \text{collector}\\ \text{potential}\end{bmatrix} + \begin{bmatrix}\text{collector-to-surface}\\ \text{retarding potential}\\ \text{at stabilization}\end{bmatrix} - 50 \text{ volts.}$$

The retarding potential is only a few volts and can usually be neglected in comparison to the other potentials involved. Varying the potential of the cathode with respect to the collector potential provides a means for controlling the energies of the bombarding primary electrons.

The first phase of the secondary emission measurement has now been accomplished since the initial energy of any bombarding primary electrons will be known. The collector will be 50 volts positive with respect to the surface at the first instant of bombardment, so that all secondaries released by the surface at the first instant of bombardment should be picked up by the collector. The next phase of the measurement is to determine the magnitudes of the secondary and primary currents at the moment when the primary electron energy is known.

Measuring the Current to the Dielectric Surface

The primary beam, having been turned off during the switching of the signal plate potential, is again turned on, causing an electron current I_p to flow to the dielectric surface. Nearly all the secondary electrons released by the surface should be attracted by the collector, thus producing an initial secondary electron current I_s away from the surface. There is a net electron flow away from the dielectric surface at the first instant equal to $I_s - I_p$. Because of the capacitance between the dielectric surface and the signal plate, an identical electron current flow to the signal plate takes place through the external network. It is this external current which is measured in order to determine the secondary emission ratio at the established primary velocity. The current to the signal plate through the external network has an initial value $I_s - I_p$ for the stabilizing and switching conditions just outlined. The signal plate current is, of course, transient in nature, for if the primary beam were left on sufficiently long the surface would be stabilized and no net current to the dielectric would exist. Observation of the signal plate current by means of a cathode-ray oscillograph is employed as a simple and relatively precise means of determining the initial value of the signal plate current.

If, after surface potential stabilization, the signal plate potential is switched more positive by 50 volts, practically all of the secondary electrons will lack sufficient energy to reach the collector at the first instant of primary electron bombardment. These secondary electrons will be repelled back to the surface from which they were emitted and the signal plate current, consequently, will be equal to the primary current I_p at this time.

The secondary emission ratio can now be calculated from the relation

$$\delta = \frac{I_s}{I_p} = \frac{(I_s - I_p) + I_p}{I_p}.$$

This ratio, in turn, can be expressed in terms of the relative beam deflections in the C.R.O. for I_p and $I_s - I_p$. Such a secondary emission ratio exists only for a primary electron energy equal to the established cathode-to-surface potential. Since only the initial values of $I_s - I_p$ and I_p are of interest, the primary beam need be pulsed on only for a very short interval during the current measurements.

Equivalent Target Circuit

The parameters of the external circuit have a bearing on the measurement method and are worth considering. Figure 3 shows the equivalent circuit associated with the target after the surface potential has been stabilized and the signal plate potential switched positive or negative by 50 volts. R_0 and C_0 are the front-to-back resistance and capacitance respectively of the dielectric surface. C_{eq} approximately represents the parallel combination of the signal plate-to-ground capacitance and the input capacitance to the video amplifier. R_{eq} represents the approximate parallel resistance combination of R and the $1M$ coupling resistor. If the time constant $R_{eq}C_{eq}$ is made very small, then a very short time after the primary beam is pulsed on for a current measurement, the voltage across R_{eq} will be proportional to either $I_s - I_p$ or I_p. This voltage is amplified and applied to the deflection plates of a cathode-ray oscillograph. The resulting beam deflections occurring in the oscillograph are proportional to $I_s - I_p$ or I_p.

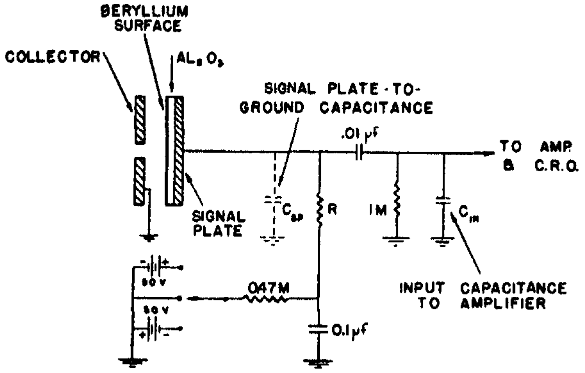

FIG. 2. Target connections and associated circuit.

A variation in the measurement method consists of making the time constant $R_{eq}C_{eq}$ large, so that when the primary beam is pulsed on to make a current measurement, the potential change across C_{eq} is proportional to the charge added to or removed from the dielectric surface. If the duration of the primary beam pulse is very short, the change of charge on C_{eq} or the change in voltage across C_{eq} will be nearly a linear function of time. In such a case, the total voltage change across C_{eq} for a given duration of primary beam pulse will be approximately proportional to the initial value of $I_s - I_p$ or I_p.

Sample oscillograph indications for both the current and charge type of secondary emission measurement are illustrated in Fig. 4.

In a typical secondary emission measurement on the surfaces studied in this investigation, representative values for the various constants were approximately as follows:

$I_p = 30$ μa.
Pulse duration = 1.0 μsec.
$C_0 = 250$ μμf.
$R_0 = 10^{12}\Omega$

	R_{eq}	Signal plate potential change for a current to or from surface of 30 μa
Current method	1000 ohms	0.03 volt
Charge method	500,000	0.3

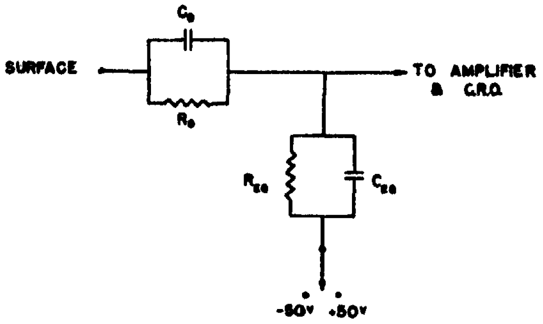

FIG. 3. Equivalent target circuit.

Since the method of measuring charge provided the greater signal plate potential change, the charge method was generally used in making measurements. If the possibility exists for an appreciable change in the current to the surface during the time of the beam pulse, then the current measurement method should be employed.

CONCLUSIONS

The dynamic secondary emission measurement technique which has been described is believed to be sufficiently precise for most purposes. As a check on the measurement technique, the following method was found useful: A special research tube was employed containing a polished nickel disk in place of the usual dielectric surface. Connection to the disk could be made through a 250-$\mu\mu f$ capacitance, thus simulating the effect of the capacitance of a target composed of a dielectric material. Consequently, a dynamic secondary emission measurement could be made on the nickel. Since a direct connection to the nickel surface was also available, a d.c. secondary emission measurement could be made. The difference between the secondary emission curves obtained for the nickel surface using both the d.c. and dynamic methods was practically indistinguishable. An advantage of the proposed method is considered to be the speed and simplicity of measurement. Since only relative deflections of the oscillograph beam are required, no calibration of the oscillograph is necessary.

It is desirable to ascertain frequently that the signal plate potential is always switched the same amount. A switching potential of 50 volts as used in this investigation is not a fixed quantity, of course. It is necessary, however, that at the positive signal plate potential practically all secondaries leaving the dielectric surface be repelled back to that surface. Similarly, at the negative signal plate potential practically all secondaries released by the surface should be picked up by the collector. The minimum signal plate switching potentials can be determined from a plot of signal plate current *vs.* switching potential. Such a curve is a prerequisite to the proper interpretation of the results of any secondary emission measurement.

The effect of surface contamination by particles from the cathode of the electron gun is certainly important. No real protection from such contamination was afforded in the type research tube used, and the effect of the contamination must be considered in evaluating the results of any measurements. Shielding the surface from the cathode is definitely a consideration for future designs of the tube used for testing surfaces.

The method is not without disadvantages. With the type of research tube employed, proper positioning of the beam into the aperture of the collector is absolutely essential in making successful measurements. The beam must also be focused as sharply as possible. If these precautions are not followed the effect of the beam striking the edge of the aperture will considerably impair the accuracy of the measurements. The beam positioning is chiefly a function of the cathode-to-collector potential, which means that positioning must be performed before each current measurement. Much of the difficulty probably can be solved, however, by proper design of the tube used for surface testing. The problem of carefully positioning the beam into the aperture for each measurement can become tedious, particularly if many readings are to be made. Even with the best positioning, some primaries must strike the edge of the aperture and affect the measurements. Although this difficulty was anticipated, the aperture plate was used because it simulated a condition under which the test surface would actually be employed. A new tube has subsequently been used which contains no aperture plate and which requires no beam positioning. A single Aquadag coating, tied to the second anode of the electron gun, serves as the secondary electron collector. Exploiting the possibilities of such a tube seems desirable since such a tube would further speed and simplify secondary emission measurements.

Provided all factors affecting secondary emission are fixed or known, the measurement method presented should be generally applicable. It is desired to emphasize, however, that this paper is merely intended to

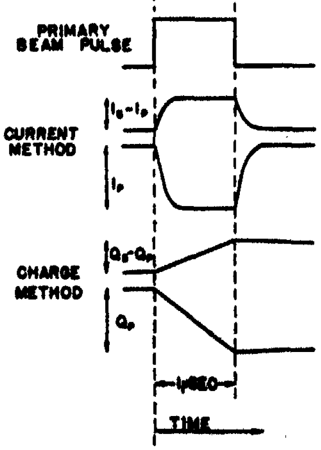

FIG. 4. Oscillograph indications obtained during the measurement of secondary emission.

present a method. Secondary emission data on a particular surface would be valuable only to those who would use the surface under the identical conditions existing when the data was obtained.

ACKNOWLEDGMENTS

The experimental work on which this paper is based was performed in the Servomechanisms Laboratory of the Massachusetts Institute of Technology. The author is sincerely grateful for the facilities and technical assistance made available to him by Mr. Jay W. Forrester, Director of Project Whirlwind, and by Mr. Patrick Youtz. Thanks are also due to Messrs. S. H. Dodd and W. J. Nolan for their many helpful suggestions and criticisms during the course of the investigation.

THE REVIEW OF SCIENTIFIC INSTRUMENTS VOLUME 21, NUMBER 7 JULY, 1950

A High Speed Expansion Valve for Cloud-Chamber Control*

R. P. Shutt and W. L. Whittemore
Brookhaven National Laboratory, Upton, Long Island, New York

(Received March 20, 1950)

In order to keep the width of cloud-chamber tracks down to less than 1 mm the time delay between passage of a ray and completion of an expansion must be 10^{-2} sec. or less. When Geiger counter control is employed it may be difficult to obtain a sufficiently fast acting expansion control valve, particularly for a large cloud chamber. A valve combining a number of principles not all used by others has been constructed. By balancing pressures the movable valve parts can be made very light despite a large valve opening, and the controlling electromagnet can be quite small. Calculations were made concerning all the important design features. Even a small electromagnet must be laminated to insure sufficiently fast decay of its magnetic field. Most of the remaining time delay is caused by the aerodynamic resistance at the valve opening. For a valve diameter of 5.6 cm expansions are completed in 8×10^{-3} sec. With a power consumption of 0.17 watt a small vacuum tube is sufficient for operation. By balancing pressures one could construct a much larger valve operating as fast as the valve described with only a slight increase in power consumption.

INTRODUCTION

A CLOUD chamber essentially consists of a cylindrical glass container sealed by a flexible diaphragm. Usually air pressure applied against the diaphragm from the outside is used to compress the gas inside the chamber. In order to expand the cloud chamber the air is released through a valve, thus allowing the internal pressure to push the diaphragm outward.

When a cloud chamber is controlled by Geiger counters, it is necessary to complete expansions in a very short time after the event setting off the counters has occurred. The accuracy of measurements of curvature and angles to be performed on a cloud chamber photograph is limited by the width and distortions of the tracks. The track width also affects the intensity and contrast of illumination necessary for photography. Tracks are distorted by turbulent motion of the cloud chamber gas during and after an expansion. This effect can be reduced to lateral deviations of considerably less than 1 millimeter by proper design and temperature control of the cloud chamber. For most applications it therefore appears to be practical to aim for a track width of somewhat less than 1 mm.

Blackett[1] has shown that in argon at approximately normal pressure a track of ions formed by a charged particle diffuses to a mean width which is proportional to the square root of the time elapsed and equal to 1 millimeter in 1/70 sec. Ion diffusion is terminated almost immediately when the supersaturation necessary for drop formation has been reached in the cloud chamber. This can be seen in the following way.

In an investigation of the growth of drops in a cloud chamber, Hazen[2] has shown that the square of the drop radius a increases proportionally to the time t after supersaturation has been reached

$$a^2 = Kt, \tag{1}$$

where the value of the proportionality constant K lies somewhere between 10^{-6} and 10^{-5} (c.g.s. units), depending on the gas and vapor used in the cloud chamber.

The mean square of the displacement $d\langle X^2\rangle_{Av}$ due to Brownian movement of the drop during the time dt is given by

$$d\langle X^2\rangle_{Av} = \frac{kTdt}{3\pi\eta a}, \tag{2}$$

where k is Boltzmann's constant, T the absolute temperature, and η the viscosity of the gas. Substituting expression (1) for the time dependent radius a in (2) and integrating one finds

---

* Work done at Brookhaven National Laboratory under the auspices of the AEC.

[1] P. M. S. Blackett, Proc. Roy. Soc. 146, 281 (1934).

[2] W. E. Hazen, Rev. Sci. Inst. 13, 247 (1942).

$$\langle X^2\rangle_{\mathrm{Av}}=\frac{2kT}{3\pi\eta K^{\frac{1}{2}}}t^{\frac{1}{2}}, \tag{3}$$

as an estimate for the movement of the growing drop. Substituting values for the constants, $T=300$°K, and $t=0.1$ sec. for the time of growth of the drop, one finds a value of approximately 10^{-3} cm for the root-mean-square of the displacement of the drop at the time it is photographed. Since this value is negligibly small as compared to the acceptable displacement caused by the diffusion of the free ions before the expansion of the cloud chamber one has to be concerned only with the delay between passage of an ionizing ray through the cloud chamber and the termination of the expansion. According to Blackett's result mentioned above this delay should be less than 10^{-2} sec. in order to obtain track widths of less than 1 mm.

The expansion valve for a cloud chamber usually consists of an electromagnet holding a valve disk against a self-sealing gasket. After passing through vacuum tube circuits in a negligibly short time, the pulse from the Geiger counters acts to decrease the field in the magnet, allowing the valve disk to be pushed open by the air pressure inside. While air escapes through the valve opening, the cloud chamber is expanding. The following time delays have to be considered. First, there is the decay time, t_1, of the field in the holding magnet. t_1 depends on the electrical constants and on the shape and structure of the magnet. The yoke of the magnet acts as a secondary winding inside which strong electric currents may be set up, delaying the decay time of the field. These currents can be made negligibly small by laminating the magnet material. Secondly, t_2 will designate the time during which air flows through the valve opening, while the valve disk is in motion and thereafter. The valve opens the faster, the smaller the mass of the valve disk assembly can be made. The aerodynamic resistance of the valve air duct is determined by its shape and size. Of course t_2 decreases as the size of the valve opening is increased, but usually t_1 increases correspondingly because of the larger size of the magnet required. Finally, the cloud-chamber diaphragm takes a certain time to fly back. However, because of their light weight the rubber diaphragms and pistons used in most designs can move practically as fast as the outflowing air slowed down by the aerodynamic resistance at the valve opening. Therefore, unless the valve opening should be made exceptionally large, only t_1 and t_2 need be considered.

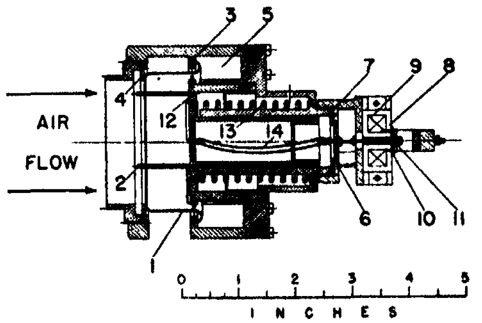

FIG. 1. Diagram of high speed expansion valve for cloud-chamber control. The whole assembly is screwed into a hole in the back compartment of the cloud chamber.

DESIGN OF EXPANSION VALVE

Various designs have been employed successfully by many workers. However, for two large cloud chambers to be used at this laboratory it appeared useful to construct a new valve combining a number of advantages not all of which have been found in previous designs. The valve to be described combines large size of the valve air duct with a short opening time, small electric power requirements, and simple operation. By applying the principles involved twice in succession one could control an even larger valve with a small amount of power and still have sufficiently fast expansions. A description of the valve will now be given. Later a number of generally applicable theoretical considerations will be used to calculate some operating characteristics of this valve for comparison with experimental data.

Reference is made to Fig. 1. The valve disk consists of a cylindrical cup with turned-out rim (1), spun of magnesium or aluminum sheet about 0.015 in. thick. The motion of the cup is guided by three pins (2), passing through small holes in the bottom of the cup. If the cup is pushed to the left against gaskets (3) and (4), air admitted into the back compartment of the cloud chamber leaks through the small holes around pins (2) in the bottom of the cup into the air chamber formed by cup (1) and container (5), thus building up equal pressure at both sides of the cup. Since the area sealed by gasket (3) at the rim of the cup is larger than the area sealed by gasket (4) at the bottom, the resultant force keeps the cup in the initial position, thus sealing the cloud chamber and air chamber (5) as long as air pressure is applied. Since the pressures at both sides of the flat bottom of the cup are equal and since the large curvature of the cylindrical section of the cup serves well to withstand the pressure difference between cloud chamber back and the outside atmosphere, one can make the cup material very thin and of light weight. The air chamber (5) is sealed by a small Lucite valve disk (6) held against gasket (7) by the magnet assembly. The yoke (8) of the magnet is made of two straight arrays of steel laminations, 0.020 in. thick, bent around a field coil (9) consisting of 3000 turns of 0.004 in. Formex-coated copper wire. The laminations are insulated electrically by a thin coat of varnish. The armature consists of two small steel strips (10), 1 in. ×0.093 in. ×0.020 in., pinned to a Lucite holder (11). 0.17 watt of power is consumed to hold this valve closed. Thus a small electronic power tube is sufficient for operation.

When the field in the magnet is decreased sufficiently the valve assembly, consisting of parts (6), (10), and (11), opens and air escapes from the air chamber (5). The small holes in cup (1) cannot pass a sufficient amount of air to keep up the pressure in (5). Thus, as soon as this pressure has dropped somewhat the forces on the cup become unbalanced, the cup is pushed to the right and air now escapes through the big opening in gasket (4), letting the cloud chamber expand. The cup flies open very rapidly because of its small mass (6 to 10 g for the present design) and also because it can move quite freely, since it is not attached to any resetting device such as a spring. In order to reset cup (1) after an expansion, piston (12) has been provided. When the cloud chamber is compressed this piston is pushed to the right by the air pressure in chamber (5), compressing spring (13). Immediately after an expansion the spring pushes the piston to the left, thus resetting cup (1) for the next compression. Due to its large mass and friction in its air seals the piston moves slowly so that it cannot interfere with the fast motion of the cup. By means of a rubber band (14) attached to the piston (12) the small valve disk (6) is also reset automatically. Two valves of this type were built and have been operated successfully for six months.

CALCULATION OF ELECTROMAGNET

In order to insure proper dimensions for the components of the valve, approximate calculations of its operating characteristics have been made. The results will be stated at this point.

First the decay time t_1 of the field in the holding magnet will be calculated. Since the yoke forms an electrical secondary circuit, one should consider the whole magnet as a transformer and solve the corresponding equations. However, we may simplify the problem by considering first the decay time t_1' of the electric current in the field coil alone and then showing separately how the decay time t_1'' of the secondary current in the iron can be kept negligibly small.

The armature is attracted by the yoke with a force F (dyne) which must be approximately equal to the force exerted by the pressure difference Δp on the valve disk. From the field energy in the magnet one finds

$$F=\frac{AB^2}{8\pi}\approx\pi r^2\Delta p, \tag{4}$$

with B (gauss) for the flux density, A (cm^2) for the constant cross section of the yoke, and r (cm) for the radius of the valve opening. One has also

$$B=\frac{4\pi}{10}\frac{ni}{(b/\mu)+x}, \tag{5}$$

where ni stands for the number of Ampere-turns in the field coil, b (cm) for the length of the magnetic circuit, μ for the permeability of the iron, and x (cm) for the sum of all air-gaps.

Finally, the e.m.f. induced in the field coil by the decaying magnetic field is

$$E=-10^{-8}nA(dB/dt). \tag{6}$$

From (4), (5), and (6) one finds

$$t_1'=2\times10^{-7}(F/P)[(b/\mu)+x], \tag{7}$$

where P (watt) is the power consumption.

In the present design we have $r=0.8$ cm, $\Delta p=0.5$ atm. For cold-rolled steel $B=4500$ gauss with $\mu\approx1000$ is quite far from saturation and leads to a practical value for $A=1.25$ cm^2. x is assumed to be 0.01 cm which is probably conservatively large. Putting $b=4$ cm enables one to accommodate a field coil consisting of 3000 turns of copper wire 0.004 in. in diameter without overheating. The coil resistance is 600 ohm. One finds $i=15$ mA, $P=0.17$ watt and $t_1'=17\times10^{-3}$ sec. This is the decay constant when the field coil is short-circuited. A series resistor or vacuum tube providing 10,000 ohm of additional resistance at the time of expansion makes $t_1'=10^{-3}$ sec. with an induced peak voltage at the coil terminals of 160 volt. A low power vacuum tube thus can be used for control of the valve.

From (7) one can see that for a desired t_1' the instantaneous power consumption P is proportional to F, and therefore to the area of the valve opening. For a large valve this leads to quite large peak currents or voltages, making fast operation rather difficult. Thus a fast cloud-chamber valve can be operated most simply if a small electromagnet is employed.

We shall now turn to the calculation of t_1'', the effect of "eddy currents" induced in the yoke material. Making use of (5) and (6) for average values only we find

$$t_1''=\frac{10^{-9}\pi wdb}{[(b/\mu)+x]\rho[(d/w)+(w/d)]}. \tag{8}$$

wd (cm^2) is the cross section of *one* of the laminations. ρ (ohm-cm) is the resistivity of the iron, the other quantities having been defined previously.

Choosing laminations $d=0.05$ cm thick and $w=0.25$ cm wide, we find $t_1''=2.2\times10^{-4}$ sec., which is small compared to $t_1'=10^{-3}$ sec. as had been mentioned above.

We conclude that the magnet constructed permits the valve disk to start moving about 10^{-3} sec. after the field coil has been deenergized, leaving a resistance of 10,000 ohm or its equivalent in series with the coil resistance. A very simple and direct measurement, making use of an oscilloscope, showed indeed a delay of 10^{-3} sec.

It may be of interest that for a ring-shaped magnet one finds

$$t_1''=\frac{4\pi10^{-9}d^2b}{\rho[(b/\mu)+x]}, \tag{9}$$

where d now stands for the width of the cross section through which the magnetic flux passes. For a large available ring magnet $t_1''=0.2$ sec. was predicted, and 0.15 sec. was found experimentally, which again shows that these simplified calculations give approximations sufficient for the purpose.

CALCULATION OF AIR RESISTANCE

Calculation of t_2, the time during which the air escapes from the rear compartment of the cloud chamber, follows. This time is determined by the aerodynamic resistance in the valve which varies as a function of time while the valve is opening. Approximately, the air pushes against the valve disk area πr^2 with a time-varying pressure difference $\Delta p(t)$. Thus we have

$$m\ddot{y}=\Delta p(t)\pi r^2, \tag{10}$$

where $m(g)$ is the mass of the moving parts of the valve and y (cm) the distance through which the valve disk has moved at the time t.

The air then passes through a cylindrical opening of area $2\pi r y$ around the edge of the valve disk. Calling $M(t)$ (g) the mass of air passing through this opening per unit time one has

$$\dot{M}(t)=2\pi r y(t)v(t)D(t), \tag{11}$$

where $v(t)$ is the velocity of the escaping air and $D(t)$ its density. Three more equations are needed to express the time dependence of $\Delta p(t)$, $v(t)$, and $D(t)$, and the integration of the problem becomes quite tedious. Therefore we make the following assumptions. For $\Delta p(t)$ and $D(t)$ we put their average values Δp and D, respectively, found from the known conditions at beginning and end of the period considered, neglecting effects, such as cooling of the air due to expansion, etc.

Referring to standard texts on frictional effects in air ducts one finds that, except for relatively long ducts, most of the losses in pressure occur at irregularities such as abrupt bends and sudden expansions and constrictions in the ducts, and that the pressure loss experienced is of the order of $Dv^2/2$ for every pronounced change in direction of flow. Therefore we shall assume that all of the change in pressure between inside and outside takes place at the valve opening and is

$$\Delta p\approx Dv^2/2 \tag{12}$$

from which the average velocity of flow can immediately be calculated once the average values for Δp and D are given.

With these simplifications (10) and (11) can easily be integrated. One finds

$$t=\frac{0.6}{r(\Delta p)^{\frac{1}{2}}}\left(\frac{Mm}{D^{\frac{1}{2}}}\right)^{\frac{1}{3}} \quad \text{for} \quad t<t_0 \tag{13}$$

$$t=\frac{2}{3}t_0+\frac{0.22M}{r^2(\Delta pD)^{\frac{1}{2}}} \quad \text{for} \quad t>t_0 \tag{14}$$

$$t_0=\left(\frac{m}{\pi r\Delta p}\right)^{\frac{1}{2}}, \tag{15}$$

where t is the time taken for the mass M of air to flow through the valve opening. t_0 is the time taken by the valve disk to open fully to a value of $y=r/2$.

By means of formulas (13)–(15), we can now predict more approximate data for our valve. For the small valve disk, held by the electromagnet, we have $m=1.4$ g and $r=0.8$ cm. The volume of the air chamber (5) is 75 cm^3. Thus the delay due to air chamber (5) amounts to $t_2'=1.5\times10^{-3}$ sec.

For cup (1) with $m=10$ g, $r=2.8$ cm, and a volume of 2400 cm^3 of air to flow out upon expansion, one finds $t_2''=5.6\times10^{-3}$ sec. Adding $t_2'+t_2''$ on has $t_2=7.1\times10^{-3}$ sec. It is of interest to note that most of this delay is due to the air resistance at the main valve opening, even though the latter is relatively large.

Finally, the total delay between breaking the current through the field coil and completion of the expansion should be $t_1+t_2=8\times10^{-3}$ sec. which was confirmed by experiment.

In a conventionally designed valve of the present size it would be difficult to make m less than 300 g, resulting in a time delay of 11×10^{-3} sec. for t_2'' alone. This is twice as long as the corresponding time delay for the present design.

ACKNOWLEDGMENT

The authors wish to express their gratitude to Messrs. F. O. Pallas, S. G. Hasselriis, and A. B. Wright for their assistance in the construction of the valves.

THE REVIEW OF SCIENTIFIC INSTRUMENTS VOLUME 21, NUMBER 7 JULY, 1950

Single Element Verniers Reading Two or Three Dimensions

ROBERT E. LEWIS
Physics Research Department, Armour Research Foundation, Illinois Institute of Technology, Chicago, Illinois

(Received October 20, 1949)

By superimposing concentric radial elements on rectangular coordinate rulings, vernier systems may be constructed reading in two or three dimensions without the necessity of any particular angular orientation.

A two-dimensional vernier may consist of one transparent element ruled with concentric circles. The observed tangencies of the circles, with regard to a rectangular grid placed in contact, provide the reading of the additional decimal of the coordinates of the fiducial center of the circles on the grid.

A three-dimensional vernier system may be established by means of a binocular optical system presenting images of spheres concentric with the locating point and images of coordinate boxes in the same space. The tangency of a vernier sphere and coordinate plane indicates the last decimal of the reading.

Angular orientation may be indicated by radial lines near the points of tangency.

I. INTRODUCTION

THE familiar linear vernier scale reading system, named after its inventor Pierre Vernier in 1631, permits linear or angular measure to a degree of accuracy many times greater than is possible by using a conventional scale. Even if the vernier device is graduated so that 10 divisions on it equal 11 or 9 divisions on the main scale, the accuracy of reading is extended by one decimal place.

The well-recognized value of a vernier rests on the sharpness of vision and accuracy of judgment of separations. Whether the vernier is read with or without magnification, the image entering the eye contains the same geometrical relations. It may then be said that the success of the vernier rests on the ability of the viewer to judge the coincidence of two end-to-end lines or ruled elements, instead of the relative position of a line some distance between two others. Furthermore, this process of coincidence recognition is assisted by the presentation of a line pattern to guide the judgment of the viewer.

A common vernier drawn on a linear or circular scale permits reading with vernier-enhanced accuracy in but one dimension. To attain two-dimensional readings, two separate sets of scales and verniers are usually used. These scales require accurately aligned sliding ways or bearings to permit translation to read various locations in a plane.

Three-dimensional measurement with common vernier scales differs only by the addition of another set of accurately aligned ways and scale with reading vernier. Thus, to read four points not in a plane, movement of vernier scales along several precision ways is required. The maintenance of alignment between ways is subject to wear as well as to numerous other problems. The cost of accurate systems for the reading of measurements in several dimensions is often measured more in terms of the labor involved in translating than in terms of the cost of the equipment. These restrictions often lead to the discarding of the vernier system, the measurer relying only on sufficient magnification of the critical dimension to permit more accurate estimation.

II. TWO-DIMENSIONAL VERNIER OF ONE ELEMENT

A basic form of the two-dimensional vernier of one element only may be developed by, what is in effect, the revolution of a one-dimensional vernier in a plane about the fiducial point. This is then superimposed on a rectangular grid of x and y coordinates. This requires that one or both of the superimposed elements be on a transparent or perforated material.

The two-dimensional vernier, therefore, may consist of ten concentric circles about a fiducial point. The radii of the circles are such that ten circles equal nine divisions on the rectangular grid. Thus, with the fiducial point at origin, vernier circle 1.0 is tangent to lines through (9,0), (0,9), (−9,0), and (0,−9). It is evident that the application of the vernier circles requires recognition of tangency which is thus viewed by eye as the coincidence of a line and arc. This corresponds in

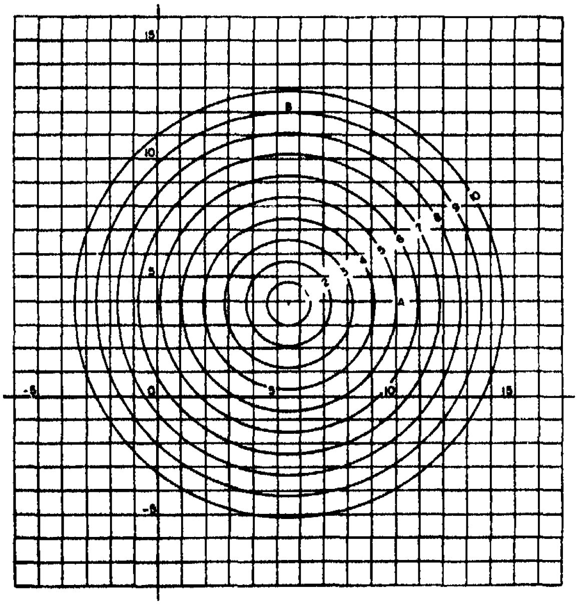

FIG. 1. A single two-dimensional vernier. The fiducial element point is set at $x=5$, $y=3$. The vernier establishes this point as $x=5.5$, $y=3.9$.

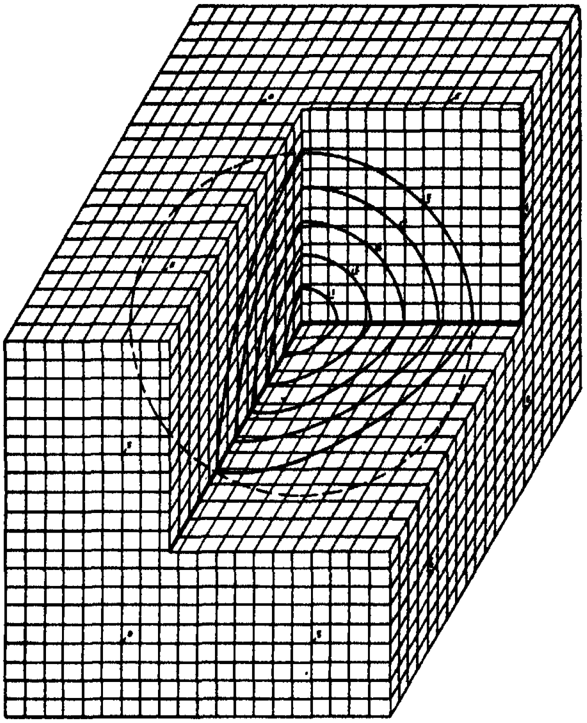

FIG. 2. A single element three-dimensional vernier, whose practical use depends on some kind of stereoscopic optical system (not shown). The cutaway shows the fiducial point at (1.3, 2.4, 0.2).

function to the recognition of the coincidence of lines in a linear vernier, and to the extent that the eye can recognize linear and tangent coincidence equally well, to the same extent the accuracy of the two-dimensional single element vernier is of the same order as the linear common vernier.

A vernier reading is tangent to two x coordinate lines separated by 180°, and likewise to two y coordinate lines separated by 180°. The tangencies in the first two quadrants represent positive vernier increments, while those in the third and fourth quadrants are negative increments. In Fig. 1 the position is read (5.5, 3.9) as the fiducial point is in the (5, 3) coordinate rectangle and the vernier is tangent at 0.5 to x coordinate lines indicated by point A, and likewise tangent to 0.9 for y coordinate lines indicated as point B. The additional negative increment readings at points opposite to A and B correspond to an ordinary linear vernier which is zero centered.

III. THREE-DIMENSIONAL VERNIER OF ONE ELEMENT

By revolving a linear vernier about a fiducial point in three-dimensional space, a set of vernier spheres is developed. These will then be read by tangency to coordinate planes in a cubical-space system. Such a system is realized by using stereoscopic methods which permit the establishment of one image within another. Recognition of tangency then becomes a problem of stereoscopic depth. Optical stereoscopic range-finders have been designed to take advantage of the increased accuracy attainable by the recognition of coincidence.

The difficulty of graphical representation of the solid shape is, perhaps, the same as that of supplying a means of identifying the surface of a sphere without obscuring another, or without obscuring the planes. Figure 2 is a cutaway drawing of a solid vernier at (1.3, 2.4, 0.2). The reduction of the number of spheres reduces the problem only by adding planes. Recognition of the surfaces involved may be assisted by presenting the spheres and planes as ruled surfaces covered with small spots much like dust particles. Careful dispersion of the spots will permit viewing through successive layers, as the binocular position of two spots in line for one eye, but in separate planes, will not produce spots in the two-eye images which are superimposed and interfering.

The application of such a system depends on the stereoscopic equipment used, details of which are beyond the scope of this paper.

IV. DISCUSSION AND CONCLUSION

The rotation of the vernier indicator has no influence on the reading of the location of the fiducial point in space. This characteristic is particularly interesting for it eliminates the necessity of translation of the reading device by means of precision ways at right angles. The right-angle relationship is maintained by the reference grid system, which construction eliminates misalignment errors that occur through wear of the ways.

Angular orientation of the vernier systems, when desired, may be indicated by polar location of the tangencies. Figure 3 shows a vernier reading (8.2, 12.4) at 60° to x axis or 150° when read on the y axis. The ac-

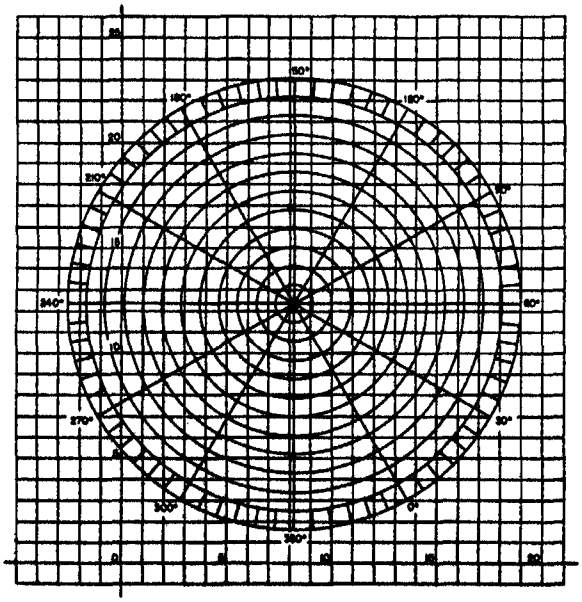

FIG. 3. A single element two-dimensional vernier ruled to indicate polar angle. The fiducial point is at $x=8.2$, $y=12.4$, polar angle $=60°$ to x axis.

curacy of interpretation of angular orientation by tangency is not the same order as that of other vernier readings. However, in certain cases, intersecting coordinate lines may permit improved accuracy.

The usefulness of the two-dimensional system is dependent on the plane-to-plane contact or equivalent of the vernier and grid. To observe the tangency characteristics of the pattern, one element must be transparent, perforated, or otherwise optically superimposed upon the other element.

The similarity between the tangency relation in reading grid and circle coincidence and the other patterns[1] suggests that finer two- and three-dimensional vernier readings may be obtained by further pattern development. Similar studies of the visibility of line elements and endings[2] may reveal higher resolution with known systems.

V. ACKNOWLEDGMENTS

The author wishes to acknowledge the suggestions and encouragement of Mr. Howard T. Betz of Armour Research Foundation of Illinois Institute of Technology. This work is a development of research originally sponsored by the Jones and Lamson Company of Springfield, Vermont.[3]

---

[1] U. S. Patent 2,475,490, Direct Reading Visual Index Forming Intersection Pattern Thread and Line Counter, Albert Gelardin.

[2] U. S. Patent 2,451,972, Optical Indicator Having Cooperating Grids, Walter P. Powers. K. W. Baker, J. Opt. Soc. Am. **39**, 567 (1949).

[3] U. S. Patent 2,484,103, Projection Comparator for Objects in Relation to Spaced Drawings on Reticles, Robert E. Lewis.

THE REVIEW OF SCIENTIFIC INSTRUMENTS VOLUME 21, NUMBER 7 JULY, 1950

Coincidence Circuit for a Scintillation Detector of Radiation

W. C. Elmore
Swarthmore College, Swarthmore, Pennsylvania

(Received March 30, 1950)

This paper describes a very simple low level coincidence circuit of moderate speed, which is suitable for use with two or more multiplier photo-tubes in a scintillation detector of radiation. The operation of the circuit is analyzed, and performance data given to show its effectiveness in eliminating spurious counts due to noise pulses in the photo-tubes. Some useful modifications of the circuit are suggested.

THE modern scintillation detector of nuclear radiation, based on a multiplier photo-tube and a suitable phosphor, has prompted the development of low level coincidence circuits that operate directly between two photo-tubes.[1] These circuits utilize the non-linear property of germanium diodes, such as the 1N34, and make it unnecessary to employ separate amplifiers with each photo-tube, although an amplifier must be used between the output of the coincidence circuit and the pulse-recording equipment. In the present report a new coincidence circuit of this type will be described, together with performance data obtained with two 931-A multiplier photo-tubes arranged to view the same sodium-iodide phosphor. The coincidence circuit in this case serves to reduce the background counting rate due to noise pulses from the photo-tubes. Its use, however, is not restricted to this application.

The version of the coincidence circuit whose performance has been studied in greatest detail is that given in Fig. 1, in which the coincidence circuit is shown connected between the anodes of two 931-A tubes. The potentiometer R_4 permits the bias currents that enter the diode-resistor network to be balanced, and the variable resistors R_5 and R_6 permit the amplifications of the two photo-tubes to be equalized. These controls are convenient in an experimental set-up, but can be omitted, or made screw-driver controls in a permanent set-up.

A qualitative notion of how the coincidence circuit operates may be had by noting that about one-tenth of the steady bias current for each branch of the circuit flows through the resistance R_3. A negative pulse of current occurring at the anode of the photo-tube T-1, for instance, serves to lower the potential of that anode, and hence to cut off one-half of the current to R_3 on account of the high back resistance of the diode D_1. Most of the missing current is then supplied through the diode D_2 from a source impedance approximately equal to R_2. Since $R_2 \ll R_3$, the potential difference across R_3 drops only slightly, giving a small anti-coincident output pulse. When pulses of current occur simultaneously at the anodes of both photo-tubes, both diodes tend to be cut off and the potential across R_3 drops an amount set by the smaller of the two current pulses, giving a much larger coincident output pulse.

A more precise account of the operation of the coincidence circuit will be based on Fig. 2, which shows the basic portion of the circuit, and Fig. 3, which shows

---

[1] G. A. Morton and K. W. Robinson, Nucleonics 4, No. 2, 25 (1949). See also Baldinger, Huber, and Meyer, Rev. Sci. Inst. **19**, 473 (1948).

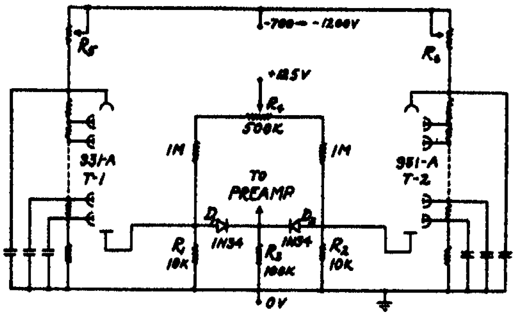

FIG. 1. Coincidence circuit connected between two 931-A multiplier photo-tubes.

experimentally determined curves relating the two currents I_1 and I_2 to the potential V_g (with respect to ground). These curves were obtained from the circuit of Fig. 2 with $R_1=R_2=10^4$ ohms and $R_3=10^5$ ohms using a portable potentiometer to measure V_g as a function of the two currents. The lack of symmetry in the characteristic curves is due to differences in the two diodes.

Let us consider first how the circuit operates leaving out of account the stray capacitance C_1, C_2, and C_3, whose presence in the circuit will be considered later. Suppose then that steady bias currents of 0.1 ma are flowing into each side of the coincidence circuit, biasing it at point x in Fig. 3, so that V_g is 0.9 volt. If now a pulse of negative current of magnitude 0.03 ma, for example, occurs at the anode of the photo-tube T-1, and none at the anode of T-2, the current I_1 is momentarily decreased 0.03 ma, whereas I_2 is unchanged in value. This situation is represented in Fig. 3 by the operating path x–y. It is clear that during the current pulse the potential V_g drops to that at point y, and then returns to its original value when the current pulse ends, causing a negative voltage pulse of about 0.07 volt to be impressed on the grid of the amplifier.

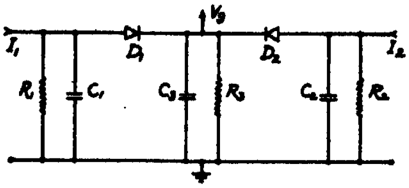

FIG. 2. Basic part of coincidence circuit, including stray capacitances.

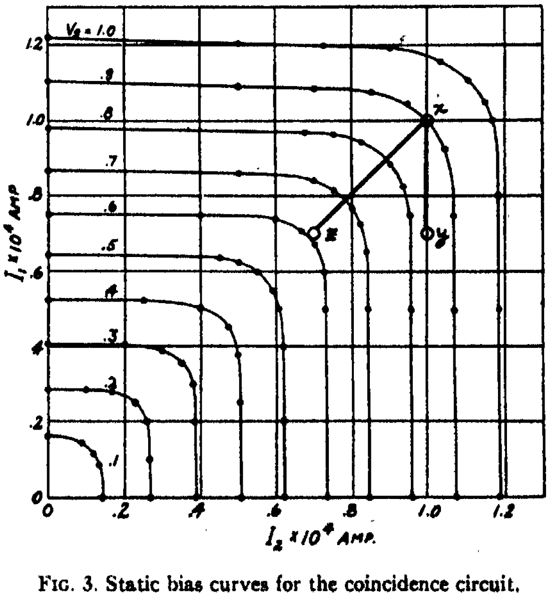

FIG. 3. Static bias curves for the coincidence circuit.

Next suppose that current pulses of 0.03 ma occur simultaneously at the anodes of both T-1 and T-2, such that an operating path x–z is followed. A negative voltage pulse of amplitude 0.29 volt is then impressed on the grid of the amplifier. The coincident pulses in general have a considerably greater amplitude than the anticoincident pulses; and can be distinguished from the latter by a conventional pulse-height discriminator after an amplification of about 250. Figure 3 enables one to estimate the amplitude of output pulses for combinations of coincident currents of differing magnitudes, provided the current pulses have a duration long compared with the RC time constants associated with the coincidence circuit, or provided the effects of the stray capacitances are taken into account. Some curves showing the output pulse amplitude as a function of the joint magnitudes of the two anode current pulses are given in Fig. 4. These curves have been derived from Fig. 3.

Let us now consider in an approximate manner how the stray capacitances $C_1=C_2$ and C_3 alter the operation of the circuit for short pulses of current. The capacitance between the electrodes of the diodes can be neglected on account of its small value. To simplify the discussion we shall assume that the diodes are ideal, i.e., that they have zero resistance when conducting, and infinite resistance when non-conducting.

Suppose first of all that large coincident pulses of current having a long duration occur simultaneously at the anodes of both T-1 and T-2, so that both anodes drop abruptly to ground potential or below. In such a case V_g drops exponentially to zero from its original value ($V_{og}=0.9$ volt) with a time constant R_3C_3, as shown by curve 1 in Fig. 5. Next assume, as might be expected under normal operating conditions, that both anodes drop in potential perhaps 0.3 volt. The output signal then has the form shown by curve 2 in Fig. 5. With $R_3=10^5$ ohms and $C_3=7.5\ \mu\mu f$, the rise time of the step (10 to 90 percent response) is about 0.3 μsec., the precise value depending, of course, on the amplitude of the pulse. When the current pulses end, the circuit recovers to its initial state with the diodes conducting, and therefore with a time constant computed from the parallel combination of resistors and capacitors in Fig. 2. For the present circuit this time constant is estimated to be about 0.15 μsec., i.e., somewhat shorter than the decay constant (0.25 μsec.) of the NaI(Tl) phosphor for which the circuit values used here have been selected.

If the current pulses at the photo-tube anodes do not cause the potential to drop as rapidly as that indicated by curve 1 in Fig. 5, then the diodes do not cut off and the transient response of the circuit is set entirely by the 0.15-μsec. time constant, and, of course, by the form of the coincident current pulses from the photo-tube anodes. For example, suppose that the current at each anode, in response to a scintillation, has the form

$$i = i_m e^{-t/T}, \quad t \geq 0$$

where T is the decay time of the phosphor. On account of symmetry in the coincidence circuit, the output pulse v_0 is found by supposing this current to flow into the capacitance $C = C_1 + \frac{1}{2}C_3$ shunted by the resistance $R = 2R_1R_3/(R_1 + 2R_3)$. A simple analysis shows that

$$v_0 = [i_m RT/(T-RC)](e^{-t/T} - e^{-t/RC}).$$

The maximum rate of change of v_0 occurs at $t=0$ and has the value i_m/C. The two diodes are cut off if this rate is greater than V_{og}/R_3C_3, which is the absolute value of the initial slope of curve 1 in Fig. 5, that is, if

$$i_m \geq (CV_{og}/C_3R_3).$$

The approximate values $C = 15\ \mu\mu$f, $C_3 = 7.5\ \mu\mu$f, $V_{og} = 0.9$ volt, and $R_3 = 10^5$ ohms give $i_m \geq 0.018$ ma, so that for currents greater that this value the diodes are temporarily cut off. Coincident scintillations from a NaI(Tl) phosphor produce output pulses having a rise time of about 0.3 μsec., with a trailing edge that decays with a 0.25-μsec. time constant. The larger pulses all have the same rate of rise.

The value 10^4 ohms for the resistances $R_1 = R_2$ has been chosen to reduce the magnitude of the current pulses required of the photo-tubes, without increasing the duration of the output pulses appreciably over that set by the decay constant of the sodium-iodide phosphor. It is also desirable that the resistance R_3 be large compared with the forward resistance of the diodes, and with R_1, but not so large that it significantly increases the rise time of the output pulses.

The speed of the coincidence circuit can be increased considerably by decreasing all resistances in proportion and increasing in the same proportion the magnitude of the output current pulses from the photo-tubes. It is found that the static bias curves of Fig. 3 very closely represent curves taken with resistances reduced tenfold, provided the current scales in the figure are increased by a factor of ten. An even greater increase in speed of the coincidence circuit should be possible before the finite forward resistance of the diodes begins to limit its effectiveness of operation.

The extent to which the circuit reduces the background counting rate due to noise pulses in the photo-tubes has been investigated by obtaining integral counting rate bias curves for various conditions of the circuit. For these measurements two 931-A tubes were selected from a group of twenty as having roughly identical sensitivities, and reasonably good signal-to-noise ratios. The sodium-iodide phosphor, contained in a sealed $\frac{3}{4}$-in. diameter quartz tube,[2] was located midway between the two photo-tubes separated 2.5 in. center-to-center. Two flat polished sheets of aluminum were mounted on opposite sides of the phosphor so as to extend from one photo-tube to the other, and thus to improve the otherwise poor optical coupling between the phosphor and the two photo-tubes. A weak Co-60 source was placed in a standard position near the phosphor as a source of γ-rays. Both the source and the phosphor were removed when background noise was measured.

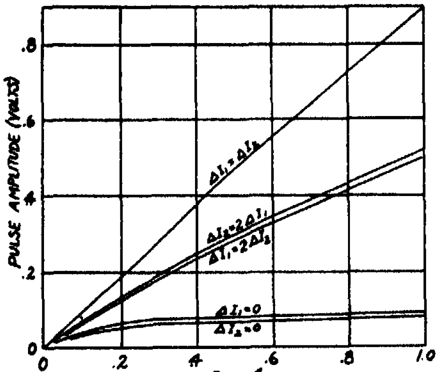

FIG. 4. Output pulse amplitude as a function of the two photo-tube currents.

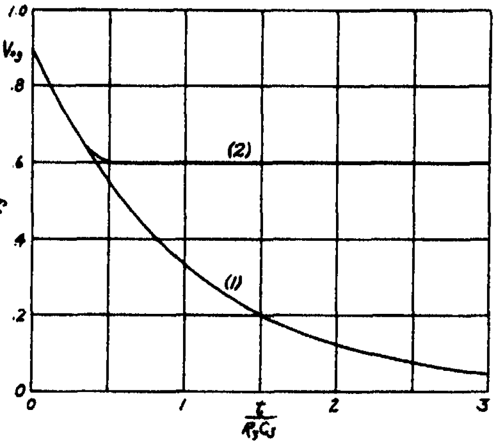

FIG. 5. Output pulse wave forms.

The amplifier, which was stabilized by inverse feedback, had a mid-band gain of 290, and a rise time of 0.08 μsec. It contained no "clipping" time constant, its frequency response extending from well below 20 kc to an upper half-power point of 4.15 Mc. To minimize capacitive loading of the coincidence circuit, the input stage (a Type 6AK5 pentode) was mounted very near the tube sockets for the photo-tubes, and coupled to

---

[2] The phosphor was kindly supplied by Dr. R. Hofstadter of Princeton University.

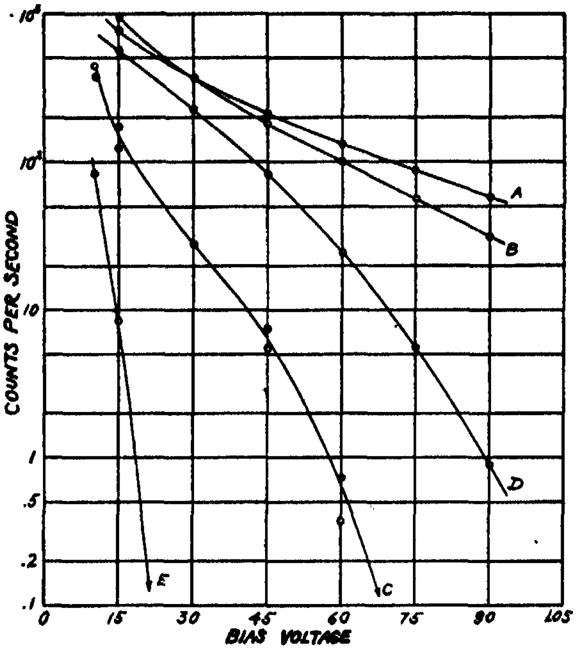

FIG. 6. Integral counting rate bias curves.

the main amplifier by a cathode follower stage. If the utmost in speed is desired, the input stage should be a cathode follower, and stray wiring capacitance kept at a minimum by a careful layout of parts.

The integral bias curves were taken using a Schmitt trigger circuit as a pulse-height discriminator or selector[3] followed by a scale-of-100 counter. The counting rates for the two photo-tubes were first equalized at a bias of 30 volts by adjusting R_5 and R_6 in Fig. 1, with the anode of first one, then the other photo-tube connected temporarily to ground. The coincidence circuit was then balanced by adjusting R_4 to give a minimum noise counting rate with the discriminator bias set at a low value. Curves A and B of Fig. 6 show the source-plus-noise bias curves for the individual photo-tubes. These curves were obtained with one or the other anode of the photo-tubes grounded, thus putting a steady coincident signal into one or the other side of the coincidence circuit. The noise bias curves were taken in a similar fashion with the phosphor and source removed, and are given by curve C which has been drawn through both sets of points. The coincidence circuit was then put into operation and curve D obtained for coincident pulses from the source, and curve E for the coincident noise pulses with the phosphor and source removed.

It is evident that the coincidence circuit is very effective in reducing the noise background provided the discriminator bias is set at about 22.5 volts, or above. According to Fig. 4, anticoincident noise pulses as great as 0.08 volt can be expected to occur, corresponding to output pulses of amplitude $0.08 \times 290 = 23.2$ volts, in agreement with this observation. Since the resolving time of the coincidence circuit described here is perhaps 0.5 μsec., a simple calculation shows that the counting rate due to accidental coincidences between noise pulses in the two photo-tubes should be negligible.

An undesirable effect exhibited by the counting arrangement tested is that the coincident bias curve (D) falls off with increasing bias more rapidly than the bias curves for the individual photo-tubes. This effect indicates that different amounts of light reach the two photo-tubes depending on the position in the phosphor at which a γ-ray makes an interaction with the phosphor. The amplitude of a coincident output pulse, of course, is set by the smaller of the two input pulses from the photo-tubes. The correlation in the amplitudes of coincident pulses could no doubt be increased by improving the optical coupling between the phosphor and the two photo-tubes. An ideal arrangement, although difficult to achieve in practice, would be one in which all the light emitted by the phosphor is gathered and then divided equally between the two photo-tubes.

A direct measurement of the resolving time of the coincidence circuit has not been made. As pointed out earlier, the resolving time of the present circuit designed for a sodium-iodide phosphor can be reduced tenfold, and possibly 100-fold by decreasing the values of the resistances in the circuit a suitable amount. For a shorter resolving time to be of practical importance, one of the faster organic phosphors must be substituted for the sodium-iodide phosphor. With these changes it would appear possible to realize a resolving time of 10^{-8} sec. or less with a coincidence circuit of the sort described.

It is worth noting that the coincidence circuit can be readily modified so that any number of photo-tubes can be connected in coincidence. Each additional tube is coupled to the resistance R_3 through a diode, with a separate bias control for each branch of the coincidence circuit. It appears possible to use the coincidence circuit for Geiger-Müller tubes of the self-quenching variety, without the need for amplification, or pulse inversion between the tubes and the coincidence circuit. Indeed, the present circuit may be considered as a low level modification of the high level diode coincidence circuits described by Howland, Schroeder, and Shipman[4] which require a separate amplifier for each G-M tube.

The author is greatly indebted to the Research Corporation for supporting his work.

---

[3] See, for example, Higinbotham, Gallagher, and Sands, Rev. Sci. Inst. **18**, 706 (1947).

[4] Howland, Schroeder, and Shipman, Phys. Rev. **18**, 551 (1947).

A 100,000,000-Frame-per-Second Camera

M. SULTANOFF
Terminal Ballistic Laboratory, Aberdeen Proving Ground, Maryland

(Received March 22, 1950)

Shock waves close to the edge of explosive charges have been successfully photographed at rates exceeding 100,000,000 frames per second. These ultra-high framing rates are obtained with a multislit focal plane shutter which is transported optically across the film plane by a rotating mirror. Linear shutter speeds up to 3000 meters per second are easily obtained, and the resulting framing rates with the proper selection of slit widths can be varied from 10^6 to 10^9 frames per second. Each individual frame is composed of a series of lines, and the degree of "discontinuity" across each frame is proportional to the total number of frames.

INTRODUCTION

THE experimental studies of the shock and detonation which accompany explosive reactions have been hampered by the lack of ultra-high speed instrumentation. Short duration optical studies are particularly required for the investigation of self-luminous detonation and shock waves.

The velocity of these transients average about 8 mm per microsecond. Therefore, usable photographic exposures of these transients must not exceed 10^{-7} sec. Kerr cell shutters[1] have been used to obtain a single or a few successive short duration exposures, while multilens cameras[2] have produced continuous short duration exposures, but at rates which are not adequately high. The O'Brien-Milne camera,[3] which is rated at 10,000,000 frames per second, but which displays poor resolving power, could not be obtained commercially, and its precise optical system made it impractical to build locally.

A motion picture camera which employs simple optical and mechanical systems to obtain up to 300 successive 4×4 in. frames at rates which can be varied from 10^5 to 10^9 frames per second, and which exhibits satisfactory resolving power, is described in this paper.

THEORY OF GRID FRAMING

The standard variable slit focal plane shutter in common use exposes a time-space record as it travels across the film plane. Although the slit moves slowly across the film, the exposure time can be made extremely short by reducing the width of the slit.

The framing grid is a focal plane shutter with a series of parallel slits placed at regular intervals across it. This shutter, therefore, is only required to move the distance between two successive slits to expose the entire film. To understand how this grid records successive frames, consider a series of optically clear slits 0.0005 in. wide, cut at 0.015 intervals across a 4×4 in. optically opaque plate. If this grid is held in a fixed position on a 4×5 in. photographic plate, a single exposure made through it would consist of a set of parallel lines which occupy only 1/30 of the total picture area with an over-all dimension of 4×4 in. A sample exposure of this type is shown in Fig. 1. By moving the grid across the film perpendicularly to the slits for a distance of 0.0005 in., and exposing a second still picture in this new position, a second series of lines lying alongside of the first set and again occupying only 1/30 of the total picture area will be produced. Thirty such single pictures will result from only 0.015 in. movement of the grid, and will expose the entire film area. To the casual observer the resulting picture will be an indistinguishable jumble. However, by proper positioning of the grid, any one of the thirty exposures can be studied separately. This type of grid framing has been used for years in animated greeting cards and photographic advertisements.

If the photographic object is moving, and if the grid

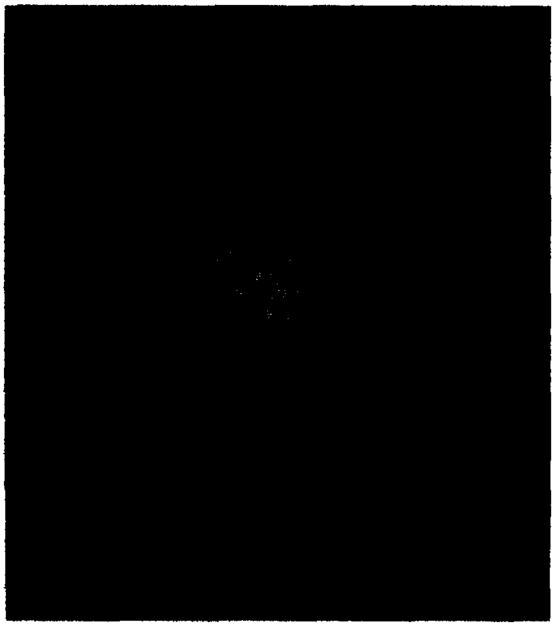

FIG. 1. Single still photograph of spherical charge in firing position, taken through 0.005 in. slit, 0.015 in. space grid.

---

[1] Zarem, Marshall, and Poole, NAVORD Report 1016 (May 14, 1948).

[2] J. Stanton, The Bowen 76 Lens Camera (a preliminary description).

[3] O'Brien and Milne, J. Soc. Mot. Pict. Eng. 52 (January 1949).

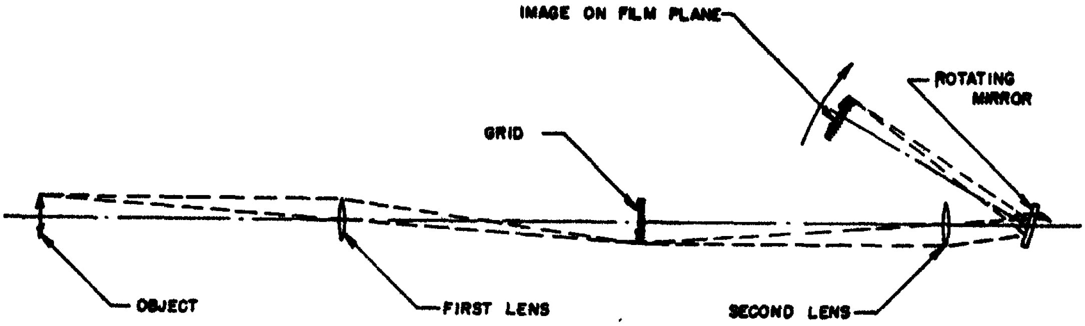

FIG. 2. Optical system of ultra-high speed camera.

is moved at a uniform rate across the film for a distance of 0.015 in., the resulting picture can be viewed through the grid as thirty separate exposures, one at a time, or, by viewing through the grid moving at any uniform speed, flickerless motion pictures will be observed. This adaptation of grid framing was described in a paper delivered by Dr. Fordyce Tuttle of the Kodak Company at the Society of Motion Picture Engineers Symposium which was held in New York City on April 6, 1949.

At this laboratory we have been successful in combining a stationary framing grid with a rotating mirror to obtain framing rates in excess of 10^8 frames per second.

THE ROTATING MIRROR GRID COMBINATION

The optimum slit width for the multi-slit focal plane shutter appears to be of the order of 0.0001 in. A shutter with 0.0001 in. slits is required to move 10,000 in. per second to produce 10^8 frames per second. It is impractical to accelerate to, maintain, and decelerate from such high velocities with a linearly moving shutter. A rotating focal plane shutter, on the other hand, has the double disadvantage of requiring tapered radial slits and the combination of a large diameter and high rotational velocity. A method for moving the image of the shutter across the film plane by reflection from a rotating mirror was obviously a simple solution to this problem. The rotating mirror optical system in a Bowen RC-3 Rotating Mirror Camera,[4] although not adequate for this application, was available at this installation, and it was modified to take a 4×4 in. multislit framing grid and a 4×5 in. camera back.

A first lens is used to image the event on the grid. The combine event-grid is then focused by a second lens, whose image, after reflection from the rotating

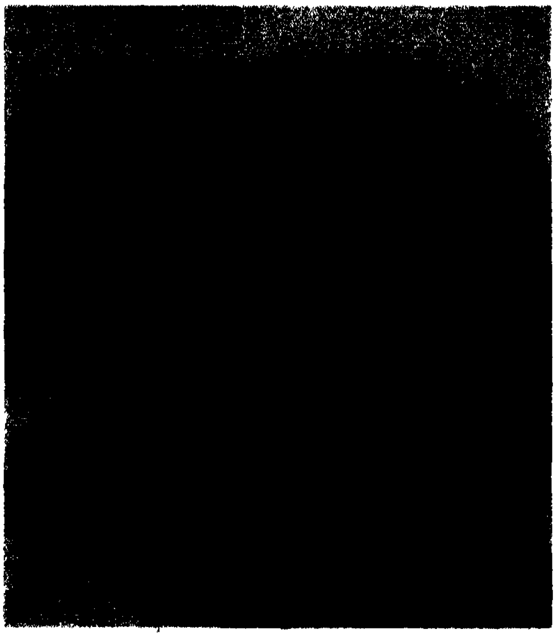

FIG. 3a. Complete exposure of detonating spherical charge. (Negative.)

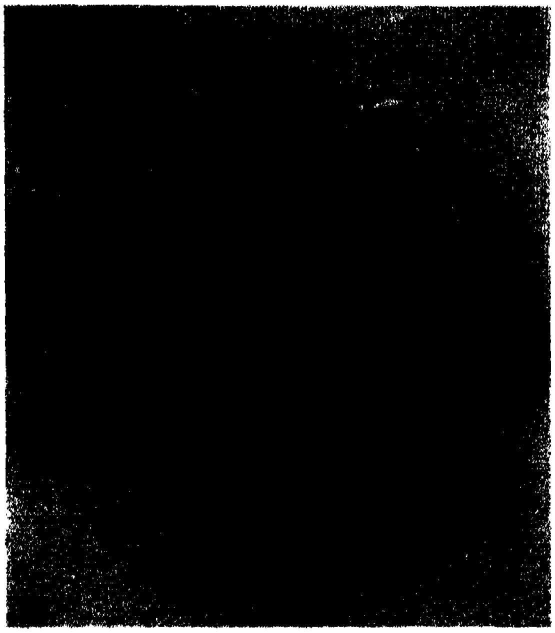

FIG. 3b. Single frame taken from Fig. 3a. (Negative.) Framing rate 1.1×10^8 frames per second.

---

[4] I. S. Bowen, *The CIT Rotating Mirror Camera* (Mod. 2) (April 27, 1945).

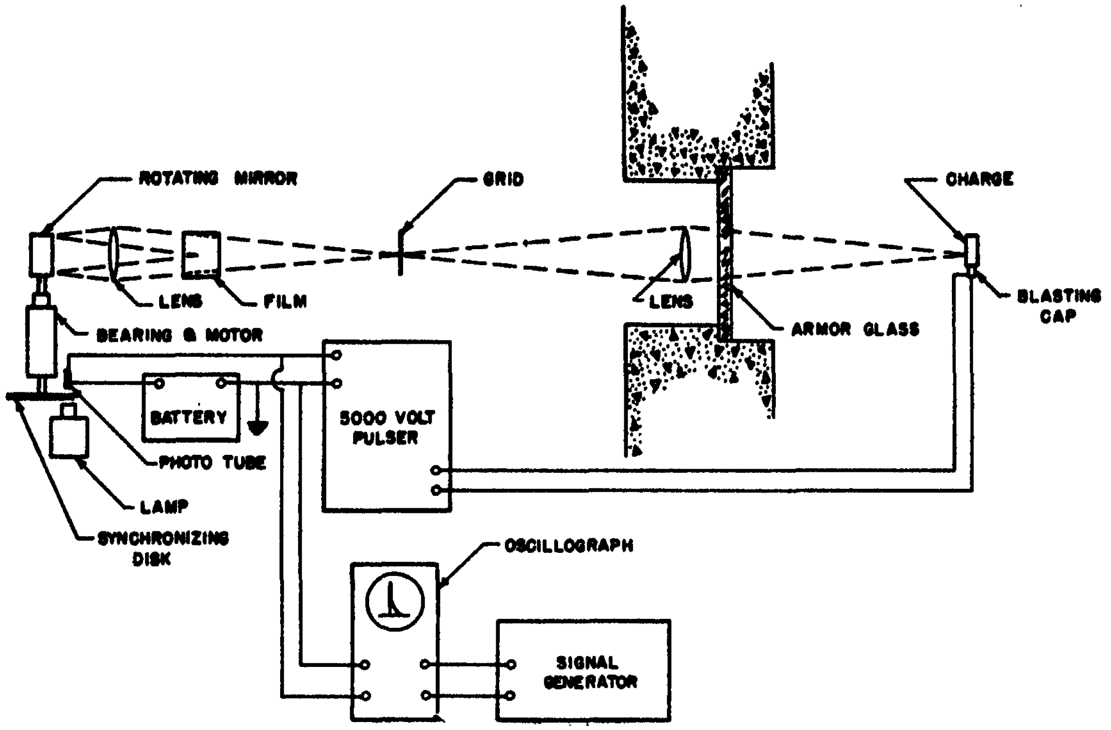

FIG. 4. Synchronizing circuit for ultra-high speed camera.

mirror, falls on the film plane as shown in Fig. 2. The photograph formed by the reflected grid differs from that formed through a grid moving across the film plane in that the latter records a varying time varying space image, while the former, by virtue of the subjects fixed position with respect to the grid, records a fixed space varying time record which is particularly suited to the studies of detonation and shock waves.

FRAMING RATE

The continuous motion of the image across the film does not form the well-defined frame of the intermittent or the rotating prism type cameras. An infinite number of viewing positions of the framing grid are possible, leaving the framing rate undetermined. However, since the exposure time of any increment of film is equal to the time it takes a slit to move its own width, the reciprocal of this time is taken as the framing rate. Thus, each consecutive frame is viewed by moving the grid one slit width per frame.

The rotational speed of the mirror being used can be varied up to 500 RPS, with a 20 in. optical arm the maximum image speed is 0.122 in. per microsecond. The exposure time with a 0.0005 in. slit at the full rotational speed of the mirror is 4×10^{-9} sec., or 2.5×10^{8} frames per second. With a 0.0001 in. slit the framing rate is 1.25×10^{9} frames per second. With suitable optics, it is believed that sufficient light will be available from detonation and shock phenomena to take pictures at the rate of one billion frames per second.

THE CONTRIBUTION OF THE GRID TO THE RESOLVING POWER AND TOTAL NUMBER OF FRAMES

The resolving power, or more exactly, the measure of the "discontinuity" across the picture because of the nature of its line structure, expressed in lines per inch, is equal to the number of slits per inch. The number of slits per inch is determined by the slit width and the number of frames required. That is, with a 0.0005 in. slit if 30 frames are desired, the space between the slits must be 30 times 0.0005 in. or 0.015 in. Such a grid will have a "resolving power" across the slits of $1/0.0005+0.015$ or about 65 lines per inch. With a 0.0001 in. slit and the same resolving power, 150 consecutive frames are obtainable.

The total exposure time, with no double exposures, is the product of the exposure time per frame and the total number of frames without double exposures. With 30 frames taken at 100,000,000 per second the total exposure time is 3×10^{-7} sec. All of the pictures taken up to the present time have been of self-luminous shock waves. Double exposures are prevented by quenching the shock wave in an atmosphere of propane at a predetermined time. However, for investigating shock velocities, it has been found convenient to get multiple exposures (Figs. 3a and 3b), which permits the measurement of distance as a function of time on each individual frame.

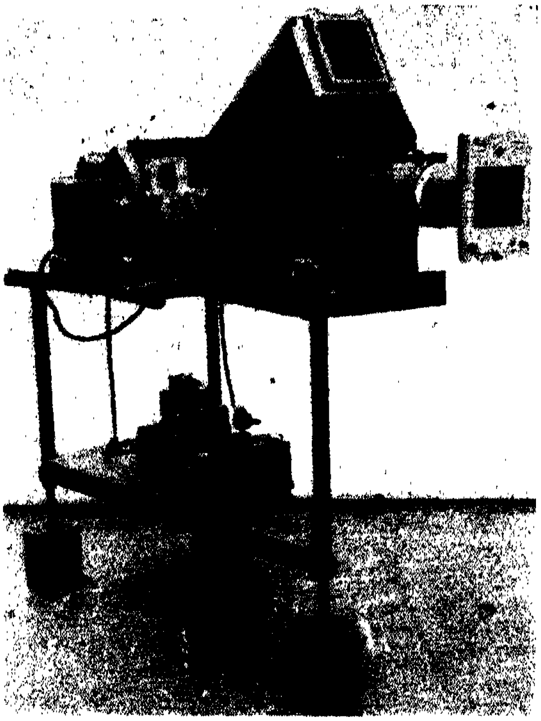

FIG. 5. ¾ front view of camera showing grid in position.

COMPONENTS OF THE ULTRA-HIGH SPEED CAMERA

The components of this camera, shown in Figs. 4 and 5 are described below.

1. First imaging lens. One of a number of high quality large aperture photograph objectives which are available is used depending on the size of the charge and the magnification of image desired at the framing grid. All of these lenses are long focal lengths (12 to 40 in.) as required by the physical set-up in the blast chamber. (Fig. 4.) 2. Framing grid. The grids most easily obtained and reasonably priced are made on opaque coated optical glass 4×4×⅛ in. by Max Levy, Photolithographers of Philadelphia. The 0.0005 in. and 0.0001 in. slits are cut with corresponding flat diamond points on a dividing engine. 3. Second imaging lens. This lens has a focal length of 360 mm. With the 1:1 magnification from the grid to the film plane the mirror can be placed to given an effective optical lever of about 20 in. Several photographic objectives with aperatures of about *f*:4.5 have been tested. A high quality process lens corrected for a flat field appears to resolve the slits most accurately. 4. Rotating mirror. The 1 in. square face octagonal mirror in the Bowen rotating mirror camera is the aperature stop of the system. A 2 in. square flat mirror designed to rotate around an axis in the plane of its face will not only take advantage of all of the light from the second lens but will eliminate the complicated form of the focal plane. 5. Film plane. A standard 4×5 in. camera back is being used as illustrated. 6. Synchronizing circuit. A hole in the wheel which drives the mirror passes a beam of light to a phototube which in turn fires a thyrotron. This thyrotron, operating at 400 volts then fires the charge directly or is used to trigger a timing circuit depending on the time requirements for the particular charge.

PHOTOGRAPHIC TECHNIQUE

Kodak Tri-X panchromatic plates have produced images of good density at exposures times of 10^{-8} sec. These plates are processed in Kodak D19 developer for 20 minutes at 60°F. Base fog "latensification" of these plates has been used to obtain good image densities with developing times as short as 8 minutes at 65°F.

REVIEWING THE FILM

Since the magnification from the grid to the film plane is 1:1, the negatives or contact printed positives can be viewed by placing the grid directly over them. Motion pictures can be observed by moving the photographic plate across the grid and frame by frame viewing is accomplished with a micrometer feed. Measurements are made at 10× magnification with a Bausch and Lomb contour projector. The sample reproductions in this report were made by enlarging through the grid properly positioned on a positive plate.

CONCLUSIONS

The fundamental features of the design described in this report indicate limitless possibilities for obtaining ultra high speed photographs of self-luminous phenomena. Probably, with the use of explosive type flash bombs, or with Edgerton type lights, non-luminous subjects can also be photographed at rates exceeding 10^8 frames per second.

Book Reviews

The Cyclotron

By W. B. Mann. Third edition. Pp. 92+xi, Figs. 31. Methuen and Company, Ltd., London; John Wiley and Sons, Inc., New York, 1948. Price $1.25.

This book is one of the series of Monographs on Physical Subjects published by Methuen and Company. It is the intention of this series "to supply readers of average scientific attainment with a compact statement of the modern position in each subject." The present volume presents a lucid and detailed account of the development and construction of cyclotrons of the prewar period. (The latest reference given is the paper published by Lawrence and his group at Berkeley in 1939 describing their 60-inch cyclotron.) In view of the fact that present attention in the accelerator fields is focused on synchrocyclotrons and cyclosynchrotrons designed to accelerate protons to energies in the billion volt range, it might have been worth while to include some remarks on these new developments in the new edition. However, as ordinary cyclotrons are and will probably continue to be widely used, the present volume is a valuable introduction to their design and operation.

The first four sentences of this book take the reader from the discovery of artificial radioactivity by Rutherford in 1919 to the development of the cyclotron and the electrostatic generator in the early 1930's. The problem of resonance acceleration is introduced with a review of the work of Wideröe and Lawrence, Sloan and others on the linear resonance accelerator for heavy ions.

The limitations of this method are discussed and serve to emphasize the ingenuity of Lawrence in overcoming these difficulties with his magnetic resonance accelerator. (It should, however, be remarked that the former method has recently been used by Alvarez to attain 32-Mev protons.) The author proceeds to describe the basic principles of the cyclotron. Some calculations and curves are given which serve to orient the reader; mention is made of the difficulties to be faced in future developments resulting from the relativistic increase in mass at high energy. Detailed consideration is then given to the design and construction of the vacuum chamber, magnet, and the r-f system. Many references are made to the work of other laboratories as well as to the work at Berkeley. The final chapter is a very brief review of typical applications of the cyclotron, or rather its products, to nuclear physics, chemistry, and medicine.

The reader who is unfamiliar with but interested in the design and operation of cyclotrons will enjoy this little (pocket-size) book. The usual textbook descriptions cannot give the reader the same appreciation of the amount of ingenuity and engineering which are necessary in order to proceed from the remarkably simple resonance formula to a beam of energetic ions.

R. Sherr
Princeton University

Kinematic Relativity

By E. A. Milne. Pp. 238+viii, 6¼×9¼ in. Oxford University Press, London, 1948. Price $5.00.

E. A. Milne's cosmological theory, named by him "kinematic relativity," stands apart from most of the generally recognized physical theories. It has been hitherto almost inaccessible, inasmuch as the earlier work, *Relativity, Gravitation, and World Structure* (Oxford University Press, London, 1935), was dated almost the day it appeared, and a series of papers by Milne which appeared in the *Proceedings of the Royal Society* and elsewhere after 1935 were very hard to read. The present volume was written at a time when the foundations of the theory had settled down, even though Milne has continued to work out its applications in various fields of physics.

Kinematic relativity as a theory is distinguished from other physical theories primarily by its almost completely abstract, *a*-physical character. The starting point of the theory is an abstract space possessing three plus one dimensions, in which every observer is at first permitted to introduce his own frame of space-time coordinates. However, by means of an exchange of light signals, two observers can, if they so wish, regraduate their clocks in such a manner that their private times become "congruent." This expression (Milne's) denotes such a graduation of clocks that each of the two observers "sees" (with the help of light signals) the other observer's clock delayed relative to his own by the same (time-dependent) amount. Or, putting it differently: Each observer can by observations express the relationship of the other observer's time to his own by means of a function:

Observer "1": $t_2=f_1(t_1)$.
Observer "2": $t_1=f_2(t_2)$.

Here t_1 is the time kept by "1"'s clock as observed by himself; t_2 is "2"'s clock time as observed by "1". Thus f_1 is the summary of the raw data assembled by "1" who observes "2"'s clock at a distance and compares the remote clock dial with his own. Analogous meanings are attached to the symbols occurring in the second line above. The state of *congruence* is achieved when the two functions f_1 and f_2 are *the same function*. By means of regraduation, *two* observers can always achieve congruence if only the initial functions f_1 and f_2 (before regraduation) are monotonically increasing.

The next question tackled by Milne is the characterization of a *set* of observers (more than two) who are in such a relationship to each other that they can achieve universal congruence, i.e., that they can regraduate their clocks so that after regraduation any two of them use congruent time in the sense defined above. A set of observers in this state are called an *equivalence*.

Milne's basic assumption is that in the physical Universe such a set of observers can be introduced and that they are connected with the individual galaxies. Granted this basic assumption, Milne can show that in his Universe there exists a certain over-all isotropy and homogeneity.

In all that follows, it is very difficult for the reader to gauge properly the roles played by the axioms and those by the deductive proofs. At first sight, many of Milne's assumptions appear innocuous and even self-evident, so-called symmetry assumptions or, at any rate, assumptions concerning qualitative aspects of nature only. On closer inspection, the assumptions turn out to be very definite quantitative assumptions. Two examples will illustrate this point.

First, let us consider the assumption that there exists an equivalence of observers as defined previously. The power of this assumption can be studied best if we discuss it in the light of some other theory of the physical Universe, and such alternatives are provided by the special and by the general theories of relativity. Let us start with the special theory, i.e., with an assumption of a flat (quasi-Euclidean) space in which the velocity of light is a universal constant. In such a space, Milne equivalences can be constructed without difficulty. As a first equivalence, take a number of observers who are all at rest relative to each other. Given any two observers A and B, both A and B will find permanently that the other observer's clock is slow compared to his own, by an amount constant in time and equal to their mutual distance, divided by c. Another equivalence can be constructed by a set of observers stationed on all the straight, time-like lines passing through one world point. If these observers calibrate their clocks so as to show proper time counting from the world point of coincidence, or any unique function of this proper time (such as the logarithm, if they wish to provide a range for the time from negative to positive infinity), the relationship between any two observers of the equivalence will again be symmetric. If the point of convergence lies in the past, we shall have, in the language of Milne, an expanding Universe; if it lies in the future, the Universe will contract.

Now consider as our theoretical vantage point the general theory of relativity, and let us assume that light rays travel along so-called zero-geodesics. (This assumption in general relativity corresponds to the adoption of geometrical optics; it is certainly well taken if we use light of sufficiently short wave-length to permit the clear-cut transmission of signals.) Let us consider in this Riemannian space-time a situation that corresponds to the so-called Schwarzschild solution; a single particle in whose neighborhood the space is strongly curved, but so that at spatial infinity the curvature tends toward zero. In this space, we can set up an equivalence again, but in a peculiar fashion. It is well known that in the Schwarzschild solution of the field equations we can introduce "static" coordinates, i.e., coordinates in terms of which the geometry is time-independent and so that $g_{i4}=0$. However, the world lines along which x, y, and z are constant are not geodesics, i.e., a free particle will not stay permanently on such a curve, but will be accelerated toward the center $r=0$. Milne's equivalence can now be set up as a set of observers who remain permanently on these world lines, and whose clocks are calibrated to show coordinate time (rather than proper time). This prescription determines both the starting time and the rate of each clock. This system of clocks is an equivalence, but, of course, each observer must be kept at his appointed place by means of an external non-gravitational force. Whether a material particle can be kept in this state is doubtful, since non-gravitational force fields, through the resulting stress, affect the gravitational field.

We are now ready to turn to the second example. Milne "derives" the dynamical behavior of a free particle from the requirement that in terms of the equivalent observers the equations of motion of the particle must contain only elements already provided by the basic conceptual framework. These elements are essentially the present location and the present velocity of the particle. With this assumption, it turns out that the particle will remain at rest with respect to any observer belonging to an equivalence if it is at rest with respect to him initially. Substantially, this proof amounts to the theorem that in a flat space the only curves definable without the introduction of *ad hoc* elements (such as the curvature vector) are the straight lines. Now let us compare Milne's results with the result of the general theory of relativity. According to the general theory of relativity, a free test particle in the field of a Schwarzschild solution will experience acceleration even when initially at rest with respect to a coincident observer of the equivalence. The discrepancy is obvious and inescapable. Its only explanation must be sought in the basic assumptions, since the syllogisms afterward are flawless.

In this reviewer's opinion, Milne's assumptions are actually, and in spite of their deceptively innocuous form, very severe assumptions concerning the nature of the physical Universe; in all probability, the real Universe does not possess the properties ascribed to it by Milne. Milne not only assumes that the Universe is on the whole isotropic and homogeneous, assumptions that might be accepted tentatively (though recent cosmological research by Hubble, Omer, and others tends to cast doubt even on these hypotheses), but he proposes to construct a physical theory in which the only properties of space-time are those determining the trajectories of light rays. Furthermore, in Milne's theory it is not the local directions of the light cones, but the *finite geometrical figures* whose sides are either light rays (zero geodesics) or material observers of an equivalence which are to describe the entire geometry and physics of physical space-time. Interesting as this point of view may be, it appears to this reviewer to be in flagrant contradiction to the known facts about fields of gravitation. Newton's law of gravitation, the observed effects of gravitational fields on the direction and the color of light waves, the precession of the Mercury perihelion, and, last but not least, the equivalence of inertial and gravitational mass, shows conclusively that the geometry of space is tied up with the gravitational potentials (otherwise the principle of equivalence remains unexplained), and that the number of these potentials is greater than one. Just as the existence of the Lorentz force in electrodynamics shows that in the face of a Lorentz transformation the electric potential cannot be a scalar, so does the Coriolis force and the effect of gravitation on light, show that the theory of gravitation cannot get along on one potential. The very fact that the "source" of the static gravitational field is not the proper mass of the particles (a scalar), but the *relativistic mass density* (one component of a tensor), suggest that the number of gravitational potentials is 10. That under these circumstances the detailed properties of physical force fields can be derived from assumptions of homogeneity and isotropy of space alone is, to say the least, not intuitively obvious.

Milne has claimed that in his theory he cannot only explain the inverse-square law of gravitation, but also some of the most important properties of elementary particles, such as the instability of the neutron. Most of Milne's arguments in the construction of his theory reduce to the requirement, reasonable in itself, that theoretical concepts should be derivable from as small a number of independent fundamentals as possible. Thus, even though most of his basic assumptions have little to recommend them to the physicist, some of his subsequent derivations may possibly become valuable components of some other theory.

The book is organized into four parts, entitled (I) "Kinematics," introducing the concepts of congruence and equivalence; (II) "Dynamics," dealing mostly with the behavior of free particles and photons; (III) "Gravitation," deriving Newton's inverse-square law and also giving a theory of spiral nebula genesis; and (IV) "Electrodynamics," discussing besides the laws of the electromagnetic field itself atomic physics and the structure of elementary particles. This part contains a concluding chapter, "General Outlook," which serves as a nice summary of the whole book and indicates in which direction Milne proposes to go.

This reviewer has found Milne's present book considerably more readable than any of his previous work, though a full appreciation and a critical appraisal remain most difficult undertakings. For the reader who wishes to study Milne's theories thoroughly and to form his own opinions, this book can be recommended as the most authoritative presentation.

Peter G. Bergmann
Syracuse University

Der Ultraschall und seine Anwendung in Wissenschaft und Technik

By Ludwig Bergmann. Fifth edition. Pp. 748+viii, Figs. 460. S. Hirzel Verlag., Zürich, 1949. Price $13.00.

It appears from the author's Preface that the fourth edition, if its publication was actually completed, was largely destroyed in the war days of 1945. The continuation of wartime difficulties into the publication of the present edition is to be noted in the very poor quality of the paper used and of the binding. The author points out his own great difficulty in attaining more than mere titles for many of the postwar papers and makes the plea that reprints be sent to him in order that he may provide a more adequate coverage of the field in the next edition. It is to be hoped that his request may bring a generous response both for the sake of the author and for the long-range enrichment of a well-established and outstanding reference work which is unique in its field.

Without access to the fourth edition, which appears incidentally not to have been entered at the Library of Congress, the reviewer can make comparison only with the earlier editions, including the third of 1942. The expansion to be noted is extreme indeed. The author calls attention in his Preface to two new sections in the first part of the book where the excitation, demonstration, and the measurement of ultrasonic waves are treated. These sections discuss the underwater whistle of Janovski and Pohlman and the ultrasonic siren of American origin and constitute the principal changes in Part I.

The expansion in many of the later sections of the book is between two- and threefold and is perhaps most marked in Chapters III and V which deal, respectively, with the immediate application to the study of the properties of materials at ultrasonic frequencies, and with applications further afield as in instrumentation generally, direction finding, testing of materials, physical and colloidal chemistry and application for their biological and medical effects. These two fields of application, one to the study of ultrasonic properties of materials, and the other to bringing about desired effects and conditions for the chemist, the biologist, the physician, and the manufacturer, occupy in the fifth edition considerably more than half of the book.

The bibliography provides some indication of the growth of the field in the years since 1942 and of the expansion of the book from the third to the fifth edition. From 1068 references the number has jumped to 2322. A spot comparison with the Analytical Subject Index to Contemporary Acoustical Literature which is included in the 1938 to 1948 Cumulative Index of *The Journal of the Acoustical Society of America* indicates good coverage by the bibliography which is under review through 1948 so far as the field of ultrasonics proper is concerned. The vast accummulation, however, of wartime and postwar papers supported by the military services in this country and dealing with the field of underwater sound particularly, which has been released in considerable part during the past two or three years, is well covered in the J.A.S.A. Cumulative Index, but appears scarcely to be touched at all in the Bergmann book.

The book is of the encyclopedic type common among German reference works in which are given brief descriptive treatments of the findings of many authors, but with little attempt at critical evaluation of their results. It is a stupendous task to treat the material of 2300 references in a 700-page book. The reviewer has made no attempt to determine what particular postwar papers might be inferred to have been unavailable to the author except in title or in abstract form, or to judge in what way such unavailability on the part of more important papers may have led to the giving of space to lesser items.

Particularly pleasing in the present edition is to find the brief appendix on Ultrasonic Waves in Nature. A practice of inserting in the text the year along with the reference number to the bibliography would be of considerable help to the reader in a work of this sort. The reviewer finds himself writing the year of the reference in the margin beside the text as he reads along after having looked up the reference in the numbered bibliographical list at the back of the book. As a final comment the reviewer regrets that the many factors which go into the pricing of such a book should result in so high a figure.

KARL S. VAN DYKE
Wesleyan University

Hyperfine Structure in Line Spectra and Nuclear Spin

BY S. TOLANSKY. Pp. 120+viii, Figs. 29. Methuen and Company, Ltd., London, 1948; John Wiley and Sons, Inc., New York, 1950. Price $1.50.

This is the postwar revision of Professor Tolansky's well-known introduction to optical hyperfine structure and its use as a tool for investigating nuclear properties. The change from "Fine" to "Hyperfine" in the title is merely one of terminology, so that the general nature of the book remains unchanged. But it has been thoroughly revised, so that the introductory chapter and those on experimental technique, isotope effect, nuclear spins, nuclear magnetic moments, and nuclear electric quadrupole moments are largely new.

After an introduction outlining the scope and purpose of the study of hyperfine structure, a chapter is devoted to the causes of line width in spectral lines and the experimental techniques of producing lines sharp enough for hyperfine structure analysis. Chapter III, on multiplicity in line spectra, develops the notation and the elements of the theory of multiplets from the viewpoint of the vector model. The effect of a nuclear spin is next considered and then extended to hyperfine structure in many-electron spectra. A chapter is devoted to the methods for deriving term interval factors from hyperfine structure patterns and the dependence of interval factor on electron configuration and term type is discussed. This is followed by a discussion of isotope effects in hyperfine structure, including both those ordinarily classed as isotope shifts and the complications due to different isotope magnetic moments. The discussion of hyperfine structure patterns is completed by a chapter on perturbations. Then the results of these and similar investigations are discussed in three chapters on nuclear spins, nuclear magnetic moments, and nuclear electrical quadrupole moments. Finally, the book has brief appendices on hyperfine structure Zeeman effect and the single-particle theory of nuclear spin.

Throughout the book, the vector model is used almost exclusively. Quantum mechanics is only mentioned occasionally when theoretical results are quoted as needed. This is, in fact, the practice usually followed in discussions of hyperfine structure experiments. It permits the presentation of a clear physical picture of the phenomena, and rapid prediction of the effects to be expected. However, in a few places, such as the chapter on perturbations, the introduction of more quantum-mechanical ideas might have simplified the discussion.

The treatment is frequently illustrated by reference to actual experimental results, including many drawn from Professor Tolansky's own researches. In this way the student can acquire a very good idea both of the types of hyperfine structures observed and of their magnitudes. In some places details of the experimental results obscure the underlying principles to some extent, but almost always the connection is clearly brought out.

In a book of this size the author is faced with a difficult problem in the selection of topics to be included, and inevitably there will be some who would have liked to see other subjects discussed. Thus the reviewer would have liked to see some mention of the Fermi-Segrè formula for the calculation of nuclear magnetic moments from hyperfine structure, and a fuller discussion of the theory of isotope shifts in the spectra of many-electron atoms. Nevertheless, one must admire the skill with which Professor Tolansky has condensed so much material into this small book without loss of clarity.

This is still the only book on hyperfine structures in English. It will provide a good introduction to the subject for those who wish to know what hyperfine structures are about, and will serve as an excellent starting point for those planning to work in the field.

A. L. SCHAWLOW
Columbia University

Engineering Mechanics

BY A. HIGDON AND W. B. STILES. Pp. 505+xvii, profusely illustrated. Prentice-Hall, Inc., New York, 1950. Price $5.00.

The authors have set themselves the task of presenting in textbook form the accumulated material and methods of their department in a particular field and at a particular level.

The field covered is broad enough to give a beginning student in Engineering Mechanics a sufficiently wide base and yet it is restricted sufficiently that the work may be adequately covered in a two-semester course. The authors even suggest that the material of the book may be covered in a one-semester course by the omission of certain specified portions.

Of the 491 pages in the book, 227 are devoted to Statics and the remaining 264 to Kinematics, Kinetics, and Mechanical Vibrations. The material covered is basic and one may well say standard; for instance, Statics deals with Basic Concepts, Resultants of Force Systems, Centroids and Center of Gravity, Equilibrium, Friction, and Moments of Inertia; Kinematics covers Absolute Motion and Relative Motion; Kinetics includes Work and Energy, Impulse and Momentum; and a final chapter covers Mechanical Vibrations.

The presentation is highly systematic. For instance, in the chapter on Resultants of Force Systems, the articles deal with Resultant of a collinear force system, Resultant of a concurrent, coplanar force system, Resultant of a parallel coplanar force system, Resultant of a concurrent, non-coplanar force system, Resultant of a parallel, non-coplanar force system, and Resultant of a non-concurrent, non-parallel, and non-coplanar force system.

The material is developed from the relatively few hypotheses of Newtonian mechanics and emphasis is clearly placed upon the student's mastering the developments of the various phases of the subject as well as upon the solution of problems through the use of formulas. The explanations and developments are brief but adequate and the summaries of the results are clear and emphatic.

There is a profusion of problems, well-illustrated by excellent diagrams, which in general are practical and of present-day interest.

Vector notation is introduced and applied to force, linear displacement, velocity, and acceleration but not to angular velocity or acceleration, or to linear or angular impulse and momentum, and in dealing with rigid body, no vector notation is employed.

The only vector manipulations appearing are those of addition and subtraction, and special symbols have been introduced for these two operations. Also the authors employ a system of arrows to indicate directions of forces and couples and sometimes carry this symbolism along with equations of a more complicated sort to indicate the directions of the contributions of the various terms.

Since force is a vector, considerable work must always be done in treating force as such, but the present authors have done this to a minimum. They rather have emphasized the analytical method of dealing with forces, once having shown their vector character. In dealing with frames, for instance, the work is first carried out from an analytical standpoint, followed by the graphic method.

The calculus is employed in such parts of the subject as the calculation of centers of mass, of moments and products of inertia, and of frictional couples. Differential equations are employed very little as, for example, in the solution of the simple harmonic motion equation and some references are made to this solution in the chapter dealing with Mechanical Vibrations.

The treatment of kinetics is based upon Newton's laws, in particular the second and third laws and upon D'Alembert's principle which is stated as follows: "The resultant of the external forces acting upon a system of particles is equal to the resultant of the effective forces (*ma* values) of the particles of the system." This is extended when needed as follows: The sum of the moments of the external forces with respect to the axis of rotation is equal to the sum of the moments of the internal effective forces.

The above principles are employed directly to show that the mass center of a system behaves as if all the external forces of the system were applied to it and that in the two-dimensional case the sum of the moments of the external forces is equal to the product of the moment of inertia and the angular acceleration for a fixed axis or an axis through the center of mass or for an axis that possesses no component of acceleration normal to the line joining it to the center of mass.

It is shown that the whole kinetic energy of a rigid body in the two-dimensional case may be regarded as the linear kinetic energy of any point plus the angular kinetic energy relative to this point plus two terms involving the component velocities of the point, the angular velocity of the body etc., and that if the point is the point is the mass center the last two terms vanish.

Linear and angular impulse and momentum are introduced and the principles of conservation of both linear and angular momentum are brought out.

The general procedure throughout the book is to give a theoretical development of some limited part of a subject, then to work an example when that would be helpful. Whenever possible specific rules for the attack and solution of problems have been listed.

In the opinion of the reviewer, the book presents a good selection of subject matter in the field of Engineering Mechanics but this is secondary to the fact that the book sets forth a process of presenting this subject matter to students at the particular level. In this attainment it would seem that the authors and their associates should be complimented.

MERIT SCOTT
Pennsylvania State College

Albert Einstein: Philosopher-Scientist

BY P. A. SCHILPP. Pp. 781+xvi. Library of Living Philosophers (Vol. 7), Northwestern University, 1949. Price $8.50.

This is the seventh in the series of volumes on living philosophers in which contemporary thinkers praise, criticize, and condemn, and in which the philosopher "replies to his critics." There is also an autobiography and a bibliography. The choice of Einstein as a philosopher was an eminently sensible one; only a mind ignorant of philosophical traditions can believe that a great theoretical physicist can fail to be an eminent philosopher as well.

The contributions of the volume are actually of three sorts. First there are papers that comment on Einstein's special and general theories of relativity *as such*; these papers consider in the main the logical structure of the relativity theories and their relationship to other theories in physics, particularly quantum theory (Sommerfeld, de Broglie, Pauli, Born, Heitler, Menger, Infeld, and von Laue). Second, there are papers that are concerned with the philosophical implications of Einstein's physical theories; these either consider the impact he had on some school (e.g., Frank on positivism, Wenzl on critical realism) or set of schools (Ushenko on contemporary philosophy), or they consider certain philosophical problems that are posed by Einstein's work (Rosenthal-Schneider, Bohr, Margenau, Reichenbach, Bridgman, Lenzen, Northrop, Bachelard, and Dingle). Finally, some contributors have offered extensions of Einstein's theories, or suggested modifications (Robertson, Milne, Lemaitre, and Gödel).

Einstein's reply, though somewhat loosely written, is extremely interesting because it presents in very lucid form his already well-known attitude with respect to quantum theory. Boiled down to its essentials, Einstein's argument runs as follows:

(1) Quantum-mechanical description is a description of *ensembles* of systems (p. 71).

(2) A *complete* description includes not only an account of ensembles, but also of individual systems (p. 667).

(3) The programmatic aim of all physics is a complete description (p. 667).

Whence, it follows that quantum mechanics does not, by itself, satisfy the aims of physics.

To judge from the contributions of Born and Heitler, the majority of the adherents to the quantum faith tend to deny (1); in effect, they object to the "classical" notion of individual systems. Specifically, they do not believe that a system can be represented in common-sense (intelligible) terms, so that the "interpretation" of what is going on cannot be expressed in terms of a difference between, let us say, a single particle and an ensemble of particles. This attitude does deny one tradition of physics: to predict intelligibly, if by "intelligible" we mean "what is generally understandable." Einstein does an excellent job of showing that there is no "intelligible" meaning of certain concepts of quantum description (e.g., time of decay of a radioactive atom), *if* quantum mechanics is not considered as a description of ensembles. But it is not clear that his argument will convince the quantum mechanist, who is presumably satisfied with a program of predictability, regardless of whether or not there is a common intelligibility to all the concepts used.

Einstein's reply is also interesting because it shows beyond any doubt his present adherence to neo-Kantianism (experience requires *a priori* categories, which, however, are not "fixed").

Finally, it is strange that not one pragmatist contributed to a volume in honor of a philosopher, the implications of whose philosophy is (to many pragmatic minds) inherently pragmatic.

C. WEST CHURCHMAN
Wayne University

The Meaning of Relativity

BY ALBERT EINSTEIN. Third edition. Pp. 150. Princeton University Press, Princeton, New Jersey, 1950. Price $2.50.

The successive editions of this well-known work differ only in that for each an appendix is added covering significant advances since the previous edition. It does not appear necessary, therefore, to review at length the main body of work, which was first published in 1922. Here the reader will find a concise, technical account of the theories of special and general relativity. An outstanding feature is the clear, although brief, presentation of the fundamental concepts from which Einstein derives his theories. The title describes this material very well indeed, provided one regards it as referring to the foundations rather than the implications of the theories.

The first appendix, added in 1945, contains brief comments on a number of advances that had been made over the preceding 22 years and a somewhat more extended discussion of the author's current views concerning cosmology. Here Einstein treats several homogeneous but non-static models of the universe based both on his feelings as to the proper form of natural laws and on experimental data.

The last appendix of 15 pages is concerned with an extension of the general theory of relativity so that it will cover both gravitational and electromagnetic phenomena. A non-symmetric tensor is used as the metric tensor and as the means of correlating the covariant and contravariant components of tensors. The absolute differential calculus needed to deal with such a situation is then treated. Finally, field equations are set up on the basis of concepts of simplicity and symmetry and the requirement that they contain the usual general theory of relativity. It then turns out that the field equations contain new terms originating from the skew-symmetric part of the metric tensor and it appears that the aim is to use these to give something that will reduce to Maxwell's equations under suitable circumstances. The reviewer feels that the average physicist will not find in this appendix any new physical ideas of the kind that made both the special and general theories of relativity so important. It appears that further research and a more extensive discussion of the meaning of the equations will probably be needed before this hope can be realized.

The publishers are to be complimented on turning out a book which is pleasing to the eye, being printed with relatively large type on good paper. However, the number of annoying, although trivial, typographical errors seems large for a third edition.

Leverett Davis, Jr.
California Institute of Technology

Magnetism

By E. C. Stoner. Pp. 136+vi, Figs. 20. John Wiley and Sons, Inc., New York, 1948. Price $1.25.

This is the fourth edition of a small book (131 pages) first published in 1930, and intended, in the words of the author, "for those to whom the subject is not new." The work, in fact, turns out to be a discussion of selected topics in the field of magnetism, essentially the same as in previous editions, and at a level suitable for graduate students in physics and research workers in related fields.

The book is divided into five chapters whose contents are briefly as follows: Chapter I takes up in very sketchy form the quantum theory of atomic energy levels, the quantum numbers n, l, m, s, j, the Landé g-factor, spectroscopic notation, and the Stern-Gerlach version of atomic beam experiments. Chapter II is devoted chiefly to the theory and measurement of the diamagnetic susceptibility of neutral and ionized atoms. A few pages are allotted to molecules and molecular crystals. Chapter III contains a discussion of paramagnetism, primarily of the transition element and rare earth ions. Chapter IV, by far the longest in the book, reviews ferromagnetic phenomena. Chapter V is entitled "Magnetic Properties of the Elements," but actually deals with metals in general, particularly with the degenerate free electron gas, and with partly bound electrons.

The good points about this book are that it has all the virtues of the earlier editions, plus some modifications, particularly the inclusion of a few references to comprehensive works and review articles which can put the student on the trial of many recent original papers. The chief criticism is that the book still is largely written from the point of view of 20 years ago, and is rarely up to date. A few instances will make this situation clear.

In discussing atomic moments, no mention is made of the Lamb and Rutherford experiments, or of the explanation for the difference between the spin and orbital magnetic moments of the electron. At the end of this section, a paragraph on nuclear moments begins, "It should perhaps be mentioned here that there is now definite evidence that the atomic nucleus may have a spin moment associated with it, as was first suggested by Pauli." In the chapter on diamagnetism, there is no mention of superconductivity. In the chapter on paramagnetism, the Weiss magneton is still used in describing experimental results, and no mention is made of microwave absorption. In the chapter on ferromagnetism, there is no mention of recent work on domain structure, or on the properties of the ferrites, or on permanent magnets. There is no mention of antiferromagnetism. In the chapter on the magnetic properties of the elements, six pages are devoted to Kapitza's work on the change of resistance of metals in strong magnetic fields, while Rabi's magnetic resonance technique and its derivatives are not even mentioned. There is nothing on the change of resistance of semiconductors in a magnetic field, or on the Hall effect.

Perhaps all this amounts to the complaint of a hungry man that the sandwich he is offered is not a multi-course dinner. But without a doubt, the bread for this sandwich was sliced quite some time ago.

F. Bitter
Massachusetts Institute of Technology

Physical Principles of Oil Production

By Morris Muskat. Pp. 922, profusely illustrated. McGraw-Hill Book Company, Inc., New York, 1949. Price $5.00.

This book deals with problems which are of paramount importance in the recovery of hydrocarbons from oil or gas reservoirs. The occurrence of hydrocarbons in oil bearing rocks is discussed and the basic types of reservoirs are explained. A description is given of the behavior of the physical properties of petroleum fluids. To those accustomed to describing fluids and gases by the classical laws, it will be interesting to learn that the hydrocarbon mixtures which occur in nature show phase diagrams with very peculiar properties. The physical constants of the rock material into which the oil is imbedded and which have a bearing on the recovery of oil are explained. The concepts of porosity and permeability for single fluids and of the relative permeability for multiphase flow are clearly set out. Based on these explanations are mathematical considerations which deal with the production or the recovery of the fluids from reservoirs. These studies are grouped depending on the origin of the energy which forces the fluids into the well bore (General Reservoir Mechanics, Gas Drive Reservoirs, and Complete Water Drive Reservoirs). The "secondary recovery" methods are discussed where water or gas is injected. The depletion of condensate reservoirs is explained and the final chapter deals with the effect of well spacing on oil recovery.

The beauty of this volume lies in the fact that it is not just an enumeration of empirical formulas. For every problem, the basic physical concepts and equations are set out. From them mathematical deductions are obtained as rigorously as possible. In many instances, of course, simplifying assumptions have to be made in order to be able to handle the complicated mathematics. Such simplifications are clearly pointed out and their influence on the rigorous solutions is estimated.

For the petroleum engineer, this volume contains an almost inexhaustible supply of information and thoughts which cannot help but stimulate. For the physicist, a glance at this volume will be an eye-opener to the multitude of problems which exist in oil production and which can be successfully handled with the tools of physics and mathematics.

Gerhard Herzog
The Texas Company

Trilinear Chart of Nuclear Species

By William H. Sullivan. John Wiley and Sons, Inc., New York, 1949. Price $2.50.

The trilinear chart of nuclear species represents the most ambitious effort so far to assemble in easily accessible form the "physical constants data for all experimentally identified nuclear species (nuclides), known from information available by approximately June, 1949." The collection of nuclear data has become a formidable task, and the preparation of the chart might not have been possible without the support received by the author from the National Research Council and the Atomic Energy Commission. On the whole, the chart is very successful. The trilinear coordinate grid chosen makes it very compact, and what is more important, it is remarkably free from error. What additions, changes, and deletions seem desirable are largely due to the very rapid progress in our knowledge of nuclear properties, even in the short time since the chart went to press. The chart is preceded by three pages of explanatory material. Each nuclide is represented by a hexagon. The naturally occurring nuclides are indicated by a pale green field on which the black print stands out very clearly. Artificially produced nuclides are shown on a lavender field. The choice of this color is not very fortunate: the black print is often rather illegible on this background. Why not simply use a white background for artificially produced nuclei, and add a dash of color, e.g., a red border, to indicate radioactive nuclei, artificially produced or naturally occurring? The chart is likely to be brought up to date at frequent intervals, and the greatest simplicity seems desirable. From this point of view, some of the data now contained in it could well be left to tabular summaries. Besides much useful information (e.g., atomic masses, spins, magnetic moments, fission yields, thermal neutron cross sections, properties of radioactive nuclides), there appear some entries which are not vital. Thus "when it is known experimentally that a naturally occurring nuclide is produced artificially, a horizontal lavender strip is placed at the bottom of the hexagon in the area reserved for showing the modes of production." Of course this is not done consistently, and if it were done we might soon expect all naturally occurring nuclides to be so distinguished, from the proton up which has recently been shown to be produced "artificially" when a neutron decays! The modes of production might well be left out in all cases where a nuclide is definitely identified as to charge and mass. The numbers of entries of this type will become too large as time goes on, and even now they represent much information which has more historical than practical value and would better be left to tables with references. The symbols A, B, $\cdots G$ denoting the degree of certainty of the information given might also be sacrificed and replaced by appropriate question marks where needed. At the same time some of the more doubtful material might be left off the chart. The space saved might be used for other important entries, e.g., the total energy release in a radioactive transformation. As a reliable and time-saving guide the trilinear chart should prove invaluable to all connected with nuclear science, be it in research or teaching.

M. Goldhaber
University of Illinois

Crystals and X-Rays

By K. Lonsdale. Pp. 199+viii, Figs. 138+xiii. D. Van Nostrand Company, Inc., New York, 1949. Price $3.75.

The author begins her Foreword: "This is not a textbook for advanced students of x-ray crystallography, although I hope that they may learn something from it. It is based on a course of public lectures given at University College, London, in the spring of 1946, and is designed to interest those who do not now use x-ray crystallography, but who might well do so; and to instruct those who do use x-ray crystallographic methods without altogether understanding the tool that has been put into their hands. If I can persuade these two classes of people to pass on from this book to textbooks which are much more thorough, much more precise and much more specialized, I shall have accomplished an even better task than I set out to perform."

Those who have heard Dr. Lonsdale lecture will remember her disarming expositions of complicated topics. According to the listener's predilection she sends him off comfortably warm with unanticipated comprehension, or else impatient to investigate the fascinating techniques and challenging problems she has suggested. This brief book is written much as the author talks, cursive, pressing continuously but without haste from one development to the next, unambiguous, ignoring no essential matter, authoritative in theory, experienced in the labor, imaginative as to the possibilities.

The seven chapters are titled: Historical Introduction; Generation and Properties of X-Rays; The Geometry of Crystals: X-Ray Methods of Investigation; Geometrical Structure Determination; Determination of Atomic and Electronic Distribution; Extra-Structural Studies; The Importance of the Study of Crystals.

The text contains almost evertything that a tutor should have to say to an acute and self-reliant beginner in x-ray diffraction research. Only perhaps in the second chapter does one sense an omission; by comparison with the detailed discussion of high voltage power supplies very little is said about cameras and spectrometers. The sloughs of tedium and the mazes of trial-and-error are pointed out in fair warning. Thus the discussion of lattice planes includes an explicit and general formula for interplanar distance in terms of crystal lattice constants; I should not like to derive or use this particular formula; yet it makes clear to the neophyte that crystal geometry is elementary, that it is complicated, and that he had better ask for a girl and a calculating machine. Many formulas are considerately presented without a mathematical derivation; but the physical principles are explained, and no reader should be left mystified as to why, for example, the intensity of reflection by a perfect crystal must be calculated with a different formula from that for a mosaic.

Thickly interspersed figures are an essential part of the discussion and sometimes extend it. Thirteen plates, most carrying six reproductions of diffraction photographs, illustrate a variety of phenomena. They are uniformly successful in retaining even the more delicate details referred to in the captions.

Only a few literature references appear in the text and none in footnotes. The legends for many of the figures do contain references. At the end of the book is a list of some 42 "Textbooks for Reference," with nothing whatever (now that his beginner's luck is used up) to help the student choose his next reading. Two or three of the books in this list one would like charitably to guess that Mrs. Lonsdale had never examined.

A number of misleading or incorrect statements appear, but mostly where they generate no further error. It is twice implied that a hot-cathode high voltage rectifier owes its low voltage drop to a vacuum inferior to that in an x-ray tube. The short wavelength limit is said to correspond "to the case where the bombarding electrons give up *all* [italics by the author] their kinetic energy in the production of x-rays." On anomalous scattering: "When an atom has been profoundly disturbed by the removal of an inner electron and is trying to readjust itself it cannot be expected to scatter 'normally'." The formula for integrated intensity on page 118 and in a minor factor that on page 116 are incorrect. Occasionally the author oversells her specialty: "The development of x-ray analysis to give electron density contour maps has led to the realization that many compounds are not completely ionic, nor are they wholly covalent."

I have recommended this book to a few members of the group to whom it is directed; for example, to a young M.D. engaged in research who is scientifically well trained, very slightly experienced in x-ray diffraction, but curious as to its usefulness for his own problems; and also to an isolated research chemist forced to employ x-ray diffraction whether trained for it or not.

Their reports reinforce my own estimate that Mrs. Lonsdale has achieved her purpose very well indeed. Her book can be recommended confidently to scientifically trained executives, research directors, and research workers who wish with the minimum physical effort to decide on sound grounds for themselves the costs and probable rewards from the use of x-ray diffraction. It should be studied also by those vicarious users of x-ray diffraction who rely on results obtained by specialists in the field. It will not often be chosen as a textbook or for reference; yet it is not out of place in the library of the specialist or the student. It is refreshing to read it through, and one is indeed almost certain to learn something.

J. H. Sturdivant
California Institute of Technology

Lehrbrich der Theoretischen Physik

By Walter Weizel. Pp. 771, Figs. 270. Verlag., Julius Springer, Berlin, 1949. In German.

Professor Weizel's textbook in theoretical physics must surely stand as one of the most impressive of its kind ever to be attempted, if for no other reason than its remarkable comprehensiveness. Merely to list the subjects covered in the first volume requires almost ten printed pages. The volume itself is 771 pages long; and a second volume is promised, whose indicated contents are such that the number of pages might very well be doubled.

The book is characterized by extreme systematization. In the first place, the division of the subject matter into two volumes is arrived at by an arbitrary rule, rather rigidly adhered to. The first volume is intended to contain all those subjects in theory which can be treated without knowing anything about the molecular or atomic structure of matter—the "macroscopic" theory of physics. The second volume is to supply the subjects here omitted. Thus, while the first volume includes special and general relativity, along with point dynamics, rigid dynamics, continuum dynamics, electrodynamics, optics, and thermodynamics, we must wait until after we learn quantum theory before we are told about the kinetic theory of gases in the second volume. This arrangement of subject matter, though unconventional, is not necessarily bad; however, one can point out places at which this preoccupation with system prejudices the understandability. For example, in going over from the electrodynamics of the vacuum to that of material media, the author simply introduces the macroscopic constants of the medium in the most arbitrary way. In text books written 40 years ago this was indeed standard practice. The result was usually a deplorable confusion about the meaning of the macroscopic fields, untold arguments about the "difference between B and H," etc. Today we know how the macroscopic fields are to be derived from the microscopic ones and we see how this procedure rips the veil of mystery that otherwise covers the subject.

Exactly the same kind of criticism may be made of thermodynamics in which the concept of entropy is used long before one studies the microscopic theory which gives the notion of entropy vivid meaning.

The book is aimed at a level of mathematical skill corresponding roughly to that of a college senior or beginning graduate student. Each section begins with a short synopsis of the material covered and a list of definitions of symbols. The text is fairly condensed; long conversational passages are rarely resorted to. The derivations are clear and well organized.

In point dynamics one learns, for example, about the translation and rotation of a rigid body, the Hamilton-Jacobi equation, the transition from the Hamilton-Jacobi theory to wave mechanics. Not much is to be found on the three-body problem or on the normal modes of vibration of general systems. In optics one finds a condensed but comprehensible treatment of the geometrical optics of compound systems, of Fresnel and Fraunhofer diffraction, and of crystal optics. These brief remarks are intended only to give some notion as to the degree of completeness with which the various fields are treated.

The work would seem to be quite useful as an "encyclopedia" —a convenient reference work for the student, where a large body of derivations and formulas are to be found. It is somewhat less useful as a textbook, at least to my taste. The author points out in an opening section that a theory is intended as a means of coordinating or ordering the experiments in a certain field. If so, then an account of a theory can hardly be complete without frequent, or continual, reference to the experiments which one is trying to describe. In fact, one finds very few such references to experiment in the book. The theory is usually put forward in an absolute, or dogmatic, way. In particular, I could not find (in my sampling of the subjects covered) any criticism of the theories presented, any observation that a given theory was weak or defective and might possibly require modification in some particular respect.

No exercises are supplied for solution by the student.

Some errors are present but they seem to be very few and do not interfere with understandability.

S. M. Dancoff
University of Illinois

Low Temperature Physics

By L. C. Jackson. Pp. 130+vii, Figs. 33. John Wiley and Sons, Inc., New York, 1948. Price $1.50.

Professor L. C. Jackson of Bristol, England, is well known in this country as one of the leading experimental physicists in the field of low temperature research on the properties of matter. Having done research at Leiden and visited many laboratories in this country and abroad, he has been able to write a monograph which contains an amazing amount of information. This little pocket edition is ideal for someone who wants to get an idea about what scientists are doing in this field of physics. It is well written and it is well balanced with respect to the several subjects which are presented. It very well represents the state of low temperature physics as the war ended.

The surprise comes to this reviewer when he thinks back to the period of the close of the war and sees the changes made in low temperature physics since then. In this country nearly 25 new laboratories have been built, and the quantity and quality of research is most exciting. Such things as the liquefaction of the isotope He_3 and of tritium, the use of microwave radiation to study low temperature conductivity and to study electronic and nuclear magnetic induction are but a few of the new steps taken. Professor Jackson would be the first to admit that his book already needs revision. Indeed, his own work on liquid helium should be included in any account of this field of physics.

In this country the liquefaction of helium is done most widely by use of the Collins cryostat which uses the Claude method. We understand now, due to the work of J. de Boer, the quantum nature of the light gases and how the virial coefficients depend on temperature. The theoretical work of Tisza on liquid helium was years ahead of that by Landau and moreover Tisza properly understood that there was to be expected a temperature wave in the superfluid phase of liquid helium. These things would appear in such a revision. The section on electrical conductivity is very good. We do not agree about the specific heat humps which have been observed having an explanation by the so-called Schottky theory. Also we do not agree that at extreme low temperatures the paramagnetic salts exhibit true ferromagnetism; rather it resembles antiferromagnetism with falling susceptibility with lowering of temperature. And of course we now know that ferromagnetism is characterized by the growth of domains, by the movement of domain walls rather than the abrupt reorientation of a given domain. Such is the nature of progress.

C. F. Squire
Rice Institute

Physiology of the Eye, Vol. I, Optics

By Arthur Linksz. Pp. 334+xii, Figs. 137. Grune and Stratton, New York, 1950. Price $7.50.

This is the first volume of a set of three by Dr. Linksz on the subject of physiological optics. It is divided into three parts, namely, physics of light, 73 pages; geometrical optics, 200 pages; and optics of the eye as an image-forming mechanism, 45 pages. Volume I contains a detailed, but rather elementary, exposition of geometrical optics followed by a discussion of its applications to the theory of ophthalmic lenses and to the lens system of the human eye. The level of presentation of the subject is about that of college physics, but each topic is discussed at much greater length than is customary in such textbooks.

The style is that of a lecturer, repeatedly arguing with an imaginary listener who has learned some optics from a standard text and supposes that he understands things only because he can name them. Dr. Linksz frequently startles this imaginary listener into attention by making use of fantastic statements which seem to contradict commonly accepted knowledge. For example, he makes much ado about a thesis that plane mirrors do not form images. After investigating what they actually do to light, he states that they merely "displace objects optically." At the conclusion of some 14 pages on the peculiar nature of this displacement, he finally concedes that one might use the common term "virtual image" to identify this effect. One assumes here that he is satisfied to have cleared up the meaning of virtual images. But, later on, he repeatedly shows an evident allergy for this common term in discussing images formed by curved mirrors and lenses. He overlooks the fact that the word "virtual" is a brief and accepted equivalent of his phrase that the light "could have come" from a certain region of space as far as an eye or other optical system is concerned which receives the rays.

In the reviewer's opinion, this kind of quibbling about accepted terminology, of which the above is one example, is overdone in this text. It repeatedly makes one wonder if the author knows what he is talking about. Usually one finds, however, after reading many pages, that he really does understand the situation, and explains it very well, but insists only on some novel terminology of his own. Without his lengthy explanations, his terms are usually more misleading than those in current usage.

In his very brief discussion of the nature of light, the author shows that he is not so well informed in regard to physical optics as he is in the field of geometrical optics. Thus he states that the success of Young's experiment depends on the production of two waves of exactly equal intensity. He also states, in connection with the two-calcite experiment, that if one ray from the first calcite is isolated by some means, it will not pass through a second calcite if its axis is at right angles to that of the first. (He should examine the Wollaston double-image prism.) Of course, such misconceptions have nothing to do with ophthalmic optics, the principal subject of this book.

The treatment of distortion by prisms and lenses is particularly good, the refraction of skew rays being explained with the aid of several excellent figures. There is a good discussion of coma and astigmatism, but a mistake is made in saying that the distance between the astigmatic foci decreases with the aperture.

On the whole, this book is an accurate, though often unconventional, treatment of geometrical optics. It is clearly and interestingly written and is copiously illustrated by good figures. It may be used profitably in the study of the simpler types of ophthalmic lenses (there is nothing on bifocals) and as a foundation for the study of physiological optics.

Joseph Valasek
University of Minnesota

Mechanics, Statics and Dynamics

By Merit Scott. Pp. 394+vi, Figs. 249. McGraw-Hill Book Company, Inc., New York, 1949. Price $4.50.

In his Preface, Professor Scott states that the purpose of his book is to provide a classroom text, as well as a reference book, able to serve as a bridge from the first-year course in college physics to work making use of mathematics going beyond calculus. The book is intended to cover a full year's course, and the 25 chapters are evenly divided into two distinct sections on statics and dynamics.

The first eight chapters of the text deal with vector algebra, conditions of equilibrium, and applications of statics, characterized by the chapter headings Frames, Work and Virtual Work, Moments and Products of Inertia, and Friction. In Chapter 9 (Elasticity) the author succeeds in elucidating the concepts of stress and strain with a minimum use of partial derivatives. The next two chapters (Strings and Rods under Normal and Shear Strains, and Structure, Beam and Column) deal with applications and accentuate the use of energy considerations. Ordinary differential equations of the fourth order of necessity occur, but their treatment is very clear. Chapter 12 (Mass Field Strength and Potential) again avoids as far as possible the use of partial derivatives and of line integrals. A chapter on stability concludes the first part on statics.

The discussion of Kinematics is followed by a chapter (15, Dynamics and Energy) of only eight pages, dealing with the principles of dynamics. Special problems are then treated in four chapters labeled Motion in One and Two Dimensions, Motion Subject to Resistance, Vibrations. Chapter 20 (Orbital Motion, Central Forces) gives an easily understood, though short, discussion of planetary motion. The conservation theorems and rigid body motion are taken up in Chapters 21 (Equations of Motion) and 22 (Kinetic Energy and Energy Equation). Interesting applications, including a discussion of vibrations of beams and of air plane resistance are touched upon in the two chapters on Oscillations and on Initial Motion, Impulses and Collisions. In the last chapter (25, Three-Dimensional Mechanics), Euler's equations are derived, and the precession of a top is dealt with. A discussion of line bound vectors is marred by the introduction on page 374 of the notion of "whole angular momentum," i.e., comprising linear as well as angular momentum of a rigid body.

The selection of topics made by Professor Scott shows his appreciation of that great tradition in mechanics which is exemplified by Lamb's three volumes on Statics, Dynamics, and Higher Mechanics.

Many problems are attached to each chapter and much space is devoted to a lucid and simple discussion of problems. Many good diagrams clarify the presentation, and all notations and abbreviations are collected and defined on the first few pages. Teachers of intermediate mechanics will welcome the wealth of answered problems; this feature, as well as ready reference to definitions, may prove valuable to men planning to use Professor Scott's book for reference purposes in their later work in technical mechanics.

In the first two-thirds of the book problems considered in the general physics course are taken up at the beginning of almost every section, and are carefully treated again by means of calculus methods, thus providing good continuity with the basic physics course. The treatment seems to be lucid, except for occasional long groups of equations caused by writing out all intermediate steps. Professor Scott's book appears to be a first-rate text for a basic mechanics course for engineering physicists or engineers given within a physics department, providing in particular excellent practice in problem work.

However, the fundamental ideas of dynamics regarding the equations of motion and the conservation principles do not stand out in his treatment, but are somehow submerged in the great mass of carefully treated special cases. A further drawback is Professor Scott's reticence about the physical basis of mechanics. On page

214 he says: "It is supposed that the reader already possesses a considerable familiarity with Newton's laws so that no comprehensive discussion is necessary," and after a few lines about the classification of forces he concludes his discussion in the basic chapter on dynamics with the words: "The philosophy of these laws is wholly untouched here, except to remark that they are generally regarded as resting upon an experimental basis . . . it is *accordingly considered that the entire subject of dynamics* springs from an experimental basis formulated as Newton's laws." No mention is made of the problems raised already by Mach and others concerning the definition of mass and force.

It is indicative for the tenor of the book that the word atom is not mentioned and that, e.g., the obvious applications of hyperbolic orbits to Rutherford scattering are not touched upon. Similarly, the term "primary frame of reference" appears only in a footnote on page 217. Apparently, the author aims to present the methods of solving dynamical problems without any regard to the development of other fields of physics during the past 50 years.

This reader feels that the value of this text would be greatly enhanced if the clear presentation of the elements of classical mechanics were complemented by some applications of mechanics to problems of interest in modern physics, and in particular, by a stronger emphasis on the ideas necessary for an understanding of the structure of mechanics. Professor Scott's approach might yet be the best way to present mechanics to students who are not primarily interested in the newer developments but who should nevertheless get acquainted with the well-established techniques of solving mechanical problems.

F. T. Adler
University of Wisconsin

The Transuranium Elements

Edited by Glenn T. Seaborg, Joseph J. Katz, and Winston N. Manning. National Nuclear Energy Series Division IV, Vol. 14B. Part I, pp. 859+xxxvi, Part II, pp. 872+xii. McGraw-Hill Book Company, Inc., New York, 1949. Parts I and II. Price $15.00 (not sold separately).

This work consists of more than 150 original research papers dealing with the transuranium elements and describes a truly Herculanean accomplishment. The papers are devoted to four of the transuranium elements, neptunium, plutonium, americium, and curium, cover investigations begun as early as 1940, and include work done in very recent months. There are many more papers concerning plutonium than the other transuranium elements and in turn more papers dealing with neptunium than americium and curium. Several papers on radium, actinium, thorium, protactinium, and uranium are included for reference convenience.

The subject matter of the papers ranges all the way from nuclear physics to analytical chemistry. In Part I twelve papers are concerned with the production of elements 93 and 94, the occurence of 94 in nature and the nuclear properties of 93 and 94. Most of the remainder of the papers have to do with various chemical aspects of plutonium, covering a diversity of topics such as absorption spectra of various plutonium solutions, magnetic susceptibility of plutonium in various oxidation states in aqueous solutions and vapor pressure of plutonium halides. Part II contains about 29 papers dealing with nuclear aspects of plutonium and neptunium and also includes several papers on nuclear properties of actinium and radium. There is also a paper which is concerned with the products of deuteron and helium ion bombardments of Pa^{231} and a paper on the half-life of thorium 227. The remainder of the papers are concerned with various chemical and physical properties of plutonium and neptunium compounds.

The papers vary considerably in the extent of their coverage of a given subject. Thus Paper 16.8, describing a 48-channel pulse-height analyser for alpha-energy measurements, by A. Ghiorso *et al.*, is some 80 pages long, lists 88 references, and has tables giving decay periods and energies for alpha-emitters, as well as complete circuits for the pulse-height analyzer. Paper 6.40, on the thermodynamic properties and high temperature equilibria of plutonium compounds, by L. Brewer *et al.*, is 25 pages in length, lists 51 references, and contains much valuable data. Some of the other papers, however, are rather too short, and not very informative. However, the general tone is excellent.

The typography is good and all figures are beautifully executed. An author index is given, and many of the articles are accompanied by extensive lists of references. However, this reviewer feels that the volumes would have been very greatly improved by a subject index which is unfortunately lacking.

The volumes should be very valuable to anyone interested in the field and will no doubt form the basis for a more integrated treatise at some future time.

Robert D. Fowler
Johns Hopkins University

Electronics-Experimental Techniques

By William C. Elmore and Matthew Sands. Pp. 417, Figs. 182. McGraw-Hill Book Company, Inc., New York, 1949. Price $3.75.

This book, one of the National Nuclear Energy Series, is concerned with the developments in the theory and practice of design of amplifiers and associated equipment that were made at the Los Alamos laboratory during the war years. No one familiar with the art of pulse amplifier construction as practiced by the average physicist before the war can deny that large advances in technique and general understanding have occurred. No small part of this advance originated at Los Alamos with the authors of the present book and their co-workers, making the present book a welcome and useful addition to the literature. It is stated in the preface that no material developed after 1946, and no circuits especially applicable to weapon technology, are included. Within these limits a well-chosen list of topics is presented. The chapter headings indicate the general scope: (1) Circuit Components and Construction Practice, (2) Circuit Elements, (3) Voltage Amplifiers, (4) Electronic Counters, (5) Oscillographs and Associated Equipment, (6) Test and Calibration Equipment, (7) Power Supplies and Control Circuits. The descriptions of the various circuits are in every case sufficiently detailed to permit construction of a working unit from the information given. In addition, a reasonable amount of theoretical background material is included.

The style is clear and readable and the book appears to be commendably free of errors and misprints. The reproduction by the lithoprinting process has no doubt contributed to this reduction of errors by reducing the number of materializations the text goes through between author and book store. The process has also resulted in a very attractive format at a welcome moderate price. Without a doubt this book belongs in the reference library of everyone concerned with the design or building of pulse amplifiers.

S. N. Van Voorhis
University of Rochester

Radioactive Tracer Techniques

By G. K. Schweitzer and I. B. Whitney. Pp. 241+vi, Figs. 13. D. Van Nostrand Company, Inc., New York, 1949. Price $3.25.

This book is intended to "serve as a guide for laboratory work and instruction in the use of radioactive tracers." The Table of Contents shows the topics treated: Chapter 1, Radioactive Hazards; Chapter 2, Operation of a Radiolaboratory; Chapter 3, Construction of a Radiolaboratory; Chapter 4, Working in a

Radiolaboratory; Chapter 5, Basic Experiments; Chapter 6, Chemical Experiments; Chapter 7, Physical Experiments; Chapter 8, Biological Experiments; Chapter 9, Special Preparations.

More than one-third of the book is devoted to the first four chapters. It appears to the reviewer that these chapters could have been condensed considerably, since there is undue repetition and unnecessary details regarding precautions in handling isotopes. K. Z. Morgan's statement, "Radiation need not be feared, but it must be respected," is referred to several times, but unfortunately, the text does little to allay the fears of the novice. Chapter 3 seems unnecessary, since the inclusion of such material as floor plans, materials for floor and wall surfaces of a radio laboratory might well be beyond the scope of the intended reader.

Experiments basic to radioactive measurements are presented in Chapter 5. The operation and use of the Lauritsen electroscope and the Geiger-Müller counter are discussed, as well as the preparation of liquid and solid samples prior to analysis. Several illustrations are included and add much to the clarity of the text. The division of each experiment into Object, Theory, Apparatus and Materials, Procedure, Calculations and Questions, and Other Suggested Experiments should be helpful in executing the experiments properly. The list of general references at the end of each experiment is adequate and pertinent.

The remainder of the book is devoted to special experiments illustrating specific chemical, physical and biological tracer methods, such as Analysis by Isotopic Dilution, Solubility Determination, Half-Life Measurements, Friction Studies, and Body Fluid Volumes. Unfortunately, the wide scope of the book does not permit a detailed presentation of each experiment. Thus, the experiments have limited value in the same sense that an inadequate organic chemistry manual is not useful beyond the exact preparation described, while a good manual will serve as an adequate reference book.

The final chapter and appendix contain information regarding preparation of special isotopes and some information of general interest.

The exposition is generally clear and simple except for the occasional occurrence of ambiguities.

This book is the first of its type in the field of radioactive tracers and may prove useful in elementary laboratory instruction. However, it will be difficult for this type of manual to compete successfully with the other available volumes intended primarily for research workers.

Martin P. Schulman
University of Pennsylvania

Electronics in Engineering

By W. Ryland Hill, Pp. 274, Figs. 205. McGraw-Hill Book Company, Inc., New York, 1949. Price $3.50.

This book is intended as a text for a one-quarter or one-semester elective course in electronics to be given to advanced students in other fields of engineering or science to acquaint them with the applications of electronic techniques to their own instrumentation problems. It is hard to review a book designed to such rigid specifications without having had the opportunity of trying it on a class; lacking this experimental check, the reviewer must defer to the author's judgment on questions of choice of material to be covered and the order of presentation. In the present instance the author has followed the introduction of each new device by discussion of illustrative applications, and has leaned heavily on graphic presentation rather than mathematical analysis.

Following an introductory chapter on electrons, ions and photons, Professor Hill takes up the topic of practical thermionic emitters and diodes, and then takes up single phase rectifiers and filters before discussing grid controlled tubes in Chapter 4, which covers triodes, the principles of voltage amplification, and tetrodes and pentodes. Next come chapters on gas-filled tubes, photosensitive devices and control circuits employing thyratrons. Polyphase rectifiers are treated in Chapter 8, followed by practical amplifier circuits, a chapter on feedback, and one on resonance and tuned amplifiers. The last five chapters cover oscillators, amplitude modulation and demodulation, the cathode-ray oscilloscope, transducers (particularly strain gauges) and the vacuum tube voltmeter. The subject of the discharge of a condenser through a resistance is treated in a brief appendix. All but two of the chapters are provided with a short list of problems which appear to require more of the student than simple substitution in a formula.

Naturally, with such an imposing list of subjects to cover in 270 pages, it is impossible to deal with each in much detail, so we find, for example, that only one type of vacuum tube voltmeter is described, though the particular one chosen is excellent for the author's purpose. However, in view of the necessity for compressing the material one wonders at the inclusion of two pages (243–4) of discussion of the ordinary Wheatstone bridge in connection with strain gauges.

The style is rather informal, but the resultant lack of rigor in many places may well be offset by the better hold on the students' attention. Nevertheless, I was a little surprised to read (page 89) that if "finer grained" control of the current through a thyratron is needed the remedy suggested is the rather impractical one of increasing the supply frequency. In discussing the effect of omitting the cathode by-pass condenser (pages 139–140) in a resistance-capacitance coupled voltage amplifier, the author states that it "does no harm" except for a reduction in gain, but fails to point out the effect on frequency response and the improvement in linearity. Also, I was disappointed to see again the old mistake (page 261) of operating a vacuum tube voltmeter at the floating grid potential. Defects of this sort would be serious only in a reference book, and, since this is definitely not a reference work but a text, perhaps they can be overlooked.

J. B. H. Kuper
Brookhaven National Laboratory

Electron-Tube Circuits

By Samuel Seely. Pp. 529+ix, Figs. 469. McGraw-Hill Book Company, Inc., New York. Price $6.00.

In this book the author has attempted to develop in the student a clear, analytical method in studying electronic circuits; to present and analyze the various classes of circuits which find widest application; and to indicate with examples how various basic circuits are combined to achieve complex operations. Sufficient material has been included for a course in radio engineering circuits and for one in non-radio electronic circuits, with an opportunity for the instructor to choose topics to satisfy almost any course requirements. A background in basic a.c. theory and basic electronics is assumed.

In arranging his material the author has been guided by the character of the analysis rather than the application, but, nevertheless, the book falls into a number of major divisions. The first four chapters are devoted to a review of the fundamental properties of vacuum tubes and their basic applications. Next comes a discussion of a variety of untuned amplifiers (including some computer circuits), occupying five chapters. The third section covers tuned circuits, including oscillators, in three chapters. Fourth comes a comprehensive treatment of rectifiers, filters, and regulators, followed by chapters on Amplitude Modulation, Demodulation, and Frequency Modulation and Detection. Finally, there are five chapters on circuits that received considerable attention in connection with radar applications. Some of these circuits have not been treated previously in such detail in any general text.

Each chapter is provided with a well-chosen bibliography and a set of problems formulated so as to require an understanding of the subject matter. Appendices give characteristic curves for the tube types used in the problems and a table of Bessel functions of the first kind. In many places the author has drawn freely on his earlier text, *Electronics*, written with J. Millman.

Considering the mass of material discussed and the great number of equations, it is to be expected that numerous errors have crept in. The author, in his Preface, calls attention to the perennial difficulties with notation, in that in many places he found the I.R.E. standard single subscript notation inadequate. Possibly the attempt to conform to this standard is responsible for some of the cases where the notation used in the text differs from that in the figures. It would have enhanced the value of the book for reference purposes if the author had provided a glossary of his notation.

This reviewer feels that there are already too many synonyms in the English language with no precise shadings of meaning and so regards the author's introduction of the terms "sinor" and "sinor diagram" for rotating vector and vector diagram as superfluous, but this may be a purely personal prejudice. A more serious objection to the book is that in some spots the writing appears to have been hasty, resulting in clumsy sentences and in occasional misstatement of fact. For example, on page 72, we are told that "blocking" may occur in an untuned amplifier when the time constant CR_g is much larger than the period of the highest frequency to be passed by the amplifier. In general the analyses of circuits are quite clearly done, but the description of the "Phasitron" tube and the analysis of the Miller integrating delay circuit stand in marked contrast. Also, the index could be much more complete.

In spite of these technical blemishes, which are not at all likely to lead the serious student astray, the book appears to be an excellent text. Certainly, it is unique in respect to the breadth of material covered, and it seems likely to prove invaluable as a reference work.

J. B. H. Kuper
Brookhaven National Laboratory

Author Index to Books Reviewed

Bergmann, L.—*Der Ultraschall* 444

Einstein, Albert—*The Meaning of Relativity* 555
Elmore, W. C. and M. Sands—*Electronics—Experimental Techniques* 777

Higdon, A. and W. B. Stiles—*Engineering Mechanics* ... 888
Hill, W. R.—*Electronics in Engineering* 999

Jackson, L. C.—*Low Temperature Physics* 000

Katz, J. J.—see Seaborg, G. T. 000

Linksz, Arthur—*Physiology of the Eye, Vol. I, Optics* 111
Lonsdale, K.—*Crystals and X-Rays* 222

Mann, W. B.—*The Cyclotron* 333
Manning, W. N.—see Seaborg, G. T. 444
Milne, E. A.—*Kinematic Relativity* 555
Muskat, Morris—*Physical Principles of Oil Production* .. 666

Sands, M.—see Elmore, W. C. 777
Seaborg, G. T., J. J. Katz, and W. N. Manning—*The Transuranium Elements* 999
Schilpp, P. A.—*Albert Einstein: Philosopher-Scientist* 000
Schweitzer, G. K. and I. B. Whitney—*Radioactive Tracer Techniques* 222
Scott, Merit—*Mechanics, Statics and Dynamics* 333
Seely, Samuel—*Electron-Tube Circuit* 444
Stiles, W. B.—see Higdon, A. 555
Stoner, E. C.—*Magnetism* 666
Sullivan, William H.—*Trilinear Chart of Nuclear Species* 777

Tolansky, S.—*Hyperfine Structure in Line Spectra and Nuclear Spin* 999

Weizel, Walter—*Lehrbrich der Theoretischen Physik* 000
Whitney, I. B.—see Schweitzer, G. K. 111

Other Books Received

An Index of Nomograms. D. P. Adams. Pp. 174+ix. John Wiley and Sons, Inc., New York, 1950. Price $4.00.

Cosmical Electrodynamics. H. Alfven. Pp. 237+viii, Figs. 78. Clarendon Press, Oxford, 1950. Price $5.00.

Electron Diffraction. R. Beeching. Pp. 107+viii, Figs. 39. John Wiley and Sons, Inc., New York, 1949. Price $1.25.

Physical Methods in Chemical Analysis, Vol. I. Edited by W. G. Berl. Pp. 664+xiii, Figs. 217. Academic Press, Inc., New York, 1950. Price $12.00.

Radiative Transfer. S. Chandrasekhar. Pp. 393+xiv, Figs. 35. Oxford University Press, London, 1950. Price $7.00.

Experimental Designs. W. G. Cochran and G. M. Cox. Pp. 454+ix. John Wiley and Sons, Inc., New York, 1950. Price $5.75.

Joseph Henry, His Life and Work. Thomas Coulson. Pp. 352. Princeton University Press, Princeton, New Jersey, 1950. Price $5.00.

Counting Tubes. S. C. Curran and J. D. Craggs. Pp. 238+xi, Figs. 119. Academic Press, Inc., New York, 1949. Price $5.25.

Physical Chemistry of the Hydrocarbons, Vol. 1. Edited by A. Farkas. Pp. 453+x, profusely illustrated. Academic Press, Inc., New York, 1950. Price $8.50.

Aerials for Centimetre Wave-Lengths. D. W. Fry and F. K. Goward. Pp. 172+x, profusely illustrated. Cambridge University Press, London, 1950. Price $3.50.

Medical Physics, Vol. 2. Edited by Otto Glasser. Pp. 1227, 978 illustrations. Year Book Publishers, Chicago, Illinois, 1950. Price $25.00.

An Introduction to the Laplace Transformation. J. C. Jaeger. Pp. 132+viii, Figs. 31. John Wiley and Sons, Inc., New York, 1949. Price $1.50.

Vector and Tensor Analysis. Harry Lass. Pp. 347+viii, Figs. 101. McGraw-Hill Book Company, Inc., New York, 1950. Price $4.50.

Threshold Signals. Edited by J. L. Lawson and G. E. Uhlenbeck. Pp. 388+xii, Figs. 150. McGraw-Hill Book Company, Inc., New York, 1950. Price $5.00.

Dipole Moments. R. J. W. LeFevre. Pp. 117, Figs. 23. John Wiley and Sons, Inc., New York, 1948. Price $1.25.

Cosmological Theory. G. C. McVittie. Pp. 103. John Wiley and Sons, Inc., New York, 1949. Price $1.50.

The Organization of Industrial Scientific Research. C. E. K. Mees and J. A. Leermakers. Pp. 383+vii. McGraw-Hill Book Company, Inc., New York, 1950. Price $5.00.

Recent Advances in Radio Receivers. L. A. Moxon. Pp. 183+ix, Figs. 88. Cambridge University Press, London, 1950. Price $4.00.

Stetige Regelvorgange. W. Oppelt. Pp. 143, Figs. 42. v. Schroedel-Siemau and Company (20a), Hannover N, Germany, 1949.

The Scientists's Ready Reckoner. W. Roman. Pp. 142+viii. Dr. W. Junk, publisher, The Hague, 13, van Stolkweg, Netherlands, 1950.

The Mathematical Theory of Communication. C. E. Shannon and W. Weaver. Pp. 117+v. University of Illinois Press, Urbana, Illinois, 1949. Price $2.50.

Microwave Electronics. J. C. Slater. Pp. 406+xiv, Figs. 91. D. Van Nostrand Company, Inc., New York, 1950. Price $6.00.

Electricity for Students of Science and Engineering. T. T. Smith. Pp. 448+ix, Figs. 234. International Textbook Company, Scranton, Pennsylvania, 1949. Price $5.00.

Elementary Pile Theory. H. Soodak and E. C. Campbell. Pp. 73+ix, Figs. 21. John Wiley and Sons, Inc., New York, 1950. Price $2.50.

Mercury Arcs. F. J. Teago and J. F. Gill. Pp. 107+viii, Figs. 50. John Wiley and Sons, Inc., New York, 1950. Price $1.50.

The General Principles of Quantum Theory. G. Temple. Pp. 120+vii. John Wiley and Sons, Inc., New York, 1948. Price $1.25.

Hyperfine Structure in Line Spectra and Nuclear Spin. S. Tolansky. Pp. 120, Figs. 26. John Wiley and Sons, Inc., New York, 1948. Price $1.50.

X-ray Optics. A. J. C. Wilson. Pp. 127+vii. John Wiley and Sons, Inc., New York, 1949. Price $1.50.

Electronics, Principles and Applications. Ralph R. Wright. Pp. 387+ix, Figs. 314. Ronald Press Company, New York, 1950. Price $5.50.

Foundations of Modern Physics. T. B. Brown. Pp. 391+xvi, Figs. 181. John Wiley and Sons, Inc., New York, 1949. Price $5.00.

Applied Experimental Psychology. Chapanis, Garner, and Morgan. Pp. 434+xi, Figs. 196. John Wiley and Sons, Inc., New York, 1949. Price $4.50.

Laboratory and Shop Notes

Energy Dependence of the Naphthalene Scintillation Detector*

Jack C. Smeltzer
National Bureau of Standards, Washington, D. C.

December 1, 1949

MEASUREMENTS of the sensitivity of a naphthalene scintillation detector for x-rays with energies of 250 to 1200 kev show that the ratio

$$S=\frac{\text{d.c. current out of photo-multiplier in } \mu\text{a}}{\text{intensity of irradiation in r/min.}}$$

is essentially independent of energy and intensity in this region. The experimental data given in Fig. 1 show that S varied less than 1.5 percent for constant irradiation with variable energy. A companion experiment showed less than two percent variation for tenfold variation of intensity at constant effective energy of 500 kev.

X-rays generated by tube potentials of 500 to 1400 kv as well as gamma-rays for cobalt 60 were used in this determination. Heavy filtration at the higher tube potentials, as shown in Table I, reduced the wide energy spread of the x-ray beam by heavily attenuating the lower energies. The effective energy was then determined from the slope of the attenuation curve[1] for the filtration employed. The effective energy so assigned thus has the same absorption coefficient as that of the filtered x-ray beam. The intensity of irradiation was measured by means of a thimble chamber calibrated against radium to ±1 percent accuracy.

A standard light source was used so that the efficiency of conversion of light to photo-multiplier current could be measured prior to each run. The change in this efficiency during a run was made negligible by holding temperature, potentials, and geometry constant, and by prefatiguing the photo-multiplier. Fatigue of the photo-multiplier[2] at light levels which give anode voltage outputs measurable directly with a potentiometer will change the sensitivity S appreciably during the time required to measure the ionization chamber current. To reduce this change in sensitivity below the probable error of measurement of intensity of irradiation, the photo-multiplier was prefatigued overnight at the light level to be expected from the crystal.

It is desired to determine the sensitivity due solely to the radiation absorbed in the crystal. The light output of the crystal depends upon the electrons traversing it. Some of these originate outside the crystal. If, for instance, a high atomic number material surrounded the crystal, too many electrons would strike the crystal surface.[3] The crystal was therefore inclosed in a shell of material with approximately the same atomic number as that of the crystal so that the electrons traversing the crystal were characteristic of the average atomic number of the crystal. To insure that no electrons generated outside the shell entered the crystal, the shell thickness was made equal to the range of the highest energy electrons in the shell material.

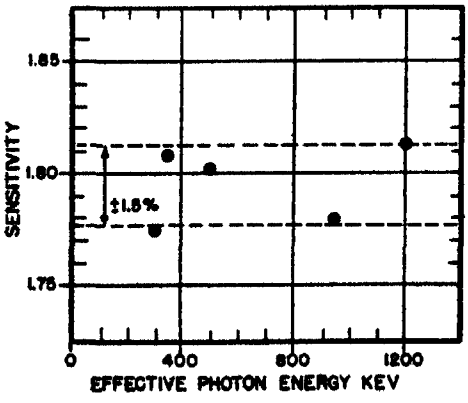

Fig. 1. Energy dependence of the RCA 931-A naphthalene scintillation detector. Sensitivity is the ratio of corrected photo-multiplier current to thimble chamber reading.

Table I.

X-ray tube kilovoltage	X-ray tube current ma	Added filter (mm lead)	Effective energy (kev)
500	1.4	0	250
800	0.5	3.35	350
1000	0.5	9.72	500
1400	0.5	27.10	950

It is estimated that the measurement of each S was acurate to ±1 percent. It is planned to extend the spectral dependence investigations to higher effective energies with the National Bureau of Standards' 50-Mev betatron.

---

* This work was performed under contract with the AEC.

[1] Wyckoff, Kennedy, and Bradford, J. Research Nat. Bur. Stand. 41, 223 (1948).

[2] Marshall, Coltman, and Bennett, Rev. Sci. Inst. 19, 744 (1948).

[3] "An ionization method for the absolute measurement of gamma-ray energy," Proc. Roy. Soc. London A156 (1936).

Modification of Electron Microscope for Electron Optical Shadow Method

J. Arol Simpson and Alan Van Bronkhorst
National Bureau of Standards, Washington, D. C.

March 6, 1950

THE detailed investigation by means of the electron optical shadow method[1,2] of magnetic and electric fields of the size predicted by domain theory is best carried out by use of a high resolution electron optical system. Such a system is readily available in the conventional transmission-type electron microscope. It is, however, necessary to have a stage mechanism capable of rotating the specimen around an axis intersecting the optical axis and a means of holding and moving a fine mesh screen axially just behind the back focus of the objective lens. Although these adjustments are sufficient, it is highly desirable that the specimen may be rotated on a second perpendicular axis and that the mesh holder also provide rotation.

The micrographs by this method are a superposition of the specimen image on a shadow image of the mesh. Maximum sensitivity to low fields is obtained by placing the mesh as near the objective lens crossover as possible. Unfortunately, this increases the mesh magnification, reducing the definition of the field. If the specimen and related field are highly magnified, the instrumental field of view is reduced below the extent of the field. In fields with an extent of the order of 100μ, and with the use of the finest available mesh, 1000 mesh per inch,[3] the best compromise between field sensitivity, field definition, and field of view is obtained by reducing magnification of both objective and projector lens. The former is accomplished by raising the object plane approximately 2 cm; the latter by removing the projector polepiece. An EMB microscope has been modified for the electron optical shadow method in such a way that there is no difficulty in reconverting it to more conventional applications. This modification is accomplished by two auxiliary devices: an object stage mechanism, and a holder and control for the fine mesh electrolytic screen.

Figure 1 shows an exterior view of the microscope column with the modified stage mechanism (A) and screen control (B) in place.

The stage mechanism mounts on the specimen control valve port and is sealed with a flat rubber gasket. Figure 2 shows the assembly of the stage mechanism. Provision is made for rotation of the specimen about two perpendicular axes, which intersect on the optical axis of the microscope. The rotations are controlled from outside the vacuum by coaxial shafts (1, 2) passing through U-cup Wilson seals (3, 4). Translation along the axis perpendicular to the optical axis is accomplished by sliding the outer shaft (2)

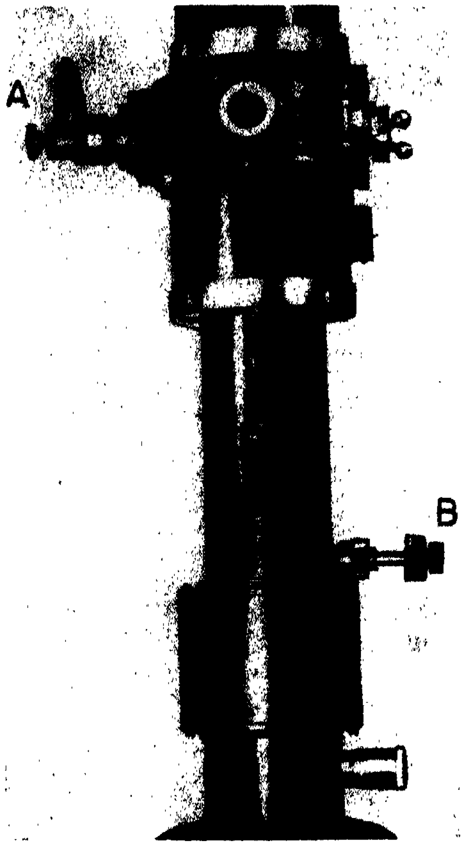

FIG. 1.

by means of a threaded nut (5). For purposes of alignment, the shafts are mounted on a flexible metallic bellows (6) which may be deformed enough to insure the intersection of the axes of rotation on the optical axis.

The screen control, which provides rotation around and translation along the optical axis, is more complicated mechanically because the only available port through which it may be controlled is located just above the projector lens while the screen must be placed some 20 cm above this port. Moreover, since the screen cannot be removed without dismantling the column, in order that the microscope be readily available for other purposes, the intermediate viewing port must not be obscured and a clear bore of at least 1 cm must be maintained.

Figure 3 shows the device finally adopted. Once again coaxial shafts (1, 2) through Wilson seals (3, 4) are used for control. The outer shaft (2) terminates in a bevel gear (5) which drives a long pinion (6). The inner shaft (1) drives, through a set of bevel gears (7), an externally threaded thin-wall tube (8); while the long pinion (6) drives the outer, internally threaded tube (9) by a spur gear (10) which slides on the pinion (6). The screen holder (11) is set on the upper end of the outer tube (12) and may be removed, by a special tool, through the object chamber port after removing the objective pole piece.

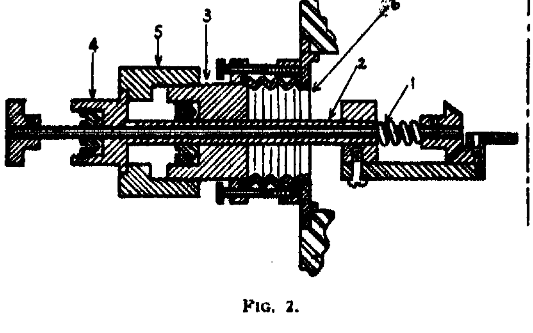

FIG. 2.

The gear ratios are so chosen that if both drives are turned together there is no relative rotation of the threaded tubes and the screen is rotated without translation. If, however, the outer drive is held fixed while the inner one is rotated, the screen is translated without rotation. The total amount of vertical movement thus provided for the screen is about 2½ in., while there is no limit to the amount of rotation.

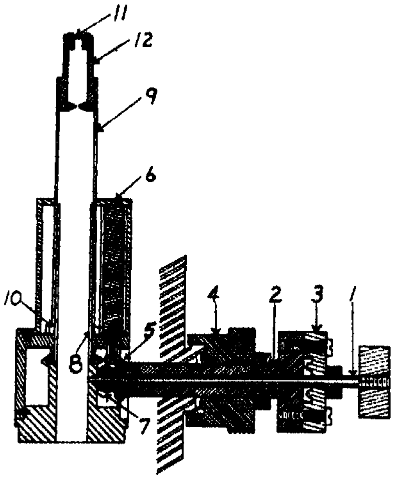

FIG. 3.

Shadowgraphs taken with this instrument of barium titanate and of cobalt crystals have been previously published.[4]

With some change in geometry, other transmission microscopes can also be adapted for this work. In fact, the conversion is probably easier due to the more convenient mechanical construction of other instruments.

---

[1] L. Marton, J. App. Phys. 19, 863 (1948).
[2] L. Marton and S. H. Lachenbruch, J. App. Phys. 20, 1171 (1949).
[3] Obtained from Dr. H. B. Law of RCA Manufacturing Company.
[4] Marton, Lachenbruch, Simpson, and Van Bronkhorst, J. App. Phys. 20, 1258 (1949).

Microtome Knife Sharpness

OSCAR W. RICHARDS
Research Laboratory, American Optical Company, Stamford, Connecticut

April 21, 1950

THE current need for cutting very thin sections of less than a micron has renewed interest in the problem of assessing the condition of the microtome knife. The cutting edge of an ideal microtome knife would be a smooth, straight line formed by the intersection of two planes, the knife facets. Such a perfect edge is not obtained, because variations in the microstructure of the steel and abrasive particles do not give a geometrical line, although modern sharpening methods and improved steels approach this ideal.

When the knife is supported by a block, Fig. 1, and illuminated at the proper angle, Fig. 2, only the light reflected from the cutting edge is seen with a microscope and this reflection is the most useful means for evaluating the sharpness of the knife.[1] A magnification of 100 to 120× should be used for routine examination and 400 to 500× for critical study of the edge. A piece of black photo paper placed on the stage of the microscope blocks light from below and gives a black background. The angle of illumination should be set to give the least reflection. A really

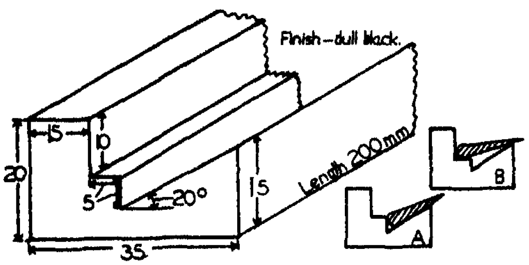

FIG. 1. Block for supporting microtome knife (dimensions in mm). A. Position for examining sharpness. B. Position for observation of polish.

sharp knife edge is seen as a straight, fine line like the left-half of Fig. 3. After some use the edge will appear as the right-half of the figure. Likewise, a poorly sharpened knife will have a broken, wavy line resembling Fig. 4, or even when incompletely sharpened a thicker line.

If the edge is not quite sharp it may be thinned and improved by stropping, but if it is properly honed sharp, then stropping can only round the edge and lessen the sharpness. Too vigorous stropping can overheat the edge and draw its temper.

The facets that produce the cutting edge should be polished smooth and their quality can be examined by placing the knife flat on the microscope stage, Fig. 5, over a piece of black paper, or placed in position B, Fig. 1. Diffused light may reveal the detail of the polish more clearly and can be obtained by placing a ground glass on the front of the illuminator. Unless the facets are smooth, the sections tend to stick and compression is increased.

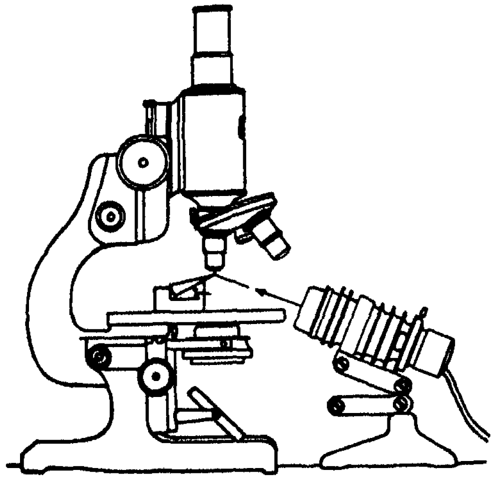

FIG. 2. Method for examining sharpness.

A good edge should be free from nicks which are easily seen if the knife in the last position is illuminated from below to silhouette the edge. They may be measured with a calibrated ocular micrometer. Photo-micrographs are useful for permanent records.

Different materials cut better with different adjustments of the clearance angle between the back facet of the knife and the surface of the block, with different room temperatures and rates of cutting.[2] The clearance angle may,[3] or may not,[4] be critical depending on these conditions, the material being cut and the embedding matrix. An edge rounded from stropping may not require as critical setting of the clearance angle as a very sharp edge. The angle of the cutting edge, between the facets, may be less for softer materials.

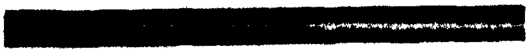

FIG. 3. Reflection from knife edge, left half sharp and right half dulled from sectioning.

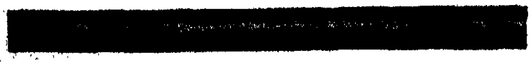

FIG. 4. Reflection from edge of poorly sharpened knife.

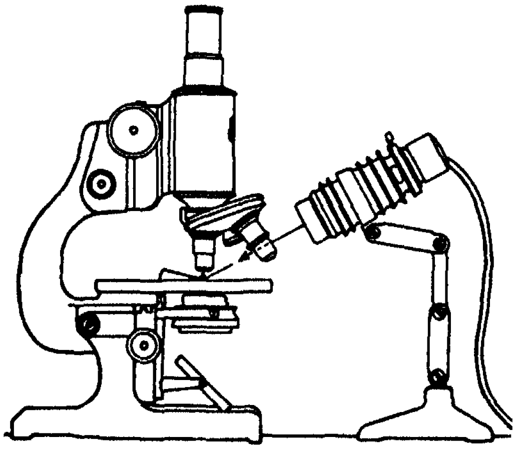

FIG. 5. Method for examining facet polish.

Reports on the problems of fractional micron sectioning will become useful only when the condition of the knife (sharpness, facet polish, facet angle, facet width) and of cutting (material and embedding matrix, temperature, clearance angle and rate of cutting) are known so that different technics and procedures from different laboratories may be compared. Adequate data should lead also to an understanding of the cutting process which will facilitate making better sections adequate for modern microscopy.

[1] H. von Mohl, Bot. Ztg. 15, 249, (1857).

[2] O. W. Richards, *The Efficient Use and Proper Care of the Microtome* (American Optical Company, Buffalo, New York, 1949), second edition, pp. 84.

[3] R. F. Baker, and D. C. Pease, J. App. Phys. 20, 480 (1949).

[4] Borsyko, Newman, and Swerdlow, J. Research Nat. Bur. Stand. 43, 183 (1949); Science 110, 66 (1949).

Glass Variable Microleaks for Gases*

JOHN J. HOPFIELD
Applied Physics Laboratory, Johns Hopkins University, Silver Spring, Maryland

May 2, 1950

GLASS variable microleaks described below have application in spectroscopy[1] and in positive ray work. The range of flow rates are fixed for any one leak but vary from one leak to another. The following are the maximum and minimum rates of air for a series of such leaks with a differential pressure of 1 atmosphere. The values in cc/hr. n.t.p. are: 9.6−0.012; 6.3−0.015; 4.2±0; 60−0.01; 4.8−0.01; 120−0.15; 40−0.03; 60±0; 4.3−0.2; 40−0.01; 3.6−0.006; 6−0.003.

Method of construction.—The leak can be made by any one experienced in glass blowing. Pyrex glass is preferred. It consists of an inner and an outer tube, with a ring seal at 6 and a spot seal at 7 (Fig. 1). Gas leaks from arm 1 to arm 2 through the crack 8 of the inner tube. The opening through the crack is continuously varied by the twist which arises from pressing arms 1 and 2 together at 3, the point of crossing, where they are left slightly separated. The dimensions shown in Fig. 1 are not critical, but a snug fit of the inner tube into the outer one is desirable. The space left between the arms at 3 for the average leak is 0.5 mm.

A unique feature of such a leak is a crack which is made in the inner tube without completely rupturing it. This may be done in the following way.

(1) Heat one end of the tube for 5 sec. in a torch and then

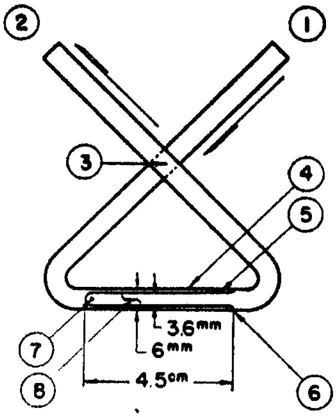

Fig. 1.

quench it by dragging it swiftly across a beaker full of water. The straight crack II,1 results.

(2) Seal off the end II,2 and while still hot quench it in light oil. This makes subsequent operations more sure. Wipe off the oil and flame the end to burn off the residual traces.

(3) Make the ring seal I,6 and bend the arms 1 and 2, leaving a space of a mm between them at the crossing I,3. A metal shim is a good spacer to use for this purpose.[2]

(4) While holding the arms squeezed against the metal spacer (a spring clothes pin with crossed grooves filed in it is a suitable clamp), make a spot weld I,7 and II,3 joining the inner and outer tubes together at this point. When the work cools, squeeze the arms carefully toward one another at the crossing point. Diagonal cracks I,8 and II,4 will lead off from the straight one. As a final step one of the arms is softened *above* the bend and the spacing I,3 reduced to about 0.5 mm for the finished leak. A modified pinch clamp may be used as a regulator for varying the space I,3 of the finished leak and controlling the leak rate. Arm I,2 is on the low pressure side.

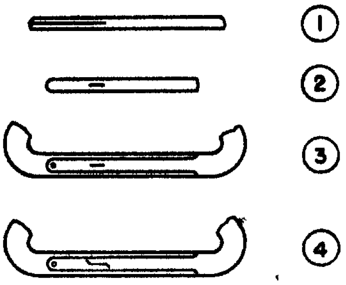

Fig. 2.

The above leak is satisfactory for work in which a tight shut-off is not essential. One can make it shut off more tightly when one springs the arms slightly apart at I,3. One then sees the diagonal crack close to optical contact and the "zero" leak is through the horizontal crack only. Too much spreading of the arms, however, is likely to start an opposite diagonal crack and spoil the leak.

Refinements.—(a) To obviate the above danger and still have the advantage of the lowered zero leak rate, one can proceed to *freeze* a *closing torque* into the finishing leak. This is done as follows: Put the finished leak with the metal spacer held in place by the spring clothes pin into a vise, using a split nut with the threads padded with asbestos to hold it, III. A helical spring attached to the arm I,2 and directly above the nut puts a slight twist in both inner and outer tubes. Now when one softens the spot weld I,7 with a blow pipe, the inner tube becomes relaxed, the left elbow softens, and the outer tube holds all the torque of the spring transmitted down arm 2. When the weld cools and the leak is unclamped, this torque is balanced by a counter torque in the inner tube, the diagonal cracks are found to be closed and can be opened by pressing the arms together as usual. In like manner one can freeze a compression in the inner tube by stretching the outer one.

(b) Another refinement is to fuse the horizontal crack and one of the diagonals permanently closed, leaving only one of the diagonals, subsequently extended if necessary, for regulation of the leak rate. To do this, one clamps the completed leak in the split nut as before, but omits the spring. The split nut is placed in position to cover the right-hand one of the diagonal cracks I,8 and to leave the rest of the crack uncovered. The spot weld is now softened with a fine pointed flame, and another not too hot flame is applied to the outer tube immediately over the crack. Because the edges of the crack in the inner tube are practically in optical contact they are fused together by this gentle heat even through the outer glass envelope. The protected diagonal remains unfused. Finally, after allowing the leak to cool, one reclamps it and freezes a closing torque in this remaining diagonal in the manner described under (a). Do not be discouraged by your first failure.

Microleaks of the last sort can be made to shut off completely and still have regulation up to their maximum rate of a few cc/hr.

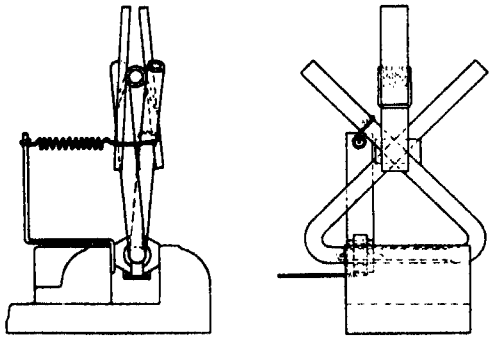

Fig. 3.

In such a leak, the closed crack is entirely invisible and when open it shows interference fringes. If left closed for a period, some of these leaks will freeze closed and refuse to open again. Therefore, it is usually preferable to leave a slight zero rate (about 0.02 cc/hr.) in the finished leak to prevent this freezing. The crack is stable and does not lengthen with use. Never flash a flame across the finished leak when fusing it to the apparatus; to do so may break it.

---

* Work finished under Navy Bureau of Ordnance Contract NOrd 7386.

[1] J. Opt. Soc. Am. and Rev. Sci., Inst. 12, 391 (1926). (The prototype of this leak was at one time commercially available. The present leak shuts off more nearly and is more stable than the prototype.)

[2] The spacing of the finished leak is half of this amount. The greater spacing gives room for initiating the diagonal cracks and overstraining the final crack about 30 percent so that it will be stable in the range of use.

Ultra-High Vacuum Ionization Manometer

J. J. Lander
Bell Telephone Laboratories, Murray Hill, New Jersey

April 20, 1950

THIS note describes an ionization manometer which indicates pressures more than two decades below the lower limit usually encountered at about 1×10^{-8} mm of Hg with other manometers.[1] This limit depends on the design of the gauge; however, values reported for various gauges do not differ much from that given above. Commonly the limit is observed as a lowest reading obtained despite recourse to more or less drastic methods of producing lower pressures, or a variety of changes in gauge design. The flash filament method of pressure measurement has been used to measure lower pressures and at the same time to indicate the lower limit of an ionization gauge.

The most generally accepted theory advanced to account for the lower limit assumes that soft x-rays, generated at the positive

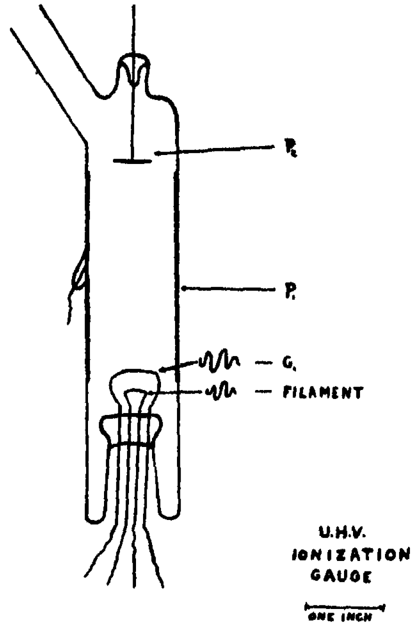

FIG. 1. Cross section of ultra high vacuum ionization gauge.

grid by electron bombardment, excite electron emission at the ion collector. At constant pressure the numbers of ions collected and photo-electrons emitted should be proportional to the ionizing electron current. The gauge fails when, with decreasing pressure, the number of ions collected becomes less than the number of photo-electrons emitted.

In a conventional gauge the positive ion collector surrounds, more or less completely, the filament and positive grid. This design is efficient and it reduces space charge effects to a minimum (ion current is proportional to ionizing electron current up to quite high currents). This design also guarantees that most of the soft x-ray radiation is intercepted by the ion collector and therefore that the lower limit of the gauge is high.

The gauge of Fig. 1 is designed with an ion collector P_2 which collects ions efficiently, but intercepts a relatively small amount of any direct radiation from G_1, which together with the filament is at the opposite end of the tube. P_1 is as efficient as the ion collector of conventional gauges and may be used in the upper pressure range or it may be omitted. The radius of P_2 is about 0.2 inch and it is about 2.7 inches from G_1. Thus P_2 intercepts about one part in 500 of the direct radiation from G_1, whereas P_1, intercepts about half of that radiation. But it has been observed experimentally that P_2, under normal operating conditions collects about ¼ of the total ion current. Thus the ratio of photo-current to ion current for P_2 should be depressed to about 1/50 of that for P_1. Furthermore, it was found that the wire support of P_2 alone is practically as sensitive as the support plus plate. Thus by removing the plate, a gain of more than two decades is to be expected.

Although current to P_1 shows little space charge effect up to ionizing currents of about 10 milliamperes, ion current to P_2 is effected by space charge. Ratios 1 $(P_1)/i(P_2)$ fall from 21 at very low current to about 3 at 10 milliamperes. The ratio has very little dependence on pressure. Data covering a wide pressure range are given in Fig. 2.

It was found that ion current to P_1 is not very sensitive to the potential on P_2 (between −48 and +24 volts) and conversely for P_1 less than −10 volt. Positive potential on P_1 increases ion current to P_2 to a maximum of about twice that obtained with P_1 at −24 volt.

The gauge was found to be about 75 percent as efficient as a D.P.I. gauge. Since it is very nearly as efficient as the D.P.I. gauge (which is relatively efficient), the estimated extension of more than two decades into the ultra high vacuum region should be realized if radiation from the electron collector is responsible for the normal lower limit.

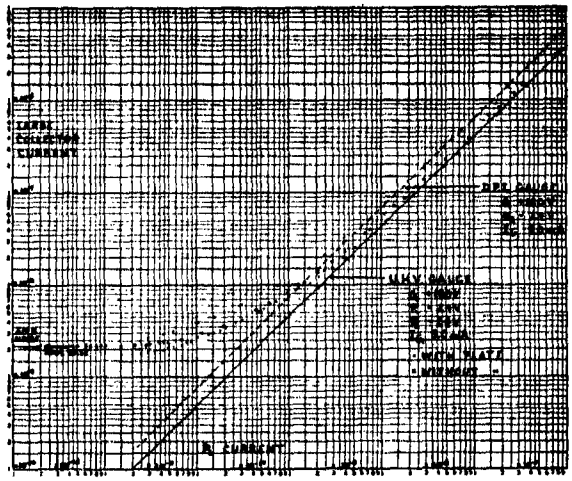

FIG. 2. Plot of ion current to collectors limited at about 2×10^{-8} amp. against current to collector P_2.

Since the wire support can be replaced by a hair-pin filament, the features of ultra high vacuum ionization manometer and flash-filament manometer can be combined in the gauge to produce a more versatile instrument.

The gauge was tested by sealing it, together with a D.P.I. gauge, to a pumping system believed capable of producing pressures well below 1×10^{-8} mm of Hg. Results are reproduced in Fig. 2. Currents to the large ion collectors are plotted against current to P_2. The lowest reading obtained from P_2 (with the plate off) is about 2×10^{-12} ampere, which should correspond to a current of about 1×10^{-11} ampere to P_1 or a pressure of about 1×10^{-10} mm of Hg if the residual gas is equivalent to air in ionization efficiency. Actually the current to P_1 reached a limit at about 2.2×10^{-9} ampere, which corresponds to a pressure of about 2×10^{-8} mm of Hg. The performance of the ion current in the D.P.I. gauge parallels that to P_1 but with a slightly higher limit.

It is to be noted that with the four lowest readings obtained with the U. H. V. gauge the base, containing filament and G_1 leads, was cooled. Either liquid air or dry ice was effective. It is concluded that the largest source of gas in the apparatus operating in the ultra high vacuum range is in the neighborhood of the hot filament.[2]

It is finally concluded that the ionization gauge described extends the useful range of pressure indication by such manometers by at least two orders of magnitude and that the success of the design may be accounted for by the soft x-ray theory for the lower limit of ionization manometers.

[1] While this note was in manuscript, a gauge of similar purpose but somewhat different design and due to R. T. Bayard, Westinghouse Manufacturing Company, was described at the M.I.T. Electronics Conference (April 1, 1950).

[2] Gettering action by the filament of a gauge has been observed by J. Blears, Proc. Roy. Soc. 188, 62 (1947).

An All-Metal Ionization Gauge

F. M. KELLY
McLennan Laboratory, University of Toronto, Toronto, Canada

April 21, 1950

THE construction of an all-metal ionization gauge for use as a rough pressure indicator in metallic vacuum systems was suggested by Kurie.[1] Such a gauge has been constructed and found to be satisfactory.

The design of the gauge is shown in Fig. 1. The outer jacket is a brass tube 2¼ in. in diameter and 4 in. long. It is cooled by water flowing in copper coils which are soldered on the outside of the jacket. The cylindrical anode is sheet monel and is mounted in a large metal-to-glass seal[2] in the side of the gauge. The nickel supports for the grid and filaments pass through and are soft soldered to Fusite terminals[3] mounted in a brass plate which covers the open end of the gauge. The grid consists of twenty turns of 15 mil tungsten wire in the form of a cylinder $\frac{5}{16}$ in. in diameter. The filament is a 2¾ in. length of 10 mil thoriated tungsten wire which is heated to operating temperatures by a potential of 4 to 6 volts across its ends. Only the lower filament support is shown in the diagram. The upper support is directly behind the filament and passes midway between the grid and the anode to a fourth Fusite terminal ¼ in. behind the central one shown in Fig. 1. The filament and grid mount is sealed in place with a Neoprene gasket and can be easily removed. Thus broken filaments can be readily replaced.

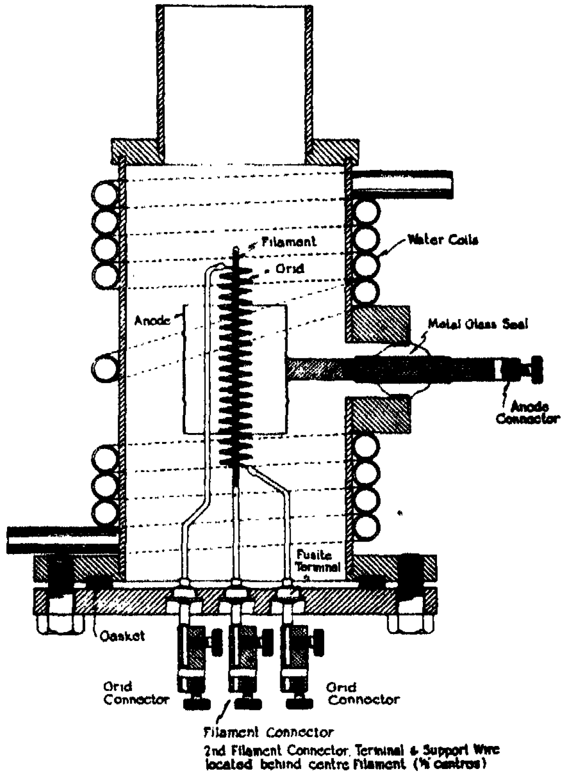

FIG. 1. Sectional elevation of metal ionization gauge.

The potentials used on the electrodes are the same as those for commercially available gauges. This gauge has been checked against the RCA ionization gauge 1949 and has been found to give comparable readings at pressures down to 10^{-5} mm of mercury. Ten to twenty minutes must be allowed for the gauge to reach a steady condition if it has been opened to the air.

The gauge is easily constructed and the parts are readily available. The ease with which filaments can be replaced makes safety devices for the protection of the gauge unnecessary. It is not suitable for accurate pressure determinations but is useful as a rough indicator and in leak hunting.

---

[1] F. N. D. Kurie, Rev. Sci. Inst. 19, 485 (1948).

[2] Type GA 95.2013 supplied by the Stupakoff Ceramic and Manufacturing Company, Latrobe, Pennsylvania.

[3] Type 107-HT supplied by the Fusite Corporation, Cincinatti, Ohio.

A Convenient Leak for Testing Helium Leak Detectors*

G. H. Jenks
Chemistry Division, Oak Ridge National Laboratory, Oak Ridge, Tennessee

May 25, 1950

IN the use of helium leak detectors, it is frequently desirable to test the sensitivity of the instruments by admitting helium gas to the system at known slow rates. The methods commonly employed in admitting the gas make use of fine capillaries of different types. The capillary leaks, however, are troublesome to use because of the ease with which they are stopped or their calibrations changed.

It should be pointed out that a "leak" which is not of the capillary type but which makes use of the permeability of glasses to helium can also be used in testing helium detectors. Thus, the rate at which helium diffuses through silica glass at room temperature is known to be about 7×10^{-11} cc/sec./cm^2/mm/cm Hg[1]. A section of the glass having an area of 1 cm^2 and a thickness of 0.1 mm will then pass about 5×10^{-8} cc of helium per second when the pressure difference is one atmosphere. This rate is about 25 times greater than the minimum rate which the commercial instruments will detect. The diffusion constant of Pyrex glass is smaller than that of silica by a factor of ten, but the amount of helium passed by a section of Pyrex of moderate dimensions is still appreciable compared with the sensitivity of the detectors. Soft glass does not pass helium at appreciable rates.

The precise rates of diffusion of helium through glasses are strongly dependent upon the temperature of the glass, varying about 3 percent per degree for both silica and Pyrex at room temperature. However, if desired, corrections for temperature changes can be applied so that the relative rates at different temperatures should be known readily to within 3 percent.

A "leak" of the diffusion type has been in use at this Laboratory for several weeks and so far has operated very satisfactorily. The design of the leak is shown in the accompanying sketch. The silica glass bulb is approximately 1 cm in diameter and has an estimated minimum thickness of 0.1 mm. Helium gas under a pressure of 1 atmosphere is sealed in the Pyrex reservoir. The rate at which helium diffuses through the leak is such that a General Electric detector registers a steady deflection of one-tenth of the most sensitive full scale deflection. Momentary deflections of much greater magnitude can, of course, be obtained by allowing helium to collect in the Pyrex envelope for several minutes and then opening the envelope to the detector.

There is no apparent reason why the leakage through the above

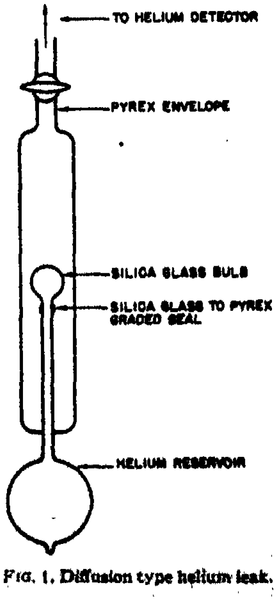

FIG. 1. Diffusion type helium leak.

leak when it is at constant temperature should change appreciably as long as the pressure of helium within the reservoir remains constant. The reservoir pressure will, of course, decrease as the helium diffuses through the silica, but the fractional decrease during a given period can be made small by choosing a sufficiently large reservoir volume. Thus, at a leakage rate of 5×10^{-8} cc/sec., about 1.5 cc/yr. will diffuse through the silica. If a reservoir having a volume of 100 cc is used, the yearly change in pressure will be 1.5 percent. Some additional leakage through the walls of the reservoir will occur, but this may be eliminated by substituting soft glass for the Pyrex.

* This document is based on work performed for the AEC at Oak Ridge National Laboratory.

[1] Richard M. Barrer, *Diffusion in and through Solids* (University Press, Cambridge, England, 1941), p. 117–142.

Preparation of Unbacked Metallic Films

F. E. Carpenter and J. A. Curcio
Naval Research Laboratory, Washington, D. C.
May 11, 1950

A TECHNIQUE has been developed for the preparation of thin unsupported metallic films. The films are strong and usually free from pinholes. Aluminum films ranging in thickness from 1000 to 3000A have been prepared, the thickness determined from weight and area measurements. Usually, the films have been placed over slots 1 mm×10 mm for use in upper atmosphere x-ray investigations. A larger film of 3000A thickness with a surface area of 3 inches×4 inches has been prepared and used to cover an aperture 2 inches in diameter.

The aluminum film is evaporated in the usual way on glass slides which have previously been coated with a water soluble film. The slides are hand dipped in a sugar-aerosal solution and dried on edge in a dust free atmosphere before evaporation. The metallic film is stripped from the glass slide by immersion in water for 20 to 30 minutes. At the end of this time the film will be sufficiently detached so that it can be peeled off and placed over the area to be covered while still under water.

The water soluble film used to cover the slides is a dilute bubble solution as given by Kuehner.[1] In our application the solution is made up of 15 grams of ordinary cane sugar dissolved in 75 ml of a one percent aerosal-water solution.

[1] A. L. Kuehner, J. Chem. Ed. 25, 211–212.

Comments on "Velocity-Acceleration Response from a Seismic Pick-Up via Controlled Damping"*

A. J. Hermont
3737 Bellaire Boulevard, Houston, Texas
May 20, 1950

AS a corollary to Jeffries' paper, the following may be of interest. Since damping is an important parameter in determining the relationship between the response of an oscillatory system and displacement-, velocity-, and acceleration-input, and since the concept of damping is linked with the transient rather than the steady state, it was thought worth while to study the transient state of the systems discussed by Jeffries. The transient solutions for the underdamped (Fig. 1) and the overdamped (Fig. 2) cases were obtained by operational means, i.e., the response (S_a) of the relative motion to a unit-step ground acceleration for the underdamped, and the response (S_v) of the relative motion to a unit-step ground velocity for the overdamped cases were derived. For the numerical value $\omega_n=100$ radians per sec. (ω_n = natural circular frequency of the system) the relative indicial responses were computed and the results are indicated in the accompanying illustration. Consider first the underdamped case, Fig. 1. If the system were a perfect "acceleration reproducer," its relative motion to a unit-step acceleration would be a unit-step (ideal). Instead, the actual response for $\delta=0.5$ and $\delta=0.7$ (δ = damping factor) is as shown. For $\delta=0.7$, the system behaves as a near-perfect acceleration reproducer at low frequencies. For high frequencies, it is a poor acceleration reproducer. This is inherent in the fact that the transient starts with zero slope (as may at once be deduced from the equation given in Fig. 1) and is manifested by the pronounced "build-up" time.

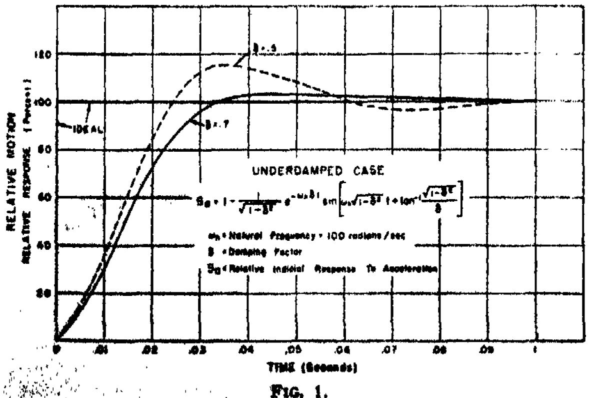

FIG. 1.

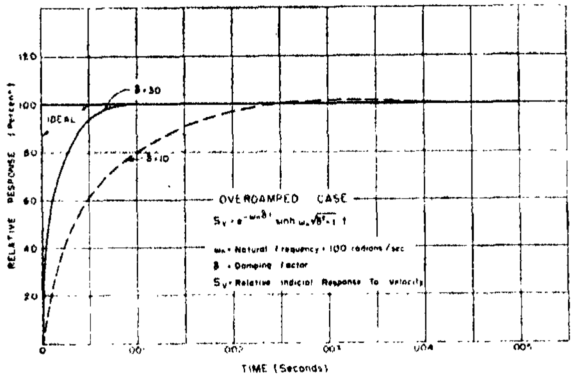

FIG. 2.

* R. J. Jeffries, Rev. Sci. Inst. 21, No. 2, 115–117 (1950).

New Instruments

W. A. Wildhack: Associate Editor
in Charge of this Section
National Bureau of Standards, Washington, D. C.

These descriptions are based on information supplied by the manufacturer and in some cases from independent sources. THE REVIEW *assumes no responsibility for their correctness.*

Principal Strain Computer

A new electronic computing instrument for automatically computing and indicating principal strains was developed and built for the National Advisory Committee for Aeronautics, and it is now in operation at Langley Field, Virginia.

This computer operates directly from strain gauge rosettes, indicating almost instantaneously the values of major principal strain, minor principal strain, and the principal angle.

Principal strains are determined experimentally by means of the strain gauge rosette which is an arrangement of 3 or 4 resistance strain gauges mounted on the surface under test at definite angles with each other. The voltage outputs of each gauge are translated into strain, and then these individual strain values are placed into equations or formulas which yield the desired values of principal strains and the principal angle. Equations differ for different arrangements of gauges in the rosette, but all equations involve

sums and differences and square roots of sums and/or differences squared.

The principal strain computer operates with equiangular rosettes, rectangular rosettes, and with TΔ rosettes. To convert from one equation to another, it is merely necessary to operate a single selector switch.

The sum and difference factors are obtained by networks, operating directly on the outputs of the individual gauges. The square root of the sum of several squares is obtained almost instantaneously by a self-balancing electrodynamometer.

The rosettes are powered by a 400-cycle carrier and all operations in the calculations are performed on this carrier without any modulation or demodulation, and wave form and frequency are not critical.

The computer contains all the oscillators, amplifiers, and power-supply equipment within one cabinet, for operation directly from a single source of 115-volt 60-cycle power. A total of 75 vacuum tubes is used.

A total of 48 rosettes, either of the 3-gauge or 4-gauge variety may be connected to the computer and each gauge properly balanced before strain determinations are made. After each increment of strain is applied, the operator can read and record the major and minor principal strains and the principal angle just as fast as he can operate the rosette selector switch and read and tabulate the results.

Built-in calibrating equipment is provided for quick and precise calibration for the rosette to the strain and angle indicators.—Hathaway Instrument Company, *1315 South Clarkson Street, Denver 10, Colorado.*

Chain Pulse Amplifier

The Model 214 Chain Pulse Amplifier has been specifically designed to amplify very fast pulses and transients. Employing fourteen 6AH6 vacuum tubes in a traveling wave circuit, it has a band width of 40 kc to 100 Mc and a gain of 30 db. The input impedance of 180 ohms is designed to match the output impedance of the Series 200 Wide-Band Chain Amplifiers for additional gain up to 60 db.

A special termination at the end of 15 inches of cable is provided for convenient use with a DuMont 5XP Cathode-Ray Tube for the viewing of high speed pulses. With an output voltage of 65 volts and a rise time of 6 millimicroseconds, 1 inch of deflection is obtained under the stiffest beam conditions. A second output is also provided for connection to high speed counters and other associated equipment. Standard connectors are used at the input and no special cable and fittings are required.

The Model 214 Chain Pulse Amplifier and power supply is housed in an aluminum chassis and can be supplied for either table or rack mounting. *This versatile amplifier finds many applications in nuclear physics, radar, high speed oscillography, television testing, and general laboratory measurements.*—Spencer-Kennedy Laboratories, Inc., *Department SI, 186 Massachusetts Avenue, Cambridge 39, Massachusetts.*

Versatile Photo-Micrographic Apparatus

This Photo-micrographic Apparatus, designed also to serve all other aspects of scientific photography, provides facilities for photo-micrography; photo-macrography; micro-projection; laboratory, clinical, and general photography; photo-copying; microfilming; x-ray photo-copying; and photo-enlarging.

The apparatus is named the Orthophot, and is used with any standard microscope. It comprises three basic units:

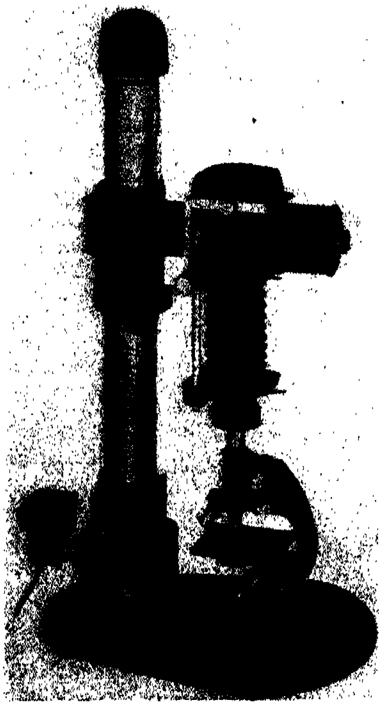

1. A base with permanently aligned built-in light source operating on the Koehler principle (balanced at 3200 K for color work) with intensity-control maintaining constant color temperature, and with built-in color filters for black-and-white photo-micrography. This unit is available separately as light source for exacting visual microscopy.
2. A self-aligning reflex camera with precision focusing device (for use with No. 120 roll film, $2\frac{1}{4}$ in.$\times 3\frac{1}{4}$ in. cut or pack film, and standard 35 mm film), automatic Rapax shutter (1 sec. to 1/200 sec., T and B); attached sensitive photoelectric exposure meter.
3. A vertical column assembly with counterbalanced elevating device for the camera, operated by rack and pinion.

These units are shown in the illustration assembled and with a microscope in position for photo-micrography. Accessories, not shown, convert the unit for photo-macrography, cine-photomicrography, general laboratory photography, photo-copying, of opaque and translucent objects, and photo-enlarging, by attaching lamp unit with double condenser which works through the basic camera unit.

The reflex camera itself is detachable and can be used on a standard tripod or hand-held for all forms of scientific or general photography.

Light source, camera, or vertical column are available separately for combination with existing equipment in the user's laboratory. A simplified version of the column can be had with adjustable camera holder to permit use with a wide variety of standard still and motion-picture cameras. Price of the standard Orthophot is $825.00.—Silge and Kuhne, *Box E, 153 Kearny Street, San Francisco 8, California.*

Microwave Signal Sources

A series of Microwave Signal Sources covering the range of 634 Mc to 8340 Mc in four units, is now available.

These reflex klystron signal sources are controlled by one dial only and frequency is read directly from a linear indicator to accuracies of ½ percent. The reflector voltage is automatically tracked with the cavity tuner. There are no klystron modes to set, no voltage settings to be made and frequency can be read directly without resorting to charts or graphs. Non-contacting shorts are used to eliminate noise and reduce mechanical wear. Terminals are provided for applying modulation to either the grid or reflector.

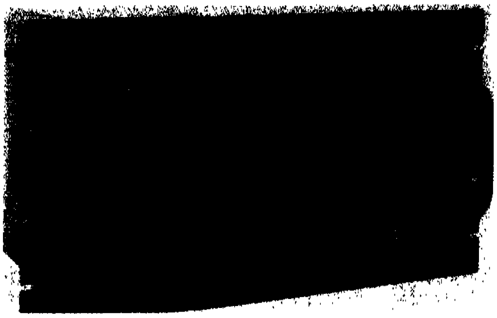

The Model SSR Microwave Signal Source covers the range from 634 to 1174 Mc; Model SSL—1140 to 2184 Mc; Model SSS—2145 to 4310 Mc; and Model SSM—4290 to 8340 Mc. The signal sources are supplied complete with tube.

A Klystron Power Unit, Model KX-1, which has been designed to minimize klystron frequency modulation due to reflector voltage variations is also available.—Polarad Electronics Corporation, *100 Metropolitan Avenue, Brooklyn 11, New York.*

New Gamma-Ray Detector

The Model 939 Scintillometer (gamma-ray detector) employs the scintillation principle, and provides a detection sensitivity over 100 times that obtainable by conventional portable Geiger counters, the actual count rate being approximately 290 times that of three popular Geiger counters tested under identical conditions. This increased sensitivity, with negligible effects from cosmic rays, permits more rapid and accurate measurements of gamma-ray field intensity.

When used for radioactive ore survey, the Scintillometer will detect deposits through greater depths of over-burden and provides information which can be correlated with geological structure, to provide accurate information on distribution and concentration of the deposit. Through the use of a special gamma-ray spectrometer feature, the Scintillometer may be used to distinguish the difference between thorium and uranium ore deposits, and will indicate the uranium concentration in an ore containing both radioactive minerals.

The Scintillometer employs only high vacuum tubes in conservatively designed circuits, is protected against vibration, shock, temperature, and humidity; will operate continuously between −20°F and +110°F, with a relative humidity of 95 percent. A removable probe is contained in the lower section of the case proper, which need only be removed for laboratory research purposes.

The instrument is housed in a weather-proof aluminum alloy case, measuring 3½ in.×11 in.×13 in., and is supplied complete with batteries, canvas carrying case, and strap.—Halross Instruments Corporation, Limited, *171 Garry Street, Winnipeg, Canada.*

Ultra Low Frequency Oscillator

A new, wide range, ultra low frequency oscillator, Model 410-A, combines the sub-audio with the normal audiofrequencies and provides both sine and square wave outputs over the entire frequency range from 0.02 to 20,000 c.p.s. Six frequency bands are provided, each covering a full decade, with continuous control of frequency. A single, 11-in., illuminated, direct-reading logarithmic scale is used on all bands.

The sub-audio range of frequencies makes the unit especially useful for design and test of servomechanisms, geophysical instruments and feedback amplifiers, for vibration checks and medical research, and in conjunction with time and production controls. The square wave output is useful for low frequency switching and triggering operations, and for checking the frequency or transient response of audio circuits.

This instrument features low distortion and hum level, constant output impedance, excellent frequency stability, and amplitude constancy over the entire frequency range. An important feature of a sub-audio electronic oscillator is its ability to recover quickly from bandswitching and similar disturbances; the sine wave output of the 410-A recovers to 90 percent of its steady state amplitude in less than 2 cycles of the dial frequency.—Krohn-Hite Instrument Company, *580 Massachusetts Avenue, Cambridge 39, Massachusetts.*

Oscillo-Tracer

The Oscillo-Tracer is an optical super-positioning device, using a newly developed double-coated lens. The arm carrying the lens is adjustable in length to fit any standard oscilloscope, and looking down through it one sees a reflection of the cathode-ray trace superimposed on the paper directly below the lens. A small lamp is provided in the base of the Oscillo-Tracer to illuminate the pencil while you trace the oscillogram. The Oscillo-Tracer has been found useful for many applications, such as detecting small, slow changes of patterns, comparing traces by the super-position

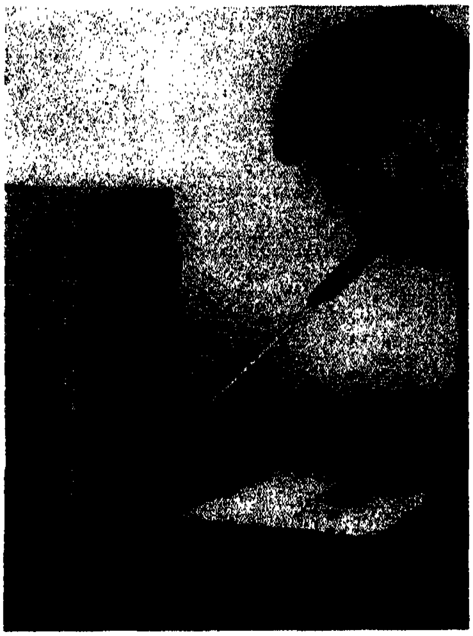

method, and so on. School and college laboratories find the Oscillo-Tracer invaluable for economical recording of experimental data in student notebooks. It is priced at $19.50.—Robert A. Waters, Inc., *4 Gordon Street, Waltham 54, Massachusetts.*

Model On-5 Oscillo-synchroscope

This new oscillosynchroscope, Model ON-5 is designed to provide wide band amplifier and versatile sweep facilities in single portable unit. It is particularly well adapted to the study of pulse and transient phenomena as well as being useful in all conventional oscillographic applications.

Vertical amplifier response is flat within 3 db from 5 cycles to 5 megacycles. Horizontal amplifier is direct-coupled with high frequency response extending to 500 kilocycles.

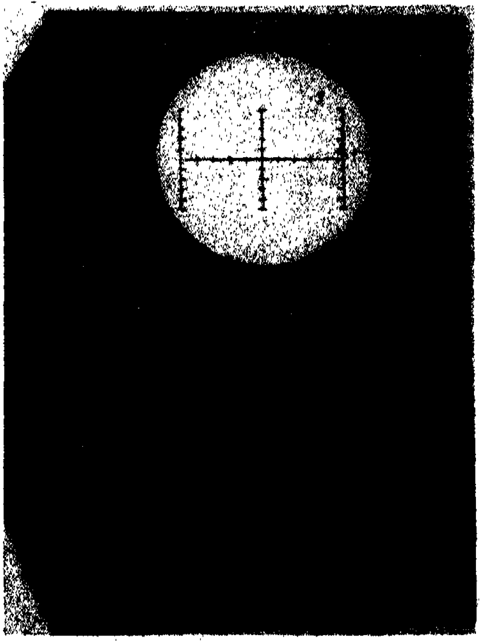

The sweep generator may be triggered or recurrent with direct reading-writing rate calibration for any internal sweep condition. Triggered sweep speeds from 1.0 microsecond per inch to 25,000 microseconds per inch and recurrent sweeps of 10 to 100 kilocycles are available.

An adjustable calibration voltage may be used for determination of vertical deflection voltage amplitudes. Either d.c. or a.c. connection may be made to all deflection electrodes. Also provided is a panel connection to the cathode-ray tube for external beam modulation. The ON-5 is housed in a steel cabinet. Dimensions: height 14¾ in., width 10 in., depth 16¾ in.; weight: 50 lbs.—Browning Laboratories, Inc., *Winchester, Massachusetts.*

Projection-Microphotometer

A double projection comparator and microphotometer, particularly applicable to rapid qualitative and quantitative spectrographic analysis, has been developed by Optica, Milan, Italy. The instrument, called "Evaluation Apparatus," serves three purposes: (1) a single plate or film projector combined with a micrometer for measuring line-to-line distance; (2) a double projector providing direct comparison of two plates or films with controls for rapid alignment of the images on a horizontal screen; and (3) a microphotometer capable of measuring the transmittances of very narrow spectral lines. The instrument ordinarily accommodates plates and films up to 9 by 24 cm but, if necessary, can be used for sizes as large as 24 by 30 cm.

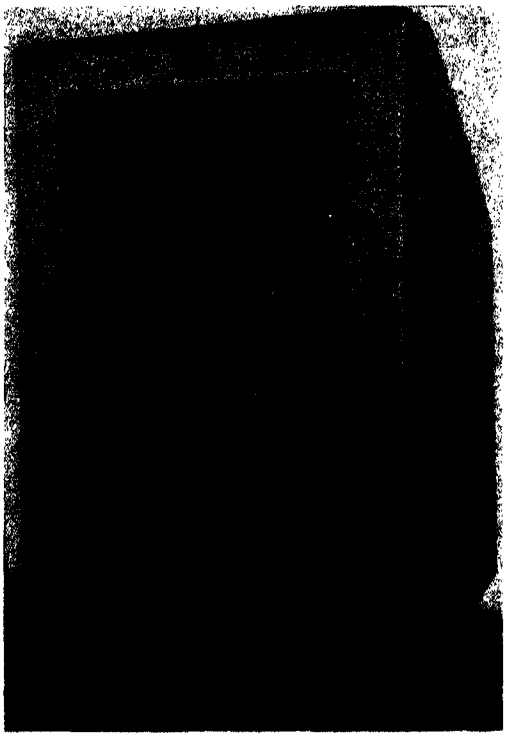

The single plates, or the two plates to be compared when the unit is used as a double projector, are placed on a slightly inclined table and images are projected on a horizontal table arranged at a suitable level in the front part of the projector. The spectrograms are quickly leveled and aligned by the controls provided. When two spectra are to be compared the images can be projected either side by side or one slightly above the other. The light intensities of the two projection systems, each being equipped with its own 6-volt, 100-watt lamp, can be adjusted individually; this permits adjusting for density differences between the two plates. When the unit used as a single projector the second field can be shielded, and the one image extended to cover the full area of the screen.

When the apparatus is to be used as a microphotometer, the white table used for comparing plate images is removed to uncover a second gray table. In the center of this table is a slit adjustable in width to 0.002-mm divisions by a drum and behind the slit is mounted an RCA 931A photo-multiplier tube fed by a constant voltage circuit. The deflections of a mirror galvanometer are observed on either of two moving scales, one linear with 1000 divisions and the other logarithmic. The system is designed to be compact by employing a scale reduced photographically to a few centimeters in length and then projecting the scale full size on the screen. The projection lamp is run on battery power when photometric measurements are made.

The whole unit is enclosed in a large metal cabinet, in front of which the operator may sit comfortably. The cabinet also serves as a light shield and, when not in use, the cabinet can be closed tightly by a curtain to protect the instrument against dust. The linearity of the photoelectric system is reported to be better than one percent.—Optica S.p.A., *Via Calatafimi, 7–9, Milan, Italy.*

Manufacturer's Literature

Measurement of Low Temperatures—Manual discusses generally the various thermometric devices employed in the determination of temperature below the boiling point of liquid oxygen. There is also a discussion of barometric corrections. An appendix of tables and graphs is also included.—Westinghouse Research Laboratories, *East Pittsburgh, Pennsylvania.*

Transformers—Bulletin 90–109 announces transformer design and manufacturing services offered to industry for developing special components to meet unusual operating requirements.—Sperry Products, Inc., *Danbury, Connecticut.*

Tracerlog—No. 26, April, 1950, features description of stainless steel cathode Geiger-Mueller tubes.—Tracerlab, Inc., *130 High Street, Boston 10, Massachusetts.*

Lapping Machine—Bulletin describes the Lapmaster, a machine for automatic high production lapping to extremely close tolerances. Also shown are Lapmaster accessories.—Crane Packing Company, *1800 Cuyler Avenue, Chicago 13, Illinois.*

Instrumentation—Vol. 4, No. 4, 32-page house organ, includes articles on television tube production, continuous specific gravity measurement, and recording mass spectrometer, and other items.—Minneapolis-Honeywell Regulator Company, *Wayne and Windrim Avenues, Philadelphia 44, Pennsylvania.*

Electric Timing Motors—Catalog No. 322 (1950) presents the company's line of electric timing motors.—Haydon Manufacturing Company, Inc., *Torrington, Connecticut.*

Experimenter—Vol. 24, No. 12, May, 1950, 12-page house organ, describes a direct-reading impedance-measuring instrument for the u.h.f. range.—General Radio Company, *275 Massachusetts Avenue, Cambridge 39, Massachusetts.*

Electric Connectors—Bulletin No. K3-1950, 48 pages, on Type K and RK connectors, designed for uses in aircraft, radio, and many types of instruments and general electrical equipment.—Cannon Electric Development Company, *3209 Humboldt Street, Los Angeles 31, California.*

Instrument Notes—No. 14, March–April, 1950, features an article on calibration of resistance bridge transducer circuits under temperature extremes, and includes short description and photograph of the Model P11 pressure transducer.—Statham Laboratories, Inc., *9328 Santa Monica Boulevard, Beverly Hills, California.*

Nuclides and Isotopes—Booklet APD-35A describes nuclides and isotopes. Included is a list of the elements, indicating atomic number and symbol. A chart of the nuclides accompanies this booklet.—General Electric Company, *Schenectady 5, New York.*

Infra-Red Recording Spectrophotometer—"Better Analysis," No. 1, 1950, 10 pages, illustrated, presents the Baird Infra-Red Recording Spectrophotometer and its applications.—Baird Associates, Inc., *33 University Road, Cambridge 38, Massachusetts.*

New Materials

Forest K. Harris: Associate Editor
in Charge of this Section
National Bureau of Standards, Washington, D. C.

Teflon Applications

Teflon (tetrafluorethylene resin) is finding electrical applications in which its electrical properties at high frequencies, its heat resistance, or both are important. Its short-time dielectric strength is 1000 to 2000 v.p.m. in 5- to 12-mil thicknesses and 400 to 500 v.p.m. in 80-mil thickness. Volume resistivity is greater than 10^{15} and surface resistivity 3.6×10^{6} at 100 percent relative humidity. Dielectric constant is 2.0 and power factor is less than 0.0005 over a frequency range from 60 to 10^{8} c.p.s. Teflon insulated wire is being used as ignition cable and for transformer leads in high voltage electronic devices. It is proving particularly useful as coaxial spacers in TV in f-m transmission lines where its low dielectric constant minimizes reflections, and its low loss factor makes the line practically the equivalent of a line with air insulation. Where machined Teflon inserts are used as insulators in coaxial connectors, the advantages are the same, and in addition the heat resistance of the material permits soldering of connections during assembly without danger of injury to the insulation.

In addition to its unique electrical, chemical, and thermal properties, Teflon has another characteristic which leads to interesting applications. Nothing sticks to it with any appreciable strength and it may be used in processes where a non-sticky surface is required, such as the jaws of heat-sealing machines and on conveyors and rolls handling sticky materials. For example, its use on bakery rolls for handling dough eliminates the need for dusting flour and for roll scrapers. Its use is under evaluation in non-adhesive applications such as bread pans, mold release agents, and conveyors.—E. I. du Pont de Nemours and Company, *Polychemicals Department, 350 Fifth Avenue, New York 1, New York.*

Silicone Molding Compound

GE-12810, consisting of a silicone resin with a glass fiber filler, is the first commercially available silicone molding compound. Its outstanding characteristic is heat resistance, continuous operation at 392°F being possible. High impact strength and excellent arc resistance, as well as good flow in the mold, are also reported. It will not support combustion and has no toxicity when burned. Applications include circuit breakers, switchgear and other parts where resistance to extreme heat and impact is needed.—Chemical Department, General Electric Company, *Pittsfield, Massachusetts.*

Aluminum-Silicone Paint

Silicone Coating Aluminum is a new aluminum paint supplied in separate compartments containing the pigment and the silicone resin vehicle. They are mixed just prior to use. The paint may be applied by brush or spray on plain or galvanized metal surfaces and affords weather protection in temperatures ranging from below freezing to 750°F. The coating is also resistant to attack by fumes. Coverage is about 1000 square feet per gallon and drying takes place in from one-half to three hours.—Dampney Company of America, *1241 River Street, Boston 36, Massachusetts.*

Silicone Rubber Sponge and Shock Mounts

Chorlastic, silicone rubber sponge, made from recently developed silicone compounds, has a more uniform cell size than previous types. Tensile strength, elongation, abrasion resistance, and tear strength have also been improved. The sponge has a volume of 25 to 35 cu.in./lb. and will resist temperatures between −100 and +500°F. It is used as a vibration damper at extreme temperatures, and as fairing strips, seals, gaskets, etc. It is available in sheet stock $\frac{11}{16}$, $\frac{1}{8}$, and $\frac{1}{4}$ in., and can also be obtained in special extrusions and molded shapes on a custom basis.

Chorlastic mountings use silicone rubber to permit vibration damping at temperatures ranging from −100 to +500°F. They will protect instruments and other apparatus under conditions of extreme cold where ordinary rubber becomes hard and brittle, and in locations where high ambient temperatures would make ordinary rubber soft and gummy. They are designed for loadings and deflections required by *AN* specifications and are available in many sizes of the *AN* instrument series. They can be designed for most services where temperature resistance is required with the vibration characteristics of a shear-type mount.—Connecticut Hard Rubber Company, *407 East Street, New Haven 9, Connecticut.*

Aluminum Wire

Polyethylene-covered aluminum line wire, for use where weatherproof or insulated electrical conductors are required, is available in a full range of sizes of solid and stranded conductors, as well as in small sizes. This wire has advantages which include light weight (one-half the weight of equivalent weatherproof copper wire); free stripping (making it easy to clean for splices and taps); resistance to abrasion and fungi; and freedom from rotting and festooning as textile coverings do. Long lengths can be readily handled because of the light weight.—Kaiser Aluminum and Chemical Sales Company, *1924 Broadway, Oakland 12, California.*

Laboratory Aids

Varniton Stopcock Lubricant has been found useful as a liquid pouring aid for screw-cap bottles, beakers, flasks, metal containers, and carboys. A small amount of the lubricant spread around the lip edge of the container acts as a barrier to prevent the spread of liquid drops, permitting pouring in a steady controlled stream. No drops form over the lip when the pouring is terminated. The lubricant is non-volatile and remains effective for a long time. It is almost completely insoluble in aqueous solutions of acids, bases, and salts so that no contamination results from its use.

Var-Clean is a high foaming laboratory detergent, containing no soap, for cleaning laboratory glassware, as well as metals, porcelain, plastic cloth, and stone surfaces. It has excellent wetting and spreading properties and is effective on oil, grease, gums, culture media, etc. It contains no strong alkali salts and is easy on hands. After rinsing, laboratory ware drains dry without wiping. The detergent is supplied in powder form in a conical dispenser which facilitates its use in narrow-necked flasks and other apparatus with restricted openings. Addition of water to the detergent makes a powerful cleaning agent.

Powdex contains the same ingredients as *Var-Clean* with the addition of a mild abrasive to facilitate the removal of waxes, stains, and carbonized material.

Nitro-Seal is a quick-drying, thick sealing cement designed for application to cold surfaces. It seals leaks in vacuum apparatus, dries fast by solvent evaporation, and leaves a smooth transparent coating. It can be employed for cementing wood, cork, metal, cloth, glass, porcelain, paper, plastics, leather, etc., and is satisfactory for insulating electric wires and protecting them from corrosion. It is resistant to dilute acids and alkalis, petroleum oils and greases, and may be removed with acetone. By adding fine wood sawdust it can be converted into a plastic wood filler.—Varniton Company, *416 North Varney Street, Burbank, California.*

Degreaser

Barco Metal Degreaser Q-200 is designed for cold application. Metals and plastics are degreased by immersion, by dipping and brushing, or by wiping with the fluid. It is also useful in removing pitch or cementing resins from ground lenses. It has been approved by the Underwriters Laboratories. Further information may be obtained from the manufacturer.—Barco Chemical Products Company, *701 South LaSalle Street, Chicago 5, Illinois.*

High Speed Hacksaw Blade

Molyflex is a high speed steel hacksaw blade which can be twisted through more than 90° without breaking. It is shatter-proof and when used in a frame is unbreakable. It is available in all popular sizes and pitches for hand-sawing.—Victor Saw Works, Inc., *Middletown, New York.*

Solder Alloys

New solder alloys for use with silver-printed or silver-plated conducting mediums are stated to eliminate danger of dissolving silver. The solder is formulated in two melting ranges: *Divco No. 233,* for applications where abnormally high temperatures are not encountered; and *Divco 276,* for use in assemblies that operate above 350°F. Both can be applied in the same manner as ordinary solders, and may be used on ceramic, plastic, Bakelite, and other base materials coated with silver. They are available in bar, solid-wire, and rosin-core shapes.—Department B-34, Division Lead Company, *836 Kinzie Street, Chicago 22, Illinois.*

Flashlight Battery

Eveready No. 1050 industrial flashlight battery has a plastic-coated cardboard-covered container with a carbon lining and a zinc vane as the central element. Unlike older type units which have a central carbon rod and a zinc container, this type of construction provides a container that is inert to electrolytic action, and that will not perforate, leak, corrode, swell, or jam in the flashlight. A metal disk at the top provides a connection to the carbon element and one at the bottom is welded to the zinc vane. This arrangement keeps the polarity the same as that in the older type cell, and the battery is completely interchangeable with all *D*-size (standard flashlight size) units. In flashlight service the new battery has more than double the useful life of any previous type.—National Carbon Division, *30 East 42nd Street, New York 17, New York.*

Welding Glass

G-S Welding Plates are guaranteed to absorb at least 99.5 percent of infra-red and 99.75 percent of ultraviolet radiations. They are graded for density and thickness in accordance with Federal Specification GGG-H-211 for welding helmets and shields. The standard size is 2×4¼ in.—General Scientific Equipment Company, *2700 West Huntingdon Street, Philadelphia 32, Pennsylvania.*

Metal-Ceramic Materials

Metal-Ceramics are a mixture of metal and ceramic materials having useful characteristics at high temperatures including high strength, good abrasion resistance, and high thermal shock resistance. They have intermediate electrical and thermal conductivities and can be machined and electroplated. Dense metal at one end and a "metal-ceramic" at the other can be incorporated. Possible uses include dies for hot forming, containers for high temperature furnace work, flux-resistant brazing and welding fixtures, electrical contacts, and spark-plug electrodes. The manufacturer is accepting sample orders for these materials to evaluate major applications.—Special Metals Division, P. R. Mallory and Company, *3029 East Washington Street, Indianapolis 6, Indiana.*

THE
REVIEW OF SCIENTIFIC
INSTRUMENTS

VOLUME 21, NUMBER 8 *AUGUST, 1950*

The Measurement of Rates of Flow of Gases by Wet Test Meters*

ROBERT L. BURWELL, JR., MAX METLAY, AND FRANK W. PFOHL
Department of Chemistry, Northwestern University, Evanston, Illinois

(Received March 20, 1950)

Rates of flow of gases may be measured to an accuracy of better than 0.1 percent with properly modified and operated wet test meters. The period of a single rotation is measured by an electric stop clock. The instrument is not an absolute one but must be calibrated by a meter prover. A suitable prover is described. Within rather wide limits the calibration is independent of flow rate. The instrument may be used for direct measurement or for calibrating other types of flow meters.

RATES of flow of vapors may be measured with considerable accuracy by condensing and weighing the amount of vapor passing through a system in fixed time. However, measurement of the rate of flow of permanent gases such as oxygen or air to an accuracy of 0.1 percent or better is attended with considerable difficulty. To achieve this end, for example, Wacker, Cheney, and Scott,[1] in determining the heat capacity of oxygen, condensed oxygen at low temperatures in light weight pressure bottles and weighed it under pressure at room temperatures.

In experiments designed to measure the heat capacities of gases and vapors by a differential method in a dual flow calorimeter, it was necessary to measure the rate of flow of a reference diatomic gas (such as oxygen, nitrogen or air) to a high degree of accuracy as a routine operation. It has been possible to adapt the ordinary wet test meter to this purpose.

At first, it was planned to calibrate a capillary flow meter against a wet test meter as a secondary standard. The wet test meter was then to be calibrated against a fundamental standard.

The three-liter wet test meter manufactured by the Precision Scientific Company has been used. To obviate non-uniformity of the rotor,[2] it appeared essential to measure the time required for one rotation rather than the change in dial reading occurring in a fixed time. This instrument is provided with binding posts one of which is connected to the rotor needle and the other to a contact located at the top of the dial. A system of relays was arranged to start a Model S-1 precision timer of the Standard Electric Time Company of Springfield, Massachusetts, on the first contact between the rotor needle and the contact and to stop it on the second. The timer reads to 0.01 second. This arrangement eliminates possible observational error and preliminary experiments indicated a surprisingly high degree of reproducibility.

For the purpose in hand, dry gas had to be passed through the capillary flow meter. It was then passed directly into the wet test meter. Since it has been shown that gases are better than 98 percent saturated on passage through a wet test meter,[2] knowing the aqueous tension one could compute the corresponding rate of flow of the dry entering gas. However, the consequent evaporation of the water in the wet test meter, changes the calibration of the meter. Therefore, calibrations of the wet test meter were interspersed among the comparisons of pressure head in the capillary flow meter against time of rotation of the wet test meter. Thus, allowance could be made for the evaporation of the confining liquid in the meter.

However, since the calibration of a wet test meter may depend upon the rate of flow, it was necessary to calibrate the meter over the range of flows to be employed. A bulb of a capacity of somewhat less than three liters was provided at opposite ends with two coaxial tubes of a cross-sectional area of 2.35 sq. cm. The tubes were provided with centimeter scales 35 cm in length. Calibration enabled one to know the volume between any point on the upper scale and any on the

---

* Supported by a Frederick Gardner Cottrell grant from The Research Corporation.

[1] Wacker, Cheney, and Scott, J. Research Nat. Bur. Stand. 38, 651 (1947).

[2] Bean and Morey, Proc. A. S. T. M. 39, 1171 (1939).

lower to 0.0005 liter. A little wetting agent was added to the water used in the bulb. A standard period of drainage, five minutes, was employed in all experiments.

In operation, the air contained in the calibrating bulb was displaced by water from a storage bottle connected to the lower tube of the calibrating bulb. Air from the compressed air line was employed for this purpose. The position of the rotor of the wet test meter was adjusted so that the needle would make contact when the water level was in the lower part of the scale of the lower tube. About 250 cc of air would flow before this would occur. The air flow was started and the scale reading taken visually when the clicking in the timer relay circuit was heard. The reading in the upper scale was similarly taken when the next clicking was heard.

Over rotation periods of 67 to 970 seconds, the calibration was constant to within the precision of measurement, about 0.001 liter save at times of less than 100 seconds in which case the precision is less owing to observational difficulties. Andersen and Friedman[3] with a one-quarter cubic foot meter have reported a constant calibration over the range of 0.1 to 0.8 c.f.m. to within 0.2 percent in mean deviation from the average.

Using the procedures outlined satisfactory calibration of capillary flow meters was achieved.

At this stage, the paper of Andersen and Friedman appeared in which they describe a device for controlling the water level of a wet test meter by the use of a depth micrometer with enlargement of the bore of the sight gauge tubing to 1.5 inches. A similar device was installed by removing the gas pressure gauge and inserting a Starrett one-inch micrometer head which was insulated from the meter body. The micrometer spindle was terminated with a tungsten rod of 1-mm diameter ground flat at its lower extremity.

In the technique of Andersen and Friedman, the end of the comparable part was dried and the water level raised until an electrical contact was indicated. In the present work, it was found that, if the rod was dipped into the liquid before use and then raised, the drop which was formed at the end of the rod was sufficiently constant to give results precise to 0.001 inch. Before this operation, gas was run through the meter for one revolution and the rotor brought to the zero position. It is important to fix the rotor needle permanently at half-way between uncupping points as otherwise serious errors enter.[2] By the use of the meter prover described above, it was found that the meter calibration changed by 25 parts in 100,000 per 0.001 inch change in water level. For their meter Andersen and Friedman reported 15 parts in 100,000 per 0.001 inch.

An enclosed plumb bob leveling device similar to that used by Andersen and Friedman was also fitted to our meters. However, it should be unnecessary where meters are mounted firmly in one place and subject to periodic recalibration.

Two meters have been found to give results equal to one another to within the experimental error of the meter prover. They have been further cross-checked by passing air from a constant pressure system through a water vapor saturator and then through the two meters connected in series. With meter I first, the following pairs of periods of rotation were determined: meter I, 161.68 sec., meter II, 161.76 sec.; 161.68, 161.58; 161.46, 161.39; 191.79, 191.64; 191.72, 191.66; and 191.81, 191.69. In another experiment, with the meters reversed, the following pairs of values were obtained: 200.05, 200.01; 200.03, 200.10; and 200.04, 200.12. It would thus appear that the flow rates are reproducible to ±0.05 percent.

In view of these developments, the wet test meters are being used directly for flow measurement and the capillary flow meters which precede them are used only for adjustment of approximate flow rates and to check upon constancy of flow. The porous ceramic biological filter thimbles manufactured by the Selas Company, Philadelphia, Pennsylvania, have advantages over conventional capillary tubes.[4] Effects due to turbulence and orifices are much reduced and the total flow follows Poiseuille's Law. Owing to the expansion of gas as it passes through the capillaries, π_0/V' should not be a constant as it would be for an incompressible fluid. Here, π_0 is the pressure drop through the capillary and V' is the volume per unit time read on the wet test meter. Rather

$$\pi_0/V'=2p/[k(2p+\pi_0)],$$

where p is the barometric pressure. Or if one feeds a stream of dry air to the capillary flow meter,

$$\pi_0/V'=2(p-a)/[k(2p+\pi_0)],$$

where a is the aqueous tension. These equations are valid for ideal gases only.

An accuracy of better than 0.1 percent may be obtained by the use of properly modified and operated wet test meters. An accuracy of 0.05 percent would require the temperature to be held constant to within 0.15°. Where location does not readily permit this, the meters would have to be thermostated. If one can afford several liters of gas for each flow determination, the modified wet test meter provides a convenient and accurate method of measurement of gas flow. Where smaller quantities of gas must be used, it provides an accurate method of calibrating capillary flow meters.

---

[3] Andersen and Friedman, Rev. Sci. Inst. 20, 61 (1949).

[4] Padovani and Monti, Giorn. chim. ind. applicata 15, 331 (1933), Chem. Abst. 27, 5581 (1933) report similar advantages for other porous materials.

THE REVIEW OF SCIENTIFIC INSTRUMENTS VOLUME 21, NUMBER 8 AUGUST, 1950

Solution of Simultaneous Equations through Use of the A.C. Network Calculator

L. M. HAUPT
Texas Engineering Experiment Station, Texas A. & M. College System, College Station, Texas

(Received December 27, 1949)

Kirchhoff's law equations may be written for any electrical network. Conversely, it is usually possible to find an electrical network whose Kirchhoff law equations are similar to the given set of simultaneous equations. The solution to the equations may then be found by measuring the corresponding quantities in this analogous network. The a.c. network calculator is adaptable to this method of solving equations. Presented here are the fundamentals of finding the correct electrical network for a given set of simultaneous equations.

INTRODUCTION

An alternating current network calculator[1] may be used to solve simultaneous linear equations. This method, where applicable, offers certain advantages over other methods. However, certain limitations prevent the general application of this method to all problems. These advantages and limitations are discussed below.

The alternating current network calculator is an adjustable electric system made up of generators, transformers, resistors, inductance coils, and condensers so arranged that any electric network, within the limitations of the calculator, may be set up for study. There are now (1949) 22 large calculators in operation or on order in the United States, a number of which are located on college campuses. They are used mostly by electric utility companies in the study of their operating and design problems. They have also proved useful in the studies of mechanical, hydraulic, thermal, and other systems for which electrical analogies have been determined.

Fundamentally, Kirchhoff's law equations may be written for any electrical network. These equations may then be solved simultaneously for the unknown quantities. Conversely, it is usually possible to find an electrical network whose Kirchhoff law equations are similar to the given set of simultaneous equations. The solution to the equations may then be found by measuring the corresponding quantities in this analogous network.

GENERAL NETWORK

The coefficients of the equations derived from physical systems often lead to determinants that are symmetrical about the principal diagonal. Analogous networks may be found on either a "loop basis" or a "node basis."[2] The general form for a set of symmetrical equations written so that an analogous electrical network may be found on the "loop basis" is

$$\begin{array}{l}
Z_{11}I_1+Z_{12}I_2+Z_{13}I_3+\cdots Z_{1n}I_n=E_1\\
Z_{21}I_1+Z_{22}I_2+Z_{23}I_3+\cdots Z_{2n}I_n=E_2\\
Z_{31}I_1+Z_{32}I_2+Z_{33}I_3+\cdots Z_{3n}I_n=E_3\\
\cdot\ \cdot\ \cdot\ \cdot\ \cdot\ \cdot\ \cdot\ \cdot\ \cdot\ \cdot\ \cdot\ \cdot\\
\cdot\ \cdot\ \cdot\ \cdot\ \cdot\ \cdot\ \cdot\ \cdot\ \cdot\ \cdot\ \cdot\ \cdot\\
Z_{n1}I_1+Z_{n2}I_2+Z_{n3}I_3+\cdots Z_{nn}I_n=E_n,
\end{array}$$

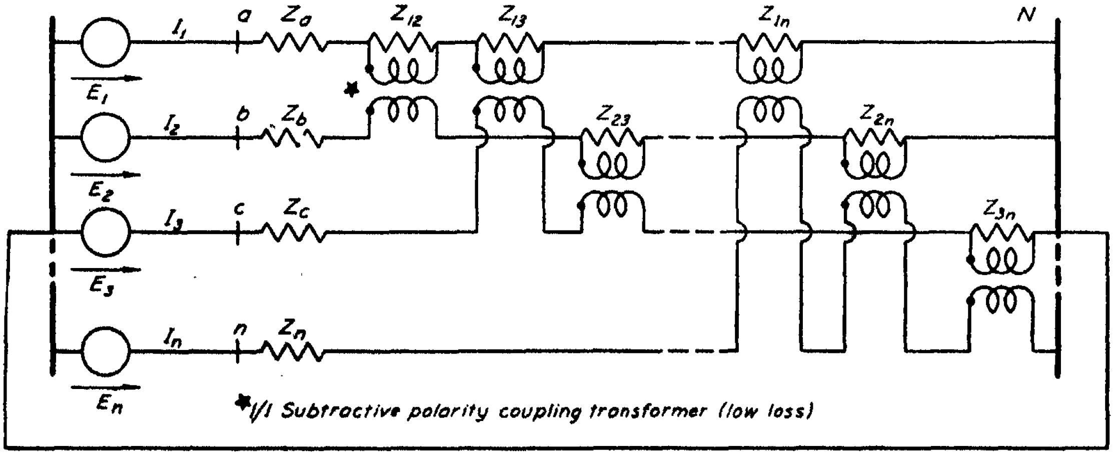

FIG. 1. General network used in the solution of simultaneous equations.

$$\begin{array}{l}
Z_a=Z_{11}-(Z_{12}+Z_{13}+\cdots Z_{1n})\\
Z_b=Z_{22}-(Z_{21}+Z_{23}+\cdots Z_{2n})\\
Z_c=Z_{33}-(Z_{31}+Z_{32}+\cdots Z_{3n})\\
\cdot\ \cdot\ \cdot\ \cdot\ \cdot\ \cdot\ \cdot\ \cdot\ \cdot\ \cdot\\
Z_n=Z_{nn}-(Z_{n1}+Z_{n2}+Z_{n3}+\cdots)
\end{array}$$

---

[1] H. A. Travers, "The network calculator brought up to date," Westinghouse Engineer, pp. 111–14 (July 1944).
[2] M. F. Gardner and J. L. Barnes, *Transients in Linear Systems* (John Wiley & Sons, Inc., New York, 1942), pp. 19–49.

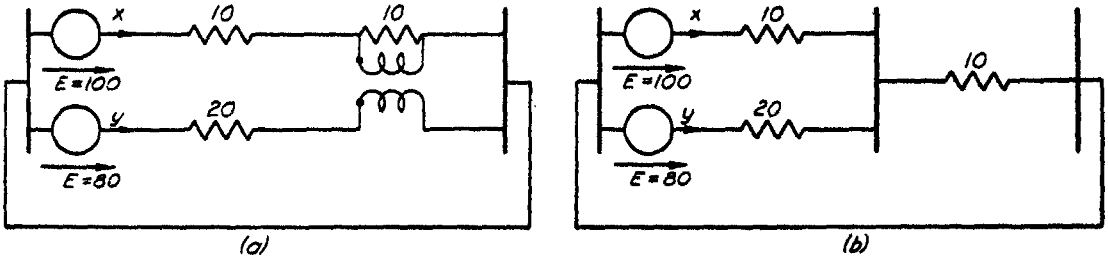

FIG. 2. Elimination of coupling transformers in a two-circuit network.

$$\begin{aligned} 20x+10y &= 100 \\ 10x+30y &= 80 \end{aligned}$$

where

$$Z_{12}=Z_{21},\ Z_{13}=Z_{31},\ \text{etc.}$$

In the above set of equations, $Z_{11}, Z_{22}, Z_{33}, \cdots, Z_{nn}$ represent the self-impedances to $I_1, I_2, I_3, \cdots, I_n$, respectively; and $Z_{12}=Z_{21}$, $Z_{13}=Z_{31}$, etc., represent the mutual impedances (coupling) between the circuits carrying I_1 and I_2, I_1 and I_3, etc., respectively. Both the currents, $I_1, I_2, I_3, \cdots, I_n$, and/or electromotive forces, $E_1, E_2, E_3, \cdots, E_n$, are adjustable in magnitude and phase relation to an arbitrary reference. This makes it possible to represent real, imaginary, or complex quantities.

The above simultaneous equations may be obtained from the network, Fig. 1.

The number of low loss coupling transformers needed to couple the circuits inductively in the general network is given by the expression

$$n=[N(N-1)/2],$$

where n is the number of coupling transformers (1/1 ratio) needed and N is the number of simultaneous equations represented by the network. However, a limited number of circuits may be conductively coupled.[3] Coefficients that are zero (or negligible) also decrease the number of coupling transformers needed in the network.

In each of the examples, Figs. 2, 3, and 4, the original set of simultaneous equations may be found from the

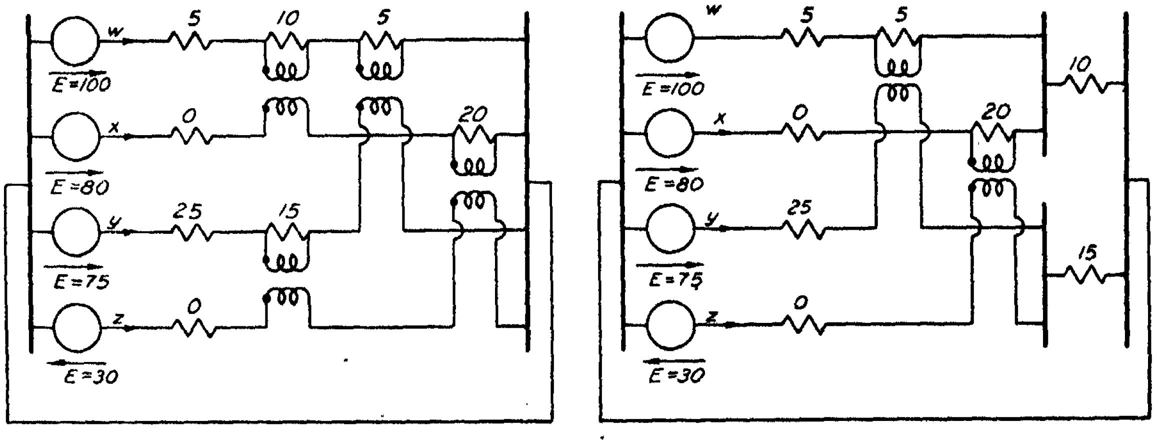

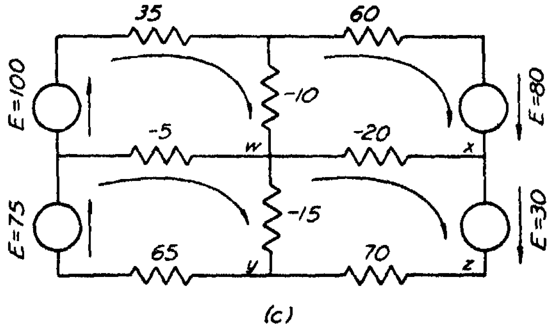

FIG. 3. Elimination of coupling transformers in a four-circuit network having a limited number of negligible coefficients.

$$\begin{aligned} 20w+10x+5y \qquad &= 100 \\ 10w+30x \qquad +20z &= 80 \\ 5w \qquad +45y+15z &= 75 \\ 20x+15y+35z &= -30 \end{aligned}$$

Note: For the general network, six coupling transformers would be needed. For this particular set of equations, the coupling transformers could be eliminated entirely, but this would necessitate the use of negative impedances (Fig. 3c) in a "mesh" network.

---

[3] Edith Clarke, *Circuit Analysis of A-C Power Systems* (John Wiley & Sons, Inc., New York, 1947), pp. 185–95.

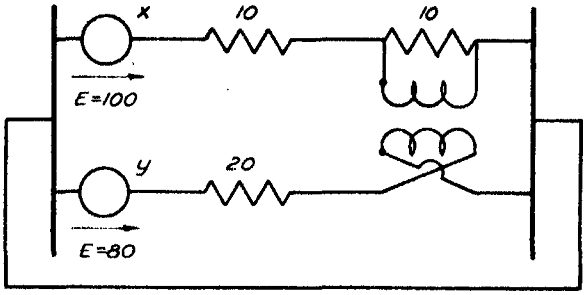

FIG. 4. Use of coupling transformers to obtain the equivalent of negative impedance. One winding of the coupling transformer is reversed.

$$20x-10y=100$$
$$-10x+30y=80$$

Kirchhoff second law equations written between the two busses from either figure.

NEGATIVE AND COMPLEX IMPEDANCES

In the solution of simultaneous equations by this method, it is often necessary to deal with negative coefficients. This involves no difficulty so long as the real component of a coefficient is positive. Resistance is used for the positive real component, inductive reactance is used for the positive imaginary component, and capacitive reactance is used for the negative imaginary component.

If the coefficients of the equations are real numbers only, inductive reactance may be used for positive values and capacitive reactances may be used for negative values. The currents that flow will, of course, lag the voltages by 90°.

It is possible to simulate negative resistance by introducing a series electromotive force in the circuit. This electromotive force is then adjusted until it is in phase with the current and equal to the product of the absolute values of resistance and current.

NONLINEAR EQUATIONS

Equations whose coefficients are not constant and equations where one or more of the unknowns are of a degree higher than one may also be solved by this method. The procedure is similar to that used for linear equations except that adjustments of the impedances in

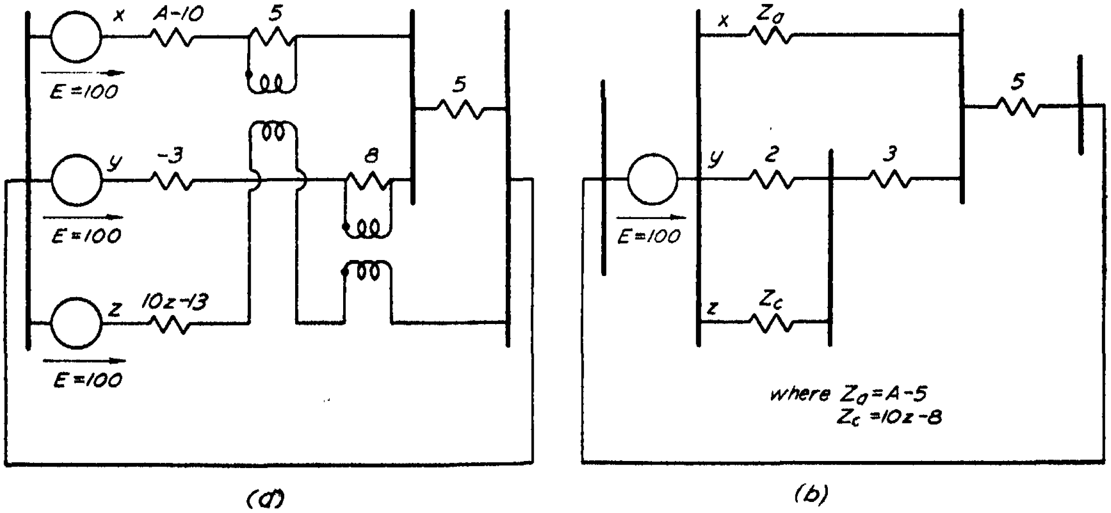

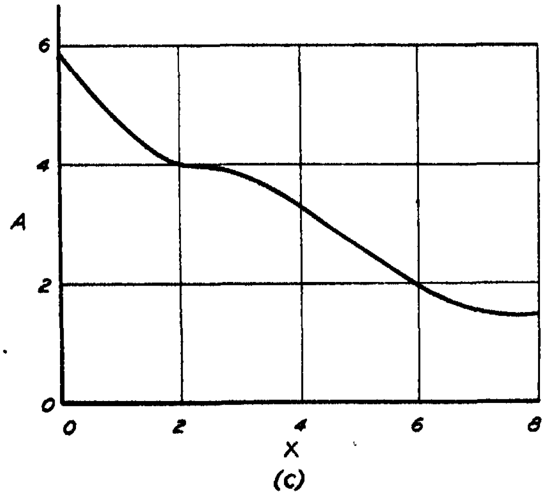

FIG. 5. Network for the solution of equations whose coefficients are not constant. The relation between A and x is given by the accompanying graph, and the network has been reduced so as to use only one generator, no coupling transformers, and no negative resistance.

$$Ax+5y+5z=100$$
$$5x+10y+8z=100$$
$5x+8y+10$[illegible]$=100$

question must be made until the conditions of the equations are satisfied. This is demonstrated in Fig. 5.

The circuit is "balanced" by adjusting Z_a and Z_c, respectively, until the given conditions are satisfied. This may be done easily by first plotting the two graphs (Z_a *vs.* x) and (Z_c *vs.* y) as a guide to the adjustments that must be made.

NONSYMMETRICAL EQUATIONS

The use of this method is not limited to simultaneous equations that are symmetrical about their principal diagonal. This is demonstrated by Fig. 6. However, the analogous network is not so easily found and sometimes may be quite complicated. Where possible, the equations should be converted into a symmetrical system.

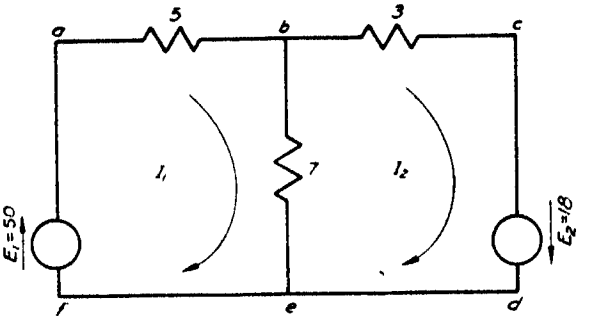

FIG. 6. Network for the solution of equations that are not symmetrical about their principal diagonal.

$$12I_1-7I_2=50$$
$$5I_1+3I_2=68$$

Note: Kirchhoff voltage equations are written around the loop *abef* and *abcdef* respectively.

APPLICATION

This method is particularly applicable where it is permissible to have a possible error of several percent in the solution and where it is necessary to find solutions of similar sets of equations which differ only in the values of one or more coefficients. This method has value in that the resulting electrical network may be considered an electrical analogy to the original physical system from which the equations were derived. This sometimes permits analysis that would otherwise be improbable. It is also possible to show clearly and easily the sensitivity of the solution to the accuracy of any coefficient by noting the effect of variation of the analogous circuit parameter.

Personal errors, i.e., error due to wrong connections, missetting of impedances, misreading instruments, etc., are reduced to a minimum through a careful systematic check. For example, the first equations of the general form could be checked from the general network, Fig. 1, by adjusting I_1 to one ampere after the other circuits have been opened at $b, c, d, \cdots, n$. The voltages from a to N, b to N, c to N, $\cdots$, n to N, should be the coefficients $Z_{11}, Z_{12}, \cdots, Z_{1n}$, respectively. The second equation could be checked by adjusting I_2 to one ampere after the other circuits have been opened at $a, c, d, \cdots, n$. The voltages from a to N, b to N, $\cdots$, n to N are now the coefficients $Z_{21}, Z_{22}, Z_{23}, \cdots, Z_{2n}$, respectively. This is repeated until all of the coefficients have been checked. The solution may be checked, of course, by substitution into the proper Kirchhoff law equation.

SUMMARY

The a.c. network calculator has been used on various occasions to solve equations involving complex numbers for zero sequence impedances,[4] for a study of intrasystem transmission loss,[5] and other problems, some purely theoretical. As a rule, the solution may be obtained in less time, with less personal error, and with greater accuracy than by other methods in which slide rule calculations are involved. For example, it required approximately four hours to set up and find a solution to simultaneous equations involving ten unknowns. After the initial solution was found, solutions to 28 similar problems (which differed only in the values of one or two of the coefficients) were found in less than one hour additional time. Only a few minutes was required to balance and find the solution of nonlinear simultaneous equations involving four unknowns.

The a.c. network calculator is a tool of many uses. It is felt that this is another application that will prove valuable to those who find it necessary to solve many simultaneous equations and who must obtain the solutions in a minimum of time.

---

[4] Westinghouse Electric & Manufacturing Company, Central Station Engineers, *Electrical Transmission and Distribution Handbook* (Westinghouse Electric & Manufacturing Company, 1944), p. 25.

[5] E. E. George, "Intrasystem Transmission Losses," A.I.E.E. Transactions 62, 153–58 (1943).

THE REVIEW OF SCIENTIFIC INSTRUMENTS VOLUME 21, NUMBER 8 AUGUST, 1950

Arithmetic Operations in a Binary Computer

ROBERT F. SHAW
Eckert-Mauchly Computer Corporation, 3747 Ridge Avenue, Philadelphia, Pennsylvania

(Received February 13, 1950)

The application of binary arithmetic in the computing circuits of a high speed digital computer is discussed in detail. The discussion covers, with numerous examples, the use of complements to represent negative numbers, the corrections necessary in the multiplication process as a result of the use of complements, and additional modifications of the process to simplify mechanization. A special division method well-adapted to automatic computer use is described, and round-off procedures are noted briefly. The article is concluded with a discussion of the storage of negative numbers as absolute values with a sign rather than in complement form.

INTRODUCTION

THE extensive development of large-scale digital computers in the past few years has naturally been accompanied by a corresponding development of the mathematical techniques required for the most efficient use of these tools of research. Probably the outstanding feature of electronic circuits, insofar as their application to digital computers is concerned, is their binary nature. It is possible, by relatively simple means, to use these essentially binary circuits for operation in the decimal system, provided the decimal digits are represented in binary coded form. There is little doubt that all significant future development of general purpose computers, particularly for use in the commercial and industrial field, will be concerned with decimal operation. Nevertheless, it is also true that many of the large-scale computers now under development both in this country and abroad are purely binary, at least in their arithmetic operations. The greater simplicity of this type of device and its slightly more efficient use of memory capacity will probably assure it a position of continuing importance in the field of small special-purpose computers such as those contemplated for industrial control applications.

While the present discussion is concerned chiefly with the arithmetic operations of the Binac, a general purpose binary computer recently completed by the Eckert-Mauchly Computer Corporation, they apply to a large degree to most of the other binary computers now under construction. The mathematical developments presented are not intended to be rigorous, but are intended more to convey as simply and clearly as possible the principles underlying the operation of the Binac's arithmetic circuits. For a more thorough and rigorous analysis of these principles, the reader is referred to the report of Burks, Goldstine, and von Neumann, on the computer being built at the Institute for Advanced Study.[1] The arithmetic operations in this computer are similar to those in the Binac, although the latter is serial in nature, while the Institute's computer is of the parallel type.

I. RANGE OF NUMBERS

The arithmetic circuits and memory of a computer are designed to handle data in units, each consisting of a fixed number of binary digits; since these units may represent either numbers or instructions,[2] they are commonly referred to as "words." The choice of word length must be a compromise among a number of factors, such as available memory capacity, operating speed, required accuracy of numerical data, and other considerations. A word length of 30 binary digits, equivalent numerically to slightly less than 10 decimal digits, was chosen for the Binac; other binary computers now in the process of construction use word lengths varying from 16 to 44 binary digits.

Placement of the binary point must next be determined. Multiplication will be simplified if the point is placed to the left of the first significant digit, since it will then be possible to form the product of two factors, each having the maximum of 30 significant digits, without exceeding the capacity of the computer, and without resorting to "floating point" methods which require the keeping of a separate record of the binary point position. Placing of the point in this position also leads to a convenient method of handling negative numbers, as will be seen later. The absolute values of numbers which the computer can represent will lie in the range $0\leqq x<1$, and, since 30 binary digits can be stored, the smallest increment which the computer can represent is 2^{-30}.

Both positive and negative numbers can be represented if one additional digit, to the left of the binary point, is used. This digit will be a 0 for positive numbers and a 1 for negative numbers; and the absolute value of the latter will actually be replaced by its complement with respect to 1; for example: $+\frac{3}{16}$ will be written 0.0011, but $-\frac{3}{16}$ will be written 1.1101. (It will be noted that if the sign is treated as if it were simply another digit, negative numbers are represented by

---

[1] Burks, Goldstine, and von Neumann, *Preliminary Discussion of the Logical Design of an Electronic Computing Instrument* (Institute for Advanced Study, Princeton, New Jersey, 1947), second edition, Part 1, Vol. 1.

[2] Instructions and numerical quantities are handled interchangeably in both the memory and arithmetic circuits, instructions being modified in the latter circuits by addition or subtraction of constants where necessary. However, an instruction differs from a quantity in that it can be interpreted by the control circuits of the computer and through those circuits can cause predetermined operations to be performed.

TABLE I.

Addends	Sum	Carryover
0 and 0	0	0
0 and 1	1	0
1 and 1	0	1

their complements with respect to 2. This statement will be further amplified in the discussion of addition and subtraction.) The total range of numbers which the computer can represent is then $-1 \leqq x < 1$.

II. ADDITION

It will next be shown that the correct algebraic sum of two quantities can be formed by an adder which will form the correct sum of two positive numbers. The basic rules of binary addition are illustrated in Table I. Since the adder must be capable of forming the correct sum even if two ones from the two addends coincide with a carryover from the preceding digit, Table II, which is developed from the basic principles in Table I, summarizes the results which the adder must produce. An adder satisfying these requirements, then, will form the correct sum of two positive numbers. Since it is not the purpose of this paper to discuss circuit details, it is sufficient to state here that these requirements can be met electronically by relatively simple means.

The significance of the statement, previously made, that negative numbers are represented by their complements with respect to 2, must now be examined. This implies that if $-1 \leqq x < 0$, x is actually written $2+x$, which obviously lies in the range between 1 and 2. Thus, in the example previously given, $-\frac{3}{16}$ (in binary form -0.0011) is written 1.1101. If the digits to the left of the sign position are ignored, any positive number $0 \leqq x < 1$ is indistinguishable from $2+x$; for example, $\frac{3}{16}$ in binary form is 0.0011; $\frac{3}{16}+2$ is 10.0011, which becomes 0.0011 again if the 1 to the left of the sign digit is ignored.

Thus, if an adder is constructed which discards carries beyond the sign digit, it should work equally well for positive or negative numbers. The following examples will illustrate this.

$$\begin{array}{rr} 0.0011 & \frac{3}{16} \\ 0.0111 & \frac{7}{16} \\ \hline 0.1010 & \frac{5}{8} \end{array}$$

$$\begin{array}{rr} 0.0011 & \frac{3}{16} \\ 1.1001 & -\frac{7}{16} \\ \hline 1.1100 & -\frac{1}{4} \end{array}$$

$$\begin{array}{rr} 1.1101 & -\frac{3}{16} \\ 1.1001 & -\frac{7}{16} \\ \hline (1)\ 1.0110 & -\frac{5}{8} \end{array}$$

TABLE II.

Addends	Sum	Carryover
0, 0, and 0	0	0
0, 0, and 1	1	0
0, 1, and 1	0	1
1, 1, and 1	1	1

(The carryover, shown in parentheses, is discarded.)

$$\begin{array}{rr} 1.1101 & -\frac{3}{16} \\ 0.0111 & \frac{7}{16} \\ \hline (1)\ 0.0100 & \frac{1}{4} \end{array}$$

(Again, the carryover is discarded.)

To summarize these results, then, it is possible to use a simple binary adder to add positive or negative numbers, provided (a) each quantity is confined to the range $-1 \leqq x < 1$ and a 2 is added to the quantity before it is sent into the machine, and (b) any digits to the left of the 2^0 position, called the sign position, are discarded, whether they result from the original addition of 2 to the number or from an addition in the course of subsequent computation.

III. SUBTRACTION

Since the addition process just described works equally well for positive and negative quantities, subtraction can be accomplished by changing the sign of the subtrahend and adding. Since the sign reversal is accomplished by determining the complement of the quantity with respect to 2, a procedure for complementing is required.

First, consider the result obtained by selecting a quantity, changing all its zeros to ones and its ones to zeros, then adding the result to the original number.

$$\begin{array}{r} 0.1101001 \\ 1.0010110 \\ \hline 1.1111111. \end{array}$$

It is evident that the result will always be a series of ones. For n digits to the right of the binary point, the result will be $2-2^{-n}$. The quantity obtained by interchanging zeros and ones is therefore the complement of the original quantity with respect to $2-2^{-n}$; that is, the new quantity $m' = 2-2^{-n}-m$. Since the result required is $2-m$, it is only necessary to add 2^{-n} to the result obtained by interchanging ones and zeros:

$$m = 0.110100$$
$$-m = 1.001011 + 0.000001 = 1.001100.$$

Complementing is thus accomplished by interchanging ones and zeros in the quantity to be complemented, and adding a one to the result in the least significant digit position.

A somewhat different subtraction method is discussed in the section dealing with storage of absolute values.

IV. MULTIPLICATION

Multiplication in the binary system is simplified by the fact that any multiplier digit can be only a one or a zero. This fact results in a process easy to mechanize, since additions and shifts alternate, whereas in the decimal and other number systems, the number of additions between shifts varies in accordance with the multiplier digits. (Of course, the case of no addition can be treated as equivalent to the addition of zero.) Multiplication of two positive binary quantities, then, consists of examining the multiplier digits in succession, starting with the least significant, adding the multiplicand into the partial product if the corresponding multiplier digit is a one, but adding zero if the multiplier digit is zero. After every such addition, the partial product is shifted one place to the right. The following example illustrates the procedure:

$$\begin{array}{rll}
0.1\,1\,0\,1 & x & \frac{13}{16} \\
0.1\,0\,1\,1 & y & \frac{11}{16} \\
\hline
0.1\,1\,0\,1 & x\cdot 1 & \\
0.1\,1\,0\,1 & x\cdot 1 & \\
0.0\,0\,0\,0 & x\cdot 0 & \\
0.1\,1\,0\,1 & x\cdot 1 & \\
0.0\,0\,0\,0 & x\cdot 0 & \\
\hline
0.1\,0\,0\,0\,1\,1\,1\,1 & xy & 143/256.
\end{array}$$

Note that a shift takes place after every addition except the last. Although the above example is written as if the multiplicand were shifted to the left, obviously this is equivalent to shifting the partial product to the right; the latter process is better adapted to computer operation.

Now suppose that the multiplicand, x, is positive and the multiplier, y, is negative. As usual, y is written $2-|y|=2+y$. Multiplying gives $x(2+y)=2x+xy$, which can be corrected to equal the product xy by subtracting $2x$. Although $2x$ is obtainable by a simple shift, nevertheless it would be more convenient if this shift could be avoided, and this turns out to be easily possible. Let x be multiplied by all digits of y except the sign digit. Since y is negative, this sign digit is 1; the result, therefore, is to multiply x by one less than before. This means the formation of the product $x(1+y)=x+xy$ instead of $x(2+y)=2x+xy$. Now, a correction of $-x$ is sufficient, and furthermore, the process is more systematic, since every addition is followed by a shift.

Thus, to take care of the cases of x positive and y either positive or negative, it is only necessary to follow the procedure outlined for both x and y positive, and, if y is negative, correct the result by subtracting x from it. The following example illustrates the procedure:

$$\begin{array}{rll}
0.1\,1\,0\,1 & x & \frac{13}{16} \\
1.0\,1\,0\,1 & y & -\frac{11}{16} \\
\hline
0.1\,1\,0\,1 & & \\
0.0\,0\,0\,0 & & \\
0.1\,1\,0\,1 & & \\
0.0\,0\,0\,0 & & \\
\hline
0.0\,1\,0\,0\,0\,0\,0\,1 & xy+x & \\
1.0\,0\,1\,1 & -x & \\
\hline
1.0\,1\,1\,1\,0\,0\,0\,1 & xy & -143/256.
\end{array}$$

From symmetry it is apparent that if x is negative and y positive, a correction of $-y$ will give the true product. As a preliminary assumption, let the sign digit of x be ignored until the correction at the end is made. This leaves only the question of how to add in the $-y$. It turns out to be convenient, as far as computer design is concerned, to examine successive digits of y by shifting y to the right a digit at a time, dropping off each digit after it has been examined. This means that by the end of the process y has been lost and is not available for use in correcting the product. Therefore, the possibility of making the correction digit by digit as the product is built up must be examined.

Suppose the numbers being used have 30 digits and a sign. Referring back to the basic multiplication process, it is noted that 30 shifts are made in building up the product; therefore, the sign digit of x during the first addition finally becomes the 30th or least significant digit of the product. Similarly, the sign digit of x on the second addition becomes the 29th digit of the product, and so on. It therefore becomes apparent that the sign digit of x during any addition occupies in the final product a position equivalent to that of the digit of y which controlled its addition into the product.

Next, note that the correction needed is the complement of y. Thus, for every 1 in y a 0 is needed in the correction term, but for every 0 in y a 1 should appear in the correction term. As usual, the complement must be corrected by adding a unit in the last place. Note further that the correction is needed only if x is negative —that is, if its sign digit is 1.

Putting together the above facts, the required procedure may be defined. If a digit of y is 1, x (without its sign digit) is added into the partial product. If a digit of y is 0, its complement, 1, must be added into the partial product, but a 1 is available, in the correct position, in the form of the sign digit of x. Thus, if a digit of y is 0, the sign digit only of x is added. Of course, this sign digit might be 0, but that would imply that x was positive and no correction was required; thus no harm is done by adding the zero. Since the additions are terminated before examining the sign digit of y, the correction term, if any, still lacks a 1 in the sign position and a 1 in the units position. Hence, if x is negative, these digits must be added to the product, as shown in the following:

$$\begin{array}{rll}
1.0011 & x & -\tfrac{13}{16}\\
0.1011 & y & \tfrac{11}{16}\\
\hline
0.0011 & (x \text{ without sign}) & \\
0.0011 & & \\
1.0000 & (\text{sign only of } x) & \\
0.0011 & & \\
\hline
0.01100001 & & \\
1.0001 & (\text{correction term}) & \\
\hline
1.01110001 & xy & -143/256.
\end{array}$$

Taking the third term of the partial product (that is, 1.0000 shifted twice to become 0.0100) and the correction term, and adding, the result 0.0100+1.0001 = 1.0101 is obtained. Thus, it is shown that the complement of y has in fact been added to the product.

Finally, the case of x and y both negative will be considered. Starting with the numerical example, and following the procedure outlined for the preceding cases:

$$\begin{array}{rll}
1.0011 & x & -\tfrac{13}{16}\\
1.0101 & y & -\tfrac{11}{16}\\
\hline
0.0011 & (x \text{ without sign}) & \\
1.0000 & (\text{sign only of } x) & \\
0.0011 & & \\
1.0000 & & \\
\hline
0.10101111 & & \\
1.0001 & (\text{correction for sign of } x) & \\
\hline
1.10111111 & xy+x & \\
0.1101 & -x\ (\text{correction for sign of } y) & \\
\hline
0.10001111 & xy & 143/256.
\end{array}$$

The correction terms added on account of the sign of x are (1) 1.0000, shifted three times to become 0.0010; (2) 1.0000, shifted once to become 0.1000; (3) 1.0001, added after all shifts are completed.

Again adding these various corrections, the result is 1.1011, which appears to be wrong, because the complement of y is 0.1011. Recalling that, up to the correction steps, signs were disregarded, and that therefore the factors behaved like $x+1$ and $y+1$, the uncorrected product obtained must be $(x+1)(y+1)=xy+x+y+1$. Hence, it is necessary to subtract 1 as well as x and y to get the true product. Since all carryovers beyond the sign are disregarded, subtracting 1 is the same as adding 1. Thus, the extra 1 which appeared in the complement of y is necessary.

The foregoing discussion covers all possible cases and shows that a single generalized multiplication process can be used to produce results which are correct regardless of the signs of the factors.

V. DIVISION

The division process used in the binary computer is the non-restoring method, analogous to that used in desk computing machines. This method has two important advantages—it eliminates time-consuming comparison operations which are necessary in the restoring method, and it requires no extra correction operations if either dividend or divisor is negative.

In the non-restoring method of division, the signs of the dividend and divisor are first examined. If they are alike, the divisor is subtracted from the dividend repeatedly until the signs become different, a unit being added into the corresponding quotient digit for each subtraction. If the signs are different, the divisor is added to the dividend repeatedly until the signs become the same, a unit being subtracted from the corresponding quotient digit each time. Thus, in the decimal system, if the signs were alike and the divisor had to be subtracted three times to cause a sign reversal, the corresponding quotient digit would be 3; if the signs were different and the divisor had to be added seven times to cause a sign reversal, the corresponding quotient digit would be −7. As soon as a sign reversal occurs, the remainder is shifted one place to the left and computation of the next quotient digit begins.

If the above process is carried out exactly as described, any quotient digit may be $\pm n$, where n is an integer in the range 1 to 10 inclusive. It is obvious, however, that if a sign reversal has not occurred after nine additions or subtractions (in the decimal system), it must surely occur on the tenth operation.[3] Thus, it is sufficient to terminate the computation of each digit of the quotient after nine operations and shift the remainder without waiting for a sign reversal. The quotient digits then may be $\pm 1, \pm 2, \cdots, \pm 9$. Suppose the quotient obtained is the sequence 1, −3, 9, 5, −4, 6. To obtain the quotient in usable form, the aggregate of the negative digits must be subtracted from the aggregate of the positive digits: 109,506−30,040=79,466. If the quotient was built up in an accumulator (i.e., a register containing an adder so arranged that after entry of a new quantity the register contains the sum of the latter and the previous contents), this process was carried out stepwise as the quotient was built up.

An accumulator must be used to hold the dividend (which becomes the remainder, of course, after the process has started), in order to provide means for adding in the divisor or its complement. It is more convenient to store the quotient digits in a simple register, which cannot add or subtract, thus avoiding the necessity of providing an additional accumulator. Returning for a moment to the decimal example, it is noted that there are 18 possible quotient digit values

---

[3] An exception to this rule occurs in the case of an improper division, i.e., one in which the dividend is larger than the divisor. In this case, no sign reversal would occur on the tenth operation in the computation of the first quotient digit; it may, in fact, be desirable to perform the tenth operation and institute an automatic corrective procedure if no sign reversal occurs.

($\pm 1, \pm 2, \cdots, \pm 9$). By the same reasoning, it follows that in the binary system there are only two values (± 1) and that only one operation (addition or subtraction, as the case may be) is necessary for each quotient digit. Thus, as in multiplication, additions (or subtractions) can alternate with shifts, and the result is a process easy to mechanize. There is still the difficulty, however, that the quotient register has no way of distinguishing -1 from $+1$. An investigation of the possibility of entering a 0 in the quotient wherever a -1 is called for immediately suggests itself, in order to see if the pseudo-quotient so obtained bears some simple relationship to the true quotient, x/y, of two binary quantities. If such a simple relationship exists, it will be reasonable to compute the pseudo-quotient and make any necessary corrections to the latter to obtain the true quotient.

Recalling that -1 should be entered in the quotient if y is added to the remainder, and $+1$ if y is subtracted, 0 is used for each addition and $+1$ for each subtraction. An expression can now be written for the new remainder, r_k, in terms of the old remainder r_{k-1}, the quotient digit p_k, and y:

$$r_k = 2r_{k-1} + (1 - 2p_k)y$$

which reduces to $2r_{k-1}+y$ if p_k is 0 and $2r_{k-1}-y$ if p_k is 1. The factor of 2 results from the fact that the old remainder was shifted to the left before the addition or subtraction of y. Multiplying through by 2^{-k}

$$2^{-k}r_k = 2^{-(k-1)}r_{k-1} + (2^{-k} - 2^{-(k-1)}p_k)y$$

gives a more convenient recursion formula. Noting that the "zeroth" remainder is actually x itself,

$$\begin{aligned} 2^{-1}r_1 &= x + (2^{-1} - 2^0 p_1)y \\ 2^{-2}r_2 &= 2^{-1}r_1 + (2^{-2} - 2^{-1}p_2)y \\ &= x + [(2^{-1}+2^{-2}) - (2^0 p_1 + 2^{-1}p_2)]y \quad \text{etc.,} \end{aligned}$$

or, in general,

$$2^{-n}r_n = x + \left(\sum_1^n 2^{-k} - \sum_1^n 2^{-(k-1)}p_k\right)y.$$

Now

$$\sum_1^n 2^{-k} = 0.1 + 0.01 + \cdots = 0.111\cdots$$

which is evidently equal to $1-2^{-n}$. Thus, making this substitution and transposing,

$$x = \left[-1 + 2^{-n} + \sum_1^n 2^{-(k-1)}p_k\right]y + 2^{-n}r_n$$

and, dividing by y,

$$x/y = \left[-1 + 2^{-n} + \sum_1^n 2^{-(k-1)}p_k\right] + 2^{-n}r_n/y.$$

The expression in square brackets, then, is the desired quotient. Now if $n=30$, the first 30 quotient digits computed by the method outlined above correspond to the sign and the first 29 digits of the pseudo-quotient. (The first digit, p_1, corresponds to the sign rather than the most significant digit because it is in the 2^0 position; ($2^{-(k-1)} = 2^0$ for $k=1$.) To convert the pseudo-quotient into the true quotient, it is necessary to add 2^{-30} and subtract one. The first of these corrections corresponds to putting a unit in the least significant digit position, a step which also coincides with the round-off procedure to be adopted. As for subtracting 1 from the result, since carries beyond the sign position are disregarded, subtracting 1 is the same as adding 1; the two corrections can therefore be taken care of by bringing the pseudo-quotient from the register where it was built up into the accumulator, simultaneously clearing out the last remainder and adding units into the sign and the least significant digits. (It may be noted that the latter position is still unfilled, since p_{31} was not computed; the correction in this position could therefore have been made in the register, but an adder is required for the sign correction.)

The reader may have been troubled by the fact that in doubling the remainder the sign digit will be lost. Actually, this does no harm. The addition or subtraction of the divisor is always such as to decrease the absolute value of the remainder; since $x<y$ to begin with, $2x-y<y$ and in general $2r-y<y$. Since $y<1$, $2r-y<1$, and therefore the result of the operation is always within the range of the machine; although the sign digit of r was shifted out of range, it could not have affected the result in any case. It should be noted that the sign of r is used to determine whether y is to be added or subtracted, however; therefore, since this sign is lost by the shift, it must be examined and compared with the sign of y before the shift takes place.

The example below illustrates the division process just described:

1.0111	$x(r_0)$	$-\frac{9}{16}$
0.1011	y	$\frac{11}{16}$
0.1110	$2r_0$	
0.1011	$+y$	
1.1001	r_1	$(p_1=0)$
1.0010	$2r_1$	
0.1011	$+y$	
1.1101	r_2	$(p_2=0)$
1.1010	$2r_2$	
0.1011	$+y$	
0.0101	r_3	$(p_3=0)$
0.1010	$2r_3$	
1.0101	$-y$	
1.1111	r_4	$(p_4=1)$
0.0010	$x/y+1-2^{-4}$	
1.0001	$1+2^{-4}$	
1.0011	$x/y+2=x/y$	$-\frac{13}{16}$

TABLE III.

Minuend	Subtrahend	Difference	Borrow
0	0	0	0
1	0	1	0
1	1	0	0
0	1	1	1

which is the exact quotient, $-9/11$, rounded off to four binary places. r_4 is discarded; the pseudo-quotient ($p_1+p_2+p_3+p_4=0.001$) and the correction term 1.0001 are added together and the result left in the accumulator.

VI. ROUND-OFF PROCEDURES

Both multiplication and division give results having more significant figures than the original numbers entering into these processes; in general, multiplication of two n-digit factors yields a product of $2n$ digits, and division yields a quotient having an infinite number of digits. Since only n digits are required for most computational processes, some round-off procedure must be followed in order to avoid the bias which would result if the remaining digits were simply dropped. The round-off procedure should fulfill two requirements: the approximation should lie as close to the true product or quotient as practical, and it should be unbiased, i.e., its mean should equal the true result.

Of the various possible round-off schemes, two are of interest here. The first and most familiar consists of adding a unit to the $n+1$st digit, allowing any resulting carries to take place, and then keeping only the first n digits. The other consists of replacing the nth digit with a 1, regardless of whether that digit was originally a 1 or a 0. It can be shown that both schemes produce results which are sufficiently unbiased in view of the fact that products and quotients themselves are not entirely unbiased.[4] The latter situation is due to the fact that the original quantities themselves are, in general, rounded-off approximations of other quantities. On the other hand, the variance of the second method is twice as great as that of the first, being 0.58 times the last digit as compared to 0.29 times the last digit for the more familiar scheme.

In spite of the larger variance, however, the second round-off scheme is used. It has the advantage of being usable even after the $n+1$st digit has been lost as the result of a right shift; thus, it is unnecessary to interrupt the multiplication process before the last step to add in the unit for round-off. Furthermore, no carries are produced; thus, the unit pulse can be put in after the adder, and the process carried out concurrently with the last complement correction. In the case of division, as has already been seen, the result obtained already conforms to this round-off procedure without further modifications; it therefore becomes unnecessary to compute the 31st quotient digit.

TABLE IV.

M	S	B	D	B
0	0	0	0	0
1	0	0	1	0
1	1	0	0	0
1	0	1	0	0
1	1	1	1	1
0	1	0	1	1
0	0	1	1	1
0	1	1	0	1

When it is necessary during computation to round off to less than 30 digits, the more precise method can be used; in most cases the procedure will be to shift right until all but one of the unwanted digits are lost, add a unit in the lowest position, and then shift right one more place.

VII. STORAGE OF ABSOLUTE VALUES

While negative quantities are stored in complement form in the Binac and most other binary computers now under construction, it is of interest to examine briefly the possibility of storing the absolute values of negative quantities, distinguishing them from positive quantities only by the difference in the sign digit; in this case it is immaterial whether 0 and 1 are used for + and −, respectively, or vice versa. There are two principal advantages to such a procedure; first, the preparation of input data and the interpretation of output data are simplified; and second, the visual interpretation of data in registers and memory is made easier, thus expediting trouble-shooting.

The effect on multiplication and division is that of simplification, since in these operations the signs can be disregarded and the operations performed on absolute values with no corrections necessary. A preliminary comparison of the signs of the operands discloses immediately the sign of the result; this is stored until the operation is complete and then appended to the product or quotient.

In the case of addition, however, the operations become more complex. Before addition can take place, the signs of the addends must be compared; if they are alike, an addition is performed; otherwise subtraction is necessary, with some provision for assuring the subtraction of the operand having the smaller absolute value from that having the larger, or for making a suitable correction which will produce the same effect. The subtraction can be accomplished in a regular adder by complementing negative quantities before sending them to the adder, but it is possible to avoid complements completely, even in the arithmetic circuits, by using a subtractor rather than an adder when such operation is indicated. The subtractor proves to be as simple electronically as an adder, since it must fulfill a set of conditions differing only slightly from those satisfied by the adder.

---

[4] See reference 1, p. 20.

For two binary digits, the rules for subtraction can be summarized as in Table III. To complete the subtraction, provision must be made for taking the "borrow" pulse and subtracting it from the next minuend digit. This is equivalent, however, to adding it to the next subtrahend digit; and the latter procedure proves to be more advantageous electronically. The full set of conditions can now be written down as in Table IV.

The preceding discussion of the storage of absolute values has been included here partly to illustrate the difficulties to be encountered in such a system, and partly because of the importance of the system in computers of the decimal type, even though the latter are not otherwise considered in this paper. Because of the complications involved, storage of absolute values is not ordinarily employed in binary computers, probably because it is felt that the inconvenience of representing quantities in binary form is not materially increased by the necessity of representing negative quantities in complement form. In decimal computers such as the Univac, however, where convenience in handling of input and output data is of great importance, the storage of complements is avoided.

THE REVIEW OF SCIENTIFIC INSTRUMENTS VOLUME 21, NUMBER 8 AUGUST, 1950

A Recording Polarimeter

GABOR B. LEVY, PHILIP SCHWED,* AND DAVID FERGUS
Research Department, Schenley Laboratories, Inc., Lawrenceburg, Indiana

(Received March 23, 1950)

A recording polarimeter has been constructed. The principle of operation is essentially the replacement of an operator in conventional visual polarimetry by a photoelectric servo system. A photo-multiplier tube is used which, in conjunction with a mechanical chopping system, delivers an alternating current signal proportional to the unbalance. The latter is filtered and amplified and actuates a servo mechanism. The precision of the system is ±0.005° for static balance and the speed about 0.5° per minute. Hence the arrangement compares favorably with ordinary visual operation. The construction of the instrument is discussed briefly and its performance is illustrated by examples.

INTRODUCTION

IN the study of chemical or biochemical reactions, it is of great advantage to select a method of analysis that is non-destructive and which does not involve sampling. Potentially, polarimetric measurements are suitable, particularly in the biochemical field, since the optical activity is frequently subject to change in the course of the reaction. However, the measurement of changing optical rotation by visual methods is tedious and of limited precision. For such applications, a recording polarimeter would be of great value.

Instruments of this type are not available, and furthermore, the existing literature gives no encouragement for success of such a scheme. For example, W. Heller[1] states: "Persons with particularly sensitive, specially trained, and well-adapted eyes can be expected, however, to surpass any photoelectric registration. . . ."

Considering the fact that measurement of fast changing rotation is far from an ideal condition for visual observation, we felt encouraged to construct a photoelectric instrument despite the statement cited. In addition, the potential value of such an instrument appeared to warrant the effort.

We have chosen the most direct approach, i.e., converting a visual instrument to photoelectric operation. The performance of the resultant instrument and its potential value in the study of optical activity seems to justify its description in some detail.

PRINCIPLES OF OPERATION

Essentially monochromatic light is passed through a conventional polarimeter. The "half-shade" image from its Lippich analyzer (with two fields) is projected onto a photo-multiplier photo-cell. Interposed is a semicircular sector which is driven by a synchronous motor. Thus the output of the photo-cell, at unbalance, is a sinusoidal alternating current whose phase is shifted by 180° when the direction of the unbalance reverses. This signal is amplified by a battery operated untuned preamplifier and further amplified by an amplifier tuned to the fixed frequency of the sector and signal. The signal, which is thus freed from noise, is fed after further amplification to one of the two coils of a differential relay, the coil energized depending on the position of the sector. This arrangement provides phase discrimination and rectification as well as further filtering. The relay actuates a reversible 60-cycle motor which is mechanically linked to the analyzer of the

---

* Now with the National Advisory Committee for Aeronautics, Cleveland, Ohio.

[1] W. Heller, in A. Weissberger, *Physical Methods of Organic Chemistry*, Vol. II (Interscience Publishers, Inc., New York, N. Y., 1946), p. 967.

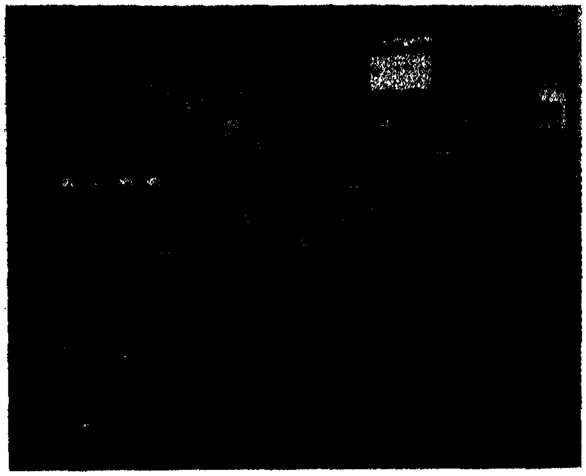

FIG. 1. The recording polarimeter.

polarimeter. An electrical link is also provided to a fast strip chart recorder.

The operation can be summarized as follows: Whenever the polarimeter analyzer deviates from zero position the two halves of the half-shade field differ in intensity. Therefore, as the semicircular chopping disk is rotated, a periodic variation of light intensity occurs which appears as alternating current in the photo-cell circuit. This alternating current, after suitable amplification, is rectified and fed into one of the coils of a differential relay, depending upon which of the two fields is the brighter. The relay switches the line voltage accordingly into a motor which drives the analyzer in the proper direction to optical balance. A recorder indicates the angular travel of the analyzer.

DETAILS OF CONSTRUCTION AND OPERATION

In constructing the instrument it was found that the design of the electrical components is not critical. The circuits used are conventional and therefore are only indicated and discussed briefly. The most important factors for successful operation proved to be the proper design and arrangement of mechanical parts and a number of small details aiding operations which are discussed in the following.

The general appearance of the assembly is shown in Fig. 1 and a schematic plan in Fig. 2. The light source (1) is a General Electric mercury vapor lamp (S-4) which is operated at about 150 watts from 250 v d.c. line voltage by use of a rheostat. The lamp housing is connected to an exhaust fan (2) and the lamp thus cooled has a life of several months. The light passes through two Corning filters (Nos. 3484 and 5120) which isolate the mercury line of 5460A. In a housing (3) together with the filters may be placed a ground glass plate so that a beam of more uniform intensity enters the polarimeter (4). The polarimeter is the research type of O. C. Rudolph and Sons which was modified slightly by providing weights to enhance its stability and leveling screws in three planes (5). The half-shade image emerging from the polarimeter enters box (6) and can be observed by means of a 45° plane mirror through a port (7). Alternately by means of a knob (8), the mirror can be swung out of the optical path thus closing the port and opening an interlocked window. This is the normal mirror position; and the light passes through a brass tube which is equipped at its exit with an adjustable knife edge blocking exactly half of the tube. The tube is mounted between two ball bearings and can be rotated by means of an external

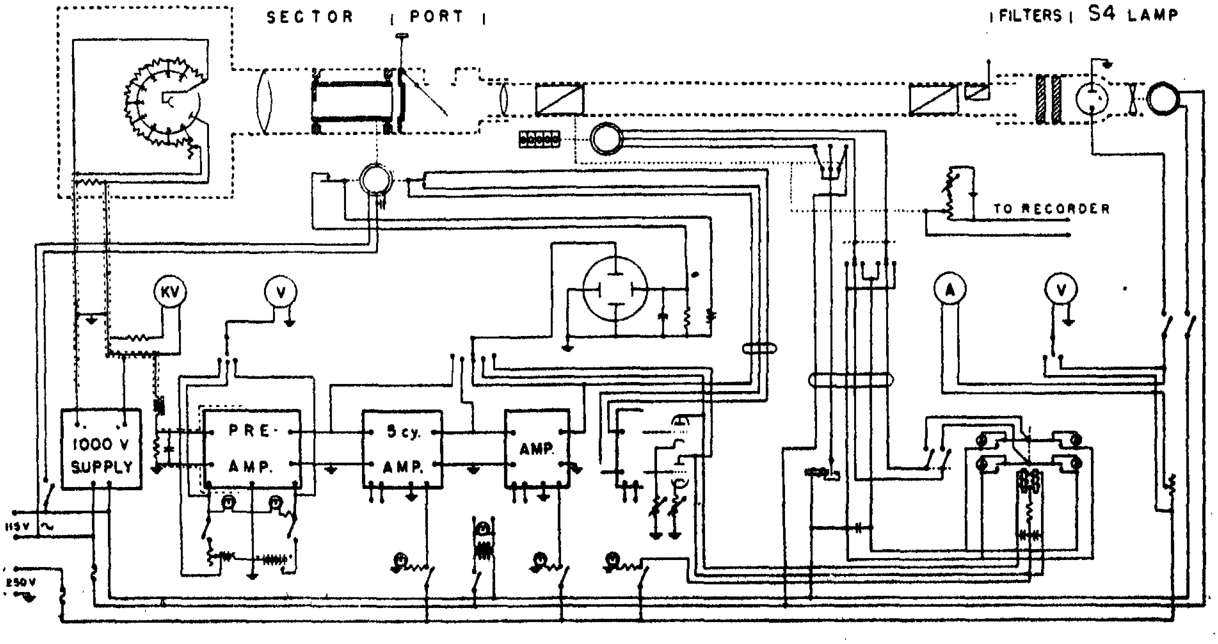

FIG. 2. Schematic diagram of polarimeter.

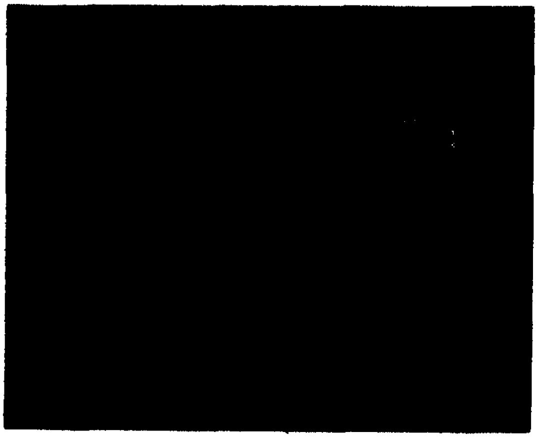

FIG. 3. Oscillogram (preamplifier circuit).

gear, gear train, and synchronous motor (9). There is also a screw mounted on the periphery of the tube which actuates a microswitch. This switch in conjunction with a dry cell, resistor, and condenser serves as a synchronized saw tooth voltage generator for the horizontal sweep of the oscilloscope (10). The tube is rotated at 5 cycles/second and serves as a chopping shutter.

The chopped light is focused by a small lens on a photo-multiplier tube which is mounted on an adjustable, well-insulated bracket at the end of box (6). Tube 1P21 is preferred although No. 931A can also serve (with some loss in over-all sensitivity). The fixed dynode resistors and a potentiometer, for a variable output, are arranged inside the box. The electrical components are contained in the console (11). The services used are: 110 v a.c. for the filament transformer and the synchronous motors, 250 v d.c. for the plate voltages and the mercury vapor lamp, 12 v d.c. from two storage batteries for the preamplifier filament (variable 6–7 v), and inside the console a tapped 45-v dry-cell for variable plate voltage for the preamplifier. The various chassis in the console contain the following units:

(1) The bottom chassis contains the power supply of 1000 v for the photo-multiplier. This is of conventional design using a 2×2 rectifier tube. It supplies approximately 100 v per dynode stage of the photo-tube while the output can be regulated, as mentioned.

(2) The next chassis contains the rheostat for the light, fuses, a filament transformer and the differential relay assembly. Four neon bulbs are wired in parallel with the four contact points of the relay. This arrangement is beneficial for the stability of the unit and at the same time provides a visual guide to the performance of each contact.

(3) The third chassis contains the preamplifier which is electrostatically shielded and shock mounted. It is a direct coupled amplifier of conventional design using two No. 5693 tubes. The tuned amplifier is of the parallel *T* type.[2] Controls are provided for both the total amplification and the sharpness of tuning of this amplifier. An untuned amplifier stage follows this unit. It

FIG. 4. Oscillogram (tuned amplifier circuit at balance ±0.015°).

provides additional amplification and is set to clip the signal to some extent (Fig. 5).

The filtered and amplified signal is fed to the pair of microswitches (12). These are mounted on alternate sides of a brass plate which also contains a bearing for a gear. The face of the gear carries a raised sector of 40° which actuates the switches. This assembly slides on the box and by withdrawing it, the gear can be made to engage the synchronized gear train in any position. Once locked in, the scanning sector, sawtooth voltage and the phase discriminator (i.e., the switches discussed) are in permanent synchronization. Each switch is associated with a No. 5692 tube, connecting the voltage passed by it to the grid of the proper tube. These tubes are biased by variable cathode resistors to deliver less than 2 milliamperes, at 0 v grid signal, which is the release point for the differential relay contained in the plate circuit.

(4) The next chassis contains the toggle switches for the multipurpose instruments, the resistor by which the filament voltage of the preamplifier is varied and the selector switches for the oscilloscope.

(5) The instrument panel permits the reading of the following: a. High voltage (photo-tube circuit). b. D.c. voltages, both of plate circuits and mercury vapor lamp. c. Current through mercury vapor lamp. d. Voltages of batteries, preamplifier plate, and filament circuits.

The line voltage switched into two branches by the differential relay drives the small motor in either

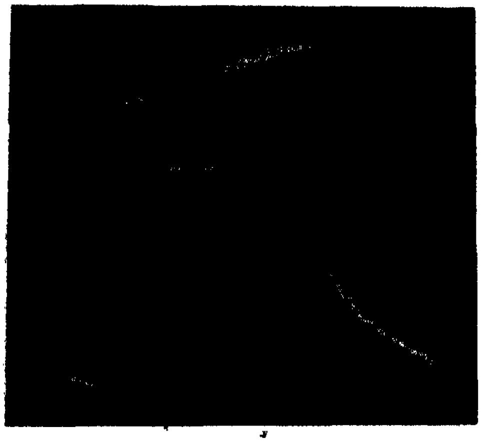

FIG. 5. Oscillogram (coupling amplifier circuit).

---

[2] M. P. Givens and J. S. Saby, Rev. Sci. Inst. 18, 342 (1947). The use of this circuit was suggested to us by Dr. Denman Shaw whose advice we gratefully acknowledge.

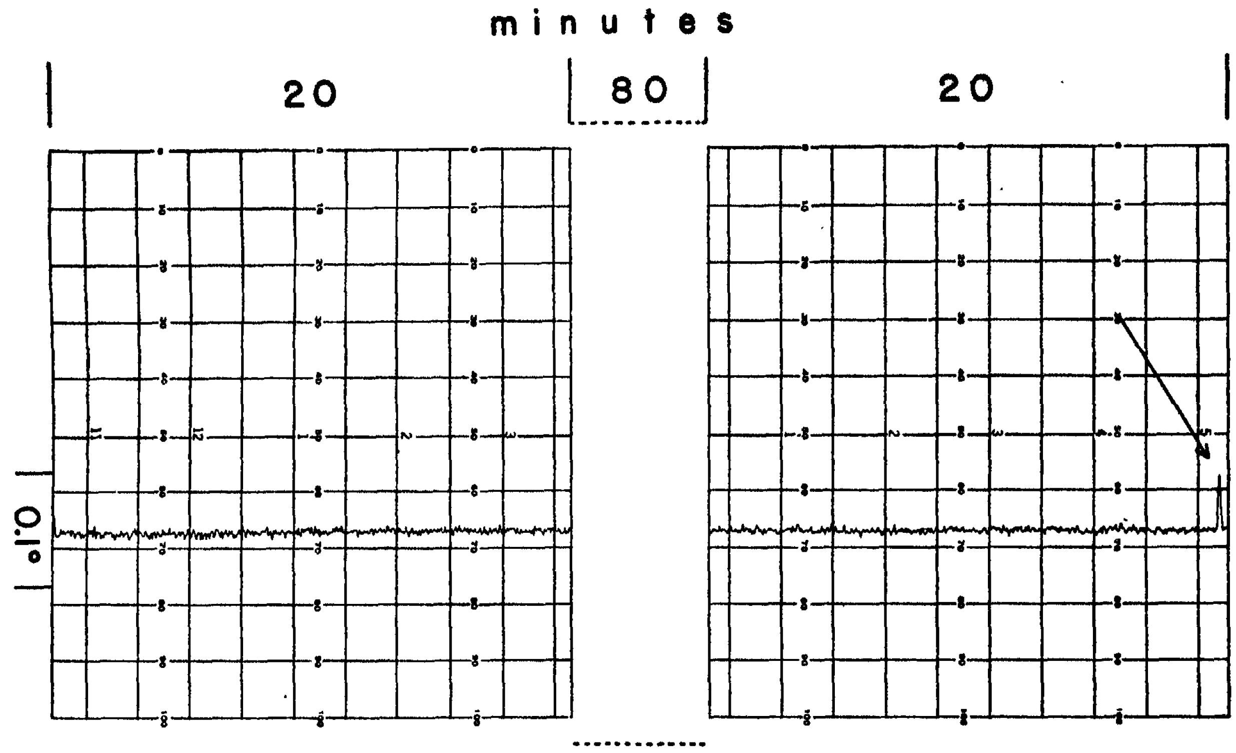

FIG. 6.

direction. This motion is transmitted to a counter (13) and also through a gear train to the fine adjustment of the polarimeter analyzer and hence to a Beckman 360° potentiometer (14). This potentiometer provides a variable voltage (0–50 mv) to the Brown Electronik recorder. The gear arrangement is such that each count of the counter corresponds to 1/1000° rotation of the analyzer† while the full rotation of the potentiometer and hence 100 divisions of the strip chart correspond to 0.5°. This arrangement provides a convenient scale expansion. A double throw switch (15) is provided by means of which the motor driving the analyzer may be controlled independently of the signal of the servo. Outside the console is the detachable oscilloscope whose function is discussed below.

In setting up the instrument for operation the procedure is as follows: The 250-v d.c. line is switched on and the mercury vapor lamp started, including the fan. After a few minutes the lamp is adjusted to about 150 watts and the filters are inserted. The half-shade angle is set between 3° and 10° and a cell containing water is inserted in the polarimeter. The position of the lamp is adjusted for proper illumination of the tube. The mirror is swung into place and the analyzer is set near the balance. Then the front panel is removed from the box and the mirror removed from the light path. The knife edge is now set to coincide with exactly half of the half-shade image. For observation of this and subsequent steps a piece of paper is held in front of the photo-cell assembly. The polarimeter is leveled to approximately the right height, and laterally so that the rotation of the shutter intersects the center of the field. Simultaneously the analyzer is focused. Then the lens is inserted and the photo-cell adjusted so that the light spot hits the center of the cathode surface. The front panel is replaced and the ground glass diffuser inserted.

It should be mentioned that alignment, as described, is only made once when setting up or after very severe mechanical shock. In daily operation only fine adjustment is made as described in the following.

The power is switched on including the synchronous motor driving the scanning sector. With the relay circuit switched off, the analyzer (with fine adjustment locked) is moved off balance and the preamplified signal observed in the oscilloscope. If properly aligned, a sinusoidal curve is observed (Figs. 3, 4). In conjunction with observing the travel of the analyzer (by means of the counter) the operation of the instrument can be gaged. Lack of sensitivity indicates improper focusing or improper operation of the amplifiers. After the suitable adjustments have been made the operation of the phase discriminator may be observed with the oscilloscope switched into the coupling amplifier circuit (Fig. 5). The drop in voltage coincides with the operation of the switches. (When setting up the instrument the gear is made to engage in such a manner that the switch operation coincides with the maxima.) The

---

† The drive is actually proportional to the tangent of the angles but no correction is necessary at the small angles in question.

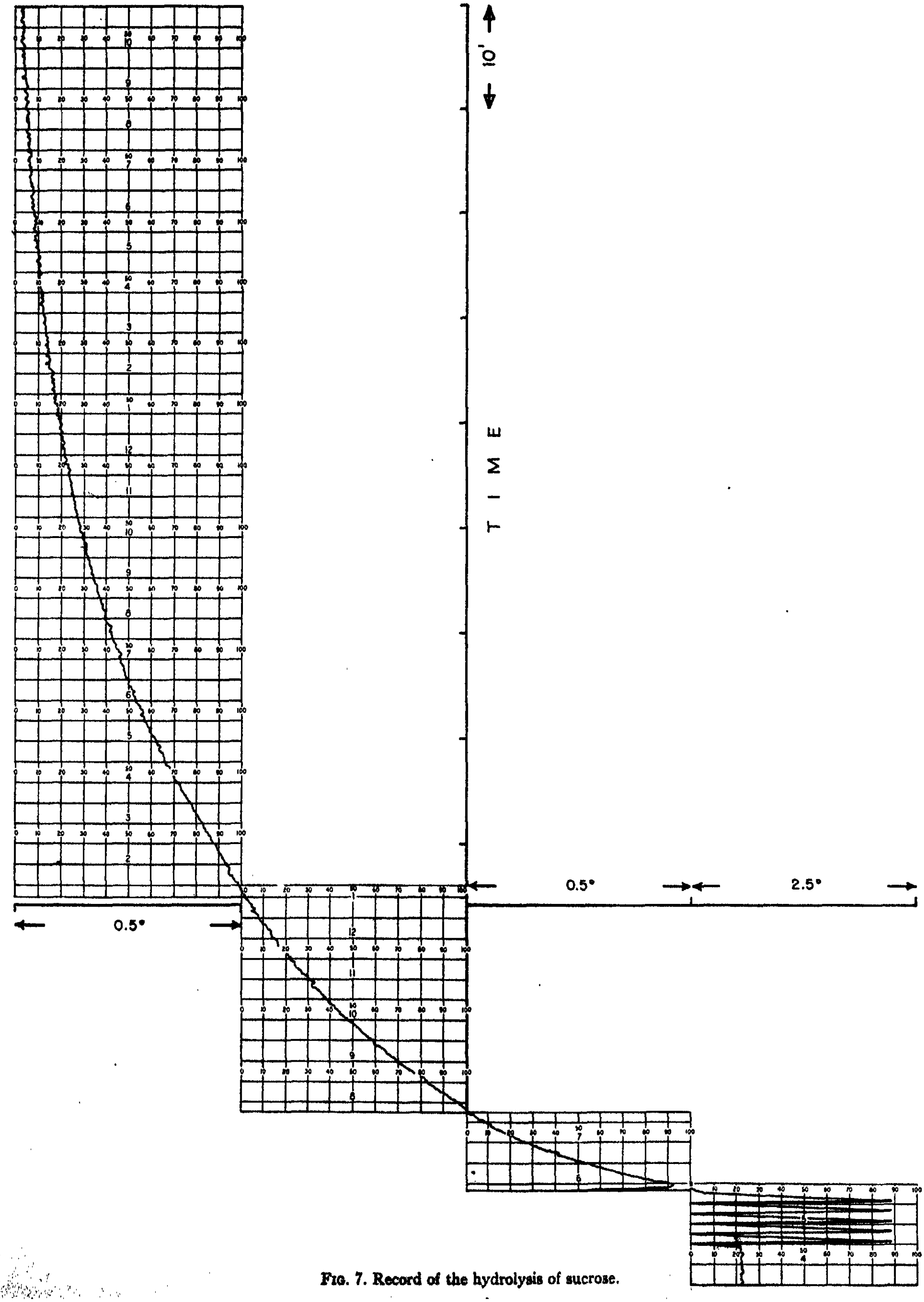

FIG. 7. Record of the hydrolysis of sucrose.

proper operation of the relay may be observed in the oscilloscope by switching to either plate circuit of the last tube. The only remaining step is to adjust the voltage in the recorder circuit so that the pen travels 100 divisions per revolution of the polarimeter fine adjustment screw.

PERFORMANCE

The performance of the instrument is shown graphically in Fig. 6. This is a record of a two-hour test run showing a scatter of less than ±0.005°. There is no measurable shift of rotation during the run. The amplification was set, as usual, so that a response commensurate with the speed of the balancing motor was achieved. This can be seen on the chart where, at the end of the run, the position of the analyzer was changed by overriding the signal; immediately the instrument readjusted itself. The slopes indicate that the travel was at maximum speed of about 0.5° minute in the reverse direction also. The ultimate limit in precision is determined by the period of the amplifier and the motor speed, which in the present arrangement is about 1/5 second and 1/120°/second, respectively, and so the limit is about ±0.002°/second.

Extensive tests were also made to determine the effect of alignment. It was found that the shift most frequently encountered was in the height of the instrument. This does not generally cause a shift in values of rotation although it does affect the sensitivity adversely. The position of the sample tube was found to cause considerable shift in values of rotation due to asymmetries in construction. This was minimized by marking the tube and by placing it always in the same angular position. The resultant reduced scatter of values was found to be of the order of 0.01°.

DISCUSSION

In planning for the construction of the recording polarimeter the preceding literature on photometric polarimetry was considered.[3] Particularly with a view toward adapting an existing design to include recording features. Previous schemes of photoelectric polarimetry were reviewed, e.g., that of Landt and Hirschmüller,[4] Ebert and Kortüm,[5] Bruhat *et al.*,[6] and Schönrock and Einsporn.[7] None of these seemed easily adaptable and therefore the more direct approach was chosen of substituting a photoelectric-servo system for the observer in the visual system of polarimetry. An advantage of this scheme was that it permitted the use of available component parts which proved expedient. The system described could probably be improved in precision by more careful mechanical design, since mechanical deficiency was found to be the limiting factor in the present arrangement. However, the present operation is adequate for most applications.

The main use of the instrument was found in the study of enzyme reactions. This work is being reported elsewhere. However, as an illustration a tracing is included Fig. 7, which represents the hydrolysis of sucrose, catalyzed by the enzyme invertase. The typical logarithmic course of the reaction is apparent.

Other possible uses include measurement of optical activity on changing product streams. In this application a careful design of the sample cell is important, as was found in exploratory experiments. The reason for this is that the appearance of schlieren materially impedes the measurement of optical activity.

In view of the precision of the instrument which compares favorably with visual observation under ordinary conditions, the use for routine determination of optical activity may also be considered. In this application the counter suffices and the use of the recorder is unnecessary.

ACKNOWLEDGMENT

The authors wish to express their appreciation of James H. Hocker for many valuable suggestions concerning the circuits used and to various members of the shops who helped in construction, particularly, C. Miller and H. Giffin. They thank Dr. G. E. Ward for his advice and encouragement, and Schenley Industries, Inc. and Dr. E. C. Williams for permission to publish this material.

---

[3] A survey of the literature by W. Heller, see reference 1.

[4] Landt and Hirschmüller, Deut. Zuckerind. 62, 647 (1947).

[5] Ebert and Kortüm, J. Phys. Chem. B13, 105 (1931).

[6] Bruhat *et al.*, Comptes Rendus 214, 615 (1942).

[7] Schönrock and Einsporn, Physik. Zeits. 37, 1 (1936).

THE REVIEW OF SCIENTIFIC INSTRUMENTS VOLUME 21, NUMBER 8 AUGUST, 1950

High Pressure Ionization Chamber Counters and Their Use

R. Wilson, L. Beghian, C. H. Collie, H. Halban, and G. R. Bishop
Clarendon Laboratory, Parks Road, Oxford, England

(Received March 6, 1950)

Certain new developments in ionization chamber technique are described. Ionization chamber counters have been designed to operate with fillings of H_2, D_2, or CH_4 to pressures of 35 atmos. with simple filling techniques. The design, characteristics, and uses of these counters are described.

ELECTRON collection makes it possible to use ionization chamber counters with fast amplifiers. We have used these counters for several experiments and therefore feel that a summary of our experimental techniques may be useful. We have used counters filled with hydrogen and methane for the detection of neutrons by proton recoil,[1] and deuterium-filled counters for investigation of the photo-disintegration of deuterium.[2] For both of these applications it is necessary to use a high gas pressure to obtain a sufficiently high counting rate and to reduce the number of protons which lose most of their energy in the walls and are not counted ("wall effect").

GAS PURITY

In order to obtain electron collection it is important to use a gas in which the formation of negative ions by electron attachment to neutral molecules is negligible; H_2, D_2, N_2, CH_4, and the inert gases do not form negative ions. But the electron attachment coefficient for such molecules as O_2, CO, H_2S, Cl_2, H_2O is so large that the presence of even small impurities can cause a considerable fraction of the electrons to form ions before collection. The electron attachment coefficients have been measured at low pressures (10 cm) (e.g. Massey)[3] and usually under different conditions from those prevailing in ionization chamber experiments, so that comparison between theory and experiment is difficult. Rough estimates, however, indicate that one part in 10^7 of oxygen, the most difficult impurity to avoid, will prevent electron collection in a counter filled to ten atmospheres pressure.

It has been the practice to mix 10 percent CO_2 with a gas such as argon in order to increase the electron mobility[4] and therefore to make the effects of impurities less serious. But above pressures of three atmospheres, this leads to loss of pulse height,[5] probably due to columnar recombination, which is high in CO_2.[6] This columnar recombination is discussed more fully later. The introduction of CO_2 reduces the average electron energy by inelastic collisions to a value where the mean free path of electrons in argon is large. (The variation of mean free path with electron energy is often called the Townsend-Ramsauer effect.)

PREPARATION OF GASES

Hydrogen, deuterium, and methane were purified by different methods. The hydrogen is obtained at 180 atmos. pressure from a large hydrogen liquefier,[7] the supply being taken after the charcoal cleaning stage.

The deuterium is prepared by electrolysis of heavy caustic soda* solution in a simple bell type cell. The electrolytic cell is run with a current of 6 amp., giving a current density at the anode of about 0.2 amp. per sq. cm. The electrodes are made of nickel and the nickel leads are welded to tungsten seals; the weld is guarded with glass so that the tungsten is not unduly corroded. The oxygen passes through two liquid air traps to the open air, one to trap heavy water vapor, the other to prevent entry of light water vapor. The hydrogen passes through a metal pressure controlling reducing valve[8] and a capillary to the catalyst tube which is normally at some pressure below atmospheric. Here any residual oxygen is recombined over a red-hot platinum spiral about 2 cm long and 1 cm diameter. Water vapor is condensed out in a liquid air trap, and the deuterium passes through 10 cm of capillary tube before it is adsorbed on charcoal immersed in liquid air. The filling continues until sufficient gas has been produced or until the pressure in the charcoal bottle rises to atmospheric pressure. The only impurity in a large concentration to be expected from this system is CD_4 from CO_2 dissolved in the caustic soda.

A second evacuated charcoal bottle equally immersed in liquid air is then connected to the first until equilibrium has been established. It is hoped that any residual impurity will not desorb from the first charcoal bottle. On removing the liquid air the pressure in the charcoal bottle rises from 1 atmos. to 60 atmos. and the gas is available for filling counters. It is important to use a material for the charcoal bottle that does not

---

[1] L. E. Beghian and H. Halban, Proc. Phys. Soc. 42, 395 (1949).

[2] Wilson, Collie, and Halban, Nature 162, 185 (1948); 163, 245 (1949).
Collie, Halban, and Wilson, Proc. Phys. Soc. 63, September, 1950.

[3] H. S. W. Massey, *Negative Ions* (Cambridge University Press, London, 1938).

[4] J. Allen and B. Rossi, M.D.D.C., 448 (1947).

[5] Bridge, Hazen, Rossi, and Williams, Phys. Rev. 74, 1083 (1948).

[6] M. Moulin, Thesis, Paris (1910).

[7] Jones, Larsen, and Simon, Research I, 420 (1948).

* Easily prepared by dissolving dry sodium peroxide in heavy water.

[8] H. Halban and R. Wilson, J. Sci. Inst. 26, 1949 (1949).

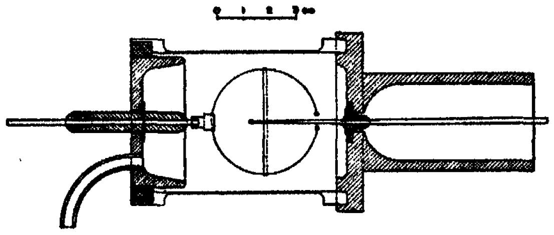

FIG. 1. Ionization chamber counter with well-defined counting volume.

become brittle at liquid air temperature. Stainless or Vibrac steel or Phosphor Bronze are satisfactory, but not mild steel.

Dr. London and Dr. Kronberger, AERE Harwell, supplied the methane, which was distilled by a fractionating column of 30 plates.[1]

We have found that when we add one part in 2×10^5 of oxygen to a deuterium gas filling there is no electron collection at 6 atmos. It is estimated that not more than one part in 10^7 of oxygen is normally present. In some preliminary experiments using impure methane, there was no electron collection. But after two months without use, electron collection was achieved, without any loss of pressure. This we attribute to adsorption of the electronegative impurity—presumably oxygen—on the counter walls. This adsorption may be hastened by operating the counter in a high gamma-ray flux with a reverse voltage. The impurities then form negative ions which drift to the outer cylinder and hence have a chance of being adsorbed. The adsorption effect has also been noticed with deuterium.

The gas purity has been sufficient to achieve electron collection at 35 atmos. for each gas.

COUNTER CONSTRUCTION

The counters we have used are all made of metal' The first were made of brass, but this was sometimes found to be porous. Subsequently we have used copper —which is reputed to act as a good "getter" for oxygen. More recently, stainless steel, and a high tensile strength aluminium alloy (No. 66E, T.I. Aluminium Ltd., Birmingham) have been used. The metal surfaces are well cleaned, before assembly, in chromic acid and then acetone; the assembly is carried out in a workshop where the risk of radioactive contamination has been kept low.

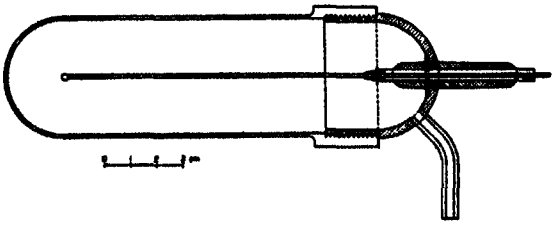

FIG. 2. Ionization chamber counter with low neutron scattering by the walls.

In order to minimize the charge induced on the collecting electrodes by heavy ions in the counter, cylindrical or spherical geometry has been used. The counters have been made in several shapes and sizes, according to the purpose to which they are to be put, but they are of two general types. The first type (Fig. 1) consists of an earthed metal vessel designed for the pressure limits required (made of stainless steel with mild steel ends) with a collecting electrode connected through a Kovar-to-glass seal coming out at one end, and a cylindrical or spherical electrode of aluminium connected through a seal at the other end. It is possible to make the sensitive volume equal to the geometrical volume of this sphere by making only a very small hole for the entry of the collecting electrode, and shielding the collecting electrode till it is inside the sphere. The uncertainty in this volume is then about 0.1 percent. The metal parts are joined with hard solder; the metal-to-glass seals are soldered in with a silver-tin alloy solder of melting point 300°C (Johnson-Matthey LM 10) and the final assembly of the counters is completed by screwing in the end cap (on which the high voltage electrode is usually mounted) and sealing with soft solder. This final seal is made without flux on previously tinned surfaces. It is not, however, easy to soft-solder to aluminium or stainless steel. In these cases the seal is made by running Cenco-Sealstix in the thread and screwing up the joint when the wax is warm.

The second type of counter (Fig. 2) uses a "guard ring" type of seal. This enables the outer pressure vessel to be also the high voltage electrode. Because the diameter is only that of the collecting electrode, the walls of the pressure vessel may then be made thinner. The disadvantages are that the counting volume is less well defined, and there is a likelihood of spurious discharges from the outside of the counter. It is often necessary to reduce the amounts of material in the immediate vicinity of the counter as much as possible to reduce neutron or gamma-ray scattering. Stainless steel or aluminium counters are then the most convenient because less massive walls may be used to withstand the same pressure. All equipment except the first valve of the subsequent amplifier is placed at a distance.

Most of the Kovar-to-glass seals used are made by Cathodeon Ltd., Cambridge, England; the guard ring type seal was made specially for us. For the counter in Fig. 1 a special low capacity seal for the collecting-electrode was made for us by B.T.H. Ltd. The small hollow seals for the proportional counter (Fig. 5) were made by Stupakoff Ceramic and Manufacturing Company, Latrobe, Pennsylvania. After assembly of the counter we usually took an x-ray photograph. This verified the alignment of the electrodes. We use x-rays from a tungsten target, and we can observe a 0.001-in. tungsten wire inside a counter.

The counters are sealed with a specially developed

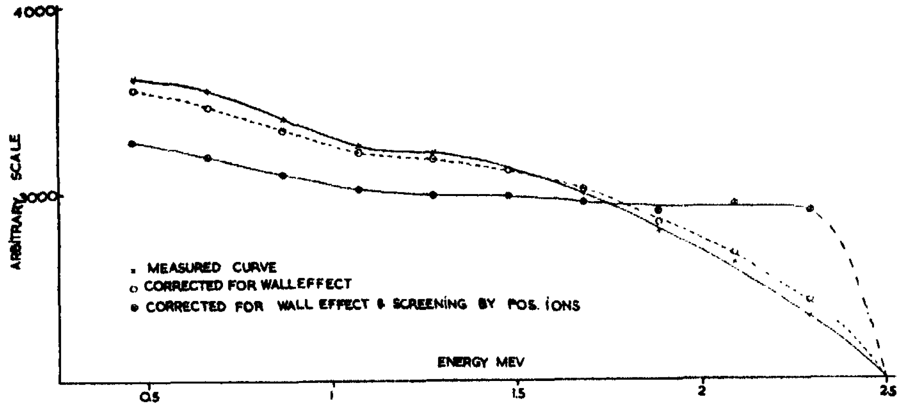

FIG. 3. Pulse-height distribution for recoil protons from 2½-Mev neutrons in the counter of Fig. 2 filled with CH_4 to a pressure of 20 atmos.

vacuum and pressure tap[8] which is also used in the filling system. The counters are joined to the filling system by a metal cone and socket join which is screwed tight and covered with Cavendish wax. The counters are outgassed by pumping for several days at a pressure of 10^{-6} mm of mercury until the pressure does not rise when the pump is disconnected. Slight heating (up to 100°C for a soft-soldered join or 50°C for a waxed join) hastens this process. For the H_2 fillings, the counters and filling tubes are washed out well with pure H_2, so that the filling tube need not be evacuated. In order to avoid wastage of D_2 or CH_4 the filling tube is carefully evacuated when using these gases. The gas pressure is measured when the counter is filled with a Bourdon gauge connected to the filling system. After use the pressure in the counter may be measured by expanding the gas into a known volume and measuring the resulting pressure accurately on a mercury manometer. An accuracy of two percent is attainable with a gauge; 0.1 percent with the expansion method.

POSITIVE ION EFFECTS

In order to make full use of a counter it is necessary to calculate the theoretical pulse height. The positive ions and electrons move in opposite directions, and as they move they induce currents on the collecting electrode. The electrons are all collected within a few microseconds, but the positive ions take longer. For many experiments it is desirable to reduce the gamma-ray background. It is then necessary to shorten the amplifier time so that secondary electron pulses do not pile up. For coincidence work it is also necessary to shorten the amplifier time constants. The amplifier will not then respond to the slowly moving positive ions. If an appreciable part of the pulse is caused by the positive ions, this will result in a loss of pulse height, and this loss will depend on the position of the initial ionization in the counter. This is especially the case for the parallel plate counters of Scherr and Petersen.[9] In the cylindrical and spherical geometry which we used this effect is considerably reduced.

It is possible to calculate how much of the pulse is caused by collection of the electrons and how much by collection of the positive ions as a function of the distance of the initial ionization from the central electrode. This calculation can be readily performed for any geometry by using a theorem due to Shockley[10] that the current induced on a conductor by a moving charge q is given by $i=qvE_v$, where v is the velocity of the charge and E_v is the component of the electric field in the direction of the velocity that would exist if the collecting electrode were at unit potential, all other electrodes earthed, and the charge removed. Calculations made in this way agree with the results of Nicodemus[11] for the special case of a cylindrical counter. The correction to be applied to a spectrum of proton recoils from monokinetic neutrons has been evaluated for the case where the positive ion contribution may be neglected (e.g., using CH_4 as a counter gas where the positive ion mobility is low). If N' are the measured number of pulses per second in an energy interval dE,

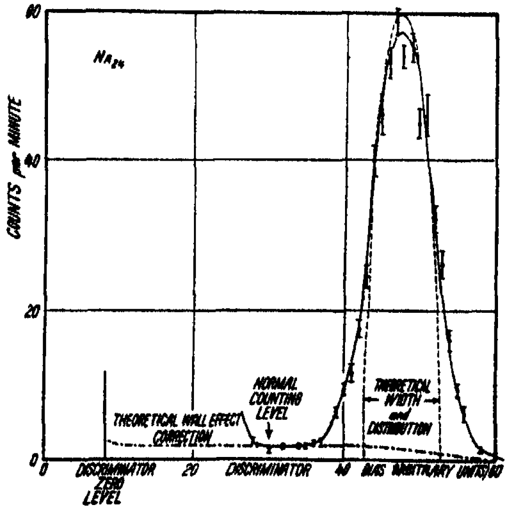

FIG. 4. Pulse-height distribution for photo-protons from 2.76-Mev γ-rays in the counter of Fig. 1 filled with D_2 to a pressure of 8 atmos.

---

[9] R. Scherr and R. Petersen, Rev. Sci. Inst. 18, 567 (1947).

[10] W. Shockley, J. App. Phys. 9, 635 (1938).

[11] D. Nicodemus, M.D.D.C., 470 (1947).

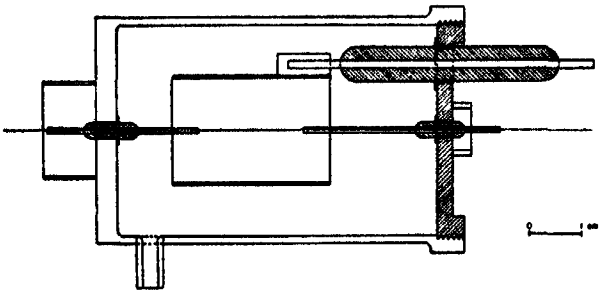

FIG. 5. Proportional counter filled to 20 atmos. of D_2.

then the number corrected for positive ion effect is given by the relation

$$N'=N\left\{1+\int_y^1 \frac{p^{(z-1)}}{z^2}dz-\frac{p^{y-1}}{y}\right\},$$

where $y=E/E_{\max}$ and $p=b/a=$ radius of outer electrode/radius of collecting electrode. An uncorrected and a corrected curve for 2½-Mev D−D neutrons are shown (Fig. 3) for the cylindrical counter of Fig. 2.

The wall effect was calculated from simple geometrical considerations using the known range energy relationship and is seen to be small in comparison with the positive ion effect. The divergence from the isotropic distribution at low energies may be caused by a small (three percent) group of inelastically scattered neutrons, or to the effect of carbon recoil atoms. It is not, however, known whether the counter voltage is sufficient to saturate the counter for the intensely localized ionization produced by the carbon recoils.

The counter shown in Fig. 2 is partly spherical and partly cylindrical. The positive ion correction is then difficult to evaluate. The correction is small for pure H_2 or D_2 at moderate pressures, where the positive ion mobility is high, because the positive ions move sufficiently quickly to contribute to the pulse. This is especially true for high fields. Figure 4 shows a typical pulse-height distribution for photo-protons, with the counter filled to 8 atmos. D_2, and with a counter voltage of 4 kv. The asymmetry in the peak is due to the positive ions and electron loss. The wall effect correction is here easy to apply and is shown dotted. This correction can be avoided altogether by using a gridded counter.[12]

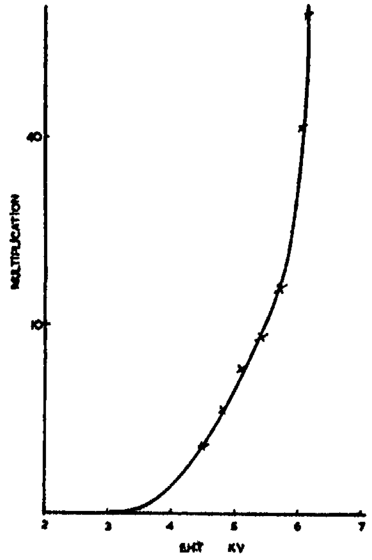

FIG. 6. Proportional counter filled with hydrogen to 20 atmos. pressure. Variation of multiplication with voltage.

PROPORTIONAL COUNTERS

For some purposes a high pressure proportional counter may be required. The design shown in Fig. 5 has been developed, but for various reasons has not yet been used for experiments. The counter wire (made of 0.001-in. tungsten) must be cleaned well before assembly, and flashed to 2000°C during the outgassing. The temperature of the wire is measured during flashing by the change in resistance. This flashing was not always found adequate to reduce spurious pulses. In these circumstances we flashed the wire to 2000°C with the counter filled and with the voltage on, a procedure which appeared to remove any points from the wire very effectively.

There is no variation of pulse height with position of the initial ionization in a proportional counter.[13] This is due to the fact that the pulse is caused by the movement of the positive ions formed in the avalanche away from the central wire, and is independent of the initial ionization. The total length of the pulse is great (10 μsec.) but the initial rise is short (0.05 μsec.) and the pulse may be sharpened in the amplifier without affecting proportionality of pulse height. This is fully discussed by Corson and Wilson.[14]

The characteristics of the proportional counter are given in Figs. 6 and 7. It was necessary to use a large amplifier band width to amplify the short pulse (0.08 μsec.), and a large amount of shot noise was introduced. The proportional multiplication was sufficient to make

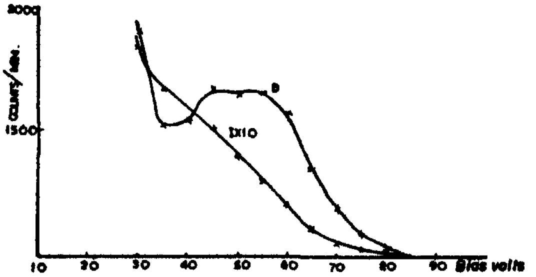

FIG. 7. Proportional counter filled with deuterium to 20 atmos. pressure. Pulse-height distribution of photo-protons from RdTh 2.62-Mev γ-ray line. Curve *I* is the integral count, Curve *D* the differential count.

---

[12] O. R. Frisch, Atomic Energy Report BR49 (1945). Buneman, Cranshaw, and Harvey, Can. J. Research 27A, 191 (1949).

[13] P. G. Koontz and T. A. Hall, Rev. Sci. Inst. 18, 643 (1947).

[14] D. R. Corson and R. R. Wilson, Rev. Sci. Inst. 19, 207 (1948).

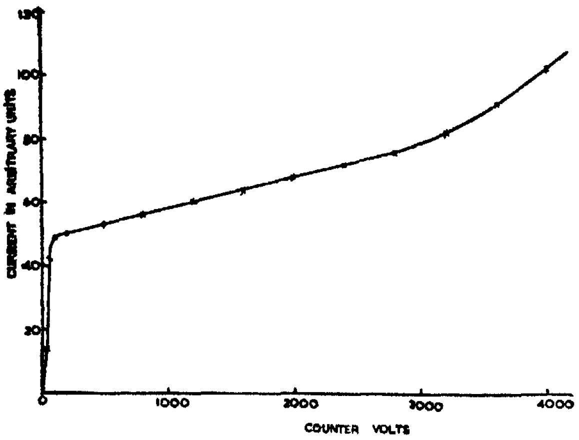

FIG. 8. Saturation curve of ionization current in photo-disintegration chamber filled to 5 atmos. pressure, due to γ-rays.

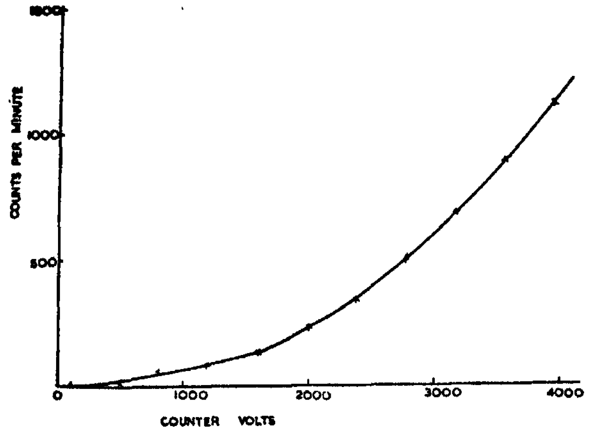

FIG. 9. Saturation curve of γ-ray background in photo-chamber of counts above a fixed bias voltage.

the effect of the shot noise small. In order to obtain the high photo-proton counting rate (20,000/min.) there was an intense γ-ray source and an intense background of secondary electrons. It was possible to discriminate against this background by using a short pulse width. This would not have been possible with an ordinary ionization chamber counter, because the increase in amplifier noise would have been too great.

COLLECTION TIME

The collection time is measured by observing the rise time of the pulses on a triggered oscilloscope. A delay line is used to delay the signal until the sweep is under way. It was noticed that the pulse rise time depends upon the type of event causing the pulse. If the ionization is localized the rise time will be the short time taken for the electrons to cross the high field region near the center wire. If, however, the ionization is along a long track crossing the counter, the pulse rise time is equal to the electron collection time.

Different cases arise. For instance, with a filling of 10 atmos. D_2 a photo-proton track from RdTh gives localized ionization, whereas some of the recoil protons from a PoBe neutron source (which have up to 9.5 Mev) will give a long track.

On the other hand, a counter filled to 30 atmos. CH_4 has a high stopping power so that all the recoil protons from a PoBe source give localized ionization. Because of the high stopping power, Compton recoil electrons will now lose sufficient energy in the counter to produce a count. Some of these electrons will have long tracks.

The pulses from events with a long track are used to measure the electron collection time. They may also be used to measure positive ion collection time by reversing the counter potential. When a slight impurity prevents electron collection, the rise time of the pulses is due to negative ion collection. A routine check of the counter filling is to observe the collection time of the negative ions in this way, with the amplifier time constants set to accept all pulses between 0.1 μsec. and 3 millisec. and to check that no pulses of rise time greater than the electron collection time occur.

With some counter fillings the collection time may be measured more accurately by measuring coincidences between the neutrons and γ-rays of a Po-Be source detected by proton recoil and scintillations, respectively. The coincidences will decrease if the coincidence resolving time is reduced below the counter collection time. The analysis is simple because the photo-multiplier has a much faster response than the ionization chamber counter.

The collection time of electrons in CH_4, at 35 atmos. pressure in the counter of Fig. 2 with 15 kv on the electrode, is found to be 1 μsec. in fair agreement with the formula of Snyder.[15] The electron collection time in D_2 at 10 atmos. found by observation of pulses in the counter of Fig. 1 and with four kv collecting potential is found to be 1 μsec. The positive ion collection time in D_2 at three atmos. at three kv is found to be 40

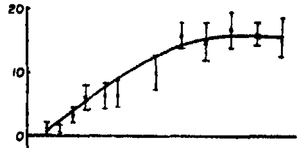

FIG. 10. Saturation curve of neutron recoil deuterons of high energy. Neutrons from Po-Be source.

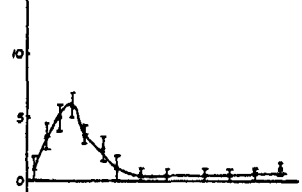

FIG. 11. Saturation curve of differential photo-proton count taken with a single-channel kicksorter with channel width of 10 kev.

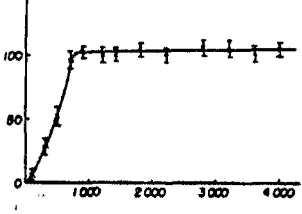

FIG. 12. Saturation curve of integral photo-proton counts, with bias set below the peak.

---

[15] T. M. Snyder, M.D.D.C., 243 (1946).

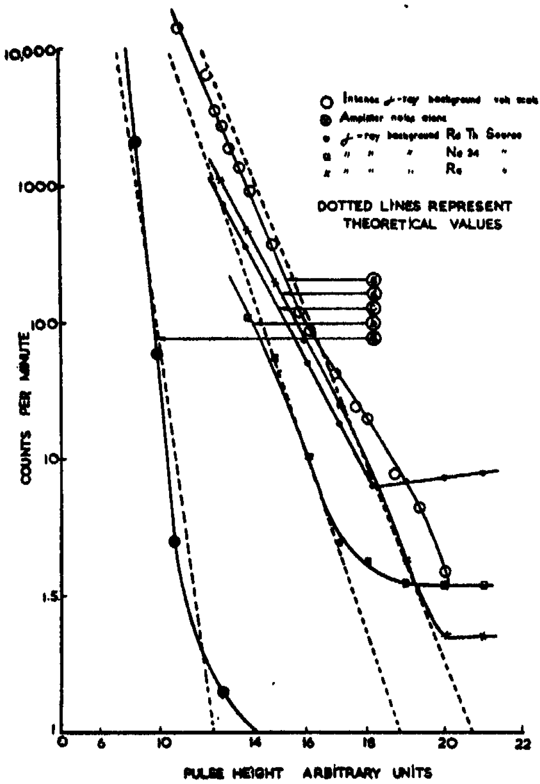

FIG. 13. Plot of $\log_e$ (counts/min.) against the square of the bias voltage V^2, for various types of background and noise.

μsec.; this suggests a positive ion mobility of 60 cm/sec./volt/cm at one atmosphere pressure which is higher than the value 10.6 recently reported.[16] This is presumably due to the different conditions of the measurements.

It is possible to take advantage of the difference in collection time for localized ionization and extended ionization to discriminate against gamma-ray background. The amplifier time constants may be adjusted so that the pulse from the desired localized ionization is just accepted, whereas a pulse from the background extended ionization, being longer, is heavily attenuated. This is the case for the proportional counter adjustment in Fig. 7.

SATURATION CURVES AND PULSE-HEIGHT LOSS

We have plotted in Figs. 8 to 12 saturation curves for a counter taken under various conditions.

Figure 8 shows that ordinary saturation takes place at 100 volts, but there is still a considerable increase in pulse height above this value. This is shown in Fig. 9; the rise in γ-ray background count is between linear and logarithmic with *HT* voltage; this is equivalent to an increase in pulse height which is less than linear at the high voltages showing approximate saturation of pulse height.

Figure 12 shows complete saturation of the counting rate of photo-protons under actual experimental conditions. Figure 11 also shows that at low *HT* voltages, the pulse height is reduced and confirms that saturation is effective for the experimental conditions of Fig. 12. Confirmation of this is also given by the distribution curve of Fig. 4, which shows that pulse height losses, if they exist, are proportional. Figure 10 shows that saturation is less easily attained for recoil deuterons than for photo-protons.

With one counter filling (20 atmos. H_2 in a counter two cm diameter, one mm inner electrode diameter, and four kv on the electrodes) the pressure was slowly reduced. It was found that there was three percent pulse height loss at 20 atmos., due presumably to initial recombination. This effect is reported to be smaller in D_2 and CH_4 and should not therefore affect most of our measurements.[17]

AMPLIFIER EQUIPMENT

We have used for this work standard amplifiers, and have found the AERE amplifier Type 1008 particularly reliable. The preamplifier used has, however, been one of especially low noise discussed elsewhere.[18] In order to test the amplifier, pulses from a pulse generator are fed through the high voltage condenser and counter. The rate of counting of noise peaks has been measured for different types of background (using a counter filled to 10 atmos. D_2) and compared with the formula of Rice.[19]

C = rate of counting of noise peaks $= \frac{1}{2}\exp(-v^2/2V_0^2)$ (expected number of zeros of the noise wave form per second) $\simeq (1/T)\exp(-v^2/2V_0^2)$, where T is the amplifier pulse width.

In Fig. 13 $\log C$ is plotted against v^2. It may be seen that the extrapolation of the curves to zero does not give the constant $1/T$ (in this case 10^6/sec.). In curve (a) of amplifier noise alone, this is attributed to some 50-cycle background of about two volts amplitude, which is difficult to observe in the presence of the noise. The existence of this 50-cycle background was verified by the change in the rate of counting of noise peaks at different parts of the 50-cycle wave form, the other parts being suppressed with a gating circuit. Once discovered, this 50-cycle background was eliminated. The failure of the law for curves (b), (c), and (d) at high counting rates is largely due to the small number of events which constitute the gamma-ray background. At low counting rates, curve (b) shows recoil protons from background neutrons, and curves (c) and (d), the wall effect from disintegration protons. The curve (e) for an intense gamma-ray background is slightly distorted at low counting rates by the presence of an unresolved group of photo-protons.

---

[16] W. H. Bennett and C. B. Thomas, Phys. Rev. 62, 41 (1942).

[17] G. H. Stafford, Nature 162, 771 (1948).

[18] Richard Wilson, Phil. Mag. 41, 66 (1950).

[19] S. O. Rice, Bell Sys. Tech. J. 23, 282 (1944); 24, 146 (1945).

The gain constancy of the whole equipment, as determined by the change in counting rate on the side of a photo-proton peak, is better than one percent over a period of a week. Tests over longer times than this have not been made.

COUNTER BACKGROUND

The spurious pulses from the amplifier are below noise level; there are some pulses from the counter which are due to breakdown in a bad seal, or high voltage condenser breakdown; we cannot distinguish between these two types of breakdown which together give detectable pulses at a rate of about 2/min., but they are of the opposite sign to the genuine pulses from the counter and can, therefore, be readily separated. Polonium contamination on the counter electrodes has led to a background as high as 5/min. But the background of a good counter filled to 10 atmos. D_2 varies from less than 1 in 20 min. at 30,000 ion pairs to 0.7/min. at 6000 ion pairs. We attribute this to cosmic rays. At higher pressures (35 atmos. CH_4) pulses due to individual secondary electrons produce a background of 100/min. at 10,000 ion pairs and 0.2/min. at 100,000 ion pairs.

ACKNOWLEDGMENTS

We gratefully acknowledge the assistance given to us by Mr. V. Round who assembled many of the counters and by Mr. Larsen in the design of the deuterium production plant. We are also grateful to Dr. J. Tuck for suggesting the use of methane, to Dr. London and Dr. Kronberger of AERE Harwell for its purification, and to Professor F. E. Simon for the use of pure hydrogen from his liquefier. We would also like to thank Lord Cherwell for extending to us the facilities of his laboratory and for his interest and encouragement.

THE REVIEW OF SCIENTIFIC INSTRUMENTS VOLUME 21, NUMBER 8 AUGUST, 1950

The Chalk River Single Crystal Neutron Spectrometer

D. G. Hurst, A. J. Pressesky, and P. R. Tunnicliffe*
Atomic Energy Project, National Research Council, Chalk River, Ontario, Canada

(Received November 1, 1949)

A single crystal neutron spectrometer has been constructed which shows improvement in resolution and intensity over previously described instruments. This has been made possible by the high flux available from the Chalk River heavy water reactor. The instrument can be operated automatically.

Mechanical design, crystals, resolution and the contamination of the spectrum by higher orders are discussed.

I. INTRODUCTION

Monochromatic neutrons in the energy range from zero to several kilovolts are used for studying nuclear energy levels, absorption and scattering cross sections, nuclear reactions, and the structure of matter. Various methods have been described for producing such neutrons. The modulated cyclotron method originated by Alvarez[1] and developed by the Columbia[2] and Cornell[3] groups permits measurements up to ten kilovolts. The mechanical velocity selector developed by Dunning *et al.*[4] and by later workers has been most useful at thermal energies. Crystal diffraction spectrometers have been described by Zinn,[5] Sturm[6] and Borst.[7] An instrument designed specifically for the study of crystal structures has been described by Wollan and Shull.[8]

The lower limit of energy of the crystal spectrometers is determined by crystal spacing and is in the neighborhood of 0.001 electron volt; the upper limit, due to loss of resolution is less definite and is approximately 50 electron volts. Such a wide range can be achieved only with extreme precautions and the intensity is low at both ends. For normal use the range is roughly from 0.02 to 10 electron volts.

The Chalk River heavy water reactor provides an intense neutron flux and is an excellent source for a crystal diffraction spectrometer. Two instruments have been built; the first is described in this paper and is a single axis spectrometer similar in principle to the spectrometer at the Argonne Laboratory described by Zinn;[5] the second, to be described in a later paper, is a double axis instrument.

II. MECHANICAL DESIGN

The instrument is large and strongly constructed to carry the massive shielding required for adequate re-

---

[*] Now at A.E.R.E., Harwell, England.

[1] L. W. Alvarez, Phys. Rev. 54, 609 (1938).

[2] J. Rainwater and W. W. Havens, Phys. Rev. 70, 136 (1946).

[3] C. P. Baker and R. F. Bacher, Phys. Rev. 59, 332 (1941).

[4] T. Brill and H. V. Lichtenberger, Phys. Rev. 72, 585 (1947); Dunning, Pegram, Fink, Mitchell, and Segrè, Phys. Rev. 48, 704 (1935); W. Selove, Phys. Rev. 76, 187 (1949).

[5] W. H. Zinn, Phys. Rev. 71, 752 (1947).

[6] W. Sturm, Phys. Rev. 71, 757 (1947).

[7] Borst, Ulrich, Osborne, and Hasbrouck, Phys. Rev. 71, 557 (1946).

[8] E. O. Wollan and C. G. Shull, Phys. Rev. 73, 830 (1948).

duction of background intensity. Also, to obtain reasonable intensities from the extended neutron source, a beam of relatively large cross section is necessary and, therefore, the distance between the crystal and counter must be large for work at small angles.

The general arrangement is shown in Figs. 1 and 1A and details are shown in Figs. 2 and 2A. The spectrometer is anchored to the floor, its axis of rotation being accurately vertical and intersecting the center line of a horizontal steel collimator inserted into one of the experimental holes of the reactor.

The main bearing of the spectrometer (Fig. 2, item 2a) is the azimuth bearing from a Bofors antiaircraft gun. Preliminary tests had shown that this bearing could support a load of 500 pounds at six feet radius with a deflection at that distance of less than 1/16 of an inch. The bearing is mounted on a structural steel platform. The arm (2b) which carries the counter and its shielding is made of two eight inch structural steel channels, welded to form a rigid beam and bolted to the upper face of the Bofors bearing. Machined ways are provided on the arm for accurate positioning of the counter.

The crystal table (2c) is fifteen inches in diameter and is machined from a rib-reinforced brass casting. It is mounted on a spindle which is centered by a precision 3-ball cone bearing (2d), the balls being equally spaced by balls of smaller diameter. The spindle is maintained vertical by a ground and lapped journal bearing at its lower end. A spring and cam actuated collet (2e) is provided to grip the lower end of the spindle to lock it to the base if required. The edge of the crystal table is graduated in 1/4 degree divisions and a vernier (2f) allows the angle to be read to 0.01 degree.

A second circle (2g), graduated as above and provided with a similar vernier, turns with the arm. This circle is mounted on the same type of bearing as the crystal table. Connection between the arm and the divided circle is made through a link which permits vertical and radial freedom of motion and embodies a tangent screw for zero adjustment.

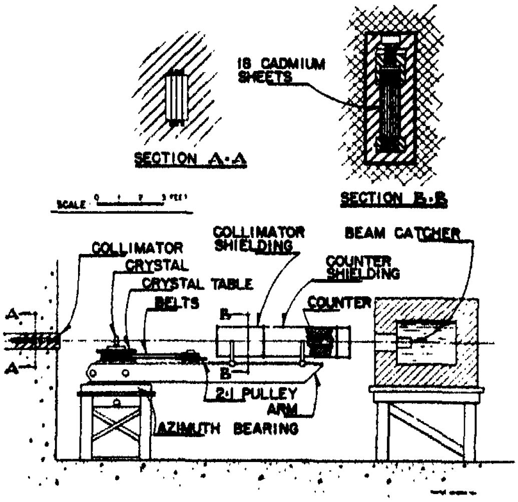

FIG. 1. General arrangement of the neutron spectrometer.

To keep the counter on the line of the diffracted beam, a 2:1 angular relationship between the rotation of the counter arm and the crystal rotation must be maintained. This is accomplished by means of steel pulleys driven by spring-tensioned steel belts (2h). A step pulley (2j) mounted on the arm is held in fixed azimuth by an equal stationary pulley (2i) with its center on the spectrometer axis. The smaller step of pulley (2j) is in 2:1 ratio with the crystal table pulley (2k) and causes it to turn at half the rate of the arm. The crystal table is connected to the pulley (2k) by a clamp and tangent screw. The pulleys are carefully machined and hardened, the edges being chromium plated and ground to a tolerance of ±0.0002 inch. The steel belts are 0.010 inch by 1/2 inch in cross section and are under a tension of 20 pounds. To allow for the effect of belt thickness, the effective pulley radius was taken as the actual radius plus 40 percent of the belt thickness. In practice the angular relationship between the arm and crystal table is held to better than 0.01 degree in a 90 degree rotation of the arm.

To take advantage of the continuous operation of the reactor means are provided for automatic operation of the spectrometer (see Section VIb). Because the belts and pulleys maintain the correct angular relationship between the crystal and counter, it is only necessary to rotate the arm to change the energy setting and a motor drive is provided to move the instrument in discrete steps (Fig. 3). The final pulley of the drive (Fig. 3, item 3a) is connected to the main bearing by crossed belts (3b). The ends of the belts are anchored, thus limiting the rotation by the automatic drive to slightly less than 90 degrees but this is more than is required in practice. Limit stops and switches prevent damage to the belts.

The pulley (3a) is mounted co-axially with the final worm wheel (3c) of the drive gear train and may be connected to it through a clutch plate (3d) which has a circle of 72 equally spaced holes drilled in it. Four equally spaced holes are drilled in the pulley on a circle matching that of the 72 holes, and to engage the clutch steel pins are inserted through a diametral pair of the holes in the pulley into a pair of holes in the clutch

FIG. 1A. A photograph of the neutron spectrometer with the counter rotated almost into line with the main neutron beam. The exit hole from the pile is on the left. A sample cell for gases can be seen mounted in front of the counter collimator both here and in Fig. 2A.

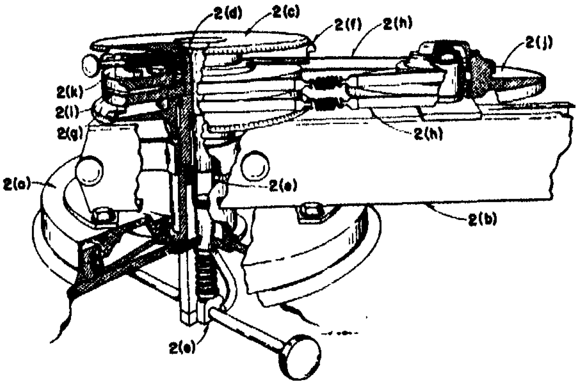

FIG. 2. Details of spindle assemblies and belt linkage.

plate. This provides preliminary arm settings at intervals of five degrees.

The shaft of the final worm carries a circular cam (3e) which operates the controlling microswitch (3f) by means of notches cut in its periphery. The gear ratio has been chosen so that one revolution of this shaft provides one degree of rotation of the arm to better than one part in a thousand. Cams with one, two, four, eight or sixteen notches provide the corresponding fractions of one degree down to 1/16 degree for each step.

For transmission measurements it is necessary to move the sample into and out of the neutron beam at each energy setting. A motor driven sample carriage, which can be seen in Fig. 2A, is attached to the front of the counter collimator shielding. The carriage runs on ballraces and the limits of its travel are determined by microswitches connected into the control system as described in Section VIb. To and fro motion is achieved by a rack and pinion drive from a reversible shaded-pole motor. A boron carbide defining aperture may be placed in front of small samples to reduce the beam to an appropriate area.

III. THE COLLIMATION SYSTEM

The angular spread of the neutron beam emerging from the reactor is limited by a steel plug 81 inches long inserted in a hole through the concrete shield. A rectangular channel (Section AA, Fig. 1) one-inch high by half an inch wide is cut along the axis of the plug. Three equally spaced vertical septa of 0.020 inch steel shim stock along the channel improve the collimation further and the resulting beam has a horizontal divergence of eight minutes of arc and a vertical divergence of about one degree. The beam is very sharply defined and has a total flux of about 4×10^7 thermal neutrons per second. The steel septa are readily removable and four times the intensity can be obtained at a sacrifice of energy resolution.

The hole extends all the way through the shielding and reflector to the walls of the reacting core. The source of neutrons is thus the flux at the outside of the heavy water. Between the inner end of the collimator and the core there is a cast iron gate which may be closed, thereby cutting off the thermal neutron beam and markedly reducing the fast neutron and gamma-radiation. This means of shutting off the beam during operation is a very useful feature of the experimental facilities of the reactor.

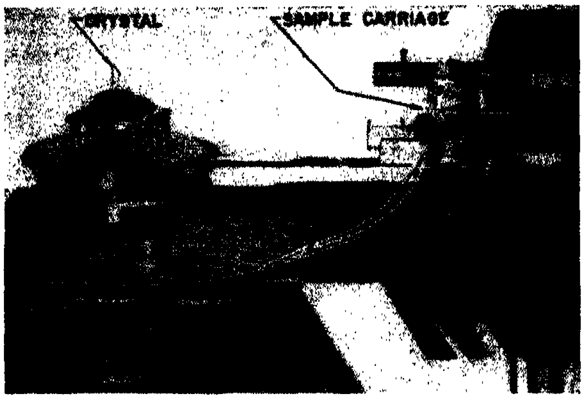

FIG. 2A. A close-up of the crystal table, belt linkage and sample carriage. Entrance to the counter is at the right.

The undeflected beam is received by a catcher (Fig. 1) consisting of a 15 gallon drum containing a saturated aqueous solution of potassium tetraborate. The drum is shielded by one layer of nine inch thick laminated steel and masonite blocks. The radiation from this beam catcher is negligible from the health point of view. It is also worth noting that although the intense beam of neutrons is accompanied by an equally intense flux of gamma radiation, it is possible to work within a foot of the axis of the beam for reasonable lengths of time.

IV. DETECTION SYSTEM

The detector is a proportional counter containing boron trifluoride enriched to 96 percent in the B^{10} isotope. The cathode, which is also the outer shell, is made from copper tubing $2\frac{1}{2}$ inches in diameter and

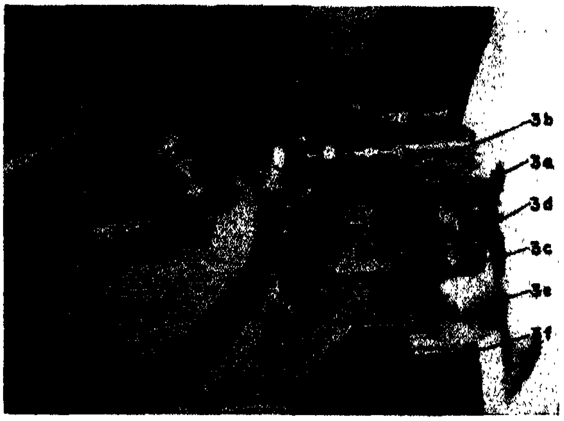

FIG. 3. The motor drive for automatic operations. The motor turns the main arm of the spectrometer by belts (b) the control being through cam (e) which operates switch (f). The pulley (a) is connected to gear (c) by a clutch plate (d).

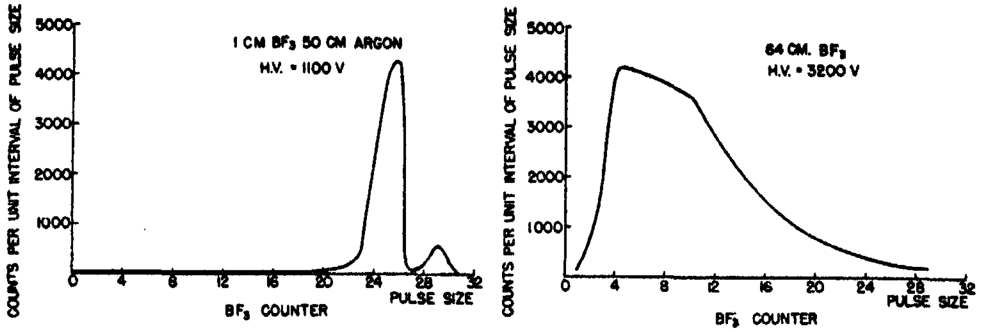

FIGS. 4 AND 5. Pulse size distributions for two pressures of BF_3 in the proportional counters. The distribution of Fig. 4 is characteristic of the boron disintegration, but Fig. 5 shows considerable deterioration of the pulses because of electron attachment in the gas.

25 inches long. The anode is a tungsten wire 0.002 inch in diameter. Neutrons enter through an end window of copper 0.010 inch thick, and pass axially along the counter.

Early studies of the distributions of pulse sizes led to results typified by Figs. 4 and 5. It was assumed that (after allowance for end effects) all disintegrations occurring in the sensitive volume of the low pressure counters could be detected, but that this might not be true for the high pressure counters. Accordingly the low pressure type was used where a knowledge of the absolute neutron flux was required, the efficiency being calculated from the BF_3 pressure, the boron cross section and the length of the anode; the high pressure type was used where maximum sensitivity was required. More recent work has yielded counters with pressures of BF_3 up to 60 cm having the "ideal" characteristic of Fig. 4. These are suitable for absolute measurements and, compared to the low pressure type, have the advantage that the efficiency is much less sensitive to errors in pressure or boron cross section over the important thermal neutron energy range. Figure 6 shows typical efficiency curves. The maximum efficiency for the high pressure type is determined by the length of the inactive region preceding the counting volume. These counters will be discussed in detail in a forhtcoming paper by Mr. I. L. Fowler and one of us (PRT).

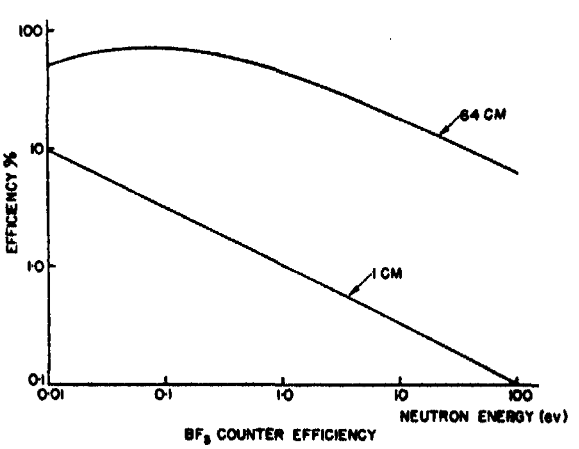

FIG. 6. Efficiency as a function of energy for the two counters of Figs. 4 and 5. The efficiency was calculated using the pressures and the known boron cross section.

The counter and its preamplifier fit inside a cylindrical shield containing a layer of one inch of boron carbide surrounded by four inches of paraffin wax. Mounted in front of the counter and inside similar shielding is a slit system, referred to as a "collimator" (Section BB, Fig. 1), the function of which is to reduce the neutron background by limiting the field of view of the counter to a small area around the crystal. This collimator consists of a steel box divided into narrow vertical apertures by eighteen flat parallel cadmium sheets 0.004 inch thick, 18 inches long and 2¾ inches high. The long edges of the cadmium strips are clamped firmly between steel spacers 1/32 inch thick, and the assembly is stretched vertically by bolts like that shown in Section BB, Fig. 1. The horizontal angular divergence is 12 minutes of arc and this does not affect the resolution of the spectrometer.

The background counting rate, with the entrance of the counter collimator closed and using the more efficient counter, ranges from one to ten counts per minute, depending on the state of neighboring experiments. With the entrance open but the crystal rotated several degrees from the Bragg position, the background is approximately one hundred counts per minute.

For the study of neutron induced nuclear reactions a sample together with the necessary counters and preamplifier may be inserted between the counter and its collimator.

V. CRYSTALS

The crystal holder (seen in Fig. 2A) permits rotation of the crystal about two orthogonal axes through a fixed point which is arranged to be the center of the neutron beam. Thus the crystal planes may be aligned with respect to the beam. All parts of the holder are below the beam and introduce no scattering.

In general the crystals are used in transmission with the advantage that they cover the full area of the beam at small Bragg angles. In some cases, e.g. lithium

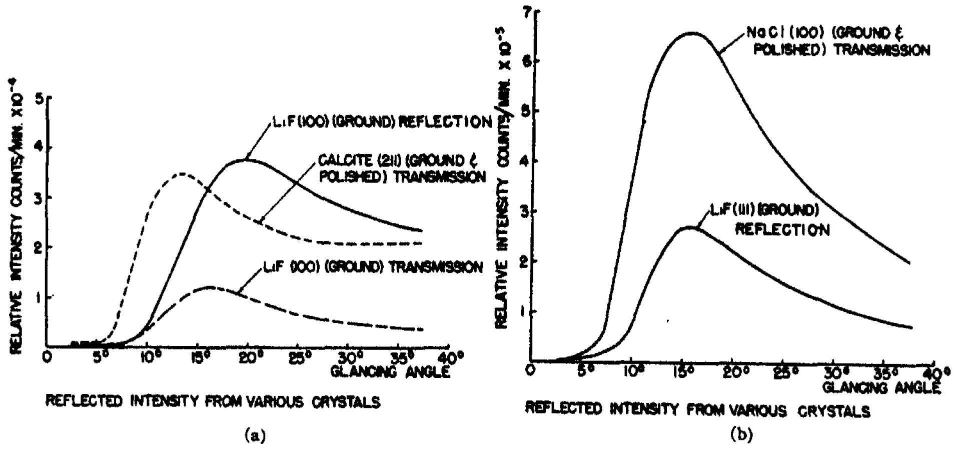

FIG. 7. Reflected intensity from various crystals.

fluoride, large absorption offsets the gain of intensity resulting from this arrangement.

A number of crystals have been prepared, e.g., NaCl, (100) and LiF, (100) (111) cut from samples grown synthetically,* and calcite (211) cut from natural calcite. Counting rates as a function of glancing angle for transmission and reflection by these crystals are plotted in Figs. 7a and 7b.

In a particular experiment choice of crystal depends on a number of factors: (a) Upper and lower energy limits, (b) intensity, (c) resolution, (d) permissible contamination by higher orders. We may group these factors in relation to the following properties of the crystal: (i) Plane spacing with reference to (a). (ii) Crystal structure, chosen planes and relative phases of neutron scattering with reference to (b) and (d). (iii) Mosaic structure with reference to (b) and (c).[9]

In general NaCl has been found to yield a much larger intensity than most crystals and is used for the majority of work at energies below a few electron volts. However, LiF (111) yields less order contamination since even orders are almost entirely absent owing to the opposite sign of scattering from successive planes. LiF (100) has the smallest crystalline plane spacing and yields the highest energy for a given angle but owing to the low reflectivity per plane the intensity is low. For high resolution calcite is used because of its negligible mosaic structure but it yields poor intensities.

We have investigated the mosaic structure of the crystals with a simple double crystal x-ray spectrometer.† The instrument is illustrated in Fig. 8 and is designed for the parallel position only. Two crystal tables, *A* and *A'*, are mounted on ball bearing shafts in dural blocks, *B* and *B'*, which rest on a heavy steel base plate. The first block, *B*, is mounted in a fixed position on levelling screws. The second block, *B'*, can slide on ways perpendicular to the incident x-ray beam. The diffracted beam is detected by an argon filled ion-chamber, *C*, mounted on the second block and connected to a vibrating reed electrometer, *D*. Micrometer heads, *E* and *E'*, serve as tangent screws for the crystal tables. The crystals, mounted on holders similar to that seen in Fig. 2A, are used in the reflection position. The output of the electrometer is connected to an Esterline-Angus recording milliammeter and the chart drive of the recorder turns the second crystal tangent screw *E'*. The instrument plots the rocking curve automatically, a typical curve being shown in Fig. 9.

We have found that most of our samples of synthetically grown NaCl and LiF have mosaic structure of about four minutes of arc width at half maximum but some samples of LiF have large areas of the crystal tilted by an appreciable fraction of a degree to each other and are therefore unsuitable for neutron diffraction work. Ground and polished calcite crystals have widths of 30 seconds which can be reduced to about 5 seconds by etching.[10]

VI. ELECTRONIC EQUIPMENT

The electronic equipment can be divided into two main sections: (a) counting section (b) control and recording section. Figure 10 is a block diagram of the equipment.

(a) Counting Equipment

Two channels of counting equipment are provided, each consisting of its own high voltage supply, linear amplifier with pulse discriminator, and scaling circuits. One channel is connected to the neutron counter and the second is available for use in the nuclear reaction studies referred to at the end of Section IV.

The scaling units are of British manufacture** with

---

* Harshaw Chemical Company, Cleveland, Ohio.

[9] Discussion of some of these points will be found in a paper by E. Fermi and L. Marshall, Phys. Rev. 71, 666 (1947).

† The use of the double crystal x-ray spectrometer for investigating the diffraction pattern of crystals is discussed by Compton and Allison, *X-Rays in Theory and Experiment* (D. Van Nostrand Company, Inc., New York, 1935), Chapter IX.

[10] K. V. Manning, Rev. Sci. Inst. 5, 316 (1934).

** Type 200 manufactured by Dynatron Radio, Maidenhead, England.

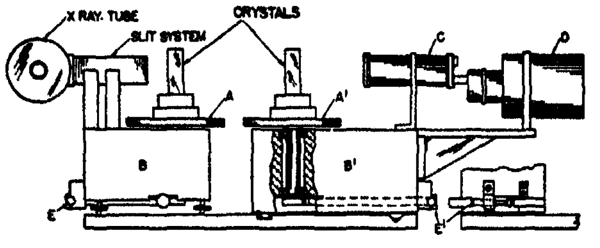

FIG. 8. Double crystal x-ray spectrometer built for checking the quality of the crystals used on the neutron spectrometer.

two scales of ten in series and a mechanical register. Connections are provided for remote control and for remote indication of the information supplied by the units and for these reasons they are eminently suitable for our purpose. By arranging units in series any decimal number of counts is available for recording or automatic control.

(b) Control and Recording System

Automatic operation of the spectrometer is controlled by a relay system connected to the scaling units. The operations are in the following sequences:

(a) Transmission measurements

- (I) sample in
- (II) count
- (III) sample out
- (IV) count
- (V) spectrometer shift and repeat

(b) Reaction rates, etc.

- (I) count
- (II) spectrometer shift and repeat

Backgrounds are determined separately.

The accumulation of a preset number of counts in one of the alternative counting channels results in operation of the register circuit of the last scaler; this energizes the control system and the appropriate motor in the sequence begins to operate. During operation of the motor the relay system automatically stops the scalers and clears any spurious counts. When the operation is completed as indicated by the cam of the main drive or by the limit switches of the sample holder, the motor stops and the scalers are brought into operation again. Overrun of the main drive induction motor is prevented by passing direct current through the motor for about one second immediately after the alternating current is switched off.

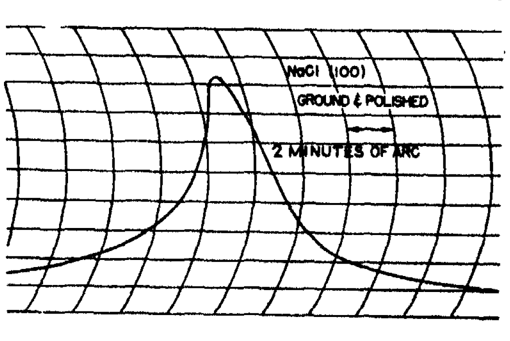

FIG. 9. Rocking curve obtained with the instrument shown in Fig. 8. This corresponds to adjusting the crystal on table *A* (Fig. 8) for Bragg reflection of the x-ray line and table *A'* so that the diffracted beam falls on the face of the second crystal. The second crystal is then turned slowly through the position of parallelism with the first crystal. The above curve is the reflected intensity as a function of angle of the second crystal. The shape of the curve is determined by the characteristics of the two crystals.

Data are fed into a ten-pen Esterline-Angus operation recorder as follows: Two pens mark the times during which each of the motors is operating; a third pen marks the position of the sample; pens are connected to the scalers to record the number of counts at convenient increments; another pen indicates when the reactor is operating at steady power and is connected to the reactor control system; a further pen can, if necessary, be used to record time intervals from a clock, but in general the chart is sufficiently accurate; several pens remain which are available for special purposes.

A record* of deviations up to 25 percent from the normal operating level of the reactor is used for conversion of counting rates to a common basis of power, the detecting instrument being a boron-coated ion-chamber placed in the thermal column of the reactor.

VII. ALIGNMENT

After the spectrometer had been adjusted so that the arm moved accurately in a horizontal plane, the axis of rotation was made to intersect the center of the beam with the aid of photographs taken on x-ray film backed by cadmium. A cadmium pointer was set up on the axis of rotation and its shadow on the photographs served as an index for alignment.

The counter and its collimator are aligned with adjusting screws which carry the supporting frame on the arm. Mechanical alignment of the height and level of this system is sufficient, but to ensure that the counter collimator points at the crystal a maximum counting rate is obtained by alternately adjusting the system and the crystal about vertical axes through their centers.

The zero of the instrument can be found in two ways. A relatively inaccurate method (±0.05°) is to reduce the main neutron beam intensity with absorbers so that the counter can be moved into the beam and a maximum counting rate found. Accuracy to the precision of the angular scale can be had by finding the position of the indium resonance absorption on both sides of zero and taking the mid point.

VIII. PERFORMANCE

(a) Intensities

The counting rates noted in Figs. 7a and 7b are representative of those obtainable with the instrument using the high efficiency counter.

(b) Resolution

When the instrument is set for diffraction at a certain angle, the diffracted beam contains a band of energies, the width of this band depending principally on the horizontal divergence of the primary beam, and to some extent on the mosaic structure of the crystal. Recalling the Bragg equation $n\lambda = 2d\sin\theta$ and that the energy E is proportional to λ^{-2}, we get

---

* The current for this is available to us through the courtesy of Dr. R. E. Bell.

$$-\delta E/E = 2\delta\lambda/\lambda = 2\cot\theta\delta\theta,$$

where $\delta\theta$, measured in radians, may be associated with the horizontal divergence and then $\delta E/E$ is the fractional spread in energy and its reciprocal is a measure of the energy resolution.

The intensity of the diffracted beam is small at high energies and a compromise must be reached between the needs for intensity and resolution. In fact, with the type of spectrometer described here, the resolution is poor above a few volts. For these energies simple differentiation is inadequate and one has to consider the two limits $\theta+\delta\theta$ and $\theta-\delta\theta$. The narrowest collimation available in the present instrument is 0.110 inch in 80 inches, i.e., $\delta\theta = 1.4\times10^{-3}$. Table I contains some examples of the energy ranges involved with this collimation. The composition of the diffracted beam has been calculated for various conditions of collimator and crystal. The case of reflection from a set of crystal planes parallel to the crystal surface is the simplest, the transmission case is complicated by uncertainty as to the behavior of the beam inside the crystal. Only an outline of the calculations and results for reflection is given.

Referring to Fig. 11, we assume a parallel sided collimator and a crystal set for reflection of the central ray at an angle θ_0. The corresponding wave-length is determined by $\lambda_0 = 2d\sin\theta_0$.

The effect of vertical divergence of the beam on the angle of incidence is small and we limit ourselves to the horizontal plane. A ray from any point P in the entrance plane YY' of the collimator meets the crystal at an angle θ. Because the source emits a continuous spectrum comprising neutrons of all relevant wave-lengths, there will be a diffracted ray BQ of wave-length λ satisfying the Bragg equation. If the crystal were perfect the wave-length λ could be diffracted only for directions extremely close to PB. However, we are interested in mosaic crystals for most of our work and this means that the crystal planes are broken up into small areas tilted at small angles about the mean direction. In other words diffraction of the wave-length λ is possible over a much wider range of direction of PB than for a perfect crystal. The diffracted intensity as a function of direction of PB is known as the "rocking curve" of the crystal. If $\pm\alpha$ is the angular range in which the intensity is appreciable then the rays within $\pm\alpha$ of PB will be diffracted, and furthermore they will be focused at Q on the plane XX', where XX' and YY' are equidistant from the crystal. This focusing action is known for powdered crystals and the mosaic is like a powdered crystal with limits $\pm\alpha$ on the orientation.

Table I. Energy spread of the diffracted neutrons.[a]

θ Degrees	E_0 Electron volts	$\frac{E_0-E}{E_0}$ %	$\frac{E-E_0}{E}$ %	$E_{\min}$ Electron volts	$E_{\max}$ Electron volts
20	0.019	0.8	0.8		
10	0.073	1.6	1.6		
5	0.29	3.1	3.3		
2	1.8	7.5	8.5	1.66	1.95
1	7.3	14	18	6.3	8.6
0.5	29	26	42	21.4	41

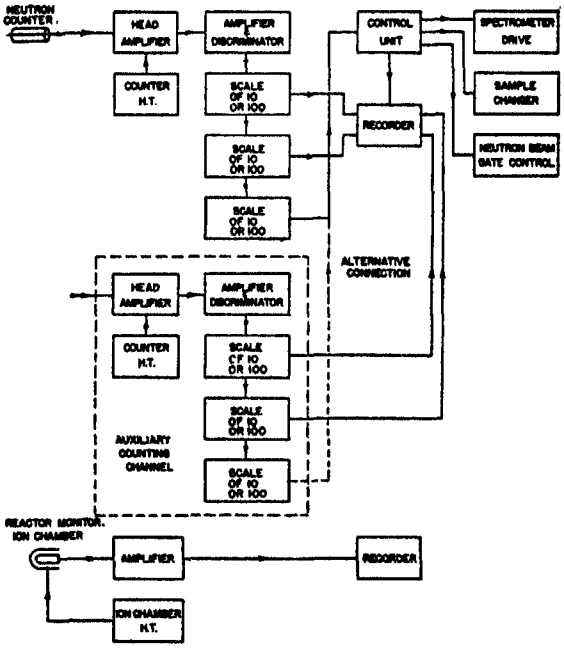

Fig. 10. A block diagram of the arrangement of the spectrometer electronic equipment.

As P is moved across the entrance of the collimator the foci Q for a chosen wave-length trace an image of the collimator entrance on XX', the extent of the image being limited by the collimator channel. The λ_0 image has maximum intensity and due to the variation of θ with λ the images for different wave-lengths are displaced along XX'. It is now clear how the structure of the diffracted beam may be calculated, and that an aperture of width $2a$, equal to the width of the collimator, placed on XX' to coincide with the λ_0 image will pass all diffracted neutrons of wave-length λ_0 but reduce the intensity and limit the range of other wave-lengths.

Using $\delta\theta = \theta-\theta_0$ as the variable which expresses deviation of wave-length (or energy) from the chosen value, the curves of intensity against $\delta\theta$ were drawn for several values of β/α, assuming a rectangular rocking curve (β being the collimator semi-angle). They are nearly triangular and are symmetrical about $\delta\theta = 0$. The effect of an aperture of width $2a$ at XX' is to narrow the triangles without reducing the peaks.

[a] θ = Bragg angle. E_0 = energy corresponding to θ for calcite (211). E = energy corresponding to $\theta\pm\delta\theta$ for calcite (211). $\delta\theta$ = 4.8 minutes of arc.

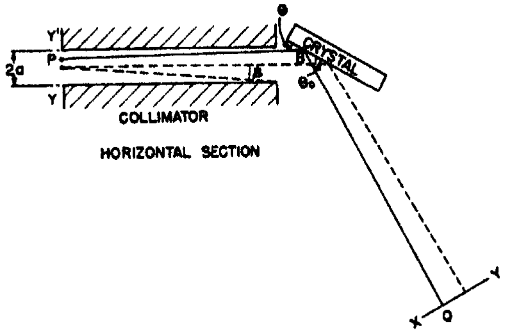

FIG. 11.

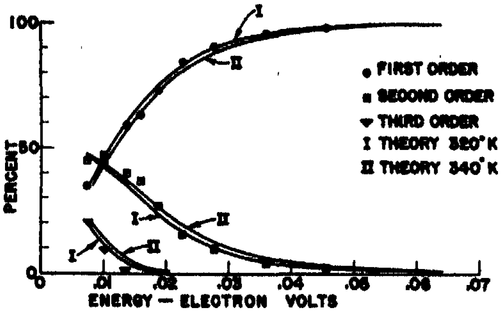

FIG. 12. Comparison of experimentally measured order contamination with the theory of Goldberger and Seitz.

The experimental measurement of such resolution functions would be very difficult. They are however directly related to what we may call the geometrical resolution function, that is, the intensity as a function of angle within the diffracted beam neglecting the effect of the width of the crystal rocking curve. This we have measured by the following method. Calcite crystals free from mosaic structure were mounted on the main axis and on an auxiliary axis behind the exit of the counter collimator. The counter and its shielding were carried on an arm rotating about the auxiliary axis thus forming a two-crystal spectrometer. In the antiparallel position the variation of intensity obtained by rocking the second calcite crystal is the geometrical resolution function and was found to be very nearly triangular in reasonable agreement with that expected.

(c) Orders

In dealing with resolution we are concerned with contamination of the chosen neutron wave-length by an undesirable spread about the chosen value. A second type of contamination arises because a series of wavelengths λ'/n satisfies the Bragg equation where λ' is the chosen wave-length and n is the integer known as the order. The higher orders are always present because of the continuous nature of the neutron spectrum from the reactor.

Sturm[6] has given a discussion of measurement of orders. He found agreement with the theory of Goldberger and Seitz[11] at 0.025 ev. Using the boron absorption method discussed by Sturm, we have measured the orders from a sodium chloride crystal [(100) planes]. The absorbers were sheets of Pyrex glass of thickness 3/16 inch, 1/4 inch and 3/8 inch. Because the same measurements have to serve to calibrate the Pyrex plates, the accuracy at low energies is poor as the calculations involve extrapolating the transmissions from the higher energies.

The results are shown in Fig. 12 together with theoretical curves based on the formula of Goldberger and Seitz. It will be seen that there is fair agreement with the 320°K curve except that the third order is too weak and the second order correspondingly too strong. This could be due to small errors in the calibrations.

The formula assumes a Maxwell distribution of neutron velocities and a perfect crystal. For energies above 0.2 ev the Maxwell distribution is negligible compared to a component of the spectrum which is proportional to E^{-1}. Using resonance absorbers 5 percent second order was found at 2 ev and this quantity does not vary rapidly with energy.

IX. ACKNOWLEDGMENTS

Credit is due Mr. Neilson of the Chalk River design section for the mechanical design of much of the instrument. Various parts were made by the NRC Workshops both at Chalk River and Ottawa and by Messrs. MacLanders and Dean in the Technical Physics Branch workshop. Thanks are due the Electronics Section for design, construction, and maintenance of electronic equipment, and to Mr. I. L. Fowler for construction and filling of our BF_3 counters.

---

[11] M. L. Goldberger and F. Seitz, Phys. Rev. 71, 294 (1947).

Ring Focus in a Thin Magnetic-Lens Beta-Ray Spectrometer*

JOSEPH M. KELLER, ERNEST KOENIGSBERG, AND ARTHUR PASKIN
Institute for Atomic Research and Department of Physics,† Iowa State College, Ames, Iowa

(Received March 28, 1950)

The paths of electrons in a thin magnetic-lens type of spectrometer are described by a non-linear differential equation. The equation was numerically integrated to obtain a set of electron trajectories originating from a point source on the axis of the instrument. Trajectories for off-axis sources were approximated. On the basis of these trajectories, the location and some properties of ring focus were studied. Theoretically calculated line shapes are compared for axial and ring focus. For reasonable values of resolution, the transmission of the spectrometer would be roughly doubled by performing the momentum discrimination by a ring focus baffle instead of by a small counter on the axis.

SEVERAL authors[1–3] have suggested the possibility of using "ring focus" in a magnetic-lens spectrometer to obtain increased intensity for a given resolution. DuMond[4] and Persico[5] have recently studied the case of ring focus in a solenoid spectrometer, which lends itself to straight-forward calculations. Our paper presents a theoretical study of the electron trajectories in a thin-lens spectrometer of the type now in use at Iowa State College.[6] Unlike the case of the solenoid, trajectories in a thin-lens spectrometer cannot readily be described by analytic expressions and must be obtained by numerically integrating a differential equation.

Ring focus may be described in several ways. If the focusing action of a thin magnetic-lens is examined, it is found that electrons with a larger initial slope cross the axis closer to the lens than electrons with the same momentum and with a smaller slope. Therefore, the trajectories of two electrons with the same momentum and slightly different initial slope intersect. The family of electron trajectories will form an envelope, which in space is an axially symmetric surface. Any point on the envelope constitutes "ring focus" for some small range in initial slopes. The envelope is clearly shown in Fig. 3, below, which is a plot of radial distance *versus* axial distance for a set of trajectories of different initial slopes and a given momentum.

There is another way of considering ring focus, which brings out its possible advantages. If we choose a point at random beyond the lens, electrons of varying momentum will pass through this point, providing they are suitably directed initially. Figure 1 shows the qualitative relation between initial slope and momentum for electrons passing through some such point. Electrons of enormously high momentum are not appreciably affected by the magnetic field. If they are aimed geometrically for the point in question, they will pass through it. All the electrons of lower momentum require a larger initial slope in order that after deflection by the magnetic field they will still pass through the point. The gradual increase of initial slope, as electron momentum is decreased, is shown by the lower branch of the curve, Fig. 1. But there must be some minimum momentum, since sufficiently slow electrons will be deflected too much ever to reach the point. That there must be another branch to the curve is implied in the crossing of trajectories, already mentioned. For every trajectory (of electron momentum greater than the minimum) that passes through the point, there must be another trajectory passing through the same point corresponding to the same momentum, but with a different initial slope. As the momentum is decreased, the two initial slopes must both approach the initial slope of the trajectory for the minimum momentum.

Suppose we consider placing a discriminating baffle at this point, so as to transmit only electrons which pass

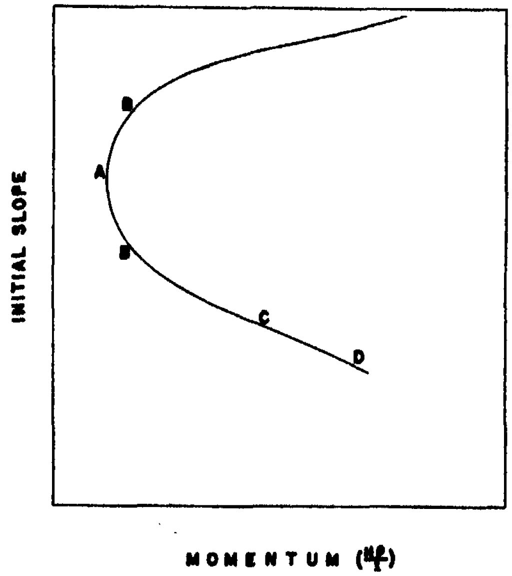

FIG. 1. A set of electrons pass through any point beyond the lens. This figure shows the relationship between initial slope and momentum for these electrons. The existence of a minimum momentum (at *A*) is essential for ring focus.

---

* Contribution No. 87 from the Institute for Atomic Research and Department of Physics, Iowa State College, Ames, Iowa.

† Work was performed at the Ames Laboratory of the Atomic Energy Commission.

[1] Clifford M. Witcher, Phys. Rev. 60, 32 (1941).

[2] S. F. Frankel, Phys. Rev. 73, 804 (1948).

[3] S. F. Frankel and E. C. Nelson, Navy Contract N6 onr-238 Task V, University of Southern California, (1948).

[4] Jessie W. M. DuMond, Rev. Sci. Inst. 20, 160 (1949).

[5] E. Persico, Rev. Sci. Inst. 20, 191 (1949).

[6] Jensen, Laslett, and Pratt, Phys. Rev. 75, 458 (1949).

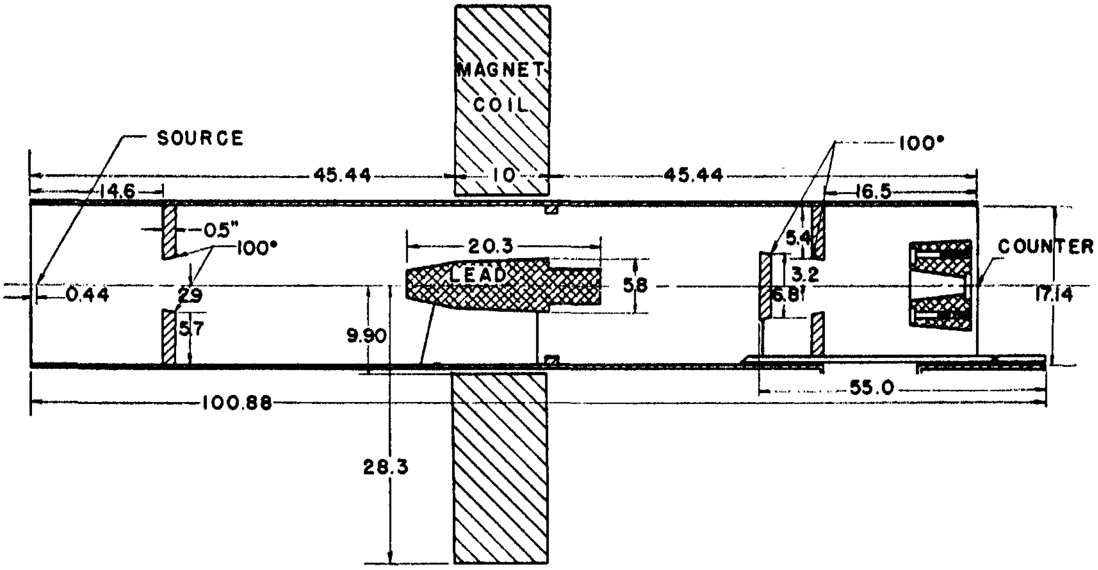

FIG. 2. Dimensions of the spectrometer at Iowa State College.

through this point. This will constitute a possible scheme for selecting electrons of a limited momentum range, providing we have an auxiliary set of baffles to limit the angles transmitted by the spectrometer. If the point has been chosen arbitrarily, then a range of momentum *CD*, determined by the angular selector, will pass through the discriminator. In this region of operation, varying the transmission of the angular selector will cause a linear variation in the "irresolution" (reciprocal resolution). This type of resolution-transmission behavior is characteristic of axial focus. If we now select the point where we place our final discriminator as the position of ring focus, this is equivalent to working at the minimum momentum of Fig. 1. Then a range of initial angles will allow the momentum interval *AB* (Fig. 1) to pass through the point. This type of operation of a spectrometer would exhibit an irresolution that should vary quadratically with the intensity. Hence, on the basis of such a crude analysis it might be expected that ring focus would yield an improvement of transmission, for a given resolution, over axial focus.

The dimensions of the spectrometer under consideration are shown in Fig. 2. The baffles indicated are those that have been used with the conventional axial-focusing selection.

TRAJECTORIES FOR A POINT SOURCE

From the equations of motion for an electron in a cylindrically symmetric magnetic field (no azimuthal component)[7,8] a single equation for an electron trajectory can be obtained. The magnetic field is described by a vector potential, which is always in an azimuthal direction. The two constants of motion—energy (or velocity) and (canonical) angular momentum about the axis of cylindrical symmetry—can be used to eliminate the time and the azimuthal variable. In particular, for any particle that starts at or passes through the axis, the angular momentum is zero, and the resulting equation for the "trajectory" (radial displacement r as a function of axial displacement z) is[9]

$$r''(k^2-A^2)/(1+r'^2)-r'A(\partial A/\partial z)+A(\partial A/\partial r)=0. \quad (1)$$

Here A is the vector potential per unit magnetizing current, and k is the electron momentum in "$H\rho$" units, also divided by the magnetizing current. Primes indicate differentiation with respect to z.

To determine the vector potential, the magnetic field was first calculated along the axis. For a coil of rectangular cross-section of axial length L, inner and outer radii a_1 and a_2, and n turns, the axial field per ampere of magnetizing current is given by[10]

$$H_0(z)=\frac{2n\pi}{10L(a_2-a_1)}(B(a_2)-B(a_1)), \quad (2)$$

where

$$B(a)=\left(z+\frac{L}{2}\right)\ln\left\{a+\left[a^2+\left(z+\frac{L}{2}\right)^2\right]^{\frac{1}{2}}\right\}$$
$$-\left(z-\frac{L}{2}\right)\ln\left\{a+\left[a^2+\left(z-\frac{L}{2}\right)^2\right]^{\frac{1}{2}}\right\}.$$

The values used were: $a_1=9.9$ cm, $a_2=28.3$ cm, $L=10$ cm, and $n=2799$. In using these values of the inner and

---

[7] H. Busch, Ann. d. Physik 81, 974 (1926); Arch. Elect. 18, 583 (1927).

[8] L. S. Goddard, Proc. Phys. Soc. (London) 56, 372 (1944).

[9] The derivation of this equation is outlined in the Appendix. See also: N. F. Verster, Applied Scientific Research B1, 363 (1950); G. Liebmann, Proc. Phys. Soc. B62, 753 (1949).

[10] Deutsch, Elliot, and Evans, Rev. Sci. Inst. 15, 178 (1944).

outer radii for computing the field on the axis it was recognized that Eq. (2) only approximated the true field intensity. The magnetic coil is not in reality a continuum of turns as required in the derivation of Eq. (2). Seventeen cooling shims, each 0.2 cm thick, are inserted throughout the magnetic coil. The effect of these shims is to make the field at the center of the lens stronger than the value calculated by Eq. (2), and to reduce the field below the calculated value at distances greater than ten cm from the center.

The vector potential at any point (r, z) was calculated from the field H_0 on the axis by the well-known expansion[10]

$$A(r,z)=\frac{r}{2}H_0(z)-\frac{r^3}{16}\left(\frac{\partial}{\partial z}\right)^2 H_0(z)+\frac{r^5}{384}\left(\frac{\partial}{\partial z}\right)^4 H_0(z)$$
$$+\cdots+\frac{(-1)^s}{s!(s+1)!}\left(\frac{r}{2}\right)^{2s+1}\left(\frac{\partial}{\partial z}\right)^{2s} H_0(z)+\cdots. \quad (3)$$

The field H_0 was calculated by Eq. (2) at 2 cm intervals, and five successive derivatives of H_0 were obtained by differences. In calculating A by Eq. (3) only three terms in the series were retained. The errors introduced by neglecting sixth differences of H_0 were studied in the region of the lens for one trajectory. The error in A was found to be less than 0.2 percent, and the error in $\partial A/\partial r$ was no greater than 0.7 percent. The over-all effect on the path was less than this because the error in curvature reversed sign at four centimeters from the center of the lens. The error in r due to the error in field calculations in the region of ring focus is estimated to be about 0.8 percent (0.023 cm).

TABLE I. Positions of ring focus.

Momentum, k gauss cm/amp.	Radius r cm	Distance past center cm
960	2.823	22.65
990	2.872	24.57
1020	2.925	26.90
1050	2.979	29.30
1080	3.033	31.97
1110	3.090	34.30
1140	3.133	36.90

It might be pointed out that we deliberately avoided the paraxial approximation as we did not feel that it would yield sufficient information for a study of ring focus.

The actual computations involved in the numerical integration of the differential equation of motion were carried out on International Business Machines. It was advantageous to use automatic computing machines because in this way we could obtain at once a large number of trajectories. All of these trajectories werg desired to obtain information such as line shape for rine focus and the behavior of ring focus for different momenta. The numerical integration was carried out using

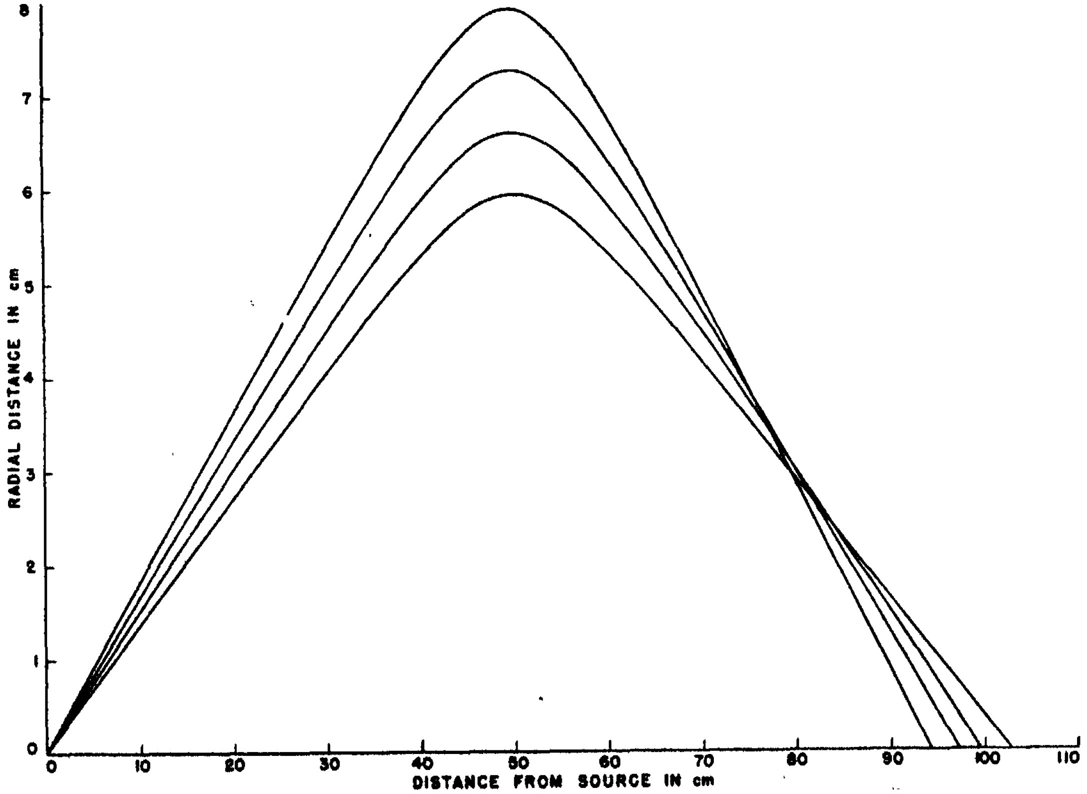

FIG. 3. Trajectories for electrons of a given momentum.

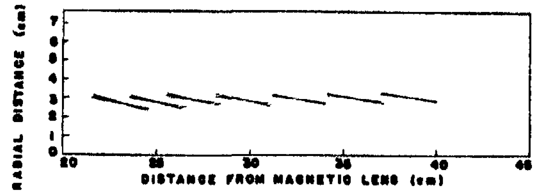

FIG. 4. Location of ring focus. The positions of ring focus are indicated by the intersection of extremal rays for different momenta. The z coordinate of the position of ring focus increases with increasing momentum.

two centimeter intervals in z (the axial distance). The method used is described in the appendix.

Forty-nine separate electron trajectories were calculated for a point source on the axis, using seven values of momentum and seven initial slopes. The selected values of initial slope and momentum were:

Initial slope (tanα)	Momentum (k) gauss cm/amp.
0.1350	960
0.1425	990
0.1500	1020
0.1575	1050
0.1650	1080
0.1725	1110
0.1800	1140

The seven trajectories for a given momentum were plotted together so that the location of ring focus could be determined (radius is plotted against axial distance from source). The set of trajectories for $k=1050$ gauss cm/amp. is shown in Fig. 3. The "aberration" of the lens which makes ring focus possible can easily be seen from this plot.

As was noted earlier, every point over a considerable region of the spectrometer is a point of ring focus for a definite momentum and some initial slope (actually for a small range of slopes). Likewise for a chosen electron momentum, every point along the envelope of trajectories for that momentum is a point of ring focus for some initial direction. A more practical way of discussing the location of ring focus than either of these is to consider a given range of initial electron directions and to describe how the position of ring focus varies with momentum for this range. Further, since we are interested in collecting electrons starting out through a finite range of solid angle, we define the point of ring focus as the intersection of the extremal trajectories. All the electrons of the chosen momentum and range of initial directions will pass between this intersection and the envelope of the trajectories. Intersections of the extreme trajectories for different momenta are shown in Fig. 4. We note that the locus of the point of ring focus approximates a straight line at nearly constant radius. The location of ring focus is tabulated in Table I.

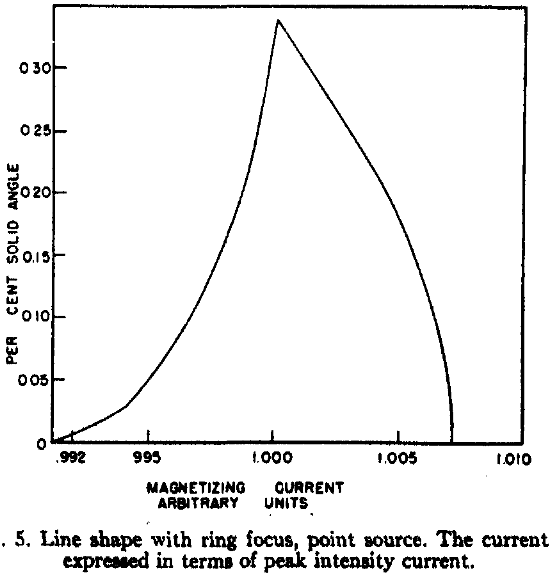

FIG. 5. Line shape with ring focus, point source. The current is expressed in terms of peak intensity current.

LINE SHAPE FOR A POINT SOURCE

The calculated trajectories contain the necessary information for determining line shape. With a monoenergetic source, for purposes of calculation, we have assumed that electrons are ejected from the source with the same intensity in all directions. Then, the intensity collected by the counter will be proportional to the difference in values of cosα (α is initial slope angle) between the extreme rays collected. We considered the ring for ring focus as an annular opening in a plane baffle perpendicular to the axis. To focus a given momentum, the width of the annulus was chosen just large enough to admit the extreme rays where they intersect, and also the envelope of trajectories of this momentum. Having chosen the axial position of the ring, we plotted, for several values of focusing current, the values of cosα as a function of the radius at which the trajectory in question crosses the plane of the annulus. In this way we determined the range in initial angles admitted by the annulus, and hence the line shape (see Fig. 5). In order to reduce the long tail on the low current end of the line, it was assumed that baffles placed between the source and the field coils eliminated all initial slopes outside of the range of values for which trajectories were calculated. These baffles do not appreciably affect the line shape near its peak. It was also assumed that the counter had a large enough window to collect all electrons passed by the baffles and the discriminating annulus.

A similar calculation was made for momentum discrimination by a 0.82 cm diameter counter placed on the axis without any annulus ("axial focusing"). The baffle system used in this calculation is shown in Fig. 2. Axial focus is somewhat more affected by baffle location than ring focus. The results are shown in Fig. 6.

To investigate the validity of Frankel's quadratic dependence of irresolution on transmission[3] for our spectrometer, line shapes were determined with various transmissions. The range of solid angle admitted was

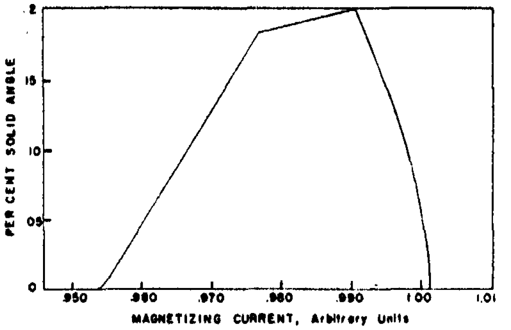

FIG. 6. Line shape with axial focus, point source. The unit of current is the same as Fig. 5.

altered by considering different minimum initial slopes, keeping the maximum initial slope fixed at 0.180. The irresolution is the full momentum width at half maximum (Δk) divided by the peak momentum (k). Intensity, Φ, is defined as the fraction of 4π-steradians transmitted. For these calculations the value of k for peak transmission was kept fixed at 1050 gauss cm/amp., requiring a shift in location of the plane of the discriminating annulus as well as changes in the radial dimensions of the annulus.[11] The results are approximated by the relation $\Delta k/k = (25\Phi)^2$.

Frankel has suggested that an optimum arrangement would be obtained using an annulus in a cone instead of a plane baffle. The cone would contain positions of ring focus of neighboring momenta for the initial angles admitted. We have found little difference in line shape between the two types of annulus for reasonable intensities.

EFFECT OF FINITE SOURCE SIZE

The effect of a finite source diameter was obtainable from the results of calculations made on an axial, point-source basis. The method of finding the trajectories of electrons originating off the axis, but still with zero angular momentum, made use of the symmetry of the magnetic lens about the mid-plane. It was only necessary to reverse any rays with a given calibration constant to obtain a new set of rays originating off the axis.

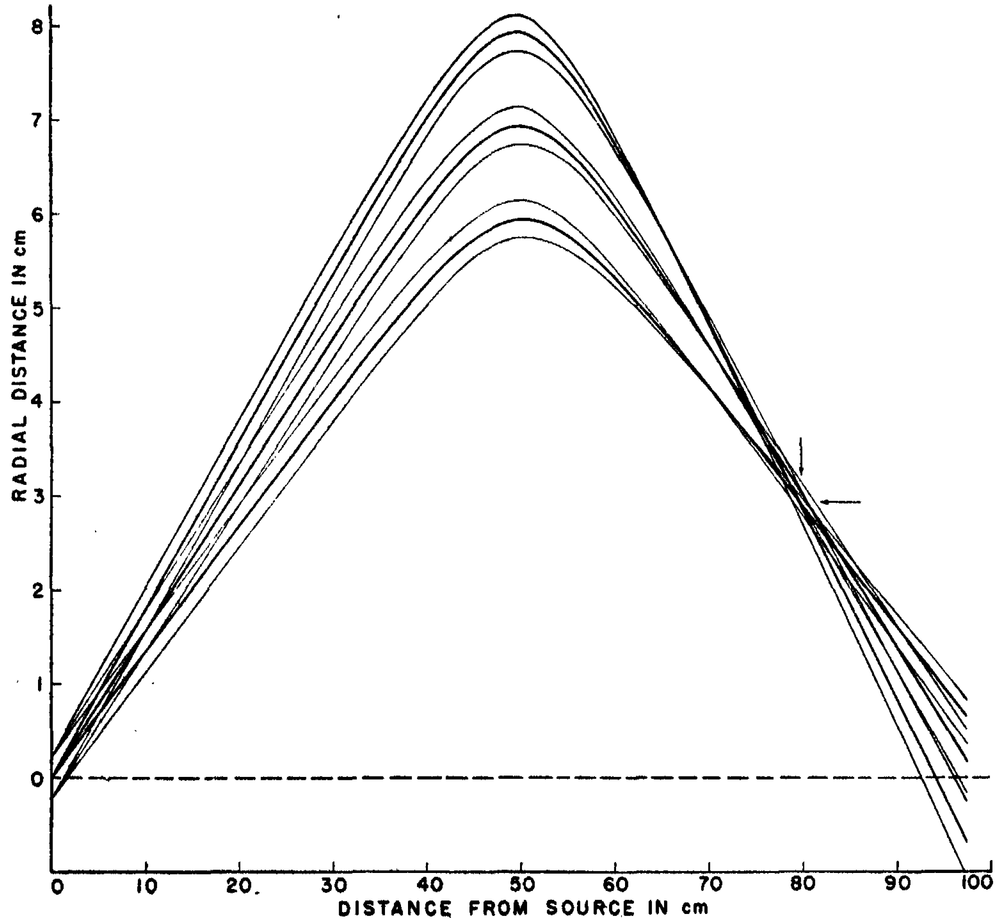

FIG. 7. Effect of finite source diameter on electron trajectories. These trajectories are for electrons with a given momentum and zero angular momentum about the central axis. Arrows indicate the location of ring focus for a point source.

---

[11] In practice one might equally well contemplate keeping the plane of the annulus fixed. This would imply a change in calibration constant (optimal value for k) as the range of the admitted angles was altered. Our choice of keeping k fixed was one of convenience. In tracking down sources of irregularities in the trajectories, we discovered that the business machines failed to perform properly one operation when the r value exceeded 6.3 cm ($r^5 > 10^4$). Working in the neighborhood of a chosen value of k required less recalculation. The trajectories for $k = 1050$ gauss cm/amp. were recomputed over the range of large r, using desk calculators. Corrections to the trajectories for $k = 1020$ and 1080 gauss cm/amp. were then estimated.

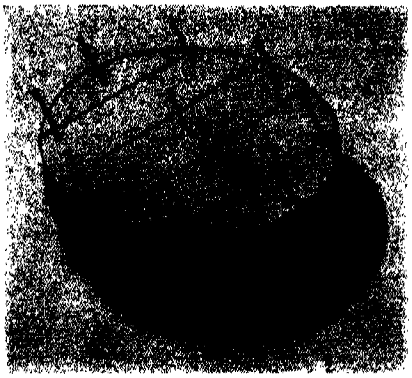

FIG. 8. The model illustrates a set of electrons starting out from an extended source in a given direction. Vectors one and five indicate electrons of zero angular momentum. The angular momentum of all electrons starting outside of the 1–5 plane is not zero. In subsequent calculations, the source was divided into zones as shown.

For rays starting off the axis, "zero angular momentum" means that if such an off-axis trajectory be extended (forward or backward) there will be at least one intersection with the axis.

A detailed examination was made of three trajectories with electron momentum $k=1050$ gauss cm/amp., initial slopes 0.1350, 0.1575 and 0.1800 (the mean and extreme rays). The entire set of trajectories of $k=1050$ gauss cm/amp. was reversed as described above. A linear interpolation was made and the three reversed rays found that had the same initial slope as the three reference trajectories. Assuming that a small displacement off the axis at the source would have only a small effect on the trajectories, a linear interpolation was made between off-axis and axial trajectories to obtain rays of a given initial slope originating from any source point.

The effect of a finite source diameter, neglecting angular momentum, is shown in Fig. 7. The two sets of off-axis trajectories were chosen to originate from points 0.225 cm off the axis.

A thorough treatment of finite source size must also take into consideration the cases where the angular momentum is not zero. This complicates the equation of an electron trajectory, but cannot change the physical behavior much. Consider electrons starting from the source in some particular direction. A finite source diameter replaces a single ray by an initially parallel beam. Let us think of the plane containing the axis and parallel to this initial direction. Displacement, in this plane, of a ray from an axial starting point gives rise to a trajectory of zero angular momentum. Displacement of a ray out of this plane gives rise to a trajectory of finite angular momentum. As the displacement which causes angular momentum is small compared to the maximum radius of the electron path, the effect of angular momentum must likewise be small. Figure 8 is a pictorial representation for the cases discussed.

The equation of an electron trajectory of arbitrary angular momentum in the presence of fields is obtained by replacing A, wherever it occurs, by $(A-pc/Ier)$, where p is the angular momentum of the focused electron, c the velocity of light, I the magnetizing current, and e the charge on the electron. The result is:

$$\frac{r''[k^2-(pc/Ier-A)^2]}{(1+r'^2)}+r'(pc/Ier-A)(\partial A/\partial z)$$
$$-(pc/Ier-A)(pc/Ier^2+\partial A/\partial r)=0. \quad (4)$$

Including angular momentum in the treatment of a finite source size has two effects. In the region of strong field, angular momentum alters the effective field slightly. In weak fields, the trajectories are approximately straight lines in space but they do not intersect the axis. When radius is plotted against axial distance, these straight lines appear as hyperbolas.

Figure 9 shows the effects of angular momentum on the sets of rays illustrated in Fig. 8. The rays were started and ended by matching them to the proper hyperbolas. Corrections through the region of strong field were aided by the fact that the trajectory of maximum angular momentum coincided, near the lens, with the axial point-source (zero angular momentum) trajectory. For clarity, in Fig. 9 only the paths for maximum angular momenta were continued beyond the point of intersection. It can be seen that the effect of angular momentum is such that only displacements of the source point in the axial plane (of zero angular momentum) containing the initial electron direction need be considered.[12]

The line shape for a finite source (0.56 cm diameter) was therefore calculated by dividing the source into sections as in Fig. 8 and weighting each section according to its area.

Line shapes for ring and axial focusing of a finite source are shown in Fig. 10 and Fig. 11. For axial focusing the same experimental arrangement (Fig. 2) was considered as for point source calculations on axial focusing. The geometry used for ring focus included, in addition to the ring selector, a set of auxiliary baffles. These were again the baffles of Fig. 2, but with their position relative to source and counter reversed. This gave a somewhat better line shape than the baffles considered for ring focus of a point source, and were convenient experimentally.

One effect of an extended source not previously mentioned is to broaden the ring focus. While a ring width of 0.12 cm passed the desired rays for a point source, twice this width seems a minimum reasonable value for the source size discussed. The line shape shown in Fig. 10 was calculated for a ring 0.36 cm wide. A still wider ring will allow our spectrometer to transmit more than twice the intensity that it passes with axial focusing, without exceeding the axial focus irresolution of approximately 3 percent.

---

[12] More generally, under the approximation that a displacement of the source point from the axis produces at any axial position z a change in radius proportional to the displacement of the source, there always exists (except where the trajectory approaches the axis) some direction in which source displacement has no effect. That this direction is nearly perpendicular to the plane of initial electron motion seems to be a property of a thin lens. A comparison of our analysis with that of DuMond[4] for a solenoid indicates that the same result would not hold in his case.

DISCUSSION OF RESULTS

Our calculated line shapes (Figs. 10, 11) agree roughly, though not in detail, with experimentally observed line shapes for internal conversion sources. In particular, the theoretical and experimental half-widths are in good agreement. Further, we have calculated a calibration constant from our line shape. From Fig. 11 we would obtain directly a value 1069.5 gauss cm/amp. The calibration constant is defined as the value of the momentum-per-unit-current k midway between the values for half-maximum transmission. This value must be corrected as follows (Appendix 3):

Effect of cooling shims in magnet coil..... 5.4.
Effect of higher differences in magnetic field. 1.8.

$$\begin{array}{r} 1069.5\\ 5.4\\ 1.8\\ \hline 1076.7\pm 4 \text{ gauss cm/amp.}\end{array}$$

The suggested uncertainty is half of the above corrections, combined with others errors discussed in the Appendix. Comparison of the theoretical constant with the best experimental value ($k=1078.5\pm 3$) gauss cm/amp. is satisfactory.

A further confirmation of our trajectories was obtained by Boley, Pratt, and Nichols,[13] who used photographic plates to detect electrons in the spectrometer and in this way were able to verify the location and width of the ring focus.

Our calculations have shown that using ring focus in a thin lens beta-ray spectrometer produces an increase in transmission of better than a factor of two for a given resolution ($\Delta k/k \leqq 3$ percent).

We would like to acknowledge the many helpful discussions with Messrs. L. J. Laslett, E. N. Jensen, W. W. Pratt, and F. I. Boley. We would also like to thank R. C. Ling for his preliminary calculations of the field and C. C. Mosier for the care with which he carried out the numerical integrations.

APPENDIX

1. Equations for the Trajectories

An axially symmetric magnetic field (with no azimuthal component) can be represented as the curl of a vector potential A_θ, whose direction is always azimuthal. The motion of a charged

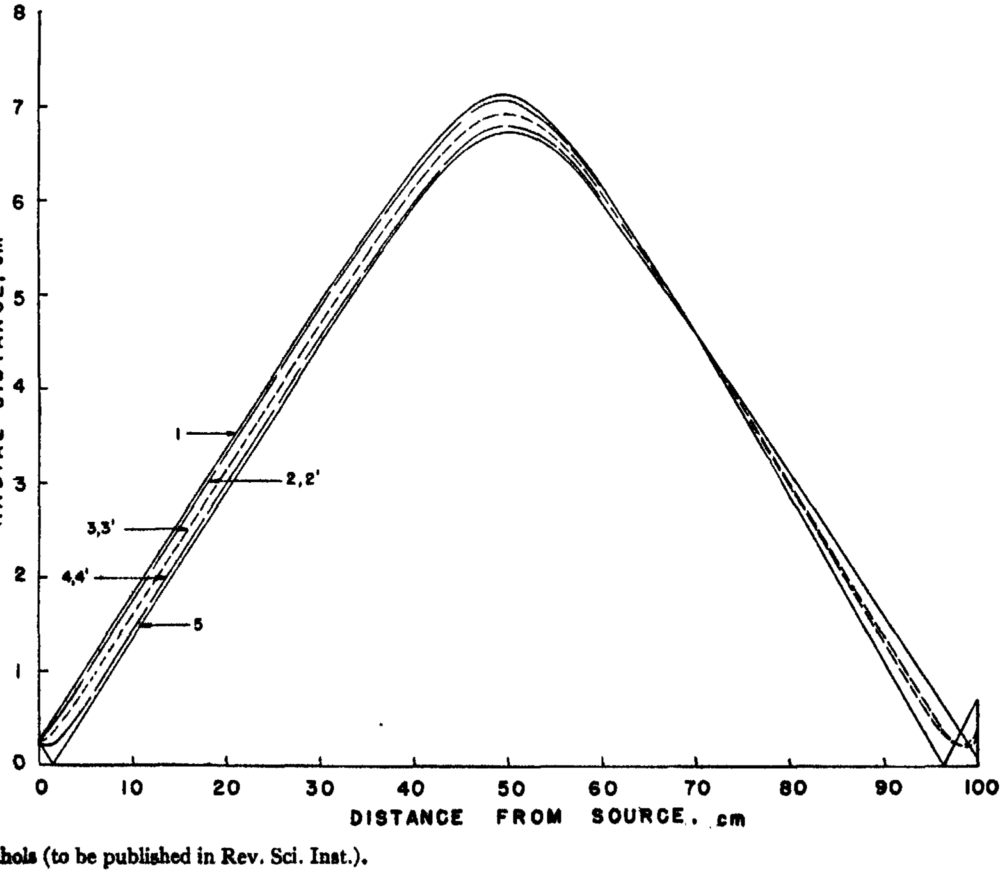

FIG. 9. Effect of angular momentum on electron trajectories. The trajectories are numbered the same as in Fig. 8. Only the rays of zero angular momentum (1,5) and maximum angular momentum (3,3') are continued past the central region.

---

[13] Boley, Pratt, and Nichols (to be published in Rev. Sci. Inst.).

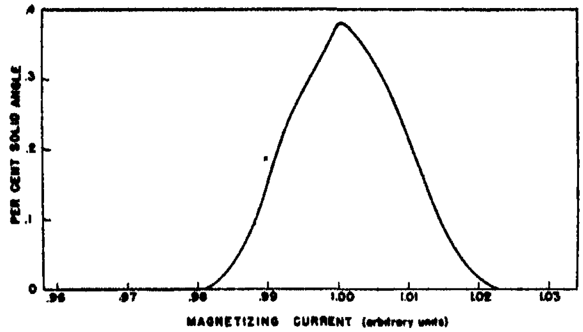

FIG. 10. Line shape with ring focus, extended source. The unit of current is the same as Fig. 5.

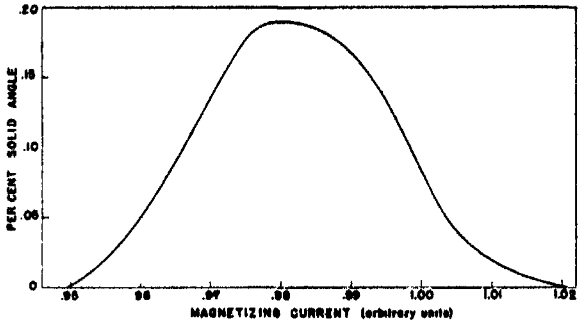

FIG. 11. Line shape with axial focus, extended source. The unit of current is the same as Fig. 5.

particle in such a field is governed by the equations

$$\begin{aligned}(d/dt)(m\dot{r}) &= mr\dot{\theta}^2+\frac{e\dot{\theta}}{c}\frac{\partial}{\partial r}(rA_0),\\ (d/dt)(m\dot{z}) &= (er\dot{\theta}/c)(\partial A_0/\partial z),\\ (d/dt)(mr^2\dot{\theta}+erA_0/c) &= dp/dt=0.\end{aligned}\tag{A-1}$$

In these equations, r, and z are the cylindrical coordinates describing the position of a particle of charge e and (relativistic) mass m at time t. A dot indicates time differentiation, and c is the velocity of light. The particle speed v and hence also the mass, is a constant of the motion, since a steady magnetic field can do no work on a charge. p, the canonical angular momentum about the symmetry axis, is also a constant of the motion. By introducing it into the first two equations, the angular velocity $\dot{\theta}$ can be eliminated, and the equations

$$\begin{aligned}(d/dt)(m\dot{r}) &= (e^2/mc^2)(pc/er-A_0)(pc/er^2+\partial A_0/\partial r),\\ (d/dt)(m\dot{z}) &= (e^2/mc^2)(pc/er-A_0)(\partial A_0/\partial z)\end{aligned}$$

result.

The equations for an orbit are obtained from the equations of motion by replacing time by some other quantity, say z, as the independent variable. The left-hand members of the last two equations will now be expressed as

$$\dot{z}\frac{d}{dz}\left(m\frac{dr}{dz}\dot{z}\right)=m\dot{z}^2\frac{d^2r}{dz^2}+m\frac{dr}{dz}\dot{z}\frac{d}{dz}(\dot{z})$$

and

$$m\dot{z}(d/dz)(\dot{z})$$

respectively. $\dot{z}$ in turn can be expressed in terms of the particle speed v by the relation

$$\begin{aligned}v^2 &= \dot{r}^2+\dot{z}^2+r^2\dot{\theta}^2\\ &= \left[1+\left(\frac{dr}{dz}\right)^2\right]\dot{z}^2+\frac{e^2}{m^2c^2}\left(\frac{pc}{er}-A_0\right)^2.\end{aligned}\tag{A-2}$$

Carrying out the indicated substitutions, we obtain the single differential equation[14]

$$\begin{aligned}r''\frac{[(mvc/e)^2-(A_0-pc/er)^2]}{1+r'^2}&-r'(A_0-pc/er)(\partial A_0/\partial z)\\ &+(A_0-pc/er)(pc/er^2+\partial A_0/\partial r)=0.\end{aligned}\tag{A-3}$$

Primes indicate differentiation with respect to z. The expression mvc/e is the momentum of the particle expressed in "$H\rho$" units. If we divide the equation through by I^2 (the square of the current), write k for mvc/eI, and A for A_0/I, as has been done in the body of the paper, Eq. (A-3) becomes Eq. (4). Setting $p=0$ reduces this to Eq. (1).

2. Numerical Integration

The trajectories, $r(z)$, were calculated at 2 cm intervals in z ($\Delta=2$ cm) by the following process. (We denote derivatives with respect to z by primes.) Assume $r(z)$, $r(z-\Delta)$, $r(z-2\Delta)\cdots$known.

1. Calculate $r'(z)$ by the approximate relationship

$$r'(z)=[3r(z)-4r(z-\Delta)+r(z-2\Delta)]/2\Delta.\tag{A-4}$$

2. Calculate A, $\partial A/\partial r$ and $\partial A/\partial z$ for the position (r, z).
3. Solve Eq. (1) for $r''(z)$.
4. Compute $r(z+\Delta)$ by the approximate relationship

$$r(z+\Delta)=2r(z)-r(z-\Delta)+\Delta^2r''(z).\tag{A-5}$$

The cycle is repeated to obtain $r(z+2\Delta)$ etc.

The integration was begun assuming no change in slope until 8 cm from the source. A and r and their derivatives were carried out to six decimal places.

3. Errors

There are two types of errors involved in the trajectory calculations: those inherent in the step-by-step method of calculating and those associated with the approximate calculation of the magnetic field. The first type of error is quantitatively much smaller than the second. It is discussed first because of the basic nature of the treatment of errors involved.

Errors Arising from Numerical Integration

(a) Replacing the differential equation by difference equations, as in Eq. (A-5), introduces a cumulative error in $r(z)$.

(b) The error in r due to (a) will produce an error in the calculated value of the second derivative since A and its derivatives will be calculated at the incorrect value of r. This will in turn produce further errors in r and its first derivative.

Since the magnetic field increases as r increases (i.e., as one approaches the field windings), at least in the strong field region, too large a value of r will produce too large a curvature. This will tend to compensate for the error in r. However, the slope of the calculated trajectories will be in error after the particle passes out of the strong field region. Errors of the types (a) and (b) have been estimated, and the correction applied to the trajectories, before any further calculations (on ring focusing, line shapes, etc.) were made.

r'' is also dependent on r' according to Eq. (1). r' is approximated by difference equation (Eq. (A-4)) and is also affected by any error in r. However, the dependence of r'' on r' is very weak, and errors in r'' due to incorrect values of r' have been neglected.

To study the propagation of errors we observe that:

$$r(z+\Delta)=r(z)+\Delta r'(z)+\Delta^2r''(z)/2!+\Delta^3r'''(z)/3!+\Delta^4r^{(4)}/4!+\cdots,$$

and

$$r(z-\Delta)=r(z)-\Delta r'(z)+\Delta^2r''(z)/2!-\Delta^3r'''(z)/3!+\Delta^4r^{(4)}/4!+\cdots;$$

then

$$\begin{aligned}r(z+\Delta)-2r(z)+r(z-\Delta)=\Delta^2r''(z)&+\Delta^4r^{(4)}(z)/12\\ &+2\Delta^6r^{(6)}(z)/(6!)+\cdots.\end{aligned}\tag{A-6}$$

---

[14] This equation also appears in the report of Frankel and Nelson, reference 3.

TABLE II. Errors.

Type of error	Error in r†		Error in calibration constant
	At ring focus	*At counter*	
1. Method Error			
(a)* and (b)*	0.0096 cm	0.016 cm	0.035%
(c)	less than 0.0003 cm	less than 0.0003 cm	negligible
2. Machine Error			
(d)*	0.03 cm	0.05 cm	0.1%
3. Field Error			
(a)	0.023 cm	0.04 cm	0.17%
(b)	0.053 cm	0.140 cm	0.50%

† Errors in r have been calculated for k 1050 gauss cm/amp.

* Errors marked with an asterisk have been corrected for in the initial calculation of the calibration constant. The values given for the error in r are for initial slope 0.180. The errors are less for lower initial slopes.

Equation (A-6) is an exact equation. In the numerical integration this is replaced by

$$r(z+\Delta)_{\text{calc.}}-2r(z)_{\text{calc.}}+r(z-\Delta)_{\text{calc.}}=\Delta^2 r''(z)_{\text{calc.}}. \qquad \text{(A-7)}$$

Subtracting Eq. (A-7) from Eq. (A-6), and denoting the correction $r(z)-r(z)_{\text{calc.}}$ by $\delta r(z)$ etc., we obtain

$$\delta r(z+\Delta)-2\delta r(z)+\delta r(z-\Delta)=\Delta^2\delta r''(z)+\Delta^4 r^{(4)}(z)/12+\cdots.$$

The left-hand side of this equation is approximately $\Delta^2(d^2/dz^2)\delta r(z)$, and dropping the . . . terms, we end up with the basic differential equation for propagation of errors:

$$(d/dz)^2\delta r(z)=\delta r''(z)+\Delta^2 r^{(4)}(z)/12. \qquad \text{(A-8)}$$

In the case that $\delta r''(z)$ arises because $r''(z)$ (or more correctly $r''(z, r)$) is calculated from Eq. (1) at an incorrect value of $r(z)$ we can approximate $\delta r''(z)$ by

$$\delta r''(z)=\delta r(z)\cdot\partial/\partial r(r''(z, r)).$$

If there were no errors, $\delta r''$, in the calculated second derivative, the principal effect of replacing the differential equation by difference equations could be obtained at once by integrating Eq. (A-8) explicitly.

$$\delta r(z)=[r''(z)-r''(z_0)-(z-z_0)r'''(z_0)]\Delta^2/12,$$

where z_0 is the value of z at which integration was begun. Since z_0 was in a nearly field free region, a good approximation, obtained by neglecting $r''(z_0)$ and $r'''(z_0)$, is given by

$$\delta r(z)=\Delta^2 r''(z)/12. \qquad \text{(A-9)}$$

In integrating the complete equation,

$$(\partial/\partial z)^2\delta r(z)=\delta r(z)(\partial/\partial r)(r''(r, z))+\Delta^2 r^{(4)}(r, z)/12,$$

expression (A-9) was used as a first trial value in the right hand member.

(c) The propagation of rounding off errors was studied by a similar equation, using as initial conditions at an arbitrary point z_0

$$\delta r(z_0)=a,$$
$$(d/dz)(\delta r(z_0))=a/\Delta;$$

a, the initial rounding off error, was taken as 10^{-6} cm.

(d) Machine Failure: The failure of the business machines to carry out correctly one operation was mentioned in reference 11. Calculations were repeated for the trajectories with $k=1050$ gauss cm/amp., corrections to the trajectories for $k=1020$ and 1080 gauss cm/amp. were estimated.

Errors Arising from Magnetic Field Approximations

(a) ***Errors due to neglecting higher order differences:*** In calculating A, $\partial A/\partial r$ and $\partial A/\partial z$, sixth and higher order differences in the magnetic field were consistently neglected. The effect of 6th order differences on r'' was calculated in the region of strong fields. Corrections to the trajectories were obtained by integration. The correction made the trajectory cross the axis of the spectrometer 0.25 cm nearer the lens. This was found to correspond to a change in calibration constant k of 0.17 percent. Here, and in the remainder of the Appendix, we are using k to mean that particular momentum-per-unit-current that the spectrometer focuses.

That this order of magnitude is reasonable follows from application of the thin lens formula. From the relation

$$1/P+1/Q=1/F,$$

where P, Q, and F are source and detector distances from the lens and "focal length" of the lens, we have that

$$dQ/Q^2=dF/F^2.$$

Since Q is approximately equal to $2F$, this equation reduces to

$$dQ/Q=2dF/F.$$

But for a thin lens

$$F\propto k^2;$$
$$dF/F=2dk/k$$

and so the fractional correction to k must be $\cong\frac{1}{4}$ the fractional change in Q.

(b) *Effect of cooling shims:* The trajectories were calculated for an idealized magnet carrying a uniform current density. For comparison of our results with experiment it was necessary to include the alteration in the field produced by the cooling shims of the experimental magnet.[6] The effect of these cooling shims was to increase the field strength in the center of the lens by about 1 percent, and to decrease it below the idealized value at distances greater than about 10 cm from the mid-plane of the instrument.

The error in k produced by neglecting the cooling shims was estimated as follows. According to the simple "very thin" lens formula[15]

$$k^2\propto\int H^2dz.$$

If, as before, we use the symbol δ to denote error ($\delta H=H_{\text{correct}}-H_{\text{calculated}}$, etc.),

$$\delta k/k\cong\int H\delta H dz\bigg/\int H^2dz.$$

By calculating δH at a few points and making a reasonable interpolation, we estimated $\delta k=0.5$ percent.

The error in r was found by calculating the error in r'' and integrating twice.

Errors are summarized in Table II.

---

[15] V. E. Coslett, *Introduction to Electron Optics* (Oxford University Press, London, 1946), p. 84.

THE REVIEW OF SCIENTIFIC INSTRUMENTS VOLUME 21, NUMBER 8 AUGUST, 1950

Lens Tester for Photographic Lenses

F. G. Back
Research and Development Laboratory, New York, New York

(Received March 30, 1950)

Testing lenses, particularly photographic lenses, in a simple, fast, and accurate manner is quite a difficult problem. One of the solutions to this problem is a lens tester which is basically a modified autocollimator with a built-in color filter arranged in conjunction with an assembly unit consisting of an adjustable microscreen and a lens holder. This latter unit may be rotated about an axis perpendicular to the optical axis of the instrument, giving an immediate reading of the tangential and sagittal foci. By means of this instrument it is possible to determine: (1) the flange focal distance, (2) the shift of axial focus with respect to the lens aperture, (3) longitudinal chromatic aberration, (4) tangential and sagittal foci for any angular distance from the axis and for any aperture, and (5) all these readings for various color bands. This new instrument makes possible the immediate reading of the results without further computation. The determination of the nodal point and the focal length for extra-axial aberrations is unnecessary. Built-in color filters allow testing for chromatic aberrations. Because of a special microscreen and reflection-free beam splitter arrangement, this instrument gives satisfactory readings also for small apertures.

Testing photographic lenses in a fast and accurate way presents a problem in many cases, especially if a great variety of lenses with different equivalent focal lengths have to be checked and the quality of the images evaluated. Very often it is not required, and even not desirable, to measure or determine the five basic aberrations separately because frequently they would not give a true picture of the real performance.

It is well known that certain aberrations mask others. On the other hand, aberrations of different kinds may appear as similar defects as far as the final photographic image is concerned. For instance, on a black and white photograph, longitudinal color and spherical aberration, especially zonal aberration, create the same fuzziness all over the image. Coma and astigmatism will show a similar fuzziness toward the edges of the frame.

It is therefore very often better to determine the combined effect of all aberrations on the actual picture quality of the photographic lens for different relative apertures and different field angles.

These measurements cannot be obtained quickly and accurately by conventional methods. The Hartman method as well as the nodal slide method, although accurate, are time consuming. The Hartman method requires photographic processing and determines axial aberrations only. The bench method necessitates a very accurate determination of the nodal point and the equivalent focal length. The results obtained by the interferometer measurements are difficult to translate into actual picture quality.

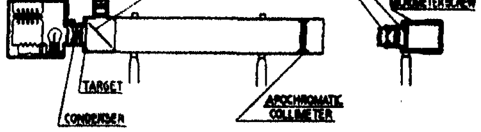

Fig. 1.

The lens tester is based on the principle of the autocollimator. This same principle has been used by Townsley and Foote[1] in their "microfocuser." The basic difference between the lens tester and the "microfocuser" lies in their different purpose. The "microfocuser" has been designed to determine the "flange focal distance," i.e., the distance between the flange of the test lens to the image plane, which is the only standardized size in motion picture optics and is therefore preferable to the customary back focal length.

The "microfocuser" also allows accurate calibration of the focusing scale of the test lens for objects at finite distances, as well as checking the coincidence of running motion picture film with the image plane of the camera lens.

All these measurements can only be made on sufficiently corrected lenses. If the lens is afflicted with heavy aberrations, the instrument cannot be focused. It is therefore self-evident that the "microfocuser" cannot be used for a quantitative measurement of lens aberrations. The lens tester, on the other hand, is primarily intended to measure lens aberrations.

Both instruments use a peculiarity of the autocollimator, namely, that the longitudinal magnification of such a system is twice as large as the longitudinal magnification of any other system of equal lateral magnification. This gives to both instruments a sensitivity which cannot be obtained with the ordinary bench method. Townsley and Foote have furnished a very elegant mathematical proof of this phenomenon which need not be repeated here.

Figure 1 shows a schematic cross section through the lens tester. It can clearly be seen that the instrument consists of two units—the collimator unit and the micrometer unit.

The collimator unit consists of:

(A) A low voltage filament lamp burning at two intensity levels: the lower level for measurements under normal conditions; the higher level for measurements with dark filters or very small apertures.

---

[1] M. G. Townsley and P. C. Foote, J. Opt. Soc. Am. 37, 42 (1947).

(B) A four-way filter disk with a white window and a red, green, and blue filter.

(C) A condenser system which images the filament on the collimator lens.

(D) A target consisting of a thin metal plate showing a transparent cross and a concentric dotted circle.

(E) A beam splitter consisting of a plano parallel glass plate with a semitransparent and semireflective coating on one side and antireflection coating on the other side, set at a 45° angle to the optical axis of the system with the semireflective coating away from the target.

[The author prefers the coated semitransparent mirror to the block glass-type of beam splitter used in the "microfocuser" because it eliminates internal reflections. These reflections are objectionable because they diminish the contrast of the image seen through the eyepiece, thus making it difficult to obtain accurate reading for small lens apertures. The anti-reflection coating on the reverse side of the semi-transparent mirror reduces the brightness of the secondary image. Whatever remains of this unwanted image is rendered harmless by the thickness of the semi-transparent mirror which provides ample separation between the primary and secondary image.]

(F) An eyepiece arranged perpendicular to the optical axis of the system in such a way that its focal plane and the target (D) are equidistant from the point where the optical axis of the system intersects the semireflective coating of the beam splitter (E).

(G) A collimator consisting of a cemented triplet corrected for primary and secondary color and designed in such a way that zonal spherical aberrations are at a minimum.

[The collimator lens of the "microfocuser" is a long focus achromatic doublet which is fully sufficient for the purposes for which the "microfocuser" was designed. On the other hand, an instrument which measures aberrations has to use a much higher corrected objective to avoid the contribution of its own aberrations to those of the lens under test. The author has succeeded in designing a sufficiently thin triplet to avoid transversal color, which is the bane of most apochromats.]

The above-mentioned components are mounted in one metal unit on the standard optical bench. This unit collimates the target at infinity and transmits a bundle of parallel rays toward the lens to be tested.

The micrometer unit comprises:

(A) A microscreen consisting of a finely ground but unpolished silver-coated first surface glass mirror arranged perpendicular to the optical axis of the test lens. This microscreen is the basic point of difference between this instrument and the "microfocuser." Although ground as fine as possible to achieve maximum resolution, the microscreen still obeys Lambert's law and therefore reflects the incident rays diffusely. The receiver of the "microfocuser," on the other hand, is a highly polished mirror. This explains why, in the presence of stronger aberrations, the "microfocuser" cannot be focused, as there are an infinite number of coincidence planes equally out of focus. A quantitative analysis of lens performance is therefore impossible with the "microfocuser."

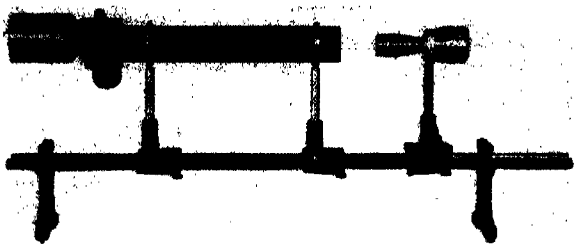

FIG. 2.

(B) A micrometer screw attached to the screen for moving it back and forth along the optical axis.

(C) An interchangeable lens mount which holds the test objective and which is dimensioned in such a way that the flange of the lens mount has the proper focal plane distance from the screen when the micrometer is set at zero.

A differential action of the aforementioned micrometer screw prevents the microscreen from rotating and at the same time permits an accurate reading.

This second unit can be rotated around an axis perpendicular to the optical axis of the system, and the angle of rotation is indicated on a dial. Since the microscreen remains always perpendicular to the optical axis of the lens to be tested, it is not necessary that this axis of rotation coincides with the transverse axis of the test objective. It is also unnecessary to keep any accurate distance between the two measuring units because the rays between the collimator and the lens are parallel.

The novel features of the aforementioned instrument give an accurate indication of the lens performance in the following readings.

(1) The distance from the lens flange to the image plane for an object at infinity in the center of the field with the iris closed to the smallest setting, measured with white light. This distance represents the flange focal distance of the lens. The flange focal distance is measured from the flange because the flange distance is the only standardized dimension on a camera and therefore most suitable as a reference point for photographic lenses.

(2) Determination of the same distance as (1), but for different iris settings. This measurement shows the shift of the focal plane caused by spherical aberration. Our measuring method integrates the total spherical aberration for that particular relative aperture and determines automatically the circle of least confusion for this iris setting.

(3) Same as (1) and (2), but measured with green, red, and blue light. These data determine the primary and secondary longitudinal color of the objective for the paraxial region as well as for the higher orders of this aberration.

(4) Distance between the flange and the two focal surfaces for objects at infinity not located on the optical axis but subtending, with the latter, various angles with the iris closed. The difference between these two distances represents the amounts of pure astigmatism with which the lens is afflicted at that particular field angle; while the difference between each of these two measurements and the flange focal length as measured according to (1) represents the tangential and sagittal field curvature.

(5) Same as (4), but for different iris settings to determine the additional influence of coma and oblique spherical aberration.

It should be noted here again that the measurements (2) and (5) do not represent the mathematical image point for that particular aperture but rather the circle of least confusion, taking into consideration the sum total of all aberrations which come into play at the image formation for that particular point of the field. The variations of these distances give a reliable measure for the evaluation of the lens performance under actual working conditions.

Figure 2 shows the instrument mounted on a standard optical bench.

It is obvious that, from the standpoint of production engineering, the necessary computations have been reduced to an absolute minimum. Nearly all data required to plot graphs of the resolution of the lens at different apertures and field angles can be directly read off from the instrument.

The instrument is also very sturdy and needs no adjustment once it is set. Like the "microfocuser," it can be operated by an unskilled worker after very short instruction.

An instrument of this type has been in practical daily use for over a year and has given most satisfactory results.

THE REVIEW OF SCIENTIFIC INSTRUMENTS VOLUME 21, NUMBER 8 AUGUST, 1950

Improvements in Mass Spectrometers for the Measurement of Small Differences in Isotope Abundance Ratios

C. R. McKinney, J. M. McCrea, S. Epstein, H. A. Allen, and H. C. Urey
Institute for Nuclear Studies, University of Chicago, Chicago, Illinois

(Received March 30, 1950)

A Nier-type mass spectrometer and its associated electronic units have been constructed for the purpose of measuring small variations in the abundances of oxygen of mass 18 and of carbon of mass 13 in carbon dioxide, and of oxygen of mass 18 in oxygen gas, to an accuracy of ±0.01 percent of the abundance of these isotopes.

The electronic units of the necessary stability for this degree of accuracy are described. A gas feed system is described which permits fast alternate introduction of the sample of gas to be analyzed and a standard gas into the mass spectrometer. All measurements of the variation in the abundance of the oxygen and carbon isotopes are made with reference to a standard.

During recent years great progress has been made in developing mass spectrometers for the measurement of the relative abundance of isotopes. Particularly sensitive instruments have been developed by Nier, Thode, and others.[1] Basically, the mass spectrometer and electronic units in our research were those described by Nier. We report only the changes we made in these that assisted us in being able to measure small differences in the abundance of the rarer isotopes in gaseous compounds. The method has been applied to carbon and oxygen in carbon dioxide and to oxygen in oxygen gas. Our success in securing this greater sensitivity depends both upon increasing the intensity of the ion beam and upon increasing the absolute sensitivity of detection. In doing this, it has been necessary to improve the stability of the beam intensity and output from the amplifiers by the use of more stable power supplies, more reliable amplification systems, and an improved emission regulator. Also, it has been necessary to use a method for rapid change of samples in order to decrease errors due to general variability of the instrument with time, and it has proved essential that a recording potentiometer be used to detect and record the state of balance of the simultaneously collected ion beams. The instrument has been constructed with the objective of measuring small differences in isotopic abundances of the oxygen isotopes as a means of measuring paleotemperatures, but the instrument and our procedures may be useful in other researches.

POWER SUPPLY FOR ELECTROMAGNET

Figure 1 shows the circuit diagram of the power supply used to furnish the current for the magnet windings and to supply some of the power requirements for the high voltage electronic unit.

---

[1] A. O. Nier, Rev. Sci. Inst. 18, 398 (1947). Thode, Graham, Ziegler, Can. J. Research B23, 40 (1945). For an excellent review of this subject, see M. G. Inghram, Advances in Electronics 1, 219 (1948).

Several measures are used to achieve good stability of the output of this power supply. The voltage to the screen of the 6L6 tubes (1V4 and 1V5) and the plate supply of the 12AU6 (1V13) amplifier tube is obtained from a separate power supply regulated by using OA2 (1V6 to 1V9) miniature voltage regulator tubes. A 5651 voltage regulator tube (1V11) is used to obtain a reference voltage. The ripple of the output is minimized by adjusting potentiometer 1P2. This potentiometer controls the balance of the bridge circuit operating through the isolating cathode follower tube (1V10) and the screen of the amplifier tube (1V13). The "*H*" network of which 1P2 is a part is designed so that the d.c. level of the output voltage is nearly independent of the setting of 1P2. This type of circuit is similar to the one described by McCrea and LeRoy.[2] Since the response of this circuit is rapid, the single condenser 1C3 provides ample smoothing of the input.

To further increase the stability of the power supply, the current for the heaters of the critical amplifier tubes (1V10, 1V12, and 1V13) is supplied by the output of the power supply itself. By using switch 1S3, the unit is allowed to warm up under reduced output voltage. Relay 1S2 protects the circuit from excessive voltage rise during operation. A properly adjusted power supply unit has an output of 250 volts and supplies a current of about 200 milliamperes. The ripple is 1.5 millivolts, peak to peak, with a noise level of about 0.6 millivolt. The internal resistance for direct current conditions is 0.35 ohm and for 60 cycle load variation about 0.6 ohm. A 1.1-volt (1 percent) variation in the alternating current input appears as a 0.000184 percent, or a 0.5 millivolt, variation in the output. The 115-volt power line is regulated by a Sola Constant Voltage Transformer.

The magnet current can be varied by varying the resistance in series with windings by means of controls 1P4 and 1P5 and switches 1S4 and 1S5. A Helipot 1P5, connected to a motor by a clutch mechanism, allows

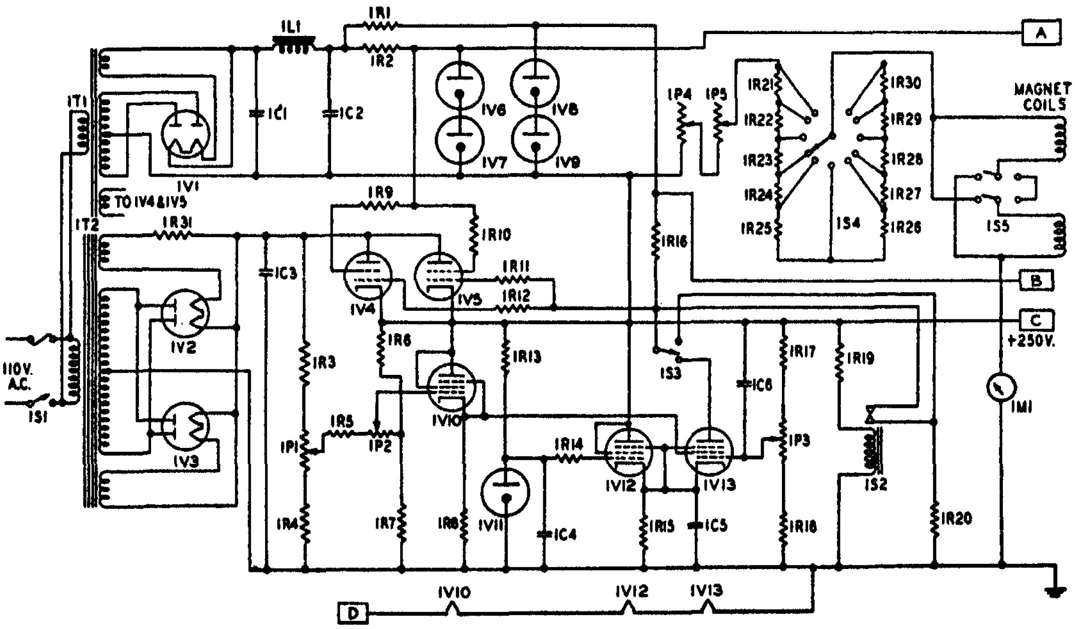

FIG. 1. Power supply (regulated).

1R1	13,500 ohms, 10 watt, wire wound
1R2	5000 ohms, 10 watt, wire wound
1R3	68,000 ohms, 1 watt
1R4	39,000 ohms, 1 watt
1R5	22 megohms, 1 watt
1R6	50,000 ohms, precision wire wound
1R7	75,000 ohms, precision wire wound
1R8	35,000 ohms, precision wire wound
1R9, 1R10	470 ohms, 1 watt
1R11, 1R12	47,000 ohms, 1 watt
1R13	60,000 ohms, 1 watt
1R14	470,000 ohms, 1 watt
1R15	15,000 ohms, precision wire wound
1R16	1 megohm, precision wire wound
1R17	50,000 ohms, precision wire wound
1R18	25,000 ohms, precision wire wound
1R19	Sufficiently small to cause relay to close in case of excessive voltage rise during operation
1R20	680,000 ohms, 1 watt
1R21 to 1R30	750 ohms, 10 watt
1R31	0.65 ohm (wound with nichrome wire)
1C1	8 mfd 600 v
1C2	12 mfd 600 v
1C3	20 mfd 600 v
1C4, 1C5	0.01 mfd 400 v
1C6	250 micro-microfarad
1V1	5Y3
1V2, 1V3	5U4G
1V4, 1V5	6L6
1V6, 1V7, 1V8, 1V9	OA2
1V10, 1V12, 1V13	12AU6
1V11	5651
1L1	5 henry 100 milliamps filter choke
1T1	Stancor power transformer type P6143
1T2	Westinghouse power transformer (Navy type No. CAY-301164)
1P1	15,000 ohms wire wound potentiometer
1P2	500,000 ohms carbon potentiometer
1P3	10,000 ohms wire wound potentiometer
1P4	800 ohms 25 watt rheostat
1P5	800 ohms 15 turn Helipot
1M1	0–200 milliampere meter
1S1	S.P.S.T. toggle switch
1S2	Single pole relay, normally open
1S3	S.P.S.T. toggle switch
1S4	Single pole 11 position rotary switch
1S5	D.P.D.T. toggle switch

---

[2] J. M. McCrea and D. J. LeRoy, Rev. Sci. Inst. 19, 692 (1948).

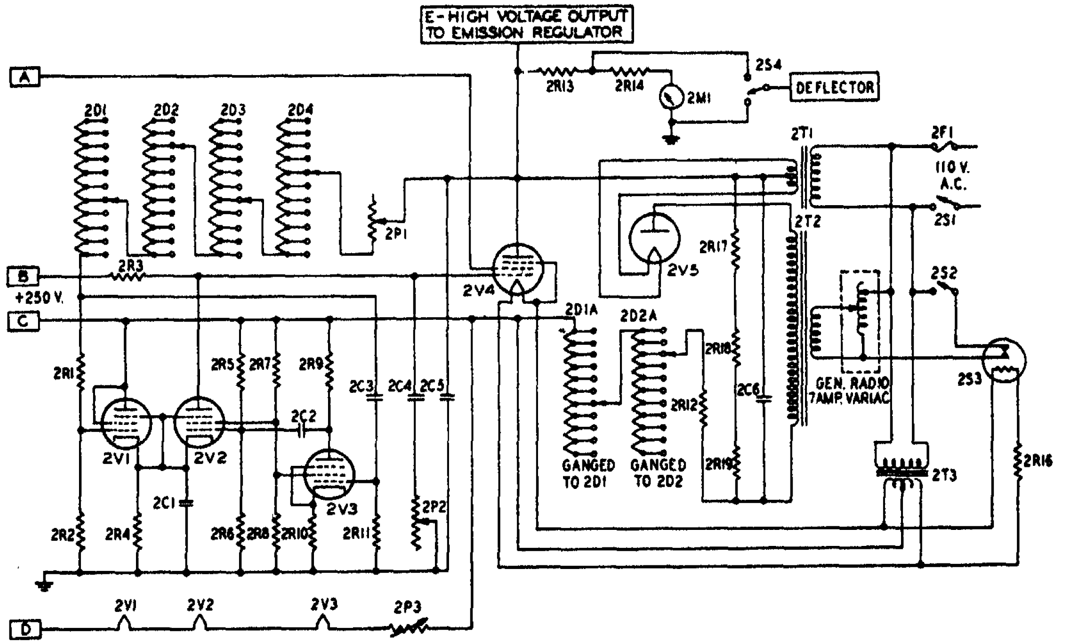

Fig. 2. Parts list for high voltage supply.

2R1	250,000 ohms, precision wire wound
2R2, 2R6, 2R8	75,000 ohms, precision wire wound
2R3	1 megohm, precision wire wound
2R4	25,000 ohms, precision wire wound
2R5	50,000 ohms, precision wire wound
2R7	35,000 ohms, precision wire wound
2R9	30,000 ohms, precision wire wound
2R10	40,000 ohms, precision wire wound
2R11	2.2 megohms carbon 1 watt
2R12	50,000 ohms, 100 watt
2R13, 2R14	2 megohms, precision wire wound
2R16	Reduces 10 v to 6 v required by 2S3 relay
2R17, 2R18, 2R19	10 megohms, 2 watt
2D1A	10 steps, 5000 ohms per step (10 watt each)
2D2A	10 steps, 470 ohms per step (2 watt each)
2D1	10 steps, 100,000 ohms per step precision wire wound
2D2	10 steps, 10,000 ohms per step precision wire wound
2D3	General Radio decade type 510E 1000 ohms per step
2D4	General Radio decade type 510D 100 ohms per step
2P1	100 ohms, wire wound potentiometer
2P2	3 megohms, carbon potentiometer
2P3	1300 ohms, 50 watt potentiometer
2V1, 2V2, 2V3	12AU6
2V4	Type 813 transmitting tube
2V5	Type 8020 high voltage rectifier
2C1	0.01 mfd 600 v
2C2	0.25 mfd 400 v
2C3	2 mfd 600 v
2C4	0.1 mfd 600 v
2C5	4 mfd 3000 v
2C6	4 mfd 4000 v
2T1	Stancor filament transformer type P-4086, 5 v c.t. 14 amp. 10,000 v insulation
2T2	Maloney Electric Company high voltage transformer part No. 5503 (Army surplus) 5600 v at 0.1 amp. (reduced to 3700 v with 1 kva Variac)
2T3	Stancor filament transformer type 6139 10 v c.t. 8 amp.
2T4	General Radio variac 7½ amp. capacity
2M1	0–1 milliamp. meter
2S1	S.P.S.T. toggle switch
2S2	S.P.S.T. toggle switch—high voltage on-off
2S3	Amperite thermostatic delay relay type 6N045
2S4	S.P.S.T. high voltage rotary switch for beam on-off

automatic magnetic scanning for the desired mass range.

HIGH VOLTAGE SUPPLY

The high voltage supply shown in Fig. 2 furnishes a continuously variable regulated voltage in the range 600 to 2200 volts for accelerating the ions in the mass spectrometer. The voltage of the output is varied by means of decades 2D1 to 2D4, which are ganged with 2D1A and 2D2A to keep the load across the rectifier and transformer nearly constant. Condenser 2C4 and resistor 2P2 are included to eliminate tendencies for oscillation. Tube 2V3 performs the function of applying part of the output ripple in a degenerative manner to the grid of 2V2 which in turn acts to reduce the ripple of the output. A 1 percent variation in the line voltage appears as a 0.001 percent variation of output at 600 volts and as 0.005 percent at 2200 volts, with internal resistances of 1 and 4 ohms respectively at these outputs.

The reference voltage of 250 volts, the heater current for control tubes 2V1, 2V2, and 2V3, and the other necessary voltages are obtained from the appropriate places in the magnet power supply (*C*, *D*, *A*, and *B*). The thermal time delay relay 2S3 protects the cathodes of 2V4 and 2V5.

THE ELECTRON EMISSION REGULATOR

The emission regulator circuit as shown in Fig. 3 consists of two parts. One part is a power supply similar to the one used in the magnet circuit. Since the requirements for this power supply are less critical than the one used for furnishing current to the magnet windings, the plate supply voltage for the amplifier tube (3V12) is obtained from the unregulated direct current from the rectifiers. This power supply provides the electron accelerating voltage and the trap voltage in the ion source.

Regulation of electron emission of the filament in the source is accomplished by the second part of the emission regulator. Electron emission currents from the filament in the ion source flows through resistors 3R10 and 3P2 and the resulting voltage drop is amplified and applied to the grid of a series control tube (3V14) which

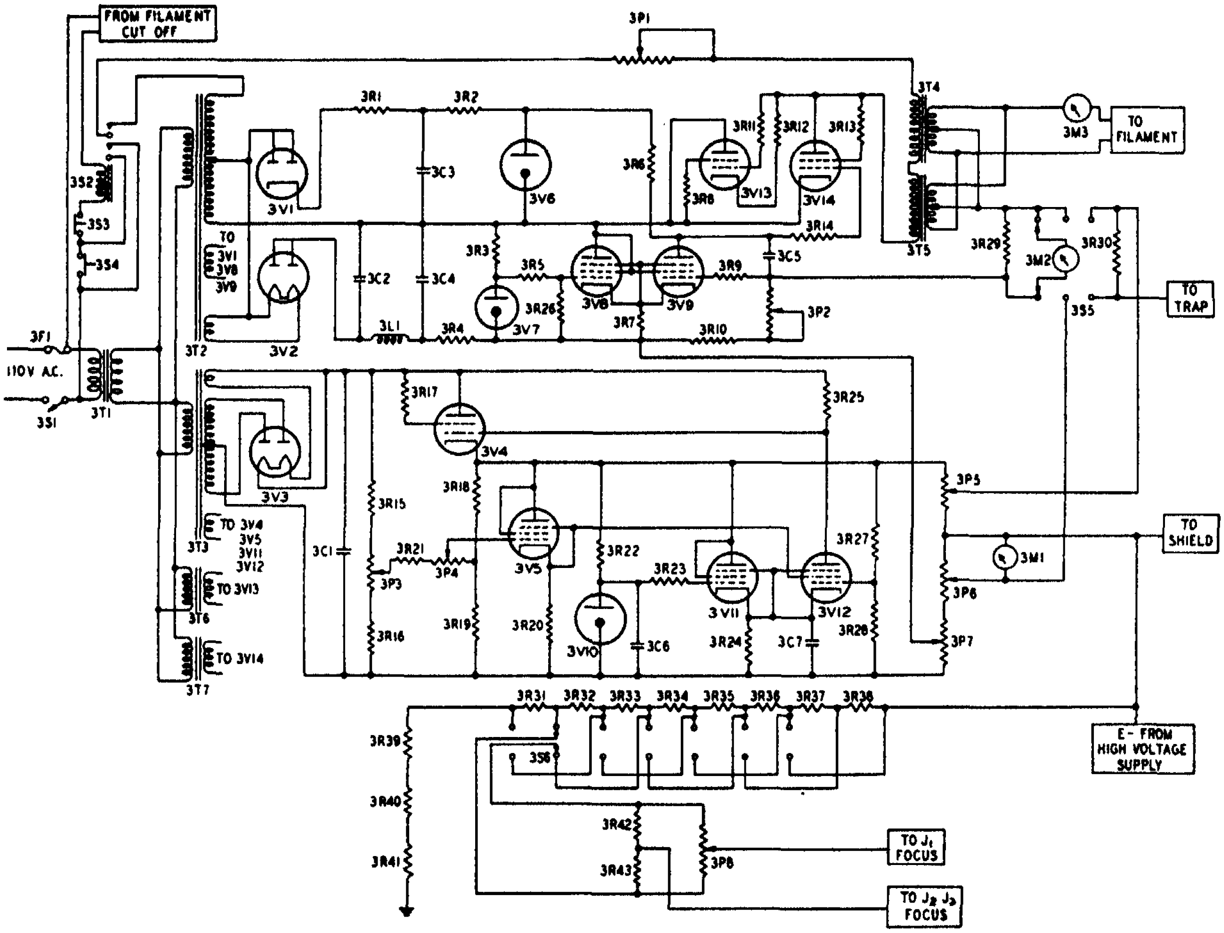

FIG. 3. Parts list for emission regulator.

3R1	300 ohms, 10 watt
3R2	35,000 ohms, 20 watt
3R3	7500 ohms, 10 watt
3R4	5000 ohms, 10 watt
3R5	25,000 ohms, precision wire wound
3R6	0.5 megohm, precision wire wound
3R7	15,000 ohms, precision wire wound
3R8, 3R13	15,000 ohms, 2 watt
3R9, 3R11, 3R14	82,000 ohms, 1 watt
3R10	150,000 ohms, 1 watt
3R12	50 ohms, 5 watt
3R15, 3R19, 3R20, 3R22	68,000 ohms, 1 watt
3R16	27,000 ohms, 1 watt
3R17	470 ohms, 2 watt
3R18	47,000 ohms, 1 watt
3R25	2.2 megohms, 1 watt
3R26	75,000 ohms, precision wire wound
3R27	50,000 ohms, precision wire wound
3R24, 3R28	35,000 ohms, precision wire wound
3R29	250 ohms, precision wire wound. Shunts meter 3M2 to read 500 microamperes full scale
3R30	1000 ohms, precision wire wound. Shunts meter 3M2 to read 200 microamperes full scale
3R21, 3R23, 3R31 to 3R38	0.47 megohm, 1 watt
3R39, 3R40, 3R41	10 megohms, 1 watt
3R42, 3R43	2.2 megohms, 1 watt
3P1	*800 ohms, 25 watt rheostat*
3P2	250,000 ohms, carbon potentiometer
3P3	15,000 ohms, wire wound potentiometer
3P4	0.5 megohm, carbon potentiometer
3P5	5000 ohms, wire wound
3P6	10,000 ohms, wire wound
3P7	5000 ohms, wire wound
3P8	3 megohm, carbon potentiometer
3T1	Thordarson No. T18V01 1:1 isolation transformer (*changes made so secondary is insulated* for 3500 v) 250 volt-ampere capacity
3T2	Acme No. T4822 power transformer
3T3	Stancor No. P6143 power transformer
3T4, 3T5	6.3 volt, 5 amperes filament transformers
3T6, 3T7	6.3 volt, 2 amperes filament transformers
3C1, 3C3	16 mfd 600 v
3C2, 3C4	8 mfd 600 v
3C5	0.05 mfd 600 v
3C6, 3C7	0.01 mfd 400 v
3M1	0–100 volts d.c. voltmeter
3M2	0–100 microampere d.c.—1000 ohms resistance
3M3	*0–10* a.c. amperes
3V1	6X4
3V2, 3V3	5Y3
3V4	6L6
3V5, 3V8, 3V9, 3V12	6AU6
3V6, 3V7	OA2 miniature voltage regulator tube
3V10	5651 miniature voltage regulator tube
3V11	6AG5
3V13, 3V14	807
3S1	S.P.S.T. toggle on-off switch
3S2	D.P.D.T. high voltage relay
3S3	Push switch normally closed
3S4	Push switch normally open
3S5	2 pole three position switch
3S6	2 pole seven position switch

controls the current flowing through the primary of transformers 3T4 and 3T5. The secondaries of these transformers supply the current to the filament in the mass spectrometer. Tube 3V13 serves to maintain proper wave form of the primary current. The controlled range of electron emission from the filament in the mass spectrometer extends from 100 to 500 microamperes depending upon the setting of 3P2. A 1 percent change in line voltage input results in a 0.02 percent change in average emission. Switch 3S5 is a three-position switch

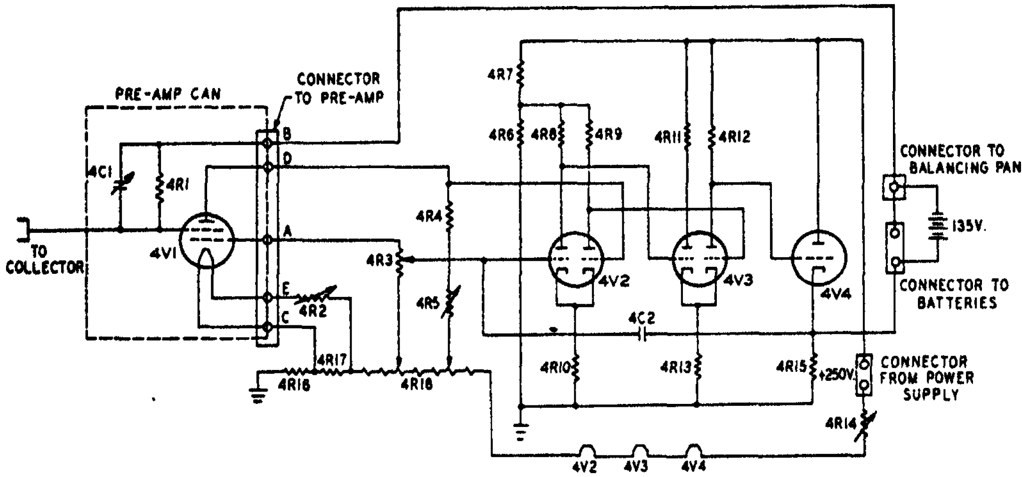

FIG. 4. Parts list for d.c. amplifier.

4R1	1.5×10^{10} ohm Victoreen Hi-Megohm obtained from Victoreen Instrument Company, Cleveland, Ohio	4R14	1000 ohms, 50 watt
4R2	30 ohm wire wound potentiometer	4R15	25,000 ohms, precision wire wound
4R3	20,000 ohms Helipot 10 turns, obtained from Helipot Corporation, South Pasadena, California	4R16	80 ohms, special wire wound
		4R17	40 ohms, special wire wound
		4R18	12 steps of 26 ohms each special wire wound
4R4	250,000 ohms, precision wire wound	4V1	VX-41A obtained from Victoreen Instrument Company, Cleveland, Ohio
4R5	100,000 ohms Helipot 15 turns		
4R6	20,000 ohms, precision wire wound	4V2	12SL7-GT
4R7	35,000 ohms, precision wire wound	4V3	12SL7-GT
4R8, 4R9	500,000 ohms, precision wire wound	4V4	12J5-GT
4R10	75,000 ohms, precision wire wound	4C1	100 micro-microfarad variable air dielectric condenser
4R11, 4R12	1 megohm, precision wire wound	4C2	0.002 mfd condenser 400 v
4R13	300,000 ohms, precision wire wound		

which allows meter 3M2 to read either trap current, total emission current or to indicate the zero adjustment of 3P6 so that meter 3M1 reads electron accelerating voltage.

ION CURRENT AMPLIFICATION

Essentially the same amplifier design as described by Nier was used initially in this research. A stable d.c. amplifier is obtained by using our previously described power supply and by using the tubes described in Fig. 4. To allow collection of currents of approximately 3.7×10^{-9} and 1.5×10^{-11} ampere for masses 44 and 46 respectively, and to get sensitivity of 0.2 permil in determining the ratio of mass 46 to mass 44, the respective sizes of the resistors 4R1 of the two amplifiers must be approximately 1.5×10^{10} and 1.5×10^{11} ohms.

Since the inherent difficulties present in sensitive d.c. amplifiers did not permit day to day use of the mass spectrometers for analyses with the accuracy required in this research, a different amplification system was tried. A vibrating reed electrometer with its associated amplifier in conjunction with a null system described by Nier, Ney, and Inghram,[3] where the vibrating reed replaces the FP54 electrometer, gave continuously satisfactory performance.

A schematic diagram of this system is given in Fig. 5.

GAS FEED AND RECORDING POTENTIOMETER

Since the amplifiers always drift with time and have a noise level as high as or higher than the sensitivity required, it is necessary to have a record of the state of balance of the potentials produced by the two peaks being compared, and it is necessary to be able to change from one sample to another very rapidly.

Two complete feed systems with gas volumes, mercury leveling reservoirs, and capillary leaks of the type previously described by Nier were attached to the mass spectrometer through a magnetically operated valve which delivered one sample to the mass spectrometer and the other to a waste vacuum line. In this way the flow of the two samples could be reversed rapidly. Since the valve is on the high vacuum side of the leaks there is a very small lag in changing from one sample to the other. The tube leading from the valve to the mass spectrometer must be fairly large in order that the hold up in this region is small. In our instrument the volume of the valve and connecting tube is about 10 cc and the internal diameter and length of the feed tube within the mass spectrometer head are 3 mm and 12 cm, respectively. The greater resistance of a 2-mm I.D. tube considerably increased the time lag. The gases replace each other in a few seconds. The construction of the valve is shown in Fig. 6. The memory effect of each gas is small and hence when samples of nearly identical composition (differing by, say, 5 permil in the ratio) are compared, this effect is insignificant. However, if samples of substantially different isotopic composition are used, say differing by a few percent in the ratio, then some minutes must elapse before steady conditions are established. If carbon dioxide containing oxygen of double the normal concentration or higher is used, the

---

[3] Nier, Ney, and Inghram, Rev. Sci. Inst. 18, 294 (1947).

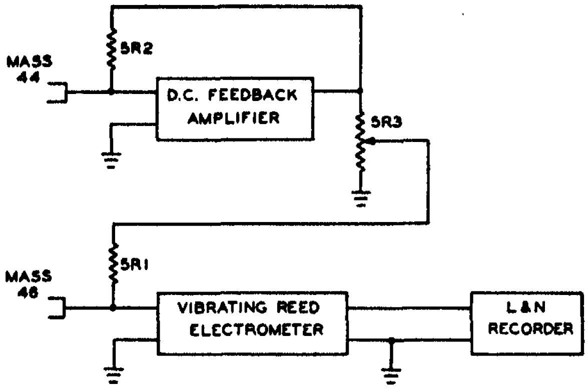

FIG. 5. Parts list for ion beam balancing circuit. 5R1—1.5×10¹¹ ohms, Victoreen Hi-Megohm resistor. 5R2—1.5×10¹⁰ ohms, Victoreen Hi-Megohm resistor. 5R3—Put and take decade resistance potentiometer, made up of General Radio decade resistance units 510A, 510B, 510C, 510D and 510E. Vibrating reed electrometer—obtained from The Applied Physics Corporation, 30 West Green Street, Pasadena, California. D. c. feedback amplifier—as shown in Fig. 4.

feed system that contained the concentrated gas will contaminate succeeding samples so that analysis to high precision, i.e., differences of the order of 0.2 permil in the ratio, cannot be made until the apparatus has been pumped and swept out for many days.

It is not possible to judge the steadiness of the balance of the two potentials by watching a galvanometer when it is desired to detect differences of the order of the unsteadiness of the potentials being observed. The galvanometer fluctuates unsteadily, and whether the mean has any reliable meaning cannot be judged. The recording potentiometer makes a trace which can be averaged over a satisfactory period of time.

We have used recording potentiometers to observe the balance between the potentials of the two peaks. The recorder draws an irregular line down the chart with negligible drift (if the instrument is in proper adjustment). If erratic fluctuations occur the instrument is unreliable. Of course, if the small but statistically regular fluctuations are too great the precision desired cannot be secured. By observing the record for some time it is possible to judge the stability of the amplifier circuits particularly as well as the mass spectrometer as a whole, and thus decide whether analyses can be made.

FIG. 6. Valve for reversing samples. 1, inlet for sample 1; 2, inlet for sample 2; 3, outlet to waste vacuum; 4, outlet to mass spectrometer; 5, coil windings; 6, soft iron washer on glass valve.

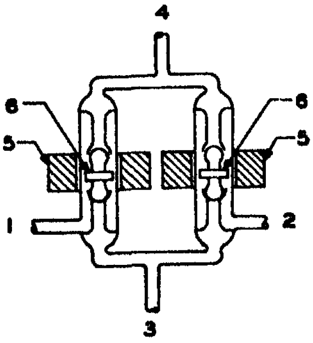

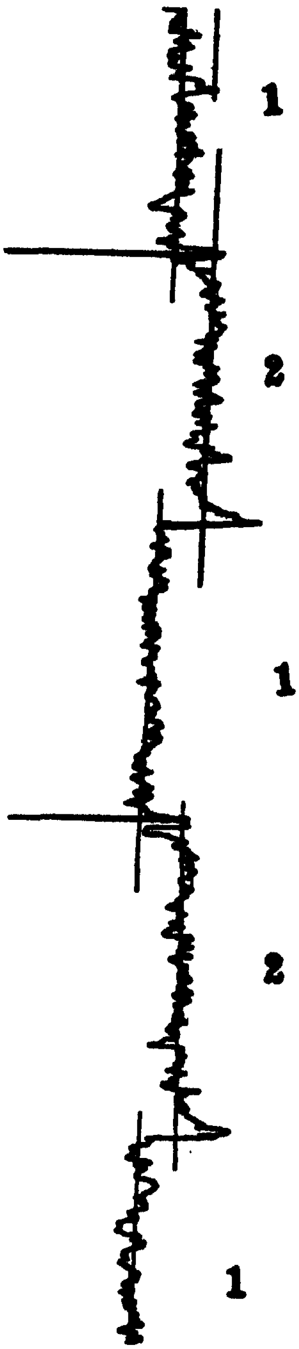

FIG. 7. Sample potentiometer record.

The use of the recording potentiometers is essential to securing differences to a precision of 0.2 permil of the oxygen isotope ratio.

The type of traces obtained are shown in Fig. 7, where trace 2 represents the null point of the standard and trace 1 represents the deviation from the null point by an increase of 0.63 permil in the intensity of ion beam of mass 46. If the deviation from the null point was large, part of the increase or decrease in mass 46 was taken up by changing the setting on the decade resistor system. Straight lines are drawn through the irregular

TABLE I.

	CO_2 gas		CO_2 gas			O_2 gas	
Sample	$\delta(O^{18})$	Date	$\delta(C^{13})$	Date	Sample	$\delta(O^{18})$	Date
1	−0.53	12/13/49	0.42	12/13/49	1	17.11	12/7/49
	−0.59	1/4/50	0.50	1/4/50		16.77	12/8/49
2	−2.98	12/20/49	1.95	12/20/49	2	0.23	2/10/50
	−2.99	1/3/50	1.75	1/3/50		−0.10	2/13/50
	−3.00	1/3/50	1.58	1/3/50			
3	−3.87	12/12/49	1.30	12/12/49	3	0.00	2/10/50
	−3.83	1/3/50	1.35	1/3/50		0.00	2/11/50
						−0.20	2/13/50
4	−2.30	12/13/49	2.30	12/13/49	4	0.44	2/10/50
	−2.56	1/4/50	2.46	1/4/50		−0.02	2/11/50
						−0.14	2/13/50
5	−2.18	12/22/49	1.73	12/22/49			
	−2.22	1/4/50	1.90	1/4/50			

curves and extended to the point where the samples were changed and the differences are read at these points. The displacement on the chart is easily calibrated in terms of the dial settings in the resistance panel. The average of some five or seven readings is then used to correct the ratio read from the resistances.

CONCLUSION

Two instruments of this type have been constructed and operated, one for 18 months, the other for 6 months. At present electronics technicians can keep the instruments in operation from 50 to 75 percent of the time. The analyses are made by laboratory technicians. Altogether some two thousand high precision comparisons of oxygen isotopic abundances in carbon dioxide, some hundreds of carbon abundances in the same gas, and perhaps a hundred comparisons of oxygen isotopes in oxygen gas have been made with these instruments. Examples of check analyses are given in Table I. The recorded figures are the differences in permils of the normal ratios between the sample and the standard working gas, i.e.,

$$\delta=\left(\frac{R_{\text{sample}}}{R_{\text{standard}}}-1\right)1000,$$

where R_{sample} and R_{standard} are the ratios of $CO^{16}O^{18}$ to CO_2^{16} for the unknown sample and reference gas respectively. These examples of analysis on carbon dioxide are taken from our working notebooks and are a group of consecutive duplicate analyses selected at random and with no omission of any results. These duplicate analyses are on different preparations of the gas from the same samples of calcium carbonate and hence the fluctuations include any variations due to the chemical preparation of the gas. (The calcium carbonate is heated to 475°C for 15 minutes in a stream of pure helium gas and the carbon dioxide liberated by reaction of the carbonate with 100 percent orthophosphoric acid.) Thus the operation of the instrument is at least as reproducible as indicated by these results. On the basis of analyses made before the vibrating reed amplifier was adapted to the instrument, we believe that variations greater than 0.2 permil are due to variations introduced by the method of preparing the gas, a subject which will be discussed elsewhere.

The first example of the oxygen gas analyses is for two preparations from a silicate rock. The last three examples are all for tank oxygen. The most recent of our analyses are given here since they represent the precision we have been able to attain in our most recent work. It is expected that this precision will be maintained and in fact improved in the future as we acquire more experience in these analyses.

Vacuum Tests of Rubber, Lead, and Teflon Gaskets and Vinyl Acetate Joints

ROBERT W. CLOUD AND SANBORN F. PHILP
Massachusetts Institute of Technology, Cambridge, Massachusetts

(Received April 10, 1950)

Rubber, Teflon, and vinyl acetate sealed systems are compared, by an approximately quantitative method, with a lead gasket sealed system which is shown to give off negligible gas at room temperature. Rubber is shown to evolve relatively large amounts of gas with an apparent vapor pressure above a micron at room temperature and about 0.1 micron at liquid air temperature. Continuous pumping for several days produces no improvement, nor does the use of metal-to-metal joints. Vinyl acetate joints are shown to improve with pumping over a period of several days, reaching a condition exhibiting an "apparent vapor pressure" of 5×10^{-7} mm of mercury, or less, at room temperature. Heating to 45°C raises the apparent vapor pressure to the 10^{-4} mm range, and heating to 100° raises the apparent vapor pressure to the micron range. If this behavior is caused by the vapor pressure of the vinyl acetate itself, continued baking in vacuum will, of course, produce no improvement.

THE experiments were designed to give a comparison of the amount of gas evolved in vacuum as a result of using rubber, lead, and Teflon gaskets and vinyl acetate in the typical application of sealing flanges in a vacuum chamber. Gas evolved in vacuum must arise from the evaporation of the vacuum materials themselves or from the desorption of gas previously occluded by the materials. The former are, of course, "condensable" gases, whereas the latter are not necessarily so. Attempt was made in each case (except that of Teflon) to determine if condensable gases were present to an important degree.

The apparatus consisted of an aluminum vacuum chamber (Fig. 1) of approximately ½ liter volume having two side ports covered by aluminum flanges and a steel flange to which was mounted a valve closing the chamber from the vacuum pump. To the side port flange was attached a glass ionization gauge. The pump was a D.P.I. MHG 50.02 pump (mercury) with a trap consisting of concentric stainless steel cylinders 15 cm and 11 cm by 60 cm. The pumping speed to the vacuum chamber was measured to be 25 liters per second (flat from about 5×10^{-6} to 10^{-4} mm of mercury).

The experimental procedure was to close the valve and observe the pressure (measured with an HK-54 used as an ionization gauge) as a function of time after closing the valve. The slope of the pressure-time curve and the known volume of the chamber may be multiplied to give a rate of gas evolution in mm-liters/sec. It is the initial rate of gas evolution calculated in this way and the equilibrium pressure of the system with the chamber valve open which constitute the basis for comparison of the materials studied.

Figure 2 shows pressure-time curves for various stated materials used to seal the vacuum chamber. "Metal-to-metal joints" refers to flanges specially designed to provide as much metal-to-metal surface between the system and the gasket as possible, thus giving a low pumping speed from the gasket to the system. In this case the metal-to-metal joints were as

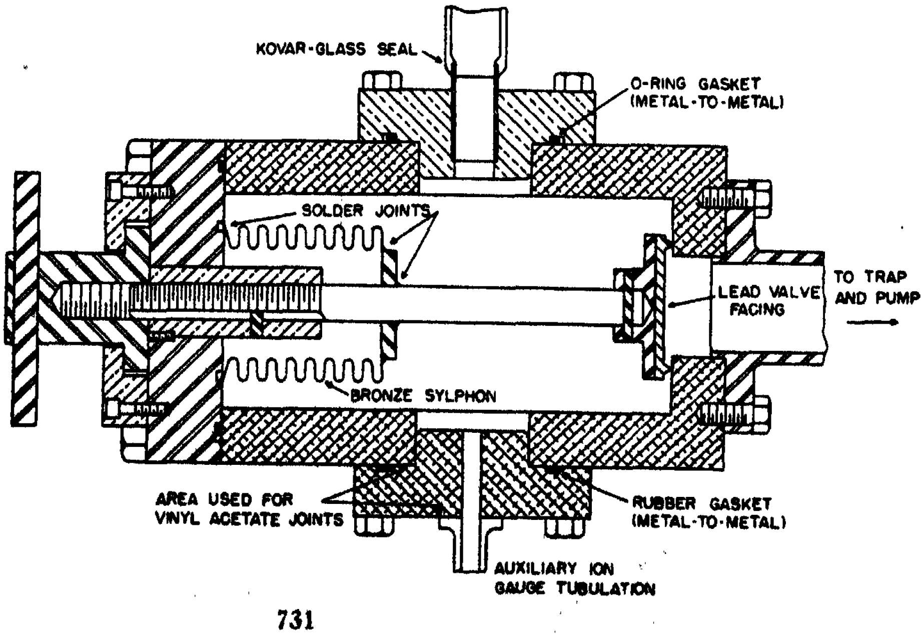
ION GAUGE TUBULATION
KOVAR-GLASS SEAL
O-RING GASKET (METAL-TO-METAL)
SOLDER JOINTS
LEAD VALVE FACING
TO TRAP AND PUMP
BRONZE SYLPHON
AREA USED FOR VINYL ACETATE JOINTS
RUBBER GASKET (METAL-TO-METAL)
AUXILIARY ION GAUGE TUBULATION

FIG. 1. Vacuum chamber (sectional view).

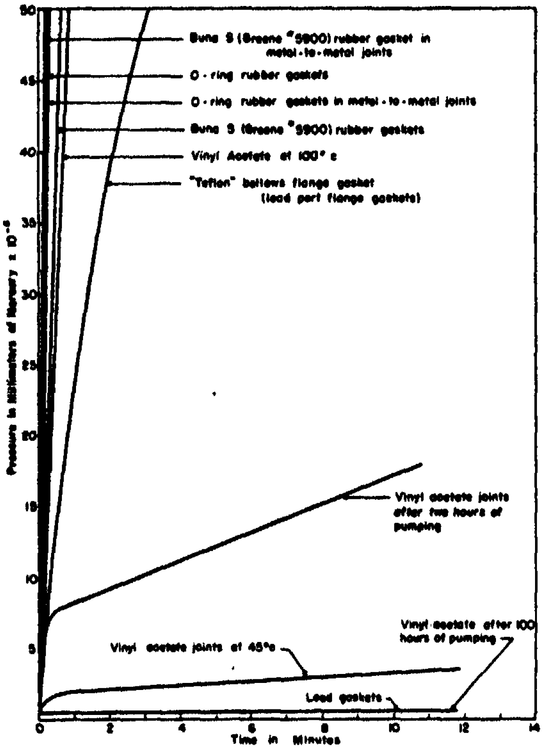

FIG. 2. Pressure in vacuum chamber as a function of time after closing chamber valve (a graph).

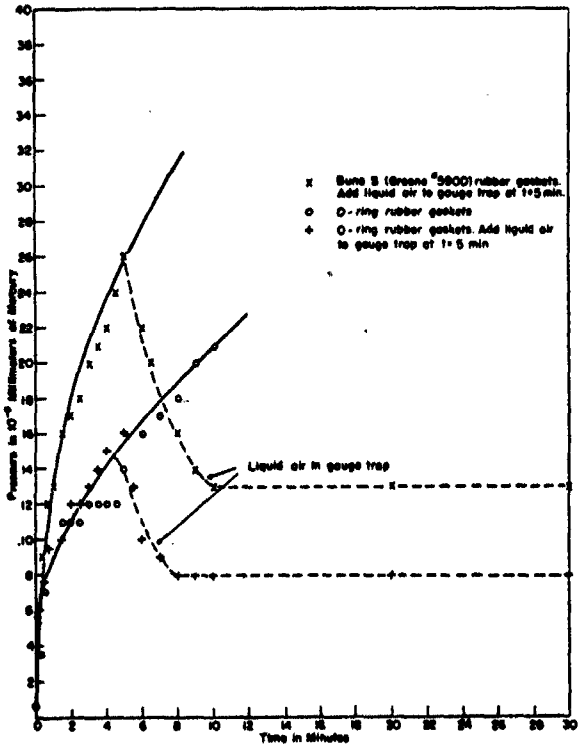

FIG. 3. Pressure as a function of time after closing valve. Chamber equipped with rubber gaskets in metal-to-metal joints (a graph).

shown in Fig. 1. In view of the inaccuracies involved, chiefly due to (1) the use of an ionization gauge and (2) the fact that the system had to be opened to the atmosphere to install each different gasket material, differences such as those which appear to exist between rubber gaskets with and without metal-to-metal joints, and between lead gaskets and vinyl acetate joints, must be regarded as insignificant. An ionization gauge reading constitutes a measure of the over-all ionization probability of the atmosphere in which the gauge is operating. It is therefore by no means an absolute measurement of pressure, although probably an effective measure of vacuum insulating strength. Furthermore, the gauge has a tendency to clean up the vacuum, as is well known. Dushman suggests that the plate collector voltage be applied only as necessary to make readings and thereby minimize the clean-up effect. This procedure was tried with both plate and grid voltages, and readings were found to be roughly 20 percent and 70 percent higher, respectively, than in the case of continuously applied voltages—a correction which is not particularly significant for this experiment. Still another effect of the ionization gauge involves the decomposition of large, complex molecules which come in contact with the filament. This could have an important effect in the case of an organic vapor from vinyl acetate. In an attempt to detect a variation in readings due to the gauge, two gauges were used to measure pressure in the chamber with the bellows coated with vinyl acetate.

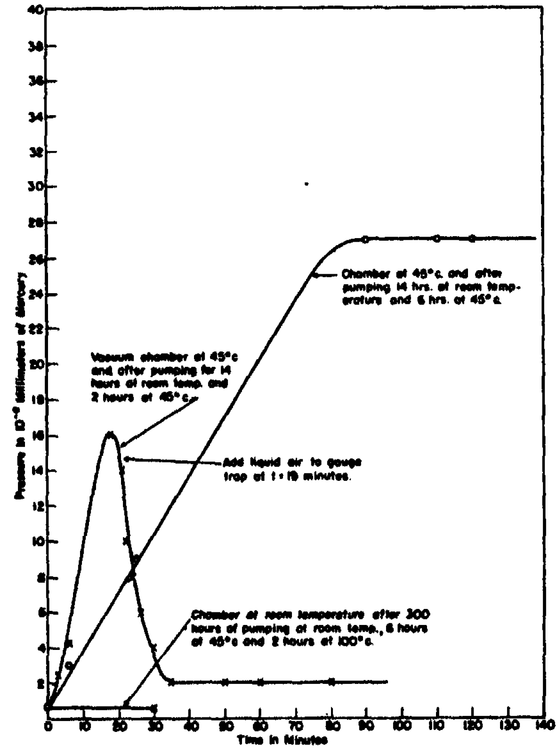

FIG. 4. Pressure as a function of time after closing valve (all joints sealed with vinyl acetate) (a graph).

TABLE I.

Flange sealing material	Total pumping time (hr.)	Equilibrium pressure (mm Hg) when pumping on chamber and in equilibrium with Dry ice	Liquid air	Apparent vapor pressure (mm Hg) 20°C	−78°C	−180°C	Approximate initial rate of gas evolution at 20°C (mm liters/sec.)
Buna S rubber gaskets (Greene No. 5900)	70	1×10^{-5}	5×10^{-6}				0.7×10^{-6}
Buna S rubber gaskets in metal-to-metal joints	60		5×10^{-6}	$>10^{-3}$	$>10^{-3}$	1.3×10^{-4}	2.5×10^{-6}
O-ring rubber gaskets	40	1×10^{-5}	5×10^{-6}				2.5×10^{-6}
O-ring rubber gaskets in metal-to-metal joints	17		7×10^{-6}	$>10^{-3}$	$>10^{-3}$	1×10^{-4}	2.5×10^{-6}
Teflon gasket (bellows flange only, lead gaskets in port flanges)	30	6×10^{-6}	2.5×10^{-6}				1.5×10^{-7}
Lead gaskets	40	1×10^{-6}	3×10^{-7}	none	none	none	10^{-9}
Vinyl acetate	2	5×10^{-6}				2×10^{-6}	1.5×10^{-7}
(chamber at 20°C)	100	2×10^{-6}		2.5×10^{-6}		1×10^{-6}	3×10^{-8}
	300 at 20°	4×10^{-7}	3×10^{-7}	5×10^{-7}		4×10^{-7}	10^{-9}
Vinyl acetate	14+2 at 45°	6×10^{-7}		2.7×10^{-5}		2×10^{-6}	7×10^{-8}
(chamber at 45°C)	14+6 at 45°						2×10^{-8}
Vinyl acetate (chamber at 100°C)	14+6 at 45°	1.8×10^{-6}		$>10^{-3}$	$>10^{-3}$	2×10^{-6}	5×10^{-7}

Presumably any variation would be magnified by the second gauge. While pumping on the chamber, each gauge reading was independent of whether the other was off or on. With the valve shut and the pressure rising in the chamber, however, results were rather inconclusive since the second gauge seemed to be "gassy." Nevertheless, readings with the second gauge were unaffected by the first gauge, which seems to indicate that decomposition effects, if any, do not seriously affect the results.

Figure 3 shows results obtained by adding liquid air to a trap located between the ionization gauge and the vacuum chamber (referred to in the graphs as the "gauge trap") a stated time after closing the valve. After addition of liquid air to the trap, a marked decrease in pressure followed by a constant pressure would seem to indicate the presence of a vapor whose vapor pressure at liquid air temperature is approximately equal to, or less than, the constant pressure obtained by condensing the vapor in the trap.

Figure 4, which shows results for the vinyl acetate sealed chamber at room temperature, 45°C, and 100°C, indicates that the gas evolved at these temperatures is likewise almost entirely vapor from the vinyl acetate. The curve for vinyl acetate joints at 45°C rises to 2.7×10^{-5} mm, and then becomes constant, apparently indicating that the vapor pressure of vinyl acetate must be of this order of magnitude at 45°C.*

Measurements were also made with a vinyl acetate covered sylphon. This exposed an area of approximately 127 cm² of vinyl acetate to the system. The equilibrium pressure (lead gaskets, liquid air in high vacuum trap) was 7×10^{-7} mm, and the rate of gas evolution 7.5×10^{-8} mm-liters/sec. after 60 hours of pumping. Generally speaking, it required two or three days of pumping on vinyl acetate to obtain a vacuum in the 10^{-7} range.

Table I summarizes the results giving comparative equilibrium pressures, "apparent vapor pressures" (i.e., the equilibrium pressures obtained in the chamber with the valve closed and under stated conditions), and the approximate initial rate of pressure rise.

Apparent differences between results which differ by no more than a factor of two are probably insignificant, and any comparison of results which differ by less than an order of magnitude must not be taken too seriously.

A leak in the vacuum chamber or in the valve which shuts the chamber off from the pump could introduce severe errors into the results. A VEECO helium leak detector was used to test the soundness of the vacuum chamber and other joints throughout the system. The tightness of the valve was checked in the following way: The chamber valve was closed and then the diffusion pump heaters turned off and the pump boiler allowed to cool. (The pump stalls in 3 to 5 min. after turning off the heaters.) The pressure on the pump side of the valve thus becomes considerably higher than in the case of leaving the diffusion pump on. The pressure-time curve taken under these circumstances was compared with readings taken closing the valve with the pump left operating during the time when the valve was shut. No significant differences were found, and its was therefore concluded that leakage through the valve was too small to affect the results.

ACKNOWLEDGMENT

This work was assisted by the joint program of the ONR and AEC.

---

* Vinyl acetate AYAT (the most highly polymerized variety commercially supplied by the Bakelite Corporation) was used for these joints, the method of application being (1) to heat the parts to be joined in 150°C and melt the solid vinyl acetate stick on to the mating surfaces, or (2) to apply a solution of one part of vinyl acetate in 10 parts of toluene by weight to the surfaces to be joined. The coating is allowed to dry, and the parts are then heated to 150°C for about ½ hour to eliminate the toluene. In either case the seal is made by raising the temperature of the abutting surfaces to 150°C. At this temperature, vinyl acetate is very plastic, and the parts must be kept clamped or bolted together until it is cool.

THE REVIEW OF SCIENTIFIC INSTRUMENTS VOLUME 21, NUMBER 8 AUGUST, 1950

Boron Trifluoride Proportional Counters

I. L. Fowler and P. R. Tunnicliffe*
National Research Council of Canada, Atomic Energy Project, Chalk River, Ontario

(Received May 4, 1950)

Boron trifluoride proportional counters of calculable efficiency for neutron beam measurements are described. It has been found possible to obtain excellent pulse-size distributions with a filling of 60 cm of purified BF_3 by "soaking" the counters for a long time (up to three months) with BF_3 before putting in the final filling. These fillings are stable. Fillings of less than 5 cm BF_3 made up to 50 cm with argon have also been studied. With these fillings the pulse-size distributions are very good for both beam and total irradiation conditions. A discussion of the counter efficiencies with particular reference to end correction is given.

I. INTRODUCTION

THE detection of slow neutrons by the exothermic reaction, ${}_0n^1+{}_5B^{10}\rightarrow{}_3Li^7+{}_2He^4$ is well known, and counters filled with boron trifluoride have long been used for this purpose.[1] The principal requirements of a neutron counter are (a) that the pulses be of uniform size to enable the efficiency to be calculated, and (b) that the sensitivity be as high as possible. In counters containing a low pressure of BF_3 the distribution of pulse sizes is sufficiently good for the number of boron disintegrations in the sensitive volume to be accurately counted. Thus "low pressure" counters can satisfy requirement (a). To satisfy requirement (b) as well, a high pressure of BF_3 is necessary, but until recently counters containing more than 20 cm Hg pressure of BF_3 have given unsatisfactory pulse-size distributions because of electron capture. Work by Steljes and Hudswell[2] at Chalk River had suggested that it was possible to prepare samples of gas, on occasion, but not reproducibly, in which electron capture was markedly reduced. For this reason the technique of filling BF_3 counters to near atmospheric pressure was pursued. The results obtained are in agreement with experimental work by Bistline[3] on electron capture in BF_3 which indicated that it should be possible to make satisfactory counters filled to near atmospheric pressure.

It has been found that the counters must be aged with a temporary filling of BF_3, for a period of up to three months for the high pressure type, before the final filling is inserted. The results on high pressure fillings have been obtained on a rather small number of counters because of this long time required in the experiments. However, publication of the results to date is felt to be justified.

The counters are intended principally for applications where a neutron beam is directed axially down the counter. The beam is admitted by a thin copper window at one end. The high pressure counter is filled to 60 cm Hg pressure, with BF_3 enriched to 96 percent in B^{10}, and shows good pulse distributions when used in applications where the neutron beam is less than one inch in diameter. The low pressure counter is filled with not more than 5 cm Hg pressure of BF_3 together with sufficient argon to bring the total pressure to about 50 cm and shows excellent pulse distributions under both beam and total irradiation conditions.

II. CONSTRUCTION

Details of the counter construction are shown in Fig. 1. The outer shell (a), which is also the cathode, is a seamless copper tube 25 in. long, 2½ in. outside diameter, with a wall thickness of 0.081 in. The threaded brass end cap (b) carries the copper-glass seal (c) which serves as an insulator for the anode lead (d). The pumping tube is attached to the copper-glass seal. A window (e) of 0.010-in. thick copper is soldered to the other end of the tube. The anode wire (f) is 0.002-in. diameter tungsten, which, at the window end, is wrapped around a heavier tungsten wire (g) and both are sealed into the end of a 3-mm diameter "Nonex" glass tube (h). A nickel tube 0.060 in. diameter (j) is assembled over the anode wire and held in the tube (h), when the seal is made (the nickel tube is held mechanically rather than sealed). A short length of 0.030-in. diameter tungsten wire (k) is sealed into the other end of the glass tube (h), and this wire is then soldered into a further short length of nickel tube (l). The nickel tube (l) is soldered to the center of the window (e) to give a sound mechanical joint and the solder is prevented from spreading over the surface of the window. The other end of the anode wire is soldered to a tungsten tension spring (m) which is attached to a heavier tungsten lead (n) sealed into the end of the glass tube (o). The nickel tube (j) and the glass tube (o) serve to define the counting volume.

All soldered joints are made with a silver solder containing no cadmium.†

After assembly the counters are thoroughly cleaned using dilute sulfuric and chromic acids. It is most important to remove all traces of the borax soldering flux. Many washings of distilled water complete the cleaning.

---

* Now at the Atomic Energy Research Establishment, Harwell, England.

[1] S. A. Korff and W. E. Danforth, Phys. Rev. 55, 980 (1939).

[2] Unpublished.

[3] J. A. Bistline, Rev. Sci. Inst. 19, 842 (1948).

† B.S.I. Grade A solder, supplied by Johnson, Matthey, and Mallory Ltd., Montreal, Canada.

Following the cleaning the counters are pumped dry with gentle heat applied and then sealed on to the filling system as soon as possible. When refilling is required, a break seal combination is used to reconnect the counters to the system.

The boron trifluoride is prepared from calcium fluoborate (a boron trifluoride-calcium fluoride complex) in a similar manner to methods already described.[3–5] The complex contains boron enriched to 96 percent of the B^{10} isotope.‡ Details of the filling apparatus and procedure are given in the Appendix.

After filling and initial test, the high pressure counters are allowed to stand for a period of up to three months. They are then reconnected to the system by means of the break seal, the initial filling is taken out, and, without further baking, the final filling inserted.

This double filling procedure with a long "soak period" in between has been found necessary due to rapid deterioration of the pulse-distribution characteristics of the high pressure counters following initial filling. It is suggested that chemical action following the initial filling produces gas with strong electron attachment properties. If a trace of water vapor is left in the counter, its action on the boron trifluoride can produce hydrogen fluoride. This will react with the silica in the glass to produce silicon tetrafluoride and water. Traces of silicon tetrafluoride have been detected in a sample of a counter filling gas by mass spectrometer analysis.

It would thus appear that in spite of extreme care in outgassing the counters and trapping of water vapor in the filling system, a trace may still be left in the counter sufficient to cause marked deterioration.

It seems possible, therefore, that "soaking" produces a wall layer which effectively prevents, or slows down very considerably, the continued production of silicon tetrafluoride following refilling.

III. METHOD OF TESTING

A preamplifier is mounted directly on to the end of the counter, and is followed by an amplifier with adjustable time constants, giving a total gain of 8000. High voltage to the central wire is supplied through a 10-MΩ resistor and the input time constant to the head amplifier is 100 μsec. The amplifier time constants are adjusted to give a pulse rise time of about 0.2 μsec. and a differentiating time as required. The counter shell is grounded. The high voltage is adjusted so that the maximum pulse size from the amplifier is about 80 volts, corresponding to a gas multiplication of approximately 20 for the low pressure counters.

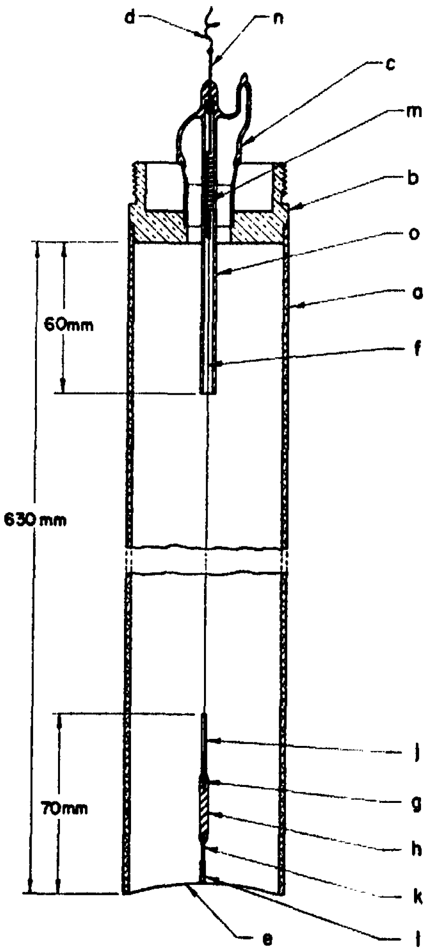

FIG. 1. Details of neutron counter construction.

The pulse distribution is measured with the aid of the 30-channel pulse analyzer described by Westcott and Hanna.[6] The counters are tested using either a well-collimated beam of thermal neutrons from the

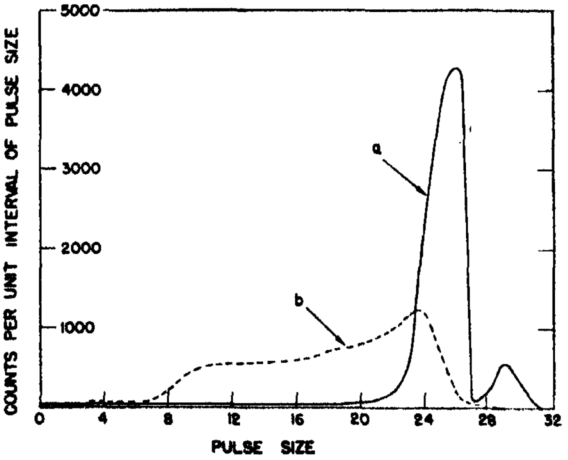

FIG. 2. Pulse distribution of a low pressure BF_3 counter, 1.1 cm BF_3, 47 cm argon, H.T. = 1100 v, 1-in. diameter neutron beam. (a) With differentiating time constant 1.6 μsec. (b) With differentiating time constant 0.16 μsec.

---

[3] C. P. Baker and J. A. Bistline, MDDC 1409, LADC 417.

[5] Hodges, Lloyd, and Weinstock, AECD 2223, LADC 450.

‡ Supplied by the Carbon and Carbide Chemical Corporation, Oak Ridge, Tennessee.

[6] C. H. Westcott and G. C. Hanna, Rev. Sci. Inst. 20, 181 (1949).

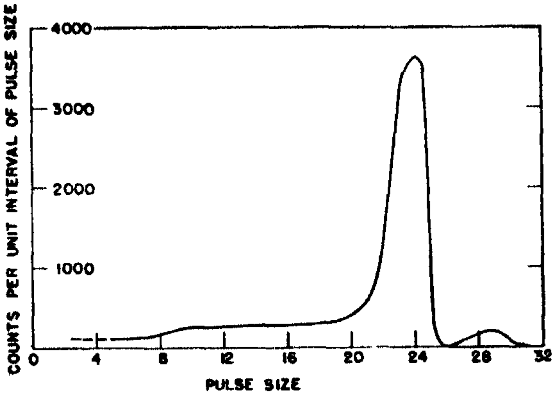

FIG. 3. Pulse distribution of the same counter as Fig. 2 under total irradiation conditions, H.T. = 1100 v, differentiating time constant 1.6 μsec.

Chalk River reactor directed axially down the counter, or a polonium-beryllium neutron source enclosed in a paraffin castle.

IV. RESULTS AND DISCUSSION

A. Low Pressure Counters

Typical pulse-size distributions for a counter containing 1 cm BF_3 and 47 cm argon tested with a 1-in. diameter neutron beam parallel to the anode are shown in Fig. 2. For a differentiating time constant of 1.6 μsec. (curve a), the pulses are confined mainly to two narrow peaks which correspond to the formation of Li^7 in the excited and ground states. The relative positions and intensities are consistent with a recent determination in this laboratory.[7] The broadening of the peak when the differentiating time constant is reduced to 0.16 μsec. (curve b) indicates that the pulse rise time is of the order of 0.5 μsec. and it is consistent with the expected rate of electron collection. The uniform distribution of small pulses in curve (a) is attributed to boron disintegrations occurring near the ends of the sensitive volume.

Figure 3 shows the pulse distribution given by the same counter as in Fig. 2 under total irradiation conditions. The distribution is similar but the number of small pulses is greater, due to disintegrations occurring near the wall.

B. High Pressure Counters

High pressure counters (60 cm BF_3) are poor and unstable if they are inadequately "soaked" with BF_3. This is illustrated in Fig. 4. The pulse distributions shown were taken using a neutron beam, (a) just after filling and (b) several weeks later. It will be seen that the distribution peak was initially very broad, and soon deteriorated until there was no sign of a peak at all.

Figure 5 shows similar results after the counter had been "soaked" at only 1 cm pressure for three months and then refilled to high pressure. It will be noted that the distribution is much better and the deterioration not so marked.

Figure 6 shows the pulse distribution given by a counter "soaked" at 60 cm pressure of BF_3 for three months and then refilled to the same pressure. No evidence of deterioration has been noted for a period of three months.

Figures 7 and 8 show the properties of this counter under different irradiation conditions. In Fig. 7 the neutron beam was reduced from 1 to ⅜ in. in diameter resulting in a marked narrowing of the pulse-distribution peak. Figure 8 shows the results obtained for total volume irradiation of the same counter at various amplifier differentiating time constants. It will be seen

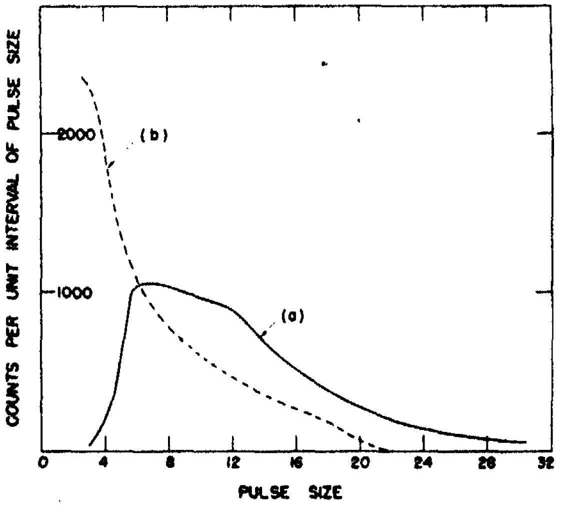

FIG. 4. Pulse distribution of a high pressure BF_3 counter (66.3 cm BF_3), 1-in. diameter neutron beam, H.T. = 3200 v. (a) Immediately after first filling. (b) Several weeks after filling.

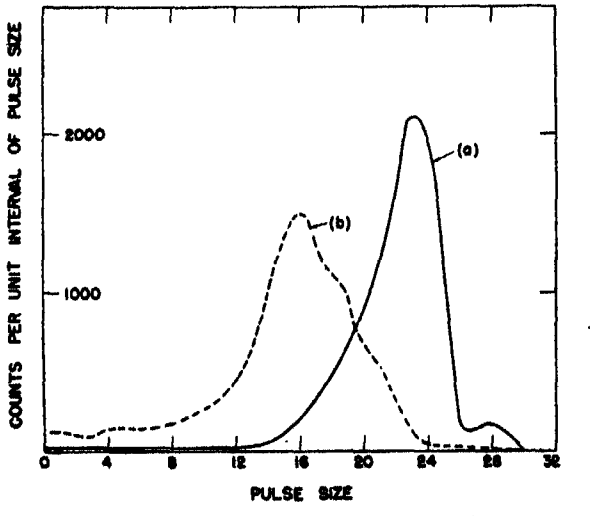

FIG. 5. Pulse distribution of a high pressure BF_3 counter (58.7 cm BF_3), 1-in. diameter neutron beam, H.T. = 2200 v, "soaked" for 3 months at 1 cm pressure BF_3. (a) Immediately after refilling. (b) Three weeks later.

---

[7] G. C. Hanna (private communication).

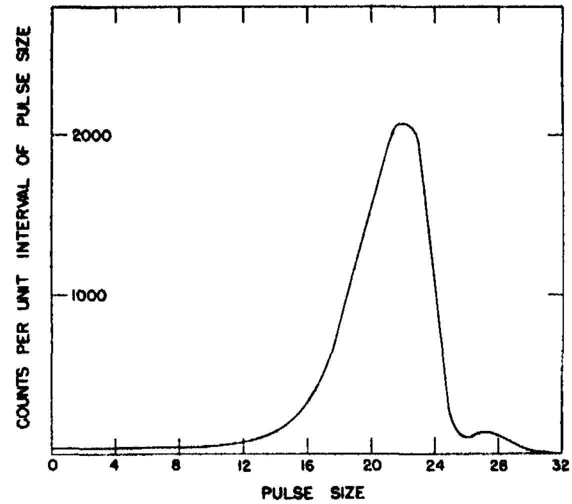

FIG. 6. Pulse distribution of a high pressure BF_3 counter (60.3 cm BF_3), H.T. = 2520 v, 1-in. diameter neutron beam, "soaked" for 3 months at 60 cm pressure BF_3, after refilling.

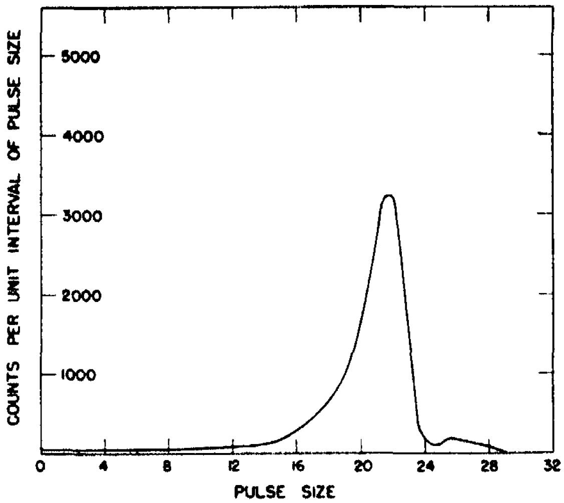

FIG. 7. The same as Fig. 6 using a ⅜-in. diameter neutron beam, H.T. = 2520 v.

that the distribution is very broad and that the maximum pulse size is markedly reduced if the differentiating time constant is reduced below 3 μsec. The broad peak and the effect of differentiation are in general agreement with the results of Bistline[3] for the mean free drift distance and drift velocity respectively of the electrons at ratios of field to pressure which exist near the counter wall. This effect is attributed to those boron disintegrations which occur within 1 cm of the counter wall.

These counters are very satisfactory for the requirements of most beam experiments, but consideration is being given to means of purifying the gas further and raising the field to pressure ratios near the wall. It is expected thereby to improve the pulse distribution under total irradiation conditions, and there is some recent evidence that increased gas purity alone may effect this. It is also considered likely that the minimum "soak" period necessary to produce satisfactory stable counters may be much less than three months with certain precautions, and this is being investigated further.

C. The Counter Efficiencies

Direct calculation of the counter efficiencies using the known boron cross section cannot be made owing to uncertainties introduced by end effects. Disintegrations occurring just within the sensitive volume can send particles into the insensitive end space, and disintegrations occurring in the insensitive end space just outside the sensitive volume can project particles into the sensitive volume. Both types of boundary disintegrations will produce small pulses and the fraction of these which is counted depends on the bias setting. In an ideal counter where the ends of the sensitive volume are so defined that there is no disturbance of the electric field distribution at the ends of the anode wire, it can readily be shown that a pulse distribution would be obtained consisting of a narrow peak together with a number of smaller pulses uniformly distributed from the peak down to zero size. This applies in the case of the boron disintegrations when there are two particles and assumes that the ionization along the tracks of the disintegration particles is uniform. It can also be readily shown in such an ideal counter that if the counting circuit discriminator bias is set at a value equal to half the pulse size in the peak the counting rate will be the same as if it were assumed that every disintegration occurring in the sensitive volume gave a pulse of uniform size, i.e., that no ionization was lost at the ends of the sensitive volume. This is still true when the variation of specific ionization with particle energy is taken into account. However, as shown previously, the pulse-distribution curve has two peaks, corresponding to the formation of Li^7 in the excited and ground states,

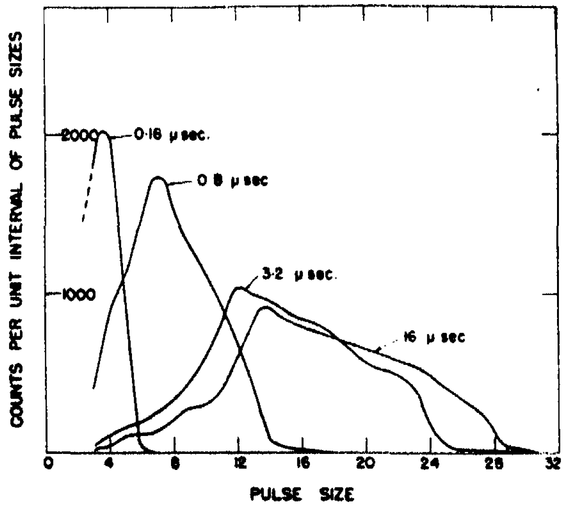

FIG. 8. The same counter as Figs. 6 and 7 but showing pulse distributions under total irradiation conditions showing the effect of various differentiating time constants 0.16, 0.8, 3.2, and 16 μsec., H.T. = 2520 v.

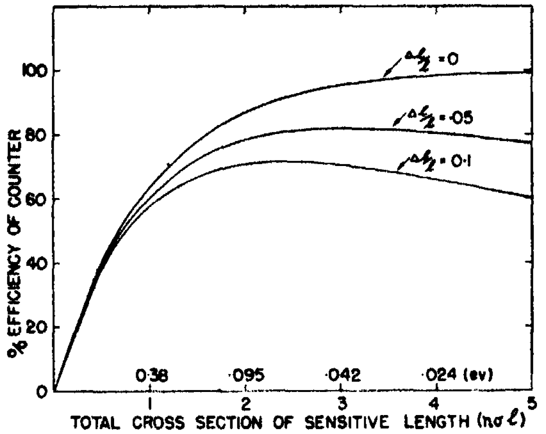

FIG. 9. Efficiency curves of BF_3 counter against total cross section of sensitive length for axial beam irradiation at various ratios of end space Δl to anode length l.

so that the discriminator bias setting for zero end correction in the ideal counter is slightly greater than one-half the pulse size of the main peak.

Ideal conditions as indicated above might be approached by mounting guard rings at the ends of the counter wire, with the potential so adjusted that there is little disturbance of the field. However, for simplicity of construction an attempt has been made to define the sensitive volume by means of the nickel tube (j) (see Fig. 1) and the glass sleeve (o). It is certain that the nickel tube has the effect of making the effective length of the counter less than the geometrical length of the exposed wire, by disturbance of the field. On the other hand, at least some of the ionization occurring in the volume nominally screened by the glass sleeve may be collected by the wire and therefore effectively increase the length. The magnitude of this latter effect will depend on the insulating properties of the glass and the amount of ionization in this region.

The behaviors of the high and low pressure counters as regards end effects are somewhat different and are discussed separately. The discussion is limited to beam applications where there is no wall effect and, in the case of the high pressure type, to beams of small diameter so that the pulse distribution approaches the ideal shape.

1. *Low Pressure Counters*

If the self-absorption of the counters can be neglected, a determination of the efficiency is in principle relatively simple. If two counters of different sensitive lengths but of otherwise identical construction and filling are successively placed in the same neutron beam and the counting rates obtained under identical operating conditions, the difference of these counting rates will represent the counting rate in an ideal counter whose length is equal to the difference between the geometrical lengths of the sensitive volumes of the two counters. The efficiency of such a counter can be calculated. The pulses from this ideal counter will all lie in the pulse-distribution peak. The effective length of one of the counters can then be found (under the given operating conditions) by comparing its counting rate with that of the "ideal" counter.

In practice the counters are not ideally thin and therefore allowance must be made for the self-absorption of the neutron beam. If this is done, the total correction to the geometrical length of the counters due to end effects may be written as

$$\delta l \approx \frac{C_2(l_1 - al_1^2/2) - C_1(l_2 - al_2^2/2)}{C_1(1 - al_2) - C_2(1 - al_1)},$$

where l_1 and l_2 are the geometrical lengths, C_1 and C_2 are the counting rates in the two counters, and $a = n\sigma$, where n = number of B^{10} atoms/cc and σ = the boron cross section.

The value of δl is of course a function of the operating conditions, in particular the setting of the discriminator bias. Two simple conditions may be chosen. The common method of extrapolation of counting rate to zero pulse size, either by means of a bias curve or a pulse-distribution curve, may be used; or the simpler condition of setting the discriminator bias at a value equivalent to half that for the distribution peak. In practice some bias must always be used to avoid spurious counts due to gamma-rays and amplifier noise.

Measurements were made using two counters of identical construction except that l_1 was equal to twice l_2. These were filled simultaneously so that the fillings would also be closely identical.

There are considerable practical difficulties in making the measurement, from fluctuations of neutron beam intensity, difficulty of accurate positioning of the counters, counting statistics, and consistency of the two fillings. The effective length was found to be within two percent of the geometrical length of the standard counter (500 mm). Further work would be required to assess the effects of the two ends separately.

For efficiency calculations it is also necessary that a sample of the filling gas be taken at the time the counters are filled for analysis on the mass spectrometer since the repeated distillations during the filling process may change the isotopic proportions slightly. In addition, the filling pressure must be measured accurately and corrections amounting to a few percent made for scattering and absorption in the window, the gas in the end space, and the glass bead supporting the anode wire.

With all these precautions, the efficiencies of the counters at a given neutron energy are calculable to an accuracy of a few percent. These low pressure counters are intended for applications where high efficiency is not necessary and they are easier to fill than the high pressure type.

2. *High Pressure Counters*

The efficiency of high pressure counters can be calculated in applications where the neutron beam is sufficiently small in diameter to yield a narrow pulse distribution. The inactive region at the window end has a marked effect on the efficiency which can be expressed as:

$$\text{Efficiency} = \exp(-n\sigma\Delta l)[1-\exp(-n\sigma l)],$$

where l = measured length of anode, n = number of B^{10} atoms/cc, σ = cross section of B^{10}, and Δl = length of inactive region at the window end. ($\Delta l/l \approx 0.1$ for the counters described.)

With the geometry and filling of these counters the efficiency is practically independent of $n\sigma l$ (the total cross section/cm² of the sensitive length) over the energy region of 0.03 to 0.1 ev. This is apparent from Fig. 9 which gives counter efficiency curves against values of $n\sigma l$ for various ratios of $\Delta l/l$.

The geometrical value of Δl is readily determined during construction. Its effective value is, however, sensitive to the end effects in the counter in the same way as the counter length. Since these counters are almost completely absorbing at near thermal neutron energies, the only important end effects will occur at the window end. Δl is a function of the bias, but if it is assumed that the nickel sleeve behaves ideally and the discriminator bias is set at the half-value point as discussed, the value of Δl will be the geometrical value. Under these assumptions the uncertainty in Δl will probably not be more than five percent leading to a much smaller error (one percent) in the calculated efficiency.

ACKNOWLEDGMENTS

The authors are indebted to Mr. G. C. Hanna and Dr. D. G. Hurst for helpful discussions and to the former for assistance in using the 30-channel pulse analyzer. They are also indebted to Dr. H. G. Thode of the Chemistry Department of McMaster University for mass spectrometer analyses of samples of counter filling.

APPENDIX. FILLING PROCEDURE

A diagram of the filling apparatus is shown in Fig. 10. The complex is contained in a flask surrounded by a small thermostatically controlled oven. Initially it is heated to 100°C under vacuum for approximately 48 hr. to remove water vapor, with dry ice surrounding trap 2, and liquid air surrounding trap 5. Little BF_3 is lost in this process and the vacuum is maintained at better than 10^{-8} mm Hg. The complex is then allowed to cool to room temperature while pumping is continued to as good a vacuum as possible before tap 1 is turned off and traps 2 and 5 removed for cleaning. Thereafter the counter filling procedure for high pressure counters is as follows.

1. The counter is sealed on, evacuated, and checked for leaks. (Liquid air surrounds trap 5 since a mercury vapor pump is used.)

2. The counter is flame baked to approximately 500°C for at least 45 min. or until the outgassing is considered complete as evidenced by the pressure while still hot. (Flame baking is used solely for convenience owing to certain physical difficulties of assembly and removal of an oven with the present set-up.)

3. Pumping is continued until a vacuum of 10^{-6} mm Hg is reached with the counter cooled to room temperature. The counter is then turned off.

4. Tap 1 is turned on, and the complex pumped for a further period of one hour while heated to 100°C.

5. Dry ice is placed around trap 1, and liquid air around trap 2. The complex temperature is raised to 250 to 300°C. The BF_3 distills into trap 2, and when almost all has come off, the complex is allowed to cool and tap 1 is closed.

6. The frozen BF_3 is pumped for 30 min. more or until a satisfactory vacuum is reached. The McLeod gauge is turned off.

7. Tap 3 is closed, trap 2 is allowed to warm up until a few centimeters pressure is recorded on the manometer. At this point tap 2 is closed and the liquid air promptly replaced around trap 2.

8. Tap 3 is slowly opened allowing the small amount of BF_3 in the system to freeze in trap 5. (This first fraction is always rejected.)

9. Tap 2 is opened, the McLeod gauge turned on, the system again pumped down, and the counter opened to the system. When as good a vacuum as possible has been obtained the McLeod gauge is again turned off.

10. Dry ice is put around trap 4, tap 3 is turned off, and then trap 2 is allowed to warm up until the pressure in the system reaches the desired pressure of BF_3. At this point tap 2 is closed and the liquid air replaced around trap 2.

11. Liquid air is placed around trap 3 and, when all the BF_3 has frozen into it, tap 3 is reopened and the system again pumped to a hard vacuum.

12. Tap 3 is again closed, trap 3 is allowed to warm up and the counter thus filled to the required pressure.

13. The counter is sealed off.

14. All remaining BF_3 is then taken over into trap 5 and from thence to storage pending recombination with ether.

The counters are tested shortly after filling and set aside to "soak" for up to three months. This "soak" period appears to be a major factor in obtaining good characteristics without serious deterioration over a period of time. Refilling following the "soak" is to be the same schedule as the original filling, with the omission of step 2.

As mentioned, the foregoing schedule applies to high pressure counters. For low pressure counters the procedure is slightly different as follows.

1 to 4. Same as high pressure schedule.

5. Dry ice is placed around trap 1 and liquid air around trap 2. The complex temperature is raised to 250°C for a short time to collect a small quantity of BF_3 in trap 2. The complex is allowed to cool and tap 1 is closed.

6. Same as high pressure schedule except that counter is opened to the system after 15 min.

7. Tap 3 is closed, trap 2 is allowed to warm up, and BF_3 enters the system and counter at a low pressure. The counter tap is closed and the counter allowed to stand overnight to "soak."

8. The BF_3 in the system is frozen into trap 5 and then taken over for storage.

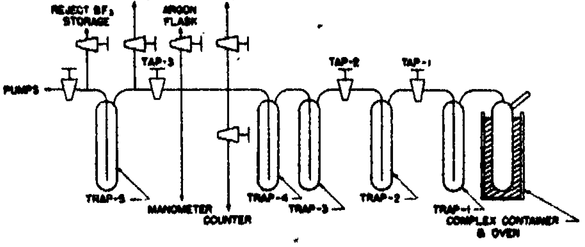

FIG. 10. Diagram of the BF_3 filling apparatus.

9. Next morning the BF$_3$ is pumped out of the counter into trap 5, and the counter pumped down to a hard vacuum.

10 and 11. Same as items 5 and 6 high pressure schedule.

12 to 14. Same as items 10 to 12 high pressure schedule.

15. Argon is admitted to make up to the total pressure to 50 cm. After several hours to allow proper mixing of the gases, the counter is sealed off.

16. Same as item 14, high pressure schedule.

A gold foil is included in the pumping line to the counter to trap residual mercury vapor. Other than those mentioned in the schedule, no special precautions are taken except those compatible with good vacuum technique. Conventional stopcocks are used and all traps can be taken apart for cleaning. Taps and the trap ground joints are greased sparingly with Apiezon *L* or *M* grease.

The amount of complex required for a given filling is calculated and a little more than this quantity put in the flask. This allows the first and last fractions to be discarded, and since all the BF$_3$ is taken off each time, each filling is comparable.

THE REVIEW OF SCIENTIFIC INSTRUMENTS VOLUME 21, NUMBER 8 AUGUST, 1950

The Design of a Magnetic Focusing Coincidence Spectrometer[*]

C. M. Fowler[**] and R. G. Shreffler[†]
Randall Laboratory of Physics, University of Michigan, Ann Arbor, Michigan

(Received April 13, 1950)

Design and operating features are described for a semi-circular magnetic focusing coincidence spectrometer. The primary function of the spectrometer is that of determining whether or not two different radiations from a radioactive sample are in the same branch of the nuclear decay scheme. Although the instrument is designed primarily for studies between conversion electron groups, it is also suitable for studies between conversion groups and beta-spectra.

A feature of the instrument is its extraordinarily good coincidence resolving power. Applications of the spectrometer to two activities are briefly discussed, and an explanation of the high resolving power is given.

1. INTRODUCTION

THE primary function of the magnetic focusing coincidence spectrometer is to determine whether or not two different electron radiations of an active element are in cascade, that is, in the same branch of a decaying nucleus. The electrons may arise from the continuous beta-spectrum of an activity and from conversion electrons. Although no experimental data is offered for the case of photo-electrons, studies could include these as well.

The basic principle of the instrument involves the magnetic focusing of electrons from one of the radiations into one Geiger tube, while those of the other radiation are focused into a second Geiger tube. If the two radiations are in cascade, then a coincidence circuit collecting the inputs of the two Geiger tubes will record true coincidences. If no true coincidences are observed, the radiations are not in cascade.

Fig. 1. Fully assembled coincidence spectrometer.

For decay schemes exhibiting gamma-radiations which are moderately or strongly converted, the spectrometer offers a useful and certain method for properly ordering the radiations. The advantage of the spectrometer over the usual absorption coincidence techniques is that the radiations may be focused and studied in pairs through their conversion electrons, thus leaving no ambiguity as to which of several radiations may be in coincidence.

Feather,[1] as early as 1940, described a coincidence spectrometer designed primarily for coincidence studies between one conversion electron group and a beta-spectrum. Feather, Kyles, and Pringle[2] first reported the results of a specific investigation of this type in 1948.

The spectrometer described here is designed primarily to study coincidences between two conversion electron groups, and as will be shown later, exhibits very high coincidence resolving power. Among other details, it differs from that described by Feather, in that the coincidence radiations focused into the two Geiger tubes both travel through the same portion of the active source, and do not pass through the sample backing. This feature accounts in part for the high resolution of the spectrometer.

Limitations to which the spectrometer is subject include: 1. Only radiations suitably converted may be studied. A rough rule (modified considerably for branched decay schemes) is that the product of the conversion coefficients of the radiations studied should not be appreciably less than 0.001. 2. Only conversion groups which can be focused two or more centimeters apart on the focal plane may be studied as a pair. This is a design limitation arising from the finite widths of the Geiger tubes. This restriction is usually only severe for high energy radiations (greater than 200 kev) or for elements of low atomic number. This is true, since for studies between gamma-radiations of nearly the same energy, by proper adjustment of the magnetic field, one Geiger tube may collect electrons from the K conversion group of one radiation, while the other tube may collect L conversion electrons from the other radiation. 3. Operational times required to build up adequate statistics are frequently quite long. This is an inherent difficulty brought about by large solid angle losses required for focusing. For activities of lifetimes less than a few days, the method becomes unfeasible unless the radiations are highly converted. 4. Two radiations delayed long with respect to the resolving time of the coincidence circuit will not yield appreciable true coincidences. It is therefore necessary to know from other investigations whether or not long delays are present in an activity before it can be assumed that two radiations are not in cascade, when they produce no true coincidences.

---

[*] Sponsored in part by ONR and the AEC (through NRC Predoctoral Fellowship Funds).

[**] Now at Kansas State College, Department of Physics, Manhattan, Kansas.

[†] Now at Los Alamos Scientific Laboratory, Los Alamos, New Mexico.

[1] N. Feather, Proc. Camb. Phil. Soc. 36, 224 (1940).

[2] Feather, Kyles, Pringle, Proc. Phys. Soc. 61, 466 (1948).

2. DESIGN DETAILS OF THE SPECTROMETER

Figure 1 is a photograph of the fully assembled coincidence spectrometer. The assembly consists of a camera, a vacuum system, a magnet, and a recording system. These components are described in the following sections:

The Camera

The design of the camera (scale drawing, Fig. 2) is based upon the principles incorporated in the photographic semi-circular spectrometer. Instead of a photographic plate, two movable Geiger tubes, controllable from outside the camera, open upon the focal plane.

The camera is constructed of $\frac{3}{8}$ in. brass plate. Bronze bolts seat the removable top on a rubber gasket, which in turn is contained in a channel milled around the top edges of the camera sides. When the camera is in proper position between the magnet pole faces, a flanged connection can be coupled to the vacuum line.

A rigid three-sided frame, supporting the sample, slit, and Geiger tube assemblies is mounted upon the camera floor, and secured by set screws. The sample and slit assemblies are shown in the plan view of Fig. 2 The slits are made of Lucite, and can be separated from 0 to 2 centimeters. Provisions are also made to allow variation of the separation of source and slit planes from one to five centimeters.

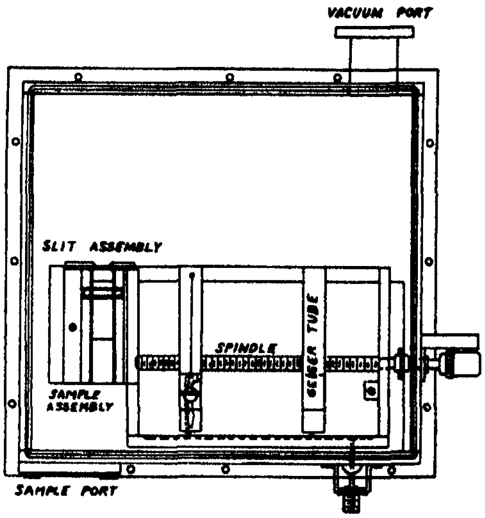

FIG. 2. Camera plan view; scale drawing.

The Geiger tubes are moved by threaded spindles, rotated by control knobs outside the camera. Veeder-Root counters, connected to the spindles, record the positions of the tubes. The control knob assembly can be separated from the drive spindles by uncoupling flanged connections, when it is necessary to remove the frame from the camera. The Geiger tubes receive their anode voltages through spring loaded contact pieces which make contact with copper bar conductors. These conductors are embedded in the Lucite rear wall of the frame. The spring loaded contacts are also mounted in Lucite pieces, which are bolted onto the ends of the Geiger tubes. Soldered to the copper conductor bars in the frame, are female sockets into which covar conductors slide, when the frame is properly placed within the camera. The covar conductors are permanently mounted on the camera, and lead through the camera walls to external amphenol fittings.

A $\frac{1}{32}$ in. celluloid lining, over all interior parts of the camera exposed to radiation, practically eliminates detectable scattering.

The Vacuum System

The vacuum system comprises two stages, a mechanical fore-pump, and a water-cooled, oil diffusion pump. Thermocouple vacuum plug units are installed in the system so that pressures within the camera, and between the two pumps can be read. A manometer, with a double stopcock arrangement, is incorporated into the system so that pressures may be built up slowly when the camera is opened. This procedure avoids undue strains on the Geiger tube windows.

Normal operating pressures of approximately one micron are used. These low pressures minimize electron air scattering and are more than sufficient to prevent the high anode voltages from breaking down within the camera.

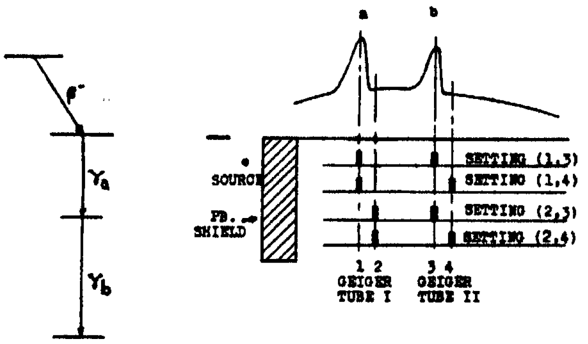

FIG. 3. Sketch illustrating offset method.

The Magnet

The chief property required of the magnet is stability. As will be shown later, the slightest drifting of the magnetic field greatly reduces the effectiveness of the instrument.

The stability required was obtained by butting a large number of Alnico No. 3 cylinders (1 in. $D \times 3$ in.) between the yoke and pole pieces. After establishing a convenient magnetic field, by pulsing current through fixed exciting coils, slight drifts up to one percent occur during the first few hours. After 24 hours, no further detectable changes are observed over periods of months.

By spacing the Alnico cylinders uniformly over the pole faces, except for a small increase in density near the face edges to help compensate for fringing flux, fields uniform out to nearly a half pole-gap width from the face edges may be obtained.

Recording System

Individual Geiger tube pulses are monitored by commercial IDL scalars. Pulses are then sent to a Rossi type coincidence circuit, including a pulse height selector discriminator circuit. Coincidences are recorded by a thyratron driven mechanical recorder. The time constant of the coincidence circuit can be varied by switching in various pairs of different valued grid leak resistors. By suitable choices of the *RC* constant of the Rossi circuit and pulse heights, the over-all circuit resolving time may be varied from 0.2 to 2 μsec.

For the Geiger tubes employed, drift time losses were found to be negligible for resolving times greater than 0.45 μsec.

3. ANALYSIS OF COINCIDENCE DATA

The procedure used in the study of two radiations sometimes varies, but the most useful one usually consists of fixing one Geiger tube at about the peak of one of the electron groups, while the other tube is set at various locations about the other line. A plot of the coincidence rates so obtained *versus* the position of the variable tube gives rise to the coincidence lines shown in Figs. 8, 9, and 10. The most noticeable feature of these lines is their sharpness, as compared to the lines seen when the instrument is operated as an ordinary non-coincidence spectrometer.

Studies to be published later will discuss the application of the spectrometer as a tool to resolve L_{I}, L_{II}, and L_{III} conversion electron groups in a more quantitative manner, as well as its use in distinguishing conversion lines arising from gamma-radiations of almost the same energies.

Observed coincidence rates consist of spurious coincidences and coincidences resulting from cascade radiations of the active isotope. Both require discussion.

Spurious Coincidences

There are two sources of spurious coincidences: accidentals and cosmic-ray coincidences.

Accidental coincidences are subtracted from all observed rates according to the well-known formula, $q_A = 2\tau n_1 n_2$, q_A being the accidental rate, τ the resolving time of the coincidence circuit, n_1 and n_2 the input counting rates entering the coincidence circuit.

Experimental studies showed that, to within the statistical accuracy of the research, hard components of cosmic radiation contributed a coincidence rate depending only upon the Geiger tube separations, the rate decreasing as the separation increases. From each observed coincidence rate, a cosmic-ray rate is thus deducted.

True Coincidences

When the spurious rates have been deducted from the observed rates, the resultant rates represent coincidences arising from nuclear cascade radiations. However, in addition to the coincidence rates sought between conversion electron groups, there exist smaller true coincidence rates between the conversion electrons focused in one Geiger tube, and portions of the continuous beta-spectrum focused in the other tube. Further, if the source shielding (see Fig. 3) is insufficient to absorb all of the lateral gamma-radiation, coincidences between the gamma-ray leakage and both conversion electrons groups and the continuous beta-spectrum will be present.

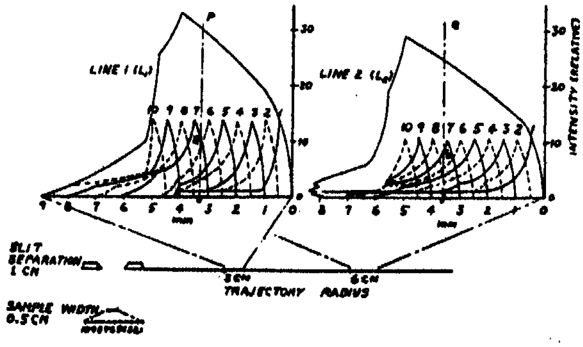

FIG. 4. Contributions of source increments to gross line densities. The number specifying the sample increment also identifies the contribution of this increment to the two gross lines.

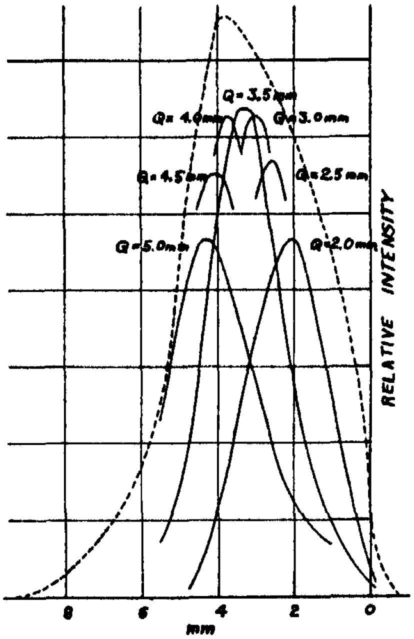

FIG. 5. Effect of fixed Geiger tube location on the shape and position of the coincidence lines. The values of Q given at the peaks of the curves locate the center of the fixed Geiger tube with respect to the leading edge of the gross density curve of line L_2. Geiger tube window widths: 1.5 mm.

The combined rates of all these cross coincidence terms may be eliminated by use of the "offset" method described below, leaving a net rate for the conversion electron coincidences alone.

In Fig. 3, let c_a and c_b represent conversion electron groups, between which coincidence studies are to be made. Suppose the positions 1 and 3 represent arbitrary points, one for each of the lines, at which the Geiger tubes are centered. Points 2 and 4 are offset points, such that the inner edges of the Geiger tube windows just clear the leading edges of the conversion lines. Then the true coincidence rate $Q(1,3)$ for the Geiger tubes centered at points 1 and 3 is given by the following equation:

$$Q(1,3)=q(1,3)-q(1,4)-q(2,3)+q(2,4). \quad (1)$$

The small q's are the coincidence rates for the pairs of settings shown in Fig. 3. These rates are supposedly corrected for spurious coincidences.

Details of the proof for this formula, and its degree of validity are discussed in the Appendix.

4. COINCIDENCE LINE SHARPENING

The high coincidence resolution is a consequence of two effects, one arising from a minimization of source scattering of the electrons (an effect which accounts in considerable part for line broadening in non-coincidence spectrometry, particularly for lower energy radiations) and the other, a so-called natural line sharpening effect.

Both of these effects have as their common source the feature that a true coincidence can result only from electrons leaving the same atom of the source.

That the relatively intense scattered line portion seen in non-coincidence spectrometry is minimized here follows since both electrons forming a possible coincidence traverse about the same portion of the source; thus if one electron is scattered from the line peak, on the average, so would the other electron be scattered from its peak. Therefore unscattered electrons focused into one Geiger tube located at a line peak would be less likely to have highly scattered electrons in coincidence with them.

Aside from the reduction of line broadening due to source scattering, the following discussion shows that a natural line sharpening effect is also present. The arguments are given for a two-dimensional spectrometer and are thus only qualitative, but the important features entering into line sharpening are brought out clearly.

Suppose L_1 and L_2 are two conversion lines between which coincidence studies are to be made. The envelopes of the curves shown in Fig. 4 give the densities of the two lines. However, rather than the complete density curves, it is necessary to know the contribution of each element of the source to the density curve. In the discussion that follows, the complete line density curve will be referred to as the gross line, in distinction to the coincidence lines to be considered later. The integration of the gross line density curve over a Geiger tube window width, results in the lines as seen by either Geiger tube as it sweeps across the gross line.

Plotted below the gross density curves in Fig. 4 are shown the contributions to the curves from small elements of the source. The method of construction of these increment curves follows a treatment previously given by the authors.[8]

The total coincidence rate between a point P of line L_1 and a point Q of line L_2 is given by the sum of the coincidence rates furnished by each element of the

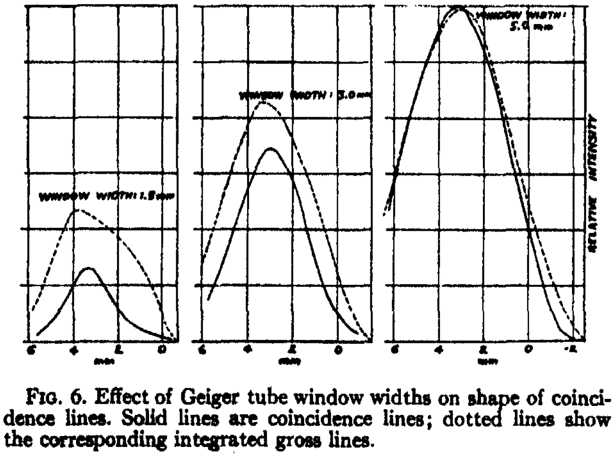

FIG. 6. Effect of Geiger tube window widths on shape of coincidence lines. Solid lines are coincidence lines; dotted lines show the corresponding integrated gross lines.

---

[8] Fowler, Shreffler, and Cork, Rev. Sci. Inst. 20, 966 (1949).

source for these two points. For example, the coincidence rate between P and Q arising from the small source element 7, is given by the product $(oa)\cdot(ob)$. Contributions from all the source elements add to give the total coincidence rate for the pair of points P,Q.

In this manner, a rectangular grid can be drawn up giving the coincidence rates between any pair of points, one being taken from each of the two lines, L_1 and L_2.

The construction of these grids (one is necessary for each pair of gross lines to be studied) greatly facilitates the integrations over the Geiger tube window widths. In practice, it is found convenient to select equal spacings between the points P and Q, of the gross lines, such that an even number of these spacings are subtended by the Geiger tube windows. The total coincidence rate observed for specified locations of the two Geiger tubes will be comprised of the contributions from all pairs of points, P, Q, falling within the window widths covering portions of the gross lines. By use of conventional numerical integration formulas, the simultaneous integration over both Geiger tube window widths is readily accomplished, using the grid described above.

As mentioned previously, one of the procedures adopted in this research for coincidence studies, involves fixing one Geiger tube on one of the two lines, while the other tube is placed at various points of the other line. The distribution of coincidence rates plotted *versus* the movable tube setting gives rise to the sharp coincidence lines.

Theoretical coincidence lines following this procedure were then studied with gross line radii of 3.0 and 6.0 centimeters. The slit spacing was one centimeter, while a very wide source of 0.5 centimeter was used. The choice of this wide source was made to see if coincidence sharpening was still appreciable, and also to lend more accuracy to the numerical studies carried out, since the source could be conveniently divided into more increments.

Figure 5 shows the predicted coincidence lines, as the movable Geiger tube traverses the line L_1. The different curves arise from selecting different locations for the fixed Geiger tube on the line L_2. In this figure, both Geiger tube windows were taken as 1.5 mm wide.

Figure 6 shows the effect of Geiger tube window widths on the coincidence lines. For all these curves, the fixed Geiger tube was centered at the same point on line L_2. Since the gross line curves, integrated over different window widths are not the same, over each of the coincidence lines is plotted the window integrated gross line.

Some of the important observations from Fig. 5 are:

(1) The coincidence line intensities are strongly dependent upon the position of the fixed Geiger tube, being greatest when this tube is located on the leading edge of the gross line somewhat past its peak.

(2) The coincidence line widths are about half that of the integrated gross line width, thus showing coincidence sharpening. Even greater calculated sharpening should be expected with exact calculations replacing the triple numerical integrations.

(3) The locations of the peaks of the coincidence lines are also dependent upon the location of the fixed Geiger tube.

Some further observations from Fig. 6 are:

(4) The line sharpening improves as the window widths are decreased. For example, the ratio of half-widths of coincidence line to gross line decreased from 0.95 to 0.52 as the window widths changed from five mm to 1.5 mm.

(5) The coincidence line peak intensities increase with the window width.

5. APPLICATIONS OF THE SPECTROMETER

The Hafnium 181 Activity

For convenience of discussion of the coincidence studies, the decay scheme for this activity is given in Fig. 7.

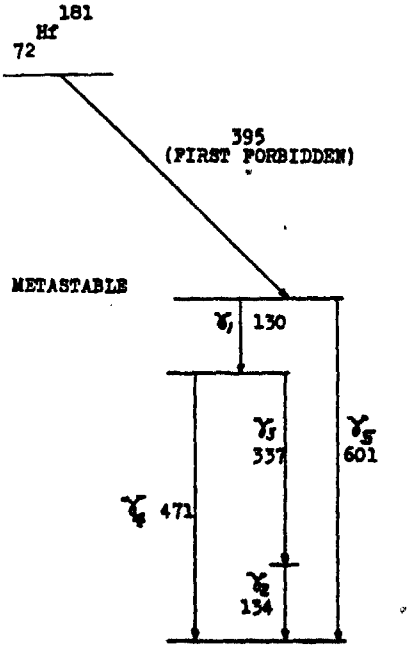

FIG. 7. Proposed decay scheme for Hf 181. All energies in kev.

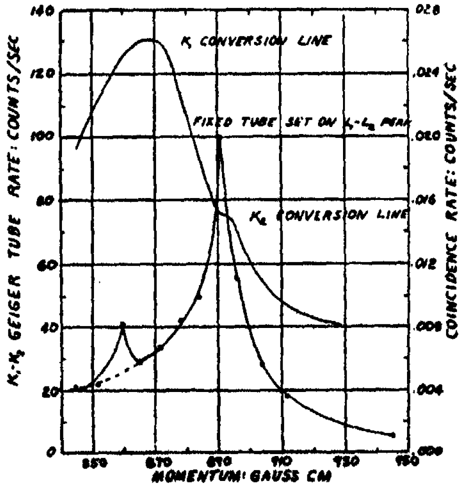

FIG. 8. Hafnium coincidence curve.

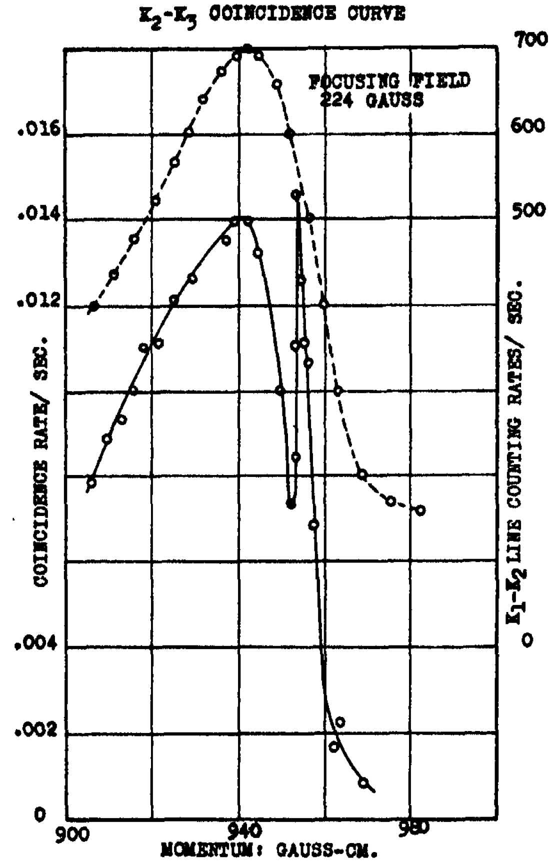

FIG. 9. Europium coincidence curve.

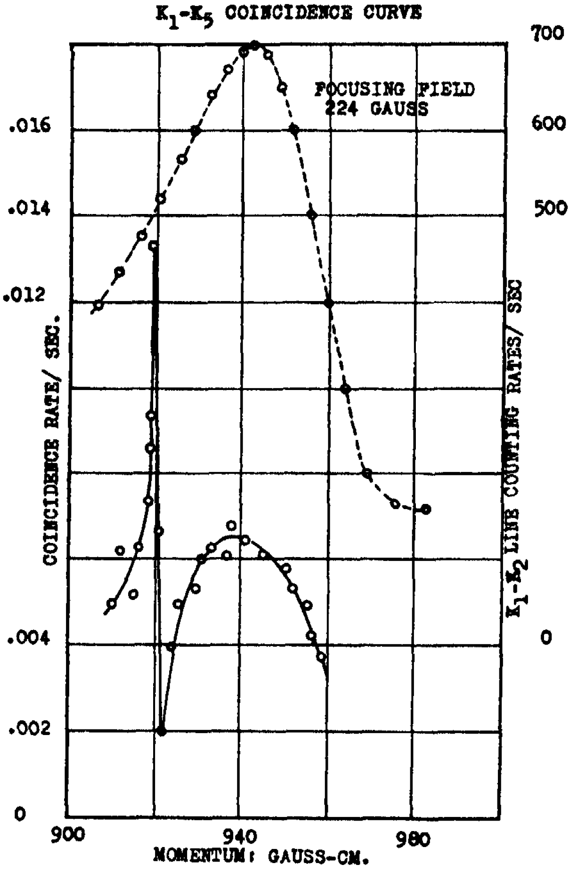

FIG. 10. Europium coincidence curve.

The initial report on the 48-day hafnium activity by Hevesy and Levi[4] has been followed by numerous papers. DeBenedetti and McGowan[5] first reported a metastable state of 22 microseconds following the initial beta-decay. Recently Chu[6] reported on the radiations from this element and proposed a decay scheme consistent with his analysis of the conversion and secondary spectra.

A preliminary survey of the conversion electron spectrum was undertaken by the authors in collaboration with E. Salmi. The results of this effort, with minor changes, agree with the report of Chu. The continuous beta-spectrum was found to be first forbidden with an end point of 395 kev; and a weak *K* conversion line corresponding to a gamma-energy of 601 kev was found with an intensity measured in units of the normalized beta-spectrum of approximately 0.0005. Chu reported the beta-spectrum to be allowed, and omitted the weak gamma-ray.

By making coincidence studies between various pairs of conversion electron groups, it was established that γ_1 is in coincidence with γ_2 and γ_3, and also that γ_2 and γ_3 are in coincidence, all in agreement with the decay scheme shown. Due to smaller coincidence intensities encountered it was difficult to show with statistical accuracy the anti-coincidence which should exist between conversion groups of γ_4 and either γ_2 or γ_3. No conversion line was found in coincidence with the continuous spectrum, establishing the previously reported position of the metastable state. Figure 8 shows a typical coincidence line. It records data confirming the coincidence between γ_1 and γ_2, and also illustrates the technique of employing the *L* conversion groups for radiations resulting from gamma-rays of nearly the same energies. Here, the fixed Geiger tube subtended portions of both *L* conversion groups, being centered at the peak of the unresolved *L* doublet.

Applications to the Long-Lived Europium Activities

When naturally occurring europium is subjected to thermal neutron bombardment, among others formed, are two long-lived activities (greater than five years) which exhibit a host of internal conversion lines.[7,8] Among these are two very intense lines of nearly the same energy: γ_1 (123 kev) and γ_2 (121 kev). Coincidence studies were made among these lines, and two of lesser intensity: γ_3 (244 kev) and γ_5 (344 kev).

---

[4] Hevesy and Levi, Kgl. Danske Vid. Sels., Math.-Fys. Medd. 15, No. 11 (1938).

[5] DeBenedetti and McGowan, Phys. Rev. 74, 728 (1948).

[6] K. Chu, Thesis (University of Michigan, 1949).

[7] Cork, Shreffler, and Fowler, Phys. Rev. 74, 240 (1948).

[8] F. Shull, Phys. Rev. 74, 917 (1948).

Figures 9 and 10 show some of the results of these studies. In both figures the dotted lines show the unresolved K conversion lines of γ_1 and γ_2, as seen by a single Geiger tube. The solid curves show the coincidence lines obtained, as the inner Geiger tube is swept across the K doublet, while the outer Geiger tube is fixed under the K conversion line of γ_3 in Fig. 9, and under the K conversion line of γ_5 in Fig. 10. Although the cross coincidence terms have not been subtracted from the data of these figures, it is clear that γ_1 and γ_5 are in coincidence, as are γ_2 and γ_3.

As an example of the "offset" method, γ_3 and γ_5 were shown not to be in coincidence. Positions 1 and 3 correspond to the two line peaks, while 2 and 4 are points such that the inner edges of the Geiger tube windows just clear the conversion lines. The observed rates, corrected for spurious coincidences, were as follows:

$$q(1,3) = 0.00345 \pm 0.00009 \text{ coinc/sec.}$$
$$q(1,4) = 0.00353 \pm 0.00012 \text{ coinc/sec.}$$
$$q(2,3) = 0.00283 \pm 0.00011 \text{ coinc/sec.}$$
$$q(2,4) = 0.00285 \pm 0.00011 \text{ coinc/sec.}$$

From Eq. (1) this leaves as the net coincidence rate between K_3 and K_5:

$$Q(1,3) = -0.00006 \pm 0.00022 \text{ coinc/sec.}$$

This result is taken as evidence that γ_3 and γ_5 are not in coincidence.

With the coincidence data obtained supplementing other information known about these activities, it has been possible to propose plausible decay schemes for these activities, incorporating such features as K-capture, the presence of an isomeric state, three beta-spectra and numerous gamma-rays.[9]

Figures 9 and 10 together show the complete separation of the K conversion lines of γ_1 and γ_2. The remarkable coincidence resolution is evident upon noting that the radii of curvature of the conversion groups are only slightly greater than four centimeters.

ACKNOWLEDGMENTS

The authors are greatly indebted to Professor J. M. Cork for many valuable suggestions, as well as for continued encouragement. Acknowledgment is also due Dr. W. C. Parkinson of the University of Michigan Physics Staff for valuable discussions concerning the line sharpening effect. Finally, thanks are due to Professor E. K. Chapin of the Kansas State Physics Department and H. B. Keller of the University of Michigan, both of whom very kindly assisted the authors in the preparation of photographs.

APPENDIX

Referring to the simple decay scheme of Fig. 3, it is seen that in the case of incomplete gamma-ray shielding, the Geiger tube counting rates are due not only to conversion electrons, but beta- and gamma-radiation as well. Thus for the setting (1,3), the total counting rates for the two tubes may be written as:

$$n_1 = n_{1c_a} + n_{1\beta} + n_{1\gamma}$$

and

$$n_3 = n_{3c_b} + n_{3\beta} + n_{3\gamma}.$$

The terms on the right represent partial rates from the conversion electrons, continuous beta-spectrum and gamma-ray leakage, respectively. The numerical subscripts refer to the positions of the Geiger tubes.

In addition to the coincidence rate between conversion electrons, which will involve the factor $n_{1c_a}n_{3c_b}$, cross coincidences between various combinations of the partial counting rates will occur, for example between the pairs $(n_{1c_a}, n_{3\beta})$ and $(n_{1\beta}, n_{3\gamma})$.

To indicate the proof of Eq. (1), the partial coincidence rate due to the cross term n_{1c_a} and $n_{3\beta}$ will be computed. Let ω_1 be the fraction of conversion electrons of group c_a collected by Geiger tube I at setting 1, and ω_3 the fraction of the continuous beta-spectrum collected by Geiger tube II at setting 3. Let N be the total source strength. Then for each particle collected by tube II, there will be ω_1 coincidences with the converted electrons focused in tube I. Since there are $N\omega_3$ beta-particles collected per second in tube II, the partial coincidence rate may be written:

$$q(1c_a, 3\beta) = N\omega_3\omega_1 = n_{1c_a}n_{3\beta}/N.$$

The contributions of all other coincidence terms for each of the settings of Fig. 3 may be computed in similar fashion.

If it is now assumed that the small offsets of the Geiger tubes shown in Fig. 3 do not change the partial rates due to the beta-spectrum and gamma-ray leakage, we can write:

$$n_{1\beta} = n_{2\beta} \quad n_{1\gamma} = n_{2\gamma} \quad n_{3\beta} = n_{4\beta} \quad n_{3\gamma} = n_{4\gamma} \tag{A.1}$$

Using these approximations, and substituting all of the cross term coincidence rates, as computed above, for the various settings of Eq. (1), the net result becomes:

$$Q(1,3) = n_{1c_a}n_{3c_b}/N. \tag{A.2}$$

The offset procedure then eliminates all coincidence combinations except that between the conversion electrons.

The method of proof may be generalized to cover more complex decay schemes, taking account of branching, Geiger tube efficiencies etc., but in all cases, the offset method leaves only the rate arising from conversion electrons.

The assumptions involved in Eq. (A.1) are ordinarily quite good, since most beta-spectra are quite flat over the narrow regions subtended by conversion lines. In all cases, if necessary, a correction factor, based upon the shape of the beta-spectrum can be applied to the observed offset rates, if the offsets are quite large as may be required in case several closely spaced lines must be skipped before arriving to a line free portion of the beta-spectrum. Measurements of gamma-ray leakage have shown that over the narrow offsets employed, the decrease in intensities are scarcely detectable.

Finally it should be remarked that, although the offset procedure correctly leaves only the coincidence rates between conversion electrons, the final formulas given by the above proof, such as Eq. (A.2) have failed to take into account the line sharpening effect existing between the conversion groups. Implicitly assumed in the above proof, was the uniformity of coincidence rates between the various cross terms over all increments of the Geiger tube windows. This assumption is essentially correct for all the combinations except that where both of the terms are from conversion lines. Here, the sharpening effect must be considered for an accurate calculation of this coincidence rate.

---

[9] Cork, Keller, Rutledge, and Stoddard, Phys. Rev. 77 848 (1950).

THE REVIEW OF SCIENTIFIC INSTRUMENTS VOLUME 21, NUMBER 8 AUGUST, 1950

A High-Low Temperature Microscope Stage

R. E. Cech
Research Laboratory, General Electric Company, Schenectady, New York

(Received May 8, 1950)

A microscope stage has been designed and constructed which permits microscopic observation of metal specimens from the temperature of liquid nitrogen to an upper temperature usually determined by the melting point of the specimen.

The stage consists of a vacuum-tight water or liquid nitrogen-cooled copper chamber in which a specimen is heated by passage of an electric current. A quartz window in the chamber permits "at temperature" observation of the specimen. Operation of this stage is described.

INTRODUCTION

USUALLY, structures stable at high temperatures are deduced from microscopic observation at room temperature on specimens which have been rapidly quenched. This technique is most useful in those instances in which the high temperature structure is retained at room temperature. In many cases, however, transformations occurring during the quench alter the microstructure and make the correct interpretation very difficult. It is possible by the use of high temperature microscopy to examine metals at temperature and in many cases determine the structure directly.

A high temperature microscope stage generally consists of a tiny furnace in which a very small sample is placed. The furnace and sample are located within a chamber which may be evacuated or contain an inert atmosphere. An observation window in this chamber permits a microscope to be focused on the specimen within the furnace.

Burgess,[1] Wright,[2] and Stadnichlenko[3] were among the first to make use of high temperature microscopy as a research tool. In their apparatuses an electrically heated strip constituted the microfurnace. Williams[4] recently has designed and built a high temperature microscope stage similar to that of Burgess but differing in that the heating current was passed directly through the specimen. This has been used in an elevated temperature study of the refractory metals and their alloys. In a number of other researches high temperature microscope stages have been constructed using, instead of a strip heater, a resistance winding on a refractory core for a microfurnace.[5–10] This type of microfurnace has the inherent disadvantage of radiating a large quantity of heat upward since the volume of furnace is large as compared to the specimen. It is difficult in this case to keep the microscope objective properly cooled. Also, with a microfurnace of this type contamination of the specimen at very high temperatures is likely to occur.

It is desirable that the microscope stage be adaptable for observations at sub-zero as well as at elevated temperatures. This requirement is necessary for a direct microscopic study of the martensite transformation when it occurs below room temperature.

The microscopic observation of metals below room temperature has been accomplished by a method parallel to high temperature studies, that is, by inserting the specimen in a stage at room temperature and cooling by conduction to a liquified gas supply. There appears to be no published work of a microscope stage capable of quenching a specimen under observation directly from a high temperature to any desired sub-zero temperature. The microscope stage described in this paper was designed to be cooled with a liquified gas if desired, thus permitting its ambient temperature to be that of the liquified gas. This type of design makes possible a microscopic investigation of martensite type transformations below room temperature by direct rapid quench from the temperature of a stable parent phase.

EXPERIMENTAL: CONSTRUCTION

The stage described in this report was constructed so as to use a specimen in the form of a strip which is heated by passage of an electric current. A separate strip heater having a specimen in thermal contact with it could also be used. Details of construction of the stage are shown in the cross-sectional view, Fig. 1. A copper tube $1\frac{1}{2}$ in. in diameter, $1\frac{1}{2}$ in. long forms the chamber. The specimen or strip heater is mounted in the end of this chamber and a quartz observation window with sealing gaskets of silicone rubber placed over it. This window is held in position by a retaining ring and the top ring of the stage turned down to form a vacuum tight seal. This top ring also serves to suspend the stage in a tank of the desired cooling medium. The chamber is sealed at the bottom with a ceramic disk through which thermocouple leads and the insulated power lead pass. The stage serves as one side of the electrical circuit, thereby necessitating only a single insulated power lead. The electrical connections to the chamber and power lead are not shown in Fig. 1. Inert gases are admitted to the stage or it is evacuated through two ⅛ in. diameter copper tubes. Provision is made to either flow a gas over the specimen surface so as to sweep away volatile materials evaporated from the metal or to direct the gas perpendicularly to the specimen surface to permit rapid gas quenching.

---

[1] G. K. Burgess, Bull. Bur. Stand. **3**, 345 (1907).

[2] F. E. Wright, J. Wash. Acad. Sci. **3**, 232–236 (April 19, 1913).

[3] R. Stadnichlenko, J. Opt. Soc. Am. **10**, 605 (1925).

[4] A. L. Williams, G. E. Research Laboratory Report, RL-230 (June, 1949).

[5] Oberhoffer, Zeits. f. Elektrochemie **15**, 634 (1909).

[6] B. A. Rogers, Trans. A.I.M.E. Iron and Steel Division, 320 (1929).

[7] Eisen and Cornelius, Stahl u. Eisen **53**, 552 (1933); Metals and Alloys **4**, 119 (1933).

[8] Swinden, Howie, and Chesters, Trans. Ceramic Soc. **38**, 245 (1939).

[9] Chalmers, King, and Shuttleworth, Proc. Roy. Soc. **193A**, 465 (1948).

[10] D. G. Nicols, J. Iron and Steel Inst. **160**, Part 4, 415 (December, 1948).

The heat generated by the electrically heated specimen or strip heater is conducted to the specimen mounts and then to the copper chamber where it is dissipated by the cooling medium used. The stage may be partly immersed in a small tank of water if a room temperature ambient is desired. When a sub-zero ambient temperature is required the stage is placed in a Dewar flask of liquified gas. It is necessary in this case to replace the observation window gaskets of silicone rubber with gaskets of "Teflon" plastic. Also, the top ring must be thermally insulated and a small auxilliary filament heater placed on top of the quartz window to prevent frost formation.

Specimens to be observed microscopically are cut to the shape of slivers $\frac{1}{32}$ in.×$\frac{3}{16}$ in.×$\frac{7}{8}$ in., polished, and mounted in slotted copper blocks as shown in Fig. 2a. These are then heated directly by passing a heavy current through them. For some specimens such as copper or silver or isolated metal particles a separate heater is needed. Platinum and molybdenum strip heaters have been used for this type of specimen. Separation of the heater and specimen is obtained by interposing a thin flake of blown quartz or by placing the specimen in a quartz capsule. These are illustrated in Figs. 2b and 2c. These heaters, of a more permanent nature, are brazed to copper mounting blocks. The stirrups in the strip increase the length of the heated portion, thus permitting greater temperature uniformity in the center section. Heaters of this type have been used in the study of the solidification behavior of small metal droplets.[11]

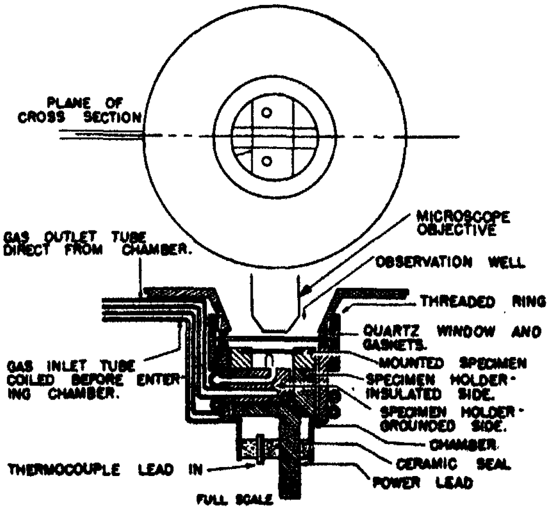
PLANE OF CROSS SECTION
GAS OUTLET TUBE DIRECT FROM CHAMBER.
MICROSCOPE OBJECTIVE
OBSERVATION WELL
THREADED RING
QUARTZ WINDOW AND GASKETS.
GAS INLET TUBE COILED BEFORE ENTERING CHAMBER.
MOUNTED SPECIMEN
SPECIMEN HOLDER-INSULATED SIDE.
SPECIMEN HOLDER-GROUNDED SIDE.
CHAMBER.
THERMOCOUPLE LEAD IN
CERAMIC SEAL
POWER LEAD
FULL SCALE

FIG. 1. Cross section of asembled stage with specimen.

After mounting the specimen between copper blocks it is mounted in the chamber as shown in Fig. 3. A rigid low resistance connection is made to the grounded side of the chamber by means of a copper wedge. Electrical contact to the other side of the specimen is made with sliding contacts on the insulated portion of the chamber interior. Mica sheet separates this insulated portion from the rest of the chamber. Electrical connection to the chamber exterior is made through the single power lead. The massive copper construction used in the specimen mounts permits rapid removal of heat from the mounting blocks, thus keeping them very close to the ambient temperature. This is necessary to obtain a rapid quench from an elevated temperature.

Power for heating the specimens is supplied by a 30:1 step down transformer controlled by a Variac transformer and operated from a constant voltage source. The temperature of the specimen is controlled manually by adjustment of the Variac setting. The power requirements of the microscope stage vary according to the type of specimen and temperature of operation. In the average specimen at a temperature of 1200°C a current of about 150 amperes at 1 volt is required. Temperature may be maintained constant within 5°C by a constant power input and constant heat loss from the stage.

Temperatures are determined by means of a 0.005-in. Chromel-Alumel thermocouple welded to the specimen in the area of microscopic observation. For temperatures above 1200°C in vacuum or inert atmosphere a 0.010-in. platinum-platinum rhodium thermocouple is used. A manually balanced portable thermocouple potentiometer is used for direct reading and a self-balancing potentiometer recorder is used when permanent records are desired. The maximum temperature of observation is limited only by the melting point of the specimen or the temperature at which rapid vaporization of metal to the window makes observation difficult. The upper temperature limit of thermocouples has thus far imposed a limit on the maximum practical temperature of observation.

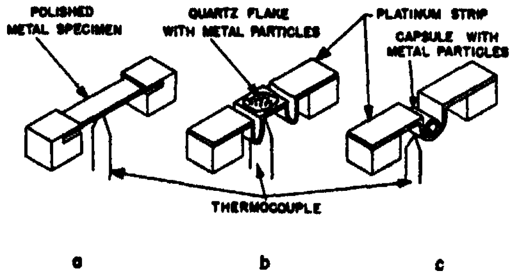
POLISHED METAL SPECIMEN
QUARTZ FLAKE WITH METAL PARTICLES
PLATINUM STRIP
CAPSULE WITH METAL PARTICLES
THERMOCOUPLE
a
b
c

FIG. 2.

The microscope stage when suspended in the tank of water for cooling is sufficiently small to be placed under a conventional metallographic bench microscope with a large working space. Photo-micrographs may be taken using a standard photo-micrographic camera for bench microscopes.

---

[11] D. Turnbull and R. E. Cech, J. App. Phys. (to be published).

PERFORMANCE AND OPERATION

The described microscope stage has been used at temperatures up to 1550°C in the study of the solidification of small metal droplets. Because of the small area of heater providing radiation upward there is little likelihood of overheating the microscope objective even upon prolonged observation. With ordinary objectives magnifications of 250× are easily obtained and with the use of the newly developed reflecting objectives magnifications of 500× or greater are possible.

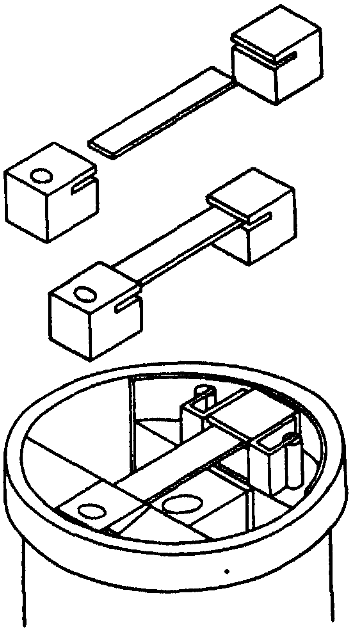

FIG. 3. Details of specimen mount.

Specimens may be heated very rapidly by applying full power to the specimen from room temperature. A rapid quench is attained by merely shutting off the power to a specimen at elevated temperature. Heat conduction to the copper mounting blocks and to the atmosphere in the chamber causes rapid cooling to take place. The rate of cooling can be further increased by forcing a blast of gas on to the specimen surface through the tube provided for that purpose. This tube is coiled around the chamber exterior to insure that the entering gas will be at the ambient temperature when entering the chamber. A rapid quench, such as is provided here, is a necessary requirement for the study of the martensite transformation.

An experimental determination of heating and cooling rates was made using a specimen of an alloy of 70 percent iron, 30 percent nickel, 0.020 in.×0.250 in. in cross section, mounted as shown in Fig. 2a. Chromel and Alumel wires 0.005 in. diameter were spot welded to opposite sides of the specimen heated portion. Thermocouple e.m.f. was recorded using a General Electric photoelectric potentiometer recorder having a period of 0.5 second.

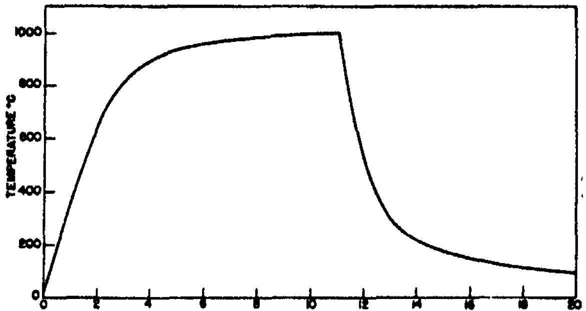

FIG. 4. Heating and cooling curve of specimen in stage.

The specimen was heated by applying full power from room temperature and cooled by switching off the power while at the same time admitting a blast of gas to the specimen surface. The heating and cooling curve obtained has been replotted and is shown in Fig. 4.

It is seen that in both the heating and cooling portions of the curve, the initial rate, extending to about $\frac{3}{4}$ of the temperature interval, is approximately 300°C per second. The rate rapidly decreases as the specimen approaches the final temperature. This is caused by the slower temperature equilibration of the mounting blocks. The resulting temperature curve is a superposition of the rapidly changing specimen temperature and the more slowly changing temperature of the mounting blocks. The temperature lag of the mounting blocks is most noticeable on quenching as the rapid quenching rate extends to only about 300°C and decreases markedly below this temperature.

To operate the microscope stage at a low ambient temperature it is assembled as described earlier and suspended in a Dewar of liquid nitrogen. As the chamber cools to −195°C power is slowly applied to the specimen to keep it at room temperature. Liquid nitrogen must be continuously added to the Dewar flask through a small tube. When the stage has cooled completely the desired heat treatment may be given the specimen while being observed or photographed. It has been possible to observe martensite formation at sub-zero temperatures after direct quench from above 1000°C by this method.

ACKNOWLEDGMENT

The author wishes to express his appreciation for the valuable assistance of Mrs. A. L. Williams and Dr. David Turnbull in the design of the high-low temperature microscope stage.

Random Coincidence Rates with Unsteady Sources

R. M. Littauer
Cavendish Laboratory, Cambridge, England

(Received May 17, 1950)

The random coincidence rate between two sets of pulses can be measured by delaying one of the sets through a time greater than twice the resolving time of the coincidence detector, thus destroying all true coincidences. A circuit using this principle for supervising the random rate continuously is described.

INTRODUCTION

When coincidence experiments are carried out with unsteady sources, whose strength is known not as a function of the time but only as a time average, it is difficult to estimate the correction for random coincidences. For instance, the source may be a target under bombardment with artificially accelerated particles whose flux is subject to periodic and random fluctuations (ripple on the accelerating voltage, random variation in beam position and intensity).

Suppose each disintegration yields two particles, A and B, coincident within the resolving time τ of the apparatus. Let there be $n=n(t)$ disintegrations per second, and let α and β be the efficiencies of detection for A and B respectively. Then the counts recorded by the two detectors in time t will be

$$S(A)=\alpha\int_0^t ndt$$

and

$$S(B)=\beta\int^t ndt,$$

while the number of true coincidences in this time is

$$C=\alpha\beta\int_0^t ndt.$$

The random coincidence rate is given by

$$r=2\tau\cdot\alpha n\cdot\beta n=2\alpha\beta\tau\cdot n^2,$$

so that the random count

$$R=2\alpha\beta\tau\int_0^t n^2dt.$$

The usual method of estimating R is to express it in terms of the measured $S(A)$ and $S(B)$; this can be done only if the shape factor $k=\langle n^2\rangle_{\text{Av}}/\langle n\rangle^2_{\text{Av}}$ is known and constant for the source used. Since

$$R=2\alpha\beta\tau\langle n^2\rangle_{\text{Av}}t$$

and

$$S(A)=\alpha\langle n\rangle_{\text{Av}}t,$$

we have in that case

$$\begin{aligned}R&=2\alpha\beta\tau k\langle n\rangle^2_{\text{Av}}t\\&=2\tau k\cdot S(A)\cdot S(B)/t.\end{aligned}$$

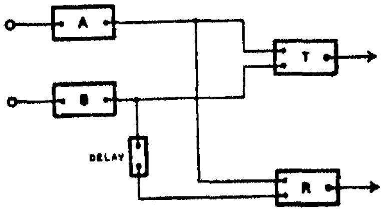

FIG. 1. Block diagram of the coincidence circuit.

For radioactive sources, k can be calculated from a knowledge of the lifetime:

$$k=\lambda t(1-e^{-2\lambda t})/2(1-e^{-\lambda t})^2,$$

where λ is the decay constant of the source ($=0.69$/half-life) and t is the time of counting. As $\lambda t\rightarrow 0$, k approaches unity, the value for a steady source.

For disintegrations produced during artificial bombardment, however, k is generally not constant, but depends on the exact adjustment of the apparatus. Thus in the case of a high tension set accelerating protons or deuterons, the shape factor of the bombarding beam striking the target usually depends critically on the exact setting of the analyzing magnet and on the instantaneous position and focusing of the beam. An experimental method of measuring R is thus required in all cases where R is not negligible compared with the true rate C.

Such a method has already been proposed by Hereward,[1] who operates two coincidence gates of resolving times τ_1 and τ_2 simultaneously from the same set of pulses A and B. If $\tau_2\gg\tau_1$, then the second gate records predominantly random coincidences, and the correction to be applied to the first gate is given by $(N_2-N_1)\tau_1/(\tau_2-\tau_1)$, where N_1 and N_2 are the counts in the two gates. The experimental difficulty in this method lies in the construction of two coincidence gates with widely different resolving times, for which the factor $\tau_1/(\tau_2-\tau_1)$, however, remains constant.

The method to be described in this paper is represented schematically in Fig. 1. The pulses from the two channels A and B are fed directly into a coincidence gate T, where the total coincidence count is recorded. They are also led to a second gate R, but in this case one of the pulses is first delayed by a time greater than twice the resolving time of the gates.

---

[1] Devons and Hine, Proc. Roy. Soc. 199A, 59ff. (1949).

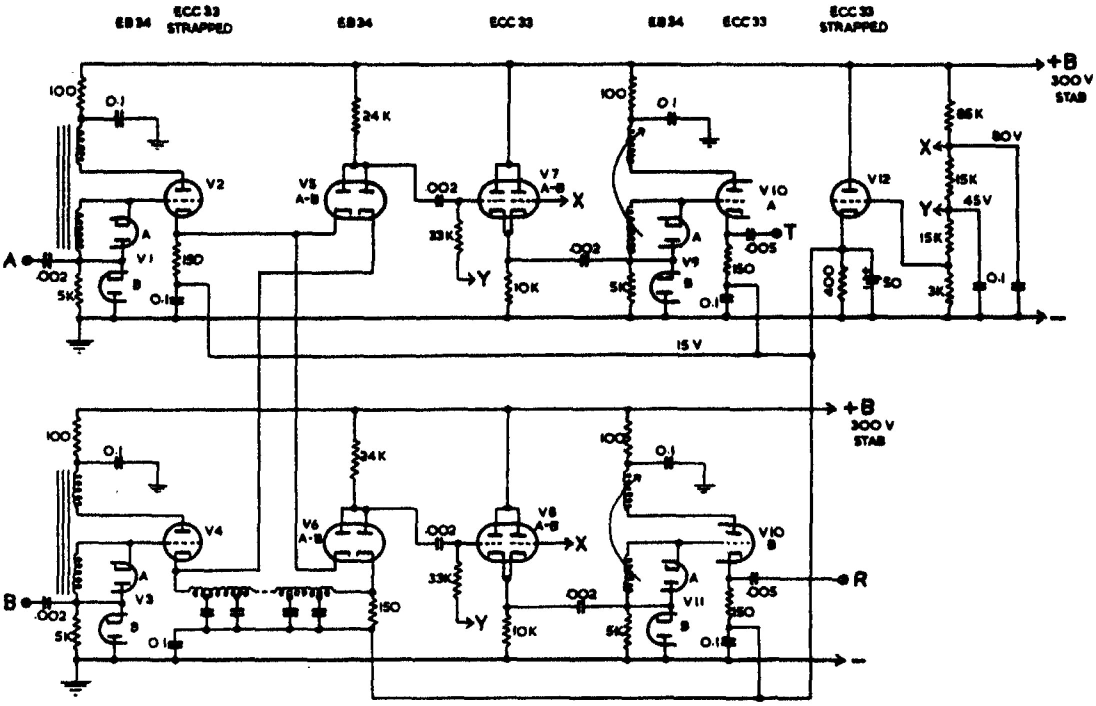

Fig. 2. Complete circuit. Resistance values in ohms, capacities in μF.
Approximate American valve equivalents:

$EB34 = 6H6$
$ECC33 = 6N7$

Pulse transformers: 45–45 turns on laminated high permeability cores, 0.5 cm^2 cross section.

This second gate records only random coincidences, since all the true coincidences have been destroyed by the delay.* If the two gates have the same resolving time, then R gives directly the random component of the coincidences recorded in T.** The advantage of the method lies mainly in this direct indication of the number of random coincidences; but also in the fact that it is not difficult to construct two coincidence gates whose resolving times remain in a constant ratio if this ratio is close to unity.

EXPERIMENTAL METHOD

Figure 2 shows the complete circuit diagram of the apparatus. The main components are as follows: two square wave generators (V_{1-4}), two diode coincidence gates (V_5, V_6), and two discriminators (V_{7-11}). V_{12} serves merely to maintain the bias line for the pulse generators at a constant potential of +15 volts.

To make the resolving times almost independent of the pulse sizes and discriminator levels, the coincidence gates are fed with nearly square pulses. These are generated in the blocking oscillators V_1, V_2 and V_3, V_4. The transformers employed have laminated cores of high permeability material, thus ensuring a coupling factor very close to unity. This is necessary in order to reduce the ratio of the time of rise of the pulse to the pulse duration. In place of the usual $R-C$ combination to give a blocking action, two diodes are employed. In this way the deadtime of the circuit after it has produced a pulse is reduced considerably.

The blocking oscillators are triggered by short positive pulses delivered from a discriminator in each counting channel. When the oscillator is fired, the current in the triode increases rapidly until it reaches such a value that the magnetizing forces due to the grid and anode currents in the transformer are almost equal and opposite. This state is maintained by the steadily rising flux in the transformer, which produces the requisite e.m.f. in the grid circuit. The reset of the pulse appears to be initiated when the iron begins to reach saturation; we have, however, no exact knowledge of the behavior of laminated cores under these high frequency conditions. With the valves used, the current in the cathode reaches 0.7A, so that a 100-volt pulse is produced across the cathode resistor of 150 ohms.

The blocking oscillator in the B channel employs a 150-ohm delay line, properly terminated, as cathode load. The line has 80 sections, giving a total delay of 4 μsec., and does not appreciably distort the shape of

---

* This assumes, of course, that the resolving time τ (and thus the delay $>2\tau$) have been so chosen that all the events to be recorded as being coincident do, in fact, occur within this time of each other.

** Strictly speaking, the number of coincidences in R will be too great in the ratio $S(A)\cdot S(B)/[S(A)-C]\cdot[S(B)-C$, but this correction can be neglected if $C \ll S(A)$, $S(B)$, which is almost always the case in practice.

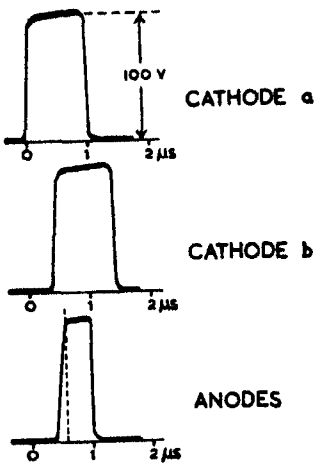

FIG. 3. Pulse shapes on the coincidence gate, V_1.

the pulses from the cathode. The square pulses are approximately 1 μsec. long, as this was the value of resolving time required in the present application.

The coincidence gates each consist of a pair of diodes. Figure 3 shows the wave forms obtained on the various electrodes when pulses with a certain time overlap are applied to the cathodes. The anode pulse rises at a rate determined by the standing current and the stray capacities attached to the anodes, provided that the cathode pulse has a leading edge steeper than this value. This is actually the case, for the anode rate of rise (with 12 mA and 18 pF) is limited to about 600 volts/μsec., while the input pulse, even after passage through the delay line, rises considerably faster than this. Thus the shape of the anode pulse is independent of the exact shape of the input leading edge. The rate of rise of 600 volts/μsec. means that a relative variation of 3 volts in the discriminator levels following the coincidence gates does not affect the resolving time by more than ½ percent. The fact that virtually the same pulses are used in the two gates ensures that the ratio of resolving times is independent of the length of the input pulses.

The discriminator following the coincidence gate consists of a cathode follower biased off by approximately 35 volts. Pulses exceeding this amplitude are passed to a further blocking oscillator, which produces the output pulse for registering in a scaling circuit. The total and random coincidence pulses appear respectively at T and R.

The ratio of the resolving times of the two channels can be measured by applying completely random pulses to the two inputs A and B; in the present instrument this ratio was found to be 1.02, and has not measurably changed in the course of the investigations so far made.

CHOICE OF SOURCE STRENGTH

When the mean source strength is under the control of the experimenter, it is desirable, apart from other considerations, to choose it in such a way that the maximum statistical accuracy can be achieved in a given counting time.

Let C, R, and T be the true, random, and total coincidence counts recorded in time t. Then, as shown in the introduction,

$$C = \alpha\beta\langle n\rangle_{\mathrm{Av}} t$$

and

$$R = 2\alpha\beta\tau\langle n^2\rangle_{\mathrm{Av}} t,$$

so that

$$R/C^2 = 2\tau k/\alpha\beta t,$$

which is independent of the source strength chosen, provided that the other quantities, especially k, remain unaffected. (k *may* depend on the absolute source strength.)

The experimentally measured quantities are T and R, from which C is deduced by putting $C = T - R$. If ΔC is the standard statistical deviation of C, we have

$$(\Delta C)^2 = (\Delta T)^2 + (\Delta R)^2 = T + R = C + 2R.$$

Thus

$$(\Delta C/C)^2 = 1/C + 2R/C^2.$$

Hence we see that the fractional error in C cannot be reduced below the value $(2R)^{\frac{1}{2}}/C$, which is a constant independent of the source strength. This strength will thus be chosen (if other considerations permit) such that $1/C \ll 2R/C^2$, i.e., that $R > C$; any further increase in source strength would not affect the statistical accuracy, but would, on the other hand, increase the errors introduced by any inequality of resolving time in the gates T and R.

Absolute Determination of the Emission Rate of Beta-Rays*†

R. K. CLARK**
Radiological Research Laboratory, College of Physicians and Surgeons, Columbia University, New York, New York

(Received May 17, 1950)

A technique for the absolute determination of the rate of disintegration of beta-particle emitters is described. The method consists of measuring the rate at which charge is carried away from the active material by the emitted electrons. The effects of ionization are eliminated by placing the material in a high vacuum. The effects of the surroundings (excluding the parts required to support the active material) are reduced by using a tank of large dimensions, and the magnitude of these effects is determined by the use of supplementary surrounding surfaces with various potentials applied to them. Some information is obtained about the effects of the source supporting structures by placing over the active side of the source supporting foil a cover foil identical to it. It is shown that this technique makes possible the measurement of beta-ray activities with high accuracy.

I. INTRODUCTION

SINCE the advent of artificial radioisotopes, the Geiger-Mueller counter has been the principal instrument used for the determination of the emission rate of beta-rays. In measuring emission rates it is used with a fixed geometry and corrections are made for solid angle, absorption, scattering, and the production of "secondaries" by the surroundings. Sometimes calibrations are made by means of a sample of another material of known activity, although this requires correction for the difference in energy spectrum. All these corrections are difficult to make, especially in the low energy regions. Methods have been devised to reduce the importance of these sources of error, one of the best (in principle) being coincidence counting.[1] Although in this case the over-all efficiencies of both the gamma-counter and the beta-counter cancel, the number of random coincidences may be an important fraction of the total if the source is quite active. When the source is weak, the background coincidences may be important. There are ways of reducing these difficulties, but when this technique is applied to activity measurements, the decay scheme must be completely known and is limited to those isotopes that yield at least one gamma-ray as well as the beta-ray.

When the radioactive material emits at least one charged particle per disintegration, a simple and direct method of measuring activity is to observe the rate at which charge is carried away from the active material by the emitted electrons. This technique requires relatively little knowledge of the decay scheme; when both positrons and electrons are emitted by the isotope, as in the case of Cu^{64} the ratio must be known; in the case of positron emission the branching ratio must be known; and the number of particles emitted per disintegration must be known. This information is easier to obtain than complete decay schemes as are required for coincidence counting, and is already completely known for practically all isotopes which emit only negative particles.

Wien[2] was the first to use this technique. Rutherford[3] and Makower[4] modified the method, and Moseley[5] improved it. The first three of these experiments are summarized by Rutherford.[6] The fourth is summarized by Rutherford, Chadwick, and Ellis.[7] These workers had three sources of inaccuracy. They were limited to natural radioactive materials, necessitating the use of absorbers to stop the alpha-rays. They were unable to produce very low pressures, having to correct for ionization effects. They did not investigate the importance of the production of secondaries in all parts of the apparatus, although the extrapolation techniques of Makower and, later, of Moseley tended to reduce the importance of secondaries from the source and its supporting structures.

The method presented in this paper is a modification and development of that described above. The principal improvements consist of a reduction of the magnitude and the determination of the various secondary contributions to the observed current.

II. PRINCIPLES OF THE MEASUREMENT

In the ideal situation where the active material has no absorber nor scatterer associated with it and there is no material of any sort around it, the current observed would be exactly that constituted by the emitted electrons and would therefore be an exact measure of the activity. In isotopes producing internal conversion electrons or Auger electrons, corrections would have to be made for the effects of these particles. Likewise, in those isotopes decaying by emitting both positrons and electrons the ratio of the numbers of the two types of

---

* This paper is based on work performed under Contracts W31-109 eng 14 and At-30-1-Gen 70 for AEC.

** Now at the Argonne National Laboratory, Chicago, Illinois.

† Extract from a thesis submitted in partial fulfillment of the requirements for the degree of Doctor of Philosophy in Physics at the University of Illinois.

[1] M. L. Wiedenbeck, Phys. Rev. 72, 974 (1947).

[2] W. Wien, Phys. Zeits. 4, 624 (1903).

[3] E. Rutherford, Phil. Mag. 10, 193 (1905).

[4] W. Makower, Phil. Mag. 17, 171 (1909).

[5] H. G. J. Moseley, Proc. Roy. Soc. A87, 230 (1912).

[6] E. Rutherford, *Radioactive Substances and Their Radiations* (Cambridge University Press, London, 1913), p. 201ff.

[7] Rutherford, Chadwick, and Ellis, *Radiations from Radioactive Substances* (Cambridge University Press, London, 1930), p. 387ff.

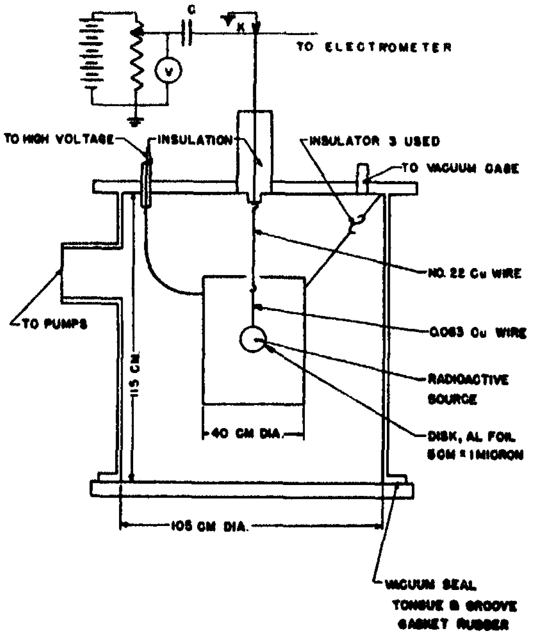

FIG. 1. Schematic diagram of apparatus. The active material is dried on the aluminum foil. Retarding or accelerating voltages are applied between the can and the foil (which is at ground potential). *The figure shows the large can in place. In determining* the effects of the surroundings (except for those involved in supporting the active material), this can was replaced by a screen of the same size, and by another can and screen each of one-half the linear dimension of the first can.

particles would have to be known, and in the case of pure positron emitters the branching ratio would have to be known. The problem is, then, one of approximating the ideal situation, and determining the magnitude of the effect of the unavoidable scattering and absorbing materials of the apparatus.

The effects of ionization can be completely eliminated by placing the active material in a highly evacuated tank. The tank walls and all structures except that supporting the active material can affect the observed current by scattering primaries and producing secondaries, some of which will be caught by the source structures. The magnitude of this effect can be reduced by the use of apparatus of large dimensions, and it can be studied by varying the dimensions and by applying retarding or accelerating potentials between the surroundings and the source structure.

The dimensions are varied by introducing in turn two "cans" of the same shape, but differing in linear dimensions by a factor of two. Two screens are also introduced in turn. One of these has the same dimensions as one "can," the other the same as the other "can." The screens thus provide a change that can be determined with precision in the number of particles from the surroundings. A change in the linear dimensions of a "*can*" does not change the total number of particles leaving it (since in any case it occupies a solid angle of 4 pi), but only changes the solid angle subtended by the source structures at a point on the can. When the can is made negative with respect to the source, some particles of energy greater than the applied voltage will be deflected so that they are caught and measured, and this "focusing" action is not a simple function of the dimensions of the can. Introducing, then, a screen in place of a can of the same dimensions does not change the focusing properties, but does change the total number of particles from the surroundings by a large factor since there is much less material to produce secondaries and reflect primaries. Thus this makes possible a more reliable computation of the magnitude of the component of the observed current due to the surrounding structures.

The resulting data show that under certain conditions the correction for the effects of the surrounding materials amounts to only a few percent of the observed current and can be determined to a few tenths of a percent of the observed current.

The material involved in supporting the active isotope will affect the observed current by producing secondaries and by absorbing primaries. These effects can be studied by varying the amount of inert material associated with the active isotope. When the observed change for doubling the amount of inert material is small, it is possible to determine the number of secondaries and to extrapolate to zero absorber by assuming that the effect of the original material is the same as that of the added material. It is true that such an extrapolation is not exactly justified, but since the observed changes are small the error is certainly small.

III. APPARATUS

In observing the current carried from the source and its supporting structures by the beta-rays, a Lindemann electrometer is used in conjunction with a "compensating condenser." One terminal of the condenser is connected to the electrometer and the source support, and the other terminal goes to a source of e.m.f. the magnitude of which can be varied easily. In use, the electrometer is kept with the needle as close to "zero" potential as possible and the mean time rate of change of voltage required to maintain this balance is determined. The desired current is then equal to the capacitance of the condenser multiplied by the average rate of change of voltage. This is known as the Townsend method.[8] Thus the observed currents are recorded in terms of volts per second. One curie gives 5.93 times 10^{-9} amperes, and with this method (in other experiments) currents of the order of 10^{-15} amperes have been observed in this laboratory. This is equivalent to about 0.17 microcuries. Thus there is more than adequate sensitivity for measuring weak sources—of the order of a hundred microcuries.

The active material is dried on an aluminum foil approximately one micron thick after the foil has been attached to an aluminum supporting ring with Aquadag. The ring is about 2 inches in diameter, 6.5 mils thick, and 30 mils wide. This assembly is then suspended in the center of the tank by means of two links of copper wire. The lower (about 6.5 mils diameter) is about 7 inches long, while the upper (No. 22 wire) is about 18 inches long.

---

[8] See reference 6, p. 103.

The materials which have been studied so far (P^{32} and Na^{22}) were applied in water solution and dried at about 60 degrees C. About one ml of solution distributes the material over an area about one centimeter in radius, and is the quantity which has usually been used. (Although the foil will support as much as two ml, it was felt that this amount of solution distributed the active material over somewhat too large an area.) This manner of preparation of the source allows the use of standard sampling methods. Thus it is possible to calibrate a solution, and to establish other instruments as secondary standards which can be rechecked as desired.

The limitations on the solution to be applied are as follows. The *p*H must be close to 7.0 so that the foil will not be attacked. The active material must be in the form of a compound that will not volatilize on drying and, especially, under the reduced pressures used in measurement. The non-volatile material (carrier, impurities, etc.) must not amount to more than about 2 milligrams per milliliter for such material as P^{32}, and should be less for lower energy emitters. This much solid does not seem to affect appreciably the activity determination for the more energetic isotopes, although it is certainly preferable to keep the solids to a minimum.

Because certain inconsistencies in the observed currents were found to be associated with the joints between the suspending wires (which were simply hooked together), all such joints were treated with Aquadag. These inconsistencies might arise either from poor conductivity or from varying contact potentials, but in any case the trouble was eliminated by the addition of the Aquadag.

A stainless steel tank 42 inches in diameter and 46 inches high is the vacuum chamber (Fig. 1). The pumping system is such that pressures as low as 1.2 or 1.3 times 10^{-6} mm of mercury have been obtained. Experiment has shown that ionization effects are completely eliminated by pressures as low as 10^{-5} mm of mercury under the conditions of these measurements.

In the center of the top of the tank is mounted the polystyrene insulated lead-through which supports the source in the center of the tank and connects to the measuring apparatus outside.

A lead-through is provided in the top of the tank for the application of potentials to whichever "can" or "screen" is in position.

Three insulating hooks ("Pyrex" tubing) are provided for suspending in the center of the tank the following structures in turn: the "small can" of galvanized iron similar in shape to the tank and one-fifth as large in linear dimension, the "small screen" of copper wire (No. 22) (with a mesh ½″×6½″, giving a transmission of about 94 percent) of the same size as the can, the "large can" of the same material as the first can but twice its linear dimension, and the "large screen" of the same construction as the first screen but the same size as the large can (and having a mesh 1″×8½″, giving a transmission of about 97 percent).

IV. RESULTS

The first question studied was the effect of changes in pressure. A Distillation Products ion gauge was used with a standard type circuit. Although the construction of these gauges is such as to make their rated sensitivity reliable, it was checked at higher pressures with a McLeod gauge (a liquid air trap was used) and satisfactory agreement was found. Preliminary measurements with none of the screens or cans present showed any change in the observed current for pressures below about 10^{-3} mm of mercury. With the small screen at zero volts, no effect was observed on changing the pressure from 2.0 times 10^{-5} mm to 8.0 times 10^{-4} mm. With the small screen at −1800 volts (with re-

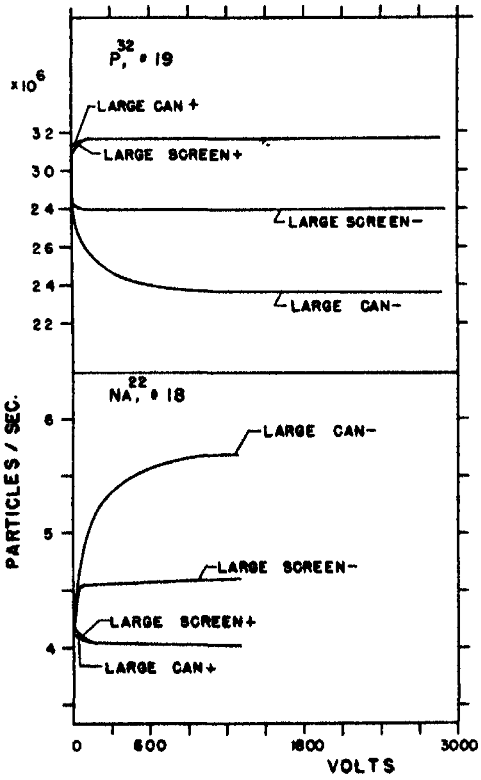

FIG. 2. Typical data. This shows the numbers of particles per second observed under various conditions with P^{32} and Na^{22} sources. A negative voltage means that the can—or screen—was negative with respect to the source.

Note the reversal of the changes due to the fact that Na^{22} is a positron emitter.

TABLE I. Summary of results. (The uncertainties attached to these figures are based exclusively on the observed internal consistency of the current measurements.)

Symbol	Number of particles/second observed under various conditions P^{32}	Na^{22}	Conditions Surrounding surface	Applied voltage (source at ground)
I_{c+}	$39.8 \pm 0.2 \times 10^6$	$3.97 \pm 0.03 \times 10^6$	Small can	+600 volts
I_{c-}	31.0 ± 0.2	6.08 ± 0.03	Small can	−600
I_{C+}	40.7 ± 0.2	4.03 ± 0.03	Large can	+600
I_{C-}	31.6 ± 0.2	5.66 ± 0.03	Large can	−600
I_{s-}	36.0 ± 0.2	4.64 ± 0.03	Small screen	−600
I_{S-}	36.2 ± 0.2	4.62 ± 0.03	Large screen	−600
Computed values of the numbers of particles leaving the source structures with an energy greater than 600 ev				
I	36.3 ± 0.2	4.52 ± 0.03	Computed from small can and small screen data.	
I_{check}	36.4 ± 0.2	4.55 ± 0.03	Computed from large can and large screen data.	
Correction factors to be applied to I_{S-} to obtain I				
	1.004 ± 0.005	0.983 ± 0.008		
Computed values of secondary and scattering effects				
b_{pos}	0.035 ± 0.005	0.000 ± 0.008	Number of particles from the small can of energy greater than 600 ev per unit I, computed from the can positive data.	
b_{neg}	0.022 ± 0.005	0.125 ± 0.008	Same as b_{pos}, except computed from the can negative data.	
c	0.126 ± 0.005	0.217 ± 0.008	Number of particles from the small can of energy less than 600 ev per unit I.	
i	0.129 ± 0.005	0.118 ± 0.008	Number of particles from the source structures of energy less than 600 ev per unit I.	

spect to the source) there was also no change observed on changing the pressure from 4.0 times 10^{-5} mm to 8.2 times 10^{-4} mm. However with the small screen at + 1800 volts, there was considerable change in the region of 10^{-4} mm. Because of this, all subsequent data were taken at pressures below 10^{-5} mm. In order to detect any unexpected effects due to pressure changes, the pressure was recorded with each observation of current throughout the data. No effects due to changes of pressure were noted other than those described above.

The effect of applying different potentials to the surrounding structures is shown in Fig. 2. The observed current was found to vary rapidly with the potential applied to either can up to about 600 volts, with essentially no change between 600 volts and 3000 volts (the present upper limit of the apparatus) for P^{32} and Na^{22}. The form of these curves justifies the division of the electrons into three groups: "low energy"—below 600 electron volts; "intermediate energy"—between 600 electron volts and 3000 electron volts; and "high energy"—above 3000 electron volts.

A detailed analysis of the situation under various conditions may be made as follows: With a can at a negative potential greater than 600 volts, the low energy group from the source structure is suppressed, the remainder being unaffected. The low energy group from the can is completely focused onto the source structure, its magnitude depending only on the efficiency of production of this group. The high energy group from the can, being unaffected by the potential, depends on the solid angle subtended by the source at a point on the can (proportional to the square of its linear dimension) and on the efficiency of production. That part of the intermediate energy group which is sufficiently focused (deflected by the applied field) to be caught by the source structure is, in effect, included with the low energy group. Since this focusing (for a particular potential) depends only on the dimensions of the can, it is the same for the screen of the same size. Thus this effect will be taken care of if the term representing the low energy group from the can is eliminated algebraically from the equations for the can and its corresponding screen.

The current observed with a screen at a negative potential greater than 600 volts includes the same terms as a can, except that the magnitude of the contribution from the screen also depends on the area of the material constituting the screen. In addition there are some particles from the tank reaching the source structure. The low energy group from the tank is suppressed by the potential on the screen. The effect of the remaining particles is small because of the large dimensions of the tank, and therefore can be approximated by neglecting the intermediate energy group, the effects of which are complicated by the fact that the screen defocuses them while they are outside it, and focuses those which pass through. The magnitude of the remaining high energy group, being unaffected by the potential, depends on the transmission coefficient of the screen (squared, since both the particles from the source and those from the tank must pass the screen), on the solid angle subtended by the source at a point on the tank and on the efficiency of production.

When a positive potential greater than 600 volts is applied to a can, none of the energy groups from the source structures is suppressed, but the low energy group from the can is now defocused so that it is not included, while the high energy group is still unaffected by the potential. The intermediate energy group from the can tends to be defocused, and is therefore partly included with the low energy group, and partly with the high energy group.

When a positive potential greater than 600 volts is applied to a screen, the effects are the same as those with a can, except that some of the particles from the tank will be included. However, the effect of a positive screen on these particles is not simple. The screen has a tendency to catch some of the particles from the source which otherwise would escape to the tank. Likewise, it catches some of the particles from the tank. In addition it will have some focusing action on those particles which miss the screen, so that some which otherwise would have missed the source structures are measured.

The currents observed with "zero" potential applied to a can or a screen are very sensitive to small changes in voltage (from the shapes of the curves) and, since differences in contact potential certainly exist, it is impossible to give any specific relation between these currents and the others.

Thus, the currents observed with each can positive (more than 600 volts) and with each can and each screen negative (more than 600 volts) can be expressed in terms of known geometrical factors and of six unknowns with the aid of the following assumption:

> The total number of particles emerging from unit area of material per particle striking the material is the same for the cans, the screens and the tank.

This assumption is roughly justified since the atomic numbers of copper, zinc and iron are roughly the same.

The six unknowns then are the three components of the current from the source structures, the efficiency of production of low energy particles in the surrounding materials, the efficiency of production of intermediate energy particles in the surrounding materials and the efficiency of production of high energy particles in the surrounding materials. These six unknowns can be reduced to four by noting: first, that there are few particles of intermediate energy leaving the source structures as indicated by the screen data; second, that even with the cans there are few particles of intermediate energy observed, so that the efficiency of production of this group in the surrounding material may be assumed to be zero. (See Table I.)

Making the following definitions:

I = number of particles of high energy leaving the source structures per unit time.

i = number of low energy particles leaving the source structures per unit "I."

b = number of high energy particles from the small can per unit "I," which are caught by the source structure (essentially the efficiency of production of measured high energy particles in the small can).

c = number of low energy particles per unit "I" from the small can which are caught by the source structure with the can negative (600 volts) (essentially the efficiency of production of measured low energy particles in the small can).

d_S = the ratio of the solid angle subtended by the source structure at a point on the large screen to the solid angle subtended by the source structure at a point on the small can. (d_S is then the square of the ratio of the radius of the small can to that of the large screen.)

d_C, d_c, d_s are defined in the same way as d_S, with the large can, small can and small screen, respectively, substituted for the large screen.

f_S = the ratio of the area of metal in the large screen to the area of the large can.

f_s = the ratio of the area of metal in the small screen to the area of the small can.

The following equations can then be written.

For the small can:

$$I_{c+}=I(1+i-b), \qquad (1)$$

$$I_{c-}=I(1-b-c). \qquad (2)$$

For the large can:

$$I_{C+}=I(1+i-d_Cb), \qquad (3)$$

$$I_{C-}=I(1-d_Cb-c). \qquad (4)$$

For the small screen:

$$I_{s-}=I(1-d_sf_sb-(1-f_s)^2d_tb-f_sc). \qquad (5)$$

For the large screen:

$$I_{S-}=I(1-d_Sf_Sb-(1-f_S)^2d_tb-f_Sc). \qquad (6)$$

The numerical values of the d's and f's are: $d_C=1/4$, $d_s=1$, $d_S=1/4$, $d_t=1/25$, $f_s=1/16.4$, $f_S=1/33.0$. The precision required of these magnitudes is not high, since they enter the most important equations (for the two screens) only through small correction terms. It is estimated that the uncertainty in these values is not greater than 5 percent, which is quite acceptable.

Since there are more equations than necessary, there is more than one way to obtain the values of the unknowns. The remaining equations are then available as a further check on the over-all internal consistency of the data. The above numerical values may then be introduced and the unknowns computed as follows:

The value of "b" may be computed from Eqs. (1) and (3) or from Eqs. (2) and (4). When computed from the first two (the can positive equations) it is termed "b_{pos}," when from the second two, as "b_{neg}." The difference between b_{pos} and b_{neg} in the case of sodium probably arises because of the difference in the focusing of the intermediate energy groups by the two cans, and by the two screens, when they are negative (the current observed with the large screen changes by about 2 percent in going from −600 volts to −1200 volts). The small difference in the case of phosphorus may arise

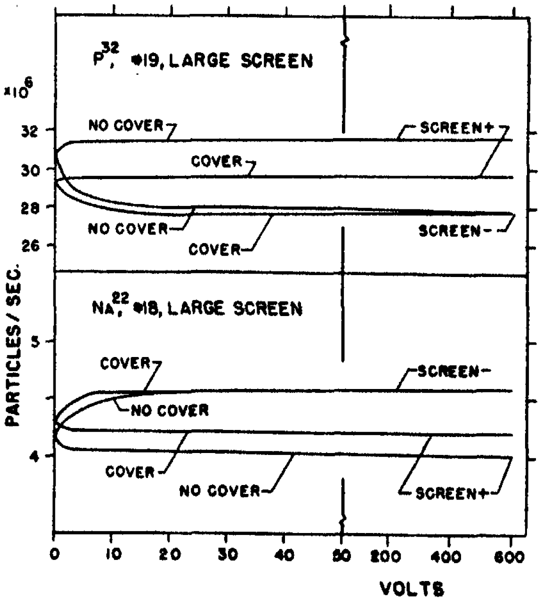

FIG. 3. Cover foil effects. This shows the numbers of particles per second observed for various potentials applied to the large screen. A negative voltage means that the screen was negative with respect to the source. The curves labeled "No Cover" were for the active material on the supporting foil with no other material associated with the source. The curves labeled "Cover" were for the same source, but with a second foil identical to the supporting foil covering the active material. (See also Table II.)

TABLE II. Effect of impurities and cover foil.* (The uncertainties attached to these figures are based exclusively on the observed internal consistency of the current measurements.)

Source number	Isotope	Approx. solids deposited	Cover foil	Computed number of particles leaving source structures: With an energy greater than 600 ev (I)	Computed number of particles leaving source structures: With an energy less than 600 ev, per unit I (i)
10	P^{32}	0.5 mg/mc	Not used	$36.4 \pm 0.2 \times 10^4$	0.129 ± 0.005
19	P^{32}	0.3	Not used	27.9 ± 0.2	0.170 ± 0.005
19	P^{32}	0.3	Used	27.8 ± 0.2	0.090 ± 0.005
29	P^{32}	0.0	Not used	3.37 ± 0.02	0.085 ± 0.005
29	P^{32}	0.0	Used	3.38 ± 0.02	0.077 ± 0.01
18	Na^{22}	0.5	Not used	4.50 ± 0.03	0.116 ± 0.005
18	Na^{22}	0.5	Used	4.52 ± 0.03	0.080 ± 0.005

* The amount of solids deposited is taken from the Oak Ridge data for the material in question, except for Na^{22}, which was estimated from the appearance of the deposit as compared to the P^{32} sources.
The cover foil is a foil identical to the foil upon which the active material was dried. When used, it was placed over the active surface of the supporting foil.

in the same way, although the change observed is not larger than the uncertainty in the observed currents.

The value of "I" can next be computed from either Eqs. (2) and (5) or from Eqs. (4) and (6). In this computation it is reasonable to pair the equations in this manner since (as discussed above) the focusing of a screen should be the same as that of a can of the same dimensions. "b_{neg}" is used since these equations are for negative potentials. The value computed from Eqs. (2) and (5) is termed "I" in Table I and that from Eqs. (4) and (6), "I_{check}." This amounts to a check on the consistency of the data from the two screens. It is thus an indication of the reliability of the determination of the magnitude of "I."

The value of "c" can be computed either from Eqs. (2) or (4), using "b_{neg}." Since these were the equations used in computing "b_{neg}," this allows no check.

The value of "i" can be computed either from Eqs. (1) or (3), using "b_{pos}." Since these were the equations used in computing "b_{pos}," this also allows no check.

Table I includes the computed values of these unknowns for P^{32} and Na^{22}. The observed numbers of particles per second listed are for typical sources of these materials, and are the values from which the unknowns listed were computed. It must be emphasized that the uncertainties attached to these figures are based exclusively on the observed variations in the observed currents.

Table I also includes the values of the correction factors by which the observed large screen negative currents must be multiplied to obtain the average of the computed "I's".

In order to determine the effect of the supporting foil on the number of particles observed, measurements were made with a "cover" foil over the active side of the supporting foil. This foil was identical to the first, including the aluminum supporting ring and the 6.5 mil copper wire. It was attached to the supporting foil by means of loops of fine wire or thread, and all points of contact were Aquadagged. The addition of the cover foil can change the number of primaries or of secondaries leaving the active side of the source structure. The number of primaries can only be decreased, of course, while the number of secondaries could either increase or decrease depending on the relative efficiency of production of aluminum *versus* that of whatever materials may be deposited with the active material. Since the added foil only affects half the particles, the change observed upon adding it will be the same, except for reflected particles, as the previously unknown effect of the original supporting foil. Because of the existence of reflected particles, this gives an upper limit to the correction for the presence of the supporting foil.

The data presented in Fig. 3 shows that the cover foil does not make any significant change in the number of particles of energy greater than about 100 ev for P^{32} or about 40 ev for Na^{22}, while there is a considerable change in the number below this energy. Table II shows that i for P^{32} varies with the amount of solids deposited, although rather erratically. Except for Source No. 29, the average thickness of the solids was of the order of 1 micron, so that the erratic behavior may be attributed to local variations in the thickness of the deposit. However, the reduction of i by the cover foil to essentially the same value as for minimal solids (Source No. 29) with no cover would indicate that most, if not all of these particles are secondaries. Since the effective atomic number and the surface condition differ for the deposited solids and the clean foil, a change in the efficiency of production of such low energy secondaries is to be expected. The interpretation of these low energy particles as secondaries is also consistent with theory[9] which shows that secondaries should be mostly of very low energy, with the number decreasing rapidly with increasing energy as Fig. 3 demonstrates. The Na^{22} data confirm this interpretation in two ways. First, since it is a positron emitter, all negative particles must be secondaries. The low energy particles from this isotope are clearly negative, from Fig. 2, and are of about the same energy distribution as for the phosphorus sources of comparable amounts of solids. Secondly, the distribution with the cover foil in place is essentially the same as for the covered phosphorus source. Thus there are very few, if any, primary particles observed of energy less than 600 ev.

Since few particles are found in the energy region between 600 ev and 3000 ev, as shown by Fig. 2, there are few secondaries of energy greater than 600 ev. This is confirmed by the observation that there is no detectable change in the number of particles in this energy range caused by the addition of the cover foil.

Because there are few, if any, primaries of energy less than 600 ev and there are at most few secondaries of energy greater than 600 ev, the current as observed with the large screen at a negative potential of 600 volts with respect to the source, corrected by the computed factor, gives an accurate measurement of the activity of these isotopes.

---

[9] H. A. Bethe, *Handbuch der Physik* 24 (1), 515 (J. Springer, Berlin, 1927).

V. DISCUSSION

In the case of P^{32} it will be seen from Table I that the observed current leaving the source structures can be corrected for the effects of the surrounding structures. Thus the magnitude of the current leaving the source can be determined with a known maximum uncertainty representing the sum of the known uncertainties. From the observed internal consistency of the measurements there is an uncertainty of about 0.5 percent. From the compensating condenser calibration, about 1 percent; from the voltmeter calibration, about 0.5 percent. Thus the maximum uncertainty in the current leaving the source is about 2.0 percent. However, this still leaves the uncertainties in interpretation of this observed current. In view of the cover foil experiments described above, the maximum error introduced by taking all particles of energy less than 600 ev as secondaries and all of energy greater than 600 ev as primaries may be estimated as about 3 percent. Accordingly the over-all accuracy in measuring the activity of P^{32} by this technique may be estimated to be about 5 percent under the conditions of this experiment.

As a check on the possible existence of systematic errors, an indirect inter-check with P^{32} was made with the Bureau of Standards. This inter-check was made near the first of November, 1948, and the agreement was well within experimental error.

For Na^{22}, the same sources of error exist as for P^{32}. However, since Na^{22} emits a gamma-ray of about 1.3 Mev as well as annihilation radiation, these must also be considered. These radiations can only affect the measurements by the production of secondary electrons. Any secondaries produced in the walls of the vacuum chamber or the large screen are automatically taken into account in the correction factor. It may be noted in Table I that the effects of the surroundings are not very different for the two isotopes, indicating that the effects of the electro-magnetic radiations are certainly small. The effects of these radiations on the source supporting structures must also be small, because, for the atomic numbers involved, the cross section for the production of secondaries by photons of these energies is much less than that of charged particles. Thus any effects of these radiations may safely be included in the 3 percent allowed for the possible existence of low energy primaries and high energy secondaries. Accordingly the over-all precision in measuring the activity of Na^{22} by this technique may be estimated to be about 5 percent under the conditions of this experiment.

In comparing this technique with counter techniques, it may be noted that here particles are included of much lower energy than counters can reliably detect. In addition, counters will also include many of the high energy secondaries which this technique records. Thus the principal source of error in this technique is also a source of error of roughly the same magnitude for counter techniques. This is in addition to the difficulty of reliably establishing the other corrections required for counter measurements of activity. Given, then, a reliable determination of the importance of the low energy primaries and the high energy secondaries, this technique allows a precision limited only by the precision with which currents of the order of 10^{-13} amperes can be measured. Using the compensation technique described in this paper, this only requires increased precision in the compensating condenser calibration and the compensating voltmeter calibration in order to achieve a precision limited only by the observed internal consistency of the data (0.5 percent for P^{32} and Na^{22}). Thus this technique makes possible a considerable improvement in the precision of measurement of beta-ray activities.

VI. ACKNOWLEDGMENTS

The author is deeply indebted to Dr. G. Failla and Dr. H. H. Rossi, each of whom participated in many helpful discussions and had independently thought of using this technique. Many useful suggestions were also contributed by Mr. N. Baily.

Electronic Pile Simulator

P. R. BELL AND H. A. STRAUS*
*Oak Ridge National Laboratory,*** *Oak Ridge, Tennessee*

(Received April 18, 1950)

A device has been made that follows the same set of kinetic equations as a chain-reacting pile. The voltage output varies as a function of time as the neutron flux would vary in a pile. A potentiometer varies the effective multiplication factor and can be considered as a control rod. Five delayed neutron periods are simulated. A high precision electronic integrator is used, and the instrument is capable of an accuracy much better than one percent.

THE neutron flux in a graphite-uranium chain-reacting pile decreases or increases when a control rod or other absorber is moved into or out of the pile. The way in which the flux increases or decreases is of some interest as one might wish to keep the pile output constant by an automatic controller or one might wish to know the change in flux with time produced by an absorber. It is possible to make an analog computer or simulator that responds exactly as a pile does to changes in absorption. Such an instrument serves admirably for the design of controllers or for demonstration or training.

If one assumes that the neutrons produced by the fission process are slowed down without absorption and are absorbed only as thermal neutrons, then the number of thermal neutrons per cm^3 (n) is given by the relation

$$dn/dt=(\delta k_{\text{effective}}/kl^*)n-(\beta/l^*)n+e^{\tau\Delta}\sum_i \lambda_i C_i+S, \quad (1)$$

where

$l^*=l/ke^{\tau\Delta}=(1/ke^{\tau\Delta})\cdot(\lambda_a/v)$ = effective mean life of the neutrons from formation by fission to absorption or loss from pile by leakage.
$k=\nu\,\Sigma_f/\Sigma_{\text{total}}$ = number of neutrons per fission × (macroscopic cross section for fission/macroscopic total absorption cross section).
k = multiplication constant that pile lattice would have if it were of infinite extent.
τ = "Fermi age" of the neutrons, a measure of the net distance traveled by a neutron while being slowed down.
Δ = Laplacian representing the relative spatial distribution of the neutron flux. This is essentially a constant with time since the flux distribution is independent of the power level of the pile.
$\delta k_{\text{effective}}$ = reactivity of the pile $=(L^2\Delta-1+ke^{\tau\Delta})$.
L = diffusion length for thermal neutrons.
β = fraction of the fission neutrons coming from all delayed neutron emitters.
λ_i = decay constant of the ith kind of delayed neutron emitter.
C_i = concentration in atoms per cm^3 of the ith kind of delayed neutron emitter.
S = source in neutrons per cm^3 per second, other than those produced from neutron induced fission.

The first term on the right-hand side of Eq. (1) represents the effect of control rods or other absorbers upon the pile flux and is zero when the pile is in equilibrium at any value of neutron flux. The second term is inserted to correct for the fraction of the fission neutrons of each generation that does not appear instantaneously, and the third term represents the contribution of each of the delayed neutron emitters. The second and third terms must be equal when the pile is in a steady state at a constant flux. The fourth term represents the contribution of spontaneous fission, cosmic rays and other neutron sources that are not affected by adjusting the control rods of the pile.

The concentration of each delayed neutron emitter is a function of time depending on the past history of the pile. The rate of change of each delayed emitter is given by Eq. (2).

$$dC_i/dt=-\lambda_i C_i+(e^{-\tau\Delta}/l^*)\beta_i n. \quad (2)$$

Here β_i represents the fraction of the total fission neutrons formed from this particular delayed emitter. It is clear that the sum of these fractions β_i must be equal to the total fraction β.

The solution of differential equations of this type with variable coefficients can generally be accomplished by the use of a feed-back equation solver, which in principle is a very quick-operating trial and error method generally employing electrical circuits. In the electronic pile simulator the number of neutrons per cubic centimeter, n, is represented by a voltage and the other quantities involved in the equation are represented by other voltages or currents or by suitable circuit constants.

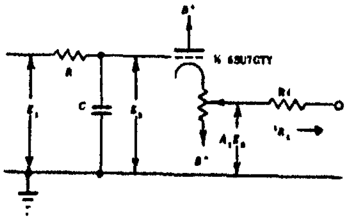

FIG. 1.

The circuit of Fig. 1 is used for the solution of Eq. (2). In this circuit

$$dE_2/dt=i/C=(E_1-E_2)/RC. \quad (3)$$

If $1/RC=\lambda_1$ and E_1 represents n, then

$$dE_2/dt=-\lambda_i E_2+\lambda_i n. \quad (4)$$

This equation is like Eq. (2) with

$$(e^{-\tau\Delta}\beta_i/l^*\lambda_i)E_2=C_i.^1 \quad (5)$$

---

* Now at Bendix Radio Corporation, Towson, Maryland.
** Contract W-35-058-eng. 71.

[1] The delayed neutron periods were taken from Table I, Bernstein, Preston, Wolfe, and Slattery, Phys. Rev. 71, 573 (1947).

The tube connected to E_2 is operated as a cathode follower. If the amplification factor (μ) of the tube is high and the load in the cathode circuit is a high resistance the gain (A) is nearly unity

$$A=1/[1+(1/gR_k)+1/\mu], \tag{6}$$

where R_k is the resistance of the load circuit measured from cathode to ground. In this instrument $A\approx 0.98$.

Potentiometers $R_{5,6,7,8,42}$ (Fig. 2) are located in the cathode circuits of the cathode followers and the gain at each potentiometer arm (A_i) includes the tube gain and the "gain" of the potentiometer. The internal resistance of the cathode follower and the potentiometer measured at the arm is so small that it can be neglected. To the arm of each potentiometer is attached the "adding" resistor R_i, and the far ends of these resistors are attached to point P which is essentially at a fixed potential. The current in each resistor is given by

$$i_{Ri}=(A_i/R_i)E_2=(A_il^*/R_i\beta_i)e^{\tau\Delta}\lambda_iC_i. \tag{7}$$

Thus if the voltage $E_1=n$, then the current given by this circuit at P is one of the elements of the sum in the third term of Eq. (1) with a scale factor $A_il^*/R_i\beta_i$. The first term in Eq. (1) can be represented very easily. Let us suppose a potentiometer is connected between a voltage representing n and a voltage representing $-n$. Then for the voltage E at the tap on the potentiometer we have

$$E=Dn, \tag{8}$$

where D is the linear scale of the potentiometer with zero at the center, $+1$ at the $+n$ end and -1 at the $-n$ end.

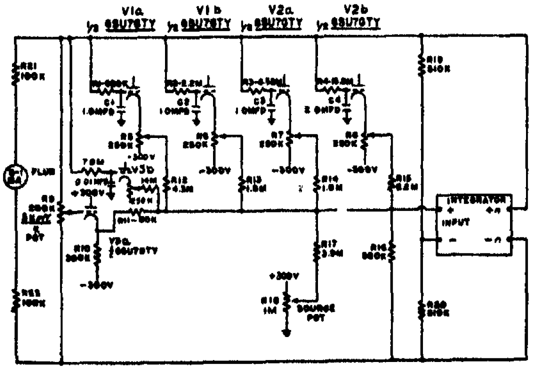

FIG. 2.

A cathode-follower circuit similar to that used in Fig. 1 is connected to the tap of the potentiometer and the current, i, in the output or adding resistor R_{11}, if the far end of this resistor is kept at a fixed potential, will be given by

$$i=(A_KD/R_{11})E$$
$$=[A_K/R_{11}(\delta k_{\text{eff. max.}}/kl^*)](\delta k_{\text{eff.}}/kl^*)n, \tag{9}$$

where A_K is the gain of the cathode follower and $(\delta k_{\text{eff.}}/kl^*)/(\delta k_{\text{eff. max.}}/kl^*)=D$. This current i represents

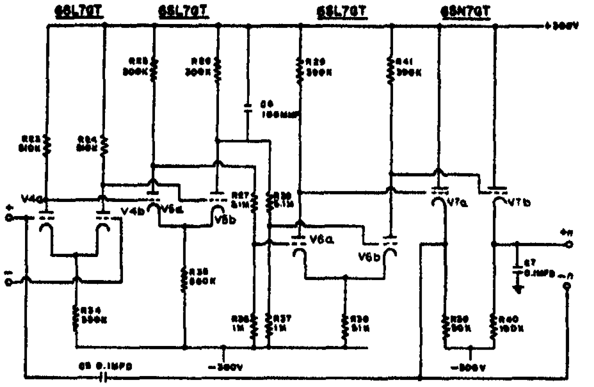

FIG. 3.

the first term in Eq. (1) with a term in brackets as a scale factor. In this instrument $(\delta k_{\text{eff. max.}}/k)$ was arranged to be ± 0.05.

The second term in Eq. (1) is obtained from a resistor (R_{16}, Fig. 2) connected to the voltage representing $-n$. The current in this resistor (if the opposite end is fixed in voltage) is

$$i=-n/R_{16}=-(l^*/R_{16}\beta)(\beta/l^*)n. \tag{10}$$

Nothing has been said, so far, about the fact that although the output of a cathode follower changes at a rate A times its input there is also a constant difference of voltage. This constant voltage difference is the bias required by the cathode-follower tube when its input is at its "zero input" or reference voltage. The reference voltage is obtained when the $+n$ and $-n$ points have no voltage difference. There are enough disposable values to allow one to arrange things so that the tubes are operating at all times on a satisfactory part of their characteristics. A potentiometer (source potentiometer) is included to represent a source of neutrons and compensates the residual constant voltage difference of the cathode followers which would by itself represent a source of neutrons. The potentiometers $R_{5,6,7,8,42}$ in the cathode follower circuits are adjusted so that the residual constant voltage difference term which must be corrected by the source potentiometer is quite small.

When the ends of the adding resistors like R_1 in Fig. 1, R_{11} and R_{14} (Fig. 2) are all connected together to a common point P there will be (if the point P is kept at a fixed voltage) a total current

$$i_{\text{total}}=[A_K/R_{11}(\delta k_{\text{eff. max.}}/kl^*)](\delta k_{\text{eff.}}/kl^*)n$$
$$+e^{\tau\Delta}\textstyle\sum_i(A_il^*/R_i\lambda_i)\lambda_iC_i-(l^*/R_{16}\beta)(\beta n/l^*)$$
$$+[(i_{\text{source}}+i_{\text{const}})/S]S, \tag{11}$$

where i_{const} is the current due to the several constant voltage differences in the cathode followers and i_{source} is the current contributed by R_{17}, the sum of these last two terms represents the source term in Eq. (1).

All that remains now is to connect point P to a circuit that will produce, as its output voltage, the time integral of the total current at P multiplied by an appropriate

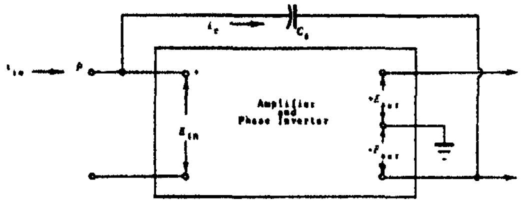

FIG. 4.

constant. This output voltage then would represent *n*. If a voltage changing equally but in the opposite direction is also produced, these voltages may then be connected to the parts of the circuit whose inputs are required to be *n* or $-n$. The whole instrument will then operate to give *n* as a function of time as required by the set of Eqs. (1) and (2). As long as the various elements of the circuit are operating in the range of voltages or currents in which their performance is satisfactory, the system approximates the relations we have assumed.

The integrator section of the instrument is the circuit whose output voltage is the time integral of its input current. The details of this section are shown in Fig. 3, and the operation may be more easily understood from the simplified diagram Fig. 4.

The point *P* is connected to a grid and one end of condenser C_6. This grid is in the negative grid region and the grid current is negligible so that the input current i_{in} at point *P* must be equal to the condenser current i_c but

$$\int i_c dt = C_6(E_{out} - E_{in}) = \int i_{in} dt. \tag{12}$$

If the voltage gain (*A*) of the amplifier in Fig. 4 is very great then E_{in} is very small compared with E_{out} and

$$\int i_{total} dt = \int i_{in} dt = C_6 E_{out} \tag{13}$$

is a good approximation.

The actual amplifier used (Fig. 3) is of the "differential" type in that it responds only to the difference in voltage between the two input grids. This effect is produced by the use of unbypassed cathode resistors.

The two nearly equal resistors, R_{19}, R_{20}, feed one of the input grids ($-$input) with one-half of the algebraic sum of the $+n$ and $-n$ output voltages, and only the difference between the voltage of this grid and the voltage at point *P* ($+$input) is amplified. This arrangement converts the circuit into a bridge and greatly reduces the effect of any errors in the phase-inverting action which produces $+n$ and $-n$; in addition if R_{19} is the right amount larger than R_{20} the effective gain of the integrator may be made infinite. A condenser C_7 is connected from the $+n$ output to ground to make the loading symmetrical.

It can be seen that the action of the integrator-amplifier opposes any change in the voltage difference between the $+$input and $-$input by supplying a current through the integrating condenser C_6. This keeps point *P* at a constant voltage relative to the algebraic sum of $+n$ and $-n$, that is, approximately constant with respect to ground as was assumed when considering the currents in the adding resistors.

Using Eqs. (13) and (11) we find

$$\begin{aligned}(C_6)dn/dt = {}& [A_K/R_{11}(\delta k_{\mathrm{eff.\,max.}}/kl^*)](\delta k_{\mathrm{eff.}}/kl^*)n \\ & + e^{r\Delta}\sum_i [A_i l^*/R_i\beta_i]\lambda_i C_i - (l^*/R_{16}\beta)(\beta n/l^*) \\ & + [(i_{source} + i_{const})/S]S. \end{aligned} \tag{14}$$

The quantities in the brackets are scale factors for each term. The condenser C_6 is 0.1 microfarad, which is the largest value for which the maximum integration current required can be supplied by tubes $V3_a$ and $V7_a$. The choice of C_6 fixes the value to which the other scale factors must be adjusted.

The errors in this instrument are mostly in the integrating circuit and these errors arise as follows:

Let us suppose that the amplifier of the integrator has an initial gain of 1000 and the resistor pair R_{19}–R_{20} is adjusted to supply just the amount of positive feedback required to make the effective gain infinite. If the differential gain of the amplifier falls to 500 at full output

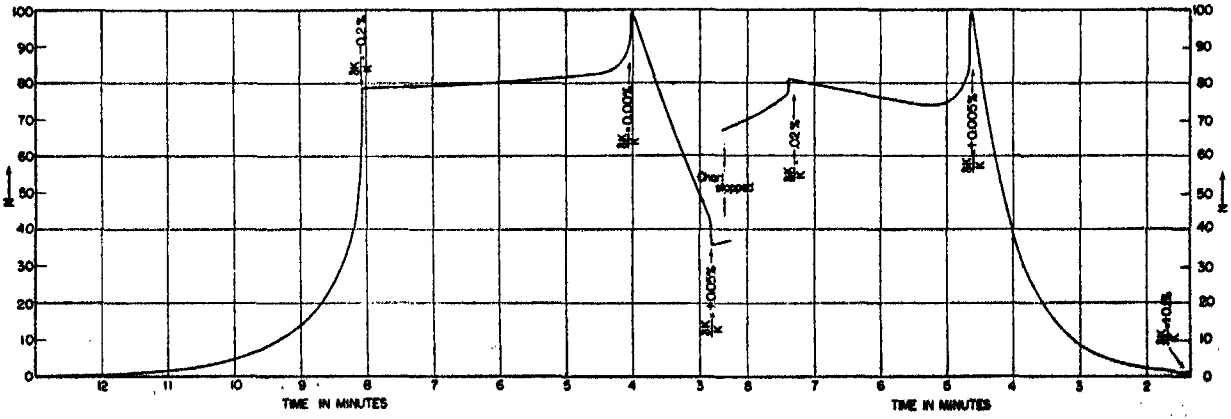

FIG. 5.

(100 volts), the signal required at the grids would be 0.2 volt, and the positive feedback would supply only 0.1 volt thus requiring the input signal to supply the remaining 0.1 volt. If the simulator output was rising initially with a 30 minute period due to a signal from the $\delta k_{\text{effective}}$ potentiometer of $\delta k/k_{\text{effective}}=0.005$ percent, the output would just cease rising when this amount of non-linearity had set in. Another kind of error due to the integrator circuit is drift or fluctuation of the output due to changes in contact potential in the first double triode. These fluctuations limit the range of n to about 5×10^3.

The last noticeable source of error is the variation in gain of the delayed neutron cathode followers. The current in these cathode followers varies about 30 percent from no output to full output. This change of current gives a variation of g of about 10 percent and results in a change of gain of about 0.03 percent. The effect due to the change of μ is still smaller. Since the total contribution of all the delayed neutron emitters is roughly 0.7 percent of the total neutrons, this small change in gain produces an error that has the same effect as a change in $\delta k_{\text{effective}}/k$ of 0.0002 percent.

The complete instrument must be adjusted experimentally to determine the exact setting of the source potentiometer, R_{18}, that represents zero source strength. It must be noted that this instrument, unlike the pile, is completely symmetrical with respect to the zero output point and may be caused to build up on either "positive" or "negative" neutrons depending on the source setting. In addition to the source zero the position of $\delta k_{\text{critical}}$ must be determined on the δk potentiometer. A satisfactory procedure is to set the δk potentiometer slightly more negative than the apparent position of $\delta k_{\text{critical}}$ and then slowly adjust the source potentiometer, allowing several minutes to elapse between each adjustment, until the n meter gives only an extremely small positive reading. The δk potentiometer should then be adjusted to cause the output to rise slowly (say 10–20 min. to reach full output) and the output plotted against time. If the δk potentiometer is at $\delta k_{\text{critical}}$ the output will rise linearly due to the small source; if the reactivity is positive the curve will bend upward; if the reactivity is negative the curve will bend downward. Slight readjustments can now be made until a very small change in the source potentiometer setting causes the output to rise or fall linearly with time. The setting on the source potentiometer is then zero source, and the setting on the δk potentiometer is $\delta k_{\text{critical}}$.

Figure 5 is a tracing made from a Brown recorder record of the output voltage n against time as the δk potentiometer, which represents the control rod of the pile, is moved as shown on the tracing. Note the transient effects whenever the control rod is moved. The output approaches a pure exponential curve as the transient dies away.

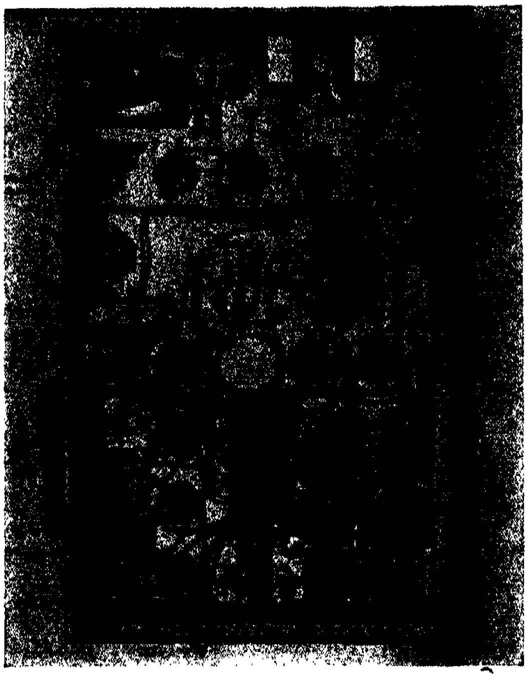

FIG. 6.

Figure 6 is a photograph of the bottom of the chassis of the simulator. The row of four tubes is the integrator section. All of the delayed neutron storage condensers except C_8 are invisible because they are above chassis. These condensers are Western Electric type D 161270 1 μf units chosen for their extremely low leakage and "soaking up" effect.

Anyone attempting the construction of an instrument of this type should place the leads with care, especially in the integrator section, and employ an oscilloscope to check the absence of high frequency parasitic oscillations. Condenser C_6 was added to suppress such an oscillation. When the δk potentiometer is mounted in a remote location it is necessary to shield separately the lead from the arm to prevent coupling between this lead and the $+n$ lead. Such coupling will produce oscillations at a high frequency.

We wish to acknowledge the valuable suggestions of F. H. Murray during the planning of this instrument.

THE REVIEW OF SCIENTIFIC INSTRUMENTS VOLUME 21, NUMBER 8 AUGUST, 1950

Physical Instruments for the Biologist

Detlev W. Bronk
Associate Editor in Charge of this Section
Eldridge Reeves Johnson Foundation for Research in Medical Physics,
University of Pennsylvania, Philadelphia, Pennsylvania

An Infra-Red Microspectrometer for Biological Research

DARWIN L. WOOD*
Mendenhall Laboratory of Physics, Ohio State University, Columbus, Ohio

(Received May 15, 1950)

The apparatus herein described consists of a totally reflecting microscope of numerical aperture 0.6 coupled with a Perkin-Elmer Model 12C infra-red prism spectrometer. The combination makes possible the recording of infra-red spectra of individual cells of biological materials over the familiar range from 1 to 15μ, and has been particularly designed for the study of muscle fibers. The techniques for producing aspheric optics used in the microscope are discussed. Some preliminary performance data are given.

VARIOUS authors have described the optics of reflecting and reflecting-refracting microscopes.[1–6] Others have described the combination of microscope and infra-red spectrometer.[6–8] In all but one of these references (7), the microscope was either of low aperture or contained refracting elements which absorbed longer wave-lengths of the infra-red. It is the purpose of this paper to describe the relatively high aperture totally reflecting aspherical system built by the author.

The optical parts of the microspectrometer are shown in Fig. 1, with the elements in the same relative positions as in the photograph of Fig. 2. On the left in front is the source unit consisting of a self-starting Nernst filament N and a high aperture spherical mirror combination (M_1 and M_2) which fills the entrance pupil of the microscope condenser (M_5 and M_6) with radiation. From the condenser (M_5 and M_6) the radiation proceeds through the tissue specimen at S to the objective (M_7 and M_8), which forms an enlarged image of the tissue on the screen *Sc*. By properly positioning the specimen on the stage of the microscope, the desired portion of the specimen is selected to fall on the aperture of the screen *Sc* and the radiation passing through the aperture is focused on the slit of the spectrometer by the mirrors M_{10} and M_{11}. The mirrors M_3, M_4, M_9, and M_{11} are plane first surface mirrors folding the optical path into a convenient shape. It should be pointed out that the mirror combination M_1 and M_2 is merely a convenience, introduced to give a uniform illumination to the whole area of the image on the screen at *Sc*. Without this pair of mirrors only a small area of the magnified image (about the size of the source) will be illuminated. It makes little difference whether these mirrors are in the system or not as far as the amount of the energy received by the detector of the monochromator is concerned. The monochromator, as is evident from the photograph of Fig. 2, is that of the Perkin-Elmer Model 12*C*. The detecting system is the 7-cycle/sec. a.c. thermocouple system which is standard equipment on the Model 12*C*. The radiation interrupter can be seen just in front of the slit in Fig. 2. It is mounted in ball bearings in a brass block and is connected to the Perkin-Elmer synchronous rectifier camshaft by a flexible cable.

The whole auxiliary optical system for the microspectrometer is mounted on a heavy aluminum casting which fits over the standard spectrometer without disturbing the optical arrangement used in making macrospectra. Indeed, for use with d.c. operation where the radiation chopper is not needed, the auxiliary system can be installed without disturbing any part of the standard spectrometer. For the a.c. operation, it is necessary to remove the smaller housing of the spectrometer so that the synchronous rectifier camshaft can be reached with the flexible cable from the chopper. The microscope assembly, which is patterned to some extent after the ordinary light microscope, can be removed as a unit from the auxiliary optical system for use by itself.

The microscope optics are aspherical and follow the design of Burch.[1] The aspherical optics are necessary if the microscope is to have a reasonably large numerical aperture, as shown in Burch's paper. The objective and condenser form a symmetrical pair of effective numerical aperture 0.6 with a magnification of about 65× at the screen *Sc* of Fig. 1. Such high magnification is perhaps more than necessary, but it is very convenient when it comes to selecting the areas of the specimen to be examined. The mirror M_{10} provides some subsequent demagnification at the slit.

The microscope mirrors M_6 and M_7 are commercially available spherical segments, convex, 6 mm in diameter, and about 4.3 mm in radius of curvature. The mirrors M_5 and M_8 are aspherical, concave, 8 cm in diameter, and roughly 5 cm in radius of curvature. The large diameter of the concave mirrors is desirable to facilitate the aspherization. It causes no difficulty in practice, although it might offend the aesthetic sense of the conservative light microscopist.

---

* This work was done under tenure of an AEC Predoctoral fellowship.

[1] C. R. Burch, Proc. Phys. Soc. London 59, 41 (1947).

[2] D. S. Grey and P. H. Lee, J. Opt. Soc. Am. 39, 719 (1950).

[3] D. S. Grey, J. Opt. Soc. Am. 39, 723 (1950).

[4] B. K. Johnson, J. Sci. Inst. 26, 148 (1949).

[5] E. H. Land *et al.*, Science 109, 371 (1949).

[6] R. C. Gore, Science 110, 710 (1949).

[7] Barer, Cole, and Thompson, Nature 163, 198 (1949).

[8] Blout, Bird, and Grey, J. Opt. Soc. Am. 39, 1052A (1949).

Tests of the objective in visible light indicate that the resolving power is quite adequate for infra-red work. Using a stage micrometer ruled with lines 10μ apart, it was deduced that the objective would resolve lines 3 to 5μ apart. The image in visible light is quite good enough to select the portions of a piece of tissue for examination, and structures smaller in dimension than the wavelength of the radiation used for the examination are, of course, not observable.

To dispel the impression that aspherical objectives are prohibitively difficult to produce, some of the production techniques used by the author will be described. Let it be said at the outset that the aspherical mirror is not more difficult to figure than, for instance, an ellipsoid of the same depth of curve, and a focal ratio not far from unity. Furthermore, for the tolerances required for the infra-red, the figuring need not be particularly precise.

To start with, it was found that a local optometric supply house was equipped to supply glass blanks ground and polished to the spherical curve most nearly approximating the finished shape, so that the problem remaining was one of figuring these blanks. To do the figuring properly one needs first a good testing procedure, and second a polishing technique with which to change and control the shape of the surface.

The testing technique used in this work was a variation of the familiar Foucault knife edge test. A diagram of the arrangement as it was set up on an optical bench is shown in Fig. 3. A small, bright source of light about 1 mm in diameter is located at A. At B a standard 1.8-mm focal length microscope objective forms a greatly reduced image of the bright source A. The aspherical mirror under test is assembled in its proper position in the reflecting microscope objective housing, and located at C, "looking" at the reduced image of the source produced by the refracting objective at B. The refracting objective must have sufficient aperture to fill the large concave mirror of the reflecting objective with light. Then at D a knife edge is arranged with a screw adjustment so that it can be moved gradually across the enlarged image produced by the reflecting objective C when focused on the virtual source formed at B. The telescope F receives light from the small convex mirror of the reflecting objective, and is focused on the surface of the large concave mirror which is being tested. The telescope shows a bright field in its eyepiece which is to go dark all at once when the knife edge is moved across the ray bundle at D. The telescope has sufficient magnification to enlarge the field of the exit pupil of the reflecting objective up to the point where the various areas of the large convex mirror can be conveniently examined. As the correction of the objective improves, the contrast of the knife edge shadow pattern can be increased by placing a pinhole in a piece of aluminum foil in front of the 1-mm diameter hole at A to diminish the size of the virtual source at B.

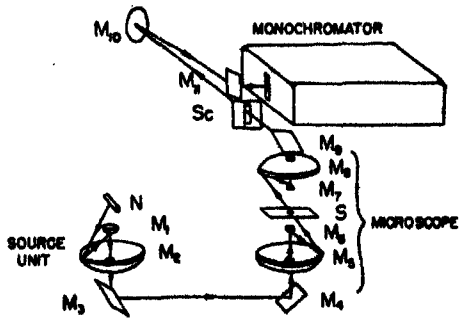

FIG. 1.

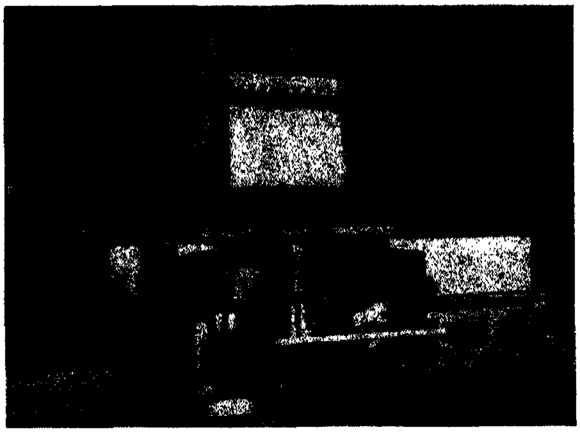

FIG. 2.

To supplement the knife edge test an eyepiece may be introduced at E, and some information about the objective may be obtained through the so-called eyepiece test. Both tests worked well with the convex mirror aluminized but the large concave mirror not coated.

The polishing technique actually involved more than just polishing, since the aspherical surface was so far from a sphere. It was found convenient to do some grinding before the surface could be brought in by polishing with rouge. The grinding and polishing operations were carried out on a rotating spindle such as commonly used by the producers of ophthalmic lenses. The only necessary deviation from ordinary optical shop practice was the use of the flexible lap in both grinding and polishing. The laps were of two kinds: a metal one for grinding, and a pitch lap for polishing. The metal lap

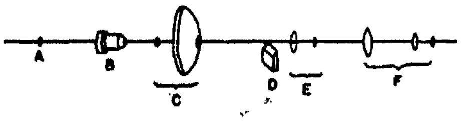

FIG. 3.

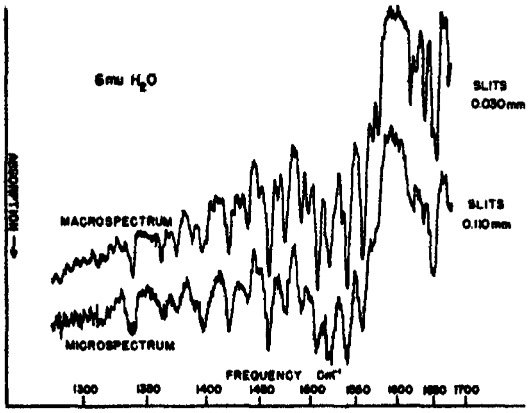

FIG. 4.

was made by casting Woods metal between the glass surface to be aspherized and a cast iron spherical form of a suitable curvature. A second cast iron spherical lap was then covered with a piece of sponge rubber about 0.125 in. thick and the cast Woods metal lap was waxed to the sponge rubber with beeswax. The metal was cut into facets about ½ in. sq. with a jeweler's saw, and the appropriate facets removed to grind down the "high" zones of the mirror. An obvious variation of this procedure came after one aspheric surface had been finished. This was to cast the Woods metal against the aspheric surface and use the rigid aspheric lap thus produced to grind in the asphericity on the second mirror. By this means it was possible to eliminate the metal flexible lap grinding step, and proceed directly to the polishing steps.

The pitch polishing lap was made in much the same way as the metal grinding lap. The pitch layer was applied directly to the sponge rubber layer on the cast iron base. Hard pitch was used, and it was formed against the surface to be polished in the usual manner. When the lap was cold, it was struck with a hammer, and a multitude of facets was thus produced. By painting the lap with a thin coating of beeswax the scratches from the hard pitch were minimized. The lap was cut down where the test showed the mirror surface to be low, and it was not disturbed where the test showed it to be high. With this lap, then, the shape of the surface was worked until the knife edge test showed sufficient correction. For the last few stages of the figuring the mirror was worked with the spindle stationary.

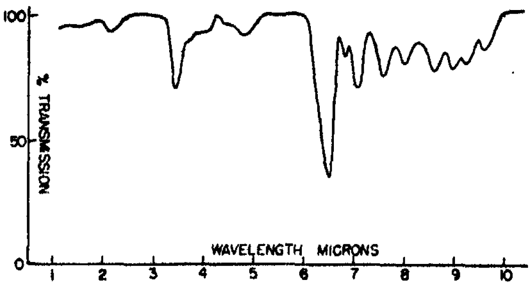

FIG. 5. Frog muscle single fiber absorption spectrum.

Typical results with the microspectrometer are indicated in Figs. 4 and 5. In Fig. 4 is shown a microspectrum of the 6μ-atmospheric water band and a macrospectrum of the same part of the same band recorded with the spectrometer in its standard form. It will be quickly seen that there is a loss in resolution because of the larger slit widths required by the microscope in the optical path. The microspectra require slits almost four times as large as those for ordinary macrospectra. The microspectrometer will be useful, none the less, over the same range as the macrospectrometer in spite of the diminished resolution.

In Fig. 5 is shown a composite microspectrum of single live frog muscle fibers supported between fluorite plates. The excessive interference of the aqueous medium and the cellular water has been partially compensated for by measuring the percent transmissions relative to the Ringer's solution just next to the muscle fiber in the preparation. It is expected that considerable information on the contractile mechanism of muscle will become available from further studies of the microspectra of muscle fibers, and muscle extractives.

THE REVIEW OF SCIENTIFIC INSTRUMENTS VOLUME 21, NUMBER 8 AUGUST, 1950

Modification of the Apparatus Used for the Baldes Thermoelectric Method of Measuring Osmotic Pressure*

V. Everett Kinsey
Howe Laboratory of Ophthalmology, Harvard Medical School, Boston, Massachusetts

(Received April 28, 1950)

The apparatus employed with the Baldes method for determining osmotic pressure has been modified by substituting a breaker-type d.c.-a.c. amplifier for a sensitive galvanometer, thereby permitting its use under conditions where galvanometers are impractical. Precise temperature control of the water bath in which the thermoelements are immersed has been shown to be unnecessary provided the bath is stirred vigorously. A switch made from one block of electrolytically pure copper provides a satisfactory current-reversing mechanism with low interfering contact potentials arising from non-thermostated portions of the circuit.

BALDES[1] has devised an excellent method for determining osmotic pressure which is applicable to quantities of fluids of the order of several microliters. More widespread application of this method has probably been lacking because of the complexity of the apparatus required. The present paper is concerned with several modifications of this apparatus which, while maintaining the accuracy of the method, offer advantages which permit measurement of osmotic pressure to be made more easily and under a wider variety of laboratory conditions.

The apparatus, as described in detail by Baldes, consists of a double thermocouple enclosed in a small water-tight chamber, the inside walls of which are lined with filter paper moistened with a solution having an osmotic pressure approximately the same as that of the solution to be determined. The chamber is immersed in a water bath the temperature of which Baldes maintained constant to 0.001°C. Leads from the thermocouples connect with a galvanometer having a sensitivity of 10^{-9} ampere through a double-throw, double-pole switch.

The two features of the method which involve the most elaborate components of the apparatus are the measurement of extremely small voltages set up by the thermocouples and the maintenance of the temperature of the water bath to within 0.001°C. A third complication is concerned with possible spurious electromotive forces arising from contact potentials in the non-thermostated double-pole, double-throw switch.

AMPLIFIER

Because the Howe Laboratory is located close to heavy city traffic it was not possible to use a sensitive galvanometer to measure the voltages without taking elaborate precautions to damp the instrument. The latter would require excessive space and expensive equipment. Direct current amplifiers are frequently unsatisfactory when great amplification is required. However, a satisfactory substitute for the galvanometer was found in a breaker-type d.c.-a.c. amplifier (Perkin-Elmer Corporation, Model 53). This instrument operates satisfactorily in a range between 0.1 and 300 microvolts and is designed to change d.c. into a.c. current by mechanical means, amplify the current in this form, and reconvert it to d.c. whence it can be measured on any common indicating instrument such as a milliameter. The sensitivity of the amplifier approaches the theoretical limit imposed by thermal agitation in the input circuit, and is particularly suited for amplification of thermal e.m.f. when both voltage and impedance are low.

Despite these desirable features, when the instrument was set for medium amplification it did not give satisfactory results when employed with the thermocouple elements because of oscillation of the needle on the milliameter. The oscillations were presumably due to the effect of slight contact noise in the room. Insertion of a capacitance (2000 mfd, 6 working volts) in parallel with the milliameter, however, completely eliminated this difficulty. In practice the gain was set so that 0.5 microvolt corresponded to full-scale deflection (1 milliampere) on the milliameter. Increased amplification could be obtained by advancing the gain but much of the advantage is offset by variations in voltage arising apparently from contact potentials from non-thermostatted parts of the circuit. The breaker-type d.c.-a.c. amplifier has been in use over a period of two years and is satisfactory except for the occasional need of replacing amplifier tubes and bias cells.

THERMOSTAT

The second modification of the apparatus involves the need for controlling the temperature constant to 0.001°C. Initially, temperature control was accomplished by constructing a copper water bath 18 inches on a side. The four sides and bottom of the tank were surrounded with one inch of cork and a five-eighths inch plywood box. The tank was then sunk in an ordinary laboratory bench and the top covered with a one-fourth inch Lucite plate. Stirring was accomplished with a one-twentieth horsepower electric motor using a two inch, three-bladed propellor. The temperature was controlled by means of a thermoregulator consisting of a twenty-foot glass helix filled with mercury, feeding into a

---

* Supported in part by a grant from the Snyder Ophthalmic Foundation, New York, New York.

[1] E. J. Baldes, J. Sci. Inst. 11, 223 (1934).

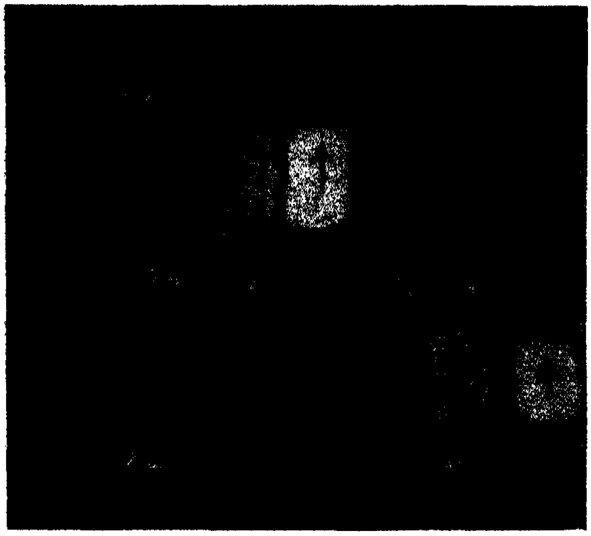

Fig. 1.

capillary. Consideration of the problems involved in controlling temperature, however, suggests that if the temperature were maintained constant to within 0.001°C over all parts of the surface of the brass jacket surrounding the thermocouples, no further precautions would be necessary. This could be accomplished presumably by stirring the bath vigorously even though the temperature of the water in the bath may vary considerably from moment to moment.

To test this idea, the water was permitted to assume the temperature of the room, stirring was continued as before, but the thermoregulator was disconnected. Measurements were made using 150 millimolar solution of NaCl on one couple and 145 millimolar solution of NaCl on the other. The difference in concentration amounting to a 5.0 millimolar solution gave rise to a reading of 0.15 milliampere (0.073 microvolt) and the greatest variation between replicate readings was ±0.015 milliampere.† This variation was no greater than that obtained when the temperature of the water bath was maintained constant to 0.001°C. To eliminate the possibility that temperature conditions might have been unusually favorable on the day in which the experiments were performed, for example, with respect to draughts, a more critical test was arranged by elevating the temperature of the bath to 32°C, or about 8° above room temperature, and another series of measurements was made (without any temperature regulation). Under these circumstances the temperature of the water in the bath fell at a rate of 0.02° per minute during the four-hour period in which measurements were made. The maximum variation in replicate determinations was the same as those obtained under the conditions prevailing during the two preceding experiments despite a change of temperature approximately five times that which would introduce a serious error had it given rise to temperature differences of this magnitude on the two sides of the brass jacket surrounding the couples. These results indicate that with adequate stirring a water bath may be used without the necessity of providing especially constant temperature control, thus permitting the use of sturdy, relatively cheap, and readily adjustable thermoregulators.

SWITCH

A third modification of the apparatus as originally described by Baldes arose from inability to procure a double-pole reversing switch which did not produce high contact potentials. At the suggestion of Dr. Ernst Bárány of Uppsala, Sweden, who had experienced a similar difficulty, a reversing switch was constructed by sawing a one-half inch block of electrolytically pure copper into several segments (Fig. 1). The copper was obtained from a local electric utility company. The switch is closed by inserting two additional blocks of copper from the same block between the center and lateral blocks of copper and reversal is made by changing the position of the blocks. The ends of the blocks to be inserted are insulated from the heat of the hand with adhesive tape, and all the edges which make electrical contact are cleaned frequently with emery paper. It is thought that contact potentials arising from the non-thermostated switch are minimized by use of metal of essentially similar composition.

ACKNOWLEDGMENT

Dr. Elek Ludvigh suggested substituting the d.c.-a.c. amplifier for the galvanometer.

---

† Incidentally, this represents a maximum variation in individual readings of ±0.5 millimole in 150 millimoles or less than 1 percent.

Laboratory and Shop Notes

The Temperature Coefficient of Resistance of Tin Oxide-Coated Electrically Conducting Glass between 1° and 300°K*

D. N. Lyon and T. H. Geballe
Chemical Laboratory, University of California, Berkeley, California

May 8, 1950

THE development, by Corning and other groups, of electrically conducting coated glass suggests that some of the problems of calorimetry in the temperature region below 10° K might be minimized if such conducting coatings could be produced with a temperature coefficient of resistance such as to make them suitable for secondary thermometers. A suitable reference thermometer should of course be reproducible during the course of an experiment, relatively insensitive to magnetic fields, independent of the measuring current, and should have as small an adsorptive capacity for helium gas as possible. A glass sample container, with a suitable heater-thermometer coating essentially an integral part of the surface might prove useful down to temperatures below which it is impossible to maintain thermal equilibrium between a sample and container (~0.2° K).

We have recently measured the properties of a number of coated conducting glass samples and although it is not yet certain that a coating satisfactory for precision thermometry can be developed, we believe the results are sufficiently promising and interesting to report here.

The samples tested were made and supplied to us by Corning Glass Works through the courtesy of Mr. W. W. Shaver. The samples were in the form of flat plates of Pyrex Brand 7740 glass, approximately 2.5 cm wide, 15 cm long and 0.4 cm thick. The coatings are produced by an incompletely disclosed process which yields a film of controllable resistivity, consisting nominally of stannic oxide with added small amounts of certain other metallic salts, on one surface of the glass. Fired silver contacts were provided at each end, to which copper lead wires were fastened. The samples were placed in a Dewar and immersed directly in baths of various refrigerants.

Samples with the following approximate surface resistivities at 295° K were tested:

No. 1—	10.5 ohms/cm square	No. 7—	670 ohms/cm square
2—	170	8—	740
3—	280	9—	1530
4—	290	10—	1470
5—	450	11—	13,000.
6—	370		

Curves of resistance *versus* temperature for samples No. 2 through 11 are shown in Fig. 1. Sample No. 1 showed practically no change in resistance with temperature below 77° K, and about a 2 percent increase in resistance between 77 and 297° K, and is not included in the figure.

Above ~14° K, those samples with appreciable temperature coefficients exhibited severe lag in the approach to final resistance following a change in temperature. When samples No. 3 to 8 were cooled from 295° K to 90° K over a period of 45 minutes and then placed directly in liquid N_2, all samples required some 20 hours to reach an equilibrium resistance. The approach to equilibrium was approximately exponential with time; the total change in resistance, between the value some 15 minutes after placing in liquid N_2 and the equilibrium value, was roughly proportional to the temperature coefficient of the sample and approximately equal to the change which would be produced by a temperature change of 0.5°. The effects persisted, although much less severe, to 4.2° K below which, if present, they were masked by instability of the bath temperatures. Upon rewarming to room temperature, all samples returned to the initial resistance at 295° K to within deviations corresponding to ± 0.2° K.

Between 297 and 77° K, all samples can be approximated by expressions of the form $R=aT^n$. Below 77° K, more elaborate expressions are required, although for sample No. 3 the expression

$$R_{\text{No. }3}=46640T^{-0.4927},$$

based upon the observations at 20.4 and 1.25° K, reproduces the measurements at 2.60 and 4.22° K to within 0.005° K, deviating at 13.95° K by 0.33° K.

The change in resistance produced by a magnetic field applied parallel to the direction of current flow was measured for a few of the samples and is shown in Table I. Although small, the effect at 20.4 and 13.95° K appeared beyond the limits of error to be opposite in sign to the effect at and below 4.2° K. Within the accuracy of the measurements, the increase in resistance of sample No. 3 was proportional to H^2 up to 9000 oersteds at 4.2° K, but at 1.25° K, the increase was less rapid that $\propto H^2$.

TABLE I. Isothermal change in resistance of Corning E-C glass samples with parallel magnetic field.

		Sample No.					
		No. 3		No. 6		No. 7	
T, °K	H_{oersteds}	R Ω	ΔR Ω	R Ω	ΔR Ω	R Ω	ΔR Ω
20.4	0	10557		21748			
	7350		−0.9		−2.1		
13.95	0	12874		28811			
	7600		−2.3		−7.1		
4.25	0	22850		76335		323450	
	6200		+5.0		+62		+200
	7150		+7.5		+81		+265
	9000		+12.5		+134		+440
1.25	0	41700					
	6200		+221				
	7150		+278				
	9100		+406				

The following data were obtained in the few tests made of conformity to Ohm's law. The accuracy of the circuits used for the larger currents (normally used for determination of energy input during calorimetry) was about 3 ohms in 25,000. The effect noticed on sample No. 3 is in the direction which would be produced due to heating slightly above bath temperature,

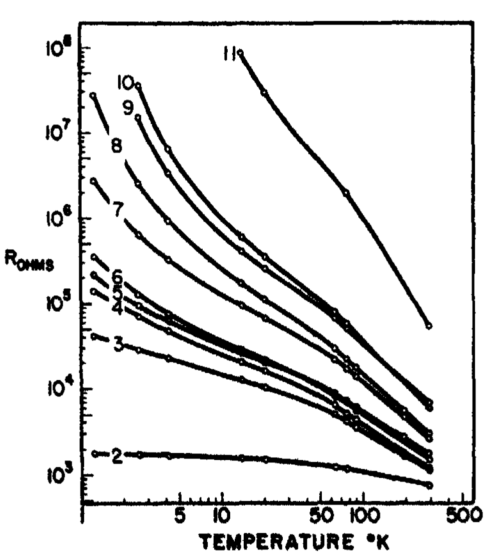

FIG. 1. Resistance *vs.* temperature for Corning electrically conducting coated glass.

TABLE II. Tests for dependence of resistance upon measuring current.

Sample No.	Temperature °K	Approximate current amp.	Resistance ohms
3	4.215	3.4×10^{-6}	22,960
		2.8×10^{-4}	22,918
		3.4×10^{-6}	22,964
	1.253	2.4×10^{-6}	41,660
		1.6×10^{-4}	41,585
		2.4×10^{-6}	41,655
5	4.215	1.8×10^{-6}	63,150
		1.0×10^{-4}	62,960
		1.8×10^{-6}	63,160
8	77.3	1.8×10^{-6}	22,998
		2.8×10^{-4}	23,000
		1.8×10^{-6}	23,008
9	77.3	2.3×10^{-6}	59,090
		1.1×10^{-4}	59,130
		2.3×10^{-6}	59,100

+0.015° at 4.215° K and +0.004° at 1.25° K. For sample No. 5 the effect at 4.215° K corresponds to +0.003° K. For sample No. 9 at 77° K, the effect is in the opposite direction to that produced by a slight heating of the sample and probably represents a real deviation from Ohm's law. The resistances of samples Nos. 8 and 9 were too large at helium temperatures to permit accurate tests. (See Table II.)

We believe these few data to be sufficiently promising to warrant further study of resistances comparable to samples Nos. 2, 3, 4 and 5.

---

* This work was supported in part by the ONR.

Improving Differential Amplifier Rejection Ratios*

RICHARD MCFEE
Heart Station, University Hospital, Ann Arbor, Michigan

March 20, 1950

A LARGE number of circuits having the differential amplifier property are known, but of these only a few have combined simple construction and operation with stable, high rejection ratios. The most important differential amplifiers are shown in Fig. 1.[1] The purpose of this note is to describe for two of these circuits some simple modifications which result theoretically in infinite rejection ratios and experimentally in rejection ratios about fifty times as great as those of the unmodified circuits. By using adjustable potentiometers in these modified circuits, their rejection ratios may be made as large as desired.

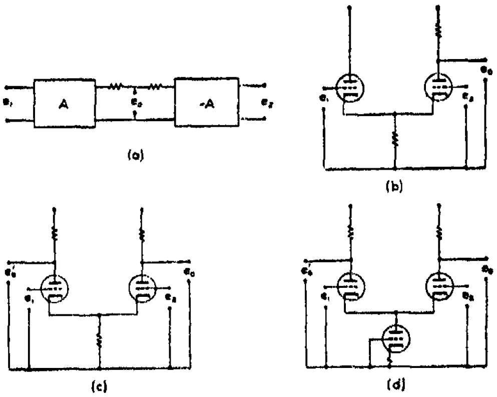

FIG. 1. Basic differential amplifier circuits.

Modification A: The first modification is shown in Fig. 2 and is obtained from the circuit of Fig. 1(b) by adding the resistor R_s. Several factors act to make the output of a modified circuit insensitive to the common-mode component of the input. There is degeneration due to cathode-follower action which reduces the effective grid voltage resulting from the common-mode component to about two percent of its actual value, and there is complete cancellation of the amplified residual e_g at the output, as can be seen from the equivalent circuit. Thus, the common-mode gain is zero, and the rejection ratio infinite. This property of the circuit is dependent only upon tube balance and equality of the cathode and shunt resistors; it is independent of the impedance of the load and the linearity of the tube characteristics.

Because tubes and resistors are in reality never precisely matched, the common-mode gain will not be exactly zero. Experimental tests indicate that using ±1 percent tolerance resistors and randomly selected 6SL7's rejection ratios from 2000 to 4000 may be expected. Of course when the d.c. plate voltages of the tubes are not the same it is necessary to change either R_s or R_k slightly to compensate for the resulting unbalance in tube gains and plate resistances, but this correction need not be variable. If a very high rejection ratio is desired, a balancing potentiometer may be added as is shown in Fig. 2(c).

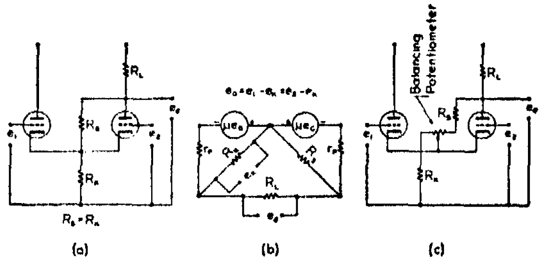

(a) (b) (c)

FIG. 2. Modification A. (a) Circuit. (b) Equivalent circuit. (c) Circuit with balancing potentiometer.

The gain of the circuit is

$$\frac{e_0}{(e_1-e_2)}=\frac{\mu R_T}{r_p+R_T},\quad R_T=\frac{R_kR_L}{2R_k+R_L}. \tag{1}$$

In the actual design of the circuit it is desirable to choose R_k and R_L so that the gain is maximum for a given tube voltage, current and plate supply voltage. It can be shown that this will occur when the d.c. voltage across the cathode resistor is one-half the total supply voltage. This condition completely determines the values of the resistors.

It is sometimes useful, in designing the circuit for use without a balancing potentiometer, to be able to calculate the common-mode gain resulting from unbalances in tube gains. An approximate equation for this is

$$\frac{e_0}{\frac{1}{2}(e_1+e_2)}=2\frac{\mu_1-\mu_2}{\mu_1+\mu_2}. \tag{2}$$

Similar equations showing the effect of mismatches in tube plate resistances and circuit resistances have been worked out.

Modification B: The second modification[2] is shown in Fig. 3 and is obtained from the circuit of Fig. 1(c) by adding the two pairs of resistors R_1 and R_2 and the resistor R_c. Zero common-mode gain results partly from cathode-follower degeneration and partly from the cancellation of the amplified residual by the bucking resistors R_2 connected from the cathode to the output. Complete cancellation occurs when

$$\frac{R_2}{R_1}=\frac{R_L}{2R_k}. \tag{3}$$

The magnitude of R_c does not affect the differential action of the circuit. It is determined by the desired tube voltages and currents, the values of the other resistors, and the plate-supply voltage.

With ±1 percent tolerance resistors and 6SL7's, rejection ratios from 2000 to 5000 are found. When an even higher rejection is desired, a balancing potentiometer may be located as is shown in Fig. 3(c).

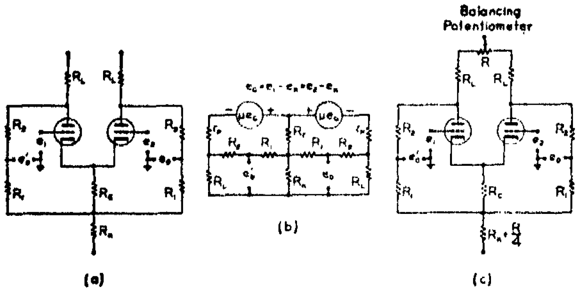

FIG. 3. Modification B. (a) Circuit. (b) Equivalent circuit. (c) Circuit with balancing potentiometer.

An equation for the gain is

$$\frac{e_0}{(e_1-e_2)}=\frac{R_1}{R_1+R_2}\frac{\mu R_T}{r_p+R_T},\quad R_T=\frac{(R_1+R_2)R_L}{R_1+R_2+R_L}. \tag{4}$$

An approximate value for the common-mode gain resulting from unbalance in tube amplification factors may be found using Eq. (2).

This circuit may be used as a differential d.c. amplifier, but it is advantageous to do so only when one stage of amplification is required, or when a single-ended output is needed. It might be noted that when $R_1=R_2$, the output is at the d.c. level of a center-tap on the plate power supply, which can be grounded. In this case the output is not affected by equal changes in the tube characteristic or emission, or by variations in the plate voltage.

Both of these circuits may be used as multipliers. Large variations of the common-mode voltage will not affect the output directly but will vary the differential gain if the tubes are nonlinear, and this variation of gain is easily used to obtain multiplication. They may also be used as simple balanced modulators.

The author is indebted to Dr. Samuel Seely of the Syracuse University Electrical Engineering Department for help in checking the equations.

---

* This work was performed under a grant from the S. S. Kresge Foundation.

[1] Differential amplifiers are discussed comprehensively in Valley and Wallman, "Vacuum Tube Amplifiers," MIT Radiation Lab. Series No. 18 (McGraw-Hill Book Company, Inc., New York, 1948), pp. 441–451.

[2] The author has learned that this circuit has been used by Dr. W. A. H. Rushton of Cambridge University, although details concerning it have not been published.

Voltage Stabilizer for 200 Kv Acceleration

J. T. DEWAN
Atomic Energy Project, National Research Council of Canada, Chalk River, Ontario, Canada

May 8, 1950

IN recent experiments with the resolved beam from a 200 kv positive ion accelerator[1] it was necessary to prevent the beam from wandering more than 0.5 mm on a target placed 100 cm from the exit face of the 90° resolving magnet. This required the accelerating voltage to be held constant to 0.1 percent despite fluctuations of 1 percent in the a.c. supply voltage.

A stabilization ratio of 40 is achieved by the method shown schematically in Fig. 1. This method is an extension of the common degenerative stabilizer[2] and is somewhat similar to that used by Parratt and Trischka[3] for stabilizing voltages up to 50 kv. Regulation is effected by a series tube capable of handling variations of several thousand volts. This is controlled by a feed-back amplifier which receives as its error signal the difference between the voltage across a small portion of the 250 megohm bleeder resistance and a stable balancing voltage. The over-all voltage constancy depends on the stability of the bleeder chain which is a precision wire-wound resistance[4] guaranteed to 0.1 percent. Power is supplied to the stabilizer from a 500 c.p.s. generator which feeds the ion source and focusing supply at the d.c. level designated G in Fig. 1.

Essentials of the regulating circuit are shown in Fig. 2, all supply voltages being referred to the cathode of the stabilizer tube. A small fraction of any output voltage variation appears across R_1, is amplified in two stages directly coupled through Type 5651 high stability neon tubes, and the amplified voltage applied to the grid of a Type 4E27 series regulating tube. As the accelerator voltage is raised from 0 to 200 kv the voltage across R_1 increases from 0 to 160 volts. Consequently a stable adjustable bucking voltage is applied, via the 6AC7 cathode follower, to allow operation of the first amplifier grid at the correct d.c. level. The magnitude of the balancing voltage is controlled by a helical potentiometer which is operated through selsyn motors from the main control panel. The stabilizer is brought into proper operation at any given accelerating voltage by simply adjusting the potentiometer until the electrostatic voltmeter across the 4E27 tube indicates 3 to 4 kv. Fluctuations in the meter up to several kv in magnitude then represent the input voltage variations which are being canceled by the stabilizer tube. In order to protect this tube and the meter from overvoltage a 6H6 diode clamp is placed at the grid of the tube. This prevents the grid being driven negative by more than 105 volts and therefore prevents the plate voltage from rising above 7 to 8 kv. The exact voltage at which the plate clamps depends on the plate current which, however, varies only between 0 and 1 ma.

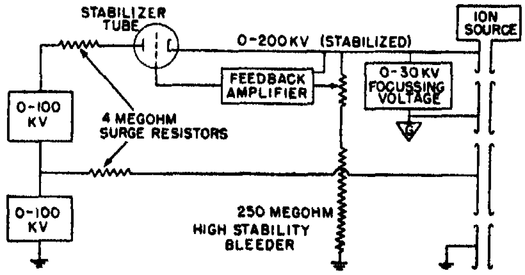

FIG. 1. Schematic diagram of the method of stabilization.

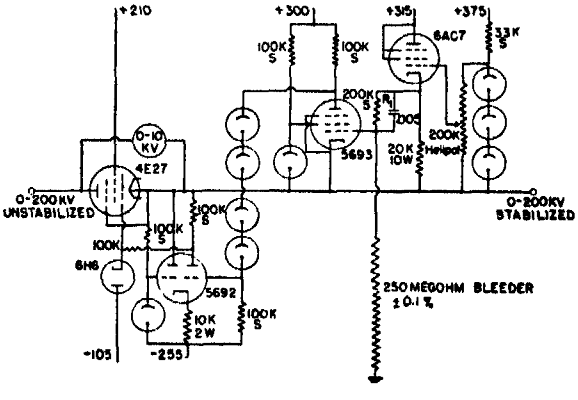

FIG. 2. Details of the stabilizer circuit. All neon tubes are Type 5651 and all resistances marked S are Nobleloy high stability 1-watt resistors.

Theoretically the stabilizer should reduce input voltage variations by a factor approximately equal to $\mu\beta G$ where μ is the amplification factor of the 4E27 tube (150), β is the feed-back factor (1/1250) and G is the gain of the amplifier (500). Thus the stabilization ratio should be 60 but in practice it is about 40. The reduction, inconsequent in this application, is caused by pick-up of stray radiation from the r-f ion source in the feed-back amplifier. With regulation, the output impedance of the accelerator is 10^8 ohms but variations in current at any given voltage are less than 10^{-4} ampere; hence fluctuations due to the high output impedance are only a few volts.

In order that the accelerator voltage should drift less than 25 volts (0.1 percent at 25 kv) over a period of about an hour it is necessary to ensure that any spurious amplifier drift referred to the 5693 grid be less than 20 millivolts. This is effected (a) by the use of iron wire ballast tubes to maintain the 5693 filament current constant, (b) by the use of high stability neon tubes to provide the bucking voltage, (c) by regulating all power supply voltages with ordinary VR tubes, and (d) by using high stability resistors wherever necessary. A final test showed the drift to be 10 millivolts in one hour.

When installed in the accelerator the circuit admirably fulfilled all requirements for regulation and simplicity of operation. Used in conjunction with a constant current supply for the beam deflecting magnet, a target spot results in which the only small fluctuations detectable may be ascribed directly to ion source variations.

---

[1] Almqvist, Allen, Dewan, Pepper, and Sanders, Phys. Rev. 79, 209 (1950).

[2] See, for example, F. V. Hunt and R. W. Hickman, Rev. Sci. Inst. 10, 6 (1939).

[3] L. G. Parratt and J. W. Trischka, Rev. Sci. Inst. 13, 17 (1942).

[4] This resistance consists of 50 XR-5 units of 5 megohms each, supplied by the Shallcross Manufacturing Company, Collingdale, Pennsylvania.

A Mass Indicator

V. J. Caldecourt
The Dow Chemical Company, Midland, Michigan
May 29, 1950

MASS spectrometers which scan by varying the magnetic field require a calibrated field measuring device to indicate the mass of the ions being recorded. The field can be measured conveniently by measuring the voltage output of a small solenoid and commutator rotated in the field by a sychronous motor. This voltage output depends on the motor speed and, if the indicating device draws current, on the commutator contact resistance.

The method shown in Fig. 1 minimizes both of these variables. To eliminate the motor speed effect, the output of the field generator of the mass spectrometer is compared to the voltage output of a permanent magnet generator driven by a second sychronous motor. Separate motor drives were used to avoid the problem of magnetically shielding the permanent magnet generator from the variable magnetic field of the mass spectrometer. The indicator actually shows the ratio of the permanent magnet field to the field of the spectrometer.

The effects of varying commutator contact resistance are negligible because the indicator is a self-balancing potentiometer with high input impedance. The modification of the Brown amplifier to attain this involves removing the input transformer and wiring the input to the first grid as shown. Since the slide wire voltage is high, no trouble from a.c. pick-up is encountered.

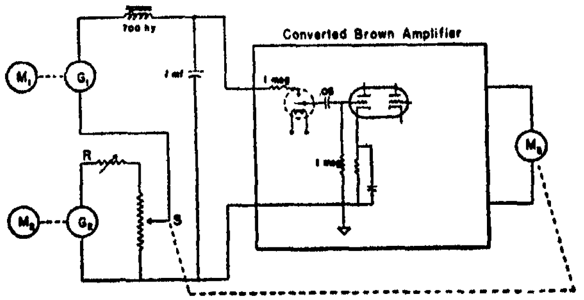

M_1, M_2—Bodine Synchronous Motors 1800 r.p.m. 1/150 hp. Type NSY-12
M_3—Brown Balance Motor
G_1—Field Generator
G_2—P.M. Generator, Elinco Type PM-2
S—Slide Wire 20,000 Ω
R—2000 Ω

FIG. 1. Mass indicator.

The mass indicator used here has a ten turn, drum-type linear slide wire, *S*, of six inch diameter with a resistance of 20,000 ohms. It is coupled to a tape scale of 35 mm film nearly ten feet long. This gives 1 cm spacing between mass 200 and 201, and the readings are steady to ½ mm. The indicator is standardized daily by adjusting *R* with the spectrometer set on a known peak.

An uncertainty results from the hysteresis effects in the spectrometer magnet in the instrument here. The flip coil is in a region of nearly uniform field and therefore is affected differently than are the ions which pass through the fringing fields as well as the uniform field between the pole faces. Probably a position could be found for the flip coil so that it also would be subject to some fringe effects, thus giving a better mass indication. In the present setup this effect causes an uncertainty of 0.2–0.3 of a mass unit if the scanning range is changed by a large factor. On running samples over the same scanning range and having standardized in that range, the indicator is accurate to one-tenth of a mass unit for the high masses and slightly better than that for the low masses.

Packless Valve Flow Regulator

Walter Rose*
Gulf Research and Development Company, Pittsburgh, Pennsylvania
May 15, 1950

THIS note describes a valve which has been found convenient to employ when low flow rates are to be controlled and when valve-stem leakage is to be avoided. Although the valve is operatable at pressures above or below atmospheric, it is implicit in the following discussion that the control of flow rate depends on maintenance of a constant pressure drop across the valve as well as on the valve plunger position determining the resistance to flow offered by the valve.

The principles of construction and operation of the valve are indicated by Fig. 1, where it is seen that the flowing fluid is directed through the porous element, *C*, fabricated from unglazed porcelain, fritted glass, sintered metal or the like. Thus, the fluid path is through entry port, *A*; thence through a portion of hole *B* drilled in the porous element; thence through a portion of the porous body, *C*; and thence out through exit port, *D*. Hole *B* opens into mercury reservoir *E*, and the position of piston, *F*, determines how much mercury will be contained in drilled hole, *B*. Obviously, if mercury completely fills the hole, no flow will occur between ports *A* and *D* unless the pressure drop between *A* and *D* is sufficient to cause the mercury to enter the pores of the porous element *C*. This critical pressure drop which must not be exceeded for the proper shut-off operation of the valve is known as the displacement pressure, and is given approximately by:

$$\text{p.s.i. displacement pressure} = \frac{2\gamma \cos\theta}{r} \times 1.45 \times 10^{-5}$$

where γ is the interfacial tension in dynes/cm between mercury and the fluid flowing through the valve, θ is the contact angle, and r is the radius in centimeters of the larger pores in the porous element, *C*. Thus, in flowing air through a valve with the porous element fabricated from 10^{-4} cm pore radius material (e.g., filtration grade porcelain) it is not difficult to achieve the positive shut-off of the valve with pressure differences between *A* and *D* of 100 p.s.i.

The operation of the valve involves changing the piston position until the mercury column position in *B* limits in the desired manner the surface area of hole *B* available to flow. Thus, for a given piston position the flow rate which obtains will be proportional to the pressure drop from *A* to *D*, to the viscosity of the flowing fluid, to the mean pressure of the fluid in *C* if the fluid is a gas, to the geometry of that portion of *C* available to flow, and to the permeability characteristics of *C*. One is enabled, therefore, to calibrate piston position *versus* flow rate for given conditions of

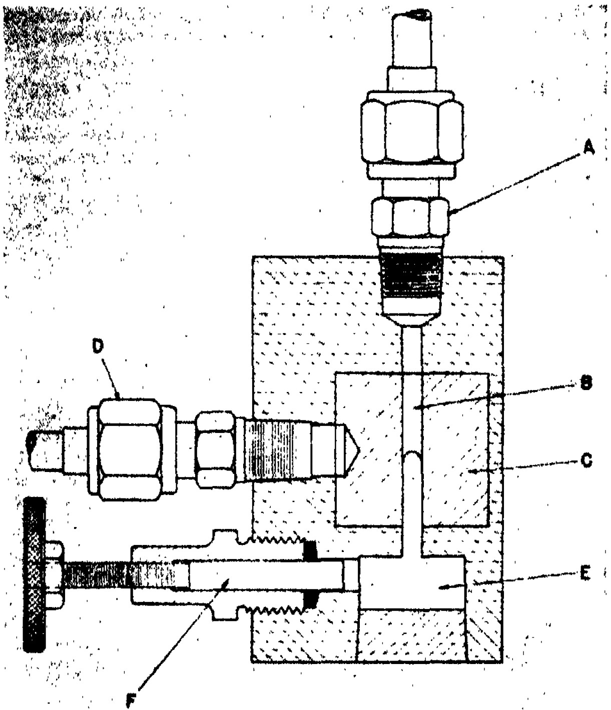

FIG. 1.

fluid viscosities and fluid pressures. It has been found possible to regulate flow rates as low as 10^{-8} cc/sec. employing filtration grade porcelain as the porous element *C*.

The valve units are comprised of porous elements molded in plastic with subsequent machining to provide for the port and piston entries. The mercury column effectively prevents fluid loss through the piston packing. When liquids are being flowed the system is evacuated initially to provide for a complete saturation of the porous element *C*. In this connection, there would be advantage in a valve assembly which would permit interchange of porous elements *C* to facilitate alternating from gas to liquid flow, as well as enlarge on the range of flow rates which could be achieved, since the flow rate is so much dependent on the permeability characteristics of the porous elements. On the other hand, no way has been found to avoid the requirement that the valve be operated in the vertical position indicated by Fig. 1, since it is necessary to prevent mercury spillage.

---

* Now with Texas Petroleum Research Committee, Austin, Texas.

New Instruments

W. A. Wildhack: Associate Editor
in Charge of this Section
National Bureau of Standards, Washington, D. C.

These descriptions are based on information supplied by the manufacturer and in some cases from independent sources. THE REVIEW *assumes no responsibility for their correctness.*

Spectrograph and Excitation Unit

A single instrument combining a large Littrow spectrograph and equipment for arc and spark excitation of spectra is available from *Optica*, Milan, Italy. The autocollimating spectrograph Model B3 has a working range from 2000 to 10,000A, obtained with quartz and glass optics easily interchangeable by means of a special revolving system. The quartz system has a working field ranging from 2000 to 3800A with reciprocal linear dispersion of 5.0A/mm at 3000A. The glass system covers the range from 3600 to 10,000A with 8.0A/mm at 5000A. The camera accommodates a 9 by 24-cm photographic plate and may be modified later to carry a film holder. Linear and wave-length scales are provided for each working range. The plate holder can be adjusted vertically by means of a lever and provision for automatic raising of the holder is available. The prism, lens, and photographic camera are automatically adjusted to the positions required for the different ranges of spectra by turning a drum. The wave-length range and central wave-length of the plate are read on a scale. The apparatus is enclosed in a metal cabinet approximately 3 meters long, which accommodates also the optical bench, arc and spark excitation equipment and a control panel.

The excitation equipment built into this instrument is also available as a separate unit. It consists of a Fuessner-type spark generator and an arc generator providing continuous and interrupted arc current. The standard model of the spark generator is equipped with 0.012 μf capacitance and a larger model with 0.024 μf capacitance. The input voltage is controlled by an adjustable transformer and the capacitance and inductance in the discharge circuit are selected by lever switches operated from the control panel. The 200-volt d.c. arc may be varied from 2 to 15 amperes, the current being obtained from a thermionic rectifier tube. The 200-volt interrupted arc is operated by a thyratron tube to supply current that may be varied from 2 to 40 amperes peak for each single impulse. The duration of each impulse is 0.001 to 0.01 second, the interval between impulses is 0.02 second, and the series of impulses can be adjusted from 1 to 200.

Optica also builds a medium quartz spectrograph, Model B2, and various accessories for spectrographic analysis and research in spectroscopy.—OPTICA S. P. A., *Via Calatafimi, 7–9, Milano, Italy.*

Gas Flow Counter

The Model 200 Gas Flow Counter is a windowless or internal-sample type Geiger counter. Samples are placed in the counting chamber by means of the circular style sample holder. Self-quenching counting gas mixture continuously flows through this chamber, through the pre-flush position chamber, and out the glass bubbler.

The Model 200 is made of stainless steel with a Teflon insulator and a platinum anode. Simple assembly and disassembly makes cleaning and thorough decontamination fast and easy. The large gas sealing surfaces are hand-lapped flat. The counting chamber is easily removable and interchangeable with other chambers. The sample holder has three positions: while one sample is being loaded, another is being pre-flushed, and a third is being counted. Because these operations are performed simultaneously rather than in sequence, the time required for the over-all counting operation is considerably less than that for single-position, straight-slide style flow counters.

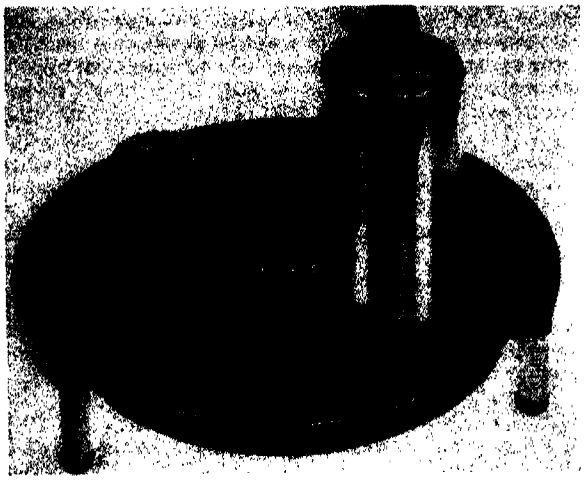

Samples up to 1⅜ in. diameter and ⅜ in. deep may be accomodated. Special stainless steel adapters will be provided to order for all smaller samples. The 1⅜ in. inside diameter of the standard counting chamber is designed to give full geometry with the maximum sample size. Special interchangeable chambers with any smaller inside diameters down to 11/16 in. will be provided upon request. By selecting a counting chamber with an inside diameter equal to your sample size, you will get the lowest background count possible without losing full geometry. The background counts without additional shielding will range approximately from 12 counts per minute with an 11/16 in. chamber to 30 counts per minute with a standard 1⅜ in. chamber. The plateau will depend upon the size counting chamber and the particular gas mixture being used. In general there will be at least 200 volts with a slope of less than 3 percent per hundred volts in the range around 1400 volts.—RESEARCH EQUIPMENT AND SERVICE, *1155 East 61st Street, Chicago 37, Illinois.*

New Stabilized D.C. Indicating Amplifier

Multi-purpose Stabilized D.C. Indicating Amplifiers just announced by Leeds and Northrup Company are useful for low level d.c. measurements as direct-reading microvoltmeters or micromicroammeters; as recorder preamplifiers to extend the range of standard Speedomax Recorders; and as high sensitivity, short-period null detectors in place of galvanometers. Amplifiers are supplied either as voltage or current type, with choice of zero-left or zero-center built-in 4-inch indicating meter.

Both gain and zero point are so highly stabilized by a combination of a.c. amplification and d.c. null-balance feedback that trimmer controls are unnecessary. Without impairing performance, the voltage amplifier can be used with sources up to 10,000 ohms resistance, and the current type with sources of 100,000 ohms and higher.

Basic range of the voltage amplifier is 0 to 50 or −25 to +25 microvolts, with scale multipliers of 1, 2, 4, 10, 20, and 40; of the current amplifier, is 0 to 1000 or −500 to +500 micromicroamperes, with multipliers of 1, 2, 5, 10, 20, 50, 100, 200, 500, 1000, and 2000. Response time of both models is 2 to 3 seconds. Output at recorder connector for full-scale input on any range is 10 millivolts at output impedance of 500 ohms.

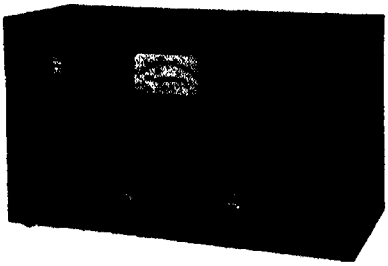

For convenience in null balance measurements, the indicating meter can be switched to non-linear response. This type of response retains full sensitivity where needed, in the region of the zero point, but gradually decreases sensitivity toward the ends of the scale, to prevent large unbalance inputs from sending the meter off scale.—LEEDS AND NORTHRUP COMPANY, *4934 Stenton Avenue, Philadelphia 44, Pennsylvania.*

Dew-Point Indicators

Three new types of dew-point indicators, designated as Types D-1, D-2, and D-3, are used for determining the moisture content of air. These instruments measure the dew point or frost point of air by indicating temperatures of a small mirror surface. The temperature is controlled automatically in a manner such that a thin film of dew or frost of constant thickness is maintained on the mirror surface at all times.

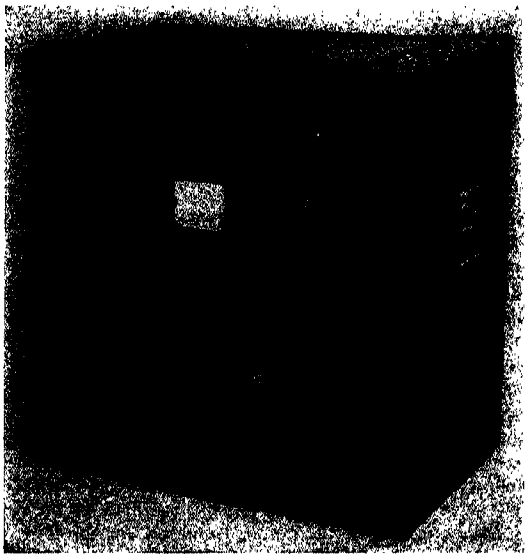

These dew-point indicators find wide application in scientific and engineering work. The Tower Unit, Type D-1, is designed for installation at airports or remote locations, such as in weather towers. It can be left unattended and is built to operate indefinitely. The Aircraft Unit, Type D-2, is made in two sections to

Dew-point indicator specifications.

	Type D-1	Type D-2	Type D-3
Response	5°C/sec.	5°C/sec.	5°C/sec.
Range	−30°C to +−40°C	−80°C to +−40°C	−80°C to +−40°C
Operation time	Indefinitely	8 hr./filling	8 hr./filling
Application	Airport and remote locations	Aircraft	Indoors
Power	110 v 60 c.p.s.	110 v 60 c.p.s.	110 v 60 c.p.s.
Weight	142 lb.	72 lb.	103 lb.
Height	23″	21″	23″
Width	21″	10″	21″
Depth	13″	15″	15″

facilitate installation in aircraft and airborne equipment. It is designed to operate for 8 hours without refilling. Laboratory Unit, Type D-3, illustrated, is most suitable for laboratory use or indoor locations and is built to operate for an 8-hour period without refilling with coolant.

Specifications on the three types of dew-point indicators are as shown in the table.

—Cook Research Laboratories, *1457 Diversey Parkway, Chicago 14, Illinois.*

Pressuregraph

The new Electro Pressuregraph has been tested and used by leading manufacturers and universities in the design and maintenance of internal combustion engines, compressors, injection pumps, and pipe lines and also in the measurement of hydraulic, gas, or explosion pressures, and the displacement of moving bodies. It accurately measures and records dynamic and static pressure variations in either gaseous or hydraulic media. Extreme versatility is made possible by its excellent frequency response and by its wide range, obtained through the use of interchangeable diaphragms. Particularly wide acceptance has been found in the Diesel and gasoline field, where its ease of installation and operation make it a cost-saving instrument in the study of intake, exhaust, and firing pressures.

The equipment consists of (1) an electronic pick-up, which is connected to the region where the pressure is to be studied; (2) an associated electronic circuit and power supply; (3) a cathode-ray oscilloscope, on whose screen the pressure-*versus*-time characteristic is presented. When used with the Syncro-Marker the Electro Pressuregraph provides three information channels on the same diagram: (a) the pressure curve which shows the pressure being measured; (b) a predetermined reference point that can be set at any angular position such as top dead-center; and (c) a choice of time or angular markers (time markers are spaced 1/60 or 1/1000 of a second; angular markers are spaced 5°).

The Pressuregraph is based on a system of carrier modulation. Carrier voltage is made to vary according to the pressure applied to the diaphragm. A 100-kilocycle carrier provides sufficiently high frequency to reproduce any pressure variations encountered in most applications. It is said to produce fullscale deflections for any pressure or vacuum from a few ounces to over 10,000 p.s.i., and to offer a wide frequency response of static to over 20,000 c.p.s. Installation is simple, requiring only a threaded hole into which the pick-up is screwed.

The Electro Syncro-Marker and Angular-Sync are designed to broaden and amplify the usefulness of the Pressuregraph by performing three important functions: 1. It makes possible quick, thorough examination of any particular portion of pressure cycles while the engine under study is in operation, and it synchronizes the horizontal time base sweep of the cathode-ray oscilloscope with rotation of the engine, making trace of the pressure phenomenon appear stationary on the screen. The synchronizer head may be rotated to trip the sweep at any position through 360°. 2. It produces 5 degree, millisecond, and reference marker signals directly on the pressure diagram. 3. It provides an identification pulse, once each revolution, which can be adjusted to coincide with that of the top or bottom dead-center, or of any other point in the rotation. This pulse may be shifted over the calibrated scale for measuring angular distances on the diagram.

The Syncro-Marker contains a 1000-cycle oscillator for generating the primary signal, electronic circuits for shaping the identification and marking signals, and for mixing these signals with the Pressuregraph output and power supply.

The Angular-Sync is a magneto-mechanical device whose shaft is coupled to that of the engine. It generates the pulse and marking signal and synchronizes the oscillograph picture with variations in the speed of the engine.—Electro Products Laboratories, Inc., *4501 North Ravenswood Avenue, Chicago 40, Illinois.*

Exposure Photometer

The SEI Exposure Photometer is a portable photometer that can be used for accurately measuring either reflected or transmitted light. No larger than a flashlight, and just about as easy to use, it makes it possible to obtain scientifically correct answers to all exposure problems. It is as valuable at the darkroom enlarging easel for determining printing exposures as it is in the studio or on location.

To the photographer and the television cameraman, the SEI Photometer offers two distinct advantages over the conventional type of exposure meter—it can be used to measure the brightness of pinpoint areas on a subject *from camera position*, and it can be used to measure brightness ranges up to one million to one. With it, a subject literally can be analyzed in terms of the reflected light as the lens sees it, and readings can be made of the deepest shadows as well as the brightest highlights.

In use, any portion of a subject—which may be only a few feet away or as much as 100 feet away from the camera—whose illumination is to be measured, is viewed through the photometer's focusable telescopic eyepiece. A dark spot is seen superimposed on the scene. The user then turns a knurled ring on the photometer's base until the brilliance of the dot, which is illuminated by a calibrated battery-powered bulb, is adjusted to match the portion of the scene or subject being measured. When the dot blends in and disappears, shutter speeds and *f*-stop openings can be read directly from scales on the photometer's main barrel.

Calibration, to compensate for battery and lamp wear, is accomplished just as easily. The light from the comparison lamp, which illuminates the dot, also illuminates a photoelectric cell connected to a microammeter mounted in the top of the photometer. Before the exposure readings, a rheostat control in the photometer's base is adjusted until the needle of the microammeter points to a central standard mark. This ability to calibrate the photometer quickly and easily eliminates the possibility of errors caused by uncontrollable variables.

The SEI Exposure Photometer is made by Salford Electrical Instruments, Ltd., England, and is now distributed exclusively in the United States by the Zoomar Corporation.—The Zoomar Corporation, *381 Fourth Avenue, New York 16, New York.*

Analascope

This new instrument provides a convenient, dependable means for measuring and continuously showing any phenomena that can be translated into electrical impulses. Heretofore, devices to measure these functions had to be custom built by researchers at considerable expense and loss of time which could be more profitably applied to their own projects.

Its possibilities as a tool of general utility in the laboratory can be appreciated from the fact that one moment it can serve as a *p*H meter which measures to 0.001 *p*H, and the next moment it can serve as an electrocardiograph, a pressure indicator, a strain analyzer, or, in fact, an instrument for measuring any phenomena converted into electrical impulses, whether static, rapidly fluctuating, or of high or low impedance.

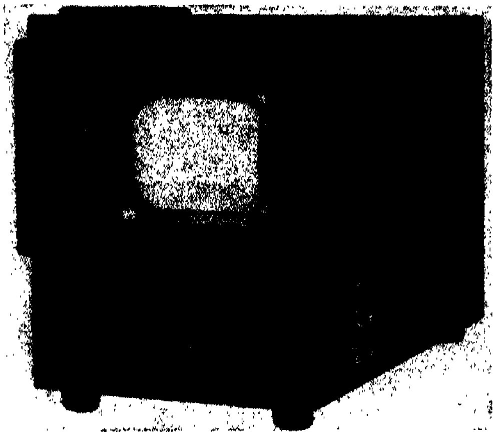

Results are displayed on the long persistence screen of a 5-in. cathode-ray tube which is an extremely flexible, indestructible indicator. It allows continuous observation of non-recurrent phenomena at sweep speeds of from 0.01 to 5 seconds. A two decade precision potentiometer calibrated with a self-contained standard cell provides direct measurements from 0.001 *p*H to 15 *p*H and 0.1 millivolt to 1.5 volts. An input attenuator of 1000 megohms provides overlapping ranges of 1 micromicroampere to 10 milliamperes and 1 millivolt to 100 volts per centimeter deflection.—Analytical Measurements, Inc., *585 Main Street, Chatham, New Jersey.*

Variable Electronic Filter

The Model 300 Variable Electronic Filter has the unusual specification of a continuously variable cut-off within the frequency range of 20 cycles per second to 200 kc. With an attenuation rate of 18 db per octave it is analogous in performance characteristics to the Constant-K inductance capacitance filter.

A range switch selects the type of section desired—high pass or low pass—as well as four decade frequency ranges. Several filters can be cascaded so that attenuation rates of 36, 54, etc. db per octave can be realized. Sections can be combined to make a variable band-pass filter.

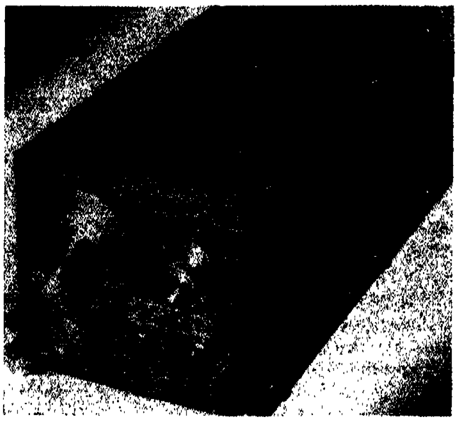

Light in weight, compact in construction, and including a regulated power supply, the Model 300 Variable Electronic Filter has many uses in the movie, radio broadcasting, television, and sound recording industries. Its low noise level and versatility make it an ideal research instrument for noise analysis or acoustic measurements in the automotive, aircraft, machine tool industry or for general laboratory use in university, commercial and government laboratories.—Spencer-Kennedy Laboratories, Inc., Department SI, *186 Massachusetts Avenue, Cambridge 39, Massachusetts.*

Manufacturers' Literature

Wheelco Comments—Vol. 9, No. 3, June, 1950, describes increased capacity on wire patenting process by use of complete automatic controls. This article won second prize in a contest sponsored by Instruments Magazine.—Wheelco Instruments Company, *Harrison and Peoria Streets, Chicago 7, Illinois.*

Special Products Digest—Vol. VIII, No. 3, June, 1950. Described and illustrated is a portable leak detector which permits inspection on the production line. It is sufficiently light and compact to be carried by an attached handle or slung on the shoulder by a strap. Among other features is a new paper tensiometer, which continuously monitors actual tension without damage to a moving sheet. For further information on above-cited and other products, write to General Electric.—General Electric, *1 River Road, Schenectady 5, New York.*

Counters—Illustrated bulletin depicting recording mechanical counters. Variable components multiply the recording possibilities for a variety of counting and timing jobs. Useful in machine shops, airports, hospitals, scientific laboratories, etc.—Streeter-Amet Company, *4101 Ravenswood Avenue, Chicago 13, Illinois.*

Controllers—Catalog 50, 28 pages, describes new developments in exhibiting and controlling flow instruments for all industries. The exhibiting instruments illustrated are flow indicators, recorders, integrators and a new pneumatic controller unit.—Fischer and Porter Company, *50 County Line Road, Hatboro, Pennsylvania.*

Servo Amplifier—A four-page folder provides details of a new servo amplifier designed to drive a control motor wound for plate to plate operation.—Transicoil Corporation, *107 Grand Street, New York 13, New York.*

Analysis Unit—Bulletin A-2, describes a quartz fiber electrometer and ionization chamber unit for measurement of radioactivity; great economy and simplicity are the principal features.—Landsverk Electrometer Company, *Pippin Road, Cincinnati 31, Ohio.*

Experimenter—Vol. XXV, No. 1, June, 1950, describes a polariscope for dynamic stress analysis, the GR Type 1534-A. Specifications are included.—General Radio Company, *275 Massachusetts Avenue, Cambridge 39, Massachusetts.*

Hewlett-Packard Journal—Vol. 1, No. 10, June, 1950, explains certain cathode-follower effects avoided with the Model 451A Bridging Amplifier, and describes the new Model 712A Regulated Power Supply.—Hewlett-Packard Company, *395 Page Mill Road, Palo Alto, California.*

CEC Recordings—Vol. 4, No. 2, 12 pages, features two new amplifiers for the Recording Measurement System D, and includes articles on improvements in velocity-type vibration pick-ups for high temperature, new 250′ oscillograph magazine, biological nitrogen fixation studies at the University of Wisconsin, and recording galvanometers.—Consolidated Engineering Corporation, *620 N. Lake Avenue, Pasadena 4, California.*

Modern Precision—Vol. 10, No. 1, Spring 1950, describes new silver-switch a.c. resistance boxes, moistureproof glass electrodes for *p*H equipment, advantages of steam treated tools, L and N Unit Load Controls, and the new Type E Electro-Chemograph.—Leeds and Northrup Company, *4902 Stenton Avenue, Philadelphia 44, Pennsylvania.*

Direct Current Multirange Kilovoltmeter—Literature states it will measure safely, accurately and at a low current drain, d.c. kilovolts up to 30 kv. It has a sensitivity of 50,000 ohms per volt with ranges of 0-3/7.5/15/30 kilovolts.—Sensitive Research Instrument Corporation, *9-11 Elm Avenue, Mount Vernon, New York.*

Cenco News Chats—No. 68, 48 pages, includes articles on the Westphal Balance, the Speedigram Balance, new Becker Balances, the use of ultraviolet in petroleum geology, a new simplified electron microscope, a new detergent for washing glassware, and other articles.—Central Scientific Company, *1700 Irving Park Road, Chicago 13, Illinois.*

Bulletin B250—Lists gearmotors, right-angle type, ⅙-hp to 5-hp-ratios, 5.8–1 to 100–1, output speeds from 17.5 r.p.m. to 302 r.p.m. Other speeds on application.—Abart Gear and Machine Company, *4828–4836 West 16th Street, Chicago 50, Illinois.*

Densichron—A booklet on the Densichron, a densitometer with a patented system of magnetic modulation, will be sent upon request to interested physicists.—W. M. Welch Scientific Company, *1515 Sedgwick Street, Chicago 10, Illinois.*

For Rent—"Rental Instruments," describes a useful service available to science and industry. Listed are such items as Recording A.C. Ammeter, Recording A.C.-D.C. Voltmeter, Recording Wattmeter, Current Transformer. Complete details with rental prices appear in the catalog, which will be mailed on request.—InstruRental Company, *411 Albee Building, Washington, D. C.*

The Perkin-Elmer Instrument News—Spring 1950, Vol. 1, No. 3, carries a description of a new technique for measuring flame temperatures in jet engines as developed for the U. S. Air Force.—The Perkin-Elmer Corporation, *Glenbrook, Connecticut.*

New Materials

Forest K. Harris: Associate Editor
in Charge of this Section
National Bureau of Standards, Washington, D. C.

Heat-Resistant Steel Castings

16–25–6 is a heat-resistant alloy containing chromium, nickel, and molybdenum, patented and trademarked by the Timken Roller Bearing Company, which has now been adapted to sand or centrifugal casting processes. Originally developed as a wrought material, the alloy has high creep resistance and rupture strength at temperatures as high as 1200–1500°F, and provides satisfactory corrosion resistance at these elevated temperatures. To keep the alloy austenitic and to assure good welding properties, the carbon content is kept to 0.12 percent or less. Comparative data on the wrought form of this alloy show a rupture time of 1000 hours under 10,000 p.s.i. stress at 1500°F, whereas the corresponding time was seven hours for 18–8 stainless steel. Exact data of a comparable nature have not been developed or the cast form of the alloy. It is of interest to note that critical materials such as columbium, cobalt, or tungsten are not used in this alloy.—Lebanon Steel Foundry, *Lebanon, Pennsylvania.*

Coated Tubing

Dekoron tubing is a low cost, corrosion-proof metal instrument tubing with a 1/32-inch coating of extruded thermoplastic. It is planned for use in laboratories and plants where there is a corrosive atmosphere. The plastic coating is stated to be unaffected by moisture, salt air, oils, acids, and alkalies. The plastic coating can be used to color-code the line. The tubing can be bent as easily as ordinary copper tubing and is available in ¼- and ⅜-inch diameters. Literature and sample lengths of tubing are available from the maker.—Samuel Moore and Company, *Mantua, Ohio.*

Coaxial Cable

Coaxitube consists of an inner conductor, a dielectric and a seamless outer tube forming an efficient coaxial cable. The components are continuous and the cable remains coaxial even when formed into intricate shapes. The dielectric can be of any commercially available material to give required electrical performance. The cable can also be used as a thermocouple, being available with an inner conductor of Copnic, Constantan or Advance wire, a suitable insulator, and a seamless copper outer conductor. Outside diameter can be controlled from 0.023 to 0.100 in. or larger.—Precision Tube Company, *3824 Terrace Street, Philadelphia 28, Pennsylvania.*

Glass Bearings

Industrial Glass Bearings are available in which glass is fused in a thickness of 5–15 mils on cast iron or low carbon steel to form an integral porcelain-enameled bearing surface. The bearing is installed with a sleeve of synthetic rubber ⅛–¼ inch in thickness, depending on service conditions. This sleeve presses over the shaft and rides in the bearing. It will operate satisfactorily with most liquids as the lubricant but should not be run dry. Custom-built bearings are available for shafts up to 12 inches in diameter to operate at speeds up to 4500 r.p.m.—Farley M. Caldwell, *1105 Richwood Avenue, Cincinnati 26, Onio.*

Coated Safety Lenses

Tuf-Cote is a preparation for coating safety lenses to make them more resistant to welding splatter and emery pitting. Its effectiveness is derived from its resilience which cushions the impact of particles striking against lens surfaces, and keeps them free from pits and scratches for a substantially longer period than is the case with untreated lenses. The process involves the patented application of a clear solution, resulting in a coating which is stated not to produce distortion, not to discolor or peel, and to afford the same degree of vision available in untreated lenses. Lenses may be recoated indefinitely so long as their surfaces are undamaged, and the coating may be applied to both surfaces of the lens. While the process is applied largely to safety glasses it may be applied successfully to prescription lenses of any curvature from −15 to +15 diopters. Lenses treated with Tuf-Cote will be available at all Bausch and Lomb sales and service divisions and affiliated offices. —Bausch & Lomb Optical Company, *635 St. Paul Street, Rochester 2, New York.*

Fluoro Carbons

Halocarbons, now in quantity production, are stabilized low polymers of chlorotrifluoroethylene in the form of oils, greases, and waxes. These products contain only carbon, fluorine, and chlorine and are inert toward corrosive agents including acids, alkalies, salts, and oxidizing agents, wet or dry. They are unaffected by prolonged heating in air at 480°F.

The presence of unstable structures and of hydrogen in the molecules of ordinary lubricants and plastics causes their decomposition by corrosive chemicals and by air at high temperatures. By synthesizing compounds containing only carbon, fluorine, and chlorine, products are obtained that are in many ways more inert than graphite itself. In addition to the well-known fluorinated refrigerants and the high melting point fluorinated plastics the present line of oils, greases, and waxes completes the range of fluorinated analogs of hydrocarbons available for industrial use. They make available a number of lubricants and coatings which are not attacked by corrosive products, and their resistance to oxidation at high temperatures permits their use, with or without inert bodying agents, as bearing lubricants in high temperature installations. Laboratory uses include inert stopcock greases, sealing cements, diffusion-pump oils, and manometer liquids. In the field of plastics their use as softeners of fluorocarbon plastics in molding and coating operations is of interest. Their use yields a molding mix which can be readily melted and formed without the decomposition usually experienced in fabricating the pure plastic. —Halocarbon Products Corporation, *2012 88 Street, North Bergen, New Jersey.*

Chemical Developments

Sterox CD is a re-wetting agent developed to increase the absorbency of paper toweling and tissues. Industrial toweling is usually strengthened with materials that reduce its absorbency. This is restored by the re-wetting agent. It may also be added to soft household toweling to prevent loss of absorbency with age and to improve moisture pick-up. This chemical, used in minute amounts as an additive, is stated to be odorless and harmless.

OS-16 is a hydraulic fluid with a favorable combination of properties. Chemically it is an ester base compound, containing no halogenated hydrocarbons, salts or water. It is non-toxic, flame-resistant and has excellent lubricating qualities. During a three-month test period it was used in a heavy-duty, hydraulically operated, coal-cutting machine on a 24-hour day, three-day week schedule. The operating pressure was 1500 p.s.i. At the conclusion of the test the machine was disassembled, and examination showed no evidences of wear in pumps and all other parts which were in contact with the hydraulic fluid. This fluid generally requires the use of special hose, packing and gasket materials. Its viscosity is 11.05 c.s. at 100°F and 2.65 c.s. at 210°F. Its flash point is 435°F.—Monsanto Chemical Company, Organic Chemicals Division, *St. Louis 4, Missouri.*

Static Eliminator

The Model B Neutra-Stat eliminator was designed to dissipate static charges from materials being weighed on delicate analytical balances. It employs polonium to irradiate the balance inclosure with alpha-particles which ionize the air and discharge all nearby surfaces. The unit can also be carried in the hand and passed over a charged object or area to remove any static charge.—E. Machlett and Son, *220 East 23 Street, New York 10, New York.*

THE
REVIEW OF SCIENTIFIC
INSTRUMENTS

VOLUME 21, NUMBER 9 *SEPTEMBER, 1950*

A Machine for Synthesizing Two-Dimensional Fourier Series in the Determination of Crystal Structures*

H. SHIMIZU, P. J. ELSEY, AND D. MCLACHLAN, JR.
Department of Metallurgy and the Engineering Experiment Station, University of Utah, Salt Lake City, Utah

(Received February 6, 1950)

An electromechanical analog machine is described which performs a two-dimensional Fourier synthesis for use primarily in x-ray crystal structure calculations,

$$\rho(xy)=\sum_h\sum_k F_{hk0}\cos 2\pi(hx+ky).$$

The analog to a term in this summation is obtained through the use of a pair of selsyns as a synchro-variable transformer somewhat similar to its use in servomechanisms. $\rho(xy)_{hk}$ is represented by the output voltage, F_{hk0} by the input voltage, and $2\pi hx$ and $2\pi ky$ are the angles of rotation of the primary and secondary rotors respectively. A system of crossed shaft and cascading gear trains turns the rotors to the appropriate angles for each selection of point (x, y) in the unit cell. The present machine handles h and k values up through 8, but provision is made for future extension through 16. Computations are shown for two known structures to indicate the results obtainable with the machine.

INTRODUCTION

Although any machine capable of synthesizing two-dimensional Fourier series may be applied to a variety of problems, such as heat flow and vibrations in thin membranes, the present machine is to be described on the basis of its utility in Fourier projections as applied in the study of crystal structures using x-ray data. It may be well to state that the data are obtained in the form of diffraction spots from the x-ray film of the moving film types of camera, such as the Weissenberg camera. From a so-called zero layer line x-ray picture the positions of the spots enable the investigator to assign two indices, h and k, to each spot, and from the intensity of each spot an amplitude factor or coefficient, F_{hk0}, is deduced. The solution of the structure of a crystal in two dimensions implies the computation of the electronic density (that is, the number of electrons per square angstrom) over the entire area of unit of projection. The computation is accomplished by introducing the x-ray data (in the form of h, k, and F_{hk0}) into a Fourier equation of the type

$$\rho(xy)=\sum_h\sum_k F_{hk0}e^{2\pi i(hx+ky)}. \tag{1}$$

In the case of centro-symmetric structures, this equation is of the form

$$\rho(xy)=\sum_h\sum_k F_{hk0}\cos 2\pi(hx+ky). \tag{2}$$

Although the machine under discussion is in the process of being extended to utilize h and k values up through 16, in its present state it is capable of handling only h and k values up through 8. Equation (2) indicates the computation which the machine performs.

Some of the principles of this machine were presented by Dan McLachlan as part of a paper before the American Society for X-Ray and Electron Diffraction at Lake George, New York, June 11, 1946, at which time a scheme was shown for mechanically coupling Maxwell's[1] variometers so that use of them may be extended to two dimensions. The present machine makes use of selsyns† instead of variometers because of their availability, small size, low cost, and adequacy of magnetic shielding.

PRINCIPLES OF THE MACHINE

In its original form, Maxwell's variometer consists of a long stationary primary coil within which are mounted

---

* This paper was prepared as a partial fulfillment of the requirements for the degree of Doctor of Philosophy for H. S.

[1] L. R. Maxwell, Rev. Sci. Inst. 11, 47 (1940).

† Selsyn is one of the trade names which has come into common usage for synchros or self-synchronous repeaters. Other trade names are Autosyn, Teletorque, Diehlsyn, etc.

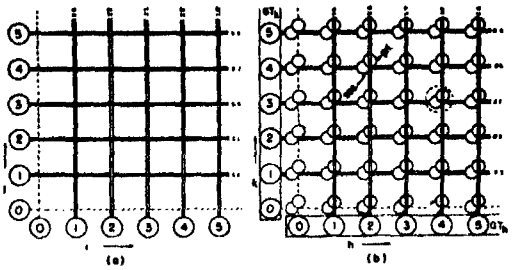

FIG. 1. The arrangement of (a) shafts for a two-dimensional array of variometers and (b) shafts and selsyns for a two-dimensional array of selsyns.

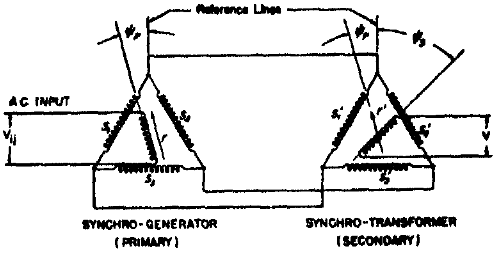

FIG. 2. The synchro-transformer system.

two identical secondary coils, one free to rotate (the rotor) and the other fixed (the stator). The output of the secondary rotor generates a potential which is a sinusoidal function of the angle of rotation while the secondary stator produces a constant potential equal to the amplitude of the rotor potential. These secondary rotor and stator coils are connected in series with each other and with those of additional variometers for the higher harmonics to obtain a one-dimensional Fourier summation of the type

$$V=\sum_{i=1}^{n} kV_i'(1+\cos i\varphi), \tag{3}$$

where V is the total output voltage, k is the inductive coefficient, V_i' is the input voltage to the primary coil of the ith variometer, and φ is the angle of rotation of the first variometer. The proposal made at Lake George extended the use of variometers to a two-dimensional synthesis of the type

$$V=\sum_i\sum_j kV_{ij}'[1+\cos(i\varphi_p+j\varphi_s)], \tag{4}$$

where i and j are integers taking values 0, 1, 2, 3, $\cdots$ with the exception $ij=00$ and where φ_p and φ_s are the angles of rotation of the first primary coils and first secondary rotor coils respectively. To accomplish this synthesis it is necessary that the primary coil also rotate about the same axis but independently of the secondary rotor. A system of parallel shafts emerging from two gear trains, one set perpendicular to the other, controls the rotations of the coils. Thus in Fig. 1(a) the variometers are mounted at the intersections of the shafts with the vertical shafts turning the primary coils to the angle $i\varphi_p$ and the horizontal shafts turning the secondary coils $j\varphi_s$.

The net shown in Fig. 1 is not new, having been suggested by Robertson[2] in connection with a machine for synthesizing two-dimensional Fourier series wherein pistons were driven sinusoidally into cylinders containing oil and the summation accomplished by measuring the total oil displaced.

In the present machine, a pair of selsyns is used in place of each variometer, see Fig. 1(b). Selsyns are essentially two-pole three-phase alternating current generators or synchronous motors and for most purposes used in pairs. Their conventional use is in remote positioning or indicating in which case the a.c. input is applied to the rotors of both selsyns, the generator whose rotor is driven and the motor whose rotor follows in synchronism. A second common use for selsyns is as synchro-control transformers used in conjunction with servomechanisms in which case the a.c. input is applied only to the rotor of the first selsyn or generator. Any voltage produced in the rotor of the second selsyn or transformer represents an error and is amplified and fed into a servo-motor which turns the transformer rotor shaft and other mechanisms to correct the error. For the purpose of the calculator, however (see Fig. 2), the selsyns are used in a third manner (as a synchro-variable transformer) in which the rotors of the generator and transformer are driven independently while a given voltage V_{ij}' (Eq. (4)) is applied to the generator rotor and the output voltage is measured. With the generator rotor in the position indicated in Fig. 2 a magnetic field r is induced in the direction of the poles of the rotor. This field causes currents in coils s_1, s_2, and s_3 of the generator which are transmitted to coils s_1', s_2',

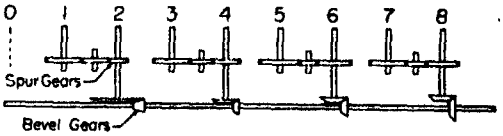

FIG. 3. The gear train.

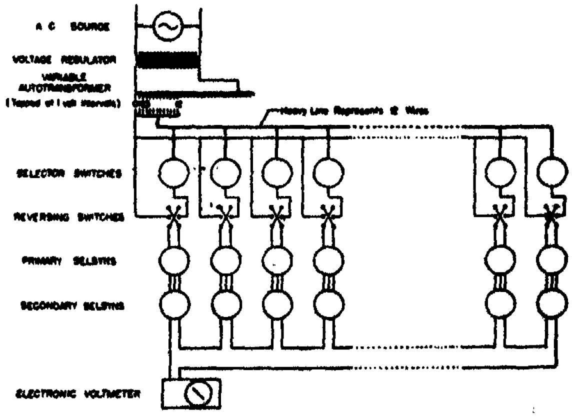

FIG. 4. The electrical circuit.

---

[2] J. M. Robertson, Phil. Mag. 13, 413 (1932).

and s_3' of the transformer which in turn induce a field r' in a direction corresponding to the field r of the generator. When the poles of the transformer rotor are in the direction parallel to r' the output is a maximum and when perpendicular the output is zero. At any position of the rotors the output voltage varies according to the equation

$$V_{ij}=kV_{ij}'\cos(i\varphi_p+j\varphi_s), \tag{5}$$

where symbols are as previously defined. This equation is directly analogous to a term of Eq. (2),

$$\rho(xy)_{hk}=F_{hko}\cos 2\pi(hx+ky), \tag{6}$$

where the output V_{ij} represents the electronic density $\rho(xy)$ due to the hk term, kV_{ij}' represents the structure factor F_{hko}, and where i, j, φ_p, and φ_s are analogous respectively to h, k, $2\pi x$, and $2\pi y$.

As mentioned for the proposed use of the variometers, a network of shafts (Fig. 1(b)) is placed so that the vertical shafts turn the primary rotors $2\pi hx$ radians and the horizontal shafts turn the secondary rotors $2\pi ky$ radians corresponding to the h and k values of each selsyn pair. For example the pair in the dotted circle of Fig. 1(b) would achieve the angle $2\pi(4x+3y)$. If separate potentials proportional to F_{hko} are applied to the primary rotors of the respective h, k selsyn pairs and if the output potentials of all the transformers are summed in series, the resulting potential will be proportional to the summation in Eq. (2). Thus through proper calibration of the voltmeter, the electronic density, $\rho(xy)$, may be obtained directly for any desired point, x, y.

Again the use of selsyns as variable transformers is not new. Booth[8] states that the use of selsyns was con-

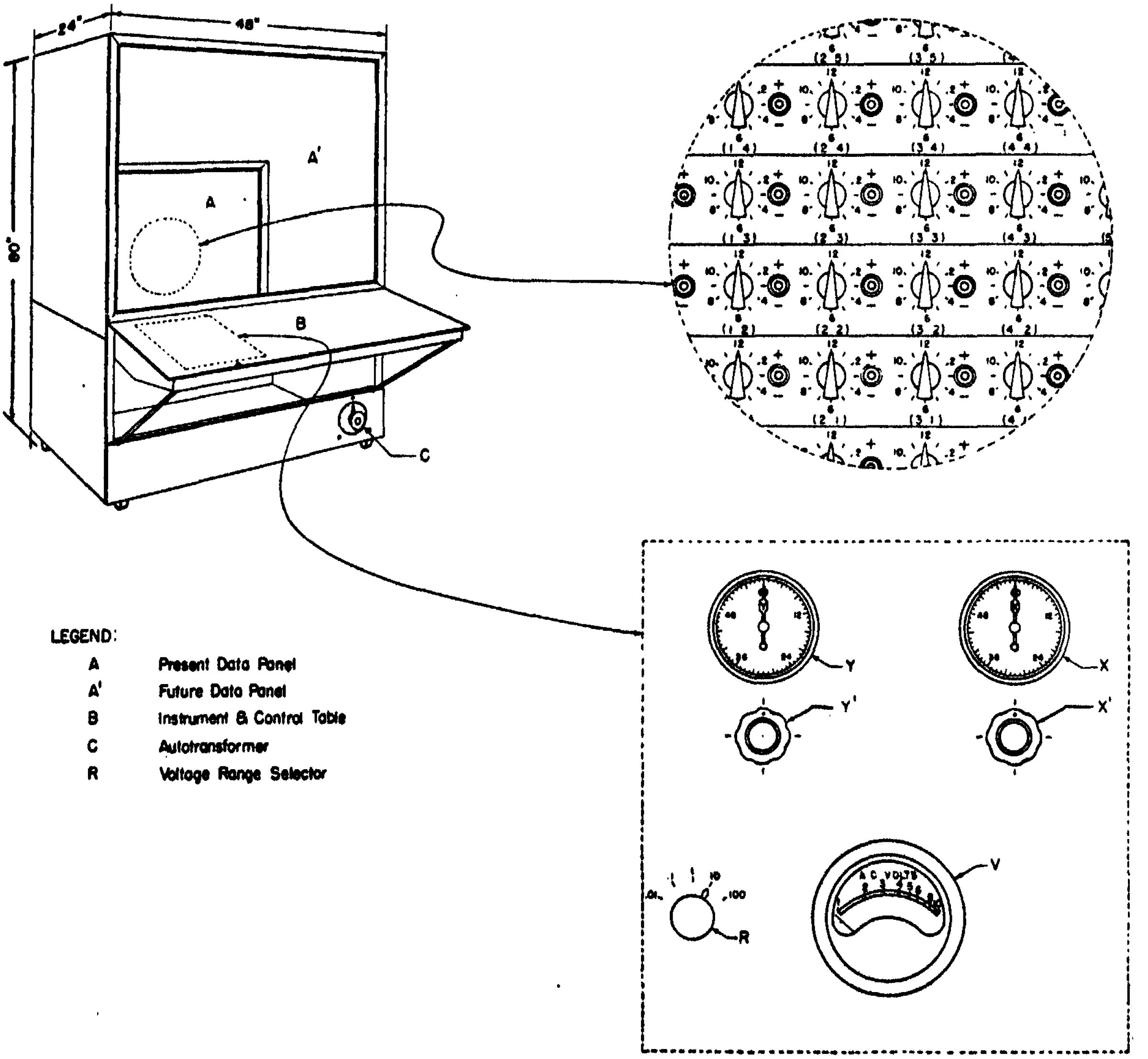

FIG. 5. An external view of the machine with dimensions.

---

[8] A. D. Booth, *Fourier Technique in X-ray Organic Structure Analyses* (Cambridge University Press, London, 1948), p. 82.

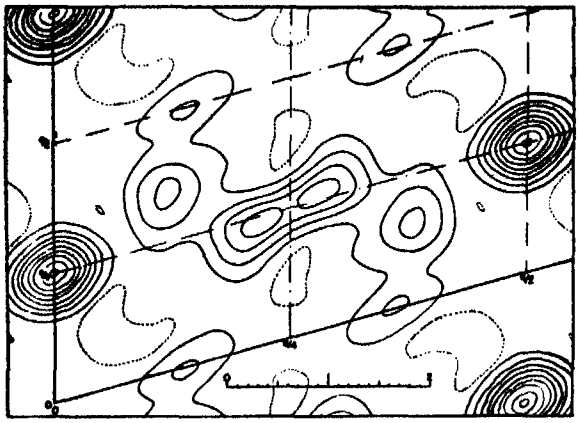

FIG. 6. The *b*-axis projection of diopside.

sidered in connection with his machine but the high cost precluded their use. Also Pepinsky[4] describes the use of selsyns in synchronizing sweep frequencies on the screen of the cathode-ray tube of his machine.

CONSTRUCTION OF THE MACHINE

The most important parts of the mechanical system of the calculator are the two nearly identical gear trains, GT_h and GT_k (Fig. 1(b)), one on the primary rack and the other on the secondary rack. The arrangement of gears is shown diagrammatically in Fig. 3 with numbers assigned to indicate ratios of shaft rotations with respect to each other. For example, all primary selsyn rotors of column 1 (Fig. 1(b)) rotate 1 revolution while those of column 2 rotate 2 revolutions, etc. All the rotors of the secondary selsyns of row 1 rotate 1 revolution and those of row 2 rotate 2 revolutions, etc. The main drive shaft of each gear train is turned manually from the instrument and control table (see Fig. 5) as a consequence of selecting positions x, y in the unit cell.

The crossed shaft arrangement as shown in Fig. 1(b) requires a separate series of selsyns for each value of h and of k in Eq. (2), the h or primary series being arranged vertically and the k or secondary series arranged horizontally in the machine. To provide this, the selsyns for each series are mounted along an angle-iron and connected by miter gears to a common shaft running the length of the angle-iron. The angle-irons are mounted in their respective positions in the primary or secondary rack and the shafts of each series of selsyns connected to their respective gear train shafts. These connections are made by means of multijaw couplers to facilitate assembly and adjustments and to provide for independent removal of each angle iron carrying its series of selsyns.

The primary and secondary racks were constructed in two separate frameworks. Cord-end plugs and sockets were used for electrical connections from the front to the primary rack and also between the primary and secondary racks, thus permitting independent removal and insertion of the entire racks. The plugs and sockets also facilitate testing and checking individual selsyns.

Figure 4 shows the basic electrical circuit for the machine. The a.c. voltage supply is held constant by means of a voltage regulator. Voltages from 0 to 12 in approximately one-volt steps, representing the structure factor coefficients, F_{hk0}, are applied to the primary rotor by means of 12 point single pole rotary switches on the data panel. The voltages are obtained from 12 taps on a variable autotransformer. The input to this transformer is through the slide contact to permit adjustment of the voltages. The input to each primary rotor can be reversed by means of a d.p.d.t. switch. The resulting 180° phase shift provides for the negative values of F_{hk0}. The "off" position of the d.p.d.t. switch serves as the "zero" which was not provided by the rotary selector switch.

The secondary selsyn rotors are connected in series so that the total voltage is the algebraic sum of all the rotor voltages. Because of the high impedance in the secondary circuit an electronic voltmeter is used to measure the output voltage.

OPERATION OF THE MACHINE

The appearance and dimensions of the machine are shown in Fig. 5. The structure factor data are applied to the machine through the rotary switches which are shown in the dotted circle insert to the panel. To the right of each rotary switch are the d.p.d.t. switches for the selection of signs and also for the "zero" structure factor not provided by the rotary swtiches. The (hk) values are marked below each rotary switch to aid the operator when setting up the machine for calculation. The structure factor values are applied as one of twelve values from a simple conversion table letting the largest F_{hk0} value assume the twelfth position of the rotary switches.

When the data have been applied and machine turned on, the voltage representing the electronic density value is read on the voltmeter V for each position (xy) which in turn is selected by knobs X' and Y' and indicated by dials X and Y of Fig. 5. These

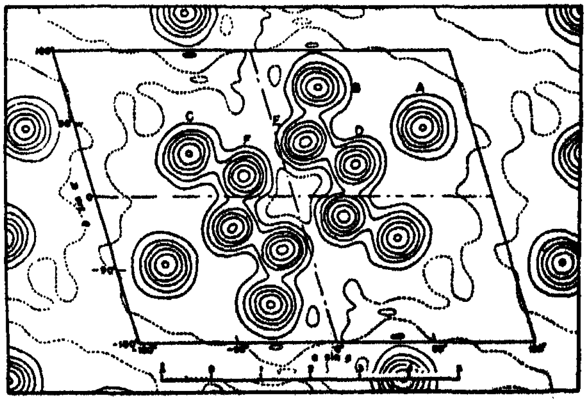

FIG. 7. The *c*-axis projection of hexamethylbenzene.

---

[4] R. Pepinsky, J. App. Phys. 18, 601 (1947).

instruments and control knobs are located on the instrument and control table as shown in the dotted rectangle inset. The dials are divided into 60 parts as a result of traversing the unit cell in 60 increments. This restriction of cell positioning may be removed at any time by disengaging a ratchet in each of the gear trains. The knob rotates a 1/4 turn for a movement of one division of the dial needle. The knobs turn the main gear train shafts directly by means of flexible shafting.

To ascertain the usefulness and accuracy of the machine, calculations were made on two known structures using the data of the original investigators. The first was that of one of the projections of diopside determined by Bragg.[5] The contour map obtained by use of the machine in a *b*-axis projection shown in Fig. 6 is in very close agreement with that of Bragg's. Although numerical comparison, point for point, cannot be made (since Bragg used intervals of 1/48 unit cell dimensions instead of 1/60), interpolation reveals satisfactory operation of the machine. As in the original work, a contour interval of 40 was used.

The second test was made on hexamethylbenzene based on the data of Brockway and Robertson.[6] Since the machine handles only Miller indices up through 8, there were two structure factor values that could not be included. However, these were of minor magnitude and the effect of omitting them is considered negligible. Figure 7 shows the *c*-axis projection of hexamethylbenzene obtained through the machine. The lines were drawn at equal density intervals from uncalibrated results, but the interval may be taken as approximately 60 with the values for the dotted lines being about 30. The carbon atom positions taken from this map are tabulated and compared with Brockway and Robertson's values in Table I.

FACTORS AFFECTING ACCURACY

The accuracy of the machine is dependent upon (a) backlash in the gears, (b) the accuracy with which the structure factors can be applied, and (c) the uniformity in the construction of the selsyns for their use as variable transformers. In adjusting the gear spacings the decrease in backlash must be weighed against the tightness of meshing to obtain optimum operating conditions. The use of only twelve discrete voltages rather than a continuous one has its effect on accuracy, but if the twelfth point of the rotary switch is used for the highest value of the structure factors, the error for the others with respect to this value is one-half of one-twelfth or about 4 percent. This is of sufficient accuracy for most structure calculations, the degree of accuracy in locating the positions of the atoms being of a much higher order. To offset the non-uniformity in the construction of individual selsyns, an attempt is made to match the selsyns to obtain equality of transformer characteristics from one pair of selsyns to another. The variations resulting from fluctuations in the line voltage are eliminated by the voltage regulator in the power supply.

TABLE I. Position of carbon atoms in hexamethylbenzene.

Atom	Brockway and Robertson x/a	y/b	Machine x/a	y/b	Difference x/a	y/b
A	0.371	0.234	0.371	0.233		−0.001
B	0.144	0.379	0.142	0.375	−0.002	−0.004
C	−0.227	0.1455	−0.226	0.147	0.001	0.0015
D	0.1775	0.111	0.178	0.113	0.0005	0.002
E	0.685	0.180	0.683	0.182	−0.002	0.002
F	−0.108	0.169	−0.110	0.070	−0.002	0.001

Since many structures require F_{hk0} values where *h* and *k* exceed eight, it is planned to extend the machine to receive values to 16 and also provide for one of the Miller indices to be negative. Also since the speed of the present machine is limited to the rate at which a person can write down the answers, a means for automatic recording of contour intervals is being developed.

ACKNOWLEDGMENTS

The authors wish to express their gratitude for a grant from The University of Utah Research Fund which made this work possible, to Dean C. J. Christensen of the College of Mines and Mineral Industries and to Dr. J. R. Lewis, Head of the Department of Metallurgy, for their continued encouragement and valuable suggestions, to Dr. J. Hugh Hamilton, Director of Utah Engineering Experiment Station, for use of tools and machine shop facilities, and to Mr. Hardy Felt for his ready assistance and suggestions.

---

[5] W. L. Bragg, Proc. Roy. Soc. 537 (1929).

[6] L. O. Brockway and J. M. Robertson, J. Chem. Soc. (London) 1324 (1939).

THE REVIEW OF SCIENTIFIC INSTRUMENTS VOLUME 21, NUMBER 9 SEPTEMBER, 1950

The Scintillation Efficiency of Anthracene for Low Energy Electrons

W. J. RAMLER AND M. S. FREEDMAN
Argonne National Laboratory, Chicago, Illinois

(Received January 11, 1950)

The efficiency of an anthracene scintillation counter used as the detector in a double magnetic lens beta-ray spectrometer for electrons in the range 0–20 kev has been determined. Monoenergetic electrons generated by an electron gun were focused on the anthracene crystal, the beam being concurrently monitored by an electron collector and electrometer. The results are shown in Fig. 4.

THE comparative efficiency for low energy electrons of a scintillation counter employing a thin anthracene crystal as scintillator has been determined. The scintillation counter has been used for over a year as the detector in the double lens β-ray spectrometer constructed in this laboratory.[1] Recent investigations of very low energy spectra[2] have shown that β's were being counted at energies as low as 500 ev. The primary purpose of the experiments described here was to obtain the relative efficiency as a function of β-energy in the experimental arrangement used in the spectrometer, which efficiency may then be applied to obtain corrected β-energy distributions.

EXPERIMENTAL PROCEDURE

The experiment was performed by counting scintillations induced in the anthracene counter by a monoenergetic electron beam and simultaneously monitoring the beam intensity with an electron collector and vibrating reed electrometer. The apparatus is shown in Fig. 1, and enlarged views of the collector and crystal in Fig. 2, and of the electron gun in Fig. 3. An electron beam is furnished by the electron gun driven by a 30-kv voltage supply, the gun being mounted in the source position in the double lens spectrometer. The gun consists of a tungsten hairpin filament shielded by a highly polished platinum cup, and a conical polished brass anode. All insulation is fused quartz. It was found that zinc vapor was evolved from a brass filament shield, which led to breakdown in a short time for accelerating voltages greater than 10 kv. At a pressure of 5×10^{-6} mm Hg, accelerating potentials of over 25 kv could be maintained with negligible field emission.

The most intense part of the electron beam is projected along the axis of the spectrometer where it is intercepted by baffles. Because of the defocusing actions of the conical electrostatic lens anode and of space charge, a small fraction of the beam diverges sufficiently to be focused by the spectrometer at the adjustable ring focus baffle, B_2. Baffle B_2 is set to a very narrow annulus, so that light from the incandescent gun filament is effectively shielded from the scintillation counter.

The focused beam impinges on the electron collector, and a fraction ($\sim$1 percent) passes through the central hole onto the anthracene crystal. The angle at which the beam enters the central hole is such that it cannot touch the wall, so no secondary electrons can reach the crystal. Secondary electrons produced in the collector tubes are recollected with an observed efficiency of >85 percent (probably greater than 98 percent) over the range 0–20 kev of primary electron energy.

The thin anthracene single crystal (0.1 mm) was grown by sublimation in a helium atmosphere, and the 1-mm thick crystal was cleaved from a large single

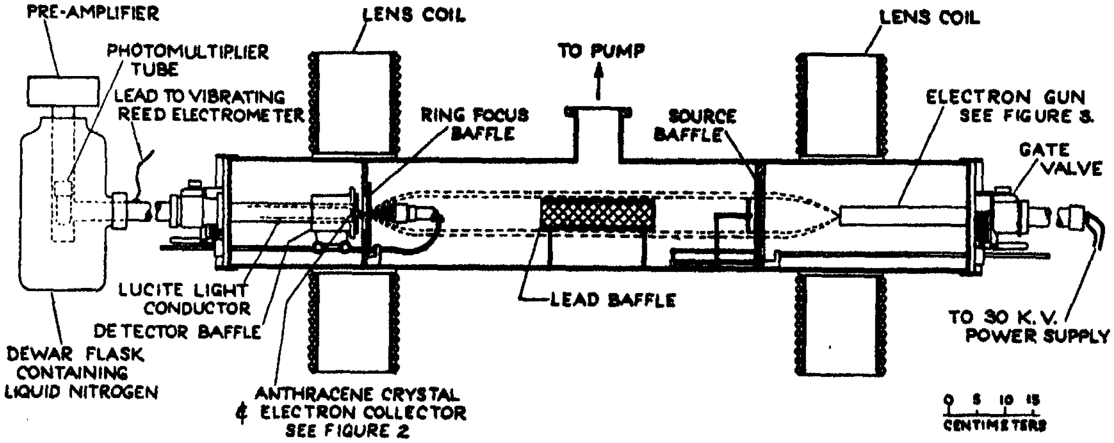

FIG. 1. Double lens β-ray spectrometer.

---

[1] To be published.

[2] To be published. $Ac^{227}-E_{max}=40.5$ kev. $Ru^{106}-E_{max}=35.7$ kev.

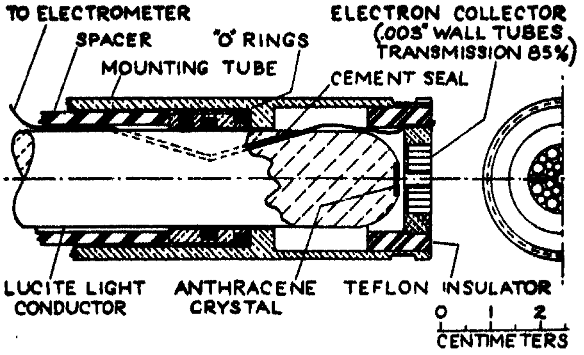

FIG. 2. Detector tube.

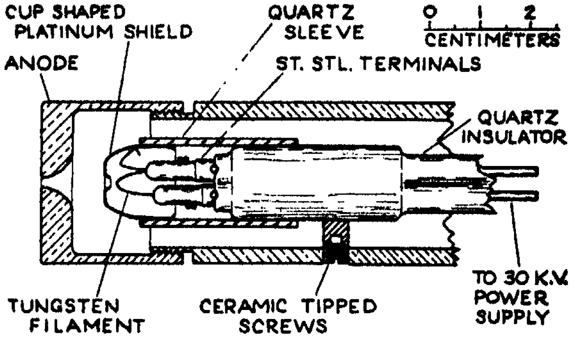

FIG. 3. Electron gun.

crystal grown from the melt. Both crystals were clear blue-white and showed only faintly the bands due to naphthacene fluorescence with either ultraviolet or x-ray excitation.[3] The crystals are cemented to the Lucite light pipe, which is shaped hemispherically[4] to collect photons ejected tangentially to the crystal surface. Photons are piped with a geometrical efficiency of ~10 percent to the 1P21 photo-multiplier, which is maintained at −196°C in a Dewar, and shielded from the magnetic field of the lens coil. Since Lucite fluoresces well at −196°C[5] and so enhances the background count due to cosmic rays, the last few inches of the light guide inside the Dewar consists of an aluminum foil cylinder. With 1200 v on the photo-multiplier, well up on the plateau for pulses due to single photo-electrons from the photo-cathode, the background is about 40 c/m. With the gun filament on, the stray light increased the background to a few hundred counts per minute.

Amplified pulses from the 1P21 are recorded by a logarithmic counting rate meter and chart recorder as is the output of the vibrating reed electrometer. As the current through the spectrometer lens coils is controlled by a motor driven potentiometer, the current may be swept continuously through the range corresponding to the energy being emitted by the gun, and the profiles of the "line" received on both scintillation counter and electron collector may be simultaneously recorded. This is necessary as it is difficult to ensure extremely steady emission from the tungsten filament. Furthermore it ensures against a change in the spatial distribution of the gun emission pattern appearing as an altered ratio of the electron current on the collector to that on the crystal, because the pattern is swept across both by the varying magnetic field. The emission is adjusted to give counting rates in the range 5000 to 35,000 c/m and collector currents of 10^{-14} to 10^{-12} amp. At all energies investigated the lines were sharp, indicating clean separation from low energy scattered electrons in the beam.

RESULTS

The relative counting efficiency, defined as the ratio of the peak counting rate to peak collector current, as a function of electron energy is shown in Fig. 4. Curve *A* is for a "thick" crystal (1 mm) which was somewhat "frosted" on its surface due to partial evaporation of the anthracene in the vacuum.[6] Curve *B* is for a thin (0.1 mm) clear single crystal. The curves are normalized to 100 percent counting efficiency at the horizontal asymptote. Data were not obtained for curve *B* for energies below 1.5 kev because of the more rapid drop in efficiency.

It was anticipated that the frosted surface of the thick crystal would result in light losses for the lower energy electrons. The higher efficiency of the thicker crystal at very low energies is thus as yet unexplained, as is the very rapid drop off in efficiency at low energy for both. It appears that the specific efficiency of the anthracene for the production of ~3-ev fluorescence photons (photons/kev) is sensitive to primary electron energy in the region of a few kilovolts.

That the sharp drop in efficiency of production of photons is due to an insensitive surface layer on the crystal seems ruled out because the surface is continually renewed by the evaporation of the anthracene. Contamination of the crystal surface from residual vapors such as silicone diffusion pump oil in the vacuum system is eliminated as the cause since there is no progressive lessening of the efficiency with time.

The data of curve *A* are shown on a log-log scale in Fig. 5. Where the efficiency is low there is only a small probability that more than one photo-electron will be ejected from the photo-cathode, so the efficiency will be closely proportional to the number of photons generated per incident electron. It may be seen from Fig. 5 that the curve is asymptotic to the relation:

Number of photons = constant $(\text{volts})^{3.8}$. Similar relations have been observed[7] for some inorganic phosphors, such as zinc orthosilicate, zinc sulfide, and calcium tungstate, with values for the exponential factor of 2.0, 2.8, and 2.0, respectively. If this relation is

---

[3] E. J. Bowen and E. Mikiewicz, Nature 159, 706 (1947).

[4] The angle for total reflection in Lucite is 42°, so all the light emitted into the Lucite from a small source on the hemispherical surface will be internally reflected down the light pipe.

[5] M. S. Freedman and B. Smaller, ANL-4288, p. 52.

[6] Anthracene crystals 1 mm thick have been found to last 3 to 4 weeks at high vacuum before complete sublimation.

[7] W. B. Nottingham, J. App. Phys. 10, 73 (1939).

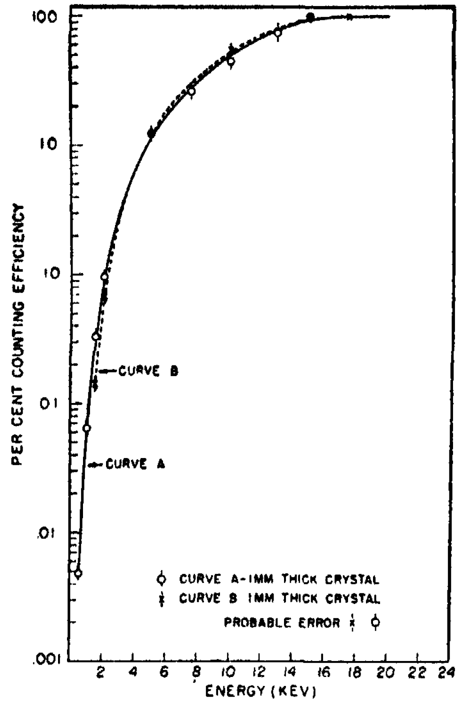

FIG. 4. Relative counting efficiency.

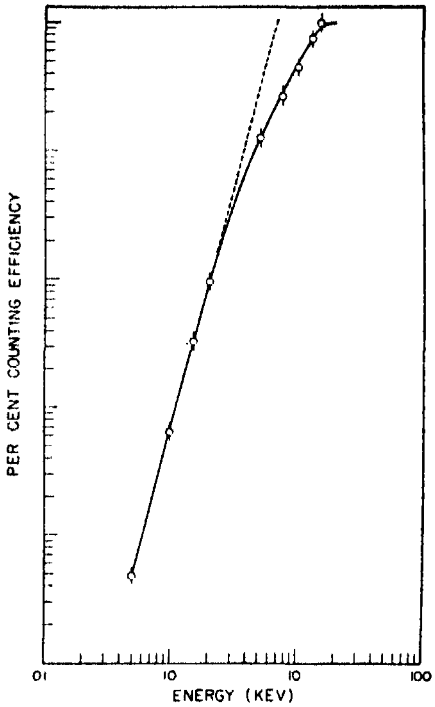

FIG. 5.

assumed to hold for energies somewhat higher than 15 kev, it follows that the counting efficiency curve will change only slightly with changes in the light-gathering efficiency, because of the rapid variation of light emission with energy.

From estimates of the light-gathering efficiency and the value of the photo-electron yield of the photomultiplier (supplied by the manufacturer) the efficiency of anthracene to electron energies in excess of 15 kev is simply calculated as ~5 percent; i.e., ~5 percent of the energy loss appears as fluorescence, or 60 ev per photon. This value compares with a value of 3 percent for energetic deuterons given by Wouters,[8] and with 64 ev per photon for electrons in naphthalene by Kallmann.[9]

We have observed that scintillation pulses generated by 5-Mev α-particles in anthracene have amplitudes about equal to those produced by 0.5-Mev electrons. It is notable that both α's and very low energy electrons have higher rates of energy loss than do energetic β's. Kallmann[9] assigns an efficiency of 960 ev per photon for α-particles in naphthalene.

The reproducible counting efficiency of 100 percent above 50 kv, with usable efficiency to below 2 kev, combined with the convenience of the scintillation counter technique makes it an attractive alternative for Geiger counters in the beta-spectrometer. If a low energy cut-off of ~50 kev is acceptable in a particular experiment, the pulse height discrimination may be raised to correspond, with the advantage that the background count is reduced essentially to zero. We have observed that if too thin anthracene crystals are used (~0.1 mm), the counting efficiency for high energy beta-rays is less than 100 percent. This result is consistent with calculations of the energy loss of energetic β's in such thicknesses based on a simple model.[10] No loss in high energy counting efficiency with 1-mm thick crystals has been found.

The low energy ends of some β-spectra have also been observed using KI (Tl) single crystals as fluorescers. Poorer low energy sensitivity than anthracene was found. In addition, KI (Tl) gives rise to spurious "single electron" counts because of the release of trapped electrons.[11] The gross efficiency of diphenyl acetylene[12] for low energy β's has also been compared with that of anthracene by D. W. Engelkemeir of this laboratory; anthracene was superior.

We are indebted to Dr. T. B. Novey of this laboratory who prepared the anthracene crystals, and to Bernard Smaller for his contributions to the adaptation of the scintillation counter for use in the beta-spectrometer.

---

[8] Louis Wouters, UCRL-116, p. 11.

[9] H. Kallmann, Scintillation Counter Symposium, Oak Ridge, Tennessee (June 3 and 4, 1949).

[10] R. Platzman (private communication).

[11] Freedman, Smaller, and May, "Scintillation studies on potassium iodide," Bull. Amer. Phys. Soc. 24, No. 7, 28 (1949); Phys. Rev. 77, 759(A) (1949).

[12] W. S. Koski and Carl O. Thomas, Phys. Rev. 76, 308 (1949).

THE REVIEW OF SCIENTIFIC INSTRUMENTS VOLUME 21, NUMBER 9 SEPTEMBER, 1950

Fabrication of a High Power Resonant Wave-Guide Window

E. V. EDWARDS AND K. GAROFF
Signal Corps Engineering Laboratories, Fort Monmouth, New Jersey

(Received May 17, 1950)

The inability of present wave-guide pre-TR and TR tube windows to withstand high transmitter power necessitates improved window design if 3000-megacycle radar systems are to continue using the conventional band pass TR protective device. The fabrication of a glass window with a loaded Q of four is described and operational tests at high line power are discussed. This construction permits the TR tube parts to be brazed in a hydrogen furnace and a more rigorous pumping schedule to be followed. A flow chart of the window processing operations and pictures of the window and pre-TR tube are included.

1. INTRODUCTION

THE band pass type of TR tube consists of a gas-filled section of wave guide containing two or three resonant gaps and closed at both ends by resonant windows. A pre-TR is a similar gas-filled tube except that it is only a quarter of a wave-length long and has no gaps. The high power from the pulsed transmitter ionizes the gas between the gaps and across the back of the window, most of the power being dissipated at the window. The heat generated in the discharge across the window reaches very high levels because of the required presence of a de-ionizing gas in the tube. It has been known for some time that window burnout would limit the maximum transmitter power handling capabilities of TR tubes now in use.[1]

The development of band pass TR tubes for high power therefore requires an improved window. An accepted method of reducing the power dissipated at the window is to increase the loaded Q of the window.[1] An additional requirement of high power TR tubes is that they be hard soldered and baked at 400°C instead of the present practice of soft soldering the windows to the tube body.[1,2] The window must therefore be capable of resisting the high brazing temperatures of the hydrogen furnace.

Before entering into the discussion of the glass window, it should be noted that the possibilities of a ceramic window have not been ignored. The techniques for bonding rectangular shaped ceramic to metal are now being investigated at this laboratory.

2. DESIGN OF A RESONANT WINDOW (Loaded $Q=4$)

The wave-guide type of TR tube described in the previous paragraph has a band pass frequency response to signal levels below the ionization potential of the gas. The band width of this response depends on the loaded Q of the resonant elements and therefore limits the increase in window loaded Q that can be tolerated. With these considerations in mind, a value of 4 was assigned as a design parameter for the loaded Q of the window. The dimensions were determined empirically for such a window to resonate at the desired frequency and fit into standard rectangular wave guide $1\frac{1}{2}\times 3\times 0.080$ inches. The Kovar of the cup is 0.060 inches thick and the glass thickness at the center of the finished window is 0.078 ± 0.001 inches. Figures 1 and 2 show views of a window made to these specifications and Fig. 3 is a pre-TR tube with the windows brazed to the tube body.

3. WINDOW PROCESSING

A flow chart has been included to show the step by step procedure for processing the window. However, some elaboration on the skeleton of the flow chart may prove helpful. It should be noted that the procedure outlined is the result of a number of attempts which will not be described here for lack of space.

Spraying the powdered glass takes some practice if an even coating of the desired thickness is to be obtained. A small DeVilbiss gun under 20 pounds pressure of tank nitrogen with the work 8 to 12 inches from the gun gives the most satisfactory results. The first coat is light and wet and permitted to dry only partially before the next coat is added. The 705*FN* powdered glass should be used as soon as possible after it is ball milled and sized, in order to minimize the moisture adsorbed by the glass. The mixture must be stirred after every minute of spraying to maintain a uniform density of the sprayed material. Methyl alcohol was found to be a very poor substitute for ethyl alcohol as a carrier for the powdered glass. However, Sylvania has reported favorably on the use of Innis Speidon and Company's Isco Algin No. 117 as a binder. The strength of the final seal is greatly improved by glazing the front of the Kovar cup as well as the edges of the iris. The glazing period is measured from the time that the furnace and the Kovar cup became the same color.

Electric motor-brush carbon is best suited for molding the glass during the sealing operation. The carbons are grooved on the surfaces that contact the softened glass to permit trapped air to escape without forming bubbles in the glass. A weight of 175 grams is placed on the carbon to bring the glass to the desired thickness in the firing time specified. This thickness is fairly critical, a 0.002-inch variation shifts the resonant frequency of the window by 30 megacycles. If required a small amount of glass can be removed by an ammonium bifluoride solution, although this has not been necessary in the 25 or more windows processed thus far.

---

[1] L. D. Smullin and C. G. Montgomery, *Microwave Duplexers*, Radiation Lab Series (McGraw-Hill Book Company, Inc., New York, 1948), Vol. 14, p. 253.

[2] M. D. Fiske, Rev. Sci. Inst. 17, 478 (1946).

4. RESULTS OF TESTS ON WINDOW

These windows have proved their ability to withstand extreme processing and operational temperatures. The former is indicated during the assembly of the pre-TR of Fig. 3 where the temperature required for brazing window to tube body is 800°C. The windows and the tube body are not preheated but pushed directly into the hot hydrogen furnace. None of the windows that were processed leaked as a consequence of the thermal shock from such treatment. In addition, some windows have withstood reheating to this temperature as many as 14 times in TR tubes that were being rebrazed. For operational tests, pre-TR tubes were used since they are simpler to construct although the window is subjected to the same gas discharge conditions as in the TR tube.

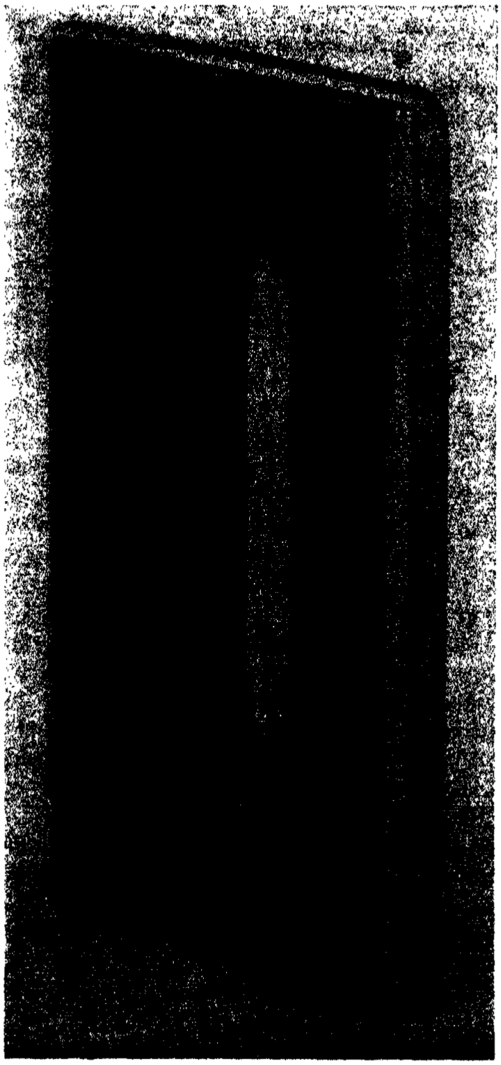

FIG. 1. 3000 mc r-f window, $Q_L = 4$. Interior view. Complete unit showing sprayed powdered glass fused to inner surfaces.

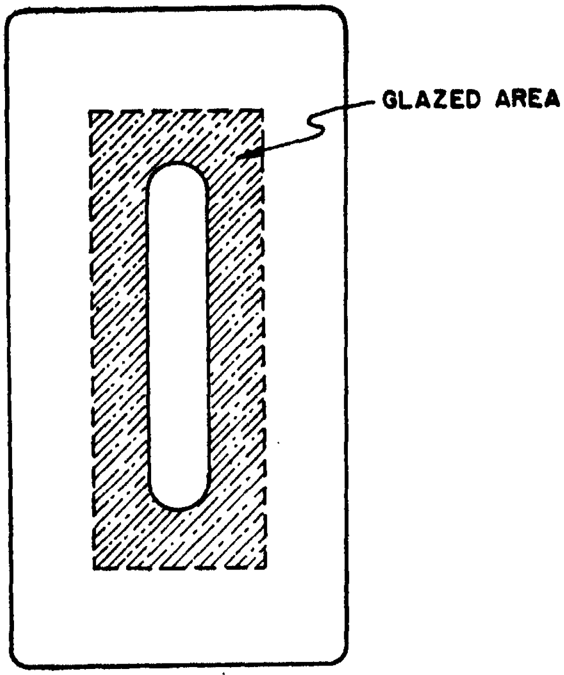

FIG. 2. 3000 mc r-f window, $Q_L = 4$. Exterior front view. Complete unit showing glass to metal type of seal.

Since tubes filled only with a de-ionizing gas will generate the hottest discharge, three pre-TR's with such gas were subjected to high peak transmitter powers. The temperature of the window as measured by a thermocouple was 160°C under these conditions with no window failure. This should be compared with the results obtained with the pre-TR tubes having a window loaded Q of unity, where the window was sucked in or cracked at about half the power used here, depending on the partial pressure of the de-ionizing gas.

5. CONCLUSION

Windows with a loaded Q of unity now being used in TR and pre-TR tubes will not be satisfactory at high transmitter power. The use of a higher Q window processed as reported, solves one of the major problems in the path of the development of conventional band pass pre-TR and TR tubes that will operate at very high power levels. The sources of r-f power available at this Laboratory at the present time cannot feed sufficient power into the pre-TR discharge to damage the high Q window.

WINDOW PROCESSING FLOW CHART

Preparation of Kovar Cup

1. Cut sheet Kovar to size and anneal in H_2 at 900°C for one-half hour.
2. Draw Kovar into rectangular cup approximately 0.400 in. deep.
3. Anneal cup at 900°C for one-half hour in H_2 furnace.

4. Mill the lip of the cup for mounting to wave-guide body and cut out the iris. Round the edges of the iris to avoid sharp corners.

5. Degrease the cup and then sandblast the inside of the cup and a narrow margin around the iris on the outside of the cup.

6. Degrease and anneal in H_2 furnace for one-half hour at 900°C.

7. Spray powdered 705*FN* glass uniformly around the inside of the cup as well as around the sandblasted margin on the front of the cup. (200 mesh 705*FN* glass—one part glass to three parts ethyl alcohol by volume.)

8. Dry thoroughly under infra-red lamp but avoid intense heat.

9. Remove powdered glass from any parts of cup where it will interfere with brazing the window to the tube body.

10. Glaze the sprayed glass in an air furnace at 940°C, keeping the cup in the furnace for two minutes after it reaches this temperature.

11. Remove the glazed cup from the furnace and cool to room temperature in a place free from drafts.

Processing the Glass Blank

1. Press 707*DG* glass cane into a ¾×2×0.100 inch blank.

2. Shape blank on the grinding wheel to 0.250×1.718 ×0.070 inches.

3. Bevel the edges on one face of the blank to permit insertion into glazed iris.

4. Clean blank with soap-water, rinse in potassium dichromate solution then distilled water and dry under infra-red lamp.

5. Examine blank for cracks, flaws or large air bubbles.

Sealing Glass Blank to Kovar

1. With the glass blank set in the iris, place the Kovar blank cup side down on a carbon block and place another carbon block, weighted by 175 grams, on the face of the window.

2. Keep in air furnace at 940°C for three minutes after work has reached temperature, then remove and allow it to cool to room temperature in draft-free place.

3. Remove oxide with "Oakite," polish with aluminum oxide and electroplate with a high conductivity metal.

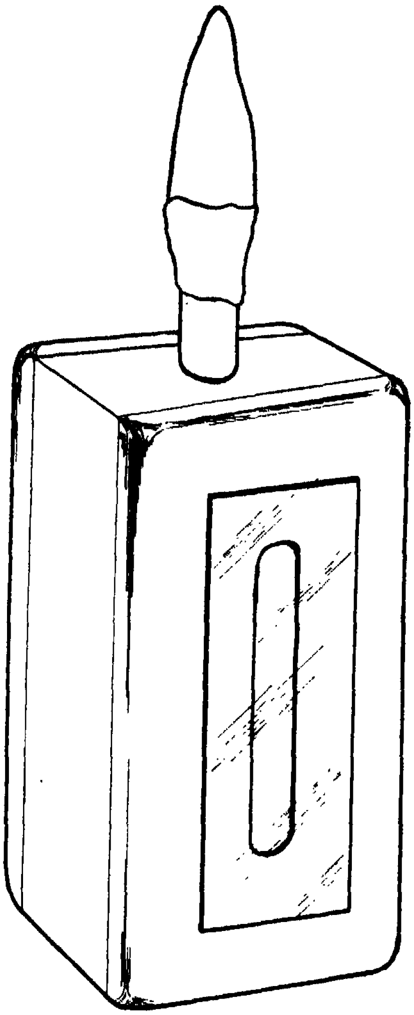

FIG. 3. 3000 mc pre-TR tube. Application of r-f windows in hard-soldered construction over-all ¾ view. Complete unit showing typical assembly and use of a window.

Erratum: Regulated Low Voltage Power Supply

[Rev. Sci. Inst. 21, 570 (1950)]

A. K. SOLOMON
Biophysical Laboratory, Harvard University, Cambridge, Massachusetts

THE lead from pin 5 of the uppermost VR 75 tube should be connected to the regulated output voltage of 225 volts, in lieu of the *incorrect* connection as indicated in Fig. 1 to the grids of the 6AS7 and plate of the 6AK5 tubes.

THE REVIEW OF SCIENTIFIC INSTRUMENTS VOLUME 21, NUMBER 9 SEPTEMBER, 1950

An Improved Resolving Time Measuring Device*

B. W. ROBERTS, JR., K. E. PERRY, AND R. G. FLUHARTY
Department of Physics and the Radioactivity Center of the Laboratory for Nuclear Science and Engineering, Massachusetts Institute of Technology, Cambridge, Massachusetts

(Received January 23, 1950)

A circuit for measuring resolving times has been developed utilizing the scheme of Curran and Rae with the addition of a delayed pulse of variable width. Any random event initiates a delayed pulse which is fed into coincidence with subsequent pulses giving rise to a sharp increase in the coincidence rate at a delay time close to the resolving time. A theory is given which predicts observed curve shapes and data is given for several counters to illustrate the operation under different counting rates and overvoltages.

INTRODUCTION

THE resolving time, ρ, of a counter or circuit is a parameter needed to obtain accurate counting results. It will be defined as the dead-time of a counter or circuit plus that part of the recovery time[1] needed for the pulse height to reach operating size.

Among the more direct methods of measuring resolving times of counters observing random events are: (1) the direct timed-sweep oscilloscope method[1] in which a pulse initiates the horizontal sweep and then records the subsequent pulse on the oscilloscope, (2) the standard two-source method and (3) the coincidence methods.

Curran and Rae[2] devised a coincidence circuit which utilized a variable width square pulse initiated by any random pulse from the counter tube. The square pulse was then differentiated, giving rise to a narrow pulse delayed a time equal to the time-width of the square pulse. This delayed pulse was fed into a mixing circuit with subsequent random pulses where coincidences were observed. A plot of the delay time against the observed coincidences gave a curve with a rise in the region of the resolving time.

A National Bureau of Standards circuit[3] used for dead-time measurements "selects, in effect, pairs of pulses with a time separation less than a selected value determined by the setting of the multivibrator controls, and one count is recorded for each pair received." A plot of counting rate *versus* gating time is then interpreted for the dead-time.

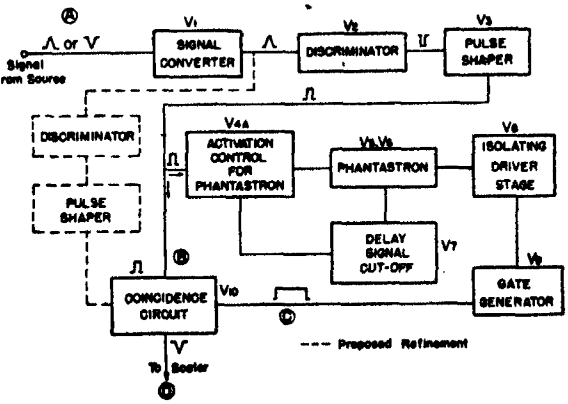

FIG. 1. Block diagram of coincidence circuit.

A British report[4] describes an electronic method where the "electronic gate is initiated by fully recovered pulses, and this automatically sets itself to the time of recovery to a pre-set amplitude. The time is then displayed on a calibrated meter." This is essentially a coincidence method with an involved circuit for directly recording the resolving time on a meter.

An interesting indirect method for measuring the resolving times of x-ray counters was devised by Pepinsky and co-workers.[5] An x-ray tube is pulsed into conduction by two sets of ½ micro-second, 1000 cycle triggers which are continuously phasable with respect to each other. The sets of x-ray pulses produce two Geiger pulse contours on the oscilloscope screen, and by reducing the time separation (phase difference) until the second pulse contour disappears, the dead-time can be directly determined. Measurements made by this technique checked favorably with those taken by Alexander[6] using the oscilloscope method.

Among the above methods, there are various limitations. The oscilloscope method requires photographic recording for best results. The two-source method does not give consistent results for mixed β- and γ-sources,[7] γ-sources and x-ray sources;[8] and a large number of counts is required to reduce statistical errors. This is objectionable both in regard to counter lifetimes and to the laboratory time required for measurement.

The British gate circuit is complicated by the large number of electronic elements. The Pepinsky method requires a pulsed x-ray source which is not always available. And the circuit of Curran and Rae requires large counting rates or long observation times to get significant results because of the narrowness of the pulses mixed for coincidences.

---

* Assisted by the joint program of the ONR and the AEC and a grant-in-aid of the National Institutes of Health.

[1] H. G. Stever, Phys. Rev. 61, 38 (1942).

[2] S. C. Curran and E. R. Rae, Rev. Sci. Inst. 18, 871 (1947).

[3] NBS Circuit, Rev. Sci. Inst. 20, 627NI (1949).

[4] "A meter for measuring dead time and recovery time in Geiger counters," A. E./T. R. E. Memo W#/M4/JLP.

[5] Pepinsky, Jarmotz, Long, and Sayre, Rev. Sci. Inst. 19, 51 (1948).

[6] L. Alexander, J. App. Phys. 20, 735 (1949).

[7] Y. Beers, Rev. Sci. Inst. 13, 72 (1942).

[8] R. P. Ghelardi, Tracerlog No. 6, p. 5 (October, 1947).

In an effort to increase the efficiency and accuracy of measuring resolving times a circuit has been designed using the basic scheme of Curran and Rae but utilizing a variable-width delayed pulse.

DESCRIPTION OF CIRCUIT OPERATION

A block diagram of this improved instrument is shown in Fig. 1 and the schematic in Fig. 3. Idealized wave forms at various points of the circuit are detailed in Fig. 2 to clarify the following text.

A positive or negative signal is received from the counter preamplifier, or other source, and is fed through the signal converter where the correct polarity is selected by a panel switch.

The initiating pulse (curve *a*, Fig. 2), being large enough to overcome the discriminator bias on V_2 (Fig. 3), triggers the pulse shaping multivibrator V_3. The shaped pulse (*b*, Fig. 2) is impressed on the grid of V_{4A}, the phantastron activation control; and on the first grid of V_{10}, the output coincidence tube; but since there is no opening gate on the third grid of V_{10} no pulse appears on the output plate. The phantastron circuit is triggered by the plate of V_{4A} through the isolating diode. The operation of the phantastron circuit (V_5, V_6) has been given by Close and Lebenbaum.[9]

A wide negative gate appears on the cathode of V_{4B} (curve *c*, Fig. 2) and another of the same duration on the cathode of V_6 (curve *d*) which faithfully reproduces the linear fall of the V_6 plate. The gate widths are determined by the quiescent d.c. voltage on the plate of V_6, which is controlled through diode V_{8B} by the linear voltage divider potentiometer which is calibrated in micro-minutes. R_1C_1 also determines the phantastron gate width; C_2 being switched in for the higher range.

V_7 constitutes a blocking tube or signal cut off which inactivates V_{4A} during the delay time and for several hundred micro-seconds thereafter. This prevents the phantastron from being triggered before it has fully recovered to its quiescent state. If this were not done the delay time would not be reliable. Curves *e* and *f* of Fig. 3 show this action. It can be seen that the cathode of V_{4A} is driven strongly positive, thus holding it far beyond cut-off until, after the recovery of the phantastron, it decays back nearly to its original voltage.

At the end of the phantastron delay a positive pulse is applied to the grid of V_8 (curve *g*), the isolating driver stage (there is a negative pulse at the beginning of the delay but since V_8 is nearly at cut-off this has no effect), causing it to trigger the gate generator multivibrator V_9 which delivers the opening gate to grid three of coincidence tube V_{10}. In V_9 it is seen that in the left triode the grid is returned through a large resistor to 75 volts positive bias so that it is held at zero bias by drawing grid current. The left-hand plate being only a few volts above ground, the right-hand triode, with cathode at plus 75 volts, is cut off. The trigger pulse cuts off the left triode, causing the circuit to flip and the plate, along with grid three of V_{10}, to go plus 75 volts (curve *h*). The plate of V_{10}, which was originally cut off by the fact that the third grid was more negative than the cathode, will, during this gating interval, conduct if a positive subsequent pulse is applied to the first grid (curve *j*).

Five dotted pulses are shown on curves *a* and *b* (Fig. 2). These represent alternative random pulses which may occur after the initiating pulse. Number 1 is too early for the particular delay setting and is not detected. Pulses 2 and 3 represent the extremes that will be detected within the coincidence gate. Pulse 4 occurs after the end of the gate but the phantastron driver is still cut off so that a new cycle is not initiated. Pulse 5 occurs just after the phantastron is ready to receive a pulse so that it initiates another delay cycle.

Thus when the delay time is less than the effective resolving time, no coincidences can occur. As the delay time is increased, a sudden rise will be observed in n_c, the coincidence rate, when the resolving time is reached. n_c is largely determined by three parameters: t the time of delay, T the delayed pulse width, and ρ the resolving time of the circuit.

THEORY

In operation of the device two extremes of counters or circuits can be encountered. The actual case will be intermediate. The first to be considered is the paralyzable type such as a pure gas non-self-quenching

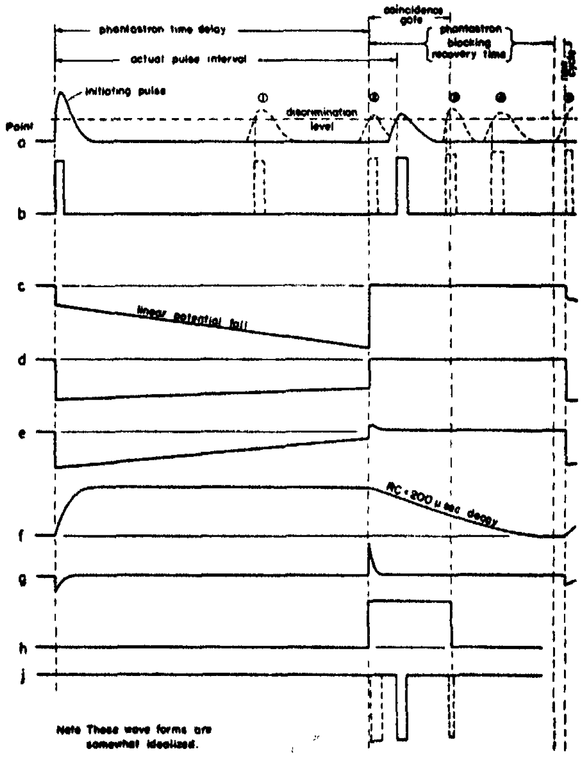

FIG. 2. Plot of time relation of pulses in circuit of Fig. 3.

---

[9] R. N. Close and M. T. Lebenbaum, Electronics 21, 100 (1948).

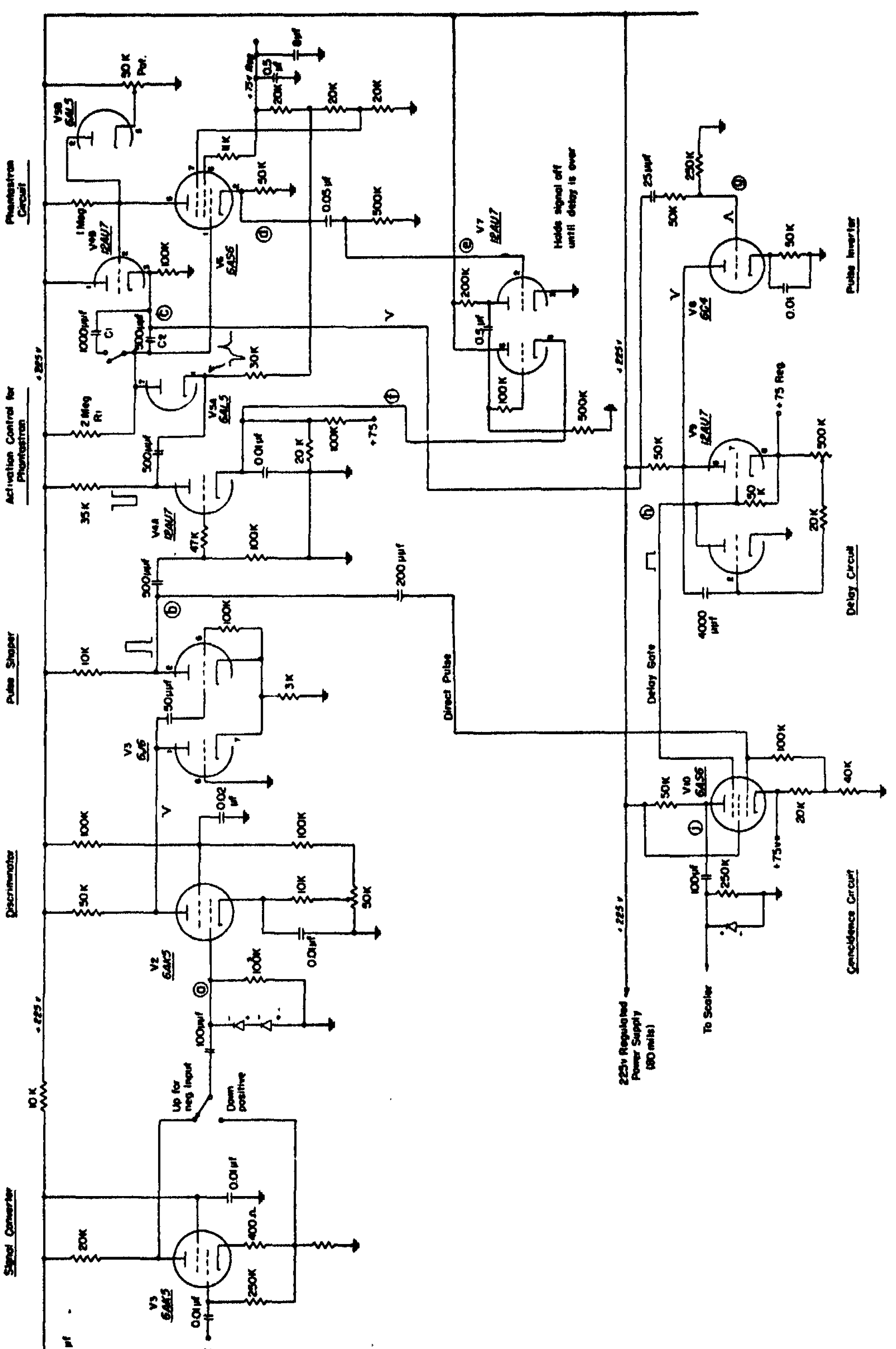

Fig. 3. Circuit design schematic of the coincidence-resolving time device.

counter where the preamplifier time constant is greater than ρ. This circuit will give a counting rate n_1 from n_0 true random events:

$$n_1=n_0e^{-n_0\rho}. \tag{1}$$

From these n_1 observed pulses, n_2 wide delayed pulses are derived. Since the delay circuit is dead during a delay time t (plus the phantastron blocking recovery time which is neglected here), the counting rate n_2 will be reduced since the circuit is inactive for a fraction of time n_2t. Thus the circuit is sensitive for a fraction of time $1-n_2t$ which is also equal to the ratio n_2/n_1. This gives for the delayed pulse rate:

$$n_2=n_1/(1+n_1t). \tag{2}$$

n_1 and n_2 are mixed in the coincidence circuit giving rise to a rate n_c. If n_1 and n_2 are assumed to consist of random events (which is untrue in both cases due to the loss of very short intervals in the distributions) the observed n_c will be:

$$n_c=n_1n_2(dt_1+dt_2), \tag{3}$$

where dt_1 and dt_2 are the pulse widths of n_1 and n_2 respectively.

Substitution of Eq. (2) in (3) and the use of Eq. (1) after replacing dt_2 by T gives:

$$n_c=\frac{n_0^2e^{-2n_0\rho}}{1+n_0te^{-n_0\rho}}(dt_1+T)\quad t\geqslant\rho, \tag{4}$$

which is a maximum when $t=\rho$ as shown in Fig. 4. In the limiting case as n_0 goes to ∞, n_c approaches zero. When $n_0\rho\ll 1$, the exponentials can be expanded and after dropping the second-order terms and permitting t to equal ρ we have:

$$n_c\approx\frac{n_0^2}{(1+3n_0\rho)}(dt_1+T). \tag{5}$$

This shows that the maximum value of n_c becomes proportional to n_0^2 as $n_0\rho$ approaches zero.

From $t=0$ to $t=\rho-T$, n_c must equal zero since no coincidences can occur. Then a sharp rise is observed as the delay pulse of width T moves across $t=\rho$, i.e. into the region where n_1 pulses can occur. This rise may be approximated for low values of n_0 by:

$$n_c=n_c(\max)\left(\frac{t-\rho+T}{T}\right)\quad \rho-T<t<\rho, \tag{6}$$

where $n_c(\max)$ is the value of n_c in Eq. (4) when $t=\rho$. Finally for the region of $\rho<t<\infty$, Eq. (4) applies. This region is described by a nearly constant relationship between n_c and t when $n_0\rho$ is very small and a $1/(1+n_0te^{-n_0\rho})$ decrease when $n_0\rho$ is large. Figure 4 shows several plots of n_c *versus* t and illustrates the expected curve shapes for low and high counting rates.

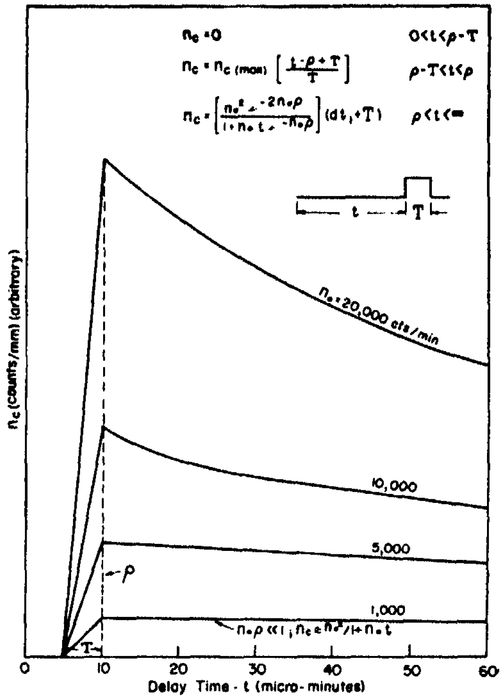

FIG. 4. Predicted coincidence curve for paralyzable apparatus.

The ordinate is arbitrary for each curve in order to plot simultaneously since $n_c(\max)$ for $n_0=1000$ counts/min. is 1/400 the value for $n_0=20{,}000$ counts/min. n_c is also directly dependent upon the value of T used in the measurement.

The non-paralyzable apparatus on the other extreme which is typified by a self-quenching counter with a very sensitive preamplifier gives rise to an equation

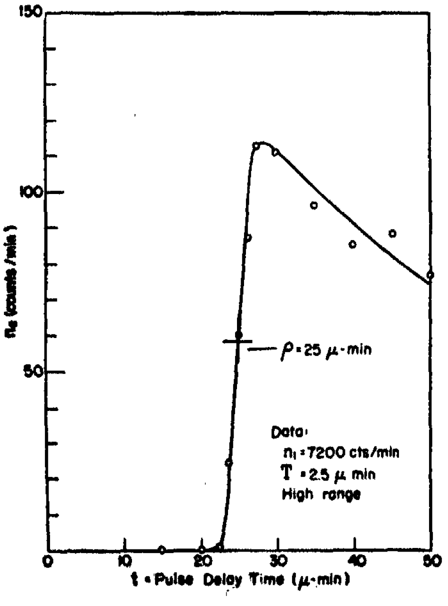

FIG. 5. Plot of n_c *versus* t for multivibrator-quenched circuit.

TABLE I. n_c and ρ as a function of pulse width T.

T micro-minutes	Rise width micro-minutes	ρ micro-minutes	n_c(max) Exper. counts/min.	n_c(max) Theory counts/min.
0.3	8.3	17.4	144	146
1.5	9.8	17.5	460	730
2.5	10.1	17.5	990	1200
3.5	9.7	16.0	1670	1700
5.0	10.1	15.6	2430	2430

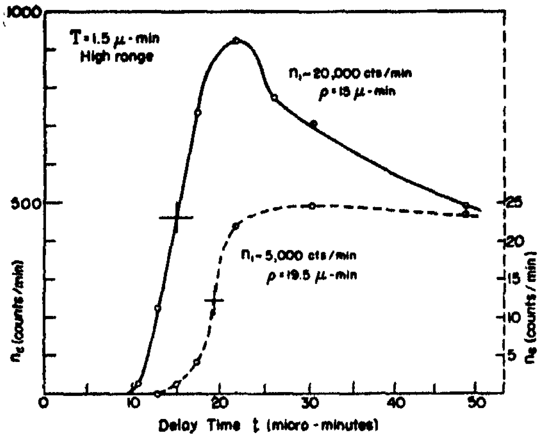

FIG. 6. Plot showing ρ as a function of counting rate.

for the coincidence rate similar to Eq. (4).

$$n_c' = \frac{n_0^2(dt_1+T)}{(1+n_0\rho)[1+n_0(t+\rho)]} \qquad t>\rho. \tag{7}$$

OPERATION

The delay time and pulse width were calibrated against the fixed time intervals on a precision synchroscope with internal calibration with intervals of about $\frac{1}{5}$ micro-minute. The delay time t had a range from 3 to 50 micro-minutes and the pulse width T varied from 0.3 to 20 micro-minutes. The input pulse height *versus* discriminator setting was found for both the scaler and coincidence circuit.

To measure ρ it is best to have the counter in an environment identical to that of normal usage to avoid effects such as counter sensitivity to light that may affect the counting rate. The counter is attached to the pre-amplifier and the prescribed operating voltage applied. A source is placed to give the desired counting rate n_1. By changing a switch the counter pulses enter directly into the scaler and a quick measure of n_1 can be made if desired. The pulses from the counter and the pre-amplifier are then fed into the coincidence circuit. The discriminator bias is adjusted to eliminate noise and other disturbances arising in the circuit for G-M counters, and the bias may usually be adjusted to maximum value for circuit resolving times since the pulses are full size and large. Next, the delayed pulse width T is adjusted to a value that gives a useful n_c. That is, an n_c value that may be quickly observed and plotted. For ρ up to 15 micro-minutes and n_1 approximately 6000 counts/min. a pulse width up to 2.5 micro-minutes was found applicable. For ρ above this range a 5 micro-minute pulse width may be used. There are two overlapping ranges of delay time. With these adjustments completed, t is varied from high to low until the abrupt drop in n_c is observed. This region is then scanned at small intervals of t over the n_c drop. A plot of n_c *versus* t is made and the half-maximum point on the curve is taken as the effective resolving time.

DISCUSSION OF MEASUREMENTS

The first determinations of resolving time were made on a high resistance multivibrator quenching pre-amplifier which had been carefully measured by the two-source method and found to be 25 micro-minutes. Figure 5 shows a plot of n_c *versus* t made at $n_1=7200$ counts/min. and $T=2.5$ micro-min. The expected abrupt rise is found and an approximately linear decrease follows. Using the half-maximum point on the plot gives 25 micro-minutes for the effective resolving time of the pre-amplifier circuit. The rise covers 5 micro-minutes which is twice that predicted since the theory gives the rise width as T. This extra width may be due to several factors, including non-ideal pulse forms in the circuit and the probable occurrence of G-M multiples in the rise region.

To observe the effects of pulse width, T, on n_c

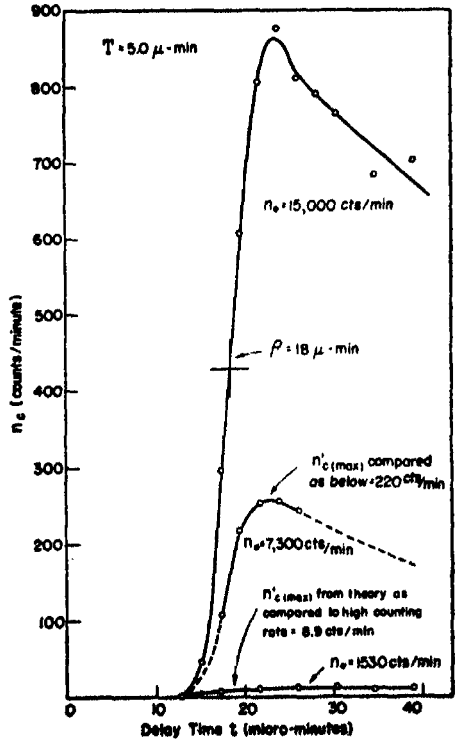

FIG. 7. Plot of n_c *versus* t to show experimental agreement with theory (multivibrator-quenched circuit in conjunction with a mica end-window x-ray counter).

and ρ, a series of measurements with a high pressure (69-cm Hg argon, 1-cm alcohol) mica end-window G-M counter were taken. A classical non-quenching pre-amplifier was used (1 megohm). From the plots the half-maxima were taken as ρ and the rise width was measured as the intercepts on a straight line along the rise from $n_c=0$ to n_c a maximum. These data are given in Table I. The pulse width does not affect ρ until a value of $T=3.5$ micro-minutes is obtained where a decrease is observed. The rise width does not show conclusive change. The maximum values of n_c are given to show the wide range obtainable with the variable pulse width T. A rough linear comparison between T and n_c is given in the last column where the n_c for $T=5$ micro-minutes was taken as the comparison point.

Figure 6 shows the effect of counting rate on ρ for a high pressure G-M counter with a classical pre-amplifier. An increase in counting rate of four times or more gives a decrease of about 20 percent. This decrease has been observed by Muehlhause and Friedman.[10] The plot also illustrates the theory roughly in that a more rapid decrease is observed for the higher counting rate after the maximum value of n_c.

In Fig. 7, three plots of n_c *versus* t are shown with their respective counting rates. The curve with $n_0=15{,}000$ counts/min. rises linearly in accord with Eq. (8) and then falls sharply. The fall is more rapid than that shown in Fig. 4 for $n_0=20{,}000$ counts/min. because the experimental ρ is nearly twice that of the theoretical curve. For the low counting rate the curve is horizontal within the dispersion of the points due to statistical error. Theoretical maximum values of n_c are shown for the two lower curves as referred to the top curve.

An interesting check was made on the variation of ρ with overvoltage on a high pressure counter (69-cm Hg argon, 1-cm alcohol) with a mica end-window. A very high fixed counting rate n_0 was used throughout with $T=0.3$ micro-minutes. The discriminator bias was reduced for the 50-volt reading due to the decrease of input pulse height (nearly a linear function of overvoltage). Figure 8 shows four plots at specified voltages above minimum operating voltage. A marked decrease of ρ is observed with increasing overvoltage. This effect has been observed and reported by Hartog.[11]

DISCUSSION AND CONCLUSION

By the addition of a wide delayed pulse to the scheme devised by Curran and Rae,[2] a flexible instrument has been designed to measure resolving times in the 3 to 50 micro-minute range. It is believed that the principle can be extended to the 10 micro-second region. The flexibility lies directly with the wide delayed pulse which permits arbitrarily large coincidence counting rates to be observed between a delayed pulse and subsequent pulses. This coincidence counting rate may be made large to the point that a rough resolving time can be read directly from a calibrated pulse delay dial.

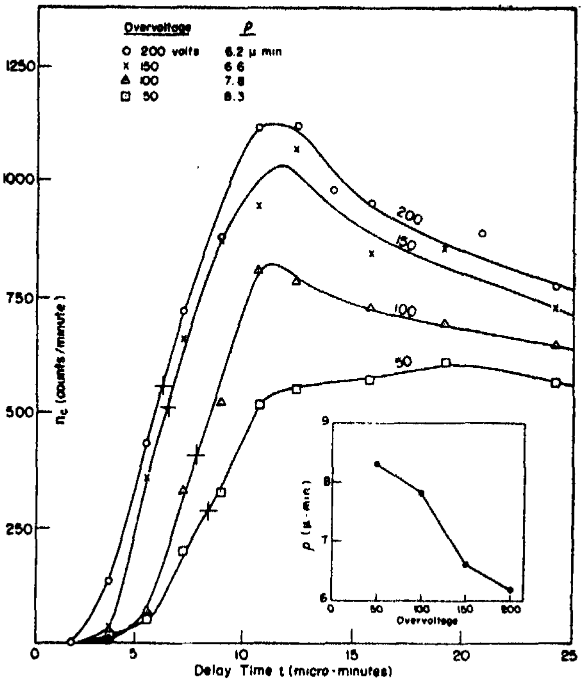

FIG. 8. Plot of n_c *versus* t for several over-voltage values.

A comparison of the observed resolving times with those measured by the two-source method indicates that the half-maximum of the coincidence curve is the best effective value of the resolving time. This contrasts with the rough theory which gives the curve maximum for the resolving time. This may be due to the neglect in the theory of small interval losses, the phantastron blocking recovery time, and the statistical nature of resolving time. Also the n_1 and n_2 pulse shapes found experimentally are not those assumed for the theory. These irregular pulse shapes would tend to make the n_c rise wider than indicated by the theory. The occurrence of G-M multiples would also disturb the curve in this manner. It is believed that a better comparison of resolving times could be made using the timed-sweep oscilloscope method.

The measured resolving time is determined both by the dead-time of the counter and by the pulse size discrimination level of the instrument for detection of the subsequent pulses. It is also true that the dead-time of the counter after any initiating (of the phantastron delay) pulse is affected by the size of this initiating pulse. That is, if the phantastron delay is initiated by one of the smaller pulses which may occur under the recovery envelope then the dead-time and the measured resolving time will be smaller. This effect can occur occasionally at high counting rates in the present instrument.

Thus it is seen that there are two functions of the discrimination level which are inseparable; the resolving time as determined by the level of selection of the subsequent pulses, and the minimum possible dead-time determined by the pulse size necessary for the delay initiation. The latter effect is not too important except at very high counting rates. In order to separate the two functions it has been suggested that a separate identical discriminator be employed as shown in Fig. 1. By this scheme the phantastron could be triggered only by full size pulses and the detection level of the subsequent pulses could be selected without the possibility of affecting the dead-time.

---

[10] C. O. Muehlhause and H. Friedman, Rev. Sci. Inst. **17**, 506 (1946).

[11] H. D. Hartog, Nucleonics **5** (No. 3), 33 (1949).

ACKNOWLEDGMENTS

The authors wish to thank Dr. Robley D. Evans for his aid in developing the theory and for his encouragement throughout the research. We also wish to thank Miss Doris McGuire and Mr. Sidney Millen for friendly aid in the measurements.

THE REVIEW OF SCIENTIFIC INSTRUMENTS VOLUME 21, NUMBER 9 SEPTEMBER, 1950

A 500-Kilovolt Linear Accelerator Using Selenium Rectifiers

WAYNE R. ARNOLD[*]
State University of Iowa, Iowa City, Iowa

(Received June 16, 1950)

A 500-kilovolt generator for use on a linear accelerator is described. This voltage is obtained by using selenium rectifiers and one microfarad condensers in 22 stages of voltage doublers. The maximum input is nine kilovolts r.m.s. at 750 cycles, and the maximum peak inverse voltage across each rectifier and each condenser is 25 kilovolts. The measured regulation is 25 kv/ma, the measured ripple (peak to peak voltage) is less than 1200 volts/ma; both independent of output voltage. The maximum load is 2.5 ma.

INTRODUCTION

THE voltage multiplier circuit usually used to give voltages of 500 kilovolts or less is a two- or three-stage multiplier using hot filament x-ray tube rectifiers. Such circuits require the use of condensers and rectifiers which must be rated at one-half to one-third of the total output voltage. They also require batteries, generators, or high voltage insulation transformers to heat the rectifier filaments. The machine described here uses selenium dry disk rectifiers so the filament heating problem does not arise. It is then convenient to use a greater number of stages of multiplication; more stages with the same output voltage results in a reduced voltage across each component. Although for a given load there is a limit to the number of stages of multiplication that can be used, proper choice of condensers and input frequency make this limitation relatively unimportant.

ELECTRICAL CIRCUIT AND COMPONENTS

The circuit used is shown in Fig. 1, and is essentially the same as used by Cockcroft and Walton[1] and by Bouwers and Kuntke.[2] The 44 condensers, used in 22 stages, are Westinghouse Inerteen Type FP rated at one microfarad and 25 kv and are all identical. Each of the selenium rectifier assemblies consists of five General Electric type 6RS5K72 selenium rectifiers placed in series to form a 25-kilovolt rectifier. These rectifiers are rated at 2.5 ma maximum and are the limiting factor on the output current. The transformer is a special 750-cycle transformer with a 250-volt primary and a 10,000-volt secondary insulated for 50 kv. This transformer is supplied through a Variac by a 750-cycle, 10-kva alternator. The 750-cycle frequency was used because this alternator was available. Lower frequencies could be used if a higher ripple voltage would not be objectionable.

The paper by Bouwers and Kuntke[2] gives an analysis of the circuit of Fig. 1, based on the assumption of perfect rectifiers and condensers. Their result, where n is the number of stages of doublers, C is the capacity of the individual condensers, i is the current drain, f is the frequency of the a.c. supply voltage, E is the peak input voltage, and V the output voltage, is

$$V=2nE-i[2n^3/3+n^2/2-n/6]/fC.$$

The terms in n^2 and n (in the bracket) may be neglected for large n. For this machine $n=22$, $C=10^{-6}$, $f=750$, $E=12.5$ kv; so for maximum input we have

$$V=550\text{ kv}-9.5i\text{ kv},$$

where i is in milliamperes.

By taking the derivative of V with respect to n, we find that the maximum voltage output (for 2.5-ma load, one-microfarad condensers, and a frequency of 750 cycles) would be obtained for n equal to 61 stages.

---

[*] Now at Los Alamos Scientific Laboratory.

[1] J. D. Cockcroft and E. T. S. Walton, Proc. Roy. Soc. 129, 477 (1930) and Proc. Roy. Soc. 136, 619 (1932).

[2] Von A. Bouwers and A. Kuntke, Zeits. f. Techn. Phys. 18, 209 (1937).

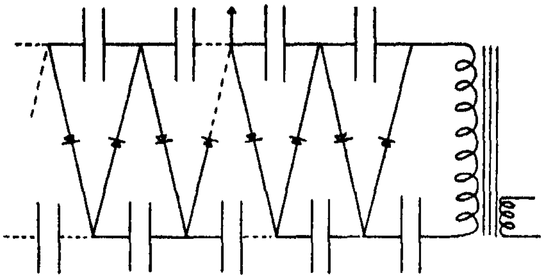

FIG. 1. Voltage multiplier circuit. The circuit below the arrow represents the usual quadrupler or two-stage multiplier.

The same theory gives

$$v=i[n^2/2+n/2]/fC$$

for the peak to peak value of the ripple. At full load on this machine the theory thus predicts a ripple of 840 volts (peak to peak). Either ripple or voltage drop under load could be minimized by using different values of capacity in the different sections, but the advantage over having all capacitors identical is negligible.

500-volt and 50-kilovolt scale models were built to check the applicability of this theory and to aid in the design of the 500-kilovolt machine. The behavior of both models was adequately explained by the theory so construction was started on the main machine.

MECHANICAL CONSTRUCTION

The manner in which the machine was assembled may be seen in the photograph of Fig. 2. The 44 condensers are arranged in four stacks of 11 condensers each. Each condenser is housed in an aluminum cylinder 18 inches in diameter, 3/16-inch wall, and nine inches high. The case of the condenser is connected by means of a strap soldered to the corona shield on which it rests, while the single insulated terminal is connected by means of an aluminum tube to the corona shield in the adjoining stack. The selenium rectifier assemblies attach to the aluminum tubes by means of fuse clips. These rectifier assemblies have five of the G.E. five kv units, inside of a one-half-inch I.D. Textolite tube, compressed by a spring. On top of each aluminum cylinder is a 26-inch disk of Textolite insulation, one-half inch thick, which in turn is covered by the 28-inch diameter corona shield. This shield forms the base for the next condenser in the stack. One of each pair of stacks has a 4¾-inch spacer at the bottom so that the condenser lead from one stack will be level with the corona shield on the adjoining stack. All four stacks are insulated from the floor to allow a voltage to be applied which will compensate for drifts in the high voltage. Mechanically the stacks were quite stable and no provision was made to prevent sideways slip. This allows a rather rapid change of components if necessary. Supported atop the four stacks is a large tank 30 inches high and with outside dimensions 84 by 90 inches, giving an over-all height of 12 feet for the machine. The main purpose of this tank is to prevent corona, but it provides more than adequate room for the voltage supplies for the ion source of the linear accelerator. This tank contains a 110-volt a.c. generator run by means of the long belt seen in Fig. 2. All wiring in the room is run through conduit for shielding.

The accelerating tube of the linear accelerator is seen at the right in Fig. 2, and consists of 23 re-entrant spinnings separated by 2½-inch porcelain insulators. Each stage of the voltage multiplier provides a constant voltage point which was connected by means of Yard-ohm (500 ohm/inch) inside of ⅜-inch Neoprene tubing to an accelerator tube spinning. This insures that the potential difference between adjacent spinnings is 1/22 of the total voltage. The extra spinning is used for focusing.

These tie lines necessitated a separate column at the edge of the accelerator tube platform. This column spaces the lines and prevents them from exerting sideways force on the accelerator tube. The column is made of Textolite tubing, six inches in diameter, with aluminum rings inside and out. In addition to the tie lines, this column also supports two three-inch copper tubes which run from the high voltage tank to the sphere atop the accelerator tube. One of these tubes is used as a vacuum pumping line for the ion source, and the other carries the wires supplying voltages for the ion source and focusing gap.

The ion source used on the accelerator tube is an Allison type source[3] modified so as to be more compact

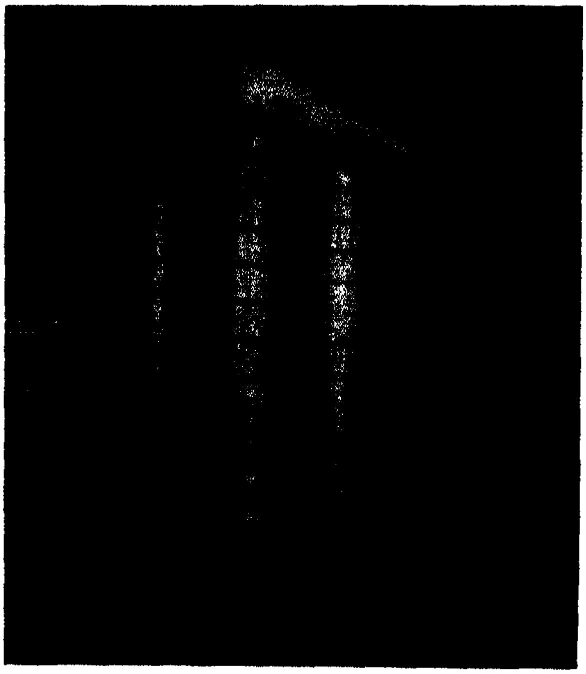

FIG. 2. The Iowa Generator. The accelerating tube is on the platform to the right.

---

[3] S. K. Allison, Rev. Sci. Inst. 19, 291 (1948).

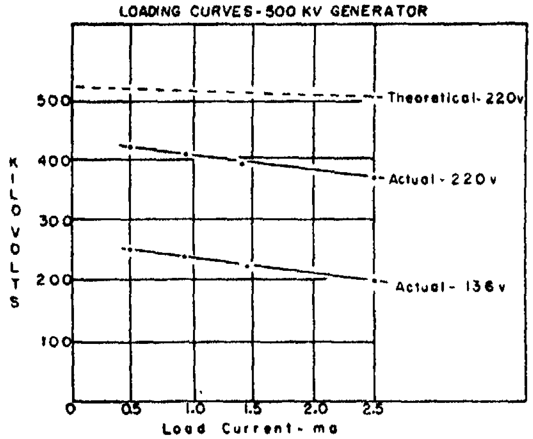

FIG. 3. Output voltage *vs.* load curves. The curves are designated by the corresponding input voltage to the supply transformer.

and having a second probe orifice to allow differential pumping.

PERFORMANCE TESTS

The performance of this generator under load was measured by means of a resistance load, since the maximum total beam current was less than 1 ma. Several $\frac{1}{8}$-inch diameter Saran tubes were run from bottles of distilled water in the large tank on top to grounded bottles on the floor, and the water allowed to syphon out of the upper bottles. Moving water was used to prevent overheating in the Saran tubing. The resistance of the water was varied by adding small amounts of NaCl. The high voltage was measured by running a beam down the accelerating tube and finding the magnetic field necessary to deflect the protons through 90°. The current was measured by a meter in the line joining the bottom of the high voltage generator to ground. The curves obtained are shown in Fig. 3. Zero load points were not obtained since the beam with which the voltage was measured drew 0.5 ma. The curves show a voltage drop under load of about 25 kv/ma, or about 2.5 times the drop predicted for perfect rectifiers. The relatively large forward resistance of the selenium rectifiers also shows up in the lower output voltage obtained for a given a.c. input voltage. This effect is relatively unimportant as the voltages are uniformly lower across all components and in practice this is compensated by merely increasing the input voltage. A curve was not obtained for maximum output voltage because the resistivity of the distilled water was too low. The machine has, however, been run at 500 kv with a 0.5-ma beam load.

The ripple was measured by placing a known resistor in series with one of the Saran tubes. The a.c. component across this resistor was measured by an oscilloscope. It was necessary to shield the resistance and oscilloscope to prevent electrical pick-up from the sharply peaked current which flows in the transformer secondary. Since this pick-up was not completely eliminated the ripple measurement is only an upper limit to the true value. The ripple measured by this method was 1200 volts peak to peak per milliampere of load. This is about 3.5 times the theoretical ripple to be expected if the rectifiers and condensers were perfect.

The over-all efficiency was measured at 350 kilovolts and a 0.5-ma load and found to be 70 percent. (The current measured was the return current and not the beam current.)

The time constant for the high voltage to fall to $1/e$ of its original value with no load and zero input is 240 seconds.

OPERATIONAL PERFORMANCE

All difficulties with corona and arc-over have been experienced at the accelerating tube and the adjoining Textolite column. Because there are no surge resistors in this machine, the arc-overs are rather violent. All wiring in the room is in conduit and only very minor damage has been caused by electrical pick-up from these surges. The most damage that has occurred was when one of the straps joining a condenser case to a corona shield came loose during a surge. Photographs taken of the arc-over showed that it took place down the Textolite column next to the accelerator tube, and experience showed that it occurred only after 30 to 40 minutes of operation at voltages above 200 kv. A flattened sphere was placed on top of the column but had no effect. Recently corona shields having an outside diameter of 12 inches were placed around the outside of the column and these appear to have eliminated the arc-over completely. These shields were added after the photograph of Fig. 2 was taken. Research was done previous to the addition of these shields by limiting the length of a run to 20 minutes and discharging the machine completely between runs. Such a procedure was possible because the beam was steady almost immediately after voltage was reached.

The machine has been in operation since July of 1949, but it was not until the spring of 1950 that trouble was experienced with the 26-inch Textolite disks used for insulation in the condenser stacks. Six of these disks have punctured so far. As much as ten minutes before one of these disks breaks down a fluctuation of about 5 to 10 kilovolts is usually noticed in the high voltage, indicating that a leakage path is set up through the Textolite prior to puncturing. These Textolites are being replaced with annealed plate glass (Herculite) three-eighth-inch thick, with one-sixteenth-inch rubber gaskets to distribute the load. No difficulty has been experienced as yet with the glass disks in the machine. There seems to be no connection between the arc-overs and the failure of the Textolite disks.

Difficulties with the selenium rectifiers have been limited to gaps opening up within individual rectifiers. This does not introduce fluctuations of more than a few hundred volts in the output voltage, but does produce a 750-cycle arc across the gap which may be picked up by high gain detection apparatus. This difficulty is due to the manner in which the five-kv rectifier units are manufactured. The individual buttons are $\frac{9}{32}$-inch in diameter and are slid into a Textolite tube of only slightly larger diameter and then compressed with a small spring. The buttons tend to bind inside of the tube and expansion and contraction with temperature occasionally results in an imperfect contact between adjoining buttons. The offending rectifier may be easily found by use of an ohm-meter and corrected by tapping the end of the unit on the bench.

The use of a large number of accelerating gaps in the accelerator tube with each spinning connected to a constant voltage point on the power supply, has resulted in a beam that is well focused and which does not fluctuate nearly as much when the machine is first brought up to voltage as do beams in tubes where corona gaps are used as voltage dividers.

Resolved beams have been obtained with 30 microamps in mass one and 100 microamps in mass 2. The limitation on the beam current appears to be in the size of the second probe button which it used to effect the differential pumping. It should be possible to overcome this limitation with a new design, and allow full use of the maximum current available in the high voltage supply. To date the maximum load that has been placed on the machine by the beam and the return electron current is less than 1 ma.

Because of the small contribution of each stage to the total output, repair of an offending component may be postponed by merely shorting out the particular stage involved. This was done, for example, for the stage involved in the open condenser strap.

CONCLUSIONS

The difficulties that have been experienced with this machine are of such a nature that it should be possible to correct them without any major changes in design. The elimination of corona gaps for voltage dividers appears to be a definite advantage in obtaining stable operating conditions. By proper design of the ion source one should be able to obtain resolved beams on the order of three to five hundred microamperes without undue ripple. By reversing the polarity of the rectifiers, this machine could be used to accelerate electrons and thereby produce rather high x-ray intensities.

ACKNOWLEDGMENTS

This machine was built under the direction of Professor James A. Jacobs. Mr. George Carson helped keep costs down by securing many of the components, in particular the condensers, from war surplus. Mr. Joseph Zijacek did most of the labor involved in the construction, and Mr. Russell K. Soderquist helped in obtaining the data on the performance of the machine.

THE REVIEW OF SCIENTIFIC INSTRUMENTS VOLUME 21, NUMBER 9 SEPTEMBER, 1950

An Electronic A.C. Differential Voltmeter

L. A. Rosenthal and H. S. Zablocki
Rutgers University, New Brunswick, New Jersey

(Received June 8, 1950)

An electronic a.c. differential voltmeter capable of giving a direct reading of the percentage change in voltage in the region of ± 10 percent for voltage levels from 1.5 to 150 volts and frequencies between 20 and 200,000 cycles, is presented. The instrument is stable in operation, and simple in design. Experimental observations and circuit details are included.

INTRODUCTION

THE need frequently arises for a voltmeter capable of measuring changes in voltage about a given reference level. If the changes are in excess of ±10 percent, they can generally be read directly on a conventional instrument. However, for small changes the accuracy becomes poor and, if this region is to be expanded, a differential voltmeter capable of reading variations of less than ±10 percent is highly desirable. In addition, the differential voltmeter must have the other necessary characteristics of vacuum tube voltmeters, outstanding of which are insensitivity to line voltage variations, aging effects, and independence to input frequency. It is also desirable that the instrument be phase sensitive to avoid ambiguity in the change measured.

The aforementioned characteristics are obtainable in the electronic differential voltmeter to be described. The instrument consists of a non-linear Thyrite[1] bridge as the differential a.c. voltage detector in an amplifier circuit that has been stabilized by a large amount of feedback.

NON-LINEAR BRIDGES

A non-linear bridge can be defined as a bridge containing one or more elements which are non-linear. The

---

[1] Thyrite is the General Electric trade name for silicon carbide non-ohmic resistors. Bulletin GEA-4138B.

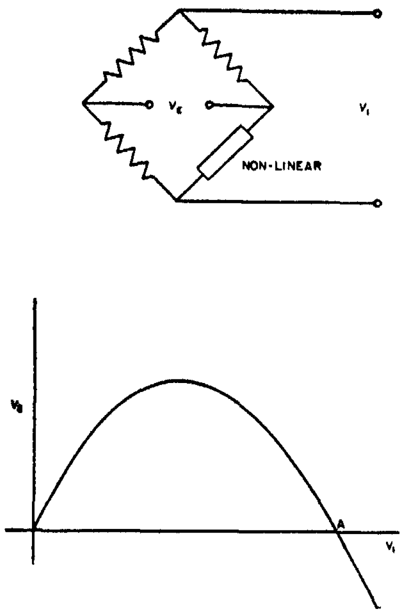

FIG. 1. Typical bridge characteristic for the indicated non-linear bridge.

element may have a resistance which varies with average power and temperature, or a resistance that varies with the instantaneous voltage applied. The former group includes lamps, barretters, and thermistors whereas the latter group includes elements such as Thyrite. If a bridge characteristic is obtained relating the error voltage as a function of the applied voltage, a curve typical to that of Fig. 1 is obtained. The point A corresponds to the balance point at which the power dissipated in, or voltage across, the non-linear element results in the critical resistance necessary to balance the bridge.[2,3] The region about A is generally linear for approximately ±20 percent of the balance voltage. For elements which are power sensitive, the voltages indicated can be a.c.[4]

There are several disadvantages in using power sensitive elements in a differential bridge. They are sensitive to ambient temperature changes, slow in response, and require an a.c. type[4] detector which is not phase sensitive. Mechanical shock may change the thermal characteristics and the balance point of the bridge. There is also a minimum balance voltage which increases at the lower frequencies due to harmonics generated by the non-linear element. A Thyrite bridge appears to be generally superior since the response is rapid, the temperature sensitivity is considerably less, and the elements are physically rugged.

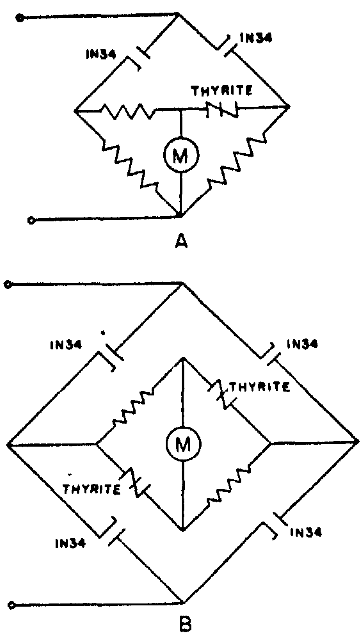

FIG. 2. Two non-linear bridge combinations. A. Half-wave single Thyrite bridge. B. Full-wave double Thyrite bridge.

The non-linear volt-ampere characteristic of Thyrite[5,6] is closely represented by

$$V = KI^n,$$

where K is a geometry constant and "n" is an exponent that generally falls between 0.2 and 0.4.

It can be shown that a non-linear symmetrical bridge, at the balance point, will have a slope,

$$s = (n-1)/2(n+1),$$

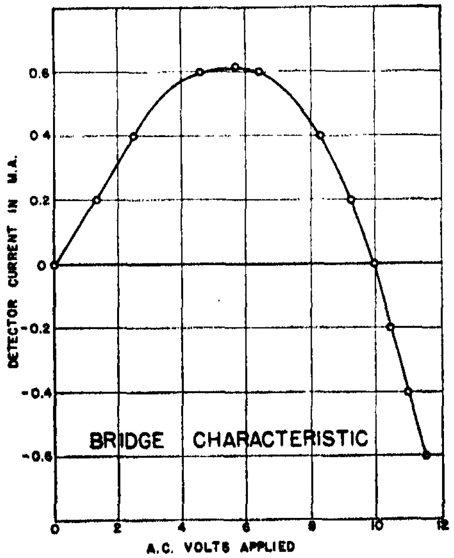

FIG. 3. Voltmeter bridge characteristics for the bridge of Fig. 2B.

---

[2] G. N. Patchett, "Theory of the non-linear bridge circuit as applied to voltage stabilizers," J.I.E.E. 93 (Pt. III), 16 (1946).

[3] G. N. Patchett, "The characteristics of lamps as applied to the non-linear bridge, used as the indicator in voltage stabilizers," J.I.E.E. 93 (Pt. III), 305 (1946).

[4] L. B. Turner, "Voltmeter for a.c. mains fluctuation," J. Sci. Inst. 14, 379 (1937).

[5] Ashworth, Needham, and Sillars, "Silicon carbide non-ohmic resistors," J.I.E.E. 93 (Pt. I), 385 (1946).

[6] T. Brownlee, "The calculation of circuits containing Thyrite," Gen. Elec. Rev. 37, 175 (April 1934), and 37, 218 (May 1934).

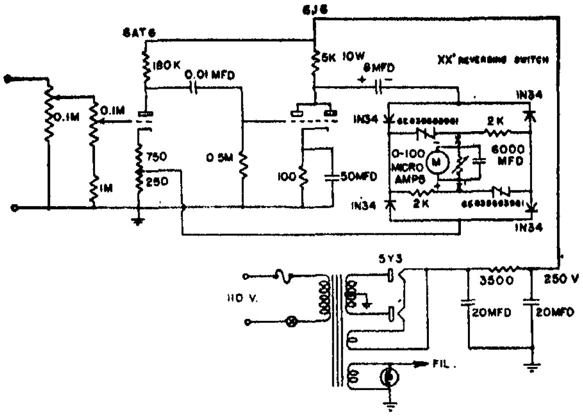

FIG. 4. Differential voltmeter circuit. Component values are as indicated.

for one Thyrite element, or if two identical elements in diagonal arms are used then,

$$s=(n-1)/(n+1).$$

If the voltage across a bridge at balance is V_A, then for a change in V_A the current that would flow through a detector is approximately

$$s\Delta V_A/(R_B+R_D),$$

where R_B is the internal bridge impedance and R_D is the detector impedance. Since the balance voltage is fixed by the operating resistance, the detector current can be calibrated as a percent change in V_A. It is apparent that operating the bridge at higher initial balance voltages will result in a greater sensitivity percentage-wise. However, Thyrite resistance decreases with increasing voltage and the entire bridge impedance will decrease, thus rapidly increasing the power requirements of the driving source. A compromise must be made between sensitivity and driving power requirements.

If instead of applying d.c., as in the foregoing analysis, the applied voltage is half or full wave rectified a.c., similar characteristics would be obtained. Figure 2 (A and B) indicates two varieties of bridges that can be used. The half wave bridge of Fig. 2A is less sensitive and more non-linear than the full wave bridge of Fig. 2B. In addition, it offers a lower impedance to the driving source. A typical over-all bridge characteristic relating d.c. detector current to applied a.c. voltage is shown in Fig. 3. The bridge is very similar to that used in the complete experimental model (Fig. 4).

THE COMPOSITE VOLTMETER

Figure 4 is a circuit diagram of the complete differential voltmeter. The circuit consists of a high μ-triode driving a twin triode in which the two sections have been paralleled. By paralleling the two sections, a g_m sufficiently large to develop over ten volts across the 2000 ohm bridge load is obtained. The bridge is in a feed-back path to the first cathode, producing high stability and good internal wave form. As shown, the feed-back factor is 0.11 and since the loop gain without feedback is approximately 500, the gain with feedback is approximately 9. A 6000 mfd condenser is placed across the meter to prevent any a.c. from passing through the meter at even the lowest frequencies. The power supply need not be regulated. A line voltage variation from 105 to 125 volts produced an indication of less than 0.3 percent. Barring the input attenuator, which was not frequency compensated, no measurable change in the input voltage necessary for balance was observed between 20 and 200,000 cycles per second. With the indicated feedback, the input voltage necessary for balance was 1.2 volts and by installing a proper attenuator the percentage change about higher voltage levels can readily be obtained. The basic sensitivity of the instrument was ±6 percent full scale but by shunting the meter movement it was preset for a convenient ±10 percent range. A low resistance shunt is provided for coarse zero setting and a reversing switch on the meter allows for positive or negative percentage readings. Figure 5 is the experimental linearity characteristic for the instrument.

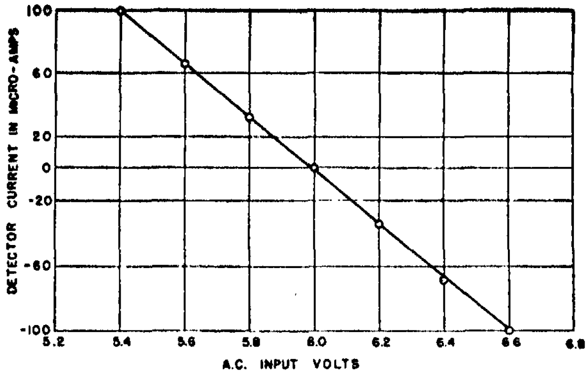

FIG. 5. Experimentally observed linearity characteristic relating meter indication to input amplitude.

ACKNOWLEDGMENT

In conclusion, the authors wish to extend their thanks to the United States Air Force, Watson Laboratories, who made this work possible under Contract No. AF28(099)-33. The assistance of Mr. W. Kurylo and Mr. G. Badoyannis is appreciated.

THE REVIEW OF SCIENTIFIC INSTRUMENTS VOLUME 21, NUMBER 9 SEPTEMBER, 1950

A Microtome Specimen Holder Advanced by Thermal Expansion

M. Eden, A. W. Pratt, and H. Kahler
National Cancer Institute, Bethesda, Maryland

(Received June 26, 1950)

A microtome specimen holder which advances the specimen by thermal expansion is described. The holder was heated by an electrical current, the value of which could be regulated to give any desired rate of heating and expansion. A quantitative comparison was made between the heating and expansion rates of the Newman, Borysko and Swerdlow CO_2 precooled instrument and the electrically heated instrument. It was found that the electrically heated specimen holder fulfilled the requirements of flexibility, reproducibility, sensitivity and linearity.

INTRODUCTION

Electron microscopy of tissue sections is successful only when the sections are of the order of 0.1-micron thick. It should be possible to study the three-dimensional structure of tissue by preparing a series of sections of a given tissue: each section having a known and uniform thickness. Preparing such a series requires a microtome advancing mechanism that will satisfy rigorous conditions of constancy and reproducibility.

Pease and Baker[1] modified a Spencer microtome by attaching a steel wedge of a smaller angle to the advance plate. They calculated the rate of advance to be one-tenth that of the standard microtome. Gettner and Hillier,[2] later studied this procedure and pointed out the extreme sensitivity to vibration and the need of reducing the friction of the ways.

Newman, Borysko, and Swerdlow[3] suggested a different advancing mechanism. The object holder, a hollow brass block about two inches in length, is pre-cooled about 25° below room temperature with expanding carbon dioxide gas. As the block warms to room temperature tissue slices are cut, the operator guessing at the time interval required to produce a suitable thermal extension of the rod.

It occurred to us that a simpler and more accurately controlled device could be built. A heavy brass rod insulated on its surface by a thin sheet of mica is wound with resistance wire. The outer surface is covered with a thick insulating wrapper. A suitable mount is machined in the end of the block to hold the specimen to be cut (Fig. 1). The power dissipated in the heating coil may be regulated by a variable transformer of suitable range.

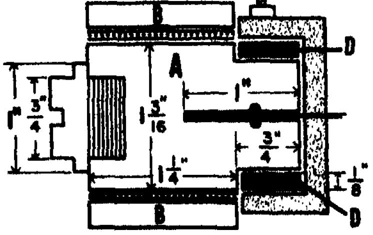

Fig. 1. Expansion assembly. Cross section of the electrically heated microtome specimen holder.

EXPERIMENTAL

A. Procedure

In order to study the performance of the Newman, Swerdlow, and Borysko[3,*] attachment and our modification, we measured two physical properties of the specimen block: temperature and the displacement between the front surface of the specimen holder and the knife holder (Fig. 2).

We determined temperature with a Copper-Constantan thermocouple using a White potentiometer to measure thermocouple voltage. We assumed that voltage varied linearly with temperature over a ten-degree range. The "cold" junction was kept at room temperature and lagged against abrupt room temperature changes by insertion into a Dewar flask. In the case of the N.B.S. attachment the other junction was usually soldered to the front surface of the specimen block. In certain runs the couple was taped to the block. In one experiment one junction of the thermocouple was soldered to the block and the other taped to the block with a gap of about a centimeter between them. No difference between the two couples greater than five microvolts (*ca.* 0.12°) was observed during a warm-up of 10°C. We measured the displacement of the specimen block by means of an unbonded strain gauge[4] mounted rigidly in the knife holder. A small piece of quartz slide was cemented to the front surface of the specimen block and the drive pin of the strain gauge was placed against it.

---

[1] D. C. Pease and R. F. Baker, Proc. Soc. Exper. Biol. and Med. 67, 470 (1948).

[2] M. Gettner and J. Hillier, J. App. Phys. 21, 68 (1950).

[3] Newman, Borysko, Swerdlow, J. Research Nat. Bur. of Stand. 43, 183 (1949).

[*] In the following, referred to as the N.B.S. attachment.

[4] The gauge used was a Statham transducer Model No. YE-4-60 manufactured by Statham Laboratories, 9328 Santa Monica Blvd., Beverly Hills, California.

The output of the gauge was measured directly by a galvanometer with a sensitivity of 0.0431 microvolts/mm. The input voltage was usually maintained at 0.750±0.002 volts. The output voltage of the strain gauge was 6.55 microvolts/micron displacement, so that the sensitivity of the complete system was 0.0065 microns/mm.

B. N.B.S. Specimen Holder

We cooled the N.B.S. specimen block to a predetermined temperature as indicated by the thermocouple. The block then warmed up to room temperature. We measured both temperature and expansion during the warm-up. Three typical runs have been plotted in Figs. 3 and 4. The block was pre-cooled about 4.5°C for run *A*, about 7.5° for run *B* and 10.5° for run *C*.

Within a ten-degree rise in temperature (curve *C*) the rate of expansion changes from 1 to 9 microns/minute. In order to cut sections 0.1 micron thick it would be necessary to cut at six second intervals at the beginning of the run and 54 second intervals at the end.

While a cutting program with increasing time intervals is feasible, a more serious difficulty is the lack of reproducibility. The data for curves *A* and *B* in Fig. 3 fit an equation of the form $X = X_0(1-\exp[-kt])$. The rate constant k is 0.93×10^{-3} for *A*, and 1.50×10^{-3} for *B*. No over-all rate constant holds for *C*. It is clear that the same cutting schedule could not be used for these three runs if slices of equal thickness were desired.

This is shown in somewhat different form in Fig. 4. Here the expansion data are plotted against temperature. To a first approximation these curves should be linear. It can be seen that the curves approach linearity as they warm to room temperature but the rate of expansion per unit temperature is different in each run. The effective length of the block has been calculated for the three runs using $L_{\mathrm{eff}} = (dL/dT)1/\lambda$; λ is the coefficient of expansion of brass; dL/dT, the change in length in centimeters per degree centigrade, determined graphically from Fig. 4. The effective lengths were found to be 5.0, 6.7, 10.0 centimeters for curves *A*, *B*, *C*, respectively.[5] It is clear that the previous treatment of the block and microtome has an important influence on the rate of warming.

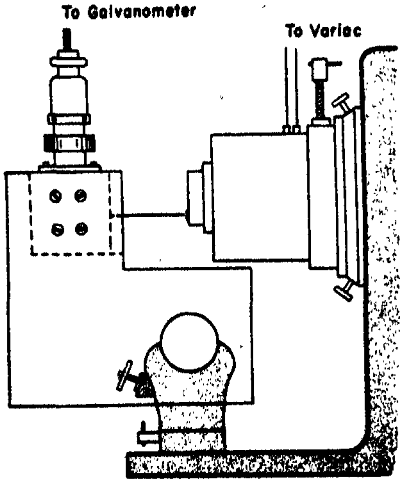

FIG. 2. The specimen holder in position in the Spencer microtome. The Statham gauge is shown mounted on the knife holder.

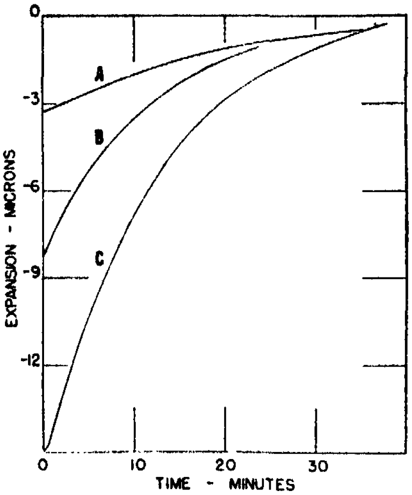

FIG. 3. A plot of three typical runs with the precooled specimen holder. Expansion *vs.* time.

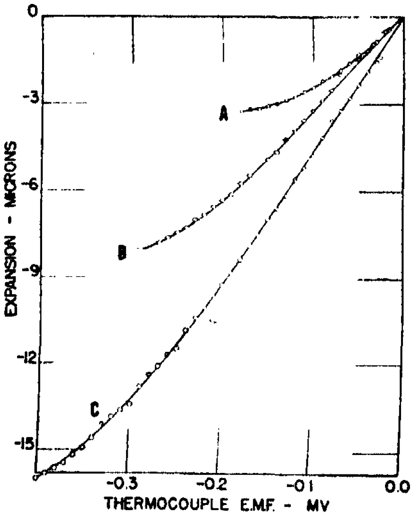

FIG. 4. A plot of three typical runs with the precooled specimen holder. Expansion *vs.* thermocouple voltage.

C. The Electrically Heated Specimen Holder

In view of these difficulties we decided to modify the N.B.S. device to satisfy the following criteria:

1. The rate of expansion should be uniform to within 20 percent for a range of at least three microns.
2. The rate of expansion should be reproducible to within five percent for a range of at least three microns.
3. It should be possible to stop the expansion for one or two minutes if need arises and then to continue with the same cutting schedule.

A plan of our modification is given in Fig. 1. A sketch of the modified specimen block mounted in the Spencer microtome is shown in Fig. 2. A brass block *A*, two inches long and $1\frac{3}{16}$ inches in diameter. was wound with

---

[5] A large measure of the lack of reproducibility could probably be eliminated by exhausting the CO_2 to the side rather than into the body of the microtome.

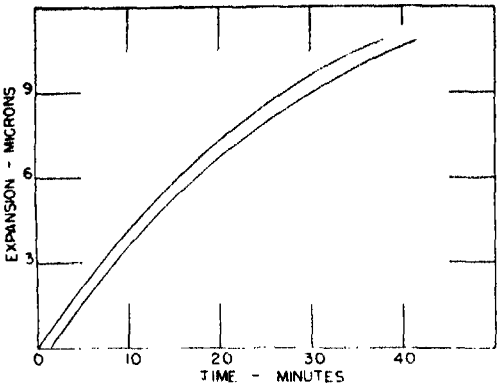

FIG. 5. A plot of two typical runs with the electrically heated specimen holder. Expansion *vs.* time.

twenty feet of B. & S. No. 30 gauge Nichrome wire (resistance 78.1 ohms). The wire was insulated from the block by a sheet of mica. The outer surface of the wire was insulated by a cylinder of Lucite, *B*, 1¼ inches long, 1½ inches i.d. and ¼-inch thick. A 0.032-inch hole, *C*, one inch deep was drilled in the rear of the specimen block. A Copper-Constantan junction was soldered into the bottom of the hole. The block was insulated from the jaws of the microtome by bakelite plates, *D*, ⅛-inch thick.

The 115-volt house line was stepped down to ten volts by a transformer. The voltage was controlled by a small Variac wired across the output of the transformer. All the measurements described below were made using 10.0 volts.

The block was heated to 10° above room temperature (0.400 mv) and measurements of temperature and displacement were made as before. Calculations were made on the basis of eleven runs performed over a period of six weeks. Two typical runs have been plotted in Figs. 5 and 6. The curves were arbitrarily separated.

A determination of the reproducibility of our device was made by comparing the slopes of each run after an expansion of 1.25 and again after 3.25 microns. The averages obtained were $7.57\pm0.16\times10^{-3}$ microns/second at 1.25 microns and $6.50\pm0.08\times10^{-3}$ at 3.25 microns.

The effective length of the block, calculated from the slope of the curve in Fig. 6, was found to be 5.04 cm. This is virtually identical with the actual length of the block, 5.08 cm. It is evident that the runs are reproducible within the error in controlling the input voltage and the instrumental errors of measurement.

The expansion of the block may be described by the equation

$$x=\frac{8.28\times10^{-3}}{5.43\times10^{-4}}[1-\exp(-5.43\times10^{-4}t)].$$

Within an interval of 4.5 microns the slope of the curve changes from 7.7×10^{-3} microns per second at two minutes to 6.0×10^{-3} at twelve minutes elapsed time. If an interval of fifteen seconds is taken between each slice, the advance of the specimen will be 0.115 microns at the beginning of the run and 0.090 microns at the end of the run. It may be possible to decrease the rate constant still further by providing better insulation.

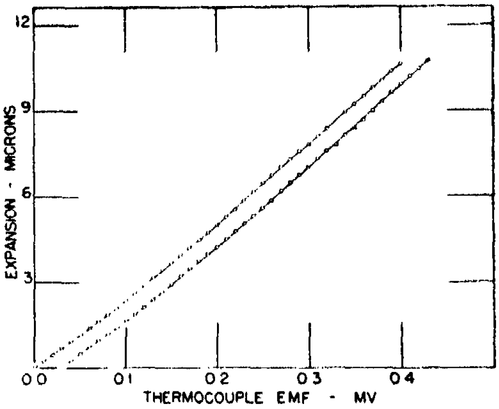

FIG. 6. A plot of two typical runs with the electrically heated specimen holder. Expansion *vs.* thermocouple voltage.

TABLE I.

Expansion-microns	1.00	2.00	3.00	4.00	5.00
Holding resistance-ohms	228	138	98	76	62

It can be seen from Fig. 6 that the specimen holder advances about one micron for each degree rise in temperature. Consequently, forty thin sections might be cut in an interval of four degrees. It is doubtful that such a small change in temperature will effect the physical properties of the specimen or the imbedding plastics.

In order to test the modified specimen block in operation, tissue specimens imbedded according to the technique of Newman, Borysko, and Swerdlow[8] were inserted in the block and cut using a twenty second time interval between slices. No attempt was made to determine the thickness of each slice but a slice was cut from the specimen with each stroke of the wheel. Disturbances such as door slamming will cause the microtome to skip only when the disturbance occurs at the instant of cutting.

Ordinarily an interval of twenty seconds leaves ample time for the operator to remove the slice from the knife and transfer it to the spreading solution. In order to introduce a little more flexibility, a holding circuit was introduced. A variable stepwise resistor was put into the circuit so that it might be inserted in series with the Variac output by means of a double-pole double-throw switch. The holding resistance was defined as the resistance in series with the heater that decreased the rate of expansion to less than 0.01 micron/minute as indicated by the displacement gauge. The holding resistance for various displacement readings is given in Table I.

THE REVIEW OF SCIENTIFIC INSTRUMENTS VOLUME 21, NUMBER 9 SEPTEMBER, 1950

Physical Instruments for the Biologist

Detlev W. Bronk
Associate Editor in Charge of This Section
Eldridge Reeves Johnson Foundation for Research in Medical Physics,
University of Pennsylvania, Philadelphia, Pennsylvania

A Differential Vectorcardiograph*

Stanley A. Briller, Nathan Marchand, and Charles E. Kossmann
*Department of Medicine, New York University College of Medicine, and the Adult Cardiac Clinic,
Third (New York University) Medical Division, Bellevue Hospital, New York*

(Received February 27, 1950)

A vectorcardiograph was designed and constructed for the purpose of separating and recording the temporal components (*P* form, *QRS* form, and *T* form) of the spatial vectorcardiogram in two planes.

The equipment consists of a network to convert the patient voltages into an orthogonal set, a three-channel low frequency amplifier, a synchronized timing unit, a dual-beam oscilloscope, a time marker, an electronically operated camera, and a simultaneous direct-writing recorder.

I. INTRODUCTION

THE usual clinical electrocardiogram is a record of the differences in potential between two points on the surface of the body caused by electromotive forces generated in the heart. These forces vary in size and direction with time, and are subject to a vector-time type of analysis. Assuming, among other things, a point source of the forces in the body, a figure may be constructed for any complete or partial cycle of electrical events occurring either in the atria or in the ventricles by connecting the heads of successive vectors. Such a figure is called a monocardiogram,[1] vectordiagram,[2] vectorcardiogram,[3] or cardiovectorgram.[4] Since two almost inverse electrical processes, excitation and recovery, occur in the normal heart in a relatively fixed sequence, it would be expected that four separate vectoral forms (loops) for each cardiac cycle could be synthesized from a study of surface leads. These have come, by usage, to bear the names of *P* form, T_a form, *QRS* form, and *T* form.

Such vectorcardiograms are three dimensional in the body. Analytical or instrumental synthesis of the spatial forms from surface leads gives rise to what is known as the spatial vectorcardiogram. This is a manifest record; the generator value of the spatial vectorcardiogram cannot be measured because of the unknown attenuating effects of the surrounding volume conductor.

From the points of view of greater simplicity in clinical recording and a newer approach to certain fundamental problems it seemed desirable to devise an instrument which would make it possible to record each of the vectoral forms independently. Vectorcardiographs with different recording principles have been designed,[1–9] but separate recording of the four forms by electrical circuits has not, to our knowledge, been achieved. To report the design and construction of such an instrument, called a differential vectorcardiograph, is the purpose of this paper.

II. GENERAL DESCRIPTION

Voltages are picked up by means of German silver electrodes placed on the arms, on the left leg, and on the back to the left of the seventh dorsal spine. The connection to the right leg is used as a ground return. The voltage expected with each heartbeat from any pair of surface electrodes consists of a group of summits and depressions which are called *P*, T_a, *Q*, *R*, *S*, and *T* (Fig. 3). The time relationships of the 4 vector forms of each heartbeat remain fixed within workable limits for any one subject, but the repetition rate of groups will change since not even the normal heart beats with perfect regularity. It is desirable then for the purpose of separation to activate all timing circuits within the group. The first voltage which is ordinarily available in each group is the beginning of the *P* wave, one of the smallest and slowest rising voltages in the human electrocardiogram.

For presentation purposes, the two planar projections utilized are the frontal (*XY*) and the sagittal (*ZY*). The time dimension is furnished by interrupting the oscilloscopic trace at intervals of 5 milliseconds. The problem of transforming the nonorthogonal voltages obtained from the patient to the classical *X*, *Y*, and *Z* projections

---

* This work was supported by grants from the Knapp Foundation and the New York Heart Association.

[1] H. Mann, Arch. Int. Med. **25**, 283 (1920).

[2] Schellong, Heller, and Schwingel, Zeits. f. Kreislaufforsch. **29**, 497, 596 (1937).

[3] F. N. Wilson, and F. D. Johnston, Am. Heart J. **16**, 14 (1938).

[4] R. Sulzer, and P. W. Duchosal, Cardiologia **6**, 237 (1942); Cardiologia **9**, 106 (1945).

[5] F. Schellong, *Grundsüge einer klinischen Vectordiagraphie des Hersens*, (Verlag. Julius Springer, Berlin, 1939).

[6] M. M. Vastesaeger and J. Rochet, Trav. Lab. Inst. Solvay Physiol. **4**, 29 (1944).

[7] W. Hollmann, and E. Guckes, Arch. f. Kreislaufforsch. **4**, 69 (1939).

[8] P. Cantonnet, and J. B. Milanovitch, C. R. Soc. de Biol. **141**, 614 (1947).

[9] P. W. Duchosal, and R. Sulzer, *La Vectocardiographie* (S. Kargen, Bâle, Switzerland, 1949).

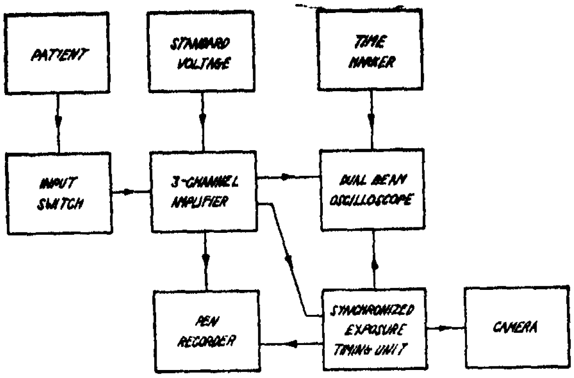

FIG. 1. Block diagram of the differential vectorcardiograph.

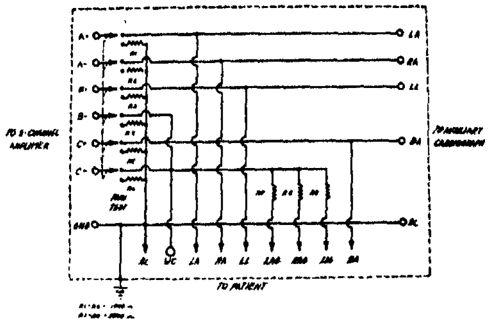

FIG. 2. Schematic circuit diagram of the input switch.

is solved by the methods of Wilson and Johnston,[8] and of Wilson, Johnston, and Kossmann.[10]

Permanent records are obtained by photographing the oscilloscopic images of successive heartbeats. This is done in a semidark room with orthochromatic film (duPont No. 201). The oscilloscope is blanked at all times except during exposure. The time of onset and the duration of exposure is determined by the synchronized exposure timing circuit. Following exposure, the film is automatically advanced in the camera by a solenoid mechanism.

In Fig. 1 is shown a block diagram of the complete instrument. The patient voltages are fed into an input switch (Fig. 2) which has a twofold function: (1) to convert the patient voltages with subsequent amplitude corrections into an orthogonal set; (2) to replace the patient with an equivalent resistive network for balancing and adjusting the circuits.

Three voltages are obtained from the input switch representing the X, Y, and Z projections of the heart voltages. The peak magnitudes of these voltages are of the order of one millivolt. These are amplified separately in a three-channel amplifier.† Each channel is a highly balanced push-pull unit with low hum level. The gain of each is individually controlled and is calibrated by the application of a standard millivolt to the input while a photograph of the oscilloscopic output is taken. The voltage gain is such that about 200 volts is available at the output for every millivolt at the input.

The three outputs of the amplifier are fed into a dual-beam oscilloscope. They are paired off on the deflection plates to create the two desired planar projections (XY and ZY). The outputs from the amplifiers are also fed into a three-channel direct-writing recorder† which furnishes a continuous simultaneous record of the three individual channel outputs.

The outputs of the amplifiers are also fed into the synchronized exposure timing unit where a switch is used to select the channel having the P wave most suited for tripping the trigger circuits. The trigger circuits which form the synchronized exposure timing unit supply two voltages, both in the form of rectangular pulses. The first of these determines the exposure time. The starting time of this exposure voltage is determined by a variable delay which can start the exposure as early as the beginning of the P wave or as late as the end of the T wave. The exposure time is also variable so that either a complete or partial vector form can be photographed. A portion of the exposure timing voltage can be applied, by means of a switch, to one of the three direct-writing units and thus furnish an accurate record of those electrocardiographic deflections actually photographed on the face of the oscilloscopic tube. The second voltage supplied by this unit is a tripping voltage coincident with the end of exposure time. This output is used to advance the film to the next frame.

The time marker voltage consists of a series of rectangular pulses of adjustable width at a constant frequency. These voltages are applied to the grids of the cathode-ray tube.

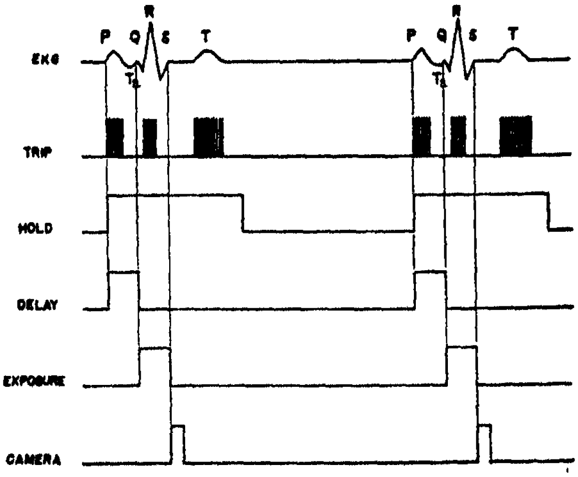

FIG. 3. Diagram illustrating the voltages generated by the synchronized exposure timing unit. The circuits have been adjusted to record the QRS deflections. All positive electrocardiographic voltages are transformed into a series of pulses by the "trip" circuit, but only the first pulse is utilized to energize the "hold" and "delay" circuits.

Simultaneous points are indicated by the vertical lines at P, Q, and S.

---

[10] Wilson, Johnston, and Kossmann, Am. Heart J. 33, 594 (1947).

† The three-channel amplifier and three-channel direct-writing recorder are those contained in the Technicon Cardiograph.

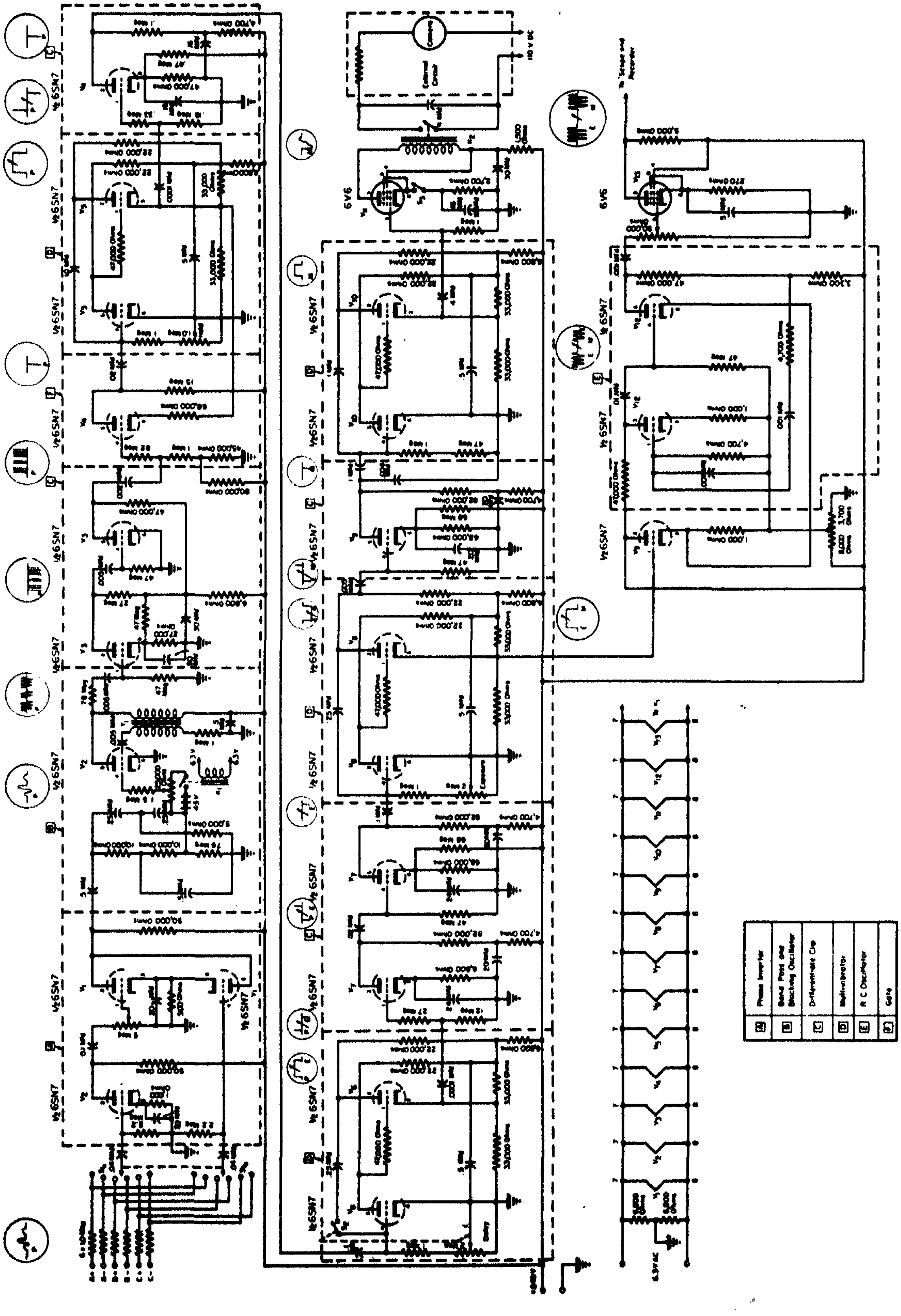

FIG. 4. Schematic circuit diagram of the synchronized exposure timing unit. Functional units of the circuit are enclosed in dashed lines and labeled to correspond to the reference table shown. Oscilloscopic traces are indicated in the circled areas. In these, "*P*" indicates the instant of rise of the *P* wave, "*E*" the beginning of the exposure period, and "*M*" onset of the pulse responsible for movement of the film.

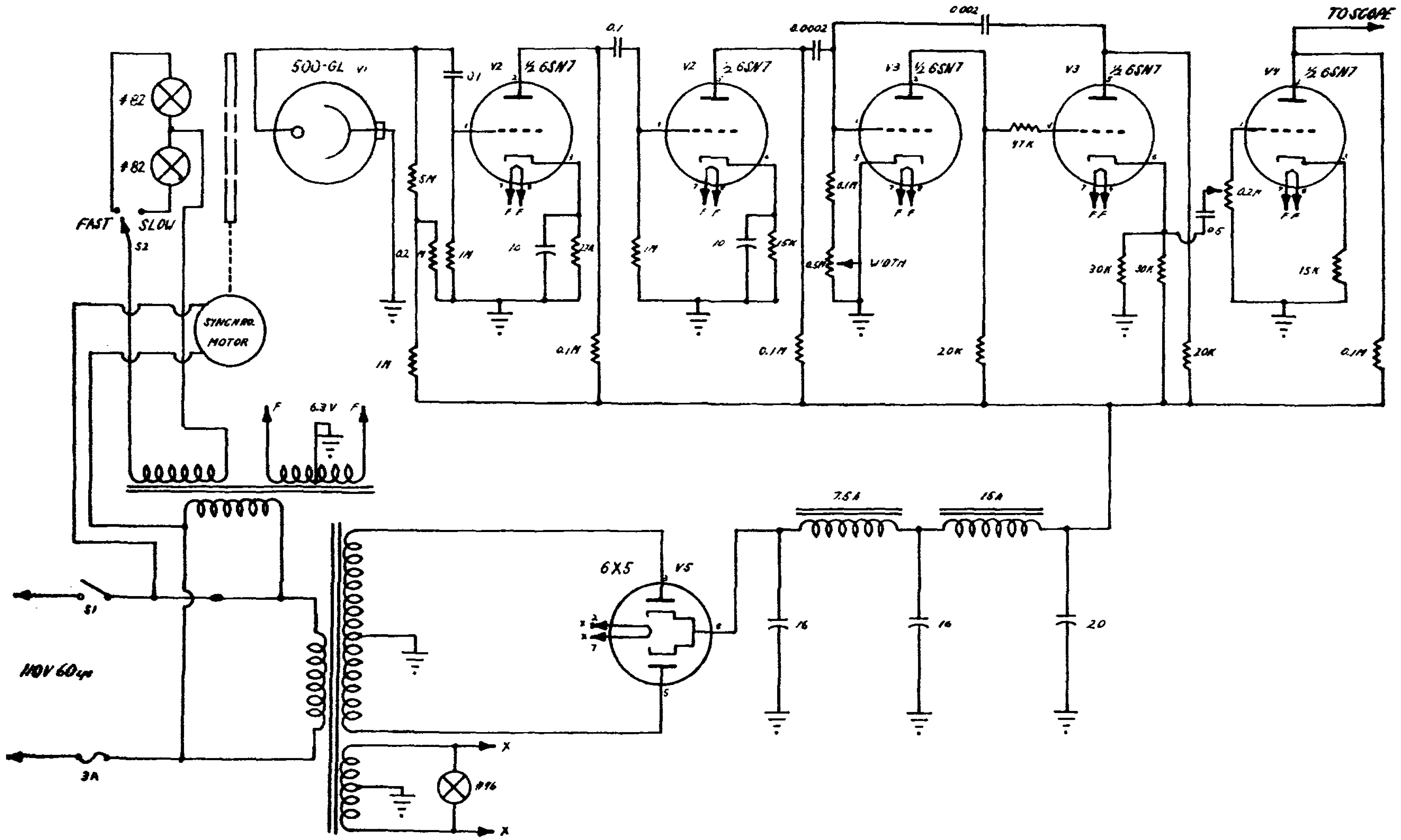

Fig. 5. Schematic circuit diagram of the time-marker unit.

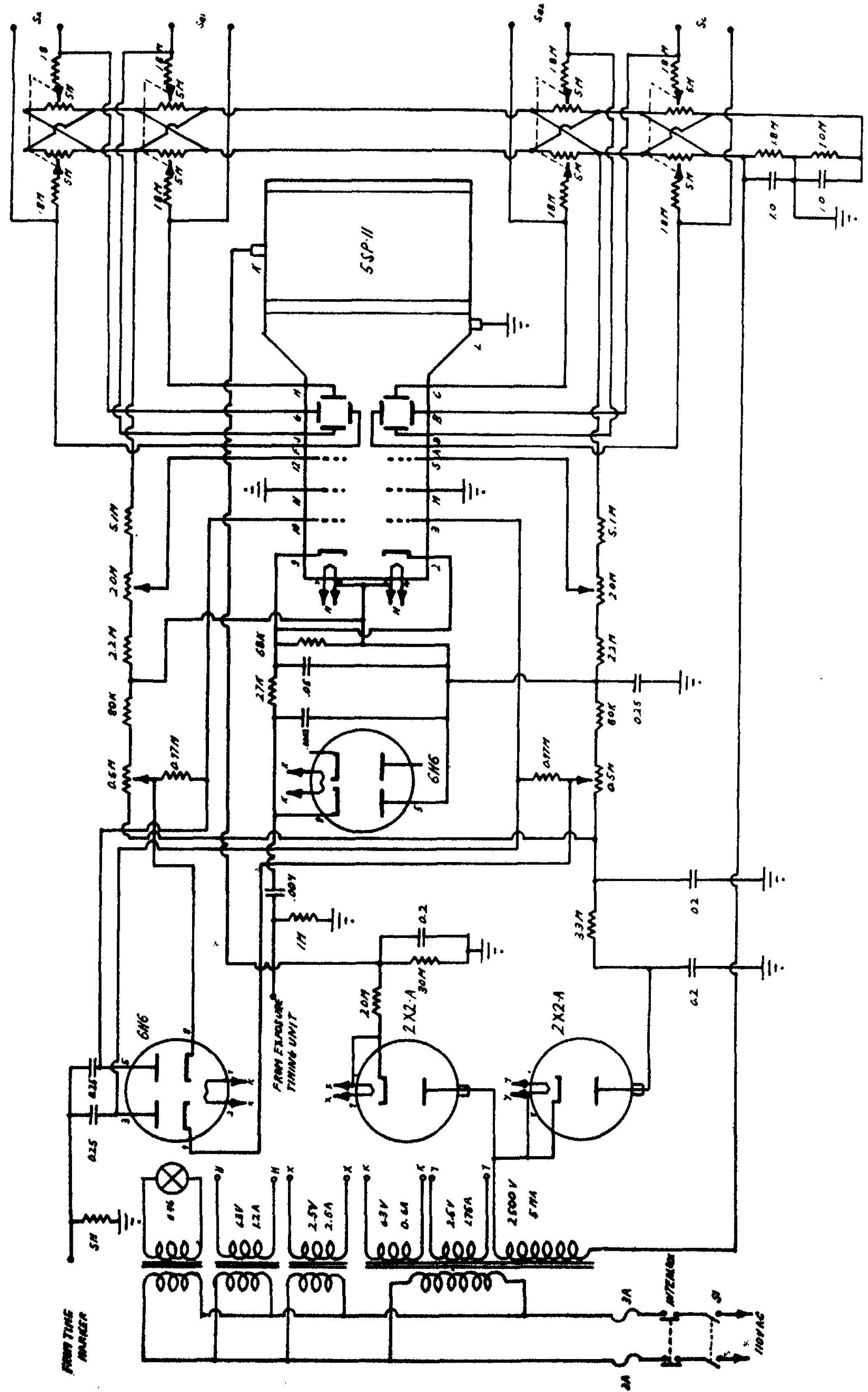

FIG. 6. Schematic circuit diagram of the dual-beam oscilloscopic indicator unit.

Individual regulated power supplies are utilized for each unit to prevent interaction and to reduce to a minimum the effect of power line fluctuations. Special care was given to filtering and decoupling, since even a slight amount of hum or coupling deteriorates the quality of the trace and interferes with the timing circuits.

III. CIRCUIT DESCRIPTIONS

1. The Synchronized Exposure Timing Unit

The time relationships of the important voltages in the synchronized exposure timing unit as compared with two typical, successive electrocardiographic complexes are shown in Fig. 3. In this instance the unit is adjusted to photograph the *QRS* form as a unit. A trip voltage is generated by the leading edge of each *P* wave. Because every other rise in voltage would similarly act as a triggering point, a hold circuit is initiated to inactivate the input until the entire cardiac cycle is completed. The leading edge of the hold voltage initiates a delay circuit and the trailing edge of this latter voltage trips the exposure voltage. The end of the exposure voltage operates the film advance circuit. The hold, delay, and exposure intervals may be varied.

A complete schematic circuit diagram is shown in Fig. 4. The transformation of the *P* wave into a sharp pulse coincident with its instant of rise is accomplished by applying the greatly amplified electrocardiographic voltage to a blocking oscillator which is biased just at cut-off. In a similar fashion, every other rise from the base line such as the *R* and *T* waves are transformed into a series of sharp pulses. To eliminate the effect of drift and pick-up, the input is applied through a band pass filter. The hold circuit allows only the first rise of a particular pulse group, namely that of the *P* wave, to pass to the timing circuits. This operation is accomplished by a gate tube biased by the hold voltage. The basic circuit employed to generate the hold, delay, exposure and camera trip voltages is the "one-shot" multivibrator. Coupling between the various stages is by conventional differentiation and clipping.

The cathode-ray tube is normally maintained at cut-off by the rectified output of a resistance-capacitance oscillator operating at a frequency of about 30 kc. Application of the exposure voltage cuts off the oscillator, gating the beam on. This method was employed to avoid d.c. coupling to a high voltage element.

The film advance circuit consists of a solenoid-operated, pull-down mechanism actuated by a relay. The inertia of the mechanism demands that the relay be held down for a finite amount of time; a separate fixed "one-shot" multivibrator performs this function.

2. The Time Marker

A metal disk driven by a synchronous motor is the basic timing unit. Equally spaced holes around the circumference of the disk interrupts a beam of light falling upon a photo-cell which generates a series of pulses. These pulses are sharpened by differentiation and clipping, and are then used to drive a "one-shot"

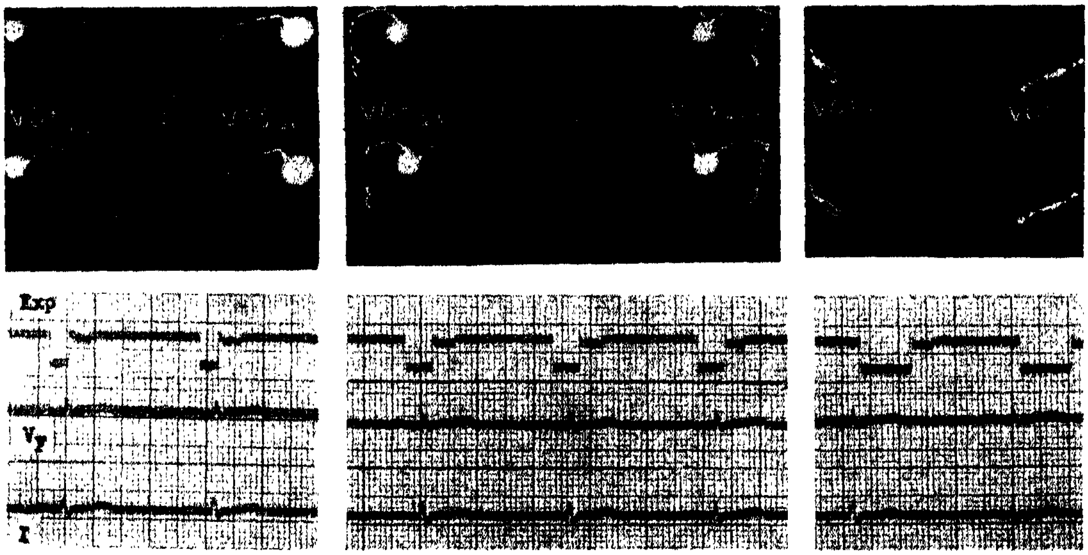

FIG. 7. Partial differential vectorcardiograms of the *QRS* and *T* forms of a normal subject in the frontal (*XY*) and sagittal (*ZY*) planes. In each instance two consecutive vectorcardiograms are shown. In the middle, the frontal (VGF_{QRS}) and sagittal (VGS_{QRS}) forms of the *QRS* complex are recorded. On the right, the frontal (VGF_T) and sagittal (VGS_T) forms of the *T* wave are shown. On the left a portion of the *QRS* is recorded in two planes to demonstrate clockwise rotation in the frontal plane (VGF_{QR}) and counterclockwise rotation in the sagittal plane (VGS_{QR}). The tracings are interrupted every 0.005 second. Below each pair of vectorcardiograms are the simultaneous records made with the direct-writing recorder. The lower record (*I*) is the difference in potential between the two upper extremities or *X* component. The middle record (V_F) is the potential of the left leg or the *Y* component divided by $\sqrt{3}$; the upper record (*Exp*) shows by a downward deflection that part of the *QRST* complex which is recorded in the vectorcardiogram. The small deflections before or after the main downward displacement in this record are artifacts.

multivibrator. For clarity of presentation, the width of the timing pulse is made variable. These pulses are impressed on the grid of the cathode-ray tube. The circuit diagram of the time marker is shown in Fig. 5.

3. The Cathode-Ray Oscilloscope

In Fig. 6 is shown a schematic diagram of the oscilloscopic indicator unit with its power supply. Because of its special requirements, it was necessary to construct rather than purchase this apparatus.

The power supply is standard and employs the 2X2 tubes in a voltage doubling circuit. The usual coupling capacitors employed to isolate the centering circuits on the deflection plates are not shown because these capacitors are incorporated in the amplifier chassis. It was found advisable to incorporate two separate blanking circuits, one for the time marker and the other for the exposure timing pulses. Since the former are short duration pulses, they are impressed upon the two cathode-ray tube grids through a pair of 0.25 microfarad capacitors. The 6H6 double diode is employed as a d.c. reinserter to prevent the grid bias from shifting as the time marker pulses are varied in size or width. Beam brightness thus is maintained constant.

The 30-kc carrier of exposure pulses is coupled into the oscilloscopic indicator unit through a 0.004-microfarad capacitor. It is rectified in one section of a 6H6 double diode and then filtered. The filtered voltage is then impressed directly on the cathodes of the cathode-ray tube.

4. The Camera

A modified Sept camera of French origin is employed to record the oscilloscopic traces. The pull-down mechanism, originally spring operated, was replaced by an electric solenoid. The shutter of the camera was removed. A stand was constructed to hold the camera conveniently in front of the cathode-ray tube. To reduce the force necessary for pull-down, the film is fed directly into a collection bag at the bottom of the camera.

5. The Amplifier Unit

The amplifier employs three push-pull resistance-capacitance stages of voltage amplification in each channel. Low frequency compensation is employed to bring the frequency response to below 0.25 c.p.s. This results in a flat frequency response from 0.25 c.p.s. to 150 c.p.s. The hum level without the patient connected in circuit is kept below an equivalent input level of 10 microvolts.

Since the cathode ray is inertia-less, no damping is necessary and no overshoot is encountered in the vectorcardiographic tracings. The standardization voltage is inserted in the cathodes of the first stages, all standardizations being impressed at once.

IV. RECORDS

Examples of differential vectorcardiograms are presented in Figs. 7 and 8. In the former, a strip of simultaneously recorded standard electrocardiograms (Lead I, x component and Lead V_F, y component/1.7) is shown. Exposure time is recorded above the electrocardiograms. Figure 7 also illustrates the method of obtaining the direction of rotation of a form (loop). By decreasing the exposure time only a portion of the loop is recorded. Comparison of this trace with any other complete loop immediately indicates the origin and hence the direction. Figure 8 shows variations of successively recorded QRS forms with respiration.

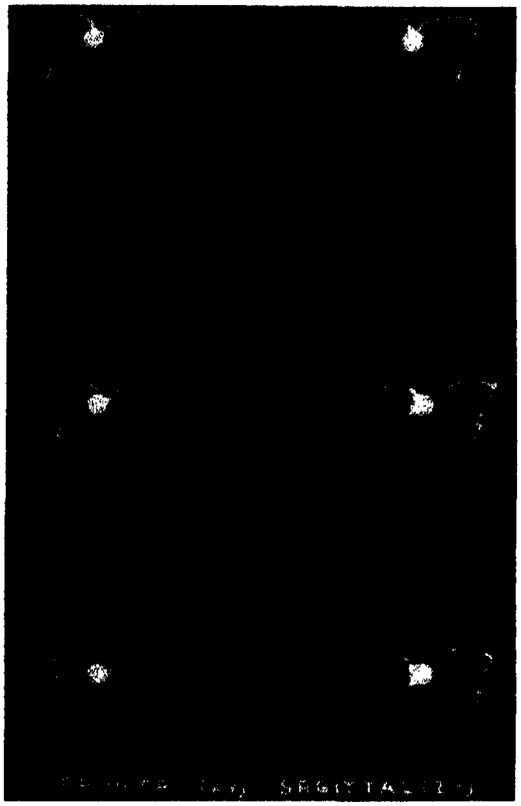

FIG. 8. Frontal and sagittal vectorcardiograms of QRS of three successive heart beats. Variations in the QRS form are due to respiration. Trace interruptions occur every 0.005 second.

V. PROCEDURE

The amplifiers are first balanced for hum and standardized for gain. A short preliminary recording is made of the orthogonal lead on the direct writer. The duration of $PQRST$ ($P-T$ interval) is observed and the calibrated hold-control set accordingly. Also from the recording the lead containing the tallest P wave is selected by means of a selector switch (switch 1 in Fig. 4) and applied to the synchronized timing circuit. Careful adjustment of the blocking oscillator bias control (Fig. 4, B) will result in reliable tripping of the timing circuits at the beginning of each P wave. The hold and exposure controls are then set to obtain the desired portions of the PQRST group under study.

THE REVIEW OF SCIENTIFIC INSTRUMENTS VOLUME 21, NUMBER 9 SEPTEMBER, 1950

Laboratory and Shop Notes

Expansion Valve for Triggered Cloud Chambers*

Jacob L. Zar
New York University, Washington Square College, New York
April 4, 1950

It has been shown that sharp tracks can only be obtained in a counter-controlled cloud chamber if the time between passage of the triggering particle and the condensation of water droplets is of the order of 0.01 sec.[1] For this type of chamber, an expansion valve and control circuit have been built which are believed to have the advantages of simplicity, ease of construction and rapidity of action.

The valve shown in Fig. 1 is a modification of the one described by Fussel,[2] in which an unsupported rubber ring is sealed against a valve disk mounted on a solenoid armature. The magnetic force on the armature in the closed gap position is sufficient to hold the valve closed; but when the exciting current is removed, air pressure against the disk provides the necessary force for rapidly opening the valve.

A commercially manufactured solenoid is used in place of the laboratory-made units that have been described.[2–4] The one that was found most suitable for a three-inch valve port was the Allen Bradley No. 4 product. Its coil is the standard one supplied for 110 v 60 c although direct current is actually used in this application. The following operating characteristics were determined with the return spring removed: Coil resistance is 25 ohms; normal operating direct current of 0.5 amp. provides 60-lb. force in the closed gap position; a direct current of 0.75 amp. is required to raise the armature against gravity with the gap fully open. In order to increase the speed of operation, the copper shading coils were removed from the face of the gap. The valve disk is three in. in diameter and, together with the solenoid armature, weighs 0.62 lb. If the air pressure acting on the valve is 4 p.s.i., its acceleration is 45 g, and it will open $\frac{1}{16}$ in. in 0.003 sec.

The operating circuit is shown in Fig. 2. The solenoid coil is connected in the "galvanometer position" of a Wheatstone bridge powered by the 110-volt d.c. line. One arm of the bridge is a 2050 thyratron. Its equivalent resistance can be obtained from the fact that its voltage drop is 12 volts when conducting. Normally the thyratron tube is off and the bridge is unbalanced. A coil current of 0.5 amp. holds the valve closed against the force of air pressure. A positive pulse arriving at the grid fires the thyratron, shuts off the coil current, and initiates an expansion. By a judicious choice of bridge resistances the solenoid current can actually be reversed slightly when the tube is conducting. This increases the speed of operation of the valve by counteracting the effect of the inductance and coercive force of the solenoid.

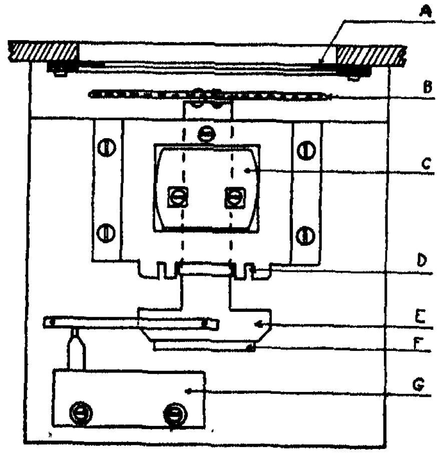

FIG. 1. The expansion valve. *A* is a rubber ring; *B* is the valve disk; *C* is the solenoid coil; *D* is the space where the shading coils have been removed; *E* is the armature; *F* is a stop plate; *G* denotes two microswitches.

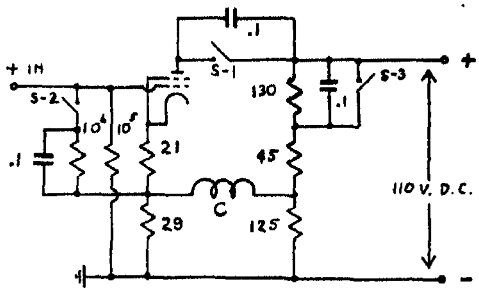

FIG. 2. Wheatstone bridge type circuit for triggering expansion valve. The tube is a 2050 thyratron. *C* denotes the expansion valve coil.

The solenoid armature also operates two microswitches by means of a pivoted link. One of these, S_1, extinguishes the thyratron; the other (not shown in Fig. 2) starts a motor-operated set of switches to prepare the cloud chamber for its next expansion. One of these switches, S_3, momentarily short circuits a section of one of the bridge resistors to increase the solenoid current for reclosing the valve. S_2 is a pushbutton that manually fires the thyratron for testing the operation of the cloud chamber.

The values given in Fig. 2 were chosen for a low resistance coil and are consequently wasteful of power. In many installations this is of little importance. However, in those instances where a d.c. power line is not available, it is advantageous to use higher values of resistance for both the Wheatstone bridge and the solenoid coil. In the Allen Bradley solenoid the coil is very easily removed and replaced with one having more turns of finer wire. The bridge may then be designed with sufficient resistance to operate from a standard *B* supply.

To test the speed of operation of this valve, a contact was mounted directly beneath the valve disk and an oscillograph used to time the delay between the arrival of a pulse and the start of an expansion. It was found that the valve was in actual motion 0.003 sec. after being triggered.

The assistance of a grant by the Research Corporation is gratefully acknowledged. Credits are also due Mr. J. Hershkowitz for valuable help in the construction of this valve, and the late Dr. I. S. Lowen who sponsored the research at the time this work was done.

---

* Assisted by the joint program of the ONR and AEC.

[1] N. N. Das Gupta and S. K. Ghosh, Rev. Mod. Phys. 18, 225 (1946).

[2] L. Fussel, Jr., Rev. Sci. Inst. 10, 321 (1939).

[3] F. S. Chu and G. E. Valley, Rev. Sci. Inst. 19, 496 (1948).

[4] W. Y. Chang and J. R. Winckler, Rev. Sci. Inst. 20, 276 (1949).

Waterproof Cable Connectors

K. Feldman
Division of Physics, National Research Council, Ottawa, Canada
March 23, 1950

The need for waterproof cable connectors sometimes arises in situations where, due to space or other limitations, commercially available connectors are unsuitable. The simple solution that was found satisfactory in one such case is described below in the hope that it may be helpful to others faced with similar problems.

It was required that a connection be made between two portions of a cable of $\frac{3}{16}$-in. diameter. The cable contained two conductors to be operated at a potential difference of about 1000 volts. The connection was to be used under a 1000-foot head of water and its diameter was not to exceed one inch.

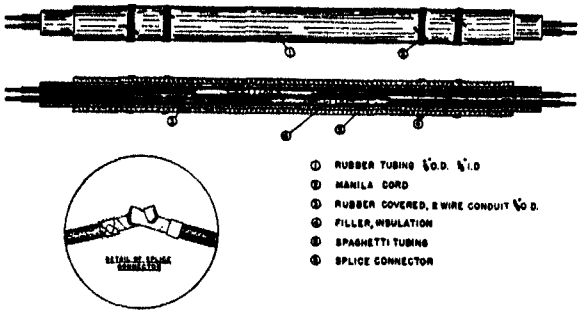
①
②
③
④
⑤
⑥
DETAIL OF SPLICE CONNECTOR
① RUBBER TUBING ⅞"O.D. ⅝"I.D
② MANILA CORD
③ RUBBER COVERED, 2 WIRE CONDUIT ½"O.D.
④ FILLER, INSULATION
⑤ SPAGHETTI TUBING
⑥ SPLICE CONNECTOR

FIG. 1.

The connection was made as follows. (See Fig. 1.) The jacket on each cable was split lengthwise for a few inches to expose the conductors. The corresponding conductors were then connected by the use of disconnect splices of the type indicated in the diagram. These connections were displaced from each other along the cable and were further insulated with spaghetti tubing. The split portions of the cable jacket were then cut back sufficiently to neatly close over the connections.

The connection was rendered waterproof by the use of a length of rubber tubing (⅝ in. i.d. by ⅛ in. wall) slipped over the joint. Suitable cord was then tightly wrapped and tied around the tubing at each of two places near each end.

Such connections have given satisfactory service in the field as well as in laboratory tests. They can be made or broken in a few minutes and practically no tools are required.

Motion within a Vacuum System

FRED A. MCNALLY
Research and Development, Jarrell-Ash Company, 165 Newbury Street, Boston, Massachusetts

July 11, 1950

IN high vacuum evaporation, motion controlled by the operator is frequently desired in order to shield unwanted films from the object. Most systems have a motion introduced by one of several mechanical arrangements. A convenient method used in this laboratory for many months makes use of a set of selsyn motors which were obtained from war surplus instruments.

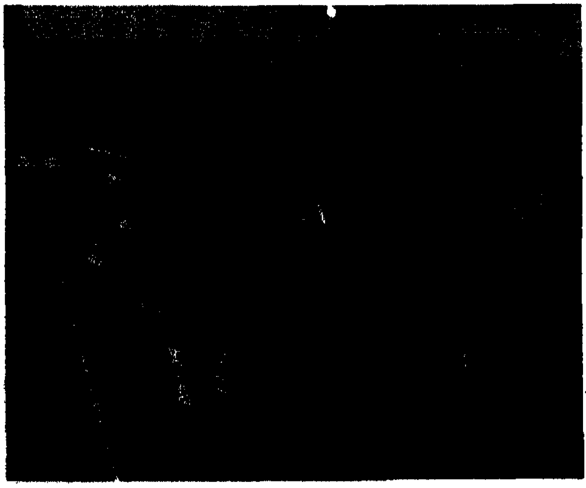

FIG. 1. Base plate arrangement.

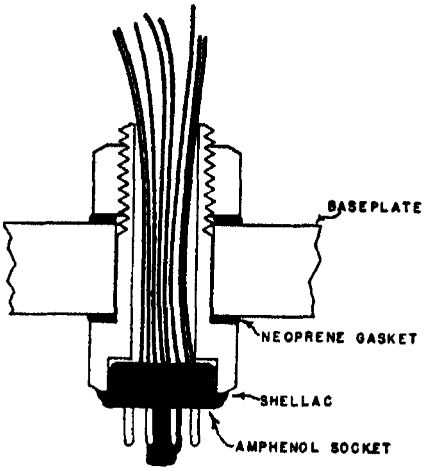

FIG. 2. Lead-in wire seal.

The vacuum system is one using an 18×30 in. belljar with a 6-in. diffusion pump. The repeater motor is centered over the baseplate as shown in Fig. 1. Holding the repeater is a brass disk which is placed high enough to prevent any loss in pumping efficiency.

Five lead-in wires are necessary and several methods of introducing them into the vacuum were tried. Finally a 1-in.-8 bolt, drilled through as suggested by Strong,[1] was fitted outside with an Amphenol PM-8 socket (Fig. 2). In addition the octal socket gives three extra leads for other purposes. Plastic insulated wire was not found to be satisfactory within the vacuum but most silk insulated wire gives no trouble.

The power requirement originally was 115 v 400 cycle and supplied a torque of approximately 54-in. ounces. The system is operated very well however at 20 v 60 cycle giving plenty of torque to rotate the 3-ounce aluminum shield.

By means of a dial on the control panel, the shield may be brought to any angle covering completely the evaporation from any of the eight filaments. The system has been useful in producing multi-layer films and partial-transmission filters.

[1] J. Strong, *Procedures in Experimental Physics* (Prentice-Hall, Inc., New York), p. 131.

A Self-Triggering Cloud-Chamber Counter

E. L. FIREMAN* AND G. M. MCHANEY†
Palmer Physical Laboratory, Princeton University, Princeton, New Jersey

June 29, 1950

A SELF-TRIGGERING cloud chamber was made by inserting open counters inside an ordinary cloud chamber. The cloud chamber triggered itself by the coincident counter pulses and the corresponding tracks were observed.[1] This type of chamber permitted the observation of rare events involving coincidences of soft particles, e.g. pairs of electrons from extremely weak sources. It was about 1200 times more sensitive for coincidence electrons than was the corresponding randomly expanding cloud chamber, and therefore was suited to investigate the previously reported possibility of double β-decay in Sn^{124}. The following is a description of this apparatus together with some preliminary results.

The cloud chamber was cylindrical, having an 8½-in. inner diameter and a 4½-in. depth. Ordinary tank argon and helium were used; it was necessary to dessicate the alcohol for good counter operation. Dried ethyl, iso-propyl, and iso-amyl alcohol were used as the condensible cloud and counter quench vapors;

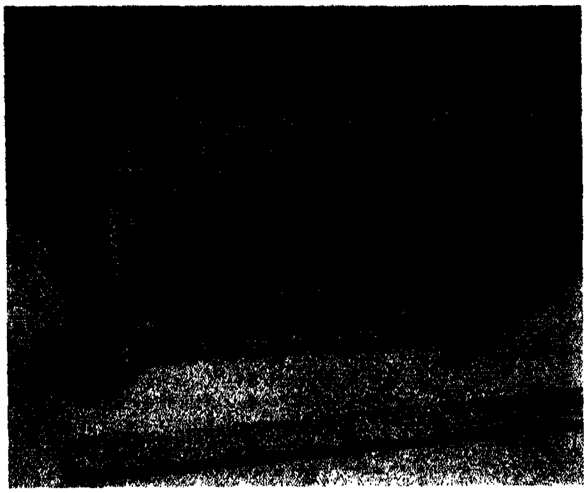

Fig. 1.

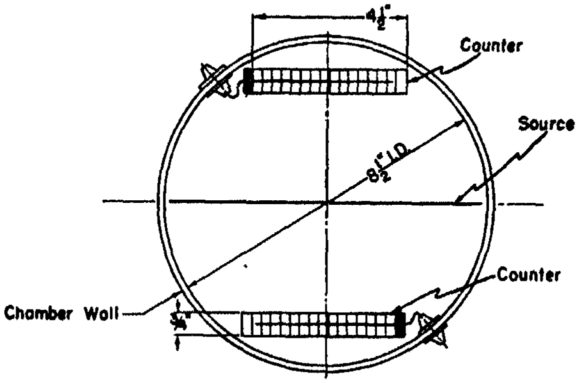

CLOUD CHAMBER COUNTER (Top View)

Fig. 2.

the heavier alcohols seemed to work slightly better. The chamber operated well at pressures between 1 and 2 atmos. No attempt was made to work at other pressures. The counters worked equally well in the proportional and Geiger regions. Since we were interested in events involving soft electrons, we took pictures only from coincident Geiger pulses.

Figure 1 is a photograph of one of the counters. Figure 2 is a diagram of two such counters in the chamber with a source between them. The rectangular copper frame in the center of the counter served to support four turns of 1 mil tungsten wire. The outer wire (No. 22) served as the counter cathode at ground potential. Although various counter sizes were used, a size of 4×4½ in. subtending a solid angle of 0.25 sterad. at the chamber center was most convenient. It was found necessary to bring the counter high voltage leads in through the cylindrical glass wall to avoid surface leakage pulses. Figure 3 shows the plateau curve of two counters having different dimensions. The threshold for Geiger action in argon was about 100 volts higher than in helium; this threshold increased by 200 volts as the pressure increased from 1 to 2 atmos. The threshold also rose slightly with the age of the counter filling (~100 volts/week). The counter pulses were normal, having an amplitude of 0.1 volt at the Geiger threshold. This amplitude increased with the voltage above the threshold. The counter voltage was removed immediately after an expansion because the reduced pressure caused the counter to count very rapidly. This in turn increased the recovery time of the chamber, i.e., the smallest permissible time between successive pictures. As our chamber was usually operated the counter voltage decreased to zero within 2 sec. after the expansion and the recovery time was 90 sec. The chamber could be operated continuously under these conditions for about two weeks before it was necessary to refill. The chamber was in a dark room with the temperature controlled to 1°C. The camera was open all the time and the pictures were taken by flashing the lamps between 3×10^{-3} and 3×10^{-1} seconds after the coincidence. Some of the positive ions from the counters drifted through the counter wires into the center of the chamber. For long lamp delays (>0.1 sec.) it was necessary to place a 1-mil cellophane sheet over the inner side of the counters to retain these ions.

This chamber was used to investigate the previously reported[3] coincidence activity from Sn with the aim of getting more definitive evidence as to whether or not it was a double β-process. Figure 4 is a self-triggered cloud chamber picture showing a pair of electrons from a 1-mil Sn foil of ordinary isotopic constitution. The chamber filling was argon with dried alcohol. Coincidence electrons were observed from various Sn samples, but the measurement of the momenta of the electrons in a field of 300 gauss was not successful because the multiple scattering in argon gave rise to curvatures as great as the magnetic field curvature in

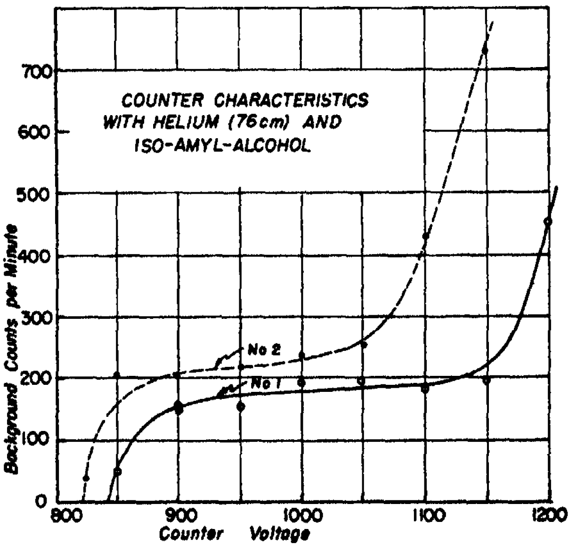

Fig. 3.

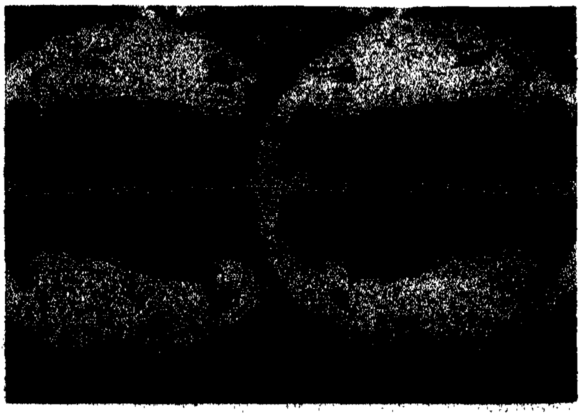

Fig. 4.

more than 50 percent of the cases. Therefore, it was not possible to say whether or not the coincidence electrons were electron-positive pairs, β-internal conversion electron coincidences, or double β-electrons. Self-triggered tracks in helium were not satisfactory even though good electron tracks were observed on random expansions. The reason for this is thought to be the rapid ionic diffusion and mobility in helium.[3] The expansion valve opened about 20×10^{-3} sec. after the coincidence. The clearing field (250 volts) was removed by a 2050 thyratron about 10^{-6} sec. after the coincidence.

In order to obtain momentum measurements of sufficient accuracy to identify with certainty the coincidence process, it would be necessary to use helium with a magnetic field of 1000 gauss or more. Since there did not remain sufficient time to make the required change here, it was decided to report on the apparatus and preliminary results at this time.

We are indebted to Professor R. Sherr for suggesting and supervising the present investigation and to Professor M. G. White whose advice and encouragement are gratefully acknowledged.

---

* AEC Postdoctoral Fellow (November 18, 1948 to November 18, 1949).

† Lt. Col. McHaney, U. S. Army.

[1] A cloud chamber triggered by big ionization pulses was built by M. J. Cohen. See Princeton thesis (1950); Phys. Rev. 74, 1244 (1948).

[2] E. L. Fireman, Phys. Rev. 74, 1238 (1948); Phys. Rev. 75, 323 (1949).

[3] P. M. S. Blackett, Proc. Roy. Soc. 146, 281-299 (1934).

A Diamond Bomb for Obtaining Powder Pictures at High Pressures

A. W. Lawson and Ting-Yuan Tang
Institute for the Study of Metals, University of Chicago, Chicago, Illinois

July 7, 1950

RECENTLY a procedure for obtaining x-ray powder diffraction patterns of materials subjected to high hydrostatic pressures has been described in this journal by N. A. Riley and one of the authors.[1] This technique involves the use of a large grain size beryllium bomb for retaining the pressure. Transmission diffraction patterns of samples retained by the bomb are obtained by traversing both the bomb and the sample with an x-ray beam consisting of 50-kv molybdenum K-α-radiation. Because of superposition of the Debye-Scherrer rings diffracted by the bomb, only five or six rings diffracted by the sample are clearly discernible. As a result, the technique is severely restricted in application.

This restriction is considerably reduced by using a single crystal bomb. Indeed, a single crystal Be bomb was constructed and it was possible to recognize fifteen or twenty rings diffracted by the sample (in this case calcite). Unfortunately, however, the Be bomb, although rather brittle at ordinary pressures, is too plastic above 10,000 atmos. to be suitable. For this reason, we have tried using a bomb constructed of diamond and found notable improvements in performance over the older technique at pressures ranging up to 25,000 atmos.

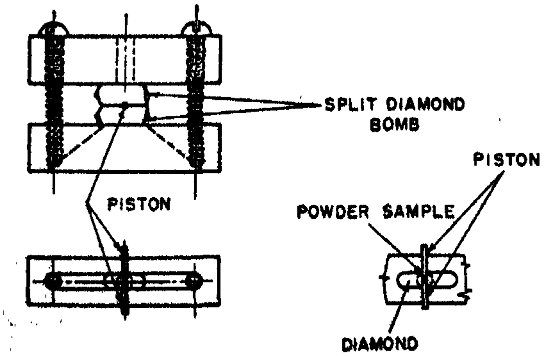

FIG. 1. Diamond bomb assembly.

The exact construction is shown in Fig. 1. The bomb consists of two diamonds, lapped together. A hole 0.015 in. in diameter is drilled through the clamped pair in the manner indicated. The clamp is machined so as to allow the x-ray beam to strike the sample and be diffracted to a cylindrical film holder of the type previously described.[1] The diamond is split to facilitate cleaning of the diamond and removal of the pistons after the application of pressure. No particular precautions were taken to orient the diamonds since, in the selection of the diamonds, size and mechanical properties were given precedence. The cutting and polishing of the diamonds was done by Arthur Crafts and Company, Chicago, Illinois. Although the diamonds were transparent, small optical flaws and even slight cracks were visible under a microscope. These flaws did not appear to grow and otherwise cause trouble even after the application of 30,000 atmospheres pressure for many hours. The upper range of pressure utilizable is limited at the present not by the strength of the bomb but by the failure of the drill rod pistons. It is hoped to extend the range by the use of carboloy pistons.

The two diamond crystals give rise to relatively few Laue spots which cause little confusion in identification of the Debye rings from the sample. As a result we are able to recognize easily at least fifteen rings from a calcite sample. The principal disadvantage of the technique is the appreciably higher friction present in the system as a result of the smaller dimensions involved. Thus, when external loading of the system indicated a peak possible pressure of 30,000 atmos., only 23,000 atmos. were generated in the sample, as determined by lattice constant measurements on AgBr.

In conclusion, because of the insulating nature of the bomb and the conducting nature of the pistons, the possibility of using this technique for exploratory investigations of the change in conductivity and photoelectric properties as a function of pressure should be noted.

---

[1] A. W. Lawson and N. A. Riley, Rev. Sci. Inst. 20, 763 (1949).

A Resistance-Temperature Relation for Low Temperature Thermometry

Harold J. Hoge
National Bureau of Standards, Washington, D. C.

May 31, 1949

THE Callendar-Van Dusen equation, a polynomial in temperature, relates the resistance of a standard platinum thermometer to the temperature in a relatively simple way. Temperatures on the International Temperature Scale (ITS)[1] are defined by this relation from 0°C down to the oxygen point ($-182.970°\text{C}=90.190°\text{K}$), and although these temperatures are not in perfect agreement with the thermodynamic scale, they are sufficiently near it to make the ITS extremely useful for practical purposes. Nothing of equivalent accuracy and simplicity has been found for use at lower temperatures. A table giving R/R_0 as a function of T may be used,[2] but each thermometer must then be calibrated at a rather large number of points in order to establish its deviation from the table.

Recently C. S. Cragoe[3] proposed the use of the linear function $y(R)=(R-R_1)/(R_2-R_1)$, where R_1 and R_2 are the resistances of a thermometer determined at two calibration points, such as the normal boiling points of hydrogen and oxygen. Instead of computing temperature directly from R, the value of y is computed as an intermediate step, after which T is obtained from a master table $T(y)$ that is used for all thermometers. The only calibration of an individual thermometer required is the determination of R_1 and R_2. A proposal to extend the ITS below 90.19°K by this method was made by the National Bureau of Standards. The Advisory Committee on Thermometry to the International Committee on Weights and Measures received this proposal,

TABLE I.

Thermometer	R_0	$R_{20.273}/R_0$	α	δ	β
53	25.56716	0.0047033	0.00392366	1.495	0.1109
48	25.55641	0.0052010	0.00392092	1.496	0.1115
58	25.56384	0.0044661	0.00392596	1.491	0.1103

prior to revision of the ITS in 1948, but did not act upon it. The method gives an adequate temperature scale between 54.363°K (oxygen triple point), and 90.190°K (oxygen boiling point) when calibrations are made at these two temperatures. If calibrations are made at 20.273°K (boiling point of equilibrium hydrogen) and at 90.190°K, results in the interval between the calibration points are not so satisfactory, and the situation is not greatly improved by shortening the range to the interval between calibration points of 20.273° and 54.363°K.

It is the main purpose of this note to propose a somewhat different method of establishing a temperature scale, which on the basis of preliminary tests offers advantages over the methods described above. The advantages are greatest below 20°K, where previously-used methods have either failed or become difficult to apply. Let $P(T)$ and $Q(T)$ be two tables giving the resistances of two platinum resistance thermometers of rather different characteristics. Values of P and Q at 1-degree intervals are adequate for this purpose. Then it is found that the resistance R of a third thermometer can be expressed as a linear combination of the two functions P and Q. That is

$$R=AP+BQ+C, \qquad (1)$$

where A, B, and C are constants to be determined by calibrating the thermometer at three fixed points. This equation has been tested by using the temperature-resistance tables of 7 previously calibrated thermometers. The thermometers selected, and the particular combinations taken to represent P, Q, and R, were chosen to give a reasonable test of the procedure rather than to put the method in the most favorable light.

Two illustrative examples taken from the results will be given, involving the thermometers for which the constants are given in Table I. Using the equation $R_{53}\text{ calc.}=0.26789R_{48}+0.73286R_{58}+0.00097$, having constants determined at 13.813°, 20.273°, and 54.363°K, the maximum value of $\Delta T=(R_{53}\text{ obs.}-R_{53}\text{ calc.})\times(dT/dR_{53})$ between the two lower calibration points was 1 mdeg. and between the two upper points, 2 mdeg. Using only two calibration points, at 20.273° and 90.190°K, the equation $R_{53}=0.32116R_{48}+0.67935R_{58}$ was derived, and for this the corresponding maximum value of ΔT was 4 mdeg. at about 56°K. On the basis of the tests made thus far, the most satisfactory method of applying Eq. (1) appears to be to use a three-constant equation similar to the first example given above for the range below 54.363°K, and to use a two-constant equation ($C=0$) with constants determined at 54.363° and 90.190° for the range between these two calibration points. It may be possible to cover the entire range with a single equation by giving the constants A, B, and C a slight temperature dependence, but this has not been investigated.

The results of the tests of Eq. (1) indicate that above 20°K it should lead to a temperature scale reproducible within ±5 mdeg., with criteria for acceptable thermometers that are no more difficult to satisfy than those now contained in the ITS. Below 20°K, Eq. (1) gives a somewhat more accurate representation of the *resistance* of a thermometer than above. Because dR/dT becomes smaller in this region, however, the reproducibility of a temperature scale defined by Eq. (1) is not as good below 20°K as above. Even so the results are much superior to those obtained when the function $y(R)$ is used.

The electrical resistivity of a pure metal may be expected to be represented by some such function of temperature as that proposed by Gruneisen.[4] This function is defined by an integral similar to that which defines the Debye specific heat function, and in fact the Gruneisen function G and the Debye function D roughly satisfy the relation $G/T\doteq D$. Hence even if the correct analytical expression for the resistivity of a pure metal were known, it would probably be expressed in tabular form as a matter of convenience.

Without knowing the correct analytical expression for the resistivity of a pure metal, it is still possible to make assumptions about how this resistivity will be modified by the introduction of a small amount of impurity. If it is assumed that the modification is roughly proportional to the amount of a given impurity added, Eq. (1) becomes quite plausible. For P and Q then represent the resistance of the pure metal as modified by the presence of two different amounts of this impurity, and by compounding P and Q in different proportions it should be possible to represent the resistance of a sample containing some other amount of the same impurity. If two impurities are present, it might be expected that they would modify the resistance-temperature relation of the pure metal in different ways. It would then be necessary to use three suitably chosen functions to represent the resistance of a sample containing arbitrary amounts of either or both impurities. From the standpoint of resistance thermometry it is rather fortunate that it seems to be possible to lump together the effects of all impurities present, and even to include the effects of any differences in mechanical strain and number of lattice defects.

---

[1] H. F. Stimson, J. Research Nat. Bureau of Stand. **42**, 209–17 (1949), RP1962.

[2] Harold J. Hoge and Ferdinand G. Brickwedde, J. Research Nat. Bureau of Stand. **22**, 351–73 (1939), RP1188.

[3] Compare Daniel R. Stull, Chem. Eng. News **27**, 2772 and 2817 (1949); also National Bureau of Standards, memorandum relative to a 5th section . . . for the ITS of 1948, Procès-Verbaux Séances Comité International Poids Mésures 21, pp. T84–T88 (1948).

[4] See for example E. F. Burton, H. Grayson Smith, and J. O. Wilhelm, *Phenomena at the Temperature of Liquid Helium* (Reinhold Publishing Corporation, New York, 1940), p. 278.

Note on Reduction of Background Fog in Nuclear Emulsion Plates

P. K. S. WANG
Betatron Section, National Bureau of Standards, Washington, D. C.

June 8, 1950

SOME difficulty has been encountered because of electron background in nuclear emulsion plates exposed directly in the x-ray beam of a betatron.[1,2] This note will describe a refixation technique that helps to reduce the electron background density of emulsions.

Because nuclear photo-disintegration cross sections are small compared with electron pair production cross sections, the number of background electrons is necessarily large when nuclear disintegrations are investigated in plates. The emulsions are usually so blackened that a special technique has to be applied to make the disintegration tracks observable. Recently we found that refixation of the processed plates in Kodak liquid x-ray fixer was very effective in reducing the dense electron background. The reduction of the silver grain density in emulsion plates by refixing is a phenomenon similar to that found in standard negative film and thoroughly investigated by Russel and Crabtree.[3] No adequate description of the basic mechanism has been given.

The refixation technique can be best described by the following experiment: Several Ilford E-1 emulsion plates, 100μ thick, were located in a cadmium box and surrounded with 14 inches of paraffin. The assembly was exposed to the x-ray beam from a betatron running at 35 Mev. The successive exposures measured with a Victoreen r-meter were 200 r, 300 r, and 500 r. The plates were first processed by a standard method and were blackened by the electron background to such an extent that they became opaque. They were then refixed by placing in a Kodak liquid x-ray fixer at room temperature for 2 hours. This comparatively long refixing time was necessitated by the unusually dense back-

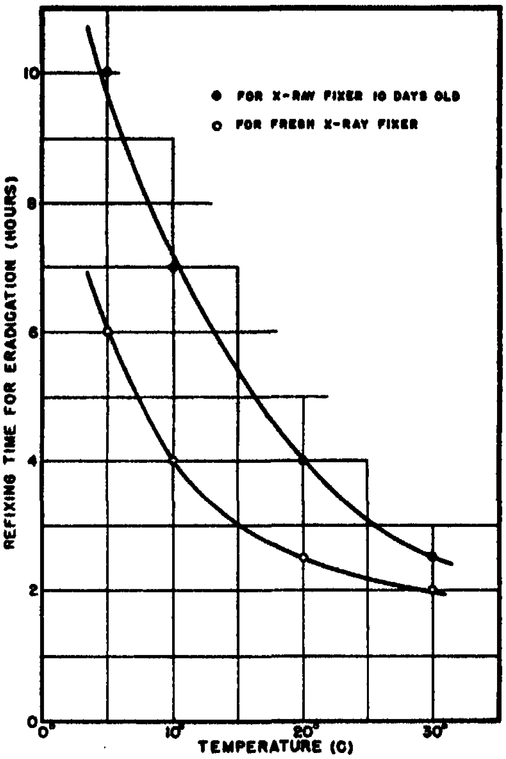

FIG. 1.

ground due to the exposures which were intentionally high. After this treatment, all the plates showed 3 and 4 pronged alpha-stars besides numerous single alpha-tracks as described by Cameron and Millar.[1] The latter used a modified Van der Grinten "grain-gradation" development which permitted them to use an exposure of 200 r. In comparison with the "grain-gradation" development, the present refixation technique has the advantage of being more flexible and convenient. The necessary refixation can be visually monitored and accomplished in small increments.

One objection to the refixing method is the alteration in track lengths which could result from the grain reduction on alpha- or proton tracks of varying grain density. However, this objection can be raised in the case of any similar technique. In order to examine quantitatively the refixing times in Kodak liquid x-ray fixer that would seriously alter heavy particle tracks, a series of tests were made. In all cases the plates used were processed Ilford C_2 emulsions. They were refixed until the proton and the alpha-tracks were made just to disappear. The minimum refixing times required to eradicate all the tracks were determined as a function of the x-ray fixer temperature and age. The results are plotted in Fig. 1 with the time in hours *versus* temperature in °C for fresh fixer and for 10-day-old fixer. With new fixer at 20°C the refixing time for disappearance of proton and alpha-tracks is 2½ hours. Therefore, plates with dense background that require more than one hour of refixing to make proton or alpha-tracks observable should be interpreted with care, because of the possible effects on the track lengths.

According to a report of the Office of Naval Research,[4] a strong ammonium-thiocyanate fixer was recommended by Franzinetti, which reduced the fixing time as compared with hypo fixer. Upon refixing some processed plates, results similar to those found with the x-ray fixer were also found with this ammonium-thiocyanate fixer. Use of the ammonium-thiocyanate fixer, or similar fixers, for work with thick emulsions where long fixing times are necessary should be made with caution in order to avoid alterations in the track lengths. This is true especially for experiments in which energy distributions of particles are involved.

The author appreciates very much Dr. H. W. Koch's constant interest and advice during the progress of this work.

---

[1] A. G. W. Cameron and C. H. Millar, Phys. Rev. 78, 337 (1950).
[2] P. K. S. Wang and M. Wiener, Phys. Rev. 76, 1724 (1949).
[3] H. D. Russel and J. I. Crabtree, J. Soc. Mot. Pict. Eng. 18, 371 (1932).
[4] Tech. Rep. OANAR 29-48, p. 11 (1948).

New Instruments

W. A. Wildhack: Associate Editor
in Charge of this Section
National Bureau of Standards, Washington, D. C.

These descriptions are based on information supplied by the manufacturer and in some cases from independent sources. THE REVIEW *assumes no responsibility for their correctness.*

Infra-Red Detector

The thermistor bolometers originally developed by the Bell Telephone Laboratories are now available for infra-red measurements from The Servo Corporation. They are rugged, sealed units suitable for spectrophotometric, industrial, and military applications.

The standard Servotherm bolometer consists of a matched pair of thermistor flakes having similar thermal and electrical characteristics. The thermistor material is a semiconductor with a high negative temperature coefficient of resistance. Positive and negative temperature bias voltages are applied to the active and compensating flakes. Radiation falling on the active flake causes a temporary change in resistance and results in an output voltage which is suitably amplified.

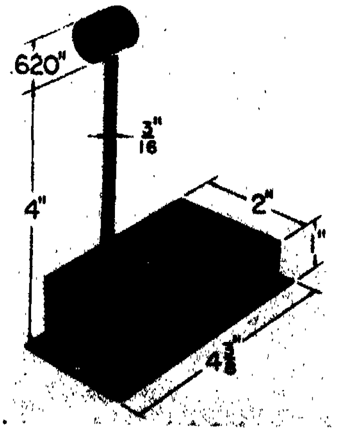

The steady state and dynamic characteristics of thermistor flakes are determined by the properties of the material itself, by their size and shape, and by the rate of thermal transfer from the thermistor flake to its surroundings. In order to have fast response to thermal radiation, the flake is mounted in close proximity to a thermal sink.

Three types of bolometers are currently available, with sensitive areas of 2.5×0.2 mm, and time constants of 3, 7 and 25 milliseconds, respectively, and noise equivalent power of the order of 10^{-9} watts.

The bolometer shown in the figure is mounted on a pre-amplifier, which provides initial amplification and reduces the impedance to permit use of flexible signal leads.—SERVOTHERM PRODUCTS DEPARTMENT, SERVO CORPORATION OF AMERICA, *New Hyde Park, New York.*

Ventilation Meter

The Air Ventimeter is a new instrument for measuring ventilation air flow. It utilizes a miniature non-directional probe $\frac{3}{8}$ in. long and $\frac{1}{8}$ in. in diameter and has an indicator for reading velocities from as low as 5 feet per minute up to 6000 feet per minute. The indicator and probe operate on the noble metal thermopile principle.

The Air Ventimeter, recently developed for the Army Quartermaster Corps to study ventilation between layers of clothing in a protective research program, has now been adapted for general commercial applications. It is especially suited for micro-climatology studies, controlled ventilation during painting, finishing, and drying processes, cooling and air flow studies in motor and machinery design, air flow measurements within small ducts and grills (probe can be inserted through $\frac{5}{32}$ in. opening) and similar applications. It is of particular value for measurements where the amount of cooling or ventilation must be determined in confined areas and where the direction of air flow is unknown or variable.

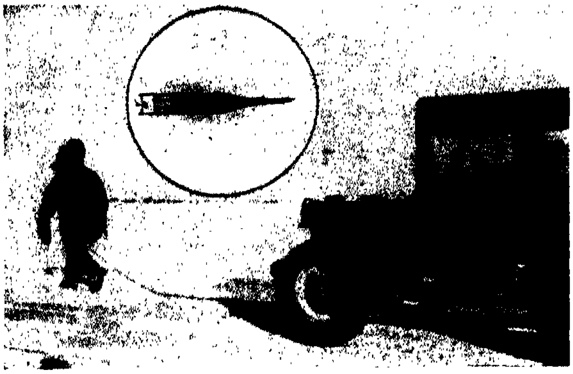

The temperature compensating feature incorporated into the Ventimeter permits accurate measurements even when extreme cases of sudden temperature changes occur.

The indicator movement is calibrated to indicate velocity readings directly in feet per minute. Indicators are available for operation on 115v a.-c. or battery power supplies. An attachment can be provided for use with a suitable recorder.—HASTINGS INSTRUMENT COMPANY, INC., *Hampton, Virginia.*

Frequency Standard

A compact, miniature tuning-fork frequency standard may be used for navigational aids, controlling gyros, firing electronic inverters, time bases, telemetering, and chronometry. It may be readily integrated into basic equipment, and may be operated under conditions of extreme temperature, humidity, and vibration. The manufacturer claims it to be an accurate, stable source for any frequency between 200 and 1500 c.p.s.; dividers and multipliers are available for other frequencies. The accuracy is one part in 100,000 and the temperature coefficient is better than one part per million per °C from 0 to 85°C.—AMERICAN TIME PRODUCTS, INC., *580 Fifth Avenue, New York 19, New York.*

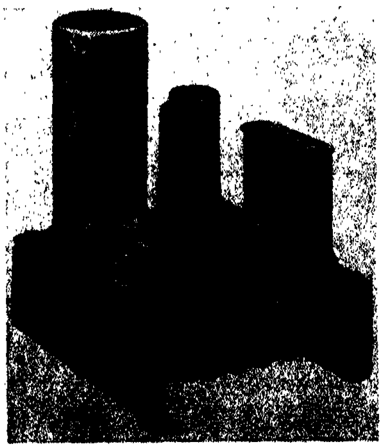

Micro Burette

A platinum-tipped micro burette, designed to deliver drops of approximately 0.01 milliliter, is being made by Kimble Glass, Division of Owens-Illinois Glass Company. It was designed by Kimble research engineers for use in the field of micro chemistry.

The platinum-alloy delivery stem is sealed into a glass tip which can be removed for cleaning. It extends inside the glass tip for a short distance so that dirt and grease cannot clog the opening.

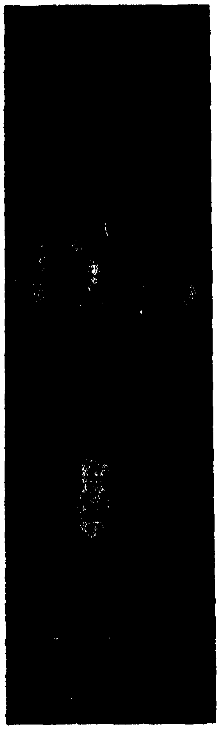

The tip has a standard Luer grinding. Where there is no significant danger of chemical reaction between the titrating liquids and hypodermic syringe needles, the latter can be used with the micro burette instead of the regular tip.

Two types of these micro burettes in each of two sizes are available through laboratory supply houses. One type has a standard-taper straight stopcock and funnel top, and the other a three-way interchangeable ground stopcock and plain top. The smaller size has a 5-ml capacity and 0.01-ml subdivisions, and the larger a 10-ml capacity with 0.02-ml subdivisions. Micro burette or tip may be purchased separately.—OWENS-ILLINOIS GLASS COMPANY, *Toledo 1, Ohio.*

Radiation Monitor

A new laboratory monitor for alpha-beta-gamma-detection has been announced by Nuclear Instrument and Chemical Corporation. Model 1615 is a general purpose count rate instrument with wide utility, which may be used for checking clothing, benches, glassware, and hands or fingertips for contamination, or for continuous monitoring of background air contamination or isotope decay. It may also be used to count samples with activities between 100 and 50,000 counts per minute where accuracy of measurement need not be better than 3 percent standard error. A

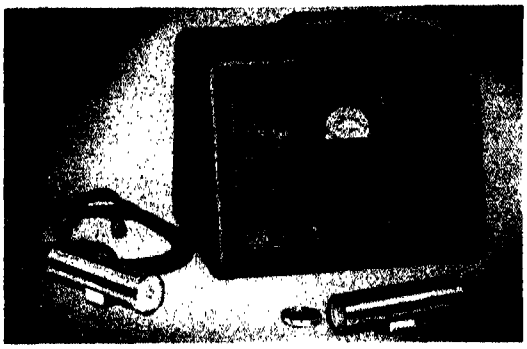

chart type recorder may be attached for maintaining a permanent written record.

A choice of five different ranges, from 500 to 50,000 counts per minute full scale, is provided. Suitable time constants in each range, in conjunction with a switch permitting choice of standard error, allow either 3 percent or 20 percent error to be read on any range if desired. The instrument incorporates a loud speaker with controllable volume and a high voltage supply which is controlled from the front of the panel.

The probe used in this instrument has an unusual mounting arrangement. It incorporates a permanent magnet which allows the probe to be mounted in any position on one side of the cabinet, and also makes possible its use on a ring stand, vacuum line, or any ferro-magnetic material.

If desired, a 10-foot cable and probe can be obtained to permit use of the "Radiation Sentinel" in clinics and hospitals for surveying a patient's body. The recording meter may also be attached in order to provide a permanent record of counts.—Nuclear Instrument and Chemical Corporation, *229 West Erie Street, Chicago 10, Illinois.*

Platinum Thermometer

The conventional precision platinum thermometer is often too bulky to fit the small opening in some types of calorimeters or other apparatus with restricted space. A new type of platinum thermometer of much smaller dimensions has been developed for precision measurements.

The sensitive tip is 5 mm o.d. and 1¼ in. long for a resistance of 25.5 ohms. The stem is 7 mm in diameter and can be several feet long if required.

The backbone of the thermometer is a heavy wire of thermometer quality platinum of .050-in. diameter and onto which a glass coating is fused. A resistance winding is placed on this coating, one end being connected to the center wire. An outside coating of Pyrex glass is fused on the winding. In this way the platinum wire is completely sealed off and protected from contamination and mechanical injury, similar to the other types of Weiller resistance thermometers. Four leaves of fine gold wire are provided.

The unit is monofilar. The characteristics of the unit are identical with those of the manufacturer's precision platinum thermometer.—Dr. Paul G. Weiller, *95 Broad Street, New York 4, New York.*

Micro-Photometer

A new Light-Scattering Micro-Photometer which measures 20 micromicrolumens of scattered light, has a sensitivity approximately 100 times greater than similar instruments.

It may be used with any of the accepted techniques for molecular weight, particle size, micro-fluorescence, depolarization, dissymmetry, and micro-turbidity measurements. Its high sensitivity opens new fields in the measurement of optical-glass scattering power and in micro-chemical turbidity analyses.

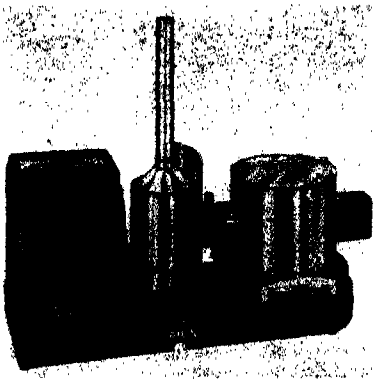

The instrument is portable and completely a.-c. operated. It employs two built-in electronic-regulated power supplies, also a d.-c. amplifier which operates the panel micro-ammeter and which may be connected directly to an external recorder. Full-scale deflections of the panel micro-ammeter are made with photomultiplier tube currents of 10, 1, .1, and .01 micro-amperes.

Details are given in Bulletin 2182, obtainable from the manufacturer.—The American Instrument Company, Inc., *Silver Spring, Maryland.*

Photographic Exposure Computer

Potentially large savings in costs of photographic film used for industrial pictures are among the possibilities of a simple, inexpensive computer with which light conditions can be accurately evaluated, especially when professional photography is not warranted. The device is low enough in cost to be distributed in quantity to field service men, for example.

The new Photographic Exposure Computer is a cooperative development of 45 national technical societies and leading manufacturers of photographic and optical equipment working through American Standards Association. It is a by-product of the war, the first edition having been used all over the world by the Armed Forces.

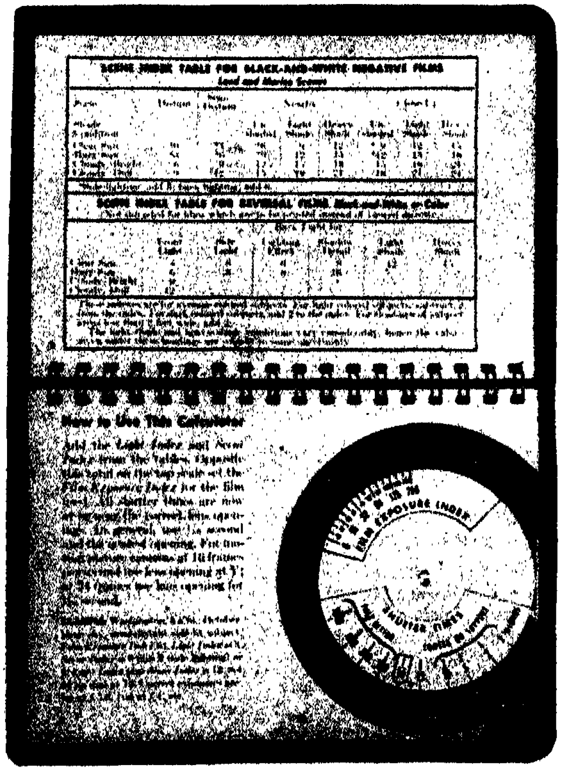

The value of the computer has now been enhanced by the addition of tables for color film, which requires more accurate exposure settings, and for transparencies or reversal materials in both black-and-white and color for projection or viewing with an illuminator. The computer is an American Standard method for evaluating light conditions. It is based not only on long-existing exposure tables, but also on data on radiant energy reaching the earth's surface. It consists of a pocket-size booklet containing 25 durable, loose-leaf pages, 3¼×4¾ in., with a flexible fabricoid cover. On one page is a circular calculator for determining shutter speed and lens stop or *f*-number with index numbers obtained from included tables and from the film used.

Index numbers allow for all lighting variables, including the altitude of the sun by latitude, date and hour; atmospheric conditions (especially clouds); spacial structure of the scene (especially distance), conditions of illumination (shade and direction of lighting); and film speed. The guide thus evaluates light intensities and luminance of scenes to be photographed. The calculator combines this index with a film exposure index to indicate proper camera adjustment for a picture. Copies of the computer are available at $1.00 each.—AMERICAN STANDARDS ASSOCIATION, *70 East 45 Street, New York 17, New York.*

Ground Resistance

Vibroground Model No. 263 is designed to provide corrosion and electrical engineers with a light, rugged, accurate instrument for measuring soil, anode, and circuit resistances and polarization effects.

It is capable of measuring the true resistance to earth of man-made grounds, irrespective of the earth resistance and conditions. Readings are not affected by the resistance of auxiliary prods or leads, or stray a.c. or d.c. currents in the earth. Accuracy is not dependent upon the meter movement, but upon a carefully calibrated resistance. The instrument circuit is such that it has the ability to discriminate in accepting only currents from its own power supply for measurement.

Ranges are selected by a separate switch at lower left of the panel. Special design features permit direct readings on the single scale of the potentiometer. All resistance values are determined by simple decimal multiplication. The ranges have been incorporated which can give the most accurate readings in soil varying in resistivities from 0 to 1,195,000 ohms per cubic centimeter at 10 feet or greater spacings.

Power is provided by eight standard flashlight batteries, with a circuit incorporating a synchronous self-rectifying vibrator having an output of 125 volts. Resistance measurements can be made by the two-, three-, or four-electrode methods.

Simplicity of operation and ease of use are outstanding features of Vibroground. No previous instruction or training period is required. Vibroground Model No. 263 is mounted in a steel case, with removable cover and quick opening battery drawer. It weighs 10¾ lbs. including cover. Over-all dimensions are 9 in.×6 in.×6¾ in. —ASSOCIATED RESEARCH, INC., *3758 W. Belmont Avenue, Chicago 18, Illinois.*

Michelson Interferometer

This latest design of a well-known laboratory instrument is an economical and accurate device for calibrating finely divided scales, strain gauges, precision dial indicators, and other length measuring equipment using the wavelength of light as the unit of measurement.

The optical system is mounted on a standard Gaertner micrometer slide with a choice of 25-mm or 1-inch range. The micrometer drum is direct reading to 0.01 mm or 0.0001 inch. Settings can be made either by means of a microscope mounted in the carriage or, in the case of dial indicators, by contact with the carriage. Measurements are made either by counting interference fringes directly or by first using them to calibrate the lead screw of the micrometer slide and then employing the divided scale and drum on the slide to obtain the measurements.

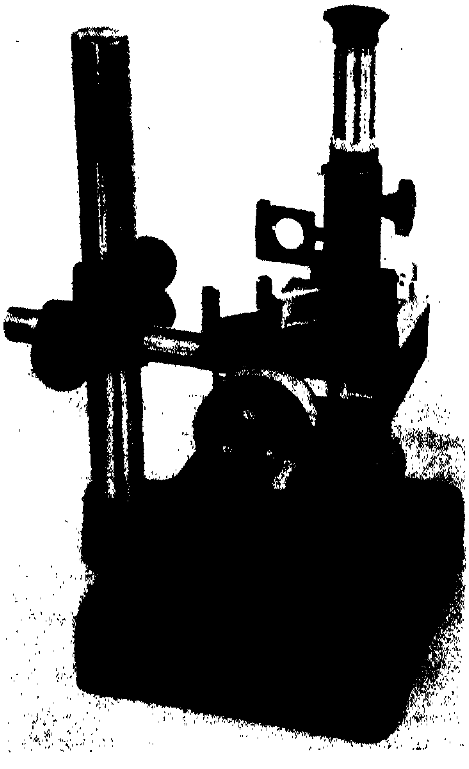

The power of the microscope can be varied over a wide range by use of interchangeable objectives. The standard eyepiece and cross-hair reticle can be replaced with a filar eyepiece micrometer which is preferable for some types of microscopic settings. The instrument is designated as M305 Interferometer Attachment.—THE GAERTNER SCIENTIFIC CORPORATION, *1201 Wrightwood Avenue, Chicago 14, Illinois.*

Electrically Controlled Camera

A new 35-mm data-recording camera, Type A-1, has been announced by Cook Research Laboratories. This camera is a completely automatic, electrically tripped instrument built for special applications. It is capable of taking pictures at any rate up to four frames per second.

Provision is made for control of the taking rate by means of an external electrical tripping pulse if desired. This feature widens the scope of usefulness of this camera and makes it adaptable to many additional problems. Large magazine capacity (200 feet) and automatic operation make the unit well suited for applications in remote locations which might be left unattended for long periods of time. The film magazine can easily be replaced with a fresh cartridge when required.

Other features of the Type A-1 Camera are as follows: 1. Film transport is effected by a precision Geneva Type intermittent. 2. All castings are of a high impact strength aluminum alloy. 3. Bearings are of a lifetime porous bronze. 4. Emphasis has been placed on ruggedness and dependability of all components.

Some of the more obvious applications of the camera include photographing of meter readings, oscillographic records, chemical reactions, and general laboratory use.—Cook Research Laboratory, *1457 Diversey Parkway, Chicago 14, Illinois.*

Manufacturers' Literature

Electronic Supplies—Aerovox General Catalog lists capacitors of many different types, many of them new; an entire section is given over to television capacitors for TV servicing. Wire-wound and carbon resistors are listed, and vibrators and test instruments.—Aerovox Corporation, *Bedford, Massachusetts.*

Fractional-Horsepower Motors—Over 200 specifications are listed to fit almost any fractional horsepower requirement—plain motors, and speed reducer motors—in all popular winding classifications. Contained also is such information as connection diagrams, dimensions, how to measure machine torque, how to increase speed reducer motor life, and a listing of typical motor applications. Copies are available upon request.—Bodine Electric Company, *2254 W. Ohio Street, Chicago 12, Illinois.*

Burrell Announcer—No. 50 6 39, describes laboratory centrifuges, "Monochromatic" Colorimeter, and other laboratory apparatus.—Burrell Corporation, *2223 Fifth Avenue, Pittsburgh 19, Pennsylvania.*

High Frequencies—Catalog 20-A, 1950, lists and illustrates a Pulse Generator for radar, nuclear, and TV circuits; Signal Generators for measuring receiver performance, standing wave ratio, gain, antenna and transmission-line characteristics; attenuators for use in measuring gain, frequency response, voltage ratios; and other laboratory instruments.—Hewlett-Packard Company, *395 Page Mill Road, Palo Alto, California.*

Springs—Catalog No. 6, lists and illustrates beryllium copper spring data, including compression, standard brush, flat, strip, etc.—Instrument Specialties Company, Inc., *Little Falls, New Jersey.*

Oxygen Equipment—Aircraft Oxygen Equipment Engineering Manual describes typical installations and recommended practices, and covers masks and accessories, regulators and flow gauges, cylinders, connections, pressure gauges, etc.—Ohio Chemical and Surgical Equipment Company (a division of Air Reduction Company, Inc.), *1177 Marquette Street, Cleveland 14, Ohio.*

Biophysics—Catalog No. 3-49, Tools for Biophysics, presents measuring and testing equipment for the experimental biologist or biophysicist.—Phipps and Bird, Inc., *303 South 6th Street, Richmond 5, Virginia.*

Biophysical Measurements—Bulletin No. 675, illustrates the "Manometricon" for micro gas reactions and the Dubnoff Metabolic Shaking Incubator.—Precision Scientific Company, *3737 W. Cortland Street, Chicago 47, Illinois.*

Electronic Instruments—Summer 1950, issue of the Cathode Press describes a rotating anode tube, a miniature ceramic triode, x-ray tubes for thickness gauging, and other electronic instruments.—Machlett Laboratories, Inc., *Springdale, Connecticut.*

New Materials

Forest K. Harris: Associate Editor
in Charge of this Section
National Bureau of Standards, Washington, D. C.

Zirconium in Surgery

Various metals and alloys have been utilized at one time or another in surgery, including gold, silver, aluminum, magnesium, tantalum, brass, steel, and vitallium. These uses have been to suture wounds with wire, to unite broken bones with plates and screws, to connect broken channels with tubes and to cover holes in the skull with plates. Materials used in these operations must conform to exacting specifications as to strength, durability, malleability, resistance to fatigue and to corrosion, etc. Materials for cranioplasty should not produce inflammation or foreign body reactions when implanted in tissue. The ideal material should be non-irritating electrically and chemically, equivalent in strength to the skull but easily adaptable to the contour of the defect, light in weight, non-absorbable, non-toxic, unaffected by therapeutic procedures of x-rays and diathermy and by the extremes of heat and cold encountered by humans, unaffected by infection, and inexpensive.

It has been suggested that stress "corrosion" may take place in alloys used as structural replacements, which are initially corrosion-resistant. Thus a bone plate, subjected to multiple stresses over a period of years may become irritating and necessitate a second operation for its removal. For this reason an element is preferable to an alloy.

Tantalum is the only element that has been used so far in surgery with any degree of safety. It is used mainly in cranioplasty (to cover holes in the skull), as small clips to stop bleeding from blood vessels in the brain and as thin sheets to wrap around cut nerves. However, there are several drawbacks to its use. It is rare, extracted with difficulty from its ores, and expensive. Plates are difficult to fashion and usually require careful time-consuming molding in advance. In view of these disadvantages it was decided to study the application of zirconium to surgery. This study was carried out at the Harrison Department of Surgical Research of the University of Pennsylvania Medical School.

Zirconium is relatively abundant, and has been available in a ductile form for a number of years. Although it is extremely active at high temperatures, it is almost completely inert and corrosion-resistant below 200°C. Fully annealed, it is soft and malleable, and can be drawn or shaped easily. Although it work-hardens to a considerable degree, it has a high work capacity and can be fully annealed in 15 minutes at 750–800°C. Chemically one of its most important properties is its corrosion-resistance. Physically, its malleability and low specific gravity are advantages. Its electrolytic action when immersed in a physiological saline solution is, like that of tantalum, minimal.

In animal experiments zirconium wire has been used as sutures in the abdominal wall. In a second experiment zirconium screws and pegs were inserted into the leg bone. Thin strips of the metal have been inserted into the brain along with tantalum and silver. Skull defects have been covered with zirconium plates. Microscopical studies in all experiments proved that zirconium caused little reaction in muscle, fascia, bone, and brain. The third experiment was considered to be a delicate method of evaluating the reaction to brain tissue, and zirconium compared favorably with tantalum. It was much better than silver which was included because it is used in neurosurgical clinics as clips to stop bleeding. Some surgeons feel that tantalum is too hard and cannot be pinched tightly enough to insure adequate compression of the vessel. It is probable that the more malleable zirconium will find use in this application.

These preliminary studies indicate that zirconium has a place in surgical procedures and that further experimental and clinical study is warranted. In addition to hemostatic brain clips, it may be used in the form of plates to cover skull defects and give adequate protection to the brain. It can be machined into screws for fixation of bone plates. It can be drawn into wire of sufficient strength and malleability for use as suture material. Zirconium tubes are being made for the repair of bile ducts. Thin sheets of the foil may be used to seal the ends of cut nerves, and the foil may be used as a burn dressing. It is possible that zirconium rods will prove adaptable for intramedullary bone pinning in which the ends of a broken bone are aligned by a metal rod passed down the central core. Zirconium powder has not been used experimentally or clinically but it will show up on x-ray and might be used to mark the location of certain operations such as intervertebral disks and frontal lobotomies. At present vitallium, 18-8-SMO stainless steel and tantalum are used in surgical operations and can be buried in human tissue for many years without undue irritation. Zirconium appears to be relatively inert and, being an element like tantalum, will also find a place in the operating room.

The above material was abstracted from an article entitled "Zirconium in the Operating Room" by Dr. J. I. Bates. This article appeared in Foote-Notes 22, No. 1, 1950.—Foote Mineral Company, *18 West Chelten Avenue, Philadelphia 44, Pennsylvania.*

Permanent Magnets

Hyflux Alnico V magnets have a guaranteed energy product of at least 5.25×10⁶ BH. This is about 16 percent more than the highest published, guaranteed value for regular Alnico V. These stronger, smaller magnets permit greater compactness in design. They are the result of a special production technique applied to regular Alnico V, not a new alloy.—Indiana Steel Products Company, *Valparaiso, Indiana.*

Static Elimination

Alphatron static eliminators are essentially bars, strips, or foils of brass or nickel on which polonium is electrochemically deposited. The active area is covered by a thin layer of electroplated gold which is finally coated with lacquer. The alpha-particles emitted by the polonium ionize the air and dissipate either positive or negative static charges. Used as a bar, the eliminator is placed about an inch from the surface of moving sheets or films to render surfaces completely neutral. Foils may be placed on the inside of nozzles or blow-guns and the ionized air blown across surfaces to remove dust. Since the surface is neutralized in the process it loses its tendency to attract further dust from the air. Attached as a strip to a brush in such a position that it leads the stroke, it facilitates the cleaning of surfaces by brushing. While it will completely neutralise a charged surface, the action is not of course permanent in that the surface could be recharged by the normal causes for the formation of static. The manufacturer states that the short-range alpha-particles emitted by the polonium do not constitute a radiation hazard.—Recco, *205 East 43rd Street, New York 17, New York.*

Diamond Abrasive Kit

A kit containing the six most widely used NBS grades of diamond compounds is offered by the manufacturer of *Dymo* brand diamond abrasives to facilitate experimental and development work with these materials. The selection is such that almost any desired finish can be produced on carbides, mold, and tool steels and other hard materials. Each grade of diamond abrasive compound is distinctly color-marked and is contained in jars with matching colored tops. The kit is in a sturdy, compact wood case with a hinged top.—Elgin National Watch Company (Industrial Products Division), *Elgin, Illinois.*

Carbide Marking Pencil

A tungsten carbide pencil is now available for permanently marking glassware. Only slightly below the diamond on the hardness scale, tungsten carbide is cheaper than diamond and comes to a definite point rather than an edge as is found on a diamond tip. The point is permanently mounted in a knurled steel pencil shaft and is protected by a cap so that the pencil may be safely carried in the pocket. The pencil is useful for a variety of laboratory tasks: sealed vials can be permanently identified; sheets of glass can be accurately scored for breaking; tubes and rods can be scored more rapidly than with a file.—Fisher Scientific Company, *717 Forbes Street, Pittsburgh 19, Pennsylvania.*

Plastic Products

Lustrex glass mat consists of styrene reinforced with random glass fibers. Molded products have all the advantages of styrene and the additional value of greatly improved strength. It is recommended for molding trays, housings for mechanical devices, paneling, structural laminates, boxes, and other containers where improved strength and chemical resistance are needed. Technical details are available in a bulletin prepared by the manufacturer.

Lauxite UF 77A is a new cold-setting urea resin glue with catalyst incorporated, having greatly improved storage stability. It was developed to meet the hot-weather storage problems of woodwork manufacturers. High standards of strength, water resistance, working life, setting speed, and color have been maintained in developing this product. It has been laboratory- and field-tested successfully both for ordinary cold gluing and for high frequency gluing.—Plastics Division, Monsanto Chemical Company, *Springfield, Massachusetts.*

Flame-Retardant Insulation

Rulan is a plastic electrical insulation that will not support combustion. Whereas flammability has been a characteristic disadvantage of plastics with good electrical properties, tests with this material have shown that it will not burn after a flame has been removed, nor will it drip when molten, a further advantage since plastic drippings can spread fires. Its electrical properties are comparable to, although not the equivalent of, those of polythene, one of the best insulating materials known for high frequency applications. It has a power factor of 0.002, and a dielectric constant of 2.5. It is non-tracking and retains its electrical properties after long immersion in water at elevated temperatures. Its mechanical properties are good and its low temperature properties excellent. It can be injection-molded and extruded on to wire at high speeds. Its use is suggested as insulation for high voltage hook-up, signal-control, lead-in, and flame-retardant line wire, and for high voltage street-lighting cables. Molded electrical parts and extruded tape are also being developed for uses where flammability is a consideration.—E. I. duPont de Nemours and Company (Polychemicals Department), *Wilmington, Delaware.*

THE
REVIEW OF SCIENTIFIC
INSTRUMENTS

VOLUME 21, NUMBER 10 *OCTOBER, 1950*

Chart Recording of Microsecond Pulse Amplitudes

J. T. DEWAN AND K. W. ALLEN
Atomic Energy Project, National Research Council of Canada, Chalk River, Ontario, Canada

(Received July 7, 1950)

A peak voltmeter circuit is described which will record, on an Esterline-Angus chart, the amplitudes of microsecond pulses generated at random in ionization chambers or similar counters. Slow response of the recording pen prohibits the resolution of pulses less than one second apart. Provision is made for selecting pulses coincident with some triggering event as the low counting rates suitable for the circuit are most often encountered in coincidence experiments. Coincidence resolving times as low as five microseconds may be attained, and the linearity is such that input pulse amplitudes from 2 to 100 volts are reproduced on the chart to within ±1 volt.

INTRODUCTION

IN many instances it is necessary to obtain the distribution in size of microsecond pulses produced in ionization chambers or proportional counters and for this purpose a multi-channel pulse analyzer is normally utilized. However, when the pulses occur very infrequently, at an average rate of a few per minute, as is often the case in coincidence experiments, a high speed pulse analyzer is a much more complex instrument than is required. Its discriminating circuits may tend to drift during the long counting periods necessary to produce good statistics, and usually it has no provision for the selection of pulses coincident with other events. Consequently a circuit has been designed which will indicate, on the chart of an Esterline-Angus 1-ma pen recorder, the magnitudes of random pulses which may, if desired, be selected by coincidence with other events. It was originally used in the study of the energy distribution of long-range α-particles which are emitted occasionally in the fission process,[1] but subsequent experience has confirmed its usefulness in other applications. The rather slow response of the Esterline-Angus pen prohibits the resolution of pulses less than one second apart, although the coincidence resolving time may be as low as several microseconds. The circuit can be readily adjusted to handle input pulses ranging from microseconds to milliseconds in duration and will reproduce on the chart pulse amplitudes from 2 to 100 volts to within ±1 volt. It is, perhaps, somewhat tedious to translate the spectrum of pulses obtained on the chart into a differential or integral bias curve, but on the other hand a permanent record is obtained showing the actual time distribution of the pulses, a feature especially useful when deviations from randomness are suspected.

DESCRIPTION OF THE CIRCUIT

The general operation of the circuit can be readily understood from the block diagram of Fig. 1. Pulses to be recorded, of positive sign and up to 100 volts in amplitude, are normally obtained from a linear amplifier. They are fed into the discriminator D_1, which eliminates amplifier noise and any small undesired pulses, and then into the coincidence gating circuit C. If a given pulse is coincident with one from the gate generator G it passes on with unchanged magnitude to the lengthener L; if not, it is suppressed in the coincidence circuit. The lengthener is a two-stage integrating circuit which, in the absence of the restorer R, would extend the duration of the input pulse from a few microseconds to several minutes thereby allowing the Esterline-Angus pen ample time to record the magnitude of

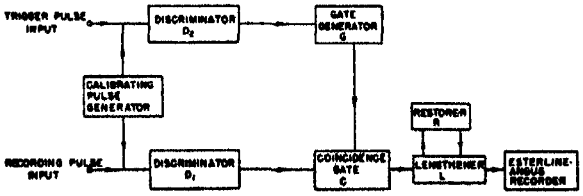

FIG. 1. Block diagram of the pulse amplitude recorder.

---

[1] K. W. Allen and J. T. Dewan, Phys. Rev. 80, 181 (1950).

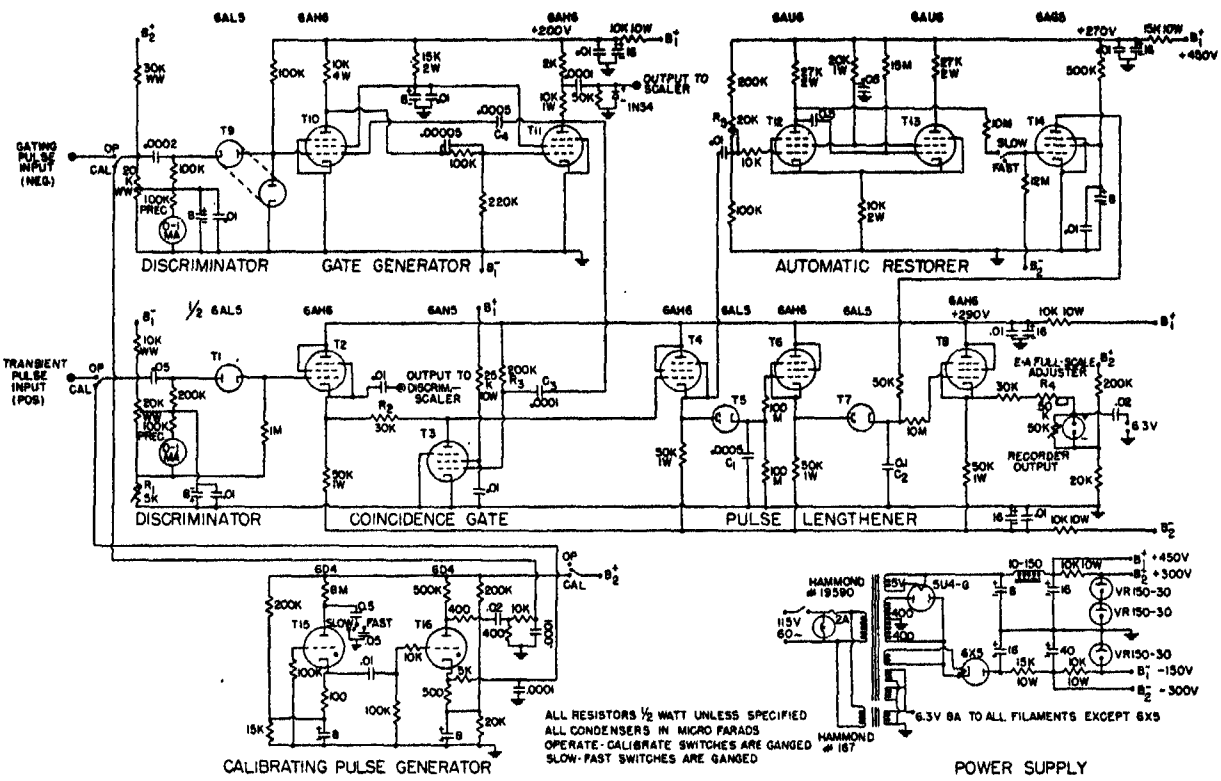
GATING PULSE INPUT (NEG.)
TRANSIENT PULSE INPUT (POS)
DISCRIMINATOR
GATE GENERATOR
AUTOMATIC RESTORER
DISCRIMINATOR
COINCIDENCE GATE
PULSE LENGTHENER
CALIBRATING PULSE GENERATOR
POWER SUPPLY
OUTPUT TO SCALER
OUTPUT TO DISCRIM.-SCALER
RECORDER OUTPUT
E-A FULL-SCALE ADJUSTER
OP
CAL
SLOW
FAST
HAMMOND #19590
HAMMOND #167
115V 60~
5U4-G
6X5
VR150-30
6.3V 8A TO ALL FILAMENTS EXCEPT 6X5
ALL RESISTORS ½ WATT UNLESS SPECIFIED
ALL CONDENSERS IN MICRO FARADS
OPERATE-CALIBRATE SWITCHES ARE GANGED
SLOW-FAST SWITCHES ARE GANGED

FIG. 2. Circuit diagram of the pulse amplitude recorder.

the pulse before it has appreciably decayed. The rectoring circuit allows the pen about one second to reach its maximum traverse and then returns it in a fraction of a second to its normal position in readiness for another pulse. The use of a restorer decreases the dead time by a large factor since, in its absence, the pen would follow a very slow exponential decay. The calibrating pulse generator provides standard pulses, simulating the transients in speed of rise, to facilitate the adjustment of the recorder and to check the linearity of the system. A complete diagram of the circuit is shown in Fig. 2 and a more detailed description follows.

Pulses with amplitudes sufficiently large to overcome the biased diode T_1 are fed into a coincidence gate circuit consisting of the cathode follower T_2 driving the load R_2 in series with the tube T_3. Normally T_3 has zero grid bias and draws a large screen current so that it has a plate to cathode resistance of about 500 ohms. Consequently only two percent of an input pulse reaches the grid of T_4 when the coincidence gate is closed. On the other hand, when a negative pulse from the gate generator drives the grid of T_3 beyond cut-off, this tube acts as a very large resistance shunted by its plate-cathode capacity, wiring capacity and the input capacity of T_4. Complete charging of these stray capacities through R_2 requires about 1 μsec.; hence if the input transient rises in a fraction of this time it must remain at maximum for a microsecond to ensure that no loss in pulse amplitude will occur in the coincidence gate. This necessitates that exponentially decaying input pulses have a total duration of about 40 μsec.

As it is difficult to predict accurately from the published data the performance of T_3 under such conditions, a number of different miniature tubes were investigated to determine their effective resistances at low plate voltages. The results are shown in Fig. 3. In each case the tube was tested at zero grid bias and sufficiently large screen voltage to produce maximum rated screen dissipation with no plate current flowing. It is evident from Fig. 3 that the 6AN5 is best suited for the application; it has a resistance of 500 ohms at plate voltages up to eight volts. Several other coincidence circuits were investigated but the one described was found to be the most satisfactory. It responds rapidly and has the advantage that small unavoidable delays in the gating pulse cause no loss in the size of coincident pulse reaching the lengthener provided that pulse remains at maximum for at least one microsecond after T_3 has been driven to cut-off.

The pulse lengthening is effected by a straightforward two-stage integrator comprising tubes T_4, T_5, T_6, and T_7.[2] Each stage consists of a cathode follower which charges a reservoir condenser through a sharp cut-off diode. The cathode follower will supply 50 ma without drawing grid current so that the first reservoir condenser

---

[2] W. C. Elmore and M. L. Sands, *Electronics: Experimental Techniques* (McGraw-Hill Book Company, Inc., New York, 1949), p. 196.

C_1 can be charged to 100 volts in a microsecond. It loses its charge in about 25 msec., while the second condenser C_2 is charged in half a millisecond and has a decay time constant of approximately five minutes. As the Esterline-Angus pen requires half a second to sweep fully across the chart, it cannot actually follow this millisecond rise but attains its full traverse before the pulse has perceptibly decayed in magnitude. The use of a "Glassmike"* condenser for C_2 is strongly recommended because of its extremely high leakage resistance. The lengthened pulse appearing across the final reservoir condenser is coupled to the Esterline-Angus recorder through the cathode follower T_8. The d.c. voltage at the cathode is balanced out by a voltage divider so that little current normally passes through the recorder. Accurate balance is not necessary because of the manual pen shift on the instrument. A variable resistor R_4 in series with the recorder is provided for adjusting the size of the pulses on the chart; usually it is arranged that 100 volt input pulses produce full scale deflection. For large pulses the recorder is critically damped by 15,000 ohms shunt resistance but small pulses appear slightly overdamped due to the friction of the pen on the chart. However a small 60-cycle voltage applied to the movement aids the pen in responding more quickly to small pulses. The oscillation caused by this a.c. voltage is barely perceptible, producing only a slight widening of the trace.

As already mentioned the function of the restoring circuit is to discharge rapidly the final reservoir condenser after the recording pen has had ample time to reach its maximum, i.e., after about one second. Otherwise the lengthener would not be ready for another pulse until condenser C_2 had completely discharged, which would require about fifteen minutes. The restoring circuit consists of the cathode-coupled trigger pair T_{12} and T_{13} and a discharge tube T_{14} which normally conducts and acts as a relatively low resistance across C_2. Positive pulses from T_4 fire the trigger pair producing negative pulses of about one second duration and of sufficient size to bias off T_{14} completely. For this interval of one second, condenser C_2 is allowed to retain the charge which it accumulates; at the end of the interval T_{14} conducts and discharges C_2 in a few milliseconds. As the coincidence gate is not 100 percent efficient, small non-coincident pulses of two volts or less can reach the lengthener. The purpose of R_5 is to ensure that these small pulses do not trigger the restorer and hence do not record on the chart. C_2 is actually charged by such pulses but loses its charge through T_{14} before the pen has had sufficient time to respond.

The gate generator was rather arbitrarily chosen to accept negative input pulses, up to 100 volts in magnitude. Pulses large enough to pass the biased diode T_9 fire the direct-coupled trigger pair T_{10} and T_{11} producing fast rising output pulses of 50 μsec. duration. The differentiating combination C_3R_3 transforms these to sharp triangular pulses causing T_3 to be biased off for a well-defined interval of time, which should be somewhat greater than the rise time of the transients under study. The load resistor of T_{11} is tapped to provide a small negative output to feed an external scaling unit. Positive pulses can be obtained equally well by reversing the 1N34 diode.

The internal calibrating pulse generator has been found extremely useful for checking the overall operation, adjusting the recorder to correct full scale deflection and testing the linearity of the transient channel. It consists of a 6D4 thyratron relaxation oscillator T_{15} providing positive pulses at two frequencies, either one every four seconds or two per second, to trigger the thyratron pulse generator T_{16}. The pulse shaping elements in the second stage may be altered at will to provide pulses with rise and decay times simulating those of the actual transients under study.

ADJUSTMENT AND CALIBRATION

The system is adjusted and checked as follows. With the internal pulse generator arranged to give pulses of the desired shape, C_3 and if necessary C_4 are adjusted so that the gate generator biases T_3 to cut-off for roughly twice the rise time of the transients under study, with a minimum of two microseconds. R_3 is then varied by screwdriver adjustment until the cathode of T_2 is at ground potential. With no input pulses to either channel and with the "Operate-Calibrate" switch on "Operate," the recorder pen is balanced to have minimum pressure on the chart consistent with proper tracing and is then brought to the proper baseline by the manual adjustment provided in the instrument. The switch is then turned to "Calibrate," which starts the internal generator operating and connects the standard pulses to the gate generator and transient channels. A discriminator-scaler, whose calibration is known to be accurate, is connected to the monitor output of T_2. With the calibrator frequency switch on "Fast" the magnitude of the pulses entering the discriminator-scaler is adjusted to be 100 volts, the frequency switch is thrown to

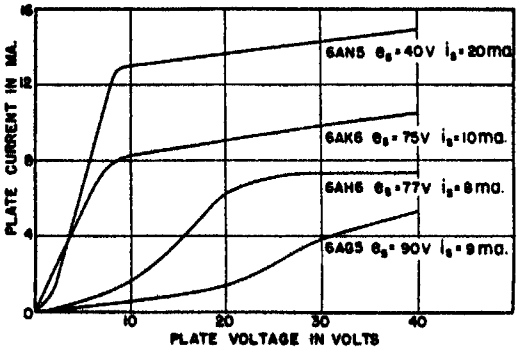

FIG. 3. Low voltage characteristics of several pentodes. Screen voltages are constant and screen currents indicated are those which obtain with zero plate current.

---

* Oil-filled plastic film capacitors supplied by Condenser Products Company, Chicago, Illinois.

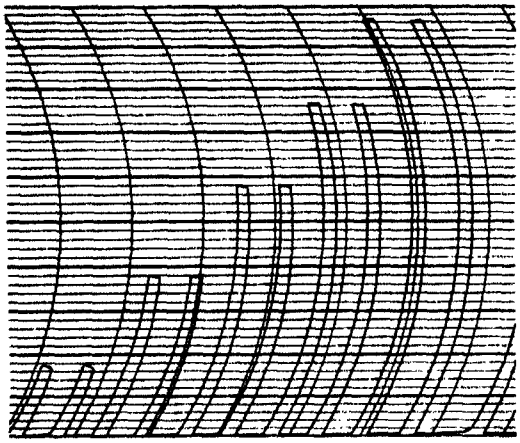

FIG. 4. Response of the recorder to test pulses of one microsecond rise time. The width of each pulse on the chart is approximately two seconds.

"Slow" and the height of the pulses recorded on the Esterline-Angus is adjusted to be full scale by means of the variable resistor R_4. The linearity of the system, as well as the satisfactory operation of the recorder, is then checked by reducing the size of the calibrating pulses in a number of steps, each time noting the pulse amplitude entering the discriminator-scaler at "Fast" frequency and the amplitude on the pen recorder at "Slow" frequency. The "Fast" frequency is provided merely to facilitate finding the cut-off point with the discriminator; this would be a very tedious process at a pulse frequency of one in four seconds. The frequency change is not sufficiently great to cause any change in pulse amplitude. Finally with 100-volt pulses at the monitor output of T_2, but with no gate pulses fed to T_3, R_5 is adjusted until no small pulses are recorded on the chart. The adjustment and checking are then completed and the "Operate-Calibrate" switch is moved to "Operate." Figure 4 shows the response of the Esterline-Angus recorder to test pulses of varying amplitudes, the rise time of the test pulses being approximately one microsecond and the decay 50 μsec.

DISCUSSION

In connection with the use of the pulse recorder one or two points are worthy of note. It is evident from the operation of the coincidence gate that the resolving time of the system for chance coincidences cannot be less than the duration of the input transients and for reasons previously given this is a minimum of 40 μsec. for an exponentially decaying pulse. A resolving time of perhaps 50 to 100 μsec. is not excessive in many experiments. If a spectrum of pulses is recorded in which a fraction of the pulses is due to chance coincidences a correction can be made by triggering the gate generator from an independent source, e.g. an external pulse generator, and subtracting the resulting spectrum of random coincidences from that previously obtained, after normalizing the two to identical counting rates.

When it is desired to achieve the minimum possible resolving time with fast-rising pulses these pulses should be preshaped into flat-topped rectangles of the same amplitudes and of about 3 μsec. duration. As the coincidence gate must remain open for at least 2 μsec. the shortest resolving time attainable is approximately 5 μsec. (If still shorter resolving times are required, coincidences must first be formed with a conventional mixer circuit whose output is then used to trigger the gate generator.) Pretreatment of the pulses may be effected by a simple one-stage integrator with restorer, very similar in nature to the circuits already described. It sometimes happens[1] that gate generating pulses, although nominally coincident with pulses to be recorded, have unavoidable delays of perhaps several microseconds. In such cases preshaping of the transient pulses is necessary because exponentially decaying pulses, unless exceedingly long, would suffer losses in amplitude in the coincidence gate by amounts depending on the delays involved. Preshaping is also necessary when one wishes to record pulses less than a microsecond or so in duration as these pulses are too short to pass through the coincidence gate properly.

If it is desired merely to record the amplitudes of all pulses entering the transient channel, the coincidence feature of the circuit can be eliminated by removing T_3 from its socket. In this case bypassing R_2 and decreasing C_1 will improve the response to pulses rising in less than a microsecond.

Indications are that the pulse recorder described in this paper will find many uses in cosmic-ray research where low counting rates are quite common. In this laboratory it has been used to record the number of counters in a tray of paralleled Geiger tubes which are fired simultaneously by the passage of a cosmic-ray particle, and is currently being used, in conjunction with a proportional counter, to study the specific ionization of mesons of selected ranges. However, it is believed that the circuit is sufficiently versatile to find application in other fields requiring peak voltmeters or pulse recorders.

Technical Apparatus for Determining Thermal Conductivity of Steels up to 500°C

Z. HORÁK AND F. KRUPKA
Department of Technical Physics, Technical University, Prague, Czechoslovakia

(Received November 1, 1949)

An apparatus for determining the thermal conductivity of metals based upon the comparison of flux of heat in a conductor in the usual form of a bar consisting of three parts of different materials has been developed. This method enables one to measure the temperature gradients by only one differential thermocouple sliding in an axial boring of the bar. In this way usually difficult measurements of thermal conductivity can be carried out very easily with sufficient accuracy for industrial purposes.

INTRODUCTION

In practice, methods of comparing the thermal conductivities in a steady state have proved to be very convenient since the difficult measurements of quantity of heat flowing through the whole cross-section area of the specimen are not necessary. Existing methods of comparison, however, require very long rod specimens which are not always at hand and they may be applied at higher temperatures only with difficulty. A new simple method somewhat similar to that developed by Van Dusen and Shelton[1] excludes these disadvantages and may be easily applied to a technical apparatus.

The apparatus described in the mentioned paper requires very difficult fitting-up (bars soldered together, thermocouples attached by peening), very careful and laborious attendance (manual adjusting of currents in the individual heating elements) etc. Under such conditions it does not appear that the comparative method would offer greater simplification and it is more advantageous to make "absolute" determinations directly. The authors intended therefore to develop an apparatus free of all these disadvantages which would enable the measurement to be performed in the simplest and easiest way with an accuracy convenient for industrial purposes.

METHOD OF COMPARING THE THERMAL CONDUCTIVITY

Consider a thermal conductor in the form of a bar consisting of three portions from which the outer ones *I* and *II* are of the same material and the middle portion *III* of another material as shown in Fig. 1. At the upper end of the bar a heater produces (continuously) per second the quantity of heat Q which flows through the bar into a water- or air-cooled receiver mounted on the lower end of the bar. In the steady state and in the case the bar is thoroughly insulated to prevent losses by radiation and convection, the flux of heat through any cross-section area of the bar will be uniform and will be given by $f=Q/A$ where A is the cross-section area of the bar. The quantity of heat Q, transferred across the area A, is given by the well-known equation

$$Q=kA(t_1-t_2)/(x_1-x_2)=f.A, \qquad (1)$$

where k is the thermal conductivity of the material. From this

$$f=k(t_1-t_2)/(x_1-x_2)=k\Delta t/\Delta x, \qquad (2)$$

where $\Delta t/\Delta x$ is the temperature gradient, i.e., the fall in temperature per centimeter. If the cross-section area A is at any point of the bar uniform, the flux of heat f also would be uniform. However, it is impossible to prevent in a perfect way losses of heat by radiation and convection, and for this reason, the average fluxes of heat in the portions *I*, *II*, *III* of the bar will be $f_I>f_{III}>f_{II}$.

When the losses in all three portions of the bar are approximately equal, the flux of heat in the bar will decrease linearly and the average flux of heat f_{III} in the middle portion will be the arithmetical mean of f_I and f_{II}, i.e.,

$$f_{III}=(f_I+f_{II})/2. \qquad (3)$$

From (2) and (3) we obtain

$$f_{III}=k_{III}\Delta t_{III}/\Delta x=(k_I\Delta t_I+k_{II}.\Delta t_{II})/2\Delta x. \qquad (4)$$

The thermal conductivity of the middle bar $k=k_{III}$ may be then computed from

$$k=(k_I\Delta t_I+k_{II}\Delta t_{II})/2\Delta t \qquad (5)$$

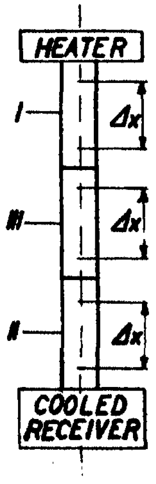

FIG. 1.

---

[1] M. S. Van Dusen and S. M. Shelton, Bur. Stand. J. Research **12**, RP 668 (1934).

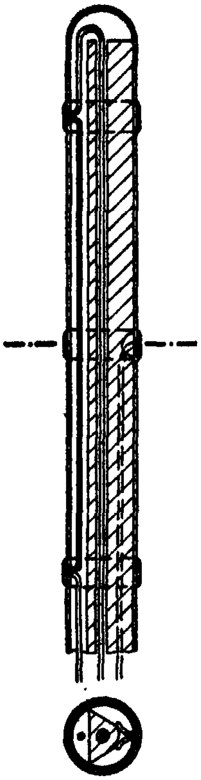

FIG. 2.

by means of observed temperature differences $\Delta t = \Delta t_{III}$, Δt_I and Δt_{II}, if the distances Δx are all equal and the conductivities k_I and k_{II} are known.

The measurement is then performed by inserting a specimen under investigation between two bars with exactly equal diameters made from a metal the conductivity of which is known and by observing the temperature differences which arise in equal distances in the specimen and in the outer bars in positions symetrical to the middle bar.

DESCRIPTION OF THE APPARATUS

In order to obtain the value of the thermal conductivity for the specimen III from Eq. (5), the sectional areas of all bars must be exactly equal. This may be reached with ease by careful machining of the cylindric specimen.

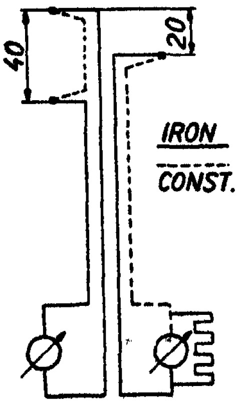

FIG. 3.

Furthermore, the distances Δx over which the temperature differences arise must be equal. It is possible to fulfil this condition perfectly by using a differential thermocouple, as shown in Fig. 2, having its junction placed in fine drill holes separated by a certain distance along the wall of a glass tube which slides in an axial boring of the bars. Besides the temperature differences, the absolute mean temperatures in the bars *I, II, III* are to be measured and for this reason two separate thermoelectric circuits (see Fig. 3) are suitable. By means of one of the circuits made up of iron-constantan wires, the temperature differences Δt in distances of 40 mm are directly read on the scale of the connected galvanometer. It will be noted from Eq. (5) that it is not necessary to graduate the scale of this instrument if the change of e.m.f. with temperature is linear. This is accomplished with the combination iron-constantan to about 500°C with sufficient accuracy. The advantage of such an arrangement is obvious. Then the absolute mean temperatures of the bars are measured by the use of the second circuit and a sensitive millivoltmeter with its scale graduated in degrees centigrade. Figure 2 illustrates the construction of the thermocouple. The fused ends of the wires placed in the wall of a glass tube are covered with 2.5 mm high copper rings fitted with putty; they are in contact with the surface of the axial boring in the bars and receive the temperature belonging to its particular position. Inside the tube the wires are insulated by means of a glass capillary shaped in the form of a three-sided prism.

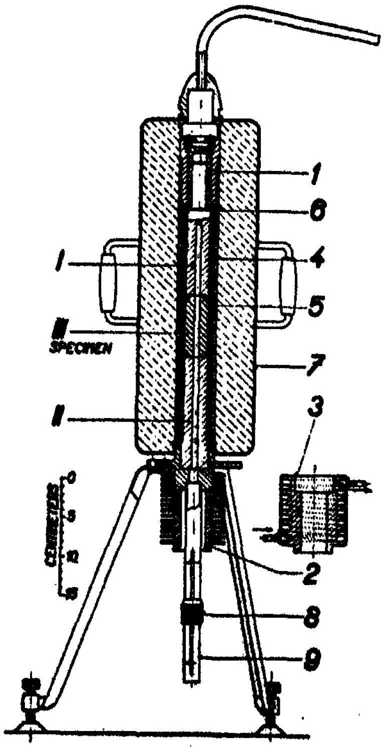

FIG. 4

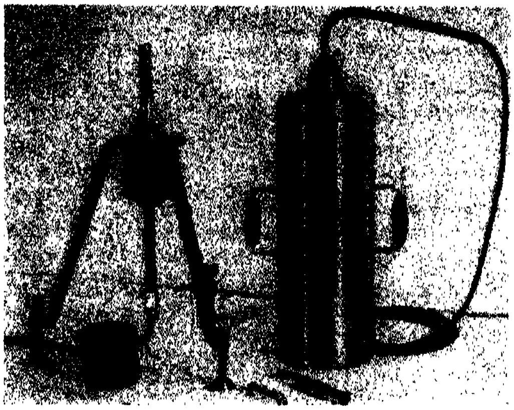

FIG. 5.

The heat transfer by the glass tubes, wires, and air column inside the boring is negligible due to the low thermal conductivity of these materials.

Equation (5) pertains to the case that the flux of heat in the middle bar is the arithmetical mean of the fluxes in both outer cylinders. This condition will be evidently fulfilled with sufficient accuracy if the radial losses are kept to a very low value in comparison to the total quantity of heat transmitted by the bar. In the apparatus the radial losses are reduced to a minimum by means of a porcelain tube 5 and a steel guard tube 4 which surround the bars *I*, *II*, *III* between the electrical heater 1 and the air- or water-cooled receiver 2 or 3, respectively, as shown in Fig. 4. Along this steel guard tube which is heated at its upper end and cooled at its lower end together with the bars *I*, *II* and *III*, a distribution of temperature arises similar to that along the bars. It is possible to adjust the temperature distribution along the steel guard tube by means of the copper tube 6 of a suitable length, joined to the top of guard tube 4. The space between cover 7 and tube 4 is then filled with glass wool and in this way the radial losses are considerably reduced. Cover 7 with guard tube 4 and heater 1 form one compact part which must be removed by drawing upward so that the cylinders will be free. The specimen may then be replaced by another (Fig. 5).

The differential thermocouple is set into position by means of sleeve 8 sliding on tube 9 (Fig. 4) in which the lower end of the thermocouple is suitably fitted. The precise position in which the temperatures are measured are fixed by the notches made in the slit along tube 9 and by a spring-pressed catch mounted in sleeve 8. In this way the required symmetry is secured.

TABLE I.

	Mean temp. deg. C	Temp. diff. div. of galv. scale	Corresp. therm. conductivity cal./cm sec. deg. C
Bar I	212.0	50.2	0.1403
Specimen III	154.5	94.2	
Bar II	99.0	47.7	0.1465

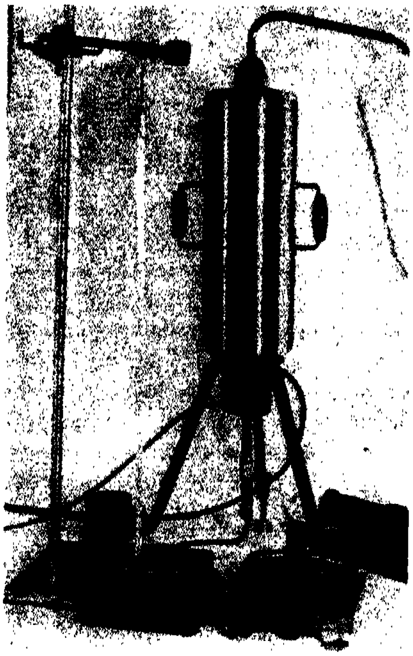

FIG. 6.

In order to exclude temperature drops in the contact areas between the bars, the ends of the specimen are provided with a screw and are screwed into the ends of bars *I* and *II*. The assembled apparatus prepared for measuring is shown in Fig. 6.

PERFORMANCE

In a certain range of thermal conductivities it is possible to adjust the fluxes of heat along the bars and steel guard tube so that an approximately linear temperature gradient is reached. In order to obtain an apparatus suitably for conductivity measurements on steels, bars *I* and *II* have been made from very pure nickel (99.521 percent), its thermal conductivity being similar to that of steels. The relationship of the conductivity to temperature of the pure nickel was given. The apparatus thus has proved to be suitable within the range about 0.18 to 0.05 cal./cm sec. deg. C and for temperatures of 40° to 500°C.

For example, a steel specimen, the chemical analysis of which showed C 0.16 percent, Mn 0.69 percent, Si 0.44 percent, P 0.014 percent, S 0.020 percent, Cu 0.20 percent, Cr 6.65 percent, Mo 0.52 percent, was investigated. The specimen was heat-treated: normalized at 900°C—one hour—cooled in still air and annealed at 750°C—one hour—cooled in still air. Table I shows data obtained in the steady state attained in about five hours.

Using Eq. (5), the thermal conductivity of this specimen at 154.5°C will be found as 0.0746 cal./cm sec. deg. C.

It will be noted that the difference between

$$k_I \cdot \Delta t_I = 0.1403 \times 50.2 = 7.05$$

and

$$k_{II} \Delta t_{II} = 0.1465 \times 47.7 = 6.98$$

amounts to about one percent. At higher temperatures this difference is of course somewhat greater but it proved to be regularly smaller than about 3 to 3.5 percent. The method of temperature measurement employed enables one to detect quite easily drops in temperature across the screwed joints of the bars which may occur. It is found, however, that if the specimen has been carefully manufactured, no remarkable drops in temperature occur which may exert an influence upon the accuracy of measurement.

SUMMARY

The apparatus described was found to be useful for measuring the thermal conductivities in the range of 0.18 to 0.05 cal./cm sec. deg. C, i.e., it is especially suitable for measuring conductivities of steels at temperatures about 40° to 500°C. The accuracy of values obtained is, of course, affected chiefly by accuracy with which the conductivity of bars *I* and *II* has been determined. The method itself is believed to be accurate to about two percent in the above-mentioned ranges assuming the specimen is manufactured carefully enough.

ACKNOWLEDGMENT

The authors wish to thank Mr. J. Junek for his excellent machine work in the construction of the apparatus.

THE REVIEW OF SCIENTIFIC INSTRUMENTS VOLUME 21, NUMBER 10 OCTOBER, 1950

Polarimeter for the Study of Low Frequency Radio Echoes

A. H. Benner and H. J. Nearhoof
Radio Propagation Laboratory, The Pennsylvania State College, State College, Pennsylvania

(Received June 8, 1950)

An instrument is described which allows the determination of the ellipticity, angle of tilt, and sense of rotation of low frequency radio waves returned from the ionosphere.

INTRODUCTION

THREE quantities are important in the observation of the reflected wave in the pulse technique method of radio sounding the ionosphere. These quantities are delay time, intensity, and polarization. The polarization of a radio wave reflected from the ionosphere, in general, is elliptical in shape, and the state of this polarization is defined by three factors. They are the ellipticity, the angle between the major axis of the ellipse and the earth's magnetic field (called the angle of tilt), and the sense of rotation of the ellipse. From a knowledge of the time variation of these factors, conclusions can be made concerning the structure of the ionospheric reflecting layer.

In conjunction with a program of ionospheric research conducted at the Radio Propagation Laboratory, an instrument has been constructed to measure the polarization of radio waves reflected from the ionosphere at low frequencies. It is the purpose of this paper to describe this equipment and its operation.

THE GENERAL SYSTEM

The equipment was designed to receive and record ionospheric echoes from a high power pulse transmitter operating at a carrier frequency of 150 kc/sec., a pulse rate of 1.5625 p.p.s., and with a Gaussian pulse shape whose width is approximately 150 microseconds. The receiving and transmitting site are separated by 4 km and synchronization is accomplished by means of an auxiliary transmitter operating on 2.398 mc/sec. which transmits a pulse 200 microseconds prior to the 150 kc/sec. pulse.

The basic ideas for a polarimeter, for operation on continuous waves, are due to Appleton and Watson Watt[1] and modifications of Martyn and Green.[2] Martyn,

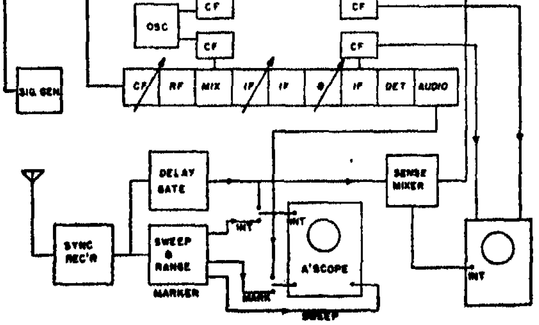

FIG. 1. Block diagram of polarimeter equipment.

---

[1] E. V. Appleton and R. A. Watson Watt, Radio Board, Wireless World p. 17 (July 8, 1932).

[2] D. F. Martyn and A. L. Green, Proc. Roy. Soc. 148, 104–121 (January, 1935).

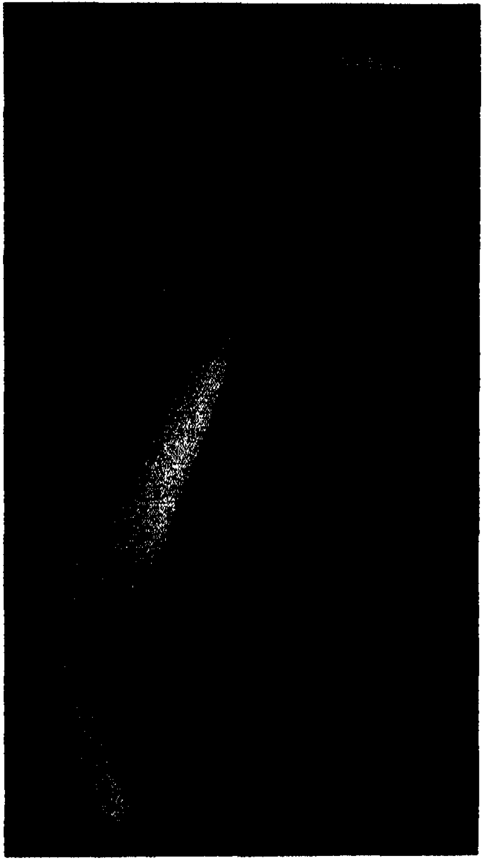

FIG. 2. Photograph of polarization ellipse of 150 kc/s echo with left-handed polarization.

Piddington, and Munro[3] applied these techniques to the pulse system of sounding.

The complete receiving installation is shown in block form in Fig. 1. Referring to the block diagram, two crossed loop antennas are connected separately to two receiver channels. The downcoming elliptical echo is resolved into two quadrature components by these crossed loops, amplified with equal gains and with equal phase, and recombined in the oscilloscope to portray the original ellipse. These receivers are of superheterodyne type with a common local oscillator. The intermediate frequency amplifiers of these channels are coupled by means of a low impedance output to the final deflection amplifiers of a type 208 DuMont Scope. These 'scope amplifiers were tuned to the receiver intermediate frequency of 1050 kc/sec. It was necessary to use such a high frequency in order to realize an adequate number of trace revolutions in the 150-microsecond pulse interval. Also, because of the very small duty cycle (about 10^{-4}), it is necessary to increase the accelerator potential to 4000 volts for greater picture intensity.

Located in the lower left-hand corner of the block diagram is a fixed tuned receiver, modified Wilcox *F*-3, which receives the synchronizing pulse from a separate remote antenna. The band width of this receiver was broadened to that adequate to preserve the synchronizing pulse shape, and noise discriminating threshold and video amplifiers were added. Both positive and negative going synchronizing pulses are available from this receiver.

The positive pulse actuates a delay gate unit whose function is to select a specific portion of the time scale for observation. The output of this unit is a positive pulse which is adjustable in both time location and in width. The negative synchronizing pulse triggers a sweep and range marker. The outputs of this unit are a sweep voltage for a type *A* presentation oscilloscope, an intensity gate for the same 'scope, and time markers.

The output from either channel of the low frequency receiver is detected and coupled to the vertical deflection amplifiers of the *A* 'scope. The pulse from the delay gate unit may be switched to the intensity grid of the *A* 'scope to select the desired portion of the time axis. The output of this unit is also fed to the intensity of the polarimeter 'scope. Thus, this tube is illuminated only during the desired time, and the ground pulse, noise, and interfering signals are not seen except when coincident with this gate pulse.

The sense mixer provides a scheme for ascertaining the direction of rotation of the ellipse. The 1.05 mc/sec. output of one receiver channel is given a 90-degree phase lag, gated by the delay gate pulse, amplified, and fed to the intensity grid of the polarimeter 'scope. It can be shown by a study of the Lissajous figures that, if the ellipse is rotating clockwise (right-hand) and lies in the second and fourth quadrants, only the top portion of the ellipse will be illuminated. If on the other hand, the ellipse lies in the first and third quadrants and is right-handed, only the bottom half of the ellipse is illuminated. In the case where the ellipse lies on either the horizontal or vertical axis, and is right-handed, only the right-half of the ellipse is observed. For left-handed rotation the results are opposite to those for the three cases mentioned above. An example is shown in the photograph of Fig. 2. A somewhat similar system was used by Martyn, Piddington, and Munro.[3]

The signal generator shown in the block diagram, Fig. 1, provides a 150 kc/sec. signal to the calibrate loop, which bisects the angle between the crossed loops. With this signal adjusted to the approximate amplitude of the desired echo, the two receiver channels are adjusted in gain and phase to give a straight line at 45° in the proper quadrants on the polarimeter 'scope. The calibrate loop is then rotated, say counter clockwise as viewed from above, and the line on the 'scope should rotate counter clockwise to assure correct alignment. The amplitude of the calibration oscillator is then varied to assure that the receiver channels do not suffer a phase change within the amplitude limits of the expected echo. After this procedure is completed, the system is ready to operate at this specific frequency and gain setting.

---

[3] Martyn, Piddington, and Munro, Proc. Roy. Soc., Series *A* 158, 536–551 (1937).

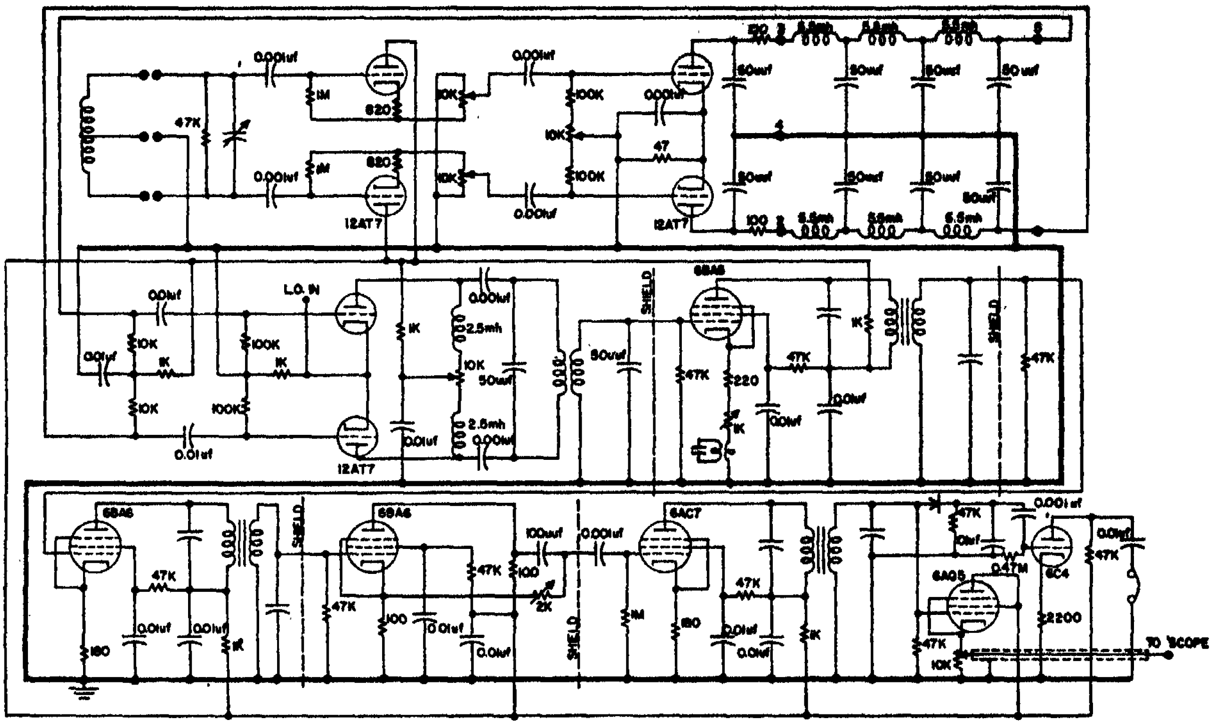

FIG. 3. Schematic diagram of one low frequency receiver channel. Note: Bypass condenser placed in B^+ and filament circuits in both receivers. (Not shown on schematic.) Polarimeter receivers, channels one and two.

In actual operation, the desired pulse as presented on the *A* 'scope, is selected by the delay gate unit. The switches are now positioned to place this gate pulse on the intensity grid of the polarimeter. This allows the observation of the desired pulse, and its ellipticity and angle of tilt may be recorded. By switching the intensity grid of the polarimeter 'scope to the sense mixer, the direction of rotation of the ellipse may be determined. A photographic record of the echoes is made with an Army Air Force Camera type 05 which has an *f* 2–3 lens and a 3 plus portra lens. Because of the very low duty cycle and the resulting low intensity picture, it is necessary to use a time exposure of at least 3 seconds.

CIRCUIT DETAILS

Since the low frequency channels are identical, only one will be discussed in detail. The schematic diagram of one channel is shown in Fig. 3. The input from the loop is coupled into balanced cathode followers. The purpose of this circuit is to facilitate amplitude adjustments without disturbing the phase to any noticeable degree. The outputs of the cathode followers are coupled through balanced, untuned r-f amplifiers to a low pass filter which is designed to attenuate above 300 kc/sec. This system was employed to avoid the difficulty of tracking problems as compared to the slight gain realized by the low *Q* tuned circuits. A push-pull mixer stage was incorporated primarily to balance the local oscillator signal out of the mixer plate circuit and prevent its passing into the I.F. strip.

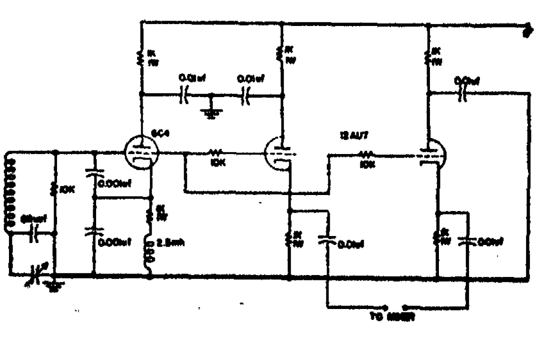

FIG. 4. Schematic diagram of the receiver common local oscillator.

A trap, tuned to the local oscillator frequency of 1200 kc/sec. (150 kc/sec. above the I.F. frequency), is placed in the cathode circuit of the first I.F. stage to eliminate any 1200 kc/sec. signal feeding through from the balanced push-pull mixers. The I.F. stages were designed to have a 40 kc/sec. band width to maintain the pulse shape.

The phase shifting network employes a cathode follower-phase inverter with a resistance-capacitance combination to obtain the desired 90° phase shift. Particular care was taken in the I.F. strip to prevent feedback by shielding each individual stage. The output of the last I.F. stage is connected to a cathode follower which provides a low impedance source to the input of the polarimeter 'scope.

The local oscillator which supplies both receiver channels is shown schematically in Fig. 4. It is a Clapp

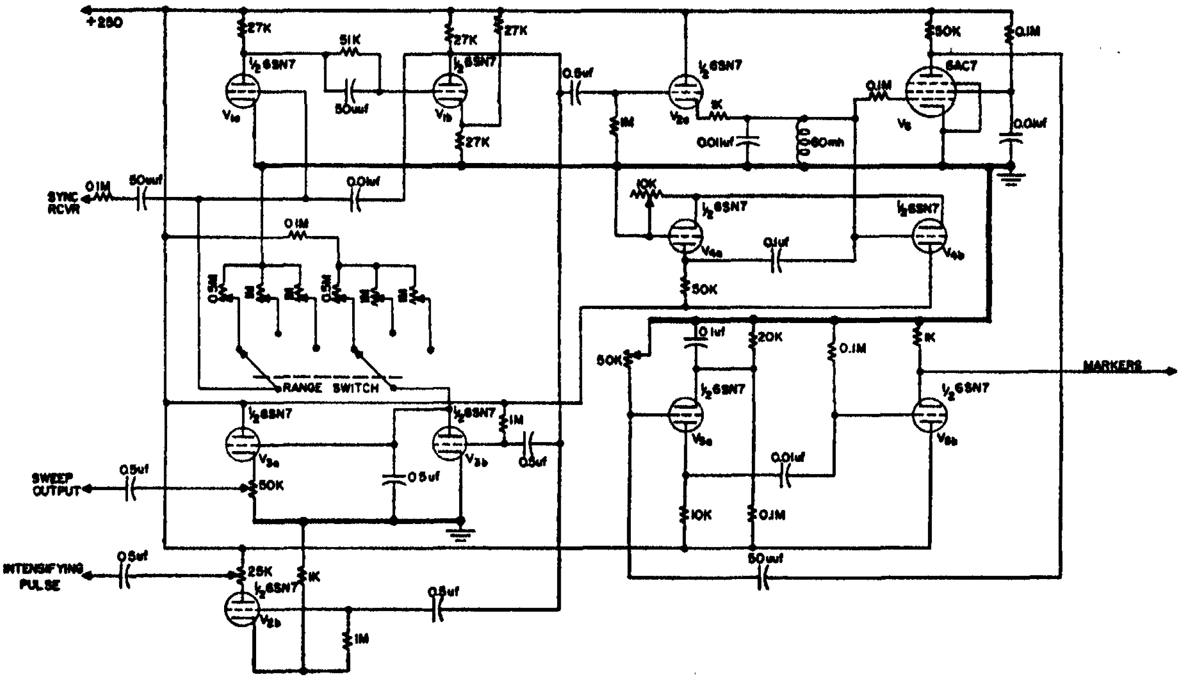

FIG. 5. Schematic diagram of the sweep and range marker.

oscillator[4] designed for good frequency stability. The oscillator is coupled to the two receivers through separate cathode followers to prevent cross-talk.

The sweep and range marker generator is of conventional design. The schematic is shown in Fig. 5. A negative pulse from the synchronizing receiver passes through a differentiating circuit to a monostable multivibrator. A negative square pulse is taken from the plate of V_{1b} and fed to the sweep generator. The saw-tooth output of the generator is coupled to the horizontal amplifier of the *A* 'scope through a cathode follower. The negative square pulse from V_{1b} also goes to V_{2b} which is an amplifier-inverter providing a positive square pulse to trigger the intensity of the *A* 'scope. Tubes V_{4a} and V_{4b} comprise a grounded grid, cathode coupled oscillator[5] whose tank circuit is placed in the cathode circuit of V_{2a}. V_{2a} is normally conducting, thereby placing a low impedance across the tank circuit of the oscillator. This prevents the oscillations until the negative pulse arrives at the grid of V_{2a}, cutting the tube off and allowing the circuit containing V_{4a} and V_{4b} to oscillate. These oscillations are squared and amplified in V_6, and differentiated and peak rectified in V_{5a}. The output of V_{5a} is a series of negative spikes. These markers are coupled to the *A* 'scope through cathode follower V_{5b}.

The positive pulse from the synchronizing receiver is connected to the delay gate unit. The schematic diagram of this unit is shown in Fig. 6. The positive pulse is differentiated and applied to the first half of the 6*SN*7, turning this tube on. The time this tube conducts is determined partially by the *RC* coupling network between plate to grid of the second half of the 6*SN*7. The negative going pulse from the plate of this tube is differentiated and the positive spike from the trailing edge of the pulse, which is adjustable, is used to actuate the second monostable multivibrator. The output of this multivibrator is a positive pulse whose width can be adjusted by the *RC* time constant of the coupling network between the plate and grid of the second 6*SN*7. This pulse is used to gate on the polarimeter 'scope for

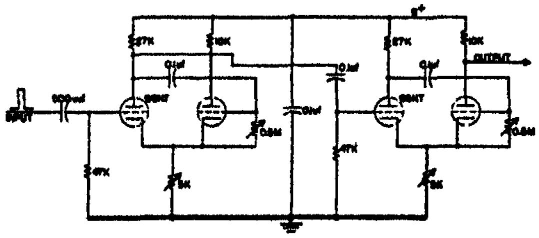

FIG. 6. Schematic diagram of the delay gate unit.

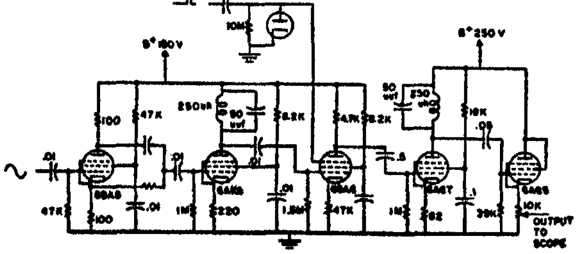

FIG. 7. Schematic diagram of the sense mixer unit.

---

[4] J. K. Clapp, Proc. I.R.E. 36, 356–358 (March, 1948).

[5] P. G. Sulzer, Proc. I.R.E. 36, 1034–1039 (August, 1948).

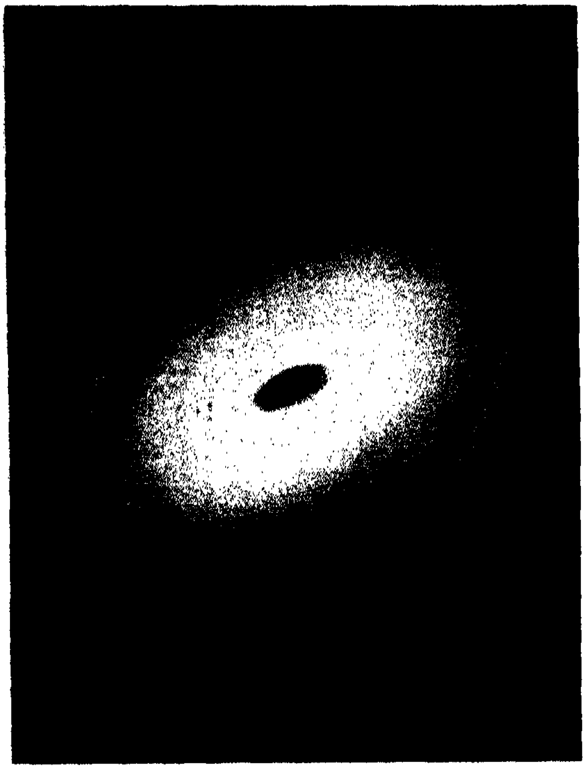

FIG. 8. Photograph of polarization ellipse taken on May 9, 1950 at 21:32 L.M.S.T., magnetic north vertical on page.

the portion of the sweep that is desired. The same pulse is connected through a switching arrangement to the sense-mixing unit.

The schematic of the sense-mixing unit is shown in Fig. 7. The 1.05 mc/sec. signal from channel one is connected to the sense-mixing unit as well as to the polarimeter 'scope. The signal is shifted 90 degrees lagging, by an identical circuit to the one employed in the 150 kc/sec. receiver. After the signal is shifted by 90 degrees, it is amplified by a tuned amplifier of the proper bandwidth. Tuned amplifiers were used to develop the necessary output voltage in order to illuminate the 'scope. This shifted, amplified signal is coupled to the grid of a *6AS6* switch tube that is biased below cut-off by the suppressor grid. The bias is obtained by the action of the biasing diode.

The positive pulse coming from the delay unit charges the 4 microfarad condenser to approximately 100 volts. When the pulse is removed, the grid is effectively placed −100 volts below ground. The *RC* time constant of the biasing diode is large due to the low duty cycle. The suppressor is held below cut-off until the next positive pulse appears, returning the grid to zero, and allowing the 1050 kc/sec. signal to pass. The 1.05 mc/sec. signal is gated in this manner and then amplified by the *6AG7*. The output is fed to the intensity grid of the polarimeter 'scope through a *6AQ5* cathode follower. The output is 40 volts peak for an input of 0.05 volts r.m.s.

EXPERIMENTAL RESULTS

Measurements have been made with this equipment in August and September, 1949, and March and April, 1950, at vertical incidence at 150 kc/sec. The results of the measurements to date have shown that the night time polarization is steady and conforms with that predicted by the theory. The state of the polarization was reported previously[6] for the early period of observation and has been confirmed by the recent experiments. An example of a typical ellipse seen at night on 150 kc/sec. is shown in Fig. 8. This ellipse, representing the electric vector, has its major axis inclined at an angle of 23° east of magnetic north, and ellipticity (defined as the ratio of the minor to major axis) of 0.563, and its sense of rotation is left handed.

At night, split or double echoes have been studied and found to have the same sense of rotation, but slightly different angle of tilt and elliptical configuration. The leading pulse of such a split is normally of the same character as described above, while the later pulse has been seen to lie at the same angle of tilt but with a tendency to be more linear. A series of measurements have been made comparing the observed ellipses for the first and second hop. All observations thus far, although not great in quantity, give an identity between the two. Other measurements have shown rather unusual and rapid changes near sunrise, while pre-sunset and sunset measurements have shown rather constant conditions; very similar to the nocturnal measurements. More complete experimental results will be presented at a later time.

The authors should like to acknowledge the assistance of Mr. P. G. Sulzer, and Mr. C. H. Grace. This work was done under the direction of Dr. A. H. Waynick and was supported in part by Contract No. *AF*19(122)-44 with the U. S. Air Force, through sponsorship of the Geophysical Research Directorate, Air Materiel Command.

---

[6] Benner, Grace, Kelso, Proc. I.R.E. (to be published).

THE REVIEW OF SCIENTIFIC INSTRUMENTS VOLUME 21, NUMBER 10 OCTOBER, 1950

The Design of Neutron Counters Using Multiple Detecting Layers

R. D. Lowde
Ministry of Supply, Atomic Energy Research Establishment, Harwell, England

(Received May 25, 1950)

A discussion is given of ion chambers in which a series of electrodes carry layers of solid detecting material. Counters of this type require low operating voltages, and can easily be miniaturized. Formulas are given for the correct layer thicknesses and for the neutron counting efficiency. The equations are applied to boron 10, and it is shown that there is a permissible tolerance of about 50 percent on the thickness of a boron layer, and a very considerable tolerance on the assumed values of the disintegration product ranges. Curves are given relating the optimum boron layer thicknesses and the efficiency to the number of layers. A miniature instrument is described having a sensitive volume of 0.4 cm^3. It operates at a thermal neutron efficiency of 24 percent with a collecting voltage of 70.

1. INTRODUCTION

RECENT experiments in nuclear physics have involved the detection of neutrons at the rate of only one every few seconds. For such work, a counter should be highly efficient, and where possible also small, so as to present a small projected area to the background flux and to require a minimum of the bulky materials used in neutron shielding. If the flux to be measured is in the form of a beam, the counter should in addition have a highly directional sensitivity.

For several purposes a suitable instrument is one which may be called a multiple-layer chamber. The neutrons are detected by a succession of solid coatings of some reacting material such as boron or uranium, on the electrodes of a series of parallel plate ion chambers. This type of counter may be made extremely compact, and may also be operated at a very low collecting voltage. Rossi and Staub[1] have already exploited these advantages of ion chamber methods by using a uranium layer coiled into a region of dimensions about 2 cm. The performance of these counters cannot be equalled by a simple ion chamber filled with detecting gas. For instance, about three atmospheres of $B^{10}F_3$ would be required in the same sensitive volume to give the efficiency of the counter described below; and for operation at this pressure, BF_3 must be purified to a degree that is difficult to achieve.

This paper deals with the theory and design of multiple-layer chambers. After discussing the relation between the layer thicknesses, the counting efficiency, and the number of detecting layers, the arrangement of the electrodes is examined. The performance of a miniature neutron counter designed on these principles is then given, and shown to be in general agreement with the theory.

2. THEORY

For the purposes of this section, a neutron beam is imagined perpendicularly incident on an arrangement of x_0 successive layers of some suitable material. Four assumptions are made: that the detecting substance is deposited with uniform thickness t on smooth thin backing foils impenetrable to the disintegration products, but not absorbing neutrons; that the generation of disintegrations is uniform throughout any one layer; that there are two detectable products of the neutron capture reaction; and that all disintegration products emerging from the surface of a layer are detected by the electronic apparatus.

The Efficiency of an Individual Layer

The counting rate of a solid layer of material depends on both the cross section of the nucleus for neutron capture, and the ranges of the disintegration products in the parent substance. These ranges are referred to throughout as R_L and R_α, with $R_L<R_\alpha$, in view of the later application to boron 10. The weaker long-range group of particles in the boron reaction is ignored.

In any given detecting layer, some of the disintegrations for which the particle tracks lie nearly parallel to the plane of the foil, pass unobserved. The total number of disintegrations taking place may be divided into two halves, according to which particle is projected in the direction of the detection chamber. If the layer is perfectly plane, and t is less than both R_L and R_α, the fraction of the particles emerging from a depth τ is easily shown to be $\frac{1}{2}-\frac{1}{2}\tau/R_L$ in one case, and $\frac{1}{2}-\frac{1}{2}\tau/R_\alpha$ in the other. The efficiency c of one layer therefore increases with t as

$$c=\tfrac{1}{2}\mu t(1-\tfrac{1}{2}t/R_L)+\tfrac{1}{2}\mu t(1-\tfrac{1}{2}t/R_\alpha), \qquad (1)$$

where μ is the linear neutron absorption coefficient. As the thickness of the layer is increased, this efficiency also increases up to $t=R_\alpha$; but at $t=R_L$ and $t=R_\alpha$ the first and second terms in (1) respectively reach a maximum and are replaced in turn by the constant terms

$$\tfrac{1}{4}\mu R_L \quad\text{and}\quad \tfrac{1}{4}\mu R_\alpha. \qquad (2)$$

Writing

$$a_1=(R_L^{-1}+R_\alpha^{-1})/4\mu;\; a_2=\tfrac{1}{2}\mu R_L,\text{ and } a_3=\tfrac{1}{2}/\mu R_\alpha, \qquad (3)$$

this efficiency is conveniently given by

$$c=\mu t[1-a_1\mu t], \qquad 0\leqslant t\leqslant R_L \qquad (4a)$$

$$c=\mu t\cdot\tfrac{1}{2}\cdot[a_2(\mu t)^{-1}+1-a_3\mu t], \quad R_L\leqslant t\leqslant R_\alpha. \qquad (4b)$$

---

[1] B. B. Rossi and H. H. Staub, *Ionization Chambers and Counters* (McGraw-Hill Book Company, Inc., New York, 1949), p. 210.

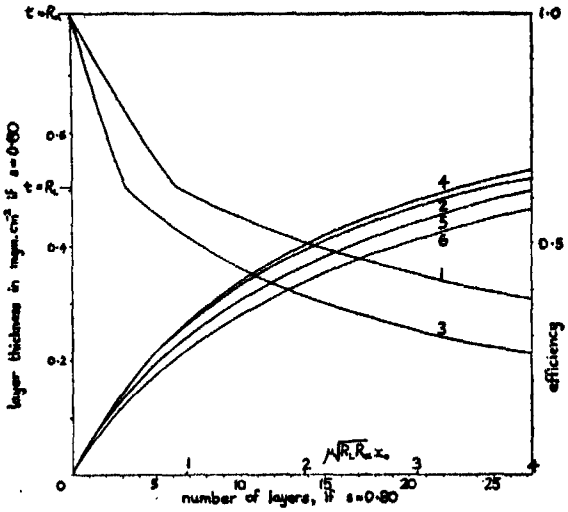

FIG. 1. Boron 10, layer thickness and counting efficiency in multiple-layer chambers. (1). The optimum thickness of boron 10 for x_0 identical layers. (2). The thermal neutron detection efficiency given by (1). (3). Curve showing the best variation of layer thickness along a counter having x_0 layers. Thicknesses are read off above the number of the layer, starting at the back of the counter. (4). The thermal neutron detection efficiency given by (3). (5) and (6). The efficiency given by the thicknesses of curve (3) multiplied by 1.6 and 0.5 respectively. In deriving these curves, the weak long-range group of disintegration products is ignored. s is the atomic stopping power of B^{10} (see Section 4).

The maximum efficiency for a single layer is obtained with $t=R_\alpha$.

Chamber with a Number of Identical Layers

With multiple-layer chambers, on the other hand, the maximum over-all efficiency is *not* obtained by putting every $t=R_\alpha$. For where there is a number of foils in succession, the layers at the front waste neutrons which would otherwise have stood a chance of being detected farther down the counter. It will therefore be profitable to reduce the thickness of the layers to an extent depending on their number, so that the initial waste of neutrons where the beam is at full intensity will be diminished, resulting in a greater total count.

Suppose x_0 identical layers are used. The factor μt in (4), which represented the fraction of the incident neutrons captured in one thin foil, must now be replaced by $(1-e^{-\mu t x_0})$; the bracketed factor in (4), which takes account of the wastage, is unaltered. This leads to an efficiency

$$c=(1-e^{-\mu t x_0})[1-a_1\mu t], \qquad 0\leqslant t\leqslant R_L, \qquad (5a)$$

$$c=(1-e^{-\mu t x_0})\tfrac{1}{2}[a_2(\mu t)^{-1}+1-a_3\mu t], \quad R_L\leqslant t\leqslant R_\alpha. \quad (5b)$$

Equations (5) may be transformed so as to have dimensionless coefficients by the new choice of variables

$$T=t/(R_L R_\alpha)^{\frac{1}{2}}, \quad X_0=\mu(R_L R_\alpha)^{\frac{1}{2}}x_0. \qquad (6)$$

This gives for boron 10 (ignoring the weak long-range group of disintegration products),

$$c=(1-e^{-TX_0})(1-0\cdot514T), \qquad 0\leqslant t\leqslant R_L, \qquad (7a)$$

$$c=(1-e^{-TX_0})0\cdot198(T^{-1}+2\cdot53-T), \quad R_L\leqslant t\leqslant R_\alpha. \quad (7b)$$

The optimum thickness, t_{opt}, giving the greatest efficiency for a given number of layers, is calculated by solving the two equations $dc/dt=0$ in the form $t_{\text{opt}}=f(x_0)$.

A graphical solution for boron 10 is shown in curve 1 of Fig. 1, and the corresponding efficiency in curve 2. The abscissa is $\mu(R_L R_\alpha)^{\frac{1}{2}}x_0$, which has been regarded as a continuous variable to give rise to a smooth curve through the points having x_0 integral. A calibration in x_0, the number of foils, has been made as accurately as measurements of R_L and R_α allow; t has also been calibrated in mg cm^{-2} subject to the same uncertainty. As the number of boron layers is increased, the optimum boron thickness decreases rapidly from the maximum value R_α to less than half that thickness for counters containing more than fourteen foils. The form of the function is different, depending on whether t is greater or less than R_L, since the relation between t and the counting rate is different in these two ranges; it is easily proved that the two branches join continuously at $t=R_L$. The rather sharp drop from R_α for one-layer counters to R_L for six-layer counters is due to this fact: so long as all the layers of a counter are thicker than R_L the waste of neutrons due to the comparative shortness of R_L is severe, and by thinning the boron deposit, advantage is gained on this ground to offset the diminished number of α-particles recorded.

It will be noticed that in this calculation, $t=R_\alpha$ corresponds to $x_0=0$ rather than $x_0=1$. This is caused by the approximation whereby Eq. (1) assumes there is no appreciable diminution of the incident neutron intensity within any one layer. At the extreme left of the graph for boron, this approximation is evidently only just valid.

The Optimum Variation of Layer Thickness

The design in which all foils carry equal deposits is open to further improvement. For when any counter containing several foils is exposed to a neutron beam, those neutrons entering it which escape capture are confronted by a shorter and shorter residual length of counter as they proceed; and it is clear from what has just been said that an improvement will be gained by thickening up the layers successively so that the highest possible detection efficiency for that residual length awaits the neutron at any point of its passage. The best variation of t will now be calculated.

Consider a hypothetical continuous counting medium of length x_0 and detector density t per unit length, instead of, as before, a counter of x_0 layers of thickness t. In a length dx of this counter, the amount tdx of detecting substance has a counting rate per unit incident intensity given by the right-hand sides of Eqs. (4) multiplied by dx. The result of this procedure approximates to a rigorous calculation when x_0 in the solution takes integral values.

The solution for boron 10, again ignoring the long-range group of particles, appears in curve 3 of Fig. 1, with the corresponding efficiency given by curve 4.

Curve 3 has been drawn such that when any number x_0 of layers has been decided on, the shape of the curve from 0 up to the appropriate value of $\mu(R_LR_\alpha)^{\frac{1}{2}}x_0$ gives the best possible distribution of detecting material; with good accuracy, the thickness of individual boron layers in a practical case can be read from the ordinates at the integral values of x_0. The rear foil in the counter should always have the thickness R_α. Again the curve gives the value $t=R_\alpha$ to $x_0=0$ rather than $x_0=1$, due to the continuous model ceasing to represent reality for counters having a small number of foils, up to about three in the boron counter.

The derivation of this function is as follows. Let $x=0$ be the back and $x=x_0$ the front of the counter. For a unit incident intensity of neutrons the intensity of the beam within the counter varies along the length as

$$I(x)=\exp-\int_x^{x_0}\mu t(x)\cdot dx. \tag{8}$$

The number of neutrons detected by the material between x and $x+dx$ is then

$$dc=-I(x)\cdot\mu t(x)[1-a_1\mu t(x)]\cdot dx, \qquad 0\leqslant t\leqslant R_L, \tag{9a}$$

$$dc=-I(x)\cdot\mu t(x)\tfrac{1}{2}[a_2\{\mu t(x)\}^{-1}+1-a_3\mu t(x)]\cdot dx, \qquad R_L\leqslant t\leqslant R_\alpha. \tag{9b}$$

Putting

$$y=\int_x^{x_0}\mu t(x)\cdot dx, \tag{10}$$

Eqs. (9) become

$$dc=e^{-y}\cdot y'[1+a_1y']\cdot dx, \qquad 0\leqslant t\leqslant R_L, \tag{11a}$$

$$dc=\tfrac{1}{2}e^{-y}\cdot[y'(1+a_3y')-a_2]\cdot dx, \quad R_L\leqslant t\leqslant R_\alpha. \tag{11b}$$

The counting rate of the whole instrument is greatest when the integral

$$\int_{x_0}^{0}dc \tag{12}$$

takes its maximum value.

This problem would be elementary, but for the fact that (11) has a discontinuity in the second partial derivative with respect to y' at $t=R_L$. That point is known to be within the range over which a solution for $t(x)$ must be found, and so the integrand (11) does not satisfy the continuity conditions for the application of Euler's equations. However, we can derive by a physical argument a class of functions containing the solution.

Consider first very short counters. The best thickness of deposit for counters of limitingly small length has already been deduced from Eqs. (1) and (2). For very short counters of finite length, the only reason for reducing $t(x)$ below R_α anywhere, is to reduce the waste of neutrons at the front, and it is easy to argue (by discussing the alternatives), that at least for short enough counters, $t(x)$ will be a continuous function, equal to R_α at $x=0$, of everywhere negative slope, and such that $R_L<t\leqslant R_\alpha$.

Thus for x_0 sufficiently small, the correct solution is obtained from (12) simply by Euler's method, using as integrand (11b) alone. This gives at once

$$t(x)/(R_LR_\alpha)^{\frac{1}{2}}=\tan[\tan^{-1}(R_\alpha/R_L)^{\frac{1}{2}}-\tfrac{1}{2}\mu(R_LR_\alpha)^{\frac{1}{2}}x]. \tag{13}$$

Now whatever the length of a counter, there will be a portion at the rear covering a range of x within the region of validity of Eq. (13). If the residual neutron beam which penetrates to this region is to be detected with the greatest efficiency, the function $t(x)$ must therefore follow (13) at the back of a long counter for some distance ξ. But at the point $x=\xi$, whose value may well depend on x_0, the detection efficiency of the rear portion becomes great enough to justify a reduction of $t(x)$ below R_L at greater x, in the interest of reducing the waste of neutrons where the incident beam is most intense.

The argument thus shows the desired solution to consist of two component counters in cascade, each having a different design based on one of the two Eqs. (11). The problem is therefore one of matching these two sections to give the maximum combined counting rate.

If the efficiency of the rear section is written $c_r(\xi)$, the total counting rate is the sum of the contributions of the front and rear sections:

$$c=\int_{x_0}^{\xi}e^{-y}\cdot y'[1+a_1y']\cdot dx+c_r(\xi)\cdot\exp-[y]^{x=\xi}. \tag{14}$$

This may be put in the form

$$c=c_r(\xi)+\int_{x_0}^{\xi}e^{-y}\cdot y'[1-c_r(\xi)+a_1y']dx. \tag{15}$$

Although the maximum value of the expression (15) contains ξ, the function y which maximizes the integral in (15) does not. The desired solution for y' in the region $0\leqslant t\leqslant R_L$ is therefore obtained by applying Euler's equations to the integrand of (15), which gives

$$t(x)=2/\mu(x+\kappa), \tag{16}$$

with κ a constant. Notice that apart from a multiplying factor and dependence on ξ, the integral in (15) is identical with that in (14), so that the solution (16) is the same function that gives the front section the greatest efficiency in itself.

ξ and κ are found by expressing the total counting rate as the sum of two integrals of the form (12) referring respectively to the front and rear sections; thus

$$c(x_0,\xi,\kappa)=\int_{x_0}^{\xi}dc+\int_{\xi}^{0}dc. \tag{17}$$

The integrands in these two integrals are separately, (11a) using (16), and (11b) using (13), in that order. The expression (17) reaches a maximum when

$$\partial c/\partial\xi = 0 = \partial c/\partial\kappa; \tag{18}$$

which yields

$$\mu(R_L R_\alpha)^{\frac{1}{2}}\xi = 4\tan^{-1}(R_\alpha/R_L)^{\frac{1}{2}} - \pi, \tag{19}$$

$$\kappa = a_2^{-1} - \xi. \tag{20}$$

Both ξ and κ are independent of x_0, so that $t(x)$ may be represented by a single function of x whatever x_0. Calculation further shows that the two branches (13) and (16) of the solution meet continuously at $t = R_L$.

Curve 3 of Fig. 1 is this function with x_0 written as the independent variable. Using (6) together with $\Xi = \mu(R_L R_\alpha)^{\frac{1}{2}}\xi$, it may be written:

$$T = \tan[\tan^{-1}(R_\alpha/R_L)^{\frac{1}{2}} - \tfrac{1}{2}X_0], \quad 0 \leqslant X_0 \leqslant \Xi, \tag{21a}$$

$$T = 2/[X_0 - \Xi + 2(R_\alpha/R_L)^{\frac{1}{2}}], \quad \Xi \leqslant X_0. \tag{21b}$$

In these equations, $X_0 = \mu(R_L R_\alpha)^{\frac{1}{2}}x_0$, with x_0 the number of boron layers; $\Xi = 4\tan^{-1}(R_\alpha/R_L)^{\frac{1}{2}} - \pi$, and $T = t/(R_L R_\alpha)^{\frac{1}{2}}$.

The Maximum Efficiency

The result of substituting (11) and (21) into (17) is an efficiency

$$c = \tfrac{1}{2}(1 + R_L/R_\alpha)/(1 + \cot\{\tfrac{1}{2}X_0\}\cdot R_L/R_\alpha), \quad 0 \leqslant X_0 \leqslant \Xi, \tag{22a}$$

$$c = [X_0 - \Xi + (R_\alpha/R_L)^{\frac{1}{2}} - (R_L/R_\alpha)^{\frac{1}{2}}]/[X_0 - \Xi + 2(R_\alpha/R_L)^{\frac{1}{2}}], \quad \Xi \leqslant X_0. \tag{22b}$$

This function is shown for boron 10 in curve 4 of Fig. 1.

The formulas (22) do not reduce to any simple criterion which will decide the most efficient detector for any given number of layers, but they may be illustrated by the following general remarks. A counter will be the more efficient, the greater the product of the neutron absorption coefficient and the geometric mean of the disintegration product ranges. It is also important that the two ranges be nearly equal, for then a thickness of coating which is efficient for the detection of one of the products will also be efficient for the detection of the other. Moreover, when the two ranges are nearly equal, the detecting layer may be deposited onto a thick electrode with little loss, because whichever of the two particles is projected in the direction of the backing plate, the other is thrown in the direction of the ion chamber with much the same probability of detection.

Tolerances on the Design Constants

A striking feature of Fig. 1 is the closeness of curves 2 and 4. Curve 4 exhibits, for any x_0, the highest efficiency obtainable with a multiple boron layer instrument, curve 2 the best efficiency of boron counters having all layers identical. Over the whole range of the figure the latter efficiency is more than 0.97 of the former, which means that any design intermediate between those given by curves 3 and 1 will give rise to a counting efficiency very close to the maximum. This result is fortunate, since thin films cannot be laid down with very great accuracy; and also because the thicker layers at the back of the counter, which are comparatively expensive to make, are shown to be unnecessary.

Curves 5 and 6 illustrate the insensitiveness of the over-all efficiency to the fine details of the function t. They allow for the possibility that the boron deposits may unintentionally be laid down too thick or too thin. Curve 5 is the efficiency of a counter whose layers have thicknesses given by curve 3 times 1.6; curve 6 is the efficiency with curve 3 times 0.5. These great errors in the practical values of t, therefore, give rise to remarkably little loss of efficiency. A glance at the form of the ideal curve shows why this is. For fairly long counters, say with $\mu(R_L R_\alpha)^{\frac{1}{2}}x_0 \sim 4$, most of the initial detection of the beam takes place in the front part of the counter, where the foils are too thin for excessive waste of neutrons; while for short counters, having say $\mu(R_L R_\alpha)^{\frac{1}{2}}x_0 < \frac{1}{2}$, thickening the boron gives an increased number of α-particles to offset the increased wastage of lithium recoils. The two factors operating together permit a wide tolerance on t over the full range of $\mu(R_L R_\alpha)^{\frac{1}{2}}x_0$.

Furthermore, some of the generous tolerance on t may be taken up as a tolerance on the assumed values of R_L and R_α. Consider curve 1. When a value of x_0 is chosen, it leads to an abscissa x, say, dependent upon the value R_α used. The graph then reads t as a certain fraction θ of R_α. Suppose the true value of the alpha-range were actually $R_\alpha + \delta R_\alpha$; then the correct thickness is given by the abscissa $x(1 + \delta R_\alpha/R_\alpha)$, for which the corresponding t is $(\theta - d\theta)(R_\alpha + \delta R_\alpha)$. Owing to the difference of sign in the two brackets, and since $t \sim \text{constant}/x_0$, this magnitude differs from the original figure θR_α by second-order quantities only. It therefore follows that the figure used for R_α may be considerably in error before it has a serious effect on the design constants; and in view of the large tolerance on t, an accuracy of 10 percent or so is quite sufficient for R_α. The chief inaccuracy introduced by an error in R_α is in the calibration of the axis of abscissae for the efficiency curves.

3. ARRANGEMENT OF THE ION CHAMBERS

When counting efficiency is important, the thicknesses of detecting material demanded by the theory introduce difficulties in detection. The particles emerging from the layers have all residual energies from the maximum down to zero, and some of the smaller pulses are consequently missed by the detecting equipment, which is set at a finite bias voltage. The need for compactness may also impose restrictions on the design. To find the best possible system taking these considerations into account, it will be necessary to devote the next paragraph to the elements of ion chamber theory.[2,3]

In a non-gridded ion chamber employing electron collection, the height of the pulse received at the amplifier depends not only upon the total amount of ionization produced by the high speed particle, but also upon the position of the original ion track inside the chamber. The peak signal voltage induced across a plane parallel plate chamber is very approximately $(Q/C)f$, where Q is the total charge carried by the electrons, C the capacity of the chamber, and f is the fraction of the interelectrode spacing travelled by the electrical center of the electrons. This is a simple consequence of integrating over the contributions of the original electrons individually. Consider ionizing particles emerging at a fixed energy from the negative electrode of a parallel plate chamber. If the filling gas pressure is so high that the ion tracks are all crowded right over to one side of the chamber, then the pulses observed will all have nearly maximum height, since the electrical centers of the electron tracks cross the chamber almost entirely. On the other hand, if the polarity were the reverse, only a greatly reduced signal would be received. With correct polarity, the curve of counting rate against bias voltage will have a plateau and the bias voltage may be set for operation at a value above noise where the dependence of counting rate upon bias voltage is very small.

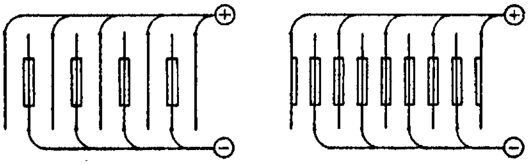

(a) (b)

FIG. 2. Electrode assemblies carrying layers of detecting material.

The ideal design therefore requires the chosen number of coated foils to be connected together and interleaved with a set of blank positive electrodes as in Fig. 2(a). This arrangement is to be contrasted with that of Fig. 2(b), which at first sight may seem superior, because the amount of detecting substance present has been doubled, while the physical size and the interelectrode capacity remain the same. The efficiencies of two boron 10 counters, one of which has twice the linear density of layers of the other, are compared in Fig. 3. Curve 4 is repeated from Fig. 1, where it represents the maximum efficiency of a multiple-layer chamber; curve 7 is identical except that the abscissa is $2\mu(R_L R_\alpha)^{\frac{1}{2}}x_0$ instead of the $\mu(R_L R_\alpha)^{\frac{1}{2}}x_0$ shown.

The counting rate with Fig. 2(b) is not simply that of Fig. 2(a) plus the contribution of the extra layers working with reversed polarity; for most of the counting rate and of the waste of neutrons, arises from the first few layers, of which the additional ones in Fig. 2(b) are working inefficiently. With an infinitely high gas pressure in arrangement (b), only those foils on the negative electrode give any count, so that the efficiency is given by curve 7 scaled down by approximately one-half. As Fig. 3 shows, this is always *less* than the efficiency of arrangement (a).

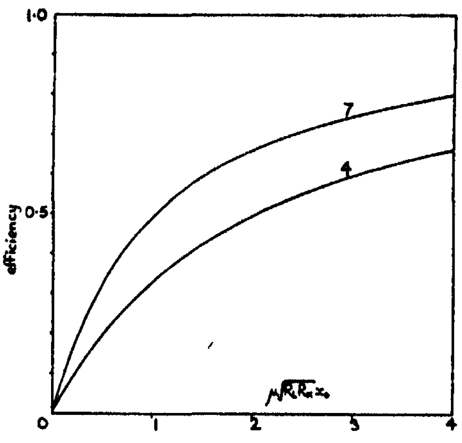

FIG. 3. Curves relating to the efficiency of multiple-layer chambers.

However, with finite gas pressures, the ion tracks extend across the chambers. With reduction of pressure, the count from the negative layers decreases, while that from the positive layers increases to a maximum; the net result is a higher counting rate than that at infinite gas pressure. The question whether a pressure can be found at which arrangement 2(b) is more efficient than arrangement 2(a) is a practical one, since the operating bias voltage is determined by valve capacity and noise. Investigation of the boron counter shows that the maximum efficiency of a counter similar to that of Section 5 below with arrangement 2(b), is only approximately equal to that with 2(a).

The disadvantages of arrangement 2(b) are, on the other hand, that it has twice the amount of boron, three times the bias curve slope, and a greater background count than 2(a).

4. THE DETECTING MATERIAL

The separated isotope B^{10} was chosen as the detecting substance for a slow neutron counter. Being of small atomic weight, this isotope is more easily isolated in a magnetic separator than a heavy substance such as uranium. The constants[4] of the disintegration $B^{10}(n, \alpha)Li^7$ are found in Table I, the reaction being spherically symmetrical. Using the interpolated stopping power 0.80 for boron, the range of the main group α-particle in B^{10} comes to 0.81 mg $cm^{-2} \equiv 3.5$ microns. (Walker[5] has used without reference a stopping power of 0.94, which leads to 0.69 mg $cm^{-2} \equiv 3.0$ microns.) The number

---

[2] D. R. Corson and R. R. Wilson, Rev. Sci. Inst. 19, 207 (1948).

[3] R. Sherr and R. Peterson, Rev. Sci. Inst. 18, 567 (1947).

[4] C. W. Gilbert, Proc. Camb. Phil. Soc. 44, 447 (1948).

[5] R. L. Walker, Phys. Rev. 76, 244 (1949).

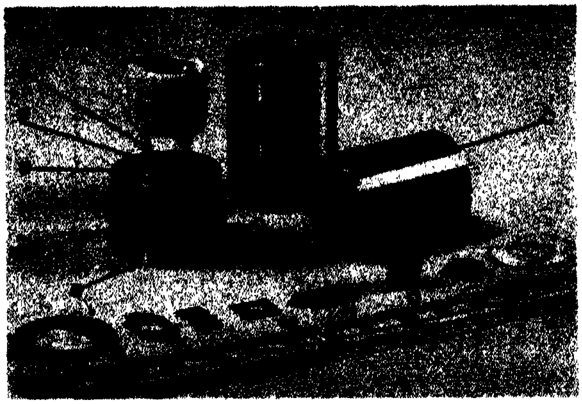

FIG. 4. A miniature neutron counter.

of B^{10} layers of thickness, say, 3 microns needed to capture 95 percent of an incident neutron beam is 19.

A further constant required by the theory of Section 2 is the ratio of the ranges in B^{10} of the recoil nucleus and the α-particle. For practical purposes, the long-range group may be considered weak enough to be ignored. For the main group, the ratio of these ranges in air is, from Table I, 0.62±0.03, and in argon, from measurements on Fig. 8 and similar curves, 0.63±0.03. The value 0.625 has been assumed for the ratio in B^{10}.

5. A MINIATURE NEUTRON COUNTER

Figure 4 shows a fully demountable neutron counter with a sensitive volume of 0.4 cm^3. It operates at a thermal neutron efficiency of 24 percent with a collecting voltage of 70 volts. The whole instrument is contained within a cylinder of length $2\frac{5}{16}$ in. and diameter $1\frac{3}{16}$ in., which is larger than a sealed-off version would need to be.

The outer case *A* screws onto the base *B*, compressing the container *C* into the groove *D* containing a Neoprene gasket *E*. The filling tube *F* passes through a cock *G*, turned by a screwdriver, which is tightened after filling the counter by the threaded ring *H* being upon a Neoprene ring *I*. The electrode assembly *J* comprises twelve ionization chambers of 1-mm spacing. Six negative electrodes *K*, stamped from 0.005-in. nickel foil, each carry two 0.005-in. aluminum squares *L* which fit into a recessed nickel foil *M* spot welded to the electrode. The aluminum squares are coated on one side in an electromagnetic separator with nominally $\frac{1}{2}$ mg cm^{-2} of boron 10, and the boron surfaces face outward through circular windows of diameter 6 mm. The seven alternate positive electrodes *N* are cut from 0.002-in. copper foil. The interelectrode distance is determined by the use of polytetrafluorethylene spacers *O*. All electrodes of the same sign are connected together, the negative ones being connected to the base *B* and the positive ones via the Kovar seal *P* to the signal cable, which enters through the hole *Q*.

The counter is filled with a pressure of 5 atmos. of argon, the counting rate not being improved by any further increase in pressure. (After testing and insertion in the shielding, the actual model of Fig. 4 is operated in a pressurized chamber to prevent eventual leaks through the miniature cock.)

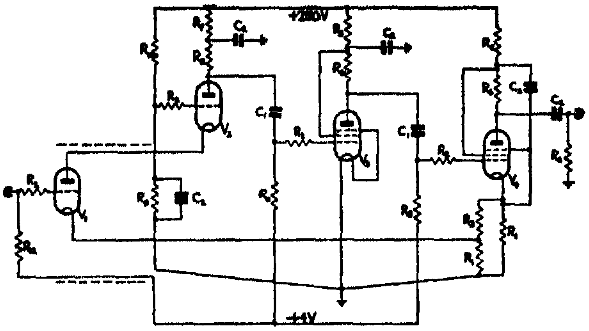

FIG. 5. Head-amplifier suitable for the counter of Fig. 4. R_1, 10Ω; R_2, 47Ω (not high stability); R_3, 100Ω; R_4, 2.7*k*Ω, $\frac{1}{2}W$; R_5, 3.9*k*Ω, 1*W*; R_6, 10*k*Ω, 1*W*; R_7, 22*k*Ω; R_8, 27*k*Ω; R_9, 100*k*Ω; R_{10}, 150*k*Ω; R_{11}, 560*k*Ω (not high stability); R_{12}, 10*M*Ω (not high stability). All resistors $\frac{1}{4}W$, five percent, high stability, except where otherwise stated. C_1, 470*pf*; C_2, 0.5*μf*; both condensers 250 v working. V_1 and V_2, *CV* 139; V_3 and V_4, *CV* 138.

A head amplifier designed by A. B. Gillespie at the Atomic Energy Research Establishment is shown in Fig. 5. It is intended to feed into an impedance of 100 ohms followed by rise and clipping time constants of 3 μsec. Two identical miniature valves in series replace the first valve of a conventional ring of three circuit, giving a stage gain comparable with that of a single pentode while the signal-to-noise ratio remains close to that of a single triode.[6] The first valve V_1, together with only two resistors, may be attached to the counter at the far end of several feet of cabling. The total input capacity of the grid of V_1, adding the capacities of the valve and the counter, is about 25 μμf. The noise voltage adds a half-width equivalent to 29 kv to the α-particle spectrum.

The bias curve obtained with an *HT* of 120 volts is shown in Fig. 6. Since for the sake of efficiency, the thickness of the boron layers has been made comparable with the range of the α-particle, there is no plateau. The counter is operated with twice the amplification of Fig. 6 at a bias voltage of 16, when the slope is 1.4 percent per volt. At this bias voltage, the dependence of counting rate on *HT* is as shown in Fig. 7.

According to Fig. 1, the efficiency of the electrode assembly should ideally be about 46 percent. The

TABLE I.

	% intensity of group	Energy of alpha-particle, Mev	Ranges in cm of standard air of alpha-particle	lithium particle
Main group	91.4 ±1.0	1.53	0.77 ±0.02	0.48 ±0.02
Long-range group	8.6 ±1.0	1.83	0.93 ±0.02	0.56 ±0.02

---

[6] R. Wilson, Phil. Mag. 41, 66 (1950).

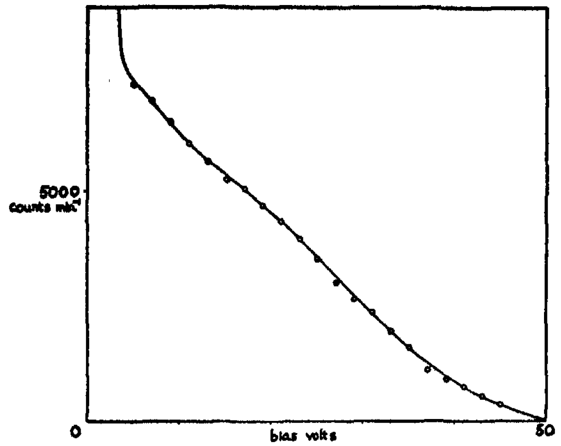

FIG. 6. Bias curve of the miniature neutron counter.

measured efficiency of the counter is reduced below that amount by a factor 0.80 due to the finite bias curve slope, and by a further 0.89 due to the neutron absorption of the counter end wall. There remains a loss of a factor of 0.73. As shown in the next section, this is caused by imperfections in the boron layers, so that an improvement in these should be capable of restoring the over-all efficiency to about 33 percent.

6. QUALITY OF THE BORON LAYERS

In practice, thin boron coatings on foils only roughly approximate to the perfect planes assumed in the theory of the preceding sections. The result of this is a reduced efficiency; for with an uneven boron layer the waste of neutrons is excessive in regions where the deposit is too thick. Indeed, it was found that layers with a visibly rippled surface gave only two-thirds the count of smooth layers of the same nominal thickness of ½ mg cm^{-2}.

A convenient way of checking the adequacy of a given boron layer is by observing the pulse amplitude distribution obtained when the layer is the negative electrode of a parallel plate ion chamber. If the layer were perfectly formed, the function obtained would agree with the theoretical one derived from the range-energy relation of the particles and the constants of the materials. The effect on counter efficiency of deviations from the calculated function is illustrated by the results below.

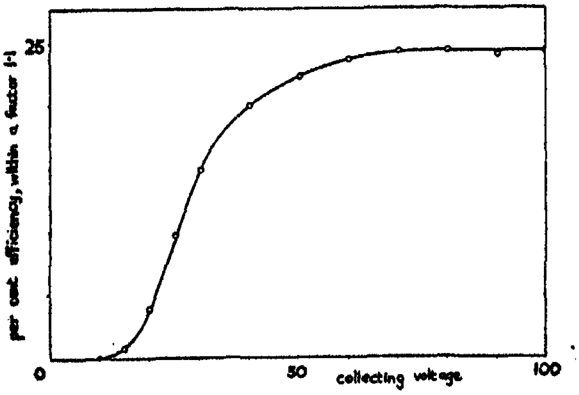

FIG. 7. Dependence of the efficiency of the miniature neutron counter on collecting voltage.

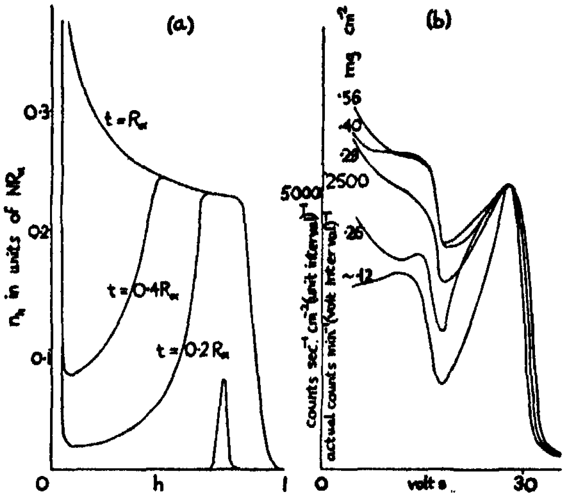

FIG. 8. (a). Theoretical pulse amplitude distribution curves for the main group α-particle component from B^{10} layers of various thicknesses in a given experimental chamber. (b). Observed distribution curves.

A theoretical pulse amplitude distribution curve for the main group α-particle component is shown in Fig. 8(a) for plane boron deposits of different thicknesses. It has been computed for an interelectrode spacing of 5 mm and a filling of 5 atmos. of argon, which were the figures for the experimental chamber, and is accurate to about four percent. Account is taken of the noise level and of the finite resolution of the actual apparatus used in the investigation; the over-all resolution when pulses were sorted into one-volt channels is indicated by the viewing function also shown in the figure.

The ordinate of Fig. 8(a) is the number of pulses having heights between h and $h+dh$; it is given in units of NR_α, where N is the number of disintegrations cm^{-2} sec.^{-1} in the boron. It will be noticed that for deposits thinner than about $\frac{1}{2}R_\alpha$, the pulses are mostly gathered into a sharp peak at the upper end of the scale; under these circumstances the bias curve, which of course is the integral of the distribution curve, has a very good plateau so far as the alpha-component is concerned. Thicker boron layers do not show a higher peak, because this peak is contributed only by the alpha-particles of nearly maximum energy which come from the shallower regions of the metal. Thickening the boron layer may be considered as a process of putting more boron behind it, which can only contribute lower energy particles. The thicker deposits therefore show a progressive filling in of the hollow between the peaks at $h=1$ and $h=0$, until at $t=R_\alpha$ the limiting shape is reached.

A real boron layer having an undulating surface may be considered as thin over some parts of its area and thick over others; the pulse histogram for the alpha-component will therefore be recognizable as a kind of average over all the possibilities shown in Fig. 8(a). Starting from the right-hand end of the diagram, the curve will rise to its peak, which should give the correct amplitude of approximately $0.23NR_\alpha$; but towards the left of this peak it will immediately curve down in a rounded manner which will not lead to any meaningful indication of t/R_α.

Typical distribution curves taken with five apparently smooth boron layers of different thicknesses prepared similarly to those used in the counter of Section 3 are shown in Fig. 8(b). For clarity, the scales of some of the curves have been adjusted by a few percent to bring all five peaks into coincidence. The lithium recoil particle spectrum appears clearly superposed on the α-particle component in each curve.

The agreement of the α-particle spectrum with Fig. 8(a) is, as expected, only qualitative. The factor by which this kind of discrepancy reduces the efficiency, may be estimated from the area underneath the curves, which is always less than the theoretical value. An approximate reading for the twelve-chamber counter of Section 5 is given by the average area under the curves for 0.40 and 0.56 mg cm^{-2}. When this is divided by the theoretical amount, taking account of the operating bias voltage, the ratio comes to about 0.6. This is more than enough to explain the observed loss factor, which from the results of Section 5 is 0.73.

7. ACKNOWLEDGMENTS

Thanks are due the Director of the Atomic Energy Research Establishment, Harwell, for permission to publish this paper; Dr. W. D. Allen and his Group at the Establishment for preparation of the boron layers; Mr. A. B. Gillespie for discussions of electronics; Messrs. A. R. Pollock and R. F. Dyer for constructional work and advice; and Dr. J. Thewlis for encouragement.

THE REVIEW OF SCIENTIFIC INSTRUMENTS VOLUME 21, NUMBER 10 OCTOBER, 1950

A System for the Collection and Purification of Radon by Remote Control*

Chester H. Shiflett,** Mark E. Steidlitz, and Wallace Davis, Jr.
Carbide and Carbon Chemicals Division, Union Carbide and Carbon Corporation, K-25 Laboratory Division, Oak Ridge, Tennessee

(Received May 20, 1950)

A plant for the collection and purification of radon has been constructed. In order to reduce the gamma-radiation level, the plant was designed to be operated entirely by remote control except for the final sealing of the radon capsule. This plant compares favorably with other collection systems both with regard to the time required for a collection and to the yield of radon obtained.

When investigations in the field of alpha-radiation chemistry were begun at the K-25 Laboratories, it became necessary to design a system for the collection and purification of radon. Due to recent radiation hazard studies, it was decided to incorporate considerable lead shielding and remote control operation in the plant in order to reduce beta- and gamma-ray exposure to the operator. This plant houses 230 milligrams of radium on loan from the Bureau of Mines.

DESIGN AND OPERATION OF PLANT

The collection system, as shown in Figs. 1 and 2, is similar to the one described by Livingston,[1] the essential difference being that all stopcocks are replaced by mercury cut-offs, which are regulated by compressed air and vacuum lines. The latter are valved at a main control panel, Figs. 3 and 4. This panel, located about 12 feet in front of the hood housing the plant, is also equipped with controls to raise and lower two Dewar flasks mounted on sylphon bellows, and to fill the traps with liquid nitrogen.

The radium chloride, in 100 cc of 0.1 N hydrochloric acid, (a), in Fig. 1, is contained in a 200 cc soft glass flask surrounded by six inches of lead shielding. As a precaution against breakage, the flask is contained in a Fluorothene beaker which in turn is placed in a Pyrex beaker. The line from the flask to the Toepler pump, (b), is shielded by one inch of lead to a point well below the mercury level at its lowest position between collections. The free volume above the radium solution is 100 cc and that of the Toepler pump is one liter.

After each collection, the plant is left as shown in Fig. 2, with cut-offs *A* and *C* closed and *B* open. Before starting a collection, a new collection tube is sealed in place at (*d*). The system is then pumped to a pressure of less than 10^{-4} mm of mercury. On obtaining this vacuum, cut-offs *A* and *C* are opened and the entire system up to the mercury in the Toepler is pumped to

---

* This document is based on work performed for the AEC by Carbide and Carbon Chemicals Corporation, at Oak Ridge, Tennessee.

** On leave from Macalester College, St. Paul, Minnesota.

[1] R. Livingston, Rev. Sci. Inst. 4, 15–17 (1933).

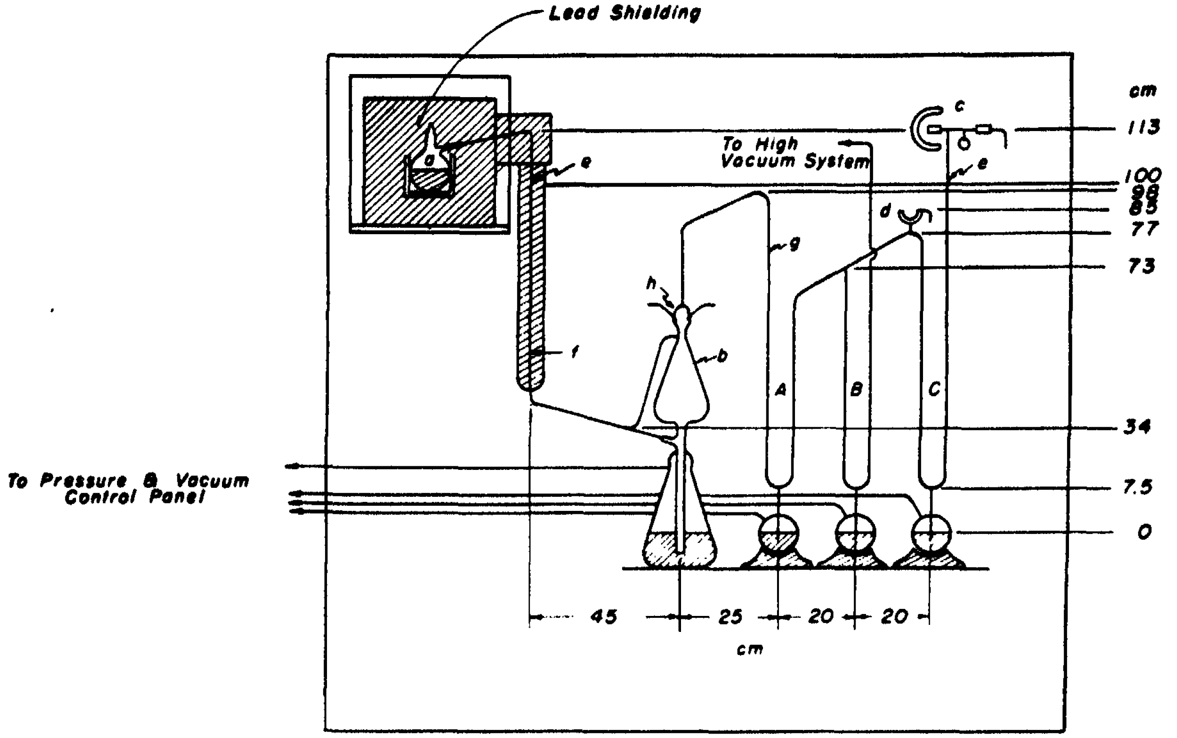

FIG. 1. Radon collection system. Schematic. a. $RaCl_2$ solution in lead safe. b. Teopler Pump. c. Chemical cleanup system. d. Built-in Dewar and collection tube. e. Mercury traps. f. Pyrex to soft glass seal. g. Capillary to six mm seal. h. Spark gap.

remove any water vapor and absorbed gases from the previous collection. Cut-off *B*, to the high vacuum system, is then closed, the mercury being raised to a point just below the junction of *A* and *B*.

Cut-off *A* is closed and the mercury in the Toepler pump is lowered to allow a portion of the accumulated gases to be drawn in. The mercury is then raised in the Toepler pump until the pressure is about 15 cm, as determined by the difference of mercury levels in cut-off *A*, following which the mixture is ignited at (*h*). These operations are repeated until the mercury level can be lowered below the junction of the radon line and the Toepler pump, allowing the gases to distribute themselves freely between the radium flask and the pump.

Before transferring the radon to the purification system, (*c*), which consists of a tube of potassium hydroxide, a tube of phosphorus pentoxide, a side-arm containing copper and copper oxide enclosed in a furnace, and a cold finger, the mercury level in the Toepler pump is lowered to reduce the pressure differential across cut-off *A*. This cut-off is then opened, and the pump and spark gap are filled with mercury, pushing all of the gas toward the clean-up system. When the purification has proceeded sufficiently, as indicated by equality of levels in cut-off *B*, cut-off *A* is closed. The Toepler pump is again used to collect radon from the flask and the whole series of operations is repeated as often as desired.

After the last portion of radon has been transferred to the purification train, the gas is condensed with liquid nitrogen into the built-in Dewar, (*d*), at the final collection point. This procedure facilitates removal of all radon from the section of tubing between the Toepler pump and cut-off *A*. The latter is then closed. The radon is warmed and transferred by condensation with liquid nitrogen into the cold finger on the purification system. After sufficient time for diffusion has elapsed, cut-off *C* is closed, the Dewar around the cold finger is lowered, and a stream of air turned on to warm

FIG. 2. Radon collection system. Photograph.

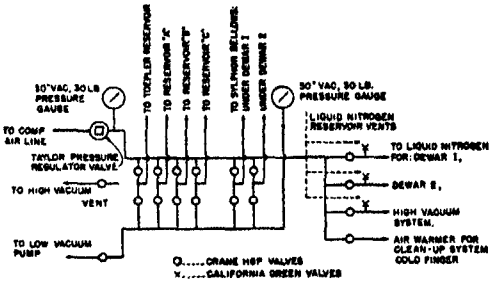
TO TOEPLER RESERVOIR
TO RESERVOIR "A"
TO RESERVOIR "B"
TO RESERVOIR "C"
TO SYLPHON BELLOWS UNDER DEWAR 1
UNDER DEWAR 2
30"VAC, 30 LB PRESSURE GAUGE
30" VAC, 30 LB. PRESSURE GAUGE
TO COMP AIR LINE
TAYLOR PRESSURE REGULATOR VALVE
TO HIGH VACUUM
VENT
TO LOW VACUUM PUMP
LIQUID NITROGEN RESERVOIR VENTS
TO LIQUID NITROGEN FOR: DEWAR 1,
DEWAR 2,
HIGH VACUUM SYSTEM.
AIR WARMER FOR CLEAN-UP SYSTEM COLD FINGER
O.....CRANE HSP VALVES
X.....CALIFORNIA GREEN VALVES

FIG. 3. Main control panel. Schematic.

the radon and allow it to circulate through the clean-up system. Again it is condensed in the cold finger and with cut-offs *B* and *C* opened, the system is pumped for about 30 seconds to remove nitrogen or other permanent gases. Cut-off *B* is then closed and the radon allowed to warm. It is next condensed at the built-in Dewar and cut-off *C* is closed. The mercury level is then raised to any desired position in the final collection section, depending on the type of collection. The liquid nitrogen is removed from the Dewar and the radon finally condensed into the collection tube. This is sealed off a short distance above the liquid nitrogen level. If traces of mercury or water vapor are undesirable in the reaction system, the built-in Dewar may be filled with a dry ice-acetone slush before the radon is condensed into the collection tube. In this case the mercury must be kept below the Dewar to prevent its freezing.

After the radon has been removed, cut-offs *A* and *B* are opened and the mercury level in the Toepler pump lowered to pump off the residual water, following which the mercury is raised through the spark gap, and up into the capillary tubing. Cut-off *A* is closed and cut-off *C* is opened to pump the clean-up system. The plant is shut down with cut-offs *A* and *C* closed and *B* open by stopping the pumps and admitting atmospheric pressure to the high vacuum system.

RESULTS

This radon plant has been in operation for more than eight months. Measurements of the radon collected indicate an efficiency of 85 to 90 percent. The time required for a collection is 30 minutes, not including either the initial or final pumping operations. This is considerably less time than is required with a comparable system using stopcocks.

SUGGESTED MODIFICATIONS

A number of improvements have suggested themselves during the operation of the plant. The entire line from cut-off *A* over to cut-off *C* should be raised to at least 85 cm, instead of the present 73 to 77 cm, above the mercury. This would allow an atmosphere of mercury on both sides of each of the cut-offs, so that the initial pumping could be started without having to exercise the caution now necessary to keep the mercury above cut-offs *A* and *C*.

FIG. 4. Main control panel. Photograph.

Another change would involve extending the capillary tubing, which now runs from the spark gap to the point (*g*), to include all but a few centimeters on the Toepler pump side of cut-off *A*. This modification would provide a smaller volume so that a higher pressure could be built up in the sparking chamber. Finally, a small bulb, on the clean-up side of cut-off *A*, would prevent excessive turbulence as the gas bubbles through the mercury.

ACKNOWLEDGMENTS

The authors wish to express their appreciation to Dr. S. C. Lind and Dr. H. A. Bernhardt for timely suggestions and help during the construction of the collection system; to Mr. C. Asmanes of the Works Laboratory Department for construction and assembly of the glassware; to Mr. W. R. Smith and Mr. W. A. Pryor of the Radiation Hazards Department of the Safety and Inspection Division for determining the necessary amount of shielding, both for the radium in the plant and the comparison standards; and to the Bureau of Mines for the loan of the radium in solution and the radium standards.

THE REVIEW OF SCIENTIFIC INSTRUMENTS VOLUME 21, NUMBER 10 OCTOBER, 1950

Precision Thermostat for High Temperatures

WILLIAM R. EUBANK*
Portland Cement Association Fellowship at National Bureau of Standards, Washington, D. C.

(Received June 5, 1950)

A precision thermostat has been developed, based upon that of Roberts, for the control of high temperatures (1000°–1550°C). With the instrument described, temperatures are readily maintained constant within ±0.1°C for several hours, and within ±1.0°C for several days.

In this method of control a thyratron is used in conjunction with an a.c. bridge and high gain amplifier. The phase angle of the unbalanced bridge regulates the firing of the thyratron. The control is highly sensitive and independent of normal fluctuations in line voltage. The thermostat is convenient to operate, easy to adjust for any temperature, and reliable for periods of continuous operation from a few minutes to several days.

INTRODUCTION

SYSTEMATIC phase-equilibrium studies have been of great value in exploring new systems involving the components of glass, refractories, Portland cement, and other industrial products. In order properly to employ this method of investigation, it is necessary that the specimen under study reach a state of equilibrium at any given temperature. To accomplish this, constant temperature must be maintained until no further change takes place in the sample under study. Even small fluctuations in temperature may be responsible for erroneous data, especially in multi-component systems.

In an attempt to obtain better temperature regulation than had been reached with regulators currently in use, the possibility of employing a thyratron regulator, based on that designed by Roberts[1] was explored.

Many temperature regulators employing thyratrons have been reported. Some of these were designed for use with oil or water baths and others for low temperature furnaces, 1000° maximum.[2] In this form of regulation a transformer is employed partly as a saturable reactor as reported also by others[3, 4] to control load currents of several amp. The output of an a.c. bridge, one arm of which serves both as a resistance thermometer and as a heater element, is amplified and applied to the control grid of a thyratron. Unbalance of the bridge results in a difference in phase between this control voltage and the applied voltage, and determines the firing period of the thyratron. The thyratron action is reflected to the primary circuit through the transformer, thus controlling the amount of energy supplied to the furnace.

Some investigators[5, 6] have employed thyratron-controlled regulators to operate in connection with conventional mercury regulators. Another[7] has employed an optical lever with a photo-tube and galvanometer. In 1938 Sturtevant[8] reported a thyratron regulator adapted from a circuit described by Henney.[3] Modifications on this regulator were later reported.[9, 10] These circuits have the heater load directly in the thyratron anode circuit and are generally designed for low power applications. In describing the performance of the above regulators, Bancroft[11] states, "Circuits in common use are apt to be somewhat erratic and to require rather critical adjustment if uniformly stable operation is to be achieved. In particular, most such devices do not behave properly when the control voltage amplifier is overloaded, as when the resistance bridge is preset for a new temperature." By elaborate tuning and filtering, Bancroft developed a more stable regulator for low temperature operation.

Penther and Pompeo[12] attribute the erratic performance of these earlier circuits to a secondary phase shift. They state, "It was found that this secondary phase shift was caused by the large current amplitudes in the off-balance conditions, overloading the tubes and transformers. . . . The limit of control is a maximum of 1 degree F." These investigators obtained improved operation for bath thermostats by using an amplifier with automatic gain control.

After consultation with Roberts, a controller based upon his original circuit, but with important modifications, was constructed and tested. The wiring diagram is shown in Fig. 1 and a photograph of the assembly in Fig. 2. Several hundred quenching experiments in the temperature range 1000° to 1550° have been successfully performed with this thermostat.

DESCRIPTION

The furnace winding is the temperature-sensitive element of the thermostat. The resistance of this winding, which consists of about 100 g of 0.8-mm platinum-20 percent rhodium wire, changes rapidly with tem-

---

[*] Research Associate at the National Bureau of Standards, representing the Portland Cement Association.

[1] H. S. Roberts, *Temperature: Its Measurement and Control in Science and Industry* (Reinhold Publishing Corporation, New York, 1941), pp. 604–610.

[2] Temperatures are expressed in degrees Centigrade.

[3] Keith Henney, *Electron Tubes in Industry* (McGraw-Hill Book Company, Inc., New York, 1934), chapter IV.

[4] H. J. Reich, *Principles of Electron Tubes* (McGraw-Hill Book Company, Inc., New York, 1942), chapter IX.

[5] A. D. Compton, Jr., Science 93, 215 (1941).

[6] W. E. Gilson and H. A. Wooster, *J. Chem. Ed.* 19, 531 (1942).

[7] W. W. Hull, Gen. Elec. Rev. 32, 213, 390 (1929).

[8] J. M. Sturtevant, Rev. Sci. Inst. 9, 276 (1938).

[9] Manson Benedict, Rev. Sci. Inst. 8, 252 (1937).

[10] J. C. Mouzon, invited paper, Am. Phys. Soc. Annual Meeting, 1947.

[11] Dennison Bancroft, Rev. Sci. Inst. 13, 24 (1942).

[12] C. J. Penther and D. J. Pompeo, Electronics 14, 20 (April, 1941).

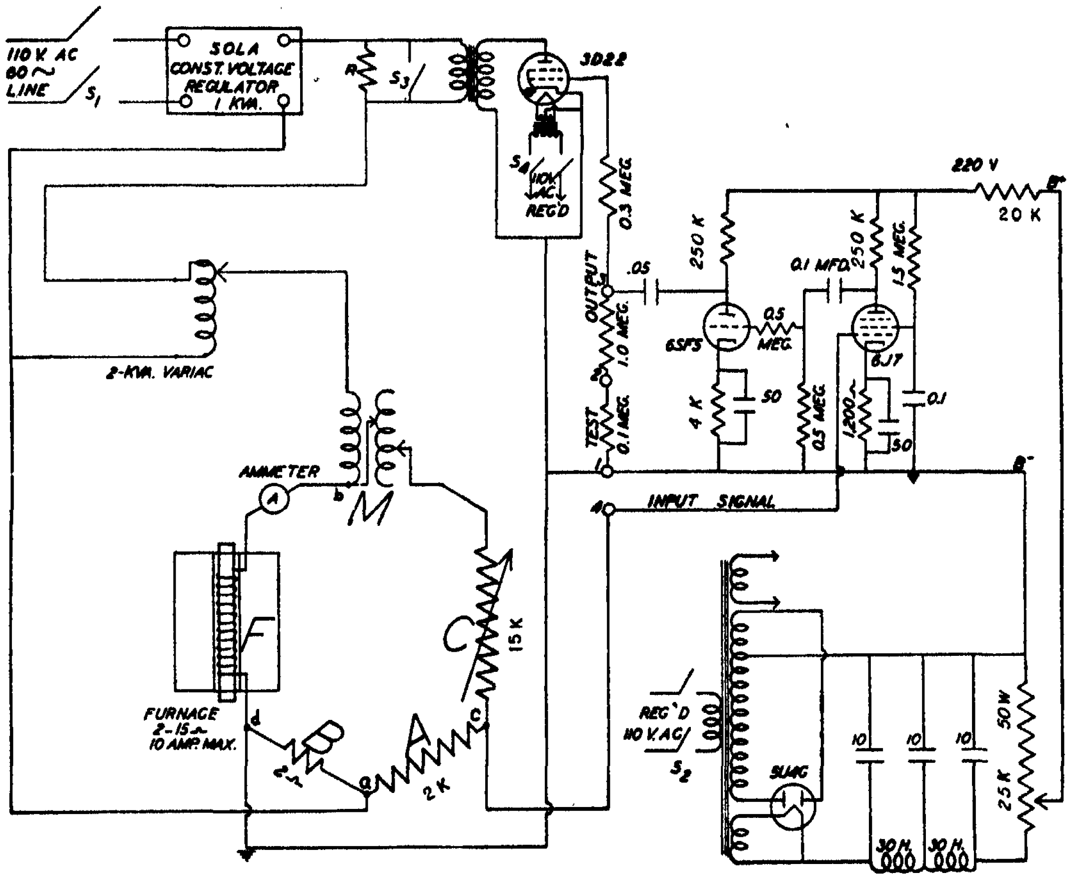

Fig. 1. Thyratron quenching furnace thermostat.

perature (above 1000°) and, except for aging effects, maintains a definite relation to the temperature.

The relation of the furnace winding to the other resistances in the bridge is shown in Fig. 1. The two sides of the bridge have a ratio of about 1000 to 1. This high ratio is possible because the amplifier is voltage-operated. The high resistance arm *C* consists of a 5000-ohm coil and a 10,000-ohm decade box in series. The resistance of the furnace varies from about 2 to 15 ohms. The remaining two arms of the bridge, *A* and *B*, are 2000 and 2 ohms, respectively. Arm *A* is a standard coil used in decade boxes while arm *B* was constructed in the laboratory. The latter carries the entire furnace current and is made of two 1-ohm sections of heavy advance ribbon wound on a core of alundum. Each section is insulated from the other by a thin layer of mica. The second winding is doubled back over the first in order that the inductances will cancel.

The response of the thyratron is determined primarily by the phase angle of the control voltage relative to the anode voltage of the thyratron. The thyratron circuit acts then as a continuously variable rheostat whose setting depends on the phase angle and amplitude of the unbalance voltage across the bridge.

With alternating current it is necessary to balance both the reactive and resistive components of the bridge. For this reason the bridge coils, except that of the furnace, are non-inductively wound. The reactance balance of the bridge is then adjusted by means of the variable secondary of the mutual inductance (*M*, Fig. 1) in arm *C*.

The primary winding of the mutual inductance is a single layer of copper wire (No. 12 *DCC*) having an inductance slightly greater than that calculated from the dimensions of the furnace winding. The primary has 43 turns and occupies 5 inches on a bakelite tube 2.5 inches in outside diameter. In order to use this controller with furnaces of various inductances, the primary winding was tapped at three points. The secondary winding, which is of fine wire (No. 24 *DCC*), occupies the *V*-shaped helical groove between the primary turns. Each of the first 11 turns of the secondary winding is tapped and connected to a point on a rotary selector switch. Turns 12 to 42 are tapped at every fifth turn and connected to a second rotary selector switch. Fine adjustment of the mutual inductance is made by means of one-half turn of $\frac{1}{16}$ inch iron strip cut from a transformer lamination rotated about an axis perpendicular to that of the bakelite tube.

The power to operate the thyratron controller is supplied by a constant-voltage transformer.[13] A variable auto-transformer is utilized to reduce the voltage output of the controller to the value needed for a particular operating range. It should be adjusted with S_3 closed so that, at the control temperature, an appropriate rate of heating results.

The resistance panel *R* consists of five coils of 5, 7.5, 15, 30 and 60-ohms resistance and a 30-volt lamp all connected in parallel. Except for the 5-ohm coil, each unit can be disconnected from the circuit by a switch. These parallel resistances should be adjusted with S_3 open and the thyratron either not firing or removed from its socket so that, at the control temperature, an appropriate rate of cooling results. The maximum drop across *R* should be limited to 25 volts for protection of the thyratron.

The action of the thyratron controls the furnace current by changing the impedance of the primary winding of a transformer connected in parallel with resistance *R*. This transformer is rated at 250 va. and has a 25-volt primary and 1000-volt secondary. If the phase of the control voltage is such that no plate current flows in the thyratron, the transformer is unloaded and the impedance is high. Consequently a negligibly small magnetizing current flows in the primary. When the thyratron fires, however, the impedance of the primary becomes low relative to *R*. The bridge current is thereby increased, nearly the whole of it passing through the primary of the transformer. Thus, this transformer reflects the high-voltage low-current characteristics of the thyratron switch into the power circuit as a low-voltage, heavy-current control. The primary voltage averages about 12.5 volts and the transformer steps up the plate voltage to about 500 volts.

The amplifier has a gain of about 6000 and is of the conventional resistance-capacity coupled type. It is desirable for protection of both thyratron and furnace that a suitable magnetic switch, not shown on Fig. 1, be added to shut down the apparatus in case the a.c. supply is interrupted, and to indicate such interruption to the operator.

The first unit of the thyratron controller was supported together with the furnace in an angle-iron framework, Fig. 2. A second unit was designed to be more compact. It fits into a 12×12×20-inch radio cabinet and is portable. The thyratron tube employed is the sensitive, four-electrode *3D22*. This tube by virtue of its inert gas content has a control characteristic which is essentially independent of ambient temperature variations over a wide range. It also has small preconduction or gas-leakage currents, low control-grid-to-anode capacitance, and low control-grid current. The *3D22* has about 50 percent more current capacity than the *FG*-17 tube used by Roberts, and is more compact and entirely base-connected.

Before the regulator is turned on, switch S_3 must be closed to protect the thyratron unless a time delay relay is placed in the anode circuit. After S_4 has been closed for at least 30 seconds and the cathode has come to operating temperature, S_3 can be opened.

The furnace is brought to approximately the desired temperature by manipulation of the variac. The variable bridge arm *C* is then set at the value found by experiment to correspond with the temperature desired. Adjustment of the control is conveniently checked by means of a 30 v 15 w lamp. The variac is adjusted so that the lamp is neither out nor fully lit, but intermediate between the two.

If an oscilloscope is available it can be connected across S_3 and the inductance *M* adjusted to give patterns like those shown in row *D* of Fig. 4. The adjustment is not critical, however. When the bridge approaches the balanced condition, the glowing lamp, *L*, usually begins to flicker at a low frequency which increases to a maximum rate of 30 per second at balance. This is a useful indication that the regulator is in satisfactory operation.

If the bridge is unbalanced greatly (e.g., in resetting to a new temperature several hundred degrees away) the regulator will lose control until balance is approached. Several manual adjustments of the furnace temperature may therefore be necessary the first time a particular setting is made.

Application of this thyratron control may be made to other furnaces and to baths and heaters operating at other temperatures. At lower temperatures, heater elements of sufficient change in resistance with temperature, such as pure nickel or certain nickel-chromium alloys, will be required.

A certain amount of distortion and constant phase shift is developed in the amplifier. However, this does

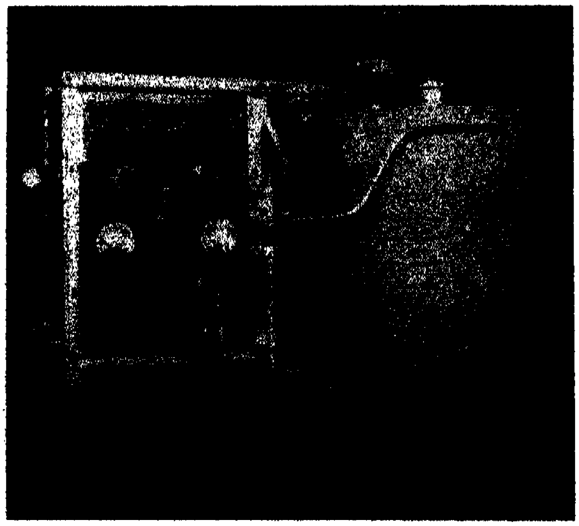

Fig. 2. Thyratron-controlled thermostat and quenching furnace. First model.

---

[13] For this purpose a 1-KVA voltage regulator manufactured by the Sola Electric Company, Chicago, Illinois, was found to be satisfactory.

not appear to interfere with the operation of the regulator. Elaborate tuning and filtering of the control voltage, as advocated by certain investigators,[11] do not appear necessary. No special shielding of the amplifier is required; however, it should be located outside any large external fields such as are produced by the voltage regulator. Proper grounding of both the amplifier and bridge as shown in Fig. 1 is essential, but this local ground is insulated from physical ground because the output winding of the constant-voltage transformer is not isolated from the input.

An advantage derived from the use of the phase-controlled thyratron regulator is gradual or proportional control as contrasted to on-off control. The thyratron circuit acts as a continuously variable valve allowing just enough current to reach the furnace to compensate for a given temperature fluctuation. Thus overshooting, which appears with on-off control, is greatly reduced.

The control characteristics of the thyratron quenching-furnace thermostat will depend on the furnace with which it is used. In the present study, the thermal sensitive element, which is also the heater element, was wound on the outside of a one-eighth-inch-wall alundum tube and the temperature read by means of a Pt-PtRh thermocouple placed inside the tube. Similar windings and tubes are generally used for quenching furnaces.

Thermocouple potentials were read to within 0.5 μv by means of a type *K*-2 potentiometer and a suspension galvanometer.

Several hundred short quenching experiments (one-half to one hour) have been made with the thermostat with average temperature variations corresponding to 1 or 2 μv (1 μv = 0.084° at 1300°). Dependability for long experiments was demonstrated by maintaining the thermostat in constant operation controlling a quenching furnace at 1300° for more than a month. The temperature of this furnace was later maintained at 1350° for three weeks. The average of 20 consecutive fluctuations occurring overnight and weekends was 5.65 μv, or less than 0.5°. These variations were about equally positive and negative. Values of 1 to 20 μv (less than 0.1° to 1.7°) were obtained, although fluctuations of as much as 12 μv (1.0°) were rare. Typical control obtained with the thyratron quenching-furnace thermostat is illustrated by the curves in Fig. 3; *A*, for a period of 60 minutes; *B*, 8 hours: *C*, 7 days at an operating temperature of 1300°. No adjustment was made to compensate for change in resistance of the winding with age.

During long periods of continuous operation the balancing resistance, *C*, in the bridge is usually adjusted at about three-day intervals to compensate for the drift in the resistance of the winding. It is well known that, at high temperature, slight deterioration and accompanying increase in resistance of all wire-wound furnaces occurs, and that this is a function of time and temperature. With no adjustment, after about three days the temperature of the furnace was found to drift downward (see curve *C*, Fig. 3).

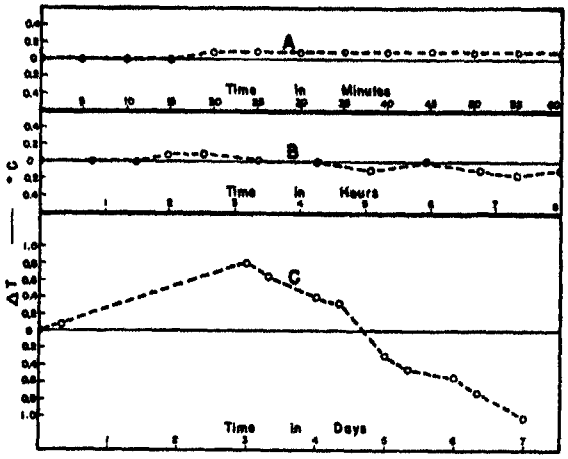

FIG. 3. Typical control obtained with thyratron quenching-furnace thermostat, *A*, for a period of 60 min.; *B*, 8 hr.; *C*, 7 days. Operating temperature was 1300°C.

OPERATION

The operation of thermo-regulators, using phase-shifting a.c. bridges in the temperature-measuring circuit and phase-controlled thyratrons as the power-regulating elements, has been discussed in some detail by Roberts and others as above indicated. The unit described here follows generally the circuit design of Roberts, and the operation is similar for conditions of decided unbalance in the temperature-sensitive bridge (such as immediately follows resetting the control). However, for normal operation in the zone near balance, this system is characterized by stable hunting at 30 c.p.s., one-half the power line frequency. This operation provides the high sensitivity and the flicker indication already mentioned.

The practical advantage of these features has been attested by the performance of the unit. No quantitative analysis of the operation has been made, but the oscillographic records of wave forms at various points in the circuit, under several balance conditions, give a reasonably clear picture of the operating principles. The oscillographs are shown in Figs. 4 through 11.

These may be interpreted in terms of the vector diagrams of Fig. 12, showing the voltage relations in the bridge. The subscripts correspond to those used in designating the circuit components in Fig. 1. The bridge includes two reactances, *F*(*L*) which is due to the self-inductance of the furnace coil, and *M* which is due to the mutual inductance coupling the high resistance bridge arms to the bridge supply current. The reactive components $E_{F(L)}$ and E_M have been purposely magnified in order to provide open diagrams. As the bridge is actually used, the reactive component voltages are on the order of one-thousandth the resistive voltages E_B and $E_{F(R)}$. The lower vectors which are in phase with bridge currents are actually almost in phase with bridge voltage, *E*. Therefore, E_{cd}, the output voltage from the

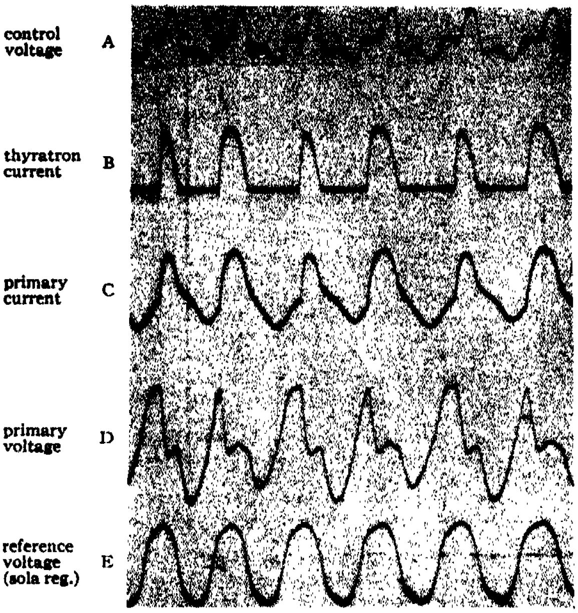

FIG. 4. Flicker indication, bridge in balance.

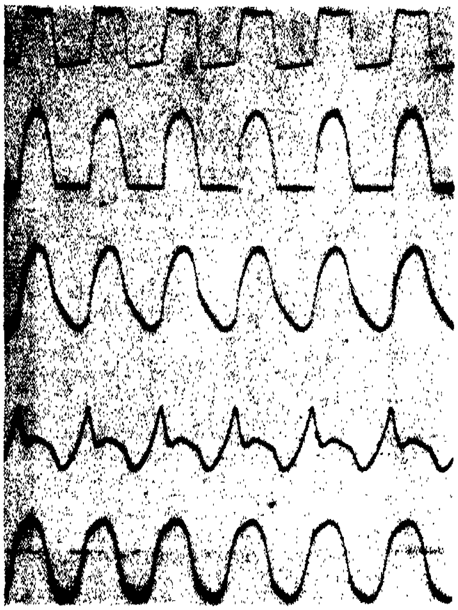

FIG. 5. Thyratron firing for most of positive cycle, bridge unbalanced by +10 ohms.

bridge, has nearly the same phase relative to both bridge voltage and furnace currents, I_F.

With variation of $E_{F(R)}$, it is seen that E_{od} varies monotonically in phase but its amplitude passes through a minimum at the resistive balance of the bridge. At minimum, $E_{cd} = -(B/B+F)\omega(L-M)I_F$. This amplitude is directly proportional to frequency, and to the reactance unbalance, $\omega(L-M)$. Unbalance voltage, E_{cd}, after amplification, and as applied to the thyratron grid, is shown in row *A* of the oscillographic records. For conditions of appreciable bridge unbalance (record *A* of Figs. 5 and 9), the control voltage is so large that its peaks are clipped by saturation of the amplifier, but conventional phase control of the thyratron obtains. The firing voltage is indicated by the notch in the control voltage record, due to grid current effect. Here the operation of the system follows that described by Roberts.

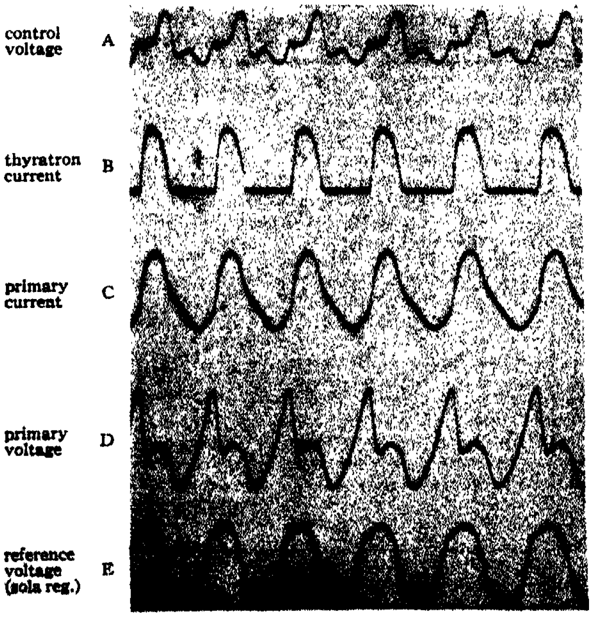

FIG. 6. Thyratron firing for about two-thirds of positive cycle, bridge unbalance less than 10 ohms.

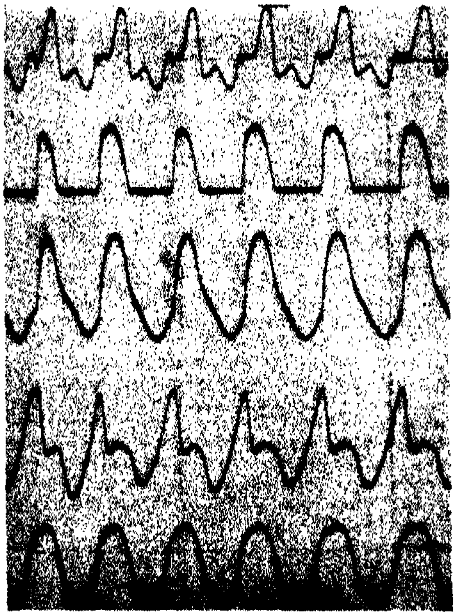

FIG. 7. Beginning of flicker indication, bridge regaining balance.

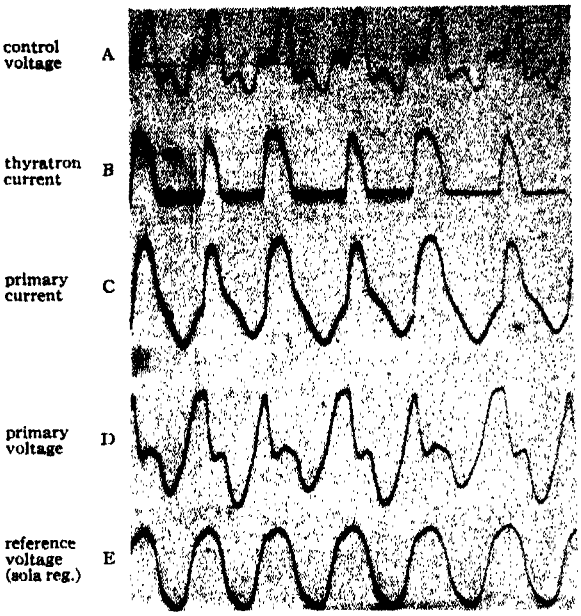

FIG. 8. Flicker indication, bridge in balance.

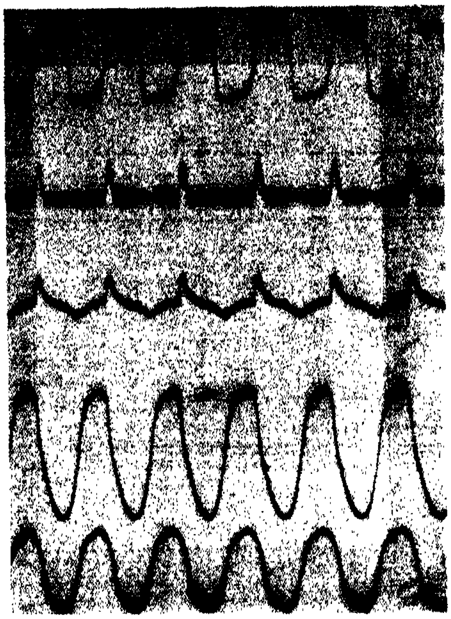

FIG. 9. Thyratron firing for little of positive cycle, bridge unbalanced by −10 ohms.

For conditions very near bridge balance, as shown in record *A* of Figs. 4, 7, 8, and 11, flicker control is obtained. The control voltage is much reduced in amplitude and contains relatively strong harmonics, particularly second and third. Their greater amplitude relative to the 60-cycle fundamental in the bridge output is due to the fact that when resistive balance is approached the output is mainly due to the unbalanced reactive component, which of course is proportional to the frequency of the harmonics.

The effect of harmonics in the bridge is difficult to analyze. The greater dependence of the higher frequencies upon the reactance unbalance of the bridge causes them to show smaller phase variation but greater relative amplitude near resistance balance. Oscillographs *A* of Figs. 4, 7, 8, and 11 indicate that there is some

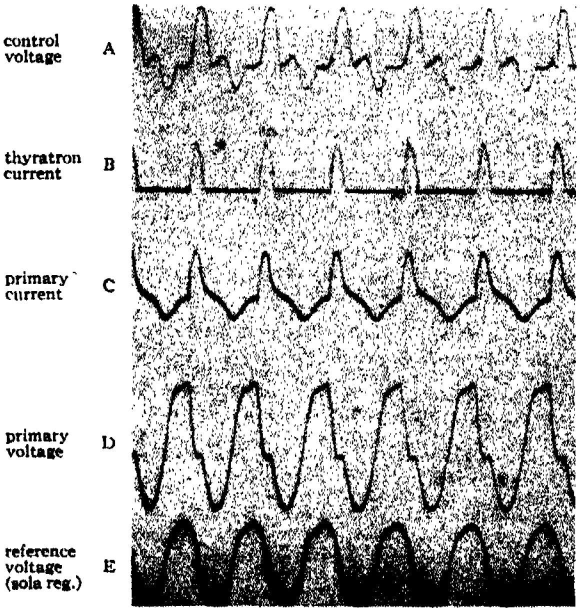

FIG. 10. Thyratron firing for about one-third of positive cycle, bridge unbalance less than 10 ohms.

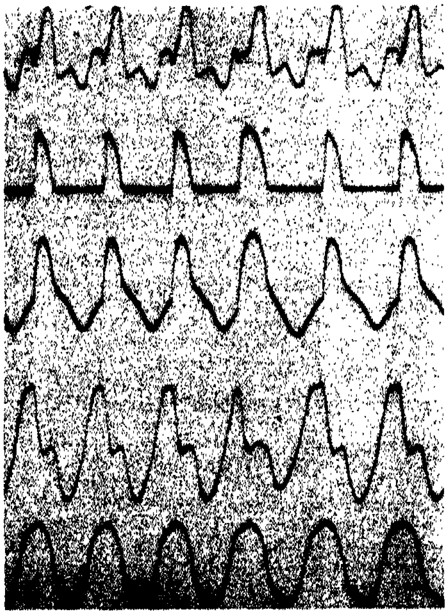

FIG. 11. Beginning of flicker indication bridge regaining balance.

differential phase shift among the harmonic components. Furthermore, the phase variation in this region is extremely sensitive. It is given by the expression

$$\frac{d\phi}{dF}=-\frac{\omega(L-M)}{(\Delta F^2+\omega^2(L-M)^2}.$$

In practice both L and M are small and by adjustment of M their difference is made very small.

In the region of flicker control at balance, as shown in records *B* of Figs. 4 and 8, the thyratron is caused to fire alternately early and late in successive positive half-cycles. This represents a stable operating condition where the average power supplied is that required for maintaining thermal balance in the furnace. In the approach to balance, Figs. 7 and 11, the thyratron fires early or late, but not alternately, in successive positive half-cycles. A flicker appears whenever a change between early and late firing occurs.

The apparent explanation of flicker control hinges upon the extremely high phase-sensitivity of the bridge near resistance balance and the tight thermal coupling between the heater and the temperature-sensitive bridge arm, since they are the same element. The thermal system has sufficiently fast response and the regulation loop has sufficiently high gain to permit an over-all oscillation at 30 c.p.s. This does not require a sharp 30-c.p.s. resonance in the system because the oscillation must be carried around the loop on the 60-c.p.s. carrier frequency.

No simple means of checking this explanation was available because the feed-back loop could not readily be opened for study. However, insertion of a 60-c.p.s. band pass filter into the amplifier circuit eliminated the flicker operation. Removal of the Sola regulator also eliminated the flicker, which suggests that harmonics generated in the regulator are essential to flicker operation.

Inherently the 30-c.p.s. flicker has no merit. It does, however, indicate that the regulation loop is operating with an over-all gain which is the maximum permitted by the phase and attenuation constants of the thermal system. Furthermore, the phase characteristics of the bridge provide a continuous reduction in the loop gain as balance is lost so that the system has excellent transient response with protection against overshoot.

The ultimate perfection of equipment of this character lies of necessity in its use by various investigators. Changes undoubtedly will be introduced involving improvements of one kind or another. Since the apparatus was completed, several minor changes have been proposed and used. They are set forth below for the benefit of those who may wish to build a thermostat.

1. Because the reactances are relatively small, M is not a necessary feature of the circuit. 2. The inability to make a physical ground connection somewhere on the amplifier and power-supply circuit is a disadvantage from a safety standpoint. If the input signal leads from points d and c on the bridge (Fig. 1) were opened, and a capacitance of suitable size inserted in the series with each, the amplifier could then be grounded. 3. If an increase in amplification of the bridge signal and isolation of the amplifier from the bridge network is desired, this could be accomplished by means of a small step-up transformer. Capacitance coupling, however, would be less expensive. 4. The maximum attainable resistance of R may be increased so that the controller can be used with lower furnace currents.

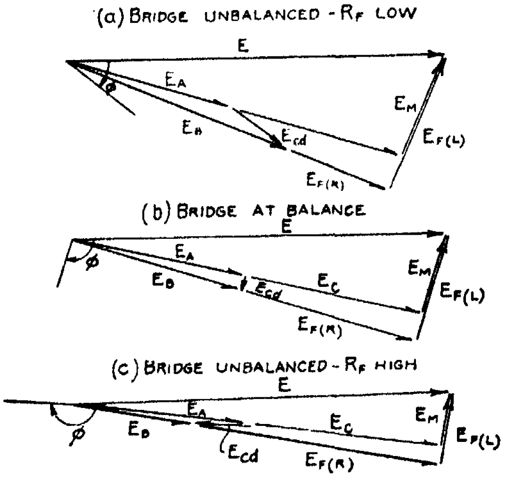

FIG. 12. Vector diagrams for the voltages in Roberts' furance control bridge.

THE REVIEW OF SCIENTIFIC INSTRUMENTS VOLUME 21, NUMBER 10 OCTOBER, 1950

A Magnetic Analyzer for Charged-Particles from Nuclear Reactions

C. W. Snyder, S. Rubin, W. A. Fowler, and C. C. Lauritsen
Kellogg Radiation Laboratory, California Institute of Technology, Pasadena 4, California

(Received June 23, 1950)

A double-focusing magnetic spectrometer for detecting and analyzing charged particles from nuclear reactions is described. The magnetic field, varying as $r^{-\frac{1}{2}}$ near an average radius of 10.5 in., extends over a semicircle yielding object and anastigmatic image positions some distance outside of the region of strong field. The acceptance solid angle is $\Omega = 0.0061$ sterad. and the momentum resolution with an 8-mm slit at the detector is $R = 128$. The ultimate resolution determined by spherical aberration and some residual astigmatism is about 1000. Applications to the study of the energy and yield of nuclear reaction products are discussed.

I. ENERGY ANALYSIS OF NUCLEAR REACTION PRODUCTS

MUCH of our present knowledge of the structure of nuclei has come from an analysis of the kinetic energies of the particles which initiate nuclear reactions or which are produced in nuclear reactions. For some time improved techniques have made possible the production of ion beams which are monoenergetic to a high degree so that detailed features of nuclear structure such as narrow, closely spaced energy levels have become observable through the study of excitation curves of nuclear processes. The equally precise analysis of the kinetic energies or momenta of the products of the reaction is a technique of equal importance which has remained completely unexploited until recently.

A reaction-product analyzer with high dispersion and energy resolution and with large solid angle has several important functions. (1). Under ideal conditions using highly resolved incident particles and thin targets, it makes possible the investigation of fine structure in the groups of particles produced in a reaction and thus of the corresponding fine structure in the energy levels of the residual nuclei. (2). It makes possible the observation of a single group of particles in the presence of a large flux of other particles of greater range. Although "differential" range techniques have been developed, they have not been successful in isolating "weak" short range groups. (3). It makes possible energy measurements of the hitherto neglected "residual nuclei" whose ranges are so short as to be practically unobservable in the usual type of range measurement. This point is particularly important with respect to neutron reactions, the direct determination of fast neutron energies with high precision (<one percent) being impossible at present. This technique has been used by Tollestrup, *et al.*[1] to infer the neutron energy in the reaction $D^2(d, n)He^3$ by analyzing the energy of the He^3. It can also be used to infer the angular distribution and excitation functions of neutrons produced in nuclear reactions. (4). The analyzer can be used with a thin target to study reaction products produced by monoenergetic incident particles even with high energy accelerators which do not produce monoenergetic beams. (5). With monoenergetic incident particles the analyzer is able to pick out charged particles produced in a thin lamina in a thick target, thus making it possible to obtain thin-target data in cases where the actual production of a thin target without backing is not feasible. This technique has been applied to determine the excitation function for elastic scattering of protons in lithium and beryllium. In addition compounds of the element of interest can be employed, the effects of other components being easily avoided. Similarly the effects of surface contaminants can be avoided.[2] (6). The analyzer can be employed for precise measurements of the differential stopping powers of various materials as a function of the energy of the incident particles. The application of such analysis to the determination of differential stopping powers for natural alpha-particles is well known.[3] (7). By the high resolution analysis of elastically scattered particles the analyzer can be used to determine the nuclear composition of thin layers of unknown materials.

II. GENERAL DESCRIPTION OF THE MAGNETIC SPECTROMETER

We have built a magnetic spectrometer[4] and have used it for analyzing the energy of particles produced in several reactions brought about by bombardment with monoenergetic protons and deuterons from an electrostatic accelerator and analyzer previously described.[5] These particles include protons, deuterons, tritons, He^3 nuclei, alpha-particles, Li^6, Li^7, Be^7 and heavier nuclei. For brevity, we shall refer only to protons in the following. The instrument is a modification of the design of Siegbahn and Svartholm[6] for electrons, employing a ring-shaped inhomogeneous magnetic field having the property of double focusing (i.e., anastigmatism). The choice of this instrument over other possible types of analyzers was dictated by two considerations: (1). the difficulty of obtaining fields sufficient to deflect million-volt protons without using iron in the circuit; it is this point which ruled out the "lens type" spectrometer so popular for electrons, and (2). the increased intensity or aperture obtainable with this design in contrast to other types of ferromagnetic spectrometers,[7] when "point" detectors of limited opening are to be employed. It is true that line detectors of sufficient extent can be employed with astigmatic spectrometers but this is often undesirable for other reasons. The high dispersion (twice that of the "180 degree" spectrometer) is also an advantage.

---

[1] Tollestrup, Jenkins, Fowler, and Lauritsen, Phys. Rev. 75, 1947 (1949).

[2] Fowler, Lauritsen, and Rubin, Phys. Rev. 75, 1471 (1949). Thomas, Rubin, Fowler, and Lauritsen, Phys. Rev. 75, 1612 (1949).

[3] S. Rosenblum, Ann. d. Physik 10, 408 (1928).

[4] Snyder, Lauritsen, Fowler, and Rubin, Phys. Rev. 74, 1564 (1948).

[5] Fowler, Lauritsen, and Lauritsen, Rev. Sci. Inst. 18, 818 (1947).

[6] K. Siegbahn and N. Svartholm, Arkiv. f. Math. Astron. Fysik. 33A, No. 21 (1946); N. Svartholm, Arkiv. f. Math. Astron. Fysik. 33A, No. 24 (1946).

Several double-focusing spectrometers for electrons have been built and the principle has been extensively discussed in recent literature.[7-10] A magnetic field is required which has cylindrical symmetry about a line (the z-axis) and mirror symmetry about a plane which we shall call the "midplane" and designated by $z=0$ in cylindrical coordinates. For an anastigmatic image, the radial component of the field must vanish in the midplane and the axial component must vary as $r^{-\frac{1}{2}}$ in the vicinity of a particular circle $r=r_0$ which we shall designate as the "midcircle." Conjugate foci lie on the midcircle separated by an angular distance of $(2\pi)^{\frac{1}{2}}$ radians or 254.56 degrees.[8] The required magnetic field shape can be obtained by adjusting the contours of the pole faces.

The proton spectrometer, shown in Figs. 1a and 1b differs from that of Siegbahn and Svartholm principally in having the pole pieces cover an angle about the axis of symmetry of only 180° so that the conjugate foci do not lie in the field. It is easily shown that a first-order focus is still obtained in this case although of course some dispersion and resolution for a given solid angle is sacrificed. In studies of prompt nuclear reactions it is advantageous to have the target or source and the reaction product detector in a field free region; for the target this is required in order not to move the incident beam on the target in a variable manner with changing field and for the detector it is important as certain types of detector components such as photomultiplier tubes, etc., do not operate properly in strong fields. The 180-degree angle was chosen in particular so that both pole faces could be machined simultaneously and it also represents a reasonable compromise between the conflicting requirements just discussed. The pole faces were fastened to a half-inch steel plate end-to-end to form a complete circle and were machined on a gap lathe. Pertinent dimensions in inches are as follows: Core: 11.25 in. diameter×6.25 in. height; yoke: 3.00 in. thick×24.0 in. diameter; pole pieces: 24.0 in. o.d.×18.0 in. i.d.; midcircle radius $r_0=10.5$ in. (26.7 cm); and maximum gap: 1.80 in. at $r=11.2$ in.

The magnetic circuit was made in five parts—two pole pieces, two yokes, and the core. For availability reasons, ordinary hot-rolled steel was used and the dimensions are by no means optimum. For example, it would have been preferable to have a core of larger diameter. The coil was designed to take the full output of a 15-kw 120-volt d.c. generator and still be adequately cooled. The seven "pancake coils" were wound individually, each consisting of two layers of 31 turns of No. 7 rectangular (0.091×0.229 in.) double cotton-covered copper wire, the winding being started at the center of the wire so that both leads are at the outside. Wire somewhat thinner and wider would have been preferable, but was not immediately available. Wrapped with 0.007-inch thick cotton tape, varnished and baked, the coils were smooth, rigid, and quite satisfactory. Two single-layer pancakes were wound to go between the ends of the spool and the end cooling plates, but it was decided to use more insulation and dispense with one of them. The inside lead for the half-pancake comes out through a slot in the adjacent cooling plate.

The cylinder and two end plates of the spool were made of steel, $\frac{1}{4}$-in. thick, and threaded for assembly. The cooling plates between the pancakes were cut from $\frac{3}{16}$-in. copper plate. Copper tubing $\frac{5}{16}$ in. in diameter was fitted into channels machined in the plates, flattened to the same thickness as the plates, and soldered in. The cooling plate design can be seen in the horizontal section in Fig. 1a. In assembly, the pancakes were daubed liberally with insulating varnish and separated from the spool and from adjacent cooling plates by a layer of varnished cambric ("empire cloth") 0.012 in. thick. The resistance between the windings or the cooling plates and the spool is in excess of 20 megohms. Water connections to the cooling plates are made with $\frac{1}{2}$-in. "Aeroquip" rubber hose fittings. Water circulates through the plates in parallel, and at 15-kw input the heating is not excessive except on the spool face adjacent to the half-pancake. Continuous operation at currents over 125 amp. is not possible because of the heating of this plate. Cooling plates adjacent to both spool ends should be incorporated. The coil has a resistance of 0.8 ohm and gives approximately 50,000 amp. turns at 15 kw.

The vacuum chamber was made in two half-shells of brass. Two $\frac{7}{8}$-in. plates were bolted side by side on the face plate of a large lathe and the two halves were carved out simultaneously so that they mated exactly. Grooves $\frac{1}{16}$ in. wide and $\frac{1}{16}$ in. deep were machined in the center of the abutting surfaces of the half shells, and these were filled with a tightly fitting brass strip to position the shells as they were soft soldered together. The ends of the box were closed with brass pieces machined to a close fit in the inside of the box and

---

[7] F. B. Shull and D. M. Dennison, Phys. Rev. 71, 681 (1947); 72, 256 (1947); E. S. Rosenblum, *ibid.* 72, 731L (1947).
[8] F. B. Shull, Phys. Rev. 74, 917 (1948).
[9] Kurie, Osoba, and Slack, Rev. Sci. Inst. 19, 771 (1948).
[10] D. Judd, Rev. Sci. Inst. 21, 213 (1950).

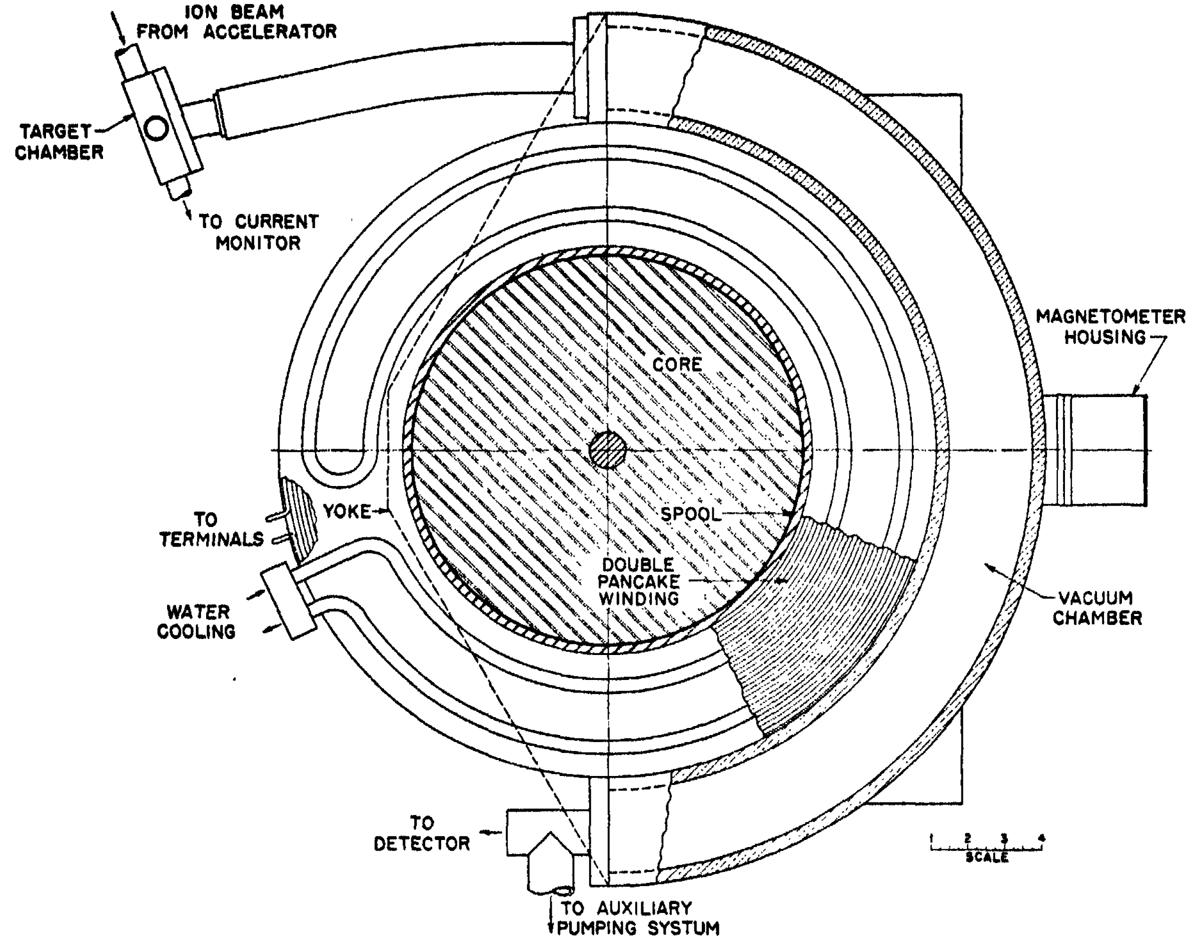

FIG. 1a. Horizontal section of Proton Spectrometer.

soldered in. The box appears to be completely vacuum tight. 0-ring joints are used for connections to the box. The interior cross section is approximately rectangular, $2\frac{1}{4}$ in. wide and $1\frac{1}{2}$ in. high with rounded corners.

The inlet end of the box leading to the target chamber is a length of brass pipe, within which is a short length of brass tubing rotatable about a vertical transverse axis. This aperture stop limits the range of scattering angles accepted by the spectrometer in cases where it is required for precision and is permitted by the intensity. At the exit end of the box, provision is made for attaching a small diffusion pump and liquid air trap. The auxiliary pump and trap are necessitated by the small size of the connections to the main vacuum system.

Shaping of the Magnetic Field

The magnetic field in the midplane can be expressed in the neighborhood of the midcircle in a series of the form[6]

$$H(r)=H_z(r)=H_0\left[1-n\left(\frac{r-r_0}{r_0}\right)+m\left(\frac{r-r_0}{r_0}\right)^2+\cdots\right], \quad (1)$$

where $H_0=H(r_0)$. The double-focusing property requires that $n=\frac{1}{2}$. The values of m and higher order coefficients affect only the aberrations and not the focal length, and they will not be considered here. If n is larger than $\frac{1}{2}$, the r-focal length (i.e., the focal length for trajectories in the midplane with r varying) is longer than the z focal length (i.e., the focal length for trajectories in the cylinder $r=r_0$ with z varying). If n is too small, the reverse is true. In either case the magnetic lens is astigmatic.

The problem of the proper shape of pole face to achieve the field described by $n=\frac{1}{2}$ does not permit of an accurate solution analytically because of the stray field and of non-linearity in the iron. A very simple analysis gives as the first approximation to the slope of the pole pieces at their center the expression

$$\tan u = n z_0/r_0, \quad (2)$$

where u = angle between pole face and midplane; z_0 = coordinate of pole face at $r=r_0$, i.e., half-spacing of pole faces at their center. That this approximation gives the correct answer in the case $n=0$ (parallel faces, uniform field) and the case $n=1$ ($1/r$ field in which equipotentials are coaxial cones with vertices at the origin)

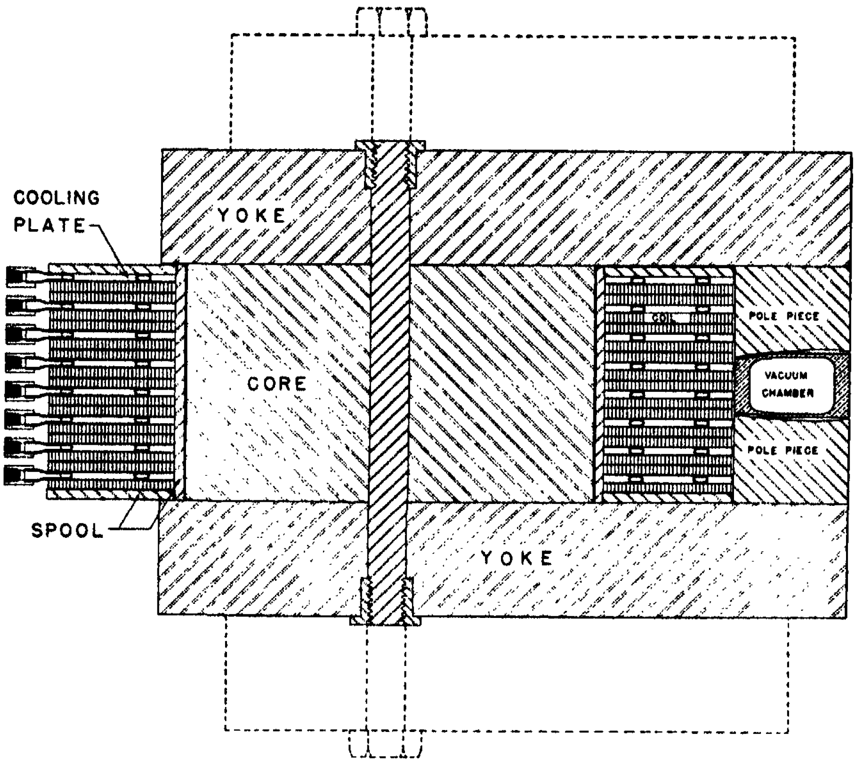

FIG. 1b. Vertical section of Proton Spectrometer.

gives some assurance that it will be valid for the intermediate case $n=\frac{1}{2}$ of interest here. For this spectrometer, it proved to be a good approximation.

Our initial estimate for the proper contour was that shown by the upper curve in Fig. 2. This shape was determined by scaling up the contour published by Siegbahn and Svartholm,[6] but because of slightly altered proportions, the scaling was not exact. The half width of the air gap at its center was 2.20 cm, so that for $n=\frac{1}{2}$ Eq. (2) gives $\tan u=1.10/26.7=0.0412$. Actually $\tan u$ was made equal to 0.0536, and it was expected that this contour might give a field falling off too rapidly with radius and make the z focal length shorter than the r focal length.

Rather than make a detailed investigation of the field shape, the focusing properties were investigated by projecting the proton beam from the electrostatic analyzer directly into the spectrometer and observing the spot produced on a quartz disk at the other end. A small alternating current electromagnet spread the beam in a plane 45 degrees from the vertical so that both radial and vertical focusing effects could be observed. The virtual source in this arrangement is at the center of the magnetic gap. With the source at 36 cm from the end of the pole pieces, the r focus was found to be more than 30 cm beyond the other end and the z focus to be 5 cm inside the gap.

The pole faces were then re-machined to the contour shown in the lower curve of Fig. 2, which was expected to give a slight overcorrection, $\tan u$ being 0.0380, somewhat slightly less than the calculated value 0.0412. Investigation revealed that, for approximately symmetrical cases, the radial focus was now shorter than the vertical focus, but that by moving the source farther away, a very good point image could be obtained. Although a slight improvement in the first-order astigmatism is to be expected from using a larger source than image distance, the improvement observed was considerably greater than that expected and is most certainly to be attributed to second-order effects or to the fringing field. Since the large stray field made it desirable to keep the source well away from the magnet in order to minimize the deflection of the incident beam, this arrangement was adopted, and no further studies of field shape or focusing properties have been made. *Note added in proof:* Field measurements have recently been made by W. D. Warters who finds $n=0.50\pm0.02$ over $r=10.5\pm0.8$ inches.

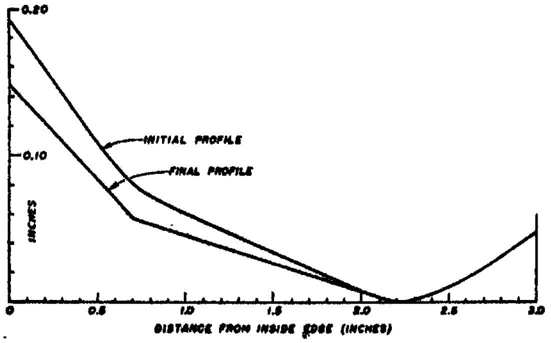

FIG. 2. Profiles of pole faces.

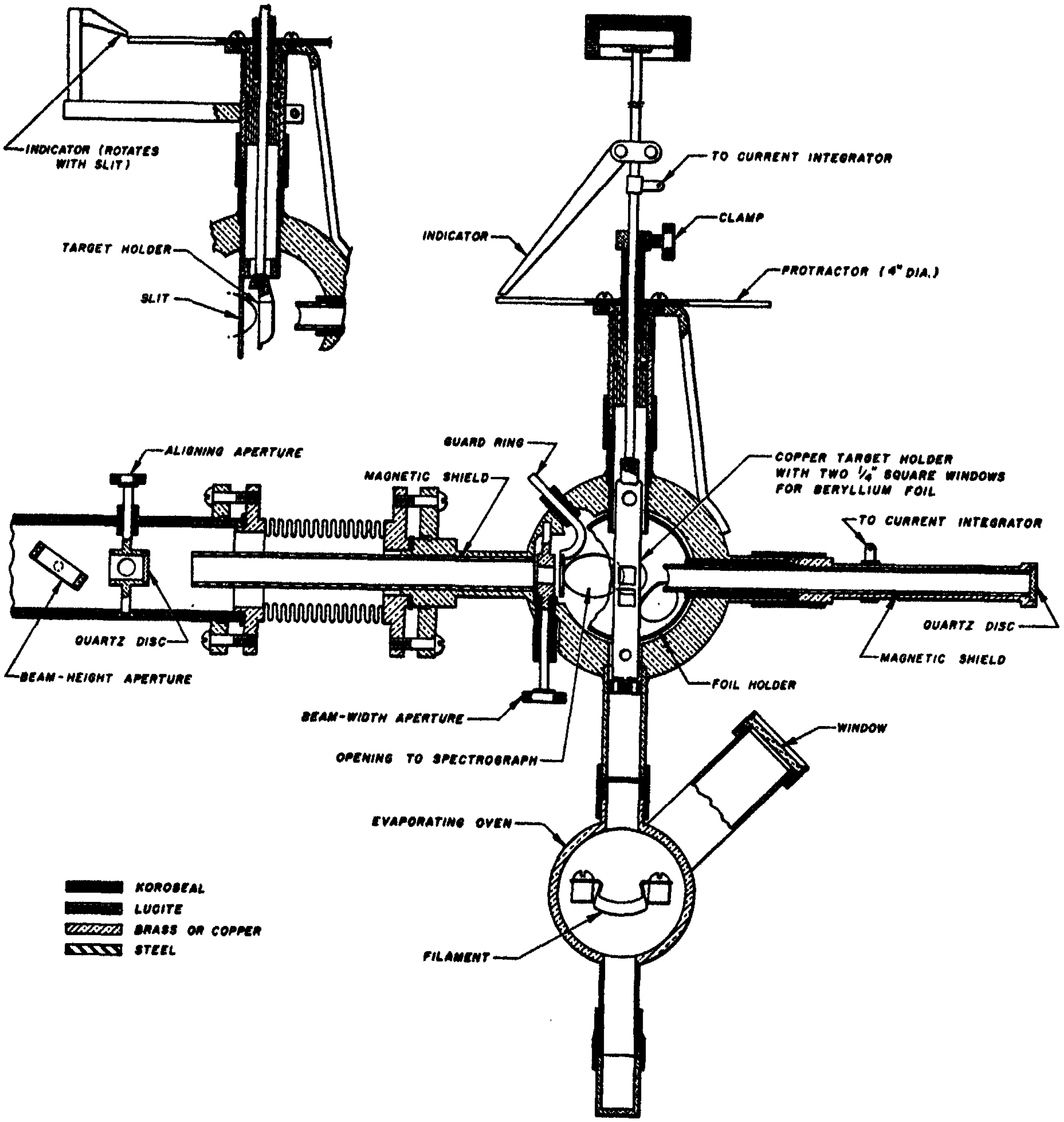

FIG. 3. The target chamber and evaporating oven.

Limitations of Present Design

The maximum field obtainable in the spectrometer with the 15 kw, 120-volt generator proved to be 7000 gauss, corresponding to 2-Mev protons. The most constricted portion of the magnetic circuit was at the intersections of the core with the two yokes. This constriction was eliminated by adding steel pieces as shown by the dashed lines in Fig. 1, but the change increased the peak field in the gap by only about five percent. The difficulty is simply that the leakage flux is very large because of the shape of the magnetic circuit so that the fraction of the total flux which goes through the pole faces is only ⅔ at low fields and less than ½ at high fields. Hence, the core, which carries all the flux, saturates too soon. It seems probable that a magnet with the present dimensions could be made to bend 4-Mev protons by winding the coils around the pole pieces themselves instead of around the core. It must be remembered, however, that the achievement of the proper inhomogenous field by shaping the pole pieces is dependent on having the permeability of the iron very high, so that the pole pieces cannot be magnetized near to saturation without introducing defocusing effects.

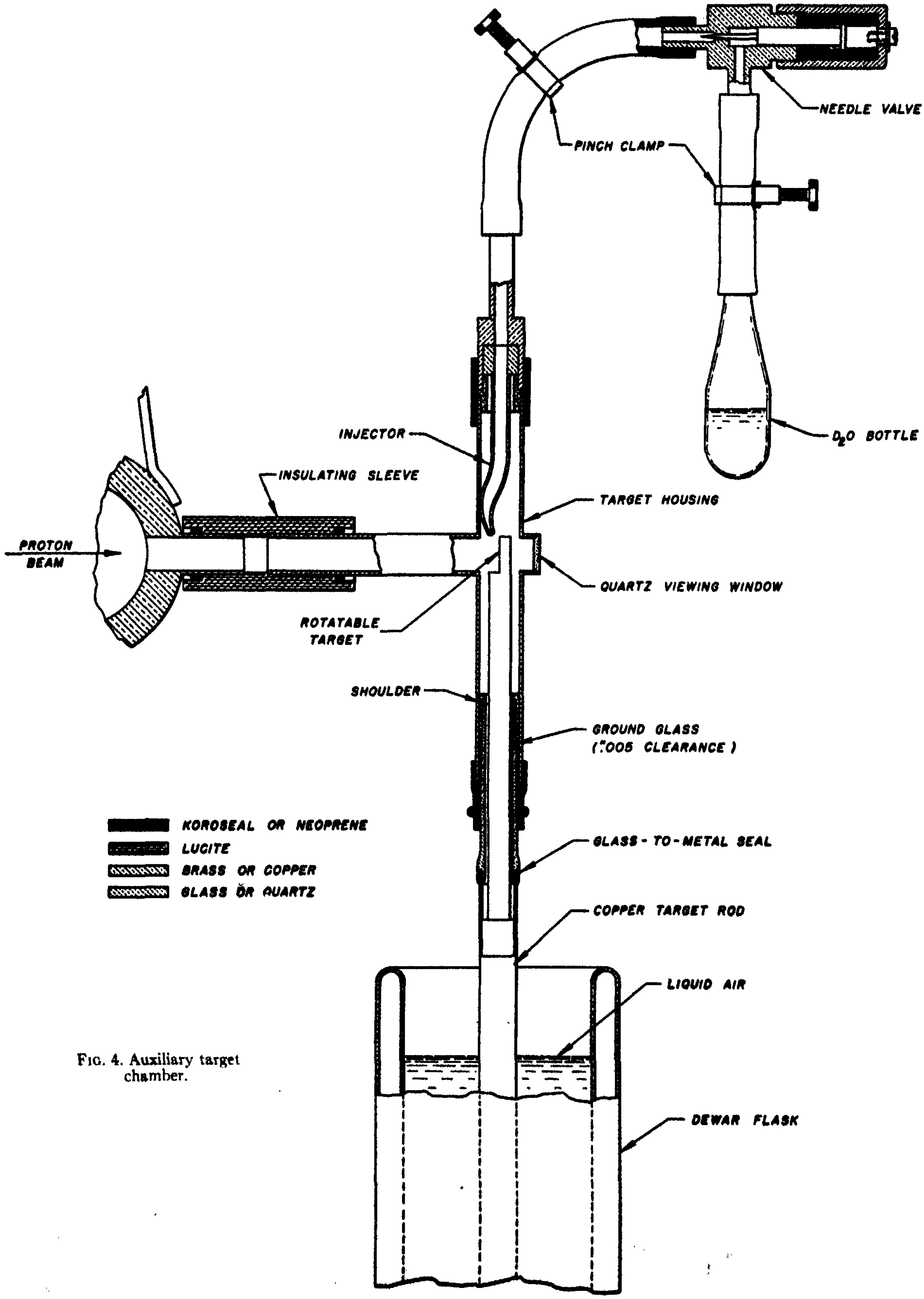

FIG. 4. Auxiliary target chamber.

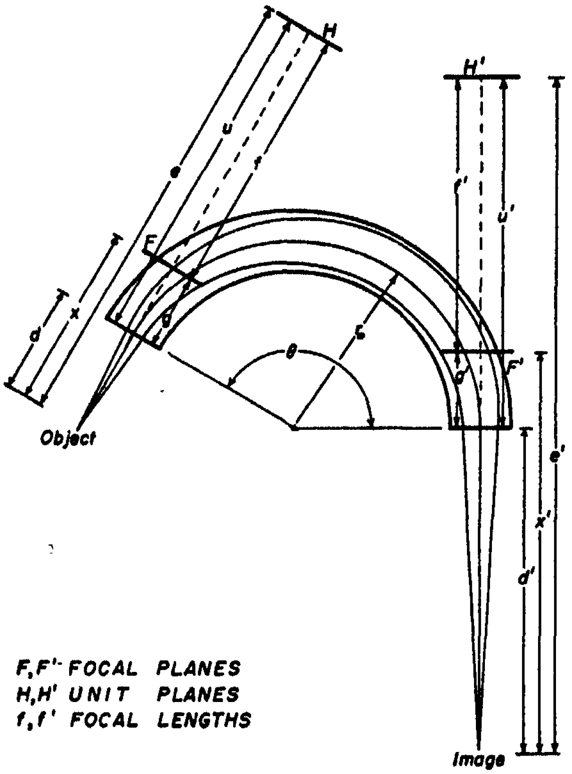

FIG. 5. Constants of the spectrometer as a magnetic lens.

An even more serious difficulty than the inability to focus high energy protons is the presence of the large stray field in the laboratory. It necessitates the magnetic shielding of the incident beam for a distance of several feet and makes the operation of certain instruments (such as photo-multiplier tubes) in the vicinity of the spectrometer very difficult. In spite of the fact that with this spectrometer source and detector are outside of the main field some difficulties remain if the fields outside the gap are not minimized. A 90-degree analyzing magnet[11] and a larger 180-degree double-focusing spectrometer ($r_0=16.0$ in.$=40.6$ cm) have recently been built in this laboratory using "kidney-shaped" coils wound around the pole pieces and having the magnetic circuit completely in iron except for the gap itself. By using flat wire, such a coil can be wound with little difficulty, and the stray field around the magnets is considerably reduced. These instruments will be described in forthcoming publications. The 16-in. double-focusing spectrometer reaches a field of 11,000 gauss (10-Mev alpha-particles and protons) with negligible field outside and has a solid angle of ~0.008 steradian and an observed resolution with a narrow slit ($\frac{1}{32}$ in.) of $p/\delta p=600$.

Fluxmeter

An important auxiliary instrument for use with any magnetic spectrometer having iron in the circuit is, of course, the field measuring device. The fluxmeter designed for this purpose has been previously described.[12] It is mounted so that approximately half the coil is between the pole faces and half in the fringing field. The current necessary to balance the fluxmeter is measured by a Leeds and Northrup Hydrogen Ion Potentiometer Number 7655 and is expressed in millivolts developed across a 1-ohm precision resistor. The readings range from 29 to 100 millivolts and are designated by I in what follows. I is inversely proportional to the magnetic field and thus proportional to the charge/momentum or non-relativistically to the charge/(energy×mass)$^{\frac{1}{2}}$ of the observed particles. The sensitivity is such that the field can be held fixed to 0.05 percent during a run. The pointer is kept on the null mark during a run by manually adjusting the field current in the generator supplying the magnet. The calibration over a period of three years has been reproducible to 0.2 percent.

Target Chamber

The design of the target chamber is shown in Fig. 3. As shown in Fig. 1, it is attached rigidly to the spectrometer through the brass inlet tube and can be moved relative to the proton beam by flexing the sylphon. The alignment of the beam is determined by intercepting it successively at the center of two quartz disks about 13 in. apart. The first disk is mounted in the end of a short length of brass tube pivoted as shown so that the beam can be intercefted by the disk or passed through the ½-in. hole into the target chamber. The other disk is mounted at the outer end of the target tube. For most of its length between these two fixed points, the beam is shielded by steel tubing to minimize curvature of its path in the stray field. The width of beam striking the target is controlled by the defining slit at the left edge of the chamber, which consists of a transverse rectangular opening in a shaft which can be rotated from outside.

The target to be bombarded can be mounted on the end of the second steel magnetic shield, which is beveled so that incident and scattered angles are equal. The tube is perforated so that pressure changes do not damage thin-foil targets and it is insulated from the target chamber by a polystyrene bushing so that it can be used to collect charge for the current integrator. In most experiments the target is mounted on a target holder which can be rotated from outside the vacuum system as shown. A pointer and a fixed protractor indicate the angular position of the target. This target support can also be lowered into a furnace where thin layers of lithium or other materials can be evaporated onto it.

An auxiliary target assembly which can be employed for other types of measurement requiring the proton beam without disturbing the spectrometer is shown in Fig. 4. In this particular assembly a heavy ice target was produced by allowing D_2O vapor to enter the target chamber adjacent to the flat face of a copper rod which was kept at liquid air temperatures. For the study of heavy ice targets with the spectrometer, the copper rod and injector system were made so that they could be inserted into the target chamber of Fig. 3 in place of the target holder and furnace shown there. This arrangement for interchanging targets and bombarding positions was found to be a very flexible and convenient one.

---

[11] D. B. Duncan, Phys. Rev. 76, 587 (1949).

[12] C. C. Lauritsen and T. Lauritsen, Rev. Sci. Inst. 19, 916 (1948).

For determining the scattering angle, the arrangement shown in the inset in Fig. 3 is used. A brass strip containing a vertical 0.003-in. slit is located so that the slit can be moved on a $\frac{1}{4}$-in. radius about the center of the target foil. Particles scattered by a copper target surface are detected. By rotating the slit so that first the incident beam and then the scattered beam pass through it, an accurate measurement of the scattering angle accepted by the spectrometer can be made.

Detection of Reaction Products

Various types of detectors can of course be used at the focus. The double-focusing spectrometer is advantageous essentially because detectors with small openings can be used with it. An ionization chamber,[13] 1 cm in diameter and 5 mm deep has been used for some experiments. The protons pass through a "Newskin" window of approximately 1-mm air equivalent mounted on a grid, and the ionization chamber reliably counts particles having about 1-mm residual range after traversing the window, so that this set-up is usable with protons of at least 150-kev energy and for alpha-particles with at least 300-kev energy.

For low energy protons a scintillation counter has been used, consisting of a small zinc sulfide screen, a hemispherical reflector and a photo-multiplier.[14] Its chief advantage is its ability to go to very low energies since no window is required, but its lack of dead time is also convenient, obviating the necessity for counting rate corrections. Excellent agreement has been found between absolute yields measured by the two types of counters for energetic particles. The pulse size of the scintillation counts relative to background noise was such that with the bias commonly used to eliminate noise, the counting efficiency was about 90 percent even for low energy particles.

Detection has also been accomplished by photographic plates and end-window proportional counters. The photographic plates are useful for searching for unknown particle groups as they allow use of a very wide slit. The proportional counters are useful in distinguishing protons and alpha-particles of the same energy and $B\rho$ by measurements of the ionization produced in short range intervals.

Source of Incident Particles

The incident beam, protons or deuterons, is obtained from the 1.5-Mev pressure-insulated electrostatic accelerator equipped with a precision electrostatic analyzer.[5] The voltage control is such that the incident proton energy relative to some assumed standard can be fixed to better than 0.2 kev at 1.0 Mev but in order to attain this precision, it is necessary to take considerable care in aligning the beam. This is particularly true since the stray field from the spectrometer magnet deflects the beam appreciably even above the electrostatic analyzer, a distance of more than two meters. The effect is compensated by means of three magnets, two with horizontal fields at right angles above the analyzer and one with a vertical field below the analyzer.

III. THEORETICAL CONSIDERATIONS

We have noted previously that in the axially-symmetric double-focusing spectrometer the conjugate foci are separated from one another by an angle $2^{\frac{1}{2}}\pi = 254.56$ degrees. In the present case, the pole pieces are only 180 degrees in extent, and to a first approximation the foci are found by linear extrapolation beyond the pole pieces of the trajectories inside the field. The spectrometer can then be considered as a "thick" spherical lens and the usual optical theory applied.

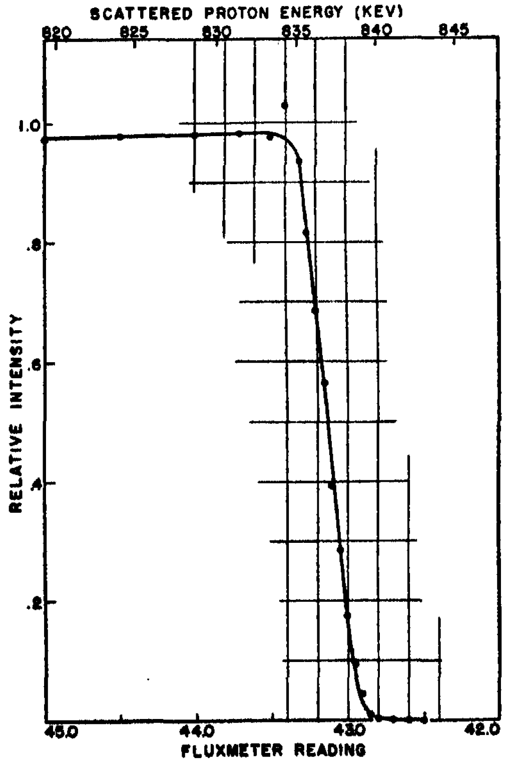

FIG. 6. The elastic scattering of 0.955-Mev protons at 137.8° by a thick copper target.

---

[13] Thomas, Rubin, Fowler, and Lauritsen, Phys. Rev. 75, 1612 (1949).

[14] A. Tollestrup, Phys. Rev. 74, 1561 (1948).

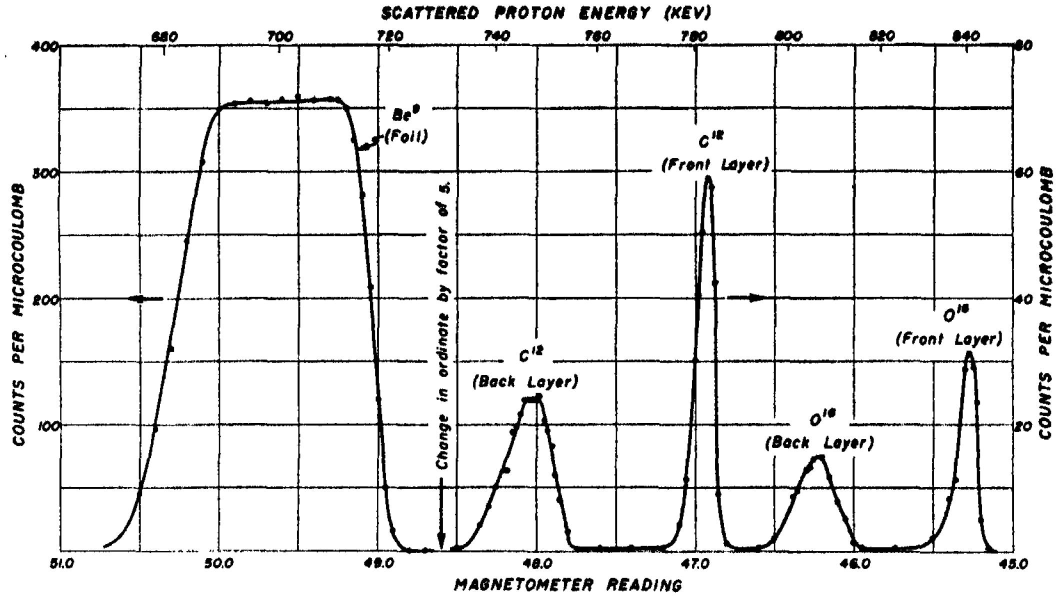

FIG. 7. The distribution in momenta of 1.066-Mev protons elastically scattered at 137.8° by a thin (∼18 kev) beryllium foil. Note the sharp peaks arising from carbon and oxygen layers approximately 50 atoms thick on the front and back surfaces of the foil. The scattering from the front layers and from the front surface of the beryllium indicates an over-all momentum resolution of ∼500. The effect of straggling in energy loss in the foil on the rear layer and rear surface scattering is noticeable.

The results for any n and any angular extent of the field, θ, have been given by Judd.[10] In what follows we first give the formulas for the anastigmatic case, $n=\frac{1}{2}$ and for any θ. The second expressions are for $\theta=\pi$ while the last expression gives the numerical value for $r_0=26.7$ cm as in the spectrometer described in this paper. The results are illustrated in Fig. 5.

Focal length (i.e. distance between focal planes and unit planes)

$$\begin{aligned} f=f'&=\sqrt{2}r_0\csc\theta/\sqrt{2}=1.78r_0 \quad \text{for} \quad \theta=\pi \\ &=47.5\text{ cm} \quad \text{for} \quad r_0=26.7\text{ cm}. \end{aligned} \tag{1}$$

Distance from ends of pole pieces to unit planes (measured inward)

$$\begin{aligned} u=u'&=\sqrt{2}r_0\tan\theta/\sqrt{2}=2.86r_0 \quad \text{for} \quad \theta=\pi \\ &=76.4\text{ cm} \quad \text{for} \quad r_0=26.7\text{ cm}. \end{aligned} \tag{2}$$

Distance from ends of pole pieces to focal planes (measured inward)

$$\begin{aligned} g=g'&=-\sqrt{2}r_0\cot\theta/\sqrt{2}=1.08r_0 \quad \text{for} \quad \theta=\pi \\ &=28.8\text{ cm} \quad \text{for} \quad r_0=26.7\text{ cm}. \end{aligned} \tag{3}$$

The conjugate focal points, object and image, can be determined from either of the standard relations:

$$1/e+1/e'=1/f \quad \text{or} \quad xx'=f^2, \tag{4}$$

where e and e' are measured from the unit planes and x and x' from the focal planes. However Judd has given the image distance, d', measured out from the pole piece directly in terms of the object distance, d, similarly measured as

$$\begin{aligned} d'&=-\sqrt{2}r_0\tan[\theta/\sqrt{2}+\tan^{-1}d/\sqrt{2}r_0] \\ &=-\sqrt{2}r_0\tan[127.28°+\tan^{-1}d/\sqrt{2}r_0] \quad \text{for} \quad \theta=\pi \\ &=-37.8\tan[127.28°+\tan^{-1}d/14.9]\text{ cm} \\ &\qquad \text{for} \quad r_0=26.7\text{ cm}. \end{aligned} \tag{5}$$

We used an object distance, $d=30.5$ cm and found the image distance experimentally to be $d'=8.6$ cm. The calculated image distance is $d'=9.4$ cm in reasonable agreement with the measured value.

The first order anastigmatic image also shows no distortion and the magnification in both the r and z directions is

$$\begin{aligned} M&=\left(\frac{d}{2^{\frac{1}{2}}r_0}\sin\theta/\sqrt{2}-\cos\theta/\sqrt{2}\right)^{-1} \\ &=\frac{d'}{2^{\frac{1}{2}}r_0}\sin\theta/\sqrt{2}-\cos\theta/\sqrt{2} \\ &=\left(0.562\frac{d}{r_0}+0.606\right)^{-1}. \\ &=0.562\frac{d'}{r_0}+0.606 \end{aligned} \tag{6}$$

For $d=30.5$ cm, $r_0=26.7$ cm, this gives $M=0.8$. Judd has also calculated the dispersion of the instrument and finds in the general case

$$D=\frac{\delta r}{r_0}\bigg/\frac{\delta P}{P_0}=\frac{\delta r}{r_0}\bigg/\frac{\delta B}{B_0}=\frac{1+M}{1-n}, \tag{7}$$

where δr is a small increment in the image position measured normal to the optic axis of the spectrometer arising from a change δP in the momentum of the particles injected into the spectrometer or from a change δB in the magnetic induction, B_0, of the spectrometer. We note that $D=2(1+M)$ for the anastigmatic spectrometer as compared with $D=1+M$ for the type with uniform field ($n=0$). For $M=1$ these become $D=4$ and $D=2$ respectively. In the spectrometer described here a magnification of 0.8 was employed for reasons previously given and the dispersion has the value $D=3.6$.

The ultimate resolving power of the instrument can be calculated if the size and shape of the image of a point source formed by the particles emitted in a finite solid angle is known. This in turn depends on higher order calculations and on fringing field effects. Practically we have found no occasion to employ the ultimate resolution as determined by the small image aberrations but have been limited to values of the resolution given by the source and collector sizes dictated by intensity considerations. This resolution in momentum can be computed from the width of the collecting slit, δr_c, by using the expression for D given above

$$R_c=\frac{P_0}{\delta P_c}=\frac{Dr_0}{\delta r_c}=\frac{1+M}{1-n}\left(\frac{r_0}{\delta r_c}\right). \tag{8}$$

In the case described here $R=3.6r_0/\delta r$. For a finite source width, δr_s, a similar expression is obtained by replacing δr_c by $M\delta r_s$ yielding

$$R_s=\frac{P_0}{\delta P_s}=\frac{1+M^{-1}}{1-n}\left(\frac{r_0}{\delta r_s}\right). \tag{9}$$

The apparent spread in momenta, δP_c or δP_s, of particles actually having the same momentum will be indicated in terms of an interval δI_c or δI_s in fluxmeter readings over which counts can be obtained.

For rectangular source and slit the apparent distribution in momentum for monoenergetic particles will be trapezoidal in shape with a width at half-maximum determined by whichever of δP_c or δP_s is the larger and the effective resolution will be determined by the smaller of R_c and R_s. The base of the trapezoid will have a width given by $\delta P_s+\delta P_c$ while the top will have a width given by $|\delta P_s-\delta P_c|$.

For a continuous distribution of particles extending up to a maximum energy as is observed for example when a thick target is used in scattering or reaction experiments, the observed distribution will show the effects of finite resolution near the upper limit. These effects are shown in Fig. 6 which illustrates the distribution in momentum of monoenergetic protons scattered by a thick Cu target. The curve shows a linear portion of finite slope symmetric about the true end point with rounded fillets at each end. If the linear portion be extended from the maximum reading to zero it will be found to cover a momentum range given by δP_c or δP_s, whichever is larger. The corresponding δI_c or δI_s divided into the reading I will give the resolution.

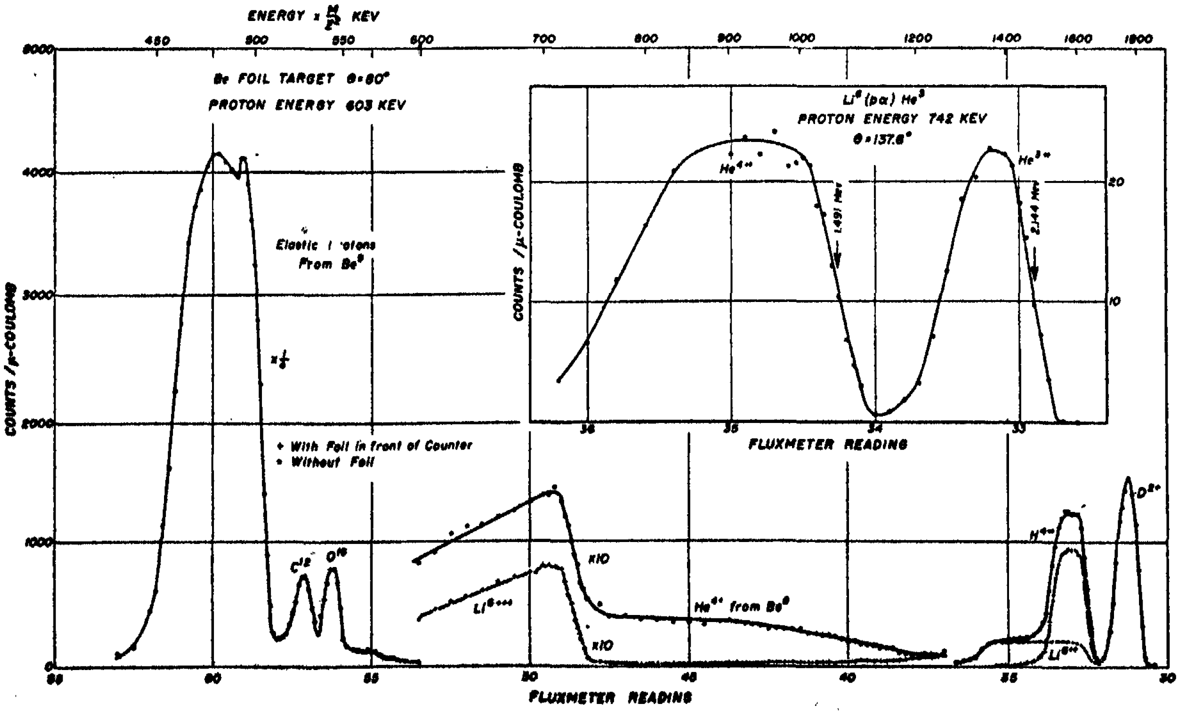

FIG. 8. Momentum analysis of the ions produced in the bombardment of Be^9 and Li^6 by protons.

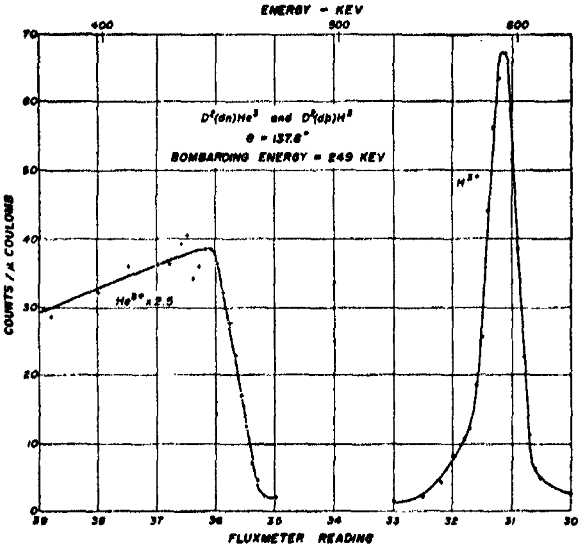

FIG. 9. Momentum analysis of the He^{3+} and H^{3+} produced in the bombardment of deuterons with 249 kev deuterons and with the angle of observation equal to 137.8°.

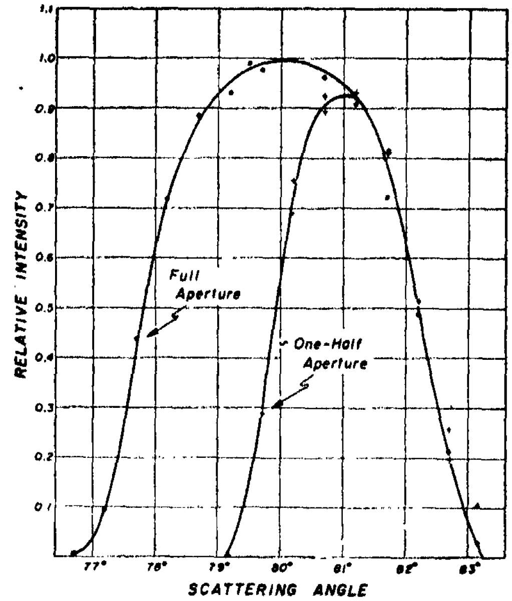

FIG. 10. Distribution in angle of the particles accepted by the spectrometer.

In the use which we have made of the spectrometer δr_c and δr_s have been determined by intensity considerations. The number of counts observed is linear in δr_c as long as the particle spread in energy is greater than that accepted by the spectrometer as is usually the case. The source width is usually determined by the beam width from the electrostatic generator and the useful current depends on the width permitted through the beam slit as long as the focused beam is larger than this slit width. In addition to the apparent spread in energy arising from (1) the source (or bombarding beam) width and (2) the collector width, (3) aberrations and (4) fluctuations in the magnetic field, there are real spreads in energy in the particles entering the spectrometer. These arise from (5) the energy spread in the incident beam (6) the angular extent of the inlet aperture[*] since the energy of a particle emitted in a nuclear reaction or scattering process depends on the angle of emission, (7) the energy loss in the target of both the incident and outgoing particles and (8) the energy straggling in the target of both particles, and (9) the thermal motion of the target nuclei.

TABLE I. The elastic scattering of protons by several materials. Incident energy = 1.2373 Mev. Angle of scattering = 137.8°. (Relativistic corrections included.)

Scatterer	Calculated energy after scattering E (Mev)	Fluxmeter reading I (mv)	Spectrometer constant for protons C_p
Li	0.7475	48.24	1.7390×10^4
Be	0.8367	45.56	1.7366
C	0.9230	43.39	1.7379
O	0.9931	41.83	1.7382
Cu	1.1704	38.52	1.7376
Mean			1.7379×10^4 ± 0.0006

The ultimate line shape can be predicted from a folding of the various contributions listed above into each other. The effect of (7) will depend markedly on whether the outgoing particles emerge into the spectrometer from the same side of the target as the incident particles enter or from the opposite side. The effect will also depend on whether the energy of the particles produced in the nuclear reaction under study decreases as the incident particle energy decreases because of energy loss in the target or whether it increases. For the so-called residual nuclei produced in a nuclear reaction the latter is often the case for angles of observation with the incident beam greater than 90°.

Items (1) to (6) and (9) discussed above make symmetrical contributions to the line shape of a group of particles under observation. Thus for very thin targets for which (7) and (8) can be neglected the observations yield a symmetrical line the midpoint of which corresponds to the momentum (or energy) of the secondary particles produced at the angle corresponding to the mean acceptance angle of the spectrometer by those particles in the incident beam having the mean energy of the beam. Usually for reasons of intensity ideally thin targets cannot be used. In energy determinations if the midpoint of the observed line is employed as a measure of the energy of the secondary particles then a correction must be made for half the energy loss in the target both for the incident and emergent particles. The method of correction will be the same whether the secondary particles emerge from the same side of the target as the primary particles impinge upon or from

---

[*] The finite source size also makes a contribution to the spread in the angle of observation. Its effect must be combined algebraically with (1).

TABLE II. The elastic scattering of protons by copper at several energies. Angle of scattering = 137.8°. (Relativistic corrections not included.)

Inc. energy $\bar{E}$ (Mev)	Scat. energy	Fluxmeter Reading H^+	HH^+	HHH^+	Spectrometer constant for protons calculated from H^+	HH^+	HHH^+
1.3314	1.2603	37.08	52.51	64.34	1.733×10^4	1.737×10^4	1.739×10^4
0.8876	0.8402	45.35	64.30		1.728	1.737	
0.4438	0.4201	64.26			1.735		
Mean						1.735×10^4 ±0.002	

the opposite side if the inclination of the target to the incident and emergent beams is properly taken into account. The contribution to the observed width of the line will of course be markedly different in the two cases. It is clear that other characteristics of the observed thin-target curves such as extrapolated end points can be employed if properly interpreted but we have found it most convenient to use midpoints representing mean energies with appropriate corrections for target energy losses.

Actually in our most accurate energy determinations with the spectrometer we have preferred to employ thick targets. It is then necessary to observe the particles emerging from the surface of the target upon which the incident particles impinge. The measurements yield a step curve (see Fig. 6 for example) which is essentially just the integral of the curve arising from contributions (1) to (6) and (9). The midpoint of the sloping front of the step is taken as the momentum of the secondary particles produced at the mean acceptance angle of the spectrometer by the particles of mean energy in the incident beam. In some cases we have employed semithick targets which do not completely stop the incident particles but which give a spread in energy large compared to that arising from (1) to (6) and (9). In this case we have also used the midpoint of the initial rise just as with thick targets but the accuracy is not as great primarily because of the effect of straggling on the peak reading obtained.

The error in the determination of the energy of a group of particles arises from the following causes with which we also list an estimate of the contribution to the probable error: (1) uncertainty in the fundamental constants, 0.01 percent, (2) uncertainty in the energy of calibration particles, 0.1 percent, (3) uncertainty in fluxmeter setting and line location, 0.2 percent, and (4) uncertainty in the particle path arising mainly from variations in the target or beam position and from saturation effects in the magnetic field, 0.05 percent. The over-all error is slightly over 0.2 percent. In the determination of the Q of a nuclear reaction in addition to (1) the error in the energy of the observed particles, errors arise from (2) uncertainty in the energy of the incident particles, (3) uncertainty in the angle of observation, (4) uncertainty in the masses of the particles involved, (5) uncertainty in the thickness of surface contamination layers on the target, and in some cases, (6) uncertainty in the interpretation of the line structure.

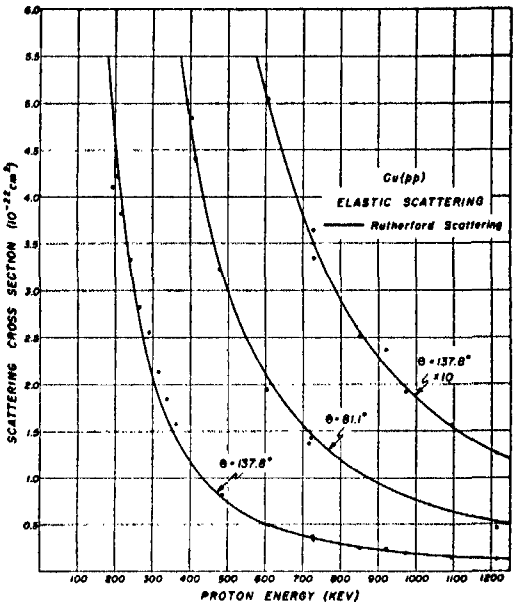

FIG. 11. The cross section for the elastic scattering of protons by copper as a function of energy. The experimental point at $E_p=610$ kev, $\theta=137.8°$ has been fitted to the Rutherford cross section (solid curves) yielding a value for the spectrometer solid angle of 0.0061 steradian.

IV. TESTS AND CALIBRATION

Energy Measurements

The characteristics of the spectrometer have been investigated by scattering protons and deuterons elastically from various targets, particularly gold, copper, oxygen, carbon, beryllium and lithium. A thin beryllium foil* gives a particularly interesting trace as shown in Fig. 7. The foil was thin enough and the bombarding energy high enough so that the scattered protons from beryllium, from carbon and oxygen contamination on the front of the foil, and from similar contamination on the back of the foil are all distinctly separated in energy. The separation occurs because of the differing amounts of recoil energy imparted to nuclei of different mass and because of the energy loss of incident and scattered protons in the beryllium. The high resolution in momentum (~500) arises from the fact that $\delta r_c=\delta r_s=0.1$ cm in these measurements. Figure 8 shows an example of what happens with a lower bombarding voltage and a wider exit slit (0.8 cm). Here the peak from the front oxygen layer is clearly apparent while the peaks from the rear oxygen layer and the front carbon layer occur at the same reading. The peak from the rear carbon layer lies atop the beryllium peak, which therefore appears to have an unusual shape. Such effects must be taken into consideration in making accurate energy measurements.

---

* This foil and others were very kindly supplied to us by Dr. Bradner of the University of California. The technique of preparing them is discussed in Rev. Sci. Inst. 19, 662 (1948).

Figure 8 also shows the nuclear reaction products obtained in the bombardment of Be^9 and Li^6 by protons. The reactions are $Be^9(p, \alpha)Li^6$, $Be^9(p, d)Be^8$, and $Li^6(p, \alpha)He^3$. The singly ionized deuterons, doubly ionized alpha-particles, doubly ionized He^3 and both the doubly ionized and the triply ionized Li^6 give definite peaks. The Be^8 produced in the second reaction breaks into two alpha-particles with random directions in the moving center of mass system yielding the continuous distribution of alpha-particles in the laboratory system which is also clearly indicated. These results have been analyzed in a previous publication.[15] Another set of measurements which have also been previously described[1] are shown in Fig. 9. Here the residual nuclei from $D(d, p)H^3$ and $D(d, n)He^3$ have been measured by bombarding heavy ice targets with deuterons. In these measurements considerable analysis was necessary to properly interpret the "thin" target curve for H^3 and the "thick" target curve for He^3 obtained using the same target and the analysis carried out along the lines discussed above is given in detail in the reference.

The results obtained by elastically scattering protons or deuterons of known energy at a known angle from various targets has been used to calibrate the momentum (or energy) scale of the fluxmeter. The energy of the incident particles is determined by means of the electrostatic analyzer calibrated at the strong gamma-resonance in $F^{19}(p, \alpha'\gamma)$ at 873.5±0.9 kev.[16] The angle of scattering was determined by means of observations with the rotating slit described previously. A record of the data taken with the slit and two settings of the entrance aperture is shown in Fig. 10. With the aperture stop completely open the mean scattering angle seen by the spectrometer as set up in this particular experiment is 80° with some particles being accepted up to 3° on either side of this. To improve the resolution some data has been taken with the aperture stop partially closed. It will be noted in Fig. 10 that for this setting the mean angle is 81° with a spread of slightly less than 2° on either side.

In Table I we present the results of the elastic scattering of 1.2373-Mev protons at 137.8° by Li, Be, C, O, and Cu. Column 2 lists the energies after scattering (E) calculated using the conservation laws of energy and momentum. Small relativistic corrections have been made. These arise in the energy determination in the analyzer and in the calculation of the energy after scattering. Column 3 lists the fluxmeter readings in millivolts (I). In column 4 are listed values of the spectrometer constant for protons as calculated from:

$$C_p = I^2E[1+(E/2M_pc^2)],$$

where M_p is the mass of the proton appearing in the second terms in brackets which is a small relativistic correction. The results for the various determinations of C_p indicate the high precision possible with the spectrometer. The average value from these determinations is $C_p = 1.738\times10^4$ for E in Mev and I in millivolts. This value for C_p holds only for protons. The constant for any other ion of charge Z and mass M can be obtained by multiplying C_p by M_pZ^2/MZ_p^2 or by Z^2/M for M in proton mass units.

In passing it is worth noting that the observation of elastic scattering peaks with spectrometers of high resolution is an excellent method for determining the nuclear composition of thin layers of unknown materials. Since the Rutherford scattering increases as the square of the nuclear charge the method is especially sensitive in detecting minute quantities of heavy nuclei. Very high resolution (10^4) and very thin targets (<100 ev) are necessary to separate the heavy nuclei even at large angles of scattering.

By using the hydrogen ion beams of masses one, two, and three with a constant setting on the electrostatic analyzer for the incident protons, one can check the linearity of the magnetic fluxmeter and establish the precision with which measurements can be made with the spectrometer. Similarly with fixed fluxmeter settings one can check the linearity of the analyzer. In Table II we give readings for three energies in the ratio 3,2,1 taken with copper as the scattering material. The calculated values for C_p are also given.

Small relativistic corrections and corrections for the electrons carried by ions of mass two and three have not been included. Even without these corrections the results show that the over-all combination of electrostatic analyzer for incident particles and of magnetic analyzer for outgoing particles gives consistent results within a probable error of 0.1 percent.

Resolution and Line Width

Very thin targets or infinitely thick ones can be used in elastic scattering experiments to yield a measure of the line width arising from source and exit slit size. In the former case the energy losses can of course be neglected while in the latter case the slope of the rise to the maximum reading can be employed to calculate the line width neglecting target losses. Using an exit slit $\delta r_e = 0.8$ cm and an entrance slit $\delta r_s = 0.2$ cm so that δr_e determines the resolution we have made careful measurements using thick Cu targets of the rise in the scattering curve. We find $\delta I/I = 0.0081$, 0.0075, and 0.0078 in measurements at 1240, 992, and 744 kev yielding an average value 0.0078 and a resolution $R = 128$. Our expression for R is the resolution in particle momenta. Since energy is proportional to momentum squared, we have $E/\delta E = \frac{1}{2}P/\delta P = \frac{1}{2}R = 64$. If we substitute $M = 0.8$, $n = 0.5$, $\delta r_e = 0.8$ cm, $r_0 = 26.7$ cm into expression 8, we obtain $R = 122$ in good agreement with the observed value. Simple calculations indicate that the spread in energy in the incident beam and in the scattered particles over the entrance aperture contribute values of $\delta I/I \sim 0.001$ and merely increase the fillets on the observed curves. The widths of the carbon and oxygen peaks shown in Fig. 7 which were obtained using 0.1-cm entrance and exit slits indicate $R \approx 500$ while the calculated value is $R \approx 1000$. In this case the contribution to line width from the angular extent of the aperture is not negligible.

---

[15] Tollestrup, Fowler, and Lauritsen, Phys. Rev. **76**, 428 (1949).

[16] Herb, Snowdon, and Sala, Phys. Rev. **75**, 246 (1949).

We have made no attempt to measure the ultimate inherent resolution of the spectrometer. However the image size due to aberrations of a point source of protons as described above was visually estimated to be of the order of 0.1 cm in size. Substitution in 8 above yields $R \sim 1000$. There is reason to believe that the recognition of detail even to better than one part in a thousand in momentum is possible with sufficiently intense sources.

Solid Angle

The solid angle of acceptance of the spectrometer can be determined by measuring the yield of elastic scattering from a substance such as copper. The measurements we have made are illustrated in Fig. 11 and show a $1/E^2$ dependence over the entire energy range showing that there are no anomalies in the Rutherford scattering. With a thick target the yield is of course proportional to the Rutherford cross section and to the target thickness in which the over-all losses are just enough to fill the exit slit of the spectrometer. This involves the instrument resolution and the stopping cross section for protons in Cu. The data shown in Fig. 11, using Mano's stopping power for Cu, are consistent with a value for $\Omega = 0.0061$ steradian or $\sim 1/2000$ of the sphere. Using the formula for Ω given by Judd we calculate $\Omega = 0.008$ steradian from the *maximum* available cross section of the spectrometer vacuum tank. That the experimental result is slightly smaller than the value so calculated is not surprising in view of the fact that other stops in the system probably determine the solid angle.

Yield Measurements

In a future paper we intend to discuss the use of the spectrometer in the measurement of the intensity of particles produced in a nuclear reaction. We note at this point that the number of counts observed in the detector, N, for a given yield, y, of particles produced at the target per unit momentum interval per 4π steradians of solid angle, is

$$N = y(\Omega \delta P_c / 4\pi),$$

where δP_c is the momentum interval corresponding to the collector slit width and Ω is the solid angle through which particles leaving the source can traverse the spectrometer and enter the detector. In terms of $R_c = P/\delta P_c$ we have

$$N = y(\Omega P / 4\pi R_c).$$

We emphasize that it is the resolution, R_c, appropriate to the collector size which appears explicitly in this expression and not the resolution, R_s, appropriate to the source, nor the resolution, R_a, arising from aberrations such as spherical aberration. It is true that in certain cases y may depend on the area of the source, as for radioactive deposits with a limiting surface activity or for targets which can be bombarded only by beams of limited concentration. Also, of course, Ω and R_a are intimately related and numerous papers have been written proposing methods for obtaining small aberrations and thus high resolution R_a for a given solid angle. In the last analysis it must be noted that it is R_c which appears in N and there are many practical cases in which to obtain sufficient counts for the maximum solid angle in the available magnetic field volume, one must reduce R_c to a value considerably below the ultimate value R_a so that the observed resolution is of the order of R_c and not of R_a. In these cases many other considerations may dictate a choice of design parameters which do not yield a high value of R_a but other desirable features such as low power consumption, ease and simplicity of construction, and so forth. Only in those cases where R_c can be matched to R_a will the practical resolution and the ultimate be approximately equal.

For the spectrometer discussed in this paper we have found

$$\frac{N}{yP} = \frac{\Omega}{4\pi R_c} = 3.80 \times 10^{-6}$$

or

$$R_c/\Omega = 21{,}000,$$

where $R_c = 128$ for the 0.8-cm collector slit which was employed in most measurements and $\Omega = 0.0061$ steradian for the full aperture. If R_c had been matched to the ultimate resolution $R_a \sim 1000$, a result eight times smaller would have been obtained which would have been impractical for applications involving nuclear processes of low probability.

In determining yields and cross sections in nuclear reactions from observed counting rates, we have

$$y(I) = \frac{4\pi R_c}{q\Omega_c} \frac{N(I)}{I} \times 1.6 \times 10^{-13}$$

$$= \frac{2R_c}{q\Omega_c} \frac{N(I)}{I} \times 10^{-12}$$

where $y(I)$ is the yield per incident singly charged particle per 4π steradians in the center-of-mass system per unit interval on the fluxmeter scale and $N(I)$ is the number of counts observed at the fluxmeter reading I when q microcoulombs strike the target. The equivalent solid angle Ω_c, in the center-of-mass system, can be calculated in a straightforward manner from Ω. *For thin targets* one can integrate over the total area under the peak corresponding to a given group of particles and obtains

$$Y=\int y(I)dI=\frac{2R_c}{q\Omega_c}\int\frac{N(I)}{I}dI\times 10^{-12}$$

which is the yield in disintegrations per incident particle per 4π steradians appropriate to the target thickness and angle of observation employed. The cross section is then given by thin target measurements as

$$\sigma=Y/nt=Y\epsilon_1/\xi_1$$
$$=\frac{2R_c\epsilon_1}{q\Omega_c\xi_1}\int\frac{N(I)}{I}dI\text{ millibarns,}$$

where n = disintegrable nuclei per cc in the target, t = target thickness parallel to the incident beam in cm, ξ_1 = energy loss of incident particles in target in ev, and ϵ_1 = stopping cross section[15] in 10^{-15} ev-cm^2 for the incident particles per disintegrable nucleus in the target molecules. *For targets thick* enough that the energy spread of the outgoing particles exceeds the total energy spread from all other causes including in particular the energy interval accepted by the spectrometer collecting slit, it is often convenient to use the maximum reading over the flat portion of the observed curve of counts *versus* spectrometer setting. Similarly for very thick targets it is convenient to use the maximum reading obtained after the initial rise. In both cases if $N_{\max}$ is this maximum reading for q microcoulombs

$$Y=2N_{\max}/q\Omega_c\times 10^{-12},$$

where Y is now the yield in disintegrations per incident particle per 4π steradians appropriate to the target thickness which just gives a spread in energy of the outgoing particles equal to that accepted by the spectrometer collecting slit. A simple calculation gives this thickness in energy units as

$$\xi_1=\frac{\epsilon_1\delta E_2}{|\epsilon_1(\partial E_2/\partial E_1)+\epsilon_2(\cos\theta_1/\cos\theta_2)|}$$
$$=\frac{2\epsilon_1 E_2}{R_c|\epsilon_1(\partial E_2/\partial E_1)+\epsilon_2(\cos\theta_1/\cos\theta_2)|},$$

where ϵ_2 = stopping cross section in 10^{-15} ev-cm^2 for the outgoing particles per disintegrable nucleus in the target molecules. E_2 = energy of outgoing particles in electron-volts. θ_1 = angle of incident beam measured from the normal to the target on the side of the incident beam. θ_2 = angle of outgoing particles measured from the normal to the target on the side of the incident beam. $\partial E_2/\partial E_1$ = variation in energy of outgoing particles with that of the incident particles calculated from the expression $E_2=E_2(E_1,\theta,Q)$ given by the application of the usual conservation laws. The cross section is thus given by thick target measurements as

$$\sigma=\frac{N_{\max}R_c}{q\Omega_c E_2}\left|\epsilon_1\frac{\partial E_2}{\partial E_1}+\epsilon_2\frac{\cos\theta_1}{\cos\theta_2}\right|\text{ millibarns.}$$

Great care must be observed in using this expression if $\partial E_2/\partial E_1<0$ as is often the case for residual nuclei or if $\cos\theta_1/\cos\theta_2<0$ as in transmission experiments. In either case straggling in energy loss of the outgoing particles may make a large contribution to their observed spread in energy and a calculation taking this into account must be made. In most of our experiments observations have been made on the light particles emitted in a nuclear reaction for which $\partial E_2/\partial E_1>0$. The one exception has been discussed in detail previously.[1] In addition, in most of our experiments we have observed on the side of the target on which the bombarding particles were incident so that $\cos\theta_1/\cos\theta_2>0$. The reason for this is that this choice is convenient for large angles of detection with the incident beam. At these angles Rutherford scattering of the incident particles is small and not considerably greater than nuclear processes as it is at forward angles. This reduces the interference from the scattered incident particles. Observations in this manner are of course the only method for targets so thick that the particles cannot emerge from the side opposite to the incident beam.

In conclusion we wish to thank Professor R. F. Christy and Dr. D. L. Judd for many illuminating discussions of this paper.

This work was assisted by the joint program of the ONR and AEC.

---

[15] Livingston and Bethe, Rev. Mod. Phys. 9, 270 (1937).

THE REVIEW OF SCIENTIFIC INSTRUMENTS VOLUME 21, NUMBER 10 OCTOBER, 1950

Physical Instruments for the Biologist

Detlev W. Bronk
Associate Editor in Charge of This Section
Eldridge Reeves Johnson Foundation for Research in Medical Physics,
University of Pennsylvania, Philadelphia, Pennsylvania

Vibrating Probe Electrometer for the Measurement of Bioelectric Potentials

O. Blüh and B. I. H. Scott*
Physics Department, University of British Columbia, Vancouver, Canada

(Received May 22, 1950)

The instrument described in this paper is intended for the measurement of bioelectric, membrane, and diffusion potentials. The principle of the method has been suggested previously and applied to the study of contact potentials and electrical properties of adsorptive films.[1] Apparently it has not been used for the purposes mentioned above.

The construction of the instrument is shown diagrammatically in Fig. 1. An insulated metallic probe is set into vibration by means of a telephone *T*, and brought close to the surfaces of the object to be investigated, in this case a plant. As long as a potential difference obtains between probe and surface, the induced charge on the former undergoes alterations with the change of capacity due to the vibration of the probe. Corresponding potential changes are produced on the grid of the electrometer tube *E*, the output of which is fed to an amplifier *A* and displayed on a C.R.O. screen as a sinusoidal curve. The amplitude of this curve depends on the potential difference between *S* and *P*. The action of the instrument can also be compared to that of a generating voltmeter.

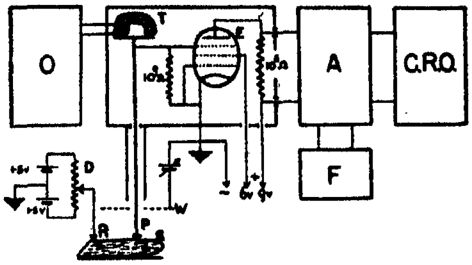

Fig. 1.

With the help of a potential divider *D* an opposing potential is introduced between surface and ground, which is varied until the trace on the C.R.O. screen is reduced to zero amplitude, when the probe and the opposite region of the surface are at equal potentials. Alternatively the compensation voltage could be introduced into the circuit between cathode and earth.

A photograph of the apparatus is shown in Fig. 2. Telephone and electrometer tube, carefully shielded from each other, are enclosed in a tinplate box which is mounted on a microscope rack allowing vertical movement of the probe with the help of the coarse and fine controls. The object is placed on the mechanical stage of a microscope, and can be moved in the horizontal plane. A reference electrode *R* is in contact with the object, and connects it to the compensating circuit *D*. Both platinum and silver-silver chloride electrodes have been used and found sufficiently stable.

The probe vibrates at a frequency of 280 sec.^{-1}. A 959-acorn tube operated at reduced potentials with *G*3 as its control grid to reduce grid currents[2] was chosen as

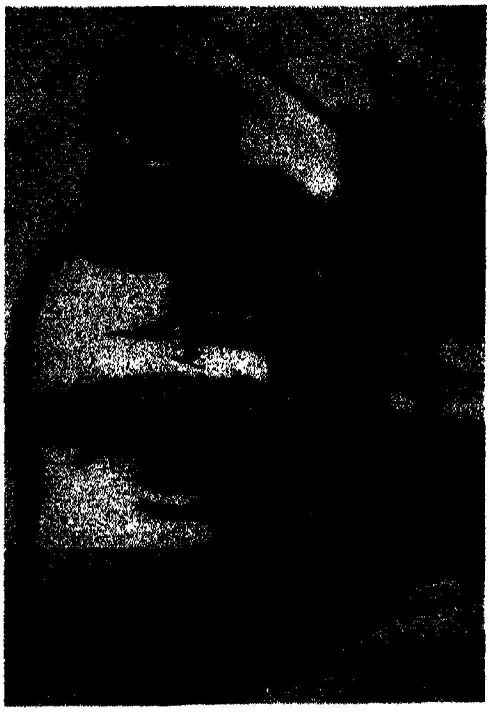

Fig. 2.

---

* On leave of absence from the University of Tasmania, Hobart, Tasmania, Australia.

[1] Zisman, Rev. Sci. Inst. 3, 7 (1932); Frost and Hurka, J. Am. Chem. Soc. 62, 3335 (1940).

[2] C. E. Nielson, Rev. Sci. Inst. 18, 18 (1947).

electrometer tube. The amplifier *A* is a three-stage battery operated General Radio Company Model 1231-A.[3] A parallel antiresonant filter *F* tuned to 280 $\mathrm{sec.}^{-1}$ is used to reduce the noise level and 60 $\mathrm{sec.}^{-1}$ alternating current interference. The object is shielded with wire gauze *W* to reduce a.c. pick-up.

One of the main advantages of the instrument is the possibility of using a.c. amplification. Further, since the probe does not make contact with the surface, no galvanic current is drawn from the source of potential and no diffusion potentials are introduced, as by the use of conventional electrodes. The possibility of producing injury potentials through the mechanical contact between electrode and object also does not arise. The use of the instrument is, of course, limited to surface measurements. The vibrating probe electrometer can be used for the investigation of resting potentials and their slow changes in time (growth, external influences), or for the study of the electric potential distribution across an extended surface; it could also be adapted for the measurement of action potentials. With the present arrangement and a probe area 2-mm^2 readings could be obtained only within 2–3 mv. It is hoped that the noise level can be still further reduced with more adequate shielding, and by using an electrometer tube of lower input capacity. This would permit the use of smaller probes, and even microprobes for the mapping of microscopic electrical structures. The instrument has been used in preliminary experiments for the mapping of surface potentials of various plant materials, and the observation of diffusion processes in ionic solutions.

---

[3] The amplifier has been placed at the disposal of one of us (O.B.) by the National Research Council of Canada in connection with another research problem.

Book Reviews

Molecular Spectra and Molecular Structure. I. Spectra of Diatomic Molecules

By Gerhard Herzberg. Second edition. Pp. 658+xv, Figs. 207. D. Van Nostrand Company, Inc., New York, 1950. Price $9.75.

The first edition of this book, published in 1939, was the leading book in its field. In fact, there was no other book to compare with it for the excellent presentation of the material, for comprehensiveness, and for the large number of references to the original literature. Although the subject of molecular structure and molecular spectra is complicated, the reader was introduced to these complexities gradually, so that he did not become aware of the complexity too soon. The book was illustrated with a wealth of spectrograms, energy level diagrams, potential energy curves, and other figures, and provided with tables, which helped to bring abstract theory down to earth and make the presentation vivid. Although this subject can be understood only with the aid of considerable theory, based on quantum mechanics, the theory was kept as simple and non-mathematical as is practical in a book of its caliber. Furthermore, it was written both for the beginner and the research worker. The sections that were not necessary for the understanding of fundamentals were put into small type, so that the reader could omit them if he wished. A great deal of the less important mathematical theory was put into small type.

The second edition is a revision of the first edition, but a rather complete and thorough revision to bring it up to date by adding new material and to improve the presentation. The general plan and character of the book is the same as before. In fact, the chapter titles are exactly the same as before, and the titles of sections are the same except that three new sections have been added.

The chief differences will now be pointed out. The book has considerably more mathematical theory than the first edition. However, most of this mathematical theory is in small type so that the reader can omit it if he wishes. This additional mathematical theory makes the book much more valuable and transforms it into a higher caliber book more useful for advanced students and research workers. It should be added, however, that the mathematical discussions are never long and extended developments, but succinct and sometimes summarizing the work of various investigators. When derivations are given, they are relatively short and simple. The book is not a book of the mathematical deductive type, in which the effort is made to prove or to indicate the proof of everything from first principles.

Twenty-six new illustrations have been added. New sections have been added on Radiofrequency (Microwave) Spectra, Hyperfine Structure, and Intensities of Electronic Transitions. Other additions have been made in sections contained in the first edition. Among these are a treatment of the Stark effect in diatomic molecules, a discussion of the polarization of resonance fluorescence, and the Hönl-London formulas. The discussion of van der Waals binding has been greatly expanded. A figure showing the simpler symmetric top eigenfunctions has been added; these are available nowhere else in the literature. Many sections have been completely rewritten. Thus the treatment of the theory of rotation and vibration has been improved by the introduction of more mathematical theory.

A very valuable feature in the appendix is a table of the vibrational and rotational constants for the electronic states of all known diatomic molecules. This covers 80 pages and evidently required an enormous amount of work to assemble. The bibliography has been brought up to date and now contains about 1600 references. The book has both a subject and author index. The subject index includes all the more important symbols and quantum numbers as well as all the molecules treated. Thus the book is a most useful reference book, both because of the wealth of material in it and the excellent index.

For anyone from beginning student to research worker this book by an outstanding authority is to be highly recommended. In fact, it is practically indispensable to anyone interested in diatomic molecules and their spectra.

Enos E. Witmer
University of Pennsylvania

Advances in Catalysis, Vol. II

Edited by W. G. Frankenburg *et al.* Pp. 292. Academic Press, Inc., New York, 1949. Price $6.80.

It is not possible to write thirty-odd pages on a particular aspect of catalysis without introducing the flavor characterizing an author, a school, or a piece of specialized research. It is not an easy task to combine nine of these flavors into a tasty book. That is, however, what the editors of *Advances in Catalysis* have done once again in their second volume and their boldness deserves encouragement. The special subjects are well chosen and provide a broad, perhaps slightly fuzzy, scanning of the field. The personal bias of each contributor is readily detectable as it should be in reviews of this kind. It is gratifying to spot the name of a solid-state physicist in the table of contents, but after reading the paper of F. Seitz, the chemist will certainly be disappointed because it treats in a very elementary style the Eyring concept of rate processes. The physical chemistry student of today is perfectly aware that "each atom consists of a central, positively charged nucleus which contains practically all the mass of the atom and which is surrounded by a cloud of electrons." A collaboration between catalytic chemists and solid-state physicists in the realm of solid appears highly desirable and further articles by the latter *on a more advanced level* would be welcome in the *Advances*. G. M. Schwab gives a brief summary of the kinetic relationships encountered in catalytic work. The exposé of O. Beeck is especially interesting because it contains much long-awaited unpublished material, presented in a "pro domo" but highly stimulating fashion. The importance of entropy of adsorption is emphasized by C. Kemball: it gives some indication of the extent to which adsorbed molecules may translate freely on the surface, of dissociation and association in a localized adsorption film and of phase changes. More about adsorption entropy will undoubtedly be heard in the near future so that Kemball's survey comes at the right moment. The more technically minded reader will find much interest in the contribution of L. Schmerling and V. N. Ipatieff, some fifty pages on the mechanism of the polymerization of alkenes. The authors review the different mechanisms which have been proposed for such reactions during the past fifteen years; they favor the carbonium ion mechanism which permits one to systematize a great deal of experimental data; they point out however that in this case "the word ion has a different connotation than it does in inorganic chemistry." No one could give a better idea of the recent progress in hydrogen fluoride catalysis than J. H. Simons whose chapter is complete and critical. Simons discusses the mechanism of HF catalysis in a careful and convincing style: in order to make a point, he even prefers to write 10,000,000,000,000 instead of the less expressive 10^{13}. T. H. James does an excellent job in reminding the catalytic chemist about the rich domain of catalytic phenomena related to photographic development; the work of Hautot *et al.*, at Liége could have been mentioned in this review, especially since it does not appear to be sufficiently known in this country. In their effort to present the many facets of catalytic research, the editors finally include an historical account of multicomponent catalysts by A. Mittasch who played a decisive role in their early study.

Summing up, the book will be a valuable acquisition to the library of an advanced worker in catalysis. It can be fully appraised only if it is considered as a part of "the compilation of papers written by competent specialists," which the editors continue to build up, it seems, with considerable success.

Michel Boudart
Princeton University

Medical Physics, Vol. II

Edited by Otto Glasser, Editor-in-Chief. Pp. 1227, 978 illustrations. The Year Book Publishers, Inc., Chicago, Illinois, 1950. Price $25.00.

In 1944, when the first volume of *Medical Physics* was published, the Editor-in-Chief listed three ideal objectives of the book and described the difficulties encountered in attempting to achieve these objectives. Dr. Glasser and his associates are working toward (1) a compendium of the knowledge in medical physics, including comprehensive bibliographical references; (2) a text for students of medical physics; and (3) a handbook of data for the use of those working on specific problems in the field. When the two volumes are examined, the magnitude of the problem of effective presentation becomes apparent, and the energy, judgment, and breadth of knowledge of Editor and authors are not only apparent, but amazing.

If any doubt the size of the problem, the following physical data on the two volumes of *Medical Physics* may be convincing: Vol. I (1944), 1792 pages each 7¼ by 10¾ in., 1382 illustrations; Vol. II (1950), 1227 pages, 978 illustrations; total weight of the two volumes, more than 12 pounds. Page size, two-column format, type, and jacket are the same for both volumes.

Volume II contains some material published in the 1944 volume, revised to bring it up to date; but the major part of Vol. II is new material comprising articles on subjects not listed in the earlier book and articles that are supplements to those appearing in 1944. Many articles published in the 1944 volume are listed by title in Vol. II to help the reader to use the two volumes together.

The need for Vol. II arises from two circumstances: first, data on some subjects—such as aviation medicine and the production and use of both stable and radioactive isotopes—were known but not available for publication in 1944; and second, the whole field of medical physics has undergone a highly accelerated expansion during the last six years. The range of subjects discussed in *Medical Physics* is extremely broad, including applications of statics, dynamics, electromagnetism, optics, quantum physics, molecular, atomic, and nuclear physics to anatomy, physiology, physical anthropology, physiological chemistry, pathology, and pharmacology; and the interrelation of these applications to medical specialties such as internal medicine, surgery, radiology, physical medicine, neurology, ophthalmology, otolaryngology, dermatology, and urology.

Topics are arranged in Vol. II—as they were in the earlier work—alphabetically, and some closely related topics are kept together by means of subtitles. An example appears at the beginning of of Vol. II. A 10-page article by M. S. Livingston entitled Accelerators: High Energy is devoted to the electrostatic generator, betatron, cyclotron, synchrotron, synchro-cyclotron, linear accelerator, and proton-synchrotron. The article on the betatron by D. W. Kerst and L. S. Skaggs is entitled Accelerators: High energy; Betatron; it occupies 10 pages and it is placed after the above-mentioned article on Accelerators by Livingston. This sounds clear-cut and orderly, but medical physics refuses to fit into a simple pattern. The article on the betatron discusses briefly but clearly the possible uses of the device in therapeutic radiology. To analyze this material effectively the reader may want to look up information on absorption phenomena for high energy x-rays in tissue, depth-dose measurements, positron-electron pair production, and biologic effects of radiation. Each of these subjects is listed in the 36-page index of Vol. II and in the 43-page index of the original volume.

Thus the user of these volumes can learn to find the articles dealing with subjects he particularly wants to investigate, and he finds relatively little duplication of information in articles on related topics. Furthermore, the reader will be amply repaid for the time and effort he devotes to finding out how the books are organized.

The relation of physics to biology and medicine might be likened to the relation of hormones to physiology: the methods of physics have stimulated the solutions of problems in biology and medicine in the most surprising and remotely separated fields. It is not surprising that it is difficult to present medical physics in a manner that is at once brief, simple, and comprehensive.

The Editor and contributing authors are to be congratulated on their notably successful efforts to achieve their objectives. They have worked together to attain two apparently mutually exclusive results: the articles on related subjects are well correlated to avoid unnecessary duplication, yet each author appears to have written independently to present his material as he thinks best. The authors of articles on subjects with which this reviewer has some familiarity are men and women who are not only extremely able investigators but also effective expositors. From this fact, and from the presence in the list of authors of the names of so many well-known scientists in other branches of medical physics, it may be inferred that this happy result has been achieved throughout both volumes.

Extensive bibliographical lists, appended to nearly all articles, and the inclusion in the Name Index of authors of articles in *Medical Physics* and of authors of reference papers in the journals, improve both flexibility and usefulness.

In universities, hospitals, government laboratories, and industry there is a potent and increasingly coherent effort to bridge gaps between the several branches of science. To recognize the strength of this development, and its scope in both the philosophy of science and in research, it is sufficient to note such diverse publications as the lists of papers prepared and issued by the U. S. Atomic Energy Commission, and the book *Cybernetics* by Norbert Wiener. *Medical Physics* is an important exponent of the trend toward interscientific research and development.

S. Reid Warren, Jr.
University of Pennsylvania

Collision Processes in Gases

By F. I. Arnot. Pp. 104+viii, Figs. 37. John Wiley and Sons, Inc. New York, 1950. Price $1.25.

This little book gave an excellent account of its subject in 1933 and nothing has been added since, although the publisher lists the monograph as "fourth edition, 1950." The last sentence refers to the "neutron recently discovered by Chadwick." For its treatment of atomic collisions up to 1933, however, this reviewer can recommend it.

Walker Bleakney
Princeton University

Wave Filters

By L. C. Jackson, Pp. 107+vii, Figs. 64. Methuen and Company, Ltd., London, and John Wiley and Sons, Inc., New York. First published in February, 1944, second edition in May, 1946, third edition in 1950. This book is one of Methuen's Monographs on Physical Subjects, a "series intended to supply readers of average scientific attainment with a compact statement of the modern position in each subject." Price $1.25.

Chapter I serves as an introduction to the broad subject of wave filters, and includes a brief review of their main applications in the fields of radio, telegraphy, telephony, and acoustics. Chapters II and III present the classical treatment of uniform, lossless ladder structures, "constant *k*" filters and "*m*-derived" filters. Examples of coupled circuits, crystal filters, and coaxial-line filters are briefly discussed in Chapter IV. Chapter V treats the effects of dissipation and of mismatched terminations on the behavior of the filters discussed in Chapters II and III. Practical suggestions regarding the design and construction of filters may be found in Chapter VI. The last chapter discusses the analogy between electrical and mechanical systems, and gives a few illustrative examples of mechanical and acoustical filters. A very brief bibliography is provided at the end of the monograph for those readers who wish to pursue further the subject of wave filters. It is unfortunate that such well-known books as Guillemin's *Communication Networks* and Bode's *Network Analysis and Feedback Amplifier Design*" are not included.

Apart from a few misleading statements, the treatment of the subject is clear and correct. It might provide an introductory (and necessarily superficial) knowledge of wave filters to a reader totally unfamiliar with the subject. This knowledge, however, would be insufficient for the solution of many practical filter problems, even outside the difficult fields of television and telephony. As an example, band-pass ladder structures of the "constant *k*" and "*m*-derived" types cannot be built in many cases because of the impractical sizes of the inductances and capacitances. Appropriate network transformations, which are not discussed in the monograph, need to be employed in such instances in order to obtain satisfactory element values.

The treatment of wave filters presented in this monograph is basically still that of the original papers published by Campbell and Zobel in the early twenties. Truly, some of the most recently developed techniques of filter design are too involved to find place in a short monograph. Still, it would be helpful to many readers to know at least that direct synthesis procedures are available which permit the solution of many practical problems for which the simpler types of filters are inadequate. Moreover, the tremendous progress in network theory that has taken place since the pioneering work of Campbell and Zobel has led to simplifications as well as to involved refinements. For instance, more general and yet simpler treatments of wave filters are possible, which should not require any more space than Chapters II, III, and IV. I am thinking in particular of the use of lattice structures for design purposes, and of the impedance-level and pass-band normalizations which simplify considerably the derivation and the evaluation of the element values.

The monograph by L. C. Jackson is intended to strike a compromise between a catalog of filter designs, and a treatise on network theory. This reviewer feels that an elementary treatment of the general properties of filter networks would constitute a more useful compromise, both as an introduction to a treatise on network theory and as a means of providing sufficient knowledge for the effective use of a filter catalog.

R. M. Fano
Massachusetts Institute of Technology

The Kinetic Theory of Gases: Some Modern Aspects

By Martin Knudsen. Third edition. Pp. 64+vii, Figs. 20. Methuen and Company, Ltd., London, 1950. Price $1.25.

This little book contains principally a clear and pleasing description of the author's own illuminating and important experiments on certain phenomena in gases at low pressures. The topics treated are evaporation and condensation, flow of gases through tubes, resistance to motion, thermal molecular pressure, the author's absolute manometer, and the coefficients of accommodation in relation to the conduction of heat and to mechanical reactions of the radiometer type. The density of the gas is in all cases kept low enough so that the molecules perform individually, with little interference by molecular collisions.

The scant attention paid here to the work of others was appropriate when the manuscript was first prepared in 1933 as a basis for three lectures given at the University of London. The designation of this as the "third edition . . . 1950," however, has converted into an error the author's statement on p. 60 that the radiometer force at high pressures is an edge effect; this surmise as to its nature has been definitely disproved.

The short title used on the cover and on a fly leaf inside, simply *The Kinetic Theory of Gases*, is grossly misleading. The full title is obviously hard to abbreviate concisely; but it seems unfair to prospective readers to imply that the book is a general treatise when in reality it covers only a few selected topics. The introductory remarks on the fundamentals of kinetic theory are adequate for the author's purpose but are very limited in scope.

E. H. Kennard
David Taylor Model Basin

Introduction to Vector Analysis

By B. Hague. Fourth edition. Pp. 122+vi, Figs. 39. Methuen and Company, Ltd., London, and John Wiley and Sons, Inc. New York, 1950. Price $1.25.

This excellent little monograph, first published in 1939, is designed as an introduction to the principles of vector analysis for physicists and engineers, who are interested in obtaining a familiarity with vector techniques and an ability to use them in their own fields. The subject matter is well chosen and well organized, and the presentation is exceptionally clear. As stated in the preface, "the outlook adopted is almost entirely physical; geometrical matters and questions of an exclusively mathematical interest are limited to essentials. Formal proofs of invariance and conditions of continuity in vector processes are replaced by an appeal to physical intuition." This point of view renders the subject matter very much more readable and understandable to students who want only a working knowledge of vector methods.

The book is more likely to satisfy the needs of engineers than of physicists. The latter will regret the omission of some very useful topics, such as a treatment of vector relations in general orthogonal curvilinear coordinates, Green's theorems, the equation of continuity, and perhaps also a brief discussion of wave motion. The section on polar coordinates should be amplified to indicate the ways in which they are applied to the solution of physical problems. Also, a brief treatment of coordinate transformations and the metric tensor would have been a valuable supplement to the chapter on linear vector functions.

It is regrettable, also, that the book does not contain a limited number of well-chosen problems to accompany and supplement the text, since only by working with vectors can readers acquire a working knowledge of vector techniques. Such a set of problems would make the book self-contained for those who are learning vector analysis for the first time, without detracting from its value as a brief and lucid review of the subject for engineers and physicists who need a refresher course. The problem set could also include a number of vector relationships to be verified, thus providing useful additional material for reference purposes.

Because of its clarity and readability this monograph will continue to be a very valuable aid in the teaching of vector analysis.

Simon Pasternack
Brookhaven National Laboratory

Practical Analysis, Graphical and Numerical Methods

By F. A. Willers. Translated by Robert T. Beyer. Pp. 422+x, Figs. 132. (A modified translation of the German edition: *Methoden der praktischen Analysis*, Berlin and Leipzig, De Gruyter, 1928.) Dover Publications, Inc., New York, 1948. Price $6.00.

The translator has rewritten Section 3 to describe the Standard American slide rules. T. W. Simpson wrote Section 6 which discusses thoroughly the features of the three standard (Friden, Marchant, and Monroe) American desk calculators and some of the more important operations that may be performed with them. The remaining 33 sections of Willers' book have merely been translated. Consequently, a large fraction of the material is chiefly of historical or academic interest. In this category can be placed many of the excellent descriptions of graphical methods and mechanical devices. The real worth and usefulness of Willers' book are results of the simply and carefully written sections on numerical methods which are replete with the solutions of illustrative problems from the fields of engineering, physics, astronomy, etc. In many of these examples, the physical data and the work sheets are given in complete detail. Each of the sections was intended to be a unit independent of the rest of the book. For the most part the author has merely separated the sections on numerical methods by interposing sections on graphical methods and mechanical devices. The uncluttered derivation and presentation of the standard formulas together with the abundance of applications make *Practical Analysis* a valuable reference work for anyone who has occasion to do computing.

Chapter I, entitled Numerical Calculation and its Aids, is divided into six sections. The material covered here is: calculation with approximate values (significant figures), graphing functions, the slide rule (with applications), linear interpolation (with a complete analysis of the error involved), nomograms, and desk calculating machines (with many short-cut methods for doing other than routine computations).

In Chapter II, Interpolation, the standard finite difference formulas for interpolation, differentiation, and integration of functions of one or more variables are derived. The discussion starts with a treatment of divided differences and is particularly to be recommended for its clarity and conciseness. In this chapter, except for the Lagrange form of the interpolation polynomial, Simpson's rule (called the Kepler barrel rule on p. 125 and elsewhere) and two formulas for cubature, the principal formulas are presented in finite difference form using only one type of difference notation (Δ-delta, in one variable). The adoption of a simple symbolism is one of the reasons that the book should be useful for reference purposes. The formulas are usually written with the remainder term.

For the most part Chapter III, Approximate Integration and Differentiation, presents the standard formulas for summation and numerical integration in terms of the ordinates of the function. The first section is devoted to a description of Coradi's integraph and of several graphical methods. On p. 170, note 7, a rather cumbersome form of the remainder term in a special Simpson's rule is derived. But, in the next section the author (following Steffensen) derives an elegant form of the remainder term for the closed-type integration formulas. The numerical integration methods of Tschebyscheff and Gauss are carefully explained. The theory of the planimeter is thoroughly developed and several models are described in the last section.

Chapter IV is entitled Practical Equation Theory. In Section 18 several methods for calculating the roots of an equation or system of equations are described (false position, iteration, Jacobi's transformation, and Newton's method). The next section treats special methods for finding the roots of a polynomial (Horner's method and various graphical methods). Section 20 discusses Descartes' rule of signs and the Sturm series for determining the number of roots of an equation. Application of the Sturm series and of various graphical methods to the location of the complex roots of an algebraic equation are made in Section 21. The next section gives a too brief account of Graeffe's method. An elimination method and several graphical methods for solving a system of linear equations is described in Section 23. This work is not especially adapted for the use of desk calculators. Some discussion of the error produced by using approximate coefficients is given. In the last section several iteration procedures for solving a system of linear equations are described.

Chapter V, entitled Analysis of Empirical Functions, is concerned mainly with the theory of least-square approximation by polynomials, harmonic analysis, period analysis, and the representation of a function as a sum of exponential functions. The last two topics are incompletely treated.

Chapter VI, Approximate Integration of Ordinary Differential Equations, is the final chapter. Several graphical methods of integrating differential equations are described and illustrated in the first section. In the next section, the Runge-Kutta and Adams-Bashforth methods are described. The method of iteration is developed with the use of two types of integration formulas. The method of Milne is not described. In Section 24 the graphical and numerical procedures to be used in the solution of differential equations of higher order are described. The last section is devoted to an interesting description of several integrators of first-order differential equations and of the Knorr integrator for equations of second order of a special type.

Each section of the book is followed by a list of references (mainly German) to the literature. There are 132 figures in the text which materially improve its readability. Some of the diagrams suffered in reproduction.

The field of computing and numerical analysis has grown since Willers wrote his book. Many of the modern techniques are therefore not to be found in *Practical Analysis*. However, any book which is well written will prove to be quite valuable until it is replaced by a later well written book. The reviewer knows of no book in the field which can match the spirit and quality of Willers' *Practical Analysis*.

EUGENE ISAACSON
New York University

The Organization of Industrial Scientific Research

BY C. E. KENNETH MEES AND JOHN A. LEERMAKERS. Second edition. Pp. 383+vii. McGraw-Hill Book Company, Inc., New York, 1950. Price $5.00.

Two well-known leaders in the field on industrial research discuss in this 383-page book a subject of utmost importance. The first edition of this book was written by Dr. Mees in 1920 and it is interesting to compare the development of industrial research in this country during the intervening 30 years of the contents, scope, and size of the book. Dr. C. E. Kenneth Mees is particularly qualified, as Director of Research of the Eastman Kodak Company, and as a recognized leader in the field of industrial research, to write on the subject.

The book is divided into three parts. Part I discusses general principles, Part II discusses agencies for the conduct of industrial research, and Part III summarizes the organization and operation of industrial laboratories.

Naturally, the organization of industrial research depends to a considerable extent on the industry it serves. Fortunately, the authors have drawn not only on their own wide experience, but have in addition canvassed numerous large and small industrial laboratories for additional pertinent information. Thus, their conclusions are not based only on the experience of the chemical industry but on that of a number of others. At the same time, their observations are not only limited to the experience gained in this country, but also include that of Great Britain, various countries of continental Europe, and some references to the Soviet Union.

Chapters I and II of Part I trace the whole development of scientific research starting from the dawn of history and concluding with the enormous effort, both in manpower and money, which developed during the Second World War. The gradual growth of industrial research, as distinguished from fundamental or basic research, is discussed in Chapter III.

In Part II the various government research agencies and laboratories are examined in detail. Subsequently, the historical development of such well-known institutes as Mellon, Battelle, and Armour, and the various regional research institutes, which serve the interest of particular regions, such as New England, Industrial Research Foundation, Mid-West, and Stanford Research Institutes are discussed. The structure and progress made at the large industrial laboratories are described in a separate chapter.

The most important part of the book is Part III, where the organization and operation of industrial laboratories are discussed in detail. In some of those chapters the authors were ably assisted by S. W. Davidson and R. Halstead of the Eastman Kodak Company and H. H. Race of the General Electric Company. This reviewer recently had had the occasion to discuss the organization and performance of one of our largest industrial research laboratories with the vice-president in charge of research. The latter outlined some of the difficulties large research organizations are running into at the present time. We have over and over again emphasized the importance of team work in research, putting much less emphasis on leadership as expressed in originality and imagination. This reviewer agrees fully with the authors of the book when they state on p. 204 that: "The efficiency and accomplishment of an industrial laboratory depends to a very large extent upon the director. It may be said of research laboratories, as of other human institutions, that they are the reflex of a man. The large industrial research laboratories have passed through a critical stage in which the founding directors are passing and are being replaced by their successors. Their experience shows to how great an extent the success of a research laboratory is dependent upon the individuality of its director. There are laboratories which have had a distinctly successful career and which, with passing of the directors who organized and developed them, have fallen into obscurity. It is extremely difficult, moreover, to find a suitable man to direct industrial laboratories. The director of an industrial research laboratory must be both a scientist and an executive, and he must have an interest in and a capacity for the commercial operations of the business in which he is engaged. The reason he must be interested in the commercial operations of his company is that he must make his laboratory pay; and if he does not know how to do that, no one else can do it for him."

As our industrial civilization grows in complexity the problems it has to solve become more complicated and intricate and this applies particularly to one of the foundations of this civilization namely, scientific research. It is thus fortunate that those individuals that have both the experience and ability to solve those problems share with us in their experience. Everyone interested in industrial research will find this book a highly desirable text and it is heartily recommended to both the business executive and the research scientist.

A. V. Grosse
Research Institute of Temple University

Mercury Arcs

By F. J. Teago and J. F. Gill. Pp. 107+viii, Figs. 50. John Wiley and Sons, Inc. New York, 1949. Price $1.50.

In this small book which represents a slight revision of an earlier first edition, the aim is to cover the important aspects of mercury arc operation including the electrical, structural, and operational. It is intended as an introduction to the subject which will permit the newcomer to orient himself in the engineering fundamentals without the confusion of detail which must ultimately form part of any thoroughgoing study—an objective which the authors attain adequately.

Their discussion of tube structure and function is illustrated with a few well-labeled drawings which clearly show what an arc tube consists of and why. The useful mercury vapor pressure range and the problem of heat removal both by air and water cooling and the effect of cooling requirements on rectifier size is gone into.

In the examination of the electrical relationships multi-phase operation and grid control are introduced at the beginning. Separate chapters are devoted to grid control of voltage and current, and one chapter examines voltage regulation in the absence of grid control with the current in any one arm assumed to follow part of a sine wave. Then current-voltage characteristics are developed on the more general basis of a sine voltage but a current obeying the usual linear first-order equation for a circuit with inductance and resistance. By a simple extension of the phasing ideas thus far developed, the authors "generalize"— this is the best expression for it—rectification into inversion and show how the two functions can be combined to give regeneration.

There follow chapters on wave-form analysis, transformer ratings, and power factor—the latter explaining the possible meaning to be attached to the term in a multi-phase rectifier circuit. Finally, there is a fairly general over-all treatment of the current and voltage relations in the presence of a load and including the rate of transfer of current from one anode to another due to inductance in each anode arm.

At a few places the book takes on briefly the role of a laboratory manual in giving a detailed description of the calibration of a McLeod gauge and the analysis of two circuits suitable for a Pirani gauge.

The treatment is clear throughout and easily followed. The authors give adequate warning regarding the limited validity of their results because of factors omitted from the calculations at some point. A comparison with actual oscillographic results would have been instructive. The book suffers from what might best be called the engineer's point of view. This shows up in two places. The complicated set of equations developed in the last chapter is solved by an approximation which leads to a minor inconsistency, which "is probably due to the fact that (certain variables) cannot be evaluated exactly." Actually, the method of successive approximations would allow these evaluations to be made as accurately as required. Of more importance is the sad unreliability of the description of fundamental arc processes in the introduction, which would make the book an unsafe starting point for someone who required an understanding of the gaseous conduction—and non-conduction—processes. But as this was not the intent of the authors, this shortcoming can be overlooked. The index is good.

Lewi Tonks
General Electric Research Laboratory

Physical Chemistry of Hydrocarbons. Vol. I

Edited by A. Farkas. Pp. 453+x, Figs. 189, 15×23 cm. Academic Press, Inc., New York, 1950. Price $8.50.

In the words of the editor "the purpose of this book is to summarize the physicochemical basis of the new techniques and methods recently adopted by the hydrocarbons industry, and to help the research worker in exploiting these procedures more extensively and more intensively." This book has the virtues and suffers from the defects of most books which consist of independent chapters written by specialists on their respective fields. The average level is high, however, and this reviewer believes that this volume will be a valuable addition to the library of anyone concerned with the more physical aspects of hydrocarbons, and it will be useful to an even wider circle of readers.

The book starts with a compact and excellently written treatment of the application of quantum mechanics to valence theory by G. W. Wheland. Attention is appropriately centered on bonds between hydrogen and/or carbon atoms and the chapter ends with a balanced presentation of the resonance concept and its use in the interpretation of hydrocarbon structures and energies. A chapter entitled The Molecular Structure of Hydrocarbons as Determined by Spectroscopy and Electron and X-Ray Diffraction by M. H. Jellinek turns out to include much less than its title suggests. The portion devoted to spectroscopy consists of a few paragraphs on infra-red absorption and one on Raman spectra. These are not only grossly inadequate but are so poorly written as to be misleading. It would have been preferable to have omitted mention of spectroscopy, especially in view of the fact that this subject is presented later in the book. The rest of the chapter, dealing with x-ray and electron diffraction, is much better.

J. J. Mitchell contributes a well-organized and quite complete chapter on Mass Spectroscopy in Hydrocarbon Analysis. The subjects of infra-red absorption, Raman, and ultraviolet absorption spectroscopy are treated by N. D. Coggeshall in two chapters, the first of which covers the theoretical and molecular structure aspects while the second is devoted to the analytical applications of these branches of spectroscopy. The title of this latter chapter, Optical Methods of Hydrocarbon Analysis, is too general because *no optical methods except the spectroscopic ones are mentioned.*

In a chapter on Electrical Properties of Hydrocarbons by A. Gemant, emphasis is laid on conductivity, and the dielectric constant and dielectric strength are treated quite briefly. The subject of Solvent Extraction of Hydrocarbons is discussed by A. W. Francis primarily in terms of various types of ternary phase diagrams. A feature of this chapter is the inclusion of two tables, one for references to nearly 600 ternary systems involving hydrocarbons, the other for critical solution temperatures for various hydrocarbons in 422 solvents. A chapter on Solid-Liquid Equilibria of Hydrocarbons by M. R. Cines treats melting points, solid-phase transitions, and associated heat effects. There is a good review of the application of melting point measurements to the determination of hydrocarbon purity by both the static (calorimetric) and dynamic (time-temperature) methods. Purification by fractional freezing or melting is also discussed.

The book ends with a chapter entitled Chemical Thermodynamic Equilibria among Hydrocarbons by F. D. Rossini. The first part of this chapter consists of a concise development of the elements of chemical thermodynamics which will be appreciated by those whose thermodynamic background is a little rusty. The remainder contains a large amount of information, in the form of graphs, on equilibrium constants and concentrations and free energies of formation and isomerization for a number of groups of hydrocarbon isomers, homologues, and compounds otherwise related.

The book is attractively printed and only a relatively small number of typographical errors were noticed.

E. J. Rosenbaum
Sun Oil Company

Dipole Moments

By R. J. W. LeFevre. Second edition. Pp. 117+v, Figs. 23, 10.5×17.5 cm. Methuen and Company, Ltd., London and John Wiley and Sons, Inc., New York, 1948. Price, $1.25.

The object of the series of monographs to which this little book belongs is "to supply readers of average scientific attainment with a compact statement of the modern position in each subject." For the benefit of readers unfamiliar with the first edition, it is desirable to indicate the contents of the book. The first chapter summarizes the theory of dielectric polarization and the methods of calculating dipole moments. An apparent misprint gives the word "Methods" instead of "Moments" in the chapter title in the table of contents. The second chapter describes a heterodyne beat and a resonance method for measuring dielectric constant, gives a number of experimental details, and mentions other methods of measurement. The third chapter gives an excellent summary of the work which had been done upon solvent effect in dipole moment measurements prior to the publication of the first edition. It devotes a brief paragraph to the Onsager equation, which is now regarded as fundamental in the treatment of the dielectric behavior of liquids, and does not mention the important work of Kirkwood on the subject. A good account of the relations of dipole moments to the structures of a variety of molecules is given in the next and longest chapter of the book. Special topics are treated in brief chapters on Intramolecular Rotation and Flexibility of Molecules, and Some Anomalous Dipole Moments, and the book closes with a two-page list of dipole moment values selected apparently from the appendix to the *Transactions of the Faraday Society*, Vol. 30, 1934. Subsequently measured values must be regarded as superseding many of those selected for this short list.

This second edition contains only two literature references later than 1938 and is virtually a reprinting of the text of the first edition. The reader will again note the smoothness, clarity, and authority of the presentation of the material evident in the first edition. The strong emphasis on the valuable work that has been done on dipole moments in England is not unnatural since, in so short a book, only a small fraction of the available material can be treated. Most of the various aspects of the relations between dipole moment and molecular structure are interestingly illustrated. Since, however, many papers in the field have appeared since the publication of the first edition, the very slight alterations introduced in the second edition have been insufficient to make it a wholly satisfactory statement of the modern position in the subject. The book remains, nevertheless, an excellent summary of valuable material which should be useful to readers seeking their first acquaintance with the subject and to investigators not wholly familiar with the field.

Charles P. Smyth
Princeton University

Elementary Pile Theory

By Harry Soodak and Edward C. Campbell. Pp. 71+ix, Figs. 21. John Wiley and Sons, Inc., New York, 1950. Price $2.50.

The modest size, scope, and price of this book do not prevent the authors from making a real and significant contribution to the open literature of the neutron chain reaction. The economy of treatment should make this a valuable reference for use within and outside of the atomic energy program.

Reactor theory is developed from first principles of diffusion theory and the physical processes of fission and absorption, to the point of application to a slow neutron reactor with reflector. The general method is to follow a neutron through its life cycle and to introduce each new physical process into the calculations. The diffusion and eventual absorption of thermal neutrons is given. The slowing down of fast neutrons is first described in terms of elastic collision, followed by an evaluation of the probability of the fast neutron reaching thermal energy without absorption. The consequences of a finite diffusion medium are introduced, and finally the complete problem is solved involving slow, fast, and intermediate energy neutrons diffusing in a reproducing medium surrounded by a neutron reflector. Critical dimensions are calculated for four cases: the one-dimensional or infinite slab, sphere, cylinder, and cube. Reflector savings are calculated for a finite aqueous reflector by the one group theory, i.e. considering thermal neutrons only. The method of attach by two groups theory, considering both fast and slow neutrons, is given but no specific calculations are made.

The latter part of the book is devoted to the time-dependent diffusion equations and the kinetics of a reactor. The effect of delayed neutrons on reactor control is developed and the transient behavior of a supercritical reactor is developed.

While the book is more brief and less descriptive than that of *The Science and Engineering of Nuclear Power*, C. Goodman, editor, it is better integrated. It makes no pretense of being complete, but rather follows a single possible line of development. In principle calculations may be made for a low power homogeneous thermal neutron reactor with small excess reactivity. The authors do not always indicate concisely the limitations of the method or the exact postulates on which the development is based.

It is to be regretted that security requirements do not permit the application of the methods to real physical systems. The authors have alleviated this situation as much as possible by taking published and hypothetical values of physical constants and evaluating hypothetical cases.

The average student would benefit by a series of problems and a glossary of symbols.

Lyle B. Borst
Brookhaven National Laboratory

The Mathematical Theory of Communication

By C. E. Shannon and W. Weaver. Pp. 117+v. University of Illinois Press, Urbana, Illinois, 1949. Price $2.50.

This book contains two sections. The first section is essentially a reprint of a paper written by Dr. Shannon and previously published in the *Bell System Technical Journal*. The importance of this work by Dr. Shannon is generally recognized in the communications field. In the second section of the book, Dr. Weaver discusses the general analytical approach to the communication problem.

During the past few years a number of new systems for modulating a carrier for the transmission of information have been proposed and developed. The "Hartley" law set down many years ago was found inadequate for dealing with these systems. The present work provides a more satisfactory method of arriving at an answer to the question of how these various systems compare insofar as the "efficiency" with which they transmit information is concerned. One of the most important results of this work is to show that without noise it is possible to transmit an unlimited amount of information in any given interval of time; with the presence of noise the amount is definitely limited.

Dr. Shannon defines the capacity of a communication "channel" for discrete systems such as the teletype in terms of the amount of choice one has of the messages he can send per unit time; and from this he derives the general formula by which the capacity can be computed for any discrete system. This is followed by a general discussion of discrete sources of information in which the theory of stochastic processes is applied and interesting illustrations are given using the English language in which the separate letters are treated as (discrete) symbols. Thus the concept of the statistical nature of communication is introduced. It is found that a useful measure of the quantity of information produced by a specific source is its "entropy." In this case the entropy is defined by direct analogy to methods used in statistical mechanics in terms of the probability of a particular message.

An important problem involved is that of encoding. In general, a message (in whatever form it may be presented) must be coded for the particular modulation system used, and the coding process can, of course, affect the efficiency of transmission. It is shown that a coding process can be devised which will provide maximum entropy with a given channel, and that in the absence of any noise in the channel it is always possible to encode an information source so that information may be transmitted at a rate which is as close as desired to the capacity of the channel. In the presence of noise, information may be transmitted at the same rate, with, however, a finite probability of errors depending on the amount of noise present. It is possible to transmit this information at a reduced rate with an arbitrarily small probability of errors.

In the case of information which is of a continuous nature (such as a speech wave) it is necessary to determine the probability of a particular wave form, for example a particular voltage given as a function of time, $s=f(t)$. It is well known that if a function $f(t)$ is limited to a band width W it can be represented over a period of time T by properly specifying the value of $2TW$ coordinates. The entropy of a source generating a group of such functions can be expressed in terms of the probability distribution of these $2TW$ coordinates; thus the methods used for discrete sources can be extended to the continuous case.

Finally, a few examples are given for the case of random noise for which quantitative formulas are developed. The application of the method to noises not of random character (such as static) which, incidentally, constitute the major source of interference to radio communications is not entirely clear; it is pointed out, however, that in comparing equivalent levels of random noise and non-random noise the random noise will in general provide a greater amount of interference.

In the second section of the book, Dr. Weaver divides the communication problem into three parts or levels as follows:

Level A. How accurately can the symbols of communication be transmitted? (the technical problem)

Level B. How precisely do the transmitted symbols convey the desired meanings? (the semantic problem)

Level C. How effectively does the received meaning affect conduct in the desired way? (the effectiveness problem)

He points out that the work done so far has been almost exclusively at level A. However, one of his main objectives is to show that there is a close interrelation between studies of the problem at the three levels such that an understanding of the problem at level A (especially as presented in the first part of the book) sheds much light on the problems at levels B and C. This discussion is perhaps shorter than it deserves to be but it contains some stimulating ideas which the communication engineer should find of interest even though, in his immediate problems, he will find his work at level A only. In addition, this part presents a rather detailed summary of the main points of the theory of the problem at level A omitting the mathematical developments and may profitably be read first. Unfortunately, the general problem is sufficiently complex so that a certain minimum knowledge of the analytic methods used is required for understanding the theory.

Ralph M. Showers
University of Pennsylvania

Physical Methods in Chemical Analysis. Vol. I

Edited by Walter G. Berl. Pp. 664, Fig. 235, Tables 65, References 875. Academic Press, Inc., New York, 1950. Price $12.00.

This two-volume publication, written for the chemical analyst, is a comprehensive guide-book on the instruments and the techniques for determining the physical constants of substances. Volume I deals with mass spectrometry and the interaction of radiation with matter. During the last quarter century, in particular, knowledge has greatly advanced in these fields. Likewise the problems of the chemical analyst are becoming so increasingly difficult that he must turn to the determination of the physical constants of complex chemical substances to give a complete picture of the material. A knowledge of the molecular arrangement and design of such substances may be of importance equal to, or greater than, the knowledge of only its quantitative chemical composition. Here these new methods are of significant help.

The apparatus required, the techniques of experimentation, and the interpretation of results for such studies are not simple. It is thus appropriate to provide for those persons interested primarily in their use as a tool, a collected, simplified, and directive treatment which will make these new developments available to them.

Volume I does this job quite successfully. It is divided into the twelve sections listed here. Each section is written by different authors. Four of these authors are university professors of physics or chemistry, four are engaged in industrial laboratories, and the others are associated with governmental agencies, such as the Bureau of Standards. At least three of them have published books dealing with the material of their sections and others are authors of papers in scientific journals.

The titles of the twelve sections and their authors are: Absorption Phenomena of X-Rays and γ-Rays, George L. Clark; X-Ray Diffraction Methods as Applied to Powders and Metals, William L. Davidson; X-Ray Diffraction as Applied to Fibers, John A. Howsmon; Electron Diffraction, L. O. Brockway; Spectrophotometry and Colorimetry, Wallace R. Brode; Emission Spectrography, J. Sherman; Infrared Spectroscopy, Harold H. Nielsen and Robert O. Oetjen; Raman Spectra, James H. Hibben; Polariscopic and Polarimetric Examination of Materials by Transmitted Light, C. D. West; Refractive Index Measurement, Leroy W. Tilton and John K. Taylor; Electron Microscopy, Robert D. Heidenreich; Mass Spectrometry, Harold W. Washburn.

As may be expected, the different sections vary somewhat in their approach and completeness. Each section starts with an outline which is indexed giving the page number of the discussion of that part of the subject matter. This is a very helpful time-saving feature. The outline is followed, in general, by a discussion of the development of the knowledge in the field leading to the derivation of working equations. Some of this material, very appropriate in its setting, could also serve as a review for the young physicist. The necessary equipment is described, including in some sections information on the sources of commercial apparatus and the characteristics of this apparatus.

The type and scope of the problems which may be successfully attacked are indicated. Several sections show how to evaluate the data. The copious set of diagrams are carefully selected and the tables are particularly useful guides of more than handbook value.

The cover carries the notation "Enough experimental and theoretical data have been assembled to minimize the need of consulting more specialized texts or the original literature." There is included, however, a large reference list of source material appended to each section, totaling some 875 references. To cover such a large field adequately in one book is an ambitious undertaking—it is most likely that the user will wish to refer also to certain of the references to fill in those gaps which space limitations necessitated.

The reader is impressed with the care and thought put into this book to make it helpful to a wide cross section of scientists. It should be available to the experimentalists in the several physical science fields.

C. J. Overbeck
Northwestern University

The General Principles of Quantum Theory

By G. Temple. Fourth edition. Pp. 120+viii. No figs. John Wiley and Sons, Inc., New York, 1948. Price $1.25.

This well-received book in Methuen's Monographs on Physical Subjects originally came out in 1934 and has gone through three editions since 1942. The object is to give an introductory account of the general principles which form the physical basis of the quantum theory. The necessary mathematical background is given in the first chapter on the theory of linear operators. This starts with complex numbers, which it is assumed are well understood by the reader, and the ideas are developed in terms of these familiar quantities. They are used to illustrate the less familiar concepts of operators, proper vectors, and proper values. Projective operators, still a familiar idea, further illustrate the development.

The second chapter on the laws of measurement in atomic physics is the core of the book's treatment and sets up the connection between the experimental observations and the quantities used in quantum mechanics. The states of a system are represented by vectors, the variables are represented by linear operators whose average values give the expectation values of the variable for the states represented by the vectors. This treatment throws light on the physical significance of the operations of quantum mechanics, and is done very smoothly, indeed so smoothly that one is almost persuaded that it is being proved that states can be represented by vectors. The elegance of the treatment notwithstanding, this is still a fundamental assumption of the theory. Furthermore, the fact that the sum of two variables is represented by the sum of the operators representing each variable alone is an assumption although the argument on p. 36 gives the impression that this is being proved. The argument, however, is not conclusive. For example, in the harmonic oscillator the squares of the momentum and the displacement are continuous, but their sum which is proportional to the energy is discrete. The operator $X+Y$ is not known *a priori;* but it may be and is assumed to represent the variable $x+y$. Otherwise Chapters 2 and 3 are a good introduction to elementary quantum mechanics, original and less complicated than the usual treatment. Anyone who will take the trouble to understand these chapters will have a firm foundation on which to build together with an insight into what is involved in quantum mechanics.

The fourth chapter introduces the spin operators including the 16 Eddington Dirac operators and their matrix representation. The last chapter treats systems consisting of more than one particle. Temple is adept at discussing the ideas behind the formalism, with a minimum of mathematical detail. The treatment of perturbation theory is a good example of this. Throughout the book familiar results are obtained with little calculation, e.g., the energy and matrix elements of the harmonic oscillator, the energy levels of the Bohr hydrogen atom, the selection rules for the dipole radiation, and Laporte's rule all fall out without effort. It is not expected that all the questions will be answered. We still do things because they give the right answers. The empirical facts of atomic and molecular structure "can be correlated with the general principles of quantum theory only by assuming that antisymmetry is characteristic of pairs of electrons or of pairs of protons." At least we know where we stand in this statement. Numerous examples for solution by the student are well chosen to illustrate and extend the developments of the theory. Even the difficult ones repay in understanding the effort required to solve them. Most of the misprints of the earlier editions have been removed, but there are still a few especially in the problems.

This excellent little book is highly recommended to anyone seeking an understanding of quantum mechanics. It must be pondered over and digested as it is elementary but abstract in its treatment. It is probably too abstract for the beginner, but it covers the meat of the matter as indicated by the books to which it acknowledges indebtedness: Dirac, Weyl, von Neumann, and Heisenberg.

C. W. Ufford
University of Pennsylvania

An Index of Nomograms

By Douglas P. Adams. Pp. 174+ix. Technology Press of M.I.T. and John Wiley and Sons, Inc., New York, 1950. Price $4.00.

Readers of this very useful *Index of Nomograms* will find references to over 1700 published nomograms in well-known periodicals such as *Aero-Digest*, *Aeronautical Engineering Review*, *American Gas Journal*, *American Machinist*, *American Journal of Physics*, *American Journal of Roentgenology*, *American Society for Metals* (*Transactions*), *Biochemical Journal*, *Civil Engineering*, *Chemical Engineering*, *Chemical Industries*, *Electronics*, *Engineering and Mining Journal*, *Engineering News-Record*, *Electrical Review*, *Food Research*, *Heating and Ventilating*, *Illuminating Engineering*, *Iron and Steel*, *Machinery Journal of Mathematics and Physics*, *Machine Design*, *Metal Progress*, *Journal of the National Cancer Institute*, *Journal of the Optical Society of America*, *Product Engineering*, *Power*, *Public Roads*, *Railway Age*, *Rock Products*, *Textile World*, *Welding Journal*, *Water Works Engineering*, and many others.

Users of the nomograms included in this index will save much time in solving equations involving three or more variables and in the repeated solution of design formulas.

The master list index includes 21 fields, i.e., mathematics, physics, hydraulics and power, aeronautics, machine tools, medicine, food, etc.

Users of the *Index of Nomograms* should examine the sections on mathematics and physics because several of the references include material that might have been listed in one of the other categories. For example, in the section on mathematics, reference 1.11, Hopper Edge Slopes, might also have been included in Section 11—building, structures, etc.

Similarly, in Section 2—physics, references 2.11 and 2.12, might also have been included in Section 5—hydraulics and power.

A brief bibliography could have been included for those readers who would be interested in the theory and design of nomograms.

A. S. Levens
University of California

Microwave Electronics

By John C. Slater. Pp. 406+xiv, Figs. 91. D. Van Nostrand Company, Inc., New York, 1950. Price $6.00.

Lest any of the following remarks be misunderstood, this writer believes that Dr. Slater's book is an extremely valuable contribution to the understanding of phenomena taking place in microwave circuits and tubes. It is much more than a unified resume of "research in microwave electronics conducted at the Bell Telephone Laboratories and at the Radiation Laboratory of M. I. T.," as the fly-leaf states. It is a logical, thorough, basic and easy-to-understand development of several topics, the understanding of which is indispensable to the serious student or research worker in this field. It is true that the book is written on a rather high level, but a reader familiar with Maxwell's theory and equipped with the mathematical background of a graduate student of physics or engineering will find himself well-prepared for its study. He will, moreover, find it to be a very good introduction to many other branches of theoretical physics. Much of the work is original with Dr. Slater, and represents his personal contributions to the rapid progress which took place in establishing microwaves as a mature branch of science and engineering. Some of this material has been published by Dr. Slater under the same title [see Rev. Mod. Phys. 18, 441–512 (1946)] and in the form of reprints, has been used as a text in graduate courses in microwaves as taught by the late Professor W. W. Hansen and his colleagues at Stanford University. There is no doubt that this book will find much use both as a text and as a reference book.

Perhaps the choice of title for this book is misleading. To this writer, a treatise on the subject of microwave electronics would imply the study of the basic *electronic* phenomena at the very high frequencies. In this category would belong such topics as the mechanism of exchange of energy between electron beams and r-f fields in the presence of space-charge; the theory of space-charge waves with given boundary conditions; the general expressions for density and velocity modulation under transit time conditions as expressed by the Llewellyn-Petersen equations; high frequency random phenomena, such as noise; and other related topics. To be sure, Dr. Slater devotes one chapter to these general problems, and does, indeed, describe the various microwave electronic devices such as the klystron, magnetron, traveling wave tube, etc. But the one chapter on the general subject, and specific topics by way of illustration, do not seem to justify the general title that this book has been given.

The first half of the book is devoted to such topics as: the wave guide with perfect and imperfect walls, standing wave ratio, impedance, and mode concepts, power and energy relations, the analogy between transmission line equations and Maxwell's equations, the theory of resonant cavities, and numerous basic concepts associated with cavities.

It is interesting to note that the treatment in this half of the book no longer begins with a consideration of lumped circuit and transmission line relations. The field concept is used immediately. Impedance, power flow, standing wave ratio, etc., are defined in terms of electromagnetic field components. The powerful tool of expansion of fields in terms of orthogonal modes serves for the analysis of wave guides and cavities. Dr. Slater has not only been pioneering in this field of applying electromagnetic theory to microwave transmission problems, he has also given us an exemplary lucid exposition of this generalization of circuit concepts. Further developments of this circuit theory given in the book include applications to more complex wave-guide circuits and wave-guide discontinuities. The reader is admirably introduced to these subjects and the methods presented may be applied to a wide class of problems. For example, Dr. Slater's analysis of discontinuities in wave guides by application of standing wave solution and the symmetry properties of the structure quickly and simply lead to equivalent circuits; moreover, the analysis predicts what laboratory information needs to be accumulated to establish the constants of these circuits. Several kinds of structure are analyzed in the text, such as an iris in a wave guide, a "T," a "Magic T," coupling loops in cavities, etc. It is not hard for the reader to use these methods to learn and to describe the behavior of other structures. This part of the book appears to be especially useful as a text. The treatment here is, however, not quite as thorough as in the earlier part of the volume. The results could well be complemented by following up the references to some of Bethe's and Schwinger's original work.

The second half of the book is devoted to electronic devices. The klystron, the linear accelerator, the traveling wave tube, the cyclotron, the synchrotron, and other devices are described and analyzed with typical clarity. All the chapters are well written and form an excellent introduction to the various applications of the microwave art. An effort has been made to bring together the various classes of devices which now appear to have a common origin. For example, Dr. Slater points out that the klystron amplifier does not need to be restricted to the conventional form of two or three resonant cavities along an electron beam. More cavities can be used, spaced closely together. This, in the limit of zero spacing between cavities, becomes the problem of continuous interaction of r-f field with a beam thus resembling both the traveling wave tube and the linear accelerator. Thus the reader is made aware from the start of the similarity among several devices which appear, at first glance, to be so radically different and unrelated.

This reviewer believes that a more generous use of references would have been helpful in the second half of the book. Since most of the work in the first half was self-contained, and often original with Dr. Slater, references were not essential. In the second half, however, the descriptions are often brief and necessarily incomplete. Greater reference to the abundant literature would have been helpful, especially where existing parallel analyses have been written from a different viewpoint and lead to conclusions which, at least on the surface, are not identical with Dr. Slater's.

Edward L. Ginzton
Stanford University

Vector and Tensor Analysis

By Harry Lass. Pp. 347+viii, Figs. 101, McGraw-Hill Book Company, Inc., New York, 1950. Price $4.50.

This book is the first to appear in McGraw-Hill's newly projected International Series in Pure and Applied Mathematics and, as such, will be greeted with interest by all those acquainted with the uniform excellence of the familiar companion series in physics.

The book is intended as a text for a course at the first-year graduate or undergraduate senior level, and is liberally interspersed with illustrative examples and with a very great number of problems. A large fraction of the text is concerned with the application of vector analysis to mathematics and to physics, there being two chapters on vector analysis proper, and chapters on Differential Geometry, Integration (Real Variable Theory), Static and Dynamic Electricity, Mechanics, and Hydrodynamics and Elasticity. The last two chapters in the book treat tensor analysis and its applications.

Because of the number of applications of vector analysis, the treatment of each field is brief and concise. Although it would be generally agreed that each of the fields of application treated would be of value to students of mathematics or physics, it would appear that the brevity of the treatments would render comprehension difficult for the average student. There are fundamental conceptual difficulties in each of the fields, and these concepts must be carefully learned before the manipulatory aspects of the field can be intelligently handled. To illustrate the techniques of vector analysis by applications to a number of fields each of which is strange and bewildering to the student would almost certainly result in an identification, in the mind of the student, of some of the mystery and strangeness with the vector analysis itself. Nor may it be expected that the students who use the text are apt to have previous familiarity with an appreciable fraction of these fields. Thus the chapter on Electricity includes such relatively advanced topics as the solution of Laplace's equation in spherical coordinates, introducing Legendre polynomials. It is to be regretted, also, that electrostatic units are used in the Electricity chapter, reversing the almost universal trend to m.k.s. units and placing an additional and unnecessary impediment in the path of those students who have had a prior course in electricity.

The two chapters on tensor analysis introduce the subject in full generality, with the repeated index convention, and in n dimensions. The applications are to differential geometry and to relativity theory. The elements of Riemannian geometry are simply and clearly introduced, and these chapters will afford the young physicist a clear and valuable introduction to this branch of tensor analysis. It is the reviewer's experience and opinion, however, that three-dimensional Cartesian tensors merit separate treatment and are best introduced before consideration of the generalized tensor analysis. Despite the popularity of the more modern fields of atomic physics, the classical fields of elasticity and mechanics are still important branches of the science, and these fields are rendered awkward at best if tensors are avoided. It indeed seems strange and anachronistic to observe the author of a book with the title of this one engaging in all sorts of devious manipulations to avoid the use of tensors in the chapters on elasticity and mechanics. The author is, in fact, essentially forced to introduce tensors prematurely in the section on the dynamics of a rigid body when the moments and products of inertia are written in a square array which, it is pointed out, "will be shown in Chapter 8 to be a tensor." Nevertheless, the whole subject of principal axes and principal moments is treated without benefit of the theory of tensor eigenvalues, and the Euler equations are presented in the complicated and untransparent form required by the avoidance of tensor notation.

Those who are apt to find the book most valuable are seniors and graduate students who happen to have sufficient background in mathematical physics to follow the chapters on applications with some ease and who will use the volume as a reference book in the elements of theoretical physics and perhaps as an introduction to generalized tensor analysis. These students will find the chapters on applications well written and well planned and will find the chapters on tensors clear, understandable, and direct.

H. CALLEN
University of Pennsylvania

Aerials for Centimetre Wave-Lengths

BY D. W. FRY AND F. K. GOWARD. Pp. 172+x, profusely illustrated. Cambridge University Press, London, 1950. Price $3.50.

This book of the Modern Radio Technique Series is a companion volume of one by R. A. Smith on *Aerials for Metre and Decimetre Wave-Lengths*. It is intended to review the wartime developments in microwave antenna technique with emphasis on the radar system requirements, basic design principles, and typical performance data. The mathematical analyses as well as the detailed design information has a fairly complete coverage on microwave antennas developed during the war. It will be a valuable reference book for a radar system engineer.

The first chapter is devoted to the functions and system requirements of microwave antennas. Methods of scanning and types of coverage determined primarily by the tactical needs are reviewed. The electrical and practical requirements are properly covered.

In the second chapter, the basic concepts of the polar diagram theory are discussed. In dealing with microwave antennas where the dimensions are large as compared to the wave-length, two simple and powerful mathematical techniques are commonly used both in analysis and synthesis. The physical optics supply the relationship between the polar diagram and the current or aperture distribution. Whenever one has to deal with divergent waves, the geometric optics usually provide the direct and satisfactory solution.

The rest of the book is divided into three parts: point sources and double-curvature focusing devices, line sources, and cylindrical focusing devices. The chapter on primary point sources is descriptive in nature. The sources are usually designed experimentally, without the benefit of reliable quantitative theory, to feed double-curvature focusing devices such as reflector and lenses. In dealing with focusing devices, emphasis is put on off-axis properties and synthesis. The subjects on line sources and cylindrical focusing devices are treated in the same way.

Many practical considerations on electrical design and construction are given which will be helpful to radar antenna engineers.

L. J. CHU
Massachusetts Institute of Technology

Elements of Heat Transfer and Insulation

BY MAX JACOB AND GEORGE A. HAWKINS. Second edition. Pp. 229+xvi, Figs. 79. John Wiley and Sons, Inc., New York, 1950. Price $4.00.

The first edition of this undergraduate engineering textbook, published in 1942, has been widely adopted; the second edition seems to be an improvement on the first. The approach is a practical one and a great many examples of typical engineering interest are given. The basic concepts involved are satisfactorily developed. A physicist confronted with a practical heat transfer problem would find this book very useful as a first reference. Presumably what is lacking here can be found in the senior author's masterwork, *Heat Transfer* ($12.00).

The new edition differs in that 16 sections have been added or completely revised; the new material is slightly more difficult (or sometimes just more detailed) than that in the first edition. The number of problems has increased from 83 to 220. There are four chapters on conduction (including the unsteady state), three on convection, a considerably revised chapter on radiation, and others on heat transfer in condensing and boiling; combined effects of conduction and convection and of conduction, convection and radiation; experimental determination of conductivities and emissivities; heat transfer in temperature measurements; and heat transfer and fluid friction.

There is a logical stress on graphical and numerical methods, and on dimensionless analysis. Units are more carefully handled than is usual in engineering texts. The British gravitational system is used throughout, save that the authors take some pains to limit their use of the word "slug," preferring instead the pound mass. In this, of course, they do not stand alone. The symbols recommended by the American Standards Association have been adopted. There is a lot of empirical information on properties of materials and the heat transfer characteristics of queerly shaped objects.

Poisson's equation is derived in one dimension and stated in three dimensions. Rigorous solutions for this equation are derived for only a few simple cases; some other solutions are given without proof. The student will need to know the elements of differential equations.

The authors differentiate between a temperature and a temperature difference, using symbols such as °C and C, respectively, for these quantities. The reviewer agrees with the need for such differentiation; perhaps the notation used for many years by the late A. G. Worthing—°C and C°—is better in that it corresponds more closely with the spoken words "degree centigrade" and "centigrade degree."

Among the examples of interest to physicists is a method (Vidmar, 1918) for determining the maximum temperature t_{max} inside a current-carrying coil from measurements of the surface temperature t_s and the mean coil temperature t_m; the latter is easily found from resistance measurements. The simple relationship $t_{\max}=t_s+1.5(t_m-t_s)$ is derived.

David Halliday
University of Pittsburgh

Analytical Absorption Spectroscopy, Absorptimetry and Colorimetry

Edited by M. G. Mellon. Pp. 618+vii, Figs. 281. John Wiley and Sons, Inc., New York, 1950. Price $9.00.

The announced purpose of this book is to present those aspects of absorptimetry and colorimetry that are "of most practical concern in a modern chemical testing and analytical laboratory." Because of the wide range of problems encountered in such laboratories, a wide variety of analytical techniques is needed. It is virtually impossible for one individual to be thoroughly informed on all of them and their associated instrumentation. A comprehensive survey of one of the most useful techniques—that of absorption spectroscopy—is therefore bound to be of value to analytical chemists, whatever their special problems or interests.

The same wide applicability that makes absorption spectroscopy of general interest also makes it difficult for one individual to write authoritatively on all the many ramifications of the subject. (This limitation applies as well to book-reviewers!) The editor of *Analytical Absorption Spectroscopy* has wisely chosen a group of nine specialists in the field to write one chapter each on his specialty. The first, M. L. Moss of the Aluminum Company of America, has written a comprehensive account of the preparation of samples for spectrophotometric or colorimetric analysis. This chapter goes far beyond sample-handling procedures, and includes an extensive discussion of chemical procedures for the development of appropriately colored compounds when the substance to be analyzed is not colored. The chapter includes many examples of these procedures, two valuable tables summarizing methods for analysis of inorganic and organic substances (with references), and a bibliography with nearly six hundred entries.

The second chapter, by the Editor, is devoted to the physical basis of the subject. Terms are defined with care, fundamental physical principles such as the laws of emission and absorption of radiation considered, sources of error are examined in general, and conventions followed by workers in the field are summarized. Then come two chapters on Color Comparimeters and Filter Photometers, respectively, by W. B. Fortune of Eli Lilly and Company, and R. H. Müller of New York University, in which these two types of instruments are treated in detail.

Spectrophotometers for the ultraviolet and visible are the subject of Chapter 5 by K. S. Gibson of the National Bureau of Standards. Here a general discussion of basic concepts, and of the elements of spectrometry and photometry is followed by a survey of typical instruments and methods. Of special value is the detailed consideration of the operating characteristics and practical modifications of two widely used instruments—the Hardy-General Electric spectrophotometer for the visible and the Beckman model DU for the ultraviolet. The chapter is completed with an examination of sources of error and an account of methods of recording data.

Next comes a brief survey of photographic methods, in which E. R. Holiday of the London (England) Hospital pays chief attention to instrumental and optical devices for getting round the many difficulties of photographic photometry. This is followed by an extensive account of the analytical applications of spectrophotometric data by E. I. Stearns of the Calco Division of the American Cyanamid Company. In the reviewer's judgment, Stearns' chapter is one of the most valuable in the book for the analytical chemist. Not only does he consider in detail the very practical aspects of the effects of temperature, concentration, *p*H, solvent, and the like on the use of absorption spectra in analysis, but also gives a remarkably thorough account of the different methods for proceeding from observed absorption data to analytical results. The chapter closes with specific examples of the use of ultraviolet and visible spectra in analysis, especially for certain natural products and dyes.

Chapter 8, Spectrophotometers: Infra-Red Region, by L. J. Brady, Air Reduction Company, is rather heavily weighted with optical and electrical material, and gives very brief treatment of infra-red analytical methods. It appears to the reviewer that when one has a budget of 76 pages to devote to the analytical uses of infra-red spectroscopy, 10 pages on elementary prism optics, and 20 pages on detectors and amplifier circuits are unwarrantedly large amounts of material on these topics. This is especially true if it leads one to devote only one page to non-dispersive infra-red gas analyzers (which are not adequately treated anywhere in the present textbook literature) and two paragraphs and a table to the highly important subject of qualitative infra-red analysis. The subject of quantitative analysis is well handled (20 pages).

The final contribution, on the measurement and specification of color, by D. B. Judd of the National Bureau of Standards, is an interesting and (for the analytical chemist) unusual chapter. It is an authoritative summary of the physiological basis of color specification, and of various practical and short-cut methods of color-specification by material standards. It should give the analyst a clearer quantitative understanding of the physics and physiology of color, and of why these subjects are of direct importance for his own work.

The reviewer has no serious adverse criticism to make. It does appear that the editing of the volume has been rather loose in the sense that the various chapters have been written by the contributors with little concern for integration. There are many instances of this: the analysis of Vitamin A is treated for four or five pages in Chapter 1 and again for four pages in Chapter 7, with no cross-reference other than that afforded by the index. The basic question of optimum solution transmittancy is discussed twice, once in Chapter 7 and once in Chapter 8. The long discussion of prism optics in Chapter 8 is applicable to other regions of the spectrum as well as the infra-red (incidentally the Cauchy index formula 8.22 on p. 450 is not generally correct for the infra-red). A complete section (5.14) of six pages is devoted to filter photometers in Chapter 5, although the preceding chapter presumably covers this topic completely.

There is some evidence that the book has been rather long in the publication stage. Although the references are quite complete up to 1946, very few since that date are cited. No discussion is given of the important Cary recording ultraviolet spectrophotometer, although this instrument has been on the market since 1947 and is in wide current use as an analytical tool. The double-beam version of the Perkin-Elmer infra-red spectrometer is not mentioned, although it was first described in the literature in 1948.

Apart from such minor matters the book is well done, and will be a worth-while addition to the library of the working analytical chemist.

Richard C. Lord
Massachusetts Institute of Technology

Author Index to Books Reviewed

Adams, Douglas P.—*An Index of Nomograms* 876
Arnot, F. I.—*Collision Processes in Gases* 870
Berl, Walter G.—*Physical Methods in Chemical Analysis. Vol. I* 875
Campbell, Edward C.—see Soodak, Harry 874
Farkas, A.—*Physical Chemistry of Hydrocarbons. Vol. I.* 873
Frankenburg, W. G., *et al.*—*Advances in Catalysis. Vol. II.* 869
Fry, D. W. and F. K. Goward—*Aerials for Centimetre Wave-Lengths* 878
Gill, J. F.—see Teago, F. J 873
Glasser, Otto—*Medical Physics. Vol. II* 870
Goward, F. K.—see Fry, D. W 878
Hague, B.—*Introduction to Vector Analysis* 871
Hawkins, George A.—see Jacob, Max 878
Herzberg, Gerhard—*Molecular Spectra and Molecular Structure. I. Spectra of Diatomic Molecules* 869
Jackson, L. C.—*Wave Filters* 870
Jacob, Max and George A. Hawkins—*Elements of Heat Transfer and Insulation* 878
Knudsen, Martin—*The Kinetic Theory of Gases* 871
Lass, Harry—*Vector and Tensor Analysis* 877
Leermakers, John A.—see Mees, C. E. Kenneth 872
LeFevre, R. J. W.—*Dipole Moments* 874
Mees, C. E. Kenneth and John A. Leermakers—*The Organization of Industrial Scientific Research* 872
Mellon, M. G.—*Analytical Absorption Spectroscopy* 879
Shannon, C. E. and W. Weaver—*The Mathematical Theory of Communication* 875
Slater, John C.—*Microwave Electronics* 877
Soodak, Harry and Edward C. Campbell—*Elementary Pile Theory* 874
Teago, F. J. and J. F. Gill—*Mercury Arcs* 873
Temple, G.—*The General Principles of Quantum Theory* 876
Weaver, W.—see Shannon, C. E 875
Willers, F. A.—*Practical Analysis* 871

Other Books Received

Elements of Internal Combustion Turbine Theory. H. T. Adams. Pp. 178+xii, Figs. 123. Cambridge University Press, London, 1950. Price $3.75.

The Physical World. Paul McCorkle. Pp. 450+vii, Figs. 289. The Blakiston Company, Philadelphia, 1950.

Smith's Introductory College Chemistry. Third edition. Pp. 511+viii, Figs. 198. Appleton-Century-Crofts, Inc., New York, 1950. Price $4.25.

Infrared Radiation Therapy Sources and Their Analysis with Scanner. Leopold Rovner. Pp. 34, Figs. 21. Chas. C. Thomas, Springfield, Illinois, 1950. Price $1.50.

Blindness. Edited by P. A. Zahl. Pp. 576+xvi, Figs. 12. Princeton University Press, Princeton, New Jersey, 1950. Price $7.50.

Wave Mechanics. H. T. Flint. Pp. 131+ix, Figs. 131. John Wiley and Sons, Inc., New York, 1949. Price $1.25.

Acceptance Sampling (a Symposium). Pp. 155. American Statistical Association, Washington, D. C., 1950.

A Bibliography in Audition, Vols. I and II. Harvard University Press, Cambridge.

Nuclear Physics. Francis Bitter. Pp. 200+viii, Figs. 99. Addison-Wesley Press, Cambridge, 1950. Price $5.50.

Radioactivity and Nuclear Physics. James M. Cork. Pp. 415+xiii, Figs. 162. D. Van Nostrand Company, Inc., New York, 1950. Price $5.00.

Atomic Physics. Wolfgang Finkelnburg. Pp. 498+x, Figs. 226. McGraw-Hill Book Company, Inc., New York, 1950. Price $6.50.

The Inelastic Behavior of Engineering Materials and Structures. Alfred M. Freudenthal. Pp. 587+xvi, illustrations. John Wiley and Sons, Inc., New York, 1950. Price $7.50.

Electricity and Magnetism. Norman E. Gilbert. Pp. 569+xv, Figs. 391. MacMillan Company, Ltd., London, 1950. Price $5.00.

Classical Mechanics. Herbert Goldstein. Pp. 339+xii, Figs. 72. Addison-Wesley Press, Inc., Cambridge, 1950. Price $6.50.

Metallurgical Applications of the Electron Microscope. Pp. 164+vi, profusely illustrated. Institute of Metals, 4 Grosvenor Gardens, London, S.W.1, England, 1950. Price $2.50.

Kleinste Drucke ihre Messung und Erzeugung. Rudolf Jaeckel. Pp. 302, profusely illustrated. Springer-Verlag, Berlin, 1950.

X-Ray Crystallography. R. W. James, Pp. 88+vii, Figs. 28. John Wiley and Sons, Inc., New York, 1950. Price $1.25.

Heavisides' Electric Circuit Theory. H. J. Josephs. Pp. 115+viii, Figs. 15. John Wiley and Sons, Inc., New York, 1950. Price $1.25.

Electromagnetic Fields, Theory and Application, Vol. I, Mapping of Fields. Ernst Weber. Pp. 590+xiv, figures and tables. John Wiley and Sons, Inc., New York, 1950. Price $10.00.

Heat and Temperature Measurement. Robert L. Weber. Pp. 422, profusely illustrated. Prentice-Hall, Inc., New York, 1950. Price $6.65.

Applications of Interferometry. W. Ewart Williams. Pp. 104+viii, Figs. 43. John Wiley and Sons, Inc., New York, 1950. Price $1.25.

X-Rays. B. L. Worsnop and F. C. Chalklin. Pp. 126+vii, Figs. 47. John Wiley and Sons, Inc., New York, 1950. Price $1.25.

Laboratory and Shop Notes

Stark Effect Absorption Cells for Microwave Spectroscopy*

D. H. Baird, R. M. Fristrom, and M. H. Sirvetz
Mallinckrodt Chemical Laboratory, Harvard University, Cambridge, Massachusetts

July 7, 1950

STARK effect absorption cells in wave-guide form have been extensively used in microwave spectroscopy; the most common type is that introduced by Dakin, Good, and Coles[1] in which the Stark field is applied between the wave guide and a central "tongue." Its principal disadvantage lies in its relatively high attenuation which increases with frequency. We have found that transmission becomes a problem with this type of wave guide at frequencies above 35,000 mc.

For operation at higher frequencies we have tested two new forms of Stark effect wave guides. The two types of guide complement each other in use; the "slotted" type is useful for searching and general work, and the "parallel plate" type is useful for the study of Stark effects.

The slotted guide[2] consists of a section of rectangular guide (usually *K*-size, ½ in. × ¼ in., because of voltage limitation) slotted along the "no current line" (see Fig. 1). The two halves are supported by insulating clamps and the edges of the guide painted with porcelain cement. This allows the two halves to be juxtaposed while still permitting the application of sufficient Stark voltages between the two halves. Transmission of a 6-foot section of this type of guide runs about 90 percent at 25,000 mc. Because of the presence of the slot it is necessary to enclose the guide in a gas-tight glass envelope with mica end plates. It is also advisable to shield[4] completely the system electrically to avoid pick-up in the detecting system.

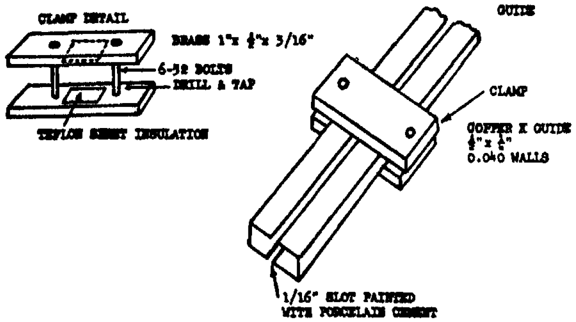

FIG. 1. "Slotted guide" construction details.

The slotted guide introduces only slight changes in the boundary conditions as seen by the dominant H_{01} mode of the microwaves, and, hence, very long lengths may be used, giving high sensitivity. Unfortunately, this end is achieved only by distorting the applied Stark field to the point where the use of Stark effects for obtaining additional information is completely lost. (At the same time, however, the advantages of Stark effect *modulation* are retained.) This guide has been operated up to 40,000 mc, and it is expected that it will allow operation throughout the millimeter region.

FIG. 2. "Parallel plate" guide construction details.

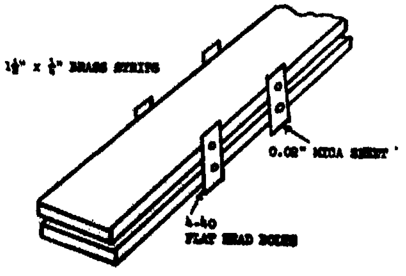

Another guide of very different physical appearance was first described by Gordy;[3,4] it is the "parallel plate" type which consists of two long flat metal plates separated by insulating posts (see Fig. 2). Microwave energy is fed into the system by means of horns. The horns have been found to transmit more than 75 percent of the energy input and are broad-banded. The most satisfactory method of construction of horns has been an electroforming process in which a form is cut from Woods metal and electroplated with silver and finally with copper until a wall of convenient thickness is formed. The Woods metal is melted out by boiling water and the horn is cleaned with steel wool and mounted. Convenient plate widths and separations (4 cm × 0.1 cm) allow satisfactory operation in the *K*-band, and increase of the width to 8 cm allows operation at 40,000 mc. As with the slotted type of guide a glass envelope should be used with an electric shield. The chief advantage of this type of guide would appear to be in the attainment of high Stark fields (by the use of closer spacings of the plates). We have attained fields as high as 20,000 v/cm and are able to resolve completely the water line at 22,235 mc $(5_{-1}\rightarrow 6_{-5})$. Transmission properties tend to depend rather critically on tuning, and for this reason the parallel plate guide seems less convenient than other types for preliminary searching operations.

We wish to acknowledge the encouragement and advice of E. B. Wilson, Jr., who suggested the work on the parallel plate guides.

---

* The research reported in this paper was made possible by Funds extended to Harvard University by the ONR under ONR Contract No. N5ori-76, T. O. V.

[1] Dakin, Good, and Coles, Phys. Rev. 70, 560 (1946); R. Hughes and E. Bright Wilson, Jr., Phys. Rev. 71, 562 (1947), McAfee, Jr., Hughes, and Wilson, Rev. Sci. Inst. 20, 821 (1949).

[2] We are indebted to Dr. B. Bleaney for suggesting that this form of guide might be used successfully.

[3] W. Gordy, Rev. Mod. Phys. 20, 668 (1948), especially p. 677.

[4] A satisfactory shield is a copper pipe completely enclosing the glass envelope grounded to the two horns feeding the system and to the Stark voltage generator.

Apparatus for Cutting Metals Strain-Free

Robert Maddin* and W. R. Asher**
The Johns Hopkins University, Baltimore, Maryland

July 31, 1950

WHEN a metallic single crystal is plastically deformed in tension, the rotations of the slip plane alter the regularity of the lattice. A simple method of measuring this disorientation or strain is to cut a disk from the single crystalline rod parallel to the active slip plane and to measure the strain by means of a glancing-angle x-ray technique.[1-3] The cutting has previously been accomplished by means of a mechanical saw[2,3] which was followed by polishing metallographically and etching to remove the distortion caused by the cutting and polishing. This technique was recently shown to be faulty[3] since, after removal of a large amount of the surface, the strain still remained. It then became apparent that no mechanical means of cutting a metallic disk from a single crystal could eliminate the extremely high local deformation which seemed to penetrate to great depths.

This present note describes a method for cutting a single crystalline disk from a rod by means of chemical attack. The etching cutter is a modification of one which has been used previously.[4] In Fig. 1 may be seen the detailed drawings of the apparatus. Figure 2 shows a photograph of the apparatus arranged for cutting a disk parallel to a specific crystallographic plane.

The unit consists of a specimen holder (1) which incorporates a simple goniometer containing a V-block upon which the specimen rests. The goniometer is so arranged that the specimen, in this case six inches long by one-half inch in diameter, can be rotated

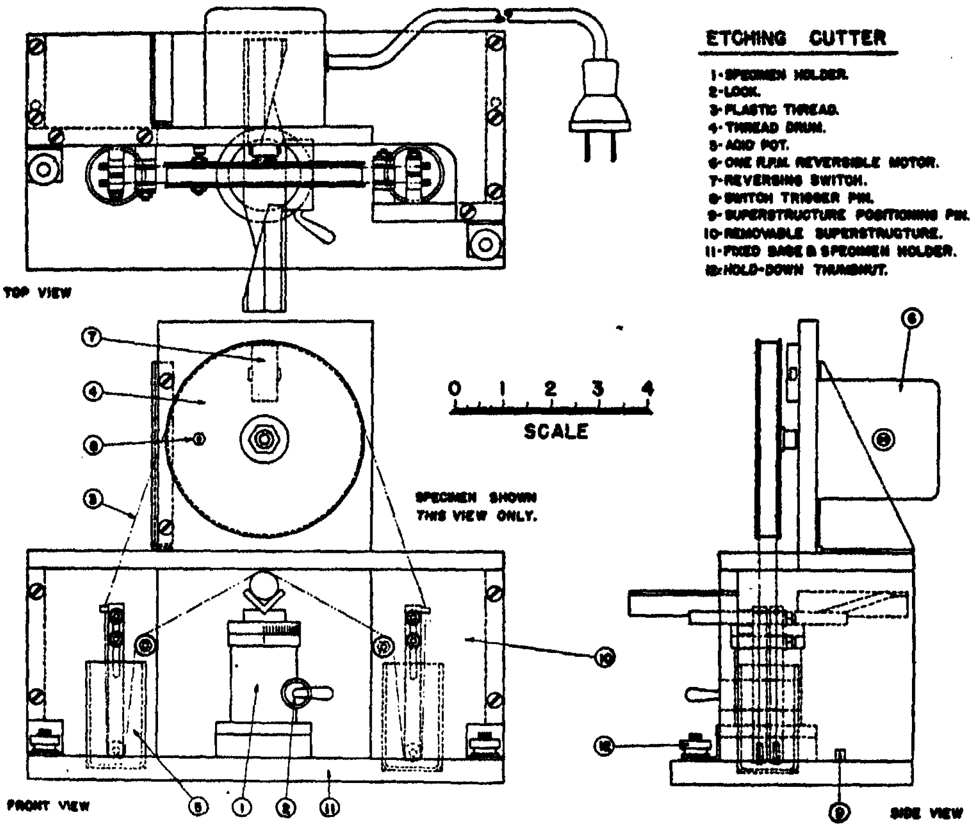

FIG. 1. Drawing for etching cutter.

FIG. 2. Etching cutter arranged for cutting three-eighths-inch disk parallel to octahedral plane of a brass single crystal.

about two axes so that any crystallographic plane may be located. Once the specific plane is located, the goniometer is locked by means of the screw arrangement shown, labeled (2). In the case of brass, a plastic thread (3) (Saran) is wound around a polystyrene drum (4) through a bath containing an eye-pulley down through a bath containing a 1:1 HNO_3 over an idling pulley. The plastic endless thread is led over the specimen over a second idling pulley, through a second tank of HNO_3 and back to the drum again. A second Saran thread is similarly arranged but is kept at a predetermined distance from the first thread by means of slots on the idling pulleys. The superstructure to which the drum is attached contains a 1 r.p.m. reversible motor (6). The drum contains a trigger pin (8) which trips a reversing switch (7) so that continuous oscillating operation may be maintained. The superstructure is composed of plastic and is held in alignment by positioning pins (9) and hold-down thumb nuts.

FIG. 3. Glancing angle photogram of the disk showing sharp Bragg reflection. $\theta = 19°30'$; monochromatic radiation; ten-hour exposure.

To measure the extent of strain induced by this type of cutting, the orientation of a single crystal of brass was determined by the back reflection x-ray Laue method, and a specific crystallographic plane was determined stereographically. The disk was then cut parallel to the $\{111\}$ plane by the apparatus described above. A beam of white radiation impinged on the c-cleavage face of a pentaerythritol crystal. The monochromatic beam was then led through a collimator onto the disk specimen. The disk was set at a theta-angle of 19.5° and was given ten hours' exposure. It may be seen in Fig. 3 that a sharp Bragg reflection results. To insure that a sharper reflection could not be obtained, the disk was annealed for twenty-four hours at 900° C, and another exposure was made. Here again, an extremely sharp Bragg reflection was obtained. This is good evidence to indicate that no strain was induced by this type of cutting.

This work was sponsored by the ONR under Contract Number N6onr 243-21 ONR 031–383.

---

*Assistant Professor, Metallurgy.

** Instrument Maker, Institute for Cooperative Research.

[1] G. I. Taylor, Trans. Faraday Soc. 121 (November, 1927.)

[2] R. Maddin and W. H. Hibbard, Jr., Metals Trans. 185, 700 (1949).

[3] J. A. Collins, Yale University Ph.D. dissertation (1939) (*cf.* also, Collins and Mathewson, Trans. A. I. M. E. *(1940) TP 1145*).

[4] T. R. McGuire, Yale University Ph.D. dissertation (1949).

A High Speed Short Resolving Time Coincidence Circuit for Use with Scintillation Counters

E. F. Shrader
Case Institute of Technology, Cleveland, Ohio

July 31, 1950

The use of non-linear circuit elements in coincidence circuits after the method of Morton[1] and Meyer *et al.*[2] is very attractive, especially when used with the scintillation-type counter. Such coincidence circuits can be made to handle directly the wide distribution of pulse heights which in many cases is characteristic of this type of counter. They can also be made to operate in the pulse voltage range of the photo-multiplier even when the photo-multiplier is operated at conservative voltages. A modification of the Meyer circuit has been developed which realizes these two advantages to a high degree. Because the details of such a circuit have not been widely published, it is felt that a description of one of the many possible variations of this circuit giving its capabilities and limitations will be of value.

The circuit schematic of the coincidence unit is shown in Fig. 1. The input tube (T_1) serves as an impedance changer operating at *essentially unity gain in both input channels.* This provides a high input impedance and insures that the diode bridges will be driven from a source impedance which is not dependent on the input circuitry. The non-linear elements (1*N*34*s*) are incorporated in two bridge circuits which have elements in common. Bridge #1 consists of R_1 and R_3 (R_3 is of course shunted by R_4 and R_2 in series with source #2 impedance) in one side and of D_1 and D_3 in the other side. The other bridge is similar to the first with R_1 being exchanged with R_3 and D_1 being exchanged with D_2. The *grid of the detector tube (T_2) is driven from the diode branch and* the cathode is driven from the resistive branch. Each bridge may be balanced so that there will be no output from the detector for a single pulse applied to either bridge. If, however, the two pulses are applied simultaneously there will be an output because of the non-linear addition of the pulses in the non-linear element D_3. As employed in this circuit the diodes are driven in the forward direction and the coincidence output of the circuit is a positive pulse. The three diodes used are carefully selected and the resistors R_1 and R_3 are matched. The variable resistor R_2 and trimmer condensers (3-12$\mu\mu f$) across the diodes are used to balance the bridges after construction. The balancing is performed using artificial pulses of 0.02μsec. duration. With sufficient care a balance can be achieved such that a single pulse required to give a certain output must be 50 times as large as two equal simultaneous pulses required to give the same output.

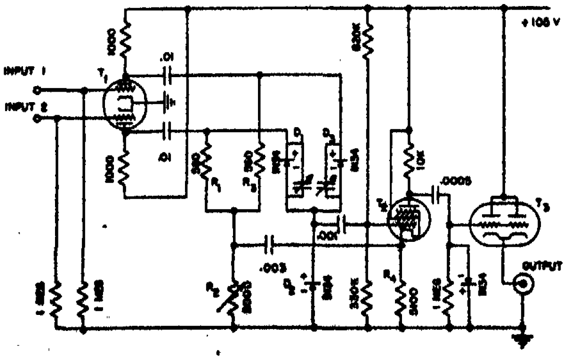

FIG. 1. Circuit schematic of coincidence unit.

In the use of this coincidence unit with the output of a photo-multiplier the scintillation pulses are shaped using the well-known shorted delay line technique. The photo-multiplier output drives a 6J6 cathode follower whose cathode load is a length of RG8U coaxial cable. This cable is shorted at the desired distance beyond the point at which the input pulse for the coincidence circuit is derived. The length of the pulse-shaping line which may be used depends on the time constant of the phosphor and the loss in amplitude of the voltage pulse which may be tolerated.

The output of the coincidence unit is amplified by a wide-band amplifier and registered on a high speed scaling unit (resolving time <0.2μsec.). Figure 2 shows the performance of the unit when tested by the following experimental arrangement. Two 931A photo-multiplier tubes are arranged with an anthracene crystal between them so that real coincidences are observed by the photo-multipliers whenever a scintillation is produced in the crystal by a weak radium source. The coincidence counting rate is plotted against the time delay introduced between the photo-multiplier and the coincidence unit. In each case the time delay required for a 50 percent decrease in counting rate corresponds to twice the length of the pulse-shaping coaxial cable. The curves were normalized to same number of coincidence counts at zero delay.

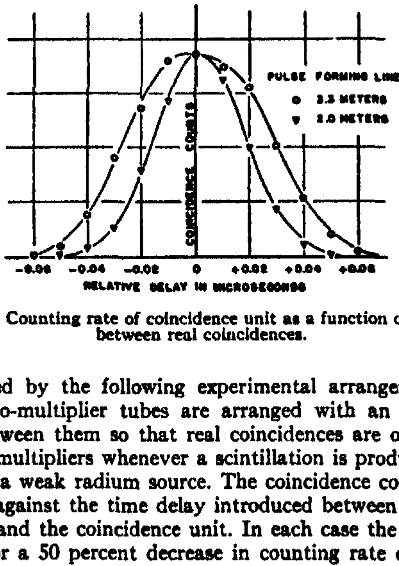

FIG. 2. Counting rate of coincidence unit as a function of delay between real coincidences.

In the above experiment the sensitivity of the over-all system was such that the minimum pulse height excepted was 0.04 volt. By increasing the gain of the amplifier, pulses as low as 0.01 volt can be used with coincidence unit. The amplitude discrimination against single pulses is maintained regardless of the operating voltage range within limits.

The main disadvantages of this type of unit are the difficulties of getting matched diodes and performing the initial balancing. The balancing is made difficult because of the temperature dependence of the diode characteristics. Fortunately, however, thermal cycling does not upset the balance at a given temperature and the stability is good after warm-up period.

This work was aided by the AEC.

---

[1] G. A. Morton, Nucleonics 4, 25 (1949).

[2] Meyer, Baldinger, Hahn, and Huber, Helv. Phys. Acta 22, 421 (1949).

Ultraviolet Photon Counting with an Electron Multiplier*

A. H. Morrish, G. W. Williams,† and E. K. Darby‡
Department of Physics, University of British Columbia, Vancouver, Canada

June 23, 1950

THE counting of single nuclear particles using some detecting device such as a Geiger-Müller or scintillation counter, together with electronic pulse counting techniques, has been in general use for years. Recently[1] the decay of some luminescent alkali halides, whose light emission intensity is very weak, was investigated by counting single visible photons. An RCA 5819, which has a large photo-sensitive cathode sensitive to light from 3100 and 6800A, was used together with a conventional pulse amplifier and scaling circuit. It was thought that a photo-multiplier sensitive to the ultraviolet might be useful in certain experiments. A multiplier, whose electrodes were fashioned from sheets of a beryllium-copper alloy after the design of J. S. Allen,[2] was investigated and found to be photo-sensitive to light of wave-length below 2900A. The tube was installed in a metal envelope which had a 3-mm quartz window situated approximately 1.75 in. in front of the first (photo) Be-Cu electrode.

This electron multiplier has been used previously as a particle counter. Allen's paper[2] gives data on its use as an electron counter. J. M. Robson[3] has investigated its use in detecting 10-kev protons and also gives a bias curve for the counting of the gamma-rays from RdTh (2.62 Mev). Several authors have investigated the tube's properties for counting other ions.[2,4] The recording equipment used in this experiment is similar to that used for particle counting, consisting of a pre-amplifier and linear amplifier with maximum gain of 5000. A commercial scale of 64 and mechanical register were used to count the pulses. The first electrode was operated at high negative potential and the collector close to ground potential.

The source of ultraviolet light was the Beckman quartz photoelectric spectrophotometer used as a monochromator with a hydrogen lamp source. Questions of design, slit widths, and stray radiant energy are discussed in papers by Cary and Beckman[5] and by Gibson and Balcom.[6] A Corning No. 9863 Red-Purple Corex A filter is provided with the instrument and was used to remove stray radiation. The filter cuts off below about 2450A.

The beam from the monochromator was fed into the electron multiplier through the quartz window, along the axis of a Bakelite tube. The precaution of using the Bakelite tube proved unnecessary, since the tube was totally insensitive to light above 3000A.

Figure 1 shows the dependence of the counting rate, measured in the scale of 64 per 2 minutes, on the voltage between successive electrodes of the electron multiplier. Light of wave-length 2500A was used. The shape is similar to the one obtained by Allen[2] for electron counting, but the plateau is reached at about 75 volts less per stage, which may be caused by a slightly different condition of the electrode surfaces. Allen found 100 percent efficiency for counting of electrons of 300-500 volts energy, indicating that it is possible to count all electrons emitted from the cathode by the *uv* photons since they are accelerated to the second electrode by a potential difference which can be of this order. With 4000 volts on the tube and the above discriminator and gain setting, the background was approximately 8 counts per minute.

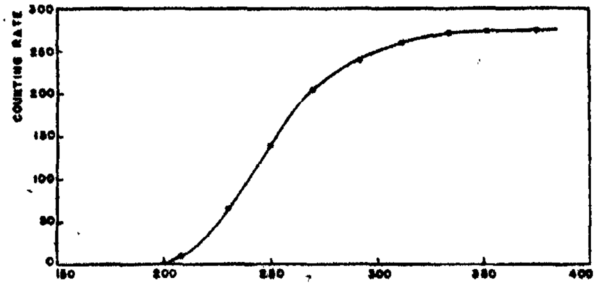

FIG. 1.

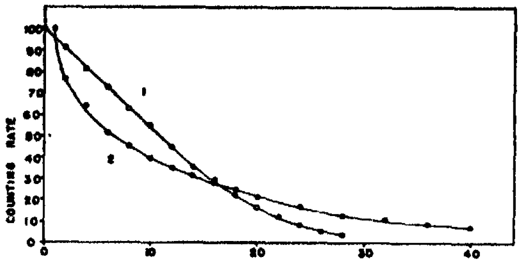

FIG. 2.

Because of the variation of the multiplication ratio for secondary emission there is a wide distribution of pulse size at the output of the electron multiplier. Curve 1 of Fig. 2 shows the counting rate in arbitrary units as a function of discriminator bias. The wave-length of the light used for this curve was 2500A. Bias curves taken for incident light of wave-length 2800A, 2400A, and 2000A coincide with this curve in shape. They, of course, had to be normalized to some point, since the absolute counting rates were different because of the different photo-sensitivity of the tube. This curve is very similar in shape to Allen's curve of the pulse distribution for the counting of electrons.

Figure 3 shows the spectral sensitivity of the tube. The counting rate is plotted on a logarithmic scale as a function of the wave-length of the incident radiation.

The assumption was made that the hydrogen lamp emitted the same number of photons in a given frequency interval from 2000 to 3000A, inasmuch as the intensity distribution from a hydrogen lamp in this region has not been determined very precisely.[7]

The curves at the right are upper edges of the sensitivity curve multiplied by a factor of 100. The dashed curves appear to show that appreciable counting rates are obtained above 3000A. This was shown to be caused by scattered radiation below 2400A, because when the red-purple filter was used the solid black curve was obtained at long wave-length settings. This curve fitted into the curve taken without the filter just below 2700A.

Fused quartz was used as the window to the multiplier, and in the Beckman, and, since quartz varies considerably in its absorption properties below 2200A, the drop in the sensitivity curve below this wave-length may have been caused by this and the assumption of constant number of photons emitted from the H_2 lamp rather than lowering of the sensitivity of the Be-Cu cathode.

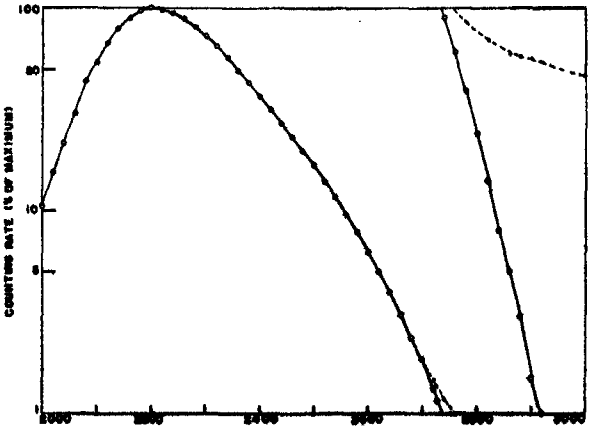

FIG. 3.

By using the value of the threshold obtained from this experiment, the work function of Be-Cu is determined to be 4.2 volts.

In order to obtain the quantum efficiency of the tube in the ultraviolet region, its response was measured using a source of thermal radiation. The light from a hot platinum wire was collimated and directed at the first electrode. The temperature of the wire was measured with an optical pyrometer. The quantum efficiency was found to be about 7×10^{-4} at the wave-length of maximum sensitivity, 2000A. The efficiency at other wave-lengths is proportionately less as indicated by Fig. 3.

The efficiency and pulse distribution for high energy photons was investigated using gamma-rays (1.17 and 1.33 Mev) from Co^{60}. A lead collimator was constructed, and the gammas were directed at the first electrode of the multiplier. From a knowledge of the strength of the source and the solid angle, the efficiency at zero bias was calculated to be 0.1 percent.

Curve 2 of Fig. 2 shows the pulse-height distribution curve for the gammas. It is similar in shape to that obtained by Robson[4] using a RdTh source of gammas (2.62 Mev). The efficiency he obtained was 0.2 percent for these gammas.

Comparison of the bias curves in Fig. 3 shows a number of pulses, caused by the gammas, bigger in amplitude than those caused by the *uv* photons. Also, there are more small pulses. Since the efficiency for the *uv* photons of 2200A and for 1.2-Mev gammas is about the same, and the bias curves are markedly different, it seems that the mechanism for the production of electrons in the two cases is different. Since the *uv* photon bias curve is similar to that obtained for electron counting, it suggests that single *uv* photons are being counted. While *uv* photons accomplish electron emission because of the photoelectric effect, those caused by the gammas are obtained by Compton collisions. The scattered electron evidently is capable of knocking out several electrons in some cases, and this will account for the large pulses. The smaller pulses may be caused by scattered gamma-rays striking electrodes other than the first and giving rise to a smaller pulse, since then a smaller number of electrodes are available for amplification of the signal by secondary emission.

It was found that the decay of luminescent CaF_2 could be detected with the tube. A CaF_2 crystal was irradiated with 55-kv 3 ma x-rays at room temperature at a distance of 4 cm for 15 minutes.

The observed counting rate was plotted as a function of the time after irradiation. The decay observed was of the form $I=at^{-n}$, where n is 1.17 in this case.

In view of the great amount of literature concerning mitogenetic radiation,[8] and conflicting views on its existence, a preliminary attempt was made to detect ultraviolet photons from onion roots. Counting rates with and without a bundle of onions placed before the quartz window were determined for the same period of time. In one experiment the counting rate was 158 counts in 16 minutes with the onion roots as compared to 152 counts without the onions in the same period of time, so that, within the limits of the sensitivity of the tube, apparently no mitogenetic radiation was observed. The authors wish to thank Professor O. Blüh for suggesting the experiment on mitogenetic radiation, and for preparing the samples of onion roots.

No suitable phosphor was found for use with the tube as a scintillation counter.

---

* This work was assisted financially by the Defence Research Board of Canada, Ottawa.

† Holder of B. C. Telephone Company scholarship.

‡ Holder of National Research Council Studentship.

[1] A. J. Dekker and A. H. Morrish, Phys. Rev. 78, 301 (1950).

[2] J. S. Allen, Rev. Sci. Inst. 18, 739 (1947).

[3] J. M. Robson, Rev. Sci. Inst. 19, 865 (1948).

[4] S. K. Allison and L. Del Rosario, Phys. Rev. 73, 1224A (1948); A. H. Morrish and J. S. Allen, Phys. Rev. 74, 1260A (1948).

[5] H. H. Cary and A. O. Beckman, J. Opt. Soc. Am. 31, 682 (1941).

[6] K. S. Gibson and M. M. Balcom, J. Research Nat. Bur. Stand. 38, 601 (1947).

[7] W. Finkelburg, *Kontinuierliche Spektren* (Julius Springer, Berlin, 1938), pp. 186–187.

[8] J. B. Bateman, Biological Revues X, 42 (1935).

Preparation of Carbon Targets

G. C. Phillips and J. E. Richardson
Rice Institute, Houston, Texas

July 7, 1950

In investigating the $C^{12}(d, n)N^{13}$ and $C^{12}(d, p)C^{13}$ reactions in this laboratory, it was found necessary to prepare thin, pure carbon targets on light silver foils. A thin backing was needed to prevent the positrons from the N^{13} from backscattering and to enable observation of the long-range protons in the forward direction. Targets prepared by depositing soot or by evaporating ceresin on silver foils were found unsatisfactory as the composition and the thickness of the soot is unknown, and the ceresin was found to evaporate under bombardment when deposited on a thin foil.

We have devised a method of cracking benzene on silver which produces a pure, uniform carbon target free from the abovementioned difficulties.

A Hubert's Model 22 Deluxe oven was used to produce the temperature necessary to crack the benzene. A three-mil silver foil was mounted on a silver disk and placed in a Vycor tube which was sealed at one end. The open end was connected to a bottle of benzene and a vacuum pump. The Vycor tube was evacuated and the pump was then applied to the benzene until all air over the benzene had been removed. The hose to the pump was closed, and the benzene vapor was allowed to fill the tube. Then the hose to the tube was closed, and the target end was inserted in the oven which had been pre-heated to 1500° F. With the oven held at this temperature, any number of targets can be prepared simultaneously in six or seven minutes. The target thickness, of course, depends upon the amount of benzene used and the time in the oven. Care must be taken that the temperature of the target has dropped below that at which carbon burns before air is admitted to the tube.

We have prepared several targets in this manner which were found to be very uniform. This uniformity was checked by comparing the observed width and shape of the $C^{12}(d; p, \gamma)C^{13}$ 1.435-Mev gamma-ray resonance[1] to the width as calculated from the thickness determined by the yield. The thickness of a target was determined by comparing its yield with that from a thin ceresin target of known thickness and with a thick graphite target. These targets were found to have a carbon deposit of about 25 μg per cm^2. This corresponds to a thickness of 8 kev for 1.4-Mev deuterons.

Isotopically enriched C^{13} targets were prepared from methyl iodide which was purchased from the Eastman Kodak Company of Rochester, New York. The methyl iodide had been enriched to 48 percent C^{13}. As the methyl iodide was quite expensive, a more efficient method of preparation than that described above was devised.

A $\frac{1}{32}$-inch thick nickel disk of 1-inch diameter was supported in a Vycor tube by means of a quartz support. The Vycor tube was placed inside a single-turn induction coil of a Model 1-A l RCA Electronic Power Generator with the disk at the center of the coil. A sylphon-bellow Hoke valve was placed between the Vycor tube and the vacuum system which included a diffusion pump and a liquid air trap. Two similar valves placed between the Vycor tube and the methyl iodide allowed known amounts of methyl iodide vapor to be sent into the tube. All vacuum seals were made with rubber "O" rings which were found not to be as readily attacked by methyl iodide as was ordinary vacuum hose. The inner seal of the methyl iodide glass container was broken by an iron cylinder which itself was sealed in a glass envelope.

After attaining a vacuum of about 5 mm of mercury, the nickel disk was thoroughly degassed by heating with the induction heater. The valve to the pump was closed, and the desired amount of methyl iodide vapor was sent into the Vycor tube. The induction heater was tuned to heat the nickel disk to red-orange heat which is sufficient to obtain a carbon deposit from the methyl iodide vapor. The cracking process actually commences at about red heat. The iodine was found to deposit on the cooler parts of the Vycor tube, but starch tests showed no traces of iodine on the targets. An additional inner sealed tube was attached to store the unused methyl iodide. The liquid was transferred to the new container by immersing the tube in liquid air.

Seven targets of different thicknesses have been prepared. Of these targets the thickest have a carbon deposit of about 60 μg per cm². Calculations show that about 30 percent of the carbon in the methyl iodide vapor is cracked onto the blank. It was found necessary in the preparation of these targets to freeze the methyl iodide by immersing the tube containing the methyl iodide in liquid air and then pumping off oxygen which was apparently sealed in the tube with the methyl iodide.

[1] Bonner, Evans, Harris, and Phillips, Phys. Rev. 75, 1401 (1949).

A Scintillation Counter for Fast Neutrons*

H. B. Frey
Servomechanisms Laboratory, Massachusetts Institute of Technology, Cambridge, Massachusetts

June 5, 1950

A SCINTILLATION counter, using two type 931 photo-multiplier tubes and a coincidence circuit, in combination with a zinc sulfide phosphor on Lucite sheet, has been used previously as a detector of fast neutrons.[1] A more sensitive instrument is now desirable because the recommended fast-neutron tolerance level has been recently reduced from 200 to 20 neutrons per square centimeter per second. The present tolerance level corresponds to only 0.38 count per minute on the earlier detector. The newer type 5819 photo-multiplier tube with its large photo-cathode on top of the tube makes greater sensitivity possible and allows more of the light from the phosphor to be collected, thereby increasing the signal-to-noise ratio and making a two-channel coincidence circuit for noise suppression unnecessary.

Two drops of thickened polystyrene coil dope[2] were placed on the cathode end of a type 5819 photo-multiplier tube and zinc sulfide powder[3] was mixed with the dope until a stiff white paste was formed. This mixture was spread over the entire photo-cathode area and allowed to dry. An aluminum foil reflector was placed over the phosphor, a Mumetal magnetic shield slipped over the tube, and the assembly enclosed in a light-tight box.

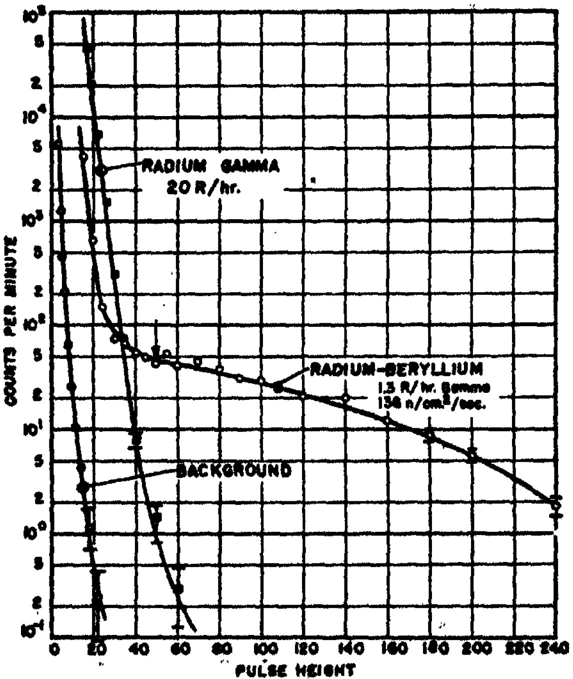

FIG. 1. Integral bias curve for fast-neutron scintillation counter. Arrow indicates pulse-height setting for normal operation.

A linear amplifier and discriminator[4] followed by a pulse counter was used to obtain the integral bias curves shown in Fig. 1. The background curve includes amplifier noise, photo-multiplier dark current, and actual gamma-counts from other sources stored nearby. When data for the radium-gamma-curve were taken, the radiation intensity at the phosphor was approximately 20 roentgens per hour. The radium-beryllium curve was obtained with the phosphor in a neutron flux of 136 neutrons per square centimeter per second and a gamma-radiation intensity of 1.3 roentgens per hour. The radium-beryllium source used had been calibrated against the standard pile at Oak Ridge National Laboratory. With a pulse-height setting of 50, a flux of 20 neutrons per square centimeter per second would correspond to an easily measured counting rate of 7.4 counts per minute.

* This work was assisted by a joint ONR, Bu Ships, and AEC program.

[1] W. G. Moulton and C. H. Sherwin, Rev. Sci. Inst. 20, 766 (1949).

[2] Amphenol Polyweld "912" (Polystyrene-Base) Coil Dope.

[3] RCA Phosphor No. 33Z20A.

[4] Atomic Instrument Company Model 204B. See also W. H. Jordan and P. R. Bell, Rev. Sci. Inst. 18, 703 (1947).

Making Small Metal Tubes by Electrodeposition on Nylon Fibers

Rolf J. E. Gezelius
Research Institute of National Defense, Stockholm, Sweden

July 7, 1950

METAL tubes with diameters from 1 mm down to 0.1 mm or less are often useful in electronics and instrument techniques. Biological injection needles, eyelets, and indirectly heated cathodes for electron tubes are examples. These small tubes are generally made either by drawing down larger tubes or by electrodeposition on a mandrel. The first method must generally be used for alloy tubes, i.e. stainless steel but the difficulties are considerable in using this method to obtain very small diameters. The electrodeposition method can be used for pure metals but in the deposition on waxed or oxidized threads it is difficult to pull out the mandrel without destroying the tube, especially with very thin walls and small diameters. A variation of the older electrodeposition method of making small metal tubes makes use of the excellent mechanical properties of the Nylon fiber as a mandrel. Drawn Nylon fibers of high strength and with very smooth surfaces are obtainable in exact dimensions.

The first step in making tubes is the silvering of the Nylon fiber by the Brashear or rochelle salt method as used for glass.[1] A better adhesion between Nylon fiber and the silver coating is obtained if the Nylon fibers before the silvering process are dipped in a solution of 1 g $SnCl_2$ in 1 liter of distilled water and then rinsed in two (not more) baths of distilled water. The silvered Nylon fiber is then plated to the necessary wall thickness with the metal desired. In order not to destroy the thin silver coating the electric circuit must be closed before the fiber is immersed in the electroplating bath. Further details on such electroplating work are given elsewhere.[2,3]

The Nylon mandrel may be removed from the metal tube by holding one end of the tube with tweezers and drawing on the free end of the Nylon fiber. The fiber will then contract without breaking and free itself from the inside surface of the tube. It can easily be drawn out. If it is necessary the thin silver coating inside the tube can be removed by short dipping in dilute nitric acid.

Tubes of several inches in length with inside diameters as small as 0.05 mm can be made in this way. Metals such as copper, silver, and nickel have generally been used. It is also possible to make hard and corrosion-resistant tubes of a nickel-cobalt alloy by simultaneous electrodeposition of these two metals.

[1] *Handbook of Chemistry and Physics*, 30th edition, p. 2537.

[2] "Modern Electroplating," published by the Electrochemical Society, New York, 1942.

[3] W. Pfanhauser, *Galvanotechnik* (Leipzig, 1941).

Volumetric Displacement Flask*

S. D. Snyder, C. J. Craven,** and D. B. Trauger
K-25 Laboratory, Carbide and Carbon Chemicals Division, Union Carbide and Carbon Corporation, Oak Ridge, Tennessee

July 10, 1950

Although many similar displacement flasks have been devised, the authors have not seen one which incorporates all of the features of the flask presented here. This unit has proven particularly useful where very precise gas volume flow measurements are required. Flasks having volumes of ½, 2, 5, and 12 liters have been constructed.

In using the flask shown in Fig. 1, the flow to be measured is first by-passed through stopcock 1 and the liquid drawn into the flask and bulb by closing stopcock 2 and opening stopcock 3 to vacuum. (Dibutyl phthalate is a suitable liquid for many gases.) After reversing the setting of cocks 2 and 3, cock 1 is turned to direct the flow into the flask simultaneously with starting a timer and the collection interval is timed until the image of the leveling point meets the leveling point as viewed from below. The damping tube prevents bubbling at the intake from creating disturbances which blur the leveling point image. Although the pressure in the flask varies throughout the collection, the inlet pressure remains nearly atmospheric and constant since the right side of the trap is open. Pressure variations of no more than ¼ cm of water are observed at the source at the beginning and throughout the collection if the bulb and arms are proportioned as indicated and the collection time exceeds two minutes. Proper leveling of the bulb is obviously important and it is recommended that it be given permanent mounting on a stand. In the larger sizes, it was advantageous to locate the arms and leveling point in a short cylindrical section of reduced diameter which was added to the bottom of the flask. (The volume of the bulb is determined by weighing the displaced liquid.)

Each of the flasks used has been compared with those of adjacent sizes using a constant source of nitrogen from a cylinder and regulator, Moore Products Regulator and critical orifice in series. When the collection time was greater than 2 minutes, the greatest difference in flow measurement was 0.1 percent. The liquid must be completely saturated with the gas if maximum accuracy is to be obtained.

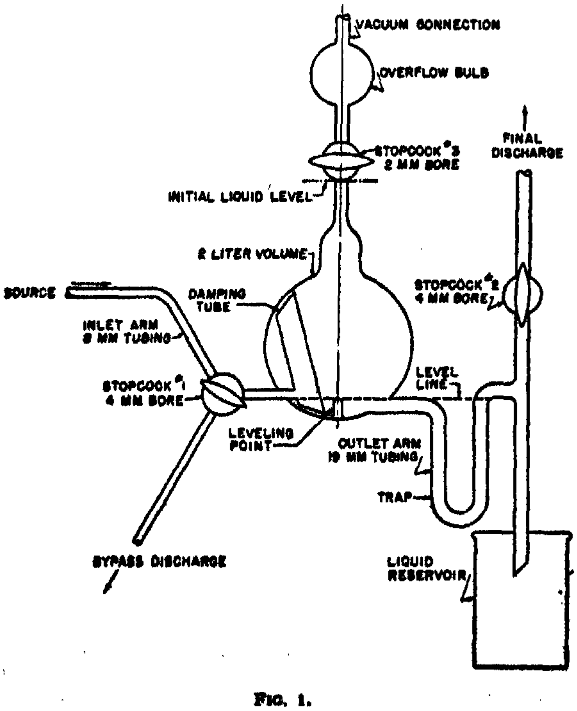

Fig. 1.

---

* This document is based on work performed for the AEC by Carbide and Carbon Chemicals Division, Union Carbide and Carbon Corporation, at Oak Ridge, Tennessee.

** Now at University of Tennessee, Knoxville, Tennessee.

New Instruments

W. A. Wildhack: Associate Editor
in Charge of this Section
National Bureau of Standards, Washington, D. C.

These descriptions are based on information supplied by the manufacturer and in some cases from independent sources. The Review *assumes no responsibility for their correctness.*

Power Level Indicator

For the measurement of non-sinusoidal or otherwise erratic wave forms, a thermocouple or other thermoelectrical device is usually employed. However, a small, robust, and portable instrument using *no* thermocouple, yet giving a similar, true r.m.s. reading regardless of wave form has now been announced.

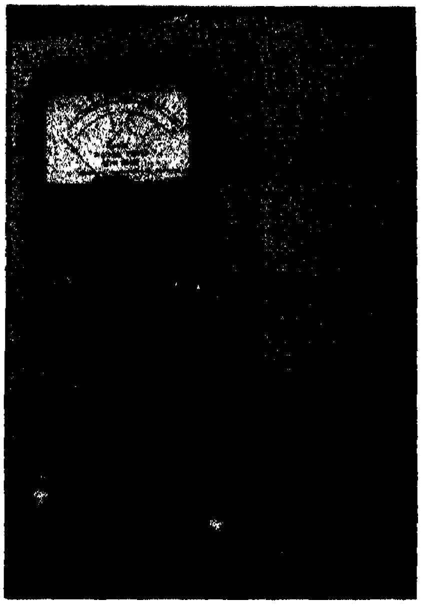

A new circuit comprising a temperature-limited diode, d.c. amplifier, and feed-back loop will maintain constant power in the diode filament. Accordingly, an unknown current introduced into the filament produces effects which depend only on its heating ability, and a root-mean-square voltmeter can be built having the accuracy associated with feed-back devices. A mathematical approximation involving an error of the order of one percent allows construction of an r.m.s. voltmeter carrying a linear scale in watts. Full-scale measurements of 1 mw, 10 mw, 100 mw, 1 w, and 10 w into 600 ohms are available in the instrument, and accurately corresponding r.m.s. voltage scales are also provided.

The portable instrument, now in production, has a case size of 6×7×12 in., and is suitable for 150-v, 50- to 60-c.p.s. operation. Rack-mounted and special types are also available, including instruments giving a true oscillographic record of power *vs.* time. Applications of this device are the measurement of noise, both the audio- and radiofrequencies, and underwater sound work.—Reed Research, Inc., *1048 Potomac Street, Washington 7, D. C.*

Laboratory Coating Unit

This instrument, designated Type 3108, is designed to meet the following requirements: (1) pump down to shadow-casting pressure (1×10^{-4} mm Hg) in ½ hr. (2) a sales price "below $1000" to be gained without loss of quality by good design, and (3) versatility and ease of operation with special emphasis on filament adjustments.

The individual requirements of various users are so diversified that it was concluded the best way to meet individual demands was to present a base unit with all of the essentials for shadowcasting and to furnish accessories for special requirements.

The basic unit consists of a neat table-top cabinet with a 9-in. glass bell jar and a pumping system using a National Research Corporation H-2-P purifying-type three-stage oil diffusion pump, offset from the bell jar by a water-cooled gooseneck manifold, to reduce oil migration into the bell jar to a minimum. This pump is capable of reaching a blank-off vacuum of 2×10^{-7} mm Hg absolute.

A mechanical pump is included in the base unit, as well as a high voltage discharge which acts as a cleaner and degasser for surfaces within the bell jar. The high voltage discharge also serves as an order of magnitude vacuum gauge to indicate when evaporation can take place. A set of high current feed-thrus is furnished with the base unit and they are connected to a 100-watt low voltage transformer for heating the filament.

The basic unit is capable of pumping down to 1×10^{-4} mm Hg in less than ½ hr. If a high vacuum valve and roughing line are added, a reduction in cycle time of 15 min. can be achieved. Two sets of filaments can be provided with the unit and adjusted to move on straight line loci 90° apart, which intersect at the center of the bell jar. The height of the filaments is also adjustable. These two adjustments permit complete control of the oblique angle used for shadowcasting. The filament holders use a new spring design which permits expansion and contraction of the filament during the evaporation cycle. This facilitates filament changes so that longer life and less breakage can be expected.—National Research Corporation, *70 Memorial Drive, Cambridge, Massachusetts.*

R-F Mass Spectrometer Tube

New progress in the field of radiofrequency mass spectrometry has been reported. Improved three-stage tubes of the design of Dr. W. H. Bennett are now commercially available, and complete spectrometers will become available soon.

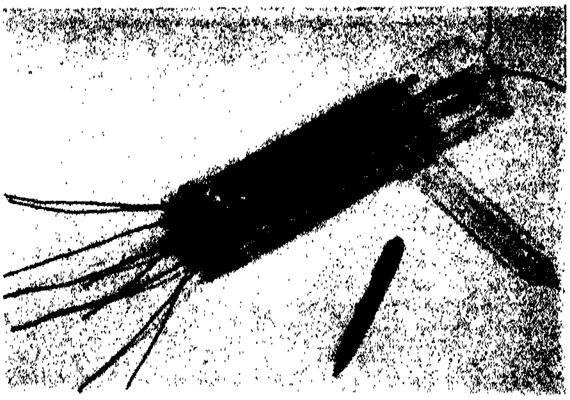

A new model of the Bennett r-f tube is shown in the accompanying photograph. The tube consists of filament, sixteen grids, and a collector plate, together with the necessary leads and supports, enclosed in an evacuated glass envelope. Masses are sorted by the principle of velocity selection, as described previously [Rev. Sci. Inst. **21**, 578 (1950)].

The grid-holding disks are drawn Nichrome V with grids of knitted ½-mil tungsten wire. Because of the large number of grids, fine wire and an open grid structure must be used to allow large usable beam currents. In the model shown only about 50 percent of the tube cross section is blocked by grid wires.

Insulation for voltages as high as 2000 v and more is provided by glass tubes, running along the outside of the grid structure to each set of grids. Grid-spacing dimensions are held to a tolerance of 0.001 in. by carefully ground spacers. In early models glass spacers have been used, but glass is being replaced by Alumina to improve resistance to shock and vibration.

New models of the tube use monel metal envelopes with ends sealed by screw caps and gaskets. Not only are these tubes less sensitive to shock and vibration, but they can be easily disassembled for inspection, adjustment, and cleaning.

The filament used in this model is a tungsten spiral coated with catephoretically deposited thoria. Emission currents of 1 ma are sufficient to get the usable beam currents of 10^{-7} to 10^{-8} amp. Signal currents from 10^{-9} to 10^{-10} amp. are readily obtained.

R-f voltages in the order of 5 v at frequencies from 0.1 to 10 Mc represent typical operating conditions. D.c. voltages from 50 to 1000 v are used for ion acceleration.

This tube shows a sensitivity of helium in air of one part in 200,000. Resolution to about mass 40 is possible with suitable circuitry. In operation the tube is apparently sufficiently stable for chemical analysis work, with low background currents. Pressure, emission, and d.c. voltage must be carefully regulated.

Uses of the new r-f mass spectrometer tubes include leak detection, process control, and analytical work. These Bennett tubes have been placed on the market to encourage various laboratories to build and test different types of r-f mass spectrometers, thus contributing to the advance of the entire field of r-f mass spectrometry.—General Electric Company, *1 River Road, Schenectady, New York.*

Spring Motor

New latitude in devising spring motors for cameras, time recorders, mechanical recording instruments, automatic reels, antibacklash mechanisms, and balancing devices is offered to design and development engineers through the Neg'ator—a new type of elastic member made from prestressed flat spring stock. Spring motors designed around the Neg'ator are characterized by two inherent attributes: (1) a constant output torque, and (2) a long running time (large numbers of turns) on a single winding.

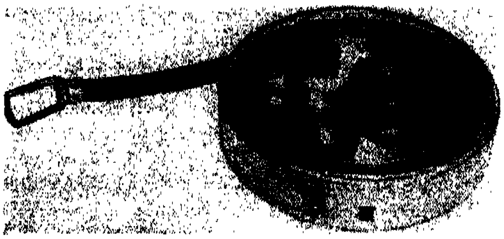

The basic Type B Neg'ator spring motor, is made up of three basic parts: the Neg'ator spring itself and two spindles or spools. The Neg'ator band coils on both spindles in opposite rotational direction.

The unusual feature of the Neg'ator which permits the design of such spring motors is its ability to exert constant—or even decreasing—force with increasing deflection. This is in contradistinction to accepted principles of design which suppose that increasing deflections of elastic members can only be accomplished by exerting greater force. This is possible because only a small increment of length of the long Neg'ator coil is being deflected from its natural position at any instant, whereas the entire length of a conventional power or spiral spring is always involved in generating that spring's torque.

Energy is stored in a Neg'ator by deflecting each increment of length—in succession—from its natural radius to a larger radius. Therefore, if a Neg'ator with a natural radius of curvature R_1 is mounted on a spindle of the same radius and forcibly wound onto a spindle of larger radius R_2, the Neg'ator will subsequently run from the larger spindle onto the smaller one when the external restraining force is released. The greater the difference in the radii of the two spindles, the greater will be the torque at the output spindle. Maximum output torque in minimum space is achieved by back-bending the Neg'ator from one spindle to the other (involving the concept of a negative radius). Neg'ator motors can be used for linear motion, recoiling, balancing, and backlash-elimination. For example, hand-power tools on an assembly line can be spring-supported without requiring the operator to fight strong retracting forces while using the tool.

The 50-ft. steel measuring tape illustrated is retracted by a single Neg'ator "B" motor that has the following specifications: small bushing radius, ¾ in.; large bushing radius, 1⅛ in.; blue tempered stock is 0.005 in. thick, ⅜ in. wide, and 250 in. long; life is 5000 cycles.—NEG'ATOR DIVISION, *Hunter Spring Company, 1 Spring Avenue, Lansdale, Pennsylvania.*

2000-M.P.H. Timing Equipment

Velocity and acceleration of objects moving at 2000 m.p.h. can be recorded and measured in a single optical image by a new Beckman & Whitley temporal sequence system based on slit-type camera techniques.

To measure optical phenomena, a slit camera records time sequence in a vertical plane passing through the optical axis of the lens. Besides photographing the event, this equipment automatically records—on the same film—numbers showing elapsed seconds and hundredths with intermediate pips spaced at thousandths of seconds. Printer dials accumulate 1000 seconds per turnover. Longer time periods are handled by an independent tally of the total number of such periods. External time-standard pulses can also be applied to synchronize the timer with events occurring elsewhere. Continuously variable film speed in either direction permits recording events progressing in either direction and at speeds up to 2000 m.p.h. Higher speeds can be accomodated with modifications.

Used optically in this manner, the camera produces a strip picture looking like a conventional stop-action photograph of two-dimensional space. Because it is made with a vertical slip instead of a shutter, the image is actually a geometric plane figure of generation with the horizontal coordinate in terms of time rather than space. Events taking place vertically in the slit plane are expanded horizontally—coordinated with the calibrated time scale. The camera can also be used to make conventional time-and-position intermittent sequence photographs indoors if the object is illuminated with a stroboscopic lamp.

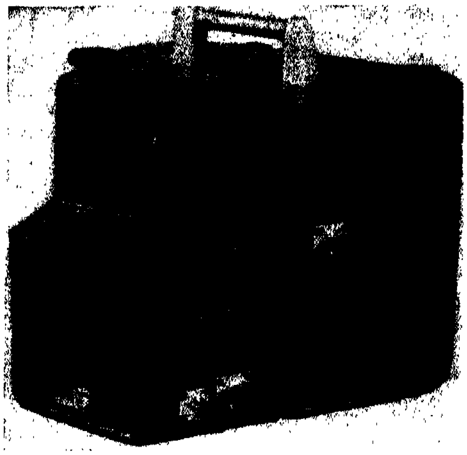

For non-optical events, electrical pulses can be fed to the system and recorded on the film in a specified relation to the printed time sequence. In addition to measuring the velocity and acceleration of high speed objects such as missiles, projectiles, etc., the apparatus is useful for the recording of oscillograph traces and other oscillations taking place vertically within the slit plane, for example, machinery parts.—BECKMAN & WHITLEY, Inc., *936 San Carlos Avenue, San Carlos, California.*

Electronic Flowmeter

The Potter electronic flowmeter comprises a flow-sensing unit having a dynamically balanced rotor and magnet rotating within a non-magnetic housing, and an external pick-up coil connected to an electronic integrator, or totalizer, or both. It features a high efficiency, free-flowing rotor, which the manufacturer claims eliminates such troubles as bearing maintenance, friction drag, and large pressure drop. Fluid flow around the rotor establishes upstream thrust components which exceed the downstream drag factor. This tends to move the revolving rotor axially upstream into an intermediate operating position where no thrust is exerted upon either upstream or downstream supports. This feature eliminates the need for thrust bearings and permits the use of a small-diameter rotor shaft and short guide bearings to journal the

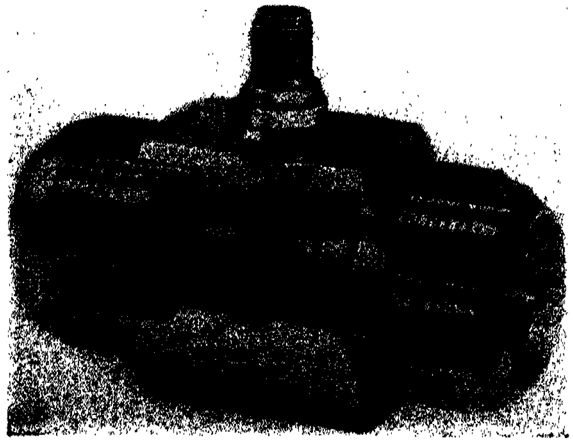

rotor. Fluid from the line is admitted into each bearing through a small vent, so that the rotor actually revolves on a film of liquid.

This design also results in an exceptionally low pressure drop through the meter. One of the major factors which influence pressure loss is blade loading. Since blade loading has been eliminated, the pressure drop is directly related to Venturi efficiency, which can be made quite high.

The housing of the sensing unit is compact (usually a standard AN fitting). It is no larger than the line into which it is installed. Three circular spring clips at each end maintain the guide bearings for the rotor shaft in center. Fluid passing through the housing turns the rotor at a speed determined by velocity of the liquid and pitch of the rotor blades. A cylindrical permanent Alnico magnet within the rotor sets up a rotating field which generates a.c. current in the pick-up coil. Frequency is equal to the speed of the rotor when the magnet is two-pole. A four-pole magnet provides twice this frequency. A single, shielded wire conducts the a.c. current to an electronic unit which either integrates it into d.c. current for operating a rate-of-flow meter, or counts and totals the cycles on an electromechanical counter of the Veeder-Root type.

Since the sensing-element output is an electrical frequency, only flow factors which affect the speed of the rotor can affect the accuracy of the meter. As long as the rotor maintains its balanced position, its blades operate no-slip. Therefore fluid viscosity, pressure, temperature, and specific gravity have very slight effect upon the volumetric flow rate.

Operating temperatures range from 4° A. to 1000°F. Standard housings withstand pressures up to 5000 p.s.i. Special housings can be supplied for pressures up to 20,000 p.s.i.—POTTER AERONAUTICAL COMPANY, *87 Academy Street, Newark, New Jersey.*

Oscilloscope Camera

The F-284 Fairchild-Polaroid oscilloscope camera adapts for oscilloscope recording the Polaroid-Land principle of a "photographic print in one minute." Because of the speed with which prints become available it offers a convenient method of recording oscilloscope traces for immediate study or future reference. No special photographic skill is required to obtain good pictures.

The complete unit consists of an adapter which can be attached to any 5-in. cathode-ray oscilloscope, a light-tight hood which automatically provides the correct focus for the camera, and a standard Polaroid-Land camera body which is equipped with a specially designed high speed *f*2.8 lens and suitable between-the-lens shutter. The camera body is also fitted with a special two-position, spring-actuated shift device which permits two images to be recorded on each photographic print. Each print is 3¼×4¼ in. in size and the recorded image is one-half the size of the scope image. Traces with speeds up to 1 in./μsec. at 3000 v have been recorded.—FAIRCHILD CAMERA & INSTRUMENT CORPORATION, *88-06 Van Wyck Blvd., Jamaica 1, New York.*

Electron-Diffraction Camera

Electron-diffraction cameras are used for the investigation of the structure of matter and particularly for the study of thin films, surfaces, and gases. The process is particularly suitable for the study of surface phenomena, due to the small penetrating power of the electrons. The ease with which electrons are scattered results in an intense diffraction pattern, and therefore exposure times of the order of seconds may be used, as compared with the hours frequently necessary with x-rays.

The Finch-Edwards electron-diffraction camera obtains a constant accelerating voltage with relatively simple equipment. Since a change in accelerating voltage alters the wave-length and consequently the diameter of the diffraction ring, the high tension system must be designed so that the accelerating voltage is highly stable. To secure stability advantage is taken of the fact that the gas pressure and current in the cathode tube and the accelerating voltage are interdependent. The gas pressure is therefore maintained constant by employing a special leak system, while a constant current is ensured by employing the saturation characteristics of a diode. The discharge pressure in the cathode chamber

is maintained at a constant value by a small diffusion pump and a fixed leak from a "leak chamber." The leakage rate is controlled by the leak chamber pressure, which can be raised by adjusting a needle valve or lowered by opening a valve to an evacuated reservoir. Cold-cathode discharge is used to give a beam of high current density, which can be employed for accelerating voltages of 15 to 80 kv.

The usual attachments are provided, and three types of plate holders are available, one of which enables three plates to be exposed without breaking the vacuum, while the second is fitted with a shutter so that the two halves of a plate can be exposed independently for comparison purposes. The third is a single-plate holder for taking one exposure only. Separate diffusion pumps are provided for the discharge and camera chambers with a common backing rotary pump. Both the rotary and diffusion pumps can be isolated from the camera while changing plates, so that only a few minutes are necessary to restore the vacuum afterward. A Pirani gauge head is provided for indicating the pressure conditions and carrying out leak detection.—W. EDWARDS & COMPANY, LTD., *Worsley Bridge-Road, Lower Sydenham, London, S. E. 26, England.*

Manufacturers' Literature

Fast Pulse Amplifier—Hewlett-Packard Journal, Vol. 1, No. 11, July, 1950, describes a new hp Model 460B amplifier, which is designed for a maximum output level of 125 volts open circuit—high enough to permit viewing on a cathode-ray tube.—HEWLETT-PACKARD COMPANY, *395 Page Mill Road, Palo Alto, California.*

Photo-micrographic Camera—Pamphlet GI-27 presents the Model "U" (Universal) camera, which features extreme versatility and convenience of operation. It can be used for micro, low power and macro work, copying, and projection. A great number of accessories are available, including a line of six objectives ranging in focal length from 20 to 250 mm, macro stage, light box for large objects, enlarger head, etc.—GAMMA INSTRUMENT COMPANY, INC., *P.O. Box 532, Great Neck, Long Island, New York.*

Magnetic Amplifiers—Bulletin, entitled "Magnetic Amplifiers—Circuits, Characteristics, Types," introduces three new types now being made available to industry: The High Performance Series, with output powers ranging from milliwatts to 385 watts, the High Gain Series, with outputs from ½ to 1200 watts, and the High Power Series, for 65 to 3660 watts.—VICKERS ELECTRIC DIVISION, *1815 Locust Street, St. Louis 3, Missouri.*

High Power Pulse Transformers—A design manual for pulse transformers, used in magnetron circuits, comprises one section of a report by Armour Research Foundation discussing the theory of pulse transformers and the Armour interleaved winding design. The design manual section permits the development of a pulse transformer to meet within narrow limits given operation requirements. Procedure for all design steps is given, and the calculations for a typical sample design are described for illustrative purposes. PB 100 478, *High Power Pulse Transformer Design and Development*, 229 pages including diagrams, graphs, and tables is available at $8 in microfilm, $28.75 in photostat. Orders should be accompanied by check or money order payable to the Librarian of Congress and addressed to the LIBRARY OF CONGRESS, PHOTODUPLICATION SERVICE, *Publication Board Project, Washington 25, D. C.*

Cost and Properties Comparator—A coat-pocket-sized, two-dial, ready reference guide to facts and figures on 12 leading plastics and 11 other structural and fabricating materials is based on the PMMA "Technical Data on Plastics," May, 1948, and the Department of Commerce Survey of Business, 1949. A quick twist of the twin dials gives comparative cost figures or condensed information on mechanical, thermal, electrical, optical, and chemical properties.—PLASTICS DIVISION, MONSANTO CHEMICAL COMPANY, *Springfield, Massachusetts.*

Management of Industrial Research—A new bulletin gives a selected and annotated bibliography on the management of research programs and projects. It has been prepared primarily from the viewpoint of the research director and of those in charge of research policy.—ARTHUR D. LITTLE, INC., *Cambridge 42, Massachusetts.*

Computers—Two bulletins, "Electrons at Work" and "Fundamentals of Electronic Calculation," describe in nontechnical language the functions of some calculating and business machines and discuss IBM services to research workers.—INTERNATIONAL BUSINESS MACHINES CORPORATION, *590 Madison Avenue, New York 22, New York.*

The Perkin-Elmer Instrument News—Summer 1950, Vol. 1, No. 4, contains a discussion of the application of polarized infra-red spectra to crystal structure determination, a progress report of the Punch-Card Committee for classification of infra-red spectra, and some abstracts of current articles in the field of electro-optical instruments.—THE PERKIN-ELMER CORPORATION, *Glenbrook, Connecticut.*

New Materials

Forest K. Harris: Associate Editor
in Charge of this Section
National Bureau of Standards, Washington, D. C.

Optical Quartz

Your editor has received a letter from which the following excerpt is quoted.

"Enclosed is a picture of a remarkable piece of optical quartz which I have recently acquired. It weighs 1000 pounds, and represents the central portion of a crystal which originally weighed four tons. This piece is flawless and wholly free of such optical defects as blue needles, Tyndall effect, bubbles, seeds, Chuva, phantoms, smokiness, or other defects visible in an arc lamp. Due to its enormous size, it has been impossible to examine it in polarized light to determine optical twinning, but as Brazilian quartz, in the

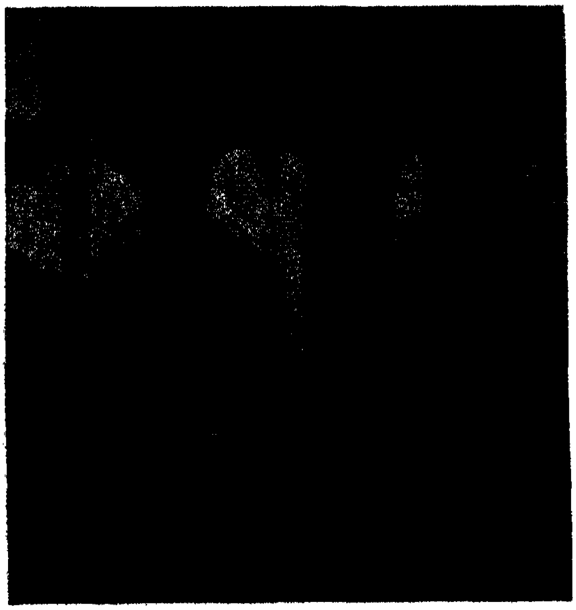

large sizes, is notably free of optical twinning near the center of the crystal, I have every hope that this piece is clean in this respect as well.

"It is my intention to saw this crystal into slabs some 6 to 12 inches thick, measuring parallel to the optic axis, and to examine these slabs in polarized light to detect optical twinning, after which the slabs will be marked off as to the clear portion and sold on the basis of such clear portion.

"This crystal is, in every way, unique and I wish to use it in the most efficient possible manner, both for the sake of monetary return and because such a crystal represents, in a sense, a trust for the benefit of the optical industry. I should, accordingly, like to enlist your help in publicizing its availability so that users who require pieces of quartz of unusual size or purity may be apprised of the availability of this piece. I hope, in this manner, to be able to cut slabs of such thickness as can be most efficiently used by the optical companies concerned."—Dan E. Mayers, *214 East 18 Street, New York 3, New York.*

Flaw Detection

Dy-Chek is an assembly of a red dye, a white liquid developer, and a cleaning and dye-removing liquid, to detect surface cracks and flaws in metal parts. In application the surface is prepared with the cleaner, the dye is applied and then removed with the cleaner and finally the developer is spread over the surface. Flaws show up as red markings where the dye has penetrated and has not been removed by the cleaner. These markings show up in sharp contrast to the white background of the developer. The liquids can be sprayed or brushed on a surface or can be applied by dipping.—Dy-Chek Company, *1513 East Broadway, Hawthorne, California.*

Vibration Isolation

Met-l-flex unit mounts are designed for mounting equipment subject to vibration or shock. They are of all-metal construction and are unaffected in spring rate or damping by extreme temperatures (−80 to 250°C), oil or moisture. High damping is provided by inter-wire friction in the woven-wire cushion, which reduces amplification at resonance and affords greater structural stability in the mounting system. Drift or permanent set in this cushion is negligible.—Robinson Aviation, Inc., *50 Industrial Avenue, Teterboro, New Jersey.*

Abrasion-Resistant Plastic

Enrup is a mixture of nitrile rubber and a thermosetting plastic which can be made in varying degrees of flexibility, and which is described as bridging the gap between soft and hard rubber. It is stated to be a high strength material which is resistant to abrasion and to chemicals and which can be formulated with physical characteristics to meet varying requirements. Tensile strength (varying with hardness) averages 4200 p.s.i.; specific gravity is about 1.3; water absorption is low; and the safe operating range is from 0 to 250°F. It has been used in high strength, low-cost gears which can be molded to close tolerances. In such applications, it is reported that Enrup gears have been in operation for more than a year where metal gears have failed within a few weeks. Other suggested applications include fuel-pump parts, battery cases, valve seats, bearings, tote boxes, electrical insulators and automotive parts. The material is available in the form of sheets, rods, tubes, gear blanks, and as molded parts.—United States Rubber Company, *Rockefeller Center, New York 20, New York.*

Decontamination

Radiacwash is a solution designed for the cleaning of surfaces contaminated by radioactivity. A number of actions, combining the physical and chemical principles of decontamination, contribute to the removal of radioactive contaminants from exposed surfaces. The liquid acts as a detergent, emulsifier, solvent, ion-extractor, surface wetter, and carrier. The maker states that in a laboratory test the radioactivity of a beaker contaminated with radio phosphorus was reduced to a value corresponding to a reading of 4.5 mr for a particular geometrical configuration of object and detector, by repeated scrubbings with water and a strong detergent. Under identical conditions the reading was reduced to 0.25 mr after 3 min. of agitation in the new cleaner.—Atomlab, *489 Fifth Avenue, New York 17, New York.*

Plastic Packing

Super-Seal plastic packing is now made with a securely vulcanized tape back as an integral part. This increases packing flexibility and permits the spiral to be twisted down to small shaft sizes and then cut into rings without breakage. Packing is available in six different styles to cover various ranges of operating conditions, which are clearly marked by different colors on the tape back for identification. These packings are resilient and homogeneous, and are composed of asbestos, antifrictional metal particles, flake graphite, and special binders. They do not harden at elevated temperatures and need not be removed as wear occurs. An added ring in the stuffing box is sufficient to maintain leakproof service. Full service recommendations are included in a booklet available from the manufacturer.—Crane Packing Company, *1800 Cuyler Street, Chicago 13, Illinois.*

Radiant Glass Panels

Pyrex 7740 heat-resistant glass is coated on one surface with a transparent conducting film for radiant heating. Backed by a metal reflector behind the film the panel will radiate 80 percent of the energy input through its uncoated surface. Mounted in a suitable frame it may be used for space heating, process drying, and electrostatic charge dissipation. A $12\times12\times\frac{7}{32}$-in. panel is available in 500- to 1500-watt rating at 110 volts and 1000 watts at 220 volts. Element temperatures range from 410 to 640°F in free air. A $16\times24\times\frac{7}{32}$-in. panel is made for 1000 and 1500 watts on 110-volt input, and 1000 to 3500 watts on 230 volts, with temperatures in free air from 356 to 600°F. Manufacturer's bulletin B-86 *Pyrex E-C Radiant Glass Panels* gives further information and data.—Corning Glass Works, *Corning, New York.*

Front-Surface Mirrors

Zeno-Kote is a process for producing front-surface mirrors having unusual durability and tarnish resistance. The reflecting surface is produced by evaporation of a special aluminum alloy under high vacuum. The reflecting surface is then protected by the deposition of an extremely hard transparent film which does not affect the reflectivity of the mirror but which permits it to be dusted or wiped without injury to the surface. Mirrors produced by this process have a reflectivity of about 93 percent in the visible spectrum, and can be made to meet any optical or dimensional tolerances. Further details can be obtained from the manufacturer.—Zenith Optical Laboratory, *123 West 64 Street, New York 23, New York.*

Metal Cleaning Sponge

A metal cleaning sponge, made of a continuous ribbon of curled monel metal, is now available. It is stated to be soft and flexible to handle, designed so that it will not splinter and injure the hands, and hard enough to insure long wear. Being rust and corrosion resistant, it can be used where other metallic or non-metallic cleaning pads might not serve. Because of its springiness and flexibility it will withstand repeated stretchings and rinsings, and the ease with which it may be cleaned helps to prevent the introduction of metallic impurities into equipment where contamination must be avoided.—Kleenette Manufacturing Company, *1269 West North Avenue, Chicago 22, Illinois.*

Low Expansion Steel

No. 430-ELC is a new stainless steel developed to have essentially the same expansion as glass. As a result it is particularly suited for use in products such as glass-steel television tubes. This steel is characterized by its relatively low cost as compared to previous compositions developed for the same purpose.—Armco Steel Corporation, *701 Curtis Street, Middletown, Ohio.*

THE REVIEW OF SCIENTIFIC INSTRUMENTS

VOLUME 21, NUMBER 11 *NOVEMBER, 1950*

Magnetic Tape Recorder for Very Low Frequency Phenomena*

PAUL E. GREEN, JR.
Research Laboratory of Electronics, Massachusetts Institute of Technology, Cambridge, Massachusetts

(Received June 23, 1950)

An apparatus is described for the recording of electrical signals of frequencies below 100 cycles per second on magnetic tape for subsequent playback. A system of wide deviation frequency modulation of an audio frequency carrier has been employed to eliminate the difficulties normally encountered in the direct recording of low frequency and d.c. signals.

GENERAL DESCRIPTION

IN certain investigations it is necessary to have permanent records of electrical signals whose frequency spectra lie below 100 cycles. Pen recorders, oscillograph cameras, and the like have provided a means of obtaining such records, but are useless when the need for playback arises. Conventional disk or tape recording procedures suffer from the inability to handle such low frequencies.

In this laboratory the problem arose as a need for a device which could record brain wave signals (1–100 cycles) and then reproduce them later as a function of time for statistical analysis by electronic means. It is the purpose of this paper to describe the equipment built for this purpose.

It was decided to use magnetic tape because of ease of handling and editing, and the possibility provided by such tapes of playing fairly long records repetitively using an endless loop arrangement. Because the analyzing equipment into which the playback output is to be fed can perform its analysis more quickly with higher frequency inputs, a speed step-up on playback is used. Two independent identical channels are provided so that two signals can be simultaneously recorded and their relative phase relations preserved.

Since the frequencies to be used are too low for direct recording, they are used to modulate a carrier of a higher, more convenient frequency. Amplitude modulation proved to be impractical because of excessive playback amplitude variations due to non-uniformity of the magnetic properties of the tape. For this reason, the recorder described here uses frequency modulation. A system somewhat similar to this has been described previously,[1] but it is felt that the details of the present equipment are sufficiently different and simplified to be of interest.

The f-m signal recorded on the tape has a center frequency of 1000 cycles per second with deviations from this of plus or minus 55 percent on modulation peaks. These large frequency swings are desirable in order that spurious tape speed variations shall not have appreciable influence. Linear tape speed is 3.0 inches per second during recording. The tape is played back at 15 inches per second into the demodulator circuit and the original signal, with all its frequencies multiplied by 5, is recovered at the output.

The tape-handling unit is an Amplifier Corporation of America Type 808-A twin track chassis modified for the new speeds and for simultaneous operation of both tracks. Conventional one-quarter-inch tape is used.

A block diagram of one of the two channels is shown in Fig. 1, with the corresponding detailed circuit diagram in Fig. 2.

RECORDING SECTION

Of the various means available for producing frequencies proportional to voltage, the most satisfactory one for the present purpose appeared to be the variable-bias multivibrator.[2] By varying the voltage to which both grids of a simple multivibrator are returned, it is possible to make the frequency vary almost linearly over a wide range, as shown in Fig. 3. (Circuit values

---

* This work has been supported in part by the Signal Corps, the Air Materiel Command, and the ONR.

[1] H. B. Shaper, Proc. I.R.E. 33, 753–760 (November, 1945).

[2] S. Bertram, Proc. I.R.E. 36, 277–280 (February, 1948).

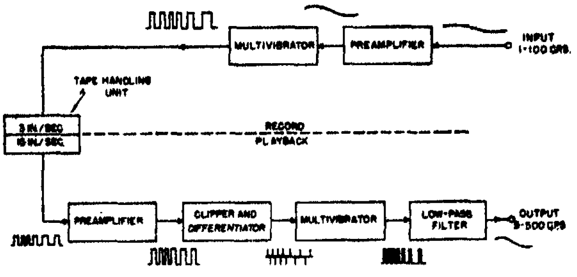

FIG. 1. Block diagram of f-m magnetic tape recording equipment.

and connections are those shown in Fig. 2.) Although the frequency *versus* voltage characteristic is steeper when the grid bias is negative, the improved linearity and convenience of power supply connection for the positive grid case made it more desirable.

The violently non-sinusoidal nature of the wave form produced by the multivibrator is of no consequence in this application, since, as will appear later, demodulation amounts merely to counting the rate at which the wave crosses the zero axis. Tape biasing and equalization are also unnecessary for the same reason. As shown in Fig. 2, the recording-playback head is energized directly by one of the plate circuits of the multivibrator. The resulting assymmetry of the multivibrator wave form has no effect.

The varying multivibrator bias voltage is obtained from the input signal by a preamplifier consisting of one stage of amplification and a cathode follower. In the present recorder, it was not necessary to have response down to d.c., so these two stages were made RC-coupled. It would be a fairly simple matter to provide for recording the d.c. level as well by substituting direct-coupled circuits instead, but then additional problems of long-time stability are encountered.

PLAYBACK SECTION

As shown in the lower halves of Figs. 1 and 2, the playback section consists of two amplifier stages, followed by a clipping and differentiating circuit, a multivibrator, and a low pass filter. The clipper is a bistable circuit which can be adjusted to change from one state to the other each time the input wave crosses the zero axis. The large rectangular pulses produced are differentiated to feed sharp triggers to the monostable multivibrator. This multivibrator generates a constant-width and constant-height pulse for each positive trigger, that is, for each cycle of the incoming f-m signal. By passing the multivibrator output through a low pass filter whose cut-off frequency is lower than the lowest excursion of the carrier, only the average value of the pulse train remains at the output. This is proportional to the instantaneous carrier frequency and corresponds therefore to the desired signal originally impressed on the carrier (with all frequencies multiplied by a factor of five due to tape speed-up).

Figure 4 shows the frequency relations involved in the demodulator circuits. The carrier center frequency is 5000 cycles, with maximum and minimum frequency excursions to approximately 7750 and 2250 cycles respectively. The low pass filter is designed to reject all components of the f-m spectrum, yet to pass modulation frequencies up to 500 cycles (corresponding to an input of 100 cycles—approximately the upper limit of the brain waves of interest here).

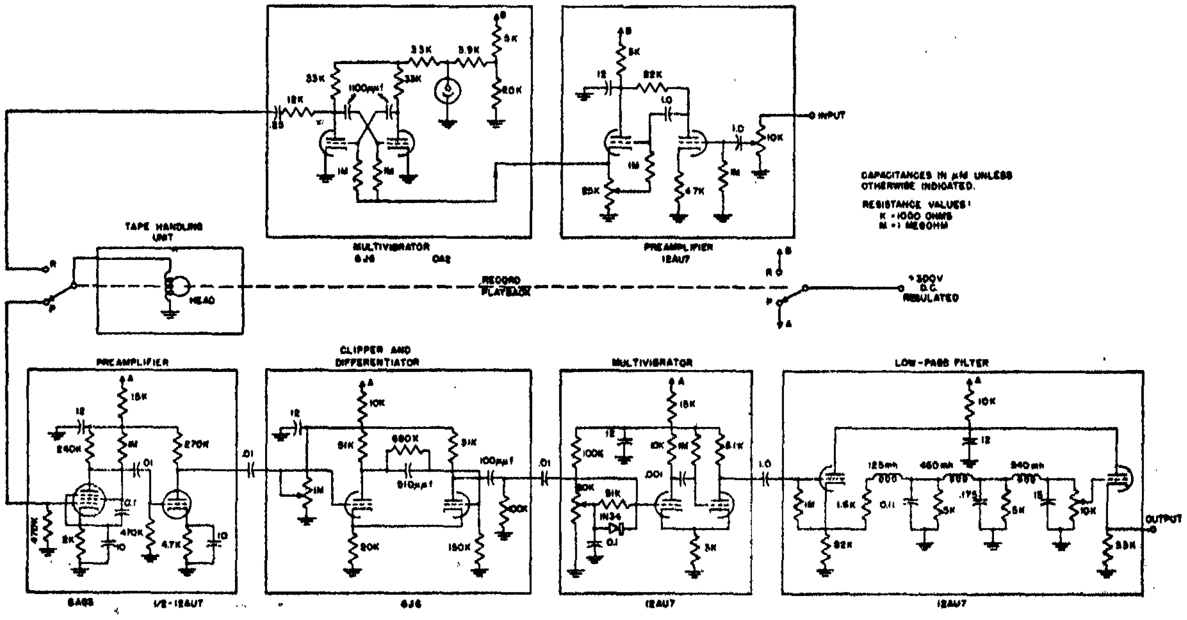

FIG. 2. Schematic diagram of tape recorder.

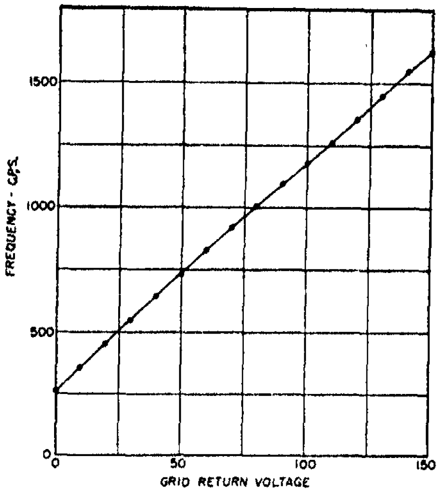

FIG. 3. Recording multivibrator frequency *versus* grid bias.

By using a recording multivibrator of five times the frequency used here, the playback could be performed at the same tape speed as that used for recording.

PERFORMANCE

The upper curve in Fig. 4 indicates the over-all frequency response of the system. The high frequency attenuation is seen to be due to the filter characteristic, whereas at low frequencies, attenuation occurs in the RC coupling circuits in recording preamplifier and demodulator multivibrator output.

Flutter in the tape transport mechanism as used is about 0.5 percent. This represents an unwanted noise component in the output giving a signal-to-noise ratio for the maximum (55 percent) carrier swings of 100 to 1, or 40 db.

The recorder is operated in conjunction with conventional electroencephalographic equipment, which is customarily employed to make pen recordings of the incoming signal.

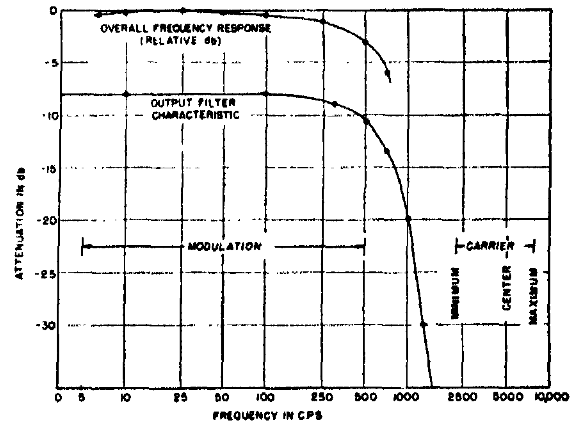

FIG. 4. Over-all frequency response and output filter characteristic.

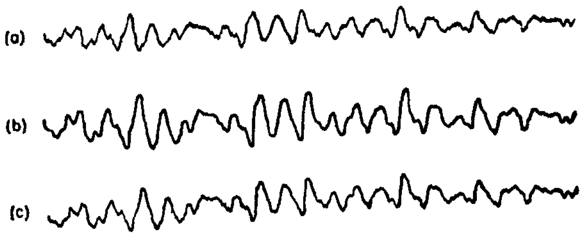

FIG. 5. Performance of one channel of the recorder with a brain wave signal. (a) Electrical input to both pen recorder and tape recorder. (b) Record made by conventional pen recorder. (c) Playback from tape recorder.

Figure 5 shows a comparison between simultaneous brain wave records made by such a pen recorder and the magnetic tape recorder described here. Aside from a loss of frequency components above about 100 cycles the system is seen to provide faithful reproduction of the original input. The frequencies above 100 cycles are usually attributed to muscle activity and are not of particular interest here. The duration of traces (a) and (b) is 2.3 seconds, and that of (c), 0.46 seconds, due to increased tape speed on playback.

ACKNOWLEDGMENT

The author wishes to express his appreciation to Professor J. B. Wiesner and Dr. O. H. Straus of the Research Laboratory of Electronics for their aid and supervision, and to Mr. James Casby of Massachusetts General Hospital for his assistance in obtaining the data presented in Fig. 5.

THE REVIEW OF SCIENTIFIC INSTRUMENTS VOLUME 21, NUMBER 11 NOVEMBER, 1950

An Apparatus for the Study of Electrets

LARRY A. FREEDMAN AND LOUIS A. ROSENTHAL
Rutgers University, College of Engineering, New Brunswick, New Jersey

(Received June 23, 1950)

An apparatus capable of continuously measuring and recording electret strength is described. It consists of a mechanically driven condenser whose induced voltage, due to the electric field of the electret, is filtered and amplified before being applied to a recorder. Some experimental observations of the transition from heterocharge to homocharge are presented.

INTRODUCTION

THE majority of electret strength measurements have been confined, in the past, to the charge transfer method. The effective electret surface charge is transferred to a charge sensitive instrument such as the electrometer, electroscope, or low capacity electrostatic voltmeter.[1,2] This method is quite tedious when numerous measurements are desired for the various time studies of electrets. Strength characteristics with time under normal conditions or with variations in temperature, pressure and humidity are of considerable interest at present. The apparatus herein described serves the obvious need for a completely automatic measuring system.

THE MEASURING APPARATUS

The measuring apparatus consists of a mechanically driven capacitor in which the electret is mounted. The voltage output of the capacitor is passed on to the associated equipment shown in block form in Fig. 1. The equipment includes a high input impedance cathode follower with a 60-cycle twin "T" filter, a standard amplifier and rectifier unit,[3] and a recorder.[4] Continuous visual indication of relative electret strength is given by the recorder.

An assembly drawing of the driven capacitor is shown in Fig. 2. It consists of a frame, a solenoid mounting and an electrode mounted on flat springs. It is designed to give electrode motion of about one-hundredth to one thirty-second of an inch at 120 cycles per second.[5] The springs are designed so that their natural resonant frequency is well above the 120 cycles per second operating frequency. They consist of 1 by $\frac{1}{8}$ in. steel 4 in. long and are fastened rigidly to the frame which is made of $\frac{1}{2}$ in. steel 4 in. wide. This gives enough mass to prevent vibrations of the whole device and is at the same time light enough to be easily portable. The solenoid is mounted on the overhead part of the frame. A brass rod is inserted at the ends of the springs with a brass collar and nuts for rigid mounting. Fastened at the top of the rod with a screw thread and nut is the iron plunger, while at the bottom is the brass electrode. The electrode consists of a circular brass disk $1\frac{5}{8}$ in. in diameter and $\frac{1}{8}$ in. thick with a collar for mounting on the brass rod.

The plunger is centered axially in the solenoid[6] and adjusted so that it is just below is normal centered-position. When it is positioned in this way, a relatively small amount of current is necessary for a usable amplittude of oscillations. The solenoid is fed with 60-cycle a.c. voltage. This voltage is controlled with a variac and may be varied over a relatively wide range. For satisfactory operation however, 100 volts is sufficient.

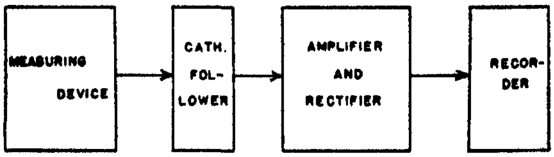

FIG. 1. Assembly drawing of the mechanically driven condenser. The solenoid is not shown, but is mounted on the upper frame for correct motion of the electrode structure.

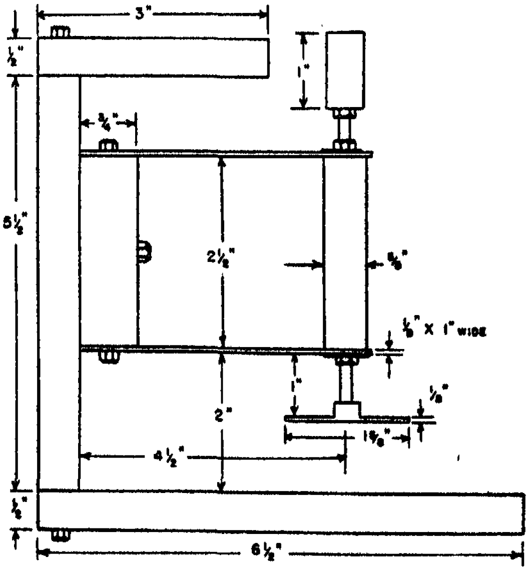

FIG. 2. Block diagram of measuring apparatus.

---

[1] F. Gutmann, Rev. Mod. Phys. 20, 457 (1948).

[2] A. Gemant, Phil. Mag. 20, 929 (1935).

[3] TAA-16EA Amplifier Serial No. 29-M.I.T. Radiation Lab. built by Electronic Corporation of America.

[4] Esterline-Angus Company—1 ma 1600 ohms.

[5] For a 60-cycle per second applied voltage, there will be a maximum field in the solenoid twice in each cycle. The plunger will be drawn toward the center position in the solenoid twice for each cycle and 120-cycle motion of the plunger will result.

[6] Solenoid from General Electric Company circuit breaker CN-1 for 110 volts a.c.

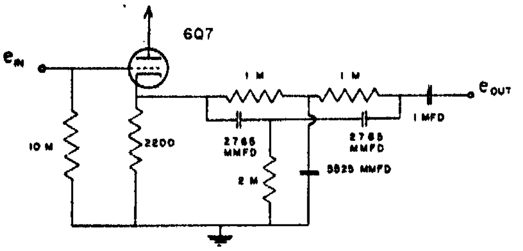

FIG. 3. The cathode follower with filter to eliminate stray 60 c.p.s. pickup.

When measurements are made, about $\frac{3}{4}$ in. of insulating material, such as polystyrene, is placed on the base of the device and on this is placed an electrode consisting of a thin sheet of aluminum or tin foil. The electret is then placed on this electrode, and the upper electrode and the frame are grounded. The lower electrode on which the electret is placed is the electrode of varying potential, and to this is attached the pick-up lead. It has also been found that copper mesh used for electrostatic shielding, when placed around the springs and the electrodes, prevents an excess of stray pick-up.

The action of the oscillating electrode above the surface of the electret is similar to the vibrating plate of the condenser microphone. As the electrode is displaced sinusoidally in the field of the electret, the potential induced on this plate varies. If a constant gradient is assumed for a very small amplitude of vibrations, the variation in potential on the plate will be sinusoidal. Stray pick-up is a serious problem so that the frame and the oscillating electrode are grounded. This causes the potential at the bottom surface of the electret to vary and it is from this surface that the variations in potential are passed on to the associated equipment.

Because of the small voltages and correspondingly small currents associated with the device, it is necessary to use an amplifier with a very high input impedance. Since the induced electret voltage is 120 c.p.s. and 60 c.p.s. pick-up may be large, it is desirable to filter the output before amplifying and recording. Since an input impedance of the order of megohms is not easily attainable with a filter a cathode follower stage was constructed with the filter across the output, as shown in Fig. 3. The triode section of a 6Q7 was employed so that a short lead could be used to the grid cap, and at the same time an input resistor of ten megohms could be used. The twin "T" filter attenuates the 60 cycle by 25 db while passing the 120 cycle with negligible attenuation.

The output of the cathode follower was fed to a standard amplifier-detector unit available in the laboratory. The amplifier had a maximum sensitivity of 100 microvolts per milliampere which gives a full scale meter reading of one milliampere for an input level of 100 microvolts. The meter and recorder movements both had a one milliampere full scale deflection so that the amplifier output could be read, or switched to the recorder for the same indication. The recorder speed is readily changed so that speeds of 0.75 inch per 15 seconds, per minute, per 15 minutes, or per hour may be used. For most long time recordings a speed of 0.75 inch per hour was used.

EXPERIMENTAL RESULTS

An electret mixture of 40 percent carnauba wax, 40 percent rosin, and 20 percent beeswax was used for testing purposes. This composition has good mechanical strength as well as the desired electrical properties.

Figure 4 is a typical recording obtained with the apparatus. Zero time represents the electret strength immediately upon removal from the charging electrodes. An apparent heterocharge is present at this point which gradually decreases to zero charge after about five hours. The zero signal level indicates a null in the electret charge.[7] This is followed by a more gradual rise after which the maximum signal level is reached in about fifteen hours. This signal level represents a homocharge and is the final strength attained by the electret; no change being evidenced in a month's time.

It is interesting to note that the transition from heterocharge to homocharge appears to take place in

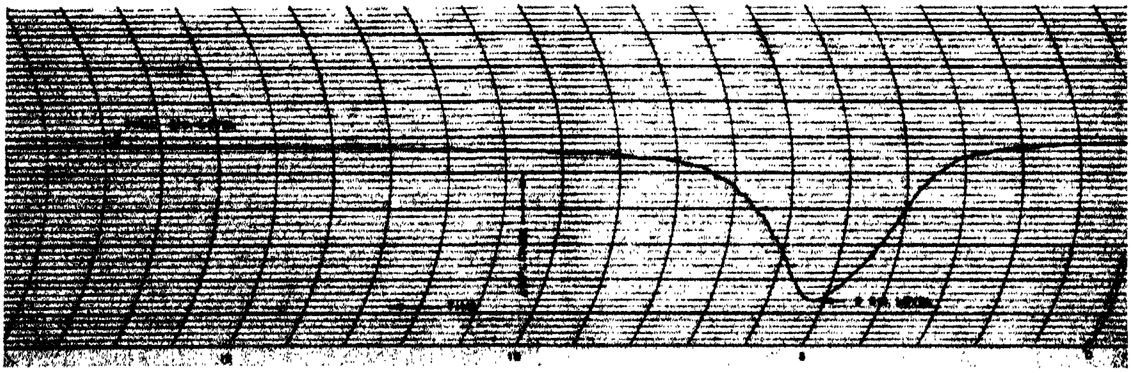

FIG. 4. The recorded strength of a newly formed electret with time. The electret was made with a field of 10 KV/cm and the chart speed is 0.75 in./hr.

---

[7] Since the detector is not polarity sensitive, the heterocharge and homocharge are recorded in the same direction.

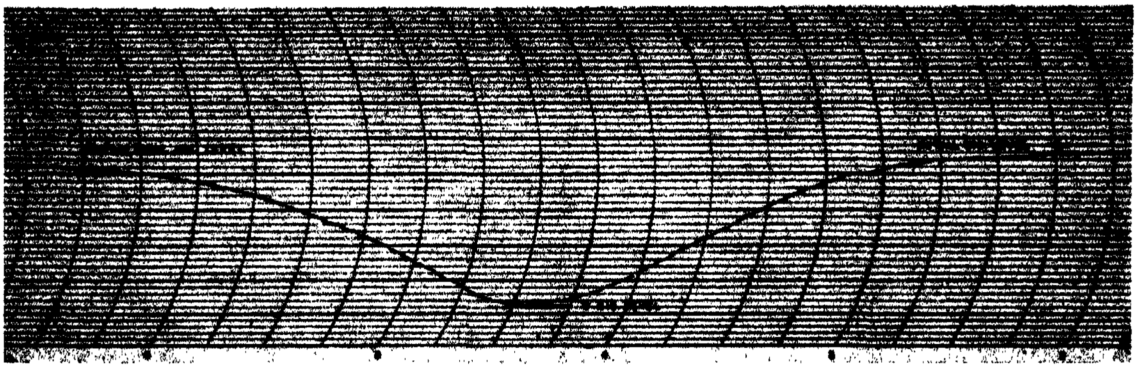

FIG. 5. The transition region is expanded by increasing the recorder speed. The electret is identical to that of Fig. 4; the chart speed has been increased to 3 in./hr.

discontinuous steps. Figure 5 shows the transition region using a faster recording speed. A speed of three inches per hour was used while only three quarters of an inch per hour was used in Fig. 4. The duration of the transition is about the same in either case but the discontinuities are more apparent at these higher recording speeds.

Other interesting and informative experiments on electrets may be performed with the aid of the apparatus described. Such variables as pressure, temperature, and humidity may be controlled and the electret strength measured. It is hoped that the device will afford a valuable tool to the experimenter in electrets.

The authors wish to acknowledge the aid and cooperation received from Professor J. L. Potter of the Electrical Engineering Department.

THE REVIEW OF SCIENTIFIC INSTRUMENTS VOLUME 21, NUMBER 11 NOVEMBER, 1950

Transmission of Beta-Rays by Nylon and Formvar*

R. B. HELLER, E. F. STURCKEN, AND A. H. WEBER
Saint Louis University, St. Louis, Missouri

(Received June 29, 1950)

The percent beta-ray transmission by thin Nylon and Formvar films (windows) was studied to obtain experimental "absorption" corrections to be used with G-M counters employing such thin windows. It was found that window "absorption" included (1) energy loss of electrons traversing the films and (2) scattering of incident electrons by the film (a geometry effect). The results are plotted in several ways to exhibit the various factors involved and to permit easy use in applying the corrections. It was found that scattering of transmitted electrons was a factor of considerable importance, whereas the energy lost in traversing the film was not very important for the range investigated. The electron energy range investigated was limited to the region in which the "absorption" correction was considerable for the window thicknesses used. A scintillation counter was used as the detector, and the source of monoenergetic electrons was an electron gun with electrostatic focusing.

I. INTRODUCTION

THE problem of "absorption" of low energy electrons in thin end-window G-M counters has become an important one, and experimental correction factors for these effects should be made if any accurate measurements are to be obtained in low energy beta-ray spectroscopy where these counters are employed for detection.

It was found in the present investigation that, for a given beta-ray energy and film (window) thickness, the apparent absorption of the window was a function of (1) the scattering of the incident electrons by the window and (2) the energy lost by the electrons in traversing the window.

The method of window thickness correction in G-M counters ordinarily applied[1] consists in extrapolating to zero window thickness (for various constant beta-energies) an experimental counting rate *vs.* window thickness curve. This method is always questionable because of the uncertainty of the extrapolation in the region of very thin films. Also, to apply such a method with the apparatus used in this investigation (scintillation counter plus electron gun with electrostatic focusing) would require maintaining constant the electron beam current, which would be difficult.

---

* This work was sponsored by the AEC, Contract No. 11-1-58.

[1] See, for example, F. A. Scott, Phys. Rev. 48, 391 (1935).

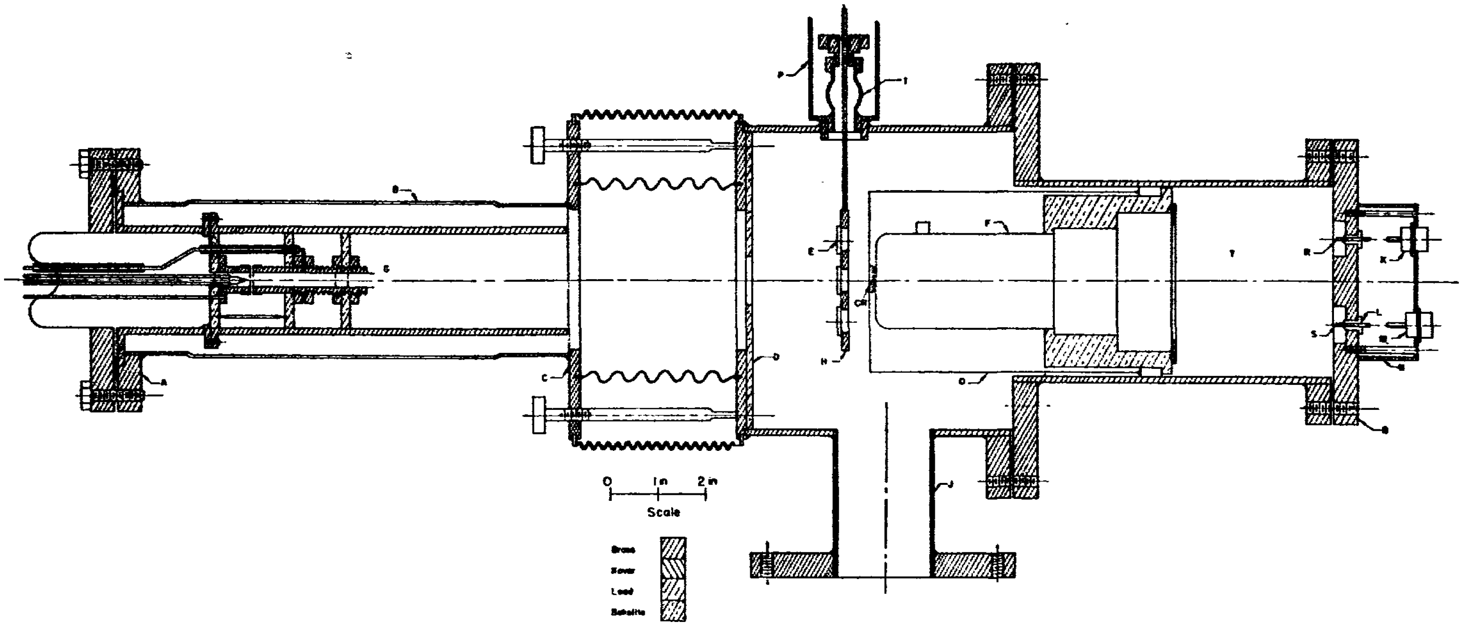

FIG. 1. Cross-sectional view of the apparatus. Solid triangles at joints indicate soft solder, open triangles silver solder. *A*, end plate to receive electron gun, with 6 holes spaced every 60° tapped for ¼-20 bolts; *B*, Pyrex insulator, sealed to Kovar, to separate second and third anodes; *C*, flexible Cu bellows with three thumb screws and springs for adjusting the electron gun; *D*, Pb diaphragm to block light from filament of electron gun; *E*, Al button for mounting films; *F*, C-7140 photo-multiplier tube; *G*, electron gun (C. T. Keogh and A. H. Weber, J. App. Phys. 19, 1077 (1948)). *H*, current collector or film holder; *I*, glass and Kovar insulator with *O*-ring sealed brass rod through center screw hole at the end of the rod for attachment of *H*; *J*, pump-out stack to oil diffusion pump; *K*, coaxial lead for photo-multiplier tube voltage; *M*, coaxial lead for output of photo-tube; *N*, brass cap for electrical shielding of output lead wires; *O*, mu-metal shield to minimize magnetic effects; *P*, shield for lead to electrometer (not shown); *Q*, end plate; *L*, polystyrene lead-through vacuum-tight bushings; *CR*, $CdWO_4$ crystal mounted on inside of mu-metal shield; *R*, lead to ground; *S*, lead to anode of photo-multiplier tube; *T*, space for resistor housing.

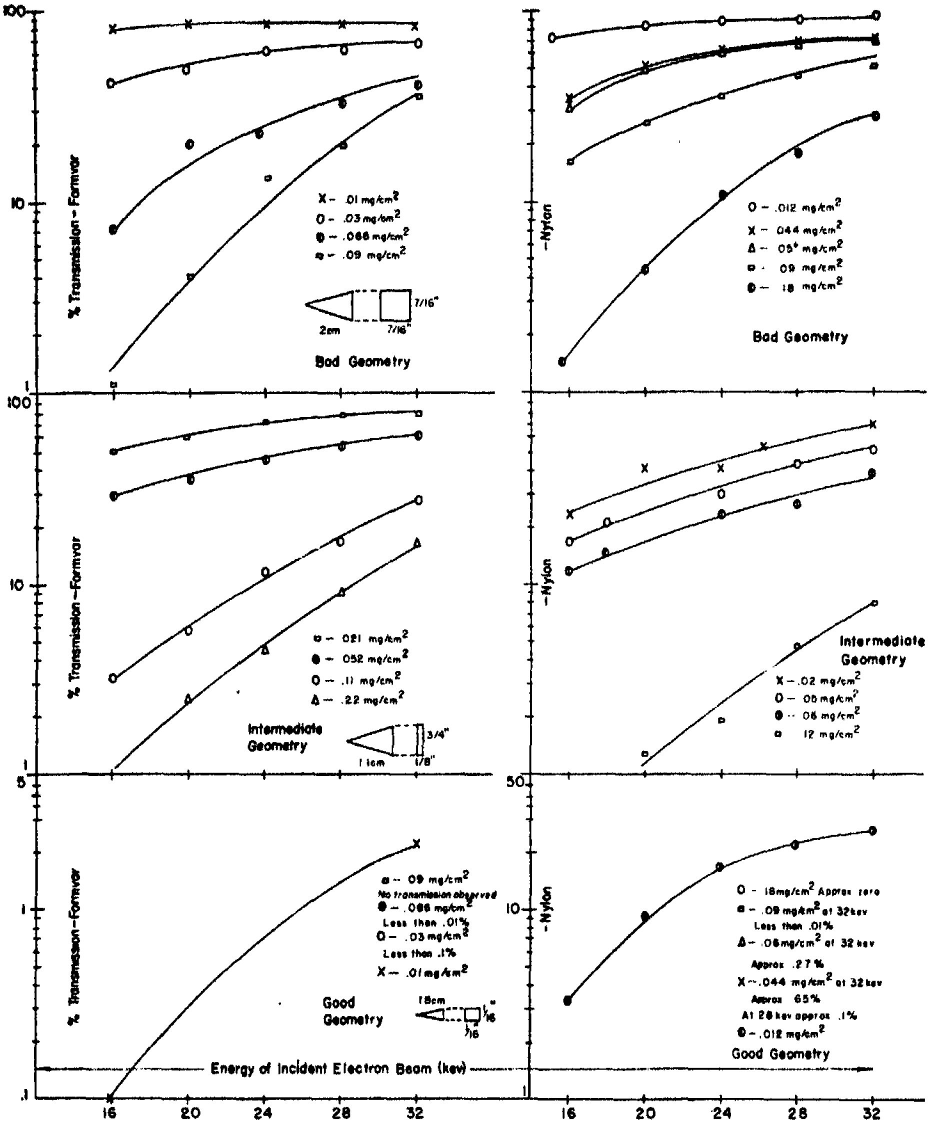

FIG. 2. Percent transmission *vs.* electron beam energy for films of Formvar and Nylon of different weights. The scaler pulse-height discriminator was set at zero for all readings. Electron gun filament current operated in the neighborhood of 1.5 amp. The geometries (*Bad*, *Intermediate*, *Good*) are defined by the diagrams so labeled; area and shape of crystal surface and distance from film are specified. Bad and good geometry data were obtained with a cadmium tungstate crystal and C-7140 RCA photo-tube; intermediate geometry data were obtained with a calcium tungstate crystal and a 1P21 RCA photo-tube.

To avoid the use of a detector which already had a window in the determination of "window corrections" and to eliminate the necessity of maintaining constant the electron beam current, it was decided to use a scintillation detector which is a "windowless" counter. The effect of scattering was studied by determining the percentage transmission[2] through thin Nylon and Formvar windows as a function of geometry (size of the crystal and its distance from the window) at distances such that the area presented by the scintillating crystal to the radiation was the important factor. The effect of energy loss on the "absorption" correction was studied by determining the change in counting rate due to a change in electron energy alone, so that the above measurements of counting rate for the transmitted beam intensity can be corrected to the same energy as the incident beam intensity and the I and I_0 measurements will be for the same energy.

It was found that scattering of transmitted electrons by the windows gave rise to a considerable part of the "absorption" correction. The electron energy range investigated is limited to the region in which the corrections are considerable for the window thicknesses used.

At approximately 50 kv the corrections considered here are negligible; extrapolation of the curves of Fig. 2 from 32 to 50 kv appears justifiable. In all transmission experiments the estimated error is at most ten percent.

II. EXPERIMENTAL

The monoenergetic electron beam was obtained from an electron gun, G (Fig. 1), using electrostatic focusing.

---

[2] The percentage transmission is defined as the ratio of the transmitted beam intensity I (the counting rate with sample minus background) to the incident beam intensity I_0 (the counting rate without sample minus background). The background was found to be negligible (less than 0.01 percent) in all cases.

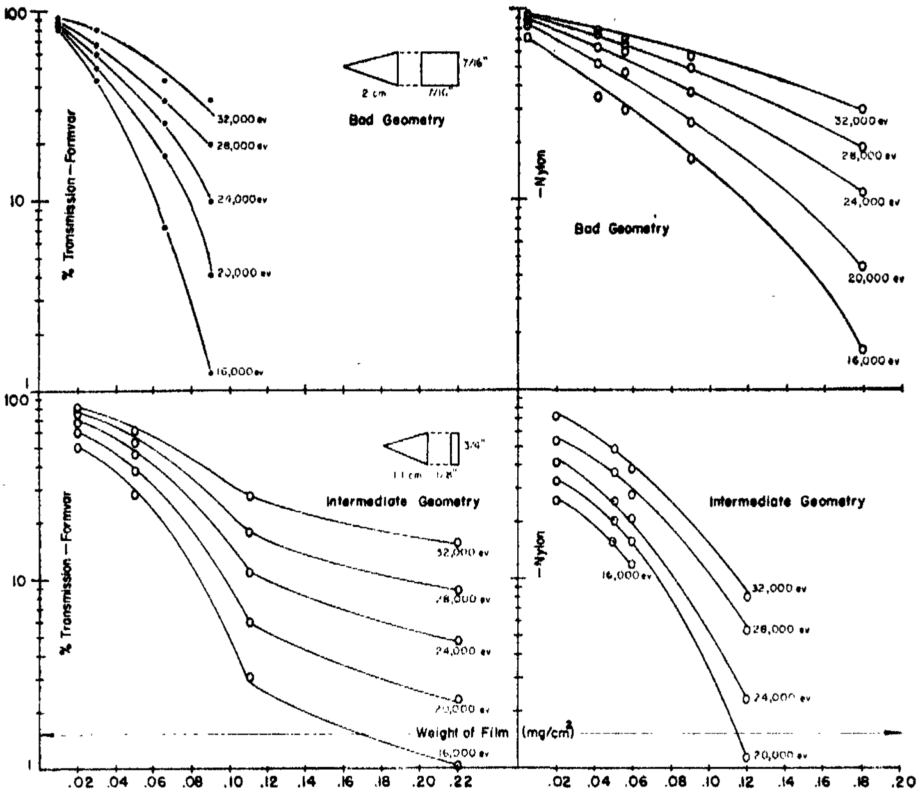

FIG. 3. Percent transmission *vs.* film weight at constant electron beam energy. These curves were plotted from the data of Fig. 2.

The voltage was varied from 16 to 32 kv in steps of 4 kv. To minimize spurious counts caused by light from the filament, four things were done: (1) the electron gun filament was operated at a temperature which would assure adequate electron emission along with minimum light output, the latter to minimize counts due to filament light; (2) a metal shield was placed around the photo-tube leaving a small hole only exposing the crystal (fluorescent[3] material was placed around the hole to facilitate locating the beam on the crystal); (3) the beam was focused off the crystal and brought on with a magnet when a run was taken (this procedure also minimized charging of the crystal); (4) a circular lead plate with a small hole, *D* (Fig. 1), was placed in the chamber. The arrangement of Fig. 1 was employed for the bad and good geometry experiments.

The intermediate geometry experiments employed the apparatus of Fig. 1, with the exception that a 1P21 photo-multiplier tube with a calcium tungstate crystal[4] mounted directly on the window of the photo-tube was used. The crystal was polished and, because of the high refractive index of calcium tungstate, was coated with evaporated aluminum[5] on parallel long sides to prevent loss of light from total internal reflection and scattering. The crystal was Aquadaged around the edges and grounded to minimize accumulation of charge.

The Nylon and Formvar windows were inserted in and out of the electron beam with an O-ring sealed probe, *H* (Fig. 1). Three- to ten-sec. counting periods were used (to avoid charging the crystal), and the average value of I_0 was controlled to give a probable error in counting of less than 0.2 percent.

The Nylon films were prepared in the usual manner.[6] Clear films 25 cm² in area were obtained by this method. A uniform piece about one cm² was selected from the film and mounted in a holder, *E* (Fig. 1), which was fastened to the end of the O-ring sealed probe for the experiment, *H* (Fig. 1). The method of preparation of Formvar films was the same as that of Nylon with the exception that ethylene dichloride was used as a solvent.

It was reported[7] that calcium tungstate had a serious "afterglow" following exposure to extreme radiation intensities, so cadmium tungstate[8] was used in the good and bad geometry experiments which were performed after the intermediate geometry experiments. An area of $\frac{7}{16}\times\frac{7}{16}$ in. of the crystal was used for the bad geome-

---

[3] RCA Fluorescent Screen Material, Zns-cds-2272, Stock No. 47655, suspended in a 50-50 (by volume) mixture of ethylene dichloride and dioxane.

[4] Memorandum on Synthetic Calcium Tungstate as a Scintillation Counter Crystal (Linde Air Products Co., 30 East 42nd Street, New York).

[5] An evaporated aluminum film was applied to the crystal by Evaporated Metal Films Corporation, Ithaca, New York.

[6] Brown, Felber, Richards, and Saxon, Rev. Sci. Inst. 19, 820 (1948).

[7] W. H. Jordan, Scintillation Counter Symposium, AECU-583, Tech. Info. Division, Oak Ridge Tennessee AEC, Oak Ridge, Tennessee; 1-18-50—700-A14181.

[8] Obtained also from Linde Air Products Co.; the crystal was a single cleaved boule section approximately $\frac{3}{16}\times\frac{1}{2}\times1\frac{1}{2}$ in.

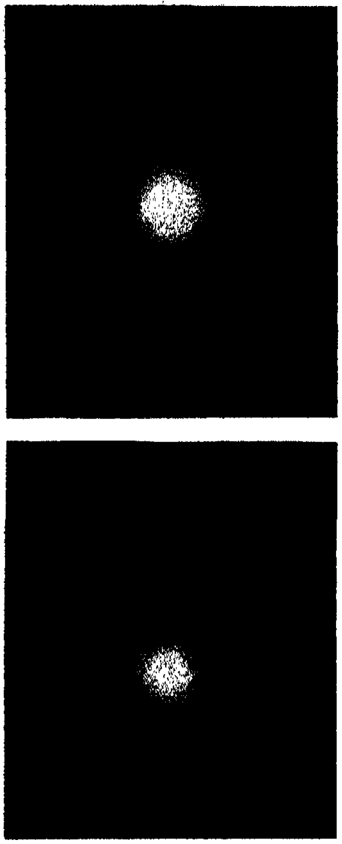

FIG. 4. Electron diffraction patterns of Formvar (lower) and Nylon (upper) films. The films were 0.01 mg/cm^2 in weight. The accelerating voltage was 20 kv. In the printing of the positives from the negatives, the exposure was varied to bring out each individual ring.

try, and the arrangement was changed to good geometry by the placing of a carbon button with a $\frac{1}{16}$-in. square hole directly in front of the crystal. The procedure for taking data was the same as for the intermediate geometry experiments, with the exception that three-sec. counting periods were used always and the beam was focused on the crystal but deflected magnetically until a reading was taken. The large surface of the C-7140 photo-tube insured good light collection.

The change in counting rate due to a change in energy alone, that is, the response of the photo-tube *vs.* electron beam energy with constant electron beam current, was measured for the 1P21 and C-7140 photo-tubes. The apparatus of Fig. 1 was used for these experiments. A current collector in the form of a brass cup coated with Aquadag replaced the holder, *H*, of Fig. 1, and an electronic electrometer connected through *P* (Fig. 1) with a sensitivity of 2×10^{-13} amp./division was used to maintain a constant beam current for various beta-ray energies. Calcium tungstate was used as the scintillator. The detailed results of these experiments are not reported here; but it was found that the energy loss of electrons in traversing the films contributed a maximum of ten percent to the "absorption" correction, and this was within the experimental error of the transmission experiments. However, for energies lower than 16 kv, the energy lost in traversing the windows would become a considerable part of the "absorption" correction and would have to be applied to the transmission curves. To estimate the energy lost in traversing a thin window, the aluminum equivalent of the window was employed in conjunction with the curve of specific energy loss for singly charged particles *vs.* kinetic energy.[9,10]

III. RESULTS

The results of the transmission experiments are shown by Figs. 2 and 3. The window thicknesses used were selected on the basis of those to be employed in G-M counters. It is to be noted that the measured transmission varied most markedly in the region of the electron energies employed in these experiments; the curves (except for good geometry) extrapolate to 100 percent transmission as the energy is increased beyond 50 kv. It is observed that Formvar and Nylon have different transmission properties. In an attempt to explain this fact, electron diffraction patterns of Nylon and Formvar windows (Fig. 4) were obtained. These patterns show that (1) Nylon has a more regular structure than Formvar and (2) there is greater incoherent scattering in Formvar than in Nylon. With these considerations it would not be expected that Nylon and Formvar would have the same transmission properties.

For the good and bad geometry experiments a magnetic shield was used; however, in the intermediate geometry experiments the beam was deflected on the crystal with a magnet and a shield was not used. Graves[11] has reported that magnetic fields affect the response of scintillation counters. In this investigation all measurements were on a relative basis, and (since the magnetic field was present in both the I and I_0 readings) the results of the transmission experiments were not affected.

It is hoped that these results will permit investigators in this field to make experimental window "absorption" corrections.

Somewhat similar experiments to those here described were performed by Schonland[12] with Au and Al films (thinnest foil 0.15 mg/cm^2, approximately). The results are also similar to those of the present work.

---

[9] Livingston and Bethe, Rev. of Mod. Phys. 9 (1937); *Nuclear Physics Laboratory Manual* (Heinicke Instrument Corp., 315 Alexander St., Rochester, N. Y.), p. 7.

[10] Aron, Hoffman, and Williams, "Range Energy Curves," AECU-663, Tech. Info. Division, ORE, Oak Ridge, Tenn., 4-20-50—675-A20779.

[11] J. D. Graves, Phys. Rev. 78, 309 (1950).

[12] B. F. T. Schonland, Proc. Roy. Soc. A104, 235 (1923).

THE REVIEW OF SCIENTIFIC INSTRUMENTS VOLUME 21, NUMBER 11 NOVEMBER, 1950

A Pulse Generator for the Millimicrosecond Range

R. L. Garwin
Institute for Nuclear Studies, University of Chicago, Chicago, Illinois

(Received June 16, 1950)

A description is given of a laboratory pulse generator producing pulses with rise and decay times less than 2×10^{-10} sec. at a repetition rate of 120/sec. Three simultaneous outputs are available, variable in amplitude from 100 microvolts to 100 volts and accurate to a few percent.

INTRODUCTION

The considerable interest evoked by a pulse generator constructed here last year has prompted publication of this paper. This instrument has proved invaluable in the testing of distributed amplifiers and very fast coincidence circuits, and in calibrating fast electronic equipment.

DESCRIPTION

The heart of the pulser is a switch which is incorporated into the center conductor of a coaxial line and is operated at 120 cycles by the 60-cycle magnetic field from a coil external to the outer conductor. In Fig. 1 both the lower flexible "reed" and the longer upper contact are ferromagnetic, so that the reed snaps from its rest position as indicated in the figure to make contact when an axial magnetic field is applied.[1]

The reed is so constructed that the contacts are continuously wet with mercury by capillary action from a drop of the metal at the base of the capsule. The liquid serves the important purpose of bridging mechanical chatter and so completely eliminates multiple pulses. A 10-atm hydrogen filling keeps the mercury clean and increases the sparking potential to some 8 kv.

If now the copper shield diameter is so chosen as to make an approximate impedance match with some common high frequency cable, and if a short open-ended section of the cable is attached to the upper contact and charged to potential V, and an essentially infinite or matched length is connected to the reed, then on closing the switch a rectangular pulse of amplitude $V/2$ and duration twice the electrical length of the pulse forming line is propagated into the infinite line.

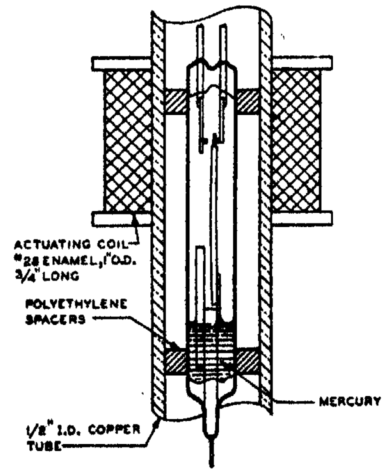

FIG. 1. Rapid coaxial switch.

The circuit of the instrument (Fig. 2) is thus clear: a connector is available to which to attach various lengths of pulse forming line (Pulse widths from 5×10^{-10} to 10^{-6} sec. are obtained from lines ranging from 5 cm to 100 m long). The relay is actuated by 6.3 v.a.c. applied to a coil wound on the copper shield. The voltage regulator tubes and the switches allow full scale output voltages from 100 v to 0.001 v in decimal steps, while the wire-wound potentiometer allows one-percent accuracy in setting pulse heights. The tee which splits the output pulse into three introduces an attenuation of a factor 3, so that the line must be charged to 600 v to produce output pulses of 100-v amplitude. The reversing switch allows either positive or negative pulses to be obtained.

TECHNIQUE

The indicated pulse heights hold, of course, only if the system is matched in impedance at each point. Thus, if an output is not being used, it must be terminated in its characteristic impedance to avoid reflections. The system impedance used in the pulser here constructed is 75 ohms, for which no constant-impedance connectors are available. Accordingly, the AN-83 series connectors

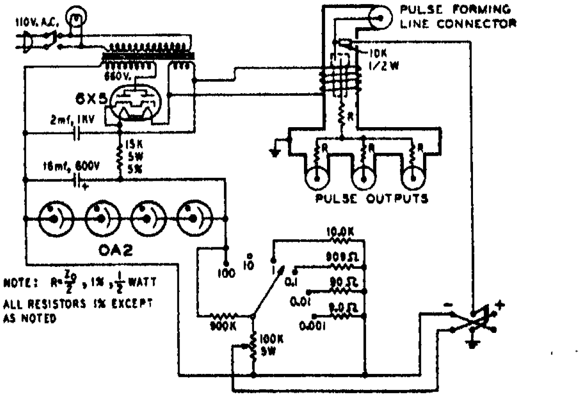

FIG. 2. Pulser schematic.

---

[1] The glass-enclosed switch is taken from a Western Electric D-168479 synchronous relay.

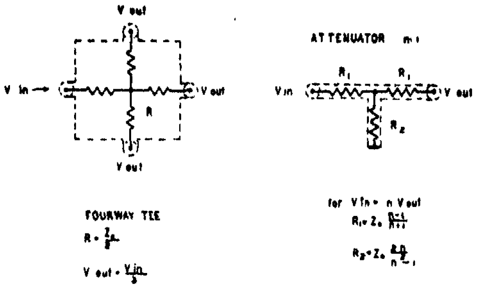

FIG. 3. Very high speed elements.

were used, introducing a time constant about 10^{-11} sec. at each junction. (The 50-ohm type *N* connectors will match a 50-ohm line into the microwave region.) It can be shown theoretically and has been observed that a connector of impedance Z and of electrical length (time) t, short compared to the pulse rise time τ, will introduce in a system of impedance Z_0 a fractional voltage reflection $t(Z-Z_0)/\tau(Z+Z_0)$. In the present instrument this is ~ 2 percent. In using this instrument it is necessary to have several connectors with resistors carefully soldered in to terminate properly non-infinite lines. Open circuited lines are approximated by the noncontacting weatherproofing plug, while shorted terminations are most conveniently obtained by inserting into the plug a small metal cylinder which efficiently shorts the line. While disk resistors have been used in some cases, it has been found that the Allen-Bradley ½-watt carbon resistors have good characteristics for rise times about 2×10^{-10} sec.

For convenience some matched tees and attenuators for a system of impedance Z_0 are shown in Fig. 3. It is best not to take an attenuation greater than 10:1 in a single attenuator as the shunt resistance becomes so low that the inductive impedance is important. In the range above 10^{-10} sec. it has been found sufficient to maintain minimum inductance by the use of closely fitting metal shields to which the connectors are attached. For higher frequencies at least two approaches are obvious: to use rod and disk resistors as the elements, or to use a lossy line.

PERFORMANCE

The operation of the pulser is perhaps best illustrated by the measurement of its apparent rise time. A long length (10 m) of 75-ohm cable was used as pulse forming line, while two other lengths led two output pulses to the intensity grid and the sweep trigger of a fast oscilloscope (a Du Mont K 1033 tube operated at a writing rate of $c/6=5\times 10^9$ cm/sec. by a triggered hydrogen thyratron). The pulse to be observed was delayed 0.15 microsecond and led to the coaxial vertical deflection plate. The rise was fully observable at 120/sec. and was from 10 percent to 90 percent in 1.5 cm, so 3×10^{-10} sec. The shape of the rise, however, checks with what one expects for the distortion of a step function through 0.15 microsecond of the cable used. It is hoped to use air dielectric delay line for a better determination of the switch characteristics. The sweep calibration in the region of interest was established by removing and adding 6-cm lengths of coaxial cable.

SUMMARY

The pulser has proved to be a very helpful accessory. A minor limitation is the impossibility of triggering the artificial pulse at an arbitrary time, but this does not decrease appreciably the utility of the instrument.

Erratum: D.C. Amplifier for Biological Application

[Rev. Sci. Inst. 21, 366 (1950)]

P. O. BISHOP, *Anatomy Department, University College, London*
AND
E. J. HARRIS, *Biophysics Research Unit, University College, London*

THERE are two errors in the values quoted for the components of the d.c. amplifier for biological application. They are: 1. In Fig. 6: R13 is 33 *k*ohm *not* 68 *k*ohm. 2. In Fig. 7: R11 is 200 *k*ohm *not* 100 *k*ohm.

THE REVIEW OF SCIENTIFIC INSTRUMENTS VOLUME 21, NUMBER 11 NOVEMBER, 1950

A Method for Measuring the Thermal Conductivity of Small Samples of Poorly Conducting Materials such as Optical Crystals*

STANLEY S. BALLARD, KATHRYN A. MCCARTHY, AND WILLIAM C. DAVIS†
Department of Physics, Tufts College, Medford, Massachusetts

(Received June 29, 1950)

Thermal conductivities of from 2 to 500×10^{-4} c.g.s. units are measured by comparing the flow of heat through a given sample with that through a standard material. On the basis of repeat runs and checks with literature values, an accuracy of about five percent is estimated for this method. The dimensions of the apparatus limit the face size of both the unknown and standard samples to a maximum of 10 millimeters square; thicknesses of 2 to 10 millimeters are suitable. Values at average temperatures between 30°C and 75°C are reported for nine materials:—sodium chloride, potassium chloride, potassium bromide, calcium fluoride, lithium fluoride (both air-grown and vacuum-grown), silver chloride, thallium bromide-iodide, thallium bromide-chloride, and fused silica.

IN the course of a program of measuring the physical properties of crystalline optical materials of importance in infra-red instrumentation,[1] it became apparent that there was no readily available method for measuring the thermal conductivity of small samples of such materials. Very often only small samples are available for test; this is especially likely to be true for new crystals which are being grown in experimental lots. Therefore it seemed that an equipment was needed which could give acceptable accuracy for samples as small as one centimeter square and a few millimeters thick. These materials are neither good conductors of heat such as the metals, nor are they very poor conductors such as insulating substances, but rather they fall into an intermediate class, with thermal conductivities in the range of 2 to 500×10^{-4} c.g.s. units (cal. sec.$^{-1}$ cm^{-1} °C^{-1}). This article describes a simple device for making these measurements, lists a few of the values that have been determined, and reports comparisons with available literature values.

The method is comparative rather than absolute in that there is a constant heat flow maintained through a standard crystal and the crystal under test, and the temperature gradients necessary to maintain this equal flow through the two crystals of unequal thermal conductivity are measured. As illustrated in Fig. 1, the two crystal blocks are placed one above the other between a heat source and a heat sink. In preparing for each measurement the heat is passed through the crystals for a sufficient time so that a steady-state condition exists. The interface temperatures T_1, T_2, and T_3 are then measured. Under these conditions the quantity of heat, Q, which flows through each material in a given interval of time is the same, and by definition of the thermal conductivity, k,

$$Q=(kA\cdot\Delta T)/t.$$

Equating Q for the standard and unknown crystals,

$$\frac{k_sA_s(T_2-T_3)}{t_s}=\frac{k_uA_u(T_1-T_2)}{t_u},$$

where k_s and k_u, A_s and A_u, t_s and t_u are the thermal conductivity, surface area, and thickness, respectively, of the standard material, s, and the unknown, u. All quantities can be measured except k_s which is taken from the literature, and k_u which is being determined.

The materials selected for use as standards in this comparative method must of course have well-established thermal conductivity values which lie in the appropriate range. Crystalline quartz, whose thermal conductivity at various temperatures has been extensively reported, is used as a basis of comparison for crystals in the upper part of the range of values being investigated. The quartz crystals are Z-cut, so the values of conductivity employed are those for heat flow parallel to the optic axis. Values from −252°C to 100°C are listed in the International Critical Tables,[2] and values from 100°C to 475°C have been determined by Knapp.[3] Plexiglas and Pyrex are used as standards in the lower part of the optical crystal range. The thermal conductivity of Plexiglas, manufactured by the Rohm and Haas Company of Philadelphia, is about one-fiftieth that of crystalline quartz; H. E. Robinson of the National Bureau of Standards has measured samples of this material using an 8-inch guarded hot-plate appa-

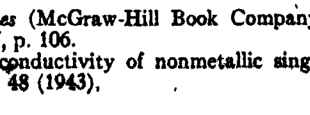

FIG. 1. Schematic design of thermal conductivity apparatus.

---

* Assisted by a grant from the Rumford Fund of the American Academy of Arts and Sciences. A brief description of this method was presented at the New York meeting of the Optical Society of America on March 9, 1950. See J. Opt. Soc. Am. 40, 256A (1950).

† Now at the Johns Hopkins University, Baltimore, Maryland.

[1] L. S. Combes and S. S. Ballard, "Measurements of the physical properties of infra-red optical materials," J. Opt. Soc. Am. 38, 1101A (1948).

[2] *International Critical Tables* (McGraw-Hill Book Company, Inc., New York, 1929), Vol. V, p. 106.

[3] W. J. Knapp, "Thermal conductivity of nonmetallic single crystals," J. Am. Cer. Soc. 26, 48 (1943).

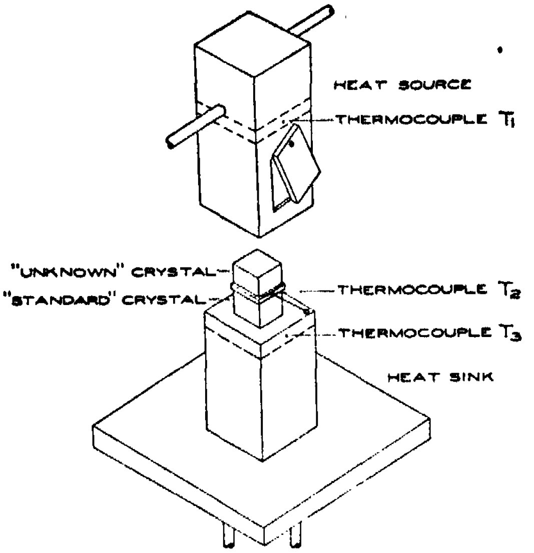

FIG. 2. Apparatus for measuring the thermal conductivity of small specimens.

ratus. The thermal conductivity of Pyrex No. 7740, as supplied by the Corning Glass Works of Corning, New York, is about one-tenth that of crystalline quartz. Stephens[4] has measured the thermal conductivity of Pyrex at temperatures from −200°C to 250°C, and reports data which are presumed to be reliable.

In the actual apparatus, which is diagrammed in Fig. 2, the heat source is a brass box with a copper bottom which is heated by steam passed through the box—copper is of course used because of its high thermal conductivity. The heat sink is a brass box with a copper top which is cooled by a stream of tap water. The heat source is located at the top of the apparatus and the sink at the bottom, so as to minimize convection currents along the sides of the crystal pile. A thin copper plate is placed between the two crystals to keep the heat flow through the crystals parallel when the crystals do not have the same cross-sectional area, and to facilitate the measurement of the interface temperature. The thermocouples are made of 32-gauge copper and constantan wire; one thermocouple is soldered in the approximate center of the copper plate between the crystals, and the other two are soldered near the surfaces of the copper plates which constitute the heat source and heat sink. A shield extends from the upper box to make thermal contact with the lower box; the air enclosed in the space between the crystal pile and the shield is thus expected to have a temperature distribution similar to that of the crystal pile. A small door is provided in the side of the shield for the inspection of the crystal pile after the apparatus has been assembled. A preliminary run of about ten minutes is generally sufficient to establish a steady state condition, with constant temperature readings.

When the copper plates are in good contact with the surfaces of the crystals, the temperature distribution over the conducting areas of the crystals is assumed to be uniform, and the flow of heat through the pile is assumed to be linear and unidirectional from the heat source at the top to the heat sink at the bottom. A possible source of error exists at the interfaces between the copper plates and the crystals, where good thermal contact must of course be established. Glycerin or vacuum-pump oil is used between the surfaces to eliminate air spaces caused by surface roughness, and weights are placed on top of the steam jacket to assist in maintaining better thermal contact. The differential heat losses from the sides of the crystal pile appear to be negligible. To study this possible source of error, tests were made in which crystalline quartz plates served both as the unknown and as the standard samples. Tests were made first with the "unknown" quartz sample in contact with the heat sink; then the crystal pile was reversed, and runs were made with the "unknown" quartz sample in contact with the heat source. The values of thermal conductivity obtained for the "unknown" quartz sample at two different average temperatures checked very closely with the literature values for those temperatures. If an appreciable amount of heat were being lost from the sides of the crystal pile, the conductivity measured at a given average temperature should not have agreed with the literature value for that temperature.

Measurements have been made only within the comparatively small range between the temperatures of steam and tap water, and the actual runs reported here have been made at average temperatures for the unknown sample of between 30°C and 75°C. By using samples of different thickness and by interchanging the positions of the unknown and the standard crystals, it is possible to obtain different interface temperatures and thus to measure values of thermal conductivity for a number of average temperatures within the range available. The face size of both the unknown and the standard materials is limited because their conducting surfaces must fit within the edges of the center copper plate, which in the present apparatus is 10 millimeters square. Sample thicknesses in the range 2 to 10 millimeters have proven satisfactory. A sample must be of constant cross-sectional area throughout its depth, and the contacting surfaces must be plane and parallel.

The materials tested to date are listed in Tables I and II. The experimental value of thermal conductivity given for each material was determined from several runs made with approximately the same temperature gradients existing. The temperature which accompanies each conductivity value in the tables is the mean of the temperatures at the two conducting surfaces of the material being tested. The test samples of the materials given in Table I are single crystals synthetically grown from the molten salt, according to the method of Bridgman and Stockbarger, by the Harshaw Chemical

---

[4] R. W. Stephens, "The temperature variation of the thermal conductivity of Pyrex glass," Phil. Mag. 14, 897 (1932).

Company of Cleveland, Ohio. Comparison of our values with those reported by other investigators[5,6] is difficult because of possible differences in the source of the crystals, some being naturally-occurring crystals, and others being synthetically grown. However, the results obtained agree with most values reported by other investigators to within five percent, except that the measurements on the synthetic lithium fluoride supplied by Harshaw differ greatly from values reported by Knapp for samples which were presumably grown synthetically by the same general method. The conductivity measured for air-grown lithium fluoride differs significantly from that measured for vacuum-grown lithium fluoride; this appears to be consistent with the differences in certain elastic properties reported by Combes and Ballard[1,7] for these two materials.

In Table II values are given for five materials whose thermal conductivity has not been previously reported, at least for the synthetic crystals. The silver chloride tested was cut from a sheet rolled from a single-crystal ingot, and supplied by Harshaw. In order to prevent the corrosive action of silver chloride on copper, the conducting surfaces of the samples were coated by evaporation with a thin protective layer of silver. The mixed crystals *KRS*-5 (thallium bromide-thallium iodide) and *KRS*-6 (thallium bromide-thallium chloride) were supplied by the Engineer Research and Development Laboratories, Fort Belvoir, Virginia. The fused silica listed in Table II is of the high optical homogeneity variety "Homosil," manufactured by the W. C. Heraeus Company of Hanau, Germany, and since its thermal conductivity has not been reported previously, it is listed with the new values.

TABLE I. Thermal conductivity of some optical materials.

Material	Experimental value c.g.s. units	Temperature °C	Literature value c.g.s. units	Temperature °C	Source
Sodium chloride	147×10^{-4}	35	167×10^{-4}	0	Eucken[a]
	130	70	150	30	Eucken[a]
Potassium chloride	156	42	167	0	Eucken[b]
	153	72			
Calcium fluoride	232	36	250	0	Eucken[a]
Lithium fluoride (air-grown)	249	36	61.3	105	Knapp[c]
Lithium fluoride (vacuum-grown)	280	34			

[a] See reference 5.
[b] See reference 6.
[c] See reference 3.

TABLE II. New values of thermal conductivity of optical materials.

Material	Experimental value c.g.s. units	Temperature °C
Potassium bromide	115×10^{-4}	46
Fused silica (Heraeus)	28.2	41
Silver chloride	27.1	52
Thallium bromide-iodide	21.3	54
Thallium bromide-chloride	17.1	56

Samples of crystals additional to those listed in Tables I and II have been obtained, and are being measured. Of particular interest are non-cubic crystals, such as sapphire and rutile, with which a study can be made of thermal conductivity as a function of crystal orientation. Plans are underway to construct a variation of the present apparatus which will make possible the extension of the thermal conductivity measurements down to temperatures well below 0°C.

The authors wish to thank David W. MacLeod and Gustave A. Larson of the Research Laboratory of Physical Electronics of Tufts College for their assistance in the construction of the apparatus and the preparation of samples, and Professor Gordon B. Wilkes of the Massachusetts Institute of Technology for his encouragement and assistance in the early days of the project.

---

[5] Smithsonian Physical Tables (Smithsonian Institution, 1933), eighth revised edition, p. 273.

[6] See reference 2, Vol. V, p. 231.

[7] L. S. Combes and S. S. Ballard, "Studies of the inelastic behaviour of optical crystals," J. Opt. Soc. Am. 40, 256A (1950).

THE REVIEW OF SCIENTIFIC INSTRUMENTS VOLUME 21, NUMBER 11 NOVEMBER, 1950

Synchrotron-Oscillation Resonance*

NELSON M. BLACHMAN
Brookhaven National Laboratory, Upton, Long Island, New York

(Received June 16, 1950)

The frequency of phase oscillation in a synchrotron is so low as to make possible resonances with harmonics of the power-supply frequency. The interaction may take place through ripple in the magnetic field or in the frequency or amplitude of the accelerating voltage, the first two interacting very strongly and the third moderately. Thus, a small ripple in the magnet power supply output, though it produces only an extremely small ripple in the magnetic field because of the magnet's inductance, may tend to cause large phase oscillations. The detuning effect of the fall in phase oscillation on frequency with increasing amplitude limits the resulting amplitude, however, and may even reduce the amplitudes of initially large phase oscillations. The ripple in the accelerating field is unlikely to be sufficient at a resonant frequency to cause trouble. In addition to ripple, there will be noise which, particularly through modulation of the frequency of the accelerating field, may result in time in considerable phase oscillations because the noise contains a wide range of frequencies, one of which is always in resonance throughout the acceleration cycle.

I. INTRODUCTION

ALTHOUGH resonances among the frequencies of vertical and horizontal betatron (free) oscillation and of revolution in a synchrotron have already been studied,[1-3] the possibility of resonance in the phase (synchrotron) oscillation has received less attention.[†] The frequency of the latter is much lower than those of the former three; in the Brookhaven proton synchrotron it will vary from 2620 to 1800 c.p.s., and resonance may occur with harmonics of the power-supply frequency. The Brookhaven magnet is powered by a nominally 60-cycle generator and 12-phase rectifier, having significant output components at multiples of 720 c.p.s.; the third gives cause for concern with phase-oscillation resonance.

II. DIFFERENTIAL EQUATIONS OF PHASE OSCILLATION

The differential equations of small phase oscillation are[3]

$$\omega d(e/\omega)/dt=-A\theta \tag{1}$$

and

$$d\theta/dt=Ke-Ch+w, \tag{2}$$

where e is the energy excess of the particles over that of the equilibrium particle, θ is its phase-angle excess, h is the amount by which the magnetic field exceeds the field H required to keep a particle of the equilibrium energy at the equilibrium radius R, and w is the amount by which the radian r-f exceeds the angular velocity of ω of the equilibrium particle. A, K and C are the slowly varying positive constants

$$A=-\partial(dE/dt)/\partial\theta=(\omega/2\pi)\epsilon V|\cos\phi|, \tag{3}$$

$$K=-\partial\omega/\partial E=\frac{\omega}{E(E^2-E_0^2)}\times\left[\frac{E^2}{(1-n)(1+4L/2\pi R)}-E_0^2\right], \tag{4}$$

$$C=\partial\omega/\partial H=\omega/[H(1-n)(1+4L/2\pi R)], \tag{5}$$

with E the total energy of the equilibrium particle, of rest energy E_0 and charge ϵ, V the amplitude of the accelerating potential, ϕ the equilibrium phase angle ($\pi/2<\phi<\pi$), n the index of the fall-off of the magnetic field with radius, and $4L$ the total length of straight sections.

If the amplitude of the r-f voltage should be excessive by the amount aV, i.e., by fraction a, Eq. (1) must be modified to read

$$de/dt=-A\theta+Da, \tag{6}$$

in which the two ω's have been canceled because the change in ω during a passage through resonance will be negligible;

$$D=V\partial(dE/dt)/\partial V=(\omega/2\pi)\epsilon V\sin\phi. \tag{7}$$

Combining (2) and (6), we get

$$\ddot{\theta}+\Omega^2\theta=-C\dot{h}+\dot{w}+\Omega^2|\tan\phi|a, \tag{8}$$

where $\Omega=(AK)^{\frac{1}{2}}$ is the radian frequency of phase oscillation.

III. FORCED OSCILLATION

The right side of (8) is a forcing term, causing θ to oscillate. For example, if h is varying sinusoidally with radian frequency W and amplitude h_0, its time derivative will have amplitude Wh_0, and θ will be forced to vary with the same frequency and amplitude

$$\theta_0=CWh_0/|\Omega^2-W^2|. \tag{9}$$

Likewise, if the accelerating frequency varies sinusoidally with frequency W and amplitude w_0, θ will be forced to oscillate with amplitude

---

* Work done under the auspices of the AEC.

[1] E. D. Courant, J. App. Phys. 20, 611 (1949).

[2] D. M. Dennison and T. H. Berlin, Phys. Rev. 69, 542 (1946); 70, 764 (1946).

[3] N. M. Blachman and E. D. Courant, Rev. Sci. Inst. 20, 596 (1949).

† N. M. Blachman, Phys. Rev. 80, 125 (1950).

$$\theta_0 = Ww_0/|\Omega^2 - W^2|, \tag{10}$$

while if the r-f voltage is amplitude modulated at frequency W with modulation index a_0, a forced phase oscillation of amplitude

$$\theta_0 = \Omega^2 |\tan\phi| a_0/|\Omega^2 - W^2| \tag{11}$$

will result.

The amplitude of forced phase oscillation (10) or (11) is of the same order of magnitude as the amplitude-modulation index or the ratio of frequency swing to phase-oscillation frequency, respectively, unless the modulating frequency resonates with the phase-oscillation frequency. However, because C is of the order of ω/H and ω is of the order of a thousand times Ω because the particles' energy gain per revolution is of the order of a millionth of their kinetic energy, a large phase oscillation (9) will result from only a very small wobble of the magnetic field. Ordinarily, though, the ripple in the magnetic field will be of a still smaller order of magnitude on account of the filtering effect of the magnet's inductance on the ripple in the magnet-supply voltage.

If the amplitude of the latter is m times the d.c. voltage, the rate of change of the ripple magnetic flux must be m times the rate of change of the d.c. flux. Assuming that these two fluxes are distributed similarly in space, we conclude that $Wh_0 = m\dot{H}$, whence

$$h_0 = m\dot{H}/W. \tag{12}$$

Substituting (12) and (5) into (9), we obtain

$$\theta_0 = m\omega\dot{H}/[H|\Omega^2 - W^2|(1-n)(1+4L/2\pi R)], \tag{13}$$

which is of the order of magnitude of m unless the ripple and phase-oscillation frequencies are nearly equal. In the latter case, because Ω is changing, it must pass through W, and resonance will occur.

IV. RESONANCE

Since the effect of Ω passing through W will be practically the same as that of W passing through Ω at the same rate while Ω remains constant, the solution to

$$\ddot{\theta} + \Omega^2\theta = f(t) \tag{14}$$

may be written

$$\theta = \Omega^{-1} \int_{-\infty}^{t} f(t') \sin\Omega(t-t')dt'. \tag{15}$$

We may write the forcing term, assumed to have amplitude F, as

$$\begin{aligned} f(t) &= F \sin\left\{ \int_0^t [\Omega + (\dot{W} - \dot{\Omega})t]dt + \psi \right\} \\ &= F \sin[\Omega t + \tfrac{1}{2}(\dot{W} - \dot{\Omega})t^2 + \psi], \end{aligned} \tag{16}$$

substitute it into (15), and then write the product of the two sines as the difference of two cosines, one having the frequency difference multiplying t' and the other the sum. The resonance occurs in the former term, which we retain, the integral of the latter being negligible so that we drop it:

$$\theta = (F/2\Omega) \int_{-\infty}^{t} \cos[\Omega t + \psi + \tfrac{1}{2}(\dot{W} - \dot{\Omega})t'^2]dt'. \tag{17}$$

Expanding the integrand as the cosine of a sum, we obtain two terms, a cosine times the Fresnel integral C and a sine times the Fresnel integral S. However, by setting $t = \infty$ and using Peirce's integral No. 487, we can find the total effect of passage through resonance without reference to Fresnel integrals, *viz.*,

$$\theta = (F/\Omega)(\tfrac{1}{2}\pi/|\dot{W} - \Omega|)^{\frac{1}{2}} \sin(\Omega t + \psi - \pi/4). \tag{18}$$

Therefore, the amplitude of the phase oscillation resulting from passage through resonance at the rate $|\dot{W} - \dot{\Omega}|$ will be

$$\theta_0 = (\tfrac{1}{2}\pi/|\dot{W} - \dot{\Omega}|)^{\frac{1}{2}} Ch_0, \tag{19}$$

$$\theta_0 = (\tfrac{1}{2}\pi/|\dot{W} - \Omega|)^{\frac{1}{2}} w_0, \tag{20}$$

$$\theta_0 = (\tfrac{1}{2}\pi/|\dot{W} - \dot{\Omega}|)^{\frac{1}{2}} |\tan\phi| \Omega a_0, \tag{21}$$

or

$$\theta_0 = (\tfrac{1}{2}\pi/|\dot{W} - \dot{\Omega}|)^{\frac{1}{2}} m\omega\dot{H}/[\Omega H(1-n)(1+4L/2\pi R), \tag{22}$$

corresponding to (9), (10), (11), and (13), respectively. The effective time interval during which the ripple resonates with the phase oscillation equals twice the square root appearing in (18) to (22). Following this period of build-up, the resulting oscillations continues, damping very slowly. These phase oscillations are limited in the amplitude to which they can build up in a way not taken into account above by the fall in phase-oscillation frequency with increasing amplitude, which hastens the passage through resonance. Thus, the danger is not from the oscillations themselves but from the protons' decreased phase stability and consequent increased vulnerability to such disturbances as noise. Ripple is able to push particles past the limits of phase stability only to the extent that Ω^2 is not $\gg\Omega$, i.e., the number of cycles of phase oscillation during resonance is finite and the growth of their amplitude is not smooth.

Sufficiently large ripple can even reduce the amplitudes of initially large oscillations by locking in their frequency. Since the phase-oscillation frequency falls with time as well as amplitude, it can remain constant and equal to the ripple frequency only if the amplitude falls. For this locking in to occur, the product of the partial derivative of the phase-oscillation frequency with respect to amplitude, $\partial\Omega/\partial\theta_0$, times the amplitude of the incremental phase oscillation produced per unit time by the ripple at resonance, $|F|/2\Omega$, must be many times the rate of change with time of the phase-oscillation frequency, $\dot{\Omega}$. In this case, there will be a stable phase-oscillation phase and amplitude, the latter falling with time, which maintains approximate equality of ripple and phase-oscillation frequencies until the amplitude has fallen to the point where $\partial\Omega/\partial\theta_0$ is no longer sufficient ($\partial\Omega/\partial\theta_0=0$ for $\theta_0=0$); then the oscillation will go out of resonance without increasing in amplitude.

An oscillation larger in amplitude than the stable amplitude would have a lower frequency and so get behind in phase. An oscillation behind in phase would be reduced in amplitude faster than the stable amplitude because it would be closer to 180° out of phase with the incremental oscillation due to ripple. Thus, particles executing phase oscillations with other than the stable phase and amplitude will oscillate in phase and amplitude about these values provided that there is sufficient ripple and amplitude dependence of the phase-oscillation frequency. To determine the latter, it is necessary to integrate the equation of finite phase oscillation[3] numerically over a cycle of oscillation.

V. APPLICATION TO BROOKHAVEN PROTON SYNCHROTRON

In the Brookhaven proton synchrotron[4] the phase-oscillation frequency will pass through resonance with the nominally 2160-c.p.s. power-supply ripple with $\Omega/2\pi=2055$ c.p.s. at the time the field $H=8500$ gauss, $\omega/2\pi=4.0$ mc/sec., $\dot{H}=14750$ gauss/sec., $\dot{\Omega}/2\pi=-1600$ c.p.s./sec., and $\dot{W}/2\pi=-100$ c.p.s./sec. on account of the slowing down of the generator due to the conversion of rotational energy into magnetic. With $m=0.5$ percent r.m.s. for this ripple, we find on substituting into (22), taking $n=0.6$ and $4L/2\pi R=0.2122$, that $\theta_0=0.64$ radian $=36°$ in amplitude, which is not small. It may be compared with the phase acceptance range of 199° corresponding to the equilibrium phase angle $\phi=152.8°$ at this resonance. The resonance will effectively last 26 msec.

The amplitude of the incremental phase oscillation produced per unit time by the ripple at this resonance is 0.64 radian/0.026 sec. = 25 radians/sec. Numerical integration of the equation of finite phase oscillation shows that for an equilibrium phase angle $\phi=150°$ the frequency of phase oscillation varies approximately as $(1-0.10\theta_0^2)$ for small θ_0. The frequency becomes zero for oscillations touching the limit of the region of phase stability. Thus, $\partial\Omega/\partial\theta_0$ is about $-411\theta_0$ c.p.s./radian, which gives a product of $-10{,}300\theta_0$ c.p.s./sec., to be compared with $\dot{\Omega}-\dot{W}=-1500$ c.p.s./sec. The former is larger in magnitude over most of the range of θ_0 during the resonance, but not sufficiently to bring about any considerable locking in of the oscillations set up by the resonance. The chief effect of the amplitude dependence of the phase-oscillation frequency in this case is to hasten the passage through resonance, reducing the resulting amplitude θ_0 to about 0.41 radian $=23°$.

From (12) we find that $h_0=0.0057$ gauss r.m.s., which is indeed small! Balancing terms on the right side of (8) to get zero, we find that this h_0 may be compensated by an appropriately phased 2055-cycle amplitude modulation with a peak swing of 7.8 c.p.s., which is equivalent to a 0.22° phase modulation. This f-m should be supplied automatically by the frequency-control system, which is designed to keep the frequency appropriate to the magnetic field, however the latter may wobble. Just as this variation in frequency of two parts in a million is enough to balance out a 23° phase oscillation, so such a variation could cause one. However, no ripple in the frequency of this order of magnitude is expected in the range of phase-oscillation frequencies. It is expected that the 2-kc amplitude modulation of the accelerating voltage will not exceed 0.1 percent, which would produce only a 5° phase oscillation.

VI. NOISE

In addition to ripple modulation of the accelerating voltage and ripple in the magnetic field, there will be modulation by the noise in the r-f control system of the frequency and amplitude of the accelerating voltage and noise in the magnetic field due to noise in the magnet supply voltage. Although this noise has no discrete frequencies like ripple to resonate with the phase-oscillation frequency, it contains components of a wide band of frequencies, including the entire range over which the phase-oscillation frequency varies. Thus, instead of resonating only during a brief passage through resonance, a part of the noise is effective throughout the acceleration cycle. The various spectral components are not coherent but produce only statistical effects much smaller in magnitude than if they were coherent like a discrete frequency; but because of the longer time of interaction, noise can produce considerable phase oscillations.

Noise may be considered to be made up of many discrete components of random phase and amplitude, the latter obeying a Rayleigh distribution (of the shape $xe^{-x^2/2}dx$) with its mean-square value given by the spectral intensity. We may resolve the noise into components whose frequencies change in the same way as the phase-oscillation frequency, so that there is one that remains in resonance throughout the acceleration cycle. It represents all components that remain coherent for this period of time, say T. They in effect occupy a band width about the phase-oscillation frequency of $2\pi/T$ in radians/second.[5] Note that ripple components at multiples of 60 cycles which are more or less uniformly small in amplitude may be regarded as noise since their effects on the particles will not be coherent.

Considering (8) again in the form (14), we suppose that $f(t)$ is a noise with spectral intensity $\Phi(\Omega)$ in the neighborhood of the phase-oscillation frequency Ω. Φ is the mean-square value of that part of $f(t)$ lying within a

---

[4] Livingston, Blewett, Green, and Haworth, Rev. Sci. Inst. 21, 7 (1950).

[5] If an undamped harmonic oscillator of resonance frequency Ω is driven by a sinusoidal force of frequency W nearly equal to Ω for a long time T ($\Omega T\gg 1$), the resulting amplitude, which is proportional to T at resonance, is readily found to be $[\sin\frac{1}{2}(\Omega-W)T]/[\frac{1}{2}(\Omega-W)T]$ times as large when $W\neq\Omega$. If the forcing frequencies W are distributed uniformly in the vicinity of Ω, the effective band width is

$$\int_{-\infty}^{\infty}[\sin\tfrac{1}{2}(\Omega-W)T]^2/[\tfrac{1}{2}(\Omega-W)T]^2dW=2\pi/T.$$

frequency band of unit width (1 radian/sec.). Thus, the mean-square value of the effective component of $f(t)$ is $2\pi\Phi/T$, and its r.m.s. amplitude is $(4\pi\Phi/T)^{\frac{1}{2}}$. Such a resonant driving force, acting for time T, excites oscillations of θ of amplitude $T/2\Omega$ times the amplitude of the driving force, i.e., phase oscillations of r.m.s. amplitude

$$\theta_0 = (\pi\Phi T/\Omega^2)^{\frac{1}{2}}, \tag{23}$$

since there is very little damping of the phase oscillations.[6] As is shown in the Appendix, the r.m.s. phase-oscillation amplitude due to noise builds up with time as $(\pi\int_0^t \Phi dt/\Omega^2)^{\frac{1}{2}}$; hence, if $\Phi(\Omega)/\Omega^2$ is not constant, its mean value must be used in (23), due account being taken of the dependence of Ω on amplitude. At the end of the acceleration cycle the amplitudes due to noise of the phase oscillations of the various particles will have a Rayleigh distribution of r.m.s. value (23), since those starting with different initial phase oscillation amplitudes will, on account of their different phase-oscillation frequencies, respond to different noise components. The particles that would execute oscillations exceeding the limits of phase stability are, of course, lost.

Noting that the spectral intensity of a derivative is the square of the angular frequency times that of the original quantity, we see that the r.m.s. amplitude of phase oscillation due to a random variation with time of the magnetic field of spectral intensity η in gauss²/(radian/sec.) is

$$\theta_0 = C(\pi\eta T)^{\frac{1}{2}}. \tag{24}$$

If the accelerating frequency varies randomly, e.g., because of noise in the r-f control system, with spectral intensity ν in (radians/sec.)²/(radian/sec.), which may be given by the spectral intensity of the latter noise times the mean-square sensitivity of the frequency-control system, the r.m.s. amplitude of the resulting phase oscillation is

$$\theta_0 = (\pi\nu T)^{\frac{1}{2}}. \tag{25}$$

If the accelerating voltage has random amplitude modulation which, expressed dimensionlessly (in percent), has spectral intensity α in (radian/second)$^{-1}$,

$$\theta_0 = \Omega|\tan\phi|(\pi\alpha T)^{\frac{1}{2}}, \tag{26}$$

while (24) in terms of noise in the magnet supply voltage which, similarly expressed, has spectral intensity μ in (radian/sec.)$^{-1}$ is

$$\theta_0 = C\dot{H}(\pi\mu T)^{\frac{1}{2}}/\Omega, \tag{27}$$

which is of the order of magnitude of $\Omega(\pi\mu T)^{\frac{1}{2}}$ and may be compared with (26).

VII. APPLICATION TO BROOKHAVEN MACHINE[4]

Values of μ or α corresponding to 0.1 percent magnet-supply noise or noise modulation, respectively, in a 10-kc frequency band correspond to a θ_0 of about a tenth of a radian for the Brookhaven machine, which should do little harm. However, the synchrotron is very sensitive to frequency modulation, because a slight change of accelerating frequency introduces an equal rate of change of particle phase (see Eq. (2)) that is effective for a time of the order of the period of phase oscillation and produces a net change of particle phase of the order of a thousand times $(=\omega/\Omega)$ the fractional change of accelerating frequency. The great sensitivity to variation in the magnetic field is due to the same effect, the relative frequency change this time being due to the shift of the equilibrium radius.

With $T=1$ second and an r.m.s. oscillator sensitivity of about 25 kc/v, 100 μv of noise in a 10-kc band feeding the frequency-control circuit along with the 0- to 300-v control voltage will result in phase oscillation of r.m.s. amplitude 0.11 radian = 6.4°, which will have only a slight effect on the life expectancy of the protons. Over half of the effect of the noise f-m, however, will have appeared by the time the protons reach 50 Mev, where the radial oscillations still require all available aperture. On reaching relativistic energies these phase oscillations will damp slowly in their customary way.

VIII. ACKNOWLEDGMENT

I want to acknowledge discussions of the present problem with Dr. Ernest D. Courant and other members of the Accelerator Project of this laboratory.

APPENDIX

Another derivation of (23) from (14). White fluctuation noise may, without loss of generality, be assumed to result from a sequence of impulses (delta-functions) that occur at random times going through a low pass system that smears out and conceals the individual impulses. We have seen that the frequency response of a particle to the driving force $f(t)$, our noise, is very sharp and would do so much of its own smearing as to hide the effects of any low pass filter. Hence, we suppose that $f(t)$ consists of a sequence of delta-functions occurring at the random times t_i.

Thus, after t_1 and before t_2, θ is given by the indicial response of (14), $\theta = \Omega^{-1}\sin\Omega(t-t_1)$. Ignoring the rather small damping of the phase oscillations, we find that after a large number N of impulses

$$\begin{aligned}\theta &= \Omega^{-1}\sum_{i=1}^{N}\sin\Omega(t-t_i)\\ &= \Omega^{-1}\sin\Omega t\sum_{i=1}^{N}\cos\Omega t_i - \Omega^{-1}\cos\Omega t\sum_{i=1}^{N}\sin\Omega t_i\\ &= \Omega^{-1}\Big[\Big(\sum_{i=1}^{N}\cos\Omega t_i\Big)^2 + \Big(\sum_{i=1}^{N}\sin\Omega t_i\Big)^2\Big]^{\frac{1}{2}}\sin(\Omega t+\psi)\\ &= \Omega^{-1}\Big[N+2\sum_{i>j=1}^{N}\cos\Omega(t_i-t_j)\Big]^{\frac{1}{2}}\sin(\Omega t+\psi),\end{aligned}$$

whence we see that the r. m. s. amplitude of oscillation of θ is $\theta_0 = N^{\frac{1}{2}}/\Omega$, for the mean value of the summation over i and j is zero. If the number of impulses per second is b, $N = \int_0^T bdt/\Omega^2$, whence

$$\theta_0 = \left(\int_0^T bdt/\Omega^2\right)^{\frac{1}{2}}. \tag{28}$$

From the fact that the Fourier transform of the delta-function is $1/\pi$ (radian/sec.)$^{-1}$, it follows that the spectral intensity of the integral of its square is $1/\pi$ sec./(radian/sec.). Hence, the power spectral intensity of the sequence of delta-functions coming at the rate b per second is b/π (radians/sec.)²/(radian/sec.), which is what we called Φ. Therefore, $b = \pi\Phi$, and (28) becomes (23).

---

[4] R. Q. Twiss and N. H. Frank, Rev. Sci. Inst. 20, 1 (1949).

THE REVIEW OF SCIENTIFIC INSTRUMENTS VOLUME 21, NUMBER 11 NOVEMBER, 1950

An Electrostatic Beta-Spectrograph*

DONALD R. HAMILTON AND LEONARD GROSS†
Palmer Physical Laboratory, Princeton, University

(Received June 16, 1950)

A beta-ray spectrograph has been constructed in which electrons move radially outward against a retarding electric field, and the current due to those electrons having more than any given energy is measured. Momentum resolution is one-third percent. The insensitivity of current collection, as compared to single particle detection, is compensated by a large tolerable source area and a large useful solid angle subtended at the source by the detector.

I. INTRODUCTION

THIS article is concerned with the design and operation of an electrostatic beta-ray spectrograph which has been used to investigate the low energy portion (0–30 kilovolts) of the spectrum of sulfur 35, as reported elsewhere.[1] Instead of single-particle detection this spectrograph uses current detection, thus obviating difficulties with the thin windows of counters. Use of electrons leaving the source in a large solid angle increases the intensity as is necessary in going to the less sensitive method of current detection. This spectrograph is thus complementary to the magnetic spectrograph and, among other things, may be used in the low energy range to test the Fermi theory[2] of beta-decay, which has proven so robust and in such good agreement with the observed spectra at all other energies.

II. DESIGN OF APPARATUS; RESOLVING POWER AND INTENSITY CONSIDERATIONS

The increase in intensity requisite to current detection is obtained by having electrons move radially outward against a spherically symmetric retarding electric field; one measures the relative number of electrons able to surmount the retarding field, i.e. having more than a given energy. The spectrum measured is thus an integral spectrum from which the

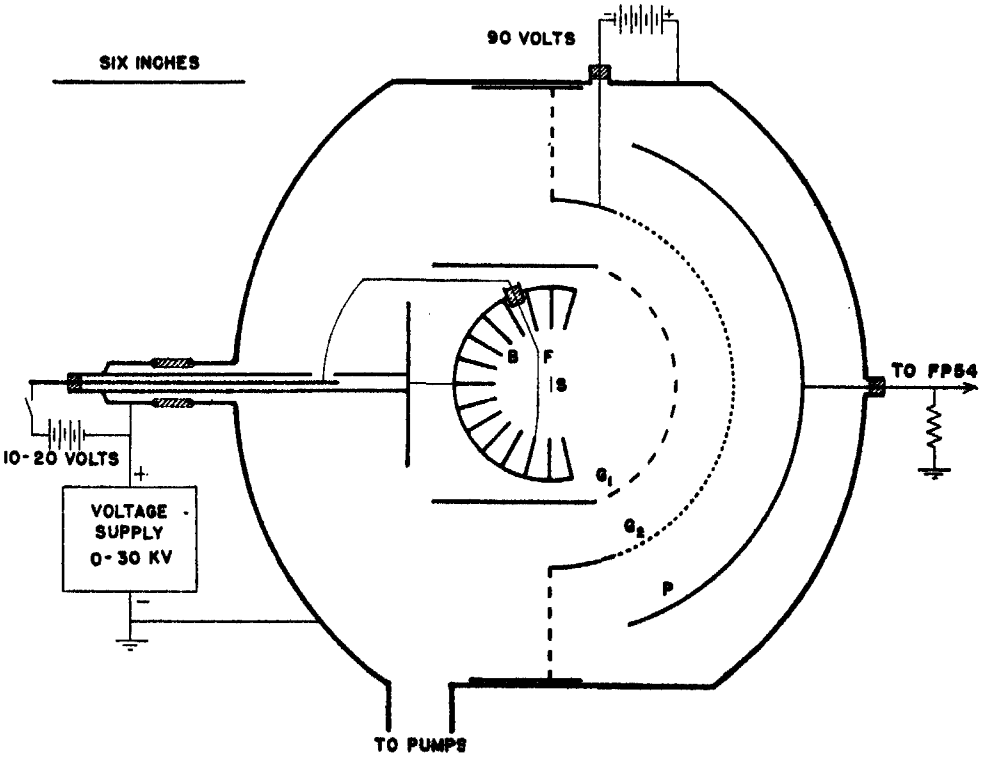

FIG. 1. Schematic diagram of electrostatic beta-spectrograph showing collector P, grids G_1 and G_2, source S, decharging filament F, and electron backstop B.

---

* This work assisted by the joint program of the ONR and AEC. This article is based upon a portion of a dissertation submitted by Leonard Gross to the Faculty of Princeton University in partial fulfilment of the requirements for the degree of Doctor of Philosophy.

† Now at Hughes Aircraft Company, Culver City, California.

[1] L. Gross and D. R. Hamilton, Phys. Rev. 78, 318 (1950).

[2] E. Fermi, Zeits. f. Physik 88, 161 (1934).

customary spectrum is obtained by differentiation. Such an instrument is not mentioned in the literature although it has apparently occurred independently to various individuals. Electrostatic spectrographs described in the literature, in which electrons move at right angles to a cylindrically symmetric electric field,[3,4] have no particular advantages over magnetic types.

The simplest electrostatic spectrograph of the present general type, consisting of two parallel planes as source and collector, is practically useless since only a small component of the initial electron momentum is on the average parallel to the retarding field. This fault is easily remedied by having a small spherical source, radius r_0, concentric with a spherical collector of radius r_2; from conservation of angular momentum it follows that a mono-energetic electron source would have an apparent total relative energy width $(r_0/r_2)^2$. This width is unaffected if the radial dependence of the spherically symmetric field is altered, as by a spherical grid of radius $r_1 (r_0<r_1<r_2)$ intermediate in voltage and space between source and collector. In particular the apparent energy width is unaffected if such an intermediate grid be at source potential and have a radius comparable to that of the collector. In addition, this last condition minimizes edge effects which arise if the collector subtends at the source a solid angle considerably less than 4π steradians.

The latter features are incorporated in the practical spectrograph shown in Fig. 1. Here the grid G_1 is maintained at the same potential as the source S. Electrons from S travel initially in a field free space and meet the retarding field between G_1 and G_2. Electrons having enough energy to pass G_2 are collected by P; since G_2 is biased 90 volts negative with respect to P, no slow secondary electrons leave P. Electrons turned back between G_1 and G_2 return toward S and are absorbed in B with, as will be discussed later, the production of very few secondaries. Electrons not initially emitted toward G_1 likewise terminate their career suddenly at B. Confinement of the retarding field to the region G_1G_2 is necessary for the prevention of electrical stress on the thin film source S; and of course since the source must for practical reasons be non-spherical and non-conducting, any retarding field which extended up to the source would be considerably distorted by the latter. The possibility of insertion of B as an electron trap is one advantage of the hemispherical arrangement of Fig. 1 over the idealized spherical arrangement; the principal additional advantage is mechanical simplicity.

In addition to the general limits set by convenience, the dimensions in Fig. 1 are set by a number of factors:

(1) The G_1G_2 spacing must be large enough to reduce sufficiently any strong-field emission of electrons from G_2 toward G_1. (2) The G_1G_2 spacing must be small enough, relative to the radii of G_1 and G_2, to keep down edge-effect distortions of the retarding field. (3) The G_1G_2 spacing must be large enough, relative to the size of the holes in G_2, to minimize loss of resolving power from coarseness of G_2. (4) The detector sensitivity sets the minimum source strength, which in turn, for a minimum source thickness, sets a minimum source area; as this area increases relative to G_1 area, resolving power gets worse.

The considerations involving resolution warrant more detailed discussion. By "resolution" we shall mean the apparent relative momentum width, $\Delta p/p = 1/2(\Delta V/E_0)$, for a source of non-relativistic monoenergetic electrons of energy E_0; here ΔV is the differential width of the range of retarding voltages within which electrons reach the collector. Hereafter V denotes retarding voltage between G_1 and G_2.

It has already been noted that for concentric spherical source and collector of radii r_0 and r_2, $\Delta V/E_0 < (r_0/r_2)^2$; a more detailed estimate for the arrangement of Fig. 1, bearing in mind that for practically all electrons the shortest distance from line of flight to center of symmetry is less than the radius of the source, gives

$$(\Delta V/E_0)_s = A/9R^2, \tag{1}$$

using the subscript s to refer to an effect arising from the source. Here A is the area of a plane circular source, R the mean radius of G_1 and G_2.

At G_2, coarseness and opposing electric fields on opposite sides of the grid mesh result in a potential barrier of variable height for different electron trajectories. The maximum variation of the barrier height from point to point, a new ΔV, could be calculated exactly. With relative dimensions of the order of magnitude of those used here, ΔV will be proportional to the separation of adjacent grid wires; several methods of estimating ΔV give

$$(\Delta V/E_0)_{G_2} = 1/10(G_2 \text{ grid wire separation}/G_1G_2 \text{ separation}) = 10^{-3}.$$

Coarseness of G_1 causes a transverse deflection of an electron passing through G_1; since the radial component of momentum is not altered, no $\Delta V/E_0$ results.

It should be noted that the values of ΔV indicated above do not combine error-wise. The finite-source effect makes monoenergetic electrons appear to have less energy, the G_2 effect more energy, than they actually have.

The resolving power of the spectrograph was checked experimentally with a monoenergetic source of electrons, provided by a wire mesh diode plate through which passed electrons accelerated from a tungsten filament by a d.c. voltage E_0 ranging from zero to 15 kilovolts. Results are summarized in Fig. 2 which shows the differential current distribution (slope of the directly observed integral spectrum) as a function of normalized retarding voltage V/E_0. The curve has a

---

[3] Rogers, McReynolds, and Rogers, Phys. Rev. 57, 379 (1940).

[4] J. G. Backus, Phys. Rev. 68, 59 (1945).

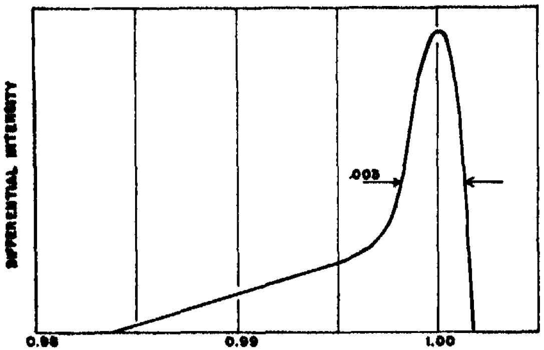

FIG. 2. Apparent momentum distribution of monoenergetic electrons.

relative voltage width at half maximum of 0.006, or a resolution $\Delta p/p=1/2(\Delta V/E_0)=0.003$, of which one-third is contributed by the region $V>E_0$(G_2 effect). These widths are about twice those calculated by the same method as above, assuming a beam 1 cm in diameter. The factor two in the finite-source effect would be explained if, as is very possible, the effective source were a quarter-inch off center.

The question of intensity is complementary to that of resolution, and is particularly important here; how much can the loss in intensity in going to current detection be compensated by the increased solid angle utilized at the source? A quantitative figure of merit involving intensity and resolving power is provided by the product

$$F\equiv(A\Omega/n)(p/\Delta p) \tag{2}$$

in which Ω is the solid angle utilized at the source, relative to 4π, and n is the detector background in electrons per second. In the present spectrograph, as in most types, F is independent of source area A since $p/\Delta p$ is proportional to $1/A$; taking A_0 as the effective sensitive area of the detector (i.e. the area of P) and $\Omega=A_0/4\pi R^2$, then by Eq. (2) $F=1.4A_0/n$. For the specific apparatus of Fig. 1, for which $A_0=430$ cm^2 (actual area times factor 2/3 for grid shadow) and $n=1000$, $F=0.6$ cm^2. The Columbia solenoidal spectrograph,[5] which seems to be the best magnetic type with respect to this figure of merit, yields about the same value; here $A=1$ cm^2, $n=1/2$, $p/\Delta p=25$ and $\Omega=0.04$, giving $F=2$ cm^2.

III. BACKGROUND ELECTRONIC EFFECTS

In addition to the primary electron current at P, a number of secondary sources of current exist and give rise to spectrum distortions. Among the masking secondary effects to be considered are secondary electron emission from electrodes, positive ion formation, and strong field emission from G_2. These will be considered in the order just given.

Secondary Electron Emission

In general this effect has been minimized by geometry and by coating all sheet-nickel surfaces, such as B and the mounts for G_1 and G_2, with aquadag (colloidal graphite). The following discussion is of necessity somewhat general since detailed effects depend on the energy spectrum of the primaries. The necessary information on secondary emission ratio (ratio of secondaries to primaries) and on energy spectrum of secondaries has been taken from a number of sources.[6-10]

(a) *Secondary Emission from Collector P*

The -90 volt bias of G_2 prevents the escape from P of the slow secondaries (<90 volts energy) which comprise at least 90 percent of the secondaries produced in carbon by primaries of less than 50 kilovolts energy. (The total secondary emission ratio from carbon varies from approximately unity at low energies to <0.1 for primary energy >70 kilovolts.) Electrode geometry is such that about one-half of the fast secondaries (>90 volts) which are not held back by G_2 can escape from P; the fast secondary emission ratio for carbon drops from 0.1 at ≤ 2 kilovolts to 0.01 at 40 kilovolts and then rises to 0.03 at 170 kilovolts. All told, secondaries from P may diminish the primary spectrum by amounts ranging from several percent to less than one percent.

(b) *Secondary Electrons from Backstop B*

Here, just as at P, the slow but not the fast secondaries are irrelevant. The geometry of this electrode is such that most secondaries are trapped; for a source one inch in diameter less than eight percent of the secondaries should be able to escape. Hence secondaries from B, as compared to those from P, have small effect.

(c) *Secondary Electrons from G_1*

Slow secondaries are irrelevant. This grid is stainless steel, 0.009-inch wire, 16 mesh, open area 73 percent. By geometry, ≤ 0.2 of the fast secondaries from G_1 head toward G_2. The fast secondary emission ratio is ≤ 0.3 for 40–100 kilovolt primaries, less for slower primaries. All told these secondaries will make at most a two percent contribution to the current at P.

(d) *Secondary Electrons from G_2*

All slow secondaries, even those initially heading toward P, will be pulled toward G_1 and are irrelevant. Although the mesh of G_2 is quite open (0.001-inch wire, 50 mesh, open area 90 percent) this is counteracted by the fact that the fast secondary emission ratio for tungsten is high, approximately 0.4–0.5 for 40–100 kilovolt primaries. Also, because of the finer mesh a larger fraction (≤ 0.4) of the fast secondaries can see P. Thus, depending on the primary spectrum, these secondaries could contribute up to two percent to the current at P.

---

[5] C. S. Wu, private communication.

[6] H. Bruining and J. H. DeBoer, Physica 5, 17 (1938).

[7] H. Bruining, Physica 5, 913 (1938).

[8] J. H. O. Harries, Electronics 17, 100 (1944).

[9] K. R. Spangenberg, *Vacuum Tubes* (McGraw-Hill Book Company, Inc., New York, 1948), p. 52.

[10] J. G. Trump and R. J. Van de Graaf, Phys. Rev. 75, 44 (1949).

To summarize, it will be noted that secondaries from P diminish, those from B, G_1 and G_2 increase, the total current at P, in an amount possibly amounting to several percent. If this percentage were independent of retarding voltage the secondaries would have no effect on the observed spectra. A more detailed estimate gives, for the primary spectrum of sulfur 35, relative errors of less than one percent in the observable part of the differential or integral spectra.

Positive Ion Current

When monoenergetic 6 kilovolt electrons are turned back just before reaching G_2, one observes at the collector 5×10^{-6} positive ions per primary electron at the standard operating pressure of 3×10^{-6} mm Hg. From data on mean free path of electrons in nitrogen[11, 12] at good vacuum, a value of 4×10^{-6} positive ions per primary electron is to be expected. The work of Filosofo and Rostagni[13] and Trump and Van de Graaf[14] seems to indicate that in comparison to ionization of residual gas at 10^{-6} mm pressure and a few cm electron path length (but not at 10^{-5} mm), positive ion liberation from clean steel electrodes is certainly negligible at 6 kilovolts and probably negligible up to 200 kilovolts. All told, these considerations indicate that positive ion current caused by action of primary electrons will be completely negligible for low energy beta-spectra.

Strong Field Emission

Electrons emitted from G_2 under the influence of the strong field in the G_1G_2 region will travel to G_1; but at G_1 some of these strong field electrons can be scattered back to G_2 with practically no loss of energy and reach P. Such an effect should be observable in the absence of source S. When this spectrograph was originally constructed with a one-inch G_1G_2 spacing, an electron current to P of 10^{-15} amp. was observed with G_1 13 kilovolts positive with respect to G_2; shrinking G_1 to make the G_1G_2 spacing two inches raised this figure to about 26 kilovolts. At a later stage the onset voltage for this current fell below 20 kilovolts. Grid G_2 (12-inch diameter) had been fabricated from 3/4-inch strips of fine tungsten mesh and had many minute whiskers; spotting these whiskers with very small amounts of polystyrene coil dope raised the onset voltage to about 26 kilovolts again. Strong field emission thus sets the useful upper limit on voltage for this spectrograph.

IV. ACCESSORY EQUIPMENT

Current Measurement

The current collected at P is measured by a split FP54 electrometer using a 10^{11} ohm grid resistor and the manufacturer's balanced circuit. The FP54 output was found to be non-linear in input grid voltage to a degree negligible for the S^{35} measurement. With a sensitive ten-second galvanometer, the sensitivity was 1.6×10^{-16} amp. per mm, with r.m.s. fluctuations of the order of one mm. However, as will be noted shortly, voltage fluctuations are introduced to the input grid of the FP54 by coupling to the G_1 voltage fluctuations via a small PG_1 capacity; this effect introduced equivalent current fluctuations some five times larger than those noted above. The P-to-ground capacity of 200 mmf gives the FP54 input circuit a 20-second time constant but helps to filter out the fluctuations coming through from G_1.

High Voltage Supply

The d.c. retarding voltage which is applied to G_1 and enclosed electrodes was supplied by a regulated r-f supply variable between 2.5 and 30 kilovolts and designed by R. H. Dicke.

The basic element in the regulation is a 300-megohm bleeder resistance which runs from high voltage to the negative terminal of a 180-volt bank of B-batteries, the other side of which is grounded. Thus, for any given power supply output voltage some point on the bleeder is at ground potential. A variable tap on the bleeder goes to the input grid of a d.c. amplifier which in turn controls the output of the voltage supply in such a way as to hold the amplifier input grid at ground and the output voltage at a constant value.

A change of the 60 cycle a.c. input voltage from 100 to 120 volts results in less than 20 volts change in output voltage. The r-f modulation on the output voltage amounts to 1/2 volt at 30 kilovolts; the 60-cycle ripple is about two volts. With the relative output voltage being read on an 8-second galvanometer (as described below) the fluctuations in output voltage in one minute were less than ±5 volts at 30 kilovolts.

As affecting knowledge of the voltage at which one is reading collector current at any given time, the variations just described are trivial; but really important is the fact that voltage fluctuations on G_1 appear as an equivalent current fluctuation in the FP54 output. A shielding grid which runs from G_2 to the wall of the vacuum chamber considerably reduces the PG_1 coupling; nevertheless in the sulfur 35 measurements the accuracy of current measurement was set by the fluctuations in the G_1 voltage.

---

[11] K. T. Compton and I. Langmuir, Rev. Mod. Phys. 2, 124 (1930).

[12] E. J. Williams and F. R. Terroux, Proc. Roy. Soc. 126A, 289 (1929).

[13] I. Filosofo and A. Rostagni, Phys. Rev. 75, 1269 (1949).

[14] J. G. Trump and R. J. Van de Graaf, J. App. Phys. 18, 327 (1947).

Voltage Measurement

The retarding voltage is measured using a Sprague 500 megohm Meg-O-Max resistor as a meter multiplier in series with a 10K decade box, the voltage across which is measured with a type K potentiometer.

Calibration of the 500 megohm resistor, and of the intermediate standards necessary for its calibration in terms of a tenth-percent megohm standard, was carried out with a series of Wheatstone bridges. The null indicator was in each case a d.c. amplifier of 10-megohm input impedance, the high impedance providing satisfactory tenth-percent bridge sensitivity.

Since the meter multiplier resistance was observed to vary somewhat over the period of several months during which data were taken with it, the resistance is quoted only as 540.6 megohms, ±1 percent.

The value of approximately 500 megohms, as set by the current capacity of the voltage supply, necessitated a carbon resistor with a correspondingly large negative temperature coefficient; this has the effect that at zero applied voltage, after reaching thermal equilibrium in still air at an applied voltage V kilovolts, the particular resistor used here has a resistance found to be given by

$$R=R_0(1-6.5\times10^{-6}V^2).$$

After any change in voltage, the new resistance is approached exponentially with a time constant of 0.7 hour; observation of the apparent rate of drift of voltage due to resistance drift allows a correction to be made, since independent measurements show that the time rate of drift of output voltage of the voltage supply is negligible by comparison.

The Meg-O-Max resistor also has an instantaneous negative voltage coefficient; the manufacturer's value for this coefficient yields the relation

$$R=R_0(1-3\times10^{-4}V)$$

for the instantaneous effect. (V is in kilovolts.) This correction is small compared to the "thermal" effect.

V. THIN SOURCE TECHNIQUES AND DATA

Backscattering in the Source

Since the present spectrograph is concerned primarily with the low energy portions of spectra, the source phenomena which limit low energy beta-spectroscopy become of more than usual importance.

Among such source phenomena are absorption and energy loss in the finite source thickness, and backscattering from the source and source backing; the former occurs for electrons which are emitted in the direction of the detector. Since the initial diminution in the intensity of an electron beam in passing through a thin foil is almost entirely due to backscattering,[15] it is apparent that for thin films, absorption and backscattering are practically equivalent phenomena which will set in below the same point in the spectrum, backscattering being predominant when the backing is thicker than the active source.

The backscattering ratio (scattered electrons per primary) increases with thickness of the scattering film until at some critical thickness t_0 it reaches an asymptotic value called the "backscattering constant" S. The value of S is proportional to Z and has little energy dependence. The critical thickness t_0 on the other hand, is always of the same order of magnitude as the thickness at which electrons passing through the film emerge completely diffusely (i.e. probable scattering angle approximately 1/2 radian);[15] and this fact, together with the relation for the probable scattering angle,[15] indicates the connection of t to the electron energy V_c by the approximate relation

$$V_c=800[(Z^2/A)t_0]^{\frac{1}{2}}. \tag{3}$$

Here V_c is in kilovolts, Z and A are atomic number and weight of the scatterer, and t_0 is thickness in g/cm^2; this relation holds true below several hundred kilovolts. Conversely, for a film of thickness t_0 the energy V_c given by Eq. (3) characterizes a transition region for backscattering; in this region the backscattering is strongly energy-dependent and at voltages above this region there is little backscattering.

These considerations furnish no guarantee that the critical backscattering voltage of Eq. (3) is the same as the voltage at which backscattering gives rise to deviations from a straight line in the Kurie plot of a beta-spectrum. But they do suggest the comparison which is shown in Fig. 3 and which refers to all data through July 1949 on negatron activities for which good information on source thickness is available.[16] The observed critical voltage for Kurie plot deviations, V_K, is shown as a function of thickness t, or rather as a function of the weighted average value of the parameter Z^2t/A for source plus backing. The letter which is encircled for each point corresponds to the corresponding subreferences in reference 16. Points with an arrow represent upper limits in that they correspond to spectra in which the initial deviations were apparently caused by counter-window rather than backscattering effects. The solid line in the figure represents the relation

---

[15] O. Klemperer, *Einfuhrung in die Electronik* (Julius Springer, Berlin, 1933), Chapter 18.

[16a] J. L. Lawson, Phys. Rev. **56**, 131 (1939);
[16b] A. W. Tyler, Phys. Rev. **56**, 125 (1939);
[16c] R. J. Haynes, Phys. Rev. **74**, 423 (1948);
[16d] D. Saxon, Phys. Rev. **74**, 849 (1948);
[16e] C. L. Peacock and R. G. Wilkinson, Phys. Rev. **74**, 289 (1949);
[16f] J. L. Berggren and R. K. Osborne, Phys. Rev. **74**, 1240 (1948);
[16h] R. D. Albert and C. S. Wu, Phys. Rev. **74**, 847 (1948);
[16i] P. W. Levy and E. Grueling, Phys. Rev. **75**, 819 (1949);
[16j] D. Saxon, Phys. Rev. **73**, 811 (1948);
[16k] C. S. Cook, L. M. Langer, and H. C. Price, Phys. Rev. **74**, 548 (1948);
[16l] C. S. Cook and L. M. Langer, Phys. Rev. **73**, 601 (1948).

$$V_K = 1700[(Z^2/A)t]^{\frac{1}{2}} \text{ kilovolts,} \qquad (4)$$

which therefore seems to provide a good empirical relation for beta-spectra and which is closely related to the equation for critical backscattering thickness deduced above.

Source Charging

The thin-film sources of low-energy beta spectroscopy become charged up as beta-particles leave them; spectrum distortion results.[17] In the present case the source is mounted on a film 1½ inches in diameter, making unfeasible some of the stratagems which work on a slit-shaped foil. The procedure used for sulfur 35 consisted of mounting one-half inch behind the source a 0.001-inch tungsten filament. When heated this filament provides a copious source of thermal electrons which will be attracted to and neutralize any charged part of the film. The filament also boils off positive ions, which, once they pass G_1, are accelerated to the collector. To avoid this positive ion background the filament was flashed and then turned off before each reading of collector current, the subsequent reading being given a small correction by extrapolating back to the moment of flashing. The charging up of the source was definitely observable over a period of a few minutes and corresponded to the rate to be expected from a source of the known activity (0.15 millicurie S^{35}) and a few micromicrofarads capacity.

Source Backing Preparation

Since the present spectrograph is not limited by counter-window thickness, and since the comparisons in Fig. 3 indicate that a fair prediction of the effects of a very thin source backing can be made, it is important both to have a source backing of minimum thickness and to know what this thickness is.

With slight modification of apparatus developed for undergraduate physical optics, it was found possible to measure reflecting power, and hence thickness, of thin films at normal incidence. A check was made of the minimum thickness obtainable by the usual technique of picking up double films from water, using solutions of zapon in zapon thinner and of Merck flexible collodion in amyl acetate. To a first approximation, the reflecting power R of a film of thickness d and index of refraction n, for monochromatic light of wave-length λ, should be given by

$$R = 4(n-1/n+1)^2 \sin^2(2\pi dn/\lambda).$$

Measurements on collodion and zapon films gave an approximately sine-squared dependence of R on concentration of the solution used to form the film. From the maximum value of R one knows n and hence, for every other value of R, the thickness d. The respective indices of refraction of zapon and collodion film were found to be 1.57 and 1.47; the film thickness varied approximately linearly with concentration of solution. For collodion the film thickness ranged from 3 to 16 $\times 10^{-6}$ cm for solutions 20 to 80 percent by volume; corresponding figures for zapon are 6 to 51×10^{-6} cm for 10 to 60 percent solutions. In each case the lowest value represents the minimum usable thickness for a 1½ inch diameter film which has to support 0.2 cc of water for an hour or so during the process of active source deposition. The thinnest collodion films seemed to gain in strength during the course of drying out for a day or two.

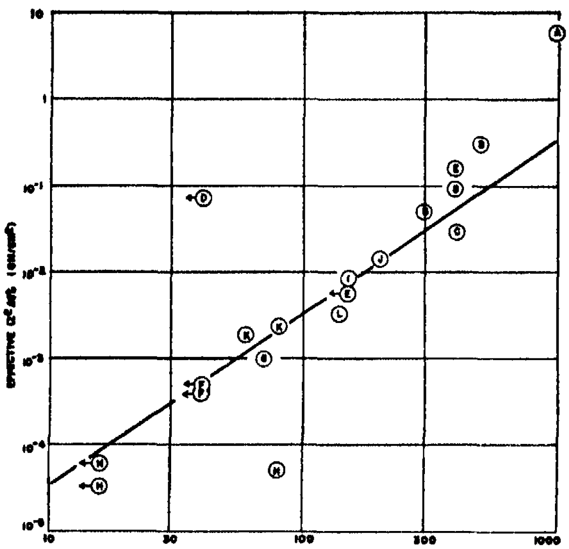

FIG. 3. Relation between source and backing thickness and critical voltage below which deviations from straight line Kurie plot occur, for a number of spectra as indicated by the corresponding letters in reference 15.

Thicknesses measured by this method checked well with values obtained by stacking up a number of films and weighing the lot.

The source backing finally used in the sulfur 35 measurements was a 3×10^{-6} cm collodion film.

ACKNOWLEDGMENTS

We are deeply indebted to Professor R. H. Dicke for the design of and advice concerning the r-f power supply described herein. One of the authors (L.G.) was the recipient of a Charles A. Coffin fellowship (1947–1948) and an AEC predoctoral fellowship (1948–1949) during the course of this work. This research has been supported in part by the joint program of the ONR and AEC.

---

[17] L. M. Langer, Rev. Sci. Inst. 20, 216 (1949).

A Note on the Geometry of Geiger Counter Telescopes

HOMER E. NEWELL, JR. AND ELEANOR C. PRESSLY
Naval Research Laboratory Washington, D. C.

(Received August 8, 1950)

The contribution of a portion of the solid angle of a two-counter telescope to the total coincidence rate is studied for both isotropic and cosine squared law radiation fields. Formulas and graphs are presented for estimating the percentage of counts due to radiation from directions near the telescope axis. The average path length traversed by particles passing through the telescope is touched upon briefly.

I. INTRODUCTION

THE geometry of a two-counter telescope was discussed in two earlier papers.[*] The coincidence rate was expressed in the form

$$N_2 = GI,$$

where G depends both upon the geometry of the telescope and upon the character of the surrounding radiation. When the radiation is isotropic, I is the unidirectional intensity in particles per unit area-unit solid angle-unit time. If the radiation intensity depends upon zenith angle ζ in accordance with a cosine squared law, then $I\cos^2\zeta$ is the intensity factor. Subject to simplifying conditions explicitly set forth in the second paper, formulas were obtained for calculating G once the effective length, diameter, and separation of the counters are known.

A brief consideration of the underlying geometry shows that the directions in the neighborhood of the telescope axis are the most effective in producing coincidences in a two-counter telescope. To make this not so, radiation from directions about the telescope axis would have to be of markedly lower intensity than that from other directions. The present paper provides formulas for estimating the relative effectiveness in producing counts of different portions of the solid angle viewed by the telescope. Some illustrative graphs are given in connection with the discussion.

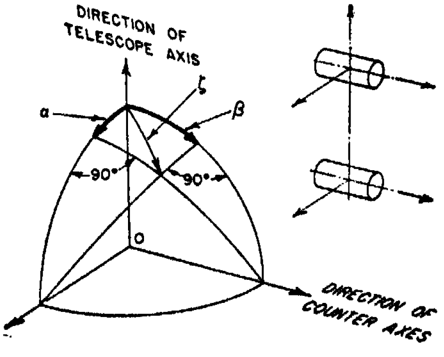

FIG. 1.

II. REVIEW

A direction in space can be specified uniquely by an ordered pair of parameters $[\alpha, \beta]$. Let $\sigma(\alpha, \beta)$ be the plane area normal to the direction $[\alpha, \beta]$ which a ray travelling parallel to $[\alpha, \beta]$ must cross in order to traverse both counters of the telescope. By Σ denote the solid angle over which $\sigma(\alpha, \beta)$ does not vanish. Then the coincidence rate of the telescope is given by

$$N_2 = \int_\Sigma\int I(\alpha, \beta)\sigma(\alpha, \beta)d\Sigma. \tag{2.1}$$

If α and β are given the meanings assigned to them in the earlier papers, and illustrated in Fig. 1, the total range of integration with respect to α and β is from $-\beta_0(\alpha)$ to $\beta_0(\alpha)$ for β, and from $-\alpha_0$ to α_0 for α, where

$$\beta_0 = \operatorname{arcctn}\{(\cos\alpha/\Delta)[\cos\alpha - (\delta^2 - \sin^2\alpha)^{\frac{1}{2}}]\}, \tag{2.2}$$

and

$$\alpha_0 = \arcsin\delta. \tag{2.3}$$

Using a, d, and l to denote, respectively, the separation of the centers, the diameter, and the length of the counters, δ denotes the ratio d/a, and Δ the ratio l/a. When $I(\alpha, \beta)$ is symmetric about the telescope axis the integration may be confined to a single quadrant of the (α, β)-plane. In such a case the region of integration would be the heavily outlined area of Fig. 2.

An expression for $\sigma(\alpha, \beta)$, valid for $-\beta_1(\alpha) \leq \beta \leq \beta_1(\alpha)$, $-\alpha_0 \leq \alpha \leq \alpha_0$, where

$$\beta_1(\alpha) = \operatorname{arcctn}\{(\cos\alpha/\Delta)[\cos\alpha - (\delta\sin\alpha - \sin^2\alpha)^{\frac{1}{2}}]\}, \tag{2.4}$$

was given in Eq. (5.2) of the first paper referred to above. Using the expression given for $\sigma(\alpha, \beta)$ and carrying out the integration over the area under the curve $\beta = \beta_1(\alpha)$ in Fig. 2, a lower bound N_{2m} to the total counting rate N_2 can be calculated.

---

[*] H. E. Newell, Jr., Rev. Sci. Inst. 19, 384 (1948); and H. E. Newell, Jr. and E. C. Pressly, Rev. Sci. Inst. 20, 568 (1949).

For fixed α, $\sigma(\alpha, \beta)$ decreases monotonically to zero as β increases from $\beta_1(\alpha)$ to $\beta_0(\alpha)$. Thus if integration of (2.1) be carried out over the entire area under $\beta=\beta_0(\alpha)$, but with $\sigma(\alpha, \beta)$ replaced by $\sigma(\alpha, \beta_1(\alpha))$ for all points lying between $\beta=\beta_1(\alpha)$ and $\beta=\beta_0(\alpha)$, the result will be an upper bound N_{2M} to N_2.

Both N_{2m} and N_{2M} serve as good approximations to N_2 in most practical cases, since the values of $\sigma(\alpha, \beta)$ at points between the curves $\beta=\beta_1(\alpha)$ and $\beta=\beta_0(\alpha)$ are quite small relative to the values associated with directions in the neighborhood of the telescope axis. The closeness with which N_{2m} and N_{2M} approximate to N_2 can be estimated by reference to Figs. 3 and 5 of the second paper.

III. RELATIVE CONTRIBUTION TO THE TOTAL COINCIDENCE RATE OF RADIATION FROM PORTIONS OF THE SOLID ANGLE VIEWED BY THE TELESCOPE

A. Formulas

The number n_2 of counts per second contributed to the total coincidence rate by a portion of the solid angle viewed by a two-counter telescope may be calculated by carrying out the integration of (2.1) over the shaded area of Fig. 2. Considering radiation from a single hemisphere only:

$$n_2(\alpha, \beta)=4\int_0^\alpha\int_0^\beta I(\alpha, \beta)\sigma(\alpha, \beta)d\Sigma. \qquad (3.1)$$

The formula is valid for all α, β in the ranges $0\leq\alpha\leq\alpha_0$, $0\leq\beta\leq\beta_1(0)$. Within these ranges the expression (5.2) of the first paper may be used for $\sigma(\alpha, \beta)$.

The counting rate $n_2(\alpha, \beta)$ forms a certain fraction of the total coincidence rate N_2 of the telescope, which fraction may be expressed in percentage form as

$$P(\alpha, \beta)=100[n_2(\alpha, \beta)/N_2]. \qquad (3.2)$$

Either $100\, n_2/N_{2m}$ or $100\, n_2/N_{2M}$ can be used as an approximation to P. The absolute error in using the latter satisfies the inequality

$$\begin{aligned} P-100\, n_2/N_{2M}&<100\, n_2(1/N_{2m}-1/N_{2M})\\ &<(n_2/N_{2M})E, \quad E=100(N_{2M}-N_{2m})/N_{2m}. \end{aligned}$$

The quantity E is precisely that plotted in Figs. 3 and 5 of the second paper. Thus the error in using $100\, n_2/N_{2M}$ for P is in the negative direction and is less than

$$100\{[(n_2/N_{2M})E]/[100(n_2/N_{2M})]\}=E$$

percent of P. The error can accordingly be estimated by reference to the graphs of E in the previous paper.

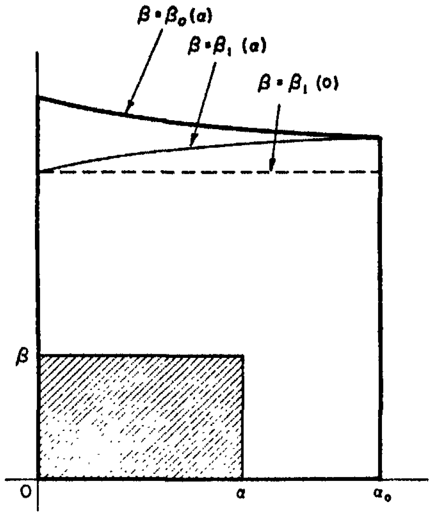

FIG. 2.

In the isotropic case the formula for n_2 is

$$n_2(\alpha, \beta)=4I\int_0^\alpha\int_0^\beta \sigma(\alpha, \beta)d\Sigma.$$

Using the relation

$$d\Sigma=\frac{\cos\alpha\cos\beta}{[1-\sin^2\alpha\sin^2\beta]^{\frac{1}{2}}}d\beta d\alpha,$$

this becomes:

Isotropic Case

$$\begin{aligned} n_2(\alpha, \beta)=2a^2I\int_0^\alpha\Big\{&\Delta(\delta-\sin\alpha)\arctan(\cos\alpha\tan\beta)\\ &+[(\Delta\operatorname{ctn}\beta-\cos^2\alpha)(\delta-\sin\alpha)+B\cos\alpha]\\ &\times\frac{\cos\alpha\sin^2\beta}{(1-\sin^2\alpha\sin^2\beta)}\Big\}d\alpha, \end{aligned} \qquad (3.3)$$

where

$$\begin{aligned} B=\frac{1}{4}\Big[&\delta^2\arccos\left(\frac{2\sin\alpha-\delta}{\delta}\right)\\ &+2(\delta-2\sin\alpha)(\delta\sin\alpha-\sin^2\alpha)^{\frac{1}{2}}\Big]. \end{aligned} \qquad (3.4)$$

When the radiation intensity factor is $I\cos^2\zeta$, the angle ζ being measured relative to the telescope axis,

$$n_2(\alpha, \beta)=4I\int_0^\alpha\int_0^\beta\cos^2\zeta(\alpha, \beta)\sigma(\alpha, \beta)d\Sigma,$$

where

$$\cos^2\zeta=\frac{\cos^2\alpha\cos^2\beta}{1-\sin^2\alpha\sin^2\beta}.$$

TABLE I. $P(\alpha, \beta)$ (Eq. (3.2)) for $\alpha/\alpha_0=\beta/\beta_0$.

	$\alpha\beta/\alpha_0\beta_0$	Isotropic case			Cosine squared law case		
d/a	l/d	0.2	0.4	0.6	0.2	0.4	0.6
0.05	3	49	75	90	49	75	90
	5	49	76	91	49	76	91
	15	50	77	92	52	79	93
	25	50	78	92	53	79	92
0.2	3	50	77	92	52	79	93
	5	50	77	92	54	80	93
	15	51	79	92	59	84	96
	25	52	79	93	60	84	95
0.6	3	52	79	93	62	86	95
	5	53	80	94	63	87	96
	15	53	80	94	64	88	96
	25	53	80	94	64	87	96
1.0	3	61	85	96	79	96	99
	5	61	85	96	79	96	98
	15	60	85	96	79	96	98
	25	60	85	95	78	95	96

Upon integration this yields:

Cosine-Squared Law Case

$$n_2(\alpha,\beta)=a^2I\int_0^\alpha\Bigg\{\Delta(\delta-\sin\alpha)\cos^3\alpha\times\left[\frac{\sin\beta\cos^3\beta}{(1-\sin^2\alpha\sin^2\beta)^2}+\frac{3\sin\beta\cos\beta}{2(1-\sin^2\alpha\sin^2\beta)}+\frac{3}{2\cos\alpha}\arctan(\tan\beta\cos\alpha)\right]+[B\cos^2\alpha-(\delta-\sin\alpha)\cos^3\alpha]\times\left[1-\frac{\cos^4\beta}{(1-\sin^2\alpha\sin^2\beta)^2}\right]\Bigg\}d\alpha. \quad (3.5)$$

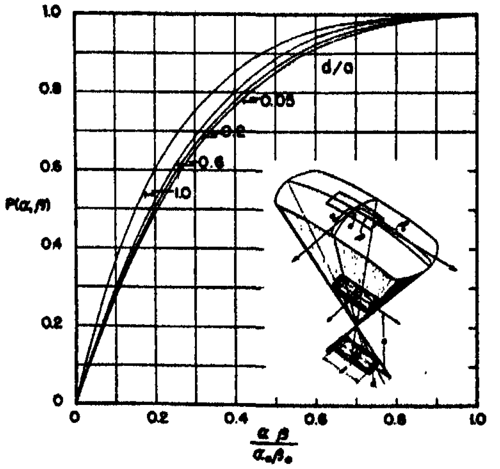

FIG. 3. Contribution of part of counter telescope's solid angle to total counting rate. Isotropic case, $n_2(\alpha, \beta)$-counting rate due to radiation from all directions (α', β') where $-\alpha\leq\alpha'\leq\alpha$, $-\beta\leq\beta'\leq\beta$, with the direction (0, 0) being taken along the telescope axis, and with $\alpha/\alpha_0=\beta/\beta_0$. N_2 = total counting rate of the telescope. $P(\alpha, \beta)=[100n_2(\alpha, \beta)]/N_2$.

In computing $P(\alpha, \beta)$ one must, of course, use the isotropic case value of N_{2M} in conjunction with (3.3), and the cosine-squared law value with (3.5).

B. Graphs

Table I gives $P(\alpha, \beta)$ for various values of d/a, l/d, and $\alpha\beta/(\alpha_0\beta_0)$, under the assumption that $\alpha/\alpha_0=\beta/\beta_0$. The approximation $(100n_2)/N_{2M}$ was used in calculating P. With $\alpha\beta/(\alpha_0\beta_0)$ and d/a fixed, P shows little variation with l/d. It seems reasonable, therefore, to average out the parameter l/d by taking, for each pair of values of $\alpha\beta/(\alpha_0\beta_0)$ and d/a, the unweighted arithmetic mean of the corresponding values of $P(\alpha, \beta)$ for l/d equal to 3, 5, 15, and 25. These average values plotted in Figs. 3 and 4 show the variation of $P(\alpha, \beta)$ relative to $\alpha\beta/(\alpha_0\beta_0)$ for four different values of d/a.

From the graphs one can see that radiation from the directions corresponding to the shaded area of Fig. 2 accounts for about 50 percent of the total coincidence rate when $\alpha=0.4\alpha_0$ and $\beta=0.4\beta_0(0)$.

The parameter $\alpha\beta/\alpha_0\beta_0$ is easily visualized and readily determined for any case in question, and for these reasons was used instead of the corresponding ratio of the actual solid angles involved. In the event that the solid angles are of interest they can be determined with some additional effort. That corresponding to the shaded area of Fig. 2 is given by

$$\Sigma=4\int_0^\alpha\int_0^\beta\frac{\cos\alpha\cos\beta}{[1-\sin^2\alpha\sin^2\beta]^{\frac{3}{2}}}d\beta d\alpha$$

$$=4\arcsin(\sin\alpha\sin\beta). \quad (3.6)$$

The total solid angle viewed by the telescope can be calculated from

$$\Sigma_T=4\int_0^{\alpha_0}\int_0^{\beta_0(\alpha)}\frac{\cos\alpha\cos\beta}{[1-\sin^2\alpha\sin^2\beta]^{\frac{3}{2}}}d\beta d\alpha, \quad (3.7)$$

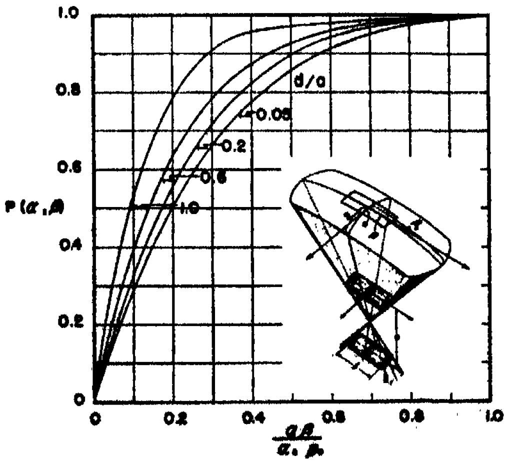

FIG. 4. Cosine-squared law case. See caption for Fig. 3 for definition of terms.

TABLE II. $P(\alpha_0, \beta)$ (Eq. (3.2)).

d/a	β/β_0 / l/d	Isotropic case 0.2	0.4	0.6	Cosine squared law case 0.2	0.4	0.6
0.05	3	36	65	85	36	65	85
	5	36	65	85	37	65	85
	15	37	66	86	40	70	89
	25	37	67	87	41	72	90
0.2	3	38	67	87	40	69	88
	5	38	67	87	42	74	90
	15	38	68	88	47	80	96
	25	38	69	89	48	81	96
0.6	3	38	68	88	46	79	94
	5	38	68	89	47	80	96
	15	38	68	89	48	82	97
	25	38	69	89	49	84	97
1.0	3	35	65	86	47	80	96
	5	35	65	86	47	80	96
	15	34	64	86	47	80	96
	25	34	64	86	46	79	95

where $\beta_0(\alpha)$ is given by (2.2). When $\alpha = 0.4\alpha_0$ and $\beta = 0.4\beta_0(0)$, the ratio Σ/Σ_T is in the neighborhood of 0.2, so that 50 percent of the total counting rate is due to radiation from roughly 20 percent of the total solid angle of the telescope. This illustrates quantitatively the fact stated earlier that most of the radiation counted by a telescope comes from directions near the telescope axis.

In practice the ratio l/d for the counters of a telescope is often fairly large. In such a case, except when the counters are close together, the angle α_0 may be considerably smaller than $\beta_0(0)$. Whereas the range of angles in the β-direction may be so large that its effect upon interpretation of data must be considered, at the same time the angular spread in the α-direction may be small enough to be negligible. When α_0 isn't too large, the variation of $P(\alpha_0, \beta)$ with β is of especial interest. The variation of $P(\alpha_0, \beta)$ with d/a, l/d, and β/β_0 is shown in Table II. Once again $P(\alpha_0, \beta)$ varies but little with l/d when the other parameters are fixed, and it is thought worth while to average out l/d before graphing $P(\alpha_0, \beta)$. The average values are plotted in Figs. 5 and 6.

The graphs of Figs. 3 and 5 covering the case of isotropic radiation provide in essence a means of judging how effective a telescope is as a collimator. This is of especial interest when the directional properties of a radiation field are under study.

IV. VARIATION OF PATH LENGTH WITH DIRECTION

When the solid angle viewed by a telescope is large, the variation in path length through the telescope may be appreciable. Suppose, for example, that an absorber of thickness t is located between the counters of the telescope. As was shown in the discussion of the preceding sections, most of the particles registering counts in the telescope approach from directions near that of the telescope axis. For such particles the path length traversed within the absorber is close to t. On the other hand some of the particles causing coincidence counts penetrate the absorber at large angles to the telescope axis. For these the path lengths through the absorber are considerably greater than t. When the average path length L through the absorber is significantly different from t, it may be important to know L.

The path length through the absorber for a particle from the direction $[\alpha, \beta]$ is $t/\cos\zeta(\alpha, \beta)$, where $\zeta(\alpha, \beta)$ is the angle made by the ray with the telescope axis. Hence the average path length L is given by

$$L = \frac{t}{N_2} \int\int_{\Sigma} \frac{I(\alpha, \beta)\sigma(\alpha, \beta)}{\cos\zeta(\alpha, \beta)} d\Sigma, \tag{4.1}$$

where N_2 is the total coincidence rate, and Σ the total

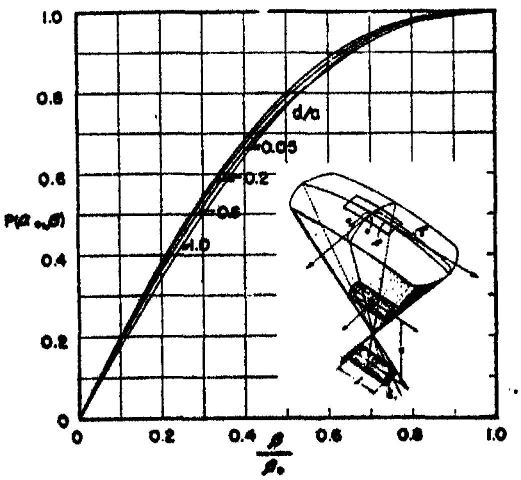

FIG. 5. Isotropic case. See caption for Fig. 3 for definition of terms.

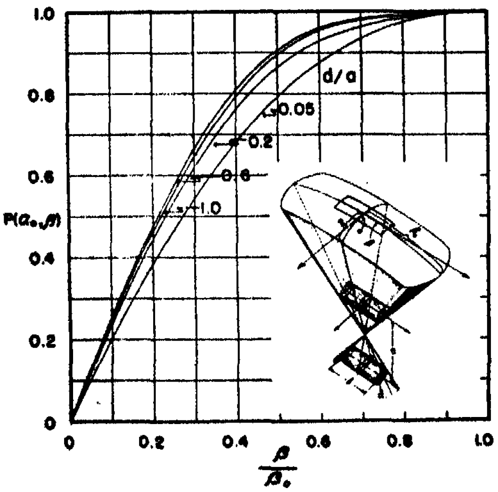

FIG. 6. Cosine-squared law case. See caption for Fig. 3. for definition of terms.

solid angle, of the telescope. Using

$$\cos\zeta(\alpha,\beta)=\frac{\cos\alpha\cos\beta}{[1-\sin^2\alpha\sin^2\beta]^{\frac{1}{2}}},$$

and the expression given previously for $\sigma(\alpha,\beta)$, one gets upon integration:

Isotropic Case

$$L\geq L_m=\frac{4tI}{N_2}\int_0^{\alpha_0}\int_0^{\beta_1(\alpha)}\frac{\sigma(\alpha,\beta)}{\cos\zeta(\alpha,\beta)}d\Sigma=\frac{4a^2tI}{N_2}\int_0^{\alpha_0}\{[(\delta-\sin\alpha)(\Delta+\operatorname{ctn}\beta_1)-B\sec\alpha\operatorname{ctn}\beta_1]$$
$$\times[\operatorname{ctn}^2\beta_1+\cos^2\alpha]^{-\frac{1}{2}}+[B\sec\alpha-(\delta-\sin\alpha)]\}d\alpha;\quad(4.2\text{a})$$

and

$$L\leq L_M=L_m+\frac{4tI}{N_2}\int_0^{\alpha_0}\int_{\beta_1(\alpha)}^{\beta_0(\alpha)}\frac{\sigma(\alpha,\beta_1(\alpha))}{\cos\zeta(\alpha,\beta)}d\Sigma=L_m+\frac{4a^2tI}{N_2}\int_0^{\alpha_0}[(\delta-\sin\alpha)(\Delta\sec\alpha\operatorname{ctn}\beta_1-\cos\alpha)+B]$$
$$\times\arctan\left[\cos\alpha\left(\frac{\operatorname{ctn}\beta_1-\operatorname{ctn}\beta_0}{\operatorname{ctn}\beta_1\operatorname{ctn}\beta_0+\cos^2\alpha}\right)\right]\times(\operatorname{ctn}^2\beta_1+\cos^2\alpha)^{-\frac{1}{2}}d\alpha,\quad(4.2\text{b})$$

for the isotropic case. Expressions for β_1, β_0, and B appear in (2.4), (2.2), and (3.3).

For the cosine-squared law case:

Cosine-Squared Law Case

$$L\geq L_m=\frac{4tI}{N_2}\int_0^{\alpha_0}\int_0^{\beta_1(\alpha)}\cos\zeta(\alpha,\beta)\sigma(\alpha,\beta)d\Sigma=\frac{4a^2tI}{3N_2}\int_0^{\alpha_0}\left\{[B\cos\alpha-(\delta-\sin\alpha)\cos^2\alpha]+\frac{3\Delta\cos^2\alpha(\delta-\sin\alpha)}{(\operatorname{ctn}^2\beta_1+\cos^2\alpha)^{\frac{1}{2}}}\right.$$
$$\left.+\frac{[(\delta-\sin\alpha)\cos^2\alpha-B\cos\alpha]\operatorname{ctn}^3\beta_1-\Delta\cos^4\alpha(\delta-\sin\alpha)}{(\operatorname{ctn}^2\beta_1+\cos^2\alpha)^{\frac{3}{2}}}\right\}d\alpha;\quad(4.3\text{a})$$

and

$$L\leq L_M=L_m+\frac{4tI}{N_2}\int_0\int_{\beta_1(\alpha)}^{\beta_0(\alpha)}\cos\zeta(\alpha,\beta)\sigma(\alpha,\beta_1(\alpha))d\Sigma=L_m+\frac{2a^2tI}{N_2}\int_0^{\alpha_0}\{(\delta-\sin\alpha)(\Delta\sec\alpha\operatorname{ctn}\beta_1-\cos\alpha)+B\}$$
$$\times\left\{\arctan\left[\cos\alpha\left(\frac{\operatorname{ctn}\beta_1-\operatorname{ctn}\beta_0}{\operatorname{ctn}\beta_1\operatorname{ctn}\beta_0+\cos^2\alpha}\right)\right]+\frac{\cos\alpha\operatorname{ctn}\beta_0}{\operatorname{ctn}^2\beta_0+\cos^2\alpha}-\frac{\cos\alpha\operatorname{ctn}\beta_1}{\operatorname{ctn}^2\beta_1+\cos^2\alpha}\right\}(\operatorname{ctn}^2\beta_1+\cos^2\alpha)^{-\frac{1}{2}}\cos^2\alpha d\alpha.\quad(4.3\text{b})$$

Erratum: The Scintillation Efficiency of Anthracene for Low Energy Electrons

[Rev. Sci. Inst. 21, 784 (1950)]

W. J. RAMLER AND M. S. FREEDMAN
Argonne National Laboratory, Chicago, Illinois

The following was omitted from the original article:

Note added in proof: To test the applicability of the efficiency correction to beta-spectra, the spectrum of Pm^{147} was measured using samples ~10 $\mu\mathrm{g/cm}^2$ thickness. Langer[18] has shown the Kurie curve to be linear for such samples down to ~8 kev. Our Kurie curve deviated below linearity below 50 kev, such that the application of a correction factor linear with energy from 50 to 20 kev, amounting to 2.0 at 20 kev in addition to the correction factor of Fig. 4 below 20 kev, gave a Kurie curve straight to ~10 kev. Thus the normalization of Fig. 4 to 100 percent at 20 kev is incorrect; the curve has a small positive slope from 50 percent at 20 kev to 100 percent at 50 kev. Such a slope is consistent with the error in the experimental points above 10 kev.

---

[18] Langer, Mott, and Price, Jr., Phys. Rev. 77, 798 (1950).

THE REVIEW OF SCIENTIFIC INSTRUMENTS VOLUME 21, NUMBER 11 NOVEMBER, 1950

Physical Instruments for the Biologist

Detlev W. Bronk
Associate Editor in Charge of This Section
Eldridge Reeves Johnson Foundation for Research in Medical Physics,
University of Pennsylvania, Philadelphia, Pennsylvania

A Continuous Flow Respirometer Utilizing the Oxygen Cathode*

FRANCIS D. CARLSON,† F. BRINK, JR., AND D. W. BRONK
Johnson Foundation for Medical Physics, The University of Pennsylvania, Philadelphia, Pennsylvania, and the Thomas C. Jenkins Laboratories of Biophysics, The Johns Hopkins University, Baltimore, Maryland

(Received June 26, 1950)

The method of construction and operating conditions are given for a respirometer suitable for determining steady-state rates of oxygen uptake by peripheral nerve. The polarographic method is used to measure the change in oxygen concentration occurring when a solution of known oxygen concentration flows at a constant, predetermined rate over a tissue sample which removes oxygen from the stream. From a knowledge of the concentration change and volume-flow rate the rate of oxygen uptake by the tissue is readily determined. Electrodes for stimulating the nerve sample and for recording the action potential are provided. By virtue of the flow system the respirometer maintains constant environmental conditions. The system is linear with respect to changes in the steady-state rate of oxygen consumption, and the sensitivity is such that, for a 10-mg sample of nerve, changes in the rate of oxygen uptake of 0.1 micromoles/g hr., (2 cu. mm/g hr.) are readily detected.

THE purpose of this paper is to present in detail the theory, the method of construction, and the operational characteristics of a flow-respirometer for the direct measurement of the steady-state rate of oxygen uptake by peripheral nerve. The present instrument is essentially the same as the earlier model mentioned by Bronk *et al.*,[1] and later described in an abstract by Carlson, Brink, and Bronk.[2] Extensive use of the instrument over the past few years has led to modifications in construction and operating technique, which in the opinion of the authors make the present model the instrument of choice for studying the steady-state rate of oxygen uptake in nerve.

Basically, the flow respirometer is a device which allows one to measure the change in oxygen concentration occurring when an oxygenated solution flows at a constant, predetermined rate over an oxygen-consuming tissue sample. From a knowledge of the concentration change and the rate of volume flow it is a simple matter to compute the rate of oxygen uptake by the tissue. The critical problem in the construction of such a respirometer is the development of a device for detecting the concentration of oxygen in a solution of electrolytes.

Brink and Davies[3,4] have described a platinum microelectrode, referred to as the oxygen cathode, which can be used as the active electrode in a polarograph[5] designed to measure oxygen concentration. The method is based on the fact that under certain specifiable conditions the rate of electrolytic reduction of oxygen at the surface of a platinum electrode immersed in a solution of electrolytes is directly proportional to the concentration of dissolved oxygen, the current in the external circuit being used as a measure of the rate of electrolytic reduction. As far as the present discussion is concerned, the important features of such a technique are its high sensitivity to dissolved oxygen concentration and its small physical size. These two features make possible the construction of the respirometer described here, since none of the existing manometric or volumetric techniques are readily adaptable for use in a flow system.

The results of previous studies have suggested to us the following specifications for a respirometer intended to measure the steady-state rates of oxygen uptake of nerve.

1. The respirometer should maintain a constant chemical and thermal environment consistent with the maintenance of a steady-state of metabolism. This requires a constant source of oxygen, and other necessary substrates, together with a sink for heat, carbon dioxide, and any other diffusable material produced by the metabolic processes.
2. The system should be capable of detecting changes in the rate of oxygen uptake of about 2.0 cu. mm/g hr. for a 5 mg to 10 mg sample of nerve tissue, and at the same time give a measure of the total amount of oxygen removed from the stream.

---

* This work was aided by grants from the American Cancer Society, recommended by the Committee on Growth, and the National Foundation of Infantile Paralysis.

† Presented to the faculty of the Graduate School of the University of Pennsylvania in partial fulfillment of the requirements for the degree of Doctor of Philosophy.

[1] Bronk, Brink, Connelly, Carlson, and Davies, Federation Proc., Vol. 6, No. 1, Part II (1947).

[2] Carlson, Brink, and Bronk, Federation Proc., Vol. 7, No. 1, Parts I and II (1948).

[3] P. W. Davies and F. Brink, Rev. Sci. Inst. 13, 524–533 (1942).

[4] P. W. Davies, Ph.D. thesis, University of Pennsylvania, 1942.

[5] J. M. Kolthoff and J. J. Lingane, *Polarography* (Interscience Publishers, Inc., New York, 1941).

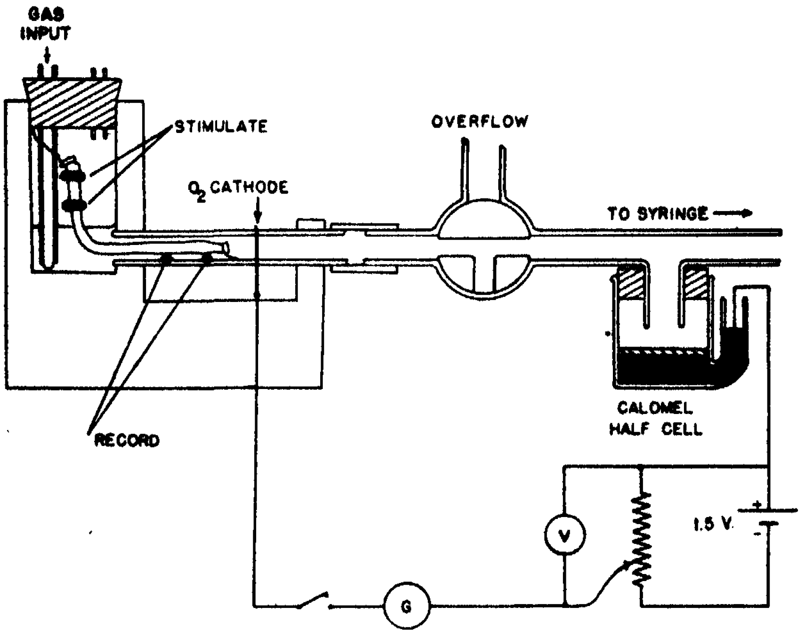

FIG. 1. Schematic diagram of flow respirometer.

3. The oxygen detecting system should be linear over the operating range with respect to the steady-state rate of oxygen uptake and the total amount of oxygen removed from the stream.

4. Adequate control experiments should be possible. For example, a tissue sample on which the effects of a metabolic inhibitor are being studied should be used as its own control.

Davies[4] has described a static respirometer in which an oxygen cathode is used to detect the change in oxygen concentration in a fixed volume of solution enclosing the respiring nerve tissue. The slope of the oxygen concentration-time curve obtained from this type of respirometer is a measure of the rate of oxygen uptake by the nerve. Subsequent work with these static respirometers has led to the following conclusions regarding their undesirable properties:

1. In the static respirometer the oxygen concentration of the solution is measured as a function of time, whereas what is really wanted is a device which measures directly the rate of removal of oxygen.
2. The steady uptake of oxygen by the nerve sample reduces the oxygen concentration in the fixed volume of solution to zero in about an hour, thereby putting a limit on the allowable time for continuous observation.
3. The oxygen cathode in the static respirometer is close to and in some cases actually touching the tissue. While this situation is satisfactory for some experiments, it is not conducive to a high degree of stability of the calibration, and introduces the possibility of the electrode current influencing the metabolic and functional behavior of the nerve.
4. In a static respirometer there exists the possibility that changes due to the accumulation of metabolic products could prevent the establishment of a steady state of metabolism.
5. The static respirometer does not permit an accurate determination of the absolute value of the rate of oxygen uptake; it can be used only to measure relative rates of oxygen uptake owing to the difficulty of determining the amount of oxygen dissolved in the nerve sample itself.

All of these considerations suggested a flow respirometer as a possible improvement.

GENERAL DESCRIPTION OF RESPIROMETER

Figure 1 is a schematic diagram of a flow respromiter. There is a reservoir containing suitable perfusion solution,‡ equilibrated by constant bubbling with a gas of known oxygen concentration. Above the level of the solution mounted in the wall of the reservoir are the platinum electrodes across which the stimulating voltage is applied to the nerve. A heavy-walled glass capillary of suitable diameter enters the reservoir. Tubes having an inside diameter of 1.4 mm are satisfactory for studies of frog and crab nerve. Sealed in the capillary wall and exposed to the lumen are two 0.003-in. platinum wire electrodes for recording the electrical activity of the nerve. Beyond the second of these is the oxygen cathode.

---

‡ The results presented in this paper were obtained with a perfusion fluid for frog's nerve of the following composition:

$CaCl_2$	1.81 millimoles/liter
NaCl	115.0 millimoles/liter
KCl	2.10 millimoles/liter
$NaHCO_3$	1.98 millimoles/liter

Equilibrate with two percent CO_2 gas giving a pH of 7.0 at 20°C.

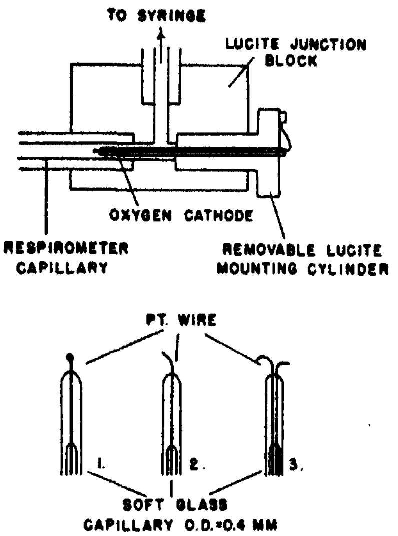

FIG. 2. Detail of oxygen cathode construction and mounting.

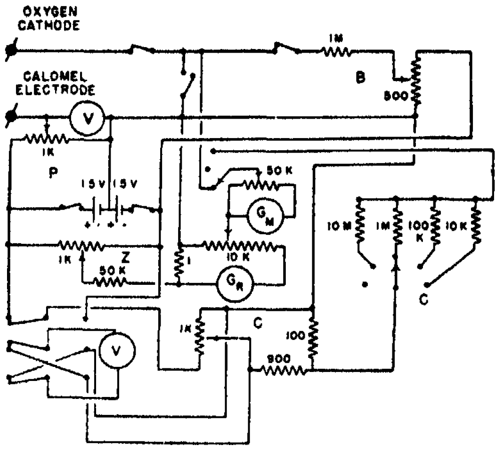

FIG. 3. Circuit diagram of polarizing circuit and auxiliary circuits. P, polarizing circuit for oxygen cathode. Z, galvanometer zero adjustment circuit. B, "bucking" circuit (see text). C, circuit for providing calibrating currents.

Two types of oxygen cathode have been used successfully, consisting of either a 0.002-in. platinum wire sealed across the lumen of the capillary (Fig. 1) or a short length of platinum wire supported on the end of a longitudinal glass rod located in the center of the stream (Fig. 2). The chief advantage of the second type of oxygen cathode is that it allows easy replacement at any time.

Following the chamber are: a three-way stopcock for refilling and cleaning purposes, and a calomel electrode. A simplified polarizing circuit is also shown in Fig. 1.

Beyond the calomel electrode a syringe draws solution from the reservoir through the capillary at a constant volume flow rate. It is obvious that such an arrangement can detect only changes in the rate of oxygen uptake associated with the portions of nerve in the capillary, since the section of nerve in the reservoir is in a region of constant oxygen concentration. In use, only the respirometer proper is placed in a temperature bath regulated to 0.1°C, while the stopcock, calomel electrode, and syringe remain outside at room temperature.

In actual operation, the oxygen cathode circuit is closed 12 seconds out of every minute. Intermittent operation of the electrode reduces the rate of drift of sensitivity. A Leeds and Northrup type *R* galvanometer is used in conjunction with motor-driven camera for recording the oxygen cathode currents. In addition, this current is monitored on a Rubicon table galvanometer placed in series with the Leeds and Northrup instrument.

Figure 3 is a circuit diagram of the polarizing and auxiliary circuits for providing calibrating currents, zero-control currents, and "bucking" currents. The polarizing circuit provides a controllable voltage for the oxygen cathode circuit, as well as a galvanometer and shunt for measuring the current in the circuit. Changes in the mechanical zero of the galvanometer are compensated by a small current from the zero-control circuit. Currents of known amounts for calibration purposes are provided by the calibrating circuit.

The "bucking" circuit shown in Fig. 3 allows one to oppose part of the oxygen cathode current flowing through the galvanometer shunt. In this way, the resulting current can be adjusted to give full scale deflection for the maximum galvanometer sensitivity. This procedure increases the over-all sensitivity of the instrument to changes in rates of oxygen consumption. In practice, fivefold increases have been obtained with a continuously operated oxygen cathode and the Leeds and Northrup galvanometer. The large initial current associated with closing the oxygen cathode circuit made it impossible to use this technique for intermittent electrode operation. In the future it is hoped that by using an electronic current-sensitive device, full use can be made of the "bucking" technique for increasing the useful over-all sensitivity to the limit set by current fluctuations due to variations in the volume flow rate.

THEORY OF FLOW RESPIRATOR

Before launching into any detailed theoretical analysis of the flow respirometer, it is worth while to state the important results obtained from such an analysis. These are the expression relating galvanometer deflection and volume flow rate to the steady-state rate of oxygen

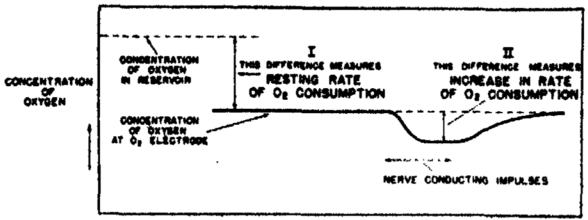

FIG. 4. Simplified record of a typical experiment.

uptake by the nerve in the capillary, and the operational conditions necessary for this expression to hold. Unless these conditions are met, it is not certain that the rate of oxygen uptake computed from the derived expression will be correct.

Figure 4 is a simplified record of a typical experiment. The ordinate is directly proportional to the oxygen concentration at the cathode, time is measured along the axis of abscissas. The difference between the oxygen concentration measured with the capillary empty and then with a resting nerve present is a measure of the resting rate of oxygen uptake by the nerve. Similarly, the difference between the oxygen concentration measured with a resting nerve in the capillary and then with a nerve conducting impulses is a measure of the increase in the rate of oxygen uptake. If the proper conditions are met, it can be shown also that the area between the broken line and the solid curve of II, Fig. 4 is a measure of the total amount of oxygen removed from the stream as a result of the nerve's activity.

The equation used to determine the rate of oxygen uptake of the nerve sample from the measured electrolysis current and the constants of the system is:

$$Q = V\cdot C_0(1 - i_1/i_0).$$

Q is the steady-state rate of oxygen uptake in micromoles/hour. V is the volume flow rate of solution through the capillary in liters/hour. C_0 is the concentration of oxygen in the reservoir in micromoles/liter. i_0 is the current in the oxygen cathode circuit when no nerve is present in the capillary and the oxygen concentration in the stream is C_0. i_1 is the current in the oxygen cathode circuit when a nerve with a rate of oxygen uptake equal to Q is present in the capillary and the oxygen concentration in the reservoir is C_0.

The first of the necessary operational conditions to be met is the constancy of C_0. In practice this is achieved by constantly bubbling a gas of known oxygen concentration through the solution in the reservoir.

It is also necessary that V be maintained at a constant known value. The syringe drive used in the present work consisted of a precision screw coupled to a 1-ml B-D Yale Tuberculin syringe. The screw was driven through a reduction gear by a Holzer-Cabot 75 in.-oz., 1 r.p.m. synchronous motor. This drive produced a volume flow rate of 2.16×10^{-4} liters/hour, constant to within one percent. A constancy of one percent is adequate for rates of oxygen uptake greater than 2.0 cm/g hr.; for rates smaller than this value a more uniform syringe drive is needed.

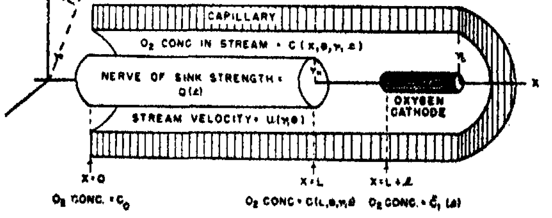

FIG. 5. Schematic diagram of respirometer capillary showing orientation of nerve and oxygen cathode with respect to the cylindrical coordinate system.

Finally, and of utmost importance in assuring proper operation of the respirometer, is the location of the oxygen cathode; it is essential that it be located at a point in the capillary where the oxygen concentration is constant across the area of the stream. This can be achieved by placing the oxygen cathode sufficiently far downstream from the end of the nerve to allow all concentration gradients existing across the stream as it leaves the end of the nerve to equilibrate. The results of the following discussion show that the oxygen cathode should be located downstream from the end of the nerve by a distance l in cm greater than $12r_c^2D/[V-(V^2+145r_c^2D^2)^{\frac{1}{2}}]$. V is the volume flow rate in ccm/sec. and D the diffusion coefficient of oxygen in water at the operating temperature in units of cm²/sec. and r_c the radius of the capillary. At this distance from the nerve the oxygen concentration across the area of the capillary will be constant to within two percent of its average value.

Although it is not necessary for the proper operation of the respirometer itself, mention should be made of the necessity for choosing the volume flow rate and initial oxygen concentration high enough to insure that no part of the nerve becomes anoxic. For a ten-milligram sample of frog sciatic nerve a volume flow rate of 2.16×10^{-4} liters/hour and an initial oxygen concentration of 265 micromoles/liter (20 percent oxygen in the equilibrating gas) was sufficient to prevent any part of the nerve from becoming anoxic even under the most extreme conditions. Anyone contemplating using this type of respirometer for studies on other tissues should first examine the extent to which the rate of oxygen uptake is dependent on oxygen concentration and choose the volume flow rate and initial oxygen concentration accordingly.

In discussing the theory of the flow respirometer it is convenient to orient the nerve and capillary with respect to a cylindrical coordinate system as shown in Fig. 5, and to introduce the following symbols and definitions:

x, r, θ = coordinates of a point in the capillary stream defined by the coordinate system shown in Fig. 5.
t = time in hours.
$C(x, r, \theta, t)$ = oxygen concentration in micromoles/liter as a function of x, r, θ, and t.
$u(r, \theta)$ = stream velocity as a function of r and θ in cm/hour.
$Q(t)$ = rate at which entire nerve sample removes oxygen from the stream in micromoles/hour as a function of time.
L = length of nerve in capillary in cm.
r_n = radius of nerve in cm.
r_c = radius of capillary in cm.
C_0 = oxygen concentration in the reservoir, $x=0$, a constant, in micromoles/liter.
$C_1(t)$ = oxygen concentration at the oxygen cathode, $x=L$, as a function of time in micromoles/liter.
V = volume flow rate through the capillary in liters/hour.

i_0 = current in microamperes in oxygen cathode circuit due to a flowing solution of oxygen concentration C_0 and volume flow rate V.

$i_1(t)$ = current in microamperes in oxygen cathode circuit due to a flowing solution of concentration $C_1(t)$ and volume flow rate V.

K = sensitivity of the oxygen cathode in (micromoles/liter) per microampere.

D = diffusion coefficient of oxygen in water at the temperature of operation, in cm²/sec.

The total amount of oxygen contained in the portion of the stream surrounding the nerve of length L at the time t is given by the integral of the oxygen concentration function over the volume. This quantity is equal to the average concentration over the volume, $\bar{C}_v(t)$, at the time t multiplied by the volume. That is:

$$\int_0^L dx \int_0^{2\pi} d\theta \int_{r_n}^{r_c} C(x, \theta, r, t) r dr = \bar{C}_v(t) \pi L (r_c{}^2 - r_n{}^2),$$

where the radii of the nerve r_n and capillary r_c are assumed constant over their length. Similarly, at the time $(t+\Delta t)$ the amount of oxygen in the stream is:

$$\int_0^L dx \int_0^{2\pi} d\theta \int_{r_n}^{r_c} C(x, \theta, r, t+\Delta t) r dr = \bar{C}_v(t+\Delta t) \pi L (r_c{}^2 - r_n{}^2).$$

The change in the amount of oxygen in this volume during the time Δt is equal to the difference between the amount which enters the volume over the annular section at $x=0$ and the amount which leaves because of both the flow through the annular section at $x=L$ and the oxygen uptake of the nerve present in the capillary. This assumes, of course, that the amount which enters and leaves by diffusion and mixing in the x-direction is small compared to the amount transported by the stream. Equating these quantities we obtain:

$$\begin{aligned}[\bar{C}_v(t) - \bar{C}_v(t+\Delta t)] \pi L (r_c{}^2 - r_n{}^2) \\ = \Delta t \int_0^{2\pi} d\theta \int_{r_n}^{r_c} u(r, \theta) C(0, r, \theta, t) r dr \\ - \Delta t \int_0^{2\pi} d\theta \int_{r_n}^{r_c} u(r, \theta) C(L, r, \theta, t) r dr - Q(t) \Delta t. \quad (1)\end{aligned}$$

The two integrals on the right of (1) are the oxygen fluxes through the section at $x=0$ and $x=L$, respectively. Division of each side of (1) by Δt and passing to the limit as Δt approaches zero yields:

$$\begin{aligned}Q(t) = \int_0^{2\pi} d\theta \int_{r_n}^{r_c} u(r, \theta) C(0, r, \theta, t) r dr \\ - \int_0^{2\pi} d\theta \int_{r_n}^{r_c} u(r, \theta) C(L, r, \theta, t) r dr \\ - \pi L (r_c{}^2 - r_n{}^2) [d\bar{C}_v(t)/dt]. \quad (2)\end{aligned}$$

Equation (2) is the general expression relating the rate of oxygen uptake of the nerve, $Q(t)$, to the concentration functions $C(0, r, \theta, t)$ and $C(L, r, \theta, t)$, the stream velocity function $u(r, \theta)$, and the time rate of change of the average volume concentration function, $d\bar{C}_v(t)/dt$. By imposing certain physically realizable conditions on the concentration function it is possible to obtain a simplification of (2) which relates $Q(t)$ to measurable quantities. If the concentration function $C(0, r, \theta, t)$ is made independent of r, θ, and t and at the same time the function $C(L, r, \theta, t)$ is made independent of r and θ, then these two functions can be taken outside of their respective integrals in (2) and we obtain:

$$\begin{aligned}[C_0 - C_1(t)] \int_0^{2\pi} d\theta \int_{r_n}^{r_c} u(r, \theta) r dr \\ - \pi L (r_c{}^2 - r_n{}^2) [d\bar{C}_v(t)/dt] = Q(t), \quad (3)\end{aligned}$$

where C_0 is the constant concentration at $x=0$ and $C_1(t)$ is the uniform oxygen concentration at the oxygen cathode, a function of time only. Further simplification of (3) results when use is made of the fact that:

$$\int_0^{2\pi} d\theta \int_{r_n}^{r_c} u(r, \theta) r dr = V,$$

where V is the volume flow rate through the capillary. Equation (3) then becomes:

$$V[C_0 - C_1(t)] - \pi L (r_c{}^2 - r_n{}^2) [d\bar{C}_v(t)/dt] = Q(t). \quad (4)$$

In practice the function $C(0, r, \theta, t)$ is made constant by constantly bubbling oxygen through the solution in the reservoir, thereby stirring it and maintaining the oxygen concentration at a constant value independent of r, θ, and t at $x=0$.

The concentration at $x=L$, $C(L, r, \theta, t)$ cannot be made uniform over r and θ directly. What can be done, however, is to place the oxygen cathode far enough downstream from the end of the nerve so that concentration gradients existing in the stream as it leaves the end of the nerve have sufficient time to be dissipated by diffusion. For the time being we will assume that the oxygen cathode has been located in that portion of the capillary where the oxygen concentration is essentially constant. The details of determining the separation between the end of the nerve and the region of constant oxygen concentration are given at the end of this discussion.

Returning to Eq. (4) we are now in a position to derive the desired relationship between the steady-state rate of oxygen uptake by the nerve and the measurable quantities. If the system is in the steady state, then all of the concentrations are constant in time; therefore, $d\bar{C}_v(t)/dt = 0$, and (4) becomes:

$$V[C_0 - C_1] = Q, \quad (5)$$

where C_1 and Q refer to the steady-state values of $C_1(t)$ and $Q(t)$, respectively.

Since the current in the oxygen cathode circuit is directly proportional to the oxygen concentration, it follows that:

$$\begin{aligned} C_0 &= K\cdot i_0, \\ C_1 &= K\cdot i_1, \end{aligned} \tag{6}$$

where K is the sensitivity of the oxygen cathode. Substitution of (6) in (5) yields:

$$Q=VC_0[1-i_1/i_0]. \tag{7}$$

Equation (7) is the desired expression relating the unknown steady-state rate of oxygen uptake to the known constants of the respirometer, V, C_0, and i_0 and the measured quantity i_1.

For the transition from one steady state to another we can derive the following useful relationship between the variables of Eq. (4). Without loss of generality, it is allowable to assume that at time $t=0$ the rate of oxygen uptake by the nerve is equal to zero, and that for all subsequent times it is given by some function $Q(t)$ which approaches the constant value Q for $t=\infty$. Under this condition the boundary values of the variables become:

$$\begin{aligned} &t=0, \quad C_1(0)=C_0 \quad \text{and} \quad \bar{C}_v(0)=C_0, \\ &t=\infty, \quad C_1(\infty)=C_1 \quad \text{and} \quad \bar{C}_v(\infty)=C_v. \end{aligned}$$

Integration of (4) with respect to time from 0 to ∞ now yields:

$$V\int_0^\infty C_1(t)dt-\pi L(r_c^2-r_n^2)[C_v-C_0]=\int_0^\infty Q(t)dt. \tag{8}$$

For the particular case in which $C_v=C_0$, the final steady state, is the same as the initial steady state, we obtain:

$$V\int_0^\infty C_1(t)dt=\int_0^\infty Q(t)dt. \tag{9}$$

Since the current in the oxygen cathode circuit is proportional to the concentration $C_1(t)$, it follows that:

$$C_1(t)=K\cdot i_1(t). \tag{10}$$

Substitution of (10) in (9) yields:

$$VK\int_0^\infty i_1(t)dt=\int_0^\infty Q(t)dt. \tag{11}$$

Equation (11) is a statement of the fact that the total amount of oxygen taken up by the nerve because of a temporary change in the rate of uptake is equal to the product of the volume flow rate, sensitivity, and time integral of the current curve.

There remains the problem of determining how far beyond the nerve the oxygen cathode must be located in order to be in a region of constant oxygen concentration. The discussion that follows is not intended to be a precise treatment of this problem but rather an approximate solution sufficiently accurate for design purposes.

It is possible to determine approximately from the theory of diffusion in moving liquids the minimum distance beyond the nerve at which the oxygen concentration is essentially constant across the stream. In the steady state, diffusion in a cylindrical stream of constant mean velocity $u_2=V/\pi r_c^2$ satisfies the differential equation:[6]

$$u_2(\partial C/\partial x)=D[(\partial C^2/\partial r^2)+(1/r)(\partial C/\partial r)+\partial^2 C/\partial x^2]. \tag{12}$$

For the portion of the stream beyond the end of the nerve, $x=L$, the following boundary conditions apply:

at $x=L$, $C=C(L,r)$
at $x=\infty$, $C=C_1$ (a constant)
at $r=r_c$, $\partial C/\partial r=0$.

The boundary condition at $x=L$ is a statement of the fact that in the steady state a radial oxygen concentration distribution $C(L,r)$ exists across the stream. It should be noted that $C(L,r)$ can never be less than zero nor greater than C_0, the oxygen concentration in the reservoir. Under the most extreme conditions of oxygen uptake by nerve tissue $C_0<2C_1$. The boundary condition at $x=\infty$ is merely a statement of the absence of radial concentration gradients and the requirement that the concentration gradient vanish at the capillary wall is demanded by its impermeability to oxygen.

Application of the above boundary conditions to the solution of Eq. (12) given by Riemann-Webers yields:

$$C(x,r)=C_1+\sum_{i=1}^{\infty} B_i J_0(r\sigma_i/r_c)e^{\xi_i(x-L)}, \tag{13}$$

where $J_0(r\sigma_i/r_c)$ are the Bessel functions of order zero and:

$$\xi_i=(u_2/2D)-[(u_2^2/4D^2)+\sigma_i^2/r_c^2]^{\frac{1}{2}},$$

σ_i are the roots of $J_1(\sigma_i)=0$; $\sigma_1=3.83$, $\sigma_2=7.02$, etc. The constants B_i are determined by the boundary conditions at $x=L$ and need not be evaluated for our purposes.

Since $C(L,r)$ is bounded by the values 0 and $2C_1$, the quantity $|C(L,r)-C_1|$ has a maximum value no greater than C_1. Furthermore, since there is no device present in the stream beyond the point $x=L$ which concentrates the oxygen above its maximum value at $x=L$, it follows that the quantity $|C(x,r)-C_1|$ falls off with increasing x, for $x>L$, in a manner determined by the exponential series of (13), that is:

$$|C(x,r)-C_1|\leqq C_1\sum_{i=1}^{\infty} e^{\xi_i(x-L)}. \tag{14}$$

---

[6] Riemann-Webers, *Differential-gleichungen der Physik* (Braunschwieg, 1927), Vol. II, page 252.

The series converges rapidly in ξ_i so the first term can be used as a good approximation, therefore:

$$|C(x,r)-C_1|/C_1 \leqq \exp[\{(u_2/2D)-[(u_2^2/4D^2)+\sigma_1^2/r_c^2]^{\frac{1}{2}}\}(x-L)], \quad (15)$$

where $\sigma_1=3.83$.

The left-hand term in the inequality (15) is the maximum fractional deviation of the oxygen concentration at a point x $(x>L)$ from its constant value at $x=\infty$. If a numerical value is assigned to this quantity, it is possible to solve the above inequality for the value of $(x-L)$ at which the fractional deviation will not exceed the assigned value.

To be sure, in the actual case the stream velocity is not constant across the cross section, but varies with the radius in the characteristic parabolic manner of Poiseuille flow. The solution of the diffusion equation for such a parabolic velocity distribution is not worth while for our purposes. If instead of using the mean velocity of the stream the peak velocity is used, the value of $(x-L)$ obtained will certainly be greater than that for a Poiseuille velocity distribution. For a Poiseuille velocity distribution the peak velocity is twice the mean velocity. Using twice the mean velocity in (15) we obtain for l, when the fractional deviation is taken as 1/50, the expression:

$$l\geqq -3.9/\{(u_2/D)-[(u_2^2/D^2)+14.7/r_c^2]^{\frac{1}{2}}\} \quad (16)$$

or,

$$l\geqq 12r_c^2D/[V-(V^2+145r_c^2D^2)^{\frac{1}{2}}]. \quad (17)$$

MEASURED PROPERTIES OF THE FLOW RESPIROMETER

The particular respirometer on which the experimental studies described below were made possessed the following dimensions and constants: r_c = radius of capillary $=7\times10^{-2}$ cm. r_n = radius of nerve sample = about 5×10^{-2} cm. V = volume flow rate $=2.16\times10^{-4}$ liters/hour $=6.0\times10^{-5}$ cm³/sec. L = length of nerve sample = 2.2 cm. l = distance from nerve to oxygen cathode = 0.4 cm. D = diffusion coefficient of oxygen in water $=3\times10^{-5}$ cm²/sec. For a respirometer with these constants one obtains a value of 0.38 cm for l, using Eq. (17) derived above. Since the actual value of l was 0.40 cm, it is reasonably certain that the oxygen concentration was constant across the stream at the oxygen cathode.

TABLE I.

Date	Oxygen cathode sensitivity in $\left(\frac{\text{micromoles/liter}}{\text{microampere}}\right)$
11/2	1075
11/4	995
11/7	991
11/10	920
11/12	894
11/15	950
Average value	971

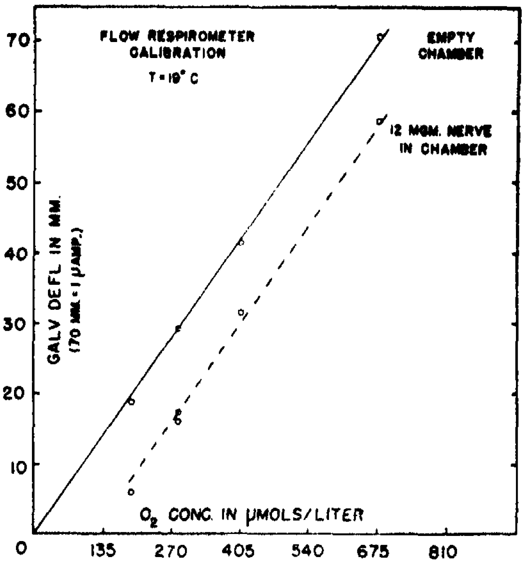

FIG. 6. Calibration curve for an oxygen cathode.

The first operational characteristic to be examined experimentally was the dependence of the oxygen cathode current on oxygen concentration. This was done both with and without a nerve present in the capillary. Figure 6 is a calibration curve showing the observed galvanometer deflection and calculated oxygen cathode current as a function of oxygen concentration. The fact that this curve is a straight line through the origin establishes the strict proportionality between oxygen cathode current and oxygen concentration. The lower curve in the figure is a calibration curve with a nerve present in the chamber. Once again a straight line is obtained with the same slope as the line for the empty chamber. This fact establishes the constancy of sensitivity with respect to the presence or absence of a nerve sample in the chamber, since the respiration of nerve is constant in this range of oxygen concentrations. The slope of both of the lines is 645 (micromoles/liter)/microampere, which is the sensitivity of this oxygen cathode.

Table I is a tabulation of the sensitivities for one of the oxygen cathodes over a two-week period. It is seen that the change in sensitivity does not exceed 10 percent during this period. If the oxygen cathode is allowed to operate continuously, there is usually an appreciable drift in sensitivity over the course of a day. This drift is greatly reduced by allowing the cathode current to flow only 12 seconds out of every minute. Intermittent operation of the oxygen cathode is easily achieved by means of a microswitch actuated by a 1 r.p.m. motor-driven cam.

In general, the calibration changes with changes in the chemical constitution of the perfusion solution. It is therefore necessary to determine the calibration curve

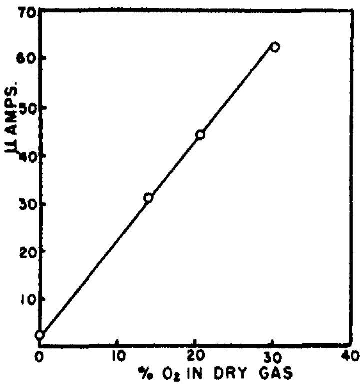

FIG. 7. Platinum sink current as a function of oxygen concentration in the entering stream.

for each new solution. Although small temperature changes (1°C) have slight effects on the calibration, it is advisable to calibrate the system at each temperature used.

While we have established the linearity of the system with respect to changes in oxygen concentration, it remains to be shown that it is linear with respect to changes in the rate of removal of oxygen by the nerve present in the chamber. To do this, a sink[§] was constructed from 2 to 3 cm of 0.001-in. platinum wire wound around a glass tube 0.7 mm in diameter and 1.9 cm long. One end of this wire was connected to a polarizing circuit and calomel electrode similar to those used in the oxygen cathode circuit. The sink was then placed in the chamber so that it occupied much the same space as would a nerve sample. With the polarizing voltage properly adjusted, such a system acts like the oxygen cathode and electrolyzes oxygen from the solution. The current through such a sink varies linearly with the concentration of oxygen in the stream (Fig. 7). Assuming that the number of electrons required to reduce an oxygen molecule at the sink electrode is independent of the oxygen concentration, we can conclude from the linear dependence of sink current on oxygen concentration that this particular sink reduces oxygen at a rate directly proportional to the oxygen concentration.

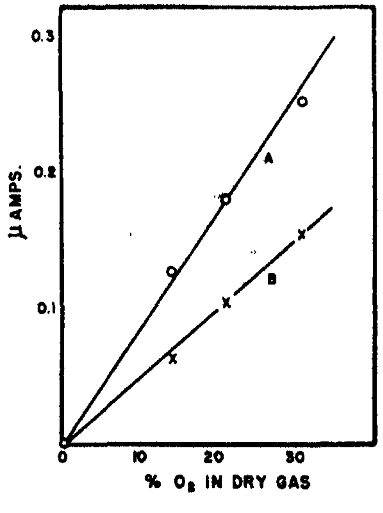

FIG. 8. Curve A, oxygen cathode current as a function of oxygen concentration in the entering stream with the platinum sink off. Curve B, oxygen cathode current as a function of oxygen concentration in the entering stream with the platinum sink on.

If the oxygen cathode current depends linearly on the strength of the sink in the capillary, a calibration made with the above described sink in operation should produce a straight line with a slope less than the calibration curve for a sink of zero strength. Figure 8 is a plot of the steady-state oxygen cathode current as a function of oxygen concentration with the sink off (curve A), and with the sink on (curve B). The sink polarizing voltage was the same for each point on curve B. The linearity of curve B proves that the current in the measuring electrode is related linearly to the rate of removal of oxygen from the flowing stream in the capillary tube.

All of the above experimental results are consistent with the existence of the necessary conditions for proper operation of the respirometer; however, none of them afford direct proof of the uniformity of oxygen concentration over the area of the stream at the oxygen cathode. If it were possible experimentally to show that the integrative relationship expressed by (11) held for the respirometer, then it would be fairly certain that the condition of uniformity of concentration had been met. Such an experiment requires a sink of accurately known strength. The sink described above is of unknown strength owing to an ambiguity in the number of electrons involved in the electrode reaction. Accordingly, it is necessary to resort to an indirect proof.

If the respirometer does satisfy the condition that the oxygen concentration at the oxygen cathode is uniform across the stream, we should expect the oxygen concentration measured at this point to be independent of the form of the oxygen cathode. To test this, the platinum wire sink was inserted in the respirometer and turned on. The oxygen concentration in the stream beyond the sink was determined first with a spherical type oxygen cathode, Fig. 2, 1. The spherical oxygen cathode was replaced with a whisker type, Fig. 2, 3, and the oxygen concentration again determined. The oxygen concentration in the first case was 195 μmoles/l., while in the second case a value of 208 μmoles/l. was obtained. The close agreement of these two values establishes the fact that measurements of oxygen concentration are independent of oxygen cathode geometry for the two types of oxygen cathodes used.

In view of the fact that the flow respirometer is primarily intended for studying steady-state rates of oxygen uptake by nerve, no detailed analysis of its transient response has been attempted. It seems certain that even if the formal expressions for the transient response were known, the computational problem of determining the actual transient behavior of a given sink from the measured response would be quite laborious.

[§] For the purposes of this discussion it is convenient to define as a sink any device which when placed in the capillary stream, can be made to remove oxygen from the stream at a constant rate. The rate of oxygen removal will be referred to as the strength of the sink.

In order to provide some criterion for deciding to what extent an observed transient is due to the response characteristics of the respirometer and to what extent it is due to the properties of the sink, a study was made of the transient response to a step change in sink strength. The platinum wire sink described above was placed in the capillary, turned on, and allowed to come to a steady state. At time $t=0$ the sink was turned off and the resultant response recorded. The open circles of Fig. 9 are the experimentally observed values for three separate experiments.

The solid line of Fig. 9 is the transient response calculated for the simplified case of a sink of constant strength per unit length in a stream of constant velocity u_1 along the length of the sink and u_2 between the sink and the oxygen cathode. It is apparent that in the steady state the average oxygen concentration falls linearly with x from the value C_0 at $x=0$ to some final value at $x=L$. If S is the sink strength per unit length, the concentration distribution is given by:

$$\begin{aligned} &C_1(x)=C_0; \quad x=0,\\ &C_1(x)=C_0-S\cdot x/V; \quad 0\leqq x\leqq L,\\ &C_1(x)=C_0-S\cdot L/V; \quad L\leqq x\leqq L+l. \end{aligned} \tag{18}$$

If at time $t=0$ the sink is turned off ($S=0$), the concentration distribution given by (18) will move to the right, past the oxygen cathode, giving rise to the transient response. By virtue of this movement the space variable x is transformed to a time variable t according to the transformation.

$$\begin{aligned} &x=L+(u_1l/u_2)-u_1t \quad \text{for} \quad 0\leqq x\leqq L,\\ &x=L+l-u_2t \quad \text{for} \quad L\leqq x\leqq L+l, \end{aligned} \tag{19}$$

where the velocities u_1 and u_2 are given by:

$$u_1=V/\pi(r_c^2-r_n^2), \quad u_2=V/\pi r_c^2.$$

Substituting the above transformation (19) for x in (18) yields the transient response:

$$\begin{aligned} &C_1(t)=C_0-S\cdot L/V \quad \text{for} \quad 0\leqq t\leqq l/u_2,\\ &C_1(t)=C_0-(S/V)[(u_1l/u_2)+L-u_1t]\\ &\qquad\qquad \text{for} \quad l/u_2\leqq t\leqq (L/u_1)+l/u_2,\\ &C_1(t)=C_0 \quad \text{for} \quad (L/u_1)+l/u_2\leqq t. \end{aligned} \tag{20}$$

The platinum-wire sink used was 1.9 cm long (L) and 3.5×10^{-2} cm in diameter (r_n); the distance between the sink and oxygen cathode (1) was 0.7 cm. Using these values together with the values for V and r_c given above in (20) the solid curve in Fig. 9 was obtained. The agreement between the experimentally and theoretically determined values for the time of initiation and the time of completion of the transient are quite good considering the many approximations made in determining the latter.

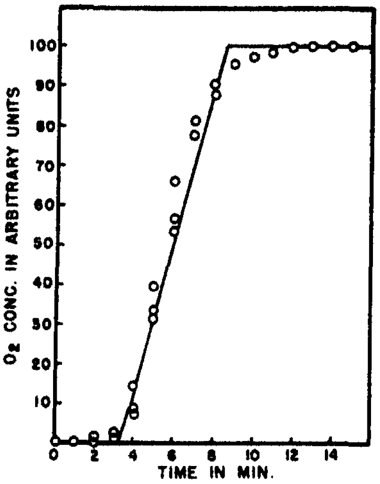

FIG. 9. Transient response of flow respirometer to a step change in sink strength. Open circles are experimentally determined points for three separate experiments. Solid line is theoretical transient response for the simplified case described in the text.

The response time of the respirometer is conveniently defined as $(L/u_1)+l/u_2$, the duration of the transient response to a step change in sink strength. Any observed transient of duration appreciably greater than $(L/u_1)+l/u_2$ is due to the transient response characteristics of the sink being studied. In the case of a nerve 2.2 cm long and 1×10^{-1} cm in diameter the value of $(L/u_1)+l/u_2$ for the respirometer described above is about 6.5 minutes.

SENSITIVITY TO ERRORS

One further aspect of the apparatus remains to be discussed, namely, the sensitivity to error. Equation (7) provides the relationship between the measured and desired quantities, that is:

$$Q=VC_0(1-i_1/i_0).$$

Q is the desired quantity. V and C_0 are constants of the system which, once determined, remain constant and do not constitute a source of error. i_1 is the measured current which can be determined to better than 1 part in 200 with no difficulty. i_0, the calibration current, cannot be determined during any one experiment without removing the nerve from the chamber. Its value can be measured before and after an experiment only. This being the case, unexpected changes in i_0 would give rise to an error in the calculated value of Q. The sensitivity of the calculated value of Q to small changes in i_0 can be ascertained as follows:

$$\partial Q/\partial i_0=V\cdot C_0 i_1/i_0^2$$
$$dQ=(\partial Q/\partial i_0)di_0.$$

Therefore:

$$dQ/Q=(\partial Q/\partial i_0)(di_0/Q).$$

Substitution yields:

$$dQ/Q = (di_0/i_0)[(i_0/i_1)-1]^{-1}.$$

The percentage error in Q is $100\times dQ/Q$ or:

$$100(dQ/Q) = 100(di_0/i_0)[(i_0/i_1)-1]^{-1}.$$

Measurements of i_0 over the course of a day's experiments show that it drifts steadily downward. For a good oxygen cathode the total change in i_0 is about 10 percent over a twelve-hour period; the mean value of i_0 would be within ±5 percent of its actual value at any time during the day. For the nerves used i_0/i_1 was never less than 3/2. Substituting this value for i_0/i_1 together with the figure of ±5 percent for the percentage change in i_0 gives ±10 percent as an upper limit for the percentage error in Q.

Studies of the way in which i_0 changes in time with no nerve in the chamber indicate that it is uniform. This being the case, one can determine from its initial and final values a correction term applicable at any time during the course of the experiment. It is likely that this corrected value is not in error by more than two or three percent, which gives ±5 percent for the error in Q. The values five percent and 10 percent are estimates of the extremes of the percent error in the value of Q determined from flow respirometer data when the calibration changes during a day's run. Under optimum conditions (no change in i_0 over the course of the experiment), the absolute error in Q is determined by the precision of measurement of V, C_0 and i_1. In work where i_0 is corrected for drift it is likely that the ±5 percent figure is applicable. More frequent calibration is necessary if greater accuracy is desired.

For the error in the increment in Q due to activity, the situation is somewhat better. Let Q_1 be the resting rate of oxygen utilization; and Q_2 the steady-state activity rate of oxygen consumption. The increment in rate of oxygen utilization is therefore:

$$[Q_2-Q_1] = VC_0(1-i_2/i_0) - VC_0(1-i_1/i_0).$$

Therefore:

$$\partial[Q_2-Q_1]/\partial i_0 = -VC_0(i_1-i_2)/i_0^2.$$

The fractional error in $[Q_2-Q_1]$ becomes:

$$d[Q_2-Q_1]/[Q_2-Q_1] = -di_0/i_0,$$

or the percentage error in the increment is equal in magnitude to the percentage change in i_0. As was previously mentioned, the percentage error in i_0 is less than five percent. In general, then, errors from two to five percent can be expected in the values for changes in Q.

SUMMARY OF METHOD

The oxygen cathode flow respirometer together with the action potential recording system described above possess the following operational characteristics:

1. Electrodes for stimulating nerves and for recording the action potential are provided which allow the establishment and monitoring of varying degrees of activity in frog sciatic nerve.
2. The respirometer provides a constant source of oxygen and constant sinks for heat, carbon dioxide, and diffusable metabolites. The pH is held constant by means of the carbon dioxide-bicarbonate buffer system, two percent carbon dioxide being supplied by the equilibrating gas.
3. Linearity with respect to changes in the steady-state rate of oxygen consumption is achieved. The total oxygen uptake during a transient change of sink strength is measured by the area under the recorded transient curve.
4. The sensitivity is such that, for a 10-mg sample of nerve, changes in the rate of oxygen consumption of 0.1 micromoles/g hr., 2 cu. mm/g hr., are readily detected.
5. Errors in absolute values and incremental values of the rates of oxygen consumption, arising from drifts in the sensitivity of the oxygen cathode, are 10 percent or less and five percent or less, respectively. These may be reduced by calibrating more than twice a day.

Laboratory and Shop Notes

Improvements in the Li^6 Technique

George R. Keepin, Jr.*
Radiation Laboratory, Department of Physics, University of California, Berkeley, California

August 15, 1950

A NUMBER of improvements have been made during the past year at the Radiation Laboratory on the Li^6 technique. The technique[1] employs measurements on alpha-particles and tritons from Li$^6(n,\alpha)$H^3 reaction in Li^6 loaded emulsions to give a precise measure of incident neutron energy without requiring collimation of the neutrons. The new developments are outlined briefly here; for those using the Li^6 technique, a detailed report including all necessary curves is available.[2]

For the Li$^6(n,\alpha)$H^3 reaction, a new Q-value of 4.78 ± 0.03 Mev has been obtained by combining recent precision Q-value determinations for the Li$^6(p,\alpha)$He^3 and H$^3(p,n)$He^3 reactions.[3,4] Neutrons from D(d,n)He^3,† H$^3(p,n)$He^3, and Li$^7(p,n)$Be^7 have been used to obtain revised range-energy relations in Ilford Li^6 loaded C-2 emulsions. Only the sum of alpha-particle and triton ranges *versus* neutron energy is required, individual calibration of R_α and R_T *vs* E_n being superfluous data for E_n determination. From this new range-energy calibration and the new Q-value, we have obtained revised curves of $R_\alpha+R_T$ *vs* E_n, parametric in both θ, the laboratory angle between the alpha and the triton, and in ϕ, the laboratory angle between the triton and the incident neutron beam (ϕ defined for collimated neutrons only).

Discrimination between the alpha-triton pairs and recoil protons has been markedly improved by use of latent image fading.[5] Artificial fading methods, though more expedient, were rejected because of the possibility of emulsion distortion. For Ilford Li^6 loaded emulsions we have found a vertical shrinkage factor of 2.9 ± 0.1 as compared with the nominal figure of 2.0 for unloaded emulsions. Our search for a fine-grained, high-contrast developer to give optimum discrimination has led to a hybrid solution which is essentially ID 19 with 12 g/liter additional KBr acting as a differential inhibitor. The Brussels group has reported that temperature of the developer is critical, the optimum for alpha-triton discrimination being 72 ± 0.5°F. Our experience has confirmed this. Figure 1 shows the alpha-triton discrimination obtainable using the new processing procedure.

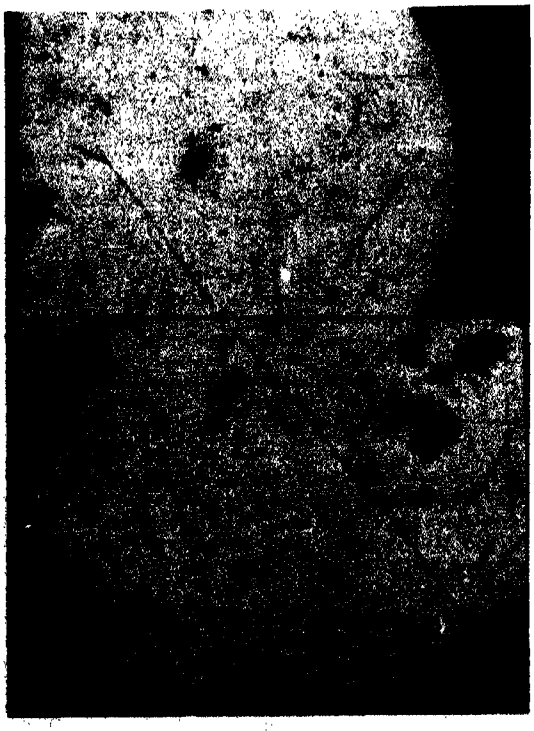

FIG. 1. Li^6 disintegration produced by D,D neutrons: $R_\alpha+R_T=124\pm1.3\mu$; $\theta=154\pm1°$; $E_n=3.8\pm.15$ Mev.

For energy measurement of non-collimated neutrons, three natural groups of track selection criteria have been established, and appropriate correction functions for each group have been developed.[2] In a given experiment, choice of the proper group depends on the energy range of the spectrum under study, the amount of data available, and the maximum energy resolution required. Under the most stringent criteria, which include $175°\leq\theta\leq180°$, resolution to better than ±70 Kev has been obtained. Though the Li^6 technique does not require neutron collimation, when good geometry is possible (ϕ known), two advantages arise: first, energy resolution is increased because E_n is a less sensitive function of $R_\alpha+R_T$ with ϕ, rather than θ, as a parameter; and, second, the θ-azimuth correction,[2] arising from measurement of projected rather than true θ angles, is eliminated. With 5° collimation, resolution to better than ±50 Kev has been obtained for $0\leq E_n\leq3$ Mev.

Exposures to neutrons produced by the Berkeley proton linear accelerator have shown the Li^6 technique to be of little value for $E_n>10$ Mev, owing mainly to the lower Li^6 cross section and to other neutron-induced reactions competing favorably at these energies. Our work has indicated an upper limit of ~5 Mev on this technique as a precision neutron spectrometer.

As a supplementary technique for use at higher energies, B^{10} impregnated plates have been developed and are now being studied. The desired B$^{10}(n,2\alpha)$H^3 reaction has a threshold near 5 Mev, giving measurable ranges of the disintegration products for $E_n>10$ Mev. The B^{10} neutron capture cross section is comparatively high in this energy range.

I am grateful to Professors E. Segrè and L. W. Alvarez for their advice and continued interest in the Li^6 program and to Mr. F. C. Gilbert for his valuable assistance.

---

* AEC Postdoctoral Fellow.

[1] G. R. Keepin, Jr., and J. H. Roberts, Phys. Rev. 76, 154 (1949); AECU 563 or LAMS 924 (1949); G. R. Keepin, Jr., and J. H. Roberts, Rev. Sci. Inst. 21, 163 (1950).

[2] G. R. Keepin, Jr., UCRL-790 (1950). This report obtainable from the Technical Information Division, Oak Ridge, Tennessee.

[3] A. Tollestrup, W. A. Fowler, and C. C. Lauritsen, Phys. Rev. 76, 428 (1949).

[4] Taschek, Argo, Hemmendinger, and Jarvis, Phys. Rev. 76, 325 (1949).

† Obtained at California Institute of Technology through the kindness of Professors C. C. Lauritsen and W. A. Fowler.

[5] L. Vermaesen and G. Occhialini, Note No. 13, Centre Nuc. Phys., Brussels (1950).

A Slide Rule for Nuclear Emulsion Calculations

Arthur Beiser
Department of Physics, New York University, University Heights, New York 53, New York

September 5, 1950

PARTICLE identifications and energy measurements from tracks in nuclear emulsions are generally made on the basis of grain counts and track ranges in the emulsion. Multiple scattering and delta-ray determinations are, because of their less exact nature and difficulty of application, of only limited utility. Range-energy, range-grain density, and distance from end of track-grain count calibration curves are generally made for the various particles recorded in a particular emulsion from identified reference tracks and from theoretical considerations; and these curves are then used in subsequent work with the emulsion.

When the above curves are plotted on logarithmic graph paper, they will appear as virtually straight lines, with the curves for the different particles being parallel on each graph. This property may be utilized to construct a slide rule that, with very little error in

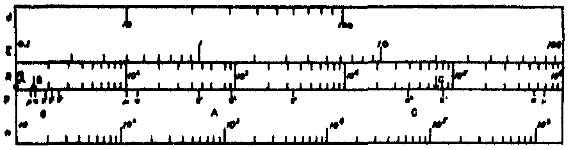

FIG. 1.

most cases, may be used to facilitate greatly work with nuclear emulsions. The scales of the slide rule are most conveniently laid out as shown in Fig. 1, being calibrated from the experimentally determined durves. The *R* (range) scale and the *E* (energy), *d* (grain density), and *n* (total grain count) scales are taken directly from the slopes of the lines on the appropriate curves. The *P* (particle) scale may then be determined by selecting a particular value of *R*, finding from the curves the value of *E*, *d*, or *n*, and setting it opposite the *R* value, with the identity of the particle appearing opposite the appropriate arrow on the *P* scale. The *A* arrow is used for *R vs E*, the *B* arrow for *R vs n*, and the *C* arrow for *R vs d*.

When the slide rule is used, the identity of the particle must first be determined. If the track ends in the emulsion, the total number of grains *n* in a distance in microns *R* from the end may be set against this value of *R*, and the identity of the particle will then be adjacent to arrow *B*. In practice this method will be accurate only if the calibration tracks had the same predevelopment history as the unknowns, and had received the same processing. However, for pre-eradicated plates from balloon and airplane flights, where all the phenomena were recorded within a comparatively short time of each other, this method is very convenient. As a check, or if the track does not end in the emulsion, the grain density *d* in grains per 100 microns at two different points in the tracks as far apart as possible should be determined. The arrow *C* may then be set against the various particles on scale *P*, and the ranges corresponding to the smaller grain density read off on *R*. The distance in microns between the two points at which the grain density was determined is then subtracted from the values for the ranges obtained as above. The arrow *C* may then be reset against *P*, and the grain densities corresponding to the new range values for the different particles determined. The one nearest to the greater measured grain density will then give the identity of the particle.

The energy of a particle ending in the emulsion may be found from the *R* and *E* scales, the arrow *A* being set opposite the particle on the *P* scale. For identified tracks not ending in the emulsion, the ranges corresponding to the smaller grain densities may be used to find the energy on the *E* scale. These energies, in all cases where both the origin and ending of the tracks are not in the emulsion, will, of course, be minimum figures.

A Geiger-Counter Mounting for Continuous Counting of Gas-Phase Radioactivity*

FRANCIS BONNER** AND ALFRED WEINSTEIN
Chemistry Department, Brookhaven National Laboratory, Upton, Long Island, New York

July 31, 1950

IN the course of a recent investigation of the carbon dioxide-carbon reaction,[1] $C^{14}O_2$ and $C^{14}O$ were pumped over charcoal by thermal syphon and the radioactivity of the gas phase was continuously monitored with an end-window Geiger tube. This tube was sealed to a vacuum system with its mica window directly over a glass chamber of about 50-ml volume. The counters used had window thicknesses of 3 to 3.5 mg/cm², thus calling for the use of relatively high activity levels of C^{14} in the system. Thinner windows could not be used because of the great mechanical stress to which they are subjected in this type of work, by flexion upon evacuation and filling of the system. Durability of counters under these severe conditions was variable; some lasted as short a time as one month, while one counter showed only slight deterioration after three months of rather hard usage.

An alternative mounting was developed and employed successfully. While it was not used extensively in the particular investigation mentioned above, the authors feel that it possesses advantages which make it worth bringing to the attention of other workers in this field. The counter, as shown in Fig. 1, is incorporated directly into the top of the male portion, or valve, of a two-way, hollow-bore stopcock. The top of the stopcock was opened and flanged so that the Geiger tube (also flanged) would fit snugly over it. A mica window of appropriate thickness was then cemented between the two flanges, the tube evacuated, filled with counting gas, and sealed. A generous nipple was left for further evacuations and fillings.

The female portion, or housing, of the stopcock is sealed directly into the vacuum system and with the stopcock assembled there are three positions available for varying needs. With the stopcock turned so that its inner portion and the vacuum system are in communication the counter may be used for continuous counting of gas flowing through the system. In the second position shown in the diagram the interior of the stopcock is by-passed altogether. This is often desirable in order to avoid wear on the mica window during pumping and filling operations which need not involve the counter and extra volume. In a third position neither pair of holes lines up with the system. This may be used for counting a static gas sample at measured pressure and volume. Intermittent sampling of a flowing gas may also be carried out without disruption of flow by quickly turning from position one to position two.

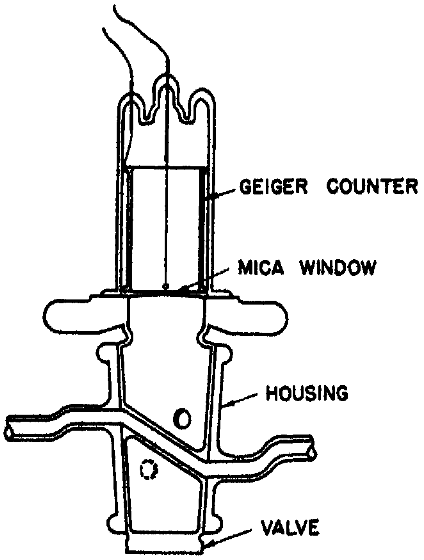

FIG. 1.

Self-absorption corrections are of utmost importance in a counting arrangement such as this, since counting response is clearly a function of gas density. The necessary corrections, carried out by measuring the variation of counting rate with pressure for a gas of fixed specific activity, are described by Bonner and Turkevich.[1]

In addition to the operational advantages already described, the counter in this arrangement can be readily removed from the system for refilling, and when the mica window gives way to flexion it can be replaced without undue difficulty.

---

* Research carried out under the auspices of the AEC.

** Present address: Department of Chemistry, Brooklyn College, Brooklyn 10, New York.

[1] F. Bonner and J. Turkevich, J. Am. Chem. Soc. (to be published).

A Reliable Pirani Vacuum Safety Circuit*

W. Franzen and J. Horton
Palmer Physical Laboratory, Princeton University
August 15, 1950

IN the operation of vacuum systems, it is frequently desirable to control the operation of valves and similar components automatically, in accordance with the pressure in the system. Requirements on a control circuit of this type are reliability, long life, freedom from "chatter," and an operating differential which is as small as possible. In addition, one would require the circuit to fail "safe" in case of a component or power failure. The circuit to be described, which was developed for use with the vacuum system of the Princeton cyclotron, is believed to fulfill these requirements, and, in view of its simplicity, may be of general interest.

The vacuum measuring device is a Sylvania Type R1111 Pirani tube which forms one arm of the bridge shown in Fig. 1.

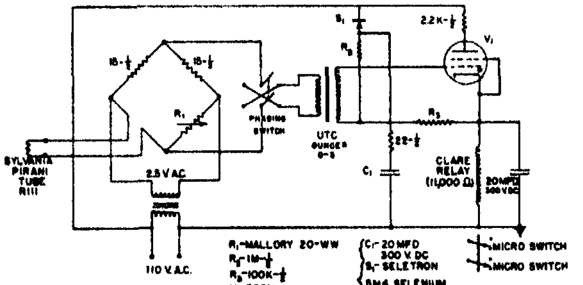

Fig. 1.

The "cold" resistance of this tube is 6.6 ohms; this increases to approximately 16 ohms when the tube is evacuated and a 100 m.a. heating current is applied. The setting of the potentiometer R_1 therefore controls the balance point of the bridge. On one side of balance, the 60-cycle a.c. signal appearing on the grid of the miniature thyratron V_1 is out of phase with the voltage applied to the plate of the tube, and the thyratron cannot fire. On the other side of balance, the two signals are in phase, and the tube will fire during each positive half-cycle provided the positive signal applied to the grid is large enough to overcome its negative d.c. bias. This bias is derived from a network consisting of the half-wave selenium rectifier S_1, the condenser C_1 and the voltage dividing resistors R_2 and R_3.

It was convenient to use a Clare d.c. relay (Navy type CRY-29161) in the cathode circuit of V_1. This relay closes on a current of 4.5 m.a. and opens when this current drops to 2.5 m.a. The switching action of the relay is performed by two micro-switches which are actuated by the moving arm of the relay. Thus the relay has a fairly large differential and a sudden action; these features result in freedom from "chatter." Nevertheless, the differential of the entire circuit is small.

Typical operating conditions in a test of the circuit allowed the relay to close at a pressure of 75 microns Hg and to open at 100 microns Hg. The life of V_1 can be prolonged by incorporating a time delay into the plate circuit of V_1 which delays the application of plate voltage relative to the application of filament heating power.

---

* Supported by the joint program of the ONR and AEC.

Ejection of the Electron Beam from a Betatron*

S. L. Fawcett,† and E. C. Crittenden, Jr.
Case Institute of Technology, Cleveland, Ohio
June 23, 1950

A MODIFICATION of a scheme proposed by Crittenden and Parkins[1] for ejecting the electron beam from a betatron has been applied to the Case biased betatron of 30 Mev maximum energy.[2] The ejected electron beam has been detected by means of the x-rays produced in the wall of a vacuum donut having no exit window.

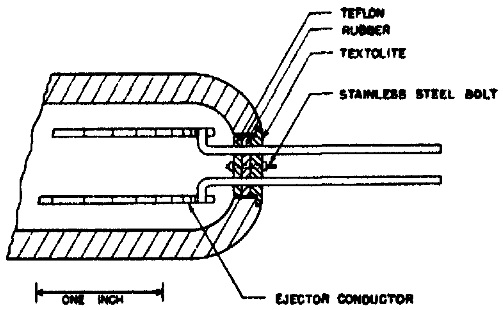

Fig. 1. Ejector conductor structure in donut.

The method utilizes the perturbing magnetic field produced by a current pulse flowing in a pair of conductors, placed above and below the orbital plane, inside the donut. The conductors are segments of circles concentric with the axis of the machine, extending over an azimuth of 40° at the outer edge of the normal region of electron stability. Figure 1 shows a section through one of the two support structures which also function as electrical leads. The general location in the donut is shown in top view in Fig. 2. The two conductors are externally connected in series and carry current in the same direction. A rectangular current pulse, variable up to 500 amp., 20μsec. wide, is applied to the ejector conductors a few microseconds before the expansion coils are pulsed. The expansion pulse is a half-sine wave of about 500 amp. peak, 20μsec. long. The expansion coils consist of one turn of litz wire on both the upper and lower pole faces, at a radius just inside the normal equilibrium orbit. The resultant ejector field is shown in Fig. 3. Calculation of the orbits described by the electrons indicates the following general principle of operation. When the ejector field is added to the normal field the effect is to produce an eccentric displacement of the beam. As the electron beam is expanded the electrons eventually become unstable and are released from the magnetic field in a diverging beam which becomes converging upon passing through the focusing region *B-C*, Fig. 3. This focusing property of the region *B-C* results because electrons passing through the inside of the region spiral out faster than ones passing through the outside of the region.

Fig. 2. Azimuthal relation of direction of x-ray beam from incident ejected electrons to injector and ejector system locations.

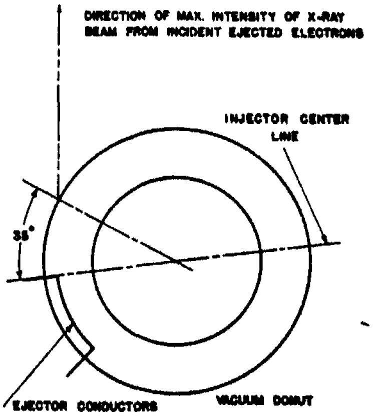
DIRECTION OF MAX. INTENSITY OF X-RAY BEAM FROM INCIDENT EJECTED ELECTRONS
INJECTOR CENTER LINE
38°
EJECTOR CONDUCTORS
VACUUM DONUT

Detection of the ejected electron beam was accomplished through the x-rays produced by the ejected electrons incident on the donut wall. Using an RCA 931A photo-multiplier tube shielded by $\frac{1}{32}$ in. brass and photographic film shielded by $\frac{1}{16}$ in. lead as detectors, the location and direction of the maximum intensity of the x-ray beam was determined to be as shown in Fig. 2, when the variable parameters were adjusted for optimum focusing.

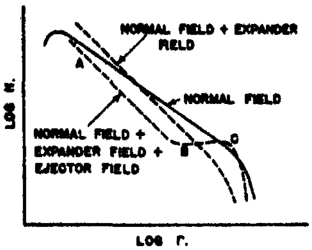

FIG. 3. Typical field shapes produced when expander and ejector fields are applied to normal betatron field.

The width of the x-ray beam was the same order of magnitude as the height, indicating a well-collimated beam. The ejection system works equally well using a conventional "outside" electron gun or an "above orbit" electron gun. The use of a conventional "outside" electron gun permits operation of the betatron as either an x-ray or electron source by switching off or on the ejection circuit. Using an outside electron gun the x-ray output due to the ejected electron beam was about equal to the x-ray output observed from the conventional target with the ejector switched off. With the ejector off the conventional target gave one Roentgen per minute at one meter as measured on a thin walled chamber. This fell to 0.5 Roentgens per minute when the ejector was operated. Difference in x-ray production efficiency between the donut wall and the conventional target makes an estimate of the ejection efficiency difficult. Observations with accelerated electron beam energies of 13 Mev, 14.6 Mev, and 15 Mev indicated no significant variations in the focusing properties of the ejector system. The possibility that the x-rays originate from incidence of electrons on some obstruction in the tube or on the ejector conductors has been ruled out by the behavior under a variety of conditions.

Since the ejector structure is non-ferromagnetic it introduces no field disturbance during injection and acceleration. In addition, operation is not limited by the magnitude of the magnetic field. Determination of more detailed properties of the ejection system awaits the completion of a donut with a window to permit emergence of the electron beam.

* Work supported by the AEC.

† AEC. Predoctoral Fellow, now at Battelle Memorial Institute, Columbus, Ohio.

[1] E. C. Crittenden, Jr., and W. E. Parkins, J. App. Phys. 17, 444 (1946).

[2] E. C. Gregg, Phys. Rev. 73, 95 (1948).

Design and Performance of a Joule-Kelvin Helium Liquefier

J. G. DASH, D. B. COOK,* M. W. ZEMANSKY,† AND H. A. BOORSE‡
Pupin Physics Laboratories, Columbia University,§ New York, New York

July 31, 1950

THE present paper describes a helium liquefier having a capacity of one liter per hour, using the Joule-Kelvin principle for liquefaction. Descriptions of such liquefiers have been published,[1] but the details of design have been largely omitted. In view of the increase in interest in low temperature research it is deemed worthwhile to outline the design procedure which was found to yield results in good agreement with calculation and which may be applied to the construction of almost any liquefaction system.

Design Features.—The design of an apparatus for gas liquefaction has a considerable latitude depending on the desired economy in refrigerants, the complexity of the apparatus, and the length of time required for precooling. In general, a short "starting time" is more desirable for laboratory equipment than maximum economy of operation. In the present case, a liquefier having an output of one liter per hour was chosen as a suitable size to operate in conjunction with our hydrogen liquefier which has an output rate of 3.5 liters per hour. The flow diagram chosen for the liquefier is given in Fig. 1. Exchanger D, omitted in some designs, is necessary to keep consumption of liquid hydrogen down to 5 liters for each liter of liquid helium produced.

The most important factor in determining yield efficiency is exchanger F. We may therefore use the design of this exchanger to illustrate the general procedure. Exchanger F is illustrated schematically in Fig. 2. Various tube arrangements[2] may be chosen to provide the necessary surfaces for heat transfer. If simplicity and ease of construction are guiding factors, a tube-in-tube arrangement is most convenient. Proceeding on this basis, the design may be carried out using equations given by Starr[3] according to the following sequence.

It is easily seen from a T-S diagram that the percentage liquefaction increases as the temperature T_i of the incoming gas at the hot end of the exchanger is lowered. The triple point of hydrogen (14°K) is a practical lower limit for T_i in the liquefaction of helium, if the convenience and excellent heat transfer properties of a liquid bath are to be used. For the maximum rate of liquefaction at this temperature, the proper value of the input pressure P_i must be found from the inversion curve. The coordinates of the inversion curve for helium may be approximately determined from published data,[4] values being given in Table I.

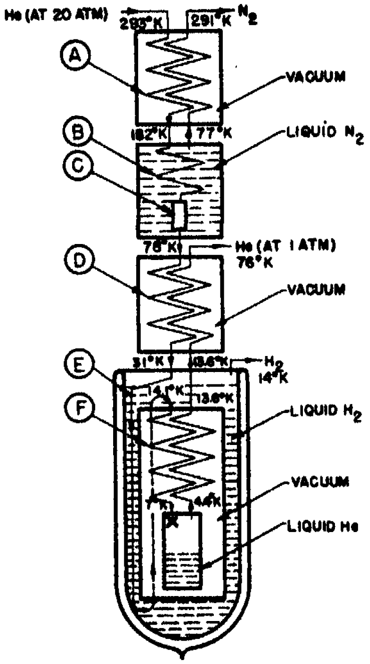

FIG. 1. Flow diagram of helium liquefier.

It is seen from Table I that the value of P_i appropriate to a value $T_i = 14$°K is 30 atmospheres. Experience at Leiden has shown[5] that a more suitable value of P is 20 atmospheres.

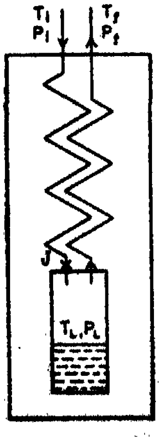

FIG. 2. Schematic diagram of heat exchanger F and liquid helium well.

TABLE I. Points on the helium inversion curve.

T°K	P (atmos.)
15	31.5
14	30
13	27.5
12	25
11	22.5
10	20

A value of P_L, the pressure at which the liquid is to be collected, is next chosen. Pressures from 1.2 to 1.5 atmospheres are usually sufficient to provide turbulent flow (Reynolds' number >2000) in the return tubes, which is necessary for efficient heat exchange. In view of the low critical pressure of helium, P_L was chosen as 1.2 atmos.; the corresponding liquid boiling temperature T_L was found from the liquid-vapor equilibrium curve to be 4.4°.

The next step was to make an arbitrary selection of the "efficiency" of exchanger F which may be expressed[3]

$$E=\frac{T_f-T_L}{T_i-T_L},$$

where T_f is the temperature of the returning low pressure gas at the hot end of the exchanger. The equation thus serves to determine the value of T_f. In the present instance E was chosen as 96 percent, and the corresponding value of T_f was found to be 13.6°.

The fraction y of the gas which will be liquified under these circumstances was then found from the well-known thermodynamic expression

$$y=\frac{h_f-h_i}{h_f-h_L},$$

where the h's are the enthalpies under the condition indicated by the subscripts. Substitution of the appropriate values shows that y is approximately 17 percent.

The heat transfer-length characteristic of the exchanger can be determined from the following relation[3]

$$UL=\frac{\dot{m}_o\bar{c}_o}{1-\dot{m}_o\bar{c}_o/\dot{m}_i\bar{c}_i}\log_e\left[\frac{1-E\dot{m}_o\bar{c}_o/\dot{m}_i\bar{c}_i}{1-E}\right],$$

where the $\dot{m}$'s refer to the flow rate of the gas in grams per second, the $\bar{c}$'s are specific heats of the gas averaged over the indicated temperature intervals, L is the length of the exchanger in cms, and U is the over-all heat transfer coefficient per unit length. The subscripts "i" and "o" refer to incoming and outgoing gas streams respectively.

To account for non-ideal conditions in the operations of exchangers, E and F and Joule-Kelvin valve, the liquefaction fraction was rounded off to 15 percent, and a liquefaction rate of 1.2 liters per hour was chosen as a basis for design. This choice of liquefaction rate and the chosen value for the liquefied fraction lead to a value of $\dot{m}_o$ equal to 0.24 g/sec. This corresponds to a value of $\dot{m}_i$ equal to 0.28 g/sec. The value of $\bar{c}_o$, obtained by averaging data from the Zelmanov diagram, was 1.43 cal./g deg. In order to calculate $\bar{c}_i$ it is necessary to find the temperature of the gas immediately before throttling. This is accomplished by determining the position of 15 percent liquid on the 1.2-atmos. isobar on the T-S diagram and following the corresponding isenthalp to the 20-atmos. isobar intersection, which occurs at 7°. With this knowledge of the correct temperature interval, the value of $\bar{c}_i$ was determined to be 1.52 cal./g deg. The product UL was then found to be 3.1 cal./sec. deg.

There remains to be determined the geometric dimensions of exchanger F, i.e., the length and diameters of the inner and outer tubes. For higher heat transfer efficiency, the inner tube is chosen for the low pressure outgoing gas stream. Convenient tube sizes are chosen and the heat transfer coefficient H per unit length is calculated for each gas stream by means of the relation[3]

$$H=0.15\bar{c}\eta^{0.25}(\dot{m}/d)^{0.75}(1+3.5d/D),$$

where η is the average viscosity in poises, d the effective diameter in cm, and D is the exchanger coiling diameter in cm. Inner and outer tube diameters were chosen as $\frac{3}{16}$ in. and $\frac{5}{16}$ in. o.d. respectively, both sizes having 0.020 in. wall thickness. To obtain favorable transverse heat transfer across the tubing walls and still minimize heat conduction along the length of the exchanger, it is necessary to use low conductivity, thin-walled tubing. Supernickel 0.020 in. wall tubing represented a good compromise and yielded a large safety factor for the high pressure gas. Computations for the coefficients gave $H_i=0.010$ cal./sec. cm deg., and $H_o=0.011$ cal./sec. cm deg. Neglecting the thermal resistance of the tube walls, we obtain the over-all coefficient

$$U=(H_i^{-1}+\mathrm{H}_o^{-1})^{-1}=0.0052\text{ cal./sec. cm deg.},$$

and by making use of the value found for UL, the value of L is found to be 590 cm. This is very close to 20 ft. which is a standard tube length and was accordingly the length used in making the exchanger.

The pressure drops in the incoming and outgoing tubes were next determined by means of the equation

$$\delta p=3.0\times10^{-4}\frac{Tm^{1.75}\eta^{0.25}L}{MPd^{4.75}}(1+3.5d/D)$$

where δp = pressure drop in lb./in.^{2}, P = average pressure in atmos., M = molecular weight, T = Kelvin temperature, and L = length of the tube in cm. Similar calculations were carried out for the other exchangers. The calculated characteristics of all exchangers are found in Table II.

TABLE II.

Characteristics	Exchanger A	B	D	E	F
o.d. of outer tube, in.	0.375	0.1875	0.3125	0.1875	0.3125
o.d. of inner tube, in.	0.250		0.1875		0.1875
Coiling diameter, in.	6.0	3.50	3.25	3.50	3.25
Temp. of incoming gas at hot end	293	182	78	31	14.1
Temp. of outgoing gas at hot end	291		76		13.6
Temp. of incoming gas at cold end	182	78	31	14.1	7.0
Temp. of outgoing gas at cold end	77		13.6		4.4
Length in feet	12	4	15	4	20
Av. incoming pressure, atmos.	20	20	20	20	20
Av. outcoming pressure, atmos.	1		1.1		1.2
Pressure drop, incoming gas, lb./in.^{2}	6.3	0.035	1.6	0.0091	0.29
Pressure drop, outgoing gas, lb./in.	0.99		1.4		0.27
Efficiency	0.99		0.968		0.960

Liquefier Construction.—A copper shell enclosed the liquid hydrogen Dewar which surrounds the liquefier assembly consisting of the heat exchangers E and F, the Joule-Kelvin valve, and the liquid helium collection well. The copper shell is equipped with Lucite windows, to permit observation of the liquid hydrogen and liquid helium levels.

The exchanger F, Joule-Kelvin valve, and liquid helium well are enclosed by a high vacuum jacket consisting of a brass cylinder for the upper section and a glass lower section, attached by means of a 3 in. diameter Kovar-to-glass seal. The liquid helium well, visible within the lower section, has a capacity of 540 cm^3, and communicates to a vacuum pumping line by means of a $\frac{1}{2}$ in. diameter stainless steel tube extending through the top plate of the liquefier. This tube also permits mechanical operations on apparatus contained within the helium well.

Pressure gauges on the control board allow observations of the helium gas pressures at the entrance to heat exchanger A and the high and low pressure sides of the expansion valve. A Bourdon gauge is used to indicate the liquid hydrogen vapor pressure. The helium gas temperature immediately before expansion is measured by means of a helium gas thermometer connected to a vacuum Bourdon gauge. Liquid helium vapor pressures are read by a mercury manometer. Helium gas for liquefaction may be supplied either by high pressure supply tanks regulated to 300 lb./in.², or a compressor.

Before liquefaction, the liquefier was cooled to 77°K by admitting liquid nitrogen to the large Dewar surrounding the vacuum jacket, the vacuum space being filled with helium gas at a few cm pressure. The liquid nitrogen was then forced out into the Dewar surrounding the heat exchanger *B*, and the liquefier Dewar filled with 7 liters of liquid hydrogen. The liquid hydrogen bath was cooled to about 14° by pumping, and as the inner parts approached equilibrium, as indicated by the gas thermometer, the vacuum jacket was opened to the pumps and thermal isolation restored.

Circulation was then started through the Joule-Kelvin valve. A cooling time of about 15 minutes was required before liquefaction, at which time the gas thermometer indicated 7°K. With $m_t = 0.28$ g/sec., the liquefaction rate was 1 liter/hour.

After liquefaction was finished, the helium well was used for experimental work. To economize on the use of liquid hydrogen, the outer bath was replaced with liquid nitrogen for thermal buffering. In this condition, it was possible to cool the liquid helium to below 1.5° by pumping. The evaporation rate was sufficiently low so that experiments of over five hours' duration could be performed with about 300 cm³ of liquid helium.

---

[*] Now at E. I. DuPont Experimental Station, Wilmington, Delaware.

[†] The City College of New York.

[‡] Barnard College, Columbia University.

[§] Assisted by ONR.

[1] W. H. Keesom, *Helium* (Elsevier Publishing Company, Inc., New York, 1942), pp. 151–156. Mechanical arrangement of the present liquefier follows descriptions given by J. G. Daunt and H. L. Johnston in Ohio State University ONR reports December 1, 1947, February 1, 1948, and April 1, 1948.

[2] R. B. Jacobs and S. C. Collins, J. App. Phys. 11, 491 (1940).

[3] C. Starr, Rev. Sci. Inst. 12, 193 (1941).

[4] J. Zelmanov, J. Phys. U.S.S.R. 8, 135 (1944).

[5] J. A. van Lammeren, *Technik der tiefen Temperaturen*, p. 128.

[||] Effective diameter is the cross-sectional area for flow multiplied by the product of $4/\pi$ and the total perimeter wetted by the gas stream.

A Simple Automatic Recording Microphotometer

R. M. Fisher and D. S. Miller
Research Laboratory, United States Steel Corporation of Delaware, Kearny, New Jersey

May 31, 1950

An inexpensive precision microphotometer has been constructed to measure electron diffraction patterns taken with the camera of the RCA EMU electron microscope. A novel feature of our photometer is that by means of a balanced optical and electronic system only the difference in photographic density between the lines and the plate background is recorded. Thus the large background changes on electron diffraction patterns do not cause the chart record to rise rapidly right off the paper but rather to remain flat (as in Fig. 2). Another advantage of the balanced system is that there is no need of regulation on the lamp voltage supply.*

We used the optical system and framework of an outmoded General Electric Company photometer as a starting point, although a similar arrangement could easily be constructed. In our instrument, the plate or film is mounted horizontally on a moveable stage and is illuminated from below with a projector lamp and condenser lens. A low power standard microscope objective is used with a prism to project a magnified image of part of the plate on a viewing screen mounted vertically. A 1-in. square hole in the center of the screen is covered with a sliding panel in which are cut four slits, which are 0.25, 0.5, 1, and 2 mm wide and can be varied in length up to 16 mm. By using either of two objectives, which produce magnifications of 9 or 22, effective slit widths of 12 to 220 microns are available in eight steps.

The plate stage, mounted on balls in flat ways, is connected by a split nut to the driving screw which is turned either by a hand wheel or by a synchronous motor. The screw was made by cutting 40 threads per inch on a ¾-in. diameter shaft and lapping it into the nut. About 4½ inches of thread on the screw gives sufficient plate travel, limiting switches serving to protect the screw. For use with a 12-second full-scale deflection recorder the plate is driven at 3 in. per hour by a 1 r.p.m. motor through a gear; a typical line 0.01 in. wide is passed over in 12 seconds. A faster recorder would permit a higher plate speed.

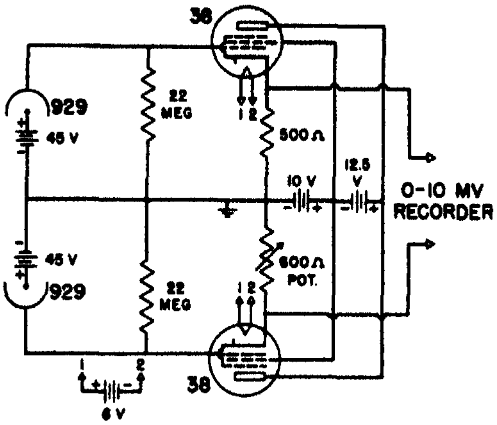

FIG. 1. Wiring diagram of amplifier circuit.

The moving plate stage, screw and motor are mounted on another stage which can be adjusted laterally to align slit and pattern and vertically to focus the image on the screen.

Two vacuum photo-tubes (Type 929) are used in the balanced cathode follower circuit shown in Fig. 1. The measuring tube mounted directly behind the viewing screen receives light passing through the slit, while the monitoring tube, mounted a few inches in front of the screen, receives scattered illumination from the projected image. Both photo-currents are amplified in the electrometer type circuit and the e.m.f. difference between the cathode resistors drives a 0–10 mv strip chart recorder. Thus, in effect, the average of the background density over several millimeters on either side of the slit is subtracted from the density right at the slit. By means of an iris diaphragm on the monitoring tube

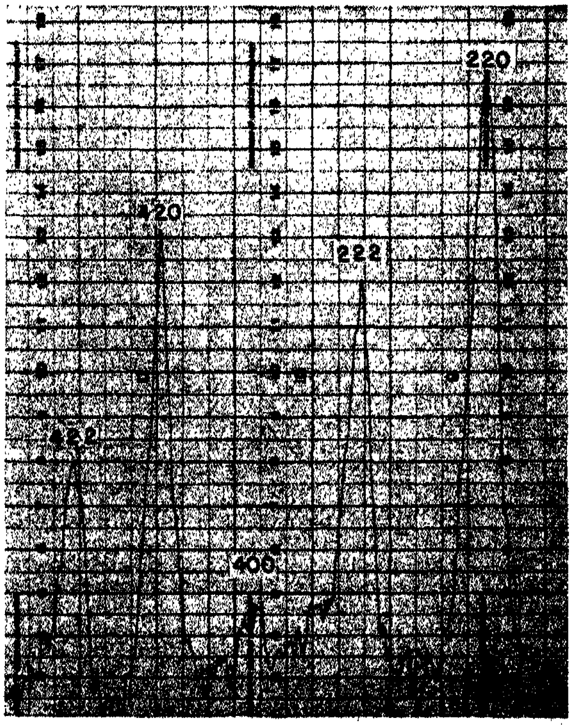

FIG. 2. Photograph of chart record.

housing and a wire-wound potentiometer as one cathode resistor, both light and circuit balance can be achieved.

After a warm-up period of about five minutes the recorder shows no objectionable drift due to resistor noise or tube grid current. The output impedance of the amplifier (1100 ohms) is not well suited to the standard recorder impedance of 400 ohms but the latter can be increased to more than a thousand ohms by removing the grid resistor of the first stage in the recorder amplifier. A still higher recorder impedance of the order of 5000 ohms can be obtained by replacing the input transformer with one of higher inductance.

Figure 2 is a typical chart record of an electron diffraction pattern of MgO taken with an effective slit width of 55 microns, a recorder impedance of 1000 ohms at a plate speed of 3 in. per hour and a chart speed of 60 in. per hour. Measurements on the complete chart give interplanar spacings within ½ percent of those calculated for the cubic structure.

* P. Rosenblum and A. DeBretteville, Jr., Rev. Sci. Inst. 20, 321 (1949).

Simultaneous Photography of Self-Luminous and Non-Self-Luminous Effects

JOHN S. RINEHART
Naval Ordnance Test Station, Inyokern, China Lake, California

STREAK photography[1] and microsecond multiflash[2] techniques have been used extensively to study high speed phenomena that occur during the breakup of explosive missiles, the flight of projectiles, etc. Generally only one or the other of the techniques is used. This note describes a test in which both techniques were employed simultaneously. The data desired could not have been obtained by employing either of the two techniques individually or successively.

In studies of the flights of the very high speed particles that are produced by shaped charges, the following information is needed: (*a*) the velocity of the particle, (*b*) variations in luminosity of the particle during its flight, (*c*) the duration of burning of the eroded material, (*d*) the spatial distribution of smoke left by the particle, and (*e*) the way in which the smoke trail changes with time. Data on (*a*), (*b*), and (*c*) can be obtained from normal streak photographs, since the effects are self-luminous. On the other hand, the smoke trail must be illuminated in order to be observed.

The experimental set-up that was used to photograph the self-luminous and non-self-luminous features of shaped charge particles is illustrated schematically in Fig. 1. A 35-mm continuous film General Radio camera was used. The smoke trails left by the particles were illuminated with four flash lamps that flashed at a rate of 1000 flashes per second. The duration of each flash was about one microsecond. The number of flashes was usually thirty or more.[3]

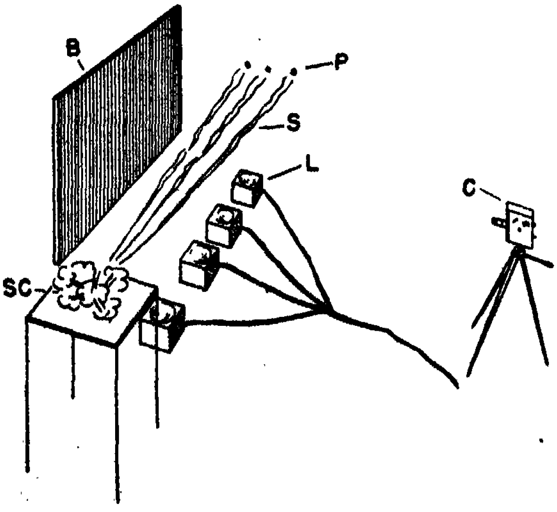

FIG. 1. Experimental set-up: SC, shaped charge; P high velocity particles; S, smoke trails left by particles; B, black screen; L, flash lamps; C, General Radio continuously moving film 35-mm camera.

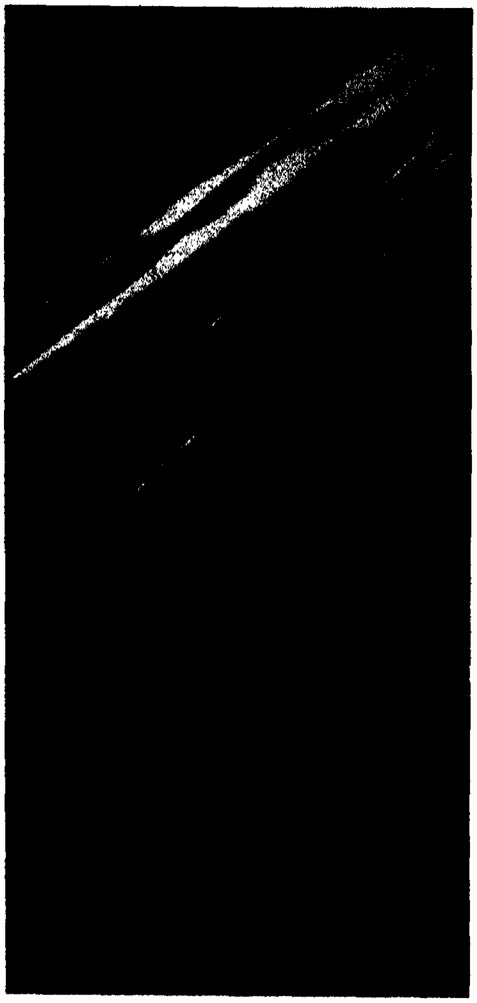

FIG. 2. Photograph of a group of high velocity particles.

The following experimental procedure is used. The camera is started, the shaped charge is fired, and flashing of the lights is begun. The final result is that both the self-luminous and non-self-luminous phenomena appear together on a single strip of film.

A typical photograph, obtained in this way, of a group of shaped charge particles is reproduced in Fig. 2. Each particle that crossed the field of view of the camera is seen as a luminous streak that runs slantwise across the film. Ten such streaks were visible on the original film. Two of the streaks are very bright. The velocity of each particle can be readily determined from film speed and camera data. The film speed in this case was about 70 ft./sec. The horizontal field of view of the camera was about 11 ft. The velocities of the two brightest particles were about 10,000 ft/sec. Variations in luminosity of the particles during flight and burning of the eroded material are also evident in the photograph.

The smoke trails left by the two brightest particles appear as horizontal lines in the photograph. The light flashed first when the uppermost particle was about two-thirds and the second particle about one-half of the way across the field of view. The second and third flashes occured at 1/1000-sec. intervals thereafter. The spatial distributions of smoke left in the wakes of the two brightest particles can be seen in the photograph. The smoke, for example, is seen to be most dense at the places along the trajectory of the particle where the particle was most luminous.

This note has been prepared primarily with the thought that the simultaneous use of streak photography and microsecond multiflash techniques can possibly be used to advantage in other investigations.

[1] G. St. J. Perrott and D. B. Gawthrop, J. Franklin Inst. 203, 103 (1927).
[2] H. E. Edgerton, J. Soc. Mot. Pict. Eng. Part II, p. 8 (March, 1949).
[3] The microsecond multiflash unit used in these tests was designed and built by Mr. E. C. Barkofsky, Naval Ordnance Test Station.

Two Beta-Gamma-Counters for Gas Samples

Rodman Jenkins
California Institute of Technology, Pasadena, California*

June 26, 1950

In connection with a study of diffusion in turbulent flow, Geiger counters of two different types were prepared for the determination of activity of a series of gas samples. In all cases the radiation originated in iodoform containing substantial quantities of iodine-131. This isotope emits several gamma-rays and a beta-ray spectrum with a maximum energy of 0.67×10^6 electron volts.[1]

The conditions of the experiment made it desirable to use Geiger tubes which recorded a large fraction of the disintegrations available. The volume of air in any given sample was restricted to a maximum of about 150 cc. Since quantitative results were an essential part of this program, it was necessary to achieve a reproducible relationship between the quantity of iodine-131 and the observed counting rate. Satisfactory plateau curves were necessary to allow a succession of analyses to be made without repetition of calibrations.

A reasonable compromise between these requirements was found in two designs, though neither was entirely satisfactory. The first design was a conventional cylindrical glass counter sealed in a concentric glass jacket. These parts were joined in the glassblowing process, and no foreign materials were introduced in the jacket chamber. Cathodes were of silver, deposited by the Rochelle salt process,[2] and gold, prepared from a commercially available solution called "Liquid Bright Gold." The anodes were prepared from 0.004-inch diameter tungsten wire, and were not heated to the glowing point. All tubes were filled with a mixture of 90 percent argon and 10 percent absolute alcohol to a total pressure of 10 cm of mercury. They were not baked out.

An experiment was performed which demonstrated the proportionality between counting rate and concentration of iodoform in the jacket. One of these counters was sealed into a vacuum system from which organic materials had been eliminated. Portions of air containing a constant fraction of radioactive iodoform were admitted to the jacket surrounding the counter at randomly varying pressures. Before entry of a given sample, the preceding one was removed by evacuation. Each time, the pressure of the air being counted was determined, and converted to pressure of the same gas at 20°C. Since some series of measurements lasted as much as 12 hours, all counting rates were corrected for the radioactive decay of the 8-day half-life iodine.

The results of these measurements are shown in Fig. 1. The number of counts taken at each point varied from 1000 to 3000, with an average of about 2200, which corresponds to a standard deviation of about 2 percent. This deviation, when obtained from the observed counting rates was found to be 2½ percent. This was considered to be a satisfactory comparison.

The second type of Geiger counter was constructed in order to record a larger fraction of the disintegrations occurring in a given sample. It consists of a ring of six commercial aluminum Geiger tubes with their cylindrical axes parallel, sealed within a close fitting stainless steel chamber. The individual counters are sealed into the chamber by means of Neoprene gaskets fitting under small flanges located near one end of each tube. Three tubes enter the chamber from each end. A follower plate which presses these flanges from the outside provides force on the gaskets.

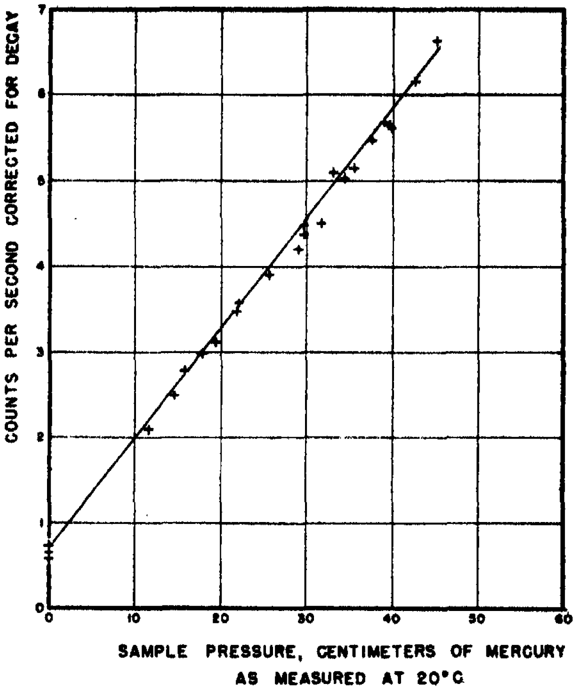

FIG. 1. Measured activity as a function of sample pressure.

The entire unit was assembled from machined parts by soft soldering. A pressure of less than one micron was easily obtained in the assembled instrument. It is estimated that with this geometrical arrangement, 35 to 40 percent of the radiation produced in a sample strikes one of the Geiger counters at an active point. The simultaneous operation of these tubes was found to give satisfactory electrical characteristics.

The writer's financial support as a National Institute of Health predoctoral research fellow during this work is gratefully acknowledged. E. W. Molloy suggested the arrangement of the Geiger tubes in the second counter described here.

* Present address: Magnolia Petroleum Company, Dallas, Texas.
[1] Downing, Duetsch, and Roberts, Phys. Rev. 61, 389, 686 (1942).
[2] J. Strong, *Procedures in Experimental Physics* (Prentice-Hall, Inc., New York, 1938), p. 157.

An Ultrasonic Projector Design for a Wide Range of Research Applications

E. J. Fry
University of Illinois, Urbana, Illinois

July 18, 1950

In research work concerned with the ultrasonic irradiation of many types of specimens it is desirable to have a flexible projector design which offers features of adaptability to different types of systems as well as possessing the inherent ability to obtain high power output levels.

Figure 1 illustrates in cross section the essential design features of such a projector in which the crystal, vibrating in thickness mode, is held in a vertical plane. The ground plate *H* is constructed so as to be readily connectable to various irradiating chambers.

One major aspect of the design is the clamping of the crystal between two small Neoprene gaskets *A* which in the undeflected position are 0.030 in. thick. The same thickness Neoprene is used for gaskets *B*. Parts *E*, *F*, and *G* are bolted together with gasket

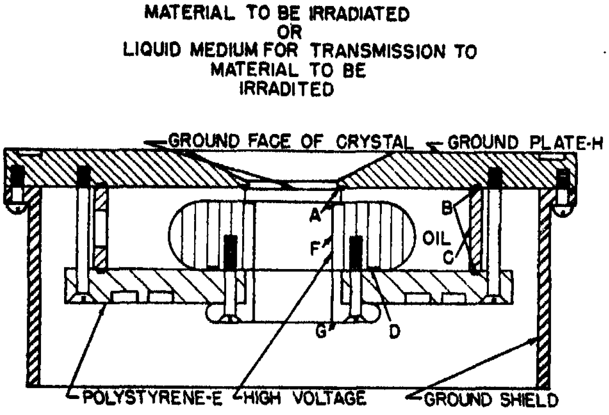

FIG. 1.

D. For assembly purposes ground plate *H* is laid in the horizontal position. Then stacked in order, on top of this plate are gasket *A*, the crystal and another gasket *A*. Gaskets *B* and ring *C* are also placed in position. Then *E*, *F*, *G* assembly is laid on top and the whole assembly is bolted together as shown. The gasket grooves in all cases are designed so that the Neoprene is not deflected too much in any tightening operation. This means that ring *C* is pulled against the ground plate and polystrene plate *E* and the gaskets *B* are not over deflected. This pulling together operation also limits the deflection of gaskets *A*.

After the assembly of the physical parts shown in the figure, the chamber surrounding the crystal edge is filled with oil for the purpose of giving a much higher voltage break down strength to the space between the two crystal faces.

Another important aspect of the design is concerned with the final electrical contacts to the crystal faces. The crystal faces are electroded to a distance from their edges equal approximately to the Neoprene gasket width. A conducting paint is then applied around the crystal faces at the gasket edges, over the gasket edges and to both the ground plate *H* and plate *F*. This produces a desirable configuration of equipotential surfaces for the electric potential.

For flexibility in changing from one crystal to another of different frequency but of the same shape in all but the thickness dimension it is only necessary to have a new length for ring *C*. Rings *C* are made beforehand for all the crystal frequencies wanted, and the limiting time for a change is then the drying time of the conducting paint which can be accelerated with warm air blasts so that only a few minutes is involved in a change of this sort.

The same design features are readily incorporated into set-ups wherein the crystal is mounted horizontally or the crystal must assume any position as in an applicator. It is also apparent that changes in crystal size of other than the thickness dimension are readily incorporated into the design. Crystals with curved shapes for focusing of the sound field can be readily handled.

Experience with eight of these projectors in which the crystals have had both horizontal and vertical mounting has been used as an indication of the general trouble free operation obtained from these design specifications.

A Float for Liquid Helium

JULIUS BABISKIN
Naval Research Laboratory, Washington, D. C.

July 31, 1950

THE density of liquid helium is much lower than that of most homogeneous solids. Therefore, a float material for liquid helium should have enclosed hollow spaces to lower its apparent density below that of liquid helium and it must be impermeable to liquid helium as well. This suggests the use of a body consisting of a continuous lattice of individual thin-walled hollow cells of low density material.

Unicellular polystyrene foam[1] was tried as a float material and has proved satisfactory for use in both liquid helium I and II. The individual cells have sufficient mechanical strength to resist collapse and the material does not crack when subjected to liquid helium temperatures. Other unicellular expanded plastics would probably also exhibit these properties.

When floating on liquid helium, it was observed that the apparent density of a ¾-in. cube of the polystyrene foam was about 0.04 g/cc. Thus it is likely that this foam will float on liquid hydrogen. The apparent density of the float is higher for shapes having a larger ratio of surface area to volume than the cube. Pieces one or two cells thick often did not float on liquid helium.

Since the unicellular polystyrene float is white, the liquid helium level in slit-silvered Dewars can be easily observed. For situations where the helium level and the white float cannot be seen, this float has sufficient buoyancy to support a thin rod of balsa wood, which can be used as the indicator. Care should be exercised in the use of balsa wood indicators, since the balsa wood shatters when warmed from liquid helium temperatures too rapidly.

[1] This material is available commercially at nominal cost. See Expanded Plastics or Styrofoam in *Modern Plastics Encyclopedia* (Plastics Catalogue Corporation, New York, 1949).

New Instruments

W. A. Wildhack: Associate Editor
in Charge of this Section
National Bureau of Standards, Washington, D. C.

These descriptions are based on information supplied by the manufacturer and in some cases from independent sources. THE REVIEW *assumes no responsibility for their correctness.*

Micromanometer The Model 23-105 Micromanometer is a sensitive device for measuring gas pressures in the 0-150 micron range. It measures the absolute pressures of condensible as well as noncondensible gases independently of their composition. The operation is based on a pressure sensitive condenser utilizing a stainless steel diaphragm as one of the plates; the gauge forms one arm of a capacitance bridge which is balanced to a null when the pressures on each side of the diaphragm are equal and close to zero microns. In operation, the gas whose pressure is to be measured is intro-

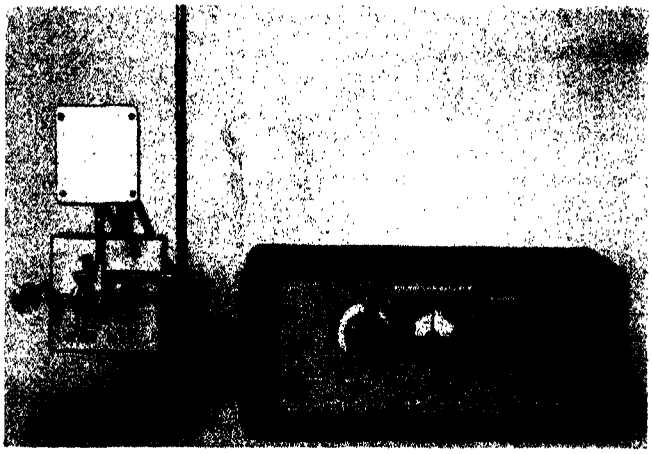

duced to one side of the diaphragm, and an electrostatic restoring force is applied by an adjustable d.c. voltage thereby rebalancing the bridge. The magnitude of the restoring voltage is read on a duodial and the reading is converted to microns of pressure by a calibration chart or simple formula.

According to the manufacturer, typical specifications of the Model 23-105 Micromanometer, when used at room temperature, are as follows: Pressure range—0.1 to 150 microns; minimum detectable pressure change—0.1 micron; reproducibility (8 hr.)—±0.3 micron, linearity—±0.2 percent; maximum overload—1 atmosphere on either side of the diaphragm; and power consumption—30 watts at 115 volts a.c.—CONSOLIDATED ENGINEERING CORPORATION, *620 N. Lake Avenue, Pasadena 4, California.*

Nuclear Fluxmeter

The Model F-6 Nuclear Fluxmeter is designed to utilize the gyromagnetic properties of the nuclei of hydrogen atoms in such a way as to reduce the measurement of magnetic field strength to a direct measurement of frequency. The instrument also provides an error signal which can be used to actuate field stabilization equipment.

The phenomenon of nuclear induction results from the interaction of nuclear spin and nuclear magnetic moment with an external magnetic field. Any species of nucleus possessing a spin also possesses a magnetic moment. Since the spin of a particular species of nucleus is always the same, and likewise the magnetic moment, any such nucleus possesses a constant gyroscopic moment similar to that of a top or gyroscope, and the magnetic poles provide a means of applying a force couple such as may be applied to a mechanical gyroscope. The result is the same in both cases: the axis precesses, swinging around in the surface of a cone. The rate of this precession, if it can be measured in relation to the applied magnetic field, will identify the species of nucleus, and conversely, if the nuclear species is known, the strength of the magnetic field may be determined. The Nuclear Fluxmeter is designed to measure this precession. Normally, the axes of the spinning nuclei point in all possible directions and under these conditions the external effects of their precession exactly cancel. In order to obtain an observable external effect, there must be a preponderance of nuclei pointing simultaneously along some particular axis, or what may be called nuclear polarization.

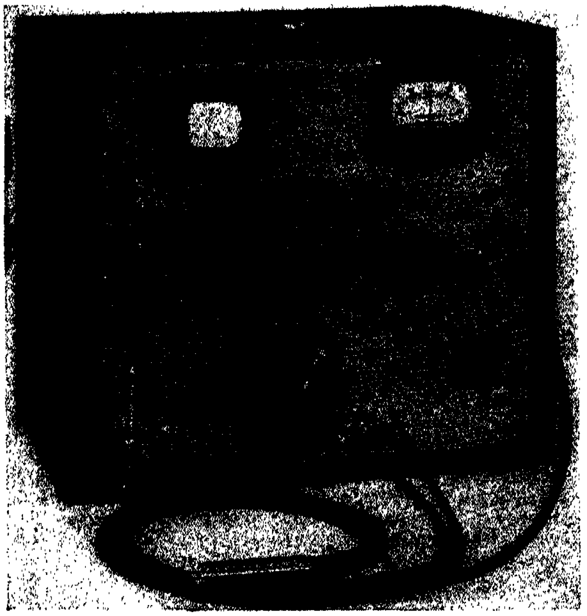

This can be accomplished by application of a constant magnetic field which will, after sufficient time for attaining equilibrium, produce the desired net polarization along an axis parallel to the magnetic field. An alternating magnetic field of suitable frequency produced by a small r-f coil perpendicular to the constant field will now produce a precession of the net polarization, and this effect may be detected by the induced voltage in a second coil located at right angles to the excited coil. The frequency of the induced voltage, i.e., the precession frequency, and the value of the gyromagnetic ratio of the nuclei serve to determine the absolute value of the constant field since they are linearly related to it. Ultimate precision is dependent on the absolute value of the gyromagnetic ratio of the proton, which is known to 25 parts per million. Frequency measurements can be made with much greater accuracy than this with comparative ease.

The standard model of the Nuclear Fluxmeter has a range of 9–18 kilogauss and accuracy of 0.005 percent in the presence of field inhomogeneities of less than 4 gauss per cm. Frequency measuring equipment is required covering the range from 38–77 mc. The probe containing the r-f coils is a metal cylinder ¾ inch in diameter and 4½ inches long. Additional equipment may be supplied to extend the range from 18–23 kilogauss and from 2–9 kilogauss. The error signal for control purposes is +50 volts for a ±1 gauss change in field strength. There are a multitude of methods of using the error signal from the Nuclear Fluxmeter to provide precision control of a magnetic field. It has been successfully used in connection with amplidyne current supplies, photoelectric current stabilizers and conventional current stabilizers, and conventional current stabilized power supplies. The method used depends on the magnet power requirements and the degree of control desired. Detailed suggestions of methods of field stabilization can be obtained for specific applications.

Another interchangeable r-f unit is available covering the range 0.5 to 24 kilogauss. This is accomplished by three sets of plug-in coils with frequency ranges of approximately 2 to 4, 4 to 8, and 8 to 16 megacycles; these frequency ranges, combined with the use of both deuterons and protons as samples, give the desired field range.

The price of the F-6 Nuclear Fluxmeter is $1,725.00 f.o.b. San Carlos, California, including any one r-f unit with its probe. R-f units with probes are available at $650.00 each.—VARIAN ASSOCIATES, *San Carlos, California.*

Bulb Temperature Pick-Ups

These instruments are based on the resistance thermometer principle and are suitable for the measurement of liquid, gas, and metal temperature. The resistance of the sensing element changes 6.2 ohms over the specified temperature range of the instrument. As a result the pick-up may be placed in a 300-ohm bridge to simulate strain gauge pick-ups having an output voltage of 5 millivolts per volt. Up to 155 millivolts may be obtained from the pick-up proper.

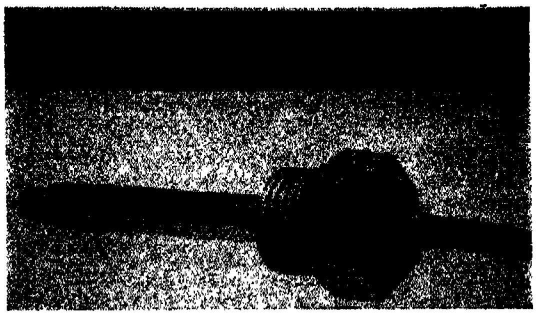

The sensing element consists of a platinum winding contained between concentric cylinders having a total wall thickness of only a few thousandths of an inch. The sensing element is located within approximately one-fourth inch of the extreme end of the structure. As a result of the unique construction, the thermometer has a thermal time constant of only 1.8 seconds in water. The pick-ups are suitable for pressurized applications and are available for use with system pressures up to 12,000 p.s.i.

The Type 19 Bulb Temperature Pick-Ups can be supplied in ranges up to 1100°C (2000°F). Units designed for ranges above 750°C (1400°F) are supplied in inconel cases.—TRANS-SONICS, INC., *Bedford Airport, Bedford, Massachusetts.*

Manufacturers' Literature

Control Motor Chart—Includes tables on physical dimensions and electrical characteristics of 25 different motors and a page of application data, such as how to connect for plate-to-plate operation, a speed-torque curve, and connections to obtain desired rotation.—TRANSICOIL CORPORATION, *1036 Broad Street Station Bldg., Philadelphia 3, Pennsylvania.*

Cellulose Esters—New 59-page book gives comprehensive and detailed information covering uses and specifications of Eastman cellulose esters, the compatibility of these esters with solvents, resins and plasticizers, and procedures of analysis.—TENNESSEE EASTMAN CORPORATION, *Kingsport, Tennessee.*

Technique—Vol. IV, No. 3, July 1950, has articles on tuning forks, a logarithmic potentiometer for use in densitometry, and some applications of the Magslip Resolver.—MUIRHEAD & COMPANY, LTD., *Beckenham, Kent, England.*

Tracerlog—No. 29, September 1950, features the SC-16 Windowless Flow Counter.—TRACERLAB, *130 High Street, Boston 10, Massachusetts.*

Precious Metal Alloys—Bulletin R-12 supplies complete data on physical properties and applications of Ney Industrial Precious Metal Alloys.—J. M. NEY COMPANY, *Hartford, Connecticut.*

Magnetic Clutch—Bulletin No. 6000 contains a brief description of the operation, characteristics, and applications of the Magneclutch and Magnebrake, including performance and dimensional data and featuring servomechanism applications.—VICKERS ELECTRIC DIVISION, *1815 Locust Street, St. Louis 3, Missouri.*

The Beckman Bulletin—Applications of the Flame Spectrophotometer.—BECKMAN INSTRUMENTS, INC., *South Pasadena, California.*

New Materials

Forest K. Harris: Associate Editor
in Charge of this Section
National Bureau of Standards, Washington, D. C.

Plastic Lenses

Armorlite is a clear plastic used for spectacle lenses. Advantages claimed over the orthodox glass lens include lightness and safety features. The plastic is stated to be clearer than optical glass, to be more resistant to fogging, and to be very much harder than previous plastic lenses. It is more resistant than glass to molten spatter, flying abrasives, and the common chemicals. It has about half the weight of glass and an impact resistance greater than that of case-hardened glass. Single-vision ophthalmic lenses are available either clear or tinted, and can be coated to reduce surface reflections.—ARMORLITE LENS COMPANY, *117 East Colorado Street, Pasadena 1, California.*

Silicone Resins

No. 81132 is a flexible silicone resin for coating glass cloth and sleeving or as an adhesive for mica-glass tape. It is supplied as a 60 percent solution in toluol, and dries without a catalyst in 30 min. to 1 hr. at 250°C. Dielectric strength is 1600 to 2000 v.p.m. in a 7-mil thickness on 3-mil glass cloth.

No. 81145 is intended for bonding and impregnating motors, generators and transformers requiring class *H* insulation. It may also be applied in bonding mica and glass combinations. It is supplied as a 50 percent solution in petroleum spirits. The film dries in 10 to 15 min. at 200°C, while thick sections in coils and windings require up to 6 hr.—GENERAL ELECTRIC COMPANY, *Pittsfield, Massachusetts.*

Neoprene Mat

Neotex is a Neoprene mat built on an expanded-fiber core to provide a flexible shock-absorbing material for covering hard surfaces where glassware is to be set down. Its open mesh assists in draining. It is soft and pliable, light in weight, and is not subject to attack by gasoline, oils, acids, and alkalis commonly encountered in laboratory service. It is available in rolls measuring 27 in. in width by 50 ft. in length, and may also be bought by the yard. It can be cut to any desired shape with ordinary scissors.—SCIENTIFIC GLASS APPARATUS COMPANY, *52 Ackerman Street, Bloomfield, New Jersey.*

Filters

A new booklet *Filters and Lens Attachments* has been published by Eastman. This catalog presents comprehensive data on the purposes, available forms, and prices of all Kodak Wratten filters and other optical attachments made by the Eastman Kodak Company. More than 200 different filters are described, of which more than 100 are of interest in science and technology. This book will be available through all Kodak dealers at 50 cents per copy.—EASTMAN KODAK COMPANY, *Rochester 4, New York.*

Stainless Steel Tubing

A new stainless steel, containing 16 percent Cr, 18 percent Ni, and less than 0.08 percent C, has been made available in round and equivalent-section tubing up to 1½ in. It is characterized by its slow work hardening and permits fabrication in forms that require severe deforming, bending, or upsetting. It can be brazed or soldered after cold-working, and can be spun, coined, or extruded. It remains non-magnetic after cold-working. It is resistant to attack by nitric acid, and to some extent by sulfuric acid, but does not stand up in contact with hydrochloric or other halogen acids.—CARPENTER STEEL COMPANY, *131 Springfield Road, Union, New Jersey.*

Miniature Storage Battery

Silvercel No. A1-HR-1 is a high efficiency, low volume alkaline storage battery using silver and zinc as active materials. Less than 1 cu. in. in volume and under 1 oz. in weight, it has a discharge rate of 5 amp. for 20 min., and can be discharged at rates up to 30 amp. It is spillproof, substantially shockproof, and completely free from corrosive fumes, vapor, or spray.—YARDNEY ELECTRIC CORPORATION, *105 Chambers Street, New York 7, New York.*

Self-Adhesive Marking Tape

Labelon tape consists of an adhesive-backed carbon paper in which the carbon faces outward and is covered with transparent plastic. Markings appear on the rear face of the plastic when its outer face is marked with a pencil or stylus. Since the marking is not exposed it cannot be obliterated by rubbing. The tape can be applied to metal, plastic, and glass surfaces and can be stripped off. It is made in ½-, ¾-, and 1-inch widths in 500-inch lengths.—WILL CORPORATION, *37–41 Russel Street, Rochester 3, New York.*

Sealing Rings

Molded *Teflon* rings are available to specification in a wide range of sizes and sections for use in packing joints in equipment for handling chemicals and petroleum products. The plastic is serviceable in the temperature range from −100 to 625°F.—CONNECTICUT HARD RUBBER COMPANY, *405 East Street, New Haven 9, Connecticut.*

Mildew Preventive

An aerosol preparation of a mold killer has been developed for home use. Two types are available, one for fabrics and the other for leathers, the latter containing oils which prevent the embrittlement of leather in addition to the mildew preventive. This product, distributed by the J. W. Johnson Company of Bellwood, Illinois under the trade name of *Formula* J, is used in the form of a fine spray emitted from its container when pressure is released. It is not considered toxic to humans.—Monsanto Chemical Company, *St. Louis 4, Missouri.*

Plastic Bonding Agent

Res-n-bond, a free-flowing water-white solvent combination originally developed for bonding acrylics, has now been modified so that is is equally effective in joining polystyrene to polystyrene. It is non-flammable, contains no acid, and may be safely handled with no precautions other than adequate ventilation. No deterioration results from long storage. Plastic objects set almost instantly due to rapid penetration of the solvents and jigs are necessary only in clamping poorly fitted seams or large sections. Handling, buffing, and other finishing operations can be carried out within an hour. Small objects are cemented by brushing the liquid on one surface and then pressing this surface into position. Larger objects are joined by a "soak" method. A flat, shallow pan is lined with a felt pad kept moist with the liquid. The plastic part is allowed to rest on the moist pad for a few seconds causing the edge of the plastic to soften and absorb the liquid, after which it is pressed into position. Cemented joints in clear polystyrene or acrylics should be optically clear and free from bubbles when these procedures are properly followed. The joint is as strong as the plastic itself and cannot be separated without fracturing the surrounding area.—Schwartz Chemical Company, *326 West 70th Street, New York 23, New York.*

Vinyl Insulation

A vinyl insulating compound (*Geon 8630*), especially designed for service up to 105°C, is being used to protect iron-constantan and copper-constantan thermocouple lead wires in applications where a conventional rubber had previously been applied. This "Geon" insulation withstands oils and most chemicals at high temperatures for longer periods than rubber, is noncorrosive toward copper, does not affect painted or varnished surfaces, and exhibits good outdoor weathering characteristics. In addition to its high temperature resistance, the new insulating compound is stated to have excellent low temperature characteristics and to be suitable for sub-zero applications.—B. F. Goodrich Chemical Company, *324 Rose Building, Cleveland 15, Ohio.*

Lead-Glass Fabric

Protective gowns are available made from a spun lead glass woven into a fabric. These gowns protect the arms, shoulders and lower legs as well as the body of the operator against x-rays and beta-radiation and yet are lighter than the ordinary type of leaded rubber apron.—Bar-Ray Products, Inc., *205 25th Street, Brooklyn, New York.*

Strippers for Organic Finishes

A folder is available describing various strippers for removing synthetic coatings including lacquers, enamels, and varnishes from metals. Strippers described include fast-evaporating strippers used at room temperature, emulsion-type materials mixed with water and used either heated or at room temperature, and brush-on strippers. The folder, listing 10 standard strippers for use in a variety of applications, is available from the manufacturer.—Enthone, Inc., *442 Elm Street, New Haven, Connecticut.*

Insulating Screws

Screws are now available which are stated to be comparable in strength to conventional metal screws, but which have the additional features of electrical insulation, vibration damping and shock resistance. A thermoplastic material is extruded on a serrated metal core, and the resulting composite rod is threaded and headed in an automatic screw machine. The type of metal core and the plastic are varied to meet the requirements of particular applications. The metal core extends the full length of the screw and supplies most of the tensile and torsional strength, while the plastic threads are said to seize and form an effective lock, eliminating the need for lock washers. Length, head size, thread pitch, and color can be varied. Currently screws are being made in diameters from No. 8 to ½ inch, with cellulose acetate, cellulose acetate butyrate, polyethylene, and ethyl cellulose insulation.—Forman Insulating Screw Company, *401 Broadway, New York 13, New York.*

Non-Crazing Plastic

Sierracin-212 is a transparent, thermosetting plastic developed for applications where crazing caused by pressure, cleaning compounds or mounting cements cannot be tolerated. It is at present used in airplane windows and enclosures, and is expected to find other industrial uses. It is stated to withstand rapid changes in temperature or pressure without adverse effects and will tolerate temperatures up to 225°F, having favorable creep properties at elevated temperatures. Other formulations are available for use at temperatures up to 400°F. A laminating cement is available with which the plastic can be cemented to other plastics, wood, metal, and glass, and it is said not to craze even when cemented to metal parts. It can be cleaned with conventional cleaners, alcohol, methl-ethyl ketone or lacquer thinner.—Sierra Products Company, *1632 East Compton Boulevard, Compton, California.*

Porous Bronze

Bost-Bronz is a line of solid and cored bar stock and plates from which bushings, thrust washers, and ways may be machined. The bronze is porous, so that it absorbs and holds oil by capillary action, delivering it uniformly over the bearing surface. Solid bar stock is available in diameters from ⅜ to 4 in.; cored stock from ⅜ to 4 in. i.d., 1 to 6 in. o.d.; and plate stock from ⅛ to 1 in. in thickness. A catalog is available with further information on stock sizes, tolerances, load ratings and prices.—Boston Gear Works, *63 Hayward Street, Quincy 71, Massachusetts.*

THE REVIEW OF SCIENTIFIC INSTRUMENTS

VOLUME 21, NUMBER 12 *DECEMBER, 1950*

Beta-Ray Spectroscopes

E. Persico* and C. Geoffrion
Université Laval, Québec, Canada

(Received June 19, 1950)

This paper is a review of the various types of beta-ray spectrographs and spectrometers. The principal theoretical results as to the resolving power and luminosity attainable under various conditions are briefly related. Finally the construction and performance data of a number of instruments described in the literature are collected, and compared by means of a graphical representation.

INDEX

I. Introduction
- A. General Outline and History 945
  - 1. Flat Spectroscopes 945
  - 2. Helical Spectroscopes 947
  - 3. Calibration 949
- B. Nomenclature and Notations 949
- C. A Few Fundamental Formulas 951

II. Theoretical Results on Flat Spectroscopes
- A. General 951
- B. First-order Single-focusing Spectroscope 952
  - 1. Focusing Properties 952
  - 2. Image of a Finite Source 952
  - 3. Dispersion and Resolving Power 953
  - 4. The Spectrograph 953
  - 5. The Spectrometer 954
  - 6. Optimum Conditions of Operation 954
  - 7. The Magnet Size 955
- C. Third-order Single-focusing Spectroscope 956
  - 1. Focusing Properties 956
  - 2. Image of a Finite Source 956
  - 3. Dispersion and Resolving Power 956
  - 4. The Spectrometer 957
  - 5. Optimum Conditions of Operation 957
  - 6. The Magnet Size 957
- D. First-order Double-focusing Spectroscope 957
  - 1. Focusing Properties 957
  - 2. Image of a Finite Source 958
  - 3. Dispersion and Resolving Power 958
  - 4. The Spectrometer 958
  - 5. Optimum Conditions of Operation 958
- E. Comparisons between the Different Flat Types 959
- F. Miscellaneous Types 960

III. Theoretical Results on Helical Spectrometers
- A. The Solenoid Spectrometer with Point Source 960
- B. The Solenoid Spectrometer with Disk Source 962
- C. The Short Lens Spectrometers 963
- D. The Long Lens Spectrometers 964

IV. Electrical and Mechanical Devices
- A. The Magnetic Field 965
- B. The Spectroscope Chamber 965
- C. The Source 966
- D. The Detector 966
- E. Magnetic Field Measurements 967

V. Some Beta-ray Spectrometers and Their Performance 967

I. INTRODUCTION

A. General Outline and History

1. *Flat Spectroscopes*

It has long been known that the β-rays emitted by a radioactive substance are a mixture of electrons of different kinetic energies. From the beginning it was realized that these electrons would be deflected in a magnetic field according to their momenta. This provided a simple method of sorting out and studying the various energies present in a given beam, since these are related to the momenta by a simple formula (4). The first experiment to this effect seems to have been made in 1910 by von Baeyer and Hahn,[1] and its principle is schematically described by the full lines of Fig. 1: S is the radioactive source (in the shape of a thin filament perpendicular to the plane of the drawing), A is a slit (*entrance slit*) limiting a narrow bundle of β-rays, and P is a photographic plate. The whole is in a vessel, evacuated to the order of 0.001 mm Hg. A uniform magnetic field, perpendicular to the plane of the drawing, bends the rays into circular paths, whose radius is proportional to the momentum. All the rays of a given momentum (two of which are shown in the figure) will be recorded on the plate as a spot L, in the shape of a rather wide

---

* Now at the University of Rome, Rome, Italy.

[1] G. Baeyer and O. Hahn, Physik. Zeits. 11, 488 (1910).

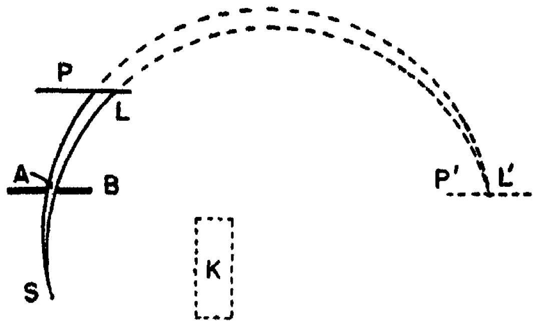

FIG. 1. Comparison of the direct deflection and the semicircular focusing spectrographs.

"line" (parallel to the slit) whose position on the plate gives a measure of the deflection and therefore of the momentum. The image formed by this (continuous or discontinuous) array of lines is called, because of its obvious optical analogy, a *β-ray spectrum*. This method of obtaining the spectrum may be compared to Newton's experiment of the analysis of a sun beam by means of a prism, which is here replaced by the magnetic field.

It is easily seen that this method cannot give a very thin line for each monokinetic radiation, because the line is necessarily wider than the slit, and the latter cannot be made very narrow without sacrificing too much of the intensity. So an enormous progress was made shortly after, when Danysz pointed out[2] that a kind of "focusing" could be obtained by making use of a very simple geometrical property of the circle (namely, that if a circle is given an infinitesimal rotation around one of its points, S, the point diametrically opposed is displaced along the tangent). So, if the two rays of Fig. 1, instead of being stopped at L, are allowed to continue their circular paths for about 180°, they meet again in L', and give rise to a very sharp line on a photographic plate P'. This is the principle of the *semicircular focusing*[3] which was immediately applied by Rutherford and Robinson[4] and, thereafter, without substantial improvements, by many others. Among other advantages on the previous one, this method gives much greater resolution for a given intensity, greater dispersion, and permits shielding the photographic plate from γ-rays from the source by means of a thick lead shield K.

This type of β-ray spectrograph, still widely employed, is described in detail in part II. Its optical analog is the prism spectrograph of Féry, in which a focusing *in the horizontal plane* is obtained by giving the prism faces a cylindrical shape. It is to be noted that no focusing is so obtained in the vertical plane: rays coming from a point of the source are vertically spread along the whole length of the spectral line (*astigmatism*). The same is true of the semicircular magnetic focusing.

The development of the Geiger-Müller counter around 1928 suggested its replacing the photographic plate in β-ray spectrographs. The apparatus so modified is called a β-ray *spectrometer*.[5] Its principle is illustrated by Fig. 2; the photographic plate of Fig. 1 is replaced by a lead diaphragm B' with a narrow slit E (*exit slit*), which allows a very small portion of the spectrum to fall on the G-M counter G. This is provided with a window W, covered with a very thin foil of metal or plastic to allow the rays to enter the counter without too much absorption. The counting rate of the counter gives the "intensity" of β-rays corresponding to the short range of momenta picked up by the slit, and therefore, if divided by this range, may be considered as a measure of the "density" of the spectrum for a given value of the momentum. The magnetic field is then slightly changed, and so another point of the spectrum falls on the slit E and its density is measured. In this way, by scanning the field in small steps and taking at each value of the field the counting rate of the G-M counter, the whole spectrum is explored and a diagram can be traced, taking as abscissa the momentum and as ordinate the "density" of the spectrum. This diagram is even more significant than a photographically registered spectrum, because in the latter the density of blackening is not always simply related to the density of β-radiation. Clearly, the optical analog of a β-ray spectrometer is a prism monochromator.

It is to be noted that the semicircular focusing on a spectral line of electrons of a given momentum in a uniform field is only approximate, and this on two accounts:

(a) For an electron leaving the source in a direction more or less inclined to the horizon,[6] the horizontal component of the momentum (which is the only one determining the deflecting force) is a little reduced: so its path, projected on the plane of the drawing, is a circle of a radius a little shorter than those shown in Fig. 1. Therefore, this ray will meet the plane of the diaphragm B' on a line a little to the left of L'. The horizontal displacement is proportional to the square of the angle of the initial momentum with the horizontal.

(b) As is made clear by Fig. 2, all the circles of a given radius passing by S do not meet the plane B' exactly at the same point: the displacements are of the order of the square of the angular aperture of the beam in the horizontal plane.

These two effects are analogous to *second-order* aberrations of the optical instruments: they both contribute to a broadening of the spectral line and therefore to a loss of resolving power (see part II). This focusing is called a *first-order* focusing because it can be said that the rays meet on the same line only if powers of the angular apertures higher than the first are neglected.

---

[2] J. Danysz, Comptes Rendus 153, 339; 1066 (1911). Le Radium 9, 1 (1911).

[3] This principle had been already utilized in 1908, by J. Classen, in order to determine the value of e/m for thermionic electrons: Physik. Zeits. 9, 762 (1908).

[4] E. Rutherford and H. Robinson, Phil. Mag. (6) 26, 717 (1913).

[5] The term *spectroscopes* is frequently employed to denote collectively the *spectrographs* and the *spectrometers*.

[6] For convenience of expression, we suppose that in the instruments of this type the magnetic field is vertical, as is usually the case today.

A further broadening is produced by the fact that the source is not a mathematical line but a wire or a strip of a certain finite width. Finally, in spectrometers, account must be taken of the finite width of the exit slit *E*, which also reduces the resolving power.

It is easily seen that all the conditions that would improve the resolving power (narrow beam aperture, source, and exit slit) would reduce the number of electrons reaching the detector, and therefore the "luminosity" of the instrument (see Section I B), so that a compromise must be made between these two opposite requirements. The same is true of all other types of β-ray spectroscopes, but the relation between the resolving power and the luminosity is not always the same. A good deal of theoretical work is being done at present in order to determine this relation for the different models, and some results of it will be given in parts II and III.

Coming back to the general description of the various types of β-spectroscopes, we must now mention those derived from the 180°-focusing spectrometer by replacing the uniform field by a non-uniform one (shaped field). The first spectrometer[7] of this kind was made in 1946 by K. Siegbahn and N. Svartholm:[8–10] in it the electron bundle coming from any point of the source describes an arc of $\sqrt{2}\pi = 254°33'$ in a field slightly decreasing toward the exterior of the orbit, and is focused again at a point, to a "first-order" approximation (see above). The main difference between this focusing and the semicircular one is that here two rays starting from a point of the source with different inclinations to the horizontal are concentrated at the same *point* of the image line, so that there is a focusing not only in the horizontal direction, but also in the vertical one (*double focusing*): one could say that such a magnetic field acts as a prism and as a convergent spherical lens (whereas the uniform field acts as a prism and as a *cylindrical* lens): it forms, therefore, on the plane of the exit slit a true image of each point of the source (without astigmatism). However, the chief advantage of this sort of spectrometer is another: if one considers electrons of a slightly increased momentum, one sees that they will travel in a weaker field, and therefore the radius of curvature of their paths will be increased on *two* accounts: the greater momentum and the weaker field, whereas in semicircular focusing only the first effect would be present. So the point of impact of these electrons on the exit slit will be displaced more than with semicircular focusing (in fact, twice as much), and this increases the resolving power for the same luminosity (see Sections II D).

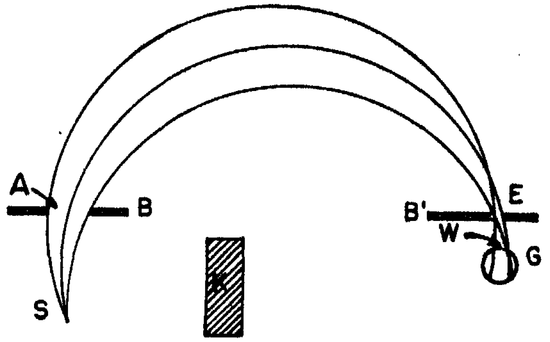

FIG. 2. The principle of the semicircular spectrometer.

Another type of shaped field has been calculated by Bock[11] and by Beiduck and Konopinski[12] so as to correct the third-order aberration due to the horizontal aperture of the beam (without correcting that due to the vertical one): one thus has "*third-order*" horizontal focusing. This permits making the beam very divergent in the horizontal plane, without too greatly impairing the resolving power (see Section II C).

In all the spectroscopes so far described, the electrons move approximately at right angle to the field in a region more or less annular-shaped. For this reason, we shall refer to all the instruments of this kind as *flat* spectroscopes.

2. *Helical Spectroscopes*

We turn now to a different family of β-ray spectroscopes which may be called *helical spectroscopes:* they are those that utilize the focusing property of an axially symmetric magnetic field for electrons coming from a source located on the axis. As is well known, this property permits the use of such a magnetic field as a convergent lens for electron rays, and is widely employed in the electron microscope and in other electron-optical devices. Figure 3a shows, in orthogonal projections, the trajectory of an electron in a uniform magnetic field (which is the simplest type of magnetic lens): the path is a cylindrical helix with the axis parallel to the direction of the field. However, the best way of representing this movement for our purpose is not by means of the orthogonal projections but by the following method, currently employed in electron optics. Imagine a rotating plane *m* always passing through the axis of symmetry *z* of the lens and through the instantaneous position of the electron (*meridional* plane): the trajectory of the electron in this plane is called its *trace* and is recorded in the drawing (Fig. 3b). Of course it does not describe completely the path in the space because it does not take into account the rotation around the axis, but since the apparatus is symmetrical around

---

[7] The shaped field can be applied in spectrometers, not in spectrographs, because only in the former is the geometry of the utilized paths the same for electrons of any momentum. These paths are like railway tracks on which, by changing the current intensity in the magnet, electrons of different momenta are conveyed in succession.

[8] K. Siegbahn and N. Svartholm, Nature 157, 872 (1946).

[9] N. Svartholm and K. Siegbahn, Arkiv. Mat. Astron. Fys. Bd. 33A (No. 4) 21 (1947).

[10] N. Svartholm, Arkiv. Mat. Astron. Fys. Bd. 33A, 24 (1947).

[11] C. D. Bock, Rev. Sci. Inst. 4, 575 (1933).

[12] F. M. Beiduk and E. J. Konopinski, Rev. Sci. Inst. 19, 594 (1948).

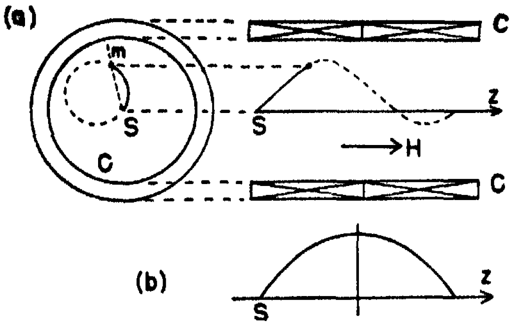

FIG. 3. (a) Two orthogonal projections of the helical path of an electron in a uniform field. (b) The "trace" of the same path in the rotating meridional plane *m*.

the latter, the trace contains just the elements relevant to the electron optics problems.

In the case of a uniform field, the trace is a sinusoid of amplitude and period double those of the orthogonal projection of the helix; in the general case of non-uniform but axially symmetrical fields the same method of representation is employed, but the trace is of course no longer a sinusoid. It is to be borne in mind that all drawings referring to helical spectrometers represent usually the traces and not the orthogonal projections of the paths.

The use of a magnetic lens for the analysis of β-rays was proposed by Kapitza in 1924[13] and realized shortly after by Tricker.[14] Its principle is the same as that of an optical experiment by Rubens and Wood, who in 1910 exploited the chromatic aberration of a quartz lens for the spectral separation of infra-red rays:[15] this principle is schematically explained by Fig. 4.

A diaphragm B, with an annular slit A, selects from the electrons of a given momentum emitted by the source S, only those whose initial directions are comprised between two cones having zz as axis and slightly different apertures. These electrons are approximately focused (full lines) on a circular hole R in the diaphragm B' and so are allowed to fall on the front window of a G-M counter of special design, G. Electrons of a different momentum (broken lines) will be focused nearer or farther and so will fall at least partially outside the hole R.

As is seen in the figure, traces of a given momentum but starting at different angles with the axis are not focused exactly at the same point, owing to the *spherical aberration*. So they will fall on a rather extended area of the plane B' and this impairs the resolving power just as does the widening of the lines in the flat spectroscopes. Therefore, substantial progress was achieved when, following Witcher,[16] the hole R was replaced by an annular slit E (Fig. 23), placed at the point (I in Fig. 4) where the bundle attains its minimum thickness before reaching the axis (*ring image*). As was pointed out by Frankel[17] and will be explained later, this improves radically the relation between resolving power and luminosity.

The magnetic lens of a helical spectrometer can be of different types:

(a) a uniform field, obtained by means of a long solenoid (*solenoid spectrometer*). The first helical spectrometer made by Tricker in 1924[14] was of this type, as was another built later (1941) by Witcher at Columbia University, where it is still in use with various alterations.[16] The chief advantages of the uniform field are the possibility of a rigorous analytical calculation of the electron paths, the easier adjustment, and the less sensitivity to external magnetic perturbations; the chief disadvantage is the necessity of considerable electric power and large dimensions if high energy β-rays are to be analyzed.

(b) a non-uniform (but axially symmetrical) field, confined to a small region between source and detector, obtained by means of a flat coil, usually without iron, similar to the conventional magnetic lenses of the electron optics. Figure 23 gives an idea of this type of instrument, which is called a "short lens spectrometer." It was built for the first time by Klemperer,[18] and later was adopted by Deutsch, Elliott, and Evans[19] and many others.

(c) a non-uniform (but axially symmetrical) field, extending throughout the paths of the electrons, and produced by several coils aligned along the same axis, with or without an iron core. Figures 24 to 26 give some examples of this type of instruments, called *"long lens spectrometers:"* the first of them was built by Siegbahn.[20]

It must be noted that, until recently, only the solenoid spectrometers had an annular exit slit: in the short and long lens instruments there was instead only a circular window on the axis (usually the entrance window of the counter). A long lens spectrometer with annular exit slit has been described in 1948 by Zunti[21] and a short lens one in 1949 by Hornyak, Lauritsen and Rasmussen[22] another one in 1950 by Verster, who has studied its theory.[23] A study for the utilization of the ring image in short lens spectrometers has been made recently by Keller, Koenigsberg and Paskin.[24] They find that in a short lens the use of an annular exit slit increases the luminosity of better than a factor of two for a given spread.

As it is seen, both flat and helical spectrometers have the same essential parts: a *magnet*, a *source*, an *entrance slit*, an *exit slit* or *window*, and a *counter*. Besides, there is usually on the axis a long lead cylinder (shaded rectangle in Fig. 4) in order to prevent gamma-rays from the source from reaching the counter, and several other baffles, variously disposed, serving not to define the electron beam but to prevent secondary and scattered beta- and gamma-rays from reaching the counter. It is to be noted, moreover, that a magnetic lens focuses at the same point positive as well as negative electrons: so, when it is necessary to discriminate between them, a further baffle is used, having a helicoidal shape as seen in Fig. 25: since the two kinds of electrons spiral in opposite directions, such a baffle lets through only one or the other of them, depending on the direction of the magnetic field. It serves also (as well as any other baffle placed on the axis) to stop the electrons that would reach the exit slit after performing more than one revolution.

---

[13] P. Kapitza, Proc. Camb. Phil. Soc. 22, pt. 3.

[14] R. A. R. Tricker, Proc, Camb. Phil. Soc. 22, 454 (1925).

[15] Berl. Berich 1910. Also R. W. Wood, *Physical Optics* (The Macmillan Co., New York, 1936), III ed. p. 523.

[16] C. M. Witcher, Phys. Rev. 60, 32 (1941).

[17] S. Frankel, Phys. Rev. 73, 804 (1948).

[18] G. Klemperer, Phil. Mag. 20, 545 (1935).

[19] Deutsch, Elliott, and Evans, Rev. Sci. Inst. 15, 178 (1944).

[20] K. Siegbahn, Arkiv. Mat. Astron. Fys. Bd. 30A, No. 1 (1943).

[21] W. Zunti, Helv. Phys. Acta. 21, 179A (1948).

[22] Hornyak, Lauritsen, and Rasmussen. Phys. Rev. 76, 731 (1949).

[23] N. F. Verster, App. Sci. Research B1, 363 (1950).

[24] Keller, Koenigsberg, and Paskin. Rev. Sci. Inst. 21, 713 (1950).

The equipment for the production and the measurement of the vacuum and of the magnetic field, the construction of the source and of the counter will be dealt with in part IV. The remaining electronic circuits (amplifier, etc.) are well known and will not be described in this paper.

3. *Calibration*

In any spectrograph or spectrometer with uniform field, an *absolute* determination of the momentum corresponding to a given line can be obtained by means of *geometrical* measurements in order to determine the radius of curvature ρ of the central path, and *magnetic* measurements to determine H (see formula 3). The latter are of course the most troublesome, and a very ingenious method of performing absolute determinations without measuring H has been devised by Siegbahn.[25] It makes use of the fact that the difference of the energies of two β-lines, originating in the conversion of the same γ-line, is simply related to the frequency of a line of the x-ray spectrum of the converter, which is known from diffraction experiments.

Another method of making absolute determination of the momentum corresponding to a β-line is based on the diffraction measurement of the wave-length of the γ-ray, whose conversion originates the said line. Many such measurements of high precision have been performed by J. W. M. DuMond and his collaborators, by means of a curved crystal gamma-ray spectrometer.[26]

With such methods the momenta of a number of "standard" β-lines (particularly of the spectrum of RaB and ThB) have been determined with an incertitude of less than 0.1 percent.

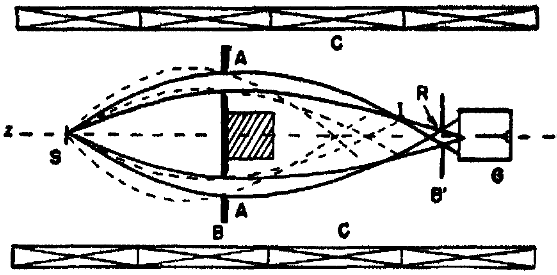

FIG. 4. The principle of helical spectrometers.

These *standard lines* are currently employed for the *relative* determination of the momentum of other lines, by means of any type of instrument. A relative determination demands, in the case of a spectrograph, only geometrical measurements, and in the case of a spectrometer only the measurement of the ratio of two successive values of the magnetic field. If the magnet has no iron core, this ratio is equal to that of the values of the exciting currents, and is easily determined: this is a great advantage of ironless spectrometers. When iron is present, the field ratio must be measured (at any point) (see Section IV E): however, if the magnet has been designed so as to keep the magnetization well under the saturation value in all sections (as is often possible, e.g. in long lens types), and if iron of low remanence has been employed, proportionality to the current can often be assumed.[27]

B. Nomenclature and Notations

The terminology in this branch of physics is far from being uniform. We summarize in this section the nomenclature and the notations adopted in this paper. Our terms are chosen, as a rule, from those used by other authors, but the choice has been guided more by considerations of perspicuity and preciseness than by current popularity. We report also, in the most important cases, some of the expressions used by different authors to denote the same thing.

Spectrograph: an instrument recording the β-ray energy spectrum on a photographic emulsion.

Spectrometer: an instrument measuring the relative number of β-particles in a short energy range, which can be gradually displaced along the spectrum.

Spectroscope: spectrograph or spectrometer.

Flat spectroscope: a spectroscope in which the central electron path lies in a plane (which will be considered as a *horizontal plane*).

Helical spectroscope: a spectroscope in which all of the paths of the particles are essentially of helicoidal shape. It is usually a spectrometer and can be a *solenoidal*, *long lens*, or *short lens* type (see Section I A).

Baffles: all the obstacles intended to prevent electrons or gamma-rays from reaching the detector directly or by scattering. Among these are the *first diaphragm* determining the *entrance slit* and the *second diaphragm*, determining the *exit slit* (in spectrometers). Both the entrance and the exit slit may have their two edges in different planes (see Fig. 16). Still other baffles act as shields against scattered radiation without contributing to the determination of the direct beam.

---

[25] K. Siegbahn, Arkiv. Mat. Astron. Fys. Bd. 30A, (No. 20) (1944).

[26] J. W. M. DuMond, Rev. Sci. Inst. 18, 626 (1947); DuMond, Lind, and Watson, Phys. Rev. 73, 1392 (1948) and 75, 1226 (1949); Lind, Brown, Klein, Muller, and DuMond, Phys. Rev. 75, 1544 (1949).

[27] K. Siegbahn, Phil. Mag. XXXVII, 162 (1946).

Momentum (p): the "quantity of motion" or "mechanical momentum" of an electron: $p=m_v v$, where v is the velocity and m_v the relativistic mass.[28]

In all formulas concerned with the magnetic deflection of electrons the momentum appears divided by the electron charge in e.m. units: this ratio will be denoted by p^*:

$$p^*=p/e_m.$$

Because of formula (3), this quantity is called by many authors "the $H\rho$ of the electron" even when there is no explicit reference to H and ρ (and even when $H=0$ and $\rho=\infty$). Its dimensions are those of a magnetic potential: so it will be expressed in "gilberts" (gauss-cm).

Total activity: The number of electrons emitted by a source in all directions per unit time.

Specific activity: The total activity of a source divided by its area.

Intensity: The number of electrons reaching the counter of a spectrometer per unit time (apart from scattered radiation) with a given source and a given magnetic field.

Transmission (T)*:* The intensity (see above) divided by the total activity of the source. Also: the fraction of all emitted electrons reaching the counter (except by scattering) with a given source and a given magnetic field.

Line profile: In a spectrometer, it is the diagram obtained, with a monokinetic source, by measuring the transmission (see above) with different values of the coils current j, and plotting it against the values of p^* which correspond to those of j according to the calibration law. In a spectrograph, it is the diagram having as ordinate the number of electrons falling per unit time and unit area at a point of the plate, with a monokinetic source of unit total activity, and as abscissa the value of p^* corresponding to that point of the plate according to the calibration law.

Half-maximum width: (Δp^*) The width of the line profile at half-maximum ordinate.

Spread: (η) The relative half-maximum width:

$$\eta=\Delta p^*/p^*=\Delta p/p.$$

The spread is usually expressed in percent and is called by different authors: "*irresolution*," "*spread*," "*resolving power*," "*inverse resolving power*," "*limit of resolution*," "*inverse momentum resolution*," "*half-intensity width*." Some authors call "*resolving power*" the quantity $\Delta E/E$, where E is the energy and ΔE is the half-maximum width of the line profile in the scale of energies: it is related to η by formula (5) in the following section.

Resolving power (P)*:* The inverse of the spread:

$$P=1/\eta=p^*/\Delta p^*=p/\Delta p.$$

This definition conforms to current usage in optics.

Base width ($\Delta_0 p^*$)*:* The width of the line profile at zero ordinate. Also called: "*total width.*"

Base spread (η_0)*:*

$$\eta_0=\Delta_0 p^*/p^*=\Delta_0 p/p.$$

Base resolving power (P_0)*:*

$$P_0=1/\eta_0=p^*/\Delta_0 p^*=p/\Delta_0 p.$$

Dispersion: In the plane of the photographic plate, or of the exit slit, let us call x the distance between an arbitrary origin and the line where electrons of momentum $p=e_m p^*$ from a point source are focused. Then $\gamma=dx/dp^*$ will be called "dispersion." Clearly, if the real image (or the ring image) of the source has a width Δx (due to the source width and to aberration) and if the width of the exit slit is X, the base width of the line profile will be approximately $\Delta_0 p^*=(X+\Delta x)/\gamma$.

Solid angle (Ω)*:* The solid angle filled by the initial directions of all the electrons of a monokinetic source leaving the center of the source (or, practically, any point of it) and passing through the entrance slit. It is also called "*angle of collection.*"

Gathering power (ω)*:* The fraction of all the emitted electrons of a monokinetic source passing through the entrance slit. For a source emitting isotropically it is given by

$$\omega=\Omega/(4\pi).$$

The gathering power is usually expressed in percent. In a spectrometer it is equal to the maximum intensity obtainable, with an exit slit wide open, with a source of unit total activity: so, it can be said that the gathering power measures the ability of the instrument to deal with sources of very low *total* activity.

Over-all gathering power: In a spectrometer the gathering power ω characterizes only the parts of the instrument up to the exit slit. The *over-all gathering power* with a given setting of the exit slit is measured by the value $T_{\max}$ of the transmission at the peak of the line profile. Clearly, $T_{\max}\leq\omega$.

Luminosity (L)*:* The gathering power multiplied by the source area: $L=\omega\sigma$. In a spectrometer, it is equal to the maximum intensity obtainable, with an exit slit wide open, with a source of unit specific activity (and of the given area). It measures therefore the ability of the instrument to deal with sources of very low *specific* activity. It will be expressed in cm^2.

---

[28] For the purpose of studying the theory of a β-ray spectroscope it is convenient to assume an ideal source emitting only electrons of a sharply defined momentum (*monokinetic* source): we shall always do so in the following, unless otherwise stated. Of course, a real source always emits a continuous spectrum, and even the lines of a so-called line spectrum (produced by internal or external conversion of gamma-rays) are only more or less sharp peaks in a continuous distribution of momenta. Their "natural" width (that is, apart from the broadening due to the imperfect resolving power of the instrument) is partly due to the width of the energy levels and partly (usually, for the most important part) to the fact that electrons coming from atoms deeply situated inside the source are slowed down by collisions before emerging from the source surface. This phenomenon will not be taken into account in the evaluation of the qualities of an instrument (similarly, the self-reversal or the pressure broadening of spectral lines is not introduced into the theory of optical spectroscopes). So the line profile of which we speak later is not the one that will be obtained with any real source, but only a limiting case of it.

Over-all luminosity (L^*): In a spectrometer, the luminosity characterizes only the parts of the instrument up to the exit slit. The *over-all luminosity* L^* with a given setting of the exit slit is measured by the peak transmission $T_{\max}$ multiplied by the source area:

$$L^* = T_{\max}\sigma.$$

Clearly, $L^* \leq L$.

Efficiency μ: The ratio of the luminosity L of a flat spectroscope to its useful pole piece area $\sum$ (as defined in Section II B). This dimensionless quantity helps the comparison between instruments of different types, by reducing them effectively to the same size.

C. A Few Fundamental Formulas

We recall here some formulas of relativistic mechanics that are basic in the theory of β-ray spectroscopes.

If m is the rest mass of the electron, m_v its mass at speed v and p its momentum, then

$$p = m_v v = m(1 - v^2/c^2)^{-\frac{1}{2}} v. \tag{1}$$

Since the magnetic deflection does not alter v, the relativistic change of mass does not introduce any complication in the movement of a *given* electron, provided the right value of m_v is taken at the start.

The radius of curvature ρ of the path of an electron moving at right angles to a magnetic field H is given by the well-known formula

$$H\rho = p/e_m, \tag{2}$$

where e_m is the electron charge in absolute e.m.u. ($e_m = 1.60199 \times 10^{-20}$). This formula suggests taking as a measure of momentum the quantity

$$p^* = p/e_m = H\rho \tag{3}$$

which will be expressed in gauss-cm (or "gilberts").

Let E be the kinetic energy (usually expressed in Mev). Its relation to p^* is most conveniently expressed by introducing the two universal constants

$$E_0 = mc^2 = 0.5107 \text{ Mev,}$$
$$p_0^* = mc/e_m = 8.125 \times 10^{-7} \text{ gilbert.}$$

Then the relation is

$$(E/E_0 + 1)^2 - (p^*/p_0^*)^2 = 1. \tag{4}$$

The relation between E in Mev and p^* in gilberts is tabulated, for instance, in "Miscellaneous Physical Tables" (Nat. Bur. of Stand. 1941).

The "spread" of an instrument (or its inverse, the resolving power), is most easily calculated in terms of momentum, but sometimes it is needed in terms of energy. To pass from the one to the other the following formula, obtained by differentiation of (4), is useful:

$$\eta = \frac{dp^*}{p^*} = \frac{dp}{p} = \frac{E + E_0}{E + 2E_0} \frac{dE}{E}. \tag{5}$$

The factor at the right-hand side is plotted against E and p^* in Fig. 5. It is to be noted that in the theory of magnetic spectroscopes all the relativistic corrections can be ignored as far as the spectrum is studied in terms of p (or p^*) rather than of E.

II. THEORETICAL RESULTS ON FLAT SPECTROSCOPES

A. General

For the discussion of the different types of flat spectroscopes, the cylindrical coordinates r, θ, and z are adopted, with the axes oriented in such a way that the central electron trajectory lies in the horizontal plane $z = 0$, the source in the plane $\theta = 0$ and centered at the point $r = a$, $\theta = 0$, and $z = 0$ (Fig. 6). The initial position of an electron leaving the source is determined by

$$r_0 = a + \delta r,$$
$$\theta_0 = 0,$$
$$z_0 = \delta z$$

and the components $\dot{r}_0$ and $\dot{z}_0$ of its initial velocity are approximately given by

$$\dot{r}_0/v = \varphi, \quad \dot{z}_0/v = \psi,$$

where φ and ψ are angles specifying the direction of the initial velocity.

We assume the magnetic field to be independent of θ and symmetrical with respect to the median plane $z = 0$; the vertical component H_z and the radial one H_r may be functions of z and r and H_θ is always zero. However for $z = 0$ and $r = a$, H_r is zero and H_z is such that an electron leaving the center of the source ($r_0 = a$, $\theta_0 = 0$, and $z_0 = 0$) with zero velocity components $\dot{r}_0$ and $\dot{z}_0$, will describe a circular trajectory of radius a. The necessary value of H_z,—called hereafter H_0—, is related to a and p^* by

$$H_0 = p^*/a.$$

The trajectory of the electron and its equation will depend on the initial position and momentum of the

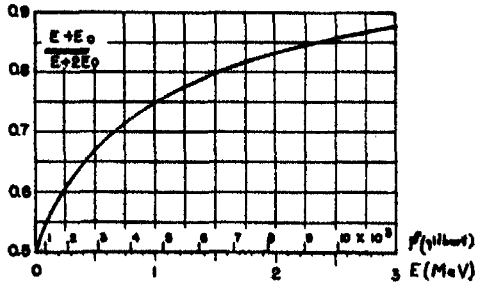

FIG. 5. The ratio between the momentum spread $\Delta p/p$ and the energy spread $\Delta E/E$ (form. 5). (E = energy in Mev; $p^* = H\rho$ = momentum divided by the electron charge in e.m.u.).

electron and also on the form of the magnetic field. It is in fact[29] the form of H_z that permits a classification of the different types of flat spectroscopes; according to this form, the kind and the degree of focusing are different. The flat spectroscopes may thus be classified in three groups:

(1) First-order single-focusing spectroscopes,
(2) Third-order single-focusing spectroscopes,
(3) First-order double-focusing spectroscopes.

In the following sections, each type will be studied; the form of the field, the equations of the trajectory, the image width, the dispersion, the resolving power, and the luminosity will be given for each, when available. The relations between the different parameters, such as source and slit dimensions and solid angle, will be investigated so as to determine the conditions of operation, —called optimum conditions—, which will result in maximum luminosity for any given radius of curvature and resolving power. Comparisons between the different types will then be possible. Attention will also be paid to the necessary size of the magnet.

B. First-Order Single-Focusing Spectroscope

1. *Focusing Properties*

This type of spectroscope is the oldest and uses a uniform magnetic field perpendicular to the central electron trajectory, i.e., in the z direction; H_z is then constant and equal to H_0 while H_r is always zero. The equations of the electron trajectory in cylindrical coordinates, as given by Shull and Dennison,[30] are approximately:

$$r=a+\left[\delta r-\frac{a}{2}(\varphi^2-\psi^2)\right]\cos\chi+\varphi(a+\delta r)\sin\chi$$
$$-\frac{1}{4a}(\delta r^2-a^2\varphi^2)\cos 2\chi-\tfrac{1}{2}\varphi\delta r\sin 2\chi$$
$$+\frac{1}{4a}(\delta r^2+a^2\varphi^2)-\frac{a\psi^2}{2}, \qquad (6)$$

$$z=\delta z+\psi a\chi, \qquad (7)$$

$$\theta=\chi-(\delta r/a)\sin\chi-\varphi(1-\cos\chi), \qquad (8)$$

where $\chi=vt/a$, and δr, δz, φ, and ψ depend on the initial conditions described before.

From these equations it is obvious that there will be no focusing in the z direction; this could be foreseen because there is no restoring force in that direction. In the r direction, on the contrary, a first-order focusing is achieved in the diametral plane through the source; the solution of Eqs. 6, 7, and 8 gives for the impact point on the $\theta=\pi$ plane:

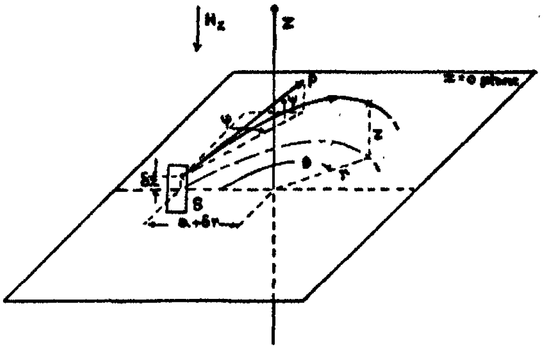

FIG. 6. Electron trajectory in a magnetic field whose main component is along the z axis of a cylindrical coordinates system (r, z, θ). The initial position of the electron on the source S is determined by $r_0=a+\delta r$, $z_0=\delta z$, and $\theta_0=0$; the dotted line is the projection of the trajectory on the $z=0$ plane.

$$r^*=a-\delta r-a(\varphi^2+\psi^2),$$
$$z^*=\delta z+\pi a\psi.$$

These two equations give the point of impact of an electron of momentum p in the plane containing the source, when it has left a source point of coordinates $r_0=a+\delta r$ and $z_0=\delta z$ in a direction making angles φ and ψ with the normal to the plane $\theta=0$. They also indicate that this type of spectroscope, semicircular with constant field, gives first-order single focusing.

2. *Image of a Finite Source*

Consider now a source of finite dimensions centered at $r=a$, $\theta=0$, and $z=0$ and extending from $a-Q/2$ to $a+Q/2$ in the r direction and from $-h/2$ to $+h/2$ in the z direction. Then, if the maximum values of φ and ψ are limited by baffles to φ_0 and ψ_0, all the electrons of the same momentum will cross the plane $\theta=\pi$ in an area whose dimensions are:

width: $Q'=Q+a(\varphi_0^2+\psi_0^2)$,
height: $h'=h+2\pi a\psi_0$.

This area may be considered as an image of the source which would be equal to it but for aberrations which are functions of φ_0 and ψ_0. The monokinetic electrons forming this image may be registered on a photographic plate or passed through an exit slit to a measuring apparatus. In the latter case, the presence of an exit slit of finite width will enlarge the line profile (for a monokinetic electron group) by the width of the latter, while in the former the line profile will be widened by the defining slit width of the microphotometer that will read the density distribution on the photographic plate. In both cases, the image is apparently increased by the width (F) of this last slit and the effective image width may be defined by

$$Q''=F+Q+a(\varphi_0^2+\psi_0^2). \qquad (9)$$

---

[29] The form of $H_z(r)$ for $(z=0)$ determines completely H, according to Maxwell's equations.
[30] F. B. Shull and D. M. Dennison, Phys. Rev. 71, 681 (1947); Phys. Rev. 72, 256 (1947).

It is this effective width Q'' that must be used in calculating the resolving power of the spectroscope.

3. *Dispersion and Resolving Power*

The dispersion γ (see Section I B) can be easily calculated: it is

$$\gamma=2\frac{dr^*}{dp}=2\frac{dr^*}{da}\frac{da}{dp}$$

and, from the preceding formulas for H_0 and r^* (neglecting second-order terms)

$$\gamma=2/H_0.$$

The base spread is, according to a preceding formula (Section I B):

$$\eta_0=\Delta_0 p/p=[F+Q+a(\varphi_0{}^2+\psi_0{}^2)]/2a. \tag{10}$$

The inverse of this formula gives the base resolving power, i.e., the resolving power for complete separation of two lines. Practically, this is not necessary because, as is well known, one may distinguish two lines even if they are partially overlapping; they are in practice said to be resolved if they are separated at half-maximum density and the resolving power of the spectroscope is usually defined with respect to this half-maximum line width. Its relation to the base resolving power depends on the shape of the profile line, which in its turn depends on the focusing properties of the apparatus, and on the relative choice of the parameters such as source and slit dimensions, and solid angle.

4. *The Spectrograph*

In a spectrograph, all the electrons of various momenta are simultaneously registered on a photographic plate while the homogeneous field is held at a constant value. The method proposed by Rutherford and Robinson[4] is still in use and may be described in the following way (Fig. 7). A rectangular source S of width Q and height h is placed in a plane parallel to the field; the divergent electron beam is limited in the plane perpendicular to the field by a slit A of width $2b$ placed in a plane parallel to the source at a distance d from it. In the same plane is located the photographic plate P on which focused monokinetic electrons form an image of width Q'. Though the photographic plate and the source do not lie in the same plane, it has been proved[31] that the image width Q' is equal as before to

$$Q'=Q+a(\varphi_0{}^2+\psi_0{}^2),$$

where φ_0 is determined by the ratio b/d and ψ_0 by $h/\pi a$ since the heights of the source and of the plate are generally made equal. The slit is larger than the source and much smaller than d; h is small enough to neglect $\psi_0{}^2$. With this design the image width Q', and consequently the spread, varies with the electron momentum. This latter value is known from the strength of the field and the radius of curvature of the path, which is given by

$$a=(1/2)[d^2+(x-Q/2)^2]^{\frac{1}{2}},$$

where d is, as before, the source-slit distance and x is the distance between the slit center and the right edge of the image or line.

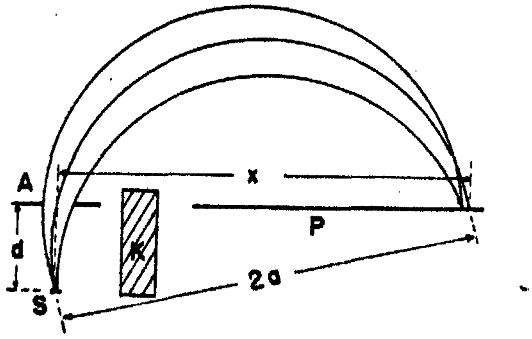

FIG. 7. Rutherford's and Robinson's design for beta-spectrograph. Electrons from the source S, going through the entrance slit A are focused on the photographic plate P; K is a lead shield.

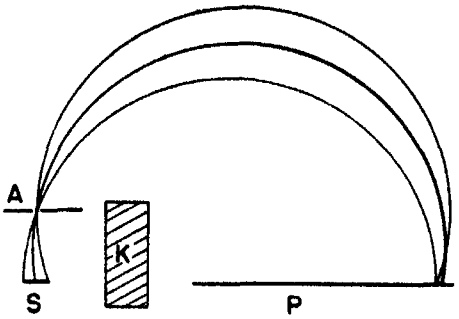

FIG. 8. Robinson's design for large source S. A and P are the entrance slit and the photographic plate and K is a lead shield.

Another design has been proposed by Robinson[32] in which the slit is very narrow and the source large (Fig. 8). This method, whose efficiency is less than that of the preceding one, is used when narrow electron sources are impractical, as for the study of secondary emission due to x-rays.

Siegbahn[26] has proposed the following design for the spectrograph (Fig. 9): the photographic plate is in the plane of the source so that the value of a is determined from a single measurement which affords greater precision. In this design also the image width, the spread and even the angle φ_0 vary with the electron momentum The method presents moreover the following disadvantage: if the spectrograph is designed for a mean radius a_m, some of the central rays whose impact points on the plate determine the value of a, may be stopped by the defining slit if their radius of curvature is much smaller or greater than a_m. This method thus limits the

---

[31] R. Arnould, Ann. de Phys. Serie 11, t. 12, 241 (1939).

[32] H. Robinson, Proc. Roy. Soc. (London) A. 104, 455 (1923).

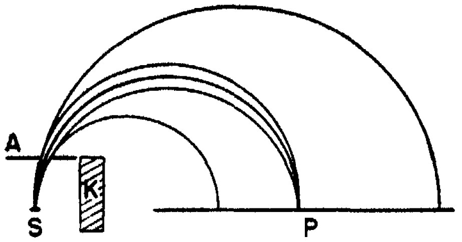

FIG. 9. Siegbahn's spectrograph design. The source S and the photographic plate P are in the same plane while the entrance slit A is in front of the source. K is a lead shield.

measurable momenta to an interval which becomes smaller as the resolving power increases.

5. *The Spectrometer*

In a spectrometer, a G-M counter is fixed at a distance $2a$ from the source and various momentum electrons are registered by varying the field (Fig. 10). The image width and the resolving power are then constant whatever may be the momentum; the base spread is given by the general formula (10) where φ_0 and ψ_0 are maximum divergence angles. The first one is determined by the width $2b$ of a diaphragm (A) placed at 90° from the source and is related to it by $\varphi_0=b/a$. The angle ψ_0 is limited by making the height h of the source, that of the diaphragm, and that of the exit slit all equal to $\pi a\psi_0$. Under these conditions, the "entrance slit" is formed by the vertical edges of the midway diaphragm and by the upper and lower edges of the exit slit; the total solid angle Ω of the beam is given by $2\varphi_0\psi_0$.

Among the advantages of the spectrometer over the spectrograph are that it requires a magnetic field over a smaller area and that the homogeneity of the field may be less perfect, since electrons of different momenta will nevertheless follow identical trajectories. The apparatus once calibrated gives the value of the momentum directly from the measurement of the field, and finally intensity measurements are more exact with a counter than with a photographic plate, even if corrections must be made for the background and for the thickness of the counter window.

6. *Optimum Conditions of Operation*

As seen before, the resolving power is a function of several parameters of which many sets of values may give the same result. However the luminosity of the apparatus, which is equal to the product of the source area by the gathering power, i.e., $L=Qh2\varphi_0\psi_0/4\pi$, depends also on the same parameters. It is evident that one should select among the possible parameter values those which for a given resolving power will achieve maximum luminosity. These conditions of operation for the semicircular spectroscope have been the subject of many papers. Wooster[33] and Li[34] first examined the advantages of various source forms, such as wires and rectangular plates, and the effects of photographic plate inclination. They also determined the resultant line profiles. From different standpoints and with different methods, Siegbahn,[26] Arnoult,[31] and more recently Owen,[35] and Fowler, Shreffler, and Cork,[36] have studied the form of the line profile as a function of various choices of parameters. In the case of spectrometers, Lawson and Tyler,[37] and Owen[35] studied similar problems and established the line profile for various operating conditions. The results contained in all of these papers are very useful to the β-ray spectroscopist. One of the most important is that for optimum conditions of operation the relative parameter choice should be $Q=a\varphi_0^2$ and $F=Q$ (for spectrometers). The angle ψ_0 which equals $h/(\pi a)$ is made small so as to make ψ_0^2 negligible in the spread formula; in practice ψ_0^2 is less than $0.1\varphi_0^2$. With these conditions, one may express the following relations:

$$\eta_0=\Delta_0 p/p=1.55\varphi_0^2 \quad \text{and} \quad L=0.05a^2\varphi_0^5,$$

and since then the line profile has a half-maximum width of 3/7 of its base width (Fig. 11), the spread is given by

$$\eta=\Delta p/p=0.665\varphi_0^2 \tag{11}$$

and the luminosity by

$$L=0.139a^2\eta^{5/2}. \tag{12}$$

In this case also, the *over-all* luminosity L^* (see Section I B) is found to be 55 percent of L, so we have finally the following relation between L^* and η:

$$L^*=0.0765a^2\eta^{5/2}. \tag{13}$$

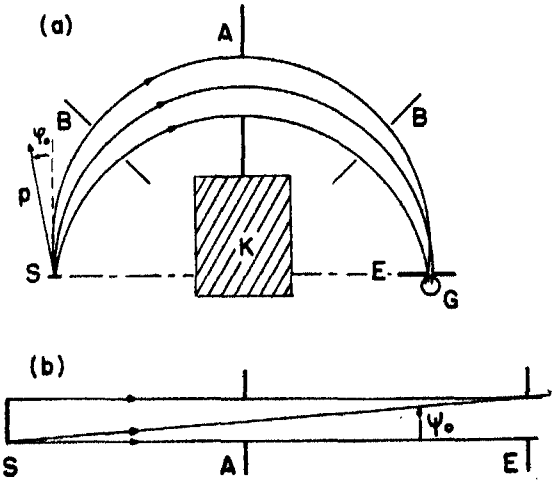

FIG. 10. First-order and third-order single-focusing spectrometers: (a) Projections on the $z=0$ plane of the central and marginal trajectories showing the maximum divergence angle φ_0, the source S, the baffles B, the entrance slit A, the exit slit E, the counter G and the lead shield K. These trajectories are all circular only with homogeneous field. (b) Development in the vertical direction of the outmost trajectories parallel to the $z=0$ plane and of the one making the maximum divergence angle ψ_0.

---

[33] W. A. Wooster, Proc. Roy. Soc. (London) A114, 729 (1927).

[34] K. T. Li, Proc. Camb. Phil. Soc. 33, 164 (1937).

[35] G. E. Owen, Rev. Sci. Inst. 20, 916 (1949).

[36] Fowler, Shreffler, and Cork, Rev. Sci. Inst. 20, 966 (1949).

[37] J. L. Lawson and A. W. Tyler, Rev. Sci. Inst. 11, 6 (1940).

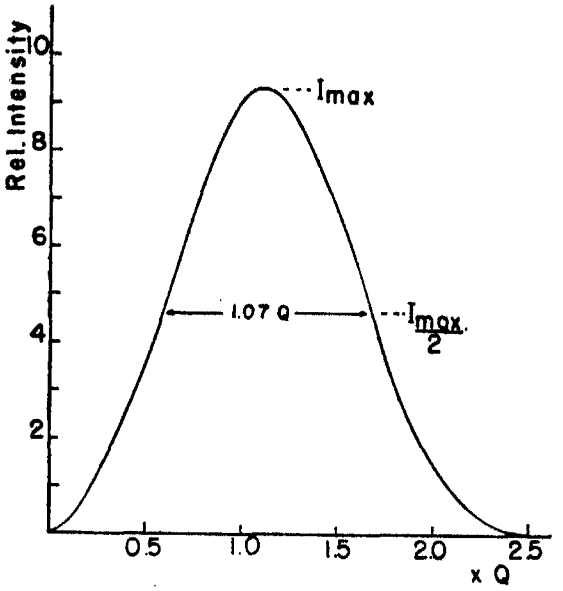

FIG. 11. Line profile for a usual type spectrometer with $Q=F=\varphi_0^2a$. Distances along the r axis are expressed in term of the source width Q.

However these are only relative optimum conditions, because the relative values of ψ_0 and h are arbitrarily fixed. A spectroscope operated under these conditions will be referred to hereafter as the "usual type."

It has been pointed out by one of us[38] that total optimum conditions could be established analytically and realized in practice. The relative choices of parameter values are then:

$$Q=2\varphi_0^2a,\quad \psi_0=2^{\frac{1}{2}}\varphi_0,\quad \text{and}\quad F=Q. \tag{14}$$

The corresponding spread and luminosity are

$$\eta=1.5\varphi_0^2\quad \text{and}\quad L=0.725a^2\eta^{5/2}. \tag{15}$$

In this case the line profile is given by Fig. 12 and the over-all luminosity L^* is 63 percent of the luminosity:

$$L^*=0.456a^2\eta^{5/2}. \tag{16}$$

A spectrometer operated under these total optimum conditions, which requires a higher source, will be called hereafter the "high source type."

Comparisons between the two types clearly show that for the same resolving power and for the same radius a, the luminosity of the high source type is greater by a factor 5.2 than that of the usual one, and that its over-all luminosity is higher by a factor 6. These advantages speak for themselves in favor of the use of total optimum conditions.

It is to be noted that these comparisons are theoretical. In practice, many designers of the usual type make ψ_0 even smaller than $\varphi_0\times10^{-\frac{1}{2}}$. Examination of some published designs of the usual type shows that the use of high source type would increase their L^* by as much as 7.5 times.

7. *The Magnet Size*

In making comparisons between various types of spectroscopes one must take into account not only the luminosity (or the over-all luminosity) at a given resolving power but also the required magnet size; the best spectroscope being the one which has the greatest ratio of luminosity (or over-all luminosity) to magnet size for a given spread. It does not seem necessary for comparison purposes to use the real magnet size; a characteristic of the magnet, such as its necessary pole piece area is quite sufficient. This area depends actually on the length of the central trajectory,[39] on the maximum beam width, and also on the maximum height of the beam since, as it is well known experimentally, the field may be considered homogeneous between parallel pole pieces in a region extending from the center to a distance from the edge equal to the air gap. Defined in that way, the necessary pole piece area is

$$\Sigma=(\text{central trajectory length})\times(\text{max. beam width}+2\text{ times beam height}).$$

This quantity gives, in our opinion, a good idea of the total size of the magnet; the height of the beam will evidently also affect the magnetomotive force required to maintain a given field in the air gap, but this is easily resolved and certainly has far less importance than the

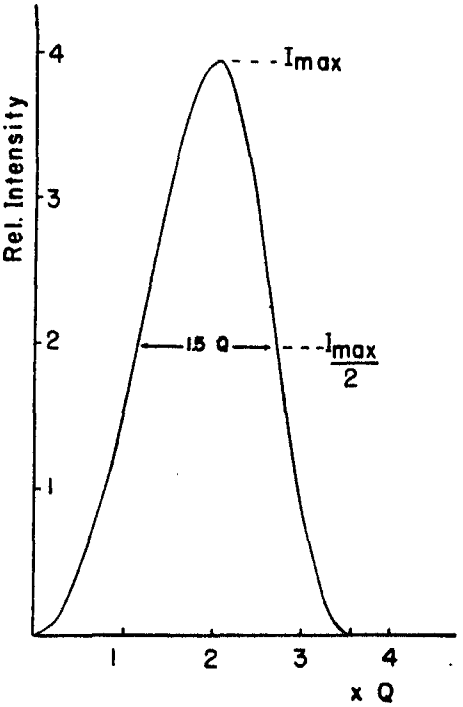

FIG. 12. Line profile for a high source type spectrometer with $Q=F=2\varphi_0^2a$ and $\psi_0=\varphi_0\sqrt{2}$. Distances along the r axis are expressed in term of the source width Q.

---

[38] C. Geoffrion, Rev. Sci. Inst. 20, 638 (1949).

[39] In the case of spectrographs, in order to make possible comparisons between them and spectrometers, we choose as the trajectory length the trajectory of mean radius between the greater and the smaller radii that the apparatus can accomodate.

pole piece area. Calculated with the preceding formula, the necessary pole piece area is for the usual type $\sum_u = 12.6a^2\varphi_0$ and for the high source type $\sum_h = 34.3a^2\varphi_0$.

The ratio of the luminosity L to the area $\sum$, which we have called the efficiency μ of the spectroscope, may be expressed by

$$\mu_u = 9.8\times 10^{-3}\eta^2 \text{ for the usual type,}$$

and

$$\mu_h = 2.59\times 10^{-2}\eta^2 \text{ for the high source type.}$$

If the ratios μ^* of L^* to $\sum$ are now calculated, the results are:

$$\mu_u{}^* = 5.4\times 10^{-3}\eta^2$$

and

$$\mu_h{}^* = 16.2\times 10^{-3}\eta^2.$$

From this study it is clear that the high source type is superior since for the same magnet size and at the same resolving power it will give a profile line with an intensity peak three times higher. From another standpoint, at the same spread and at the same intensity the usual type requires a magnet whose pole piece area is three times greater and whose total size is consequently about 5.2 times bigger than for high source type.

C. Third-Order Single-Focusing Spectroscope

1. Focusing Properties

The necessary field for this type of focusing has been studied by Bock[11] and Beiduck and Konopinski.[12] The latter derived the shape of the field so as to meet the general requirements mentioned in the beginning of this part II and also the following requirement, namely that it focuses perfectly the electrons emerging from a point source and confined in the median plane $z=0$. They found that in the median plane the H_z component of the field, which equals H since H_r is zero in that plane, should be:

$$H_z(r,0) = H_0\left[1-\frac{3}{4}\left(\frac{r-a}{a}\right)^2+\frac{7}{8}\left(\frac{r-a}{a}\right)^3 -\frac{9}{16}\left(\frac{r-a}{a}\right)^4+\frac{51}{320}\left(\frac{r-a}{a}\right)^5\cdots\right] \quad (17)$$

where H_0, r, and a have the same meanings as before.

Using for the field in the median plane the approximation $H_z(r,0)=H_0[1-(3/4)(r/a-1)^2]$ they obtain for the horizontal component $H_r \approx -(3/2)H_0 z(r-a)/a^2$, and for the vertical component $H_z \approx H_0\{1-(3/4)[(r-a)^2 - z^2]/a^2\}$.

These determine the orbit equations for an electron leaving a point source of coordinates $r_0 = a+\delta r$, $z_0=\delta z$ and $\theta=0$, with an initial velocity forming angles φ and ψ with the normal to the plane $\theta=0$.

These equations are found to be:

$$\begin{aligned}
\theta &= \chi-(\delta r/a)\sin\chi-\varphi(1-\cos\chi),\\
z &= \delta z + a\psi\chi - (3\varphi\psi a+3\delta z\delta r/2a)+(\psi\delta r-\varphi\delta z)(3\chi/2)\\
&\quad +(3\varphi\delta z/2-3\psi\delta r+3\varphi\psi\chi a/2)\sin\chi\\
&\quad +[3\varphi\psi a+3\delta r(\delta z/a+\psi\chi)/2]\cos\chi,\\
r &= a+\delta r\cos\chi+\varphi a\sin\chi+\psi^2 a\\
&\quad +5(\varphi^2 a+\delta r^2/a)/8-3(\delta z+\psi a\chi)^2/4a\\
&\quad +(3/2)(\varphi\delta r+\psi\delta z)\sin\chi\\
&\quad +(3\delta z^2/4a-\delta r^2/4a-\varphi^2 a-\psi^2 a)\cos\chi\\
&\quad +(3/8)[(\varphi^2 a-\delta r^2/a)\cos 2\chi-2\varphi\delta r\sin 2\chi].
\end{aligned}$$

From these equations it is seen that there will be no focusing in the z direction but a very good focusing in the r direction for $\theta=\pi$. The corresponding value of χ is $(\pi+2\varphi)$ and the coordinates r and z becomes for this value of θ:

$$\begin{aligned}
r^* &= a-\delta r+\delta r^2/2a-5.41\psi^2 a-1.5\delta z^2/a-4.71\psi\delta z\\
&\quad -4\varphi^2\delta r-6\varphi\psi\delta z-3\pi\varphi\psi^2 a-5\varphi^4 a
\end{aligned}$$

and

$$z^* = \delta z+\psi\pi a-3\delta z(\delta r+\pi\varphi a/2)/a-4\varphi\psi a.$$

The formulas for r^* and z^* give the point of impact of an electron of momentum p in the plane containing the source when it has left the source point of coordinates $r_0=a+\delta r$ and $z_0=\delta z$ in a direction forming angles φ and ψ with the normal to the source. They also indicate that at 180° from the source a field of such a shape gives a third-order focusing with respect to φ (for $\psi=0$ and $\delta r=0$).

2. Image of a Finite Source

In this type, the image of a finite source has the following dimensions:

$$\begin{aligned}
\text{width: } Q' &= Q+5.41\psi_0{}^2 a+1.5h^2/4a+4.71\psi_0 h+4\varphi_0{}^2 Q\\
&\quad +6\varphi_0\psi_0 h+6\pi\varphi_0\psi_0{}^2 a+5\varphi_0{}^4 a,\\
\text{height: } h' &\cong h+2\psi_0\pi a,
\end{aligned}$$

where Q and h are source dimensions, and φ_0 and ψ_0 are maximum divergence angles, fixed by baffles. This image is defined for monokinetic electrons having such a momentum that their radius of curvature in a field H_0 is a. In this case also the line profile is enlarged by the exit slit and its final width is:

$$\text{effective image width: } Q''=Q'+F.$$

3. Dispersion and Resolving Power

For this spectrometer, the dispersion is again $2/H_0$, while the base spread may be expressed (see Section I C) by:

$$\begin{aligned}
\eta_0 = \Delta_0 p/p &= (F+Q)/2a+11.86\psi_0{}^2\\
&\quad +2\varphi_0{}^2 Q/a+18.8\varphi_0\psi_0{}^2+2.5\varphi_0{}^4.
\end{aligned}$$

The relation between the spread and the base spread depends on the relative choice of parameters, and the focusing properties of the field; it should be determined for each mode of operation.

4. *The Spectrometer*

A spectrometer utilizing the previously mentioned shaped field and possessing the focusing properties described above has been built by Langer and Cook[40] and by Bruner and Scott.[41] As we have seen, the source and detector are placed 180° apart (Fig. 10); the divergence of the electron beam in the median plane is limited by a diaphragm (A) located midway on the trajectories, i.e., at $\theta=\pi/2$. Its width $2b$ is related to φ_0 by $b=a\varphi_0$ (in first approximation). On the other hand, the beam divergence in a vertical plane is fixed by the height h of the source and that of the exit slit which are made equal; ψ_0 is then given by $\psi_0=h/\pi a$. The entrance slit is thus formed partly by the midway diaphragm and partly by the exit slit and the total solid angle Ω is $2\varphi_0\psi_0$.

5. *Optimum Conditions of Operation*

The optimum conditions of operation of this recent type of spectrometer have not yet been published. An attempt to determine them in a manner identical to that used for the homogeneous field spectrometer[38] gives, to a first approximation, the following results:

$$Q=13.6a\varphi_0^4 \quad \text{and} \quad \psi_0=0.965\varphi_0^2$$

when $h=\pi a\psi_0$. Under these conditions the parameters determining both luminosity and base spread are fixed such as to produce maximum luminosity at any given base resolving power. However the value of the exit slit width F is not fixed and since the determination of its optimum choice is not easy, we fix it to be equal to Q. This choice is not completely arbitrary because in all optical spectrometers and many electron focusing devices optimum conditions of operation are reached when the exit slit is as large as the image of the source without aberrations. With this choice of the various parameters, the expressions for the base spread and for the luminosity become:

$$\eta_0=29.6\varphi_0^4$$

and

$$L=4.65\times10^{-8}\eta_0^{9/4}.$$

The relation between the base spread and the spread (at half-intensity), the form of line profile with these optimum conditions and the corresponding value of L^* as a function of L are not known theoretically. The experimental results given by Langer and Cook[40] together with their operating conditions enable us to calculate, in their case, the base width of the line profile and compare it to its half-intensity width, as taken from an experimental graph. The ratio of the spread (at half-intensity) to the base spread is then found to be $\frac{1}{6}$; this value is quite small when compared to the value 3/7 of the same ratio for the homogeneous field type. This low ratio was to be foreseen since, due to the high degree of focusing, most of the electrons are focused near the right edge of the image (Fig. 13).

If this ratio $\frac{1}{6}$, which should be approximately the same for the proposed optimum conditions, is used, the following important results are obtained:

$$\eta=4.94\varphi_0^4 \quad \text{and} \quad L=0.17\eta^{9/4}.$$

6. *The Magnet Size*

In this case also, the pole piece area can be used to characterize the magnet size; the formula established for the homogeneous field type to calculate this area may serve here since it depends also on the beam length, maximum width and height. The Langer and Cook magnet has a pole piece area which corresponds exactly with the one calculated with this formula under their operating conditions.

The value of this area $\sum$ is, for the third-order single-focusing spectrometer (under optimum conditions),

$$\sum=3\pi a^2\varphi_0.$$

The efficiency of the apparatus for a given spread is given for this type by:

$$\mu=L/\sum=2.68\times10^{-2}\eta^2.$$

Unfortunately we do not have enough information to express the ratio of the over-all luminosity to $\sum$, which is a better criterion of efficiency.

D. First-Order Double-Focusing Spectroscope

1. *Focusing Properties*

This type proposed by Svartholm and Siegbahn[9] has been also studied by Shull and Dennison[30] in a more general theory of which we shall give the most important features. In this theory, the vertical component of the field, H_z, as measured in the median plane, is taken to have the form

$$H_z(r,0)=H_0[1-\alpha(r-a)/a+\beta(r-a)^2/a^2-\cdots]$$

where H_0, a, r, and z have the same meanings as before

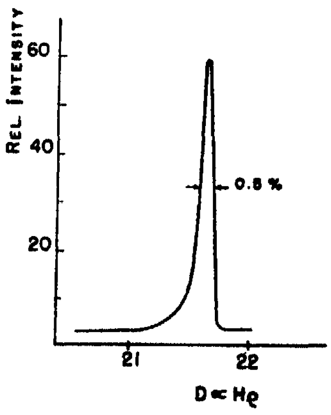

FIG. 13. Experimental line profile for the third-order single-focusing spectrometer as determined by Langer and Cook (see reference 40). The various parameters were then: $a=40$ cm, $h=2.5$ cm, $Q=F=0.4$ cm, and $\omega=0.1$ percent.

---

[40] L. M. Langer and C. S. Cook, Rev. Sci. Inst. 19, 257 (1948).

[41] J. A. Bruner and F. R. Scott, Rev. Sci. Inst. 21, 545 (1950).

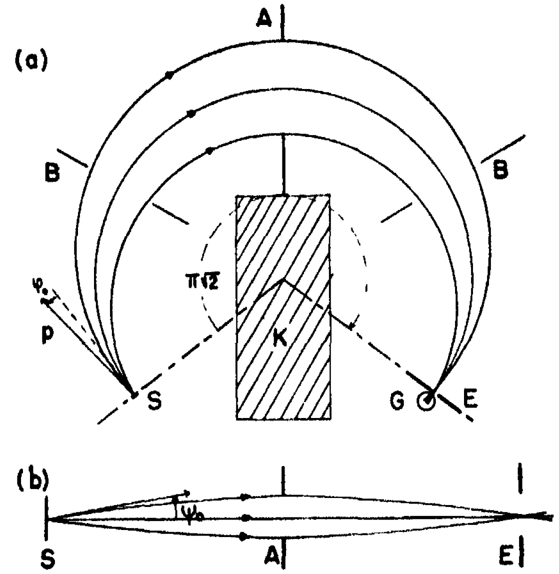

Fig. 14. Double-focusing spectrometer. (a) Projections on the $z=0$ plane of the central and marginal trajectories, showing the maximum divergence angle φ_0, the source S, the baffles B, the diaphragm A, the exit slit E, the counter G and the lead screen K. (b) Developments in the vertical direction of the central and outmost trajectories of electrons leaving a point of the source; the focusing action and the maximum divergence angle ψ_0 in the z direction are indicated.

and where α and β are arbitrary dimensionless constants. The magnetic field outside the median plane turns out to be

$$H_r(r, z)=zH_0[-\alpha/a+2\beta(r-a)/a^2]$$

and

$$H_z(r, z)=H_0[1-\alpha(r-a)/a \\ +\beta(r-a)^2/a^2-z^2(\beta-\alpha/2)/a^2]$$

where the value H_0 is such that an electron of momentum p will describe a circular path of radius a in that field. The study of electron orbits in such a field shows that there is simultaneous first-order focusing in both r and z directions for $\theta=\sqrt{2}\pi$ if the value of the parameter α is $\frac{1}{2}$. The corresponding values of the two other coordinates are

$$r^*=a-\delta r+\delta r^2(2-4\beta)/3a+\delta z^2(4\beta-3)/3a \\ +a\varphi^2(2-16\beta)/3+a\psi^2(16\beta-6)/3,$$
$$z^*=-\delta z+8\beta\delta r\delta z/3a+(32\beta-12)a\varphi\psi/3.$$

These equations, in which all terms have the same meanings as before, give the point of impact in the plane $\theta=\pi\sqrt{2}=254°33'$ of an electron which has left a point source determined by $r_0=a+\delta r$, $z_0=\delta z$ and $\theta_0=0$ with an initial velocity forming angles φ and ψ with the normal to the $\theta=0$ plane; they also indicate the double-focusing property.

2. *Image of a Finite Source*

The image of a source $(Q\times h)$ given by this type of field, if the angles are limited to φ_0 and ψ_0, has the following dimensions:[42]

width: $Q'=Q+|4\beta-3|h^2/12a$
$+|2-16\beta|a\varphi_0^2/3+|16\beta-6|a\psi_0^2/3,$
height: $h'=h+4\beta Qh/3a+4|16\beta-12|a\varphi_0\psi_0/3.$

3. *Dispersion and Resolving Power*

Svartholm and Siegbahn[9,10] have determined the dispersion of the double focusing spectrometer; they found it to be twice that of a semicircular one, i.e., $4/H_0$. The base spread formula gives in this case:

$$\eta_0=Q/4a+F/4a+|4\beta-3|h^2/48a^2 \\ +|2-16\beta|\varphi_0^2/12+|16\beta-6|\psi_0^2/12.$$

This relation indicates that η_0 will be a function of β and that for $\beta=\frac{1}{8}$ it will be independent (to the second order) of φ_0, and for $\beta=\frac{3}{8}$ of ψ_0. If one compares the base spread of this instrument with that of the homogeneous field spectrometer, it appears that the spread of the former is smaller by a factor of about two which is due to its double dispersion. On the other hand the double-focusing action increases the solid angle and consequently the luminosity by a factor of two $(L=Qh\varphi_0\psi_0/\pi)$; thus at the same resolving power this new type has a luminosity gain, over the homogeneous type, due to both its double focusing and double dispersing properties.

From experimental data of Shull,[43] the spread may be taken as half the base spread; unfortunately the ratio of L^* to the luminosity is not given.

4. *The Spectrometer*

Spectrometers of this type have been built by Svartholm and Siegbahn,[9] Shull,[43] and Kurie, Osoba, and Slack;[44] they differ by the use of different values of the field parameter β which is $\frac{3}{8}$ for Siegbahn and $\frac{1}{8}$ for Shull and Kurie. They have in common the general design (Fig. 14): the source and detector are located 254°33′ apart and the entrance slit is placed midway on the electron trajectories. The divergence angles are both determined by its dimensions; the width equals $2\sqrt{2}a\varphi_0$ and the height $2\sqrt{2}a\psi_0$.

5. *Optimum Conditions of Operation*

Shull[43] studied the line profile due to a point source when different forms of diaphragm are used and with values of β equal to $\frac{1}{4}$ and $\frac{1}{8}$. He has not however indicated any optimum relation between the different parameters. An attempt to determine such relations leads us to the following results (with the same methods as before):[38]

(1) For β equal or near $\frac{3}{8}$, the value of φ_0 is arbitrary, but for optimum conditions the following ratios must be

---

[42] It is to be noted that each term contained in the formula of the image dimensions must be positive. The absolute values of parenthesis should then be taken.

[43] F. B. Shull, Phys. Rev. 74, 917 (1948).

[44] Kurie, Osoba, and Slack, Rev. Sci. Inst. 19, 771 (1948).

realized:

$$\frac{Q}{4a}=\frac{5h^2}{48a^2}=\tfrac{2}{3}\psi_0{}^2=\tfrac{1}{3}\eta.$$

The luminosity is then

$$L=2.14a^2\varphi_0\eta^2.$$

(2) For β equal or near $\frac{3}{8}$, ψ_0 is arbitrary and the ratios are

$$\frac{Q}{4a}=\frac{1}{16}\frac{h^2}{a^2}=\tfrac{2}{3}\varphi_0{}^2=\tfrac{1}{3}\eta,$$

which gives for luminosity

$$L=2.83a^2\psi_0\eta^2.$$

(3) For β equal or near $\frac{3}{4}$, h is arbitrary and the ratios are

$$\frac{Q}{4a}=\frac{5}{3}\varphi_0{}^2=\psi_0{}^2=\tfrac{2}{3}\eta.$$

The luminosity then becomes

$$L=0.44ah\eta^2.$$

(4) For other values of β, the luminosity will be a maximum if the various parameters take the following values:

$$\psi_0=\left(\left|\frac{1-8\beta}{3-8\beta}\right|\right)^{\frac{1}{4}}\varphi_0,\quad h=\left[\left|\frac{8(1-8\beta)}{4\beta-3}\right|\right]^{\frac{1}{4}}\varphi_0,$$

$$Q=\frac{4a}{3}|1-8\beta|\varphi_0{}^2.$$

The value of the spread and of the luminosity are then

$$\eta=0.58|1-8\beta|\varphi_0{}^2$$

and

$$L=4.57a^2\eta^{5/2}[|(4\beta-3)(1-8\beta)(3-8\beta)|]^{-\frac{1}{4}}.$$

In all these four cases, the exit slit width F is chosen equal to Q, since the magnification is one, and the ratio η_0/η is taken equal to 2 as determined from Shull's[48] data on line profile (Fig. 15).

The optimum value of β is still to be determined; it is evident from the last formula (case 4) that L becomes infinite at β equal $\frac{1}{8}$, $\frac{3}{8}$, and $\frac{3}{4}$ for which the formula is not valid. It is also obvious that since the parameters h, φ_0 and ψ_0 are always finite and small, the mentioned values of β will never be optimum values. The choice of β must in this case be made with respect to some practical desiderata. For example, if one chooses a square diaphragm ($\varphi_0=\psi_0$) the optimum value of β is $\frac{1}{4}$; if he chooses the source, the diaphragm, and the exit slit to be all of the same height, then the optimum value of β is $\frac{1}{2}$. Other criteria may be used such as the ratio of L to the maximum beam cross section, which reaches its maximum value for $\beta=\frac{1}{2}$, or the ratio of L to the pole piece area (the efficiency defined for the other types) for which $\beta=\frac{3}{16}$ gives a very high value (but not a maximum). This last value, for which, furthermore, the necessary air gap is one of the smallest, is in our opinion to be chosen. The efficiency $\mu(=L/S)$ is then given by:

$$\mu=\frac{0.28\eta^2}{(|4\beta-3|)^{\frac{1}{4}}[(|8\beta-3|)^{\frac{1}{4}}+2(|1-8\beta|)^{\frac{1}{4}}]}.$$

(We have supposed that magnet pole pieces could be shaped to give any desired value of β; that may not be done so easily in practice.)

E. Comparisons between the Different Flat Types

A useful criterion for comparing the relative merits of the different flat spectroscopes is the efficiency μ as defined by the ratio of the luminosity to pole piece area for a given spread. This criterion may not be the best; the ratio (μ^*) of the over-all luminosity L^* to the same area is probably a better indication of the efficiency, but we were unfortunately unable to determine it due to the lack of theoretical data on the line profile. It is our opinion that comparisons between various μ^*'s should not differ very much from those between μ's as we define it and that this one gives to a first approximation a good idea of the usefulness of the apparatus.

In Table I are given the theoretical values of the luminosity, of the efficiency and of the gathering power as functions of the spread for the three classes of spectrometers studied. In the case of the double-focusing type, these values have been determined for β equal to $\frac{1}{2}$, $\frac{1}{4}$, and $\frac{3}{16}$ at total optimum conditions and for β equal to $\frac{1}{8}$ and $\frac{3}{8}$ with optimum conditions limited by the condition $\psi_0=\varphi_0$.

This table indicates clearly the relative merits of the various types and the advantage of the double focusing with $\beta=\frac{3}{16}$. The tabulated functions are also graphically represented in Fig. 31 together with the corresponding values for existing models.

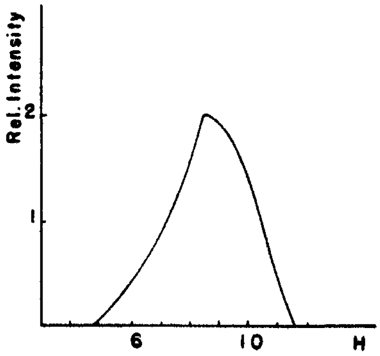

FIG. 15. Theoretical line profile for a double focusing spectrometer as determined by Shull (see reference 43). The various parameters where then: $a=170$ mm, $\beta=\frac{1}{2}$, $Q=0.3$ mm, $F=2$ mm, h (source) $=15$ mm, h' (exit slit) $=0.75$ inch, $\varphi_0=\psi_0\cong0.1$ rad. Experimental points are in close agreement with the theoretical line.

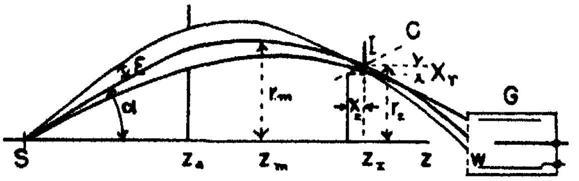

FIG. 16. *Notations employed in the theory of the helical spectrometers*: α = emission angle; ϵ = half-aperture; S = source, and origin of coordinates; z_a = abscissa of the admission slit; I = ring image; G = Geiger counter; w = front window of the counter.

F. Miscellaneous Types

The use of electrostatic fields has also been proposed for beta ray spectrometers: these apparatus, whose theory has been given by Rogers,[45] unfortunately require very high voltages, except for the low energy spectrum. For this reason they are not often used.[46]

A generalized theory of the focusing properties of magnetic spectrometers has recently been published by Judd[47] and by Rosenblum.[48] In their papers, they suggest the use of a spectrometer in which both the source and the detector are outside the field which is shaped and gives double focusing. They also study the optical properties of the system and show the possibility of increasing the resolving power without loss of intensity; it is our opinion that beta-ray spectrometers, as well as mass spectrometers, could be improved through the use of these authors results.

Other types for special use have been built such as a double spectrometer for the direct determination of the charge of the beta-particle[49] and a sextupole spectrometer for the study of the K^{40} spectrum.[50] Siegbahn and Slätis[51] have also recently built a "limegraph" for the study of the upper limit of β-spectra and of the γ-radiation.

Coincidence spectrometers which register simultaneously two monokinetic electron beams of different energy have been designed by Feather[52] and Fowler and Schreffler.[53] Their function is to determine whether or not two different radiations from a radioactive sample are in the same branch of a nuclear decay scheme.

III. THEORETICAL RESULTS ON HELICAL SPECTROMETERS

A. The Solenoid Spectrometer with Point Source

This is the spectrometer for which the theory is most advanced, because in it the "traces" of the electron paths are of a very simple shape (sinusoidal). Figure 16 shows three of them and explains the meaning of many of the symbols we shall employ in the following sections.

TABLE I.*

No.	Type of spectrometer	$L\times a^{-2}\eta^{-3/2}$	$\mu\times\eta^{-2}10^3$	$\omega\times\eta^{-1}$
1	1st-order, single-focusing, usual type	0.139	0.98	0.076
2	1st-order, single-focusing high source type	0.725	2.59	0.15
3	3rd-order, single-focusing	$0.17(\eta)^{-\frac{1}{2}}$	2.68	$0.51\eta^{-\frac{1}{2}}$
4	1st-order, double-focusing, $\beta=\frac{1}{2}$	2.67	6.29	0.31
5	1st-order, double-focusing, $\beta=\frac{1}{4}$	3.24	6.61	0.54
6	1st-order, double-focusing, $\beta=\frac{3}{16}$	3.60	7.10	0.63
7	1st-order, double-focusing, $\beta=\frac{1}{3}$ and $\psi_0=\varphi_0$	2.14	5.66	0.16
8	1st-order, double-focusing, $\beta=\frac{2}{3}$ and $\psi_0=\varphi_0$	2.78	6.70	0.16

* The figures recorded in the third and fifth columns are the values of Φ and Ψ defined in Section V.

It is convenient to consider only electrons of a given momentum $p=e_mp^*$, emitted isotropically by the point source S. If we call H the field intensity, the length

$$D=2p^*/H \tag{18}$$

(equal to the diameter of the circle that would be described by an electron emitted at right angles to the field) is the only dimensional parameter entering in the theory.[54] The trace starting at an "emission angle" α is a sinusoid of amplitude $r_m=D\sin\alpha$ and the abscissa of its (first) maximum is $z_m=(\pi/2)D\cos\alpha$.

To study a spectral line, the field H, and therefore D, must be varied in a small interval around a typical value H_0 (and D_0), which we define as that for which the central trace of the beam just grazes the outer edge of the exit slit. All the linear dimensions of the apparatus can be expressed solely in terms of D_0.

Consider now two infinitely near traces, started at "emission angles" α, $\alpha+d\alpha$: they cross each other at a point I, whose coordinates z_I, r_I are functions of α. This means that if the "aperture angle" 2ϵ were infinitely small, and a plane screen were placed at $z=z_I$, the electron beam would design on it a circle of radius r_I, which can be called a "*ring image*" of the source (some-

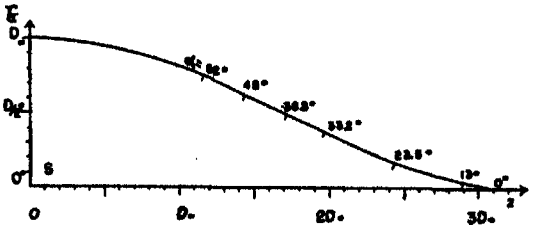

FIG. 17. The "caustic" of the uniform magnetic field.

---

[45] F. T. Rogers, Rev. Sci. Inst. 8, 22 (1937); 11, 19 (1940); 14, 217 (1943).

[46] J. Backus, Phys. Rev. 68, 59 (1945).

[47] D. L. Judd, Rev. Sci. Inst. 21, 213 (1950).

[48] E. S. Rosenblum, Rev. Sci. Inst. 21, 586 (1950).

[49] Y. Beers, Phys. Rev. 63, 77 (1943).

[50] Dzelepow, Kopjova and Vorobjov, Phys. Rev. 69, 538 (1946).

[51] K. Siegbahn and H. Slätis, Arkiv. f. Mat. Astron. Fys. B.36A, 22 (1949).

[52] N. Feather, Proc. Camb. Phil. Soc. 36, 224 (1940).

[53] C. M. Fowler and R. G. Shreffler, 21, 740 (1950).

[54] For this reason, all these problems may be studied equally well by assuming a monokinetic source and a variable field, or a source emitting a continuous uniform spectrum and a fixed field. We choose the first method.

times called a "*ring focus*"). Its position determines the location of the exit slit.

To calculate the position of the ring image, it is convenient to introduce the function $\beta(\alpha)$ defined by

$$\tan\beta = (\pi - \beta)\tan^2\alpha, \quad 0 \leq \beta \leq \pi/2. \tag{19}$$

The diagram of this function is given in Fig. 2, reference 55: it is also tabulated (with the notation $\pi - \beta = \psi_i$) in reference 56. Then one has

$$z_I = D(\pi - \beta)\cos\alpha, \quad r_I = D\sin\alpha\sin\beta. \tag{20}$$

The locus of the point I for a given D and for α varying between 0 and $\pi/2$ is analogous to the *caustic* of optical lenses: it is shown in Fig. 17.

Now suppose that H, and therefore D, is varied slightly, keeping unchanged the abscissa z_a and the radius r_a of the (infinitely narrow) entrance slit.[57] Then the point I is displaced along a (practically straight) line C. The conical surface of which C is the meridional section is the analog of the plane of the photographic plate in the flat spectrograph (in fact, on it the different lines of a heterokinetic source would be simultaneously focused). Clearly, the two edges of the exit slit must be located on this cone, and this defines the ratio X_r/X_z (*slope* of the exit slit). If the entrance slit is very near the source, where the traces are almost rectilinear, ($z_a \ll z_m$), a change in D_0 does not change the value of α: in this case, as was first pointed out by Frankel,[17] the line C is directed toward S and the edges of the slit must be placed on a cone with the vertex in the source. If the entrance slit is located farther from S (as it is usually), the slope of the exit slit may be different and even negative. In the rather frequent case that the entrance slit is placed at the point where r is maximum ($z_a = z_m$) the slope X_r/X_z is always negative and is given, as a function of α, by the lower curve of Fig. 18. By placing the entrance slit at a convenient abscissa z_a, the exit slit can be made exactly "horizontal" ($X_r = 0$), that is, the two edges of the slit can be of equal diameter, with the advantage that, by making the inner one longitudinally movable, the width of the slit can be altered without changing its slope. The necessary value of z_a/z_m is given as a function of α by the upper curve of Fig. 18.[58]

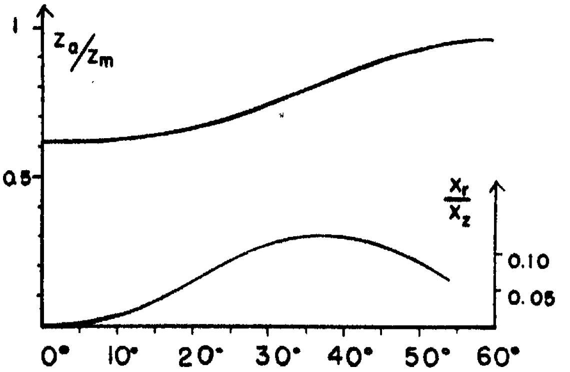

FIG. 18. *Upper curve:* abscissa z_a of the admission slit (as a fraction of the abscissa z_m of maximum r) for which the curve C of Fig. 16 is horizontal (exit slit parallel to the axis) (for a solenoid spectrometer). *Lower curve:* slope X_r/X_z of the exit slit when the admission slit is at the point of maximum r (for a solenoid spectrometer).

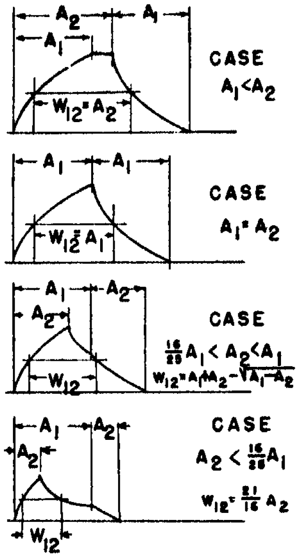

FIG. 19. Form of the line profile for a solenoid spectrometer with point source, for different widths of the exit slit A_1 = aberration width of the beam, A_2 = width of the exit slit, W_{12} = width of the line profile at half-maximum intensity. (DuMond, reference 56.)

If the aperture 2ϵ is not infinitely small, all of the traces of the beam will not pass through the same point I but will pass at a distance from I of the order of ϵ^2, (as is shown in Fig. 16): on a screen placed at z_I the beam would design a ring of a certain width, with a sharp exterior edge of radius r_I (where the electron density would be infinite). This broadening of the ring, due to the "spherical aberration," determines the width to be given to the exit slit. In fact[56] the most favorable line profile is obtained by making the exit slit as large as the aberration width, so that for $D = D_0$ the beam just grazes the two edges of the slit. In this case, the line profile has the shape shown in Fig. 19 (case $A_1 = A_2$). The same figure, taken from reference 56, shows the line profiles obtained with a larger or narrower exit slit.

The gathering power is easily calculated: it is

$$\omega = \sin\alpha\sin\epsilon \cong \epsilon\sin\alpha,$$

and the *over-all* gathering power is the same.

The half-maximum width of the line profile is proportional to ϵ^2 and is a rather complicated function of α[55]: therefore for a given α and variable ϵ the spread $\eta = \Delta p/p$ is proportional to the square of the gathering power ω:

$$\eta = \omega^2/f(\alpha),$$

---

[55] E. Persico, Rev. Sci. Inst. 20, 191 (1949).

[56] J. W. M. DuMond, Rev. Sci. Inst. 20, 160 (1949).

[57] Sometimes the two edges of the admittance slit are placed in different planes. This introduces some complications in the theory, and doubtful advantages in practice.

[58] E. Persico (to be published).

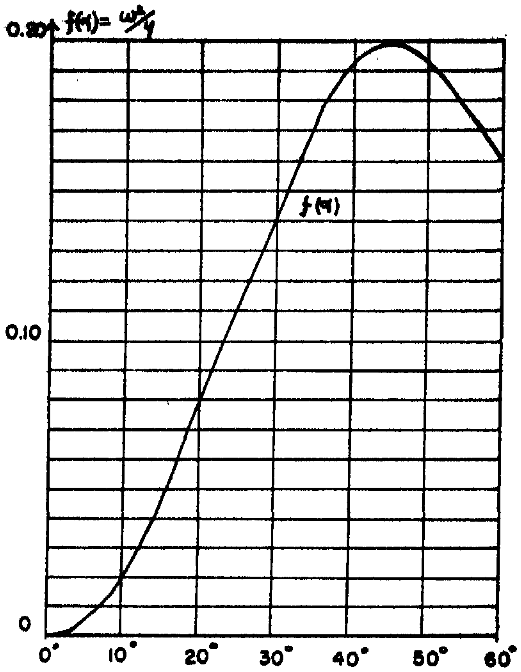

FIG. 20. The ratio $f(\alpha)=\omega^2/\eta$ as a function of the average emission angle α, for a point source solenoid spectrometer (ω = gathering power, η = spread). This ratio is the square of the figure of merit Ψ defined in Section V.

where

$$f(\alpha)=2(3+\cos^2\alpha\,\tan^2\beta)^{-1}\sin^2\alpha. \tag{21}$$

The function $f(\alpha)$ is plotted in Fig. 20. This curve has a maximum at $\alpha=45°37'$, where $f=0.197$. The existence of this maximum suggests, as was pointed out by one of us,[59] giving α a value much bigger than those usually adopted before (which were around 18°): however, as the maximum is rather flat, not much is lost if, for convenience of construction, α is kept a little below the optimum value. In the optimum conditions for a point source, η and ω are related by:[55]

$$\eta/\omega^2=5.07. \tag{22}$$

An interesting modification of the solenoid spectrometer has been recently proposed by P. Hubert.[60] In it the entrance and the exit slit are no longer completely distinct: the beam is limited internally by a unique baffle placed at the ring image, and externally by two or more other baffles. In this way, according to the author, the resolving power could be increased by a factor of about 4/3 with the same peak transmission.

B. The Solenoid Spectrometer with Disk Source

If the source cannot be made of negligible dimensions compared with X_r, then the beam falling on the exit slit is thickened not only by the spherical aberration but also by the width of the source, and the line profile is changed in shape.

Suppose the source is a disk of radius s and of uniform specific activity. In many practical cases it is the specific activity, and not the total activity, that is important; for instance, because of the necessity of reducing the broadening of the spectral line by the thickness of the radioactive layer; see Section IV. In these cases the performance of the spectrometer is measured not by the gathering power but by the *luminosity* $L=\pi s^2\omega$, and s, ω and α must be determined so as to get the maximum resolving power for a given luminosity. This problem has not yet been rigorously solved, but it seems probable that the following conditions, illustrated by Fig. 21, are not far from the optimum:[61]

$\alpha=40°25'$ $s=2.84D_0\epsilon^2$
Entrance slit: $z_a=1.02D_0$ $r_a=0.630D_0$ $h=0.881D_0\epsilon.$
Exit slit: $z_f=1.63D_0$ $r_f=0.544D_0$ $X_s=12.3D_0\epsilon^2.$

Minimum radius of the counter window: $w=1.74D_0\epsilon^2$.

The position of the entrance slit has been chosen so as to have an exit slit exactly "horizontal" (see preceeding section): therefore $X_r=0$.

The gathering power is $\omega=0.648\epsilon$, the luminosity $L=16.5D_0^2\epsilon^5$ and the spread $\eta=3.56\epsilon^2=8.46\omega^2$. The value of D_0 must be chosen according to the availability of electric power and the acceptable weight and bulk of the instrument. By choosing the aperture 2ϵ one can adjust the luminosity to the source specific activity. The spread and the luminosity are related by

$$\eta=1.16(L/D^2)^{2/5}=2.32(L/l^2)^{2/5}. \tag{23}$$

where $l=2z_m=2.39D_0$ is the distance between source and counter.

If we assume for the line profile the shape of Fig. 22 (calculated by DuMond for $\alpha=45°$ and a "vertical" exit slit) the *over-all luminosity* turns out to be $L^*=0.60L=9.83D_0^2\epsilon^5$, and is related to the spread by

$$\eta=1.43(L^*/D^2)^{2/5}=2.86(L^*/l^2)^{2/5};$$

the base spread is approximately $\eta_0=2.5\eta$.

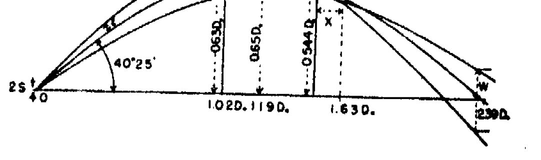

FIG. 21. Optimum conditions for a solenoid spectrometer with disk source. The admittance slit has been placed so as to have the exit slit parallel to the axis. The aperture 2ϵ has been arbitrarily chosen equal to 12°, corresponding to a spread $\eta=4$ percent and a luminosity $L=0.215\times10^{-5}D_0^2$.

---

[59] E. Persico, Phys. Rev. 73, 1475 (1948).

[60] P. Hubert, Comptes Rendus 230, 1464 (1950).

[61] They are calculated by taking for α the optimum value for a *disk* source as calculated by Persico (see reference 55), and for s the value which minimizes the *half-maximum* width of the line profile following DuMond (see reference 56). The position of the entrance slit has been so chosen as to have the exit slit parallel to the axis (that is $X_r=0$, $X_s=X$).

A precision solenoid spectrometer which will realize very nearly the optimum conditions is at present being built by DuMond (private communication).

C. The Short Lens Spectrometers

In these instruments the source and the counter are outside the region where the field is appreciable, so that the traces of the electrons are composed of two straight lines joined by a sharply bent curve (Fig. 23). These traces cannot, in general, be calculated analytically but must be determined by numerical computation.[62] For this reason, not very much has been published till now on the theory of these instruments. As we have noted in the introduction, the ring focus exit slit has been adopted in short lens spectrometers only very recently.

A simplified theory of the short lens spectrometer with circular exit window has been made by Deutsch, Elliott, and Evans:[19] we give here the essentials of this theory, using the notations explained in Fig. 23 (where the ring slit E must now be supposed absent).

Let us call u the distance of the source from the symmetry plane of the lens, and 1 the distance between the source and the exit window: then $M=(l-u)/u$ is the "magnification" of the lens. In addition, let s be the source radius, w the exit window radius, and r_1, r_2 the internal and external radii of the entrance slit. Neglecting spherical aberration, Deutsch, Elliott, and Evans have shown that the highest peak-intensity for a given resolving power is obtained when the window is large as the source image ($w=Ms$) and r_2/r_1 is equal to $\sqrt{2}$. Under these conditions, one finds that the "base spread" is given by

$$\eta_0=2.42\frac{M}{M+1}\frac{s}{r_2}$$

and the "luminosity" L (as defined by us) by

$$L=0.54(M+1)^2s^2r_2^2/l^2,$$

$$L=0.092\frac{(M+1)^4}{M^2}\frac{r_2^4}{l^2}\eta_0^2,$$

which can be written, if we introduce the average[63]

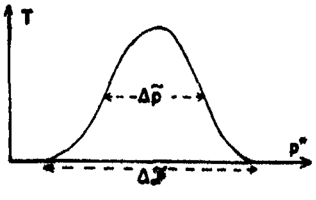

FIG. 22. Shape of the line profile with a disk source.

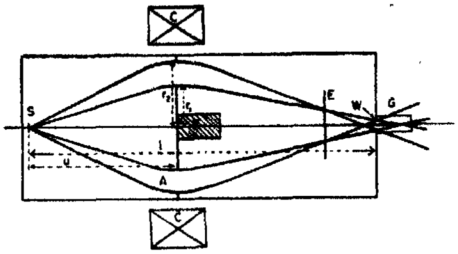

FIG. 23. Scheme of a short lens spectrometer (S=source; C=coil; G=Geiger counter; K=lead shield against direct radiation; A=admission slit; E=exit slit; W=counter window (acting as exit slit if E is absent).

emission angle $\alpha\cong r_2/u$ (supposed $\ll 1$), as:

$$\eta_0=3.3M\alpha^{-2}(L/l^2)^{\frac{1}{2}}.$$

This last formula shows that, given α, the magnification M must be made as small as conveniently possible. However, if the activity of the sources available is so great that a loss of luminosity is no objection, the authors advise making $M=1$, since this symmetrical arrangement minimizes some of the causes of spread, such as inaccuracy of alignment, aberrations, and stray magnetic fields.

The last formula also shows that α must be as large as possible, but if it is made larger than a few degrees the spherical aberration can no longer be neglected and the ratio L/η_0^2 becomes much smaller than indicated by the formula (in instruments of this type, α is usually not larger than 12°).

When an annular exit slit is used, it is possible to give α a larger value and to achieve a much greater luminosity for a given resolving power. A theory of the short lens with annular exit slit has been given very recently by Grivet.[64] He finds that for a given α and a disk source of the optimum radius, the luminosity is proportional to $\eta_0^{5/2}$, as in the solenoid type (see Section III B). A comparison with the latter type shows that the short lens can give the same resolving power and luminosity than the uniform field, with less expenditure of electric power. However, when the radioactive substance can be concentrated in a source of negligible dimensions, the solenoid spectrometer is the more advantageous.

In all the short lens spectrometers, to insure that the axes of the various baffles coincide *in direction* and *in position* with the symmetry axis of the field, one connects the source, the baffles and the counter rigidly to the walls of the vacuum chamber: this rigid unit can be slightly displaced with respect to the coils, by means of micrometer screws, to get the proper alignment. This adjustment is very critical and can be made by trial and error, or by a method described by Verster.[23] It may be noted that in the solenoid spectrometer the adjustment is much easier, because in it only the direction of the

---

[62] The technique of these calculations is described in various books on electron optics, for instance: Zworykin *et al.*, *Electron Optics and the Electron Microscope* (John Wiley and Sons, New York, 1945).

[63] The curvature of the traces in the vicinity of the lens compensates almost exactly for the difference between r_2 and $(r_1+r_2)/2$.

[64] P. Grivet, Comptes Rendus 230, 936 (1950). Also private communication.

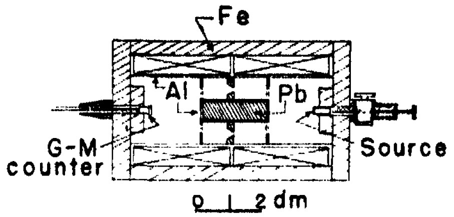

FIG. 24. A long lens spectrometer with "closed" magnet (Siegbahn, reference 27).

axis must be adjusted: parallel displacements are of no consequence.

D. The Long Lens Spectrometers

Attempts to reduce the spherical aberration of lens spectrometers by means of a suitable distribution of the field have lead to the consideration of other arrangements.

In the usual magnetic lenses the spherical aberration may be defined as follows. Call $z(\alpha)$ the distance, from the source, of the (first) intersection with the axis of the trace with emission angle α: if this function is developed in MacLaurin's series, it gives

$$z(\alpha)=z(0)+\alpha^2z''(0)/2+\cdots$$

because, by reason of symmetry, $z'(0)=0$. The "longitudinal aberration" is $z(\alpha)-z(0)=\alpha^2z''(0)/2$. The "tranversal aberration" (that is, the ordinate r of the intersection of the trace with the plane $z=z(0)$) is, in the same approximation, $r=\alpha^3z''(0)/2$. It is the latter that limits the resolution in a spectrometer if a *circular window* is used instead of a ring exit slit and if α is not very large. It has been proved[65] that an axially symmetric magnetic field for which the aberration coefficient $z''(0)$ is zero must have some singularities on the axis, so that it cannot be produced by coils placed at the exterior of the electron beam.[66] However, it is possible to approach this field by a regular one, obtainable by such coils, and so to reduce appreciably the spherical aberration. This approximate field varies, along the axis, in such a way that its diagram as a function of z is a curve *concave* upward.

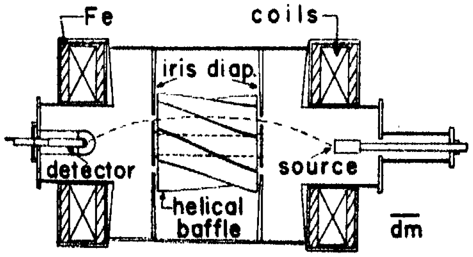

FIG. 25. The long lens spectrometer of Agnew and Anderson (reference 68).

One method of obtaining such a "concave" field of reduced aberration is the "closed" cylindrical magnet first devised by Siegbahn,[27] a section of which is shown in Fig. 24. It is a cylindrical iron tube, closed at the ends by iron disks bearing at the center two pole pieces directed inward: the coils are inside the tube.

Another method of obtaining a concave field is by means of two equal flat coils, placed on the same axis some distance apart. This method has been recently applied by Lauritsen and Christy,[67, 28] who, by varying the separation between the coils, have investigated the effects of various shapes of the concave field. On the same principle, Agnew and Anderson,[68] have constructed a long lens spectrometer in which the source and the counter are each at the center of the two equal coils, and the entrance and exit slit (both annular) are symmetrically located with respect to the median plane (Fig. 25). The traces shape is particularly favorable to the suppression of scattered radiation.

A new, and very promising, type of long lens spectrometer is that with "intermediate image" constructed by Slätis and K. Siegbahn[69] (Fig. 26). In it the magnet is of the "closed" type, and the field is such that the traces form a ring image midway between source and detector and then concentrate again on a point of the axis, where a small G-M counter is located. The entrance slit is rather near the source, and the exit slit is located at the median plane, where the intermediate ring image is formed. The performance of this instrument is very remarkable (see part V). Two interesting modifications of it have been proposed by Bothe[70] and by Grivet.[71] A theory of the two coils long lens spectrometers has been made by G. Paquien and P. Grivet[72] and a more general theory, with application to the Slätis and Siegbahn instrument, by P. Grivet.[72]

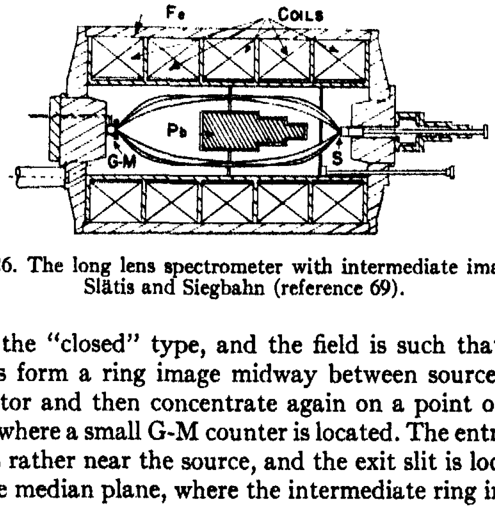

FIG. 26. The long lens spectrometer with intermediate image of Slätis and Siegbahn (reference 69).

We must finally mention a different principle that can be used to build a magnetic lens spectrometer: to utilize not the "chromatic aberration" of the lens, but the *rotation* of the image, which is a phenomenon typical of magnetic lenses. If the source (at $z=0$) is a line normal to the lens axis, its image (at $z=z'$) is a similar line but rotated of an angle Θ, given (for small α values) by

---

[65] G. Scherzer, Zeits. f. Physik **101**, 593 (1936).

[66] With an interior coil such a field can be obtained (E. Persico, Rend. Lincei **7**, 191 (1950)).

[67] T. Lauritsen and R. F. Christy, Phys. Rev. **73**, 536 (1948).

[68] H. M. Agnew and H. L. Anderson, Rev. Sci. Inst. **20**, 869 (1949).

[69] H. Slätis and K. Siegbahn, Phys. Rev. **75**, 1955 (1949).

[70] W. Bothe, Nature **37**, 41 (1950).

[71] Private communication.

[72] G. Paquien and P. Grivet, Comptes Rendus **230**, 64 and 196 (1950). P. Grivet, Comptes Rendus **230**, 1048 and 1652 (1950).

$$\Theta=\frac{1}{2p^*}\int_0^{z'} H(z)dz$$

where $H(z)$ is the value of the magnetic field on the axis. If a slit of the proper orientation is placed at the plane $z=z'$, it will select electrons of a given p^* (of course, the source must not extend in the vicinity of the axis). The principle of this spectrometer has been discussed by Butt[73] and by Georgesco[74] (who enumerates many of its advantages). Very recently it has been utilized for registering the pairs of positive and negative electrons produced by very hard gamma-rays: the two electrons of a pair are rotated by 90° in opposite directions and received on two G-M counters, whose coincidences are recorded.[75]

IV. ELECTRICAL AND MECHANICAL DEVICES

A. The Magnetic Field

The necessary field for beta spectrum analysis is achieved through the use of solenoidal coils, iron magnets or Helmholtz coils. The first ones are used in helical types; if a homogeneous field is needed, the homogeneity is insured over the whole electron path by designing the solenoid longer than the necessary length[16] or by correcting the end effects with auxiliary coils. For non-homogeneous fields in helical spectrometers, one or more flat coils or a closed magnet can be used (see Section III C, Fig. 24).

Most of the flat types utilize iron magnets; in spectrographs a permanent magnet is often used in which part of the yoke is of Alnico.[76] The exciting coils are used to establish a residual field of a desired value which may be changed at will; the great stability of the field and the simplification in auxiliary equipment compensate for any minor inconvenience in operation. In spectrometers, the variable magnetic field is obtained in the usual way; though circular pole pieces[37] are very common, recent spectrometer designs favor the annular form (Fig. 27) with the coils in the center (double mushroom magnet), as first used by Cockroft for an alpha-spectrometer. This form which allows a larger radius without increasing the magnet size, necessitates lower fields; it is also perfectly suitable for the shaped field models.[40, 41, 44] Here designers make use of the fringing field to obtain the desired field shape. The pole pieces may be machined in different manners, in a continuous or discontinuous surface (Figs. 27 and 28).

The iron used is not necessarily of high grade since with relatively large radii high fields are not required.

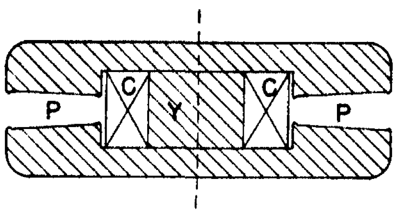

FIG. 27. Double-mushroom type magnet with bevelled pole pieces P. The coil C is wound around the central part of the yoke Y.

One must take care however that the first part of the yoke to saturate be that surrounded by the coils; the contrary may cause inhomogeneity or variations in the field shape. Another practical rule to insure constancy of the desired field shape is to have the pole piece width equal to the maximum beam width plus twice the air gap.[77] Variations from the ideal field of one part in a thousand may be tolerated, although for the spectrograph field, where various momentum electrons follow different trajectories, the homogeneity should be better.

The exciting coils are made either of a great number of small diameter wire turns or of a small number of large diameter wire turns; both methods require the same power and the first one, which requires less current, is more practical with an electronic power supply, while the second one is more suitably supplied from batteries since it requires less voltage.

A different method of obtaining the magnetic field is the use of Helmholtz coils.[31, 78] This method gives, however, only weak fields and is utilized in spectrometers designed for the study of low energy spectra.

B. The Spectroscope Chamber

The spectroscope chambers must be vacuum tight and are usually made of brass or even of aluminium; with an annular magnet, the pole pieces are often used as the upper and lower sides while the vertical sides are made of brass with special joints for vacuum sealing.[9, 44]

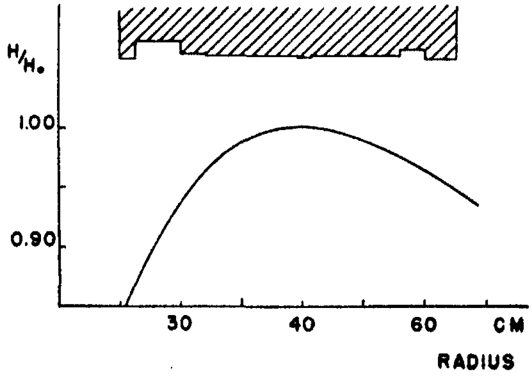

FIG. 28. Shaped pole pieces of Langer's and Cook's magnet (see reference 40).

---

[73] D. K. Butt, Proc. Phys. Soc. London B62, 551 (1949).

[74] M. Georgesco, Comptes Rendus 229, 297 (1949).

[75] K. Siegbahn and S. Johansson, Rev. Sci. Inst. 21, 442 (1950).

[76] Plesset, Harnwell, and Siedl, Rev. Sci. Inst. 13, 351 (1942).

[77] N. D. Coggeshall, J. App. Phys. 18, 855 (1947).

[78] Langer, Motz, and Price, Jr., Phys. Rev. 77, 798 (1950).

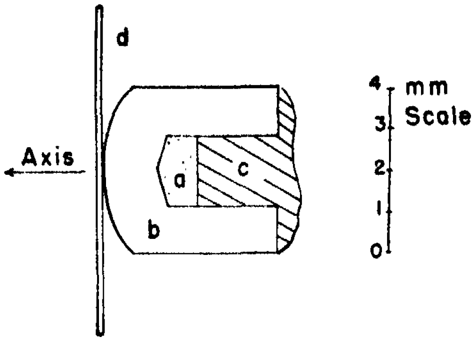

FIG. 29. Deutsch's design of a secondary β source (see reference 19): a, gamma-source; b, brass or copper capsule; c, wax; d, radiator.

The baffles contained in the chamber are generally made of Lucite or aluminium, or of lead coated with these materials, so as to diminish wall scattering, which causes distortion in beta-ray spectra,[79] and to absorb the most energetic electrons. The slit apertures are adjusted through vacuum-tight doors and in many cases a Wilson seal or other special device[80] allows the source to be changed without affecting the chamber vacuum.

Spectroscopists generally employ a diffusion pump backed by a mechanical pump to maintain the vacuum in the chamber;[81] various types of flanges with grease, or rubber *O*-rings insure vacuum-tight doors and tube joints.[82] Vacuum measurements are made with thermocouple and ionization gauges together with adequate circuits;[83] a vacuum of at least 10^{-4} mm Hg is required so that the electron mean free path, a few meters, be much longer than the electron trajectory. In this way, scattering from the residual gas will be minimized.

C. The Source

One of the most important causes of error in beta-spectrum analysis may be the source; its thickness, unevenness, and support modify the electron energies disproportionately and so influence the spectrum shape particularly at low energies.[84] The influence of the source thickness has been studied recently by Langer, Motz, and Price;[78] they found that for a source of less than 11 micrograms/cm^2, the deviation of the shape occurs at 8 kev and that it rises as the source thickness increases.[85]

Homogeneity of the source is also desirable since local concentrations of radioactive material produce electrostatic effects due to local charges; however this homogeneity is difficult to realize as pointed out by the same authors. They found in fact that sources chemically prepared and apparently uniform showed variations of intensity of as much as one hundredfold; they described a technique by which they were able to reduce these variations 25 times.[78]

To diminish the total charging effects, thin foils of nickel or aluminium have been used as source supports; however their thickness is always too great and produces backscattering.[84] Thin films of zapon, Nylon, Formvar, or collodion are now prefered as source backing since their backscattering is practically negligible, if thicknesses of a few micrograms/cm^2 [78, 86] are employed. The electrostatic effects are then reduced by framing the source with aluminum strips.

Special sources have also been designed[19] for the energy measurement of gamma-rays by their photo-ejected electrons (Fig. 29). The gamma-source is placed in a dense metal cup such as copper which absorbs all the primary betas; the filtered gamma-beam then radiates a thin foil of a heavy element such as Au, and the energy of the emitted secondary electrons is measured. To obtain the correct gamma-energy, one must correct the measured electron energy for its atomic binding energy, which varies with the radiated substance, and for the loss of energy due to the electron source thickness, which in this case is greater than for the beta source in order to secure sufficient efficiency of secondary electron production; the latter correction, however, is a minor one.

For analyzing very hard gamma-rays it is more convenient to utilize the materialization pairs, instead of the photoelectrons, registering them by means of a coincidence spectrometer (see, e.g., the end of Section III D).

D. The Detector

In a spectrograph the spectrum is registered on a photographic plate and the relative blackening of the plate, as measured by a microphotometer, is translated into an electron intensity distribution.[87] The photographic action of beta-rays on different types of plates has been studied particularly by Plesset, Harnwell, and Seidl[76] who concluded that a linear relationship exists between electron intensities and the relative blackening they produce, for all practical purposes. Cranberg and Halpern[88] have also made calibration of photographic emulsions for low energy electrons. With the uses of special plates recently developed in America and in England this method is thus perfectly suitable for beta-ray analysis.

---

[79] G. E. Owen and C. S. Cook, Rev. Sci. Inst. **20**, 768 (1949).

[80] R. R. Wilson, Rev. Sci. Inst. **12**, 91 (1941); A. E. Shaw and W. Hall, Rev. Sci. Inst. **18**, 278 (1947).

[81] H. M. Sullivan, Rev. Sci. Inst. **19**, 1 (1948); J. Strong, *Procedures in Experimental Physics* (Prentice-Hall, New York), 1947, pp. 93–150.

[82] F. N. D. Kurie, Rev. Sci. Inst. **19**, 485 (1948). R. W. Cloud and S. F. Philp, Rev. Sci. Inst. **21**, 731 (1950).

[83] J. Rainwater, Rev. Sci. Inst. **13**, 118 (1942).

[84] R. D. Albert and C. S. Wu, Phys. Rev. **74**, 847 (1948); Curran, Angus, and Cockroft, Phil. Mag. **40**, 53 (1949); Langer, Moffat, and Price, Phys. Rev. **76**, 1725 (1949); G. E. Owen and C. S. Cook, Phys. Rev. **76**, 1726 (1949).

[85] For methods of correcting source distortion effects, see: G. E. Owen and H. Primakoff, Phys. Rev. **74**, 1406 (1948); Rev. Sci. Inst. **21**, 447 (1950).

[86] B. P. Burtt, Nucleonics, August, 29 (1949); J. Backus, Phys. Rev. **68**, 59 (1945); R. D. Albert and C. S. Wu (reference 71).

[87] W. Langendijk and Ornstein, Physica **7**, 475 (1940).

[88] L. Cranberg and J. Halpern, Rev. Sci. Inst. **20**, 641 (1949).

In spectrometers, the detector most commonly used is the Geiger-Müller counter; the use of scintillation counters and of electron multipliers is just at its start, owing to the difficulty of operating them in a magnetic field. Usually the counters require no special features[89] except for the thin window wall. This can be a side window or, especially in helical spectrometers, a front window; in this case, the anode is a rigid wire held at one end only. The window wall must be as thin as possible to avoid absorption at low energies, uniform enough to avoid gas diffusion through it and also strong enough to support the counter gas pressure. All of these requirements are met in windows of thin mica foil[90] or of several layers of very thin films of Nylon, zapon, or collodion.[78, 86] Thicknesses as small as a few micrograms/cm^2 are realized for window walls; for large window apertures fine copper grids (such as Lektromesh[78]) are often used to reinforce the film. A few authors have employed a gas ballast tank to compensate for gas loss by diffusion.

Windowless counters have been used[78] with success; the counter pressure was dynamically maintained and the equivalent window thickness of the diffused gas was of the order of one microgram/cm^2. In order to register low energy electrons, which are absorbed by the counter window, accelerators have been designed[40] in which electrons coming through the exit slit are accelerated to 20 kev before reaching the counter and being registered.

Besides the beta-ray counter, one or many gamma-ray counters may be used either near the source for coincidence measurement[91] or close to the beta-counter in order to diminish the background effect by anti-coincidence methods.[92]

E. Magnetic Field Measurements

Absolute magnetic field measurements are always delicate and in most cases not necessary, as pointed out in Section I A3; this is fortunate since differential measurements always afford higher accuracy than absolute ones.

Measurement of the magnetic field with a search coil is frequently employed by spectroscopists. The electrical pulse from a flip coil may be measured directly with a fluxmeter or a ballistic galvanometer,[44] or compared to the pulse coming from a standard mutual inductance whose secondary is rotated simultaneously with the search coil; the necessary primary current together with instrument characteristics permits calculation of the field strength. The second method is more accurate than the first and allows field measurements of one part in a thousand.[31]

Other methods have been recently perfected: continuously rotating coils with which changes of 0.01 gauss can be observed,[93] vibrating wires driven by a quartz crystal,[94] a fluxball allowing point measurement,[95] a search coil with electronic fluxmeter,[96] a null reading fluxmeter,[97] an alternating probe current utilizing the permalloy incremental permeability,[98] and a magnetic field strength meter employing the Hall effect in germanium.[99]

The bismuth spiral does not seem to be popular, probably due to its temperature sensitivity and to the relatively small values of the magnetic field to be measured: for the same last reason the very accurate nuclear resonance method, so adequate for high field measurements, does not seem to have yet been applied in beta-ray spectroscopy.

V. SOME BETA-RAY SPECTROSCOPES AND THEIR PERFORMANCE

In this section, we have collected the more relevant data on some of the beta-ray spectroscopes of which a description has been available. This collection does not claim to be complete nor to include all of the most important instruments. Some of the recorded values have been calculated by us on the basis of other data contained in the original paper or have been deduced from drawings. Since any spectrometer can usually work under different conditions (as to aperture, source dimensions, etc.) only one or a few of the possible sets of data have been recorded.

The meaning of the symbols in Tables II and III is the following:

Type: Sh.l. = short lens; L.l. = long lens; Sol. = solenoid; Spg. = 1st-order focusing spectrograph; Spm. = 1st-order single-focusing spectrometer; 3 s.f. = 3rd-order single-focusing spectrometer; D.f. = double-focusing spectrometer. The letter *r* indicates a ring exit slit.

Iron: y = yes; n = no;

$E_{\max}$ = maximum energy of electrons that can be focused (in Mev);

l = distance, along the axis of a helical type, between source and counter (in cm);

a = radius of curvature of the median trajectory, for flat types (in cm);

α = average emission angle;

ϵ = half-range of emission angles (half-aperture);

$\eta = \Delta p/p$ = spread in the momentum scale (at half-maximum of the line profile);

$\omega = \Omega/4\pi$ = gathering power;

$L = \sigma\omega$ = source area × gathering power = luminosity;

$T_{\max}$ = peak transmission (or over-all gathering power);

$L^* = \sigma T_{\max}$ = over-all luminosity.

---

[89] D. R. Corson and R. R. Wilson, Rev. Sci. Inst. 19, 207 (1948).

[90] Wu, Meaker, and Glassford, Rev. Sci. Inst. 18, 693 (1947).

[91] N. Feather, Proc. Camb. Phil. Soc. 36, 224 (1940).

[92] L. Feldman and C. S. Wu, Phys. Rev. 76, 180 (1949) and private communication (1950).

[93] Cork, Shreffler, and Shull, Rev. Sci. Inst. 18, 315 (1947). L. M. Langer and F. R. Scott, Rev. Sci. Inst. 21, 522 (1950).

[94] D. M. Chapin, Rev. Sci. Inst. 20, 945 (1949).

[95] W. F. Brown, Jr. and J. H. Sweer, Rev. Sci. Inst. 16, 276 (1945).

[96] R. H. Dicke, Rev. Sci. Inst. 19, 533 (1948).

[97] C. C. Lauritsen and T. Lauritsen, Rev. Sci. Inst. 19, 916 (1948).

[98] E. C. Gregg, Jr., Rev. Sci. Inst. 18, 77 (1947).

[99] G. L. Pearson, Rev. Sci. Inst. 19, 264 (1948).

TABLE II. Data on some flat spectroscopes.

No.	Authors	Year	Reference	Type	Iron	$E_{\max}$ Mev	a cm	η %	ω %	$L\times10^3$ cm²	$\Phi\times10^3$	$\Psi\times10^3$
1	Li	1937	a	Spg	y	—	6	0.63	0.0067	0.020	18	1.1
2	Arnoult	1939	b	Spg	n	0.26	13.5	0.2	0.011	0.00022	0.74	5.5
3	Lawson and Tyler	1939	c	Spm	y	3.1	12	1.6	0.10	0.50	11	6.3
4	Neary	1940	d	Spm	y	—	(a)7	1.0	0.041	0.052	11	4.1
							(b)10	1.26	0.041	0.052	2.8	3.3
5	Towsend	1941	e	Spm	y	—	8	1.6	0.10	0.38	19	6.3
6	Plesset, Harnwell, and Seidl	1942	f	Spg	y	10	11.4	0.2	—	—	—	—
7	Siegbahn	1944	g	Spm	y	—	12	0.17	0.029	0.00073	4.2	17
8	Svartholm and Siegbahn	1946	h	D.f.	y	5.6	12.5	0.27	0.134	0.022	38	50
9	Langer and Cook	1948	i	3 s.f.	y	8.7	40	0.5	0.089	0.89	8.2	4.7
10	Shull	1948	j	D.f.	y	6.0	17	0.35	0.32	0.14	69	92
11	Kurie, Osoba and Slack	1948	k	D.f.	y	5.0	24.3	0.66	0.115	0.29	15	17
12	Langer, Motz, and Price	1950	l	Spm	n	0.23	5	2.6	0.10	0.20	7.3	3.9
12′	Bruner and Scott	1950	m	3 s.f.	y	4.0	20	0.7	0.127	0.76	13	5.3
12″	Hedgram, Siegbahn, and Svartholm	1950	n	D.f.	y	—	50	—	—	—	—	—

The values of Φ and Ψ for the third order single focusing spectrometers should be compared only between themselves, but not with corresponding values of other types.

[a] See reference 34.
[b] See reference 31.
[c] See reference 37.
[d] G. J. Neary, Proc. Roy. Soc. (London) **175**, 71 (1940).
[e] A. A. Townsend, Proc. Roy. Soc. (London) **177**, 358 (1941).
[f] See reference 76.
[g] See reference 25.
[h] See reference 9.
[i] See reference 40.
[j] See reference 43.
[k] See reference 44.
[l] See reference 78.
[m] See reference 41.
[n] Hedgram, Siegbahn, and Svartholm, Proc. Phys. Soc. (London) **63** (1950).

In Tables II and III we have entered two dimensionless quantities Φ and Ψ, that can be considered as *figures* of *merit* of a spectrometer and are defined as follows:

$\Phi=\eta^{-5/2}L/a^2$, $\Psi=\eta^{-1}\omega$, for all flat types except third-order focusing types;

$\Phi=\eta^{-9/4}L/a^2$, $\Psi=\eta^{-3/4}\omega$, for third-order focusing types (Section II C);

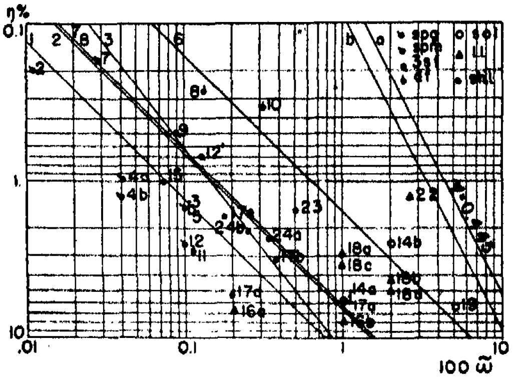

FIG. 30. Spread (η) *versus* gathering power (ω). Straight lines represent the behavior of the various types under optimum conditions: curve numbers refer to flat types of corresponding numbers of Table I; curve letters refer to (a) the solenoid helical type with point source and to (b) the solenoid helical type with a disk source. Point numbers refer to the existing models tabulated in Tables II and III. Note that the positive direction of the η-axis is downward. See the text for more details.

$\Phi=\eta^{-5/2}L/l^2$, $\Psi=\eta^{-1/2}\omega$, for all helical types with ring exit slit.

In a few cases in which the over-all luminosity L^* and the over-all gathering power $T_{\max}$ were known, instead of L and ω, we have replaced Φ and Ψ by Φ^* and Ψ^* defined in the same way except for the substitution of L^* and $T_{\max}$ in the place of L and ω.

The choice of these definitions has been suggested by the following considerations. If the specific activity of the source is the limiting factor, and if the source and exit slit dimensions are chosen according to the optimum conditions, it has been proved in Section II B 6, II C 5, II D 5, III B that the quantities Φ and Φ^* are independent of the aperture. If, instead, the total activity is the limiting factor and the source can be made of negligible dimensions, the quantities Ψ and Ψ^* are independent of the aperture. In addition, all four of these quantities are independent of the geometric scale of the instrument.

The maximum theoretical values for Φ and Ψ for flat types have been given in Table I (Section II E); those for an ideal solenoid spectrometer of optimum emission angle are given by formulas (23) and (22): $\Phi=2.32^{-5/2}=0.12$, $\Phi^*=2.86^{-5/2}=0.072$; $\Psi=5.07^{-1/2}=0.445$ (point source). For a point source solenoid spectrometer with arbitrary α the value of Ψ is given by formula (21) or Fig. 20, where $f(\alpha)=\Psi^2$.

In the case of helical spectrometers with non-uniform fields we have adopted the same form of Φ and Ψ as for

TABLE III. Data on some helical spectrometers.

No.	Authors	Year	Reference	Type	Iron	E_{max} Mev	l cm	α deg.	ϵ deg.	η %	ω %	$L\times10^3$ cm^2	$\Phi\times10^4$	$\Psi\times10^2$
13	Cosslett	1940	a	Sh.l.	*y*	15	130			40	0.032			0.05
14a	Witcher	1941	b	Sol.r.	*n*	4.44	90	18	5.5	6.0	1.0	31	42	4.2
14b	Haggstrom	1942	c	Sol.r.	*n*	4.44	90	13.8	4.9	2.5	2.0	4.0	50	12.5
15	Siegbahn	1942	d	Sh.l.			58	7	0.35	1.0	0.075	0.12	2.7	0.75
16a	Siegbahn	1944	e	L.l.	*y*	7	60			6.7	0.2			0.77
16b	Siegbahn	1944	e	L.l.	*y*	7	60			7.7	1.0			3.6
17a	Deutsch, Elliott, and Evans	1944	f	Sh.l.	*n*	3.5	100	11.5	2.9	6.0	1.0	2.0	2.2	4.0
17b	Deutsch, Elliott, and Evans	1944	f	Sh.l.	*n*	3.5	100	8.1	1.6	3.2	0.39	0.5	2.7	2.2
17d	Deutsch, Elliott, and Evans	1944	f	Sh.l.	*n*	3.5	100	6.3	1.0	5.4	0.19	3.9	5.8	0.85
17e	Deutsch, Elliott, and Evans	1944	f	Sh.l.	*n*	3.5	100	9.0	0.6	1.7	0.18	0.22	5.8	1.4
18a	Siegbahn	1946	g	L.l.	*y*	4	50	22.2	1.5	2.9	1.0	1.25	35	5.9
18b	Siegbahn	1946	g	L.l.	*y*	4	50	20.5	3.15	4.3	2.0	2.5	26	9.7
18c	Siegbahn	1946	g	L.l.	*y*	4	50	22.2	1.5	3.5	1.0	5.0	87	5.3
18d	Siegbahn	1946	g	L.l.	*y*	4	50	20.5	3.15	5.0	2.0	10	72	9.0
19	S. Jnanananda	1946	h	Sol.r.	*n*	0.25	28			6.5	5.0	3.5	4.2	19.5
20	Miller and Curtiss	1947	i	Sh.l.	*n*	2.5	100			2.0				
21	Rall and Wilkinson	1947	j	Sh.l.	*n*	3				2.0				
22	Zünti	1948	k	L.l.r.	*y*					1.3	2.7	0.15		24
23	Hornyak, Lauritsen, and Rasmussen	1949	l	Sh.l.r.	*n*	3	114	13		1.5	0.5	3.55	100	4.1
24a	Jensen, Laslett, and Pratt	1949	m	Sh.l.	*n*	3.4	102	8	1.4	2.3	0.34	1.22	14.6	2.2
24b	Jensen, Laslett, and Pratt	1949	m	Sh.l.	*n*	3.4	102	8.5	1.0	2.1	0.24	0.95	14.5	1.7
											T_{max} %	$L^*\times10^3$ cm^2	$\Phi^*\times10^4$	
25a	Agnew and Anderson	1949	n	L.l.r.	*n*	2.8	96			1	1.4	1.75	150	
25b	Agnew and Anderson	1949	n	L.l.r.	*n*	2.8	96			9	11.0	585	260	
26	Slätis and Siegbahn	1949	o	L.l.r.	*y*					4	8.0	16	160	
27	Feldman and Wu	1950	p	Sol.r.	*n*		34	38		9	0.31	10	35	

[a] V. E. Cosslett, J. Sci. Inst. **17**, 259 (1940).
[b] See reference 16.
[c] E. Haggstrom, Phys. Rev. **62**, 144 (1942).
[d] K. Siegbahn, Arkiv. Mat. Astron. Fys. **28A**, 4, No. 17, 27 (1942).
[e] K. Siegbahn and A. Johansson, Arkiv. Mat. Astron. Fys. **34A**, No. 10, 19 (1940).
[f] See reference 19.
[g] See reference 27.
[h] Swami Jnanananda, Phys. Rev. **71**, 321 (1947).
[i] L. C. Miller and L. F. Curtiss, J. Research Nat. Bur. Stand. **38**, 359 (1947).
[j] W. Rall and R. G. Williamson, Phys. Rev. **71**, 321 (1947).
[k] See reference 21.
[l] See reference 23.
[m] Jensen, Laslett, and Pratt, Phys. Rev. **75**, 458 (1949).
[n] See reference 68.
[o] See reference 69.
[p] See reference 92.

the solenoid type, although their independence of aperture has not been proved in this case. When a circular exit window is used instead of a ring slit, this independence is certainly not true: we have nevertheless also calculated Φ and Ψ for such instruments.

Some of the data of Tables II and III are graphically represented, in doubly logarithmic diagrams, in Figs. 30–32: in all of these we have plotted as ordinates the quantity $-\log\eta$ (that is the logarithm of the resolving power). In Fig. 30, we have taken as abscissas $\log\omega$: so, this diagram may serve to compare the performance of various instruments (or various modifications of the same) as far as the attainable intensity is limited by the total activity of the source. In Fig. 31 which refers to flat spectrometers, the abscissae are $\log L/a^2$, and in Fig. 32, which refers to helical types, $\log L/l^2$: both these diagrams serve for comparisons in which the specific activity of the source is the limiting factor. When the value of L^* replaces that of L, we have enclosed the number of the apparatus in brackets.

As it is seen from the definitions of Φ and Ψ, the lines $\Psi=$const. in the first diagram, and $\Phi=$const. in the other two, are straight lines of different slope, depending on the type: we have traced a few of them, corresponding to optimum conditions. By changing the aperture of an instrument (with the corresponding alterations in the source and exit slit dimensions) its representative point could be displaced (within certain limits) along a straight line having the slope that corresponds to its type.

ACKNOWLEDGMENTS

The authors wish to express their sincere appreciation to Drs. L. Feldman and C. S. Wu, Dr. S. Frankel, Dr. F. H. Schmidt, Dr. L. Slack, and Dr. P. Grivet, who

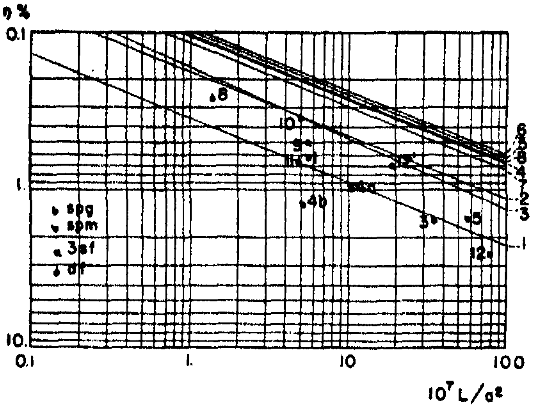

FIG. 31. Spread (η) *versus* luminosity L over the square of the curvature radius (a) in flat types. Straight lines represent the behavior of the various flat types under optimum conditions; curve number refer to types of corresponding number of Table I. Point numbers refer to flat types whose data are included in Table II. Note that the positive direction of the η-axis is downward. See the text for more details.

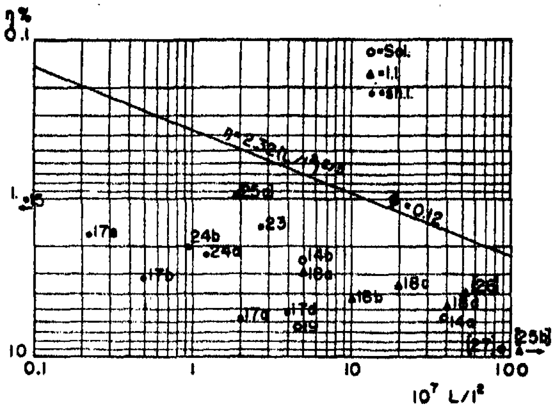

FIG. 32. Spread (η) *versus* luminosity L over the square of the distance (l) between the source and the detector in helical types. The straight line represents the behavior of the solenoidal type under optimum conditions (with a disk source). Point numbers refer to existing models whose data are given in Table III. Note that the positive direction of the η-axis is downward. See the text for more details.

have kindly made available unpublished results. They are indebted to Drs. M. Deutsch, L. G. Elliott and R. D. Evans, J. W. DuMond, K. Siegbahn, H. Slätis, H. M. Agnew and H. L. Anderson, L. M. Langer and C. S. Cook, and F. B. Shull for permission of reproducing some illustrations. They have also appreciated the assistance of Professor G. Hall in compiling the bibliography and of Dr. L. Kerwin for linguistic advice.

An Orbit-Bender to Assist Injection into Betatrons

LEVERETT DAVIS, JR.
California Institute of Technology, Pasadena, California

(Received July 18, 1950)

It is suggested that the fraction of the beam in a betatron or synchrotron that is lost by striking the injector might be decreased by a suitable transient bending of the steady-state orbit during injection.

THE motion of an electron in a betatron or synchrotron is usually described as being a harmonic oscillation about a circular (or race-track shaped) orbit called the instantaneous circle.[1] A more accurate description, that allows for deviations from the ideal magnetic field, replaces the instantaneous circle by the steady-state orbit, that closed orbit for which the path taken on the second revolution is identical with that taken on the first. No static bending of the steady-state orbit will assist injection, since the electrons oscillate about it with an amplitude at least as great as the distance of the injector from the steady-state orbit. Thus the amplitude is always great enough so that after a few revolutions the electrons strike the injector and are removed from the beam unless the oscillations are rapidly damped or unless the steady-state orbit is shifted away from the injector. Hence it is necessary to make some significant change in the situation during injection. Among the changes that have been used or considered are an increase of the main field[1] (which both shifts the steady-state orbit and damps oscillations), the use of an orbit contractor,[2] the exploitation of mutual interactions as electrons are added to or removed from the beam[2,3] (which has the same effect as an orbit contractor), and the use of transient inhomogeneities in the magnetic field[4,5] (thus damping oscillations having a favorable phase without shifting the phase so far that oscillations are amplified). The purpose of this note is to suggest that a transient bending during injection of the steady-state orbit in the neighborhood of the injector by magnetic or electric fields might be an efficient and convenient means whereby one could increase the fraction of the electrons that do not strike the injector of a betatron or synchrotron.

Two ways in which this could be done are suggested by Fig. 1, which is drawn for an injector placed in the straight section of a race-track machine, although the procedure could be adapted to any machine. S represents the normal position of the steady-state orbit and I the position of the injector when the orbit-bender is not used. S' represents the position of the steady-state orbit when it is given the maximum bending by means of the magnetic fields caused by currents in the coils M M M or by means of electric fields caused by the condensers E E E. During the injection process the excitation of the orbit-bender is varied from its maximum value to zero so that for the first electrons injected the steady-state orbit is at S', while for the last it is at S. Thus the steady-state orbit is continuously receding from the injector, which could perhaps be placed at I'. The amplitude of the oscillations about the steady-state orbit is not appreciably increased by its motion; hence the recession will make it less likely that an electron will strike the injector. The shifting shown could be either radial or axial, or both.

The production of a maximum deflection Δ in an orbit-bender whose total length is L requires the use of subsidiary fields at least strong enough to produce, acting alone, the radius of curvature

$$R=(L^2/16\Delta)[1+(2\Delta/L)^2] \tag{1}$$

in the beam at injection. It is easy to estimate the fields required. If one uses magnetic fields produced by the current loops M M M (or by a more complicated system that confines the lines of force and produces better focusing properties), the average field must be

$$B=B_I R_S/R, \tag{2}$$

where B_I is the magnetic field needed at injection to produce the radius of curvature R_S in the steady-state orbit. On the other hand, electrostatic fields caused by condensers E E E placed inside the doughnut could be used to bend the steady-state orbit. The potentials required would be of the order of

$$V_E=\frac{V_I t}{R}\frac{(V_I+2V_R)}{(V_I+V_R)}, \tag{3}$$

where V_I is the injection voltage, t is the distance

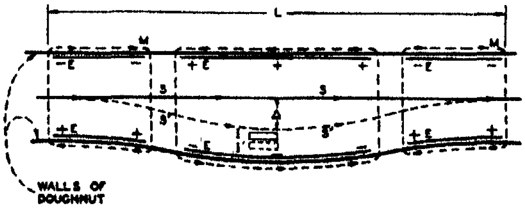

FIG. 1. Schematic representation of an orbit-bender.

---

[1] D. W. Kerst, Phys. Rev. 60, 47 (1941).

[2] D. W. Kerst, Phys. Rev. 74, 503 (1948).

[3] D. L. Judd, Thesis (California Institute of Technology, Pasadena, California).

[4] Jones, Krats, Lawson, Regan, and Voorhies, Phys. Rev. 78, 60 (1950).

[5] L. Davis, Jr., and R. V. Langmuir, Phys. Rev. 75, 1457 (1949).

between the plates of the condenser, and eV_R/c^2 is the rest mass. It probably would be necessary to control the shape of the electric field by longitudinal conductors at intermediate potentials along the top and bottom of the doughnut inside the condensers. In this way the electric fields could be given both radial and axial focusing if desired. Deflection by means of electric fields has the disadvantage that high potentials will be required unless L is long. The use of magnetic fields might lead to difficulties with eddy currents or with getting rapid enough changes in the field.

It does not appear profitable to discuss here details of design such as dimensions, the distance that the steady state-orbit must shift for each revolution, the accuracy of the timing required, and the voltages and currents needed, since to do this a specific machine would have to be considered. It is obviously desirable that the design allow as many revolutions as possible before a collision with the gun would be expected in the absence of any bending of the orbit.

The orbit-bender suggested in Fig. 1 has the advantage that S and S' coincide throughout most of the orbit, thus allowing the use of a doughnut of relatively small cross section except in the bender. If one uses a large enough doughnut so that S' can be shifted from S everywhere, then one can use one set of coils, or condenser, instead of three. With a circular machine and for n in the usual range, it then appears best to place the single orbit-bender 180° around the machine from the injector, since the maximum deflection of the steady-state orbit then seems to occur 180° from the orbit-bender.

It is interesting to speculate on the possibility that transient electrostatic charging of the walls of the doughnut during injection and transient currents in the trimming coils may have produced effects similar to those discussed above in some operating machines.

The author is indebted to Professor R. V. Langmuir and Mr. M. A. Ruderman for helpful discussions and suggestions.

THE REVIEW OF SCIENTIFIC INSTRUMENTS VOLUME 21, NUMBER 12 DECEMBER, 1950

An Improved Electrical Network for Determining the Eigenvalues and Eigenvectors of a Real Symmetric Matrix

ABRAHAM MANY
Department of Physics, The Hebrew University, Jerusalem, Israel

(Received July 31, 1950)

An electrical computor for determining the eigenvalues and eigenvectors of real symmetric matrices up to the tenth order is described. It is an enlarged and an improved form of a computor described in a previous paper. The time required for solution is considerably reduced, and the accuracy is ten times higher. The solution of a matrix of the tenth order takes four hours, as compared to a hundred hours by computational methods. The accuracy of the eigenvalues is about 0.01 percent of the difference between the greatest and smallest eigenvalues, and the accuracy of each eigenvector is better than one percent of its greatest component.

INTRODUCTION

In a previous paper[1] an electrical network for determining the eigenvalues and eigenvectors of real symmetric matrices up to the fifth order was described. We shall henceforth refer to it as paper I. The network consisted of five LC-circuits, each one coupled to each of the others by two equal condensers. The values of the condensers were adjusted according to the elements of the matrix. The network was excited by a variable frequency source. It was shown that the eigenvalues were given by the resonance frequencies of the network, and the components of the eigenvectors by the voltages across the coils.

The instrument as constructed was primarily intended for studying the behavior of the network, and was inadequate for routine work. In this paper an improved instrument is described, capable of solving matrices up to the tenth order. The electrical network of the new instrument is essentially the same as that described in paper I, but the mechanical construction has been improved leading to a considerable reduction in the time required for solution. In addition, new methods of operating procedure have been developed, rendering higher accuracy obtainable.

CONSTRUCTION

In order to realize a matrix in the electrical network, the values of the network condensers should be adjusted according to the elements $a_{\alpha\beta}$ of the given matrix (see Eqs. (5) in paper I). As these adjustments constitute a major part of the time required for solution, the instrument was constructed in view of making this time as short as possible. The capacitors used are of the molded mica type (Cornell Dubilier) having values from 100 mmf to 1000 mmf (in steps of 100 mmf), and from 1000 mmf to 10,000 mmf (in steps of 1000 mmf). All the capacitors were brought to the same geometrical dimensions (23 millimeters square and 8 millimeters thick), by inserting them in suitable formers. Two metal rings were fitted to the ends of each capacitor and soldered to the terminals. In this way the capacitors can easily be plugged into the network.

---

[1] A. Many and S. Meiboom, Rev. Sci. Inst. 18, 831 (1947).

The capacitors forming each network condenser are plugged into a "capacitor holder." Each of the capacitor holders intended for the diagonal elements consists of a pertinax plate fitted with two prongs and carrying two vertical metal T-shaped frames. Each frame contains six spring clamps similar to fuse holders, so that six capacitors can be plugged into the pair of frames. In addition a mica trimmer, whose value may be varied from 100 mmf to 200 mmf, is connected at the top of the two frames. By suitably choosing the capacitors and adjusting the trimmer, any value between 100 mmf and 50,000 mmf can be obtained.

The two sets of capacitors corresponding to an off-diagonal element are plugged into a similar capacitor holder, provided with four prongs, and carrying four vertical metal T-shaped frames. A trimmer is connected on top of each pair of frames. Every frame contains three spring clamps, so that three capacitors can be plugged into a pair of frames, and any value between 100 mmf and 20,000 mmf can be obtained for each condenser. A photograph of such a capacitor holder is shown in Fig. 1.

By introducing these fittings, a great deal of time is saved. The suitable capacitors are quickly plugged into the holders, and the latter plugged into the bridge and adjusted. The adjustment of each network condenser is performed in less than one minute.

The capacitor holders are plugged into a series of jacks mounted on a horizontal pertinax plate, 70 centimeters square and 0.8 cm thick. The jacks are arranged and connected in a similar manner to that shown in paper I (Figs. 2 and 3). But in the present instrument the bridge for adjusting the condensers is incorporated in the plate in order to facilitate the adjustments. Moreover, in the eleventh isolated *LC*-circuit used for measuring the eigenvalues, the condenser C consists of a decade with a trimmer connected in parallel, and so may be varied continuously from 100 mmf to 80,000 mmf. An eigenvalue is given by the value of C at a resonance frequency, and may be measured by switching to the bridge without removing the decade from its position.

Ten toggle switches are fitted along the diagonal of the plate, by means of which each coil can be short-circuited (see next section).

ACCURACY

In this section we shall discuss the methods employed to increase the accuracy of the new instrument. Equations (5) in paper I were obtained by assuming that the coils of the network were identical. This cannot be attained in practice, and the coils used by us differ among themselves by as much as 0.3 percent. However the theory can readily be adapted to this case. Let $L_1, L_2, \cdots, L_{10}$ denote the values of the self-inductances of the ten coils, and let L denote the self-inductance of the eleventh isolated coil. The equations governing the behavior of the network at resonance (Eqs. (4) in paper I) now become:

$$\begin{aligned}\{2C_\alpha+{\textstyle\sum_\beta}'(A_{\alpha\beta}+B_{\alpha\beta})-2/\omega_i^2L_\alpha\}V_\alpha&\\ +{\textstyle\sum_\beta}'(A_{\alpha\beta}-B_{\alpha\beta})V_\beta=0,\quad \alpha=1,2,\cdots,10&\end{aligned}\tag{1}$$

where the term $2/\omega_i^2L_\alpha$ is different for different values of α. Multiplying each equation by $(L_\alpha/L)^{\frac{1}{2}}$, it can readily be seen that the equations obtained become identical with Eqs. (1) in paper I if

$$\begin{aligned}a_{\alpha\alpha}&=(L_\alpha/L)[2C_\alpha+{\textstyle\sum_\beta}'(A_{\alpha\beta}+B_{\alpha\beta})]\\ a_{\alpha\beta}&=(L_\alpha L_\beta/L^2)^{\frac{1}{2}}(A_{\alpha\beta}-B_{\alpha\beta}),\quad(\alpha\neq\beta)\\ \lambda_i&=2/\omega_i^2L,\quad x_k=(L/L_k)^{\frac{1}{2}}V_k.\end{aligned}\tag{2}$$

It is essential to determine L_α/L accurately. It was found that the measured ratios L_α/L vary slightly with frequency, the reason for this being the inequality of the stray capacities of the windings of the different coils. In order to measure these stray capacities, we determined the resonance frequency of each coil when tuned with its own stray capacity only. The resonance frequencies of the coils by themselves were approximately 25,000 cycles. The self-inductance of each coil being about 88 mh, we inferred that the stray capacities in each coil have the approximate value of 450 mmf. We added to each coil a small capacitor so that all the coils resonate at the same frequency (25,000 cycles). Let $C(L_\alpha)$ and $C(L)$ denote the stray capacities of the coils L_α ($\alpha=1, 2, \cdots, 10$) and L, respectively, together with the added capacitors, then:

$$C(L)/C(L_\alpha)=L_\alpha/L.\tag{3}$$

Next we connected in parallel with each coil L_α a capacitor C_α, and in parallel with the eleventh coil L a capacitor C, such that all the eleven *LC*-circuits obtained resonate at the same frequency. It is seen that

$$L_\alpha/L=[C+C(L)]/[C_\alpha+C(L_\alpha)],$$

and using (3) we obtain

$$L_\alpha/L=C/C_\alpha.\tag{4}$$

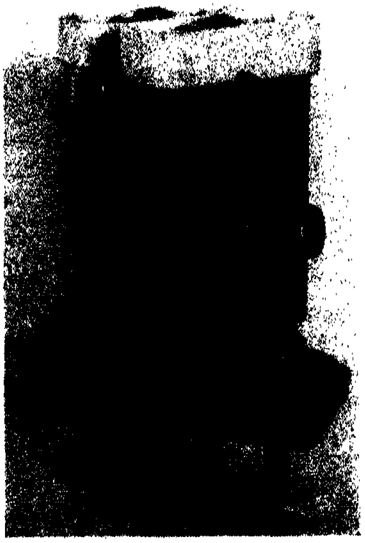

FIG. 1. A photograph of a capacitor holder.

This ratio is now independent of frequency. By measuring C and C_α in the bridge we got the required values of L_α/L correct within one part in 10,000.

It is necessary to correct for the stray capacities of the wirings of the network. Most of these capacities are in parallel with the diagonal condensers and may cause an error of about one part in a thousand in the measured eigenvalues. This can be corrected for by reducing the diagonal condensers by corresponding amounts; to determine which we employ the above mentioned toggle switches. After adjusting all the network condensers to the values given by (2), according to the elements of the given matrix, we short-circuit all the coils except one, say the αth coil. In this way we obtain an LC-circuit consisting of the coil L_α and the condenser $C_\alpha+C(L_\alpha)+C_\alpha'+\frac{1}{2}\sum_\beta' (A_{\alpha\beta}+B_{\alpha\beta})$, where C_α is the diagonal condenser, $C(L_\alpha)$—the stray capacity of the coil's windings, C_α'—the effective capacity across the coil caused by the stray capacities of the wirings of the network, and $\frac{1}{2}\sum_\beta' (A_{\alpha\beta}+B_{\alpha\beta})$—the capacity arising from the coupling condensers corresponding to the matrix elements in the αth row (see Fig. 2 in paper I). The resonance frequency ω_α of this LC-circuit is determined, and keeping the oscillator at this frequency, it is applied to the eleventh isolated LC-circuit; the condenser C is adjusted until resonance is again obtained. We then have

$$1/\omega_\alpha^2 L=C+C(L),$$
$$1/\omega_\alpha^2 L_\alpha=C_\alpha+C(L_\alpha)+C_\alpha'+\tfrac{1}{2}\textstyle\sum_\beta' (A_{\alpha\beta}+B_{\alpha\beta});$$

using (3) and (2) we obtain

$$C_\alpha'=(L/L_\alpha)(C-\tfrac{1}{2}a_{\alpha\alpha}). \tag{5}$$

In practice the correction for the stray capacities of the wirings is performed as follows: we adjust the condenser C on the bridge to the value $\frac{1}{2}a_{\alpha\alpha}$, and then determine the resonance frequency of the eleventh LC-circuit. Keeping the oscillator at this frequency, it is applied to the αth coil, and the diagonal condenser C_α is reduced until resonance is obtained. This procedure is repeated for each row of the network.

Two important factors determine the accuracy of the measured eigenvalues and eigenvectors. The first factor is the losses in the coils. By taking these losses into account, it was shown in paper I that in matrices where the eigenvalues are widely separated, the losses involve an error of order D^2 in the eigenvalues, and an error of order D in the eigenvectors, where $D=1/Q$. A more rigorous treatment showed that these estimates for the errors are not quite accurate. It was found that the maximum fractional error $\Delta\lambda/\lambda_i$ involved in the measurement of an eigenvalue λ_i is the smaller of the two terms $g(\lambda_i/|\lambda_i-\lambda_i'|)D^2$ and D, where g is usually smaller than unity, though its maximum possible value is $n-1$ (n being the order of the matrix), and λ_i' is the nearest eigenvalue to λ_i. The value of D over the range of frequencies used in exciting the network (2000 to 6000 cycles) is lower than 0.005. In ordinary matrices the roots are widely separated, and the error is given by the first term, and usually amounts to less than one part in 10,000. The same error is obtained for a truly multiple eigenvalue. In this case λ_i' denotes the nearest eigenvalue to the multiple eigenvalue λ_i. For matrices whose eigenvalues become closer (but do not coincide) the error increases, but is never larger than D, i.e., 0.5 percent. This error is obtained for eigenvalues lying so close together that the difference between the corresponding resonance frequencies is of the same order of magnitude as the resonance width. It is thus seen that if $\Delta\lambda/\lambda_i$ is plotted as a function of $|\lambda_i-\lambda_i'|$, the curve will show a maximum, whose value is 0.5 percent, for $|\lambda_i-\lambda_i'|=\lambda_i D$, and will decrease on both sides of this point to a value of about 0.01 percent.

The error involved in the measurement of a component of an eigenvector belonging to λ_i, in the case of ordinary matrices, was found to be $g(\lambda_i/|\lambda_i-\lambda_i'|)D$, which usually amounts to less than one percent. In the case of quasidegenerate eigenvalues, the eigenvectors belonging to such roots are very labile and large errors are involved in their measurement.

The second factor affecting the accuracy of the results is the accuracy with which the given matrix is realized in the network. This realization consists of the adjustment of the condensers according to (2), and the correction for the stray capacities. The ratios L_α/L are correct within an accuracy of 0.01 percent, and the adjustment of the condensers on the bridge is made with the same accuracy. Hence, after the correction for the stray capacities, the values of the condensers are correct within an accuracy of about one part in 10,000.

From the above discussion we can expect that in ordinary matrices, the accuracy of the eigenvalues will be mainly determined by the accuracy of adjustment of the condensers, while in matrices having close eigenvalues the errors caused by the losses in the coils will predominate. In the first case we obtained for the eigenvalues an accuracy of about 0.01 percent of the difference between the greatest and smallest eigenvalues. As for the eigenvectors, we obtained for their components an accuracy of better than one percent of the greatest components.

CONCLUSION

At present the instrument described is extensively employed in our department for the solution of matrices arising from spectroscopic problems. The solution of a matrix of the tenth order takes about four hours as compared to a hundred hours by computational methods.

This paper and paper I are a summary of a dissertation submitted to the Senate of the Hebrew University in Jerusalem in fulfilment of the requirements for the degree of Doctor of Philosophy.

The author wishes to acknowledge his indebtedness to Professor G. Racah for his continued assistance during this work, and to Dr. E. Alexander for his interest and encouragement.

THE REVIEW OF SCIENTIFIC INSTRUMENTS VOLUME 21, NUMBER 12 DECEMBER, 1950

Distributed Coincidence Circuit

CLYDE WIEGAND
Radiation Laboratory, University of California, Berkeley, California

(Received July 31, 1950)

A coincidence circuit using the traveling wave principle as applied to distributed amplification is described. The resolving time is about 10^{-8} sec. when the device is used in connection with scintillation detectors.

AN electronic coincidence circuit employing the traveling wave concept as applied to distributed amplification[1] has been developed and used in the Radiation Laboratory. When the circuit is used in connection with scintillation crystal detectors, photo-multiplier tubes, and distributed amplifiers, the resolving time is about 10^{-8} sec. The response to single pulses in either channel is satisfactorily small and is independent of the height of the single pulses.

The circuit employs conventional miniature pentagrid converter tubes (type 6BA7) and makes use of the fact that their plate current can be practically cut off by biasing either of the two control grids a few volts negative with respect to their cathodes. Consequently, a positive pulse on either grid alone will not allow plate current to flow, whereas if positive pulses are applied simultaneously to both control grids, plate current will flow during the time both grids are sufficiently less negative with respect to the cathode.

The principle of distributed amplification is applied by using a series of tubes and connecting separate artificial transmission lines to each set of control grids. The schematic circuit is shown in Fig. 1. The grid-to-other tube-elements (ground) capacitances serve as the shunt capacitances of the transmission line sections. The plates are connected to a third transmission line in the usual manner of distributed amplifiers.

Type 6BA7 tubes were chosen because the two control grids and the plate are quite well shielded from each other and thus interaction among the grid and plate lines is minimized. The type 6BA7 was preferred to type 6BE6 because of the higher current and transconductance ratings and only slightly increased capacitances.

A coincidence circuit for particle counting should ordinarily have the two input channels equal to each other. The circuit is thus required to be symmetrical so that its behavior is unchanged upon interchanging the two input leads 1 and 2. However, the input capacitances of the two control grids are not equal and their effectiveness in controlling the plate current is different. Therefore, the staggered connection is used as indicated in the schematic diagram where one input grid line is shown connected alternately to grids No. 1 and No. 3 and the capacitances are made equal by adding external condensers to the No. 1 grids.

Two other requirements should be met to assure effective traveling wave amplification. These are that the velocity of the waves be equal on the grid and plate lines and that there should be no discontinuities in the value of the impedance upon which the waves are incident. Neglecting losses the velocity of propagation of the waves will be equal when

$$L_{g1}C_{g1}=L_{g2}C_{g2}=L_pC_p,$$

where L_g refers to the series inductance and C_g the shunt capacitance of the grid line sections and likewise L_p and C_p refer to the plate line.

The corresponding impedances are

$$Z_{g1}=\left(\frac{L_{g1}}{C_{g1}}\right)^{\frac{1}{2}},\quad Z_{g2}=\left(\frac{L_{g2}}{C_{g2}}\right)^{\frac{1}{2}},\quad Z_p=\left(\frac{L_p}{C_p}\right)^{\frac{1}{2}}.$$

In order for the circuit to be symmetrical we must have $Z_{g1}=Z_{g2}$. It is not necessary that $Z_{g1}=Z_p$, since the plate line will generally work into an arbitrary impedance such as a pulse-height discriminator stage.

The coincidence circuit has thus far been used in connection with distributed amplifiers having output impedance values of 200 to 400 ohms. The grid lines should be designed to match the output impedance of the amplifiers. The coincidence circuit can then be coupled directly to the amplifiers. Present designs incorporate the amplifiers and coincidence circuit on a common chassis.

A typical design makes use of m-derived[2] filter networks as suggested in reference 1. The coils are wound on $\frac{1}{4}$-in. diameter pregrooved polystyrene rods with bare copper wire of about 0.015-in. diameter. The coil con-

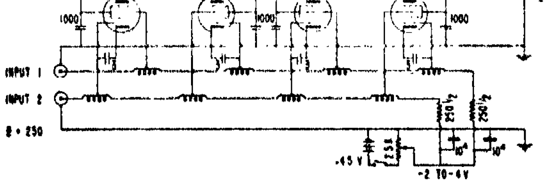

FIG. 1. Schematic diagram of the coincidence circuit. Capacitances are ceramic type with values indicated in micro-micro-farads. Resistance values are in ohms.

---

[1] Ginzton, Hewlett, Jasberg, and Noe, Proc. I.R.E. 36, 956 (1948).

[2] See, for example, L. C. Jackson, *Wave Filters* (Methuen and Company, Ltd., London, 1950).

TABLE I. Sample coil data.

	C μμfd	L_1μH	L_2μH	n	turns/inch	m	Z_0 ohms
Grid line	10.5	0.25	0.63	12	40	1.27	250
Plate line	9.3	0.31	0.76	14	40	1.24	290

stants were calculated by the formula for the inductance of a single layer solenoid (Handbook of Chemistry and Physics). The values of the shunt capacitances are those of the tube manufacturer plus an allowance of 1 μμfd for socket capacitance. Effort was made to maintain inductances to ±10 percent of the calculated values.

A sample of the coil data is presented in Table I. L_1 refers to the inductance of half of the coil, L_2 to the whole coil. n is the total number of turns and m is the parameter of the m-derived filter. $Z_0=(L_2/C)^{\frac{1}{2}}$ is the nominal iterative impedance.

The lines should be terminated by a resistance equal to their iterative impedance. Ordinary carbon resistors are satisfactory, although some improvement might be realized by using half-sections at the terminations. Satisfactory operation has resulted for grid biases of −2 to −4 volts when using a minimum pulse input level to the coincidence circuit of about 10 volts. The non-linearity of the coincidence circuit provides sufficient discrimination against small pulses.

For further discussion of the design and adjustment of distributed amplifiers the reader is referred to a paper by G. G. Kelley[3] on the construction of a high speed synchroscope.

This work was performed under the auspices of the AEC.

---

[3] G. G. Kelley, Rev. Sci. Inst. 21, 71 (1950).

THE REVIEW OF SCIENTIFIC INSTRUMENTS VOLUME 21, NUMBER 12 DECEMBER, 1950

A Continuously Sensitive Cloud Chamber

T. S. NEEDELS* AND C. E. NIELSEN
Mendenhall Laboratory of Physics, Ohio State University, Columbus, Ohio

(Received July 20, 1950)

A particularly simple cloud chamber is described that is continuously sensitive to ion tracks. The chamber operates on the principle of vapor diffusion from a hot to a cold surface. The sensitive region is a shallow horizontal layer near the cold surface. The chamber has been placed in a magnetic field and curved tracks of β-particles from a radioactive source have been photographed. Pictures of such electron tracks are shown.

EXPANSION chambers as invented by C. T. R. Wilson have always suffered from the essential intermittency of their expansion-recompression mechanism. One would like a chamber that maintains a continuously supersaturated region in which tracks form and fall out to be replaced by tracks from the next event with no insensitive period or dead time ever intervening. A notable attempt in this direction was made by Langsdorf[1] but his rather complex apparatus has never come into use. We have been studying this problem and recently we have set up a particularly simple device. We have used the principle of vapor diffusion from a hot to a cold surface employed by Langsdorf. This diffusion mechanism produces a shallow region between these two surfaces that remains continuously supersaturated.

The chamber we have set up consists of a glass beaker that sits on a cake of dry ice (cold surface) and is covered with a cardboard wet with alcohol that stays at room temperature (hot surface). The wet cardboard provides the vapor, which can be either ethanol or propanol, or mixtures of either of these with water. Ion tracks of excellent quality are observed in a shallow layer near the cold bottom of the beaker. Sharp tracks of both electrons and protons are seen in air.

Our experience with this simple beaker chamber has been that best operation is obtained when a clearing field is placed across the sensitive region. Both horizontal and vertical fields have been tried and a vertical field works best. Here, of course, the clearing field cannot sweep old ions away as in a Wilson chamber but, instead, it forces additional tracks from above and below into the permanently sensitive region. This adds more ionizing events to those occurring originally in this thin layer. The additional ion load helps keep the supersaturation from increasing to the fog limit and makes chamber operation much more satisfactory. We have used fields of about 50 to 100 volts/cm with equal results.

For better seeing from above (through a 4-in. diameter hole cut in the cardboard and covered with a glass plate) we have put a piece of black velvet cloth in the bottom of the beaker; and to keep any white frost from forming on top of the velvet we have added alcohol sufficient to cover the velvet. This arrangement provides a very satisfactory black background that stays black at dry ice temperatures. Incidentally, the thickness of the cold alcohol layer can be varied so as to vary the temperature attainable at its upper surface. This in turn determines the maximum supersaturation attained in the sensitive region, giving some control of the optimum track load. Reducing the maximum supersaturation, however, also makes the sensitive layer thinner; and this may or may not be an advantage in a particular experiment.

---

* Now at Los Alamos, New Mexico.

[1] A. Langsdorf, Rev. Sci. Inst. 10, 91 (1939).

After one first puts the beaker on the dry ice cake, a thin fog forms near the cold bottom and the fog particles grow and gradually fall out *in a very few minutes.* This fog is due to the dust, present in ordinary air, that must be removed before one can see ion tracks. Tracks begin to show usually about five to ten minutes after the beaker is first put on the dry ice. Those who have operated Wilson cloud chambers, and have struggled with making the air dust-free by tedious repeated slow expansions, will recognize here another remarkable property (besides the simplicity) of this type of chamber. Tracks continue to be visible after this short dust-clearing period as long as one keeps the cardboard wet and the dry ice supply adequate. We find that if the dry ice block covers less than about two-thirds of the beaker bottom, operation begins to deteriorate and the tracks become fragmentary and diffuse.

We have put this chamber with its horizontal ion tracks into a vertical magnetic field (air core coils, $H\simeq 1000$ oersted) and observed the characteristic circular paths of electrons and positrons of energies up to a few Mev. (See Fig. 1.) With a γ-ray source we have enjoyed watching the development in the chamber gas of ion clusters and longer range recoil electrons from the Compton process, and some events that look like electron-positron pairs. With a 5 mc Po-Be neutron source outside the beaker at the level of the sensitive region we have observed many sharp bright straight tracks of proton recoils and an occasional nuclear reaction occurring in the chamber gas. A proton recoil frequently shows its characteristic sharp small angle bend near the end of its range. The nuclear reactions are distinguished from the protons by the appearance of a short bright track that has a large angle bend near one end. In this case the apex of the bend always faces the neutron source.

We have found this beaker chamber to be useful for looking at samples of very weak radioactive isotopes made in the cyclotron. The weak sample spread thin behind a zapon film is merely lowered on a string through the hole in the top cardboard all the way to the level of the sensitive region. Any electrons, positrons or γ-rays from the sample make themselves immediately evident. We have put also a bit of uranium oxide into a tiny zapon bag, lowered it on a string into the sensitive layer, and watched the α-particles shoot out from the bag.

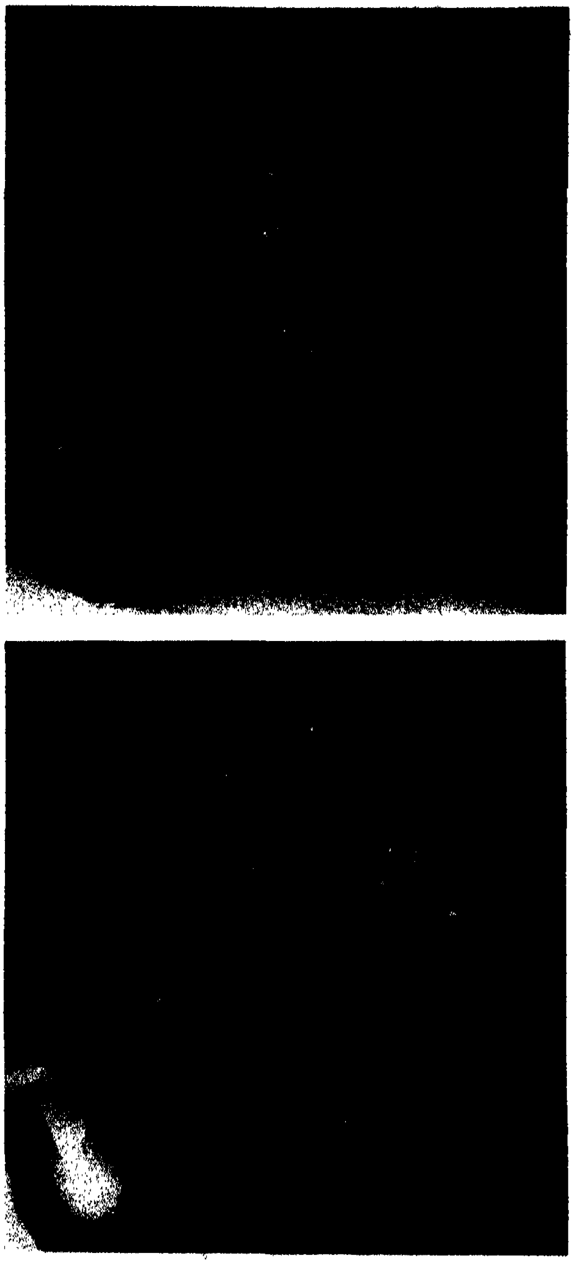

FIG. 1. Two photographs of β-particles from $Sr^{90}+Y^{90}$. The active material is evaporated on zapon film and placed at the level of the sensitive region. The active source is the diffuse object at the left in each photograph. In addition to the β-particles, there are present stray diffuse tracks of electrons from cosmic ray background. In most of the pictures we have obtained, these stray electrons can be distinguished easily from the β-electrons.

The different radiations produced by a β^+-emitter that emits also x-rays from K-capture may readily be distinguished because the positrons describe circular arcs in the magnetic field which originate at the *surface* of the sample whereas any γ's or x-rays form Compton recoils at random distances from the sample. It is interesting to note that the sensitive region is sensitive to ions very close to the sample surface. As far as we can tell, the visible tracks of β-particles start at most about 1 mm from the sample. Moreover, the observation of what is coming from a radioactive sample is continuous because we have found that it disturbs nothing to leave an incandescent light source focused on the sensitive region all the time. Thus the detection by the continuous cloud chamber of just what radiations are being emitted from radioactive substances becomes especially simple and satisfying.

THE REVIEW OF SCIENTIFIC INSTRUMENTS VOLUME 21, NUMBER 12 DECEMBER, 1950

A Semi-Automatic Device for Analyzing Events in Nuclear Emulsions

MARIETTA BLAU,* ROBERT RUDIN, AND SEYMOUR LINDENBAUM
Columbia University, New York City

(Received June 16, 1950)

An apparatus is described the basic element of which is a microscope with a motor-driven stage. The operator controls the direction and speed of motion by a steering wheel and an accelerator pedal and drives the track to be analyzed through a target. Range, grain density, and geometrical orientation of tracks, etc., are automatically recorded on charts. Methods of measurements and results are discussed.

I. INTRODUCTION

NUCLEAR emulsion techniques have become quite important in modern physics. A wide range of commercially available emulsions together with suitable development procedures make possible the registration of all charged particles crossing the emulsion, and under favorable conditions also their identification. One obtains all the useful information about the tracks making up an event by determining the geometrical history of the tracks and the grain density along the tracks. Although for many purposes it is necessary only to identify certain types of particles, which an experienced worker can do by mere observation, it is necessary in other problems to measure accurately grain density, range, scattering, and also the exact geometrical orientation of tracks, especially those connected with an event. The various methods of performing these measurements are very well known to workers in this field, and it is, furthermore, well known that these methods are intrinsically lengthy, exacting, to a certain degree subjective, and also require experienced observers. Therefore, we felt that there is a need for an apparatus which simplifies the various measuring procedures necessary in nuclear emulsion experiments. We achieved this by incorporating in the apparatus mechanical, photoelectric, and recording devices which minimize manual operations and personal error while at the same time increase the speed and ease of measuring.

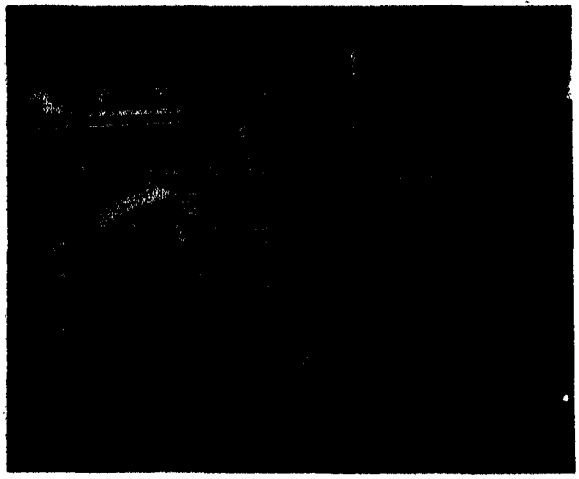

FIG. 1. A general view of the apparatus.

II. DESCRIPTION OF THE APPARATUS

The whole instrument (see Fig. 1) is built around a microscope with a motor-driven stage, moved by selsyn motors in two dimensions (x and y). The accuracy of the gears, feedscrews, etc., is such that dimensions can be measured to within 0.2 of a micron. These selsyn motors are fed from identical selsyn generators which are driven by a steering unit so that the photographic plate under observation can be moved in any direction and with any desired speed, up to approximately 25 microns per second. For convenience the arrangement is such that the direction of movement is controlled by a steering wheel (like the steering wheel of an automobile) and the speed is adjusted by a foot pedal. The schematic diagram (Fig. 2) shows how this steering arrangement works: a d.c. motor M with permanent field magnet is fed from a rectifier connected to the secondary winding of a variac transformer. This transformer is controlled by the foot pedal against the torque of a spring so that it delivers zero voltage when the pedal is released and increases voltage when the pedal is depressed. The motor M drives two turntables T (the figure shows only one of two identical units). A friction wheel F is connected to the shaft of a selsyn generator S, and can be displaced along the diameter of the turntable T by a crank C. It is clear that the direction and speed of the rotation of the generator depends on the relative position of T and F, and disregarding for the moment second-order differences, the speed of the generator is proportional to the sine of the angle α, the displacement of the crank. The generator S_1 drives a selsyn motor S_2 which moves by gears G_x the feedscrew for the x-movement of the mechanical stage, and a counter which gives number of revolutions to the nearest tenth. Therefore, the magnitude of the movement of the stage is proportional to the product of the speed (V_M) of the motor M and the sine of the angle α. The ratio of the gear and worm drive to the feedscrew was chosen so that one revolution of the selsyns corresponds to a stage movement in any direction of 1 micron.

---

* Now at Brookhaven, National Laboratory, Upton, Long Island, New York.

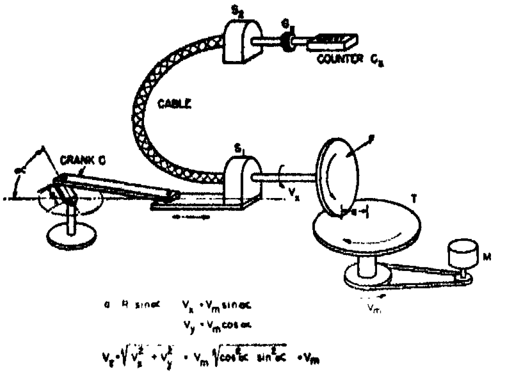
S2
C2
COUNTER C2
CABLE
CRANK C
α
S1
Vx
F
T
M
Vm
a = R sin α   Vx = Vm sin α
Vy = Vm cos α
Vt = √(Vx² + Vy²) = Vm √(cos²α + sin²α) = Vm

FIG. 2. A schematic drawing of the driving unit.

A second identical set of turntables, friction wheel, selsyns, feedscrew, etc., is driven by a second crank, but with a displacement of 90° between the two cranks; the two cranks are driven by the steering wheel. Obviously the movement of the stage in the y direction is proportional to the cosine of α and we can write: $V_x = V_m \sin\alpha$, $V_y = V_m \cos\alpha$. The resulting speed of the stage and therefore of the photographic plate or the event under observation is $V_e = (Vx^2 + Vy^2)^{\frac{1}{2}} = V_m(\sin^2\alpha + \cos^2\alpha)^{\frac{1}{2}} = V_m$. That means that the speed with which an event in the emulsion, for instance a trajectory of a particle passes through the eyepiece, is independent of the angular displacement of the crank and the position of the steering wheel determines the direction of travel.

Because of the finite length of the connecting rods between crank and selsyn generator, the movement is not a pure sine movement in this schematic setup. In the model constructed (Fig. 3) the simple crank drive is replaced by a planetary gear arrangement, consisting of a stationary inside gear and a planetary gear of one-half of the diameter; when the inner gear rotates and rolls along the inside of the stationary gear, a certain point of the pitch-circle moves in a straight line with a pure sine movement. The photograph (Fig. 3) shows the working model of the steering unit using the planetary gear drive.

The recording chart is moved by a selsyn motor connected to a selsyn generator which rotates with the speed V_m of the turntables. The movement of the chart is thus proportional to the stage movement, and the gearing is such that the chart speed is 2000 times that of the stage; therefore 2 mm on the chart correspond to 1 micron in the photographic plate.

The image of the plate is observed by the operator through an eyepiece and at the same time projected upon a small slit before a photo-multiplier tube. The position of the slit coincides with an optical target in the eyepiece and one merely needs a short training period to learn to steer the track under investigation through the center of the target (consisting of two concentric circles) (Figs. 4, 5), while the photo output is recorded on the moving chart (Fig. 6). The chart records also the angular position of the steering wheel and the vertical movement of the objective (Fig. 6). The operator of the apparatus has to follow the track in three dimensions and therefore must also keep the image in focus. Since the chart is driven with a speed proportional to the track displacement in the x-y plane and the z-movement is recorded by a displacement of a steady line across the moving sheet, the length of this line, when measured for instance by a map reader, determines the three-dimensional length of the track.

For some investigations, especially measuring of straight line lengths, angles, scattering, etc., another set of selsyn generators is used driven by individual motors governed by the accelerator pedal, whereby the movement goes only in the x or y direction, and the direction is chosen by a four position switch. The movements of the three selsyn motors connected with the stage (x, y, and z components) are measured by counters connected to these motors. One revolution of the counters corresponds to a movement of 1 micron and as the first number wheel contains 10 figures, a reading can be made to 1/10 of a micron of plate displacement.

To make it unnecessary for the operator to shift his eyes from the microscope to the counter and write down readings, another set of three selsyns with counters is connected in parallel to the stage motors and these auxiliary counters arranged side by side. A simple photographic arrangement pictures the counter readings on a sheet of pack film through a slot. A button control moves the film for the width of the slot, so that fifteen exposures can be made on a sheet of film. After development the coordinates of these fifteen points can

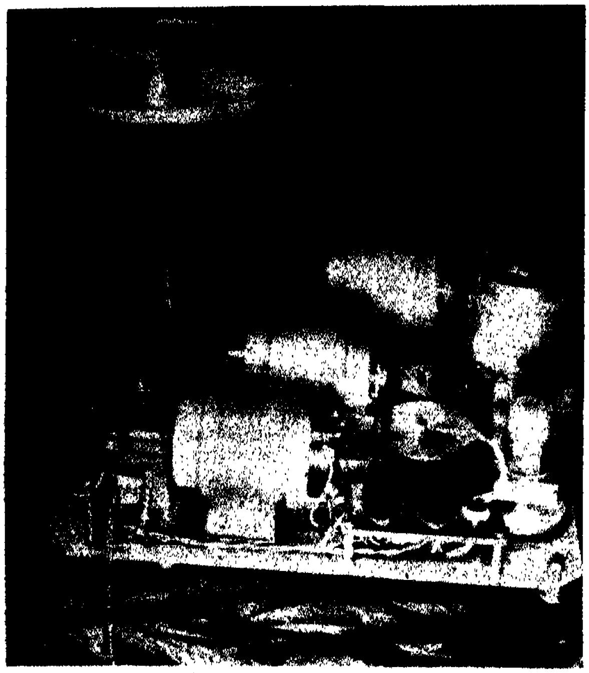

FIG. 3. Photograph of the driving unit.

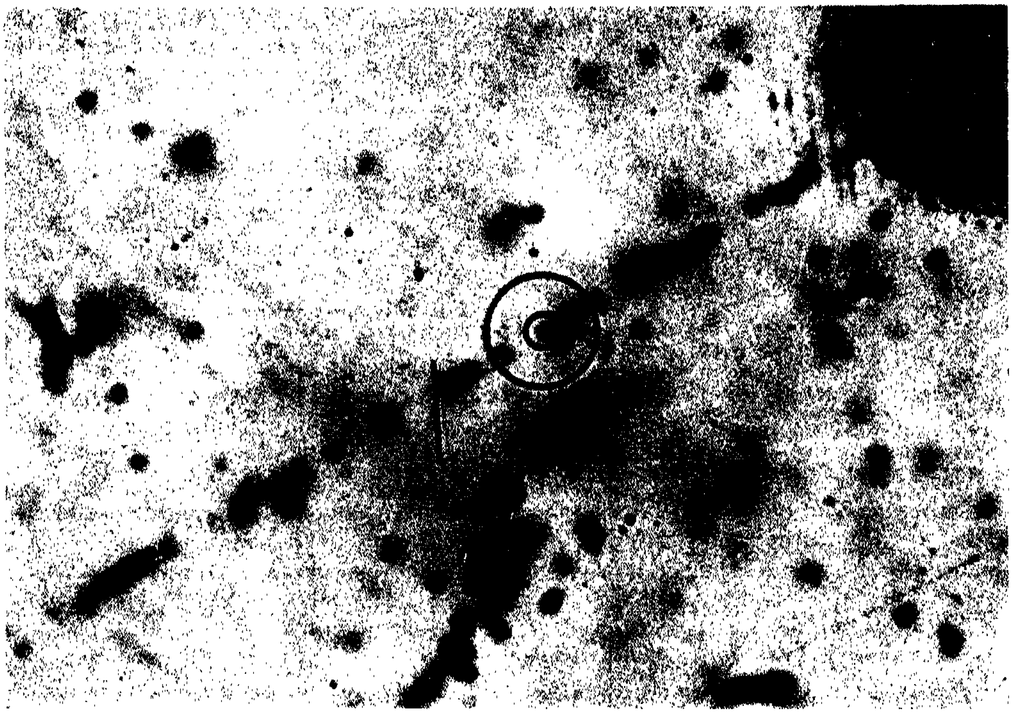

FIG. 4. A microphotograph of a track going through the bull's eye target.

be read easily. This counter photographing device is useful for taking the coordinates of various points of a track and calculating curvature and scattering.

For counting grains, the slit before the photo-multiplier is positioned across the track. This is accomplished by mounting two small pins connected with the observation eyepiece, which can be rotated to be approximately parallel to the track and by an arrangement of bevel gears which simultaneously rotate the slit to its proper position.

The smallest slit used up to now is 1 mm long and 0.03 mm wide, covering an area of the plate of approximately 0.7×0.02 microns (for the 2-mm immersion objective). This slit yields good resolution and with it the recording chart shows a distinct fine structure even for overlapping grains. The use of still smaller slits could not improve the resolution because of optical limitations.

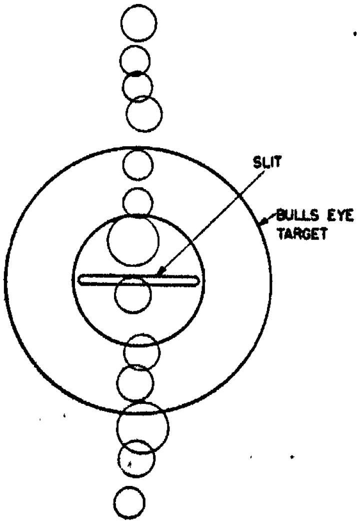

FIG. 5. A schematic drawing depicting the operation of the grain counting slit.

In cases where the accumulation of grains in the track is too heavy to be analyzed by counting individual grains (heavy tracks, dense shower cores), the apparatus can be used for direct photometric comparison of the track against the surrounding background.

This instrument as it stands now is only an experimental model. Improvements to increase ease of operation, extend the automatization, reduce over-all size, etc., have already been planned to be incorporated in another model.

III. RANGE AND GRAIN DENSITY OF TRACKS

Measurements of range and grain density of tracks are performed in the following way. First, a magnification is chosen, sufficient to give satisfactory resolution. Then a rectangular slit is placed in the image plane before the photo-cell. The width of the slit is a small fraction of the grain diameter in the image plane; the length corresponds to about several grain diameters. The slit can be rotated and is positioned so that its length is perpendicular to and bisected by the track. In the eyepiece we have a centered bull's eye target; the inner circle corresponds to the length of the slit. Therefore the track is projected through the slit on to the photo-cell as long as it is positioned within the inner circle of the target (Fig. 5).

With the mechanism previously described the track is driven through the bull's eye and simultaneously the photo-cell output is traced on the moving chart by a Brush pen motor which moves proportionally to the amplified photo-cell output in a direction perpendicular to the chart motion. Since, as previously explained, the chart movement is proportional to the stage displacement, which in this case is equal to the length driven along the track, we obtain the photo-cell output as a function of this length or range interval. Since, as previously mentioned, the width of the slit is only a fraction of the grain diameter, we can expect to get a clear distinction in the photo-cell output for every grain passing through the slit. Figure 7 gives 4 charts of the same proton track, driven by different operators including one driven in the opposite direction. Figure 8 gives 3 charts of the same meson track. These comparisons show how reproducible the results are. The narrow peaks in these charts correspond to individual grains which can be resolved under high magnification. The wider peaks correspond to groups of grains which are not individually resolvable. An estimate of the number of grains in such groups must be made, using both the fine structure and the width of these peaks as

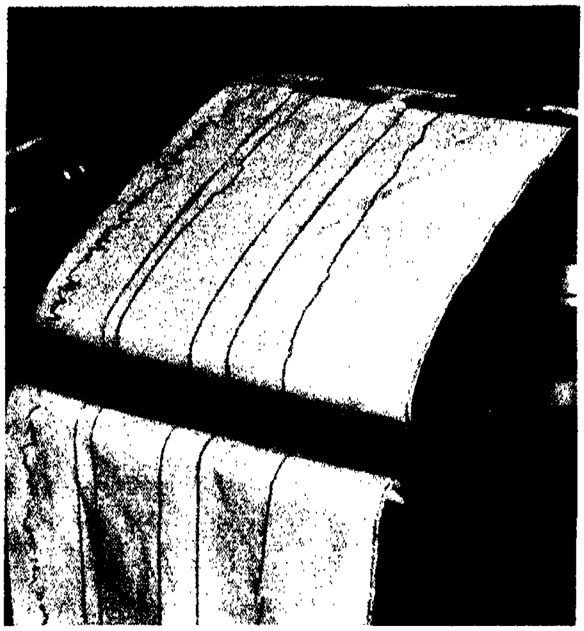

Fig. 6. A photograph of the recording chart, the length of which is 2000 times the projection of track length in the $x-y$ plane. The upper curve is the photo-multiplier output. The middle curve is the variation of driving angle (a). The bottom curve is the variation of focusing movement.

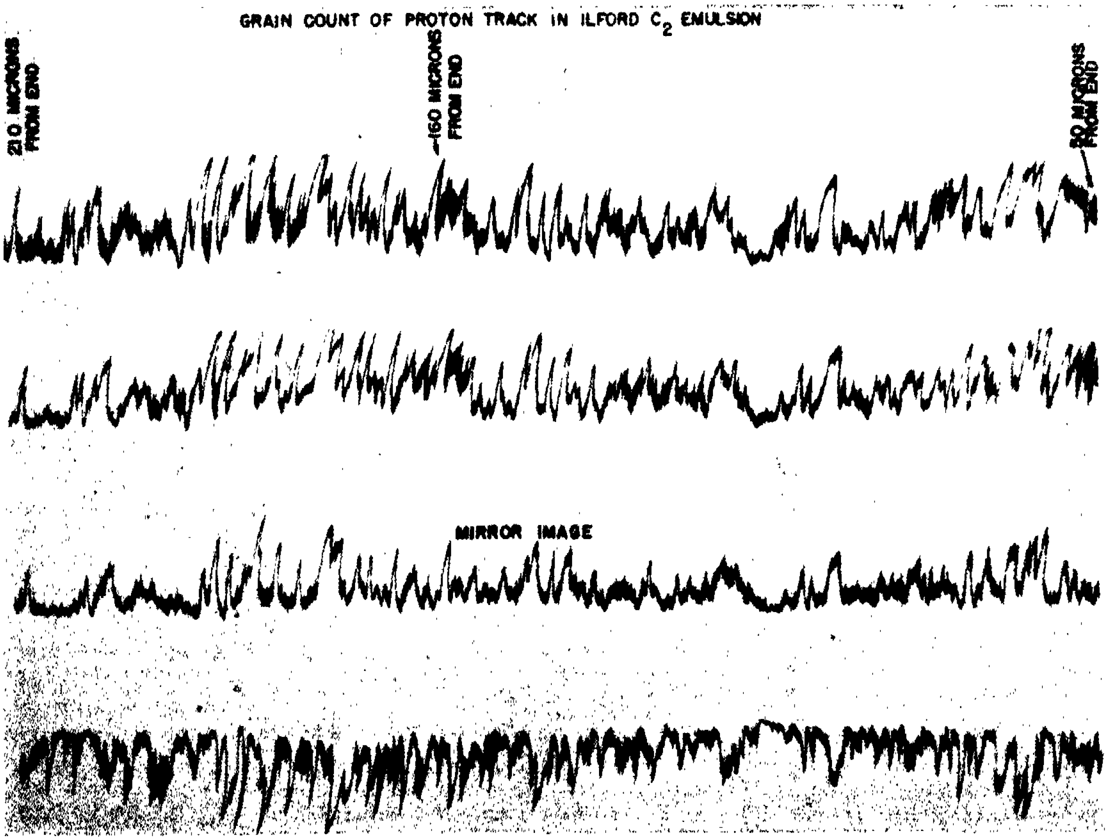

Fig. 7. Grain density record of proton track.

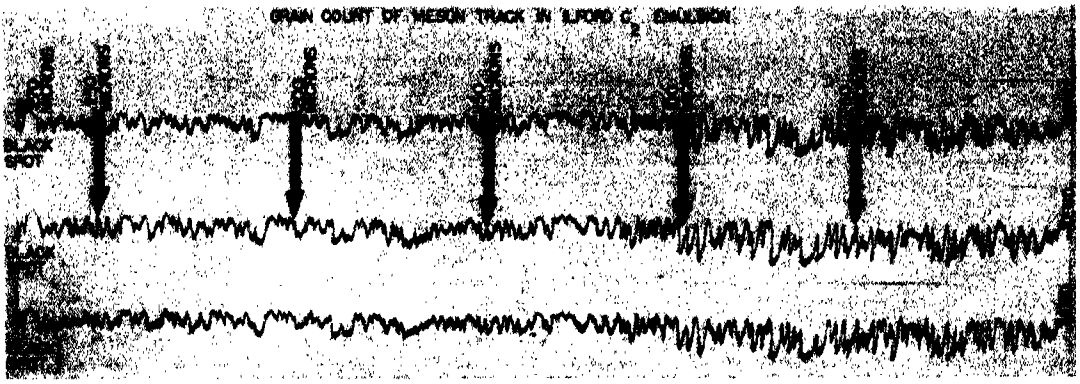

FIG. 8. Grain density record of meson track.

criteria. Grain counts of the same tracks by both our method and the conventional microscope method were in good agreement. It is obvious that in both cases background grains increase the grain count. The length of the slit used here corresponds to about two grain diameters so that the conditions for adding background grains are similar to those in usual grain counting methods. A correction could be made in our case by running along the background in the vicinity of the track.

One advantage of our method is the reproducibility of the results which do not depend on the experience of the operator. The only requirement is that he learn how to drive. His driving abilities can be easily checked by inspecting the record of the steering angle and focusing movements which are also given automatically by our charts (Fig. 6). Another advantage is the objectivity with which interpretation criteria can be established and applied to the charts; these can be inspected by any number of people at any time.

The measurements can be done quite rapidly and easily. For example, a conservative estimate of the driving time for a grain density record of a 2000μ-track is about 10 minutes. The evaluation of the chart can be done at any convenient time and simply involves counting and weighing of peaks on the regions of the chart one is interested in. In many cases merely an inspection of the patterns as a function of range will be sufficient for the identification of the particle.

The reproducibility, accuracy, and speed of our method is especially convenient if one wants to obtain large statistics, for instance upon the relation between grain density and energy loss.

In case the identity of the particle causing the track is known and only range measurements are necessary for determining the energy, the driving speed can be increased appreciably because the limiting speed factor in grain density measurements is the frequency response of our recording system and the necessity of using high magnification. It may be that at higher speeds one does not follow the track exactly; however, as long as one drives smoothly so that the maximum angle formed with the direction of the track is small, the error introduced is not appreciable. For instance, if one continuously wanders across the track with an angle of 10°, the error introduced is $1\frac{1}{2}$ percent.

IV. ACCURATE DETERMINATION OF COORDINATES

The counters connected with the x, y, and z movements read to 1/10 of a micron. We have found that we can center one grain in our bull's eye, record its coordinates, then wander around the plate at random, and recenter the same grain so that the difference between the coordinates is not greater than 0.2 micron. The deviation read on the counters connected with the stage movement is mainly due to the difficulty in judging the center part of a grain.

The counters are therefore used to determine the coordinates of a series of points connected with tracks, if highest accuracy is needed. Such problems are present in measurements of multiple scattering of tracks. From the coordinates which we record with the photographic system mentioned before, the data necessary for mean scattering angles can be determined. Because of the motor-driven stage and automatic recording, these measurements can be done fairly easily. Coordinate intervals can be selected and preset by utilizing microswitches on the stage driving selsyns. This procedure can be further simplified by using punching counters instead of photographic recording and then analyzing the charts by machines.

Another method used for scattering measurements[1] can be incorporated in our apparatus. In this case we install a line in the eyepiece which by rotation is aligned along the track and the angle of rotation is magnified and recorded together with the coordinates. Furthermore, to increase the accuracy of alignment we intend to introduce a slit in the image plane before the photocell, rotating parallel and simultaneously with the eyepiece line and use the photo-cell output maximum as indicator for alignment.

It is clear that large angle scattering or any geometrical relationship between track directions in stars can be calculated after having obtained a suitable sequence of coordinates.

---

[1] Y. Goldschmidt-Clermont, Como Conference, September, 1949, Nuovo Cimento (to be published).

V. PHOTOMETRIC MEASUREMENTS

There are cases in which counting of individual grains is not necessary or may even be impossible because of an excessively high grain density. In order to identify the particle it is necessary to determine the rate of decrease of grain density along the track. In these cases we use a slit before the photo-cell having in the image plane a width equal to about two grain-diameters and a length corresponding to about 6–10 grains. We then drive the longer side of the slit parallel to the track and record the photo-cell output along the track (V_{track}) using a proportional amplifier. In order to obtain the amount of light absorbed by the track, the photo-cell output on either side of the track corresponding to the empty background is also recorded ($V_{\text{background}}$). The ratio $\frac{V_{\text{track}}-V_{\text{background}}}{V_{\text{background}}}$ determined from the charts with the aid of a planimeter is a function of the grain density within the track and its variation along the track a measure for the change in energy loss with the range of the particle.

VI. HEAVY TRACKS

The photometric method is especially indicated in investigations of heavy tracks.[3] The tracks produced by heavy charged particles ($3 \leqslant Z \leqslant 26$) have in addition to the usual track core (single line) a conglomeration of many grains on both sides extending out from the center, due to the ejected electron tracks (δ rays). In analyzing these tracks one needs to determine the number of δ-rays[2] per unit length along the track, since this count is a function of the charge and velocity of the particles. The number of δ-rays in a given energy and geometric interval is proportional to Z^2 and increases with decreasing velocity up to a maximum value. The velocity where the maximum occurs depends upon the δ-ray interval chosen. As the velocity continues to decrease, the number of δ-rays drops; furthermore, the particle captures electrons and the track thins down (thin down length).

Visual δ-ray counting is lengthy and quite subject to personal judgment. Therefore we have attempted to develop a rapid photometric method of analyzing heavy tracks. We drive along the track with a wide slit or set of slits placed before the photo-multiplier, so that only selected regions of the track cross section are visible to the photo-cell.

Thereby one can choose the δ-ray interval one intends to measure (choice of slit) and determine its photometric density which will be a function of the number of δ-rays and the geometry of the slit. The output from the photo-multiplier is linearly amplified and automatically recorded on the chart moving with a speed 2000 times the driving speed. Thus we obtain a record of the amount of light transmitted by the track through the slit as a function of the length of the track. We then drive along the empty background on both sides parallel to the track and obtain the light transmitted by the background.

With the cooperation of Dr. H. Bradt and Dr. B. Peters of Rochester University we were able to perform a preliminary investigation using some of the heavy tracks found and analyzed by these authors.

With a 4-mm objective (650 times magnification) and a slit which projected on the object plane which defines an opening 18 microns long and 6 microns wide, we measured the percentage of light transmitted by 10 tracks ranging from carbon to iron, all having $\beta = v/c = 1$. In Fig. 9 the percentage of light absorbed is plotted *versus* the number of δ-rays per unit length, determined by Bradt and Peters. The relationship appears to be linear within the possible experimental accuracy. It is clear that the percentage of light absorbed by the track should be an increasing function of the number of developed grains which fall within the area covered by the slit. Provided that saturation, packing, and contagious development effects are negligible, it is to be expected that both the number of grains and the percentage of light absorbed should be linearly related to the visual δ-ray count. The fact that we get an approximately linear relationship shows that in the case of heavy particles with high velocity these effects do not enter, at least not in the type of emulsion and development chosen by Bradt and Peters. The Y-intercept or percentage of light absorbed for zero δ-ray count represents the average contribution of the grains within the core of the tracks.

While the δ-ray count by Bradt and Peters is averaged over track lengths extending through several plates, our results are based on track lengths in only one plate (average length approximately 500 microns). Since we include in our measurements the very great number of short δ-ray tracks, which cannot be counted visually, our statistics per unit track length are greatly increased, and hence it is not too surprising that the results, with the exception of two points, do not scatter too much, considering the short track lengths measured. These two

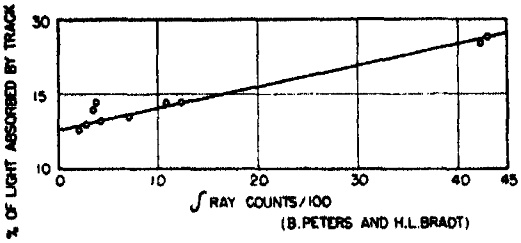

FIG. 9. Percentage of light absorbed by a heavy track as a function of δ-ray counts.

---

[3] H. L. Bradt and B. Peters, Phys. Rev. 74, 213 (1948); Phyllis Freier *et al.*, Phys. Rev. 74, 213 (1948).

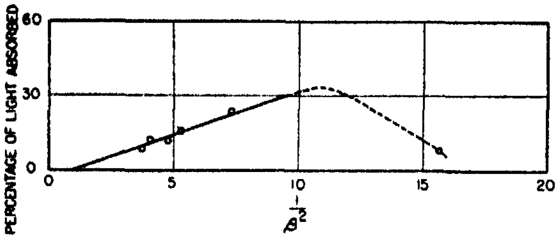

FIG. 10. Percentage of light absorbed by an iron track as a function of $1/\beta^2$.

points may be due to our erroneous identification of tracks measured by Peters and Bradt.

As shown above, saturation effects etc. are small for even iron tracks, if the particle velocity is high, and therefore with a suitable calibration our measurements (percentage of light absorbed) are directly related to the δ-ray counts and can thus be substituted in calculations based on δ-ray count.

It was clear that with lower velocities saturation effects could enter and obscure the relationship between photometric measurements and δ-ray count. Therefore we investigated an iron track starting at $\beta=0.525$ and stopping after passing through 12 plates. We found, using the slit previously described, that the photometric values did not follow the expected $1/\beta^2$ law to the maximum but saturated rather early exhibiting a wide plateau.

We felt that if we excluded the core and the immediate densely blackened neighborhood and measured the δ-rays beyond this region we could obtain the expected relationship. Therefore we used a double slit blocking out a center region of approximately 3 microns and extending 4.7 microns to both sides of the blocked out region. The light absorbed by the δ-rays within this double slit was again compared with the light absorbed in background measurements.

The results for an iron track measured at the average velocities $\beta^2=0.27$, 0.26, 0.25, 0.21, 0.187, 0.138, 0.064 (the intermediate plates were developed differently and therefore not taken into consideration) are plotted *versus* $1/\beta^2$ in Fig. 10. We find an approximate linear relationship up to the maximum. The scattering of the data can be explained by occurrence of staining effects on some of the plates. Unfortunately we do not have a measured point near the maximum; however, it lies within the region to be expected on the basis of calculations taking into account our slit geometry. After the maximum the photometric value drops rapidly to zero due to the contraction of the δ-ray pattern. However, with the single slit previously described we can measure towards lower velocities and accurately determine the thin down length.

Although our investigation has been only of a preliminary nature, it seems reasonable to expect that the proper combination of slits (single slit for low ray density, double slit for higher density) together with suitable calibration curves provides all the information one obtains from visual δ-ray counts. In addition the position of the maximum and the thin down length[*] can be determined. Grain counting along lightly ionized tracks of heavy particles which is sometimes helpful for their analysis can be rapidly done with the arrangement described in Section II.

A great advantage of our method for heavy particles in comparison with visual δ-ray counts is the speed with which the measurements can be performed. The actual measuring time for a track 2 mm long is about 5 to 6 minutes with an additional ten minutes necessary for evaluation of the charts.

The results of the analysis in visual δ-ray counting depend upon the judgment of the observer; furthermore because of the lengthy and exacting nature of the observations the statistics cannot be increased beyond a certain point. On the other hand our method gives reproducible results, and since both the time factor and eyestrain are materially reduced, the statistics and therefore the accuracy can be increased.

It is clear that the photometric method gives the best results when the emulsions are uniformly developed without stain or other inequalities. However, to some degree these fluctuations in transparency are averaged out through background measurements in the immediate vicinity of the track.

If confronted with a problem involving the accurate analysis of a great number of heavy particle trajectories, the above described method is of definite advantage.

SUMMARY

It has been our purpose to develop a measuring apparatus for nuclear emulsions which permits the operator of the machine to follow as simple a procedure as possible and thereby have all the necessary measurements performed and recorded automatically. By this procedure we hoped to achieve reproducibility, speed, accuracy, and a reduction of the fluctuations due to personal judgment. Although the apparatus herein described is only an experimental model, it has proved useful for rapid accurate measurements of range, grain density, delta-ray density (photometric method), multiple scattering, and geometrical relationship of trajectories in emulsions.

Since all the measured quantities are indicated by mechanical movements and electrical voltages, it is clear that we can also utilize computing machines etc. to calculate desired results. Furthermore, we are at present considering an extension of its use by incorporating automatic scanning and recording features for selected events.

---

[*] The thin down length is determined from the chart of photometric value *versus* length which exhibits a marked drop over the effective thin down length.

ACKNOWLEDGMENTS

The authors are indebted to Dr. B. Peters and Dr. H. L. Bradt of Rochester University for their cooperation and helpful discussions on the heavy particle work.

We wish to thank Dr. J. R. Dunning and Dr. P. Mitchell of Columbia University for their interest in the development of the apparatus.

This work was jointly sponsored by AEC Contract AT-30-2-Gen 16 Subcontract S-62 and ONR Contract N6 ONR 110, Task Order No. 1.

THE REVIEW OF SCIENTIFIC INSTRUMENTS VOLUME 21, NUMBER 12 DECEMBER, 1950

A Double Thin Lens Beta-Ray Spectrometer*

C. M. Van Atta,† Sydney D. Warshaw,‡ Joses J. L. Chen,§ and Samuel I. Taimuty
University of Southern California, Los Angeles, California

(Received July 31, 1950)

The description of the performance of a double thin magnetic lens beta-ray spectrometer is given. A detailed investigation of the separate distortions introduced by chamber misalignment, internal scattering, charged source and poor resolution has been made, and the results are presented qualitatively. An alignment procedure is presented, and also the arrangement of baffles to minimize scattering.

A. INTRODUCTION

THE purpose of this communication is first, to describe the construction of a new beta-ray spectrometer, and second to indicate, more or less precisely, some of the more pronounced sources of error in the use of this instrument for the measurement of beta-ray spectra.

Neither the basic design nor the interpretation of errors and distortion is original with us. The instrument itself has been patterned after a design first given by Quade and Halliday[1] which, in turn, was a modification of the original thin lens design of Deutsch and his coworkers.[2] Since the first-mentioned authors have not, to our knowledge, published any measurements made with their instrument, we think that such a description and discussion is worth while as a measure of the performance of the design.

Many authors (to be referred to in the text) have indicated the sources of error common to all kinds of magnetic spectrometers: the thick source, window absorption, effect of the earth's field, scattering in the chamber, and charged source all play a role in introducing distortions. However, it seems useful to repeat these observations for a single spectrum and on a single instrument, both to make the interpretation easier and to collect these data in a single paper for convenient reference. For these purposes the Cs 137 spectrum was chosen because its shape is accurately known;[3] the strong and conveniently located conversion line has been precisely measured[4] and the prominent Auger lines at low energy offer a further convenience.

B. DESCRIPTION OF THE INSTRUMENT

Figure 1 shows a schematic layout of the spectrometer. The chamber proper consists of a 54-in. long brass tube, 8-in. i.d. mounted inside a brass sleeve 9-in. i.d. The mounting was effected simply by allowing the inner chamber to ride on four leveling screws placed at both ends of the sleeve. This allows the inner chamber to be moved with respect to the sleeve (which also serves as a mounting for the coils) and gives an additional degree of freedom which proved to be useful in the alignment process.

The baffle system inside the main chamber is somewhat more elaborate than is customary in instruments of this type. Baffle L in the figure is a lead assembly for gamma-ray shielding. Mounted on it are three thick aluminum disks which serve to define the inner limit of the electron trajectories. At each end of the tube are installed the cone baffles; these are constructed of four

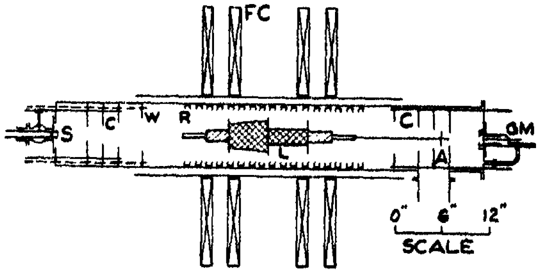

FIG. 1. Schematic diagram of the spectrometer. S, source and Lucite holder; GM, counter with replaceable thin window; FC, field coils; C, cone baffles; W, limiting baffle; R, rim baffles; L, lead baffle with aluminum disks and brass handles; A, axial baffle.

---

* This work was assisted by the joint program of the ONR and AEC.

† Now at the Radiation Laboratory, University of California, Berkeley.

‡ Now at the Institute of Radiobiology and Biophysics, University of Chicago.

§ Fellow of the China Foundation for the Promotion of Education and Culture.

[1] E. A. Quade and D. Halliday, Rev. Sci. Inst. 19, 234 (1948).

[2] Deutsch, Eliot, and Evans, Rev. Sci. Inst. 15, 178 (1944).

[3] H. Agnew and H. L. Anderson, Rev. Sci. Inst. 20, 86 (1949).

[4] L. M. Langer and R. D. Moffat, Phys. Rev. 78, 74L (1950).

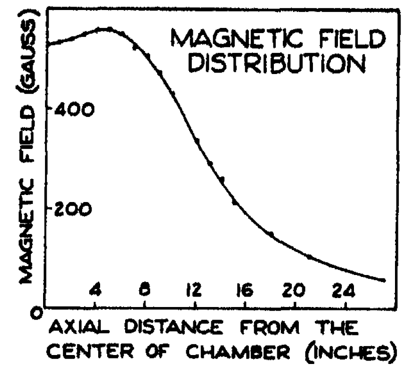

FIG. 2. Magnetic field distribution on the axis of the chamber.

aluminum disks each mounted perpendicular to the chamber axis and several inches apart. They limit the extreme peripheral rays from the source and their net effect is to put the source at the apex of a cone of angle about 22°. The central portion of the chamber is lined with a series of rim baffles in the form of circular channels placed $\frac{3}{8}$ in. apart and projecting $\frac{3}{8}$ in. into the chamber. These were formed of $\frac{1}{32}$-in. aluminum sheet bent to fit the inside of the tube snugly. In addition a single axial aluminum disk was installed at the counter end of the chamber 5 in. from the counter window.

The four field coils are placed in two pairs as shown in the figure. These are constructed of $\frac{1}{2}$-in. copper tubing, spiral wound in two layers and water cooled. The current is supplied by a 12-kw welding generator the field of which is excited by four thyratrons connected in parallel as a full wave rectifier. Stabilization is obtained by comparing the generator output with the voltage of a 24-volt storage battery and feeding the error signal to a direct coupled amplifier which controls the thyratron grid potentials. The coil current is measured in terms of the voltage drop across a shunt by means of a type K potentiometer.

With the coils placed as shown, the field distribution was measured (to about five percent accuracy) with a flip coil on the chamber axis. According to Quade and Halliday[1] this type of field distribution results in relatively small aberration. The field plot is given in Fig. 2.

Since there is no closed form solution of the ray equation for this type of field distribution it is necessary to use numerical methods to compute the trajectories. However, since the ray equation is appropriate only to obtain those paths which lie very close to the axis, and not for obtaining more useful information (like the amount of aberration) it was felt that a simple estimate of the refracting power as calculated from the ray equation with a variational principle would suffice for a design criterion. The more essential information was obtained empirically and by scaling the dimensions of Quade and Halliday's instrument. If one puts $H=hI$ gauss for the magnetic field on the axis, where I is the coil current, and for the momentum of an electron moving close to the axis $p=kI$ gauss-cm, then the ray equation becomes:

$$d^2r/dx^2=-h^2/4(u/k)^2r. \tag{1}$$

Here u is the object distance measured from the center of the lens system, r is the radial distance from the axis to the trajectory, and x is distance on the axis in units of u. In this equation the eigenvalues give directly the value of the constant of the instrument, k; a well-known modification of the Rayleigh-Ritz variational method gives

$$\frac{1}{4}\left(\frac{u}{k}\right)^2=\frac{\int_0^1 (dr/dx)^2dx}{\int_0^1 h^2r^2dx}. \tag{2}$$

Any value of k, calculated with some trial function for r in Eq. (2) will be smaller than the value calculated with the true eigenfunction. If trial functions like $\cos\pi x/2$ (the solution for the solenoid case) or $(1-x)$ (bending through a very small region) are used in (2) the result is a value for k which is much lower than the observed value. The usual thin lens formula can be obtained from (2) by noting that for this case the factor r^2 is slowly varying and, in these units, cancels the numerator; that is

$$\left(\frac{k}{u}\right)^2=\frac{1}{4}\int_0^1 h^2dx. \tag{2'}$$

Using $u=68.6$ cm and applying Simpson's rule for numerical quadrature, one gets $k=43.4$, which is quite close to the measured value. Hence the designation of the instrument as an equivalent thin lens seems justified.

The calculations were used only as a point of departure. The calibration was achieved with the Cs 137 K conversion line momentum value given by Langer[4] and cross-checked with the most recent measurement[5] on the conversion lines of In^{114}, using a rather thick In source. A further check was obtained using several lines from a lead radiator in front of a radon seed. All of the values for k, so measured, clustered around the Cs 137 line value to better than 0.5 percent.

The image rotation, as calculated from the thin lens formula, is about 102° as compared with the measured (see below) 122° for focused rays.

The source is introduced into the chamber through a vacuum lock assembly and is mounted on a thin Lucite shell which supports the Nylon source backing. The counter is a conventional pressure-seal, end-window type with the seal provided quite satisfactorily by an 0-ring. The thin Nylon window, the Nylon films made according to the recipe of Brown *et al.*,[6] is supported on a brass grill consisting of a hexagonal array of 0.040-in. diameter drilled holes which provides about 75 percent transmission. The counter is connected through Saran tubing to a pressure regulating system[7] to compensate for any loss of counter mixture due to window porosity and normally operated with an argon-10 percent alcohol mixture at about 5 cm Hg, although pressures as low as 3 cm can be used without loss of efficiency.

---

[5] Mei, Mitchell, and Zaffarano, Phys. Rev. 76, 1883L (1949).

[6] Brown, Felber, Richards, and Saxon, Rev. Sci. Inst. 19, 818 (1948).

C. PERFORMANCE OF THE INSTRUMENT

1. Scattering

With a reasonably thin source mounted on a very thin Nylon backing and supported by a thin Lucite shell, the whole assembly being loaded with Aquadag to prevent charging up, the Cs 137 spectrum was run with the result shown in Fig. 3a. At this point, the only adjustments of the instrument were an initial lining up by means of an electron gun, and the only baffles installed were a central (peripheral) baffle and the lead baffle. Note that on this curve, the Auger lines are quite indistinct and the resolution is poor. If this curve at the low energy end is compared with the good measurement made by Agnew[2] there is a pronounced deviation which may be partially explained by scattering. The first step in the adjustment was to eliminate the scattering distortions. C. S. Cook[8] has already indicated that this distortion can be removed by defining the beam by a sufficient number of baffles. In the present case enough baffles were introduced one at a time in such a way that, finally, the only straight line more than about 6 in. long that could be drawn starting from the counter window, without intersecting a baffle, was essentially in the direction of the trajectory. As partially indicated in the curves of Fig. 3 each addition of a baffle assembly had a definite and pronounced effect on the entire appearance of the spectrum, in particular, on the low energy end. All of these curves were run with the same thin source. Not all of the individual steps of improvement due to the separate additions are shown. In particular, the baffles fixed to the lead shield and the central peripheral baffle were originally made of brass. The simple device of replacing these with aluminum made a noticeable improvement, indicating a degree of scattering from the edges of the baffles themselves. Installation of the "rim-baffles" (*R*) also improved the low energy spectrum by preventing scattering from the chamber wall proper. An alternative method for eliminating chamber wall scattering by making the diameter of the chamber very large was followed by Agnew and Anderson.[3]

The two conical baffle assemblies (*C*) are mounted on ¼-in. aluminum rods which pass through Wilson seals on the chamber end plates. The position of these baffles was varied until the electron trajectories, defined by the small annular opening at the center, just missed grazing the edges of the disks. On the source end, there is also a movable baffle (*W*) mounted on similar rods which pass through both *C* and the chamber end-plate which can be used to vary the solid angle. (For the dimensions used, the variation produced in this way is too small to be very useful.) The final baffle was the small central disk (*A*) mounted axially on a rod projecting from the lead shield toward the counter and placed a few inches in front of *GM*. No special provision, like the use of a helical baffle, or a sector baffle was used to eliminate higher harmonics. Rather than reduce the already low transmission of the instrument, we simply note that the second harmonic has a node at the center of the lead shield, and the third harmonic should be (and apparently was) reduced by the smaller annular opening left by baffle *A*. The final result is shown in Fig. 3b. The almost complete absence of scattering was further confirmed by photographic means, a technique which was primarily used for the alignment of the chamber axis with the magnetic axis.

For indicating alignment of the chamber with the magnetic field a photographic plate, placed at the position of the counter window, recorded the image of the source. A comparative microdensitometer study of this image and a radioautograph of the source (neither of these are shown) indicated that the aberration was quite small and the scattering negligible, since the image was very sharply defined and actually slightly smaller (although with the same outline) than the autograph of the object. The image spot was taken using the coil current that corresponded to the *K*-conversion line. With about 100 microcuries activity the Eastman 103a-0 *UV* plates used required about a three-hour exposure for a good image. The solid angle was about 0.4 percent of a sphere.

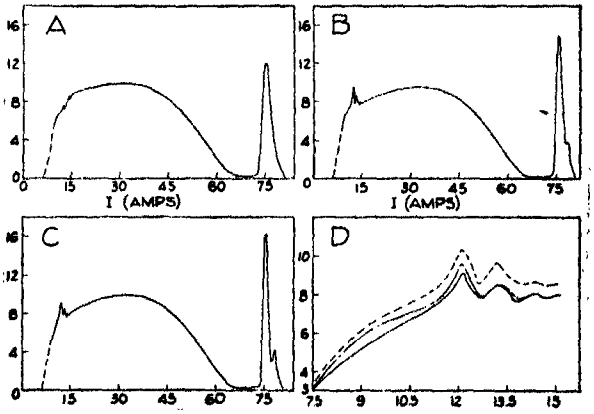

FIG. 3. A set of curves showing the improvements due to additional baffles and final alignment of the chamber. *A*, before adding baffles *C*, *R*, *A*; *B*, after adding baffles *C*, *R*, *A*; *C*, after final alignment of the chamber; *D*, low energy portion (10–50 kev) showing successive improvements: .... before adding axial baffle *A*, —·—·— after adding axial baffle *A*, ——— after final alignment. (Dashed lines in *A*, *B*, *C* indicate no window correction.)

---

[7] Ter-Pogassian, Robinson, and Townsend, Rev. Sci. Inst. **20**, 289 (1949).

[8] G. E. Owen and C. S. Cook, Rev. Sci. Inst. **20**, 768 (1949).

2. Alignment and the Effect of Earth's Field

The instrument has been so placed that the axis of the chamber is lined up with the direction of magnetic north. Quade and Halliday[1] have shown that for this arrangement, the correction to the focusing coil current is just one-half the difference of the currents required to focus a line spectrum with the field aiding and then bucking the earth's field. This correction they showed to be a constant for all focusing currents. For the arrangement described in this paper the correction is found to be 0.20 amp., which is quite insignificant compared to the rather large currents that were used; e.g., Cs 137 conversion line is focused at about 75 amp. However, the vertical component of the earth's field is quite important with respect to the proper behavior of the electron trajectories, especially for the lower energy groups. For its compensation a set of Helmholtz coils of rectangular shape is mounted about the chamber, symmetrically with respect to the axis of the chamber. These coils are 3 ft.×16 ft., spaced 3 ft. apart. Each coil is made of a six-conductor cable connected to give six turns in series. The current source is a set of storage batteries of high capacity, and the current may be varied continuously with a rheostat. A current of 5.9 amp. in the coils gave complete compensation of the earth field at the center of the chamber, while the error in the off-center region within the chamber is computed to be less than 2.3 percent of the vertical field at the center.

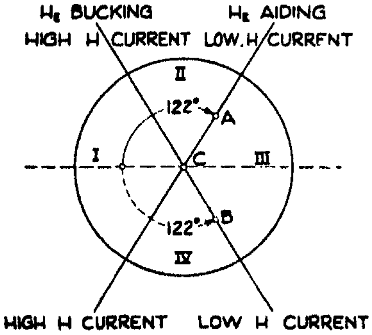

FIG. 4. Image space sketch showing the effect of sweeping Helmholtz coil current.

During the initial alignment of the focusing field, by making slight changes in the orientation of each of the four field coils, the Helmholtz coil field was found to be a convenient tool. The monoenergetic beam from an electron gun was used to give a focused image on a fluorescent screen at the detector end. Sweeping the Helmholtz coil current (hereafter the *H* current) through its compensating value moved this spot across the screen. The same observation was then repeated for reversed focusing field. The swept lines are shown in Fig. 4 which is drawn from observation and later confirmed by measurement on the burned marks on the inside surface of the fluorescent screen. The inclination of these lines with the horizontal axis corresponds to a rotation of 122°. The point of intersection of the two lines is taken as the center of the image plane after proper adjustment of the field coils. It should be understood that the precision of this method is limited by the finite size of the image and the necessity for the use of visual judgment of intensity.

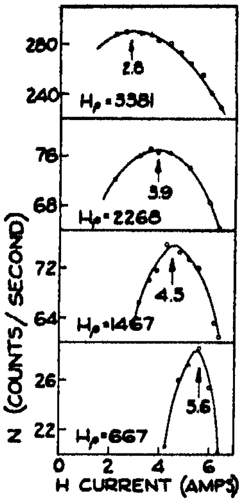

FIG. 5. Energy dependence of *H* current setting indicating imperfect alignment.

When the baffles and detector were completely installed, the possible existence of a slight misalignment was then sought for by a systematic variation of the *H* current. First the focusing current was set on a convenient point of the familiar Cs 137 spectrum, and the number of counts at the detector plotted against *H* current. This was repeated for a few points of the spectrum. If the maximum of this curve appears at a different value, in general, than the *H* current needed for exact compensation, then this indicates that the magnetic axis of the coils and the axis of the chamber are not identical. Further, a comparison of the maxima for different focusing fields will show an energy dependence as is illustrated in Fig. 5. With the field reversed the procedure was repeated to help in the approximate location of the apparent focal spot relative to the center of the counter. For example, if for the focusing field both aiding and bucking the earth's horizontal field, the maxima appear at higher *H* currents, the apparent focal spot is in region *I* of Fig. 4 and the chamber should be adjusted to shift the counter toward that region. The actual adjustment was accomplished by means of the set screws which support the chamber in the sleeve. At each adjustment the counts *versus H* current curve for a given focusing field was plotted. A correct move was indicated by both an increase in the number of counts at peak and an approach of the *H* current for peak to the correct compensating value. A few typical curves taken in the process of adjustment are shown in Fig. 6. Here the direction of motion of the counter for each move is indicated on the line connecting the maxima of the two associated curves. After final adjustments, a complete set of curves like those in Fig. 5 but with no energy dependence of the maxima (both for the aiding and the bucking case) were taken

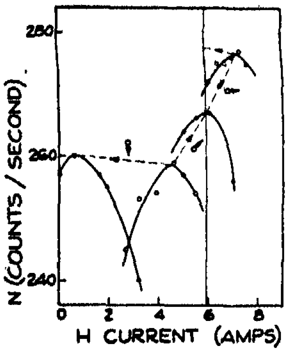

FIG. 6. Some maximizing curves taken during final alignment of the chamber.

to confirm the satisfactory centering of the detector with respect to the magnetic axis. An improvement of some 0.25 percent (out of 2.5 percent) in the resolution was obtained after this adjustment. The final check on the alignment was obtained by the photographic method mentioned above, with the addition of a reticle, drawn on the edges of the plate before exposure, and accurately located with respect to the center of the end plate of the chamber.

3. Resolution

As noted above, the final figure for the resolution was 2.1 percent with a solid angle of 0.4 percent of a sphere. At present the solid angle can be increased at the expense of resolution only by replacing the central baffle system or by reducing the distance between source and counter. Therefore, with the present arrangement, the only possibilities of increasing the number of detector counts are an increased total activity with a corresponding increase in source thickness and an increased total activity with an increased source diameter. Several authors[9] have pointed out the undesirability of the thick source. For low energy spectra, a thick source may make an unambiguous interpretation of the result impossible. This leaves only the possibility of increasing the source diameter, while keeping the thickness as small as possible; in effect this spoils the resolution and a correction must then be made. To check on the amount of distortion produced in this way, we ran several curves with the source diameter varied from about 4 mm to about 15 mm and with a corresponding variation in the counter window opening. (Deutsch[8] has shown that the optimum condition for unit magnification is to have the source size and the window size the same.)

In Fig. 7 the uncorrected spectrum is given for the 15-mm source, of about three-quarters the total activity of the source used in the 2.1 percent resolution case (Fig. 2). The resolution was now 5.4 percent (twice the half-width at half-maximum). While this resolution figure is not excessive, Owen and Primakoff[9] have emphasized that the distortion in the continuous spectrum that can be produced by this is not negligible.

If the poor resolution curve of Fig. 7 is normalized to the "good" curve of Fig. 2 (normalization at about 2580 gauss-cm, as explained below) it is found that the necessary correction is less than two percent except very near the end point, and that the "poor" curve is higher than the good curve for momenta greater than the normalization point and lower for smaller momenta. For the quantitative correction at least two, not unrelated, methods are available. As formulated by Owen and Primakoff[9] the number of counts at the detector, $M(p)$, per unit momentum interval is given by

$$M(p)=\int_0^\infty N(p')K(p,p')dp', \tag{3}$$

where $N(p)$ is the true momentum distribution, and K, the kernel of the integral equation, is obtained from a study of the shape of an internal conversion line. In the case where source thickness may be neglected, K is simply the transmission function of the instrument. For an arbitrary line shape the integral equation cannot be solved in closed form. Owen and Primakoff express the true counts N in terms of M and its derivatives and the moments of K about its maximum. In the case they first investigated, they used a 180° spectrometer for which the line shape was asymmetric and represented by an exponential. In our own case the line is very nearly represented by a Gaussian function (Fig. 8). For this symmetric shape, the first moment vanishes, making the distortion smaller for this type of instrument. A good fit to the line is obtained with $\exp-(p-p_0)^2/2a^2$, and with $a=0.0155p_0$, $p_0=3381$ gauss-cm. Although the width was not measured for any lower energy line, this value of a is not inconsistent with the shape of the Auger lines at the low end of the spectrum. If we put $a=0.0155p_0+b$, where b may be a roughly constant addition to the width due to, e.g., scattering, it is found that b is no more than seven percent of a at as low a value of energy as 26 kev. The Owen-Primakoff correction is then

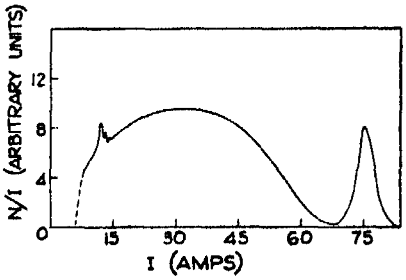

FIG. 7. Cs 137 spectrum with "poor" (5.4 percent) resolution.

$$N(p)=M(p)\left[1-(0.0155p)^2\frac{M''}{M}\right], \tag{4}$$

---

[9] G. E. Owen and C. S. Cook, Phys. Rev. 76, 1726 (1949); Langer, Moffat, and Price, Phys. Rev. 76, 1725 (1949); G. E. Owen and H. Primakoff, Phys. Rev. 74, 1406 (1948), and Rev. Sci. Inst. 21, 447 (1950). In particular, note footnote 8 in the last paper.

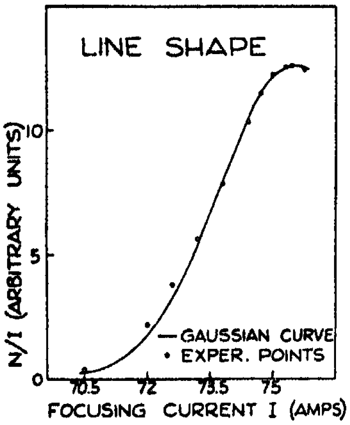

FIG. 8. Line shape for 5.4 percent resolution.

where the second derivative is obtained by numerical methods. For the 5.4 percent case the measured curve has an inflection point at about 2580 gauss-cm where the correction factor is therefore unity; the application of this factor in general results in a satisfactory fit of the poor resolution case to that with good resolution. (In the 2.1 percent case the correction is of course, about one-sixth that of the situation with 5.4 percent resolution.) The alternative correction is a graphical "cut-and-try" method first used by Hughes and Alburger[10] for the measurement of the low activity Be^{10}. Here the end point is first determined and then a plausible assumption is made about the shape of the true spectrum, $N(p)$. The integral in Eq. (3) is then calculated graphically by using the actual rather than an analytically fitted line shape. The result is a prediction of the distortion produced in a definite theoretical spectrum by the resolution used. The value of N at a point, divided by the predicted value of M is then taken to be the correction factor which multiplies the observed value of M. The application of this method to the 5.4 percent curve gave a correction very nearly equal to that given by the analytical method, but somewhat larger near the end point. Probably the small (but not statistical) discrepancy is due to the neglected contribution of the low intensity high energy group of the Cs 137 spectrum. In the case of an unknown degree of forbiddenness (the first-forbidden correction factor was used here) the procedure is repeated using different correction factors until a straight line Fermi plot results. There is, therefore, some uncertainty in whether at least part of the "distortion" is real, i.e., produced by some unknown degree of forbiddenness, or whether it is experimentally produced by poor resolution. The analytical method, although it involves a number of mathematical approximations that restrict its validity, seems to be more straightforward.

4. Charging-Up of the Source

The erratic behavior of a charged source is well known.[11] For a systematic study we deliberately made some sources on ungrounded film and/or ungrounded holder, while a control source of identical size and activity was mounted on a well-grounded backing—the Lucite shell holder painted with Aquadag in alcohol, and the back side of the Nylon film smeared with a foggy coating of Aquadag in dilute insulin solution—the resistance across the support being about 100 megohms. The sources were about 20 μc in activity and 0.2 mg/cm^2 in thickness. The ungrounded source usually gave a nearly correct transmission curve for the K conversion line (with the L line on the upper side) when a reading was taken right after introducing the source through the vacuum lock. With an improperly grounded Lucite shell, a second curve taken after a short time was similar except for a definite shift of both K and L peaks downward of about 50 gauss-cm (corresponding to about 13 kev in energy), and a corresponding distortion of the continuous spectrum. After longer intervals of time, the peaks shift slightly further. Generally if the Lucite holder is well grounded but the Nylon is not, the shift of peaks will be gradual, taking many hours to reach equilibrium value. Evidently in the former case the surface conductivity of the Lucite holder is the main factor, while in the latter the aging of the Nylon film in vacuum seems to decrease its conductivity. It is certain that even for a weak source the charging-up effect will disturb not only the low energy portion but the whole spectrum to the extent of 10 kev or more, depending on the source activity and the insulation property of the backing materials.

ACKNOWLEDGMENT

It is a pleasure to acknowledge the assistance given by Dr. Alfred W. Einarsson for the design and construction of the field control circuit and field calibration and to Mr. John M. Leffler for participation in the design and construction of the instrument.

---

[10] Hughes, Eggler, and Alburger, Phys. Rev. 77, 726 (1950). Dr. Alburger kindly sent us the unpublished details of this technique.

[11] See, for example, L. M. Langer, Rev. Sci. Inst. 20, 216 (1949).

THE REVIEW OF SCIENTIFIC INSTRUMENTS VOLUME 21, NUMBER 12 DECEMBER, 1950

Continuously Sensitive Diffusion Cloud Chambers*

E. W. COWAN
California Institute of Technology, Pasadena, California

(Received August 20, 1950)

The following types of continuously sensitive diffusion cloud chamber have been built and successfully operated: a chamber designed to be photographed through the top for use with a particle accelerator; a chamber designed to be photographed from the side for cosmic-ray studies; and a very simple chamber for demonstration purposes. The construction and best operating conditions are described.

SEVERAL models of cloud chambers are described here which are of the same general type of continuously sensitive diffusion chamber described by Langsdorf.[1] Supersaturation is obtained by the diffusion of alcohol or water vapor from the warm roof of the chamber downward through an inert gas to the cold floor. Condensation occurs on ions in a sensitive layer of several inches depth near the floor of the chamber. Considerable simplification in the design and also some improvement in the results have been obtained.

The following general considerations apply to all of the specific types that will be described later. A pad of black velvet or other cloth soaked with alcohol and warmed by contact with a metal plate that forms the top of the chamber has been found to be the best vapor source. The deepest sensitive layers have been obtained with mixtures of methyl alcohol, ethyl alcohol, and water. However, since the composition of the mixture changes with evaporation, and since methyl alcohol alone gives very good results, pure methyl alcohol usually has been used.

As the temperature of the roof is increased, the depth of the sensitive layer increases until an optimum temperature is reached above which the sensitive volume splits into two layers. Since the exact temperature depends upon the dimensions of the chamber and the vapor used, numerical values will be given later only for specific instances. Droplets which form about ions in the upper sensitive layer grow very rapidly because the concentration of vapor is greatest near the source of vapor at the top of the chamber. These droplets fall to the bottom, and remove vapor that would otherwise increase the supersaturation of the lower part of the chamber so that below the top layer the supersaturation is not sufficient for ion condensation, except in a shallow layer near the bottom where the temperature gradient is large. As the temperature of the top plate approaches the value at which the vapor pressure of the liquid nears the total pressure in the chamber, which might appear at first sight to be the best temperature, the upper layer approaches the top of the chamber and fills the chamber with a general rainfall. The very rapid growth of droplets in the top layer results in a competition for vapor in which only a relatively few of the ions near the top of the layer are in regions of sufficient supersaturation to form droplets. No recognizable tracks are formed in this layer, and the fact that the condensation is actually on ions can be ascertained only by careful observation of the effect of an electric sweep field. A pulsed electric field, of one of the types to be described later, is of some value in preventing the splitting of the sensitive layer.

This type of general rainfall may have been the cause of some of the difficulties with Langsdorf's chamber attributed to droplet nuclei produced by the vapor source.[1] Although a general rainfall is produced by heating the vapor source above the boiling point, at the normal operating temperature "streamers" of droplets which sometimes appear have been traced to leaks that permit contaminated air from the outside to enter

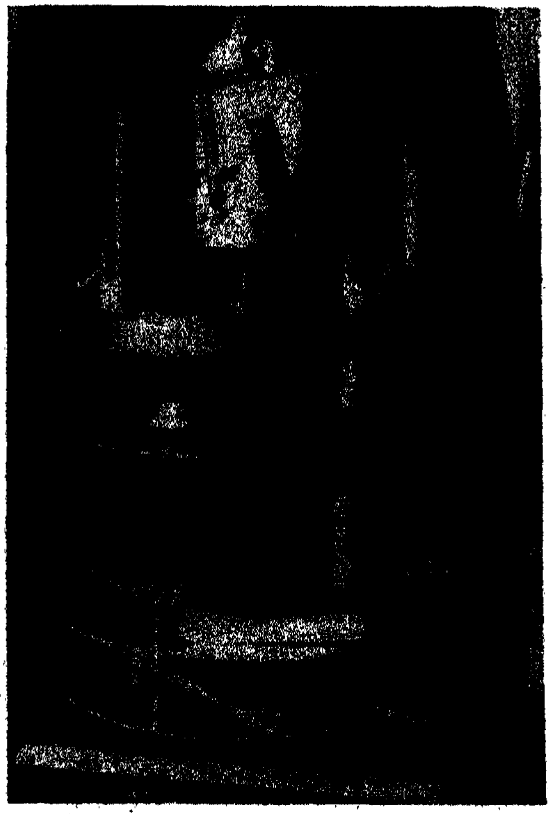

FIG. 1. Continuous chamber with camera mounted above.

---

* This research was assisted by the joint program of the ONR and AEC.

[1] Alexander Langsdorf, Rev. Sci. Inst. 10, 91 (1939).

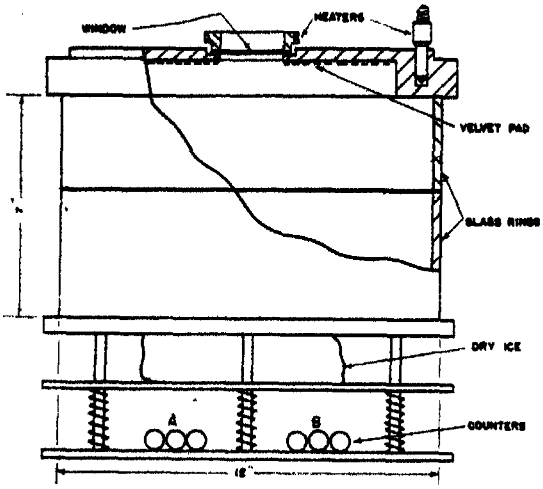

FIG. 2. Construction of chamber shown in Fig. 1.

the chamber, or to corona from fine points if a high sweep voltage is used. Streamers resulting from the circulation of contaminated air through leaks, which are especially likely to occur when the top is cooling, appear like small waterfalls in the chamber and may be stable over considerable periods of time. Brass, aluminum, rubber, Neoprene, and several types of cloth have all been placed in direct contact with the liquid in the top of the chamber without causing any apparent trouble.

Air may be used as the inert gas in the chamber, although argon gives better results, especially if ethyl alcohol is used in the mixture. If the molecular weight of the vapor is heavier than the molecular weight of the inert gas, there will be some unstable motion of the gas near the top of the chamber, resulting in considerable condensation on the walls of the chamber. However, the lower layers of gas in the chamber will still be stable, and tracks have been observed even using combinations such as helium and ethyl alcohol. Experiments made to determine the optimum pressure in the chamber showed that in the range of 0.1 to 2 atmospheres the difference in performance, which was difficult to measure because the optimum temperature and height vary with pressure, was not sufficient to justify the added difficulty in operating at a pressure different from one atmosphere.

The floors of the chambers have been made of aluminum blackened by an anodizing process or of black Bakelite. When the bottom becomes covered with alcohol, the black surface makes an excellent background for photography or viewing if the source of illumination is arranged so that its reflection is not

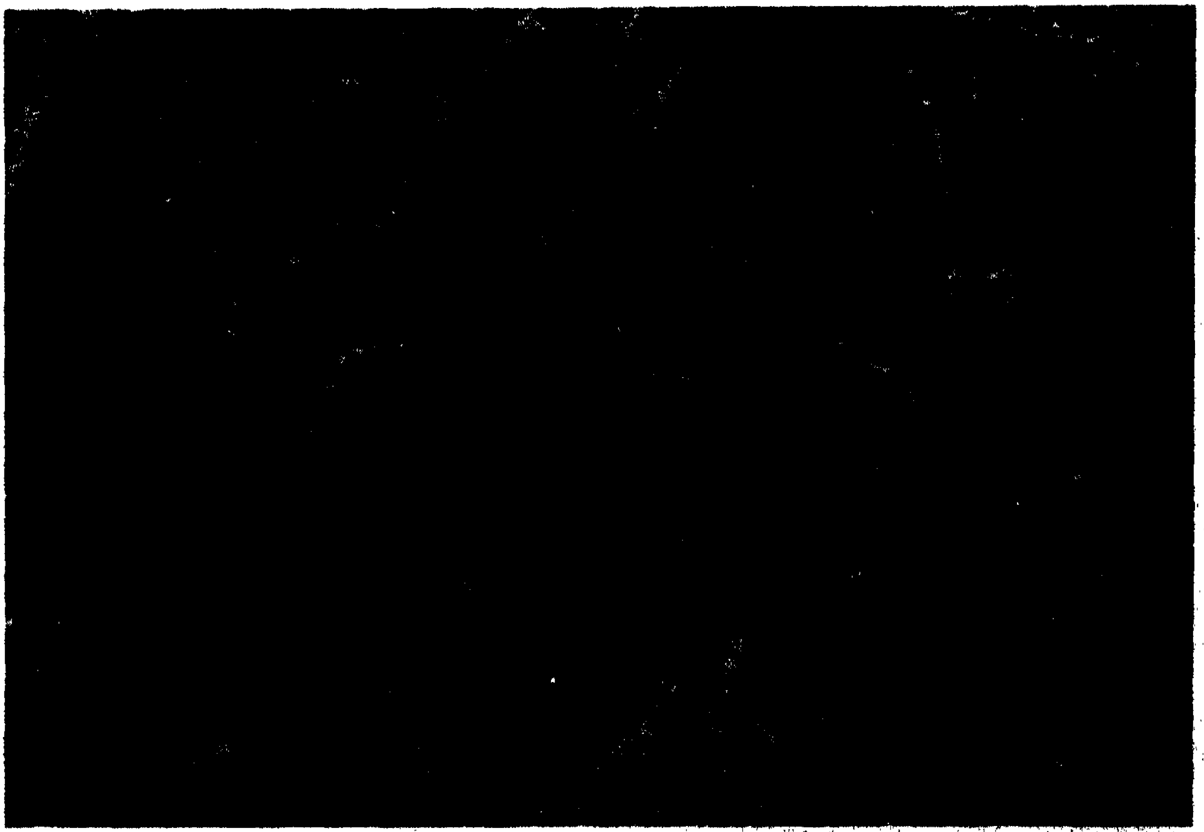

FIG. 3. Tracks produced in chamber by exposure to radium source.

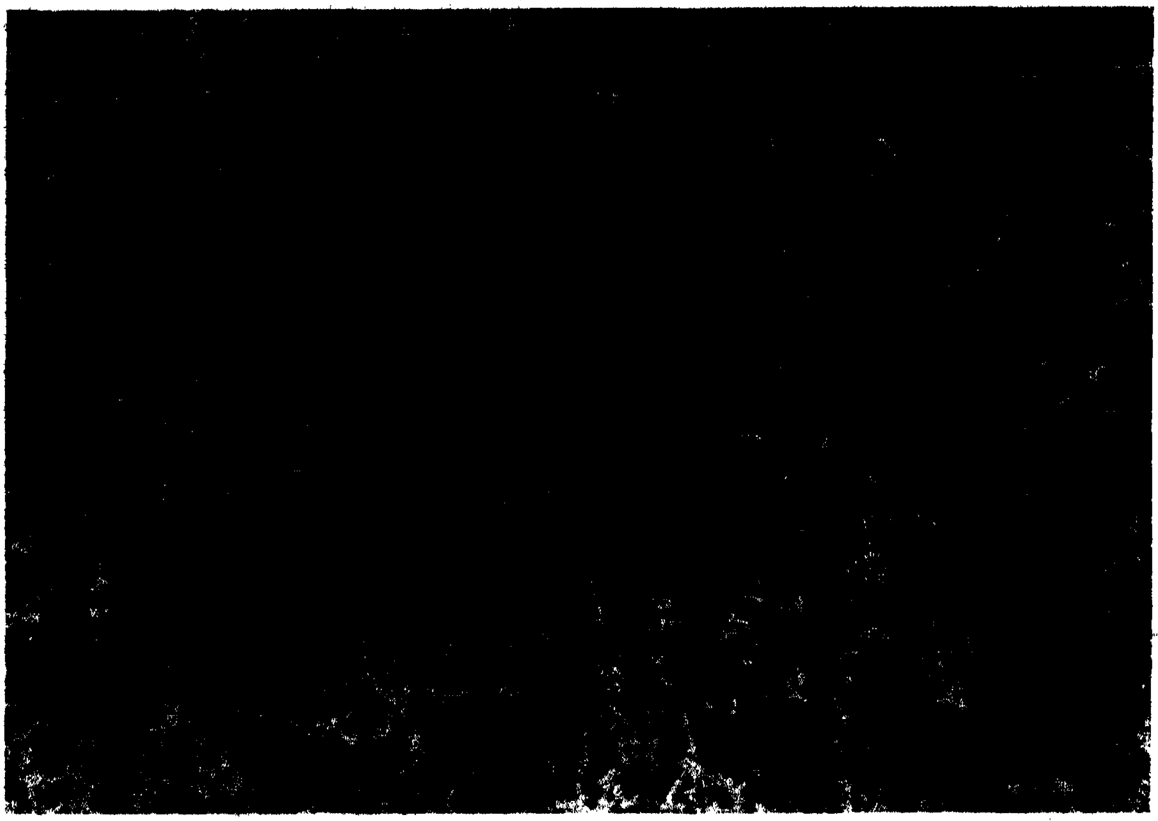

FIG. 4. Photograph of chamber after heavy exposure to radium source.

visible in the bottom. The temperature of the floor of the chamber is not at all critical. Tracks are first observed as the temperature is lowered below about −30°C, and below −70°C (with methyl alcohol) droplets begin to form without ion nuclei, producing a thin cloud layer about one-eighth of an inch deep on the floor. The most convenient method of cooling the bottom is by direct contact with a block of dry ice (−78°C). If the illumination is such that the cloud layer on the floor forms an objectionable background, a thin heat insulator between the dry ice and the bottom may be used to raise the bottom temperature slightly. Another method of cooling is by partially submerging the bottom of the chamber in a bath of alcohol and dry ice, which gives a temperature just above that necessary for the cloud layer on the floor to form.

With a pressure of one atmosphere in the chamber, the height of the chamber giving the deepest sensitive layer is about eight inches. If the diameter is considerably larger than this height the sensitive layer is uniform in depth except near the walls. With a diameter about the same as the height, the layer becomes mound shaped with the greatest thickness at the center.

The chamber shown in Figs. 1 and 2 was designed with the idea of possible use with the synchrotron now under construction at the California Institute of Technology. A camera with a wide-angle lens of 28-mm focal length is mounted above a small window in the top of the chamber, which has a cylindrical glass wall. The construction is shown in Fig. 2. A velvet pad with a hole in the center is sewed to a piece of perforated sheet aluminum that is in turn fastened to an aluminum top plate, which is sealed to the glass ring forming the walls of the chamber. This plate is heated by three pencil-type soldering iron tips inserted into holes around the edge of the metal plate. About 40-watts power is needed for normal operation. A small additional heater is wound around the clamping ring for the top window to prevent vapor from condensing on the window.

The alcohol is contained in a reservoir and fed through a needle valve to the velvet pad, over which the alcohol becomes uniformly distributed. The bottom of the chamber is made of anodized aluminum, and dry ice is held in contact with it by a spring-supported plate. The cylindrical glass wall is made of two twelve-inch diameter glass rings, the lower one being four inches high and the upper three inches high. These rings are separated by a conducting rubber gasket which is one of the sweep-field electrodes. The other sweep-field electrode is formed by the top and bottom of the chamber connected electrically. This arrangement removes the ions from the upper part of the chamber without pulling them down into the sensitive layer.

Rubber gaskets are used to seal the rings to the top and bottom of the chamber, which may be pulled tightly against the rings by Bakelite rods running from the top to the bottom. When the chamber is used at atmospheric pressure the Bakelite rods may be omitted and the chamber clamped together only by the weight of the top plate. If the rings are accurately ground the leaks are small enough not to disturb the operation of the chamber seriously, although the displacement of inert gas out of the chamber by vapor may change the operating conditions. The outside of the lower ring occasionally must be wiped with a cloth moistened with alcohol to remove the frost that accumulates.

When the chamber is used with the synchrotron, it is planned to pulse the sweep field by applying a voltage to remove the ions after each burst of particles from the synchrotron. The photograph in Fig. 3 was taken after the chamber was exposed to a sudden pulse of radiation from a radium source. With a properly synchronized sweep-field voltage pulse of about 600 volts amplitude, the chamber will recover sufficiently fast to be sensitive to a large pulse of radiation, such as shown in Fig. 4, at intervals of three or four seconds. Although a continuous background of ionization reduces the height of the sensitive layer, the chamber operates satisfactorily with a background several times the normal background ionization at sea level.

With argon and methyl alcohol in the chamber, the sensitive layer is about three inches deep in the center of the chamber at the optimum roof temperature of 39°C. With air and methyl alcohol the sensitive layer is about three inches deep at a roof temperature of 44°C, but there is some turbulence near the top of the chamber which limits the depth of the sensitive layer. The addition of water to the alcohol causes the droplets to grow more slowly. With a liquid mixture of about equal parts of methyl alcohol, ethyl alcohol, and water, it is possible to obtain a sensitive layer five or six inches deep after a pulse of sweep voltage. The tracks in the upper part of the layer, however, are diffuse, indicating that the supersaturation is barely sufficient for ion condensation, and, except for a small time after the pulse of sweep voltage, the sensitive layer divides into the two parts mentioned earlier. A roof temperature of 55° to 65°C is best for the mixture given above when using argon in the chamber.

This chamber also has been operated with the coincidence-counter arrangement shown in Fig. 2, which tends to select cosmic-ray showers of two or more particles. A coincidence between any counter in group *A* and any counter in group *B* triggers a flash lamp after a 180-millisecond delay. Figure 5 shows a small cosmic-ray shower photographed with this type of counter control. Since the tracks are very sharp this arrangement operated at high altitudes could provide an

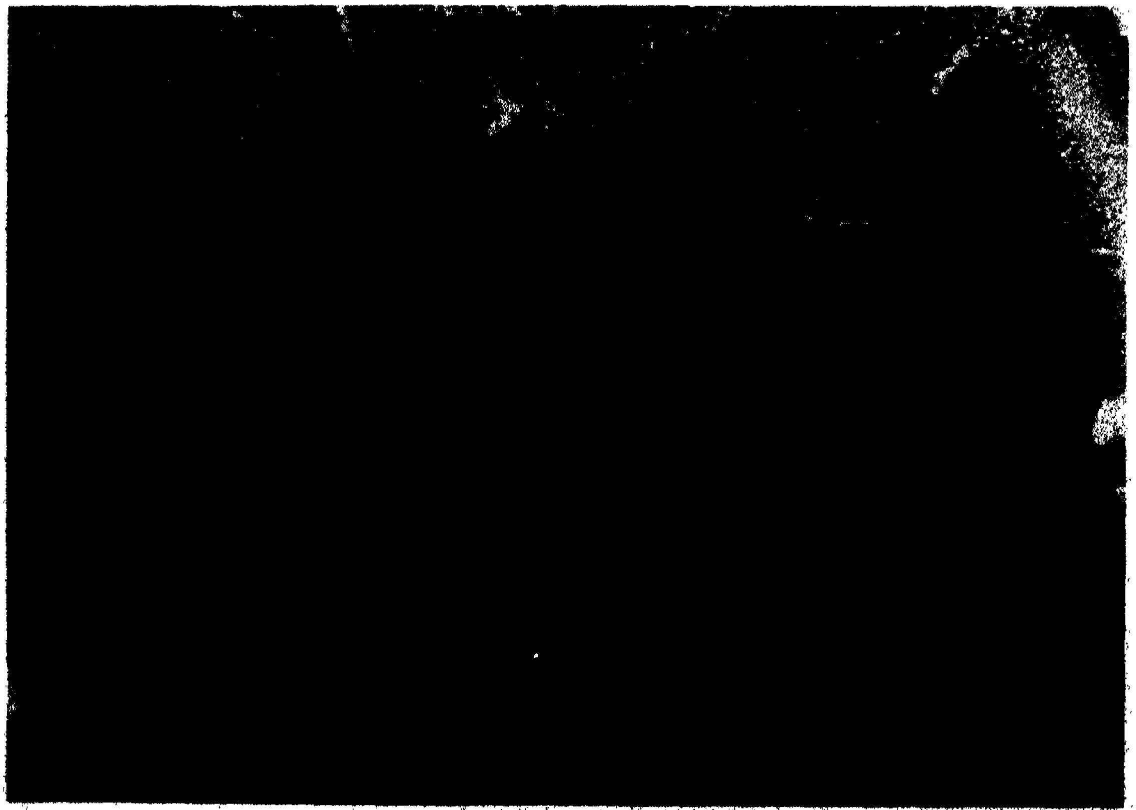

FIG. 5. Small cosmic-ray shower photographed with counter control.

FIG. 6. Sharp cosmic-ray track photographed with 20-msec. light delay (actual projected length of track as viewed by camera about 6 cm). Crooked track was made by low energy electron at an earlier time, and droplets have separated while falling.

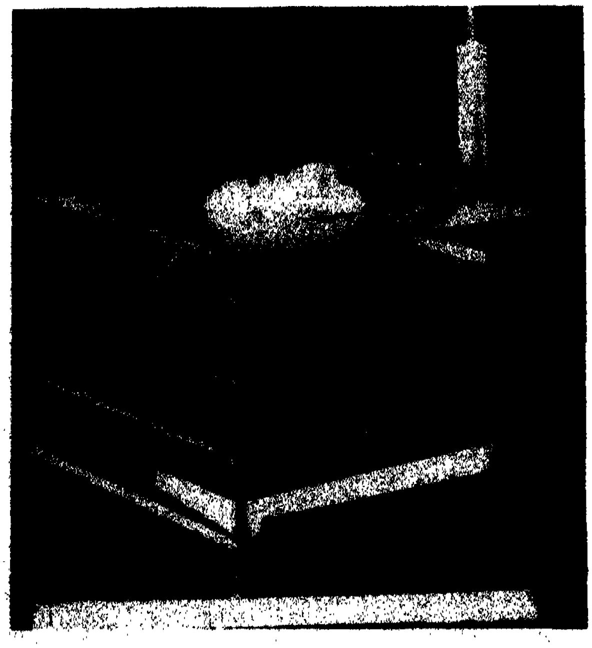

FIG. 7. Continuous chamber designed to be photographed from side.

effective means of studying the cores of large air showers.

The flash lamp is a General Electric Type FT-422, connected to 250 μf charged to a voltage of 2000 volts. Only the region from $\frac{1}{4}$ in. to $2\frac{3}{4}$ in. above the floor is illuminated by the flash. A lens aperture of f/8 gives adequate exposure on Linagraph Pan or Linagraph Ortho film. Under these conditions the photograph may be taken as soon as twenty milliseconds after the counters are tripped, although a very short delay is not essential since the diffusion chamber is not troubled, as is the expansion-type cloud chamber, by the diffusion of ions before droplet growth begins. The stable atmosphere of the diffusion chamber also alleviates the problem of distortion. Figure 6 is an enlarged photograph of a sharp cosmic-ray track photographed 20 milliseconds after the counters were tripped. When the chamber is operated with counter control, a sweep voltage pulse of 1.5 seconds duration and 600 volts amplitude is applied every 45 seconds.

The rectangular chamber shown in Fig. 7 was designed to be photographed from the side for studies of cosmic rays. With the thought in mind that this chamber might be used later in a magnetic field, the smallest dimensions consistent with good results were used. The inside dimensions are 9×9×5 in. high, and the maximum depth of the sensitive layer, using methyl alcohol and argon, is 2½ in. with a roof temperature of 34°C. A window of black glass in the back provides a background for taking a photograph through the front window, and the sensitive volume is illuminated through the side windows. The windows are mounted in Bakelite frames that are held together with screws and Bakelite cement to form the walls of the chamber.

The construction of the top and bottom of the chamber is very similar to that of the first chamber described except that the heater consists of the heating element from a coffee percolator clamped to the center of the top. A pulsed sweep voltage of 600 volts is applied between the top and bottom plates.

The continuously sensitive diffusion chamber makes an ideal demonstration unit, both because the continuous operation makes the tracks easy to observe, and because of the simplicity of construction. A glass ring resting on a black Bakelite base placed on a cake of dry ice makes a very simple demonstration chamber. The vapor source may be a doubled layer of black cloth tied over the top and saturated with warm alcohol. If operation for a considerable time is desired, a metal plate warmed by a flat iron may be placed on top of the cloth. The chamber floor should be covered with a layer of alcohol to seal the bottom to the glass ring and to provide a good viewing background. A battery of several hundred volts may be connected by clip leads between the cloth and the Bakelite (with the clip in contact with the alcohol puddle around the ring) to provide a sweep-field, although this is not essential. With a good source of parallel light projected horizontally through the chamber, a large group can observe the tracks from all directions except when looking directly into the light. A continuously sensitive demonstration chamber has been used for several lectures, and for several months it has been one of the regular demonstrations shown visitors to this laboratory.

I would like to express my appreciation for the encouragement and advice in this work by Dr. C. D. Anderson, who, in 1936, made some of the first investigations of this type of chamber.

THE REVIEW OF SCIENTIFIC INSTRUMENTS VOLUME 21, NUMBER 12 DECEMBER, 1950

A Rapid Method for Calculating and Using Platinum Thermohm Tables

R. A. Buerschaper
Taylor Instrument Companies, Rochester, New York

(Received July 18, 1950)

A method is described whereby resistance-temperature tables can be calculated in a few hours using punched cards. The method is much simpler and quicker to use than the "platinum temperature" tables. An example is given for reducing resistance measurements to temperature and a method for checking bridge and thermohm drift with respect to the tables is proposed.

THE THERMOHM AS THE INTERPOLATION INSTRUMENT

THE International Temperature Scale of 1948 defines the temperature °C from the ice point to the antimony point by the formula

$$R_t = R_0(1 + At + Bt^2),$$

and from the oxygen point to the ice point by the formula

$$R_t = R_0(1 + At + Bt^2 + C(t-100)t^3).$$

R_t is the resistance of the thermohm at any temperature t°C and R_0 is its resistance at the ice point. The constants A, B, and C are obtained by measuring R_t at the steam, sulfur, and oxygen points. The constants for any thermohm may be obtained by having the thermohm certified at the National Bureau of Standards. From these constants, a table may be calculated of values of R_t/R_0 *vs.* t°C and t°F whereby the resistance may be converted to temperature. The thermohm and its table, together with a Mueller Bridge, form one of the primary temperature standards from the oxygen point to the antimony point.

CALCULATIONS FROM THE OXYGEN POINT TO THE ICE POINT

The following constants were obtained from a National Bureau of Standards Certificate for one of two thermohms in use at present.

$$A = 3.9821 \cdot 10^{-3};$$
$$B = -5.862 \cdot 10^{-7};$$
$$C = -4.351 \cdot 10^{-12}.$$

Write the formula as

$$\begin{aligned} R_t/R_0 &= 1 + At + Bt^2 + C(t-100)t^3 \\ &= 1 + At + Bt^2 + Ct^4 - 100Ct^3. \end{aligned}$$

By setting $t = 0, -1, -2, -3, -4$, and -5°C in the expression for R_t/R_0, we may obtain the successive differences. The fourth difference is a constant as the equation is of the fourth order.

t°C	R_t/R_0	X_1	X_2	X_3	X_4
0	1				
		$-A+B+C+100C$			
−1	$1-A+B+C+100C$		$2B+14C+600C$		
		$-A+3B+15C+700C$		$36C+600C$	
−2	$1-2A+4B+16C+800C$		$2B+50C+1200C$		$24C$
		$-A+5B+65C+1900C$		$60C+600C$	
−3	$1-3A+9B+81C+2700C$		$2B+110C+1800C$		$24C$
		$-A+7B+175C+3700C$		$84C+600C$	
−4	$1-4A+16B+256C+6400C$		$2B+194C+2400C$		
		$-A+9B+369C+6100C$			
−5	$1-5A+25B+625C+12500C$				

X_1, X_2, X_3, and X_4 are the first, second, third, and fourth differences.

At this point it may be well to list the punch card machines used in calculating and tabulating the results: (1) Key Punch Machine which is a hand machine to punch the information into the cards, (2) Reproducing Summary Gang Punch Machine which reproduces, punches common information in cards and also summarizes totals from a group of cards, and (3) Tabulating Machine which adds, subtracts, and prints. With the aid of these machines the sets of differences and the function R_t/R_0 may be calculated and tabulated.

The steps in using the punched cards and machines are given below for the fourth-order equation.

The fourth difference, X_4, must be calculated first using data from the certificate.

$$24C=-104.424\cdot 10^{-12}.$$

This value is gang punched into 200 cards to cover the range 0 to −200°C.

Calculate the first, third difference, X_3

$$X_3=36C+600C=-2767.2\cdot 10^{-12}.$$

This value is now key punched into a lead card of another color and the 200 fourth-difference cards precede the third-difference cards, tabulate and summary punch. Mathematically this step is equivalent to subtracting algebraically the fourth difference from the first third difference 200 times, to form a set of third differences.

Next, calculate the first, second difference $2B+14C+600C$.

$$X_2=2B+14C+600C=-1.1751\cdot 10^{-6}.$$

This value of the first X_2 is key punched into a lead card of a still different color. Precede the third-difference cards (X_3) with this second difference and tabulate and summary punch. Again this step is mathematically equivalent to subtracting algebraically the set of third differences from the first second difference.

The next step is to calculate the first, first difference, X_1.

$$X_1=-A+B+C+100C=-3982.7\cdot 10^{-6}.$$

Precede the X_2 or second difference set with the X_1 lead card, tabulate and summary punch. Gang a 1 and a 1.8 in the summary cards. This step is equivalent to subtracting algebraically the set of second differences, X_2, from the first, first difference. The 1 and 1.8 ganged in the summary cards are for the differences in °C and °F, respectively, for which the function R_t/R_0 is to be given.

Now, key punch a 1 in the lead card of the function R_t/R_0 and a 0 for °C and a 32 for °F. These are the starting temperatures in this table. Precede the first difference cards with this function card and tabulate. This step is, in effect, subtracting algebraically the values of the set of first differences in sequence from 1, which is the value of R_t/R_0 at the ice point and also subtracting 1 from zero and 1.8 from 32 each time. This tabulation gives the values of R_t/R_0 for every °C and every 1.8°F from 0 to −200°C or 32 to −328°F.

CALCULATIONS FROM THE ICE POINT TO THE ANTIMONY POINT

The constants for the equation are given above. The calculations are made in the same manner as for the fourth-order equation. The calculations are simpler as we are now dealing with an equation of the second order.

$$R_t=R_0(1+At+Bt^2)$$
$$R_t/R_0=1+At+Bt^2.$$

Set $t=0$, 1, and 2 in the equation above and obtain the various differences in terms of the constants A and B.

t°C	R_t/R_0	Y_1	Y_2
0	1		
		$A+B$	
1	$1+A+B$		$2B.$
		$A+3B$	
2	$1+2A+4B$		

Y_1 and Y_2 are the first and second differences. Here the second difference is a constant as the equation is of the second order.

Calculate the second difference, Y_2

$$Y_2=2B=-1.1724\cdot 10^{-6}.$$

Gang punch this value, $2B$, in 500 cards to cover the range 0 to 500°C. Also, gang punch a 1 and 1.8 in these cards.

TABLE I.

Date	Benz. acid cell No.	Thermohm No.	R_t/R_0	°C	Benz. acid freezing pt. °C	Corr. to benz. acid pt.
9/ 1/49	N.B.S. 15	446899	1.478463	122.357	122.359	+0.002°C
1/31/50	N.B.S. 15	446899	1.478443	122.352	122.359	+0.007°
5/ 5/50	N.B.S. 15	446899	1.478448	122.353	122.359	+0.006°
6/23/49	N.B.S. 15	671634	1.478570	122.360	122.359	−0.001°
3/ 3/50	N.B.S. 15	671634	1.478573	122.361	122.359	−0.002°
7/ 6/50	N.B.S. 15	671634	1.478566	122.359	122.359	0.000°

Next, calculate the first, first difference $A+B$.

$$Y_1 = A+B = 3981.5\cdot 10^{-6}.$$

Key punch this value of $A+B$ in a card of another color and key punch a 1 and a 1.8 for the increments of °C and °F in this card. Precede the 500 second-difference cards with the first difference card, tabulate and summary punch. This step is equivalent to adding algebraically the 500 values of the second difference to the first, first difference to form the set of first differences.

Now, key punch a card with 1, the value of R_t/R_0 at 0°C or 32°F. Also, key punch a 0 and 32 in this card for the initial temperatures. This is the function card.

Precede the first difference cards with this function card and tabulate. The results are tabulated values of R_t/R_0 *vs.* °C and °F from 0° to 500°C. As the thermohms were not guaranteed above 500°C, the tables were terminated at 500°C, and not the antimony point. The tables may be checked at convenient temperatures by direct substitution in the equations, using the constants from the N.B.S. Certificate.

VALUES OF R_t AND R_0 CONVERTED TO TEMPERATURE

Assume the resistance of the thermohm to be measured with a Mueller Bridge and that the corrections to the bridge are already applied to the values of the resistances given below.

Let $R_0 = 25.5358$ ohms.

Let $R_t = 37.6311$ ohms.

$$\text{Then } R_t/R_0 = \frac{37.6311}{25.5358} = 1.473660.$$

From the table, we have

°C	°F	R_t/R_0	Diff.
121	249.8	1.473254	
			0.003840
122	251.6	1.477094	

Interpolating, $1.473660 - 1.473254 = 0.000406$.

$$\text{Then } t\text{°C} = 121 + \frac{0.000406}{0.003840} = 121.106\text{°C}.$$

In using the table, R_0, the resistance at the ice point, should be measured at the time of test.

CHECK OF THERMOHM DRIFT

The drift of the thermohm, with respect to the table, must be checked at some point other than the ice point as the resistance at the ice point is already explicitly used. The freezing point of benzoic acid is a good one to use. Benzoic Acid Cells may be purchased from the National Bureau of Standards, certified to ±0.003°C. The freezing point is about 122.36°C. Freezing point checks may be made with these cells every 3 to 4 months and the temperature as calculated from the thermohm table compared with the freezing point temperature for that particular cell. Table I shows the history of two thermohms and the deviation of the temperature calculated from the certified temperature of the Benzoic Acid Cell.

The largest correction to date is +0.007°C for thermohm 446899. Assuming straight line error curve with zero error at the ice point, we would have an extrapolated error at 500°C of 0.029°C for the top of the range and 0.015°C error at the low end of the range, −200°C. This error is due to drift with respect to the table. To date, the rate of drift of this thermohm is 0.004°C per 8 months or 0.0005°C per month. Thermohm 671634 shows no apparent drift. The drift, with respect to the table, may be due to the change in resistance of the components of the Mueller Bridge as well as a change in resistance of the thermohm. It is good practice to certify the Mueller Bridge yearly.

CONCLUSION

The method described for calculating the tables of R_t/R_0 *vs.* t can be accomplished in a few hours as against several weeks for the former method of direct computation of the successive differences, using a calculator and having two people independently compute the tables. This type of table is easier and quicker to use than the tables involving the "platinum temperature" as there are no successive approximations involved as are in the latter table. The Benzoic Acid Cell furnishes an accurate and reproducible point for checking the drift from the table. This error due to drift may be extrapolated to the extreme temperatures of the table using the error at the Benzoic Acid Point and zero or negligible error at the ice point. This zero or very small error at the ice point assumes the R_0 was measured in a precision ice bath.

ACKNOWLEDGMENT

The author wishes to thank Mr. T. J. Price of the Taylor Instrument Companies Tabulating Dept. for his help and cooperation in preparing the tables.

THE REVIEW OF SCIENTIFIC INSTRUMENTS VOLUME 21, NUMBER 12 DECEMBER, 1950

An Electronic Recording Analytical Balance

IDAS W. LOHMANN
Southern Regional Research Laboratory, New Orleans, Louisiana*

(Received September 5, 1950)

An electronic recording analytical balance is described which is free of mechanical connections with the balance beam, direct reading, sensitive, and rapid. All mechanical and electrical contactors have been eliminated from the instrument proper, using electronic means as a substitute for mechanical. A relay and two cam-operated microswitches are, however, used in the range extender. The construction is simple, being made up, for the most part, of available standard commercial units. For work requiring a continuous record of changes in weight with respect to time, the instrument should prove to be most valuable.

IN the course of physical studies of the mechanics of impregnated resins, an instrument was needed which would automatically record, with respect to time, changes in weight due to volatilization. An electronic recording analytical balance designed and built by R. H. Müller and R. L. Garman[1] suggested a ready means whereby this might be accomplished. Ewald,[2] Oden,[3] Svedberg and Rinde,[4] and others have designed and built recording balances. Desirable features of the instrument to be described are that there are no mechanical or electrical connections with the beam of the balance, the recordings are linear, the chart speed is uniform and accurately timed, the chart speeds can be changed easily, the sensitivity of the balance can be varied (a knob control), slow or fast rates of changes of weight can be recorded, and a minimum number of controls is used. This instrument is operated through a servo mechanism, and although the idea is not new, it is presented as a means for accomplishing this task.

The balance may serve many other purposes besides the one specifically mentioned such as to follow the rate of sorption, desorption, evaporation, oxidation, and decomposition by automatically weighing the substance placed on the pan with the pan in normal position or with the pan suspended in a conditioned chamber below the balance.

A general view of the instrument is shown in Fig. 1. A standard 36-inch relay rack provides the framework for supporting the chainomatic balance and the accompanying amplifier and servomechanism. The recorder is wall-mounted in close proximity to the balance. Necessary controls are at a minimum and mounted on the front panel. The rear glass window of the balance is replaced by a one-quarter inch plywood panel. This acts as a support for the photo-tube, light shield, and also the range extender mechanism.

The assemblage consists essentially of the following parts—optical system, discriminator, amplifier, balancing mechanism, recording potentiometer circuit, recorder, and range extender.

The optical system (Fig. 2) is simple, requiring only a reflector (B) at the source (A), a tubular light shield (C), and a photo-tube (F). All parts were painted black where necessary to reduce light reflections. The target is so cut that when the balance is in equilibrium about one-half of the light from the source falls on the photo-tube. Compensation for ageing of the light source and the photo-cell is accomplished by varying R_6 (Fig. 3). Variations in light on the photo-tube owing to movement of the pointer of the balance actuate the balancing mechanism. In order to detect these changes a discriminator is used.

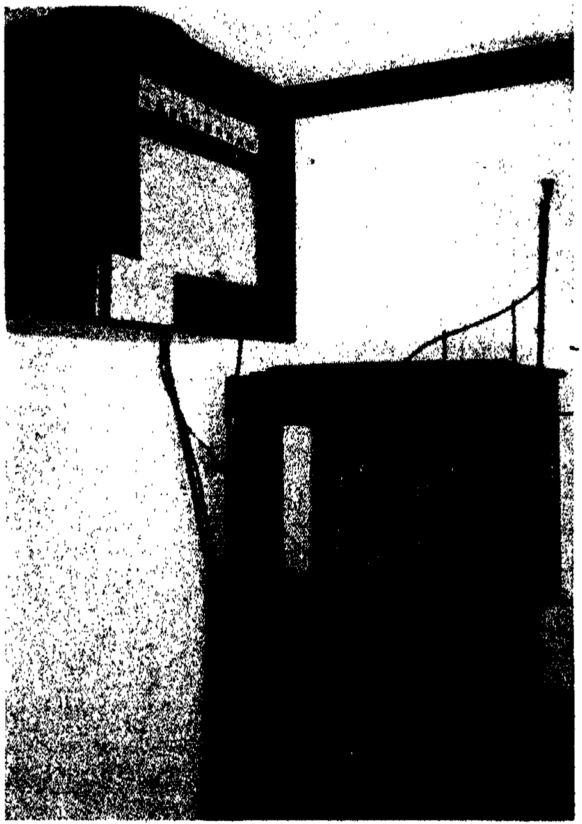

FIG. 1. Electronic recording analytical balance.

---

* One of the laboratories of the Bureau of Agricultural and Industrial Chemistry, Agricultural Research Administration, U. S. Department of Agriculture.

[1] R. H. Müller and R. L. Garman, Ind. Eng. Chem., Anal. Ed. 10, 436 (1938).

[2] P. Ewald, Ind. Eng. Chem., Anal. Ed. 14, 66 (1942).

[3] S. Oden, Trans. Faraday Soc. 17, 327 (1921).

[4] T. Svedberg and H. Rinde, J. Am. Chem. Soc. 45, 943 (1923).

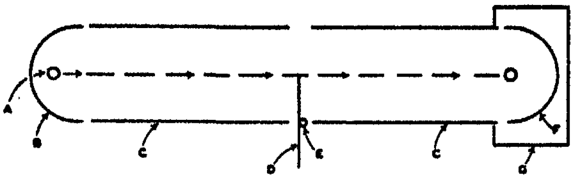

FIG. 2. Optical system. A. Light source at focus of reflector. B. Reflector (flashlight). C. Light shield, brass tube, 1-in. diameter. D. Target, aluminum foil glued to balance pointer. E. Balance pointer. F. Photo-tube. G. Photo-tube light shield.

The discriminator (Fig. 3) functions in the following manner. When the balance is in equilibrium, the current flow in the plate circuit of each No. 89 tube (V_1 and V_2) is such that the voltage drops across R_a and R_b (see Fig. 3) are equal. The bias for the tubes is furnished by the photo-tube (V_3) through a resistance network. When the equilibrium of the balance is disturbed, the bias on the tubes is changed through the variation in the amount of light falling on the photo-tube. This bias change causes the plate current to vary thereby making the voltage drops across R_a and R_b unequal. The direction in which the bias changes determines whether the voltage drop across R_a or R_b will be the larger. The difference in the voltage drops across R_a and R_b is the signal voltage input to the servo-amplifier (A). The amplitude of this signal voltage is dependent upon the amplitude of the change in bias on the No. 89 tubes. Any pentode power output tube will serve the purpose as well as the No. 89 tube. Batteries were used to offset the effect of line voltage fluctuations and for simplicity.

The signal voltage is fed into a servo-amplifier,†‡ which converts the input voltage into an alternating output voltage. The phase and magnitude of the output voltage are dependent upon the polarity and magnitude of the input voltage. The 2-phase balancing motor (M) has one leg excited by the servo-amplifier and the other by the 60-cycle line. Thus, a change in phase (or polarity of input voltage) means a change in direction of the motor's rotation. This amplifier† responds to a signal of about 50 microvolts and has provision for reducing this sensitivity when necessary. This two-phase motor is the driving force for the balancing mechanism.

The balancing mechanism is controlled by the balancing motor which has been geared down to increase the sensitivity of the instrument. The gear reduction allows the motor to make several revolutions in order to compensate for a small change in weight and return the balance to equilibrium. The reduction gear makes only one revolution for a weight change of one hundred milligrams on the balance. To accomplish this, sprocket gears connected through a ladder chain are attached to the crankshafts of the balance and the reduction gear. The ratio of the gears is slightly greater than the number of turns of the balance crank as a stop is placed on the reduction gear which permits about a 350° revolution in either direction.

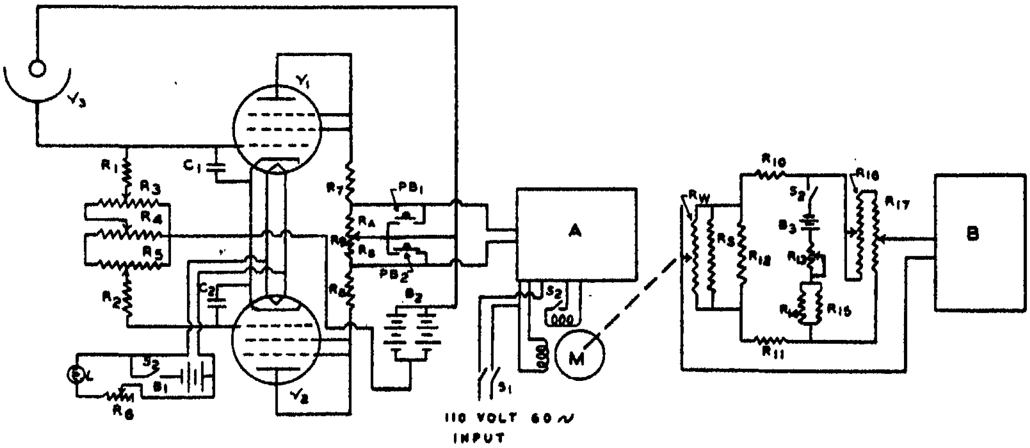

FIG. 3. Circuit diagram. R_1, R_2—4.7 megohms, ½ watt. R_3—1000-ohm helipot. R_4—50,000-ohm potentiometer. R_5—25,000-ohm potentiometer. R_6—25 ohms, 25 watts. R_7, R_8—22,000 ohms, 1 watt. R_9—100 ohms, 10 watts, variable tap, R_a and R_b form R_9. R_{10}, R_{11}—20 ohms, 1 watt, wire wound, non-inductive. R_{12}—6 ohms, 1 watt, wire wound, non-inductive. R_{13}—10,000-ohm potentiometer (variable sensitivity control). R_{14}—5000 ohms, 1 watt, wire wound, non-inductive. R_{15}—1000 ohms, 10 watts, wire wound. R_{16}—5-ohm potentiometer (fine zero control). R_{17}—190-ohm potentiometer (coarse zero control). R_w, R_s—Slidewire R_w shunted by R_s to 20 ohms. C_1, C_2—0.01 mfd, 1600 volts, oil-filled. V_1, V_2—No. 89 tube. V_3—No. 919 photo-tube. PB_1, PB_2—Pushbutton, S.P.S.T. B_3—2 1½-volt "A" batteries connected in series. B_2—2 45-volt "B" batteries connected in parallel. B_1—6-volt storage battery. S_1—Toggle switch, D.P.D.T., 5 amperes, 125 volts. S_2—Toggle switch, T.P.D.T., 5 amperes, 125 volts. A—Servo-Amplifier, from Brown Instrument Recorder Model No. 851325. B—Recording potentiometer, 7.5-mv range, strip chart, 12 sec. full-scale travel. M—Two-phase balancing motor. L—Lamp, Mazda No. 31, 6.2 volts, 0.3 ampere (optical light source).

---

† Servo-amplifier from Brown Instrument Recorder Model No. 851325.

‡ The mention of firms' names or trade products does not imply that they are endorsed or recommended by the Department of Agriculture over other firms or similar products not mentioned.

The drive cable pulley is also attached to the reduction gear so that balancing the analytical balance and moving the contact on the recording potentiometer circuit's slidewire is accomplished simultaneously. Thus as the reduction gear is moved to place the balance in equilibrium, the output of the potentiometer bridge network is varied and is at all times directly proportional to the movement of the reduction gear. The output of this network is fed to the recorder. Provision is made in this circuit for "zeroing" (both coarse and fine controls) the recorder and also for adjusting (expanding) the range when calibrating. This facilitates calibrating the instrument. This potentiometer circuit, including the slidewire, is the bridge network from a Brown Instrument recorder† in which the following changes were made. On the resistor terminal board, resistors Nos. 5 and 6 (Brown Instrument numbers) were removed and a thousand-ohm ten-watt resistor soldered across terminals 4A and 4B. The two 500-microfarad 6-volt electrolytic condensers were also removed. The recorder (B) input connections were made between the movable contact on the slidewire and the movable contact on the coarse "zero" control.

The output of the recording potentiometer network is fed into a null-balance type strip recorder§ with a sensitivity of 7.5 millivolts for full-scale deflection and a pen speed of 12 seconds for full-scale travel. This gives a direct reading in milligrams so that no interpolation is necessary. If the changes in weight are greater than 100 milligrams, it becomes necessary to use the range extender.

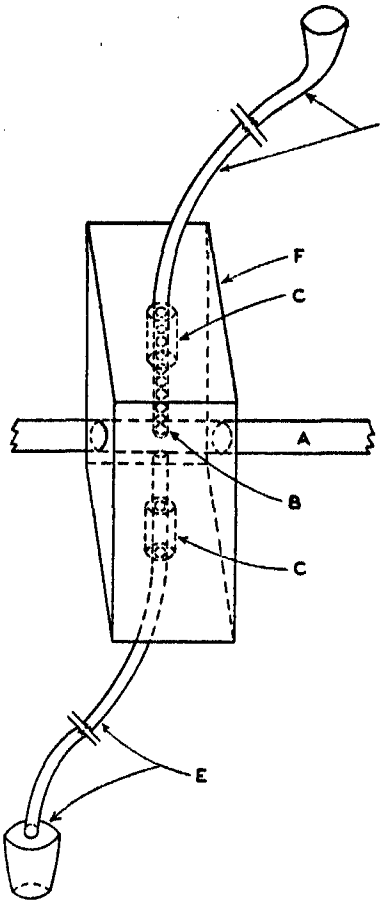

FIG. 4. Range extender. A. $\frac{1}{4}$-in. drill rod used for shaft, driven by 4-r.p.m. motor. B. Hole $\frac{3}{32}$-in.+0.005-in. diameter and $\frac{3}{32}$-in. depth in shaft. C. Hole $\frac{3}{32}$-in.+0.005 in., upper and lower portion cut $\frac{1}{8}$-in. deep to fit outer diameter of copper tubing used for storage and guide. D. Copper tubing, storage and funnel. E. Copper tubing guide to thimble. F. Brass block 1×$1\frac{1}{4}$×2 in.

The range extender (Fig. 4) is so designed that should a change in weight exceed that of the balance chain, a small stainless steel ball would be deposited in a cup (a thimble) supported by the pan hanger. This ball is deposited when the vernier on the balance indicates zero. The weights (balls) are always added to the left-hand pan. The stainless steel balls are $\frac{3}{32}$-in. in diameter and weigh 55 milligrams. Two identical thimbles were used for equilibrium and symmetry, the left-hand thimble being the holder for the balls. The drive mechanism for the range extender is a small synchronous motor whose speed was reduced to 4 revolutions per minute. The motor drives a shaft (A) of $\frac{1}{4}$-in. drill rod with a hole (B) $\frac{3}{32}$-in. deep and 5 thousandths of an inch larger than the $\frac{3}{32}$-in. ball. As the shaft rotates, it removes balls one at a time from the upper tube (D) and drops them into the lower tube (E) which causes them to drop into the thimble. The motor's operation is controlled by a latching relay which in turn is controlled by two microswitches. These microswitches are operated by a cam which is also attached to the reduction gear shaft. They are so mounted that when additional weight is needed to bring the balance into equilibrium, the motor is energized by causing a microswitch to close. After the weight (ball) is added, the system tends to balance itself. In so doing, it opens the first switch, and shortly thereafter closes the second switch momentarily, then opens the second microswitch again to remove power from the relay coil. The motor does not stop until the second microswitch is closed. The delay is used so that the range extender will be almost ready to drop another ball when needed instead of having to wait approximately fifteen seconds. When another weight is needed, the same operation is repeated.

OPERATION

The operational controls mounted on the front panel are the main power switch, balancing motor switch, coarse balance control, fine balance control, "up" push button, and "down" push button. (The push buttons are used only when the beam is off the knife edges.)

The main power switch is turned on and the instrument allowed to heat up for at least 30 minutes. The balance beam is then lifted off the knife edges and the balance switch is turned on. With the fine balance control at about the middle of its range (about 5 turns from either end as it is a 10-turn helical wound potentiometer), the coarse control is used to bring the balancing mechanism to a stop, or as close to a stop as possible, anywhere on the scale. After the coarse control has been adjusted, the fine control is then used to make the final adjustment. With the fine control adjustment, no motion of the chain occurs for about 1 turn of the fine control. When the movement of the chain has been stopped, the fine control is then turned about one-half turn from this point. This places the fine control halfway between operating points. The recorder is then checked against the balance scale. The "down" push button is depressed until the balance scale reads zero; if the recorder does not read zero, the "zero control" (located with range sensitivity just inside of the small door in the rear) is adjusted to give the correct reading. Then the "up" push button is depressed until the balance reads some convenient point on the upper portion of the balance scale. If recorder fails to agree, the range sensitivity control is adjusted. It is then necessary to check "zeroing" again as these controls are interdependent. The balance is now ready for weighings. The balance motor switch is turned off and sample is placed on the balance pan. The equilibrium of the balance is adjusted as closely as possible, with use of standard weights and the beam rider to within 100 milligrams. The balancing motor switch is turned on. The instrument will then automatically keep the balance in equilibrium and will also record the time rate of change of weight of the sample on the chart.

---

§ Brown Instrument recording potentiometer, model No. 153 ×11V—x—27.

CALIBRATION AND REPRODUCIBILITY

The performance of the recording balance was checked by placing 10-milligram weights on the balance pan and allowing the instrument to automatically balance itself. The maximum recorded deviations were of the order of 0.15 milligram.

As a check on the reproducibility of the results, a 10-milligram weight was weighed, removed, then weighed again for a total of 10 times with a maximum deviation of 0.125 mg. This was repeated again with a 20-milligram load and the deviations were within the same range. In checking the constancy of the instrument two different loads were used, one at the lower and the other at the upper end of the recorder scale. There was no observable variation on the chart for the two loads over a period of time, the trace being a straight line. The instrument appears to be free from the effects of line voltage variations, as none has been observed in all the weighings.

RANGE

With the present arrangement, weight changes up to ±11.1 grams may be made automatically. This is accomplished through the use of 200 stainless steel balls weighing 55 milligrams apiece in the range extender.

THE REVIEW OF SCIENTIFIC INSTRUMENTS VOLUME 21, NUMBER 12 DECEMBER, 1950

A Capacitance Bridge for High Frequencies*

J. S. Mendousse,† P. D. Goodman, and W. G. Cady
Wesleyan University, Middletown, Connecticut

(Received July 31, 1950)

A type of bridge for measurements at frequencies in the megacycle range is described, containing two fixed capacitors and a variable capacitor. The unknown impedance is connected in the fourth arm as a "load." The unbalanced high frequency e.m.f. is rectified by a germanium crystal rectifier and measured as a small d.c. voltage. The bridge is "balanced" by varying the variable capacitance until the ratio of output d.c. to input h-f voltage is at a minimum. The impedance of the variable capacitor is then numerically equal to that of the load.

In a second and perhaps more important application, the bridge is used for examining vibrational modes and measuring the Q of piezoelectric crystals or transducers. Here the variable capacitor is set at a fixed value equal to the parallel capacitance of the crystal, and the output voltage is observed, or recorded graphically, while the frequency is slowly varied over the resonance range. Some graphical records are shown, illustrating the performance of crystals at various frequencies and under different mechanical loads.

The theory of the bridge is given, and sources of error are discussed.

INTRODUCTION

1. First designed as a mode analyzer for piezoelectric crystals, this device has proved to be useful also for measuring the Q of crystals and crystal transducers and the acoustic resistances of liquids. At present it is also playing a part in a new type of acoustic interferometer for measuring velocities and absorption coefficients. With a given crystal in the load arm the bridge requires practically no retuning over the range from 1 to 50 Mc. Although a balance is more difficult at lower frequencies, the bridge has been used as a mode analyzer down to 35 kc.

---

* This work was done under contract with the ONR (N6onr-262, T.O. 1) at Wesleyan University, Middletown, Connecticut. The original manuscript appeared as *Technical Report No. 6*, February 1, 1950, under the contract. The present paper, except for a few changes and omissions, is identical with that report.

† Now at The Catholic University of America, Washington, D. C.

The distinguishing feature is the use of a crystal rectifier and direct current voltmeter to measure the potential difference across the bridge. A procedure is described whereby the error caused by non-linearity of the rectifier is eliminated.

Although somewhat similar types of bridges have been described by others,[1–5] the present device differs from them in arrangement of components, purpose, and operation, and requires a different theoretical treatment.

2. A diagram of the bridge is shown in Fig. 1. C_3 and C_4 are fixed capacitors, C_2 a variable capacitor. The load is at Z, in parallel with C_0, the capacitance of the jack to which the load is plugged, together with associated stray capacitances. V_0 is the h-f input voltage. If the load Z contains a resistance, there is no value of C_2 that makes the voltage drop V_{AB} across AB vanish. It is possible, however, to set C_2 so as to make the ratio V_{AB}/V_0 a minimum. As will be shown in the theory, when $C_3=C_4$, X_2, the reactance of C_2, is then equal to the impedance in the load arm DB, that is, the combination of Z with C_0. C_2 is calibrated so as to include the stray capacitance in the arm BE. G is a germanium rectifier, V the d.c. output voltage measured with a vacuum tube voltmeter, C_5 a by-pass capacitor to keep h-f currents from V, while r_1 and r_2 are high resistances. The output circuit between A and B is described in Section 7.

3. In its present form the bridge is in a metal cabinet, 10×5×3 in., containing the capacitors C_3 and C_4, each of approximately 24 $\mu\mu$f; the variable capacitor C_2 with a range up to 36 $\mu\mu$f; a high resistance germanium rectifier; and resistors of one megohm each in the leads from points A and B to the output voltmeter. The input voltage V_0 is taken directly from a signal generator having a maximum output of 5 volts. For higher voltages an amplifier is used. V_0 is measured with a vacuum tube voltmeter.

The usual range of values of V_0 is from a few hundredths of a volt to about 10 volts. Values as high as 60 volts have been used. With a load of high Q, the output voltage may be several times as great as V_0. When Q is small, V may be less than a thousandth of V_0.

In the first tests a microammeter was used to measure V. It was replaced later by a d.c. amplifier, which is more sensitive, has a higher impedance, and can be used with a graphic recorder or sensitive external meter.

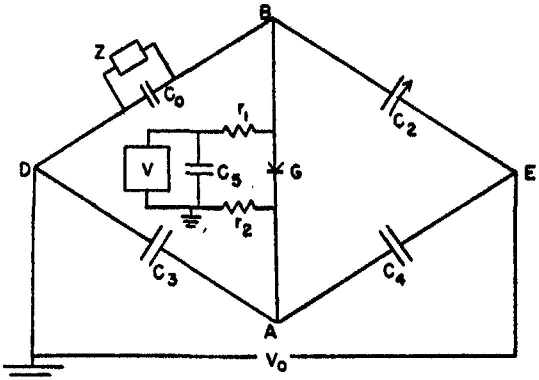

FIG. 1. Schematic diagram of the capacitance bridge.

THEORY OF THE BRIDGE

4. The bridge network is shown in Fig. 2, in which the notation agrees with Fig. 1. For definiteness the load is represented as a piezoelectric resonator or transducer with the customary $RLCC_1$ network. C_1 includes the capacitance C_0 of the arm DB. The expression $Z_s=R_s+jX_s$ used below is applicable, however, to any sort of load.

At present we consider only the ideal case in which the impedance across the branch connecting A and B is infinite. For this reason the rectifying circuit is not shown in Fig. 2.

The following symbols will be used, in which all V's and I's are vectors:

R_s, X_s = equivalent series resistance and reactance of load, including C_0 and r_1 (Fig. 1).
$Z=R_s+jX_s$.
X_2 = reactance of C_2.
Z_5 = impedance of rectifying system between A and B.
V_0 = input voltage.
V_A = potential at $A=jI_3X_3=I_3/j\omega C_3$.
V_B = potential at $B=I_1Z=I_1(R_s+jX_s)$.
$V_{AB}=V_A-V_B$ = potential drop across AB.
V = d.c. rectified output voltage (Section 7).
M = absolute value of V_{AB}/V_0.

We have

$$V_A/V_0=C_4/(C_3+C_4) \tag{1}$$

and

$$\frac{V_B}{V_0}=\frac{Z}{Z+jX_2}=\frac{R_s+jX_s}{R_s+j(X_s+X_2)}. \tag{2}$$

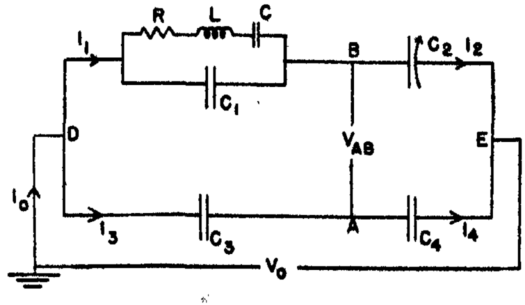

FIG. 2. The basic network of the bridge.

---

[1] August Hund, *High-Frequency Measurements* (McGraw-Hill Book Company, Inc., New York, 1933), pp. 430–431.

[2] E. Burstein, Rev. Sci. Inst. 18, 317–327 (1947).

[3] E. B. Armstrong and K. G. Emeleus, Proc. I. E. E., Part III, Radio and Communication Engineering 96, 390–394 (1949).

[4] D. D. King, Proc. I.R.E. 38, 37–39 (1950).

[5] Warren P. Mason, *Piezoelectric Crystals and Their Application to Ultrasonics* (D. Van Nostrand Company, Inc., New York, 1950), p. 48.

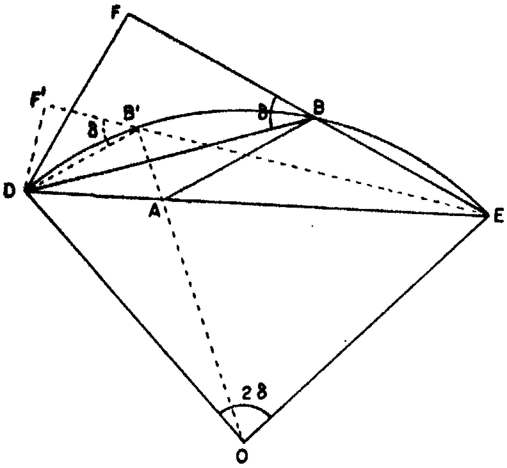

FIG. 3. Vector diagram showing distribution of e.m.f. components.

Hence,

$$\frac{V_{AB}}{V_0}=\frac{C_4}{C_3+C_4}-\frac{R_s+jX_s}{R_s+j(X_s+X_2)}. \qquad (3)$$

5. Equation (3) is general, holding for all loads and for all values of C_2, C_3, and C_4. It can be interpreted by reference to the vector diagram (Fig. 3), drawn for the case in which the absolute value of Z is less than that of X_2. Here $DE=V_0=DA+AE=I_3X_3+I_3X_4$. DE is also the vector sum of DF and FE, where $DF=I_1R_s$ and $FE=FB+BE=I_1X_s+I_1X_2$, with $X_2=-1/\omega C_2$, and $DB=I_1Z$. Then AB represents the potential drop V_{AB}.

The loss angle δ for the load is given by

$$\tan\delta=R_s/X_s=DF/FB. \qquad (4)$$

Since δ is independent of C_2, it follows that when C_2 is varied while DE remains constant, the point B must move along a locus such that the angle $DBE=180°-\delta$ is constant. This locus is a circular arc of radius $OE=V_0/(2\sin\delta)$. When C_2 is varied so that B coincides with B', on the radius passing through A, C_2 has the value that makes V_{AB}/V_0 a minimum. This is because AB' is the shortest distance from A to a point on the arc. At this adjustment for minimal V_{AB}/V_0, the lengths DB', DF', and $F'B'$ are respectively proportional to Z, R_s, and X_s.

If the fixed capacitances C_3 and C_4 are equal, the point A falls midway between D and E, as shown in Fig. 4. The shortest distance from A to the arc is now AB perpendicular to DE, so that B corresponds to the value of C_2 for minimal V_{AB}/V_0, and $DB=BE$. V_{AB} and V_0 differ in phase by 90°. From the geometry of the diagram it is seen that the angle $BDA=\delta/2$.

The fact that $DB=BE$ means that the moduli of X_2 and Z are equal, or

$$|Z|=|X_2|. \qquad (5)$$

In terms of admittance,

$$|Y|=|B_2|. \qquad (6)$$

Equations (5) and (6) show that when $C_3=C_4$ the bridge is "balanced" when the impedances in the other two arms are numerically equal. Owing to the difference in phase between I_1 and I_2 in Fig. 1, however, the balancing consists in bringing V_{AB} to a minimum. V_{AB} becomes zero at balance only when Z is a pure capacitance.

Making $C_3=C_4$ offers the double advantage of expressing the load impedance Z immediately in terms of C_2 by the use of Eq. (5), while at the same time making AB in Fig. 4 (and hence the minimal ratio V_{AB}/V_0) greater than the corresponding distance (as AB' in Fig. 3) for any other ratio of C_3 to C_4. Thus V_0 can be made quite small while still permitting a precise determination of the minimum of V_{AB}/V_0 as C_2 is varied.

In all that follows it will be assumed that $C_3=C_4$. Equation (3) now becomes simplified to

$$\frac{V_{AB}}{V_0}=\frac{1}{2}-\frac{R_s+jX_s}{R_s+j(X_s+X_2)}. \qquad (7)$$

Equation (5) can be derived from (7) by minimizing the modulus with respect to X_2.

6. The following relations, which will also be used later, serve to illustrate the performance and limitations of the bridge. Letting M stand for the minimum of $|V_{AB}/V_0|$ obtained by varying C_2 while V_0 is constant, we have

$$M=\min|V_{AB}/V_0|=\tfrac{1}{2}\tan(\delta/2). \qquad (8)$$

We have also the general relation

$$\tan\delta=R_s/X_s=G/B, \qquad (9)$$

where G and B are the conductance and susceptance of the load.

When the power factor is low enough to permit the approximation $\tan\delta\approx\delta$, we may write

$$M\approx\delta/4\approx R_s/4X_s\approx G/4B. \qquad (10)$$

The smaller δ is, the flatter is the arc in Fig. 4, and the more sharply can the minimum of V_{AB}/V_0 be determined. When $R_s=0$, $\delta=0$, and $V_{AB}=0$. We have then a pure capacitance bridge of the usual type.

On the other hand, as δ increases, the point 0 moves up toward A, the setting of C_2 for minimal V_{AB}/V_0 becomes less sharp, and when $\delta=90°$, $X_s=0$, 0 coincides with A, and the arc is a semicircle. The output voltage

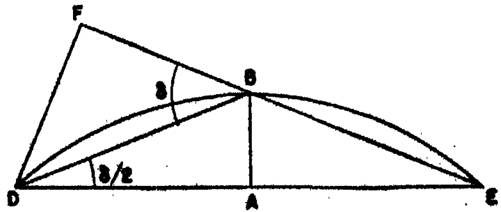

FIG. 4. Distribution of e.m.f.'s after C_2 has been adjusted to make AB/DE a minimum.

V_{AB} is then constant for all values of C_2. Varying C_2 changes the *phase* of V_{AB} with respect to V_0. If C_2 could be varied from zero to infinity the phase would change from $-90°$ to $+90°$. The bridge can thus be made to serve as a constant-voltage phase regulator at any frequency.

When X_s, which is negative as long as the load is capacitive, passes through zero and becomes positive, we have the case of an inductive load which, dropping the former subscripts, may be expressed simply as $Z=R+j\omega L=R+jX_L$. The point 0 is now located *above* A (*cf.* Fig. 3), and the arc is greater than a semicircle, approaching a complete circle as R approaches zero.

This case is illustrated in Fig. 5, where $DF=I_1R$, $FB=I_1X_L$, $DB=I_1Z$, and $BE=I_2X_2$. In contrast to the case represented in Fig. 4, where the load was capacitive, it is no longer possible to set C_2 for a minimum of $V_{AB}/V_0=AB/DE$. On the contrary, it is when this ratio is a *maximum* (point B in Fig. 5) that the absolute values of Z and X_2 are equal. This maximal setting is not sharply defined, as may be seen from the fact that B can move over a considerable range around the circle without greatly changing the distance AB. It should be noted that in setting C_2 for maximal V_{AB}/V_0 we have approximated the condition for series resonance between Z and X_2. When R/X_L is small, DF is almost as large as DE, almost the entire input voltage V_0 acts across R, and the current I is relatively very great.

The capacitance bridge is best adapted to measuring capacitive loads with loss angles not much over 45°.

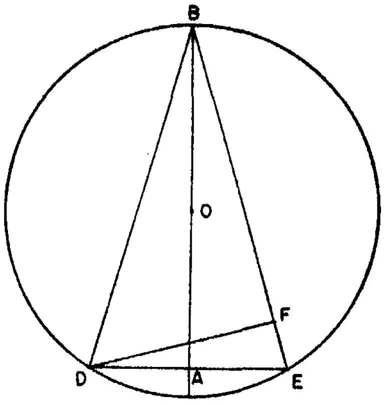

FIG. 5. E.m.f. diagram for inductive load.

THE DIRECT-CURRENT MEASURING CIRCUIT

7. Thus far the potential difference V_{AB} between points A and B (Figs. 1 and 2), has been treated as if there were infinite impedance in the output circuit between these points. Account must now be taken of the impedances in this circuit.

For a rectifier, germanium was chosen on account of its high rectification efficiency, low capacitance, and nearly linear characteristic for all but the lowest voltages. The present unit has nearly constant efficiency (ratio of d.c. output voltage to peak input voltage) for input above 0.05 volt, diminishing rapidly for voltages less than this. When the rectifier is in the bridge, its input voltage is the V_{AB}' of Eq. (11), which in practice may be much less than 0.05 volt. The rectifier then operates on the non-linear part of its characteristic. The rectifier described here has an effective resistance of the order of 30,000 ohms (depending somewhat on frequency and input voltage), shunted by its capacitance of about 0.5 $\mu\mu$f. At 15 Mc the impedance is therefore around 20,000 ohms.

The rectifier is shown at G in Fig. 1. It is connected through resistances r_1 and r_2 of one megohm each and condenser C_5 of a few hundred $\mu\mu$f (located close to G in the bridge cabinet), to an output jack. From here a concentric cable runs to the d.c. vacuum tube voltmeter V. The total impedance between A and B is designated by Z_5. Since this quantity includes the rectifier it is non-linear. Moreover, it depends somewhat on frequency and on V_{AB}. Nevertheless, its value in ohms can be roughly estimated, and it serves as a measure of the ratio of V_{AB}', the actual voltage between A and B, to the ideal voltage V_{AB} for infinite Z_5.

Let Z_t be the impedance of the entire bridge network as seen from AB (Fig. 1). The internal impedance of the input generator may usually be considered as zero. It can be shown that

$$V_{AB}\approx V_{AB}'[1+(Z_t/Z_5)]. \tag{11}$$

Since in general Z_t and Z_5 are complex, V_{AB}' differs from V_{AB} in both magnitude and phase.

For example, in the bridge described here, at 15 Mc, Z_t and Z_5 are of the order of 400 and 20,000 ohms respectively, so that $|V_{AB}'|$ is within about two percent of $|V_{AB}|$.

The current that becomes rectified is $I_5=V_{AB}'/Z_5$. The d.c. output voltage V is a function of V_{AB}', say $V_{AB}'=f(V)$. Then from Eq. (11),

$$V_{AB}=|1+(Z_t/Z_5)|f(V). \tag{12}$$

In the methods described below it is unnecessary to know the form of the function $f(V)$. It is enough to know that it is monotone increasing, so that a minimum of V_{AB} is indicated by a minimum of V.

BRIDGE CALIBRATION

8. For C_3 and C_4 two equal capacitors are symmetrically located in the cabinet. Their values do not appear in the final equations, but for maximum sensitivity they should be of the same order of magnitude as C_2.

C_0 (Fig. 1) is best determined by temporarily severing the connection between C_2 and E and that between G and the junction-point for r_2. When the load jack is connected to a measuring network, C_0 can be measured with C_2 set at various values. The slight dependence of C_0 upon C_2, which is inevitable unless C_2 is well sheilded, is thus determined.

To calibrate C_2 it is only necessary to balance the bridge with various known capacitances C in the load arm. A curve can then be plotted relating the dial setting of C_2 to the total capacitance between B and E (Fig. 1), which is $C_2=C+C_0$.

For measuring an unknown impedance and for obtaining resonance curves and values of Q, no further calibration is necessary.

C_0 can also be measured without severing any connections, by the use of two known loads with two different known loss angles.[6] Owing to the presence of small differences in the formula it is difficult to obtain accurate results, especially for the dependence of C_0 upon C_2.

MEASUREMENT OF THE COMPONENTS OF AN IMPEDANCE

9. In Sections 5 and 6 it was shown that the absolute admittance of an unknown load Y_x can be measured in terms of C_2 when the bridge is balanced; and that the precision is best with capacitive loads in which the loss angle is not too large. To determine the components G_x and C_x of the load one can use a substitution method, as described in reference 6. A second method consists in observing C_2 for balance with the given load, and C_2' when a known capacitance C has been connected in parallel with the load. These data yield two equations from which G_x and C_x can be found.

Enough measurements of various loads have been made to demonstrate the limitations and the possibilities of bridges of this type for absolute measurements. With the present model a precision of from two to five percent in the measurement of a total impedance is attained, but the determination of components with like precision would demand refinements such as are mentioned in Section 12. On the other hand the present model serves well in relative determinations, as in comparing the acoustic resistances of different liquids.

RESONANCE CURVES

Theory

10. With its d.c. voltage V connected to a graphic recording instrument, the capacitance bridge with a crystal in the load arm can be made to serve two useful purposes. The first is to function as a mode analyzer, the second is to furnish a means for measuring the crystal constants. In both cases the bridge is first balanced at a frequency well below resonance by setting C_2 for minimal V/V_0. This adjustment can be made very precisely, since the crystal is now nearly a pure capacitance, and V/V_0 becomes practically zero, unaffected by Z_5. When balance has been achieved, $C_1=C_2-C_0$ (see Section 8). In the equations that follow C_1 will signify the parallel capacitance of the crystal plus C_0. Then, at this low frequency, $C_1/C_2=C_3/C_4$.

The frequency is then slowly varied over the resonance range, while C_2 is left constant. Near any resonant frequency the crystal admittance undergoes characteristic changes which are automatically recorded. Since the delineating of a complete record requires only a few minutes, an exact comparison can be made in a short time between different crystals, or between the effects produced by different mountings or different mechanical loads on the same crystal.

As stated in Section 3, the input to the bridge is taken directly from a signal generator. From the bridge output a short cable runs to the amplifier, which in turn drives the pen of a 5 ma d.c. recorder. The frequency-control shaft of the signal generator is connected by a chain drive to a slow-speed synchronous motor. By this means the change in frequency in one minute with a d.c. recorder can be varied in steps from 0.6 to 10 percent. Since the paper of the recorder is also driven by a synchronous motor, the signal generator and the paper are accurately synchronized, so that successive recordings can be made with exactly the same frequency scale.

Resonance curves can of course also be obtained by a point-by-point method. At each frequency the input voltage V_0 and the d.c. output voltage V are observed; if V_0 is constant, a curve can be plotted for V against frequency. Although slow, this method offers the advantage of enabling the observer to hold V_0 constant at all frequencies. A still greater advantage is the possibility of holding V constant while V_0 is varied, thus yielding a $V_0{:}f$ curve free from distortion due to nonlinearity in the rectifier. This latter method works well over the resonance range. For points far from resonance V_0 becomes inconveniently large.

In the present case it is most convenient to express the output voltage V_{AB} by considering the potentials at A and B with respect to the point E in Fig. 1. Equation (18) below is then easily derived; as in the case of Eq. (3), the assumption is made that Z_5, the impedance of the output circuit, is infinitely great. It is also assumed that V_0 is constant. In the present apparatus the reaction due to the load is negligible, but the characteristics of the signal generator are such that V_0 varies somewhat with frequency. This variation is easily taken into account in determining Q.

$$\frac{V_{AB}}{V_0}=\frac{C_3}{C_3+C_4}-\frac{jX_2}{R_e+j(X_e+X_2)}=\frac{C_3}{C_3+C_4}+j\frac{Y_2'}{\omega C_2}, \quad (18)$$

where $Y_2'=1/[R_e+j(X_e+X_2)]=$ admittance of the crystal and C_2 in series. Equation (18) is only another way of writing Eq. (3). It holds at all values of C_2.

When the network $RLCC_1$ in Fig. 1 is in series with C_2, the combination is equivalent to the series chain $R'L'C'$ in parallel with a capacitance C_1', where, calling

---

[6] For details see Technical Report No. 6, cited above.

$(C_1+C_2)/C_2=n$, we have[7]

$$\left.\begin{array}{l} R'=n^2R \quad L'=n^2L \quad C'=\dfrac{C}{n^2[1+C/(C_1+C_2)]} \quad C_1'=C_1/n \\ Z'=1/Y'=R'+jX' \quad X'=\omega L'-(1/\omega C') \end{array}\right\}. \tag{19}$$

The admittance of $RLCC_1C_2$, expressed in terms of $R'L'C'C_1'$, is

$$Y_2'=\frac{R'-jX'}{Z'^2}+j\omega C_1'\equiv Y'+j\omega C_1'. \tag{20}$$

From Eqs. (18) to (20),

$$\frac{V_{AB}}{V_0}=\frac{C_3}{C_3+C_4}+j\frac{Y'}{\omega C_2}-\frac{C_1'}{C_2}$$

$$=\frac{C_3}{C_3+C_4}-\frac{C_1}{C_1+C_2}+j\frac{Y'}{\omega C_2}. \tag{21}$$

If, as stated above, the bridge is so adjusted that $C_1/C_2=C_3/C_4$, it follows that

$$\frac{V_{AB}}{V_0}=j\frac{Y'}{\omega C_2}. \tag{22}$$

Finally, if, as is the case with the bridge described here, $C_3=C_4$, it follows that $C_1=C_2$, so that Eq. (22) may be written as

$$\frac{V_{AB}}{V_0}=j\frac{Y'}{\omega C_1}. \tag{23}$$

Thus when the ratio V_{AB}/V_0 and ωC_1 (or ωC_2) are known, Y' can be found at any frequency.

The components of Y' could be found at once if we knew the phase relation of V_{AB} to V_0. Since in general this is not known, we take the modulus of Eq. (23). By use of Eqs. (19) and (12) it is found that

$$M=\left|\frac{V_{AB}}{V_0}\right|=\frac{f(V)}{V_0}\left|1+\frac{Z_t}{Z_5}\right|=\frac{|Y'|}{\omega C_1}$$

$$=\frac{1}{C_1}\left[\omega^2R'^2+\left(\omega^2L'-\frac{1}{C'}\right)^2\right]^{-\frac{1}{2}}. \tag{24}$$

The ordinates of recorded curves are proportional to V. As the frequency varies, $Y'/\omega C_1$ varies, and these variations are accompanied by corresponding changes in V. The relation between V and $Y'/\omega C_1$ is approximately parabolic when V is very small, approaching linearity with increasing V.

Equation (24) is for an idealized resonance curve. It is subject to two practical limitations. In the first place it is valid only over a frequency range within which R', L', and C' can be regarded as constant. The frequency spectrum of an actual crystal with small damping usually contains a large number of peaks, one of which can be identified as the main peak to which Eq. (24) especially applies. Still, the equation can be used also for deriving the equivalent constants for any "peak" or vibrational mode sufficiently isolated for R', L', and C' to be considered as constant over a reasonable range.

The second limitation is that in the actual bridge the impedance Z_5 of the output circuit is finite, involving the sources of error discussed in Section 7. Nevertheless this circumstance distorts the curve by no more than a few percent, at least as long as V is greater than 0.05 volt. By the procedure described in the next section, this source of error is eliminated in the determination of Q.

When the crystal radiates into a liquid the damping is so great that a very broad resonance curve results, in which the separate peaks usually lose their identity. In this case Eq. (24) is, to a good approximation, applicable over a wide frequency range.

Whether the damping is large or small, for any peak sufficiently isolated for R', L', and C' to be regarded as constant, we can find the peak frequency f_M by equating to zero the derivative of Eq. (24) with respect to ω. The result is

$$\omega_M^2=\omega_0'^2[1-(1/2Q'^2)], \tag{25}$$

where, if C_1 differs from C_2, with $(C_1+C_2)=nC_2$,

$$\omega_0'^2=\frac{1}{L'C'}=\left(1+\frac{C}{C_1}\frac{n-1}{n}\right)\omega_0^2=4\pi^2f_0'^2. \tag{26}$$

In Eq. (25) Q' is the quality factor of the crystal in series with C_2, defined by

$$Q'=\frac{\omega_0'L'}{R'}=\frac{\omega_0'}{\omega_0}\frac{\omega_0L}{R}=\frac{\omega_0'}{\omega_0}Q \tag{27}$$

where Q is the quality factor for the RLC series chain. The difference between Q' and Q is extremely small.

When, as in the present case, $n=2$, Eq. (26) becomes

$$\omega_0'^2=[1+(C/2C_1)]\omega_0^2. \tag{28}$$

From Eqs. (25) to (28) f_M can be expressed in terms of f_0, the series resonant frequency for RLC, for the case where $C_2=C_1$:

$$f_M\approx\left(1+\frac{C}{4C_1}-\frac{1}{4Q'^2}\right)f_0. \tag{29}$$

---

[7] W. G. Cady, *Piezoelectricity* (McGraw-Hill Book Company, Inc., New York, 1946), pp. 335, 358, and 359.

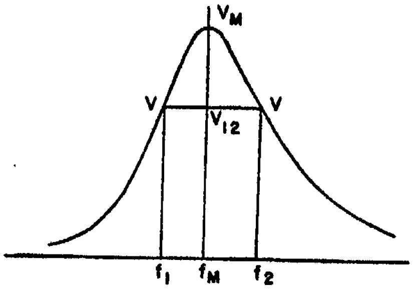

FIG. 6. Resonance curve, illustrating procedure for measuring Q.

Example: for a certain X-cut quartz plate radiating into water at 15 Mc, $C_1/C=144$, $Q=15$, so that from Eq. (29) $f_M=(1+0.00063)f_0$.

In all cases f_M is very close to f_0. For crystals of large Q, $f_M\approx(1+C/4C_1)f_0$. This value is midway between f_0 (series resonance) and $(1+C/2C_1)f_0$, the commonly used expression for antiresonance. The expression for f_M is also almost identical with that for $f_0'=1/2\pi(L'C')^{\frac{1}{2}}$, the frequency for series resonance of the combination $RLCC_1C_2$. As Q decreases, for example by increasing the mechanical load on the crystal, f_M also decreases, and becomes less than f_0 when $Q'^2<C_1/C$.

Measurement of Q

Method 1

11. With a crystal or transducer in the load arm of the bridge, the frequency f_M is found at which the d.c. output voltage V is a maximum, say V_M, while V_0 is constant. With V_0 at the same value, two frequencies f_1 and f_2 are selected at which V is the same, this value being anywhere from half to three-quarters of that at the peak. Then the frequency is again set at f_M, and the input voltage V_0 is decreased until the output voltage is diminished from V_M to the same V that was previously observed at the frequencies f_1 and f_2. The advantage in this method is that the effect of nonlinearity between V and V_0 is eliminated.

This procedure is illustrated in Fig. 6, in which $V_{12}=V$ is the value of the output voltage at frequency f_M after V_0 has been decreased from its original value to one that we will call $(V_0)_{12}$.

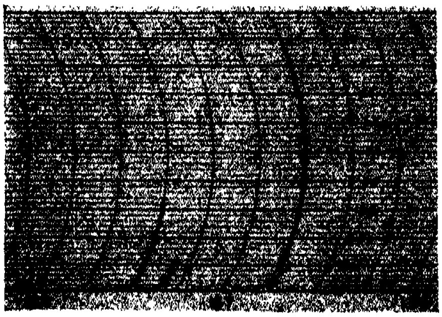

FIG. 7. 1.67 Mc crystal free in air. Diameter 1.27 cm, fully plated on one side, diameter of plated area on other side 0.95 cm.

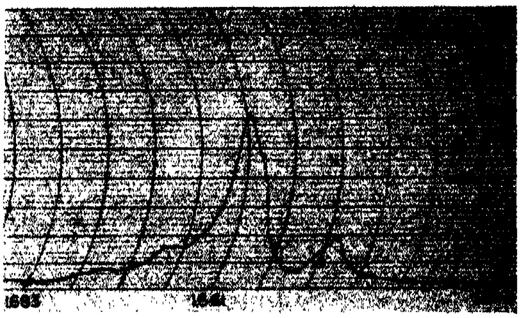

FIG. 8. Same crystal as in Fig. 7, but in cartridge. Note decrease in Q due to clamping.

Method 2

If a resonance curve at constant V_0 is drawn by a recording instrument the same procedure is followed, suitable marks being made on the curve. Two or more pairs of points may of course be selected, V_0 being reduced in each case to the appropriate value at frequency f_M.

Whichever method is used, Q is to be expressed in terms of V_0, $(V_0)_{12}$, f_1, f_M, and f_2. The admittance Y' of the $R'L'C'$ series chain described in Section 10 is

$$Y'=\frac{1}{(R'^2+X'^2)^{\frac{1}{2}}}\approx\frac{1}{\{R'^2+[2L'(\omega-\omega_0')]^2\}^{\frac{1}{2}}}\tag{30}$$

where ω_0' is the angular frequency for maximal Y', according to Eq. (26). Maximal Y' is $Y_m'=1/R'$. From the foregoing, calling $\omega_0'L'/R'=Q'$, and Y' the admittance at f_1 and f_2, it is found that

$$Q'\approx\frac{f_0'}{f_2-f_1}\left[\left(\frac{Y_m'}{Y'}\right)^2-1\right]^{\frac{1}{2}}.\tag{31}$$

Since in the present case the output V is the same at f_1 and f_2, it follows from Eq. (11) that V_{AB} is also the same. Therefore from Eq. (24), in terms of moduli,

$$M=\frac{V_{AB}}{V_0}=\frac{Y_1'}{\omega_1C_1}=\frac{Y_2'}{\omega_2C_1},\tag{32}$$

FIG. 9. Same crystal as in Fig. 7, free, in air, at third harmonic (5 Mc).

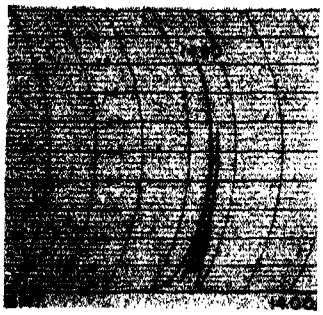

FIG. 10. Crystal 1.9 cm diameter, mounted in a special cell, air on both sides. One side fully plated, diameter of plated area on other side 1 cm.

where Y_1' and Y_2' are the admittances at f_1 and f_2. Y_1' and Y_2' are not quite equal, but they approach the common value Y' when $\omega_2-\omega_1 \ll \omega_M$. In this case $V_{AB}/V_0 \approx Y'/\omega_M C_1$.

At the frequency f_M we have maximal output voltage. As stated above, f_M is also almost exactly the frequency f_0' at which Y' has its greatest value Y_M'. Therefore $V_{AB}/(V_0)_{12} \approx Y_M'/\omega_M C_1$. Moreover, Eq. (27) shows that $Q \approx Q'$. Equation (31) can therefore be written in the form

$$Q \approx Q' \approx \frac{f_M}{f_2-f_1}\left[\left(\frac{V_0}{(V_0)_{12}}\right)^2-1\right]^{\frac{1}{2}}. \tag{33}$$

POSSIBLE REFINEMENTS TO THE BRIDGE

12. It should be stated first that capacitors rather than resistors were chosen for the ratio arms C_3 and C_4 owing to the difficulty in obtaining reactance-free resistors at megacycle frequencies.

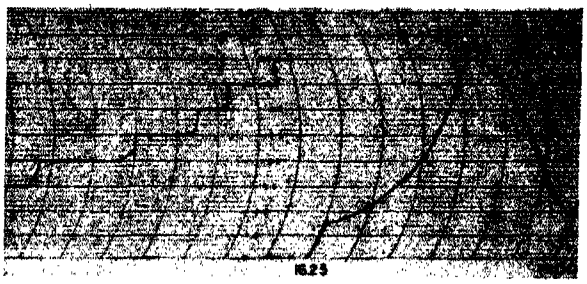

FIG. 11. Carbon tetrachloride in contact with crystal on one side. The left-hand portion of the figure shows how Q is measured according to Method 2, Section 11. Owing to the sources of error mentioned in Section 7 the measured values of Q varied from 14.7 to 15.4 with varying V_0.

If the bridge is to be used only as a mode analyzer, one terminal of C_2 can be grounded by interchanging C_2 and C_3, Fig. 1. For measuring impedances and their components the circuit has to be as in Fig. 1.

In the construction of a model for more precise measurements all parts of the bridge should be properly shielded. Insulation should be of the best. Means should be sought for a more accurate measurement of voltages. When these matters have been cared for, the chief source of error for which correction must be made will be the finite impedance of the rectifying circuit, discussed in Section 7.

RECORDINGS OF RESONANCE CURVES

13. Figures 7 to 11 are reproductions of original recordings with X-cut quartz crystals. Frequencies are given in Mc/sec. Ordinates are approximately proportional to $Y'/\omega C_1$ (Section 10).

Transmission Line Reflection Doubling Amplifier*

JOHN MARSHALL
Institute for Nuclear Studies, University of Chicago, Chicago, Illinois

(Received October 7, 1950)

A pulse amplifier has been constructed using voltage doubling by reflection at the open end of a transmission line. Cathode followers are used to couple the output of one line into the input of the next. An amplifier using in each stage the four triode units of two 6J6's in parallel driving 16 feet of 100-ohm line has theoretically a voltage gain of 1.32 per stage. With appropriate grid series compensation the gain can be made constant, theoretically, to 100 megacycles. Experimentally the gain is 1.3 per stage with a rise time less than 6×10^{-9} sec. Below 50 volts, distortion is not serious for pulses shorter than twice the transmission time of the line. Pulses up to 150 volts can be handled by the amplifier.

INTRODUCTION

A WIDE-band pulse amplifier has been constructed using the principle of voltage doubling by reflection at the open end of a transmission line. In essence, the amplifier is a series of lengths of coaxial line driven at the input end of each line by a cathode follower, and driving at the unterminated output end the grid of the next cathode follower. At frequencies where the grid has a high impedance relative to that of the line, the pulse amplitude is doubled at each grid, and the gain per stage is twice that of the cathode follower operating into line impedance.

The circuit of the amplifier is shown in Fig. 1. A description of the circuit is given below.

GENERAL CONSIDERATIONS

The gain of a cathode follower operating into a resistive load is, at low frequencies,

$$A=\frac{g_m}{g_m+(1/R_p)+(1/R_L)},$$

where g_m is the transconductance of the tube, R_p is its plate resistance, and R_L is the load resistance.

At high frequencies, the interelectrode capacitances become important and the gain is

$$A=\frac{g_m+j\omega C_{gk}}{g_m+(1/R_p)+(1/R_L)+j\omega(C_{kp}+C_{gk})},$$

where ω is 2π times the frequency, C_{kp} is the cathode-plate capacity which here includes the capacity between cathode and filament. C_{gk} is the grid-cathode capacity.

The admittance of the grid of a cathode follower, assuming that it never goes positive with respect to the cathode, is

$$Y=j\omega[C_{gp}+(1-A)C_{gk}],$$

where C_{gp} is the grid-plate capacity, A is the gain of the cathode follower which in general is a complex quantity smaller than one. The quantities A and Y can be derived easily using the equivalent circuit shown in Fig. 2.

If the output of a cathode follower is fed into the end of a lossless line of infinite length, the cathode follower behaves as if its load impedance were a resistor of value Z_0, the characteristic impedance of the line. If the line is finite in length, this condition still holds true provided that the pulse is shorter than twice the transmission time of the line. After this time, the signal reflected from the far end may interfere with the operation of the cathode follower.

Suppose a wave of amplitude E_1 to be traveling along a line the end of which is loaded with an impedance Z. A reflected wave is generated at Z with amplitude

$$E_2=E_1\frac{Z-Z_0}{Z+Z_0}.$$

E_2 is complex and contains the phase of the reflected

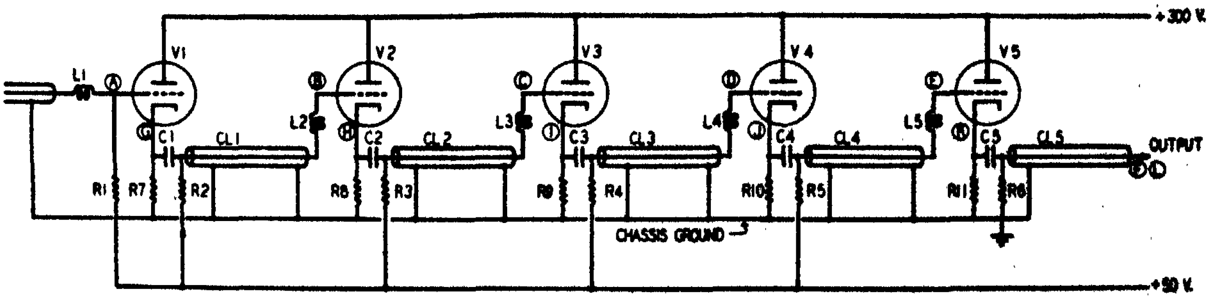

FIG. 1. Circuit diagram of 5-stage amplifier. Parts list: V1–V5—4 triode units of two 6J6's in parallel, R1–R5—56 K ½-watt resistors. R6—100-ohm ½-watt resistor. R7–R11—2.2 K 2-watt resistors. L1–L5—0.05 μh self-supporting helical coils. C1–C5—0.01 μf ceramic condensors. CL1–CL5—16-foot sections of RG7U 100-ohm coaxial cable.

---

* This work was done with the joint support of the ONR and AEC.

wave as well as its amplitude. The voltage generated across Z is the sum of E_1 and E_2.

$$E_0=E_1+E_2=E_1\left(1+\frac{Z-Z_0}{Z+Z_0}\right)=E_1\frac{2Z}{Z+Z_0}.$$

Now consider an inductance L to be placed between the line and the grid of a cathode follower, the grid impedance of which is $1/Y$. The voltage appearing at the grid of the tube will be

$$E_g=\frac{1E_0/Y}{(1/Y)+j\omega L}=\frac{2E_1}{1+Y(Z_0+j\omega L)}.$$

The voltage gain per stage is

$$G=\frac{2A}{1+j\omega[C_{gp}+(1-A)C_{gk}][Z_0+j\omega L]},$$

where

$$A=\frac{g_m+j\omega C_{gk}}{g_m+(1/R_p)+(1/Z_0)+(1/R_k)+j\omega(C_{gk}+C_{kp})}.$$

The expression for A has changed here slightly in that $1/R_L$, the load conductance, has been replaced by $(1/R_k)+(1/Z_0)$ since it is necessary to have a cathode resistor in parallel with the input of the line to carry direct current.

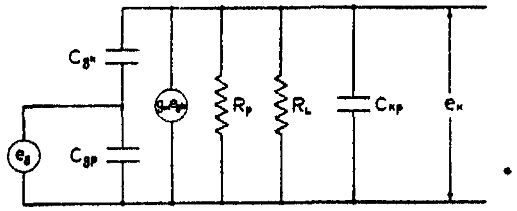

FIG. 2. Equivalent circuit for cathode follower.

The value of G has been calculated as a function of frequency assuming the following circuit constants: $g_m=21{,}200$ micromhos; $R_p=1500$ ohms; $C_{gk}=8.8$ pf.; $C_{kp}=12$ pf. including C_{kf}; $C_{gp}=6.4$ pf.; $R_k=2200$ ohms; $Z_0=100$ ohms.

The tube constants are the published values for the four triode units of two 6J6's in parallel. The other constants are those used in the amplifier, the circuit of which is shown in Fig. 1. The calculated values of G are given in Table I, and the absolute values are plotted in Fig. 3. Several values of the series inductance, L, have been used in the calculations. Inspection of Fig. 3 shows that, theoretically, the gain can be made approximately constant at about 1.3 per stage up to 100 Mc by using a series inductance of 0.05 microhenry in each grid circuit. The gain is a complex quantity, of course, because of phase shifts in the cathode follower and in the line termination. The phase shift is approximately linear with frequency, being about 45° for $L=0.05$ microhenry at 100 megacycles.

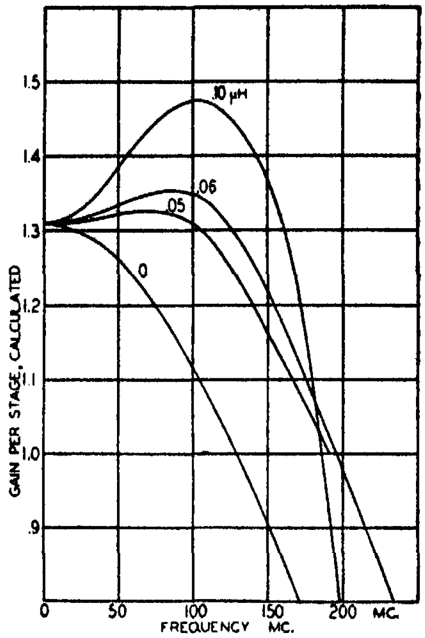

FIG. 3. Gain per stage *vs.* frequency for various values of grid series inductance.

DISCUSSION OF CIRCUIT

The tube type used is the 6J6 because of its high transconductance and ability to handle large bursts of cathode current. Two amplifiers were constructed, the first one using the two units of one 6J6 in parallel driving 20 feet of 250-ohm line for each stage. This amplifier performed satisfactorily, but was quite bulky and rather expensive because of the type line used. It had a gain of about 1.4 per stage which agreed quite well with the theoretical value.

A second amplifier was constructed using RG7U coaxial cable in 16-foot lengths. At this impedance level (100 ohms), it is necessary to use a transconductance greater than that afforded by a single 6J6. In consequence, two 6J6's were used in parallel in each stage. At first there was some trouble from high frequency oscillations in the parallel tube circuits. This trouble was overcome by orienting the tubes so that the connecting leads were as short as possible and by isolating the plates of the two 6J6's from each other with separate 10-ohm resistors to the +300 volt bus.

To make the gain as high as possible, it is necessary to use a cathode resistor large compared with the impe-

TABLE I. Gain per stage, as function of frequency and grid series inductance.

Frequency megacycles	$L=0$	0.05 μh	0.06 μh	0.10 μh
0	1.310	1.310	1.310	1.310
50	1.18 −0.45j	1.25 −0.48j	1.24 −0.49j	1.29 −0.52j
100	0.86 −0.71j	0.93 −0.92j	0.93 −0.97j	1.13 −0.95j
150	0.50 −0.76j	0.33 −1.12j	0.25 −1.20j	−0.23 −1.35j
200	—	—	−0.27 −0.94j	−0.52 −0.58j

dance of the transmission line. 2200-ohm resistors are used and, because of this high resistance, it becomes necessary to bias the grids positively. A grid bias of 50 volts above ground is used which gives a current of about 13 milliamperes per 6J6. Condensers and grid resistors are used to isolate each grid from direct connection to the cathode of the previous tube and to provide grid bias. Ceramic condensers are used with a capacity of 0.01 microfarad, and the grid resistors are 56,000 ohms to make them large compared to line impedance.

Some thought was given to the problem of reducing the effect of the filament-cathode capacity. If this capacity were reduced to zero, the gain of the cathode follower would increase with frequency and the amplifier would be able to handle faster pulses. Isolation of the filaments from ground with chokes is rather difficult because of distributed capacities in the chokes. It might be possible to heat the filaments with radiofrequency current through low capacity transformers, but neither of these methods was tried.

In principle, it should be possible to achieve a larger gain by using tapered lines. For instance, the central wire of the transmission line could be tapered in diameter so that the impedance would be 100 ohms at the cathode end and 200 ohms at the grid. This would give an additional voltage doubling besides that given by open end reflection. This was not tried because of the complication of preparing tapered lines. There would be certain disadvantages in the method because the frequency cut-off of the amplifier is due principally to reactive mismatch at the grid at high frequencies. This mismatch is worse with a high impedance line.

PERFORMANCE

The behavior of the amplifier was investigated with pulses from a Kay Megapulser. Its shortest pulse has a total length of about 0.04 microsecond and a rise time of about 0.015 microsecond. The pulses were reduced in amplitude with a resistor network so that they were barely visible on the screen of an oscilloscope.

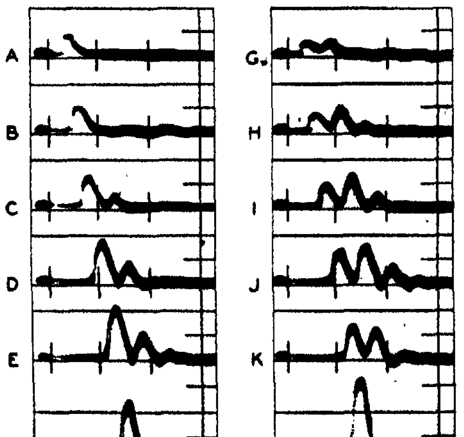

FIG. 4. Pulse of 0.04-μsec. length traced through amplifier with probe. A to E—grids 1 to 5; G to H—cathodes 1 to 5; F—end of output cable; L—output cable directly into oscilloscope. Sweep speed—0.1 μsec. per division.

A triode inverter probe was constructed to make it possible to observe pulse height and shape at various points in the amplifier without serious loading. A 6J6 was used with its two units in parallel. The cathode drove a terminated 173-ohm line connected to one deflection plate of the oscilloscope, while the plates were connected to the other deflection plate through an equal length of line also terminated. The grids were connected to a short, stiff length of wire which could be used as a probe. Appropriate blocking condensers and bias were used so that the tube could be operated with 300 volts on the plates.

Figure 4 is a composite photograph of the oscilloscope screen with the probe connected to a number of points in the amplifier. The encircled letters in Fig. 1 correspond to the labeling of the different traces of Fig. 4. Traces *A* through *E* were obtained at the grids of the successive amplifier stages. *G* through *K* are the cathodes of the same stages. The oscilloscope sweep speed was approximately 0.1 μsec. per division along the horizontal axis. The cathode pulses can be seen to have generally a two-peak structure, consisting of the original cathode pulse plus a reflection from the grid of the next stage. The grid pulses have an amplitude which increases from stage to stage by a factor of approximately 1.32 which agrees very well with the theoretical value as given in Fig. 3.

Trouble is to be expected from pulses reflected again from the cathode of a previous tube. The cathode impedance of a tube looking toward it from a line is approximately the reciprocal of its transconductance for small pulses or for pulses whose current direction is that in which d.c. can be transmitted through the tube. For small pulses, then, the line is terminated at the cathode end with a resistance of about $1/g_m$ or 50 ohms for the tubes used. This would be expected to produce reflections of one-third the amplitude and of opposite sign from the pulse arriving at the cathode. The grid of the next stage, then, receives first a positive pulse and then a negative one of one-third the amplitude arriving later by twice the transmission time of the line.

For large pulses, the situation is different. In this case, the reflected pulse coming back to a cathode from the grid of the next tube drives the cathode beyond cut-off so that the resistive impedance becomes very large. The result is that for large pulses, the later pulses arriving at the grid of a tube as a result of reflection from the cathode end of the line are characteristic of reflection from a high impedance termination. In other words, they are of the same sign as the first pulse. These secondary pulses are fed through successive stages where they blend with reflections in those stages.

The amplifier, then, at large amplitudes, transmits secondary pulses of the same sign as the first one. These pulses arrive later by integral multiples of twice the transmission time of the line and fall off rather rapidly in amplitude as the order of the reflection increases. In general, the size of the reflected pulses is relatively larger when the amplifier is handling high voltage signals than when the amplitude is small.

It is undesirable, of course, to have secondary pulses following the primary one. It is possible, by the sacrifice of a small amount of gain to remove, almost completely, the secondary pulses in the output circuit of the amplifier. This is done by terminating the cathode end of the output line, which for this purpose must be of the same length as the between stages lines, with a resistor of such a value that reflections from this cathode and transmitted reflections from previous stages cancel each other. The far end of the output line must of course be terminated in roughly the same way as the between stages lines are terminated by the grids. This has been done in the amplifier described here. It was found that the best termination was achieved with a 100-ohm resistor, the characteristic impedance of the line. The result can be seen in traces *F* and *L* of Fig. 4. In *F*, the triode inverter probe was connected to the end of the output line CL5. In *L*, the oscilloscope is driven directly by CL5.

The deflection sensitivity of the oscilloscope photographed in Fig. 4 is such that one vertical division is about 12.5 volts. The output pulse, then, was about 40 volts high. Pulses of considerably more than 100 volts in height can be handled by the amplifier. In general, however, there is more distortion at the higher pulse sizes. Up to 60 volts, there is no noticeable distortion attributable to excess amplitude.

The rise time of the amplifier was investigated using a mercury switch pulse generator designed by R. L. Garwin. This pulse generator has a rise time of less than 10^{-9} sec. so that it can be considered instantaneous as far as this amplifier is concerned. An oscilloscope photograph of the output of the amplifier which is reproduced in Fig. 5 shows a rise time of about 6×10^{-9} sec. from the beginning of the pulse to the top of the rise. It is possible that the rise time of the amplifier might be somewhat less if viewed on an oscilloscope designed for really fast pulses. The one used is a Tektronix type 511-A. The sweep speed in Fig. 5 is approximately 0.05 μsec. per division.

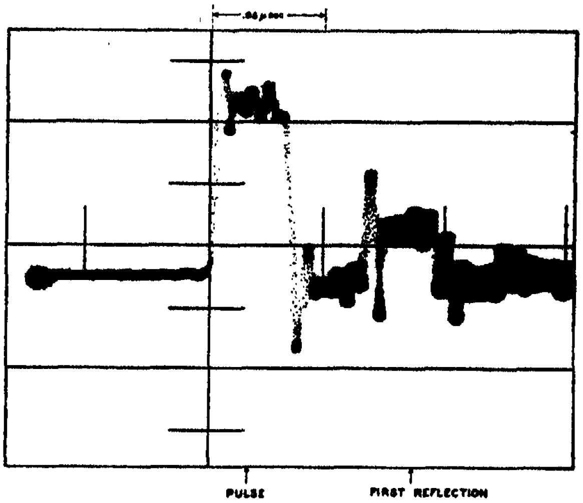

FIG. 5. Response of system to pulse of rise time less than 10^{-9} sec. Sweep speed 0.05 μsec. per division.

The behavior of the amplifier for pulses long compared to the line transmission time is roughly that the amplifier reproduces faithfully the part of the pulse up to 0.04 μsec. and then comes down sharply with reflections that vary very slightly depending on the length of the pulse.

CONCLUDING REMARKS

The line reflection amplifier is extremely simple to construct with no precise adjustments or critical conditions to meet. It is capable of handling pulses at quite high amplitudes and at low impedance levels. In these respects it is superior to the distributed amplifier. On the other hand the distributed amplifier can have a somewhat higher frequency response and can handle pulses of much longer duration.

The writer wishes to thank Mr. R. H. Miller and Mr. P. Shevick for helpful discussions of the properties of the amplifier. Mr. R. E. Mueller and Mr. H. W. Lamberty were responsible for a large part of the actual construction and mechanical design.

THE REVIEW OF SCIENTIFIC INSTRUMENTS VOLUME 21, NUMBER 12 DECEMBER, 1950

A Frequency Meter for Microwave Spectroscopy *

JOHN D. ROGERS, HENRY L. COX, AND PAUL G. BRAUNSCHWEIGER
The Mendenhall Laboratory of Physics, The Ohio State University, Columbus, Ohio

(Received July 10, 1950)

A frequency meter using known absorption lines as microwave frequency standards has been developed. By mixing signals of unknown microwave frequency f_s, standard microwave frequency f_0, and known radio-frequency signals nf_c from a crystal-controlled harmonic generator, it is possible to obtain a set of "beat" frequencies f_r which can be detected by a calibrated radio receiver. From the relation

$$f_r = \pm m(f_s - f_0) \pm nf_c$$

it is possible to determine values for the unknown microwave frequency f_s. Tests on methanol absorption lines with ammonia lines as microwave frequency standards show that microwave frequencies can be determined to ±0.03 mc/sec. Advantages of this device over other frequency meters are discussed; the accuracy is ultimately limited by the uncertainties in the value of the standard frequency f_0.

TWO distinct types of high precision frequency meters have been described earlier. The first type[1] involves the use of a series of frequency multipliers to obtain standard microwave frequencies from the standard radio frequencies broadcast from station WWV. Frequency meters of this type have been used to make careful measurements of certain strong absorption lines, which can now be used as secondary frequency standards for the microwave region. The second type[2] of frequency meter employs these spectral lines to stabilize microwave oscillators, which are then used to produce frequency markers in the microwave region. In the present paper we wish to describe a precision frequency meter that uses the carefully measured ammonia lines as secondary frequency standards but avoids the intermediate step of using the lines to stabilize a microwave oscillator. This meter is being used successfully in studies of microwave absorption spectra.

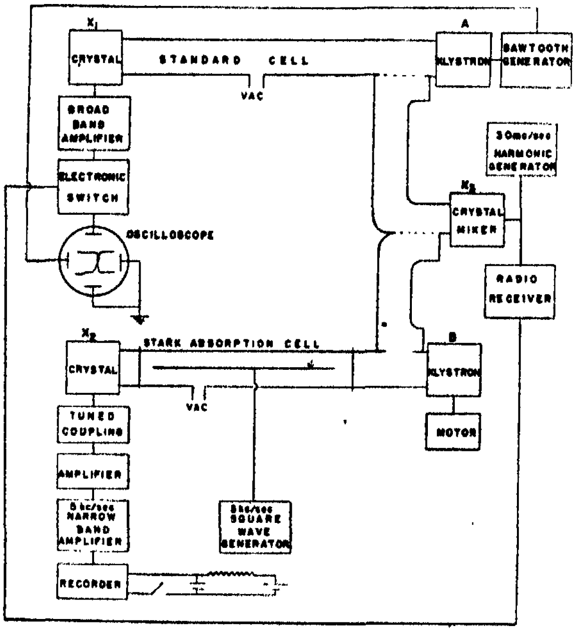

FIG. 1. Block diagram of frequency measuring system.

A block diagram of the circuits involved is given in Fig. 1. Two spectrographs are employed. A sweep-type[3] spectrograph A is used for observing one of the accurately measured lines in the inversion spectrum of ammonia. Application of a 60-cycle sawtooth voltage to the reflector sweeps the klystron frequency through a range containing the ammonia absorption line. The resulting output signal from crystal X_1, is amplified and applied through an electronic switch to the vertical deflection plates of an oscilloscope; the sweep for the horizontal deflecting plates is furnished by the 60-cycle sawtooth voltage applied to the reflector of klystron A. In cases where it is desirable to use some gas other than ammonia as the standard it is desirable to use a Wilson-type Stark-modulation spectrograph[4] utilizing a square-wave voltage biased to ground.

The search spectrograph B is of the type using Stark modulation, a narrow band-pass amplifier and detector, and a recorder for displaying the observed spectra on a chart.[5] A small amount of power can be fed from each klystron by means of a directional coupler to a crystal mixer X_3. The resulting "beat" frequencies are fed into a communications receiver, the output of which is displayed on the oscilloscope along with the ammonia line. This may be accomplished by means of the electronic switch as shown in Fig. 1, thus obtaining a double trace, or by applying the receiver output to the "Z-axis" terminal of the oscilloscope, thus using intensity modulation on the single trace showing the ammonia line. The

---

* The research reported here has been made possible through support and sponsorship extended by the Geophysical Research Directorate of the Air Force Cambridge Research Laboratories under Contract AF 19 (122) 13. It is published for technical information only and does not represent recommendations or conclusions of the sponsoring agency.

[1] M. W. P. Strandberg *et al.*, Phys. Rev. 71, 326 (1947), W. E. Good and D. K. Coles, Phys. Rev. 71, 383 (1947). R. R. Unterberger and W. V. Smith, Rev. Sci. Inst. 19, 580 (1948).

[2] Townes, Holden, and Merritt, Phys. Rev. 74, 113 (1948).

[3] W. E. Good, Phys. Rev. 70, 213 (1946).

[4] R. H. Hughes and E. B. Wilson, Jr., Phys. Rev. 71, 562 (1947).

[5] "A Recording Stark-Effect-Modulation Spectrograph for the Microwave Region" by William J. Pietenpol and John D. Rogers, *Symposium on Molecular Structure*, The Ohio State University, June, 1949.

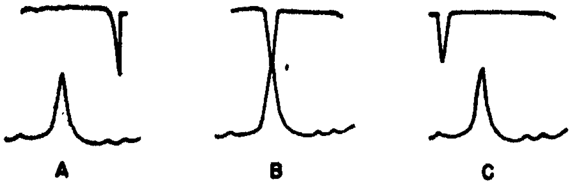

FIG. 2. Tracings of photograph of oscilloscope patterns. As klystron A is slowly tuned mechanically, the pip on the upper trace moves slowly toward the left. (Note: Separation of main ammonia line and its inner satellite is about 1.7 mc/sec. Width of main line at half-height is about 0.4 mc/sec.)

receiver output appears as a "pip" whenever one of the beat frequencies from crystal X_3 corresponds to the frequency f_r to which the communications receiver is tuned.

When the pip from the receiver coincides with the ammonia line on the oscilloscope screen, the frequency f_x of the search klystron B can be obtained from the relation

$$f_r = \pm m(f_0 - f_x),$$

where f_0 is the frequency of the ammonia line and m is an integer. In the present apparatus the search klystron is tuned mechanically by means of a drive operated from a synchronous motor and the pip moves slowly across the screen as shown in Fig. 2. A frequency marker is made on the recorder paper by a manually operated pulsing circuit or by a mechanically operated pen when the pip and the ammonia line coincide on the oscilloscope; for convenience and for somewhat improved precision, an electronic coincidence triggering switch may be used to actuate the marking device.

With only the signals from klystrons A and B reaching crystal mixer X_3, microwave frequencies within a range of at least a hundred mc/sec. from the ammonia frequency f_0 can be measured. In order to extend the frequency range of measurement with respect to a given standard absorption line, the output of a harmonic generator operated from a 30 mc/sec. crystal-controlled oscillator may also be applied to crystal mixer X_3 as shown in Fig. 1. When this arrangement is employed, the frequency relation applying when the pip and ammonia line are in coincidence is

$$f_r = \pm m(f_0 - f_x) \pm n f_c,$$

where f_c is the frequency of the crystal-controlled oscillator as measured in terms of WWV and n is an integer. Observable pips can be obtained when f_0 and f_x differ by as much as 4000 mc/sec. When frequencies f_x remote from f_0 are being measured, it is desirable to employ a resonant-cavity wave meter to give an approximate value of f_x so that m and n can be determined unambiguously.

TABLE I. Frequencies of several methanol lines.

	Frequency (mc/sec.)	
Line	Cole's value	Value obtained by present method
$J=5$	24,959.08	24,959.02±0.014
6	25,018.14	24,018.20±0.023
7	25,124.88	24,124.89±0.025
27	23,854.25	23,854.23±0.015

The accuracy of the frequency measurements made with the present device depends upon the sharpness of the standard spectral line, the frequency and amplitude of the sawtooth voltage applied to klystron A, the pass band of the communications receiver, the speed of the motor drive of klystron B, and, ultimately, the accuracy of the original measurement of the standard frequency f_0. The ammonia lines can be observed at low pressures and furnish highly satisfactory sharp standard lines. The *SX* 42 receiver calibrated by means of a signal generator checked against WWV has been employed and, when used as a broad band receiver, gives no distortion of the pips produced by a 60-cycle sawtooth voltage of amplitude sufficient to give a total frequency excursion of 3.7 mc/sec. for the low frequency bands and 37 mc/sec. for the high frequency bands.

In order to test the frequency meter with the Stark modulation spectrograph shown in Fig. 1, two somewhat inexperienced observers used it to make measurements of several hindered-rotation lines of methanol. The results obtained are shown in Table I along with the values reported by Coles.[6] The values given in Table I are the averages obtained from sixteen independent measurements of each line with the 3,3 ammonia line as the standard. The uncertainties given are the probable errors and hence give only a measure of the internal consistency of the data. The uncertainty in the frequency of the standard ammonia line is ±0.02 mc/sec. and, as stated above, this sets the ultimate limitations on accuracy with which frequencies can be measured. Including this uncertainty, we obtain a limit of approximately ±0.03 or ±0.04 mc/sec. for the methanol frequencies.

Although the frequency meter described above has been tested only in spectroscopic applications, it should be noted that it can be used to measure the frequency f_x of any *CW* microwave radiation.

---

[6] Private communication. An accuracy of ±0.1 mc/sec. is claimed.

THE REVIEW OF SCIENTIFIC INSTRUMENTS VOLUME 21, NUMBER 12 DECEMBER, 1950

Apparatus for Concentration of He^3 by Thermal Diffusion*

O. F. Schuette, Jr.,† A. Zucker, and W. W. Watson
Sloane Physics Laboratory, Yale University,‡ New Haven, Connecticut

(Received June 29, 1950)

A multistage thermal diffusion apparatus for the concentration of He^3 is described. Included is a novel three-stage, all-metal column based on a G. E. Calrod heater. Concentration was carried only to a He^3/He^4 ratio of 0.05 percent, a factor of 3.3×10^3. The performance indicates the importance of having the hot wall in concentric cylinder columns made of metal of good thermal conductivity to minimize azimuthal temperature gradients which can markedly increase parasitic remixing of the gas if a metal such as stainless steel is used.

DESPITE the extremely low value of 1.5×10^{-7} for the He^3/He^4 ratio in well helium, the thermal diffusion method is one of the possible ways of concentrating the rare and important He^3 isotope. Some details of the construction and operation of thermal diffusion apparatus for this purpose have been given by McInteer, Aldrich, and Nier.[1] Along with a complete development of the theory of isotope separation by thermal diffusion, Jones and Furry[2] calculated the design of a multistage helium apparatus. Our construction differs somewhat from the recommendations of Jones and Furry, but our calculations of critical dimensions and operating conditions are all based on the relations given in their article. Although the performance of our columns has not come up to expectations, we believe that we have the explanation for the deficiencies. A brief description of our experience may be helpful to others constructing similar apparatus.

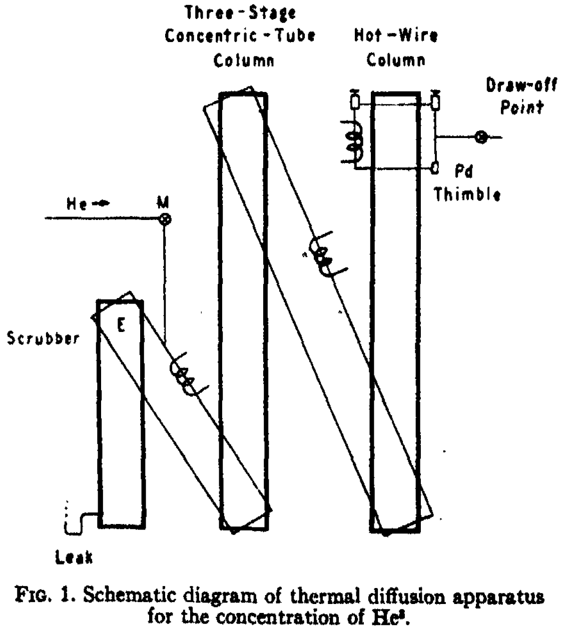

FIG. 1. Schematic diagram of thermal diffusion apparatus for the concentration of He^3.

DETAILS OF APPARATUS

Figure 1 is a schematic representation of our metal columns which were operated at that helium gas pressure, 4.5 atmos., calculated to give maximum separation factor in the hot-wire column. In addition to these columns, we have employed a single 3-meter, hot-wire glass column to recycle, batchwise, the gas enriched in He^3 from the top of the metal hot-wire column. Both the scrubber and the three-stage column have for the hot wall a G. E. Calrod heater with chrome steel sheathing. Many of the construction features of these two columns, such as the use of two-ply sylphon bellows to take up the differential expansion of the hot and cold surfaces, thin stainless steel end sections to minimize heat loss by metallic conduction, convective coupling between columns, etc., are similar to those of another thermal diffusion apparatus recently described in this journal.[3] The total consumption of power is 7 kw and of cooling water 3 gal/min.

Operation of the first column as a scrubber in order to make more effective use of the rare isotope in the original gas is in agreement with the Jones and Furry design. The Calrods are both 0.6 inch in diameter; that in the scrubber has a heated length of 130 cm and is mounted concentrically inside a 1⅛-inch o.d. copper pipe, so that the gap space $2w$ is 0.932 cm. Helium gas enters through a tee in one of the first coupler pipes while gas depleted in the light isotope is valved off at the bottom of the scrubber at the rate of 1.5 cm^3/sec. We compute that about half the He^3 in this ejected gas has been removed and transported up the longer separating column. The scrubber and this separation column may be considered as a single column with the gas entering the system between the two and flowing toward both ends.

The longer second column has a novel construction (Fig. 2), there being three sections with decreasing gap space in the order bottom to top, so designed as to match roughly the transport of the light isotope in the three stages. By such construction one should be using a long column at highest efficiency. At intervals of 50 cm, sets of thin stainless steel spacers in groups of four project from the copper cold wall to hold the heater accurately centered.

---

* A portion of this research constituted a part of a dissertation submitted by O. F. Schuette, Jr. to the Faculty of the Graduate School of Yale University in partial fulfillment of the requirements for the degree of Doctor of Philosophy.

† Now at William and Mary College, Williamsburg, Virginia.

‡ Assisted by the AEC.

[1] McInteer, Aldrich, and Nier, Phys. Rev. 74, 946 (1948).

[2] R. C. Jones and W. H. Furry, Rev. Mod. Phys. 18, 151 (1946).

[3] Watson, Onsager, and Zucker, Rev. Sci. Inst. 20, 924 (1949).

In the choice of gap spaces in concentric cylinder columns, one is limited by available sizes of copper tubing for the cold wall; but the pressure is a variable that can then be adjusted to make for most efficient operation. Our choice for the scrubber column was made by calculating the transport coefficients H, K_c, and K_d (reference 2), assuming the remixing coefficient K_p due to parasitic convection to be $0.3K_c$, and taking the hot wall temperature to be the stated operating temperature of the heater in air (1200°F or 980°K for 2 kw input). This calculation indicated that the convenient gap space of 0.932 cm should give maximum efficiency at a pressure of 5.3 atmos.

From preliminary experiments with this shorter column plus calculations on the heat conduction through the gas, we could calculate that, for the available spaces of 0.932 cm, 0.773 cm, and 0.643 cm for a three-stage column based on the Calrod heater with heated length of 289 cm, the hot-wall temperatures for the rated power input of 5 kw are 985°K, 952°K, and 920°K, respectively. Calculation for balanced transport (cf. reference 2) between stages then showed that for stages 1 and 2 the lengths should be 92.5 cm and 57.5 cm, respectively. It was decided to make the remainder of the column into a final stage, for with any available gap space less than 0.643 cm there would be a much lowered hot-wall temperature plus probable increased parasitic convection from small absolute values of the error in centering of the hot wall.

We have also used the scrubber column with argon gas to measure by the method of Onsager and Watson[4] the Reynolds number at which the lamellar convective flow of the gas between the hot and cold walls becomes turbulent. At hot-wall temperatures of 1180°K and 805°K this Reynolds number is 89 and 40, respectively. These values are much smaller than those obtained for pure pressure flow through pipes, but are in agreement with other recent measurements with thermal diffusion columns.[4,5] Since the Reynolds number for the onset of turbulence should be about the same for all gases, we compute that for the scrubber column filled with helium a pressure of about 100 atmos. would be required to produce the necessary density to cause turbulence. Even higher pressures are required to produce turbulence in the smaller gap spaces of our long Calrod column. We are sure, then, that at the pressures of 6.5 atmos. or less the flow of the helium gas in these columns is lamellar.

The all-metal, hot-wire column is 3 meters long and consists of a copper pipe 9/16 inch i.d. surrounded by the usual water jacket and carrying a 15-mil Pt-Ir alloy wire down its axis. A direct current of 4.85 amperes produces a wire temperature of 1100°K. To keep this wire centered, crosswires are spotwelded on to it at 75-cm intervals. These crosswires carry quartz sleeves of 1-mm o.d., which are longer than the wires so that the latter cannot touch the metal cold wall. The current is led in and out by means of Stupakoff seals soldered to the metal end-fittings. Rubber O-rings used as gaskets make tight pressure seals between these fittings and the pipe ends. The wire carries at its lower end a 50-g weight, which connects to the bottom Stupakoff seal through an accordion-pleated copper ribbon made of copper cold-rolled to a thickness of 0.001 inch. The lower end-fitting which contains this weight-and-ribbon assembly is made of a brass tube lined with a glass tube for electrical insulation. This type of construction for a high pressure hot-wire column has proved successful in operation for considerable periods both in this apparatus for He^3 concentration and in another for separating the argon isotopes.

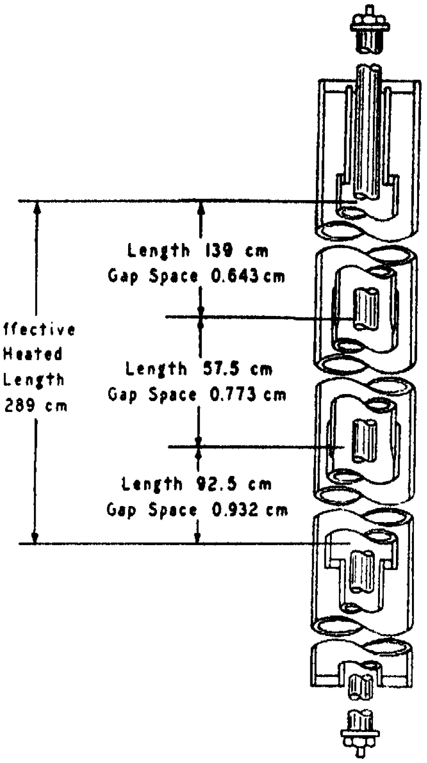

FIG. 2. Internal construction of three-stage all-metal thermal diffusion column based on a G. E. Calrod heater.

The end volume at the top of this hot-wire column consists of a rectangle of standard ½-inch o.d. copper tubing. Connections to the top of the column are made through sylphon bellows-type valves having clear ½-inch diameter openings. Convective circulation is maintained in this end volume, which contains upon closure of the two valves just one standard liter of gas.

To eliminate the hydrogen impurity, which is well concentrated in this end volume by the combined thermal diffusion and thermal siphoning action, a palladium thimble is silver-soldered re-entrant into one corner. This thimble is heated by means of a hot air blast to 200°C. As the gas in the end volume circulates continuously past the thimble, the hydrogen is effectively lost by diffusion through the palladium wall and is carried away by the air blast.

---

[4] L. Onsager and W. W. Watson, Phys. Rev. 56, 474 (1939).

[5] R. Simon, Phys. Rev. 69, 596 (1946).

In order to make more accurate analyses with our mass spectrometer, which has a limit of sensitivity of 0.01 percent for He^3/He^4, we concentrated further with an available 3-meter hot-wire glass column the helium in this end volume, after a 40-day run had just consumed the contents of one large helium cylinder. The hot wire in this recycling column is made of 20-mil tungsten and the diameter of the glass cold wall is 2 cm. The wire was kept at 1200°K and the "heavy" end volume was so constructed that the one liter of enriched gas from the metal columns just brought this glass column to atmospheric pressure. One can compute with these data in the hot-wire approximation of Jones and Furry[2] that $H=8.43\times10^{-6}$ g/sec.; $K_c=1.73\times10^{-5}$ g-cm/sec.; $K_d=1.03\times10^{-3}$ g-cm/sec.; $2AL=2.44$; the equilibrium separation factor, $q=11.47$; and the time for equilibrium is but a few hours.

PERFORMANCE

In one of our first runs without the metal hot-wire column, the system was operated at a pressure of 6.5 atmos., and enriched gas was drawn off at the top of the three-stage column at a rate of 300 cm^3/day ($\sigma=6\times10^{-7}$ g/sec.). This gas was stored in an oil-sealed Toepler pump from which it could be pushed back into the (evacuated) main column for recycling after 40 days of collection at this rate. A sample of the once-through helium taken before the start of this stripping process was kindly analyzed for us by A. O. Nier who reported the He^3/He^4 ratio to be 6×10^{-6}. This corresponds to an experimental enrichment factor of 40.

With this datum, and assuming the transport to be balanced in this three-stage column, the thermal diffusion coefficients were computed for these operating conditions. These were introduced into the transport equations integrated for the case in which the concentration of the desired isotope is everywhere small, giving about 45 as the experimental equilibrium separation factor of the three stages. The product of the equilibrium separation factors $q=e^{(H/K)L}$ for the three stages, on the other hand, is 3240. We can account for practically the whole of this discrepancy by the assumption that in our theoretical analysis we underestimated the remixing coefficient K by a factor of 2. The most probable source of a remixing coefficient larger than expected is the presence of parasitic convection arising from azimuthal variation in temperature of the hot surface. From the analysis in reference 2, we compute that for our smallest gap space the coefficient of parasitic convection K_p equals the remixing coefficient for longitudinal convection K_c if an azimuthal temperature difference of about 7° exists on the surface of the hot wall.

It is possible that the small gap space in helium, a gas of high thermal conductivity, together with the fact that the sheath of the Calrod is made of stainless steel, a material of relatively low thermal conductivity, would permit such azimuthal thermal gradients to be maintained. Poor centering of the heater wire in the Calrod might be the cause of the gradients. We recommend, then, that the hot wall in thermal diffusion columns always be made of a metal of good conductivity, such as copper.

With this clear indication that a marked increase in the separation factor of the apparatus was needed, the metal hot-wire column described above was convectively coupled to the top of the three-stage column. To determine the gas pressure for maximum separation factor, it is only necessary to maximize the constant $2A=H/(K_c+K_d)$. The transport H is a function of the square of the pressure p, K_c varies as p^4, and K_d is independent of p. By numerical evaluation $2A$ is found to be a maximum for $p=4.5$ atmos., with $H=4.33\times10^{-5}$ g/sec., $K_c=4.86\times10^{-4}$ g-cm/sec., and $K_d=5.3\times10^{-4}$ g-cm/sec. This gives a theoretical separation factor of 3.6×10^5, a figure much larger than can be realized in practice because of the limitation imposed by the small amount of He^3 in the original gas. Of the 1 cm^3 of He^3 in the contents of a large cylinder of well helium consumed in 40 days of operation, we estimate that half is valved-off at the bottom of the scrubber. If the other half in its entirety were concentrated in the liter of helium gas in the "light" end volume, the He^3/He^4 ratio there would be 0.05 percent. The indication from our mass spectrometer analyses, however, was that the He^3 content of this enriched gas was somewhat less than 0.01 percent.

After recycling this liter of helium gas for 12 hours in the glass hot-wire column, three samples totaling 25 cm^3 were withdrawn from the top of the column. These samples averaged 0.050±0.005 percent for the He^3/He^4 ratio, and so the over-all separation factor for these operations is $5\times10^{-4}/1.5\times10^{-7}$ or 3.3×10^3. Upon considering the factor (11.5) of this glass column and the volumes involved, the He^3/He^4 ratio in the end volume of the metal columns is indicated to be about 0.005 percent.

We conclude that it would definitely be feasible by improvement of some of our design features and by operation of more columns in series-parallel combination to produce any reasonable amount of highly concentrated He^3; but, since this isotope has been made available by the AEC, the thermal diffusion method need not be further developed at present. Experience here detailed is, however, applicable to other isotope and gas-mixture separations for which thermal diffusion is the preferred method.

THE REVIEW OF SCIENTIFIC INSTRUMENTS VOLUME 21, NUMBER 12 DECEMBER, 1950

Gas Flow through the Mass Spectrometer Viscous Leak

R. E. HALSTED AND ALFRED O. NIER
Department of Physics, University of Minnesota, Minneapolis 14, Minnesota

(Received August 11, 1950)

An approximate expression for the flow of a binary gas mixture through a mass spectrometer "viscous" leak has been derived and compared with experimental data. The factors important in the design and use of the leak are determined from this result.

THE design of gas inlet systems for mass spectrometers must be such that the composition of the gas in the spectrometer bears a known relation to the composition of the sample to be analyzed. Two types of gas inlet systems which satisfy this criterion are commonly employed. The simplest of these employs a "molecular" leak. Its operation has been described by Honig.[1] The sample is placed in a large bulb at a pressure below 100 microns. Flow into the mass spectrometer is through a pinhole so small that the mean free path is much larger than the diameter of the hole. The flow through the hole is molecular. This is also true of the flow of gas out of the mass spectrometer tube. Hence the absolute pressure in the ionizing region of the mass spectrometer of any constituent of the gas sample is directly proportional to the absolute pressure of that constituent in the gas sample. The constant of proportionality is the same for all gases and all constituents regardless of the composition of the sample.

The second type of gas inlet system employs a "viscous" leak.[2] It has the virtue that the sample is admitted to the mass spectrometer from a high pressure region (several cm Hg, or more). This simplifies the inlet system and makes possible in a simple manner continuous gas analyses from, for example, a process stream.[3] Inghram[4] has discussed its use, but the literature contains no references on experimental tests or its performance. The present paper derives an approximate equation for the flow of a binary gas mixture through such a leak and compares it with experiment. Some general conclusions concerning the design and performance of viscous leak systems can be drawn from this result.

Figure 1 is a schematic diagram of a viscous leak gas flow system. For convenience in theoretical treatment, this system is divided into the three following flow regions: A. Flow through the spectrometer; B. Flow through the constriction; C. Flow through the capillary tubing on the high pressure side of the constriction. Equations are obtained for the flow of one component of a gas mixture through each of these regions. Since the gas flow through the system is continuous, these three flow equations may be equated. With suitable approximations one can then solve for the partial pressure of one component of a gas mixture in the mass spectrometer ion source in terms of its partial pressure in the sample. Finally, the ratio of the two such expressions obtained for a binary mixture gives one an expression for the variation in measured sample composition with sample pressure.

A. Flow through the Spectrometer

The pressure in the spectrometer itself is so low that the mean free path of a molecule is much larger than spectrometer dimensions. Therefore, between two points in the vacuum system, such as 3 and 4, the flow is molecular and can be described by the equation

$$Q_{a34} = (k_{34}/M_a^{\frac{1}{2}})(P_{a3} - P_{a4}), \tag{1}$$

where Q_{a34} = flow of component a of a gas mixture between points 3 and 4 expressed as the time rate of change of pressure-volume product; k_{34} = constant dependent upon the geometry and temperature in the region between points 3 and 4; M_a = molecular weight of component a; and P_{a3}, P_{a4} = partial pressures of component a in regions 3 and 4, respectively.

B. Flow through the Constriction

In the constriction the flow cannot be so simply described. If the pressure behind the constriction is lowered to the point where molecular mean free paths are much larger than constriction dimensions, the description must reduce to one of molecular flow. At high pressures the description should change to the form of Poiseuille's law for viscous flow. Knudsen[5] has given a rather complicated semi-empirical equation which meets

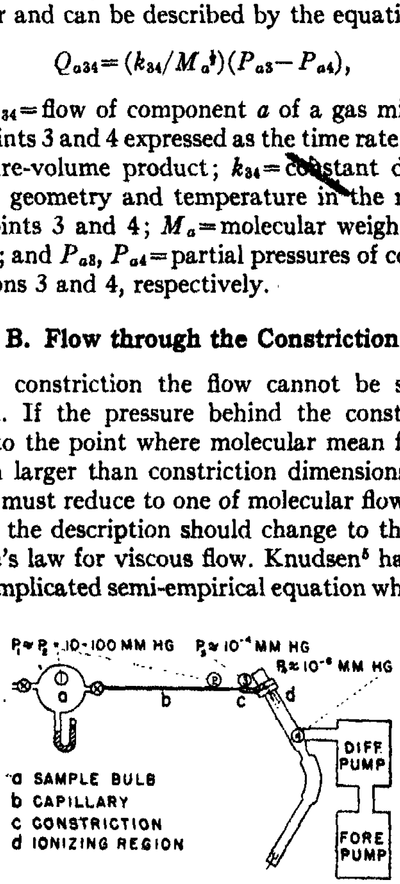

FIG. 1. Schematic diagram of spectrometer gas flow system with approximate pressure levels indicated.

---

[1] R. E. Honig, J. App. Phys. 16, 646 (1945).

[2] A. O. Nier, Rev. Sci. Inst. 18, 398 (1947).

[3] A. O. Nier *et al.*, An. Chem. 20, 188 (1948).

[4] M. G. Inghram, *Advances in Electronics* (Academic Press, Inc., New York, 1948), Vol. I, p. 232.

[5] M. Knudsen, Ann. d. Physik [IV] 28, 75 (1909).

these requirements and accurately describes the flow over the entire pressure range through cylindrical tubes. However, the geometry of the constriction is not so well defined. A simple sum of molecular and viscous flow terms is used here as an approximate form of the Knudsen equation. For the flow of one component of a gas mixture through the constriction

$$Q_{a23}=(k_{23}/M_a^{\frac{1}{2}})(P_{a2}-P_{a3})+v(P_{a2}/P_2)\bar{P}(P_2-P_3), \quad (2)$$

where k_{23} = constant dependent upon the geometry and temperature in the constriction; $\bar{P}=(P_2+P_3)/2$; v = coefficient of viscous flow, proportional to $1/\eta$; and η = coefficient of viscosity of gas mixture.

C. Flow through Capillary Tubing

The variation of flow with mass, indicated by the first term of Eq. (2), would tend to change the composition of a gas mixture adjacent to the high pressure side of the constriction and establish concentration (or partial pressure) gradients along the capillary. The function of the capillary tubing is to create a mass flow of gas toward the constriction with a velocity sufficiently great to overcome any back diffusion which would result from such a gradient. The flow through the tubing is therefore described by competing mass flow and diffusion terms. For one component one can write with fair approximation

$$Q_{a12}=VAP_{a1}-AD_{ab}[(P_{a2}-P_{a1})/L], \quad (3)$$

where V = average velocity of mass flow along the capillary; A = cross-sectional area of capillary; D_{ab} = diffusion coefficient for a mixture containing two components a and b, and L = length of capillary behind the constriction.

In practice the pressure dependence of Eqs. (1) and (2) is simplified by the fact that $P_2 \gg P_3 \gg P_4$. Also the difference between P_1 and P_2, though finite to permit mass flow in the capillary, is sufficiently small to permit replacement of P_2 by P_1 in Eqs. (1) and (2). Equating the flow equations and solving for P_{a3} in terms of P_{a1}.

$$k_{34}P_{a3}=P_{a1}\frac{[VA+(AD_{ab}/L)][k_{23}+(VM_a^{\frac{1}{2}}P_1/2)]}{(k_{23}/M_a^{\frac{1}{2}})+vP_1/2+(AD_{ab}/L)}. \quad (4)$$

The expression which would be obtained for the b component is given by replacing the subscript a by b wherever it occurs alone. Noting that the ion current is in general directly proportional to the partial pressure of any particular gas in the ionizing region of the spectrometer (ionizing electron energy and intensity constant) one obtains for the ratio of ion currents

$$\frac{I_a}{I_b}=\frac{P_{a3}}{P_{b3}}=\frac{P_{a1}}{P_{b1}}\left\{\frac{[k_{23}+vM_a^{\frac{1}{2}}P_1/2][(k_{23}/M_b^{\frac{1}{2}})+v_1P_1/2+AD_{ab}/L]}{[k_{23}+vM_b^{\frac{1}{2}}P_1/2][(k_{23}/M_a^{\frac{1}{2}})+v_1P_1/2+AD_{ab}/L]}\right\}, \quad (5)$$

where I_a and I_b equal the ion currents from components a and b respectively.

Since D_{ab} = constant$/P_1$; as $P_1 \to 0$, Eq. (5) reduces to

$$(I_a/I_b)\to(P_{a1}/P_{b1}). \quad (6)$$

Here the gas inlet system has introduced no mass discrimination and has behaved like a molecular leak. However, as P_1 gets large,

$$(I_a/I_b)\to(M_a/M_b)^{\frac{1}{2}}(P_{a1}/P_{b1}). \quad (7)$$

This situation results when there is viscous flow through the capillary and constriction, and separation of components occurs only in the molecular flow through the source region.

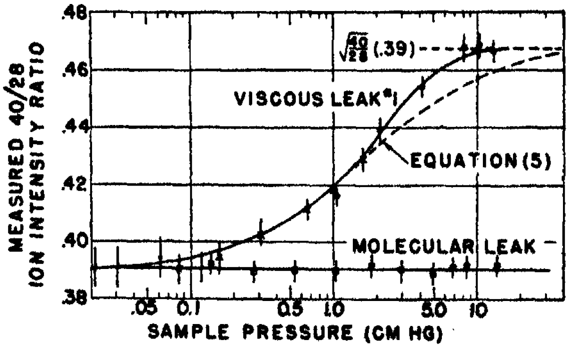

FIG. 2. Comparison of Eq. (5) with experiment for a mixture of argon and nitrogen (A/N$_2$ abundance ratio = 0.39) using viscous leak No. 1. Molecular leak data is plotted such that points along abscissa indicate same total gas flow through both leaks.

Within the pressure range of transition between Eqs. (6) and (7), a viscous leak would introduce an uncertain mass discrimination. Therefore, it is important to know where this change occurs for any given leak, and to design the leak in a manner which will remove the transition from the desired sample pressure range.

In order to compare Eq. (5) with experiment the quantities k_{23} and v must be determined. At pressures low enough for the viscous flow term of Eq. (2) to be neglected, $k_{23}=M^{\frac{1}{2}}Q_{23}/P_1$ for pure gases. One can obtain the value of k_{23}, therefore, if the relationship between the gas flow, Q, and the ion current is known. This relationship can be determined from the rate of depletion of a known quantity of sample from a constant volume under molecular flow conditions, for, making use of a molecular flow equation and the fact that I is proportional to P_3,

$$Q_{13}dt=(k_{13}/M^{\frac{1}{2}})P_1dt=-V_1dP_1.$$

Therefore,

$$Q_{13}=-(V_1P_1/\Delta t)\ln(P_{1f}/P_{1i})$$
$$=-(V_1P_1/\Delta t)\ln(I_f/I_i), \quad (8)$$

where Δt is the time difference between initial and final ion current measurements I_i and I_f, respectively.

The relationship between v and k_{23} for a given pure gas is chosen to fit an experimental curve for the equation

$$(I/P_1) \propto (k_{34}P_3/P_1) = k_{23} + (vM^{\frac{1}{2}}P_1/2), \tag{9}$$

obtained from Eqs. (1) and (2). For other gases v can be calculated since it is inversely proportional to the coefficient of viscosity. Unfortunately, this coefficient for even a binary gas mixture is not simply related to the coefficients of its components, so an approximate value must be used where exact values are not available. It might be noted here that at pressures where the viscous flow term of Eq. (2) predominates, $Q \propto v \propto (1/\eta)$. Therefore the total flow of a gas mixture through the leak is subject to the same variations, often unpredictable, with composition as the coefficient of viscosity. Equation (7) shows, however, that relative abundance measurements are not affected by variations in η.

Figure 2 gives one example of the degree of agreement between Eq. (5) and experiment, a mean v being used in this case. A consideration of the approximations involved in replacing P_2 with P_1 and assuming Eqs. (2) and (3) shows that a more elaborate treatment would improve the fit. The preceding development remains useful, however, for its simple physical picture of the gas flow.

Equation (5) suggests that the most feasible way of improving a leak of this design (i.e., extending the viscous flow portion of the curve to lower sample pressures) would be to decrease the cross-sectional area and/or increase the length of the capillary behind the leak. Figure 3 illustrates the effect of changing each in this manner by a factor of 2 for a frequently encountered type of isotope analysis. By changing each by the same factor the time response (i.e., transit time of gas through capillary) of the leak in the above example was essentially unchanged.

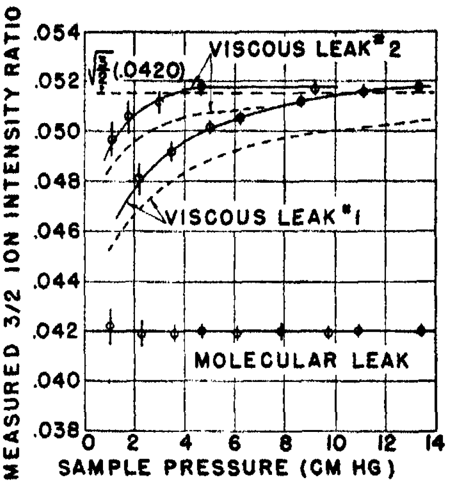

FIG. 3. Variation in measured $\frac{3}{2}$-ion intensity ratio as a function of sample pressure for several leaks. HD/H_2 abundance ratio for sample $=0.0420$. For viscous leak No. 1: $L=50$ cm; average i.d. $=0.010$ in. For viscous leak No. 2: $L=100$ cm; average i.d. $=0.007$ in. The constrictions were adjusted to give equal pumping speeds of 9×10^{-5} cm^3 sec.$^{-1}$ for N$_2$. Broken curves give Eq. (5) for each leak. Molecular leak data are plotted such that points along abscissa indicate same total gas flow through all leaks.

In practice, area reduction is limited by the requirement that the diameter of the capillary must be sufficiently greater than the mean free path to obtain viscous flow. An increase in length, without a corresponding reduction in cross section, will increase the time response. Therefore the leak dimensions for optimum performance will vary somewhat with application.

This research was supported in part by a grant provided by the Experiment Station of the Hawaiian Sugar Planters Association.

Erratum. Tektronix Advertisement

The Tektronix advertisement in the July issue, publicizing their Type 514-*D* Cathode Ray Oscilloscope, erroneously listed the sweep range as being ".01 usec/cm to .01 sec/cm." This should have read ".1 usec/cm to .01 sec/cm." They sincerely regret any inconvenience they might have caused to any of the readers of *The Review of Scientific Instruments*.

THE REVIEW OF SCIENTIFIC INSTRUMENTS VOLUME 21, NUMBER 12 DECEMBER, 1950

Physical Instruments for the Biologist

Detlev W. Bronk
Associate Editor in Charge of this Section
The Johns Hopkins University, Baltimore, Maryland

Detection of Tritiated Compounds in Paper Chromatography

IRVING GRAY,* SABURO IKEDA, ANDREW A. BENSON, AND DAVID KRITCHEVSKY
Radiation Laboratory,[1] *University of California, Berkeley, California*

(Received June 16, 1950)

A windowless tube has been developed which can be used to detect tritium activity on paper, glass, or aluminum. The tube is of glass, with a nichrome anode and a copper sulfide coated copper cathode, and utilizes a stream of helium saturated with alcohol. This device is convenient for detection of tritiated compounds in paper chromatography.

LOCATION of tritiated compounds in paper chromatography has posed a problem because of the difficulties involved in the detection of the active spots. Because of the low energy of its emitted β-rays, the assay of tritium has usually been done in the gaseous phase. This procedure does not lend itself to the location of tritiated compounds on paper. A possible method, which has been tried in this laboratory, involves cutting of the paper into squares and counting each square in a windowless counter such as the "Nucleometer." This method has the disadvantage that it renders the paper useless for further work. A counting tube has been developed which will measure the radiation from the spots in question easily and accurately.

The counting apparatus (Fig. 1) consists of a windowless Scott tube,[2] a gas flow regulator, and a source of helium saturated with alcohol at 0°C. The tube is wrapped in lead foil to minimize background radiation and to add ballast, so that a constant resistance to gas flow through the paper is maintained.

A rate of gas flow of 300 ml/min. was maintained. This rate insured a reproducible counting rate. At this rate of flow, the system showed the following characteristics: Starting voltage, Plateau, Optimum operating voltage, 1125 volts; 1200–1400 volts; 1350 volts.

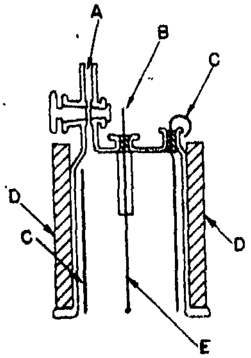

FIG. 1. Windowless counting tube. A. Gas flow inlet. B. To scaler. C. Cathode, CuS-coated copper. *D*. Lead shield. E. Anode, glass-tipped nichrome wire.

For scanning, the tube is allowed to rest on the paper and is slowly moved over the paper in a definite pattern. Where a particular area is to be counted, the tube is flushed for at least thirty seconds, after which a count is made.

This apparatus has been used to scan and count papers on which compounds containing either C^{14} or tritium have been adsorbed. Table I summarizes the results obtained using various types of counters. For counting in the "Nucleometer," papers were cut into 1¼-inch squares.

TABLE I. Comparison of the values obtained by counting the same sample by various counting devices. All data given as counts per minute.

Sample	Scott tube	Windowless tube	Nucleometer
Background	138	49	70
T^a (on paper)	…[c]	12,288±45	10,815±1280
T (on glass plate)	…[c]	7,488±64	12,224± 704
T (on aluminum plate)	…[c]	3,008±26	5,952± 26
C^b (on paper)	4032±64	6,080±51	10,752± 128

[a] Denotes tritium containing compound (tritiated cholesterol).
[b] Denotes C^{14} containing compound (stearic acid-1-C^{14}).
[c] No measurable activity.

Once the active spots have been located on the paper, it is desirable to make a radiogram of the paper in order to have an accurate outline of the active area.[3] Here again, the low energy of tritium radiation (0.018 Mev) and the high self-absorption indicated the necessity of altering the usual procedure. We have found, however, that a satisfactory image of an area containing a tritiated compound is obtained on Eastman "No-Screen" X-ray film in twenty-four hours if the area has an activity of 15,000 counts/min./cm² as recorded by the windowless tube. (C^{14}, 0.16 Mev, requires a recorded activity of about 200 counts/min./cm² in order to give a satisfactory image in twenty-four hours.)

ACKNOWLEDGMENTS

The authors wish to acknowledge the kind interest shown by Professor Melvin Calvin and Dr. Bert M. Tolbert during the course of this investigation.

---

* Major, Medical Service Corps, U. S. Army. Present address, Brooke Army Medical Center, Fort Sam Houston, Texas.

[1] The work described in this paper was sponsored by the A.E.C.

[2] Differs from drawing only in that it has a thin mica end window, *ca.* 1.5 mg/cm². This tube was developed by Dr. Kenneth Scott of this laboratory.

[3] A. A. Benson, *et al.*, J. Am. Chem. Soc. **72**, 1710 (1950).

Laboratory and Shop Notes

BRIEF contributions in any field of instrumentation or technique within the field of the journal can be accorded earlier publication if submitted for this section.

A Simplified Percent Transmission Computer

A. L. McClellan* and G. C. Pimentel
Department of Chemistry, University of California, Berkeley, California

July 20, 1950

THE use of any single beam spectrometer requires the transformation of the spectra measured by the instrument into the related and more useful percent transmission curves normally reported in the literature. This task can be lightened to some extent with a device reported by Gershinowitz and Wilson[1] but this conversion remains a tedious and time consuming portion of spectral analysis.

The electric analog computer first reported by Fuoss and Mead[2] and modified by Zerwekh[3] can be further simplified to provide a rapid, reasonably accurate method of making these calculations. An alternative solution to the problem is the more arduous task of converting the single beam instrument into one using a split beam.

The basic changes reported here eliminate the need for a second recorder and avoid the use of specially wound coils. This allows construction of the computer as a compact unit attached directly to the door of the spectrometer recorder. The door is swung open to permit normal use of the recorder.

The electrical circuit is essentially the same as, and the component designation is identical, with that of Zerwekh. The values of the components used were $R_1 = RI_0 = 50{,}000\Omega$; $R_2 = RI = 100\Omega$; $R_3 = 500\Omega$; a 2 v battery. Beckmann Helipots, linear to 0.1 percent, were used for R_I and RI_0 as substitutes for the specially wound coils used by Zerwekh. Figure 1 shows a top view of the actual computer (not to scale).

Attached to each potentiometer is an extending shaft which is threaded in the center section and has a crank at the outer end. A flexible wire, fastened in the threads and over a pulley at the other end of the computer, is attached to a carriage sliding on a rail of rectangular cross section. As the crankshaft is turned, the wire moves the carriage. The diameter of the shaft in the threaded section is such that a pointer mounted on the sliding carriage moves over the entire range of the recorder scale as the resistance of the Helipot is varied from zero to maximum. The guide rail is rectangular to minimize vertical motion of the pointer. The other Helipot is connected, in a like fashion, at the opposite end of the computer to a second carriage on the same guide rail.

The same recording instrument used to register the spectra can be used to plot the I/I_0 curve. Jack connections must be placed in the input circuit of the recorder so that either the spectrometer signal or the computer signal can be received by the recorder.

The background and desired spectrum are superimposed as usual. The paper in the recorder is then turned back to the beginning of the two spectra. The computer output is substituted for the spectrometer signal by means of the appropriate jack connections and the power supply circuit closed. With the two Helipots set on zero resistance the zero adjustment clamps are loosened and the two carriages moved until both pointers are set on the no-signal reference line of the two spectra. Now the two pointers are placed together at the center of the scale and the value of R_3 is changed so that the pen records 100 percent transmission when the pointers are together. In the case that the two spectra do not have a common reference line, the independent zero-adjustments of R_I and RI_0 permit separate settings. The R_3 adjustment would then be made with the pointers not together but at equal distances from their respective reference lines.

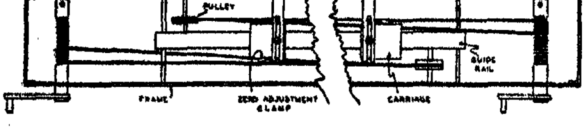

FIG. 1 Top view of computer.

The recorder is started and while the two cranks are manipulated so that the pointers follow the curves, the pen traces I/I_0. This latter curve will necessarily be displaced from the spectra since there must be clearance between the pointers and the pen. Adjustment screws are provided on the pointers so that this offset can be made a convenient amount. If the background is not perfectly aligned with the sample spectra, correction can be made with these screws.

In some spectra it may be difficult to record the background and sample spectra with the same amplification (e.g. solid spectra in which reflection loss is significant). If a standard test signal is recorded at the time of the experiment, the amplification need not be identical for both runs. In this case R_3 is adjusted so that the pen records the ratio of the test signal deflections when the pointers are together.

The ease of operation and accuracy of this computer are the same as those of the instrument described by Zerwekh.

---

* Present address, Department of Metallurgy, Massachusetts Institute of Technology.

[1] H. Gershinowitz and E. B. Wilson, J. Chem. Phys. 6, 200 (1938).

[2] R. M. Fuoss and D. J. Mead, Rev. Sci. Inst. 16, 223 (1945).

[3] C. E. Zerwekh, Rev. Sci. Inst. 20, 371 (1949).

Note on Crystals Suitable for Double Crystal X-Ray Spectroscopy in the Region 3 to 15A*

S. T. Stephenson and D. L. Martin
The State College of Washington, Pullman, Washington

July 26, 1950

THE problem of finding crystals of large enough grating space to be useful in the vacuum region above 3A has been considered from time to time. Typical of studies on crystals suitable for single crystal x-ray use in vacuum spectrometers was that of Stenstrom[1] who found mica, gypsum, beryl, sugar, $CaSO_4$ and $K_4Fe(CN)_6$ to be satisfactory. Double crystal work imposes more stringent requirements on the crystals than does single crystal work because the x-ray beam is of the order of a hundred times broader in the double crystal arrangement and correspondingly larger areas of the crystal faces are used. Thus one is limited to compounds for which large crystals are available and for which the crystal faces are relatively perfect. The test of perfection is the width of the parallel rocking curve obtained by rocking the second crystal about the position (1, −1) in which it is parallel to the first crystal, since the narrower the rocking curves, the higher the

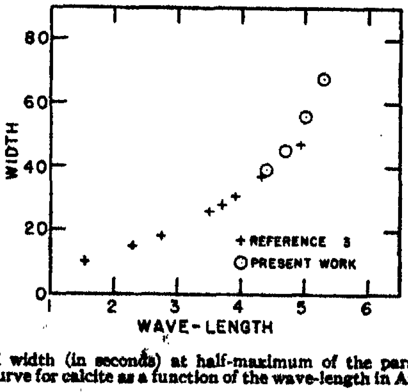

FIG. 1. Full width (in seconds) at half-maximum of the parallel rocking (1, −1) curve for calcite as a function of the wave-length in Angstroms.

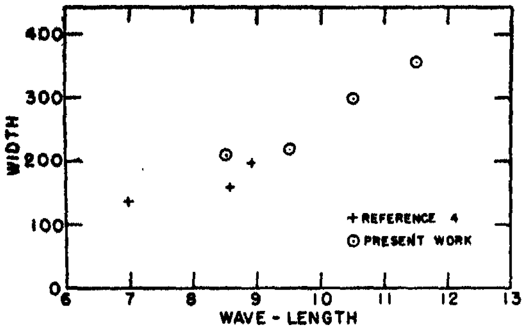

FIG. 2. Full width (in seconds) at half-maximum of the parallel rocking (1, −1) curve for beryl as a function of the wave-length in Angstroms.

resolution the crystals will achieve in the (1, +1) position. An additional requirement for the spectrometer used in this laboratory[2] is that the crystals must have properties suitable for use in a vacuum which is essentially as good as that in the x-ray tube itself, because there is no film covering the window between the x-ray tube and the spectrometer chamber.

As far as we are aware the only studies of the parallel rocking curves in this wave-length region are those of Parratt[3] who obtained curves on calcite out to 4.94A and on quartz out to 7A, and those of Munier, Bearden, and Shaw[4] who used beryl at wave-lengths up to 8.9A. It was the purpose of the present investigation to extend these results to longer wave-lengths and to determine if crystals of other compounds might be useful.

The results for calcite[3] and beryl[4] have been verified in the present work and have been extended to 5.3A and 11.5A, respectively. The data are presented in Figs. 1 and 2. It is evident that the resolution offered by calcite is excellent for use out to 5.3A which is about as far as one can go with the small grating space. Beryl offers satisfactory resolution out to 11.5A. Beryl had so low a reflecting power at wave-lengths shorter than the AlK edge as to be useless in this region. The calcite surfaces were cleaved and etched lightly with dilute HCl whereas the beryl surfaces were natural (10 $\bar{1}$0) faces. The radiation was the continuous spectrum from a tungsten target and the x-ray tube was operated at a voltage low enough so as not to produce second-order radiation for the particular glancing angle being studied.

An effort was made to find other crystals of large grating space which would be useful at these wave-lengths in the double crystal spectrometer. Other crystals investigated were mica, gypsum, quartz, and topaz. Mica and gypsum seemed particularly promising because of the large grating space for the natural cleavage faces and because these faces are easily available with large area. Many attempts were made to secure parallel rocking (1, −1) curves for two mica crystals, but without success. Thin crystals, thick crystals, and thin crystals pasted onto optical flats were all tried but no (1, −1) curves were obtained. Presumably this was because of macroscopic waviness of the natural mica crystal surfaces, which was reduced almost to microscopic waviness upon cementing to flat surfaces but was not eliminated; thus portions of the two crystal faces were parallel to each other over large rocking angles and no sharp (1, −1) peak was produced. Gypsum did not have suitable vacuum properties for use in an x-ray vacuum. The pumps did not achieve an operating vacuum even after prolonged pumping and the crystals gradually turned white. Presumably water of crystallization was slowly given off and plaster of Paris was formed. Coating the crystals with glyptal proved ineffective. Quartz and topaz were found to have too low a coefficient of reflection to be useful. Sugar and $K_4Fe(CN)_6$ were not tested because they were not available in large enough size. Gratings built up by successive dipping in a proper organic liquid have not as yet been tried nor would they appear to offer much promise because of the stringent requirements which double crystal work makes on the perfection of the grating.

---

* Supported in part by the ONR.

[1] W. Stenstrom, Ann. d. Physik 57, 347 (1918).

[2] S. T. Stephenson and F. D. Mason, Phys. Rev. 75, 1711 (1949).

[3] L. G. Parratt, Phys. Rev. 41, 561 (1936); Rev. Sci. Inst. 5, 395 (1934); Rev. Sci. Inst. 6, 387 (1935).

[4] Munier, Bearden, and Shaw, *Phys. Rev.* 58, 537 (1940).

A Greaseless Gas Flow Valve

R. E. HONIG*
Socony-Vacuum Laboratories, Research and Development Department, Paulsboro, New Jersey

August 25, 1950

IN experiments where appreciable pressures (1 mm Hg$<p<1$ atmos.) of highest purity samples are to be introduced into a high vacuum system, the following greaseless valve has been found very useful. In essence, it consists of a small volume that terminates in three sintered glass disks (Corning grade *F*) and is partially filled with Hg (see Fig. 1). Disk *A* connects to the gas sample, disk *B* to the vacuum system, and disk *C* to a manipulating vacuum-pressure line. The valve is closed when *C* is at atmospheric pressure (Fig. 1a). Gas will flow from the sample bulb through disks *A* and *B* into the vacuum system as soon as the pressure above disk *C* is reduced sufficiently to pull the mercury up (Fig. 1b). It is readily seen that this occurs when

$$p_c \leq p - \Delta h.$$

This valve will operate satisfactorily under all conditions if the following requirements are met:

1. When the valve is closed, the Hg level in the manipulating arm should lie above a (Fig. 1a), thereby keeping the pressure to the right of disk *B* somewhat above atmospheric. This will prevent air from bubbling from the system through disk *B*, the mercury, and disk *A* into the sample bulb at times when the system is let up to air and the sample is partially depleted. This requirement is met by arranging the three disks as shown in Fig. 1a and filling the tube to the level of disk *A*.

2. Disk *C* should be mounted in such a way that disk *B* is completely bared when the valve is open. At the same time, the bend of the *U*-tube should lie below level *b* to prevent part of the sample from bubbling through into the manipulating arm.

The valve may be thoroughly degassed at elevated temperatures before the mercury is distilled into it. In this respect it is more versatile than the simpler gas introduction system described by Taylor and Young[1] who obtain flow by making contact between two movable sintered disks in a pool of Hg. Because the gas flow rate through fine sintered disks is relatively slow, it is easy to time the valve manipulation so as to admit any desired pressure to the vacuum system.

In a simpler version of this valve, the mercury is moved mechanically by a stainless steel bellows (see Fig. 2) which is attached to a manipulating screw. While this method is not amenable to

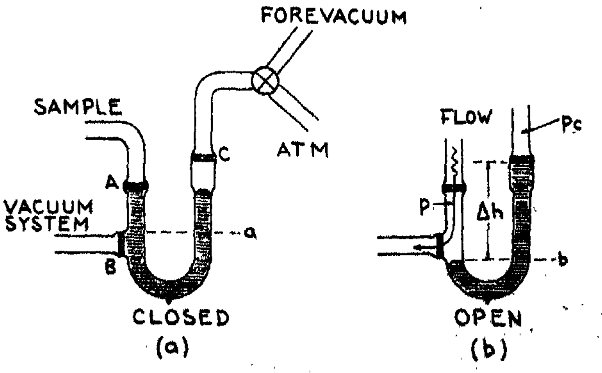

FIG. 1. Essential parts of sintered glass valve.

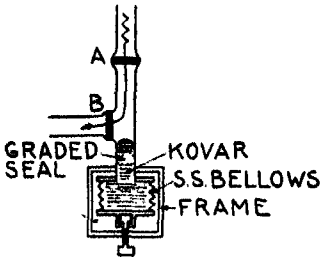

FIG. 2. Sintered glass-bellows valve.

thorough outgassing, it does eliminate the vacuum-pressure manipulating line and it is spill-proof.

---

* Now at RCA Laboratories, Princeton, New Jersey.

[1] Taylor and Young, Ind. Eng. Chem. Anal. Ed. 17, 811 (1945).

Zero Inefficiency Anticoincidence Circuit

M. DEGALLIER
Laboratoire de Recherches Nucleaires, Ecole Polytechnique, Université de Lausanne, Lausanne, France

September 12, 1950

LET us consider a mixing circuit composed of two pentodes, one being normally conductive, receiving the negative coincidence pulse (*C*) formed somewhere else, and the other, normally cut off, receiving the positive square pulses (*S*) from the anticoincidence counters. Any *C*-pulse not accompanied by an *S*-pulse thus gives rise to a positive pulse which is termed anticoincidence ($A=C-S$).

A 100 percent efficiency has been claimed in the literature for such a circuit using a flip-flop to generate the *S*-pulses. That is not exactly true, though the inefficiency may be small enough to be negligible in certain experiments; in others it can be very harmful and intolerable. It is due to the existence of the recovery time of the flip-flop. The expression giving the inefficiency has been calculated in the following way:

Let n_c, n_s, n_{sa} be respectively the rates of pulses *C*, *S*, and spurious anticoincidences, and φ the dead time of the flip-flop, defined as the shortest interval between the end of a pulse and the front of the next one.

Thus every *C*-pulse falling in that interval will give rise to a spurious anticoincidence, the rate of which is therefore $n_{sa}=n_c\cdot n_s\cdot\varphi$. The resulting inefficiency is consequently $n_s\cdot\varphi$, and the only way to get rid of it is to design the circuit in order to have $\varphi=0$.

The proposed circuit for generating the anticoincidence pulses *S* (Fig. 1), similar to that of Putman, [Proc. Phys. Soc. 61, 312 (1948)] satisfies this demand: its essential characteristic is that it can be re-excited at full pulse duration inside or outside its cycle. At each positive input pulse on the grid of *T*1, the condenser *C* is fully discharged (this is true only if the input pulse is sufficiently long) and then recovers while generating the exponential timing wave which determines the duration of the *S* pulse.

This circuit, developed for very low inefficiency measurements of counters, has been tested by feeding the *S* input terminal from 17 counters counting altogether at 170 c.p.s. while the *C* input terminal was fed only from the pulses of one of these counters (4 c.p.s.). The pulses from the single counter were, of course, coincidences and not a single anticoincidence has been registered for 10^5 coincidences.

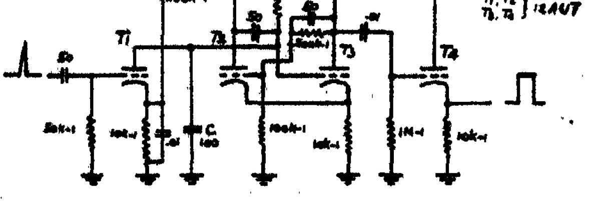

FIG. 1.

Varying Nuclear Emulsion Sensitivity with Altitude

ARTHUR BEISER
Department of Physics, New York University, University Heights, New York, New York

September 12, 1950

IN reviewing cosmic-ray detection techniques, Korff[1] points out that a major deficiency in nuclear emulsion work is the continuously sensitive property of emulsions, rendering uncertain the circumstances attendant upon the recording of a particular event. Methods of eradicating previous phenomena in a nuclear emulsion before use have been described[2] and are frequently helpful, but a process for sensitizing and desensitizing plates at prescribed times would be of very much greater value.

The dependence of the sensitivity-reducing action of photographic desensitizers on oxygen concentration[3] suggests the possibility of limiting the sensitivity time of nuclear emulsions by the use of such agents. The dyes used for this purpose apparently act as catalysts for the oxygen in its reaction with the emulsion, and are capable of preventing the formation of a latent image while not ordinarily sufficient to attack an existing one. Since the density of atmospheric oxygen varies with altitude, the use of desensitizers is of especial interest in connection with balloon and perhaps also airplane and rocket flights with nuclear plates.

To determine the degree of desensitization attainable and the magnitude of its reduction under the conditions of a balloon flight, preliminary experiments were performed with pinakryptol green (1:5000), Eastman Kodak NTB emulsions and a polonium alpha-particle source. It was found that the desensitized plates, irradiated and processed with a standardized procedure, exhibited an optical density at the area of exposure approximately ten percent that of untreated control plates. The tracks themselves were very faint, from one-half to two-thirds shorter than the control tracks, and exhibited a grain structure along almost all of their length, while the controls showed no grain structure beyond the first few microns of track length.

The simulated balloon flight occupied one hour, with the pressure in a chamber containing the desensitized plate and the source being reduced to 2.5 cm Hg (corresponding to ~75,000 ft. or 23,000 m altitude), where it was held for five minutes. After processing, the plate had a density almost three times that of a control, exposed for the same length of time outside of the chamber. Reduced pressures had no influence on plates not desensitized. Examination of the tracks revealed two distinct kinds, with relatively few transitional ones: a background of weak tracks identical to the ones in the control, and a number of heavier tracks as long as those in the non-desensitized plates but with a slight grain structure for part of their length. The latter tracks were presumably recorded at the lower pressures and account for the increased density. This moderately complete separation of the tracks in two classes would seem to indicate the existence of a discontinuity in the desensitizer action. Such a discontinuity, or cut-off region, if its dependence on altitude and rate of ascent can be determined, would be extremely desirable, making possible both fairly reliable measurements of recorded phenomena and their correlation with altitude.

A series of experiments is in progress to investigate the variation of the sensitivity of desensitized emulsions with the above factors and on the nature and concentration of the desensitizer and the emulsion composition and thickness. The ultimate utility of this method will depend largely on the magnitude of the sensitivity increase with altitude and on the existence and nature of a cut-off region. It is hoped that some conclusions may be reached on these points.

[1] S. A. Korff, Rev. Mod. Phys. 20, 327 (1948).
[2] H. Yagoda, *Radioactive Measurements with Nuclear Emulsions* (John Wiley and Sons, Inc., New York, 1949), p. 108; M. Wiener and H. Yagoda, Rev. Sci. Inst. 21, 39 (1950).
[3] M. Blau and H. Wambacher, Nature 134, 538 (1934).

Cathode-Follower Fallacies*

Paul I. Richards
Brookhaven National Laboratory, Upton, Long Island, New York

October 19, 1950

It is often stated[1] in the literature that the low output impedance of a cathode follower offers the best solution to the problem of rapidly driving a large capacity or low impedance line. While the cathode follower is indeed an excellent driver for these loads and has certain definite advantages in many applications, the statement as it stands is somewhat oversimplified and has led to the use of cathode followers in circuits where they are unnecessary and some times even unsuited. Actually the ability to drive these loads rapidly is not a unique attribute of the cathode follower. Let us examine more carefully the relative properties of the cathode follower and conventional amplifier; various quantities of interest are listed in Table I. Note that the output capacity of the tube can safely be omitted because it will either be small compared to a large load capacity or, across a low impedance line, will affect the rise time less than preceding or succeeding stages.

Considering first the problem of driving a low impedance line, it is often stated that the low output impedance of the cathode follower is required to match the sending end of the line. But it is not always important to match the sending end, for if the far end is terminated by the proper resistor, the reflections will in many applications not be serious. In *such* applications, then, the problem reduces to obtaining maximum signal voltage across the low impedance without unduly loading earlier stages. With a given tube and given load resistance Z_0, greater gain is invariably obtained with the "amplifier" circuit (Table I). This gain, of course, will be unity or less with presently available tubes and coaxial lines, but it will still be greater than that obtained from cathode connection; moreover the low gains involved result in input capacities for the two circuits which differ, even for a triode, by less than might at first be expected. Therefore, in applications where maximum gain is desired, the amplifier circuit may be preferred.[2] The two circuits, of course, have opposite output polarity and this consideration alone will often save one (inverting) tube in such applications.

With a largely capacitative load, the situation is somewhat more deceptive. It might appear that the low output impedance of the cathode follower is required to give a reasonably fast rise time. If, however, C_L is given and G_L may be varied (the usual situation), Table I shows that the gain band-width product is the *same* for the cathode follower as for the amplifier. Physically, the greater "inherent" gain of the amplifier circuit allows one to use a lower resistor across C_L thereby compensating for the higher output impedance and resulting in the same final rise time for the same gain. However, it will be noted that a given tube (that is, a given maximum plate current) cannot develop as large a maximum output voltage across the lower shunt resistance as it could with cathode connection. In other words, although the *gain* band-width products are the same for the two connections, the maximum-output-voltage-band-width products are not. Again the gains involved are low in any case, and previous remarks apply to input capacities. Thus, in those applications where large voltages are not required, the difference in output polarity of the two connections may lead to the choice of the amplifier.

TABLE I.*

	Amplifier	Cathode follower
Output impedance	r_p	$\frac{r_p}{1+\mu}\approx 1/gm$
Gain $=A$	$\frac{\mu}{1+r_pY_L}$	$\frac{\mu}{1+\mu+r_pY_L}$
Rise time	$\frac{C_L(2\pi)^{\frac{1}{2}}}{G_L+1/r_p}$	$\frac{C_L(2\pi)^{\frac{1}{2}}}{G_L+(1+\mu)/r_p}$
Mid-band gain / rise time	$g_m/C_L(2\pi)^{\frac{1}{2}}$	$g_m/C_L(2\pi)^{\frac{1}{2}}$
Input capacity	Triode: $C_gK+C_{gp}(1+A)$ Pentode: $C_gK+C_{gS_c}$	Triode: $C_{gp}+C_gK(1-A)$ Pentode, triode-connected $C_{gS_c}+C_gK(1-A)$ Pentode-connected $(C_{gS_c}+C_gK)(1-A)$

* Notation: r_p = plate resistance. μ = amplification factor. gm = transconductance. $Y_L=G_L+j\omega C_L$ = load admittance. C_L = load capacitance. C_gK = grid to cathode capacitance. C_{gp} = grid to plate capacitance. C_{gS_c} = grid to screen capacitance. A = gain.

Some general remarks on the preceding observations must be made. First, a *pentode-connected* cathode follower has a lower input capacity than any of the other circuits; if input capacity is the prime consideration the pentode-connected cathode follower is definitely indicated. Secondly the cathode follower, being a feed-back circuit, has a slight edge as regards linearity and/or stability although the feed-back factor is not very large in those cases where $R_L\approx 1/gm$. Finally, as already noted above, the cathode connection will drive a large capacity to a higher maximum voltage than any other connection with the same rise time and the same tube.

Thus the cathode follower has a definite superiority in the more exacting applications, but many less critical circuits can be unnecessarily complicated by its use.

As a simple example, suppose that a triggering pulse of 3 volts must be sent down a very long line of 100 ohms characteristic impedance and that the circuit to be triggered will not respond to pulses less than about ½ volt. If the line is terminated by a 100-ohm resistor the reflections will usually be very much less than ½ volt, so there will be no need to match the input of the line. Suppose further that the available trigger comes out of its generating circuit at a level of 4 volts. If half of a 5687 tube ($gm=10{,}000$, $\mu=20$, $r_p=2000$) is available to drive the line, the amplifier connection will give a gain of 0.95 or an output pulse of 3.8 volts which is quite sufficient; the input capacity will be 10.2 $\mu\mu$f. Cathode-follower connection would give a gain of 0.5 or an output of only 2 volts, so that additional amplification would be required; the input capacity would be 5.1 $\mu\mu$f. If, instead, an amplitude of 2 volts were sufficient but the generator gave negative pulses while a positive trigger were required, the cathode follower would again require an extra tube to invert the signal whereas the amplifier alone would suffice.

As an example involving a large capacity, suppose that the layout of complicated equipment forces one to send a small signal (say 0.1 volt or less) through a length of cable (say 5 feet having a capacity of 60 $\mu\mu$f) to another chassis where the input capacity is 10 $\mu\mu$f. Suppose further that a rise time no greater than 0.05 μsec. is required and that the polarity must be inverted. It might seem that a cathode follower preceded by an inverting amplifier would be required. If, however, gain is not needed, a tube may be saved by using an amplifier to feed the cable directly. Thus a 6AK5 pentode ($gm=5000$, $r_p=\frac{1}{2}$ meg) with a 200-ohm plate resistor will feed the 70-$\mu\mu$f load at a rise time of 0.04 μsec. with a gain of unity and an input capacity of 4 $\mu\mu$.

Thus it appears that there are many non-critical applications where a low gain amplifier is actually preferable to a cathode follower. While none of the material here presented is especially new, it is hoped that the discussion will be of help particularly to those who are not electronics experts but who must often design their own circuits for experimental equipment.

* Work done at Brookhaven National Laboratory under the auspices of the AEC.

[1] For example, F. E. Terman *Radio Engineers Handbook* (McGraw-Hill Book Company, Inc., New York, 1943), pp. 430–432.
[2] Note that a large coupling condenser can be avoided by feeding the plate voltage through the terminating resistor.

Electron Optical Disk

L. Marton and J. Arol Simpson
National Bureau of Standards, Washington, D. C.

September 19, 1950

THE electron optical literature, while not abounding in descriptions of devices for the determination of the optical constants of axially symmetrical systems, lists some electron optical benches.[1] We were unable to find, however, a description of a device for the direct study of deflecting systems. There are a number of analog models which may be used for electrostatic deflection but none for magnetic systems of large aperture. Moreover, since these are but analog models, their usefulness and accuracy is rather limited. Because of this situation we decided to construct a simple electron optical device based on the analogy with the well-known optical disk now widely used in the teaching of elementary physics. This device in its usual form utilizes a beam at grazing incidence to a diffusing surface upon which the beam path may be observed as it is reflected or refracted. This apparatus permitted us not only to study magnetic deflection but also avoided most of the difficulties inherent in models since electrons form the beam.

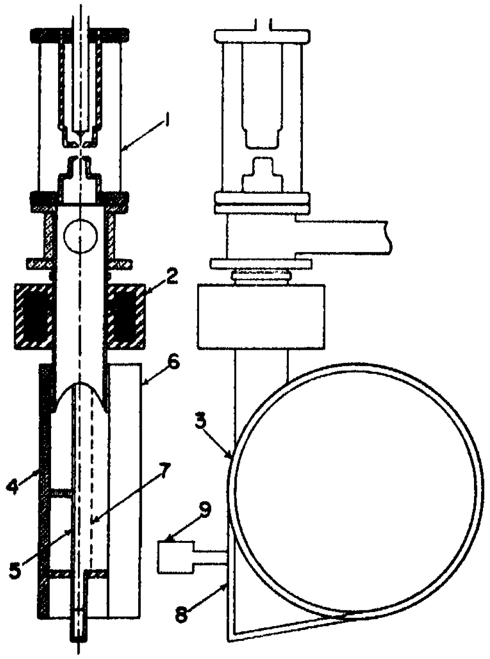

Fig. 1.

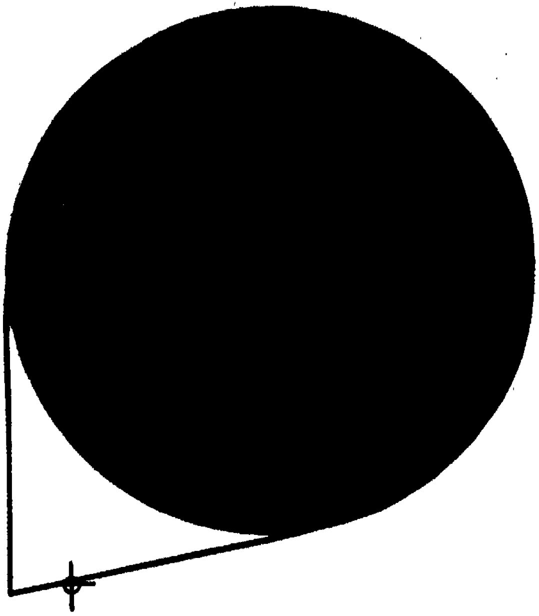

Fig. 3.

The electron optical analog is shown in Fig. 1. On Fig. 1, (1) is a 3-electrode electron gun of conventional construction; (2) is a focusing coil in an iron shield which fits over the $2\frac{1}{8}$-inches o. d. copper tubing supporting the gun; (3) is the body of the instrument. This latter consists of a 3-inch length of 10-inch wrought iron pipe grooved at each end for an *O*-ring vacuum seal. One end of the pipe is closed with a dural disk (4) which supports the phosphor screen (5) on a threaded rod. By means of this thread the screen may be accurately positioned in the median plane of the

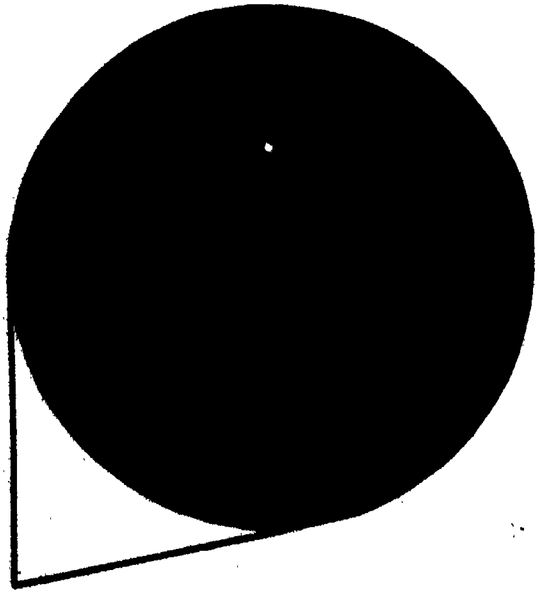

Fig. 2.

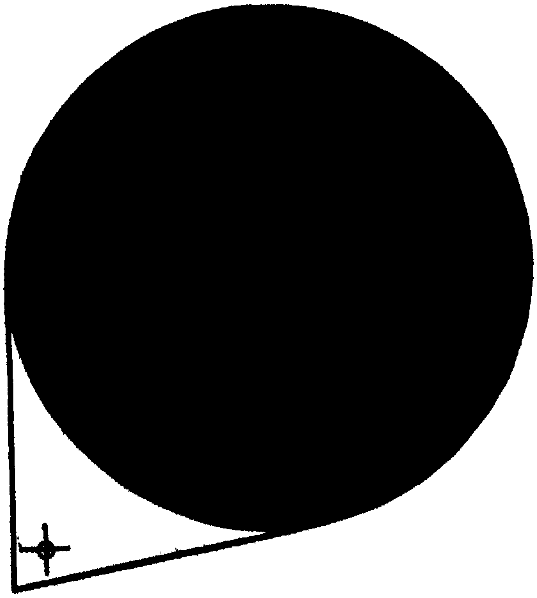

Fig. 4.

beam, or displaced a known amount if desired. In the present design this adjustment cannot be made from outside the vacuum. If this feature were desired it would easily be provided for by use of a "Wilson Seal." The other end is closed with a ¼-inch transparent plastic disk (6) which serves as an observation window. To prevent accumulation of surface charge on the plastic, a piece of bronze window screen (7) is inserted just outside the beam. The appendix (8) made of ⅛-inch brass and silver soldered, allows external positioning of the magnetic pole pieces being investigated. The pole pieces are energized by an electromagnet which is so constructed that pole pieces of various profiles may be conveniently interchanged. The optical disk is mounted on a pump wagon provided with an oil diffusion pump and a fore pump together with associated ion and thermocouple gauges.

The electrical circuit is conventional using a commercial 30 kv dc supply for the high voltage and an insulated transformer for heating the gun filament. The supply for the focus coil can deliver 400 ma into the 200-ohm load and is stabilized by negative feedback using 6 AS7's as series tubes.

It was originally planned to use a multiple slit diaphragm inserted through the "Wilson Seal" (9) to break up the electron beam into "rays." It was discovered, however, that the beam formed by the gun had observable structure so that this diaphragm was unnecessary. *Figures 2, 3, and 4 are examples of the quality of* results obtainable with this apparatus.

Figure 2 shows the convergent beam of the gun and focus coil; Fig. 3 shows the focusing pattern obtained after deflection by the field formed by parallel faced pole pieces; and Fig. 4 shows the focusing action of a dipole fringe field. The crosses in the lower left of Figs. 3 and 4 mark the center of the pole pieces, which consisted of 1-inch and ¾-inch cold-rolled rods, respectively.

In these photographs, the cross-overs are clearly visible and, although the caustic reproduces poorly, it is visible on the original photograph and may be used to estimate the order of magnitude of the axial and lateral aberrations.

To study the focusing action along the axis parallel to the field, the screen is displaced along this axis and a series of photographs give various cross sections of the beam.

The electron optical disk has proved valuable both as a research tool and as a striking demonstration of the properties of electron beams.

---

[1] J. H. Reisner and R. G. Picard, Rev. Sci. Inst. 19, 556 (1948), describes an example of such a bench. Another of unusual flexibility has been constructed in this laboratory and will soon be described in detail elsewhere.

A New Method for the Measurement of Hall Coefficients*

B. R. Russell and C. Wahlig
Randal Morgan Laboratory of Physics, University of Pennsylvania, Philadelphia, Pennsylvania

September 5, 1950

For the precise determination of Hall coefficients, the usual method is to measure the d.c. Hall voltage with reversed magnetic fields and average to eliminate misalignment and thermal voltage effects. The reversal of the magnetic field and the additional voltage measurement may require several minutes of valuable time in which the sample composition or temperature may be changing. We have been primarily interested in the Hall effect as a function of temperature and of necessity have developed a method of continuously recording Hall voltages.

If an alternating current I is passed through a sample and an alternating magnetic field H of a different frequency is produced externally perpendicular to the current, then the Hall voltage V created along the third axis consists of two parts, the sum and difference frequencies. We filter out the higher frequencies and measure the low beat frequency with the aid of a commercial ten-cycle amplifier. The output of the amplifier can be used, if desired, to drive a standard commercial recorder. Figure 1a illustrates the typical circuit. Power consideration dictates the use of sixty cycles for the magnetic field, and the high cut-off filter efficiency and availability of commercial ten-cycle amplifiers suggest that the sample current be seventy cycles.

The Hall coefficient may be calculated by means of the formula:

$$R=\frac{2V_{\text{rms-10 cycle}}\,t}{I_{\text{rms-70 cycle}}H_{\text{peak-60 cycle}}}\ \frac{\text{volt}-\text{cm}}{\text{ampere-gauss}},\tag{1}$$

where t is the sample thickness. A peak value of 2000 gauss is obtainable with our present a.c. magnet by neutralizing the inductance with a bank of condensers.

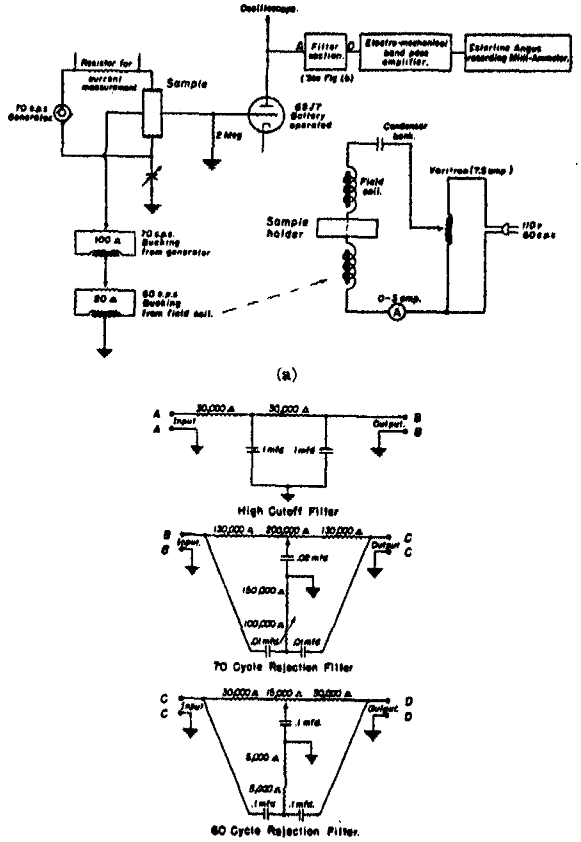

(a)

(b)

FIG. 1. Hall effect circuit.

The major difficulty is that the mixing of the sample current frequency and the magnetic field frequency in any part of the circuit will also produce a voltage of the same frequency as the Hall voltage. With the aid of the bucking sections, as shown in Fig. 1a, additional voltage of each frequency can be supplied at the sample in the proper phase so that this mixing is minimized. The adjustment of the sample current and Hall leads for minimum 60-cycle magnetic field pick-up first is essential, and then the bucking section is adjusted. The cancellation can be observed on the scope attached to the plate circuit of the first tube. Low resistance samples prove to be the more troublesome in the matter of pick-up.

The presence of the bucking section has an added advantage in that one can determine the sign of the Hall coefficient with it. Upon shifting the phase of the bucking voltage in one sense, the recorded Hall voltage increases, while a shift in the opposite direction decreases the observed voltage. With the use of a sample of known Hall coefficient sign, the bucking coil adjustment may be labeled so as to yield information about the sign of the Hall voltage for all following samples.

The magnitude of the recorded Hall voltage is determined by a calibration procedure. A known amount of ten-cycle voltage is fed into the grid of the 6SJ7 tube from a precision potential divider.

This calibration need be performed only at the beginning and the end of each temperature run.

We have made temperature runs as high as 600°C with semiconductors such as zinc oxide, copper oxide, and germanium with uniform success. These runs involved changes of Hall coefficients by factors of ten to ten thousand in the cases of zinc oxide and copper oxide, respectively. The sample resistances ranged from one ohm to three thousand ohms. The Hall coefficients observed upon decreasing the temperature repeat the ascending temperature coefficients closely. This is only possible, we believe, because of the advantageous time element.

The values of the Hall coefficients observed by this new method check within 5 percent of the measured d.c. values of the same samples at room temperature, and we believe it possible to measure Hall coefficients corresponding to sample mobilities of 1 cm^2/volt-sec.

---

* We wish to thank the Bureau of Standards for support of this work.

Electrical Resistance of Platinum at High Temperatures

H. E. Bennett
Johnson, Matthey & Co., Limited, London, England

September 5, 1950

In a note on "A Temperature-Controlled Resistance Furnace for High Temperature Measurements," Schneider and Hollies[1] record that the resistance of a coil of platinum wire, of "commercial" or "thermocouple" purity, wound on a grooved alundum rod and supported in the center of a furnace, reached a maximum at about 1575°C and progressively decreased as the temperature was further increased up to about 1650°C. This is described as "a property of the platinum wire."

There is no reason to expect such an inflection in the resistance-temperature curve of platinum and the curve has been re-determined in order to check these results. A loop of pure platinum wire, with platinum current and potential leads attached, was freely suspended in the center of a rhodium-wound furnace using pure fused alumina insulators outside of the heated zone. Temperature measurements were made with a platinum/platinum-rhodium thermocouple and resistance measurements were taken at temperatures up to the melting point of platinum (1769°C) at which temperature the sample fused. The resistance of the platinum increased in a uniform manner up to the point of fusion in accordance with the usual equation.

It is suggested, therefore, that the inflection observed by Schneider and Hollies is caused by changes in the electrical resistivity of the alundum rod. It is well known that the electrical resistivity of most refractories decreases greatly at high temperatures and it would appear that at about 1575°C the resistance of the alundum rod decreased to so low a value that appreciable current leakage occurred between the turns of the platinum coil. By the use of a different refractory the temperature-control method described might be used at temperatures higher than 1550°C.

---

[1] W. G. Schneider and N. R. S. Hollies, Rev. Sci. Inst. 21, 94 (1950).

New Instruments

W. A. Wildhack: Associate Editor
in Charge of this Section
National Bureau of Standards, Washington, D. C.

These descriptions are based on information supplied by the manufacturer and in some cases from independent sources. The Review *assumes no responsibility for their correctness.*

Shaker The Model 44 Shaker has an armature weight of 8.25 lb., and a frequency range of 3 to 500 c.p.s. It will produce a 50 g acceleration with a mass load of ½ lb. or less and 20 g with up to 14 lb., except

at the lower end of the frequency range where displacement limits are imposed. Weight of the Shaker, with base included, is about 630 pounds, and its price is $2730. A trunnion mounting is incorporated for vertical or horizontal operation. It has a 1-in. total armature stroke with an automatic overtravel cutout. There is one flexure resonance in the operating range to 500 c.p.s. A signal generator attached directly to the table is supplied as optional equipment. The Model 45 power supply is a coordinated design capable of supplying the Model 44 Shaker at its rated output and consists of two motors, four generators, and a control console. The system operates from a 220- or 440-volt 3-phase line, and has a 2- to 500-c.p.s. frequency range with an output of 1.5 kva above 60 c.p.s. and proportional to frequency below 60 c.p.s. The rotary equipment weighs 3125 lb. and is priced at $3670. The control console houses all controls, indicators, condensers for power factor correction, circuit overload and short-circuit protection, and switchgear, exclusive of the magnetic motor starter furnished as a separate unit. It weighs 275 lb. and is priced at $1580.—The Calidyne Company, *751 Main Street, Winchester, Massachusetts.*

Torque Motor The Type 35-1 Torque Motor is an electromechanical device that utilizes an electrical current to produce a backlash-free translational motion, such as is suitable for displacing the piston on a hydraulic amplifier. By utilizing this torque motor design, electrohydraulic servomechanisms with natural frequencies as high as 100 c.p.s. have been constructed.

The Type 35 Torque Motor is characterized by high speed of response, high force output, and low required driving power. It provides a linear motion of ±0.004 in. and will move approximately 0.001 in. per mamp. of signal current. The locked-rotor force output is 4 lb. for a differential current of 5 mamp. When used with a normal pilot-valve load (0.02 lb.), the device has a response time of approximately 1 msec. The input of the torque motor may be connected directly to the plate circuit of a push-pull amplifier, and a pair of subminiature vacuum tubes are sufficient to provide full output from the motor. Weight 17 ounces, volume 12 cubic inches.—TRANS-SONICS, INC., *Bedford Airport, Bedford, Massachusetts.*

Differential Pressure Switch

The new "Meletron" 427 differential-pressure actuated switch senses a difference between a variable and a reference pressure. It will make or break a circuit at any preset point within the adjustable range on increasing or decreasing pressure difference. Because the switching element is in contact with the reference pressure, air or an inert gas must be used. Six adjustable ranges are provided from 3 inches of water to 80 p.s.i. with proof pressures to 120 p.s.i.

A pressure-sensing diaphragm actuates a single-pole, double-throw, snap-action switch when a variable pressure on one side of the diaphragm differs by the preset amount from the reference pressure on the other. It incorporates an Underwriter's Laboratory approved SPDT switch rated for a.c. and d.c. circuits. It is ideal for maintaining a liquid level in a tank with respect to surface pressure on the liquid, for use on blower, ventilating, and heating ducts to sense a pressure difference, or to maintain a constant pressure in a system with respect to any reference pressure. The switches have two pressure ports and the housing is completely sealed by "*O*" rings; housing dimensions are 3 in. in diameter and 4¾ in. over-all. Its weight is 12 ounces. Pressure connections are to ⅛-27 internal threads and electrical connections are made through ¾-in. conduit connector.—BARKSDALE VALVES, *4905 Santa Fe Avenue, Los Angeles 58, California.*

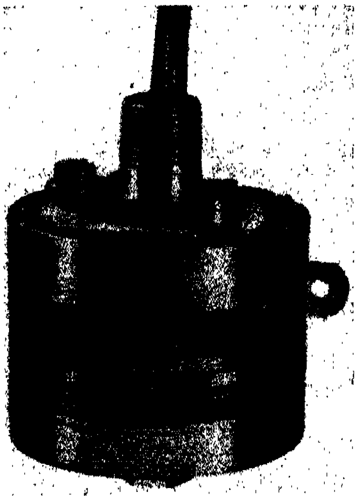

Data Recording Camera

Features of this new 35 mm motion picture camera include remote selection of from four to sixteen frames per second, with constant exposure rate regardless of frame speed. Provisions are made for single frame operation, triggered either manually or by intervalometer. Integral counting circuits afford a remote means of making frame identification. The camera mounts interchangeable Mitchell magazines of 400-ft. or 1000-ft. capacity for loading standard 35-mm motion picture film.

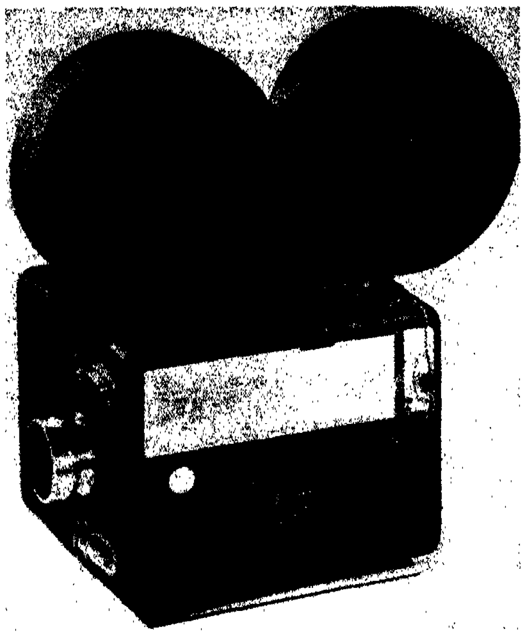

Recommended lenses are situated in a focus-calibrated mount and have been selected for sharp definition, high resolution, and light transmitting qualities. A precision dovetail mounting slide is provided to insure exact camera indexing during removal and replacement. The Fairchild Data Recording Camera is of aircraft quality throughout and has been subjected to exhaustive tests throughout a temperature range of from minus 60°F to plus 160°F; at accelerations up to 12 g; and at altitudes ranging from 0 to 60,000 ft. Power requirements are 28 volts or 110 volts, optional. Further information on special models, high speed adaptations, or cyclic variations may be had on request.—THE FAIRCHILD CAMERA AND INSTRUMENT CORPORATION, *West Coast Division, 53 West Union Street, Pasadena 1, California.*

Metallograph

Designed as a routine control instrument, this new metallograph offers convenience and simplicity of operation together with good optical performance.

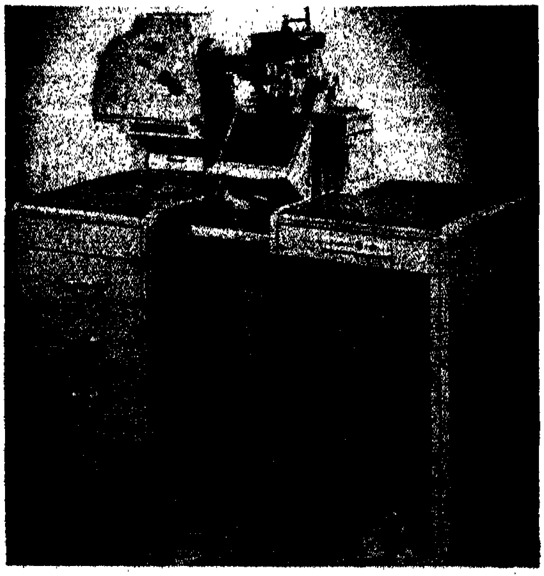

Directly in front of the operator are the 5×7 in. camera, the monocular or binocular microscope eyepieces, and the ball-bearing mechanical stage. Within easy reach is the electrical control panel for the arc and visual lamps. The four objectives on rotating turret, the photographic eyepieces mounted on a quick-change slide, the camera shutter and the color filters . . . all are operable from a sitting position.

The optical systems for photography and visual observations are coupled to permit all focusing to be done through the visual system, eliminating the necessity of ground glass focusing.

Grain size measurements, ferrous or non-ferrous, are compared directly on the ground glass with standard grain size charts. Case depth and linear measurements are easily made with an accessory micrometer rule. Selection of magnification is a very rapid procedure; no tables or charts are required. The objective, eyepiece, and camera bellows setting are all identified by the standard A.S.T.M. magnifications; these range from 50× to 1500× with 2000× available on special request. Monocular or binocular bodies are available. A built-in visual lamp reduces the use of the arc lamp to photography only. Either a ribbon filament tungsten lamp or fully automatic motor-driven arc lamp may be selected to suit individual needs.

The AO Metallograph is equipped with a standard Graflex camera back using inexpensive double plate holders. An Autofocus coarse adjustment stop on the stage eliminates possible damage to optics. "Apergon" objectives are infinity-corrected, balanced for high contrast and good color correction.—American Optical Company, *Instrument Division, Buffalo, New York.*

Microvoltmeter

A full scale sensitivity of 10 μv with an input impedance of 1000 ohms is claimed for the new mv-15A d.c. microvoltmeter. This instrument makes use of a new contact-type d.c. chopper with a condenser, which is charged by the d.c. voltage to be measured and then discharged through a pair of contacts and a tuned transformer. An oscillatory pulse which is set off in this manner, is then amplified, rectified, and metered. The new modulator not only increases the sensitivity of d.c. carrier-type amplifiers, but also eliminates to a considerable extent contact hazards commonly found in ordinary chopper circuits. Suggested applications for the new microvoltmeter include micro temperature changes, slowly changing strains and stresses, null detection in extremely sensitive bridges, medical research, geophysics, meteorology, chemical and nuclear research, as well as measurement of the output of high frequency vacuum thermocouples, bolometers, and crystal diodes. This instrument and the company's d.c. millivoltmeter and micro-microammeter are also available in combination with the Sanborn inkless recorder.—Millivac Instrument Corporation, *P. O. Box 3027, New Haven, Connecticut.*

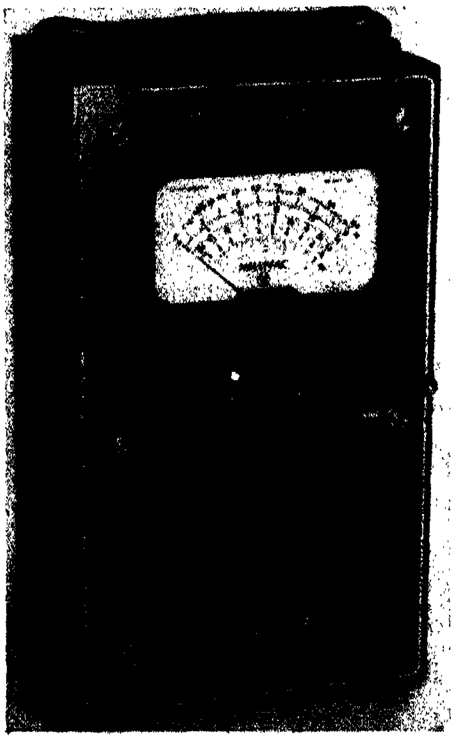

Zeiss Instruments

Carl Zeiss Scientific Instruments now available in this country include the "Lumipan," a binocular research microscope with built-in illuminator (see figure), and the new Model "*G*" Abbe Refractometer. The microscope features a revolving substage with Pancratic System new type triple condenser; the Pancratic System permits the path of light used for illuminating the slides to be varied as desired and adjusted in accordance with the numerical aperture of the objective used. Thus the light is fully utilized for all objectives, increasing their efficiency. The Pancratic System makes the "Lumipan" particularly suitable for phase contrast examinations. The refractometer is provided with a stationary reading microscope, in place of the former movable magnifier, and is designed for maximum convenience, speed, and ease of operation. —Ercona Corporation, *Scientific Instrument Division, 527 Fifth Avenue, New York 17, New York.*

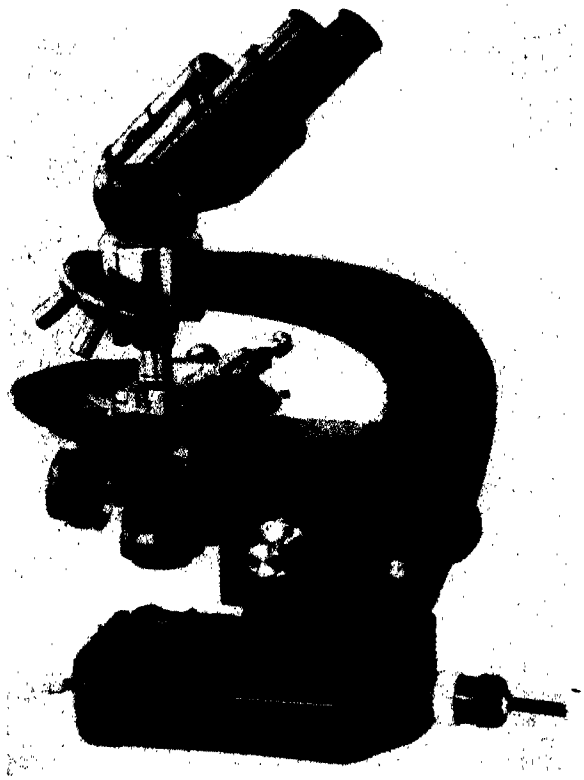

Manufacturers' Literature

Control—Instrumentation, Vol. 4, No. 6, Third Quarter, 1950, contains articles on instrument operating principles, spray drying, research in supersonics at Princeton University, and similar subjects.—Minneapolis-Honeywell Regulator Company, *Industrial Division, Wayne and Windrim Avenues, Philadelphia 44, Pennsylvania.*

Plasticizers—Technical Bulletin O-70, September 15, 1950, discusses vinyl film and sheeting formulations, plasticizers, and stabilizers, and lists 23 suppliers of raw materials.—Monsanto Chemical Company, *Organic Chemicals Division, St. Louis 4, Missouri.*

Koldwelds—Illustrated brochure describes new applications of cold pressure welding, including several trap welds.—Koldwell Corporation, *10 East 40th Street, New York 16, New York.*

Determination of *Q*—"Laboratory Report No. 2" explains the series resonance method for the determination of *Q* by means of a *Z*-angle meter and describes the type 500A wide-band decade amplifier with specifications and prices.—Technology Instrument Corporation, *1058 Main Street, Waltham, Massachusetts.*

Tape Recording—"Elements of single and dual track magnetic tape recording and 1001 applications," Second Edition, 144 pages, by A. C. Shaney, gives a technical discussion of the subject, illustrates typical mechanisms and schematic and block diagrams of circuits used in magnetic recording. Available postpaid upon receipt of $1.00.—Twin-Trax Division, *Amplifier Corporation of America, 398-30 Broadway, New York 13, New York.*

Cinemicrographic Focusing Unit—4 page brochure describes a focusing unit made by Cooke, Troughton & Simms, Ltd., of York, England, for the Vickers Projection Microscope to provide for normal or delayed motion pictures of translucent objects on 16-mm or 35-mm film.—Lovins Engineering Company, *8203 Cedar Street, Silver Spring, Maryland.*

Radio-Isotope Instruments—Directory of British Atomic Instrument Meanufacturers and their products produced in collaboration with the Atomic Energy Research Establishment, Harwell, England, includes a discussion of instrument requirements for tracer techniques.—Scientific Instrument Manufacturers' Association, *17 Princes Gate, London, S.W. 7, England.*

Experimenter—No. 5, Vol. XXV, October, 1950, contains a description of a Variac Phase-Shift Circuit, and accompanies a catalog supplement, Form 744-A, which illustrates and briefly describes the Company's new instruments announced since the publication of Catalog L.—General Radio Company, *275 Massachusetts Avenue, Cambridge 39, Massachusetts.*

New Materials

Forest K. Harris: Associate Editor
in Charge of this Section
National Bureau of Standards, Washington, D. C.

Borocarbon Film Resistors

The addition of boron to pyrolitically deposited carbon-film resistors has been found to give good stability, and considerably lower temperature coefficients than those of plain carbon-film resistors. In addition the borocarbon resistors provide access to resistance ranges previously impossible to attain in stable, accurate film-type resistors. Pyrolytic carbon resistors, known also as "cracked carbon" or "high stability carbon film" resistors, are composed of very thin films of microcrystalline carbon formed on ceramic surfaces. The carbon film is deposited by the thermal decomposition or pyrolysis of hydrocarbon vapors. The film-type of resistor is not only particularly useful at high frequencies as a result of the absence of skin effect, but is also well cooled by reason of its intimate contact with the ceramic core so that it can dissipate large amounts of power per unit area. Other characteristics include stability in use, relatively small and predictable temperature coefficient of resistance, low noise level, and tolerances to better than one percent attainable in production.

Pyrolytic carbon films are composed of minute graphite-like crystallites that are so closely and randomly packed as to lose all resemblance to graphite. Structural and analytical studies have shown that each crystallite is surrounded by a skin or layer of complex hydrocarbons separating it from its neighbors. This hydrocarbon skin increases the specific resistance and temperature coefficient of pyrolytic carbon relative to graphite. Decrease in the thickness of the skin or in the total volume it occupies results in a decrease in the specific resistance and in the temperature coefficient of the pyrolytic film. The temperature coefficient of resistance of the film, always negative, increases from about 180 p.p.m./°C in thick films to 750 p.p.m./°C for thin films having a resistance per square of 20,000 ohms. This variation results in part from film stresses due to the different thermal expansions of the film and its support. The average temperature coefficient of resistance of pyrolytic carbon resistors is about 300 p.p.m./°C. This large temperature coefficient has been a deterrent to their general use, even though a precision as good as 1 p.p.m./°C is attainable in matching coefficients. However, study has shown that the addition of boron to the carbon film greatly decreases the temperature coefficient of resistance and increases its stability.

Borocarbon films are produced by pyrolytic decomposition of boron and carbon from suitable gaseous compounds. Temperature coefficient depends on film thickness and boron content. By suitable variations in these, temperature coefficients as low as 20 p.p.m./°C are achieved. One-half-watt borocarbon resistors of 10 megohm values can be produced with temperature coefficients less than 100 p.p.m./°C while resistors of 250,000 ohms or lower have coefficients less than 50 p.p.m./°C. The specific resistance of borocarbon films depends on boron content, and films having a very high resistance per square can be produced by suitable variation of composition. Values of 500,000 ohms per square are readily obtained, and values in excess of 1 megohm per square have been studied. Temperature coefficients for these high resistance films are larger than for low resistance films but in the extremely high resistance ranges made available through use of these films, temperature variations are generally of lesser importance.—Bell Telephone Laboratories, *463 West Street, New York 14, New York.*

Industrial Noble-Metal Alloys

A new catalog and data book, available from the manufacturer, contains comprehensive technical and application data on Ney precious-metal alloys for industrial use. Various alloys are described for sliding contacts, brushes, wipers, slip-rings, commutator segments, resistance wire, and non-corrosive wear-resistant parts in electrical and other industrial components. In addition to data on physical properties and uses of individual alloys, the publication describes standard contacts and formed brush shapes now being manufactured, as well as details of the research, testing, and manufacturing facilities available for special application developments.—J. M. Ney Company, *71 Elm Street, Hartford, Connecticut.*

Micro-Burettes

Kimble Exax micro-burettes, with platinum-alloy delivery stems, are designed for microchemical work, and will deliver drops as small as 0.01 ml. The metal delivery tube, fused to a detachable glass tip holder, is easily cleaned; while the use of the metal eliminates the possibility of damage present in small glass tips. The tip is attached to the body of the burette by a ground joint of the size used for hypodermic syringes, and lugs are provided so that rubber bands can be used to help hold the tip in place. The platinum delivery tube extends a short distance inside the holder, so that dirt or grease tend to collect around this end rather than entering and clogging the opening. Hypodermic syringe needles can be substituted for the platinum-alloy delivery tube where there is no risk of contamination.—BURRELL CORPORATION, *2223 Fifth Avenue, Pittsburgh 19, Pennsylvania.*

Brazing Alloy

Genie is a new alloy rod for brazing aluminum without the need for a separate flux. In application the surfaces are first brushed under heat from a torch, to break up the surface oxide. The metal is then heated sufficiently to flow the brazing rod and tin the surfaces. As a third operation, the tinned surface is brushed under heat to fill all open pores. Finally enough of the brazing material is flowed in with the torch to fill the joint. The melting point of the brazing alloy is 732°F.—ALLADIN ROD AND FLUX MANUFACTURING COMPANY, *1302 Burton Street, Grand Rapids 7, Michigan.*

Self-Locking Screws

Spin-Lock screws have a ring of ratchet-like teeth on the under face of the head which will bite into the head-seat when the screw is driven tight. The screw is carburized so that the teeth do not flatten and so that they will dig into softer metal. No separate lock washer is required, and final tightening will produce an oil- and water-tight fit under the head. Flat, truss, and pan head screws are available from No. 4 to ⅜ inch, and hexagonal head screws from No. 4 to ½ inch. Self-tapping screws are available in all head styles. —RUSSELL, BURDSALL, AND WARD BOLT AND NUT COMPANY, *50 Midland Avenue, Port Chester, New York.*

Pyrex Sight Glasses

A line of sight-glasses, made from polished Pyrex plate glass, is available for high temperature service. The glass will also resist attack by chemicals other than hydrofluoric acid and strong hot caustic solutions. Circular units up to 16 in. diameter, or any rectangular or other shape that can be made from a 24×60 in. blank, can be made to order. Thicknesses range from ¼ to 1 in. Glasses can be supplied with cut or ground edges in thicknesses up to ¾ in., and with ground edges above ¾ in.—SWIFT LUBRICATOR COMPANY, *24 James Building, Elmira, New York.*

Polyethylene Pipe

Agaline plastic pipe is made of polyethylene and is designed for use at temperatures below 150°F. It is available in 4-foot lengths in diameters from 2 to 36 inches. The pipe is joined for runs of any desired length by chamfering an end and then heating a 5-inch section by immersion in water at 200°F. This causes the section to become flexible so that an unheated end can be inserted into it. The joint seals on cooling. The same treatment can be used for making bends.—AMERICAN AGILE COMPANY, *5804 Hough Avenue, Cleveland 3, Ohio.*

Refractory Material

A mullite refractory for furnace construction and repair is now in volume production. The material is being made into firebrick under the trade name of "Allmul." It is also available in bulk grain and in a ramming mix. Its melting point is 3335°F, and it has excellent resistance to deformation at 3050°F when loaded at 25 p.s.i. for 1½ hours. Spalling does not occur when the brick is heated to 3000°F for 24 hours and then subjected to 12 cycles of chilling in an air-water blast and reheating to 2550°F. Crushing strength is 3400 p.s.i.—BABCOCK AND WILCOX COMPANY, *85 Liberty Street, New York 6, New York.*

Corrosion Proofing

Ferro-Pak is a packaging paper which is treated on both sides with a volatile corrosion-inhibiting chemical to afford protection for ferrous articles wrapped in the paper. The wrapped product is ready for use without cleaning when the paper is removed. The coating evaporates slowly and does not flake off or stick to the wrapped product. Protection is maintained with the paper either wet or dry, and can extend into years. Sheets or rolls are regularly supplied, and bags, pouches or shrouds can be made to order.—CROMWELL PAPER COMPANY, *4803 South Whipple Street, Chicago 32, Illinois.*

Author Index to Volume 21

References with (L) are to Laboratory and Shop Notes

Abele, R. K. (see Glass, F. M.)—493

Abrahams, S. C., R. L. Collin, W. N. Lipscomb, and T. B. Reed. Further techniques in single-crystal x-ray diffraction studies at low temperatures—396(L)

Accardo, Carl A. (see Kallmann, Hartmut)—48

Adams, G. D. (see Kerst, D. W.)—462

——, **R. W. Dressel, and F. E. Towsley.** Small milligaussmeter—69

Adler, F. T. Book review—664

Allen, H. A. (see McKinney, C. R.)—724

Allen, K. W. (see Dewan, J. T.)—823

Allred, J. C., A. N. Phillips, L. Rosen, and F. K. Tallmadge. On the use of photographic plate detectors in neutron experiments—225

Alpert, Daniel (see Bayard, Robert T.)—571(L)

Amsterdam, M. F. and W. E. Danforth. High power pulsed magnetron with replaceable cathode—398(L)

Anderson, Scott, William J. Anderson, and Martin Krakowski. Water-proofing rocksalt for infra-red absorption cells —574(L)

Anderson, William J. (see Anderson, Scott)—574(L)

Andrews, Howard L. Nomogram for G-M counter resolving-time corrections—191(L)

Arnett, Raymond L. Book review—388

Arnold, Wayne R. 500-kilovolt linear accelerator using selenium rectifiers—796

Arons, A. B. and R. H. Cole. Design and use of piezoelectric gauges for measurement of large transient pressures—31

Asher, W. R. (see Maddin, Robert)—881(L)

Åström, Björn. Decade pulse counter for Geiger-Müller tubes —323

Axelbank, M. Rotary McLeod gauge—511

Ayer, Frederick, II. Suppressing mercury vapor in vacuum systems—496(L)

Babiskin, Julius. Float for liquid helium—941(L)

Back, F. G. Lens tester for photographic lenses—722

Baird, D. H., R. M. Fristrom, and M. H. Sirvetz. Stark effect absorption cells for microwave spectroscopy—881(L)

Baker, W. R. (see Panofsky, W. K. H.)—445

Ballard, Stanley S., Kathryn A. McCarthy, and William C. Davis. Method for measuring the thermal conductivity of small samples of poorly conducting materials such as optical crystals—905

Ballentine, R. (see Bernstein, W.)—158

Barkow, A. G. (see O'Connell, T. C.)—573(L)

Baron, Morton L. and A. de Bretteville, Jr. Combination two-circle goniometer and x-ray spectrometer—458

Bayard, Robert T. and Daniel Alpert. Extension of the low pressure range of the ionization gauge—571(L)

Bayly, J. G. An analog computer—228

Beal, R. J. Apparatus and method for testing radium or thorium capsule seals—400(L)

Beams, J. W. Magnetic suspension for small rotors—182

Becker, Robert A. Errata: Note on sealing Nylon films to Geiger counters—270(L)

Beghian, L. (see Wilson, R.)—699

Beiser, Arthur. Slide rule for nuclear emulsion calculations—933(L)

—— Varying nuclear emulsion sensitivity with altitude—1025(L)

Bell, P. R. (see Kelley, G. G.)—330

—— **and H. A. Straus.** Electronic pile simulator—760

Benner, A. H. and H. J. Nearhoof. Polarimeter for the study of low frequency radio echoes—830

Bennett, H. E. Electrical resistance of platinum at high temperatures—1029(L)

Benson, A. (see Gray, I.)—1022

Benzinger, T. and C. Kitzinger. 4π-radiometer—599

Bergmann, Peter G. Book review—657

Berman, Arthur I. Method for increasing the safe power input of x-ray tubes—275

Berman, M. (see Hine, G. J.)—362

Bernstein, W. and R. Ballentine. Gas phase counting of low energy beta-emitters—158

Bird, F. F. and K. S. Lion. Ultrasonic tissue disintegrator —189(L)

Birnbaum, George. Recording microwave refractometer—169

Birnbaum, Milton (see de Packh, David C.)—451

Bishop, G. R. (see Wilson, R.)—699

Bishop, P. O. and E. J. Harris. D.c. amplifier for biological application—366

Bitter, F. Book review—661

Blacet, Francis E. (see Crane, Robert A.)—259(L)

Blachman, Nelson M. Synchrotron-oscillation resonance—908

Blasco, E. and L. Miranda. New Pirani-type vacuum gauge—494(L)

Blau, M., I. W. Ruderman, and J. Czechowski. Photographic methods of measuring slow neutron intensities—232

Blau, Marietta, Robert Rudin, and Seymour Lindenbaum. Semi-automatic device for analyzing events in nuclear emulsions—978

Bleakney, Walker. Book review—870

Blewett, J. P. (see Livingston, M. S.)—7

Bloom, H. and G. W. Butler. An electron tube potentiometer method for use in circuits involving very high resistance —274

Blüh, O. and B. I. H. Scott. Vibrating probe electrometer for the measurement of bioelectric potentials—867

Bockris, J. O'M. (see Tomlinson, J. W.)—507

Boehmer, H. W. and J. E. Coolidge. Instrument for directiona studies of cosmic-ray intensity—633

Boisvert, M. (see Bricout, P. A.)—98(L)

Bonner, Francis and Alfred Weinstein. Geiger counter mounting for countinuous counting of gas-phase radioactivity—934(L)

Boorse, H. A. (see Dash, J. G.)—936(L)

Borst, Lyle B. Book review—874

Boudart, Michel. Book review—869

Bowen, I. S. Book review—85

Boyd, C. A. (see Eckstein, N. A.)—398(L)

Bradfield, R. D. (see Bromley, D. A.)—190(L)

Braunschweiger, Paul G. (see Rogers, John D.)—1014

Bricout, P. A. and M. Boisvert. Measurement and amplification of minute displacements by frequency modulation —98(L)

Briller, Stanley, Nathan Marchand, and Charles E. Kossmann. Differential vectorcardiograph—805

Brink, F., Jr. (see Carlson, Francis D.)—923

Bromley, D. A. and R. D. Bradfield. Reprojection method for studying cloud-chamber photographs—190(L)

Bronk, D. W. (see Carlson, Francis D.)—923

Brooks, Herbert B. Best arrangement of resistors in a series group—491(L)

Broussard, Leo. Improved double-crystal spectrometer for small angle scattering measurements—399(L)

Brown, Sanborn C. and Claudine Maroni. Study of plateau slopes in self-quenching Geiger-Müller counters—241

Bruner, Joseph A. and F. R. Scott. High resolution beta-ray spectrometer—545

Budlong, W. A. and Bruce C. Lutz. An automatically synchronized electronic switch—167
Buerschaper, R. A. Rapid method for calculating and using platinum thermohm tables—996
Burton, Alan C. and James T. Nichol. Design of a simple microflowmeter for biological perfusion experiments—485
Burwell, Robert L., Jr., Max Metlay, and Frank W. Pfohl. Measurement of rates of flow of gases by wet test meters—681
Butler, C. P. and F. E. Carpenter. Motor for use in vacuum systems—103(L)
Butler, G. W. (see Bloom, H.)—274

Cady, W. G. (see Mendousse, J. S.)—1002
Caldecourt, V. J. Mass indicator—772(L)
Callen, H. Book review—877
Cannon, C. V. and G. H. Jenks. Microcalorimeter suitable for study of easily absorbed nuclear radiations—236
Carlson, Francis D., F. Brink, Jr., and D. W. Bronk. Continuous flow respirometer utilizing the oxygen cathode—923
Carpenter, F. E. (see Butler, C. P.)—103(L)
—— **and J. A. Curcio.** Preparation of unbacked metallic films—675(L)
Cech, R. E. High-low temperature microscope stage—747
Chase, R. L. (see Kuper, J. B. H.)—356
Chen, Joses J. L. Test of rupture strength of thin plastic films—491(L)
—— (see Van Atta, C. M.)—985
Chu, L. J. Book review—878
Churchman, C. West. Book review—660
Cioffi, P. P. Recording fluxmeter of high accuracy and sensitivity—624
Claffy, Esther W. and Joseph G. Schumacher. An improved electrode cutter for spectrographic laboratories—575(L)
Clark, R. K. Absolute determination of the emission rate of beta-rays—753
Clifton, Donald F. Low temperature x-ray diffraction apparatus—339
Cloud, Robert W. and Sanborn F. Philp. Vacuum tests of rubber, lead, and Teflon gaskets and vinyl acetate joints—731
Cole, R. H. (see Arons, A. B.)—31
Collie, C. H. (see Wilson, R.)—699
Collin, R. L. (see Abrahams, S. C.)—396(L)
Collyer, Louis G. Detaching device for balloon flights—496(L)
Cook, D. B. (see Dash, J. G.)—936(L)
Coolidge, J. E. (see Boehmer, H. W.)—633
Conrad, Carl M. (see Segal, Leon)—431
Corak, W. S. (see Wexler, A.)—259(L)
—— (see Wexler, Aaron)—583
Cork, J. M. Book review—85
Cowan, E. W. Continuously sensitive diffusion cloud chambers—991
Cox, Henry L. (see Rogers, John D.)—1014
Crain, C. M. Apparatus for recording fluctuations in the refractive index of the atmosphere at 3.2 centimeters wavelength—456
Crane, H. R. Book review—390
Crane, Robert A. and Francis E. Blacet. Series parallel linear thermopile with interchangeable receiving units—259(L)
Craven, C. J. (see Snyder, S. D.)—887(L)
Creely, Joseph J. (see Segal, Leon)—431
Crittenden, E. C., Jr. (see Fawcett, S. L.)—935(L)
Cunningham, G. T. (see Wexler, A.)—259(L)
Curcio, J. A. (see Carpenter, F. E.)—675(L)
Curtiss, L. F., R. D. Evans, Warren Johnson, and Glenn T. Seaborg. Units of radioactivity—94(L)
Custer, Robert (see Steingiser, Samuel)—109
Cutter, P. R. (see Heston, B. O.)—608
Czechowski, J. (see Blau, M.)—232

Dancoff, S. M. Book review—662
Danforth, W. E. (see Amsterdam, M. F.)—398(L)
Darby, E. K. (see Morrish, A. H.)—884(L)
Dash, J. G., D. B. Cook, M. W. Zemansky, and H. A. Boorse. Design and performance of a Joule-Kelvin helium liquefier—936(L)
Davis, Leverett, Jr. Orbit-bender to assist injection into betatrons—971
—— Book review—660
Davis, Wallace, Jr. (see Shiflett, Chester H.)—842
Davis, William C. (see Ballard, Stanley S.)—905
Davis, William O. (see Pavalow, Melvin)—529
Dazey, Mitchell H., Jack V. Franck, A. C. Helmholz, Craig S. Nunan, and Jack M. Peterson. Synchrotron radiofrequency system—436
deBretteville, A., Jr. (see Baron, Morton L.)—458
Degallier, M. Zero inefficiency anticoincidence circuit—1025(L)
Delsasso, L. A. Book review—86
de Packh, David C. and Milton Birnbaum. Theory of the capture process in a betatron-injected synchrotron—451
Dewan, J. T. Voltage stabilizer for 200-kv acceleration—771(L)
—— **and K. W. Allen.** Chart recording of microsecond pulse amplitudes—823
Dieke, G. H. Book review—388
Dodd, E. E. (see Loeb, Leonard B.)—42
Dolecek, Richard L. (see Henry, Warren E.)—496(L)
Dollmann, Elsie M. Variation of grain density with temperature of exposure in nuclear emulsions—118
Domenicali, C. A. Null-coil pendulum magnetometer—327
Dorsey, J. (see Hall, T. A.)—177
Dressel, R. W. (see Adams, G. D.)—69
Drickamer, H. G. (see Huse, E. S.)—60
—— (see Timmerhaus, K. D.)—261(L)
Duckworth, Henry E. Large Dempster-type double-focusing mass spectrograph—54
Duffield, R. B. (see Timmerhaus, K. D.)—261(L)
DuMond, Jesse W. M. Point-focus x-ray monochromators for low angle diffraction—188(L)

Eckstein, N. A., J. W. Fitzgerald, and C. A. Boyd. Method of making glass-metal seals—398(L)
Eden, M., A. W. Pratt, and H. Kahler. Microtome specimen holder advanced by thermal expansion—802
Edwards, E. V. and K. Garoff. Fabrication of a high power resonant wave-guide window—787
Eldredge, K. R. High resolution recording with soot—199
Elkind, M. M. (see Hine, G. J.)—362
Elliot, J. O., S. H. Liebson, R. D. Myers, and C. F. Ravilious. Duration of scintillations from organic phosphors—631
Ellis, S. G. Laboratory modifications in the RCA model EMC electron microscope—255
Elmore, W. C. Coincidence circuit for a scintillation detector of radiation—649
Elsasser, W. M. Book review—389
Elsey, P. J. (see Shimizu, H.)—779
Emigh, C. R. Wire recorded magnetic pulse timing circuit—142
Engelkemeir, A. G. and W. F. Libby. End and wall corrections for absolute beta-counting in gas counters—550
English, William N. (see Loeb, Leonard B.)—42
Epstein, S. (see McKinney, C. R.)—724
Eubank, William R. Precision thermostat for high temperatures—845
Evans, R. D. (see Curtiss, L. F.)—94(L)

Fair, W. F., Jr. Book review—92
Fano, R. M. Book review—870
Farnsworth, H. E. Simple contamination-free electron gun—102(L)

Fawcett, S. L. and E. C. Crittenden, Jr. Ejection of the electron beam from a betatron—935(L)
Fein, M. L. (see Ratchford, William P.)—188(L)
Feldman, K. Waterproof cable connectors—812(L)
Fergus, David (see Levy, Gabor B.)—693
Finkelstein, Nisson Ascher. High intensity ultraviolet continuum source for use in spectrophotometry—509
Fireman, E. L. and G. M. McHaney. Self-triggering cloud-chamber counter—813(L)
Fisher, R. M. and D. S. Miller. Simple automatic recording microphotometer—938(L)
Fitzgerald, J. W. (see Eckstein, N. A.)—398(L)
Fluharty, R. G. (see Roberts, B. W., Jr.)—790
Fowler, C. M. and R. G. Shreffler. Design of a magnetic focusing coincidence spectrometer—740
Fowler, I. L. and P. R. Tunnicliffe. Boron trifluoride proportional counters—734
Fowler, Robert D. Book review—665
Fowler, W. A. (see Snyder, C. W.)—852
Fox, William. Convenient cell-stage for fluid profile measurements—499(L)
Franck, Jack V. (see Dazey, Mitchell H.)—436
Franzen, W. and J. Horton. Reliable Pirani vacuum safety circuit—935(L)
Fred, Mark S. and Everett G. Rauh. Liquid air level control—258(L)
Freedman, Larry A. and Louis A. Rosenthal. Apparatus for the study of electrets—896
Freedman, M. S. (see Ramler, W. J.)—784
Frey, H. B. Scintillation counter for fast neutrons—886(L)
Fristrom, R. M. (see Baird, D. H.)—881(L)
Fritz, James J. and Herrick L. Johnston. Design and operation of liquid nitrogen-cooled solenoid magnets—416
Fry, E. J. Ultrasonic projector design for a wide range of research applications—940(L)
Fusfeld, Herbert I. Apparatus for rapid measurement of internal friction—612
Futch, A. H. (see Quinnel, E. H.)—400(L)

Garoff, K. (see Edwards, E. V.)—787
Garwin, R. L. Differential analyzer for the Schrödinger equation—411
—— Pulse generator for the millimicrosecond range—903
—— Useful fast coincidence circuit—569(L)
Geballe, T. H. (see Lyon, D. N.)—769(L)
Geoffrion, C. (see Persico, E.)—945
Gezelius, Rolf J. E. Making small metal tubes by electrodeposition on Nylon fibers—886(L)
Giller, E. B. (see Timmerhaus, K. D.)—261(L)
Gillette, R. H. Calcium and cadmium tungstate as scintillation counter crystals for gamma-ray detection—294
Ginzton, Edward L. Book review—877
Glass, F. M. and R. K. Abele. High megohm bridge—493(L)
Glenn, E. E., Jr., and Norman Hackerman. Positive displacement pump for corrosive fluids—148
Goldhaber, M. Book review—662
Goldin, A. S., E. R. Rohrer, and R. L. Macklin. Scintillation type alpha-particle detector—554
Goodman, P. D. (see Mendousse, W. G.)—1002
Gráf, Tibor. Construction and performance of a multiple gamma-ray counter of high efficiency—285
Graves, J. D. and G. E. Koch. Photo-multiplier gamma-ray detector—304
Gray, I., S. Ikeda, A. Benson, and D. Kritchevsky. Detection of tritiated compounds in paper chromatography—1022
Green, G. K. (see Livingston, M. S.)—7
Green, Paul E., Jr. Magnetic tape recorder for very low frequency phenomena—893
Gross, Leonard (see Hamilton, Donald R.)—912
Grosse, A. V. Book review—872
Grundfest, Harry, Robert W. Sengstaken, Walter H. Oettinger, and R. W. Gurry. Stainless steel micro-needle electrodes made by electrolytic pointing—360
Gurry, R. W. (see Grundfest, Harry)—360
Gutenberg, B. Book review—385

Hackerman, Norman (see Glenn, E. E., Jr.)—148
Hagstrum, H. D. and H. W. Weinhart. New porcelain rod leak—394(L)
Halban, H. (see Wilson, R.)—699
Halford, Ralph S. (see Savitzky, Abraham)—203
Hall, T. A., S. D. Warshaw, and J. Dorsey. Integrator for small beam currents—177
Halliday, David. Book review—878
Halsted, R. E. and Alfred O. Nier. Gas flow through the mass spectrometer viscous leak—1019
Hamilton, Donald R. and Leonard Gross. Electrostatic beta-spectrograph—912
Hamm, F. A. and F. C. Snowden. Vibration studies: related to electron microscopy—426
Hansen, J. W. (see Kunkel, W. B.)—308
Harris, E. J. (see Bishop, P. O.)—366
Hartman, C. D. (see Molnar, J. P.)—394(L)
Harvalik, Z. V. Simple method to seal liquids of high vapor pressure into glass or quartz capillaries—260(L)
Haupt, L. M. Solution of simultaneous equations through use of the a.c. network calculator—683
Havens, R., R. Koll, and H. LaGow. New vacuum gauge—596
Haworth, L. J. (see Livingston, M. S.)—7
Hays, E. E. (see Richards, Paul I.)—99(L)
Heinrich, Edward Oscar. Book review—85
Heller, R. B., E. F. Sturcken, and A. H. Weber. Transmission of beta-rays by Nylon and Formvar—898
Helmholz, A. C. (see Dazey, Mitchell H.)—436
Henry, Warren E. and Richard L. Dolecek. Metal Dewar for liquid helium—496(L)
Hermont, A. J. Comments on "Velocity-acceleration response from a seismic pick-up via controlled damping"—675(L)
Herzog, Gerhard. Book review—661
Heston, B. O. and P. R. Cutter. Molecular diffraction attachment for RCA microscope—608
Hett, J. H. and R. W. King, Jr. Frequency modulation pressure recording system—150
Heydt, Howard L. Measurement of secondary electron emission from dielectric surfaces—639
Highhouse, Frederick and Julius White. Convenient gas sample tube holder and break-off applicable to mass spectrometers—101(L)
Hill, R. D., J. W. Mihelich, and M. T. Pigott. Use of secondary electrostatic focusing in a magnetic beta-ray spectrograph—498(L)
Hine, G. J., M. Berman, and M. M. Elkind. Automatic isodose recorder with scintillation counter as gamma-ray detector—362
Hofstadter, Robert and John A. McIntyre. Note on the detection of coincidences and short time intervals—52
Hoge, Harold J. Resistance-temperature relation for low temperature thermometry—815(L)
Hollies, N. R. S. (see Schneider, W. G.)—94(L)
Honig, R. E. Greaseless gas flow valve—1024(L)
Hopfield, John J. Glass variable microleaks for gases—671(L)
Hopke, E. R. (see Sears, G. W.)—570(L)
Hopkins, J. S. (see Miller, R. D.)—263(L)
Horák, Z. and F. Krupka. Technical apparatus for determining thermal conductivity of steels up to 500°C—827
Horton, J. (see Franzen, W.)—935(L)
Hunt, F. V. and O. D. Sledge. Design of logarithmic voltage dividers—332
Hurst, D. G., A. J. Pressesky, and P. R. Tunnicliffe. Chalk River single crystal neutron spectrometer—705

Huse, E. S., D. J. Trevoy, and H. G. Drickamer. Diaphragm cell for thermal diffusion measurements—60

Isaacson, Eugene. Book review—871
Ikeda, S. (see Gray, I.)—1022

Jeffries, Robert J. Velocity-acceleration response from a seismic pick-up via controlled damping—115
Jenkins, Rodman. Two beta-gamma-counters for gas samples—940(L)
Jenks, G. H. Convenient leak for testing helium leak detectors—674(L)
—— (see Cannon, C. V.)—236
Johansson, Stig. (see Siegbahn, Kai)—442
Johnson, Warren (see Curtiss, L. F.)—94(L)
Johnston, Herrick L. (see Fritz, James J.)—416
Jones, Robert N. Book review—91
Jordan, W. H. (see Kelley, G. G.)—330
Judd, David L. Focusing properties of a generalized magnetic spectrometer—213

Kahler, H. (see Eden, M.)—802
Kallmann, Hartmut and Carl A. Accardo. Coincidence experiments for noise reduction in scintillation counting—48
Keepin, George R., Jr. Improvements in the Li^6 technique—933(L)
—— **and James H. Roberts.** Measurement of fast neutron energies by observation of Li^6(n, α)H^3 in photographic emulsions—163
Keller, Joseph M., Ernest Koenigsberg, and Arthur Paskin. Ring focus in a thin magnetic-lens beta-ray spectrometer—713
Kelley, G. G. High speed synchroscope—71; Erratum:—264(L)
——, **W. H. Jordan, and P. R. Bell.** Electron component in Geiger discharge—330
Kelly, F. M. All-metal ionization gauge—673(L)
Kennard, E. H. Book review—871
Kerst, D. W., G. D. Adams, H. W. Koch, and C. S. Robinson. 80-Mev model of a 300-Mev betatron—462
Kerwin, Larkin. New type mass spectrometer—96(L)
Kessler, John A. Book review—390
King, R. W., Jr. (see Hett, J. H.)—150
King, Robert B. Book review—386
Kinsey, V. Everett. Modification of the apparatus used for the Baldes thermoelectric method of measuring osmotic pressure—767
Kirkwood, John G. Book review—90
Kitzinger, C. (see Benzinger, T.)—599
Knight, W. D. (see Pound, R. V.)—219
Koch, G. E. (see Graves, J. D.)—304
Koch, H. W. (see Kerst, D. W.)—462
Koenigsberg, Ernest (see Keller, Joseph M.)—713
Koll, R. (see Havens, R.)—596
Korn, Granino A. Design and construction of universal function generating potentiometers—77
Kossmann, Charles E. (see Briller, Stanley A.)—805
Krakowski, Martin (see Anderson, Scott)—574(L)
Krieger, K. A. Book review—87
Kritchevsky, D. (see Gray, I.)—1022
Krupka, F. (see Horák, Z.)—827
Kunkel, W. B. and J. W. Hansen. Dust electricity analyzer—308
Kuper, J. B. H. Book review—666
—— Book review—666
—— **and R. L. Chase.** Monitor for low intensity gama-rays—356

LaGow, H. (see Havens, R.)—596
Lander, J. J. Ultra-high vacuum ionization manometer—672(L)
Langer, L. M. and F. R. Scott. Measurement of the magnetic field in a nuclear spectrometer—522
Laufer, Arthur R. Electric field in a Geiger counter—252
—— Time lags in Geiger counters—244
Lauritsen, C. C. (see Snyder, C. W.)—852
Law, Harold B. Erratum: Formation of insulating layers by the thermal decomposition of ethyl silicate—270(L)
Lawson, A. W. and Ting-Yuan Tang. Diamond bomb for obtaining powder pictures at high pressures—815(L)
Leblond, C. P. Book review—391
Leet, L. Don. Book review—87
Levens, A. S. Book review—876
Levitt, I. M. Book review—91
Levy, Gabor B., Philip Schwed, and David Fergus. Recording polarimeter—693
Lewis, Lloyd G., James G. Robinson, and John Toll. Linear preamplifier for driving a long coaxial cable—593
Lewis, Robert E. Single element verniers reading two or three dimensions—647
Libby, W. F. (see Engelkemeir, A. G.)—550
Liebson, S. H. (see Elliot, J. O.)—631
Lindenbaum, Seymour (see Blau, Marietta)—978
Lion, K. S. (see Bird, F. F.)—189(L)
Lipscomb, W. N. (see Abrahams, S. C.)—396(L)
Littauer, R. M. Random concidence rates with unsteady sources—750
Livingston, M. S., J. P. Blewett, G. K. Green, and L. J. Haworth. Design study for a three-Bev proton accelerator—7
Loeb, Leonard B., James H. Parker, E. E. Dodd, and William N. English. Choice of suitable gap forms for the study of corona breakdown and the field along the axis of a hemispherically capped cylindrical point-to-plane gap—42
Lohmann, Idas W. Electronic recording analytical balance—999
Longsworth, L. G. Tests of flowing junction diffusion cells with interference methods—524
Lord, Richard C. Book review—386
—— Book review—879
Lowde, R. D. Design of neutron counters using multiple detecting layers—835
Lutz, Bruce C. (see Budlong, W. A.)—167
Lyon, D. N. and T. H. Geballe. Temperature coefficient of resistance of tin oxide-coated electrically conducting glass between 1° and 300°K—769(L)

Macklin, R. L. (see Goldin, A. S.)—554
Madansky, Leon and R. W. Pidd. Some properties of the parallel plate spark counter. II—407
Maddin, Robert and W. R. Asher. Apparatus for cutting metals strain-free—881(L)
Madorsky, Samuel L. Tungsten helical spring balance—393(L)
Makowski, M. W. Erratum: A slide rule for radiation calculations—336
Many, Abraham. Improved electrical network for determining the eigenvalues and eigenvectors of a real symmetric matrix—972
Marchand, Nathan (see Briller, Stanley A.)—805
Maroni, Claudine (see Brown, Sanborn C.)—241
Marshall, F. R. (see Zarem, A. M.)—514
Marshall, John. Transmission line reflection doubling amplifier—1010
Martin, D. L. (see Stephenson, S. T.)—1023(L)
Masket, A. V. (see Slessler, W. M.)—494(L)
McCarthy, Kathryn A. (see Ballard, Stanley S.)—905
McClellan, A. L. and G. C. Pimentel. Simplified percent transmission computer—1023(L)
McCrea, J. M. (see McKinney, C. R.)—724
McDonald, Donald. Analog computers for servo problems—154

McFee, Raymond H. Method of supplying low pressure gases on a vacuum system—100(L)
McFee, Richard. Improving differential amplifier rejection ratios—770(L)
—— Trigonometric computer with electrocardiographic applications—420
McHaney, G. M. (see Fireman, E. L.)—813(L)
McIntyre, John A. (see Hofstadter, Robert)—52
McKinney, C. J., J. M. McCrea, S. Epstein, H. A. Allen, and H. C. Urey. Inprovements in mass spectrometers for the measurement of small differences in isotope abundance ratios—724
McLachlan, D., Jr. (see Shimizu, H.)—779
McNally, Fred A. Motion within a vacuum system—813(L)
Mendousse, J. S., P. D. Goodman, and W. G. Cady. Capacitance bridge for high frequencies—1002
Metlay, Max (see Burwell, Robert L., Jr.)—681
Meyerhoff, W. E. Book review—90
Mihelich, J. W. (see Hill, R. D.)—498(L)
Miller, D. S. Recording torque magnetometer—605
—— (see Fisher, R. M.)—938(L)
Miller, R. D. and J. S. Hopkins. Electronic water-level control—263(L)
Miranda, L. (see Blasco, E.)—494(L)
Mitchell, James M. Power supply for the Cenco concentrated-arc lamp—497(L)
Molnar, J. P. and C. D. Hartman. Data on porcelain rod leak—394(L)
Montgomery, C. G. (see Saltzmann, H.)—548
—— (see Willard, D.)—520
Moore, Benjamin L. Pentode counting or control ring—337
Morrish, A. H., G. W. Williams, and E. K. Darby. Ultraviolet photon counting with an electron multiplier—884(L)
Mortensen, Tage A. An improved Schlieren apparatus employing multiple slit-gratings—3
Munson, Ivan K. Microwave power stabilizer—622
Myers, R. D. (see Elliot, J. O.)—631

Nearhoof, H. J. (see Benner, A. H.)—830
Needels, T. S. and C. E. Nielsen. Continuously sensitive cloud chamber—976
Nereson, Norris and Frederick Reines. Nuclear emulsions and the measurement of low energy neutron spectra—534
Newell, Homer E., Jr., and Eleanor C. Pressly. Note on the geometry of Geiger counter telescopes—918
Nichol, James T. (see Burton, Alan C.)—485
Nielsen, C. E. (see Needels, T. S.)—976
Nier, Alfred O. (see Halsted, R. E.)—1019
Nilsson, Ingvar. Device for measuring the high voltage for a photo-multiplier tube—396(L)
Novey, Theodore B. RaDEF standard sources for beta-disintegration rate determinations—280
Nunan, Craig S. (see Dazey, Mitchell H.)—436

O'Brien, Brian. Book review—88
O'Connell, T. C. and A. G. Barkow. Circumferential recording microphotometer—573(L)
Oettinger, Walter H. (see Grundfest, Harry)—360
O'Neill, L. H. and J. L. West. Direct reading phasemeter—271
Overbeck, C. J. Book review—875
Owen, George E. and Henry Primakoff. Relation between apparent shapes of monoenergetic conversion lines and continuous beta-spectra in a magnetic spectrometer. II—447

Page, Harold T. (see Snowden, F. Curtis)—179
Panofsky, Wolfgang K. H. Book review—383
—— **and W. R. Baker.** Focusing device for the external 350-Mev proton beam of the 184-inch cyclotron at Berkeley—445
Parker, James H. (see Loeb, Leonard B.)—42
Parsons, Jonathan. On adapting a powder x-ray diffraction camera for reflection patterns—185
Paskin, Arthur (see Keller, Joseph M.)—713
Pasternack, Simon. Book review—871
Pavalow, Melvin, William O. Davis, and William P. Staker. Balloon-borne instrumentation for neutron detection—529
Perrine, Eugene L. Optical centering system for x-ray diffraction samples—262(L)
Perry, K. E. (see Roberts, B. W., Jr.)—790
Persico, E. and C. Geoffrion. Beta-ray spectroscopy—945
Peterson, Jack M. (see Dazey, Mitchell H.)—436
Petropoulos, G. M. Experimental KVAH-meter—187(L)
Pfohl, Frank W. (see Burwell, Robert L., Jr.)—681
Phillips, A. N. (see Allred, J. C.)—225
Phillips, G. C. and J. E. Richardson. Preparation of carbon targets—885(L)
Philp, Sanborn F. (see Cloud, Robert W.)—731
Pidd, R. W. (see Madansky, Leon)—407
Pigott, M. T. (see Hill, R. D.)—498(L)
Pimentel, G. C. (see McClellan, A. L.)—1023(L)
Pollard, E. C. Book review—86
Pound, R. V. and W. D. Knight. Radiofrequency spectrograph and simple magnetic-field meter—219
Pratt, A. W. (see Eden, M.)—802
Pressesky, A. J. (see Hurst, D. G.)—705
Pressly, Eleanor C. (see Newell, Homer E., Jr.)—918
Price, Fraser P. and Paul D. Zemany. Simple recording manometer—261(L)
Primakoff, Henry. (see Owen, George E.)—447
Pringle, Robert W., Kenneth I. Roulston, and Harry W. Taylor. Scintillation counter as a low resolution gamma-ray spectrometer—216

Quinnel, E. H. and A. H. Futch. Automatic level controller for liquid nitrogen—400(L)

Ragazzini, John R. and Lotfi A. Zadeh. Wide-band audio phasemeter—145
Ramler, W. J. and M. S. Freedman. Scintillation efficiency of anthracene for low energy electrons—784
Ratchford, William P. and M. L. Fein. Simple low power electronic relay—188(L)
Rauh, Everett G. (see Fred, Mark S.)—258(L)
Ravilious, C. F. (see Elliot, J. O.)—631
Reed, T. B. (see Abrahams, S. C.)—396(L)
Reines, Frederick (see Nereson, Norris)—534
Richards, Oscar W. Microtome knife sharpness—670(L)
Richards, Paul I. Cathode-follower fallacies—1025(L)
—— **and E. E. Hays.** Scintillation-type ion detector—99(L)
Richardson, J. E. (see Phillips, G. C.)—885(L)
Ridenour, Louis N. Book review—385
Rinehart, John S. Simultaneous photography of self-luminous and non-self-luminous effects—939(L)
Roberts, B. W., Jr., K. E. Perry, and R. G. Fluharty. An improved resolving time measuring device—790
Roberts, James H. (see Keepin, George R., Jr.)—163
Robinson, C. S. (see Kerst, D. W.)—462
Robinson, C. V. Small probing Geiger-Müller counters—82
Robinson, Charles F. Observations on some properties of ultra-high frequency gas discharges—617
Robinson, James G. (see Lewis, Lloyd G.)—593
Rogers, G. L. Book review—88
Rogers, John D., Henry L. Cox, and Paul G. Braunschweiger. Frequency meter for microwave spectroscopy—1014
Rohrer, E. R. (see Goldin, A. S.)—554
Rojansky, V. Book review—90
Rose, Walter. Packless valve flow regulator—772(L)
Rosen, L. (see Allred, J. C.)—225
Rosenbaum, E. J. Book review—873
Rosenblit, George J. (see Steingiser, Samuel)—109

Rosenblum, Earl S. Sector-type double-focusing magnetic spectrometer—586
Rosenthal, Louis A. Low frequency sinusoidal voltage source —302
—— (see Freedman, Larry A.)—896
—— **and H. S. Zablocki.** Electronic a.c. differential voltmeter —799
Roulston, Kenneth I. (see Pringle, Robert W.)—216
Rubin, S. (see Snyder, C. W.)—852
Ruderman, I. W. (see Blau, M.)—232
Rudin, Robert (see Blau, Marietta)—978
Rudolph, O. B. Precision selector for voltage-regulator tubes —497(L)

Saltzmann, H. and C. G. Montgomery. Velocity of propagation of the discharge in Geiger-Müller counters—548
Samuel, A. L. Book review—387
Sasaki, Nobuji. New method for surface-temperature measurement—1
Savitzky, Abraham and Ralph S. Halford. Ratio-recording double beam infra-red spectrophotometer using phase discrimination and a single detector—203
Schawlow, A. L. Book review—659
Schneider, W. G. and N. R. S. Hollies. Temperature-controlled resistance furnace for high temperature measurements—94(L)
Scholander, P. F. Volumetric plastic micro respirometer—378
Schuette, O. F., Jr., A. Zucker, and W. W. Watson. Apparatus for concentration of He^3 by thermal diffusion—1016
Schulman, Martin P. Book review—665
Schumacher, Joseph G. (see Claffy, Esther W.)—575(L)
Schwed, Philip (see Levy, Gabor B.)—693
Scott, Arnold H. An instrument for mechanically differentiating curves—397(L)
Scott, B. I. H. (see Blüh, O.)—867
Scott, F. R. (see Bruner, Joseph A.)—545
—— (see Langer, L. M.)—522
Scott, Merit. Book review—659
Seaborg, Glenn T. (see Curtiss, L. F.)—94(L)
Sears, G. W. and E. R. Hopke. Effective vacuum cut-off—570(L)
Seemann, Herman E. Spectral sensitivity of two commercial x-ray films between 0.2 and 2.5 angstroms—314
Segal, Leon, Joseph J. Creely, and Carl M. Conrad. Rotating specimen mount for use with x-ray spectrometer in measuring crystallite orientation of cellulosic and other textile fibers—431
Selvin, G. J. (see Stang, L. G., Jr.)—97(L)
Seitz, Frederick. Book review—382
Seiwell, H. R. New mechanical autocorrelator—481
Sengstaken, Robert W. (see Grundfest, Harry)—360
Sessler, W. M. and A. V. Masket. High speed electronic scaler—494(L)
Shankland, Robert S. Book review—387
Shapiro, Jennie E. Method of preserving specimen grids for electron microscopy—500(L)
Sharbaugh, A. Harry. Design and construction of a Stark-modulation microwave spectrograph—120
Shaw, Robert F. Arithmetic operations in a binary computer —687
Sherr, R. Book review—657
Sherwood, Jesse E. Remote-control method of opening ampoules of active materials—570(L)
Shiflett, Chester H., Mark E. Steidlitz, and Wallace Davis, Jr. System for the collection and purification of radon by remote control—842
Shimizu, H., P. J. Elsey, and D. McLachlan, Jr. Machine for synthesizing two-dimensional Fourier series in the determination of crystal structures—779
Shoupp, W. E. (see Sun, Kuan-Han)—395(L)
Showers, Ralph M. Book review—875
Shrader, E. F. High speed short resolving time coincidence circuit for use with scintillation counters—883(L)
—— (see Strough, Robert I.)—575(L)
Shreffler, R. G. (see Fowler, C. M.)—740
Shutt, R. P. and W. L. Whittemore. High speed expansion valve for cloud-chamber control—643
Siegbahn, Kai and Stig Johansson. An electron pair spectrometer of lens type for hard gamma-radiation—442
Silver, L. M. and J. B. Warren. Behavior of rectangular and square section transparent beta-counters—95(L)
Simpson, J. A., Jr. Theory and properties of low voltage radiation counters—558
Simpson, J. Arol and Alan Van Bronkhorst. Modification of electron microscope for electron optical shadow method—669(L)
Sirvetz, M. H. (see Baird, D. H.)—881(L)
Sledge, O. D. (see Hunt, F. V.)—332
Smeltzer, Jack C. Energy dependence of the naphthalene scintillation detector—669(L)
Smith, Lloyd P. Book review—386
Smith, Otto J. M. Thermistors. Part I. Static characteristics —344
—— Part II. Dynamic characteristics—351
Smoluchowski, R. (see Turner, R. W.)—440
Smyth, Charles P. Book review—874
Snowden, F. C. (see Hamm, F. A.)—426
—— **and Harold T. Page.** Electronic circuit which extracts antilogarithms directly—179
Snyder, C. W., S. Rubin, W. A. Fowler, and C. C. Lauritsen. Magnetic analyzer for charged-particles from nuclear reactions—852
Snyder, S. D., C. J. Craven, and D. B. Trauger. Volumetric displacement flask—887(L)
Solomon, A. K. Regulated low voltage power supply—570(L); Erratum—789
Squire, C. F. Book review—663
Staker, William P. (see Pavalow, Melvin)—529
Stallings, Donald W. (see Weigl, John W.)—395(L)
Stang, L. G. Jr., and G. J. Selvin. Improved method of directing liquid flow in a closed system—97(L)
Steidlitz, Mark E. (see Shiflett, Chester H.)—842
Steingiser, Samuel, George J. Rosenblit, Robert Custer, and Chas. E. Waring. Precision Faraday effect apparatus—109
Stephenson, S. T. and D. L. Martin. Note on crystal suitable for double crystal x-ray spectroscopy in the region 3 to 15A—1023(L)
Stewart, Albert B. Degassing extended glass systems—258(L)
Stewart, H. J. Book review—384
Strauss, H. A. (see Bell, P. R.)—760
Strough, Robert I. and Erwin F. Shrader. Pulsed air core-series disk generator for production of high magnetic fields —575(L)
Sturcken, E. F. (see Heller, R. B.)—898
Sturdivant, J. H. Book review—662
Sullivan, H. M. Book review—381
Sultanoff, M. 100,000,000-frame-per-second camera—653
Sun, Kuan-Han and W. E. Shoupp. Scintillation counter for neutrons—395(L)
Sutton, Richard M. Book review—89
Swenson, C. A. Simple pressure balance—22

Taimuty, Samuel I. (see Van Atta, C. M.)—985
Tallmadge, F. K. (see Allred, J. C.)—225
Tang, Ting-Yuan (see Lawson, A. W.)—815(L)
Taylor, Harry W. (see Pringle, Robert W.)—216
Timmerhaus, K. D., E. B. Giller, L. H. Tung, R. B. Duffield, and H. G. Drickamer. High pressure fitting for scintillation counting—261(L)
Tisza, L. Book review—88
Toll, John (see Lewis, Lloyd G.)—593

Tomlinson, J. W. and J. O'M. Bockris. Vacuum furnace for use in the temperature range 1000–2000°C—507
Tonks, Lewi. Book review—873
Torrey, H. C. Book review—381
Towsley, F. E. (see Adams, G. D.)—69
Trauger, D. B. (see Snyder, S. D.)—887(L)
Trevoy, D. J. (see Huse, E. S.)—60
Tung, L. H. (see Timmerhaus, K. D.)—261(L)
Tunnicliffe, P. R. (see Fowler, I. L.)—734
—— (see Hurst, D. G.)—705
Turner, R. W., T. L. Wu, and R. Smoluchowski. X-ray determination of slip planes and slip directions—440

Ufford, C. W. Book review—384
—— Book review—389
—— Book review—876
Urey, H. C. (see McKinney, C. R.)—724

Valasek, Joseph. Book review—664
Van Atta, C. M., Sydney D. Warshaw, Joses J. L. Chen, and Samuel I. Taimuty. Double thin lens beta-ray spectrometer—985
Van Atta, L. C. Book review—383
Van Bronkhorst, Alan (see Simpson, J. Arol)—669(L)
Van Dyke, Karl S. Book review—658
Van Voorhis, S. N. Book review—665
Vonnegut, Bernard. Vortex thermometer for measuring true air temperatures and true air speeds in flight—136

Wang, P. K. S. Note on reduction of background fog in nuclear emulsion plates—816(L)
Waniek, Ralph W. Automatic equipment for electrolyzing heavy water—262(L)
Waring, Chas. E. (see Steingiser, Samuel)—109
Warren, B. E. Bent crystal x-ray monochromators—102(L)
Warren, J. B. (see Silver, L. M.)—95(L)
Warren, S. Reid, Jr. Book review—870
Warshaw, S. D. (see Hall, T. A.)—177
—— (see Van Atta, C. M.)—985
Watson, W. W. (see Schuette, O. F., Jr.)—1016
Watts, Richard J. Pulse type regulated high voltage supply for G-M tubes—342
Weber, A. H. (see Heller, R. B.)—898
Weigl, John W. and Donald W. Stallings. Rubber tubing pump—395(L)
Weinhart, H. W. (see Hagstrum, H. D.)—394(L)
Weinstein, Alfred (see Bonner, Francis)—934(L)
Weinzierl, Peter M. New method for the measurement of inhomogeneous magnetic fields—492(L)
Werner, F. D. Investigation of the possible use of the glow discharge as a means for measuring air flow characteristics—61
Wertz, John E. Manometer leveling procedure—263(L)
West, J. L. (see O'Neill, L. H.)—271
Wexler, Aaron and William S. Corak. Transfer device for low boiling liquids—583
——**, W. S. Corak, and G. T. Cunningham.** Low temperature gasket—259(L)
White, John U. Simple variable space infra-red absorption cell—629
White, Julius (see Highhouse, Frederick)—101(L)
Whittemore, W. L. (see Shutt, R. P.)—643
Wiegand, Clyde. Distributed coincidence circuit—975
Wiener, Martin and Herman Yagoda. Background eradication in thick-layered nuclear emulsions—39
Wildhack, W. A. Versatile pneumatic instrument based on critical flow—25
Willard, D. and C. G. Montgomery. Method of measuring spurious counts in Geiger-Müller counters—520
Williams, G. W. (see Morrish, A. H.)—884(L)
Wilson, R., L. Beghian, C. H. Collie, H. Halban, and G. R. Bishop. High pressure ionization chamber counters and their use—699
Witmer, Enos E. Book review—869
Wood, Darwin L. Infra-red microspectrometer for biological research—764
Wu, T. L. (see Turner, R. W.)—440

Yagoda, Herman (see Wiener, Martin)—39

Zablocki, H. S. (see Rosenthal, L. A.)—799
Zadeh, Lotfi A. (see Ragazzini, John R.)—145
Zar, Jacob L. Expansion valve for triggered cloud chambers—812(L)
Zarem, A. M. and F. R. Marshall. Multiple Kerr-cell camera—514
Zemansky, M. W. (see Dash, J. G.)—936(L)
Zemany, Paul D. (see Price, Fraser P.)—261(L)
Zucker, A. (see Schuette, O. F., Jr.)—1016

THE REVIEW OF SCIENTIFIC INSTRUMENTS VOLUME 21, NUMBER 12 DECEMBER, 1950

Analytic Subject Index to Volume 21

References with (L) are to Laboratory and Shop Notes

Amplifier Circuits
  D.c. amplifier for biological application, P. O. Bishop and E. J. Harris—366
  Improving differential amplifier rejection ratios, Richard McFee—770(L)
  Linear preamplifier for driving a long coaxial cable, L. G. Lewis, J. G. Robinson, and J. Toll—593
  Transmission line reflection doubling amplifier, John Marshall—1010
Anemometers
  Vortex thermometer for measuring true air temperatures and true air speeds in flight, Bernard Vonnegut—136
Biophysical Instruments
  Automatic isodose recorder with scintillation counter as gamma-ray detector, G. J. Hine, M. Berman, and M. M. Elkind—362
  Continuous flow respirometer utilizing the oxygen cathode, Francis D. Carlson, F. Brink, Jr., and D. W. Bronk—923
  D.c. amplifier for biological application, P. O. Bishop and E. J. Harris—366
  Design of a simple microflowmeter for biological perfusion experiments, A. C. Burton and J. T. Nichol—485
  Detection of tritiated compounds in paper chromatography, I. Gray, S. Ikeda, A. Benson, and D. Kritchevsky—1022

Differential vectorcardiograph, Stanley Briller, Nathan Marchand, and Charles E. Kossmann—805
4π-radiometer, T. Benzinger and C. Kitzinger—599
Infra-red microspectrometer for biological research, Darwin L. Wood—764
Making small metal tubes by electrodeposition on Nylon fibers, R. J. E. Gezelius—886(L)
Modification of the apparatus used for the Baldes thermoelectric method of measuring osmotic pressure, V. Everett Kinsey—767
Small probing Geiger-Müller counters, C. V. Robinson—82
Stainless steel micro-needle electrodes made by electrolytic pointing, Harry Grundfest, Robert W. Sengstaken, Walter H. Oettinger, and R. W. Gurry—360
Trigonometric computer with electrocardiographic applications, Richard McFee—420
Ultrasonic tissue disintegrator, F. F. Bird and K. S. Lion—189(L)
Vibrating probe electrometer for the measurement of bioelectric potentials, O. Blüh and B. I. H. Scott—867
Volumetric plastic micro respirometer, P. F. Scholander—378

Book Reviews
Adams, Douglas P., An index of nomograms—876
Andronow, A. A. and C. E. Chaikin, Theory of oscillations—389
Arnot, F. I., Collision processes in gases—870
Beranek, Leo L., Acoustic measurements—387
Bergmann, Ludwig, Der ultraschall und seine anwendung in wissenschaft und technik—658
Bergmann, Peter G., Basic theories of physics: mechanics and electrodynamics—383
Berkeley, Edmund C., Giant brains, or machines that think—385
Berl, Walter G. (edited by), Physical methods in chemical analysis, Vol. I—875
Bloom, William, Histopathology of irradiation from external and internal sources—391
Bonney, E. Arthur, Engineering supersonic aerodynamics—384
Campbell, Edward C. (see Soodak, Harry)—874
Candler, C., Practical spectroscopy—388
Chaikin, C. E. (see Andronow, A. A.)—389
Cox, Parker (see Habell, K. J.)—88
Dangl, J. R. (see Randall, H. M., R. G. Fowler, and N. Fusion)—388
Del Mar, W. A. (see Pender, H.)—387
Dieke, G. H. and A. B. F. Duncan, Spectroscopic properties of uranium compounds—386
Dobie, W. B. and Peter G. Isaac, Electric resistance strain gauges—88
Don Leet, L., Earth waves—385
Duncan, A. B. F. (see Dieke, G. H.)—386
Einstein, Albert, The meaning of relativity—660
Elmore, William C. and Matthew Sands, Electronic-experimental techniques—665
Farkas, A. (edited by), Physical chemistry of hydrocarbons, Vol. I—873
Fowler, R. G. (see Randall, H. M., N. Fusion, and J. R. Dangl)—388
Frankenburg, W. G., V. I. Komarewsky, and E. K. Rideal (edited by), Advances in catalysis and related subjects, Vol. I—87
——, Advances in catalysis, Vol. II—869
Frayne, John G. and Halley Wolfe, Elements of sound recording—390
Friedlander, G. and J. Kennedy, Introduction to radiochemistry—85
Frolich, H., Theory of dielectrics—90
Fry, D. W. and F. K. Goward, Aerials for centimetre wavelengths—878
Fusion, N. (see Randall, H. M., R. G. Fowler, and J. R. Dangl—388
Garlick, G. F. J., Luminescent materials—386
Gatterer, A. and J. Junkes, Spectra of the rare metals and some metalloids—384
Gill, J. F. (see Teago, F. J.)—873
Glasser, Otto (edited by), Medical Physics, Vol. II—870
Goward, F. K. (see Fry, D. W.)—878
Green, Henry, Industrial rheology and rheological structures—92
Gutenberg, B. and C. F. Richter, Seismicity of the earth—87
Guthrie, A. and R. K. Wakerling (edited by), Vacuum equipment and techniques—381
Habell, K. J. and Parker, Cox, Engineering optics-The principles of optical methods in engineering measurement—88
Hague, B., Introduction to vector analysis—871
Ham, Lloyd B. (see Schneider, Walter A.)—91
Harnwell, Gaylord P., Principles of electricity and electromagnetism—90
Hawkins, George A. (see Jacob, Max)—878
Herzberg, Gerhard, Molecular spectra and molecular structure. I. Spectra of diatomic molecules—869
Higdon, A. and W. B. Stiles, Engineering mechanics—659
Hill, W. Ryland, Electronics in engineering—666
Hull, Gordon Ferrie, Elementary modern physics—389
Isaac, Peter G. (see Dobie, W. B.)—88
Jackson, L. C., Low temperature physics—663
—— Wave filters—870
Jacob, Max and George A. Hawkins, Elements of heat transfer and insulation—878
Junkes, J. (see Gatterer, A.)—384
Katz, Joseph J. (see Seaborg, Glenn T. and Winston N. Manning)—665
Kennedy, J. (see Friedlander, G.)—85
Knudsen, Martin, The kinetic theory of gases: some modern aspects—871
Komarewsky, V. (see Frankenburg, W. G. and E. K. Rideal)—87
Lang, Ruth (compiled and edited by), Laboratory and workshop notes—86
Lass, Harry, Vector and tensor analysis—877
Le Corbeiller, P., Matrix analysis of electric networks—381
Leermakers, John A. (see Mees, C. E. Kenneth)—872
LeFevre, R. J. W., Dipole moments—874
Leverenez, Humboldt W., An introduction to the luminescence of solids—382
Linksz, Arthur, Physiology of the eye, Vol. I, Optics—664
Lonsdale, K., Crystals and x-rays—662
Mann, W. B., The cyclotron—657
Manning, Winston N. (see Seaborg, Glenn T. and Joseph J. Katz)—665
Mees, C. E. Kenneth and John A. Leermakers, The organization of industrial scientific research—872
Mellon, M. G. (edited by), Analytical absorption spectroscopy, absorptimetry, and colorimetry—879
Menzel, Donald H., Our sun—91
Milne, E. A., Kinematic relativity—657
Moore, Charlotte E., Atomic energy levels, Vol. I—85
Muskat, Morris, Physical principles of oil production—661
O'Hara, Charles E. and James W. Osterburg, An introduction to criminalistics—85
Osterburg, James W. (see O'Hara, Charles E.)—85
Palm, A., Elektrische messgerate und messeinrichtungen—90
Pender, H. and W. A. Del Mar (edited by), Electrical engineers' handbook of electric power—387
Randall, H. M., R. G. Fowler, N. Fusion, and J. R. Dangl, Infrared determination of organic structures—388
Richter, C. F. (see Gutenberg, B.)—87

Book Reviews (continued)
- Rideal, E. K. (see Frankenburg, W. G. and V. I. Komarewsky)—87
- Rossi, Bruno B. and Hans H. Staub, Ionization chambers and counters—390
- Rothmann, S. C. (edited by), Constructive uses of atomic energy—89
- Rushbrooke, G. S., Introduction to statistical mechanics—88
- Sands, Matthew (see Elmore, William C.)—665
- Schilpp, P. A. Albert Einstein: philosopher-scientist—660
- Schneider, Walter A. and Lloyd B. Ham, Experimental physics for colleges—91
- Schweitzer, G. K. and I. B. Whitney, Radioactive tracer techniques—665
- Scott, Merit, Mechanics, statics, and dynamics—664
- Seaborg, Glenn T., Joseph J. Katz, and Winston N. Manning, The transuranium elements—665
- Seely, Samuel, Electron-tube circuits—666
- Shannon, C. E. and W. Weaver, The mathematical theory of communication—875
- Siri, William E., Isotopic tracers and nuclear radiations with applications to biology and medicine—86
- Slater, John C., Microwave electronics—877
- Smith, R. A., Aerials for metre and decimetre wavelengths—383
- Soodak, Harry and Edward C. Campbell, Elementary pile theory—874
- Staub, Hans H. (see Rossi, Bruno B.)—390
- Stiles, W. B. (see Higdon, A.)—659
- Stoner, E. C., Magnetism—661
- Sullivan, William H., Trilinear chart of nuclear species—662
- Tolansky, S., Hyperfine structure in line spectra and nuclear spin—659
- Teago, F. J. and J. F. Gill, Mercury arcs—873
- Temple, G., The general principles of quantum theory—876
- Valasek, Joseph, Introduction to theoretical and experimental optics—386
- Wakerling, R. K. (see Guthrie, A.)—381
- Weaver, W. (see Shannon, C. E.)—875
- Weizel, Walter, Lehrbrich der theoretischen physik—663
- Whitney, I. B. (see Schweitzer, G. K.)—665
- Willers, F. A., Practical analysis, graphical and numerical methods—871
- Wolfe, Halley (see Frayne, John G.)—390

Bridge Circuits
- High megohm bridge, F. M. Glass and R. K. Abele—493(L)
- Capacitance bridge for high frequencies, J. S. Mendousse, P. D. Goodman, and W. G. Cady—1002

Centrifuge
- Magnetic suspension for small rotors, J. W. Beams—182

Chemical Analysis
- Precision Faraday effect apparatus, Samuel Steingiser, George J. Rosenblit, Robert Custer, and Charles E. Waring—109

Cloud Chambers
- Continuously sensitive cloud chamber, T. S. Needels and C. E. Nielsen—976
- Diffusion cloud chambers, E. W. Cowan— 991
- Expansion valve for triggered cloud chambers, Jacob L. Zar—812(L)
- High speed expansion valve for cloud-chamber control, R. P. Shutt and W. L. Whittemore—643
- Reprojection method for studying cloud-chamber photographs, D. A. Bromley and R. D. Bradfield—190(L)
- Self-triggering cloud-chamber counter, E. L. Fireman and G. M. McHaney—813(L)

Computing Devices and Techniques
- Analog computer, J. G. Bayly—228
- Analog computers for servo problems, Donald McDonald—154
- Arithmetic operations in a binary computer, Robert F. Shaw—687
- Differential analyzer for the Schrodinger equation, R. L. Garwin—411
- Electronic circuit which extracts antilogarithms directly, F. Curtis Snowden and Harold T. Page—179
- Electronic pile simulator, P. R. Bell and H. A. Straus—760
- Instrument for mechanically differentiating curves, Arnold H. Scott—397(L)
- Integrator for small beam currents, T. A. Hall, S. D. Warshaw, and J. Dorsey—177
- Machine for synthesizing two-dimensional Fourier series in the determination of crystal structures, H. Shimizu, P. J. Elsey, and D. McLachlan, Jr.—779
- New mechanical autocorrelator, H. R. Seiwell—481
- Nomogram for G-M counter resolving-time corrections, Howard L. Andrews—191(L)
- Note on the geometry of Geiger counter telescopes, H. E. Newell, Jr. and E. C. Pressly—918
- Random coincidence rates with unsteady sources—R. M. Littauer—750
- Rapid method for calculating and using platinum thermohm tables—R. A. Buerschaper—996
- Ratio-recording double beam infra-red spectrophotometer using phase discrimination and a single detector, Abraham Savitzky and Ralph S. Halford—203
- Recording fluxmeter of high accuracy and sensitivity, P. P. Cioffi—624
- Relation between apparent shapes of monoenergetic conversion lines and continuous beta-spectra in a magnetic spectrometer. II, G. E. Owen and H. Primakoff—447
- Simplified percent transmission computer, A. L. McClellan and G. C. Pimental—1023(L)
- Single element verniers reading two or three dimensions, Robert E. Lewis—647
- Slide rule for nuclear emulsion calculations, Arthur Beiser—933
- Solution of simultaneous equations through use of the a.c. network calculator, L. M. Haupt—683
- Trigonometric computer with electrocardiographic applications, Richard McFee—420

Cosmic Rays
- Balloon-borne instrumentation for neutron detection, M. Pavalow, W. O. Davis, and W. P. Staker—529
- Detaching device for balloon flights, Louis G. Collyer—496(L)
- Instrument for directional studies of cosmic-ray intensity, H. W. Boehmer and J. E. Coolidge—633

Counters and Counter Circuits
- Behavior of rectangular and square section transparent beta-counters, L. M. Silver and J. B. Warren—95(L)
- Boron trifluoride proportional counters, I. L. Fowler and P. R. Tunnicliffe—734
- Calcium and cadmium tungstate as scintillation counter crystals for gamma-ray detection, R. H. Gillette—294
- Chart recording of microsecond pulse amplitudes, J. T. Dewan and K. W. Allen—823
- Coincidence circuit for a scintillation detector of radiation, W. C. Elmore—649
- Coincidence experiments for noise reduction in scintillation counting, Hartmut Kallmann and Karl A. Accardo—48
- Construction and performance of a multiple gamma-ray counter of high efficiency, Tibor Gráf—285
- Decade pulse counter for Geiger-Müller tubes, Björn Åström—323
- Design of neutron counters using multiple detecting layers, R. D. Lowde—835
- Detection of tritiated compounds in paper chromatography, I. Gray, S. Ikeda, A. Benson, and D. Kritchevsky—1022

Distributed coincidence circuit, Clyde Wiegand—975
Duration of scintillations from organic phosphors, J. O. Elliot, S. H. Liebson, R. D. Myers, and C. F. Ravilious——631
Electric field in a Geiger counter, Arthur R. Laufer—252
Electron component in Geiger discharge, G. G. Kelley, W. H. Jordan, and P. R. Bell—330
Electron pair spectrometer of lens type for hard gamma-radiation, Kai Siegbahn and Stig Johansson—442
End and wall corrections for absolute beta-counting in gas counters, A. G. Engelkemeir and W. F. Libby—550
Gas phase counting of low energy beta-emitters, W. Bernstein and R. Ballentine—158
Geiger counter mounting for continuous counting of gas-phase radioactivity—Francis Bonner and Alfred Weinstein—934(L)
High pressure fitting for scintillation counting, K. D. Timmerhaus, E. B. Giller, L. H. Tung, R. B. Duffield, and H. G. Drickamer—261(L)
High speed short resolving time coincidence circuit for use with scintillation counters, E. F. Shrader—883(L)
Improved resolving time measuring device, B. W. Roberts, Jr., K. E. Perry, and R. G. Fluharty—790
Method of measuring spurious counts in Geiger-Müller counters, D. Willard and C. G. Montgomery—520
Nomogram for G-M counter resolving-time corrections, Howard L. Andrews—191(L)
Note on the detection of coincidences and short time intervals, Robert Hofstadter and John A. McIntyre—52
Note on the geometry of Geiger counter telescopes, H. E. Newell, Jr. and E. C. Pressly—918
Pentode counting or control ring, Benjamin L. Moore—337
RaDEF standard sources for beta-disintegration rate determinations, Theodore B. Novey—280
Random coincidence rates with unsteady sources, R. M. Littauer—750
Scintillation counter as a low resolution gamma-ray spectrometer, Robert W. Pringle, Kenneth I. Roulston, and Harry W. Taylor—216
Scintillation counter for fast neutrons, H. B. Frey—886(L)
Scintillation counter for neutrons, Kuan-Han Sun and W E. Shoupp—395(L)
Scintillation efficiency of anthracene for low energy electrons, W. J. Ramler and M. S. Freedman—784
Scintillation type alpha-particle detector, A. S. Goldin, E. R. Rohrer, and R. L. Macklin—554
Scintillation-type ion detector, Paul I. Richards and E. E. Hays—99(L)
Self-triggering cloud-chamber counter, E. L. Fireman, and G. M. McHaney—813(L)
Small probing Geiger-Müller counters, C. V. Robinson—82
Some properties of the parallel plate spark counter. II, Leon Madansky and R. W. Pidd—407
Study of plateau slopes in self-quenching Geiger-Müller counters, Sanborn C. Brown and Claudine Maroni—241
Theory and properties of low voltage radiation counters, J. A. Simpson, Jr.—558
Time lags in Geiger counters—Arthur R. Laufer—244
Transmission of beta-rays by Nylon and Formvar, R. B. Heller, E. F. Sturcken, and A. H. Weber—898
Two beta-gamma-counters for gas samples, Rodman Jenkins—940(L)
Useful fast coincidence circuit, Richard L. Garwin—569(L)
Velocity of propagation of the discharge in Geiger-Müller counters, H. Saltzmann and C. G. Montgomery—548
Zero inefficiency anticoincidence circuit, M. Degallier—1025(L)

Dielectrics
Measurement of secondary electron emission from dielectric surfaces, Howard L. Heydt—639
Recording microwave refractometer, George Birnbaum—169

Diffusion
Diaphragm cell for thermal diffusion measurements, E. S. Huse, D. J. Trevoy, and H. G Drickamer—60
Diffusion cloud chambers, E. W. Cowan—991
Tests of flowing junction diffusion cells with interference methods, L. G. Longsworth—524

Dilatometers
Measurement and amplification of minute displacements by frequency modulation, P. A. Bricout and M. Boisvert—98(L)

Electrical Conductivity
Temperature coefficient of resistance of tin oxide-coated electrically conducting glass between 1° and 300°K, D. N. Lyon and T. H. Geballe—769(L)

Electrical Machinery
Motor for use in vacuum systems, C. P. Butler and F. E. Carpenter—103(L)
Pulsed air core series disk generator for production of high magnetic fields R. I. Strough and E. F. Shrader—575(L)

Electrical Measurements
Chart recording of microsecond pulse amplitudes, J. T. Dewan and K. W. Allen—823
Direct reading phasemeter, L. H. O'Neill and J. L. West—271
Dust electricity analyzer, W. B. Kunkel and J. W. Hansen—308
Electronic a.c. differential voltmeter, L. A. Rosenthal and H. S. Zablocki—799
Electron tube potentiometer method for use in circuits involving very high resistance, H. Bloom and G. W. Butler—274
Experimental KVAH-meter, G. M. Petropoulos—187(L)
Frequency meter for microwave spectroscopy, J. D. Rogers, H. L. Cox, and P. G. Braunschweiger—1014
Wide-band audio phasemeter, John R. Ragazzini and Lotfi A. Zadeh—145

Electrical Networks
Analog computers for servo problems, Donald McDonald—154
Best arrangement of resistors in a series group, Herbert B. Brooks—491(L)
Cathode-follower fallacies, Paul I. Richards—1025(L)
Design and construction of universal function generating potentiometers, Granino A. Korn—77
Design of logarithmic voltage dividers, F. V. Hunt and O. D. Sledge—332
Improving differential amplifier rejection ratios, Richard McFee—770(L)
Solution of simultaneous equations through use of the a.c. network calculator, L. M. Haupt—683

Electronic Instruments
Apparatus for rapid measurement of internal friction, Herbert I. Fusfeld—612
Apparatus for the study of electrets, L. A. Freedman and L. A. Rosenthal—896
Automatically synchronized electronic switch, W. A. Budlong and Bruce C. Lutz—167
D.c. amplifier for biological application, P. O. Bishop and E. J. Harris—366
Decade pulse counter for Geiger-Müller tubes, Björn Åström—323
Differential vectorcardiograph, Stanley A. Briller, Nathan Marchand, and Charles E. Kossmann—805
Direct reading phasemeter, L. H. O'Neill and J. L. West—271
Distributed coincidence circuit, Clyde Wiegand—975
Electronic a.c. differential voltmeter, L. A. Rosenthal and H. S. Zablocki—799

Electronic Instruments (continued)
- Electronic circuit which extracts antilogarithms directly, F. Curtis Snowden and Harold T. Page—179
- Electronic recording analytical balance, Idas W. Lohmann—999
- Electronic water-level control, R. D. Miller and J. S. Hopkins—263(L)
- Frequency modulation pressure recording system, J. H. Hett and R. W. King, Jr.—150
- High speed electronic scaler, W. M. Sessler and A. V. Masket—494(L)
- High speed synchroscope, G. G. Kelley—71
- Improved electrical network for determining the eigenvalues and eigenvectors of a real symmetric matrix, Abraham Many—972
- Integrator for small beam currents, T. A. Hall, S. D. Warshaw, and J. Dorsey—177
- Low frequency sinusoidal voltage source, Louis A. Rosenthal—302
- Magnetic tape recorder for very low frequency phenomena, Paul E. Green, Jr.—893
- Measurement and amplification of minute displacements by frequency modulation, P. A. Bricout and M. Boisvert 98(L)
- Monitor for low intensity gamma-rays, J. B. H. Kuper and R. L. Chase—356
- Precision selector for voltage-regulator tubes, O. B. Rudolph—497(L)
- Radiofrequency spectrograph and simple magnetic-field meter, R. V. Pound and W. D. Knight—219
- Ratio-recording double beam infra-red spectrophotometer using phase discrimination and a single detector, Abraham Savitzky and Ralph S. Halford—203
- Regulated low voltage power supply, A. K. Solomon—570(L)
- Reliable Pirani vacuum safety circuit, W. Franzen and J. Horton—935
- Simple low power electronic relay, William P. Ratchford and M. L. Fein—188(L)
- Useful fast coincidence circuit, R. L. Garwin—569(L)
- Wide-band audio phasemeter, John R. Ragazzini and Lotfi A. Zadeh—145

Electron Microscope
- Laboratory modifications in the RCA model EMC electron microscope, S. G. Ellis—255
- Method of preserving specimen grids for electron microscopy, Jennie E. Shapiro—500(L)
- Modification of electron microscope for electron optical shadow method, J. Arol Simpson and Alan Van Bronkhorst—669(L)
- Molecular diffraction attachment for RCA microscope, B. O. Heston and P. R. Cutter—608
- Simple automatic recording microphotometer, R. M. Fisher and D. S. Miller—938(L)
- Ultrasonic tissue disintegrator, F. F. Bird and K. S. Lion—189(L)
- Vibration studies: related to electron microscopy, F. A. Hamm and F. C. Snowden—426

Electron and Ion Optics
- Beta-ray spectroscopes, E. Persico and C. Geoffrion—945
- Design of a magnetic focusing coincidence spectrometer, C. M. Fowler and R. G. Shreffler—740
- Double thin lens beta-ray spectrometer, C. M. Van Atta, S. D. Warshaw, J. J. L. Chen, and S. I. Taimuty—985
- Electron pair spectrometer of lens type for hard gamma-radiation, Kai Siegbahn and Stig Johansson—442
- Electrostatic beta-spectrograph, D. R. Hamilton and L. Gross—912
- Focusing device for the external 350-Mev proton beam of the 184-inch cyclotron at Berkeley, W. K. H. Panofsky and W. R. Baker—445
- Focusing properties of a generalized magnetic spectrometer, David L. Judd—213
- High resolution beta-ray spectrometer, J. A. Bruner and F. R. Scott—545
- Laboratory modifications in the RCA model EMC electron microscope, S. G. Ellis—255
- Magnetic analyzer for charged-particles from nuclear reactions, C. W. Snyder, S. Rubin, W. A. Fowler, and C. C. Lauritsen—852
- Method for increasing the safe power input of x-ray tubes, Arthur I. Berman—275
- Relation between apparent shapes of monoenergetic conversion lines and continuous beta-spectra in a magnetic spectrometer. II, G. E. Owen and H. Primakoff—447
- Ring focus in a thin magnetic-lens beta-ray spectrometer, Joseph M. Keller, Ernest Koenigsberg, and Arthur Paskin—713
- Sector-type double-focusing magnetic spectrometer, Earl S. Rosenblum—586
- Simple contamination-free electron gun, H. E. Farnsworth—102(L)
- Use of secondary electrostatic focusing in a magnetic beta-ray spectrograph, R. D. Hill, J. W. Mihelich, and M. T. Pigott—498(L)

Electron Tubes
- All-metal ionization gauge, F. M. Kelly—673
- High power pulsed magnetron with replaceable cathode, M. F. Amsterdam and W. E. Danforth—398(L)
- New method for the measurement of inhomogeneous magnetic fields, Peter M. Weinzierl—492(L)
- Ultra-high vacuum ionization manometer, J. J. Lander—672(L)

Errata
- Formation of insulating layers by the thermal decomposition of ethyl silicate, Harold B. Law—270(L)
- High speed synchroscope, G. G. Kelley—264(L)
- Note on sealing Nylon films to Geiger counters, Robert A. Becker—270(L)
- Regulated low voltage power supply, A. K. Solomon—789
- Slide rule for radiation calculations, M. W. Makowski—336

Gas Discharges
- Choice of suitable gap forms for the study of corona breakdown and the field along the axis of a hemispherically capped cylindrical point-to-plane gap, Leonard B. Loeb, James H. Parker, E. E. Dodd, and William N. English—42
- Electric field in a Geiger counter, Arthur R. Laufer—252
- Electron component in Geiger discharge, G. G. Kelley, W. H. Jordan, and P. R. Bell—330
- Investigation of the possible use of the glow discharge as a means for measuring air flow characteristics, F. D. Werner—61
- Observations on some properties of ultra-high frequency gas discharges, Charles F. Robinson—617
- Study of plateau slopes in self-quenching Geiger-Müller counters, Sanborn C. Brown and Claudine Maroni—241
- Theory and properties of low voltage radiation counters, J. A. Simpson, Jr.—558
- Time lags in Geiger counters, Arthur R. Laufer—244
- Velocity of propagation of the discharge in Geiger-Müller counters, H. Saltzmann and C. G. Montgomery—548

Gas Handling and Measurement
- Convenient gas sample tube holder and break-off applicable to mass spectrometers, Frederick Highhouse and Julius White—101(L)
- Data on porcelain rod leak, J. P. Molnar and C. D. Hartman—394(L)
- Gas flow through the mass spectrometer viscous leak, R. E. Halsted and A. O. Nier—1019

- Glass variable microleaks for gases, John J. Hopfield—671(L)
- Greaseless gas flow valve, R. E. Honig—1024(L)
- Measurement of rates of flow of gases by wet test meters, Robert L. Burwell, Jr., Max Metlay, and Frank W. Pfohl—681
- Method of supplying low pressure gases on a vacuum system, Raymond H. McFee—100(L)
- System for the collection and purification of radon by remote control, Chester H. Shiflett, Mark E. Steidlitz, and Wallace Davis, Jr.—842
- Volumetric displacement flask, S. D. Snyder, C. J. Craven, and D. B. Trauger—887(L)

Goniometry
- Combination two-circle goniometer and x-ray spectrometer, M. L. Baron and A. deBretteville, Jr.—458

High Voltage Techniques
- Device for measuring the high voltage for a photo-multiplier tube, Ingvar Nilsson—396(L)
- Pulse type regulated high voltage supply for the G-M tubes, Richard J. Watts—342
- Voltage stabilizer for 200-Kv acceleration, J. T. Dewan—771(L)

Infra-Red Technique
- Infra-red microspectrometer for biological research, Darwin L. Wood—764
- Ratio-recording double beam infra-red spectrophotometer using phase discrimination and a single detector, Abraham Savitzky and Ralph S. Halford—203
- Simple variable space infra-red absorption cell, John U. White—629
- Water-proofing rocksalt for infra-red absorption cells, Scott Anderson, William J. Anderson, and Martin Krakowski—574(L)

Ionization Chambers
- Boron trifluoride proportional counters, I. L. Fowler and P. R. Tunnicliffe—734
- Design of neutron counters using multiple detecting layers, R. D. Lowde—835
- High pressure ionization chamber counters and their use, R. Wilson, L. Beghian, C. H. Collie, H. Halban, and G. R. Bishop—699
- Monitor for low intensity gamma-rays, J. B. H. Kuper and R. L. Chase—356

Ion Sources
- Automatic equipment for electrolyzing heavy water, Ralph W. Waniek—262(L)

Laboratory Techniques
- Automatic equipment for electrolyzing heavy water, Ralph W. Waniek—262(L)
- High resolution recording with soot, K. R. Eldredge—199
- Improved method of directing liquid flow in a closed system, L. G. Stang, Jr. and G. J. Selvin—97(L)
- Liquid air level control, Mark S. Fred and Everett G. Rauh—258(L)
- Low temperature gasket, A. Wexler, W. S. Corak, and G. T. Cunningham—259(L)
- Making small metal tubes by electrodeposition on Nylon fibers, R. J. E. Gezelius—886(L)
- Method of making glass-metal seals, N. A. Eckstein, J. W. Fitzgerald, and C. A. Boyd—398(L)
- Packless valve flow regulator, Walter Rose—772(L)
- Positive displacement pump for corrosive fluids, E. E. Glenn, Jr. and Norman Hackerman—148
- Preparation of unbacked metallic films, F. E. Carpenter and J. A. Curcio—675(L)
- Remote-control method of opening ampoules of active materials, Jesse E. Sherwood—570(L)
- Rubber tubing pump, John W. Weigl and Donald W. Stallings—395(L)
- Simple low power electronic relay, William P. Ratchford and M. L. Fein—188(L)
- Simple method to seal liquids of high vapor pressure into glass or quartz capillaries, Z. V. Harvalik—260(L)
- Stainless steel micro-needle electrodes made by electrolytic pointing, Harry Grundfest, Robert W. Sengstaken, Walter H. Oettinger, and R. W. Gurry—360
- Test of rupture strength of thin plastic films, Joses J. L. Chen—491(L)
- Volumetric displacement flask, S. D. Snyder, C. J. Craven, and D. B. Trauger—887(L)
- Waterproof cable connectors, K. Feldman—812(L)
- Water-proofing rocksalt for infra-red absorption cells, Scott Anderson, William J. Anderson, and Martin Krakowski—574(L)

Light and Radiation Sources
- High intensity ultraviolet continuum source for use in spectrophotometry, Nisson A. Finkelstein—509
- Improved electrode cutter for spectrographic laboratories, Esther W. Claffy and Joseph G. Schumacher—575(L)
- Power supply for the Cenco concentrated-arc lamp, James M. Mitchell—497(L)

Low Temperature Technique
- Automatic level controller for liquid nitrogen, E. H. Quinnel and A. H. Futch—400(L)
- Design and operation of liquid nitrogen-cooled solenoid magnets, James J. Fritz and Herrick L. Johnston—416
- Design and performance of a Joule-Kelvin helium liquefier, J. G. Dash, D. B Cook, M. W. Zemansky, and H. A. Boorse—936
- Float for liquid helium, Julius Babiskin—941
- Further techniques in single-crystal x-ray diffraction studies at low temperatures, S. C. Abrahams, R. L. Collin, W. N. Lipscomb, and T. B. Reed—396(L)
- High-low temperature microscope stage, R. E. Cech—747
- Liquid air level control, Mark S. Fred and Everett G. Rauh—258(L)
- Low temperature gasket, A. Wexler, W. S. Corak, and G. T. Cunningham—259(L)
- Low temperature x-ray diffraction apparatus, Donald F. Clifton—339
- Metal Dewar for liquid helium, Warren E. Henry and Richard L. Dolecek—496(L)
- Resistance-temperature relation for low temperature thermometry, Harold J. Hoge—815(L)
- Transfer device for low boiling liquids, Aaron Wexler and William S. Corak—583

Luminescence
- Calcium and cadmium tungstate as scintillation counter crystals for gamma-ray detection, R. H. Gillette—294
- Duration of scintillations from organic phosphors, J. O. Elliot, S. H. Liebson, R. D. Myers, and C. F. Ravilious—631
- Energy dependence of the naphthalene scintillation detector, Jack C. Smeltzer—669(L)

Magnetism
- Design and operation of liquid nitrogen-cooled solenoid magnets, James J. Fritz and Herrick L. Johnston—416
- Focusing properties of a generalized magnetic spectrometer, David L. Judd—213
- Magnetic suspension for small rotors, J. W. Beams—182
- Measurement of the magnetic field in a nuclear spectrometer, L M. Langer and F. R. Scott—522
- New method for the measurement of inhomogeneous magnetic fields, Peter M. Weinzierl—492(L)
- Null-coil pendulum magnetometer, C. A. Domenicali—327
- Pulsed air core series disk generator for production of high magnetic fields, R. I. Strough and E. F. Shrader—575(L)

Magnetism (continued)
  Radiofrequency spectrograph and simple magnetic-field meter, R. V. Pound and W. D. Knight—219
  Recording fluxmeter of high accuracy and sensitivity, P. P. Cioffi—624
  Recording torque magnetometer, D. S. Miller—605
  Small milligaussmeter, G. D. Adams, R. W. Dressel, and F. E. Towsley—69
Mass Spectrograph and Mass Spectrometer
  Convenient gas sample tube holder and break-off applicable to mass spectrometers, Frederick Highhouse and Julius White—101(L)
  Gas flow through the mass spectrometer viscous leak, R. E. Halsted and A. O. Nier—1019
  Improvements in mass spectrometers for the measurement of small differences in isotope abundance ratios, C. J. McKinney, J. M. McCrea, S. Epstein, H. A. Allen, and H. C. Urey—724
  Large Dempster-type double-focusing mass spectrograph, Henry E. Duckworth—54
  Mass indicator, V. J. Caldecourt—772
  New type mass spectrometer, Larkin Kerwin—96(L)
  Scintillation-type ion detector, Paul I. Richards and E. E. Hays—99(L)
Mechanics
  Apparatus for rapid measurement of internal friction, Herbert I. Fusfeld—612
  Comments on "Velocity-acceleration response from a seismic pick-up via controlled damping," A. J. Hermont—675(L)
  Tungsten helical spring balance, Samuel L. Madorsky—393(L)
  Velocity-acceleration response from a seismic pick-up via controlled damping, Robert J. Jeffries—115
Micro Manipulation
  Design of a simple microflowmeter for biological perfusion experiments, A. C. Burton and J. T. Nichol—485
  Microtome specimen holder advanced by thermal expansion—M. Eden, A. W. Pratt, and H. Kahler—802
  Volumetric plastic micro respirometer—P. F. Scholander—378
Microwave Spectroscopy
  Design and construction of a Stark-modulation microwave spectrograph, A. Harry Sharbaugh—120
  Frequency meter for microwave spectroscopy, John D. Rogers, Henry L. Cox, and Paul G. Braunschweiger—1014
  Stark effect absorption cells for microwave spectroscopy, D. H. Baird, R. M. Fristrom, and M. H. Sirvetz—881(L)
Microwave Techniques
  Apparatus for recording fluctuations in the refractive index of the atmosphere at 3.2 centimeters wave-length, C. M. Crain—456
  Fabrication of a high power resonant wave-guide window, E. V. Edwards and K. Garoff—787
  Frequency meter for microwave spectroscopy—J. D. Rogers, H. L. Cox, and P. G. Braunschweiger—1014
  Microwave power stabilizer, Ivan K. Munson—622
  Recording microwave refractometer, George Birnbaum—169
Multiplier, Electron
  Device for measuring the high voltage for a photo-multiplier tube, Ingvar Nilsson—396(L)
  Photo-multiplier gamma-ray detector, J. D. Graves and G. E. Koch—304
  Ultraviolet photon counting with an electron multiplier, A. H. Morrish, G. W. Williams, and E. K. Darby—884(L)

New Instruments
  Aerolog wind recording system—193
  Air-cooled high vacuum pump—194
  All-purpose scaler—502
  Alpha-counter—193
  Analascope—776
  Audiomatic generator—197
  Bulb temperature pick-ups—942
  Cartesian manostat—266
  Chain pulse amplifier—676
  "CO-AX" very low capacitance cables and flexible feeders—196
  Data recording camera—1030
  D.c. integrator motor—403
  D.c. magnetic amplifier—192
  D.c. power supply—192
  Dew point indicators—774
  Differential pressure switch—1030
  Diffusion pump—196
  Diode modulator for video frequencies—579
  Earth resistivity apparatus—403
  Electrically controlled camera—820
  Electron-diffraction camera—890
  Electronic blackboard—268
  Electronic flowmeter—889
  Electron microscope—576
  Electrostatic generator—578
  Exposure photometer—775
  Film tape sound recorder—105
  F-m generator—265
  F-m signal generator and amplitude modulator—403
  Frequency standard—818
  Gamma-survey meter—192
  Gas flow counter—773
  Ground resistance—820
  H-42 strainalyzer—502
  Improved RCA-1P21 multiplier photo-tube—105
  Improved ultra-sensitive d.c. amplifier—401
  Industrial electron tubes—194
  Industrial Rouy-Photrometer—402
  Industrial television—501
  "Infinite life" counters—196
  Infra-red detector—817
  Infra-red spectrophotometer—503
  Interference cooler filter—401
  Ionization gauge—502
  Labmarkers—195
  Laboratory coating unit—888
  Logarithmic attenuator—404
  Manufacturers' literature—106, 197, 268, 405, 504, 580, 679, 776, 821, 891, 1031
  Metallograph—1031
  Michelson interferometer—820
  Micro burette—818
  Micro manometer—580
  Micromanometer—941
  Microphotometer—265
  Micro-photometer—819
  Microvoltmeter—1030
  Microwave signal sources—677
  Miniature seismograph—501
  Miniature speed changes—404
  Mini-chopper—576
  Model F-1 oscillograph—404
  Model On-5 oscillosynchroscope—678
  New gamma-ray detector—677
  New stabilized d.c. indicating amplifier—774
  Nuclear fluxmeter—942
  Oscillograph—103
  Oscillo-tracer—677
  Oscilloscope camera—890
  Photographic exposure computer—819
  Platinum thermometer—819
  Power level indicator—887

Pressuregraph—775
Principal stain computer—675
"Printed-circuit" TV tuner—577
Projection-microphotometer—678
Proportional counters—194
Pulse generator—501
Pulse rise time indicator—503
Radiation monitor—818
R-F mass spectrometer tube—888
"Ruggedized" electrical instruments—267
Shaker—1029
Spectrograph and excitation unit—773
Spectrophotometer—264
Spectrum analyzer—503
Spring motor—888
Square wave generator—265
Subminiature electrometer type CK5889—577
Super-brilliant light source—105
Synchronous camera—268
Temperature control—579
Temperature pick-up—106
Thermocouple and ionization type vacuum gauge—402
A Three-stage non-magnetic mass spectrometer—578
Torque motor—1029
2000-MPH timing equipment—889
TV amplifier—267
Ultra-low frequency oscillator—401
Ultra low frequency oscillator—677
Ultra-sensitive d.c. current measuring device—579
Ultrasonic equipment—103
Ultrasonic generator—104
Ultrasonic soldering iron—195
Universal monochromator—104
Vacuum fusion apparatus—266
Vacuum gauge—105
Vacuum gauge—195
Variable electronic filter—196
Variable electronic filter—776
Variplotter—402
Ventilation meter—818
Versatile photo-micrographic apparatus—676
VHF signal generator—504
Volometer—193
Zeiss instruments—1031

New Materials

Abrasion-resistant plastic—892
Aluminum-silicone paint—679
Aluminum thermal insulation—406
Aluminum wire—680
Carbide marking pencil—822
Cellulose acetate cement—198
Centrifugal bronze castings—107
Chemical developments—778
Coated safety lenses—778
Coated tubing—777
Coaxial cable—777
Conducting rubber vee-belts—198
Copying film—198
Core material—198
Decontamination—892
Degreaser—680
Diamond abrasive kit—822
Electrosensitive recording paper—269
Flame retardant insulation—822
Flashlight battery—680
Flaw detection—892
Flexible stainless tubing—270
Fluoride lens coating—107
Fluorocarbon plastic—582
Fluoro carbons—778
Front-surface mirrors—892
Glass bearings—778
Glass building blocks—406
Glass orifice plates—506
Heat insulation—582
Heat-resistant steel castings—777
High speed hacksaw blade—680
Heat treating material—582
Hydrophobic starch—270
Insulating screws—944
Interlocking lead bricks—506
Knitted metal—581
Laboratory aids—680
Lead-glass fabric—944
Low expansion steel—892
Mercury battery—582
Mercury filter—405
Metal-ceramic materials—680
Metal cleaning sponge—892
Mildew preventive—944
Molding compound—582
Molybdenum lubricant—269
New organosilicons—107
Nickel-clad copper—505
Non-crazing plastic—944
Nuclear track emulsions—506
Nylon thread-lock plug—270
Oil-proof flexible conduit—582
Optical quartz—891
Permanent magnets—822
Pipe insulation—198
Plastic bonding agent—944
Plastic lenses—943
Plastic packing—892
Plastic products—822
Porous bearing—581
Porous bronze—944
Powdered stainless steel—581
Precision casting alloy—107
Printed circuits—198
Protective tape—582
Radiant glass panels—892
Rolled gold plate—506
Rust inhibitor—198
Rust preventive—107
Sapphire gauge points—270
Sealing rings—943
Self-adhesive marking tape—943
Silicone molding compound—679
Silicone rubber—506
Silicone rubber sponge and shock mounts—680
Silicone sealing compound—270
Silicone-treated paper—582
Silver storage battery—270
Solder alloys—680
Stainless steel—581
Static elimination—822
Static eliminator—778
Strippers for organic finishes—944
Surface-active chemical—198
Synthetic mica—406
Teflon applications—679
Teflon gaskets—406
Teflon rods and tubes—506
Teflon tape—506
Vibration isolation—892
Vibration isolator—582
Vinyl insulation—944
Vacuum pump fluid—506
Welding glass—680
Woven glass fabric—198
Zirconium in surgery—821

Non-linear elements
- Thermistors, Part I. Static characteristics, Otto J. M. Smith—344
- ——, Part II. Dynamic characteristics, Otto J. M. Smith—351

Nuclear Machines
- *Betatrons*
  - 80-Mev model of a 300-Mev betatron, D. W. Kerst, G. D. Adams, H. W. Koch, and C. S. Robinson—462
  - Ejection of the electron beam from a betatron—S. L. Fawcett and E. C. Crittenden, Jr.—935(L)
  - Orbit-bender to assist injection into betatrons, Leverett Davis, Jr.—971
- *Cyclotrons and Synchrotrons*
  - Design study for a three-Bev proton accelerator, M. S. Livingston, J. P. Blewett, G. K. Green, and L. J. Haworth—7
  - Focusing device for the external 350-Mev proton beam of the 184-inch cyclotron at Berkeley, W. K. H. Panofsky and W. R. Baker—445
  - Synchrotron-oscillation resonance, N. M. Blachman—908
  - Synchrotron radiofrequency system, M. H. Dazey, J. V. Franck, A. C. Helmholz, C. S. Nunan, and J. M. Peterson—436
  - Theory of the capture process in a betatron-injected synchrotron, D. C. dePackh and M. Birnbaum—451
- *Linear Accelerators*
  - 500-kilovolt linear accelerator using selenium rectfiers, Wayne R. Arnold—796

Nuclear Technique
- Apparatus for concentration of He^3 by thermal diffusion, O. F. Schuette, Jr., A. Zucker, and W. W. Watson—1016
- Background eradication in thick-layered nuclear emulsions, Martin Wiener and Herman Yagoda—39
- Beta-ray spectroscopes, E. Persico and C. Geoffrion—945
- Chalk River single crystal neutron spectrometer, D. G. Hurst, A. J. Pressesky, and P. R. Tunnicliffe—705
- Construction and performance of a multiple gamma-ray counter of high efficiency, Tibor Gráf—285
- Design of a magnetic focusing coincidence spectrometer, C. M. Fowler and R. G. Shreffler—740
- Design of neutron counters using multiple detecting layers, R. D. Lowde—835
- Electron pair spectrometer of lens type for hard gamma-radiation, Kai Siegbahn and Stig Johansson—442
- Electrostatic beta-spectrograph, D. R. Hamilton and L. Gross—912
- Gas phase counting of low energy beta-emitters, W. Bernstein and R. Ballentine—158
- Improvements in the Li^6 technique, G. R. Keepin, Jr.—933(L)
- Magnetic analyzer for charged-particles from nuclear reactions, C. W. Snyder, S. Rubin, W. A. Fowler, and C. C. Lauritsen—852
- Measurement of fast neutron energies by observation of $Li^6(n,\alpha)H^3$ in photographic emulsions, George R. Keepin, Jr., and James H. Roberts—163
- Microcalorimeter suitable for study of easily absorbed nuclear radiations, C. V. Cannon and G. H. Jenks—236
- Note on reduction of background fog in nuclear emulsion plates, P. K. S. Wang—816(L)
- Nuclear emulsions and the measurement of low energy neutron spectra—N. Nereson and F. Reines—534
- On the use of photographic plate detectors in neutron experiments, J. C. Allred, A. N. Phillips, L. Rosen, and F. K. Tallmadge—225
- Photographic methods of measuring slow neutron intensities, M. Blau, I. W. Rudarman, and J. Czechowski—232
- Photo-multiplier gamma-ray detector, J. D. Graves and G. E. Koch—304
- Preparation of carbon targets, G. C. Phillips and J. E. Richardson—885(L)
- Scintillation counter as a low resolution gamma-ray spectrometer, Robert W. Pringle, Kenneth I. Roulston, and Harry W. Taylor—216
- Scintillation counter for neutrons, Kuan-Han Sun and W. E. Shoupp—395(L)
- Scintillation-type in detector, Paul I. Richards and E. E. Hays—99(L)
- Semi-automatic device for analyzing events in nuclear emulsions, Marietta Blau, Robert Rudin, and Seymour Lindenbaum—978
- Slide rule for nuclear emulsion calculations, Arthur Beiser—933(L)
- Variation of grain density with temperature of exposure in nuclear emulsions, Elsie M. Dollmann—118
- Varying nuclear emulsion sensitivity with altitude, Arthur Beiser—1025(L)

Optical Instruments
- High-low temperature microscope stage, R. E. Cech—747
- Improved Schlieren apparatus employing multiple slit-gratings, Tage A. Mortensen—3
- Lens tester for photographic lenses, F. G. Back—722
- Microtome knife sharpness, Oscar W. Richards—670(L)
- Multiple Kerr-cell camera, A. M. Zarem and F. R. Marshall 514
- Optical centering system for x-ray diffraction samples, Eugene L. Perrine—262(L)
- Precision Faraday effect apparatus, Samuel Steingiser, George J. Rosenblit, Robert Custer, and Charles E. Waring—109
- Recording polarimeter, Gabor B. Levy, Philip Schwed, and David Fergus—693
- Reprojection method for studying cloud-chamber photographs, D. A. Bromley and R. D. Bradfield—190(L)
- Simple automatic recording microphotometer, R. M. Fisher and D. S. Miller—938(L)
- Tests of flowing junction diffusion cells with interference methods, L. G. Longsworth—524

Oscilloscopes
- High speed synchroscope, G. G. Kelley—71

Photography
- Background eradication in thick-layered nuclear emulsions, Martin Wiener and Herman Yagoda—39
- Dust electricity analyzer—W. B. Kunkel and J. W. Hansen—308
- High resolution recording with soot, K. R. Eldredge, 199
- Measurement of fast neutron energies by observation of $Li^6(n,\alpha)H^3$ in photographic emulsions, George R. Keepin, Jr., and James H. Roberts—163
- Multiple Kerr-cell camera, A. M. Zarem and F. R. Marshall—514
- Note on reduction of background fog in nuclear emulsion plates, P. K. S. Wang—816(L)
- Nuclear emulsions and the measurement of low energy neutron spectra, N. Nereson and F. Reines—534
- On the use of photographic plate detectors in neutron experiments, J. C. Allred, A. N. Phillips, L. Rosen, and F. K. Tallmadge—225
- 100,000,000-frame-per-second camera, M. Sultanoff[illegible]
- Photographic methods of measuring slow neutron in[illegible]ties, M. Blau, I. W. Ruderman, and [illegible]
- Semi-automatic device for analyzing [illegible] sions, Marietta Blau, Robert Ru[illegible] denbaum—978
- Simultaneous photography of self-luminous and non-self-luminous effects, J. S. Rinehart—939
- Slide rule for nuclear emulsion calculations, Arthur Beiser—933(L)

Spectral sensitivity of two commercial x-ray films between 0.2 and 2.5 angstroms, Herman E. Seemann—314
Variation of grain density with temperature of exposure in nuclear emulsions, Elsie M. Dollmann—118
Varying nuclear emulsion sensitivity with altitude, Arthur Beiser—1025(L)

Photometry
Circumferential recording microphotometer, T. C. O'Connell and A. G. Barkow—573(L)

Piezoelectricity
Design and use of piezoelectric gauges for measurement of large transient pressures, A. B. Arons and R. H. Cole—31

Polarimetry
Polarimeter for the study of low frequency radio echoes, A. H. Benner and H. J. Nearhoof—830

Potentiometers
Electron tube potentiometer method for use in circuits involving very high resistance, H. Bloom and G. W. Butler—274

Pressure Measurement and Technique
All-metal ionization gauge, F. M. Kelly—673(L)
Design and use of piezoelectric gauges for measurement of large transient pressures, A. B. Arons and R. H. Cole—31
Diamond bomb for obtaining powder pictures at high pressures, A. W. Lawson and Ting-Yuan Tang—815(L)
Extension of the low pressure range of the ionization gauge, R. T. Bayard and D. Alpert—571(L)
Frequency modulation pressure recording system, J. H. Hett and R. W. King, Jr.—150
High pressure fitting for scintillation counting, K. D. Timmerhaus, E. B. Giller, L. H. Tung, R. B. Duffield, and H. G. Drickamer—261(L)
Investigation of the possible use of the glow discharge as a means for measuring air flow characteristics, F. D. Werner—61
Manometer leveling procedure, John E. Wertz—263(L)
New vacuum gauge, R. Havens, R. Koll, and H. LaGow—596
Rotary McLeod gauge, M. Axelbank—511
Simple method to seal liquids of high vapor pressure into glass or quartz capillaries, Z. V. Harvalik—260(L)
Simple pressure balance, C. A. Swenson—22
Simple recording manometer, Fraser P. Price and Paul D. Zemany—261(L)
Ultra-high vacuum ionization manometer, J. J. Lander—672(L)
Versatile pneumatic instrument based on critical flow, W. A. Wildhack—25

Radiation and Radiometry
Automatic isodose recorder with scintillation counter as gamma-ray detector, G. J. Hine, M. Berman, and M. M. Elkind—362
Energy dependence of the naphthalene scintillation detector, Jack C. Smeltzer—669(L)
4π-radiometer, T. Benzinger and C. Kitzinger—599
Series parallel linear thermopile with interchangeable receiving units, Robert A. Crane and Francis E. Blacet—259(L)

Radioactive Techniques
[illegible] determination of the mission rate of beta-rays, [illegible] K. Clark—753
[illegible]ratus and method for testing radium or thorium cap[illegible]le—400(L)
[illegible] compounds in paper chromatography, I. Gray, [illegible]keda, A. Benson, and D. Kritchevsky—1022
End and wall corrections for absolute beta-counting in gas counters, A. G. Engelkemeir and W. F. Libby—550
RaDEF standard sources for beta-disintegration rate determinations, Theodore B. Novey—280
Scintillation type alpha-particle detector, A. S. Goldin, E. R. Rohrer, and R. L. Macklin—554
System for the collection and purification of radon by remote control, Chester H. Shiflett, Mark E. Steidlitz, and Wallace Davis, Jr.—842
Transmission of beta-rays by Nylon and Formvar, R. B. Heller, E. F. Sturcken, and A. H. Weber—898
Units of radioactivity, L. F. Curtiss, R. D. Evans, Warren Johnson, and Glenn T. Seaborg—94(L)

Refraction and Refractometry
Apparatus for recording fluctuations in the refractive index of the atmosphere at 3.2 centimeters wave-length, C. M. Crain—456
Tests of flowing junction diffusion cells with interference methods, L. G. Longsworth—524

Secondary Emission
Measurement of secondary electron emission from dielectric surfaces, Howard L. Heydt—639

Seismology and Seismographs
Comments on "Velocity-acceleration response from a seismic pick-up via controlled damping," A. J. Hermont—675(L)
Velocity-acceleration response from a seismic pick-up via controlled damping, Robert J. Jeffries—115

Servo Mechanisms
Electronic recording analytical balance, Idas W. Lohmann—999
Microwave power stabilizer, Ivan K. Munson—622
Recording polarimeter, Gabor B. Levy, Philip Schwed, and David Fergus—693
Regulated low voltage power supply, A. K. Solomon—570(L)
Voltage stabilizer for 200-Kv acceleration, J. T. Dewan—771(L)

Shop Technique
Apparatus for cutting metals strain-free, Robert Maddin and W. R. Asher—881(L)
Improved electrode cutter for spectrographic laboratories, Esther W. Claffy and Joseph G. Schumacher—575(L)

Spectroscopy and Spectrometer Technique
Design and construction of a Stark-modulation microwave spectrograph, A. Harry Sharbaugh—120
Simple variable space infra-red absorption cell, John U. White—629

Thermal Diffusion
Apparatus for concentration of He^3 by thermal diffusion, O. F. Schuette, Jr., A. Zucker, and W. W. Watson—1016

Thermodynamics
Convenient cell-stage for fluid profile measurements, William Fox—499(L)
Design and performance of a Joule-Kelvin helium liquefier, J. G. Dash, D. B. Cook, M. W. Zemansky, and H. A. Boorse—936(L)
Method for measuring the thermal conductivity of small samples of poorly conducting materials such as optical crystals, Stanley S. Ballard, Kathryn A. McCarthy, and William C. Davis—905
Microcalorimeter suitable for study of easily absorbed nuclear radiations, C. V. Cannon and G. H. Jenks—236

Thermoelectricity and Thermal Properties of Matter
New method for surface-temperature measurement, Nobuji Sasaki—1
Series parallel linear thermopile with interchangeable receiving units, Robert A. Crane and Francis E. Blacet—259(L)

Thermometry and Temperature Control
Electrical resistance of platinum at high temperatures, H. E. Bennett—1029

Thermometry and Temperature Control (continued)
New method for surface-temperature measurement, Nobuji Sasaki—1
Precision thermostat for high temperatures, William R. Eubank—845
Rapid method for calculating and using platinum thermohm tables, R. A. Buerschaper—996
Resistance-temperature relation for low temperature thermometry, Harold J. Hoge—815(L)
Technical apparatus for determining thermal conductivity of steels up to 500°C, Z. Horak and F. Krupka—827
Temperature-controlled resistance furnace for high temperature measurements, W. G. Schneider and N. R. S. Hollies—94(L)
Vacuum furnace for use in the temperature range 1000–2000°C, J. W. Tomlinson and J. O'M. Bockris—507
Versatile pneumatic instrument based on critical flow, W. A. Wildhack—25
Vortex thermometer for measuring true air temperatures and true air speeds in flight, Bernard Vonnegut—136

Time measurement
High speed short resolving time coincidence circuit for use with scintillation counters—E. F. Shrader—883(L)
Improved resolving time measuring device, B. W. Roberts, Jr., K. E. Perry, and R. G. Fluharty—790
Multiple Kerr-cell camera, A. M. Zarem and F. R. Marshall—514
Nomogram for G-M counter resolving-time corrections, Howard L. Andrews—191(L)
Note on the detection of coincidences and short time intervals, Robert Hofstadter and John A. McIntyre—52
100,000,000-frame-per-second camera, M. Sultanoff—653
Some properties of the parallel plate spark counter. II, Leon Madansky and R. W. Pidd—407
Time lags in Geiger counters, Arthur R. Laufer—244
Useful fast coincidence circuit, R. L. Garwin—569(L)
Wire recorded magnetic pulse timing circuit, C. R. Emigh—142

Ultrasonics
Ultrasonic projector design for a wide range of research applications, E J. Fry—940(L)
Ultrasonic tissue disintegrator, F. F. Bird and K. S. Lion—189(L)

Vacuum Technique
All-metal ionization gauge, F. M. Kelly—673(L)
Convenient leak for testing helium leak detectors, G. H. Jenks—674(L)
Data on porcelain rod leak, J. P. Molnar and C. D. Hartman—394(L)
Degassing extended glass systems, Albert B. Stewart—258(L)
Effective vacuum cut-off, G. W. Sears and E. R. Hopke—570(L)
Extension of the low pressure range of the ionization gauge, R. T. Bayard and D. Alpert—571(L)
Glass variable microleaks for gases, John J. Hopfield—671(L)
Method of making glass-metal seals, N. A. Eckstein, J. W. Fitzgerald, and C. A. Boyd—398(L)
Motion within a vacuum system, Fred A. McNally—813(L)
Motor for use in vacuum systems, C. P. Butler and F. E. Carpenter—103(L)
New Pirani-type vacuum gauge, E. Blasco and L. Miranda—494(L)
New porcelain rod leak, H. D. Hagstrum and H. W. Weinhart—394(L)
New vacuum gauge, R. Havens, R. Koll, and H. LaGow—596
Reliable Pirani vacuum safety circuit, W. Franzen and J. Horton—935(L)
Rotary McLeod gauge, M. Axelbank—511
Suppressing mercury vapor in vacuum systems, Frederic Ayer, II—496(L)
Ultra-high vacuum ionization manometer, J. J. Lander—672(L)
Vacuum furnace for use in the temperature range 100 2000°C, J. W. Tomlinson and J. O'M. Bockris—507
Vacuum tests of rubber, lead, and Teflon gaskets and vin acetate joints, Robert W. Cloud and Sanborn F. Philp—731

X-Ray Diffraction
Bent crystal x-ray monochromators, B. E. Warren—102(L
Circumferential recording microphotometer, T. C. O'Connell and A. G. Barkow—573(L)
Combination two-circle goniometer and x-ray spectrometer, M. L. Baron and A. deBretteville, Jr.—458
Diamond bomb for obtaining powder pictures at high pressures, A. W. Lawson and Ting-Yuan Tang—815(L)
Further techniques in single-crystal x-ray diffraction stud at low temperatures, S. C. Abrahams, R. L. Collin, W. Lipscomb, and T. B. Reed—396(L)
Improved double-crystal spectrometer for small an scattering measurements, Leo Broussard—399(L)
Note on crystal suitable for double crystal x-ray spectroscopy in the region 3 to 15A, S. T. Stephenson and D. L. Martin—1023(L)
On adapting a powder x-ray diffraction camera for reflection patterns, Jonathan Parsons—185
Optical centering system for x-ray diffraction samples, Eugene L. Perrine—262(L)
Point-focus x-ray monochromators for low angle diffraction, Jesse W. M. DuMond—188(L)
Rotating specimen mount for use with x-ray spectrometer in measuring crystallite orientation of cellulosic and other textile fibers, L. Segal, J. J. Creely, and C. M. Conrad—431
X-ray determination of slip planes and slip directions, R. W. Turner, T. L. Wu, and R. Smoluchowski—440

X-Ray Equipment and Technique
Method for increasing the safe power input of x-ray tubes, Arthur I. Berman—275
Spectral sensitivity of two commercial x-ray films between 0.2 and 2.5 angstroms, Herman E. Seemann—314

I.A.R.I. 75

INDIAN AGRICULTURAL RESEARCH
INSTITUTE LIBRARY, NEW DELHI.

Date of Issue	Date of Issue	Date of Issue
23.12.63.		
30.7.64		
19.7.65		
22.11.65		
4.9.70		

GIPNLK—H-40 I.A.R.I.—29-4-55—15,000